Franco Pirajno



Hydrothermal Processes and Mineral Systems

Springer

Hydrothermal Processes and Mineral Systems

Hydrothermal Processes and Mineral Systems

Franco Pirajno
Geological Survey of Western Australia, Perth, WA, Australia

Foreword by Peter A. Cawood

Springer
Geological Survey of Western Australia

Franco Pirajno
Geological Survey of Western Australia
100 Plain St.
East Perth WA 6004
Australia
franco.pirajno@doir.wa.gov.au

ISBN: 978-1-4020-8612-0 e-ISBN: 978-1-4020-8613-7

Library of Congress Control Number: 2008933283

© Springer Science+Business Media B.V. 2009
No part of this work may be reproduced, stored in a retrieval system, or transmitted
in any form or by any means, electronic, mechanical, photocopying, microfilming, recording
or otherwise, without written permission from the Publisher, with the exception
of any material supplied specifically for the purpose of being entered
and executed on a computer system, for exclusive use by the purchaser of the work.

Cover illustration: Fig. 3.1 in this book. Figure designed and produced by Murray C. Jones.

Printed on acid-free paper

9 8 7 6 5 4 3 2 1

springer.com

To my wife

Foreword

The Earth is a complex and dynamic system that over 4.5 billion years has evolved to form the environment we live in and the resources we depend on. Franco Pirajno's book "Hydrothermal Processes and Mineral Systems" provides an authoritative and comprehensive overview of hyrdrothermally controlled major mineral resources that have developed in this dynamic system, and where appropriate their links with the development of life and extraterrestrial hydrothermal systems.

Discovery and recovery of mineral resources are fundamental to sustaining human society. Yet the discovery of world-class to giant mineral deposits has declined alarmingly over the last few decades. It is only through a comprehensive understanding of current systems that we can hope to find future deposits. This book provides an unparalleled overview of the principal features of the major mineral systems and the role of fluid circulation in their development, including: the variety of water sources that participate in hydrothermal circulation systems (Chapter 1), the alteration patterns associated with hydrothermal circulation in selected mineral systems (Chapter 2), the link with tectonic settings and interaction between the lithosphere, hydrosphere and biosphere (Chapter 3), the major mineral system types including intrusion-related (Chapter 4), porphyry and epithermal, skarn (Chapter 5), sedimentary exhalative (SEDEX) Mississippi valley-type (MVT)(Chapter 6), submarine (Chapters 7 and 8), amagmatic and other hydrothermal systems (Chapter 9) and uranium systems (Chapter 13). The book also looks the interrelationship between hydrothermal systems and life, detailing the ecosystems that develop (Chapter 10), the hydrothermal systems driven by the thermal energy from meteorite impacts (Chapter 11) and possible hydrothermal systems on other planets in the solar system (Chapter, 12). This is truly a comprehensive treatment of hydrothermal processes and mineral systems.

Franco Pirajno commenced his academic studies in his native Italy where he obtained a Doctorate in Geological Sciences from the Vesuvius Volcano Observatory of Federico II University in Naples. He has had a diverse career in industry, government and academia that included 19 years in mineral exploration with the Anglo-American Corporation of South Africa, the Chair of Economic Geology at Rhodes University, South Africa, and since 1993, the Geological Survey of Western Australia. He has held visiting professorships at

Peking University and China University of Geosciences and currently has honorary appointments at the Astrobiology Centre, University of New South Wales, Sydney, and the China University of Geosciences, Beijing. Franco Pirajno is the author of two books, authored or co-authored a monograph and more than 100 peer-reviewed papers and 19 geological maps in Western Australia, Namibia and Greenland. Throughout his career, which has included work in Europe, southern Africa, South East Asia, New Zealand, the southwest Pacific, China, Greenland and Australia, he has integrated experience in tectonics, ore deposit geology and mineral exploration. It is this wealth of firsthand experience, including the little known mineral systems in China, which Franco Pirajno weaves with a distillation of relevant literature into his comprehensive overview of "Hydrothermal Processes and Mineral Systems".

The University of Western Australia, Perth Peter A. Cawood
May 2008

Acknowledgments

I owe a debt of gratitude to several colleagues and friends. In no special order I thank Martin Van Kranendonk of the Geological Survey of Western Australia (GSWA) for stimulating discussions and for reviewing Chapter 10; other reviewers included Peter Cawood of the University of Western Australia (Chapter 5), Richard Langford (GSWA; Chapters 1 and 6), Doug Kirwin (Ivanhoe Mines; Chapter 4); Simon Johnson (GSWA; Chapter 13). Murray Jones, Arthur Hoffman, Michael Prause and Dellys Sutton (all with GSWA) drafted the figures; Murray and Arthur gave their time even when under pressure for other jobs. Nell Stoyanoff (GSWA) typed most of the tables, especially the complex ones. Jean Johnston and Chris Hocking performed the unenviable task of editing the references. Brian Knyn and Eunice Cheung (Department of Industry and Resources library) managed to meet with my never-ending appetite for books and papers, often at short notice. Tim Griffin, Executive Director of GSWA, supported the writing of this book, and on behalf of GSWA funded the cost of colour figures. I thank my Chinese friends and colleagues for their hospitality and support for the numerous field trips in China and their patience with the idiosyncrasies of a Westerner: Chen Yanjing (Peking University), Mao Jingwen (Institute of Mineral Resources, Chinese Academy of Geological Sciences, Beijing), Zhang Shihong and Han Higuy (China University of Geosciences, Beijing), Xiao Long (China University of Geosciences, Wuhan).

Once again, I dedicate this book to my wife and lifelong companion, unwavering in her support, even when faced with harsh conditions in the field, abroad and in outback Australia.

Contents

1 Water and Hydrothermal Fluids on Earth 1
1.1 Introduction 1
1.2 Origin of Water; Sea and Surface Waters 5
1.2.1 Seawater. 9
1.2.2 Surface Water 13
1.2.3 Groundwater 15
1.3 Structure and Properties of Water; Hydration and Hydrolysis . 17
1.4 Hydrothermal Fluids 18
1.4.1 Solubility and Boiling 22
1.4.2 Acid-Base Nomenclature. 23
1.4.3 Redox Potential. 24
1.4.4 Chemical Potential, Chemical Activity, Fugacity, Oxygen Fugacity. 26
1.4.5 Hot Springs 30
1.4.6 Fluid Inclusions. 38
1.4.7 Dissolved Constituents and Metals Partitioning in Hydrothermal Solutions 42
1.4.8 The Role of Complex Ions and Ligands in Hydrothermal Fluids. 44
1.4.9 Complex Ions in Hydrothermal Solutions 47
1.4.10 Precipitation of Solutes and Metal Deposition. 50
1.4.11 Isotopic Tracers. 51
1.5 Concluding Remarks 64
References 65

2 Hydrothermal Processes and Wall Rock Alteration 73
2.1 Introduction 73
2.1.1 The Main Components of a Hydrothermal System 74
2.1.2 Magma Degassing and Magmatic Hydrothermal Systems 80
2.2 Role of Volatiles in Granitic Magmas 86
2.3 Hydrothermal Alteration 90
2.3.1 Hydrogen Ion Metasomatism (Hydrolytic Alteration) and Base Cation Exchange 91

2.3.2 Styles and Types of Hydrothermal Alteration 94
2.4 Intrusion-Related Alkali Metasomatism 104
2.4.1 Sodic Metasomatism and Albitites 104
2.4.2 Potassic Metasomatism and Microclinites 105
2.5 Alkali Metasomatism (Fenites) in Anorogenic Ring Complexes 106
2.5.1 Fenites 107
2.6 Alteration in Porphyry Systems 111
2.6.1 Lowell-Guilbert and Breccia Pipe Models 114
2.6.2 Diorite Model 117
2.6.3 Hydrothermal Alteration in Climax-Type Porphyry Mo Systems 117
2.7 Skarns 119
2.8 Alteration in Epithermal Systems 120
2.8.1 Siliceous Precipitates, Self-Sealing and Hydrothermal Breccias 122
2.9 Hydrothermal Alteration in Submarine Mineral Systems 124
2.9.1 Hydrothermal Alteration in Kuroko-Type Mineral Systems 125
2.9.2 Oceanic Crust Hydrothermal Metamorphism 126
2.10 Other Types of Alteration 131
2.10.1 Tourmalinisation 132
2.10.2 Serpentinisation and Talc-Carbonate Alteration 133
2.10.3 Hematitisation and Fe-Rich Alteration 135
2.10.4 Carbonatisation and Dolomitisation 136
2.11 Metamorphism of Hydrothermally Altered Rock 137
2.12 Geochemical Signatures and Isotopic Tracers 143
2.12.1 Geochemistry 143
2.12.2 Isotopic Tracers 151
2.13 Detection of Hydrothermal Alteration from Spectral Remote Sensing 153
2.14 Concluding Remarks 156
References 157

3 Tectonic Settings, Geodynamics and Temporal Evolution of Hydrothermal Mineral Systems 165
3.1 Introduction 165
3.2 Tectonic Settings and Geodynamics of Mineral Systems 166
3.2.1 Convergent Plate Boundaries; Arc and Back-Arc Settings, Collision Tectonics, ... 171
3.2.2 Divergent Plate Boundaries; Mid-Oceanic Ridges, Passive Margins and Continental Rifting 178
3.2.3 Mantle Plumes Tectonics and Hydrothermal Systems 187
3.3 Metallogeny and Geodynamics 188
3.4 Temporal Evolution of Ore Systems, Supercontinent Cycles and Global Metallogeny 192

3.5 Concluding Remarks 199
References 199

4 Intrusion-Related Hydrothermal Mineral Systems 205
4.1 Introduction 205
4.2 Intrusion-Related Hydrothermal Mineral Systems and Granitic Magmatism 207
4.3 Greisen Ore Systems 218
4.3.1 Greisenisation Processes 220
4.3.2 Geochemistry 227
4.3.3 Greisen-Style Mineral Systems 227
4.3.4 Sn and W Geochemistry in the Greisen System and Deposition of Cassiterite and Wolframite 228
4.3.5 Tin Deposits Associated with the Felsic Phase of the Bushveld Igneous Complex, South Africa 230
4.3.6 The Sn-W Deposits of Southwest England, Cornwall and Portugal 238
4.3.7 The Greisen Systems of the Tasman Fold Belt System . . 244
4.3.8 The East Kemptville Sn Greisen, Nova Scotia, Canada . 248
4.3.9 The Brandberg West Greisen Vein Systems, Namibia . . 250
4.3.10 The Kalguta Mo-W-Be-Bi Greisen System, Southeastern Altai (Russia) 258
4.4 Intrusion-Related Gold, Polymetallic and Uraniferous Vein Systems and Breccia Pipes 260
4.4.1 Scheelite Dome, an Intrusion-Related Au Deposit, Yukon, Canada 262
4.4.2 The Kidston Breccia Pipe, Queensland, Australia 269
4.4.3 Uraniferous Vein Systems 272
4.4.4 Sabie-Pilgrim's Rest, South Africa 273
4.4.5 Capricorn Orogen Structurally Controlled Hydrothermal Vein (Base and Precious Metals), Western Australia 275
4.4.6 Polymetallic Vein Systems of the Altai (Siberia) and Northwestern Mongolia (Yustid Rift Zone) 277
4.5 Hydrothermal Systems Associated with Alkaline Magmatism and Anorogenic Ring Complexes 280
4.5.1 Tectonic Settings, Ages and Controls of Intracontinental Alkaline Magmatism in Africa 283
4.5.2 Ore Systems of Alkaline Ring Complexes 285
4.6 Iron Oxide-Copper-Gold-Rare Earth Elements-Uranium Mineral Systems 306
4.6.1 Olympic Dam, South Australia 312
4.6.2 Vergenoeg Fe Oxides-Fluorite Deposit, South Africa . . 322
4.6.3 The Palabora Complex (South Africa) 326
4.6.4 Bayan Obo REE-Nb-Fe Deposit, Inner Mongolia, China 328

4.6.5 Candelaria, Punta Del Cobre District, Chilean Coastal Belt . . . 336
4.7 Concluding Remarks . . . 339
References . . . 340

5 Porphyry Systems; Fossil and Active Epithermal Systems . . . 355
5.1 Introduction . . . 355
5.2 Porphyry Systems . . . 356
5.2.1 Porphyry Systems of Convergent Margins . . . 367
5.2.2 Porphyry Systems in Intracontinental Extensional Tectonic Settings and Volcanic Rifted Margins . . . 390
5.2.3 The Oldest Porphyry Systems . . . 419
5.3 Fossil and Active Epithermal Systems . . . 422
5.3.1 Fossil Epithermal Systems . . . 426
5.3.2 Ladolam Epithermal System, Lihir Island, Papua New Guinea . . . 442
5.3.3 Hauraki Goldfield, Coromandel Peninsula, New Zealand 448
5.3.4 The Epithermal Systems of the Biga Peninsula, Northwestern Anatolia . . . 456
5.3.5 Epithermal Systems in the South China Fold Belt . . . 463
5.3.6 The El Indio-Pascua Wpithermal Belt, Chile . . . 475
5.3.7 Epithermal Systems in the Northern Great Basin, USA. 481
5.3.8 The Oldest Epithermal Systems, Archaean Pilbara and Yilgarn Cratons, Western Australia . . . 486
5.4 Active Epithermal Systems (Geothermal Fields) . . . 493
5.4.1 Kamchatka Peninsula and Kurile Islands . . . 497
5.4.2 Geothermal Systems of the Taupo Volcanic Zone, New Zealand . . . 500
5.4.3 Geysers-Clear Lake Geothermal System, California, USA . . . 505
5.4.4 The Yellowstone National Park Geothermal System, USA . . . 507
5.4.5 Salton Sea . . . 513
5.4.6 Lake Tanganyika . . . 515
5.5 Concluding Remarks . . . 516
References . . . 517

6 Skarn Systems . . . 535
6.1 Introduction . . . 535
6.2 Copper Skarns . . . 546
6.2.1 Bingham . . . 548
6.2.2 Yerington . . . 549
6.3 Sn-W and W Skarns . . . 550
6.3.1 Moina Sn-W Deposit . . . 551
6.3.2 King Island Scheelite Deposit . . . 552

6.4 Proterozoic W Skarns in the Gascoyne Complex, Western Australia . . . 553
6.5 Gold Skarns . . . 558
6.5.1 Navachab, Namibia . . . 560
6.5.2 Gold Skarns in China . . . 565
6.6 Zinc Skarns . . . 567
6.7 Molybdenum Skarns . . . 568
6.8 Iron Skarns . . . 569
6.9 Iron, Au, Cu-Mo Skarns in the Yangzte (Chiangjiang) River Valley, China . . . 570
6.10 The Geodynamic Setting of Skarn (and Porphyry) Metallogenesis in China . . . 573
6.11 Concluding Remarks . . . 576
References . . . 577

7 Submarine Hydrothermal Mineral Systems . . . 581
7.1 Introduction . . . 581
7.2 Physiography of the Ocean Floor . . . 583
7.2.1 Mid-Ocean Ridges . . . 584
7.2.2 Transform Faults and Fracture Zones . . . 586
7.2.3 Seamounts and Volcanic Chains . . . 588
7.3 Birth, Life and Death of an Ocean Basin . . . 589
7.4 Oceanic Lithosphere and Ophiolites . . . 592
7.4.1 Ophiolites . . . 596
7.5 Submarine Hydrothermal Systems: Spreading Centres, Island Arcs and Seamounts . . . 599
7.5.1 Hydrothermal Processes, Nature of Submarine Hydrothermal Fluids and Anatomy of a Seafloor Sulphide Deposit . . . 603
7.5.2 Hydrothermal Systems at Spreading Centres . . . 610
7.5.3 Subduction-Related Submarine Hydrothermal Systems (Island Arcs, Intraoceanic and Intracontinental Back-Arc Basins) . . . 632
7.6 Oceanic Crust-Related (Ophiolite) Hydrothermal Mineral Systems in the Geological Record . . . 649
7.6.1 Massive Sulphide Deposits of the Samail Ophiolite, Oman . . . 649
7.6.2 The Cu Deposits of Cyprus Island . . . 652
7.6.3 The Besshi-Type Cu Deposits of the Matchless Amphibolite Belt, Namibia . . . 655
7.7 Volcanic-Associated Massive Sulphide Ore Systems (VMS) . . . 662
7.7.1 Kuroko-Type Mineral Systems . . . 665
7.7.2 The Kuroko Deposits of Japan . . . 679
7.7.3 Noranda or Abitibi-Type Type Massive Sulphide Deposits . . . 683

7.7.4 The VMS Deposits of Tasmania, Australia 687
7.7.5 The Iberian Pyrite Belt Massive Sulphide Deposits 693
7.7.6 The Oldest VMS: Pilbara Craton, Western Australia 705
7.8 Concluding Remarks 713
References 715

8 Metalliferous Sediments and Sedimentary Rock-Hosted Stratiform and/or Stratabound Hydrothermal Mineral Systems 727
8.1 Introduction 727
8.2 Basin Formation and Volcano-Sedimentary Successions in Continental Rifts 731
8.3 Fluid Dynamics in Sedimentary Basins 736
8.4 The East African Rift System 741
8.4.1 Lake Tanganyika 748
8.4.2 The Afar Triangle 750
8.5 Red Sea Brine Pools 751
8.5.1 The Atlantis II Deep 756
8.5.2 Mechanisms for the Formation of the Red Sea Metalliferous Sediments 760
8.6 Stratiform and Stratabound Sedimentary Rock-Hosted Disseminated Cu Sulphides Ore systems 761
8.6.1 The Central African Copperbelt 766
8.6.2 Stratabound Cu-Ag Deposits of the Irumide Belt in Southern Africa 773
8.6.3 Genetic Models 778
8.7 SEDEX Ore Systems 781
8.7.1 SEDEX Systems in Australia 786
8.7.2 SEDEX Systems in Southern Africa 809
8.8 Stratabound Carbonate Rock-Hosted Ore Systems 815
8.8.1 Mississippi Valley-Type Deposits of the Viburnum Trend (USA) 819
8.8.2 Alpine-Type Deposits 821
8.8.3 Irish Midlands Deposits 823
8.8.4 Models of Ore Genesis for MVT Ore Systems 825
8.8.5 The Pb-Zn-Cu-Ag-V Deposits of the Otavi Mountain Land, Namibia 828
8.8.6 MVT Deposits of the Lennard Shelf, Western Australia 840
8.8.7 MVT Deposits in the North Sea? 843
8.9 Iron Formations and Manganese Deposits 843
8.9.1 Iron Formation Ore Systems and Genetic Models 850
8.9.2 Granular Iron Formation of the Palaeoproteroroic Earaheedy Basin, Western Australia 857
8.9.3 Manganese Oxide Ores 861

8.10 Metalliferous Sediments on Seafloors 864
8.11 Concluding Remarks 866
References 867

9 Orogenic, Amagmatic and Hydrothermal Mineral Systems of Uncertain Origin 885
9.1 Introduction 885
9.2 Orogenic and Metamorphism-Related Lode Systems 887
9.2.1 Metamorphism and Fluid Generation; Metamorphogenic Hydrothermal Systems 895
9.2.2 Fluid Paths: Shear Zones, Faults and Thrust Faults 904
9.2.3 Veins in Metamorphic Rocks 907
9.2.4 Oxygen and Hydrogen Isotope Systematics 909
9.3 Orogenic Lodes 909
9.3.1 Yilgarn Craton, Western Australia 915
9.3.2 Hemlo Au-Mo Deposit, Abitibi-Wawa Greenstone Belt, Superior Province, Canada 920
9.3.3 Muruntau, Uzbekistan 925
9.3.4 Sukhoi Log Au-PGE Deposit of the Lena Goldfield, Russia; Multi-Stage Origin with a Late Metamorphic Overprint 929
9.3.5 Orogenic Au Lodes of the South Island, New Zealand . 935
9.3.6 Precious Metal Lode Deposits in the North China Craton 944
9.3.7 Orogenic Lodes and Lamprophyres 963
9.4 Carlin-Type Gold Deposits 965
9.4.1 Carlin Deposits of Nevada, Western USA 966
9.4.2 The Carlin Deposit 969
9.4.3 Genetic Models 971
9.5 Metalliferous Black Shales 974
9.5.1 Mo-Ni-V-PGE-Au in Black Shales, Southern China: Seafloor Venting, Seawater Precipitation, or Impact-Related? 976
9.6 Nonsulphide Mineral Systems 981
9.6.1 Classification and Genetic Models 982
9.6.2 Magellan Pb Deposit, Western Australia 985
9.6.3 Skorpion, Namibia 989
9.7 Amagmatic Hydrothermal Systems Related to High Heat Producing Granites 990
9.7.1 Southwest England and Cornwall High Heat Producing Granites and Associated Hydrothermal Systems 992
9.7.2 Central Australian Heat Flow Province 995
9.8 An Unusual Amagmatic Mineral System in Inglefield Land, NW Greenland 997
9.8.1 Mineralisation in Northeastern Inglefield Land 1000

9.8.2 Origin of the Rust Zones and Ore Genesis: A New Mineralisation Style? 1002
9.9 Concluding Remarks 1007
References 1009

10 Hydrothermal Systems and the Biosphere 1025
10.1 Introduction 1025
10.2 The Emergence of Life on Earth 1026
10.2.1 Panspermia 1030
10.2.2 Synthesis of Prebiotic Molecules, Organic Soups and Warm Little Ponds? 1032
10.2.3 Sulphide Bubbles in Seafloor Hydrothermal Vents. . . 1033
10.2.4 Models Based on Minerals Other than Sulphides 1036
10.2.5 The First Signs of Life on Earth and the Great Oxidation Event 1037
10.2.6 Is Life Being Created Today? 1044
10.3 Hydrothermal Systems and the Biosphere; the Role of Bacteria in Ore Genesis. 1046
10.3.1 High-Temperature Ecosystems Associated with Mineralisation 1050
10.3.2 Microbes Inside Rocks and in the Deep Subsurface . . 1062
10.3.3 Role of Bacteria in the Weathering Profile 1064
10.4 Gas Hydrates, Mud Volcanoes, Seafloor Seeps, Methanogens and Chemosynthetic Communities. 1065
10.4.1 Hydrate Ridge 1068
10.4.2 Mud Volcanoes and Gas Hydrate Constructs in the Geological Record 1071
10.5 Hydrothermal Ecosystems in the Geological Record 1073
10.5.1 The Rio Tinto Basin, Spain 1073
10.5.2 Cretaceous Polymetallic Ore Deposit in Georgia 1077
10.5.3 Mid-Palaeozoic Hot Spring Deposits and Associated Ecosystems, Queensland, Australia 1077
10.5.4 Palaeo- to Mesoarchaean Ecosystems Associated with Hydrothermal Activity in the East Pilbara Terrane . . 1079
10.6 Concluding Remarks 1087
References 1088

11 Hydrothermal Processes Associated with Meteorite Impacts 1097
11.1 Introduction 1097
11.2 Asteroid and Cometary Impacts and Hydrothermal Circulation 1098
11.2.1 A Working Model 1100
11.3 Mineral Deposits and Impact Structures 1102
11.3.1 The Sudbury Hydrothermal System 1103
11.3.2 The Lockne Impact Structure 1105

11.3.3 The Vredefort Meteorite Impact and the Case for Witwatersrand Gold 1106
11.4 Australian Examples of Impact-Related Hydrothermal Activity 1111
11.4.1 Shoemaker Impact Structure 1112
11.4.2 Yarrabubba Impact Structure 1118
11.4.3 Woodleigh Impact Structure 1121
11.5 Concluding Remarks 1126
References 1126

12 Hydrothermal Processes and Systems on Other Planets and Satellites: Clues for the Search of Extraterrestrial Life 1131
12.1 Introduction 1131
12.2 Extraterrestrial Water 1131
12.3 Mars 1133
12.3.1 Volcanism, Rifting and Mantle Plumes 1139
12.3.2 The Findings by the Spirit and Opportunity Rovers 1145
12.3.3 The Findings of the OMEGA Mission and Their Implications 1149
12.3.4 Water and Potential Hydrothermal Systems on Mars 1152
12.3.5 Impact Craters 1162
12.4 Europa, Ganymede, Enceladus and Titan 1163
12.4.1 Europa 1164
12.4.2 Ganymede 1170
12.4.3 Enceladus 1174
12.4.4 Titan 1177
12.5 Where to in the Search for Extraterrestrial Life? 1181
12.5.1 Where There is Water There is Life? 1182
12.5.2 The Search for Extraterrestrial Life 1183
12.6 Concluding Remarks 1201
References 1203

13 Uranium Hydrothermal Mineral Systems 1213
13.1 Introduction 1213
13.2 Uranium Geochemistry and Decay Schemes 1214
13.2.1 Organic Geochemistry of Uranium 1216
13.2.2 Decay Schemes 1218
13.3 Uranium Hydrothermal Mineral Systems 1220
13.3.1 Plutonic Associations 1224
13.3.2 Unconformity-Related U Deposits 1229
13.3.3 Sandstone-Hosted/Roll Front U Deposits 1235
13.3.4 Time-Bound Character of U Mineral Systems 1237

13.4 Concluding Remarks 1238
References 1239

Index 1243

Introduction

In this book I discuss and describe examples of hydrothermal mineral systems and of individual deposits, whose choice and geographic provinciality is based partly on personal experience and/or knowledge of the deposit(s) in question, partly on features of some specific ore systems and aspects thereof that I consider important for illustrating models of ore genesis, which may be useful as a knowledge base. I have drawn heavily from published literature and from my own publications. The reader will also note that some examples of ore systems are described at greater length than others. The reason for this inbalance is that some mineral systems and/or deposits are especially suitable in providing insights that have more general applications. One reviewer noted that in some chapters I dwell at some length in the discussion of some aspects of Chinese geology and mineralisation. I make no apologies for this occasional predilection. For the past fourteen years I have been increasingly involved in the study of the tectonics and mineral deposits of China, together with Chinese colleagues from a number of research institutions (see Acknowledgments).

In this Introduction and before outlining the nature and contents of this book, I think it appropriate to discuss some issues of definitions and classification of ore deposits.

Definitions and Classifications of Ore Deposits

The terms mineral deposit, ore deposit, mineral occurrence, prospect, mine, reserves and resources are familiar, but more rigorous definitions are often needed for scientific accuracy and/or legal requirements.

Cox and Singer (1986) defined **mineral deposits** as occurrences of a valuable commodity (e.g. copper) or mineral (e.g. barite) that are of sufficient size and concentration (grade) that they might, under favourable circumstances, be considered to have potential for economic exploitation. An **ore deposit** is a mineral deposit that has been tested and discovered to be of sufficient size, grade and accessibility to allow it to be extracted at a profit. Guilbert and Park (1986) considered **ores** as rocks or minerals that can be mined, processed and

delivered to the market place or to technology at a profit. **Mineral deposit** carries no necessary profitability implications and usually denotes subeconomic or incompletely evaluated occurrences of ore minerals. **Mineral occurrences** or ore-mineral occurrences are uneconomic, but still anomalous concentrations of minerals that may form ores elsewhere.

Reserves include orebodies in production, or known by drilling or other specific measurements, to exist. Reserves are subdivided into measured, indicated and inferred, following the regulations set out by the JORC Code (2004). **Resources** include reserves and all other potentially viable mineral deposits that are either unknown or uneconomic at present, but can still be reasonably expected to exist.

Definitions set out in Cooper et al. (1998) are applied by the Geological Survey of Western Australia and these include **prospect** as any working or exploration activity that has found subeconomic mineral occurrences, and from which there is no recorded production. **Operating mines** are workings that are operating, including on a care-and-maintenance basis, or that are in development leading to production.

In every day practice, and in the majority of recent publications, the general term **ore deposit** is used a broader sense to include both economic and non-economic mineral deposits. **Mineral system** or **ore system** are terms used interchangeably in this book. The concept of a mineral (ore) system is analogous to that of a petroleum system, but owing to the nature of ore deposits and host rocks, a mineral system is far more diverse and complex. The formation of an ore deposit requires a source of metals, a mode of transport (usually a hydrothermal fluid, but also can be a magma) and a site of deposition or accumulation, where commodities become concentrated to enable economically viable extraction during a given period. A mineral system includes all geological and geodynamic factors, at all scales, that control the inception, evolution and preservation of ore deposits, *sensu lato*. Thus, the study of mineral systems necessarily must integrate;

(1) local studies on recognised deposits, including such factors as;

- local geology, rock types and structural controls
- location of potential accumulation sites
- the physico-chemical processes leading to deposition;

with

(2) regional scale studies including

- geodynamic (tectonic) controls on timing and location of ore deposits (space-time distribution)
- terrane-scale physico-chemical processes that determine how ore deposits are formed;
- the evolution of magmas and other energy sources and fluids at the scale of mineralising systems that influence the location of individual deposits
- regional context

Classifications and Models

The systematic classification of ore deposits is inherently fraught with many difficulties. These stem from a large number of variables (lithological, structural, chemical and tectonic), all of which interact to make the observed data difficult to interpret. Frimmel (2007), referring to Au deposits, stated that "*a given deposit may be classified according to host rock (e.g. sediment-hosted), or according to a preferred genetic model (e.g. orogenic), the classification may emphasize a specific* metal *association (e.g. iron oxide copper gold), or it may be based on a comparison with a large prototype (e.g. Carlin type)*".

The recently recognised role of meteorite megaimpacts as an important geological process adds to an already complex scenario. Any classification scheme has to take into account that ore deposits are formed by one or more of three fundamental processes, namely: magmatic, hydrothermal, mechanical and residual. Each can be further subdivided as follows:

- MAGMATIC
  - Layered intrusions
  - Alaskan zoned intrusions
  - Mafic lavas
  - Sill complexes
  - Dykes
  - Pegmatites
- MAGMATIC-HYDROTHERMAL
  - Porphyry
  - Epithermal
  - Skarns
  - Intrusion-related
  - VMS (Volcanogenic massive sulphides), Kuroko and Besshi types
  - Spreading centres sea-floor smokers; Cyprus type
  - Alkaline complexes, greisens, pegmatites
  - Iron Oxide Copper Gold Uranium and REE (IOCG); Olympic Dam style
- SEDIMENTARY-HYDROTHERMAL
  - Sedimentary exhalative (SEDEX)
  - Copperbelt and Kupperschiefer types
  - Metalliferous sediments; Red Sea brines
  - Mississippi valley type (MVT)
  - Iron formations (banded IF, granular IF) and Mn oxides
- AMAGMATIC OR UNCERTAIN ORIGIN
  - Orogenic lodes
  - Black shales

  - Carlin type
  - Associated with high-heat producing granites
  - Meteorite impact structures

- MECHANICAL/RESIDUAL/WEATHERING
  - Placers
  - Laterites

If geological processes are used to classify ore deposits, they necessarily rely heavily on genetic factors; however, ore genesis can be extremely complex because it usually involves a number of interactive processes. Genetic classifications lend themselves to mis-interpretations. In fact, variations within the same class of ore deposits can be extreme. For instance, the class of Cu-Au-U-REE-Fe (IOCG) deposits includes Olympic Dam (South Australia), the Fe deposits of the Kiruna district (Sweden), Fe-REE deposits of Box Bixby and Pea Ridge (Missouri, USA) and possibly the REE-rich Bayan Obo (Mongolia), the Palabora carbonatite-hosted Cu and the Vergenoug Fe-F deposit (South Africa). When examined in detail all of these deposits are remarkably different. Nevertheless, they all have a common theme: anorogenic mafic to alkaline magmatism in rift settings, with many, but not all, of Proterozoic age.

The alternative is to use a non-genetic classification scheme. This can be done by using host rocks and/or geological environments. However, here too there are problems. For example, Ni and Cu deposits hosted in layered mafic-ultramafic rocks in the interior of cratons, comprise such a great variety of types and styles, ranging from primary magmatic to hydrothermal. Another possibility is to consider ore deposits on a combination of descriptive features, such as host rocks and dominant economic metal(s), and genetic features, such as mechanism of fluid movement, temperature of formation, alteration and extent, if any, of magmatic involvement. Some students of ore deposits adopt a descriptive classification based upon the dominant economic metals and then modify individual categories based upon compositional, tectonic, or genetic variations. An example is the classification of porphyry deposits into porphyry copper-gold, porphyry copper-molybdenum, and porphyry tin types.

In reality, none of the above schemes (genetic, non-genetic or mixed genetic-non-genetic) are adequate because they are open to all sorts of debates.

Holistic studies of ore deposits and their classification can be divided into two groups: studies done before plate-tectonics was recognised as a global geological process, and those done afterwards. In the former are the works of Lindgren (1933), Bateman (1967), Stanton (1972), Smirnov (1976) and Jensen and Bateman (1979). To the second group belong Mitchell and Garson (1981), Hutchison (1983), Sawkins (1990), and Guilbert and Park (1986).

Lindgren's (1933) classification of ore deposits remains a landmark achievement. For example, his ideas of epithermal, hypothermal and telethermal are still valid concepts today. Stanton (1972) although focussing on ore petrology,

which is the title of his book, did provide a useful classification by considering ore deposits in terms of lithological associations, as detailed below:

- Ores of mafic-ultramafic association
- Ores of felsic association
- Iron and manganese concentrations of sedimentary affiliation
- Stratiform sulphides of marine and volcanic association
- Stratabound ores of sedimentary affiliation
- Ores of vein association
- Ores of metamorphic affiliation

Guilbert and Park (1986) adopted a similar approach, by considering ore deposits related to

- Mafic igneous rocks
- Oceanic crust
- Intermediate to felsic intrusions
- Subaerial volcanism
- Submarine volcanism
- Submarine volcanism and sedimentation
- Chemical sedimentation
- Clastic sedimentation
- Weathering
- Regional metamorphism
- Solution-remobilisation
- Doubtful igneous connection

Cox and Singer (1986) preferred to classify ore deposit models by geological-tectonic environment, thereby devising a tree-like diagram such as those used in life-sciences. In this way, they consider a first division into: igneous, sedimentary, regional metamorphic and surficial. Mitchell and Garson (1981) were amongst the first to enthusiastically espouse the idea that plate tectonics offered a double solution in the difficult task of systematising ore deposits. The idea, with which we are all now familiar, is that plate tectonic processes are responsible for generating ore deposits, therefore ore deposits are effectively an expression of the tectonic setting in which they are formed, but not necessarily the tectonic setting in which they occur. Conversely, a specific type of ore deposit can (and does in many cases) help in unravelling the tectonic setting of a geological terrane. Examples are ophiolite-hosted metal deposits. Some are formed in oceanic crust at a mid-ocean ridge and later tectonically transported onto a continental margin, but the same ophiolite rocks may also host hydrothermal mineralization resulting from deformation and metasomatism during a collision event.

The relationship of ore deposits to plate tectonics led to the formulation of ore deposit models. An ore deposit model describes the essential features (geological, host rocks, wall rock alteration, geochemical/metal associations, spatial distribution, grade, size, ore mineralogy, regional metallogenic

framework, tectonic setting) of a group or class of deposits. Ore deposit models effectively are sets of data that best describe a deposit or family of deposits, which share similar features and which contain common geological attributes and are formed in similar tectonic environments. A model can be empirical based entirely on facts, such as field observations, geochemical and geophysical data, or theoretical based on conceptual ideas generally borne out of experience and knowledge of, and extrapolation from known mineral districts. Ore deposit models ranges from simplistic (very limited database) to complex (large database); in the same way as few data points define a smooth curve, whereas many points usually define a more complex curve. But, as is the case for a curve derived from many data points, this can be smoothed to obtain a fairly accurate overall picture. This is the one of the keys to understanding ore deposits and their genesis: filter out the noise and home in to a general model that fits within a regional framework and that adequately explains the observations. Another important factor is that an ore deposit can be modified, perhaps more than once, by subsequent geological processes (e.g. collision tectonics, meteorite impacts). The literature on ore deposit models is abundant; some of the more popular works include Roberts and Sheahan (1988), Kirkham et al. (1993) and Du Bray (1995).

Overall the new plate tectonics paradigm fostered the modelling of ore systems, which turned out to be very useful in mineral exploration because of their predictive capacity, although the difficulty of obtaining a classification of ore deposits that completely satisfies both genetic and non-genetic conditions remains. Nevertheless, building a mineral system genetic model provides insights into the geodynamic environment of ore formation and, importantly, allows a degree of predictability that can assist in exploration targeting. A thematic issue of the Australian Journal of Earth Sciences is devoted to conceptual exploration targeting (Groves 2008).

Several other books deal with various aspects of ore deposits. These include: Lindgren (1933), Bateman (1967), Park and MacDiarmid (1970), Smirnov (1976), Mitchell and Garson (1981), Hutchison (1983), Guilbert and Park (1985), Sawkins (1990), Pirajno (1992), Evans (1993), Barnes (1997), Pirajno (2000), Misra (2000), Solomon and Groves (2000) and a recent and very comprehensive treatise by Laznicka (2006). The 100th Anniversary Volume of Economic Geology (Hedenquist et al. 2005) provides excellent and in-depth reviews of both magmatic and hydrothermal mineral systems which include: (1) Magmatic ore deposits (2) porphyry deposits, (3) skarns, (4) granite-related ore deposits, (5) precious metal deposits in metamorphic terranes, (6) Carlin-style deposits, (7) epithermal precious and base metals, (8) sediment-hosted Pb-Zn, (9) sediment-hosted stratiform deposits, (10) iron-formations, and (11) the hydrothermal model for the Witwatersrand Au-U deposits. In addition, regional metallogeny and earth environments and processes are discussed in some detail. More recently, the Geological Association of Canada published an extremely well-illustrated book (Goodfellow 2007), which although focussing on the mineral deposits of Canada, does provide excellent reviews of ore systems that are applicable world wide.

This Book

This book is about Hydrothermal Processes and Mineral Systems and where appropriate links with life. The book consists of 13 chapters, which can be considered on a "stand-alone" basis. In Chapter 1, I discuss the different sources of water that participate in hydrothermal activity and circulation systems. Hydrothermal fluids can be juvenile-magmatic or derived from seawater, metamorphic, meteoric, connate waters or a mix of two or more of these. I briefly look into solubility, boiling and redox processes. A brief overview is presented on hot springs because they, whether subaqueous or subaerial, are the surface expression of hydrothermal systems. Next I discuss fluid inclusions and isotopic tracers, which provide the means of investigating the nature and composition of the fluids that are involved in ore making processes. Water is a powerful solvent, but the transport of metals in solution is aided and promoted by complex ions ligands. This aspect, together with the precipitation of metal compounds, is also examined in Chapter 1.

The interaction of hydrothermal fluids with wallrocks and/or the hydrosphere and changes in their composition through time and space, contribute to the formation of a wide range of mineral deposit types and associated wallrock alteration. Chapter 2 looks at hydrothermal alteration processes of selected mineral systems, such as anorogenic ring complexes, porphyry, epithermal and skarns and presents examples of types of alteration, such as tourmalinisation, serpentinisation and talc-carbonate. Briefly, I also discuss the effects of metamorphism on hydrothermally altered rocks and the geochemical and isotopic signatures of alteration. A very brief panoramic is provided on the use of spectral remote sensing for the detection of hydrothermal alteration.

As metioned above, an ore system is the product of a set of geodynamic events and as such it bears the signature of these events. This is not easily unravelled, but the constantly improving geochronological techniques are providing the means for distinguishing these tectonic signals. Conversely, knowledge of a tectonic setting can and does afford important clues for understanding a mineral system and also for providing vectors to finding new deposits. In Chapter 3 tectonic settings and associated hydrothermal processes are examined. Hydrothermal processes on Earth have played an important role in the evolution of our planet. These processes link the lithosphere, hydrosphere and biosphere in continuously evolving dynamic systems. Terrestrial hydrothermal processes have been active since water condensed to form the hydrosphere, most probably from about 4.4 Ga. The circulation of hot aqueous solutions (hydrothermal systems) at and below the Earth's surface is driven by internal heat. Hydrothermal systems form beneath the oceans (e.g. spreading centres, oceanic plateaux), in lakes, intracontinental rifts, continental margins and magmatic arcs. Tectonic settings have evolved with geological time from mantle plume tectonic-dominated regimes in the Archaean, to a more "buoyant" style tectonics in the Proterozoic, to modern plate tectonics in the Phanerozoic, reflecting the trend of a cooling Earth.

Therefore, the evolution of hydrothermal processes through geological time is ultimately related to planetary cooling and the mode of heat transfer from the mantle towards the surface (e.g. mantle plume events, associated tectonism, continental volcanism, oceanic magmatism). Thus, some hydrothermal systems and related mineral deposits are strictly time-dependent, for example uranium mineralisation and the huge accumulation of banded iron-formations. The latter reached a peak during the Palaeoproterozoic and were associated with an evolving oxygenated atmosphere and the delivery of large quantities of ferrous Fe from seafloor hydrothermal venting, possibly associated with mantle superplume events.

The descriptions and discussions on mineral systems commence with intrusion-related deposits in Chapter 4. In this chapter I begin with an overview of granitic magmatism and intrusion-associated hydrothermal and ore-making processes, before embarking on the description of specific intrusion-related systems, which includes classic cases of Sn-W mineralisation, the less known polymetallic Mo-W-Be-Bi deposits in Siberia, Au and polymetallic veins and hydrothermal systems in alkaline complexes. In this same chapter I have included the Fe oxide copper-gold (IOCG) systems. The inclusion of IOCG systems in this chapter may be disputable, but I find that in spite of the diversity of IOCG deposits, a common link seems to be that they are all related to A-type anorogenic intrusions and magmatism.

Porphyry and epithermal systems are presented in Chapter 5. I may be forgiven for the unusual length of this chapter, but this was somewhat unavoidable due to the common and close link between porphyry and epithermal systems. An important point that I have endeavoured to emphasise is that porphyry and epithermal systems are not necessarily related to subduction settings. Indeed, there is abundant evidence for some porphyry deposits to occur in intraplate rift settings and volcanic rifted margins associated with mantle plume tectonics. I have also included in Chapter 5, the oldest porphyry and epithermal systems that are known from the Pilbara Craton in Western Australia, which were also formed in an intraplate setting. Although, also commonly linked with porphyry intrusions, skarns are described in Chapter 6. Skarn systems generally form in carbonate rocks, are typically mineralogically zoned, characterised by mineral assemblages that reflect decreasing temperatures in a dynamic evolving regime away from the contact with the causative intrusions. Skarns provide a wide array of Sn, W, Fe, Au and base metal ores in tectonic settings ranging from steep to shallow subduction to continental rifting. Skarn systems in eastern China provide a spectrum of mineralisation types and styles that range from veins to disseminated, massive magnetite and sulphides in endoskarn and exoskarns, which in many cases appear transitional to intrusion-related, porphyry and even IOCG systems. These mineral system are controlled by major tectonic boundaries and linked to the activity of asthenopsheric upwellings.

In Chapter 7, I discuss hydrothermal systems in the submarine environments. Truly another fascinating field that has captivated the life science and

geoscientific communities with the discovery of unsuspected ecosystems that not only thrive in the absence of oxygen and hot temperatures, but also actively participate in precipitating metalliferous compounds. These submarine hydrothermal systems, in my opinion, give us a glimpse on what the early Earth may have been like and on the environments where life may have been generated. Chapter 7 also looks into the physiography of the ocean floor and provides an overview of what hydrothermal systems are like at spreading centres, island arcs and seamounts, giving us invaluable insights on ancient mineral systems that may have originated on the seafloor. Kuroko and Abitibi types massive sulphides deposits are the classic representative of submarine hydrothermal systems in the geological record and again we have examples of the most ancient ones in the Pilbara Craton, where evidence of early life is undeniably present (Chapter 10). Other ancient deposits are more difficult to pigeon-hole and may represent either a unique case or a new system type. In this category I include the Iberian Pyrite Belt, arguably the world's largest metal accumulation, and the unusual Abra deposit in Western Australia.

There is a transition from oceanic seafloor hydrothermal systems, the metalliferous sediments that accumulate well away from hydrothermal vents and hydrothermal systems that actively form in incipient oceanic settings, such as the Red Sea. These are discussed in Chapter 8, in which volcano-sedimentary basins in intracontinental rift settings are the main topic with examples from the great East African Rift System. The East African rifts and the Red Sea together may well present a modern analogue of the variability of rift settings in which giant and world-class sedimentary exhalative (SEDEX) deposits were formed. In this chapter I have included the disseminated Cu-Co sulphides of the Central African Copperbelt and the world-class SEDEX deposits of Australia and South Africa. Mississippi valley-type (MVT) are included in Chapter 8 as part of the stratabound mineral systems, although these may also have been incorporated in Chapter 9. Iron (and Mn) formations (banded and granular) not only constitute giant accumulation of Fe (and Mn) but, in the 21st century, are in high demand by the emerging economies resulting in unprecedented prosperity in the supplying countries. Iron formations are time-dependent and effectively confined to passive margins that resulted from supercontinent breakup in the Palaeo-Mesoproterozoic. The deposition of Fe oxides occurred because of changes in oxygen levels in the biosphere-hydrosphere-atmosphere system.

Chapter 9 deals with amagmatic and hydrothermal systems of uncertain origin, amagmatism intended as lack of, unproven or doubtful involvement of magmas. In reality, amagmatism is not entirely proven for the class of orogenic lodes, which continue to defy us on whether there was or not direct or even indirect involvement of magmas. If and where there is such a link then the relevant orogenic lodes can be considered as intrusion-related systems. It is, however, well established that compression in collision orogen and metamorphic devolitilsation processes were implicated in the making of these ore systems. Carlin-type or better Carlin-style deposits too present a challenge in

that a clear link with magmatic activity remains elusive and fall into a category best considered of uncertain origin. Similarly for black shales, also discussed in this chapter and whose metal endownment's origin is not entirely clear. The example given in this book is that of southern China, where highly mineralised black shales exhibit unusual textures and metal association (Mo-Ni-V-PGE-Au). Given the age and nature of these deposits, I cannot help but wonder if there is a link with a large meteorite impact, with a possible candidate being the Acraman structure in South Australia. Nonsulphide mineral systems, the result of palaeo-weathering processes that have operated on MVT deposits, are dealt with in this chapter. Also in Chapter 9, I discuss hydrothermal systems powered by high heat producing granites (HHP) and conclude with an unusual amagmatic mineral system from northwest Greenland.

On Earth, sites of hydrothermal activity support, both at surface and in the subsurface, varied ecosystems based on a range of chemotrophic micro-organisms. An intriguing question is whether primitive life is still being created in present-day hydrothermal systems, or did it occur only in the ancient geological past? These are some of the issues discussed in Chapter 10. Also in this chapter the role of bacterial communities in ore genesis are examined with recent and ancient examples being discussed. On the way, I thought it appropriate to make a brief mention of gas hydrates and associated seafloor seeps and mud volcanoes.

Chapter 11 looks into the role of meteorite impacts as a source of thermal energy for hydrothermal circulation. Accounts of hydrothermal systems associated with meteorite impacts are mostly confined to a somewhat restricted group of geoscientists or "impactologists", who tend to publish in specialist journals. The fact is that large and small meteorite impacts do have a major role in setting up hydrothermal citculation, but because of the poor preservation record of many of the large impact structures, it is difficult to provide tangible proof of impact involvement for some ore systems (for instance the above-mentioned polymetallic black shales in southern China). The Witwatersrand conglomerates, the largest accumulation of Au in the world, may have been preserved and/or locally re-distributed by hydrothermal fluids, generated by the large and oldest known impact structure ($\sim$2.02 Ga; Vredefort). An intriguing hypothesis, difficult to prove, due to the succession of thermal events that affected the Witwatersrand basin.

It is also possible that hydrothermal processes operate or operated on other planets, such as Mars, where liquid water is, or was present and even in some of the satellites of the Jovian planets. These are examined in Chapter 12. The recent and on-going space missions continue to supply astonishing large amounts of data that will take years to completely absorb and assess. NASA reports are regularly posted on web sites, often reporting new finds. Maintaining a connection with these web sites is akeen to each time opening a window on a new view. Our vision of the "cradle of life" has surely changed, life, as we know it, needs water and planet Earth must have been a very different place 3.5–4 billion years ago when life first appeared. The Earth must have had far greater lengths of deep sea ridges, volcanoes and submarine hydrothermal vents releasing large quantities

of nutrients, than in later ages. In spite of frequent meteoritic bombardment, there must have been several well protected "hydrothermal ponds" where microbial life thrived. The challenge now is to find these "hydrothermal ponds" on other planets, with Mars being the best candidate, but certainly not excluding the very far away Galilean satellites, where deep oceans may exist beneath a crust of ice. Chapter 12 examines Europa, Ganymede, Enceladus and Titan as these possible candidates.

Chapter 13 is the last in this book and it deals exclusively with uranium mineral systems. Nuclear energy is a politically sensitive subject in many countries, but one which sooner or later needs to be accepted. Canada and Australia have large uranium resources, mostly contained in unconformity-related ore systems. In Australia, substantial resources are also contained in IOCG systems, such as Olympic Dam, discussed in Chapter 4. I have included in this chapter the alaskite-hosted U deposits, with the best example being provided by Rössing in Namibia.

Finally, I take full responsibility for the contents of this book. If I have misrepresented or misquoted some of the concepts or ideas obtained from the literature, this was unintentional and in no way reflects a disregard for the original author(s)' work.

Spelling is English Australia (Moore 2000), except in references where original spelling is maintained. Unless otherwise explained, the abbreviations and symbols used in this book (e.g. Mt for million tonnes, t for tonnes, element symbols, such as Cu for copper, Ag for silver and so forth, ~ for circa, wt% for weight percent, ppm for part per million, g/t grams per tonne, kbar for kilobar etc) should be familiar to all Earth scientists.

References

Barnes HL (ed) (1997) Geochemistry of hydrothermal ore deposits, 3rd edn, John Wiley & Sons, New York, 972 pp

Bateman AM (1967) Economic mineral deposits. John Wiley & Sons, New York, 916 pp

Cooper RW, Langford RL, Pirajno F (1998) Mineral occurrences and exploration potential of the Bangemall Basin. Geol Surv West Aust, Report 64

Cox D, Singer DA (eds) (1986) Mineral deposits models: US Geol Surv Bull 1693

Du Bray EA (ed) (1995) Preliminary compilation of descriptive geoenvironmental mineral deposits models: U. S. Department of the Interior, U S Geol Surv Open File Rep 95–831

Evans AM (1993) Ore geology and industrial minerals – An introduction. Blackwell Scientific Publ, Oxford

Frimmel HE (2007) Earth's continental crust gold endowment. Earth Planet Sci Lett, doi:10.1016.j.epsl.2007.11.022

Goodfellow WD (ed) (2007) Mineral deposits of Canada – A synthesis of major deposit types, district metallogeny, the evolutionof geologicalprovinces and exploration methods. Geol Ass Can Sp Publ 5

Groves DI (ed) (2008) Coceptual mineral exploration. Aust J Earth Sci 55(1)

Guilbert JM, Park CF (1986) The geology of ore deposits. Freeman, San Francisco

Hedenquist JW, Thompson JFH, Goldfarb RJ, Richards JP (eds) (2005) Economic Geology One Hundreth Anniversary Volume. Soc Econ Geol, Littleton, Colorado

Hutchison CS (1983) Economic deposits and their tectonic settings. The MacMillan Press Ltd, London, 355 pp
Jensen M L, Bateman AM (1979) Economic mineral deposits: John Wiley & Sons, New York
JORC Code (2004) Australasia code for reporting of exploration results, mineral resources and ore reserves. Austral Inst Min Metall, Aust Inst Geosci, Min Council Aust
Kirkham RV, Sinclair WD, Thorpe RI, Duke JM (eds) (1993) Mineral deposit modeling: Geological Association of Canada Special Paper 40
Laznicka P (2006) Giant metallic deposits; future sources of industrial metals. Springer, New York
Lindgren W (1933) Mineral deposits. McGraw-Hill Book Co, New York
Misra KC (2000) Understanding mineral deposits. Kluwer Academic Publishers, Dordrecht
Mitchell AHG, Garson MS (1981) Mineral deposits and global tectonic settings. Academic Press, London
Moore B (ed) (2000) The Australian Oxford dictionary. Oxford Univ Press, Oxford
Park CF, MacDiarmid RA (1970) Ore deposits, 2nd edn, W. H. Freeman & Co, San Francisco
Pirajno F (1992) Hydrothermal mineral deposits – principles and fundamental concepts for the exploration geologist. Springer-Verlag, Berlin, 709 pp
Pirajno F (2000) Ore deposits and mantle plumes. Kluwer Academic Publishers, Dordrecht
Roberts RG, Sheahan A (1988) Ore deposit models: Geoscience Canada Reprint Series 3
Sawkins FJ (1990) Metal deposits in relation to plate tectonics, 2nd edn, Springer-Verlag, Berlin
Solomon M, Groves DI (2000) The geology and origin of Australia's mineral deposits. Centre for Ore Deposit Research and Centre for Global Metallogeny, Univ West Austr Publ 32
Smirnov VI (1976) Geology of mineral deposits. MIR Publishers, Moscow
Stanton RL 1972, Ore petrology: McGraw-Hill Book Co

Chapter 1
Water and Hydrothermal Fluids on Earth

1.1 Introduction

In this Chapter I introduce aspects of the physics and chemistry of water that are relevant to the basic understanding of hydrothermal solutions, hydrothermal processes and systems. Given the context of this book, this introduction is perhaps somewhat elementary and by no means exhaustive, but for the reader who wants to further his/her knowledge I provide a list of a range of useful and/or essential published works. Water is an oxide of hydrogen, composed of two H and one O atoms forming a polar molecule, meaning that the H atoms posses a weak positive charge and the O atom a weak negative charge and. This polarity is extremely important because it makes water a good ligand for cations, enabling processes of hydration and hydrolysis (Section 1.4.8). Pure water dissociates according to:

$$H_2O \rightarrow H^+ + OH^-$$

The OH^- ion is known as the hydroxyl group, which commonly enters the structure of a large number of minerals, such as amphiboles, micas and clays.

Water is used as a standard for physical constants, it is a powerful solvent, which carries and deposits substances, and in which life abounds. As mentioned previously, life, in the sense that we understand it, originated in water and to remind us of this, water is the major constituent of all living organisms. The ubiquitous biological property is that of being water-based and this together with other bioelements, C, N, P and S is about all that there is in all living organisms from bacteria and archaea to humans. I return to that most elusive topic, life, in Chapter 12.

Water on our planet is found in all three phases of liquid, solid (ice) and vapour. At and near the surface water exists in the liquid state, as in the oceans, rivers, lakes, underground in the pores of the solid surface materials (groundwater); as a vapour in the atmosphere and in volcanic emissions; as a solid in the polar ice caps, mountain glaciers and as permafrost. Water is also, and importantly, in the context of this book, a major chemical constituent of many minerals, which are qualified by the adjective hydrous. All functioning terrestrial biological systems

F. Pirajno, *Hydrothermal Processes and Mineral Systems*,

© Springer Science+Business Media B.V. 2009

consist predominantly of water. Life on Earth arose in water. In addition, water is undoubtedly the most valuable resource today, and obtaining and maintaining fresh water supplies for human consumption has become a priority in many countries, as sources of potable and clean water are becoming scarcer due to ever increasing demands. There is little doubt that the first organic molecules were first synthesised in aqueous solutions and that the most primitive biota was likely to have arisen near or at sites of hydrothermal discharges. Indeed, as pointed out by Bada (2004), the two fundamental requirements for life, as we know it, are liquid water and polymers (nucleic acids and proteins). Water with its unique properties as a solvent and the wide range of temperatures under which it maintains its liquid state, make it an ideal medium for chemical reactions to occur (Bada 2004).

Water participates in two major cycles: (1) the endogenic cycle, which derives its energy from the interior of the Earth and becomes involved in tectonic, igneous and metamorphic processes; (2) the exogenic cycle, which derives more than 99% of its energy from the Sun, and promotes the interactions between the hydrosphere, atmosphere and geosphere (hydrologic and weathering cycles). Comprehensive articles on the hydrologic cycle and the global ocean circulation can be found in Maurice (2000) and Ingle (2000). Juvenile water is that which has never been part of the exogenic cycle. Its existence is difficult to prove because of obvious contamination with recycled water. Although the detection of juvenile water can be made in mineral phases that originate in the deep mantle and for which a unique isotopic composition can be postulated (Ohtani 2005), the possibility of contamination from the surface, such as descending subduction slabs, cannot be discounted. Hydrous mineral phases that are likely to exist in the mantle are listed in Table 1.1.

Table 1.1 Selected hydrous mineral phases postulated to exist in the mantle (after Ohtani 2005; Williams and Hemley 2001)

Mineral phase	Formula	H_2O wt%
Chlorite	$Mg_5Al_2Si_3O_{10}(OH)_8$	13
Serpentine	$Mg_3Si_2O_5(OH)_4$	14
Chondrodite	$Mg_5Si_2O_8(OH)_2$	5.3
Hydroxylclinohumite	$Mg_9Si_4O_{16}(OH)_2$	3
Phase A	$Mg_7Si_2O(OH)_6$	12
Phase B	$Mg_{12}Si_4O_{19}(OH)_2$	2.4
Phase D	$Mg_{1.14}Si_{1.73}H_{2.81}O_6$	14.5–18
Phase E	$Mg_{2.3}Si_{1.25}H_{2.4}O_6$	11.4
Wadsleyite	Mg_2SiO_4	<3
Ringwoodite	Mg_2SiO_4	1.0–2.2
Topaz-OH	$Al_2SiO_4(OH)_2$	10
Diaspore	AlOOH	15
Phase II	$Al_3Si_2O_7(OH)_3$	9
Phase EGG	$AlSiO_3OH$	7.5
Phase δ	AlOOH	15
Lawsonite	$CaAl_2Si_2O_{10}H_4$	11.5

Ringwood (1966, 1975), who pioneered the study of mineral phases in the mantle, estimated that the mass of water in the mantle would be roughly three times the total mass of the present day oceans. Mantle degassing began immediately the Earth was formed, with an early period of degassing in the first 500 Myr producing the equivalent of one ocean mass (Schubert et al. 2001).

The history of the hydrosphere and atmosphere is essentially the result of the interplay of volcanic activity, asteroid impacts, tectonism and the increasing role of biological activity (Holland 1984, 2003). Volcanism, both subaerial and submarine, is the major geological process responsible for the transfer of water and other volatile elements and compounds from the interior of the planet to the atmosphere. Estimates of water fluxes from submarine and subaerial volcanic eruptions are in the order of 1.4×10^{11} kg yr^{-1} from magmatic arcs and 0.6×10^{11} kg yr^{-1} from mid-ocean ridges (Peacock 1990; Le Cloarec and Marty 1991; Bodnar 2005), giving a total amount of water outgassed from the mantle to the surface of about 2.0×10^{11} kg yr^{-1} (Ohtani 2005). The imbalance between water returned by subduction and outgassed water is not fully explained, but it has been suggested that some of the water recycled into the mantle may be consumed in hydration reactions (Peacock 1990). Water returns from the surface to the Earth's deep interior mostly via subduction zones. It is estimated that water returned to the mantle from pelagic sediments transported along a subducting slab is 0.7×10^{11} kg yr^{-1} and about 8×10^{11} kg yr^{-1} from the oceanic crust, thus the total amount is about 8.7×10^{11} kg yr^{-1} (Peacock 1990, Ohtani 2005). The water cycles, deep and shallow endogenic and meteoric, are schematically illustrated in Fig. 1.1. Dehydration of subducting slab is particularly effective in transferring water back to the surface via partial melting and volcanism. Dehydration of a subducting slab through the decomposition of hydrous minerals takes place in four main regions (Ohtani 2005, Fig. 1.2): (1) upper mantle with dehydration of minerals such as serpentine, chlorite, phengite; these hydration processes transfer water to the mantle wedge above the subduction zone triggering partial melting, resulting in arc magmatism (Fig. 1.1); (2) in the transition zone with the decomposition of Phase E and wadsleyite (see Table 1.1); (3) in the lower mantle with decomposition of Phase B; (4) and in the deep mantle, at depths > 800 km, with decomposition of Phase D.

Water is not an uncommon constituent in the outer planets of the Solar System (Jupiter, Saturn, Uranus and respective satellites), where it is abundant as water-ice. By contrast, the terrestrial planets (Mercury, Venus, Earth and Mars) are comparatively dry, where water may not be present at all or it exists only in the vapour state, or as ice in the subsurface or forms a thin film on the surface, as is the case for the Earth. In fact, although two thirds of the surface of the Earth is covered by water, which constitute our oceans, this is only a thin film because in terms of planetary mass it represents less than 0.03% of the total mass of the planet.

Below the surface at depth, water becomes hot and saline; in continental basins water may contain up to 40 wt% total dissolved solids (TDS) and have temperatures greater than 100°C. These waters are also known as basinal

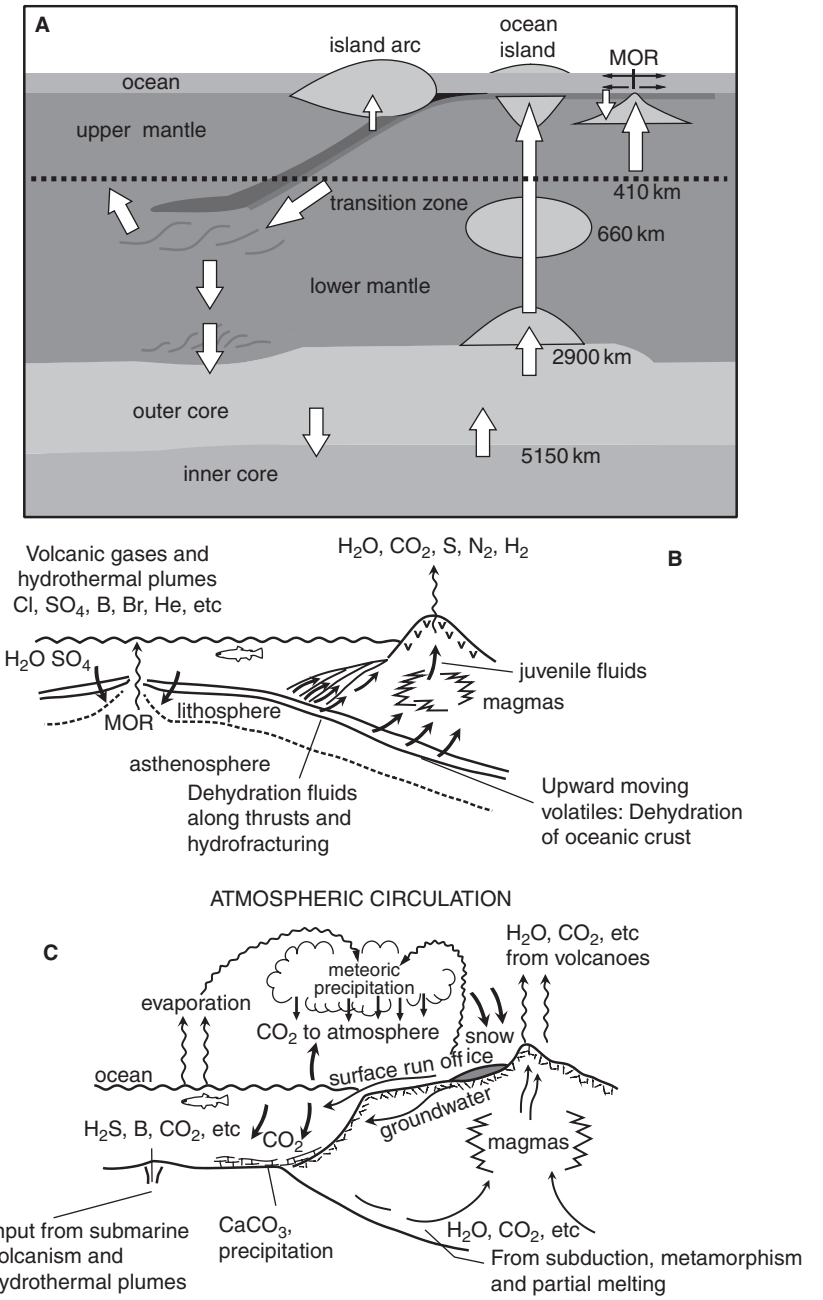


Fig. 1.1 Models of terrestrial water circulation; (**A**) Global circulation (after Williams and Hemley 2001; Ohtani 2005); (**B**) Circulation of water and other volatiles in a mid-ocean ridge and volcanic arc systems; (**C**) Endogenic and meteoric water cycles. (**B** and **C**) are from modified Pirajno (1992) and Press and Siever (1982)

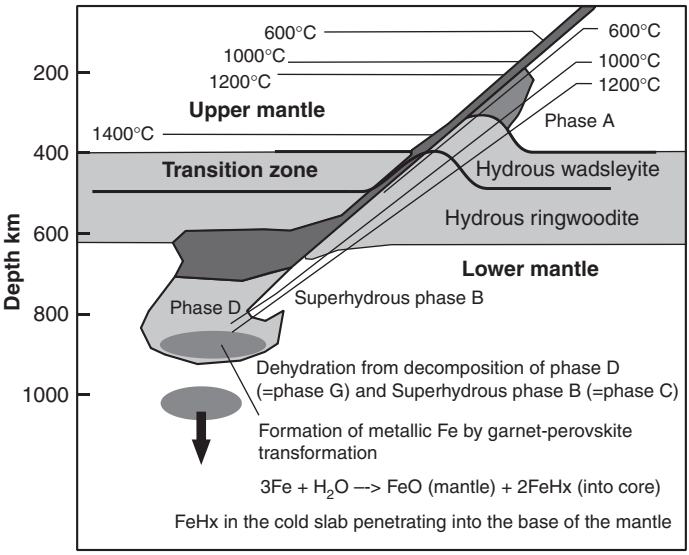


Fig. 1.2 Water generation by dehydration and decomposition of hydrous mineral phase in a subducting slab (after Ohtani 2005)

brines, which play a very important role in the formation of sedimentary-hosted hydrothermal mineral deposits, as is discussed in Chapter 8.

In the following sections of this Chapter, partly summarised from Pirajno (1992) augmented with more recent data, I review the principal facets of the origin, history and physicochemical properties of water that are relevant for the geological and hydrothermal processes that constitute the topic of this book.

1.2 Origin of Water; Sea and Surface Waters

The Earth was formed approximately 4.6 Ga ago. Studies in the dating of minerals by SHRIMP (sensitive high resolution ion microprobe) U-Pb techniques suggest that some form of continental crust must have been in existence since 4.4 Ga (Wilde et al. 2001). The presence of sedimentary rocks as old as 3.8 Ga indicate that a hydrosphere and atmosphere must have been well-established by that time. The atmosphere and hydrosphere together make up the gaseous-liquid envelope of the Earth, and, as outlined here, were first formed by a combination of the early outgassing of the planet and water delivery by cometary and meteoritic impacts. Condensation of liquid water and its accumulation in low-lying areas, or protobasins, formed the early oceans, which explains the discontinuity of the liquid envelope around the Earth.

The hydrosphere comprises all the waters at the surface of the Earth, oceans, lakes, rivers and ice. Present-day oceans cover approximately 366×10^6 km^2, or 70.8%, of the surface of the Earth. The mass of present day seawater is calculated to be 1.4×10^{21} kg, constituting roughly 98% of the total hydrosphere, with fresh waters taking up the remaining 2%, of which about 22% is groundwater. Approximately 77% of the fresh water is locked up in ice, and less than 1% is surface meteoric water. As emphasised earlier, this makes water a precious commodity, with the effects of the ever increasing human demand, waste and pollution beginning to exact a toll on our water resources.

The planets of the solar system closest to the Sun (Mercury, Venus, Earth-Moon system, Mars and the asteroid belt), are rocky and volatile-poor compared to the outer planets. The planets were formed by the collision and cold accretion of nebular grains and larger bodies known as planetesimals, whose compositions differed at different distances from the parent solar nebula, according to their density. The solar nebula is the raw material of our system, and is estimated to consist of a 98% mixture of H_2 and He, less than 2% volatiles (H_2O, CH_4, NH_3, etc.), and approximately 0.5% solids containing SiO_2, MgO, FeO, FeS etc. (Lewis and Prinn 1984). Calculations show that one tonne of interstellar cloud, from which a solar nebula is derived, consists of 984 kg of H and He, 11 kg of ices, 4 kg of rocky material, and less than 1 kg of metal (Wood 1999). Metals, oxides and silicates dominate in the region between Mercury and the asteroids, whereas further beyond water-ice, methane, ammonia and other light materials are more abundant. However, comparatively small amounts of these volatiles were present in the accreting rocky debris at the time of the Earth's formation.

Recently, it has been suggested that some or much of terrestrial water was a contribution of cometary impacts during the first 500 or 600 Ma (4.6–4.0 Ga) of Earth's geological history (Pinti 2005). Comets are essentially made up of water ice and ice and other volatile constituents, such as CO_2, CH^+, CN^+, N_2, C^+, Ca^+, NH_3, CN, CH_4, C_2H_2, C_2H_6, H_2S as well as elements like Na, Fe, K, V, Cr, Mn, Co, Ni, Cu, Si, Mg, Al and Ti (Brandt 1999). A detailed paper on the nature and composition of comets can be found in Despois and Cottin (2005). Delsemme (1999) suggested the possibility of cometary contributions to the volatile and organic inventory of the atmosphere and hydrosphere. In addition to comets, carbonaceous chondrites can contain up to 22 g of H_2O per 100 g of rock (Kerridge 1985). Hydrous carbonaceous chondrites provide the largest amount of extraterrestrial material currently reaching the Earth with about 40 000 t per year (Pinti 2005). The deuterium and hydrogen ratios (D/H; see Section 1.4.11) can further constrain the likely extraterrestrial contribution. Ocean water has a D/H value of 155.7×10^{-6}, the range of values for the whole Earth are $149–153 \times 10^{-6}$. These values are sufficiently close to the average D/H of carbonaceous chondrites ($149 \pm 6 \times 10^{-6}$). The D/H measured in the Halley, Hyakutake and Hale-Bopp comets are $316 \pm 34 \times 10^{-6}$, $290 \pm 100 \times 0^{-6}$ and $320 \pm 120 \times 10^{-6}$, respectively (Pinti 2005 and references therein). These values are 10–20 times larger than modern seawater and therefore, Pinti (2005)

suggested, comets would not have been a major source of extraterrestrial water, and based on mass balance calculations they probably only contributed about 10% of the total delivered estraterrestrial water. However, other authors (Delsemme 1999) pointed out that the comets for which the D/H was measured may not be representative because they could have originated from other regions (e.g. Uranus-Neptune) of the solar system. Instead, it is more probable that comets delivering water would have come from the Jupiter region. Pinti (2005) conceded that the problem remains unsolved, even though, based on current data, the hypothesis that chondrites delivered about 90% of the Earth's water is more popular. Indeed, the existence of an early terrestrial hydrosphere requires discrimination between volatile and organic constituents introduced from endogenous sources and extraterrestrial contributions. The possibility of extraterrestrial contributions of organic and volatile constituents also brings about the fundamental question regarding the origin of life. The "panspermia" hypothesis, originally suggested by Lord Kelvin in 1865, advocates inter-stellar and inter-planetary transport of organic molecules and even of primordial life forms (Folsome 1979; Hoyle and Wichramasinghe 1980; Dyson 1985; Chyba and Sagan 1996). I return to this topic in Chapter 10.

The newly-formed terrestrial planets were subsequently heated through three main processes: impact energy, gravitational compression and radioactivity. As heat was produced far more rapidly than it could flow out into space, melting began to take place. This initial melting led to the differentiation of the planetary bodies into a series of shells with progressively lighter materials towards their surfaces. On Earth, Al, Si, K and Na accumulated as a slag to form the outer-most shell (crust) towards the surface, followed by an inner shell (mantle) composed of Fe and Mg silicates with denser and more closely packed crystal structures. The sinking of heavier metallic materials in turn gave rise to the formation of an innermost shell (core), believed to consist mostly of a Fe-Ni alloy. A natural consequence of heating and partial melting is volcanic activity, that is the expression of the transfer of heat and mass out and onto towards the surface. It is here that the process of volatile release took place, as it does today through volcanoes and at mid-ocean ridges. Outgassing of water and volatiles, including CO_2, CO, H_2S, H_2, N_2, CH_4, NH_3, HF, HCl, and noble gases (He, Ar, Ne etc.), occurred at a great rate during this early period of differentiation. Planetary bodies with sufficient gravity, such as the Earth and Venus, and to a lesser extent Mars, were able to retain most of these volatiles, with the exception of H_2 and He, which escaped into space. Degassing of the Earth's interior is substantiated by noble gas isotope systematics, in particular the anomalous enrichment of the isotope ^{3}He detected at mid-ocean ridges. The analyses of primordial noble gases in mantle-derived igneous rocks and xenoliths together with the discovery of extinct radionuclides indicates that catastrophic degassing occurred during the first 100 Ma after initial accretion of the Earth (Pinti 2005 and references therein). As discussed above the delivery of water could have been made by both comets and carbonaceous chondrites. Pinti (2005) proposed a model of the formation of the Earth's oceans as follows. The stage is set at the

beginning of Earth's accretion at about 4.56 Ga, with segregation of the core and the first interior degassing between 4.5 and 4.45 Ga while at the same time impacts by carbonaceous chondrites delivered extraterrestrial water and possibly organic molecules. During this asteroids bombardment much of the volatile input would have been dispersed into the primitive atmosphere, some would have been partitioned into the molten Earth's surface. In addition, it is also calculated that about 50% of the water delivered at this time could have been dissociated into H and O through the action of ultraviolet radiation. At about 4.5 Ga, collision with a Mars-size asteroid occurred, with the ensuing debris forming the moon. This collision dramatically raised the temperature of the Earth to about 2000°C, causing melting of the surface materials. Any water on the surface would have been instantly vaporised. This is a momentous time because the collision with the Mars-size asteroid caused the formation of a dense atmosphere of gaseous silicates, which rapidly cooled and precipitated in a few thousands of years. This resulted in a residual atmosphere enriched in water vapour, CO_2 and lesser N_2. Pinti (2005) reasoned that if we assume that the amount of water vapour was that of the present day oceans (1.4×10^{21} kg H_2O), then atmospheric pressure would have been 270 bars. To this value a CO_2 partial pressure of at least 40 bars must be added, assuming that the amount of C available is that preserved in carbonates, continental sediments and the biosphere (3.65×10^{21}; 1.12×10^{21}; 2.6×10^{17} moles, respectively). The present day mantle inventory of CO_2 is calculated at 2.5×10^{22} moles, and if this amount was all in the primordial atmosphere then this would have been a mixture of 270 bars of H_2O and between 40 and 210 bars of CO_2, which is similar to the composition of present day Venus. This stage with a massive H_2O-CO_2 atmosphere heralds a new phase, which was characterised by a runaway greenhouse effect. The surface of the Earth began to cool to form a rind of solid mafic crust, which separated the atmosphere from the hot interior. This cooling down period allowed condensation of atmospheric water vapour, because at high atmospheric pressure (100s of bars) water vapour will start condensing at 326°C. Both on Earth and Mars condensation of water must have contained much CO_2 in solution, and the leaching of other elements from the surface materials. It is suggested that terrestrial oceans were established in less than 1000 years following a deluge of heavy rains with rates as high as 7000 mm/year (Abe 1993). This water collected first of all into pools and then into larger basins to form the oceans. It has been proposed that these larger basins were mare-type basins, such as those formed on the Moon, initially formed by the flux of asteroid-size objects (Frey 1977). Most of the Earth's water took up residence in the oceans, and CO_2 in carbonate rocks, while the other volatiles formed a gaseous shell enveloping the entire planet (atmosphere). At 4.40–4.35 Ga the newly formed oceans were nevertheless very hot and the development of life, even by hyperthermophiles (heat loving micro-organisms within a temperature range of 80–110°C), would have been unlikely. However, by 4.3–4.2 Ga the oceans were stable and the temperature cool enough to allow the survival of the first hyperthermophilic micro-organisms. Nevertheless heavy asteroid and cometary bombardment continued unabated and

this would have caused local increased temperatures and vaporisation of seawater, followed by recondensation, till about 3.9 Ga when the flux of large meteorite impacts decreased substantially. The oceans become stable as water bodies by the end of the Hadean (3.9 Ga).

It is difficult to obtain temperature values for the ancient oceans, and various attempts by calculating the temperature from measurements of $\delta^{18}O$ in Archaean chert for example, are fraught with difficulties because in this specific case the cherts are of hydrothermal origin and therefore fluid inclusions would reflect the temperature of hot fluids and not of the ambient seawater. Homogenisation temperature of primary fluid inclusions taken from hydrothermal iron oxides (iron pods of de Ronde et al. 1997) suggest a calculated oceanic surface temperature of 39°C, which is much lower than the 70°C obtained from $\delta^{18}O$ data in Archaean chert (Knauth and Lowe 1978). But even the iron pods data have raised concern, because Lowe and Byerly (2003) and Hren et al. (2006), on the basis of stable isotopes and rare earth element evidence, suggested that the goethite of the iron pods may have been deposited by Quaternary subaerial hot springs.

The Archaean ocean was probably in equilibrium with a CO_2 rich atmosphere and therefore must have had a pH below 6 (present day oceans pH is 8.2). With the gradual decrease of the CO_2 in the atmosphere there was a change in the pH values. An acidic ocean would have been conducive to the deposition of iron formations mostly composed of silica, hematite and siderite, a topic that I examine more fully in Chapter 10. For the present purpose it will suffice to say that Fe^{2+} is soluble in a reduced, anoxic and low-pH environment. Precipitation of Fe^{3+} as oxide or hydroxide will occur in alkaline and oxygenated water like that of present seawater. Therefore, the precipitation of the Proterozoic iron formations from about 2.5 Ga may reflect the change from a predominantly anoxic, low pH, acidic ocean to an oxic and alkaline ocean. This change was accompanied by the progressive atmospheric oxygenation. An anoxic and acidic ocean would also require that much of the sulphur added to the hydrosphere in the Hadean and Archaean would have been removed as sulphides. As pointed out by Pinti (2005) this indeed seems to be the case, because sulphates, such as barite and anhydrite, are only locally present in Archaean rocks (e.g. Van Kranendonk and Pirajno 2004; Van Kranendonk 2006), where volcanic SO_2 reacted with H_2O at temperatures below 400°C to produce H_2S and H_2SO_4, without requiring oxygen.

1.2.1 Seawater

The principal characteristic of the water in the Earth's oceans is their salinity. Salinity largely derives from two sources: (1) hydrothermal discharges and (2) weathering of continental crust materials. Evidence from both terrestrial and marine environments indicates that the salinity of the early oceans had already been established since the formation of the first large bodies of water more than

4 Ga ago. Thus the primeval oceans must have contained significant concentrations of Cl^-, Na^+, Ca^{2+} and Mg^{2+}, with Na^+ and Cl^- being the dominant cation and anion respectively (Holland 1984, 2003).

A history of the composition of seawater through geological time is provided by Holland (2003). This author examined the evidence from the rocks in the Archaean (4.0–2.5 Ga), such as the 3.87 Ga Isua greenstone belt in Greenland, in which banded iron formation (BIF) deposits are preserved. Holland (2003) reasoned that, although metamorphosed, these BIF must have been deposited in seawater because, as mentioned above, Fe^{2+} and the silica required to form these rocks must have been dissolved in seawater after being cycled through oceanic crust. However, it must be pointed out that some of the field evidence from the Isua greenstone belt that has been regularly used for proposing early life and seawater compositions was reappraised by Myers (2004), who cautioned that the preserved examples of biogenic and sedimentary structures may not be primary but could have resulted from later deformation events. During the Mesoarchaean (3.7–3.0 Ga) the early oceans must have been saline. This is corroborated by the presence of sedimentary deposits of evaporitic origin in rock sequences of Archaean age, such as those of the Warrawoona group (3.5 Ga) in Australia (Van Kranendonk and Pirajno 2004, Van Kranendonk 2006). In the rocks of this group, well-developed, rosette-shaped minerals replaced by silica are interpreted to represent casts of evaporite minerals such as gypsum. In fact, the only evidence that could give clues as to the composition of Mesoarchaean seawater is provided by the mineralogy and composition of the rocks from that period (Holland 2003). Minerals such as calcite, dolomite and aragonite were dominant carbonate minerals in the Mesoarchaean. Siderite, on the other hand, was scarce and only found in BIF. The presence of these carbonates suggests that seawater was supersaturated with respect to $CaCO_3$ and $CaMg(CO_3)_2$. The lack of siderite in Archaean carbonate sequences implies higher Fe^{2+} content of limestones and dolomites, which in turn implies a low-oxygen atmosphere (Holland 2003). In the Neoarchaean (3.0–2.5 Ga) rocks of the Fortescue and Hamersley Groups in the Pilbara Craton of Western Australia also provide us with some clues. Although, the presence of microbial biota (cyanobacteria) indicate the presence of a localised photic zones, the atmosphere must have had little or no oxygen because of detrital grains of pyrite, uraninite, gersdorffite and siderite in siliciclastic sediments of the Pilbara Craton (Rasmussen and Buick 1999), which means that the seawater must have been largely anoxic. Again, this is confirmed by the mineralogy of BIF with the dominance of Fe^{2+} minerals, greenalite and siderite, which were deposited in shallow seas (subtidal, lagoonal and near-shore). The Proterozoic McArthur rift basin in Australia, which contains giant stratabound Pb-Zn-Ag ore deposits (see Chapter 8), contains sedimentary rocks (1.7–1.6 Ga, McArthur Group) with pseudomorphs of anhydrite and gypsum nodules and crystals, halite casts as well as remnants of sulphate minerals. Like for the Warrawoona Group in the Pilbara, these evaporitic minerals were formed by evaporation of seawater in shallow marine environments. The presence of these evaporitic minerals in

the McArthur Group sediments indicates that the salinity of seawater then was much the same as it is today.

However, some scientists believe that the composition of seawater has not remained constant throughout the geological ages. Spencer and Hardie (1990), for example, consider that the composition of seawater is controlled by the mixing of two major inputs, namely Na-HCO_3-SO_4 from rivers and Ca-Cl from hydrothermal discharges at mid-ocean ridges, oceanic plateaux and back arc settings. Therefore the concentration of these ionic species in the sea could have varied with time as a function of the intensity of hydrothermal discharges from mid-ocean ridges and climatic changes. These authors argue that a smaller development of mid-ocean ridges would result in lesser fluxes of Ca and Cl and higher solubilities of Na^+, Mg^{2+}, SO_4^{-2} and HCO_3^- from river input and viceversa in the case of larger mid-ocean ridges. This would also affect the composition of marine evaporites, in which aragonite rather than calcite and Mg-rich salts would predominate for smaller fluxes, whilst calcite and K-rich salts would predominate in the other case. Secular variations in seawater chemistry have been modelled by Spencer and Hardie (1990) and Demicco et al. (2005). The major controls of seawater chemistry depend on the rate of input of solutes from rivers, cycling rates of seawater at mid-ocean ridges and rates of carbonate production to return seawater (Demicco et al. 2005).

The composition of seawater is defined by salinity, which is the total amount of dissolved solids per kilogram of water. For the student of hydrothermal ore deposits it is important to be aware of the dissolved solids in seawater, bearing in mind that these may have changed with time and may change in specific environments, as for example, lagoonal, evaporitic ponds, anoxic deep basins. Table 1.2 gives an average composition of seawater. The precipitates obtained

Table 1.2 Seawater composition; values on the left are from Goldberg (1972); those on the right are from Seibold and Berger (1982)

Ion	Part per million (ppm)	Ion	Part per million (ppm)
Ca^{2+}	410	Ca^{2+}	400
Mg^{2+}	1350	Mg^{2+}	1272
Na^+	10500	Na^+	10561
K^+	390	K^+	380
Cl-	19000	Cl-	18980
SO_4^{2-}	2700	SO_4^{2-}	2649
HCO_3^-	142	SO_4^{2-}	140
Br^-	67	HCO_3^-	65
Sr^{2+}	8	Br^-	13
SiO_2	6.4	SiO_2	1
B	4.5	B	26
F	1.3	F	0.01
Total	34579	Total	34487

Table 1.3 Salts (chlorides and sulphates) of marine evaporites

Chlorides	**Formula**
Halite	$NaCl$
Sylvite	KCl
Carnallite	$KMgCl_3{\cdot}6H_2O$
Sulphates	**Formula**
Kainite	$KMgClSO_4{\cdot}3H_2O$
Anhydrite	$CaSO_4$
Gypsum	$CaSO_4.2H_2O$
Polyhalite	$K_2MgCa_2(SO_4)_4{\cdot}H_2O$
Kieserite	$MgSO_4{\cdot}H_2O$

from the evaporation of seawater (evaporites) can constitute important non-metallic orebodies. Leaching of ancient evaporites may influence the composition and precipitation of sulphide species, as is the case for the sulphide brines formed in the Red Sea (see Chapter 4). Table 1.3 lists some of the more common and important salts of marine evaporites.

One of the most remarkable characteristics of the oceans is that the concentration of those elements that may be harmful to living organisms (e.g. As, Se, Hg, Pb etc.) does not increase, as might be expected from the annual input from the rivers. Whitfield (1982) explained the chemical budget of the oceans in terms of a steady-state model; in other words, material is added and removed at a constant rate. He also suggested that while the composition of seawater is largely controlled by geological processes, the biotic masses may also influence modern-day seas in their control the elements' distribution, as indicated by the correlation between the biological importance of an element and its concentration.

Seawater also contains gases in solution (O_2, N_2, CO_2, Ar, H_2S) as well as a host of other elements including Li, C, Al, Si, P, Ti, V, Mn, Fe, Co, Ni, Cu, Zn, As, Se, Rb, Mo, I and Ba (Nightingale and Liss 2003). Elements such as Au, Ag, Hg, Pb and U are present in even lesser quantities than carbonate and sulphide species. H_2S may be locally abundant, especially in stagnant organic-rich bottom waters (e.g. Black Sea), and in the areas of mid-ocean ridges and submarine volcanoes, where gas emission from seafloor hydrothermal vents is common (discussed in Chapter 7). The material added to the oceans by the rivers is augmented by that from submarine volcanism along the active mid-ocean ridges, oceanic plateaux and volcanic islands, which inject the most common anions into the sea (Cl^-, SO_4^{2-}, B and Br). To determine the budget of dissolved matter, it is important to know the average length of time that each element remains in the sea (residence time). This is calculated by dividing the total amount of any one element in solution by the amount introduced each year by terrestrial waters. Elements with the highest abundance (Na, Cl, Mg, Ca and K) are found to have the longest residence time, whereas those with lowest abundance (e.g. Fe, Al, Zn, Cu, Mn, Pb, Au and Ag) have the shortest residence time.

Kennett (1982) provides details of oceanic circulation, geology, geophysics, biological and sedimentological aspects of the oceans. The chemistry, composition and physical-chemical properties of seawater are discussed by Turekian (1969), McSween et al. (2003), Brewer (2000) and Millero (2003).

Seawater may be an important component of hydrothermal systems, such as those that occur along mid-ocean ridges, back-arc basins, in rift basins, in oceanic plateaux and submarine volcanoes. Volcanic calderas in back-arc settings form volcanic-hosted sulphide deposits (VHMS), whereas hydrothermal exhalations in the seafloor of rift basins form sedimentary hosted sulphide deposits (SEDEX). Chimneys and sulphide mounds at mid-ocean ridges are almost entirely driven by the circulation of seawater. The mineral deposits that result from seawater hydrothermal systems are treated in Chapter 7.

1.2.2 Surface Water

Meteoric, or terrestrial waters, though minor components of the hydrosphere, are important in that they are responsible for most of the weathering, erosion and transport of material from the land masses. Figure 1.1 shows the hydrologic cycles from ocean to atmosphere, to land and back to ocean. It is estimated that meteoric water carries some 27.4×10^{14} g of dissolved matter per year. The Danube River in Europe is estimated to carry about 108×10^6 tonnes of matter each year from a catchment basin area of 0.8×10^6 km^2; the Nile carries some 54×10^6 tonnes from a catchment area of 2.75×10^6 km^2; the Mississippi river with a catchment area of 3.11×10^6 km^2 carries about 406×10^6 tonnes of solids and dissolved matter (Gortani 1959). Compared with seawater, rain water has a strong leaching action on rocks because of its low salt concentration and higher CO_2 content, especially where abundant rainfall is charged with much organic matter. Consequently, carbonates are dominant in river waters and in excess over sulphates and chlorides, although the latter tend to prevail in arid regions.

The average salinity of river water is about 100 ppm. Table 1.4 gives the average composition of dissolved solids in river water. The amount of dissolved solids carried by the rivers annually is but a small fraction of the total mass of solids contained in the sea (49.5×10^{21} g). Ca^{2+} and HCO_3^- are the ions that are dominant in river waters.

Table 1.4 Average composition of dissolved solids in river water in parts million (ppm); after Turekian (1969)

Ion	ppm	Ion	ppm
HCO_3^-	58.4	Mg_2^+	4.1
SO_4^-	11.2	Na^+	6.3
Cl^-	7.8	K^+	2.3
NO_3^-	1.0	Fe	0.67
Ca_2^+	15.0	SiO_2	13.1
		Total	120

Lakes form when runoff or river water build up in a depression. Deep lakes, such as Lake Baikal (southern Siberia) or Lake Tanganyika (east Africa), are of tectonic origin. Lake Baikal is the deepest in the world (maximum depth is 1620 m) and contains 20% of the world's fresh water. By contrast, shallow lakes, like Lake Chad in Africa and Lake Eyre in Australia, form in crustal sags. Other lakes can form along coastal regions and in fluvial wetlands or in deltas. Some large lakes are ephemeral, like Lake Eyre in Australia, which only fills up after unusual rain falls. Lakes can be closed if there is no outlet or open if they have an outlet. Lakes cover about 2% of the Earth's surface, and although some lakes are saline, most constitute a major repository of much needed fresh water. Crater lakes, as the name implies, occupy the craters or caldera structures of quiescent or extinct volcanoes (e.g. Lake Taupo in New Zealand). Examples of caldera and crater lakes are shown in Fig. 1.3. Crater lakes are also common in monogenetic volcanoes (e.g. maars). Hydrothermal discharges can occur in lakes, as for example in the East African tectonic lakes and in crater lakes.

In Antarctica more than 100 subglacial lakes have been identified. One of these, and probably the largest, is Lake Vostok, which is some 4 km beneath the surface of the ice, occupies a subglacial topographic hollow, and is about 250 km long, 50 km wide and 1 km deep. Its discovery has generated much scientific interest, particularly as a potential habitat for microbial life (Siegert et al. 2001; Siegert 2005). The water of Lake Vostok is kept warm, relative to the surroundings, by geothermal heating (Siegert 2005). The exciting aspect of the Antarctic



Fig. 1.3 Examples of crater lakes; (**A**) Kelimutu volcano, Flores Island, Indonesia (**B**) Tongariro volcano in Taupo Volcanic Zone, New Zealand (**C**) Tofua caldera, with active cone on east side; Tonga archipelago, southwest Pacific

subglacial lakes is that they may provide an analogue of the Jovian satellite Europa, where a 10–100 km crust of ice may overlie an ocean of liquid water. Extraterrestrial life in the subglacial oceans of Europa becomes a possibility, as indicated by studies of Lake Vostok, where current research hinted at the presence of microbial life (Petit et al. 2005). I return to the Europa case in Chapter 12. Equally important is the possibility of geothermal activity and hence of hydrothermal systems on the floor of Lake Vostok (Petit et al. 2005).

1.2.3 Groundwater

On reaching the surface of our planet rain water or snow and ice melt, part runs off down slope to form or feed streams and rivers and is ultimately discharged into the sea, part evaporates and is returned to the atmosphere (Fig. 1.1), part is taken up by vegetation. The remainder percolates through the soils into the bedrock to form groundwater, or phreatic water. Groundwater can penetrate deep into the subsurface and travel for considerable distances, especially if gravity-driven by steep topographic gradients. Groundwater from the Rocky Mountains in the USA travels for about 1600 km to discharge as saline springs, with about 3 wt% salinity, in the state of Missouri (Cathles and Adams 2005). Similarly, rain falling on the Great Dividing Range in eastern Australia travels 1200 km westward through sedimentary horizons with 20% porosity forming artesian aquifers. This groundwater travels at a rate of about 0.5–1 m/yr, taking approximately 1–2 million years to travel the distance.

The percolation and retention of groundwater is dependant on porosity and permeability. Permeability is the property that allows the passage of a fluid through the interconnected pore spaces in a rock, without displacement of the rock particles. Permeability is measured in *darcy*, which is the rate of flow of a fluid that passes through a cm^2 for the length of 1 cm in a second (permeability coefficient k = cm/s). Porosity is the sum total of available spaces between rock particles or grains and is expressed as a percentage (porosity coefficient n) of the total volume of the rock. Porosity can be primary if it is a relic of deposition, such that the space between grains was not completely eliminated by compaction or subsequent chemical changes, or secondary when there is partial dissolution at grain margins, fracturing or chemical changes. Figure 1.4 illustrates types of porosity. Permeability, therefore, controls the rate at which fluids flow through connected pore spaces in a porous medium (Cathles and Adams 2005). Cathles and Adams (2005) distinguished two types of permeability: intrinsic and dynamic. Intrinsic permeability is defined by the property of the medium at standard temperature and pressure; dynamic permeability is that which the medium might have under non-standard conditions. An example of the former is provided by sandstone and quartz arenites, which are composed of quartz and feldspar grains, and their permeability decreases with increasing proportions of feldspars and rock fragments. Another example is clay coatings and oil

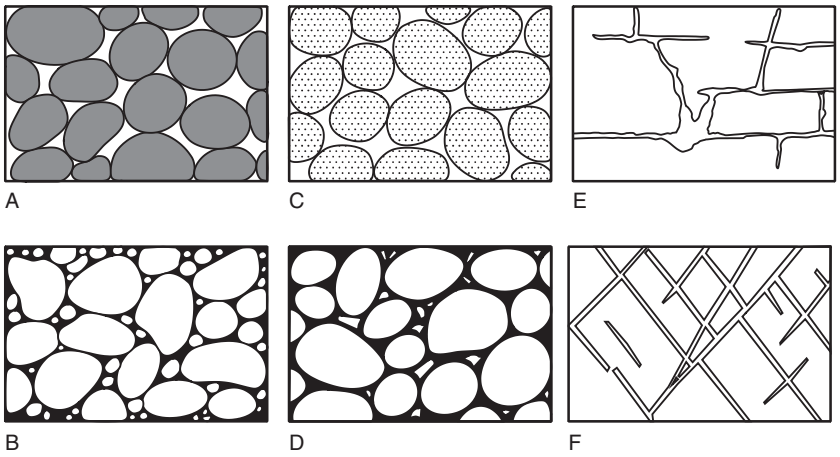


Fig. 1.4 Types of pore spaces and permeability in sedimentary rocks; (**A**) well sorted sandstone with high permeability; (**B**) poorly sorted sandstone with low permeability; (**C**) well sorted sandstone with porous clasts, permeability is very high; (**D**) well sorted sandstone with interstitial cementing material, poor permeability; (**E**) and (**F**) fractured carbonate rocks, permeability is high (after Desio 1959)

staining of the component grains, which inhibit compaction and therefore tend to preserve permeability. Fluid pressure and temperature control dynamic permeability, as for example thermal contraction at the margins of an igneous intrusion. This will induce fracturing that will increase permeability. In sedimentary basins permeability is dynamically controlled where, for example, pore pressures hydraulically fracture the rocks, or where there is thermal expansion and positive volume changes through chemical reactions (Cathles and Adams 2005).

Groundwater is known to contain bicarbonates, sulphates, chlorides and alkali metals, with their amount depending on the composition of the surrounding rocks and the length of time that the water has been in contact with them. Groundwater is the "meteoric" water of economic geologists, and in regions of high geothermal gradients it will activate as a meteoric hydrothermal system as it rises along fractures or faults. Where it reaches the surface this water becomes a hot spring (see Section 1.4.5). Meteoric hydrothermal systems in volcanic regions are generally heated by subjacent magmas, and may reach temperatures above 350°C. During their upward flow they become solutions that deposit metals and sulphides. Where they discharge at or near the surface these meteoric waters are known as geothermal fields, such as those of Rotorua in New Zealand, or the Yellowstone National Park in the USA. Examples of hot springs and geothermal fields are shown in Fig. 1.7; hot springs are discussed more fully in Section 1.4.5. Fluids of these geothermal systems usually have near neutral pH, low S and salinity.

Subsurface flow of groundwater can be very important for the formation of some ore deposits, such as roll-front U deposits (Ingerbritsen and Sanford

1998). In the case of roll-front U deposits, oxidised groundwater leaches U^{6+} from the rocks through which it travels and precipitates U^{4+}, where these waters encounter a reducing medium (redox front).

1.3 Structure and Properties of Water; Hydration and Hydrolysis

The structure of the water molecule is of special importance to its physico-chemical behaviour, as discussed in Franks (1982) and Neilson and Enderby (1986). It has been determined that the structure of water-ice is analogous to that of tridymite, and that the oxygens in ice are tetrahedrally coordinated (the tetrahedron being the building block of all silicate minerals in the Earth's crust). Therefore water appears to have a pseudo-crystalline arrangement similar to the quartz structure, which possibly serves to explain its higher density relative to ice (Paton 1978). The oxygen ion in a water molecule is much larger than the hydrogen ion, with the result that the molecule can be described as a sphere that, though neutral, has a positive charge on the side of the two hydrogens and a negative charge on the side of the oxygen. Consequently, the isolated molecule has a polar character and behaves in solution like a small magnet. This polar character is the key to the hydration and hydrolysis of silicate minerals, and thus important in weathering and hydrothermal alteration processes. In the process of hydration, water molecules are attracted to and, by virtue of their polar charges, become orientated around other attracting ions, forming hydration shells (Brimhall and Crerar 1987). Dissolution occurs when successive layers of water molecules completely surround the ion. Polar water molecules can enter crystal lattices and orientate themselves against charged mineral surfaces. Where these molecules come into mutual contact, a lubricated surface is produced, for example clays which become slippery when wet. Water of crystallisation is part of the mineral lattice, as in gypsum ($CaSO_4{\cdot}2H_2O$). On heating, this water is given off without breaking the lattice, and can be restored to reform the mineral.

Hydrolysis is the effect of the dissociation of water molecules into H^+ and OH^- ions. The process of hydrolysis is responsible for the breakdown of silicate minerals, and involves the addition of H^+ and OH^- to bonding sites in the mineral lattice. Hydrolysis is defined as the reaction between water and the ion of a weak acid or a weak base (Krauskopf 1979, p. 37). An example of hydrolysis is the reaction of fayalite with water at neutral pH:

$$2FeSiO_4 + 4H_2O \leftrightarrow 2Fe^{2+} + 4OH^- + 2H_2SiO_4$$

Or the hydrolysis reaction of atmospheric SO_2 to form sulphurous acid

$$SO_2 + H_2O \rightarrow H_2SO_3 \rightarrow H^+ + HSO_3^-$$

Hydrolysis reactions tend to be accelerated under conditions of low pH, as for example in the vicinity of oxidising sulphide ore bodies. The presence of H^+ ions in acid waters promotes the attack on silicate minerals resulting in the liberation of cations. These cations may remain in the vicinity and become fixed as stable secondary mineral assemblages, while others go into solution and are transported elsewhere. The mobility of these cations under different physico-chemical conditions has important implications for exploration geochemistry and for the evaluation of gossans (Taylor and Eggleton 2001).

Thus, hydrolysis is dependent on the concentration of H^+ ions, and any process which affects their concentration will also affect the speed and intensity of the hydrolysis process. The breaking of molecular bonds by water in a silicate melt, and consequent lowering of viscosity and consolidation temperature, is a similar process. Hydrolysis of silicate minerals is very important for hydrothermal alteration because the hydrogen ions penetrate the silicate lattices where they compete with cations (K, Ca, Na etc.) to attach to oxygen ions. The larger concentration of the charge in the hydrogen ions predominates, resulting in the displacement of the cations which are transferred from the silicate into the solution, while H^+ enters the silicate structure, producing in it drastic changes that convert the parent silicate into a new mineral, such as sericite or illite. In silicate minerals the presence of the various ions tends to consume more hydrogen than hydroxyl ions, so that if the reaction is to proceed more H^+ ions have to be supplied. Volcanic gases (HCl, CO_2, H_2S) can provide these H^+ ions and are major acidifying agents during processes of hydrothermal alteration.

1.4 Hydrothermal Fluids

A hydrothermal fluid can be defined as a hot ($\sim$50 to $> 500^\circ$C) aqueous solution, containing solutes that are commonly precipitated as the solution changes its properties in space and time. It must be pointed out at the outset that the terms fluid and solution are used interchangeably, although fluid *sensu stricto* refers to a phase at supercritical temperature in which a liquid no longer exists. In physics the term fluid refers to a substance that can flow and by its very nature it will include liquids and gases, although strictly speaking there are fluids, such as glass, that behave like solids over comparatively short periods of time. Fluids (and hydrothermal solutions) are subject to variations in temperature, pressure and density, three very important parameters in the study of hydrothermal systems. Temperature hardly needs an introduction, but in our context it is useful to be acquainted with the Zeroth law of thermodynamics and the temperature scales. If a body A feels cold to the hand and an identical body B feels hot and these are placed in contact with each other, after a time A and B will give the same temperature sensation; A and B are said to be in thermal equilibrium. This is basically the Zeroth law of thermodynamics, which states: if A and B are in

thermal equilibrium with a third body C, then A and B are in thermal equilibrium with each other. Three scales are used to measure temperatures, Celsius (°C; or centigrade), Kelvin (K) and Fahrenheit (F). The Celsius and Kelvin scales have the same numerical intervals and

$$°C = K - 273.15°$$

The K temperature is defined by the triple point of water (liquid-ice-vapour; 273.16°), which corresponds to 0.01°C; the 0 K corresponds to – 273.15°C, which is the absolute zero. The F scales has 32.02 F corresponding with 0°C and 0 K or –273.15°C corresponding to –459.67°F. The F scale is no longer used in scientific literature, being practically obsolete. Pressure p is a scalar quantity and is the magnitude of normal force acting per unit surface area. The SI unit of pressure is the *pascal*, abbreviated to Pa ($kg\ m^{-1}\ s^{-2} = N\ m^{-2}$); other units commonly used are the *bar*, where 1 bar = 100 kPa, 1 mbar = 0.1 kPa, the atmosphere (*atm*), where 1 atm = 1.01×10^5 Pa, and the *torr* (millimetres of mercury), where 760 mm Hg = 760 torr = 1 atm. The density ρ of a homogeneous fluid is mass divided by volume, and is dependant on many factors such as temperature and pressure to which the fluid is subjected. As is intuitive, for liquids the density varies little over wide ranges in temperature and pressure, whereas for gases density is very sensitive to changes in temperature and pressure.

The water of hydrothermal solutions can be derived from the following sources: seawater, meteoric, connate, metamorphic, juvenile or magmatic. Most hydrothermal solutions are of mixed origin in which one or more of the above sources can predominate. Meteoric waters include rain water, lake and river waters, and groundwaters. These waters can penetrate deep into the crust and may become heated and mineralised, thereby acquiring the properties of hydrothermal solutions. Stable isotope systematics indicate that in volcanic regions the waters of hot springs and pools are largely, if not exclusively, of meteoric origin. Oceanic crust, in and around mid-ocean ridges, allows penetration of sea water to several kilometres below the seafloor. As a result, the sea water is heated, transformed into a fluid highly enriched with metals and driven by convection, and is subsequently discharged at the seafloor as a submarine mineral-depositing hot spring. Water trapped during the deposition of sediments and produced during diagenetic reactions is known as connate water, or formation water. It is calculated that some 20% by volume of unmetamorphosed sediments in the Earth's crust consist of pore water (Hanor 1979). It is also widely recognised that hydrothermal fluids can develop during burial diagenesis, and attain high salinities and temperatures. This water is essentially unbound water, which is not bound in the lattice of rock-forming minerals. Removal of interlayer water from clays, gypsum and organic matter is an important aspect of diagenetic processes. Expulsion of fluids during burial and diagenesis takes place as a result of reduction of porosity, and the volume of water released can be considerable. An average shale can yield 3.5×10^3 litres

of water for every 1 m^3 of solid material deposited. Temperatures during diagenesis may range from a few degrees below 0°C up to 250–300°C, but water expulsion during diagenetic changes occurs at temperatures between 90 and 120°C (Hanor 1979). During the evolution of a sedimentary basin, expulsion of fluids takes place and they migrate upward and towards the margins of the basin. Where sulphur is added from any source (for example, organic matter), precipitation of sulphides may occur at favourable sites.

Metamorphic waters are derived from the dehydration of hydroxyl-bearing minerals (bound water) through rising pressure and temperature (metamorphic dewatering). The presence of volatile-rich fluids liberated during metamorphism is commonly accepted, and they can be considered as dilute brines generally containing H_2O, CO_2 and CH_4. Direct observation of waters of probable metamorphic origin comes from the Kola peninsula, where one of the world's deepest well was drilled to a depth of 12 000 m. Between 4500 and 9000 m the well intersected a zone of disaggregated metamorphic rock, within which abundant hot and highly mineralised water was found. At such depths, this water is likely to be of metamorphic origin released from bound water in rock-forming minerals. Also present in the well were abundant gases such as He, H_2, N_2, CH_4, CO_2 and various hydrocarbons, most of which are also believed to have been liberated by deep metamorphic processes (Koslovsky 1984). It is interesting to note that the dehydration of rocks at those depths is accompanied by microfracturing or hydraulic disaggregation. Temperatures of around 180°C were measured at 10 000 m, whereas sulphur isotopic determinations indicate an origin of the sulphur from the mantle. A surprising finding from these results is that the well intersected the Conrad Discontinuity (where density rise from 2.5 to 2.75 g/cm^3 and velocity of seismic waves from 5 to 6 km s^{-1}), which is taken to mark the transition from upper (granitic) to lower crust. This discontinuity, however, is found to be the lower boundary of the disaggregation and hot metamorphic water zones, where the rock returns to its normal density for that depth and water is no longer present. It was further established that in the zone of disaggregation, rock fragments are cemented by sulphides of Cu, Zn, Ni, Fe and Co. These discoveries indicate that gas-water-rock interactions are active at great depths, and that conditions exist for the formation of hydrothermal ore deposits entirely powered by metamorphism (Chapter 9).

Some geoscientists consider juvenile water as that which is assumed to be derived from the mantle. Magmatic waters are those that separate from melts upon cooling, generating a magmatic-hydrothermal system, which is perhaps the most powerful ore-depositing agent. In addition to water, other volatile constituents that may be present in magmas include H_2S, CO_2, SO_2, SO_4^-, HCl, B, F and H_2. Water contents of magmas range from as little as 0.2% to as much as 6.5% by weight. The presence and abundance of these volatiles in a magma is generally related to its composition and the source region from which it originated. It is possible, for example, that a B-rich granite may have derived from melts that have interacted with tourmaline-rich metasedimentary rocks. Further, the relative abundance of one volatile over another (e.g. B/F) may be

very important in determining the type of ore deposit that may be formed on exsolution of the volatile fractions from the late stages of consolidation. I return to discuss in some detail magmatic waters and the evolution of a magmatic-aqueous phase during the solidification of a hydrous magma in Chapter 2.

Hydrothermal fluids are generally assumed to be liquid solutions in which water is the solvent. Ore-forming fluids may occur as either molecular or colloidal solutions. The circulation of hydrothermal fluids in the Earth's crust results in the inception and development of hydrothermal systems.

A true or molecular solution is defined as a homogeneous system containing a dissolved substance (solute) distributed uniformly in a dissolving substance (solvent). Solutions can exist in all three states of matter: gas, solid or liquid. All gas mixtures are solutions (air, for example); whereas solid solutions are characterised by the substitution or interposing of foreign atoms, or ions, in the lattice sites, or between the lattices of mineral-forming elements. Solids or gases become solutes when dissolved in liquids. If both components are liquid, it is usual to call the more abundant component the solvent. A solution is said to be saturated if it is in equilibrium with the undissolved solute. Therefore, an undersaturated solution is characterised by a lower concentration of solute with respect to the saturated solution; a supersaturated solution, on the other hand, contains more than the equilibrium concentration of solute. This latter type is usually unstable. There are two types of solute in water: non-electrolytes and electrolytes. In non-electrolytic water solutions the solute dissolves as molecules and therefore they do not conduct electric current. Examples of non-electrolytic solutions are methyl alcohol or sugar in water. Electrolytic solutions conduct electric current through the dissolved substances which are present as electrically charged ions. NaCl is a typical example that, when dissolved in water, dissociates into its constituent ions:

$$NaCl(s) \rightarrow Na^{+}(aq) + Cl^{-}(aq)$$

Other examples are:

$$Na_2SO_4(s) \rightarrow 2Na + (aq) + {SO_4}^{2-}(aq)$$

$$HCL(aq) \rightarrow H^{+}(aq) + Cl^{-}(aq)$$

The concentration of solutes in aqueous solutions is expressed as moles of solutes per litre of solution, defined as molarity or molar concentration, and indicated as "M". A mole is the number of a given element's molecules, or atoms, contained in its unit molecular or atomic mass. For example, one mole of O_2 contains 6.022×10^{23} O_2 molecules (called Avogadro's number) in exactly 32 g ($2 \times$ atomic mass 16), and one mole of H_2O contains 6.022×10^{23} H_2O molecules in 18.02 g of H_2O (2.016 + 16.00 atomic masses of H_2 and O respectively). A one-molar solution (1 M) therefore contains one mole (1 mol) of solute per litre of solution. Gill (1989) provided details of the chemistry of aqueous solutions.

A colloidal solution is made up of a dispersed phase (solid, liquid or gas) diffused in a medium that can be solid, liquid or gas. A review of the general properties of colloidal systems can be found in Krauskopf (1979, p. 120–139), from whom I have summarised the following. In ore-forming colloidal systems, solid phases are dispersed in liquid (sol), or gaseous media. The size of the particles is in the range of 10^{-3}–10^{-6} mm (1000–1 μm). Colloidal particles have a very high surface area to volume ratio and behave as electrically charged particles. Their charge is due to adsorption of ions, making colloidal particles repel each other, so that settling is difficult or impossible. The addition of an electrolyte to the system will neutralise the colloidal particle to enable flocculation (precipitation). When a colloid containing a certain adsorbed ion on its particles is added to an electrolyte solution consisting of different ions, some of these electrolytic ions will be adsorbed, displacing the original ions, which will then pass into the solution. This is the phenomenon of ion exchange, and an important mechanism in explaining the distribution of cations between solutions and wall rocks. The high concentration of metals in manganese ores can be attributed to adsorption of cations on manganese dioxide sols. Ions that are also commonly adsorbed are H^+ and OH^-. In general, sulphides, silica and manganese dioxide sols are negatively charged, whereas oxide and hydroxide sols are positively charged. Temperature is an important parameter for colloids in hydrothermal solutions. High temperatures favour flocculation because increased kinetic movements allow the particles to come into contact with one another, and the larger particles thus formed will flocculate (although this is not always true, because gold sols are stable at temperatures of up to 150°C). On a geological time scale colloids are unstable and tend to crystallise, so that the materials examined may not show their pristine colloidal state. Amorphous or cryptocrystalline substances with colour banding may have had a colloidal origin. Certain textures of metallic ores in hydrothermal veins and some finely crystalline ores in open cavities are also thought to form from colloidal solutions. Silica in hot springs may also be of colloidal origin. At the Sleeper bonanza Au deposit in Nevada (USA) evidence of colloidal solutions, responsible for the transport of Au and silica, is provided by alternating bands of barren colloform quartz and mineralised opaline quartz (Saunders 1990).

1.4.1 Solubility and Boiling

Boiling and solubility are instrumental in the separation of components from the solutions, and therefore of great importance in the deposition of ores from hydrothermal fluids. The solubility of ionic substances is the result of interaction between polar H_2O molecules and the dissolving ions. Solubility depends on: (1) the force of attraction between H_2O molecules and the ions of the solid, which tends to bring the solid into solution; and (2) the force of attraction

between oppositely charged ions, which will tend to prevent the solid from going into solution. Generalised solubility rules are (Masterton et al. 1981):

NO_3^- All nitrates are soluble
Cl^- All chlorides are soluble, except for AgCl, Hg_2Cl_2
SO_2^- All sulphates are soluble except $CaSO_4$, $SrSO_4$, $BaSO_4$, $PbSO_4$, Ag_2SO_4
CO_2^- All carbonates are insoluble except those of Group elements (I, Na, K, etc.)
OH^- All hydroxides are insoluble except Group I elements, $Sr(OH)_2$ and $Ba(OH)_2$
S_2^- All sulphides are insoluble, except Groups I and II elements

Both temperature and pressure have major effects on solubility. Usually the dissolution of a solid is an endothermic process, brought about by the necessary absorption of heat to break down the crystal lattice. Hence an increase in temperature increases the solubility, and the reaction given below moves to the right:

$$\text{solid} + \text{solvent} \leftrightarrow \text{solution}$$

Dissolving a gas into a liquid evolves heat (exothermic), so that:

$$\text{gas} + \text{liquid} \leftrightarrow \text{solution}$$

This means that gases become less soluble as temperature increases. Pressure can also have major effects on gas-liquid systems: for a given temperature an increase in pressure increases the solubility of a gas. A pressure rise increases the concentration of molecules in the gas phase, which in turn is counteracted by more molecules entering the solution. The equilibrium of the second equation above also moves to the right. Conversely a drop in pressure will cause the gas to exsolve from the solution. Boiling of a common liquid occurs at a temperature at which its vapour pressure equals the pressure above it. Boiling of a hydrothermal solution takes place for the same reason, with the immediate result that dissolved gases and other volatile compounds, such as CO_2 and H_2S, are removed from the solution. The process of boiling hydrothermal solutions is important because it results in the precipitation of ore elements (e.g. Au, As, Sb, Ag).

1.4.2 Acid-Base Nomenclature

A substance is said to be an acid if it produces hydrogen ions (H^+) in water solution, and a base if it produces hydroxide ions (OH^-). Water, whether pure or in solution, dissociates into a hydrogen cation (H^+) and a hydroxyl anion (OH^-). The dissociation constant of water (Kw) at 25°C is given as:

$$\text{Kw} = (\text{H}+) \times (\text{OH}^-) = 1.0 \times 10^{-14}$$

The product $(H^+) \times (OH^-)$ is constant for all water solutions, which at 25°C is always 1.0×10^{-14}; thus the concentration of H^+ or OH^- can be calculated and the acidity or alkalinity of a solution specified (Krauskopf 1979). A neutral solution has equal concentrations of H^+ and OH^-, which is 10^{-7} MH^+. A strong acid has 1 H^+, and a strong base 10^{-14} MH^+. It is more convenient to express acidity in terms of pH rather than H^+, and this is calculated using a negative logarithmic exponent of the hydrogen concentration according to the formula:

$$pH = -\log_{10}[H^+] = \log_{10} 1/[H^+]$$

Thus a strong acid has a pH of 0, a neutral solution 7, and a strong base a pH of 14.

This terminology is not to be confused with the geological usage of acid, basic and alkaline. Silica, being the principal oxide constituent of all rock systems, serves as a basis to determine the acidity of a rock. Thus a high concentration of SiO_2 (> 66 wt%) defines an acid rock. An intermediate rock contains between 52 and 66 wt% SiO_2, whereas values of less than 52 wt% define basic rocks. The basicity of a rock can also be determined by the abundance of metal oxides, such as MgO and FeO; the alkalinity of rocks by the oxides of Na and K. The above geological usage originated many years ago when SiO_2 was considered an acid oxide, and MgO, FeO etc. as basic oxides. This terminology is well-entrenched in the current geological language and is considered useful for practical purposes.

1.4.3 Redox Potential

The redox potential is an important parameter for characterising aqueous solutions and the oxidising and reducing conditions of a geological environment. Redox is an abbreviation of reduction and oxidation. A reduction-oxidation reaction is one in which transfer of electrons takes place from one element to another.

A relevant example in the context of this book is the case of Fe. This element has two oxidation states, Fe(II) (ferrous) and Fe(III) (ferric); metallic Fe is symbolised Fe(0). A reaction in which Fe increases its number of electrons that become bonded with other atoms is an oxidation reaction, as shown in the reaction:

$$\underset{\text{olivine}}{2Fe_2SiO_4} + O_2 + 4H_2O \leftrightarrow \underset{\text{hematite}}{2Fe_2O_3} + 2H_4SiO_4$$

with the opposite being the process of reduction, in which the oxidised element, Fe, receives back some or all its bonding electrons (Gill 1989).

Redox reactions commonly include the actual exchange of O_2 between the mineral phases, as in the example below (McSween et al. 2003):

$$2Fe_3O_4 + 1/2O_2 \leftrightarrow 3Fe_2O_3$$

magnetite

But, as pointed out by McSween et al. (2003), it would be quite misleading to emphasise the role of O_2, because it is more important to highlight the significance of electron exchange between reactants and products. Thus, the above reaction becomes:

$$2Fe_3O_4 \leftrightarrow 3Fe_2O_3 + 2H^+ + 2e^-$$

In which,

$$Fe^{2+} \leftrightarrow Fe^{3+}$$

This is an oxidation step that is of fundamental importance in banded iron ore systems (Chapter 8).

The process by which certain elements lose electrons while others gain them can be quantitatively measured. This can be done by assigning a potential difference to half-reactions, choosing as a standard the half-reaction of the hydrogen couple:

$$H_2 \rightarrow 2H^+ + 2^{e^-}$$

To this half-reaction potential is assigned the arbitrary value of 0 (E = 0.00 V). If the sign is positive, the half-reaction has a greater tendency to release electrons than does the reaction shown above, and the converse is true if the sign is negative. Thus, Cu with an oxidation potential of +0.16 displaces Ag with a potential of +0.22, whereas Zn (–0.76) will displace Cu (+0.16). This means that Zn will release electrons to both Cu and Ag, but Cu only to Ag.

The term redox potential is used as a synonym for oxidation potential and is given the symbol Eh. Conventionally, it is assumed that a high Eh indicates an oxidising system, whereas a low Eh indicates a reducing system. Thus, oxidation involves the loss of electrons, and reduction the gain of electrons. If a copper wire is immersed in a solution of silver nitrate ($AgNO_3$), the copper will dissolve and metallic silver will precipitate. The copper wire releases electrons (e^-) which combine with silver cations in the solution to precipitate neutral metallic silver. This reaction involves oxidation-reduction (redox) and is shown thus:

$$Cu(s) = Cu^{+2} + 2e^-;$$
$$2Ag^+(aq) + 2e^- = 2Ag(s)$$

The net reaction is:

$$Cu(s) + 2Ag^{+}(aq) = Cu^{+2}(aq) + 2Ag(s)$$

The first equation above is a half-reaction in which electrons are lost, and is therefore oxidation; the second equation is the half-reaction in which electrons are gained, and is reduction. The net result, expressed in the third and last equation, is therefore the oxidation-reduction reaction, in which Cu is the reducing agent and is oxidised, and Ag is the oxidising agent that is reduced. The same can be said for oxidation numbers, where a fictitious charge is given to an ion. Thus, for the net reaction above, Cu is oxidised because its oxidation number is increased from 0 to +2; reduction, on the other hand, results from a decrease in oxidation number, and so Ag is reduced with a decrease in its oxidation number from +2 to 0. Eh and pH are two important variables that control the mobility of elements in a geological system, and consequently Eh-pH diagrams are useful to show conditions under which processes of oxidation and reduction can occur in nature. Standard redox potentials are given in Table 1.5 and examples of Eh-pH diagrams are given in Fig. 1.5.

1.4.4 Chemical Potential, Chemical Activity, Fugacity, Oxygen Fugacity

The terms chemical potential, chemical activity and fugacity are frequently used in discussions of hydrothermal alteration involving aspects of physical chemistry, chemical equilibria and thermodynamics. The chemical potential indicates the capacity of one compound to react with another, and represents a particular energy level for the given compound in a phase. The chemical potential is analogous to gravitational potential energy, in which the stable state is at the lowest potential. The chemical potential can be expressed by the formula:

$$\mu_a = (dG/dXa)_{P,T}, X_b, X_c \text{ etc.}$$

In the equation above, the chemical potential μ_a of a substance *a* equals the change of an extensive state function G (internal energy, volume, mass) resulting from the addition of small amounts of a, while P, T and all other substances b, c etc remain constant (Best 1982). In a hydrous silicate melt at equilibrium the chemical potential μa of water equals the potential of water vapour, which in turn equals the potential of water in the hydrated minerals (Best 1982). The activity of a chemical species is denoted by *a* and is approximately proportional to concentration and is expressed as moles

Table 1.5 Redox potentials. After Milazzo et al. (1978) and Bard et al. (1985)

Half-reaction		E^{-o} (volts)
Oxidizing agent	*Reducing agent*	
$Li^+ + e–$	⇄ Li	–3.05
$K^+ + e–$	⇄ K	–2.93
$Ba^{2+} + 2e–$	⇄ Ba	–2.91
$Ca^{2+} + 2e–$	⇄ Ca	–2.76
$Na^+ + e–$	⇄ Na	–2.71
$Mg^{2+} + 2e–$	⇄ Mg	–2.38
$Al^{3+} + 2e–$	⇄ Al	–1.68
$Mn^{2+} + 2e–$	⇄ Mn	–1.18
$2H_2O + 2e–$	⇄ $H_2(g) + 2OH^-$	–0.83
$Zn^{2+} + 2e–$	⇄ Zn	–0.76
$Cr^{2+} + 2e–$	⇄ Cr	–0.74
Fe^{2+} 2e–	⇄ Fe	–0.44
$Cr^3 + e–$	⇄ Cr^{2+}	–0.42
Cd^{2+} 2e–	⇄ Cd	–0.40
$Co^{2+} + 2e–$	⇄ Co	–0.28
$Ni^{2+} + 2e–$	⇄ Ni	–0.25
$Sn^{2+} + 2e–$	⇄ Sn	–0.13
$Pb^{2+} + 2e–$	⇄ Pb	–0.13
$Fe^{3+} + 3e–$	⇄ Fe^{2+}	–0.04
$2H^+ + 2e–$	⇄ $H_2(g)$	0.00
$S + 2H^+ + 2e–$	⇄ $H_2S(g)$	+0.14
$Sn^{4+} + 2e–$	⇄ Sn^{2+} (*aq*)	+0.15
$Cu^{2+} + e–$	⇄ Cu^+ (*aq*)	+0.16
$SO_4^{2-} + 4H^+ + 2e–$	⇄ $SO_2(g) + 2H_2O$	+0.17
$Cu^{2+} + e–$	⇄ Cu (*s*)	+0.34
$2H_2O + O_2$ 4e–	⇄ $4OH^-$	+0.40
$Cu^+ + e–$	⇄ Cu (*s*)	+0.52
$I_2 + 2e–$	⇄ $2I^-$ (*aq*)	+0.54
$O_2(g) + 2H^+ + 2e–$	⇄ H_2O_2 (*aq*)	+0.70
$Fe^{3+} + e–$	⇄ Fe^{2+} (*aq*)	+0.77
$NO_3 + 2H^+ + e–$	⇄ $NO_2(g) + H_2O$	+0.80
$Ag^+ + e–$	⇄ Ag (*s*)	+0.80
$Hg^{2+} + 2e–$	⇄ Hg(*l*)	+0.85
$(AuCl_4) + 3e^-$	⇄ Au(*s*) + $4Cl^-$ (*aq*)	+0.93
$NO_3 + 4H^+ + 3e–$	⇄ NO(g) + $2H_2O$	+0.96
$Br_2(l) + 2e–$	⇄ $2Br^-$ (*aq*)	+1.07
$O_2(g) + 4H^+ + 4e–$	⇄ $2H_2O$	+1.23
$MnO_2 + 4H^+ + 2e–$	⇄ Mn^{2+} (*aq*) + $2H_2O$	+1.23
$Cr_2O_7{}^2 + 14H^+ + 6e–$	⇄ $2Cr^{3+}$ (*aq*) + $7H_2O$	+1.36
$Cl_2(g) + 2e–$	⇄ $2Cl^-$ (*aq*)	+1.36
$MnO_4 + 8H^+ + 5e–$	⇄ Mn^{2+} (*aq*) + $4H_2O$	+1.51
$Co^{3+} + e–$	⇄ Co^{2+} (*aq*)	+1.92
$F_2(g) + 2e–$	⇄ $2F^-$ (*aq*)	+2.87

Increasing oxidizing ability ↓

Increasing reducing ability ↑

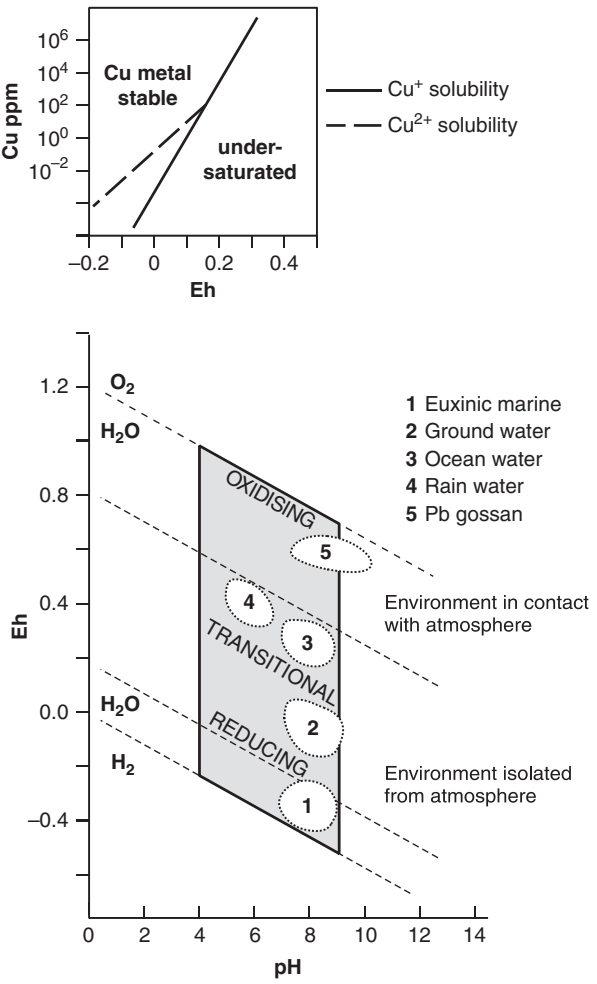


Fig. 1.5 Examples of Eh-pH diagrams; (**A**) solubility of Cu as a function of Eh; (**B**) Eh and pH limits of some natural environments. After Rose et al. (1979) and Krauskopf (1979)

per litre. In solid solutions, or mixtures of liquids, chemical activity is related to the mole fraction of the constituent. In gases, chemical activity can be approximated by partial pressure (Rose et al. 1979), and is expressed by:

$$a = m$$

where m is the concentration and a is the activity coefficient (Hemley and Jones 1964).

Fugacity is a measure of the escaping tendency of a vapour or gas and its departure from ideal behaviour. In a mixture of gases the fugacity f of a gas is

proportional to its mole fraction X, or concentration in the mixture, and to the total pressure, according to the relation:

$$f = X_{PT}$$

Fugacity is not restricted to gases, but is also accepted as a measure of flow of matter from high to low potentials of solids and liquids. For a detailed and comprehensive treatment of this topic, the reader should consult Carmichael et al. (1974) and Carmichael and Ghiorso (1990).

Oxygen fugacity (f_{O2}), first defined by Eugster and Wones (1963), is a variable controlling oxidation potential in terms of partial pressure of oxygen. Oxygen fugacity is of petrological importance and essentially relates to the potential of Fe to occur in a more oxidised or reduced state. Oxygen fugacity is usually calibrated using buffers, such as fayalite-magnetite-quartz (FMQ) or nickel-nickel oxides (NiNiO). At very low f_{O2}, Fe is present in the native state (Fe°), as in meteorites, and presumably in the core. At higher f_{O2}, Fe is divalent, as in the reaction below, known as QIF (Frost 1981):

$$Fe_2SiO_4 \leftrightarrow 2Fe^{\circ} + SiO_2 + O_2$$

fayalite

At higher f_{O2}, Fe is in both ferrous and ferric states and forms magnetite (reaction FMQ):

$$2Fe_3O_4 + 3SiO_2 \leftrightarrow 3Fe_2SiO_4 + O_2$$

and at even higher f_{O2}, ferric Fe forms hematite (reaction MH):

$$6F_2O_3 \leftrightarrow 4Fe_3O_4 + O_2$$

In the system Fe-O-SiO_2, the reactions FMQ and IQF are the upper and lower f_{O2} limit for fayalite and MH is the upper f_{O2} limit for magnetite. The reactions IQF, FMQ and MH are referred to as oxygen buffers.

Oxygen fugacity is also important in determining the composition of fluids associated with igneous and metamorphic rocks (Frost 1981). The Fe content of magmas determines the oxidised or reduced character of magmatic fluids, which in turn determines the type of ore system. The oxidation state of intrusions is largely based on the abundance of magnetite or ilmenite, and can be classified as reduced (ilmenite series or S type) or oxidised (magnetite series or I type) (Lang and Baker 2001). The diagram of Fig. 1.6 shows the relationship of the Fe content versus f_{O2} and the position of reduced, mantle derived alkaline magmas with Sn and W mineralisation and of oxidised calc-alkaline magmas with Cu-Mo, or Cu mineralisation (Lang and Baker 2001). I return to discuss

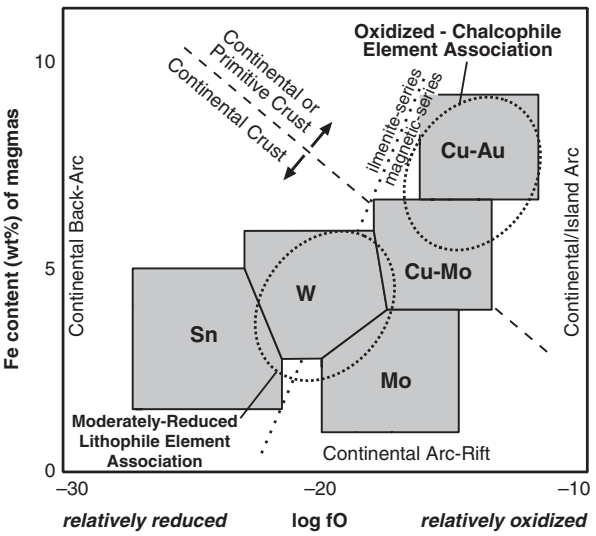


Fig. 1.6 Diagram showing relationships between oxidation state of magmas, their Fe content and associated metal assemblages. After Lang and Baker (2001)

the topic of oxidation state of magmas and their relationship to intrusion-related ore systems in Chapter 4.

1.4.5 Hot Springs

"*What is a hot spring*?" is the title of the first article in a special issue of the Canadian Journal of Earth Sciences (Renaut and Jones 2003). The article in question by Pentecost et al. (2003) reviews the results of a questionnaire sent to a number of geoscientists. The definitions returned include: (1) hot springs; water issuing at temperatures above 36.7°C, referring to the definition of hot or cold in relation to the human body; (2) thermal springs defined as mean water temperature higher than mean air temperature; (3) temperature above local mean air, but above 36.7°C (normal temperature of the human body); (4) cold spring defined by water temperature less than 36.7°C. Pentecost et al. (2003) acknowledged the difficulty in using the above definitions because cold, warm and hot are relative terms. The final recommendation was that the use of the term "hot spring" is more acceptable and should be applied to waters issuing at or above 36.7°C, preferably measured at the point where it emerges from the ground. This is the definition used in this book.

Subaerial and subaqueous (submarine and sublacustrine discharges) hot springs and degassing volcanoes are evidence of hydrothermal activity. Subaqueous hot springs are very common in volcanic and tectonic lakes (e.g. East African lakes, Lake Taupo in New Zealand), and on the seafloor along mid-ocean ridges and in volcanic islands. During the last 25 years, studies of the

ocean floor by manned and unmanned submersible crafts have led to some of the most astonishing scientific discoveries. Amongst these discoveries are active vent sites on the seafloor, commonly depositing ore minerals in the submarine valleys of spreading ridges and on the flanks of volcanic islands, as well as the previously unsuspected existence of thriving ecosystems. These submarine hot spring systems are of great importance for a number of reasons, including the fact that they can be considered as modern analogues of ancient ore systems that are now exposed on land and constitute exploitable ore deposits, as well as providing valuable insights into the origin of life and possible life forming processes. In this section, however, I focus on subaerial hot springs and return to relevant aspects of submarine hot springs in Chapter 7.

Subaerial hot springs are generally found in areas of high geothermal gradients in both orogenic (convergent margins) and non-orogenic areas (divergent margins, intracontinental rifts). Anomalous geothermal gradients are related to on-going or residual magmatic activity (e.g. cooling magmas at depth) or anomalous crustal conditions, such as tectonic uplift of slices of hot lower crust close to the zone of meteoric waters (e.g. Alpine Fault zone in New Zealand, or Himalayan collision zone). Hot springs can also result from regions of anomalous heat flow due to high concentration of radioactive elements in the crust or in high-heat producing granites. Hot springs and associated hydrothermal systems that can be related to high heat flow due to radioactivity have been called amagmatic and have been reported in the literature (Neumann et al. 2000; Brugger et al. 2005). I return to this topic in more detail in Chapter 9.

There are several types of hot springs on land (Renaut and Jones 2003), including acid-sulphate, alkaline, and carbonate-rich. Acid-sulphate springs are generally low in chlorides and are characterized by low pH, due to oxidation of H_2S to H_2SO_4. Other volatiles that may be present include CO_2, NH_3, B, as well as metals such as Hg, Bi, As, Au, Sb, W, Tl and Sn. Acid-sulphate thermal waters are generated by condensation of steam and vapours as they rise through cracks and fissures at temperatures below 400°C (Ellis and Mahon 1977). Acid-sulphate hot springs occur more commonly on volcanic slopes and in crater lakes than in basins or caldera structures and are generally associated with fumaroles and mud pools (Fig. 1.3). Alkaline near neutral chloride thermal waters are characterised by the presence of Na, K chlorides, silica, bicarbonates, fluoride, ammonia, As, Li, Rb, Cs and boric compounds. The pH, though generally near neutral, can range from 5 to 9 (Ellis and Mahon 1977). These hot springs are generally found in caldera settings, because the convective column is within easy reach of the ground surface. Siliceous sinters are usually well developed in areas of chloride springs, due to precipitation of amorphous silica as opal-A, which later changes to cristobalite and finally quartz. Siliceous sinters may take on a variety of colours due to Fe oxides and the growth of algae, and their deposits can form spectacular features such as cascades, terraces and mounds (Fig. 1.7). Siliceous sinters may contain Au, Ag, W, Sb, As, Tl, as exemplified by the famous Champagne Pool at Waiotapu, Taupo Volcanic Zone, in New Zealand. Alkaline chloride thermal springs are also associated



Fig. 1.7 Waimangu geothermal area in the Taupo Volcanic Zone, New Zealand (**A**) Panoramic view of Champagne Pool; orange precipitate contains anomalous abundances of Au and Sb (see Table 1.6) (**B**) Waimangu hot spring and algal mats pink and greenish colours; material from this pool assayed 4% W (**C**) Waiotapu sinter deposit

with geysers, such as those in the Yellowstone National Park in the U.S. and the Taupo Volcanic Zone. Siliceous sinters (including geyserite) are perhaps the most common product of hot spring precipitates. The precipitation mechanisms of the silica can be abiotic or biotic (Guidry and Chafetz 2003). The former includes processes such as rapid cooling, evaporation and pH changes. Biotic precipitation is by microbial mediation with two main pathways (Guidry and Chafetz 2003): active and passive. In the active pathway microbes can induce the precipitation of silica by changing the pH of the solution, as for example by sulphate reduction. In the passive mechanism, microbes would promote silica precipitation by simply providing a suitable organic substrate. In addition, active silicification of microbes is quite rapid and may occur while they are still alive (Renaut et al. 1998). The silica precipitated from hot springs generally consists of opal-A ($SiO_2{\cdot}nH_2O$), of which there are many variations depending on water content and mode of precipitation (Jones and Renaut 2003). For example, geyserite from the Whakarewarewa geothermal area in New Zealand can contain up to 15 wt% water, although the siting of this water changes according to the morphologies of the precipitate (Jones and Renaut 2003). Opal-A may form spherical bodies, spicules, rods, tubules, lenticular shapes

or can replace organic substrates, such as microbes or plant material. Of the microbes, cyanobacteria are especially prone to silicification and, as reported by Jones and Renaut (2003), can be partially silicified while still alive. In this way, microbes with tell-tale filamentous shapes are preserved and for this reasons when these shapes are detected in ancient siliceous chemical sediments, the possibility of microbial life is inferred (Chapter 10). In addition to opal-A, other minerals that can be found in siliceous sinters include kaolinite, clays, jarosite, alunite, Fe oxyhydroxides, pyrite and native S (Jones and Renaut 2003).

As mentioned above, siliceous sinters may contain ore-grade metalliferous concentrations of Au, Ag, W, Sb, As, Tl and Hg. For example, the sinter shelf that borders Champagne Pool in New Zealand (Fig. 1.7), which is a mixture of amorphous silica, silicates, sulphate, organic materials and sulphides rich in Au (110 ppm) and Ag (330 ppm). However, much of the anomalous trace element abundances (see Table 1.6) found in sinters are not associated with sulphides or other mineral species, but appear to be bound to the opal-A that precipitates around filamentous bacteria (Jones and Renaut 2003). Table 1.6 shows metal contents of hot springs and related chemical precipitates. Other elements such as Cu, Pb, Zn, Te and Bi are by contrast concentrated at deeper levels of the geothermal system. Thus, it is clear that geothermal systems can have distinct metal zonations with respect to depth, as discussed in Chapter 5. The striking

Table 1.6A Metal analyses of surface deposits at Broadlands, New Zealand. After Weissberg et al. (1979)

Element (Values in ppm or %)	Au	Ag	As	Sb	Tl	Pb	Zn	Hg
Champagne pool – orange precipitate	80	175	2%	2%	320	15	50	170
Sinter material	<0.02	<0.2	50	5	1.0	<5	5	0.03
Geiser sinter	0.05	0.5	20	5	10	–	–	2
Yellow-orange mud	0.08	1.0	12%	800	110	–	–	13
Sulphur mounds	0.05	0.5	10%	285	130	25	15	18
Sinter terrace	2.35	2.0	5500	440	40	5	5	16
Silicified breccia	0.02	–	2.3	80	9	1	580–6450	0.03
Silicified breccia	0.05	2.5	100	55	5	2600	1.3%	1.0
Wallrock	0.05	1.5	–	5	–	3000	4100	–

Table 1.6B Selected metal analyses of fumarolic sublimates at Merapi Volcano, Indonesia. After Kavalieris (1994)

Element (Values in ppm or %)	Au	Ag	Mo	V	W	Pb	Zn	As
Blue and red-green sublimates	100	61.8	3.18%	4800	4390	1.84%	2010	3600
as above	12.1	50	1.08%	488	1470	1.64%	2870	966
as above	24	9.1	0.14%	222	460	0.11%	1510	2720

Table 1.7 Relative Concentrations of Gold, Silver, and other trace elements from Sinter Samples around Champagne Poo land from the Artists Palette ($mgkg^{-1}$ unless otherwise indicated). After Pope et al. (2005)

Description	Au	Ag	B	Co	Cu	Zn	Ga	Ge	As %	Mo	Sb %	Cs	W	Tl	Pb
Orange precipitate	543	745	252	2.7	411	492	1290	20.2	12.1	7.74	45.9	1120	310	8640	55.3
Orange-yellow sulfurous precipitate	295		3310	15.9	6480	3120	1770	317	13.5	26.5	11.1	3790	13352	655	7.8
Dark organic(?) material											8.97	2130	788	463	88.0
Yellow-orange sulfurous precipitate	94.6		3000	10.8	886	741	796	187	11.7	10.9	4.15	2870	3114	384	296
White silica-rich sinter	51.5		572	3.7	123	402	426	13.3	3.65	0.88	4.16	1930	65	539	34.4
Silica-rich sinter	9.2		8180	2.3	94.7	227	156	148	0.90	2.68	0.70	1.80	299	70.0	7.8

feature of these discharge waters is their poor metal content compared with the strong concentration in the precipitates (by a factor of up to 10^6), as may be the case for Au and Ag. As previously mentioned, some of the critical factors for this enrichment must be time and depositional rates, as well as the presence of microbial life. In this respect an interesting calculation first published by Weissberg et al. (1979) shows that the discharge water of one borehole contained 0.04 ppb Au, or 0.00004 ppm, so that 32×10^6 g of Au would be contained in 800 km^3 of discharge water (1 tonne of H_2O = 1 m^3). Given that a natural discharge rate of 1.6×10^6 kg/h (or 0.014 km^3 yr^{-1}) was recorded at Wairakei, then some 800 km^3 of thermal water would pass through the system in 57 000 years. In 300 000 years a total of 4200 km^3 of water would circulate through the system, and given a suitable rate of deposition, an orebody containing 168×10^6 g of Au could result. Similar calculations carried out by Browne (1986) indicate that those of Weissberg et al. may, in fact, be conservative. On the basis of the Au content in scales deposited during discharge from a well, Browne (1986) estimated a concentration of 1.5 g/t Au in the aquifer, and envisaged that it would take only 1500 years to transport 32×10^6 g of Au through the system. Studies of fumarolic gases of Colima volcano (Mexico) by Taran et al. (2000) revealed the presence of several mineral precipitates, including Au crystals up to 40 μm in size, in silica tubes that had been inserted into 800°C fumarolic vent. The mineral precipitates that these workers found in the inner walls of the experimental silica tube reflected complex temperature zones, namely: (1) 380–450°C amorphous silica, cristobalite, hematite and various Na-K-V-Zn-Cu-S phases; (2) 450–550°C Au, cristobalite, hematite, Fe-Ti oxides, tenorite, chalcopyrite; (3) 600°C Au, amorphous silica, cristobalite, hematite, tenorite, WO_3, barite, anglesite and various K-Cu-Pb-V-Cl-S phases; (4) 680°C cristobalite, tridymite, hematite, rutile, plattnerite (PbO_2), anglesite, Cu-Sn-Zn-Cl phases; (5) 740°C tridymite, hematite, fluorite, wolframite, K-Na-Pb-Zn-s phase; (6) 828°C, tridymite, hematite, bunsenite, fluorite, Na-K-Pb-Cu-S phases, Na-K-Ca-S phases, Fe-Ti-u-S phases, As-Sb-S phase and W-V-Co phase. Gold was found to have precipitated within a narrow temperature range of 550–600°C. Taran et al. (2000) calculated that within the above temperature range, Au precipitation at high f_{SO2} corresponds to a Au concentration of about 1 ng/kg. Since geothermal fields are known to have been active for between 1 and 2 million years, the implications of these estimates, even if taken conservatively, in consideration of less efficient deposition rates, are obvious.

The exploration for geothermal energy received great impetus in the 1960 s and 1970 s as a result of the increased oil prices and the political uncertainties in the oil-producing countries. The result of this exploration, particularly in New Zealand, the USA, southern Europe and Japan, was of incalculable benefit to our knowledge of hydrothermal activity, processes of solution, transport and deposition of metallic elements, effects of water-rock interaction, and in a broader sense, the ore-forming processes related to the geothermal systems. There is much literature on the subject, but for the present purpose the reader is

referred to White (1981), Weissberg et al. (1979), Ellis (1979), Ellis and Mahon (1977), Seward (1979a,b) and Henley and Ellis (1983). Similarities between the active geothermal systems and epithermal precious and base metal ore deposits were noted many years ago by Lindgren (1933). It is now widely recognised that epithermal deposits are essentially the result of the interaction of geothermal waters with wall rocks, and that many epithermal deposits in the geological record are in fact the fossil equivalent of ancient geothermal systems. Nowhere is this in greater evidence than in New Zealand, where subduction-related volcanic arcs, such as the active Taupo Volcanic Zone and the Coromandel peninsula volcanics of Miocene-Pliocene age and associated Hauraki goldfields, afford a unique opportunity for examining active and fossil epithermal systems geographically adjacent to one another.

In general, discharge of fluids at the surface is represented by near-neutral chloride-rich hot spring waters, or it may be characterised by acid-sulphate boiling pools. The latter are generally related to steam that separates from deeper chloride-rich boiling fluids in vapour-dominated systems resulting in fumarolic activity containing CO_2 and H_2S. Bicarbonate-rich waters are common in areas where carbonate rocks are present. Deeper in the system, beneath the levels of boiling and atmospheric oxidation, waters are usually slightly alkaline (pH 6–7) and weakly saline. Isotope systematic indicate that the waters of geothermal systems are dominantly of meteoric origin with a possible minor component being derived from magmatic sources. For the Yellowstone geothermal system i*t* is estimated that all the chloride waters discharged by the hot springs could be derived from about 0.2–0.4% magmatic and 99.6–99.8% meteoric waters (Fournier 1989).

Carbonate-rich thermal waters are normally found in areas underlain by calcareous rocks. Travertine is the $CaCO_3$ sinter, its deposition due to exsolution of CO_2 from the waters as they reach the surface. Travertine deposits are abundant in the Latium region, central Italy, from where the name originated (*Lapis tiburtina*). Low-chloride waters may contain bicarbonate in areas of H_2S and CO_2–bearing seam. Bicarbonates are formed by reactions with wall rocks.

The study of degassing volcanoes has gained considerable momentum, particularly since the catastrophic CO_2 eruption in 1986 from Lake Nyos (a crater lake) in Cameroon. In this eruption CO_2 gas welled up from the lake killing about 1700 people and 5000 cattle. Fumaroles have been studied for nearly 130 years on Mount Vesuvius, where analyses carried out in the late 19th century revealed high amounts of Cu, Pb, Fe and Sn, but the realisation of a link with ore-forming systems is comparatively recent. In this respect the work of Hedenquist et al. (1994) is of considerable importance. These authors studied the flux of volatiles from the Satsuma Iwojima volcano in Japan, and estimated a total discharge of about 5×10^6 tonne/year of S, with 6×10^4 tonnes/year being from high temperature fumaroles, whereas the flux of metals (Cu, Pb, Zn, Mo) in the vapour of acidic springs is from 0.1 to 10 tonnes/year and that of Au is from 10^{-5} to 10^{-3} tonnes/year. Fumarolic metal discharges (including Au) have also been observed for the Galeras volcano in Colombia, in which up to

0.5 kg of gold/year is released into the atmosphere, while at the same time it is calculated that some 20 kg/year is deposited inside the volcanic edifice (Goff et al. 1994). Crater lakes of quiescent volcanoes actively release volatiles that derive from degassing magmas at depth (Brantley et al. 1993). Some of these crater lakes contain the most acidic natural waters with pH = 0. Monitoring of the acid lake of the Volcán Poás in Costa Rica revealed volatile release rates of about 0.78 Gg/yr^{-1} of F, 15 Gg/yr^{-1} of Cl, and 13 Gg/yr^{-1} of S, with a power output of 200 MW during degassing between 1988 and 1989 (Brantley et al. 1993). The Merapi volcano in Indonesia has high temperature (800°C) fumaroles with sublimates that assay up to 3% Mo, 1.8% Pb, 100 ppm Au and 60 ppm Ag (Kavalieris 1994; see also Table 1.6). Fumarolic fluids from island volcanoes mix with sea water, resulting in ore-forming reactions. It may be of interest to know that during the Mount Pinatubo eruption of June 1991, about 38 Mt of CO_2 and 17 Mt of SO_2 are estimated to have been belched out, while Mount Etna, when quiescent, emits about 1000 tonnes of greenhouse gases each day. Astonishingly, Mount Etna discharges Au into the atmosphere at the rate of 0.1–1.0 tonne per year; White Island (New Zealand) fluxes an estimated 10 million tonnes of Cu and 45 tonnes of Au over a 10 000-year life of its hydrothermal system (Einaudi 2000). In some fumaroles, ammonium chloride (NH_4Cl) may be so abundant that it can be commercially exploited, as is native S, which is formed by the oxidation of H_2S according to:

$$2H_2S + O_2 \rightarrow 2H_2O + 2S^\circ$$

$$2H_2S + SO_2 \rightarrow 2H_2O + 3S^\circ$$

Boric acid, known as sassolite, $B(OH)_3$, was extracted from the geothermal fields of Larderello in Italy. Sassolite is also found in the crater of Vulcano in the Aeolian Islands. The origin of the element B in the Larderello fumaroles may be related to evaporitic sedimentary rocks in the region.

Intense and high temperature, up to 940°C, fumarolic discharges are recorded from the Kamchatka-Kurile volcanic arcs, between the Okhotsk Sea and the Pacific Ocean (Glasby et al. 2006). Here, the 996 m high basaltic-andesitic Kudryavy volcano on the island of Iturup discharges a large quantity of volatiles, including some 10^6 t of water and elements such as Pb, W, Cd, As, Mo, Bi, Sn. In, Se, Re and Te, as well as native elements such as Si, Ti, Fe and Pt. Interesting to note, especially in these days of intense preoccupation of human-induced CO2 emissions, is the fact that the Kudryavy volcano alone emits some 18000 t yr^{-1} of CO2 to the atmosphere, of which it is estimated that 67% and 21% are derived from subducted marine carbonates and organic matter respectively, and some 12% from the mantle (Glasby et al. 2006).

As a matter of general interest I point out to the reader that volcanic fumaroles are commonly studied by inserting silica tubes into the fumaroles. This induces sublimate precipitation inside the tube with the sublimates forming at different levels in the tube, depending on the precipitation-temperature of the

mineral phases (Quisefit et al. 1989). These experiment have show that magnetite, molybdenite and wolframite form at temperatures $> 500°C$, whereas chalcopyrite, galena, pyrite and sphalerite precipitate at temperatures $< 450°C$. Native Au precipitation at temperatures between 450 and 550°C was also observed in silica tube experiments by Taran et al. (2000) from the Colima volcano in Mexico (see also Chapter 5 for more information on volcanic sublimates and fumaroles).

Hot springs and hydrothermal systems may also be formed in complex meteorite impact craters. In this case, the heat source results from the conversion of kinetic to thermal energy, which in turn causes thermal perturbations and heat release particularly in the central structural uplifts where deeper and hotter crust is brought to near the surface. I return to this extraterrestrially-induced type of hydrothermal venting in Chapter 11.

All types of hydrothermal systems on Earth harbour life in the form of varied microbial communities that employ different metabolic pathways to obtain food and energy. These include photosynthetic cyanobacteria and chemoautotrophs, such as sulphur reducing bacteria and sulphur oxidising bacteria. The 70 000 km-long mid ocean ridge systems harbour deep and anoxic ecosystems with an abundance of chemoautotrophic, thermophylic life forms. The East African Rift System, Yellowstone (USA) hot springs, New Zealand and Iceland provide well-documented examples of on-land hydrothermal systems that foster microbial communities (Farmer 2000; McCollom and Shock 1997; Konhauser and Ferris 1996; Siegert et al. 2001). Microbial habitation of fossil hydrothermal systems is present in the ancient geological record from the Sulphur Springs (3.24 Ga) and North Pole (3.49 Ga) areas of the Pilbara Craton, Western Australia, as described in Chapter 10.

1.4.6 Fluid Inclusions

A brief mention of fluid inclusions is appropriate in the present context. Well known publications on fluid inclusions are Roedder (1984), Shepherd et al. (1985), De Vivo and Frezzotti (1995), and Shepherd and Rankin (1998). Reviews for the use of fluid inclusions studies in hydrothermal ore systems can be found in Roedder and Bodnar (1997), Wilkinson (2001) and Van den Kerkhof and Hein (2001). The present discussion is based largely on the works cited above.

Fluid inclusions are droplets of fluid trapped in crystals at the time of their growth, or introduced along microcracks and cleavages after crystallisation of the host mineral. Fluid inclusion chemistry indicates that major solutes of hydrothermal fluids are cations of Na, K, Ca, Mg, Fe, Ba, Mn, anions of Cl, S, C, N, P, Si, metals such as Au, Ag, Cu, Pb, Zn, U, gaseous species (CO_2, CH_4, N_2, SO_2, H_2S) and hydrocarbons. They represent samples of hydrothermal fluids, and range in size from a single water molecule up to several millimetres,

with an average of about 0.01 mm (Roedder 1979). The number of inclusions in any one crystal can be very high, with a maximum of 10^9 inclusions having been estimated in 1 cm^3. Fluid inclusions have many practical uses for the student of ore deposits, providing information on the temperature, pressure, density and composition of the fluids that originated the mineralisation. The study of fluid inclusions can have direct application to mineral exploration. For example, the spatial distribution of Th in a region or mining district may give an indication of temperature gradients and thus predict the direction in which new deposits can be found. Fluid inclusions provide direct evidence of the nature and composition of hydrothermal solutions. They are easily observed under the microscope in plane polarised light and at medium or high power. The size of fluid inclusions ranges from 1μ to centimetres. There are main three types of fluid inclusions (Fig. 1.8A):

- Primary: formed during growth of the host mineral; they occur isolated or in small clusters and may define growth zones
- Secondary: formed after growth of the host mineral is completed; they cut across growth zones and even crystal boundaries
- Pseudosecondary: formed in fractures within a single crystal and do not cross mineral boundaries

However, these definitions are somewhat simplistic, and it is often difficult to distinguish between, say, secondary and pseudosecondary, or primary and pseudosecondary inclusions.

Some of the abbreviations used in fluid inclusions studies are temperature of trapping Tt, temperature of homogenisation Th, temperature of decrepitation Td and eutectic temperature Te. Clathrate is a mixture of H_2O with gas (H_2S, CO_2 and CH_4). Tables of empirical criteria for the identification of the genetic types of fluid inclusions are given in Roedder (1979, 1984). A fluid inclusion contains one or more phases:

- L = liquid (e.g. H_2O, hydrocarbons)
- V = vapour (e.g. H_2O, CO_2, CH_4)
- S = solid (e.g. NaCl, KCl, carbonates, sulphides)

A fluid inclusion is heated on heating-freezing stage mounted on a petrological microscope until the vapour and liquid phases homogenise. Homogenisation of the liquid and gas phases will be seen to occur at a given temperature on heating of the inclusions, when observed under the microscope. This homogenisation temperature is a lower limit having been obtained at atmospheric pressure, and therefore a pressure correction for the original depth at which the fluids were discharged is necessary. The Th is plotted on a P-T diagram to determine the range of pressure at which the inclusion may have been trapped. Salinity is measured in terms of NaCl wt% equivalent and is based on freezing point depressions, determination of Te and Raman spectroscopy. The salinity of the

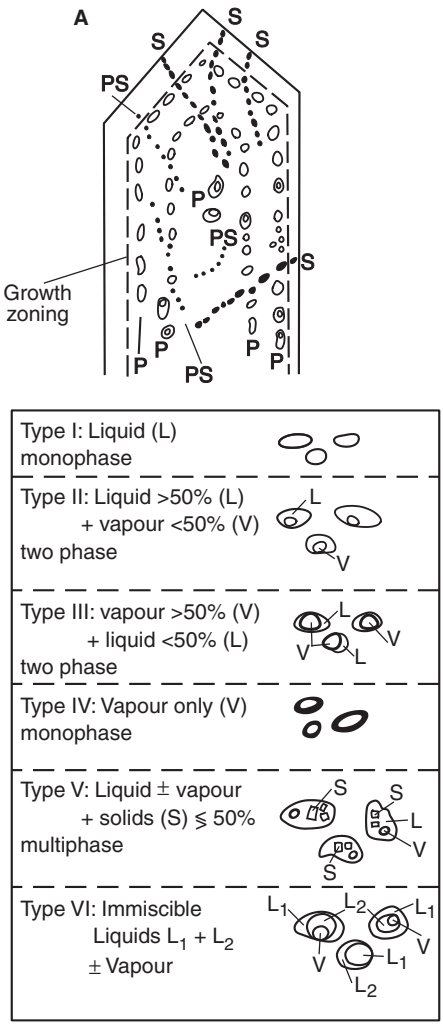


Fig. 1.8 Schematic representation of types and classification of fluid inclusions (**A**) Primary (P), secondary (S) and pseudosecondary (PS) fluid inclusions in a quartz crystal (**B**) Classification of fluid inclusions as observed at room temperature. Both (**A** and **B**) after Sheppard et al. (1985)

inclusion is determined by first freezing the inclusion and then raising the temperature of the stage, and observing the first and final melt temperatures ($T_{m\text{-}ice}$). The first melt temperature indicates the type of salt (NaCl or MgCl, for example), while the temperature of the last melt indicates the degree of salinity, usually measured in equivalent NaCl. Decrepitation temperatures are obtained by crushing and bursting of inclusions by heating.

Fluid inclusions usually occur in combination, such as L + V, L + V + S, V1 + V2, L1 + L2 etc. Co-existing L-rich and V-rich inclusions are indicative of either boiling or mixing. The classification scheme of Shepherd et al. (1985) is given below, and diagramatically shown in Fig. 1.8B.

1. Monophase inclusions: entirely filled with liquid (L).
2. Two-phase inclusions: filled with a liquid phase and a small vapour bubble (L + V).
3. Two-phase inclusions: in which the vapour phase is dominant and occupies more than 50% of the volume (V + L).
4. Monophase vapour inclusion (V): entirely filled with a low density vapour phase (generally mixtures of H_2O, CH_4 and CO_2).
5. Multiphase inclusions containing solids (S + L + /–V): contain solid crystalline phases known as daughter minerals. These are commonly halite (NaCl) and sylvite (KCl), but many other minerals may occur including sulphides.
6. Immiscible liquid inclusions: contain two liquids, usually one H_2O-rich and the other CO_2-rich (L1 + L2 = /–V).

In general, the coexistence of types 2 (L + V) and 3 (V + L) may indicate that the fluid was boiling at the time of entrapment. In the case of boiling of a one-component system, the gas bubble is the vapour phase of the host liquid; or, in the case of a heterogeneous system, the gas phase exsolves by effervescence. However, it must be cautioned that the presence of a gas bubble may also indicate immiscibility. This is the case with CO_2, which if present in the fluids, will separate on cooling (Roedder 1979). In systems that contain volatiles such as CO_2 it is more appropriate to use the term effervescence rather than boiling. Boiling or effervescence result in the partitioning of a vapour phase from a residual liquid that is more saline. Phase separation and mixing of fluids are important processes in several hydrothermal ore deposits. For example, sulphur and metals are generally transported by separate fluids and precipitation of sulphides occurs when these two fluid mix.

The presence of daughter minerals, on the other hand indicates that solids nucleated from an oversaturated liquid solution. It is found that in these hypersaline fluids, Na^+, Cl^-, Mg^{2+} and Ca^{2+} are the most common dissolved ions. The concentration of the salts in the solutions ranges from less than 1 wt% to greater than 50 wt%. The diagram in Fig. 1.9 reflects the range of salinities (wt% equivalent) and homogenisation temperatures of a range of hydrothermal mineral deposits (Large et al. 1988).

The composition of inclusion fluids is becoming increasingly more accurate using Raman spectroscopy, proton-induced X-ray emission (PIXE), synchroton X-ray fluorescence (SXRF), secondary ion mass spectrometry (SIMS) and cathodoluminiscence (CL) techniques. A discussion of these techniques is beyond the scope of this book, but for a useful review the reader should consult Boiron and Dubessy (1995).

The halogen content and their ratios in inclusion fluids can be used to characterise different hydrothermal fluids (Wilkinson 2001). Ratios and plots commonly used are Cl/Br versus Na/Br and Cl versus Br, which can provide clues as to the origin of fluids (e.g. seawater, continental brines). Other useful elements in the study of inclusion fluids are the noble gases, He, Ar, Kr, Xe. He isotopes are especially useful to trace fluids that may either derive form the

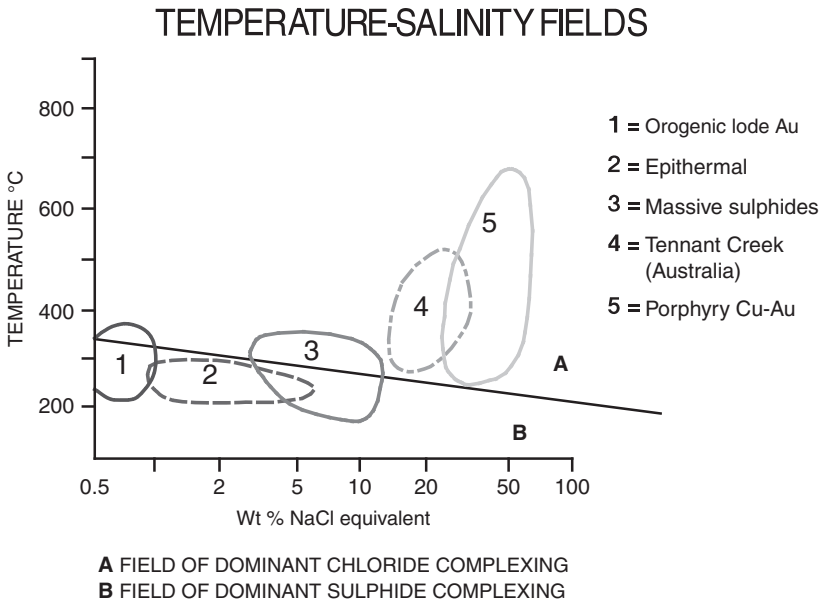


Fig. 1.9 Temperature-salinity fields and mean gradient curve for a range of hydrothermal ore systems: (1) Archaean orogenic Au; (2) Epithermal Au-Ag; (3) volcanogenic massive sulphides; (4) Tennant Creek Au-Cu, Australia; (5) Porphyry Cu-Au. After Large et al. (1988)

mantle or have a link with mantle degassing. The $^3He/^4He$ ratio can discriminate whether or not fluids originate from the mantle ($^3He/^4He > 1.4 \times 10^{-6}$), from the crust ($^3He/^4He < 1.4 \times 10^{-6}$) or are of atmospheric origin ($^3He/^4He = 1.4 \times 10^{-6}$). However, as pointed out by Wilkinson (2001), the presence of a mantle contribution as revealed by the $^3He/^4He$ in a hydrothermal system does not necessarily mean that the fluids are directly derived form the mantle, but may simply be an indication of mantle heat contribution, or degassing. This is an important aspect and I discuss this further in Section 1.4.11 in which some case studies are examined.

1.4.7 Dissolved Constituents and Metals Partitioning in Hydrothermal Solutions

From the study of fluid inclusions, hot springs and fluids encountered during drilling operations in geothermal areas and oilfields, it is apparent that the amount of dissolved solids in hydrothermal solutions varies from approximately $< 1\%$ to $> 50\%$ by weight.

Some typical compositions are given in Tables 1.8 and 1.9. From the values in these Tables the following two observations can be made: (1) Na, K, Cl and

Table 1.8 Composition of modern and ancient hydrothermal solutions. Data from various sources published in Skinner (1979). All values in parts per million (ppm) unless stated otherwise

Element	Salton sea	Cheleken	Ancient hydrothermal solutions determined from fluid inclusions		
Cl	15.5%	15.7%	8.7%	4.65%	2.95%
Na	5.04%	7.61%	4.04%	1.97%	1.52%
Ca	2.8%	1.97%	8600	7500	4400
K	1.75%	409	3500	3700	6.7%
Sr	400	636	–	–	–
Ba	235	–	–	–	–
Li	215	7.9%	–	–	–
Rb	135	1.0	–	–	–
Mg	54	3080	5600	570	–
B	390	–	<100	185	–
Br	120	526	–	–	–
I	18	32	–	–	–
NH_4	409	–	–	–	–
SO_4	5	309	1200	1600	1.1%
Fe	2290	14	–	–	8000
Mn	1400	46.5	450	690	–
Zn	540	3.0	1.09%	1330	–
Pb	102	9.2	–	–	–
Cu	8	1.4	9100	140	–

Table 1.9 Analyses of geothermal waters. Data from various sources published in Ellis and Mahon (1977). (1) Iceland; (2) Philippines; (3) Japan; (4) New Zealand; (5) Mexico; (6) Taiwan; (7) Italy. All values in parts per million (ppm), unless stated otherwise

Element	1	2	3	4	5	6	7
Cl	197	1.44%	1219	1625	1.6%	1.34%	4.28%
Na	212	7800	846	950	9062	5490	7.89%
Ca	1.5	219	9.9	28	520	1470	106
K	27	2110	1005	80	2287	900	4.83%
Li	0.3	40	4.5	12.2	38	26	380
Rb	0.04	12.5	1.8	0.8	–	12	450
Mg	0.0	0.28	0.02	–	1	131	17
Mn	0.0	–	0.0	0.02	–	40	0.1
Fe	0.1	–	0.5	0.1	0.3	220	0.7
F	1.9	–	3.8	0.8	2	7.0	100
Br	0.45	–	2.5	–	31	–	–
SO_4	61	32	214	17	6	350	16.3%
As	–	28	2.3	–	0.5	3.6	8.3
B	0.6	313	20.51200	14	106	2650	–
SiO_2	480	995	425	460	1250	639	–
NH_3	0.1	6.4	0.1	46	21	36	82
CO_2	55	27	56	61	56	2	5850
°C	216	324	200	2340	340	245	250
pH	9.6	6.7	8.4	7.4	7.7	2.4	8.5
Depth(m)	650	1947	350	585	1285	1500	1415

Ca are in almost all cases the major components of the solutions; minor components are Sr, Fe, Zn, Mg, Fe, Mn, CO_2, SO_2, H_2S and NH_3; (2) with few exceptions, the most striking feature is that the actual concentration of ore-forming metals in these waters is generally low. From these Tables it can thus be deduced that metal concentrations in the hydrothermal fluids need not necessarily be high in order to form an ore deposit, and therefore the critical factors for ore deposition must therefore be time and deposition rate. Although difficult to identify with absolute certainty, it is fair to assume that the source of these constituents can be the cooling magmas and/or the rocks through which the solutions pass. The case for Pb is instructive. In a classic study by Doe and Delevaux (1972) of the sources of Pb in galena ores in southern Missouri, based on the isotopic compositions for this metal, it was found that the Pb is probably derived from the Lamotte Sandstone, which is the main aquifer for the hydrothermal solutions in the district. The Pb is thought to have been transferred from solid solution in the feldspars to the hydrothermal fluid by rock-hot water interactions. Other metals such as Zn, Cu, Sn and W are present in various amounts in micas, pyroxenes and amphiboles. Sn and W concentrations of up to 500 ppm have been found in biotites and muscovites (Ivanova 1969). The release of the metals may take place either during specific reactions with production of a new mineral phase from the original host or simply by a process of ion-exchange reactions.

In summary, evidence suggests that hydrothermal fluids acquire their dissolved constituents by one or both of two fundamental processes, where: (1) the constituents are released to a fluid by a crystallising magma, and (2) constituents derive from the rock through which the hot aqueous solutions circulate. Finally, Skinner (1979) questioned whether or not a rock mass need be abnormally rich in certain elements in order to serve as a source for the elements. For those elements that have crustal abundances of 0.001–0.01% (10–100 ppm), the rocks need not be enriched. An example is the Lamotte Sandstone, above, in which its feldspars provided the Pb to the solutions. Volcanic piles with predominant rhyolite-dacite components will produce Pb-rich ores because of the abundance of feldspars relative to mafic silicates; yet if andesite-basalt predominate, with an abundance of olivines and pyroxenes, they will yield Cu-rich ores. For those elements such as Sn and Ag, which have very low crustal abundances (less than 10 ppm or 0.001%), a pre-concentration would probably be necessary before solution extraction takes place, although a paucity of reliable data makes this an uncertain point.

1.4.8 The Role of Complex Ions and Ligands in Hydrothermal Fluids

A complex ion is a "*charged species in which a metal ion is joined by co-ordinate covalent bonds to neutral molecules and/or negative ions*" (Masterton et al. 1981). A complex can also be defined as a coordination compound, where a central

atom or ion, M, unites with one or more ligands, L, to form a species $ML_iL_jL_k$ (Cotton et al. 1999, cited in Rickard and Luther 2006). For example, in the complex Cu $(NH_3)_4{}^{2+}$, where one Cu^{2+} ion combines with four neutral NH_3 molecules, each of the NH_3 contributes a pair of unshared electrons to form a covalent bond with the Cu^{2+} ion. The structure is shown in Fig. 1.10A. Metals that have the tendency to form complex ions are those that are placed towards the right of the transition series (i.e. Ni, Cu, Zn, Pt, Au, Co, Cr, Mo, W), while non-transition metals (Al, Sn, Pb) form a more limited number of complex ions. The central ion in a complex is a metal cation, and the neutral molecules or anions bonded to the cation are called ligands. The number of bonds formed by the central ion is the co-ordination number. In the case illustrated in Fig. 1.10A, Cu has a co-ordination number of four. Charged complex ions, such as $Cu(NH_3)_4{}^{2+}$ or $Al(H_2O)_6{}^{3+}$, cannot exist in the solid state unless the charge is balanced. Thus, $Cu(NH_3)_4Cl_2$, for example, is a complex ion balanced by 2 Cl ions. Therefore the complex ion acts in this case as a cation. Other examples are:

$$Pt(NH_3)_4{}^{2+} + 2Cl = Pt(NH_3)_4Cl_2 \text{ (complex cation);}$$
$$Pt(NH_3)Cl_3^- + K = Pt(NH_3)Cl_3K \text{ (complex anion)}$$

If a ligand has more than one bond then it is called a chelating agent (from the Greek chelate, meaning hard). Ligands usually contain atoms of the

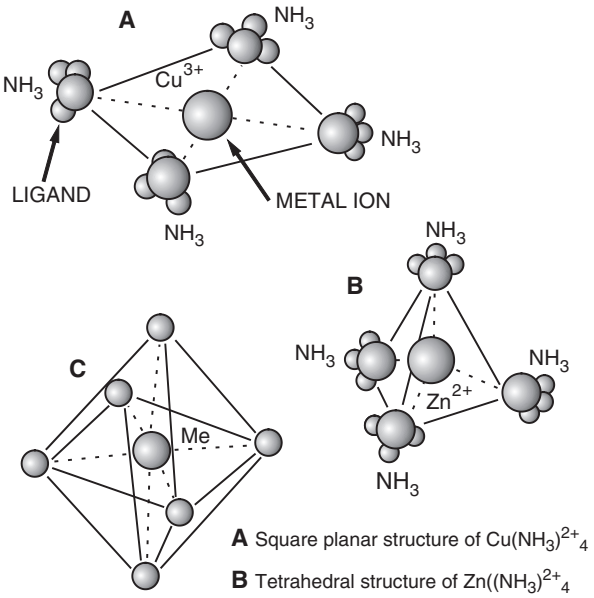


Fig. 1.10 Molecular structures of complex ions. Details in text. After Masterton (1981)

electronegative elements (C, N, O, S, F, Cl, Br, I). The most common ligands are NH_3, H_2O, Cl^-, OH^- and HS^-. Co-ordination numbers are usually 6, 4 and 2, in that order of frequency. Odd co-ordination numbers are very rare. The co-ordination number also determines the geometry of the complex ions. Thus, for complex ions in which the central ion forms only two bonds the ligands are linear with the bonds directed at 180°.

Metal complexes with co-ordination numbers of 4 form either tetrahedral structures or square planar structures (Fig. 1.10A, B), whereas the octahedral geometry is obtained for ion complexes in which six ligands surround a metal ion (Fig. 1.10C).The interpretation of the nature of the bonding in complex ions is beyond the scope of this book; suffice it to say that two models are considered, based on the electronic configurations of the ion in question. One is the valence bond model and the other is the crystal-field model, the nature of the bonding in the latter case being essentially electrostatic. Details on the nature of complex ions and their role in the transport of transitional metals in hydrothermal solutions can be found in Brimhall and Crerar (1987) and Crerar et al. (1985).

Metal-ligand interactions are similar to acid-base reactions, with the metal being an electron acceptor and the ligand an electron donor. Metals and ligands can be classified into two important classes: class A, or hard, and class B, or soft. In the former, metals and ligands are highly charged, small and slightly polarisable. Class B, or soft type, is characterised by species that are large, of low charge and are highly polarisable. An important aspect of this classification is that soft metals tend to bind with soft ligands, and hard metals with hard ligands. Table 1.10 lists those metals and ligands that are important in hydrothermal processes, according to their soft or hard behaviour. From Table 1.10 it can be seen that HS^- is a soft ligand and will therefore form strong complexes with Au, Ag, Hg, Cu and Sb (soft metals); whereas weaker complexes will be formed with Pb and Zn, and even weaker still with Sn and Fe. Transition metals show increased hardness at higher temperatures and therefore complexes with intermediate hard ligands such as Cl^- and OH^- become more stable at a given higher temperature. This behaviour is corroborated by experimental evidence

Table 1.10 Classification of metals and ligands; hardness decreases to the right. After Brimhall and Crerar (1987)

	Hard	Borderline	Soft
A	H^+ Li^+ Na^+	Fe^{2+} Co^{2+} Ni^{2+}	Cu^+ Ag^+ Au^+
C	K^+ Rb^+ Cs^+	Cu^{2+} Zn^{2+} Sn^{2+}	Cd^{2+} Hg^+ Hg^{2+}
I	Ca^{2+} Mg^{2+} Ba^{2+}	Pb^{2+} Sb^{3+} Bi^{3+}	M° (metal atoms)
D	Ti^{4+} Sn^{4+} MoO^{3+}	SO_2	
S	WO^{4+} Fe^{3+} CO_2		
A	NH_3 H_2O OH^-	Br^-	CN^- CO
S	CO_3^{2-} NO_3^-		H_2S HS^-
E	PO_4^{3-} SO_4^{2-}		I^-
S	F^- Cl^-		

that indicates the high stability of chloro complexes at high temperatures, as shown later. Electronegativity, ionic potential and the ligand field stabilisation energy (LFSE; energy that affects the stability and behaviour of transition metal ions in hydrothermal solutions) are considered to be important parameters for the behaviour of transition metals in hydrothermal solutions.

Brimhall and Crerar (1987) find that of the 30 transition metals only Mn, Fe, Cu, Zn, Mo, Au, Ag, W, Hg and Co commonly form sizable hydrothermal deposits, even though this array of elements does not correlate with their crustal abundances. A possible explanation for this is the availability of tetrahedral and octahedral sites in crystallising magmas. High Al_2O_3/alkali ratios appear to favour the octahedral sites in residual melts and hence the concentration of metals in the hydrothermal fluids (Feiss 1978). This ratio, in turn, may be influenced by the presence of volatiles in the magma.

1.4.9 Complex Ions in Hydrothermal Solutions

Two classes of complexes are important for the transport of ore metals in hydrothermal solution, namely: sulphide (HS^- and H_2S) and chloride (Cl^-). Both these complexes are capable of transporting large quantities of metals in natural aqueous systems. A comprehensive review on metal sulphide complexes can be found in Rickard and Luther (2006).

Other ligands, which are less common, though also important, include OH-, NH_3, F^-, CN^-, SCN^-, SO_2^{-4} and also some organic complexes (i.e. humic acid). The comprehensive review of the solubility of ore minerals and complex-forming ligands by Barnes (1979) provides the basis for the discussion that follows. The ore-carrying capacity of the fluids is largely determined by the activity of these ligands, rather than the abundance of the metals to which they are bonded. This activity is a function of concentration temperature, ionic strength, pH and Eh. Very important complexes for the solubility of metal sulphides in hydrothermal fluids are H_2S and the hydrosulphide ion HS^- (Rickard and Luther 2006). Species such as $Zn(HS)_3^-$ and $HgS(HS)^-$ have been shown to be transported in solution in large amounts. Studies of active hydrothermal systems and epithermal Au deposits indicate that thio-sulphide complexing $(HS)^-$ is one of the dominant mechanism of transport for Au. Here, Au^+ is complexed by the sulphur ligand HS, which was shown by Seward (1979a,b) at Broadlands, New Zealand, to predominate over chloride complexes at near neutral pH. Furthermore, Pope et al. (2005) in their study of Au abundances in the Waiotapu springs (also in New Zealand) have shown that Au-HS complexes are several orders of magnitude more abundant than any other complexing ligands. Thio-complexes of Au^+ up to 300°C and 1500 bar, with pH 3–10 are found to be stable. Gold thio-complexing at near neutral pH is defined thus:

$$Au + H_2S + HS^- = Au(HS)_2^- + 1/2H_2$$

Stefánsson and Seward (2004) taking into account the solubility of Au at 500°C, suggested that for most pH conditions $[Au(HS)_2]^{-1}$ is the dominant sulphide species. With sulphide complexing, however, the concentration of reduced sulphur atoms in solution must be far greater than that of the metals if the complexes are to remain stable (Krauskopf 1979; Skinner 1979). It follows that loss of H_2S caused, for example, by boiling, cooling, oxidation or sulphide precipitation will result in an increase in pH, decrease in HS activity, and subsequent precipitation of sulphides and Au, providing this metal is present in sufficient quantities. Deposition from sulphide complexing can be written as:

$$Me(HS)_3^- = MeS + HS + H_2S(aq)$$

The importance in some hydrothermal systems of chloride complexing is indicated by the abundance of NaCl in fluid inclusions. Aqueous species such as $ZnCl_2$, $CuCl_2^{-3}$ and $AgCl_2^-$ form in chloride-rich solutions. Both Barnes (1979) and Krauskopf (1979) showed that there is evidence that chloride complexes are more stable than sulphide complexes at higher temperatures (above 350°C). The predominance of sulphide complexing at lower temperatures and chloride complexing at higher temperatures, and their relationships to certain types of ore deposits, ranging from skarns (high temperature) to hydrothermal veins (low temperature), is illustrated in Fig. 1.11. In the case of Au, its solubility in chloride solutions is defined thus:

$$Au + H^+ + 2Cl^- = AuCl^{-2} + 1/2H_2$$

This type of complexing for the transport of Au is probably valid in the deeper and hotter regions of magmatic and hydrothermal systems, and in hydrothermal fluids originating during metamorphic dewatering. Deposition of sulphides from chloride- complexed metals takes the form:

$$MeCl_2(aq) + H_2S(aq) = MeS + 2H+ + 2Cl^-$$

The greater stability of chloride complexes at higher temperatures with respect to sulphide complexing is corroborated by the modelling studies of Ag/Au ratios in hydrothermal solutions by Cole and Drummond (1986). They found that $AuCl^-_2$ complexes dominate at temperatures higher than 250°C and low to moderate pH, thus favouring high Ag/Au ratios in the solution. At temperatures below 250°C sulphide complexing with more Au than Ag predominates, causing lower Ag/Au ratios in the solution. According to Barnes (1979), deposition of metals from chloride complexes may be due to the following:

1) Increased H_2S concentration;
2) Increased pH (caused by boiling for example);
3) Decreased chloride concentration and decreasing temperature.

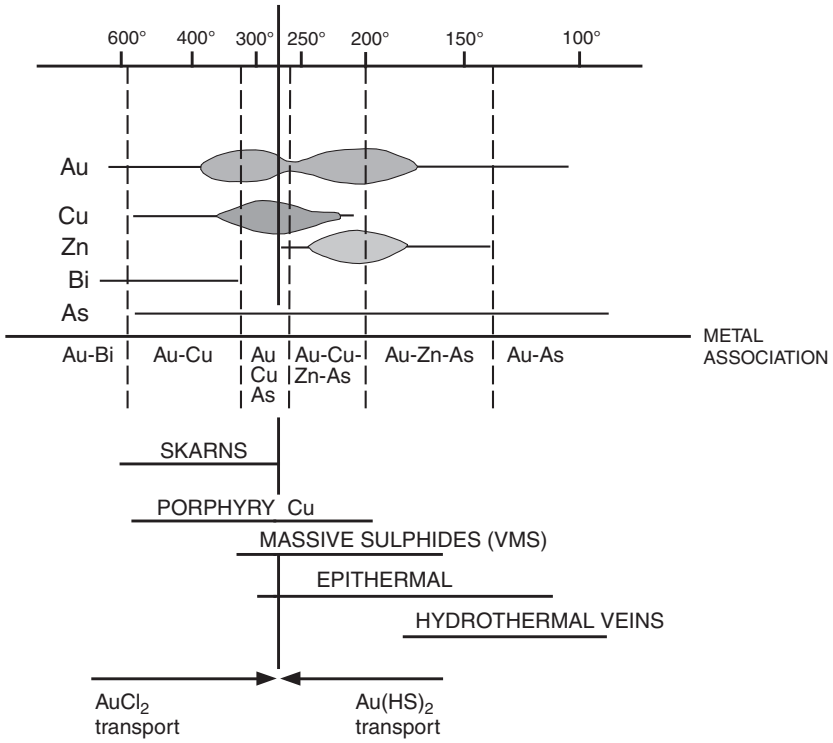


Fig. 1.11 Temperature range of AuCl and AuHs metal transport diagram and associated mineral systems. After Huston and Large (1989)

The causes of deposition from sulphide complexes are:

1) Pressure release and boiling;
2) Oxidation, which decreases the sulphide contents and the pH.

Evans (1987) pointed out that the actual mechanism of metal transport via complex-forming ligands is by no means clearly understood. One problem is that in order for sulphide complexes to be stable, high concentrations of H_2S are necessary in the fluids. However, it is possible that S may enter the system at a later stage, for example by reduction of sulphates by organic compounds. If this is true, a mixing model could be considered whereby both chloride and sulphide complexes may be important as transporting agents for the metallic elements. Sulphide deposition could hence take place according to the reaction:

$$PbCl_2 + H_2S = PbS + 2H^+2Cl^-$$

in which galena precipitates on addition of H_2S (Henley et al. 1984; Evans 1987).

The study of mineral precipitates from fumarolic gases of the previously mentioned Colima volcano (Mexico) provided some insights into the transport and complexing of Au in oxidised gas systems, in which little H_2S is available (Taran et al. 2000). Taran et al. (2000) suggested that in the Colima fumaroles Au is released from the magma as volatile AuS(g) or AuH(g) complexes, where g is gas. In the high oxidation environment of the summit crater the following reactions would take place:

$$AuS(g) + 2H_2O \rightarrow Au(g) + 2H_2 + SO_2$$
$$2AuH(g) \rightarrow 2Au(g) + H_2$$

The AuS(g) and AuH(g) are stable at around 600°C and, as mentioned above, Au precipitates between 500 and 600°C.

1.4.10 Precipitation of Solutes and Metal Deposition

Precipitation of the dissolved constituents in hydrothermal fluid can occur as a result of temperature variations, pressure changes and boiling, reactions between wall rocks and solutions and chemical changes due to mixing of fluids. Temperature changes affect the solubility of sulphides and oxides, as well as the stability of the complex ions. And it is believed that a fall of just 20°C may be sufficient to cause precipitation (Skinner 1979). Temperature changes can be caused by mixing of hot solutions with cold near surface waters. This is particularly common and evident at sites where hydrothermal solutions discharge on the seafloor. Here the hot rising fluids with temperatures of up to 350°C mix with sea water of only a few degrees Celsius above zero, resulting in immediate sulphide precipitation, which in turn gives rise to the so-called black smoker chimneys (see Chapter 7). Adiabatic decompression (throttling) also causes rapid temperature drops over short distances, and occurs when the pressure changes from lithostatic to hydrostatic (Skinner 1979). An adiabatic process is one in which no heat flows either into or out of a system sealed off from its surroundings. Since flow of heat in rocks takes time, any process can be adiabatic if sufficiently fast. Thus, rapid compression causes a rise in temperature and, by the same token, rapid decompression results in a temperature drop. Pressure changes also cause solubility changes, but need to be substantial (about 1000 bar) for precipitation to occur. One of the most important pressure-controlled phenomena is boiling. Boiling is the result of a sudden increase in the concentration of the solution and the removal of the volatile constituents, which leaves a residue that is less capable of keeping constituents in solution. It is very important for the precipitation of Au in geothermal systems. In these situations, self-sealing due to mineral deposition (sinter) may be a cause of

boiling. Other causes are increase in temperature or build up of volatiles. If the seal is suddenly breached, say by an earthquake, the immediate drop in pressure results in violent boiling. During boiling H_2, CO_2, etc. go into the vapour phase:

$$HCO_3 + H^+ = CO_2(g) + H_2O$$

and

$$HS + H^+ = H_2S(g)$$

also fO_2 increases, and oxidation ($HS \rightarrow H_2S \rightarrow H_2SO_4$) and destruction of thio-complexes ($Au(HS)_2^-$; $Au^{+2}(HS)$) will take place due to the rapid disappearance of the ligands HS.

Thus, oxidation within and above the zone of boiling results in the formation of sulphuric acid (H_2SO_4), decrease in pH and acid leaching (argillic alteration). During this process, electrons are released that reduce the Au^+ to its neutral state Au^0 causing its precipitation as a native metal. Other important mechanisms for the precipitation of the dissolved constituents are chemical reactions between the solutions and wall rocks. Skinner (1979) lists three types of reactions that can be considered important, and which are explained below.

When a hydrothermal solution is acidic, as are the majority, extraction of hydrogen ions from the solution takes place through hydrolysis of feldspars (see Chapter 2) and other silicates, which are then transformed into clays (argillic alteration). The loss of H^+ from the solution reduces the stability of chloride complexes and causes precipitation of sulphides, providing S is present to react with the metals liberated from the metasomatised silicates. Another type of wall-rock reaction is the change of oxidation, or valency state, of some metals, most notably Fe, Cu and N. It is known that Fe^{2+} can be transported in solution and that a change from Fe^{2+} to Fe^{3+} causes its precipitation as Fe_2O_3. This is the mechanism invoked for the deposition of banded iron formations (BIF), whatever the causes for oxidation of Fe. Another example is provided by U. This metal is transported in solution as the uranyl ion $(UO_2)^{2+}$, and precipitation occurs when the solutions enter a reducing environment, so that reduction of $UO_2{}^{2+}$ to UO_2 takes place corresponding to a change in valency from U^{6+} to U^{4+}. Additions of wall-rock components to the solution are a third type of reaction during which precipitation of sulphides may take place. Chemical changes due to mixing of fluids of different components lead to ore deposition.

1.4.11 Isotopic Tracers

There are several isotopic systems that can be used, not only for age determinations of rocks and ores, but also to trace the source or sources of metals and

ore-making fluids. Frequently used radiogenic isotopic systems are: ^{235}U-^{207}Pb, ^{238}U-^{206}Pb, ^{232}Th-^{208}Pb, ^{40}K-^{40}Ar, ^{187}Re-^{187}Os, ^{87}Rb-^{87}Sr, ^{147}Sm-^{144}Nd. Non-radiogenic isotopic systems (stable isotopes) include: ^{34}S-^{32}S, ^{13}C-^{12}C, ^{18}O-^{16}O and ^{2}H. Stable isotopes are especially suitable for the study of temperature ore systems, the origin, evolution and nature of ore-making fluids, sources of the ore materials (e.g. sulphur and carbon) and mechanisms of ore deposition. However, it is important to realise that in most cases the complexity of fluid-rock interactions makes most isotope tracers non-diagnostic in terms of sources of metals and fluids. Indeed, in any large scale hydrothermal system all rocks that interact with the fluids are likely to contribute to a greater or lesser extent metals and other cations. Therefore, isotope systematics can only be useful if well constrained within a robust geological and tectonic framework.

It is well beyond the scope of this book to elaborate or provide details of these radiogenic and non-radiogenic isotope systems, and the interested reader is referred to Faure (1986 and 2001), Heaman and Ludden (1991), Taylor (1979, 1997), Ohmoto and Goldhaber (1997) and Hoefs (2004) for detailed treatment of the subject, and to Rollinson (1993) for an overview. Case studies relating to individual ore deposits are described, where appropriate, in the chapters that follow. Analyses of stable (non-radiogenic) isotopes provide useful data for the understanding of the origin, nature and evolution of hydrothermal fluids and their interaction with wall rocks, and for this reason here I briefly discuss the stable H and O isotopic system. A section is devoted to noble gases (He, Ar, Ne) because these are especially useful for providing important information into the role of the mantle as the primordial source(s) of volatile components of hydrothermal fluids. The last sections of this chapter briefly introduce the sulphur, lead and carbon isotopic systems. In the chapters that follow, I will not be repeating abbreviations of the reference standards, such as SMOW, CDT and PDB (see below). They are implied, unless otherwise stated.

1.4.11.1 Oxygen and D Systematics

Water on Earth is a mixture of isotopes of H and O. Hydrogen has three isotopes, ^{1}H (protium, or simply referred to as hydrogen), ^{2}H (deuterium) and ^{3}H (tritium). All have one proton, but the addition of one neutron makes deuterium, and of two neutrons makes tritium. ^{1}H and ^{2}H are stable isotopes, ^{3}H is radiogenic and their natural abundances are 99.9844%, 0.0156% and 10^{-18}, respectively. Oxygen has three isotopes too, ^{16}O, ^{17}O and ^{18}O, with 99.763%, 0.0372% and 0.1995% abundances, respectively. The $^{18}O/^{16}O$ ratio in nature exhibits a range of variation due to fractionation resulting from the mass difference of the two isotopes. Thus, the partitioning of isotopes or isotopic fractionation between two co-existing phases results in different ratios in the two phases. The mechanisms that explain isotopic fractionation are (Misra 2000):

- Isotope exchange reactions, involving the redistribution of isotopes of an element between phases that contain the element in question, without any change in the overall chemistry of the phases in the reactants and products
- Bacteriogenic reactions, such as bacterially mediated reduction of sulphate to sulphide
- Mass differences due to evaporation, condensation, melting, crystallisaton, adsorption and diffusion processes

The enrichment or depletion of ^{18}O relative to a standard is given in the δ notation as a permil (‰). The usual standard is Standard Mean Ocean Water (SMOW) as further explained below. Isotopic notations use the delta (δ) value, which is the difference in the ratio of the isotope compared to the standard, thus:

$$\delta A = (R_A - R_{std}) \times 10^3‰/R_{std}$$

where $A = {}^{18}O/{}^{16}O$, in the specific case, but equally valid for other stable isotopic systems such as $^{34}S/^{32}S$ for example. Isotope exchange reactions are important particularly for estimates of temperature and water/rock ratios. In natural systems an isotope exchange reaction is of the type:

$$H_2O + 1/2Si^{16}O_2 = H_2{}^{16}O + 1/2Si_{18}O_2$$

The fractionation factor is called alpha (α) and is:

$$\alpha = ({}^{18}O/{}^{16}O)SiO_2/({}^{18}O/{}^{16}O)H_2O$$

In the case of oxygen isotopes the relationship below allows calculation of the temperature:

$$1000 \ln \times (\text{mineral}-\text{water}) = -3.7kT^2$$

where ln is the logarithm, T is the temperature and k is a constant.

In general the δD and $\delta^{18}O$ of meteoric waters vary systematically and plot on a line, termed the meteoric water line. In meteoric waters δD and $\delta^{18}O$ vary with latitude and altitude, because the δD and $\delta^{18}O$, tend to be depleted in the vapour phase. Magmatic waters have a fairly well-defined range (+ 5 to + 10‰ $\delta^{18}O$ and –40 to about –80‰ δD). Metamorphic waters, assumed to be in equilibrium with their host rocks, tend to vary widely from 0 to 70‰ δD and + 3 to + 20‰ $\delta^{18}O$. Formation or connate waters of sedimentary basins are characterised by high salinity and low to moderate temperatures, so that δD and $\delta^{18}O$ values increase with salinity and plot in lines that extend away from the meteoric water line. A classic work on the application of oxygen and hydrogen isotopes studies to hydrothermal ore deposits that still makes worthwhile reading is that of Taylor (1974).

Since oxygen is the most abundant element, and hydrogen its companion in the water molecule, the ratios of $^{18}O/^{16}O$ and D/H, where D is deuterium ($^{2}_{1}H$), the heavy isotope of hydrogen, constitute powerful indicators or tracers of the nature and source of hydrothermal fluids. The theoretical, experimental aspects, measurements technology and reviews of studies of the O and D isotope systematics can be found in a number of excellent publications. The interested reader is advised to consult Valley et al. (1986), Nesbitt (1996) and Taylor (1997).

The isotopic values are reported as deviations from an arbitrary standard, which in the case of hydrogen and oxygen is taken to be oceanic water (standard mean ocean water, SMOW) with $\delta^{18}O = 0$ and $\delta D = 0$. This deviation, indicated by δ, is given by the formula:

$$\delta = (\text{Rsample}/\text{Rstandard} - 1) \times 1000$$

where R is the ratio of the isotopes being considered (e.g. D/H and $^{18}O/^{16}O$). Thus, positive or negative values represent enrichment or depletion with respect to the standard. Sea water, meteoric water and juvenile water are considered to be reference waters, in that they have defined isotopic characteristics at their source. Consequently, geothermal, connate, metamorphic and magmatic waters are re-cycled from one or more of these reference waters (Ohmoto 1986). In the study of hydrogen and oxygen isotope systematics, it is important to take into account the meteoric water line (MWL). Meteroic waters have linear relationship between δD and $\delta^{18}O$, which is defined by:

$$\delta D = 8\,\delta^{18}O + (\text{in permil, ‰})$$

Isotopic variation of meteoric waters is dependent on latitude and elevation, with δD and $\delta^{18}O$ values being lower towards higher elevations and higher latitudes. This is due essentially to less evaporation and therefore less vapour-fluid fractionation, which tends to favour the partitioning of the lighter isotopes into the vapour phase, leaving the fluid enriched in the heavy isotopes. Thus, water condensing from a vapour is enriched in ^{18}O and D relative to the vapour, so that air masses become progressively depleted in the heavy isotopes relative to the initial condensate (Taylor 1979, 1997). In addition, O and D isotopic compositions are dependant on the extent of interactions between wallrocks and fluids. This is known as water/rock ratio (w/r), which is the total mass of water that interacts with a given mass of rock (Nesbitt 1996). Extensive isotopic exchange takes place at values of $w/r > 1$ and the wallrocks will tend to equilibrate with the fluids; whereas if w/r are < 1 the isotopic composition of the fluids will tend to equilibrate with the wallrocks (Nesbitt 1996).

Taylor (1997) presented details of how to calculate the amounts of water and the w/r in hydrothermal systems, providing that the δD and $\delta^{18}O$ of unaltered rocks are known. For example the initial $\delta^{18}O$ values of basaltic and andesitic

rocks are ~ 6.5 ± 1‰ and those of mid-ocean ridge basalts ~ 5.8±0.3‰ (Taylor 1997). Studies of the isotope characteristics of natural waters by Taylor (1979, 1997) and Sheppard (1986) reveal that present-day ocean waters are relatively uniform with δD of +5 to –7‰ and $\delta^{18}O$ of +0.5 to 1.0‰ , and with mean values close to 0‰ for both D and ^{18}O (SMOW standard). Isotopic values of ancient sea water, as determined through the analysis of minerals that equilibrated with fossil sea water hydrothermal systems, show a progressive increase of $\delta^{18}O$ of the sea water since Archaean times (–8 to –12‰). From 2.5 Ga ago it is calculated that the $\delta^{18}O$ values were between 0 and –3‰, and δD of 0 to –25‰. Although in no instance can it be stated that truly juvenile water (or for that matter magmatic water) has ever been identified (Taylor 1997), the nearest D and ^{18}O values are obtained from unaltered igneous and mantle rocks and minerals, using mineral-water isotopic fractionation factors at high temperatures (>700°C). These give δD values of approximately –50 to –90‰ and $\delta^{18}O$ of +5.5 to +10‰ (Sheppard 1986). The main fields of δD- $\delta^{18}O$ compositions of natural waters are shown in Fig. 1.12.

The isotopic composition of geothermal waters and of hot springs indicates in all cases a strong meteoric component. The δD values of geothermal waters are more or less the same as those of the local meteoric waters. Modern

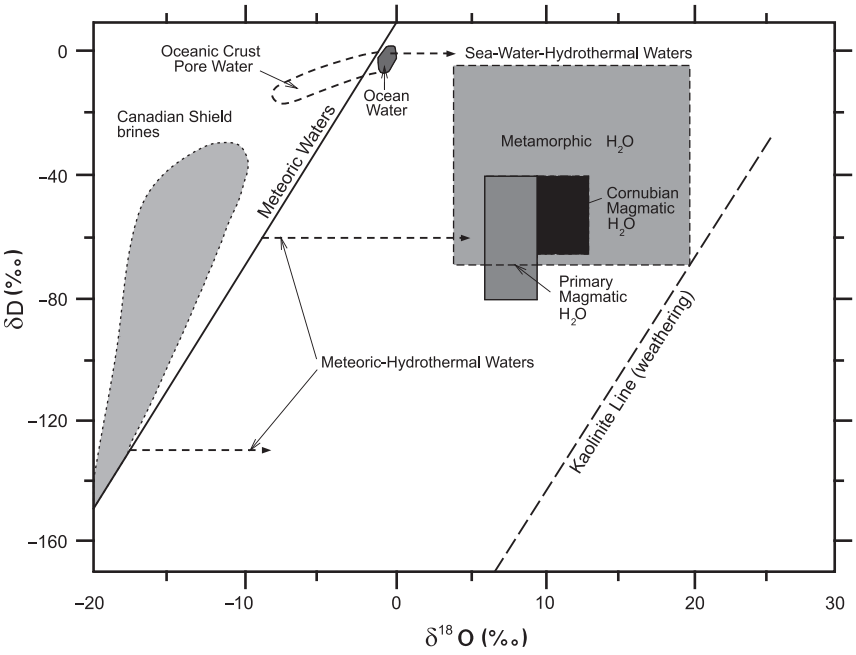


Fig. 1.12 Fields of isotopic compositions of natural waters (magmatic, metamorphic, ocean waters); note overlap between magmatic and metamorphic waters (see discussion in text). After Sheppard (1986)

geothermal waters show a positive shift from the meteoric water line (MWL) in $\delta^{18}O$ (^{18}O shift) due to isotopic exchange with wall rocks, which usually have $\delta^{18}O$ values $> +5.5$ (Fig. 1.12). The amount of the $\delta^{18}O$ shift increases with temperature and salinity of the fluids, and this probably means that the fluids acquired their heat, and dissolve solids, by interaction with deeply buried and hot rocks (Ohmoto 1986). The amount of shift may range from 1 or 2‰ in areas of high water/rock ratios, to +15‰ for hot waters in high latitude areas (Taylor 1997). The $\delta^{18}O$ enrichment is accompanied by a depletion of ^{18}O in the wall rocks. I return to this important aspect of O and D isotope systematics in Chapter 2 with a discussion of the isotopic effects during hydrothermal alteration processes and their utilisation in mineral exploration. The D/H values, on the other hand, are not controlled by water-rock exchanges (Taylor 1997). This is largely due to the fact that rocks contain very little hydrogen compared to circulating fluids. Therefore the δD values tend to remain constant, roughly identical to local meteoric waters (Taylor (1979, 1997).

Connate and formation waters show a wide range of $\delta^{18}O$ and δD. The D values of connate waters show a decrease with latitude, as with meteoric waters. The variations in δD and $\delta^{18}O$ of pore fluids and connate waters are largely dependent on whether the original fluid was sea water or meteoric water. Generally, in pore fluids of oceanic rocks, there appears to be a decrease in $\delta^{18}O$ with increasing depth and salinity. Measurements taken from samples of ocean floor suggest that alteration of basalt with sea water is responsible for this isotopic characterisation of pore fluids (Ohmoto 1986). The δD and $\delta^{18}O$ values obtained from sedimentary basin fluids by contrast show a wide range of values ($\delta D = +20$ to –150‰; $\delta^{18}O = +10$ to –20‰). Also, in basin brines there seems to be an overall increase in the isotopic values with salinity and temperature, so that brines with the lowest temperature approach the isotopic composition of present-day local meteoric waters.

Metamorphic waters, like juvenile water, are still somewhat unconstrained isotopically. They are derived from dehydration of mineral phases during prograde regional metamorphic events (Chapter 9). Nevertheless, here too the isotopic composition is clearly dependent on the orginal rock type and its history of interaction with fluids. Ohmoto (1986) points out that if volcanic rocks are first altered by sea water, at temperatures less than 200°C, and then undergo metamorphism, their final $\delta^{18}O$ values could be as high as 25‰. On the other hand, if volcanic rocks are altered by meteoric waters, then subjected to high-grade metamorphism, the δD and $\delta^{18}O$ values could be much lower. Metamorphic waters have a range of δD values from 0 to about –70‰l, and a range of $\delta^{18}O$ from +3 to about 25‰. Taylor (1979) attributes the wide range of $\delta^{18}O$ to the original values in the metamorphosed rocks.

Magmatic waters, like metamorphic waters, are not well constrained and may have a range of δD and $\delta^{18}O$ values, depending on the source region of the magma in question, as well as the possible isotopic exchanges with wall rocks during the cooling stages of the melt. Primary magmatic water is a somewhat arbitrary term and is the calculated H_2O in equilibrium with magmas at

$T \geq 700^{\circ}C$ (Taylor 1997). The $\delta^{18}O$ values for volcanic and plutonic igneous rocks range from + 5.5 to 10.0‰, with corresponding δD values of –50 to –85‰ (Taylor 1997). Isotopic values, determined on the basis of experimental studies of fractionation factors between melts and water, give a range for magmatic waters of δD = –30 to –75‰ and, $\delta^{18}O$ = + 7 to + 13‰ (Ohmoto 1986). While the range of δD and $\delta^{18}O$ for primary magmatic water remains valid it must be borne in mind, as cautioned by Taylor (1997), that the isotopic range O and D within the magmatic water box (Fig. 1.12) by no means signifies that natural water is of magmatic origin. The similarities of the D/H ratios in minerals of igneous and metamorphic rocks make it impossible to distinguish between magmatic and metamorphic waters on the basis of δD values alone (Taylor 1997). Furthermore, there are cases where volcanic rocks have high $\delta^{18}O$ values (+ 16‰), as in the Roman magmatic province (Italy), due to contamination of the magma by sedimentary rocks with high $\delta^{18}O$. These isotopically anomalous magmas will therefore have magmatic water well outside the normal range (Taylor 1997).

In the final analysis, O and D isotope systematics of hydrothermal fluids can only be realistically evaluated in conjunction with other data, including fluid inclusion measurements, petrography and, importantly, field relations.

1.4.11.2 Noble Gas Isotope Systematics

Geochemical studies of noble gases in water and gases from hot springs can help in the detection of their origin. For example, studies of He isotopic systematics conducted for springs and associated travertine deposits in the Grand Canyon (Arizona, USA) helped in assessing the role of mantle degassing in supplying CO_2 for the deposition of travertine (Crossey et al. 2006).

The standard for noble gas measurements is the composition of the atmosphere, which apart from N_2 (21%) and O_2 (78%), in the remaining 1% has an inventory that comprises CO_2, CH_4, H_2, N_2O, CO, and the noble gases Ar, Ne, He, Kr, Xe and Rn. The noble gas isotope composition of the atmosphere is shown in Table 1.11. ^{3}He can be produced by the reaction

$$6Li(n, \alpha)^{3}H(\beta) \rightarrow^{3} He$$

Where n, α and β represent neutron, alfa and beta emissions, respectively. This reaction can occur by interaction with cosmic rays or Li in the crust. Of the three stable natural isotopes of Ar, ^{36}Ar, ^{38}Ar, ^{40}Ar, (Table 1.11), the first two are produced by cosmic rays, whereas ^{40}Ar is a decay product of ^{40}K.

He and Ar are the more widely used noble gases in the study of hydrothermal fluids, but isotopes of Kr and Xe together with halogens (Cl, Br, I) are also used to fingerprint fluid sources, especially where there is involvement of seawater, evaporites and organic-rich materials (Ballentine et al. 2002). Potentially serious difficulties in the study of noble gases isotope systematics include atmospheric contamination as well as post-entrapment processes that can modify the

Table 1.11 Noble gas isotopes and their abundances in the atmosphere. After Porcelli et al. (2002)

Isotope	Relative abundance	% molar abundance
^{3}He	$1.399\pm0.013\times10^{6}$	0.000140
^{4}He	1	100
^{20}Ne	9.80±0.09	90.50
^{21}Ne	0.0290±0.0003	0.268
^{22}Ne	≡1	9.23
^{36}Ar	≡1	0.3364
^{38}Ar	0.1880±0.0004	0.0632
^{40}Ar	295.5±0.5	99.60
^{78}Kr	0.6087±0.0020	0.3469
^{80}Kr	3.9599±0.0020	2.2571
^{82}Kr	20.217±0.004	11.523
^{83}Kr	20.136±0.021	11.477
^{84}Kr	≡100	57.00
^{86}Kr	30.524±0.025	17.398
^{124}Xe	2.337±0.008	0.0951
^{126}Xe	2.180±0.011	0.0887
^{128}Xe	47.15±0.07	1.919
^{129}Xe	649.6±0.9	26.44
^{130}Xe	≡100	4.070
^{131}Xe	521.3±0.8	21.22
^{132}Xe	660.7±0.5	26.89
^{134}Xe	256.3±0.4	10.430
^{136}Xe	217.6±0.3	8.857

inclusion fluids, as explained below. Noble gases in hydrothermal fluids derive from one or more of the following sources (Burnard et al. 1999): (1) air, both modern and from palaeoatmosphere, or (2) air saturated water (ASW; seawater, meteoric or connate waters); (3) mantle and (4) crust.

The Ar isotope atmospheric composition is:

$$^{40}\mathrm{Ar}/^{36}\mathrm{Ar} = 295.5$$

The ^{3}He/^{4}He ratio in air is:

$$\mathrm{R_A} = {}^{3}\,\mathrm{He}/^{4}\mathrm{He}\ \text{of air}\,(1.4\times10^{-6})$$

Since ^{3}He is not produced in significant amounts in the Earth, the only source of terrestrial ^{3}He is the mantle, as determined from the study of basalts in mid-ocean ridges and oceanic volcanic islands (Graham 2002). Thus, the presence of ^{3}He/^{4}He ratios greater than $\mathrm{R_A}$ in volcanic gases, hydrothermal fluids or volcanic rocks may be indicative of mantle degassing. The suboceanic asthenospheric mantle has $^{3}\mathrm{He}/^{4}\mathrm{He} = 8\pm1\ \mathrm{R_A}$ (Craig and Lupton 1976); in

general mantle volatiles have 7–9 R_A. Mantle derived Ar, dominated by ^{40}Ar, has $^{40}Ar/^{36}Ar$ greater than 40 000; crustal values of $^3He/^4He$ are ≤ 0.1 R_A and $^{40}Ar/^{36}Ar$ ratios are $\geq 45\,000$ (Burnard et al. 1999). Noble gas isotope chemistry can be represented as plots of $^3He/^4He$ and $^{40}Ar/^{36}Ar$ ratios, as shown in the example of Fig. 1.13. Thus, by comparing the He-Ar isotopic composition of a sample with the He-Ar composition of the possible sources of He and Ar, outlined above, the origin of these gases in the hydrothermal fluid can be determined. He from mantle fluids is obtained from the following:

$$He_M = [(R - R_C)/(R_M - R_C)]$$

Where R_C, R_M are the $^3He/^4He$ ratios in the crust and mantle respectively, and R is the measured $^3He/^4He$ ratio.

Noble gases isotope chemistry can be examined in ancient hydrothermal fluids that are released from fluid inclusions providing, as already mentioned, that these have not been subsequently modified. These post-entrapment modifications relate to noble gases released from fluid inclusion trapped in mineral grains and may include (Burnard et al. 1999): (1) He and Ar produced by radiogenic decay from U and/or K that may be present in the fluid inclusion; (2) diffusion of He into the inclusion, from radiogenic decay of U, Th or K from

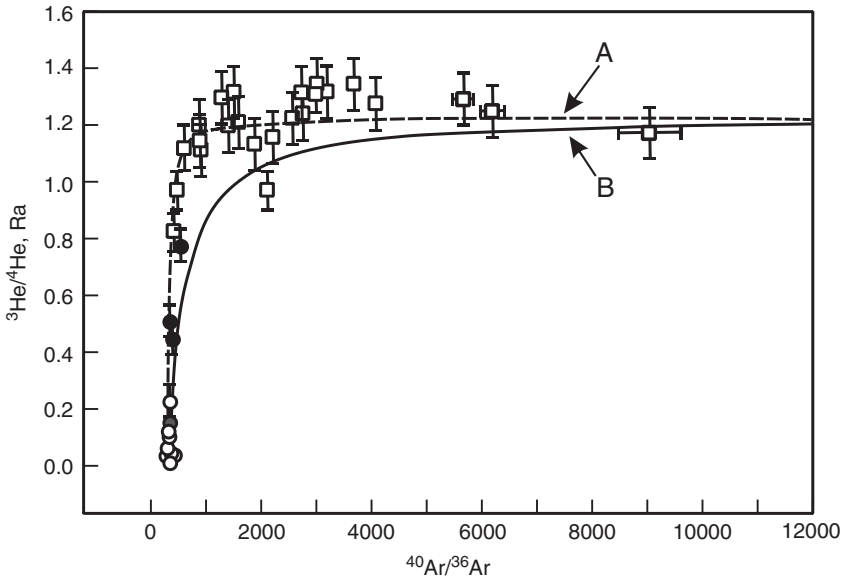


Fig. 1.13 Example of $^3He/^4He$ vs $^{40}Ar/^{36}Ar$ diagram, showing mixing of a magmatic fluid with a fluid dominated by atmospheric $^{40}Ar/^{36}Ar$. This example is from the Ailaoshan Au deposits, Yunnan Province, China, reported by Burnard et al. (1999). ^3He-rich is magmatic, ^{36}Ar-rich is atmospheric or modified ASW (air saturated water). Line A is for R = 1400; line B is for r = 140, where R = ($^4He/^{36}Ar$)magmatic/($^4He/^{36}Ar$)modified ASW

outside the inclusion; (3) release of lattice trapped gases, again from the decay of U, Th or K, during extraction of the fluids; (4) post-crystallisation production of ^{3}He by the action of cosmic rays. These post-entrapment effects can be effectively minimised by crushing the mineral grains rather than use step heating or fusion techniques for the release of the gases and by collecting samples from well below the surface, since the action of cosmic rays is confined to the first 1–15 m of the Earth's surface.

From the numerous examples provided in the recent literature, the following case studies of He and Ar isotope systematics are described here. Stuart et al. (1995) in their work on hydrothermal fluids from the Dae Hwa W-Mo vein deposit in South Korea, pointed out that the conservative behaviour of the He, Ar and Ne gases in the crust and mantle are invaluable in constraining the origin of the fluids and their mixing. Stuart et al. (1995) used correlations between He and Ar isotopes in fluid inclusions, in conjunction with $\delta^{18}O$ data, to identify mantle and crustal end member components. The noble gases were extracted from the crushing of primary fluid inclusions in scheelite ($CaWO_4$) crystals. These inclusions are of two types: Type I characterised by aqueous liquid with a vapour bubble and gas-rich type II. Homogenisation temperatures, together with data from δD and $\delta^{18}O$ systematic, show that the mineralising fluids had a temperature range from about 400°C (early) to 230°C (late). The scheelite crystals examined exhibit up to nine colour zones, which reveal a systematic decrease of homogenisation temperature and salinity from the core to the edge of the crystals. Similarly, the $\delta^{18}O$ of the aqueous fluid (denoted as $\delta^{18}O_{H_2O}$) decreases from +3.2‰ to –2.6‰ from core to edge. The measured $^{3}He/^{4}He$ ratios (R) of the released gases range from 1.5 to 0.1 R_A, with $^{3}He/^{36}Ar$ ratios from 0.003 to 0.012 being higher than air (2.4×10^{-7}) thereby eliminating the possibility of atmospheric contamination. Bearing in mind that the R can be influenced by cosmogenic nuclear activities ($R_C = \sim0.1$) in the upper 1–1.5 m of the Earth's surface, the authors ruled out this possibility because the samples examined were collected from a mine depth of about 100 m. The $\delta^{18}O_{H_2O}$ trend reflects dilution of a magmatic-dominated fluid ($\delta^{18}O_{H_2O} > +8‰$, T = 400–500°C) to meteoric-dominated fluids ($\delta^{18}O_{H_2O} > -10‰$) with lower temperatures in the hydrothermal system. The $\delta^{18}O_{H_2O}$ trend is matched by a progressive decrease in the $^{3}He/^{4}He$, $^{3}He/^{36}Ar$ and $^{40}Ar/^{36}Ar$ ratios, which also record a dilution from fluids with more primordial and radiogenic He and Ar to meteoric fluids enriched in radiogenic He and atmospheric Ar. Stuart et al. (1995) calculated an undiluted magmatic fluid $^{3}He/^{4}He$ ratio of between 0.9 and 2 R_A and $^{3}He/^{36}Ar > 0.01$ and $^{40}Ar/^{36}Ar > 1000$ for the Dae Hwa W-Mo hydrothermal system. The authors concluded that the above values are below typical mantle values and therefore they are likely a mixture of radiogenic and mantle values.

Zhang et al. (2002) studied the noble gas isotopes of the Denggezhuang, Jiaojia, Pengjiakuang, and Fayunkuang orogenic gold deposits. Their results show that the $^{3}He/^{4}He$ ratios of inclusion fluids in pyrite are 0.40–2.36 Ra. More specifically, the $^{3}He/^{4}He$ ratios of Denggezhuang (quartz vein-type) and

Jiaojia (fracture-type) are 1.64–2.36 R_A, and 0.43–0.79 R_A for the breccia type in the Pengjiakuang-Fayunkuang deposits. The helium isotope systematics suggests that mantle-derived fluids were involved in the metallogenic process. Accordingly, in a model of two-member mixed system of mantle and crust, 20–30% of ore-forming fluids are from the mantle in the quartz vein-type and fracture-type gold deposits. Similarly, a mantle fluid component for the Mesozoic Au deposit (Dongping) on the northern margin of the North China Craton, was detected on the basis of $^3He/^4He$ ratios (2.1–5.2 R_A) in inclusion fluids from ore zone pyrite (Mao et al. 2003). These results suggest that the ore forming fluids had a strong mantle component, thereby reinforcing the idea of mantle upwelling during the Mesozoic along the eastern regions of China to account for the widespread magmatism and hydrothermal ore deposits of that age (Mao et al. 2007). Helium isotopic analyses of inclusion fluids of ore veins from the Tongkeng-Changpo Sn deposit in the Dachang ore field in southern China showed $^3He/^4He$ ratios ranging from 1.2 to 2.9 R_A, which combined with a positive relationship with $^{40}Ar/^{36}Ar$ data are suggest that the ore fluids represent a mixture of both mantle and crustal components (Cai et al. 2007).

However, the usefulness of $^3He/^4He$ ratios as tracers of mantle sources was thrown into doubt by Stroncik et al. (2007). These workers studied He and Ne isotopes from volcanic glasses of lavas of off-axis seamounts of the the Mid-Atlantic Ridge and suggested that He isotopes are susceptible to decoupling from elements such as Ne. The combined He, Ne and Ar isotopic data from these lavas showed that there was a preferential loss of He compared to Ne and Ar, and that only ^{22}Ne preserved evidence of a primitive mantle component.

1.4.11.3 Sulphur Isotopic System

There are four stable isotopes of S (with natural abundances in parenthesis): ^{32}S (95.02%), ^{33}S (0.75%), ^{34}S (4.2%) and ^{36}S (0.017%). One radiogenic isotope, ^{35}S, has a short half life of 88 days. The isotopic ratio that is most frequently used in the study of ore systems is $^{34}S/^{32}S$, which is measured in $\delta^{34}S$ permil (‰), according to:

$$\delta^{34}S = {}^{34}S/^{32}S(\text{sample}) - {}^{34}S/^{32}S(\text{standard})/^{34}S/^{32}S(\text{standard}) \times 1000$$

where the international standard is an iron meteorite, Cañon Diablo Troilite (CDT), which has a value of 0.0450045 (Ohmoto and Goldhaber 1997). The principal S-bearing compounds include sulphides, sulphates, H_2S and SO_2, and these are found in both magmatic and hydrothermal ore deposits, with the S originating from three main isotopically distinct reservoirs (Rollinson 1993): (1) mantle, with $\delta^{34}S$ values of about 0‰; (2) sea water with $\delta^{34}S$ (today) of about + 20‰, and (3) sedimentary, with large negative $\delta^{34}S$ values. The main mechanisms that control the fractionation of S isotopes are (Rollinson 1993): (1) igneous processes (fractionation of ^{34}S between sulphides and melt); (2) bacterial reduction of sulphate to sulphide; (3) bacterial oxidation of sulphide to

sulphate; (4) non-bacterial reduction of sulphate to sulphide (thermochemical sulphate reduction); and (5) evaporite deposition. In general, biological activities produce the largest fractionations, as exemplified by up to 80‰ fractionation between seawater sulphate and biogenic sulphides since the beginning of the Phanerozoic, resulting in ^{34}S enrichment in seawater sulphate, averaging from $+10$ to $+30$‰.

For sulphides and sulphates of hydrothermal systems, the $\delta^{34}S$ values are controlled by temperature, the isotopic composition of S in the fluids and the ratio of oxidised (SO_4^{2-}) to reduced S (H_2S) in the ore fluids, which are in turn dependant on pH and f_{O2} of the ore fluids. However, as Rollinson (1993) pointed out, the $\delta^{34}S$ of a hydrothermal fluid cannot be simply estimated from the values of sulphide minerals, unless temperature, pH and f_{O2} are known.

Figure 1.14 illustrates a range of $\delta^{34}S$‰ for sulphides from selected ore systems, compared with meteorites, seawater and igneous sulphides.

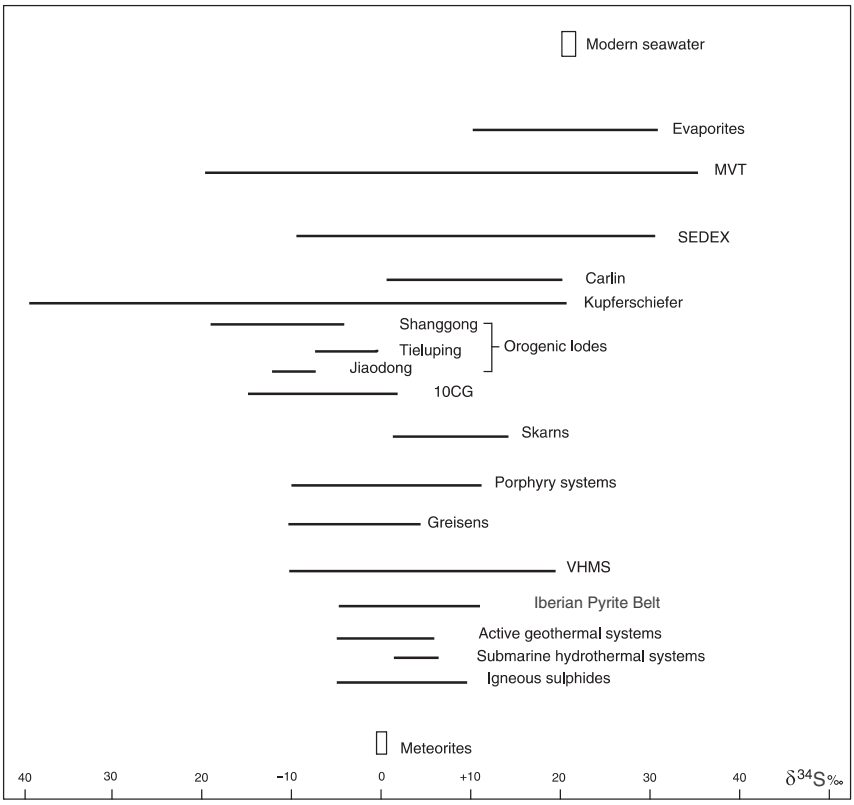


Fig. 1.14 Range of $\delta^{34}S$‰ of sulphides in selected ore systems and reservoirs. Data are taken from the various ore systems desribed in the chapters of this book

1.4.11.4 Lead Isotopes

A brief discussion is warranted to explain the principles of Pb-isotope systematics and their role in the discrimination of deposit types and, consequently, as a tool in the understanding of hydrothermal mineral systems (Young 1995). There are numerous papers that deal specifically deal with Pb isotope systematics applied to mineral systems. For the interested reader, a good example is provided by Frimmel et al. (2004). Lead isotopic ratios can provide information not only on the age, but also on the origin of hydrothermal deposits. There are in nature four isotopes of Pb, namely: ^{208}Pb, ^{207}Pb, ^{206}Pb and ^{204}Pb. The first three are the products of the radioactive decay of ^{232}Th, ^{235}U and ^{236}U respectively, whereas ^{204}Pb is non-radiogenic. The half-life of a radionuclide is a measure of the time it takes for half of the original nuclides to decay (see also Chapter 13 and Faure 1986 for details). Th and U, which have half-life rates comparable to the age of the Earth, are therefore suitable for dating purposes. A fundamental equation, which describes radioactive decay is:

$$P = P_0 e^{-\lambda t}$$

where P is the amount of parent now, P_0 parent at start of decay, λ is the decay constant an t is the elapsed time since the start of decay; half life is given by:

$$t_{1/2} = \ln 2/\lambda = 0.693/\lambda$$

A growth curve represents the variation of the radiogenic Pb with time, the starting point being the primordial value as deduced from meteoritic measurements. Points that fall on the growth curve therefore indicate a single-stage evolution. However, the Pb-isotopic ratios from hydrothermal mineral deposits usually do not fall on the growth curve, because in most cases the Pb-bearing ores would have experienced more than one stage of evolution. In this case data points form a line that intersects the growth curve at two points. The lower intercept measures the age of the source rocks; the upper indicates the age of the mineralisation. Allsopp et al. (1981), however, also pointed out that a linear trend can be obtained if there is mixing of two or more isotopic compositions. In other words, the hydrothermal fluids would have leached Pb from different sources with different Pb compositions related to the rocks with which the solutions interact. In this case a linear trend, would indicate mixing in varying proportions of two end members.

1.4.11.5 Carbon

Carbon has two stable isotopes, ^{12}C (98.89%) and ^{13}C (1.11%) and the commobnly used parameter is δ^{13}C, according to the formula:

$$\frac{(^{13}C^{12}C)\text{sample} - (^{13}C^{12}C)\text{std}}{(^{13}C^{12}C)\text{std}} \times 10^3$$

The reference standard is the Peedee Belemnite (PBD; *Belemnitella Americana*, Cretaceous Peedee Formation of South Carolina, USA).

Carbon isotope systematics are commonly used to assess whether the C of carbonate samples have igneous or biogenic signatures. $\delta^{13}C$ values in igneous rocks, if oxidised range from + 2.9 to –18‰ and if reduced from –20 to –28‰ (Faure 1986). Enrichment in ^{12}C or $\delta^{13}C$ values ranging from –15 to –40‰ PDB suggest a photosynthetic origin (Faure 1986; Hoefs 2004) whereas values raging from –20 to –65‰ PDB is indicative of derivation from microbial degradation of organic matter. Deep seatedIn the chapters that follow reference is made to C isotope systematic in a number of examples. Carbon isotopic compositions are especially useful to determine the source of C in hydrothermal fluids and for the recognition in the geological record of microbial communities associated with hydrothermal vents and gas hydrate seeps.

1.5 Concluding Remarks

In this first Chapter I have introduced the reader to some essential data on the universal solvent, water. Water, apart from its biological importance, is the chief constituent of hydrothermal solutions, from which ore metals and non-metals are deposited in a great variety of mineral systems, from subaerial and subaqueous hot springs to deep seated magmas. Important elements in the understanding of hydrothermal fluids are structure and properties of water, controls on solubility, redox and chemical potential.

The main kingdoms of terrestrial waters are oceans, meteoric water, connate, basinal water, juvenile and magmatic waters, metamorphic water. An interesting, and difficult to resolve aspect, is the ultimate origin of water; endogenic (mantle-derived) or extraterrestrial (brought in by cometary impacts), or both. Therefore one way to classify hydrothermal systems is in terms of water sources, namely metamorphic, seawater, magmatic, metamorphic, basinal and combinations thereof, depending on local geological and tectonic conditions. I return to this topic in later chapters. The boundaries between some of the above mentioned kingdoms (e.g. magmatic-meteoric, juvenile-magmatic) are by no means always clearly defined, even where isotopic tracers are used. Isotope systematics can be ambiguous and difficult to interpret. Often, field geological relations and the "big picture" context, help in giving useful insights and may provide reasonable answers to what may turn out to be an intractable problem.

Hot springs provide us with a window in the geometry and the end-stage in the evolution of a hydrothermal system. The discharge of hot aqueous fluids to the surface provide students of the Earth and Life sciences with a stupendous natural laboratory. The spectacular hot springs on the seafloor have captured

the imagination of many scientists, especially following the discovery of unsuspected ecosystems that thrive in these anoxic and high temperature environments. In many instances, microbial life of these ecosystems participates in mediating metal deposition by reducing sulphates to sulphides. This is one of the topics treated in Chapter 10.

Inclusion fluids continue to provide the geoscience community with a wealth of data. Particularly important are the isotopic analyses of the D and ^{18}O system in these fluids, and more recently the use of He and Ne as isotopic tracers. The latter having delivered some surprises, in that mantle He has been found to be involved in subaerial hot springs and in metal-depositing hydrothermal systems.

References

Abe Y (1993) Physical state of the very early Earth. Lithos 30:223–235
Allsopp HL, Welke HJ, Hughes MJ (1981) Shortening the odds in exploration. Nucl Act 24:8–12
Bada JL (2004) How life began on Earth: a status report. Earth Planet Sci Lett 226:1–15
Ballentine C J, Burgess R, Marty B (2002) Tracing fluid origin, transport and interaction in the crust. Geochem Soc Mineral Soc Am Rev Mineral 47:539–614
Bard AJ, Parsons R, Jordan J (eds) (1985) Standard potentials in aqueous solutions. Int Un App Chem, Marcel Dekker, New York
Best MG (1982) Igneous and metamorphic petrology. Freeman, San Francisco, 630pp
Barnes HL (1979) Solubilities of ore minerals. In:Geochemistry of hydrothermal ore deposits, 2nd edn. John Wiley & Sons, New York, pp 404–410
Bodnar JR (2005) Fluids in planetary systems. Elements 1:9–12
Boiron M-C, Dubessy J (1995) Determination of fluid inclusions compositions: microanalytical techniques. In: de Vivo and Frezzotti (eds) Fluid inclusions in minerals: methods and applications, Virginia Polytech Inst and State Univ, pp 45–71
Brandt JC (1999) Comets. In: Beatty JK, Petersen CC, Chaikin A (eds) The new solar system, 4th edn. Sky Publishing Corp & Cambridge Univ Press, Cambridge, pp 337–350
Brantley, SL, Ágústsdóttir AM, Rowe GL (1993) Crater lakes reveal volcanic heat and volatile fluxes. GSA Today 3(7):173–178
Brewer PG (2000) Chemical oceanography. In: Ernst WG (ed) Earth Systems; processes and issues. Cambridge University Press, Cambridge, 182–193
Brimhall GH, Crerar DA (1987) Ore fluids: magmatic to supergene. In: Carmichael ISE, Eugster HP (eds) Thermodynamics and modelling of geological materials: minerals; fluids and melts. Reviews in mineralogy, vol 17. Min Soc Am, pp 235–321
Browne KL (1986) Gold deposition from geothermal discharges in New Zealand. Econ Geol 81:979–983
Brugger J, Long N, McPhail DC, Plimer I (2005) An active amagmatic hydrothermal system: the Paralana hot springs, northern Flinders Ranges, South Australia. Chem Geol 222:35–64
Burnard PG, Hu R, Turner G, Bi XW (1999) Mantle, crustal and atmospheric noble gases in Ailaoshan gold deposits, Yunnan province, China. Geochim Cosmochim Acta 63:1595–1604
Cai MG, Mao JW, Ting L, Pirajno F, Huang HL (2007) The origin of the Tongkeng-Changpo tin deposit, Dachang metal district, Guanxi, China: clues from fluid inclusions and He isotope systematics. Miner Deposita 42:613–626

Carmichael ISE, Ghiorso MS (1990) The effect of oxygen fugacity on the redox state of natural liquids and their crystallising phases. Mineral Soc Am Rev Mineral 24:191–212
Carmichael ISE, Turner FJ, Verhoogen J (1974) Igneous petrology. Mc-Graw Hill Book Co, New York, 739pp
Cathles LM, Adams JJ (2005) Fluid flow and petroleum and mineral resources in the upper (<20-km) continental crust. Econ Geol 100th Anniv Vol: 77–110
Chyba CF, Sagan C. (1996) Comets as the source of prebiotic organic molecules for the early Earth. In: Thomas PJ, Chyba CF, McKay PC (eds) Comets and the origin and evolution of life. Springer-Verlag, New York, pp 147–174
Cole DR. Drummond SE (1986) The effect of transport and boiling on Ag/Au ratios in hydrothermal solutions: a preliminary assessment and possible implications for the formation of epithermal precious metal ore deposits. J Geochem Expl 25:45–79
Cotton FA, Wilkinson G, Murillo CA, Bockman M (1999) Advanced inorganic chemistry. 6th edn. John Wiley
Craig H, Lupton JE (1976) Primordial neon, helium and hydrogen in oceanic basalt. Earth Planet Sci Lett 31:369–385
Crerar DA, Wood S, Brantley S, Bocarsly A (1985) Chemical controls on solubility of ore forming minerals in hydrothermal solutions. Can Mineral 23:333–351
Crossey LJ, Fischer TP, Patchett PJ, Karlstrom KE, Hilton DR, Newell DL, Huntoon P, Reynolds AC, de Leeuw GAM (2006) Dissected hydrologc system at the Grand Canyon: interaction between deeply derived fluids and plateau aquifer waters in modern springs. Geology 34:25–28
Delsemme AH (1999) The deuterium enrichment observed in recent comets is consistent with a cometary origin of seawater. Planet Space Sci 47:125–131
Demicco RV, Lowenstein TK, Hardie LA, Spencer RJ (2005) Model of seawater composition in the Phanerozoic. Geology 33:877–880
Desio A (1959) Geologia applicata all'ingegneria, 2nd edn. Ulrico Hoepli, Milan, 1058pp
Despois D, Cottin H (2005) Comets: potential sources of prebiotic molecules for the early Earth. In: Gargaud M, Barbier B, Martin H, Reisse J (eds) Lectures in Astrobiology, vol I. Springer, Berlin, pp 289–352
De Ronde CEJ, Channer DMDR, Faure K, Bray C, Spooner TC (1997) Fluid chemistry of Archean seafoor hydrothermal vents: implications for the composition of circa 3.2 Ga seawater. Geochim Cosmochim Acta 61:4025–4042
De Vivo B, Frezzotti ML (eds) (1995) Fluid inclusions in minerals: methods and applications: Short course of the working group (IMA), Siena, September, 1994, Virginia Polytech Inst State Univ
Doe RB, Delevaux MA (1972) Sources of lead in southwest Missouri galena ores. Econ Geol 67:409–425
Dyson F (1985) Origins of life. Cambridge Univ Press, Cambridge
Einaudi MT (2000) Mineral resources: assets and liabilities. In: Ernst WG (ed) Earth systems – processes and issues. Cambridge University Press, Cambridge, pp 346–372
Ellis A J (1979) Explored geothermal systems. In: Barnes HL (ed) Geochemistry of hydrothermal ore deposits. John Wiley & Sons, New York, pp 632–683
Ellis AJ, Mahon WAJ (1977) Chemistry and geothermal systems. Academic Press, New York, 392pp
Eugster HP, Wones DR (1963) Stability relations of the ferruginous biotite, annite. J Petrol 3:82–125
Evans AM (1987) An Introduction to ore geology, 2nd edn. Blackwell, Oxford
Farmer JD (2000) Hydrothermal systems: doorways to early biosphere evolution. GSA Today 10:1–9
Faure G (1986) Principle of isotope geology, 2nd edn. John Wiley & Sons, New York
Faure G (2001) Origin of igneous rocks – The isotopic evidence. Springer, Berlin

Feiss P G (1978) Magmatic sources of copper in porphyry ÿcopper deposits. Econ Geol 73:397–404
Folsome CE (1979) The origin of life. WH Freeman and Company, San Francisco, 168pp
Fournier RO (1989) Geochemistry and dynamics of the Yellowstone National Park hydrothermal system. Ann Rev Earth Planet Sci 17:13–53
Franks F (ed) (1982) Water A comprehensive treatise. Plenum, New York, 484pp
Frey H (1977) Origin of the Earth's ocean basins. Icarus 32:235–250
Frimmel HE, Jonasson IR, Mubita P (2004) An Eburnean base metal source for sediment-hosted zinc-lead deposits in Neoproterozoic units of Namibia: Lead isotopic and geochemical evidence. Mineral Depos 39:328–343
Frost BR (1981) Introduction to oxygen fugacity and its petrologic importance. Rev Mineral 8:1–9
Gill R (1989) Chemical fundamentals of geology. Unwin Hyman, London, 291pp
Glasby GP, Cherkashov GA, Gavrilenko GM, Rashidov VA, Slovtsov IB (2006) Submarin hydrothermal activity and mineralisation on the Kurile and western Kamchatka island arcs, NW Pacific. Marine Geol 231:163–180
Goff F, Stimac JA, Larocque ACL, Hulen JB, McMurtry GM, Adams AI, Róldan-M A, Trujillo PE, Counce D, Chipera, SJ, Mann, D, Heizler M (1994) Gold degassing and deposition at Galeras volcano, Colombia. GSA Today 4(10):241–248
Goldberg ED (1972) The fkuxes of marine chemistry. Proceed Roy Soc Edin, Sec B 72:357–364
Gortani AR (1959) Compendio di geografia generale. Casa Editr Giuseppe Principato, Milano, 540pp
Graham DW (2002) Noble gas isotope geochemistry of mid-ocean ridge and ocean island basalts: characterisation of mantle source reservoirs. Geochem Soc and Mineral Soc Am, Rev Mineral 47:247–318
Guidry SA, Chafetz HS (2003) Anatomy of siliceous hot springs: examples from Yellowstone National Park, Wyoming, USA. Sedimen Geol 157:71–106
Hanor JS (1979) The sedimentary genesis of hydrothermal fluids. In: Barnes HL (ed) Geochemistry of hydrothermal ore deposits, 2nd edn. John Wiley & Sons, New York, pp 137–168
Heaman L, Ludden JN (eds) (1991) Short course handbook on applications of radiogenic isotope systems to problems of geology. Mineral Ass Can 19, 423pp
Hedenquist JW, Aoki M, Shinohara H (1994) Flux of volatiles and ore-forming metals from the magmagtic-hydrothermal system of Satsuma Iwojima volcano. Geology 22:585–588
Hemley J, Jones WR (1964) Chemical aspects of hydrothermal alteration with emphasis on hydrogen metasomatism. Econ Geol 59:538–569
Henley RW, Ellis AJ (1983) Geothermal systems ancient and modern: a geochemical review. Earth Sci Rev 19:1–50
Henley RW, Truesdell AH, Barton PB, Whitney JA (1984) Fluid-mineral equilibria in hydrothermal systems. Rev Econ Geol 1, Soc Econ Geol, 267pp
Hoefs J (2004) Stable isotope geochemistry. 5th edn, Springer, Berlin
Holland HD (1984) The chemical evolution of the atmosphere and the oceans. Princeton Univ Press, Princeton, 582pp
Holland HD (2003) The geological history of seawater. In: Elderfield H (ed) The oceans and marine geochemistry. Treatise on Geochemistry, Elsevier, Amsterdam, pp 583–625
Hoyle F, Wichramasinghe NC (1980) Comets and the origin of life. Reidel, Dordrecht, 227pp
Hren MT, Lowe DR, Tice MM, Byerly G, Chamberlein CP (2006) Stable isotope evidence for recent ironstone pods within the Archean Barberton greenstone belt, South Africa. Geochim Cosmochim Acta 70:1457–1470
Huston DL, Large RR (1989) A chemical model for the concentration of gold in volcanogenic massive sulphide deposits. Ore Geol Rev 4:171–200

Ingerbritsen SE, Sanford WE (1998) Groundwater in geologic processes. Cambridge Univ Press, Cambridge, 341pp
Ingle JC (2000) Deep-sea and global ocean circulation. In: Ernst WG (ed) Earth systems: processes and issues. Cambridge University Press, pp 169–181
Ivanova GF (1969) Conditions of concentration oftungsten during greisenisation. Geokhimya 1:22–36 (in Russian)
Jones B, Renaut RW (2003) Hot spring and geyser sinters: the integrated product of precipitation, replacement and deposition. Can J Earth Sci 40:1549–1569
Kavalieris I (1994) High Au, Ag, Mo, Pb, V and W content of fumarolic deposits at Merapi Volcano, central Java, Indonesia: J Geochem Expl 50:479–492
Kennett J (1982) Marine Geology. Prentice-Hall, Inc, Englewood Cliffs, 813pp
Kerridge JF (1985) Carbon, hydrogen and nitrogen in carbonaceous chondrites: abundances and isotopic compositions in bulk samples. Geochim Cosmochim Acta 49:1707–1714
Knauth LP, Lowe DR (1978) Oxygen isotope geochemistry of cherts from the Onverwacth Group (3.4 billion years), Transvaal Group, South Africa, with implications for secular variations in isotopic compositions of cherts. J Geol 41:209–222
Konhauser KO, Ferris FG (1996) Diversity of iron and silica precipitation by microbial mats in hydrothermal waters, Iceland: Implications for Precambrian iron formations. Geology 24:323–326
Koslovsky YEA (1984) The world's deepest well. Sci Am 251:106–113
Krauskopf KB (1979) Introduction to geochemistry, 2nd edn. McGraw-Hill Kogakushu New York, 617pp
Lang JR, Baker T (2001) Intrusion-related gold systems: the present level of understanding. Mineral Deposita 36:477–489
Large R, Huston D, McGoldrich P, McArthur G, Ruxton P (1988) Gold distribution and genesis in Paleozoic volcanogenic massive sulphide systems. In: Bicentennial Gold 88. Geol Soc Aust Abst Ser 22:121–126
Le Cloarec MF, Marty B (1991) Volatile fluxes from volcanoes. Terra Nova 3:17–27
Lewis JS, Prinn RG (1984) Planets and their atmospheres; origin and evolution. Academic Press, new York, 470pp
Lindgren W (1933) Mineral deposits. McGraw-Hill Book Co, New York
Lowe DR, Byerly GR (2003) Ironstone Pods in the Archaean Barberton greenstone belt, South Africa: Earth's oldest seafloor hydrothermal vents reinterpreted as Quaternary subaerial springs. Geology 31:909–912
Mao JW, Li YQ, Goldfarb R, He Y, Zaw K, (2003) Fluid inclusion and noble gas studies of the Dongping gold deposit, Hebei province, China: a mantle connection for mineralization? Econ Geol 98:517–534
Mao JW, Wang YT, Li HM, Pirajno F, Zhang CQ, Wang RT (2007) The relationship of mantle-derived fluids to gold metallogenesis in the Jiadong Peninsula: evidence from D-O-C-S isotope systematics. Ore Geol Rev, doi: 10.1016/j.oregeorev.2007.01.003
Masterton WL, Slowinski EJ, Stanitski CL (1981) Chemical principles, 5th edn. Holt-Saunders International Editions, Saunders, Philadelphia, 641pp
Maurice PA (2000) The hydrologic cycle. In: Ernst WG (ed) Earth systems: processes and issues. Cambridge University Press, pp 135–151
McCollom TM, Shock EL (1997) Geochemical constraints on chemolithoautotrophic metabolism by microorganisms in seafloor hydrothermal systems. Geochim Cosmochim Acta 61:4375–4391
McSween HY, Richardson SM, Uhle ME (2003) Geochemistry – pathways and processes, 2nd edn. Columbia Univ Press, New York, 359pp
Milazzo G, Caroli S, Sharma VK (1978) Tables of standard electrode potentials. Wiley, Chichester
Millero FJ (2003) Physico-chemical controls of seawater, in Treatise on Geochemistry, Elsevier, Amsterdam pp 1–21

Misra KC (2000) Understanding mineral deposits. Kluwer Academic Publ, Dordrecht
Myers JS (2004) Isua enigmas: illusive tectonic, sedimentary, volcanic and organic features of the >3.7 Ga Isua Greenstone Belt, southwest Greenland. In: Eriksson PG, Altermann W, Nelson DR, Mueller WU, Catuneanu O (eds) The Precambrian Earth: tempos and events. Developments in Precambrian Geology vol 12, Elsevier, Amsterdam, pp 66–73
Nesbitt BE (1996) Applications of oxygen and hydrogen isotopes to exploration for hydrothermal mineralization. SEG Newsletter 27:1–13
Neilson GW, Enderby JE (1986) Water and aqueous solutions. Hilger, Bristol, 349pp
Neumann N, Sandiford M, Foden J (2000) Regional geochemistry and continental heat flow: implications for the origin of the South Australian heat flow anomaly. Earth Planet Sci Lett 183:107–120
Nightingale PD, Liss PS (2003) Gases in seawater, in Treatise on Geochemistry, Elsevier, Amsterdam, pp 49–81
Ohmoto H (1986) Stable isotope geochemistry of ore deposits. In: Valley JW, Taylor HP, O'Neil JR (eds) Stable isotopes in high temperature geological processes. Rev Mineral Min Soc Am 16:491–559
Ohmoto H, Goldhaber MB (1997) Sulfur and carbon isotopes. In: Barnes HL (ed) Geochemistry of hydrothermal ore deposits, 3rd edn. John Wiley & Sons, New York, pp 517–612
Ohtani E (2005) Water in the mantle. Elements 1:25–30
Paton TR (1978) The formation of soil material. Allen & Unwin, 143pp
Peacock SM (1990) Fluid processes in subduction zones. Science 248:329–337
Pentecost A, Jones B, Renaut RW (2003) What is hot spring? Can J Earth Sci 40:1443–1446
Petit JR, Alekhina I, Bulat S (2005) Lake Vostok, Antarctica: exploring a subglacial lake and searching for life in an extreme environment. In: Gargaud M, Barbier B, Martin H, Reisse J (eds) Lectures in Astrobiology, vol I. Springer, Berlin, pp 227–288
Pinti DL (2005) The origin and evolution of the oceans. In: Gargaud M, Barbier B, Martin H, Reisse J (eds) Lectures in Astrobiology, vol I. Springer, Berlin, pp 83–112
Pirajno F (1992) Hydrothermal mineral deposits – Principles and fundamental concepts for the exploration geologist. Springer-Verlag, Berlin, 709pp
Pope JG, Brown KL, McConchie DM (2005) Gold concentrations in springs at Waiotapu, New Zealand: Implications for precious metal deposition in geothermal systems. Econ Geol 100:677–688
Porcelli D, Ballentine C J, Wieler R (eds) (2002) Noble gases in geochemistry and cosmochemistry. Mineral Soc Am Rev Miner Geochem 47, 844pp
Press F, Siever R (1982) Earth, 3d edn. Freeman, San Francisco, 613pp
Quisefit JP, Toutain JP, Bergametti G, Javoy M, Cheyet B, Person A (1989) Evolution versus cooling of gaseous volcanic emissions from Momotombo volcano, Nicaragua: thermochemical model and observations. Geochim Cosmochim Acta 53:2591–2608
Rasmussen B, Buick R (1999) Redox state of the Archean atmosphere: Evidencxe from detrital heavy minerals in ca. 3250–2750 Ma sandstones from the Pilbara Craton, Australia. Geology 27:115–118
Renaut RW, Jones B, Tiercelin JJ (1998) Rapid in-situ silicification of microbes at Loburu hot sprngs, lake Bogoria, Kenya rift valley. Sedimentology 45:1083–1104
Renaut RW, Jones B (eds) (2003) Sedimentology of hot spring systems. Can J Earth Sci 40(11)
Rickard D, Luther GW (2006) Metal sulfide complexes and clusters. Rev Mineral Geochem 61:421–504
Ringwood AE (1966) The chemical composition and origin of the Earth, in Hurley PM (ed) Advances in Earth Sciences. The MIT Press, Cambrdige, USA, pp 287–356
Ringwood AE (1975) Composition andpetrology of the Earth's mantle. Mc-Graw Hill, New York, 618pp
Roedder E (1979) Fluid inclusions as samples of ore fluids. In: Barnes HL (ed) Geochemistry of hydrothermal ore deposits, 2nd edn. John Wiley & Sons, New York, pp 684–731
Roedder E (1984) Fluid inclusions. Rev Mineral 12, Min Soc Am, 644pp

Roedder E, Bodnar RJ (1997) Fluid inclusion studies of hydrothermal ore deposits. In: Barnes HL (ed) Geochemistry of hydrothermal ore deposits, 3rd edn. John Wiley & Son, New York, pp 657–697

Rollinson H (1993) Using geochemical data: evaluation, presentation, interpretation. Longman Scientific & Technical, John Wiley & Sons, New York

Rose AW, Hawkes HE, Webb S (1979) Geochemistry in mineral exploration, 2nd edn. Academic Press, New York, 657pp

Saunders JA (1990) Colloidal transport of gold and silica in epithermal precious metal systems: evidence from the Sleeper deposit, Nevada. Geology 18:757–760

Schubert G, Turcotte DL, Olson P (2001) Mantle comvection in the Earth and Planets. Cambridge University Press, Cambridge, 940pp

Seibold E, Berger WH (1982) The seafloor. Springer-Verlag, 288pp

Seward TM (1979a) Hydrothermal transport and deposition of gold. In: Glover JE, Grove DI (eds) Gold Mineralisation. Univ W Aust Extens Serv Publ 3:45–55

Seward TM (1979b) Modern hydrothermal systems in New Zealand and their relation to gold mineralisation processes. In: Glover JE, Grove DI (eds) Gold Mineralisation. Univ W Aust Extens Serv Publ 3:56–64

Shepherd TJ, Rankin AH (1998) Fluid inclusion techniques of analysis: Rev Econ Geol 10:125–150

Shepherd TJ, Rankin AH, Alderton DHM (1985) A practical guide to fluid inclusion studies. Chapman and Hall, New York, 239pp

Sheppard SMF (1986) Characterization and isotopic variations in natural waters. In: Valley JL, Taylor HP, O'Neill JR (eds) Stable isotopes in high temperature geological processes. Rev Mineralogy Min Ass Can 16:165–183

Siegert MJ (2005) Lakes beneath the ice sheet: the occurrence, analysis and future exploration of Lake Vostok and oter Antarctic subglacial lakes. Ann Rev Earth Planet Sci 33:215–245

Siegert MJ, Ellis-Evans JC, Tranter M, Mayer C, Petit J-R, Salamantin A, Priscu JC (2001) Physical, chemical and biological processes in Lake Vostok and other Antarctic subglacial lakes. Nature 414:603–609

Skinner BJ (1979) The many origins of hydrothermal mineral deposits. In: Barnes HL (ed) Geochemistry of hydrothermal ore deposits, 2nd edn. John Wiley & Sons, New York, pp 3–21

Spencer RJ, Hardie LA (1990) Control of seawater composition by mixing of river waters and mid-ocean ridge hydrothermal brines. Geochem Soc Spec Publ 19:409–420

Stefánsson A, Seward TM (2004) Gold(I) complexing in aqueous sulphide solutions to 500°C at 500 bar. Geochim Cosmochim Acta 68:4121–4143

Stroncik NA, Niedermann S, Haase KM (2007) Neon and helium isotope as tracers of mantle reservoirs and mantle dynamics. Earth Planet Sci Lett. doi: 10.1016/j.epsl.2207.03.046

Stuart FM, Burnard PG, Taylor RP, Turner G (1995) Resolving mantle and crustal contributions to ancient hydrothermal fluids: He-Ar isotopes in fluid inclusions from Dae Hwa W-Mo mineralisation, South Korea. Geochim Cosmochim Acta 59:4663–4673

Taran YA, Bernard A, Gavilanes JC, Africano F (2000) Native gold in mineral precipitates from high-temperature volcanic gases of Colima volcano, Mexico. Applied Geochem 15:337–346

Taylor HP (1974) The application of oxygen and hydrogen isotope studies to prblems of hydrothermal alteration and ore deposition. Econ Geol 69:843–883

Taylor HP (1979) Oxygen and hydrogen isotope relationships in hydrothermal mineral deposits. In: Barnes HL (ed) Geochemistry of hydrothermal ore deposits, 2nd edn. John Wiley & Sons, New York, pp 236–277

Taylor HP (1997) Oxygen and hydrogen isotope relationships in hydrothermal mineral deposits. In: Barnes HL (ed) Geochemistry of hydrothermal ore deposits, 3rd edn. John Wiley & Sons, New York, pp 229–302

Taylor G, Eggleton RA (2001) Regolith geology and geomorphology. John Wiley & Sons Ltd, Chichester, 375pp
Turekian KK (1969) The oceans, streams and the atmosphere. In: Wedepohl KH (ed) Handbook of Geochemistry. Springer-Verlag, Berlin, pp 297–323
Valley JL, Taylor HP, O'Neill JR (eds) (1986) Stable isotopes in high temperature geological processes. Reviews in Mineralogy Min Ass Can 16:570
Van den Kerkhof AM, Hein UF (2001) Fluid inclusion petrography. Lithos 55:27–47
Van Kranendonk MJ (2006) Volcanic degassing, hydrothermal circulation and the flourishing of early life on Earth: A review of the evidence from c. 3490–3240 Ma rocks of the Pilbara Supergroup, Pilbara Craton, Western Australia. Earth-Science Rev 74:197–240
Van Kranendonk MJ, Pirajno F (2004) Geological setting and geochemistry of metabasalts and alteration zones associated with hydrothermal chert±barite deposits in the ca. 3.45 Ga Warrawoona Group, Pilbara Craton, Australia. Geochem: Explor Envir Analys 4:253–278
Weissberg BG, Browne PRL, Seward TM (1979) Ore metals in active geothermal systems. In: Barnes H L (ed) Geochemistry of hydrothermal ore deposits. John Wiley & Sons, New York, pp 738–780
White DE (1981) Active geothermal systems and hydrothermal deposits. Econ Geol 75th Anniv Volume, pp 392–423
Whitfield M (1982) The salt sea, accident or design? New Scient 94:14–17
Wilde SA, Valley JW, Peck WH, Graham CM (2001) Evidence from detrital zircons for the existence of continental crust and oceans on the Earth 4.4 Gyr ago. Nature 409:175–178
Williams Q, Hemley RJ (2001) Hydrogen in the deep earth. Ann Rev Earth Planet Sci 29:365–418
Wilkinson JJ (2001) Fluid inclusions in hydrothermal ore deposits. Lithos 55:229–272
Wood JA (1999) Origin of the solar system. In: Beatty JK, Petersen CC, Chaikin A (eds) The new solar system, 4th edn. Sky Publishing Corp & Cambridge Univ Press, Cambridge, pp 13–22
Young LE (1995) Empirical applications of common lead-isotope ratios to exploration/ SEG Newslett 22:1–12
Zhang LC, Shen YC, Li HM, Zeng QD, Li GM, Liu TB (2002) Helium and argon isotopic compositions of fluid inclusions and tracing to the source of ore-forming fluids for Jiaodong gold deposits. Acta Petrol Sinica 18:559–565 (in Chinese with English abstract).

Chapter 2
Hydrothermal Processes and Wall Rock Alteration

2.1 Introduction

In this chapter, I discuss the effects that hydrothermal fluids derived from internal processes have on the ambient lithologies. I begin by describing the main components of a hydrothermal system and models of magmatic-related hydrothermal processes. Circulation of these hydrothermal solutions or fluids, produces physico-chemical changes in the rocks through which they circulate. This is what is commonly referred to as hydrothermal alteration. When these fluids come into contact with rocks they set off chemical reactions, which tend to approach equilibrium and through processes of dissolution and precipitation develop new mineral assemblages There are different types and styles of hydrothermal alteration, depending on the nature, chemistry, temperature and pressure of the circulating fluids as well as the nature and composition of the rocks through which the fluids circulate. Although there are transitional types and continua in many of the alteration processes, it is convenient to describe these as end members. Alteration processes can be described solely in terms of their chemistry and mineralogy, as for example potassic or argillic alteration. Alternatively, potassic and argillic alterations and their characters can be described in the context of the mineral system of which they are part. For example, potassic alteration of porphyry systems, or potassic alteration of alkaline ring complexes (also called fenitisation). Hydrothermal alteration is very important for mineral exploration, because it extends well beyond the limits of the ore, thereby allowing to focus exploration activity towards smaller targets. In the pages that follow, I draw from an earlier book of mine (Pirajno 1992), augmented by more recent data from the literature. There are not many books or other publications that deal with hydrothermal alteration, apart from special issues of journals devoted to specific ore systems. A classic paper is that of Meyer and Hemley (1967). The books by Guilbert and Park (1986) and Lentz (1994) provide a wealth of good information on alteration processes and systems. Atlases of alteration can be found in Thompson and Thompson (1996) and that of Eilu et al. (1999) on orogenic lodes. Gifkins et al. (2005) produced an excellent and superbly illustrated book on alteration of submarine volcanic systems.

F. Pirajno, *Hydrothermal Processes and Mineral Systems*,

© Springer Science+Business Media B.V. 2009

Hydrothermal alteration patterns and associated mineral assemblages are discussed under the relevant mineral systems in the chapters ahead. In this chapter, I review the general aspects of hydrothermal alteration processes in intrusion-related, porphyry and epithermal systems, skarns and alteration (or hydrothermal metamorphism) of oceanic crust at spreading centres, inevitably with some repetition, with the aim of providing a "road map" for field-based studies. Indeed, the mapping of alteration mineral assemblages can be very useful for the identification of hydrothermal conduits, which in turn may lead to the discovery of buried ores. In addition, I examine the overprint of regional metamorphism on hydrothermally altered rocks, considering that there are instances in which it may difficult to separate the two, because the same mineral phases can be formed (e.g. chlorite, biotite, calcite, garnet, amphibole, etc.), under conditions of regional metamorphism and hydrothermal circulation. I conclude with overviews on the use of geochemistry and stable isotope systematics in the study of hydrothermal processes and the detection of regional alteration patterns from spectral remote sensing.

2.1.1 The Main Components of a Hydrothermal System

It is said that Leonardo da Vinci thought that there are two cycles of water on Earth. One is the surface cycle (evaporation, precipitation, runoff), the other is an internal cycle. Although Leonardo was not a geologist, he probably suspected that water issuing from springs had something to do with internal processes. A hydrothermal system can be loosely defined as the distribution of hot fluids circulating, laterally and vertically at various temperatures and pressures, below the Earth's surface. The presence and movement of these fluids, whether or not they discharge at the surface, constitute hydrothermal activity. More rigorous definitions would have to include the geological environment within which the circulation of fluids is generated and maintained for a period of time long enough to form an anomalous concentration of metallic minerals. Whether this anomalous concentration constitutes an orebody or not, is generally an artificial parameter dictated by the global and/or local social, economic and political framework of organised human societies, at a given time. A hydrothermal system consists of two essential components: a heat source, which provides the necessary energy (magmatic, geothermal gradient, radiogenic decay, metamorphism), and a fluid phase, which includes solutions derived from magmatic/juvenile fluids, metamorphic fluids, meteoric, connate waters or seawater. A hydrothermal system necessitates a plumbing structure (fault, fracture, permeable lithologies) that focuses the solutions to a depositional site. An actively convective hydrothermal cell will consist of: a recharge system, a circulation cell and a discharge system. A hydrothermal mineral deposit is formed by the circulation of warm to hot fluids (about 50 to $> 500^{\circ}C$) that leach, transport and subsequently precipitate their mineral load in response to

changing physico-chemical conditions. Mineral deposits are usually formed at the discharge site, whether this is a single conduit, or a series of channelways, or a fine network of small fractures. Seen in a different perspective, a hydrothermal system can be considered in terms of a fluid flow regime. In this view, shown in Fig. 2.1, the development of a hydrothermal mineral system requires that fluids are transported from a large-volume reservoir through progressively smaller pathways to a depositional site. Cox (2005) envisaged in this hydrothermal mineral system an upstream part flow regime and a downstream part flow regime (Fig. 2.1). The depositional sites are faults, fractures networks and shear zones.

The rocks within which the deposit is formed undergo varying degrees of hydrothermal alteration, the intensity of which as a rule decreases away from the discharge site(s), and hence from the mineralised body. As mentioned

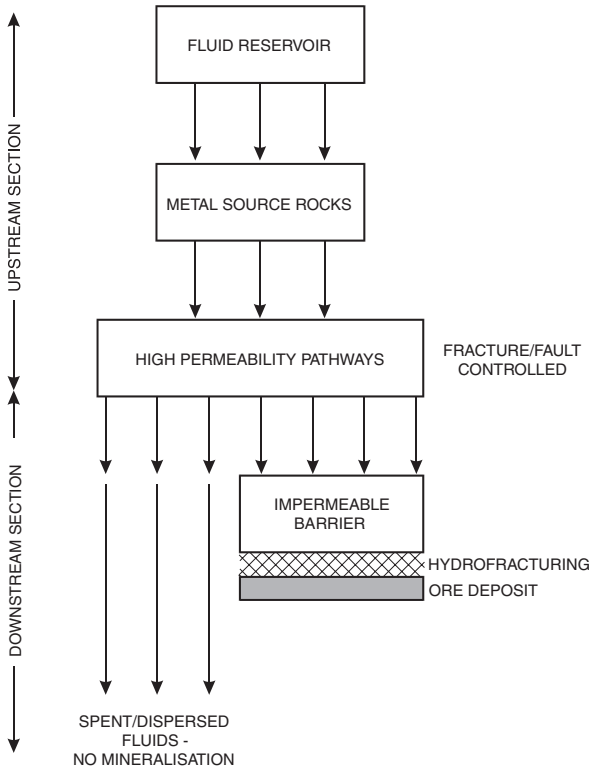


Fig. 2.1 Fluid flow in a fracture-controlled hydrothermal system; the upstream section consists of a large volume fluid source from which the fluids are channelled along progressively smaller pathways, to interact with a metal(s) source rocks, to a downstream section where fluids may encounter an impermeable barrier, which will preclude the upward flow resulting in a pressure build up, followed by effervescence or boiling, hydrofracturing and metal deposition; if the fluids do not encounter a barrier, then it is possible that these fluid become dispersed or spent and produce no mineralisation. Modified after Cox (2005)

above, alteration takes place because the mineral assemblages in the wall rocks are in physico-chemical disequilibrium with the hydrothermal fluids, and tend to re-equilibrate by forming new mineral assemblages that are stable under the new conditions. In this respect it may be appropriate to make a distinction between mineral assemblages and mineral associations (Seedorff et al. 2005). A mineral assemblage refers to a group of minerals that formed more or less at the same time and are stable together. A mineral assemblage essentially defines the physico-chemical conditions of the system. A mineral association, on the other hand, is a group of minerals that occurs together, but are not necessarily in equilibrium and did not form at the same time.

A "fossil" hydrothermal system is the result of "frozen-in" hydrothermal activity in a given geological and tectonic setting. Although there may be different opinions amongst geologists as to details of the workings of such a system, there is little doubt that the hydrothermal activity, in a porphyry Cu-Au deposit for example, was started by magmatic events relating to the emplacement of a volcano-plutonic complex. Quartz veins are the "fossil" expression of the discharge of fluids along a narrow structure or channel. Many of the volcanic-associated precious and base metal deposits (e.g. volcanogenic massive sulphides, VMS; Chapter 7), both in the subaerial and submarine environments, represent "frozen-in" hydrothermal systems, with their analogues being observed in areas of active venting at modern convergent and divergent plate boundaries. Similarly, some of the Proterozoic-aged, sediment-hosted massive sulphide deposits or SEDEX, represent a geological record analogue of sulphide muds accumulating in the brine pools of the axial zone of the Red Sea. However, not all of the hydrothermal mineral deposits preserved today have a modern equivalent. For example, some of the ore deposits of Archaean and Palaeoproterozoic age have no modern analogue. This is because they were the product of hydrothermal systems activated during particular geodynamic, metallogenic and/or biogenic and atmospheric conditions, which have not since been repeated. Amongst these I cite the Witwatersrand Au-U deposits in South Africa, formed when the atmosphere was clearly O_2 poor or the Fe ores of the banded iron-formation (BIF) formed during a transition to a rise in the levels of O_2 in atmosphere. In other instances, hydrothermal activity occurs at depths beyond our direct observation. Deep drilling in the continental crust has, however, indicated the presence of hydrothermal fluids circulating along major shear zones at depths of several kilometres (see Chapter 9).

2.1.1.1 Hydrothermal Veins

Hydrothermal veins are the best indicators of hydrothermal fluid flow and as such can also be considered an expression of the conduits or fractures through which fluids circulate. Textural variations and morphology of vein crystals (usually quartz and carbonates) and other silica precipitates (e.g. opal, chalcedony) provide valuable information on the nature of the hydrothermal system from which the veins were sourced. Much of microthermometric measurements of fluid inclusions

are carried out on vein quartz and carbonate minerals. Hydrothermal veins have a very wide size range from submicroscopic to several km in length. Giant quartz veins from the Abitibi greenstone belt are estimated to have formed from 1×10^{18} g of fluids, precipitating 9×10^{14} g of Si, 9×10^{13} g of CO_2 as carbonate, and 1×10^{13} g of K (Jia and Kerrich 2000). Hydrothermal veins mostly form from silica-bearing fluids that originate from (Jia and Kerrich 2000): (1) igneous intrusions; (2) deeply convecting meteoric fluids; (3) metamorphic devolatilisation; (4) mantle-derived fluids. Quartz veins are commonly found in low-grade rocks, typically within or above the brittle-ductile crustal stress field, forming around 2–3 kbar and 200–350°C (Bons 2001). Hydrothermal veins can be syntectonic to post-tectonic.

Bons (2001), using an example from intrusion-associated quartz veins in western New South Wales, Australia, proposed an interesting model of veins forming by rapid ascent of batches of fluids along hydrofracture systems. This author reasoned that quartz should precipitate close to the source as the ascending fluids cools because the solubility of silica dramatically decreases with temperature. Instead quartz veins are observed in the upper crustal levels at and above the brittle-ductile transition. This indicates that silica-bearing fluids move very fast and, because of this, these fluids would have no time to equilibrate with cooler and lower pressure environments. Bons (2001) proposed that silica-bearing fluids do not flow through the fracture, but move with a water-filled hydrofracture which, according to this author, can move at speeds of 1 m/s and therefore propagate 10 km in about 3 hours. Ascending microfractures are likely to arrest their movement once they enter the brittle regions in the upper crust, where pore fluid pressure is lower than lithostatic pressure. The region of brittle-ductile transition and above it is where quartz veins are formed. Hydrofractures move by stress concentration at the upper fracture tip, which is where the fluid is overpressured. In this way the hydraulic fracture propagates upward and its contained fluid moves with it. Tectonic stresses determine the orientation of the hydrofracture that, as explained in Chapter 9, tend to form along the least compressive stress σ_3.

Much of the hydrothermal mineral systems that are associated with igneous intrusions are primarily characterised by vein systems that are spatially and genetically associated with these intrusions. Mineralised vein systems that are formed in the metamorphic environment by devolitilisation reactions are treated in some detail in Chapter 9.

Vearncombe (1993) examined vein morphologies from Archaean Au deposits, based on growth direction of quartz and listed seven categories, namely: (1) face-controlled, characterised by quartz addition along crystallographic axis; (2) displacement-controlled, characterised by growth along trace of incremental opening; (3) parallel controlled, characterised by bands parallel to the vein margins; (4) radiating, characterised by growth from a point; (5) non-directional controlled, characterised by unrestricted and homogeneous growth; (6) replacement, characterised by quartz replacing earlier textures; and (7) modified, characterised by deformation. Figure 2.2 schematically

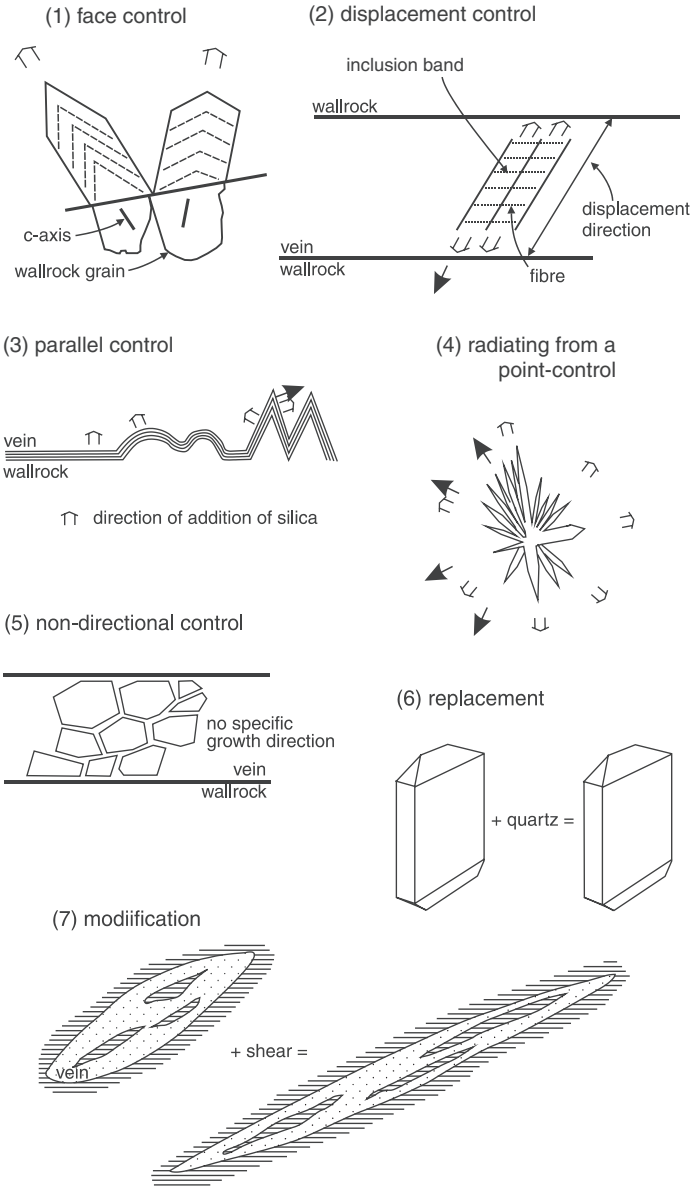


Fig. 2.2 Seven categories of quartz that form in quartz veins, according to Vearncombe (1993): (1) face-control refers to unidirectional growth, in this example along the c-axes; (2) displacement-control with quartz addition along the direction of the vein opening, inclusion bands are left behind at each incremental opening; (3) parallel-control with addition of parallel growth bands, with banding mimicking the shape of the host surface; (4) radiating growth from a single point, forming quartz/chalcedony rosettes; (5) non-directional control, quartz crystals nucleate randomly; (6) replacement textures, in which a pre-existing mineral, other than quartz, is replaced by silica; (7) modification texture, in the example shown a pre-existing quartz vein is sheared with its original inclusions of wall rock, which form ribbons

illustrates Vearncombe's seven categories. Vein textures that can be recognised in the field are very important because these can help in assessing not only the nature and origin of the vein, but also the associated mineral system. Vein textures and corresponding explanations are listed in Table 2.1.

Table 2.1 Quartz vein textures, modified after Vearncombe (1993)

Vein texture	Explanation
Antitaxial fibre	Displacement-controlled; fibres in optical continuity from the vein margins; growth is from the centre outwards; some wall-parallel of wallrock slivers may be present
Syntaxial fibre	Displacement-controlled; material filling vein is compisitonally similar to vein wall; fibres form two groups, each crystallographically related to a corresponding wall; growth is from wall to centre; see also section
Breccia	Quartz clasts, cemented by silica or other materail; commonly due to hydraulic fracturing or to multiple generations of quartz
Buck or bull quartz	Coarse-grained and typically white quartz
Cockade	Parallel-controlled, concentrically banded
Colloform	Parallel-controlled, concretionary, mammillary, reinform and spherical textures; bands at various scales (Fig. 2.3a)
Comb	Face-controlled, long axis of quartz crystals perpendicular to cavity or wall rocks; crystals have rhombohedral terminations; zoning
Comb spider veinlets	Network of veins cutting host quartz; mostly clear fine, euhedral quartz with c-axis oriented perpendicular to vein margins
Composite fibre	Displacement-controlled; two mineral species fill the vein and are zonally arranged; crystals adjacent to vein margins are compositionally and crystallographically related to host rocks
Crack-seal	Texture that derives from an accretionary process, which involves increments of microcrack opening and sealing. Generally forms in metamorphic environments and may be typical of orogenic lodes (Chapter 9)
Crustiform	Parallel-controlled; successive bands parallel to vein wall; defined by variable grain form and size
Drusy	Face-controlled; growth in cavity or geode
Laminated or ribbon	Wall rock mm- or cm-thick laminae; multiple parallel veins containing slabs, slivers of wall rock, formed by opening and reopening of the vein material (type 1); deformed parallel bands of ribbons also including slivers of wall rock, but deformed or sheared
Lattice and replacement	Silica replacement of calcite crystals, resulting in a "bladed" texture; this is generally due to boiling fluids (Fig. 2.3b)
Plumose	Feathery, radial or flamboyant quartz (Fig. 2.3a)
Rosette	Radiating crystal growths
Saccharoidal	Crystals of uniform grain size and habit; no matrix
Stretched fibre	Face- and displacement-controlled; material fllling the vein is compositionally similar to vein wall, but fibres form a crystallographic continuum with wall rocks
Stylolite	Zones of dark residue; saw-tooth cross-section; product of pressure solution



Fig. 2.3 **(a)** Concretionary and feathery, radial quartz; from a vein system in the Skirmish Hill area, West Musgrave, Western Australia; (**b**) bladed quartz from the Hes Daba Au epithermal occurrence in the Ethiopian flood basalts, Djibouti (photo courtesy of Murray Surtees)

2.1.2 Magma Degassing and Magmatic Hydrothermal Systems

As a prelude to the pages ahead, I describe two models of intrusion-related magmatic-hydrothermal systems. The first was proposed by Burnham (1979). The second model, which I believe important because of its implications for understanding of porphyry-epithermal systems, is that of William-Jones and Heinrich (2005).

2.1.2.1 Burnham's Model

Burnham (1979) examined in detail the magmatic hydrothermal system generated during the cooling of a hypothetical granodiorite intrusive stock containing 3 wt% water. In the discussion that follows, based on Burnham (1979, 1997), reference must be made to the sketches in Fig. 2.4. Cooling of the intrusive body is assumed to have taken place in a subvolcanic environment. Therefore, it is implied that during the initial stages of cooling the system is open, allowing the escape of volatiles through fractures above the pluton. At a later stage, the intrusive body becomes a closed system by developing a solidified shell. This stage is shown in Fig. 2.4A, where line S1 represents the boundary outside which the stock is below the solidus temperature. Burnham (1979) further assumed that the maximum temperature in the interior of the stock is 1025°C, that the 1000°C isotherm extends to a depth of 2.5 km, and that this isotherm encloses the portion of the body which is still 90% melt. Upward and outward from the 1000°C isotherm, the H_2O content of the residual melt increases to a zone where the melt is saturated with H_2O at 3.3 wt%. At this level and up to the solidus line S1, the system is made up of a crystalline assemblage containing pyroxene, a residual melt of granitic composition and an aqueous fluid phase. At greater depths, and always outward from the 1000°C isotherm, hornblende and biotite remain stable at temperatures between 800–900°C and 780–850°C, respectively. Biotite forms by reaction of the residual melt with hornblende, and as a result, silica is enriched

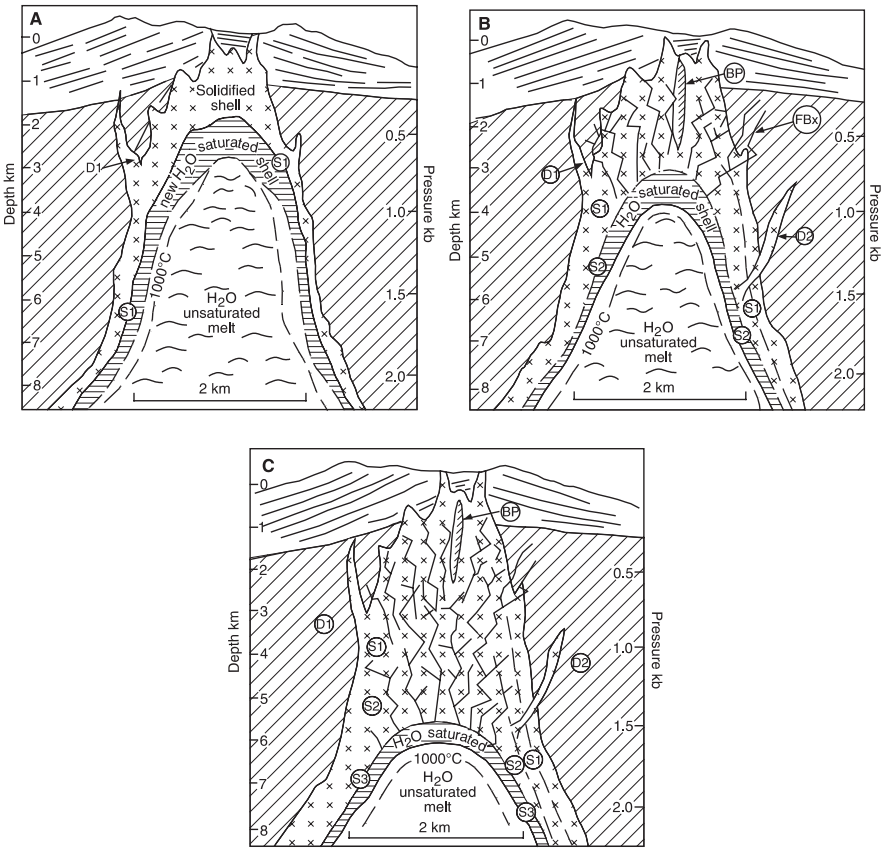


Fig. 2.4 Evolution of a magmatic-hydrothermal system during cooling of a porphyry intrusion; the sequences (**A**), (**B**) and (**C**) are explained in the text. After Burnham (1979)

in the residual melt and quartz crystallises. These processes lead to saturation with H_2O of the remaining interstitial melt, while the rest of the stock is still largely molten and H_2O unsaturated. This molten portion becomes enveloped by a zone of H_2O saturated interstitial melt, which is in turn enclosed by a solidified shell (or carapace in the terminology of Burnham's). The thickness of this H_2O saturated zone decreases with depth, forming a barrier to the movement of volatiles towards the solidified wall rocks, thus increasing the vapour pressure within the magma. In the upper portion of the H_2O saturated zone second boiling occurs, leading to the development of an abundant aqueous phase (Fig. 2.4B).

As illustrated in Fig. 2.4B, the mechanical energy developed by the increased vapour pressure overcomes the tensile strength of the rock, as well as the confining pressure, resulting in rapid expansion with fracturing and brecciation (FBx) of the crystalline shell above the H_2O saturated zone. A further result of this process is the reduction of the fluid pressure, which causes more of the H_2O

saturated interstitial melt to crystallise and to evolve more aqueous fluid phase. This fluid phase will penetrate the overlying fractures, further extending them out and upward by hydraulic fracturing. The near-vertical attitude of the fractures is related to the local stress field, with its maximum principal stress being vertical so that expansion occurs in the direction of the least principal stress, in the horizontal plane. Continued cooling will cause the retreat of S1 to S2 and the H_2O saturated zone to the deeper levels of the stocks. If the breaching of the H_2O saturated zone occurs in the thickened upper portions of the zone, where large volumes of aqueous fluid would ordinarily have accumulated, then the formation of breccia pipes is likely (BP in Fig. 2.4B, C). Breaching in the thinner and deeper parts of the H_2O saturated zone, on the other hand will cause plagioclase and hornblende-bearing dykes to emanate from the central and still molten part of the stock (D2 in Fig. 2.4B, C). In the stage depicted in Fig. 2.4B, the magmatic hydrothermal system has been restored to a situation similar to that prior to fracturing, the only difference being that now the H_2O saturated one lies at a greater depth. The stockwork zone developed during the stage of second boiling becomes healed by precipitation of silica. Further cooling of the magma leads to a repetition of the processes described above. In the final stage, a complex fracture system is developed above the stock (Fig. 2.4C), and this acts as a major channelway for ore-bearing fluids and heat from the underlying and still cooling igneous body. The ore minerals are concentrated in the fluid phases and transported into the network of fractures. Mineralisation is usually associated with late pulses of magmatic hydrothermal activity, and repeated pulses that will lead to the formation of large orebodies. It is theorised that the H_2O-saturated zone can expand up to 30% upon complete crystallisation at a depth of 3 km, but not more than 5% at a depth of 5 km (Burnham 1979, 1997). Most of these hydrothermal systems are restricted to the upper parts of the Earth's crust, where rocks are capable of yielding by brittle fracture and penetration of meteoric waters can occur. Collapse of the hydrothermal system, is followed by the influx of, and is dominated by meteoric water, which overprint and may obliterate the signatures of the preceding magmatic-hydrothermal system.

2.1.2.2 William-Jones and Heinrich's Model

William-Jones and Heinrich (2005), based on extensive experimental studies on the stability of metallic species in aqueous vapours, integrated with studies of inclusion fluids, drew attention to the role of magmatic vapours rather than aqueous fluids in the making of magmatic-hydrothermal ores. Herein their model is described and reference must be made to Fig. 2.5. These authors proposed that aqueous vapour phases are potentially very important agents for the transport of metallic elements in hydrothermal systems, beyond the usually accepted role of boiling fluids. At this point and before proceeding further it is necessary to provide the reader with some key definitions (taken from Table 1 of William-Jones and Heinrich 2005): A vapour is considered a water-rich, salt-bearing fluid with a density below the critical density of the

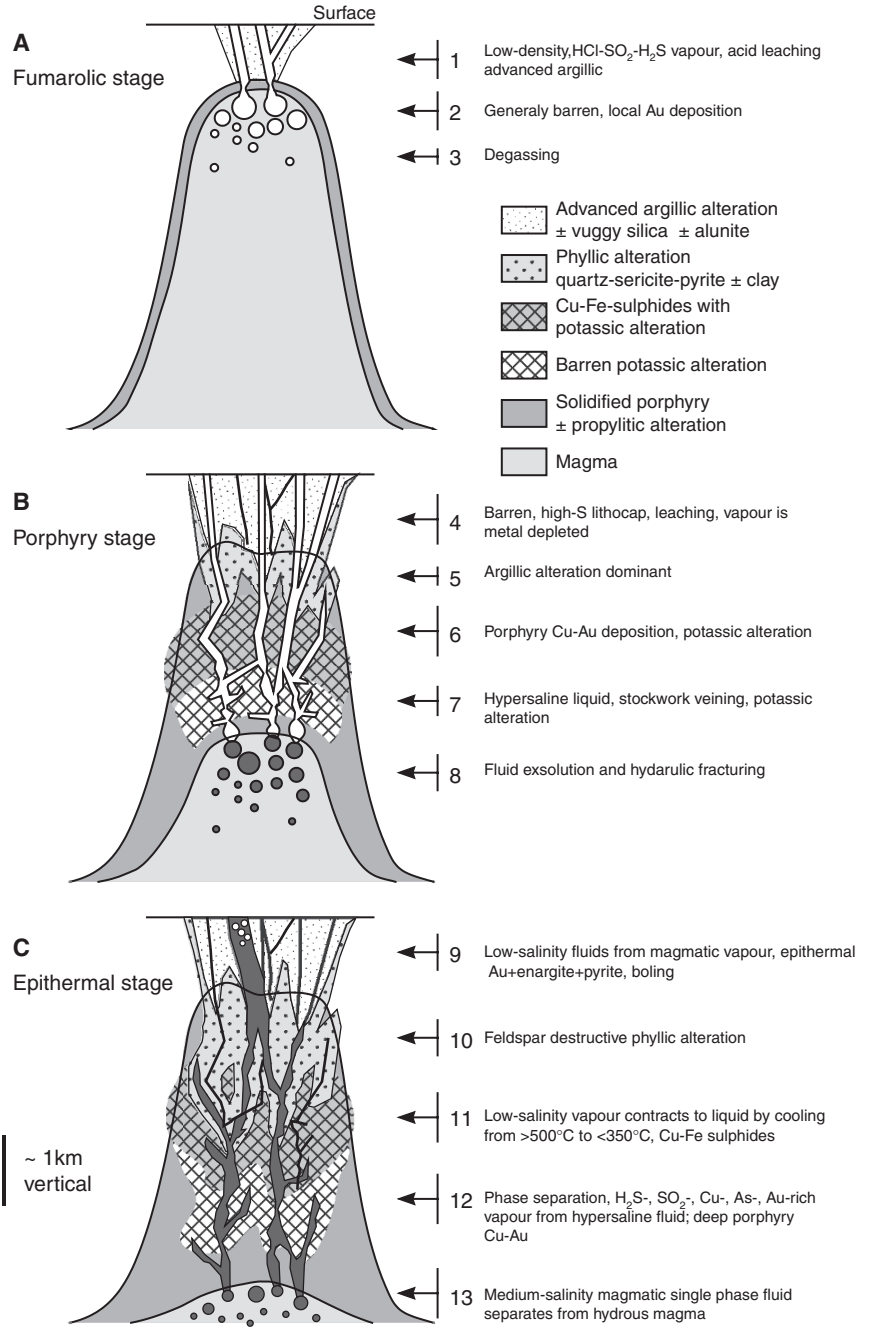


Fig. 2.5 Evolution of hydrothermal fluid regimes, within and above a magma chamber, leading to the development of intrusion-related mineral systems, in this case porphyry and epithermal. Note successive overprinting of hydrothermal processes during fluid evolution in the system. The sequences (**A**), (**B**) and (**C**) are explained in the text. After William-Jones and Heinrich (2005)

solution being considered; a liquid can be a brine (hypersaline) or aqueous, with the former having > 26 wt% NaCl equivalent, the latter having < 26 wt% NaCl equivalent at a temperature below that of the critical point. A liquid is generally a H_2O-rich, salt bearing fluid and a fluid is any mobile phase containing volatiles such as H_2O, CO_2, SO_2, H_2S, N_2 with variable amounts of dissolved components such as chloride salts.

The vapour phase in a hydrothermal system becomes increasingly dense with increasing temperature and pressure, while at the same time the co-existing aqueous liquid expands, and at the critical point of 374°C and 225 bars, the two phases become indistinguishable with water being a supercritical fluid. Volcanic sublimates found around fumaroles provide direct evidence of the role of vapours in transporting significant amounts of metallic elements. These sublimates show that apart from H_2O, other important components are H_2O, CO_2, H_2S as well as HCl, CO and H_2. The concentration of metallic elements in volcanic vapours is variable and depends on the composition and nature of the source magma. For example, basaltic magmas are especially enriched in Cu, Zn, Pb, Sb, A, Ag, Au, whereas andesitic magmas tend to yield high abundances of Cu, Pb, Zn, As, Mo and Hg; felsic magmas have lower abundances of the above elements but higher concentrations of Sn and Mo. Fumarolic fields around many volcanoes provide spectacular examples of a great variety of sublimates. Active subaerial and submarine geothermal systems provide us with another source of data for constraining the physico-chmeical characteristics of magmatic-hydrothermal systems. Subaerial geothermal systems are characterised by near-neutral pH and the co-existence of liquid and vapour, whereas submarine systems are clearly dominated by heated sea water and for this reason have different behaviour and evolution than the subaerial systems, although there is evidence of liquid-vapour co-existence also in submarine systems. Phase separation in black smokers (Chapter 7) occurs near the critical point of sea water (407°C and 298 bars) resulting in two fluids that only differ slightly in salinity from that of sea water. The vapour phase in submarine hydrothermal vents is typically enriched in CO_2, H_2S and $B(OH)_3$, but with metallic abundances not substantially different in vapour and liquid phases, instead metal abundances are proportional to the availability of chloride ligands which, understandably, are readily available from sea water. In all cases, however, high-temperature volcanic vapour, from both continental and submarine geothermal systems have a significant capacity to concentrate and transport metallic elements.

William-Jones and Heinrich proposed that major mass-transfer with vapour as metal-transporting agent in magmatic-hydrothermal systems, is particularly efficient for metal deposition in fumaroles, porphyry Cu, Cu-Mo, Cu-Au and Au-Cu epithermal systems. They pointed out that a key factor is the depth at which fluids exsolve from the hydrous magma and the pressure-temperature path followed by the fluids en-route to the surface, with fluid regimes that could develop independently at different depths above the magma chamber and result in different ore systems (e.g. fumarolic, porphyry, epithermal), or these regime may follow in succession in the same locale and overprint one another. These

three fluid systems of fumarolic, porphyry and epithermal are discussed in some detail below and schematically shown in Fig. 2.5).

Fumarolic deposits of active volcanoes or subvolcanic intrusions have salt-poor, but SO_2-, H_2S-, HCl-rich vapours, which result in a residual hypersaline liquid (Fig. 2.5A). The vapour phase condenses on cooling forming a liquid that contains HCl and H_2SO_4 and therefore with a very low pH, generally producing haloes of advanced argillic alteration characterised by minerals, such as pyrophyllite and alunite accompanied by intense leaching. This type of alteration is commonly observed around fumaroles and in high-sulphidation epithermal systems. These vapours also transport ore metals and may result in economic ore deposits by precipitation either directly from the gaseous fluids or from their condensation in meteoric waters. Examples of vapour-dominated magmatic-hydrothermal systems include the Ngawha geothermal field in New Zealand where Hg precipitates as cinnabar and liquid native metal in swamp sediments that contain abundant organic material. High-sulphidation systems produce Au-Cu-As deposits, described in Chapter 5.

The porphyry stage in Fig. 2.5B, shows exsolution of magmatic volatiles from a crystallising hydrous magma (see and compare with Burnham's model above). Exsolving fluids under supralithostatic pressure initiate hydrofracturing, flow upward and hypersaline liquids condense from the vapour phase to form stock-work veining and pervasive potassic alteration. Low- to medium-salinity S-rich vapours coexisting with lesser hypersaline brines produce a porphyry Cu-Au system. Studies of inclusion fluids from the Bingham Cu-Au porphyry deposit show that low-salinity vapours are the principal agent of metal transport. The Bingham data suggest that a single phase fluid ascended from the magma chamber beneath the porphyry system condensing a small brine fraction but with the vapour phase continuing its upward flow. The two coexisting fluids (vapour and brine) cooled below 425°C with precipitation of bornite and chalcopyrite from the vapour phase. This is because these sulphides are accompanied by dissolution of quartz, owing to the fact that silica solution is retrograde in low-salinity fluids, whereas in high salinity fluids (brines) silica solution is prograde and no dissolution would have occurred. The simultaneous transport of S, Cu and Au in the magmatic vapour system suggests that the availability of S is the important factor in the generation of economic porphyry systems. The final phase of this porphyry stage is that the metal-depleted expanding vapour produces advanced argillic alteration at the top of the system, as shown in Fig. 2.5B.

In the epithermal stage (Fig. 2.5C) medium-salinity magmatic fluids separates as a single phase from the hydrous magma and is followed by H_2S-, SO_2-, Cu-, As- and Au-rich vapour phase that separates from a condensing hypersaline fluid that is rich in $FeCl_2$. The magmatic vapour contracts to an aqueous liquid and by cooling from 500°C to < 350°C induces Cu-Fe sulphide precipitation, while Au would remain in solution. The derived low-salinity fluid will precipitate epithermal Au, enargite and pyrite in the upper levels of the system (Fig. 2.5C). Consequently, this stage provides the link between porphyry and epithermal systems, in which the Cu-Au-As deposition is effected by a low-salinity acidic

aqueous fluid and not by vapour, accompanied by intense acid leaching of the wall rocks. The high-sulphidation epithermal low-salinity and acid liquids are commonly interpreted as being derived form meteoric waters with only a small magmatic contribution. But, William-Jones and Heinrich (2005) pointed out that there are several lines of evidence, including stable isotope systematics, to show that fluids that induce advanced argillic alteration can be of magmatic origin. The authors quoted the example of a Au-Ag-Te epithermal deposit in Transylvania (Alderton and Fallick 2000), in which magmatic-epithermal liquid, was originally derived from a vapour of the same composition. This vapour initially separates from brines at near-magmatic temperatures and pressures, but with cooling the vapour contracts to an aqueous liquid. This is supported by fluid inclusion studies which, according to these researchers, can generate a weakly saline vapour with Cu, As and Au abundances that are much higher than those of geothermal liquids. The important question to consider is how the brine-vapour separation at high temperatures (~450–600°C) and pressures (400–100 bars) affects the composition of the vapour and its capacity to transport ore metals. William-Jones and Heinrich suggested that this is largely a function of the relative concentrations of $FeCl_2$ and H_2S in the vapour system. If $FeCl_2$ in the high temperature fluid exceeds that of H_2S, precipitation of sulphides leads to exhaustion of reduced S, thereby reducing the capacity of the low-salinity fluid to transport Au in the epithermal environment. If, however, $FeCl_2$ partitions into a high-salinity brine, this would increase the H_2S/Fe ratio in the high temperature vapour, which condenses into a low-salinity fluid that is capable of carrying comparatively large amounts of Au. Thus, the temperature-pressure evolution of brines and vapour lead to the observed differences in the epithermal system and associated alteration patterns.

In the final analysis, William-Jones and Heinrich (2005) concluded that porphyry Cu-Au and epithermal Au-Ag systems can be considered as the products of a continuous process that is linked to the evolution and cooling of a hydrous magma.

2.2 Role of Volatiles in Granitic Magmas

The fundamental importance of the role of volatiles in granitic melts is two-fold. Firstly, they modify the physico-chemical behaviour of the melt and its crystallisation products. Secondly, as a result of the volatiles' tendency to partition into the residual fluid phases, they are instrumental in the complexing and transporting of metallic elements, and thus also important in the understanding of ore genesis processes. The addition of volatiles (B, F, Cl, H_2O) to a mineral assemblage undergoing high-grade metamorphism lowers the melting temperature of the assemblage, and the addition of volatiles to a melt phase has the effect of lowering its solidus temperature. The behaviour of volatiles (B, F, Cl) in a melt is similar to that of water, in that they react with the bridging oxygens

of the silicate tetrahedra by breaking the Si-O bridges and depolymerising the melt (Burnham 1979). In order to fully understand this behaviour, it is necessary to first discuss the relationship of the physical properties of a magma in relation to the atomic structure of silicate melts. Details on this topic may be found in Best (1982), from whom this information is obtained. The physical properties of liquids are intermediate between crystalline and gaseous states, and any changes in one of the three states, solid, liquid or gas, is a reflection of the thermal energy of the system. With increasing thermal energy, the motion of the particles increases until loss of cohesion takes place from the crystalline state to the liquid and gas states. Since silicate melts have high electrical conductivity, it is surmised that loosely bound ions must be present in the structure. Thus, a silicate melt is interpreted to be formed by arrays of ions, arranged to form links of Si^{4+} and Al^{3+} in tetrahedral co-ordination with O^{2-} ions, and creating a silicon-aluminium network, or what is commonly known as a "polymerised structure".

Liquid SiO_2 is formed by a network of Si-O chains, called polymers, and in the Si-O tetrahedra each O bridges two Si ions, and all tetrahedra are interconnected to form a highly polymerised structure. The Si ions are therefore said to be network-forming. In other silicate liquids, such as pyroxenes, there are, in addition to the Si (network-forming cation), network-modifying ions (such as Ca, Mg, Fe, Al etc.). Another difference with the liquid silica is that in liquid pyroxene the Si-O polymers are not as long, because many O do not bridge between two Si, and therefore it is less polymerised, or in other words less viscous. The effect of H_2O dissolved in a silicate liquid is related to the vapour pressure of H_2O in the system with a reaction of the type:

$$H_2O + O^{2-} \rightarrow 2(OH)^-$$

In this H_2O combines with O to form non-bridging hydroxyl ions (OH), breaking the Si-O chain of the melt and reducing polymerisation. The result is a reduction of the viscosity so that the melt then becomes more fluid. High temperatures produce the same effect, where the silicate melt structure is loosened as a result of the greater motion of the atoms, which can break free from nearby atoms. In addition, the strong bonds of a highly polymerised melt (high in silica) may be broken under highly applied stress, thus allowing flow. The presence of volatiles, other than H_2O, in melt has more or less the same effect as that of water. Both F and Cl produce a distortion of the alumino-silicate structure, resulting in an increase in co-ordination sites that allow large, highly charged cations to form new and high-order structures. Distortion of the Si-O frameworks by F, B, Cl produces octahedral sites capable of accommodating other elements such as Ni, Co, V, Cr etc., although they may already have been incorporated in the early mafic phases. Fractionation processes tend to concentrate volatiles and incompatible elements, such as Sn, W, Mo, Th, U, Zr, Ta, Nb, Hf, and sometimes also Cu, Zn, Pb, in the residual melts for the reasons outlined above. Thus the increase in volatiles not only depolymerises the melt but also provides ligands for complexing trace elements.

In the presence of volatiles the composition of a melt tends to be more alkaline than that formed under volatile-poor conditions. Experimental work reported by Pichavant and Manning (1984) shows that at 1 kbar and near-liquidus temperatures, the addition of B and/or HCl results in a decrease in the Si/alkali and Al/alkali ratios. Therefore both B and HCl cause a transfer of alkalies from the melt to the vapour/fluid phase, although the Na/K ratio may vary. This indicates that Na is leached from melts co-existing with B-bearing vapours, producing in turn an Al- or K-rich silicate melt. In the Q-Ab-Or-H_2O system, changes in the melt composition by addition of B (or F) in a source region undergoing melting are reflected by the shift of the melt composition towards the Q-Or side of the ternary system. There is also experimental evidence that the solubility of H_2O in magmas may be enhanced in B-rich melts (Pichavant 1981), whereas F-rich systems do not appear to have the same effect. The experiments carried out by Pichavant and Manning (1984) indicate that progressive addition of F (between 1 and 4%) and B (between 1 and 4.5%) causes the ternary composition to shift towards the albite (Ab) corner. In other words, in the case of magmatic systems that during fractionation and crystallisation are progressively enriched in B, F and Li, there is a concomitant enrichment in the Ab component, while the liquidus temperature is also depressed. Thus, with progressive crystallisation of the volatile-rich melt Na and Si enter easily into a residual fluid phase. The opposite trend may be observed if the volatiles are removed from the crystallising melt. In this case Ab, or peraluminous minerals, crystallise and the residual melt becomes progressively enriched in quartz (Q) and orthoclase (Or). This is the K-rich assemblage that appears under subsolidus conditions (potassic metasomatism). The removal of the volatiles from the melt can take place either by second boiling or through the opening of the system by fracturing and adiabatic decompression, leading to boiling and volatile partitioning into the vapour phase. The nature of potassic metasomatism is therefore dependent on the rate of melt-fluid separation. In a closed-system potassic metasomatism is slow, and coarse-grained crystals are likely to form (microcline megacrysts). In a system that has become open by rapid decompression, on the other hand, a pressure-quenched intergrowth of quartz + K-feldspar would result, producing the type of granophyric texture that is so often observed in granitic systems associated with hydrothermal activity (see below). The effect of F extraction from the melt would be similar to that of B extraction, producing a Na(K)-, Si-, B(F)-rich aqueous fluid.

In summary, increasing volatile content during crystallisation enriches the melt in the Ab content, while the fluid phase is enriched in K (decreasing Na/K in the fluid phase), resulting in transfer of K from fluid to the wall rocks. Conversely when volatiles are lost from the system, the residual melt becomes enriched in Or, while Na is transferred to the fluid phase. K-feldspar crystallises from the melt and Na in the fluid is transferred to the wall rocks. The evolution of an alkali-rich residual fluid phase from a nearly consolidated igneous body, results in a series of post-magmatic and subsolidus growth of minerals (Bowden 1985). Such changes are largely dependent on the intensity of the rock-fluid

interaction. The subsolidus processes include: cationic exchange reactions in feldspars, Na for K, or, K for Na (albitisation and microclinisation); changes in the structural state of feldspars. Other changes involving increasing amounts of H_2O (H^+ metasomatism) and/or dry volatiles include: changing compositions of pyroxenes and amphiboles, growths of tri-octahedral micas, aegirine and riebeckite, as well as a series of F- or B-rich mineral assemblages. It must be pointed out that many of the replacement features of subsolidus changes can also be explained by magmatic crystallisation, or unmixing of solid solutions. However, subsolidus reactions are especially developed in the apical zones of plutons, and along fractures or in pods and lenses. Eaxmples of post-magmatic alteration in granitic rocks and their spatial association with the apical regions of an igneous body are shown in Figs. 4.3 and 4.6.

In igneous rocks there are at least three types of textures that can be attributed to alkali metasomatism. These include: replacement coronas, granophyric textures and perthitic textures. Replacement coronas refer to the replacement along the margin, and crystal boundaries of ferromagnesian silicates by Na-amphiboles, such as arfedsonite or riebeckite, resulting from the breakdown of fayalite. There is good evidence from field relationships and geochemical data that granophyric textures, formed by intergrowths of quartz and K-feldspar and encountered in many igneous rocks, are of metasomatic origin. These peculiar intergrowths are usually distinguished by the turbidity of the K-feldspar component. Examples of alkali ion metasomatism are provided by the granophyric intergrowths developing as a result of devitrification of glassy material in ash-flow tuffs and acid lavas. Perthitic textures of feldspar may in some cases also be indicative of alkali metasomatism, rather than unmixing during cooling of a two-phase assemblage. Replacement of Na for K in feldspars is shown by the presence of albite inclusions in the K-feldspar host. These inclusions can occur either as irregular shapes, or as veinlets, and do not follow crystallographic directions, as would be the case for solution unmixing. Microclinisation and K-silicate alteration show features that range from the generation of intermediate to ordered microcline to micas. Order-disorder relationships in alkali feldspar refer to the distribution of Al and Si in the unit cell and its departure from the monoclinic towards triclinic symmetry (obliquity). This obliquity decreases with decreasing temperature and the K content increases. Thus K increases with ordered structures (e.g. towards a sanidine composition), whereas in passing from the ordered towards the disordered structure, Na migrates into the lattice to form distinct domains, giving rise to the perthitic texture. The structure can change back again towards a K-rich domain to form microcline with further decreasing of the temperature. Thus the sequence from high to low temperature feldspar is as follows:

$$\text{sanidine} \rightarrow \underset{\text{Na-metasomatism}}{\text{orthoclase}} \rightarrow \underset{\text{K-metasomatism}}{\text{perhite (orthoclase + albite)}} \rightarrow \text{microcline.}$$

Albitites, microclinites, fenites and the core zones of potassic alteration in porphyry systems are the most common products of alkali metasomatism. The

sections ahead focus on albitites, microclinites and fenites, while potassic alteration of porphyry and volcanic systems is examined in Chapter 5.

2.3 Hydrothermal Alteration

Hydrothermal alteration is a complex process involving mineralogical, chemical and textural changes, resulting from the interaction of hot aqueous fluids with the rocks through which they circulate, under evolving physico-chemical conditions. Alteration can take place under magmatic subsolidus conditions by the action and infiltration of supercritical fluids into a rock mass. At lower temperature and pressure, exsolution of gas and aqueous phases constitute hydrothermal fluids which act on the surrounding rocks, producing changes as the result of disequilibrium, largely due to H^+ and OH^- and other volatile constituents (e.g. B, CO_2, F). In essence, hydrothermal fluids chemically attack the mineral constituents of the wall rocks, which tend to re-equilibrate by forming new mineral assemblages that are in equilibrium with the new conditions. The process is a form of metasomatism, i.e. exchange of chemical components between the fluids and the wall-rocks. Therefore, it is also likely that the fluids themselves may change their composition as a result of their interaction with the wall rocks. The main factors controlling alteration processes are: (1) the nature of wall rocks; (2) composition of the fluids; (3) concentration, activity and chemical potential of the fluid components, such as H^+, CO_2, O_2, K^+, H_2S and SO_2. Henley and Ellis (1983) suggested that alteration products in epithermal systems do not depend so much on wall-rock composition but more on permeability, temperature and fluid composition. They cited, for example, that in the temperature range of 250–280°C, similar mineral assemblages (e.g. quartz-albite-K-feldspar-epidote-illite-calcite-pyrite) are formed in basalts, sandstone, rhyolite and andesite. Other workers, however, emphasised the fundamental role played by the nature and composition of wall rocks in hydrothermal alteration processes, particularly in porphyry systems.

The action of hydrothermal fluids on wall rocks is by infiltration and/or diffusion of chemical species (Rose and Burt 1979). Hydrothermal circulation and related alteration, generally involve large quantities of fluids that pass through a given volume of rocks, which therefore must have considerable permeability in the form of fractures, or connected pore spaces. Small quantities of fluids have lesser, or even negligible effects, as exemplified by metamorphic hydrothermal systems in which the amount of fluids in relation to the rock, i.e. the water/rock ratio (w/r; defined as the total mass of water that passes through the system, in the unit time, divided by the total mass of rock in the system considered), is small, and the resulting mineral deposits have small or negligible wall-rock alteration. Thus the interaction between H_2O and rocks, and the intensity of alteration is, inter alia, a function of the water/rock ratio (w/r). This ratio is an important parameter because it affects the degree of exchange with the wall- rocks. In hydrothermal systems, w/r ratios may range from 0.1 to 4,

with a lower limit obtained when all free water is absorbed as hydrous minerals (Henley and Ellis 1983). Exchange of oxygen isotopes during water/rock interaction allow to calculate the w/r ratios, as discussed by Taylor (1997) for various granitic rocks, in which meteoric waters circulate through a very large volume of rocks. Within this volume the w/r ratio is calculated at between 0.1 and 3.0.

2.3.1 Hydrogen Ion Metasomatism (Hydrolytic Alteration) and Base Cation Exchange

Hydrolysis and hydration are introduced in Chapter 1. Here, these terms are defined in the context of hydrothermal alteration processes. Hydrolysis, or hydrogen ion metasomatism or hydrolytic alteration, is a very important phenomenon involving the ionic decomposition of H_2O into H^+ and OH^-. In hydrothermal alteration, H^+ (or OH^-) is consumed during reaction with the silicate minerals, so that the ratio H^+/OH^- changes. The source of H^+ ions can be subsolidus reactions during alkali metasomatism, water, or acids in the hydrothermal solution. The conversion of anhydrous silicates to hydrous ones (e.g. micas or clays) is a reaction which consumes H^+ and releases metal ions into the solution. This in turn affects the pH of the solution and its power to dissolve or to keep cations in solution. This is related to the dissociation of complexes containing H^+, the degree of association of compounds such as NaCl, and consequently the formation of chloride complexes and the solubility of metallic elements (Guilbert and Park 1986). A typical example of hydrolytic decomposition of feldspar is:

$$\underset{\text{K-feldspar}}{1.5KAlSi_3O_8} + H_2O \rightarrow \underset{\text{K-mica}}{0.5KAl_3Si_3O_{10}(OH)_2} + K^+ + \underset{\text{quartz}}{3SiO_2} + OH^-;$$

$$H^+ + OH^- \rightarrow H_2O$$

The sum of the first and second reactions gives:

$$1.5KAlSi_3O_8 + H^+ \rightarrow 0.5KAl_3Si_3O_{10}(OH)_2 + K^+ + 3SiO_2.$$

It can be seen from this reaction that K^+ is released and H^+ is consumed. Hydration, the transfer of molecular water from the fluid to a mineral, often accompanies hydrolysis.

Reactions where a cation is replaced by another in a mineral are called base exchanges, as for example in the conversion of microcline to albite, Na replaces K, which goes into solution:

$$\underset{\text{microcline}}{KAlSi_3O_8} + Na^+ \rightarrow \underset{\text{albite}}{NaAlSi_3O_8} + K^+$$

In summary, hydrogen ion metasomatism, hydration and base exchange control the stability of silicate minerals, the pH of the solution, and the transfer of cations into the solution. They are responsible for propylitic, argillic, sericitic or phyllic, and potassic mineral assemblages, which are so typical of hydrothermal mineral deposits. Areas of intense hydrolytic decomposition, or hydrogen ion metasomatism, of silicates, are usually surrounded by propylitic alteration in which hydration phenomena (addition of water and CO_2) are dominant.

2.3.1.1 Reactions in Feldspars and K-Mica

Hemley and Jones (1964) conducted experimental studies with aqueous chloride solutions on K- and Na-bearing systems. These experimentally determined reactions are described below:

(a) K_2O-Al_2O_3-SiO_2-H_2O system:

The formation of sericite can be expressed by the following:

$$\underset{\text{microcline}}{3KAlSi_3O_8} + 2H^+ \rightarrow \underset{\text{K-mica}}{KAl_3Si_3O_{10}(OH)_2} + 2\,K^+ + \underset{\text{quartaz}}{6SiO_2}$$

$$\underset{\text{andesine}}{0.75Na_2CaAl_4Si_8O_{24}} + 2H^+ + K^+ \rightarrow \underset{\text{sericite}}{KAl_3Si_3O_{10}(OH)_2} + 1.5Na^+ + 0.75Ca^{2+} + 3SiO_2$$

Other reactions are:

$$\underset{\text{K-mica}}{KAl_3Si_3O_{10}(OH)_2} + H^+ + 1.5H_2O \rightarrow \underset{\text{kaolinite}}{1.5Al_2Si_2O_5(OH)_4} + K^+;$$

$$\underset{\text{K-mica}}{KAl_3Si_3O_{10}(OH)_2} + 3SiO_2 \rightarrow \underset{\text{pyrophyllite}}{1.5Al_2Si_4O_{10}(OH)_2} + K^+;$$

(b) Na_2O-Al_2O_3-SiO_2-H_2O system:

$$\underset{\text{albite}}{1.5NaAlSi_3O_8} + H^+ \rightarrow \underset{\text{paragonite}}{0.5NaAl_3Si_3O_{10}(OH)_2} + 3SiO_2 + Na^+;$$

$$\underset{\text{paragonite}}{NaAl_3Si_3O_{10}(OH)_2} + H^+ + \underset{\text{quartz}}{3SiO_2} \rightarrow \underset{\text{pyrophyllite}}{1.5Al_2Si_4O_{10}(OH)_2} + Na^+;$$

$$\underset{\text{albite}}{1.17NaAlSi_3O_8} + H^+ \rightarrow \underset{\text{Na-montmorillonite}}{0.5Na_{.33}Al_{2.33}Si_{3.67}O_{10}(OH)_2} + 1.67SiO_2 + Na^+;$$

$$\underset{\text{kaolinite}}{3Na_{.33}Al_{.33}Si_{3.67}O_{10}(OH)_2} + H^+ + 3.5H_2O \rightarrow \underset{\text{Na-montmorillonite}}{3.5Al_2Si_2O_5(OH)_4} + 4SiO_2 + Na^+.$$

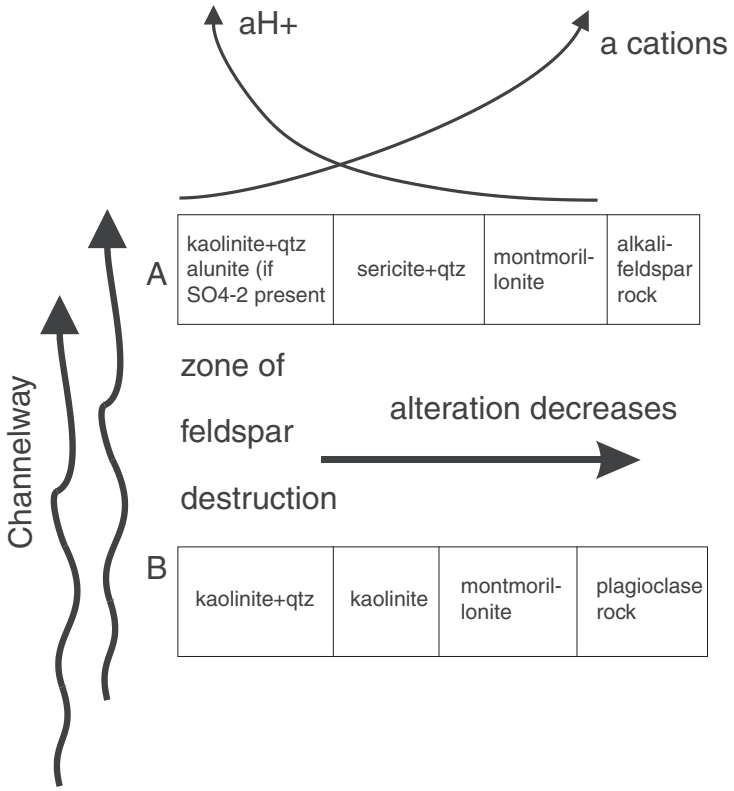


Fig. 2.6 Diagrammatic representation of hydrothermal alteration in rocks containing (**A**) dominant alkali-feldspar and (**B**) dominant calcic plagioclase (After Hemley and Jones 1964)

All of these reactions consume H^+ and release cations such as Na^+ and K^+, as well as other metallic elements that may substitute for them in the lattices of the altering silicates. These reactions are sensitive to pressure and temperature changes and the ratios of the components' activities. The overall patterns of wall rock alteration containing dominant feldspars and quartz are shown in Fig. 2.6. The silica derived by the hydrolytic alteration of silicates does not crystallise at the site of alteration, but diffuses towards the channelways, while parts of it may remain in the zone of sericite development.

(c) K_2O-Al_2O_3-SiO_2-H_2O-SO_3 system:

Oxidation of H_2S leads to the formation of sulphuric acid (H_2SO_4), a powerful leaching agent, particularly active in the lower temperature regimes of volcanic and subvolcanic environments. Acid leaching is responsible for argillic alteration commonly seen in epithermal mineral deposits and many porphyry systems. Hemley et al. (1969) experimentally studied the above five-component system, involving the stability relations of K-feldspar, muscovite, kaolinite and alunite as a function of H_2SO_4 and K_2SO_4 activities. Alunite is a key mineral in

the system considered, being an important and common component found in high-sulphidation epithermal systems. Alunite is therefore commonly found associated with hot springs, mud pools and fumaroles in volcanic terranes, where it forms veins, lenticular bodies and masses of rocks almost entirely replaced by it. Spectacular examples of alunite formation can be seen in the Phlegrean fields near Naples and at La Tolfa north of Rome (Italy). Alunite is generally associated with opal, kaolinite, dickite, sericite, pyrophyllite and diaspore. Because of the intense leaching associated with the presence of alunite, a leached zone may be present that is typically porous and siliceous. This vuggy silica, however, is residual and should not be confused with sinter material (see Chapter 5). Relevant reactions are:

$$\underset{\text{K-mica}}{KAl_3Si_3O_{10}(OH)_2} + 4H^+ + 2SO_4^{2-} \rightarrow \underset{\text{alunite}}{KAl_3(SO_4)_2(OH)_6} + 3SiO_2;$$

$$\underset{\text{kaolinite}}{3Al_2Si_2O_5(OH)_4} + 2K^+ + 6H^+ + 4SO_4^{2-} \rightarrow \underset{\text{alunite}}{2KAl_3(SO_4)_2(OH)_6} + 6SiO_2 + 3H_2O;$$

$$\underset{\text{K-mica}}{2KAl_3Si_3O_{10}(OH)_2} + 2H^+ + 3H_2O \rightarrow \underset{\text{kaolinite}}{3Al_2Si_2O_5(OH)_4} + 2K^+.$$

2.3.2 *Styles and Types of Hydrothermal Alteration*

The terms used to describe and classify hydrothermal alteration can be expressed as a function of: (1) recognised mineral assemblage(s) and (2) chemical changes. In the former, the recognition of mineral assemblages is primarily carried out through extensive thin section studies. This leads to a listing of minerals in order of abundance, as shown by Rose and Burt (1979) and Gifkins et al. (2005), or by general descriptive terms reflecting the dominant mineralogy (assemblages), such as argillic, potassic, sericitic etc. Chemical changes indicating the type of chemistry of the fluids involved in the alteration process would include hydrogen ion metasomatism, alkali metasomatism, fluorine and boron metasomatism etc. In addition, the style of alteration takes into account the intensity, form and character of the phenomenon. Here the terminology becomes a little confusing because of its inherent subjectivity. Terms, such as weak, moderate, strong, extensive, pervasive, non-pervasive, are well known and frequently used. These terms essentially refer to the state of preservation of the original rock, how far the alteration process has advanced, both at the single mineral scale and at the regional scale, the overall geometry of the alteration halo and so forth. Gifkins et al. (2005) recommended a "*multi-faceted*" approach for describing alteration facies in volcanic rocks, based on four variables mineral intensity, distribution, texture and mineral assemblage, as follows:

$$4 + 3 + 2 + 1$$

Where, the intensity variable (4) can be subtle, weak, moderate, strong or intense, the distribution variable (3) can be local or regional, on the footwall, hanging wall, pipe, stratabound etc., the texture variable (2) is usually described from hand specimen or thin section and includes shape, grainsize, fabric and can be selective, pervasive or vein halo. Finally, the mineral assemblage variable (1) lists the minerals and in order of decreasing abundances, for example quartz > sericite > K-feldspar. Alteration intensity refers to how much a rock has been affected by alteration. The intensity of alteration, though perhaps a little more subjective, is generally used as a convenient field term. Weak, or low, intensity would mean that only a few of the original minerals have been replaced with little or no modification of the original textures. Qualitative estimates can be made using thin sections.

The main styles of alteration are "pervasive", "selectively pervasive" and "non-pervasive". Pervasive alteration is characterised by the replacement of most, or all, original rock-forming minerals. This results in the partial or total obliteration of the original textures. Selectively pervasive alteration refers to the replacement of specific original minerals, e.g. chlorite replacing biotite, or sericite replacing plagioclase. In this case the original textures are preserved. Non-pervasive alteration means that only certain portions of the rock volume have been affected by the altering fluids. An empirical approach recommended by Guilbert and Park (1986), proposes the use of symbols to characterise the type of alteration. Selective pervasiveness and pervasiveness would be indicated on scales from 1 to 10, so that 1 would mean that alteration is confined to a veinlet or a thin fracture, whereas 10 would indicate that the entire rock is permeated by the alteration effects. For example, a notation like S-10-4 means a rock in which the minerals susceptible to sericitisation (S) are all affected in about 40% of the rock volume. Clearly, then, selectively pervasive alteration falls in this category, as well as fracture or veinlet-controlled alteration. In the latter, the alteration minerals are confined to within a certain distance from a vein or a fracture. The alteration style around the controlling vein or fracture can be pervasive or selectively pervasive.

Alteration types and patterns of specific hydrothermal deposits are dealt with in the chapters that follow. Here I examine in a general way, types of alteration resulting from the interaction of hydrothermal solutions with wall rocks as revealed and understood from a great variety of hydrothermal ore deposits, and therefore each type discussed may be applicable only if the proper setting and related deposit type are considered. The effects produced on the wall rocks by interaction with and the chemical changes in a hydrothermal solution as a result of variations in the aK^+/aH^+ ratio; i.e. the activities of the K^+ and H^+ ions in the system. This ratio decreases as the system evolves towards lower temperatures and pressures. In other words, with increasing H^+ metasomatism alteration processes would move from alkalic to argillic in a theoretically continuous evolving system. This concept is schematically shown in Fig. 2.7A, B. Consequently, the types of alteration discussed will be in order of decreasing aK^+/aH^+ (increasing H^+ metasomatism), and are: (1) alkali metasomatism and potassium silicate alteration; (2) propylitic; (3) phyllic, or sericitic, alteration and greisenisation; (4) intermediate argillic; (5) advanced argillic (Fig. 2.7B).

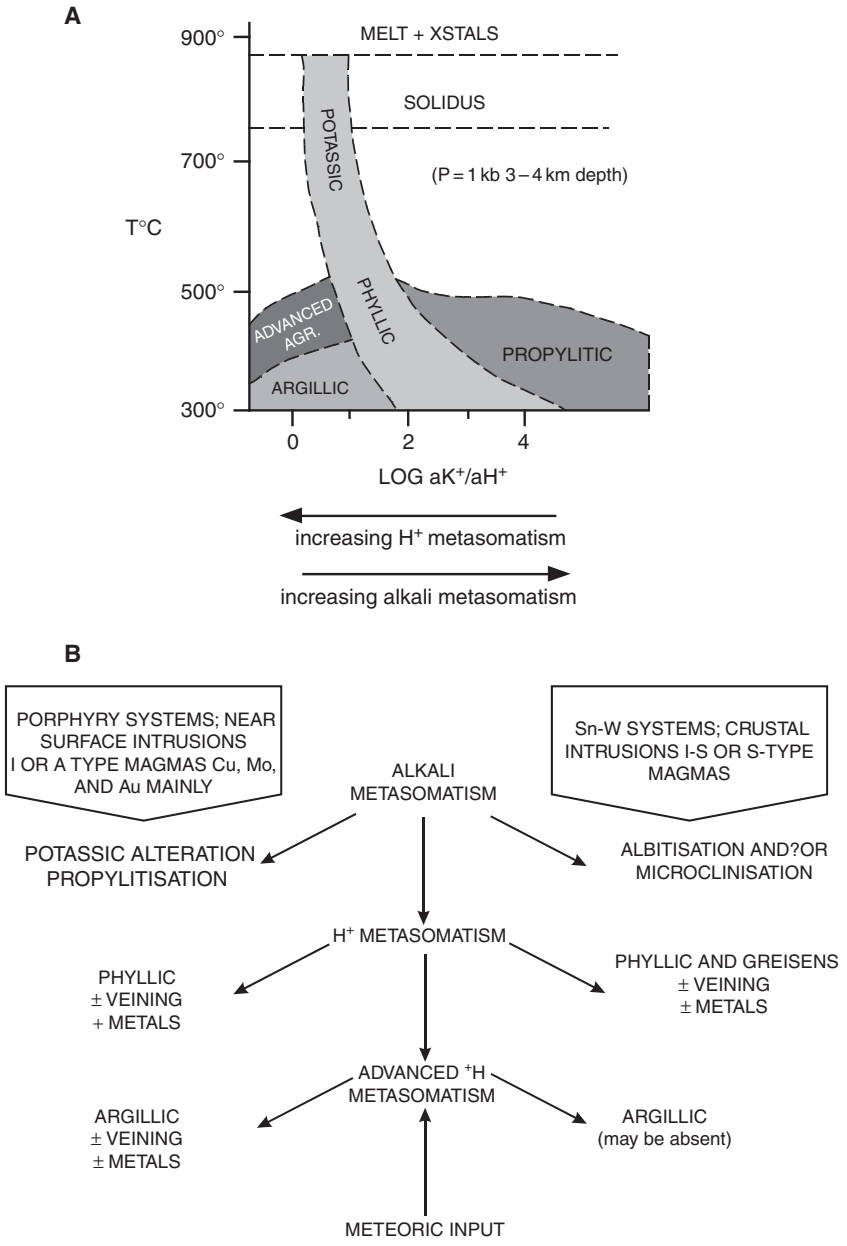


Fig. 2.7 Idealised evolutionary alteration sequence. (**A**) Illustrates types of alteration as a function of temperature, K^+ and H^+ activities (After Guilbert and Park 1985; Burnham and Ohmoto 1980). (**B**) Alkali metasomatism liberates H^+, resulting in decreasing alkali/H^+ ratios, and subsequent destabilisation of feldspars and micas, with growth of new mineral phases (greisen and phyllic stages). Advanced H^+ metasomatism is due to meteoric water input into the system, with oxidation and further H^+. Acid leaching and argillic alteration result from this stage

The interaction with a residual fluid phase evolving from a nearly consolidated igneous mass, results in a series of post-magmatic, or subsolidus, changes both within the igneous body and the surrounding country rocks, if they are fractured (open system). These are early high temperature fluids in the range of about 800–600°C, which are derived from a melt in its late stages of crystallisation, and they result in the subsolidus growth of new minerals and exchange reactions. Subsolidus processes include: (1) base exchange reactions in feldspars, specifically Na for K, or, K for Na; (2) changes in the structural state of feldspars; (3) albitisation; (4) microclinisation; (5) growth of tri-octahedral micas. In anorogenic tectonic settings mineralogical changes may include a series of Na-rich amphiboles and F- or B-rich assemblages. I return to this aspect of alkali metasomatism in Chapter 4. Here it will suffice to say that alkaline and highly saline fluids develop during the final stages of consolidation of an igneous mass, resulting in widespread potassic or sodic alteration.

Tables 2.2 and 2.3 show examples of alteration terminology, types and associated mineral systems, taken and modified from Gifkins et al. (2005)

2.3.2.1 Potassic and Propylitic Alteration

Potassic alteration is especially common and important in porphyry and epithermal mineralising systems, where it occurs in the high temperature core zones. The minerals characteristic of this alteration are K-feldspar and biotite in porphyries, and adularia in epithermal systems. Potassic alteration is usually accompanied by sulphides (chalcopyrite, pyrite, molybdenite). Anhydrite is a common associated mineral in porphyry environments. Biotite is often green in colour and Fe-rich. Potassium silicate alteration is formed as a replacement of plagioclase and mafic silicate minerals, at temperatures in the region of 600–450°C. Common assemblages are K-feldspar-biotite-quartz, K-feldspar-chlorite, K-feldspar-biotite-magnetite, accompanied by varying quantities of other minerals such as albite, sericite, anhydrite, apatite, and also occasionally rutile, derived from the breakdown of biotite. The K-feldspars of the potassic zones are characteristically reddish in colour due to minute hematite inclusions. Fig. 2.8 illustrates examples of potassic alteration.

Propylite is an old term used to describe altered volcanic rocks. Propylitic alteration is characterised by the addition of H_2O and CO_2, and locally S, with no appreciable H^+ metasomatism. Typical minerals are epidote, chlorite, carbonates, albite, K-feldspar and pyrite. In places sericite, Fe-oxides, montomorillonite and zeolite may also be common. The well-defined pressure and temperature stability fields of zeolite mineral species make them important monitors of temperature and depth. This feature is particularly useful in epithermal systems, as it enables monitoring the proximity to the heat source and boiling zone where higher grades of gold mineralisation may be found. In some situations, there can be intense albitisation, chloritisation or carbonitisation, which Meyer and Hemley (1967) considered separately, reserving propylitisation for weaker H^+ metasomatic effects. Propylitic alteration tends

Table 2.2 Hydrothermal alteration terminology, after Gifkins et al. (2005 and references therein)

Generic terminology	Alteration mineral assemblage (*main assemblage in italic*)*s*	Ore system
Argillic	*Kaolinite (or halloysite, or dickite) + montmorillonite* ± sericite (or muscovite) ± chlorite	Porphyry Cu, high-and low-sulphidation epithermal, geothermal
Advanced argillic	*Pyrophyllite + kaolinite (or dickite)* ± quartz ± sericite ± andalusite ± diaspore ± alunite ± topaz ± zunyite ± enargite ± tourmaline ± pyrite ± chalcopyrite ± hematite	Porphyry Cu, high-sulphidation epithermal, geothermal
Intermediate argillic	*Chlorite + sericite* ± kaolinite ± montmorillonite ± illite-smectite ± calcite ± epidote ± biotite ± pyrite	Porphyry Cu, high-sulphidation epithermal
Phyllic (or sericitic)	*Sericite + quartz + pyrite* ± biotite ± chlorite ± rutile ± leucoxene ± chalcopyrite ± illite	Porphyry Cu
Sericitic (or Phyllic)	*Sericite + quartz + pyrite* ± K-feldspar ± biotite ± calcite ± dolomite ± chlorite ± andalusite ± chloritoid ± albite ± pyrrhotite	Porphyry Cu, low-sulphidation epithermal, geothermal, VHMS, sediment hosted massive sulphide
Propylitic (or saussuritization)	*Epidote (or zoisite or clinozoisite) + chlorite + albite* ± carbonate ± sericite ± montmorillonite ± septachlorite ± apatite ± anhydrite ± ankerite ± hematite ± pyrite ± chalcopyrite	Porphyry Cu, high-sulphidation epithermal, low-sulphidation epithermal, geothermal
Potassic	*K-feldspar (orthoclase) + biotite + quartz* ± magnetite ± sericite (or muscovite) ± albite ± chlorite ± anhydrite ± apatite ± rutile ± epidote ± chalcopyrite ± bornite ± pyrite	Porphyry Cu
Greisen	*Muscovite (or sericite) + quartz + topaz* ± tourmaline ± fluorite ± rutile ± cassiterite ± wolframite ± magnetite ± zunyite ± K-feldspar	Porphyry Cu, porphyry Sn
Skarn		
Calcic skarn (or tactite)	*Pyroxene + garnet + wollastonite* ± epidote (or zoisite) ± actinolite-tremolite ± vesuvianite ± pyrite ± chalcopyrite ± sphalerite	Porphyry
Magnesian skarn	*Forsterite + diopside + serpentine + talc* ± actinolite-tremolite ± calcite ± magnetite ± hematite ± chalcopyrite ± pyrite ± sphalerite	Porphyry, skarn
Retrograde skarn	*Calcite + chlorite* ± hematite ± pyrite	Porphyry, skarn
Jasperoid	*Quartz + pyrite + + hematite*	Sedimented-hosted Au, VHMS

Table 2.3 Examples of alteration terminology applied to selected mineral systems, after Gifkins et al. (2005)

Dominant mineral	Mineral assemblage	Composition	Generic
VMS			
Silicic	Quartz + sericite + pyrite ± chlorite	Si-metasomatism	Not used in
Chloritic	± K-feldspar	Mg-metasomatism	VHMS
Sericitic	Chlorite _ pyrite + sericite ± quartz	K-enrichment	literature
Albitic	Sericite ± quartz ± chlorite ± pyrite	Na-depletion	
Carbonate	Albite + sericite ± quartz	Ca, Mg, or Mn-	
	Dolomite/siderite/ankerite ± quartz ± sericite ± chlorite ± pyrite	=metasomatism	
Porphyry			
Kaolinitic	Kaolinite + montmorillonite ± sericite	K, Ca, Mg-	Argillic
Pyrophyllitic	± chlorite	metasomatism	advanced
Kaolinitic	Pyrophyllite + kaolinite ± quartz ±	K, Ca, Mg-	argillic
	sericite	metasomatism	Intermediate
Sericitic	Kaolinite + chlorite + sericite ±	K, Ca, Mg-	argillic
Feldspathic	montmorillonite ± illite-smectite ±	metasomatism	Phyllic
Biotitic	calcite ± epidote ± biotite	Na, Ca, Mg-	Potassic
	Sericite + quartz + pyrite ± chlorite ± biotite	metasomatism	
Chloritic	K-feldspar ± biotite ± quartz + sericite ± albite ± anhydrite ± epidote	K-metasomatism	Potassic
	Biotite + K-feldspar _ magnetite ± quartz ± albite ± anhydrite	K-metasomatism	Propylitic
	Chlorite _ epidote _ albite ± carbonate ± sericite ± montmorillonite ± pyrite	Ca-Mg-metasomatism	
Epithermal			
Silicic	Quartz ± chalcedony ± alunite ± barite	Si-enrichment	Silicic
Alunite	± pyrite	Ca, Mg, Na-depletion	Advanced argillic
K-mica or kaolinite	Alunite+ kaolinite/dickite + quartz/ cristobalite ± pyrophyllite ±diaspore ± pyrite ± topaz ±andalusite	K, Ca, Mg, Na-metasomatism	Intermediate argillic
Chloritic	Kaolinite/dickite + illite-smectite ±	Ca, Mg-	Propylitic
Sericitic	quartz ± pyrite	metasomatism	Argillic
	Chlorite + calcite + epidote + albite ± pyrite	K-metasomatism	
	Sericite + illite-smectite ± quartz ± calcite ±dolomite ±pyrite		
SEDEX			
Silicic			
Silicic	Quartz + pyrite + hematite		Jasperoid
Tourmaline	Quartz ± muscovite ± carbonate ± pyrite ± pyrrhotite		Tourmalinite
Carbonate	Tourmaline ± muscovite ± quartz ± pyrrhotite		
Sericitic	Ankerite/siderite/calcite + quartz ±		
Albitic	muscovite ±pyrrhotite		
	Sericite + chlorite + quartz ± pyrrhotite ± pyrite ± albite		
	Albite + chlorite + muscovite ± biotite		

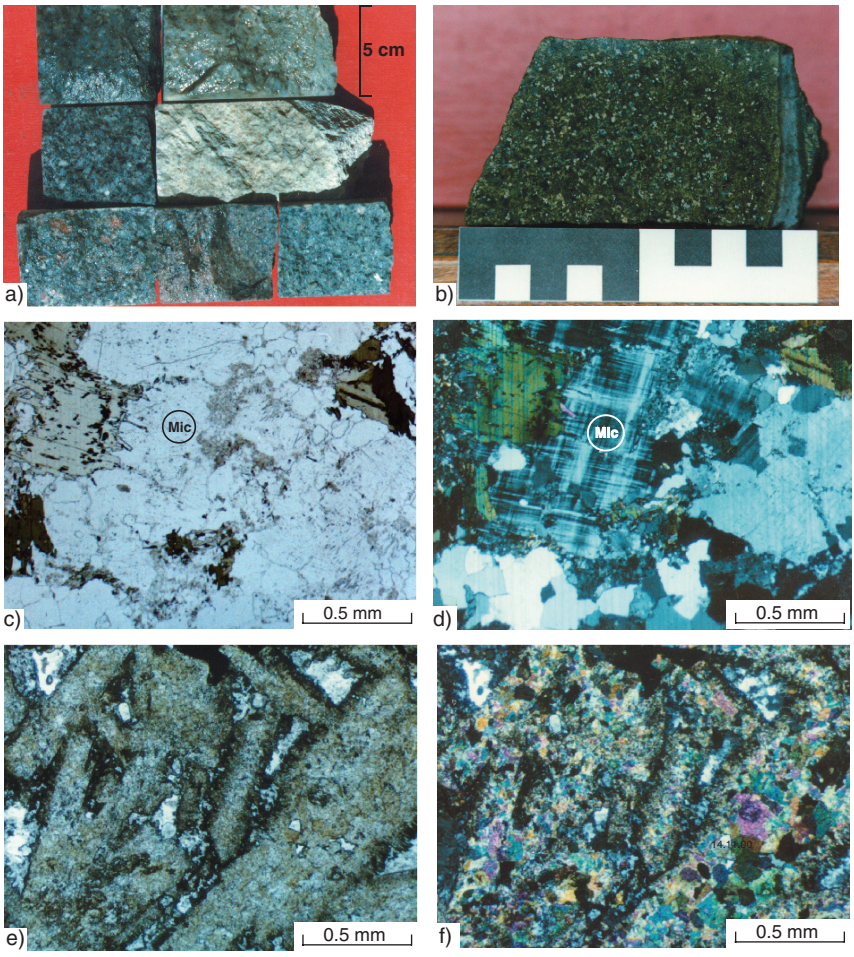


Fig. 2.8 (**a**) Hydrothermal alteration exhibited by core specimens of quartz-porphyry rock from the 2.0 Ga Haib Cu-Mo deposit in southern Namibia. *Bottom row* shows mainly potassic alteration; *reddish-brown spots* in specimen at bottom are K-feldspars; specimen in centre has mainly hydrothermal biotite; specimen at right has potassic alteration overprinted by sericitic alteration. Specimens in the centre exhibit mainly sericitic alteration; *light-coloured specimen at right* exhibits pervasive quartz-sericite-pyrite alteration; specimen in *top row* are affected by intense silicification (note patches of bluish opaline quartz); (**b**) Sample of feldspar-porphyry from the Haib CuMo deposit in Namibia showing pervasive propylitic alteration, the *green* colour is due to the presence of chlorite and epidote. Scale bar is in cm; (**c**) Photomicrograph in plane polarised light showing hydrothermal biotite (coloured) and microcline feldspar (*light coloured*). Both these minerals are the products of potassic metasomatism and alteration of a quartz-porphyry rock (Haib CuMo deposit, southern Namibia); (**d**) Same as 1b, but with crossed nicols. Mic is microcline; (**e**) Photomicrographs, in plane polarised light, of thin section from specimen in b showing plagioclase phenocrysts pervasively replaced by an aggregate of chlorite epidote and quartz; (**f**) Same as in e, but with crossed nicols

to be more pervasive towards the inner zones of a hydrothermal deposit or, in other words, towards the heat/hydrothermal source. Outward propylite alteration grades into unaltered rocks or, where metamorphism is present, into greenschist facies rocks with which propylitic assemblages are equivalent. Examples of propylitic alteration are shown in Fig. 2.8.

2.3.2.2 Phyllic (Sericitic) Alteration and Greisenisation

Phyllic, or sericitic, alteration is typified by the assemblage quartz-sericite-pyrite (QSP) (Fig. 2.9). Mineral phases usually associated with QSP alteration are K-feldspar, kaolinite, calcite, biotite, rutile, anhydrite and apatite. This alteration grades into the potassic type by increasing amounts of K-feldspar and/or biotite, and into the argillic type by increasing amounts of clay minerals.

Increasing amounts of topaz, tourmaline, quartz and zunyite herald a transition to greisen-type alteration. QSP alteration is one of the most common types of hydrothermal alteration, as it is present in almost all hydrothermal mineral deposits, from Archaean volcanogenic massive sulphides and gold quartz lodes to recent epithermal systems. Sericite refers to fine-grained dioctahedral white micas (muscovite, paragonite, phengite, fuchsite, roscoelite). Although, it has been pointed out that sericite is not a fine-grained variety of muscovite, but a petrographic term used to indicate fine-grained micaceous and potassic material and that its characterisation by XRD and TEM remains somewhat ambiguous (Fleet 2003). Under the microscope sericite may be confused with pyrophyllite, or even phlogopite, and X-ray or microprobe analyses may be necessary to make positive identification. Hydromuscovites and illites are also associated with this type of alteration; in the former, higher H_2O and K_2O contents are present, whereas the latter is a mica interlayered with clay-type minerals (see Fleet 2003). Sericitic alteration is essentially due to the destabilisation of feldspars in the presence of H^+, OH^-, K and S, to form quartz, white mica, pyrite and some chalcopyrite (sulphide content can be up to 20% by volume). In the process Na, Mg, Ti, Fe and also K are leached out.

Greisen, an old Cornish miners' term, refers to a coarse-grained assemblage of quartz-muscovite with varying amounts of topaz, tourmaline, fluorite, oxides (cassiterite, hematite), wolframite, scheelite, and sulphides of Fe, Cu, Mo, Bi, and Cu-Bi-Pb sulphosalts. Although greisen alteration is common in continental porphyry systems, its most favourable environment is a granite stock or sheet emplaced within argillaceous-arenaceous rock sequences, and associated with Sn-W mineralisation. The physico-chemical processes of greisenisation are not entirely understood. In these situations greisen alteration is usually preceded by Na metasomatism (albitite), during which H^+ ions are produced, which then initiate the process of greisenisation. This involves the destabilisation and destruction of feldspars and biotites to form the assemblage of quartz + muscovite. The process may be more complicated in mineralised systems, in which there is introduction of B, F, Li. This will result in new series of reactions that may take place to form topaz, tourmaline, and oxide minerals (Fig. 2.9). Silicification may

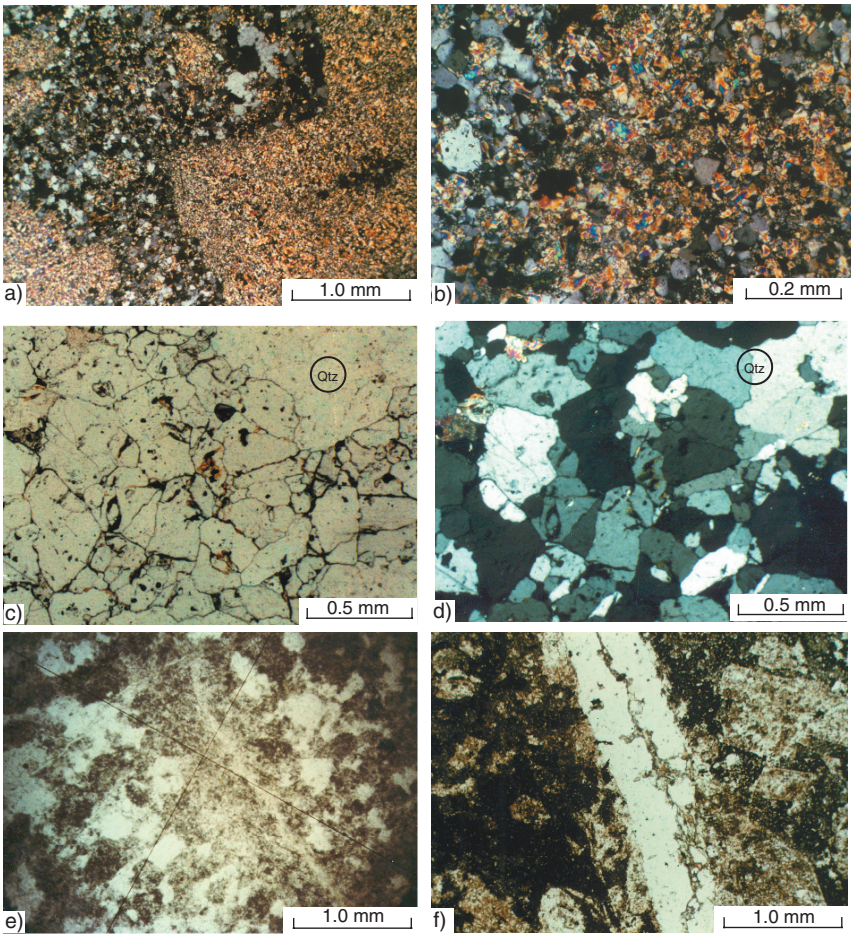


Fig. 2.9 (**a**) Photomicrograph taken at crossed nicols, showing pervasive quartz-sericite alteration of a feldspar porphyry rock. The porphyritic igneous texture is still recognisable; (**b**) Photomicrograph taken at crossed nicols, showing pervasive quartz sericitic alteration of the same porphyry rock shown in (**a**). Here the original igneous texture is no longer recognisable; (**c**) Photomicrographs (plane polarised) showing a quartz-topaz greisen assemblage (*left* and *upper* portion of photo is mostly topaz, quartz has lower relief and is on the *upper right* (Qtz), resulting from the replacement of a precursor granitic rock (Krantzberg tungsten deposit, Namibia); (**d**) Same as (**c**), but with crossed nicols. Qtz is quartz; (**e**) Photomicrograph in plane polarised light showing veinlet-controlled argillic alteration (brown material) of porphyry rock (Henderson Mo deposit, Colorado, USA); (**f**) Photomicrograph in plane polarised light showing pervasive argillic alteration of andesite rock and cut by a quartz veinlet. Feldspar phenocrysts are still recognisable on the right, adjacent to the veinlet (Namosi porphyry Cu deposit, Fiji). After Pirajno (1992)

accompany greisen alteration during and after, evidenced by the common quartz flooding of the greisen altered rocks. Muscovite preferentially replaces the biotites, and during this process cations locked in the biotite lattice are released into the system, and are possibly responsible for the paragenetically, later associated, metallic mineralisation. Quartz + muscovite greisens may be followed by progressive stages of F- and/or B-metasomatism, and in the latter case the development of tourmaline may be so extensive that quartz-tourmaline assemblages may dominate altogether. Subsequent to greisen alteration, sericitic and argillic types may follow by increased H^+ activity.

2.3.2.3 Argillic Alteration

Argillic alteration (argilla means clay in Latin) is characterised by the formation of clay minerals due to intense H^+ metasomatism and acid leaching, at temperatures of between 100 and 300°C. This alteration inwardly grades into phyllic zones, whereas outwardly it merges into propylitic ground. This type of alteration is common in porphyry systems, although in older terranes, for instance the Haib porphyry Cu-Mo deposit in Namibia (Chapter 5), erosion may eliminate evidence of this alteration type. Epithermal environments are typified by extreme acid leaching, and therefore argillic alteration provides a very useful guide to mineralisation. Base leaching of alumino-silicates may result in silica enrichment, so that argillic alteration may in fact grade into zones of silica-rich material. Clay minerals replace principally the plagioclases and the mafic silicates (hornblende, biotite). Amorphous clays, such as allophone, are also present and replace the alumino-silicate phases. Examples of argillic alteration are shown in Fig. 2.9.

Intermediate argillic alteration is defined by the presence of montmorillonite, illite, chlorite, kaolin group clays (kaolinite, dickite, halloysite, hallophane) and minor sericite, while K-feldspar may remain unaltered, and K, Ca, Mg, Na not entirely leached out. Zoning within the intermediate argillic alteration may be present with kaolinite being closer to the phyllic zone, whereas montmorillonite clays occur in the outer zones.

Advanced argillic alteration is due to intense acid attack, and more or less complete leaching of the alkali cations with complete destruction of the feldspars and mafic silicate phases. Dickite, kaolinite, pyrophyllite, barite, alunite and diaspore are the typical mineral phases of this alteration type. In addition, sulphides, topaz, tourmaline and a range of amorphous clays may be present. Sulphide minerals can include covellite, digenite and enargite (high sulphur to metal ratios). Base leaching above 300°C will produce assemblages containing pyrophyllite, andalusite, quartz, topaz and pyrite. Other associated minerals may include minor amounts of sericite, diaspore, kaolinite, rutile, anhydrite, corundum, zunyite, durmotierite, chloritoid. Amorphous clays (e.g. allophane) are common in the supergene environment. Advanced argillic alteration is found in porphyry systems, in the inner zones of hydrothermal base and precious metal-bearing veins, and most typically in the high-sulphur

epithermal systems. Alunitic alteration is part of advanced argillic alteration, and in the presence of abundant sulphate ions and Al-rich protoliths may become a dominant phase, as mentioned earlier. Alunite group minerals include alunite, natroalunite (Na replaces K), and jarosite (Fe replaces Al). Accompanying minerals are kaolinite, sericite, jarosite, pyrite, barite, hematite, chalcedony and opal.

2.4 Intrusion-Related Alkali Metasomatism

2.4.1 Sodic Metasomatism and Albitites

This aspect of metasomatism is characterised by Na-bearing minerals, which are clearly in replacement relationships with primary magmatic minerals. The replacement of alkali feldspar by albite (albitisation or Na-feldspathisation) is the more common form of sodic metasomatism. This replacement may proceed from pre-existing perthites, or by direct replacement of K-feldspar with newly formed albites (Pollard 1983). The albitisation of K-feldspar (Na replacing K) reaction is shown in Section 2.3.1.

The development of albite-rich rocks is usually associated with rare element mineralisation (Nb, Ta, Sn, W, Li, Be). Na-enrichment is accompanied by concentrations of Fe, U, Th, Zr, Nb, Sn, Zn and HREE. Also, Na-metasomatised rocks tend to be enriched with respect to K-metasomatised rocks in Rb, Th, Nb, La, Ce, Hf, Zr, Y (Kinnaird 1985). Several types of albitites have been recognised according to their mineralogy and rock type affected. In general terms albitite is a leucocratic rock made up of albite and quartz and containing some residual primary feldspars. Albitisation can affect a large mass of rock, and in some cases the albitised material can be injected as apophysis into the country rocks (see Chapter 4).

In peraluminous granites, sodic metasomatism is manifested by textural and colour changes, due to coarsening domains in perthite and development of the so-called chessboard texture. Growth of new micas, such as siderophyllite, also takes place. Geochemically the rock is enriched in Nb, Zr, U, Th and REE. Sodic metasomatism in peralkaline granites brings about textural and colour changes, due to growths of aegirine and arfvedsonite, and replacement of K in perthite by Na (Fig. 2.10), which leads to the development of albitites. Geochemically, an enrichment in the same elements as for the peraluminous granites is noted. Albitisation is followed by incipient H^+ metasomatism, usually characterised by the growth of sericite and varying amounts of fluorite and topaz. Experimental work on silicate systems with volatile components such as Li, F, H_2O, and fluid inclusion studies of quartz from sodic granites, can be used to estimate the temperature-pressure conditions of sodic metasomatism. Results indicate a range of temperatures of between 400 and 600°C approximately, at pressures of 1 kbar or less (Pollard 1983).

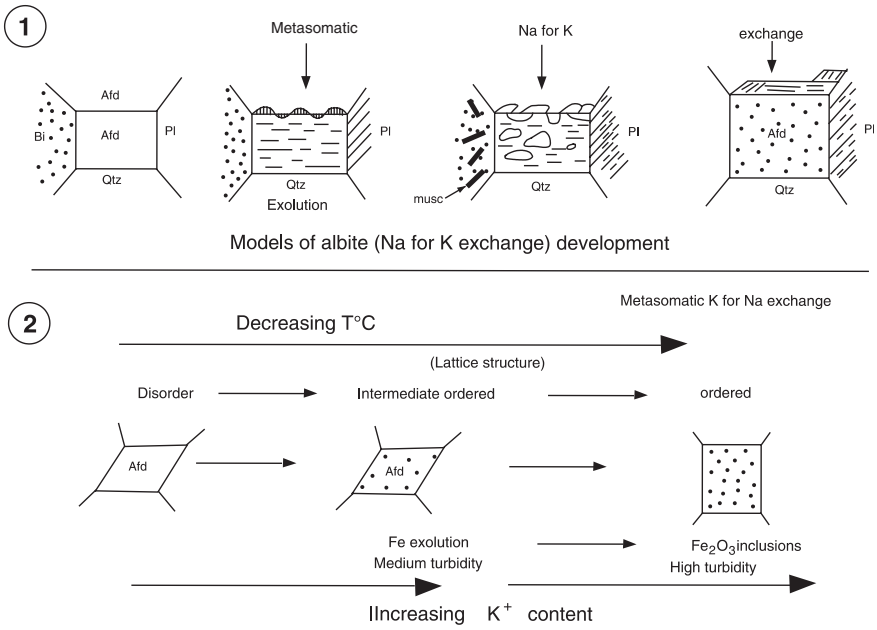


Fig. 2.10 Alkali metasomatism of alkali feldspar crystals. (1) Metasomatic Na for K exchange with development of albite domains; (2) Metasomatic K for Na exchange with development of microcline; turbidity results from the presence of minute exsolved hematite inclusions (After Haapala 1986; Kinnaird 1985)

2.4.2 Potassic Metasomatism and Microclinites

Potassic metasomatism (or K-feldspathisation or microclinisation) involves K for Na exchange mineral reactions, and is typically represented by the replacement of albitic plagioclase by microcline or orthoclase (Fig. 2.10). Other products of K for Na exchange reactions include the growth of new micas with compositions ranging from annite (Fe^{2+}-rich phlogopite) and amphibole compositions characteristic of Fe^{2+}-rich members (ferroedenite and ferroactinolite) (Bowden 1985). K-feldspathisation is believed to assume regional proportions and leads to the development of microclinites. Field and petrographic evidence from Nigeria (Bowden et al. 1984) also shows, however, that K-feldspathisation may post-date Na-metasomatism, is generally confined to fractures in the roof zones of granitic plutons, and is related to early stages of vapour separation. Microclines typically develop in pockets or pods in the roof zones of plutons. Extreme K-feldspathisation may result in a vuggy-textured microclinite as a result of desilication (Kinnaird 1985). K-metasomatism is characterised by the presence of an intermediate to ordered microcline. Also, during the K for Na exchange, Fe is released from the lattice and oxidised to form minute hematite inclusions which give the microclines a distinct reddish

colouration in hand specimens (Kinnaird 1985), whereas in thin-section this phenomenon is manifested by the turbidity of the feldspar crystals.

Fluid inclusion work, supported by textural evidence, for the Nigerian complexes suggests that CO_2 effervescence takes place in the system which enhances the K/H ratio of the remaining fluid, resulting in the development of K-feldspar at the expense of albite (Kinnaird 1985). In an ongoing process of alteration, potassic metasomatism is followed by incipient hydrolytic alteration characterised by the growth of siderophyllite or zinnwaldite aggregates, chlorites, and in some cases kaolinite. Temperature-pressure conditions for K metasomatism are not well known, but a minimum temperature of 630°C in the Q-Ab-Or system at 1 kbar, with 4% F, is considered possible (Manning 1982; Pollard 1983). Studies of fluid inclusions in K-feldspars indicate a range of temperatures from 320 to 700°C, at 1.2 to 2 kbar. During K-metasomatism Rb, Li, Zn are enriched and Na depleted.

2.5 Alkali Metasomatism (Fenites) in Anorogenic Ring Complexes

Magmatism in tensional zones of plate interiors is called anorogenic (Chapter 4). The nature of this magmatism is generally alkaline with a bimodal range of products (mafic-felsic). Notable examples of magmatic provinces containing anorogenic ring complexes include: Niger-Nigeria (Bowden et al. 1984), Corsica (Bonin 1986), Oslo Graben (Neumann et al. 2004) and the Damara alkaline province in Namibia (Pirajno 1994). The products of continental alkaline magmatism are volumetrically small. They have high concentrations of incompatible elements and volatiles, especially CO_2, B, F, Cl. The origin of these magmas is by no means certain, except that they are known to form in regions characterised by a thick lithosphere by small degrees of partial melting. It is also envisaged that these magmas may derive from metasomatised parts of subcontinental lithospheric mantle. This metasomatism may be linked with mantle outgassing of CO_2 with high halogen contents (Bailey 1978). This volatile flux through mantle material lowers the solidus so that liquids would result either from a drop in pressure, or through a local increase in temperature. Mantle plumes and associated lithospheric thinning accompanied by rifting and pressure release are the mechanisms invoked. These mechanisms could account for the generation and rise of these asthenospheric liquids through conduits that are usually long-lived or re-activated crustal fractures. The enrichments of the alkaline magmas in non-hydrous volatiles, such as CO_2 and halogens, lead to the concentration in the residual melts, during fractionation, of the volatile constituents and elements such as Zr, Y, Nb, U and Th.

Typical rock associations of alkaline magmatism include: kimberlites, mafic ultrapotassic rocks, syenite-pyroxenite-ijolite-carbonatite assemblages, alkali basalts and peralkaline granite-syenite-gabbro assemblages (Mutschler et al. 1985). Bowden (1985) grouped, ring complexes into: granitic (alkaline

granite-syenite-gabbro), alkalic (ijolite-carbonatite) and basaltic-gabbroic ring complexes. Figure 4.29A, B illustrates idealised cross-sections of alkaline ring complexes of the syenite-pyroxenite-ijolite-carbonatite association, and of the alkaline granite type, respectively. Details of the petrology of the alkaline rocks in general, and ring complexes in particular, are beyond the scope of this discussion. For these the reader is referred to Black and Bowden (1985), Bonin (1986) Woolley (1987, 2001) and the collection of works edited by Fitton and Upton (1987). Ring complexes are generally eroded volcanic centres with a circular shape and characterised by caldera-forming events. The erosion level of the complexes is reflected by the rock types exposed as indicated in Fig. 4.29. In the more deeply eroded structures only the sub-volcanic magma chambers and/or conduits are left exposed.

During the crystallisation and differentiation of the ring complex magmas, peralkaline fluid phases develop that can be retained within the magma or expelled into the country rocks. The interaction of fluids with the surrounding rocks at subsolidus temperatures induces the metasomatic changes, which may extend from a few hundred metres up to several kilometres away from the complex. Studies of the metasomatic and mineralised systems related to ring complexes can be of great importance in the understanding of the geological and geochemical processes related to the partitioning of metals from the alkaline magmas into subsolidus fluids and hydrothermal solutions. Especially important from this point of view are syenites and alkaline granites. These belong to the spectrum of A-type granites (anorogenic, alkaline, or meta- to peraluminous) (Collins et al. 1982), as distinct from the classic I and S-types of Chappell and White (1974); (see discussion in Chapter 4).

2.5.1 Fenites

One of the most interesting cases of anorogenic alkali metasomatism is that which takes place around alkaline complexes in stable continental areas. This phenomenon is known as fenitisation, and the rocks affected are called fenites. The name fenite is derived from the Fen carbonatite in Norway where this type of alteration was first documented by Brogger (1921). Fenitisation is type of alkali metasomatism and is a consequence of Na and/or K-rich fluids related to the cooling of carbonatites or ijolite intrusions. Le Bas (1987) stated that "*products of fenitization are mineralogically syenitic, with the result that they are sometimes misidentified as igneous syenites*". A plethora of complicated names have been adopted by different authors to describe fenitic rocks. Verwoerd (1966) proposed that the naming of fenitic rocks should be prefixed by the principal mineral components followed by fenite (e.g. orthoclase-aegirine-augite fenite). Kresten (1988) considered three styles of fenites: (1) aureole fenites; (2) vein fenites; (3) contact fenites. Aureole fenites are characterised by incipient growths of K-feldspar and sericite; alkali amphiboles occur in higher temperature aureole fenites. Vein fenites comprise riebeckite and

K-feldspars. Contact fenites are characterised by almost complete replacement of original minerals by K-feldspar, alkali amphibole, sodic pyroxene and carbonate.

Fenites are formed through progressive metasomatism in the country rocks surrounding alkaline complexes. This usually involves the elimination of free quartz (desilication) and the development of alkali mineral phases. Carmichael et al. (1974) attributed these metasomatic effects to residual alkali-rich fluids deriving from the fractionation of alkaline magmas. The fluids are in strong disequilibrium with the country rocks, producing haloes of alteration products which, as mentioned above, in some cases may resemble primary igneous rocks. The process is thought to be a solid state transformation due to expulsion from the igneous complex of hot, highly reactive volatiles and their subsequent infiltration into the country rocks. The spatial relationships of alkaline and carbonatite magmas and their fenitised envelopes are illustrated in Fig. 4.30.

The composition of fenites is dependent on both the nature of the country rocks affected and the igneous complexes from which the fenitising fluids evolve. Fenitic envelopes occur mainly around carbonatites, but other alkaline complexes are also surrounded by alteration haloes with a fenitic character. Since most anorogenic alkali complexes and allied rocks occur in stable continental areas, fenite envelopes are for the greater part found within granitoids and/or basement gneisses. However, fenitisation has also been noted in mafic igneous rocks and sedimentary rocks (Verwoerd 1966). Two main styles of fenitisation are recognised, one associated with carbonatites; the other with ijolites. Carbonatites form intense K-feldspar fenitisation, whereas ijolite magma is preceded by Na-K fenitisation with the production of aegirine-bearing rocks (Le Bas 1977).

Prins (1981) studied the chemical and mineralogical changes in the fenitic aureoles of the Kalkfeld and Okorusu alkaline-carbonatite complexes (Namibia). The findings of this author, reported here, are useful for the understanding of the genesis of mineralisation and alteration associated with intraplate anorogenic magmatism. The Kalkfeld syenite-carbonatite complex developed extensive fenitisation both within a primary syenite and within the granitic wall rocks. The fenitisation of the granitic rock is characterised by the replacement of quartz by aegirine-augite and Na-amphibole along fractures. The syenite reveals a re-crystallised texture and consists of orthoclase and aegirine-augite. The main changes involve the enrichment of Na, Al, Mg and total Fe with decreasing Si contents (advancing fenitisation), whereas K and Ca remain nearly constant. Here two important observations were made by Prins (1981). One, that the "trachytic" dykes may, on the basis of their low Si and high Na, represent mobilised fenites. Two, that the sum of Si + Al + Na + Total Fe is constant for the granitic rocks, leading this author to suggest that this type of metasomatism involves substitutions between the elements so as to preserve the charge balance. The chemical variations at Okorusu refer to a metasomatic pyroxenite (pyroxene-fenite) and its parent material, which is a calcareous feldspathic sandstone. Here increases in Na, Mg, total Fe, and decreases in Ca and Al versus

decreasing Si concentrations are recorded. Feldspathic dykes and breccias (feldspathisation stage), show strong Si depletions and are also interpreted as reflecting re-mobilisation.

The Okorusu nepheline-syenite carbonatite complex, by contrast, developed its fenitic envelope in sedimentary wall rocks, which in their unaltered form contain quartz, feldspar, biotite, calc-silicate and calcite. Fenitisation converted these rocks into a "massive alkali pyroxenite", which retained the sedimentary structures. The pyroxene-fenite consists of alternating bands or layers of pyroxene; calcite + quartz. Apatite + pyrite + titanomagnetite are also present. During a later stage of alteration biotite and Na-amphibole formed at the expense of the pyroxene. The new pulse of metasomatism introduced K (feldspathisation), resulting in the transformation of pyroxene-fenite and syenite into a K-feldspar-limonite-calcite fenite. The new feldspar forms large crystals, has a maximum ordered structure with a composition of Or_{90-95}, and shows turbidity due to minute hematite inclusions. Flow-structured dykes containing feldspar, limonite, calcite and fluorite are interpreted as mobilised feldspathised rocks. The transfer of elements and the related mineralogical changes associated with the transformation of the unaltered sediments at Okorusu to pyroxene-fenite were calculated by Prins (1981), who used for his calculations the composition-volume equations given by Gresens (1967) and Babcock (1973). For the first set of mineralogical changes and transfer of elements, relating to the early Na-dominated fenitisation (pyroxene-fenite), he assumed constancy of volume. It was found that during metasomatism total Fe, Mg, Na and P were added, whereas K, Mn, Al and Ti remained constant. With some surprise, only a little Si was abstracted, whereas a large amount of Ca was removed and redistributed. The weak depletion of Si during the pyroxenisation of the sediments is at odds with the usual desilication observed in fenitised rocks. The author explained the phenomenon by suggesting that the increase, or decrease, of Si is dependent on the degree of saturation in Si of the fluid relative to the invaded wall rocks. Thus, it is reasoned that if the fluids enter a Si-oversaturated rock body, desilication will occur to establish equilibrium, whereas the opposite will take place if the wall rocks are undersaturated with respect to the matasomatising fluids. The mineralogical changes and element transfer that took place during the Na-dominated stage (pyroxene fenite) at Okurusu, as calculated by Prins (1981, p. 213), are given below.

$$\begin{aligned}2\text{anorthite} + 8SiO_2 + 5Fe^{3+} + 4Na^+ + Mg^{2+} + 4H_2O \rightarrow \text{aegirine-augite} \\ + 2\text{albite} + Fe_3O_4 + Ca^{2+} + 8H^+;\end{aligned}$$

$$\begin{aligned}\text{biotite} + 5\text{calcite} + 12\text{quartz} + 3Fe^{3+} + 6Na^+ + 3PO_4^{3-} + 4H_2O \rightarrow \text{apatite} \\ + 6\text{acmite} + 2\text{orthoclase} + Fe_3O_4 + 5CO_2 + 11H^+\end{aligned}$$

The second stage of fenitisation was K-dominated and allowed the formation of orthoclase. Mass transfer equations were calculated allowing a 20% volume increase for the transformation of the pyroxene-fenite to a feldspathic

fenite. Aluminium, K and CO_3 were added, while Fe, Ti, Mg, Na, P remained constant, and Si and Ca were removed. Here feldspathisation is taken to be accompanied by desilication because, as mentioned above, of the contrast between the invading fluid (Si-undersaturated) and the host lithology (Si-oversaturated). Silica is therefore removed but is locally re-distributed as chalcedonic breccia fillings associated with calcite. The equations representing the mineralogical changes and element transfer associated with feldspathisation are (Prins 1981, p. 217):

$$\text{aegirine-augite} + 6\ \text{quartz} + Fe_3O_4 + 4Al^{3+} + 2K^+ + 8CO_2 + 8OH \rightarrow 2\text{albite} + 2\text{orthoclase} + 5FeOOH + 6FeCO_3 + CaCO_3 + MgCO_3 + 3H^+;$$

$$\text{aegirine-augite} + 2\text{calcite} + 7\text{quartz} + 4Al^{3+} + 2K^+ \rightarrow 2\text{orthoclase} + 2\text{albite} + 2\text{siderite} + Si^{4+} + Mg^{2+} + 3Ca^{2+}.$$

Precise temperature, pressure and composition of fenitising fluids are not well understood, but from available data (Woolley et al. 1972; Ferguson et al. 1975; Siemiatkowska and Martin 1975; Verwoerd 1966; Le Bas 1977; Prins 1981), it can be surmised that the composition of the fenitising fluids ranges from Na + K + CO_2-rich (carbonatitic magmas) to saline brines enriched in Na and/or CO_2. Temperatures of the fluids, based on mineral equilibria, range from 450°C up to 700°C (alkaline magmas) with pressure from a few hundred bars up to 5 kbar.

An example of large-scale fenitisation can be found in Western Australia in an area intruded by the carbonatitic rocks and ultrabasic sills of the Gifford Creek Complex. The carbonatitic suite consist of ferrocarbonatite-magnetite veins and aegirine-phlogopite-apatite-magnetite-pyrochlore sills. The Complex, with poorly constrained ages of ~1.68–1.25 Ga, was emplaced in the ~2.0 Ga Gascoyne Complex and was investigated in detail by Pearson et al. (1995) and Pearson and Taylor (1996). The Gascoyne Complex is located between the northwestern Archaean Yilgarn Craton and the Mesoproterozoic Ashburton Formation in the north. The Complex consists of a suite of Neoarchaean to Palaeoproterozoic granite gneisses that are interpreted as basement to various Proterozoic granitic rocks (2.0–1.9 Ga Dalgaringa Supersuite, 1.68–1.97 Ga Durlacher Supersuite, 1.83–1.62 Ga Moorarie Supersuite) and metasedimentary sequences. Details of the geology of the Complex can be found in Sheppard et al. (2007). The Gifford Creek Complex is a suite of high-level alkaline ultrabasic rocks (mostly lamprophyres) and carbonatite sills, dykes, veins, associated with quartz and massive Fe oxide veins. This is a field of REE and U mineralisation (Flint and Abeysinghe 2000), hosted in sinuous veins of carbonatite and Fe oxides that intrude porphyritic granites of the Durlacher Supersuite. The carbonatite-Fe oxides veins form a regional-scale stockwork-like system. These veins have margins of Fe carbonates (ankerite; siderite) and are associated with zones of alteration that have a fenitic character. The fenitic haloes are characterised by the presence of feldspars and/or amphiboles and

magnetite, locally with monomineralic feldspar (orthoclasite) zones. Fenitisation of the country rock granitoids can form zones (aureoles) up to 2–4 km across, in which the granitic rocks exhibit sericitisation of primary feldspars and growth of new K-feldspar. Around the lamprophyre rocks, the granitic roks show progressive replacement of the constituent minerals by K-feldspar, sericite and alkali amphibole. Pearson and Taylor (1996) noted "stock-like" zones of syenite, which they attributed to intense and pervasive fenitisation. Following the classification of Kresten (1988), these authors also recognised vein fenites consisting of riebeckite and cutting across the above-described larger zones (aureole fenites). Pearson et al. (1995) suggested that the Gifford Creek Complex and the associated extensive fenitisation of the intruded country rocks may represent the upper levels of unexposed major alkaline ring complexes.

2.6 Alteration in Porphyry Systems

Hydrothermal alteration and mineralisation form more or less concentric shells centred on the intrusions associated with porphyry mineral systems. The effects of hydrothermal alteration and mineralisation extend into a large volume of wall rocks around and above the intrusives. Seedorff et al. (2005) discussed hydrothermal alteration of porphyry systems in some detail and considered that the processes leading to alteration in porphyry systems are: volatile addition (propylytic alteration), hydrolysis (sericitic, advanced argillic and intermediate argillic), alkali exchange (potassic, sodic-calcic alteration) and addition of silica. The principal variables in alteration processes are: temperatures, pressure, fluid composition and composition of possible external fluids (meteoric, seawater, evaporites). Phase diagrams of the system K_2O-Al_2O_3-SiO_2-H_2O-KCl-HCl were constructed by Hemley and Jones (1964) and Meyer and Hemley (1967) to define the boundaries of alteration types and mineral phases, progressively from 700°C through to 150°C (see also Seedorff et al. 2005). A simplified phase diagram is shown in Fig. 2.7A, and an idealised evolutionary alteration sequence, applicable to most porphyry systems is presented in Fig. 2.7B.

Seedorff et al. (2005) provided a detailed list of alteration types and related mineral and sulphide assemblages in porphyry systems, shown in Table 2.4.

Sheppard (1971) and Taylor (1974, 1997) examined the D/H and $\delta^{18}O$ isotopic composition of key minerals in order to determine the origin of the H_2O involved in the mineralising solutions. These studies revealed that most hydrothermal biotites exhibit an isotopic composition indicative of an igneous origin, but in some biotites there is evidence of later exchange with meteoric waters. It was also found that the oxygen and hydrogen isotopic composition of clay minerals and sericite is dependent on their geographic position, leading to the conclusion that they were formed by fluids with a strong meteoric component. The action of magmatic and meteoric fluids in porphyry systems was described by Guilbert and Park (1986, p. 199) as the "*summation of many*

Table 2.4 Alteration types and mineral assemblages in porphyry systems. After Seedorff et al. (2005)

Alteration type	Silicate mineral assemblages (minor phases or not necessarily present) ± quartz	Principal sulphide-oxide assemblages
Potassic	K-feldspar, biotite (albite, topaz, tourmaline, chlorite)	Bornite + digenite + magnetite; chalcopyrite + pyrite, magnetite±chalcopyrite, magnetite, molybdenite, titanite, ilmenite
Transitional potassic-sericitic	K-feldspar, biotite, sericite (albite, topaz, tourmaline, chlorite)	Bornite + chalcopyrite + magnetite, chalcopyrite + magnetite, chalcopyrite + pyrite, molybdenite, titanite, rutile
Sericitic (phyllic, quartz-sericite-pyrite)	Sericite, chlorite	Chalcopyrite + pyrite + molybdnite, pyriute, tennantite, sphalerite, galena, hematite, rutile
Transitional potassic-advanced argillic	K-feldspar, biotite, andalusite, albite (topaz, tourmaline, cordierite, corundum)	Chalcopyrite, molybdenite, magneitte, ilmenite
Transitional potassic-sericitic-advanced argillic	K-feldspar, biotite, andalusite (topaz, tourmaline, cordierite, albite)	Bornite + chalcopyrite ± magnetite; chalcopyrite + pyrite ± magnetite; molybdenite + chalcopyrite ± pyrite; titanite
Transitional sericitic-advanced argillic	Sericite, andalusite, pyrophyllite, kaolinite-dickite, diaspore, alunite, (albite) ±topaz, tourmaline, durmotierite	Pyrite + bornite; chalcopyrite, pyrite, enargite, rutile
High-T advanced argillic	Andalusite, diaspore, topaz, dumortierite, cordierite, (corundum, albite)	Pyrite, rutile
Moderate-T advanced argillic	Pyrophyllite, diaspore, topaz, dumortierite, zunyite (albite)	Covellite, digenite, chalcocite, bornite, enargite, pyrite, hematite, rutile
Low-T advanced argillic	Kaolinite-dickite, diaspore, (albite) ±topaz, dumortierite, zunyite	Covellite, digenite, chalcocite, bornite, enargite, pyrite, marcasite, hematite, rutile, anatase, brookite?
Intermediate argillic	Sericite-illite, kaolinite, montmorillonite, chlorite	Chalcopyrite, pyrite (pyrrhotite), hematite, cassiterire, stannite, bismuthinite, hematite, rutile
Propylitic	Albite, sericite-illite, montmorillonite, chlorite, (zoisite, clinozoisite, zeolite, actinolite) (biotite), zircon	(Bornite, chalcopyrite, pyrite, pyrrhotite, molybdenite, galena, tennantite, tetrahedrite, hematite, magnetite, titanite, rutile)
Silicic	Quartz, tourmaline?	(molybdnite, zircon)
Sodic-calcic	Actinolite, epidote, (plagioclase)	Titanite, rutile
Sodic	Allbite, chlorite, epidote, tourmaline, vermiculite	Pyrite, rutile, (titanite)

Table 2.4 (continued)

Calcic-potassic	K-feldspar, (albite), biotite, garnet, dioptase, actinolite, epidote	Bornite + magnetite
Sodic-ferric	Amphibole, plagioclase	Magnetite, magnetite + bornite; chalcopyrite, ilmenite, titanite

continuous, time-staged processes rather than a single event". Magmatic waters are first exsolved from the crystallising porphyry intrusion (Section 2.1.2). These early magmatic-hydrothermal fluids form at temperatures ranging from 750 to 450°C and at depths of between 5 and 1 km below the surface. The activity of these fluids is essentially confined to the apical portions of the intrusive stock and immediate surrounding areas. The early magmatic-hydrothermal fluids are generally succeeded by convective fluids of meteoric origin, with which they mix until the magmatic component relating to that particular intrusion tends to disappear completely. Meteoric-hydrothermal fluids of porphyry systems have temperatures ranging from 450 to 250°C and form at depths of between approximately 1 and <0.5 km, grading upward to epithermal regimes. The study of fluid inclusions in porphyry systems indicates that there are, broadly speaking, three classes of fluids (Beane and Titley 1981): (1) hypersaline fluids with up to 40 wt% NaCl equivalent and homogenisation temperatures of 750°C or greater; (2) high salinity fluids, with approximately 10–25 wt% NaCl equivalent and homogenisation temperatures of between 600 and 250°C; and (3) low salinity fluids with less than 10 wt% NaCl equivalent and homogenisation temperatures of between 400 and 200°C. Integration of isotopic, fluid inclusion, petrological and field data suggest that the hypersaline fluids are largely magmatic-derived. Fluid inclusion data also suggest that boiling and condensation occurred within these hypersaline magmatic fluids. From these studies the picture emerges that the earliest fluids are exsolved from cooling magmas over a protracted period of time, and they ascend and circulate through both the producing cooling intrusive and adjacent fractured wall rocks. During this time increasing amounts of meteoric-derived convective waters are drawn into the system, at first mixing with the magmatic fluids and later dominating the entire hydrothermal system. It is important to realise in this context that the permeability of the wall rocks controls the access of the convecting meteoric fluids. The action of the hydrothermal fluids on the surrounding rocks produces the alteration-mineralisation patterns of porphyry systems, which depends on the nature of the fluids, wall rock and intrusive compositions, and, as mentioned above, permeability.

Lowell and Guilbert (1970) and Guilbert and Lowell (1974), using examples of porphyry deposits in North America, detailed the configuration of spatial and temporal alteration patterns of porphyry systems (see also Chapter 4). The Lowell-Guilbert model is well known in the literature, although in detail alteration patterns may differ substantially due to the different compositions

of the individual intrusions (silica-rich and alkalic or alkalic-calcic). Hollister (1978) proposed a model of alteration associated with breccia pipes linked to porphyry systems and a diorite model. The work of these authors remains very useful to this day, especially for field-based mappable features and petrographic studies. These main-stream models are described below.

2.6.1 Lowell-Guilbert and Breccia Pipe Models

The essential features of the Lowell-Guilbert model are shown in Fig. 2.11A, B. The hydrothermal alteration zones form more or less concentric shells around a core zone of potassic alteration, around which are distributed the phyllic or quartz-sericite-pyrite zone, the argillic zone and the propylitic zone. The chief minerals that typify the potassic zone are orthoclase and biotite. The potassic zone contains assemblages consisting of various combinations of: quartz + K-feldspar + biotite + sericite + anhydrite + pyrite + chalcopyrite + bornite ± magnetite ± molybdenite. Such an assemblage is ascribed to late-magmatic-hydrothermal fluids. This alteration is generally pervasive and characterised by the replacement of primary biotite and feldspars. K-feldspar forms microveinlet fillings as well as replacement of primary feldspars. Hydrothermal biotite occurs as microfracture fillings accompanied by chalcopyrite and anhydrite, as sparse to massive replacement of plagioclase, as euhedral crystals almost identical to primary biotites, and as pervasive replacement of groundmass feldspars. The altered porphyries display a smokey-grey colour and the ore shell is typically contained within the outer limits of the potassic core.

The phyllic zone, also known as quartz-sericite-pyrite (QSP) zone, surrounds and overlaps the potassic zone. Contacts between the phyllic and potassic zones are gradational. This alteration is caused by the leaching of Na, Ca and Mg from the alumino-silicate minerals (Titley and Beane 1981). Phyllic alteration is characterised by the assemblage of quartz + sericite + pyrite ± chlorite ± rutile ± chalcopyrite. Iron is leached out of the primary mafic silicates to form mainly pyrite. Sericite predominates in the inner portions of the zone, whereas clay minerals and hydromicas become more abundant towards the outer portions. Sericite pervasively replaces all the primary silicates often forming a felted texture; faint vestiges of cleavage and twin planes, in places, indicate the presence of former silicates, although towards the inner margins of the zone relics of K-feldspars may still be recognisable. Pyrite can reach up to 30% by volume and forms veinlets and granular disseminations. Chalcopyrite may be present in subordinate amounts. Silicification is prominent and, according to the authors, well beyond that expected from the breakdown of primary minerals, suggesting perhaps that some silica comes in with later fluids. Contacts between the phyllic and argillic zones are gradational and indistinct.

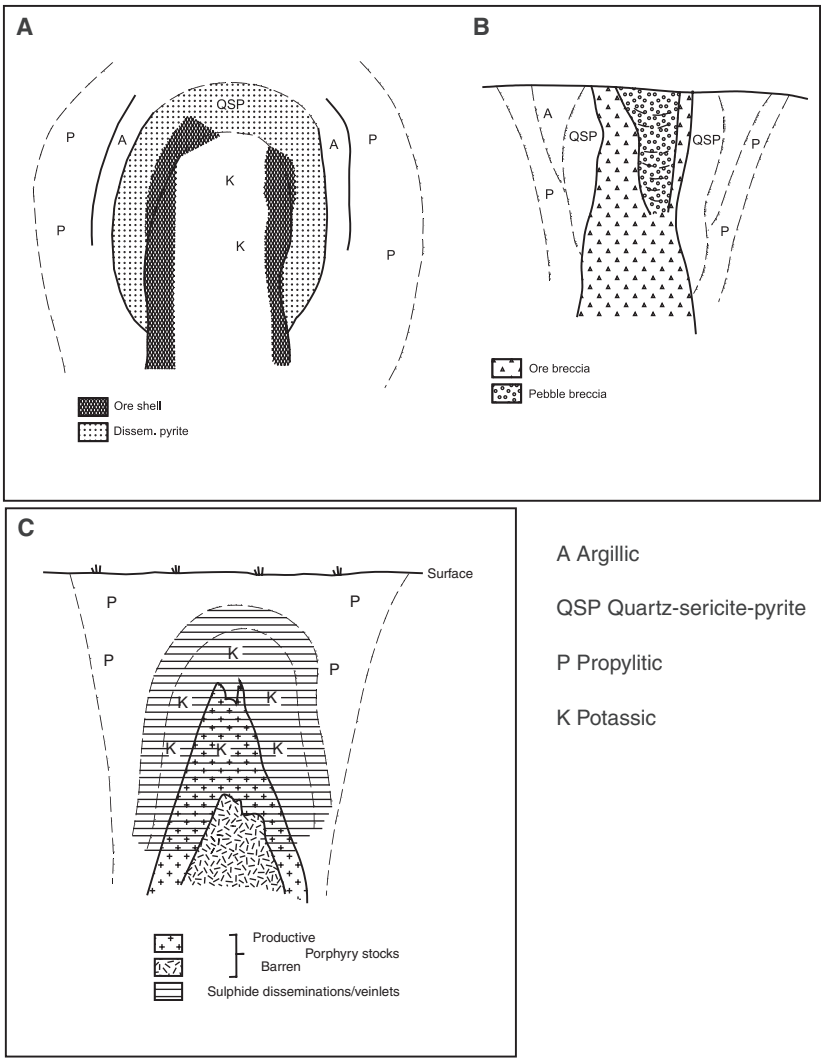


Fig. 2.11 Lowell-Guilbert models of alteration-mineralisation patterns (not to scale) in (**A**) quartz-monzonite porphyry system and (**B**) a breccia-type porphyry systems. After Lowell and Guilbert (1970); (**C**) diorite model after Hollister (1978)

The argillic zone is characterised by the presence of clay minerals, such as illite, kaolinite and montmorillonite. During this phase of alteration acid conditions prevail and leaching of cations is extensive. Plagioclase is converted to kaolinite near the ore shell and to montmorillonite further away. K-feldspar shows minor replacement by kaolinite and/or sericite. Pyrite, though less

common than in the phyllic zone, may also be present. Intermediate argillic alteration refers to the presence of minerals such as montmorillonite, illite, chlorite, hydromicas and, locally, kaolinite. The formation of these minerals is related to the availability of limited amounts of K, Ca and Mg (Beane and Titley 1981). Advanced argillic alteration refers to more or less complete acid attack with the formation of kaolinite-dickite and varying amounts of diaspore, alunite, amorphous silica, more rarely corundum and pyrophyllite. Beane and Titley (1981) pointed out that in many cases the argillic alteration reported for some porphyry deposits is in fact supergene alteration, and this is often associated with chalcocite mineralisation. Pyrite, chalcopyrite and bornite are the main sulphide species associated with the argillic alteration.

The propylitic zone is the largest of the alteration shells forming a wide halo (can reach a few kilometres in extent) in the country rocks around the porphyry intrusives, and as such is relatively easy to detect in the early stages of mineral exploration. The propylitic zone grades into the argillic zone. The propylitic assemblage consists of chlorite + epidote + pyrite + calcite ± clay minerals. Chlorite and carbonate generally replace biotite along cleavages, whereas epidote and calcite occur as fine granules in plagioclase, or associated with montomorillonite replacing amphiboles. Pyrite is abundant and chalcopyrite rare.

Tourmaline may be present in some porphyry deposits of the quartz-monzonite type and is usually associated with breccia pipes (Chapter 4). Although present in the North American and some of the Pacific deposits, breccia pipes are characteristic of the Andean region where they may be economically important. At El Teniente (Chile) two tourmaline breccia pipes, up to 1.3 km in diameter, contain Cu and Mo ore. Tourmaline may also occur in the argillic, propylitic, phyllic and potassic zones where it preferentially replaces the ferromagnesian minerals.

Hollister (1978) considered a model of porphyry system that he called "breccia-type" (Fig. 2.11B). The alteration-mineralisation is related to a large breccia pipe in which B-bearing fluids may play an important role and are responsible for the introduction of early tourmaline + quartz + pyrite, followed by Cu mineralisation. The alteration sequence is similar to the Lowell-Guilbert model (central potassic zone followed by phyllic, argillic and propylitic zones). The potassic minerals (orthoclase and biotite) and sulphides characteristically may occur as cementing material for the breccia clasts. A pebble breccia may be present within the central portions (Fig. 2.11B) and is characterised by extensive argillic alteration, crude graded bedding and the presence of rounded fragments which include ore material. Pebble breccias are formed during a post-mineral stage by continuing meteoric-hydrothermal activity. Apart from the quartz associated with the alteration mineral assemblages discussed above, silica is an important constituent of porphyry systems. It occurs as quartz veins and veinlets, as jasper and/or chalcedony replacing silicate minerals and carbonate country rocks.

2.6.2 Diorite Model

Porphyry systems associated with intrusives of dioritic or syenitic composition have alteration-mineralisation patterns that differ substantially from systems associated with more felsic granitic rocks to which the Lowell-Guilbert model is more applicable. The mafic character of both the intrusive rocks and the surrounding comagmatic volcanics plays an important role in the mineralogical and geochemical aspects of hydrothermal alteration and mineralisation. Thus, for example, the phyllic alteration is either lacking or poorly developed, whereas potassic and propylitic alteration zones are more prominent. This type of porphyry system is usually found in island arcs built on oceanic or thin continental crust. The alteration-mineralisation patterns of diorite-model porphyries are characterised by potassic and propylitic zonal sequences related to the effects and role played by the K^+ and H^+ ions in systems of high Na_2O/K_2O ratios and generally low in silica (Hollister 1978). The diorite model, shown in Fig. 2.11C, consists of two successive shells of potassic (inner) and propylitic (outer) alteration. The potassic alteration is characterised by dominant biotite and chlorite with little or no K-feldspar. Chlorite replaces sericite in the diorite model, while albite, which may be present, takes the place of orthoclase. Phyllic alteration, if present, is generally weakly developed. Propylitic alteration is characterised by the assemblage chlorite + epidote + albite + carbonate, is paragenetically later than, and replaces the potassic assemblages. In diorite-type porphyries chalcopyrite disseminations are important and tend to accompany the potassic zone. The chalcopyrite to pyrite ratio is close to unity, whereas the chalcopyrite to bornite ratio is equal to, or less than, 2 (Hollister 1978). Magnetite is a common constituent of diorite-type porphyries, and pyrrhotite may also occur.

2.6.3 Hydrothermal Alteration in Climax-Type Porphyry Mo Systems

The zones of hydrothermal alteration of the Climax-type deposits (Hollister 1978; Guilbert and Park 1986) are as follows: (1) greisen zone; (2) quartz-K-feldspar, quartz-topaz; (3) phyllic with a topaz-magnetite subzone; (4) argillic; (5) propylitic. Climax-type porphyry Mo deposits have, in addition to the usual alteration-mineralisation shells, greisen-type alteration, which is spatially and genetically related to a late granitic intrusion. Alteration patterns of the Climax-type porphyry system are shown in Fig. 2.12. Details of Climax-type hydrothermal alteration are best known from comprehensive studies of the Henderson deposit at Red Mountain, where five major zones of alteration are recognised (White et al. 1981). A potassic alteration zone coincides with the 0.3% Mo cut-off boundary of the Henderson ore and is characterised by the total replacement of plagioclase by K-feldspar, giving rise to an equigranular groundmass of K-feldspar and quartz. K-feldspar veinlets are locally present. A quartz-sericite-pyrite zone has a bell

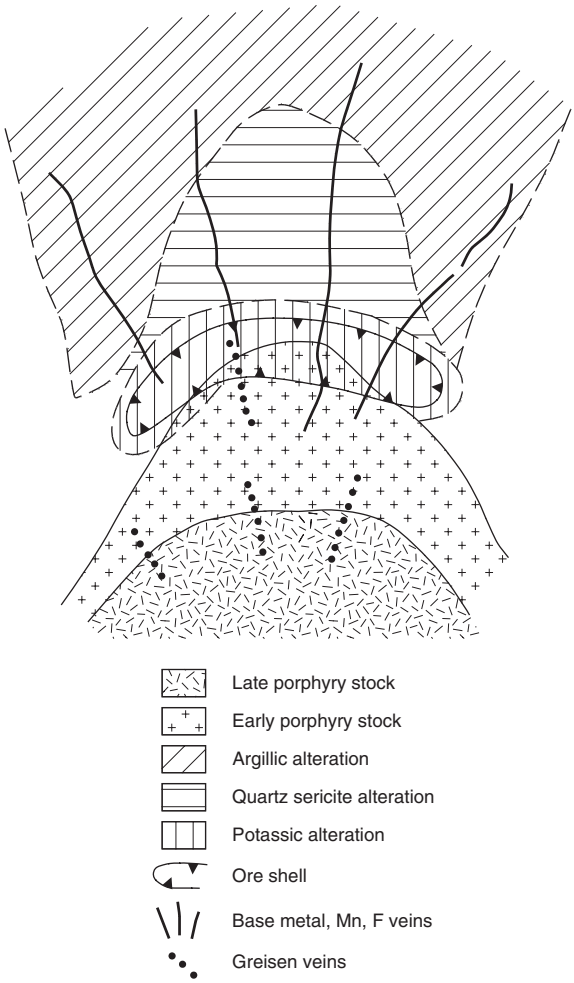


Fig. 2.12 Idealised model of porphyry Mo system and associated hydrothermal alteration (after Mutschler et al. 1981). Patterns of alteration-mineralisation in these porphyry systems are complex due to the superposition of multiple intrusive and hydrothermal events. This model depicts only one event

shape possibly reflecting temperature variations during the alteration process. This zone is characterised by the replacement of K-feldspar and plagioclase by sericite, by the presence of optically continuous quartz overgrowth and by abundant pyrite. Where pervasive the original igneous textures are completely destroyed. An upper argillic zone displays selective replacement of plagioclase by montmorillonite, kaolinite and sericite, while K-feldspar remains relatively unaltered; biotites are replaced by sericite, rutile, pyrite, carbonate and fluorite. A lower argillic zone occurs at the base of the orebody and is represented by the replacement of all

K-feldspars by kaolinite. The propylitic zone is well developed in the Precambrian Silver Plume granite. This alteration zone is typified by the mineral assemblage chlorite + epidote + calcite + clay + sericite. The outer boundary of the propylitic zone is taken to be where primary biotite is replaced by chlorite. Five additional alteration zones of lesser extent are: vein and pervasive silica zones, magnetite-topaz zone, garnet zone and a greisen zone. The latter contains quartz-muscovite and topaz as the main minerals and occurs around quartz-molybdenite veinlets and below the Henderson ore zone. The garnet zone (spessartine) is associated with a late stage of Pb-Zn-Mn hydrothermal event (Fig. 2.12).

2.7 Skarns

Skarns are calc-silicate rocks formed by replacement of carbonate lithologies either during regional metamorphism or by contact metasomatic processes related to igneous intrusions. Many skarns are associated with porphyry systems, where the porphyry stock intruded carbonate lithologies. As also mentioned in Chapter 5, Dilles and Einaudi (1992) published an interesting paper on the Ann-Mason porphyry-skarn system in Nevada; Lexa et al. (1999) provided an overview of porphyry, skarn and epithermal vein ore systems associated with a stratovolcano in the Carpathian magmatic arc (Slovakia). Skarns are very important because they host a great variety of ores and constitute a distinct class of mineral deposits, whose general characteristics and alteration patterns are reviewed in Chapter 6. In this section, I briefly discuss the process of replacement of carbonate rocks by silicate minerals, generally through the addition of silica, as in the following reactions:

$$\underset{\text{dolomite}}{CaMg(CO_3)_2} + 2SiO_2 \rightarrow \underset{\text{diopside}}{(CaMg)Si_2O_6} + 2CO_2$$

$$\underset{\text{calcite}}{CaCO_3} + SiO_2 \rightarrow \underset{\text{wollastonite}}{CaSiO_3} + CO_2$$

The addition of large quantities of silica produces a wide variety of calc-silicate minerals. Alteration mineral assemblages of skarn rocks include Ca, Fe, Mg, Mn silicates, such as epidote, clinozoisite, garnet, clinopyroxene, wollastonite, diopside, vesuvianite, tremolite–actinolite, andradite, grossularite, phlogopite and biotite. Skarns are developed at the contact between plutons and the invaded country rocks, the latter generally being carbonates and, less commonly, Ca-rich silicate rocks. Skarn genesis essentially involves isochemical contact metamorphism and metasomatism (prograde skarns), entirely due to the transfer of heat, fluids and metals from a cooling plutonic body to the surrounding wall rocks. Skarn alteration systems are typically zoned in response to temperature variations and fluid evolution outward from the intrusive stock or pluton. This

zonation begins from the endoskarn within the intrusion to proximal and distal exoskarns that develop in the country rocks. Generally the carbonate rocks at and around the contacts of the intrusion, are metamorphosed to marble (marmorised) or calc-silicates, in the case of impure carbonates. The contact, proximal or prograde skarns are characterised by various combinations and volumetric abundances of garnet (grossularite-andradite), pyroxene, vesuvianite, wollastonite and rhodonite. Retrograde stages of alteration occur towards the final stages of cooling, resulting in more intense hydrothermal activity, local mixing with meteoric waters and precipitation of sulphides and oxides, especially nearer the pluton's contacts, and overprinting of prograde assemblages. Mineral assemblages of retrograde skarns typically include hydrous phases, such as amphibole, biotite, epidote and chlorite although, as cautioned by Meinert et al. (2005), the presence of hydrous mineral phases does not necessarily imply retrograde processes. As mentioned above, retrograde minerals reflect decreasing temperature and salinity of the fluids, leading to a trend from amphibole-epidote → biotite → muscovite-chlorite → sulphides → carbonates (+fluorite or scheelite or powellite) (Kwak 1994). Common skarn minerals are listed in Table 6.2.

2.8 Alteration in Epithermal Systems

Hydrothermal mineral phases that develop in epithermal systems are a function of temperature, pressure, rock type, nature of the circulating fluids (such as pH, activities of CO_2, H_2S) and water/rock ratios. Hydrothermal alteration in epithermal systems can be considered in terms of interaction of (1) acidic fluids; (2) near-neutral chloride fluids; and (3) alkaline fluids (Fig. 2.13). The recognition of mineral assemblages is crucial in distinguishing low-sulphidation, high-sulphidation, intermediate sulphidation and alkalic types of epithermal systems.

In the lower temperature range ($< 180^{\circ}C$) the chief mineral phases related to acid-sulphate geothermal fluids are kaolinite, alunite, cristobalite, gypsum, opal, native S, quartz and sulphides. Pyrophyllite, diaspore and andalusite are stable at temperatures in excess of $250^{\circ}C$ and possibly even greater than $350^{\circ}C$, as in the case of andalusite. Barite, anhydrite and hydrated Fe oxides may also be present in the lower temperature range. These mineral phases constitute the advanced argillic alteration assemblage and a characteristic feature, easy to recognise in the field, is the so-called vuggy quartz, which is a silica residue resulting from extreme acid leaching (see example discussed in Chapter 5, Section 5.3.4). The advanced argillic alteration halo changes outward to illite, illite-smectite (Fig. 2.13). Above the groundwater table, steam-heated alteration, due to oxidation of H_2S, produces cristobalite, kaolinite and alunite, which are low temperature acid-stable minerals. These minerals generally form a zone of alteration above low-sulphidation systems but, importantly,

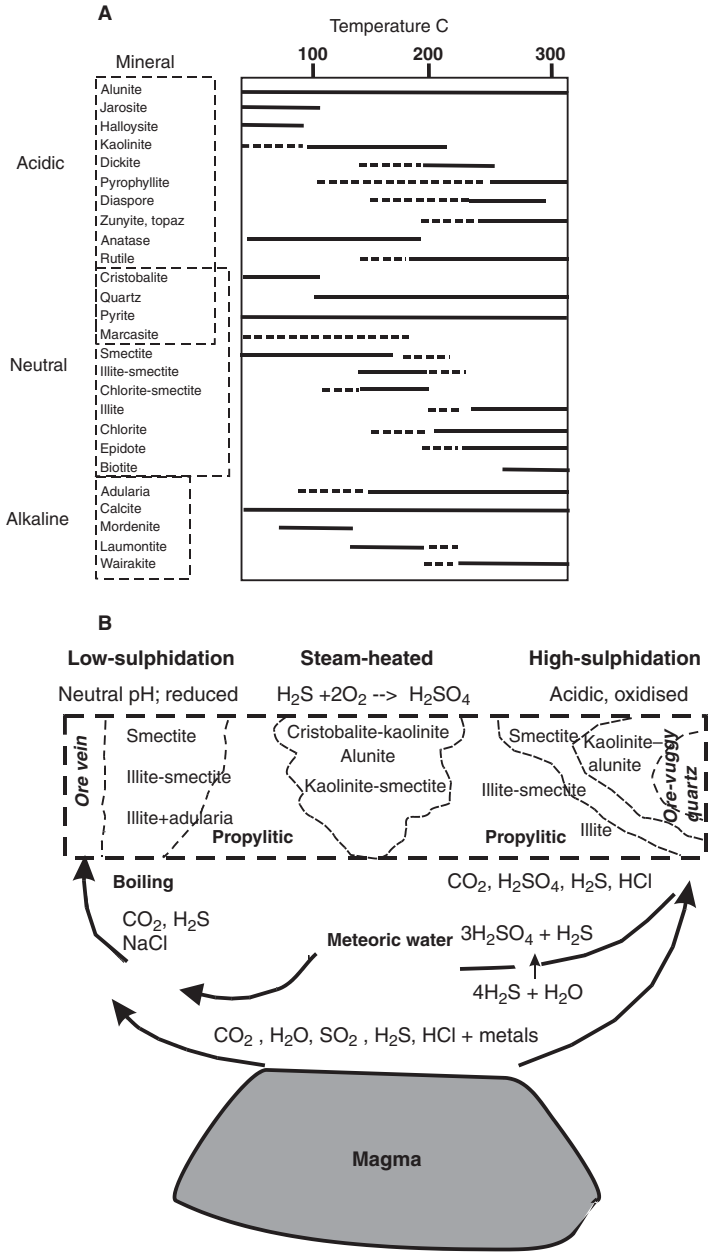


Fig. 2.13 (**A**) Temperature and pH range of hydrothermal mineral phases in epithermal systems; (**B**) Simplified scheme of the distribution of hydrothermal minerals in low- and high-sulphidation epithermal systems; steam-heated alteration can occur in both types, but it is especially common in low-sulphidation systems, where silica sinters develop where hot springs discharge. After Hedenquist et al. (1996)

they may extend downward along fractures and overprint the low-sulphidation system (White and Hedenquist 1995). In addition, erosion and collapse of the epithermal system may result in steam-heated alteration overprinting the ore (Hedenquist et al. 1996).

Common alteration assemblages related to deep chloride-rich and near-surface CO_2-rich geothermal fluids that interact with intermediate to felsic volcanic wall rocks are albite + adularia ± wairakite ± sericite ± epidote usually derived from plagioclase precursors. Biotites alter to chlorite ± sphene ± epidote, pyroxenes and amphiboles alter to mixtures of sericite + chlorite + sphene + quartz ± pyrite. Groundmass material may change to aggregates of quartz + sericite + calcite ± zeolites ± sulphides ± chlorite. Fracture and vein filling minerals include quartz, calcite, sericite, adularia, zeolites (laumontite, wairakite), chlorite, epidote and sulphides, such as pyrite and pyrrhotite. The detailed studies of active geothermal systems by Hedenquist (1986) and Hedenquist and Browne (1989) indicate that adularia and albite do not appear at depths where the temperature is less than 180°C, and that increasing alteration (e.g. increasing water/rock ratios) tends to produce a progression from unaltered plagioclase through albite to adularia. Sericite, white mica or hydromuscovite and quartz are common alteration products of both primary and hydrothermal feldspars, of groundmass material and of mafic phenocrysts. Hedenquist and Browne (1989) found that the K content of the sericites tends to increase with depth and temperature, thus approaching the composition of muscovite. Zeolites include species such as mordenite, laumontite and wairakite and are temperature-sensitive, as discussed later. Calcite, present especially in cavities and fractures, also occurs as fine to large blades (up to several centimetres), which in many instances are replaced by silica ("bladed silica"). This platy, or bladed, habit of calcite in epithermal systems is indicative of deposition from a boiling fluid. In alkaline systems, adularia and zeolite minerals (wairakite, mordenite, laumontite) become more relevant than in other systems (Fig. 2. 13). Laumontite has been found to predominantly occur in the outer zones of alkali epithermal systems, and can be considered as an important vector to the hotter parts of the systems and the ore (Chen et al. 2003).

2.8.1 Siliceous Precipitates, Self-Sealing and Hydrothermal Breccias

Precipitation and re-distribution of silica is one of the most common features of hydrothermal activity, as discussed in Section 2.1.1.1. The behaviour of silica in hydrothermal solutions was investigated in detail by Fournier (1989). In general the solubility in water of various forms of silica (amorphous silica, opal, cristobalite, chalcedony and quartz) increases with temperature in the range of 10 to 100 ppm for temperatures of < 50–100°C, and up to 1000 ppm above 300°C; thereafter, solubility of silica decreases. The silica of epithermal environments is largely derived

from alumino-silicate minerals, quartz and volcanic glass. Supersaturated silica solutions are facilitated by rapid cooling, such as that due to decompressional boiling, or by dissolution of siliceous rocks by acid solutions (Fournier 1989). Silica supersaturation promotes precipitation of amorphous (opaline) silica at temperatures of approximately 140°C, and near-neutral chloride-rich solutions generally deposit at the surface large quantities of amorphous silica, forming aprons of sinter material. Amorphous silica is unstable and with time forms chalcedony, or fine-grained quartz. Present-day sinters typically show finely banded or non-planar laminated structure (Fig. 2.14). Other small-scale structures perpendicular to the laminae may also be present. These have tubular or columnar shapes have been interpreted as having originated from the growth of bacterial stromatolites (Walter et al. 1972; Pentecost 2003; Bonny and Jones 2003). Clearly, then, the presence and recognition of sinter material are indicative of a paleosurface and therefore of a fossil geothermal system. Addition, or re-distribution, of silica in boiling zones, together with calcite and feldspar, may result in the development of an impermeable barrier or, as is commonly known, the system becomes self-sealed (Facca and Tonani 1967). An impermeable barrier created by self-sealing is considered to be a major cause of hydrothermal eruptions. This is achieved by a combination of the gradual build-up of volatile pressure and of seismic activity

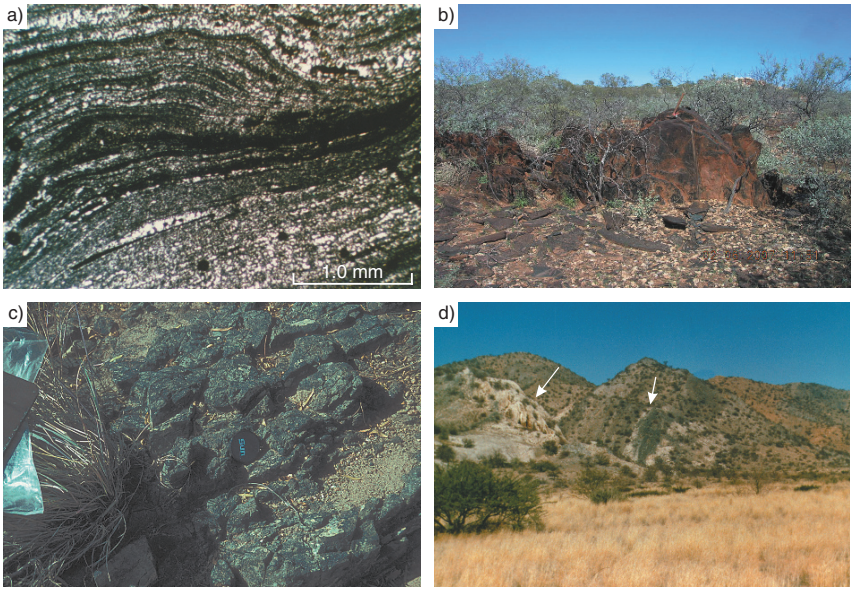


Fig. 2.14 (**a**) Photomicrograph of sinter material, Coromandel Volcanic Zone, New Zealand; (**b**) pervasive tourmalinisation of metasedimentary rocks in the Gascoyne Complex, Western Australia; (**c**) pervasive hematitic alteration of re-worked conglomerate, both pebbles and matrix are hematitised or hematitic from Vergenoeg F-Fe pipe deposit, South Africa); (**d**) dolomitisation of marble units of the Karibib Formation, Namibia, near the Navachab Au skarn deposit (Chapter 6)

which induces rupturing of the sealed zone, resulting in sudden decompression and subsequent eruption. Many breccia pipes are thought to form in this way. Hydrothermal fracturing is a manifestation of the same phenomenon at greater depths, where fractures form as a result of the decompression of high fluid pressure when this exceeds the confining pressure by an amount equal to the tensile strength of the rock (see Chapter 9). Hedenquist and Henley (1985), who have studied in some detail the origin of hydrothermal eruptions and their relationship to deposition of minerals and precious metals, did not favour large-scale self-sealing in a geothermal field, but rather envisaged localised sealing. This would result in the diversion of the fluid flow through fractures, kept open by tectonic activity, either within or laterally to the zone of sealing. These authors, however, contended that local sealing can produce eruptions in a sequence which they subdivide into a pre-eruption phase, a crater-formation phase and a post-eruption phase. In the first of these three phases the hot geothermal fluid cools and depressurises as it rises towards the surface, until at a given temperature and pressure it boils. Silica is deposited as quartz below approximately 100 m and as chalcedony above this depth. During boiling, volatiles such as CO_2 and H_2S partition into the vapour phase. CO_2 (and H_2S) loss leads to a pH increase in the residual fluids which causes precipitation of calcite. There is discussion on boiling in Chapter 1. Thus, the precipitation of quartz, calcite and other phases (e.g. adularia), results in decreasing permeability in the upper sectors of the system, although as mentioned previously, continuing tectonic activity keeps channels open for most of the time. Nevertheless when localised sealing occurs, exsolved gases accumulate below the seal until the total pressure exceeds the lithostatic pressure plus tensile strength of the rocks inducing hydraulic fracturing. This can rapidly expand and propagate upward, eventually triggering an eruption. The hydrothermal conduit and crater become a locus for the deposition of precious metals, even in the aftermath of the eruption, and an ore deposit, spatially and temporally associated with hydrothermal breccias, may thus form.

2.9 Hydrothermal Alteration in Submarine Mineral Systems

Hydrothermal alteration of seafloor mineral systems is generally characterised by intense K and Mg metasomatism, which results in alteration assemblages dominated by chlorite, quartz and sericite. Silicification and zones of clay alteration are also prominent and may grade away from the mineralisation into regional greenschist metamorphic assemblages. In this section, I focus on hydrothermal alteration of Kuroko-type mineral systems, as representative examples of the volcanogenic massive sulphide class (VMS) and the hydrothermal metamorphism of seafloor (oceanic crust) around hydrothermal vents (smokers). As in the preceding sections, here too the aim is to provide the reader with a "road map" for the assessment of the spatial-temporal distribution of alteration assemblages in order to establish genetic models and exploration guidelines.

2.9.1 Hydrothermal Alteration in Kuroko-Type Mineral Systems

Shirozu (1974) distinguished four main zones of alteration which, from the margins towards the core of the mineralisation, are: zone I, characterised by the assemblage montomorillonite + zeolite + cristobalite; zone II, consists of sericite + sericite-montmorillonite + Fe-Mg chlorite + albite + K-feldspar + quartz; zone III is characterised by clay alteration within and around the mineralisation, and contains sericite + interstratified montomorillonite + sericite + Mg-chlorite and quartz; zone IV, surrounds the central part of the mineralised body and it displays strong silicification, with quartz + sericite + Mg-rich chlorite. This simplified spatial disposition of zones I to IV around the massive sulphides, shown in Fig. 2.15, can be useful in a first-pass appraisal of a Kuroko-type ore system.

Pisutha-Arnond and Ohmoto (1983) proposed a time-space model of hydrothermal alteration, as discussed herein. From the margins towards the core of the mineralisation, alteration zones and mineral assemblages consist of: (a) a zeolite zone with Mg-Na montmorillonite, clinoptilolite, mordenite, saponite and crystobalite; (b) a zeolite zone with first appearance of analcime, calcite, illite, and quartz; (c) a Mg-Ca montmorillonite zone; (d) a transitional mixed-layer illite-montmorillonite zone; and (e) a zone of sericite and Mg-rich chlorite. The two zeolite zones (a and b) are interpreted to be the product of diagenesis, with zone (a) changing to zone (b) at deeper stratigraphic levels. The early diagenetic stages are primarily due to pore sea water reacting with the glass component of the volcanic rocks, resulting, according to Pisutha-Arnond and Ohmoto (1983), in a substantial increase of total dissolved salts in the fluids. Following this diagenetic stage and with the onset of hydrothermal activity, the zeolite zone assemblages change laterally towards the core zone (e.g. towards

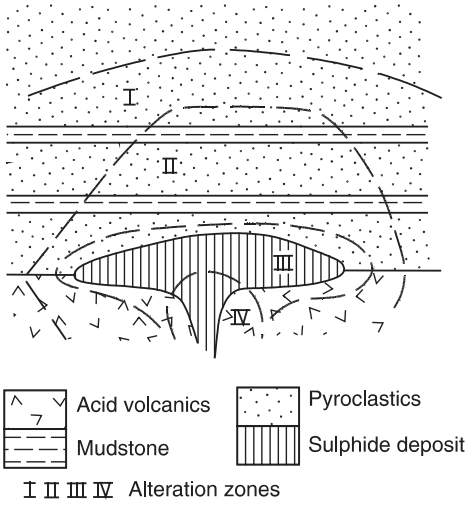


Fig. 2.15 Alteration zones associated with a kuroko massive sulphide deposit. Explanation of zones (I to IV) are given in the text (After Shirozu 1974)

the main central conduit and massive sulphides), to the assemblages outlined in (c), (d) and (e). The spatial arrangement (a) to (e) also reflects a time sequence, with assemblage (a) being the earliest and (e) the latest at a given point. These mineralogical characteristics, together with the related chemical changes, are the result of heated sea water-rock interactions. Hydration and cation exchange reactions typify the alteration zones, and the stability relations between alteration minerals are largely a function of pH, temperature and the activities of the cations involved (e.g. Mg, Ca and Na). Cation exchanges between smectite and fluids result in the increase of Ca and decrease of K and Mg in the pore fluids. The Ca gained by the fluids is then used to form sulphates and carbonates. In the late diagenetic to early hydrothermal stages and with increasing temperature, the organic matter present in the marine sediments may release CO_2 which further enhances the formation of carbonate.

As the hydrothermal system becomes more active, high temperature fluids ascend through fractures towards the discharge zone, reacting with the zeolite minerals present, to form the mineral assemblages of the Mg-Ca montmorillonite zone. This process results in a halo of Na depletion around the deposits. With further increase of the temperature ($> 250^{\circ}C$) of the fluids, Ca-montmorillonite becomes unstable and is replaced by expandable mixed-layer clays, montmorillonite, illite and sericite. At this point sulphide minerals are precipitated on the seafloor. They are the black ore (kuroko in Japanese), consisting predominantly of sphalerite and galena, with minor quantities of tetrahedrite, barite and chalcopyrite. As the temperature reaches approximately $300^{\circ}C$, with the introduction of hotter fluids, all of the montmorillonite and most of the plagioclase are converted to sericite and sericite + chlorite. The fluids of this stage are Cu-rich and therefore the dominant sulphide becomes chalcopyrite, or yellow ore (oko in Japanese). Chalcopyrite replaces the earlier sulphides in the lower parts of the sulphide deposit. The ingress of fluids with temperatures in excess of $300^{\circ}C$ results in the deposition of pyrite, which dissolves the earlier chalcopyrite and forms the pyrite-rich lowermost portion of the massive sulphide deposit. As the fluids become cooler, precipitation of ferruginous cherts and barite takes place at the top of the massive sulphide deposit. The distribution of the alteration-mineralisation zones is therefore clearly related to a time-space continuum of fluid discharge, and the mineralogical and metal zoning is generally well defined for most Kuroko systems, although it must be realised that not all of the zones described are necessarily present in a given deposit. This may be further complicated in systems where more than one episode of mineralisation has taken place.

2.9.2 Oceanic Crust Hydrothermal Metamorphism

Hydrothermal activity in sub-sea-floor environments involves the penetration of sea water through fractures in the oceanic crust. This water becomes heated,

producing a series of reactions, involving mostly hydrolytic alteration, which causes the fluids to become progressively reduced and enriched in metals removed from the rocks. These metals pass into the solution generally as chloride complexes. The permeability of the oceanic crust facilitates penetration of the sea water over vast areas, so that apart from the actual mineralising system low intensity reactions (especially hydration) result in prograde ocean floor metamorphism, ranging from zeolite to greenschist facies assemblages containing chlorite, smectite, actinolite, serpentine etc. The metalliferous fluids are then discharged on the seafloor by hot springs through fractures and vents. In this way disseminated and massive sulphide bodies are formed within the fractured oceanic crust rocks, where one set of reactions occurs, and at, or close to, the sea water-rock interface where another set of reactions take place, depositing in addition to sulphides, Fe and Mn oxides in response to contact of the hydrothermal fluids with cold and oxygenated sea water.

A scheme of hydrothermal reactions in a sub-sea-floor environment and their products is illustrated in Fig. 2.16, taken from Edmond and von Damm (1983). In this figure, sea water containing the ions indicated at point 1, penetrates the oceanic crust to form sulphate ($CaSO_4$, point 2). At point 3, several kilometres under the seafloor, reactions occur with the hot mafic rocks. These involve addition of Mg to the mafic rocks, and hydration to form serpentine minerals. In the course of these reactions H^+ is produced, and hydrogen ion metasomatism of the basaltic rocks now takes place, in which H^+ displaces the cations (Fe^{2+}, Mn^{2+}, Cu^{2+}, Zn^{2+} etc.) from the Fe-Mg and alumino-silicate rock-forming minerals, which consequently change to chlorite, clay-type minerals and zeolites. The sea water, in the scheme of Edmond and von Damm, is initially an oxygenated electrolyte solution containing the anions Cl^-,Br^-, CO_3^{2-}, SO_4^{2-}. During descent, this water becomes more and more reduced and reacts with the rock-forming silicates. A typical reaction is:

$$\underset{\text{fayalite}}{11Fe_2SiO_4} + 2SO_4^{2-} + 4H^+ \rightarrow \underset{\text{magnetite}}{7Fe_3O_4} + \underset{\text{pyrite}}{FeS_2} + 11SiO_2 + 2H_2O;$$

Other reactions between H^+ ions, SO_4^{2-} ions and Fe-silicates produce pyrite and magnetite (point 4), and a solution is subsequently developed that is hot, acidic and contains metals (point 5). The solution thus formed rises towards the seafloor where it encounters cold and oxigenated sea water, and precipitation of sulphides and sulphates occurs with the formation of the so-called chimneys (point 7). Some of the Fe-sulphide is carried upwards as a "black smoke", whereas Mn^{2+} and more Fe^{2+} remain in solution to become oxidised and to precipitate laterally away from the smoker's vent, eventually forming metalliferous sediments (Chapter 8).

Exposure of the basaltic rocks to cold sea water results in their oxidation and the subsequent production of zeolites. Zeolite facies rocks occur at the margins of the ocean ridges where hydrothermal processes take place at temperatures of less than 200°C. In the upper parts of the oceanic crust there are extreme

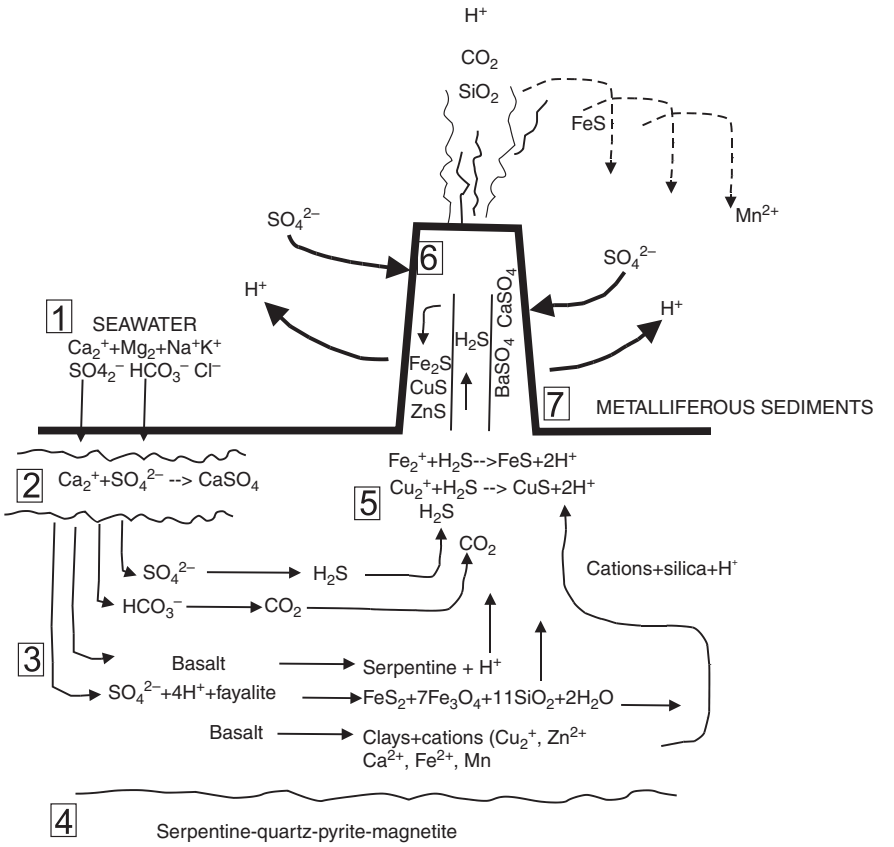


Fig. 2.16 Reactions at a spreading centre. See text for detailed explanation. After Edmond and von Damm (1983)

variations in hydrothermal alteration at and near the hydrothermal vents and distally from these vents, both in the horizontal and vertical sense. Greenschist facies assemblages are generally confined to the axial regions of spreding centres where the temperature of hydrothermal processes is in excess of 200°C and can reach up to 400°C. Greenschist facies mineral assemblages (albite, chlorite, epidote, calcite, prehnite, quartz, titanite) are also present in the deeper section of oceanic crust and in the sheeted dykes (layer 2) where temperature increases and water/rock ratio decreases.

Experimental studies on basalt-sea-water interaction, conducted using a range of temperatures and water to rock ratios, corroborate that substantial mass transfer occurs. This is characterised by cation fixation and hydrolysis reactions which increase in intensity with increasing temperature and water/rock ratios

(Mottl 1983; Rosenbauer and Bischoff 1983; Seyfried and Janecky 1985). Transfer of Mg, SO_4^{2-}, Na and Cl occurs from sea water to oceanic crust, whereas leaching and mass transfer of Li, K, Rb, Ca, Ba, Cu, Fe, Mn, Zn and Si takes place from the oceanic crust to the fluids (Rona 1984). One of the most important aspects of basalt-sea-water interaction is the removal of Mg^{2+} from sea water, after which this cation becomes included in mineral phases such as smectite, chlorite and tremolite-actinolite. The transfer of Mg^{2+} takes place as $Mg(OH)_2$, and after its reaction with the rock-forming silicates, H^+ is liberated and enters the fluid, increasing its acidity (pH decreases). This, in turn, produces further changes, during which the H^+ exchanges for cations, such as Ca and K, releasing them into the hydrothermal fluid (see above for more details of H^+ metasomatism). In addition to Mg^{2+}, Na^+ is also removed from sea water, generally at temperatures less than 300°C and water/rock ratios of between 5 and 10 (Mottl 1983). The transfer of Na^+ to the fluid is largely responsible for the formation of analcime and albite. Removal of Mg^{2+} and Na^+ is counterbalanced by the leaching of Ca^{2+} from the basalt. At temperatures greater than 150°C, K^+ and SiO_2 are leached from the mafic rocks. Experimental evidence indicates that SiO_2 exceeds quartz saturation at temperatures from 150 to 500°C, causing precipitation of quartz. Some typical metasomatic reactions that take place during the hydrothermal metamorphism of basaltic rocks, produce talc, epidote minerals and albite, as shown below (Seyfried et al. 1988):

Mg metasomatism:

$$3Mg^{2+} + 4SiO_2 + 4H_2O \rightarrow \underset{\text{talc}}{Mg_3Si_4O10(OH)_2} + 6H^+$$

Ca metasomatism:

$$\underset{\text{anorthite}}{3CaAl_2Si_2O_8} + Ca^{2+} + 2H_2O \rightarrow \underset{\text{clinozoisite}}{Ca_2Al_3Si_3O_{12}(OH)} + 2H^+$$

Na metasomatism:

$$2Na^+ + 4SiO_2 + CaAl_2Si_2O_8 \rightarrow \underset{\text{albite}}{2NaAlSi_3O_8} + Ca^{2+}$$

The changes in the oceanic mafic rocks are dominated in cation exchange of Ca for Na resulting in albite-rich rocks, epidosite and quartz-epidote-chlorite assemblages. Other mineral reactions in sea-floor rocks are discussed in Chapter 7 and shown in Fig. 2.16. Metamorphosed mafic rocks derived from hydrothermal metamorphism were known as "spilites" a term which is still in use, and refers to rocks showing a basaltic texture in which a greenschist mineralogy is developed by secondary processes (Coleman 1977). Spilitic lavas consist of sodic plagioclase, augite or its altered products (actinolite, chlorite-epidote) and titanite. The classic spilites of the old literature were often cited together with rocks of sodic rhyolitic composition, known as keratophyres. These terms are somewhat obsolete, but are still widely used in non-English literature.

As stated above, hydrothermal metamorphism is related to the convective circulation of heated sea water, the effects of which increase progressively downward in the crust and as such can be considered as a form of prograde thermal metamorphism, distinct from the dynamo-metamorphic effects which take place during the tectonic emplacement of the oceanic crust onto a continental margin. This is an important facet that must be kept in mind when examining ophiolitic sequences. The products of hydrothermal metamorphism of oceanic crust, from layer 2 (pillow lavas) to the upper portions of layer 3 (gabbro), range from zeolite to greenschist to epidote-amphibolite facies. Oxygen isotope systematics from the Semail ophiolite complex (Arabia) indicates that only small amounts of sea water reach the base of layer 3, where the fluids reach a temperature of about 400°C and about 400 bar pressure (Taylor 1983; Seyfried et al. 1988). According to the findings of Taylor (1983) in the Semail ophiolitic rocks, a general depletion in $\delta^{18}O$ values is noted with depth. Large variations of $\delta^{18}O$ are observed from their magmatic value of + 5.7‰, to values in excess of + 12‰ near the base of the section. These variations are interpreted as due to a wide range of water/rock ratios and therefore hydrothermal metamorphism of the rocks. The distribution of the metamorphic minerals with depth and increasing temperature is shown in Fig. 2.17.

Characteristically, oceanic crust rocks tend to preserve their original igneous textures after being altered. Considering a primary mineral assemblage of the

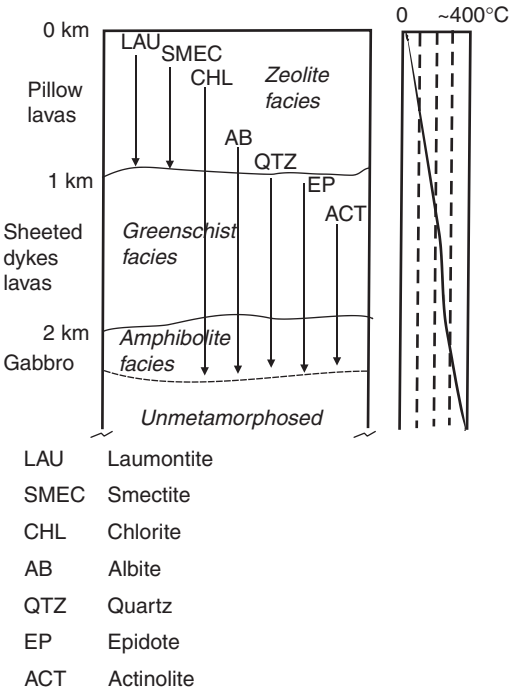


Fig. 2.17 Mineral species that characterise the hydrothermal metamorphism in oceanic crust rocks as a function of depth and temperature; after Coleman (1977 and references therein)

mafic rocks represented by glass-olivine-clinopyroxene-plagioclase, the changes that occur during hydrothermal metamorphism were determined by Kawahata and Furuta (1985) for oceanic rocks at the Galapagos spreading centre. They distinguished three zones of metamorphism as a function of depth and temperature. The mineralogy of these zones is described below. Glassy material is replaced by smectite in zone 1 (surface to a depth of about 900 m), and by chlorite with minor actinolite, serpentine and talc in zones 2 and 3 (900–1100 and 1100–1350 m respectively). Olivine is replaced by saponite in zone 1, and by chlorite in zone 2, while serpentine and talc are present in zone 3. Clinopyroxene remains as a relic in zone 1, but is replaced by actinolite and chlorite in zones 2 and 3. Plagioclase relics persist throughout zone 1 and are replaced by chlorite, albite and quartz in zones 2 and 3. Abundant vein material is also formed, especially in zones 2 and 3, and includes smectite, chlorite, Ca-zeolites, quartz and chlorite. By comparison, the metamorphic mineral assemblages as determined in a sequence of ophiolitic rocks from Liguria, Italy, allow us to see deeper into the crust (probably bottom of layer 2 and top of layer 3). They include (Spooner and Fyfe 1973): (a) albite + smectite + hematite + calcite + sphene ± chlorite; (b) albite + chlorite + pumpellyite + hematite + calcite + titanite ± smectite; (c) albite + chlorite + pumpellyite + sphene ñ hematite ± calcite; (d) albite + epidote + pumpellyite + actinolite + chlorite + titanite ± hematite ± calcite; (e) albite + epidote + pumpellyite + actinolite + hornblende + chlorite + magnetite + titanite ± calcite. Assemblages (a) to (d) refer mainly to layer 2, whereas assemblage (e) refers to the lower parts of layer 2 and upper portions of layer 3. Studies of ophiolites also indicate that epidote-rich zones (epidosites) may form at the base of the sheeted dyke complex and near the presumed top of the magma chambers (Seyfried et al. 1988 and references therein). These epidote-rich rocks also contain quartz and chlorite and are characterised by the complete obliteration of the igneous textures. The above authors considered that epidosites represent the fossilised residue of a reaction zone, permeated by hot and ascending hydrothermal fluids with high water/rock ratios.

The Salton Sea geothermal field in the Gulf of California is a present-day case of hydrothermal metamorphism (see Chapter 5 for more details). In this field geothermal recrystallisation produced a succession of minerals from the appearance of (1) epidote at 600 m and 234°C; (2) the appearance of biotite at 1135 m and 325°C; (3) to the appearance of andradite garnet at 2120 m and 360°C (Kornprobst 2002).

2.10 Other Types of Alteration

In the following I describe other types of hydrothermal alteration that are commonly encountered in several types of hydrothermal systems, namely: tourmalinisation, serpentinisation and talc-carbonate alteration, hematitisation and Fe alteration, dolomitisation and carbonitisation.

2.10.1 Tourmalinisation

Tourmaline is a complex B-bearing mineral with the general formula $XY_3Z_6B_3Si_6O_{27}(O,OH,F)_4$, where the X site may be taken by Ca or Na, the Y site by Mg and/or Fe^{2+}, (Al + Li) or Fe^{3+}, whereas Al^{3+}, Fe^{3+} or Cr may occupy the Z site (Dietrich 1985). The three end-members of the Mg-Li-Fe tourmaline solid solution series are schorl (Fe-rich), elbaite (Al, Li-rich) and dravite (Mg-rich). The composition of tourmalines may be indicative of the environment in which they originated. For example, the Fe/Mg ratio tends to decrease with increasing distance from a granitic source (Pirajno and Smithies 1992). In general, Fe-rich tourmalines are associated with Sn-W deposits of greisen affinity, whereas Mg-rich tourmalines are found with massive sulphide deposits and stratabound W deposits. Tourmalinite is the name given to rocks containing in excess of 15% tourmaline, and can be associated with exhalative ore deposits in rift settings (Plimer 1987). A detailed account of tourmaline, its association with and relationship to hydrothermal mineral systems can be found in Slack (1996).

Pervasive to selectively pervasive tourmalinisation usually occurs associated with Sn-W deposits and breccia pipes. In many cases the country rocks surrounding greisenised granite cupolas have disseminated tourmaline, which tends to be particularly abundant in zones of fracturing. Quartz-tourmaline-dominated assemblages form pervasive replacements as well as cross-cutting veins and veinlets. The replacements can be on a very fine scale, so that the smallest features and textures are perfectly preserved. This type of tourmaline alteration is linked to the emplacement and crystallisation of B-rich granitic magmas, with the possibility that the B-enrichment may have been inherited in a source region containing evaporites or tourmaline-rich protoliths. Tourmaline breccia pipes may also be associated with the crystallisation of geochemically specialised granitic magmas, and they result from high volatile pressure exceeding the lithostatic load. At the Krantzgerg W deposit in Namibia, tourmalinisation of the country rocks, hydraulic fractures infilled by tourmaline and breccia pipes are common (Chapter 4). These features are related to the emplacement of the B-rich Erongo granite, a peraluminous anorogenic granite (Pirajno and Schlögl 1987). Tourmaline breccia pipes occur associated with porphyry copper deposits, vein type Sn deposits, and as small polymetallic pipes containing W, Cu, Bi, As and Au. Fluid inclusion data indicate that they form at depths ranging from between 1 and 3 km and at temperatures in excess of 300°C from highly saline fluids (Kirwin 1985). At Rooiberg, Transvaal (South Africa; Chapter 4) highly mineralised Sn-bearing orbicular pockets occur in sedimentary slabs engulfed in the granitoids of the felsic phase of the Bushveld Complex. These pockets contain abundant tourmaline and carbonate minerals, replacing quartz and plagioclase of the host sedimentary rock.

Stratiform tourmalinites are widespread in Proterozoic and Paleozoic sedimentary sequences associated with sediment-hosted massive sulphide deposits, as for example at Sullivan in British Columbia, where a fine-grained

quartz-tourmaline rock underlies the ore deposit. Tourmalinites are also present in the Broken Hill areas (Australia), and in Namaqualand (South Africa) (Slack et al. 1984; Plimer 1987). These tourmaline-rich rocks are thought to be the result of submarine exhalations in rift environments, and are therefore neither epigenetic nor of the replacement type. Although this is invariably the case for many of these occurrences, the reader is cautioned against the interpretation of tourmaline-rich rocks, as fine-scale replacements can be deceptive and lead to erroneous conclusions.

Extensive tourmalinisation can be found in the previously mentioned Gascoyne Complex in Western Australia, where tourmaline-replaced granitic and metasedimentary rocks are spatially associated with 1.0 Ga granitic intrusions and pegmatites (Fig. 2.14; Sheppard et al. 2007).

2.10.2 Serpentinisation and Talc-Carbonate Alteration

Serpentinisation and talc-carbonate are the most common type of alteration of ultramafic rocks. Serpentine minerals (antigorite, chrysotile and lizardite) are formed from olivine and pyroxene by introduction of copious amounts of H_2O and CO_2 with an exothermic reaction. A typical example is the conversion of olivine to serpentine, according to:

$$\underset{\text{olivine}}{2Mg_2SiO_4} + H_2O + 2H^+ \rightarrow \underset{\text{serpentine}}{Mg_3Si_2O_5(OH)_4} + Mg^{2+}.$$

Serpentinisation usually is pervasive and may affect entire rock masses. The temperatures of serpentinisation processes range from as low as $<100^{\circ}C$ for lizardite, to as high as $500^{\circ}C$ for antigorite. Commonly, pseudomorphs of serpentine after olivine and pyroxene can be easily recognised because they tend to retain the shape of the original crystals.Ultramafic rocks at spreading centres undergo serpentinisation as a result of penetration and reaction with sea water. The widespread and regional scale of this phenomenon is such that serpentinisation can be considered to be a regional metamorphic process. Tectonic transport of mafic-ultramafic complexes from spreading ridges to continental margins results in high deformation and pressure-related metamorphic processes and the emplacement of ophiolite sequences (Chapter 7). The serpentinites of ophiolitic rocks contain the assemblage of lizardite + chrysotile + brucite ± magnetite. The latter is a common by-product of serpentinisation and is due to expulsion and oxidation of Fe from the silicate lattice. Serpentinite is extremely ductile and is easily transported during tectonic movements. Serpentinisation of ultramafic rocks is also common in Archaean greenstone belts, in which serpentine minerals replace olivine in dunite and komatiites (e.g. Ni-Cu Marriot deposit in the Yilgarn Craton; Pirajno unpublished data). Other important by-products of serpentinisation are metasomatic processes such as albitisation, and the formation of peculiar rocks known as rodingites. Rodingites occur as

dykes commonly found in the Dun Mountain ophiolite belt in New Zealand (the name derives from the Roding river near the town of Nelson, New Zealand). Rodingites consist of calc-silicate assemblages (garnet, clinopyroxene, tremolite-actinolite, epidote) and together with albitites may occur along contacts between serpentinites and country rocks (Carmichael et al. 1974). In some cases rodingite and carbonated serpentinites may be associated with Au, Ag and Co mineralisation (Leblanc and Lbouabi 1988).

During serpentinisation, reduction of water by oxidation of Fe^{2+} will produce H_2 and magnetite:

$$3FeO + H_2O \rightarrow Fe_3O_4 + H_2$$

and the H_2 may combine with carbon to produce CH_4 and perhaps other hydrocarbons, although some authors argue that much or part of the CH_4 may derive from mantle outgassing. This is the conclusion reached by Proskurowski et al. (2008), who using carbon isotope analyses of hydrocarbons emitted in fluids venting at Lost City (see Chapter 7), suggested abiotic synthesis of hydrocarbons in the presence of ultramafic rocks, seawater and heat. Palandri and Reed (2004) gave details of experimental simulations at temperatures ranging from 25 to 300°C and pressures of 0 to 100 bar for the formation of serpentinite and rodingite. These author simulated reactions of mafic rocks (basalt or gabbro) with hyperalkaline Ca- and Al-rich fluids at 300°C to produce assemblages typical of rodingite (grossular, clinozoisite, vesuvinaite, chlorite and diopside).

Hydrothermal talc is known to be deposited on the seafloor of the Gulf of California, where it is associated with smectite clays and sulphides. Talc is also present in the Red Sea metalliferous sediments. Talc + carbonate ± magnetite assemblages of replacement-alteration origin are commonly found in hydrothermal mineral deposits of Archaean greenstone belts. An outstanding example is provided by the Sb-Au mineralisation in the Murchison greenstone belt in South Africa (Antimony line). Here, the Sb-Au mineralisation is associated with massive and widespread structurally controlled talc-chlorite-carbonate alteration (Pearton and Viljoen 1986) The talc-chlorite-carbonate alteration is thought to have originated from metamorphic fluids that were channelled along major structural breaks resulting in the replacement and alteration of the host metavolcanic and metasedimentary rocks.

Introduction of vast quantities of H_2O and CO_2 into major structural breaks (shear zones) is possibly a major cause of the widespread regional-scale alteration in Archaean settings. Along these structural breaks every stage of replacement and alteration by sericitisation, albitisation, steatitisation (talc) and carbonate (dolomite, ankerite, magnesite) is observed, together with local concentration of pyrite, arsenopyrite and gold. Talc-carbonate and talc-chlorite alteration processes are therefore due to introduction of H_2O and CO_2. Reactions leading to talc-carbonate alteration are:

$$\underset{\text{tremolite}}{} + 4CO_2 = 2\underset{}{\text{dolomite}} + \underset{\text{talc}}{H_2Mg_3Si_4O_{12}} + 4SiO_2,$$

Talc and dolomite may also form directly from serpentinite:

$$2\text{serpentine} + 1.23CaO + 2.46CO_2 = \text{talc} + 1.23\text{dolomite} + 1.77MgO + 3H_2O;$$
$$2\text{serpentine} + 3CO_2 = \text{talc} + 3\text{magnesite} + 3H_2O$$

Anther example of Archaean talc-carbonate-chlorite alteration-mineralisation include the Epoch Ni deposit in Zimbabwe, where sulphide mineralisation is contained in talc-carbonate and talc-chlorite rocks derived from the alteration of serpentinite and dunite (Pirajno, unpubl. data). The talc-carbonate assemblage includes talc, chlorite, magnesite and dolomite. Talc is by far the most abundant mineral phase.

2.10.3 Hematitisation and Fe-Rich Alteration

Hematite, Fe-carbonates (ankerite, siderite), Fe-rich chlorite and Fe-rich amphiboles can be dominant alteration products in a number of important ore deposit types. Hematite impregnations, disseminations and veinlets are associated with the late stages of hydrothermal activity in Sn-W greisen-affiliated mineralising systems. Hematite and chlorite are important gangue and alteration minerals in Iron Oxide Copper Gold ore systems (IOCG), such as the giant Roxby Down (Olympic Dam) deposit in South Australia (Chapter 4). Particularly interesting is the association Fe-F, (actinolite-fluorite; siderite-magnetite-quartz-fluorite-sulphides), forming unusual mineralising systems related to the felsic phase of the Bushveld Complex (South Africa). These mineral deposits are interpreted as distal products of Bushveld granite-related hydrothermal systems. The Vergenoeg hematite and fluorite deposit (Chapter 4) is an outstanding example of Fe and F metasomatism on a large scale. The Fe-rich lithologies and mineralisation at Vergenoeg and other localities nearby appear to be the product of a combination of plutonic, volcanic exhalative and metasomatic activities, whose nature is not clearly understood. At any rate, the large and regional scale Fe enrichments observed in these areas (Fig. 2.14) have led Crocker (1985) to consider a general trend of Fe-Ca-F-CO_2 enrichment, perhaps initially due to immiscibility of magmatic fractions. Exsolution and degassing of HF may have been the leading factor responsible for the massive Fe-F alteration in the region. As HF passes through formerly Fe-rich lithologies (e.g. mafic rocks of the Bushveld Complex), it would leach out Ca and Fe to form fluorite, chlorite, Fe-actinolite and hematite in the uppermost sectors of the system. By pressure loss Fe-actinolite plus HF, CO_2, and O_2 would form magnetite, siderite and fluorite. One of the possible reactions proposed by Crocker (1985) is:

$$\underset{\text{ferroactinolite}}{4Ca_2Fe_5Si_8O_{22}(OH)} + 16HF + 6O_2 \rightarrow 8\text{fluorite} + 10\text{hematite} + 32\text{quartz} + 10H_2O$$

Hematite and chlorite alteration is associated with unconformity-type uranium deposits. This alteration may be accompanied by clay, dolomitisation, silicification and even ourmalinisation. At the Rabbit Lake deposit in Canada (Nash et al. 1981), alteration is characterised by chloritisation (Fe-rich) of mafic minerals, followed by Mg and B-metasomatism, silicification and hematitisation. In the Alligator uranium fields in the Northern Territory (Australia), zones of massive chlorite, quartz and hematite, which are fault-controlled, occur associated with the mineralisation (Chapter 13).

In the Brandberg areas (Damara Orogen, Namibia) Sn-W vein deposits are locally associated with extensive tourmaline, sericite and hematite alteration. The latter appears to be related to the final stages of the hydrothermal activity. Ferruginisation (mainly siderite) of marble units intercalated with the metapelites hosting the vein mineralisation is also a conspicuous feature (Pirajno and Jacob 1987). Fe-carbonate alteration is commonly found in the wallrocks of the orogenic Au vein deposits. Porphyroblast-like growths of siderite and ankerite give the wallrocks a spotted appearance. Fe-carbonate alteration and chloritisation are also common in gold deposits of Archaean age.

2.10.4 Carbonatisation and Dolomitisation

Carbonate alteration of both Ca-rich and silicate rocks involves two basic processes: dolomitisation and carbonatisation. The former is a very common type of alteration of limestones in which cation metasomatism and base exchange take place, in which Mg^{2+} substitutes for Ca^{2+}, and $CaCO_3$ becomes $CaMg(CO_3)_2$. From the mineralisation point of view, it is important to realise that dolomitisation reactions involve loss of volume (between 6 and 13%, Morrow 1982a), which enhances the porosity of the rock and hence makes it more receptive to the mineralising fluids. There are several models that attempt to explain dolomitisation and, while it is beyond the scope of this section to provide a detailed review (see e.g. Morrow 1982a,b; Hardie 1987), these include one theory, which considers that dolomite is an evaporite mineral, and that dolomites are therefore formed by the action of hypersaline brines with high Ca/Mg ratios. In evaporitic environments algae may influence this process, during which dolomite replaces calcite and other evaporite minerals. The mixed waters (known as "dorag", Persian for mixed blood) model envisages dolomite being formed by mixing of fresh water with sea water. A third possibility is dolomitisation by burial diagenesis, during which migration of Mg-rich brines and mixing with near-surface brines would take place. A critical appraisal of these theories reveals that none are completely satisfactory (Hardie 1987), but it is nevertheless clear that dolomitisation has an important association with many types of hydrothermal mineral deposits. Dolomitisation is commonly associated with the low temperature Mississippi Valley-type Pb-Zn deposits, where this type of alteration seems to have preceded and perhaps favoured the

deposition of sulphide minerals (Evans 1987). Large-scale dolomitisation of marble units of the Karibib formation, Damara sequence, may be related to Au mineralisation in the Central Zone of the Damara orogen in Namibia (Fig. 2.14). Although the origin of this very extensive dolomitisation remain uncertain, it may be related to release of CO_2 during metamorphism. Reaction of CO_2 with impure marbles containing actinolite-tremolite minerals, in turn due to high temperature prograde metamorphism, could have produced the dolomite:

$$3\text{calcite} + \text{tremolite-actinolite} + 7CO_2 = 5\text{dolomite} + 8SiO_2 + H_2O.$$

The above reaction is deduced from the mineral associations and relationships present in the dolomitised rocks (Pirajno and Jacob 1987). The relationship of this alteration to Au mineralisation is discussed in Chapter 6. At Mt.Isa (Australia), bodies of silica-dolomite are associated with Cu-Pb-Zn mineralisation, although it seems that this rock is the recrystallised product of siliceous dolomites (Chapter 8). Mineral deposits of Mississippi Valley affiliation in the carbonate platform zone of the Damara orogen (Namibia), such as Tsumeb and Kombat, have spatial relationships with fracture-controlled calcitisation of dolomite, locally accompanied by hematite alteration and silicification (Chapter 8). These alteration features are used as exploration criteria. Carbonate alteration of silicate rocks, in contrast to dolomitisation, occurs by anion metasomatism with introduction of CO_2. Carbonitisation of mafic rocks is a common type of alteration in the mafic rocks of the Archaean greenstone belts, where orogenic auriferous quartz veins are present. An outstanding, large-scale carbonate (and Fe), alteration of this type is that of the Golden Mile dolerite in the Kalgoorlie district of Western Australia (Chapter 9; Phillips 1986). The hydrothermal alteration of the lithologies of the Golden Mile is divided by Phillips (1986) into three main zones: (1) chlorite zone (chlorite + calcite + ankerite); (2) carbonate zone (ankerite + siderite); (3) pyrite zone (ankerite + muscovite + quartz + albite + pyrite and gold). This alteration is thought to be due to syn- to post-metamorphic H_2O-CO_2-rich fluids of low salinity (<2 wt% NaCl equivalent), at temperatures of between 350 and 400°C, and pressures of 0.8–2 kbar (Phillips 1986). The Golden Mile alteration-mineralisation is examined in Chapter 9.

2.11 Metamorphism of Hydrothermally Altered Rock

Many hydrothermal mineral assemblages are in first approximation identical to those that occur in greenschist and amphibolite metamorphic facies, whose mineral assemblages may be the same as those of hydrothermal minerals of altered rocks. Thus, certain metamorphic assemblages, especially if confined to restricted areas, may indeed represent the metamorphic equivalent of hydrothermal precursor minerals. It is quite likely that in metamorphosed hydrothermally altered wall rocks, analyses of individual mineral species would reveal subtle compositional differences, such as the Fe/Mg of chlorites, or the Ba content of

feldspars. Many processes normally interpreted to the result of regional metamorphism, are in fact hydrothermal alteration effects. Notably this is the case of "sea-floor metamorphism", discussed in Section 2.6.2. Although this can be regarded as a case of semantics, after all hydrothermal alteration is a type of metamorphism, it is advisable to try and separate the traditional metamorphic facies from the effects of mineral changes in response to interaction of the rocks with hot fluids. The distinction, however, is not always clear, as for instance in the extensive, regional scale talc-carbonate, carbonate and sericitic alteration of rocks in Archaean greenstone belts. For the present purpose, therefore, metamorphism refers to solid state changes that take place at the regional scale during tectonic and thermal events. The reader is referred to the books of Spear (1993), Bucher and Frey (2002) and Kornprobst (2002) for details on metamorphism and metamorphic reactions.

Most mineral deposits, even the more recent ones that have gone through an orogenic cycle, are metamorphosed to a greater or lesser extent. In the lower grades of metamorphism (up to greenschist facies), the hydrothermal minerals are already equilibrated to the conditions of temperature and pressure, and mineral changes, if any, are not anticipated to be substantial. The propylitic zone (chlorite + epidote ± carbonate ± pyrite) of a porphyry system would be difficult to detect in an area of greenschist facies metamorphism. However, the presence of unusually abundant pyrite, mineral assemblages transitional into sericitic zones, and their restriction to particular areas, may give away the true origin of the minerals in question. Considerably more difficult is the detection of hydrothermal alteration at higher grades of metamorphism (amphibolite to granulite facies). In these conditions it is sometimes difficult even to decide whether a given ore deposit is pre-, syn-, or post-metamorphic. The situation may become even more confused where retrograde metamorphism has taken place. In environments of medium to high-grade metamorphism, fabric and textural studies of the ore minerals and the enclosing lithologies are obviously very important. These studies can establish whether or not the ore minerals were subjected to the same deformation and metamorphic events as the enclosing rocks, taking into due consideration effects of re-mobilisation and re-crystallisation of the more ductile components (e.g. galena) during metamorphism. Equally important in the search for evidence of hydrothermal alteration in metamorphic rocks of upper greenschist to amphibolite facies, are studies of whole rock geochemistry patterns and mineral chemistry. For example, low K + Na and Al enrichment would be expected in a metamorphosed acid-sulphate alteration zone. Certain key minerals, such as garnet, magnetite, muscovite, chlorite, may reveal unusual concentration and/or ratios of elements (Zn, Ba, Mn, Fe/Mg) which may be indicative of a hydrothermal environment.

Metamorphism and remobilisation of ores was investigated by Marshall et al. (2000), who focussed on processes of modification and remobilisation of ore minerals during metamorphism and deformation. Amongst these changes are the conversion of pyrite to pyrrhotite, the formation of Pb-rich feldspar under conditions of high-grade metamorphism and the release of a number of

trace elements (e.g. Te, Ni, Sb, Ag, Bi) that become included in various base metal sulphides (Marshall et al. 2000 and references therein). Structural remobilisation of disseminated and massive sulphide ores occurs under conditions of intense deformation and medium-grade metamorphism, as illustrated by the base metal sulphide deposits of the Matchless Amphibolite Belt, described in Chapter 7. In this section, however, I focus on modification of hydrothermal alteration assemblages brought about by metamorphism, rather than the actual ores. A special volume on ores and metamorphism can be found in Spry et al. (2000). Other publications that can be useful to consult for the modification of ores during metamorphism include Boyle (1993) and Frost et al. (2002).

The problem of the effects of metamorphism on hydrothermal assemblages has been investigated for many years by Stanton (1972, 1982, 1983), who concentrated his efforts on the sedimentary rock-hosted stratiform massive sulphide deposits. Stanton's work therefore refers to "hydrothermal sediments", rather than wallrock "epigenetic" alteration. Nevertheless, from his work and that of others cited below, some inferences can be made that may apply to epigenetic alteration.

Stratiform ore deposits are generally concordant, lens-shaped, and are commonly hosted by metapelitic lithologies with distinctive metamorphic mineral assemblages. The ore minerals are considered as chemical precipitates deposited with the original sediments. Table 2.5, compiled from Stanton (1982), lists a range of minerals usually found in medium-grade metamorphic environments, together with their possible hydrothermal precursors.

In a later paper, Stanton (1989) dealt with the topic of the effects of regional metamorphism on chemical sediments. On the basis of detailed geological, mineralogical and geochemical observations, this author explained the intimate relationships in metamorphosed exhalites, between bedded silicate minerals, oxides, sulphides and carbonates, in terms of a "precursor principle". The theory of the precursor principle suggests that the regionally metamorphosed bedded oxides, carbonates, sulphates, sulphides and silicates are derived directly from in situ, low-temperature, sedimentary-diagenetic-alteration precursor minerals and materials and not from Barrovian prograde metamorphic reactions. As the precursor principle applies to the economically important family of SEDEX ore deposits, I briefly review Stanton's ideas on this topic. Exhalative activity on the floor of seas, lakes and lagoons leads to the stratiform accumulations

Table 2.5 Metamorphic minerals, their possible precursors and original hydrothermal materials. After Stanton (1982)

Metamorphic minerals	Possible precursors	Possible origin
Chlorite	Montmorillonite	Altered volcanic glass
Muscovite	Illite	Diagenetic illite derived from kaolinite, or epithermal alteration
Almandine garnets	Chamosite	Hydrothermal sediments, oolites
Sillimanite, kyanite, and alusite	Kaolinite, alumino-silicate clays	Acid leaching of sulphate-bearing solutions, epithermal systems
Fibrolite	Halloysite, gibbsite	

containing various amounts of Fe, Zn, Cu, Pb sulphides, Fe hydrooxides, Ba and Ca sulphates, carbonates, hydrous silica gels as well as a number of clays, chlorites, mixed layer clay-chlorite and zeolites. These accumulations form what is generally known as exhalites or chemical sediments. These chemical sediments are subsequently subjected to diagenetic changes and in many cases to regional metamorphism. During the diagenetic and metamorphic phenomena the sulphide, oxides, sulphates and carbonate undergo grain growth and coarsening. Thus, fine cherts or quartzites are derived from the dehydration of hydrous silica gels, whereas Fe oxides such as hematite and/or magnetite are derived from Fe hydroxides. Common examples of precursor chemical sediment or exhalite and corresponding metamorphosed exhalite include (see also Table 2.6): (1) hydrous forms of silica (possibly a gel) in seafloor exhalations changing to cherts; and (2) Fe hydroxides changing to hematite and/or magnetite. In the latter case the dehydration-reduction sequence envisaged is as follows (Stanton 1989, p. 545):

$$\underset{\text{limonite}}{Fe(OH)_3} \rightarrow \underset{\text{goethite}}{FeO.OH} + H_2O;$$

$$\underset{\text{goethite}}{2FeO.OH} \rightarrow \underset{\text{hematite}}{Fe_2O_3} + H_2O;$$

$$Fe_2O_3 + H_2O + Fe^{2+} \rightarrow \underset{\text{magnetite}}{Fe_3O_4} + 2H^+$$

Table 2.6 Facies and metamorphic assemblages of the Gamsberg deposit, South Africa, and their possible pre-metamorphism precursors. After Rozendaal and Stumpfl (1984)

Facies	Metamorphic assemblage	Precursor mineralogy
Oxide	Quartz, apatite, magnetite hematite, barite	Chert, magnetite, cellophane hematite, barite
Carbonate-silicate	Pyroxenoid, garnet, amphibole quartz, pyrrhotite, magnetite	Fe-Mn carbonate, chamosite, chert, quartz, Fe sulphide
Silicate ± carbonate ± sulphide	Quartz garnet, amphibolite, chalcopyrite, pyrite, pyrrhotite	Chert, quartz, chamosite, Mn-Fe carbonate, Fe sulphide
Sulphide	Quartz, garnet, amphibolite, orthopyroxene, pyroxenoid, olivine, apatite, pyrrhotite, sphalerite, graphite	Pyrrhotite, sphalerite, galena, chert, quartz, Fe-Mn Carb., chamosite, organic material
Sulphide	Quartz, sillimanite, muscovite, K-feldspar, pyrite, sphalerite, graphite	Quartz, chert, pyrite, sphalerite, illite, kaolinite, organic material, detrital K-feldspar(?)
Silicate	Quartz, garnet, K-feldspar, clinopyroxene, amphibole, pyrrhotite, pyrite	Quartz, chert, chamosite, Mn-Fe carb., illite, Fe sulphide detrital K-feldspar(?)
Carbonate ± silicate	Calcite, rhodocrosite, quartz, garnet, K-feldspar, clinopyroxene, amphibole, magnetite, pyrrhotite	Fe-Ca-Mn carb., chert, quartz, illite, kaolinite, chamosite, magnetite, Fe sulphide

In this way the magnetite of banded iron formations and magnetite-quartzites (a common exhalite in many metamorphic terranes) may be formed from the transformation of in situ limonite and goethite. Garnet is commonly a component of banded quartz-magnetite rocks and as such it may have been formed from a precursor mineral, which could have been a sedimentary-diagenetic Fe-Mn chlorite chamosite. The exhalites of the Broken Hill Pb-Ag-Zn deposits in Australia, are associated with metamorphic minerals such as sillimanite, which may have derived from kaolinite, and gahnite ($ZnAl_2O_4$) derived from a kaolinite with adsorbed Zn and muscovite from illite. The common intergrowths of cordierite-sillimanite are explained as the result of isochemical, in situ metamorphism of clay-chlorite with minor kaolinite-gibsite. In the same way many spinels, of which gahnite referred to above is an example, would be formed from clay precursors with adsorbed cations such as Fe^{2+}, Zn^{2+} and Mn^{2+}.

The mechanisms that may be important to explain the regional metamorphic changes of precursor materials are: (1) coarsening and ordering of sedimentary/diagenetic materials such as carbonates, sulphides, clays etc. (2) gel-solid changes, that is the growth of ordered crystal structures from amorphous materials, such as silica gels to cherts, gel goethite to hematite/magnetite; and (3) solid-solid changes of mixed-layer crystal structures that formed during exhalations and diagenesis, such as illite \rightarrow muscovite, kaolinite-gibsite mixed layers \rightarrow sillimanite, kaolinite \rightarrow sillimanite, chamosite \rightarrow almandine garnet. Stanton (1989) regarded the materials under (1) as simple precursors and those under (2) and (3) as complex precursors.

The polymetallic, sedimentary rock-hosted, exhalative massive sulphide (SEDEX) deposits of Aggeneys-Gamsberg in South Africa occur within the Namaqua Metamorphic Complex. The geology and mineralisation of these important deposits are discussed in Chapter 8. Here it will suffice to mention that the original host sequences may have included rhyolitic rocks, volcanic sediments and cherts. At Gamsberg these rocks are metamorphosed to include quartzites, quartz-biotite-muscovite-sillimanite schist, garnet-pyroxene-amphibolite-magnetite, quartz-sericite-sillimanite schist, quartz-grunerite-garnet, magnetite-quartz-barite (Gams Formation), amphibolites and quartz-muscovite schist. At Aggeneys the ore formation contains quartzite, quartz schist, garnet quartzite, magnetite-quartz-amphibolite, magnetite-barite and baritic quartz schist. Of particular interest is the garnet quartzite (+ cordierite + sillimanite + biotite), because this unit is thought to be the metamorphic equivalent of a siliceous-aluminous precursor feeder zone (McGregor 1986). The mineralised rocks (galena, sphalerite, chalcopyrite, pyrrhotite and pyrite) and their associated mineral assemblages at Aggeneys are therefore the metamorphic equivalent of hydrothermal exhalites of silicate, oxide and sulphide facies. The interpretation of the silicate mineral assemblages of the Gams Formation, and their pre-metamorphic precursors, are given in Table 2.6.

The precursor principle may be applied to epigenetic hydrothermal mineralisation and this may be of great importance in the exploration of volcanogenic base metal and precious metal deposits in terranes of high-grade metamorphism. Aluminous minerals such as clays and chlorite are common products of the hydrothermal alteration of wall rocks. The occurrence of these minerals in restricted zones implies the presence of hydrothermal fluid conduits (alteration pipes) which underlie volcanogenic deposits. Following deformation and metamorphism it becomes extremely difficult to recognise what could have been an alteration pipe. During metamorphism, the aluminous hydrothermal alteration minerals change to aluminous metamorphic assemblages, which include garnet, cordierite and staurolite. Therefore, the recognition of localised high-grade aluminous assemblages may indicate an ancient hydrothermal pipe. This topic is taken up again in Chapter 7, in the discussion of the massive sulphide deposits on the Matchless Amphibolite Belt in Namibia.

McLeod and Stanton (1984) worked on the mineral chemistry of phyllosilicate assemblages (chlorite + talc ± phlogopite ± biotite and chlorite + muscovite) associated with some of the Palaeozoic Pb-Zn massive sulphide deposits of New South Wales and Tasmania (Woodlawn, Captain's Flats, Rosebery, Que River). These deposits are thought to represent the ancient and metamorphosed (greenschist facies) equivalent of the Japanese kuroko-type ores. The authors concluded that these phyllosilicate assemblages derived from precursor clay minerals, such as montmorillonite and illite. More specifically, they considered that crystallisation of chlorite and muscovite could be derived from a reaction of the types: kaolinite + mixed layer illite-montmorillonite, to produce mixed layer illite-dioctahedral chlorite and finally chlorite + muscovite; or, montmorillonite + kaolinitic clay to form illite hydromica + muscovite. An example of metamorphosed epigenetic hydrothermal alteration comes from a 2000-Ma-old hydrothermal system, in the felsic volcanic rocks of the Rooiberg group (Transvaal, South Africa). Here a zone of alteration is characterised by the assemblage dickite-pyrophyllite-quartz-diaspore-zunyite-pyrite. The presence of pyrophyllite and diaspore is interpreted as being due to the low-grade metamorphism of a zone of advanced argillic alteration in an ancient epithermal system (Martini 1988). Another example of documented metamorphism of hydrothermal deposits is provided by the Fe-Mn-rich lithologies associated with massive sulphide deposits in the southern Appalachians (Georgia, USA). These rocks were subject to deformation and metamorphism during the Early Ordovician and the Carboniferous, following a collision event. The Fe-Mn-rich rocks, Fe formations and enclosing mafic schists are metamorphosed to garnet, kyanite and sillimanite grades. The petrology and geochemistry of the Fe-Mn-rich rocks, including the so-called coticules or garnet-bearing quartzites, and garnet-bearing Fe formations, were investigated by Wonder et al. (1988). They found that these rocks originated by the metamorphism of hydrothermal sediments deposited by hot springs on the seafloor. The precursor materials probably contained clays, and Fe and Mn oxides (e.g. todokorite, goethite).

2.12 Geochemical Signatures and Isotopic Tracers

Geochemistry and mineralogical studies are commonly used to describe and classify hydrothermal alteration, whereas isotopic tracers are used to constrain the source of the fluids and metals. Quantitative estimates can be made using alteration indices from geochemical data, calculated in weight percent (wt%) or as part per million (ppm) and can be useful as exploration vectors (Gifkins et al. 2005). Alteration indices are calculated to gauge components that were added (numerator) and those that were lost (denominator) during the alteration process, so that the highest value characterises the most altered rock. Examples of alteration index are given below, with more details on the geochemical quantification of hydrothermal alteration given in the section that follows. It is by now accepted practice that a combination of all or part of the above is normally used in studies of alteration, with emphasis being given to one or the other in accordance with the investigator's methodology, approach and type of research.

2.12.1 Geochemistry

Studies of equilibria between minerals and hydrothermal fluids necessitate research on thermodynamics. The presentation of mineral equilibria involves the use of variables such as pressure, temperature, Eh, pH and chemical potential. Acidity-salinity (chemical potential) diagrams have been employed by Burt (1981) to quantify alteration mineral equilibria in greisens and porphyry systems. Activity-activity diagrams are considered to be particularly useful because they allow comparisons between key ions which can be normalised to H^+ (Guilbert and Park 1986). A comprehensive and concise review of the use of activity diagrams in studies of hydrothermal alteration can be found in Rose and Burt (1979). In general, hydrothermal alteration can be relatively easily quantified and described by using mineralogical and geochemical data. Studies of hydrothermal alteration should be conducted on three fronts. The first is detailed field mapping and core logging (if available), during which representative specimens of fresh and altered materials are collected. The second comprises mineralogical studies including thin section, X-ray diffraction (XRD) and microprobe analysis, for the identification of the key mineral assemblages. The third includes major and trace element geochemical analyses. The data obtained in this way can then be evaluated and presented in the form of two-dimensional diagrams.

A useful way of representing alteration data is by plotting gains and losses as percentages relative to the unaltered rock. In this method analytical values and specific gravity determinations are obtained for individual samples, and a horizontal line represents the assumed unaltered rock composition. Gains plot above the horizontal line and losses below it. A quantitative measure of hydrothermal alteration used by Ferry (1983) is the calculation of an alteration

index (AX). The AX is defined as the total volume of the alteration mineral assemblage, divided by the total volume of all the mineral phases present (including the hydrothermal minerals). This measure of volume percentages is made by point counting of thin sections. AX values may range from 0 in the unaltered rock to as much as 0.8 or 0.9 for a pervasively altered rock with a few relicts of unaltered minerals. The AX index can then be plotted against suitable geochemical parameters. Studies of mass transfer accompanying metasomatic processes were conducted by Gresens (1967) and Babcock (1973). They considered composition-volume relationships by developing a set of equations to quantify gains and losses of matter by metasomatic exchanges. Gresens' equations allow the calculation of gains and losses in the system by using geochemical analyses and specific gravities of the rocks and minerals in question, rather than the theoretical formulae. In the simplest case of two minerals and two components the following equations were obtained:

$$100 \times [\mathrm{fv}(\mathrm{gB}/\mathrm{gA})\ \mathrm{c1}^{\mathrm{B}} - \mathrm{c1}^{\mathrm{A}})] = \mathrm{X}_1,$$

$$100 \times [\mathrm{fv}(\mathrm{gB}/\mathrm{gA})\ \mathrm{c2}^{\mathrm{B}} - \mathrm{c2}^{\mathrm{A}})] = \mathrm{X}_2$$

where A is the original mineral, B its alteration product, $\mathrm{c1}^{\mathrm{A}}$ the weight fraction of component 1 for mineral A (e.g. TiO_2 wt%), and fv the volume factor. This factor can be greater than 1 in the case of replacement with volume gain, equal to 1 for volume by volume replacement, and less than 1 with volume loss; gA and gB are the specific gravities of minerals A and B; X_1 and X_2 represent the material lost or gained ($X = X_1 + X_2$). The equations above have three variables (fv, X_1, X_2) and if it is considered that replacement is isovolumetric (fv = 1), then only X_1 and X_2 remain to be solved. A simple variation of Gresens' method, using a spreadsheet readily simplifying manipulation of the data, was proposed by Grant (1986). The procedures outlined in Grant (1986) monitor the change in the concentration of a component (ΔCi) relative to its concentration prior to alteration (Ci), (equation 6 of Grant 1986):

$$\Delta\mathrm{Ci}/\mathrm{Ci} = (\mathrm{C}_{\mathrm{Al_2O_3}}{}^{\mathrm{o}}/\mathrm{C}_{\mathrm{Al_2O_3}}{}^{\mathrm{A}})(\mathrm{Ci}^{\mathrm{o}}/\mathrm{Ci}^{\mathrm{A}}) - 1$$

where $\mathrm{C}_{\mathrm{Al_2O_3}}{}^{\mathrm{o}}$ is the concentration of Al_2O_3 in the unaltered rock (o for original rock), $\mathrm{C}_{\mathrm{Al_2O_3}}{}^{\mathrm{A}}$ is the concentration of Al_2O_3 in the altered rock (A for altered), Ci^{o} is the concentration of the component in the unaltered rock and Ci^{A} is the concentration of the component in the altered rock. The results are expressed in decimal numbers, such that 1 = 100% gain of an element and –1 = 100% loss of an element. The relative mass loss or gain of the altered samples, assuming immobile Al_2O_3 during alteration, is calculated by:

$$[1 - (\mathrm{C}_{\mathrm{Al_2O_3}}{}^{\mathrm{o}}/\mathrm{C}_{\mathrm{Al_2O_3}}{}^{\mathrm{A}})] \times 100$$

A measure of the degree of alteration for Kuroko deposits was proposed by Ishikawa et al. (1976), who defined an alteration index in terms of the ratio between elements enriched and elements enriched plus depleted; for example:

$$\mathrm{AI} = \frac{\mathrm{MgO} + \mathrm{K_2O}}{\mathrm{Na_2O} + \mathrm{K_2O} + \mathrm{CaO} + \mathrm{MgO}}$$

Other indeces include the silicification index:

$$\mathrm{SI} = \frac{100 \times \mathrm{SiO_2}}{\mathrm{SiO_2} + \mathrm{Al_2O_3}}$$

and the chlorite-carbonate-pyrite index (Large et al. 2001):

$$\mathrm{CCPI} = \frac{100 \times (\mathrm{MgO} + \mathrm{FeO})}{\mathrm{MgO} + \mathrm{FeO} + \mathrm{Na_2O} + \mathrm{K_2O}}$$

The CCPI index is useful to trace the role of the more common alteration minerals (chlorite, Fe-Mg carbonates and pyrite) in volcanogenic massive sulphide (VMS) ore systems. High CCPI values will reflect intense Fe and Mg alteration but, as pointed out by Gifkins et al. (2005), this index is not useful for monitoring alteration in mafic rocks because these will typically have high primary MgO and FeO abundances. However, if the CCPI is used together with the AI (CCPI vs AI) it will nicely discriminate VMS alteration assemblages form diagenetic or metamorphic feldspar-bearing assemblages (see Gifkins et al. 2005 for details).

2.12.1.1 Lithogeochemical Variations

The distribution of major and trace elements, both at the regional and local scale, shows useful systematic variations with respect to the central core zone of the mineralised system, as would be expected in view of the distinct mineral and metal zoning that characterise for example porphyry or VMS deposits.

Geochemical work carried out by Lambert and Sato (1974), showed that silica is strongly enriched and Na depleted in the innermost zones (zones III and IV of Shirozu 1974; see Fig. 2.15); K on the other hand is usually enriched in zones II, III and IV, so that a progressive increase in the K/Na ratios is observed towards the mineralised areas over distances of hundreds of metres. These geochemical variations can be particularly useful in tropical areas where intense weathering often makes it difficult to recognise hydrothermally altered rocks, as illustrated in the following example.

Van Kranendonk and Pirajno (2004) examined the major and trace element geochemistry and REE systematics of metabasaltic rocks associated with chert and barite horizons of an ancient epithermal system in the 3.53–3.42 Ga Warrawoona Group (Pilbara Craton, Western Australia; see Chapter 5 for

details). The Warrawoona Group consists of chert units from three formations, Dresser, Marble Bar Chert and Strelley Pool Chert, overlying the Apex Basalt. An outline of this work is presented here to illustrate the use of lithogeochemistry to monitor hydrothermal alteration. In this section, I discuss the major and trace element data; in the next section the use of REE systematics in the same units is examined. To carry out this work Van Kranendonk and Pirajno (2004) first had to discriminate between the effects of recent weathering of the basalt and hydrothermal alteration. A good measure of the degree of rock weathering is the Chemical Index of Alteration, based on the immobility of Al during weathering processes:

$$\mathrm{CIA} = \mathrm{Al_2O_3}/(\mathrm{Al_2O_3} + \mathrm{Na_2O} + \mathrm{K_2O} + \mathrm{CaO})),$$

in which high CIA values (>0.80) commonly result from recent, intense weathering and from feldspar-destructive, chloritic or advanced argillic alteration (Nesbitt and Young 1982). Nesbitt and Young (1982) also suggested that this calculation should incorporate only the amount of CaO in the silicate fraction of the rock and that a correction factor for apatite and carbonate minerals be applied. Samples of altered metabasalts from stratigraphically 1–2 km below, from just below, and from just above each of the studied chert horizons were analysed in order to characterise the geochemical characteristics of different alteration types and element mobility. Generally, metabasalts from stratigraphically above the cherts and those from well below the cherts have relatively unaltered geochemistry. Basalts sampled from immediately beneath the chert horizons, however, show marked changes in geochemical composition from relatively unaltered metabasalts above and below the cherts. These changes include large positive increases in SiO_2 values (from ~47 to ~75 wt%) and the almost complete removal of FeO (from ~9 wt% to 0), MgO (from 5.5 to 0.2 wt%) and CaO (from between 7 to 11 wt% to 0.1 wt%) from all of the samples. The white clay altered pillow basalt from the Dresser Formation is dominated by SiO_2, Al_2O_3, and TiO_2.

The highly altered nature of the basaltic rocks from immediately beneath the chert horizons is evident from ternary A-CN-K and A-CNK-FM plots (Fig. 2.18a, b). The carbonate-altered and relatively unaltered metabasalts from the North Pole Dome (Strelley Pool Chert) mostly plot within a narrow range on the A-CN tie-line in Fig. 2.18a, indicating that these metabasalts had not been subjected to subaerial weathering, consistent with the CIA data. The three samples that plot towards the CN apex of Fig. 2.18 are from the distinctive group of komatiitic basalts with low Al_2O_3 and high CaO and MgO. This shift reflects the high-Mg character of these rocks and the primary mineralogical control of olivine and/or clinopyroxene on bulk composition. Figure 2.18a, b shows that rocks from immediately beneath the chert horizons plot near the A corner, indicating the near complete removal of alkalis and Fe and Mg during alteration. Clay-altered pillow lava from the Dresser Formation (sample 177897 in the figure), altered basalts from both above and below the Apex

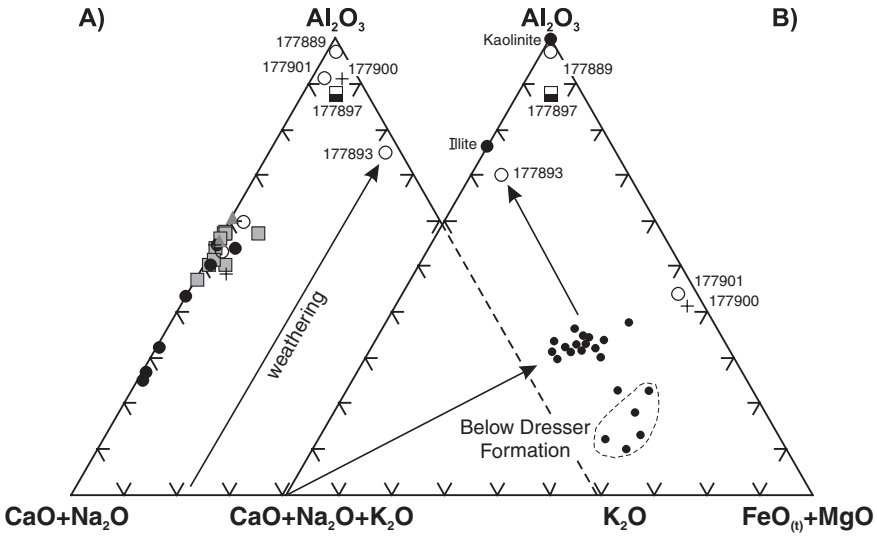


Fig. 2.18 Ternary Al_2O_3-$CaO+Na_2O$-K_2O (A-CN-K) and Al_2O_3-$CaO+Na_2O+K_2O$-FeO_T+MgO (A-CNK-FM) diagrams of metabasalts of the Warrawoona Group; in (**A**) samples from below (*circles*), within (*triangles*) and above (*squares*) the Dresser Formation, plot on the A-CN tieline suggesting no effects from weathering, whereas samples that plot near the A corner suggest extensive hydrothermal alteration, the arrow indicates modern chemical weathering trend; in (**B**) metabasalts form below the Dresser Formation have high Mg and are not affected by alteration, whereas metabasalts in and above the Dresser Formation (*dots*) are all affected by propylitic hydrothermal alteration (*left* to *right arrow*) and either phyllic alteration (samples at the A corner) or by weathering (*illite dot*). After Van Kranendonk and Pirajno (2004)

chert (samples 177900 and 177901), and the quartz-pyrophyllite schist from below the Strelley Pool Chert (locality 1, North Pole Dome, sample 177889) all plot close to A in the A-CN-K diagram, despite widely differing mineralogy and have CIA values of 0.88 to 0.91 indicating extreme alteration by hot seawater or by later, non-seawater derived fluids that leached all CaO and Na_2O and caused slight addition of K_2O and Al_2O_3. The K_2O-enriched sample of altered pillow basalt from beneath the Strelley Pool Chert at locality 2 (177893) is the only sample that lies along the trend of weathering on the A-CN-K plot. Although this weathering may have occurred in recent times, rocks a similar distance stratigraphically above the subvertically dipping chert (sample 177895) do not show this K_2O alteration and suggest that the weathering may have occurred during subaerial exposure of these rocks in the Archaean, as is characteristic of Archaean weathering profiles. Figure 2.18b shows that the metabasalts have been affected by two distinct alteration trends. The first is a trend away from the CNK apex, reflecting the effects of stripping of alkalis by hydrothermal propylitic alteration (chlorite-carbonate-epidote). This is particularly evident for the altered basalts beneath and above the Apex chert (samples 177900 and 177901),

which plot close to the A-FM tie-line. The second trend has affected the sample of clay-altered metabasalt (weathered; saprock) in the Dresser Formation and samples from both localities of the Strelley Pool Chert. This trend, related to phyllic (quartz-sericite-pyrite), argillic (kaolinite) and/or advanced argillic (kaolinite-pyrophyllite-alunite-barite) alteration and/or surface weathering, has caused the samples to plot neat the A apex of the A-CNK-FM diagram, reflecting crystallization of illite and/or kaolinite.

2.12.1.2 Rare Earth Elements (REE) in Hydrothermal Alteration Processes

Rare earth elements (REE) include those elements with an atomic number between 57 (lanthanum) and 71 (lutetium). Their similar chemical behaviour is related to the decrease in their atomic volume with increasing atomic number, the so-called lanthanide contraction. Yttrium (atomic number $Z = 39$) is often considered together with the REE because of its similar ionic radius to holmium ($Z = 67$). REE with lower atomic numbers are referred to as light REE (LREE), and those with higher atomic numbers as heavy REE (HREE). REE are contained in more than 200 minerals including various phosphates, carbonates, oxides and silicates. Common rock-forming mineral phases containing REE are apatite, zircon, monazite and xenotime. A detailed review of REE geochemistry is clearly beyond the scope of this book, but the interested reader is recommended to consult the work of Hanson (1980) for a good documentation on the topic of REE studies of igneous systems, the informative article by Henderson (1996) on REE systematics, Mariano (1989) and Taylor and Pollard (1996) for REE mineral systems, and Smith et al. (2000) for the behaviour of REE during hydrothermal processes.

For the purpose of graphical presentation, REE abundances are usually normalised to chondritic meteorite abundances, i.e. each element value in the sample is divided by the corresponding element value in chondrites (normalising factors are usually taken from Sun and McDonough 1989). The REE abundances in chondritic meteorites are taken to be the base values, and therefore the abundances in the primordial mantle form a horizontal line in the diagram, because it is assumed to be unfractionated. It follows that the REE abundances in the various rock systems show variably shaped curves above that of the primordial mantle, reflecting varying degrees of fractionation. In cases of cogenetic rocks it may be more expedient to normalise the REE to one of the rocks in the sequence, generally the least fractionated (Hanson 1980). In geological processes REE are variably enriched in magmas, their consolidation products and their residual fluids. Studies of REE abundances in rock systems are especially valuable in the investigation of petrogenetic models. Generally speaking LREE tend to be concentrated in pegmatites and carbonatites, whereas HREE are concentrated in granitic magmas. Michard (1989) has studied the REE content of hydrothermal fluids from a number of geothermal fields. She found that the REE concentrations of the hydrothermal fluids

are usually very low, but they tend to increase as the pH decreases; also, in chloride-rich fluids the REE patterns show distinct positive Eu anomalies.

REE distribution in unaltered and altered rocks is useful monitors of changing fluid conditions from dominantly magmatic to dominantly meteoric. Changes in REE abundances during potassic alteration in a porphyry system are usually characterised by LREE increase and HREE depletion, with the ratio of REE abundances in mineralised to unmineralised rocks showing a decrease from LREE to HREE, and a positive Eu anomaly, indicating this element's enrichment in the hydrothermal fluids (Taylor and Fryer, 1982, 1983). From the propylitic to the phyllic stage of alteration or in other words with decreasing K^+ activity and increasing H^+ metasomatism, the pattern of REE abundances changes. From the potassic to the initial stages of the propylitic event there is overall depletion of REE, but less so for the LREE than for the HREE. In the more advanced stages, however, the heaviest REE are enriched. From the propylitic to the phyllic stage there is further depletion of the total REE, indicating progressive leaching of the REE with increasing fluid/rock ratios and decrease in pH (increasing H^+). This decrease is more pronounced for the LREE than for the HREE, which are consequently relatively enriched (Taylor and Fryer 1982, 1983). In summary, and in agreement with Hanson (1980) and Michard (1989), it is found that in hydrothermally altered rocks the REE abundances are significantly affected only if fluids flushed through the system several times. This has important implications, because if the REE patterns may not sufficiently different from those of the unaltered rocks. Lottermoser (1990) investigated the mobility of REE during fluid-wallrock interaction in the large and active gold epithermal system in Lihir Island in Papua New Guinea. This system, which is discussed in some detail in Chapter 5, is characterised by: (1) a lower potassic-propylitic zone; and (2) argillic and advanced argillic zones. These zones are capped by a sulphide-free oxide zone. Lottermoser's work established that the REE patterns of alteration assemblages in the wall rocks and vein materials display strong mobilisation and fractionation during the hydrothermal processes that characterise an active volcanic ore-generating system. The results of this work, however, show results which contrast with those obtained by Taylor and Fryer (1982, 1983), because at Lihir there is progressive addition of LREE from the potassic-propylitic to the argillic zone, with high mobilisation and concentration of HREE characterising the higher levels of the alteration profile. Thus, in the Lihir epithermal system the magmatic-hydrothermal component is LREE-enriched, whereas LREE and HREE both are enriched in the meteoric acid sulphate component of the system. As previously suggested, this mobilisation of REE occurs under conditions of large scale fluid flow.

In the Warrawoona Group, mentioned in the previous Section, the REE systematics of highly altered rocks from immediately beneath the studied chert horizons are variable relative to those for overlying and underlying metabasalts (Fig. 2.19a–d). For the Dresser Formation and Apex chert, highly altered metabasalts immediately beneath the chert horizons have preferentially lost light rare

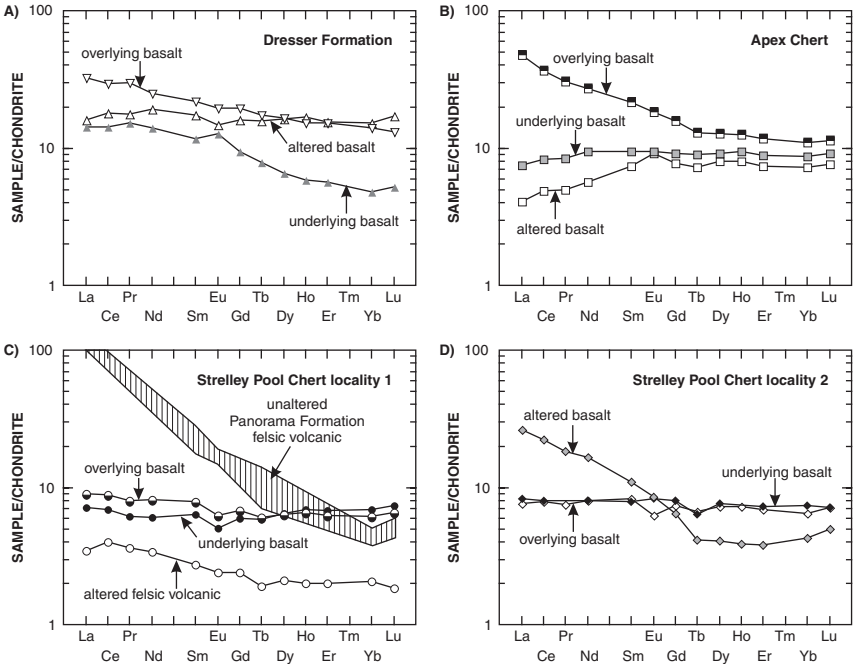


Fig. 2.19 Chondrite-normalised rare earth elements (REE) plots of unaltered and altered metabasalts from (**A**) Dresser Formation, (**B**) Apex Chert, (**C**) Strelley Pool Chert locality 1 and (**D**) Strelley Pool Chert locality 2. After Van Kranendonk and Pirajno (2004)

earth elements (LREE: Fig. 2.19a, b). In contrast, the metabasalt from above the Apex chert (sample 177900) shows significant LREE enrichment, which may be the result of high fluid-rock ratios in a low-temperature hydrothermal alteration environment. At the Strelley Pool Chert localities, the underlying and overlying metabasalts have almost identical, flat REE patterns (Fig. 2.19c, d), whereas the immediately underlying altered rocks show quite different REE patterns. At locality 1 (Strelley Pool Chert), the pyrophyllite-quartz-sericite schist has generally lower overall REE abundances (Fig. 2.19c), reflecting dilution by silica during low-temperature hydrothermal alteration that transformed this basaltic protolith into pyrophyllite-quartz-sericite schist. Unlike the metabasalts of the Dresser and Apex Basalt Formations, this sample has preferentially lost HREE. That the schist was derived from a basaltic protolith is confirmed by its different REE profile to that of altered felsic volcanic rocks (quartz-sericite) of the Panorama Formation (Fig. 2.19c). At Strelley Pool Chert locality 2, the pattern of REE alteration is different from all other localities, being characterised by LREE-enrichment and HREE- and some middle REE-depletion (Fig. 2.19d), a pattern similar to that produced by advanced argillic alteration in the Rodalquilar gold alunite deposit in Spain (Arribas et al. 1995) and the Western Tharsis Cu-Au deposit, Mt Lyell, Tasmania (Huston 2001).

2.12.2 Isotopic Tracers

The use of stable and radiogenic isotopes is very common with many papers being published each year that almost exclusively report on isotopic systems as tracers for the source of hydrothermal fluids and ore elements, as the various examples in the chapters ahead demonstrate. Definitive results are rarely obtained and ranges of values or variations in isotope systems usually reflect differences in the composition of fluid source area, of pathways used by the fluids, fractionation effects during unmixing and so forth. It is not unusual for the same data to be open to different and contradicting interpretations. Results of isotopic analyses can be equivocal. Therefore, isotopic systems must be used with a great deal of caution and interpretations not solely based on isotope systematics, but need to be constrained by field and petrographic relationships and geochemical data. In this section I briefly examine the use of stable (H, D, O) in attempting to understand the complexity of hydrothermal mineral systems. The reader who might wish to acquire greater knowledge on the topic, the works of the following authors are all especially useful in the context of this book: Faure (1986, 2001), Nesbitt (1996), Taylor (1997) and Hoefs (2004).

The study of isotopic compositions is based on systematic variations that occur in natural materials as a result of fluid and rock interactions and temperature. Isotope exchange reactions take place between fluids and between these and wall rocks (see Chapter 1). Nesbitt (1996) listed three applications in the use of stable isotope systematic for the study of hydrothermal mineralisation and mineral exploration. The first is the presence of whole rock haloes that surround or are associated with ores; the second is the identification of mineral zonations and the third is the possibility of distinguishing mineralised from unmineralised systems. In the study of hydrothermal ore systems stable isotopic analyses can be conducted on individual hydrothermal alteration minerals, altered wall rocks, or on fluids extracted from fluid inclusions. The essential principle that governs these studies is that the stable isotopic values of a mineral phase are a function of the $\delta^{18}O$ value of the fluid and the temperature of mineral formation (Nesbitt 1996).

The fractionation factor α is given by the ratio of the isotopes (e.g.$^{18}O/^{16}O$) in the two substances (1 and 2) considered, and determines how much one isotope is enriched in one substance relative to another in permil fractionation. Since isotope fractionations are temperature-dependent, while independent of pressure, this allows the determination of isotopic temperatures using fractionation curves. Thus, if two mineral phases equilibrate oxygen with a common fluid, at a given temperature, the difference in their $\delta^{18}O$ is a function of the temperature (Faure 1986). Studies of combined hydrogen and oxygen isotope systematics in hydrothermal systems rely on the different abundances of H and O in rocks and water. This enables the quantification and characterisation of the water-rock interaction, in terms of the H and O exchange between fluid and mineral phases. Therefore, the D/H ratio of the system will be controlled by the water, whereas the $^{18}O/^{16}O$ value is determined by the exchange

with mineral phases in which H is only a trace constituent. Consequently, the oxygen isotopic composition is affected by the mineral-water interaction resulting in an ^{18}O shift of the fluids from the original value, usually towards higher values (see Fig. 1.12). This shift is due to the water attempting to equilibrate with the ^{18}O-rich wall rocks. The amount of shift is related to the ratio of oxygen in the minerals to that of water, to the mineral-fluid fractionation factor, and hence temperature, and the original isotopic composition of either of the phases (Sheppard 1986). Isotopic interactions are also considered in terms of a closed system (mineral co-existing fluid), or open system (external fluid with increasing fluid to rock ratios) (Gregory and Criss 1986).

Hydrothermal alteration of rocks is accompanied by variations in $\delta^{18}O$ and δ D which tend to form zoning patterns around the ore deposit. These patterns are important in determining the geometry of the hydrothermal cell, as well as the size and location of the discharge area (Ohmoto 1986). Taylor (1974) pioneered this type of investigation with his work on the igneous rocks of the Cascade Range (Oregon, USA). This geoscientist analysed hydrothermal minerals and fluid inclusions for their $^{18}O/^{16}O$ and D/H values, and found that shallow intrusions into highly fractured and therefore permeable, country rocks act as "gigantic heat engines" throughout their evolutionary history. The isotopic signature of the hydrothermal fluids consistently indicated their derivation from meteoric waters. Calculated water/rock ratios show that high ratios are associated with areas of intense alteration and low $\delta^{18}O$ in the rocks. Where less permeable, less meteoric water is available and a larger magmatic component associated with potassic alteration is found to be present. In the particular case of the Tertiary volcanic and intrusive rocks of the Cascade Range, Bohemia mining district, the results of Taylor's work indicated a regular and concentric pattern of $\delta^{18}O$, from low values at the centre to progressively higher values towards the periphery. The areas of lowest $\delta^{18}O$ values coincide with zones of propylitic alteration. Another instructive example comes from the Lake City caldera, in the mineralised San Juan volcanic field in Colorado. Here a study of stable isotope systematics carried out by Larson and Taylor (1986) revealed the presence of a large fossil hydrothermal system. This work showed pronounced $\delta^{18}O$ depletions along the western rim of a ring fracture, and inside the caldera in an area of rhyolitic resurgent volcanism. These areas correspond to a deeply eroded part of the caldera with intense chloritic and sericitic alteration. The lowest $\delta^{18}O$ values occur along the highly permeable ring fault zone, and also along the southwestern parts of the caldera where epithermal mineralisation is present. High $\delta^{18}O$ values occur in hydrothermal quartz in a quartz-latite dome in the eastern portions of the volcanic structure. High water/rock ratios, calculated from the isotopic data, are coincident with the zones of low $\delta^{18}O$.

Isotopic studies of whole rock and hydrothermal minerals of volcanics and sediments from the Fukazawa-Kosaka area in Japan, the site of Kuroko-type mineral deposits, carried out by Green et al. (1983) revealed systematic variations of $\delta^{18}O$ and δ D with alteration and temperature of the sea water

interacting with the rocks. The $\delta^{18}O$ values vary from 6.7‰ in the sericite-chlorite zone (highest temperature of interaction with sea water from about 200–400°C), to 11.1‰ in the montmorillonite zone (temperature of about 150–300°C), to 16.9‰ in the zone of zeolitic alteration with the lowest temperature of 25–200°C. A concentric zoning pattern is also found in the footwall rocks, with $\delta^{18}O$ values of 8‰ in the sericite-chlorite zone up to 500 m from the ore, followed by 8–14‰ in the montmorillonite zone up to 3 km away, and finally to values in excess of 14‰ in the peripheral zeolite zone (Green et al. 1983). The authors found that these isotopic variations form a much larger halo than do the distribution of anomalous Cu, Zn, Pb, Mg values in the rocks. Other examples are provided by Nesbitt (1996) in relation to epithermal and porphyry systems, Kuroko-type VMS, Carlin-type and orogenic Au deposits.

Thus, hydrothermal alteration results in a consistent depletion of $\delta^{18}O$ in the rocks, usually matched by a corresponding enrichment in the hydrothermal fluids, although Criss and Taylor (1986) cautioned that due to the large fractionation factors between mineral and water, the $\delta^{18}O$ in the low temperature regimes could actually increase by interaction with low temperature fluids. The isotope systematics of fluid-rock exchange are ultimately dependent on the initial composition of the fluids and rocks, temperature and water/rock (w/r) ratios. If w/r are greater than 1, extensive isotopic exchange will occur between fluids and rocks and therefore the isotopic value of the rocks will approach that of the fluid. If the w/r is less than unity, then the isotopic composition of the rocks will not change, whereas that of the fluid will approach equilibrium with the rocks (Nesbitt 1996).

2.13 Detection of Hydrothermal Alteration from Spectral Remote Sensing

Spectral remote sensing is an important tool for the detection of hydrothermal alteration. The theory of spectral discrimination of rocks and minerals is beyond the scope of this book; for principles and details the reader should consult the books on remote sensing by Lillesand and Kiefer (1987), Drury (1987) and Gupta (1991). Other useful publications include: Ninomiya (2002), Volesky et al. (2003) and Mauger et al. (2007) and the web site http://www.gds.aster.ersdac.or.jp (accessed January 2008). Details of spectral reflectance of rocks and minerals in the visible to thermal infrared wavelength region are known from field and laboratory work, by recording data with a spectrophotometer. The detection of spectral reflectance is also obtained from aircraft and spacecraft. The spectral features of altered rocks are a function of electronic and vibrational processes involving Fe and the OH group respectively. Each displays curves with characteristic slopes and absorption bands that are diagnostic of the surface materials.

Spectral features due to vibrational processes are especially useful, as they report OH-bearing minerals that are normally present in hydrothermally altered rocks. For this reason, the short wavelength region between 1.0 and 2.5 μm is ideal for the detection of clays and zones of acid-sulphate alteration with alunite present. Portable short wavelength infrared (SWIR) spectrometers are used, mostly by exploration companies, sensitive to OH, H_2O, NH_3, CO_2 and cation-OH bonds (Al-OH, Mg-OH and Fe-OH) (Thompson et al. 1999).

The successor to Landsat TM imagery is the Advanced Thermal Emission and Reflection Radiometer (ASTER), a cooperative venture between NASA and Japan's Ministry of Economy Trade and Industry. The following overview is extracted from the work of Gozzard (2006). The ASTER instrument collects data in 14 bands across a spectral region from visible near infrared (VNIR, bands 1 to 3), to short wave infrared (SWIR, bands 4 to 9) to thermal infrared (TIR, bands 10 to 14). ASTER multispectral data can be used in a variety of geological mapping programs with commercially available image processing and analysis software, such as ER Mapper (http://www.ermapper.com accessed January 2008). In the SWIR bands, minerals that can be identified are:

- alunite–pyrophyllite — significant in mineral exploration because they can define areas of argillic alteration. Landsat TM cannot discriminate these minerals;
- kaolin-group minerals — also significant in mineral exploration because they are useful in helping to define argillic alteration and in mapping regolith;
- illite–muscovite–smectite — common minerals in the surficial environment and useful for mapping regolith. They are also associated with both phyllic and argillic alteration;
- Mg-OH minerals and carbonates — major components of many lithological units. Landsat TM cannot discriminate these minerals.

For details of how to obtain and process ASTER images, the reader is referred to the excellent work of Gozzard (2006), which is written for non-specialists. Identifying diagnostic spectral features in the ASTER data and creating suitable band ratios based on those spectral features enables the extraction of information about mineral groups. Table 2.7 lists the common features relating to mineral groups that are frequently mapped using ASTER Level 1B imagery. The following example of mineral group images shows the potential value of extracting such information. The Relative absorption-Band Depth (RBD) image, bands (5 + 7)/6, highlights the AlOH (sericite–white mica) content based on its main spectral absorption feature at 2.2 μm (Fig. 2.20A). This image principally highlights the playa lake complex of Lake Annean in Western Australia. However, subtle compositional banding is evident in some of the mafic–ultramafic outcrops, suggesting that the higher levels of white mica may be associated with the more ultramafic lithologies. When this image is interpreted in combination with the colour ratio composite image of 5/6:7/6:7/5, further variations in the compositional nature of the AlOH mineralogy and its

Table 2.7 Commonly mapped features for alteration studies; after Gozzard (2006)

Feature	Ratio or RBD
Alunite-kaolinite-pyrophyllite	(4 + 6)/5
Carbonate-chlorite-epidote	(7 + 9)/8
Dolomite	(6 + 8)/7
Ferric iron (Fe^{3+})	2/1
Ferrous iron (Fe^{2+})	5/3 + ½
Kaolinite	7/5
MgOH-carbonate	(6 + 9)/8
Muscovite	7/6
Phengite	5/6
Quartz abundance	13/10
Sericite-muscovite-illite-smectite	(5 + 7)/6
Vegetation	(3–2)/(3 + 2)

chemistry are evident. These variations may not only be related to the original lithological variation of white mica, but may, in part, be related to potential hydrothermal alteration (Gozzard 2006). The abundance of MgOH group of minerals (chlorite, epidote, hornblende) on the other hand can be examined by using the bands (6 + 9)/8 RBD image (Fig. 2.20B), which is based on the 2.33–2.35 μm absorption feature that is typical of the above-mentioned mineral groups.

An example of a comprehensive alteration and mineral system study employing a suite of hyperspectral methods is by Mauger et al. (2007). These authors examined the Tarcoola goldfield in South Australia using spectral data from five instruments: Hyperion, HyMap, PIMA II, ASD Field Spec Pro and HyLogger. The Tarcoola field is characterised by Au-and sulphide-bearing quartz veins that cut through Palaeoproterozoic granites (Paxton Granite) and metasedimentary rocks (Tarcoola Formation). The Au mineralisation is

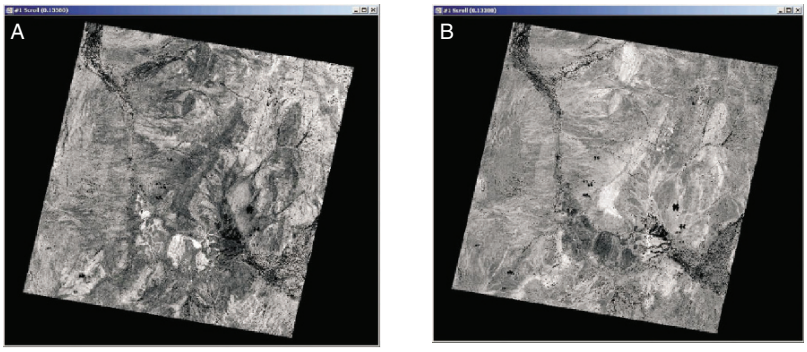


Fig. 2.20 ASTER images, (**A**) bands (5 + 70/6 RBD greyscale image; (**B**) bands 13/10 ratio greyscale image. Images courtesy of Bob Gozzard (Gozzard 2006, Figs. 10 and 11)

associated with hydrothermal alteration, which can be resolved into distal, medium proximal and proximal. Distal alteration consists of varying degrees of sericitisation of plagioclase and chloritisation of hornblende and biotite in the granitic rocks and newly formed magnetite. Increasing alteration towards the vein system is characterised by the destruction of magnetite, increased chloritisation, seriticisation and hematite dusting of K-feldspar. Proximal nearly pervasive alteration (sericite-chlorite) is next to the quartz veins, with nearly complete removal of the Fe oxides. The spectral data employed by Mauger et al. (2007) is complementary, in that the data from each instrument furnish different signatures, which can all be integrated to obtain clear mineral zonations. Samples were collected and examined using the PIMA II and ASD, whereas the HyLogger was used to map drillcore. The HyLogger system uses the principles of visible and infrared spectroscopy (wavelength range of 400–2500 nm), to measure reflectance spectra of drillcore and detect Fe oxides, OH-bearing minerals (clays, micas, smectites, pyrophyllite, chlorites, talc, amphiboles as well as sulphates and carbonates. The instrumentation is developed and used by CSIRO Exploration & Mining (Australia) for the mineralogical and alteration analysis of drillcore (for details visit http://www.csiro.au/org/HyLoggingSystemsGroup.html, accessed January 2008). The HyLogger identified in the Tarcoola field smectite and goethite, associated with high-grade Au mineralisation; phengite in the footwall and alunite associated with increasing Au contents. The Hyperion instrument discriminates between various Al(OH) minerals, but for the Tarcoola goldfield this proved unsuccessful till noise removal was carried out, resulting in the successful highlighting of fine-grained micaceous/illitic sedimentary rocks associated with the Au mineralisation. The HyMap data provided good results highlighting variations in the wavelengths related to various Al(OH) hydroxyl bonds; areas of kaolinite absorption spectrum appear green, whereas those of illite/mica appear red to orange, as also shown by the Hyperion data. Mauger et al. (2007) concluded that the spectral techniques used were very useful for the identification of mica/illite and phengite, bearing in mind that illite forms from sericite through weathering processes. Spectral logging enables to resolve weathering products from alteration mineralogy, in addition to defining the extent of weathering, thereby providing clues for targeting supergene Au enrichments.

2.14 Concluding Remarks

In this chapter I focused on hydrothermal alteration, following a brief overview of magma-generated fluids, their activity and effects on wall rocks. The many aspects and types of hydrothermal alteration range from anhydrous, partly anhydrous to fully hydrous or hydrolytic, with varying amounts of meteoric water inputs. Potassic, propylitic, sericitic, argillic, advanced argillic hydrothermal alteration types apply to most hydrothermal deposits, with the porphyry-epithermal ore

system probably being the best representative of this alteration sequence. Porphyry-epithermal and skarn systems exhibit alteration patterns and mineral assemblages that are to varying degrees common to all mineral deposit of that type. Anorogenic alkaline complexes provide unusual alteration types, generally encompassed under the general term of fenites. In contrast to porphyry-epithermal-skarn systems, anorogenic intrusions produce fenitic alteration patterns that can be widely different in their mineralogical assemblages in individual intrusion and the surrounding country rocks. Unlike porphyry-epithermal systems, the composition of the wall rocks may play an important role in determing the type of mineral assemblages. Like porphyry and epithermal system, alteration of oceanic crust rocks, or hydrothermal metamorphism, is quite predictable in its representative mineral phases.

Studies of hydrothermal alteration must include careful field and petrographic work. Thin sections represent "ground truth" at the microscopic scale, a first approximation identification of mineral phases and their textural relationships are all very important, before proceeding with equally important major and trace element analyses. Stable isotope systematic can only be interpreted in the light of these data. At the regional and local scale ASTER can be a very powerful tool, not only for mineral exploration purposes, but also for research studies of hydrothermal mineral systems. ASTER data enable to gauge the extent of alteration and its relationship to regional structures and intrusive bodies.

References

Alderton DHM, Fallick AE (2000) The nature and genesis of gold-silver-tellurium mineralization in the Metalliferi Mountains of western Romania. Econ Geol 95:495–515

Arribas A, Cunningham CG, Rytuba JJ, Rye RO, Kelly WC, Podwysocki MH, Mckee EH, Tosdal RM (1995) Geology, geochronology, fluid inclusions, and isotope geochemistry of the Rodalquilar gold alunite deposit, Spain. Econ Geol 90:795–822

Babcock RS (1973) Computational models of metasomatic processes. Lithos 6:270–290

Bailey DK (1978) Mantle metasomatism, continuing chemical changes within the Earth. Nature (London) 296:525–530

Beane RE, Titley SR (1981) Porphyry copper deposits. Part II. Hydrothermal alteration and mineralization. Econ Geol 75th Anniv Vol: 235–269

Best MG (1982) Ignneous and metamorphic petrology. WH Freeman and Co, New York

Black R, Bowden P (eds) (1985) Alkaline ring complexes in Arica. J Afr Earth Sci 3(1/2)

Bonin B (1986) Ring complex granites and anorogenic magmatism. North Oxford Academic, London

Bonny S, Jones B (2003) Microbes and mineral precipitation, Miette Hot Springs, Jasper National Park, Alberta, Canada. Can J Earth Sci 40:1483–1500

Bons PD (2001) The formation of large quartz veins by rapid ascent of fluids in mobile hydrofractures. Tectonophysics 336:1–17

Bowden P (1985) The geochemistry and mineralization of alkaline ring complexes in Africa (a review). J Afr Earth Sci 3:17–40

Bowden P, Kinnaird JA, Abaa SI, Ike EC, Turaki UM (1984) Geology and mineralization of the Nigerian anorogenic ring complexes. Geol Jahrb B 56:1–65

Boyle AP (ed) (1993) Sulphide Metamorphism and Deformation – introduction. Mineral Mag 57, Iss 386

Brogger WC (1921) Die Eruptivgesteine des Kristianiagebiets IV. Das Fengebiet in Telemarken, Norwegen. Nors Vidensk Akad Oslo Skr Nat Kl 9:408
Bucher K, Frey M (2002) Petrogenesis of metamorphic rocks, 7th edn. Springer, Berlin
Burnham CW (1979) Magmas and hydrothermal fluids. In: Barnes LH (ed) Geochemistry of hydrothermal ore deposits, 2nd edn. John Wiley & Sons, New York, pp 71–136
Burnham CW (1997) Magmas and hydrothermal fluids. In: Barnes HL (ed) Geochemistry of hydrothermal deposits, 3rd edn. Wiley, New York, pp 63–123
Burnham CW, Ohmoto H (1980) Late stage processes of felsic magmatism. Soc Min Geol Jpn 8:1–11
Burt DM (1981) Acidity-salinity diagrams – Application to greisenand porphyry deposits. Econ Geol 76:832–843
Carmichael IS, Turner FJ, Verhoogen J (1974) Igneous petrology. McGraw-Hill, New York
Chappell BW, White AJR (1974) Two contrasting granite types. Pac Geol 8:173–174
Chen YJ, Bao JX, Zhang ZJ, Chen HY, Liu YL (2003) Laumontitization as an exploration indicator of epithermal gold deposits; a case study of the Axi and other epithermal systems in West Tianshan, China. Chinese J Geochem 22:289–301
Coleman RG (1977) Ophiolites. Springer, Berlin, Heidelberg, New York
Collins WJ, Beams SD, White AJR, Chappell BW (1982) Nature and origin of A-type granites with particular reference to south-eastern Australia. Contrib Mineral Petrol 80:189–200
Cox SF (2005) Coupling between deformation fluid pressures, and fluid flow in ore-producing hydrothermal systems at depth in the crust. Econ Geol 100th Ann 1905–2005:39–75
Criss RE, Taylor HP (1986) Meteoric-hydrothermal systems. In: Valley JW, Taylor HP, O'Neil JR (eds) Stable isotopes in high temperature geological processes. Rev Mineral 16. Min Soc Am 373–424
Crocker IT (1985) Volcanogenic fluorite-hematite deposits and associated pyroclastic rock suite at Vergenoeg, Bushveld Complex. EconGeol 80:1181–1200
Dietrich RV (1985) The tourmaline group. Van Nostrand Reinhold, New York
Dilles JH, Einaudi MT (1992) Wall-rock alteration and hydrothermal flow paths about the Ann-Mason porphyry copper deposit, Nevada – a 6-km vertical reconstruction: Econ Geol 87:1963–2001
Drury SA (1987) Image interpretation in geology. Allen & Unwin, Boston
Edmond JM, von Damm K (1983) Hot springs on the ocean floor. Sci Am 248:70–85
Eilu PK, Mathison CI, Groves DI, Allardyce WJ (1999) Atlas of alteration assemblages, styles and zoning in orogenic lode-gold deposits in a variety of host rock and metamorphic settings. UWA Ext, Univ West Aust Publ 30
Evans AM (1987) An introduction to ore geology, 2nd edn. Blackwell, Oxford
Facca G, Tonani F (1967) The self-sealing geothermal field. Bull Volcanol 30:271–273
Faure G (1986) Principles of isotope geology, 2nd edn. John Wiley & Sons, New York
Faure G (2001) Origin of igneous rocks – The isotopic evidence. Springer, Berlin
Ferguson J, McIver JR, Danchin RV (1975) Fenitization associated with the alkaline carbonatite complex of Epemba, South West Africa. Trans Geol Soc S Afr 78:111–122
Ferry JM (1983) Regional metamorphism of the Vassalboro Formation, south-central Maine, USA: a case study of the role of fluid in metamorphic petrogenesis. J Geol Soc London 140:551–576
Fitton JG, Upton BGJ (eds) (1987) Alkaline igneous rocks. Geol Soc Spec Publ 30. Blackwell Scientific Publ, Oxford
Fleet ME (2003) Sheet silicates: Micas. In: Deer WA, Howie RA, Zussman J (eds) Rock-forming minerals, vol 3A, Geol Soc, London
Flint D, Abeysinghe PB (2000) Geology and mineral resources of the Gascoyne region. Geol Surv West Aust Record 2000/7
Fournier RO (1989) Geochemistry and dynamics of the Yellowstone National Park hydrothermal system. Ann Rev Earth Planet Sci 17:13–53
Frost BR, Mavrogenes JA, Tomkins AG (2002) Partial melting of sulfide ore deposits during medium- and high-grade metamorphism. Can Mineral 40:1–18

Gifkins C, Herrmann W, Large R (2005) Altered volcanic rocks – A guide to description and interpretation. Centre Ore Depos Res, Univ Tasmania, Hobart
Gozzard JR (2006) Image processing of ASTER multispectral data. Geol Surv West Aust Rec 2006/9
Grant JA (1986) The isocon diagram – A simple solution to Gresens' equation for metasomatic alteration. Econ Geol 81:1976–1982
Green GR, Ohmoto H, Date J, Takahashi T (1983) Whole-rock oxygen isotope distribution in the Fukazawa-Kosaka area, Hokoruku District, Japan, and its potential application to mineral exploration. Econ Geol Monogr 5:395–411
Gregory RT, Criss RE (1986) Isotopic exchange in open and closed systems. In: Valley JW, Taylor HP, O'Neil JR (eds) Stable isotopes in high temperature processes. Rev Mineral 16, Min Soc Am 91–128
Gresens RL (1967) Composition-volume relationships of metasomatism. Chem Geol 2:47–65
Guilbert JM, Lowell JD (1974) Variations in zoning patterns in porphyry ore deposits. Can Inst Min Metall Bull 67:99–109
Guilbert JM, Park CF (1986) The geology of ore deposits. Freeman, New York, San Francisco
Gupta RP (1991) Remote sensing geology. Springer-Verlag, Berlin
Haapala I (1986) Origin of albites in mineralised granites. Proceedings of joint meeting of working group Gp2-4. IGCP Proj 220. BMR Rec 1986/10:22–23
Hanson GN (1980) Rare earth elements in petrogenetic studies of igneous systems. Annu Rev Earth Planet Sci 8:371–406
Hardie LA (1987) Dolomitisation: A critical view of some current views. J Sediment Petrol 57:166–183
Hedenquist JW (1986) Geothermal systems of the Taupo Volcanic Zone: their characteristics and relation to volcanism and mineralisation. R Soc N Z Bull 23:134–168
Hedenquist JW, Browne PRL (1989) The evolution of the Waiotapu geothermal system, New Zealand, based on the chemical and isotopic composition of its fluids, minerals and rocks. Geochim Cosmochim Acta 53:2235–2257
Hedenquist JW, Henley RW (1985) Hydrothermal eruptions in the Waiotapu geothermal system, New Zealand: origin, breccia deposits and effect on precious metal mineralization. Econ Geol 80:1640–1666
Hedenquist JW, Izawa E, Arribas A, White NC (1996) Epithermal gold deposits: styles, characteristics and exploration. Poster, Soc Res Geol Sp Publ 1
Hemley JJ, Jones WR (1964) Chemical aspects of hydrothermal alteration with emphasis on hydrogen metasomatism. Econ Geol 59:538–569
Hemley JJ, Hostetler PB, Gude AJ, Mountjoy WT (1969) Some stability relations of alunite. Econ Geol 64:599–612
Henderson P (1996) The rare earth elements: introduction and review. In: Jones AP, Wall F, Williams CT (eds) Rare earth minerals – chemistry, orgin and ore deposits. Chapman & Hall, London, pp 1–20
Henley RW, Ellis AJ (1983) Geothermal systems ancient and modern: a geological review. Earth Sci Rev 19:1–50
Hoefs J (2004) Stable isotope geochemistry, 5th edn. Springer, Berlin
Hollister VF (1978) Geology of the porphyry copper deposits of the western hemisphere. Am Inst Min Metall Pet Eng
Huston DL (2001) Geochemical dispersion about the Western Tharsis Cu-Au deposit, Mt Lyell, Tasmania. J Geochem Expl 72:23–46
Ishikawa Y, Sawaguchi T, Iwaya S, Horiuchi M (1976) Delineation of prospective targets for Kuroko deposits based on modes of volcanism of underlying dacite and alteration halos. Mining Geol 26:105–117
Jia YF, Kerrich R (2000) Giant quartz vein systems in accretionary orogenic belts: the evidence for a metamorphic fluid origin from $\delta^{15}N$ and $\delta^{13}C$ studies. Earth Planet Sci Lett 184:211–224

Kawahata H, Furuta T (1985) Sub-sea-floor hydrothermal alteration in the Galapagos spreading center. Chem Geol 49:259–274
Kinnaird JA (1985) Hydrothermal alteration and mineralisation of the alkaline anorogenic ring complexes of Nigeria. J Afr Earth Sci 3:229–252
Kirwin DJ (1985) Tourmaline breccia pipes. Unpublished Msc Thesis, James Cook Univ, N Queensl, 139 pp
Kornprobst J (2002) Metamorphic rocks and their geodynamic significance. Kluwer Acad Publ, Dordrecht
Kresten P (1988) The chemistry of fenitisation: examples from Fen, Norway. Chem Geol 68:329–349
Kwak TAP (1994) Hydrothermal alteration in carbonate-replacement deposits; ore skarns and distal equivalents. In: Lentz DR (ed) Alteration and alteration processes associated with ore-forming systems. Short Course Notes 11, Geol Ass Can 381–402
Lambert IB, Sato T (1974) The kuroko and associated deposits of Japan: a review of their features and metallogenesis. Econ Geol 69:1215–1236
Large RR, Gemmell JB, Paulick H (2001) The aleration box plot – a simple approach to understanding the relationship between alteration mineralogy and lithogeochemistry associated with volcanic-hosted massive sulphide deposits. Econ Geol 96:957–971
Larson PB, Taylor HP (1986) $^{18}O/^{16}O$ relationships in hydrothermally altered rocks from the Lake City caldera, San Juan Mountains, Colorado. J Volcanol Geothermal Res 30:47–82
Le Bas MJ (1977) Carbonatite nepheline volcanism. John Wiley & Sons, New York
Le Bas MJ (1987) Nephelinites and carbonatites. Geol Soc London, Sp Publ 30:53–83
Leblanc M, Lbouabi M (1988) Native silver mineralisation along a rodingite tectonic contact between serpentinite and quartz-diorite (Bon Azzer, Morocco). Econ Geol 83:1379–1391
Lentz DR (ed) (1994) Alteration and alteration processes associated with ore-forming systems. Short Course Notes 11, Geol Ass Can, Waterloo, Ont, 467pp
Lexa J, Štohl J, Konecny V (1999) The Banska Stiavnica ore district: relationship between metallogenic processes and the geological evolution of a stratovolcano. Miner Depos 34:639–654
Lillesand TM, Kiefer RW (1987) Remote sensing and image interpretation, 2nd edn. John Wiley & Sons, New York
Lottermoser BL (1990) Rare-earth element and heavy metal behaviour associated with the epithermal gold deposit on Lihir Island, Papua New Guinea. J Volcanol Geothermal Res 40:269–289
Lowell JD, Guilbert JM (1970) Lateral and vertical alteration-mineralization zoning in porphyry ore deposits. Econ Geol 65:373–408
Manning DC (1982) An experimental study of the effects of fluorine on the crystallization of granite melts. In: Evans AM (ed) Metallization associated with acid magmatism. John Wiley & Sons, Chichester, pp 191–203
Mariano AN (1989) Economic geology of rare earth elements. Rev Mineral 21:309–337
Marshall B, Vokes FM, Larocque ACL (2000) Regional metamorphic remobilization: upgrading and formation of ore deposits. Rev Econ Geol 11:19–38
Martini JEJ (1988) As-Zn mineralisation associated with a Proterozoic geothermal system in the Rooiberg Group. S Afr J Geol 91:337–345
Mauger AJ, Keeleing, JL, Huntington JF (2007) Alteration mapping of the Tarcoola Goldfield (South Australia) using a suite of hyperspectral methods. Trans Inst Min Metall, App Earth Sci B 116:2–12
McGregor GJ (1986) Geology of the Black Mountain orebody. In: Abstr Geocongress '86, Johannesburg. Geol Soc S Afr 1025–1028
McLeod RL, Stanton RL (1984) Phyllosilicate and associated minerals in some Paleozoic stratiform sulfide deposits of south-eastern Australia. Econ Geol 79:1–22
Meinert LD, Dipple GM, Nicolescu S (2005) World skarn deposits. Econ Geol 100th Anniv Vol: 299–336

Meyer C, Hemley JJ (1967) Wall rock alteration. In: Barnes HL (ed) Geochemistry of hydrothermal ore deposits, 1st edn. Holt Rinehart & Winston, New York, pp 166–235
Michard A (1989) Rare earth element systematics in hydrothermal fluids. Geochim Cosmochim Acta 53:745–750
Morrow DW (1982a) Diagenesis 1. Dolomite – Part 1: the chemistry of dolomitisation and dolomite precipitation. Geosci Can 9: 5–13
Morrow DW (1982b) Diagenesis 2. Dolomite-Part 2: dolomitizing models and ancient dolostones. Geosci Can 9:95–107
Mottl MJ (1983) Metabasalts, axial hot springs, and the structure of hydrothermal systems at mid-ocean ridges. Geol Soc Am Bull 94:161–180
Mutschler FE, Wright EG, Ludington S, Abbott JT (1981) Granite molybdenite systems. Econ Geol 76:874–897
Mutschler FE, Griffin ME, Scott Stevens D, Shannon SS (1985) Precious metal deposits related to alkaline rocks in the north American Cordillera- An interpretive view. Trans Geol Soc S Afr 88:355–377
Nash JT, Granger HC, Adams SS (1981) Geology and concepts of genesis of important types of uranium deposits. Econ Geol 75th Anniv Vol: 63–116
Nesbitt BE (1996) Applications of oxgen and hydrogern isotopes to exploration for hydrothermal mineralization. Soc Econ Geol, SEG Newsletter 27:1–13
Nesbitt HW, Young GM (1982) Early Proterozoic climates and plate motions inferred from major element chemistry of lutites. Nature, 299:715–717
Neumann ER, Wilson M., Heeremans M, Spencer EA,Obst K, Timmerman MJ, Kirstein L (2004) Carboniferous-Permian rifting and magmatism in southern Scandinavia, the North Sea and northern Germany: a review. Geol Soc, Lond Sp Publ 223:11–40
Ninomiya Y (2002) Mapping quartz, carbonate minerals, and mafic–ultramafic rocks using remotely sensed multispectral thermal infrared ASTER data. In: Thermosense XXIV Maldagueand XP, Rozlosnik AE (eds), Proceed SPIE — Int Soc Opt Eng 4710:191–202
Ohmoto H (1986) Stable isotope geochemistry of ore deposits. In: Valley JW, Taylor HP, O'Neil JR (eds) Stable isotopes in high temperature geological processes. Rev Mineral 16, Min Soc Am 491–560
Palandri JL, Reed MH (2004) Geochemical models of metasomatism in ultramafic systems: Serpentinization, rodingitization and seafloor carbonate chimney precipitation. Geochim Cosmochim Acta 68:1115–1133
Pearson JM, Taylor WR, Barley ME (1995) Geology of the alkaline Gifford Creek Complex, Gascoyne Complex, Western Australia. Aus J Earth Sci 43:299–309
Pearson JM, Taylor WR (1996) Mineralogy and geochemistry of fenitized alkaline ultrabasic sills of the Gifford Creek Complex, Gascoyne Province, Western Australia. Can Miner 34:201–219
Pearton TN, Viljoen MJ (1986) Antimony mineralisation in the Murchison greenstone belt. In: Anhaeusser CR, Maske S (eds) Mineral deposits of Southern Africa. Geol Soc S Afr 1:293–321
Pentecost A (2003) Cyanobacteria associated with hot spring travertines. Can J Earth Sci 40:1447–1457
Phillips GN (1986) Geology and alteration in the Golden Mile, Kalgoorlie, Econ Geol 81:779–808
Pichavant M (1981) An experimental study of the effect of boron on a water saturated haplogranite at 1kbar vapour pressure. Contrib Mineral Petrol 76:430–439
Pichavant M, Manning D (1984) Petrogenesis of tourmaline granites and topaz granites; the contribution of experimental data. Phys Earth Planet Int 35:31–50
Pirajno F (1992) Hydrothermal mineral deposits – Principles and fundamental concepts for the Exploration Geologist. Springer-Verlag
Pirajno F (1994) Mineral resources of anorogenic alkaline complexes, Namibia: a review. Aus J Earth Sci 41:157–168
Pirajno F, Jacob RE (1987) Sn-W metallogeny in the Damara Orogen, South West Africa/ Namibia. S Afr J Geol 90:239–255

Pirajno F, Schlögl HU (1987) The alteration-mineralisation of the Krantzberg tungsten deposit, South West Africa/Namibia. S Afr J Geol 90:499–508
Pirajno F, Smithies RH (1992) The FeO/Feo + MgO ratio of tourmaline: a useful indicator of spatial variations in granite-related hydrothermal mineral deposits. J Geochem Expl 42:371–382
Pisutha-Arnond V, Ohmoto H (1983) Thermal history, and chemical and isotopic compositions of ore-forming fluids responsible for kuroko massive sulfide deposits in the Hokoruku district of Japan. Econ Geol Monogr 5:523–558
Plimer IR (1987) The association of tourmalinite with stratiform scheelite deposits. Mineral Depos 22:82–291
Pollard PJ (1983) Magmatic and postmagmatic processes in the formation of rocks associated with rare element deposits. Trans Inst Min Metall 92:B1–B9
Prins P (1981) The geochemical evolution of the alkaline and carbonatite complexes of the Damaraland igneous province, South West Africa. Ann Univ Stellenbosch Ser A1 Geol 3:145–278
Proskurowski G, Lilley MD, Seewald JS, Früh-Green GL, Olson EJ, Lupton JE, Sylva SP, Kelley DS (2008) Abiogenic hydrocarbon production at Lost City hydrothermal field. Science 319:604–607
Rona PA (1984) Hydrothermal mineralization at seafloor spreading centers. Earth Sci Rev 20:1–104
Rose AW, Burt DM (1979) Hydrothermal alteration. In: Barnes H L (ed) Geochemistry of hydrothermal ore deposits. John Wiley & Sons, New York, pp 173–227
Rosenbauer RJ, Bischoff JL (1983) Uptake and transport of heavy metals by seawater: a summary of the experimental results. In: Rona PA, Bostrom K, Laubier L, Smith KL (eds) Hydrothermal processes at seafloor spreading centers. Plenum, New York, pp 177–198
Rozendaal A, Stumpfl EF (1984) Mineral chemistry and genesis of Gamsberg zinc deposit, South Africa. Trans Inst Min Metall 93:B161–B175
Seedorff E, Dilles JH, Proffett JM, Einaudi MT, Zurcher L, Stavast WJA, Johnson, DA, Barton MD (2005) Porphyry deposits: characteristics and origin of hypogene features. Econ Geol 100th Anniv Vol: 251–298
Seyfried WE, Janecky DR (1985) Heavy metal and sulfur transport during subcritical and supercritical hydrothermal alteration of basalt: Influence of fluid pressure and basalt composition and crystallinity. Geochim Cosmochim Acta 49:2545–2560
Seyfried WE, Berndt ME, Seewald JS (1988) Hydrothermal alteration processes at mid-ocean ridges: constraints from diabase alteration experiments, hot spring fluids and composition of the oceanic crust. Can Mineral 26:787–804
Sheppard SMF (1971) Hydrogen and oxygen isotope ratios in minerals from porphyry copper deposits. Econ Geol 66:515–542
Sheppard SMF (1986) Characterization and isotopic variations in natural waters. Rev Mineral 16, Min Soc Am 165–183
Sheppard S, Rasmussen B, Muhling JR, Farrell TR, Feltcher IR (2007) Grenvillian-aged orogenesis in the Palaeoproterozoic Gascoyne Complex, Western Australia: 1030-950 Ma reworking of the Proterozoic Capricorn Orogen. J Metam Geol 25:477–494
Shirozu H (1974) Clay minerals in altered wall rocks of the kuroko-type deposits. Min Geol Spec Issue 6:303–311
Siemiatkowska KM, Martin RF (1975) Fenitization of the Mississagi quartzite, Sudbury area, Ontario. Bull Geol Soc Am 86:1109–1122
Slack JF (1996) Tourmaline associations with hydrothermal ore deposits. Rev Mineral 33:559–641
Slack JF, Herriman N, Barnes RG, Plimer IR (1984) Stratiform tourmalinites in metamorphic terranes and their geologic significance. Geology 12:713–716
Smith MP, Henderson P, Campbell LS (2000) Fractionation of the REE during hydrothermal processes: constraints from the Bayan Obo Fe-REE-Nb deposit, Inner Mongolia, China. Geochim Cosmochim Acta 64:3141–3160

Spear FS (1993) Metamorphic phase equilibria and pressure-temperature-time paths. Mineral Soc Am Monogr Ser, 799pp
Spooner ETC, Fyfe WS (1973) Sub-sea-floor metamorphism, heat and mass transfer. Contr Mineral Petrol 42:287–304
Spry PG, Marshall B, Vokes FM (eds) (2000) Metamorphosed and metamorpogenic ore deposits. Rev Econ Geol 11, 310pp
Stanton RL (1972) Ore petrology. McGraw-Hill, New York, 713 pp
Stanton RL (1982) An alternative to the Barrovian interpretation? Proc Australas Inst Min Metall 82:11–32
Stanton RL (1983) The direct derivation of sillimanite from a kaolinitic precursor: evidence from the Geco Mine, Manitouwadge, Ontario. Econ Geol 78:422–437
Stanton RL (1989) The precursor principle and the possible significance of stratiform ores and related chemical sediments in the elucidation of processes of regional metamorphic mineral formation. Phil Trans R Soc London A 328:529–646
Sun SS, McDonough WF (1989) Chemical and isotopic systematics of oceanic basalts: implications for mantle compositions and processes. Geol Soc Sp Publ 42:3131–3145
Taylor HP (1974) The application of oxygen and hydrogen isotope studies to problems of hydrothermal alteration and ore deposition. Econ Geol 69:843–883
Taylor HP (1983) Oxygen and hydrogen isotope studies of hydrothermal interactions at submarine and subaerial spreading centers. In: Rona PA, Bostrom K, Laubier L, Smith KL (eds) Hydrothermal processes at sea-floor spraeding centers. Plenum, New York, pp 83–139
Taylor HP (1997) Oxygen and hydrogen isotope relationships in hydrothermal mineral deposits. In: Barnes HL (ed) geochemistry of hydrothermal ore deposits, 3rd edn. John Wiley & Sons, New York, pp 229–302
Taylor RP, Fryer BJ (1982) Rare earth element geochemistry as an aid to interpreting hydrothermal ore deposits. In: Evans AM (ed) Mineralisation associated with acid magmatism. John Wiley & Sons, New York, pp 357–365
Taylor RP, Fryer BJ (1983) Rare earth element lithogeochemistryof granitoid mineral deposits. CIM Bull 76:74–84
Taylor RP, Pollard PJ (1996) Rare earth element mineralization in peralkaline systems: the T-zone REE-Y-Be deposit, thor lake, Northwest Territories, Canada. In: Jones AP, Wall F, Williams CT (eds) Rare earth minerals – chemistry, orgin and ore deposits. Chapman & Hall, London, pp 167–192
Thompson AJB, Thompson JFH (eds) (1996) Atlas of alteration – A field and petrographic guide to hydrothermal alteration minerals. Min Depos Div, Geol Ass Can, Mem Univ Newfoundland, St John's Newfoundland
Thompson AJB, Hauff PL, Robitaille AJ (1999) Alteration mapping in exploration: Application of short-wave infrared (SWIR) spectroscopy. SEG Newslett 39:1–27
Titley SR, Beane RE (1981) Porphyry copper deposits. Part I. Geologic settings, petrology, and tectogenesis. Econ Geol 75th Anniv Vol: 214–235
Van Kranendonk MJ, Pirajno F (2004) Geochemistry of metabsalts and hydrothermal alteration zonesassociated with c. 3.45 Ga chert and barite deposits: implications for the geological setting of the Warrawoona Group, Pilbara Craton, Australia. Geochem Expl Envir Anal 4:253–278
Vearncombe JR (1993) Quartz vein morphology and implications for formation depth and classification of Archaean gold-vein deposits. Ore Geol Rev 8:407–424
Verwoerd WJ (1966) Fenitization of basic igneous rocks. In: Tuttle DF, Gittens J (eds) Carbonatites. Wiley Interscience, New York, pp 295–308
Volesky JC, Stern RJ, Johnson PR (2003) Geological control of massive sulfide mineralization in the Neoproterozoic Wadi Bidah shear zone, southwestern Saudi Arabia, inferences from orbital remote sensing and field studies. Precambr Res 123:235–247
Walter MR, Bauld J, Brock TD (1972) Siliceous algal and bacterial stromatolites in hot springs and geyser deposits of Yellowstone National Park. Science 178:402–405

White NC, Hedenquist JW (1995) Epithermal gold deposits: styles, characteristics and exploration. SEG Newsletter 23:1–13
White WH, Bookstrom AA, Kamilli RJ, Ganster MW, Smith RP, Ranta DA, Steininger RC (1981) Character and origin of Climax-type molybdenum deposits. Econ Geol 75th Anniv Vol: 270–316
William-Jones AE, Heinrich CA (2005) Vapor transport of metals and the formation of magmatic-hydrothermal ore deposits. Econ Geol 100:1287–1312
Woolley AR (1987) The alkaline rocks and carbonatites of the world. Part 1: North and South America. British Mus Nat Hist, Univ Texas Press
Woolley AR (2001) Alkaline rocks and carbonatites of the world. Part 3: Africa. Geol Soc, Lond
Woolley AF, Symes RF, Elliot CJ (1972) Metasomatised (fenitized) quartzites from the Barralam Complex, Scotland. Mineral Mag 38:819–836
Wonder TD, Spry PG, Windom KE (1988) Geochemistry and origin of manganese rich rocks related to iron-formation and sulfide deposits, Western Georgia. Econ Geol 83:1070–1081

Chapter 3
Tectonic Settings, Geodynamics and Temporal Evolution of Hydrothermal Mineral Systems

3.1 Introduction

The topic of tectonic settings and mineral deposits was addressed by the well-known books by Mitchell and Garson (1981), Hutchison (1983) and Sawkins (1990). Condie (1997, 2005) examined the tectonics and crustal evolution of the Earth. Review papers on tectonic settings of mineral systems include Kerrich et al. (2005) and Groves and Bierlein (2007). For the first part of this chapter I draw from these works and discuss the tectonic environment of mineral systems. In the second part I discuss the temporal evolution and distribution of mineral systems. It is difficult to avoid including magmatic ore systems in these discussions, because they and hydrothermal mineral deposits within the same tectonic setting may be interrelated. An example is provided by the Bushveld Igneous Complex, where magmatic, magmatic-hydrothermal and hydrothermal deposits are part and parcel of the same event and related tectonic setting.

Some mineral systems, taken together with igneous and other lithotectonic data, are diagnostic of specific tectonic settings. Conversely, most mineral systems can usually be assigned to defined tectonic settings, providing that the geodynamic evolution of the host terranes is reasonably well established. Other ore systems, such as some of the SEDEX and MVT, may occur in extensional settings that are associated with the inboard of subduction zones and therefore it remains difficult to precisely allocate them to a specific tectonic setting. Tectonic settings are also linked to supercontinent cycles, for example extension and divergent margins, which occur during supercontinent break-up and convergent margins associated with amalgamation of terranes and assembly. The temporal evolution of supercontinent cycles, assembly to break-up, provides the basis for understanding the temporal distribution of ore systems. This aspect is taken up in more detail in Section 3.4.

F. Pirajno, *Hydrothermal Processes and Mineral Systems*,

© Springer Science+Business Media B.V. 2009

3.2 Tectonic Settings and Geodynamics of Mineral Systems

Condie (1997, 2005) considered the following: ocean ridges, settings related to mantle plumes, continental rifts, cratons and passive margins, arc systems and orogens. Others considered tectonic settings in terms of convergent and divergent plate environments (Sawkins 1990), or continental rifts and hot spots, passive margins and interior basins, oceanic settings, subduction-related settings, collision-related settings and transform faults Mitchell and Garson (1981). An excellent book that describes tectonic settings from Archaean to present is that of Windley (1995). In an earlier book (Pirajno 1992), I discussed extensional (spreading centres and intracontinental rifts), passive margins and interior basins, compressional settings (subduction, continental collision, thrust belts) and transform tectonic settings. Table 3.1 presents another version that I put together in occasion of a short course for Honours students at the University of Western Australia in 2007. Table 3.1 is not meant to show a classification or mineral systems, but only provide a view of tectonic settings of ore deposits, with some notable examples and element associations. Figure 3.1 shows a cartoon depicting a segment of the Earth's lithosphere, main tectonic settings and regions of the crust where hydrothermal activity occurs.

Groves and Bierlein (2007) considered the geodynamic settings of ore systems in terms of (1) intracratonic magmatism; (2) mantle mafic magmatism; (3) deep alkaline magmatism; (4) intracontinental rifting or continental break-up; (5) divergent margins; (6) convergent margins; and (7) sediment-hosted deposits of non-diagnostic geodynamic setting. A synopsis of their work is presented here. Continental crust of intracratonic settings can be characterised by anomalous mantle magmatism above a thick subcontinental mantle lithosphere (SCML). This mantle plume-type magmatism is possibly related to weak extension, due to failed supercontinent break-up. According to Groves and Bierlein (2007), this is a geodynamic setting that is conducive to PGE in large layered intrusions (e.g. Bushveld Complex, South Africa), diamondiferous alkaline pipes and iron oxide-copper-gold (IOCG) associated with A-type magmas. Mantle mafic magmatism produces large layered mafic-ultramafic intrusions with a well defined magmatic stratigraphy (ultramafic base and mafic upper layers). Chromitite seams, PGE and Fe-Ti-V magnetite layers occur at predictable stratigraphic position within these layered intrusions. The Bushveld Complex, the Great Dyke of Zimbabwe and the Stillwater Complex (USA) are typical examples. Furthermore, these complexes tend to occupy central positions within Archaean cratons and the authors suggested that the preservation and centralised position of these large magmatic masses in cratonic areas are made possible by the thick and buoyant subcontinental lithospheric mantle (SCLM). Thick and buoyant SCLM mostly underlies Neoarchaean and Palaeoproterozoic terranes, which is where most of the large layered complexes are emplaced. Deep mantle-derived alkaline magmatism is also largely located in Archaean cratons. The origin of these alkaline magmas is attributed to the impingement of mantle plumes

Table 3.1 TECTONIC ENVIRONMENTS OF ORE SYSTEMS; summary tabulation

PLATE TECTONIC ENVIRONMENT	TECTONIC AND/OR GEOLOGICAL ENVIRONMENT	ORE DEPOSIT TYPE	METAL ASSOCIATION	Chapters in this book, where applicable
INTERPLATE / CONVERGENT PLATE / SUBDUCTION	Back arc rifts	Intrusion-related polymetallic systems Volcanic-hosted massive sulphides (Kuroko and Abitibi types) Iberian Pyrite Belt (Rio Tinto) Contact metasomatic Polymetallic veins	Au, Sn, W, Mo, Cu, Mo, U, Hg, F Cu, Pb, Zn, Ag, ±Au Zn, Cu, Pb, Ag Cu, Pb, Zn, Ag, Au W, Au, Sb, Hg, (±Mo, Be), F Ni, Cu, Ag, au, PGE, Co Zn, Pb, Cu, Ba, F	4 7 7 6 4
	Foreland basins	Mississippi Valley Type (MVT)		9
	Magmatic Arc	Intrusion-related polymetallic systems Porphyry Cu-breccia Skarn Volcanic-hosted epithermal - High sulphur - Low sulphur - Alkalic type	Cu, Au, Ag,Sn,W, Bi, As, Sb, Te, Mo Cu±Mo, Au, Ag, Pb, Zn Cu, Mo±W Fe, Sn, W, Cu, Pb, Zn, Au Au, Ag, Hg, Sb, W, S (Pb, Zn) Au, Ag, Hg, Tl, Ba Au, Ag, Te, Mo, As, Hg	4 5 6 7
	Intraoceanic, continental	Hot springs (McLaughlin)	Au, W, Sb, Hg	
	CONTINENTAL COLLISION ENVIRONMENTS: Accreted terranes, Fold-and-Thrust belts	Orogenic Mesothermal lodes	Au, W, Sb, As, Bi	9
	Collision-granitoids	Stockwork veins, vein complexes, or single veins, skarns, greisens, pegmatites, alaskites	Sn, W, Li, Bi, Be, U (Nb, Ta), Mo	4,6,13
	Obducted oceanic crust Ophiolites	Massive sulphide (Cyprus-type) Podiform Cr in dunite	Cr, Fe-Cu-Zn, Au	7
TRANSFORM FAULTS	'Leaky' transforms Oceanic transform	Salton Sea, McLaughlin hot spring-type?	Cu-Zn, Au, As, Sb, Hg, Ba, W Ba-, Fe-, Mn-oxides and hydroxides	7
SEA-FLOOR SPREADING	Ocean floor, Mid-ocean ridges	Ferromanganese nodules Metalliferous sediments 'Black smokers'/'white smokers'	Fe, Mn, ±Ni, Co Fe, Mn, Cu Pb Zn Ba, Fe, Zn, Cu ±Co, Pb, Au, Ag	8 7 7
	Gulf of California setting	Sediment-volcanic-hosted massive sulphides (Besshi-type)	Cu, Zn, Co, Au, Ag	
DIVERGENT PLATE BOUNDARIES / ADVANCED STAGES	Red Sea type rift	Exhalative (sea-floor) Red Sea type brine pools Volcanic hosted massive sulphide (Bathurst-type)	Fe, Mn, Cu, Pb, Zn, Ba ± Ag Fe, Gu,Pb, Zn, Ba Pb, Zn, Ag ± Cu	7 8 7
	Passive margins	Chemical Sediment/Exhalative/Basinal brines Iron formation (Superior-type; Precambrian only) Black shales Carbonate rocks-hosted (Mississippi Valley-type; eg Lennard Shelf)	Fe, Mn Fe, Mn, P Au, Mo, Ni, PGE Zn, Pb, Cu, Ba, F	8 8 9 9
EARLY CONTINENTAL RIFTING, AULACOGENS		Breccia pipes, fissure lodes, veins	Cu, Au, Ag-Co-Ni-As	4
		Rift-related porphyry-epithermal systems	Mo, Au	5
		Stratiform sedimentary rock-hosted (SEDEX): Shale/Sandstone host (Zambia/Kupferschiefer) Evaporites Unconformity-related (Mid-Prot.)	Cu, Co, Fe, Pb, Zn, Se, Ag ± Au, Ba Pb, Zn, ±Cu, Ni, Co, V, Ba U, PGE, Mo, Co	8 13
INTRAPLATE / INTRACONTINENTAL HOTSPOTS; ANOROGENIC		Anorogenic granites Greisen, quartz veins, pipes, disseminations Breccias pipes, replacement bodies, pegmatites A-granitoids (Olympic Dam-style) Anorthosite massifs	Sn, Nb, Ta, W, U Th, Be, Zn, Cu Sn, W, Li, Be Fe, Au, U, REE, Cu, Ba, F Fe-Ti-V	4 4 4 4
		Komatiite (Archaean only)	Ni, Cu, Ag, Au, PGE, Co	
	Layered igneous complexes/Flood basalts	Bushveld-Stillwater-types Continental flood basalts, Noril'sk-type Voisey's Bay – troctolite	Cr, PGE, V, Fe, Ti, Cu, Ni, Co Ni, Cu, PGE Ni, Co, Cu	
	Alkaline igneous rocks	Carbonatites Kimberlites, Lamproite Peralkaline complexes (breccia pipes)	Nb, Fe, Ti, Cu, REE, P, F, U Diamond Nb, Fe, Ni, Cu, Co, REE, P, F, U	4
INTERIOR BASINS; SURFICIAL DEPOSITS	Weathering environment	Laterite-, karst-, reworked sedimentary bauxite Weathered ultramafics → Laterite Calcrete-host Regolith Sandstone-hosted/roll front Evaporite-related deposits	Al Ni U Au U Salts	13
	Placer	Mechanical concentration of heavy minerals	Au, Sn, Diamonds, ilmenite, rutile, zircon	
	Palaeoplacers	Witwatersrand, Late Archaean conglomerates	Au, U	

beneath the SCML, triggering melting of metasomatised lithospheric mantle material, or newly metasomatised by volatiles derived from the mantle plume. Consequently these magmas have complex isotopic and geochemical signatures. Conditions near the base of the SCML of relatively low T and high P, are required for the presence of diamonds, brought to the surface by kimberlitic and lamproitic melts. The IOCG systems, treated in Chapter 4, include a widely

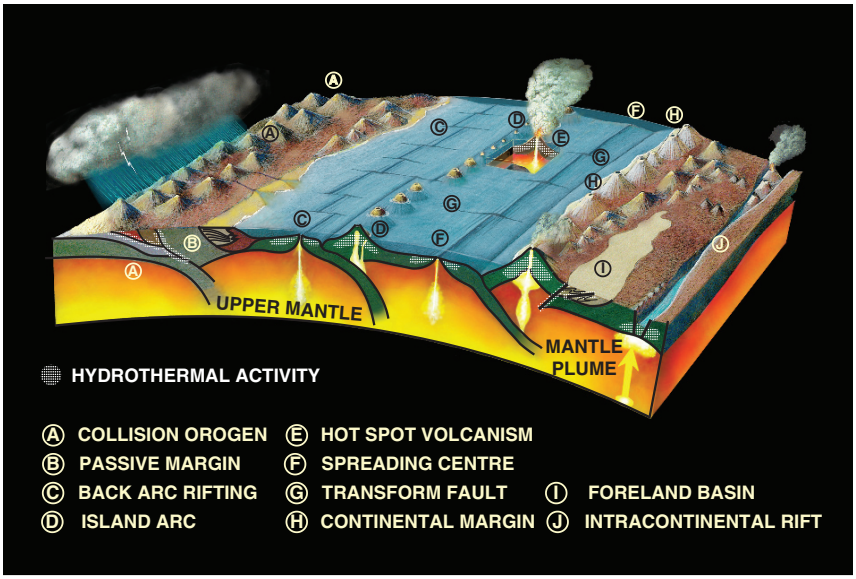


Fig. 3.1 Cartoon (not to scale) showing tectonic settings and regions where hydrothermal activity occurs. More details in text. This cartoon was drafted by Murray Jones (Geological Survey of Western Australia)

diverse group of ore systems. However, Groves and Bierlein (2007) pointed out that if only IOCG of Precambrian age are considered, then the IOCG family becomes easier to define, both as deposit style and in terms of geodynamic setting. Precambrian IOCG tend to occur near the margins of Archaean cratons or at the boundary between Archaean cratons and Proterozoic belts. These IOCG are all related to anorogenic alkaline and/or A-type magmatism associated with the impingement of mantle plumes and partial melting of SCML, previously metasomatised by subduction processes.

Ore systems related to continental break-up are sited in rifted cratonic margins and intracratonic rift basins. Orthomagmatic Ni-Cu-(PGE) deposits in mafic-ultramafic intrusions of large igneous provinces are related to rifting caused by mantle plume activity. Examples of these ore systems include the world-class Noril'sk (Siberian Traps), Voisey's Bay in Canada, Jinchuan in China. Other magmatic systems in this setting are the Fe-Ti oxides of anorogenic anorthositic magmatism (anorthosite massif type), common in the Mesoproteorozoic Columbia supercontinent, again possibly related to large scale decompression melting that produced large volumes of basaltic magmas and thick anorthositic crust through the activity of mantle plumes. Giant sedimentary rock-hosted mineral systems, discussed in Chapter 8, are formed in intracontinental rift basins. These include the stratabound Cu-Co Copperbelt type deposits of southern-central Africa, the SEDEX Pb-Zn and Broken

Hill type deposits of Australia and South Africa. Their genesis may be linked to basinal brines circulating in the host sedimentary succession, or perhaps to replacement by hydrothermal fluids and/or fluids discharged on the seafloor. The giant Australian deposits (Mt Isa, McArthur River, Century) were developed at 1.65–1.6 Ga, following the assembly of the North Australian, South Australian and Western Australian cratons, within the framework of the Columbia supercontinent. Broken Hill type deposits are similar to and coeval with SEDEX but with higher Pb and Ag contents, and are associated with bimodal volcanic sequences.

In divergent margin settings there are large-scale sedimentary deposits of Fe and Mn (banded iron formations; BIF), generally formed between 2.65 and 1.85 Ga in passive margins of continents. The largest accumulations of Fe in iron formations are found in the Hamersley province of Western Australia, Carajas in Brazil and the Sishen Fe deposits and Kalahari Mn oxides in South Africa. Volcanogenic massive sulphides (VMS) typically form at spreading centres in oceanic back arcs (e.g. Lau Basin in the Pacific Ocean) and at mid-ocean ridges. In the geological record, some of these deposits are preserved in ophiolitic terranes emplaced by obduction onto continental crust. Fore-arc settings can also produce VMS deposits, caused by extension, thinning of the SCLM, due either to slab roll-back or mantle plumes, which channel hot asthenospheric material through the rift sustaining high temperature submarine hydrothermal activity.

Far back-arc settings include Sn-W deposits in S-type granites, usually associated with continent-continent collisional orogens that close an internal ocean (e.g. Tethys and the Alpine-Himalayan orogen). Far back-arc settings also include W skarns and the Sn-W deposits of the Tasman orogen in eastern Australia. Intrusion-related ore systems are found in similar geodynamic settings of far back-arc or continent-continent collisional orogens, exemplified by the Tintina province of northwestern North America and discussed in Chapter 4. Carlin-type sedimentary rock-hosted Au systems (Chapter 9) were formed in a similar tectonic setting as the intrusion-related systems. They occur in shelf sedimentary rocks near the North American cratonic margin, are associated with extensional tectonism and are typically capped by thick siliciclastic successions, which may have acted as seals to hydrothermal fluids. The origin of Carlin-type systems, as discussed in Chapter 9, remains inconclusive and hotly debated, but again as pointed out by Groves and Bierlein (2007), the Carlin district is spatially associated with magmatic-hydrothermal metallogenic provinces that include porphyry and epithermal systems. The large Cripple Creek epithermal Au deposits in Colorado are related to magmatism in extensional tectonics within an overall convergent margin setting that characterises the North American Cordillera. Similarly, alkalic epithermal Au systems (Chapter 5), such as Ladolam, Emperor in Fiji and Porgera in Papua New Guinea are probably associated with back-arc settings. The source of the Au-rich alkalic melts is thought to be metasomatised lithospheric mantle.

Convergent margin tectonic settings are well endowed with a great variety of ore systems, including arc-related hydrothermal deposits, such as porphyry and epithermal systems, discussed in Chapter 5. Orogenic Au lodes, spanning ages from the Archaean to Tertiary formed by major compressional and/or transpressional deformation events in fore-arcs and back-arcs at convergent margins. Orogenic lode systems (Chapter 9) appear to form at all crustal depths perhaps to about 20 km, thereby having a good preservation potential. These systems originate from the flow of deep-sourced fluids caused by dehydration reactions (Fig. 3.2) and in some cases from asthenospheric upwelling in a thinning SCML probably associated with far-field stresses. A good example of this setting are the Cretaceous orogenic lodes of the Jiaodong Au field in northeastern China. Mineral systems of foreland basin include placers, palaeoplacers and Pb-Zn-Ba of Mississippi Valley Type (MVT) and unconformity-related U deposits. Giant

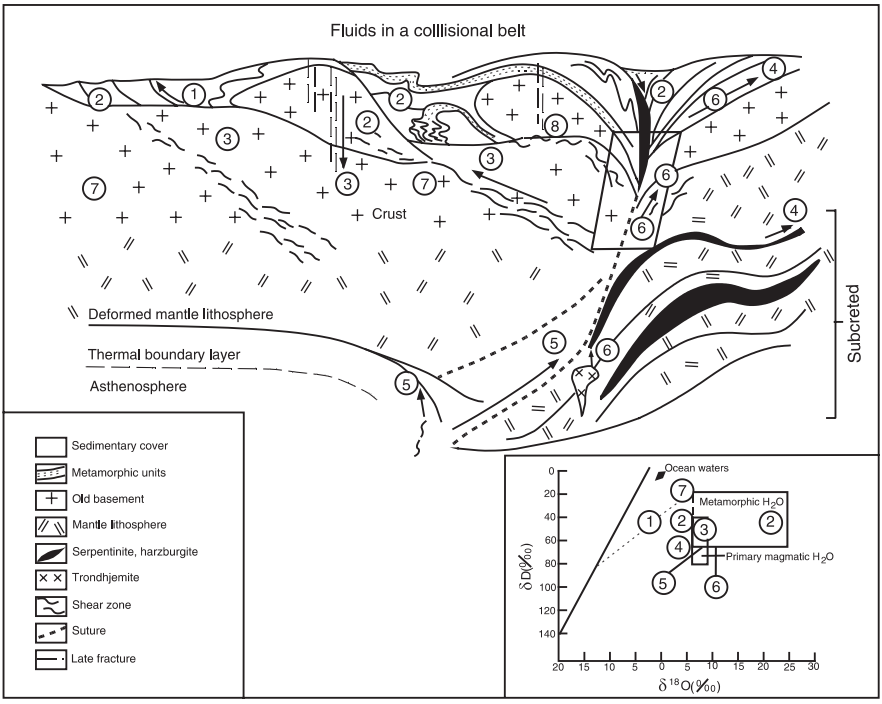


Fig. 3.2 Fluid sources in a collisional orogen and/or transpressive geodynamic regime and associated stable isotopic compositions, after Kerrich and Cassidy (1994) and Kerrich et al. (2000); (1) formation waters expelled from thrust packages and channelled along faults; (2) syntectonic veins; (3) metamorphic fluids from basement rocks; (4) metamorphic fluids from dehydration of accreted oceanic slab; (5) advection of mantle fluids; (6) magmatic fluids generated from melting of the accreted oceanic slab; (7) formation brines that penetrated basement during extensional regimes; (8) low δ18O meteoric water; inset shows stable isotopic compositions associated with the settings 1–7

placer deposits were formed from convergent margins around the Pacific Rim when rapid uplift resulted in the denudation of orogenic lodes (e.g. Alaska, New Zealand, eastern Australia). The richest and most famous palaeoplacers are those of the Witwatersrand basin of South Africa. Models have been proposed that suggest a hydrothermal event(s) for the Witwatersrand Au, but the placer origin remains the best explanation for the world's largest Au province. The geochronology of detrital zircons have demonstrated that the Witwatersrand conglomerate units were deposited in a retro-arc foreland basin on a thick continental crust. The Witwatersrand Au-bearing conglomerates contain rounded pyrite (called by South African geologists, buckshot pyrite) and uraninite grains, whose presence in these sediments is a clear indication of an oxygen-poor atmosphere or at least, climatic conditions, which have been suggested to be related to a CO_2-rich atmosphere, during degassing of frequent mantle plume activity during Archaean times (Pirajno 2007). Mississippi Valley Type (MVT) ore systems form in foreland basins related to convergent margins. These are stratabound ore systems that form by large-scale basin wide fluid flow, which migrates from a zone of compression (e.g. thrust-and-fold belt) towards the undeformed margins of the continental shelf, where carbonate reefs occur (Chapter 8). Unconformity-related U deposits contribute a substantial proportion of the world's U production. These hydrothermal deposits form in siliciclastic sequences near to unconformities (hence the name) in foreland basins and are common in northern Australia and North America. The unconformity U systems may be linked to supercontinent assembly at 1.8–1.7 Ga, which resulted in the deposition of thick sedimentary successions (Chapter 13).

In the sections that follow, I briefly discuss convergent margins and arc settings, settings related to mantle dynamics in which I include intracontinental rifting, delamination tectonics and post-orogenic environments. I conclude with synopses on metallogeny and geodynamics and the temporal evolution of mineral systems.

3.2.1 Convergent Plate Boundaries; Arc and Back-Arc Settings, Collision Tectonics

Convergent plate margins are characterised by a higher density tectonic plate subducting beneath a lower density plate. Convergence generates a continental magmatic arc where oceanic lithosphere subducts a continental margin (e.g. Andean arc), or an island arc where older oceanic crust subducts younger and less dense oceanic crust. Convergent plate margins have landward of a deep trench, a subduction-accretion complex, a magmatic arc and a foreland thrust belt. Configurations of subduction-trench-arc-back-arc systems and associated ore systems are shown in Fig. 3.3. The relationship of the angle of descent of oceanic crust (dip of the Benioff zone) to plate motions, stress

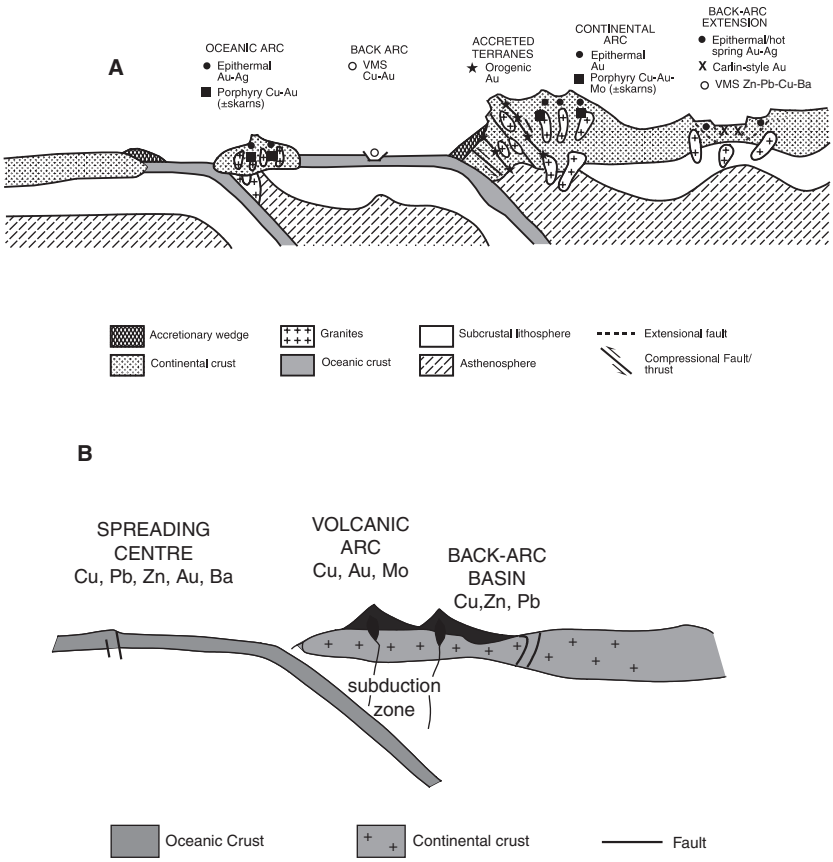


Fig. 3.3 (**A**) This figure was first published in Groves et al. (1998) referring to epigenetic Au-rich mineral deposits. The tectonic settings shown in this figure, however, effectively apply to a wide range of subduction- and back arc-related ore systems; (**B**) subduction, back arc and continental rift and associated ore systems

field and magma generation is instrumental in the type of ensuing magmatism and metallogenesis. A steep angle of descent, as is the case for the modern-day Mariana, or Tonga-Kermadec subduction systems, is conducive to creating an extensional stress field which would promote the formation of a mafic-dominated volcanic arc, in which porphyry-high-sulphidation epithermal systems develop, an intra-arc rift systems with spreading centres (e.g. the Lau Basin), in which massive sulphide deposits of kuroko affinity may form. By contrast, a shallower subduction zone, such as that occurring under the South American active margin (Andean-type), would result in the development of a shallower trench and a compressive regime behind the intermediate to felsic magmatic arc. This is the domain of large porphyry Cu-Mo and epithermal

deposits. Furthermore, it is important to note that in Andean-type subduction systems, accretionary sedimentary prisms in the trench area are well developed, whereas they may be absent in the Mariana-type trench. The implications of this difference in terms of metallogenesis are extremely important, because the presence of a sedimentary accretionary prism is relevant to the formation of orogenic Au-bearing quartz vein lodes. Active magmatic arc settings are characterised by seismic activity, high heat flow and calc-alkaline volcanism. Intraoceanic island arcs develop on the overriding plate, parallel to the plate boundary, and those of Phanerozoic to Recent ages may range from hundreds to thousands of kilometres long, and up to 100 km wide. Magma generation occurs in the asthenospheric wedge above the dehydrating subducting slab, producing plutonic rocks ranging in composition from dioritic to granodioritic (I-type magmas). These magmas vent at the surface producing a range of volcanic products ranging from basaltic to andesitic to dacitic and rhyolitic. The igneous rocks tend to become more enriched in alkalies and incompatible elements away from the trench, forming a sequence from tholeiites, low-K andesites, dacites (calc-alkaline series) to shoshonites. Andean-type subduction settings form magmatic arcs thousands of kilometres long. Here, too, volcanic rocks are of calc-alkaline affinity, but are more silicic and intermediate in composition, with basaltic rocks being less abundant than in island arcs. The Andean magmatic arcs are characterised by tall strato-volcanoes that consist of andesitic and felsic lavas with abundant and large aprons of pyroclastic rocks. Plutonic rocks comprise a range from tonalites, granodiorite, to quartz-monzonite. Andean-type igneous rocks tend to become more evolved and enriched, with distance from the trench, in alkalies and incompatible elements, reflecting increasing depth to the Benioff zone and increasing thickness of the continental crust. The source and petrogenesis of magmas of subduction zones have great importance not only for the evolution of the magmatic arc in space and time, but also for its metallogenesis. Details on subduction geodynamics and magmatism can be found in Prichard et al. (1993), Tatsumi and Eggins (1995) and Leat and Larter (2003).

Continent-continent, arc-continent, arc-arc, amalgamation of drifting microcontinents, oceanic plateaux, ridges and seamounts and their accretion on to continental margins have all been recognised in the Phanerozoic geological record, especially from the breakup of Gondwana onward. Collision events are considered to be a major factor in uplift and mountain building. Young collision belts are characterised by mountains, fold and thrust belts, zones of intense deformation and metamorphism, obducted ophiolites, and intrusion of post-collision crustally-derived granitoids. The entire Alpine-Himalayan orogenic belt was largely formed by the closure of the Tethys oceanic basins, and the collision of a number of microcontinental fragments from the northern edge of the Gondwana continent with the Laurasian continent. Similarly, the great Central Asian Orogenic Belt (CAOB) represents a giant collage of island arcs and continental fragments (see references and discussion in Chapter 5). Most of the North American cordilleras were formed by the collision and accretion of a

number of terranes that may have originated from the eastern margin of Gondwana. Allochthonous fragments of oceanic and continental material are regarded as important additions to the growth of continents. Allochthonous terranes originate by rifting and dispersion from a larger landmass, during drifting the fragments may amalgamate before accretion on to a continental margin. From here, however, they can be dispersed and moved along major strike-slip fault systems. The closing of oceanic basins, and the accretion of allochthonous terranes, may result in the emplacement of ophiolites by the obduction process. In many old terranes, all that remains of a former suture is either a line of small slivers of mafic-ultramafic bodies, or, in extreme cases, only a zone of shearing. Ophiolites are discussed more fully in Chapter 7.

Collision can take many forms depending on the nature of the leading edges (arc-continent, continent-continent, accretionary), resulting in the development of orogens or orogenic belts. Windley (1995) proposed two types of orogens: collisional (continent-continent) and accretionary (or Cordilleran type, also called Turkic type; Sengör and Natal'in 1996). Collision of two continental plates is typically marked by ophiolitic suture zones, resulting from the closure of an intervening ocean. Accretionary or Cordilleran orogens, as mentioned above for the CAOB, develop from the assembly and accretion of tectonostratigraphic terranes, mostly fragments of island arcs, oceanic plateaux and microcontinental fragments, all of which assemble to form accretionary prisms. For accretionary orogens, Condie (1997) considered two end-members: simple orogen and complex orogen. The former is characterised by accretion of juvenile terranes, whereas the latter, in addition to juvenile terranes, includes exotic microcontinents. Commonly in accretionary orogens, collision is oblique and not orthogonal and characterised by extensive lateral and vertical accretion above a subducting slab (Kerrich et al. 2005). The degree and nature of the oblique collision also results in the suture zones developing major thrust and/or strike-slip faults, such as those that characterise the Tian Shan orogenic belt in central Asia. These structures can become sites of orogenic Au lodes, due to extensive fluid flow resulting from seismic pumping (Kerrich and Wyman 1990; Goldfarb et al. 2005).

Other important features to note are the retro-arc, fore-arc basins and subduction complex, or accretionary prism of highly deformed sediments interleaved with slivers of oceanic crust. On collision, the sedimentary packages of these basins will form thrust belts, with severely deformed and metamorphosed rocks. These geodynamic effects are of great importance because many orogenic lode deposits originate through the deformation and metamorphism of these sedimentary piles, whereas thrust faults often act as major avenues for mineralising fluids. Another important aspect, from the metallogenic point of view, is the generation of magmas during the evolution of a collision orogen. Harris et al. (1986) recognised four major groups of igneous rocks as follows: (1) pre-collision igneous rock of calc-alkaline chemistry related to subduction; (2) syn-collision peralluminous leucogranites, derived from the hydrated bases of thrust sheets; (3) late to post-collision calc-alkaline intrusions; (4) post-collision

intrusions of alkaline chemistry (A-type magmatism), probably related to upwelling asthenosphere, as discussed further in below. The nature and development of granitic magmatism during collision and subduction processes are addressed more fully in Chapter 4.

3.2.1.1 Orogenesis, Post-Orogenesis and Hydrothermal Fluids

Convergence and collision of continental plates result in the formation of collisional orogens. The shortening of the crust and lithosphere is accompanied by uplift and is followed by extensional collapse. Dewey (1988) envisaged five main stages in the geodynamic evolution of collisional orogens. Stage 1 is the shortening phase, characterised by crustal thickening, development of thrusts, comparatively low geothermal gradients, lack of significant magmatism, and high pressure metamorphism. Stages 2 and 3 involve thermal re-equilibration causing a rise in geothermal gradients, rapid uplift and prograde high temperature metamorphism, accompanied by post-tectonic granitic magmatism. Towards the end of Stage 3, extension begins, which leads to lithospheric thinning and collapse of Stage 4. This extensional collapse engenders the rise of asthenopsheric mantle, induced by the detachment and sinking of pieces of lithospheric mantle in the process of delamination tectonics. The rise of asthenospheric mantle in turn causes a rapid rise in the geothermal gradient and post-orogenic bimodal magmatism. Finally, post-extensional thermal recovery, decreasing geothermal gradients with concomitant decrease of igneous activity and retrograde metamorphism takes place during Stage 5. The nature of granites in collisional orogens generally reflect changes from crustal to mantle derived partial melts, which in turn reflect changes in evolutionary geodynamics. This results in the emplacement of peraluminous granites (two-mica granites of crustal origin) during compression, potassium-rich (metaluminous and calc-alkaline granites of mixed crustal and mantle origin in transitional stages, and finally A-type granites of mantle origin (Barbarin 1999). The latter are commonly followed or accompanied by bimodal alkaline igneous suites, which typically develop in extensional settings (Turner et al. 1996).

Pirajno and Chen (2005), Chen and Pirajno (2005) and Chen et al. (2004) proposed a model, schematically shown in Fig. 3.4, in which four stages, each being the end member of a time-continuum, are considered. These four stages roughly correspond to the first four evolutionary stages of collision and collapse of an intracontinental orogenic system of Dewey (1988). The clockwise *PTt* paths of collisional orogens, reveal a regime from crustal thickening and incipient compression (stage 1) to compression (Pmax, low T; stage 2), through a transition from compression to extension (decreasing P and increasing T; stage 3) to extension (Tmax, low P, stage 3). In stage 1 (Fig. 3.4A) crustal shortening-thickening develops from continent to continent collision with the underthrusting of a continental slab (A-type subduction), imbricate stacking of crustal slices, uplift, high P metamorphism and absence of igneous activity. In stage 2

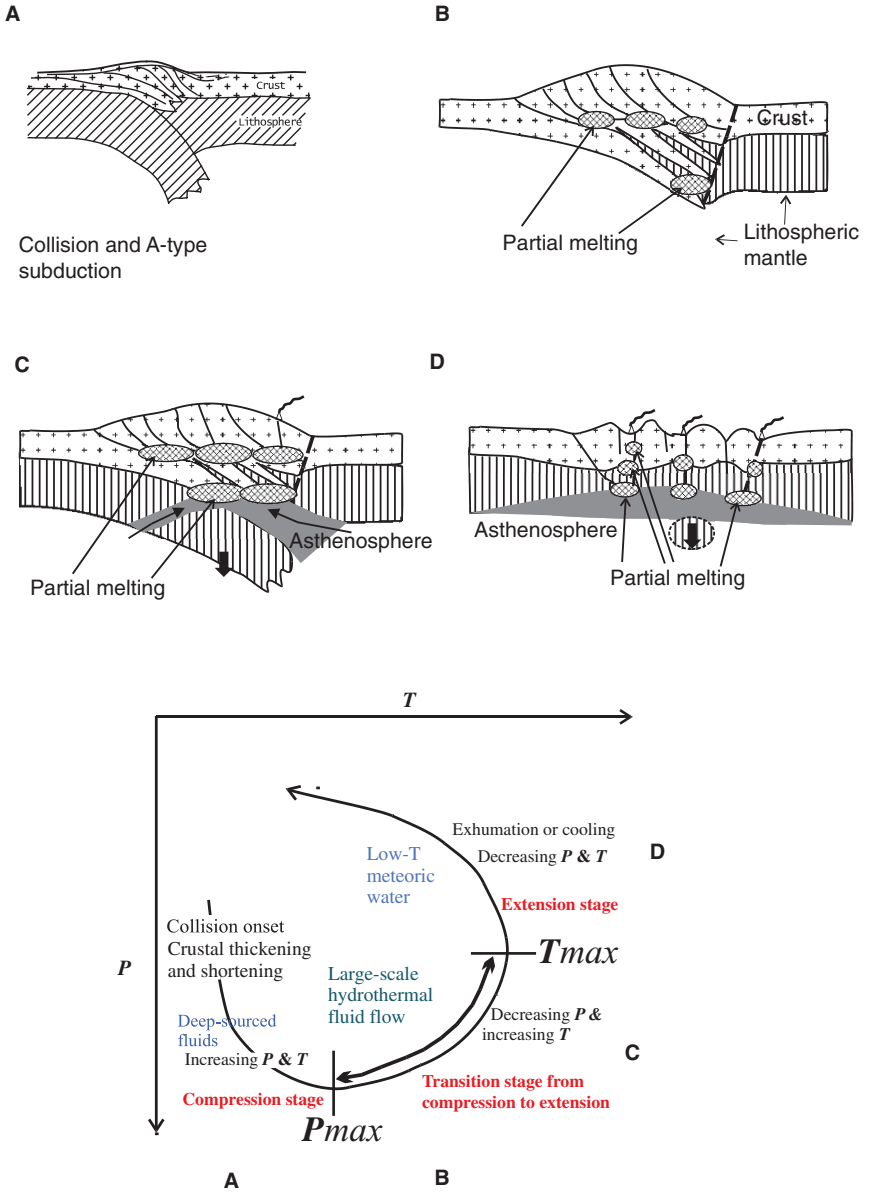


Fig. 3.4 Generation of melts and hydrothermal fluids in collisional orogens; see text for explanation, see also Fig. 9.24. After Chen et al. (2005, 2008) and Pirajno and Chen (2005)

(Fig. 3.4B), slowing down of the convergence and thermal re-equilibration occurs and prograde metamorphism begins from high P/T towards higher T/P. During these early phases, processes of fluid generation begin and are deeply-sourced. However, fluid movement is restricted due to comparatively low geothermal

gradients and lack of suitable channels and structures, because of the dominant compressive regime. At this point heating of the crust can produce S-type granitic melts, represented by muscovite-bearing peraluminous granites, as defined by Barbarin (1999). In stage 3 (Fig. 3.4C), the lithospheric root and the continental subducting slab tend to sink, either by convective thinning and removal of subcontinental mantle lithosphere or by delamination processes. In either case, upwelling of asthenospheric mantle tends to replace the space created by the sinking lithosphere. This results in partial melting of the subcontinental mantle lithosphere and of lower crust. As the tectonic regime begins to change from compresson to extension, the downgoing slab also begins to melt aided by decompression. These melts result in the emplacement of K-rich and calc-alkaline granites, reflecting increasing levels of mantle contribution (Barbarin 1999; see also Table 4.1). The upwelling asthenospheric mantle will produce a large thermal anomaly and the beginning of extension, both of which combine to promote a giant circulation system of hydrothermal fluids. Large amounts of fluids are contributed by devolatilisation reactions. This stage from compression to a predominantly extensional regime is characterised by P-T conditions with peak metamorphic temperatures and decompression melting in the deep levels (i.e. from Pmax to Tmax in response to decompression and rising geothermal gradients; Fig. 3.4C), providing further thermal energy and fluids. Structures would dilate due to regional (terrane or orogen-scale) decompression and uplift providing good conduits for fluid circulation. The spatial and temporal association between intrusive rocks and hydrothermal ore systems is readily explained because in this regime, both fluids and melts move upward at the same time. These upward flowing and deeply-sourced fluids progressively mix with downward flowing, shallow-sourced, fluids along fractures and other favourable conduits. Upon mixing, the upward-flowing deep-sourced fluids and the downward-flowing and shallow-sourced fluids, change their physico-chemical character. This change results in rapid deposition of ore-forming elements, resulting in a stage of intensive mineralisation. Therefore, in this model, the ore-forming fluids are most active during the middle (compression-extension transition) and late (extension) stages of the geodynamic evolution of the orogen.

In the last "snap shot" (stage 4 Fig. 3.4D), extension is now fully established, with a regime chracterised by exhumation, cooling and retrograde metamorphism. It is at this stage that low-T meteoric fluids percolate downward and continue mixing with the deeply-sourced fluids. Retrograde metamorphism is now concentrated along faults and shear zones, as observed in many terranes with orogenic lodes. In this final stage, post-collisional shoshonitic magmatism will be generated and is typically represented by high K alkaline series volcanism in rift basins. Examples of this tectonic setting and related alkaline magmatism are provided by the Mesozoic-Cenozoic rift basins of eastern China and Mongolia (Tian et al. 1992). During this late extensional stage and thermal relaxation (after Tmax, Fig. 3.4D), heat energy and the mobilised ore components become less and the deeply-sourced fluids become negligible, with only the shallow-sourced fluid systems acting weakly and restrictedly. In these late

stages, with decreased P and T, meteoric fluids predominate and fluid flow takes place at lower temperatures, resulting in the deposition of low-temperature minerals, such as carbonates. The nature of the hydrothermal fluids and of complex ions and ligands (e.g. sulphur, chlorides), during the extensional collapse (stages 3 and 4) is not only dependant on temperatures, but also on the nature and composition of the downgoing crustal slab during the A-type subduction. Chen et al. (2004) suggested that these ore systems form a metallogenic zoning, inboard from the collision front, from orogenic-style lodes to porphyry to breccia pipes (see Chapter 9). This regional metallogenic zoning may be the consequence of progressive metamorphism, crustal and asthenopsheric mantle contributions, zonal melting and composition of fluids with depth. Furthermore, the presence of porphyry systems associated with breccia pipes in collisional orogens is indicative of volatile-rich conditions that may have ultimately derived from both the downgoing crustal slab and asthenospheric mantle. This is supported by the fact that several continental rift-associated porphyry systems are Mo-F rich and associated with A-type magmas (see Chapter 5).

3.2.2 Divergent Plate Boundaries; Mid-Oceanic Ridges, Passive Margins and Continental Rifting

Divergent plate boundaries are also called constructive margins, because of the addition of juvenile material from the mantle to the lithosphere and crust. Divergent plate boundaries include spreading centres (mid-ocean ridges) and continental rift systems.

3.2.2.1 Spreading Centres (Mid-Oceanic Ridges) and Passive Margins

At spreading centres, new lithosphere is formed, which consists of mafic material welled up from partially molten asthenosphere, and which forms magma chambers just below the spreading centre. This part of the lithosphere, or oceanic crust, consists of an uppermost layer of basaltic pillow lavas and associated pelagic sediments, underlain and intruded by sheeted dyke systems, passing downward into gabbroic, peridotitic, dunitic and harzburgitic rocks. Once the oceanic crust moves away from the spreading centre it is either consumed in a subduction zone, or it may be accreted to continental margins, or island arcs, forming an ophiolitic sequence.

Spreading centres also form in back arc marginal basins (a modern-day example being the Sea of Japan). Although geochemical discrimination has been attempted to differentiate between mid-ocean centres and marginal basin spreading centres, the distinction in ancient systems is by no means clear. Typical cross-sections depicting oceanic crust are shown in Fig.7.2 and 7.3, bearing in mind that the overall structural configuration of a mid-ocean ridge

system depends on the rates of spreading. Present-day mid-ocean ridges have fracture-controlled black and white smokers, and surrounding metalliferous aprons, with metal association of Fe-Cu-Zn-Pb-Ba-Au-Ag. In the geological record these are represented by ophiolite-hosted stratiform massive sulphide and epigenetic stockwork feeder zone (Cyprus-type). In the Guaymas basin (Gulf of California) smokers vents and metalliferous aprons are buried in terrigenous sediments with a metal association of Cu-Zn-Co-Ag. In the geological record these are represented by Besshi-type massive sulphide deposits, exemplified by the Matchless belt in Namibia and the Sambagawa belt, Japan.

Passive continental margins develop from continental rifts that evolve into oceanic basins. Typical examples are the North American Atlantic margin in its advanced evolutionary state with a continental shelf, slope and rise and the incipient Red Sea margins. Between 2.5 and 1.8 Ga, banded iron formations and granular iron formations developed on passive margins resulting from continental break ups. For more details on tectonic and depositional processes of passive margins, the reader is referred to the thematic issue of the Journal of the Geological Society (Roberts and Kusznir 1997).

3.2.2.2 Continental Rifts

In this section I discuss continental rifting and associated basins, modern and ancient, for which several lines of evidence imply an origin related to lithosphere thinning linked to mantle plume activity. Rift basins are important repository of a wide range of ore systems from magmatic to hydtothermal. One of the earliest and perhaps most comprehensive works on plume-related rifting is that of Burke and Dewey (1973). These authors examined 45 triple junctions (see below) and associated rifting, ranging in age from about 2 Ga to present-day, including the Afar and several sectors of the East African Rift System, the Lake Baikal rift, the North Atlantic rift system, the Proterozoic rift systems of North America (e.g. Mid-continent Rift System). Burke and Dewey (1973) proposed an evolutionary scheme of plume-generated triple junctions from a three-arm rifting stage (triple junction or rrr junction), to the opening and spreading of two arms, with one arm remaining inactive (or failed arm, termed aulacogen), their closure and eventually collision to form a fold-and-thrust belt. These authors proposed an evolutionary sequence shown in Fig. 3.5. In this sequence, rifts evolve into basins, in which sedimentary accumulations can reach thicknesses of more than 10 km. As emphasised by Burke and Dewey (1973), these sedimentary successions commonly host base metal deposits and hydrocarbon reservoirs. McKenzie (1978) suggested that the mechanisms that cause subsidence of the crust and development of a basin can be related to stretching of the lithosphere (rapid extensional subsidence), followed by slow thermal subsidence, as the asthenospheric material beneath the basin cools and sinks to isostatic equilibrium. Pysklywec and Mitrovica (1998) using numerical simulation, modelled large-scale subsidence of

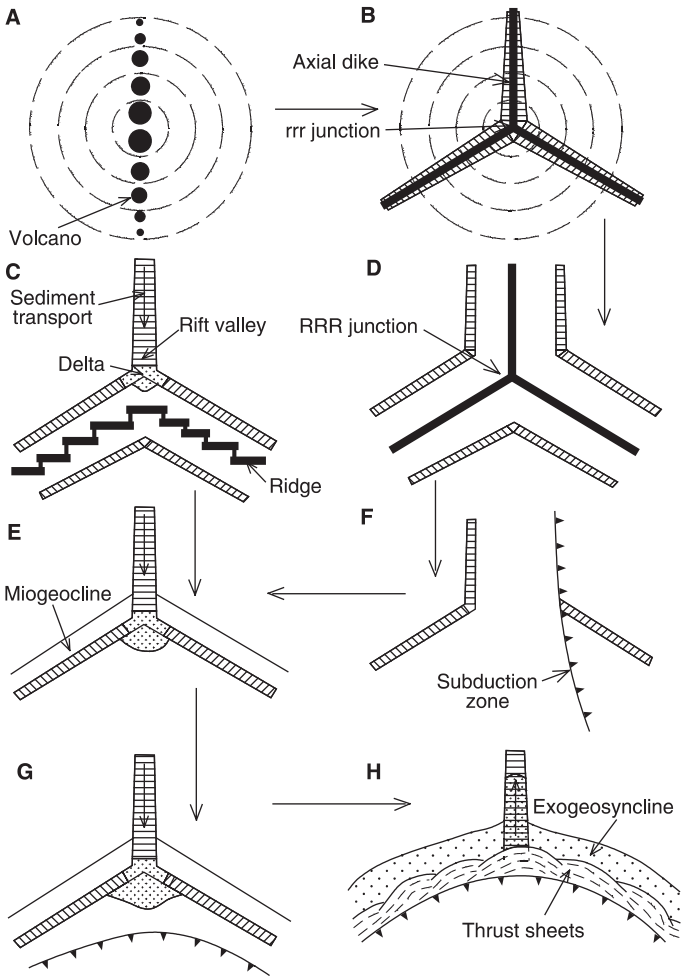


Fig. 3.5 Burke and Dewey (1973) scheme of the origin and evolution of plume-related triple junctions and associated basin structures. (**A**) Alkaline volcanoes developing on a crustal uplift caused by the impact of a mantle plume; (**B**) the rift-rift-rift (rrr) junction and the inception of a three-arm rift system; (**C**) two of the rift arms separate, with limited development of oceanic crust, while a third arm fails and is infilled with fluvial and/or lacustrine sediments; (**D**) and RRR (oceanic rifts) develops if all three rifts open to form oceanic crust; (**E**) Atlantic type rift margins, with growth of a delta at the end of the failed arm; (**F**) spreading and subduction zone impinges on rift arm on which a volcanic arc forms; (**G**) Atlantic-type margin with failed rift arms approaching a subduction zone; (**H**) rifted continental margin collides with a subduction zone, while in the failed arm sediment provenance reverses. See also Fig. 4.9

continental interiors. They concluded that topographic deflections of at least 1 km and up to 1000 km in extent can persist over time scales of 100–150 Ma and may be due to the collapse of mantle plumes.

More than a century of geological studies has focused on basin tectonics and rifting, starting with the early seminal works of Suess (1880) and Gregory (1896). Modern works concerning continental rifts and volcano-sedimentary basins include Allen and Allen (2005), Einsele (2000), Busby and Ingersoll (1995) and Olsen (1995). The geodynamics of rifting in Europe, Asia, the Americas and Africa were addressed in thematic issues of Tectonophysics edited by Ziegler (1990a,b, 1992). Geodynamic processes linked to the evolution of rifted basins are discussed in detail by Ziegler and Cloetingh (2004). A continental rift, or tectonic basin has been defined as a "*fault-bounded basin produced by extension of continental crust*" (Condie 1997) and a rift system as a "*tectonically interconnected series of rifts*" (Olsen and Morgan 1995). More precise definitions of rifts present some difficulties, but for a good review of terminology and classification the reader is referred to Olsen and Morgan (1995). There is a vast array of rift types and terms that describe continental rifts. Graben is commonly used interchangeably with rift. Sengör and Natal'in (2001) defined rifts as fault-bounded elongate troughs, identified some 290 rifts and provided a comprehensive list of rifts of the world. A classification of rift basins, adapted from Busby and Ingersoll (1995) and Einsele (2000), is presented in Table 8.2.

Continental rifting has been a major geological process on planet Earth at least since the Neoarchaean. Some examples of these early rift structures which led to basins infilled with thick volcano-sedimentary successions include, the Witwatersrand, Ventersdorp and Transvaal intracratonic rift basins in South Africa, the Capricorn Orogen rift basins in Western Australia, the Athapuscow, Bathurst, Belt-Purcell and Mid-continent Rift System in North America, the rift structures developed between the Anabar and the Aldan shields in the Siberian craton (e.g. Udzh, Iagor-Norilsky, Kjuntigdin, Viliuy and Ygatinsky aulacogens; Zoneshain et al. 1990). Most modern continental rifts contain lakes and are in fact lacustrine rift basins, the best modern-day examples being the East African lakes (e.g. Tanganyika, Malawi, Turkana) and Lake Baikal in Siberia, which is also the deepest in the world at 1640 m. A continental rift, can evolve into a proto-oceanic basin and eventually, by advanced seafloor spreading, to an oceanic basin. Thick successions of sediments and/or volcanic products accumulate in rift basins, regardless of whether or not the rifting process evolves to form oceanic crust. The lacustrine rift systems of East Africa contain up to 5 km of syn-rift sedimentary fill; whereas Lake Baikal contains up to 8 km of syn-rift sediments.

There are cases, in which lithosphere thinning and rifting occur in response to crustal thickening and delamination processes of the lithospheric mantle. These processes result in a style of basin structure and topography referred to as Basin-and-Range, from the example in western USA, where this style was first documented in the Great Basin, which is a major repository for epithermal and

Carlin-type deposits (Chapters 5 and 9). Basin-and-Range style tectonics are now recognised in other parts of the world, most notably in northeastern China, where Mesozoic to Cenozoic volcanic products fill basin-and-range style depressions (Wang et al. 2006; Xu et al. 2005) and low-sulphidation epithermal systems are present (Pirajno, unpublished data).

The origin of stratabound and/or stratiform sedimentary-rock hosted mineral deposits is intimately associated with the evolution of the host basin for which, in turn, a link with mantle plumes and rifting processes is assumed. These mineral systems are discussed in Chapter 8.

3.2.2.2.1 Rift Dynamics: Passive and Active

The main mechanisms that cause lithospheric rifting are: thermal thinning, mechanical thinning and asthenospheric diapirism. Ruppel (1995) modelled the extensional processes of the continental lithosphere in terms of mechanical, thermal, rheological and temporal factors. This author considered five categories of rifting and associated basins: (1) passive margins (e.g. North Atlantic); (2) discrete intracontinental rifts (e.g. Baikal); (3) diffuse rifts (e.g. Basin-and-Range); (4) strike-slip (or pull apart; e.g. Dead Sea); and (5) compression-related rifts (e.g. Tibetan grabens). The timing of extension, igneous activity, uplift or subsidence, determines the nature of the rifting process, which can be active or passive. The former involves the active participation of asthenospheric mantle, whereas the latter involves plate boundary forces. Ruppel (1995) pointed out that the active and passive mechanisms are difficult to delineate, owing to the fact that in both active and passive modes mantle upwelling is implicated, which results in many cases with having the same geophysical and geological signatures. But, as noted above, some distinctions can be made based on timing of key events, such as uplift and volcanism.

Many rifts are associated with crustal topographic swells, as exemplified by the Baikal, Rio Grande and the East African rift systems (Lipman et al. 1989), however whether or not these systems have been initiated by upwelling mantle plumes or by plate boundary processes is still debated. The active and passive models for the initiation of rift structures are in many instances the geological equivalent of the age-old "chicken and egg" problem. Nevertheless, it is fair to say that some rifts appear to have a closer association with far field tectonics than others. For example, the Baikal and the Rhine grabens (part of the Cenozoic European rifts system) are rift structures that could well be related to the Alpine-Himalayan collision orogens, although this is disputed (e.g. Zhao et al. 2006; Ritter and Christensen 2007). By contrast, the East African and the Mid-continent Rift Systems, with their histories of prolonged volcanicity are best explained by the active model.

Passive rifting results from far field lithospheric stresses, generated either by plate boundary forces (ridge push, slab pull, continental collision), or by forces resulting from mantle convective drag at the base of the lithosphere.

Plate boundary stresses are transmitted to plate interiors, generally taking advantage of pre-existing lines of weakness. In the passive rifting process, an upward flow of hot, buoyant asthenospheric material rises to fill the space created by the thinning of the lithosphere. In other words, the upwelling asthenosphere is not involved in the actual rifting process. The upward flow of the asthenosphere results in decompression melting, magmatic underplating and eruption of continental flood basalts. A model of passive rifting is shown in Fig. 3.6A.

One of the consequences of this asthenospheric rise is the development of thermal gradients between the extended and unextended regions. The rise of hot mantle material causes melting of the overlying crust and associated high grade lower crustal metamorphism. Conductive heating of the lithosphere above the rising plume may lead to thermal buoyancy and subsequent uplift. Thus, the passive rifting model begins with thinning of the lithosphere, which results in an initial sag of the crust. This may be followed by upwelling of mantle material, uplift and rupture of the overlying crust, magmatic underplating and accompanying igneous activity. In this case, the geological record would show a shallow water sedimentary succession, such as siliciclastic sediments associated

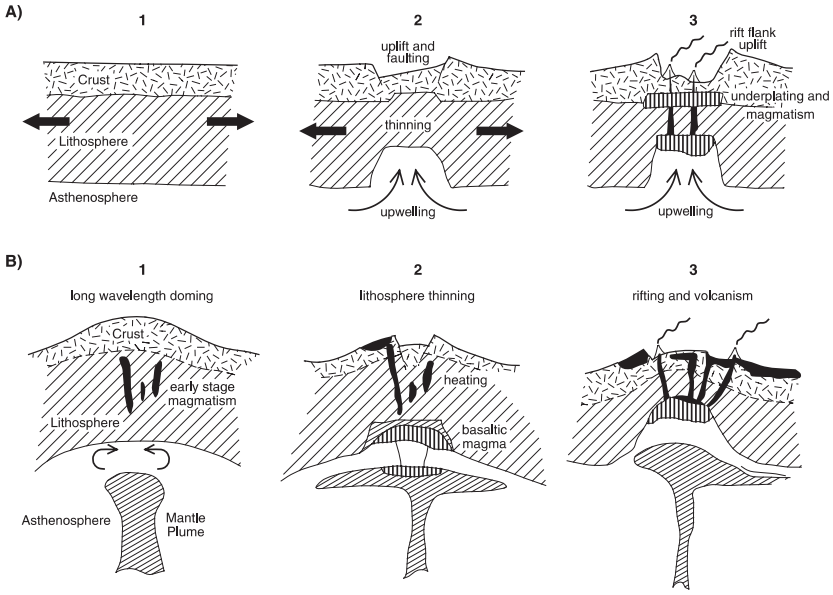


Fig. 3.6 Models of passive (**A**) and active (**B**) rifting processes, after Ruppell (1995). In (**A**) the crust and lithosphere extend as a result of plate boundaries forces; (1) incipient rifting, (2) far field stresses thin the crust and lithospheric mantle, hot asthenospheric mantle passively enters the thinned area, (3) adiabatically melts, causing magmatic underplating; volcanism may occur in the rift area. In (**B**) a rising mantle plume forces doming of the crust (1), thinning of the crust and lithosphere follow with adiabatic melting and underplating (2), rifting at the crest of the domed crust and volcanism (3)

with evaporites, followed by basaltic volcanism, subsidence and deep-water sedimentation. An example of this sequence of geological events has been documented in the Palaeoproterozoic Yerrida Basin in central Western Australia (Pirajno et al. 2004).

The theory of active rifting advocates that rupture of the crust can be initiated and largely controlled by the rise of a mantle plume. The impact of the plume on to the base of the lithosphere results in doming of the crust, followed by rupture and igneous activity, then rifting and subsidence. Courtillot et al. (1999) suggested that models of active rifting, or "*hot*" rifting, are linked to mantle plume activity and are supported by the temporal coincidence of rifting, emplacement of flood basalts and continental breakup. The progression of events from doming to final subsidence is suggestive of deformation which has its origin beneath the crust and ultimately to mantle dynamics. In addition to the mechanical uplift caused by the upward pressure of the mantle plume, thermal buoyancy of the heated lithosphere adds to the uplift component. After active rifting, thermal decay follows and results in subsidence of the newly created rift structure. A chronology of events, as observed by piecing together the geological history of modern and ancient rift structures, suggests that doming of the crust occurs several millions of years before the onset of volcanism and that rifting follows volcanism, again by several millions of years. A model of active rifting is shown in Fig. 3.6B. In this model, melts pond at the base of the lithosphere, from which basaltic melts rise through fracture to produce flood basalts.

The Neoproterozoic intracontinental Centralian Basin (Australia) is an example of an ancient rift system initiated by a mantle plume (Walter et al. 1995). Similarly, the intracontinental branch of the Damara Orogen is an example of an rift system that developed into an ocean and a number of graben systems and was probably caused by a mantle plume (Pirajno 2000).

3.2.2.2.2 Rifting and Basin Formation Related to Delamination Tectonics

As mentioned above, rifting and basin-forming processes may be linked to subcontinental lithosphere and asthenospheric mantle dynamics in regions of compression and crustal thickening. Ruppel (1995), considered three situations. In the first, zones of continental thickening may develop rift structures because of vertical stresses exceeding horizontal compressive stresses in high plateau regions (e.g. Tibet). In this way, normal faults develop in the high plateau, and bound a zone of rifting, whereas along the margins of the thickened crust, thrust faults form in response to compression. In the second, zones of extension develop behind a subduction-related magmatic arc. This is the well-known back-arc rifting, commonly linked to subduction roll-back, during which the overriding plate must extend in order to accommodate the retreating slab. Melt generation and convection take place in the mantle wedge above the slab, resulting in the bimodal magmatism that characterises back-arc rift zones.

The third situation was suggested to explain the extensional collapse that affects the late stages in the evolution of orogenic systems in continental collision zones. This scenario involves removal of the lithospheric root, beneath thickened continental crust. Initially, the thickened crust has a low plateau with a deep Moho and a deep lithospheric root that protrudes into hot asthenosphere. Convective instability causes the colder root to break and sink into the hot mantle, creating a flow of asthenosphere to fill the gap. Interestingly, Kröner (1983) suggested that, since the upper part of the mantle beneath continental crust is cooler and denser than normal mantle lithosphere under oceanic crust, the subcontinental lithosphere is negatively buoyant. This results in the sinking of the subcontinental lithosphere into the hot and less dense asthenosphere, which spreads laterally, intrudes and underplates the crust. The delamination of the lithosphere may, according to Kröner's hypothesis, initiate a form of subduction (A type) through the downward pull of the sinking lithospheric segment.

Two models have been proposed for rifting of thickened crust: delamination and convective downwelling (e.g. Seber et al. 1996). In the delamination model the lower lithosphere (thermal boundary layer) detaches itself from the overlying mechanical boundary layer, sinking into the asthenospheric mantle, which then flows into the space provided by the delamination. In the second model the thickened lithosphere, as a whole, detaches and sinks into the asthenospheric mantle. In many works, the term delamination is used for both models, although Seber et al. (1996) recommended that the distinction be made. Both models predict that cold lithosphere is replaced by hot and less dense asthenospheric material and this causes uplift, due to isostatic re-adjustment, followed by extensional collapse, rifting and magmatism. The important point is that continental collision, a compressional episode, may result in lithospheric thinning, rifting and heating of the lower crust (Houseman 1996). The asthenospheric flow into the space left by the sinking lithosphere has essentially the same effects as a mantle plume, in that dynamic and thermal lifting of the crust results in the formation of a high plateau followed by rifting and by alkaline magmatism. This is illustrated in Fig. 3.7.

The mechanics of convective removal of the lithosphere has been investigated in detail by Platt and England (1993), who emphasised that convective removal and thinning of the lithosphere will produce distinctive igneous activity, metamorphism and tectonism. The space left by the removal of the lower lithosphere is replaced by asthenospheric mantle, so that the latter is in contact with the cooler and mechanically stronger part of the lithosphere. This cooler lithosphere may be metasomatised and its partial melting, either by adiabatic decompression or conductive heating, will produce alkaline magmas, as observed in the Tibetan Plateau (Turner et al. 1996). Platt and England (1993) pointed out that the melts formed within the metasomatised lithosphere, would be chemically and isotopically distinct from melts that form during adiabatic decompression of the asthenospheric

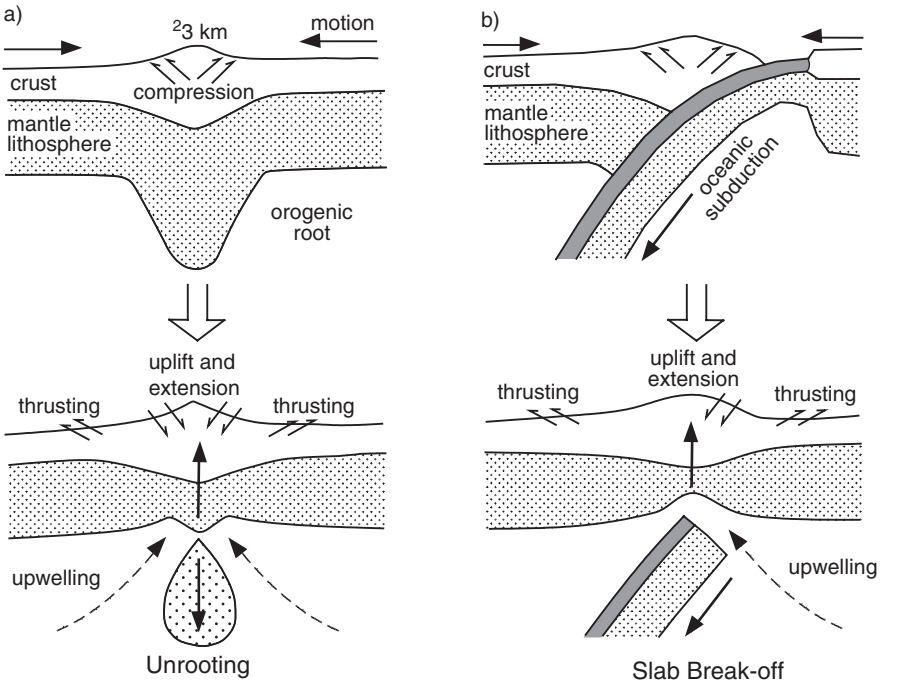


Fig. 3.7 Conceptual models of lithospheric delamination and slab break off, after Nelson (1992), Platt and England (1993) and Houseman (1996). In model (**a**), thickened lithospheric mantle, beneath a thickened crust becomes gravitationally unstable, breaking and foundering into a less dense and hot asthenospheric mantle. (**b**) shows oceanic subduction followed by slab break off and upwelling asthenospheric mantle in the space created by the delaminating slab

mantle. The other important effect of convective removal of the lithosphere is metamorphism, which in this case is related to the rise in temperature at the base of the mechanical boundary layer. The "*wave of temperature increase creates a thermal pulse*" (Platt and England 1993) that transmits upward through the overlying material, resulting in prograde metamorphism. However, the rate and duration of extension are important in determining the duration and style of metamorphism. Geological examples quoted by Platt and England (1993), where convective removal of lithosphere may have occurred, in addition to the Tibetan plateau, include the Basin-and-Range province in the USA and eastern China.

In summary, the consequences of lithospheric delamination may be similar to those of mantle plumes. The distinction being in their respective tectonic settings, with the former being related to crustal thickening associated with collisional regimes, the latter with intraplate rifting associated with an extensional regime.

3.2.3 Mantle Plumes Tectonics and Hydrothermal Systems

The wider link between hydrothermal ore deposits and mantle plumes is briefly discussed in this section. In addition to direct generation of magmas, thermal anomalies associated with deep mantle plumes or the upwelling of asthenospheric mantle, constitute powerful heat sources in the crust. These are responsible for crustal scale hydrothermal circulation and high-T and low-P metamorphism, which may result in a wide range of ore deposits in rift systems that form as result of these mantle processes. The geological record shows several rift systems associated with plume-related intraplate igneous provinces, at least since the Neoarchaean-Palaeoroterozoic (~2.7–2.5 Ga; e.g. rift systems of the Fortescue, Western Australia, and Ventersdorp, South Africa). Examples of rift systems that are well-endowed with hydrothermal ore deposits are, the 1.1 Ga Mid-Continent rift system (USA; Nicholson et al. 1992), the Jurassic Limpopo-Sabi-Lebombo triple junction rifts (southern Africa; Pirajno 2000), the Mesozoic Panxi rift and the mid-Proterozoic Langshan-Bayunobo rift (both in China; Gilder et al. 1991), which hosts the world-class Bayan Obo REE deposit (Chapter 4). Volcano-sedimentary successions of rift basins host a great variety of hydrothermal ore deposits as well as hydrocarbon reservoirs. Sn-W exoskarns, formed in carbonate successions and typically associated with intrusion-related greisen style alteration, are generally associated with rifting of stable cratons due to impacting mantle plumes (Meinert et al. 2005). Sedimentary-rock hosted metalliferous ore deposits (e.g. Pb-Zn-Ba-Cu-Au-Ag; SEDEX) typically occur in intracontinental rift basins. Well-known examples of SEDEX deposits of rift basins have been mentioned in the preceding pages. Although the origin of these intracontinental rift basins may be linked to back-arc rifts or delamination tectonics associated with far field stresses, it is interesting to note that the majority of SEDEX deposits formed between the early and mid-Proterozoic (~1.9–1.0 Ga), which coincide with global or superplume events at 1.9, 1.6, 1.2–1.3, 1.1 Ga (Ernst and Buchan 2002). A modern analogue of metallifeous sediments is provided by Red Sea brine pools (Chapter 8). The Red Sea can be considered as the northern arm of the great, 5000 km-long, East African Rift System (EARS). The EARS provides a window into what must be a giant intracontinental ore making environment, comparable to present-day oceanic spreading centers. The tectonic and magmatic environments of the EARS are schematically illustrated in Fig. 8.6. The EARS includes sulphide deposits in the Red Sea brine pools, hydrothermal sediments deposits in rift lakes, and I suggest, perhaps on a more speculative note, that deep-seated anorogenic magmatic systems may exist beneath the rift floors.

Some low-sulphidation adularia-sericite and alkalic epithermal systems are now becoming increasingly recognised in other geotectonic settings, such as continental volcanic provinces. The Great Basin (Basin-and-Range province) in the western USA is a high plateau terrain, formed by extensional tectonics, which extends from the western USA to Mexico. Magmatic activity in the

province began about 55 Ma ago, and, although highly variable in its products, it is typically bimodal. Various lines of evidence, including gravity and seismic data, suggest that the Basin-and-Range was caused by a mantle plume, which accounts for the nature and composition of the volcanism, its elevated topography and the ongoing hydrothermal activity. Low-sulphidation Au epithermal systems have been recently recognised in the Djibouti region of the Afar triple junction in the Horn of Africa (Pirajno unpublished data; see also Fig. 2.3).

3.3 Metallogeny and Geodynamics

Kerrich et al. (2005) discussed the metallogeny and geodynamics of Archaean greenstone terranes, spreading centres, intraoceanic and continental margin arcs, Cordilleran orogens, continent-continent orogens, foreland basins, intracontinental rifts, passive margins, anorogenic magmatic belts, and of mantle plume and lithospheric interactions. In the following I summarise the salient points of Kerrich et al.'s paper.

Archaean terranes essentially consist of a gneissic basement, greenstone belts (mafic-felsic volcanic and sedimentary rocks), and late granitic intrusions. The gneissic basement rocks represent the earliest juvenile crust and these rocks are commonly referred to as TTG (tonalite-trondhjemite-granodiorite; Martin et al. 2005). Archaean granite-greenstone terranes exhibit both differences and similarities with terranes of later ages. Uniquely typical of Archaean greenstones are komatiitic successions that formed from the ancient hot mantle at temperatures of about 1650°C. Komatiites and high-Mg basalts of Archaean age are thought to represent oceanic plateaux or continental flood basalts related to mantle plume events. Mafic-ultramafic magmatism of Archaean age is well known for its association with Ni-Cu-PGE orthomagmatic deposits. Subduction-accretion complexes and magmatic arc complexes of Archaean age are similar to those of the Phanerozoic and potentially have the same endowment of hydrothermal ore systems, but with a low preservation potential due to deep erosion. Kerrich et al. (2005) suggested that Neoarchaean greenstone belts are Cordilleran-style collages of oceanic island arcs and oceanic plateaux, as exemplified by the Superior province in Canada. These accretions and ensuing metamorphism and devolatilisation reactions are responsible for the abundance of orogenic Au lode systems of this age.

Submarine volcanogenic massive sulphide (VMS) deposits form in oceanic spreading centres and back-arc rifts. The latter produce some of the largest VMS (generally Abitibi type in the Archaean and Kuroko type in the Phanerozoic), associated with bimodal magmatism and submerged calderas. Cyprus-type deposits, on the other hand, are generated at mid-ocean ridges and end up as part of obducted ophiolite fragments. Intraoceanic and continental margin magmatic arcs are subduction-related, resulting in plutonic and

volcano-plutonic complexes with which porphyry and epithermal systems are genetically associated. As pointed out by Kerrich and co-workers, porphyry systems have the clearest relationship to plate tectonic processes than any other ore system. The essential element here is that during subduction the hydrated oceanic slab releases water and other volatiles, such as S, Cl and alkali elements into the overlying mantle wedge. This fluid release reaches a maximum at depths of about 100 km, at which breakdown of serpentine, chlorite and amphibole occurs. Magma generation from the metasomatised mantle wedge, results in the formation of mafic melts with relatively high concentrations of chalcophile and siderophile elements. Exsolution of hydrothermal fluids takes place in the final stages of magma evolution in the upper crust (see Chapter 2). In general, island arc systems are associated with more mafic magmas (dioritic), whereas continental arcs have more felsic magmas with the result that the former tend to be Au rich and the latter Mo rich. High-sulphidation epithermal systems are linked to porphyry volcano-plutonic activity and may be transitional to porphyry mineralisation (Chapter 5). The level of exposure of a volcano-plutonic complex is instrumental in the preservation or erosion of epithermal deposits. The presence of high level argillic and advanced argillic alteration may provide clues to underlying epithermal deposits. On the other hand if a porphyry system is now exposed, the overlying epithermal system has most likely been destroyed by erosion. Low-sulphidation epithermal systems are not necessarily associated with subduction-related volcanism. Indeed, many low-sulphidation epithermal systems are found in zones of crustal extension and intraplate magmatism, as in the Basin-and-Range of the Great Basin in western USA and in eastern China.

Codilleran orogens may expose rocks that have been metamorphosed and deformed at deeper crustal levels. Prograde metamorphism affects the fore arc region and the accretionary prism above a subduction zone and in front of a formerly active magmatic arc. High heat flow and intense fluid regimes are important elements of Cordilleran orogens, with peak prograde metamorphism causing dehydration and fluid generation. The heat generated in the deeper levels of Cordilleran orogens may have multiple origins, such as radioactivity, shear heating, crustal thickening and slab roll back followed by asthenospheric upwelling. Mantle-derived melts may participate in fluid generation and crustal melts intrude the accreted rocks, resulting in the well established spatial association with orogenic lodes. Fluids that are released during these phases of prograde metamosphism are dominated by H_2O, CO_2, CH_4 and N_2 with H_2S being produced by desulphidation reactions. Metallic elements, such as Au, As, Hg, Sb and W are also mobilised, together with silica, and metalliferous fluids are focused along major shear zones in the fore arc to form orogenic vein systems, commonly associated with large but barren quartz veins. The world-renowned Otago (New Zealand), Victorian (Australia) and Juneau gold fields, all fit into this general scheme. However, evidence from the Pacific margin of China suggests that destrutction of sublithospheric mantle, delamination and progressive asthenospheric upwelling have produced intense magmatism and hydrothermal activity during the Cretaceous (~130–90 Ma; Yanshanian

tectonothermal event, see Chapters 5 and 9) with the development of orogenic lode systems, as well as porphyry, skarns and epithermal systems that are not related to subduction.

Placer Au deposits result from the erosion of uplifted orogens and are mostly formed in the catchment areas of fore and back-arc regions. Famous placer deposits are those of the Russian Far East, Otago, the Mother Lode and Klondike in North America. The huge Witwatersrand palaeoplacers may have originated from the erosion of orogenic gold veins, although there is controversy as regarding the role of erosion and hydrothermal fluids in the genesis of the Witwatersrand Au (see Frimmel et al. 2005; Law and Phillips 2005).

Continent-continent orogens do not tend to form new ore deposits. According to Kerrich et al. (2005), reworking of older and already devolatilised crust and limited development of magmatic arcs during these collisions are not conducive to the formation of ore systems, except for Sn-W deposits associated with highly fractionated, ilmenite-type or S-type granites. These granite are highly enriched in incompatible and volatile elements (Rb, Th, U, Ta, Sn, W, Mo, B, F) and generated in the thickened crust that results from the collision of two continents. Continent-continent orogens have some of the largest Sn-W provinces, such as southwest England and Panasqueira (Portugal) of the Variscam Orogen (see Chapter 4). Proterozoic foreland intracontinental basins are the main repositories of unconformity-related U deposits and hosted in siliciclastic successions of sedimentary basins that developed on cratonic blocks, following the assembly of the supercontinent Columbia between ~2.0 and 1.8 Ga. The Athabasca (Canada) and McArthur foreland basins hosting the largest unconformity-related U deposits, owe their U endowment to brines with dissolved aqueous U^{+6} and reducing fluids, which caused the precipitation of U minerals, where these fluids mixed near and along an unconformity (Chapter 13). Continent-continent collisions produce uplift which in turn results in topographically-driven fluid flow through aquifers in the foreland basins, generating Mississippi valley type base metal deposits.

As mentioned above, intracontinental rifts are quite prolific in generating giant ore systems, such as sedimentary exhalative (SEDEX), stratiform and stratabound (Chapter 8) and Fe oxide-Cu-Au-U (IOCG, Chapter 4). The age span of these ore systems is ~1.8–1.1 Ga, which would correspond with the assembly and dispersal of the supercontinent Columbia, followed by the assembly of Rodinia. Important at this time is the activity of mantle plumes or asthenospheric material advected to the base of a thinned lithosphere, resulting in mafic and anorogenic magmatism, with the intrusion of A-type granites in siliciclastic and volcanic sequences, as is the case for the giant Olympic Dam IOCG in South Australia. Other deposits in the same class, but with substantial variants that probably reflect a spectrum of crustal depths include the Cloncurry district in northern Australia, the Fe-rich Vergenoeg in South Africa and Kiruna in Sweden. SEDEX seems to be linked with rifting in response to the fragmentation of the Columbia supercontinent, whereas stratiform and stratabound (Copperbelt or Kupferschiefer types) are linked to failed intracratonic

rift systems (aulacogens; see Fig. 3.5). The common feature of the Copperbelt and Kupferschiefer deposits is their association with organic-rich lithologies, such as black shales representing marine transgression over oxidised clastic sequences (red beds). Kerrich and co-workers suggested a link between hydrocarbon maturation, flow of oxidised brines and subsequent precipitation of sulphides due to the interaction of the brines with the reduced organic-rich shales.

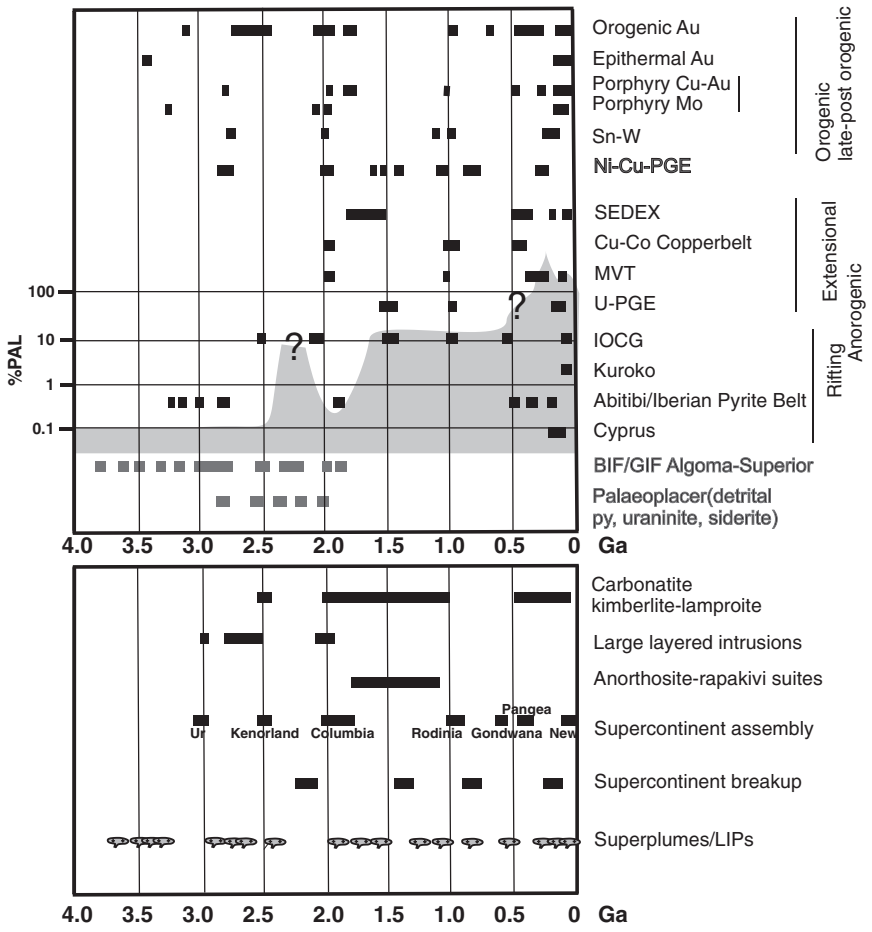


Fig. 3.8 Mineral systems, superplume events and supercontinent assembly through geological time. This diagram is based on data from Barley and Groves (1992), Rogers and Santosh (2004), Ohmoto (2004), Groves et al. (2005a,b) and Groves and Bierlein (2007); atmospheric oxygen curve is shown in light grey shading and is after Canfield (2005); PAL present atmospheric level, BIF/GIF and Archaean palaeoplacers, which contain detrital pyrite, uraninite and siderite are shown in red to highlight their dependence on oxygen-poor atmospheric conditions. Data bars and points do not imply relative size. Details in text

Passive margins are formed during dispersal of supecontinents. The Kenorland supercontinent developed passive margins between ~2.4 and 2.2 Ga, with the deposition of banded and granular iron formations peaking at 1.9–1.8 Ga. Phosphate accumulation occurred on passive margins during the dispersal of Rodinia at ~0.6–0.5 Ga. These Fe and P accumulations require oxygen and are thought to be related to sea high level stands associated with maxima of mantle plume activity (Fig. 3.8 and Chapter 8). The peak of extensive BIF accumulation is at 2.5–2.4 Ga, with the Hamersley and Transvaal BIF, which may have been deposited in a single Vaalbara (Kaapvaal-Pilbara) superbasin (Cheney 1996). Mantle plumes and delamination tectono-thermal events were responsible for widespread anorogenic magmatism that culminated with the emplacement of the A-type granites and gabbro-anorthosite complexes at 1.75–1.55 Ga and 1.0 Ga. These complexes are associated with Olympic Dam style mineralisation (IOCG), anorthosite-hosted Fe-Ti-V as well as Sn, W, Zn late stage mineralisation.

Mantle plume and continental lithosphere interactions are invoked to explain the temporal distribution of Ni-Cu sulphides and PGE deposits in mafic-ultramafic complexes and continental flood basalts. These include the Archaean Kambalda-type komatiite-hosted Ni-Cu deposits. These orthomagmatic ore systems require S saturation induced by increase of SiO_2 and/or crustal assimilation of S by the parental liquids (Naldrett 2004). Superplume events at 2.7–2.8 Ga and 2.05–2.06 Ga resulted in the emplacement of large layered intrusions, such as the Stillwater Complex (Montana, USA), the Windimurra Complex in Western Australia and Great Dyke and Bushveld Igneous Complex, respectively. Also linked with superplume events are the emplacement of kimberlite and lamproites at ~280 Ma and 120–80 Ma in Asia, North America and Africa.

3.4 Temporal Evolution of Ore Systems, Supercontinent Cycles and Global Metallogeny

Terrestrial planets evolve through time by progressive heat loss, involving stages of mantle convection. Plate tectonics, mantle plumes, accretionary and collision tectonics are ultimately manifestations of planetary cooling and mantle dynamics (Pirajno 2007). The Earth's crustal and mantle evolution through geological time resulted in the changing of dominant tectonic regimes and consequently of mineral deposit systems. In this section I examine some concepts that were put forward by Meyer (1981, 1988), and subsequently elaborated on and expanded by Barley and Groves (1992), Barley et al. (1997, 1998), Groves et al. (2005a,b) and Groves and Bierlein (2007). These concepts are based on the premise that perturbations within the solid Earth are caused by variations in heat transfer and dissipation from the interior of the planet towards the surface, which are manifested as tectonic and magmatic activity.

Consequently, the temporal distribution of ore deposits can be regarded as a function of these activities. This is reflected by the frequency of certain metals in the geological record. A diagram showing the distribution of ore deposits through time is shown in Fig. 3.8.

It is commonly agreed that the evolution of the Earth's crust can be divided into three major stages, which in turn reflect the dominance of certain tectonic styles and lithotectonic assemblages. The generally accepted chronological boundaries of these three stages, or eons, are: Archaean 3800–~2600 Ma, Proterozoic ~2600–570 Ma and Phanerozoic 570 Ma-present. The frequently cited Hadean (~4500–3800 Ma) is not yet officially ratified by the International Commission on Stratigraphy (ICS) and the International Union of Geological sciences (IUGS) (see www.stratigraphy.org). The first two boundaries are based on the predominance of greenstone belts (Archaean), and the development of epicontinental sedimentation in basins and continental rifting (Proterozoic). The third is essentially based on the first appearance of exoskeletal invertebrates and the radiation of complex life forms, a phenomenon that occurred more or less in conjunction with the predominance of large scale subduction systems and modern style plate tectonics. The nearly contemporaneous Cambrian explosion and the inception of modern style plate tectonics are suggestive of a link. This link is perhaps associated with changes in the configuration of continents and oceans that characterise the Phanerozoic, which may have engendered environmental complexity that in turn increased biological diversity, thereby accounting for the Cambrian explosion and subsequent comparatively rapid evolutionary processes and mass extinctions. The "large" Proterozoic supercontinents would not have promoted biodiversity as would smaller continental masses and intervening oceans. However, these traditional and indeed convenient divisions are not entirely coincident with global thermal events. Condie (1997), taking into consideration age distributions in juvenile continental crust, relates them to time-integrated evolution of thermal regimes in the mantle. These thermal regimes began with layered convection and buoyant subduction, or Stage 1 of Condie (1997), and evolved to catastrophic mantle overturns between 2.8 and 1.3 Ga and finally to whole mantle convection. Furthermore, in his analysis of global age data Condie's (1997) suggested that: (1) the first cratonic passive margins and rifting were developed by 3.2–3.0 Ga; (2) there are three groups of ages – 2.7–2.6, 1.9–1.7 and 1.3–1.0 Ga, indicating times of major juvenile crust production; and (3) greenstone development age minima at 2.5–2.2 and 1.65–1.35, correlate with the assembly of supercontinents. Pirajno (2007), on the other hand, proposed five evolutionary stages, based on crustal magmatic and mantle plume dynamics, as follows: (1) >3000–2800 Ma; (2) 2800–2400 Ma; (3) 2400–2100 Ma; (4) 1000–600 Ma and (5) 600 Ma-present.

In summary, it is appears that what we see in the crust, in terms of geological history, tectonic and magmatic features, is closely linked with mantle dynamics and a gradually cooling Earth. Unfortunately, the further we go back in time, the more blurred and poorly constrained our data become, and as such we can

only speculate. Condie (2005) proposed that there are two types of mantle plumes: long-lived and short-lived. The former, called shielding superplumes, (>200 Ma duration) are the result of the shielding effect of a supercontinent, which will cause upwelling of mantle plumes followed by the fragmentation of the supercontinent: these do not appear to be linked to production of large volumes of juvenile crust. The short-lived plume events (<100 Ma duration), called catastrophic superplume events, are associated with accretion of volcanic arcs and addition of juvenile crust. A decrease in the frequency of mantle plume activity with time is demonstrated by the progressive decrease in the thickness and geotherms of the sub-continental mantle lithosphere (SCML; Groves et al. 2005a,b; O'Reilly et al. 2001). Thus, an evolution from mantle plume dominated regime in the Archaean, to a more buoyant style tectonics in the Proterozoic, to modern plate tectonics in the Phanerozoic, clearly reflects the trend of a cooling Earth (Groves et al. 2005a,b).

The superplume concept suggests some form of plate tectonic cyclicity. Barley et al. (1997) considered that cycles of mantle plume breakouts have occurred since the Archaean, through to and including the Phanerozoic. Thus, plume "breakouts" can be linked to assembly and rifting of continents, and expansions or contractions of oceans (Gurnis 1988; Barley and Groves 1992; Barley et al. 1997). A wider implication is that tectonic cyclicity has a direct relationship to metallogeny, because of the interaction between continents, orogenic and anorogenic tectono-thermal activity, biotic evolution and eustasy (Barley and Groves 1992; Barley et al. 1997). The idea that supercontinents have been cyclically forming and fragmenting throughout most of Earth's geological history is not new. One theory (Nance et al. 1988) holds that the aggregation of a supercontinental mass results in the accumulation of heat in the mantle beneath it. This eventually leads to heat dissipation by means of rifts that break the supercontinent into fragments. The fragments then drift and coalesce through collision processes and a new supercontinent is then assembled. The entire cycle would take about 450 Ma to complete.

In the context of mantle plumes, fragments of continental crust tend to aggregate above plume downwellings to form supercontinents. These supercontinents, with their large mass, inhibit mantle cooling and promote the build-up of heat at the base of the crust. In this way, convective upwellings form, and result in the uplift of the lithosphere, injection of melts into the crust and melting of the crust. This is accompanied by continental rupture and dispersal of continental fragments, which then reaggregate over mantle downwellings to start another cycle. This is followed by collision, suturing and the re-assembly of a new supercontinent, until new hot upwelling forms beneath the supercontinent, and the cycle begins again (Gurnis 1988). The duration of the full cycle is envisaged to take approximately 360 Ma (Barley et al. 1997). Barley and Groves (1992), Barley et al. (1997, 1998) proposed a relationship between mantle plumes to supercontinent aggregation and dispersal, and the distribution of metalliferous ore deposits through geological time. Solomon and Sun (1997) reviewed the relationship between Earth's geological evolution

and its mineral resources, and they too considered ore deposits either as orogenic or anorogenic, linked to mantle plume activity, extension and convergent tectonic regimes. They referred, in particular, to the development of iron-formations in the geological record, a topic that is taken up in some detail in Chapter 8.

The basic idea is that groups of ore deposits appear to be associated with cycles of aggregation and dispersal of continental masses (Barley and Groves 1992), which in turn may be linked to mantle upwellings (or plumes) and downwellings. Ore deposits that form during continental rifting can be considered as anorogenic. Collisional tectonics can be related to mantle downwellings, in which case the associated ore deposits can be considered as orogenic.

One of the unresolved issues of our planet's geological history is whether increased cratonisation at the end of the Archaean, coupled with a changed mantle convection system of more regular cells, led to the onset of Wilson tectonic cycles and the assembly of supercontinents. It is well-established, however, that during the Proterozoic there was development of large sedimentary basins or platforms, supporting the idea of widespread cratonisation and the presence of large continental masses. I have mentioned that there is evidence, although not too well constrained and with different configurations by different authors, that supercontinents have been cycliclically assembling and fragmenting (Rogers and Santosh 2004). In this context, I discuss the concept of Barley's and co-workers and Groves and co-workers more fully.

The Phanerozoic eon is characterised by the breakup of the supercontinent known as Rodinia, a re-assembly to form Pangea between 400 and 200 Ma and its subsequent breakup (Fig. 3.8). The breakup of Pangea was heralded by the emplacement of continental flood basalts, layered intrusions and related magmatic Ni and PGE mineralisation. Continuing breakup and dispersal of continental fragments led to the inception of subduction systems, magmatic arcs, and metal deposits that are typically formed at convergent margins, such as porphyry and epithermal systems. Barley and Groves (1992) pointed out that the preservation in the geological record of ore deposits is dependant on whether these are part of interior or peripheral orogens, as defined by Murphy and Nance (1991). Peripheral orogens are those that form at continental margins, adjacent to an ocean, as for example along the Cordilleran and Andean side of the Americas. Interior orogens, develop during closure of oceanic basins and continental collision, resulting in crustal thickening and uplift, of which the Alpine-Himalayan and Central Asian orogenic systems are examples. It follows that the preservation potential for ore deposits in the upper portions of interior orogens is limited, due to erosion that inevitably accompanies strong uplift. This is generally the case for epithermal systems.

Barley et al. (1997) reasoned that what is true for Pangea and the Phaneorozoic, probably happened also in the preceding eras. They recognised global tectonic cycles that appear to last about 360 Ma, and which can be seen as 180 Ma cycles of ocean opening and closure. The 180 Ma cycles may be related

to what the authors called "mantle plume breakouts". Barley et al. (1997, 1998) suggested that plume breakouts and similar full cycles are apparent for the Archaean too, between 2.77 and 2.59 Ga, and for the late Archaean and Palaeoproterozoic, between 2.8 and 1.6 Ga. The breakup of the late Archaean Pilbara-Kaapvaal continent and the aggregation of a large continental mass at approximately 2.6 Ga, are associated with global production of komatiites between 2.72 and 2.69 Ga, relating to both plume activity and arc magmatism. Linked with the emplacement of komatiitic magmas are major Ni ore deposits (plume-related komatiites) and volcanogenic massive sulphide (Zn-Cu) deposits. On the basis of ore deposit styles, another cycle of assembly of cratons can be inferred to have occurred at approximately between 2.0 and 1.8 Ga. This is suggested by the emplacement of the Bushveld and Molopo Farms layered complexes and associated PGE and Cr ore deposits, and the occurrence of the giant SEDEX deposits, such as those in South Africa, Australia and Siberia (Chapter 8). The temporal distribution of giant SEDEX deposits (Fig. 3.8) is confined to ~1.65–1.6 Ga in Australia, linked to the assembly of Proterozoic Australia at 1.75–1.7 Ga, itself part of the Columbia supercontinent assembly at ~1.85–1.8 Ga that involved Laurentia, Baltica and Siberia (Fig. 3.8). It is also envisaged that the formation of the Australian SEDEX may have been associated with high heat flow and the emplacement of high heat producing granites, with the heat being produced by radiogenic decay of U, Th and K^{40} (HHP granites, Chapter 9).

In the Rodinia supercontinent, metallogeny occurred in geotectonic settings related to assembly and to breakup (Pirajno and Cooke 1998). Mineral deposits that formed in Rodinian orogenic zones include sedimentary-rock-hosted polymetallic massive sulphides (e.g. Trilogy in the Albany-Fraser orogen of Western Australia), magmatic Cu-Ni-PGE in layered mafic-ultramafic intrusions (e.g. Voisey's Bay in Canada) and Fe-Ti-V deposits in anorthosites (Fig. 3.8). The latter are associated with a belt of anorogenic volcanic and plutonic rocks, that extends for thousands of km from California to Labrador, southern Greenland and Scandinavia (Windley 1995). This is a magmatic event that took place between 1.5 and 1.3 Ga and preceded the Grenville orogeny. Large resources of W, U, REE and Mo are contained in the huge pegmatite belts in western South Africa-and Namibia (Orange River pegmatite belt; Namaqua orogen), Sri Lanka and Madagascar. These belts may also be related to Rodinian continental collisions. During assembly, in other parts of the incipient supercontinent rifting was taking place at the same time, probably related to mantle plume events. The Mid-continent Rift System contains metalliferous deposits that include Cu-Ag in Keweenawan tholeiitic lava flows of the Coppermine River Group in northwest Canada and in the Lake Superior region (e.g. White Pine). Also related to this rift system are 1.29–1.27 Ga layered intrusions that host Cu-Ni-PGE mineralisation (e.g. Duluth and Muskox complexes). To a similar extensional episode may be related the U, Th, REE mineralisation in the Ilimaussaq 1.3–1.0 Ga alkaline complexes in South Greenland. The breakup of Rodinia at ~800 Ma was heralded by a major rifting zone that split Laurentia,

Baltica, Siberia and the South America blocks from East Antarctica, India, and Australia (Li et al. 1999). In Australia, the Adelaide Geosyncline may belong to this major rift zone. This is supported by the presence of the northwest-trending, ~820 Ma Gairdner dyke swarm (Zhao et al. 1994), which may have been sourced from the same mantle plume that fed mafic dykes and sheets in western North America (Park et al. 1995) and the giant Ni-Cu-bearing Jinchuan intrusions in northwest China. Another failed rift system that could be linked to the breakup of Rodinia is the Lufillian orogen in central Africa, host to the stratiform copperbelt deposits (Cu-Co) of Zambia and the Congo. Similarly, the northeast-trending intracontinental troughs and basins that form the Irumide-Kibaran orogens, could also be related to the breakup. The Irumide belt extends from south-central Namibia, from where it may connect with the Namaqua Province, across northern Botswana to the northern margin of the Zimbabwe craton. In south-central Namibia, the Irumide belt hosts the Cu-Ag Klein Aub and Witvlei stratabound deposits. Large mineral sands deposits were formed along several Rodinian rift margins, as for example, along the east coast of South Africa (e.g. Richards Bay), Mozambique and eastern India (Pirajno and Cooke 1998).

Groves et al. (2005a,b) examined in some detail the secular mineral system distribution in relation to tectonic styles. Orogenic Au lodes have a wide temporal distribution (Fig. 3.8) and reflect fluxes of deeply-sourced fluids during orogenic processes at convergent margins. The earliest orogenic lodes are recorded from the Pilbara Craton (Western Australia) with ages ranging form 3.4 to 3.1 Ga. The development of later orogenic deposits peaks at 2.65 and 2.1–1.75 Ga, with a marked decrease between 1.7 and 0.6 Ga, and a resurgence from about 0.6 Ga to 50 Ma. Groves et al. 2005a suggested that the Archaean and Palaeoproterozoic peaks reflect growth of continental crust and perhaps plume-related tectonics. Giant placer Au deposits result from erosion of uplifted orogenic belts and for this reason they are deposited in foreland basins and are abundant in Mesozoic-recent convergent margins, such as those of the Pacific Rim. Similarly, the giant Witwatersrand palaeoplacers, must have been deposited in a retro-arc foreland basin (Groves and Bierlein 2007). Both gold and pyrite round particles (buckshot pyrite) have Re-Os ages that well predate sedimentation. The tectonic control of porphyry and epithermal systems is dominated by convergent margin settings and they form at high crustal levels with high rates of uplift and as such are subject to poor preservation in the geological record. As mentioned earlier, there are, however, porphyry-epithermal systems that develop geodynamic settings associated with lithospheric thinning and mantle upwellings (see Chapter 5). These have a better chance of preservation in the geological record, because the rates of uplift are not as strong as in convergent margins. Volcanic-hosted massive sulphide deposits (VMS) show a temporal distribution with peaks at 2.7 and 1.9 Ga and again in the Phanerozoic at ~350 Ma (Iberian Pyrite belt) and in the Neogene (Kuroko systems). Kuroko-style VMS are associated with felsic submarine volcanism in back-arc rift settings, whereas the mid-ocean ridges VMS

deposits have no preservation possibility, unless tectonically transported and emplaced at convergent margins in ophiolite complexes. Iron oxide Cu-Au-U (IOCG) systems show a temporal pattern with peaks in the late Archaean (~2.6 Ga), the Palaeoproterozoic (~2.05 Ga) and the Mesoproterozoic (~1.6 Ga). Most of the IOCG appear to be associated with mantle plume events, A-type alkaline magmatism and flood basalts (Chapter 4; Pirajno 2000). Furhermore, as pointed out in Groves et al. (2005a), the location of giant IOCG is near cratonic margins (e.g. Gawler Craton in South Australia), which suggests that the alkaline magmatism is related to small degrees of partial melting in the subcontinental lithospheric mantle, previously enriched with incompatible elements (metasomatised), such as K, Th, Au, REE, during mantle plume events.

Finally, the roles of the biosphere, hydrosphere and the evolution in the composition of the Earth's atmosphere need to be mentioned, because of the importance of oxygen in controlling the solubility of redox-sensitive ore minerals and systems, as for example U. The oxygen level in the atmosphere through geological time has been a controversial issue for decades, but it is generally agreed that at about 2.3 Ga the oxygen level arose quite rapidly (Great Oxidation Event; Chapter 10), reaching a pO_2 of 0.1–0.15 PAL (Fig. 3.8). Groves et al. (2005a), citing Ohmoto et al. (2001), subdivided the evolution of the atmosphere and hydrosphere in the following: (1) oxygen-free pre-cyanobacteria stage; (2) at about 2.7 Ga there was an anoxic deep hydrosphere, oxic shallow hydrosphere, but pO_2 of atmosphere still below 0.001 present atmospheric level (PAL); (3) PAL in atmosphere increased to 0.1–0.5 pO_2 at about 2.3–2.2 Ga; (4) at about 0.6 Ga the deep hydrosphere was oxygenated, except for localised anoxic basins, PAL in atmosphere greater than 0.5 pO_2. The mineral systems that are most sensitive to the evolution and oxygen changes in the atmosphere and hydrosphere are Fe and Mn formations and U deposits. Banded and granular iron formations (BIF and GIF; see Fig. 3.8 and Chapter 8) were deposited at passive margins and/or platform basins, with the Fe and silica being sourced from hydrothermal effluents on the seafloor, again possibly linked to mantle plume activity. Manganese, like Fe, is soluble as Mn^{2+} and is deposited through oxidation reactions to Mn^{3+} or Mn^{4+}. Redox reactions change the easily transported Fe^{2+} to Fe^{3+} causing its precipitation as oxides or oxyhydroxides. Uranium has two oxidation states (Chapter 13): U^{+6} and U^{+4}, with precipitation occurring at redox boundaries, when oxidising fluids transporting uranyl complexes are reduced by C-rich organic materials and precipitate a range of U oxides. This is the origin of unconformity-related U deposits, in which the redox boundary is at the unconformity between basement rocks and the overlying sedimentary successions. Uraninite, on the other hand, having U^{+4} is unstable in oxygenated conditions can only exist in a reducing environment. Uraninite is one of the main ore minerals in the Witwatersrand palaeoplacers, again supporting the view of a reduced atmosphere in the late Archaean.

3.5 Concluding Remarks

Ore systems form in all tectonic regimes from convergent margins to divergent plate boundaries, such as spreading centres in oceanic basins and rift systems. Ore systems can provide clues as to the tectonic setting in which they were formed. In this respect, porphyry and epithermal systems are mostly generated in subduction-related magmatic arcs. However, caution needs to be exercised, because there are also porphyry and epithermal systems in extensional tectonic settings unrelated to subduction, as discussed in Chapter 5. Rifting can occur in both convergent margins, following post-orogenic collapse, in back arc settings, or in intraplate (intracontinental) environments. The East African Rift System is the longest continental rift on Earth and is the site of on-going hydrothermal activity, covering a wide range of mineral systems from the brine pools in the Red Sea to subaqueous hydrothermal venting in lakes and, presumably, given the youth of the rift system, unexposed magmatic-hydrothermal deposits. As indicated in the text above and speculatively shown in Fig. 8.6, the East African rift could well be a major present day ore factory. The East African rift is the result of mantle plume(s) activity and the role of mantle plumes could be equally important in ancient rift systems, which hosts some of the largest SEDEX deposits and mineral systems associated with anorogenic intraplate magmatism, such as IOCG. Geodynamic settings can be complex. For example an extensional setting can be associated with a mantle plume event, or be associated with a far field collision event. The giant SEDEX deposits in Australia, could have formed through a combination of factors involving radiogenic heat from intraplate granites linked to mantle dynamics and far field tectonics that created back-arc basins.

The temporal distribution of mineral systems is clearly a complex issue, in which several factors need to be taken into account, such as evolutionary trends in the atmosphere, hydrosphere and biosphere, geodynamic settings and erosion levels. An oxygen-poor atmosphere allowed the accumulation of detrital pyrite, gold and uraninite in the Witwatersand basins, whereas the rapid rise of atmospheric oxygen between 2.0 and 1.8 Ga was probably associated with microbial metabolic processes and photosynthesis, leading to the abundance of banded iron formation during that period. The rise of atmospheric oxygen also permitted metallogenic processes that are governed by redox boundaries, such as U deposition at unconformities.

References

Allen PA, Allen JR (2005) Basin analysis: principles and applications, 2nd edn. Blackwell Scientific Publ, Oxford

Barbarin B (1999) A review of the relationships between granitoid types, their origins and their geodynamic environments. Lithos 46:605–626

Barley ME, Groves DI (1992) Supercontinent cycles and the distribution of metal deposits through time. Geology 20:291–294

Barley ME, Pickard AL, Sylvester PJ (1997) Emplacement of a large igneous province as a possible cause of banded iron formation 2.45 billion years ago. Nature 385:55–58
Barley ME, Krapez B, Groves D, Kerrich R (1998) The Late Archaean bonanza: metallogenic and environmental consequence of the interaction between mantle plumes, lithospheric tectonics and global cyclicity. Precambr Res 91:65–90
Burke K, Dewey JF (1973) Plume-generated triple junctions: key indicators in applying plate tectonics to old rocks. J Geol 81:406–433
Busby CJ and Ingersoll RV (eds) (1995) Tectonics of sedimentary basins. Blackwell Science, Oxford
Canfield DE (2005) The early history of atmospheric oxygen: homage to Robert M. Garrels. Ann Rev Earth Planet Sci 33:1–36
Chen YJ, Pirajno F, Sui YH (2004) Isotope geochemistry of the Tieluping silver-lead deposit, henan, China: a case study of orogenic silver-dominated deposits and related tectonic setting. Mineral Depos 39:560–575
Chen YJ, Pirajno F (2005) Linking the CMF model to metallogenic zoning in the east Qinling Orogen, central China. In: Mao J-W, Bierlain F (eds) Mineral Deposits Research: Meeting the global challenge 2:905–908. Proceedings SGA 2005 Beijing
Chen YJ, Pirajno F, Qi JP (2005) Origin of gold metallogeny and sources of ore-forming fluids, Jiaodong Province, Eastern China. Int Geol Rev 47:530–549
Chen YJ, Pirajno F, Qi JP (2008) The Shanggong gold deposit, Eastern Qinling Orogen, China: Isotope geochemistry and implications for ore genesis. Asian J Earth Sci. doi: 10.1016/jseas.2007.12.002
Cheney ES (1996) Sequence stratigraphy and plate tectonic significance of the Transvaal succession of southern Africa and its equivalent in Western Australia. Precambr Res 79:3–24
Condie KC (1997) Plate tectonics and crustal evolution, 4th edn. Butterworth Heinemann, Oxford
Condie KC (2005) Earth as an evolving planetary system. Elsevier, Amsterdam
Courtillot V, Jaupart C, Manighetti I, Tapponier P, Besse J (1999) On causal links between flood basalts and continental breakup. Earth Planet Sci Lett 166:177–195
Dewey JF (1988) Extensional collapse of orogens. Tectonics 7:1123–1139
Einsele G (2000) Sedimentary basins – evolution, facies and sediment budget. Springer, Berlin
Ernst RE, Buchan KL (2002) Large mafic magmatic events through time and links to mantle plume heads. Geol Soc Am Spec Pap 352:483–576
Frimmel HE, Groves DI, Kirk J, Ruiz J, Chesley J, Minter WEI (2005) The formation and preservation of the Witwtaersrabd gold fields, the world's largest gold province. Econ Geol 100th Anniv Vol: 769–797
Gilder SA, Keller GR, Luo M, Goodell PC (1991) Timing and spatial distribution of rifting in China. Tectonophysics 197:225–243
Goldfarb RJ, Baker T, Dubé B, Groves DI, Hart CJR, Gosselin P (2005) Distribution, character, and genesis of gold deposits in metamorphic terranes. Econ Geol 100th Anniv Vol: 407–450
Gregory JW (1896) The great rift valley. Murray, London
Groves DI, Goldfarb RJ, Gebre-Mariam M, Hagemann SG, Robert F (1998) Orogenic gold deposits: a proposed classification in the context of their crustal distribution and relationship to other gold deposit types. Ore Geol Rev 13:7–27
Groves DI, Vielreicher RM, Goldfarb RJ, Condie KC (2005a) Controls on the heterogeneous distribution of mineral deposits through time. Geol Soc Lond Spec Publ 248:71–101
Groves DI, Condie KC, Goldfarb RJ, Hronsky JMA, Vielreicher RM (2005b) Secular changes in global tectonic processes and their influence on the temporal distribution of gold-bearing mineral deposits. Econ Geol 100:203–224
Groves DI, Bierlein FP (2007) Geodynamic settings of mineral deposit systems. Geo Soc, London, 164:19–30

Gurnis M (1988) Large-scale mantle convection and the aggregation and dispersal of supercontinents. Nature 332:695–699
Harris NBW, Pearce JA, Tindle AG (1986) Geochemical characteristics of collision zone magmatism. Geol Soc Spec Publ 19:67–81
Houseman G (1996) From mountains to basins. Nature 379:771–772
Hutchison CS (1983) Economic deposits and their tectonic settings. MacMillan Press, London
Kerrich R, Wyman D (1990) Geodynamic setting of mesothermal gold deposits: an association with accretionary tectonic regimes. Geology 18:882–885
Kerrich R, Cassidy KF (1994) Temporal relationships of lode gold mineralisation to accretion, magmatism, metamorphism and deformation – Archean to Present: à review. Ore Geol Rev 9:263–310
Kerrich R, Goldfarb R, Groves D, Garvin S, Jia YF (2000) The characteristics, origins, and geodynamic settings of supergiant metallogenic provinces. Sci in China, Ser D 41:1–68
Kerrich R, Goldfarb RJ, Richards J (2005) Metallogenic provinces in an evolving geodynamic framework. Econ Geol 100th Anniv Vol: 1097–1136
Kröner A (1983) Proterozoic mobile belts compatible with the plate tectonic concept. Geol Soc Am Mem 161:59–74
Law JDM, Phillips GN (2005) Hydrothermal replacement model for Witwtaersrabd gold. Econ Geol 100th Anniv Vol: 799–811
Leat PT, Larter RD (eds) (2003) Intra-oceanic subduction systems: tectonic and magmatic processes. Geol Soc Lond Spec Publ 219, 352pp
Li ZX, Li ZH, Kinny PD, Wang J (1999) The breakup of Rodinia: did it start with a mantle plume beneath South China? Earth Planet Sci Lett 173:171–181
Lipman PW, Logatchev NA, Zorin YA, Chapin E, Kovalenko V, Morgan P (1989) Intracontinental rift comparisons – Baikal and Rio Grande rift systems. Eos 70:578–588
Martin H, Smithies RH, Rapp R, Moyen JF, Champion D (2005) An overview of adakite, tonalite-trondhjemite-granodiorite (TTG) and sanukitoid: relationships and some implications for crustal evolution. Lithos 79:1–24
McKenzie D (1978) Some remarks on the development of sedimentary basins. Earth Planet Sci Lett 40:25–32
Meinert LD, Dipple GM, Nicolescu S (2005) World skarn deposits. Economic Geology 100th Anniv Vol: 299–336
Meyer C (1981) Ore-forming processes in geologic history. Econ Geol 75th Anniv Vol: 6–41.
Meyer C (1988) Ore deposits as guides to geologic history of the Earth. Ann Rev Earth Planet Sci 16:147–171
Mitchell AHG, Garson MS (1981) Mineral deposits and global tectonic settings. Acdemic Press, London
Murphy JB, Nance RD (1991) Supercontinent model for the contrasting character of Late Proterozoic orogenic belts. Geology 19:460–472
Naldrett AJ (2004) Magmatic sulphide deposits: Geology, geochemistry and exploration. Springer, Berlin
Nance RD, Worsley TR, Moody JB (1988) The supercontinent cycle. Sci Am 259:44–52
Nelson KD (1992) Are crustal thickness variations in old mountain belts like the Appalachians a consequence of lithospheric delaminations? Geology 20:498–502
Nicholson SW, Cannon WF, Schulz KJ (1992) Metallogeny of the Midcontinent rift system of North America. Precambr Res 58:355–386
Olsen KH (ed) (1995) Continental rifts: evolution, structure, tectonics. Devlpmt Geotect, Elsevier, Amsterdam
Olsen KH, Morgan P (1995) Introduction: progress in understanding continental rifts. In: Olsen KH (ed) Continental rifts: evolution, structure, tectonics. Devlpmt Geotect, Elsevier, Amsterdam, pp 3–26

Ohmoto H (2004) Archean atmosphere, hydrosphere, and biosphere. In: Erickson PG, Altermann W, Nelson DR, Mueller WU, Catuneanu O (eds) The Precambrian Earth: Tempos and events, Develpm Precambr Geol 12, Elsevier, Amsterdam, pp 361–368

Ohmoto H, Watanabe Y, Yamaguchi KE, Ono S, Bau M, Kakegawa T, Naraoke H, Nedochi M, Lasaga AC (2001) The Archaean atmosphere, oceans, continents and life. In: Cassidy KF, Dunphy JM, Van Kranendonk MJ (eds) 4th Int Archaean Symp Ext Abs, AGSO Record, pp 19–21

O'Reilly SY, Griffin WL, Poudjom-Djomani YH, Morgan P (2001) Are lithospheres forever? Trakcing changes in subcontinental lithopsheric mantle through time. GSA Today 11:4–10

Park JK, Buchan KL, Harlan SS (1995) A proposed giant radiating dyke swarm fragmented by the separation of Laurentia and Australia, based on palaeomagnetism of ca. 780 Ma mafic intrusions in western North America. Earth Planet Sci Lett 132:129–139

Pirajno F (1992) Hydrothermal mineral deposits – principles and fundamental concepts for the exploration geologist. Springer-Verlag, Berlin

Pirajno F (2000) Ore deposits and mantle plumes. Kluwer Academic Publishers, Dordrecht

Pirajno F (2007) Ancient to modem Earth: the role of mantle plumes in the making of continental crest crest, *in* Van Kranendonk MJ, Smithies RH, Bennett V (eds) Earth's oldest rocks. Elsevier, Amsterdam, pp 1037–1064

Pirajno F, Cooke A (1998) Metallogeny of the Rodinia supercontinent. Geol Soc Aust Abs 50:45–48

Pirajno F, Jones JA, Hocking RM, Halilovic J (2004) Geology and tectonic evolution of Palaeoproterozoic basins of the eastern Capricorn Orogen, Western Australia. Precambr Res 128:315–342

Pirajno F, Chen YJ (2005) Hydrothermal ore systems associated with the extensional collapse of collision orogens. In: Mao J-W, Bierlain F (eds) Mineral Deposits Research: Meeting the global challenge 2:1045–1048. Proceedings SGA 2005 Beijing

Platt JP, England PC (1993) Convective removal of lithosphere beneath mountain belts: thermal and mechanical consequences. Am J Sci 298:307–336

Prichard HM, Alabaster T, Harris NBW, Neary CR (eds) (1993) Magmatic processes and plate tectonics. Geol Soc Lond Spec Publ 76, 526pp

Pysklywec RN, Mitrovica JX (1998) Mantle flow mechanism for the large-scale subsidence of continental interiors. Geology 26:687–690

Roberts AM, Kusznir NJ (eds) (1997) Tectonic, magmatic and depositional processes at passive continental margins. J Geol Soc, London, 154

Rogers JJW, Santosh M (2004) Continent and supercontinents. Oxford University Press, Oxford

Ruppel C (1995) Extensional processes in continental lithosphere. J Geophys Res 100:24187–24215

Ritter RR, Christensen UR (eds) (2007) Mantle plumes – a multidisciplinary approach. Springer

Sawkins FJ (1990) Metal deposits in relation to plate tectonics. Springer-Verlag, Berlin

Seber D, Barazangi M, Ibenbrahim A, Demnati A (1996) Geophysical evidence for lithospheric delamination beneath the Alboran Sea and Rif-Betic mountains. Nature 379:785–790

Sengör AMC, Natal'in BA (1996). Paleotectonics of Asia: fragments of synthesis. In: Yin A, Harrison TM (Eds) The Tectonic Evolution of Asia. Cambridge Univ Press, Cambridge, pp 486–640

Sengör AMC, Natal'in BA (2001) Rifts of the world. Geol Soc Am Spec Pap 352:389–482

Solomon M, Sun SS (1997) Earth's evolution and mineral resources, with particular emphasis on volcanic-hosted massive sulphide deposits and banded iron formations. AGSO J Geol Geophys 17:33–48

Suess E (1880) Über die vermeintlichen säcularen Schawkungen einzelner Theile der Erdoberfläche. Vehr K Geologische Reichanst, Wien

Tatsumi Y, Eggins S (1995) Subduction zone magmatism. Blackwell Scince, Oxford

Tian ZY, Ping H, Xu KD (1992) The Mesozoic-Cenozoic East China rift system. Tectonophysics 208:341–363

Turner S, Arnaud N, Liu J, Rogers N, Hawkesworth C, Harris N, Kelley S, Van Calsteren P, Deng W (1996) Post-collision, shoshonitic volcanism on the Tibetan Plateau: implications for convective thinning of the lithosphere and the source of ocean island basalts. J Petro 37:45–71

Walter MR, Veevers JJ, Calver CR, Grey K (1995) Neoproterozoic stratigraphy of the Centralian Superbasin, Australia. Precambr Res 73:173–195

Wang F, Zhou XH, Zhang LC, Ying JF., Zhang YT, Wu FY, Zhu RX (2006) Late Mesozoic volcanism in the Great Xing'an Range (NE China): timing and implications for the dynamic setting of NE Asia. Earth Planet Sci Lett 251:179–198

Windley BF (1995) The evolving continents, 3rd edn. John Wiley & Sons, Chichester

Xu YG, Ma JL, Frey FA, Feigenson MD, Liu JF (2005) Role of lithosphere-astenosphere interaction in the genesis of Quaternary alkali and tholeiitic basalts from Datong, western North China Craton. Chem Geol 224:247–271

Zhao JX, McCulloch MT, Korsch RJ (1994) Characterisation of a plume-related ~800 Ma magmatic event, and its implications for basin formation in central-southern Australia. Earth Planet Sci Lett 21:349–367

Zhao DP, Lei JH, Inoue T, Yamada A, Gao SS (2006) Deep structure and origin of the Baikal rift zone. Earth Planet Sci Lett 243:681–691

Ziegler PA (ed) (1990a) Geodynamics of rifting, volume I. Case history studies on rifts: Europe and Asia. Tectonophysics 208:1–3

Ziegler PA (ed) (1990b) Geodynamics of rifting, volume II. Case history on rifts: North and South America and Africa. Tectonophysics 213:1–2

Ziegler PA (ed) (1992) Geodynamics of rifting, volume III. Thematic discussions. Tectonophysics 215:1–2

Ziegler PA, Cloetingh S (2004) Dynamic processes controlling evolution of rifted basins. Earth-Sci Rev 64:1–50

Zoneshain LP, Kuzmin MI, Natapov LM (1990) Geology of the USSR: a plate tectonic synthesis. Am Geophys Union, Geodyn Series 21, 242pp

Chapter 4
Intrusion-Related Hydrothermal Mineral Systems

4.1 Introduction

Circulation of hydrothermal fluids in the Earth's crust takes place under various tectonic regimes and geological situations, within which a complex array of transitional conditions can lead to a large number of ore deposit types and mineralisation styles that effectively defy a rigorous classification. For this reason descriptions of hydrothermal mineral systems, by necessity, must be regarded as end members or parts of a continuum. This simplification is an expedient to help in the understanding of what are obviously very complex natural systems. Also, it must be remembered that the same geological situation may occur in a number of different tectonic settings. For example, felsic plutonic rocks occur in magmatic arcs related to subduction and in anorogenic rift settings. It follows that intrusion-related magmatic-hydrothermal systems, the topic of this chapter and the one that follows, can be activated in both these situations and even produce similar styles of mineralisation.

In all cases, hydrothermal ore systems that are associated with magmatism result from the emplacement of melts in the Earth's crust, their crystallisation evolution, exsolution of aqueous fluids and their interaction with the invaded rocks and their possible mixing with external (meteoric) waters. The evolutionary paths of magmatic-hydrothermal fluids exsolved from a crystallising magma are introduced in Chapter 2. The nature and redox conditions of an intrusion determine the composition and characteristics of exsolved aqueous fluids and hence the type of the derived hydrothermal ore system. Peralkaline intrusions, for example, because of their inherently high alkali abundances tend to host lithophile elements such as Nb, REE and U. Oxidised, I-type alkaline and calc-alkaline magmas, on the other hand, have a greater capacity to carry and concentrate base metals, Au, Cu and Mo, whereas reduced, S-type magmas evolve aqueous fluids that transport Sn, W and Mo. The source of the metals is difficult to assess and contentious, but in general rock-forming minerals contain metals in their lattices, (e.g. Ni in olivine, V, Fe and Mg in pyroxene; W and Ti in micas; Nb and Ta in rutile), which are released following the breakdown of the host mineral during magmatic-hydrothermal processes. In addition, the exsolved magmatic-hydrothermal fluids have the capacity to dissolve and

F. Pirajno, *Hydrothermal Processes and Mineral Systems*,

© Springer Science+Business Media B.V. 2009

transport metals from the surrounding rocks. Furthermore, crustal materials that contain pre-existing mineral deposits can also provide a rich source of metals during episodes of partial melting. Tomkins and Mavrogenes (2003) examined this aspect of igneous-related metallogeny and pointed out that regions or provinces that are well endowed with certain metals may owe their metal speciation to the presence of disseminated or massive sulphide deposits in parts of the crust undergoing anatexis. A notable example of a metal-specific region is provided by the Southeast Asian Sn belt (Schwartz et al. 1995; Lehmann 1982). During anatexis of crustal rocks containing a sulphide deposit, polymetallic melts are entrained into the leucosome that eventually coalesce to form granitic plutons. Tomkins and Mavrogenes (2003) suggested that during ascent the mixed melt, begins to dissolve the entrained sulphides, as the magma source becomes increasingly undersaturated with respect to sulphur. With addition of H_2O to the melt, during its upward migration, the metal solubility will further increase. Once the melt approaches water saturation and the magma reaches its site of emplacement, the silicate melt exsolves a metal-rich hydrothermal fluid (Tomkins and Mavrogenes 2003). Chlorine and fluorine are two major components that form halide ligands for stable metal complexes and are responsible for the transport of metals in solution (see Chapter 1). Again these components may derive from lithologies already enriched in these elements.

In this chapter, I describe intrusion-related shallow to deep-seated, plutonic magmatic hydrothermal systems, mostly in intraplate continental settings. Examples of ore deposits related to intrusion-associated hydrothermal systems include greisens, vein systems, mineral systems associated with anorogenic ring complexes, ore systems related to A-type granitic magmas (e.g. Fe oxide-Cu-Au-U) and some breccia pipes and vein deposits that may be peripheral to large intrusions. In some cases there may be a continuum of spatial, temporal and genetic relationships with porphyry systems and some epithermal systems. These are treated in Chapter 5.

Following a brief introduction into the relationship of intrusion-related ore systems and granitic magmatism, in the following sections I discuss:

- Greisen
- Intrusion-related mineral systems
- Hydrothermal systems associated with anorogenic ring complexes
- Fe oxide-Cu-Au-U (IOCG) and A-type granites associated systems

Greisen and skarn systems can be intimately associated, but are discussed separately, greisens in this Chapter and skarns in Chapter 6. Some skarn types are also intimately associated with porphyry systems. Greisen and skarn systems, as well as those associated with ring complexes, provide us with a closer view of sub-solidus magmatic and magmatic-hydrothermal processes, mainly because these systems are somewhat less contaminated by the large meteoric influxes that commonly characterise other hydrothermal systems (e.g. porphyry and epithermal systems).

4.2 Intrusion-Related Hydrothermal Mineral Systems and Granitic Magmatism

Several hydrothermal ore deposits are formed within and at some distance from felsic to intermediate igneous intrusions. In this category probably fall the majority of hydrothermal ore systems, although a direct genetic link with these intrusions is not always clear, but usually inferred due to spatial alteration patterns and mineralogical associations as well as geological context.

Intrusion-related hydrothermal systems are almost invariably linked with granitic magmas. A classification of granitic magmas is well beyond the scope of this book, but before embarking on the topic of this chapter it is appropriate to make a very brief mention of the more common classification schemes of granite magmas that have spawned since the I- and S-type classification was first reported in a short paper by Chappell and White (1974). At least 20 petrogenetic types, or as aptly put it by Hannah and Stein (1990), the granite "alphabet soup", have been recognised. Granite typology that is more commonly mentioned in the literature include I-, S-, M-, A-types and magnetite and ilmenite series, which effectively describe the redox states of the granites. There are a large numbers of papers on the topic; here I cite Pearce (1996), Petford et al. (2000), and the latest ideas on granite generation proposed by Vigneresse (2004, 2007). For information on I- and S-type granites the reader is referred to Chappell and Stephens (1988), Chappell et al. (1998), a special issue on I- and S-type granites published by the Australian Journal of Earth Sciences (Allen 2001) and Clemens (2003) to mention a few. For a comprehensive textbook on granite geology, the interested reader is referred to Pitcher (1993). In addition, it is worth mentioning some classic textbooks, such as those of Didier (1973), Raguin (1965) and Atherton and Gribble (1983). In the following, I focus on the work of two authors, Barbarin (1999) and Vigneresse (2007), because their views on granite typology and generation have an important bearing on the topic of this chapter and Chapter 5.

Barbarin (1999) proposed a "synthetic" granite typology based on field, petrographic, geochemical and isotopic characteristics (Table 4.1), which in turn can be related to geodynamic settings and the proportions of crustal and mantle contributions (Fig. 4.1). According to this author, granitic rocks can be classified into six main types (Table 4.1). Granitic rocks that are of crustal origin, that is form by melting of continental crust, include muscovite-rich peraluminous leucogranites (MPG), which typically contain tourmaline, garnet and monazite and corresponding to S-types. These granites form in collision orogens (Fig. 4.1), as exemplified by the Himalayan leucogranites and those of the Hercynian belt of Western Europe. Also dominantly of crustal origin are peraluminous granites that contain biotite, cordierite, associated with sillimanite (CPG), also with tourmaline, garnet and monazite, but in contrast to the Himalayan granites, CPG tend to be deep-seated S-types as exemplified by the granites of the Lachlan Fold Belt of southeastern Australia. Increasing mantle

Table 4.1 Petrogenetic granite types, crust-mantle contributions and geodynamic environments (see also Fig. 4.1). After Barbarin (1999)

Granite typology	Acronym	Dominant mineralogy	Sr_i	ΣNd	Origin	Geodynamic environment
Muscovite-bearing peraluminous	MPG	Muscov. ± biot.	0.706–0.760	–4 to –17	Crustal	Continental collision
Cordierite-bearing peraluminous	CPG	Biot ± cordier.	70.708	–6 to –9	Increasing mantle contribution	
K-rich calc-alkaline high K, low Ca	KCG	K-fd ± amph.	0.706–0.712	–4 to –9		Transitional
Amphibole-bearing calc-alkaline low K, high Ca	ACG	Ca amph. ± Ca px	0.706–0.708			Subduction
Arc-tholeiitic	ATC	Ca amph. ± Ca px	0.706–0.708			
Mid-ocean Ridge tholeiitic	RTG	Amph. + px	<0.704	+ values	mantle	Oceanic spreading or Continental rifting
Peralkaline and alkaline	PAG	Na – amph. Na – px	0.704–0.712			

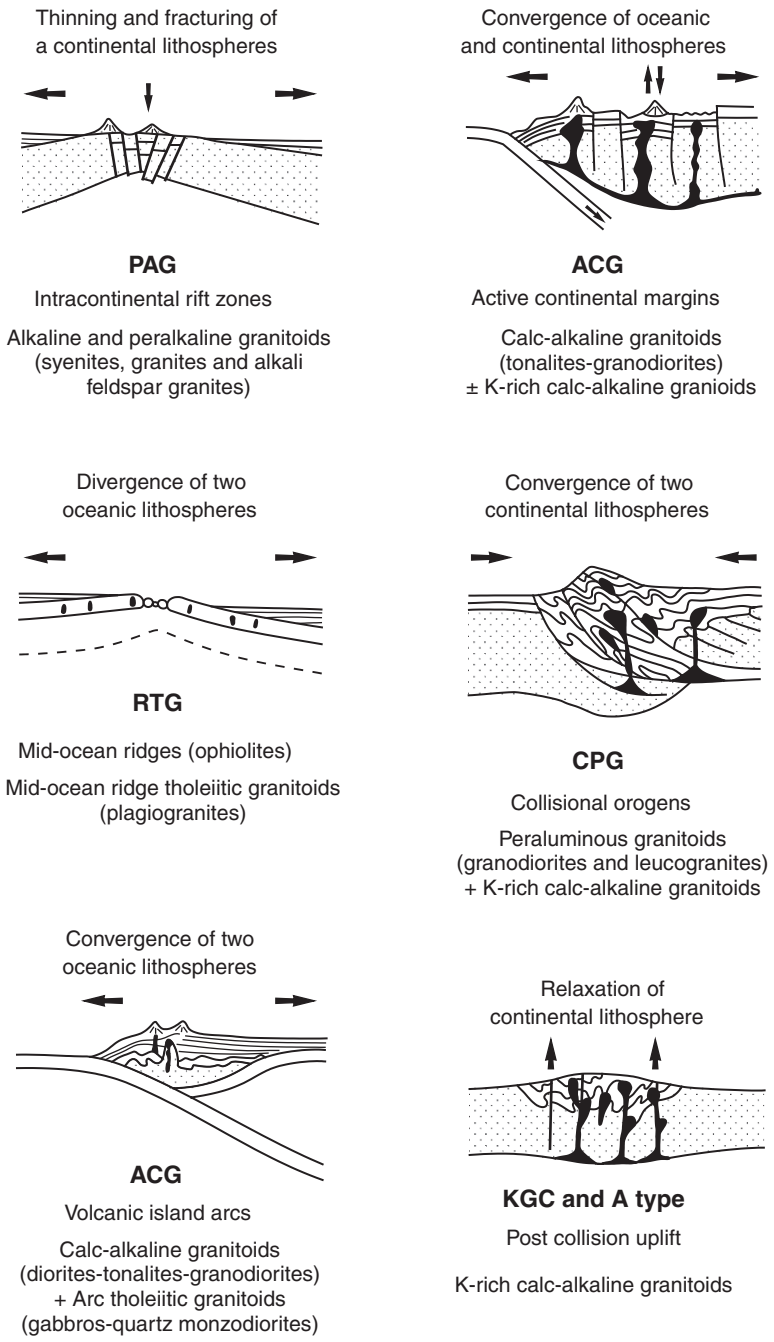


Fig. 4.1 Granite types and associated tectonic settings (see also Table 4.1). After Barbarin (1999)

contributions lead to granites that typically have K-feldspar megacrysts (monzogranites) and may contain amphibole (K-rich calc-alkaline; KCG), generally found in Caledonian plutons of northern Britain and the Hercynian belt of Western Europe. These generally form during post-collisional relaxation of continental lithosphere and may be associated with PAG types (Fig. 4.1). The nature of granites in collisional orogens (Fig. 4.1) generally reflect changes from crustal- to mantle-derived, which in turn reflect changes in the evolutionary geodynamics. The granite typology is associated with collisional tectonic settings, changes from syn-collisional peraluminous granitoids (two-mica granitoids of crustal origin), through potassium-rich calc-alkaline KCG, mixed crustal and mantle contribution types, and finally A-type granitoids (dominantly mantle source). A-type granitoids, are commonly followed by alkaline basalts, and develop in rifting or extensional settings, which indicate an important change in the final stages of the geodynamic evolution of a collisional orogen. Heating of the crust would produce S-type granitic melts, represented by muscovite-bearing peraluminous granitoids, defined as MPG (Fig. 4.1). Granodiorites and tonalites with calcic amphibole, pyroxene and titanite + magnetite (amphibole-rich calc-alkaline; ACG), form in Cordilleran type active margins, exemplified by the large Andean batholiths that are topped by andesitic volcanoes. Arc-tholeiite granodiorite, tonalitic granitic and gabbroic rocks (ATG; Fig. 4.1) occur in active continental margins and volcanic arcs, whereas the plagiogranites, trondjhemites and tonalites occur within oceanic crust of mid-ocean ridges (RTG; Fig. 4.1), and have well-defined mantle origins. Lastly, and of distinct alkaline to peralkaline comnpositions are the perthitic alkali feldspar granites to syenites (PAG; Fig. 4.1) that commonly occur as ring complexes topped by caldera and alkaline lavas and largely correspond to A-type granites. These granitic types typically have Na-bearing pyroxene and amphibole. Rapakivi granites would fall into this category. The PAG have mantle sources, in most cases related to asthenospheric upwelling or mantle plumes.

A-type granites deserve a special mention, because of the increasing recognition of their particular geodynamic and mineralisation importance. Loiselle and Wones (1979) started the concept of A-type granitic rocks, which they defined as those that occur within plate rift settings and are geochemically characterised by high alkalies, high abundances of Nb, Zr, REE but with a negative Eu anomaly and low CaO and MgO. Commonly, A-type granitoids have high Y/Nb ratios and high halogen contents, suggesting that volatiles have an important role in their petrogenesis (Whalen et al. 1987; Eby 1990). Collins et al. (1982) pointed out that A-type granites are enriched in large highly charged cations such as Ga, Nb, Sn, Zr and REE and that high Ga/Al ratios can be diagnostic and able to discriminate A-type from I-type granites. Collins et al. (1982) also suggested that A-type granites are the product of residual melts that previously formed I-type granites. This residual source would be enriched in F, which may be included within the biotite and hornblende structures. Creaser et al. (1991) on the other hand proposed that A-type granites can be derived

from partial melting of crustal rocks of tonalitic to granodioritic compositions. Eby (1992) reviewed the main features of A-type magmatism and further subdivided them into A1 and A2 groups, based on Rb/Sr and Y/Nb ratios, which are lower for A1 types and higher for A2 types. Moreover, Eby (1992) and Wu et al. (2002) proposed that A1 granitoids are geochemically similar to ocean-island-basalt (OIB) and were emplaced during intraplate rifting and related to mantle plume events. By contrast A2 granitoids have mixed geochemical signatures of continental crust and island arc and are considered to form in a post-orogenic setting (Eby 1992; Wu et al. 2002), perhaps as result of asthenospheric upwelling following the collapse of collisional orogens. Nevertheless it is also pointed out by Eby (1992) that discriminant ratios, such as Y/Nb, can change if the magma interacts with crustal materials. Martin (2006) proposed a model in which a variety of A-type magmas form in continental rift settings, from the degassing of a rising asthenospheric plume. The plume would produce a steady stream of volatiles that variably metasomatise or fenitise the lower crust transforming it into an A-type granitoid, which is then melted to give rise to anatectic A-type felsic melts of varying compositions depending on the proportion of volatiles. At the same time, Martin (2006) suggested that mantle-derived basaltic melts can fractionate to give rise to A-type magmas. A recent review of A-type magmatism is provided by Bonin (2007) who concluded that A-type granites come from mantle-derived alkaline mafic to intermediate magmas. Bonin et al. (2002) suggested that A-type granites are not confined to Earth systems, but have been recorded from the Moon and may also occur on Mars. The role of A-type magmatism in the inception of hydrothermal systems is examined again in the following sections.

Vigneresse's (2004, 2007) new paradigm for the generation and emplacement evolution of granitoids, envisaged that a pluton is built by a succession of pulses or batches of melts, spaced in time and each with distinct mineralogical, geochemical and isotopic signatures. This contrasts with the MASH model (melting-assimilation-storage-homogenisation; Hildreth and Moorbath 1988, see also Chapter 5), which proposes that a granite body is formed through melting, segregation, ascent and differentiation. The two concepts are illustrated in Fig. 4.2. Vigneresse's model has implications for the genesis of granite-related ore systems and for this reason I discuss its salient aspects. The source regions of granitic magmatism are the mantle, lower and upper crust. Dehydration melting is very effective in producing granites in continental settings and water is liberated from the breakdown of hydrous rock-forming minerals, such as hornblende, biotite and muscovite. Dehydration melting of hornblende begins at $\sim$1000°C and 800 MPa, the ensuing melt has tonalitic composition with Na abundances greater than K. Biotite breaks down at temperatures of between 950 and 820°C, with the mineral becoming progressively more Mg rich and releasing Fe, Mn, Ti and Rb. Muscovite has the lowest melting temperature at $\sim$700°C in low pressure conditions. Some granites have abundant mafic enclaves suggesting that some mixing process occurs deep in the crust, perhaps by successive pulses of mafic melts. Water in granitic melts plays an important role and determines the level

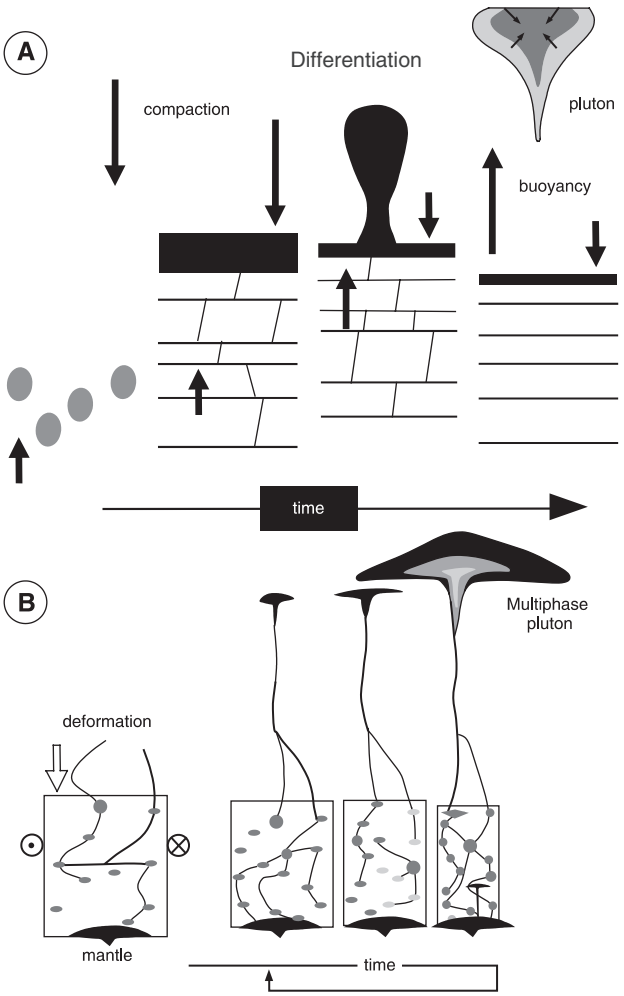


Fig. 4.2 (**A**) The MASH (melting-assimilation-storage-homogenisation) model of granite generation with four phases of melting, segregation, ascent and emplacement, leading to fractional crystallisation of a granitic body; (**B**) the new paradigm for granite generation suggests that there is cyclic segregation-ascent-emplacement of melts, so that the final granitic body is made up of a succession of magma inputs, including mafic magmas, with various chemical, mineralogical and isotopic characeters. After Vigneresse (2007)

that the melt can reach in the crust during its ascent. Water-rich (muscovite-bearing) granites reach the solidus between 17 and 5 km, whereas melts generated by the dehydration of biotite and amphibole contain less water and therefore reach high levels, 4–2 km and in fact may erupt to the surface. Recently, a new concept of hot and cold granites based on zircon saturation temperatures was introduced by Miller et al. (2003). Cold granites form at low temperatures ($<850^{\circ}C$), and therefore need the input of large amounts of fluids for melting to occur. These fluids could derive, according to the authors, from dehydration of underthrust sedimentary rocks in collisional settings, or hydrous mafic silicates. They would form in collision settings and with crustal thickening. Hot granites ($>850^{\circ}C$) form through de-hydration melting (biotite and/or hornblende) and

require large inputs of heat in the crust; these granites can erupt. These probably form in rift/extensional settings, and may be associated with mantle plumes (A and I types). Crustal melt segregation paths begin at and follow mineral grain boundaries and microfractures, from which melts coalesce to form small pockets. Mantle-derived melts, on the other hand, first form small pockets that infiltrate grain boundaries and are oriented along ambient stress patterns. Magma pockets are then extracted from the deforming source rocks resulting in a kind of mush, leading to bursts or cycles of magma that develops from the segregation of small amounts of melts. Vigneresse (2007) suggested that these cycles may last from 300 to 30 ka, leading to a "discontinuous motion of melt out of its matrix". These felsic melts ascend by a combination of fracture propagation and buoyancy, in strike-slip or compressional environments and/or in an extensional regime, which would facilitate ascent. As mentioned above, the emplacement of a granitic pluton is completed through successive and variously evolved melt inputs. The normal zoning that characterises a pluton, less evolved along the margins and more evolved at the core, is interpreted not as the result of chemical differentiation, but of successive batches of magma. These batches are emplaced into the core pushing the softer and less resistant earlier batch aside. Reverse zoning occurs when the latest batch of magma cannot force its way into a solidified core and the younger and more evolved melt moves to the margins (Fig. 4.2B). Vigneresse (2007) concluded that felsic plutons are built by successive intrusions of variously evolved melts, exhibiting geochemical and isotopic variations, ending up with compositional heterogeneity. These successive and discontinuous magma inputs have implications for ore genesis, because of temperature contrasts between inputs as for example when a mafic melt (1200°C intrudes a cooler felsic magma chamber 600°C). In this case the contact between them could reach a temperature of 900°C. These temperature variations induce changes in oxygen fugacity, creating severe disequilibrium conditions and changing metal partitioning between minerals and melt. This is documented for W and Mo partitioning between ilmenite and silicate melts (references cited in Vigneresse 2007). Preferential partitioning of S into mafic melts is suggested by the large quantities of SO_2 released during some volcanic eruptions. Thus, the input of a mafic melt into a felsic magma chamber results in the sudden exsolution of a fluid phase as the magma becomes oversaturated in S, leading to explosive volcanism.

Crystallising magmas exsolve aqueous fluids, which are usually channelled through fracture systems within the higher portions of an intrusive body, and/or within the surrounding wall rocks. As the role of H_2O in magmas is very important, a brief digression is appropriate at this point, and the reader is referred to Best (1982) for further details on this topic. Water is by far the most abundant volatile constituent of magmas, especially felsic. Other constituents include H_2S, CO_2, HCl, HF, H_2. The H_2O content of felsic-intermediate magmas with which hydrothermal activity is connected may range from 2.5 to 6.5 wt%. The presence of H_2O in a melt has the effect of considerably lowering its viscosity due to the depolymerisation phenomenon. Water-rich silicic melts can be as fluid as basaltic melts. Silicate melts have structures formed by

Si^{4+} and Al^{3+} in tetrahedral co-ordination with O^{2-} ions, these ions being commonly shared (bridging) between neighbouring tetrahedra. This linking through the bridging oxygens constitutes a polymerised structure which resembles the crystalline state. H_2O (and other volatiles like B, F, Cl) breaks the oxygen bridges and therefore depolymerises the structure. The bridging is then accomplished by replacing the O_2^- with $2OH^-$, according to Best (1982):

$$H_2O(a) + O_2^-(m) \rightarrow 2OH^-(m),$$

where a = aqueous phase and m = melt phase. Thus, H_2O is effectively not held in solution as neutral water molecules, but forms hydroxyl OH ions. Acid volatiles such as H_2S, HCl and HF behave similarly to H_2O in a silicate melt, while CO_2, SO_2 and H_2 do not generally have a solution mechanism like that of water and do not depolymerise melts. Thus, the solubility of CO_2 in alumosilicate melts is very low compared with that of H_2O and other acid volatiles. Addition of H_2O to the melt not only breaks the oxygen bridges, but also increases the expansibility of the liquid, consequently allowing entry of the larger CO_2 molecules. Thus CO_2 solubility increases with increased H_2O contents. Best (1982) summarised the behaviour and role of H_2O in silicate melts as follows: (1) it depolymerises the melt and reduces its viscosity; (2) it increases diffusion rates; (3) it depresses crystallisation temperatures; (4) it exsolves and expands in the magma, in certain instances causing explosive volcanism. In terms of hydrothermal activity the following points are important: (1) H_2O in subsolidus systems, promotes alteration of higher temperature minerals; (2) retrograde boiling and separation of an aqueous solution in confined plutonic systems produces pegmatites and mineralised veins.

The concept of boiling in magmas is also very important for hydrothermal mineral systems. First boiling is that which occurs in a magma during decompression, causing exsolution of the volatiles due to their decreased solubility resulting from the lowered pressure. Second or retrograde boiling takes place as a result of the enhanced concentration of volatiles due to the effects of crystallisation. The continuous increase of H_2O in the residual melt during crystallisation is such that, at some stage, the pressure in H_2O becomes equal to the confining pressure and retrograde boiling takes place. This retrograde boiling has the effect of creating a separate aqueous phase (i.e. a hydrothermal solution).

Conceptual models of intrusion-related multiple styles of Au and polymetallic hydrothermal systems have been proposed by Sillitoe (1996), Sillitoe and Thompson (1998), Lang et al. (2000), and Lang and Baker (2001) amongst others. Figure 4.3, schematically depicts a combination of these models, from an intrusion-related environment, to a greisen-skarn complex. Although the emphasis is commonly on Au, these intrusion-related hydrothermal systems exhibit a spectrum of polymetallic ore assemblages, with the causative intrusions being surrounded by regional aureoles, from 2 to >5 km wide, characterised by arrays of polymetallic veins (Cu-As ± Au ± Ag; Zn-Pb-Ag ± Au; Au-Sb-As ± Bi;

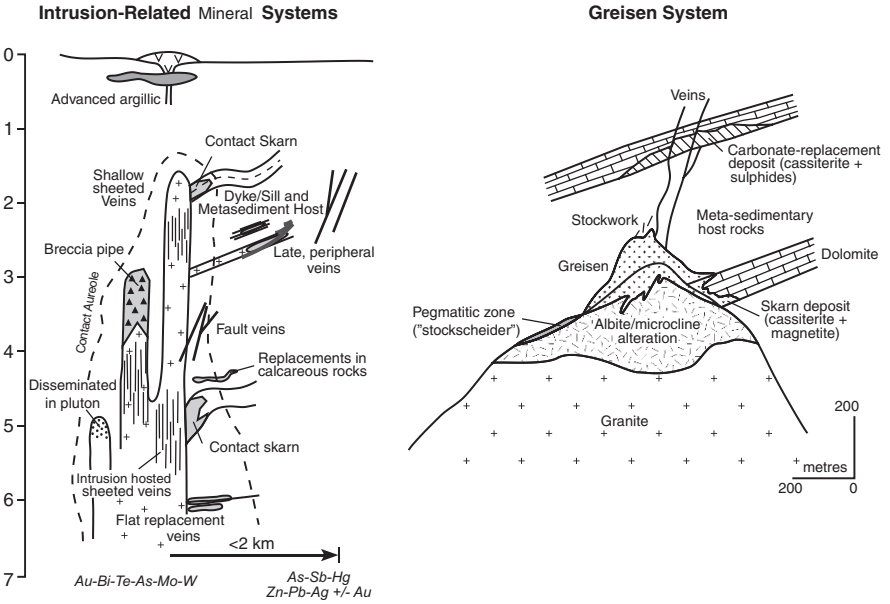


Fig. 4.3 Schematic illustrations of lateral and vertical mineralisation styles and types of intrusion-related hydrothermal ore systems (*left*) and greisens (*right*); after Lang and Baker (2001), Lang et al. (2000), and Sillitoe (1996)

Au-Bi-Te-Mo-W), replacement (Au-As ± Bi ± W; Au-Bi-As-W ± Mo), breccia pipes (Au-Cu-Mo-W-Bi ± Te ± As), disseminated (Au-Mo-Bi-Te ± W ± As), sedimentary rock-hosted (Au-As-Sb ± Hg) to greisen and skarn (Sn-Fe; W-Bi ± Au ± Mo; Cu-Au) systems. The causative intrusions have intermediate to felsic compositions (I-, S- and A-type granitoids), range from metalluminous to alkalic, are reduced to relatively oxidised (Fig. 4.4) and, in contrast to Fe oxides-Cu-Au systems, are usually characterised by reduced ore mineral assemblages (arsenopyrite, pyrrhotite, pyrite) and tend to lack in oxidised minerals, such as magnetite or hematite (Lang and Baker 2001).

The tectonic settings of intrusion-related systems include intrusions emplaced in arc and back-arc, as well as post-collisional plutons (Sillitoe and Thompson 1998), to which I add plutons emplaced in post-orogenic rift systems. Sillitoe and Thompson (1998) stressed that it is important to take into account the fact that it is sometimes difficult to distinguish orogenic lodes from intrusion-related vein systems, because of the uncertain, if any, genetic relationships of the lodes with plutonic rocks. However, Lang and Baker (2001) mentioned that a point of difference between orogenic lodes and intrusion-related vein system is regional scale zonation with Au-rich sheeted and stockwork veining within the intrusion to more base metal-rich vein systems outside the intrusion. This feature is especially valid in porphyry systems (see Chapter 5). The spectrum of deposit styles reflects the spatial relationships with the

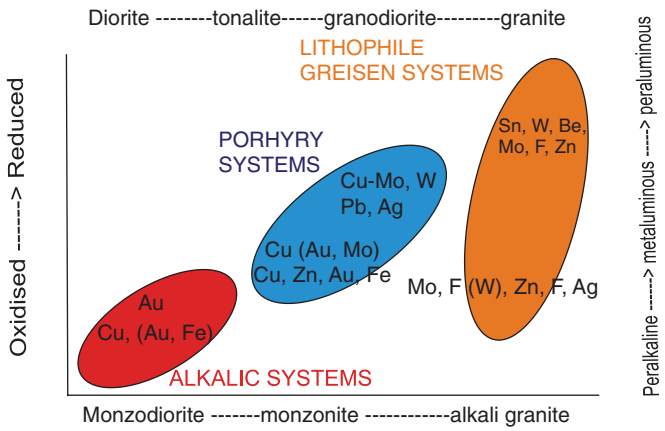


Fig. 4.4 Ore systems and metal associations in relation to the nature of felsic-intermediate intrusions and redox conditions. After Barton (1996), Thompson et al. (1999) and Lang and Baker (2001)

intrusive centre, from intrusion-hosted to proximal to distal (Lang and Baker 2001). These authors outlined the features of the style of ore systems as follows (Fig. 4.3): (1) intrusion-hosted systems sheeted or lesser stockworks generally with a metal assemblage of Au-Bi $\pm$ Te $\pm$ As $\pm$ Mo $\pm$ W and with mineralisation commonly sited in miarolitc cavities of the causative pluton and/or in pegmatitic bodies; (2) proximal deposits are found within the metamorphic aureole of the intrusions and generally have metal assemblages of W $\pm$ Cu $\pm$ Au and Cu-Bi-Au $\pm$ W skarns, Sn-bearing and Cu-rich breccia pipes and diatremes as well as disseminated deposits in sedimentary rocks; (3) distal deposits occur beyond the metamorphic aureole and have a metal assemblage of Au-As-Sb $\pm$ Hg, with the Carlin style deposits being perhaps the best representative but also including quartz-sulphide veins and base metal-bearing breccias. However, the origin of Carlin style deposits is controversial and links to putative intrusions by no means established. I return to discuss Carlin style deposits in Chapter 8. Clearly, there are problems in attempting to link distal deposits with intrusions and for this reason Lang and Baker (2001) focus on intrusion-hosted and proximal mineral systems stating that these exhibit the most characteristic features of the class. These features include alteration patterns that tend to be fracture-controlled feldspathic (sodic and/or potassic), sericitic, greisen, calc-silicate, argillic and silicic. Alteration of intrusion-hosted deposits is usually confined to narrow envelopes around veins, although these may coalesce into more extensive zones. One of the features of the intrusion-related ore systems is a dichotomy in fluid evolution in that whereas porphyry systems are characterised by several pulses of hydrothermal fluids, in cases other than porphyries fluid evolution appears to be unidirectional (Lang and Baker 2001).

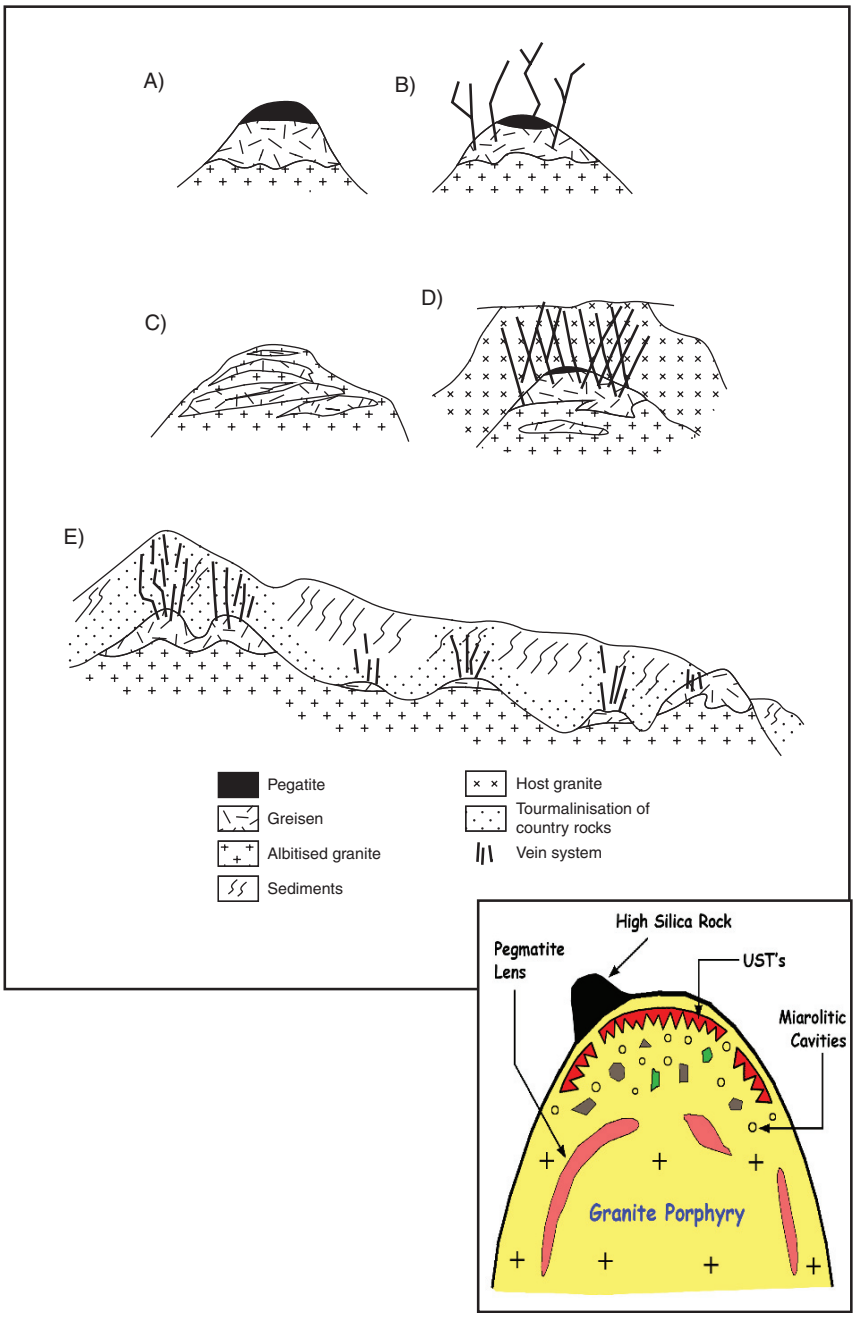


Fig. 4.5 Types of greisen systems, associated with high-level granitic cupolas; (**A**) and (**B**) are after Pollard et al. (1988), (**C**) and (**D**) after Taylor and Pollard (1988), (**E**) after Pirajno and Bentley (1985), inset at *bottom right* shows the development of unidirectional solidification textures (UST) and miarolitic cavities in a granitic cupola (after Kirwin 2005)

Some of typical features that characterise closed magmatic systems that produce intrusion-hosted deposits are miarolitic cavities and unidirectional solidification textures, which form ahead of a crystallisation front in volatile-rich melts. Miarolitic cavities are round to irregularly shaped and usually filled with a variety of crystals, such as quartz, feldspar, mica, beryl, topaz, tourmaline, fluorite and epidote. The cystals nucleate first along the walls of the cavity, the left over spaces are then filled with low temperature minerals that precipitate from hydrothermal fluids (e.g. calcite, chlorite). Miarolitic cavities form from vapour bubbles released from the granitic melt (Candela 1997). Unidirectional solidification textures (UST) are primary magmatic textures that consist of parallel to sub-parallel bands of quartz and quartz + feldspar crystals (Fig. 4.5; Kirwin 2005). These precipitate at the top of granitic cupolas and are a result of fluid pressure fluctuations. UST form zones from few metres to tens of metres in extent and 2–3 m thick. UST are commonly found in W-Mo greisen deposits and in porphyry Cu-Au-Mo systems, such as Oyu Tolgoi in Mongolia, discussed in Chapter 5. Kirwin (2005) provided an excellent documentation of UST from Mongolian mineral systems.

4.3 Greisen Ore Systems

These ore systems are usually generated by H_2O-rich magmas, such as muscovite-bearing granitoids (>8 wt% H_2O). These magmas tend to crystallise at depths ranging from a few kilometer to over 10 km, and do not usually vent at surface, although they may, at certain stages, intrude into wet crustal rocks and interact with connate or metamorphic waters. For the present purpose we are concerned only with the case of a closed system, that is, hydrothermal fluids generated entirely within the body of a cooling magma. As the magma cools and crystallises, H_2O, other volatiles and incompatible elements remain largely excluded from the consolidating mass. Volatile components are at first randomly distributed throughout the upper and central regions of the magmatic body. In this respect Taylor and Pollard (1988) envisaged that during the late stages of magmatic crystallisation, fluids are contained in the interstices of the granitic minerals, in much the same way as "oil in a sandstone ... whose movement and accumulation may be controlled by the evolving permeability" (Taylor and Pollard 1988). Eventually, the residual fluid phases may coalesce and concentrate into zones to induce autometasomatism of the igneous parent. In other words, the newly consolidated igneous body "stews in its own juice". This usually begins with a stage of alkali metasomatism (Chapter 2). The aqueous and gas phases exsolved from the magma will form a hydrothermal solution. This leads to a stage of hydrogen-ion metasomatism during which greisen-related deposits may form (Chapter 2). With decreasing temperature and pressure, and the presence of channelways, the fluids may eventually escape into the surrounding country rocks, where they form mineralised quartz vein systems.

The term greisen refers to an assemblage of quartz + muscovite, accompanied by varying amounts of other distinctive minerals such as fluorite, topaz and tourmaline. Greisenisation was defined by Shcherba (1970) as the high temperature, post-magmatic alteration of rocks by volatile-rich solutions associated with the cooling of granitic intrusives. Burt (1981, p. 832) defined greisenisation as "hydrothermally altered granitic rock consisting of a mixture of quartz and mica (normally lithian), with variable topaz, tourmaline, fluorite or other F- or B-rich minerals". More specifically, Burt (1981) distinguished quartz-topaz, quartz-muscovite or mica-fluorite greisen, defined in terms of the activities of HF and alkalies in alumino-silicate systems. Greisen systems result from complex, and as yet not completely understood, late- to post-magmatic metasomatic processes that affect and take place within a nearly consolidated granitic mass and the adjacent country rocks. These processes involve the concentration of volatile components such as F, B, Li, and the progressive concentration and activity of Na^+, K^+ and H^+ ions in a cooling granite body. Greisen systems are normally associated with Sn, W, U, Mo, Be, Bi, Li and F mineralisation.

Greisenisation is typically linked with highly fractionated magmas that have intruded into crustal depths ranging from 3 to 5 km, and takes place in the apical portions of granitic intrusive bodies (cupolas), emanating from deep-seated granite batholiths. The highly evolved granitic melts that promote the development of greisenisation phenomena and associated mineralisation are strongly enriched in volatile components, Cl, B, F, and the above mentioned metallic elements. The consolidated enriched products of these magmas are said to be "geochemically specialised". The cause of this specialisation or enrichment is a topic of much debate, with two main schools of thought contending processes of fractional crystallisation versus "geochemical heritage". Magmatic differentiation and fractional crystallisation have been advocated by Lehmann (1982) and Groves and McCarthy (1978). The idea put forward by this school is that in situ fractionation is largely responsible for the significant concentrations of volatiles and trace elements in the residual liquids. These would then accumulate into sheet-like zones in the roof of the fractionating granitic mass. The other school is advocated by Taylor, Pollard and coworkers of James Cook University in Queensland (Australia) (Pollard et al. 1983, see also Eugster 1984). These authors envisaged geochemical heritage as the main cause of the strong enrichment in volatiles, alkalies and trace elements. Indeed, there are many reasons to believe that the "geochemical specialisation" may have been inherited, or acquired, from the source region where partial melting occurs. In other words, the geochemical heritage is essentially due to the melting of crustal material containing protoliths with unusual contents of Sn, W, U, or, perhaps, containing evaporite sequences enriched in B. It is conceivable that the two theories can be reconciled by postulating that both processes may be operative, i.e. partial melting of enriched crustal material, followed by differentiation and crystal fractionation to further concentrate the volatiles and trace elements in the residual melts.

Greisen systems form in the apical portions (cupolas) of felsic and highly fractionated granites, and are commonly associated with vein systems (Černý

et al. 2005). The main features of a number of greisen systems are shown in Fig. 4.5. There are two end members: one in which the greisenising fluids are contained within the granitic cupola (closed system, or endogreisen where UST form), and one in which the fluids are channelled along fractures and faults, from within the parent cupola into the country rocks (open system or exogreisens). Transitional situations do exist, and may in fact represent the more common types of greisen systems. Russian geologists and geochemists have studied greisen rocks in detail, of which good English language publications are provided by Beus and Zalashkova (1964), Shcherba (1970) and Smirnov (1976). Ivanova (1969) studied the metallic content of greisenised granites and their mineral constituents, while more comprehensive accounts of greisens can be found in Taylor (1979) and Pollard et al. (1988). In this chapter I examine the main features of greisenisation processes, and the main mineralogical and geochemical attributes of greisen systems. A number of greisen-related mineral deposits are discussed here. These include the deposits formed in F-rich systems in the anorogenic intracontinental setting of the Bushveld Igneous Complex in South Africa, Sn-W deposits in collision-related settings (Panasqueira in Portugal, in Cornwall and southwest England), and the complex endo- and exogreisen systems of Mount Bischoff in Tasmania. The latter is a great natural laboratory in which both greisen and skarn systems are present, thereby providing important insights into magmatic and magmatic-hydrothemal processes.

4.3.1 Greisenisation Processes

According to Shcherba (1970), the sequence of greisenisation events include an early alkaline stage, a greisenisation stage and a vein-depositing stage. Smirnov (1976) subdivided the sequence of mineralogical transformations in the endogreisen environment into a progressive stage and a regressive stage, in response to temperature and pH regimes. In endogreisens the earliest stages are typified by alkali metasomatism (see Chapter 2), in which albitisation has an important role. In general, greisen systems evolve by decreasing alkali/H^+ ratios, resulting in the destabilisation of K-feldspar, plagioclase and micas, and leading to the greisen stage sensu stricto with the replacement of these minerals by quartz and muscovite. In some cases muscovite may be very coarse and may form thick monomineralic selvages along fractures. Other common mica compositions generated by the greisenising fluids include lithian siderophyllite, protolithionite, zinnwaldite and lepidolite (Kinnaird 1985). Silicification usually takes place during and after greisenisation, and is evidenced by intense quartz flooding and replacements. Muscovite characteristically replaces feldspars and biotite, and the reactions (assuming Al to be immobile) may be written as follows:

$$3(KAlSi_3O_8) + 2H^+ = KAl_3(Si_3O_{10})(OH)_2 + 2K^+ + 6SiO_2$$
microcline muscovite

$$3K(Fe, Mg, Ti)_3AlSi_3O_{10}(OH)_2 + 20H^+ = KAl_3Si_3O_{10}(OH)_2 + 2K^+ + 6SiO_2$$
biotite muscovite
$$+ 9(Fe^{2+}, Mg^{2+}, Ti^{4+}) + 12H_2O;$$

$$3KFe_3AlSi_3O_{10}(OH)_2 + 2HCl = KAl_3Si_3O_{10}(OH)_2 + 3Fe_3O_4 + 6SiO_2 + 2KCl + 3H_2$$
biotite muscovite

At this point it is pertinent to focus attention on the possible role played by the reactions shown above, in releasing metals into the system. Shcherba (1970), for example, noting that plagioclase and mica are the principal "carriers of rare metals", considered the leaching of the metallic elements from their original sites, in the lattices of these rock-forming minerals, to have occurred during greisenisation processes by virtue of the presence of F and Cl species in the fluids. Taylor (1979) commented on the Sn content of mineral phases of stanniferous granites (sphene 230–260 ppm, ilmenite 15–80 ppm, biotite 50–500 ppm); whereas, according to Eugster (1984), ilmenites may contain up to 1000 ppm Sn, 100 ppm Mo, 60 ppm W, 1000 ppm Nb, and biotite 1000 ppm Sn, 10 ppm W, 60 ppm Mo, and 100 ppm Nb. Eugster (1984) and Barsukov (1957) asserted that the conversion of biotite to muscovite (see reactions above) is of fundamental importance for the genesis of Sn-W deposits, emphasising the role played by both biotite and muscovite as "excellent hosts" for elements such as Sn, W, and Mo. The release of these elements from the lattice of micas to form ore minerals is documented by the presence of sulphide and oxide minerals in the cleavage and/or microfractures of the micas in the greisenised granites. Taylor (1979) explains that "a corollary to this concept should be that in the lower zones of Sn-systems the altered rocks should be depleted in Sn values". Indeed this was found to be the case for a greisenised granite in New Zealand (Pirajno 1982, 1985). The structural relationships between the greisenised cupolas and the enclosing country rocks, and their degree of fracturing, determines the type of endo-exogreisen system (Fig. 4.6). Types of greisen alteration within the cupola (endogreisen) and in the country rocks above and around the greisenised granite rocks are shown in Fig. 4.6. A greisenised cupola lodged in a sedimentary sequence containing pelitic and psammatic rocks will form a narrow aureole of contact metamorphism, usually identifiable by the presence of porphyroblastic biotite and, closer to the contacts, cordierite. Spotted schists are a common feature in sedimentary sequences intruded by granitic rocks. Greisenisation overprints thethermal mineral assemblages and is in most cases characterised by the nucleation of muscovite, albite and locally tourmaline. Quartz-sericite, albite and adularia, all of which may occur along fractures, may be associated with quartz vein material containing sulphides and oxides (e.g. pyrite, chalcopyrite, cassiterite, wolframite, scheelite, arsenopyrite, molybdenite etc.). Mineral assemblages generated during greisen alteration of granitic rocks are listed in Table 4.2.

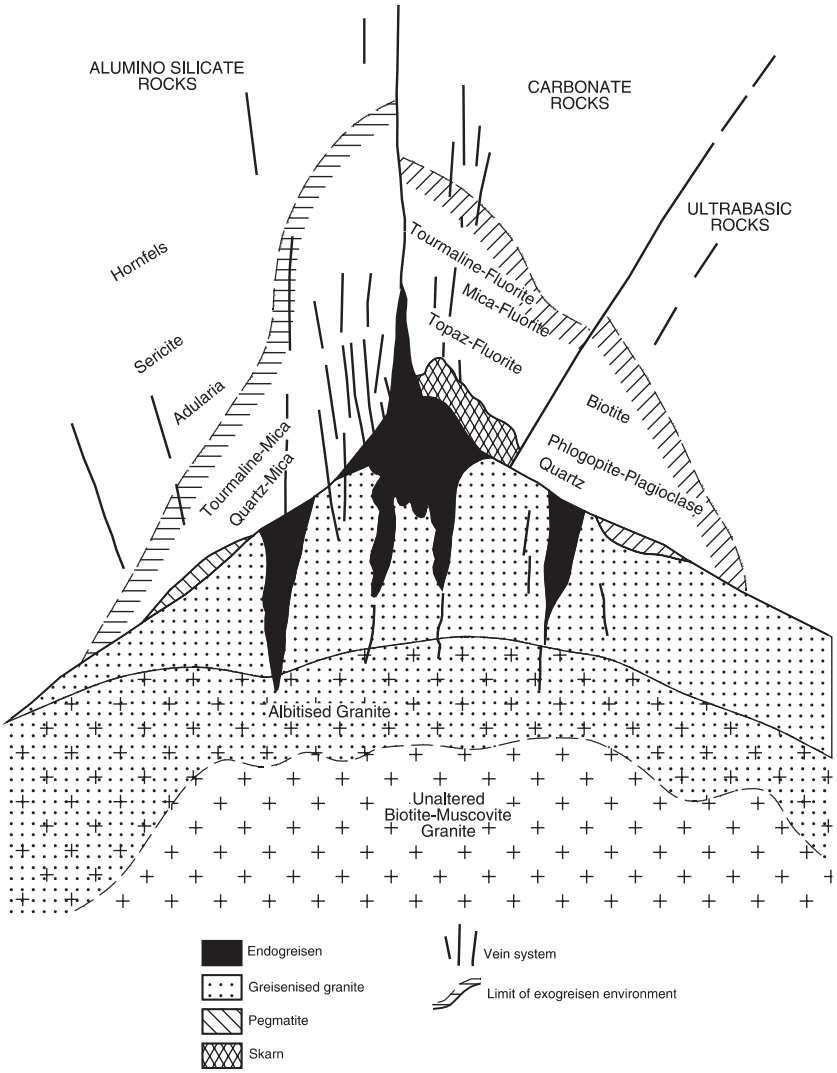


Fig. 4.6 The endo- and exogreisen systems in aluminosilicate, carbonate and ultramafic rocks. After Shcherba (1970); the endogreisen may have unidirectional solidification textures (UST; Kirwin 2005)

In mafic rocks greisenisation is characterised by the presence of chlorite-talc, phlogopite-actinolite, quartz-plagioclase and quartz-muscovite. Although typical skarns are usually associated with porphyry systems (Chapter 5), some skarns are spatially and genetically associated with greisen-related systems with which all gradations may be observed (Rose and Burt 1979). Greisen alteration of carbonate rocks usually takes place after their skarnification.

Table 4.2 Greisen alteration assemblages from precursor granitic rocks; after Kinnaird (1985)

Precursor rock	Greisen assemblage
Porphyritic plagioclase granite	Chlorite, fluorite, quartz, Li-Fe siderophyllite
Biotite-perthite granite	Chlorite, siderophyllite-protolithionite mica, quartz
Albitised biotite granite	Sericite, fluorite, siderophyllite-protolithionite mica, quartz, cryolite
Albitite	Fluorite, cryolite, siderophylllite-zinnwaldite-lepidolite mica, topaz, montmorillonite
Microclinite	Li-siderophyllite-protolithionite mica, chlorite, quartz, kaolinite

The greisen solutions are neutralised on contact with the carbonate lithologies, as the anionic species (e.g. F, OH) become fixed by Ca and Al to form fluorite and topaz. An example of greisenised carbonate rock (dolomite) is described in a later section which deals with the Mount Bischoff Sn mineralisation. The sequence of late-post-magmatic processes leading to greisenisation is shown in Fig. 4.7. In this scheme, worked out by Pollard (1983), K-feldspathisation takes place as a result of separation of fluids from a residual granitic melt. This phase leads to a concentration of Na in the melt, resulting in the crystallisation of a Na-rich rock, usually with a high F content. Pollard (1983) distinguished two stages each for K-feldspathisation and Na-feldspathisation, one magmatic and one post-magmatic. Pegmatites and UST may also form at the top of the granite cupolas, and while their relationship to the greisenising fluids is unclear (Pollard et al. 1988), in many cases the pegmatitic material is

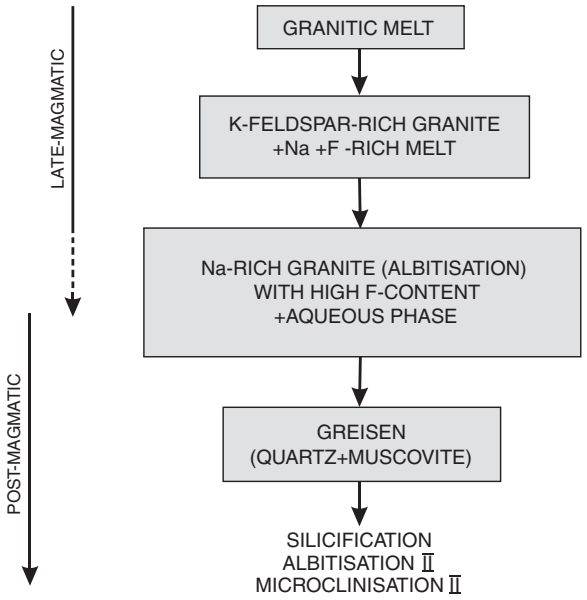


Fig. 4.7 Schematic illustration of late- to post-magmatic trends that are characteristic of greisenisation processes; the later post-magmatic minerals commonly overprint the earlier phases. After Pollard (1983)

greisenised and therefore it must be assumed that it forms during a late-magmatic stage, prior to alkali and greisen metasomatism. The enrichment of the residual melt in Na and F results in post-magmatic Na-feldspathisation, or albitisation, which is most common in the uppermost zones of the cupolas and along fractures, where in fact albitites may occur. According to Pollard (1983), this may be due to the enhanced F content, and perhaps influence of CO_2, which lower the solidus, and in so doing allows an extended period of crystallisation that in turn allows the exsolution of an aqueous phase to develop and collect in the apical parts of the granitic cupola. Greisenisation follows the stage of Na metasomatism (Fig. 4.7) during which the circulating hydrothermal fluids are characterised by enhanced activities of H^+ and of HF, and in which there is wholesale destruction of the granitic mineral components to form greisen assemblages. The silica released by the greisen-forming reactions precipitates to form granular quartz aggregates, quartz flooding and veins. Greisen alteration is the equivalent of quartz-sericite-pyrite alteration of the porphyry systems, and indeed in many porphyry deposits, an early greisen alteration may be present (e.g. at Climax in Colorado), merging into a later quartz-sericite-pyrite so that a clear boundary between the two is not always discernable. Following the phase of greisen alteration, second phases of Na- and K-metasomatism may occur, as indicated by the replacement of greisen minerals (e.g. topaz, muscovite) by albite and new growths of K-feldspars with the notable absence of perthitic feldspars (Pollard 1983). Post-greisenisation alteration is generally related to enhanced hydrothermal activity that is increasing H^+ metasomatism, in which meteoric waters may play a substantial role. This subsequent activity results in quartz-sericitic and argillic alteration with illite $\pm$ kaolinite, chlorite and carbonate minerals. Fluid inclusion studies of greisen deposits generally confirm the magmatic origin of the hydrothermal fluids, even though there are cases which have been interpreted by mixing of magmatic with meteoric waters. A classic review of salinities and homogenisation temperature of fluid inclusions from greisen-related mineral deposits can be found in Roedder (1984). According to the type of greisen-related deposit (e.g. endogreisen to exogreisen and quartz veins) the nature of the greisenising fluids varies from high (600–400°C and >40 wt% NaCl equivalent) to low (ca 200°C and 10–15 wt% NaCl equivalent) temperatures and salinities respectively. Dissolved species include mainly NaCl, KCl and CO_2, but phases such as anhydrite and borax have also been identified. Burt (1981) studied greisen mineral equilibria in the system K_2O-Al_2O_3-SiO_2-H_2O-F_2O, in terms of the activities of HF (acidity) and KF (salinity). The exsolution of a supercritical fluid phase, its ascent and evolution, marks the inception of the magmatic-hydrothermal activity in a granitic system. An increase in HF activity (μHF) brings about a tendency towards peraluminosity in the magma, and H^+ metasomatism (e.g. greisenisation) in the hydrothermal fluids. The opposite is obtained by increasing the salinity (expressed by μKF), during which there is increased peralkalinity in the magma, and alkali metasomatism (e.g. feldspathisation) in the fluids. The

separation of a liquid phase from a vapour phase (boiling) results in the concentration of the heavier saline species (KCl, NaCl etc.) in the former, and the lighter species (HCl, HF etc.) in the latter. Consequently, according to Burt (1981), the concentration of acid volatiles in the vapour phase is greatly increased, and this is considered to be the main cause of greisenisation phenomena. These fluids can at various stages be modified by diluting meteoric waters, as testified by the common occurrence of clay minerals, such as in the Cornwall greisen-related mineral deposits. Burt also draws attention to the importance of adding new elements to the system, for example Ca and W. In this case the activity of HF determines the stability of scheelite (lower μHF) or wolframite (higher μHF) in the system. At low HF activity the formation of scheelite could be as follows:

$$H_2WO_4 + Ca^{2+} = CaWO_4 + 2H^+$$

with increasing HF activity scheelite may convert to wolframite according to the following reaction:

$$\underset{\text{scheelite}}{CaWO_4} + FeO + 2HF = \underset{\text{wolframite}}{FeWO_4} + \underset{\text{fluorite}}{CaF_2} + H_2O$$

Also in his work, Burt shows that the anorthite content of plagioclase and other calcic phases (e.g. sphene) decreases or becomes unstable as the F-content of the system increases, thus making Ca available to form fluorite. This is confirmed by direct field and mineralogical observations, for example in a low-F greisen-related Sn-W deposit in the Karamea Batholith in New Zealand, where it is shown that the Ca of the plagioclases was utilised to form scheelite (Brathwaite and Pirajno 1993). In vein-type greisens the hydrothermal processes are at lower temperatures and there appears to be no evidence of boiling. Thus, in the case of greisenisation without boiling, F-bearing micas and topaz would form at high HF activity. Under conditions of very high F-activity topaz greisens form as a result of the instability of muscovite in the presence of HF as indicated by the reaction shown below for the topaz-rich greisens of Mount Bischoff (Tasmania) (Wright and Kwak 1989):

$$\underset{\text{muscovite}}{K_2Al_4(Si_6Al_2O_{20})(OH)_4} + 6HF = \underset{\text{topaz}}{3Al_2(SiO_4)(OH, F)_2} + 3SiO_2 + 2K^+ + 4H^+$$

Increase in the activity of H_2O during cooling of the hydrothermal fluids would result in the breakdown of topaz and feldspars to release large quantities of HF, with formation of muscovite and quartz. The release of F, together with the muscovitisation and chloritisation of the biotites at depth, would result in the leaching of metals and their complexing with F and subsequent transport upward in the evolving system. In low-pressure environments, such as in subvolcanic to

volcanic areas, the separation of aqueous phases from F-rich magmas causes low-pressure greisenisation. This results in the formation of greisen mineral assemblages, as indicated by the formation of topaz and fluorite in cavities of rhyolitic volcanics and ash-flow tuffs (Burt 1981). So far, I have considered only the presence of F in a greisen system. However, Li and B also occur, and the main features of B-rich systems as opposed to those enriched in F have been investigated by Pollard et al. (1987). These authors first pointed out that such environments can occur at either at the local or regional scale, and also that there may be mixed situations. The general features of the F-rich and B-rich greisen systems are shown in Fig. 4.8A, B. As previously outlined, F-rich greisen systems are characterised by the presence of fluorite and/or topaz as well as Li-rich micas (e.g. lepidolite or protolithionite). B-rich greisen systems, on the other hand, are manifested by abundant tourmaline which tends to form clots or nests in the cupola and are generally not mineralised. In open systems (Fig. 4.8A), this mineral occurs in, and is associated with, breccia pipes, stockworks and veins. These are generally the result of developing high B-rich volatile pressures during

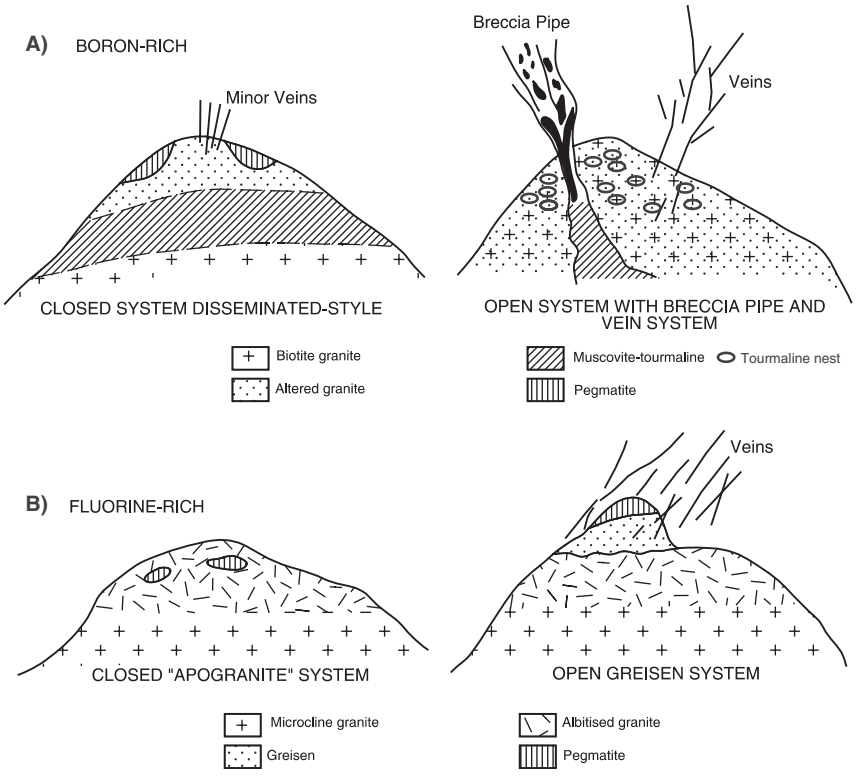


Fig. 4.8 (**A**) Boron-rich and (**B**) fluorine-rich greisen systems; see text for details. After Pollard et al. (1987)

the crystallisation of B-rich magmas. In closed systems the granitic cupola contains disseminations of tourmaline and greisen minerals (Fig. 4.8A). In both F- and B-rich systems, other components such as CO_2, Cl and of course H_2O assume importance in terms of granitic melt behaviour during crystallisation and exsolution of hydrothermal fluids.

4.3.2 Geochemistry

Greisenised granitic rocks are generally characterised by increases in Si, and losses in Al, K and Na, with respect to the parent unaltered granitic body. The breakdown of feldspars during greisenisation processes is thought to be largely responsible for the Na and Al losses and the increase in Si (Kinnaird 1985). The K liberated by the greisenising reactions is taken up by the hydrothermal fluids, probably to generate second-stage K-metasomatism. Kinnaird (1985), in her work on the greisen systems of Nigeria, reported increases in Li, Th, Ce, Y, Sn, Pb, Zn, Fe, W and Cu, as well as enrichment in light REE, in the greisenised rocks. Greisenisation of the Cligga Head granite in Cornwall is also characterised by enrichments in Ca, F, B, Li, Rb, Sn, W and Zn, and depletions in Na, Al, Ba and Sr (Hall 1971).

4.3.3 Greisen-Style Mineral Systems

Greisen systems are typically associated with Sn and W mineralisation, usually accompanied by numerous other ore elements such as Cu, Zn, Bi, Mo, U, F. Common ore minerals are cassiterite, stannite, wolframite, scheelite, arsenopyrite, pyrite, chalcopyrite, molybdenite, sphalerite, bismuth and bismuthinite. Other important minerals are topaz, fluorite and apatite. Most greisen-affiliated Sn and W deposits are spatially and genetically related to S-type granitic rocks, or the ilmenite-type of Ishihara (1977), forming dome-like (cupolas), or ridge-like intrusions. Details of Sn and W deposits of greisen affiliation can be found in Taylor (1979) and in a collection of papers edited by Hutchison (1988). The general features of greisen-related Sn mineralisation have been discussed by Pollard et al. (1988) and Hosking (1988). This mineralisation occurs as lenses, generally subparallel to the arcuate contacts of the granitic intrusion with the enclosing country rocks. In open systems, fracture-controlled, sheeted veins, and stockworks, emanate from the greisenised granite into the country rocks (Fig. 4.5). Greisen mineral systems may have distinct metal zonations. These are usually manifested by a lower zone of Sn + Mo, extending upward and sometimes laterally through W + Bi to Cu, Zn, and Pb. In some cases Au may also be present, as for example at Kirwans Hill in New Zealand (Pirajno and Bentley 1985) and the Au-Mo association in the Timbarra

Tablelands pluton in New South Wales (Australia; Mustard 2004). However, these zonations are somewhat idealised, having no general validity, and thus each case has to be assessed separately. Time-paragenetic sequences of greisen-related ore assemblages, on the other hand, appear to follow some general rules that may be applicable to most greisen deposits. Deposition of the ore minerals usually starts with an oxide phase (cassiterite, wolframite), followed by sulphides (pyrite, chalcopyrite, pyrrhotite, arsenopyrite, molybdenite, bismuthinite), and a late, lower temperature, carbonate-oxide stage characterised by calcite, siderite and iron oxides. At Panasqueira (Portugal), for example, the paragenetic sequence consists of an early oxide-silicate stage, a sulphide stage and late carbonate stage (Kelly and Rye 1979).

4.3.4 Sn and W Geochemistry in the Greisen System and Deposition of Cassiterite and Wolframite

The geochemical specialisation of the Sn-bearing granites is, inter alia, thought to be controlled by the oxidation state of Sn in the melt, with respect to conditions of high or low oxygen fugacity as determined by the Fe^{+3}/Fe^{+2} ratios. Ishihara (1977, 1981) and Ishihara et al. (1979) classified granitic rocks into a magnetite series (more or less equivalent to I-types), and an ilmenite series (more or less equivalent to S-types). The hypothesis proposed by these authors with regard to the behaviour of Sn in the granitic melts, is that in the case of magnetite-series granites, characterised by high Fe^{+3}/Fe^{+2} ratios, Sn is in the tetravalent state (Sn^{+4}) and as such may substitute for Ti or Fe, thus entering the lattice of the early crystallising, rock-forming minerals (e.g. sphene, magnetite, hornblende, biotite). Its availability in the remaining liquid fraction would hence be limited, with the further consequence that accumulation of Sn in the residual melt would be insufficient to produce an ore deposit. In the case of the ilmenite-series granites (low Fe^{+3}/Fe^{+2}), Sn is in the divalent state (Sn^{+2}) and as such cannot enter the lattice of the early rock-forming minerals. Under these conditions Sn would be more readily available for accumulation in the residual melts, leading to a Sn-rich, and hence specialised, highly fractionated leucocratic granite. It is of interest to note in this context that studies of worldwide Sn-W and porphyry metallogeny has indicated that I-type/magnetite-series granitoids are generally associated with Cu-Mo porphyry mineralisation, and generated either in the upper mantle or lower crustal levels. On the other hand S-type/ilmenite-series granitoids, which are generally associated with Sn-W mineralisation, are either generated in crustal environments, or, may interact with C-bearing metasedimentary rocks (reducing conditions, low oxygen fugacity; see also Fig. 4.3). The world distribution of the Sn-W deposits of greisen affiliation tends to form either in collisional tectonic settings or in anorogenic intraplate settings (Mitchell and Garson 1981).

Cassiterite is the chief ore mineral of Sn and is commonly associated with fluorite and/or tourmaline, suggesting a cogenetic relationship between these minerals and the transporting hydrothermal fluids. Various mechanisms have been proposed for the dissolution and transport of Sn in hydrothermal solutions. According to Paterson et al. (1981) Sn^{+2} readily complexes with F^-, OH^- and Cl^-. Sn transport as a consequence of hydroxyl and hydroxyfluoride complexing is thought to take place in high temperature, alkaline fluids (Eadington 1983). Fluoride and chloride complexes are more significant for the transport of Sn in hydrothermal solutions. It appears that F is more likely to transport Sn in highly saline solutions. Sn is considered to be readily transported as a stannous chloride complex ($SnCl^-$) under conditions of low pH and low f_{O2} (Paterson et al. 1981). Precipitation of cassiterite due to the destabilisation of the transporting complexes would then occur either by f_{O2} increase, an increase in pH, a decrease in temperature or a combination of these physico-chemical factors. Generally speaking, the conditions which cause precipitation of cassiterite are similar to those for wolframite (discussed below), and it appears that in a Sn-W-bearing solution cassiterite and wolframite would precipitate earlier under slightly more acidic conditions, while scheelite would precipitate later at slightly higher pH levels (neutral to alkaline). Precipitation of cassiterite also depends on the nature of the rocks with which the fluids interact. The metal chloride solutes are converted to oxides and/or sulphides and HCl and H^+ released (Eugster 1984). Neutralisation of the acid greisenising fluids is readily achieved by their penetration of carbonate rocks; precipitation of cassiterite may be represented as follows (Eugster 1984):

$$SnCl_2 + CaCO_3 + H_2O \rightarrow SnO_2 + CaCl_2 + CO_2 + H_2O.$$

In pelitic rocks it is the conversion of feldspar and biotite to muscovite that may induce precipitation of cassiterite, as previously mentioned. A possible reaction proposed by Eugster (1984) is:

$$\underset{\text{biotite}}{SnCl_2 + 3KFe_3AlSi_3O_{10}(OH)_2} + 2H_2O \rightarrow SnO_2 + \underset{\text{muscovite}}{KAl_3Si_3O_{10}(OH)_2} + 6SiO_2 + 3Fe_3O_4 + 2KCl + H_2.$$

In nature W is found almost exclusively in a hexavalent state (W^{+6}) with oxygen compounds. Thus, there are two principal groups of tungstate compounds known as minerals, namely, wolframite [$(Fe,Mn)WO_4$] and scheelite ($CaWO_4$). Wolframite forms a solid solution series with ferberite ($FeWO_4$) and hubnerite ($MnWO_4$). Experimental data indicate that W is mobilised in chloride-bearing hydrothermal solutions. Foster (1977) postulated that molecular hexalides (WCl_6) are probably present at near-magmatic temperatures, but with

decreasing temperatures and increasing hydration, W is transported as molecular H_2WO_4. With further decreasing temperatures the major W species are ionic $(H_3W_6O_{21})^{-3}$; $(HW_6O_{21})^{-5}$; $(WO_4)^{-2}$. Under these conditions the parameters controlling W transport and deposition are, apart from temperature, f_{O2}/f_{S2}, the activities of Ca^{2+}, Fe^{2+} and Mn^{2+} and the pH of the solution (Foster et al. 1978). Scheelite deposition at supercritical (over 500°C and 100 bar) and near-critical temperatures is a function of the temperature variations and the activity of the ratio Ca^{2+}/Fe^{2+}. Assuming a Cl^{-}-rich brine, with high Ca^{2+}/Fe^{2+} ratios, scheelite would be deposited. However, at high f_{O2} levels, and where the activity of Fe^{2+} is greater than that of Ca^{2+}, wolframite would be preferentially deposited, whereas at lower f_{O2}, sulphides will form (Foster et al. 1978) The role of F is more important for Sn than it is for W; however, oxyfluoride complexes may be responsible for the transport of W at low temperatures (±300°C), in cases where the concentration of F in the solution is high (Foster 1977). The role of F in the hydrothermal transport and deposition of W may be influenced by the activities of HF and KF, as proposed by Burt (1981). Under conditions of low HF and KF activities scheelite will form, whereas wolframite occupies a field of higher HF and KF values as discussed earlier. This would explain the common association of fluorite and topaz with wolframite mineralisation. Westra and Keith (1981) further substantiated this relationship, noting that scheelite is common (without cassiterite) in calcic magma series which have low F, while in F-enriched calc-alkaline magmas wolframite or hubnerite occur together with Mo and Sn.

Major wolframite deposits occur in southeast China and north-central, where total resources of 5.5 Mt W account for 50% of the world's tungsten endownment (Laznicka 2006).

4.3.5 Tin Deposits Associated with the Felsic Phase of the Bushveld Igneous Complex, South Africa

The Bushveld Igneous Complex (BIC) is the largest layered intrusion of its kind in the world, comprising vast mineral resources of a number of strategically important commodities (e.g. Cr, PGE). The BIC underlies an area of approximately 65 000 km^2, although of this about 55% is covered by younger sedimentary rocks. Comprehensive reviews on the BIC can be found in Vermaak and von Gruenewaldt (1986) and Eales and Cawthorn (1996). The lithostratigraphy of the BIC consists of three main suites. The Rashoop Granophyre Suite, emplaced about 2090 Ma ago, includes complex lithologies that have formed during an earlier silicic phase, and during the emplacement of the basic rocks (Walraven 1985). The Rustenburg Layered Suite, which is the main, mafic portion of the Complex, was intruded into the sediments and volcanics of the Transvaal Supergroup some 2050 Ma ago. The Lebowa Granite Suite with approximate ages ranging from 2050 to 2024 Ma comprises a series of cogenetic granitic

rocks which intrude all other lithologies and are responsible for the greisen systems discussed in the pages ahead. The BIC mineral systems can be classified into two major groups: (1) Magmatic deposits associated with the Rustenburg Layered Suite containing platinum group elements ($\pm$Au, $\pm$Ni, $\pm$Cu), Cr and Ti-V; (2) Hydrothermal deposits associated with the Lebowa Granite Suite, containing Sn, F Cu and minor Au. The Sn mineralisation is of interest in the present context and is discussed in the pages ahead. The Lebowa Granite Suite represents the final phase of the magmatic activity of the BIC, and its relationship to the BIC lithologies is shown in Fig. 4.9. It was emplaced as an intrusion of batholithic dimension generally along, or close to, the contact between the Rustenburg Layered Suite rocks and the roof rocks represented by the 6-km thick sequence of felsic volcanic rocks of the Rooiberg Group (Buchanan et al. 2004). The Lebowa Suite includes the Nebo Granite, Bobbejankop Granite, Klipkloof Granite and Lease Granite. The Nebo granite is the most abundant, all the others being considered as late-stage fractionated variants (Walraven 1985). The Nebo Granite, which is coarse-grained, is made up of K-feldspar, quartz, plagioclase and hornblende in its lower portions and biotite in its uppermost portions. The Bobbejankop granite is a variety of the Nebo Granite and distinguishable by its reddish colour, miarolitic texture, and the presence of tourmaline clusters. The endogranitic Sn deposits of the BIC occur mostly within the Bobbejankop granite and its roof facies. At Rooiberg, Sn mineralisation is hosted in sedimentary rocks and is associated with exogreisen alteration. The Sn deposits of the BIC are grouped into six main camps (Fig. 4.9A), and their postulated relationships with the granitic rocks and surrounding lithologies are shown in Fig. 4.10. The nature of this mineralisation has been reported by Crocker (1986), Coetzee (1986), Pollard and Taylor (1986) and Rozendaal et al. (1986).

4.3.5.1 Zaaiplaats Endogreisen

The Zaaiplaats Sn deposit is situated some 25 km northwest of the town of Potgietersrus in the Transvaal region (the former Transvaal administrative province is now divided into Gauteng, Northern Province and Mpumalanga) (Fig. 4.9A). The mineralisation is confined to the upper portions of the Bobbejaankop Granite and within its fine-grained marginal and apical phase, the Lease Granite. The Bobbejankop pluton was intruded as a sheet-like body roughly along the contact between the Rustenburg Layered Suite and its roof rocks represented by the Rashoop Granophyre Suite and the felsite of the Rooiberg Group. The Bobbejaankop Granite is deep red in colour, medium-grained, containing quartz and alkali feldspars as patch perthites, with variable proportions of microcline and albite, which are thought to represent Na- and K-metasomatism of earlier magmatic feldspars (Pollard and Taylor 1986). Biotite is present and invariably altered to chlorite. The Lease Granite is a volatile-rich differentiate of the Bobbejaankop granite, and is typically a microgranite with a low content of mafic minerals, which are also chloritised. This

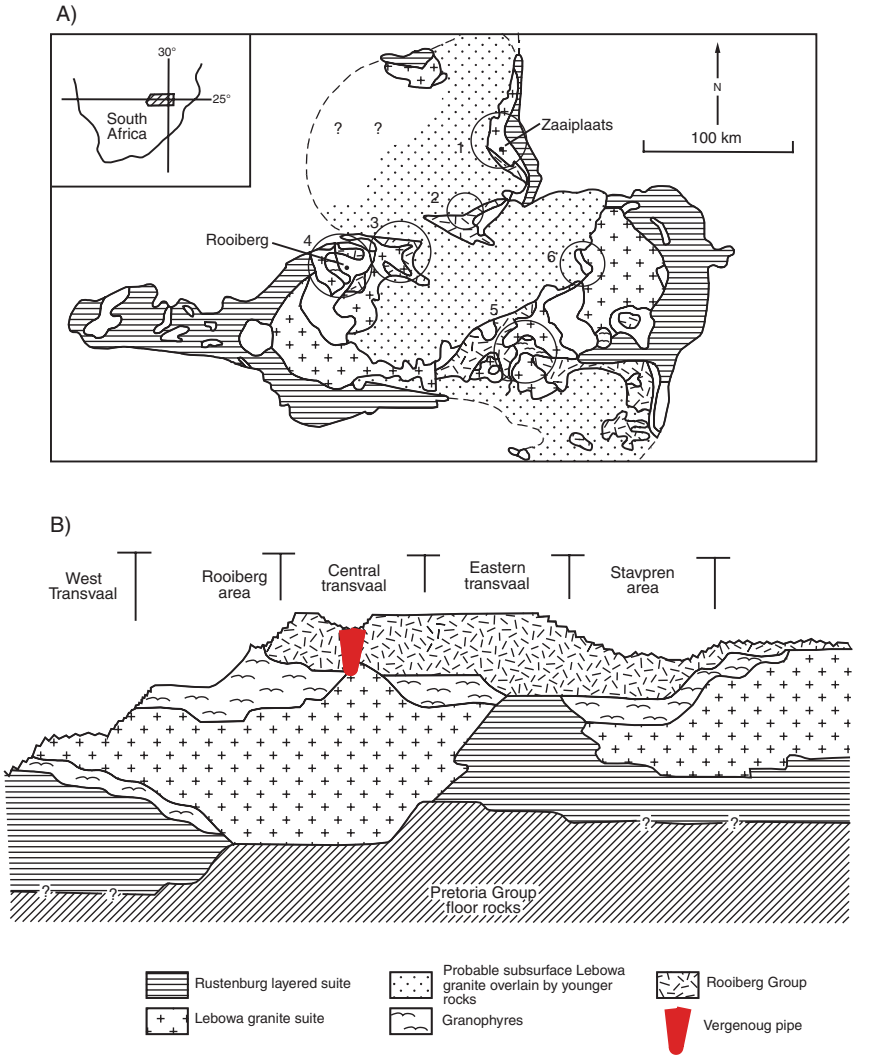


Fig. 4.9 Greisen systems in the Bushveld Igneous Complex (BIC) in South Africa; (**A**) simplified geology of the BIC and distribution of main areas of greisen-associated Sn mineralisation, 1 Zaaiplaats, 2 Union tin, 3 Elands, 4 Rooiberg, 5 Moloto, 6 Stavoren (Walraven 1985; Crocker 1979). The Vergenoug Fe-F pipe is located within 5 (see Section 4.6.2); (**B**) schematic cross-section of spatial relationships between the main lithostartigraphic units (Walraven 1985)

granite is bi-textured, that is, it has a coarse-grained phase interlocking with a fine-grained phase. The interlocking coarse materials coalesce to form the overlying pegmatitic zone. The Lease Granite also contains miarolitic cavities, filled with sericite, chlorite and tourmaline, and decreasing with depth. A zone

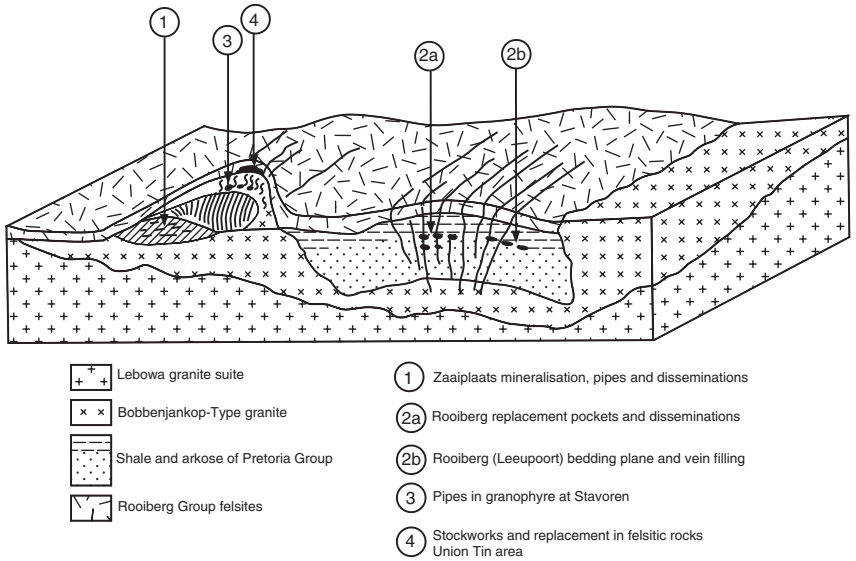


Fig. 4.10 Idealised model showing the styles of greisen-related Sn deposits in the granites of the Bushveld Igneous Complex; 1 Zaaiplaats pipes and disseminated mineralisation, 2 Rooiberg deposits (**a**) replacement pockets, (**b**) bedding plane and vein deposits, 3 pipes in the Stavoren granophyres, 4 stockworks and replacements in felsite rocks at Union Tin. See also Fig. 4.14. After Stear (1977)

of pegmatite bodies is present on the roof of the Lease Granite at, and near to, the contact with the overlying rocks of the Rashoop Granophyre. The pegmatites are characterised by large quartz and feldspar crystals orientated perpendicular to the contact, providing a good example of unidirectional solidification textures (UST). The presence of roof pegmatites and the bi-textured nature of the Lease Granite may be indicative of a closed mineralising system. Three different styles of endogranitic mineralisation are present at Zaaiplaats, including: disseminated orebodies, lenticular orebodies and pipe orebodies. A simplified representation of these three styles is shown in Fig. 4.11. Most orebodies have associated sulphides (chalcopyrite, arsenopyrite, galena and bismuthinite), wolframite, scheelite and even Au. Silver is found in grades of up to 150 g/t in the tailing concentrates. The bulk of the production was obtained from a zone of disseminated cassiterite ore, which is developed within the Bobbejaankop Granite some distance below its contact with the Lease Granite. The thickness of this ore zone, as defined by the cut-off grade, is about 10 m, and its average grade about 0.15% Sn. The granite is altered to an epidote-chlorite-sericite assemblage often associated with irregularly shaped vugs up to 25 cm in diameter. These vugs are infilled with cassiterite, scheelite, fluorite, chlorite, tourmaline and sericite. The lenticular orebodies (called “lily pads” by the local miners) occur within the Lease Granite at the base of the pegmatite

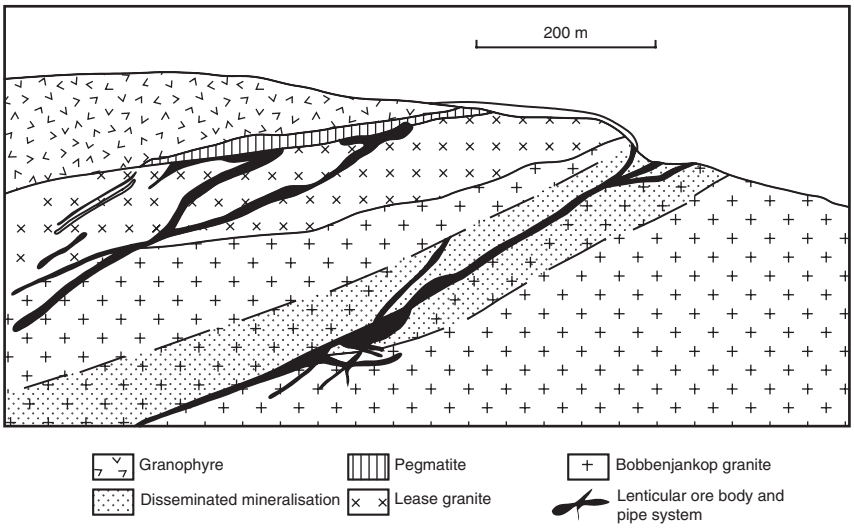


Fig. 4.11 Schematic cross-section depicting the Zaaiplaats mineralisation styles. Sketch based on Mine handout and Pollard et al. (1988)

zone. The lenticular orebodies contain relatively rich mineralisation, with grades of about 0.4–0.5% Sn. Extensive albite-sericite and chlorite alteration present within the bodies are considered to have formed by replacement of the Lease Granite by the developing hydrothermal fluids, with the pegmatite having acted as a barrier to the upward movement of the fluids. The lenticular orebodies tend to be funnel-haped and in places taper downwards into high-grade pipes of small diameter (about 50 cm). Pipe-like orebodies, which occur both in the Lease Granite and in the Bobbejaankop Granite can be exceptionally rich with grades of up to 30% Sn. The pipes have sharp contacts with the surrounding granite, and range in diameter from several centimetres up to 13 m, the average being 1–2 m. Although they have been traced for lengths of up to 1000 m, they are erratic both in distribution and strike and variable in composition. The pipes ramify and exhibit swellings and constrictions. However, there is a tendency for the overall plunge to be in a northwesterly direction, suggesting a vague structural control, and for the more productive pipes to cluster in certain areas of the granite, indicating a relationship between the cassiterite-bearing portions of the pipes and the zones of disseminated mineralisation that are traversed by the pipes (Fig. 4.11). The pipes display a strongly zoned, annular structure, generally consisting of a cassiterite-impregnated sericite-illite core, followed by an intermediate ring of tourmaline, a dark tourmaline (luxullianite)-quartz-feldspar annular zone, grading through a thin albitised zone into the relatively unaltered granite. Close examination of the pipes reveals inward-pointing euhedral quartz crystals developed between the albitised granite zone and the luxullianite zone, which is taken to be indicative of open-space

filling. Geochemical studies by von Gruenewaldt and Strydom (1985) revealed a distinct geochemical zonation of trace elements around the pipes, with Sn restricted to the pipes, and Cu, Pb, Zn, W and As forming well-defined dispersion haloes around the pipes. The enigmatic pipes at Zaaiplaats probably represent channelways along which hydrothermal fluids moved upwards towards the upper portions of the granite body. Taylor (1979) considered the formation of the pipes to be a possible result of immiscibility of an aqueous phase from the crystallising magma. This aqueous phase would have formed bubbles that trailed upwards within the crystallising silicate melt, to become "entrapped by crystallisation before reaching an overlying plumbing system" (Taylor 1979, p. 173). Pollard et al. (1989) presented a model of pipe formation. Their detailed investigation of the mineralogy and textural relationships in one of the main Zaaiplaats pipes has shown that the host granite was subjected to a process of leaching whereby quartz and to some extent feldspar, were removed by very hot solutions. Although the nature of these solutions is not certain, the authors postulated that they were weakly alkaline and contained alkali chloride, fluoride or carbonate complexes that exsolved from the magma in the subsolidus range of temperature and pressure. The dissolution of the quartz and feldspars created zones of permeability, largely formed by vugs, which allowed the movement of the developing hydrothermal fluids. The vugs created by the dissolution process were later infilled by a host of hydrothermal minerals. Minerals deposited in the vugs include quartz, tourmaline, albite, chlorite, cassiterite, scheelite, fluorite, synchisite (a fluorocarbonate containing rare earth elements), calcite and sulphides.

Pollard and Taylor (1986) and Taylor and Pollard (1988) explained the evolution of the magmatic-hydrothermal fluids responsible for the Zaaiplaats mineralisation as follows. The presence of vugs, which occupy 1–4% by volume of the granitic rock, and the pervasively altered nature of the granite containing disseminated cassiterite, are evidence of exsolving hydrothermal fluids immediately subsequent to the main crystallisation phase of the silicate melt. Work done by the Taylor-Pollard team in the Herberton tin field of Queensland in Australia indicates that in general magmatic-hydrothermal fluids are developed in situ during the very late stages of crystallisation. At Zaaiplaats hydrothermal fluids occupied an extensive system of interstitial cavities, grain boundaries and microfractures, so that the upper portions of the granitic body became a reservoir of magmatic-hydrothermal fluids.

Fluid inclusion studies indicate homogenisation temperatures in the range of 300–600°C for highly saline brines, whereas oxygen isotope determinations gave results consistent with fluids of magmatic origin having exchanged with granitic rocks at temperatures of about 350°C (Pollard and Taylor 1986). The model of a magmatic fluid reservoir, as envisaged by these workers, implies that hydrothermal fluid movement is essentially a question of permeability. This in turn is related to the amount and degree of fracturing within the granitic rocks and the adjacent country rocks. Clearly Zaaiplaats is a closed system in which, because of poor permeability, the fluids were contained within the granitic mass

(endogreisen). The development of fractures within the entire system may be related either to fluid pressure causing hydraulic fracturing, or to tectonic activity, or both. In orogenic areas both are likely to take place and the development of vein systems is perhaps more frequent than in anorogenic systems. Fracturing, according to the model outlined above, would result in the tapping of the magmatic-hydrothermal fluids and the establishment of exogreisen vein systems. In orogenic areas, meteoric waters are also more likely to participate in the evolution of the mineralising event by mixing with the fluids of magmatic-hydrothermal origin.

4.3.5.2 Rooiberg Exogreisen

The Rooiberg Sn field, situated about 65 km west of Warmbaths (Transvaal) (Fig. 4.12A), was once the largest Sn producer in South Africa. Until 1986 production was from four mines, Hartbeestfontein ("A" Mine), Nieuwpoort ("B" Mine), Leeuwpoort ("C" Mine) and Vellefontein (Fig. 4.12A). These mines, together with the Union Tin deposit near Naboomspruit, accounted for nearly 60% of the production in the Bushveld province. Up to 1998, total metallic Sn produced by the Rooiberg mines was about 84 000 t (du Toit and Pringle 1998) The Sn field occurs within the so-called Rooiberg fragment, a gigantic segment or roof pendant of sedimentary and volcanic rocks of the Transvaal supergroup (Pretoria and Rooiberg groups), intruded by the Bushveld granites (Lebowa Granite Suite). The Rooiberg Sn mineralisation was described by Rozendaal et al. (1986, 1995). The intrusion of the sedimentary and volcanic rocks by successive influxes of granitic magma gave rise to horizontally disposed stress fields within and adjacent to the Rooiberg fragment (Stear 1977). Structurally, the Rooiberg Sn field has the form of a broad east-northeast trending arch, with a superimposed northwest-trending synclinal structure. On the northwestern and southwestern limbs of the arch are two prominant dislocation zones (Kwarriehoek Wrench and South Parallel Fault), one of which, the South Parallel Fault, was probably the main feeder channel for the mineralising fluids. The most important mineralisation occurs within cross-bedded arkosic rocks (Boshoffsberg Quartzite Member) and in the overlying shaly quartzite rocks below the Blaauwbank Shale Member. The latter is thought to have acted as an impermeable barrier to the ascending fluids. Rozendaal et al. (1986) classify the Rooiberg Sn deposits as either conformable or uncomformable. Included in the former are the spectacular pockets, bedded lodes and stringers, and bedding-plane orebodies, while the uncomformable deposits comprise mineralisation of open-space filling style along fractures and faults. The bulk of the production comes from the pocket orebodies, which are best developed at the "A" Mine and confined to a stratabound zone (the "tin" zone), located within a complex of intersecting fissures. These pockets, of varying shape, size and mineral content, are formed along discontinuities in the host rock, including steep hairline fractures, low-angle bedding and/or cross-bedding planes, from which chemical replacement diffused outward. With regard to their shape and stage of development the

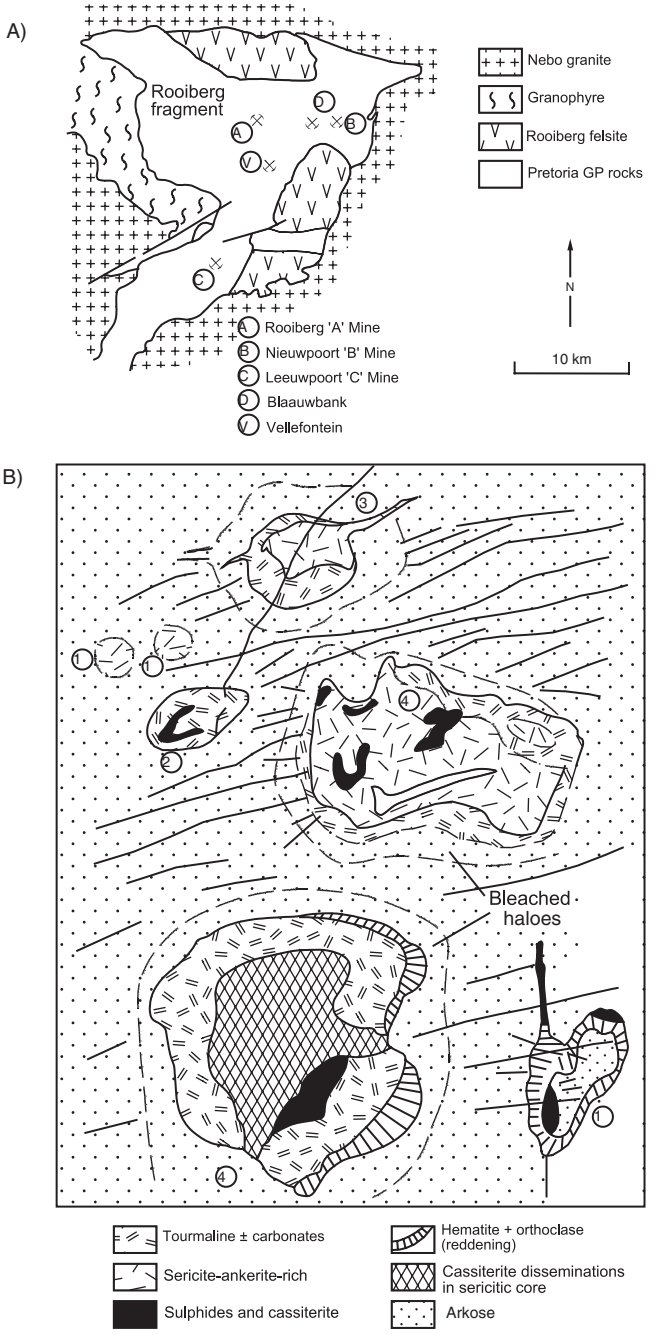


Fig. 4.12 (**A**) Simplified geology of the Rooiberg area and distribution of Sn deposits; (**B**) The Rooiberg "A" mine pockets showing various stages of development, 1 embryonic, 2 nodular, 3 orbicular, 4 complex. After Mine handout and Rozendaal et al. (1986)

pockets are referred to as embryonic or incipient, nodular, orbicular (when zoned), or complex (Fig. 4.12B). The alteration-mineralisation associated with the pockets is highly variable. Tourmaline, ankerite, cassiterite and pyrite constitute the main mineral phases, and smaller quantities of chlorite, sericite, chalcopyrite and quartz are also present. Reddening (due to K-feldspar and hematite) of the host arkosic rocks may mark the site of an incipient pocket. The host rocks of the tin zone are extensively albitised. Bedding-plane mineralisation is characterised by fine-grained concentrations of cassiterite, hematite, tourmaline, pyrite, chlorite and ankerite along bedding planes of the arkosic rocks. Bedded lodes are economically important and occur as sheet-like, conformable bodies of about 10–15 cm thickness. At Vellefontein the cassiterite-bearing bedded lodes are typified by spectacular hydraulic breccias, stockworks and stringers. A typical lode is composed of ankerite, tourmaline lenses and country rock fragments. Stringers are filled with carbonate, cassiterite, pyrite and chalcopyrite. Stear (1977) noted that the bedded lodes generally exhibit imperfect mineral banding, with relatively coarse cassiterite and orthoclase usually forming the margins of the lode. Various combinations of the gangue minerals (quartz, ankerite, pyrite, chalcopyrite, chlorite and hematite) constitute the bulk of the lodes. The conformable lodes are spatially related to the unconformable orebodies. Steeply dipping fractures are characterised by alteration of the wallrocks and networks of tourmaline-rich, locally cassiterite-bearing, hairline fractures, (Rozendaal et al. 1986, 1995).

The Rooiberg mineralisation is generally regarded as the product of a granite-related hydrothermal system derived from the Lebowa Granite Suite rocks; in other words, a system not so dissimilar from that at Zaaiplaats, except that in the Rooiberg area the magmatic-hydrothermal fluids had access to the outside in what must have been a large, open system of fractures that probably extended down into the plutonic rocks to tap the magmatic-hydrothermal fluids. Repeated phases of fracturing, perhaps enhanced by the intruding granite, allowed the tapping of continually evolving fluids. Although the origin of the Sn is generally attributed to the Bushveld granitic rocks, it is possible that at least part of the Sn mineralisation may have been leached from the sedimentary and volcanic rocks traversed by the fluids.

4.3.6 The Sn-W Deposits of Southwest England, Cornwall and Portugal

The Hercynian fold belt (Variscan orogen) of Western Europe marks the site of a major convergence between two continental plates that took place from the Late Devonian to the Upper Permian (a time span of about 150 Ma). The vast amount of geological information accumulated for Western Europe is distributed in many journals and written in many languages, making the integration of existing knowledge a daunting task. To compound the problem, many areas of

the Hercynian belt in Europe have either been covered by younger rocks, or have been re-activated during the Alpine orogeny from the Triassic to the present. The interested reader should consult Windley (1995), for an overview of the Hercynian (Variscan orogen) events. For the present purpose it is important to stress that Sn-W, as well as U, deposits formed during the Hercynian orogeny are primarily associated with late to post-orogenic batholiths generated during the collisional phases of the geodynamic evolution of the belt.

The Hercynian batholiths consist of calc-alkaline granitoids with associated porphyry feeder dykes and rhyolitic lavas. An important period of granite emplacement appears to have been between 330 and 280 Ma ago. An assessment of major and trace element geochemical data led Floyd et al. (1983) to conclude that the bulk of the Hercynian granitoids were derived from anatexis of lower crustal material, in particular widespread melting of poorly hydrated garnet-bearing granulite which produced large volumes of essentially dry granitic magma. Subsequently, through the assimilation of wet country rock, this magma became water-saturated and crystallised below the surface to form the granite batholiths. The range of compositions seen in individual plutons is explained by local, but minor, variations in source rock composition and/or the degree of melting, together with later differentiation and metasomatism. In general the granites have a restricted compositional range, high K/Na ratios, low Fe_2O_3/FeO ratios, and high to intermediate Sr isotope ratios, and a deficiency in hornblende, sphene and magnetite. Therefore the Hercynian granitoids have S-type and/or ilmenite-series affinities in south-west England and Cornwall, the granitic rocks are probably related to collision tectonics, whereas elsewhere in Western Europe it appears that thrust tectonics of the Himalayan type provided the necessary environment to generate granites. The granites of southwest England and Cornwall are also high heat producing (HHP) granites due to radioactivity generated by U, Th and ^{40}K, which can generate hydrothermal systems, a topic discussed in Chapter 9.

4.3.6.1 Southwest England and Cornwall

This classic area, along the northern boundary of the Hercynian fold belt, and known as the Cornubian tin field, occupies an area of some 3800 km^2 and coincides with the Cornubian granite batholith (Fig. 4.13). The area has produced over 2 Mt of Sn, 1.3 Mt of Cu, 350 000 t of Pb, 250 000 t of As and 1200 t of W, in addition to minor quantities of Zn, Au, Ag, Sb, U, Ni, Bi, Mo, F, Ba, Sb and Co. The large Redruth-Camborne district contained 310 000 t of Sn and 850 000 t of Cu (Laznicka 2006). The distribution of the Sn mineralisation is shown in Fig. 4.13

The mineralisation is spatially related to the roof and border zones of a series of high level, post-tectonic granitic plutons belonging to the Cornubian

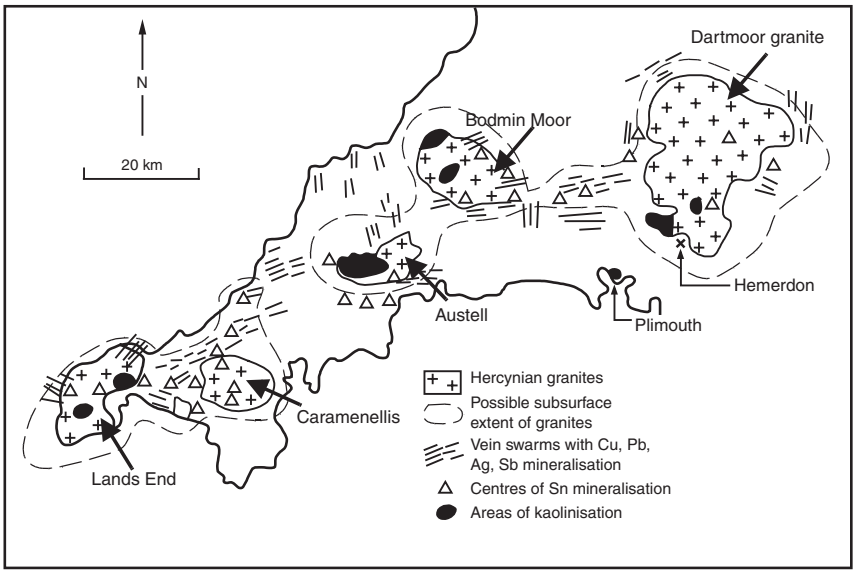


Fig. 4.13 Distribution of granitic rocks and mineral systems in southwest England and Cornwall. After Moore (1982)

batholith and emplaced within turbidite-type metasediments, known locally as "killas". The intrusion of these granites was accompanied by a period of hydrothermal alteration and mineral deposition during which quartz veins containing ores of Sn, Cu, Pb, Mo, As and W were formed. At least six major and several minor masses of granite are discernible, which were emplaced passively by cauldron subsidence and block stoping, and partly by forceful injection. The plutons are composite in nature, roughly circular or ellipsoidal in shape, and have sharp and discordant contacts with the surrounding country rocks. The age of emplacement is 300–260 Ma, with a Rb/Sr isochron of 285 ± 12 Ma. The main stage of mineralisation, which was late (about 270 Ma), was associated with pegmatitic veins and granite porphyry dykes. Major fracture systems developed in the roof and margins of the principal intrusions as a result of superimposed hydraulic and existing stress fields, soon after batholith emplacement. These fracture systems controlled the movement of the hydrothermal fluids. Thus vein and fissure systems, together with irregularly shaped replacement deposits of Sn, W, Cu, As, Pb and Zn, are formed. The above-mentioned mineralisation styles characterise four principal geological environments, namely: (1) Roof of the intrusion: sheeted vein systems, fissure veins, replacement bodies of quartz and tourmaline with cassiterite, wolframite, pyrite, chalcopyrite and arsenopyrite. Intense greisenisation and vein-controlled phyllic alteration; (2) Flank of the intrusion: important for mineralised fissure systems. These are typified by fissure veins with complex

multi-stage parageneses of quartz, cassiterite, sulphides with polyphase phyllic, chloritic, tourmaline and feldspathic alteration haloes; (3) Granite contacts: these are important for fissure veins, stockworks and replacement bodies; (4) Outer aureole: areas 2000–200 m outside the granite contacts host mineralised fissure systems with cassiterite, sulphides, tourmaline and phyllic alteration haloes. Mineral zoning within the vein systems can be very complex, as minerals may have been repeatedly emplaced in some vein systems at different structural levels, with earlier ores being commonly re-mobilised by later hydrothermal fluids. Despite the complexity, a sequence of alteration events can be summarised as follows. Alkali metasomatism (magmatic-hydrothermal fluids), consisting of K-metasomatism followed by Na-metasomatism (albitisation), occurred within and at the margins of the granites. This phase was followed by acid metasomatism (H^+ ion), resulting in greisen development, and by phyllic or sericitic alteration in the more advanced stages. Tourmalinisation was a very important process. Tourmaline replaces the feldspars and biotites and locally overprints the sericitic alteration. Tourmalinisation and silicification are commonly linked. Isotopic evidence indicates that the hydrothermal circulation was dominated by meteoric waters, and followed a phase of separation by second boiling of hydrous fluids from the plutons, resulting in the fracturing along the flanks of the intrusion. Fluid inclusion studies indicate that the fluids had moderate to low salinities (10–20 wt% NaCl equivalent) and temperatures ranging from 280 to 480°C.

An outstanding example of an endogreisen system is that of the Hemerdon W-Mo deposit. Hemerdon Ball is a 215 m-high hill about 2 km east-northeast of the city of Plymouth in southwest England (Fig. 4.13). Mining records in this area date back to the 16th century, and by the 19th century five mines were operating within 3 km of the Hemerdon township. Sn, Cu and Pb were all produced from vein deposits. Since the discovery of China clay deposits (kaolinised granite) around Hemerdon in the 19th century, clay has been extracted almost continuously to the present day. The presence of wolframite at Hemerdon was discovered in 1867, and the deposit was mined during the two World Wars with a total production of about 220 000 tonnes of ore. Resources at Hemerdon are 42 Mt grading 0.144% W (Laznicka 2006). The mineralisation (Pirajno unpubl. data and Hemerdon mine geologists) is contained within a dyke-like granitic body protruding from the Hemerdon Ball granite outcropping on the southern flank of the larger Dartmoor granite, to which it is probably connected. These granites belong to the Cornubian batholith referred to earlier, and intrude metasedimentary rocks and altered volcanics (killas). It is thought that many of the granite bodies in the area are connected beneath the killas which are, in most cases, considered as roof pendants. The mineralised granite dyke has a northeast trend, is approximately 650 m long and 120–150 m wide, and is entirely emplaced within killas country rocks, represented by metamorphosed turbidite sediments of Devonian age. The granite dyke is made up of K-feldspar, plagioclase, quartz, biotite and Li-rich muscovite. Sericite, chlorite, kaolinite and illite are alteration products replacing the

primary mineral assemblage. This altered granite is traversed by three mineralised sheeted vein systems, which locally transgress into the surrounding metasediments. The latter are tourmalinised, contain hematite and are intensely fractured. Wolframite and molybdenite are the main ore minerals, and there are minor quantities of cassiterite and arsenopyrite. The cassiterite tends to occur within the greisenised borders of the quartz veins, and is possibly the earliest ore mineral. This is followed by deposition of quartz + feldspar with wolframite. Minor amounts of pyrite, fluorite and arsenopyrite occur in the southern region of the granite dyke.

4.3.6.2 Panasqueira Sn-W Deposit, Portugal

The Panasqueira Sn-W deposit is situated about 60 km east of the university city of Coimbra, in the Beira Baxia province. Mining in the area dates back to Roman times, but W mineralisation was discovered in 1886. The production of W concentrates from Panasqueira between 1927 and 1976 was about 13 500 tonnes. In 1978 the Panasqueira mine, which was the largest producer of W in Western Europe, produced 1450 tonnes of W concentrate (75% WO_3), 62 tonnes of Sn concentrate (75% SnO_2) and 1100 tonnes of Cu concentrate (22% Cu). The Panasqueira mining district lies along the southern border of Hercynian granitoids within the so-called Luzo-Oretan geotectonic zone of the Iberian Meseta (Ellenberger and Tamain 1980). The Luzo-Oretan zone is characterised by a substratum of Lower Paleozoic sediments that were subjected to folding and low pressure metamorphism during early compressive stages of the Hercynian orogeny. The precursor rocks in the Panasqueira district were argillites, greywackes and sandstones. Regional metamorphism converted these rocks into biotite-chlorite schist, phyllite and quartzite, grouped under the name of Beira Schists. Thermal contact metamorphism, associated with the emplacement of the Hercynian granites, produced a regionally extensive aureole characterised by "spotting" in the schist rocks. The spots are best developed in the more aluminous units, such as the metapelites, and consist of biotite and chlorite, with lesser cordierite and chiastolite. Calc-alkaline granodioritic to granitic rocks, which are part of the great Hercynian batholith, extend in an arcuate belt from northwestern Portugal, through central Portugal and across to western Spain as far as Segovia. This magmatic event is linked with some of the most important metallogeneses in Europe, including, as well as Sn-W, Cu, Pb-Ag and Pb hydrothermal vein-type deposits (Ziserman et al. 1980).

Mineralisation in the Panasqueira area is typically of greisen affiliation, probably related to a buried greisenised granite cupola. The Panasqueira ore zone consists of more than 1000 W-Sn-bearing subparallel and nearly horizontal quartz veins, from a few millimetres to greaer than 1 m in thickness (Neiva 2007). Whilst the general features of the Panasqueira mineralisation are much like other greisen-affiliated hydrothermal vein deposits, it has some unique characteristics the most conspicuous of which is the flat, or nearly flat-lying,

attitude of its vein system. Kelly and Rye (1979) comprehensively described the geology of the Panasqueira deposit and reported on the result of detailed studies of fluid inclusions and isotopic work. The mineralised veins of the Panasqueira deposit range in thickness from a few millimetres to 1 m, can be traced laterally for up to 100 m and cut across strata of Cambrian schist-metagreywacke sequence. The veins are associated with Hercynian muscovite granites, ranging in age from 336 to 287 Ma (Neiva 2007). As mentioned, the veins occupy nearly horizontal joint fractures and form a mineralised package over a vertical zone from 100 to 300 m thick. It is thought that the horizontal pre-ore joints were formed by decompression due to erosional unloading. The fissures were occupied by the hydrothermal fluids and opened by hydraulic pressure. The vein system is linked at a depth of about 220 m below the surface, with a greisenised granite cupola. This cupola was probably emplaced through magmatic stoping of the country rocks, as numerous angular fragments of the hornfelsed schists occur within this granite. The cupola consists of a porphyritic biotite-muscovite granite with K-feldspar megacrysts up to 1 cm long. The porphyritic texture tends to disappear upward and the granitic rock grades into an equigranular endogreisen (quartz + muscovite). A quartz cap occurs at the apex of the cupola, and was interpreted by Kelly and Rye (1979) as a hydrothermal filling of a void formed during contraction of the granitic magma while still in the molten state. Minerals present in the veins include Fe-rich wolframite (ferberite), arsenopyrite, pyrite, pyrrhotite, sphalerite, molybdenite, cassiterite and scheelite. Numerous other mineral species are present such as oxides, tungstates, carbonates, silicates and even phosphates. Zoning of the ore minerals within the veins is as follows (Kelly and Rye 1979): (1) An inner wolframite + cassiterite zone close to the cupola; (2) An intermediate zone of wolframite mineralisation overlying zone 1 and extending radially outward; (3) An outermost zone of second generation wolframite + cassiterite. According to Kelly and Rye (1979), the mineralisation sequence in the veins can be subdivided into four main stages: (1) Oxide-silicate stage: quartz, muscovite and tourmaline; accompanied by the main ore minerals, wolframite and cassiterite ± arsenopyrite. Economically, the oxide-silicate stage is clearly the most important since it includes the ore minerals as well as most of the quartz, which comprises 90% of the vein material. Within this stage two substages are recognised: an early muscovite-rich vein selvage, containing minor amounts of tourmaline, cassiterite, topaz and arsenopyrite, and a vein-filling substage, comprising most of the coarse-grained quartz, muscovite wolframite and arsenopyrite. (2) Main sulphide stage: arsenopyrite, pyrite, pyrrhotite, sphalerite, chalcopyrite and stannite. Apatite is also present. (3) Pyrrhotite alteration stage: siderite and marcasite are the main minerals. Minor quantities of sphalerite and pyrite may also occur. (4) Late carbonate stage: dolomite and calcite are the main minerals of this stage. Sulphides may also be present. Cassiterite is found in stages 3 and 4, and wolframite in stage 3. There is a general trend from oxide-dominated to base metal sulphide-dominated. There is some evidence that He trapped in cassiterite and wolframite may have been sourced from the mantle and that

magmatic fluids were also derived from the mantle Neiva (2007); Burnard and Polya (2004). The veins are surrounded by three zonesof hydrothermal alteration, namely: 20–30 cm wide tourmaline-mica schist adjacent to the veins, followed by a muscovite-rich zone and farther from the veins a zone of chlorite-muscovite (Neiva 2007).

Fluid inclusion studies indicate that the mineralising solutions were NaCl-dominated aqueous brines of moderate salinity (5–10 wt% NaCl equivalent), with temperatures in the range of 230–360°C. During the late carbonate stage, the temperature of the fluids decreased from 120 to 70°C with salinity values below 5 wt% NaCl equivalent. $\delta^{34}S$ values of the sulphide minerals from the first three stages fall within a narrow range (–0.1 to –0.9‰), interpreted to indicate an H_2S-dominated hydrothermal solution of magmatic origin (Kelly and Rye 1979). Neiva (2007) suggested that the conversion of granite feldspar to muscovite is the main factor for the precipitation of cassiterite, with wolframite being precipitated from younger and more oxidised fluids.

4.3.7 The Greisen Systems of the Tasman Fold Belt System

The Tasman Fold Belt System (TFBS) is an Andean type orogenic zone that accreted eastward between the Early Cambrian and the Early Mesozoic and is part of the greater 18 000 km long Terra Australis Orogen that developed along the Pacific Ocean margin of Gondwana through rifting of Rodinia and plate convergence (Cawood 2005). In the TFBS deposits include endogranitic greisens, exogranitic sheeted vein systems and breccia pipes, distributed in several Sn-W mineral provinces extending from northern Queensland to the island of Tasmania in the south (Solomon and Groves 1994). Ore fluids in these deposits, as reported by Solomon and Groves (1994 and references therein), are acid, reduced and contain CO_2, CH_4, NaCl, $MgCl_2$, $FeCl_2$, H_2O, $CaCl_2$ and with temperatures ranging from about 300–500°C and pressures of about 1–1.5 kbar. Good representative Sn-W greisen style deposits are the Heberton field (Murray 1990), Mount Carbine (Forsythe and Higgins 1990), Cooktown (Jones et al. 1990). Tasmania is particularly well-endowed with a variety of greisen style deposits of which Mount Bischoff, discussed next, is perhaps the most complex and interesting, because it provides an example of both greisen and skarn type ore systems.

4.3.7.1 Mount Bischoff, NW Tasmania

The Mount Bischoff Sn deposit is located in the Waratah district in northwest Tasmania (Australia). From 1871, when the mineralisation was first discovered, up to 1978, about 62 000 tonnes of Sn metal were produced at an average grade of 1% Sn. The published works of Groves and Solomon (1964), Groves et al. (1972), Wright and Kwak (1989), Solomon and Groves (1994) and Halley and

Walshe (1995), augmented by personal observations taken during a drilling programme in the old mine area (Pirajno, unpubl. data), form the basis of the following account.

The Mount Bischoff area is underlain by a sedimentary sequence of Upper Precambrian age, forming an inlier within rocks of the Dundas Trough. The Precambrian rocks form an anticlinal structure, whose flanks are overlain by Cambrian sediments, in turn overlain by flat-lying sediments and mafic volcanics of Neogene age. The Mount Bischoff inlier is located between two major Precambrian structural units: the Rocky Cape nucleus to the northwest, and the Tyennan nucleus to the southeast. In the area of the deposit, the stratigraphic sequence from the base upward consists of interbedded shales and sandstones (footwall rocks), followed by a sequence of massive to finely bedded and fine-grained dolomitic rocks (Mount Bischoff dolomite), overlain by interbedded carbonaceous shales, siltstones and sandstones (hanging wallrocks). The Mount Bischoff Sn deposit is characterised by both endo- and exogreisen mineralisation related to granitic intrusives of Devonian age (Meredith Granite Batholith). The adjacent areas, within a radius of about 2 km, contain hydrothermal deposits of Pb-Zn, Pb-Zn-Sb, and Zn-Sn-F, and it is likely that these are genetically related to the same regional mineralising system that gave rise to the Sn mineralisation at Mount Bischoff. Therefore, the distribution of these metal deposits may represent a regional zoning pattern centred on Mount Bischoff. The Meredith Granite Batholith (about 300 km^2) intruded the Precambrian and Cambrian sedimentary rocks between 350 and 360 Ma (end of the Devonian). The batholith is of adamellitic composition, having approximately equal amounts of K-feldspar and plagioclase, with accessory zircon, topaz and tourmaline. The intrusion of the batholith resulted in the emplacement of a number of leucogranite cupolas, one of which is believed to be emplaced at depth below Mount Bischoff into the hinge of the anticlinal structure. It is postulated that quartz-porphyry dykes emanated from the cupola to intrude along tensional fractures (Fig. 4.14A). The Mount Bischoff ~342 Ma quartz-K-feldspar porphyry dykes, are from 5 to 30 m thick and up to 1300 m long. They are preferentially oriented along east-west, northwest and northeast trends and form a kind of radial pattern centred on the crest of the east-west oriented antiform, referred to above. These dykes are associated with tourmaline-bearing hydrothermal breccias, which are thought to be related to ore fluids. Mineralisation is associated with the intense greisenisation of both the quartz-feldspar dykes and the Mount Bischoff dolomite, forming endogreisen and exogreisen respectively. The intensely greiseinised dykes are characterised by having topaz, pyrite, sphalerite, cassiterite and minor wolframite. Solomon and Groves (1994) distinguished four main ore types: (1) greisen-type altered porphyry dykes and sills containing topaz, pyrite, sphalerite, cassiterite and minor wolframite; (2) skarn-type stratabound, massive pyrrhotite- and cassiterite-rich ore that replaced dolomitic rocks; (3) fissure veins, up to 7 m thick, containing quartz, pyrite, sphalerite, arsenopyrite, jamesonite, fluorite, topaz, cassiterite and wolframite; (4) thin quartz-cassiterite veins in jointing structures in the

sedimentary rocks. In general, vein fillings vary considerably, with some common assemblages consisting of quartz + cassiterite, quartz ± tourmaline or topaz, quartz + pyrite + topaz + fluorite + carbonate + sulphides and cassiterite. The greisen phase of alteration was accompanied by cassiterite and minor wolframite mineralisation, and followed by a post-greisen phase of phyllic-type alteration, accompanied by abundant sulphide mineralisation. The distribution of the greisenised rocks is shown in Fig. 4.14B. The altered quartz-porphyry (endogreisen) is characterised by three main mineral assemblages (Wright and Kwak 1989), whose chief components are: (1) muscovite + quartz + fluorite + tourmaline ± sphalerite; (2) quartz + topaz ± fluorite ± cassiterite and (3) quartz ± topaz or fluorite. The endogreisen assemblage (2) also contains rare Mg-Na-Al fluoride species, such as sellaite (MgF_2), whereas assemblage (3) is quartz-rich. The endogreisens were formed through the action of acid fluids, by dissolution and replacement of the quartz and K-feldspar from the dyke material. This acid dissolution, also postulated for the above described Zaaiplaats deposit, created enough permeability to facilitate penetration of the solutions through the dyke rock. The sulphide minerals overprint the greisen assemblages, and, as already mentioned, were precipitated during a post-greisen stage of phyllic alteration, characterised by the incoming of phyllosilicates such as chlorite, and clay minerals in addition to the sulphides. Sulphide minerals include pyrrhotite, arsenopyrite, chalcopyrite, stannite, pyrite, marcasite and bismuthinite.

The exogreisen (skarn-type) is developed by the replacement of the dolomitic rocks in contact with and adjacent to the greisenised dykes, as shown in Fig. 4.14B. Wright and Kwak (1989) recognise two main exogreisen assemblages: (1) quartz + sellaite + topaz + cassiterite ± fluorite or pyrrhotite; and (2) tourmaline + sellaite + fluorite + quartz ± cassiterite, phlogopite or hambergite [$Be_2BO_3(OH)$]. The first assemblage (also known as topaz exogreisen) is found in close spatial association with the greisenised dyke. Cassiterite is particularly abundant at the endogreisen-exogreisen contact. Sulphide minerals associated with the topaz-exogreisen are pyrrhotite, arsenopyrite, chalcopyrite, stannite, pyrite, bismuthinite, marcasite and native bismuth. Talc, chlorite and phengite replace the greisen mineralogy and are part of the post-greisen phyllic alteration phase. The second exogreisen assemblage (also called tourmaline exogreisen) surrounds the topaz-exogreisen and is mainly formed by tourmaline + sellaite + fluorite + pyrrhotite, cassiterite, or, quartz and sellaite + pyrrhotite ± cassiterite, fluorite or tourmaline. The tourmaline-greisen is also characterised by a texture known as "wrigglite" which is a fine-scale layering (or banding) that occurs as a result of alternating mineralogies (see also Chapter 6). The tourmaline exogreisen is overprinted by pyrrhotite, talc, phengite, siderite and fluorite, as part of the post-greisen phase of alteration. A more recent model proposed for the genesis of the mineralisation at Mount Bischoff is that of Wright and Kwak (1989). They envisage that the porphyry dykes acted as the main conduit for the hydrothermal solutions, possibly emanating from both the postulated underlying

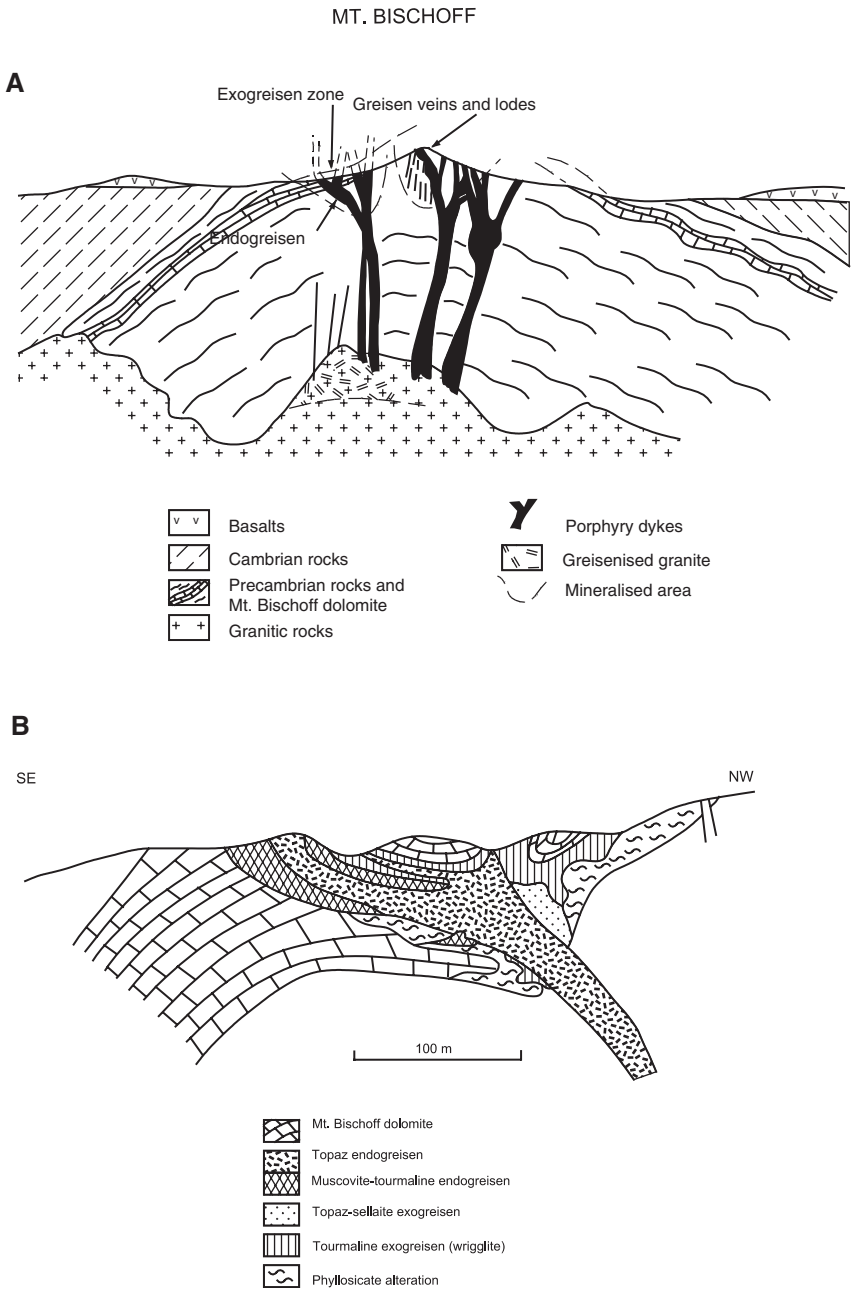


Fig. 4.14 (**A**) Schematic cross-section through the Mount Bischoff greisen system, although not to scale the depth to the roof of the causative granite cupola is in the order of 1–2 km (Groves and Solomon 1964; Wright and Kwak 1989); (**B**) simplified cross-section of the Mount Bischoff Sn deposit and distribution of greisen alteration (Wright and Kwak 1989)

leucogranite cupola (fragments of leucogranite are found in the dykes) and the dykes themselves. Homogenisation temperatures of fluid inclusions range from 220 to 420°C for the greisen assemblages and from 120 to 190°C for the overprinting assemblages. Fluids have salinities of 30–50 wt% NaCl equivalent and consist of brines with H_2O-NaCl-KCl-$CaCl_2$-$FeCl_2$-CO_2 and hydrocarbons. Sulphur isotopic data from pyrrhotite indicate $\delta^{34}S$ values ranging from –1.9 to + 5.2‰, with early-stage sulphides having values close to 0‰. The bimodal distribution of the $\delta^{34}S$ values indicates a magmatic source for the values close to 0‰, whereas the heavier isotopic values are indicative of a sedimentary source. The greisenised porphyry dykes contain pyrite with $\delta^{34}S$ values ranging from –0.2 to 1.7‰, again suggesting a magmatic source for the ore fluids. Interaction of magmatic fluids with sedimentary rocks is further documented by isotopically heavy $\delta^{18}O$ values of hydrothermal carbonates, which range from 16.4 to 19.3‰. The dykes acted as conduits for magmatic fluids originating from a buried F-rich, granitic cupola (Fig. 4.14A). The ore fluids moved upward along the margins of the dykes, forming the hydrothermal breccias, and spread out into the dolomitic rocks, with cassiterite being precipitated together with talc (Solomon and Groves 1994). The cassiterite associated with the talc, was precipitated at temperatures of around 365°C. In the dykes the fluids boiled and moved into the dolomitic rocks, creating a network of hydrothermally induced fractures and forming the exogreisen assemblages. Wright and Kwak (1989) envisaged that concentrated residual fluids derived from boiling replaced the dolomite with F- and B-rich minerals and gave rise to the observed wrigglite textures. The temporal evolution of the hydrothermal solutions led to a reduction in both temperature and acidity, and produced the post-greisen assemblages. The Sn mineralisation is regarded as a consequence of the neutralisation of the solutions by the dolomite rock with consequent destruction of the topaz phase and deposition of cassiterite.

Halley and Walshe (1995) proposed a two-stage ore-forming process for Mount Bischoff greisen-skarn mineral system. Their first stage involved late stage fractionation of a cupola intrusion emanating from the Meredith batholith, with enrichement in F, Sn, and B, forming the greisen style mineralisation. In the second stage, reduced non-magmatic fluids mixed with magmatic fluids, reacted with the greisenised granite, leaching the Sn and F. These fluids, driven by the residual heat in the granite, were channelled along the dykes and reacted with dolomite to form skarn-type or exogreisen mineralisation.

4.3.8 The East Kemptville Sn Greisen, Nova Scotia, Canada

The East Kemptville Sn greisen deposit is located some 300 km southwest of Halifax in Nova Scotia and had pre-production reserves of 58 Mt with about 0.17% Sn. Details of the geology of the East Kemptville deposits can be found

in Richardson et al. (1990) from whose work the following is extracted. The East Kemptville deposit is part of the Sn-rich Carboniferous Davis Lake Complex, which belongs to the a large peraluminous granitic batholith that contains greisen and vein-style Sn, U and W deposits. The Davis Lake Complex is a porphyritic coarse-grained biotite monzogranite, altered biotite-chlorite-muscovite monzogranite and a leuco-monzogranite with greisen zones. Rb-Sr isotopic data from the greisen yield an age of 317 ± 16 ma and Sr_I ratio of 0.7333 ± 0.005, whereas the leucomonzogranite yields an age of 321 ± 26 Ma and Sr_I ratio of 0.731 ± 0.002. The Kemptville leucomonzogranite contains pegmatitic segregations, which contain ore minerals such as cassiterite, sphalerite, fluorite, pyrrhotite and molybdenite.

The Kemptville Sn deposit consists of two main mineralised zones, the Main and Baby, which occur near the contact with metasedimentary rocks. Massive greisen forms zones that are texturally and mineralogically distinct, namely: quartz-topaz rock, quartz-mica greisen, and green muscovite greisen. The quartz topaz rock contains cassiterite, chalcopyrite, sphalerite, pyrite and forms the high-grade ore (up to 6% Sn). The quartz-mica greisen surrounds the topaz-quartz zone and is characterised by green and silver-coloured micas with much less topaz and cassiterite and has between 0.5 and 1% Sn. The green muscovite zone contains cassiterite, quartz, sphalerite and fluorite, but no topaz. Greisen veins protrude from the massive greisen zones into the surrounding rocks. Cassiterite mineralisation is characterised by large crystals (up to 3 cm) or aggregates 1 cm across, and is associated with the topaz in the massive greisen zones. Other ore minerals include sphalerite, chalcopyrite, pyrrhotite, pyrite, molybdenite, wolframite and arsenopyrite. Typically, the ore minerals are fractured and brecciated.

Richardson et al. (1990) suggested that the Kemptville leuco-monzogranite crystallised from a highly differentiated portion of a vertically zoned magma chamber, where elements such as Sn, F and P had been concentrated in the magma prior to crystallisation. The presence of pegmatitic segregations is indicative of a melt that was H_2O-saturated, with low viscosity and high diffusivity due to the presence of F in the melt. The authors further suggested that the abundance of F that was partitioned in the aqueous ore fluid at the end of the crystallisation process, created a very aggressive HF-rich ore fluid, capable of replacing and greisenising the monzogranitic rocks. During this greisenisation process, Si, Al and alkalies were released from the leuco-monzogranite to the F-rich ore fluid, precipitating topaz. This decreased the F, Al and Si content of the fluids resulting in the quartz-topaz rock, concurrently cassiterite was also precipitated as the fluids were reduced. Copper, Zn, W, As and Fe were also removed to form sulphide minerals. With continuing decrease of the F content of the ore fluids the greisen system changed from the topaz-stable field to the muscovite-stable field, giving rise to the mica greisen zones that surround the quartz-topaz rock. Ultimately, the main controls of the Kemptville Sn greisen system were the magmatic processes and the primary enrichment of the magma in Sn and F.

4.3.9 The Brandberg West Greisen Vein Systems, Namibia

Numerous Sn, Sn-W and W deposits are present within the Neoproterozoic Pan African Damara orogen. These deposits were studied by Pirajno and Jacob (1987) and Pirajno et al. (1987), who geographically grouped them into three major zones. The northernmost of these, the Brandberg West-Goantagab area, is located in the northern coastal arm of the Damara Orogen (Miller 1983, 1992). Brandberg West-Goantagab is an excellent example of intrusion-related mineral system, providing the full range of proximal to distal greisen style mineralisation, from albitites developed at the top of highly differentiated granitic cupolas, to a sheeted greisen vein system, to progressively higher level vein systems, to Fe-rich replacement bodies in carbonate rocks, which acted as a barrier to the mineralising fluids.

This area occupies the lower Ugab river region, northwest of the Brandberg granite ring-type complex, and extends in an east-northeast direction for some 80 km (Fig. 4.15). The area is characterised by two tectonostratigraphic domains: Lower Ugab and Goantagab. The Lower Ugab consists of 1700 m thick turbidite-facies metasediments with intercalated thin marble bands, divided into five lithostratigraphic units, three dominantly siliciclastic and two dominantly carbonate rocks. Metamorphism is of regional greenschist facies and thermal metamorphism up to mid-amphibolite facies (Macey and Harris 2006). The Goantagab domain consists of upper greenschist facies pelitic schist and marble of the Swakop Group. These metasedimentary rocks are intruded in the east by a large syn- to post-tectonic granitic mass of batholithic proportions, with smaller granite plutons intruding the area in a number of places. These granites are of S-type affinity and their age is ca. 590–530 Ma (Macey and Harris 2006 and references therein). Wide thermal aureoles, up to 15 km wide, developed around some of these granitic intrusions. Thermal metamorphism appears to have, at least in part, also driven regional metamorphism (Macey and Harris 2006). Metamorphic assemblages in metapelitic rocks, with increasing grades, are biotite-muscovite, biotite-andalusite, and closer to granite contacts, cordierite-andalusite hornfels. In marly carbonate rocks mineralogical changes range from muscovite to phlogopite, actinolite, zoisite to diopside near granite contacts (Macey and Harris 2006). Metamorphic (combined regional and thermal) temperatures vary from 350 to ca. 600°C at granite contacts, with pressures estimated at 1.5–3.2 kbar (Macey and Harris 2006).

The Brandberg West-Goantagab area is characterised by a number of Sn-W and Sn ($\pm$ Ag and base metals) deposits in quartz vein systems and Fe-rich replacement bodies (Pirajno 1992; Macey and Harris 2006). These mineralised systems clearly post-date Damara-age fabrics in the host rocks. Circular structures, visible on LANDSAT imagery, are present and are associated with quartz veins and, in places, breccias and thermally metamorphosed schists. The simplified geology of the Brandberg West-Goantagab area, the distribution of the

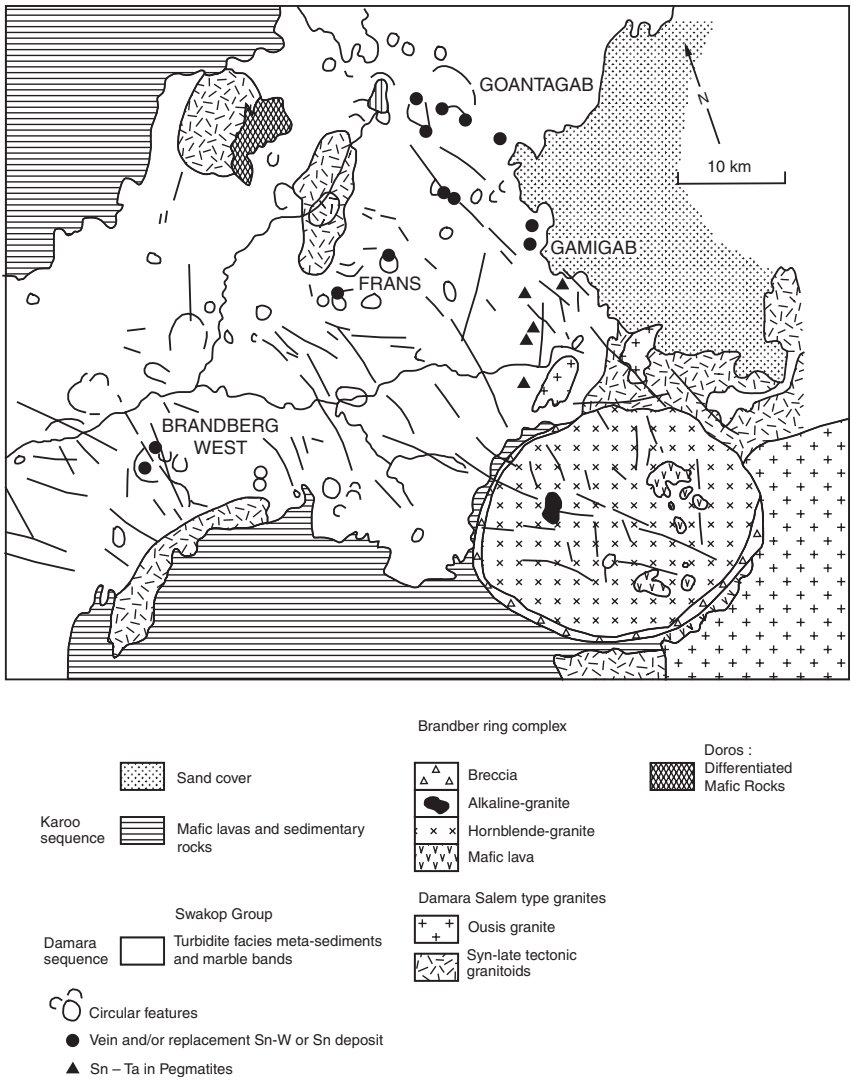


Fig. 4.15 Simplified geology of the Brandberg West area, Namibia, and distribution of proximal and distal Sn and Sn-W greisen style deposits and occurrences. After Pirajno (1992)

main deposits and circular structures are shown in Fig. 4.15. It is of interest to note that the association of circular structures with mineralisation has been reported from many areas around the world (see for example, Norman 1982; Artamonov and Vostokov 1982). Circular structures are common in the Hercynian orogenic areas in northern Portugal, where they also occur in turbiditic terranes intruded by granitic rocks, and are spatially associated with hydrothermal Sn-W mineralisation (Goinhas and Viegas 1983), such as Panasqueira

discussed above. In New Zealand, where calc-alkaline granitic stocks of the Karamea batholith of I-type affinity host porphyry Mo and greisen W deposits, are spatially associated with well defined circular structures (Eggers 1979). Apart from the spatial association, the precise nature of the relationship with the mineralisation is not known, although a possible caldera-style fracturing mechanism generated by the updoming of cupola-like granitic intrusions and a structural control for the flow of hydrothermal fluids is a possibility. The character of the hydrothermal Sn-W mineralisation of Brandberg West is consistent with a granitic source, and is most probably the result of greisenisation phenomena related to a hidden granitic cupola at depth. On the basis of Fe/Mg ratios of tourmaline, this mineralisation is considered to be proximal (high Fe/Mg) with respect to other similar occurrences to the east (lower Fe/Mg ratios) (Pirajno and Smithies 1992). Figure 4.16 illustrates the model envisaged for the genesis of the Sn-W deposits of the Brandberg West-Goantagab area.

The Brandberg West Sn-W mineralisation is hosted in anastomosing quartz-vein systems that extend for at least 4 km in a general northeast direction (Fig. 4.17). Mining was carried out as an open-cast operation from 1957 to 1980, during which time some 14 000 tonnes of concentrate were produced, grading about 32% Sn and 19% WO_3. The main lithologies in the area consist of two schist units (Zebraputz and Brak River Formations of the Swakop

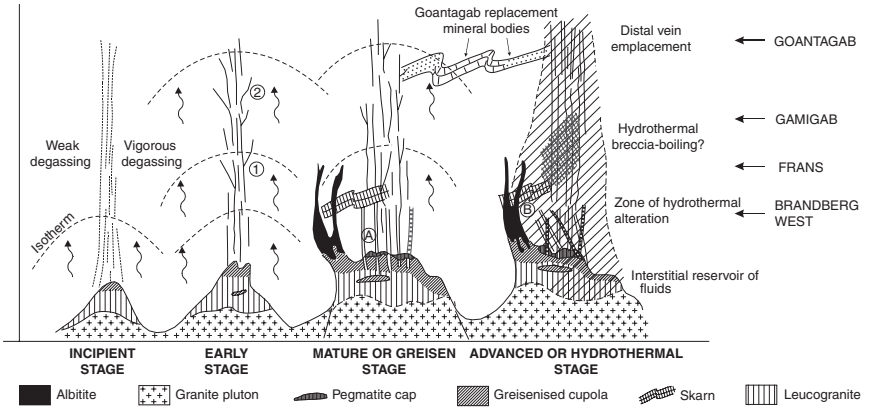


Fig. 4.16 Conceptual genetic model, first proposed by Pirajno (1992) and later modified by Macey and Harris (2006), illustrates the different styles of intrusion-related greisen deposits of Brandberg West (proximal) and the progressively distal Frans, Gamigab and Goantagab (see Fig. 4.15). In this model, volatile-rich granitic cupola-like intrusions are emplaced in siliciclastic and carbonate metasedimentary rocks. Albitites and pegmatitic caps develop as a result of extreme fractionation and Na metasomatism (see Chapter 2 for details of this process) at and near the *upper portions* of a cupola. Stages of degassing and fluid evolution range from incipient through to advanced, from *left* to *right* in the figure, resulting in different levels of mineralisation-alteration above the causative intrusions. 1 and 2 represent cordierite and biotite boundaries of thermal metamorphism, respectively; **A** and **B** represent the two alteration events at Brandberg West, greisen and quartz-sericite. See text for details

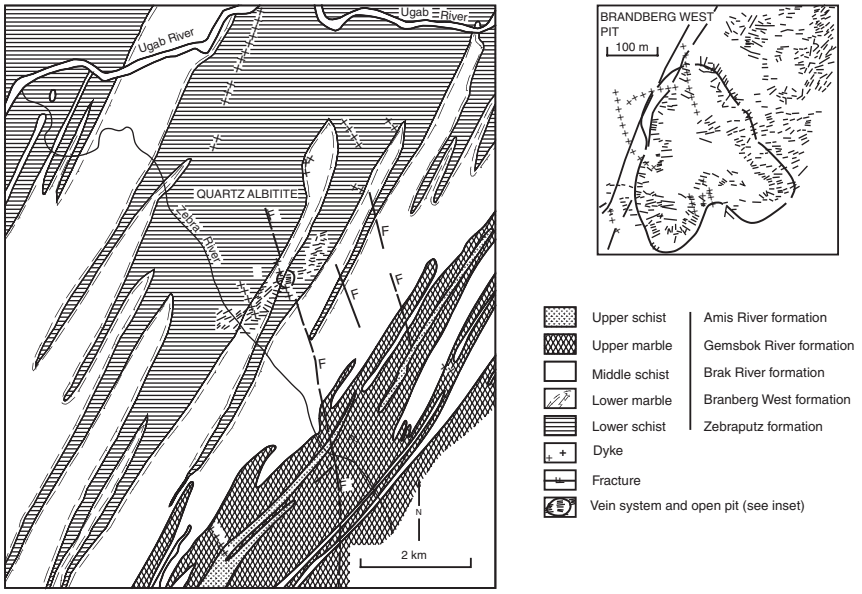


Fig. 4.17 Simplified geological map of the Brandberg West area and distribution of the vein system. After Pirajno (1992)

Group), separated by a marble unit (Brandberg West Formation) (Fig. 4.17). The base of the sequence is the Zebraputz Formation, also known as Lower Schist, which consists of quartz-biotite schists with minor calc-silicates and quartzite layers. The overlying Brandberg West Formation is represented by the Lower Marble, whereas the Brak River rocks are mainly metagreywacke. In the area surrounding the open pit, the mineralisation is primarily associated with a sheeted vein system that can be traced for some 900 m and is about 300 m wide. The quartz veins generally occur in the quartz-biotite schist of the Zebraputz Formation, most of them terminating against the overlying marble unit of the Brandberg West Formation. The veins have variable strikes, lengths and thicknesses, and were formed during at least three pulses of ore-bearing fluids and related alteration stages. The first comprises early syn-orogenic quartz-muscovite-fluorite-tourmaline veins; the second are greisen veins, which host the mineralisation and consist of quartz-muscovite with cassiterite, wolframite, scheelite, fluorite, tourmaline, beryl, graphite, hematite and some sulphides; the third set of veins are hematite-bearing quartz, and quartz-calcite, representing the last stage of hydrothermal activity. A typical ore-bearing quartz vein is usually, though not always, bounded by a selvage zone, up to 0.2 m wide, of quartz + muscovite (greisen). Fluorite, topaz, hematite, graphite and cassiterite may also be present. The greisen selvage zone grades into the wallrock through a tourmaline-rich zone. A diagrammatic representation of a quartz vein and the accompanying wall rock alteration is shown in Fig. 4.18.

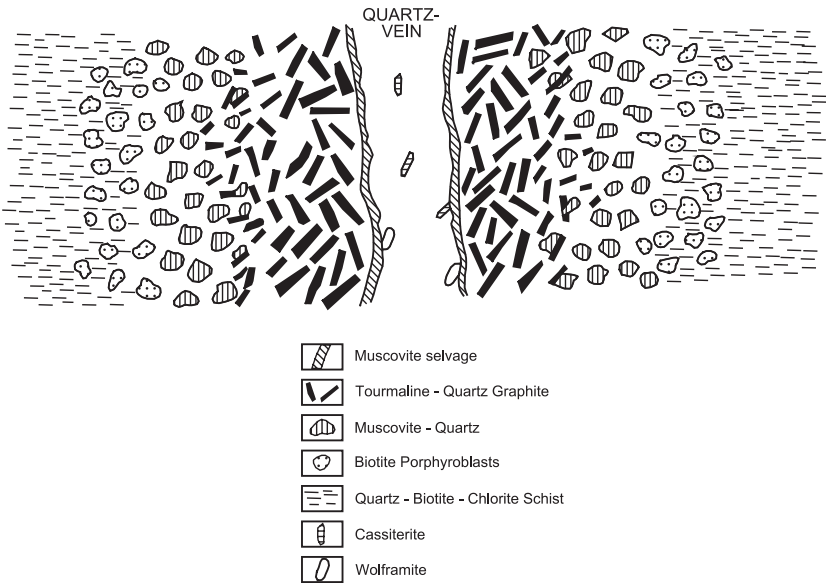


Fig. 4.18 Sketch illustrating a typical mineralised quartz vein at Brandberg West (not to scale); with greisen alteration (quartz-muscovite) of the quartz-biotite schist wall rocks, the biotite porphyroblasts are interpreted as an earlier stage of K metasomatism along the original fracture along which the vein quartz was emplaced. After Pirajno (1992)

Based on mineralogical, petrological and geochemical studies, a sequence of alteration-mineralisation events envisaged by Pirajno (1992) is as follows: (1) Thermal metamorphism is induced by hidden granitic cupolas. Effects of this metamorphism can be seen in the spotting of the schist rocks in the area; (2) K-metasomatism, manifested by fracture-controlled development of biotite porhyroblasts (Fig. 4.18); (3) Greisen stage, characterised by quartz-muscovite $\pm$ tourmaline along the same fractures (Fig. 4.18); (4) Formation of ore-bearing veins (cassiterite $\pm$ wolframite); (5) Extensional tectonic event with intense fracturing and dyke emplacement along E-W trends; (6) Renewed hydrothermal activity, characterised by intense H^+ ions activity and resulting in quartz-sericite alteration, re-opening of the earlier quartz veins, dissemination of cassiterite and fluorite particularly near and along the marble-schist contact and in the marble rocks. Deposition of sulphide minerals also took place during this stage; (7) A concluding stage of hematitisation and carbonate alteration followed, possibly as the result of opening of the system to oxidising meteoric fluids.

Macey and Harris (2006) described the alteration-mineralisation sequence into three stages (their figure 9): (1) regional metamorphism, quartz veining and deformation, followed by post-tectonic granite intrusion; (2) early post-tectonic veins followed by greisen vein system; (3) hydrothermal stage with widespread alteration.

The extent of the Brandberg West vein systems indicates that hydrothermal activity was operative on a large scale. The northeast-trending vein system transgresses the lithologies, and was mainly formed by the action of greisenising fluids that were controlled by a north-northwest-trending fracture, as well as the marble band, which acted as a barrier to the fluids (Fig. 4.19). The greisenising fluids most probably emanated from one or more granitic cupolas at depth.

Other deposits in the area include Frans (Sn-W), Goantagab (Sn-Ag-Zn) and Gamigab (Sn) (Pirajno and Jacob 1987; Pirajno et al. 1987). The Frans deposit consists of quartz vein stockworks within the limb of a tight fold in the Lower Ugab domain. The Frans vein system extends for abourt 3 km along a

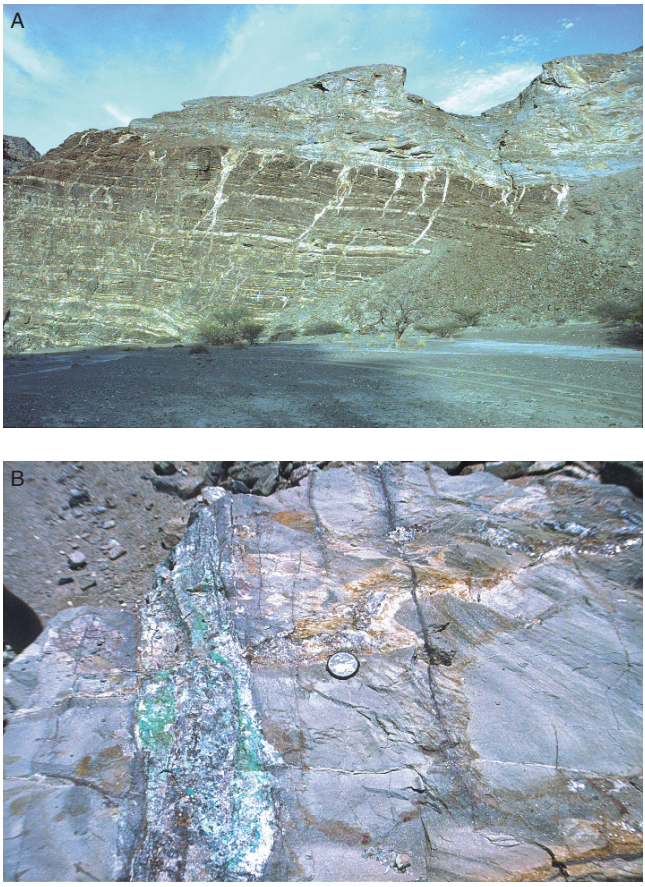


Fig. 4.19 (**A**) Quartz veins in the Brandberg West area cutting across quartz-biotite schist and terminating against the overlaing marble beds; (**B**) a mineralised quartz vein at Brandberg West pit, cutting through an earlier folded quartz vein, *green* staining is malachite, *dark line* to the *left* of the camera lens is a tourmaline vein

NNE-trending zone. The quartz veins contain cassiterite, wolframite tourmaline, muscovite, hematite, pyrite and chalcopyrite. The Goantagab deposit, about 30 km NE of Brandberg West, is hosted in marbles and phyllites of the Karibib Formation and is characterised by Fe oxides-rich cassiterite lenses and pods, which are replacement bodies in marble rocks. The Gamigab deposit comprises Sn mineralisation in E-W-trending quartz veins hosted in quartz-biotite phyllites of the Orusewa Formation. The Gamigab mineralised system is capped by Karibib Formation marbles, which have acted as physico-chemical barrier to the ore fluids.

Macey and Harris (2006) carried out fluid inclusion and stable isotope systematic studies of the Brandberg vein systems. Fluid inclusion from the greisen veins include type Ia aqueous, type Ib aqueous + CO_2 and type II carbonic inclusions (30–40% CO_2). Microthermometric data show that type I have homogenisation temperatures ranging from about 150 to 230°C with salinity values ranging from about 1.8 to 12 wt% NaCl equivalent. NaCl was considered to be the most likely dissolved salt in the system. Type II inclusions decrepitate at 350°C, before homogenisation is reached. The two type of inclusions, I and II, may reflect unmixing of a homogeneous fluid in the system H_2O-NaCl-$CaCl_2$-CO_2, giving rise to aqueous and carbonic fluids, respectively.

Stable isotopic data (O and H) from granitic rocks and quartz veins can provide valuable information on the nature and characteristics of the ore-forming fluids. The metasedimentary rocks of the Ugab and Goantagab domain have $\delta^{18}O$ values ranging from 10.3 to 19.1‰ with a mean of 13.6‰ (1σ); δD values vary between –95 and –40‰ (mean 68‰, 1σ), which are typical of greenschist facies metamorphosed sedimentary rocks. The quartz veins hosted in siliciclastic rocks have $\delta^{18}O$ values ranging from 10.3 to 19.9‰ (mean 15.5‰, 1σ), with most of the data between 14 and 18‰. Quartz veins hosted in carbonate rocks have $\delta^{18}O$ values from 17.6 to 24.8‰ (mean 20.0‰, 1σ). Macey and Harris (2006) found that the lowest $\delta^{18}O$ values are in veins in thermal aureoles closest to the granite contacts and also reported a weak increase of $\delta^{18}O$ with increasing distance from the granites. The granitic rocks (Pan-African Salem granites) have $\delta^{18}O$ values between 10.8 and 14.8‰ (mean 12.4‰), which are interpreted to be close to the boundary between I-type and S-type granites. The $\delta^{18}O$ values of the ore minerals are similar with 2.9 and 5.2‰ for wolframite, 2.7 and 2.9‰ for cassiterite and 1.8 and 2.0‰ for hematite. Isotope geothermometry, based on oxygen isotope fractionation between vein quartz and muscovite, enabled an estimation of the temperature of greisen vein formation. The calculated temperatures range from 415 to 521°C with an average of 455°C. Using quartz-hematite pairs, isotope thermometry gives temperatures between 444 and 490°C. The quartz-hematite thermometry for Goantagab suggests a lower temperature of about 330°C. Furthermore, a decrease of $\delta^{18}O$ values is observed from the centre towards the marging of the sheeted vein system and this would suggest a change of temperature of

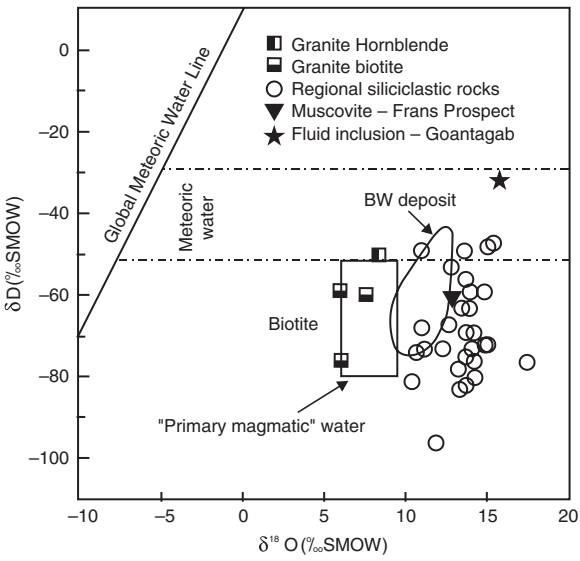


Fig. 4.20 Plot of $\delta^{18}O$ versus δD of Brandberg West, Frans, Goantagab, and country rocks (siliciclastic and granitic). The meteoric water band represents the present day latitude of Brandberg West at 530 Ma. After Macey and Harris (2006 and references therein)

deposition during fluid evolution. The $\delta^{18}O$-δD plot for the Brandberg West greisen Sn deposits is shown in Fig. 4.20. This plot shows that the δD values of Brandberg West are similar to the hydrous minerals from the granite, which supports a magmatic origin of the ore-forming fluids. Sulphur isotopic determinations, reported by Pirajno et al. (1993), show $\delta^{34}S$ values (relative to CDT) of 0.9‰ for pyrite, 1.3‰ for chalcopyrite from Brandberg West, and 4.8‰ and 6.3‰ for pyrite, sphalerite and pyrrhotite from Goantagab. These values are close to those reported for granite-related mineralisation of the Damara Orogen (Pirajno et al. 1993) and the Brandberg West values are close to magmatic values (0‰).

It is generally recognised that Sn concentration in magmas are the result of partial melting of metal-enriched sedimentary protoliths (Burnham 1997). Geochemical work on the Damaran metasedimentary rocks confirms that they are enriched in rare metals and tin and their anatexis would have led to the Sn-rich Salem S-type granites in the Brandberg West area, so that Sn-rich residual magmatic fluids would have evolved from them. An alternate possibility is that circulation of magmatic fluids could have leached Sn from the metasedimentary rocks. However, O and H isotopic data, together with $\delta^{34}S$ values of sulphides, support a magmatic origin for the Brandberg West-Frans-Goantagab-Gamigab greisen style ore system. As illustrated in Fig. 4.16, the mineralisation was formed at different levels above their granite cupola. The Brandberg West greisen veins are closest to a causative intrusion, whereas the Frans, Gamigab and Goantagab occurrences were formed at progressively increasing distances (Pirajno 1992; Macey and Harris 2006).

4.3.10 The Kalguta Mo-W-Be-Bi Greisen System, Southeastern Altai (Russia)

The southeastern Altai is part of the great Central Asian Orogenic Belt (CAOB, introduced in Chapter 5). The southeastern Altai (also spelt Altay) contains at least three terranes of Early- to Mid-Palaeozoic ages, representing fragments of oceanic crust, accretionary prisms and volcano-sedimentary successions, overlying a Late Proterozoic basement, which is probably part of the Altai-Mongolian microcontinent (Annikova et al. 2006). The region was affected by three thermal events with mafic and felsic magmatism in the Early Palaeozoic, Mid-Palaeozopic and Permian-Triassic. The latter event spans ages ranging from 280 Ma to 202 Ma and is associated with the greisen mineral systems described in this section (Vladimirov et al. 1998) and with polymetallic veins systems, described in Section 4.4.6. Igneous complexes include the Kurai gabbro-dolerite and the Chuya alkaline complex, which consists of 240–236 Ma granite, syenite and monzodiorite accompanied by kersantite, minette and bostonite dykes with ages ranging from 243 to 245 Ma (Borisenko et al. 2006).

The Kalguta (or Kalguty) Mo-W-Be-Bi greisen system (Fig. 4.21) is associated with the Chindagatui-Kalguty granite complex, which consists of anorogenic porphyritic biotite granite (main phase), leucogranite and subvolcanic quartz-feldspar porphyry dykes and stocks, called ongonites or kalgutites. These are typically highly enriched in Li, P, F, Cl, Ba and Cs and are characterised by a mineral assemblage of quartz, K-feldspar, sodic plagioclase, muscovite and apatite in a fine-grained quartz-muscovite matrix. The age range of these highly evolved granitic rocks is ~216 to ~202 Ma (Annikova et al. 2006). The Kalguta mineral system comprises greisen-related stockworks and sheeted veins, representing at least three stages of ore formation. The first stage is the called "core pegmatite" by local geologists, containing molybdenite; the second stage is represented by greisen *sensu stricto* (quartz-muscovite) and magmatic-hydrothermal breccias with chalcopyrite, molybdenite and wolframite. The third stage is characterised by thin (0.1–0.5 m) veins that are temporally associated with the ongonite dyke swarm (Fig. 4.21), containing molybdenite, wolframite, bismutite and beryl. Other ore minerals are pyrite, chalcopyrite, sphalerite, gold and scheelite. It is of interest to note that, as is the case for Brandberg West and other areas mentioned above, the Kalguta ore field too is characterised by the presence of nested circular structures.

Geophysical data (gravity and magnetics) can trace the main phase Kalguta granitic body to depths of >10 km, with stocks of leucogranites and greisens in the upper parts, all cut by the ongonite dyke swarm. These stocks represent the products of a closed system fractionation processes in a deep-seated magma chamber. The ongonites probably represent the last stage of this differentiation, culminating with an unusually high concentration of volatiles (B, F. Li). The sequence of magmatism, metasomatism and

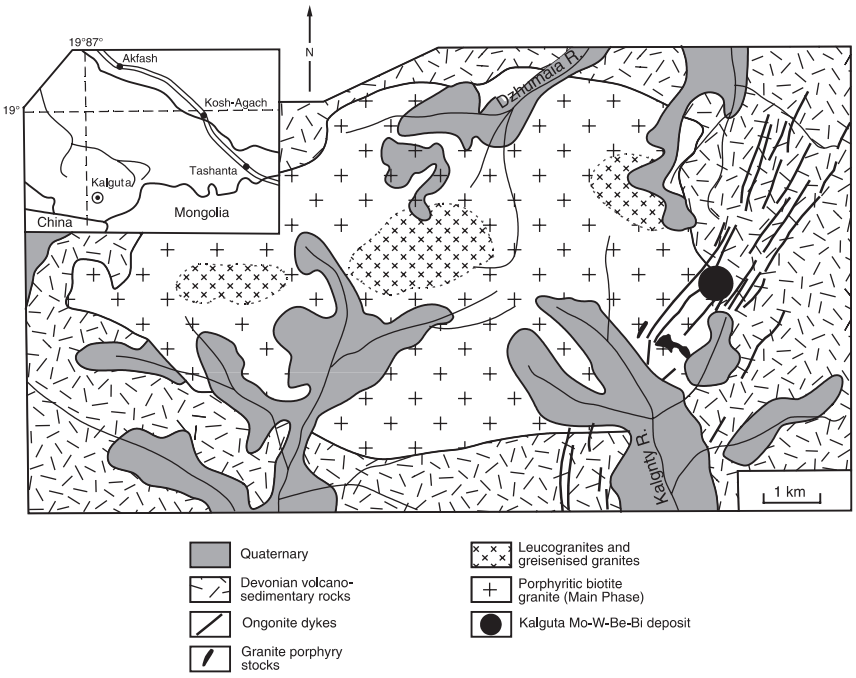


Fig. 4.21 Simplified geology of the Kalguta area. After Annikova et al. (2006) and Vladimirov et al. (1998)

mineralisation, as envisaged by Russian geologists (Annikova et al. 2006; Vladimirov et al. 1998 and references therein) is as follows. The emplacement of the main phase biotite granite was accompanied by quart-tourmaline-wolframite veins and the formation of pegmatites, in which the pegmatite quartz-molybdenite core is located. This quartz-molybdenite core is surrounded by a greisen zone (quartz-muscovite). The molybdenite of the core has a Re-Os age of 220 Ma. This was followed by the intrusion of a porphyritic granite and microgranite associated with greisen and magmatic-hydrothermal breccias containing disseminated pyrite, molybdenite, chalcopyrite and wolframite with a Re-Os age of about 213 Ma. Emplacement of ongonite, kalgutite dykes and stocks followed at 204–202 Ma. Roughly coeval or postdating the ongonites are rare metal quartz veins with wolframite, molybdenite, beryl, bismutite and chalcopyrite. Melt inclusions in quartz of kalgutites show temperatures ranging from 610 to 580°C. Sm-Nd isotopic data of the Kalguta igneous rocks show negative $\varepsilon_{Nd}(T)$ ranging from –3.7 to –9.9 and low radiogenic Pb isotopic ratios ($^{206}Pb/^{204}Pb$ = 18.305–18.831; $^{207}Pb/^{206}Pb$ = 15.527–15.571), which Annikova et al. (2006) interpreted as mantle derived. The Kalguta magmatic-ore system is therefore considered as the result of a fractionation processes in a deep crustal magma chamber.

4.4 Intrusion-Related Gold, Polymetallic and Uraniferous Vein Systems and Breccia Pipes

In this section I discuss polymetallic hydrothermal veins that have a clear spatial and, in many cases temporal, association with granitic rocks (Figs. 4.2 and 4.3). A genetic link, however, is less clear. Intrusion-related vein systems occur in the roof zones of plutons, or near their apices, or in their aureoles in the surrounding country rocks. At least two classes of granite-associated polymetallic veins have been recognised so far. One, containing gold and a range of other metals, appears to be associated with subalkalic intrusions of felsic to intermediate composition (Lang et al. 2000; Lang and Baker 2001). They are generally referred to as intrusion-related vein deposits (e.g. Sillitoe and Thompson 1998). Examples of this category include Fort Knox and True North in Alaska, Dublin Gulch and Scheelite Dome in Canada, all part of the Tintina gold province, one of the best studied, and Kidston in Queensland (Australia), both discussed below. This class of granite-associated vein deposits include sheeted quartz-sulphide vein systems with metal association such as Ag-Pb-Zn-Au, W-Cu-Zn-Au, Au-Bi-Cu, and even more complex assemblages as Au-Bi-Te-Pb-As-Sb-Ag-Mo-Co-Cu, although many of these metal associations are transitional. Some of these vein deposits can attain high grades and tonnages (e.g. Dongpin in China has 16 Mt at 6 g/t gold; Sillitoe and Thompson 1998). In addition to the above, these intrusion-related vein systems are associated with: (1) carbonic fluids; (2) a generally low sulphide content, typically of a reduced nature dominated by pyrrhotite, arsenopyrite and pyrite, with almost complete lack of hematite and magnetite; (3) have weak to spatially limited alteration haloes; (4) a continental tectonic setting, inboard of convergent margins, and characterised by alkaline, metalluminous calc-alkaline or peraluminous magmatism (Lang and Baker 2001). Most of the intrusion-related vein deposits appear to be of Phanerozoic age, but Proterozoic and Archaean examples have been proposed, such as the monzonite-syenite-associated Au deposits of the Abitibi greenstone belt in Canada (Robert 2001). In Western Australia, a Au deposit similar to those of the Abitibi belt, is at Wiluna, in the northern part of the Norseman-Wiluna greenstone belt of the Yilgarn Craton (Pirajno, unpublished data, but see Cassidy et al. 1991 for an overview). The Granites-Tanami Au district in Australia is possibly a Proterozoic example of distal intrusion-related veins, where a variety of mineralisation styles are temporally linked to the emplacement of ~1800 Ma granites (Huston et al. 2007).

In the class of intrusion-related polymetallic veins also belong the arrays of gold and/or sulphide-bearing vein in the country rocks that surround many porphyry systems generally associated with highly oxidised, I-type granitoid plutons of dominantly intermediate composition. In fact, this feature is often used by exploration geologists to guide them towards the larger and more profitable porphyry deposit. Indeed and apart from porphyry intrusions, a wide spectrum of intrusion-related vein deposits occurs both within and in the

aureoles of individual intrusions. Sillitoe and Thompson (1998) examined this wide range of intrusion-related vein deposits, within tectonic settings of magmatic arcs, back arc and accretionary orogens. However, many of these vein systems are considered within the orogenic mesothermal gold lode deposits category by Groves et al. (1998). The interested reader should consult also the special issue of Ore Geology Reviews (Ramsay et al. 1998).

The other class of polymetallic hydrothermal veins, recently proposed by Thompson and Newberry (2000), is characterised by a more specific metal association (Au + Bi + Te + As ± W ± Mo ± Sb). These veins are spatially and temporally associated with reduced granitoids, in continental arc, back-arc and collisional settings, where also Sn-W-bearing granites are found. They are of moderate size (<150 t of Au) and include well known examples, such as those found at Kidston in Queensland (Bi, Mo, Sb, As, Ag) and the sheeted vein systems in the Bohemian massif in Eastern Europe (Thompson and Newberry 2000). Other examples are those of the southeastern Altai and northwestern Mongolia, discussed in Section 4.4.6. The intrusion-related vein systems discussed in this section are therefore quite distinct from those that are typically associated with porphyry-epithermal systems (Chapter 5), orogenic lodes and Carlin-style (Chapter 8).

Processes that are responsible for the generation of intrusion-related veins systems begin in regions of the subcontinental lithosphere and/or asthenosphere where partial melting occurs and where CO_2 plays an important role. From this deep-seated source of partial melts, magmas rise through the crust, where significant contamination and fractional crystallisation take place. In the final stage, plutons rise to higher crustale levels, where further fractionation and exsolution of CO_2-rich volatile phase, lead to the formation of a magmatic-hydrothermal system. The ore fluids are essentially magmatic with only a minimum late input from non-magmatic fluids (Lang and Baker 2001).

The intrusion-related veins systems can be categorised in terms of their spatial relationship to individual plutons (Hart et al. 2000), as follows (see Fig. 4.3). Intrusion-hosted systems, characterised by sheeted and/or stockwork veins with a Au-Bi ± Te ± As ± Mo ± W metal assemblage; proximal systems, located in country rocks adjacent to the pluton and within the thermal metamorphic aureole with W ± Cu ± Au and Cu-Bi-Au ± W skarns and replacement deposits, as well as Sn- or Cu-rich breccia pipes and veins; distal deposits lie beyond the thermal aureole and include a wide range of mesothermal to epithermal quartz-sulphide vein deposits and with a typical metal association of Au-As-Sb ± Hg. This latter category is comparable with or perhaps merges with Carlin style Au systems, but as mentioned already, an unambiguous genetic relationship is far from established. I return to this topic in Chapter 9, when discussing amagmatic ore systems. Deposit styles in distal systems include fissure veins, replacement of calcareous rocks, stringers and veins adjacent to dykes and sills (Lang et al. 2000).

Hydrothermal alteration of intrusion-related ore systems is typically fracture-controlled and consists of feldspathic, sericitic, silicic, greisen, calc-silicate (skarn

type) and argillic assemblages (Lang and Baker 2001). Feldspathic alteration is represented by albite and/or K-feldspar. Gold and accompanying metals (see above) are generally associated with stages of sericitic alteration. An important difference, pointed out by Lang and Baker (2001), with porphyry systems is that the hydrothermal fluid flow of intrusion-related veins is typically unidirectional and lacks the multiple passes of porphyry and other hydrothermal systems. As briefly mentioned above, the sources of the ore fluids, based on fluid inclusion and isotopic data, are dominantly magmatic. The composition and origin of the ore fluids is discussed in some detail in Lang et al. (2000 and references therein). These fluids are CO_2-rich but evolving to aqueous brines, with other components, such as CH_4, N_2, H_2S, being more significant in proximal deposits. Temperature and pressure have a rather broad range of <200 to $>600^{\circ}C$ and 0.5 to >3.0 kbar, as may be expected from proximal to distal systems.

Many metalliferous lodes and veins owe their origin to regional anorogenic metamorphism and dewatering of rock sequences, where the heat energy is provided by deep-seated large intrusions. An example of this situation is the Sabie-Pilgrim's Rest district (South Africa), where numerous Au with minor base metal lodes are related to hydrothermal circulation powered by heat induced by the emplacement of the Bushveld Igneous Complex. These have been referred to as mesothermal ore deposits (Anderson et al. 1992; Boer et al. 1995), but are different from the orogenic mesothermal lode Au deposits as defined by Groves et al. (1998). In Western Australia in the Palaeo- and Mesoproteozoic Edmund and Collier Basins host swarms of polymetallic vein systems, which may be related to the circulation of hydrothermal fluids driven by heat energy associated with the emplacement of 1076 Ma mafic sills of the Warakurna large igneous province (Pirajno 2004).

4.4.1 Scheelite Dome, an Intrusion-Related Au Deposit, Yukon, Canada

The Scheelite Dome mineral system is part of the Jurassic-Cretaceous large Tintina province (also called Tombstone-Tungsten belt), which form a huge belt that extends for 2000 km between Alaska and central Yukon (Fig. 4.22). Comprehensive studies of the Tintina province and its magmatic belts include Goldfarb et al. (2000), Hart et al. (2002, 2004) and a more specific study on Scheelite Dome by Mair et al. (2006) make this deposit a good example of an intrusion-related ore systems. The review presented here is extracted from the above-cited authors.

The Tintina gold belt contains the Tombstone, Mayo and Tungsten plutonic suites that extend for 550 km in a west-northwest-trending zone. The intrusion-related deposits of the Tungsten suite are, as the name implies, W-rich and Au-poor and include the Cantung and Mactung skarn systems. By contrast, the

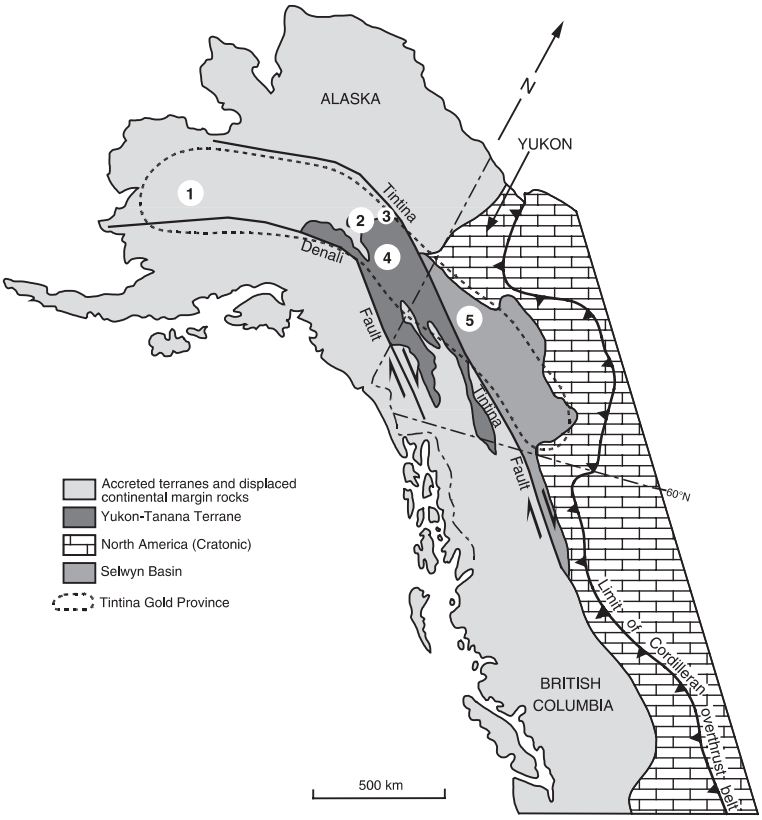


Fig. 4.22 Regional setting of the Tintina province, Alaska and Yukon, in the Cordilleran Orogen; gold districts are 1 Kuskokwim; 2 Fairbanks, which contains the intrusion-related Fort Knox; 3 Circle, also with intrusion-related deposits; 4 Goodpaster and 5 The Tombstone gold belt with the Scheelite Dome and Dublin Gulch intrusion-related systems. After Mair et al. (2006)

deposits of the Mayo and Tombstone plutonic suites are Au-rich and include Scheelite Dome, Dublin Gulch and Fort Knox. The mineralisation style of the Au-rich systems are sheeted, low-sulphide quartz veins in the apices (or cupolas) of the intrusions and veins, reduced skarns and disseminations in the thermal aureoles within the country rocks. The metal association is Au-W-Bi-Te-As $\pm$ Sb $\pm$ Mo, but in some cases enrichments of Pb, Zn and Ag are also observed.

The Scheelite Dome deposit lies in the western part of the epicratonic Selwyn Basin, which was developed at a passive margin during the Proterozoic rifting of the northwestern margin of cratonic North America. The basin was involved in collision and accretion with oceanic terranes of the Farallon plate with the North American cratonic western margin, during the Triassic-Cretaceous. This collision resulted in northward thrusting and complex ductile deformation,

culminating with the intrusion of felsic to intermediate post-collisional plutonic suites between 112 and 90 Ma. The Tombstone-Tungsten magmatic belt is the youngest and and was emplaced inboard of the accreted terranes, at ~93 Ma in an extensional setting. A change in plate motions by 85 Ma produced large scale dextral transcurrent movements, which offset the plutonic belts by up to 450 km, along the Tintina Fault (Fig. 4.22). The metasedimentary rock packages of the western Selwyn Basin are juxtaposed along a series of imbricate thrusts and are regionally metamorphosed to low-mid greenschist facies. The Mid-Cretaceous post-collisional Tombstone and Mayo plutonic suites that intruded the western Selwyn Basin outcrop as a series of small (usually <5 km across), isolated clusters of plutons and dykes, approximately parallel to the Tintina Fault. These intrusion are mostly monzogranite, quartz-monzonite and quartz-monzodiorite. The Tombstone plutonic suite is characterised by plutons of alkaline and metaluminous affinity and include six main intrusions accompanied by swarms of sills, dykes and stocks (Hart et al. 2004). The Tombstone plutons are nearly circular in plan view and concentrically zoned. Dominant rock types are alkali-feldspar syenite and quartz syenite, locally with marginal pyroxenite and hornblende diorite, and with central monzogranite and granite phases, nested in the syenitic rocks. Dominant mafic minerals are augite, aegirine, hornblende, arfvedsonite, and accessory magnetite, titanite, fluorite, apatite, zircon. Initial Sr ratios range from 0.717 to 0.737 and εNd_T between –13 and –15 (Hart et al. 2004). The Mayo plutonic suite, of which Scheelite Dome is part, is characterised by small (1–5 km^2) to large (125 km^2) isolated plutons dominated by porphyritic quartz-monzonite, locally cut by monzonite and diorite stocks and dykes, as well as a variety of aplites, pegmatite and lamprophyre dykes. The quartz-monzonite has K-feldspar phenocrysts, biotite and lesser hornblende and clinopyroxene, with accessory titanite, allanite, apatite and zircon. Initial Sr ratios range from 0.7115 to 0.7140 and εNd_T between –8 and –13 (Hart et al. 2004).

In the Scheelite Dome area (Fig. 4.23), two monzogranite intrusions are exposed, the Morrison Creek and the Scheelite Dome stocks, associated with numerous other intrusive bodies of porphyritic granodiorite and lamprophyre dykes, which are considered to be apophyses emanating from the plutonic suites. The monzogranite rocks, apart from the main phases of alkali feldspar and plagioclase, contain biotite and clinopyroxene as the mafic silicates with accessory hornblende, apatite, titanite, allanite and zircon. The Morrison Creek and Scheelite Dome stocks are surrounded by well developed thermal aureoles, with the inner hornfelsic halo as far as 500 m from the intrusive contact and containing biotite, andalusite and K-feldspar porphyroblasts in pelitic rocks and wollastonite, plagioclase and diopside in calcareous rocks. These inner hornfelsic assemblages are partially retrograded to actinolite, muscovite, calcite and chlorite. The outer zone of hornfels contains biotite porphyroblasts.

The Scheelite Dome mineralisation includes sheeted W-rich quartz veins, Ag-Pb-Zn-Sb-rich quartz veins, W- and Au-rich skarns. The W-rich sheeted quartz veins are from 1 to 3 cm thick and contain scheelite as the main ore

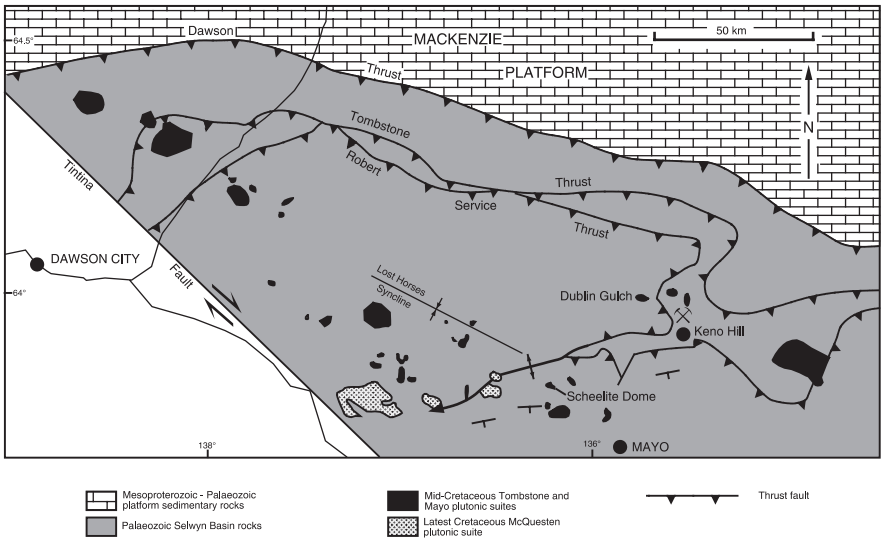


Fig. 4.23 Simplified geology of the western Selwyn Basin, showing post-collision Mid to late Cretaceous plutonic suites, discussed in text. After Mair et al. (2006)

mineral with traces of arsenopyrite and molybdenite. These thin veins may attain densities of 10/m, but have very small alteration selvages of albite and sericite, replacing feldspar and biotite respectively. In addition to W, the veins have anomalous Au contents (up to 100 ppb). Gold-rich veins, usually hosted by hornfels with only minor occurrences in the stock, have eastr-west and northwest trends and occupy tensional fractures and faults. Tension veins are from 0.5 to >10 cm thick, with a high density in the more competent rocks. Fault veins, on the other hand, are up to 1 m thick and are spaced hundreds of metres apart. Fault veins commonly exhibit multiple stages of growth. Alteration is subtle and more prominent in phyllite and calc-silicate rocks. This alteration is dominated by muscovite with lesser carbonate, quartz and sulphides. There are two end-members of Au-rich veins: (1) veins with a higher sulphide content (arsenopyrite and pyrite, about 4%) and a gangue of quartz, albite, ankerite, microcline, tourmaline and muscovite; (2) veins with less sulphides (<2%), about 90% quartz and minor muscovite and carbonate. Silver-Pb-Zn-Sb (polymetallic) veins form late stage mineralisation fills in both tension and fault zones. These veins contain between 10 and 20% sulphides in a gangue of quartz and ankerite. Sulphide species are stibnite, boulangerite, sphalerite, jamesonite and chalcostibite.

The skarns associated with the Scheelite Dome stock, as mentioned above, are W-rich, Au-poor and Au-rich. The former are hosted in pyroxene-plagioclase skarn with scheelite as the chief ore mineral. The skarn assemblage, apart from clinopyroxene and plagioclase, consists of quartz, K-feldspar, ilmenite, allanite and some arsenopyrite. Hydrous W-skarns have more sulphides (>15%) and

consist of zoisite, quartz, tourmaline, calcite, salite, K-feldspar with trace scheelite. Pyrrhotite is the dominant sulphide of the hydrous skarns, locally intergrown with chalcopyrite. Gold-rich skarns locally overprint the hydrous W-rich skarns. The gangue minerals of anhydrous skarns include diopside, plagioclase, quartz and ankerite with minor apatite, titanite and scheelite. Hydrous skarns have actinolite and biotite. In the anhydrous skarns, pyrrhotite is also the dominant sulphide, accompanied by lesser chalcopyrite and arsenopyrite. Gold occurs as the native element and may be associated with native Bi and Bi tellurides. Biotite skarns are massive and contain biotite, quartz, scheelite and apatite with arsenopyrite and as the dominant sulphide. The absence of pyrrhotite may be indicative of lower temperatures or higher sulphidation state. Native Au occurs in the biotite skarns and is associated with Bi-Pb-Sb sulphosalts, Bi tellurides and Bi selenides.

Fluid inclusion studies conducted on vein quartz revealed three types A, B and C. Type A are most abundant with predominantly primary and pseudosecondary three-phase aqueous-carbonic, type B are two-phase carbonic and type C are two-phase aqueous-carbonic with clathrate. All three types are found in secondary inclusions that cut grain boundaries and all contain H_2O-CO_2-NaCl $\pm$ $CH_4 \pm N_2$ fluids. Fluid inclusions of Au-rich anhydrous skarns are all of type A with 40–70% vapour phase at room temperature, homogenised to a liquid at temperatures of 370–380°C. The W-rich veins, mostly with pseudosecondary type A, are both vapour-rich and –poor homogenising at at temperatures between 300 and 325°C. Fluid inclusions in Au-rich veins, mostly pseudosecondary type A and vapour-rich, homogenised between 280 and 380°C, liquid-rich inclusions homogenised over a wider range between 220 and 360°C. The Ag-Pb-Zn-Sb-rich veins also have abundant type A fluid inclusions with both vapour-rich and liquid-rich homogenising at temperatures between 280 and 300°C. Primary and pseudosecondary inclusions in quartz of miarolitic cavities in granodiorite dykes that cut the Scheelite Dome stock have total homogenisation temperatures of 330 and 365°C. The salinity of most inclusions could not be determined due to the presence of CH_4 and N_2, but inclusion fluids in quartz of miarolitic cavities, which have negligeable CH_4 and N_2, contain between 2.5 and 3.5 wt% NaCl equivalent.

Oxygen isotopic data show $\delta^{18}O$ values ranging from 13.8 to 16.5‰ for sedimentary rocks of the Selwyn Basin, which are consistent with clastic sedimentary rocks derived from an igneous precursor. Calc-silicate rocks yielded $\delta^{18}O$ values of 8.8–11.1‰, reflecting high-temperature thermal metamorphism. Least altered intrusive rocks of the Scheelite Dome stock produced whole rock values of 9.7–12.8‰, whereas the $\delta^{18}O$ of quartz range from 13.8 to 15.2‰ for W-rich veins, 14.1–19.0‰ for Au-rich veins and 19.2–20.0‰ for the polymetallic veins. Sulphur isotopes determinations show a wide range of $\delta^{34}S$ values, –5.8 to –5.4‰ for arsenopyrite in W-rich veins, –10.9 to –7.1‰ for arsenopyrite in Au-rich veins and –10.1 to –6.8‰ for stibnite in the polymetallic veins. Gold-rich skarns have $\delta^{34}S$ values ranging from –7.3 to –2.4‰. Temperatures of the ore fluids, based on fluid inclusions and geothermometric data from

arsenopyrite and oxygen isotope fractionation factors indicate a range from 716 to 280°C, distributed as follows: W-rich veins 300–340°C; Au-rich veins 290–380°C; polymetallic veins 280–300°C; W-rich skarns 630–540°C; Au-rich skarns 716–480°C; biotite Au skarns 510–420°C; diopside Au skarns 610–570°C; amphibole Au skarns 540–480°C.

The presence of CO_2-rich fluids is recognised as an important characteristic of volatile exsolution from plutonic complexes. Furthermore, Mair et al. (2006) suggested that the high CO_2 contents may be linked with magmas that have assimilated sedimentary rocks and that the $\delta^{18}O$ values of W- and Au-rich skarns and the polymetallic veins are consistent with derivation of water from magmas. On the other hand, the variations in $\delta^{34}S$ values are explained by postulating two sulphur reservoirs, one igneous and the other sedimentary.

Mair et al.'s (2006) model for the Scheelite Dome magmatic-hydrothermal system is shown in Fig. 4.24. In this model, monzogranite magma intrudes the clastic and carbonate sedimentary succession of the western Selwyn Basin at a depth of approximately 6–8 km. Cooling of the magma formed a crystalline carapace (see Burnham's model in Chapter 2), with exsolution of CO_2-rich, low

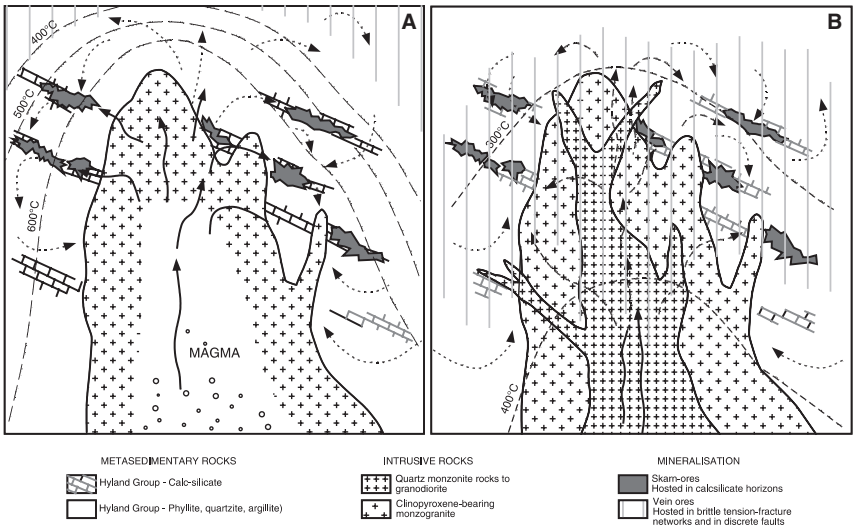


Fig. 4.24 Conceptual model illustrating the formation of the Scheelite Dome intrusion-related mineral system; (**A**) cooling and inward crystallisation of monzogranite magma, forming an outer carapace and exsolution of low-salinity H_2O-CO_2 fluids; metals partitioned into the volatile phase and transported by sulphur complexes; magmatic fluids flowed into the surrounding hornfels rocks, interacted with graphitic metapelites and cooled with deposition of Au and W in reduced skarn assemblages; continued cooling then led to the formation of Au-rich and polymetallic veins. (**B**) Further cooling above the cupola is associated with brittle fracturing forming an interconnected fault-fracture mesh into which magmatic fluids migrated from progressively greater depths. These fluid deposited type 2 W- and Au-rich veins. After Mair et al. (2006)

salinity fluids. Metals were partitioned from the melt into the volatile phase, transported by the fluid system as reduced S complexes. Fluids were modified by interaction with the graphitic units in the hornfels, were reduced and deposited W and Au in skarn lithologies. In the more brittle units of the hornfels fluid flow was restricted to fractures and faults and to more reactive lithologies, such as calc-silicates. Progressive cooling below 380°C the modified fluids formed type 1-end member Au-rich veins and at <300°C formed the polymetallic veins. Fluid flow was enhanced by a fault-fracture mesh. Magmatic fluids continued to be exsolved from the deeper parts of the plutonic complex, migrated upwards through the crystallisation front, equilibrated with the intrusive rocks with decreasing temperatures and deposited W- and Au-rich type 2 veins.

4.4.1.1 Metallogeny in the Tombstone-Tungsten Belt

Hart et al. (2004) discussed the general features of intrusion-related metallogeny from the Tombstone-Tungsten belt and the three plutonic suites, Tombstone, Mayo and Tungsten. The mineralisation styles include skarns, stockworks, disseminated veins, sheeted vein systems and replacements. Dominant metal assemblages are Au-Cu-Bi, W and W-Cu for skarns, Ag-Pb, Au-Bi-W, Au-As-Sb for veins and stockworks, Au-As for replacement bodies and U-Th-F for disseminated veins. The vein systems are generally peripheral to the plutons and appear to be related to the final phases of the magmatic-hydrothermal activity. The Mayo intrusions are more associated with Au and have Au-Bi-Te-W quartz-alkali feldspar sheeted vein arrays (Dublin Gulch) and Au-As quartz vein (Scheelite Dome). The Tombstone-Tungsten plutonic suites have geochemical features, such as negative Nb-Ti anomalies, indicative of melts from subduction settings, with the more evolved phases resulting from fractionation and crustal assimilation. This is suggested by the >70 silica, highly fractionated, tourmaline-bearing quartz-rich intrusions, all with high U, Th and Zr abundances. The presence of inherited zircons, radiogenic Sr and the negative εNd_T values further confirm a sedimentary crustal component. In addition, deep seismic profiles show the Proterozoic sedimentary package at the Moho boundary.

Intrusion-related magmatic-hydrothermal systems the partitioning behaviour of metals are governed by the oxidation state of the magma, as shown in Fig. 4.4. This oxidation state can be monitored by the presence of magnetite or ilmenite. Hart et al. (2004) pointed out that a high oxidation state prevents the early sequestration of chalcophile elements and the development of magmatic sulphides, thereby making Cu-Au and Mo available to late fractionating melts and magmatic-hydrothermal fluids. Tungsten and Sn enrichments are generally associated with reducing conditions. On the other hand, the redox controls of Au, Bi and Te are somewhat equivocal because they are associated with both reduced and oxidised systems. Gold is a siderophile element but with strong chalcophile tendency. This means that in a reduced system the segregation of early sulphides would sequester Au, diminishing its concentration in

residual melts. On the other hand, oxidised magmas do not segregate early sulphides allowing Au to be concentrated in residual melts and making it available for magmatic-hydrothermal fluids. Seen in this light, the Tombstone suite is associated with mineralisation dominated by Cu-Au-Bi and U-Th and therefore sufficiently oxidised. The Tungsten suite is reduced and therefore associated with large W deposits, with only minor Cu, Mo and Zn. The Mayo intrusions have intermediate redox state and consequently have an intermediate metal association, characterised by enrichments in Bi, Te and As, with the W being present but in lesser amounts than in the Tungsten intrusions.

4.4.2 The Kidston Breccia Pipe, Queensland, Australia

The Permo-Carboniferous calc-alkaline volcanic and plutonic rocks of the North Queensland Magmatic Province (Tasman Fold Belt), form ring complexes and batholithic intrusions, comprising I-, S- and A-type granitoids and co-magmatic felsic volcanic rocks (see Scheibner and Veevers 2000, for a good overview of this province; Bain and Draper 1997 for detailed descriptions). This magmatic province is well endowed with porphyry Cu-Mo, Sn-W and U-rich deposits and Au-bearing breccia pipes, such as Leyshon and Kidston. The Kidston Au deposit, hosted in a sub-volcanic breccia pipe at the contact between granodiorite rocks (Silurian-Devonian Oak River Granodiorite) and metamorphic rocks, is one of the largest in Australia with about 60 tonnes of contained gold metal. The brief account presented here is taken from Baker and Tullemans (1990), Baker and Andrew (1991) and Solomon and Groves (1994).

The Kidston pipe is spatially and temporally associated with rhyolite and quartz-feldspar porphyry dykes and plugs (Fig. 4.25). Rb-Sr dating of sericite at Kidtson yielded an age of ca. 321 Ma. The sub-volcanic pipe is trapezoid in shape, has dimensions of 1100 $\times$ 900 m narrowing downward and contains several breccia types with clasts derived from the metamorphic and granitic country rocks. The size of the clasts can reach 100 $\times$ 200 m in area and are separated by rock flour. The formation of the breccia pipe, characterised by three phases of brecciation, is shown in Fig. 4.26. The first phase involved the development of stockwork veins in the porphyritic rhyolite and the wall rocks above, with formation of UST textures and quartz-tourmaline cemented breccia. This phase continued with the build up of volatiles and fluids during crystallisation of the underlying granodioritic batholith. Phase 2 is the development of the main breccia, due to collapse of the overlying rocks caused by magma withdrawal and/or escape of volatiles and fluids. Phase 3 breccia was then produced within phase 2 breccia by continuing escape of fluids, either from the rhyolitic melt or by the explosive interaction between this melt and hydrothermal fluids. This was followed by the intrusion of a post-breccia rhyolite into the lower parts of the pipe. This resulted in the formation of inward-dipping concentric fractures and sheeted veins, which contain the economic Au

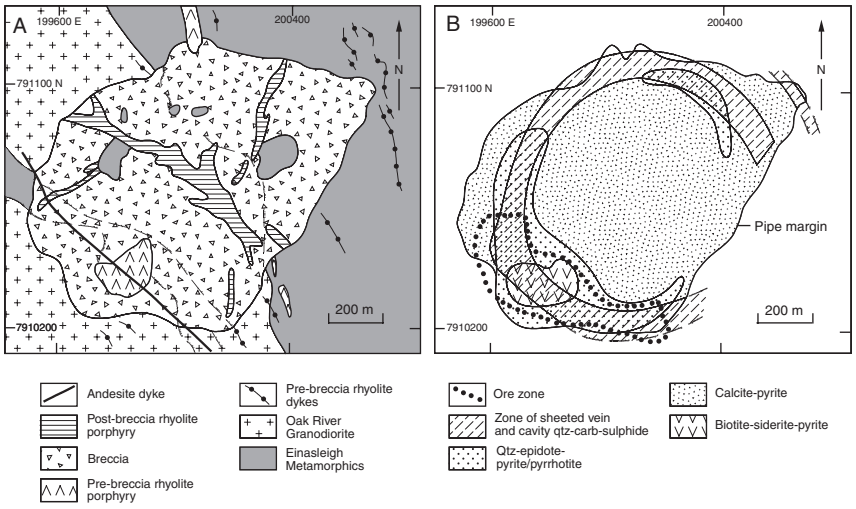


Fig. 4.25 Simplified geology (**A**) and alteration zones (**B**) of the Kidston breccia pipe. After Baker and Andrew (1991) and Solomon and Groves (1994)

mineralisation. Similarly, the mineralisation-alteration at Kidston comprises two main stages: (1) a pre-breccia; and (2) post-breccia.

The pre-breccia stage is characterised by dyke-like zones in the central parts of the pipe (Fig. 4.25A) containing quartz-magnetite-pyrite stockworks, cemented by a matrix of quartz-tourmaline; quartz-pyrite-molybdenite ± arsenopyrite ± chalcopyrite veinlets in clasts also occur in this stage. The alteration of this stage consists of weak silicification and muscovite-carbonate replacement of the plagioclase in the rhyolitic rocks. The post-breccia stage is characterised by quartz-epidote infilling open spaces in the concentric structures forming sheeted veins along the periphery of the breccia pipe (Fig. 4.25), with calcite-pyrite ± pyrrhotite infills in the pipe and a complex alteration assemblage containing K-feldspar and albite as the main minerals. The alteration is typically confined to the rims of the clasts and the breccia matrix. This stage is further subdivided into three substages, early, transitional and late. The early stage has mineral assemblages of quartz-epidote ± pyrite ± pyrrhotite and quartz-K-feldspar ± pyrite ± pyrrhotite, infilling cavities and within an inverted funnel-shaped zone around the periphery of the pipe. Alteration assemblages are quite complex with K-feldspar and albite and various combinations of muscovite-calcite-chlorite. Isolated patches of biotite-siderite-pyrite and biotite-magnetite-pyrrhotite occur in the southwest margin of the pipe (Fig. 4.25). There is an outward progression from the quartz-epidote ± sulphides to calcite ± sulphides filled cavities. The transitional stage shows zoning from an outer quartz-epidote-sulphides or quartz-K-feldspar-sulphides to an inner assemblage of quartz-ankerite-pyrite ± pyrrhotite ± base metals. This transitional stage is characterised by muscovite-ankerite overprinting the

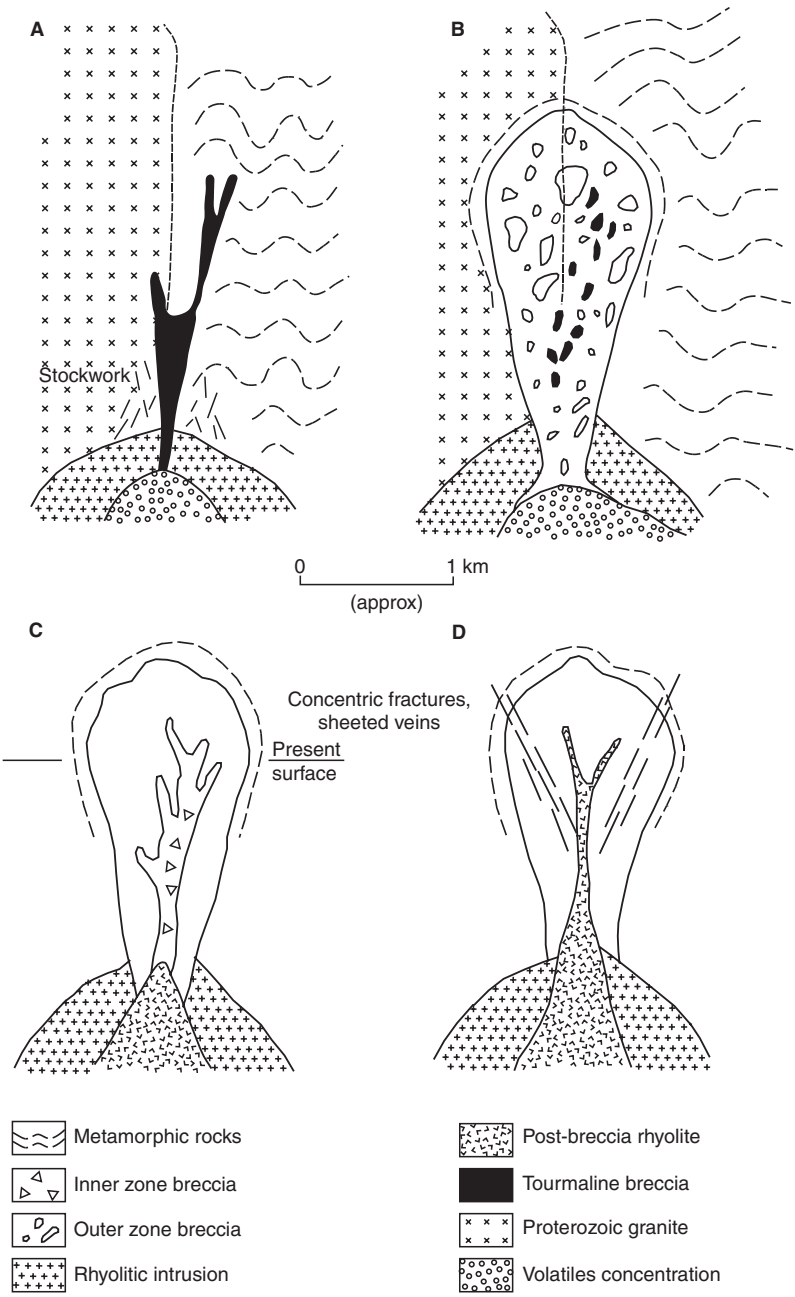


Fig. 4.26 Evolutionary stages of the Kidston breccia pipe, (**A**) pre-breccia stage with quartz-tourmaline; (**B**) formation of main breccia; (**C**) more breccia in the core of the main breccia pipe; (**D**) final stage with emplacement of rhyolite dykes and Au-beraing sheeted vein system. After Solomon and Groves (1994)

early stage K-feldspar-albite-muscovite-calcite assemblages. The late stage post-breccia consists of cavity and sheeted vein filling by quartz-calcite-ankerite and sulphides with which the bulk of the Au mineralisation is associated. The sulphides within the sheeted veins exhibit a zoning pattern, with pyrite-galena-sphalerite-chalcopyrite in the highest parts (Wises Hill), outward and downward, through pyrite-pyrrhotite-galena-sphalerite-chalcopyrite-arsenopyrite to pyrite-pyrrhotite-galena-sphalerite and molybdenite. The Au mineralisation is mostly contained in the upper levels. Hydrothermal alteration of this phase is phyllic (muscovite-quartz-calcite-ankerite), overprinting all previous stages, and the ore is mainly represented by an annular zone on the southwest side of the pipe, where it is spatially associated with a zone of biotite-siderite-pyrite (Fig. 4.25). Most of the gold (about 90%) is in free form, with the remainder being locked in sulphides.

Baker and Andrew (1991), on the basis of fluid inclusions and stable isotopes data, suggested that the pre-breccia fluids were of magmatic origin evolved from a rhyolitic magma, of high temperature (>500°C) and highly saline (40–50 wt% NaCl equivalent), with later stages of cavity infills by lower temperature fluids (170–300°C) with which the economic Au mineralisation is associated. Fluid overpressure was the main cause for explosive expansion that formed the breccia pipe. The sulphide assemblages suggest a magma with Mo > Cu, similar to the porphyry systems in the province and compatible with more fractionated magmas with high water content (Solomon and Groves 1994). The Au mineralisation was formed from a dilute brine that condensed from magmatic vapour, exsolved from the rhyolitc melt.

4.4.3 Uraniferous Vein Systems

The behaviour of U in magmatic-hydrothermal fluids is related to the large size of the its atoms and their positive valencies, U^{4+}, U^{6+}, U^{3+} and U^{5+} which causes them to be precluded from entry into the common rock forming minerals of igneous rocks (see Chapter 13 for more details). Therefore U (and Th) are concentrated in late stage silicate melts or hydrous and gaseous fractionates and tend to be taken up by accessory minerals, such as apatite, monazite, titanite and rutile. For this reason U occurs in trace amounts in those igneous systems that contain the above mineral phases. Igneous intrusions that contain U minerals (uraninite, uranothorianite, uranothorite) include alaskite, quartz-monzonite, carbonatite and peralkaline syenite. Alaskite is a megacrystic quartz-monzonite and alkali feldspar granite with a pegmatitic texture and locally uraniferous. In Namibia, alaskites host U mineralisation, mined at Rössing, but also present at other localities such as Goanikontes, Ida Dome and Valencia. Ore minerals include uraninite, betafite, uranophane, carnotite and niobates. The origin of these uraniferous alaskites is linked to partial melting of U-enriched basement rocks in the Damara Orogen (Pirajno 1998).

Intrusion-related hydrothermal veins that contain U minerals are common and are usually polymetallic, with Ni, Co, Bi, Ag, Cu, Pb, Zn, Mo, As in various combinations of metal associations. Dahlkamp (1993) considered uraniferous vein systems in terms of granite-related: intragranitic and perigranitic. Intragranitic veins, as the name implies, are stockworks or sheeted vein systems hosted in granitic rocks. These are highly differentiated two-mica leucogranites that are enriched in Be, Li, F, Sn, W, Th and of course U. The type example, cited by Dahlkamp (1993) is Limousin in the Massif Central (France), which are one of the most important sources of uranium in Europe. The veins occur within or peripheral to two-mica granites of Hercynian age, which contain anomalous U abundances (15–20 ppm) and are more fully described in Chapter 13, together with more details on uranium, radioactive decay schemes, geochemistry, and mineral systems.

4.4.4 Sabie-Pilgrim's Rest, South Africa

The sedimentary rocks of the Transvaal Supergroup, host important epigenetic Au mineralisation which is coeval with the emplacement of the Bushveld Igneous Complex (Transvaal Drakensberg gold field; Ward and Wilson 1998). The Sabie-Pilgrim's Rest goldfield has produced about 186 000 kg of gold since its discovery in 1873. There are several works that discuss various aspects of the Sabie-Pilgrim's Rest mineralisation, including the detailed work of Ash and Tyler (1986), Anderson et al. (1992), Harley and Charlesworth (1994), Boer et al. (1995) and Tyler and Tyler (1996).

The Sabie-Pilgrim's Rest goldfield is located on the eastern margin of the Palaeoproterozoic Transvaal Basin (Fig. 4.27). The lodes are referred to as reefs, some of which are veins that cut through the basement, others are parallel to bedding within the Transvaal Basin sedimentary rocks. The sedimentary succession in the region includes the Wolkberg Group that lies unconformably on Archaean basement, followed upward by the Black Reef Quartzite Formation and the carbonate units of the Malmani Dolomite. The Wolkberg Group is interpreted as an early rift phase of the Transvaal Basin. This was followed by a phase of thermal relaxation, and the deposition of the quartz-arenite of the Black Reef Formation, which is 25–30 m thick. The overlying Malmani Dolomite Subgroup is a thick succession of shales and chemical sediments that varies in thickness from 700 m in the Pilgrim's Rest area, to 350–400 m in the Sabie area. The overlying sedimentary rocks of the Pretoria Group are about 7000 m thick in the region. The regional dip of the sedimentary rocks is only a few degrees to the west. Pre- to post-Bushveld sills considerably thicken the sedimentary package. In addition, north-northeast-trending dyke swarms of Bushveld Complex age are present. The dykes were probably emplaced in deep-seated crustal structures that in the basin's sedimentary succession are manifested as sets of joint and fractures. Bedding-parallel shearing and thrusting are common in the shale and dolomite rocks.

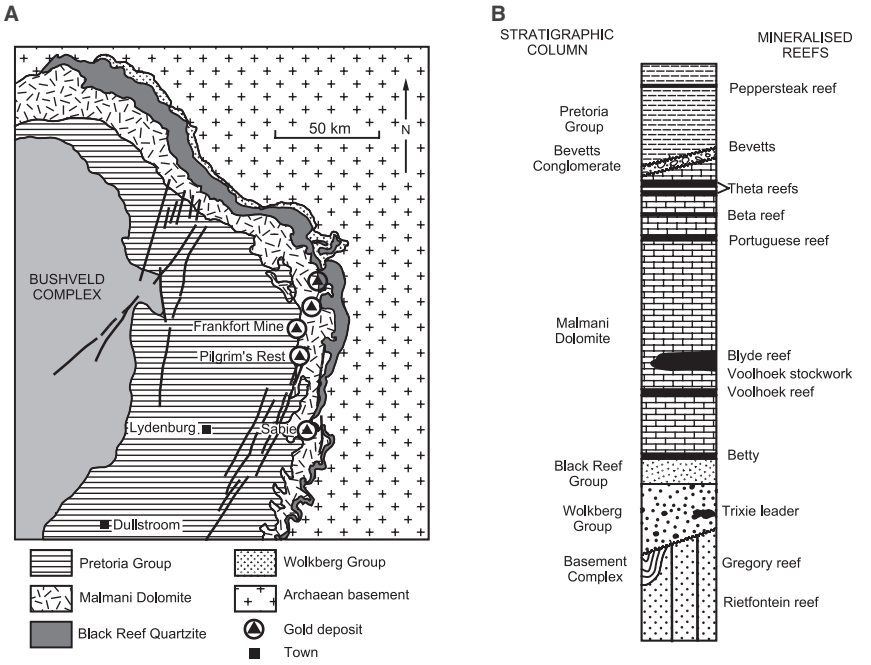


Fig. 4.27 (**A**) Simplified geology of the eastern part of the Transvaal Basin, showing principal gold deposits of the Sabie-Pilgrim's Rest goldfield; (**B**) schematic stratigraphic column of the Lower Transvaal Supergroup, showing position of selected auriferous reefs. After Tyler (1986)

The reefs range from stratiform (flat reefs), to discordant transgressive leaders, vertical lodes to irregular bodies. Flat reefs are sheet-like veins that follow near-horizontal bedding planes and bedding-plane shear zones. Many of the reefs in the Malmani Dolomite are developed along carbonaceous shaley horizons, which are thought to have been deposited in lagoonal settings. Locally, relic algal structures are discerneable. The mineralogy of the flat reefs includes an early assemblage of quartz, carbonate, pyrite and subordinate scheelite, arsenopyrite and galena. These early phases are commonly ruptured by later bedding-plane movements and introduction of gold, chalcopyrite, bismuthinite, tetrahedrite and galena. Leader reefs are transgressive veins that usually emanate as off-shoots from flat reefs. Vertical lodes occur mostly in the Archaean basement and the overlying Wolkberg Group rocks. They are quartz veins that have great lateral and vertical extent and are emplaced along faults, joints, dykes and shear zones, generally striking north-south. One vertical lode, Bokwa Stotz Reef, is 47 km long and cuts through 1000 m of stratigraphy (Harley and Charlesworth 1994). Irregular bodies include stockworks, pockets and lenses. The reefs of the Sabie-Pilgrim's Rest goldfield have grades averaging from 3 to 8 g/t Au.

Fluid inclusion studies, carried out by Ash and Tyler (1986) and Anderson et al. (1992), revealed that the fluids contained variable amounts of CO_2, CH_4, H_2O, NaCl, KCl and $CaCl_2$. Measured salinities range from 15 to 30 wt% NaCl equivalent and homogenisation temperatures from about 100 to about 400°C. Interestingly, samples of fluid inclusions from stratigraphically deeper deposits homogenised at 300–400°C, whereas measurements from stratigraphically shallower deposits gave results in the range 100–200°C.

On the basis of their results, Anderson et al. (1992) proposed that the Sabie-Pilgrim's Rest mineralisation was formed by mixing of fluids at various stratigraphic levels. Low-temperature chloride-rich basinal brines of high to moderate salinity migrated and interacted with higher-temperature CO_2-rich and Au-bearing fluids. These CO_2-rich fluids may have originated from the devolitilisation of the carbonate rocks, due to high heat flow related to Bushveld magmatism. The source of the gold is as yet unknown, and leaching of the precious metal from the underlying basement lithologies is a possibility. Boer et al. (1995) also invoked the Bushveld magmatism as the thermal event responsible for the hydrothermal convection that produced the Sabie-Pilgrim's Rest goldfield. Their evidence is based on several key features. One is age relationships, which show that vein systems cut pre-Bushveld mafic intrusions, but Bushveld pyroxenite dykes cut the mineralisation. Another is the heterogenous nature of the fluids, a component of which was probably from a deep-seated source. Boer et al. (1995) classified the Sabie-Pilgrim's Rest mineralisation as a type of mesothermal gold deposit, and acknowledged that the Sabie-Pilgrim's Rest goldfield has a clear spatial association and age relationship with the Bushveld Complex.

Finally, Harley and Charlesworth (1994) compared the Sabie-Pilgrim's Rest mineralisation to that of the Neoproterozoic Telfer (Western Australia) and the Meso-Neoproterozoic Passagem de Mariana (Minas Gerais, Brazil). In making this comparison, they pointed out the stratiform nature of the quartz reefs, the association with carbonaceous lithologies, ore mineralogy and metal association (Au-Cu-Bi-As) and magmatic fluid sources.

4.4.5 Capricorn Orogen Structurally Controlled Hydrothermal Vein (Base and Precious Metals), Western Australia

The Capricorn Orogen is a Proterozoic tectonic zone, situated between the Pilbara Craton in the north and the Yilgarn Craton in the south (Cawood and Tyler 2004; see inset of Fig. 4.28). The Orogen is the site of the convergence and collision of these cratonic blocks and is characterised by low- to high-grade metamorphic terranes (Gascoyne Complex, discussed in Chapter 6), the deformed margins of the two cratons that have been affected by the convergence-collision and a number of variably deformed sedimentary and volcano-sedimentary basins. The youngest of these basins are the Edmund and Collier basins

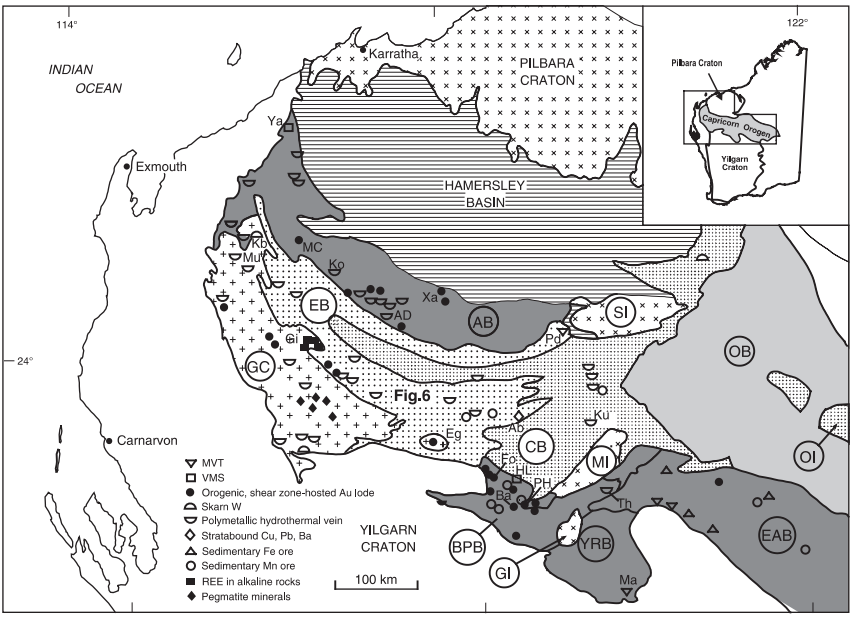


Fig. 4.28 Tectonic units of the Capricorn Orogen; and distribution of selected mineral deposits and occurrences, modified after Tyler et al. (1998). Sl Sylvania Inlier; Ml Marymia Inlier; Gl Goodin Inlier; Ol Oldham Inlier; AB Ashburton, Blair and Bresnahan basins; EB Edmund Basin; CB Collier Basin; GC Gascoyne Complex; BPB Bryah and Padbury Basins; YRB Yerrida Basin; EAB Earaheedy Basin; OB Officer Basin. Some key mineral deposits are: Ab Abra; AD Ashburton Downs; Eg Egerton; Gi Gifford Creek; Fo Fortnum; HL Horseshoe Lights; Ko Kooline; Kb Kilba Well; Ku Kumarina; Ma Magellan; MC Mount Clement; Mu Mundong Well; PH Peak Hill; Pd Prairie Downs; Th Thaduna; Xa Xanadu-Mt Olympus; Ya Yarraloola. MVT is Mississippi Valley-type, VMS is volcanogenic massive sulphides. *Inset* shows position of Capricorn Orogen

(Edmund and Collier Groups, respectively forming part of the Bangemall Supergroup; see Martin and Thorne 2004 for details of these basins).

Structurally-controlled polymetallic veins are commonly found throughout the tectonic units of the Capricorn Orogen and post-date Capricorn orogeny structures. Most of these vein deposits are found in the Edmund and Collier basins (Fig. 4.28), but they cannot be related to the 2.0-1.83 Ga (Glenburgh and Capricorn orogenies), the 1.79–1.76 Ga (Yapungku orogeny) and the 1.68 Ga (Mangaroon orogeny) tectonic events (Cawood and Tyler 2004; Sheppard et al. 2005), because these basins are younger. Pirajno (2004) suggested that high geothermal gradients linked to the 1.45-1.07 Ga continental mafic magmatism (Wingate et al. 2004), may have favoured large scale circulation of hydrothermal fluids, which would have been responsible not only for the emplacement of the vein and lode deposits in the Edmund and Collier basins, but also in the modification and remobilisation into pre-existing structures of earlier syngenetic and/or epigenetic deposits. In the Edmund and Collier Basins, hydrothermal fluids

were channelled along basin-margin parallel structures, such as the Tangadee lineament (Cooper et al. 1998), and associated faults, resulting in a variety of structurally-controlled polymetallic lodes and veins. Many of the 1.45-1.07 Ga mafic intrusions are spatially associated with lode style mineralisation, particularly along sheared contacts with the country rocks, which provided an easy channelway for fluids. As noted previously, the emplacement of numerous mafic sills and dykes must have advected considerable heat into the crust and the sedimentary successions, generating large-scale circulation of hydrothermal fluids. This hydrothermal activity could have been responsible for the much of the post-Capricorn structurally-controlled mineralisation.

4.4.6 Polymetallic Vein Systems of the Altai (Siberia) and Northwestern Mongolia (Yustid Rift Zone)

Intrusion-related polymetallic vein mineral systems dominated by Ni-Co-As, Ag-Sb, Au-Ag-Hg, Sb-Hg metal assemblages are common in the Altai region of central Asia, located between the southeastern Altai Republic (Russian Federation) and northwestern Mongolia (Fig. 4.29). These vein systems have been extensively studied by Russian geoscientists, with most publications in Russian, but with increasing works now being published in English (Borisenko et al. 1999; Pavlova et al. 2004; Seltmann et al. 2007 and references therein). In this section I focus on the Yustid rift zone and the Asgat-Ozernoe vein system, which I visited in August 2007. Details of the Asgat-Ozernoe polymetallic veins can be found in Seltmann et al. (2007 and references therein).

The Yustid rift zone contains thick (~9 km) sedimentary and volcano-sedimentary successions of Devonian age (Yustid Series). The lower units comprise felsic volcanic rocks and beds with carbonates and gypsum (possibly evaporites). The uppermost Baguchin Formation comprises fossiliferous black shales with coal and fossil ferns. These Devonian rocks were intruded by the 355 Ma Yustid composite batholith (see below) and dykes and stocks of alkaline affinity at ~246–240 Ma. The Yustid 355 Ma polyphase granitic batholith consists of gabbro, diorite, granodiorite, megacrystic hornblende granite and leucocratic granite. The Yustid ore cluster comprises skarns, greisen-related Mo-W (described in Section 4.3.10), Sn-W deposits with ages corresponding to that of the Yustid batholith. Exoskarns and hornfels formed in sedimentary rocks along the margins of the granitic intrusions. An example is the Karakul Cu-Co-Bi-W skarn deposit, with resources of 800 000 tonnes Cu and 50 000 tonnes Co, with by-product Au. The ore minerals include pyrite, chalcopyrite, cobaltine, arsenopyrite, scheelite and sulphosalts of Bi. The polymetallic vein systems surrounding the batholith, however, were formed later between 250 and 230 Ma, more or less coeval with the inception of the alkaline magmatism referred to above.

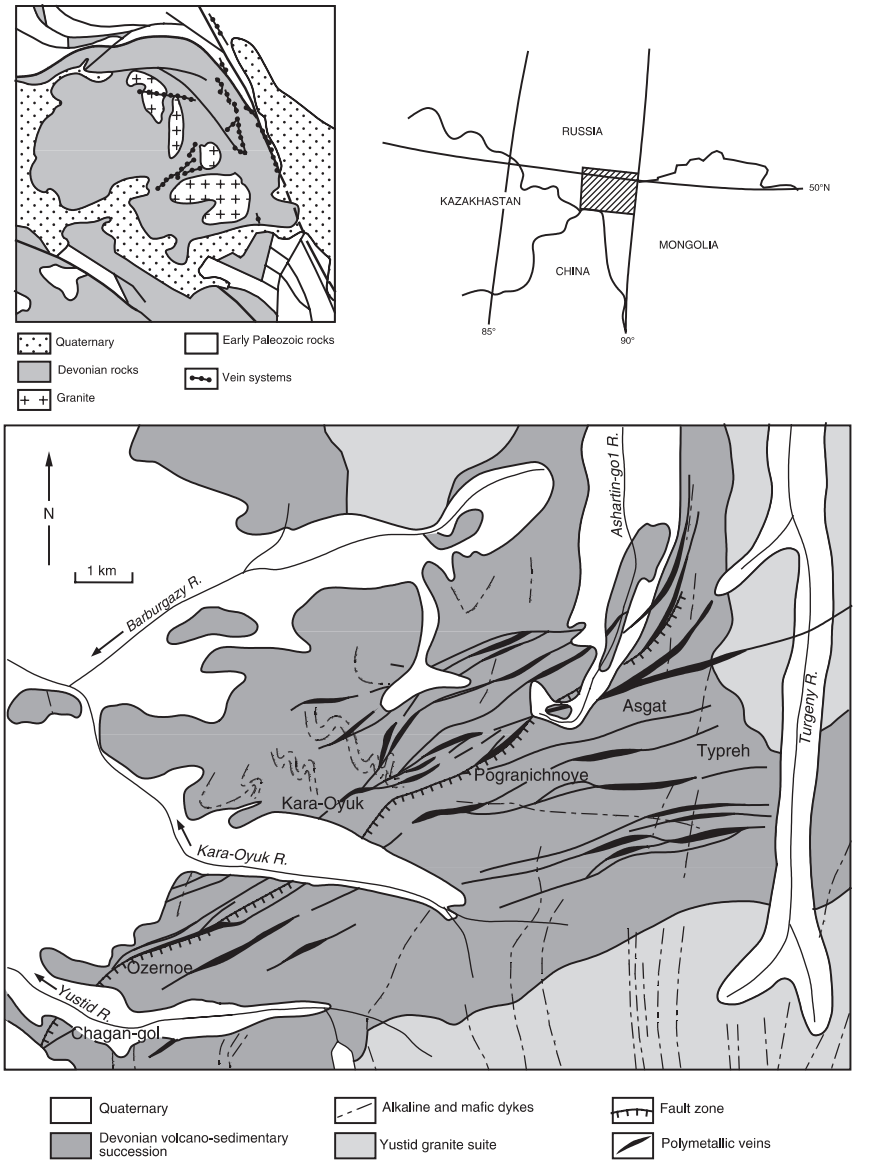


Fig. 4.29 Simplified geological map of the Asgat-Ozernou region and distribution of the polymetallic sheeted vein system; inset above *left* shows the spatial relationship of the vein systems in the region with faults and the granitic intrusions. After Borisenko et al. (1999)

4.4.6.1 Asgat-Ozernoe Ag-Sb Vein System

The Asgat-Ozernoe Ag-Sb vein system, with Ar-Ar ages ranging from ~240 to 236 Ma, is spatially associated with granitic rocks of the Yustid batholith and is

characterised by sheeted veins that strike eastnortheast and northeast and extend for about 12 km mainly contain quartz and siderite and are hosted by the Devonian sandstone-black shale rift succession (Fig. 4.29). The Asgat-Ozernoe vein system is polymetallic and comprises numerous individual deposits that, apart from Asgat and Ozernoe, include Askhatin, Kara-Oyuk, Chagangol, Mogenburen, Munguntaiga, Pogranichnye (Borisenko et al. 1999). The Asgat deposit, has resources of 12 000 tonnes of Ag (grading about 300 g/t), 16 000 tonnes of Bi, 80 000 tonnes of Sb and 150 000 tonnes of Cu. The mineralised veins are flanked by intensive stockworks and breccias, associated with chlorite and sericite, as alteration minerals. The subvertical vein-stockwork zones are 15–20 m thick, with individual veins from 0.5 to about 1 m thick. The Ozernoe deposit contains about 1000 tonnes of Ag and consists of 20 ore zones that extend for 520 m along strike and with individual veins from 0.5 to 2.5 m thick, enclosed in hydraulically fractured rocks cemented by siderite, quartz and ore minerals. The ore minerals of the Asgat-Ozernoe polymetallic vein system are many and complex, with more than 40 species identified so far and including sulphides, sulphoarsenides, arsenides and native metals. The main species are tetrahedrite, chalcopyrite, chalcostibite, freibergite, bournonite, semseyite, zinkenite, arsenopyrite-loellingite, sphalerite, bismuthinite, stibnite, native Bi and Sb. A complex paragenesis is from early siderite ± sulphides to sulphosalts to late sulphides and native metals. The first stage is quartz-siderite with calcite, barite, hematite, some pyrite and chalcopyrite. The second stage is dominated by arsenopyrite-loellingite and is associated with a period of tectonic disturbance. This stage also includes mineral species, such as pyrite, pyrrhotite, marcasite, native Sb, native Bi, and is associated with quartz, Fe-carbonates, chlorite as alteration minerals. The third stage is dominated by siderite and sulphosalts with an association of siderite II, tetrahedrite, chalcostibite, bournonite, ankerite, chalcopyrite, calcite, native Bi and Sb, semseyite, stibnite, sphalerite, galena, freibergite, bismuthinite. Fluid inclusion studies of quartz, siderite, calcite and barite have recognised two groups of pseudosecondary inclusions, liquid-vapour (L + V) and vapour-liquid-halite (V + L + S), with homogenisation temperatures ranging from 200 to 70°C. Interestingly, the earlier inclusions in the central parts of the examined crystals have lower homogenisation temperatures (110–70°C) than the inclusions in later growth zones (up to 200°C). At Asgat, the temperatures increase with depth from 178–70°C in the lower levels to 152–70°C at higher levels. Salinities, in terms of NaCl equivalent, range from 20 to 36 wt%. In addition, gas phases, established by Raman spectroscopy, include CO_2, N_2 and CH_4. Sulphur isotopic composition of siderite is nearly identical to that of pyrite from the host black shales ($\delta^{34}S$ of + 5–6‰), suggesting that this sedimentary pyrite provided the sulphur.

A lateral zonation between Asgat in the east and Ozernoe in the west is recognised. The composition of the ore changes from predominant tetrahedrite-chalcostibite (Asgat), to zinkenite (Kara-Oyuk), bournonite (Ozernou) to galena-sphalerite (Chagan-gol) (Fig. 4.29). This change is accompanied by a

decrease in the thickness of the ore veins and temperatures, with maximum temperatures at Asgat (200°C), Kara-Oyuk (130–70°C), Ozernoe (120–70°C) and Chagan-gol (<100°C). Thermodynamic modelling of ore depositional processes, based on parameters obtained from fluid inclusions, suggest that there were two types of fluids: neutral-weakly alkaline fluid (<5 wt% NaCl) and acid chloride fluid with concentrations of up to 30 wt% NaCl equivalent (Pavlova et al. 2006). The second type of fluid is of a later stage, overprints the first and contains Cu, Ag, Pb and Zn.

4.4.6.2 Ore Genesis

The polymetallic vein systems in the southeastern Altai (Russia) and northwestern Mongolia are numerous and extensive and have been compared with the vein systems in the ancient mining districts of the Erzgebirge, Cornwall (Section 4.3.6) and the Slovakian Republic in Europe (Seltmann et al. 2007), which are associated with intracratonic post-orogenic, possibly A-type, granites (Laznicka 2006). The age data from the granitic rocks and associated greisen systems (~355 Ma; Section 4.3.10) and the vein systems discussed here (Ar-Ar, ~240 Ma) indicate a substantial time gap between the emplacement of the granite and the formation of the polymetallic veins. As mentioned above, the age of the vein mineralisation is close to that of the alkaline intrusives, suggesting that a link, not necessarily genetic, may be inferred. It is possible that the intrusion of the 355 Ma batholith may have first provided the thermal energy to activate hydrothermal circulation. The country rocks (e.g. black shales) may have supplied the variety of metals in the hydrothermal system (Ni, Co, Bi, Sb and Ag). Intrusion of ~240 Ma alkaline magmas may have caused reactivation of the hydrothermal system and have induced influx of meteoric waters along major structures overprinting the first stage of hydrothermal activity and resulting in the observed complex mineralogy and metal assemblages. Borisenko et al. (1999) and Seltmann et al. (2007) suggested that this polymetallic, Ag-Sb-dominated, mineralisation is associated with mantle-derived magmatism (alkaline intrusions) that is ultimately related to the widespread mantle plume events in central Asia at around 250–240 Ma (e.g. Siberian traps; see Borisenko et al. 2006 and Dobretsov 2005).

4.5 Hydrothermal Systems Associated with Alkaline Magmatism and Anorogenic Ring Complexes

Anorogenic magmatism is generally alkaline in composition and is associated in space and time with extensional tectonics and more specifically with rifting events. Magma genesis in rift environments is thought to be related to the ascent of mantle plumes, which interact with subcontinental mantle lithosphere (Pirajno 2000). The main products of rift magmatism are fissure-fed tholeiitic

basalts (continental flood basalt, CFB), layered mafic-ultramafic intrusions, and respective feeders represented by dyke swarms, A-type granitic rocks referred to in Section 4.1 and alkaline complexes (Pirajno 2000). The latter includes volcano-plutonic ring complexes, carbonatite, kimberlite, lamproiite, and central-vent alkaline volcanoes (e.g. Mt Kilimanjaro, Kenya, in the East African Rift System). Anorogenic alkaline complexes are generally H_2O-poor, and characterised by unusual concentrations of non-hydrous volatiles (CO_2, B, F), REE and LILE incompatible elements, (P, Zr, Ba, Nb, U, Th, Sn, Ta and W). These elements may form their own minerals, or they may enter the lattice of rock-forming minerals (e.g. micas), that have crystallised in the subsolidus range of pressure and temperature. The processes that lead to the enrichment of these elements are linked with the activity of residual alkali-rich fluids. Consequently, their concentration, either in rock-forming minerals or in their own mineral species, is largely dependent on the original magma composition and the nature of the source regions where partial melting occurred.

Important rock associations of alkaline magmatism are: kimberlites, mafic ultrapotassic rocks, syenite-pyroxenite-ijolite-carbonatite assemblages, alkali basalts and peralkaline granite-syenite-gabbro assemblages. These rocks occur as dykes, pipes, hypabyssal and subvolcanic intrusions and as central volcano-plutonic structures, many of which form ring complexes. Most economic mineral deposits (excluding diamonds in kimberlites and ultrapotassic mafic rocks) occur associated with central vent-type complexes of which two main groups are recognised (Bowden 1985): (1) alkali-granite-syenite (saturated-oversaturated); and (2) ijolite-carbonatite (undersaturated). They are schematically illustrated in Fig. 4.30. The idealised cross-sections shown in Fig. 4.30 also illustrate the importance of the level of erosion, in terms of the preservation potential of the contained mineral deposits. Alkaline magmatism usually occurs during the early phases of rifting events, in which direct links are assumed with melt generation by mantle plume upwellings beneath thinned lithosphere (e.g. Latin et al. 1993). Details of alkaline magmatism associated with extensional tectonics are available in Fitton and Upton (1987), Kampunzu and Lubala (1991) and Storey et al. (1992).

The classification of alkaline rocks is essentially based on alkali content (Na_2O and K_2O), and their saturation with respect to silica. For a comprehensive review of this rather difficult subject the reader is referred to Sørensen (1974). Alkaline rocks are commonly associated with central volcanoes, or form volcano-plutonic ring complexes, composed of saturated and unsaturated igneous rocks, or are exposed as small hypabyssal plugs, isolated or in clusters, or as small dyke swarms. Alkaline magmatism is rather peculiar for the following interrelated reasons. First, alkaline magmas are strongly enriched in incompatible elements, such as Ti, P, Y, Nb, Ba, K, Na, Rb, Sr, Th, U, F, REE; secondly, because of the high abundances of incompatible elements, alkaline rocks can be an important resource of Cu, REE, phosphate, Au and diamonds; thirdly, the products of alkaline magmatism are petrogenetically complex, a factor that has led to a plethora of confusing names. These features make

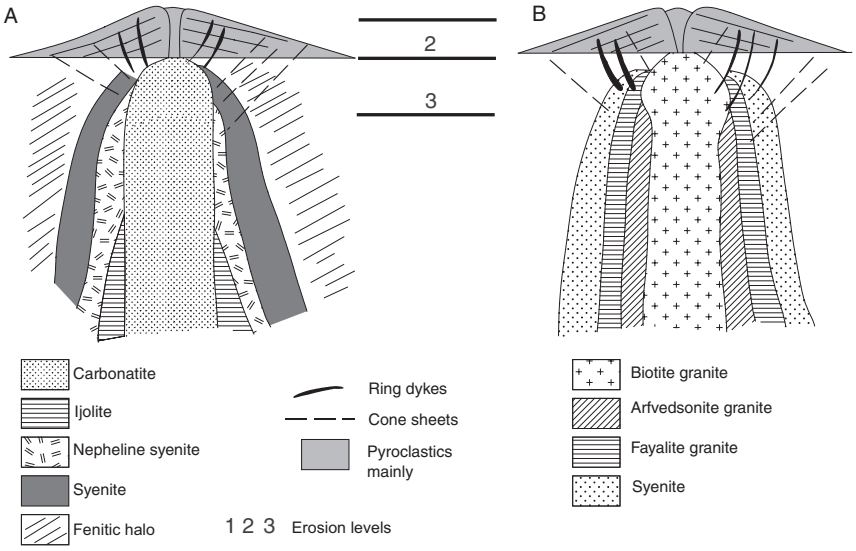


Fig. 4.30 Schematic cross-sections of alkaline ring complexes (**A**) carbonatite and undersaturated-type; and (**B**) alkaline granite and syenite-type. After Bowden (1985)

alkaline rocks disproportionately important in relation to their volume, which is very minor compared to other forms of magmatism (e.g. intraplate or subduction-related magmatism).

There is evidence that the source of continental rift alkaline magmas is metasomatised lithospheric mantle. Bailey (1983, 1987) pointed out that large quantities of CO_2, F and Cl are emitted from modern rifts such as the East African Rift System, suggesting that rifts are the sites of upwelling asthenospheric melts rich in Cl, F, C, P etc. These melts penetrate the lithosphere, metasomatising it and causing further partial melting and developing thermal anomalies. This phenomenon of mantle degassing and metasomatism, as envisaged by Bailey (1983, 1984, 1987), may also explain the origin of kimberlites and lamproites, which may be carriers of diamonds. It is probably for this reason that numerous breccia pipes, the expression of catastrophic volatile exsolution, are associated with alkaline magmatism. In some cases breccia pipes are nested, that is they are formed during a number of events. A special issue of Economic Geology (Sawkins and Sillitoe 1985) is devoted to mineralized breccias and breccia pipes.

A connection with mantle plumes is by no means certain, but it may be that thermal perturbation of anomalously hot mantle triggers melting, particularly in region of thinned or weakened lithosphere, even if these are a long distance away. A link with mantle plumes is invoked by a number of workers. For example, Ebinger and Sleep (1998), suggested that a mantle plume may focus its flow towards craton-mobile belt boundaries, where at depths of >150 km

small volumes of melt can be produced by decompression. The Late Jurassic-Early Cretaceous Damaraland alkaline igneous province in Namibia (discussed in Section 4.5.2.1), may have been linked to the Tristan da Cunha plume, from which the Paraná-Etendeka flood basalts were generated. The province may be due to lithospheric melting in response to the thermal perturbation caused by this plume (Ewart et al. 1998a, b). Ultrapotassic magmatism in the western USA has been linked to the Yellowstone plume (Edgar 1983). In other cases, as in Tibet and eastern China, alkaline volcanism appears to be related convective removal of lithospheric mantle, leading to extension and upwelling of asthenospheric mantle. The Tibetan alkaline (potassic) volcanic rocks were probably derived from a metasomatised subcontinental lithospheric mantle (see also Chapter 5; Arnaud et al. 1992).

4.5.1 Tectonic Settings, Ages and Controls of Intracontinental Alkaline Magmatism in Africa

Many examples of anorogenic magmatic systems are from Africa, mainly because this continent probably contains more alkaline complexes than anywhere else in the world, possibly because the African plate has been stationary for the past 65 million years (Burke 1996), and also for the reason that alkaline complexes in Africa locally well-studied (Kinnaird and Bowden 1987a; Black and Bowden 1985). A comprehensive volume on alkaline rocks and carbonatites in Africa is provided by Woolley (2001). In treating this topic I focus primarily on examples from southern Africa. Figure 4.31 shows the distribution of the alkaline complexes in Africa, including those in the Arabian shield prior to the opening of the Red Sea rift. The disposition of these complexes follows modern and ancient intraplate rift structures and other zones of lithospheric structural weakness, usually along the boundaries of cratonic provinces. Many of the complexes are arranged in broadly parallel linear groups, locally associated with dyke swarms, whilst others form clusters following en echelon structures.

African alkaline complexes span a very wide range of ages, from the 2050 Ma Palabora intrusion, through the 1350 Ma Pilanesberg (Ferguson 1973), the 500 Ma Kuboos-Bremem province (South Africa; Smithies and Marsh 1998), the Mesozoic and Neogene volcano-plutonic complexes in Nigeria, Angola and Namibia, to the modern volcanic centres along the East African Rift System.

Although there seems to be no specific pattern which can be related to the age of the complexes, there is a general grouping in the Proterozoic, early-mid Palaeozoic, the Mesozoic and the Cainozoic. There is also a pattern of migrating magmatism through time, at least in some instances. This is exemplified by the Aïr-Nigeria alkaline province in West Africa (Kinnaird and Bowden 1987b) (Fig. 4.31), where a southwesterly younging direction from the Cambrian to the Neogene is evident. This migrating magmatism is similar to that observed for

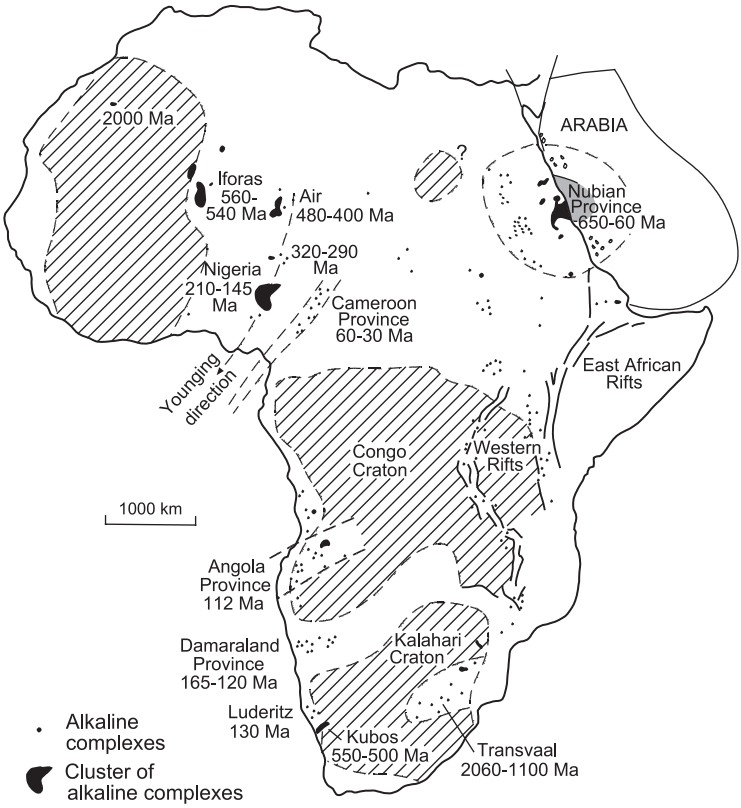


Fig. 4.31 Distribution of alkaline complexes in Africa, showing spatial relationship to crustal fractures and cratonic areas. After Black et al. (1985)

the Emperor Seamount chain in the Pacific Ocean, and it may be related to a hotspot trace, and therefore the movement of a lithospheric plate over a mantle plume. Many, if not most of the structures that are associated with the African alkaline complexes are ancient zones of lithospheric structural weakness, which have been repeatedly reactivated following a tectono-thermal event, such as the Panafrican. These structures may extend deep into the crust. Thus, several alkaline provinces are localised along crustal scale shear zones, along the margins of Archaean cratons, within Proterozoic mobile belts, and along reactivated zones of faulting and rifting.

Many alkaline magmas are mafic, rather than ultramafic, and in many cases, prolonged lithospheric and/or crustal residence time results in a wide range of rock types, including felsic derivatives. The rock types range from mafic to felsic and usually contain feldspathoids (e.g. nepheline, sodalite) and/or alkali-pyroxene and alkali-amphibole. The silica-oversaturated rocks (quartz-bearing) range

from monzonite to syenite, alkali-syenite and alkali-granite and volcanic equivalents. As mentioned earlier, nomenclature for the silica-undersaturated rock types (generally feldspathoid-bearing) is often confusing with many locality-based names.

The relationship between alkaline magmatism, thermal anomalies in the mantle and extensional tectonics has been mentioned above. Whether rifting is a passive or active process, the end result is thinning of the crust and upper lithosphere, which causes the asthenosphere to upwell. This may result in: (1) decompression melting of the rising asthenospheric mantle; (2) transfer of volatiles into the lower crustal regions; (3) melting of the lower crust due to the addition of heat through underplating, coupled with the possible effects of introduced volatiles. The amount of magma generated depends on the temperature of the upwelling mantle and the amount of thinning, which are also related to the rate of extension. High rates of extension (e.g. continental breakup) are commonly associated with voluminous production of basaltic magmas (continental flood basalts; CFB). Lower rates of extension (e.g. intracontinental rift/graben structures) result in lower degrees of partial melting, and more alkaline and silica-undersaturated magmas. It is common for alkaline complexes to consist of both silica-undersaturated and silica-oversaturated rocks, as is the case for many of the non-carbonatitic complexes of southern Africa. The relationship between these has long been a point of extensive debate. Two separate magma types have been invoked to explain the presence of silica-undersaturated and silica-oversaturated rocks in these complexes. The silica-oversaturated rocks have commonly been regarded as products of crustal, rather than mantle, melting (Smithies 1991). Isotopic evidence supports a mantle origin for the silica-undersaturated rocks, but does not always show the silica-oversaturated rocks to be of crustal derivation. Some processes of compositional evolution, both within and between different magma series, are illustrated by the wide range of rocks, as found for example in the Grootpenseiland and Marinkas Kwela complexes, of the Kuboos-Bremen Line, in southern Africa (Smithies and Marsh 1998).

4.5.2 Ore Systems of Alkaline Ring Complexes

Mineralisation in alkaline rocks is formed through at least three principal ore-forming processes, namely: (1)primary magmatic, in which the ore minerals are precipitated from residual fluids in the subsolidus range of temperature an pressure; (2) hydrothermal, from late-stage fluids evolved from (1) and their mixing with heated meteoric waters; hydrothermal mineralisation commonly overprints the primary magmatic; (2) supergene, usually developed in the weathering profiles of carbonatite in tropical climates and under conditions of high Eh and low pH. The mineralising fluids associated with alkaline complexes develop during the late stages of crystallisation and differentiation of the

melts. These late-stage fluids have an alkaline to peralkaline chemistry. Depending on the permeability of the country rocks (porosity, fractures, faults, shear zones), they are expelled from the cooling magma inducing metasomatic changes from a few hundred metres to several kilometres away from the complex (Pirajno 1992, 1994). Hydrothermal alteration related to alkaline complexes is dominated by alkali metasomatism, which in the specific case of alkaline complexes is also known as fenitisation (see Chapter 2 for details). The origin of mineral systems therefore, is related to the development, composition and evolution these late stage fluids, their interaction (and disequilibrium) with the wallrocks, and meteoric waters. Mineral systems of alkaline complexes occur in: (1) saturated-oversaturated complexes (Fig. 4.30A); and (2) undersaturated complexes (Fig. 4.30B). The saturated-oversaturated complexes tend to be enriched in Sn, W, U, Mo, Bi, As, Y, Li, Ta, Zr, La, Ce and Nb (pyrochlore), the undersaturated complexes in Sr, Ba, Th, Nb, Ti, Fe (magnetite) and P (apatite) (Pirajno 1994).

In Namibia, the Brandberg granitic complex has considerable resources of REE, Zr, Nb and Y. The Erongo volcanic complex contains W, Sn and U mineralisation associated with a late B-rich granitic ring dyke. The Okorusu carbonatite complex is characterised by intense brecciation and fenitisation of the wall rocks, which host veins and replacement bodies of fluorite, apatite and limonitic Fe ore. Ore reserves are estimated at 6 Mt averaging 56% CaF_2 and 0.5% P_2O_5 (Premoli 1993). Other carbonatite complexes (e.g. Kalkfeld) have disseminations and veins containing apatite, barite, monazite, strontianite, pyrochlore and pyrite (Pirajno 1994).

Carbonatites and associated alkaline complexes in the Indian subcontinent have abundant resources of P (apatite), Fe (hematite and magnetite), Nb-U (pyrochlore), F (fluorite), REE, Th, U and Ba (Krishnamurthy et al. 2000). Some of the Indian carbonatite-alkaline complexes are present within northeast-trending rift structures in the charnockite mobile belts in the south and east of the subcontinent, others are part of the Deccan continental flood basalt province. Here, the Amba Dongar carbonatite complex contains reserves of about 12 Mt of ore, with an average of 30% CaF_2, making it one of the largest fluorite deposits in the world (Krishnamurthy et al. 2000). A selection of these mineral systems is examined below.

Alkaline mafic-ultramafic ring complexes of Palaeozoic age are abundant in the Kola peninsula (NW Russia) and just across the international border in Finland, forming the Kola Alkaline Province (Kogarko et al. 1995).

Most important for economic mineral deposits in southern Africa are kimberlites, carbonatite and alkaline volcano-plutonic complexes. Carbonatites are especially significant because they constitute a major source of Nb, Zr, Ti, Th, Sr and REE. Table 4.3 shows some of the more important alkaline complexes in southern Africa known to contain significant mineral resources.

Table 4.3 Selected alkaline complexes in southern Africa known to contain significant mineral resources

Commodity	Locality and/or complex
Precious metals	Kruidfontein (2)
Cu and other base metals	Palabora (1), Glenover (1,3), Spitskop (1,3), Nooitgedacht (1,4), Ondurakorume (1)
Th, U	Palabora (1), Pilanesberg (4), Salpeterkop (1), Erongo (5), Brandberg (6)
Nb	Pilanesberg (1), Nooitgedacht (1,3), Glenover (1,3), Ondurakorume (1), Kalkfeld (1), Salpeterkop (1), Brandberg (6)
Ti	Goudini (1), Phalaborwa (1,3)
REE	Pilanesberg (1), Glenover (1), Ondurakorume (1), Palaborwa (1), Brandberg (6)
Sr	Ondurakorume (1)
Fe ore	Palabora (1), Kalkfeld (1,6), Okorusu (1,6)
Zr, Hf	Palabora (1), Tweerivier (1)
P (phosphate)	Palabora (1), Glenover (1), Schiel (3), Tweerivier (1), Spitskop (3), Dorowa (3), Kalkfeld (1,6), Ondurakorume (1,6), Okorusu (1,6)
W, Sn, U	Erongo (5)
F and Ba	Goudini (1), Kruidfontein (7,2), Okorusu (1,6), Pilanesberg (4), Erongo (5), Brandberg (6)

(1) Verwoerd (1966); (2) Pirajno et al. (1995); (3) Verwoerd (1986); (4) Lurie (1986); (5) Pirajno (1990); (6) Pirajno (1994); (7) Clarke (1989).

- Oversaturated complexes: Styles of mineralisation that characterise the deposits of saturated complexes include (Kinnaird and Bowden 1991): (a) pegmatitic pods (Be, U, topaz); (b) metasomatic disseminations in the roof zones of subvolcanic intrusions (Ta, Nb, Th, REE); (c) hydrothermal stockworks, veins and sheeted veins (Sn, W, Mo, Pb-Zn); (d) Greisen deposits (Sn, W, Bi). Alluvial and eluvial concentrations are not uncommon and are found around granitic cupolas unroofed by erosion (e.g. Spitzkoppe in Namibia, Pirajno 1994). In this section, I discuss the geology and mineralisation of the Erongo Volcanic Complex in the Damaraland province.
- Undersaturated complexes: Undersaturated complexes may occur associated with saturated ones. As mentioned above, carbonatites are by far the most important in terms of economic mineralisation. The main economic elements include: Cu, Fe, P, F, Ba, Nb, U, Sr, Au, Pb, Zn and REE. Styles of mineralisation are principally disseminations, late-stage replacement bodies, hydrothermal veins and lenses. Important deposits in southern Africa are the Palabora complex (Section 4.6.3), Glenover, Kruidfontein, Pilanesberg, Schiel (all in South Africa), Dorowa (Zimbabwe), Okorusu, Kalkfeld, Ondurakorume (Namibia). Epithermal-style deposits, including hot spring types, are known to occur in those alkaline complexes which are geologically young (e.g. Auas province and Regenstein diatreme complex in Namibia; Pirajno 1994), or those that are remarkably well-preserved such as the Kruidfontein Complex in South Africa, discussed below.

Some of the most common ore minerals, which occur in mineral deposits of alkaline rocks are: allanite (Ca, Al, Ce, Di, La silicate), apatite (CaF, $Ca_4(PO_4)_3$), fluorite (CaF_2), arsenopyrite (FeAsS), bastnaesite ($CeFCO_3$), britholite (complex Ce, P, Ca silicate-phosphate), vermiculite, cassiterite (SnO_2), chalcopyrite (CuS_2), columbite-tantalite (solution series of niobate-columbite and tantalate-tantalite), baddeleyite ($ZrHfO_2$), barite ($BaSO_4$), bismuthinite (Bi_2S_3), florencite (Ce phosphate), galena (PbS), gold (Au), ilmenite ($FeOTiO_2$), magnetite ($FeOFe_2O_3$), molybdenite (MoS_2), monazite [(Ce, La, Di)(PO_4)], pyrochlore (complex niobate), rutile (TiO_2), scheelite-powellite (Ca, $MoWO_4$), sphalerite (ZnS), thorite ($ThSiO_4$), topaz [$Al(F, OH)_2$ $AlSiO_4$], uraninite (La, Y, Pb, Th uranate), wolframite (Fe, $MnWO_4$), xenotime (YPO_4), yttrofluorite (Y-bearing fluorite), zircon ($ZrSiO_4$).

4.5.2.1 Carbonatites, Kimberlites and Lamproites

Carbonatite magmatism is a notable feature of the alkaline provinces of southern Africa (Fig. 4.31). The origin of carbonatite magma is controversial, and at the heart of the controversy is the relationship between carbonatites and the silica-undersaturated rocks with which they are commonly associated. Three main theories attempt to explain the origin of carbonatite:

- carbonatites evolve via crystal fractionation, at crustal pressures, of a mantle-derived alkali-rich silicate melt (Watkinson and Wyllie 1971);
- carbonatites are a direct result of melting of dolomite-peridotite within the mantle (e.g. Gittins 1989); and
- carbonatites are derived via immiscible separation of a liquid from an originally homogeneous carbonated silicate melt, the stage of separation determining the composition of both conjugate magmas (e.g. Le Bas 1989).

For a comprehensive work on carbonatites the reader is referred to Bell (1989). Special issues of the South African Journal of Geology (Verwoerd 1993) and the Journal of Petrology (Bell et al. 1998) are devoted to carbonatites magmatism. Harmer and Gittins (1998) presented isotopic (Pb, Sr, Nd) and experimental evidence to suggest that liquid immiscibility is unlikely in mantle melts and conclude that carbonatites derive from primary calcitic and dolomitic melts in the subcontinental lithospheric mantle. On the basis of isotopic and trace element analyses of peridotite xenoliths from the ocean islands of Western Samoa and Austral Islands, Hauri et al. (1993) suggested that carbonatitic melts may well be present in the source region of plume-related basalts. A study by Bell and Simonetti (1996), based on Nd, Pb and Sr isotopic systematics from Oldoinyo Lengai, a 2200 m high nephelinite-phonolite-carbonatite volcano in the East African Rift (northern Tanzania) support a mantle plume source. They envisaged that carbonatites and associated nephelinitic magmas are derived from a two-stage process, linked to a mantle plume. In the first stage, melts are generated directly from an upwelling mantle plume. Volatiles released from the plume itself cause intense metasomatism of the overlying lithosphere. In the second stage, low degrees of partial melting in the metasomatised

subcontinental lithosphere produce the carbonatite-nephelinite volcanic activity that characterises the Gregory Rift in East Africa.

Kimberlites and lamproites are volatile-rich, potassic and continental igneous rocks. Melnoites and monchiquites, also belong to this family of potassic rocks. Definitions, based on mineralogical, textural and geochemical criteria can be found in Mitchell (1989, 1995). These rocks are well known for being diamondiferous, although not all carry diamonds. For details of kimberlite and lamproite geology the reader should consult the two volumes on Kimberlites and Related Rocks (Ross et al. 1989) and the special issue of the Journal of Geochemical Exploration (Griffin 1995).

In southern Africa, all diamondiferous kimberlites are restricted to cratonic interiors, whereas in South Africa and Australia diamondiferous lamproites tend to occur along the margins of cratonic areas. An important distinguishing feature between kimberlites and lamproites is the morphology and nature of the pipes. An idealised (non-eroded) kimberlite is characterised by a pyroclastic apron forming a small crater infilled with sediments. In contrast, lamproites have a pyroclastic crater filled with lavas. Lamproites and kimberlites can also be distinguished on the basis of their TiO_2 and Zr contents, with the former having higher TiO_2 and Zr. Kimberlites are grouped into two subsets, group I and group II, both of which may or may not be diamondiferous. Group I kimberlites are micaceous, and relative to non-micaceous Group II, are depleted in incompatible elements.

Lamproites and Group II kimberlites originate from within metasomatised subcontinental lithosphere, at depths of approximately 200 km, whereas Group I kimberlites have their beginnings in a highly enriched and asthenospheric metasomatised upper mantle, from depths greater than 200 km. Diamonds in kimberlites are known to be more than 2 Ga old. They are passengers ripped out from near the base of the lithosphere during ascent of the volatile-rich melts. Major kimberlite events are recorded at 1.1 Ga, 440–410 Ma, 250–320 Ma, 200 Ma, 80–120 Ma and 50 Ma (Haggerty 1997). Many of the southern African kimberlites were emplaced during the 80–120 Ma event (Cretaceous). Based on this, White (1997) suggested that a thermal perturbation brought about by a mantle plume supplied the necessary heat and volatiles, to trigger partial melting. Haggerty (1997) pointed out that diamondiferous kimberlites (and perhaps also lamproites) are not related to arc, rift or collision settings, and therefore their heat sources must be sought in thermal anomalies in the mantle beneath continents. Haggerty (1997) favoured a mantle plume origin for these unusual igneous rocks. The origin of lamproites may involve a subduction component for their volatile content, which would explain their restriction to cratonic margins.

4.5.2.2 The Damaraland Alkaline Province, Namibia

In Namibia, alkaline complexes include a wide variety of types, such as plugs, pipes, dykes, subvolcanic intrusions and large ring complexes (Pirajno 1994). The Namibian complexes are distributed in well-defined provinces that tend to

be aligned along east-northeast trends that are probably related to pre-existing crustal zones of weakness (Figs. 4.32 and 4.33).

In this section, I examine the Damaraland alkaline province, which is one of the largest and best known and is also important from the point of view of mineral resources. The Damaraland province (Figs. 4.32 and 4.33) extends for approximately 350 km from the Atlantic coast, in a general northeast direction towards the interior. The province contains at least 21 complexes, ranging from granitic through layered basic complexes and carbonatite to peralkaline types. Recent age determinations, based on Rb-Sr and $^{40}Ar/^{39}Ar$ systems, indicate that the Damaraland complexes were emplaced between 137 and 124 Ma (Milner et al. 1995; Verwoerd et al. 2000; Pirajno et al. 2000; Wigand et al. 2004). The complexes are closely associated with the early Cretaceous Paraná-Etendeka continental flood basalt (CFB) province, the opening of the South Atlantic Ocean and have been linked with the Tristan da Cunha mantle plume (Ewart et al. 1998a; Trumbull et al. 2004). Several of the Damaraland complexes are silicic (>67% SiO_2) and have characteristics typical of A-type magmatism (Trumbull et al. 2004). One of the best studied of the Damaraland alkaline complexes is the Messum Igneous Complex, also known as Messum crater, for which a connection with the Etendeka CFB is well-established

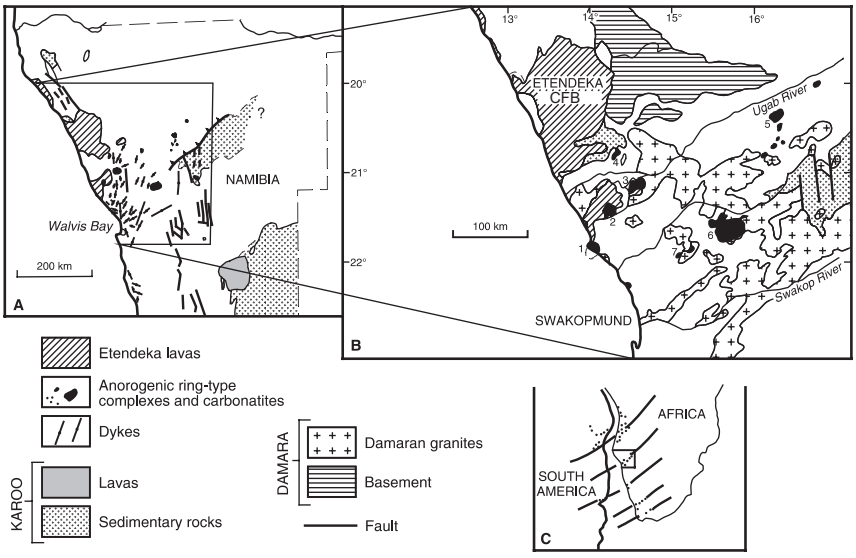


Fig. 4.32 (**A**) Schematic illustration showing distribution of Etendeka and Karoo CFBs and associated dyke swarms in north-central Namibia; (**B**) Distribution of Etendeka lavas and associated anorogenic ring-type alkaline complexes and carbonatites; selected complexes named in this figure are 1 Cape Cross, 2 Messum, 3 Brandberg, 4 Doros, 5 Paresis, 6 Erongo and 7 Spitzkop; (**C**) Relationship of alkaline complexes in southwestern Africa and the east coast of South America to transform directions (after Marsh 1973)

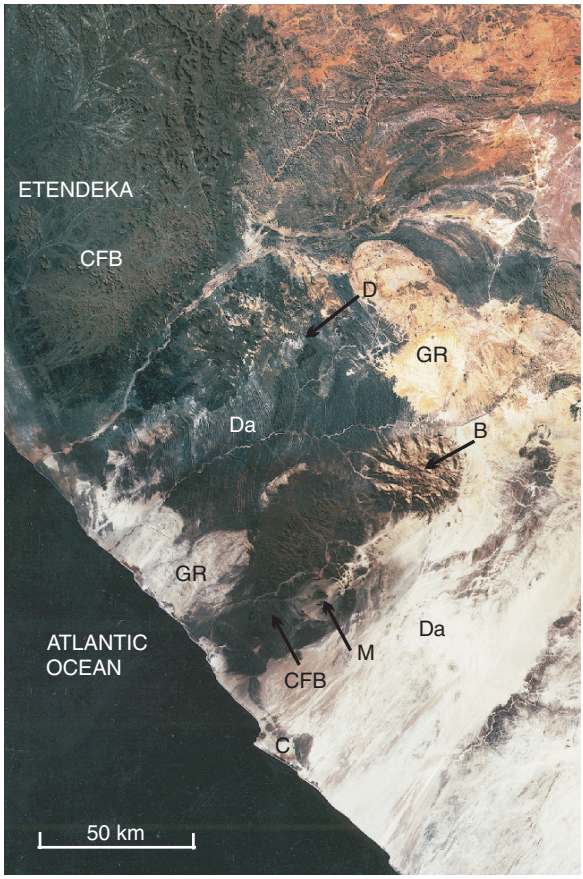


Fig. 4.33 Composite of Landsat images covering a portion of northwestern Namibia. This composite image clearly shows the three major igneous events in the region: 1 intrusions of granitic plutons (GR) into rocks of the rift-related Damara Sequence (Da), 2 the Etendeka CFBs and 3 the alkaline ring complexes (B Brandberg, M Messum, D Doros, C Cape Cross. View this figure together with Fig. 4.31

(Ewart et al. 1998a, b). This complex forms a well-defined circular structure, approximately 18 km in diameter, with the outer ridges and early magmatic phase consisting of basaltic rocks, intruded by xenolith-rich granitic veins and dykes. The central parts, or core of the complex are characterised by volcanic breccias and rhyolitic lava domes, that are in turn intruded by microsyenite, dolerite and granite. Other intrusions in the complex are various bodies and sheets of diorite, monzonite, quartz-syenite and granitic rocks with abundant mafic enclaves (Ewart et al. 1998a). The Messum Igneous Complex was emplaced through a succession of quartz latite and basalts of the Etendeka Group (Milner et al. 1995), forming in the Messum area the Goboboseb Mountains (Ewart et al. 1998a). Strong Na and K metasomatism and silicification affects the Messum rocks, and it was suggested by Korn and Martin (1954) that some of the syenitic rocks may be entirely of metasomatic origin. These authors also recognised a carbonatite vein in the core of the complex. The mafic

lavas of the Goboboseb Mountains and the Messum complex are characterised by two series that are similar to the low-Ti and -Zr basalts of the Etendeka CFB to the north, but distinguished by their higher and lower Ti/Zr ratios. Because of this, Ewart et al. (1998a) divide the lavas into higher Ti/Zr, and lower Ti/Zr. The former lavas (olivine + clinopyroxene) are more magnesian than the latter (clinopyroxene-dominant + FeTi oxides), and are considered to be mantle plume melts. The lower Ti/Zr lavas, on the other hand, show evidence of fractionation and have arc-like geochemical signature, which may be indicative of crustal contamination. Other complexes of the Damaraland province are: the Okonjenja, a well-exposed ring structure, rising about 1000 m above the surrounding country, and containing a tholeiitic suite (e.g. layered gabbros) and rocks of an alkaline series arranged in three concentrically arranged rings; the Paresis Igneous Complex, of dominantly peralkaline composition (Pirajno et al. 2000); the Brandberg alkaline complex, some 26 km in diameter and the highest mountain in Namibia (ca. 2600 m above sea-level) and characterised by arfvedsonite-granite with U-Th, REE and F mineralisation, fayalite-hedenbergite, edenite-biotite-granite, and variably metasomatised hornblende granite; the Erongo Volcanic Complex, the largest of the Namibian complexes, and a well-preserved volcano-plutonic caldera structure (Pirajno 1990; Pirajno et al. 2000), associated with Sn, W and U mineralisation. I return to discuss the Erongo complex more fully below.

At least six carbonatite complexes belong to the Damaraland province: Okorusu, Kalkfeld, Ondurakorume, Osongombo, Kwaggspan and Otjisazu (Pirajno 1994). Of these the Okorusu, is formed by a number of concentric intrusions of carbonatite, syenite, foyaite, ijolite and tinguaite. The country metasedimentary rocks are strongly fenitised around the carbonatite, and are also mineralised with fluorite.

4.5.2.2.1 The Erongo Volcanic Complex

The Erongo Volcanic Complex (EVC) is a well-preserved caldera structure, surrounded by a granitic ring dyke and a mafic cone sheet (Fig. 4.34). The EVC is the largest of the Damaran alkaline ring complexes, with the caldera structure having a diameter of approximately 30 km, but if the cone sheet is included the diameter is more than 50 km. The geology of the Complex was described in detail by Pirajno (1990) and Pirajno et al. (2000).

The EVC is emplaced through a basement of fault-bounded blocks of granitic rocks and metasedimentary rocks of the Swakop Group (Damaran Orogen). The EVC magmatism is characterised by two phases: (1) an early mafic phase, which consists of a succession of tholeiitic lavas, dykes and the above-mentioned cone sheet; and (2) a later felsic phase, which consists of pyroclastic flows of dacitic to rhyolitic composition. A first estimate of the age of the EVC was a whole-rock Rb-Sr isochron from a sample of ring dyke granite (Erongo Granite), which yielded an age of 143.6 ± 2 Ma (Late Jurassic;

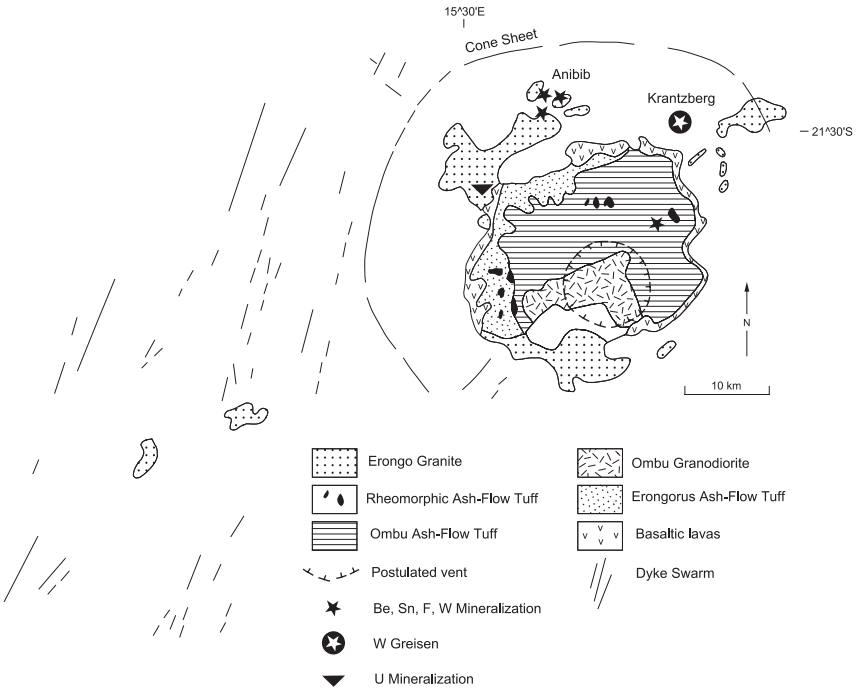


Fig. 4.34 Simplified geology of the Erongo Volcanic Complex and distribution of mineral deposits and occurrences. After Pirajno (1990)

McNeill 1989). Our new U-Pb SHRIMP dating of zircons from the Ombu Ash Flow Tuff (OAFT) yielded a mean age of 135.3 $\pm$ 3.2 (1σ) Ma.

The early mafic phase is the result of voluminous effusions of tholeiitic lavas, which formed a platform, whose areal extent may have been much greater than the present-day distribution and could be part of the Etendeka CFB. This is suggested by the presence of the Krantzberg lava outlier to the northeast, which is spatially associated with greisen style mineralisation. The thickness of the lava succession is between 200 and 300 m and on this lava pile, the subsequent felsic volcanic products accumulated. The feeders of these lavas may have been the cone sheet and a number of radial dykes that outcrop to the south and the northeast of the caldera. In addition, a swarm of north-trending mafic dykes cut through the Damaran basement to the west of the EVC (Fig. 4.34). In the upper parts of the lava pile, the composition becomes trachytic and the lavas become intercalated with the earliest pyroclastic units, suggesting that these uppermost trachyitic lava flows heralded a change in the composition of the magma towards a more felsic type.

Rocks of the felsic phase are dominated by voluminous pyroclastic deposits, which based on stratigraphic, petrographic and geochemical evidence can be

subdivided into three distinct sequences (Pirajno 1990). From oldest to youngest, they are: Erongorus ash-flow tuff (EAFT), Ombu ash-flow tuff (OAFT) and rheomorphic rhyolitic rocks (RHEOR). The EAFT rocks represent the first explosive event of the Erongo Complex, characterised by having only juvenile material, no lithics, abundant vesicles and lithophysae. The thickness of the EAFT sequence is estimated at between 200 and 370 m, and the composition ranges from andesitic in the lower levels to rhyodacitic at the top. The OAFT is volumetrically the major rock type of the EVC, reaching a thickness of at least 500 m. In the east, northeast and southeast the OAFT rests on the basal tholeiitic lavas, whereas in the central and western areas it overlies the EAFT. OAFT rocks are characterised by having abundant crystal and lithic fragments and have compositions ranging from dacitic to rhyodacitic. RHEOR rocks form isolated outliers that generally overlie EAFT and OAFT units. Field relationships, however, indicate that the RHEOR were emplaced on a rugged topography, most probably the outer slopes of the volcanic edifice, which were cut by deep valleys. RHEOR rocks have a rhyolitic composition and are characterised by fine laminations, interpreted as due to flowage. Tourmaline is present as fine overgrowths and along microfractures. The presence of tourmaline in the RHEOR rocks and their chemistry suggest that they may be genetically related to the tourmaline-rich Erongo Granite.

Subvolcanic rocks of the EVC include the Ombu Granodiorite and the Erongo Granite. The Ombu Granodiorite is in the south-central EVC, where it is expressed as a topographic depression. The Ombu Granodiorite is a coarse to fine-grained monzogranite to granodiorite rock, charged with numerous xenoliths of the same nature as the lithic fragments in the OAFT. On the basis of field relationships, geochemical and petrographic data, the Ombu Granodiorite is the subvolcanic equivalent of the OAFT rocks (Pirajno 1990). The topographic depression that the granodiorite occupies is interpreted as the outline of the vent through which the felsic phase of the EVC erupted. The Ombu Granodiorite locally exhibits hydrothermal alteration, of which two trends can be recognised: potassic (K-feldspar + biotite) and phyllic-propylitic (sericite + chlorite + tourmaline). The Erongo Granite forms plutons distributed between the ring dyke and the caldera structure. The plutons are interpreted to represent the remnants of a ring dyke. The main rock type is a coarse-grained biotite granite, containing abundant topaz and tourmaline, minor apatite and fluorite. Geochemical analyses of Erongo Granite indicate a A/CNK (defined as $Al_2O_3/CaO + Na_2O + K_2O$ mol. Wt%) ratio of between 1.08 and 1.17 and is therefore peraluminous.

A prominent feature of the Erongo Granite is the presence of disseminated quartz-tourmaline nests, up to 30 cm in diameter, veins and stringers, all of which tend to increase in intensity and to coalesce towards the upper parts of the plutons. In addition to tourmaline and quartz, the nests also contain topaz, fluorite, apatite and cassiterite. Quartz-tourmaline breccias and dyke-like bodies cut through and locally replace the country rocks of the Central Zone of the Damara orogen that surround the EVC. In the northeast of the EVC,

lamprophyre dykes crop out and converge towards a cluster of small (up to 100 m in diameter), undersaturated mafic plugs. This area is coincident with a positive gravity anomaly.

The EVC contains deposits and occurrences of W–F–Sn, W, Be, Sn, F, and U, all of which are spatially and genetically related to the Erongo Granite. The distribution of the principal deposits is shown in Fig. 4.34.

Beryllium and Sn mineralisation, hosted by a quartz-albite rock containing numerous tourmaline veins and nests, is present in the north of the EVC. This mineralisation is associated with quartz-muscovite (greisen) alteration containing minor cassiterite disseminations. Drusy pegmatitic pods with crystals of beryl and tourmaline are also present. The quartz-albite rock is probably an alteration zone in a high level (cupola) facies of the Erongo Granite. Rocks around the mineralised locality are brecciated and are cut by veins of tourmaline, attesting to hydraulic fracturing induced by B-rich fluids. About 1 km west of the Be–Sn occurrence, a northwest-trending, 50 m long mineralised fracture in Damaran granite contains a core of quartz-sericite with symmetrical bands of quartz-tourmaline rock. Wolframite is present within the quartz-sericite material. To northwest of the EVC, along the contact zone between Erongo granite and Damaran granitic rocks, there is a zone of intense brecciation and tourmalinisation associated with albitisation. This area contains Sn (cassiterite), W (unknown mineral phase) and fluorite mineralisation. Low-grade U mineralisation is present in the Erongo Granite, particularly in the northwest and southwestern areas. Secondary U minerals are associated with jointing in areas of primary U enrichment. It is probable that this mineralisation is due to oxidising meteoric waters that have leached U from the fresh Erongo granite rock in areas of high permeability due to close-spaced jointing.

The old Krantzberg W–F–Sn deposit was a major tungsten producer in Namibia. Mining operations ceased in 1979 and subsequent exploration did not define economically feasible grades and tonnages. Mineralisation at Krantzberg consists of W (ferberite), F (fluorite), minor Sn (cassiterite), Mo, Fe, and Cu sulphides. This mineralisation is hosted in replacement-type greisen rocks and quartz-tourmaline breccias. The style of the Krantzberg deposit is shown in Fig. 4.35. The Krantzberg is a prominent hill of rocks of the Swakop Group that was protected from erosion by an overlying cap of clastic sedimentary rocks of Karoo age, and an outlier of EVC basaltic rocks (Figs. 4.34 and 4.35). There are three main zones of alteration-mineralisation, all formed by the pervasive greisenisation of Damaran granites. The Krantzberg greisen alteration is interpreted to be the result of acid fluids that emanated from the subsurface apical portions of fractionated Erongo granite cupolas. The mineralising fluids were also B- and F-rich and induced extensive selective replacement of pre-existing granite lithologies by quartz, sericite, topaz, and tourmaline. Late-stage veins contain ore minerals such as ferberite, scheelite, and minor sulphides.

Breccia pipes on the southeastern slopes of the Krantzberg contain fragments of volcanic rocks cemented by quartz and tourmaline. Cassiterite occurs

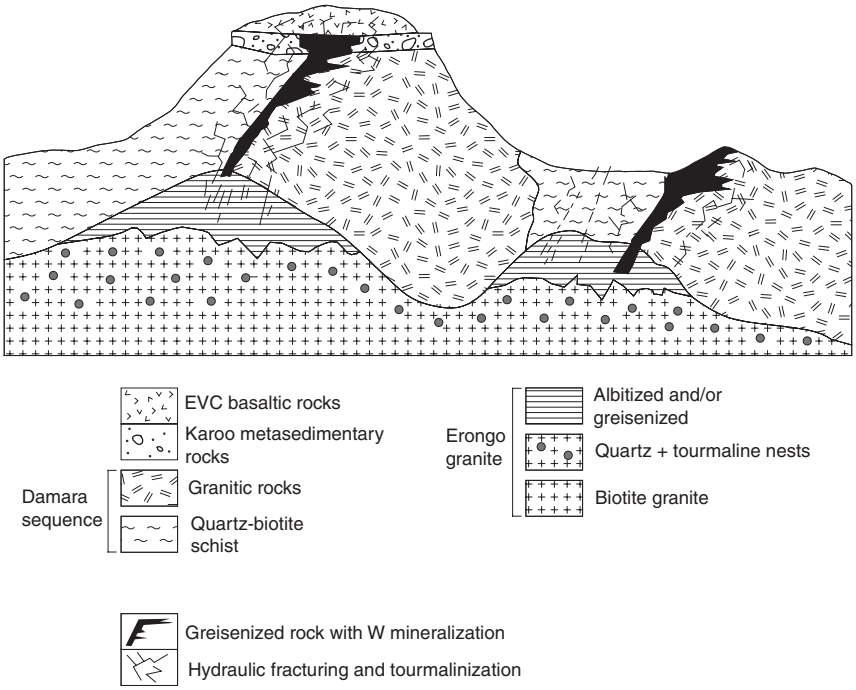


Fig. 4.35 Schematic cross-section of the Krantzberg greisen-stylle W deposits (not to scale). After Pirajno et al. (2000)

as fine disseminations or as patches along the periphery of the breccia bodies. These breccias are interpreted as a type of hydraulic fracturing due to streaming of B-rich fluids.

4.5.2.3 Mineralisation in Ring Complexes of the Ijolite-Carbonatite Association

Undersaturated alkaline ring complexes are commonly associated with a core of carbonatite rocks (Fig. 4.30). At least four types are recognised (Le Bas 1977): (1) calcite-carbonatite (coarse-grained varieties are known as sovites); (2) dolomite-carbonatite or berfosite; (3) ferrocarbonatite (ankerite-rich); (4) natrocarbonatite (mainly Na-Ca-K carbonates). Carbonatites usually occur as small plug-like bodies, or as dykes, veins, cone sheets and lavas. That they are of igneous origin is without doubt because they have been observed to occur as lava flows (eruptions of Oldoinyo Lengai in Tanzania). In general, carbonatite complexes show a sequence of nephelinite through ijolite to carbonatite (see Fig. 4.30A). The parental carbonatite magma is thought to exsolve out of a phonolitic-nephelinitic melt by liquid immiscibility (Bowden 1985). Alkali metasomatism is therefore instrumental in the production of carbonatites and

their contained mineralisation. This mineralisation, however, usually evolves into epithermal systems during the late stages of the magmatic activity. Thus, processes of alkali metasomatism are followed in a continuously evolving system by hydrothermal activity with the development of low-temperature (epithermal) aqueous fluids producing vein-type mineralisation along fractures.

Mineralisation in carbonatite complexes (see Bowden 1985 for a review and Mariano 1989a) include Ti (perovskite, ilmenite), Zr (zircon), Ba (barite), F (fluorite), P (apatite), Th and U (e.g. uranothorianite), as well as a range of REE minerals such as bastanaesite ($REE(CO_3)F$), britholite [$(REE, Ca)_5 (SiO_4, PO_4)_3$ (OH, F)], ancylite [$(SrCe(CO_3)_2(OH)H_2O)$], parasite [$(REE)_2Ca(CO_3)F_2$], synchisite [$(REECa(CO_3)_2F)$] and monazite. They can also be an important source of Al (nepheline-rich rocks) and, less commonly, Cu, Pb, Zn, Mo and Cu. Carbonatites are also enriched in LREE (light rare earth minerals). There are, according to Bowden (1985), two main associations: (1) apatite-magnetite usually related to sovites and also containing pyrochlore, and (2) REE association with late-stage enrichments of barite, usually found in ankeritic rocks, without magnetite and pyrochlore. REE mineralisation in carbonatite complexes is formed from hydrothermal fluids. Commonly associated with carbonatite complexes are hot springs from which fluids are discharged that are enriched in Ba, F, Sr, REE and Th (Mariano 1989a). Hydrothermal mineralisation of carbonatites is generally in veinlets, open space fillings and as fine-grained disseminations. Alkaline complexes and carbonatite are also a major source of Nb, mostly in the form of pyrochlore, which occurs as disseminations and veins in the carbonatite rocks. Apatite is another important mineral phase of ring complexes of the ijolites-carbonatite association, where in some cases the apatite content can exceed 50% by volume. In the Kola peninsula, the Salmagorskii mafic-ultramafic and ijiolite-carbonatite ring complex is unusual in that, as for Palabora (Section 4.6.3), it contains Cu sulphide mineralisation (Korobeinikov et al. 1998).

Supergene REE mineralisation forms where the carbonatites are subjected to chemical weathering (Mariano 1989b). Carbonate minerals are easily dissolved, with Ca and Mg removed resulting in the residual enrichment of the less mobile elements. The Araxá carbonatite (Minas Gerais, Brazil) is a Cretaceous alkaline ring complex of approximately 4.5 km in diameter, which was deeply weathered and has strong residual enrichement. This enrichement forms a laterite deposit reported to contain ca. 0.8 Mt of 13.5% REO, and 460 Mt of 3% Nb_2O_3 (Mariano 1989a). In Western Australia, the 2064 Ma Mount Weld carbonatite, which intrudes Archaean granite-greenstone rocks of the Eastern Goldfields in the Yilgarn Craton, has considerable resources in the overlying regolith, with 250 Mt at 18% P_2O_5 and 270 Mt at 0.9% Nb_2O_5 and 145 Mt at 0.034% Ta_2O_5 (Duncan and Willett 1990; Duncan 1992).

Good examples of carbonatite complex-related mineralisation can be found in the USA (Mountain Pass), in Brazil (Goiás, Tapira and the above-mentioned Araxá), in India (Amba Dongar) and in Namibia (Okorusu) and South Africa. For references on these deposits and reviews the interested reader can consult

Mariano (1989a) and Woolley (2001). Here I discuss selected South African examples from the Bushveld province and in Section 4.6.3 the Palabora carbonatite complex.

4.5.2.3.1 The Bushveld Province, South Africa

A number of undersaturated, alkali and carbonatite complexes of Mid Proterozoic age (about 1.4 Ga) intrude rocks of the Transvaal basin and Bushveld Igneous Complex (Fig. 4.36). These complexes are concentrated in the central and western areas of the Bushveld Complex-Transvaal basin and their emplacement may have been controlled by a number of northwest-, northeast- and north-northeast-trending, intersecting lineaments or fracture zones. Crocker et al. (1988) published a review dealing specifically with the fluorite resources of the complexes, but also providing the only comprehensive treatise on the associated mineral commodities. It is from their work that most of the information given here is taken. These authors distinguish mineral deposits in alkali complexes (Pilanesberg, Pienaars), and those occurring in carbonatites (Kruidfontein, Goudini and Glenover). In terms of ore type they distinguish the following associations: (1) fluorite-apatite ores of the magmatic-pegmatitic stage; (2) fluorite-apatite-carbonate ores transitional between the magmatic and hydrothermal stages; (3) fluorite-carbonate, fluorite-barite and monomineralic fluorite of hydrothermal vein type. The first and in part, second associations are essentially related to alkali metasomatism and are hence dealt with in this section. The third type of ore association is clearly related to late epithermal activity that resulted in the development of hydrothermal convection cells and the deposition of quartz vein material, with open space fillings of barite, fluorite and sulphide mineralisation. No apatite is present in this type of mineralisation.

The Pilanesberg Complex, which intrudes the western lobe of the Bushveld Igneous Complex, consists of a central zone of white and red foyaite, surrounded by concentric zones of lavas and pyroclastics, followed by a ring of red syenite. Within the Complex there are more than a dozen mineral occurrences, one of which is the Whydhoek deposit containing fluorite and apatite. This mineralisation is associated with coarse-grained (pegmatitic) K-feldspar and aegirine, and is contained in a cylindrical zone developed at the contact between pyroclastics and the red foyaite. In one place the ore is distinctly zoned with an inner fluorite-apatite-aegirine assemblage and an outer pegmatitic apatite-aegirine assemblage. The ore is composed of approximately 40–60% fluorite and 20–30% apatite, with traces of sulphides. In other places fluorite can be seen to occur as an interstitial constituent between the laths of orthoclase in coarse-grained foyaite. Based on textural evidence, Crocker et al. (1988) considered that the fluorite may have crystallised from a low-temperature magmatic melt. Mineralisation of the fluorite-apatite-carbonate association is present at a number of localities. This mineralisation is characterised by lenses, stringers, veinlets and breccia dykes (or tuffisites, thought to be the result of gas streaming). Carbonate minerals are dolomite and calcite. The Pilanesberg

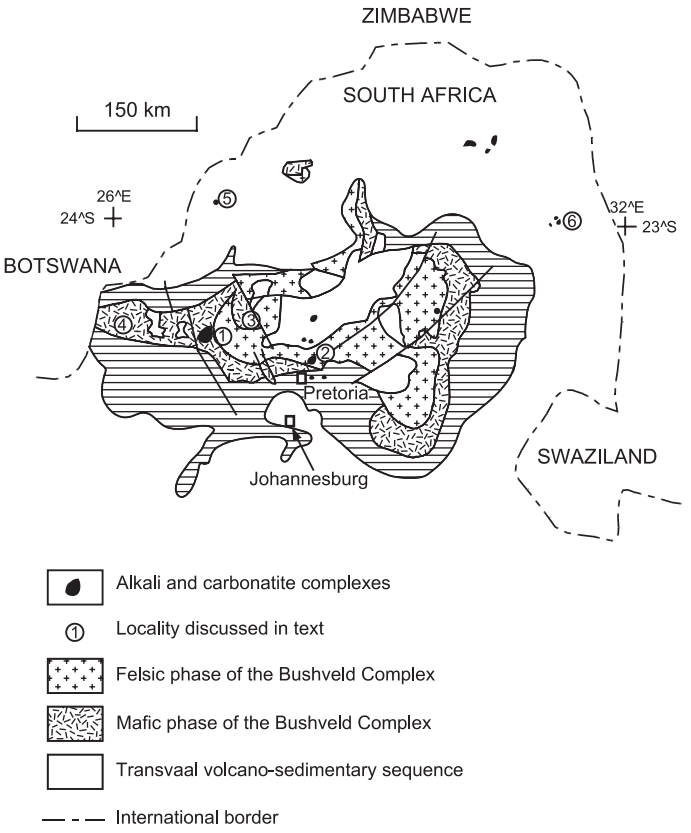


Fig. 4.36 Distribution of alkaline and carbonatite complexes in northern South Africa and in the area of the Bushveld Igneous Complex. Numbered localities are 1 Pilanesberg; 2 Pienars River; 3 Kruidfontein (discussed in text); 4 Goudini; 5 Glenover; 6 Palabora. After Pirajno (1992)

Complex also contains REE mineralisation in the form of the primary mineral britholite. This mineralisation occurs in veins along the contact between a tinguaite ring dyke and a foyaite. The latter also contains disseminated ore. Analysis of concentrates gave 1.56% ThO_2, 0.02% U_3O_8, and 58% of REE oxides (mainly Ce, La, Nd and Pr) (Coetzee 1976).

The Pienaars River Complex is formed by trachytic rocks, various pyroclastic units, syenites, foyaites, phonolites and some minor carbonatite. These rocks are subdivided into three suites, namely: Roodeplaat, Leeuwfontein and Franspoort. Several mineral occurrences are present mostly within the trachytic rocks. At one locality (Wallmannsthal) the mineralisation consists of intergrown fluorite and apatite with minor disseminated pyrite and chalcopyrite; at another, lenses of fluorite-apatite mineralisation are present (Zeekoegat). They are associated with an intrusive foyaite plug emplaced into a quartzite,

which as a result was brecciated and alkali-metasomatised with development of orthoclase laths. The fluorite-apatite mineralisation occurs as interstitial grains and clusters up to a few centimetres in size, within the foyaitic rock, which is composed of orthoclase and nepheline set in a matrix of feldspars and amphiboles. In the quartzite rock the fluorite-apatite occurs along the edges of the brecciated fragments.

Other carbonatite complexes studied by Crocker and coworkers are the Goudini Volcano and the Glenover carbonatite complex. In both these complexes metaberfosite rocks are present as a result of strong carbonatitic and alkali metasomatism. In the Goudini volcano metaberfosite contains albite, ankerite and aegirine with subordinate apatite and pyrite. The Glenover complex has apatite-bearing biotite-pyroxenite as well as berfosite-containing fluorite, barite, ankerite, dolomite, calcite, hematite and pyrite. In one area of the Glenover complex, within the alkali-metasomatic zone, are dykes of fluidised material containing fluorite, apatite and ferric hydrates. This fluidisation is thought to have occurred as a result of degassing along fissures from the underlying magma.

The Kruidfontein Carbonatite Complex (KVC) is a remarkably well-preserved Mid-Proterozoic caldera structure of approximately 5 km diameter. A simplified geological map of the KVC is shown in Fig. 4.37. The volcanic history of the complex consists of two main eruptive episodes. An earlier episode was dominated by undersaturated silicate lavas and pyroclastics, whereas a later episode was characterised by carbonatitic volcanism. Thus, the KVC consists of an outer ring, approximately defining the caldera structure, containing variably altered and metasomatised silicate lavas and pyroclastics that were probably erupted from a central vent. Phonolitic and nephelinitic rocks are recognised within this outer zone. An inner ring contains carbonatitic pyroclastic products, including bedded tuffs, ash-flow tuffs and vent breccias. The bedded tuffs are interpreted as air-fall, water-lain and surge deposits (Clarke 1989; Clarke and Le Bas 1990; Pirajno et al. 1995). The carbonatite pyroclastics generally have geochemical compositions similar to the intrusive carbonatites, although some have undergone recrystallisation and ankeritic alteration. It is worthy of note that the ankerites have high Mn contents (up to 3.6%; Clarke 1989). Carbonatite plugs and dykes intrude the central portions of the inner ring. Clarke (1989) classified the KVC carbonatites into three types: sovite (coarse-grained), alvikite (medium- to fine-grained) and fluorite-rich carbonatite.

The fresh KVC carbonatites, as seen in drillcores, are generally fine-grained, grey to brown in colour, and composed of ferroan calcite (approx. 60–70%), fluorite (approx. 10–30%), hematite, pyrite and chalcopyrite (approx. 5–10%) (Clarke 1989; Pirajno et al. 1995). An important feature of the KVC is the presence of an almost monomineralic K-feldspar-rich rock (orthoclasite of Clarke 1989). This is interpreted as the product of K-metasomatism (fenitisation) of pre-existing silicate rocks, which resulted in the development of the characteristically brick-red, orthoclasite and/or microclinite rock. Evidence of hot spring activity is indicated by the occurrence of siliceous and Fe-rich sinter

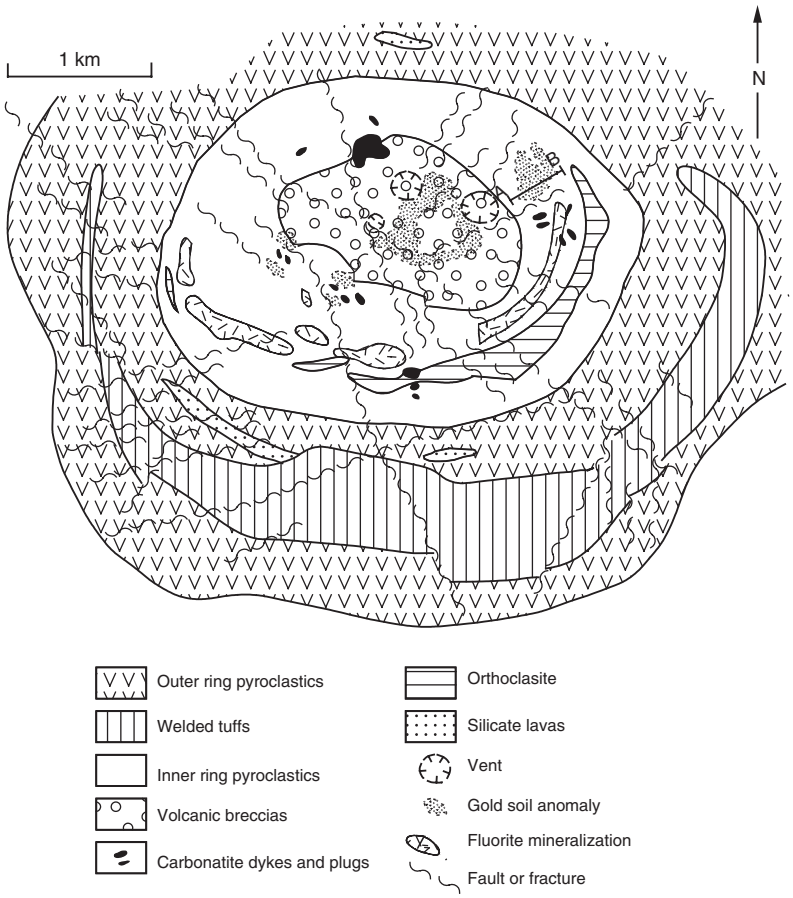


Fig. 4.37 Simplified geology of the Kruidfontein Complex (modified after Clark 1989)

material at two localities in the inner ring. Zones of disseminated fluorite are possibly associated with ring faults. This fluorite mineralisation was formed during a late-stage hydrothermal event (Crocker et al. 1988; Clarke 1989). At least three types of fluorite mineralisation are present: (1) primary fluorite, forming disseminated grains in the sovite rocks, and reaching average grades of about 20% CaF_2; (2) secondary fluorite mineralisation is present as replacement bodies in the metaberfosite rocks, where it may reach concentrations of up to 60% CaF_2; and (3) quartz-fluorite veins and fissure fillings. Ore-grade (up to 3.8 g/t) and anomalous Au occur in the weathered carbonatitic pyroclastics within the inner ring of the KVC close to vent areas and is bound by north-trending and east-northeast-trending faults (Fig. 4.37). It can therefore be assumed that the mineralisation has a structural control. In an attempt to explain the KVC gold mineralisation Pirajno et al. (1995) considered two

genetic models: (1) a supergene origin and (2) a hypogene-hydrothermal origin for the mineralising fluids.

In the supergene model, the oxidised zone is interpreted as a lateritic profile. This consists of a surficial ferruginous zone (up to 25 m), a Fe- and Mn-rich oxide zone (25–50 m), mottled clay zone and ferruginous saprolite (50–77 m) and saprolite to about 150 m. Gold, Mn, and Y behave sympathetically and are concentrated in the upper 80 m of the profile. This distribution resembles the accumulation of Au seen in the upper horizons of lateritic profiles in humid tropical environments in which gold is closely associated with Fe and, locally, Mn oxides (e.g. Santosh and Omana 1991; Gray et al. 1992). However, the thickness of the zone of Au enrichment is far greater than reported elsewhere. Lateritic ferruginous zones are rarely more than 5–15 m thick, even in profiles developed on carbonatites, and the Au enrichment is commonly confined to this zone and the immediately underlying mottled clay horizon, again only a few metres thick. It possible that the greater thickness of the ferruginous zones (laterite and mottled zone) at Kruidfontein is due to the unusually ferruginous parent lithology, but this does not necessarily explain the enrichment of Au. Lateritic supergene enrichment implies secondary accumulation of Au from a precursor similar to that of the underlying fresh carbonatites. Such enrichment, together with any vertical or lateral dispersion, is by both physical and chemical mechanisms. Two considerations are important. Firstly, what mechanisms are involved and, secondly, whether the precursor is a suitable protore.

Particulate Au accumulates residually, as other rock components are removed in solution, and may be dispersed laterally, by sheetwash or minor solifluction, and vertically by illuviation and bioturbation. Near-surface leaching of Au, and its reprecipitation with Fe oxides is a common feature of lateritic profiles (Davy and El-Ansary 1986; Enzweiler and Joekes 1990; Benedetti et al. 1990). Such mobility is considered to be the result of complexation by ligands derived from the breakdown of organic matter (Gray et al. 1992; Bowell et al. 1993), occurring under the humid conditions that prevail during lateritic weathering. The principal enriched zone at Kruidfontein, however, is at 40–50 m depth but, if this is supergene, it is improbable that downward enrichment. Enrichments at similar depths are a feature of lateritic regoliths in semi-arid environments, as exemplified by the Yilgarn Block of Western Australia (Butt 1989). This redistribution of Au deep in the profile is considered to be an arid phase modification, perhaps due to mobilisation due to complexation by chloride ions. The third principal ligand capable of mobilising Au during weathering is thiosulphate ion. This is generated by sulphide oxidation in alkaline conditions. Weathering of a carbonatite such as that at Kruidfontein, which contains disseminated sulphides in a carbonate matrix, would be highly favourable for generating thiosulphate ions and it is therefore possible that thiosulphate complexation could have resulted in considerable redistribution of Au. In conclusion, therefore, it is possible that Au mobility as a thiosulphate complex could have given rise to some redistribution and local concentration of Au in the

upper 80 m, but it is considered improbable that it could have been derived from rocks similar to the underlying fresh carbonatites.

An alternative hypothesis proposed by Pirajno et al. (1995) is that the Au mineralisation was formed through the action of hydrothermal fluids. In this model the hydrothermal fluids, activated by cooling magma at depth, ascended along faults, leaching out Au from a postulated Au-rich protolith at depth. Fluid-rock interaction resulted in Fe-rich alteration and Au deposition close to the palaeosurface. Progressive decrease of Fe enrichment eastward from a fault zone is seen to occur in the altered pyroclastics. Perhaps the solutions vented forming hot springs and depositing barren silica at surface, as suggested by the presence of sinter-like deposits in the area. The Au may have been transported as sulphide complexes and precipitated in the carbonatitic pyroclastic unit which was, at a later stage, subjected to weathering and lateritisation. These later supergene processes could have further enhanced the Au mineralisation.

4.5.2.3.2 Other Carbonatite-Related Deposits

Notable alkali metasomatism and carbonatite-related deposits containing apatite, fluorite, pyrochlore, baddelyite, bastnaesite and barite include: the Khibina ring complex in the Kola peninsula (Russia) (Gerasimovsky et al. 1974; Zaitsev et al. 1998); Jacupiranga in Brazil, where apatite ore was concentrated by weathering processes; and one of the largest known repositories of REE in the world, the Sulphide Queen carbonatite body in the Mountain Pass district in southern California (USA), which contains 31 Mt of 8.86% rare earth oxides (REO) (Mariano 1989b). The 1.4 Ga Mountain Pass carbonatite complex in the Basin-and-Range province consists of carbonatite and ultrapotassic shonkinite intrusions and dykes (Haxel 2005). The shonkinite rocks are phlogopite-rich and are associated with amphibole-biotite syenite and alkali granite stocks and dykes. The Mountain Pass carbonatite rocks comprise calcite, dolomite, siderite and ankerite (about 60%), barite and celestite (20%), quartz (10%) and 10% of bastnaesite (a rare earth fluorocarbonate) with minor monazite (Haxel 2005).

Other places where this type of mineralisation may also be found are in the Canadian shield, where some 50 carbonatite complexes contain large reserves of Nb (pyrochlore) (see Hutchison 1983 for a brief review). In Inner Mongolia (China) the Bayan Obo deposit is reported to be the largest in the world with reserves of approximately 37 Mt of REO (Mariano 1989b; Drew et al. 1990). The Bayan Obo mineral system is treated more fully in Section 4.6.4.

4.5.2.4 Mineralisation of Alkali Metasomatic Origin in the Nigerian Ring Complexes

The hydrothermal mineral systems discussed in this section are genetically related to phases of alkali and H^+ metasomatism (greisen systems; discussed in Section 4.3) in granitic rocks that are part of, and intrude into, ring complexes. These are

a class of complexes characterised by rocks of alkaline and felsic compositions. The granitic rocks are generally of A-type affinity, i.e., they are anorogenic, anhydrous and alkaline (Collins et al. 1982). Mineralisation appears to be entirely connected with post-magmatic activity, in the subsolidus range of pressure and temperature, following the consolidation of nearly all of the magmatic mass (Pollard and Taylor 1986). The temperatures involved in these post-magmatic processes range from 500 to 700°C. The fluids are highly saline with about 15 wt% NaCl equivalent, and contain Na, K, Ca and Cl. The mineralising system, however, at some stage may open to the outside, e.g. through fracturing of the roof rocks, evolving further by increasing H^+ metasomatism and input of meteoric waters. Thus, through intermediate stages of H^+ metasomatism (greisen), the mineralising system may reach phases of hydrothermal activity with deposition of fracture-controlled vein quartz and sulphides. The anorogenic ring complexes of Nigeria and their related mineral deposits have been studied in detail by Bowden et al. (1984), Bowden and Kinnaird (1984a, b), Bowden (1985), Kinnaird and Bowden (1987a, b). These publications constitute the basis of the information given below on the geology and alkali metasomatism-related mineralisation of the Nigerian province.

Alkaline anorogenic magmatism took place between the Ordovician (~430 Ma) and the Jurassic (~110 Ma) in Nigeria (Jos Plateau) and Niger (Air), forming a large magmatic province some 1600 km long and 200 km wide (see Fig. 4.31). The age range and progressive younging from north to south are taken to indicate the drift of the African plate over a sublithospheric magmatic plume or hot spot. The emplacement of the complexes was probably controlled by a series of rifts and fractures along northerly and northeasterly trends. Neogene and Recent volcanic activity is present along a northeasterly trend between the island of Sao Tome' and the Cameroun (Fig. 4.31). There are more than 50 ring complexes in Nigeria, which vary in size from 2 to 25 km in diameter, are of Jurassic age and were intruded into a basement formed by metamorphic rocks, calc-alkaline and subalkaline granitic rocks and pegmatites (Older Granites) of Pan-African age (900–450 Ma). The ring complexes represent the roots of volcanic centres, and consist of mafic to felsic lavas and pyroclastic rocks, the latter being mostly rhyolites and ignimbrites. Rocks of the volcanic pile were intruded by cogenetic, subvolcanic rocks including volcanic feeders (generally quartz-porphyries), cone sheets and ring dykes (rhyolites, porphyries and microgranites), and granitic rocks (Younger Granites). Discordant high-level granite intrusions were emplaced by stoping through the collapse of a central block, which formed a caldera structure. Younger Granite intrusions appear either as circular stocks, ring dykes or as horizontal sheeted structures, depending on the level of erosion. The granitic rock suite includes about 5% intermediate to basic rocks, which usually form small intrusions ranging in composition from olivine-gabbro to quartz-syenite. At least three granite types have been recognised by Bowden and Kinnaird (1984a, b), namely: (1) peralkaline granite and related syenites, with alkali or calcic amphiboles; (2) peraluminous biotite-alkali

feldspar granites and biotite syenogranites; (3) metaluminous fayalite and hornblende-bearing granitic rocks. A distinct feature of the Younger Granites is their lack of tourmaline. The work of the Bowden-Kinnaird team has shown that late stage, subsolidus and post-magmatic alteration processes consist of alkali metasomatism, represented by sodic metasomatism in peralkaline and peraluminous granites, whereas potassic metasomatism appears to dominate the late stages of consolidation in the biotite granites. These phases of alkali metasomatism are followed by increasing degrees of acid (H^+) metasomatism, represented by greisenisation, phyllic and even argillic alteration processes. Accordingly, the styles of mineralisation, and the mineral associations related to the metasomatic activity of the Younger Granites in the Nigerian ring complexes, can be subdivided into two distinct groups. One group is almost exclusively associated with alkali metasomatism, comprising late pegmatitic pods with beryl and topaz, and pervasive disseminations of columbite or pyrochlore with cassiterite. The hydrothermal stages, sensu stricto, involving H^+ metasomatism, are characterised by oxide-sulphide assemblages with cassiterite and wolframite in quartz-vein lodes, greisens, stockwork and replacement bodies.

Potassic metasomatism is most noticeable within pods in the cupola zones of biotite granites. It is characterised by the presence of microcline, and red in colour due to the release of Fe from the feldspar lattice. Minor disseminations of cassiterite and wolframite, accompanied by monazite, zircon and rutile, are associated with this alteration process. Pegmatitic pods and vugs, formed by smokey quartz and alkali feldspar, are not particularly important in economic terms. They also appear to be related to K-metasomatism, are usually small in size, and are sporadically developed along the marginal zones of the granites. They may contain gem-quality minerals such as topaz and aquamarine. Late magmatic to post-magmatic disseminations related to sodic metasomatism are concentrated in the apical regions of peralkaline and peraluminous biotite granites. This process results in the pervasive alteration of K-feldspar to albite, formation of aegirine and riebeckite, and desilication and enrichment in REE with the introduction of Nb-bearing fluids. The pyrochlore-columbite $\pm$ cassiterite association is of economic importance in Nigeria, largely because of the development of eluvial and alluvial deposits formed during the erosional unroofing of the granites. Although pyrochlore and columbite occur together, the former is dominant in peralkaline granites, whereas columbite predominates in peraluminous biotite granites. Pyrochlore mineralisation is characterised by disseminations of honey-coloured, U-rich (up to 5% U_3O_8) pyrochlore octahedra, accompanied by Th-rich monazite, U-Th-Hf-enriched zircons, amblygonite, astrophyllite and cryolite (a fluoride of Na and Al). The columbite-bearing granites are more common than those containing dominant pyrochlore. Cassiterite is also present. In some localities columbite is accompanied by REE and U-enriched thorite, xenotime and monazite, as well as zircon, magnetite and ilmenite. In these granites Na metasomatism is characterised by albitisation leading to an albite-protolithionite rock with a fine-grained sugary texture.

4.5.2.5 Alkaline Ring Complexes of the Arabian Shield

The Arabian-Nubian Shield (Fig. 4.31) is a Neoproterozoic accretionary orogen that includes tectonostratigraphic terranes (island arcs, oceanic plateaux and continental fragments), whose amalgamation was probably completed by the ~570 Ma Pan-African tectono-thermal event (Kröner and Stern 2005). The shield occupies extensive areas of northeastern Africa (eastern Egypt, Sinai, northeastern Sudan, parts of Ethiopia and Somalia) and the western side of the Arabian peninsula. It comprises a number of geologically distinct terranes, and the general consensus is that the shield represents a mosaic of accreted Late Proterozoic island arcs (see Kröner 1985; Pallister et al. 1987 and Kröner and Stern 2005 for details of the geology of the shield).

There are over 70 intrusions of alkali granites and associated ring complexes in the Arabian Shield, and about 40 in Sudan (Nubian Province). The mechanism of emplacement and structure of the ring complexes are similar to those in other parts of the world: building of a central volcanic complex with eruption of initial basic volcanism followed by dominant ignimbrite flows and rhyolitic lavas; and subsequent collapse which forms a caldera with accompanying intrusions of porphyritic ring dykes and stocks of granitic rocks. In Saudi Arabia, Jackson et al. (1985) recognised the following styles of Nb-Zr-REE mineralisation, all related to phases of alkali metasomatism: (1) disseminations in porphyritic alkali microgranite plutons and stocks; (2) disseminations in aplite-pegmatite sheets in the apical zones and flanks of alkali granite plutons; (3) disseminations in siliceous and pegmatitic pods, as well as veins and breccias in roof zones and wall rocks of the alkali granite plutons. The principal ore minerals are: pyrochlore, columbite-tantalite, monazite, cassiterite, bastnaesite, thorite and zircon. In the Eastern Desert (Egypt) several 535–571 Ma anorogenic A-type and fluorite-bearing granites occur as small ring complexes and plutons, emplaced at shallow crustal levels in pull-apart zones (Mohamed and El-Sayed 2007).

4.6 Iron Oxide-Copper-Gold-Rare Earth Elements-Uranium Mineral Systems

In this section I discuss the general features of a broad class of ore systems referred to as Fe oxide-Cu-Au (U-REE), commonly known as IOCG, which includes the deposits of the Cloncurry district and the giant Olympic Dam deposit in Australia, Candelaria in Chile and the Solobo deposit in the Carajas district in Brazil. However within this class other ore systems are included, with diverse metal endownments, but all sharing some common features of intrusion-related hydrothermal systems of anorogenic magmatic regimes in extensional tectonic settings. Deposits such as Kiruna Fe in Sweden, Fe-Cu mineralisation at Boss-Bixby and Pea Ridge (Missouri, USA) and the giant Bayan Obo REE-Nb-Fe deposit of Inner Mongolia, Vergenoeg Fe-F and

Palabora Cu-REE in South Africa, although controversial are included in the IOCG class. Two volumes devoted to IOCG are those of Porter (2000, 2002), whereas a more recent overview can be found in Williams et al. (2005); Lentz (2007) edited a special issue of Exploration and Mining Geology on IOCG systems. A clear definition of IOCG is difficult, but Williams et al. (2005) provided some empirical guidelines, as follows: (1) presence of Cu, with or without Au; (2) hydrothermal veins, breccias and/or replacement mineralisation styles; (3) abundant Fe oxides (magnetite, hematite); (4) Fe oxides have low-Ti contents; (5) a general absence, with some exceptions however (e.g. Palabora and Olympic Dam) of a clear spatial association with igneous intrusions. To these may be added a relationship to deep-seated megastructures in intracontinental rifts and the presence of highly fluidised breccias (D. Kirwin, pers. comm. 2007).

The general theme of the IOCG deposits, apart from the enrichment in the above listed elements, is the widespread alkali metasomatism in the host rocks (Hitzman et al. 1992; Oreskes and Hitzman 1993; Williams and Skirrow 2000). Typically, IOCG hydrothermal systems form in shallow crustal environments (4–6 km) and are the expression of volatile-rich, alkaline magmas (Hitzman et al. 1992). Ore-forming temperatures range from ca. 600°C for the Fe oxides and silicate phase, to 500–200°C for Cu-Au mineralisation, with high salinities of the ore fluids (up to 50 wt% NaCl equivalent), low pH oxidising aqueous fluids, co-existing with CO_2-rich fluids (Reeve et al. 1990; Davidson and Large 1998).

To understand IOCG systems it is necessary to unravel the spatial and genetic relationship between the various mineralised manifestations, their depths of formation, and their erosion level (Fig. 4.38). Genetic models of IOCG range from magmatic to non-magmatic. The general consensus is for magmatic models linked to I- or A-type granitoids or strongly alkaline-carbonatitic magmas, of either intracratonic or distal arc settings, from which oxidised and S-poor metalliferous fluids are released. The presence of CO_2, detected in fluid inclusions of IOCG ores, plays an important role for fluid release and influences the partitioning of alkalies between silicate melts and fluids, generating brines with high Na/K ratios that are ultimately responsible for the widespread sodic alteration in the country rocks surrounding IOCG systems (Pollard 2001, 2006; Williams et al. 2005). The $\delta^{34}S$ values of IOCG deposits in the coastal belt of Chile (see below) cluster around 0‰, which are consistent with a magmatic source (Sillitoe 2003). Groves and Vielreicher (2001) listed the evidence in favour of magmatic models: (1) high temperature and high salinity of the early fluids; (2) oxidising nature and low pH of the ore fluids; (3) element associations and the pipe to ring-like geometry of the mineralised breccias, resembling those that are typical of explosive alkaline intrusions, as shown by the cross-sections of Olympic Dam and Vergenoeg; (4) the timing of ore formation with anorogenic magmatism; and (5) mantle Nd isotope signatures; (6) the coincident magnetic and gravity anomalies that can be interpreted to reflect a mafic body at depth.

Pollard (2001, 2006) suggested that IOCG and porphyry systems may represent a spectrum of intrusion-related magmatic-hydrothermal systems, although

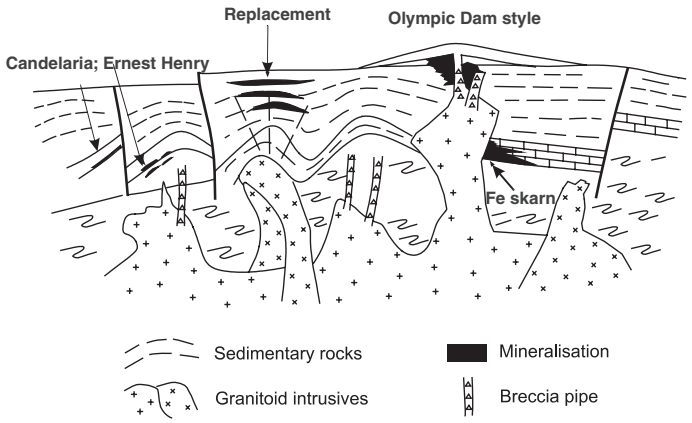


Fig. 4.38 Conceptual model of IOCG ore systems linked to Proterozoic anorogenic magmatism (not to scale); in this figure IOCG styles shown include breccias, Fe oxide skarns and replacement bodies. After Pirajno (2000); see also Fig. 8.6)

they occur in different tectonic settings and emplacement levels. The intrusions that are temporally associated with IOCG systems are magnetite-series alkaline to subalkaline, ranging in composition from diorite to syenogranite, with evidence of mafic-felsic mingling. IOCG and porphyry systems share the same oxidation state and degree of fractionation (Pollard 2006). Porphyry Cu-Au systems are associated with magnetite-series, calc-alkaline to high K calc-alkaline granitoids, ranging in composition from diorite to monzogranite (see Chapter 5). It is important to remember that the oxidation state of the magma and degree of fractionation determine the nature of the mineral system (Fig. 4.4; Lehmann 1990). In reduced magmas, Cu, Au, Pb, Zn, Mo, Co, Ni can be removed from the melt in early sulphides (pyrrhotite), whereas in more oxidised magmas, the high SO_2/H_2S ratio allows partitioning of S in the aqueous phase in hydrous melts. The intrusions linked with IOCG systems were emplaced at depths from 15 to 6 km, and therefore they are significantly deeper than porphyry systems. For this reason, Pollard (2006) suggested, the IOCG fluids, which develop at greater depths, are unable to break the host rocks and have to be channelled out along pre-existing fractures, intersection of structures, lithological boundaries, dilational jogs in trascurrent faults. Moreover, an important difference between IOCG and porphyry systems is the mechanism of fluid evolution (Pollard 2006). In porphyry systems magmatic fluids are saline and H_2O-rich, separating upon boiling into a vapour phase and a hypersaline brine. In IOCG systems, hypersaline brines coexist with CO_2-rich fluids, formed by unmixing. These differences, according to Pollard, are responsible for the different alteration styles of IOCG and porphyries. In the deeper levels of IOCG systems successive stages are characterised by sodic or sodic-calcic alteration with albite $\pm$ pyroxene and potassic alteration with

biotite ± K-feldspar, followed by amphibole and/or epidote stages, and non-silicates such as Fe oxides, sulphides and carbonates. Significantly, deep alteration of IOCG systems is similar to to that of alkaline and carbonatite complexes. At shallower levels, IOCG have K-feldspar and sericitic (muscovite-chlorite-carbonate) alteration, plus Fe oxides and sulphides, but always lacking quartz stockworks and clay assemblages. In porphyry systems, silicate alteration is characterised by biotite ± K-feldspar, followed by sericite ± chlorite and finally to clay-rich assemblages heralding increasing acidity and input of meteoric water. Indeed, Sillitoe (2003) pointed out that porphyry and IOCG systems can be readily distinguished in terms of potassic alteration and Cu-Au mineralisation, because in the case of porphyry systems these are essentially confined to the porphyry stocks, whereas these are absent from the latter. In addition, and as mentioned above, the chalcopyrite-bearing quartz veinlets and the pyrite-bearing quartz-sericite alteration are absent in IOCG.

Non-magmatic models for the genesis of IOCG systems include two categories: (1) fluids derived from surface or shallow basin; (2) metamorphic fluids passing through Cl-rich rocks or derived from deep basins. An alternative view is that of Barton and Johnson (1996), who proposed that the saline fluids responsible for these deposits are sourced from evaporites. They cited examples of Holocene hydrothermal Fe oxides formed from evaporitic sources and the correlation of the Fe oxide-Cu-Au-REE-U of Mesozoic age with zones of low-latitude as revealed by continental reconstructions. The evaporitic source model of Barton and Johnson (1996) suggests that circulation of hydrothermal fluids is caused by magmatic heat, and that the source of the metals is provided by igneous rocks, but that the metal transport is effected by chlorides supplied by evaporitic deposits. In addition, the widespread sodic alteration associated with the deposits may also be related to evaporites, which would have supplied large amounts of Na to the hydrothermal fluids. Examples of IOCG deposits that may be linked to an evaporitic source include the Mid-Neogene Cerro de Mercado (Mexico), the Jurassic Humboldt Complex, in the Basin-and-Range (USA), the Permo-Triassic Korshunovsk and Tagar in the Siberian platform (Russia) and the Bafq mining district in central Iran (Barton and Johnson 1996).

An overall and idealised hydrothermal alteration zoning, as viewed by Hitzman et al. (1992), is as follows: a zone of sodic alteration (albite-magnetite-actinolite) is surrounded by a halo of dominantly potassic alteration (K-feldspar-sericite-magnetite). This deeper and higher-temperature sodic-potassic system is followed towards the surface by a zone of sericitic alteration (sericite-hematite-carbonate-chlorite-quartz), with lenses of massive Fe oxides (hematite or magnetite). Dykes or pipes of hematite-quartz breccia may locally cut through the system.

The space-time distribution, as discussed by Williams et al. (2005), shows that IOCG span ages ranging from the Archaean to the Phanerozoic. A selection of IOCG systems from the Cenozoic to the Archaean is given in Table 4.4

North America and Australia have some of the largest and better known IOCG of Mesoproterozoic age and these may relate to the assembly of the Proterozoic supercontinents, which may have acted as a large insulation

Table 4.4 Selected IOCG districts and deposits. After Williams et al. (2005; Appendix)

Age/region	Geological setting	Deposit/occurrence name	Total resources (metal)
Cenozoic			
Andean margin (Chile, Argentina, Bolivia)	Volcanic centres in closed basins	El Laco (Chile), Pacheekala (Bolivia), Arizaro (Argentina)	500–1500 Mt (500 Mt) Feox ± Cu, Au, Co
SW USA	Continental basins with felsic to alkalic volcanism	Iron Springs (Utah), El Capitan (New Mexico), Copperstone, Planet (Arizona)	>2000 Mt (450 Mt) Feox ± Cu, Au, U
Mexico	Mid-Neogene continental felsic volcanic centres	Cerro de Mercado, El Vulcan, La Perla, Hercules	>300 Mt (>100 Mt) Feox ± REE, Cu
Mesozoic			
SW USA and western Mexico	Jurassic-Cretaceous arc and back-arc extensional mafic or felsic volcano-plutonic complexes	Humboldt complex, Cortez Mts, Yerington, Eagle Mt	>1000 Mt (>75 Mt) Feox ± REE, Cu, Au
Chilean coastal belt	Jurassic-Cretaceous extensional arc, mafic-intermediate volcano-plutonic complexes	Candelaria, Manto Verde, Romeral, Teresa de Colmo	>3000 Mt (350 Mt) Feox ± Cu, Au, Co, REE
Peruvian coastal belt	Cretaceous extensional arc, mafic-intermediate volcano-plutonic complexes	Marcona, Pampa de Pongoo, Raul-Condestable, Monterossas	>2500 Mt (>1400 Mt) Feox ± Cu
Siberian Traps	Permian intrusions in continental flood basalt province	Korshunovsk, Tagar, Krasnoyansk	>3000 Mt (>650 Mt) Feox ± Cu
Palaeozoic			
Turgai province (Kazakhstan)	Carboniferous mafic-intermediate arc volcano-plutonic complexes	Kachar, Sarbai, Sokolovsk	>5000 Mt (>2500 Mt) Feox ± Cu, Co
Altai-Sayan Mts, central Asia	Devonian mafic-felsic volcano-plutonic complexes	Teyskoe, Ampalyshoe, Tashtagol	>2000 Mt (>375 Mt) Feox ± Cu, REE, U
Central Iran, Bafq district	Cambrian anorogenic felsic volcanics	Chogart Chadomalu, Anomali, Gole Gohar, Hamadan	>1500 Mt (>500 Mt) Feox ± Cu, REE
Neoproterozoic			
Lufillian arc, Copperbelt region to Damara (Namibia)	Pan African mafic-felsic volcanic and plutonic complexes	Kalengwa, Kasempa, Malundwe, Chimiwungo	>1000 Mt (200 Mt) Feox ± Cu, Au, Co

Table 4.4 (continued)

Age/region	Geological setting	Deposit/occurrence name	Total resources (metal)
Northeastern North America, Adirondack highlands	Anorogenic intermediate-felsic suite	Benson, Minevillem Lyon Mt, New York	>1000 Mt (200 Mt) Feox ± REE, Cu, U
Mesoproterozoic			
Wernecke and Olgivie Mts (NW Canada)	Mafic-intermediate igneous intrusions into continental margin sedimentary rocks	Pagisteel, Dolores Creek	>200 Mt (30 Mt) Feox ± REE, Cu, Au, Co
Gawler Craton, Curnamona Craton, Australia	Anorogenic volcano-plutonic complexes	Olympic Dam, Acropolis, Mt Painter, Moonta, Wirrda Well, Manxman	>3000 Mt (>2000 Mt) Feox ± REE, Cu, Au, U
Cloncurry district (Mount Isa inlier), Australia	Anorogenic intermediate to felsic plutonic suites	Ernest Henry, Starra, Osborne	>350 Mt (>175 Mt) Feox ± REE, Cu, Au, U, Pb, Zn
Mid-continent USA (SE Missouri)	Anorogenic felsic caldera	Pea Ridge, Boss-Bixby, Pilot Knob, Bourbon	>1000 Mt (>300 Mt) Feox ± REE, Cu, U, Au,

blanket on sublithospheric mantle flow, resulting in accumulation of heat, rise of mantle diapirs, anatectic melting, rifting of the continental crust, and finally the inception of regional-scale hydrothermal systems at shallow levels in the crust (Fig. 4.38). Mesozoic to Cenozoic IOCG are found in the North American cordillera and the Chilean and Peruvian Andean margins. Economically significant IOCGs are: the Proterozoic Olympic Dam and Ernest Henry in Australia; the Archaean Salobo in the Carajas district in Brazil, the Mesozoic Candelaria-Punta del Cobre in the coastal belt of Chile. Unlike the Australian IOCG, the South American deposits are related to extensional settings in a continental convergent margin and there is some doubt that these may actually be considered as true IOCG deposits.

In the sections that follow I provide a brief account of four examples: (1) Olympic Dam, the key representative of the Proterozoic IOCG ore deposits and the less typical, but nevertheless interesting, (2) Vergenoeg Fe-F deposit in the Bushveld region (South Africa); (3) Palabora (South Africa); (4) Bayan Obo in Inner Mongolia and Candelaria-Punta del Cobre in Chile. Palabora and Bayan Obo are carbonatites and more controversial as to whether or not they can be considered part of the IOCG class.

4.6.1 Olympic Dam, South Australia

The world-class Olympic Dam deposit was discovered in 1975 and is located approximately 520 km north-northwest of Adelaide, along the eastern margin of the Gawler Craton, in South Australia. The deposit was discovered after many years of detailed investigations and study by Western Mining Corporation geologists (Woodall 1993; Haynes 2006). The initial concept was to locate a stratabound sedimentary rock-hosted copper deposit in a Proterozoic basin, in which the presence of thick basaltic successions would be the source of metals. This first study was integrated with geophysical data, and focused on gravity and magnetic anomalies on the Stuart Shelf, interpreted as possible buried basalts (Gawler Range Volcanics). At the same time, analyses of tectonic lineaments by O'Driscoll (1985) revealed the presence of well-defined structural corridors along areas of coincident gravity and magnetic anomalies. A synthesis of the data, integrated with field observations led to the siting of the first diamond drillhole in 1975, on a coincident gravity, magnetic and tectonic target. The initial model was incorrect, but the Western Mining Corporation's exploration team was quick to realise that something new and exciting had been discovered. Since its discovery much has been published about the deposit. Information for the short review presented here, is derived from Reeve et al. (1990), Oreskes and Einaudi (1992), Cross et al. (1993) and Haynes et al. (1995). An interesting history of the events that led to the discovery of this giant ore deposit is provided by Haynes (2006). Olympic Dam lies beneath 300–400 m of sedimentary cover, in a basement represented by the ca. 1590 Ma Gawler Range Volcanics and the coeval Hitalba Suite granitic rocks. These rocks are important for a clearer understanding of the tectono-thermal environment, tectonic setting and the origin, not only of the Olympic Dam deposit, but also for several other Proterozoic IOCG systems. For this reason, I provide a short review of the Gawler Range Volcanics and the Hitalba Suite granitoids.

The Mesoproterozoic Gawler Range Volcanic province covers more than 25 000 km^2 and consists of bimodal and high-K volcanic rocks that are part of a stable platform on the margins of the Gawler Craton of South Australia (Fig. 4.39). Uranium-Pb zircon dating of basalt yielded an age of 1592 ± 2 Ma; $\varepsilon Nd_{T=1590}$ range from –1.0 to 2.5 for basalts and –1.0 to –8.0 for felsic volcanics (Solomon and Groves 1994 and references therein). These volcanics are co-magmatic with high level, post-tectonic A-type alkali-feldspar granites of the Hitalba Suite, to which the Roxby Downs Granite, host of the Olympic Dam deposit, belongs. The Hitalba Suite has a U-Pb zircon age of ca. 1600 Ma and the Roxby Downs granite has $\varepsilon Nd_{T=1590}$ ranging from –3.7 to –3.1 (Solomon and Groves 1994 and references therein). The Gawler volcanics together with the Hitalba batholith cover an area in excess of 40 000 km^2, suggesting that very large volumes of mafic-felsic magmas were generated. A comprehensive review of the Gawler Range Volcanics and Hitalba Suite can be found in Blissett et al. (1993) and Flint (1993), respectively.

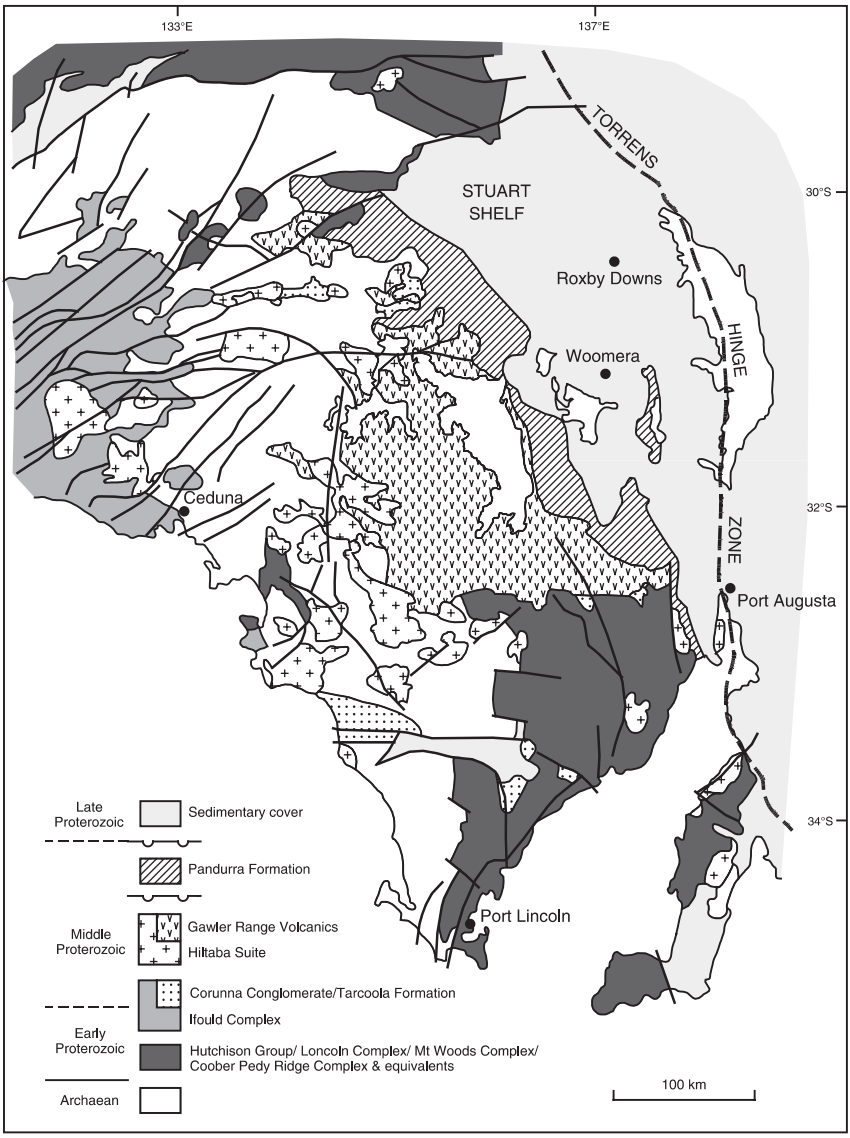


Fig. 4.39 Simplified subsurface geology of the Gawler Craton of South Australia and position of the Olympic Dam IOCG deposit. After Daly et al. (1998) and Reynolds (2000)

The Gawler Range Volcanics are subdivided into two successions, comprising basalt and rhyolite in the lower parts of the succession and dacitic and rhyolitic units in the upper parts (Blissett et al. 1993). The volcanics largely comprise thick ignimbritic dacites and rhyolites, locally interlayered with basaltic lavas. Erosional windows expose thick (ca. 400 m) successions of subaerial

basaltic lavas, which Giles (1988) divided into a lower suite and an upper, more differentiated suite. These basaltic rocks are overlain by sheets of voluminous felsic dacitic to rhyolitic ash-flow tuffs, such as the Yardea Dacite. The Yardea Dacite is an extensive ignimbrite sheet, which covers about 12 000 km^2, is over 100 m thick (Giles 1988) and overlies a succession of felsic volcanics that include crystal tuffs and lavas, and is intruded by the Hitalba granitic rocks. The Yardea Dacite is estimated to have been erupted at temperatures of 950–1000°C (Creaser and White 1991). High-temperature (ca. 1000°C) ash-flow tuffs are typically found in continental flood volcanic provinces, such as the Paraná-Etendeka. In the bimodal Etendeka province in Namibia these ash-flow tuffs (quartz-latites) are intercalated with basalts (Milner 1988), as in the Gawler province. Milner (1988) recognised that the quartz-latite units represent high-temperature ash-flows (also called rheoignimbrites, Milner et al. 1992), derived from the melting of continental crustal materials of mafic to intermediate composition, by the ponding of basaltic melts in the lower crust. In the Gawler region, no eruptive vents or caldera have been recognised, although the nature of the explosive volcanism indicates that these may have been present. Rhyolitic domes intrude and overlie the dacitic ash-flow tuffs, extend for over 50 km in an E–W direction suggesting that these were erupted along a fissure. The rhyolitic domes are overlain in turn by the Bunburn Dacite ash-flow tuff and more pyroclastic units, mostly lithic-crystal tuffs. These explosive eruptions were interrupted by short periods of erosion and sedimentation.

Giles (1988) using major and trace elements and REE data interpreted the geochemical fingerprints of the Gawler volcanics as calc-alkaline, although several felsic rocks are strongly alkaline. Giles' AFM plot shows this extreme alkali enrichment with the dominat trend towards the A corner. Total REE show increasing concentrations with increasing silica values and chondrite-normalised patterns show negative Eu anomalies. The normalised REE patterns of two basalts show that one sample is strongly fractionated REE ($La/Yb = 30.7$) compared to the second ($La/Yb = 9.6$), excluding derivation of the more evolved basalt from the more primitive one (Giles 1988). One sample of Hitalba Suite has the highest total REE and the largest negative Eu ($Eu/Eu^* = 0.14$) anomaly in the entire Gawler province, indicating feldspar fractionation from a more mafic parent. Models of petrogenesis for the Gawler volcanics, proposed by Giles (1988), include: (1) calc-alkaline fractionation series; (2) mixing of mafic and felsic magmas; and (3) coeval, but unrelated mantle-derived mafic magmas and crustal-derived felsic magmas. The bimodal nature of this volcanism and the geochemical evidence led Giles (1988) to conclude that the most likely explanation for the origin of the volcanics is that they are not related by crystal fractionation and are therefore derived from distinct sources (mantle mafic and crustal felsic). As such, the Gawler province volcanics do not conform to a subduction-related calc-alkaline series. Furthermore, the geochemistry of the basalts is consistent with shallow (<60 km), hydrous melting of an upper mantle source in an intracratonic setting and therefore likely to have been caused by elevation of the geothermal gradient in response to mantle upwelling and

subsequent underplating of mafic magmas. Thus, the underplated mafic magmas may also have generated the felsic magmas by partial melting of the lower crust (Fig. 4.40).

The Hitalba Suite comprises anorogenic granitic batholiths and plutons that intrude the Gawler Craton (Flint 1993; Daly et al. 1998). As for the Gawler Range Volcanics, the Hitalba Suite is also bimodal comprising granite, hornblende-quartz monzonite, granodiorite, gabbro and diorite intrusions. Uranium-Pb zircon dating yielded ages ranging from 1600 to 1585 Ma; the Roxby Downs granite gave a U-Pb zircon age of 1588 ± 4 Ma which, within error, are indistiguishable from those recorded for the Gawler Volcanics (1592 ± 2 Ma). Major and trace elements data suggest that the source of the Hitalba Suite was formed by 15–40% partial melting of crustal igneous rocks of tonalitic to granodioritic composition.

A schematic model for the origin of the ca. 1600 Ma igneous rocks in the Gawler volcano-plutonic province is shown in Fig. 4.40. The model envisages an early stage of mafic underplating, possibly initiated by a mantle plume, from which mafic intrusives are emplaced in the crust and mafic volcanics erupted at surface (Fig. 4.40A). A second stage follows with partial melting of the lower crust due to thermal energy from the underplated magmas; this forms magma

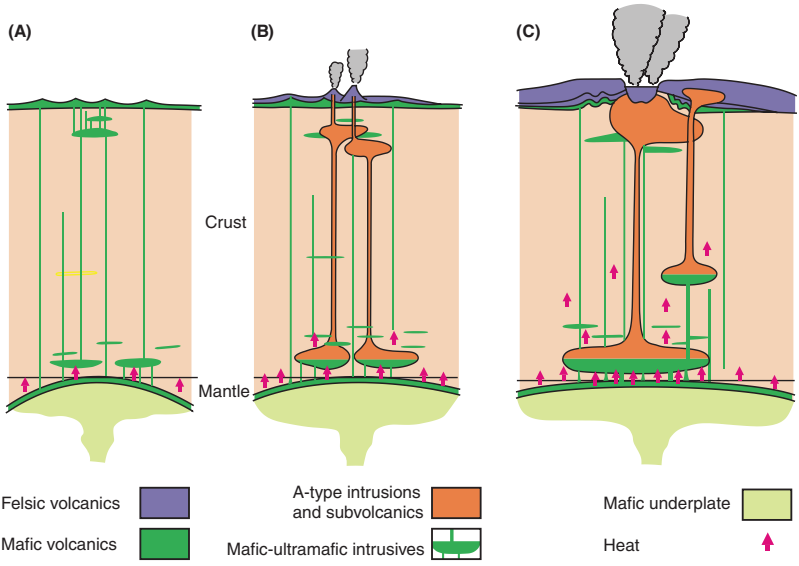


Fig. 4.40 Schematic evolution of the Gawler Range Volcanics and associated Hitalba Suite intrusives; (**A**) Early stage of mafic underplating, with mafic intrusions and basaltic volcanism; (**B**) Underplating continues and beginning of lower crust partial melting, resulting in A-type granitic intrusions and eruption of felsic volcanics; (**C**) Extensive partial melting of the lower crust leads to the generation of batholiths and the formation of silicic calderas. See text for more details. After Blissett et al. (1993)

chambers in the lower and upper crust, which fractionate and locally erupt felsic volcanics (Fig. 4.40B). The final stage relates to extensive partial melting of the crust with the formation of larger magma chambers that originate batholiths, plutons (Hitalba Suite) and perhaps erupt to the surface through large calderas producing ignimbrites.

4.6.1.1 The Olympic Dam Deposit

The Olympic Dam deposit contains ore reserves greater than 600 Mt averaging 1.8% Cu, 500 g/t U_3O_8, 0.5 g/t Au, and 3.6 g/t Ag (Reynolds 2000) and a global resource of 31 810 Mt @ 1% Cu, 0.5 g/t Au and 400 g/t U_3O_8 (Williams et al. 2005). The deposit is hosted by the Olympic Dam Breccia Complex (ODBC) in the ~1590 Ma Roxby Downs Granite of the Hiltaba Suite, which is a coarse-granite syenogranite with A-type affinities (Creaser 1989; Reeve et al. 1990; Johnson and Cross 1995). ODBC and the Roxby Downs Granite form a basement high that is buried 300 m beneath subhorizontal Neoproterozoic and Cambrian sedimentary rocks of the Stuart Shelf (Fig. 4.41). Reeve et al. (1990) give detailed descriptions of the ODBC. The deposit is characterized by a number of large Cu-, Au-, Ag-, U-, REE-bearing hematite-quartz dyke-like breccia bodies. Copper is present as chalcopyrite, bornite and chalcocite, gold and silver form native metals, the main U minerals are coffinite, pitchblende and brannerite, and the REE minerals are monazite, xenotime, bastnaesite and floencite. The abundance of REE correlates with increasing hematite content of the breccia. The breccia bodies are up to 100 wide, form a NW-trending zone that is around 5 km long and 1.5 km wide, and typically consist of brecciated granite at the edge of the deposit, passing into a heterolithic breccia and hematite-quartz microbreccia in central portions. The heterolithic breccia consists of fragments that are generally less than 100 mm across. The fragments consist of hematite (some of which is bedded or perhaps fluidised), crushed and altered granite in a matrix of quartz-hematite-sericite-siderite-chlorite, fluorite, siderite, barite (some of which is laminated), pyrite, and volcaniclastic rocks. The heterolithic breccia grades into the hematite microbreccia and fine-grained massive hematite-quartz (Cross et al. 1993; Haynes et al. 1995). The formation of the breccias implies large-scale movements of high-pressure fluids (Fig. 4.41). Furthermore, the presence of sedimentary barite and hematite in the upper parts of the deposit suggests a phase of exhalative activity (Haynes et al. 1995).

Textural relationships and the distribution of sulphides indicate that they were deposited during the late stages of the mineralising event. The sulphides are zonally arranged around a central hematite core. From this core outward, a bornite + chalcopyrite assemblage changes to chalcopyrite + pyrite. Alteration patterns at Olympic Dam begin with weakly sericitic and hematitic alteration within a fractured granite. This becomes gradationally more intense towards the breccia bodies, where sericite, chlorite, epidote and hematite tend to become dominant, until hematite becomes more abundant and overprints all other phases. Late silicification appears to be associated with higher Au grades.

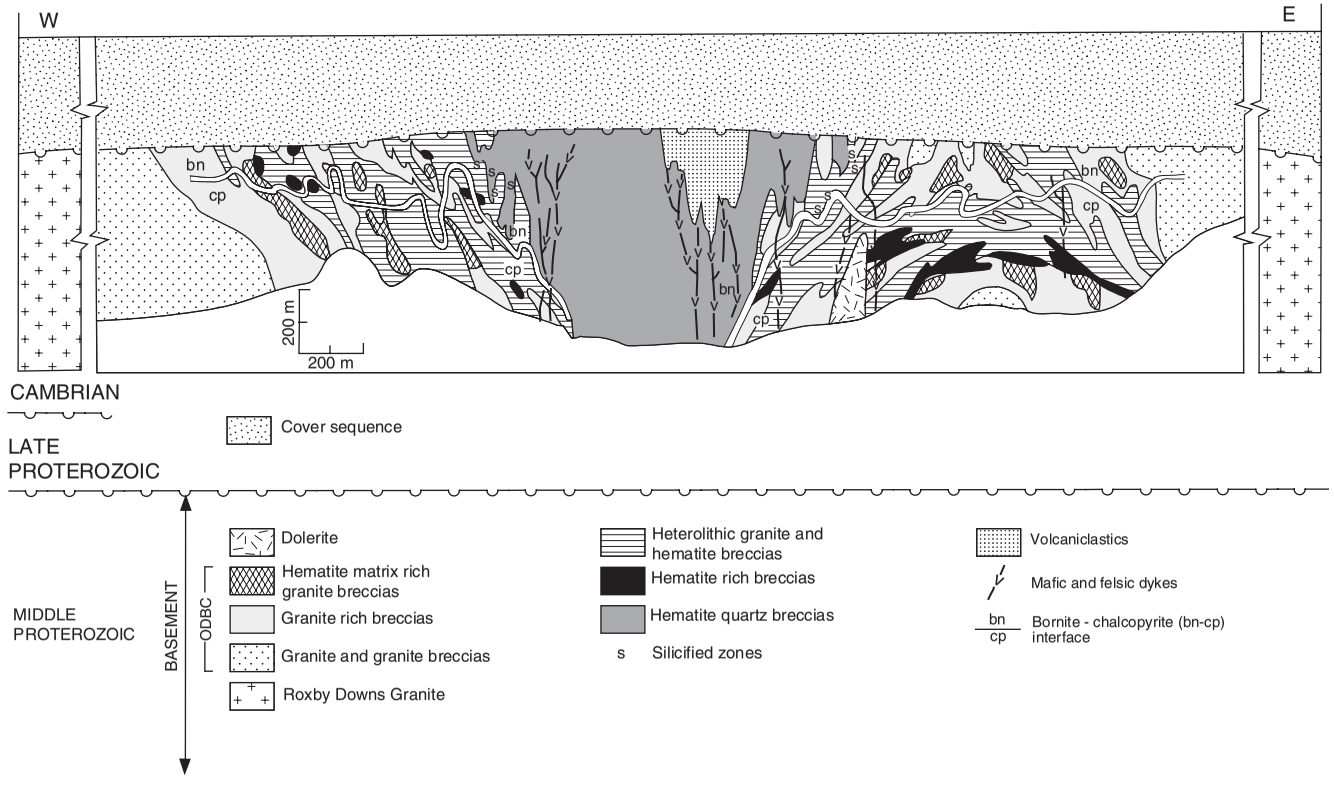


Fig. 4.41 East–west cross section through the Olympic Dam Breccia Complex (ODBC); important to note that the granite-ODBC contacts are gradational over 100s of metres (D. Kirwin, pers. comm. 2007). After Reeve et al. (1990) and Reynolds (2000)

The extensive Fe metasomatism of the Olympic Dam granite and the large-scale hematite replacement and deposition was accompanied by fluorite, barite and REE-bearing mineral phases. The hydrothermal fluids were channelled upward along faults, while tectonic activity was ongoing and caused erosion of the breccia bodies and the altered granite. Supergene enrichment, with precipitation of chalcocite, took place as result of surface weathering during the Proterozoic. Finally, about 700 Ma ago the Olympic Dam deposit was buried by sediments, allowing its preservation (Fig. 4.41). Collapse of upper parts of the breccia system was accompanied with deposition of sulphides (Haynes et al. 1995). Two sources of the mineralizing fluids have been recognized (Oreskes and Einaudi 1992). An early fluid interpreted to be of magmatic origin and produced most of the magnetite in the ore system. This fluid had a high $\delta^{18}O$ of 10‰ and a high temperature of around 400°C. Later meteoric or seawater fluids deposited hematite, with $\delta^{18}O$ of <9‰, temperatures between 200° and 400°C and salinities ranging from 7 to 42 wt% NaCl equivalent (Oreskes and Einaudi 1992).

Davidson (2002) suggested that the mineralisation at Olympic Dam is probably related to decompression of metalliferous, saline fluids in regions of lower permeability along highly permeable faults and breccias, in regions with higher geothermal gradients, and in over-pressured regions below fault seals. Skirrow (2006) suggested that IOCGs around Olympic Downs are characterized by: high paleogeothermal gradients associated with high-temperature K-rich A-type granites that were coeval with mafic and ultramafic intrusives; a regional-scale Na(-Ca-Fe) alteration up to 10 km wide; a regional to local-scale K-Fe(-carbonate) alteration and Cu-Au mineralisation; local-scale hematitic alteration and Cu-Au(-U) alteration; and hypersaline high-temperature brines (associated with magnetite alteration) and lower salinity lower temperature brines containing various concentrations of CO_2.

Oreskes and Einaudi (1992), on the basis of fluid inclusions and stable isotope systematics, recognised two sources of fluids. An early fluid, of magmatic origin, produced most of the magnetite. This fluid is characterised by high $\delta^{18}O$ (about 10‰) and high temperature (about 400°C). Later fluids deposited hematite and are associated with the Fe-rich breccias. Stable isotope studies show that these late fluids have $\delta^{18}O$ of less than 9‰ and temperatures between 200 and 400°C. Fluid inclusions indicate salinities ranging from about 7 wt% to 42 wt% NaCl equivalent.

Models that attempt to explain the origin of the Olympic Dam deposit were proposed by Oreskes and Einaudi (1990) and Haynes et al. (1995). In the model of Oreskes and Einaudi (1990), a rift basin formed on a basement of the 1.6 Ga Roxby Downs Granite, and was filled with clastic and volcanic sediments. Intense and widespread hydrothermal activity caused brecciation of the Roxby Downs Granite and pervasive metasomatism along graben faults. Fluids were exhaled at and near the surface with further infiltration of Fe-rich fluids into the sedimentary pile, and as faulting and hydrothermal activity continued, there was collapse of the central parts. The deposits were then eroded to the

unconformity level (now about 300 m below the surface), where deposition of new sediments protected the mineralised rocks from erosion (Fig. 4.41). In the model, proposed by Haynes et al. (1995), Olympic Dam began its history as a maar volcano, within which the Olympic Dam Breccia Complex developed; several pulses of oxidised and cooler meteoric water mixed with hotter deeply-sourced fluids with a main magmatic component, to form the ore zones.

Haynes et al. (1995) also performed numerical modelling of the Olympic Dam hydrothermal system and concluded that fluid mixing was the dominant process for the origin of the ores. This mixing involved fluids of magmatic origin, deep meteoric fluids and cooler, near-surface, oxidised meteoric water. The main Cu-Au-U orebody was formed within a reservoir of saline groundwater. This groundwater introduced the Cu, Au, U and S into the breccia complex and mixed with hotter water, which introduced Fe, F, Ba and CO_2. Their model suggests that the precipitation of the Fe oxides and sulphides was the result of sulphate reduction and ferrous iron oxidation ($Fe^{2+} \rightarrow Fe^{+3}$).

U-Pb zircon dating of the Olympic Dam fragmental rocks, tuffs and cross-cutting dykes (1584–1597 Ma) cannot be distinguished from the age of the host Roxby Downs granite. On the basis of these age constraints, Campbell et al. (1998) suggested that Roxby Downs-like granitoids are the product of large-scale crustal melting due to emplacement of mantle melts in a rift setting (Fig. 4.40). The rifting episode affected the Gawler Craton (South Australia) and may have been related to a mantle plume (Campbell et al. 1998).

4.6.1.2 Other Australian Examples of IOCG

Other Australian examples of IOCG deposits include Ernest Henry, Osborne, Starra in the Cloncurry district (Mount Isa), and a number of deposits in the Tennant Creek Inlier (Fig. 4.42). Several other deposits of the same class are present in the Curnamona Province of South Australia (e.g. Prominent Hill, Portia, Kalkaroo, White Dam, Mundi Mundi; Williams and Skirrow 2000). These regions are characterized by extensive Na-Ca(-Cl)- or K-metasomatism, and intrusions that are similar in age to the ore deposits (Barton and Johnson 1996; Williams et al. 2005). The review that follows is taken from Pirajno and Bagas (2008).

The Ernest Henry deposit is in the Cloncurry district at the eastern margin of the Mount Isa Inlier in Queensland, where 1760–1660 Ma metasedimentary (clastic-carbonate-evaporite) and bimodal metavolcanic rocks are intruded by 1550–1500 Ma alkaline to subalkaline A type granitic rocks. The rocks in the region are characterised by extensive Na and Na-Ca alteration, which is broadly synchronous with the granite intrusions (Mark et al. 2000). The Cu-Au ore at Ernest Henry deposit is the largest in the district, with a resource of 167 Mt at 1.1 Cu% and 0.54 g/t Au (Ryan 1998; Mark et al. 2000), and it has a complex metal association of Cu-Au-Co-Ag with trace amounts of As-Se-Mo-Sn-Sb-Te-U-LREE-W-Hg-Bi (Williams 1998a, b). The ore is hosted in a structurally controlled hydrothermal breccia vein or pipe-like body that has gradational contacts

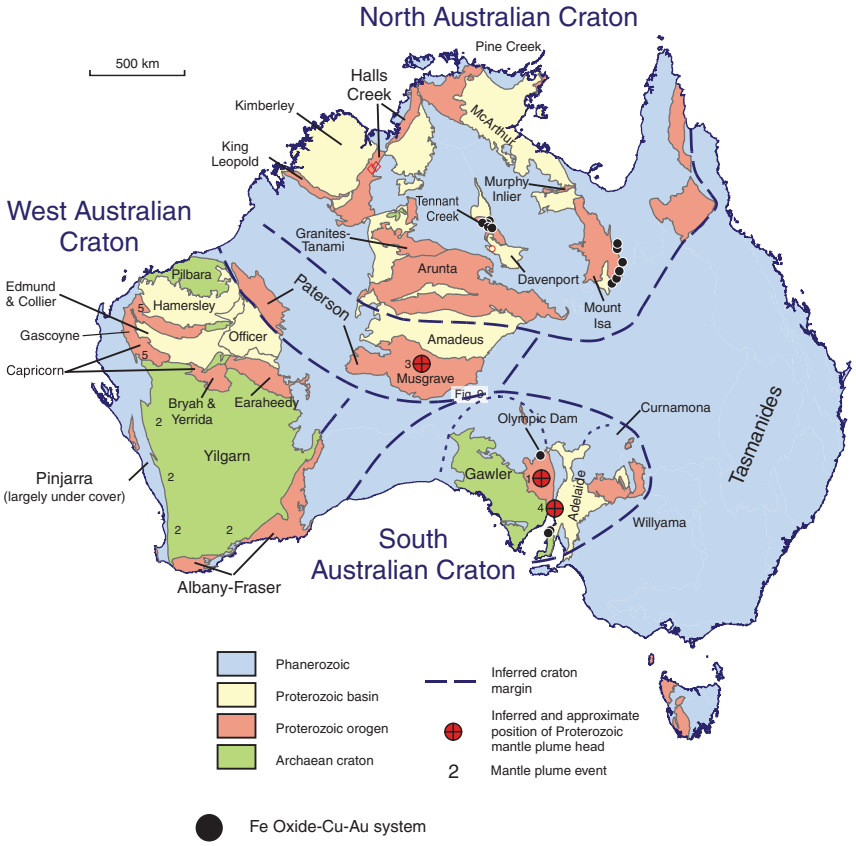


Fig. 4.42 Simplified map of Australia with Phanerozoic, Proterozoic and Archaean terranes and distribution of IOCG mineral systems of Proterozoic age (based on and modified from Pirajno and Bagas, 2008). Proterozoic mantle plume events: 1 ca. 1580 Ma Hitalba-Gawler Range; 2 ca. Marnda Moorn dyke swarm; 3 ca. 1080 Ma Warakurna; 4 ca. 830 Ma Gairdner dyke swarm; 5 ca. 755 Ma Mundine dyke swarm

with a crackle breccia (Mark et al. 2000, 2005; Ryan 1998). An important feature of the Ernest Henry mineral system is the complexity of multiple generations of veins, brecciation events and hydrothermal alteration that formed at temperatures between 400° and 550°C (Mark et al. 2000). These can be considered in terms of regional Na-Ca alteration, pre- and early mineralisation and alteration, Cu-Au mineralisation, and post Cu-Au mineralisation events (Mark et al. 2000). Na-Ca metasomatism is characterised by assemblages containing albite, actinolite, titanite, quartz, magnetite, overprinted by K-feldspar, hematite, epidote, and quartz (Williams 1998a; Mark et al. 2000). Alteration associated with the mineralisation typically consists of biotite-magnetite and garnet-K-feldspar-biotite-pyrite assemblages. Mineral species, including ore minerals, are magnetite,

hematite, chalcopyrite, pyrite, pyrrhotite, barite, fluorite, titanite, garnet, molybdenite, arsenopyrite, sphalerite, galena, monazite, scheelite, and REE-rich fluorocarbonate. In the weathering profile, ore minerals are cuprite, native Cu, chrysocolla, chalcocite covellite, and bornite (Williams 1998a, b).

The Paleoproterozoic (~1870 Ma) Warramunga Province in the Tennant Creek Inlier (Fig. 4.42) contains Au-Cu-Bi deposits associated with massive magnetite-quartz or hematite-quartz (ironstone) bodies included in the Tennant Creek goldfield. The Paleoproterozoic (ca. 1830–1815 Ma) Davenport Province in the southern part of the Tennant Creek Inlier (Fig. 4.42) contains a variety of small mineral occurrences including W, Au, Sn, Cu, Pb-Zn, Ni, Ta and Nb. The Tennant Creek mineral field is hosted by the lower greenschist facies clastic sedimentary and volcaniclastic rocks (ca. 1870 Ma Warramunga Formation). Pre- to syn-orogenic monzogranite, granodiorite and porphyry sills were predominantly intruded between ~1870 and ~1830 Ma (Stolz and Morrison 1994). The province is also intruded by late- to post-orogenic (late Paleoproterozoic) granite, porphyry, and lamprophyre (Ahmad et al. 1999).

Most IOGC deposits in the Tennant Creek mineral field are associated with ironstone bodies that are irregular in shape, flattened, ellipsoidal and pipe-shaped with long axes pitching steeply in an early (S_1) cleavage plane (Ahmad et al. 1999; Skirrow and Walshe 2002). The ironstones are discordant to bedding and many form lines of lodes that trend east (Ahmad et al. 1999). Of the 700 or more ironstone bodies recorded in the Tennant Creek goldfield, less than 200 are known to contain mineral occurrences, and only 25 have recorded productions of over 100 kg of Au (Ahmad et al. 1999). Skirrow and Walshe (2002) have modelled the Tennant Creek Au-Cu-Bi deposits and suggested that the ores formed at temperatures of around 350–400°C and consisted of a range of mineral systems from a reduced end-member to an oxidised end-member. The former being dominated by pyrrhotite, magnetite and pyrite, with salinities in the range of 3–10% NaCl eq., S isotope compositions of 0–5‰, and $CH_4(g) + N_2(g)$ in the fluids. In contrast, the oxidised end-member is dominated by pyrite, hematite, and magnetite; with salinities in the range of 12–20% NaCl eq.; S isotope compositions of –15 to + 5‰; and $CO_2(g) + N_2(g)$ rich fluids. Mixing of the reduced with oxidised fluids engendered high Au-grades.

The main minerals in the ores of the Tennant Creek deposits are magnetite, chalcopyrite, pyrite, hematite, gold, bismuthinite, bismuth sulfosalts, chlorite, quartz, talc, dolomite, sericite, pyrrhotite, marcasite, bornite, galena, sphalerite, bismuth, cobaltite, uraninite, scheelite, stilpnomelane, minnesotaite, greenalite, actinolite, and cosalite (Large 1975; Large and Mumme 1975; Solomon and Groves 1994). Gold is concentrated in magnetite-chlorite(-muscovite) zones in the ironstone bodies at their base, footwall or along their contact with the host rocks (Ahmad et al. 1999).

A conceptual model depicting the possible origin and paths of ore fluids for IOCG systems in the Gawler Craton and Tennant Creek Inlier is shown in Fig. 4.43).

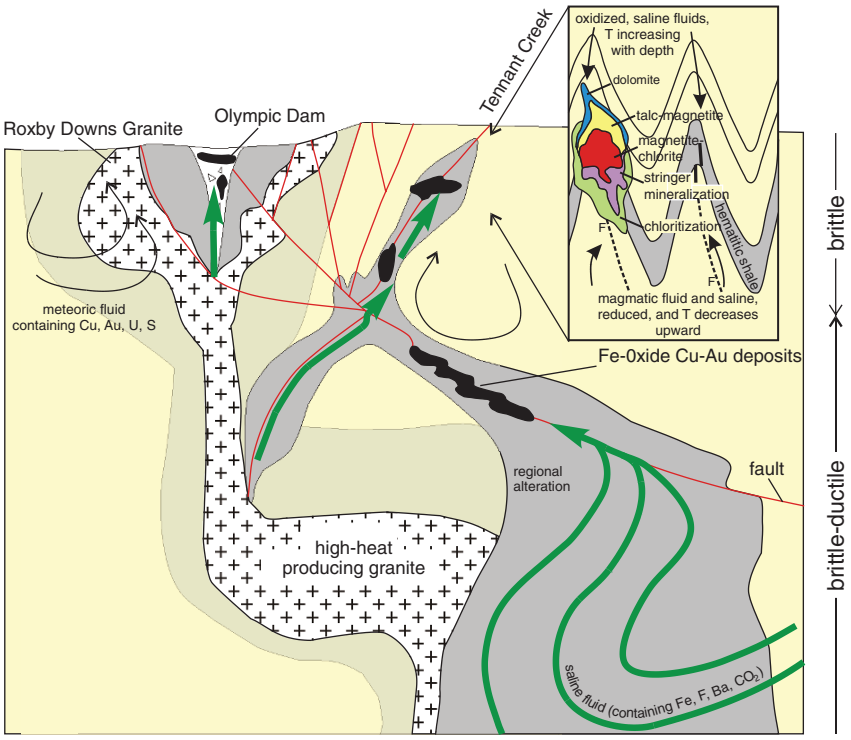


Fig. 4.43 Conceptual model for the formation of Fe oxide-Cu-Au deposits at different crustal levels. After Pirajno and Bagas (2008; adapted after Large 1975; Wedeking et al. 1989; Davidson 2002)

4.6.2 Vergenoeg Fe Oxides-Fluorite Deposit, South Africa

The Vergenoeg deposit, containing Fe oxides (hematite, magnetite, and supergene goethite), fluorite and sulphides, is hosted by rhyolitic pyroclastic rocks of the Rooiberg Group (Section 4.3.5.2) and is located almost in the centre of the four lobes of the Bushveld Igneous Complex (see Fig. 4.9). The eruption of the Rooiberg rhyolitic rocks took place at about 2.06 Ga. The deposit was studied in detail by Crocker (1985), whilst more recent works can be found in Borrok et al. (1998), Martini and Hammerback (1998) and Fourie (2000). Other and possibly coeval and genetically associated deposits in the region, include a fluorite-magnetite-Cu-Au at Slipfontein hosted by Bushveld granite (Bobbejaankop granite), the Buffalo Fluorspar deposit and the Zwartkloof fluorite-magnetite-fayalite veins, also hosted by Rooiberg rhyolitic rocks.

The Vergenoeg deposit consists of a pipe-like body, with a diameter of about 900 m at the surface, decreasing to about 400 m, at a depth of 600 m (Martini and Hammerback 1998). The Vergenoeg mineralisation consists of a series of

horizontally stacked lenses. The pipe contains magnetite, siderite, fayalite and fluorite, cutting through the Vergenoeg Pyroclastic Suite (Crocker 1985). The Vergenoeg suite comprises a sedimentary unit, hematite and hematite-fluorite units, a breccia agglomerate and ignimbrite, forming a north–south elongate body of about 8–9 km, within which is the volcanic pipe that was formed by a gas-vapour volcanic eruption. Hematite-fluorite, magnetite-fluorite and magnetite-fayalite assemblages make up about 90% of the mineralogy (Fourie 2000). Other ore minerals are apatite, monazite, xenotime and Fe and minor Cu sulphides. The fluorite has high P contents suggesting the presence of xenotime and monazite, and for this reason it also has high abundances of Th and U. Fluorite bodies are locally brecciated, with large fluorite crystals in a matrix of fine-grained fluorite, siderite, pyrite, quartz, goethite, limonite. Siderite is present in all rock types and at all depths. It occurs as veinlets and stringers that cut through the host rocks. Magnetite occurs associated with lesser quantities of ilmenite and Ti-magnetite. A plug of massive magnetite is in the centre of the Vergenoeg pipe and is surrounded by a halo of pyrite and fluorite. Fayalite is at the deepest levels of the pipe. Pyrite and pyrrhotite may be locally abundant, accompanied by lesser arsenopyrite, chalcopyrite, molybdenite, galena and sphalerite.

In the upper parts of the pipe, a porous hematite-goethite gossan, containing up to 20% fluorite, minor cassiterite, apatite and REE minerals, constituted the main orebody from which fluorite was extracted. The gossan cap grades through a transition zone into unoxidised ore. Minor sulphides (pyrite, chalcopyrite, arsenopyrite and sphalerite) are present in the deeper levels of the pipe. Ore grades ranged from 20 to 40% CaF_2 and 50–60% Fe_2O_3 (Martini and Hammerback 1998).

The Vergenoeg pipe is a volcanic vent, from which the pyroclastic material was erupted. An apron of fluorite-hematite-rich fragmental rocks (agglomerates, breccias, epiclastic rocks) surrounds the pipe. These rocks are divided into a basal massive quartz-feldspar felsite unit (possibly an ignimbrite), overlain by a massive fluorite-hematite and a breccia-agglomerate unit. The massive fluorite-hematite unit is interpreted as a lava flow of immiscible Fe-rich magma (Borrok et al. 1998). The breccia and agglomerate rocks contain large fragments of rhyolite and hematite enclosed in a matrix of hematite and fluorite. Also present is a rock that consists of irregular masses of cryptocrystalline silica with inclusions of hematite and fluorite. This rock type can be interpreted as a siliceous sinter deposit. At the top of the pyroclastic suite is a fine-grained banded iron-formation-like rock, with mud cracks and ripple marks. A schematic section through the Vergenoeg pipe is shown in Fig. 4.44. Borrok et al. (1998) recognised an assemblage of primary minerals in the lower part of the pipe. The primary assemblage consists of fluorite, fayalite, ilmenite, apatite, allanite and pyrrhotite. Early and late secondary assemblages developed by alteration of the primary assemblage. The early secondary assemblage contains ferroactinolite, grunerite, titanian magnetite, quartz and sulphides. The late secondary assemblage is formed by alteration of the primary and early

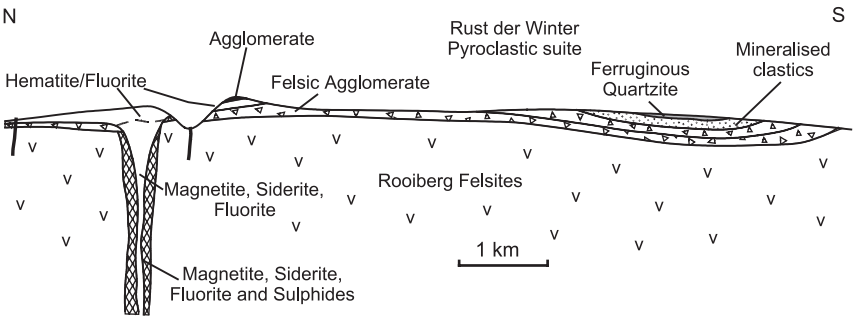


Fig. 4.44 Schematic section showing stratigraphic relationships between the Vergenoeg volcanic pipe, its pyroclastic ejecta and epiclastic sediments

assemblages and consists of magnetite, stilpnomelane, biotite, hematite, siderite, sphene, apatite and REE minerals.

The iron-rich nature of the Vergenoeg lithologies and other localities nearby appear to be the result of plutonic, volcanic exhalative and metasomatic activity, whose precise nature and relationships are poorly understood. Similar Fe oxide deposits occur in the Bobbejaankop Granite (see Section 4.3.5.1) supporting a genetic link between Vergenoeg and this granite, as postulated by Crocker (1985). This large-scale and nearly pervasive Fe enrichment was considered by Crocker (1985) as a general trend of Fe-Ca-F-CO_2 enrichment due to immiscibility of Fe-oxide-rich magmatic fractions. Exsolution and degassing of HF may have been an important factor, responsible for the pervasive Fe-F alteration in the region. In Crocker's model, HF-rich fluids flowing through a Fe-rich protolith, such as the mafic rocks of the Bushveld Igneous Complex, leach Ca and Fe to form fluorite, chlorite, Fe-actinolite and Fe oxides. As the fluids move upward and loose pressure, magnetite, siderite and fluorite are precipitated. One of the reactions proposed is:

$$4Ca_2Fe_5Si_8O_{22}(OH)(\text{Fe-actinolite}) + 16HF + 6O_2 \rightarrow 8\text{fluorite} + 10\text{hematite} + \text{Fe-actinolite} + 32\text{quartz} + 10H_2O$$

However, based on fluid inclusion and stable isotope studies, Borrok et al. (1998), dispute Crocker's model of immiscible oxide melts, instead they suggested that the Vergenoeg mineralisation was formed by Fe-rich, high-temperature and high salinity magmatic hydrothermal fluids. The fluid inclusion assemblages recognised by Borrok et al. (1998) are both primary and pseudosecondary. Primary inclusions are of two types: liquid-rich with halite, Fe chloride and sylvite daughter minerals, and CO_2-rich vapour with Fe chloride and halite daughters. There are five types of pseudosecondary inclusions: liquid-rich with a single daughter (halite), liquid-vapour, liquid-rich with hematite daughters, liquid-rich with no daughters and CH_4-rich with no daughters. Primary

inclusions are saline (35–68 wt% NaCl equivalent) and have homogenisation temperatures ranging from 482 to 290°C for type 1 and 485–435°C for the CO_2-rich inclusions. The pseudosecondary inclusions show a range of salinities form as low as 1% (liquid-rich, no daughters) to 29–35 wt% NaCl equivalent for liquid-rich with daughters, and a range of homgenisation temperatures from 120 to 540°C. Inclusion fluids from fluorite were used to determine the $\delta^{18}O$, δD and $\delta^{13}C$ compositions. $\delta^{18}O$ values range from –0.9 to –10.8‰, and δD from –91 to –53‰. The $\delta^{13}C$ compositions, determined from the CH_4 and CO_2-rich fluids, show values of about –28‰ (CH_4) and –12.7 to –1.9‰ (CO_2). Borrok et al. (1998) interpreted the stable isotope data to reflect fluids largely of magmatic origin, although they do no exclude some mixing with oxygenated fluids, probably meteoric. This is supported by the fact that the upper 200–300 m of the pipe are dominated by magnetite and hematite with no fayalite, suggesting that the primary fayalite must have been oxidised by an external source.

The intrusion-related geological setting, the association with felsic igneous rocks, occurrence of magnetite and hematite, the pipe-like geometry of the ore system, and the association with similar systems, although with different metal assemblages (e.g. Slipfontein Cu-Au) and the range of salinities and homogenisation temperatures that fit in with Olympic Dam, Cloncurry and Pea Ridge (Fig. 4.45) suggests that the Vergenoeg deposit is a type of IOCG.

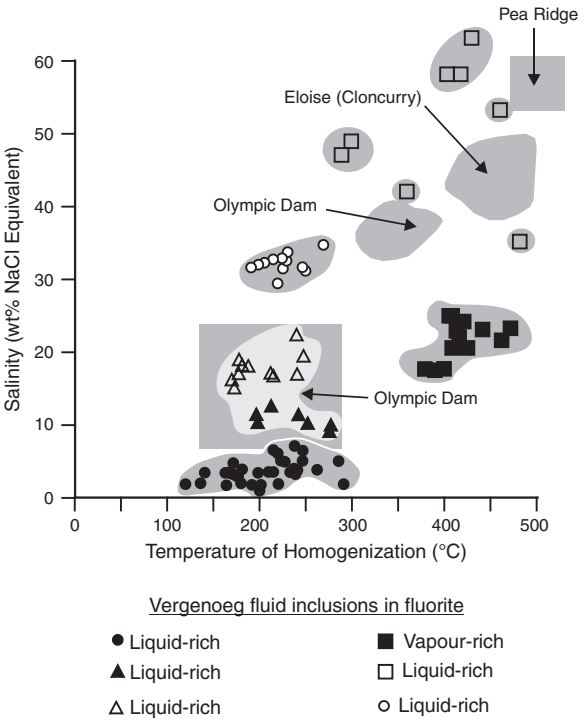


Fig. 4.45 Plot of homogenisation temperatures vs. salinity of fluid inclusions in wt% NaCl equivalent, measured for fluorite in the Vergenoeg deposit; compared with Olympic Dam and Cloncurry in Australia and Pea Ridge in the US (*shaded boxes*). After Borrok et al. (1998 and references therein)

4.6.3 The Palabora Complex (South Africa)

The Palabora carbonatite complex hosts one of the largest Cu mine in South Africa, also producing rare earths, uranium, iron and precious metals (Wilson 1998). The mine is located about 550 km northeast of Johannesburg, near the Mocambique border. The Palabora (also spelt Phalaborwa) Complex, in northeastern Transvaal, South Africa, was emplaced at about 2047 Ma into a basement of Archaean gneisses. The Complex is unusual in that its carbonatite member hosts economically viable Cu mineralisation, with U and Hf being recovered as by-products, and for this reason aptly named by Woolley (2001) as the most important carbonatite complex in the world. Phosphate is also extracted from apatite disseminations within the pyroxenite members. Publications that describe the Palabora Complex include Frick (1975), Verwoerd (1986), Eriksson (1989), Wilson (1998) and Woolley (2001). A simplified geological map of the Complex is shown in Fig. 4.46. The Complex is elongated in a north–south direction and is essentially formed by phlogopite-bearing pyroxenites, pegmatoids and a central carbonatite complex (Lolekop), surrounded by a rock known as "foscorite" (or phoskorite) and composed of serpentinised olivine, magnetite, apatite and minor phlogopite. Smaller intrusions of carbonatite breccias and syenitic rocks occur throughout the Complex. It is not clear whether these syenitic rocks were formed through the action of late magmatic fluids or whether they are the products of magmatic differentiation. Frick (1975) suggested that the highly potassic syenitic rocks were formed by differentiation via a trachytic lineage, and also that the carbonatite, was formed by a process of liquid immiscibility from a fractionating magma. The pyroxenite rocks consist of clinopyroxene, phlogopite, apatite and microcline, with a range of types from solely pyroxene-bearing to phlogopite-only rocks, called glimmerite. Where the grain size exceeds 5 mm, locally up to 1 m in size, the rocks are called pegmatoids.

The Palabora mineralisation consists of Cu with magnetite, urano-thorianite and baddelyite (ZrO_2) with traces of Hf, all of which are extracted from the central Lolekop carbonatite, originally forming a hill now completely removed by mining operations. Apatite and vermiculite are also mined. The Lolekop carbonatite is a vertical pipe, so far traced to least 1 km below the surface, surrounded by foscorite, in turn enveloped by a pegmatoidal rock. This central carbonatite comprises two generations, earlier banded carbonatite arcuate sheets, cut by a later transgressive east-west trending body, from which dykes and veins emanate. The banded carbonatite is coarse-grained, with 20% magnetite, forming layers, calcite with dolomite exsolution lamellae, phologopite, minor olivine, monazite, and some sulphides (dominantly bornite). The transgressive carbonatite also has abundant magnetite and phlogopite, apatite, but the carbonate is more magnesian (ca. 14% $MgCO_3$) than in the banded carbonatite. The Cu mineralisation occurs disseminated within the foscorite and the carbonatites, with grades ranging from 0.48 to 1%. Copper mineralisation is represented by

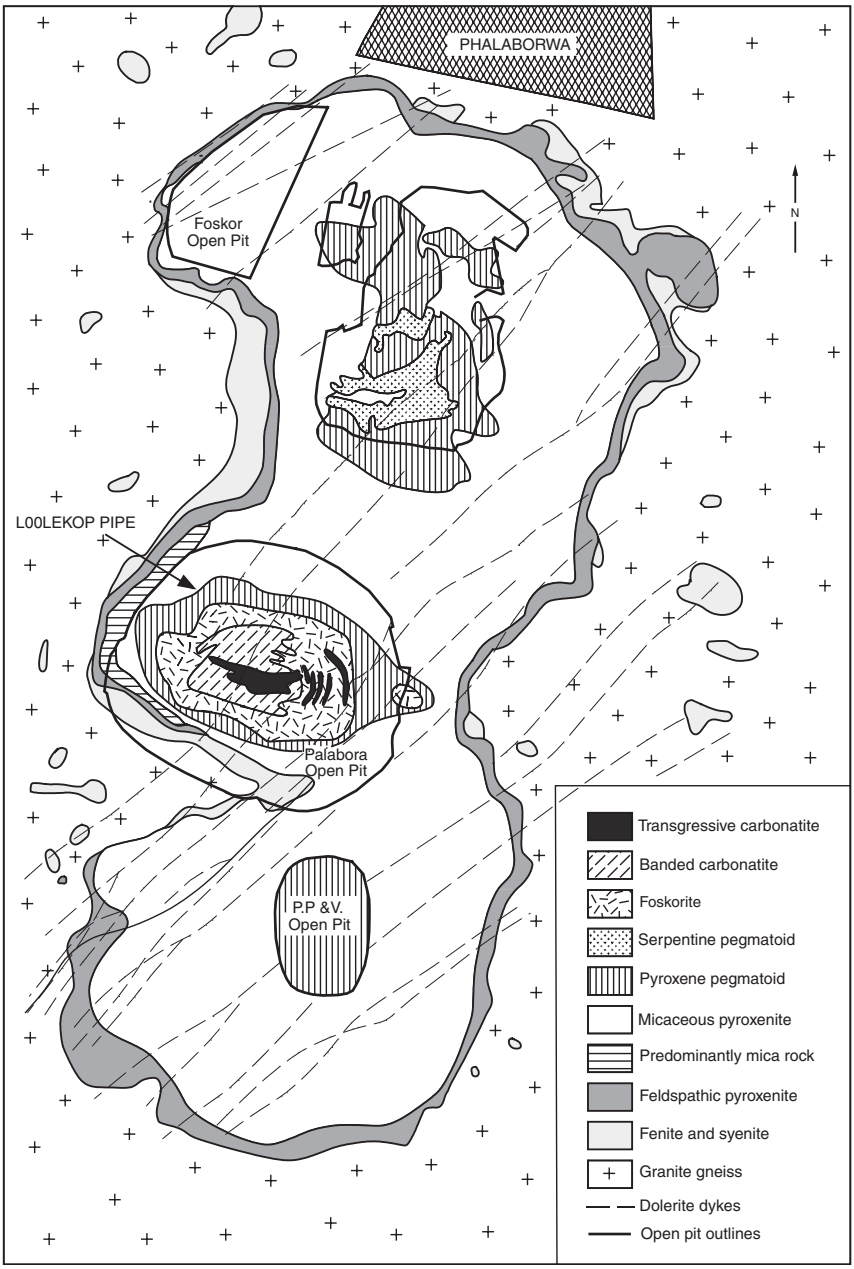


Fig. 4.46 Simplified geology of the Palabora Complex. After Wilson (1998)

chalcopyrite and bornite, with minor cubanite, pyrrhotite and other sulphides of Cu, Pb, Co and Zn. Vallereite is also present as a late stage phase, mainly along shear zone cross-cutting the orebody. Apatite occurs within the phlogopite-bearing pyroxenite, while magnetite forms up to 50% of the foscorite and is invariably titaniferous, and zoned around the Cu mineralisation.

Stable, Sr, Nd and Pb isotope compositions were determined by Eriksson (1989) from carbonatite and pyroxenite samples. Whole-rock carbonatites have $\delta^{18}O$ of 7.7–8.6‰ and for pyroxenites 7.26–7.53‰. The $\delta^{13}C$ values for carbonatites are –5.1 to –3.6‰. These stable isotope values were interpreted as due to mixing of two carbonatite magmas. The depleted mantle signature shown by the $^{143}Nd/^{144}Nd$ ratios (0.50961–0.50977) of the carbonatites are significantly different from those of other carbonatites, whereas the Pb isotopic compositions show different Pb ratios for the carbonatites ($^{206}Pb/^{204}Pb$ = 19.026–34.655; $^{207}Pb/^{204}Pb$ = 15.935–17.993), which suggest a homogeneous crustal source of common Pb. The $\delta^{34}S$, quoted in Eriksson (1989) show values of –1 to + 5‰, which are within the range of magmatic values.

Groves and Vielreicher (2001) proposed the Palabora ore system as an end-member of the IOCG class; a model with which I concur and for this reason I have placed Palabora in this section. A compendium of the features of IOCG listed by these authors include: (1) high tonnage; (2) dominant Fe oxides; (3) low-S Cu minerals; (4) lack of quartz veins; (5) pervasive alteration; (6) an Fe-Cu-Au metal association with variable amounts of REE, F, P, U, Ba, Co, Mo, As, Ag, Nb, Th, Ni; (7) high salinity ore fluids (>50 wt% NaCl equivalent); (8) a general zoning trend with hematite in the upper levels and magnetite in the lower levels, as observed at Ernest Henry in Australia, Carajas in Brazil and the above-discussed Vergenoeg, and from shallow level carbonates through actinolite to grunerite or fayalite at deeper levels (e.g. Vergenoeg). The pipe-like structures of Vergenoeg and Olympic Dam strongly resemble those that are common in anorogenic alkaline intrusions and the general association and timing with continental anorogenic alkaline magmatism support a similar setting and a common origin, with the differences explained in terms of distal (Olympic Dam) to proximal (Vergenoeg).

4.6.4 Bayan Obo REE-Nb-Fe Deposit, Inner Mongolia, China

The Bayan Obo REE-Nb-Fe deposit in Inner Mongolia contains a resource of 57.4 Mt with grades ranging from 5.17 to 6.19% REE_2O_3, Nb reserves estimated at about 2.2 Mt with average grades from 0.126 to 0.141% Nb_2O_3 and 1.5 Bt of Fe at an average grade of 35% (Drew et al. 1990; Fan et al. 2005). Bayan Obo contains the largest rare earth element (REE) resource so far discovered, representing about 70% of the world's total. This unusual deposit was discovered in 1927 by Ding Daoheng and has been, and still is, the object of numerous studies of which, in addition to the above, I cite those of Chao et al.

(1997), Smith and Henderson (2000), Smith et al. (2000), Yang and Le Bas (2004), Fan et al. (2004a, b), Fei et al. (2005) and Smith (2007). I have drawn from these works for the account that follows.

The Bayan Obo, located on the northern margin of the North China Craton, is an extremely complex, hydrothermal, stratabound mineral system hosted in carbonate rocks of the Mesoproterozoic Bayan Obo Group (Fig. 4.47). This Group is a ~1850 m thick package of clastic and carbonate rocks deposited in graben structures that formed in the Archaean basement (Fig. 4.48). The Bayan Obo Group is deformed as a series of northwest-dipping thrust slices and duplex structures. Granitic rocks of Carboniferous-Permian age intruded into the basement and the sedimentary rocks and comprise diorite, granodiorite, biotite granite and leucogranite. Gold-bearing quartz veins are associated with some of these granites. Importantly, as further discussed below, is that other

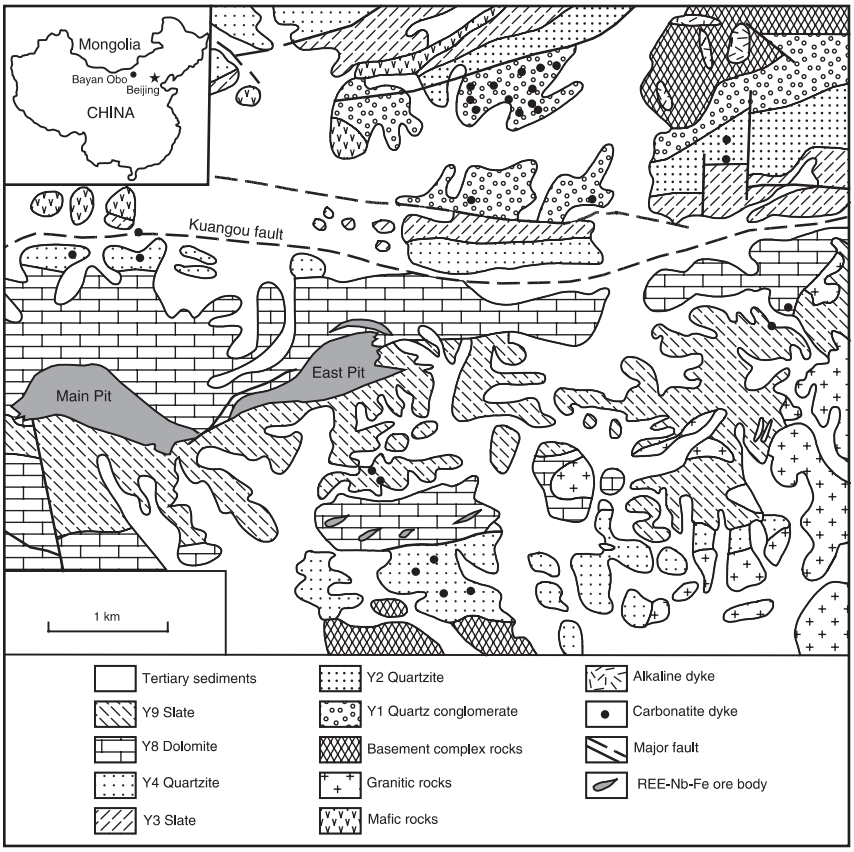


Fig. 4.47 Simplified geological map the Bayan Obo area, distribution of ore zones and carbonatite dykes, shown as *dots* because their length (ca. <60 m) is too small to be represented at this scale. After Fan et al. (2004b)

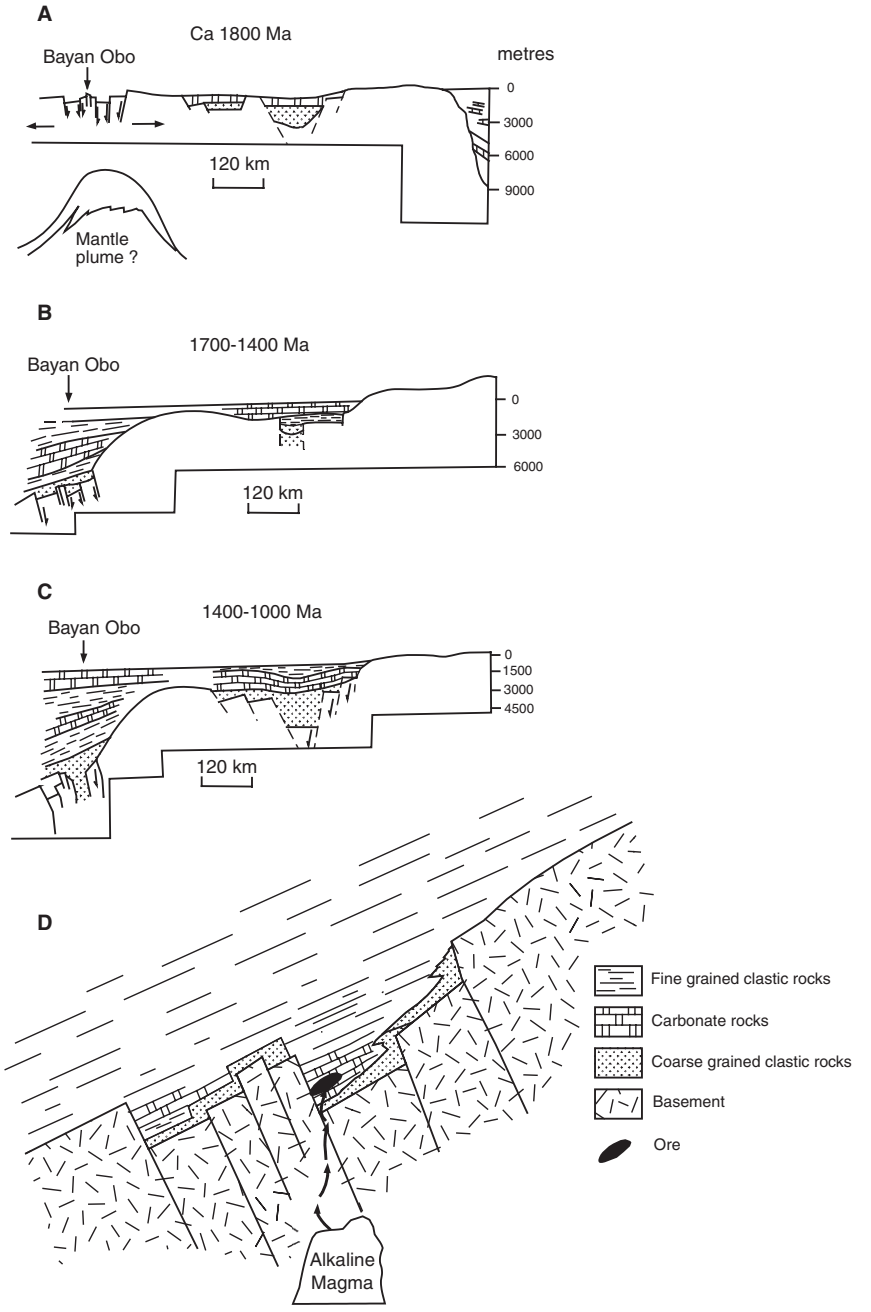


Fig. 4.48 Evolution of the Bayan Obo rift, between ca. 1800 Ma and ca. 1000 Ma on the northern margin of the North China Craton, according to Drew et al. (1990). At 1800 Ma a major thermal event occurred in the region, possibly due to a mantle plume; details in text

igneous rocks in the area include at least two suites of carbonatite dykes, with fenitised (Na-amphibole-albite-phlogopite) country rocks.

The Bayan Obo Group consists of a number of sedimentary units, variably labelled Y, H or Hb in the literature (here I use Y). These consists of a basal conglomerate and sandstone (Y1 unit), overlain by a succession of carbonaceous shale, arkosic sandstone and quartzite (Y2–Y7 units), followed by limestone and dolomite beds (Y8 unit hosting the mineralisation), black shale (Y9), capped by white and grey limestone (Y14–Y18 units). Drew et al. (1990) emphasised that the palaeoenvironmental setting of the base of Y8 is very important for the understanding of the origin of the Bayan Obo system. These authors interpreted the base of Y8 as representing a barrier island sequence with numerous tidal channels, from 1 to 3 m across and 0.5 to 1 m deep, filled with clastic sediments. This sequence was disrupted by thrust faulting resulting in misinterpretations that suggested that the jumbled sedimentary beds were due to stoping by carbonatitic magma. The 350 m-thick Y9 shale is conformable on the Y8 unit and it probably acted as a seal to the hydrothermal fluids. This shale is extensively brecciated and altered by potassic metasomatism in the core of the syncline where the orebodies are located. Volcanic rocks, possibly of Carboniferous age, within a fault-bounded tectonic slice comprise rhyolitic flows, domes, breccia and pyroclastics, hosting a volcanogenic massive sulphide deposit of the kuroko style (Chapter 6). As mentioned above, the structural setting of the Bayan Obo area is very complex and this complexity has hindered a clearer understanding of the mineral system. The complex deformation is the result of continent–continent collisional events that affected the northern margin of the North China Craton, with tectonic transport from northwest to southeast. A large synclinal structure contains the Y8 unit that hosts the mineralisation. According to Drew et al. (1990), the entire deformed package is now a gigantic roof pendant (6–8 km across) in the Carboniferous-Permian granitic rocks. The Carboniferous-Permian granitic rocks were emplaced during the collision event.

There are three main orebodies: Main, East and West, all characterised by an Fe-rich zone, dolomite, aegirine, riebeckite, biotite and fluorite zones. The ore material is hosted by coarse-grained dolomitic marble of the Y8 unit, which is banded and consists of recrystallised dolomite, apatite, magnetite, with minor pyrochlore and Na-amphibole. Ore minerals include monazite [$(Ce,La,Nd)PO_4$], bastnaesite [$(Ce,La,Nd)(CO_3)F$], huanghoite [$Ba(Ce,La,Nd)CO_3)_2F$], parasite [$(Ce,La,Nd)_2CaCO_3)_3F_2$], cebaite [$Ba_2Ce_2(CO_3)_5F_2$] for the REE ores, columbite ($FeNb_2O_6$), pyrochlore [$(Ca,Na)_2Nb_2O_6(OH,F)$], fergusonite ($YNbO_4$), aeschynite [$(Ce,Ca,Fe,Th)(TiNb)_2(O,OH)_6$] for the Nb ores and magnetite, hematite, ilmenite, martite and goethite for the Fe ores (for a comprehensive list of hydrothermal REE minerals, see Gieré 1996). Barite, fluorite, apatite, cerianite, aegirine, arfvesdsonite, riebeckite, albite and microcline are common gangue minerals. Carbonate minerals, apart from dolomite, include benstonite [$(Ca,Sr)_6Ba_6Mg(CO_3)_{13}$], norsethite [$BaMg(CO_3)_2$], barytoclacite ($BaCa(CO_3)_2$ and strontianite ($SrCO_3$).

Sulphide gangue minerals are pyrite, pyrrhotite, sphalerite, galena and chalcopyrite. The hydrothermal system that formed Bayan Obo is responsible for widespread alteration over an area of ca. 50 km^2 in both Archaean migmatites and sedimentary rocks. Drew et al. (1990) distinguished footwall and hanging wall alteration. Calcite-barite-magnetite-albite-monazite veins, up to 3 m wide, cut the footwall migmatite rocks forming alteration haloes containing aegirine, Na amphibole, albite and K-feldspar. Thinner veins and stockworks cut the Y7 and Y6 units and have the same mineralogy as those that cut the migmatites. The Y8 unit in the synclinal structure is pervasively altered as the clastic rocks and migmatites described above. Sodic amphibole, micas (annite, biotite and phlogopite) and Fe oxides are the dominant minerals. Magnetite and hematite are disseminated in the host carbonate rocks, locally forming lenses up to 20 cm thick along bedding planes in economically viable concentrations. In the hanging wall, the Y9 shale acted as an impermeable cap rock focusing the fluids derived from the reactions that replaced the Y8 dolomite, along the contact between Y8 and Y9, resulting in the emplacemet of the REE-Nb-Fe orebodies. The base of the Y9 shale is brecciated and cut by small veins and stockworks, which exhibit a zonation of alteration minerals, outward from fluorite to biotite to K-feldspar. K-feldspar is dominant alteration phase in the matrix of the brecciated material. The paragenesis of the Bayan Obo ore is extremely complex with 11 stages proposed by Chao et al. (1997), from deposition to metamorphism and mineralisation, to granite intrusions. This was simplified by Smith and Henderson (2000) and Smith et al. (2000), with a paragenetic sequence, shown in Fig. 4.49, comprising five stages of mineral deposition.

As mentioned above and shown in Fig. 4.47, the Bayan Obo mineral system is located on the rifted margin of the North China Craton. The North China Craton was subjected to rifting events that affected both its northern and southern margins, beginning about 1800 Ma. Rift systems were formed within the Trans-North China Orogenic Belt, which separates the Eastern and Western blocks of the North China Craton (Zhao et al. 2004, 2005; Kusky and Li 2003). There is evidence that this rifting was associated with the emplacement of continental flood basalts and giant dyke swarms (Peng et al. 2005, 2008). In the north, the Taihang Mountains mafic dyke swarm and the Xiong'er Volcanic Province belong to this 1800 Ma thermal event that affected the North China Craton and have been linked to the breakup of the Columbia supercontinent (Wang et al. 2004; Peng et al. 2005). Peng et al. (2005) working on the geochronology of dyke swarms in the North China Craton, identified four dyke suites with SHRIMP U-Pb ages of 2147 ± 5 Ma, 1929 ± 8 Ma, 1834 ± 5 Ma and 1778 ± 3 Ma. On the basis of this geochronology, Peng et al. (2005) suggested that the older group of dyke suites could relate to the amalgamation of the North China Craton to the Columbia supercontinent (Rogers and Santosh 2002), whereas the younger suites are related to the breakup of Columbia and a mantle plume event at 1830–1750 Ma. This mantle plume would have been implicated in a triple-junction rifting at the southern margin of the North China Craton at ca. 1.78 Ga, leading to its breakup from the

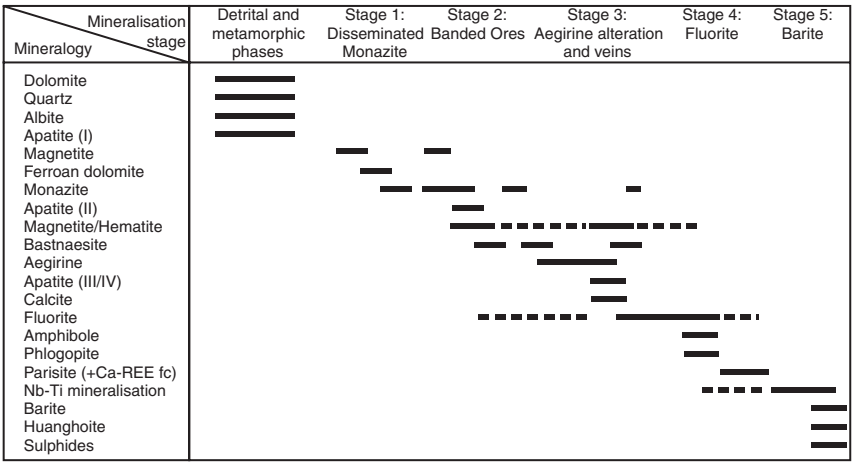


Fig. 4.49 Simplified paragenesis and mineralisation stages at Bayan Obo. After Smith et al. (2000)

Dharwar Craton in India (Peng et al. 2005; Fig. 4.50). U-Pb SHRIMP dating by Zhao et al. (2004) bracketed the Xiong'er volcanism between 1.8 and 1.75 Ga and suggested that this magmatism may represent the Palaeoproterozoic breakup of the North China Craton, which agrees with Peng et al. (2005). The Xiong'er volcanic rocks include basaltic andesite, andesite, trachyandesite, dacite, rhyodacite and rhyolite, with minor sedimentary intercalations and pyroclastic units. In this scenario, the Bayan Obo Group was deposited in a rift system with graben structures on the northern margin of the North China Craton (Fig. 4.47), estimated to have occurred between 1800 and 1350 Ma. The age of the mineralisation is controversial and uncertain. The K-Ar and $^{39}Ar/^{40}Ar$ isotopic systems provide a range of ages from 1200 Ma, 900–800 Ma, 555–474, 430–420 Ma (Chao et al. 1997) to ages of 311–306 Ma for early stage granites (mainly granodiorite) and 258–234 Ma for late stage biotite K-feldspar granites (Fan et al. 2004a and references therein). Chao et al. (1997) distinguished three periods of regional metamorphism and metasomatism: (1) 890 Ma, with recrystallisation of the Y8 carbonate to marble; (2) 425–395 which would have formed metasomatic-metamorphic sodic amphibole; (3) Hercynian event at ca. 300 Ma. Dating of monazite, using ^{232}Th-^{208}Pb chronology, yielded ages ranging from 555 to 420 Ma, with peaks at 430–420 Ma (Wang et al. 2004). Given the wide range of ages it is likely that the Bayan Obo mineral system is the product of multiple tectonothermal events, beginning at ca. 1800 Ma that progressively overprinted the preceding ones.

Fan et al. (2004a, 2005) reported on fluid inclusion data. These authors found three types of fluid inclusions: two-phase aqueous liquid-vapour (L-V),

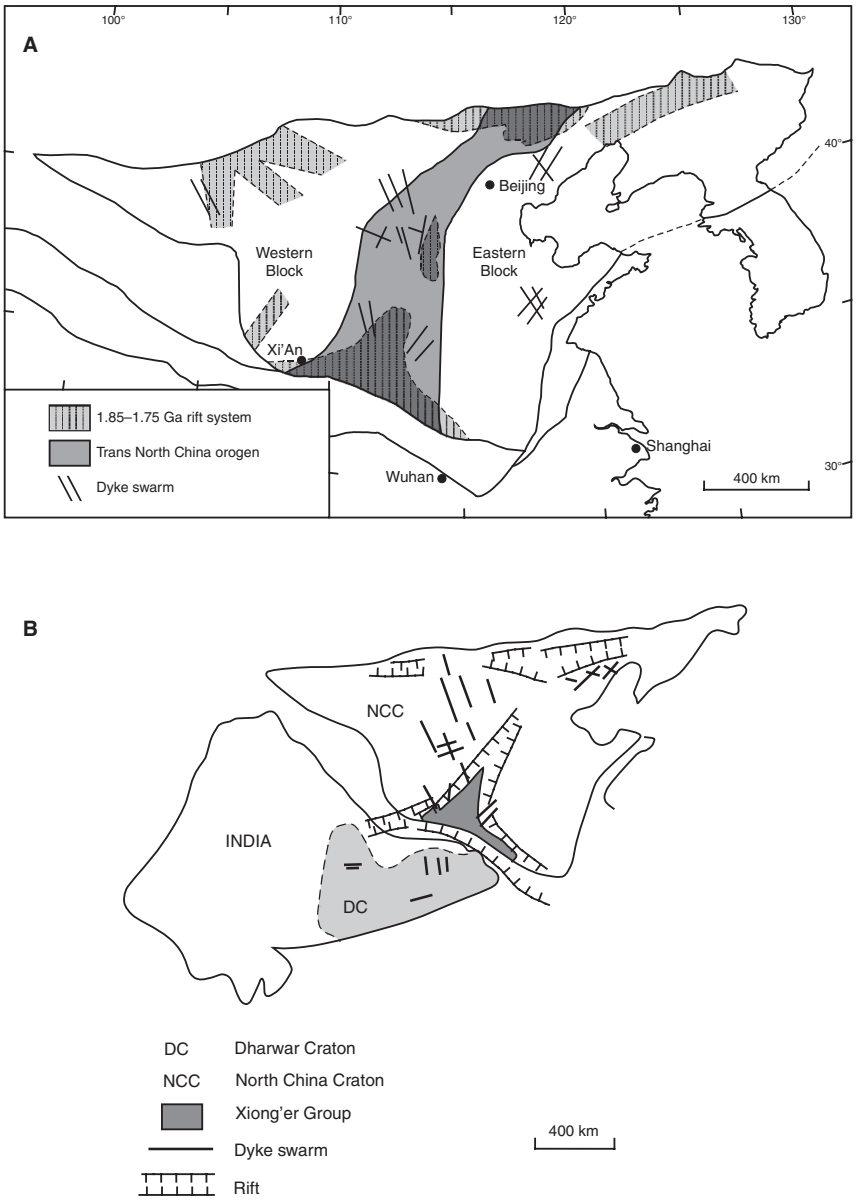


Fig. 4.50 (**A**) The rift system in the northern margin of the North China Craton is where Bayan Obo is located. The Xiong'er Group is represented by continental flood lavas of bimodal composition, dyke swarms occur north of the Xiong'er rift and are of the same age (ca. 1800 Ma), which led Peng et al. (2005) to postulate the activity of a mantle plume (see also Chapter 9); (**B**) possible join between the Dharwar Craton (India) and the North China Craton prior to breakup and postulated three-arm Xiong'er rift system (After Peng et al. 2005)

two to three-phase, almost pure, CO_2 (C) and three-phase liquid-vapour-solid (L-V-S). In the latter, daughter minerals are REE-carbonates (cebaite and bastnaesite), halite, sylvite, barite and calcite were identified by SEM and EDX analyses. Homogenisation temperatures of 480–420°C and 250–220°C were obtained from heating-cooling experiments on the L-V-S inclusion fluids. Salinities ranging from 1 to 15 wt% NaCl equivalent were obtained by Smith and Henderson (2000). In another paper, Fan et al. (2004b) reported on fluid inclusions from the contact zone between the Y8 dolomite and granitic rocks. Fan et al. (2004b) refer to this zone as a skarn because of the mineral assemblages and Fe mineralisation. The Y8 dolomite was subjected to strong metasomatism with the formation of typical skarn minerals, such as diopside, tremolite, garnet, humite, phlogopite, quartz, fluorite and magnetite. The fluid inclusions from this skarn are of three types too: two-phase primary CH_4-rich, three-phase L-V-S and two-phase aqueous. Microthermometric measurements on the CH_4-rich inclusions revealed homogenisation temperatures ranging from 344 to 280°C; L-V-S from 280 to 200°C, whereas aqueous inclusions showed a range from 180 to 140°C. Fan and co-authors suggested that the CH_4-rich inclusion fluids were derived by interaction of magmatic fluids with graphitic country rocks (black shales).

Thus, the genesis of the Bayan Obo mineral system, like its age, is controversial. Ore genesis models included synsedimentary and exhalative deposition or epigenetic hydrothermal linked to granite magmatism or A-type alkaline magmatism and/or carbonatite magma. The main question hinges on the origin of the ore-hosting Y8 dolomitic marble, with ideas ranging from sedimentary, hydrothermal, skarn to being a carbonatite. The skarn hypothesis has problems because of the age gap between the granitic rocks (~311–306 and 258–234 Ma) and the age of the monazite (555–420 Ma; Wang et al. 1994). The presence of carbonatite and albitite dykes that cut the sedimentary package a few km north and south of the orebodies (Fig. 4.46) and the composition of the dolomite support the carbonatite hypothesis. Yang and Le Bas (2004) showed that the Y8 dolomitic marble in the ore zone has a geochemical composition (MnO and SrO contents higher than 0.15 wt%) similar to that of the carbonatite dykes. Therefore, the ore-hosting dolomitic marble has carbonatitic affinities and is not part of the Y8 sedimentary carbonate sequence (Yang and Le Bas 2004). The carbonatite model seems feasible and could be considered within the framework of intraplate A-type magmatism, linked to a mantle plume. Considering the regional context, the Bayan Obo sedimentary package, the rift setting, subsequent collision and extensional events that affected the North China Craton and the accompanying magmatism, it is possible that some of these magmas could have been linked to the mantle plume that originated the rifts and caused the continental volcanism and dyke swarms in the North China craton at ~1800 Ma (see also Chapter 9, Section 9.3). The complex paragenesis of the ores, the wide range of ages could be interpreted to reflect overprinting of the subsequent thermal, tectonic and metamorphic events.

4.6.5 Candelaria, Punta Del Cobre District, Chilean Coastal Belt

The Candelaria deposit is the largest in the Punta del Cobre district where several other (Las Pintadas, Alcaparrosa, Trinidad, Carola, Mantos de Cobre etc.) but smaller IOCG systems are present in a mineral belt along the eastern margin of the Copiapó batholith in northern Chile. The Punta del Cobre belt is part of a larger belt that extends, discontinuously from near Lima (Peru) to near Santiago (Chile), for some 3000 km and containing IOCG deposits of Mid-Late Jurassic and Early Cretaceous (Fig. 4.51). In this region, IOCG systems cover a wide range of styles, such as veins, hydrothermal breccias, replacement bodies and skarns, with more than one style being present in some deposits (Sillitoe 2003).

The Candelaria deposit, has reserves of 470 Mt at 0.95% Cu, 0.22 g/t Au and 3.1 g/t Ag and was described by Marschik et al. (2000, 2003), Sillitoe (2003) and Williams et al. (2005), from whom the following is extracted. The IOCGs of Punta del Cobre are hosted by Early Cretaceous volcanic and volcaniclastic rocks formed in a back-arc basin. The Copiapó granite batholith intruded the back-arc succession between 199 and 97 Ma and comprises plutons of diorite, granodiorite, tonalite, monzodiorite and quartz-monzonite. These granitic rocks belong to the magnetite series, I-type, and are of subalkaline to alkaline affinity, with initial $^{87}Sr/^{86}Sr$ ranging from 0.7031 to 0.7032, initial $^{143}Nd/^{144}Nd$ from 0.51273 to 0.51278. To the west of the Candelaria deposit, the monzodioritic San Gregorio plutonic complex, contained between two north-northwest trending faults, was emplaced by roof uplift in an extensional tectonic regime (Arévalo et al. 2006) has a $^{39}Ar/^{40}Ar$ age of ca. 120 Ma, consistent with ages from nearby plutons. The orebodies form lenses, veins and replacements hosted by andesite and dacite volcanic rocks of the upper parts of Punta del Cobre Formation, or at the contact between the volcanics and overlying greywacke rocks and intercalated breccia and volcanics. These ore zones are structurally controlled, being emplaced at the intersection of northwest and north-northwest faults with volcanic rocks. The Cu-Au ores are mainly sulphides in veins, in the matrix of breccias or stringers and veinlets in hydrothermally altered rocks. Sulphides also overprint the massive magnetite replacement bodies. The ores consist of at least three main assemblages (Arévalo et al. 2006): (1) chalcopyrite-pyrite-magnetite ± pyrrhotite veins; (2) chalcopyrite-pyrite-magnetite in the matrix of breccias; and (3) chalcopyrite ± pyrrhotite in mylonitic biotite schist. Gold occurs as inclusions in the chalcopyrite, filling microfractures in pyrite or as Hg-Au-Ag alloys. Minor amounts of pyrrhotite, sphalerite, molybdenite and aresnopyrite are present in places. As in all IOCG systems, mineralisation-alteration was multistage and complex, with various alteration styles, lateral and vertical zonations. Nearly pervasibe Na-Ca metasomatism with alteration of volcanic, intrusive and sedimentary rocks is widespread at the district scale and represented by albite or Na plagioclase and/or scapolite and locally Ca amphibole, Ca pyroxene and epidote. Potassic ± Ca (biotite and K-feldspar)

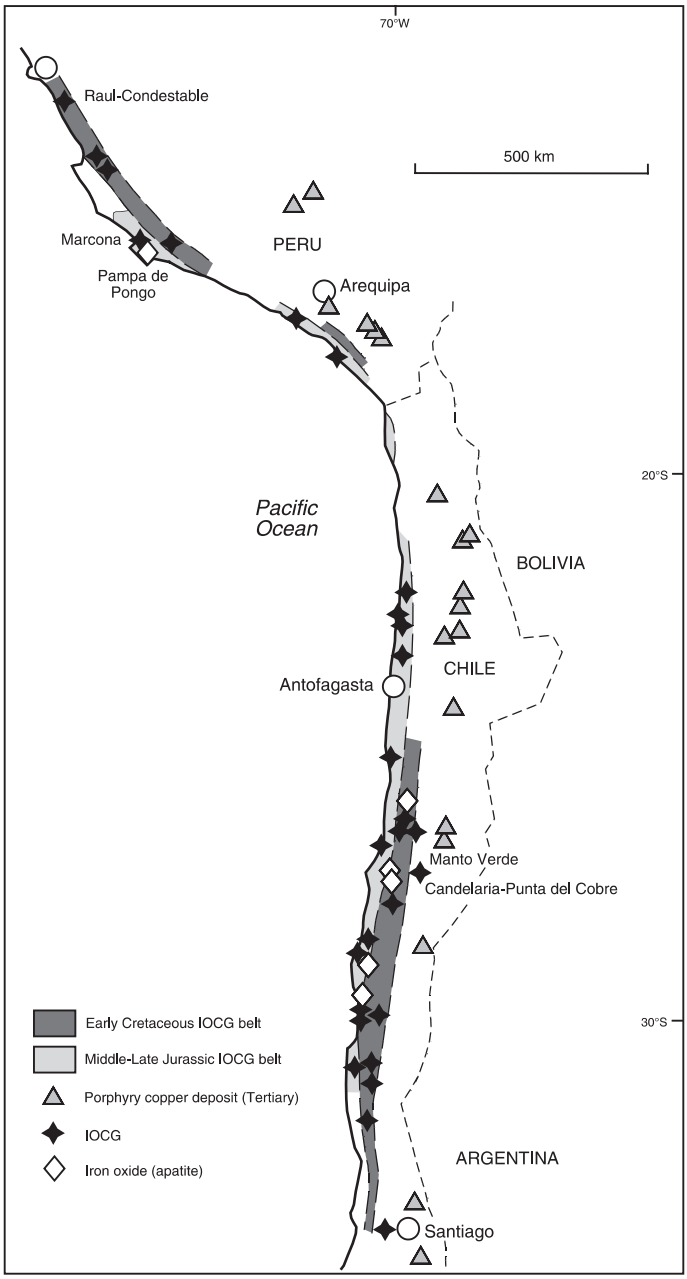


Fig. 4.51 The central Andean porphyry-IOCG province, extending from southern Peru to northern Chile. After Sillitoe (2003) and Williams et al. (2005)

alteration locally affects large volume of rocks. The Cu-Au orebodies are associated with these alteration types. A paragenetic sequence, as worked out by Reynolds (2000), is shown in Fig. 4.52.

There are at least three mineralisation-alteration stages. One is prograde and is characterised by magnetite replacing hematite, pervasive magnetite-quartz-biotite alteration at temperatures of about 600–500°C. The second stage is sulphide-dominated (chalcopyrite-pyrite) with temperatures from 500 to 300°C, followed by late-stage hematite-calcite at temperatures of <250°C Sulphur isotopic compositions range from +3.1 to –3.2‰ $\delta^{34}S$, with higher values from the late stages on the margins of the ore zones. As previously mentioned, the $\delta^{34}S$ data are consistent with a magmatic origin for the ores, perhaps with some minor contribution of sedimentary materials from the peripheral zones. Homogenisation temperatures of vapour-liquid (V-L) hypersaline fluid inclusions in quartz-chalcopyrite range from >440 to 370°C and <180°C in V-L inclusions in late calcite. Calculated temperatures obtained from $\delta^{18}O_{SMOW}$ (values of +5.9 to +8.9‰) range from 440 to 370°C confirming the figures obtained fluid inclusion data. Similarly, fluids in equilibrium with late calcite have $\delta^{18}O_{SMOW}$ values from –5.4 to +1.3‰ at temperatures of 180–100°C.

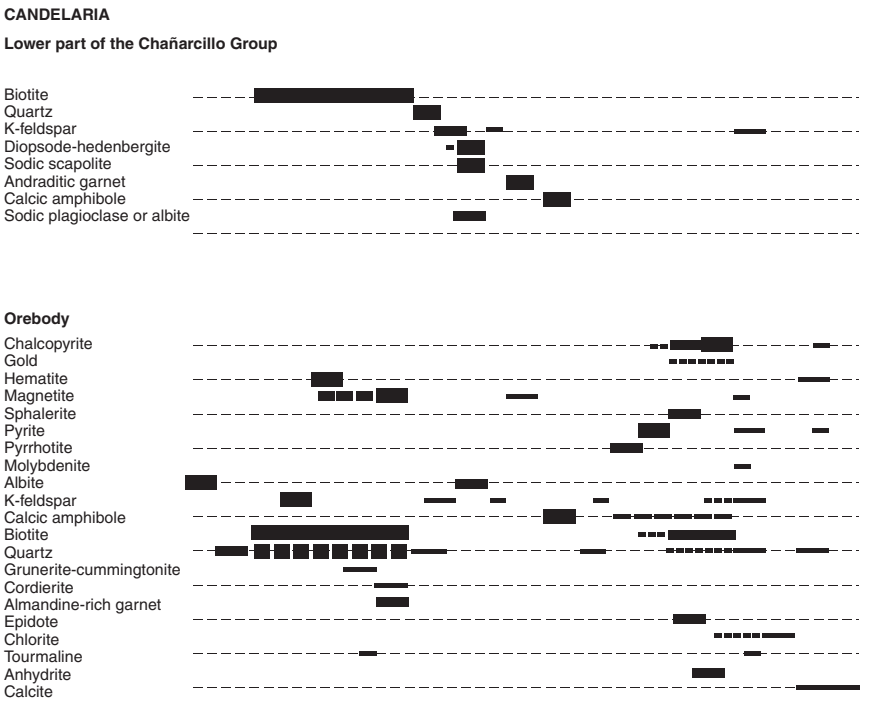


Fig. 4.52 Paragenetic sequence of mineralisation-alteration minerals from the Candelaria IOCG system. After Reynolds (2000)

A model of ore genesis for the formation of the Candelaria IOCG system suggests that magmatic near neutral pH and oxidising fluids ascended along structural conduits. These fluids cooled and possibly mixed with non-magmatic fluids in the upper parts of the system, resulting in the deposition of ore minerals near the volcanic-sedimentary rock contacts (Reynolds 2000). Furthermore, the Candelaria orebody is linked to a syn-plutonic, low-angle shear zone (Candelaria Shear Zone) and a set of ductile-brittle faults. The textural features in the ore zone and the host rocks show that the opening of the structures that contain the mineralisation, the formation of the veins and breccias was simultaneous with the deformation of the host rocks (Arévalo et al. 2006). This together with the isotopic age data from syntectonic biotite in the Candelaria Shear Zone which is indistinguishable from the age of the above mentioned San Gregorio pluton, suggested to Arévalo et al. (2006) that this pluton may have been responsible for the Candelaria IOCG system.

4.7 Concluding Remarks

In this chapter I described the salient aspects of ore systems that originate from magmas emplaced in the crust. Magmatic-hydrothermal and hydrothermal fluids are directly linked to cooling magmas, resulting in a wide variety of mineral deposits, from within the magma itself, or above it and around it in the thermally metamorphosed country rocks. Greisens, vein systems and the range of hydrothermal deposits that form in anorogenic alkaline complexes that also include greisens and skarns have been discussed.

Much of the Sn and W mineral endowment is largely due to greisenisation processes, with key ore minerals such as cassiterite, wolframite and scheelite. The Bushveld Igneous Complex, the largest mafic-ultramafic layered intrusion in the world, is accompanied by felsic magmatism, effectively forming a gigantic bimodal magmatic system. The Bushveld magmatic system contains some of the largest mineral resources of PGE, Cr, Ti and V in the world, and is also endowed with large amounts of Ni, Cu, Sn, Au, Co, F, Fe mostly linked either directly to the felsic components of the system, or to hydrothermal convection driven by the thermal energy produced by the cooling magmas. Other greisen-associated Sn-W deposits are described, ranging from the historic deposits of southwest England and Cornwall, to Panasqueira in Portugal, East Kempville in Canada, Mount Bischoff in Tasmania and finally the very interesting Brandberg West-Goantagab-Frans in the Damara Orogen of Namibia. This is a particularly useful region because it provides, within a comparatively small area, a range of mineral systems, from proximal greisen veins, probably formed very close to the roof of highly evolved granitic intrusions, to progressively distal veins and replacement bodies in marble rocks.

Gold, polymetallic and uraniferous hydrothermal vein systems and breccia pipes include a variety of deposits, at least in terms of metal associations, such

as W-Cu-Zn-Au, Au-Bi-Cu, Au-Bi-Te-Pb-As-Sb-Ag-Mo-Cu-Co, to name a few. The described examples (Scheelite Dome and Kidston) are very interesting and provide the reader with two quite diverse intrusion-related ore systems from two highly mineralised regions. As we approach the end of the first decade of the 21st century, nuclear energy is becoming increasingly important for environmental, practical and perhaps also political reasons in attempting to reduce the heavy dependence on oil and coal. For this reason, I decided to include in this chapter a short section on vein uranium systems. Unconformity-related U deposits and a discussion on uranium geology, geochemistry and deposit types is provided in Chapter 13.

Intracontinental alkaline magmatism, anorogenic ring complexes and carbonatites are typically found in rift systems linked to mantle plume events. Africa is perhaps one of the best studied in the world for this type of magmatic activity, although alkaline magmatic products are common in many other regions of the world, especially northeast Europe, Siberia and parts of central Asia. I have chosen to describe the Damaraland alkaline province in Namibia and the alkaline systems of the Bushveld province, mainly because of my direct involvement in research in those regions.

Iron oxide-Cu-Au-REE-U or IOCG systems remain an ill-defined class of ore deposits, spanning ages from the Proterozoic to the Phanerozoic, and including well known deposits, such as Olympic Dam in South Australia, responsible for sparking off the recognition of and the subsequent enlargement of the IOCG class. IOCG deposits are typically found in intraplate, cratonic margins and anorogenic settings. Others, like Candelaria are related to continental margins, but whether these can be considered as true IOCG is not entirely certain. Classic Australian examples, including Olympic Dam, are discussed, together with two important South African example (Vergenoeg and Palabora). Bayan Obo in Inner Mongolia is still somewhat of an unknown entity, and may not be an IOCG after all. Indeed, the reviewer of this chapter disagreed with the inclusion of carbonatite deposits (Palabora and Bayan Obo in the IOCG class. I find fascinating the tectonic history and settting of Bayan Obo on the margin of the North China Craton. The Palaeoproterozoic to Mesozoic geodynamic evolution of this craton may have affected the Bayan Obo deposit with several thermal and mineral events overprints.

References

Ahmad M, Wygralak AS, Ferenczi PA (1999) Gold deposits of the Northern Territory. Northern Territory Geol Surv Rep 11

Allen CM (ed) (2001) Thematic issue – 25 years of I and S granites. Aust J Earth Sci 48(4)

Anderson MR, Rankin AH, Spiro B (1992) Fluid mixing in the generation of mesothermal gold mineralisation in the Transvaal Sequence, Transvaal, South Africa. Eur J Mineral 4:933–963

Annikova IY, Vladimirov AG, Vystavnoi SA, Zhuravlev DZ, Kruk NN, Lepekhina EN, Matukov DI, Moroz EN, Palesskii SV, Ponomarchuk VA, Rudnev SN, Sergeev SA (2006)

U-Pb and 39Ar/40Ar dating and Sm-Nd and Pb-Pb isotopic study of the Kalguty molybdenum-tungsten ore-magmatic system, southern Altai. Petrol 14:81–97
Arévalo C, Grocott J, Martin W, Pringle M, Taylor G (2006) Structural setting of the Candelaria Fe oxide Cu-Au deposit, Chilean Andes. Econ Geol 101:819–841
Arnaud NN, Vidal PH, Tapponier P, Matte PH, Deng WM (1992) The high K_2O volcanism of northwestern Tibet: geochemistry and tectonic implications. Earth Planet Sci Lett 111:351–367
Artamonov MA, Vostokov YN (1982) Ring structures of the Baltic-Scandinavian region. Inter Geol Rev 24:643–645
Ash JP, Tyler N (1986) A preliminary investigation of fluid inclusions in the Pilgrim's Rest goldfield, eastern Transvaal. Econ Geol Res Unit, Univ Witwatersrand, Inf Circ 180
Atherton MP, Gribble CD (eds) (1983) Migmatites, melting and metamorphism. Shiva Publ Ltd, Nantwich
Bailey DK (1983) The chemical and thermal evolution of rifts. Tectonophysics 94:585–598
Bailey DK (1984) Kimberlite: "the mantle sample" formed by ultrametasomatism. In: Kornprobst J (ed) Kimberlite and relate rocks. Elsevier, Amsterdam, pp 232–333
Bailey DK (1987) Mantle metasomatism – perspective and prospect. Geol Soc Spec Publ 30:1–14
Bain JHC, Draper JJ (eds) (1997) North Queensland geology. Australian Geological Survey Organisation Bulletin 240 Geol Surv Queensland, Queensland Geol 9
Baker EM, Tullemans FJ (1990) Kidston gold deposit. In: Hughes FE (ed) Geology and mineral deposits of Australia and Papua New Guinea, The Aus I MM, Monogr 14, vol 2, pp 1461–1465
Baker EM, Andrew AS (1991) Geologic, fluid inclusion, and stable isotope studies of the gold-bearing breccia pipe at Kidston, Queensland, Australia. Econ Geol 86:610–830
Barbarin B (1999) A review of the relationships between granitoid types, their origins and their geodynamic environments. Lithos 46:605–626
Barsukov VL (1957) The geochemistry of tin. Geokimiya 1:41–53
Barton MD (1996) Granitic magmatism and metallogeny of southwestern North America. Trans Geol Soc Edinb, Earth Sci 87:261–280
Barton MD, Johnson DA (1996) Evaporitic source model for igneous-related Fe oxide-(REE-Cu-Au-U) mineralization. Geology 24:259–262
Bell K (ed) (1989) Carbonatites – genesis and evolution. Unwin Hyman, London
Bell K, Simonetti A (1996) Carbonatite magmatism and plume activity: implications from the Nd, Pb and Sr isotope systematics of Oldoinyo Lengai. J Petrol 37:1321–1339
Bell K, Kjarsgaard BA, Simonetti A (eds) (1998) Carbonatites into the twenty-first century, a volume in honour of John Gittins. J Petrol 39(11–12)
Benedetti M, Boulegue J, Hieronymous B, Kotschoubey B, Pinto da Silva E (1990) Present behaviour of gold in lateritic environment, Salobo (State of Para-Brazil). Geochemistry of the Earth's surface and of mineral formation. 2nd Int. Symp., Aix-en-Provence, pp 27–29
Best MG (1982) Igneous and metamorphic petrology. WH Freeman and Co, New York
Beus AA, Zalashkova NY (1964) Post-magmatic high temperature metasomatic processes in granitic rocks. Int Geol Rev 6:668–681
Black R, Bowden P (eds) (1985) Alkaline ring complexes in Africa. J Afr Earth Sci 3(1/2)
Black R, Lameyre J, Bonin B (1985) The structural setting of alkaline complexes in Africa (a review). J Afr Earth Sci 3:5–16
Blissett AH, Creaser RA, Daly SJ, Flint RB, Parker AJ (1993) Gawler range volcanics. In: Drexe JF, Preiss WV, Parker AJ (eds) The geology of South Australia. Geol Surv South Australia Bull 54: 107–124
Boer RH, Meyer FM, Robb LJ, Graney JR, Vennemann TW, Kesler SE (1995) Mesothermal-type mineralization in the Sabie-Pilgrim's Rest gold field, South Africa. Econ Geol 90:860–876
Bonin B (2007) A-type granites and related rocks: evolution of a concept, problems and prospects. Lithos, doi:10.1016/j.lithos.2006.12.007

Bonin B, Bébien J, Mason P (2002) Granite: a planetary point of view. Gondwana Res 5:261–273
Borisenko AS, Pavlova GG, Borovikov AA, Obolenskiy AA (1999) Ag-Sb deposits of the Yustid depression, eastern Russia and northwest Mongolia. Int Geol Rev 41:639–664
Borisenko AS, Sotnikov VI, Izokh AE, Polyakov GV, Obolensky AA (2006) Permo-Triassic mineralization in Asia and its relation to plume magmatism: Russian Geol Geophys 47:166–182
Borrok DM, Kesler SE, Boer RH, Essene EJ (1998) The Vergenoeg magnetite-fluorite deposit, South Africa: supportr for a hydrothermal model for massive iron oxide deposits. Econ Geol 93:564–586
Bowden P (1985) The geochemistry and mineralization of alkaline ring complexes in Africa (a review). Jour African Earth Sci 3:17–40
Bowden P, Kinnaird AJ (1984a) Petrological and geochemical criteria for the identification of (potential) ore-bearing Nigerian granitoids. Proc 27th Int Geol Congr Moscow, vol 9. VNU Sci Press, Utrecht, pp 85–119
Bowden P, Kinnaird AJ (1984b) The petrology and geochemistry of alkaline granites from Nigeria. Phys Earth Planet Interiors 35:198–211
Bowden P, Kinnaird JA, Abaa SI, Ike EC, Turaki UM (1984) Geology and mineralization of the Nigerian anorogenic ring complexes. Geol Jahrb B56:1–65
Bowell RJ, Gize AP, Foster RP (1993) The role of fulvic acid in the supergene migration of gold in tropical rainforest soils. Geochim Cosmochim Acta 57:4179–4190
Brathwaite RL, Pirajno F (1993) The metallogenic map of New Zealand. Inst Geol Nuclear Sci Monogr 3
Buchanan PC, Reimold WU, Koeberl C, Kruger FJ (2004) Rb-Sr and Sm-Nd isotopic compositions of the Rooiberg Group, South Africa: early Bushveld-related volcanism. Lithos 29:373–388
Burke K (1996) The African plate. S Afr Jour Geol 99:341–409
Burnard PG, Polya DA (2004) Importance of mantle derived fluids during granite associated hydrothermal circulation: he and Ar isotopes of ore minerals from Panasqueira. Geochim Cosmochim Acta 68:1607–1615
Burnham CW (1997) Magmas and hydrothermal fluids. In: Barnes HL (ed) Geochemistry of hydrothermal deposits, 3rd edn. Wiley, New York, pp 63–123
Burt DM (1981) Acidity-salinity diagrams – application to greisen and porphyry deposits. Econ Geol 76:832–843
Butt CRM (1989) Genesis of supergene gold deposits in the lateritic regolith of the Yilgarn Block, Western Australia. Econ Geol Monogr 6:460–470
Campbell IH, Compston DM, Richards JP, Johnson JP, Kent AJR (1998) Review of the application of isotopic studies to the genesis of Cu-Au mineralization at Olympic Dam and Au mineralization at Porgera, the Tennant creek district and Yilgarn Craton.Aust J Earth Sci 45:201–218
Candela PA (1997) A review of shallow, ore-related granites: textures, volatiles and ore metals. J Petrol 38:1619–1633
Cassidy KF, Barley ME, Groves DI, Perring CS, Hallberg JA (1991) An overview of the nature, distribution and inferred tectonic setting of granitoids in the late-Archean Norseman-Wiluna belt. Precamb Res 51:51–83
Cawood PA (2005) Terra Australis Orogen: Rodinia breakup and development of the pacific and Iapetus margins of Gondwana during the Neoproterozoic an Paleozoic. Earth-Sci Rev 69:249–279
Cawood PA, Tyler IM (2004) Assembling and reactivating the Proterozoic Capricorn Orogen: lithotectonic elements, orogenies and significance. Precambr Res 128:201–218
Černý P, Blevin PL, Cuney M, London D (2005) Granite-related ore deposits. Econ Geol 100th Ann Vol: 337–370

Chao ECT, Back JM, Minkin JA, Tatsumoto M, Wang JW, Conrad JE, McKee EH, Hou ZL, Meng QR, Huang SG (1997) The sedimentary carbonate-hosted giant Bayan Obo REE-Fe-Nb ore deposit of Inner Mongolia, China: a cornerstone example of a giant polymetallic ore deposits of hydrothermal origin. USGS Bull 2143

Chappell BW, White AJR (1974) Two contrasting granite types. Pacific Geol 8:173–174

Chappell BW, Stephens WE (1988) Origin of infracrustal (I-type) granite magmas. Trans Roy Soc Edinb Earth Sci 79:71–86

Chappell BW, Bryant CJ, Wyborn D, White AJR, Williams IS (1998) High- and low-temperature I-type granites. Resour Geol 48:225–235

Clarke LB (1989) The geology of the Kruidfontein Volcanic Complex, Transvaal, S. Africa. Unpubl. PhD Thesis, Univ Leicester, 167 pp.

Clarke LB, Le Bas MJ (1990) Magma mixing and metasomatic reaction in silicate-carbonate liquids at the Kruidfontein carbonatitic volcanic complex, Transvaal. Mineral. Mag 54:45–56

Clemens JD (2003) S-type granitic magmas – petrogenetic issues, models and evidence. Earth-Sci Rev 61:1–18

Coetzee CB (1976) Rare earths. In: Coetzee CB (ed) Mineral resources of the Republic of South Africa. Geol Surv Handb 7:199–201

Coetzee J (1986) The Lease Granite – a granophyric, miarolitic mineralized granite at the apical region of a tin-tungsten system. Trans Geol Soc S Afr 89:335–345

Collins WJ, Beams SD, White AJR, Chappell BW (1982) Nature and origin of A-type granites with particular reference to southeastern Australia. Contrib Miner Petrol 80:189–200

Cooper RW, Langford RL, Pirajno F (1998) Mineral occurrences and exploration potential of the Bangemall Basin. Geol Surv West Aus Rept 64

Creaser RA (1989) Geology and petrology of Middle Proterozoic felsic magmatism of the Stuart Shelf, South Australia. Unpubl. PhD Thesis, LaTrobe University, Melbourne, Australia.

Creaser RA, Price RC, Wormald RJ (1991) A-type granites revisited: assessment of a residual source model. Geology 19:163–166

Creaser RA, White ARJ (1991) Yardea Dacite – large volume, high-temperature felsic magmatism from the Middle Proterozoic of South Australia. Geology 19:48–51

Crocker IT (1979) Metallogenic aspects of the Bushveld granites: fluorite, tin and associated rare metal carbonatite mineralization. Geol Soc S Afr Spec Publ 5:275–295

Crocker IT (1985) Volcanogenic fluorite-hematite deposits and associated pyroclastic rock suite at Vergenoeg, Bushveld Complex. EconGeol 80:1181–1200

Crocker IT (1986) The Zaaiplaats tin field, Potgietersrus district. In: Anhaeusser CR, Maske S (eds) Mineral deposits of southern Africa. Geol Soc S Afr 2: 1287–1299

Crocker IT, Martini JEJ, Sonhnge APG (1988) The fluorspar deposits of the Republics of South Africa and Bophuthatswana. Department of Mineral and Energy Affairs. Geol Surv Handb 11

Cross KC, Daly SJ, Flint RB (1993) Mineralisation associated with the GRV and Hiltaba Suite Granitoids. Olympic dam deposit. In: Drexel JF, Preiss WV, Parker AJ (eds), Geol South Aust. Bull. 54:132–138.

Dahlkamp FJ (1993) Uranium ore deposits. Springer-Verlag, Berlin

Daly SJ, Fanning GM, Fairclough MC (1998) Tectonic evolution and exploration potential of the Gawler Craton, South Australia. AGSOJ Aus Geol & Geophys 17:145–168

Davidson GJ (2002) The shallow to mid-crustal family of iron oxide copper-gold deposits: size, alteration and mechanisms of formation. In: Cooke DR, Pongratz J (eds), Giant ore deposits: characteristics, genesis and exploration, CODES Spec Publ 4, pp 79–102

Davidson GJ, Large RR (1998) Proterozoic copper-gold deposits. AGSO J Aust Geol & Geophys 17:105–113

Davy R, El-Ansary M (1986) Geochemical patterns in the laterite profile at the Boddington gold deposit, Western Australia. Jour Geochem Expl 26:119–144

Didier J (1973) Granites and their enclaves – the bearing of enclaves on the origin of granites. Elsevier Scient Publ Co., Amsterdam
Dobretsov NL (2005) 250 Ma large igneous province of Asia: Siberian and Emeishan traps (plateau basalts) and associated granitoids. Russian Geol & Geophys 46:870–890
Drew LJ, Meng Q, Sun W (1990) The Bayan Obo iron-rare earth-niobium deposits, Inner Mongolia, China. Lithos 26:43–65
du Toit MC, Pringle IC (1998) Tin. In: Wilson MGC, Anhaeusser CR (eds) The mineral resources of South Africa, Council Geoscie Handbk 16, pp. 613–620
Duncan RK (1992) Geology and mineralization of the Mt. Weld rare earths deposit, Laverton, Western Australia. TMS-Australas Inst. Min. Metall. Joint Sympos. San Diego, California
Duncan RK, Willett GC (1990) Mount Weld carbonatite. In: Hughes FE (ed) Geology and mineral deposits of Australia and Papua New Guinea, Aus Isnt Min Metall Monogr 14, pp 591–598
Eadington PJ (1983) A fluid inclusion investigation of ore formation in a tin-mineralized granite, New England, New South Wales. Econ Geol 78:1204–1221
Eales HV, Cawthorn RG (1996) The Bushveld complex. In: Cawthorn RG (ed) Layered intrusions, Elsevier, Develpm Petrol 15, pp 181–230
Ebinger CJ, Sleep NH (1998) Cenozoic magmatism throughout east Africa resulting from impact of a single plume. Nature 395:788–791
Eby GN (1990) The A-type granitoids: a review of their occurrence and chemical characteristics and speculations on their petrogenesis. Lithos 26:115–134
Eby GN (1992) Chemical subdivision of the A-type granitoids: petrogenetic and tectonic implications. Geology 20:641–644
Edgar AD (1983) Relationship of ultrapotassic magmatism in the Western USA to the Yellowstone plume. Neues jahrbuch Miner. Abh1 47:35–46
Eggers A (1979) Large scale circular features in north Westland and west Nelson, New Zealand, possible structural control of porphyry molybdenum-copper mineralization? Econ Geol 76:2064–2065
Ellenberger F, Tamain ALG (1980) Hercynian Europe. Episodes 1980:2–27
Enzweiler J, Joekes I (1990) Adsorption of colloidal gold on colloidal iron oxides. J Geochem. Expl 40:133–142
Eriksson SC (1989) Phalaborwa: a saga of magmatism, metasomatism and miscibility. In: Bell K (ed) Carbonatites – genesis and evolution. Unwin Hyman, London, pp 221–254
Eugster HP (1984) Granites and hydrothermal ore deposits: a geochemical framework. Mineral Mag 49:7–23
Ewart A, Milner SC, Armstrong RA, Duncan AR (1998a) Etendeka volcanism of the Goboboseb Mountains and Messum Igneous Complex, Namibia. Part I: geochemical evidence of Early Cretaceous Tristan plume melts and the role of crustal contamination in the Paraná-Etendeka CFB. J Petrol 39:191–225
Ewart A, Milner SC, Armstrong RA, Duncan AR (1998b) Etendeka volcanism of the Gobobobesb Mounatins and Messum Igneous Complex, Namibia. Part II: voluminous quartz latite volcanism of the Awahab magma system. J Petrol 39:227–253
Fan HR, Xie YH, Wang KY, Tao KJ, Wilde SA (2004a) REE daughter minerals trapped in fluid inclusions in the giant Bayan Obo REE-Nb-Fe deposit, Inner Mongolia, China. Int Geol Rev 46:638–645
Fan HR, Xie YH, Wang KY, Wilde SA (2004b) Methane-rich fluid inclusions in skarn near the giant REE-Nb-Fe deposit at Bayan Obo, northern China. Ore Geol Rev 25:301–309
Fan HR, Hu FF, Wang KY, Xie YH (2005) Aqueous-carbonic-REE fluids in the giant Bayan Obo deposit, China: implications for REE mineralization. In: Mao JW, Bierlein FP (eds) Mineral deposits research: meeting the global challenge, vol 2. Springer, pp 945–948
Fei HC, Xiao RG, Cheng L, Wang CH (2005) Geochemical characteristics and genesis of Na-rich rocks in the Bayan Obo REE-Nb-Fe deposit, Inner Mongolia, China. In: Mao JW,

Bierlein FP (eds) Mineral deposits research: meeting the global challenge, vol 1. Springer, pp 385–388
Ferguson J (1973) The Pilanesberg Alkaline Province, southern Africa. Trans Geol Soc S Afr 76:249–270
Fitton JG, Upton BGJ (eds) (1987) Alkaline igneous rocks. Geol Soc Spec Publ 30. Blackwell Scientific Publ, Oxford
Flint RB (1993) Hitalba Suite. In: Drexe JF, Preiss WV, Parker AJ (eds) The geology of South Australia. Geol Surv South Australia Bull 54: 127–131
Floyd PA, Exley CS, Stone M (1983) Variscan magmatism in Southwest England – discussion and synthesis. In: Hancock PL (ed) The Variscan Fold Belt in the British Isles. Bristol, pp 178–185
Forsythe DL, Higgins NC (1990) Mount Carbine tungsten deposit. Australas Inst Min Metall Monogr 14(2):1557–1560
Foster RP (1977) Solubility of scheelite in hydrothermal chloride solutions. Chem Geol 20:27–43
Foster RP, Mann AG, Armin T, Burmeister B (1978) Richardson's Kop wolframite deposit: a geochemical model for the behaviour of tungsten. In: Verwoerd WJ (ed) Mineralization in metamorphic terranes. Van Schaik, Pretoria, pp 107–128
Fourie PJ (2000) The Vergenoeg fayalite iron oxide fluorite deposit, South Africa: some new aspects. In: Porter TM (ed) Hydrothermal iron oxide copper-gold & related deposits: a global perspective. Aus Miner Found, Adelaide, pp 309–320
Frick C (1975) The Phalaborwa syenite intrusion. Trans Geol Soc S Afr 7:201–214
Gerasimovsky VI, Volkov VP, Kogarko LN, Polyakov AI (1974) Kola peninsula. In: Sorenson H (ed) The alkaline rocks. John Wiley & Sons, New York, pp 206–221
Gieré R (1996) Formation of rare earth minerals in hydrothermal systems. In: Jones AP, Wall F, Williams CT (eds) Rare earth minerals – chemistry, origin and ore deposits, Chapman & Hall, pp 105–150
Giles CW (1988) Petrogenesis of the Proterozoic Gawler Range Volcanics, South Australia. Precambr Res 40/41:407–427
Gittins J (1989) The origin and evolution of carbonatite magmas. In: K. Bell (ed) Carbonatites. Genesis and evolution. Unwin Hyman Ltd, Lond, pp 580–600
Goinhas J, Viegas L (1983) Fractional crystallisation and the origin of tin deposits in granitoids. Mineral Depos 13:11–26
Goldfarb RJ, Hart CJR, Miller M, Miller L, Farmer GL, Groves DI (2000) The Tintina gold belt-a global perspective. In: Tucker TL, Smith MT (eds) The Tintina gold belt: concepts, exploration, and discoveries, British Columbia and Yukon Chamber Mines Spec Vol 2, pp 5–34
Gray DJ, Butt CRM, Lawrance LM (1992) The geochemistry of gold in lateritic terrains. In: Butt CRM, Zeegers H (eds), Regolith exploration geochemistry in tropical and subtropical terrains. Handb Expl Geochem 4, Elsevier, Amsterdam, pp 461–482
Griffin WL (ed) (1995) Diamond exploration: into the 21st century. J Geochem Expl 53(1–3)
Groves DI, Solomon M (1964) The geology of the Mt Bischoff district. Proc R Soc Tas 98:1–22
Groves DI, Martin EL, Murchie H, Wellington HK (1972) A century of mining at Mt. Bischoff, 1871–1971. Tasm Geol Surv Bull 54:310 pp
Groves DI, McCarthy TS (1978) Fractional crystallization and the origin of tin deposits in granitoids. Mineralium Dep 13:11–26
Groves DI, Godlfarb RJ, Gebre-Mariam M, Hagemann SG, Robert F (1998) Diversity within a unified model for Archaean gold mineralisation in the Yilgarn Craton of Western Australia: an overview of the late-orogenci, structurally-controlled gold deposits. Ore Geol Rev 13:29–64
Groves DI, Vielreicher NM (2001) The Phalaborwa (Palabora) carbonatite-hosted magnetite-copper sulfide deposit, South Africa: an end member of the iron-oxide-copper-gold-rare earth element deposit group? Mineral Depos 36:189–194

Haggerty SE (1997) The superplume model for kimberlites, mantle metasomatism and diamond. In: Hatton CJ (ed) PPM '97 Abs Vol, Inter Symp Plumes, Plates and Mineral, Pretoria, pp 39–42
Hall A (1971) Greisenisation in the granite of Cligga Head, Cornwall. Proc Geol Ass 82:209–230
Halley SW, Walshe JL (1995) A re-examination of the Mount Bischoff cassiterite sulfide skarn, Western Tasmania. Econ Geol 90:1676–1693
Hannah JL, Stein HJ (1990) Magmatic and hydrothermal processes in ore-bearing systems. Geol Soc Am Spec Pap 246:1–10
Harley M, Charlesworth EG (1994) Structural development and controls to epigenetic, mesothermal gold mineralisation in the Sabie-Pilgrim's Rest goldfield, Eastern Transvaal, South Africa. Expl Mining Geol 3:231–246
Harmer RE, Gittins J (1998) The case for primary, mantle-derived carbonatite magma. J Petrol 39:1895–1903
Hart CJR, Baker T, Burke M (2000) New exploration concepts for country-rock-hosted, intrusion-related gold systems: Tintina gold belt in Yukon. In: Tucker TL, Smith MT (eds) The Tintina gold belt: concepts, exploration and discoveries. British Columbia and Yukon Chamber Mines Spec Vol 2, pp 145–172
Hart CJR, McCoy DT, Goldfarb RJ, Smith M, Roberts P, Hulstein R, Bakke AA, Bundtzen TK (2002) Geology, exploration and discovery in the Tintina gold province, Alaska and Yukon. Econ Geol Spec Publ 9:241–274
Hart CJR, Mair JL, Goldfarb RJ, Groves DI (2004) Source and redox controls on metallogenic variations in intrusion-related ore systems, Tombstone-Tungsten belt, Yukon Territory, Canada. Trans Roy Soc Edinb, Earth Sci 95:339–356
Hauri EH, Shimuzu N, Dieu JJ, Hart SR (1993) Evidence for hotspot-related carbonatite metasomatism in the oceanic upper mantle. Nature 365:221–227
Haxel G (2005) Ultrapotassic rocks, carbonatite and rare earth element deposits, Mountain Pass, southern California. USGS Bull 2160
Haynes D (2006) The Olympic Dam ore deposit – discovery – a personal view. SEG Newslett 66:1–15
Haynes DW, Cross KC, Bills RT, Reed MH (1995) Olympic Dam ore genesis: a fluid mixing model. Econ Geol 90:281–307
Hildreth W, Moorbath S (1988) Crustal contributions to arc magmatism in the Andes of central Chile. Contr Miner Petr 98:455–489
Hitzman MW, Oreskes N, Einaudi MT (1992) Geological characteristics and tectonic setting of Proterozoic iron oxide (Cu-U-Au-LREE) deposits. Precambr Res 58:241–287
Hosking KFG (1988) The world's major types of tin deposits. In: Hutchison CS (ed) Geology of tin deposits in Asia and the Pacific. Springer, Berlin, Heidelberg, New York, pp 3–49
Huston DL, Vandenberg LC, Wygralak A, Mernagh T, Bagas L, Crispe A, Lambeck L, Cross A, Fraser G, Williams N, Worden K, Meixner T, Goleby B, Jones L, Lyons P, Maidment D (2007) Lode gold mineralisation in the Tanami region, northern Australia. Mineral Depos 42:175–204.
Hutchison CS (1983) Economic deposits and their tectonic settings. MacMillan, New York
Hutchison CS (ed) (1988) Geology of tin deposits in Asia and the Pacific. United Nations Economic and Social Commission for Asia and the Pacific. Springer, Berlin, Heidelberg, 718 pp
Ishihara S (1977) The magnetite-series and ilmenite-series granitic rocks. Min Geol 27:293–305
Ishihara S (1981) The granitoid series and mineralization. Econ Geol 75th Anniv Vol, 458–484
Ishihara S, Sawata H, Arornsuwan S, Busaracome P, Bungbrakearti N (1979) The magnetite series and ilmenite series granitoids and their bearing on tin mineralisation, particularly of the Malay peninsula region. Geol Soc Malay Bull 11:103–110

Ivanova GF (1969) Conditions of concentration of tungsten during greisenization. Geokhimiya 1:22–32
Jackson NJ, Drysdall AR, Stoeser DB (1985) Alkali granite related Nb-Zr-REE-U-Th mineralisation in the Arabian Shield. In: High heat producing (HHP) granites, hydrothermal circulation and ore genesis conference, St. Austell, Cornwall, England, Inst Min Metall. pp 479–487
Johnson JP, Cross KC (1995) U-Pb geochronological constraints on the genesis of the Olympic Dam Cu-U-Au-Ag deposit, South Australia. Econ Geol 90:1046–1063
Jones TR, Moeller T, Truelove AJ (1990) Collingwood tin deposit. Australas Inst Min Metall Monogr 14(2):1549–1556
Kampunzu AB, Lubala RT (eds) (1991) Magmatism in extensional structural settings – the Phanerozoic Africa plate. Springer, Berlin
Kelly WC, Rye RO (1979) Geologic, fluid inclusion, and stable isotope studies of the tin-tungsten deposits of Panasqueira, Portugal. Econ Geol 74:1721–1822
Kinnaird JA (1985) Hydrothermal alteration and mineralization of the alkaline anorogenic ring complexes of Nigeria. J Afr Earth Sci 3:229–252
Kinnaird JA, Bowden P (eds) (1987a) African Geology Reviews. Geol J 22(Spec Iss)
Kinnaird JA, Bowden P (1987b) African anorogenic alkaline magmatism and mineralization – a discussion with reference to the Niger-Nigerian province. Geol J 22:97–340
Kinnaird JA, Bowden P (1991) Magmatism and mineralization associated with Phanerozoic anorogenic plutonic complexes of the African plate. In: Kampunzu AB, Lubala RT (eds) Magmatism in extensional structural settings – the Phanerozoic African plate, Springer-Verlag, pp 410–485
Kirwin DJ (2005) Unidirectional solidification textures associated with intrusion-related Mongolian mineral deposits. In: Seltmann R, Gerel O, Kirwin DJ (eds) Geodynamics and metallogeny of Mongolia with a special emphasis on copper and gold deposits, IAGOD Guidebk Ser 11, pp 63–84
Kogarko LN, Kononova VA, Orlova MP, Woolley AR (1995) Alkaline rocks and carbonatites of the world. Part 2: Former USSR. Chapman & Hall, London
Korn H, Martin H (1954) The Messum igneous complex in South West Africa. Trans Geol Soc S Afr 57:83–124
Korobeinikov AN, Mitrofanov FP, Ehör S, Laajoki K, Pavolov VP, Mamontov VP (1998) Geology and copper sulphide mineralization of the Salmagorskii ring igneous complex, Kola Peninsula, NW Russia. J Petrol 39:2033–2041
Krishnamurthy P, Hoda SQ, Sinha RP, Banerje DC, Dwivedy KK (2000) Economic aspects of carbonatites in India. J Asian Earth Sci 18:229–235
Kröner A (1985) Ophiolites and the evolution of tectonic boundaries in the late Proterozoic Arabian-Nubian shield of northeast Africa and Arabia. Precambr Res 27:277–300
Kröner A, Stern RJ (2005) Pan-African orogeny. Encyclopedia of geology 1, Elsevier, Amsterdam, pp 1–12
Kusky TM, Li JH (2003) Paleoproterozoic tectonic evolution of the North China Craton. J Asian Earth Sci 22:383–397
Lang JR, Baker T, Hart CJR, Mortensen JK (2000) An exploration model for intrusion-related gold systems. SEG Newslett 40:1–15
Lang JR, Baker T (2001) Intrusion-related gold systems: the present level of understanding. Miner Deposita 36:477–489
Large RR (1975) Zonation of hydrothermal minerals at the Juno Mine, Tennant Creek Goldfield, central Australia. Econ Geol 70:1387–1413
Large RR, Mumme WG (1975) Junoite, "wittite", and related seleniferous bismuth sulfosalts from Juno Mine, Northern Territory, Australia. Econ Geol 70:369–383
Latin D, Nory MJ, Tarzey RJE (1993) Magmatism in the Gregory rift, East Africa: evidence for melt generation by a plume. Jf Petrol 34:1007–1027
Laznicka P (2006) Giant metallic deposits – future resources of industrial minerals. Springer

Le Bas MJ (1977) Carbonatite nepheline volcanism. John Wiley & Sons, New York
Le Bas MJ (1989) Diversification of carbonatite. In: Bell K (ed) Carbonatites. Genesis and evolution. Unwin Hyman Ltd, Lond, pp 428–447
Lehmann B (1982) Metallogeny of tin: magmatic differentiation versus geochemical heritage. Econ Geol 77:50–59
Lehmann B (1990) Metallogeny of tin. Lecture notes in Earth Sciences. Springer, Berlin
Lentz DR (ed) (2007) Special issue on iron oxide copper-gold deposits. Expl Min Geol 16(3–4)
Loiselle MC, Wones DR (1979) Characteristic and origin of anorogenic granites. Geo Soc Am Abs with Programs 11:468
Lurie J (1986) Mineralization of the Pilanesberg Alkaline Complex. In: Anhaeusser CR, Maske S (eds) Mineral deposits of Southern Africa, Vol II, Geol Soc S Afr, pp 2215–2228
Macey P. Harris C (2006) Stable isotope and fluid inclusion evidence for the origin of the Brandberg West area Sn-W vein deposits, NW Namibia. Mineral Depos 41:671–690
Mair JL, Goldfarb RJ, Craig AJ, Hart CJR, Marsh EE (2006) Geochemical constraints on the genesis of the Scheelite Dome intrusion-related gold deposit, Tombstone gold belt, Yukon, Canada. Econ Geol 101:523–553
Mariano AN (1989a) Nature of economic mineralization in carbonatites and related rocks. In: Bell K (ed) Carbonatites – genesis and evolution. Unwin Hyman, London, pp 149–176
Mariano AN (1989b) Economic geology of rare earth elements. In: Lipin BC, McKay CA, (eds) Geochemistry and mineralogy of rare earth elements. Rev Mineral 21. Min Soc Am, pp 309–337
Mark G, Oliver NHS, Williams PJ, Valenta RK, Crookes RA (2000) The evolution of the Ernest Henry Fe-oxide-(Cu-Au) hydrothermal system. In: Porter TM (ed) Hydrothermal iron oxide copper-gold and related deposits: a global perspective, Aust Min Foundation, Adelaide, pp 123–136
Mark G, Wilde A, Oliver NHS, Williams PJ, Ryan CG (2005) Modeling outflow from the Ernest Henry Fe oxide-Cu-Au deposit: implications for ore genesis and exploration. Geochem Expl 85:31–46
Marschik R, Leveille RA, Martin W (2000) La Candelaria and the Punta del Cobre district, Chile: early Cretaceous iron-oxide Cu-Au(-Zn-Ag) mineralization. In: Porter TM (ed) Hydrothermal iron oxide copper-gold & related deposits: a global perspective. Aus Miner Found, Adelaide, pp 163–175
Marschik R, Fontignie D, Chiaradia M, Voldet P (2003) Geochemical and Nd-Sr-Pb-O isotope characteristics of granitoids of the early Cretaceous Copiapó plutonic complex (27° 30' S), Chile. J South Am Earth Sci 16:381–398
Marsh JS (1973) Relationship between transform directions and alkaline igneous rock lineaments in Africa and South America. Earth Planet Sci Lett 18:317–323
Martin RF (2006) A-type granites of crustal origin ultimately result from open-system fenitization-type reactions in an extensional environment. Lithos 91:125–136
Martin D McB, Thorne AM (2004) Tectonic setting and basin evolution of the Bangemall Supergroup in the northwestern Capricorn Orogen. Precambr Res 128:385–409
Martini JEJ, Hammerback ECI (1998) Fluorspar. In: Wilson MGC, Anhaeusser CR (eds) The mineral resources of South Africa, Council Geoscie Handbk 16, pp 269–279
McNeill GW (1989) A geochemical study of three Namibian igneous complexes. Unpubl BSc Hons thesis, Univ St Andrews
Miller McGR (ed) (1983) Evolution of the Damara orogen of South West Africa/Namibia. Geol Soc S Afr Spec Publ 11
Miller McGR (1992) Stratigraphy. In: The mineral resources of Namibia. Geol Surv Namibia, 1st edn, pp 1. 2–1.34
Miller CF, McDowell Meschter S, Mapes RW (2003) Hot and cold granite? Implications for zircon saturation temperatures and preservation of inheritance. Geology 31:529–532
Milner SC (1988) The geology and geochemistry of the Etendeka Formation quartz-latites, Namibia. Unpubl PhD thesis, University of Cape Town

Milner SC, Duncan AR, Ewart A (1992) Quartz-latite rheoignimbrite flows of the Etendeka Formation, northwestern Namibia. Bull Volcanol 54:200–219
Milner SC, le Roex AP, O'Connor JM (1995) Age of Mesozoic igneous rocks in northwestern Namibia and their relationship to continental breakup. J Geol Soc London 152:97–104
Mitchell AHG, Garson MS (1981) Mineral deposits and global geotectonic settings. Acad Press, New York, London, 405pp
Mitchell RH (1989) Aspects of the petrology of kimberlites and lamproites: some definitions and distinctions, in Kimberlites and related rocks, Proceed 4th Int Kimberlite Conf, Perth, 1986, Geol Soc Aus Spec Publ 14, pp 7–45.
Mitchell RH (1995) Kimberlite, orangeites, and related rocks. Plenum Press, New York
Mohamed FH, El-Sayed MM (2007) Post-orogenic and anorogenic A-type fluorite-bearing granitoids, Eastern Desert, Egypt: petrogenetic and geotectonic implications. Chem Erde Geochem, doi:10:1016/j.chemer.2007.01.001
Moore McM (1982) Mineral zonation near the granitic batholiths of southwest and northern England and some geological analogues. In Evans AM (ed) Metallization associated with acid magmatism, vol 6. John Wiley & Sons, Chichester, pp 229–241
Murray CG (1990) Tasman Fold Belt in Queensland. Aust Inst Min Metall Monogr 14(2):1431–1450
Mustard R (2004) Textural, mineralogical and geochemical variation in the zoned Timbarra Tablelands pluton, New South Wales. Aust J Earth Sci 51:385–405
Neiva AMR (2007) Geochemistry of cassiterite and wolframite from tin and tungsten quartz veins in Portugal. Ore Geol Rev, doi:10.1016/j.oregeorev.2006.05.013
Norman JW (1982) The origin of metals: a speculation. Min Mag 146:226–229
O'Driscoll EST (1985) The application of lineament tectonics in the discovery of the Olympic Dam Cu-Au-U deposit, Roxby Downs, South Australia. Global Tect Metall 31:43–57
Oreskes N, Einaudi MT (1990) Origin of REE-enriched hematite breccia at the Olympic Dam Cu-U-Au-Ag deposit, Roxby Downs, South Australia. Econ Geol 85:1–28
Oreskes N, Einaudi MT (1992) Origin of hydrothermal fluids at Olympic Dam: preliminary results from fluid inclusions and stable isotopes. Econ Geol 87:64–90
Oreskes N, Hitzman MW (1993) A model for the origin of Olympic Dam-type deposits. Geol Assoc Can Spec Pap 40:615–633
Pallister JS, Stacey JS, Fischer LB, Premo WR (1987) Arabian shield ophiolites and late Proterozoic microplate accretion. Geology 15:320–323
Paterson DJ, Ohmoto H, Solomon M (1981) Geologic setting and genesis of cassiterite-sulfide mineralization at Renison Bell, western Tasmania. Econ Geol 76:393–438
Pavlova GG, Gushchina LV, Borovikov A, Borisenko AS, Obolensky AA (2004) Silver and antimony in hydrothermal solutions of Ag-Sb deposits. Russian Geol & Geophys 45:1186–1197
Pavlova GG, Gushchina LV, Borovikov A, Borisenko AS, Palyanova G (2006) Forming conditions for Au-Sb and Ag-Sb ore according to thermodynamic modelling data. J Mater Sci 41:1557–1562
Pearce J (1996) Sources and settings of granitic rocks. Episodes 19:120–125
Peng P, Zhai M, Zhang HF, Guo JH (2005) Geochronological constraints on the Paleoproterozoic evolution of the North China Craton: SHRIMP zircon ages of different types of mafic dikes. Inter Geol Rev 47:492–508
Peng P, Zhai MG, Ernst RE, Guo JG, Liu F, Hu B (2008) A 1.78 Ga large igneous province in the North China Craton: the Xiong'er Volcanic Province and the North China Dyke Swarm. Lithos 101: 260–280
Petford N, Cruden AR, McCaffrey KJW, Vigneresse JL (2000) Granite magma formation, transport and emplacement in the Earth's crust. Nature 408:669–673
Pirajno F (1982) Geology, geochemistry, mineralisation and metal zoning of the McConnochie greisenised granite, Reefton district, Westland, New Zealand. N Z J Geol Geophys 28:187–191

Pirajno F (1985) Porphyry Mo and greisen W metallogeny related to the Karamea Batholith, South Island, New Zealand. N Z J Geol Geophys 28:187–191
Pirajno F (1990) The geology, geochemistry and mineralisation of the Erongo Volcanic Complex, Namibia. S Afr J Geol 93:485–504
Pirajno F (1992) Hydrothermal mineral deposits – principles and fundamental concepts for the exploration geologist. Springer, Berlin
Pirajno F (1994) Mineral resources of anorogenic alkaline complexes, Namibia: a review. Aus J Earth Sci 41:157–168
Pirajno F (1998) Geology and mineral deposits of Namibia. Aus Inst Geoscie Bull 25:61–66
Pirajno F (2000) Ore deposits and mantle plumes. Kluwer Academic Publishers, Dordrecht
Pirajno F (2004) Metallogeny in the Capricorn Orogen, Western Australia, the result of multiple ore-forming processes. Precambr Res 128:411–440
Pirajno F, Bagas L (2008) A review of Australia's Proterozoic mineral systems and genetic models. Precambr Res Sp Iss, doi:10.1016/j.precamres.2007.05.008
Pirajno F, Bentley PN (1985) Greisen-related scheelite, gold and sulphide mineralisation at Kirwans Hill and Bateman Creek, Reefton District, Westland, New Zealand. N Z J Geol Geophys 28:97–109
Pirajno F, Jacob RE (1987) Sn-W metallogeny in the Damara Orogen, South West Africa/Namibia. S Afr J Geol 90:239–255
Pirajno F, Petzel VFW, Jacob RE (1987) Geology and alteration-mineralisation of the Brandberg West Sn-W deposit, Damara Orogen, South West Africa/Namibia. S Afr J Geol 90:256–269
Pirajno F, Smithies RH (1992) The FeO/(FeO + MgO) ratio of tourmaline: a useful indicator of spatial variations in granite-related hydrothermal mineral deposits. J Geochem Expl 42:371–381
Pirajno F, Kinnaird JA, Fallick AE, Boyce AJ, Petzel VWF (1993) A preliminary regional sulphur isotope study of selected samples from mineral deposits of the Damara Orogen, Namibia. Comm Geol Surv Namib 8:81–97
Pirajno F, Butt CRM, Winter E (1995) Gold enrichment in weathered carbonatite pyroclastics of the Kruidfontein Volcanic Complex, South Africa. S Afr J Geol 98:319–325
Pirajno F, Phillips D, Armstrong RA (2000) Volcanology and eruptive histories of the Erongo Volcanic Complex and the Paresis Igneous Complex, Namibia: implications for mineral deposit styles. Commun Geol Surv Namibia 12:301–312
Pitcher WS (1993) The nature and origin of granite. Blackie Academic & Professional, London
Pollard PJ (1983) Magmatic and postmagmatic processes in the formation of rocks associated with rare-element deposits. Trans Inst Min Metall 92:B1–B9
Pollard PJ (2001) Sodic(calcic) alteration in Fe oxide-Cu-Au districts: an origin via umixing of magmatic H_2O-CO_2-NaCl ± $CaCl_2$-KCl fluids. Mineral Depos 36:93–100
Pollard PJ (2006) An intrusion-related origin for Cu-Au mineralization in iron oxide-copper-gold (IOCG) provinces. Mineral Depos 41:179–187
Pollard PJ, Taylor RG, Cuff C (1983) Metallogeny of tin: magmatic differentiation versus geochemical heritage – a discussion. Econ Geol 78:543–545
Pollard PJ, Taylor RG (1986) Progressive evolution of alteration and tin mineralization: controls by interstitial permeability and fracture-related tapping of magmatic fluid reservoirs in tin granites. Econ Geol 81:1795–1800
Pollard PJ, Pichavant M, Charoy B (1987) Contrasting evolution of fluorine- and boron-rich tin systems. Mineral Depos 22:315–321
Pollard PJ, Taylor RG, Cuff C (1988) Genetic modelling of greisen-style tin systems. In: Hutchison CS (ed) Geology of tin deposits in Asia and the Pacific. Springer, Berlin, pp 59–72
Pollard PJ, Taylor RG, Tate NM (1989) Textural evidence for quartz and feldspar dissolution as a mechanism of formation for Maggs pipe, Zaaiplaats tin mine. Mineral Depos 24:210–218

Porter TM (ed) (2000) Hydrothermal iron oxide copper-gold & related deposits: a global perspective. Aus Miner Found, Adelaide, Aust
Porter TM (ed) (2002) Hydrothermal iron oxide copper-gold & related deposits: a global perspective. Aus Miner Found, vol 2, Adelaide, Aust
Premoli C (1993) Mineral potential of Namibia. Aust Inst Min Metall Bull 3:22–27
Raguin E (1965) Geology of granite. Interscience Publishers and John Wiley & Sons, London
Ramsay WHR, Bierlein FP, Arne DC (1998) Mesothermal gold mineralisation in space and time. Ore Geol Rev Sp Iss 13 (1–5)
Reeve JS, Cross KC, Smith RN, Oreskes N (1990) The Olympic dam copper-uranium-gold-silver deposit, South Australia. In: Hughes F (ed) Geology and mineral deposits of Australia and Papua New Guinea. Aust Inst Min Metall Monogr 14: 1009–1035
Reynolds LJ (2000) Geology of the Olympic Dam Cu-U-Au-Ag-REE deposit. In: Porter TM (ed) Hydrothermal iron oxide copper-gold and related deposits: a global Perspective, Aus Min Foundation, Adelaide, pp 93–104
Richardson JM, Bell K, Watkinson DH, Blemkisop J (1990) Genesis and fluid evolution of the East Kemptville greisen-hosted tin mine, southwestern Nova Scotia, Canada. Geol Soc Am Spec Pap 246:181–203
Robert F (2001) Disseminated syenite-associated gold deposits in the Abitibi greenstone belt, Canada. Mineral Depos 36:503–516
Roedder E (1984) Fluid inclusions. Reviews in Mineralogy, vol 12. Min Soc Am, 644pp
Rogers JJW, Santosh M (2002) Configuration of Columbia, a Mesoproterozoic continent. Gondwana Res 5:5–22
Rose AW, Burt DM (1979) Hydrothermal alteration. In: Barnes HL (ed) Geochemistry of hydrothermal ore deposits, 2nd edn. John Wiley & Sons, New York, pp 173–235
Ross J, Jaques LA, Ferguson J, Green DH, O'Reilly SY, Danchin RV, Janse AJA (eds) (1989) Kimberlites and related rocks, vol 1 & 2. Geol Soc Aus Spec Publ 14
Rozendaal A, Toros MS, Anderson JR (1986) The Rooiberg tin deposits, West-Central Transvaal. In: Anhaeusser CR, Maske S (eds) Mineral deposits of southern Africa, vol 2. Geol Soc S Afr, pp 1307–1328
Rozendaal A, Misiewicz JE, Scheepers R (1995) The tin zone: sediment-hosted hydrothermal tin mineralization at Rooiberg, South Africa. Mineral Depos 30:178–187
Ryan AJ (1998) Ernest Henry copper-gold deposit. In: Berkman DA, Mackenzie DH (eds) Geology of Australian and Papua New Guinea mineral deposits. Australas Inst Min Metall Monogr 22:759–768
Santosh M, Omana PK (1991) Very high purity gold from lateritic weathering profiles of Nilambur, southern India. Geology 19:746–749
Sawkins FJ, Sillitoe RH (eds) (1985) A special issue devoted to ore-hosted breccias. Econ Geol 80(6)
Scheibner E, Veevers JJ (2000) Tasman fold belt. In: Veevers JJ (ed) Billion-year earth history of Australia and neighbours in Gondwanaland, GEMOC Press, Sydney, pp 154–234
Schwartz MO, Rajah SS, Askury AK, Putthapiban P, Djaswadi S (1995) The Southeast Asian tin belt. Earth-Sci Rev 38:95–293
Seltmann R, Borisenko AS, Pavlova GG (2007) Metallogeny of the southeastern Altai (Russia) and northwestern Mongolia ore district, Permian-Triassic boundary. Russian Academy of Sciences, IAGOD Guidebook of Field Excusion A, Int Symp Large Igneous Prov Asia, Novosibirsk.
Shcherba GN (1970) Greisens. Int Geol Rev 12:114–255
Sheppard S, Occhipinti SA, Nelson DR (2005) Intracontinental reworking in the Capricorn Orogen, Western Australia: the 1680–1620 Ma Mangaroon Orogeny. Aus J Earth Sci 52:443–460
Sillitoe RH (1996) Granites and metal deposits. Episodes 19:126–133
Sillitoe RH (2003) Iron oxide-copper-gold deposits: an Andean view. Mineral Depos 38:787–812

Sillitoe RH, Thompson JFH (1998) Intrusion-related vein gold deposits: types, tectono-magmatic settings and difficulties of distinction from orogenic gold deposits. Res Geol 48:237–250

Skirrow R (2006) Craton-scale controls and time-space distribution of IOCG and gold systems in the Gawler Craton. IOCG Workshop, Adelaide, 24 Feb 2006 http://www.ga.gov.au/image_cache/GA7791.pdf (last opened in April 2008)

Skirrow RG, Walshe JL (2002) Reduced and oxidized Au-Cu-Bi iron oxide deposits of the Tennant Creek Inlier, Australia: an integrated geologic and chemical model. Econ Geol 97:1167–1202

Smirnov VI (1976) Geology of mineral deposits. MIR, Moscow, 520 pp

Smith MP (2007) Metasomatic silicate chemistry at the Bayan Obo Fe-REE-Nb deposit, Inner Mongolia, China: contrasting chemistry and evolution of fenitising and mineralising fluids. Lithos 93:126–148

Smith MP, Henderson P (2000a) Preliminary fluid inclusion constraints on fluid evolution in the Bayan Obo Fe-REE-Nb deposit, Inner Mongolia, China. Econ Geol 95:1371–1388

Smith MP, Henderson P (2000b) Preliminary fluid inclusions constraints on mineralising fluid composition and evolution in the Bayan Obo Fe-REE-Nb deposit, Inner Mongolia. Econ Geol 95:1371–1388

Smith MP, Henderson P, Campbell LS (2000) Fractionation of the REE during hydrothermal processes: constraints from the Bayan Obo Fe-REE-Nb deposit, Inner Mongolia, China. Geochim Cosmochim Acta 64:3141–3160

Smithies RH (1991). The geochemical evolution of three alkaline complexes in the Kubos-Bremem igneous province, southern Namibia. Unpubl. PhD Thesis, Rhodes University

Smithies RH, Marsh JS (1998) The Marinkas Quellen Carbonatite Complex, southern Namibia; carbonatite magmatism with an uncontaminated depleted mantle signature in a continental setting. Chem Geol 148:201–212

Solomon M, Groves DI (1994) The geology and origin of Australia's mineral deposits. Clarendon Press, Oxford

Sørensen H (ed) (1974) The alkaline rocks. J Wiley & Sons, New York

Stear WM (1977) The stratabound tin deposits and structure of the Rooiberg fragment. Trans Geol Soc S Afr 80:67–78

Stolz AJ, Morrison RS (1994) Proterozoic igneous activity in the Tennant Creek region, Northern Territory, Australia, and its relationship to Cu-Au-Bi mineralization. Mineral Depos 29:261–274

Storey BC, Alabaster T, Pankhurst RJ (eds) (1992) Magmatism and the causes of continental breakup. Geol Soc Lond Spec Publ 68

Taylor RG (1979) Geology of tin deposits. Elsevier, Amsterdam

Taylor R, Pollard PJ (1988) Pervasive hydrothermal alteration in tin-bearing granites and implications for the evolution of ore-bearing magmatic fluids. Can Inst Min Metall Spec Vol 39:86–95

Thompson JFH, Sillitoe RH, Baker T, Lang JR, Mortensen JK (1999) Intrusion-related gold deposits associated with tungsten-tin provinces. Miner Deposita 34:323–334

Thompson JFH, Newberry RJ (2000) Gold deposits related to reduced granitic intrusions. Rev Econ Geol 13:377–400

Tomkins AG, Mavrogenes JA (2003) Generation of metal-rich felsic magmas during crustal anatexis. Geology 31:765–768

Trumbull RB, Harris C, Frindt S, Wigand M (2004) Oxygen and neodymium isotope evidence for source diversity in Cretaceous anorogenic granites from Namibia and implications for A-type granite genesis. Lithos 73:21–40

Tyler IM, Pirajno F, Bagas L, Myers JS, Preston WA (1998) The geology and mineral deposits of the Proterozoic in Western Australia. AGSO J Geol & Geophys 17:223–244

Tyler N (1986) The origin of gold mineralization in the Pilgrim's Rest goldfield, eastern Transvaal. Econ Geol Res Unit, Univ Witwatersrand Inf Circ 179

Tyler R, Tyler N (1996) Stratigraphic and structural controls on gold mineralization in the Pilgrim's Rest gold field, eastern Transvaal, South Africa. Precambr Res 79:141–169
Vermaak CF, Von Gruenewaldt G (1986) Introduction to the Bushveld complex. In: Anhaeusser CR, Maske S (eds) Mineral deposits of southern Africa, vol 2. Geol Soc S Afr, pp 1021–1030
Verwoerd WJ (1966) The carbonatites of South Africa and South West Africa. Geol Surv S Afr Handbk 6
Verwoerd WJ (1986) Mineral deposits associated with carbonatites and alkaline rocks. In: Anhaeusser CR, Maske S (eds) Mineral deposits of Southern Africa, Geol Soc S Afr, pp 2173–2191
Verwoerd WJ (1993) Special issue on carbonatites. S Afr J Geol 96(3)
Verwoerd WJ, Retief EA, Prins P (2000) The Etanenoberg alkaline complex, Namibia. Commun Geol Surv Namibia 12:291–300
Vigneresse JL (2004) A new paradigm for granite generation. Trans Roy Soc Edin Earth Sci 95:11–22
Vigneresse JL (2007) The role of discontinuous magma inputs in felsic magma and ore generation. Ore Geol Rev 30:181–216
Vladimirov AG, Vystavnoi SA, Titov AV, Rudnev SN, Dergachev VB, Annikova IYu, Tikunov YuV (1998) Petrology of early Mesozoic rare-metal granites of southern Gorny Altai. Russian Geol Geophys 39:909–924
Von Gruenewaldt G, Strydom JH (1985) Geochemical distribution patterns surrounding tin-bearing pipes and the origin of the mineralizing fluids at the Zaaiplaats tin mine, Potgietersrus district. Econ Geol 80:1201–1211
Walraven F (1985) Genetic aspects of the granophyric rocks of the Bushveld Complex. Econ Geol 80:1166–1180
Wang J, Tatsumoto M, Li X, Premo WR, Chao ECT (1994) A precise ^{232}Th-^{208}Pb chronology of fine grained monazite: age of the Bayan Obo REE-Fe-Nb ore deposit, China. Geochim Cosmochim Acta 58:3155–3169
Wang YJ, Fan WM, Zhang YH, Guo F, Zhang HF, Peng TP (2004) Geochemical, ^{40}Ar/^{39}Ar geochronological and Sr-Nd isotopic constraints on the origin of Paleoproterozoic mafic dikes from the southern Taihang Mountains and implications for the ca. 1800 Ma event of the North China Craton. Precambr Res 135:55–47
Ward JHW, Wilson MGC (1998) Gold outside the Witwatersand Basin. In: Wilson MGC, Anhaeusser CR (eds) The mineral resources of South Africa, Council Geoscie Handbk 16, pp 350–386
Watkinson DH, Wyllie PJ (1971) Experimental study of the join $NaAlSiO_4$-$CaCO_3$-H_2O and the genesis of alkali rock-carbonatite complexes. J Petrol 12:357–378
Wedeking MR, Large RR, Williams B (1989) Controls on high-grade mineralization at Tennant Creek, Northern Territory, Australia. Econ Geol Monogr 6:168–179
Westra G, Keith SB (1981) Classification and genesis of stockwork molybdenum deposits. Econ Geol 76:844–873
Whalen JB, Currie KL, Chappell BW (1987) A–type granites: geochemical characteristics, discrimination and petrogenesis. Contrib Miner Petrol 95:407–419
White RS (1997) Mantle plume origin for the Karoo and Ventersdorp flood basalts, South Africa. S Afr J Geol 100:271–282
Wigand M, Schmitt A, Trumbull RB, Villa IM, Emmermann R (2004) Short-lived magmatic activity in an anorogenic subvolcanic complex: 40Ar/39Ar and ion microprobe U-Pb zircon dating of the Erongo, Damaraland, Namibia. J Volc Geoth Res 130:285–305
Williams PJ (1998a) Metalliferous economic geology of the Mt Isa eastern succession, Queensland. Aust J Earth Sci 45:329–341
Williams PJ (1998b) An introduction to the metallogeny of the McArthur River-Mount Isa-Cloncurry minerals province. Econ Geol 93:1120–1131

Williams PJ, Skirrow RG (2000) Overview of iron oxide-copper-gold deposits in the Curnamona Province and Cloncurry District (Eastern Mount Isa Block), Australia. In: Porter TM (ed) Hydrothermal iron oxide copper-gold & related deposits: a global perspective. Aus Miner Found, Adelaide, pp 105–122

Williams PJ, Barton MD, Johnson DA, Fonbote L, De Haller A, Mark G, Oliver NHS, Marschick R (2005) Iron oxide copper-gold deposits: geology, space-time distribution and possible modes of origin. Econ Geol 100th Ann Vol:371–406

Wilson MGC (1998) Copper. In: Wilson MGC, Anhaeusser CR (eds) The mineral resources of South Africa, Council Geoscie Handbk 16, pp 209–227

Windley BF (1995) The evolving continents. 3rd edn, John Wiley & Sons, Chichester

Wingate MTD, Pirajno F, Morris PA (2004) The Warakurna large igneous province: a new Mesoproterozoic large igneous province in west-central Australia. Geology 32:105–108

Woodall R (1993) The multidisciplinary approach to successful mineral exploration. SEG Newslett 14:1–11

Woolley AR (2001) Alkaline rocks and carbonatites of the world – part 3: Africa. Geol Soc, Lond

Wright JH, Kwak TAP (1989) Tin-bearing greisens of Mount Bischoff, northwestern Tasmania, Australia. Econ Geol 84:551–574

Wu FY, Sun DY, Li HM, Jahn BM, Wilde S (2002) A-type granites in northeastern China: age and geochemical constraints on their petrogenesis. Chem Geol 187:143–173.

Yang XM, Le Bas MJ (2004) Chemical composition of carbonate minerals from Bayan Obo, Inner Mongolia, China: implications for petrogenesis. Lithos 72:97–116

Zaitsev AN, Sinai YUM, Shakhmuradya NAR, Lepekhina EN (1998) Association of pyrrhotite and pyrite in carbonatite series rock of Khibina alkaline massif. Zap Vser Mineral Obshchest 127(4):110–119 (in Russian)

Zhao GC, Sun M, Wilde SA, Li SZ (2004) A Paleo-Mesoproterozoic supercontinent: assembly, growth and breakup. Earth-Sci Rev 67:91–123

Zhao GC, Min S, Wilde SA, Li SZ (2005) Late Archean to Paleoproterozoic evolution of the North China Craton: key issues revisited. Precambr Res 136:177–202

Ziserman A, Bertraneu J, Jaujou M (1980) European mineral wealth. Episodes 1980:33–35

Chapter 5
Porphyry Systems; Fossil and Active Epithermal Systems

5.1 Introduction

Porphyry, skarns and epithermal mineral systems are part of the broader class of intrusion-related systems discussed in Chapter 4. However, I have chosen to describe porphyry, skarns and epithermal systems in separate chapters mainly to avoid crowding the preceding chapter.

Porphyry ore systems originate from high-temperature magmatic-hydrothermal fluids and are called porphyry because of the porphyritic texture of the mineralised intrusions. Porphyry deposits are characterised by large tonnages, but low grades and the sulphides typically occur as disseminations and/or in stockworks and veins. Hydrothermal alteration is fairly uniform in the porphyry family, forming distinct envelopes within and around the mineralised intrusion, with the outer propylitic envelope extending for several kilometres in the country rocks. Porphyry systems are generally classified according to their dominant metal assemblages. Some porphyry grade upward into high-sulphidation epithermal systems, thereby representing a continuum from subvolcanic magma chambers, to epithermal veins within a volcanic edifice through to hot springs at surface. In fact, many porphyry stocks may be sited below stratovolcanoes and the uppermost sectors of the porphyry intrusive are transitional upward to epithermal mineralisation and laterally to skarn deposits, discussed in Chapters 5 and 6, respectively. An overview of porphyry, skarn and epithermal vein "ensemble" associated with a stratovolcano in Slovakia (Carpathian arc) is provided by Lexa et al. (1999). Dilles and Einaudi (1992) described in detail a cross-section through the Ann-Mason porphyry-skarn system in Nevada.

Epithermal systems are defined as those formed at low to moderate temperatures (between approximately 50 and 350°C) and pressures, from dominantly weakly saline (<1 to approximately 5 wt% NaCl equivalent) meteoric fluids. Although epithermal deposits are mostly volcanic-hosted and clearly related to volcano-plutonic activity, there is nevertheless a category of sedimentary rock-hosted epithermal systems, which do not appear to have a clear connection to igneous activity. These are best exemplified by Carlin-style ore systems, discussed in Chapter 9. Epithermal mineralisation has a number of

F. Pirajno, *Hydrothermal Processes and Mineral Systems*,

© Springer Science+Business Media B.V. 2009

common and distinctive features, such as the presence of fine-grained chalcedonic quartz, calcite, quartz pseudomorphs after calcite (probably indicative of boiling fluids), and hydrothermal breccias. The elemental association is also characteristic, with ore elements such as Au, Ag, As, Sb, Hg, Tl, Te, Pb, Zn and Cu. Ore textures include open-space filling (characteristic of low pressure environments), crustifications, colloform banding and comb structures. The deposits, which are formed from the surface to approximately 1.5 km below the surface, are typified by veins, stockworks and disseminations. These features, which may occur either together or as single entities, constitute deposits generally easy to mine as open cast or shallow underground operations, with relatively large tonnages and low Au + Ag grades, or small tonnages and high Au + Ag grades.

In regions of high heat flow, thermal convection dominates the behaviour of groundwaters or sea water in permeable and/or fractured crust, thus generating geothermal systems. Terrestrial geothermal systems are effectively active epithermal systems, derived from air-saturated meteoric waters which penetrate the crust to regions influenced by cooling magmas. Submarine geothermal systems are, by contrast, characterised by sea water convection cells which are also heated by cooling magmas at depth. This chapter takes a look at terrestrial geothermal systems, whereas submarine systems related to submerged volcanic structures at convergent plate boundaries and geothermal activity associated with mid-ocean ridges are treated in Chapter 7.

5.2 Porphyry Systems

Porphyry systems encompass a wide variety of types that can be characterised in terms of tectonic setting, metal contents, hydrothermal alteration patterns and the nature of the associated granitoids. As briefly mentioned in the Introduction, porphyry systems are universally characterised by three main features:

- Large volumes of rocks are affected by hydrothermal alteration-mineralisation (Fig. 5.1)
- The mineralisation is spatially and genetically related to intrusive bodies, of which at least one has a distinct porphyritic texture, hence the name porphyry
- Presence of veins and veinlets forming stockworks, within which are disseminated sulphides of Fe, Cu, Mo, Pb and Zn, as well as native Au, and minerals of W, Bi and Sn (Fig. 5.1)

Comprehensive reviews of porphyry systems include Titley and Hicks (1966), Titley and Beane (1981), Beane and Titley (1981), Titley (1993), Sillitoe (1993), Seedorff et al. (2005) and a special issue of Economic Geology on giant porphyry deposits (Cooke et al. 2005). Laznicka (2006) listed 112 porphyry giants with details of metal resources, whereas a database of some 600 porphyry

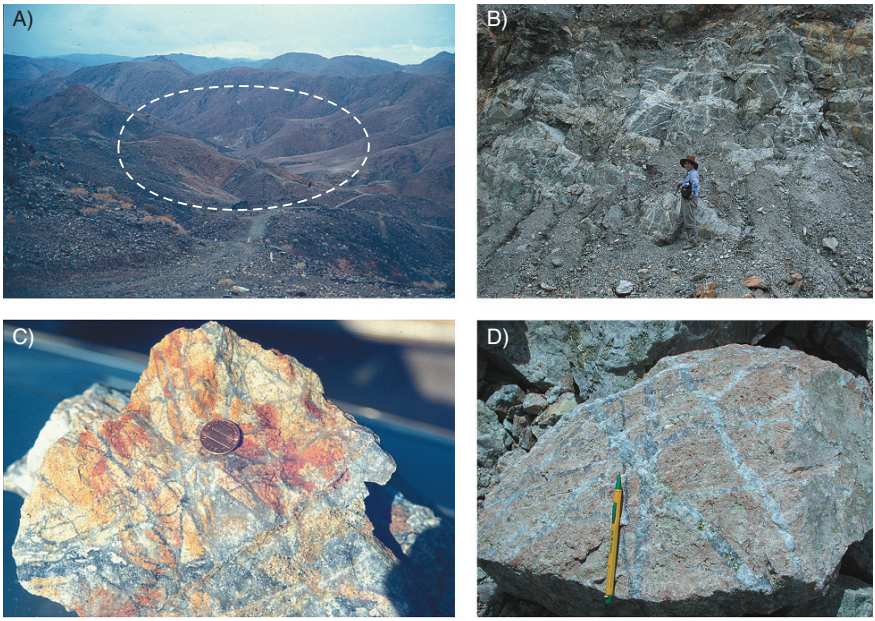


Fig. 5.1 Field photographs of some typical aspects of porphyry systems; (**A**) view of the ~2.0 Ga Haib porphyry deposit in southern Namibia, marked lighter brown area is the zone of hydrolitic alteration; (**B**) ~138 Ma Jinduicheng porphyry Mo in the Qinling orogen, Shanxi Province (central China), stockwork veining in hornfelsed country rocks; (**C**) fine stockwork veining from Climax porphyry Mo deposit in Colorado; (**D**) Jinduicheng porphyry Mo, fine stockworks in host granite cutting through earlier potassic alteration (pink-brown patches)

Cu deposits worldwide can be found in Singer et al. (2005). Seedorff et al. (2005) divided porphyry systems into five classes, based on contained metal: (1) porphyry Cu; (2) porphyry Mo; (3) porphyry W; (4) porphryry Sn and (5) porphyry Au. These are further subdivided into subclasses, as shown in Table 5.1.

The size of porphyry systems may vary from several million tonnes up to a few billion tonnes, with grades ranging from as little as 0.2% Cu up to 2% Cu (Cu porphyry), 0.01–0.5% Mo (Mo porphyry), and for those containing Au, this metal's tenors range from fractions of ppm up to a few ppm. The country rocks intruded by the igneous bodies may include carbonate units, which as a result of thermal and metasomatic exchanges with the fluids that emanate from the intrusions will form skarn ore deposits. Not all skarns are affiliated with porphyry systems, here I describe both porphyry- and non-porphyry-associated skarn deposits. In addition, porphyry-skarn systems are commonly surrounded by polymetallic vein systems, which can extend for several kilometres from the causative intrusion(s). These are known as intrusion-related vein deposits and can attain economic grades and are described in Chapter 4.

Table 5.1 Classification of porphyry systems based on dominant metals. Modified after Seedorff et al. (2005)

Class	Porphyry Copper			
Metal(s)	Cu±Au±Mo	Cu±Mo	Cu±Mo±Au	Cu±Au
Intrusive(s) type	Tonalitic-granodiorite porphyry	Quartz-monzodioritic-granite porphyry	Monzonitic porphyry	Syenitic porphyry
Class	Porphyry Molybdenum			
Metal(s)	Mo±Au	Mo	Mo–Cu	Mo
Intrusive(s) type	Monzonitic porphyry	Syenitic porphyry	Quartz-monzonite-granitic porphyry	Granite porphyry; trondhjemite porphyry; rhyolitic porphyry
Class	Porphyry gold	Porphyry tungsten	Porphyry tin	
Metal(s)	Au	W–Mo	Sn	
Intrusive(s)	Dioritic porphyry	Rhyolitic porphyry	Rhyodacitic porphyry	

Porphyry systems are found along the Pacific Rim, in the central Asian collages of island arcs and in the Carpathian arc in eastern Europe (Fig. 5.2). Large concentrations of porphyry deposits occur in the southwestern USA, along the Andean continental margin of South America and the southwest Pacific islands. A comprehensive list of porphyry deposits from Alaska to Chile can be found in Long (1995). Porphyry systems consist of composite stocks with typical porphyritic textures and a complex array of plugs, diatremes, breccias and dykes (Fig. 5.3). They have a small areal extent (0.5–2 km^2) but large vertical dimensions (km-scale). Potassic, phyllic and propylitic alterations are developed as shells around the intrusions. Mineralisation tends to form concentric shells: a weakly mineralized core, in which pyrite is a dominant sulphide, is surrounded by successive zones dominated by molybdenite, chalcopyrite and finally pyrite.

The strato-volcano-associated porphyry system (Fig. 5.3) represents the near-surface expression of granitic rocks that have intruded a cogenetic volcanic pile. There are calc-alkalic and alkalic types. Calc-alkalic types are represented by small plugs (0.2–10 km^2), sheets or dykes emplaced in a subvolcanic environment. These igneous bodies have a small core of potassic alteration with phyllic and/or argillic alteration developed locally, whereas propylitic alteration is widespread. Mineralisation is predominantly Cu–Mo, forming lenses or irregularly shaped orebodies. The ore contains chalcopyrite, bornite and molybdenite. The alkalic types are characterised by high-level plugs generally linked to underlying mesozonal batholiths. Alteration is potassic overprinted

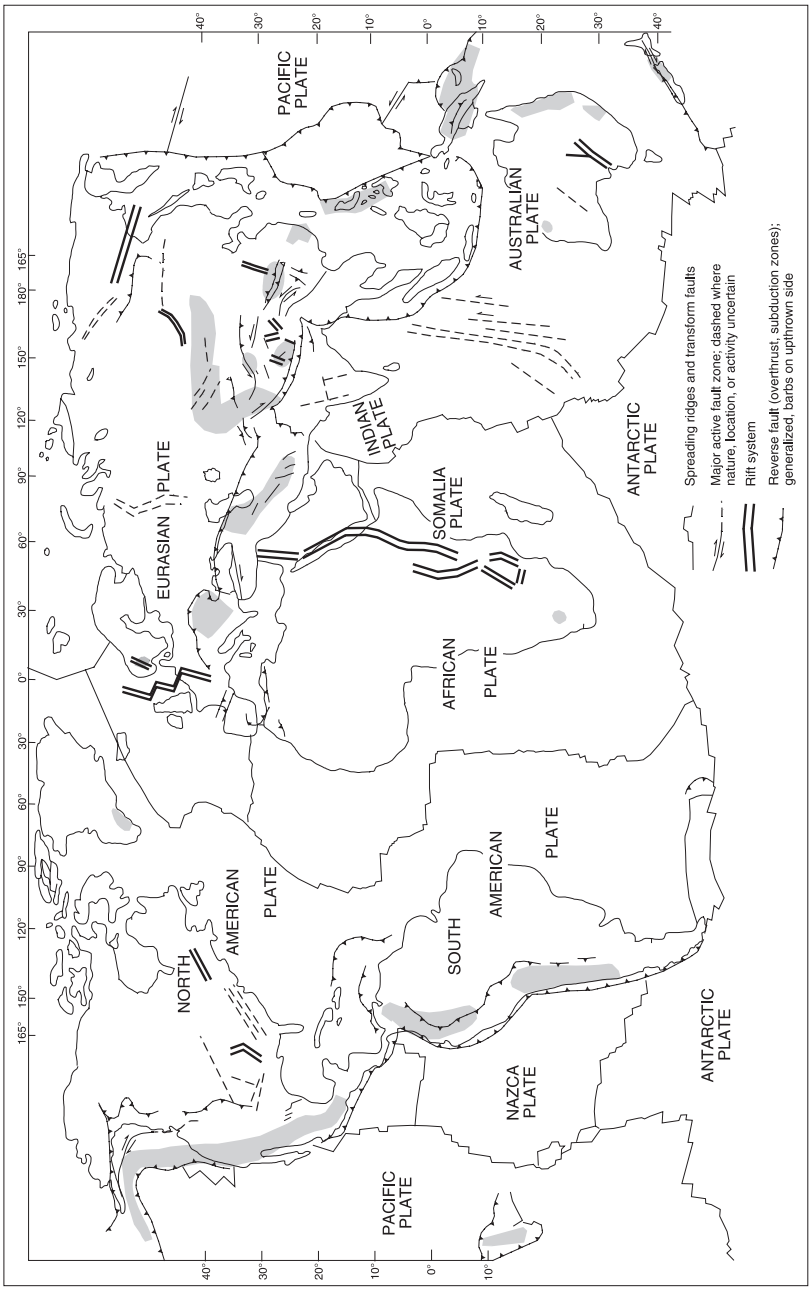


Fig. 5.2 Distribution of porphyry provinces of the world

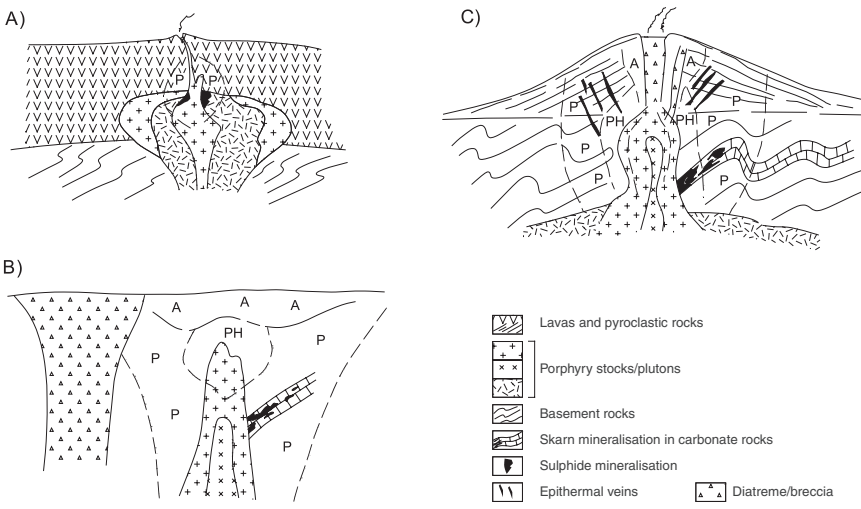


Fig. 5.3 Schematic models of porphyry systems (drawings not to scale). (**A**) plutonic type, depth of plutons is approximately 5–6 km (Pirajno 1992); (**B**) porphyry stock and associated diatreme pipe; the vertical extent of the porphyry stock may be approximately 0.5–1.5 km; (**C**) classic type volcano-plutonic system with peripheral veins and skarns, vertical extent from the top of the volcanic edifice to the upper parts of the porphyry stock may be approximately 3–4 km (after Sillitoe 1973); here the porphyry system may be transitional to a high-S epithermal system. Alteration: A argillic, P propylitic, PH phyllic

by propylitic, followed again by alkali metasomatism, which is mainly sodic and/or potassic. These are generally Cu–Au deposits in breccias and/or highly fractured rocks. Locally there may be development of magnetite and apatite. Mineral zoning consists of chalcopyrite + magnetite and bornite grading outwards to a pyrite halo.

The activity of magmatic and meteoric fluids in porphyry systems can be reconstructed on the basis of fluid inclusion studies and stable isotope systematics. Magmatic waters are first exsolved from the crystallising porphyry intrusion. These early magmatic-hydrothermal solutions develop at temperatures ranging from 750 to 450°C and at depths of between 5 and 1 km below the surface. The action of these fluids is essentially confined to the apical portions of the intrusive stock and immediate surrounding areas. The early magmatic-hydrothermal fluids are generally succeeded by convective fluids of meteoric origin, with which they mix at first until the magmatic component relating to that particular intrusion tends to disappear completely. Meteoric-hydrothermal fluids of porphyry systems have temperatures ranging from 450 to 250°C and circulate at depths of between approximately 1 and < 0.5 km. The study of fluid inclusions in porphyry systems indicates that there are, broadly speaking, three classes of fluids: (1) hypersaline fluids, with up to 40 wt% NaCl equivalent and homogenisation temperatures of 750°C or greater; (2) high salinity fluids, with

approximately 10 to 25 wt% NaCl equivalent and homogenisation temperatures of between 600 and 250°C; and (3) low salinity fluids, with less than 10 wt% NaCl equivalent and homogenisation temperatures of between 400 and 200°C. Integration of isotopic, fluid inclusion, petrological and field data suggest that the hypersaline fluids are largely magmatic-derived. Fluid inclusion data also suggest that boiling and condensation occurred within these hypersaline magmatic fluids.

Some of the most significant contributions to the understanding of porphyry mineral deposits are the works of Lowell and Guilbert (1970) and Guilbert and Lowell (1974), who formulated the well-known and still valid Lowell-Guilbert model, and Sillitoe (1986, 1993, 1995, 1997, 2002). The Lowell-Guilbert model is based on the San Manuel-Kalamazoo porphyry system in Arizona, augmented by observations carried out in 27 other porphyry deposits in North America. There are, however, many variations of, and departures from the Lowell-Guilbert model, due to the different compositions of the intrusive porphyry bodies, whether they are silica-rich and alkalic or alkalic-calcic, or silica-deficient and more calcic. Thus, two main models may be considered: the Lowell-Guilbert model (or quartz-monzonite model) and the diorite model of Hollister (1978). The chief characteristics of these models are given in Table 5.2 and discussed in more detail in Chapter 2 and shown in Fig. 10.4A,B. The alteration-mineralisation of carbonate wall rocks constitute the skarn-type deposits with distinct mineral assemblages and zoning patterns, to be discussed below.

There are many types of porphyry systems on the basis of tectonic setting, morphology and structure, composition and patterns of alteration-mineralisation, and therefore it is almost impossible to formulate any one model to generally describe a porphyry system. Each type of system, however, is a variation of the same theme, this being the intrusion of a high level porphyritic granitoid body. The differences and unique features exhibited by individual deposits reflect the influence of regional and local geological variables. With this in mind some generalisations can nevertheless be made, and the models described here serve as a good starting point. Sutherland Brown (1976) and Nielsen (1976) classified porphyry systems of the Canadian cordillera on the basis of their morphology and position in the crust into: (1) plutonic; (2) hypabyssal; and (3) volcanic.

Table 5.2 Main characteristics of Lowell-Guilbert and diorite models of porphyry systems (after Hollister 1978)

	Lowell-Guilbert model	Diorite model
Intrusive type	Quartz-monzonite porphyry; quartz-diorite porphyry	Syenite; diorite
Alteration	Potassic (orthoclase-biotite, orthoclase-sericite); phyllic (quartz-sericite-pyrite); argillic (kaolinite); propylitic (chlorite, epidote, calcite)	Potassic (biotite-orthoclase, orthoclase-chlorite); propylitic (chlorite-epidote-albite)
Mineralisation	Pyrite, chalcopyrite, bornite, molybdenite, rare gold	Pyrite, magnetite, chalcopyrite, bornite, rare molybdenite, important gold

Following the same criteria, McMillan and Panteleyev (1980) classified porphyry systems into: plutonic, volcanic and classic, and this classification is also shown in Fig. 5.3). The plutonic system (Fig. 10.3 A) is characterised by a lack of obvious concentric mineral zoning and has broad, diffuse zones of weak mineralisation. The plutons are multiphase and form large batholitic complexes of calc-alkaline chemistry. Breccias are common and are associated with late-stage dykes. Tourmaline may be common in the breccias. Alteration is fracture-controlled to pervasive and characterised by well-developed phyllic and argillic types, whereas potassic alteration is localised. Mineralisation is typically associated with stockworks and sulphide zoning shows progressive Fe-enrichment outward from chalcopyrite to bornite to outlying pyrite-rich zones. Molybdenite contents are variable.

Classic systems (Fig. 5.3B) consist of post-orogenic composite stocks with typical porphyritic textures and a complex array of plugs, diatremes, breccias and dykes. They have a small areal extent (0.5–2 km^2) but large vertical dimensions. Potassic, phyllic and propylitic alterations are developed as shells around the intrusions. Mineralisation also occurs as shells, with a weakly mineralised core in which pyrite is a dominant sulphide, surrounded by successive zones dominated by molybdenite, chalcopyrite and finally pyrite. The volcanic type (Fig. 5.3C) represents the near-surface expression of orogenic granitic rocks that have intruded a cogenetic volcanic pile. McMillan and Panteleyev (1980) also distinguished calc-alkalic types and alkalic types. Calc-alkalic types are represented by small plugs (0.2–10 km^2), sheets or dykes emplaced in a subvolcanic environment. These igneous bodies have a small core of potassic alteration with phyllic and/or argillic alteration developed locally, whereas propylitic alteration is widespread. Mineralisation is predominantly Cu–Mo, forming lenses or irregularly shaped orebodies. The ore contains chalcopyrite, bornite and molybdenite. The alkalic types are characterised by high-level plugs generally linked to underlying mesozonal batholiths. Alteration is potassic overprinted by propylitic, followed again by alkali metasomatism, which is mainly sodic and/or potassic. These are generally Cu–Au deposits in breccias and/or highly fractured rocks. Locally there may be development of magnetite and apatite. Mineral zoning consists of chalcopyrite + magnetite and bornite grading outwards to a pyrite halo. Finally, a category of porphyry systems, first proposed by Sillitoe et al. (1975), is that of subvolcanic-related Sn–Ag mineralisation in Bolivia, which is also dealt with in this chapter. Volcanic-associated Sn mineralisation considered to be of the porphyry Sn-type. The chief characteristic of these systems is the absence of potassic alteration and the complex metal associations such as Sn–Ag–Sb–Pb.

A holistic model showing all the principal features of a porphyry system with accompanying vein and skarn systems, passing upward into the volcanic edifice to both low-sulphidation and high-sulphidation epithermal systems is presented in Fig. 5.4. The genesis of a porphyry system is illustrated in Fig. 5.5 (see also Chapter 2). Although subduction zones are not uniquely favourable for the generation of Cu–Au ore systems, magmas formed above subduction

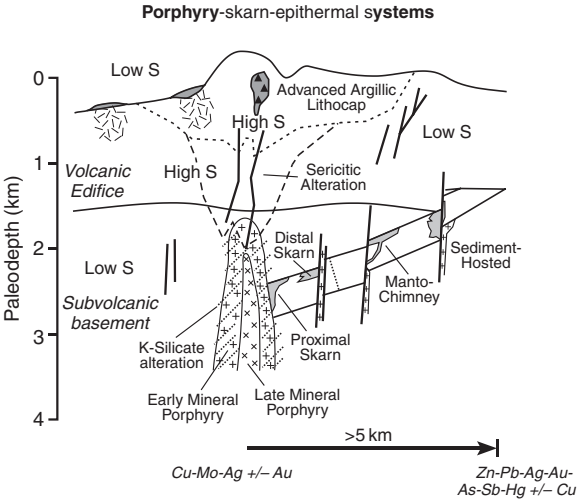


Fig. 5.4 Holistic and idealised model of a porphyry-epithermal-skarn system, based on and modified from Sillitoe (1995) and Lang et al. (2000)

zones are commonly associated with abundant porphyry-epithermal systems. In subduction zones the magma-forming process begins with dehydration of the subducting oceanic crust at the blue schist-eclogite transition, at depths ranging from approximately 50 to 150 km, which results in the transfer of solute-rich aqueous fluids from the slab to the overlying wedge of asthenospheric mantle (Richards 2003; Fig. 5.6). In this way, the asthenospheric wedge becomes metasomatised that is enriched in volatiles, silica, sulphur, and large ion lithophile elements (LILE; Rb, K, Ba, Sr, Cs). Partial melting of the asthenospheric wedge is thus facilitated by these additions, with the melt products consisting of primitive tholeiitic basalts bearing the geochemical fingerprint of slab materials (Arculus 1994). Therefore, water transported into the mantle by the hydrated subducting plate is the principal cause of magma generation above the slab. Kawakatsu and Watada (2007) used seismic waves to image reflectivity profiles beneath northeast Japan and found that the water expelled from the slab hydrates mantle peridotite to form hydrous serpentinite. They proposed that this serpentinised mantle forms a layer above the subducting slab and is the pathway through which water is transported down along the subducting slab into the mantle. This would form the pathway of water (and presumably other volatiles), which then triggers partial melting to generate arc magmas (Kawakatsu and Watada 2007).

Subduction zone basalts are volumetrically minor in continental magmatic arcs (e. g. Andean margin), where andesite and dacite predominate, whereas in oceanic arcs, eruption of this primitive basalt is more common. Subduction zone basalts underplate or pool beneath the lower crust in the subcontinental mantle lithosphere, inducing multiple stages of crustal melting and assimilation and resulting in the formation of andesitic magmas, by processes called MASH (melting-assimilation-storage-homogenisation; Hildreth and

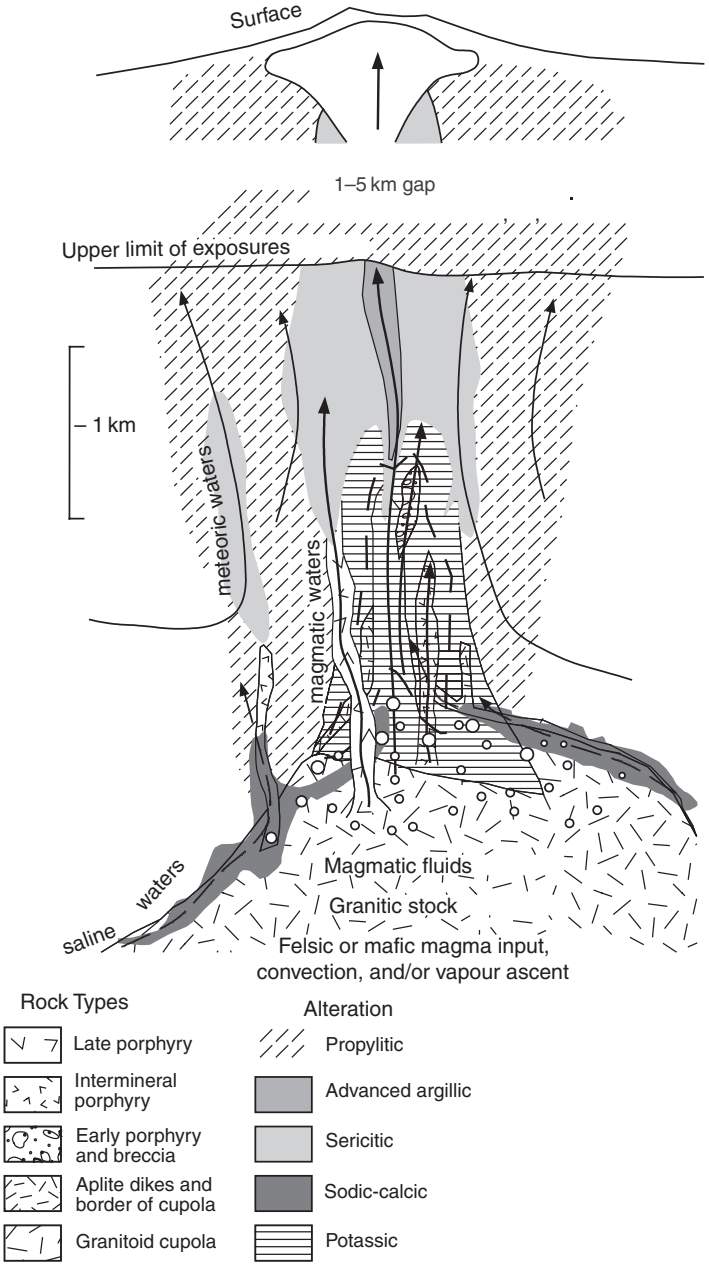


Fig. 5.5 Idealised cross-section of a porphyry system showing erosion surfaces, timing of intrusions, flow paths of magmatic-hydrothermal and meteoric fluids and alteration zones. The upper parts of the advanced argillic alteration zone, within the volcanic edifice, correspond to a high-S epithermal system. Modified after Seedorff et al. (2005)

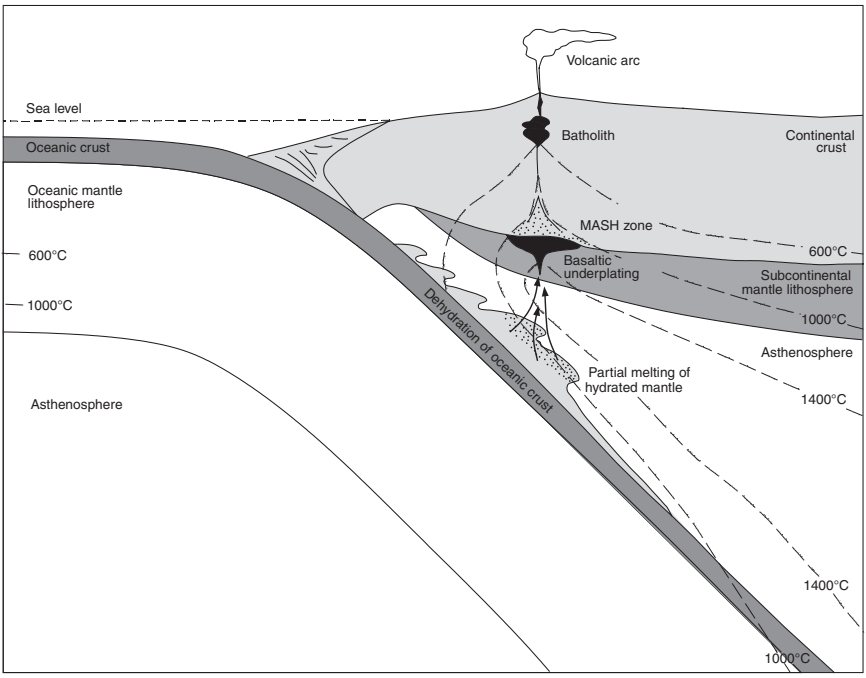


Fig. 5.6 Idealised section through a subduction-related continental magmatic arc; dehydration of subducting oceanic plate transfers volatiles to the overlying mantle wedge causing partial melting; hydrous basaltic melts underplate the base of the lower crust fractionate and partially melt crustal materials (MASH zone); andesitic magmas rise to erupt at surface as stratovolcanoes in which porphyry and epithermal systems form in the subvolcanic and volcanic environments. More details in text. Modified after Richards (2003)

Moorbath 1988) and AFC (assimilation-fractional-crystallisation; DePaolo 1981, and Wilson 1989 for an overview). For this reason, andesitic volcanic rocks and intrusive of intermediate composition dominate arc settings, where the majority of porphyry systems occur. The MASH zone combines intrusions, dykes and sills, with siginifcant exchange of heat and mixing with partially melted crustal rocks (Hildreth and Moorbath 1988). This may result in complex geochemical and isotopic signatures reflecting the varieties of this mixing. The volume of basaltic magma that ponds at the base of the crust constitutes a significant input of thermal energy, which is released as the magma fractionates to more evolved and volatile-rich members (Richards 2003). Furthermore, the release of the thermal energy will cause partial melting and assimilation of the crustal rocks in the MASH zone (Fig. 5.6), producing hybrid magmas of andesitic and dacitic compositions, further enriched in volatiles, sulphur and incompatible elements. An important factor is the comparatively high oxidation state of the magma, which allows sulphur to

be dissolved as a sulphate, which means that sulphide-compatible elements, such as Cu and Au, will not form sulphides but will be incorporated in the evolving liquids to become available in the later hydrous granitic fractionates.

Halter et al. (2002) have suggested that sulphide liquids are first segregated in the magma and subsequently released to ore-forming magmatic-hydrothermal fluids. These authors, based on microanalyses of melt inclusions, proposed that sulphide melts contribute heavily to the metal endownment of porphyry systems and would be essential to ore formation. The exsolution of chloride-rich volatile phases, destabilises the sulphide liquid effecting the transfer of Cu, Mo and Au, and other metals, as well as sulphur to the magmatic-hydrothermal fluids. On the other hand, Mungall (2002) suggested that arc magmas will have high potential to generate Cu–Au ore systems, if these magmas have high oxidation states (see Fig. 4.4). In order to achieve a high oxidation state subduction magmas must have a component of melted oceanic crust, because slab-derived melts carry volatiles that are released from the wet oceanic crust and the overlying sediments (see Chapter 7 for details on oceanic crust). Mungall (2002) reasoned that for a silicate magma to carry significant amounts of Au and Cu, a sulphide melt must be absent from the mantle source. If sulphides are present they can be removed through oxidation processes, such as:

$$\mathrm{FeS(liq)} + 2\mathrm{O_2(fluid)} \rightarrow \mathrm{FeO(melt)} + \mathrm{SO_3(melt)}$$

Aqueous fluids and other soluble elements (e. g. K, Rb, U) are released by slab dehydration, metasomatising the overlying mantle wedge lowering its solidus temperature and causing partial melting. Potassic supercritical fluids generate magmas with high f_{O2}, which can destabilise mantle sulphides and release Cu and Au from sulphides, and become potentially amenable to form Cu–Au ore systems. This is the case for many of the porphyry-epithermal systems, such as El Indio, Chuquicamata, Ladolam and Panguna.

The hybrid andesitic and dacitic magmas that form in the MASH zone rise, as dykes and diapirs through fractures in the more brittle upper crust, by a combination of buoyancy and magma pressure, aided by the tectonic stress field (Richards 2003). Porphyry systems are generated in the magma pockets or chambers in the upper levels of the crust, where they feed volcanic fields. A magma chamber from which a porphyry (and epithermal) system develops, is an open system which is frequently recharged with new batches of melts, subject to mixing, fractionation, crystallisation, degassing and erupting (Seedorff et al. 2005). Volatile exsolution and the generation of an aqueous phase form magmatic-hydrothermal fluids, which extract metals from the silicate liquid and collect in the upper parts of the chamber. This can be repeated several times as each new batch of magma is emplaced. The evolving fluids interact with the partly consolidated magma and the surrounding rocks progressively and upward spatially evolving sodic-calcic, potassic, sericitic, propylitic and argillic alteration zones (Seedorff et al. 2005). In this open system,

mixing with descending meteoric fluids is common, producing or participating in the formation of argillic alteration envelopes. This scenario and the general geometry of the system are shown in Fig. 5.5. Finally, a brief mention is given on the unusual situation created by flat subduction of young and hot oceanic crust. This causes melting of the oceanic crust slab producing magmas called adakites. Adakites are therefore different from calc-alkaline magmas, generated by the mantle wedge melting referred to above, but are similar to the tonalite-trondhjemite-granodiorite (TTG) of Archaean terranes (Martin et al. 2005). I return to discuss the effects of flat subduction in Section 5.3.6.

The tectonic settings of porphyry systems are plate margins, both continental and oceanic, major transcurrent fault systems of collision zones and rift environments. The majority and the more classic porphyries are found along plate margins, where initial compression prevents the ascent of magmas and their eruption to surface. This enables fractionation to occur with volatile saturarion and the generation of magmatic-hydrothermal fluids. Upon stress relaxation, rapid uplift and extension take place, which enable the movement of fluids (Cooke et al. 2005 and references therein). There also appears to be some correlation of giant porphyry systems with zones of low angle or flat-subduction, perhaps due to subduction of oceanic ridges, as is the case for the Juan Fernández Ridge against the Chilean margin with subsequent crustal thickening, followed by uplift and extension (Cooke et al. 2005).

In the pages ahead, brief descriptions of a selection of porphyry systems are presented. The examples given are representative of island-arc settings (Panguna and Ok Tedi in Papua New Guinea), continental Andean-type margin (Chuquicamata and El Teniente in Chile and the porphyry Sn deposits of Bolivia), the Oyu Tolgoi and Tuwu porphyries in Palaeozoic volcanic arcs in central Asia, continental rift settings (the porphyry Mo systems of Climax and Urad-Henderson in Colorado and the Oslo Rift, Norway), extensional environments resulting from post-collisional orogenic collapse (Qinling orogen in China) and in transtensional environments related to collision (Tibet porphyry belt). Reviews of porphyry-related skarns in the western USA, Sn and W skarns in Tasmania are discussed in Chapter 6.

5.2.1 Porphyry Systems of Convergent Margins

The world's distribution of porphyry deposits (Fig. 5.2) clearly show that the majority are sited along ancient and modern convergent plate margins. These are the porphyry systems that are generated in magmatic arcs above subduction zones, by the mechanisms outlined in the preceding section. The largest known and most abundant porphyry systems are along the circum-Pacific rim (Sillitoe 1997). Special issues of Economic Geology described the porphyry systems of the southwest Pacific island arcs (Gustafson and Titley 1978) and those of the Chilean margin (Dilles and Camus 2001).

5.2.1.1 Panguna Porphyry Cu–Au Deposit, Bougainville, Papua New Guinea

The Panguna Cu–Au deposit is located in the southwest Pacific island of Bougainville, within a consuming margin between the Indo-Australian and the Pacific plates (Fig. 5.7). The tectonic setting of the region is characterised by a complex interplay of a number of small plates to the north and northeast of mainland Papua New Guinea, such as the Caroline plate, the Manus Basin and Solomon plate (Fig. 5.7). Subduction, formation of volcanic arcs, continental collision with the northern margin of Australia and the accretion of island arcs and interaction with the Manus Basin spreading ridge, are part of the complex tectonic history of the region. Flat-subduction due to collision with the north of the Papua New Guinea trench may have been associated with the formation of large porphyry and epithermal systems, such as Grasberg, Ok Tedi and Lihir (Cooke et al. 2005). The porphyry intrusions are all of calc-alkaline affinity, including diorite, quartz-monzonite and granodiorite intruding in most cases their own andesitic to dacitic volcanic piles, and only locally sedimentary rocks. While numerous porphyry systems have been discovered in the Papua New Guinea region, only a few are currently operating mines. Nevertheless, all of these deposits are of considerable scientific interest as they are geologically very young all having been formed from the Miocene to Recent.

The Papuan region is subdivided into a number of tectonic provinces (Dow 1975, Hill and Hegarty 1987) which are, from south to north: the Australian Platform, the Papuan Fold Belt, the New Guinea Mobile Belt and the Northern Volcanic Province (Fig. 5.7). The Australian Platform constitutes a stable

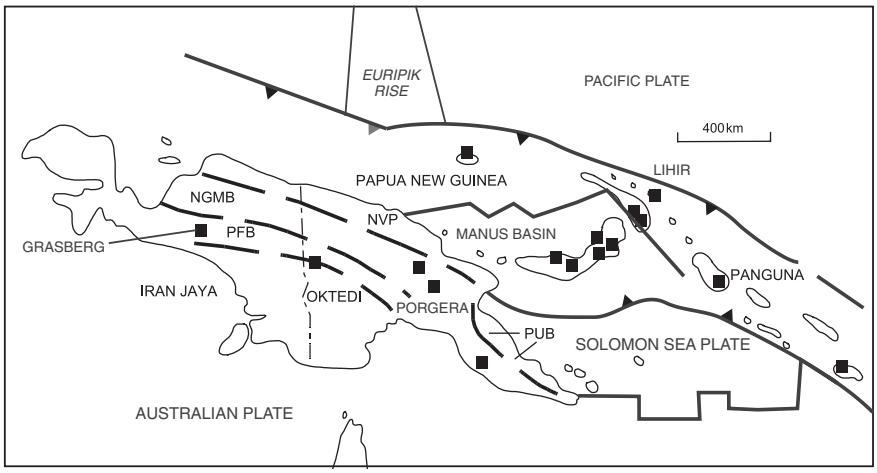


Fig. 5.7 Simplified tectonic plates and distribution of selected porphyry deposits in the Irian Jaya and Papua New Guinea region. NVP Northern Volcanic Province, NGMB New Guinea Mobile Blet, PFB Papuan Fold Belt, AP Autsralian Platform, PUB Papuan Ultramafic Belt. Modified from Pirajno (1992)

Precambrian to Paleozoic basement of granitic and metamorphic rocks overlain by shallow marine and lacustrine sediments of Jurassic to Holocene age. The Papuan Fold Belt, which is included in this subdivision, lies along the northern margin of the platform. Many porphyry Cu deposits are associated with this Belt. The New Guinea Mobile Belt contains a thick sequence of sedimentary rocks intruded by mafic to felsic plutonic rocks. This belt is part of a collision zone between the Australian continent in the southwest and island-arc systems to the northeast. Ophiolitic rocks mark the site of collision and obduction with the Northern Volcanic Arc to the north. The Northern Volcanic Arc continues eastward into the New Britain and Solomon island arcs which are part of the Melanesian oceanic province (Dow 1975). A comprehensive work on the geology and mineral deposits of Papua New Guinea can be found in Rogerson and McKee (1990).

*Panguna:*This is one of the largest Au-rich porphyry Cu deposit known, discovered in 1964 following regional and detailed geochemical sampling (Baumer and Fraser 1975). The deposit has resources of 1.4 Bt, grading 0.53% Cu and 0.63 g/t Au (Laznicka 2006). Details of the Panguna deposit can be found in Ford (1978), Eastoe (1978) and Clark (1990).

Panguna is located on Bougainville Island which is part of the Solomon Islands, a Late Cenozoic volcanic arc. Bougainville is underlain by Cenozoic andesitic and basaltic rocks, associated volcaniclastics and limestones. A number of younger dioritic and granodioritic stocks intruded this sequence during the Pliocene and Pleistocene. The Panguna deposit is centred on a complex of three porphyritic quartz-diorite and granodiorite bodies which are intrusive into the Panguna Andesite member. The intrusive stocks are marginal differentiates of the large equigranular Kaverong quartz-diorite, with ages of 4–5 Ma, itself containinig weak fracture-controlled alteration-mineralisation. The leucocratic quartz-diorite, the biotite-granodiorite and the biotite-diorite are the three strongly fractured, altered and mineralised stocks, while the Biuro granodiorite (3.4 Ma) and the plug-like Nautango andesite (1.6 Ma) post-date the mineralising event. Approximately one third of the ore is contained within the Panguna andesite member, the remainder being in the three intrusive stocks in which well-mineralised intrusive and collapse breccia zones are present. Ore minerals are chalcopyrite, lesser bornite and associated Au and Ag. Au occurs as submicroscopic particles of the native metal and Au values vary sympathetically with Cu. Other sulphide and oxide species include pyrite, magnetite, hematite and traces of molybdenite. The ore minerals occur associated with steeply dipping veins and fracture fillings, and as fine disseminations in the altered rocks. Detailed studies indicate that most of the Au is contained within the lattice of chalcopyrite and bornite. In general terms the Cu ore tends to increase with an increase in the proportion of veining, whereas disseminated ore increases with the more pervasive alteration. Also in the Panguna andesite the Cu content tends to decrease with distance from the intrusive contacts. The sulphide mineralisation is associated with the zone of potassic alteration, where in fact the highest grades are present.

Reconstruction of hydrothermal alteration geometry is complicated by the presence of multiple and overlapping alteration types. Potassic and propylitic alteration are dominant features, while argillic and phyllic alteration are important only in small areas. Potassic alteration forms a zone, within which are the higher Cu grades, and which is centred on the mineralised biotite-granodiorite and the leucocratic quartz-diorite. Potassic alteration in the Panguna andesite is mainly represented by a zone of secondary biotite surrounding the porphyries. The Kaverong quartz-diorite and the intrusive stocks display potassic assemblages of biotite + chlorite + K-feldspar + magnetite ± anhydrite, or biotite + K-feldspar + chlorite, as in the leucocratic quartz-diorite. Phyllic and argillic alteration is confined to the biotite-granodiorite and consists of chlorite + sericite + clay minerals. Propylitic alteration surrounds the potassic zone, and in the Panguna andesite consists of chlorite, epidote, pyrite, calcite, albite and K-feldspar.

The alteration-mineralisation events began with a magmatic-hydrothermal stage with potassic alteration and Cu mineralisation, followed by an influx of a cooler meteoric-dominated hydrothermal fluid which was feldspar-destructive and caused phyllic and argillic alteration. The distribution of the alteration-mineralisation zones indicates that a magmatic-hydrothermal zone was later surrounded by a cooler meteoric-hydrothermal system. Fluid inclusion data show two main mineralisation phases (Eastoe 1978). The first, associated with the Kaverong quartz-diorite, involved magmatic-hydrothermal fluids of very high salinity fluids (46–76 wt% NaCl equivalent) and high temperature ($\sim$700°C). The Cu and Fe sulphides were deposited by boiling of these magmatic-hydrothermal solutions. After this early systems cooled to about 350–400°C, it was invaded by low salinity meteoric-dominated fluids ($<$10 wt% NaCl) with further mineralisation associated with the emplacement of the leucocratic quartz-diorite. The salinity, temperature and composition (NaCl + KCl) of the fluids indicate pressures of 200–300 bar, equivalent to approximately 2–3 km of depth. The meteoric-dominated fluids resulted in the deposition of pyrite, quartz and clay minerals at a temperature of approximately 300°C. Supergene oxidation produced a number of secondary minerals such as chrysocolla, dioptase, malachite, cuprite, chalcocite, covellite and native Cu. The secondary ore grades are only a little higher than the primary ore.

5.2.1.2 Porphyry Cu–Mo Deposits in Chile (Andean Continental Magmatic Arc)

The Andean continental margin contains numerous Cu–Mo, Cu–Au porphyry deposits and high-sulphidation epithermal systems (Fig. 5.8). I have mentioned that these porphyry systems are genetically related to calc-alkaline magmatism in response to subduction of oceanic crust under the continental margin of the South American continent. The spatial and temporal

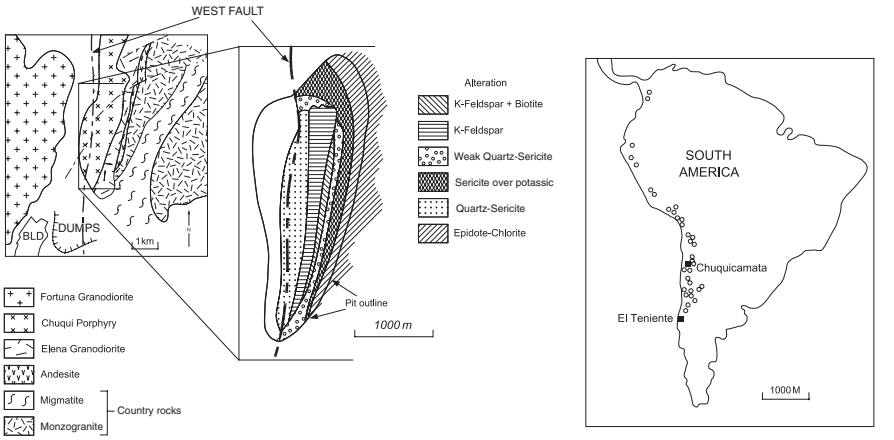


Fig. 5.8 Simplified geology and hydrothermal alteration zones of the Chuquicamata porphyry Cu deposit. Inset shows the distribution of porphyry systems along the Andean margin. Modified after Ambrus (1978)

relationships of mineralising systems in the Andean margin have been discussed by Frutos (1982), Sillitoe (1986) and in Dilles and Camus (2001). The geological evolution of the central and southern Andes from the Paleozoic onward is characterised mainly by the development of a magmatic arc at a convergent margin formed by the Farallon, Nazca and American plates. The entire magmatic system evolved from the initial stages of an ensimatic arc in the Lower Paleozoic to advanced and present-day stages of a magmatic arc of continental affinity. During the Mesozoic and Cenozoic, a migration of the magmatism towards the east occurred along belts parallel to the coast and hence to the trench and subduction zone. The emplacement of the Chilean porphyry deposits is therefore related to Mesozoic and Cenozoic, calc-alkaline magmatic activity which resulted in a continuous belt of granodioritic intrusions, andesitic lavas and associated lithologies. Initial $^{87}Sr/^{86}Sr$ ratios of between 0.703 and 0.706 in the Chilean calc-alkaline rocks are indicative of a strong mantle component and tend to confirm mantle and/or lower crust involvement. By comparison the porphyry deposits of the North American Cordillera (including Climax types) have initial $^{87}Sr/^{86}Sr$ ratios of between 0.705 and 0.710 (White et al. 1981). The two largest deposits are Chuquicamata (stockwork type) and El Teniente (breccia-type), which together contain approximately 60% of the total reserves, and are described in this section. Other important deposits in Chile are El Salvador, La Escondida, Los Pelambres and Rio Branco-Los Bronces. The total metal endownment of the Andean margin, from Colombia, through Peru, Chile to Argentina is around a staggering 528 Mt of copper metal, almost 10 Mt of molybdenum metal and 3 Mt of gold. In the Chilean deposits the Cu/Mo ratios vary from 100:1 to 10:1 and therefore Mo is recovered as a by-product.

5.2.1.2.1 Chuquicamata

This deposit (and the nearby Exotica deposit) is located in northern Chile, 240 km northwest of the town of Antofagasta in the Atacama desert. Although records of mineralisation in the region date back to the time of the Spanish conquistadores, it was not until 1915 that the first mining operations commenced. The discovery of the Exotica orebody (Mortimer et al. 1977), some 3 km to the south, was made accidentally while drilling the waste dumps for the recovery of leached Cu (Ossandón et al. 2001). Remaining resources at Chuquicamata are in the region of 6450 Mt at 0.55% Cu and 0.12% Mo, making it one of the largest porphyry deposits in the world. A comprehensive description of the Chuquicamata deposit by Ossandón et al. (2001), is summarised here.

The primary Cu–Mo mineralisation occupies an area 12 km long and approximately 800 m wide, within an elongate granodioritic porphyry complex (Chuqui Porphyry Complex) which intruded into Jurassic granodiorites and Paleozoic granitic and metamorphic rocks during the Early Oligocene (Fig.5.8). To the east the Chuqui porphyries grade into the Elena Granodiorite, and the orebody to the west is separated from the Fortuna Intrusive Complex by a major fault structure known as the West Fault (formerly the West Fissure), which may have played an important role during and after the emplacement of the Chuqui porphyries. The West Fault is a zone of brecciated quartz-sericite material. The Fortuna Intrusive Complex contains low-grade mineralisation and is made up of three units: Fiesta Granodiorite, San Lorenzo porphyries and Tetera porphyry aplite. The first is volumetrically dominant and is intruded by smaller bodies of the other two units. The Fortuna complex is weakly mineralised with chalcopyrite±bornite disseminations and veinlets, lesser chalcopyrite±magnetite and some molybdenite along fractures. The Chuqui Porphyry Complex effectively constitutes the entire Chuquicamata orebody and is in contact with the Jurassic-Cretaceous Elena and East granodiorite. The Chuqui complex consists of four units: East, Fine Texture, West and Banco porphyries. The mineral assemblage of the unaltered rocks is plagioclase, quartz, K-feldspar, biotite and hornblende, with accessory titanite and magnetite. $^{40}Ar/^{39}Ar$, U-Pb single and multigrain dating and Re-Os dating of molybdenite yielded ages of 35–36 Ma for these intrusions and associated mineralisation. Stages of hypogene alteration and mineralisation consist of an early stage, a quartz-molybdenite stage, a main stage and a late stage. Hydrothermal alteration zones eastward from the West Fault (Fig. 5.8), comprise quartz-sericite, potassic and propylitic zones. Dominant sulphide zones from the West Fault eastward are: enargite, covellite, chalcocite, chalcocite-covellite, covellite, chalcopyrite and chalcopyrite-bornite. The early stage has a quartz- K-feldspar assemblage with some biotite and anhydrite. This potassic alteration is quite distinctive in that the biotite is almost always replaced by the quartz-K-feldspar assemblage and the texture is typically cataclastic. The early stage quartz-feldspar does not seem to be associated with sulphide mineralisation. This

cataclastic deformation is associated with albitisation which preceded the potassic alteration event. The quartz-K-feldspar alteration zone spatially corresponds with and is overprinted by a zone of bornite-digenite-chalcopyrite mineralisation. The eastern margin of the potassic zone grades into a propylitic zone of alteration with chlorite, epidote and hematite and low-intensity chalcopyrite-pyrite mineralisation. The quartz-molybdenite stage is characterised by molybdenite in quartz veins and as coarse-grained, curved and elongated bunches of crystals along fracture surfaces. The so-called blue veins have a narrow halo of "feldspar-destructive" alteration with fine disseminations of molybdenite. Composite quartz veins up to 0.5 m in thickness contain coarse molybdenite and grade into irregular quartz masses and pods. The main stage comprises quartz-sericite alteration and pyretic veins, which overprint all earlier mineral assemblages. Alunite is locally present. The main stage carries most of the primary (hydrothermal) Cu, which together with that from supergene enrichment makes up most of the Chuquicamata resources. Eastward and upwards, quartz-sericite overprints the potassic alteration and is accompanied by chalcocite and covellite. The main vein assemblages are: pyrite-chalcopyrite-bornite, pyrite-bornite-digenite±enargite, pyrite-digenite-covellite±enargite. Fluid inclusions studies of the main stage quartz showed temperatures ranging from 250 to 350°C and a salinity of 2–20 wt% NaCl equivalent. The late stage consists of covellite in coarse quartz veins, locally associated with hypogene hematite and anhydrite. Covellite also occurs in fractures and veinlets. An important feature of this stage is the presence of sphalerite rims on chalcopyrite, forming a zone with fairly high Zn values (>0.08%), which at depth correlate with high As values (~0.1%). Finally, supergene enrichement of oxide Cu ore (the largest in the world but mostly mined out) is accompanied by kaolinitic clay. Chalcocite is the principal supergene ore mineral. Large amounts of Cu were leached from the supergene blanket and were deposited in gravels providing some 300 Mt of ore. Leaching, oxidation and secondary enrichment were important ore-forming processes, and much of the production of Cu metal was in fact derived from the zone of supergene enrichment. The supergene zone occupied an area of 3.5 km in a north-south direction, with an average width of 500 m and thickness of approximately 400 m. A leached cap with less than 0.10% Cu is followed by irregular masses of antlerite, brocantite and atacamite (approximate grade of 1.5% Cu). This is underlain by enrichment zones of chalcocite and chalcocite + covellite (approximately 18% Cu), and finally an elongate and deeper covellite enrichment zone (10–15% Cu) which appears to be spatiallly associated with the West Fault. Many of the supergene minerals at Chuquicamata are unique and owe their preservation to the unusual and extreme arid conditions of the Atacama desert. A number of sulphates, nitrates, chlorides, iodates and iodides occur within a few metres from the surface. Oxidation of molybdenite leads to lindgrenite [$Cu_3(Mo_4)_2(OH)$] which, as the most important Mo oxide, is more abundant in zones where the Cu oxides are stable. In the upper levels extreme acid conditions result in the leaching of lindgrenite to ferrimolybdite [Fe (MoO_4)38H_2O] (Ambrus 1978).

5.2.1.2.2 El Teniente

The El Teniente deposit owes its name to the discovery by a fugitive Spanish army lieutenant in 1706, but the first official records of production are dated at 1819 (Howell and Molloy 1960). It is the largest underground Cu mine in the world with resources of 12.4 Bt grading 0.62% Cu and 7.8 Bt at 0.018% Mo (Cannell et al. 2005). The present account is based on Camus (1975), Cannell et al. (2005) and Klemm et al. (2007).

El Teniente is situated approximately 90 km southeast of Santiago (Fig. 5.8 inset) within a major north-south-trending volcano-sedimentary belt of Cretaceous age intruded by quartz-diorite plutons and related dacitic volcanic rocks. Although the deposit is characterised by a variety of magmatic-hydrothermal breccia pipes it has many features of a porphyry system.

The mine area is underlain by great thicknesses of lava flows, pyroclastics and sediments which are intruded by calc-alkaline intermediate to felsic intrusions between 12 and 7 Ma. Detailed mapping of the El Teniente district has revealed the presence of four volcanic centres, associated with subvolcanic andesitic intrusions. The oldest formation is Coya-Machali (Upper Cretaceous), which consists of folded sediments, andesite and pyroclastics some 3000 m thick. Above this is the Farellones Formation (mid-late Miocene) which is subdivided into three members in the mine area. The lowest member is from 1400 to 1000 m thick, is made up uniquely of andesitic rocks which are also the main host of the mineralisation; the middle member is 800 m thick and made up of epidotised andesites and intercalated lacustrine sediments; the upper member consists of basalt and andesite lavas with some pyroclastics. The intermediate to felsic intrusions are part of the 8.9–5 Ma El Teniente Complex comprising the Sewell Tonalite and diorite intrusions. The youngest intrusions in the mine area are dacite and latite porphyry dated at 5.7 Ma, and lamprophyre dykes (3.8–2.9 Ma). The El Teniente deposit is located near the intersection of two major structures: the Codegua and the Teniente faults. A recent re-interpretation of the El Teniente andesitic host rocks by Cannell et al. (2005) shows that they consist of an andesitic sill and stock complex, with the sills having intruded andesitic lava flows and volcaniclastic rocks of the Farallones Formation. The sill and stock complex include coarse- and fine-grained andesite porphyries and stocks of gabbro and diorite porphyry, andesite dykes and suvertical biotite breccia zones. As series of calc-alkaline, felsic to intermediate units intrude the andesitic sill and stock complex. The oldest and pre-mineralisation intrusion is the 7.4–7.1 Ma Sewell Tonalite, followed by the intrusion of dacite pipes and dykes with ages ranging from 5.50 to 5.28 Ma. The dacitic rocks are temporally and spatially associated with Cu- and Mo-bearing veins and potassic alteration. The central part of the deposit is occupied by the late to post-mineralisation 4.7 Ma Braden Pipe, with an inverted cone geometry and a diameter varying from 1300 m at surface to 650 m at a depth of 1600 m below surface. The Braden Pipe comprises two units: a monomict clast-supported mineralised marginal breccia and a barren central unit. The central unit

consists of rounded to subangular mineralised fragments, ranging in size from a few centimetres to 3 m and set in a rock-flour matrix. No clast-size preferential distribution is recognised, but graded bedding is seen in the upper levels of the pipe. The surrounding marginal breccia is made up of angular fragments cemented by a tourmaline-quartz-sulphide matrix. Fragments of this marginal belt are also found in the central pipe.

Cannell et al. (2005) reported that the 0.5% Cu contour outlines a zone about 2.5 km long, 1.8 km wide and 0.8 km deep. These authors recognised a pre-mineralisation stage (type 1 veins), a late magmatic stage (type 2 veins), a principal hydrothermal stage (type 3 veins) and a late hydrothermal stage (type 4 veins). Type 1 veins contain quartz, magnetite, sericite, actinolite, plagioclase and tourmaline and may be related to the emplacement of the Sewell Tonalite. The late magmatic stage with type 2 veins correlates with the emplacement of the dacite porphyries and is associated with potassic alteration (biotite, K-feldspar), grading to distal chloritic and sericitic alteration. Type 2 veins are represented by quartz-anhydrite-sulphide stokcworks. These veins contain quartz, chalcopyrite, bornite, molybdenite, anhydrite, chlorite, Na-K-feldspar, biotite, sericite. Subvertical, matrix-supported biotite breccias may belong to this event. The late magmatic veins are zoned around the dacite porphyries and three domains can be distinguished with distance from the dacitic pipes: (1) proximal biotite-bearing (potassic) zone; (2) biotite-sericite-chlorite (transitional potassic-propylitic) zone; (3) chlorite or propylitic zone. Within the dacite intrusions, however, the dominant alteration phase is a Na-K-feldspar. The principal hydrothermal stage and type 3 veins overprint the veins of the late magmatic stage veins and are associated with haloes of phyllic alteration, comprising an assemblage of quartz-sericite-chlorite. The veins have quartz and anhydrite as dominant gangue minerals and sulphides (chalcopyrite, pyrite, molybdenite). The late hydrothermal stage and type 4 veins are spatially and temporally associated with the emplacement of the Braden Pipe and latite intrusions. The type 4 veins have a diverse and complex mineralogy with tourmaline, anhydrite, gypsum, barite, chalcopyrite, bornite, pyrite, tennantite-tetrahedrite, molybdenite, and minor sphalerite, galena, enargite, stibnite.

Three hypogene alteration phases and one supergene phase have been recognised. The hypogene phases are: potassic, phyllic and propylitic. The supergene phase is mainly argillic. Potassic alteration affects a large portion of the deposit and is characterised by K-feldspar and biotite. The mineralisation is mainly associated with this phase of alteration. Phyllic alteration affects all rocks, but it is best developed in the quartz-diorites, where quartz and sericite are the chief minerals; tourmaline, anhydrite, chlorite and pyrophyllite may also be present. The propylitic zone contains chlorite, epidote, calcite, magnetite, anhydrite and tourmaline. Tourmaline, an important component of the El Teniente alteration assemblages, is related to two distinct events: (1) the emplacement of the quartz-diorites and (2) the emplacement of the breccia pipe. It occurs as fine to coarse disseminations, as fracture fillings and as matrix in the breccias. Hypogene

sulphides form a zonal pattern in the north and central parts of the orebody with bornite at the core surrounded by a zone of chalcopyrite ± pyrite grading into a marginal zone of pyrite. Other sulphides and ore minerals are molybdenite, tennatite, hematite, magnetite and enargite. Molybdenite which is associated with quartz veins, occurs throughout the deposit but is most highly concentrated at the intrusive contacts.

Klemm et al. (2007) recognised ten fluid types, based on petrographic and microthermometric data. They found that there was a transition from a two-phase vapour-dominated fluid at ~410°C and 300 bars (stage 2), to a low-salinity fluid at < 350°C and 200 bars (stage 3), derived from the cooling of the magmatic vapour phase. The Cu mineralisation was formed from the vapour phase and its derived low-salinity fluids, whereas the Mo mineralisation was largely derived from residual brines and extensive boiling.

A structural model proposed by Cannell et al. (2005) envisaged the following: emplacement of a large, deep-seated felsic pluton below the current mine level from which dacite porphyry intrusions derived. Fluid exsolution from the pluton led to the formation of veins and stockworks of the late magmatic and principal hydrothermal stage, with widespread potassic alteration. This was followed by a period of relaxation, quiescence, subsidence and magma withdrawal, accompanied by the formation of steeply dipping concentric fractures. Finally, a stage of uplift and magma resurgence occurred; marginal breccia zones, late hydrothermal veins were emplaced in the concentric fractures. The explosive emplacement of the Braden Pipe caused de-pressurisation and cooling, accompanied by the late hydrothermal stage.

In summary, the genesis of the El Teniente mineralisation is related to the emplacement of stocks, their cooling, retrograde boiling, hydraulic brecciation and the activities of magmatic and meteoric hydrothermal systems. Metals were probably transported in highly saline brines and deposited in the veins and veinlets within the surrounding fractured rocks. As with other porphyry systems the potassic phase of alteration-mineralisation is linked to the activity of a magmatic hydrothermal system, while the phyllic, argillic and perhaps the propylitic phases were genetically related to influx of meteoric waters.

5.2.1.3 Porphyry Sn–Ag Systems in Bolivia

The Bolivian Sn belt extends for about 800 km throughout the length of the Eastern Cordillera of Bolivia and parts of southern Peru and northwest Argentina (Fig. 5.9). The Eastern Cordillera is a plutonic arc of granodioritic to granitic batholiths which were emplaced during two magmatic events. One took place in the Early Mesozoic (199–180 Ma), the other in the Neogene (19–8 Ma) (Schneider and Lehmann 1977). These two magmatic events are also responsible for two main episodes of mineralisation in the Cordillera. The first, of Triassic-Jurassic age, consists of auriferous quartz veins, W–Sb–Hg mineralisation and base metal and Sn deposits. The second is of Miocene-Pliocene age and is represented by Sn–Ag mineralisation.

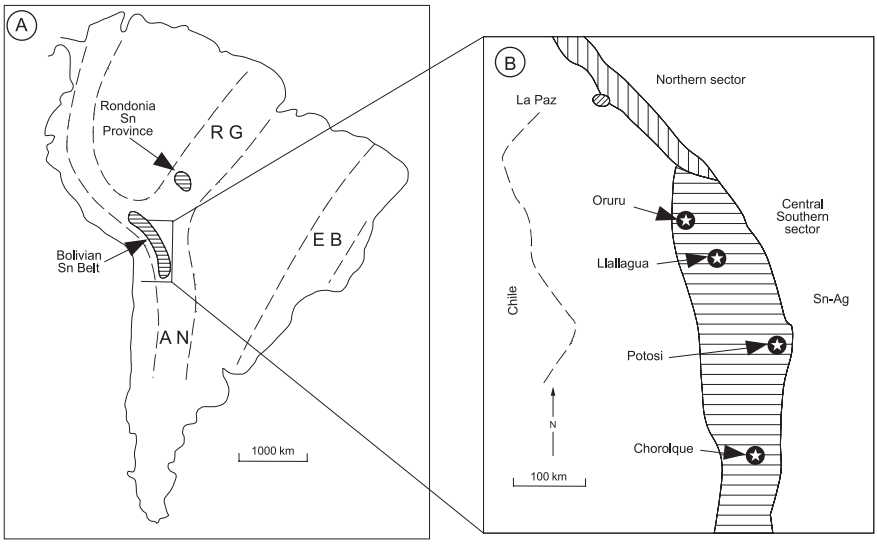


Fig. 5.9 (**A**) South American porphyry tin belts (Schneider and Lehmann 1977); (**B**) Distribution of main deposits in the Bolivian tin belt (Sillitoe et al. 1975)

The Sn belt can be subdivided into a northern sector, or Cordillera Real region, and a central-southern sector (Fig. 5.9; Sillitoe et al. 1975), separated by the so-called Arica's elbow where the eastern Andean Cordillera changes from a northwest to a north-south trend. The northern sector, characterised by Mesozoic batholithic Sn–W mineralisation, is more deeply eroded than the central-southern sector which has only exposed the later Neogene igneous rocks and is therefore characterised by Sn–Ag subvolcanic mineralisation. In the Bolivian Sn belt three main types of deposits have been identified (Schneider et al. 1978): (1) manto-type (stratabound) deposits of Lower Paleozoic age, in the northern and southern sectors; (2) vein deposits (Triassic-Jurassic age) confined to the northern sector and hosted within a Lower Paleozoic sedimentary sequence intruded by the Mesozoic batholiths; (3) Neogene Sn deposits in the southern sector associated with subvolcanic intrusions which are further divided into two subtypes (Villapando 1988): one includes vein deposits characterised by complex Bi–As–Pb–Zn–Cu parageneses; the other, which is the main subject of this section, consists of breccia pipes and vein systems characterised by Ag-rich parageneses. The Bolivian porphyry Sn–Ag deposits exhibit features of both porphyry and epithermal systems.

The porphyry Sn deposits in the central-southern sector of the Bolivian Sn belt account for about 75% of that country's tin production. In this region the igneous rocks form small isolated stocks, dykes and larger volcanic structures. Ignimbrite sheets of peraluminous chemistry are present but post-date the mineralisation (Ericksen et al. 1990). The major deposits are those of Llallagua, Potosi, Oruru and Chorolque (Fig. 5.9). Sillitoe et al. (1975) compared these

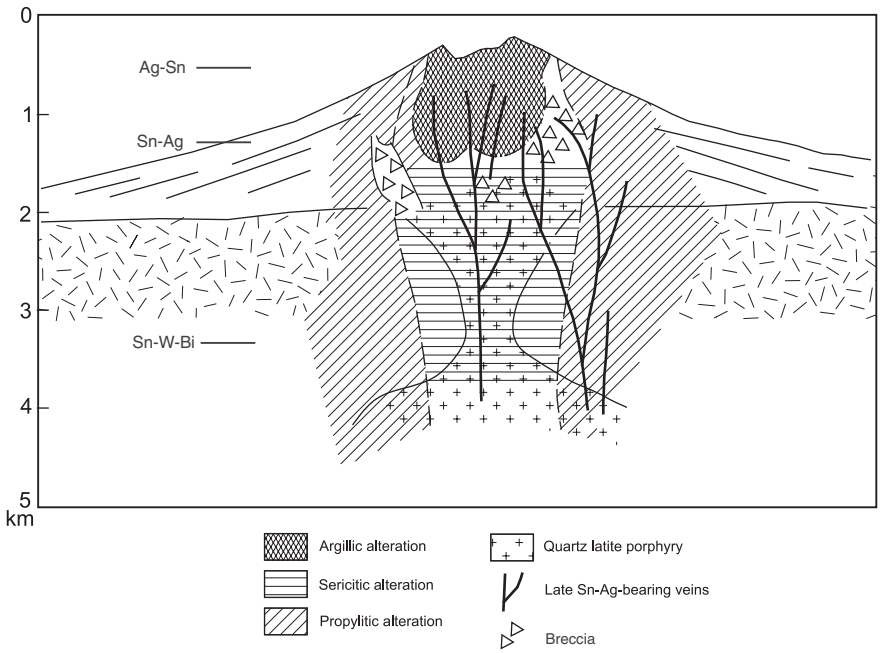


Fig. 5.10 Idealised model of subvolcanic porphyry Sn deposit of the Bolivian tin province and levels of dominant metal associations. After Sillitoe et al. (1975)

deposits to porphyry copper systems and concluded that the two types share many similarities. An idealised model of the porphyry Sn deposits according to the above authors is shown in Fig. 5.10. These deposits are centred on small calc-alkaline stocks of intermediate composition and have the form of inverted cones. Coeval volcanics are locally preserved adjacent to some deposits. Stockworks were probably formed by hydrothermal brecciation processes which overlapped in time with pulses of mineralising events. The stocks and adjacent wall rocks have undergone pervasive hydrothermal alteration in which a mineralised core of veins and breccias with quartz-tourmaline is surrounded by a zone of sericite, pyrite and tourmaline with minor cassiterite. This assemblage gives way to an outer zone of propylitic alteration characterised mainly by chlorite. Argillic alteration and silicification may occur in the upper portions of the system within remnants of the volcanic edifice. In contrast to porphyry Cu systems, potassic alteration is absent in the porphyry Sn deposits. In most deposits the stockwork mineralisation is cross-cut by a system of veins that carry high-grade Sn and other metals, notably Ag, as for example at Cerro Rico which in Spanish means "rich hill".

The Cerro Rico deposit, near the town of Potosi, is polymetallic (Sn-Ag-W-Bi-Pb-Zn), has resources of 143 Mt, grading 0.1–0.25% Sn and 174 g/t Ag (Bartos 2000). Cerro Rico is characterised by a shallow-level, funnel-shaped 13.8 Ma

dacite porphyry stock (Cunningham et al. 1996). The Cerro Rico quartz-latite stock is approximately 1700 × 1200 m at the surface, conical in shape and pinches out to a dyke at depth. The unaltered dacite consists of phenocrysts of quartz, plagioclase, K-feldspar and biotite in a fine-grained groundmass of the same minerals. The dacite porphyry intruded a 400 m-thick pile of air-fall tuffs, volcanic breccias (possibly phreatomagmatic) and sedimentary rocks, laid down in an ephemeral lake. The Cerro Rico volcanic system lies on a basement of Ordovician shales. There is field evidence that the Cerro Rico stock was intruded near a ring fault associated with the major Kari Kari caldera complex (Bartos 2000). The mineralisation is contained in 35 veins and lesser branches in the upper parts, grading downward into five principal veins. The vein ores are zoned, spatially and temporally, with Ag–Sn rich veins at the top, to Sn–Ag-rich veins to Sn–W–Bi veins at depth (Fig. 5.10). The earliest stages of lode mineralisation consisted of quartz, pyrite, cassiterite, arsenopyrite, with wolframite and bismuthinite in the deeper levels. This was followed in turn by quartz-sulphide veins with stannite, sphalerite, chalcopyrite, tetrahedrite, vein fillings of pyrite, sphalerite, tetrahedrite, galena, andorite ($Pb_9Ag_7Sb_{23}S_{48}$) and matildite ($AgBiS_2$), and last jamesonite and boulangerite. Ore mineral paragenesis (Sillitoe et al. 1975) indicates an early stage of quartz + pyrite + cassiterite with minor arsenopyrite and wolframite + bismuthinite at deeper levels; an intermediate stage with cassiterite + chalcopyrite + tetrahedrite + stannite and a late stage containing cassiterite and "ruby silver" (pyrargyrite), jamesonite + boulangerite. Hydrothermal alteration is mainly hypogene acid-sulphate, characterised by porous vuggy quartz in the upper 250 m of the Cerro Rico structure (Fig. 5.10). This porous altered rock contains almost 95% SiO_2 by almost complete removal of feldspar by extreme leaching by acid solutions with pH values of < 2 (see also Section 5.3.1), resulting in feldspar-shaped vugs that are lined with alteration minerals (quartz, jarosite, hematite and clays). The vuggy silica of Cerro Rico forms a massive blanket that overlies a 150 m-thick alteration zone of quartz-dickite-illite-kaolinite-pyrophyllite, which grades downward into quartz-sericite-pyrite and finally into a quartz-tourmaline zone at depth. The vuggy silica is very rich with Ag, with abundances ranging from 200 to 350 g/t. Bartos (2000) reported that much of this Ag-rich material was eroded and deposited as talus deposits, called pallacos, which can be economically exploited for their silver content. The vuggy silica zone is replaced by jasperoid and chalcedonic quartz and barite in the upper 10–20 m. Sillitoe et al. (1998) referred to the vuggy silica zone at Cerro Rico as "lithocap", a term first used by Sillitoe (1995) to indicate remnants of palaeosurface characterised by advanced argillic and argillic alteration that formed above subvolcanic intrusives. This is a feature that is typical of high-sulphidation epithermal systems. An example of lithocap-associated epithermal mineralisation is described in Section 5.3.4.1.

Alteration is pervasive throughout the stock with sericitic and tourmaline alteration at depth and silicification near the surface. Clay and alunite occur as a late stage alteration in the form of veinlets that cut the mineralised veins. Mineralised veins form a sheeted system containing Sn and Ag ores.

Assuming similarity between porphyry Cu systems and porphyry Sn deposits then a similar genetic model is deemed appropriate. It is probable, however, that the porphyry Sn deposits were emplaced at shallower depths than the porphyry Cu, because they have features indicative of a volcanic environment. Fluid inclusion data indicate depths of formation between 800 and 5000 m, depending on the proportions of lithostatic and hydrostatic pressure, but, for the above reasons, a depth of approximately 1000–2000 m is favoured (Sillitoe et al. 1975). Ore genesis involved the evolution of high temperature (±500°C) and high salinity (±30–40 wt% NaCl equivalent) magmatic fluids, later followed by meteoric hydrothermal convection systems. The extreme acidity of the solutions that are responsible for the lithocaps of advanced argillic alteration (vuggy silica) is due to the HCl and SO_2 volatile species, with HCl condesing directly and SO_2 disproportionating to H_2S on cooling and producing sulphuric acid (disproportionation is a process of simultaneous oxidation and reduction). The earliest hydrothermal activity produced widespread brecciation and intense hydrothermal alteration. This was followed by vein emplacement with at least three main stages of mineralisation, namely: (1) quartz-cassiterite stage, during which cassiterite deposition appears to have taken place at temperatures of between 300 and 250°C; (2) sulphide stage; and (3) a stage of late veinlets with clay minerals or fluorite and siderite.

Dating of the different types of deposits indicates metallogenic epochs of Sn mineralisation within the Bolivian belt as a whole. These deposits appear to be genetically related, with the manto type representing the precursors to vein deposits formed during the Mesozoic magmatic event, and to the subvolcanic porphyry types formed during a later tectono-magmatic reactivation in the Neogene (Schneider and Lehmann 1977; Villapando 1988). The question of the origin of the Sn, however, still remains. Figure 5.9 shows that the distribution of the Sn deposits falls within three main belts: (1) the Andean belt of which the Bolivian deposits are part; (2) the East Brazilian belt; (3) the Rondonia-Guyana belt. The Bolivian belt is situated near the intersection of the Andean and Rondonia-Guyana belts. It is possible that the manto-type deposits were derived from this mineralisation by erosion of the uplifted Precambrian shield during the development of the Andes (Schneider and Lehmann 1977). The concept of "metallogenic heritage" would appear to be substantiated by systematic variations of elements such as W, Zr and Hf in the cassiterites (Schneider et al. 1978). Furthermore, Hutchison (1983) noted that the intersection of the Bolivian belt with the Rondonia-Guyana belt may represent a triple junction, with the latter representing a possible aulocogen structure. Magma generation in this area could therefore have involved Sn-enriched protoliths. This possibility is corroborated by recent studies conducted on the peraluminous igneous rocks of the Bolivian Sn province (Ericksen et al. 1990). The results of these studies suggest that Sn-rich magmas were responsible for the emplacement near the surface of the peraluminous igneous rocks with which the Sn mineralisation is genetically associated. It may also be speculated

that there is a similarity between the South American situation and that of the Pan-African Damara orogen in Namibia, where Sn-bearing pegmatites (and U-bearing alaskites) are present in the intracontinental branch of the orogen close to a postulated triple junction that formed as a result of the impimgement of a mantle plume (Pirajno 2000)

5.2.1.4 Porphyry Systems of the Central Asian Orogenic Belt

The great Central Asian Orogenic Belt (CAOB; Jahn 2004, Windley et al. 2007) or Altaid orogenic collage (Sengör and Natal'in 1996), or Central Asian Orogenic Supercollage (Yakubchuk 2004, Yakubchuk et al. 2005) extends from the Uralides in the west to the Pacific Ocean margin of eastern Asia and is bounded to the north by the Siberian Craton and to the south by the Tarim-North China cratonic blocks (Fig. 5.11). The CAOB is a complex collage of fragments of ancient microcontinents and arc terranes, fragments of oceanic volcanic islands (e. g. seamounts), perhaps also volcanic plateaux, oceanic crust (ophiolites), and successions of passive continental margins. The amalgamation of these terranes occurred at various times in the Palaeozoic and Mesozoic and was accompanied by phases of magmatism, ranging in age from Neoproterozoic to Triassic-Cretaceous (~220–120 Ma) that resulted in the emplacement of large volumes of K-rich granitic intrusions (Jahn 2004) and mafic volcanic rocks (Zhu et al. 2005), accompanied by lesser volumes of mafic-ultramafic systems. A-type granitic and peralkaline intrusions in the CAOB are common and are associated with post-collisional tectonism. Elsewhere, northeastern China and Mongolia, A-type granites are associated with extensive Mesozoic and Neogene volcanism (Jahn 2004). Nd–Sr isotope systematics indicates that these A-type and peralkaline granites are juvenile and of mantle origin (Jahn 2004). The CAOB contains three major magmatic arcs, the Kipchak, Tuva-Mongol and Mugodzhar-Rudny Altai, bent as oroclines and separated by sutures (Yakubchuk 2004), some with back-arc ophiolitic rocks, and overprinted by new generations of magmatic provinces, some of which may be subduction-related and others related to intraplate magmatism. The CAOB includes terranes of the Urals, Tian Shan, Altai, Kazakhstan, southern Gobi, northeastern China, Kuznetsk and Sayan (Yakubchuk et al. 2005).

The CAOB is endowed with a wide range of mineral systems that include volcanogenic massive sulphides (VMS), intrusion-related vein systems, porphyry and epithermal systems and sedimentary-hosted sulphides (SEDEX), as well as orogenic Au deposits (Yakubchuk et al. 2005). A number of porphyry systems (e. g. Erdenetuin-Obo associated with trachybasaltic magma; Berzina and Borisenko 2007) are present in terranes of the Central Asian Orogenic Belt with ages ranging from 258 to 240 Ma, which are within the time span of mantle plume magmatism in northwest Siberia (Siberian traps) and in southwest China (Emeishan) Borisenko et al. 2006).

In this section I examine two porphyry systems, Oyu Tolgoi in Mongolia and Tuwu in northwest China (Xinjiang Province) (Fig. 5.11). The Oyu Tolgoi

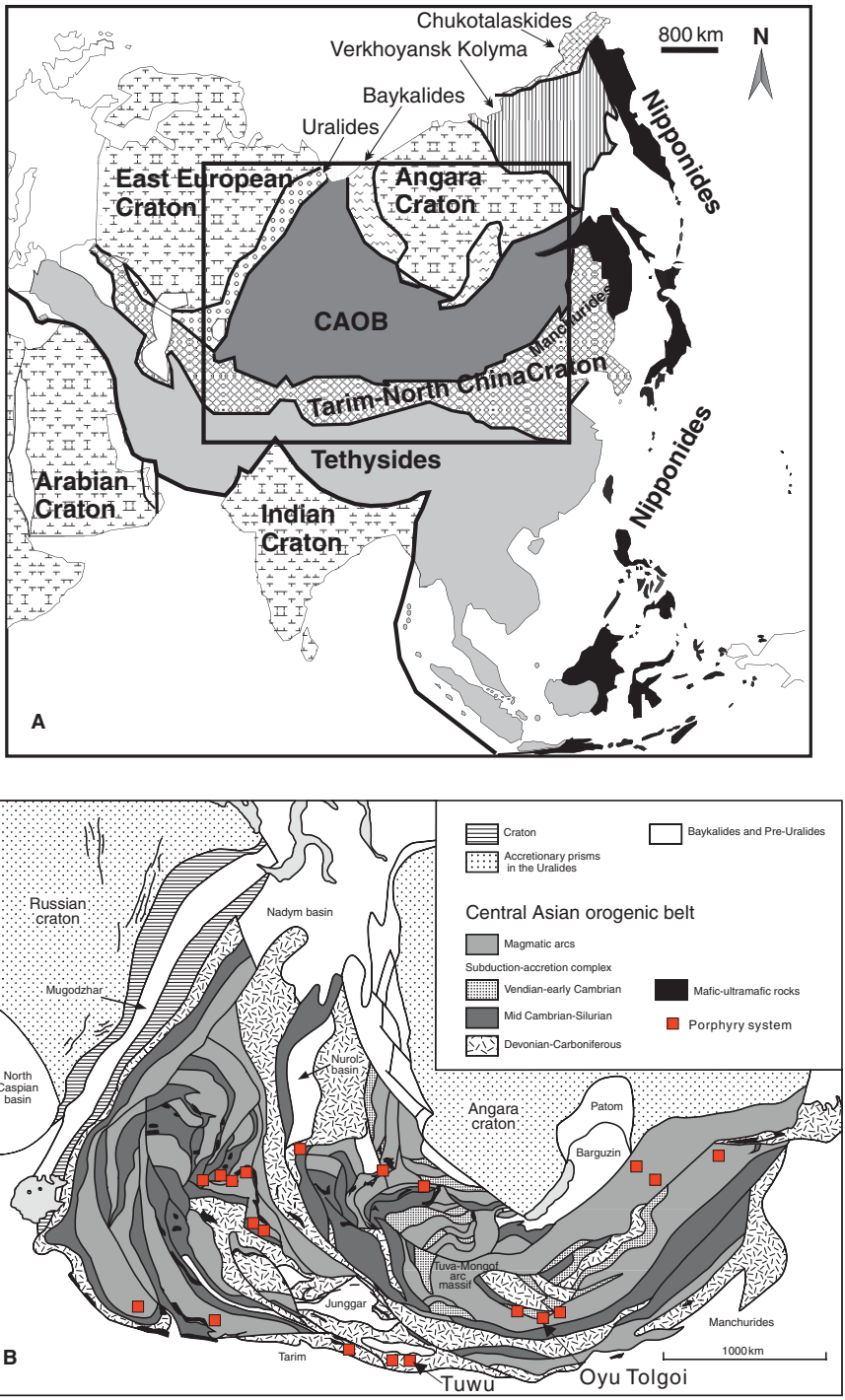


Fig. 5.11 (continued)

system is emplaced in a Mid-Late Paleaeozoic island arc setting (Gurvasayhan terrane; Khashgerel et al. 2006). The Tuwu system is also located in an ancient island arc (Dananhu-Tousuquan) in the eastern Tian Shan orogenic belt (Han et al. 2006).

5.2.1.4.1 The Oyu Tolgoi Porphyry Cu–Au System

The Oyu Tolgoi porphyry Cu–Au system is hosted in Mid-Late Palaeozoic island arc rocks of the Gurvasayhan terrane, which is part of the Kazakh-Mongol arc system (Fig. 5.11). The Gurvasayhan terrane is structurally complex and contains metasedimentary rocks and basalts, intruded by diorite and monzonite plutons that are related to the porphyry system (Yakubchuk et al. 2005). The geology and isotope systematics of this porphyry system was reported by Khashgerel et al. (2006) from whom the following account is taken.

The porphyry mineralisation extends along a north-northeast trending zone for about 6 km and comprises five deposits, namely: South Oyu Tolgoi, Southwest, Central, Hugo Dummett North and South, each of which is related to a separate intrusion of Late Devonian age. Published resources (as at May 2005; Khashgerel et al. 2006) are 1.15 Bt (billion metric tonnes) at 1.3% Cu and 0.47 g/t Au, using a 0.69 wt% Cu equivalent; Mo is less than 100 ppm. The local stratigraphy consist of augite basalt, dacitic ash flow tuff, basaltic flow breccia, volcanogenic sandstone and intercalated clastic rocks of the Alagbayan Group, aggregating about 1700 m in thickness and unconformably overlain by basaltic tuff, andesitic ash-flow tuff and clastic rocks of the Sainshandhudag Formation, about 400 m thick. The Alagbayan Group is intruded by quartz-monzodiorite and biotite granodiorite with U-Pb ages ranging from 362 to 378 Ma. The porphyry system is characterised by an extensive hypogene zone of hydrolytic (phyllic and argillic) alteration, buried beneath the younger Sainshandhudag Formation. A series of small quartz-monzodiorite intrusions occur along the margins of a larger and unmineralised monzodiorite body. The quartz-monzodiorite intrusions are of K-rich calc-alkaline and of I-type affinity and are typically porphyritic with 35–50% vol% feldspar phenocrysts. The South Oyu Tolgoi consists of a mineralised subcircular zone of quartz veins about 660 × 400 m, in with bornite, chalcopyrite and pyrite. The Southwest Oyu Tolgoi is a pipe-like zone about 250 m in diameter and 700 m high, centred on a small quartz-monzodiorite stock; chalcopyrite and lesse bornite and pyrite are the main sulphides. Central Oyu Tolgoi is an inverted cone forming a

Fig. 5.11 (continued) (**A**) Main orogenic systems of Asia and the Central Asian Orogenic Belt (CAOB; after Sengör and Natal'in 1996); (**B**) shows the CAOB terrane collage, main suture zones marking boundaries between terranes, this figure is after Sengör and Natal'in (2004), distribution of selected porphyry systems is taken from Yakubchuk (2004) and Yakubchuk et al. (2005)

subcircular zone of about 600 m in diameter with pyrite-covellite, chalcocite and bornite at depth and capped by a 40 m thick blanket of supergene chalcocite. Hugo Dummett North and South form an elongate NNE-trending zone greater than 2.6 km, with the mineralisation centred on a zone of intense quartz veining (90% by vol.). Sulphides are bornite-chalcopyrite, chalcocite, and lesser enargite and tennantite.

The Oyu Tolgoi quartz veins are typically contorted and anastomosing with textures indicative of a dominant ductile regime. Fluid inclusion studies suggest temperatures $> 450^{\circ}C$ and a palaeodepth of around 2.5–3 km. By contrast the Au-rich quartz-monzodiorite has undeformed quartz veins. Hydrothermal alteration is dominated by advanced argillic assemblages, including alunite, pyrophyllite, diaspore, zunyite, topaz, corundum, andalusite, kaolinite and dickite, which affect to a greater extent more receptive units such as ash flow tuffs and to a lesser extent the monzodiorite and basalts. Supergene alunite is also present. An early potassic alteration is recognised at depth and consists mainly of biotite, locally retrograded to Mg-chlorite. In basaltic rocks biotite alteration is zoned outward to a propylitic assemblage of epidote-chlorite-illite-pyrite for a distance of about 600 m from a high-grade Cu–Au zone. K-feldspar was probably the main potassic phase in the quartz-monzodiorite, but intense overprinting by muscovite has largerly destroyed the K-feldspar. Interestingly, it was noted that augite crystals in basaltic rocks are commonly replaced by actinolite or actinolite + biotite, suggesting that this alteration preceded the potassic phase. Hydrothermal magnetite is present as early thin veins and as late disseminations and open-space fillings. The early magnetite is thought to be associated with the potassic alteration phase. Muscovite alteration typically affects the quartz-monzodiorite intrusions, post-dating early biotite, magnetite and albite, but pre-dating advanced argillic alteration. Muscovite is considered to be the final stage of potassic alteration. Albite is common and occurs as vein selvages and is associated with veins and sulphides. Its pink colouration is attributed to fine hematite dusting. Chlorite alteration is a widespread late phase and it affects both quartz-monzodiorite and basalts. There are two types of chlorite, one is part of the above-mentioned retrograde alteration of biotite, the other is a dark green chlorite that occurs as a late filling in quartz veins, fractures, quartz-monzodiorite and basalts. Carbonate alteration is represented by siderite, associated with lesser fluorite, is pervasive or fracture-controlled. Calcite is common as fracture filling and dolomite is present in the high-grade mineralised zones.

Copper-Au mineralisation is primarily tied with the chalcopyrite-bornite assemblage, which together with gold, appears to be paragenetically late. A less important high-sulphidation assemblage consists of enargite-covellite±pyrite±tennantite, hosted by dacitic tuff and quartz-monzodiorite. As outlined above, some variations of the sulphide assemblages are recognised in individual deposits. In general a high Au content correlates with a dominant chalcopyrite mineralogy.

The Hugo Demmett North and South deposits are characterised by a high concentration (>90% by volume) of mineralised quartz veins, called Qv90 for this reason. The main sulphide minerals are bornite and chalcopyrite, with lesser tennantite and chalcocite. Gold is more abundant in Hugo Demmett North, although this deposit is cut by post-mineral granodiorite intrusions resulting in a reduction of the mineralised material. Alteration at Hugo Demmett North consist of quartz-muscovite, mostly in the monzodioritic rocks, and stages of advanced argillic alteration for which the following paragenesis (early to late) was recognised: (1) andalusite; (2) diaspore; (3) residual quartz; (4) alunite and Al-phosphate-sulphate minerals; (5) zunyite; (6) topaz; (7) pyrophillite; (8) kaolinite; (9) dickite. This advanced argillic alteration has sharp transitions, upward and outward, to relatively unaltered rocks. Tuff rocks acted as a lithological barrier to extreme hydrolytic alteration, characterised by the presence of topaz, with discrete zones up to 10 m wide. The above mentioned quartz-muscovite alteration is feldspar destructive and intensive, resulting in an aggregate of fine muscovite with corroded quartz. At Hugo Demmett South, the top of the monzodioritic pluton is altered to quartz-muscovite overprinted by advanced argillic alteration, which is dominated by pyrophyllite, although locally muscovite alteration is seen to overprint the advanced argillic minerals. Sulphide mineralisation has a zoning pattern, outward and upward, from bornite-chalcopyrite to chalcopyrite to pyrite-enargite. The latter is usually associated with the advanced argillic alteration. The paragenetic sequence of alteration-sulphide mineralisation indicates two stages: (1) early alteration with advanced argillic assemblages, accompanied by pyrite-enargite-tennantite, and (2) a later muscovite-dominant alteration accompanied by high-grade bornite-chalcopyrite. This suggests a trend from intermediate-high sulphidation (enargite-tennantite) to progressively lower sulphidation states (bornite-chalcopyrite, ending with chalcocite).

Khashgerel et al. (2006) also conducted a study of stable isotope ($\delta^{18}O$–δD and $\delta^{34}S$) systematics for the Oyu Tolgoi system (Fig. 5.12). $\delta^{18}O$ values of alteration minerals range from –4.1 to + 10.9‰ for sulphates, 11.8 to 20.1‰ for alunite, 2.0 to 12.9‰ for anhydrite and 3.6 to 5.2‰ for gypsum. δD values of alteration minerals are from –90 to –140‰ (muscovite and pyrophillite), but much lower for alunite (–43 to –98‰). The low δD values are compatible with recharge by meteoric waters at high elevation, which could have been due to a tall stratovolcano above the present porphyry system. $\delta^{34}S$ values of sulphides range from –16 to + 6.0‰ (CDT). Sulphur isotopic data show a range of values similar for all individual deposits, with all sulphate minerals being isotopically heavy and sulphides isotopically light, as is usually the case for most magmatic-hydrothermal systems. The observed O, D and S isotopic trends are consistent with the mixing of sulphate from magmatic sources with sulphate derived from the oxidation of H_2S. Using various fractionation equations (referenced in Khashgerel et al. 2006) the advanced argillic minerals formed at temperatures from < 260 to 350°C. The authors suggested that a D-enriched aqueous fluid exsolved from a melt, while volcanic vapour also D-enriched separated from a

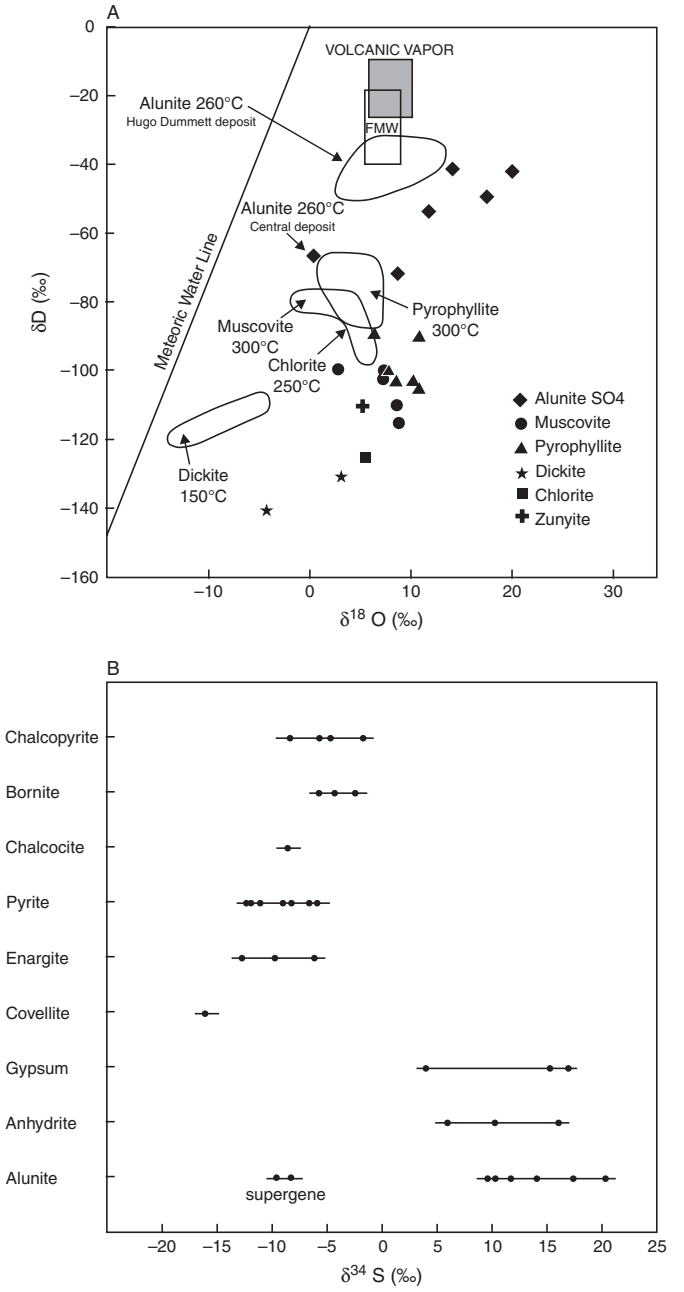


Fig. 5.12 Stable isotopic compositions of minerals from the Oyu Tolgoi porphyry system; (**A**) δ18O versus δD plot, symbols indicate measured oxygen and hydrogen isotopes, calculated fluid temperatures, using fractionation equations provided in Khashgerel et al. (2006), are shown by closed fields for each mineral; FMW field of felsic magmatic water; (**B**) $\delta^{34}S$ data for sulphide and sulphate minerals. Modified after Khashgerel et al. (2006)

hypersaline fluid at depth. The vapour ascended to near surface forming an acidic fluid, resulting in intense hydrolytic alteration and base leaching, perhaps also venting to the surface as fumaroles.

Geological observations, the dominant advanced argillic alteration and stable isotope systematics, all point to a Cu–Au porphyry system that is intrusion-centred and was formed from condensed magmatic vapours, although with a meteoric component. The Oyu Tolgoi porphyry system was formed at a depth of about 1 km below the palaeosurface.

5.2.1.4.2 Tuwu Porphyry Cu, Eastern Tian Shan, Northwest China

The northwest China region encompasses terranes and tectonic units that are part of the great Central Asian Orogenic Belt. The Tian Shan orogenic belt can be divided into North, Central and South Tian Shan, separated by major E-W-trending faults (Fig. 5.13). The North Tian Shan, best represented in the Bogda Shan range east of Xinjiang's capital city, Urumqi, consists of Carboniferous calc-alkaline volcanic and sedimentary rocks, intruded by mafic and intermediate-felsic plutons. The Bogda Shan, together with the Kanggur terrane (called

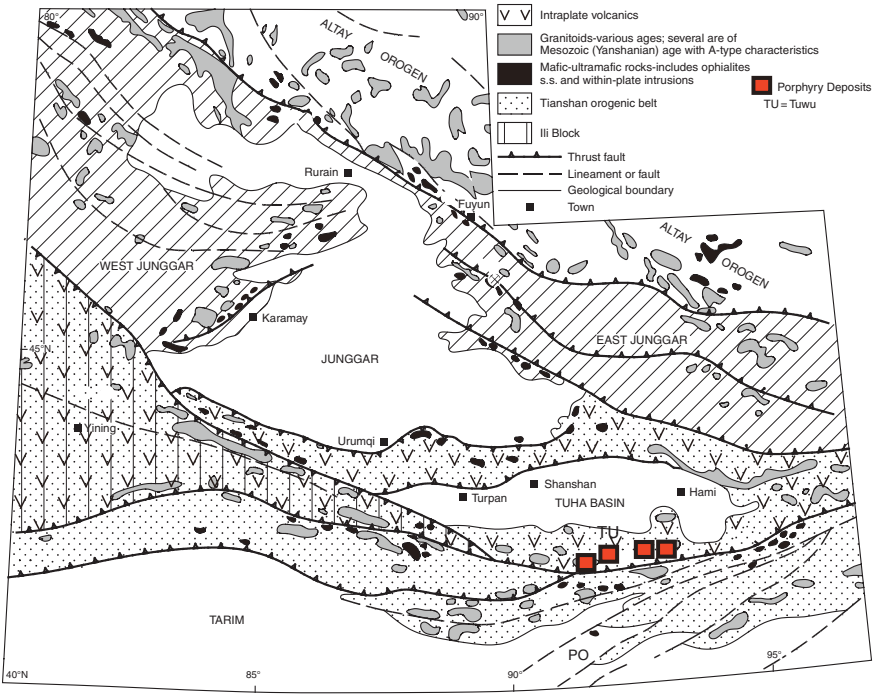


Fig. 5.13 Simplified geological map of NW China, showing parts of the Tian Shan orogenic belt and distribution of porphyry systems in the north Tian Shan. After Pirajno et al. (2008)

by local geologists Jueluotage belt or terrane), are interpreted as volcanic arcs, which could have formed either as north-directed or as a south-directed subduction of oceanic crust and separated by an ocean from other island arcs, such as the Aqishan-Yamansu arc and the Dananhu-Tousuquan arc. The latter hosts a series of porphyry systems, namely Yandong, Tuwu, Linglong and Chihu (Fig. 5.13). The Central Tian Shan is a wedge-shaped zone comprising, from north to south, a forearc melange, a Carboniferous volcanic arc and a Silurian-Devonian volcanic arc. The Central Tian Shan also contains basement inliers of Late Proterozoic age, which may have been part of an earlier microcontinent (i.e. Ili block or microcontinent) (Zhang et al. 1984). The South Tian Shan contains fragments of oceanic crust material in fault contact with sandstone, shale, chert and limestone of Mid-Silurian to Mid-Carboniferous age, which were possibly deposited on a passive margin on the north side of the Tarim block (Carroll et al. 1995). The South Tian Shan belt consists of Carboniferous felsic to intermediate volcanic and volcaniclastic rocks attributed to volcanic arcs, and Silurian volcanogenic sedimentary rocks, deposited in a back arc setting. These rocks are separated from the North Tian Shan by a major E-W-trending suture, the Kanggur Fault. The Central Tian Shan collided with a north-facing passive margin on the north side of the Tarim during Late Devonian-Early Carboniferous. In this way, the South and Central Tian Shan were amalgamated with the Tarim Block. Between the Late Carboniferous and Early Permian, the intervening ocean between the North Tian Shan arcs and the amalgamated Tarim-South-Central Tian Shan tectonic unit closed and the North Tian Shan arc was accreted to the Central Tian Shan orogen (Windley et al. 1990). Granitic rocks intrude the island arc successions and consist of a number of batholiths that include granodiorite, diorite and monzonitic granite. U-Pb dating of these granitic intrusions yielded ages ranging from 333 to 389 Ma (Han et al. 2006 and references therein).

The Tuwu porphyry Cu system was studied by Han et al. (2006) and much of the following discussion comes from this source. The Tuwu porphyry is hosted in Carboniferous rocks of the Qi'eshan Group of the Dananhu-Tousuquan arc, which mainly contains basaltic, andesitic and rhyolitic lavas and clastic sedimentary rocks. The deposit contains a total resource of 2.04 Mt of Cu metal, was discovered in 1997, briefly exploited between 1998 and 2002 and with a new mining operation beginning in 2003. The ore-hosting plagiogranite porphyry and diorite porphyry were emplaced into the volcano-sedimentary succession and at least 23 stocks and plugs have been identified in the area. Re–Os dating of molybdenite yielded an age of 323 Ma (Rui et al. 2002), whereas U-Pb ages of the plagiogranite porphyry range from 333 to 334 Ma (Han et al. 2006). The plagiogranite porphyry has a distinct porphyritic texture with quartz phenocrysts, plagioclase and biotite. This alteration changed the plagiogranite into an albite-granite porphyry with up to 55% by volume of albite. The diorite porphyry contains anorthite and biotite as phenocrysts in a matrix of anorthite, biotite, hornblende and quartz with accessory magnetite, apatite and zircon. The plagiogranite porphyry is characterised by strongly fractionated

chondrite-normalised REE patterns (ΣREE from 45 to 75 ppm), with LREE enrichment and HREE depletion, with slight positive Eu anomalies. MORB-normalised trace element patterns show depletions in Nb and Y. These patterns have been interpreted as being similar to those of subduction-related calc-alkaline magmatic arcs. The diorite porphyry has almost flat chondrite-normalised REE patterns with a slight LREE enrichement and no Eu anomalies, whereas the MORB-normalised trace element pattern shows negative Ba, Nb, and Y anomalies, HFSE depletion and LILE enrichment. These geochemical features have been interpreted as due to a suprasubduction setting.

The Tuwu deposit contains two ore zones; Tuwu and Eastern Tuwu. The former is elongated in the E-W direction and in cross-section is wedge shaped and using a 0.50% Cu cutoff grade it has a length of 900 m and an average width of 25 m. The Eastern Tuwu ore zone is about 1300 m long with widths varying from 30 to 85 m. The style of the mineralisation includes disseminations and disseminated veinlets (stockworks). Ore minerals are dominantly chalcopyrite and pyrite with lesser bornite, digenite, sphalerite, magnetite, hematite and rickardite (Cu_4Te_3). The ores have large amounts of hematite and magnetite. The ore zones are hosted in lithic sandstone and conglomeratic tuffs in contact with the plagiogranite porphyry. Five alteration zones are present, from the core outwards: quartz core, chlorite-biotite, phyllic, argillic and propylitic. The chlorite-biotite zone occurs as pods and veins and is associated with pyrite and chalcopyrite; the biotite is Mg-rich. The phyllic zone is mainly represented by the quartz-sericite assemblage and is associated with the bulk of the sulphide mineralisation. The propylitic zone is composed by chlorite, epidote and albite and is the most widespread alteration.

Six stages of alteration-mineralisation have been recognised, as follows: (1) Mg-rich biotite is accompanied by albite and K-feldspar (alkali metasomatism) with the sulphide assemblage of chalcopyrite-pyrite-bornite; (2) phyllic alteration (quartz-sericite, epidote-chlorite) and veins of chalcopyrite-pyrite-bornite; (3) quartz-molybdenite veins as well as chalcopyrite-pyrite-bornite and continuing phyllic alteration; (4) gypsum and anhydrite and calcite-laumontite are introduced, with lesser sulphide veinlets; (5) continuing calcite-laumontite alteration with sulphide precipitation waning; (6) supergene alteration with malachite and limonite mainly.

Fluid inclusion data show homogenisation temperatures (Th) ranging from 101 to 409°C, with a peak at 175°C and salinities of 0.35 to 16.4 wt% NaCl equivalent, with a peak at 7.5 wt% equivalent. Oxygen and deuterium isotopic compositions show $\delta^{18}O$ values ranging from 7.70 to 9.70‰ in quartz and chlorite. The $\delta^{18}O_{H2O}$ values for the fluid are between –5.37 and 6.62‰, using quartz-water and chlorite-water fractionation equations. δD values of quartz and chlorite range from –45 to –63‰. Sulphur isotopic compositions measured on chalcopyrite and pyrite have a narrow range from –0.9 to 1.3‰, suggesting magmatic and mantle sources for the sulphur. The ore-bearing porphyry rocks have initial $^{87}Sr/^{86}Sr$ ratios in the range of 0.7039–0.7067, suggesting that ore material was derived from the upper mantle.

Han et al. (2006) interpreted the formation of the Tuwu, and other porphyry systems in the region, as being related to one of the calc-alkaline island arcs that developed between the Junggar (Angaran) and the Tarim plates (Fig. 5.13). The Dananhu-Tousuquan island arc was formed by north-dipping subduction with some characteristics of adakites (high-Mg andesites), which are melts were derived from a subducted slab. Flat subduction induces slab melting, a feature common in the Neoarchaean but less common today (Martin et al. 2005). Therefore, adakites are different from calc-alkaline magmas, which are generated by partial melting of a metasomatised mantle wedge above the subducting plate. For this reason flat subduction and adakitic magmatism are unlikely to produce porphyry systems. Han et al. (2006) suggested slab roll back and break off with multiple new pulses of granitic magmatism, due to asthenospheric upwelling, which produced the Tuwu porphyry system.

5.2.2 *Porphyry Systems in Intracontinental Extensional Tectonic Settings and Volcanic Rifted Margins*

In this section I discuss porphyry systems that are not related to a subduction system. However, while in some cases the geodynamic environments of these deposits are not entirely clear, these mineral systems do form in extensional environments in continental settings characterised by bimodal volcanism and intrusions of highly evolved granitoids. The association of these porphyry systems with extensional tectonics and bimodal magmatism points to magmas generated by partial melting of metasomatised subcontinental lithospheric mantle, perhaps by addition of heat from rising mantle plumes, with volatiles degassing (e. g. CO_2). Several porphyry Cu–Mo mineral systems are associated with the mantle plume event that formed the Siberian traps in northwestern Siberia. One of these is the Bolgokhtokhskoe deposit in the Taimyr peninsula on the northwestern margin og the Siberian traps (Berzina and Borisenko 2007). Other porphyry Cu–Mo systems in central Asia are associated with alkaline and sub-alkaline granitic rocks in rift settings and have ages (Triassic-Permian) that suggest a link with mantle plume activity (Berzina and Borisenko 2007). The Kudara Cu–Mo porphyry system in western Transbaikalia has an Ar–Ar age of 232 Ma (Borisenko et al. 2006). In eastern China, along the lower Chiangjian (Yangtze) River valley numerous porphyry systems and associated skarns (see Chapter 6) are present and are associated with granite plutons of Mesozoic age and related to the larege scale Yanshanian tectono-thermal event (Pan and Dong 1999).

Xenoliths carried from the mantle in volcanic rocks provide a good understanding of metasomatic processes in the subcontinental mantle lithosphere. Xenoliths include lherzolites, harzburgites, websterite and clinopyroxenite, cut by veins containing hydrous minerals, such as amphibole. These form by

percolation of metasomatising fluids through fracture systems, resulting in enrichement of volatiles and incompatible trace elements (Bailey 1987). As in metasomatised suprasubduction mantle wedges, the enriched subcontinental lithospheric mantle can attain high f_{O2}, resulting in the removal of metals from sulphides, which then become incorporated in partial melts that give rise to continental porphyry systems. Commonly, these porphyry systems have Mo as one of the main metals and metal associations, such as Cu–Mo, Mo–W, Mo–Sn–W, Mo–Bi and Mo–Nb (Carten et al. 1993). There are two major classes of porphyry Mo deposits: high-silica rhyolite and monzogranite, with the former typically found in continental rifts and the latter usually associated with continental margins, such as the Andean magmatic arc. Hou et al. (in press) have examined the main geochemical differences between subduction-related and intracontinental extension-related porphyry systems. The K_2O content (at SiO_2 = 65%; K_{65}) of calc-alkaline island earc-related porphyry systems ranges from 1.2 to 2.74, those of Andean type continental margin arcs have K_{65} of between 2.74 and 3.6. The intracontinental, extension-related porphyry systems have a high K calc-alkaline and shoshonitic compositions, with K_{65} values ranging from 3.6 to 8.6 (Hou et al. in press). Furthermore, intracontinental porphyry systems exhibit enriched light REE patterns (La/Yb_N of 10 to 42), no significant Eu anomalies and strong enrichements in large-ion incompatible elements (Rb, K, Ba). According to Hou et al. (2004a) these intracontinental magmas have affinity with adakites (high-Mg andesites), which are considered to represent subducted slab melts (Martin et al. 2005). However, the intracontinental porphyry rocks studied by Hou et al. (2004a; in press) have K_2O and MgO contents (1.2–8.5% and 0.4–3.5%, respectively) and $\varepsilon Nd(t)$ values (+3 to –10) that distinguishes them from slab-derived adakites, but have more affinity with adakites derived from basaltic lower crust. Melting of the basaltic lower crust and generation of magmas with adakitic affinity could have occurred by upwelling of asthenospheric mantle during lithospheric delamination or slab break-off (Turner et al. 1993; Maheo et al. 2001).

In this section, I examine a range of porphyry systems that occur in collision- and rift-related provinces, from the giant Climax-type deposits in the Rio Grande rift of Colorado, the Mo deposits in the Oslo Rift (Norway), the porphyry deposits in the collision orogens of East Qinling of central China, Tibet and southwest China, to the Malmbjerg deposit in the volcanic-rifted margin of east-central Greenland.

5.2.2.1 Porphyry Mo Deposits of the Colorado Mineral Belt

The porphyry Mo deposits of the Colorado Mineral Belt are situated at the northern end of the Rio Grande rift system and constitute a class of their own, known as Climax type, characterised by highly evolved, fractionated porphyry intrusives enriched in silica, fluorine and alkalies and with an A-type affinity. They are therefore distinct from the subduction-related quartz-monzonite-hosted

porphyry Cu–Mo systems, such as those of the Andean continental margin, or those of the North American cordillera. In the Colorado Mineral Belt there are three major groups of porphyry Mo deposits: Urad-Henderson, Climax and those of the Mt. Emmons area (Fig. 5.14). The Cenozoic Rio Grande rift system is north-south trending and extends for approximately 900 km across the states of Colorado and New Mexico. For details of this great rift system the interested reader is referred to Baldridge et al. (1995). The famous Valles Caldera is located roughly at mid-way in the rift system in New Mexico (Fig. 5.14). In the Colorado sector the Rio Grande rift comprises a narrow, northern zone (Arkansas Valley) and a wider southern basin (San Louis Basin), which borders the San Juan volcanic field. These basins are filled with mafic lavas and pyroclastic beds intercalated with alluvial material. Large volumes of basaltic andesite, rhyolitic ash-flow sheets, with high initial Sr-isotope ratios, and therefore a lower crustal origin, developed in localised areas between 35 and 26 Ma. This was followed by a pause in the volcanic activity during the Mid Miocene (20–12 Ma), after which volcanism increased and was concentrated. This volcanism is typically bimodal (basalt-rhyolite) with low initial Sr-isotope ratios.

In this section the Urad-Henderson and Climax deposits are described briefly using the works of Wallace et al. (1978), White et al. (1981) and Seedorff and Einaudi (2004a,b). The Colorado Mineral Belt is approximately 400 km long and 15–60 km wide, extending in a northeast-southwest direction across Precambrian and Phanerozoic rocks (Fig. 5.14). Magmatic activity during the Laramide orogeny resulted in a series of events which culminated in the emplacement of a variety of volcanic, subvolcanic and plutonic rocks, penetrating both Precambrian basement and Phanerozoic sequences. Metallogeny in the region is associated with these magmatic episodes, which are thought to be related to a back-arc rift tectonic setting (Sawkins 1990) or to an environment of intraplate continental rifting (Carten et al. 1993), perhaps associated with either a mantle plume or lithospheric delamination and asthenospheric mantle upwelling. The Laramide magmatic activity came in two major pulses, one in the Cretaceous, and one in Oligocene times, during which lines of weakness in the old Precambrian crust were reactivated, providing the pathways to the ascending magmas. The mineralising events are all related to granitoid stock intrusions of Neogene age. The origin of the ore-forming magmas is not clear, but on the basis of initial Sr isotope ratios, this may be related to source regions of mantle partial melting, as well as the interaction of mantle-derived melts with the lower crust. Differentiation of enriched A-type magmas results in the formation of highly fractionated fluorine-rich melts which separate and intrude into upper crustal levels. High fluorine contents enable the development of late stage hydrous and potassic melts into which Mo and other incompatible elements are partitioned (White et al. 1981). Vapour saturation results in the formation of stockworks above the intrusion, and large amounts of incompatible-enriched (e.g. Mo, F, Si and S) fluids are therefore directly exsolved from the magmas, released into fractures within

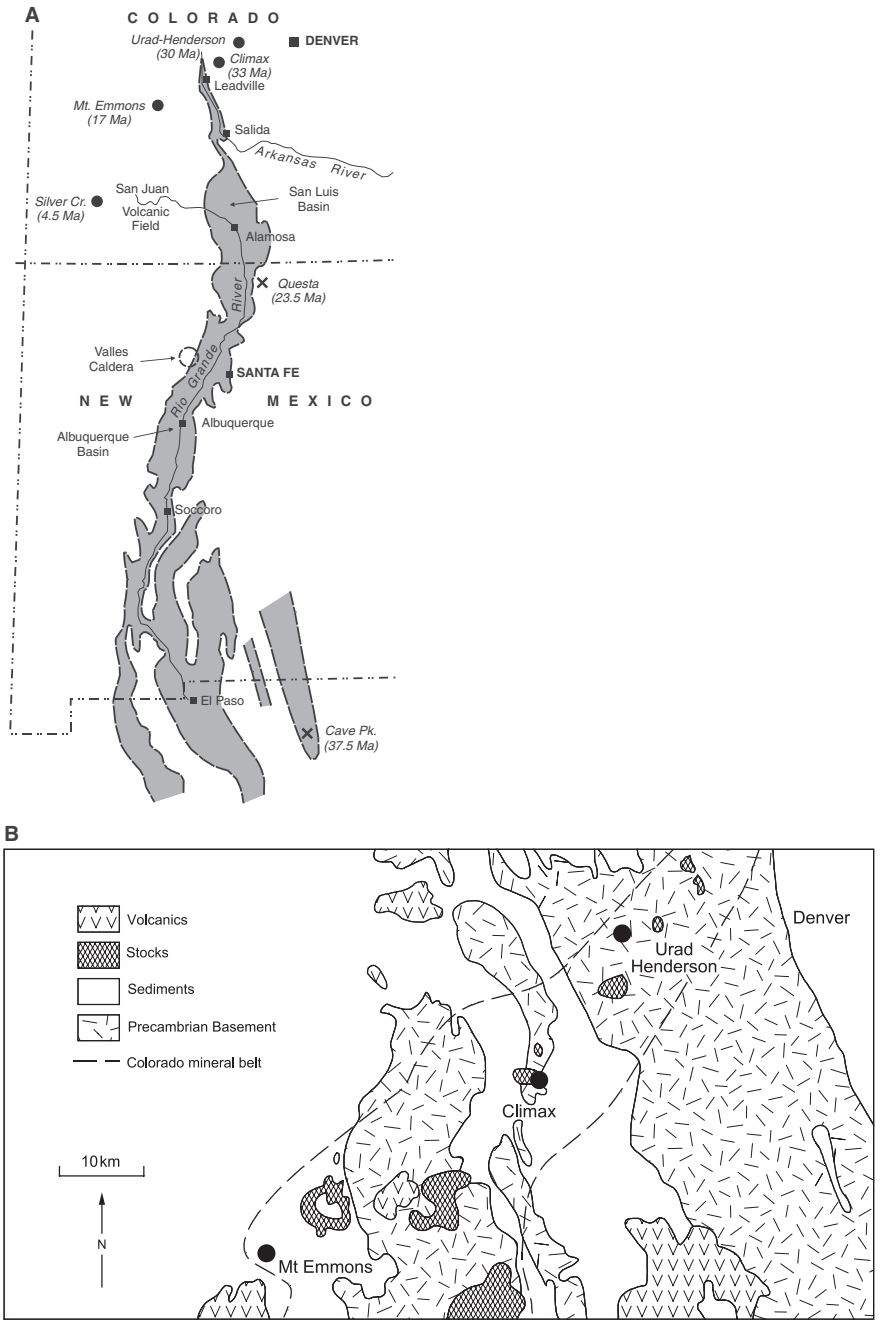


Fig. 5.14 (**A**) The Rio Grande rift system and position of Climax, Urad-Henderson and Mt Emmons porphyry systems in Colorado; modifies after Wallace (1995); (**B**) Simplified geology of the Colorado mineral belt and location of main porphyry Mo deposits. After Wallace et al. (1978)

the intruding stocks and the surrounding rocks. Various lines of evidence indicate that the fluids were expelled at depths ranging from approximately 600 to 3000 m below the surface (White et al. 1981).

5.2.2.1.1 Urad-Henderson

The Urad-Henderson Mo deposit, located some 75 km west of Denver, contains the world's second largest concentration of Mo metal, with resources of 727 Mt grading 0.17 % Mo (Laznicka 2006). Urad and Henderson form two separate and stacked orebodies, but the Urad orebody was partially destroyed by geological events following its development, and the remaining reserves of approximately 12 Mt at 0.2% Mo have been mined out. The Henderson orebody occurs deep within the Red Mountain at about 1200 m below the summit. The surface expression of the Urad mineralisation had been recognised since the early 1900s through the presence of ferrimolybdite staining along a mineralised fault which cuts the orebody. The geological events that led to the development of the Urad-Henderson porphyry Mo system include a complex sequence of igneous and hydrothermal activities. The igneous bodies in order of emplacement were called by Wallace et al. (1978) as follows: Tungsten Slide unit, East Knob unit, Square quartz-porphyry, Red Mountain porphyry, Urad porphyry, Primos porphyry and Henderson granite. All are aged between 27 and 21 Ma and intrude the Precambrian Silver Plume granite (1.4 Ga). The Urad orebody may have extended for at least 1000 m in the vertical sense, but was destroyed by the intrusion of the Red Mountain high-silica porphyry stock. Mineralisation consists of fine-grained molybdenite with minor fluorite, pyrite, galena, sphalerite and huebnerite, contained in veinlets from 1 to 20 mm wide forming extensive stockworks.

The recent works of Seedorff and Einaudi (2004a, b) recognised at least 12 high-silica rhyolitic stocks from three intrusive centres below Red Mountain and named, from oldest to youngest and deepest: Henderson, Seriate and Vasquez. The Henderson orebody has three overlapping ore zones, each related to an intrusion centre from which individual stocks developed their own ore shells. The Henderson intrusion centre comprises five stocks, called Phantom, Berthoud, Henderson, Primos and Arapaho as well as dykes and breccias. The focus of intrusive activity moved to the east-northeast with the emplacement of the East Lobe, Seriate, Ruby and Nystron stocks of the Seriate centre. At deeper levels the stocks of the Vasquez centre, Vasquez, Dailey and Ute, were emplaced.

Seedorff and Einaudi (2004a, b) recognised that magmatic-hydrothermal alteration is complex and is typified by a rich variety of assemblages reflecting not only the nature of the fluids but also that of the wall rocks affected. These authors pointed out that fluid flow and the evolution of the magmatic-hydrothermal systems was not unidirectional, as in the more classic porphyry systems, but involved a series of cycles, each associated with the emplacement of a

rhyolitic stock. This alteration, can be considered in terms of temperature of formation, as high, moderately high, moderate and low. The temperature-related alteration assemblages are complex and can be summarised as follows. The high temperature alteration assemblages are spatially and genetically related to the emplacement and crystallisation of individual stocks and are represented by two types of vein fillings: (1) a silicic type with quartz-fluorite ± molybdenite and (2) a potassic type with K-feldspar + fluorite ± quartz ± molybdenite ± biotite. The moderately high temperature assemblages are dominantly quartz, K-feldspar, fluorite, topaz, pyrite, wolframite, magnetite and lesser molybdenite. The moderate temperature assemblages contain quartz, fluorite, pyrite, topaz, magnetite and sericite. The low temperature assemblages comprise quartz, fluorite, pyrite, pyrrhotite, clay minerals, garnet, sphalerite, galena, chalcopyrite, rhodochrosite.

Unlike the comparatively simple model of Wallace et al. (1978), the evolution of the Urad-Henderson magmatic-hydrothermal system appears to be substantially more complex, subdivided in twelve time frames. In the first, ore and alteration shells formed above the Henderson stock, with cycles of high and moderate-high temperature assemblages. In the 2nd and 3rd time frames, the Henderson centre continues its intrusions, again with cycles of high and moderate-high temperature assemblages alteration shells. Emplacement of stocks from the Seriate centre follow, producing overlapping ore-alteration shells with high temperature veins (4th and 5th time frames). After all stocks of the Seriate centre had been emplaced, cooling produced moderate temperature alteration shells (time frames 6 and 7, dominated by sericite-pyrite, topaz-pyrite assemblages). Intrusion of the Vasquez stock followed, with a repeat of high temperature assemblages and associated ore shell, with initial development of sphalerite mineralisation. The final three time frames (10–12) refer to cooling events of the Vasquez intrusions, with garnet, rhodochrosite and continuing development of sphalerite.

Temperatures and salinities as determined from fluid inclusions (mostly liquid-rich and several with daughter minerals) show a range from 400 to 600°C for moderately high-moderate assemblages, with salinities ranging from about 30–65 wt% NaCl equivalent. Low temperature assemblages have homogenisation temperatures ranging from 200 to 380°C and salinities of 28–35 wt% NaCl.

5.2.2.1.2 Climax

The Climax Mo "super-giant" deposit is located on the Continental Divide about 160 km by road from Denver. Although mineralisation in the area was first discovered in 1879, it was not until World War I, when Mo became a useful alloy metal that mining began. Past production plus current resources total about 1,125 Mt grading 0.24% Mo and 0.025% W (Laznicka 2006). Tungsten, Sn and pyrite have been recovered as by-products. A comprehensive description of Climax can be found in Surface et al. (1978). The Climax igneous complex

(33–24 Ma) includes a series of four major intrusive pulses, each of which was accompanied by magmatic-hydrothermal activity. These intrusions were emplaced into a Proterozoic basement of biotite gneiss and quartz-monzonite rocks. Hydrothermal alteration associated with each intrusion is characterised by a core of silica-rich rock, grading to a topaz greisen, a potassium silicate zone and an outer zone of quartz-sericite-pyrite. Three distinct orebodies related to the first three intrusions were generated. These are, in order of decreasing age: the Ceresco orebody, most of which has been eroded off, and the Upper and Lower orebodies, forming shells around and over the top of the intrusive stocks. Taken together the ore shells have the geometry of an inverted cone with a height of about 450 m (Laznicka 2006). Post-mineralisation movement along the Mosquito Fault to the west was up to about 2600 m and it is believed that perhaps part of the Ceresco orebody might be located at depth along the west side of the fault. The mineralisation in the two upper orebodies consists of two ore zones each, an upper W-rich zone and a lower Mo-rich zone. In the upper ore zone W and Mo mineralisation overlap. Ore minerals are molybdenite, huebnerite ($MnWO_4$), cassiterite and pyrite. Quartz-molybdenite veinlets, which also contain topaz and fluorite, form the famous Climax stockwork system (Fig. 5.1). The stockworks are most common in the zones of potassic alteration, although the two events are separated in time. In a typical quartz-molybdenite veinlet (range of thickness is from 0.5 to 20 mm) molybdenite is irregularly distributed along the margins of the veinlet, whereas the centre is occupied by a closely packed mosaic of fine quartz grains. Some veinlets consist almost entirely of molybdenite and pyrite. Pegmatites pods and dykes are common in the Climax-type system and occur near the roof zones. They include accessory minerals such as fluorite, molybdenite and REE minerals.In this respect the presence of pegmatites in the roof zones is a feature similar to that of the Sn–W systems (Chapter 4).

5.2.2.2 Porphyry Mo Mineralisation in the Oslo Graben, Norway

One of the many Permo-Carboniferous rift systems in northern Europe is the Oslo Rift (Neumann 1994, Neumann et al. 2004). In the Oslo Rift, porphyry Mo mineralisation is associated with the porphyritic phase of biotite granites at several localities (Geyti and Schonwandt 1979; Schonwandt and Petersen 1983). The Oslo Rift has a N-S trend, extends for about 200 km and its southern part is submerged (Skagerrak Graben) (Fig. 5.15). The Rift comprises six sectors, namely: Oslo Graben, Skagerrak Graben, Scania, Bornholm, North Sea and NE German Basin. Tectono-magmatic activity in the Oslo Rift began about 305–300 Ma and continued till 240 Ma and this activity has been divided into five stages (Neumann et al. 2004). A pre-rift stage recorded eruption of lavas on fluvial and lacustrine sediments. A rift stage 1, is characterised by intrusion of 304–294 Ma sills and dykes of trachyandesite-rhyolitic composition, the onset of the formation of the Oslo Graben and the eruption of basaltic lavas. Rift

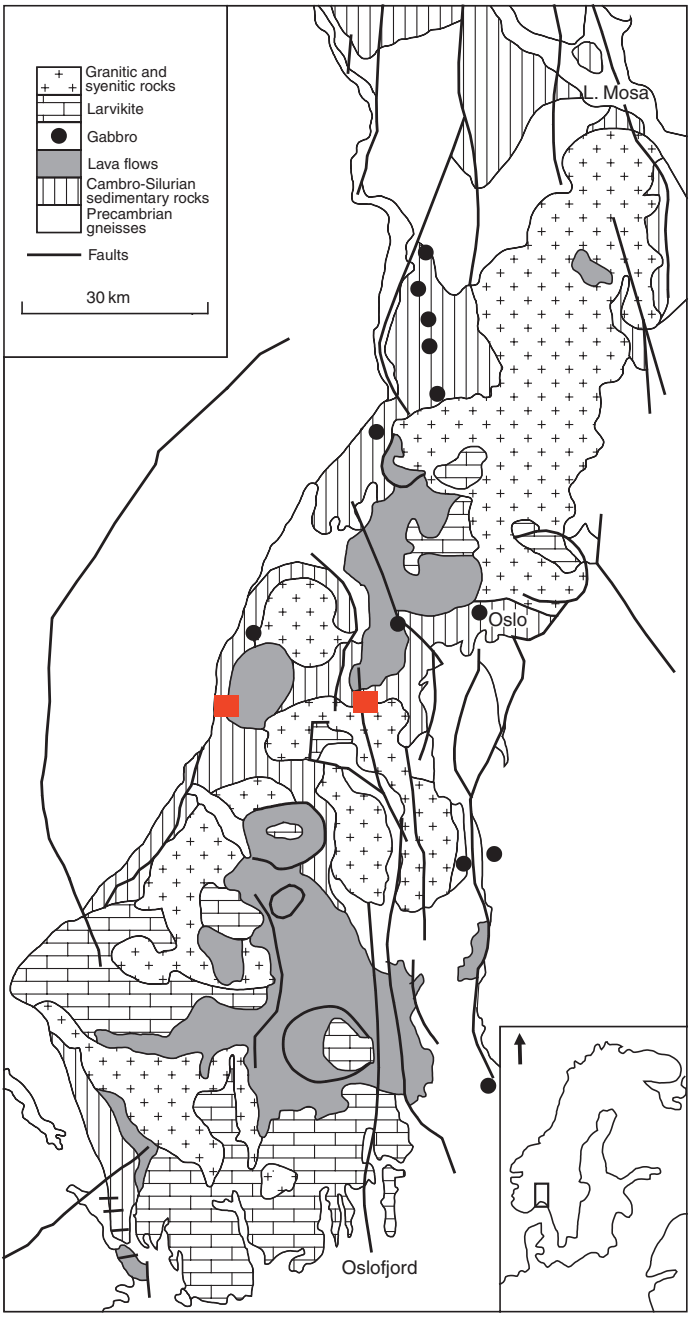


Fig. 5.15 Simplified geology of the Oslo Rift, modified after Neumann et al. (2004 and reference therein); squares indicate position of porphyry Mo deposits

stage 2 is the main rifting phase with the full development of the Oslo Graben, which was accompanied by widespread fissure eruptions of trachyandesite and basaltic lavas. Also during this stage monzonite and nepheline-syenite intrusions with U-Pb ages from 299 to 292 Ma were emplaced. During rift stage 3 central volcanoes with caldera collapse and ring dykes were developed; Rb–Sr ages of 274–243 Ma were obtained from rocks of the ring dykes. Stage 4 is dominated by the emplacement of composite batholiths, mostly syenite and granite, with Rb–Sr isochron ages ranging from 270 to 240 Ma. The formation of the Oslo Rift is thought to be related to decompression and lithospheric thinning at the margin of the Baltic Shield in response to far field tectonics. However, geochemical and Nd–Sr isotopic data indicate that the alkaline magmatism in the Rift had a source located in the enriched (metasomatised) lithospheric mantle, whereas the more depleted magmatic products were sourced from within the convecting mantle. Neumann et al. (2004) suggested the possibility that a mantle plume may have been involved in triggering the Permo-Carboniferous magmatism in northern Europe, of which the Oslo Rift is part. An alternative view was forwarded by Slagstad (2006) who, on the basis of thermo-rheological modelling, suggested that the Oslo Rift was formed by weakening of the lithosphere as a result of heat from the radioactive decay of U, Th and K in high-heat-producing Proterozoic granites (more details on this topic are presented in Chapter 9). This thermal weakening, provided by radiogenic heat, would have made the crust susceptible to passive rifting during the regional tensional stress field in northern Europe in Permo-Carboniferous times.

Hydrothermal alteration and Mo mineralisation were discovered as a result of mineral exploration which was started on the basis of a conceptual model of porphyry-style mineralisation (Geyti and Schonwandt 1979). A number of occurrences are being evaluated at the time of writing, such as Hurdal (Nordii), first discovered in 1979. At Hurdal 9000 m of drilling outlined ore zones with a potential resource of 200 Mt at an average grade of 0.11% Mo, with the highest grades in the zone of potassic alteration within a multi-stage intrusive stocks (cited by Crew Gold London News Release 2005, www.crewgold.com and http://www.crewgold.com/minerals_hurdal.php; last accessed April 2008). This is considered the largest Mo deposit in Europe. Two important localities of porphyry Mo mineralisation are in the Glitrevann and Hurdal igneous complexes where the mineralisation is closely associated with granitic rocks (Schonwandt and Petersen 1983). The mineralisation of the Glitrevann complex is briefly discussed below.

The Glitrevann complex is a ring-type volcano-plutonic structure consisting of rhyolite and rhyolitic ignimbrite associated with basaltic volcanics. The eruption of voluminous ash-flow tuffs caused the collapse of the volcanic structure and the formation of the Bordvika cauldron. This was followed by further eruption of rhyolite porphyries basaltic lavas and ash-flow tuffs. A phase of intrusive activity followed with the emplacement of syenitic ring dykes and the intrusion of a composite granitic stock (Schonwandt and

Petersen 1983). This stock consists of three units, namely: aplitic granite, and black and grey quartz-feldspar porphyries. Mo mineralisation is associated with hydrothermal alteration at Bordvika where the host rocks are rhyolite and quartz-feldspar ignimbrite which acted as a cap to the underlying aplitic granite. Molybdenite, accompanied by pyrite and fluorite, occurs in quartz vein stockworks within a zone of sericitic alteration. Geyti and Schonwandt (1979) mapped four zones of alteration (potassic, sericitic, argillic and propylitic) and likened the system to the Climax porphyry Mo deposit type. At Bordvika potassic alteration is not common and consists of K-feldspar veinlets associated with quartz, pyrite and molybdenite. Sericitic alteration with up to 10% by volume of pyrite is very prominent and widespread. Where pervasive, the original feldspars are completely destroyed and the sericitised rock becomes fine-grained and white in colour. Sericitic alteration is also found as millimetre-wide haloes around mineralised veins. Argillic alteration is mainly kaolinite and montmorillonite occurring as dusty replacements of feldspar crystals. Where sericite completely replaces feldspars and constitutes a substantial proportion of the groundmass the rocks are considered to be affected by sericitic alteration. Intense "dusty" replacement of feldspars with little or no replacement of groundmass material is taken to indicate argillic alteration. Propylitic alteration, which occurs outside the zone of argillic alteration and is poorly developed, is characterised by the assemblage of chlorite + calcite + epidote ± fluorite in veinlets and as cavity fillings.

5.2.2.3 Porphyry Systems in the Qinling Orogen, Central China

The Qinling or Qinling-Dabie orogen extends across China for more than 2000 km and is part of the central China orogenic belt that separates the Tarim-North China cratonic blocks from the Yangtze Craton, merging with the Qilian and Kunlun orogens to the east on the margins of the Tibetan plateau, and terminating to the east along the ultra high-pressure (UHP) Dabie terrane and the Tanlu Fault. The Qinling orogen hosts porphyry Mo and W-Mo porphyry deposits. In the West Qinling, is the world-class Jindui-cheng porphyry Mo, one of the largest in China, and Shijiawan; in the East Qinling are the Leimengou porphyry Mo, associated with Au-bearing breccia pipes at Qiyugou, and the Nannihu porphyry Mo field, associated with skarns.

The Qinling orogen was formed by the interaction of the North China Craton and the Yangtze Craton and a series of tectonothermal events and (Fig. 5.16). Tectonic units of the orogen are variably labelled, depending on authors, as North, South, East and West Qinling. The geological framework, geodynamic evolution and tectonostratigraphy are detailed in Meng and Zhang (1999) and Ratschbacher et al. (2003). A brief version, especially applicable to the East Qinling, taken from Chen et al. (2000; 2004) is provided here.

The tectonic history of the area of the Qinling orogen from ca 2.5 Ga to the Triassic-Jurassic, involved subduction, rifting, accretion and collision events,

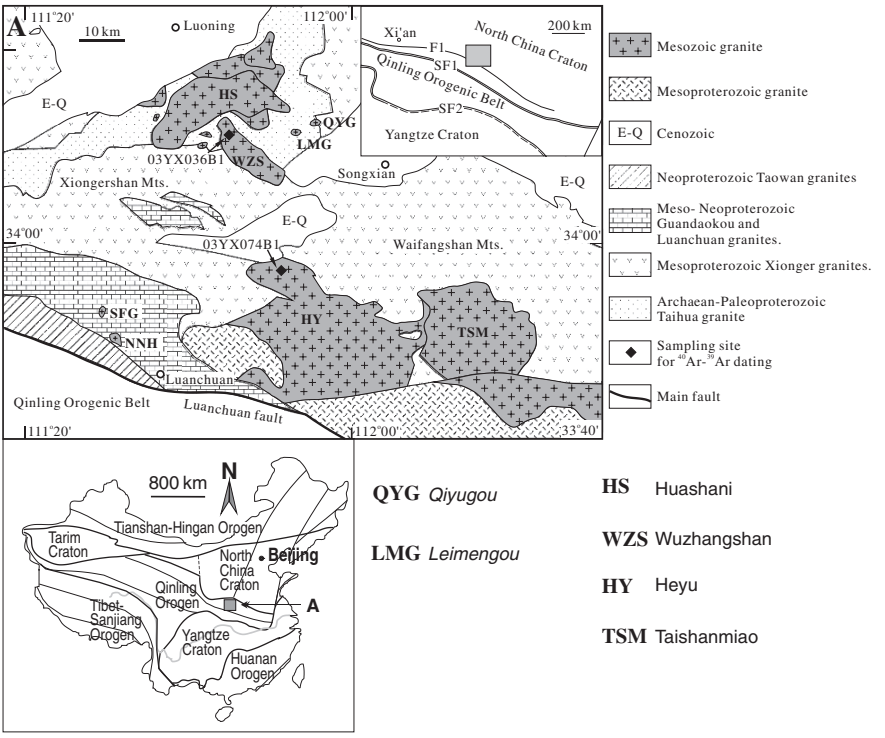


Fig. 5.16 Simplified geological map of the Xiongershan–Waifangshan region, western Henan; WZS Wuzhangshan pluton, HS Huashanni pluton, HY Heyu pluton, TSMTaishan-miao pluton. LMG Leimengou porphyry Mo, QYG Qiyugou breccia pipes, NNH Nannihu Mo–W, SFG Shangfanggou, SF1 Shangdan suture zone, SF2 Mianlue suture zone, F1 Luanchuan fault. After Han et al. (2007)

culminating with intense granitic magmatism in the Cretaceous, during the Yanshanian tectono-thermal event that affected much of the eastern margin of Asia. The Triassic-Jurassic continental collision between the North China Craton and the Yangtze Craton, resulted in north-dipping thrusts bounding the various terranes and slab-stacking. Finally, post-collision extension and lithospheric thinning occurred during the above mentioned Yanshanian event in the Cretaceous, during which magmas, ranging in composition from gabbro to granitic rocks and A-type alkaline rocks, were intruded. Large scale metallogenesis is linked with the Yanshanian tectono-thermal event, leading to the formation of Carlin-like Au deposits, the Xiaoqinling-Xiong'ershan belt of orogenic precious metal lodes, vein systems and the porphyry systems. I return to discuss in some detail the Xiaoqinling-Xiong'ershan belt of orogenic precious metal (Au and Ag) lodes in Chapter 9.

There is evidence that the Yanshanian Mesozoic granitic rocks in the Qinling orogen were emplaced in three stages (Han et al. 2007). $^{40}Ar/^{39}Ar$

dating of granitic rocks in the Xiong'ershan-Waifangshan region (Fig. 5.16) shows that there are three types of granites: high Ba–Sr, I-types emplaced in two stages ca 157 Ma and ca 130 Ma, and A-type alkaline granite emplaced at ca 115–110 Ma. The 157 Ma high Ba–Sr granitic rocks include monzogranite and granodiorite, typified by the Wuzhangshan pluton; the 130 Ma Heyu pluton is a megacrystic biotite monzogranite; the A-type, 120 Ma Taishanmiao pluton is also a K-feldspar megacrystic, containing mostly perthite albite-oligoclase and quartz (Fig. 5.16). Geochemically these granites are clearly distinguished by their major, trace and REE contents. The high Ba–Sr I-type granitic rocks have SiO_2 between 68 and 72 wt%, and K_2O/Na_2O ratios close to 1, whereas the Tainshanmiao A-type granite has higher silica contents (75–77 wt%) and K_2O/Na_2O ratios of 1.1–1.8. The high Ba–Sr I-type granites have ca 2300 ppm Ba and Sr/Y ratios of ca 70 and with chondrite-normalised REE patterns that are LREE enriched and HREE flat. The A-type granites have pronounced negative Eu anomalies and typically high 10 000*Ga/Al ratios, which are some of the parameters that identify A-type granites (eg Whalen et al. 1987).

The intrusion of these three types of granites reflects different tectonic regimes, from transitional to extensional. Han et al (2007) suggested that the decreasing trends of the Eu/Eu* and Sr/Nd ratios for the granites in western Henan support a lithospheric delamination model. Based on inversion of rapid cooling rates of ultra-high-pressure rocks and granites in the Dabieshan region, combined with seismic tomography results, Li et al. (2002) proposed that post-collisional lithospheric delamination events occurred twice in the Dabieshan region, corresponding with large-scale magmatism at 170 Ma and 130∼110 Ma. The geochronological data show that the high Ba–Sr I-type granites in western Henan have a cooling history that supports a model of rapid uplift and erosion, probably linked to post-collisional lithosphere delamination (see Chapter 3). The lithospheric delamination in the southern margin of the North China Craton may have taken place just before the emplacement of the Wuzhangshan granite, which is coeval with the delamination event in the Dabieshan region (∼170 Ma) (Li et al. 2002). Petrological and geochemical data show that the early stage high Ba–Sr I-type granites in western Henan have both characteristics of the KCG (K-rich calc-alkaline granitoids) and ACG (amphibole-bearing calc-alkaline granitoids) in the classification of Barbarin (1999; Chapter 4 and Fig. 4.3), representing the transition between the two types. The middle stage I-type granites belong to the KCG. These reflect a post-collisional tectonic regime transition from compression to tension between 157 and 125 Ma. The A-type granites in western Henan (Taishanmiao pluton and related porphyries; Fig. 5.16) indicate an intraplate anorogenic and extensional tectonic setting around 115 Ma. These events are important in terms of metallogenesis in the region, but before elaborating further on this aspect, I briefly describe two key porphyry systems: Jinduicheng and Leimengou-Qiyugou.

5.2.2.3.1 Jinduicheng Porphyry Mo System, East Qinling

The East Qinling molybdenum belt contains the world-class Jinduicheng and the Shijiawan Mo porphyry systems, the Nannihu Mo–W skarn-porphyry system (Li et al. 2004), as well as the unusual Huanglongpu carbonatite-related Mo–Pb deposit (Huang et al. 1985), all associated with the Mesozoic granitic intrusions of the Yanshanian event. A comprehensive review of the Jinduicheng and Nannihu deposits can be found in Huang et al. (1990). These porphyry deposits share many features with the Climax Mo deposits of the Colorado mineral belt discussed in Section 5.2.2.1. Here I discuss the Jinduicheng porphyry system. The geology of the Jinduicheng Mo deposit was reported by Nie (1994) and Stein et al. (1997). The Jinduicheng deposit has resources of 907 Mt grading 0.1% Mo. Stein et al. (1997) using the Re–Os isotopic system, determined the age of the mineralisation at ca 138 Ma. The mineralisation is associated with a stock of porphyritic granite that protrudes from the Laoneushan biotite monzogranite batholith, intruded into the Archaean Taihua Group and the Palaeoproterozoic Xiong'er Group. The porphyritic granite has silica contents between 71 and 75 wt%, is 1.8 km long and about 400 m wide. The Jinduicheng granite porphyry consists of orthoclase, perthite, plagioclase, quartz and biotite with accessory ilmenite, pyrite, magnetite, apatite and fluorite.

The Mo mineralisation is contained in vein stockworks both within the stock and the country rocks (Fig. 5.1) and consist of quartz + K-feldspar ± pyrite ± fluorite; the veins also contain minor quantities of magnetite, chalcopyrite, sphalerite, galena, cassiterite, bismuthinite, sericite, biotite, beryl, topaz, calcite and apatite. Hydrothermal alteration is well zoned with silicification and K-feldspar in a core zone, followed by phyllic and propylitic alteration with increasing distance from the intrusion. Phyllic and propylitic assemblages in the basaltic country rocks consist of epidote-albite-chlorite-calcite and montmorillonite-kaolinite-pyrophyllite, respectively. Sulphur isotopic compositions show $\delta^{34}S$ values of 3.7–5.5‰ for pyrite and 3.8–4.5‰ for molybdenite (Stein et al. 1997). These values, although somewhat above the mantle range for $\delta^{34}S$, suggest a ^{34}S-enriched magmatic source. Initial $^{87}Sr/^{86}Sr$ isotopic signature for the Jinduicheng and the Shijiawan granite porphyry and the Laoneushan batholith show a range from 0.7087 to 0.7095, suggesting a crustal source for the granitic rocks. This is supported by Pb isotope systematics with $^{206}Pb/^{204}Pb = 17.410$; $^{207}Pb/^{204}Pb = 15.428$; $^{208}Pb/^{204}Pb = 37.702$) that Stein et al. (1997) explained as due to melting of lower crust. Stable isotope studies of the Jinduicheng altered rocks were reported by Nie (1994). The $\delta^{18}O$‰ values for quartz in the potassic alteration zone ranges from +5.0 to +9‰, which is similar to that of magmatic water (see Chapter 1). The $\delta^{18}O$‰ and $\delta^{34}S$ values of potassic-altered rocks suggest that the ore fluids were mainly of magmatic origin during the early stages. The $\delta^{18}O$‰ values from the zones of hydrolytic alteration have a range of +10.5 to +3.4‰ (mean +11.6‰); the $\delta^{34}S$ values for pyrite in the same zone range from –5.5 to –2.4‰ (mean –3.6‰). The isotopic composition

of the hydrolytic zone indicates that meteoric waters predominated over the magmatic fluids (Nie 1994). The Jinduicheng granite porphyry is enriched in F, Rb, K and HREE and depleted in LREE, Ba and Sr. The chondrite-normalised REE patterns show a distinct negative Eu anomaly.

As noted above, the Junduicheng and other companion systems in the Qinling molybdenum belt have similarities with the porphyry systems of the Colorado belt (Climax type). Stable isotope systematics (O, D and S) indicate oxidising magmas and transfer of magmatic sulphur. Stein et al. (1997) pointed out that the REE patterns of the East Qinling granitic intrusions bear striking similarities to the contrasting REE patterns of the quartz-monzonites and Climax-type granites in Colorado. In the Colorado mineral belt, the Neogene monzonites have distinct REE patterns from the Climax-type granites, which have marked negative Eu anomalies as do the Jinduicheng granitic rocks, whereas the granitic rocks of the Laoneushan batholith show REE patterns similar to the Colorado monzonites. These differences are attributed to a change from subduction-related magmas to extension-related crustal melting. The highly evolved Climax-type granites in Colorado and the Qinling granites are comparable, suggesting similar tectonic regimes. I return to this topic when discussing the Leimengou-Qiyugou ore system.

5.2.2.3.2 Lemeingou-Qiyugou Mo–Au Porphyry-Breccia Pipe System

In the Xiong'ershan region, a cluster of breccia pipes is present in the Qiyugou and the Leimengou area near the eastern margin of the Mesozoic Huashani granite pluton (Fig. 5.16). The Leimnegou-Qiyugou area is located 100 km south of the historic city of Luoyang.

The Leimengou porphyry Mo deposit, discovered in 1979, is a large porphyry style deposit with reserves of 0.34 Mt tonnes of Mo metal at a cut-off grade of 0.075% Mo, and with sulfur as byproduct at an average grade of 2.07% (No. 1 Geological Team of Henan 1983, unpublished data). There are no published detailed studies on this deposit, except for Luo et al. (2000) and a PhD study by Zhang (2006) that focused on the Leimengou-Qiyugou district. The ore bodies are lensoid in shape and subhorrizonal and are developed along the contact zone between the porphyry granite and the gneissic rocks of Taihua Group. The mineralized stocks are characterized by porphyritic fine-grained biotite granite and hornblende monzonite. The chemistry of the porphyry granite indicates that it is an A-type alkaline granite. Some breccia pipes are developed along the margins or around the granite stock. Quartz fluid inclusions from the breccia cement show second boiling temperature and salinity in the range from about 500 to 600°C, and 5–35 wt% NaCl eq., respectively (Luo et al. 2000).

The deposit has typical stockworks developed in granitic rocks with abundant molybdenite and pervasive hydrothermal alteration. The alteration styles of the Leimengou Mo deposit conforms with the classic model for porphyry systems. The potassic K-feldspar, quartz-sericitic and minor chlorite + argillic

alteration zones are recognized from the center of the intrusion stock towards the margins (Luo et al. 2000). The quartz sericitic stage is associated with the mineralisation. Vein, stockwork and minor replacement ores occur above the intrusion. Ore minerals are mainly pyrite, molybdenite, and minor chalcopyrite, sphalerite, and galena. Quartz-sericite-pyrite and potassic alteration can be recognised in outcrops and material in the dumps outside portals. Three stages of mineralisation and temperature are recognized (Luo et al. 2000): (1) K-feldspar-quartz, 380–420°C for quartz; (2) sulphide-quartz, 350–410°C for quartz and pyrite; (3) fluorite-sulphide, 290–385°C for K-feldspar and fluorite. The isotopic composition of sulphur ranges from –2.8 to + 3.72 per mil, average about + 2.08 per mil (Luo et al. 2000).

The Qiyugou breccia pipes lie about 2 km east of the Leimengou porphyry Mo–Au deposit (Fig. 5.17). There are 35 pipes in the area, of which seven are

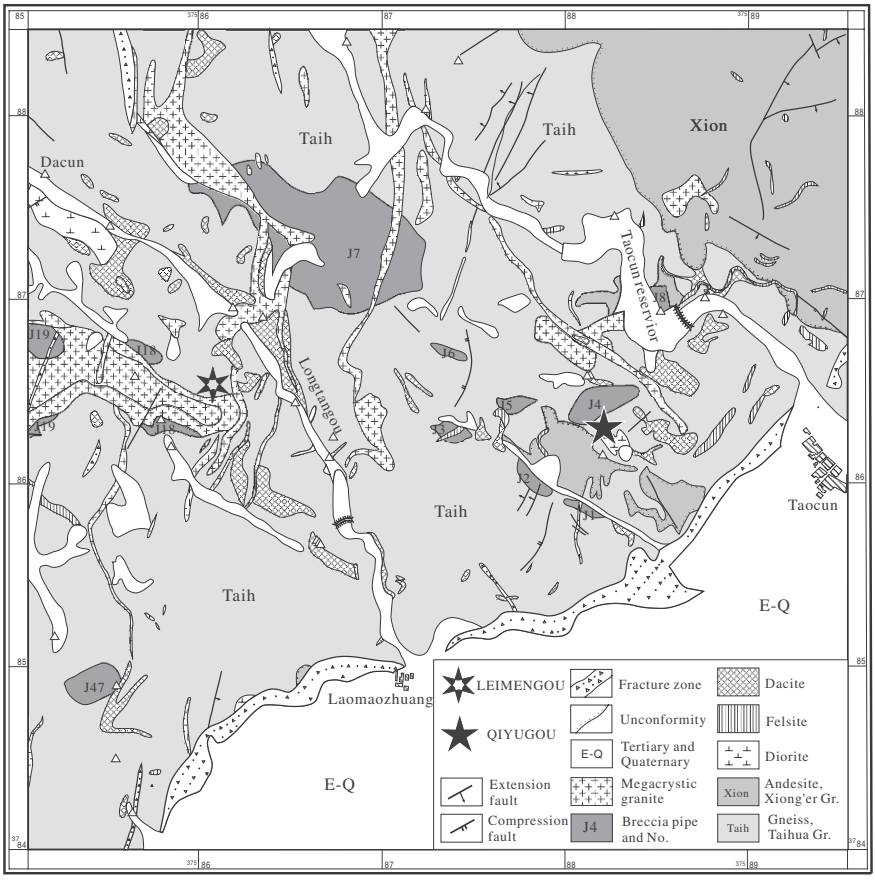


Fig. 5.17 Simplified geological map of the area around the Leimengou porphyry and Qiyugou breccia pipes. After Zhang (2006) and Zhang et al. (2005)

auriferous, with No. 2 and No. 4 being the main producers with total reserves of about 40 t (Mao et al. 2002). Gold has been mined in the region since ancient times, reaching a peak during the Han dynasty about 2200 years ago (Gernet 1999). The mineralisation of the Qiyugou pipes was reported by Mao et al. (2002) and Zhang et al. (2005, 2007). The pipes are clustered along east-west trending zones and have spindle or elliptical shapes in plan view with long axes ranging from less than 40 m to over a km and have been traced vertically for more than 300 m (Fig. 5.18). Ore grades range from 3 to 5 g/t and can reach values of up to 7 g/t, with the higher gold grades in zones of complex alteration and of greater clast population. The breccia pipes contain clasts of Archaean basement rocks, Palaeoproterozoic Xiong'er volcanic rocks and Mesozoic granitic rocks. The clasts range in size from a few cm to metres and have angular shapes with jigsaw-fit type breccia to round shapes, suggesting multiple phases of volatile activity from hydraulic fracturing to fluidisation processes (round clasts). The mineralisation styles include vein, disseminations and stockworks, arranged in subparallel sheets that are nearly perpendicular to the walls of the pipes. Most of the gold ore is associated with subhorizontal pyrite and quartz veins that contain adularia and pyrite. The principal ore minerals are pyrite, chalcopyrite, galena and native gold. Sphalerite, electrum, molybdenite, chalcocite and magnetite are present in lesser quantity. There are two alteration styles in the pipes: (1) pervasive; (2) vein and open space filling. The pervasive stage consists of chlorite, actinolite, green biotite, epidote, quartz, adularia, calcite and sericite. Vein and open space filling is represented by quartz, adularia with calcite and minor sericite. This alteration affects not only the breccia clasts, but also the matrix. Textural relationships indicate that gold mineralisation is paragenetically associated with adularia-calcite and pyrite. Adularia is a low-temperature variety of orthoclase ($KAlSi_3O_8$), commonly found in low-sulphidation volcanic related epithermal ores (Section 5.3.1.1).

In geothermal and low-sulphidation epithermal systems, the presence of adularia is indicative of boiling fluids (Hedenquist et al. 2000). The principal control on fluid pH is the concentration of CO_2 in solution, together with the salinity. Thus, boiling and loss of CO_2 to the vapour results in an increase in pH, which then causes a shift from illite or sericite to adularia stability. The loss of CO_2 also leads to the deposition of calcite with some key reactions as follow (Dong and Morrison 1995; Hedenquist et al. 2000):

$$K^+(aq) + Al(OH)^-{}_4(aq) + 3SiO_2(aq) \rightarrow KAlSi_3O_8(\text{adularia}) + 2H_2O(aq)$$

$$K^+(aq) + 2H^+(aq) + 3Al(OH)^{-4}(aq) + 3SiO_2(aq) \rightarrow KAl_3Si_3O_{10}(OH)_2(\text{sericite}) + 6H_2O(aq)$$

$$HCO_3^- + H^+ \rightarrow H_2CO_3 \rightarrow CO_2 + H_2O$$

$$6SiO_2(aq) + KAl_3Si_3O_{10}(OH)_2(\text{sericite}) + 2\,K^+(aq) \rightarrow 3KAlSi_3O_8(\text{adularia}) + 2H^+(aq)$$

$$HCO_3^- + Ca^{2+} \rightarrow CaCO_3 + CO_2 + H_2O$$

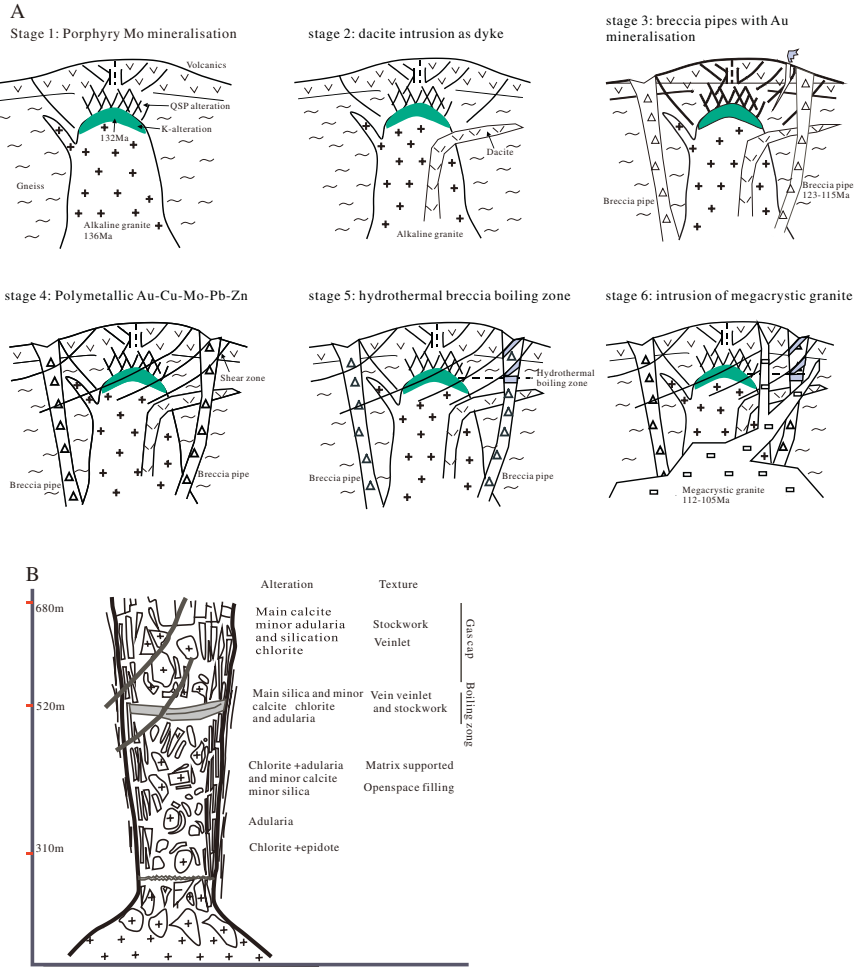


Fig. 5.18 (**A**) Conceptual model showing a six stage emplacement of volatile-rich granitic magma and related development of a porphyry-breccia pipe magmatic-hydrothermal system; stage 1 emplacement of an alkali-rich granite at 136 Ma, porphyry Mo mineralisation forms at 132 Ma; stage 2 intrusion of dacite dykes; stages 3 and 4 breccia pipes are emplaced at about 120–115 Ma with Au and base metal mineralisation; stage 5 fluid evolution continues in the breccia pipes leading to boiling and the formation of a adularia-Au epithermal system; stage 6 intrusion of 112–105 Ma megacrystic granite. Figure courtesy of Dr Zhang Yuanhou, Institute of Mineral Resources, Chinese Academy of Geological Sciences, Beijing. (**B**) Model of a breccia pipe, from its roots in a volatile-rich granite pluton (modified from Kirwin 1985)

Chen and Fu (1992 and references therein) and Fan et al. (2000) studied fluid inclusions in samples from Qiyugou and recognised three stages of homogenisation temperatures: (1) 430–330°C; (2) 338–240°C; (3) 200–170°C. Salinities range from the early 12–34 wt% equivalent NaCl, mid 7–9 wt% equivalent NaCl , to late stage less than 5 wt% NaCl equivalent. Inclusion fluids from

Au-bearing quartz have $\delta^{18}O$ values ranging from 1.4 to 7.0‰ and δD values from –52 to –74 (Mao et al. 2002). The O–D isotopic data suggests involvement of magmatic water. The sulphur isotopic composition ($\delta^{34}S$) of the Qiyugou sulphides ranges from –1.8 to + 2.7‰ for pyrite, –2.3 to –1.0‰ for chalcopyrite and –3.5 to –2.1‰ for galena (Mao et al. 2002). The sulphur isotopic data suggest a strong magmatic component, whereas the homogenisation temperatures and salinities indicate interaction between magmatic and meteoric fluids.

5.2.2.3.2.1 Origin of Auriferous Breccia Pipes and Associated Porphyry Mo Deposit

The genesis of the breccia pipes and breccia-hosted ores was reviewed by Sillitoe (1985), who listed six possible mechanisms of breccia formation: (1) release of magmatic-hydrothermal fluids during second boiling; (2) magmatic heating of meteoric pore fluids; (3) interaction of groundwaters with magmas causing phreatomagmatic explosions; (4) eruption from the top part of a magma chamber due to sudden decompression, leading to fragmentation of the roof rocks; (5) mechanical disruption of wall rocks during subsurface movement of melts; (6) tectonic brecciation.

On the basis of the geological, alteration and mineralogical features that characterise the Qiyugou breccia pipes, their origin is consistent with the first type. Release of magmatic fluids during second boiling and decompression is common in porphyry systems, in which a wide range of breccia types accompany the intrusions (Sillitoe 1985). The mechanisms of breccia formation in the porphyry-epithermal environment are associated with the emplacement of hydrous melts near the surface. Exsolution of the aqueous phase during second boiling and subsequent decompression will cause expansion and the exsolution of more fluids leading to the formation of breccia pipes (Burnham 1985). Pulses of volatile release and gas streaming will result in the full range of jigsaw breccias and fluidisation breccias, where the gas/solid ratios are very high (McCallum 1985). Fluidisation results in the upward transport, mixing and milling of fragments and production of rock flour (Sillitoe 1985, McCallum 1985). Fluidisation is a term that describes a bed of particles or clasts with fluid-like properties due to the flow of interstitial gas, forming a gas-solid mixture (Walters et al. 2006). Breccia pipes develop due to the degassing of a volatile-rich intrusion, but it is possible that in some cases the development of a pipe does not run to completion due to local exhaustion of volatiles discharge. This may resume at a later stage, but the pipe developes along a different channel or pre-exisiting fracture or fault. A model of breccia pipe is shown in Fig. 5.18. Considered together, the Leimengou porphyry Mo and the auriferous Qiyugou breccia pipes conform to an alkalic-type intrusion-related mineral system (Richards 1995). I return to this topic in Section 5.4 when discussing epithermal systems.

A holistic and schematic model of a porphyry-breccia pipe system, proposed by Zhang (2006) is shown in Fig. 5.18). In this model the breccia pipes formed after the emplacement of the Leimengou porphyry Mo deposit. This is

confirmed by the age data, which indicate that the porphyry intrusion has a SHRIMP U-Pb age of 137±2 Ma, the Mo mineralisation has Re–Os ages ranging from 131.4±1.4 to 116±1.7 Ma (Mao et al. 2008) and the breccia pipes have K-Ar ages ranging from 128 to 126 Ma. These age relationships find further confirmation in the No. 7 breccia pipe in which there are clasts of altered granite with stockworks and molybdenite. With reference to Fig. 5.18, the intrusion of an alkaline granite at 137 Ma was followed by degassing and development of magmatic-hydrothermal fluids, which resulted in the formation of a porphyry Mo deposit at about 131 Ma in the apical regions of the intrusion (Stages 1 and 2). With continuing degassing magmatic gases were channelled along conduits, fluidising material along the way and developing breccia pipes between 125 and 115 Ma (Stage, 3). Shear zones and faults formed and channelled metalliferous hydrothermal fluids from the pipes to form polymetallic (Au–Cu–Mo–Pb–Zn) ores (Stage 4). Boiling occurred, perhaps due to partial unroofing and lowering of pressure, which resulted in the formation of subhorizontal ore zones with adularia and calcite (Stage 5). The last event is the intrusion of barren megacrystic granite at 112–105 Ma (Stage 6; Zhang 2006).

The numerous breccia pipes in the Qiyugou area, the proximity of the Leimengou porphyry Mo deposit, together with the common presence of calcite, are indicative of a large scale hydrothermal system that was driven by frequent volatiles exsolution. This would suggest interaction of magmas with a volatile-rich source. Chen et al. (2004) working on the orogenic lode deposits of the Xiong'ershan proposed that the collision between the Yangtze and North China Cratons that formed the Qinling orogen, between 240 and 140 Ma, resulted in a complex stack of north-verging thrust slabs. This underthrusting or A-type subduction was accompanied by metamorphic devolatilisation of sedimentary rocks that included carbonate-shale-chert successions of the Guandakou and Luanchan Groups, south of the Maochaoying fault (Fig. 5.16). Northward underthrusting, crustal shortening and thickening was followed by extensional collapse and the emplacement of granitic magmas during the late Cretaceous phase of the Yanshanian orogeny. Based on robust isotopic and fluid inclusions evidence, Chen et al. (2004) further proposed that metallogeny in the east Qinling area, which comprises precious metal orogenic lodes, as well as the porphyry and the breccia pipes, exhibit a spatial and temporal zoning from the Maochaoying fault in the southwest to the northeast, from orogenic lodes to porphyry systems. Three stages of granite intrusions, ca 157 Ma, ca 130 Ma and ca 115 Ma, reflect changes in tectonic regimes from compressional (157 Ma) to transitional (130 Ma) to extensional (115 Ma). The porphyry mineralisation was formed during the second stage, whereas the associated breccia pipes came later. The magmas interacted with the volatile-rich sedimentary rocks thereby resulting in the emplacement of high level plutons from which porphyry-epithermal systems developed. The volatile-rich nature of the hydrothermal fluids was conducive to the formation of the numerous breccia pipes in the region. The weakly negative $\delta^{34}S$ values for the Qiyugou sulphides could be derived from a "memory" of a sedimentary source,

as postulated for similar values obtained from the orogenic lodes in the region (Chen et al. 2004).

5.2.2.4 Porphyry Systems in Tibet and Southwest China

The Tibet and southwest China regions are part of the great India-Eurasia collision complex and were (and still are) affected by compressional, strike-slip and extensional tectonic processes due to this Cenozoic collision (Sengör and Natal'in 1996). These processes formed the Tibetan plateau and activated major E-W, NW–SE and northerly-trending fault systems, such as the Altyn Tagh and the Jinshajiang-Red River, as well as re-activating and uplifting pre-existing orogenic belts, such as the Tian Shan, some 2000 km to the north of the collision front (Fig. 5.19). These Cenozoic tectonic movements reflect changes in deformation regimes from eastward-extrusion dominated indentation tectonics to crustal thickening tectonics (Windley 1995). Some authors suggested that the Baikal rift system (Fig. 5.19) was also formed in response to the India-Asia collision (Tapponier and Molnar 1979), but more recent work indicates that the Baikal rift and the Mongolian plateau are the result of a mantle plume (Windley and Allen 1993). The Tibet and southwest China regions are a collage of accreted terranes, from south to north: Lhasa, Qiantang, Songpan-Ganze and Qaidam, bound by major faults and/or sutures (Fig. 5.20). These are bound by the Himalayan orogen in the south, the Tarim Block in the north and the Yangtze and South China blocks to the east (see inset of Fig. 5.16). Reviews on the tectonics and stress patterns of the Indo-Asian collision can be found in Harrison et al. (1996), Ratschbacher et al. (1996), Yin (2000) and Chung et al. (2005).

It is important to note that a series of N-S trending rifts are present in Tibet due to active E-W extension of the plateau. These rifts may record delamination of mantle lithosphere beneath the region in the Late Miocene and Pliocene, removal of dense lithosphere may have caused uplift, as sinking cold lithosphere is replaced by hot and buoyant asthenosphere. This upwelling of hot asthenosphere may have induced crustal melting and be responsible for the intrusion-related mineral systems in the Tibet and southwest China regions. An alternative view was proposed by Xiao et al. (2007) who, on the basis of geophysical and structural data, suggested that the underthrust Indian lithosphere split in two slabs, a northward moving high-angle western slab underlying the western sector of the plateau and a northeastward moving low-angle eastern slab penetrating the eastern sector. The boundary between the two sectors is the Yadong-Anduo-Golmud tectonic corridor (Fig. 5.20). Studies of Cenozoic syn- and post-collisional igneous rocks emplaced in the Tibetan crust shows that the YAG corridor separates significant geographic variations in both the ages and types of magmatism. Miocene and Quaternary potassic volcanism predominate west of the Yadong-Anduo-Golmud corridor in the Qiangtang terrane, whereas Eocene-Oligocene volcanism predominates east of the Yadong-Anduo-Golmud corridor. Within the Lhasa terrane,

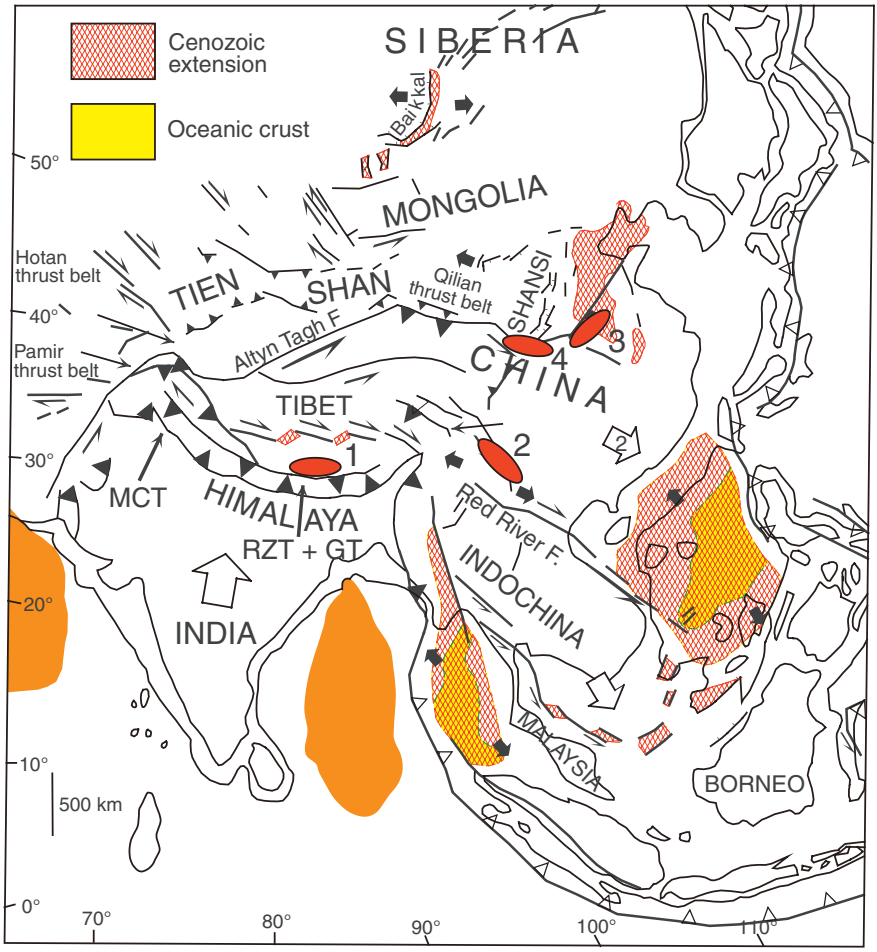


Fig. 5.19 Schematic tectonic map of Asia with major Cenozoic features, adapted from Yin and Nie (1996 and references therein); (1) Gangdise porphyry belt; (2) Jinshajiang-Red River porphyry belt (see Fig. 5.20 for more details); (3) Lower Yangtze River valley and (4) Qinling metallogenic belts

voluminous Paleogene volcanic rocks and minor Cretaceous and Eocene granites occur west of the YAG corridor. In contrast, Cretaceous and Eocene granites, with only minor Paleocene volcanic rocks, are more abundant in the eastern sector of the terrane. In addition, the western sector of the Lhasa terrane also contains earlier Miocene potassic and ultra-potassic volcanic rocks, whereas only sparse younger Miocene (<17 Ma) volcanic rocks occur in its eastern sector (Turner et al. 1996, Miller et al. 1999, Williams et al. 2001, Nomade et al. 2004). High-K and shoshonitic volcanic and intrusive rocks

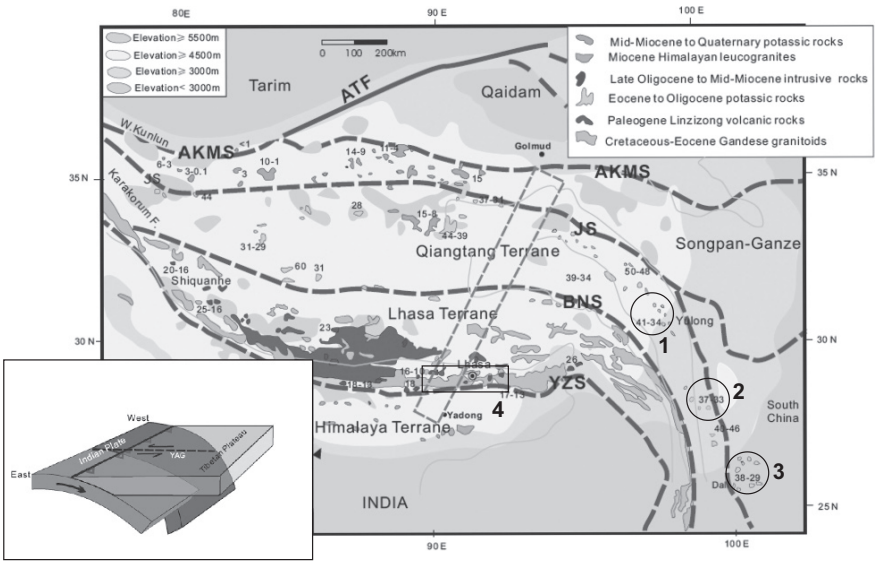


Fig. 5.20 Simplified geology of the Tibet and SW China regions; ages of post-collision alkaline magmas shown as numerals; after Xiao et al. (2007 and references therein). Inset shows the Xiao et al.'s model of split subducting plate manifested in the Tibetan plateau as the Yadong-Anduo-Golmud (YAG) tectonic corridor (see text for details). Circles indicate porphyry belts in the Jinshajiang-Red River fault zone, (1) Yulong, (2) Tongchan; (3) Machangqing; (4) Gangdise belt is shown by the rectangle

dominate in the western sector, whereas the eastern sector contains mostly potassic and calc-alkaline rocks (Chung et al. 2005, Hou et al. 2004a).

The eastern part of the great Himalayn-Tibetan orogen is host to numerous hydrothermal ore systems. In southwest China, the Sanjiang Tethyan Metallogenic Domain (STMD, Hou et al. 2007a), where volcanogenic massive sulphides, Ag-polymetallic, Sn greisen and porphyry systems are present. Hou et al. (2007a) provided a comprehensive listing of the mineral deposits in the STMD. Several porphyry copper and gold deposits in the eastern Qiantang terrane are located along the Jinshajiang and Red River fault systems (Hou et al. 2004a,b; Wang et al. 2005a). These ore deposits are associated with alkaline intrusions emplaced at 40–30 Ma. Porphyry copper and gold deposits associated with 18–10 Ma shoshonitic and potassic calc-alkaline (adakitic) intrusions are located along the Gangdise thrust in the Lhasa terrane, with most occurrences within the Yadong-Anduo-Golmud corridor and the western sector of the Plateau, between Lhasa and Xigate (Hou et al. 2004a). Geothermal fields tend to cluster within the Yadong-Anduo-Golmud corridor and in the eastern sector (Blisniuk et al. 2001). High-temperature geothermal fields and hot springs caused by exceptionally high heat flows are located within the

Yadong-Anduo-Golmud corridor. This suggests that the corridor hosts a thermal anomaly as well as a seismic discontinuity. This thermal anomaly could be due to the upwelling of buoyant and hot asthenosphere into the gap provided by the split slab. This asthenopsheric mantle could also flow laterally along major lithospheic breaks, represented by the fault systems (Gangdise, Jinshanjiang-Red River, Kunlun), where partial melting of crustal material occurs producing the intrusion-related Au and Cu hydrothermal mineral systems discussed in this section.

These mineral systems include: (1) the Gangdise porphyry Cu belt (Hou et al. 2004b); (2) the Jinshanjian-Red River alkaline intrusion-associated Au and porphyry Cu belt (Yulong, Tongchang, Machangqing; Wang et al. 2005a, b, Hu et al. 2004, Hou et al. 2003, 2007b). The distribution of these mineral systems is shown in Figs. 5.19 and 5.20. Below I discuss the Gangdise and the Jinshanjian-Red River mineral systems, condensed from the above cited authors.

5.2.2.4.1 The Gangdise Porphyry Belt

The Gangdise Cu porphyry belt is 350 km long and lies in the Lhasa terrane (Figs. 5.19 and 5.20), which contains Ordovician to Triassic shallow marine clastic rocks and the Gangdise magmatic province that consists of Late Palaeocene to Early Eocene calc-alkaline volcanic rocks and is intruded by granite batholiths rocks of Cretaceous to Neogene age, with peak ages around 55–45 Ma and 30–24 Ma, conciding with the timing of the India-Asia collision and Gangdise thrusting, respectively. East-west extension followed with the development of north-south-trending rifts across the Gangdise belt. It is at this time (18–10 Ma) that potassic calc-alkaline volcanism and shallow level emplacement of granite porphyry occurred within the notth-south-trending rift structures. These granitic rocks intruded the earlier batholiths and are associated with the porphyry systems in the Gangdise belt, which is characterised by a regional metal zoning. From west to east, the belt contains porphyry Cu–Au, Cu–Mo and Cu. In addition, lithogeochemical surveys have shown several areas of strongly anomalous Au (Li et al. 2001).

The ore-bearing porphyries consist of monzonite and quartz-monzonite composed of quartz, andesine-oligoclase, K-feldspar and minor biotite and hornblende. Re–Os dating of molybenite from the Gangdise belt gives model ages of about 14 Ma (Hou et al. 2004a, b). The porphyry have silica contents > 56 wt% and a range of K_2O from 2.6 to 8.7 wt% with an overall shoshonitic and/or potassic calc-alkaline composition, quite different from syn-collisional granites in the same belt. Furthermore, the porphyry also have adakitic affinities as indicated by high Sr/Y ratios, lack of Eu anomalies and negative anomalies of Nb, Ta, P and Ti. Initial $^{87}Sr/^{86}Sr$ vary from 0.7047 to 0.7069 and $^{143}Nd/^{144}Nd$ values from 0.51230 to 0.51290; these compositions lie within the mantle array (Gao et al. 2003). The adakitic affinity, as previously mentioned, refers to melts that derive from hot subducted lithosphere.

The Gangdise Cu porphyries were controlled by the N-S-trending rifts, associated with regional uplift and extensional tectonics, following the underthrusting of the Lhasa terrane beneath the Qiangtang terrane at 24–30 Ma. This post-collision extensional regime provided the conduits for the emplacement of the porphyries and associated mineralisation. The porphyry intrusions resulted from partial melting of the lower crust and lithospheric mantle, related to upwelling of asthenopheric material, whether by delamination or slab breakoff or, as outlined above, by flowing into the gap of slit subducting slab and along fault and fracture systems.

5.2.2.4.2 The Jinshanjian-Red River Fault Porphyry Systems

The eastern margin of the Tibet Plateau is marked by major strike-slip faults that bound several terranes, such as the Songpan-Ganzi, Qiantang and Lhasa terranes (Fig. 5.20). These terranes were juxtaposed in the Mesozoic, but following the India-Asia collision and eastward extrusion or escape tectonics (Tapponier and Molnar 1976), a complex array of strike-slip faults developed along the weak terrane boundary zones (see Chapter 3 for details on indentation tectonics). One of these fault systems is the NW–WNW-trending left-lateral Jinshanjian-Red River fault (Figs. 5.19 and 5.20) or Ailao Shan-Red River fault (Tapponier et al. 1990), extending for well over 2000 km into the South China Sea. Along this fault zone, is a 1000 km-long and 50–80 km wide magmatic belt of alkaline igneous rocks, with ages ranging from about 29 to 41 Ma, and spatially associated with rift and/or strike-slip pull-apart basins in the Qiangtang terrane (Hu et al. 2004). The basin contain up to 4000 m of gypsum-bearing clastic sediments intercalated with alkaline volcanic rocks. The igneous rocks, both extrusive and intrusive, range in composition from basaltic to rhyolitic and with an ultrapotassic or shoshonitic character, highly enriched large-ion lithophile elements (LILE) and LREE and depleted high-field strength elements (HFSE) (Hu et al. 2004). These alkaline rocks cluster into five groups, of which at least three, Machangqing, Tonchang and Yulong, are associated with Cu and Au mineralisation (Fig. 5.20). The Yulong district alone contains over 100 porphyry intrusions. Their geochemical composition, together with Sr and Nd isotopic systematics, support a source from a metasomatised lithospheric mantle, contaminated by a subducted oceanic slab (Hou et al. 2003). Furthermore, the presence of rift basins indicates that these alkaline rocks were emplaced in a post-collisional extensional tectonic setting. The $^{3}He/^{4}He$ ratios of pyrite from Yulong and the Machanqing, range from 0.3 to 2.5 Ra, where Ra represents the ratio of air (see Chapter 1), and $^{40}Ar/^{36}Ar$ ratios of 316–1736. Thus, He and Ar isotope systematics deposits confirm a mantle source for both magmas and ore fluids. Wang et al. (2005b) determined ages of 34.4±1.6 and 33.9±0.5 Ma for the mineralisation, using the Re–Os system in molybdenite.

The Machanqing ore field comprises three Cu–Au±Mo deposits: Machanqing, Yao'an and Beiya, where the alkaline intrusions mainly consist of syenite

porphyry with alteration zoning, outward, from K silicate, quartz-sericite, argillic to propylitic. The mineralisation style is stockwork veins containing chalcopyrite, molybdenite, bornite, pyrite and galena. Average copper grades are about 0.8%, with 4–6 g/t Au in 0.25 Mt Cu metal (Hu et al. 2004 and references therein). Temperatures of the ore fluids range from 120 to 430°C (Hu et al. 2004). Local gold mining takes place in Silurian carbonaceous limestones intruded by the syenites and in bauxitic material developed in karst cavities (my field observation, 2003).

The Yulong ore belt is 150 km long and 25–40 km wide, with more than 20 mineralised porphyry intrusions. A comprehensive paper by Hou et al (2003) provides up-to-date information of this ore belt, which is summarised as follows. These porphyry intrusions are emplaced into Triassic volcanic and sedimentary rocks and were emplaced within 1–3 km from the palaeosurface. The porphyry bodies are near-vertical pipe-like, with small individual outcrop (<1 km^2), with breccia pipes along their margins, associated with quartz-tourmaline veins and sulphides. The breccia pipes suggest intensive degassing of a magmatic-hydrothermal system. The Yulong ore belt contains a number of polymetallic deposits, but always with Cu as the main economic metal. These deposits are listed in Table 5.3.

Potassium-Ar ages of the Yulong belt show three peaks of porphyry intrusions: 52, 40, and 33 Ma. SHRIMP U-Pb zircon dating supports these ages within analytical error. Below I briefly discuss the two largest deposits of the Yulong belt: Yulong and Malasongduo. Other deposits in the Yulong porphyry Cu belt include Duoxiasongduo, Zhanage and Mangzong (Table 5.3), plus several minor prospects and occurrences. Liang et al. (2006) using U–Th–Pb laser ICPMS spectrometry were able to determine an age progression from Yulong (oldest at 41.2 Ma), Zhanaga (38.5 Ma), Mangzong (37.6 Ma), Duoxiaosongduo (37.5 Ma) to Malasongduo (36.9 Ma) and suggested separate pulses of magmatism along the Jinshanjian-Red River fault. Liang et al. (2006) suggested that left-lateral transcurrent movements had a significant vertical component, which pushed one side of a continental block deep into the lithospheric mantle causing partial melting. However, the model does not clearly explain the age progression, which is thought to be related to the southeastwards movement of one plate along the fault over a local melting zone. Liang et al. (2006) also used the Ce^{4+}/Ce^{3+} ratios of zircons to distinguish ore-bearing intrusions from barren ones. The Ce^{4+}/Ce^{3+} ratio is largely controlled by oxygen fugacity (see Chapter 1) and temperature of crystallisation. Ore-bearing granitic rocks have Ce^{4+}/Ce^{3+} ratios measurably higher than those from barren granitoids, thereby suggesting that the former derive from more oxidised melts. The oxygen fugacity of a melt controls the oxidation state of sulphur, so that high-oxygen fugacity melts will have SO and SO_2 sulphur species, whereas sulphur in low-oxygen fugacity melts occurs as S^{2-}. The transition from S^{2-} to SO and SO_2 impedes the formation of a immiscible sulphide phase, making this metal available for enrichment during differentiation and partition into a hydrothermal fluid (Liang et al. 2006). The porphyry rocks of the Yulong area all have Ce^{4+}/Ce^{3+} ratios higher than barren shoshonites from the same region (Liang et al. 2006).

Table 5.3 Main Cu deposits in the Yulong ore belt and their sulphide and metal associations. After Hou et al. (2003, 2007b)

Deposit name	Rock type	Wall rocks	Tonnage (Cu metal) and grade	Sulphide assemblage	Metal association
Yulong	Monzogranite and quartz monzonite	Triassic limestone	6.22 Mt; 0.99% Cu, 0.028% Mo, 0.35 g/t Au	Chalcopyrite + molybdenite + pyrite±bornite±tetrahedrite ±cubanite±Au	Cu + Mo± Au±Ag±Re± Pt±Pd± Co±Pb±Zn
Malasongduo	Monzogranite and syenogranite	Triassic rhyolites	1.0 Mt; 0.44% Cu, 0.14% Mo, 0.06 g/t Au	Chalcopyrite + molybdenite + pyrite±galena±sphalerite± bornite±tetrahedrite	Cu + Mo±Au ±Ag±Re±Pt ±Pd
Duoxiasongduo	Alkali feldspar granite, monzogranite	Triassic mudstone	0.5 Mt; 0.38% Cu, 0.04% Mo, 0.05 g/t Au	Chalcopyrite±molybednite± magnetite±galena±pyrite± sphalerite	Cu + Mo± Au±Ag
Mangzong	Monzogranite	Triassic mudstone	0.25 Mt; 0.34% Cu, 0.03% Mo, 0.02 g/t Au	Chalcopyrite + pyrite± molybdenite±galena± sphalerite±tennantite± chalcocite	Cu + Mo± Au
Zhanaga	Monzogranite and syenogranite	Triassic mudstone	0.3 Mt; 0.36% Cu, 0.03% Mo, 0.03 g/t Au	Chalcopyrite + molybdenite + pyrite±magnetite±chalcocite ± bismuthinite	Cu + Mo± Au–Ag

The Yulong Cu–Mo–Au deposit is the largest in the region, with a resource of 630 Mt (Table 5.3). The Yulong intrusion is multiphase, but dominantly consisting of monzogranite porphyry. Hydrothermal alteration is well zoned comprising an inner K-feldspar zone, followed by quartz-sericite grading to argillic and propylitic envelopes. The sedimentary wall rocks are hornfelsed, with skarns developed in limestone units. From fluid inclusion studies, three main stages of alteration-mineralisation are recognised (Li et al. 1981, cited in Hou et al. 2003): (1) early K-silicate stage with temperatures of 440–700°C, associated with a main phase of Cu–Mo mineralisation; (2) quartz-sericite with temperatures of 200–500°C, associated with Cu–Mo-Fe; (3) a final stage of argillic and propylitic alteration at a temperature of about 230°C and associated with high sulphidation Cu–Au mineralisation (Hou et al. 2007b). The ore zones include a pipe-like porphyry Cu–Mo orebody, surrounded and overlain by a ring-shaped high-grade Cu–Au zone. The Cu–Au high sulphidation ore is a hydrothermal breccia zone formed as a result of fluid boiling near the roof of the porphyry stock. The alteration associated with the Cu–Au orebody is texture-destructive advanced argillic, consisting of quartz, kaolinite, dickite, montmorillonite and some alunite. Sulphides include chalcocite, tennantite, covellite, bornite and pyrite. This orebody is overlain by a blamket of supergene chalcocite-malachite (Hou et al. 2007b).

The second largest deposit is Malasongduo with a resource of 230 Mt (Hou et al. 2003; Table 5.3). The Malasongduo monzogranite porphyry is also a multistage intrusion which was emplaced in Early Triasic rhyolitic lavas and pyroclastics. The alteration pattern is smilar to that of the Yulong porphyry system. The mineralisation is laterally and vertically zoned. Laterally an inner Cu zone, grades to a Cu–Mo zone and an outer Ag–Pb–Zn zone; vertically a disseminated veinlet ore zone grades upward to a fine veinlet Cu zone to a supergene enriched zone. In this deposit, four generations of veinlets are recognised: (1) quartz-sulphide veins, mainly quartz-pyrite-chalcopyrite, quartz-pyrite-bornite, quartz-chalcocite; (2) biotite-chalcopyrite; (3) calcite-quartz-pyrite-chalcopyrite; and (4) tourmaline-quartz-chalcopyrite-pyrite-molybdenite.

Geochemical studies by Hou et al. (2003) show that the Yulong intrusions are characterised by high K_2O, Rb and Ba contents. In the monzogranite porphyry, initial $^{87}Sr/^{86}Sr$ ratios range from 0.7065 to 0.7077, $^{143}Nd/^{144}Nd$ values of 0.512451 to 0.512495 and with $^{206}Pb/^{204}Pb$ values of 18.75 to 18.89, $^{207}Pb/^{204}Pb$ 15.49 to 15.68, $^{208}Pb/^{204}Pb$ 38.53 to 39.12. These Sr–Nd–Pb isotopic compositions fall in the type II enriched mantle (high radiogenic Sr and low non-radiogenic Nd) space and transitional type II enriched mantle and MORB space, leading Hou et al. (2003) to conclude that the Yulong porphyries derived from a mantle source metasomatised by hydrous fluids sourced from a wet subducted oceanic slab. However, the Yulong porphyry system has not a primary relationship to a subduction margin, as have the porphyry Cu–Au of the western Pacific region or the those of the Andean belt in South America. The Yulong porphyries (and those in the Gangdise belt) are in a intracontinental setting and were formed during post-collision extensional tectonics and, quite possibly, as a result of asthenospheric upwellings into lithospheric

windows created by slab splitting or breakoff or delamination, followed by partial melting of lower crustal and/or metasomatised lithospheric materials.

5.2.2.5 Porphyry Systems in the East Greenland Volcanic-Rifted Margin

Brooks et al. (2004) reported on the age and tectonic setting of porphyry systems from the rifted continental margin of East Greenland and the outline that follows is taken from their work. The East Greenland porphyries include the Malmbjerg and Mellempas deposits hosted by the Werner Bjerge Complex and the Flammefjeld deposit hosted by the Kangerlussuaq Alkaline Complex (Fig. 5.21). Malbjerg is listed in the category of giant deposits with 150 Mt grading 0.15% Mo. The East Greenland volcanic rifted margin is part of the North Atlantic Igneous Province and was formed as a result of continental

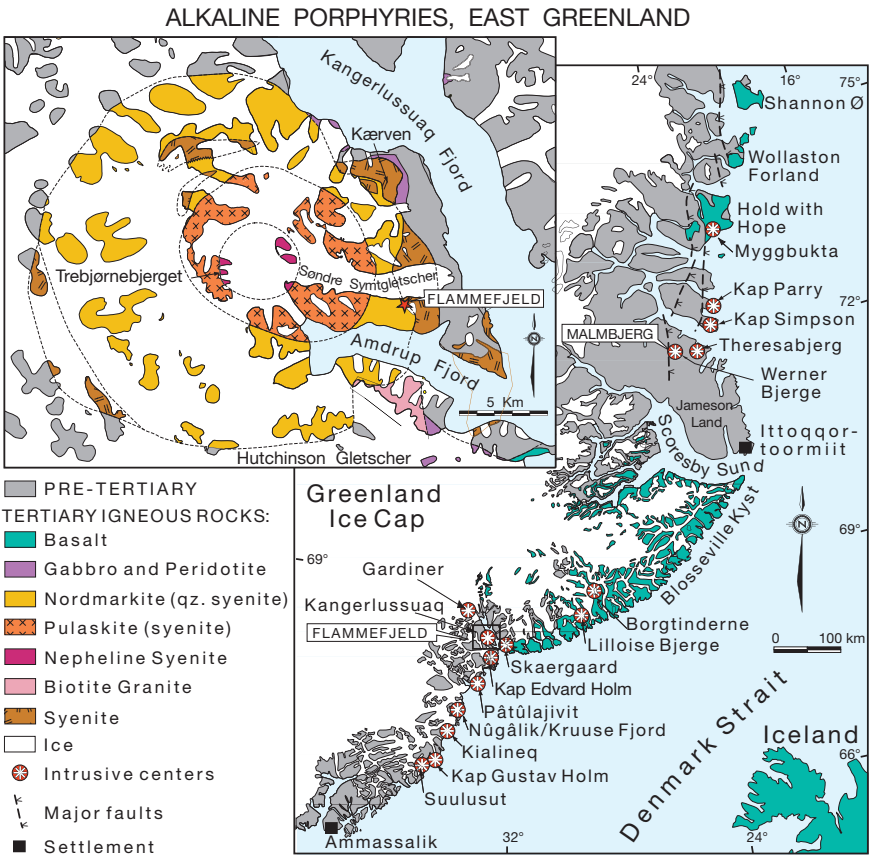


Fig. 5.21 Simplified geology of the East Greenland rifted margin and distribution of alkaline porphyry systems. Figure reproduced from Brooks et al. (2004) and by permission of Economic Geology and the Society of Economic Geologists

breakup above the Iceland mantle plume, accompanied by the eruption of flood basalts at 62–52 Ma, followed by the intrusions of mafic, felsic plutons and coast-parallel dyke swarms, between 52 and 26 Ma. For details of the North Atlantic Igneous Province and the East Greenland rifted margin, the reader should consult Jolley and Bell (2002) and Tegner et al. (1998), respectively.

The Werner Bjerge Complex consists of alkali gabbro, granite and syenitic rocks and is one of several, including the renowned and well-studied Skaergaard and Kap Edvard Holm intrusions that dot the east coast of Greenland and are associated with Neogene flood basalts. A few km west of this Complex is the Malmbjerg granite stock, which consists of perthite granite and quartz-feldspar porphyry intruded by porphyritic aplite. Most of the MoS_2 mineralisation is contained by the quartz-feldspar porphyry and the contacts with sedimentary rocks. The Malmbjerg mineralisation is of three types: (1) network of veins in the roof of the stock defining an inverted bowl shape; (2) horizontal greisen veins; (3) minor base metal mineralisation hosted by vertical argillised fractures. The Mellempas deposit is hosted by the Werner Bjierge Complex where it is associated with biotite granite. Re–Os dating of molybdenite from the Malmbjerg deposit yielded an age of ~26 Ma.

The Flammejeld complex, about 500 km south of Werner Bjerge, intrudes rocks of the ~50 Ma Kangerlussuaq zoned intrusion, which contains from the core towards the periphery: nepheline syenite, pulaskite, nordmarkite (quartz-syenite) and syenite (Brooks et al. 2004). The Flammefjeld complex consists of syenite, aplite, quartz-feldspar porphyry, rhyolitic dykes and intrusive breccias. The Flammefjeld porphyry system was first described by Geyti and Thomassen (1984). The Mo mineralisation is only exposed as granitic, quartz feldpspar and granophyre blocks of a breccia pipe, which exhibit quartz stockworks, dense networks of veinlets and fractures filled with molybdenite. It is assumed that these breccia pipes tore off blocks of mineralised material from an underlying porphyry system. The molybdenite mineralisation is accompanied by minor quantities of pyrite and chalcopyrite. Peripherally to the area of stokwork mineralisation there are veins with base metal sulphides, such as galena, sphalerite, chalcopyrite, tetrahedrite and some arsenopyirte. These veins are up to 5 m thick. Assays of grab samples averaged 3.9% Cu, 2.4% Zn, 0.9% Pb, 556 ppm Ag, 0.9 ppm Au, 418 ppm Bi, 1.1% Sb (Geyti and Thomassen 1984). The syenite around the Flammefjeld complex locally contains disseminated pyrite and quartz veinlets. Hydrothermal alteration typically consists of fracture-controlled quartz-sericite-pyrite and clay minerals (argillic). Potassic alteration is minimal and represented by biotite; no K-feldspart was observed.

As mentioned above, the magmatic events in East Greenland are related to rifting, the Icelandic mantle plume and seafloor spreading. The East Greenland margin was uplifted more or less contemporaneously with the latest intrusive phases of the ~26 Ma Werner Bjerge Complex (Brooks et al. 2004). The ~40 Ma Flammefjeld intrusive activity is also interpreted to be linked with

the strong uplift of East Greenland coastline, locally reaching elevations of 3000 m a.s.l. This regional uplift may be due to thick underplating of mafic-ultramafic bodies, as indicated by seismic and gravity data. The uplift event is coincident with the production of alkaline magmas, due to decompression and crustal and subcrustal lithospheric melting, which produced the high level porphyries (Brooks et al. 2004).

5.2.3 The Oldest Porphyry Systems

In this section I discuss porphyry systems from three regions: the Archaean Pilbara Craton in Western Australia, which boasts the oldest porphyry (and epithermal, see Section 5.3.8) systems in the world, and Palaeoproterozoic porphyries from India and Namibia. Porphyry systems of Proterozoic age are present in Finland (1.8–1.9 Ga Vlojarvi and Kopsa deposits), in Sweden (1.8 Ga Tallberg) and in Canada (2.7 Ga Don Rouyn).

5.2.3.1 Spinifex Ridge, East Pilbara, Western Australia

The Archaean North Pilbara terrain of the Pilbara Craton (Western Australia) consists of five terranes (Van Kranendonk et al. 2002, 2006a): (1) East Pilbara granite-greenstone Terrane and (2) Roeburne Terrane; (3) Sholl Terrane; (4) Regal Terrane and (5) West Pilbara granite-greenstone terrane (see Fig. 7.40). These terranes exhibit different structural and tectonic styles. The 3.5–3.2 Ga East Pilbara Terrane is characterized by a typical dome-and-basin structural pattern, with dome-shaped granitic complexes and intervening synclinal greenstone belts (Hickman 2004). By contrast the 3.3–3.0 Ga West Pilbara Superterrane is characterized by elongate northeast-trending structural patterns, not unlike those of the Yilgarn Craton in Western Australia (Hickman 2004). These two terranes testify to two different tectonic regimes and geodynamic evolutionary histories (Hickman 2004). The structure and horizontal-type tectonism of the West Pilbara Superterrane are consistent with seafloor spreading, subduction zones and arc settings, similar to Phanerozoic plate-tectonic style, whereas the East Pilbara terrane has a "vertical" or gravity-driven style of tectonism (Van Kranendonk et al. 2004) and its growth and geodynamic evolution was caused by a series of mantle plume events at 3.53–3.42 Ga (Warrawoona event), 3.35–3.29 Ga (Kelly event), and 3.27–3.24 Ga (Sulphur Springs event) (Huston et al. 2007a,b). Each event resulted in deposition of ultramafic–mafic and felsic volcanic rocks and intrusion of granites (see Fig. 7.43).

The East Pilbara Terrane contains a number of deposits that formed at high crustal levels in the porphyry-epithermal environment prior to 3200 Ma, the most significant of which is the Spinifex Ridge (also called Coppin Gap) porphyry Mo–Cu(Ag–W) deposit (Huston et al. 2007a,b) (Fig. 7.40). Other

porphyry Mo–Cu(W) deposits include the Gobbos, McPhee Creek East and Lightning Ridge deposits, all of which are located in the McPhees Dome (Barley 1982), and Copper Hills, which is located in the Kelly greenstone belt. The Spinifex Ridge porphyry system is related to the 3314 Ma Coppin Gap granodiorite intrusion emplaced into a sequence of bimodal volcanic rocks with a 500 Mt resource grading 0.06% Mo and 0.09% Cu. The emplacement of the Coppin Gap granodiorite created a fault system into which younger granodiorite intrusions were emplaced and produced the Mo–Cu mineralisation. The Coppin Gap granodiorite is typically subhorizontal and has produced an extensive alteration halo of potassic and argillic alteration with molybdenite-bearing quartz stockworks with subordinate chalcopyrite, scheelite and galena (Van Kranendonk et al. 2006b). The deposit has shapes from an inverted cup to cylindrical to an irregular geometry. The mineralisation is hosted by basaltic lavas, rhyolites, dacites, feldspar-porphyry, komatiites and the causative granodiorite itself. The mineralisation is represented by multiphase quartz stockwork veins with Mo and Cu sulphides, which have a general preferred orientation to the northwest and northeast, forming a conjugate set. Potassic alteration is represented by K-feldspar veins and pervasive biotite alteration at the periphery of the mineralised core. The biotite alteration is especially well developed in the mafic rocks (Van Kranendonk et al. 2006b). Phyllic alteration is the dominant alteration assemblage with sericite, which surrounds and overprints a large part of the potassic envelope. Pyrrhotite is associated with this phyllic alteration. Propylitic alteration consists of chlorite and epidote.

5.2.3.2 Malanjkhand Porphyry Cu–Mo–Au, Central India

The 2.5 Ga Malanjkhand porphyry Cu–Mo–Au in Madhya Pradesh, central India, was disovered in 1966 and is in the category of giant deposits with an estimated 470 Mt of ore grading 0.9% Cu, 0.025% Mo, 3.5 g/t Ag and 0.14 g/t Au (Sarkar et al. 1996; Stein et al. 2004). The origin and nature of the deposit has been debated with models considering that it may be an orogenic lode-style, vein or exhalative fracture-filling deposit (see Stein et al. 2004 and references therein for an overview of the various proposed models). In this book, I take the view of Stein et al. (2004) that the Malanjkhand deposit is a porphyry system. The brief overview of the deposit in this section is taken from Sarkar et al. (1996) and Stein et al. (2004). Stein et al. (2004) dated the Malanjkhand molybdenite using the Re–Os system, obtaining an age 2490±8 Ma.

The Malanjkhand region has a basement of Late Archaean and Proterozoic granitic rocks and mafic volcanics, overlain by Mesoproterozoic platform type clastic sedimentary rocks. Granitic rocks are granodioritic to tonalitic in composition, with aplite, gabbro and dolerite included within these granitic rocks. A U-Pb zircon age of ~2.48 Ma was determined for the Malanjkhand granites (Panigrahi et al. 2002, cited in Stein et al. 2004). Felsic volcanic rocks

are present south of the ore zone and include dacite and andesite. Sarkar et al. (1996) divided the Malanjkhand granites into four groups, which they labelled G1–G4. G1 is a coarse-grained porphryritic granite with K-feldspar megacrysts; G2 and G3, also coarse-grained, comprise tonalite, granodiorite and trondhjemite; G4 is an aplite intruding G2 and G3 granites. Magnetite is a common accessory to all of these granites, in places associated with lesser pyrrhotite, pyrite, molybdenite, apatite, ilmenite and allanite.

The Malanjkhand mineralisation is primarily hosted by the G2 granites and is associated with a zone of silicification, which grades towards the upper levels into a north-northeast-trending, large and massive arcuate quartz vein or reef, 3 km long and up to 265 m wide. In addition, there are a number of Cu–Mo–Au occurrences throughout the Malanjkhand granitic rocks. The orebody is contained in quartz ± K-feldspar ± biotite veins of two generations. First generation veins are stockworks and veinlets that surround the main quartz reef, which represents the second generation of vein quartz. The ore minerals are chalcopyrite, pyrite, molybdenite, sphalerite and magnetite. Trace amounts of cassiterite, galena, various tellurides and native gold. Apart from the above-mentioned silicification, hydrothermal alteration is manifested by alkali feldspars, biotite, epidote and chlorite replacements of primary minerals. The reddish-pink colouration of the host granitic rocks is attributed to potassic alteration due to K-feldspar dusted with hematite.

Sulphur isotopic data show $\delta^{34}S$ values ranging from –0.38 to +2.90‰, suggesting a magmatic source. A detailed fluid inclusion study of the Malanjkhand vein quartz is provided by Panigrahi and Mookherjee (1997), who reported Type I, II and III inclusions with aqueous to aqueous-carbonic to pure carbonic fluids with homogenisation temperatures ranging from $<$100 to 380°C and salinities from 4 to 12 wt% NaCl equivalent.

As mentioned above, Stein et al. (2004) consider the Malanjkhand mineralisation as a porphyry system and interpret the large quartz reef as the silicic top of a 3–5 km porphyry. Deeper levels exposed in the north seem to confirm this interpretation because disseminated molybdenite increases as do the exposures of altered and mineralised and altered granitic rocks.

5.2.3.3 Haib Cu–Mo Porphyry System, Southern Namibia

The ~2.0 Ga Haib is located in the Richtersveld Andean-style magmatic arc in Namibia, on the northern margin of the Namaqua province and the southwestern margin of the Kalahari Craton. This border region between South Africa and Namibia is characterised by tectono-stratigraphic terranes of the 2.0–1.8 Ga Orange River Orogen, of which the Richtersveld magmatic arc is part. The Haib Cu–Mo porphyry system has resources of about 560 Mt at 0.32% Cu with by-product Mo averaging 0.10% copper equivalent (Schneider and Seeger 1993). The Haib deposit, located in the Orange River valley, was described by Minnitt (1986). The ~2.0 Ga Orange River Group, an 8 km-thick

succession of calc-alkaline volcanics (Haib Subgroup) intruded by the co-magmatic Violsdrif Plutonic Suite, emplaced into the volcanic succession at 1.96–1.81 Ga. The Haib Subgroup consists of basaltic andesite, andesite, dacite and rhyolite associated with cogenetic pyroclastic rocks. Intrusive rocks of the Violsdrift suite comprise granodiorite, adamellite, diorite, tonalite, and leucogranite. These plutonic and volcanic rocks are intruded by quartz-feldspar porphyry dykes and stocks, and one of these stocks is associated with the porphyry mineralisation.

At the Haib, the mineralised quartz-feldspar porphyry stock extends along an east-west trend for about 11 km and is about 3 km wide. This quartz-feldspar porphyry is characterised by round, bluish, opalescent quartz phenocrsyts and subhedral plagioclase phenocrysts in an aphanitic matrix. Accessory minerals include apatite, rutile, pyrite, chalcopyrite and molybdenite. The mineralised rocks are fractured and have vein stockworks and intensely hydrothermally altered (Figs. 5.1 and 2.8). Hydrothermal alteration exhibits the classic three zones of dominant assemblages of potassic (K-feldspar and biotite) in the core, surrounded by a phyllic (quartz-sericite-pyrite) and a propylitic (chlorite, epidote, calcite) envelopes. However, this classic alteration pattern was overprinted by a second event of phyllic alteration, which is associated with and surrounds the mineralised fracture system. Argillic alteration is not observed at Haib, but this may be due to its elimination by erosion. Sulphide minerals are dominantly pyrite and chalcopyrite, accompanied by minor bornite, covellite, tennantite, molybdenite, galena, sphalerite, arsenopyrite and pyrrhotite. On the surface the mineralisation is oxidised to malachite and chrysocolla forming conspicuous staining covering a large area of 2 km $\times$ 1.2 km, which led early German explorers to its discovery late in the 19th century. This supergene zone is at least 40 m thick.

5.3 Fossil and Active Epithermal Systems

In regions of high heat flow, thermal convection dominates the behaviour of groundwaters or sea water in permeable and/or fractured crust, thus generating geothermal systems. Terrestrial geothermal systems are derived from air-saturated meteoric waters which penetrate the crust to regions influenced by cooling magmas (Henley and Ellis 1983). Submarine geothermal systems are, by contrast, characterised by sea water convection cells which are also heated by cooling magmas at depth. In this section I describe terrestrial geothermal systems, both ancient (fossil) and present-day. Submarine systems related to submerged volcanic structures at convergent and divergent plate boundaries are discussed in Chapter 7. In terrestrial geothermal systems the circulation of hot waters can reach depths of approximately 5 km, lasting from a few thousands up to about 2 million years. Near-surface temperatures are approximately 50–100°C, reaching 350–400°C in the subsurface environment. These low to

moderate temperatures, together with pressure, are the main reason for the use of the term epithermal, with which the mineral products, ore deposits and occurrences produced during these geothermal activities are widely known. The thermal energy which is transferred towards the surface is derived in part from the cooling magmas and in part from cooling of the wall rocks. Most solutes are transferred to the circulating waters from the wall rocks through which they pass, whereas most of the gas components are probably derived from the underlying cooling magmas.

Active geothermal systems are commonly found in areas of recent tectonic and igneous activity at plate boundaries. Most geothermal fields are in fact associated with volcanic structures, in particular calderas, at convergent margins (volcanic arcs) and intracontinental rift systems. In volcanic areas the preferred association is with andesitic, dacitic and rhyolitic centres rather than basaltic (Ellis 1979). Geothermal systems may or may not vent at surface. Some of the surface expressions include hot springs, geysers, mud pools and fumaroles. The subsurface geometry of the hydrothermal circulation in a geothermal system varies according to the geological setting, local and regional structures, and the availability of permeable and impermeable lithologies. Convective flow is usually vertical or near-vertical and is generally controlled by faults and/or fractures, although in the presence of flat-lying permeability barriers the circulating fluids may be forced to move laterally. In general, discharge of fluids at the surface is represented by near-neutral chloride-rich hot spring waters, or it may be characterised by acid-sulphate boiling pools. The latter are generally related to steam that separates from deeper chloride-rich boiling fluids in vapour-dominated systems resulting in fumarolic activity containing CO_2 and H_2S, as further elaborated below. Bicarbonate-rich waters are common in areas where carbonate rocks are present and these may form vast deposits of carbonate sinters, known as travertine. Deeper in the system, beneath the levels of boiling and atmospheric oxidation, waters are usually slightly alkaline (pH 6–7) and weakly saline. Isotope systematics show that the waters of geothermal systems are dominantly of meteoric origin with only a minor component being derived from magmatic sources. Metal-rich precipitates in many cases characterise the surface expressions of the geothermal systems, as for example in the Taupo geothermal fields in New Zealand, and the Steamboat Springs geothermal area in Nevada (USA). These surface precipitates may contain ore-grade metalliferous concentrations of Au, Ag, W, As, Sb and Tl, and are generally associated with relatively large deposits of amorphous siliceous material (sinters) which form around chloride-rich hot springs. Elements such as Cu, Pb, Zn, Te and Bi are by contrast concentrated at deeper levels. Thus, it is clear that geothermal systems have distinct metal zonations with respect to depth, as discussed later. Sinters form by precipitation of SiO_2 from hot water discharging at the surface as springs or geysers, due to cooling and subsequent loss of silica solubility, so that the solution becomes supersaturated with respect to quartz and to other more soluble silica species (White et al. 1991). However, it must be borne in mind that microbial mediation can

and does actively and/or passively induce precipitation of silica in hot springs, by modifying the pH regime or by providing an organic substrate that is used as a template for precipitation (Guidry and Chafetz 2003). Silicification of microbial substrates in hot springs can be a rapid process. Examples of metal contents of geothermal discharge water and chemical precipitates are provided in Table 1.6 in Chapter 1. At Wairakei, on the basis of the Au content in scales deposited during discharge from a well, Browne (1986) estimated a concentration of 1.5 g/t Au in the aquifer, and envisaged that it would take only 1500 years to transport 32 x 10^6 g of Au through the system. Since geothermal fields are known to have been active for between 1 and 2 million years, the implications of these estimates, even if taken conservatively, in consideration of less efficient deposition rates, are obvious.

The exploration for geothermal energy received considerable impetus in the 1960s and 1970s as a result of the increased oil prices and the political uncertainties in the oil-producing countries. The result of this exploration, particularly in New Zealand, the USA, southern Europe, Philippines and Japan, was of incalculable benefit to our knowledge of hydrothermal activity, processes of solution, transport and deposition of metallic elements, effects of water–rock interaction and, in a broader sense, the ore-forming processes related to the geothermal systems. There is abundant literature on the subject, but for the present purpose the reader is referred to, Ellis and Mahon (1977), Weissberg et al. (1979), Ellis (1979), White (1981), Henley and Ellis (1983), Barnes and Seward (1997) and the special volume of the Society of Economic Geologists (Simmons and Graham 2003). Now, history is about to repeat itself in that the near-panic, mostly felt in the political establishment, caused by global warming is driving more research into alternative "green and clean" sources of energy, which includes geothermal, both volcanic and non-volcanic (e. g. high heat producing rocks, discussed in Chapter 9).

Similarities between the active geothermal systems and epithermal precious and base metal ore deposits were noted many years ago by Lindgren (1933). It is now widely recognised that many epithermal deposits in the geological record are in fact fossil geothermal systems. Nowhere is this in greater evidence than in New Zealand, where subduction-related volcanic arcs, such as the active Taupo Volcanic Zone and the Coromandel peninsula volcanics of Miocene-Pliocene age and associated Hauraki goldfields, afford a unique opportunity for examining both active and fossil epithermal systems geographically adjacent to one another.

Epithermal systems, like porphyries, are temporally and genetically related to volcano-plutonic activity of calc-alkaline affinity at convergent margins. Like for porphyries, the magmas are oxidised and generated in the mantle wedge above the subduction zone, as discussed in Section 5.2. Epithermal mineral deposits are also found in back-arc and continental rift settings where they are associated with reduced magmas with bimodal compositions, a prime example of which are the epithermal deposits of the Great Basin in the USA, briefly described in Section 5.3.7 Also associated with rifting are epithermal

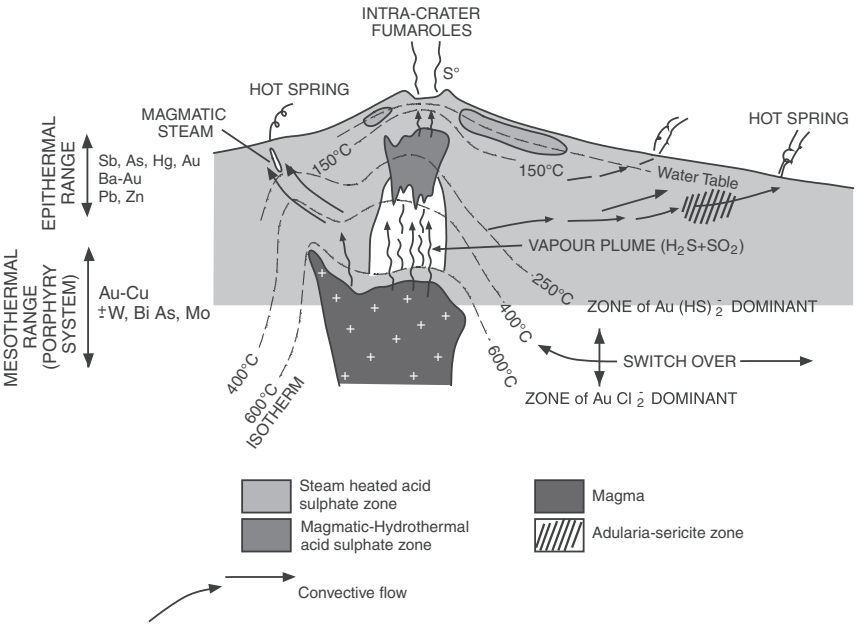


Fig. 5.22 Schematic illustration of a stratovolcano with porphyry and epithermal range of ore systems; the epithermal systems include low-S and high-S. the high-S (acid sulphate epithermal) forms above the vapour plume that emanates from the cooling porphyry magma, whereas the low-S (adularia-sericite epithermal) wil form distally from the heat source, below the water table. Note the switch from Cl-dominated to S-dominated metal complexing and resulting metal zonations. Based on Hedenquist and Lowenstern (1994), White and Hedenquist (1995) and Hedenquist et al. (2000)

mineral systems that contain Te, which are closely related to alkaline magmatism, as exemplified by the precious metal epithermal deposits of Cripple Creek in the USA and Emperor in Fiji. Some low-sulphidation adularia-sericite and alkalic epithermal systems are now becoming increasingly recognised in continental flood volcanic provinces (large igneous provinces; LIPs). Examples of low-sulphidation systems that are associated with LIPs can be found in NW China and in silicic LIPs. Silicic LIPs contain low-sulphidation precious metal epithermal systems, as in the Sierra Madre Occidental in Mexico, where more than 800 epithermal occurrences are known (Camprubi et al. 2003). Another economically important epithermal Au–Ag mineral district occurs in the siliceous Chon Aike province in Argentina. Bryan (2007) noted that the epithermal systems in siliceous provinces tend to occur in volcanic collapse structures, caldera-bounding faults and along extensional faults of rift structures.

In this section, following descriptions of the various types and styles of epithermal systems and a discussion on the transport of precious metals in the epithermal environment, I describe a selection of epithermal mineral deposits.

These include the Au–Ag epithermal deposits of the Coromandel peninsula in New Zealand, Papua New Guinea, Chile, the Great Basin in the USA, southeastern China, and northwest Turkey. Many of these epithermal systems are transitional to porphyry environments. The Far SouthEast-Lepanto porphyry and epithermal deposits and the Palinpilon geothermal field in the Philippines, provide good examples of the spatial relationship between porphyry and epithermal systems, as well documented by Hedenquist et al. (1998) and Rae et al. (2003), respectively. Figures 5.4 and 5.22 illustrate the structure of a stratovolcano and associated spatial relationships between a subvolcanic porphyry system, overlying and laterally sited epithermal systems and hot springs. These models are based on Sillitoe (1995), Lang et al. (2000), Hedenquist and Lowenstern (1994) and White and Hedenquist (1995). Figure 5.22 also shows the metal zonations that typically characterise the stratovolcano porphyry-epithermal environment and their dominant Cl and S complexing agents. Finally, some of the major active geothermal areas (Taupo Volcanic Zone in New Zealand, Yellowstone in USA, the geothermal fields of Kamchatka-Kurile volcanic arcs) are also briefly examined.

5.3.1 Fossil Epithermal Systems

Fossil geothermal systems are known as epithermal, a term coined by Lindgren (1933). Here I define epithermal systems and associated ore deposits as those formed at low to moderate temperatures (between ~50 and ~300°C) and pressures (<500 bar or depth equivalent of <1–1.5 km), from dominantly meteoric hydrothermal (but also contain HCl, CO_2 and H_2S, of magmatic derivation), and weakly saline fluids (<1 to ~5–15 wt% NaCl equivalent).

Although epithermal deposits are mostly volcanic-hosted and clearly related to volcano-plutonic activity, there is nevertheless a category of sedimentary-rock-hosted epithermal deposits which do not appear to have a clear connection to igneous activity (Chapter 9). Epithermal mineralisation has a number of common and distinctive features, such as the presence of fine-grained chalcedonic quartz, calcite, quartz pseudomorphs after calcite (indicative of boiling fluids), and hydrothermal breccias. The elemental association is also characteristic, with ore elements such as Au, Ag, As, Sb, Hg, Tl, Te, Pb, Zn and Cu. Ore textures include open-space filling (characteristic of low pressure environments), crustifications, colloform banding and comb structures. The deposits, which are formed from the surface to approximately 1.5 km below the surface, are typified by veins, stockworks and disseminations. These features, which may occur either together or as single entities, constitute deposits generally easy to mine as open cast or shallow underground operations, with relatively large tonnages and low Au + Ag grades, or small tonnages and high Au + Ag grades. Owing to the surface and near-surface environment of this mineralisation, the high relief of volcanic arcs with continuing tectonic uplift, followed by

rapid erosion, the preservation potential of epithermal systems in the ancient geological record is generally poor, although there are exceptions (see below). For this reason, most exposed and known epithermal systems are of Cenozoic age and, like porphyry deposits, they are especially abundant all along the Pacific Rim. A comprehensive list of epithermal gold deposits of the southwest Pacific is given by White et al. (1995); porphyry-epithermal deposits discovered in the last 30 years in the Indonesian islands are presented in an excellent collection of papers in van Leeuwen et al. (1994). Examples of epithermal deposits in the Alpine-Himalayan orogen can be found in Italy, Spain, Turkey and the Carpathian districts in Europe. Epithermal deposits of Paleozoic and Mesozoic age are found in the Central Asian Orogenic Belt, referred to in Section 5.2.1.4. Cooke and Simmons (2000) and Simmons et al. (2005) provided up-to-date reviews of epithermal ore systems. Simmons et al. (2005) listed more than 70 epithermal deposits world-wide.

Classification schemes of epithermal systems are numerous, but the more recent ones are based on alteration minerals, oxidation and sulphidation states. Table 5.4 provides a list of the more recent and used classification schemes and related diagnostic mineral species that are diagnostic of epithermal ore systems.

Einaudi et al. (2003) have drawn attention to the "sulphidation" terminology, in view of its common use as various synonyms (e. g. high-sulphur sulphides, sulphidation, sulphur fugacity, sulphidation state). They stressed that sulphidation state is not a function of the S content of a sulphide mineral, but considered "sulphidation state' in the reference frame of temperature and S_2 fugacity, as is the case for O_2. The sulphur (or oxygen) fugacity of a system, at any temperature, is compared to the reactions of pyrrhotite to pyrite and magnetite to hematite, respectively as follows:

$$2FeS + S_2 \rightarrow 2FeS_2$$
$$4Fe_3O_4 + O2 \rightarrow 6Fe_2O_3$$

In essence S can occur in the oxidised state (SO^{2-}_4, higher temperature) or in the reduced state (H_2S, lower temperature) and sulphide and sulphate minerals are precipitated from reduced S and from oxidised S, respectively, therefore sulphidation state controls the deposition of ore minerals (Seedorff et al. 2005). This means that ore-forming fluids contain S in valence or oxidation states that are greater or less than S_2 ($n = 0$, with SO^{2-}_4, $n = 6$ and H_2S, $n = 2$). The phase diagram that defines the sulphidation state of hydrothermal fluids is shown in Fig. 5.23. From the diagram of Fig. 5.23, five bands of sulphidation state can be defined from very low to very high, with a complex transition from porphyry (500–350°C) to high- and low-sulphidation (<350°C) environments .

The two end-members high- and low-sulphidation epithermal systems exhibit similarities and differences. It is important to be able to distinguish between them in order to accurately assess the economic potential of the ore system. One of the most important aspects of epithermal deposits is alteration

Table 5.4 Evolution of classification schemes of epithermal systems (after and modified from Simmons et al. 2005 and Sillitoe and Hedenquist 2003)

		Hot-spring type	
High sulphur	Low sulphur		Alkalic deposits
Acid sulphate		Adularia-sericite	
High sulphidation		Low sulphidation	
Alunite-kaolinite		Adularia-sericite	
	Type 1 adularia-sericite		Type 2 adularia-sericite
High sulphidation		Low sulphidation	
High sulphidation	Intermediate sulphidation	Low sulphidation	Alkalic
Au–Ag–Cu, As–Sb in oxidised magmas; Ag–Sn, Sb, Bi, W in reduced magmas; vuggy quartz; pyrophyllite-sericite alteration; barite common	Ag-Au-base metals; Mo, As, Sb; Tellurides may be common; vein filling, crustiform and comb quartz	Au-Ag deposits with calc-alkaline volcanics; crustiform and colloform chalcedony; quartz-carbonate replacement textures	Au-Ag, with alkaline and subalkaline volcanic rock; tellurides and selenides abundant; barite, celestite, fluorite
Minerals of various pH, sulphidation and oxidation states (modified from Simmons et al. 2005 and references therein)			
Acid pH		*Neutral Ph*	
Alunite, kaolinite (dickite), pyrophyllite, residual vuggy quartz		Quartz-adularia ± illite±smectite, calcite	
High sulphidation	*Intermediate sulphidation*	*Low sulphidation*	
Pyrite-enargite, ± luzonite, covellite-digenite, famatinite, orpiment	Tennantite, tetrahedrite, hematite-pyrite-magnetite, pyrite, chalcopyrite, Fe-poor sphalerite-pyrite	Electrum,arsenopyrite-loellingite-pyrrhotite, pyrrhotite, Fe-rich sphalerite-pyrite, tellurides	
Oxidised		*Reduced*	
Alunite, hematite-magnetite		Magnetite-pyrite-pyrrhotite, chlorite-pyrite	

mineralogy and zoning. Details of hydrothermal alteration of epithermal systems are given in Chapter 2, examples of epithermal mineral deposits (McLaughlin, Hishikari, Round Mountain, Kelian, Rodalquilar, El Indio-Tambo, Paradise Peak) are well illustrated in a poster published by the Society of Resource Geology (Hedenquist et al. 1996). Examples of selected deposits are discussed in the sections below.

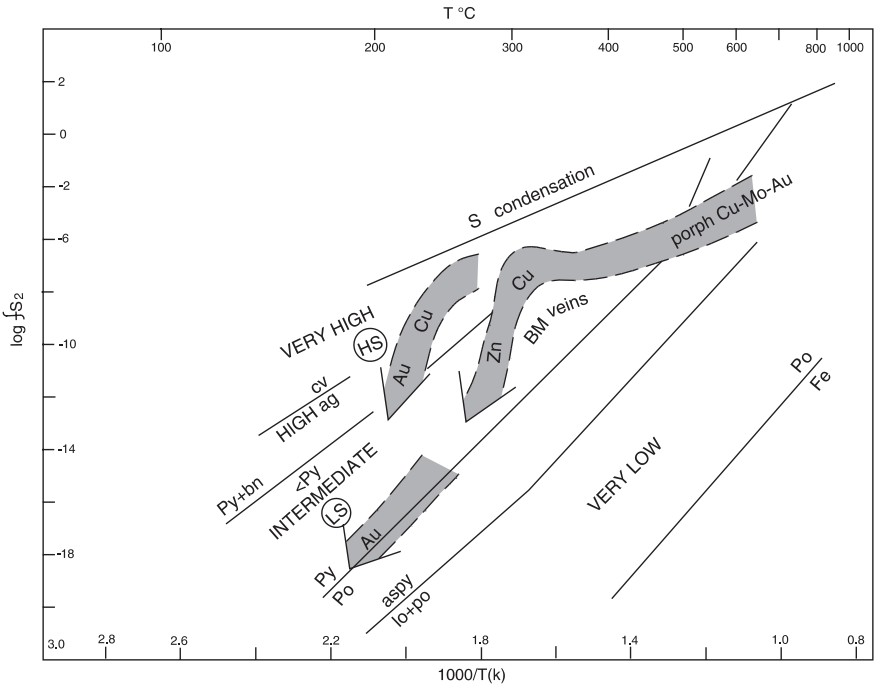


Fig. 5.23 Phase diagram of Log fS_2 versus temperature, defining sulphidation state of hydrothermal fluids and evolutionary and cooling paths of porphyry (500–350°C) → base metal veins (<350°C) → LS low-sulphidation and HS high sulphidation epithermal systems (<300°C); note that HS has an early Cu-rich high-sulphidation assemblage, followed by a later Au-rich intermediate-sulphidation assemblage. po pyrrhotite, lo loellingite, aspy arsenopyrite, py pyrite, cpy chalcopyrite, cv covellite, dg digenite, HS high-sulphidation, LS low-sulphidation, BM base metals. The diagram is after Einaudi et al. (2003) and Barton (1970)

5.3.1.1 Low-Sulphidation (LS) Systems

These are generally reduced and with a near neutral pH. The LS environment is dominated by meteoric waters, although magmatic gases may be present, these being mainly CO_2, SO_2, and HCl. Boiling may occur at shallow depths and this results in the generation of CO_2– and H_2S-rich vapours, which may eventually condense near the surface to form steam-heated acid-sulfate waters (HS system). LS deposits are characterised by open-space veins, breccias and stockworks. The ore and gangue minerals include: pyrite, arsenopyrite, sphalerite, galena, gold, electrum, quartz, chalcedony, calcite, adularia, illite, barite (see also Table 5.4). The LS veins commonly show textures such as colloform banding, hydraulic fracturing, lattice-textured bladed calcite or quartz. LS deposits are generally poor in Cu and other base metals. LS mineralisation forms distally from the heat source (magma) and the fluids have temperatures of 200–300°C, and hydrostatic pressures. There are Au-rich and Ag-rich

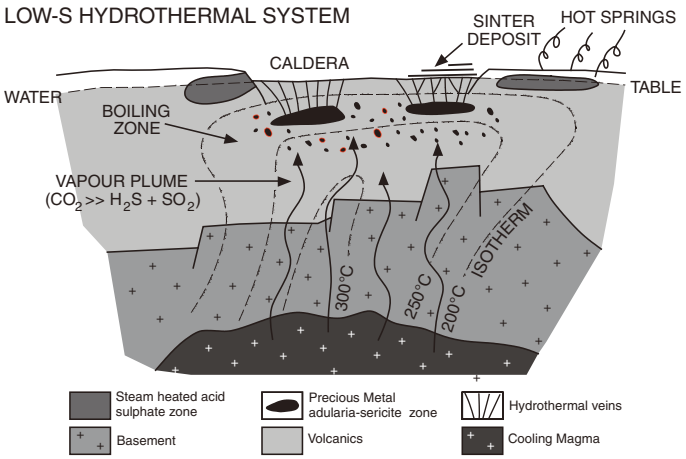


Fig. 5.24 Model of low-sulphidation epithermal system in a caldera setting, with fumaroles, hot springs and sinter deposits, below which are zones of fluid boiling with deposition of precious metals. Courtesy of MJ Van Kranendonk, modified from Henley and Ellis (1983)

systems, each with different fluid characteristics. Au-rich systems are base metal-poor and are characterised by low salinity (1–2 wt% NaCl equivalent), gas-rich fluids (CO_2 and H_2S mainly) and Ag/Au ratios ranging from 1 to 10. Ag-rich systems, by contrast, have high salinity fluids (10–15 wt% NaCl equivalent), high Ag/Ag ratios (~100) and by virtue of the high salinity, contain associated base metals. A model showing an LS system is shown in Fig. 5.24.

5.3.1.2 High-Sulphidation (HS) Systems

HS systems result from the ascent of high-temperature magmatic volatiles. These fluids mix with descending meteoric waters, forming a highly acidic solution, containing HCl, SO_2, H_2S, etc. The SO_2 and the H_2S oxidise and react with H_2O forming sulphuric acid (H_2SO_4), with reactions of the type:

$$H_2S + 2O_2 \rightarrow H_2SO_4, \text{or}$$
$$4SO_2 + 4H_2O \rightarrow 3H_2SO_4 + H_2S$$

Sulphuric acid attacks the wall rocks, causing strong leaching (advanced argillic alteration; Chapter 2). The fluids are oxidised, highly acidic, have temperatures of around 200–300°C, with a pH ranging from 0 to 2. Salinity of the fluids is from 2 to 5 wt% NaCl equivalent. The salinity of the fluids, however, tends to increase with depth, reaching values of 20–30 wt% NaCl equivalent below the ore zone. HS deposits are characterised by disseminated ore minerals, replacement ores and minor stockworks or veins. HS deposits commonly contain Cu–As ore minerals, such as enargite or luzonite. Pyrite is ubiquitous. Electrum is

not a common ore component, whereas native Au is. Diagnostic of HS systems are alteration minerals such as kaolinite, alunite, barite, dickite, pyrophyllite and diaspore (Table 5.4). The ore zone is characterised by a porous, vuggy residual silica (due to strong leaching). It is important to remember that advanced argillic alteration (kaolinite and/or alunite) is not necessarily indicative of economic mineralisation. This alteration can also be caused by downward percolation of steam heated waters, which are not related to the mineralising fluids and which cause an argillic overprint in the rocks affected.

5.3.1.3 Alkalic Systems

Alkalic-type epithermal systems are typically associated with alkali basalt, phonolite, trachyte and coeval alkaline monzonitic and/or syenitic rocks with breccia pipes, disseminations, veins and stockworks, with multiple stages of vein deposits, associated with hot (up to 500°C), saline (30–40 wt% NaCl equiv.), CO_2–bearing fluids. Alteration styles are characterised by K-metasomatism (with adularia as one of the main alteration minerals), quartz, fluorite, carbonate and regional propylitic alteration. Stages of base metal sulphides, quartz-fluorite-pyrite-hematite-rutile and Au deposition follow with decreasing temperatures and more dilute fluids (Richards 1995). An important feature of alkalic epithermal systems is the presence of tellurides (Au–Ag, Pb, Hg), base metal sulphides, sulphosalts, stibnite and rutile. Gangue minerals include quartz, chalcedony, roscoelite, barite, fluorite, adularia, celestine, kaolinite (Richards 1995). According to Richards (1995), alkalic magmas have the potential to generate Au-rich epithermal deposits and this may be due to this metal becoming progressively enriched in the residual melt because of sulphur undersaturation. Hydrothermal breccia pipes are common in alkalic epithermal systems and there is some evidence to suggest that they are distal expressions of porphyry Mo–Cu, as exemplified by the Qiyugou breccia pipes in central China, described in Section 5.2.2.3 and Fig. 5.18. Other examples of alkalic porphyry-epithermal systems include Cripple Creek (Colorado, USA), Porgera and Ladolam (Papua New Guinea) and the Emperor deposit in Fiji (Richards 1995); Sillitoe and Hedenquist 2003). All are linked with extensional tectonic regimes, generally associated with tectonic collapse following continental collisions. A model of alkalic Au–Ag epithermal deposit is shown in Fig. 5.25B.

5.3.1.4 Epithermal Styles

Ore minerals and alteration assemblages, host lithologies and associated volcanic rocks assist in defining the types and styles of epithermal mineralisation. In this respect the works of Buchanan (1981) and Berger and Eimon (1982) are important in providing a workable classification and general characteristics of epithermal mineralisation. Epithermal styles can be classified into hot-spring type and open-vein type, possibly forming a continuum from surface chemical precipitates to deep veins and fissure fillings. Erosion plays an important role in

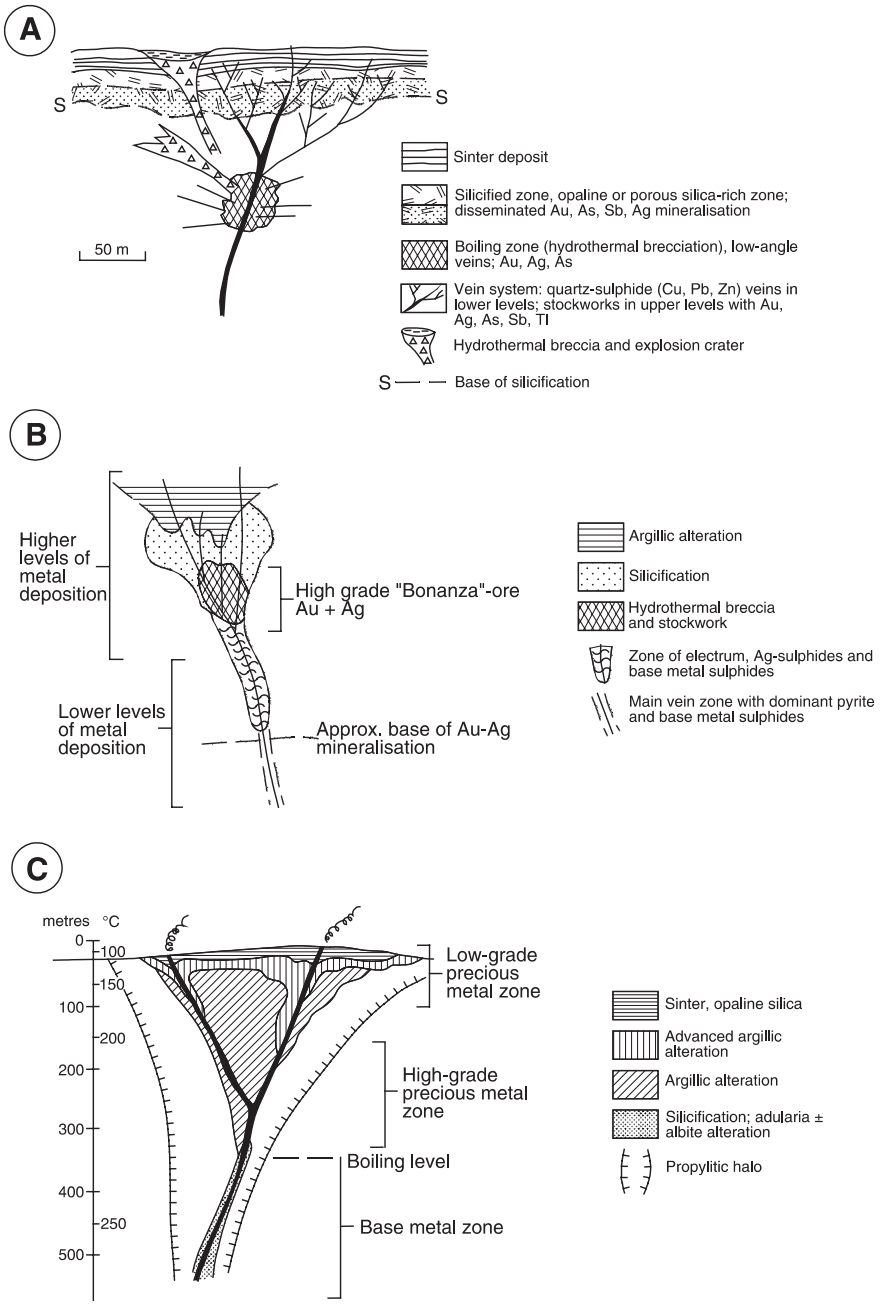


Fig. 5.25 Models of epithermal styles; (**A**) hot spring; (**B**) open vein with two levels of mineralisation; (**C**) hot spring depositional model grading downward into an open veins style. A and B after Berger and Eimon (1982), C is after Buchanan (1981)

that commonly only a few veins are exposed, representing the remnants of what could have been a more extensive epithermal system. Much of the following discussion comes from the above-cited sources.

5.3.1.4.1 Hot Spring Style

Hot spring epithermal style are formed at or near the surface and are characterised by siliceous cappings (sinter) passing downward into a zone of silicified material and stockwork veins, and into a zone of hydrothermal brecciation. Hydrothermal breccias are formed as a result of boiling or hydrothermal eruptions. The silica cap is usually brecciated, and in places explosion craters or maars are present with associated fall-out sedimentary aprons. Figure 5.25A shows a schematic cross-section of a hot spring type epithermal deposit. Dominant element association is Au–Ag–As–Sb–Hg–Tl with minor Cu–Pb–Zn in the deeper levels. The mineralisation is low grade and in the form of disseminations and stockworks just below the silicified cap, although it can reach high grades in hydrothermal breccias and associated vein systems corresponding to the boiling zone. The upper portions of the silica cap are usually barren, but some native sulphur, Au and cinnabar mineralisation may be present. Below the zone of silicification hydrothermal alteration is of the argillic type. Free Au occurs with quartz and adularia in veins, stockworks and disseminations in permeable host rocks. This mineralisation is characterised by its fine-grained size and low overall sulphide content and therefore scarcity of base metals. Episodes of brecciation are important in hot spring deposits because they can be related to rapid pulses of precious metal deposition. Explosive brecciation occurs wherever the silica cap acts as a seal. This allows the fluids to reach sufficient pressure to rupture the cap, the sudden pressure release causing the fluids to boil, with subsequent mineral deposition and re-sealing of the cap, so that the process may start again. For this reason it is often difficult in trying to work out the number of brecciation episodes that have taken place in a hot spring deposit. Examples of hot spring epithermal mineralisation include the Round Mountain Au deposit in Nevada (Tingley and Berger 1985) and the McLaughlin Au–Sb–Hg deposit in California (Sherlock 2005; see Section 5.4.5).

5.3.1.4.2 Open Vein and Breccia Style

The downward extensions of hot spring deposits, or in other words their feeder zones, are an example of open vein style epithermal deposits, which are also known as bonanza, vein and lode type (Silberman and Berger 1985). They differ from the hot spring type in that mineral deposition occurs at deeper levels, has higher sulphide and base metal contents, substantial vein widths, higher grades but lower tonnages. Dominant element association is Au–Ag–As with varying amounts of Se, Te, Cu, Pb and Zn. Figure 5.25B illustrates a model of epithermal vein system with two levels of mineralisation, and Fig. 5.25C depicts a combined hot spring vein style epithermal deposit. In general the veins are

vertically zoned. A typical vein may consist of agate and clay near the surface, passing downward into quartz, calcite, adularia and precious metals. The precious metal ore zone has a restricted vertical interval, usually between 100 and 350 m. At the base the ore grade decreases while the base metal contents increase, and minerals such as galena, sphalerite and less commonly chalcopyrite and/or pyrrhotite become important mineral phases at depth. Quartz continues to be present while calcite is reduced in volume. In alkalic epithermal systems, the veins within the precious metal zone typically consist of quartz, calcite and adularia, and may contain ore minerals such as pyrite, arsenopyrite, native gold, argentite, electrum and tellurides. Other minerals which may be present in various amounts include: tetrahedrite, fluorite, barite, stibnite, realgar, rhodocrosite, as well as the above-mentioned base metal sulphides. Native gold constitutes the most important ore mineral, followed by the tellurides, while other complex Au minerals are of lesser importance. The sulphide minerals, in particular pyrite and arsenopyrite, may contain important amounts of Au, which tends to increase towards the surface. In the open-vein epithermal systems the bulk of the mineralisation is confined to major veins, with low-grade stockwork and disseminated zones commonly found in the upper sectors of the system, usually where there is a major change in the attitude of the veins. The ore shoots (a payable zone within the vein in which a combination of width and grade allow stoping), which rarely fill the entire vein structure, usually form isolated zones within the vein (Buchanan 1981). Most of the precious metal epithermal deposits of the Hauraki goldfield in New Zealand, discussed below, can be considered as examples of open vein type.

5.3.1.5 Transport of Au and Ag in Hydrothermal Fluids, Boiling and the Formation of Epithermal Deposits

The role of complex ions and ligands in the dissolution, transport and deposition of metals is introduced in Chapter 1. Experimental geochemistry applied to problems of ore deposition has contributed a great deal to the understanding of the mechanisms involved in metal speciation and solubility in hydrothermal fluids. In addition to the works cited below, the reader is also referred to Wood (1989) and Seward and Barnes (1997). Dominant, and geologically important, ligands for metal transport are Cl^- (chloride), HS^- (thio-sulphide) and OH^-. Minor ligands, in the sense that they are either of low abundance, unstable or weak, are NH_3, SO_4^{2-}, F^- and HCO_3^-. The last two, however, become important ligands for the transport of metals, such as Sn in greisen systems (F^-) and U in the weathering environment (HCO_3^-). The most common and efficient ligands for the dissolution and transport of metals are the chloride and sulphide complexes. Chloride complexes predominate in high salinity fluids and at high temperatures (in fact their solubility increases with increasing temperature) and tend to complex base metals and Ag. Sulphide complexing, on the other hand, predominates in low salinity fluids (i.e. geothermal fluids), is less dependent on temperature and is especially favourable for complexing Au and, depending on

physico-chemical conditions, Ag (see below). The "soft", or class A, and the "hard" or class B, behaviour of metals and ligands (also discussed in Chapter 1) predicts that strong complexes are formed by complexing agents and metals of the same class. Precipitation of metals from hydrothermal solutions takes place whenever the transporting complex is destabilised and as a result the solubility of the metal in question is greatly reduced. A number of factors induce destabilisation of metal complexes, including: (1) temperature decrease; (2) pressure loss and/or boiling; (3) changes in the redox state of the solution; (4) reduced activity of complexing ions (i.e. S or Cl). Hydrothermal breccias and fluid inclusion studies have shown that boiling is a very important process for ore deposition in epithermal systems. It must be remembered, however, that fluid mixing is also an important process for the deposition of ore minerals. Boiling temperatures increase with salinity and decrease with increasing concentration of volatiles in the fluid. The important effects of boiling are the partitioning of volatiles (CO_2, H_2S, SO_2, CH_4 etc.) into the vapour phase. The release of CO_2 causes a rise of the pH in the remaining solutions, while their salinity increase as a result of H_2O steam loss. Loss of H_2S destabilises sulphide complexes and changes the oxidation state of the remaining liquid, as for example:

$$H_2S(aq) \rightarrow H_2S(g) \text{ and } Me(HS)_3 \rightarrow MeS + HS^- + H_2S(g);$$

where MeS is metal sulphide.

Oxidation processes involve the following reactions (Barnes 1990):

$$2HS^- + 2O_2 \rightarrow H_2S + SO_4^{2-};$$
$$H_2S + 2O_2 \rightarrow 2H^+ + SO_4^{2-};$$
$$HS^- + 2O_2 \rightarrow H^+ + SO_4^{2-};$$
$$Me(HS)_3^- + 4O_2 \rightarrow MeS + 3H^+ + 2SO_4^{2-}.$$

The pH increase associated with loss of CO_2 results in the decrease in the concentration of metals, therefore boiling and pH changes are effective depositing mechanism for chloride-complexed metals which are subsequently deposited as mineral phases, while metals that are sulphide-complexed are deposited as native metals (Cole and Drummond 1986). Transport of Au and Ag in hydrothermal solutions occurs dominantly as chloride and sulphide complexes. In epithermal systems Au is transported in the $+1$ and $+3$ states as either chloride or bisulphide complexes. Complexing reactions for Au in the $+1$ state are (Seward 1979):

$$Au^+ + H^+ + 2Cl^- \rightarrow AuCl_2^- + 0.5H_2;$$
$$Au^+ + H_2S + HS^- \rightarrow Au(HS)_2^- + 0.5H_2;$$

Loss of H_2S during boiling, results in increased activity of S^{2-} and HS^- in the remaining solutions, which in turn leads to more dissolution of Au and its transport in solution by sulphide complexing. A reaction that promotes gold deposition by boiling is of the type:

$$Au(HS)_2^- + H^+ + 0.5H_2 \rightarrow Au + 2H_2S$$

The continuing oxidation of H_2S meanwhile forms H_2SO_4 which attacks alumino-silicates (acid-leaching), releasing electrons into the system which destabilise the sulphide complex (e.g. Au^+ gains electrons), according to the reaction shown below:

$$Au(HS)_2^- \rightarrow Au^0 + 2HS^-$$

The cycle discussed above is schematically illustrated in Fig. 5.26. In epithermal systems Ag is transported in the +1 state as a chloride complex (AgCl-2) and is deposited either as Ag^0 or as a sulphide. The ratios of Ag/Au are important in determining the type of dominant complexing and the expected nature of the epithermal system (Cole and Drummond 1986). Thus, systems with Ag/Au ratios less or equal to 1 tend to be dominated by native Au and electrum, sulphide complexing of Au is dominant, and temperatures are less than 250°C. Systems where Ag/Au ratios are greater than 1 are characterised by argentite, base metal sulphides, sulphosalts, and electrum, with only minor Au. In this case chloride complexing is dominant and the temperatures are greater than 250°C. In summary, precipitation of Au takes place in response to changes in temperature, pressure, pH, Eh and the activity of reduced S. It is possible that the same type of complexing may also be prevalent for other metals such as As, Sb and Hg. Chloride complexing is also important for Ag and base metals (Pb, Zn, Cu) in higher temperature regions. Figure 5.27 illustrates the dominant conditions in which Au and Ag

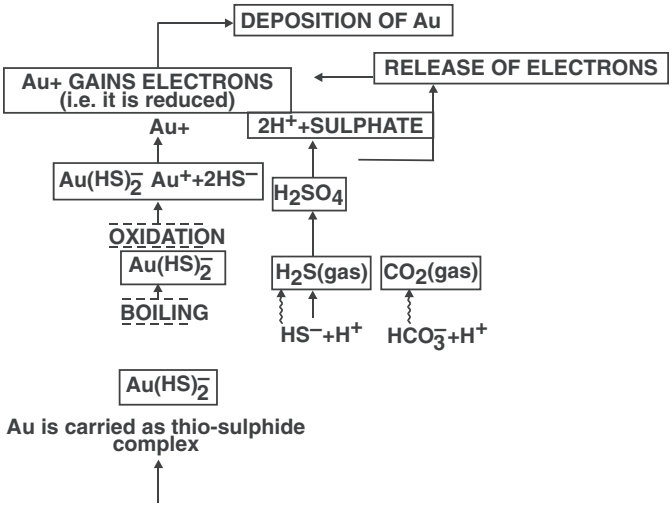


Fig. 5.26 Schematic sequence showing the breakdown of Au-carrying thiosulphide complexes. After Pirajno (1992)

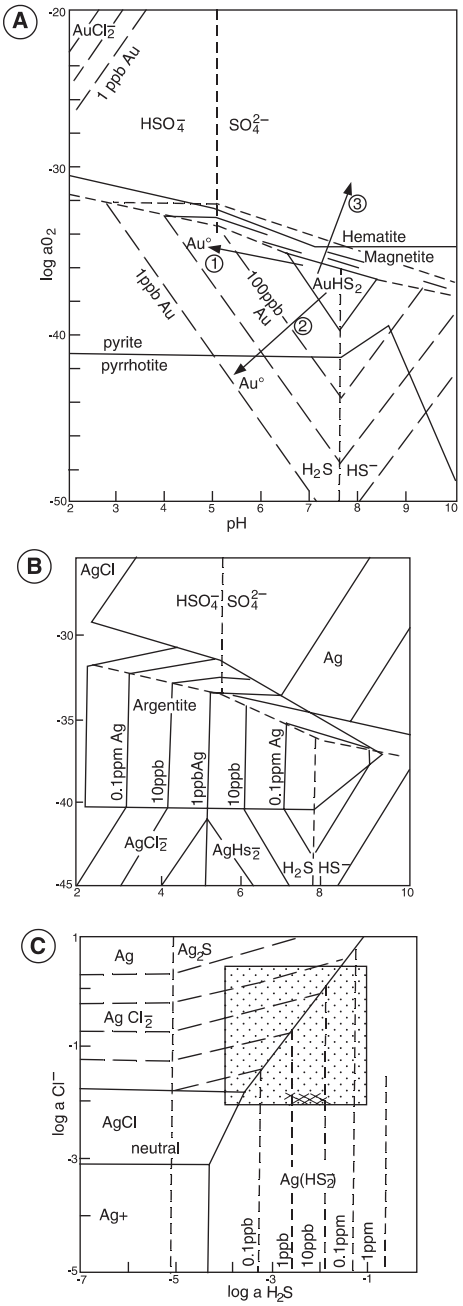


Fig. 5.27 Phase diagrams of dominant chemical conditions (oxidation state, pH, S and Cl activities) for the transport of Au and Ag in hydrothermal systems. (**A**) Diagram constructed at 250°C, total sulphur activity = 0.01 m and total chloride activity = 0.1 m, corresponding to a salinity of about 2 wt% NaCl equivalent. Note that the highest solubility of Au is attained by $Au(HS)^{2-}$ complexing in the stability field of pyrite and at pH values between 7 and 8; Au is also soluble as $AuCl^{2-}$ but at high O_2 fugacity (hematite stability field) (after Shenberger and Barnes 1989). (**B**) Solubility of Ag at 250°C, as a function of pH and oxidation state, total sulphur and chloride activities as at (**A**); minimum solubility is at pH 5 at the boundary between chloride (lower pH) and sulphide complexes (higher pH), also note that the maximum solubility field is in equilibrium with the argentite (Ag_2S) field (after Gammons and Barnes 1989). (**C**) Silver solubility at 250°C, pH = 6, as a function of chloride and H_2S activities, whose limits in natural systems are indicated by the shaded area; the cross-hatched field indicates the range for epithermal deposits; note that native Ag and argentite can precipitate at high chloride activity (upper left corner of diagram) (After Gammons and Barnes 1989)

are transported. The diagrams were constructed for a temperature of 250°C, considering S and Cl activities that best approximate natural conditions in geothermal systems (Gammons and Barnes 1989; Shenberger and Barnes 1989). It can be seen from Fig. 5.27 that Au is highly soluble as $AuCl_{2-}$ when in equilibrium with hematite, and that the $Au(HS)_{2-}$ complex is stable under alkaline conditions, however, a drop in pH (arrow 1), or in O_2 (arrow 2), will cause destabilisation and Au precipitation. In this diagram it is also important to note that the highest solubility field for Au coincides with the stability field of pyrite, indicating that this metal is transported in equilibrium with pyrite. This is corroborated by the observed common association in nature of pyrite and Au (Shenberger and Barnes 1989). Consequently, precipitation of Au may occur by mixing of a reduced fluid with oxygenated waters (i.e. meteoric), or with any other oxidised environment. Au deposition by oxidation is given by:

$$2Au(HS)_2^- + H_2O + 7.5O_2 \rightarrow 2Au + 6H^+ + 4SO_4^{2-}.$$

Reduction, on the other hand, may take place if the fluid interacts with graphite- or organic material-bearing rocks. As mentioned earlier, another cause of Au precipitation is a reduction in the activity of the S species in the system due, for example, to boiling and/or precipitation of sulphide minerals (Shenberger and Barnes 1989). At 100°C the stability field of $Au(HS)^-_2$ is much smaller than that shown in Fig. 5.27 for 250°C, which implies that the solubility of the metal is reduced, and hence precipitation may also take place during cooling of the solution. The phase diagrams shown in Fig. 5.27 refer to the stability conditions of Ag as a function of pH, the activities of Cl and S, and oxidation state, at a temperature of 250°C. In Fig. 5.27 it is seen that in high oxidation states and low pH, chloride complexing is dominant, and that $Ag(HS)_{2-}$ is stable under more reducing conditions and pH values ranging from near-neutral to alkaline (Gammons and Barnes 1989). Figure 5.27 shows that the predominance of chloride versus sulphide complexing depends on the relative activities (and hence concentrations) of Cl and S species in the system. The shaded area illustrates the likely field for natural ore solutions (Gammons and Barnes 1989).

5.3.1.5.1 Boiling Depths, Mineral and Metal Zoning

In this section I discuss the effects of boiling in terms of Ag/Au ratios and related metal zoning, following the theoretical modelling carried out by Cole and Drummond (1986), who assume a constant pressure gradient of 175 bar per 1 km of depth. Boiling is dictated by the initial temperature, salinity, volatile concentration and pH. Their calculations show that an Au ore grade of 30 g/t requires "10^6 m of boiling solution" for a system with 10% porosity, densities of 1.0 and 2.7 g/cm^3, for solution and rock, respectively, and an Au enrichment

of 1 ppb/m of boiling solution. Thus, if the flow path to the point of deposition is 1 km, it would require 1000 cycles of fluid turnover associated with the boiling process to produce the above tenors of Au mineralisation. However, if boiling is violent as in a hydrothermal eruption, then metal deposition would occur instantly on a small volume of rock. The depth of boiling becomes shallower with either decreasing temperature and/or CO_2 concentration for a given salinity. For example at a content of tot CO_2 of 1 mol, salinity of 1 mol, initial boiling depth is 1050 m at 300°C, 930 m at 250°C and 850 m at 200°C, assuming a constant pressure gradient of 175 bar/km. If, on the other hand, tot CO_2 is lowered, the fluid pressure is also lowered and the depth of boiling decreased. Thus, for example, for a solution at 250°C, pH = 5, salinity 1 mol and total CO_2 of 0.1 mol, the boiling depth is 290 m. The important point to consider here, as a result of these calculations, is that there is a general increase in the rate of Au and Ag deposition towards the top of the boiling interval, and this coincides with a change in Au complexing from chloride to sulphide. The result is the well-known metal zoning of epithermal systems. The modelling results of Cole and Drummond show that boiling systems with low CO_2 exhibit mineralisation along a narrow vertical interval, but with high Ag and Au grades and small alteration haloes, because of the lower volatile concentrations and therefore less acid leaching. Thus, the relationships of vertical ore extent, CO_2 and grade show a distinct zoning pattern: a zone of precious metals above a zone of base metal sulphides, which is consistent with observations. Above the zone of precious metal deposition the exsolved gases (CO_2 and H_2S) and H_2O vapour either continues to rise and emerge out of the system as hot springs and/or fumaroles, or they condense and mix with groundwaters. Silica deposited by the boiling solutions occurs above the mineralised intervals to form the surface sinter deposits.

Henley and Ellis (1983) reported on mineral zoning with increasing temperature. They quoted an example of the alteration of volcanic glass which, with increasing temperature, is altered to opal, smectite, calcite and zeolite to mixed layer clays. The composition of zeolite minerals is affected by successively high temperature, from heulandite at about 100°C, through laumontite (150–200°C) to wairakite (up to 300°C). The temperature range of hydrothermal minerals is shown in Fig. 5.28A. Bird et al. (1984) have shown that mineral zoning with increasing temperature and depth reflect progressive dehydration of calc-silicate minerals, whereby the amount of zeolitic and structural water in the calc-silicate assemblages decreases. These authors found systematic changes in the mineralogy and texture of deltaic sediments (Cerro Prieto and Salton Sea, see Section 5.4.5) which have interacted with geothermal fluid. In order of increasing depth and temperature the following zones occur: (1) montmorillonite + kaolinite (150°C); (2) illite + chlorite zone (150–180°C to 230–250°); (3) calc-silicate zone with epidote, prehnite, actinolite, Ca-pyroxene (230–250°C to > 350°C); (4) biotite zone (325–350°C). The geometry and boundaries of the alteration zones closely follow the configurations of the isotherms of the geothermal system, and the general zoning patterns are similar to those that

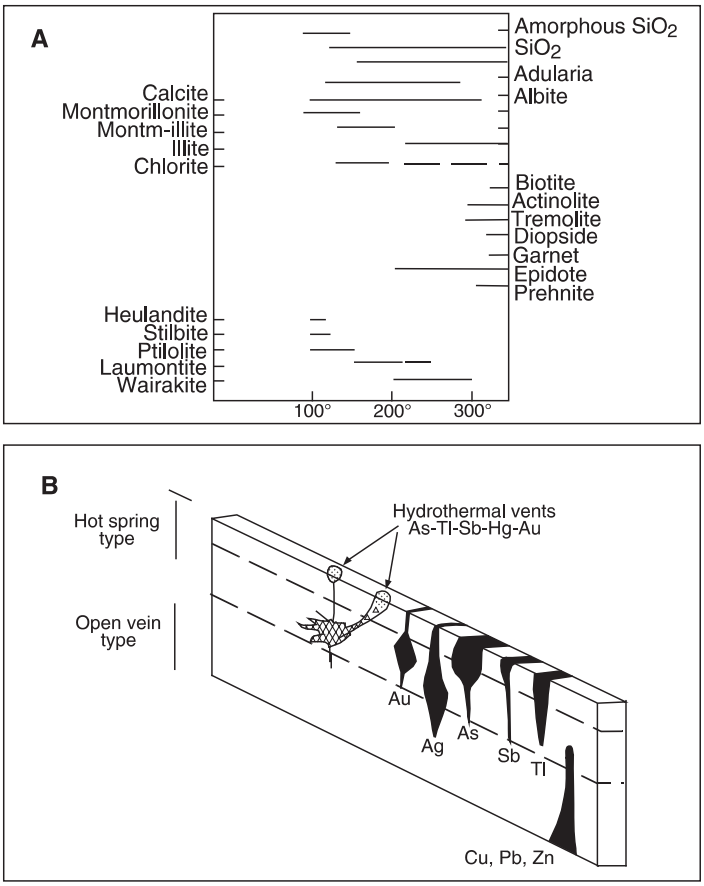


Fig. 5.28 (**A**) Temperature range of alteration minerals in epithermal systems. After Henley and Ellis (1983); (**B**) Schematic representation of metal zoning in epithermal systems. After Berger and Eimon (1982)

form in low-pressure contact metamorphic rocks (Bird et al. 1984). Epithermal deposits display characteristic metal zoning with depth. Base metal sulphides (Cu, Pb and Zn) in the deeper parts of the system grade upward to zones containing Au–Ag at or near the surface As–Sb–Hg–Tl, as previously indicated (Figs. 5.22 and 5.25). Figure 5.28B shows a typical metal zonation in epithermal systems.

5.3.1.6 Stable Isotope Systematics

Hydrothermal activity that produces epithermal deposits is ultimately driven by magmas and the sources of the circulating fluids are the magmas themselves, meteoric water and connate waters from the lithologies with which the magmas

interact. Stable isotopes facilitate the tracing of the source of water in hydrothermal systems. Figure 5.29 shows the O and D composition and variation of crustal waters, such as mid-ocean ridge, continental and oceanic volcanic arcs and water of porphyry and epithermal hydrothermal systems, relative to Standard Mean Ocean Water (SMOW; see Chapter 1). With reference to Fig. 5.29A, felsic magmas in continental crust have higher H isotopic ratios

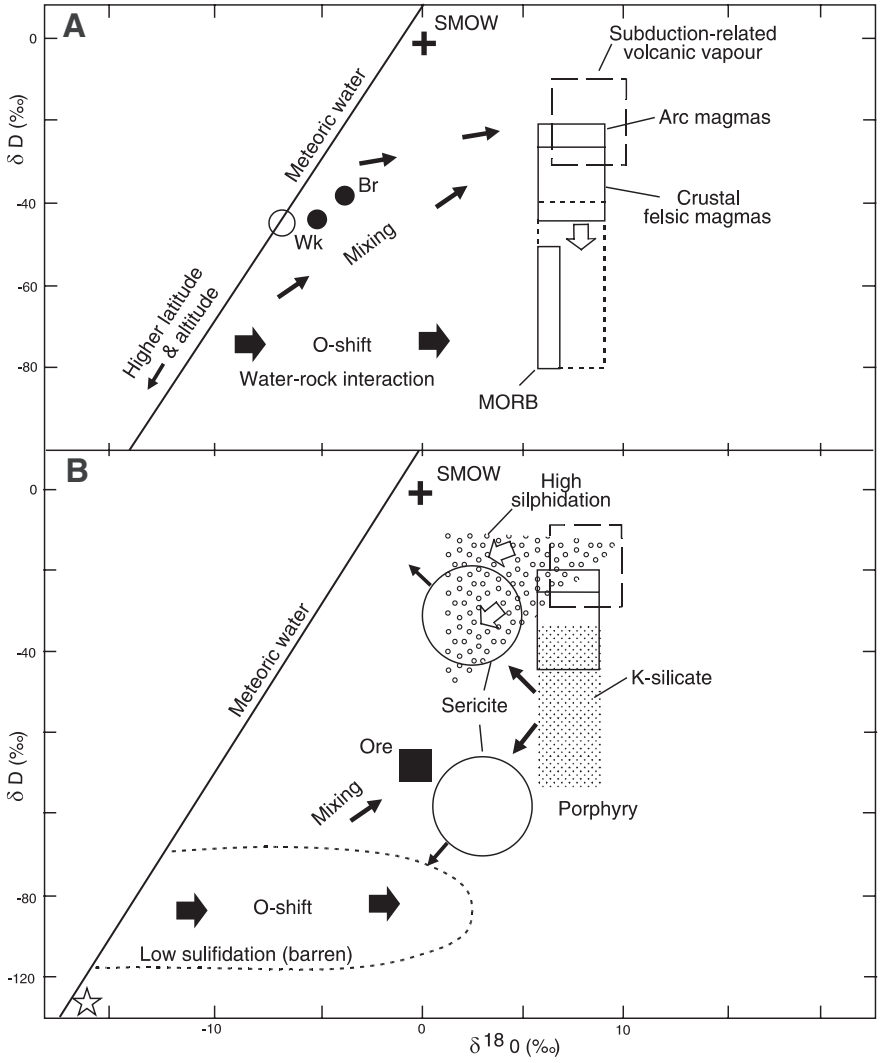


Fig. 5.29 Variations and trends of δO and δD values of magmas and hydrothermal fluids of porphyry and epithermal systems; (**A**) Crustal fluids; (**B**) Ore-related fluids. Details in text. After Hedenquist and Lowenstern (1994) and Hedenquist (1997)

than those of island arcs, probably because of contamination from crustal materials. The isotopic fingerprint of vapours outgassed from arc volcanoes have a fairly narrow range, partly overlapping with arc magmas, but clearly enriched with respect to the latter, due to fractionation during degassing, while at the same time the degassed residual melt attains lighter δD values (Hedenquist and Lowenstern 1994; Hedenquist 1997). Note the composition of the Wairakei geothermal waters (Taupo geothermal field, New Zealand), which plot close to the meteoric line. The stable isotopic composition of fluids from porphyry and epithermal systems (Fig. 5.29B) can be monitored from the composition of the high temperature K-silicate alteration minerals, from which two distinct O–D spaces for the lower temperature sericitic alteration relate to a mix of magmatic and meteoric water, which is latitude and altitude dependent. High sulphidation waters have a O–D isotopic composition similar to that of volcanic vapours, because advanced argillic alteration is a product of the condensation of volcanic gases. Barren quartz low sulphidation systems show a strong shift of the δO values towards the meteoric water line, whereas high-grade ore shown by the square in Fig. 5.29B shows a shift in the opposite direction due to magmatic fluids (Hedenquist 1997).

5.3.2 Ladolam Epithermal System, Lihir Island, Papua New Guinea

Lihir Island is one of the volcanic islands of the New Ireland province, where a number of shoshonitic alkaline volcanoes were formed during the Miocene to Recent, as a result of a southwest subducting oceanic plate (Figs. 5.7 and 5.30). Lihir is part of the Tabar to Feni group of Pliocene-Pleistocene volcanic islands which lies some 50 km northeast of New Ireland. A large low-sulphidation epithermal Au deposit was first discovered in 1982 on coastal bluffs along the eastern side of the island. A detailed drilling programme was implemented soon after, and subsequently, an open-cutable Au deposit, called Ladolam, was outlined with total reserves of oxide and sulphide ore of approximately 173 Mt, grading between 2 and 3.5 g/t Au. Total resources, including past production, are estimated at 442 Mt grading 3.14 g/t Au (Laznicka 2006). Ladolam is quite unique because it is, not only one of the giant Au deposits in the world, but is also an operating mine established on an active hydrothermal system, with hot springs in Luise Harbour currently venting and depositing sulphides and gold. For this reason, the deposit is of considerable interest and has attracted the attention of many researchers (e. g. Davies and Ballantyne 1987, Plimer et al. 1988, Moyle et al. 1990, Müller et al. 2002, Carman 2003), Simmons and Brown 2006). On Lihir Island five volcanic centres are recognised: Wurtol, Londolovit, Kinami, Huniho and Luise, all of which were built on older basaltic volcanic rocks. The Luise volcano hosts the Ladolam deposit and is characterised by an elliptical crater open to the sea, forming the Luise

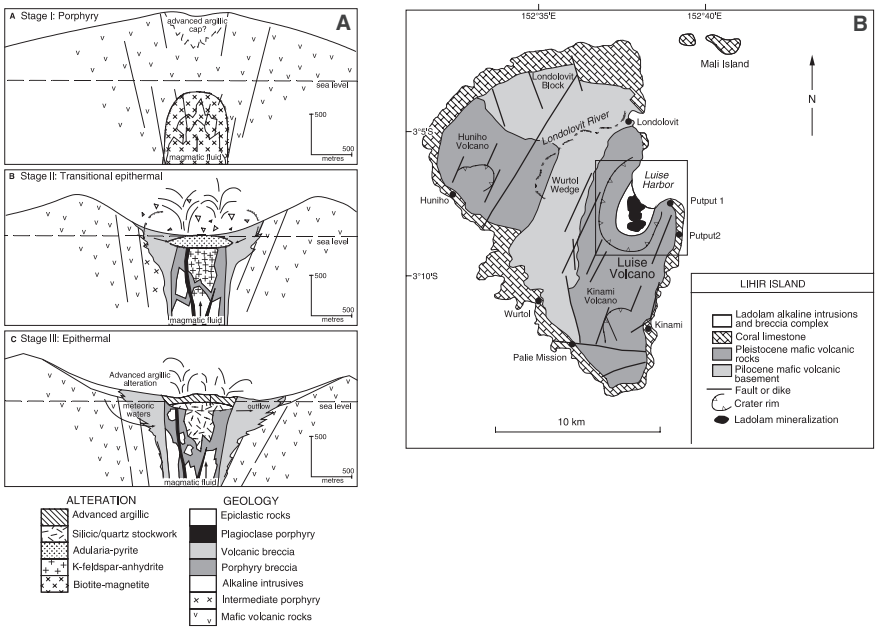


Fig. 5.30 (**A**) Schematic model showing the hydrological evolution of the Ladolam system; (**B**) Simplified geology of Lihir Island and position of the orebodies. After Carman (2003)

Harbour. About 10 km south of Lihir Island is Conical Seamount, a shallow (~1050 m water depth) submarine basaltic volcanic construct. This is also mineralised with Au, Zn, Pb and Ag and I return to mention Conical Seamount in Chapter 7 as a possible transitional system to volcanic-hosted massive sulphide deposits. The following description of the Ladolam deposit is taken from Carman (2003).

The Luise stratovolcano is characterised by an elliptical crater, measuring about 5.5 x 3.5 km, in which the northeastern margin has collapsed into the sea, due to slope failure of the original volcanic edifice. This led to a sudden pressure release and the formation of hydraulic breccias saturated with hydrothermal fluids. Rock types at Ladolam comprise three main units, from oldest to youngest, they are: mafic volcanic rocks, alkaline rocks and the Ladolam breccia complex. The mafic volcanic rocks form the flanks of the Luise stratovolcano and consist of alkali basalt trachybasalt, trachyandesite, trachyte and phonolite lavas interbedded with minor volcaniclastic rocks. Alkaline intrusions comprise a series of leucogabbro, monzonite, diorite and syenite stocks, all of which are overprinted to varying degrees by brecciation and alteration. The Ladolam breccia complex is a 3 km-diameter pipe-like body that crosscuts the alkaline intrusions and is associated with the mineralisation. The breccia pipe is partially submerged at its northeastern end and has in its central parts a number of vent breccias and hydrothermal pipes. The orebodies within these breccias are called

Lienetz (north), Minifie (south), Kapit and Coastal. The breccia complex consists of two types, referred to as porphyry breccia and volcanic breccia. The former is poorly sorted and contains fragments and clasts of biotite-altered alkaline intrusions in a rock-flour matrix that consists of anhydrite, K-feldspar and minor biotite matrix. Locally, a monomictic porphyry breccia consists of a crackle-brecciated monzonite with clasts supported by anhydrite cement. A polymictic porphyry breccia contains clasts of monzonitic rocks again in anhydrite cement. The anhydrite exhibits pronounced subhorizontal layering. The volcanic breccia is the most widespread, forming a shell around the porphyry breccia and the alkaline intrusions, and contains angular clasts of volcanic rocks up to several metres across. It is poorly sorted and matrix supported. The matrix is rock flour altered to carbonate and chlorite. Fluidised vertical structures are also present. An interesting aspect of the volcanic breccia is that some clasts exhibit veinlets that do not extend into the matrix, thus indicating a pre-breccia hydrothermal event. The Au ore at Minifie is in a vent phreatomagmatic breccia, grading downward into the porphyry breccia. At Lienetz there is a subhorizontal silicic breccia, thought to have formed by silica replacement of anhydrite. The Ladolam breccias are interpreted to represent the upper parts of a volcanic-hydrothermal diatreme complex that developed within the Luise crater following its collapse, which probably triggered violent gas exsolution due to the sudden pressure drop.

At Ladolam, porphyry and epithermal alteration-mineralisation are present and overprint an older porphyry system. The ore mineralogy of the Ladolam deposit is dominated by pyrite and marcasite, occurring as disseminations and veinlets. Other, but minor, ore minerals include magnetite, rutile, chalcopyrite, pyrrhotite, galena, sphalerite, covellite and arsenopyrite. A little molybdenite is present in the zone of potassic alteration. Sulphosalts are also present and are represented by tetrahedrite, tennantite, luzonite, and enargite. Golc occurs as particles included in pyrite, chalcopyrite and arsenopyrite. Free Au is present in the oxide ore.

Five key hydrothermal assemblages are present, which from oldest to youngest are: potassic (stage 1), propylitic and adularia (stage 2), silicic and advanced argillic (stage 3). The adularia and silicic assemblages (stages 2 and 3) are part of the epithermal system and overprint the porphyry assemblages (stage 1). The Minifie orebody is associated with the adularia alteration, whereas the Lienetz orebody is associated with the silicic alteration. Potassic alteration is dominantly biotite, which is generally confined to the alkaline intrusive stocks and is locally pervasive; orthoclase±albite occur as replacement of the plagioclase, with minor muscovite, tremolite, chlorite, tourmaline, magnetite and apatite. Stage 1 veins are relicts of a porphyry system and occur in fragments of the porphyry breccia and consist of phlogopitic biotite-K-feldspar-anhydrite ± magnetite ± tremolite ± pyrite ± chalcopyrite ± molybdenite. Propylitic alteration (stage 2) is transitional to the epithermal stage, is most extensive and consists of chlorite-calcite-albite-K-feldspar-K-mica-actinolite-pyrite-rutile ± epidote ± phlogopite. This alteration surrounds the biotite-altered intrusions

at Lienetz. Adularia alteration (stage 2) is characterised by two assemblages. One is adularia-anhydrite-pyrite-rutile-illite-vernmiculite and does not carry Au. The other is at a shallower depth, is sulphide rich and consists of adularia-pyrite-leucoxene-illite and forms most of the Minifie orebody. Anhydrite-bearing assemblages change upward to pervasive adularia-pyrite alteration and are associated with high Au grades. Stage 2 veins and breccia cavity fillings consist of anhydrite-adularia-pyrite-vermiculite with minor sphalerite, galena, pyrrhotite, chalcopyrite and molybdenite. Again anhydrite is the most abundant alteration phase. In ore-related breccias, adularia-pyrite alteration is intense and pervasively replaces all previous primary and alteration minerals. Silicic alteration (stage 3) comprises quartz-mixed layer clays-pyrite-leucoxene ± adularia ± calcite; the associated quartz and calcite stokworks and veins, exhibiting typical epithermal textures, such as colloform banding. Quartz-sulphide ± barite ± celestine veins are present at Lienetz and are associated with high grade Au mineralisation. Gold occurs as electrum and is associated with pyrite and marcasite. Silicic breccias are tabular in shape and form an important ore component at Lienetz. Advanced argillic alteration is barren of Au (stage 3) is of steam-heated origin and consists of kaolinite-smectite-pyrite ± marcasites ± alunite and is the youngest alteration evemt at Ladolam. Advanced argillic alteration forms a cap that is locally up to 200 m thick.

K–Ar and Ar–Ar age determinations of altered intrusions yielded ages ranging from ~0.9 to 0.34 Ma. Adularia samples returned ages of ~0.61 to 0.52 Ma and an alunite-rich sample gave an age of 0.15 Ma.

5.3.2.1 Fluid Inclusions and Isotopic Data of the Ladolam System

Fluid inclusion studies recognised (primary and pseudosecondary): type 1 multiphase inclusions (L + V + S), where S = halite and daughter minerals; type 2 (L + V + S), where S = hematite ± pyrite; type 3 two phase liquid rich (L + V); type 4, also two phase vapour rich (V + L). Homogenisation temperatures (T_h) for stage 2 types 2 and 3 inclusions from Minifie range from 180 to 320°C, with salinities from 1 to 22 wt% NaCl equivalent; from Lienetz T_h ranges from 100 to 300°C with salinities from 1 to 15 wt% NaCl equivalent. Fluid inclusions in stage 3 veins have T_h ranging from 150 to 250°C with corresponding salinities of 1.7 to 7.8 wt% NaCl equivalent. Stage 2 and 3 salinity and T_h exhibit a wide spread, interpreted by Carman (2003) as due to open system boiling. Stage 3 T_h-salinity data indicate a mixing trend of moderate salinity (5–0.5 wt%) and temperature (~230°C) with dilute water at 170°C.

Stable isotope data reported by Carman (2003) include S, O–D and C. The $\delta^{34}S$ values of sulphides from stage 1 veins range from –1.4 to +2.2‰, from stage 2 pyrite from +0.6 to +1.8‰, and –5.3 to +0.4‰ for pyrite and pyrrhotite. Pyrite from Minifie returned $\delta^{34}S$ values of –7.1 to +1.7‰. Stage 3 sulphides from the Au ore returned values of –12.9 to –1.8‰ and marcasite and pyrite from the argillic zone gave –13 to –3.4‰. Anhydrite veins

have $\delta^{34}S$ values of about 13‰. The early-formed sulphides have $\delta^{34}S$ values near 0‰, suggesting a magmatic origin. The shift of $\delta^{34}S$ to lighter values in auriferous sulphides suggests a change in depositional conditions interpreted to represent the effects of boiling and ^{34}S partitioning into aqueous sulphate, leaving behind a lighter component in the residual liquid phase from which sulphides precipitated. It is of interest to note that Carman (2003) pointed out that the S isotopic data indicate that there was no involvement of seawater sulphate and therefore seawater could have been present only in the uppermost parts of the Ladolam hydrothermal system. The light $\delta^{34}S$ values from stage 3 sulphides in the tabular silicic and advanced argillic ore zones are explained by increasing oxidation due to boiling fluids. The silicic ores are interpreted as having formed by mixing of rising fluids with descending steam-heated acid-sulphate waters (Plimer et al. 1988). This mixing model is confirmed by Carman's work.

Whole rock $\delta^{18}O$ values of propylitic altered rocks gave $+7.9$‰, whereas igneous and hydrothermal biotite gave values of $+5.6$ and 6.2‰. Adularia returned $\delta^{18}O$ values ranging from $+8.1$ to $+13.6$. Calcite samples gave $\delta^{18}O$ and $\delta^{13}C$ values ranging from $+9.9$ to $+19.1$‰ and -5.2 to $+3.3$‰, respectively. Temperatures estimated from $\delta^{18}O$ of water in equilibrium with biotites, using mineral-water fractionation factors range from 600 to 500°C. Oxygen and C isotope systematics, together with fluid inclusion data, seem to indicate mixing of a magmatic fluid with water of meteoric origin and not seawater. The O–D isotopic compositions, together with pH and temperature, of the modern deep geothermal fluids and hot springs at Ladolam were also determined. The $\delta^{18}O$ and δD values range from -6.0 to $+7.4$‰ and -40.6 to -6.5‰, respectively (local seawater gave $+0.4$‰ $\delta^{18}O$ and -1.4‰ δD). The deep geothermal fluids are neutral pH, Na chloride-sulphate brines with a salinity of ~5.5 wt% NaCl equivalent. Active thermal acid-sulphate springs present in the Luise caldera, have a pH of 1–2 and contain CO_2, N_2, O_2, H_2S and H_2. Sinter deposits are formed from these springs and consist of opaline silica-kaolinite-alunite-native S-marcasite. Sinter material precipitated from near-neutral chloride springs consists of pyrite-opaline silica. Analyses of fluid samples revealed an Au content less than 1.5 ppb, while scales from pipes assayed up to 2.8 ppm Au.

5.3.2.2 Ore Genesis and Au Deposition

Moyle et al. (1990) regarded the Ladolam mineralisation as a volcanic-hosted epithermal deposit sharing the characteristics of both acid sulphate and adularia-sericite type. They suggested that the Au mineralisation was formed by the circulation of large volumes of S-rich neutral chloride fluids, which on boiling exsolved H_2S and deposited Au. The evolution of the system comprises three stages. In the first stage the Luise stratovolcano was intruded by alkaline stocks whic caused the formation of porphyry-type hydrothermal alteration with weak Cu–Mo ± Au mineralisation. Stage two was characterised by the formation of the caldera structure (possibly due to an explosive event) and the

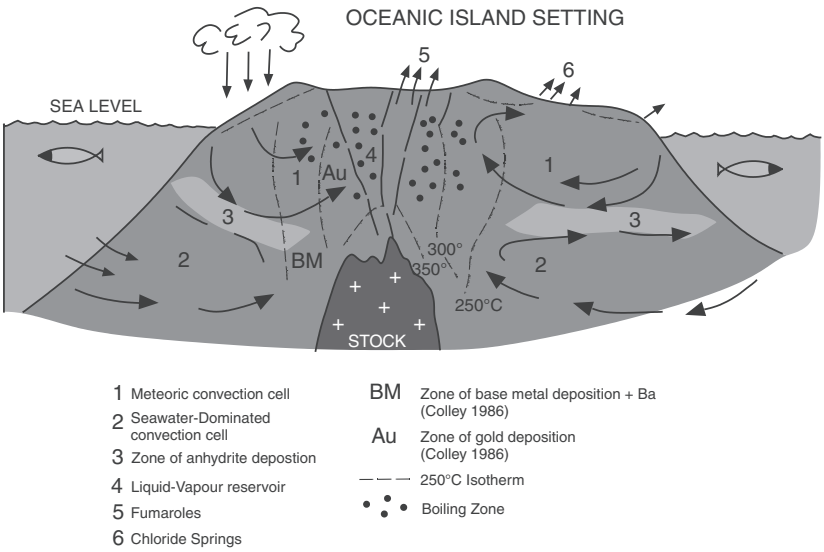


Fig. 5.31 Hydrothermal systems generated in a volcanic island, such as Lihir. After Pirajno (1992), based on Bogie and Lawless (1987)

anhydrite-calcite breccia. The sudden release of pressure caused by the caldera-forming event caused boiling of the fluids and precipitation of Au. Breaching of the caldera by sea water resulted in the cementing of the brecciated rocks by anhydrite and calcite. The main geothermal system was developed during stage three as a result of sealing of the breccia from the sea, so that recharge of the system was mainly by meteoric waters. The geothermal system thus formed resulted in the dissolution of the anhydrite-calcite stockwork, increasing permeability and continued hot spring activity with boiling and Au precipitation. The final present-day scenario is that of a roughly layered system constituted, from top to bottom, by zones of advanced argillic, argillic, phyllic alteration overlying a zone of epithermal veins and stockworks consisting of quartz-calcite-adularia-illite and sulphides formed associated with repeated pulses of hydrothermal brecciation, above a porhyry-style zone of potassic alteration. Boiling probably caused Au deposition with a reaction of the type, shown above in Section 5.3.1.5.

The entire epithermal system to the top of the porphyry zone is approximately 200 m thick. The subhorizontal geometry of the anhydrite ore body is attributed to the interaction between a hot magmatic fluid and cool surficial meteoric and/or seawater (Carman 2003). The discharge of hot springs in the Coastal area and the Luise harbour is the result of upwelling sulphate-chloride, neutral pH brines of magmatic origin mixing with meteoric waters in the upper parts of the system.

Simmons and Brown (2006) sampled the deep geothermal brines in wells that penetrate beneath the Lienetz orebody and were able to determine the flux rate

of Au in the system. These authors reported that the Ladolam active hydrothermal system has an estimated heat flux of 50–70 MW with hot water rising at a rate of ~50 kgs^{-1}, with a Au flux estimated at 24 kg/year. On the basis of this estimates and assuming constant Au concentration, fluid flow and 100% depositional rate, it is suggested that about 55 000 years would be required to account for the known Au in the Ladolam orebodies. This flux is less than that estimated at White Island in New Zealand with 37 kg/year and at Mount Etna with a staggering 80–1200 kg/year (Simmons and Brown 2006 and references therein). These authors pointed out that the deep Ladolam geothermal system is capable of forming a giant Au deposit in a geologically very short time span. A model depicting the evolution of the Ladolam porphyry-epithermal systems in shown in Figs. 5.30 and 5.31 illustrates the type of hydrothermal system that may develop in an oceanic island, such as Lihir.

5.3.3 Hauraki Goldfield, Coromandel Peninsula, New Zealand

A number of porphyry and epithermal precious and base metal deposits, as well as porphyry deposits are distributed across the Coromandel peninsula (North Island, New Zealand) for a total distance of approximately 200 km (Fig. 5.32). The Coromandel peninsula is bounded to the west by a graben structure (Hauraki rift) filled with sediments and volcanics of Quaternary age. An excellent account, both historical and geological, on the geology, mineralisation of the Hauraki Goldfield in the Coromandel Volcanic Zone and of individual deposits can be found in Williams (1974). Other important works on the mineral deposits include Kear (1989), Brathwaite et al. (1989), Brathwaite and Pirajno (1993), the recent monograph edited by Christie and Brathwaite (2006) and Christie et al. (2007).

The Coromandel Volcanic Zone (CVZ) is one of several magmatic arcs of Miocene age (~15–6 Ma) that characterise the northern and central parts of the North Island, and was formed during stages of subduction between the Pacific plate in the east and the Indian plate in the west. The CVZ consists of a thick pile of felsic-intermediate volcanic, associated pyroclastic and intrusive rocks of calc-alkaline affinity, which were emplaced on a faulted basement of Jurassic greywackes and argillites of the Manaia Hill Group. The volcanic succession of the CVZ comprises the Coromandel Group, divided into the Waiwawa and Kuaotunu Subgroups, of Lower Miocene to Lower Pliocene age, including dioritic intrusives, andesitic and dacitic volcanics, and porphyry dykes. These are overlain by, but locally overlap in time with, rocks of the Whitianga Group of Upper Miocene to Pliocene age, comprising predominantly ignimbrites, dome-forming rhyolites, and various pyroclastics and sediments. At least five major caldera structures have been recognised in the CVZ and one of these is the Waihi caldera (Fig. 5.32), which contains the Martha Hill Au–Ag epithermal vein deposit, discussed below. The regional and dominant trend of the Peninsula is north-northwest, with main fault directions along northeast and northwest trends.

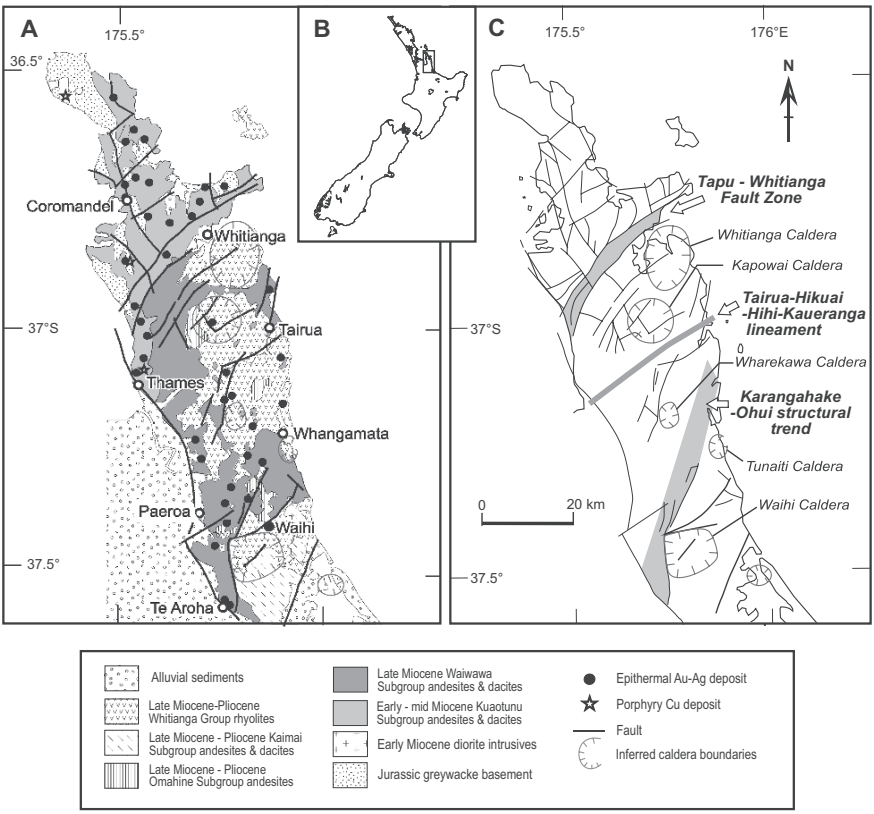


Fig. 5.32 (**A**) Simplified geology of the Coromandel peninsula, North Island, New Zealand (see inset) and distribution of porphyry and epithermal mineral systems; (**B**) main structures and calderas. After Christie et al. (2006); figure reproduced unchanged by permission of the authors and The Australasian Institute of Mining and Metallurgy

5.3.3.1 Hauraki Epithermal Systems

The mineralisation of the CVZ comprises about 50 low-sulphidation (adularia-sericite) epithermal Au–Ag vein deposits and porphyry Cu deposits. The epithermal deposits of the Hauraki field have produced 320 000 kg of Au and 1.5 million kg of Ag since 1862 (Christie et al. 2007). The mineral systems in the Hauraki field are distributed in two K–Ar and Ar–Ar age groups: a northern province with ages ranging from 16 to 10 Ma and a southern province with ages between 7 and 5.7 Ma (Christie et al. 2006). The porphyry mineralisation is the oldest (∼16 Ma) and can be found in the Great Barrier Island, at Paritu almost on the northernmost tip of the Coromandel peninsula, and further south near Thames on the western side of the peninsula (Fig. 5.32). This porphyry mineralisation is associated with quartz-diorite and granodiorite dykes and stocks which have been exposed owing to uplift and erosion along the western part of the Hauraki region. Copper mineralisation consists of chalcopyrite and pyrite

disseminations and veinlets, locally forming stockworks. Molybdenite and wolframite may occur as minor ore constituents. Near the town of Thames, the Ohio Creek Cu–Mo–Au mineralisation is hosted in a dacite porphyry stock, with zones of potassic alteration overprinted by argillic assemblages and an upper part of the argillic zone overprinted by a core of quartz-aunite-dickite, surrounded by pyrophyllite-diaspore-dickite-kaolinite assemblage (Christie et al. 2006). This very interesting spatial association between a typically porphyry alteration assemblage with acid-sulphate or high-sulphidation alteration zones at Ohio Creek are part of the same hydrothermal systems and represent the spatial and genetic porphyry-epithermal link (see Fig. 5.4). At Paritu, quartz-diorite and granodiorite plutons which have intruded rocks of the basement are accompanied by numerous cogenetic dykes. Hydrothermal alteration is locally pervasive and includes propylitisation, silicification and chloritisation of both intrusive and country rocks. The porphyry system in the Great Barrier island is located in the north (Miner's Head) where basement rocks consisting of highly contorted greywacke and argillite have been intruded by small stocks and dykes of intermediate to acid composition. The mineralisation, which was known since 1837, and hosted in brecciated greywacke adjacent to a dacitic stock, consists of pockets and veinlets of pyrite and chalcopyrite. During the period between 1857 and 1867 some 50 000 tonnes of ore were worked giving 2300 tonnes of hand-picked ore assaying 15% Cu. The Hauraki Goldfield has been a target of exploration and mining since the 1850s and to this day remains the most mineral rich region in New Zealand, with an historical production of more than 320 000 kg of Au and 1.5 million kg of Ag (Christie et al. 2006). Figure 5.33 shows groupings of the Coromandel epithermal systems, characterised by a collection of similar features. Apart from the world class Martha Hill, other economically important epithermal systems in the Hauraki field include Ohui, Broken Hills, Onemana, Neavesville, Golden Cross, Karangahake and Favona, all described in papers in the monograph edited by Christie and Brathwaite (2006).

The adularia-sericite epithermal systems of the Hauraki Goldfield are of the quartz vein type, the majority of which are hosted in andesite and pyroclastics and to a lesser extent in rhyolitic rocks. The veins are widest in massive andesites, whereas in rhyolitic rocks thin quartz veinlets and silicified breccia zones are more common. The quartz veins of the Hauraki epithermal systems are open-space fissure fillings, commonly displaying crustiform banding. Vein minerals apart from quartz include calcite, quartz pseudomorphs after calcite, manganiferous carbonates, adularia, siderite, barite and anhydrite. Pyrite is a common sulphide mineral; electrum and native Au constitute the chief economic ore minerals. Acanthite, pyrargyrite, Au and Ag selenides and tellurides are locally present. The veins are structurally controlled along fracture and fault systems with dominant northeasterly and northerly trends. The longest vein has a strike of approximately 4.5 km, while the widest is the Martha lode (Waihi deposit) attaining a thickness of 30 m in places. The more common dimensions, however, are in the order of a few hundred metres of strike length and from a

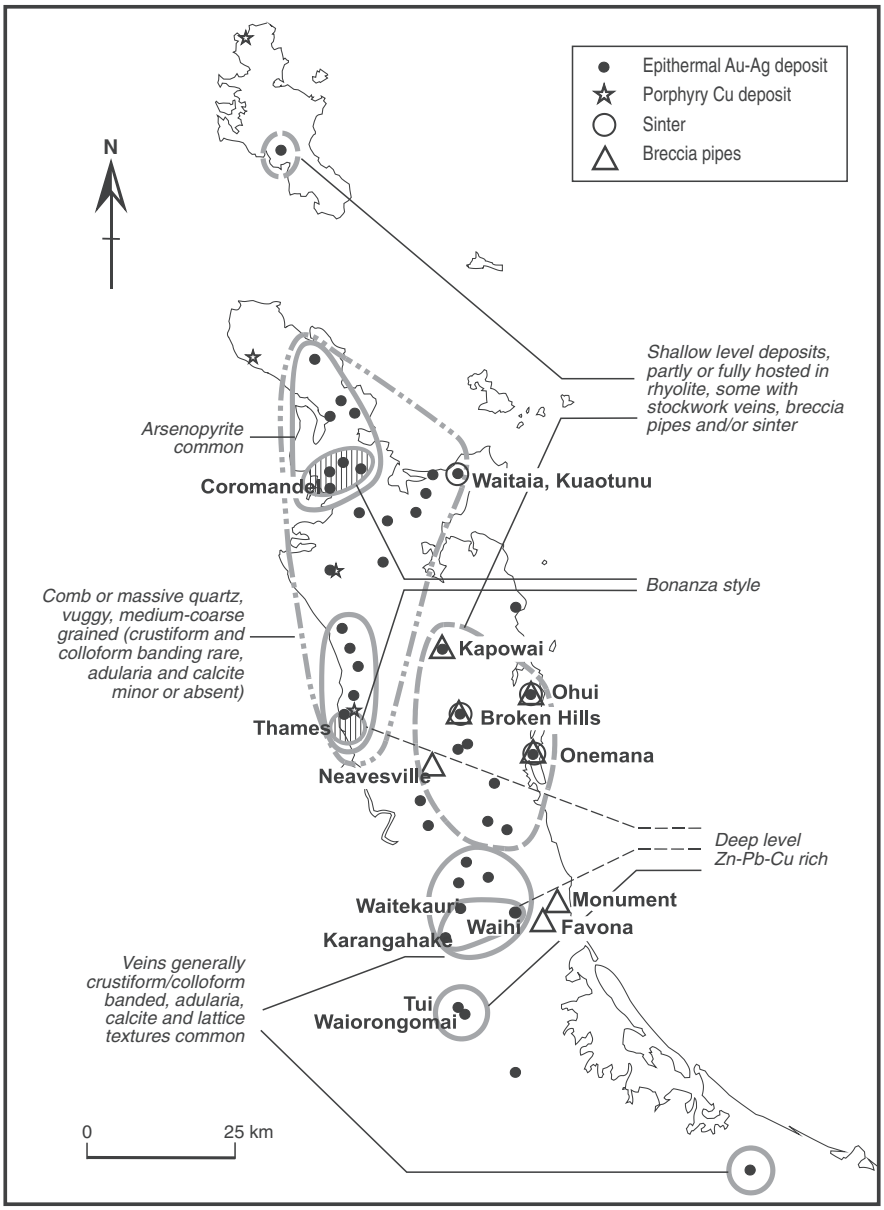


Fig. 5.33 Groups of epithermal systems in the Coromandel Volcanic Zone with common features; these groupings enhance the mineral prospectivity analysis of the region. After Christie et al. (2006); figure reproduced unchanged by permission of the authors and The Australasian Institute of Mining and Metallurgy

few centimetres to about 5 m wide. Although some deposits form isolated quartz veins, most form systems of subparallel veins. In the deeper levels, and consistent with the general character and zoning of epithermal mineralisation, the veins may contain ignificant quantities of base metal sulphides such as sphalerite, chalcopyrite and galena, as well as pyrite. Other ore minerals include arsenopyrite, Sb, Bi, Se, Te sulphides and sulphosalts. The vein mineralisation is accompanied by non-pervasive to pervasive hydrothermal alteration of the wall rocks. Extensive zones of propylitic and clay alteration commonly surround the veins. Propylitic assemblages include chlorite and calcite, whereas argillic assemblages are characterised by interstratified illite-montmorillonite, illite and chlorite. Quartz, adularia and sericite can be found in the altered country rocks adjacent to the veins. Pyrite and sphene are ubiquitous minerals.

Rabone (1975) mapped in detail zones of progressive alteration in andesitic rocks in the Waitekauri area. Relating these zones to north-northeast-trending faults, he recognised four main zones of progressive alteration based on mineralogical changes which are easily discernable under the microscope. Rabone's results, being of general application, are described. In Zone 1, unaltered to weakly altered andesite is composed of hypersthene, augite and plagioclase phenocrysts in a groundmass of andesine microlites, pyroxene and intergranular felsitic material. At this stage the hypersthene is partially or totally altered to chlorite. In Zone 2 the andesitic rock is weakly to moderately altered. Chlorite develops from both hypersthene and augite, with total to partial replacement of these mineral phases. In a more advanced stage carbonate replacement of chlorite begins to take place. Plagioclase shows incipient alteration along cleavage planes to chlorite and clay minerals. The chloritisation process releases silica which is deposited in the groundmass. Moderate to strong alteration occurs in Zone 3, where augite is totally replaced by clay minerals, sericite, epidote and carbonate. Locally, microfractures are filled with albite. Hydrothermal biotite appears here, whereas in the more advanced stages chalcedonic quartz begins to replace the carbonate. In dacitic rocks hornblende is at first replaced by carbonate and later by quartz and hematite. Intense alteration characterises Zone 4 in which the original textures are almost completely obliterated. Quartz, clay minerals and pyrite are the dominant minerals in andesite, while in dacite the earlier hydrothermal minerals are replaced by quartz and hematite, and plagioclase by adularia. The intensity and frequency of the carbonate minerals is taken to be an indication that the altering solutions are CO_2–rich. These alteration zones usually follow the trend of the veins, the alteration being pervasive and strong where a vein system occurs.

Fluid inclusions and stable isotope systematics suggest that the epithermal systems of the Hauraki Goldfield were generated by deep circulating hydrothermal fluids of low salinity (~4 wt% NaCl equivalent), with temperatures in the order of 200–300°C (Christie et al. 2006). Oxygen isotope ratios of fluid inclusions indicate that this hydrothermal fluid was probably meteoric water similar to that circulating in the geothermal fields of the Taupo Volcanic Zone. A magmatic input for the Hauraki hydrothermal fluids has been inferred from

the C isotopic ratios of calcites as well as the presence of CO_2 in the fluid inclusions. Thus, the overall model for the Hauraki mineralisation is that of meteoric convective cells with a minor magmatic component, driven by the thermal energy provided by subjacent subvolcanic intrusions of acid to intermediate composition. More detailed information from stable isotope systematics is provided in the section describing the Martha Hill Au–Ag deposit.

In the following section I provide a description of the world class Martha Hill (Waihi) epithermal Au–Ag deposit, abridged from the works of Brathwaite and McKay (1989), Brathwaite and Faure (2002) and Brathwaite et al. (2006).

5.3.3.1.1 The Martha Hill Au–Ag-Base Metal Epithermal Vein Deposit

The Martha Hill deposit is situated at Waihi, in the southern sectors of the Coromandel peninsula (Fig. 5.32). The Martha Hill mine was closed in 1952 after approximately 12 Mt of ore had been extracted since 1889. A total of 2.4×10^8 g of Au and 8.1×10^8 g of Ag was recovered during this time. The recognition of mineralised quartz vein stockworks between the nearly mined out lodes led to a re-appraisal of the mine in the 1980s and its reopening in 1988. Latest evaluations have resulted in a total resource (including ore mined out since 1988) of about 16 Mt of ore grading between 2.9 and 7.5 g/t Au and 26–28 g/t Ag.

The deposit is located on the rim of a circular structure that may represent a buried caldera (Fig. 5.32). The mine area is underlain by andesitic, dacitic and rhyolitic lavas and pyroclastics of the Coromandel Group which hosts the vein system.These lithologies are overlain by felsic volcanic and pyroclastic rocks of the Whitianga Group. The quartz vein system, hosted by the Late Miocene (8–7 Ma) altered andesite of the Waipupu Formation, has a general northeasterly trend, and consists of a number of subparallel quartz veins which locally develop into an anastomosing pattern (Fig. 5.34). Stockworks and smaller veins occur between the major lodes. There are four main sub-parallel lodes, Martha, Welcome, Empire and Royal, with the largest being the Martha Lode, roughly 1600 m long and up to 30 m wide (Fig. 5.34). Another, blind and large vein system was recently discovered only 2 km to the east of the Martha deposit. This is the Favona Au–Ag epithermal deposit, described by Torckler et al. (2006), highlighting the fact that even after over 100 years of mineral exploration in a comparatively small area, new discoveries can still be made. The Martha epithermal vein system represents an extensional fault-fracture mesh and has been interpreted as a dilational jog, between en echelon sections of a strike-slip fault zone. The veins are sulphide-bearing, consisting mainly of milky quartz, banded chalcedonic quartz and calcite. Sulphide minerals include pyrite, sphalerite, galena, chalcopyrite and acanthite. Electrum is the Au-bearing mineral with an average Ag content of about 38%. Three stages of vein minerals have been recognised: (1) early stage with platy calcite, quartz, adularia and pyrite; (2) main stage with quartz, chlorite, adularia and sulphides with pyrrhotite-sphalerite-galena in the lower levels and pyrite-sphalerite-galena-chalcopyrite-acanthite-electrum in the upper levels; (3) a late stage with amethyst.

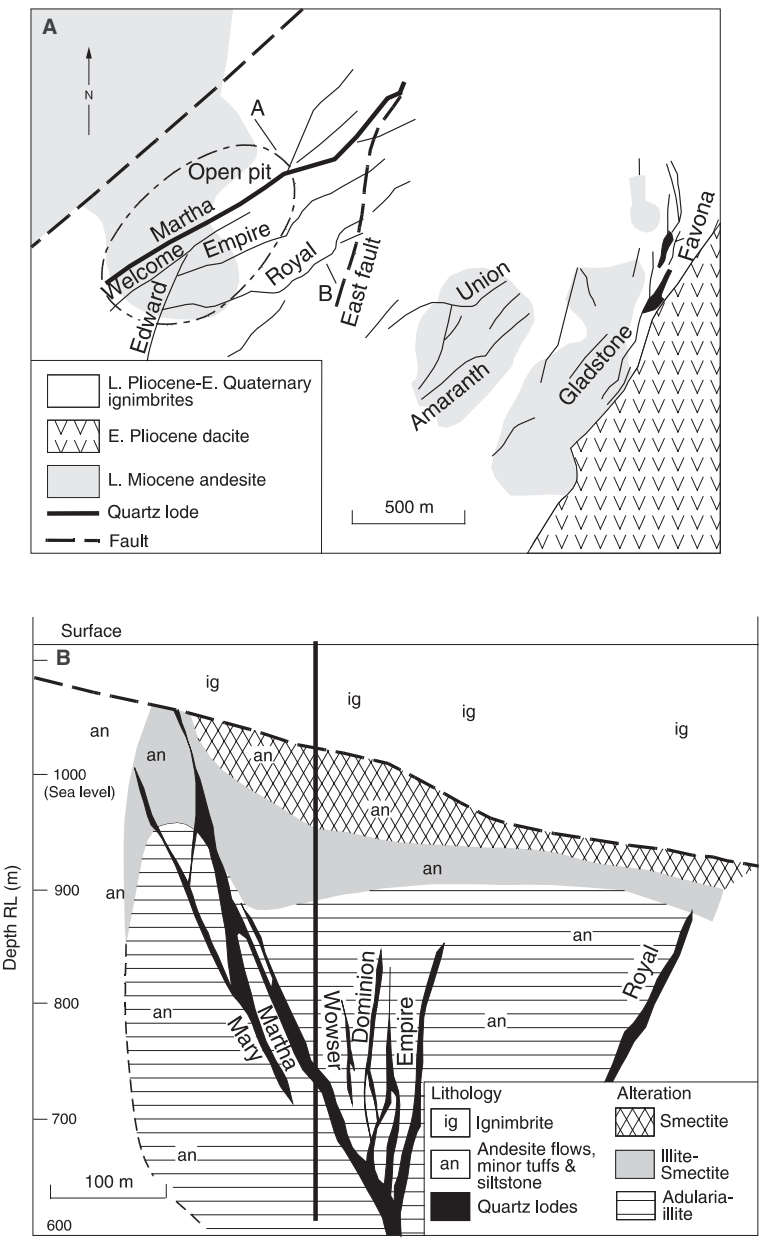


Fig. 5.34 (**A**) Plan view of the Martha Hill and Favona epithermal vein systems; (**B**) cross-section A–B of the Martha Hill deposit showing the distribution of the mienralised lodes. Modified after Brathwaite et al. (2006)

Hydrothermal alteration is closely associated with the vein system. There are three main alteration types in the Martha Hill deposit: potassic, argillic and propylitic. The potassic type is represented by the assemblage quartz + adularia + illite + pyrite ± chlorite ± albite; the argillic type has illite + smectite + chlorite + pyrite; the propylitic type quartz + calcite + chlorite + illite + pyrite. Potassic alteration forms an envelope around the quartz vein system and is in turn surrounded by the propylitic alteration. Argillic alteration overprints both and is confined to the upper parts of the vein system, on the hangingwall of the Martha Lode.

Microthermometric studies of fluid inclusions indicate that the main stage quartz was precipitated at temperatures ranging from 190 to 273°C, from dilute fluids with salinities of less than 1.7 wt% NaCl equivalent. Gas analyses of fluid inclusions revealed, apart from water, the presence of CO_2 and CH_4. Temperature of homogenisation and salinity versus depth plots show broad trends of increasing values with depth, to about 800 m below a calculated palaeosurface. Salinity values for late stage amethyst show considerable scatter but with a tendency to increase towards the surface. This was interpreted as due to localised and protracted boiling resulting to a salinity increase in the residual fluid.

Stable isotope systematics (O, D and C) for main stage quartz and calcite show $\delta^{18}O$ values from 2.3 to 11.2‰; microcrystalline quartz from the Martha Lode has heavier $\delta^{18}O$ values from 8.2 to 9.1‰ and quartz from electrum-sulphide bearing microcrystalline quartz bands show $\delta^{18}O$ values from 7.6 to 8.4‰. These variations in mm-thick quartz bands are interpreted to reflect fluctuations in composition and temperature of the fluids. Estimated temperatures for the deposition of these quartz bands are in the range of 190–255°C, in accordance with the fluid inclusion data. Measured δD, derived from fluid inclusion water, show considerable variations from –29 to –64‰, these are low values compared to present-day values of waters in the region. These low δD values are comparable with those of organic matter in carbonaceous siltstones (lake deposits intercalated within the volcanic sequence) that are present in the area. The $\delta^{18}O$ values of main stage quartz and late stage amethyst plotted against depth and temperature show consistent increase towards the surface, whereas the $\delta^{18}O$ values of water in equilibrium with main-stage quartz and late-stage amethyst show variable trends due to mixing of chloride fluids with steam heated groundwaters, boiling and water–rock interactions. The $\delta^{13}C$ values for calcite have a narrow range from –6.6 to 8.9‰, which falls within the range of other Hauraki epithermal systems. The $\delta^{13}{}_{CO2}$ are similar to those of geothermal fluids in the Taupo Volcanic Zone (see below).

In conclusion, the evolution of the Martha Hill epithermal fluids can be summarised in three stages: (1) initial vein filling; (2) a main stage vein filling of quartz and sulphides; and (3) a final stage of amethyst deposition in the veins. These were associated with contemporaneous proximal potassic alteration (adularia-quartz-pyrite), in which the adularia is indicative of alkaline conditions, boiling and loss of CO_2 gas in the deep fluid, as suggested by the platy calcite. The overprinting of the potassic assemblage by clay minerals suggests

that deep fluids are then mixed with slightly acidic waters produced by steam condensation. The final amethyst stage, which shows a higher salinity trend towards the surface, rules out a magmatic origin for the fluids, instead and as mentioned above, the amethyst was probably derived from the same fluids as the main stage quartz in a protracted open system boiling.

Gold and Ag are transported as sulphide complexes at temperatures of 200–250°C, whereas Pb, Zn and Cu are transported by chloride complexes at temperatures of about 300°C. The precipitation of Au and Ag is therefore likely to be promoted by precipitation of the sulphide minerals and/or loss of H_2S by boiling (see Section 5.3.1.5). A scheme or ore genesis, according to Brathwaite and Faure (2002), involves the rise of hot deep fluids along a mesh of fractures. These fluids deposited Zn, Pb, Cu sulphides first, then mixed and diluted with steam-heated groundwaters upward precipitating Zn, Pb, Cu sulphides and precious metals, interacting with wallrocks and forming breccias and sinters near the surface.

5.3.4 The Epithermal Systems of the Biga Peninsula, Northwestern Anatolia

The Biga peninsula, in northwestern Anatolia, Turkey, is underlain by volcanic and intrusive rocks ranging in age from the Oligocene to the Pliocene, on a basement of Palaeozoic metamorphic rocks. These rocks have a calc-alkaline to alkaline chemistry and are tectonically linked to episodes of subduction and extension, related to the northward movement of the African–Arabian plate. In this environment, hydrothermal precious metals mineral occurrences and deposits were formed. Many of the mineral deposits in northwestern Turkey were exploited since ancient times, with archaeological records dating back to at least 3200 year BP near the town of Cannakale and ancient Troy. Low-sulphidation epithermal systems are present near the town of Bergama (Yilmaz et al. 2007). Yigit (2006) reviewed the Au deposits of Turkey and their link with the Alpine-Himalayan orogenic system. Details of the geodynamic evolution of northwestern Turkey and the various models proposed for the broader Anatolian-Eastern Mediterranean region can be found in Robertson and Dixon (1985), Sengör and Yilmaz (1981) and Sengör (1992). Pirajno (1995) described high-sulphidation epithermal systems in the Biga peninsula and the following is taken from this work.

The Cannakale Volcanic Field (CVF) is an informal name given to an area underlain by volcanic rocks and associated intrusives in a portion of the Biga peninsula (Fig. 5.35). Studies on the volcanic rocks of western Turkey include Seyitoglu and Scott (1992) and Yilmaz (1989, 1990). The volcanic rocks of western Turkey range in age from Oligocene to Pliocene and occupy areas along the coast between Izmir and Canakkale and extend approximately 200 km inland. To the west, the volcanics continue into some of the Greek islands (e.g. Lesvos, Linnos, Imbroz), with lesser areas of exposure in European Turkey (Fig. 5.35). Geochemically, these volcanics can be subdivided into two

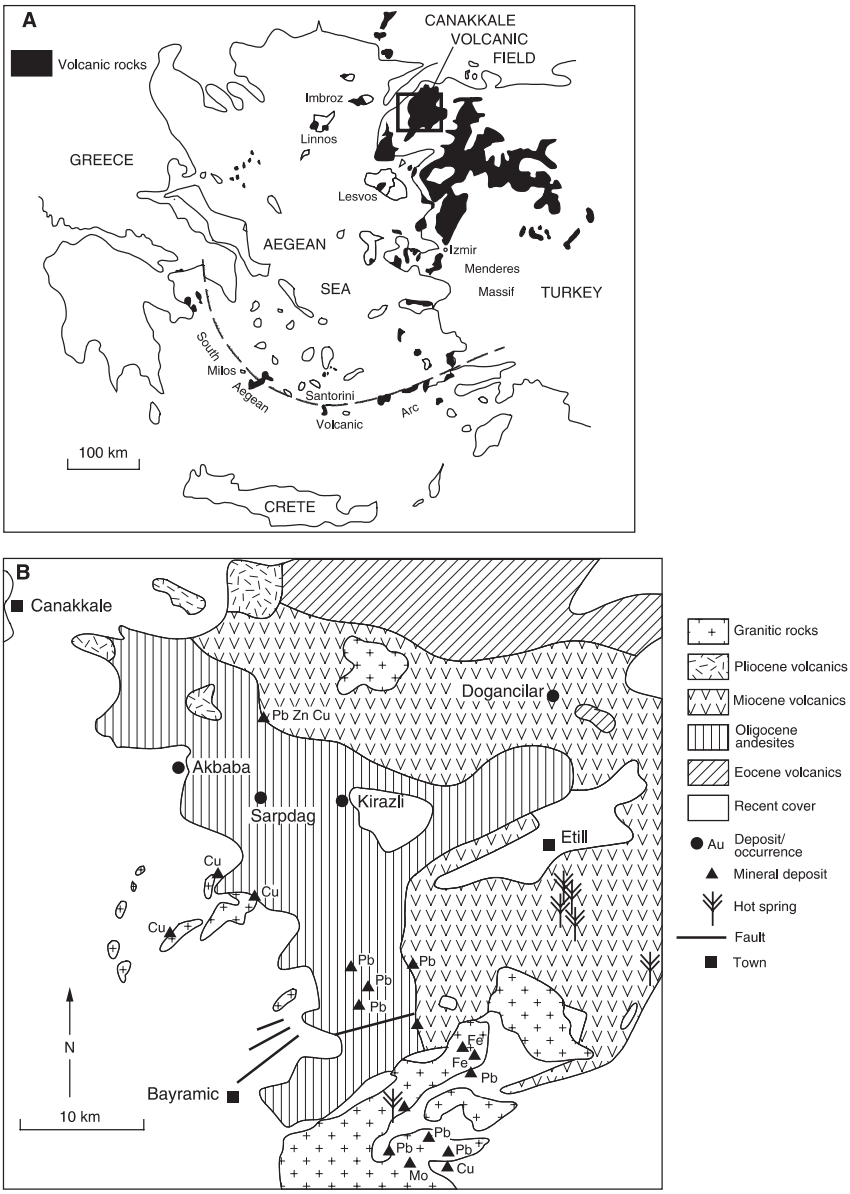


Fig. 5.35 (**A**) Simplified geology of northwestern Anatolia and distribution of main mineral occurrences; (**B**) within the Cenozoic volcanic rocks in the eastern Mediterranean and nortwestern Turkey, position of the Cannakale Volcanic Field is outlined in A. After Pirajno (1995)

associations: calc-alkaline and alkaline (Yilmaz 1989, 1990). Rock types include basalt, andesite, dacite, rhyodacite, rhyolite, alkali basalt, trachybasalt, trachyte and trachyandesite. These form lavas, domes and extensive pyroclastic deposits (e.g ignimbrites, airfalls, debris flows). The earliest volcanism began in the Late Cretaceous to Palaeocene as a result of the north-dipping subduction of the leading edge of the Neo-Tethys oceanic crust beneath the Pontide arc. In the Palaeocene, the northern Tethys had closed, but north-dipping subduction of a segment of Neo-Tethys branch, beneath the microcontinental fragment of Sakarya, was well developed. It is likely that a substantial portion of the CVF was formed during this phase. The strong north-south compression, along the entire Turkish orogen continued between the Eocene and the Early Miocene with crustal thickening and possible delamination of subcontinental lithosphere, followed by partial melting of the lower crust to produce anatectic granitic melts in western Anatolia and in the Aegean islands. Volcanism continued with the production of calc-alkaline volcanics in western Anatolia and the Aegean islands. From the Pliocene to the Present a regime of north-south extension occurred in western Anatolia, due to the "westward" escape of the Anatolian plate. This westward escape is thought to be the result of the northward push exerted by the Arabian plate in the southeast, which forced this part of Turkey to move westwards into the more ductile eastern Mediterranean oceanic floor (Sengör and Yilmaz 1981). It is suggested that the change of tectonic regime from compressional to extensional, resulted in a change from a dominantly calc-alkaline volcanism to a dominantly alkaline volcanism (Yilmaz 1989, 1990). This view, however, was challenged by Seyitoglu and Scott (1992) who, on the basis of trace element geochemistry, related the change in the nature of the volcanism not to the regional tectonic regimes (compressional-extensional) but to a thinned, extended lithosphere and increasing contributions from the asthenosphere. Seyitoglu and Scott (1992) envisaged two distinct magma sources to account for the calc-alkaline and alkaline volcanoplutonic products. Calc-alkaline magmatism was related to the beginning of extensional tectonism between the Late Oligocene and the Early Miocene, and the source is considered to have been a lithospheric mantle metasomatised by earlier subduction. Later, during more advanced stages of extension between the Late Miocene and the Pleistocene, the dominantly alkaline magmatism was sourced from the asthenosphere. It is interesting to note that Seyitoglu and Scott (1992) compared the northeastern Aegean and western Anatolia region to the Basin and Range province in the U.S.A., whereas other authors (Okay et al. 1994) compared it to an Andean-type continental margin.

The CVF is endowed with numerous occurrences and deposits of precious and base metal mineralisation, most of which are spatially associated with extrusive and intrusive rocks. The distribution of these occurrences is shown in Fig. 5.35. Low-pH, hot and ambient-temperature mineral springs also occur in the area testifying to ongoing hydrothermal activity. Hydrothermal alteration and silicification are widespread and affect all rock types to varying degrees. Silicification (chalcedony, opaline silica, crystalline quartz) is

particularly common and it can be seen to form sub-horizontal sheets, usually along hill tops. This silica is normally barren, but at a number of localities is associated with precious metal mineralisation. The significance of this silica is discussed in Section 5.3.4.2. Apart from silicification, hydrothermal alteration styles include propylitic (epidote, chlorite, calcite, pyrite, gypsum, ankerite) phyllic (sericite, pyrite, illite, quartz), argillic (kaolinite, dickite, smectite, illite), and advanced argillic (pyrophyllite, alunite). Hydrothermal breccias are present and appear to be spatially and perhaps, genetically, associated with Au mineralisation. The Au prospects in the Biga region belong to the category of high-sulphur epithermal type. They include hydrothermal veins (Akbaba), stockworks (Dogancilar) and a combination of stockworks, breccia, disseminated and replacement systems (Kirazli, Sarpdag) (Fig. 5.35). The rugged topography of the region allows a rare insight into the vertical geometry of epithermal systems, as illustrated in the section that follows on the Kirazli and Dogancilar epithermal mineralisation.

5.3.4.1 Kirazli and Dogancilar

The Kirazli prospect is located approximately 1.5 km south of the village with the same name (Fig. 5.35). Two ore zones are present: a high-grade oxide zone and a low-grade sulphide zone. The high-grade oxide ore forms a sub-horizontal zone, approximately 200 m long x 100 m wide x 5 m thick, grading from 2 to 20 g/t Au. The low-grade sulphide ore zone, is approximately 200 m long x 30 m wide x 75 m in thickness. The mineralisation is hosted in altered pyroclastic units of the andesitic series. Field observations, petrological and mineralogical work have revealed a complex pattern of hydrothermal events. Multi-phase silicification, brecciation, sericitic, argillic and advanced argillic alteration have occurred, resulting in several stages of overprinting. There are no significant quartz veins at Kirazli. Textural relationships indicate that a vertical and temporal pattern (possibly temperature-related) of quartz-sericite-pyrite alteration (below 700 m a.s.l.) is overprinted and followed upward (700–730 m a.s.l.) by a phase of hydrothermal brecciation with an alteration assemblage of quartz-pyrophyllite-epidote and of clay-barite-alunite-pyrite. XRD analyses show that the clay minerals are mainly kaolinite and dickite. These assemblages are, in turn, followed towards the surface by a second influx of silica-saturated fluids, resulting in an upper zone of chalcedonic hydrothermal breccia. This zone is of regional extent, forming prominent ridges or cliffs and can be shown to have been formed by the replacement of permeable pyroclastic units. At Kirazli pyrite occurs in two different modes, as disseminated grains and as veinlets. In addition, at least three morphological types or phases are recognised. The most common pyrite occurs as disseminated euhedral crystals or masses, normally associated with the quartz-sericite alteration assemblage. Pyrite veinlets fill microfractures and are associated with hydrothermal breccias and the clay-barite-alunite alteration assemblage. A third morphological type, is represented by tiny spheroids (<0.1–0.25 mm in diameter), which occur isolated

or as aggregates up to 1 mm long. The spheroids consist of a round central nucleus, surrounded by a shell of radially arranged crystallites. Textural relationships indicate that the pyrite spheroids are late and overprint the euhedral pyrite. Similar pyrite spheroids have been recorded in epithermal environments elsewhere (e.g. Drake Cu–Au field in New South Wales, Australia; England and Oswald 1993). It is interesting to note that the mineralogical investigations revealed that 70 % of the pyrite is of the first type (euhedral) and is As-rich and Au-poor. The pyrite spheroids are, by contrast, As-poor and Au-rich.

In summary it appears likely that late, lower-temperature fluids precipitated Au-rich pyrite in a high-sulphur hydrothermal system. The same hydrothermal system also produced the quartz-pyrophyllite alteration at lower levels, and hydrothermal breccias with advanced argillic, barite-alunite-clay alteration and pyrite veinlets alteration at higher levels. This event(s) overprinted an earlier one in which quartz-sericite-pyrite and silicification had occurred. Gold also occurs as free particles associated with Fe oxyhydroxides (goethite, limonite). The association of the gold with Fe oxyhydroxides suggests its dissolution from a primary site (e.g pyrite spheroids) and reprecipitation in the weathering environment under conditions of low pH. Remobilisation of Au from sulphides and its subsequent association with late Fe oxyhydroxides is a feature also found in the epithermal deposits of the Nansatsu district in Japan (Hedenquist et al. 1994). A multi-stage origin of pyrite and its association with Au is also discussed in Chapter 9.

The Dogancilar prospect is located approximately 3 km from the village of the same name, some 19 km east-northeast of the Kirazli-Sarpdag area (Fig. 5.35). The area affected by alteration-mineralisation covers approximately 20 km^2 and is characterised by the prominent Karadag hill formed by extensively silicified pyroclastic units. In addition to this silicification, Au-bearing stockworks, barite and sulphide-bearing veins and a site, interpreted as a fossil fumarole, are also present. Gold mineralisation has been noted to be associated with Cu and Ba (barite) in the Bakirlik vein and a stockwork zone, at elevations of 500–550 m a.s.l., where values of between 4 and 10 g/t Au and up to 2.8 % Cu have been recorded. The Bakirlik vein is hosted in hydrothermally altered andesitic volcanics. Alteration assemblages include quartz-sericite and illite-montmorillonite. Near the top of a hill, a west-northwest-trending structure contains significant Ag (120 ppm), As (10 000 ppm) and Pb (3840 ppm) at an elevation of approximately 720 m a.s.l. From the 550 m a.s.l. contour to the top of the hill, there are outcrops of intensely silicified material. This silicification consists primarily of chalcedonic quartz with colloform textures. Brecciated zones are present and locally display hydraulic fracturing and/or fluidisation textures. Silicification is gradational and it ranges from stockwork veinlets in clay-altered volcanics to progressively more abundant silica veining until the entire rock mass is replaced by chalcedonic quartz, brecciated and healed by multiple influxes of silica. Barite is locally present and associated with at least one of the silica phases. The “Silica Mine” is a locality approximately 1.5 km east of Karadag, where silica is mined for industrial uses. In this area total replacement of a pyroclastic unit has occurred. The replaced rock consists of a dense, fine, granular, quartz aggregate with very

fine pyrite disseminations. Spring waters (ambient temperature) near this quarry are mineralised with Fe hydroxides and have pH values ranging from 4.3 to 3.5.

In the southeast of the area, at an elevation of approximately 390 m a.s.l., veins containing sphalerite and galena occur. The veins are less than 2 m wide and have an approximate E-W strike. The wallrocks are fractured and pervasively altered to an assemblage of quartz, kaolinitic clay and pyrophyllite. Pyrophyllite selectively replaces phenocrysts and is in turn replaced by the kaolinite clay. About 170 m south of these veins a structurally-controlled zone of pervasive alteration occurs. Here, pyroclastic rocks are hydraulically fractured, have thin quartz stockworks and show pervasive clay + pyrite alteration. These altered rocks also exhibit encrustations of native sulphur. The alteration is characterised by halloysite and kaolinitic clays, locally with illite intergrowths, replacing groundmass and phenocrysts. Pyrite occurs as fine disseminations. This locality is interpreted as the site of ancient fumarolic activity. Pirajno (1995) postulated a vertical zonation from Ba–As–Ag–Pb ± Sb in the upper levels, Ba–Cu–Au in the middle to Pb–Zn ± Au in the lower levels.

5.3.4.2 Genetic Model

An important hydrothermal feature of regional extent in the CVF is the presence of sub-horizontal silicified zones, usually barren of mineralisation and forming topographic highs or cliffs. Field and petrological evidence indicates that these silicified zones are formed by varying degrees of replacement of pre-existing lithologies, generally high-permeability pyroclastics units, resulting in pervasive silicification. Chert, chalcedony and opaline silica are the main phases of this silicification. In places, this silica is strongly leached and a cavernous or vuggy residue is left behind (see Section 5.3.4.1 and Table 5.4). This type of leaching by acid fluids is commonly observed in high-sulphur epithermal deposits (Hedenquist et al. 1994). A regional vertical zonation, related to the lowering of the water table due to ulift, was proposed by Pirajno (1995). One of the main features of this zonation are that quartz, sericite, pyrite, epidote, alunite and pyrophyllite all occur below 750 m a.s.l. and towards the upper levels this assemblage is overprinted by a later phase of silica alteration. At Dogancilar there is field evidence that the regional silicification is very thick (approximately 250 m). The regional sub-horizontal zones of silica replacement of pyroclastic units, is interpreted to represent a silica-saturated paleoaquifer which formed the upper portions of a very extensive hydrothermal system, powered by volcanic heat. This paleoaquifer was pervasively silicified during ongoing hydrothermal activity. A similar situation is thought to have occurred in the Early-Middle Miocene, high-sulphur epithermal systems of northern Chile (Sillitoe 1991) and more specifically in the El Indio-Pascua belt, discussed in Section 5.3.6. The paleoaquifer was topographically controlled and, as the area underwent rapid tectonic uplift, the aquifer progressively descended, so that now one can observe several levels of regional silicification. This is seen at Dogancilar, where pervasive tabular silicification occurs some 250 m below the

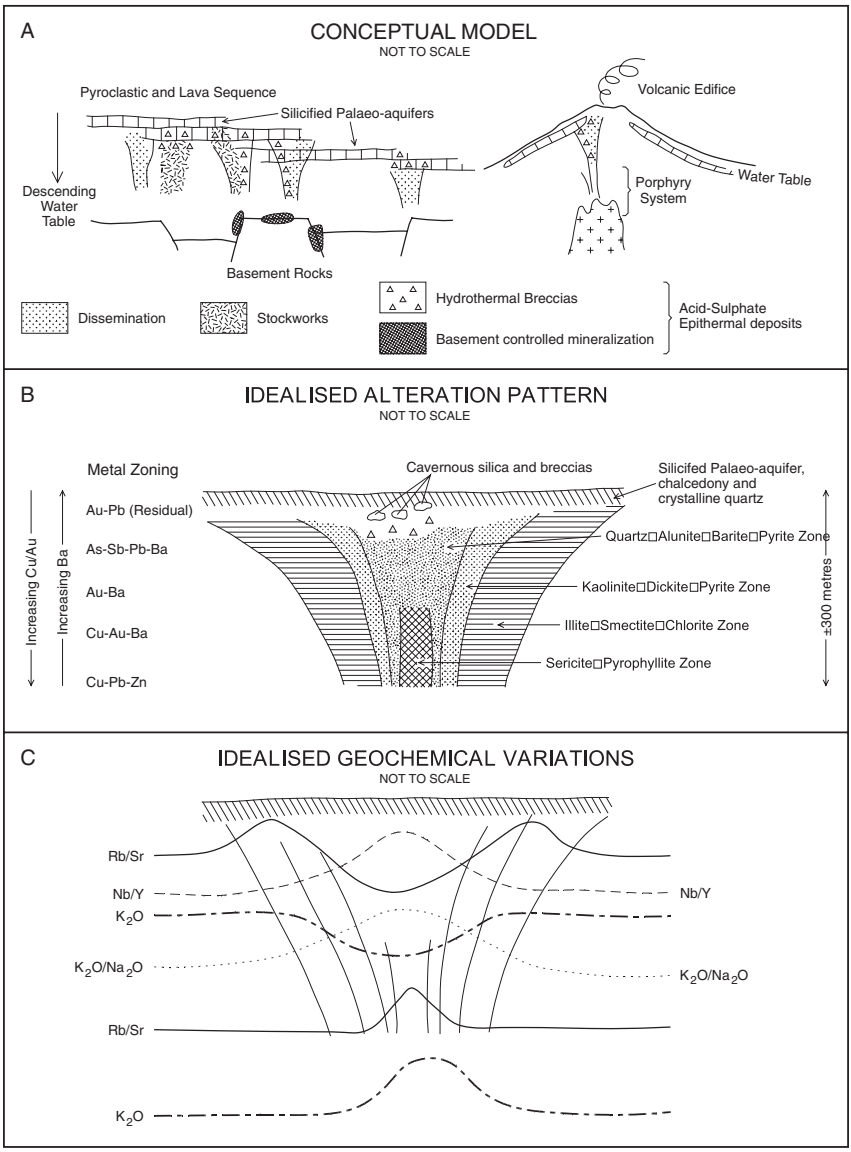


Fig. 5.36 Genetic model (not to scale) of the epithermal systems in the Biga peninsula, northwestern Anatolia. (**A**) the epithermal systems are within volcanics and pyroclastics associated with a hypothetical strato-volcano; (**B**) Idealised alteration patterns and (**C**) associated geochemical variations. After Pirajno (1995)

top of Karadag hill. The silicified aquifer, at various stages, acted as an impermeable barrier to continuously rising hydrothermal fluids. In a number of places the fluids broke through this barrier, whenever the fluid pressure exceeded the tensile strength of the overlying siliceous barrier. This resulted in

extensive brecciation, locally accompanied by precipitation of gold. Fumarolic activity continued, even after erosion began dismantling the upper silicified paleoaquifer levels and exposed the lower portions of the underlying epithermal deposits. This is shown at Dogancilar, where acid leached rocks, encrusted with native sulphur, occur alongside Pb–Zn-bearing veins. Low-pH mineral springs still issue at a number of places, between Kirazli and Dogancilar, testifying to this ongoing hydrothermal activity. The proposed genetic model is shown in Fig. 5.36, together with schematic, qualitative representations of alteration patterns and geochemical trends, both in the vertical and horizontal sense. In this model the epithermal deposits of the CVF were formed at the interface between basement rocks and the overlying volcanic cover, and in the highly permeable pyroclastics predominantly as stockworks and disseminations, owing to the weakly competent and porous nature of these rocks. Alteration ranged from argillic to advanced argillic in a predominantly acid-sulphate environment. Supergene Fe oxyhydroxides, derived from the oxidation of the abundant disseminated pyrite, commonly accompany the argillic zones and display enhanced gold values, probably due to chemical reconcentration of the metal under low pH, weathering conditions. The quartz-alunite-barite-pyrite grades downward into quartz-sericite-pyrophyllite and laterally to kaolinite-dickite-pyrite and illite-smectite to propylitically altered rocks (Fig. 5.36B). Ledges of vuggy silica, commonly seen at Kirazli for example, are indicative of extreme acid leaching, which left behind residual silica and hydrothermal breccias containing most of the gold mineralisation.

5.3.5 Epithermal Systems in the South China Fold Belt

The South China Fold Belt (or Huanan Orogen, see inset of Figs. 5.16 and 6.13) is part of the South China Block, which is the result of multiple tectonic and magmatic events that formed a collage of accreted Proterozoic and Phanerozoic terranes (see Wang H et al. 2005, for an overview of China's geology). The Jurassic to early Cretaceous Yanshanian period (208–90 Ma; see also Chapter 6), a time of major tectono-thermal events that affected much of eastern and southeastern China, is of great metallogenic importance in the fold belt. This period is linked to subduction of the Pacific plate beneath the Eurasian continent, and is manifested by voluminous volcano-plutonic activity of predominantly calc-alkaline and alkaline affinity.

The South China Fold Belt (SCFB) is well endowed with numerous Sn, W, Mo, Pb–Zn, Cu, Sb, mostly hydrothermal vein-type, as well as Au and Au–Ag epithermal mineral deposits. In this section I focus on the epithermal Au–Ag metallogeny in the SCFB, taken from Pirajno et al. (1997) and Pirajno and Bagas (2002). The gold resources of the SCFB are estimated at around 2–3% of the total gold resources of China (about 4500 t according to Zhou et al. 2002, and 3832 t according to Nie 1997). Mineralizing events in the SCFB occurred

during the Neoproterozoic through to the late Mesozoic. In this long span of geological time, precious metal deposits were formed and re-worked during lithospheric plate movements and microcontinent collisions.

The southeastern part of China is formed by the Yangtze Craton, and the ~1.8–1.4 Ga Cathaysia Block (Fig. 5.37), which are in contact along a tectonically complex zone interpreted as a crustal suture, which contains an ophiolitic-type

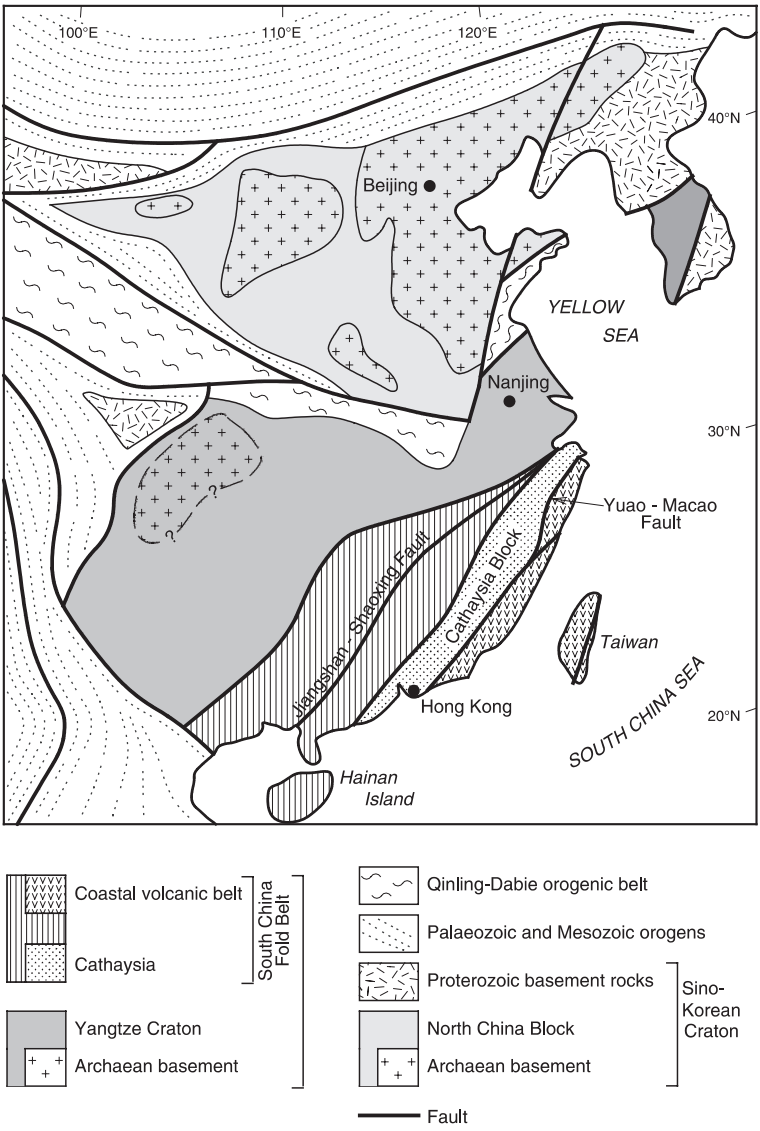


Fig. 5.37 Main tectonic units of eastern and southeastern China. After Pirajno and Bagas (2002). See also Fig. 5.33

melange and high-pressure metamorphic rocks (Sengör and Natal'in 1996). The amalgamation of the Yangtze Craton with the Cathaysia, first occurred during the 1.0–0.85 Ga Jinning Orogeny. This was followed by a rifting episode around 800 Ma during the Sinian, and a second collision event during the Caledonian (Zhou et al. 2002). Details of the tectonic evolution of the South China region are complex and still largely unresolved, although various lines of evidence (e. g. Li ZX 1998) suggest that it formed through a series of continent-continent collisions with closure of intervening segments of oceanic crust since Proterozoic time (Ye et al. 1998). More recently, Li and Li (2007) proposed a flat-subduction model for the geodynamic evolution of the SCFB between 250 and 190 Ma, with subsequent slab breakoff, roll-back and its foundering.

The SCFB is exposed along the southeastern side of mainland China, on Taiwan, and on Hainan Island, and is that part of the South China Block that was affected by Yanshanian deformation and magmatism (Wu et al. 1998; Wang H et al. 2005). Several northeast-trending fault zones traverse the SCFB, including the Jiangshan-Shaoxing Fault Zone (Fig. 5.49) and the Yuao-Macao fault zone, both of which constitute major crustal-scale structures. The Jiangshan-Shaoxing and Yuao-Macao fault zones delineate two structural and tectonostratigraphic domains (A and B in Fig. 5.38). These domains are also broadly defined by the distribution of initial $^{87}Sr/^{86}Sr$ ratios (Sr_i) of volcanic and plutonic rocks (Pei and Hong 1995), which increase from less than 0.708 in the coastal areas (domain B, Fig. 5.38) to between 0.708 and 0.724 in the interior (domain A, Fig. 5.38). The domains identified by the Sr_i values also coincide with the regional distribution of granitoid rocks, from dominantly I-type along the coast in domain B (Zhejiang-Fujian-Guandong coastal belt; < 0.708 Sr_i) to dominantly S-type in the interior belt in domain A (Hunan-Jiangxi-Guandong transitional belt and Hunan-Guangxi intracontinental belt; $0.708 < Sr_i > 0.724$). The distribution of initial $^{87}Sr/^{86}Sr$ ratios and the nature of the associated magmatism (I-type, magnetite-series versus S-type, ilmenite-series; see overview in Chapter 4) may be explained by lithospheric domains, from mantle-dominated (I-type; domain B) to accreted crustal rocks (S-type; domain A). This in turn would reflect in the nature of the associated mineralisation. Indeed, Pei and Hong (1995) defined a regional metal zonation, from a dominant Pb–Zn–Ag–Au metal association in domain B to an Au–Mo–Cu metal association in domain A.

The structural and tectonostratigraphic region between the Jiangshan-Shaoxing and Yuao-Macao fault zones (domain A), is characterized by the presence of Proterozoic inliers of orthogneiss and paragneiss that are exposed through Yanshanian cover sequences of felsic-intermediate volcanic, volcaniclastic and plutonic rocks (Fig. 5.38). The inliers consist of rocks metamorphosed to the greenschist to upper amphibolite facies, which are considered part of the Cathaysia Block. The rocks of the inliers formed part of the Neoproterozoic Shuangxiwu and Chencai island-arcs or back-arcs and are interpreted to

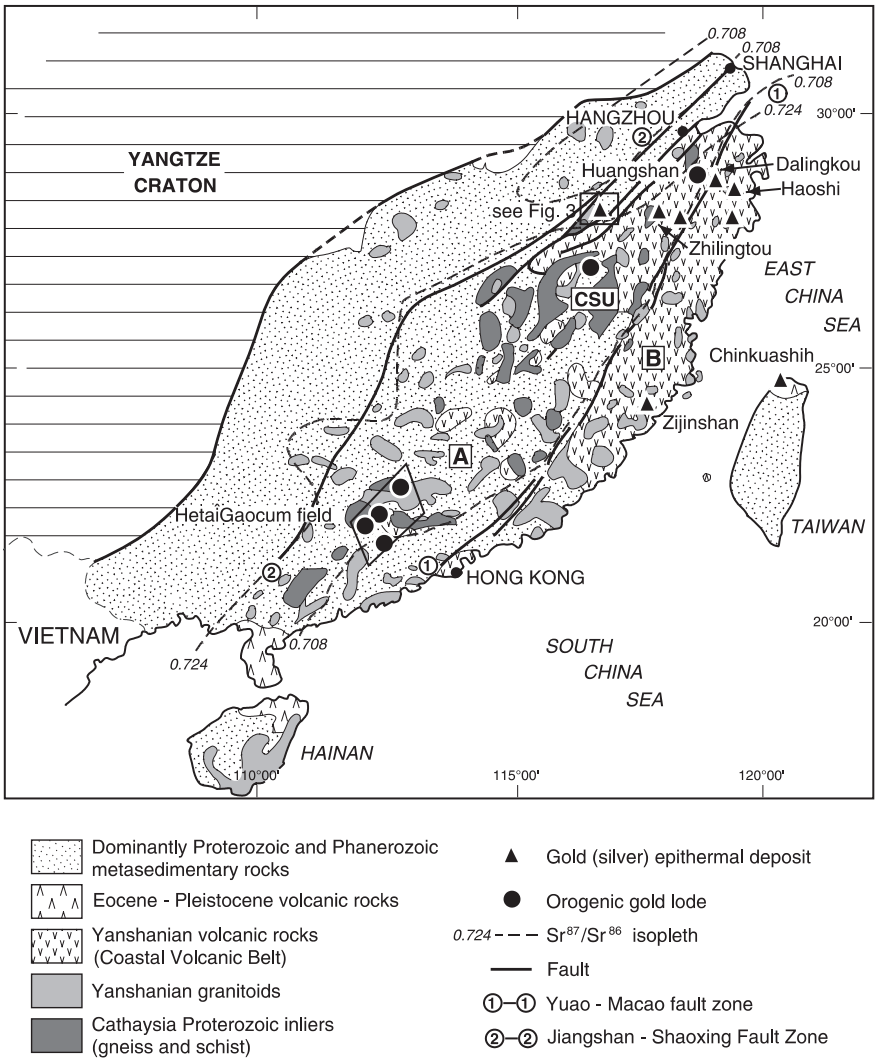


Fig. 5.38 Simplified geological map of the South China Fold Belt and distribution of selected epithermal Au–Ag deposits, east of the Jiangshan-Shaoxing Fault; $^{87}Sr/^{86}Sr$ contours are taken from Pei and Hong (1995). The Yuao-Macaoo and Jiangshan-Shaoxing faults delimit two structural and tectonostratigraphic domains, A and B. A represents structural uplifts and tectonic windows (inliers) of older rocks (Cathaysia), between the Yuao-Macao and Jiangshan-Shaoxing faults; B represents the Cretaceous Coastal Volcanic Belt east of the Yuao-Macao fault

be remnants of microcontinental fragments that were first accreted to the Yangtze Craton during the Neoproterozoic. The Jiangshan–Shaoxing Fault marks the suture between these ancient arcs (Xu G et al. 1994) that collided and together were accreted onto the eastern margin of the Yangtze Craton between

950 and 800 Ma (Jinning Orogeny; Zhou et al. 2002).The exposure of the Cathaysia inliers is the result of orogenic uplift, which is related to convergence tectonics that occurred in the Yanshanian, along the western Pacific margin. One of these uplifted areas in the Zhejiang Province is termed the Chencai-Suichang Uplift (CSU); others are found further to the southwest in Fujian and Guandong Provinces. These uplifted blocks and associated inliers are economically important because they host significant Au–Ag deposits, such as the Zhilingtou, Huangshan and the Hetai deposits in the Zhejiang and Guandong Provinces (Fig. 5.38), discussed in this section.

The Yanshanian tectono-thermal events began in the Early Mesozoic at ~208 Ma and terminated ~90 Ma (Zhou et al. 2002). It resulted in the establishment of a broad magmatic zone, as much as 1000 km wide and 3000 km long, along the eastern margin of China. The Yanshanian event in its various manifestations is utimately linked to the oblique subduction of the Pacific plate under the Eurasian plate, affecting the continental margin of eastern Asia (Sengör et al. 1993). In southeastern China, the Yanshanian magmatic zone is subparallel to and overlaps in space with magmatic belts of Caledonian-Variscan and Indosinian ages. This overlapping pattern has been attributed to successive phases of oceanic crust subduction beneath an active continental margin (Jahn et al. 1990), or to the flat subduction of Li and Li (2007).

The main phases of Yanshanian tectono-magmatic activity began in the mid-Jurassic between ~180 and 140 Ma and peaked with extensive I-type plutonism in the Cretaceous between ~120 and 90 Ma (Jahn et al. 1990; Chen CH et al. 2000). Chen CH et al. (2000) and Zhou and Li (2000) noted the presence of Cretaceous A-type plutonic rocks with the extensive high-level I-type plutonic rocks. They related this plutonism to a geothermal gradient greater than 40° C/km, large-scale underplating of basaltic magma, and a high exhumation rate. Zhou and Li (2000) further suggested that the slab-dip angle of the early Pacific oceanic plate subduction beneath southeastern China increased from a low angle to a moderate angle between 180 and 80 Ma. The consequence of this change in angle was that magmatic activity migrated some 800 km southeast towards the coastal regions of the Zhejiang and Fujian provinces. The flat subduction model proposed by Li and Li (2007) provides a good explanation for these migrating magmatic events that occurred between ~250 and 155 Ma. Post-orogenic A-, I-type granites and rift-related syenites, show a coastward younging trend suggesting both extensional and subduction-related magmatic arc environments. According to Li and Li (2007), the uplift of the coastal region in southeast China is associated with the Mid-Permian North China-South China collision. These authors interpreted the anorogenic I- and A-type magmatism to reflect the beginning of slab breakoff and asthenospheric upwelling, resulting in a Basin-and-Range topography (see Section 5.3.7). The younging of this magmatism towards the coast is interpreted as due to successive phases of slab roll-back that produced a combination of arc-related and bimodal rift-related volcanism.

Basaltic underplating and magma fractionation resulted in the release of magmatic fluids and the possible introduction of metals such as Sn, Mo and W (Zhou and Li 2000). The magmatic activity continued, however, through to the Early Neogene (Himalayan Orogeny) along the entire continental margin of eastern Asia (Sengör et al. 1993). East of the Yuao-Macao fault zone (domain B; Fig. 5.38), Yanshanian volcanic and plutonic rocks that form the Coastal Volcanic Belt (CVB) extend for approximately 1200 km from northern Zhejiang Province, across Fujian Province and through to southwest Guandong Province. The CVB volcanic and plutonic rocks consist predominantly of rhyolite, dacite, andesite and cogenetic granitoid rocks (Pei and Hong 1995). The volcanic rocks that outcrop on the islands of Hainan and the western side of Taiwan are of Eocene and Pleistocene age, and belong to the Himalayan Orogeny (< 90 Ma), and it is worthy of mention that the important 1 Ma dacite-hosted Chinkuashih epithermal gold deposit on the northern tip of Taiwan (Fig. 5.38) is the largest epithermal deposit in China (Tan 1991). A genetic link between Yanshanian magmatism and mineralisation in eastern China is well accepted (see Section 5.2.2.3). In southeastern China, most gold deposits in the Cathaysia Block inliers, and all of the hydrothermal Au, Ag, Sn, W, Sb, Pb, Zn, and Cu deposits in the CVB (Fig. 5.38), are spatially associated with Yanshanian volcanic structures, granitic dykes and subvolcanic intrusions. There are two distinct metallogenic provinces, corresponding to the structural and tectonostratigraphic A and B domains, referred to previously (Fig. 5.38). These are the areas in which the Cathaysian inliers are exposed (e. g. CSU, and other scattered uplifts to the southwest shown in Fig. 5.38), and where Yanshanian volcano-plutonic rocks define the CVB. Gold, silver and polymetallic deposits, hosted in Cathaysian inliers, are typically localised along shear zones. The deposits have a range of styles and types that include mesothermal and epithermal replacement lodes, veins and stockworks. A large number (> 200) of Au, Ag, fluorite or polymetallic (mainly Pb–Zn±Au±Ag, Cu–Mo) dominated occurrences are present in the coastal areas of the Zhejiang Province. From the descriptions given in the available literature (Pirajno et al. 1997; Pirajno and Bagas 2002 and references therein), all of these deposits represent epithermal and/or porphry systems.

5.3.5.1 Zhilingtou and Huangshan Epithermal Systems, Chencai-Suichang Uplift, Zhejiang Province

Zhilingtou is a low-sulfidation epithermal Au–Ag deposit, and is the largest and economically most important in Zhejiang Province (Fig. 5.38). The deposit located in the CSU, contains an in situ resource of approximately 2 Mt, grading 12 g/t Au and 306 g/t Ag. Quartz-dominated veins and stockworks in the mineralized zone are sulphide-rich and can be classified as Au–Ag, Pb–Zn, or Cu–Pb–Zn–Ag types. Precious metal-bearing phases include electrum, native and sulphide-hosted gold, acanthite, hessite and calaverite. Other ore minerals are pyrite, sphalerite, galena, chalcopyrite, pyrrhotite and tellurobismuthite.

Gangue minerals include adularia, rhodochrosite, rhodonite and colloform quartz. Hydrothermal alteration zones surrounding the vein system include sericite, epidote, chlorite, and Mn-carbonates. The orebodies occur as jigsaw-fit veins and stockworks, veins with open-space filling textures and locally replacement zones. A 900 m drill hole intersected propylitically-altered felsic and intermediate igneous rocks and zones of quartz stockworks with molybdenite in silicified and sericitized quartz-porphyry rocks. These features led Pirajno et al. (1997) to suggest that the Zhilingtou deposit could be spatially and genetically related to a porphyry system at depth. Zheng and Liu (1987) and Xu G. et al. (1995) carried out studies of fluid inclusions of mineralized quartz-vein material at Zhilingtou. These authors measured homogenisation temperatures ranging from 160 to 400° C, with the main hydrothermal stage at about 270°C. Calculated salinities are from 5 to 8 wt% NaCl equivalent; no CO_2–rich inclusion were found. These temperature and salinity values are consistent with those that are considered typical for the circum-Pacific epithermal systems (Hedenquist and Lowenstern 1994, White and Hedenquist 1995).

Xu B (1988) showed that the Zhilingtou "early" ore veins have narrow ranges of δD and $\delta^{18}O$ (–62 to –53‰ and +1.0 to +4.7‰ respectively). On this basis he concluded that the early ore-forming fluids originated from "syngenetic metamorphic water", perhaps hinting at a mineralizing event not related to Yanshanian magmatism, but inherited from pre-existing Proterozoic basement mineralisation. Late ore-veins at Zhilingtou have a wider spread of δD and $\delta^{18}O$ values (–73 to –58‰ and –4.9 to –2.1‰ respectively) (Fig. 5.39A). Other authors (cited in Xu G. et al. 1995), using O, H and Si isotope systematics concluded that an earlier stage of mineralisation resulted from fluids of metamorphic origin at Zhilingtou. It has also been suggested that this early mineralisation may be related to the second collision event between the Yangtze Craton and the Cathaysia Block forming the South China Block during the Caledonian (Zhou et al. 2002). Sulfur isotopic determinations on sulphides (Xu B et al. 1994, 1995) indicate that most of the δS^{34} values at Zhilingtou cluster around +4 to +6‰ (Fig. 5.39B) and overlap those of the Mesozoic volcanic rocks, which range between –1 and +5‰.

Evidence from K-Ar and Rb-Sr isochron dating on the auriferous quartz veins in the Zhilingtou mine suggests that epithermal vein formation was linked to the Yanshanian tectono-magmatic event within at least three distinct gold-mineralizing events at 227, 164–152 and 107–82 Ma. Furthermore, the high $^{87}Sr/^{86}Sr_i$ ratio of 0.72496 for the 160 Ma date and the high $^{87}Sr/^{86}Sr_i$ ratio of 0.72889 for the 127 Ma date indicate a crustal source for the mineralisation (Chen and Xu 1997).

The Huangshan deposit (Figs. 5.38 and 5.40) contains a lode about 400 m long and up to 9 m wide, with an average grade of 8.8 g/t Au. The ore minerals are native gold, petzite, calaverite, pyrite, chalcopyrite and galena, hosted by vein-quartz lenses within strongly sheared quartz-diorite. Hydrothermal alteration assemblages surrounding the lode consist of quartz-carbonate- sericite, and quartz-albite-muscovite-carbonate-chlorite. Tourmaline, carbonate, pyrite and galena are in cleavage planes parallel to the regional foliated fabric of the

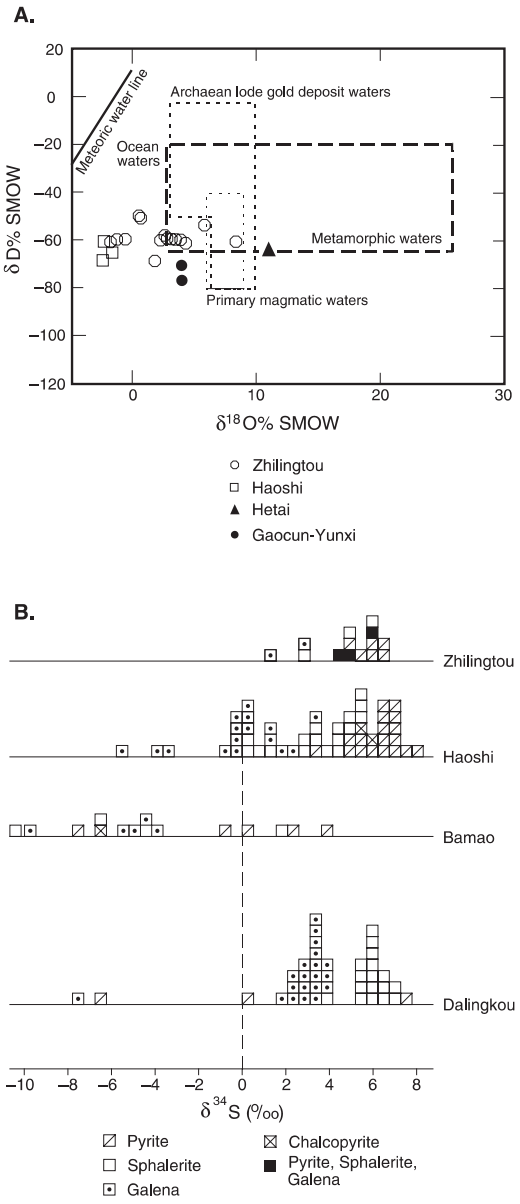


Fig. 5.39 (**A**) δ18O-δd plot for the Zhilingtou, Hetai, Gaocun, Yunxi and Haoshi mineral deposits; Hetai is an orogenic lode deposit and its O–D composition plots close to the metamorphic water box (Wang et al. 1997); Zhilingtou exhibits a trend from metamorphic to porphyry-epithermal, whereas Haoshi forms a cluster within the epithermal range. The magmatic and metamorphic boxes are from Sheppard (1986). (**B**) histogram of $\delta^{34}S$ values for Zhilingtou, Dalingkou and Haoshi (data from Xu B et al. 1994, 1995); the S isotopic data suggest mixing of magmatic (near 0‰) and crustal sources (heavier $\delta^{34}S$ values). After Pirajno and Bagas (2002 and references therein)

mylonite zone, and gold fills late dendritic fractures in the pyrite. Rubidium-Sr isochron dating of auriferous quartz yielded an age of 397 ± 34.5 Ma, with $^{87}Sr/^{86}Sr_i$ ranging from 0.7042 to 0.7053 (Chen and Xu 1997). Other operating gold mines in the area include Miaoxifan, Mali, Xipai and Xingsheng (Fig. 5.40), all hosted in strongly sheared mafic rocks (Pirajno et al. 1997).

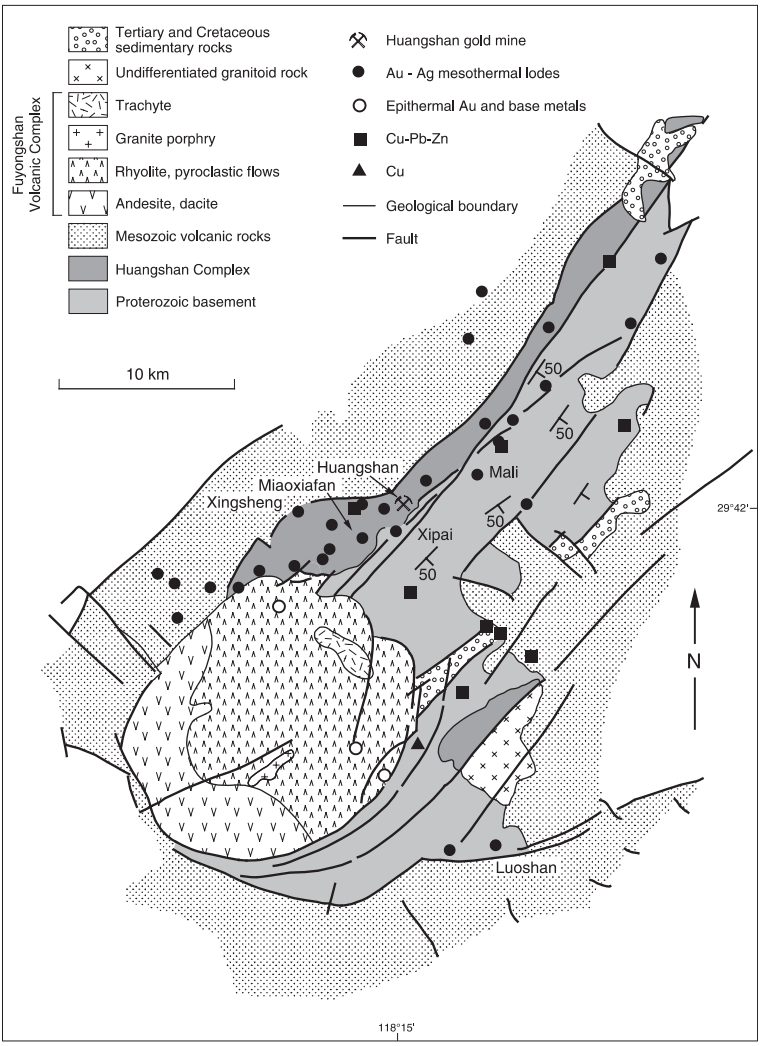


Fig. 5.40 Simplified geology of the Huangshan area and distribution of precious metal deposits, which are lithologically (Fe-rich), structurally controlled and spatially associated with the Fuyongshan volcanic complex. After Pirajno and Bagas (2002)

The distribution of the mineral deposits and occurrences in the Huangshan district indicates a strong structural and iron-rich lithological control. There are approximately 30 gold deposits and occurrences, most of which are found in the ~808 Ma Huangshan Complex, with a few in Mesozoic volcanic rocks (Fig. 5.40). The Huangshan Complex is an intermediate-mafic-ultramafic layered intrusion about 34 km long and 4 km wide, emplaced within the Jiangshan-Shaoxing Fault Zone. The complex is interpreted as part of an

ophiolite melange suturing the Yangtze Craton and Cathaysia Block (referred to above). Copper, Pb–Zn and Cu–Pb–Zn occurrences are also present in the basement and Mesozoic volcanic rocks in addition to gold (Fig. 5.40). An important and major feature in the Huangshan area is the Fuyongshan volcanic complex, which is approximately 14 km in diameter and is possibly a caldera (Fig. 5.40). Small Au, Cu and epithermal fluorite occurrences are present within and around the volcanic complex.

5.3.5.2 Zijinshan Epithermal-Porphyry Systems

The Fujian Province contains Au–Cu high-sulfidation epithermal mineralisation at the Zijinshan mining district (Fig. 5.38), and at least five other Au–Cu prospects in the district ranging from epithermal to porphyry styles. The Zijinshan deposits have a resource of about 17 t, with an average grade of 4.2 g/t Au and 1 Mt with an average grade of 1% Cu (So et al. 1998). So et al. (1998) described in detail the hydrothermal alteration and mineralisation of the Zijinshan area. The brief account that follows is taken from these authors. The Zijinshan ore is characterised by northwest-trending breccia bodies and veins within a Cretaceous (105–100 Ma) volcanic pipe of dacitic composition. Hydrothermal alteration and mineralisation are typically zoned, with quartz-sericite-pyrite in the deeper part of the system, to dickite-quartz-pyrite-zunyite in the middle levels, to alunite-quartz-pyrite between 350 and 1200 m from the surface. At levels shallower than 350 m, intense silicification dominates and is associated with Au–Ag mineralisation. Metal zoning within the alunite and silica zones is from Cu–Pb–Zn to Au–Ag–As near the surface. Fluid inclusion studies indicate mineralizing temperatures of 300–380°C in the deeper porphyry sector of the system, 320–250°C in the alunite zone, and 100–180°C in the shallow silica – gold zone (epithermal sector). So et al. (1998) suggested that the zone of alteration with dominant alunite was formed by mixing of high salinity fluids (10–22 wt% NaCl equivalent) with groundwater, whereas the near surface silica-rich auriferous zone was formed from low salinity acidic gas condensates (< 2 wt% NaCl equivalent).

5.3.5.3 Mineralisation in the Coastal Volcanic Belt

Epithermal systems in the CVB include polymetallic Ag-rich and low-sulfidation veins and/or stockworks. (e.g., Haoshi, Dalingkou in Zhejiang Province), and high-sulfidation Cu–Au deposits (e.g., Zijinshan in Fujian Province) hosted by Late Jurassic to Early Cretaceous dacite and rhyolite (domain B in Fig. 5.38).

The Haoshi and Dalingkou polymetallic low-sulfidation epithermal veins are sulphide-rich, with pyrite, sphalerite, galena and chalcopyrite. Precious metal-bearing ore minerals include freibergite, electrum, argentite, pyrargite and stephanite. The silver-rich mineralisation is present as veinlets or disseminations in vein-quartz and dacitic dykes that are hosted by north- and east-trending faults associated with the Yuao-Macao fault zone. No reliable data are

available for the metal resources at Haoshi and Dalingkou, but Wu et al. (1993) reported ore grades for Dalingkou of about 112 g/t Ag and 0.3 to 4.8 g/t Au, with Pb and Zn credits. The mineralisation is accompanied by silicic, pyritic, chloritic and sericitic wallrock alteration. The main hydrothermal alteration phases are quartz, chalcedony, sericite, rhodochrosite, muscovite and kaolinite (Wu et al. 1993). Fluid inclusion studies on the Haoshi deposit reveal a range of homogenisation temperatures from 70 to 300°C in gas-liquid inclusions, hosted by quartz, sphalerite, calcite and fluorite (Xu B et al.1995). These authors identified: (1) a quartz-pyrite mineralizing stage at 300–230°C; (2) a quartz-carbonate-sulphide mineralizing stage at 220–200°C; and (3) a quartz-fluorite-carbonate-sulfate mineralizing stage at 70–180° C. The gaseous and liquid composition of the inclusions in quartz and sphalerite include H_2O, Na^+, K^+, Ca^{2+} and Cl^{2-}, but no or little CO_2. Whole-rock Rb–Sr and K–Ar dating of sericite from altered wallrock at Haoshi and Dalingkou yields ages ranging from 130 to 95 Ma (Li C et al. 1993). The $^{87}Sr/^{86}Sr_i$ of 0.711 for the mineralized quartz suggests that the mineralizing fluid was probably of a mixed crustal-mantle source derived from the Mesozoic volcanic rocks in the region (Chen and Xu 1997). Sulfur isotope compositions of pyrite, sphalerite, galena and chalcopyrite from Haoshi and Dalingkou range from –7 to +7 ‰ δS^{34}, which is similar to those from Zhilingtou (–1 to +5 ‰ δS^{34}; Fig. 3B) from the CSU.

5.3.5.4 Epithermal Ore Genesis in the South China Fold Belt

A conceptual model of multiple stages of ore-forming events related to Jinning, Caledonian and Indosinian-Yanshanian tectono-thermal activities is shown in Fig. 5.41. In this model, Pirajno and Bagas (2002) envisaged that during tectonic events of Neoproterozoic (Jinning, ca. 850–900 Ma), Late Caledonian (ca. 400 Ma) and Indosinian (ca. 200 Ma) ages, island-arcs collided and were accreted to the eastern margin of the Yangtze Craton. These events were characterized by an active continental margin, subduction of oceanic crust and accretion of trench sediments. It is possible that during deformation and metamorphism, related to compression along the active margin, structurally controlled orogenic lode gold deposits were formed. In the SCFB, examples of mineralisation related to these events are the lode gold deposits of possible Caledonian age (ca. 400 Ma) hosted by the Huangshan Complex. The Caledonian event records the final amalgamation of the Yangtze Craton with the Cathaysia Block. The mylonite-hosted orogenic lode gold deposits of the Hetai-Gaocun field (Fig. 5.38) are considered to have an age of ca. 200 Ma. If this age is correct, the Hetai mesothermal lodes may be linked to Indosinian tectonic events and the collision of the North and South China Blocks along the Qinling-Dabie orogen (Wang et al. 1997). In a later ore-forming event, a continental margin was again active, during the latter part of the Indosinian and the Yanshanian tectono-thermal events, which resulted in the formation of the magmatic arc of the CVB, perhaps as a result of the flat-subduction, proposed by Li and Li (2007). The volcanic-hosted epithermal Au–Ag

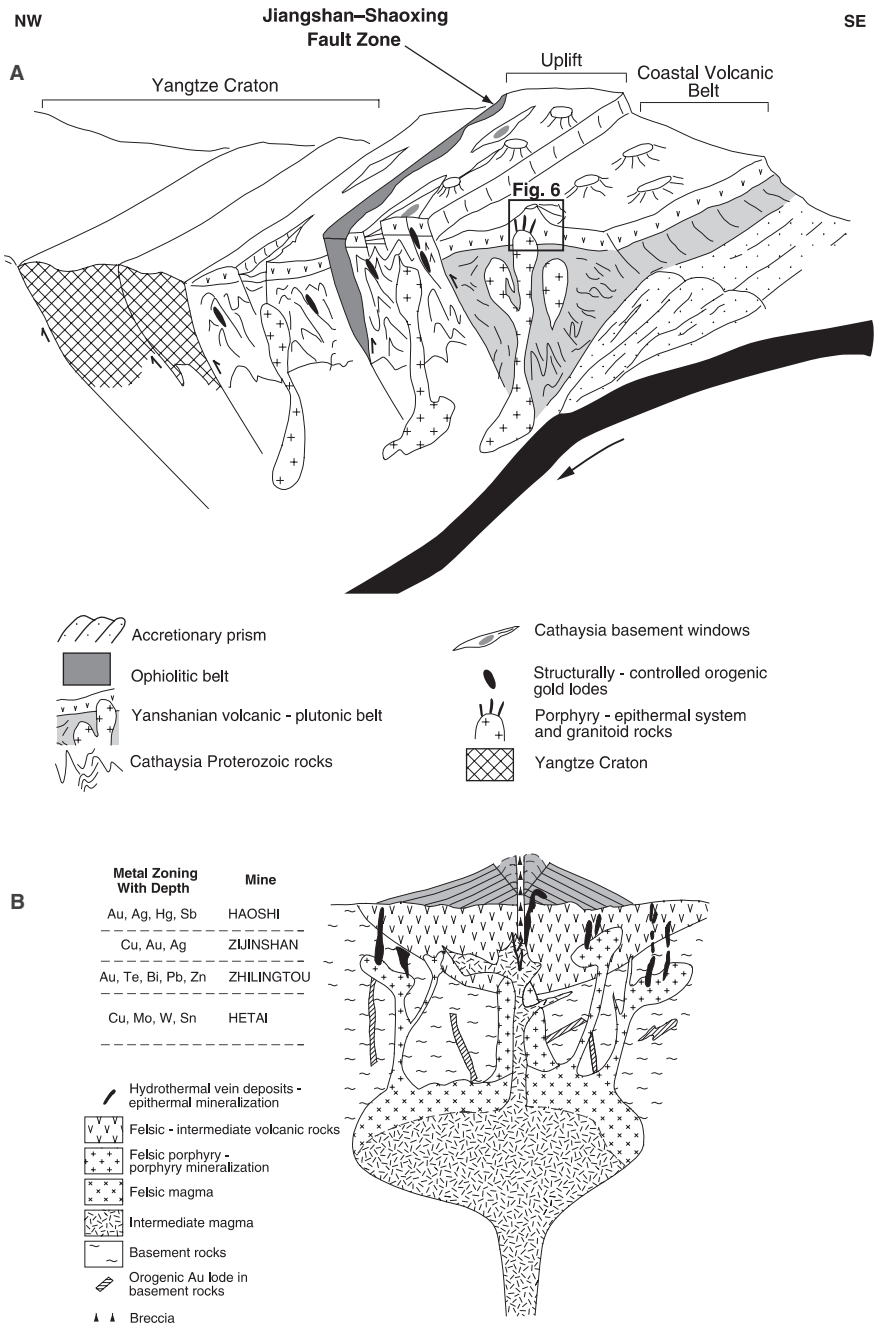


Fig. 5.41 (continued)

(e.g., Haoshi, Dalingkou, Zijinshan) and associated porphyry mineralisation was probably formed at this time.

The spatial relationship of Au–Ag mineralisation with uplifted basement rocks has also been noted in other parts of China that were affected by the Yanshanian magmatism (Miller et al. 1998). The uplifts probably formed because of compressional tectonics related to subduction and collision along the eastern continental margin of southeastern China. Hydrothermal circulation associated with Yanshanian magmatism resulted in epithermal-style deposits in Cathaysian basement rocks and within and around the overlying volcanic edifices. Stable isotope systematics from Zhilingtou show O- and H-isotopic compositions within the trends of low-salinity magmatic vapour and of neutral-pH geothermal waters, as defined in Hedenquist and Lowenstern (1994). However, the range of $\delta^{18}O$ and δ D provide some evidence of pre-existing lodes in Cathaysian basement rocks, formed during earlier (Neoproterozoic and Caledonian) mineralizing events. If this concept is correct, modification and reconcentration of precious metals at the site of the pre-existing orogenic lodes would have occurred as a result of the input of thermal energy during the Yanshanian magmatism. This may have been the case for the Zhilingtou field and perhaps in parts of the Huangshan field.

To conclude, in the model proposed in Pirajno and Bagas (2002) the Au and Ag metallogeny of the SCFB is the consequence of multiple ore-forming events. These events are linked to a series of tectono-thermal events spanning about 700 Ma and responsible for the collision and amalgamation of the Yangtze Craton, Cathaysia Block, followed by subduction of the Pacific Plate under the South China margin.

5.3.6 The El Indio-Pascua Epithermal Belt, Chile

The El Indio-Pascua belt, a fascinating major Au producing region of the central Andes (Fig. 5.42) contains the world-class Au–Ag–Cu high-sulphidation

Fig. 5.41 (continued) (**A**) Conceptual model of geodynamic setting for the South China Fold Belt and associated metalogeny; in this model subduction beneath a continental margin (Cathaysia) builds a magmatic arc, within which regional scale hydrothermal systems are activated due to magmatic heat and forming porphyry and epithermal systems. Compression along the arc causes uplift of basement blocks, such as the Chengai-Suichang Uplift (SCU) and exposed the ophiolitic rocks of the Huangshan Complex. Earlier collision events, such as the accretion of the Cathaysia Block against the Yangzte Craton, would have produced orogenic lode deposits, some of which were modified during the Cretaceous magmatic event, and some Au of epithermal systems, such as Zhilingtou, could have been sourced from prexisting lodes. (**B**) Idealised representation of a volcano-plutonic complex in the South China Fold Belt, with associated porphyry-epithermal mineral systems (e. g. Zhilingtou and Zijinshan) and depth-related metal zoning, older orogenic lodes are in the basement rocks

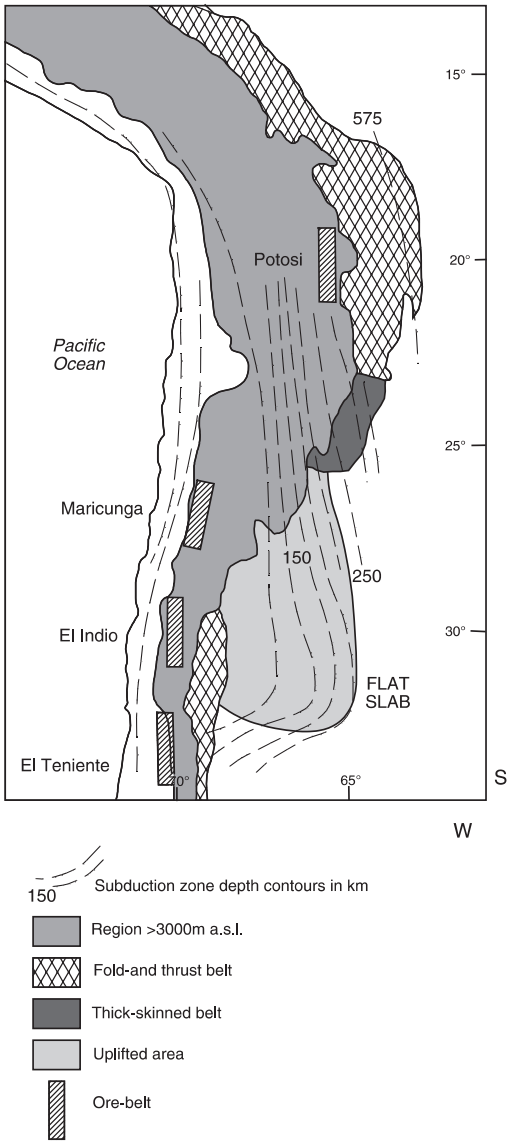


Fig. 5.42 Distribution of ore belts in the central Andean region; Potosí, El Indio-Pascua and El Teniente are described in this book. Based on Kay and Mpodozis (2002)

epithermal deposits of El Indio, Tambo, Pascua, La Coipa and Veladero (in Argentina), with a total resource of 1358 tonnes of Au, 28 746 tonnes of Ag and 2 Mt of Cu (Laznicka 2006). The overview of the mineral systems in the El Indio-Pascua belt is taken from the works of Jannas (1995), Jannas et al. (1999) and Bissig et al. (2002), Chouinard et al. (2005) and Deyell et al. (2005). The tectonic setting and geodynamic evolution of the central Andes were described by Kay and Mpodozis (2001).

The El Indio-Pascua belt is in the Main Cordillera of the Andes, straddling the border between Chile and Argentina, forming a north-trending graben of Oligocene-Miocene andesitic-dacitic volcanic and pyroclastic rocks and dioritic to granodioritic intrusions. The region was built by eastward subduction of the Nazca plate, which gradually flattened to almost near horizontal during the Miocene, leading to a geodynamic sequence of events related to slab geometry, crustal thickness, deformation, volcanism and mineralisation (Kay and Mpodozis 2001). It must be noted that the belt lies between 27° and 34° S latitude, which is at the present time non-magmatic and associated with a zone of flat subduction, separating a central volcanic zone from a southern volcanic zone, whereas the giant porphyry systems (including El Teniente described in Section 5.2.1.2), overlie the steeper part of the Andean subduction zone. An important aspect is that all mineralising events occurred before slab flattening, a topic to which I return later in this section. Equally important in the El Indio-Pascua district is the relationship between landscape evolution and the epithermal processes, as eminently documented by Bissig et al. (2002), also to be discussed later.

The epithermal systems of the El Indio-Pascua belt were formed between 9.4 and 6 Ma, but no contemporaneous igneous units have been documented in the El Indio and Tambo areas. In the El Indio-Tambo district the mineralisation is hosted by the 27–23 Ma Tilito Formation, a ~1200 m succession of dacitic and rhyodacitic pyroclastic rocks, volcaniclastic rocks and minor basalt with coeval hypabyssal diorite and granodiorite stocks. The dacite and rhyolite rocks host the orebodies and are extensively hydrothermally altered, mostly argillised and silicified. Alunite is both hypogene and supergene and may occur with jarosite, native S and gypsum.

The intensity of this magmatism steadily decreased with time till a Late Miocene (~8 Ma) phase of magmamatism of dacite porphyries associated with large scale hydrothermal breccia pipes in the Pascua area. No strato-volcanoes have been recognised in the region. The El Indio Au–Ag–Cu mineralisation is characterised by veins, locally exceeding 20 m in thickness, dominated by both high- and intermediate-sulphidation assemblages. The former represented by pyrite-enargite-alunite, the latter by quartz associated with subordinate tennantite-chalcopyrite-galena-sphalerite, tellurides, calcite, ankerite and rhodicrosite. Tennantite is associated with the Au mineralisation, replacing enargite and indicating a shift towards lower sulphidation states. There are two Cu–Au ore-forming stages (Jannas 1995). An earlier deeper stage is characterised by a systems of anastomosing veins and stockworks of massive pyrite and enargite, with minor chalcopyrite, sphalerite, galena, tennantite and calaverite. The younger stage is characterised by quartz veins with alunite, pyrophyllite and free Au forming "bonanza" ore shoots. The Tambo mineralisation is of a different style, being largely hosted by hydrothermal breccias within an area of advanced argillic alteration, mostly barite-alunite-quartz. A cap of friable and fine-grained alteration consisting of alunite-kaolinite-cristobalite-native S and native Au is in the higher parts of the Tambo deposit and was formed by steam-heated acid-sulphate waters.

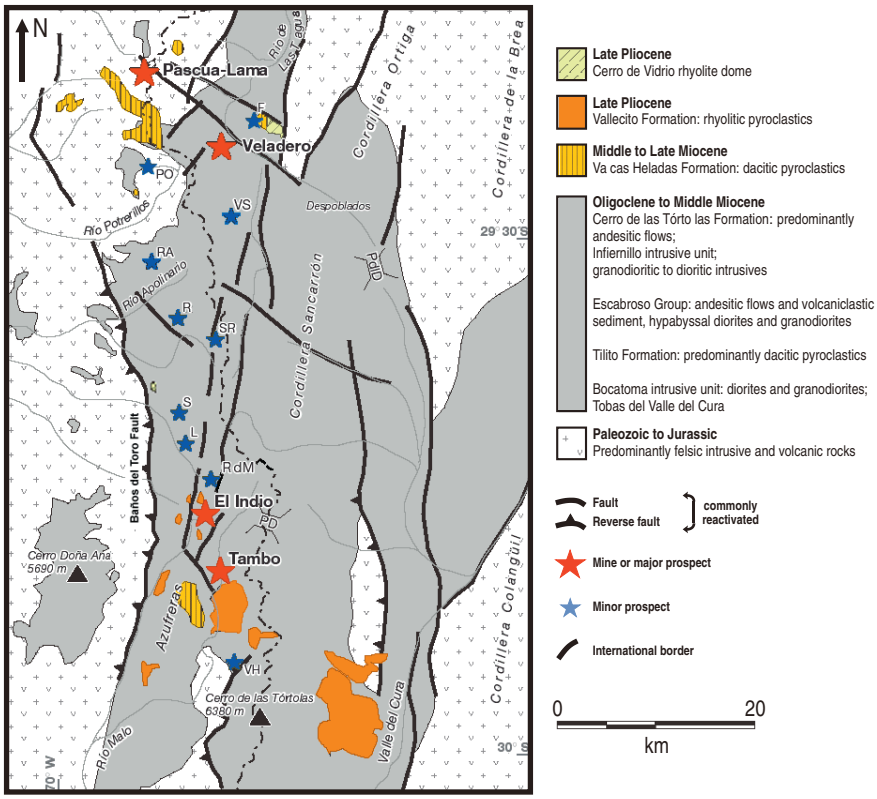


Fig. 5.43 Simplified geology of the El Indio-Pascua belt and location of ore deposits. Modified after Deyell et al. (2005) and Bissig et al. (2002)

The Pascua Au–Ag deposit is about 50 km north of El Indio-Tambo district (Fig. 5.43) and consists of irregularly shaped hydrothermal breccia bodies and adjacent stockworks, that intrude Mesozoic granites (Pascua-Lama complex) and pre-Mesozoic basement rocks. Intrusions of Neogene age (33 Ma) in the area are mainly diorites, whilst rhyodacitic quartz-feldspar porphyry and lamprophyre dykes are common and have an age of ~7.85 Ma. The ore zones tend to form a tabular body at elevations of 4800 m a. s. l., with more breccia bodies higher up showing silicification and a crude stratification. Native S is locally present. A large Au–Ag-mineralised breccia pipe is the Brecha Central contains clasts of previously altered and mineralised rocks and is subdivided into a central zone of heterolithic matrix-supported breccia, a marginal zone of monomictic, matix and/or clast-supported breccia and a surrounding stockwork zone. Post-brecciation stockworks contain quartz, alunite, pyrite, enargite and barite. Hydrothermal alteration is extensive and widespread and three stages have been recognised. Stage 1, pre-Brecha Central, is dominantly advanced argillic, with quartz, alunite, pyrite, rutile, pyrophyllite, some

kaolinite and dickite. Minor vuggy silica, argillic (illite) and propylitic (quartz, chlorite, illite, epidote, gypsum, kaolinite) alteration are also present. Stage 2 alteration includes advanced argillic, which postdates the emplacement of the Brecha Central pipe and is characterised by haloes of quartz and alunite surrounding veins. Vuggy silica alteration is characterised by leached and massive silicified rocks. Also in stage 2 is steam-heated argillic alteration (quartz-kaolinite) at the top of the system, at elevations >4950 m a. s. l. The Pascua principal ore minerals are pyrite and enargite, which contain Au, as well as some native Au. Four stages of Au–Ag–Cu mineralisation, developed after the emplacement of the Brecha Central, have been identified and are: (1) alunite-pyrite-enargite, in which enargite contains inclusions of native Au, calaverite ($AuTe_2$), stibnite, cassiterite, muthmannite [(Ag, Au)Te], goldfieldite [$Cu_{12}(Te, Sb)_4S_{13}$] and yuanjingite (AuSn); (2) pyrite; (3) pyrite-szomolnokite ($FeSO_4{\cdot}H_2O$), with Au, Ag an Cu as inclusions in pyrite; and (4) native Au, is in the vuggy silica zone, where the Au is hosted in gray quartz veinlets.

The sequence of events at Pascua began at about 9 Ma with stage 1 alteration and minor Au mineralisation. This was followed by a more complex series of stage 2 of intense leaching alteration at 8.76 Ma, representing the main Au–Ag–Cu mineralisation event. A late stage of mineralisation may have followed with Ag-rich minerals. The ore-forming events are terminated with the intrusion of the dacitic quartz-porphyry dykes, at 7.84 Ma.

I mentioned earlier the work of Bissig et al (2002) on the evolution of the Miocene landscape in the El Indio-Pascua belt. Erosional landforms in the region developed in response to tectonic uplift influencing the activity of the hydrothermal systems through the lowering of the water table, in a similar fashion as recorded in northwest Turkey (Section 5.3.4). In the El Indio-Pascua area Bissig et al. (2002) recognised three erosional landforms, reasonably well dated through associated intrusive rocks. The earliest surface is the ~17–15 Ma Frontera-Deidad surface (Stage 1), with present elevations of 4650–5250 m a.s.l. The second is the ~14–12.5 Ma Azufreras-Torta (Stage 2), at present elevations of 4300 to 4950 m a.s.l., incised into the first, following uplift. Fluvial clastic sediments were deposited in the Azufrera tableland. The third erosional surface is the 10–6 Ma Los Rios (Stage 3), extensively developed on the eastern side of the El Indio-Pascua graben (the Argentinian side), and only confined to narrow apron pediments, incised by glacial and fluvial erosion. As recorded for the Biga peninsula of northwestern Turkey, albeit on a smaller scale, the El Indio-Pascua epithermal systems were effectively controlled by uplift, which in turn controlled landscape evolution. In this way, high-temperature barren potassic assemblages formed first and are at the highest levels (Stage 1), progressively followed at lower levels by intermediate-temperature assemblages to lower-temperature hypogene quartz-alunite and supergene steam-heated (alunite-kaolinite-native S) Au–Ag–Cu mineralised alteration systems, associated with the Stage 3 Los Rios surface. Ore formation was related to episodic intrusion of dacitic porphyries in the Pascua area, whilst in the El Indio side there was episodic release of fluids

from a hidden magma chamber, over a period of about 1.5 Ma. The lowering of the water table in response to uplift influenced hydrothermal fluid evolution, by increasing lateral flow of ground waters, fluid boiling and mixing, which resulted in ore deposition. By contrast, the earlier barren vein and alteration systems were formed from non-boiling, volatile-rich, predominantly magmatic fluids.

5.3.6.1 Tectonic Setting and Geodynamic Evolution of the Central Andean Ore Belt

Kay and Mpodozis (2001), based on a model developed by Isacks (1988) and REE geochemistry of lavas, examined the geodynamic evolution of the central Andean ore belt, between 22° and 34° S latitude, where some of the world's largest and richest ore belts, between the Potosi Sn–Ag porphyries to the north, through the El Indio-Pascua epithermal systems to the El Teniente porphyry deposit to the south, are located (Fig. 5.42) These authors suggested that magmatism and ore formation in the central Andean belt were controlled by the inclination of the subducting slab and related changes in crustal and lithospheric thickness. Seismic data show that the subducting Nazca plate beneath the South American plate can be divided into a central segment of nearly flat dip with no volcanic activity, flanked by steeper segments associated with volcanism. The flat slab segment is between 33° and 28° of latitude, which is where the El Indio-Pascua belt is situated. By contrast, the El Teniente area is above the southern transition to a steeper dip and the Potosí district above the northern steeper segment. The dip of the subducting Nazca plate changed through time, with steep dips between ~23 and ~10 Ma, characterised by mafic to andesitic volcanism to progressive flattening between ~7 and <3 Ma, characterised by dacitic volcanism to lack of volcanic activity in the last stage. Rare earth element data show a small range of La/Sm and wide variations in the Sm/Yb ratios, which reflect changing pressure conditions from clinopyroxene to amphibole to garnet in the residuum of the evolving magmas, which in turn reflect crustal thicknesses from <35 km (clinopyroxene), to 30–45 km (amphibole) to >45–50 km (garnet).

The giant Miocene ore systems of the central Andes were formed during stages of shallowing subducting zone geometry, during compression and crustal shortening, near the end, or at the start of, a volcanic episode. The model is shown in Fig. 5.44. Magmas that are formed in the mantle wedge above a steep subduction zone (see Fig. 5.6), erupt through a normal thick crust and have anhydrous residual mineral assemblages and do not produce hydrothermal systems. As the slab begins to flatten, the thin asthenospheric wedge above the slab inhibits arc magmatism, but as the slab dehydrates and the breakdown of the amphibole releases large amounts of fluids during melting, resulting in hydrous magmas that crystallise amphibole and are intruded into a thickened crust. This is the stage when ore systems are developed. Furthermore, oxidising conditions prevent the early removal of

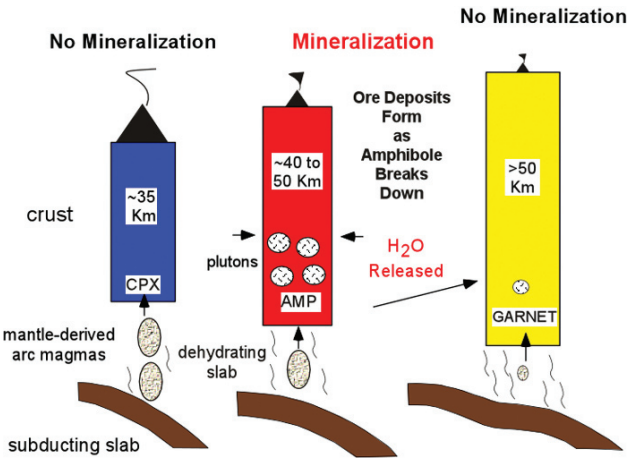


Fig. 5.44 Flat slab model of Kay and Mpozodis (2001) for the formation of the central Andean porphyry and epithermal ore systems. During stage 1 mantle-derived arc magmas are developed from the mantle wedge over a steep subduction zone, with no mineralisation being generated; during stage 2 the subducting slab begins to flatten and dehydrate producing hydrous melts and hydrothermal fluids, which generate the ore systems in the region, in this situation the crust contains; the present-day slab is nearly horizontal, resulting in no volcanism and no mineralisation, the crust is now thick and dry with no fluids being produced. Figure reproduced unchanged by permission of the authors and the Geological Society of America

sulphides in the hydrous magmas, thus allowing metals to be concentrated in the residual fluids of the cooling magmas. Kay and Mpodozis (2001) also emphasised that another important factor in fluid generation is the thickening of the crust under compression, which tends to trap magmas at depth. These magmas further promote crustal melting and increase crustal ductility, thereby increasing compression which leads to over-pressured fluids being expelled from the crystallising plutons.

Further crustal thickening and flattening of the subducting slab result in a thicker and dry crust (garnet stability; granulite facies metamorphism), leading to cessation of volcanism and the fluids necessary for hydrothermal activity are no longer available.

5.3.7 Epithermal Systems in the Northern Great Basin, USA

The Great Basin is part of the Basin-and-Range province, which is the largest area of continental extension in the world, with its structural style of tilted and faulted blocks, listric normal faulting, strike-slip faulting and general broad arching. The physiography of the Basin-and-Range province is typically a system of elongate mountain ranges and valleys, 15–20 km across. The Basin-and-Range is now an internationally accepted term for the description of

similar structural and physiographic features. The Basin-and-Range province is about 800 km wide and extends from the western USA southward into northern Mexico, a distance of about 1500 km. This region is characterised by high heat flow, seismic activity and low upper mantle velocity, rich in mineral resources, especially precious metals (e.g. the world-class Carlin style Au deposits described in Chapter 9) and active geothermal fields (Section 5.4.4). Cenozoic extensional tectonics exhumed metamorphic and igneous rocks forming metamorphic core complexes and was accompanied by extensive calc-alkaline and bimodal (rhyolite-basalt) magmatism. An explanation for the extension that resulted in the inception of the Great Basin and the Basin-and-Range province, is hotly debated but generally falls into two main models: back-arc rifting and rifting related to the impingement of a mantle plume. Extension and crustal thinning above a mantle plume may ultimately have been responsible for much of the Late Cenozoic magmatism in the western USA (Basin-and-Range, Western Great Basin, Colorado Plateau and the Great Plains; see Fitton et al. 1991, for a comprehensive review). Dickinson (2006) provided an overview of the geodynamic history of the Great Basin.

John (2001) studied low-sulphidation (adularia-sericite) and high-sulphidation (quartz-alunite) epithermal Au–Ag deposits of Mid-Late Neogene age in the northern parts of the Great Basin (Fig. 5.45). The low-sulphidation epithermal systems can be further divided into two subtypes based on mineralogy and associated magmatism, intermediate low-sulphidation and end-member low-sulphidation (Hedenquist et al. (2000); John 2001 and references therein). Calc-alkaline magmatism related to subduction of the Pacific plate beneath western North America occurred in the Mid-Late Jurassic, the Cretaceous and in the Mid-Cenozoic and may have resulted in back-arc type of extension. Porphyry Cu–Mo systems and the above-mentioned Carlin-style Au deposits were formed during this time. John (2001) divided the Cenozoic magmatism of the northern Great Basin into three assemblages: (1) Eocene-Early Miocene interior andesite-rhyolite; (2) Early Miocene-Early Pliocene western andesite; and (3) Mid-Miocene to Holocene bimodal basalt-rhyolite. The first assemblage began at around 43 Ma with volcanic activity migrating southwestward and forming a succession of arcuate belts. The andesite-rhyolite assemblage consists of dacite and rhyolite ash flow tuffs, flow dome and more than 50 caldera complexes with andesitic, dacitic and less commonly basaltic lava flows. Intrusive rocks include mostly granodiorite with associated porphyry Mo systems. Rocks of the andesite-rhyolite assemblage are calc-alkaline and related to delamination of the subducted Farallon plate, resulting in upwelling of asthenospheric mantle, decompression melting, formation and ponding of basaltic melts and partial melting of lower crust (John 2001 and references therein; see also delamination tectonics in Chapter 3). The western andesite assemblage is a 22–16 Ma high-K calc-alkaline series characterised by hornblende-pyroxene andesite and biotite-hornblende dacite, rhyolitic intrusions and minor amounts of basaltic rocks. This assemblage is part of a continental margin magmatic arc extsnding from Canada to northern Mexico, and related to subduction of

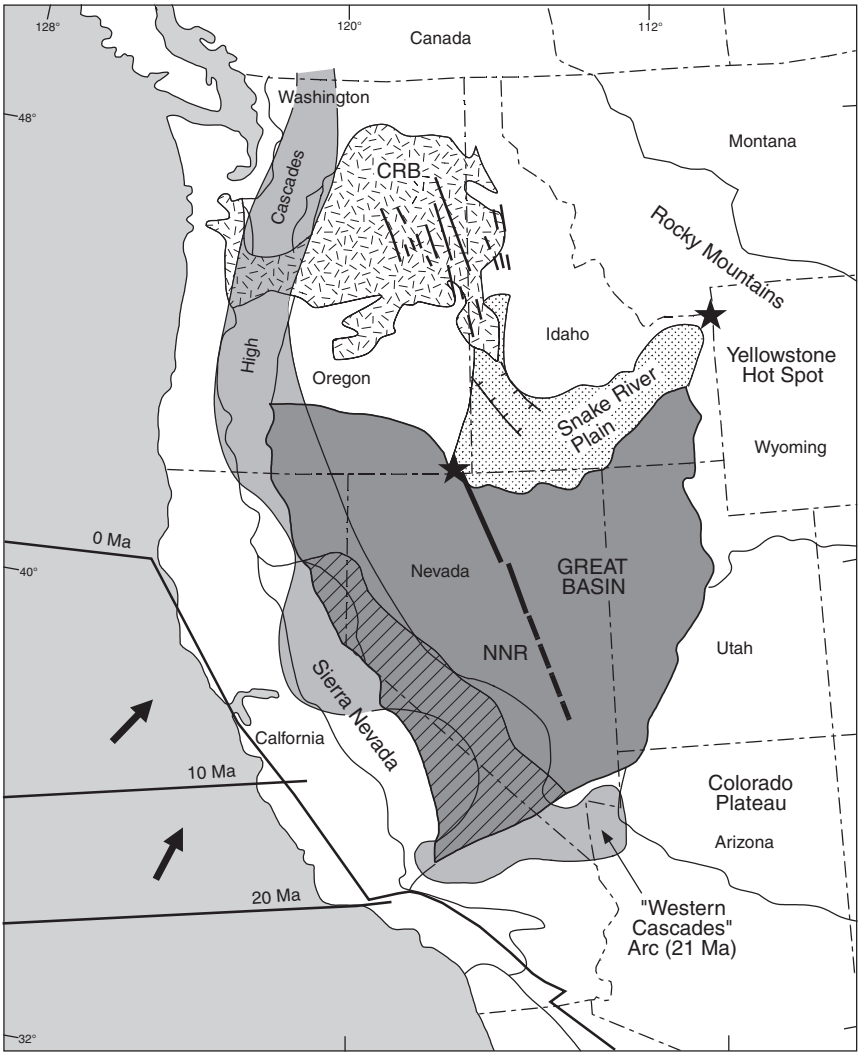


Fig. 5.45 The Great Basin in western USA; the heavy line represents the northern Nevada rift, with the 16.5 Ma Yellowstone hot spot at its northern end shown by the star, the other star at the northeast end of the Snake River Plain is the present-day position of the Yellowstone hot spot; further to the north are the Columbia River Basalt (CRB) and associated dyke swarm. After John (2001)

oceanic crust beneath the North America. The youngest volcanism in the Great Basin began around 16.5 Ma and is represented by the bimodal basalt-rhyolite assemblage, which includes olivine basalt, pyroxene andesite and basaltic andesite, with sub- and peralkaline rhyolites being most common. The basalt-rhyolite assemblage is a K-rich tholeeitic series, typically with anhydrous minerals,

suggesting low-water contents in the parent magmas. The basalt-rhyolite assemblages were erupted in a continental rift setting associated with the extension of the Basin-and-Range province. Furthermore, and as mentioned above, a mantle plume (Yellowstone plume) may have been the cause of lithospheric extension and rifting.

John (2001) noted some striking differences in the petrology between the bimodal and western andesite assemblages. The petrology of these more or less coeval suites show that the western andesite is derived from magmas that are more water–rich and oxidised than those that produced the bimodal basalt-rhyolite suite, which either lack or only sparsely contain hydrous minerals, such as biotite and hornblende. At the same time these differences reflect variations in the tectono-magmatic environment that produced the western andesite and basalt-rhyolite assemblages. The latter is characterised by thin lava flows, cinder and spatter cones and continental shield volcanoes, high-temperature and peralkaline pyroclastic ash-flows associated with the formation of large calderas (see Section 5.4.4). Rocks of the western andesite suite tend to form stratovolcanoes, dome fields, subvolcanic and granitic intrusions. The western andesite rocks are generally porphyritic and commonly contain biotite and/or hornblende phenocrysts. John (2001) suggested that the western andesite suite was erupted during the oblique subduction of the Farallon plate along the western coast of North America. The Farallon slab dehydrated, released volatiles to the overlying mantle wedge, producing volatile-rich partial melts that ascended to pond at the base of the lithosphere in the MASH (melting-assimilation-storage-homogenisation) zone (Figs. 5.6 and 5.46A). The bimodal suite, on the other hand, is associated with continental rifting and extensional faults, which allowed the rapid ascent of mafic magmas, forming monogenetic volcanoes, subvolcanic intrusions, dyke swarms and calderas (Fig. 5.46B). The volcanic activity of the bimodal suite was generally of short duration (1–2 Myrs) compared to that of the western andesite. The composition and isotopic features of the bimodal rocks are indicative of a subduction-enriched lithospheric mantle source (see also Fitton et al. 1991). The silicic ash-flow tuffs were produced by partial melting of lower crustal materials due to lithospheric underplating of basaltic melts (Fig. 5.46B).

5.3.7.1 Low-Sulphidation Epithermal Au–Ag Systems

The Great Basin hosts numerous Miocene-early Pliocene high- and low-sulphidation epithermal systems that include world class deposits, such as the Comstock Lode. The low-sulphidation epithermal systems of the western andesite have oxidation and sulphidation states that are intermediate or transitional to those of the low-sulphidation of the bimodal suite and the high-sulphidation systems of the western andesite. As mentioned above, this feature led to a further subidivision of low-sulphidation systems into an intermediate or type 1 and end-member or type 2 epithermal deposits (John 2001; Hedenquist et al. 2000). The low-sulphidation of the western andesite formed in subduction-related

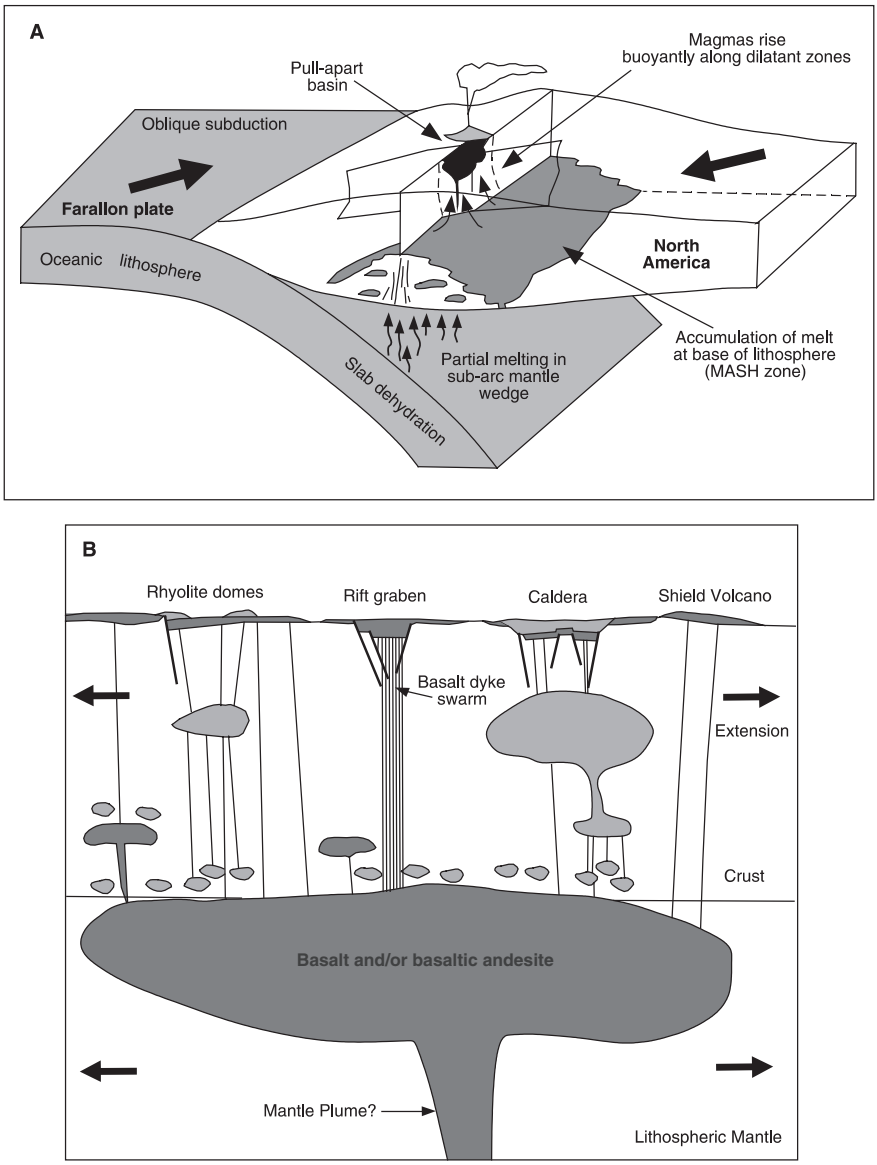


Fig. 5.46 John's (2001) models for the tectonic and magmatic setting of the calc-alkaline western andesite suite and the basalt-rhyolite bimodal assemblage; (**A**) the former developed along the western side of the Great basin (see Fig. 5.45) by the oblique subduction of the Farallon plate; magmas produced in the mantle wedge above the subduting plate accumulate at the base of the lithosphere in the MASH zone and rise into dilatant zones; (**B**) the bimodal assemblage resulted from the ponding of mafic melts at the base of the crust, probably derived from a mantle plume; these rise to the surface to erupt as basalt lavas in shield volcanoes or form subvolcanic intrusions, whilst crustal melts (high-silica water-poor rhyolites) form calderas and domes

volcanic settings, in transtensional zones related to strike-slip faults and associated with andesite and dacitic stratovolcanoes and dome fields (Fig. 5.46A). The low-sulphidation deposits related to the bimodal assemblage formed in extensional environments typical of rift settings and are related to magmas that are enriched in lithophile elements, Hg and U and are affiliated with reduced Mo–Sn–W porphyry systems. The epithermal systems of the bimodal suite are of the end-member or type 2, spatially and temporally associated with rhyolite flows, mafic flows and dykes. These epithermal systems typically have zones of smectite-illite alteration with inner zones of silica-illite-adularia and peripheral calcite-chlorite-epidote (propylitic) zones. Key metal and elemental signatures are Au–Ag–Hg–As–Sb–Se–Mo–Tl–W. Ore minerals include pyrite, marcasite, arsenopyrite, electrum, native Au, stibnite, selenides, pyrrhotite, with minor sphalerite, galena, chalcopyrite, tetrahedrite. The temperature of ore formation is generally $\leq$200°C, with fluids of neutral pH, very low salinities ($\leq$ 2 wt% NaCl equivalent), low f_{O2} and low f_{S2}. The western andesite low-sulphidation systems belong to type 2 or intermediate style. The mineralisation is characterised by rhythmically banded and comn textured veins, regional propylitic (calcite-chlorite-epidote) alteration, zones of adularia-sericite and argillic alteration. Quartz-carbonate-adularia veins are a common feature as are zones of barren steam-heated argillic alteration, overlyng boiling zones. Metal assemblage is Au–A–Cu—Pb–Zn–Ba–Mn–Se and ore minerals include pyrite, electrum Ag sulphides and sulphosalts, sphalerite, galena and chalcopyrite. The nature of the ore fluids is neutral pH, low to moderate f_{O2} and f_{S2}, salinities ranging from 1 to 6 wt% NaCl equivalent. Temperatures of ore formation range from 280 to 200°C.

In conclusion, the low-sulphidation epithermal systems of the Great Basin can be divided into those that formed in a subduction-related setting (western andesite assemblage), associated with stratovolcanoes, high-sulphidation and Cu–Au porphyry systems, and those that formed in a continental rift setting. The latter may be related to a plume event, with eruption of basaltic lavas, formation of large calderas and hig-silica ash flow tuffs, reflecting underplating of basaltic magmas and partial melting of the lower crust. These systems are typically of a bonanza vein type formed in comparatively short time, and associated with porphyry Mo systems.

5.3.8 The Oldest Epithermal Systems, Archaean Pilbara and Yilgarn Cratons, Western Australia

Archaean epithermal systems have been recognised in the Pilbara Craton and in the Yilgarn Craton in Western Australia. Those of the Pilbara Craton occur in the East Pilbara Terrane, briefly introduced in Section 5.2.3 and therefore not repeated here. The key features of the East Pilbara Terrane is that it is made up of a series of mantle plume related mafic-felsic successions, mostly forming oceanic plateaux which, given the presence of stromatolites, would have

been partially emerged and have had shallow lagoons. The Yilgarn Craton is well known for its abundance of orogenic lodes (Chapter 9), related to accretionary and collision tectonics, a geodynamic regime most unfavourable for the preservation of the high-level epithermal mineral deposit. Nevertheless, as explained below, relics of ancient epithermal systems have been recognised in eroded sedimentary products. The interested reader can find an excellent overview of the geology of the Yilgarn Craton in Myers and Swager (1997).

5.3.8.1 Epithermal Systems of the Warrawoona Group, East Pilbara Terrane, Western Australia

The 3.53–3.42 Ga Warrawoona Group (Pilbara Supergroup) in the East Pilbara Terrane contains volcanic-hosted massive sulphides (VHMS) and epithermal systems (Huston et al. 2000; 2007a, b; Van Kranendonk and Pirajno 2004). The following discussion is taken from these sources. The Warrawoona Group is a thick (about 18 km) succession of basaltic rocks interbedded with horizons of felsic rocks, including numerous chert beds (Fig. 5.47; see also Figs. 7.40 and 7.41). The Warrawoona Group is divided into four subgroups, each with a sequence of lower ultramafic-mafic volcanic rocks, overlain by felsic volcanic rocks and capped by a chert unit. Van Kranendonk and Pirajno (2004), on the basis of field and geochemical data, interpreted the Warrawoona Group to represent an ancient oceanic plateau, built on sialic basement and overlain by flood basalts of the Kelly Subgroup (Euro Basalt). They compared it with the modern-day Kerguelen oceanic plateau, where subaerial silicic caldera complexes are present in its emerged portions of the Kerguelen archipelago in the Indian Ocean (Bonin et al. 2004). The Warrawoona Group bears evidence of extensive geothermal activity, probably related to caldera-forming processes and responsible for a wide range of mineralisation types, from polymetallic veins, volcanogenic massive sulphides and epithermal deposits.

The Warrawoona chert units (bedded fine-grained silica-rich rocks) represent distinct stratigraphic horizons, from oldest to youngest including (Fig. 7.41): (1) Dresser Formation with up to five chert + barite + carbonate + jasper interbedded with pillow basaltic lavas; (2) the jaspilitic Marble Bar Chert Member and the Apex chert comprising several thin chert units overlying the Apex Basalt; and (3) silicified carbonate rocks of the Strelley Pool Chert containing stromatolites, at the top of the Panorama Formation and base of the overlying Kelly Group. The basalt stratigraphy contains numerous other, thinner, chert horizons of various protolliths that were replaced by silica. These chert horizons are associated with hyrdothermally altered footwall basalts, silica and barite veins. The cherts of the East Pilbara Terrane are well known for hosting relics of the earliest life as well as the oldest stromatolite colonies (Van Kranendonk 2006). This topic is taken up in more detail in Chapter 10.

The alteration mineral assemblage (quartz, alunite-jarosite, barite, kaolinite, sericite, chlorite, carbonate) in the footwall basalts of major bedded chert

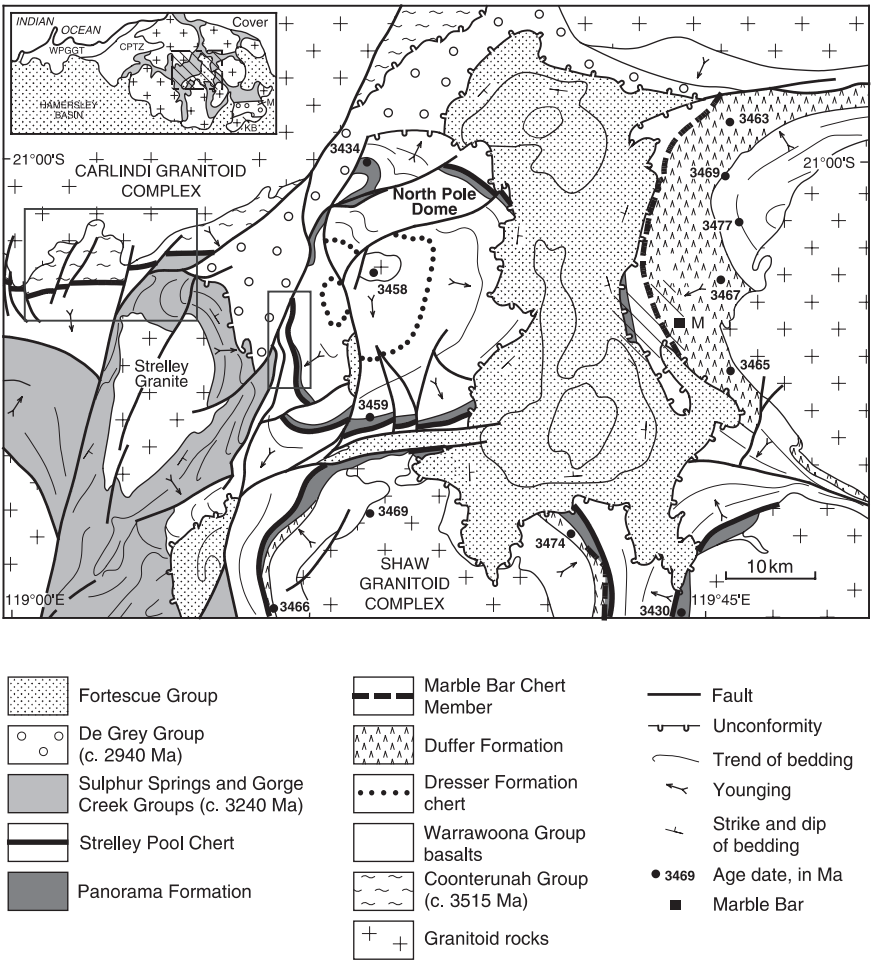


Fig. 5.47 Schematic geological map of the East Pilbara Terrane. Numbered rectangles refer tosubsequent figures. Circled numbers refer to Localities 1 and 2 of the Strelley Pool Chert discussed in the text. After Van Kranendonk and Pirajno (2004)

horizons and associated generations of amorphous silica ± barite veins in the Warrawoona Group suggests an epithermal environment of formation for the cherts, the vein swarms and the alteration. The restriction of the alteration assemblages and hydrothermal vein swarms to footwall rocks stratigraphically underneath the bedded chert deposits in these moderately to steeply dipping rocks indicate that alteration occurred at the time of accumulation of the stratigraphy at not after the rocks had been deformed; i.e. the alteration is not related to recent weathering. Three main types of alteration have been recognized associated with the different chert horizons: (1) alunite-kaolinite-barite in the Dresser Formation and Apex Chert, indicative of advanced argillic

alteration); (2) carbonate-chlorite in the Dresser Formation; and (3) Apex Chert, indicative of propylitic alteration; quartz-sericite alteration in the Strelley Pool chert localities, indicative of phyllic alteration.

The chert horizons of the Dresser Formation and Apex Chert represent episodes of exhalite deposition from acidic, high-sulphidation epithermal systems during hiatuses in mafic volcanism, including deposition of syngenetic chemical sediments (bedded chert horizons) from hot springs and replacement of host rocks along fluid pathways. The evidence for multiple phases of alternating silica- and/or barite-rich fluids in feeder veins to bedded chert-barite units in the Dresser Formation and the presence of hydrothermal chert breccias with hydrothermal kaolinite supports the data from alteration geochemistry studies that the clay altered pillow basalts beneath the major chert horizons in the Dresser Formation, although also affected by recent weathering, originated through steam-heated alteration in a high-S system. The weathering may even be the result of supergene alteration, as is common in more recent epithermal systems.

A similar scenario may apply to the Apex chert, although at a smaller scale. In the Apex chert, bedded felsic tuff and chert deposits are preserved as lenses, interpreted to represent small basins developed on relict topography in the underlying basalt that is partly controlled by long-lived growth faults. The presence of barite, alunite-jarosite and high trace metal contents in these rocks indicates a similar acid-sulphate epithermal environment as the Dresser Formation. This system differs from the Dresser Formation, however, in that it contains associated felsic rocks that probably originated as a small volume of fractionated melt from the dominantly basaltic magma chamber. Individual radiating swarms of feeder veins underlie the chert-felsic tuff lenses, and the heat energy for at least some of the hydrothermal circulation appears to be subvolcanic dolerite sills. Hydrothermal alteration of basalt overlying the Apex chert probably occurred at the end of the next overlying basalt flow, when a subsequent period of chert deposition and associated fluid circulation occurred.

The chert $\pm$ barite horizons of the lower Warrawoona Group are associated with an alteration mineral assemblage that is related either to venting of low-temperature fluids with high concentrations of H_2S, SO_4^{2-} and Si, or to distal sulphate-rich facies of high-temperature hydrothermal systems. The presence of cherts associated with minerals such as sericite, quartz, barite, alunite, jasper, and hydrothermal kaolinite is similar to the distally precipitated exhalites or chemical sediments of the Phanerozoic Kuroko-style volcanogenic massive sulphide deposits (VHMS; discussed in Chapter 7). Kuroko style deposits are well represented in the Phanerozoic as well as in the Archaean (e.g. Noranda district in Canada). The main difference between the Phanerozoic and Archaean Kuroko-style deposits is their metal association, with the former being Pb-rich and the latter Zn-rich (see Pirajno 1992; Misra 2000 and references therein). The dominance of Zn–Cu metals in the Warrawoona cherts is suggestive of a Noranda-type Kuroko environment. In these environments, massive sulphides are associated with chemically precipitated sedimentary

rocks, which may either cap the sulphide bodies or occur distally and laterally away from the sulphides. The full range, from massive sulphides and chemical sediments to chemical sediments with no sulphides, formed in a subaqueous caldera setting. Alternatively, the Dresser Formation is known to have low total sulphides and thus it may be similar to the high-level, low temperature area of disseminated Au deposits that formed near volcanic fumaroles. The extensive barite deposits and the evidence for chert-barite deposition and vein emplacement during the formation of normal growth faults, indicates alteration in a steam-heated acid-sulphate volcanic caldera-type geothermal system (Figs. 5.24, 5.48 and 5.49).

In contrast to the hydrothermal systems in the lower Warrawoona Group, the phyllic alteration associated with the Strelley Pool Chert formed from a low-sulphidation epithermal system. Field evidence shows that the Strelley Pool Chert was deposited as a succession of siliciclastic rocks and dolomite in a subaerial to shallow marine environment across a regional unconformity and then silicified after deposition. The distinctive high K_2O signature of altered footwall basalts beneath the Strelley Pool Chert may reflect Archaean weathering processes during the period of subaerial exposure, enhanced by the effects of phyllic hydrothermal alteration that may have been caused by low temperature fluids circulating beneath the overlying basalt.

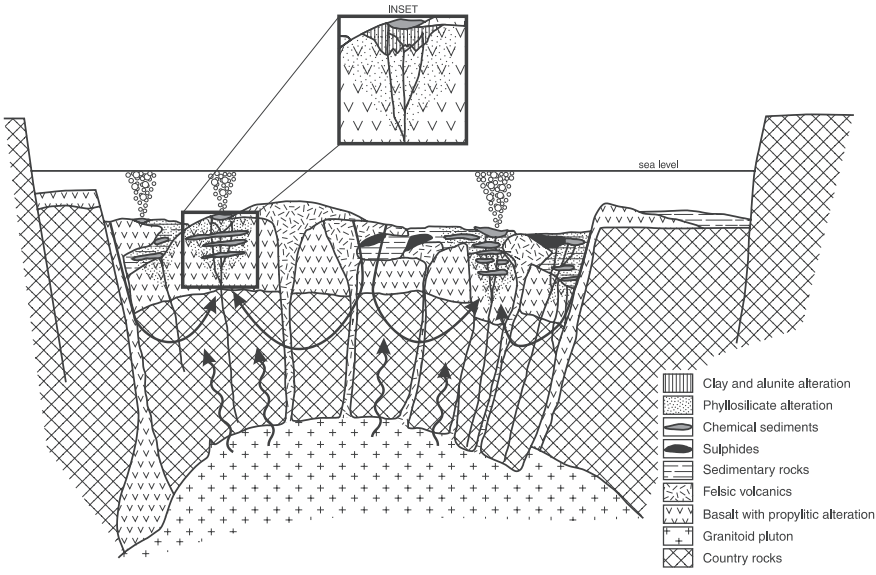


Fig. 5.48 Model of a submarine caldera setting, the inferred tectonic environment for the hydrothermal systems of the Dresser Formation and Apex chert. Inset shows idealized alteration patterns associated with a single hydrothermal circulation event and deposition of bedded chert. Note background propylitic alteration in the basaltic footwall rocks after Van Kranendonk and Pirajno (2004)

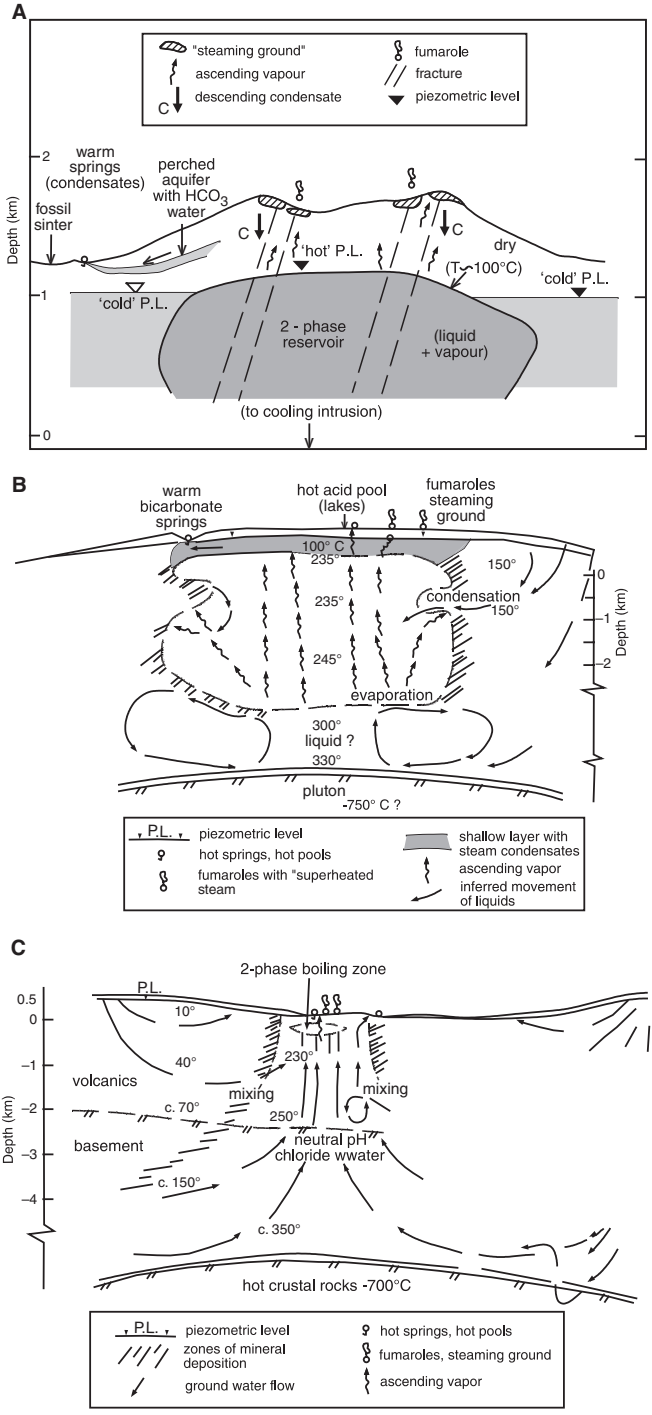


Fig. 5.49 (continued)

5.3.8.2 The Fossil Epithermal System of the Kanowna Belle Au Deposit, Yilgarn Craton, Western Australia

The Kanowna Belle Au deposit, about 18 km northeast of the town of Kalgoorlie in Western Australia, is a Late Archaean orogenic lode-gold deposit as defined in Groves et al. (1998) and the following is derived from Beckett et al. (1998) and Ross et al. (2001, 2004).

The Kanowna Belle deposit is in the Eastern Goldfields Province of the Yilgarn Craton (Fig. 9.10), which is a Late Archaean granite-greenstone terrane, characterised by deformed and metamorphosed volcano-sedimentary rocks intruded by granitic and high-level porphyry intrusions. The deposit is within the Boorara Domain of the Kalgoorlie Terrane in the easternmost part of the Yilgarn Craton, is hosted by 2.66 Ga felsic volcaniclastic rocks of the Black Flag Group, intruded by felsic and mafic sills, monzogranites and felsic porphyries. The hangingwall succession of the Kanowna Belle mine comprises the Grave Dam Grit, overlying the QED Rudite, a felsic volcanic and volcaniclastic-dominated conglomerate, a re-sedimented syn-eruptive volcaniclastic rock, and the Golden Valley Conglomerate, a volcanogenic sedimentary rock. In the footwall is a package of heterolithic volcanogenic conglomerate, with lenses of arkosic sandstone (Golden Valley Conglomerate and Cemetery Sandstone). These sedimentary units are intruded by dacitic porphyries, differentiated into four units (Kanowna Belle Porphyry, Lowes Porphyry, West Wall Porphyry, Hanging wall Porphyry, with ages of ~2.65–2.66 Ga).

The Kanowna Belle deposit had remaining resources in 1996 of 19.8 Mt at 5.9 g/t Au and its Au mineralisation is contained in four lodes, Hilder Shoot, Troy Shoot, Hangingwall Shoot and Lowes Shoot, all mined out except for the latter. The mineralisation occurs in altered clasts, quartz-carbonate dilational veins and at lithological contacts. The Lowes Shoot is hosted by the Kanowna Belle porphyry and Lowes sandstone. The ore fabric is characterised by microfracturing, veining and alteration of the host rocks. Ore is associated with silicified zones containing abundant quartz-carbonate-pyrite veins and minor breccias. The main alteration minerals are sericite, ankerite and pyrite, with localised narrow and discontinuous zones of silicification and albitisation. Three alteration assemblages are recognised: outer sericite-carbonate to carbonate-chlorite, intermediate sericite-carbonate-pyrite and inner pyrite-albite-silica. Zones of pervasive carbonate-sericite alteration extend up to 300 m from the defined mineralisation.

Fig. 5.49 (continued) Conceptual models of surface manifestations and subsurface circulation patterns of liquid and steam geothermal systems; (**A**) High-temperature steaming ground linked to a liquid-vapour reservoir; (**B and C**) liquid-dominated geothermal systems. After Hochstein and Browne (2000)

The presence of altered and Au-bearing clasts and fragments of veins in the Black Flag volcaniclastic rocks led Ren and Heithersay (1998) to suggest that the Kanowna Belle mineralisation was first generated in an epithermal-porphyry environment that was subsequently remobilised into structural sites during regional deformation events. Geochemical fingerprinting of free Au from a lode vein and of Au from a mineralised clast showed that clast Au has higher Cd/Cu and lower Te/Cu and Pb/Cu ratios than lode Au. These geochemical differences, including several other elements and key ratios (Au/Ag, Au/As, Au/Sb, Au/Te) have been interpreted to signify two generations of Au from two mineral systems: one derived from an eroded low-sulphidation epithermal deposit, the other is consistent with lode deposits elsewhere in the Yilgarn Craton. However, Ross et al. (2001) pointed out that the contribution of this epithermal Au to lode Au was probably minor. Nevertheless, the presence of a "fossil" epithermal mineral system, prior to 2.68 Ga and preserved in clastic beds, provides good evidence of early low-sulphidation epithermal mineralisation in Archaean granite-greenstone terranes.

5.4 Active Epithermal Systems (Geothermal Fields)

The convective circulation of meteoric water in areas of high heat flow, whether or not these vent to the surface, constitute a geothermal field. Generally, but not always (see Chapter 9), subaerial geothermal fields are found in regions of volcanic activity, at convergent margins, intracontinental rift zones and hot spots. The surface expressions of geothermal systems are commonly thermal and/or mineral springs, solfataras and fumaroles. The heat energy that powers the convective circulation of meteoric waters is in all cases provided by shallow intrusions. Overviews of geothermal systems can be found in Goff and Janik (2000) and Hockstein and Browne (2000) from whom I have drawn the following narrative.

Geothermal systems have three important elements: (1) a permeable reservoir; (2) water in the reservoir that transports heat to the surface; and (3) a heat source (see also Chapter 2). Geothermal systems can be considered on the basis of temperature at an arbitrary depth of 1 km. Hockstein and Browne (2000) distinguished: (1) high-temperature, $>225^{\circ}C$; (2) intermediate temperature, 125–225°C; and (3) low temperature, $<125^{\circ}C$. The amount of heat that is carried by a fluid is calculated by measuring its mass flow rate and the heat content or enthalpy. Thus, the heat discharge rate Q is given in joules/second or more commonly in megawatts (MW), where 1 MW = 10^6 W. A high-temperature geothermal system would have an output of between 3 and 300 MW.

Goff and Janik (2000) listed five types of geothermal systems, two of which are artificially induced by pumping water into the ground, and then out to "harvest" the transported heat. Three natural systems include: young igneous, tectonic and geopressured.

In young igneous systems, thermal energy is provided by volcanism and associated shallow magma chambers. Meteoric waters percolate into the ground and are heated by the intrusions and convectively circulate as shown in Figs. 5.49 and 5.22. These intrusion-driven geothermal systems are the hottest with temperatures $\leq$370°C and reservoir depths generally around $\leq$1.5 km, but can be deeper, as in the case of Larderello in Italy, where the geothermal system is at depths of about 7 km.

Circulating waters become enriched in Cl, SO_4, HCO_3, F, B, Br, Si and metals by reactions with the wallrocks, while magmatic volatiles (CO_2, HCl, Hg) are transferred to the fluids. In the deepest levels reduced, chloride and near-neutral pH waters are dominant. Dissolved gases are mainly CO_2 and H_2S, which separate from the liquid to vapour as a result of boiling, and rise to the surface, where they are absorbed into ground waters, together with condensed water vapour to form steam-heated waters (Simmons et al. 2005). Steam-heated CO_2-rich waters alter rocks to argillic assemblages (illite, illite-smectite, smectite, kaolinite), calcite and siderite, at temperatures of ~150°C (Simmons et al. 2005). Steam-heated acid-sulphate waters contain H_2S, which at contact with atmospheric oxygen, oxidises to H_2SO_4, thereby becoming very acidic (pH ~2, or less) and altering the surrounding rocks to advanced argillic assemblages (opal, alunite, kaolinite, pyrite). Neutral pH-chloride fluids tend to flow outward where they feed hot springs that can be several km away from the heat source. Acid-sulphate and neutral-chloride waters can mix to form hybrid solutions. Alkaline chloride thermal waters are characterised by the presence of Na, K chlorides, silica, bicarbonates, fluoride, ammonia, As, Li, Rb, Cs and boric compounds. The pH, though generally near neutral, can range from 5 to 9. These hot springs are commonly found in caldera settings, because the convective column is within easy reach of the ground surface. Siliceous sinters are usually well developed in areas of chloride springs, as the dissolved silica is precipitated for the reasons previously outlined (see also Chapter 1 and Fig. 1.7). Larger and longer-lasting geothermal systems are associated with caldera settings, such as Yellowstone and Taupo. Caldera settings also provide an optimal environment for the development of porphyry-epithermal systems, as exemplified in Fig. 5.50.

Tectonic geothermal systems occur in rift valleys, such as those of the East African Rift System, commonly occupied by lakes and where hot mantle material is the primary driving energy source generating high geothermal gradients. Here deep-circulating meteoric waters will form reservoirs in permeable stratigraphic horizons, as discussed in Chapter 8. Fluids rise along graben faults and may vent as hot and/or mineral springs at surface or in lakes. In the East African Rift System, Lake Natron (Tanzania) and Lakes Magadi and Bogoria (Kenya) have hot, saline springs discharging at 40–80°C. Strong evaporation results in large evaporite deposits (see Chapter 8). These are ideal settings for the formation of sedimentary-hosted ore systems, described in Chapter 8. Geopressured systems are typically found in sedimentary basins

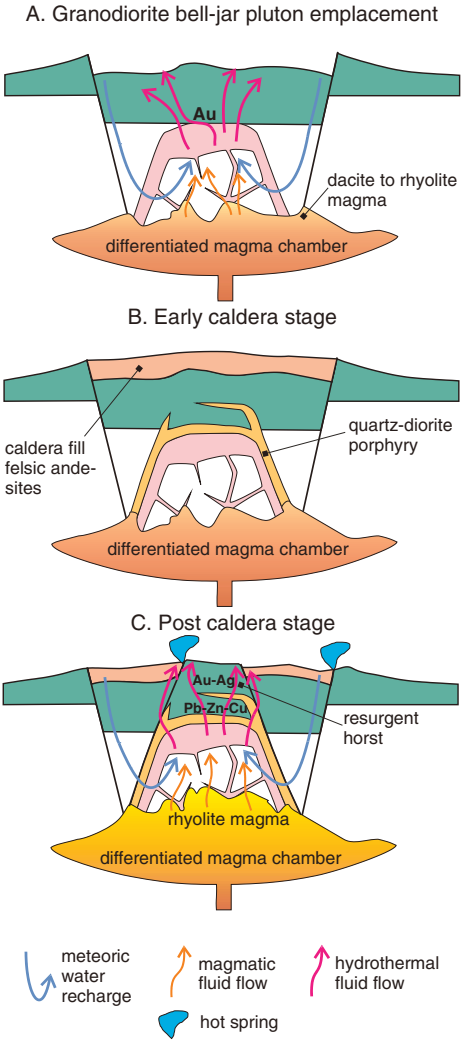


Fig. 5.50 Evolutionary stages of a geothermal system in a caldera setting with associated precious and base metal porphyry and epithermal mineralisation as exemplified in the "granodiorite bell-jar pluton emplacement" model for the Banská Štiavnica volcano in the Apuseni Mountains (Romania) of Neubauer et al. (2005) and Lexa et al. (1999). Reproduced as is by permission of the authors

where deep burial of aquifers resulted in overpressured reservoirs. Depths and temperatures range from 1.5 to 3 km and 50 to 190°C.

Hockstein and Browne (2000) considered geothermal systems as: (1) liquid-dominated high-temperature in partially eroded volcanic complex; (2) high-temperature two-phase (liquid-vapour) system (Fig. 5.49A); (3) vapour-dominated system, shown in Fig. 5.49B; and (4) liquid-dominated in flat terrain, shown in Fig. 5.49C. Surface manifestation of liquid-dominated geothermal systems are related to ascending steam that discharges as fumaroles or produces diffuse steaming ground, hot mud pools, geysers, hot acid-sulphate springs referred to above, bicarbonate (HCO_3) waters that deposit layers of carbonate,

called travertine (see Chapter 1 for details on hot springs). Geysers are jets of steam-heated groundwater that deposit terraces of siliceous material called geyserite. In geysers, the water column reaches temperatures in excess of 100°C at its base without boiling due to the high hydrostatic pressure at the given depth; when the heated water convectively rises and expands, the boiling point is then reached and the water is jetted out, falls back and the cycle starts again. Geysers are abundant in the Yellowstone National Park, where there are over 200, in New Zealand and Iceland. They are also found in Tibet near Lake Tengri Nur at 4800 m above sea level, and in the crater of the Socompo volcano in the Atacama region at 6080 m above sea level.

Extensive steaming ground is the dominant surface manifestations of two-phase systems, with lesser warm springs and fumarolic activity. Vapour-dominated systems commonly form steaming ground, fumaroles, hot pools, acid lakes and geysers.

The anatomy of a vapour-dominated geothermal reservoir, consists of a zone of convective heat transfer by thermal waters (brines), above which there is a vapour-dominated reservoir enriched in other gases (H_2S, CO_2). The vapour-dominated reservoir tends to migrate downward as excess pore water is vaporised. Channels of inflowing groundwaters from the margins of the hydrothermal chamber are continuously narrowed by mineral precipitation (mainly calcite and anhydrite). The vapour-dominated reservoir passes upward into a zone of steam condensation, where clay minerals are being formed and tend to clog pore spaces and channels. However, part of this condensate may move up to the water table, or to the surface as acid-sulphate springs, or may form pools of boiling mud. In addition, vapour from the vapour-dominated reservoir may escape directly to the surface forming solfataric fumaroles. In this dynamic system there is net loss of liquid water, due to diminished inflow caused by mineral deposition (sealing) at the margins of the reservoir, so that liquid water is constantly being replaced by vapour. Continued boiling below the vapour-dominated reservoir tends to produce brines by concentration of solute matter during boiling. Boiling of the brine is also likely to produce superheated steam with respect to pure water at the same pressure. This causes the brine to become a highly effective agent for heat and mass transfer, because steam boiling off from a brine is superheated by several degrees, depending on and increasing with the concentration of the solutes. Steam-heated aquifers are important for the exploitation of geothermal energy and for the formation of precious metal deposits.

Sublimates commonly seen in fumarolic fields are evidence that vapours dissolve and transport metals. The importance and effects of the vapour phase as agent of metal transport in hydrothermal systems was experimentally studied in detail by Williams-Jones and Heinrich (2005; see Chapter 2 for details). These authors investigated the temperatures of metal-bearing sublimates artificially induced in silica tubes inserted in active fumaroles. Mineral phases deposited included Cu, Cd, Mo, Fe, Pb and Zn sulphides, Fe and W oxides and Au, at temperatures ranging from 900 to nearly 100°C, thereby

providing a clear indication of the great variety of metals that are transported by volcanic vapours.

There are several geothermal fields in the world, some of the better known include those in the Taupo Volcanic Zone and White Island in New Zealand, the grandiose Yellowstone, Steamboat Spring and the Geysers-Clear Lake fields in the USA, the Phlegrean Fields and Larderello (where the first geothermal power station was built in 1904) in Italy, Palinpinon and Mount Cagua in the Philippines, El Tatio in northern Chile, Mutnovsky and Uzon in Kamchatka (Far East Russia). Fresh water lakes occupy the rift structures where these geothermal fields occur, such as Lake Taupo and the Yellowstone Lake, Lake Baikal in central Asia, and Lake Tanganyika in the East African Rift System. The on-land geothermal fields extend into these lakes providing examples of sublacustrine hydrothermal vents. In the following sections, I briefly discuss Kamchatka-Kurile Islands, Taupo-White Island, Yellowstone and Lake Tanganyika. Many geothermal systems are utilised for power generation in countries such as the USA, Philippines, Mexico, New Zealand, Italy, Japan, Iceland, El Salvador, Nicaragua and Costa Rica. Geothermal exploration, development and power generation are beyond the scope of this book and the interested reader is referred to Goff and Janik (2000 and references therein) and Arnórsson (2000) for overviews and the web site http://www1.eere.energy.gov/geothermal/powerplants.html (last accessed in April 2008).

5.4.1 Kamchatka Peninsula and Kurile Islands

The Kamchatka-Kurile (also spelt Kuril) volcanic arc extends for about 2000 km and is related to the northwest margin of the subducting Pacific plate, which is part of the great circum-Pacific subduction system (Chapter 7, Fig. 7.1). The Kamchatka-Kurile arc contains more than 100 active volcanoes and is characterised by an almost continuous string of Late Pleistocene and Holocene stratovolcanoes and calderas (Fig. 5.51). Publications that deal with various aspects of the geology of the region include Hochstaedter et al. (1994), Taran et al. (1995, 1997), Bindeman et al. (2004) and references cited therein. In the Kamchatka peninsula (Far East Russia) volcanic centres are grouped into three volcano-tectonic zones: Eastern Volcanic Front, Central Kamchatka Depression and Sredimy Range, about 200 km behind the modern volcanic front. Magmatism generally decreases westward, but the most voluminous Recent volcanism is in the Central Kamchatka Depression, which hosts some of the largest volcanoes in the world. Large volcanic centres include the Holocene Mutnovsky and Ksudach volcanoes, Karymsky calderas, and the Pleistocene Uzon, Akademy Nauk, Maly Semyachik calderas. The volcanic rocks of the Kamchatka-Kurile arc comprise a calc-alkaline range of compositions from rhyolite to tholeiite and rocks of the shoshonite series, with most volcanics being andesitic. Major caldera-forming eruptions occurred between the Pleistocene and Holocene, during which time the region also experienced glaciation.

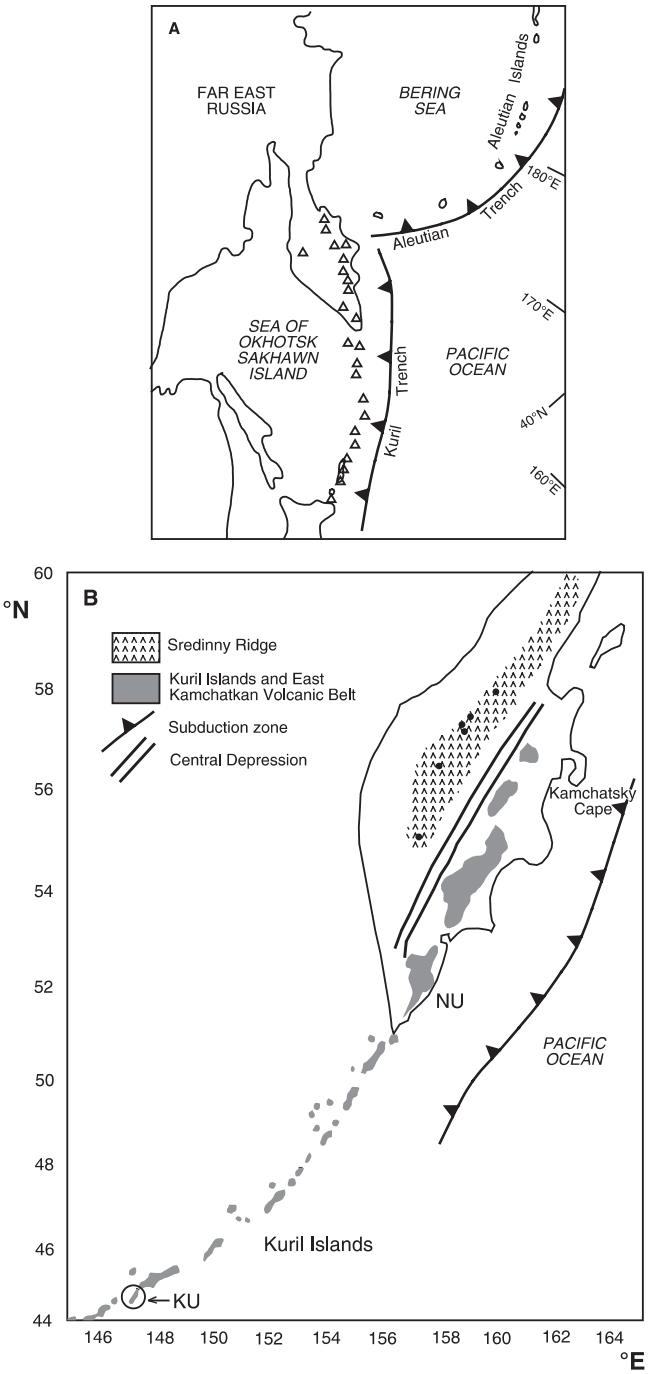


Fig. 5.51 (**A**) Kamchatka and Kuril volcanic arcs locality map; KU is the island of Kuril discussed in text; (**B**) Kuril islands and East Kamchatka volcanic belt

The Kamchatka region is host to some of the most extensive geothermal areas in the world. One of these is the geothermal system of the Mutnovosky volcano, covering an area of 30 km^2, and investigated by Taran et al. (1992, 1997). A group of steam vents and fumarolic fields are present in this volcano, with vent temperatures up to 420°C. Pools of boiling very acidic water are encrusted with native S (S^0), and locally have domes of S^0, up to 2 m high. The Upper Field fumaroles had temperatures of around 230–320°C and high concentrations of CH_4 and NH_3, with low $^3He/^4He$ ratios. The Northern Area and Bottom Field fumaroles have abundant S^0, which forms dome structures and small pools of molten S. Intense gas activity was recorded in the Active Funnel, a bowl-shaped structure about 150 m deep and from 100 to 150 m wide. Here, temperatures of up to 600°C have been measured in fumaroles that discharge more than 200 t/day of SO_2, and also contain HCl, HF and H_2. The Active Funnel first formed in 1848–1854, during a phreato-magmatic eruption and was considered by Taran et al. (1992) as an open magmatic system that is a channel connected at depth with to a magma body.

The Mutnovosky area, about 60 km south of the capital city of Petropavlosk, and Rodnikovy and Aschinsky to the north and southwest, respectively form a metalliferous province with numerous epithermal precious and base metal deposits, reported by Lattanzi et al. (1995). The Mutnovosky district has north-trending subvertical epithermal veins, extending for 3.5 km and traceable at least for 300 m vertically. There are "low-sulphide" veins which grade into "massive sulphide" veins, composed of quartz and/or chalcedony. Sulphides are pyrite, sphalerite with lesser galena and tetrahedrite. Some veins are carbonate-rich (calcite and/or rhodochrosite). Gold occurs as native Au, electrum and associated with calaverite and petzite. Alteration comprises propylitic, sericitic, hypogene and supergene acid-sulphate. Sulphur isotopic data show $\delta^{34}S$ values ranging from 0.5 to 4.5‰, more or less comparable to the values obtained for H_2S from the Mutnovosky fumaroles (–2.5 to –0.9‰ by Taran et al. (1992). Lattanzi et al. (1995) concluded that the Kamchatka base metal-rich epithermal systems are similar to and probably are a continuation of the western Pacific porphyry-epithermal ore belts.

The Uzon caldera, about 300 km north of the town of Petropavlosk, contains numerous geothermal fields. Crowe et al. (2006) used ASTER and Qickbird images (panchromatic and VNIR bands) to examine reflectance spectra signatures and compared them with existing databases to distinguish mineral zonations around active thermal pools. Crowe et al. (2006) found that reduced mineral phases, such as pyrite, are located in the vicinity of the pools, whereas oxidised phases (hematite, alunite) tend to occur further away. Hot springs of the geothermal fields of the Uzon caldera also have layers of algal mats, separated by siliceous layers. These layers are around the springs' vents in the central crater lake and have been described by Orleansky et al. (1994).

Kudriavy volcano, in the north of Iturup Island in the Kurile volcanic arc (Fig. 5.51), has numerous high-temperature (700–940°C) fumarolic fields covering an area of 2.6 km^2 (Korzhinsky et al. 1994; Taran et al. 1995; Botcharnikov et al. 2003). The volcano is of basaltic andesite composition and is on the

western flank and is part of the Medvezhya caldera, which include rhyolite and dacite domes. The fumaroles are water–rich (92–98 mole%), but also contain varying amounts of gases such as CO_2, SO_2, H_2S, HCl, HF and CH_4. The low NaCl content of these fumarolic vapours was attributed to separation of hpersaline fluids from the vapour phase at depth. The distribution of the Kudriavy fumaroles and their composition have been interpreted to be related to a stable plumbing system of convecting and degassing magma conduit in which gases exsolve and ascend to the surface (Taran et al. 1995). In addition, a pure Re sulphide, with a theoretical composition of ReS_2, was discovered in the sublimates of the Kudriavy fumaroles (Korzhinsky et al. 1994).

5.4.2 Geothermal Systems of the Taupo Volcanic Zone, New Zealand

The Taupo Volcanic Zone (TVZ) is a 25–50 km-wide tectonic depression, which extends for about 300 km north-eastwards across the central part of the North Island of New Zealand. The TVZ is the currently active volcanic arc and back-arc of the Taupo-Hikurangi arc-trench system, related to the subduction of the Pacific plate beneath the Indian plate along the Hikurangi trench off the east coast of the North Island (Cole 1984). The TVZ is also the southern extension of the Havre Trough and the Tonga-Kermadec arc-trench system, (Figs. 5.52 and 7.18). Gravity data indicate that this depression has been down-faulted between 2 and 4 km. The geology, tectonism and volcanic history of the TVZ is described in Cole (1984, 1986, 1990) and Cole and Lewis (1981). A collection of papers dealing with the TVZ geothermal fields can be found in Henley et al. (1986). The Broadlands-Ohaaki geothermal system, on the eastern side of the TVZ was studied by Simmons and Browne (2000) who discussed the epithermal environments of this geothermal field.

The TVZ comprises calc-alkaline volcanics that have been erupted from five major centres such as Rotorua, Okataina, Maroa and Taupo with dominantly felsic volcanics and the Tongariro volcano at the southwest end (Fig. 5.52). Lake Taupo is at the southern end of the TVZ sited in a rhyolitic caldera and has one of the few freshwater geothermal fields at the Horomatangi Reefs. Other freshwater active geothermal fields are found in Lake Baikal, the Yellowstone Lake and Lake Tanganyika (see Section 5.4.5). The TVZ continues off-shore to the northeast, with a number of volcanoes such as White Island and Whale Island (see Fig. 7.18). Rhyolites and ignimbrites are predominant in the felsic volcanics with minor andesite, dacite and basalts all less than 1 Ma old. Major structures of the TVZ are north-northeast-trending active normal faults, which are probably related to subsidence of the Mesozoic greywacke basement. Other structures include northwest-trending faults probably related to the Hauraki volcanic region to the northwest and ring faults which are related to the multiple

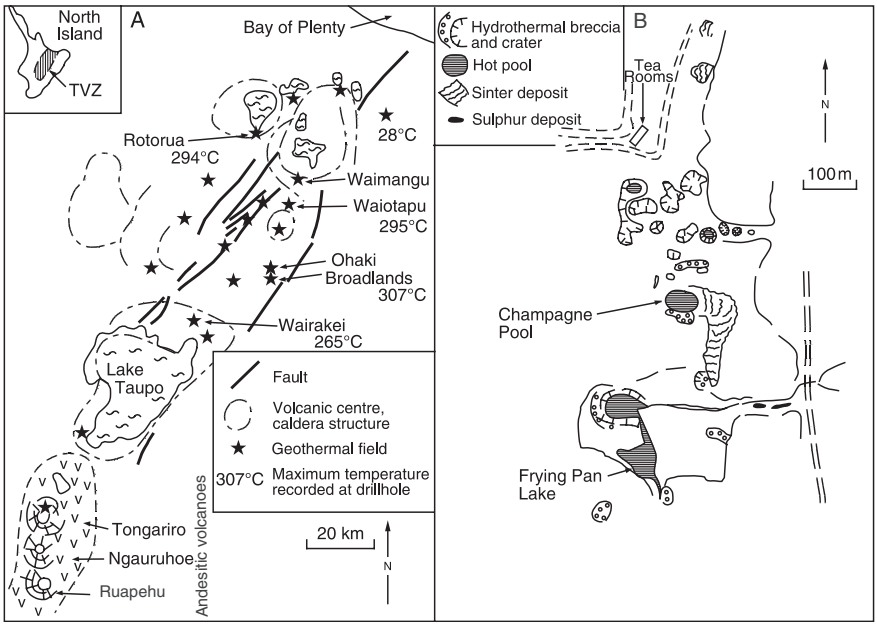


Fig. 5.52 (**A**) Taupo Volcanic Zone (TVZ), North Island, New Zealand, and its geothermal fields; (**B**) Part of the Waiotapu geothermal field, an active ore-making system. After Weissberg (1969) and Hedenquist (1983). Inset shows position of the TVZ within the Hikurangi-Kermadec-Tonga subduction system (see also Fig. 7.18)

calderas of the rhyolitic volcanic centres. The central part of the TVZ is characterised by an average heat flow several times greater than normal, which is caused by hydrothermal convection systems that are manifested at the surface as geothermal fields (Fig. 5.52). In turn, these convection systems are probably the result of thermal energy derived either from the cooling of underlying magmas, or by mantle material intruded below the attenuated crust of the marginal basin. The TVZ has at least 20 geothermal fields, spaced about 10–20 km apart in which deposits of Au and Ag are actively forming in hot springs and geothermal wells (Grieve et al. 2006; Simmons et al. 2006). The geothermal fields on the eastern side are the youngest (Broadlands-Ohaaki), whereas those on the western side are either extinct or nearly extinct. The surface manifestations include hot springs, geysers, mud pools, steaming ground and fumaroles. One of these extinct fields is Ohakuri, where a low-sulphidation epithermal system contains a resource of 126 Mt grading 0.38 g/t Au (Ohakuri North) and 42 Mt grading 0.41 g/t Au (Ohakuri South) (Grieve et al. 2006).

At Wairakei, 8 km north of Lake Taupo, geothermal steam is utilised to generate electricity. Precious metal ore-grade precipitates are actively forming from hot springs, as well as drillhole discharges in a number of these fields such

as those of Waimangu, Waiotapu, Broadlands-Ohaaki and Rotokawa, as detailed in the classic papers by Weissberg (1969) and Weissberg et al. (1979) and Hedenquist and Henley (1985). By contrast, the geothermal waters are neutral to slightly alkaline and have low metal concentrations (see Table 1.6). Although stable-isotope studies have shown that these geothermal fluids are primarily of meteoric origin, it has been pointed out that a contribution of magmatic fluids, perhaps of up to 10%, would be isotopically undetectable. Such a contribution, if originally at approximately 2 wt.% NaCl, could account for all of the chloride and up to 30% of the heat budget for a system like Wairakei (Henley and Ellis 1983).

A major feature of the Broadlands-Ohaaki geothermal field is a 60 m diameter thermal pool, filled with water of neutral to mildly alkaline pH at a temperature of about 95°C of a dilute NaCl-bicarbonate composition. The pool is lined by a greyish-white sinter material. In 1957 a flocculent red-orange precipitate appeared in these waters and was eventually incorporated into the marginal sinter. This precipitate was found to be composed of an amorphous Sb sulphide with anomalous concentrations of Au, Ag, Tl and As (Weissberg et al. 1979).

At Broadlands a greywacke basement is overlain by subhorizontal layers of ignimbrite, pumice breccia, dacite, rhyolite and other pyroclastic deposits (Huka Fall Formation). Thermal activity in the area commenced approximately 0.5 Ma ago, with maximum temperatures in the order of 300°C. Ewers and Keays (1977) found the following metal zoning: (1) higher concentrations of Tl, As, Au and Sb near the surface; and (2) greater abundance at depth of Bi, Se, Te, Ag; with Pb, Cu and Zn increasing towards the higher temperature zones. Sulphides are represented mainly by pyrite and smaller quantities of sphalerite, galena and chalcopyrite. The sulphides occur as veinlets in the more massive and impermeable rocks, and as disseminations in the more porous and permeable lithologies. Extensive zones of propylitisation, silicification and argillic alteration surround fissures and fractures through which the fluids move. Propylitic alteration is characterised by dominant chlorite and calcite, and the argillic zones have interstratified illite-montmorillonite. Vein and vein margin material include quartz, adularia and sericite. Pyrite and sphene are ubiquitous in all alteration types. The Broadlands-Ohaaki field was investigated in detail by Simmons and Browne (2000) who documented alteration and mineralisation of an active low-sulphidation epithermal system. Common hydrothermal minerals are quartz and various silica polymorphs, illite, smectite and kaolinte clays, albite, adularia, carbonates and calc-silicates (epidote and wairakite mainly). Subsurface mineralisation is in vugs and veinlets with sphalerite, galena and chalcopyrite but, as also established by Ewers and Keays (1977), base metal sulphides tend to be restricted to deeper levels, generally below 800 m. Geothermal scales and precipitates in wells contain chalcopyrite, sphalerite, galena, magnetite and pyrite and have in excess of 5 wt% Au and 17 wt% Ag (Simmons et al. 2006). Sudden pressure and temperature drops in back-pressure plates of geothermal wells apparently caused the precipitation of

these metals. Simmons et al. (2006) calculated that a rate of 100 kg/sec upflow of fluids in the Broadlands-Ohaaki field would have a total Au flux of 4700 g/year, which would translate to 30 t of Au in 6400 years.

Covering an area of roughly 18 km^2, the Waiotapu geothermal field (Fig. 5.52B) is the largest in New Zealand, and its major features include Champagne Pool, sinter deposits and several craters formed by hydrothermal eruptions (Hedenquist 1983). The area is underlain by ignimbrites, air-fall pyroclastics and lake sediments. Dacitic and rhyolitic volcanic structures are also present. Thermal activity comprises discharges of acid-sulphate and chloride-rich (Champagne Pool) waters as well as mixed acid-sulphate-chloride springs (Frying Pan area). Mineralisation is especially prominent at Champagne Pool where an orange precipitate has high concentrations of As, Sb, Au and Ag (see Table 1.6). The Pool fills a hydrothermal eruption crater at least 40 m deep from which, according to Hedenquist (1983), the eruption is believed to have occurred some 900 years ago.

As mentioned above, the Waiotapu field is characterised by numerous craters and pools which represent vents from which hydrothermal eruptions have occurred in the past. While some of these vents continue to discharge thermal waters (Champagne Pool), others have been flooded by groundwaters (Ngakoro Lake) (Hedenquist and Henley 1985). The vents are surrounded by deposits of eruption breccias which are typified by variable clast abundance, size and angularity as well as a poorly sorted matrix-supported texture and absence of primary volcanic material. These eruptions occur when self-sealing takes place, which allows an increase in fluid pressure. Hedenquist and Henley (1985) proposed a mechanism in which it is envisaged that a seal need only develop locally, with the boiling fluids being diverted to surface via open fractures. In this situation gases which collect in the fracture beneath the seal become compressed so that the pressure at the seal increases (see also Chapter 9). Rupture of the seal occurs either by hydraulic fracturing or by tectonic activity, the compressed gases rapidly expand and an eruption takes place.

The previously mentioned the Horomatangi Reefs in Lake Taupo have an active sublacustrine geothermal system that was studied by de Ronde et al. (2002). Here two hydrothermal vents have been identified, Te Hoata and Te Pupu, which emit gases and hot water ($\sim$45°C) with dilute concentrations of SO_4, Cl, SiO_2 and Na. The vents are characterised by chimney structures up to 30 cm high and with a suite of epithermal elements including S, Hg, As, Sb and Tl. In addition, the walls of the chimneys are coated with silicified filamentous bacteria and bacterial mats surround the vents. On the basis of gas geothermometry, de Ronde et al. (2002) suggested that there may exist a high temperature hydrothermal reservoir beneath the lake floor.

The TVZ geothermal systems, as documented and modelled by Simmons et al. (2006), consist of a convective cell of meteoric water circulating to depths of approximately 5 km and heated by a cooling magma. Below the water table and at depths of 1–2 km, the upflow zone attains temperature and pressure close

to hydrostatic boiling and at shallower levels the fluid flow laterally to discharge as hot springs and depositing sinters. Simmons et al. (2006) suggested that the surface manifestation represents about 10% of the total area underlain by the circulating fluids. There are thre end-member water types (Simmons et al. 2006): (1) near neutral pH chloride, derived by interaction of meteoric water with magmatic components, such as H_2O, CO_2, SO_2, H_2S and HCl. The H_2S is especially important for the complexing and transport of Au in the fluids, with boiling causing the precipitation of Au (see reaction in Section 5.3.1.5); (2) steam-heated ground waters, derived from the condensation of steam that separated from boiling fluids; (3) acid-sulphate steam heated waters, derived from the oxidation of H_2S.

5.4.2.1 White Island

The hydrothermal system of the White Island active andesitic-dacitic volcano (Fig. 7.18) may represent an intermediate stage between the TVZ continental back-arc system and the oceanic Havre Trough of the Tonga-Kermadec subduction zone, discussed in Chapter 7. White Island, located in the Bay of Plenty, about 50 km from the coast, rises 700 m from the seafloor to a height of 300 m a.s.l. Although an island, the volcanic-hydrothermal system is isolated from sea water by sealed zones within fine-grained volcaniclastic sediments (Hougton and Nairn 1991). Publications on volcanic and hydrothermal features of White Island that constitute the present database include Hougton and Nairn (1991), Hedenquist et al. (1993), Giggenbach et al. (2003) and Simmons et al. (2006). The fumaroles of White Island have fluctuating temperatures from 100 to 800°C, in response to variations in degassing rates of the magma during heating and cooling stages. These temperature variations, in turn, correlate with changes in the abundances in the discharges of H_2O, CO_2 and HCl, with the magmatic vapours condensing to form an envelope of hydrothermal fluids that surround a shallow magma chamber. Sulphur isotopic compositions of co-existing sulphate and sulphide minerals (alunite, anhydrite and pyrite) range from a $\delta^{34}S$ of –11 to –8.6‰ for pyrite and + 7.4 to + 6.5‰ for the sulphates. The measured isotopic fractionation between co-existing sulphate and sulphide minerals gives a temperature of ~380°C. The S isotopic composition of SO_2, H_2S and native S show $\delta^{34}S$ values ranging from 6.6 to –6.3‰, with a mean isotopic composition of total S of 4.6‰. These values indicate no interaction with marine sulphates. In the zone of co-existing vapour-liquid, SO_2 reacts with water to form sulphuric acid and H_2S, which together with HCl are the dominant acids in the fluids, resulting in strong H^+ activity in the hydrothermal system. Hedenquist et al. (1993) calculated the metal fluxes of the White Island volcanic-hydrothermal system, based on an average SO_2 flux of 350 t/day. They suggested that hot springs discharge about 340 g/day of Cu, with a total subsurface deposition of Cu of 6 kg/day or ~20 000 t in 10 000 years. The amount of Au degassed into the atmosphere was calculated at 4.5 kg/year, which amounts to 45 t over 10 000 years.

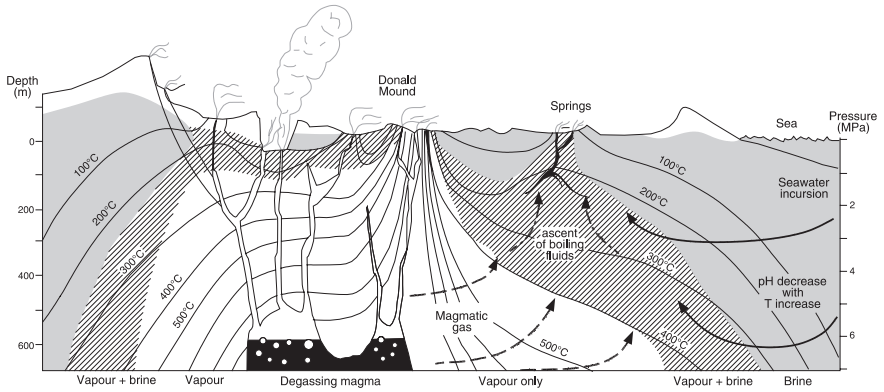


Fig. 5.53 White Island volcanic-hydrothermal system. See text for details. After Giggenbach et al. (2003)

A model of the White Island hydrothermal system is shown in Fig. 5.53, in which magmatic gases ascend, condense, boil and discharge as hot acid springs. Where these fluids enter the sea, Fe oxides and hydroxides are deposited. The White Island active volcanic-hydrothermal system is conducive to the formation of a high-sulphidation Cu–Au epithermal deposit.

5.4.3 Geysers-Clear Lake Geothermal System, California, USA

The Geysers-Clear Lake geothermal system, located in the northern Coast Ranges in California, includes active hot springs and recently active epithermal systems that belong to the same geothermal complex. Epithermal deposits of the Geysers-Clear Lake region include the McLaughlin Au–Sb–Hg, Wilbur Springs and the Sulphur Bank S-Hg deposits (Laznicka 2006; Sherlock 2005). The following is summarised from Sherlock et al. (1995) and Sherlock (2005).

The Geysers-Clear Lake region is underlain by the Cretaceous-Jurassic Coast Range ophiolite, the Great Valley sequence and the Franciscan Complex, the latter being part of an accretionary prism related to the subduction of the Pacific plate beneath North America. The Coast Range ophiolite is a fragment of oceanic crust (see Chapter 7), which forms the basement to the sedimentary rocks of the Great Valley sequence. These tectonostratigraphic packages are tectonically interleaved and have been affected by thrusting and strike-slip movements. The Neogene Sonoma Volcanic Suite and Clear Lake Volcanic Suite of Quaternary age, consisting of mafic and felsic extrusive and intrusive rocks, were emplaced into the Mesozoic package.

The Geysers steam field was one of the largest geothermal power facilities in the world, with power production attaining a peak of 2000 MW. The steam reservoir is contained in greywacke and serpentinite rocks associated with extrusive and intrusive rocks of the Clear Lake Volcanic Suite. The steam

field is about 40 km west of the McLaughlin deposit, is vapour-dominated, discharges Hg and hydrocarbons, and is spatially associated with a number of Hg deposits and hot (>60°C) and mineral springs in the general area, all with varying degrees of Au–Hg mineralisation. Where present, Hg mineralisation is in quartz and magnesite-hydrocarbon veins that cut silica-carbonate altered serpentinite rocks. In addition, there are narrow quartz and chalcedony veins, which predate the argillic-sulphur alteration and containing adularia, sulphides and sulphosalts, with anomalous values of Au, As, Sb and Hg. Bladed calcite is present in some veins and is indicative of boiling fluids. The Geyser field is associated with a granitic intrusion that is thought to be the intrusive equivalent of rhyolites of the Clear Lake volcanics. The surface expression of the Geysers geothermal system is characterised by extensive areas of argillic alteration, small mounds of native S and boiling mud pools. Calculated temperatures, based on oxygen fractionation between sulphate and water, range from 241 to 249°C. The distribution of hot and mineral springs in the Geysers-Clear Lake area are all controlled by major northwest-trending fault zones.

The Sulphur Bank Hg deposit is a hot spring that is actively precipitating HgS (cinnabar), but no Au. The mineral springs, although cooler, are related to the hot springs and are characterised by silica-carbonate alteration of the serpentinite rocks. The deposit has been labelled as a "geochemical giant" with about 7000 t of Hg (Laznicka 2006). In addition, to cinnabar, pyrite and marcasite are present in rokcs that are altered to silica, smectite and zeolites.

The McLaughlin Au–Sb–Hg hot spring mineral system consists of a sheeted vein complex, capped by siliceous sinter material, emplaced between a mélange unit and pillow basalts and is estimated to contain 93 Mt, grading 5.21 g/t Au, with Hg and Sb credits (Laznicka 2006). The deposit is zoned with cinnabar in surface sinter, followed at depth by Au–Sb. Potassium-Ar dating of the Clear Lake volcanic rocks (basaltic andesite) in the area of the McLaughlin deposit, yielded an age of ~2.2 Ma. The basaltic andesite occurs as flows and is associated with phreatomagmatic breccias and hypabyssal intrusions along a west-trending structure. The siliceous sinter material, initially mined for Hg, consists mainly of chalcedonic quartz forming a subhorizontal terrace about 30 m thick and is interbedded with hydrothermal breccias. This sinter terrace contains fossil filamentous bacteria and alunite at its base, dated by K–Ar at 0.75 Ma. This sinter was, at various times, mined for Hg till the discovery of Au–Ag mineralisation within the upper 350 m of the system. Gold occurs as electrum and Ag in sulphosalts. Below 350 m the mineralisation consist of quartz veins with base metal sulphides, thus providing a good example of epithermal vertical zoning. Sherlock et al. (1995) studied fluid inclusions of the McLaughin deposit and reported average salinities of ~2.4 wt% NaCl equivalent, with maxima of up to 14.5 wt%; homogenisation temperatures range from 121 to 263°C, with the highest temperatures in the deepest parts of the system. Gases trapped in the fluid inclusions include CO_2 and CH_4, which tend to increase with depth. Stable isotopic data are consistent with interaction of meteoric fluids with sedimentary rocks; the average of calculated values of $\delta^{18}O_{H2O}$ being 9.3‰

and of $\delta D \sim -60$ ‰. Hydrothermal alteration is characterised by the presence of adularia, silicification and silica-carbonatisation of the host rocks. Argillic alteration is present in fracture planes. Cinnabar and native Hg are commonly associated with hydrocarbons and sulphides and are also found in fractures.

The origin of the fluids in the Geysers-Clear Lake geothermal system has long been debated and considered in terms of mixing models between connate, meteoric and metamorphic fluids. However, Sherlock (2005) suggested that dominantly meteoric fluids evolved into a vapour-dominated system due to decreased permeability of the reservoir rocks, as well as decreased recharge and increased heat flow. The McLaughlin epithermal system is most likely the inactive equivalent of the Geysers field.

5.4.4 The Yellowstone National Park Geothermal System, USA

The famous Yellowstone caldera is located on the northern margin of the Basin-and-Range Province and at the eastern end of the Snake River province, in the northwest corner of the state of Wyoming and along the borders with Idaho and Montana (Fig. 5.54). The Yellowstone caldera is situated on a high plataeau that predominantly consists of felsic lavas and pyroclastic rocks dated from about 2.2 to 0.6 Ma (Bonnichsen et al. 1989, Fournier et al. 1994a, Bindeman 2006). Volcanic activity is characterised by three cycles of dominantly explosive volcanic activity, with basaltic and rhyolitic lavas and associated volcaniclastics. Each cycle ended with voluminous rhyolitic ash flows erupted from ring fractures, which induced collapse of the roof of the magma chamber and the formation of a large caldera, as explained in more detail below (Bonnichsen et al. 1989, Fournier et al. 1994a). These eruptions were exceedingly voluminous with the latest occurring about 640 000 years ago (lesser eruptions have occurred about 80–70 000 years ago), earning Yellowstone the title of super-volcano (Bindeman 2006). The Yellowstone caldera is one of the Earth's largest active volcanic fields and hosts the largest known crustal-scale hydrothermal system, with a heat flow 40 times the global average and was also the first national park in the world, established in 1872 (Fournier 1989, Fournier et al. 1994a, b). The Yellowstone National Park has been the subject of multidisciplinary studies for almost 200 years.

The Yellowstone National Park geothermal system is for the most part confined within the ring fractures that define the caldera and along the margins of two resurgent domes north and northwest of Yellowstone Lake (Fig. 5.54). Boiling springs and geysers discharge large quantities of near-neutral pH to slightly alkaline, chloride-rich waters, but where the caldera is filled with nearly impermeable ash-flow tuff, vapour-dominated conditions form fumaroles, mud pools and acid-sulphate springs. Bicarbonate, carbonate and Ca-, Mg-rich waters are also present. Along a 40 km-long north-south subsidence structure, called Norris-Mammoth corridor, exceptional fluid discharges were recorded by Kharaka et al. (2000). The discharges occur in geothermal areas, such as

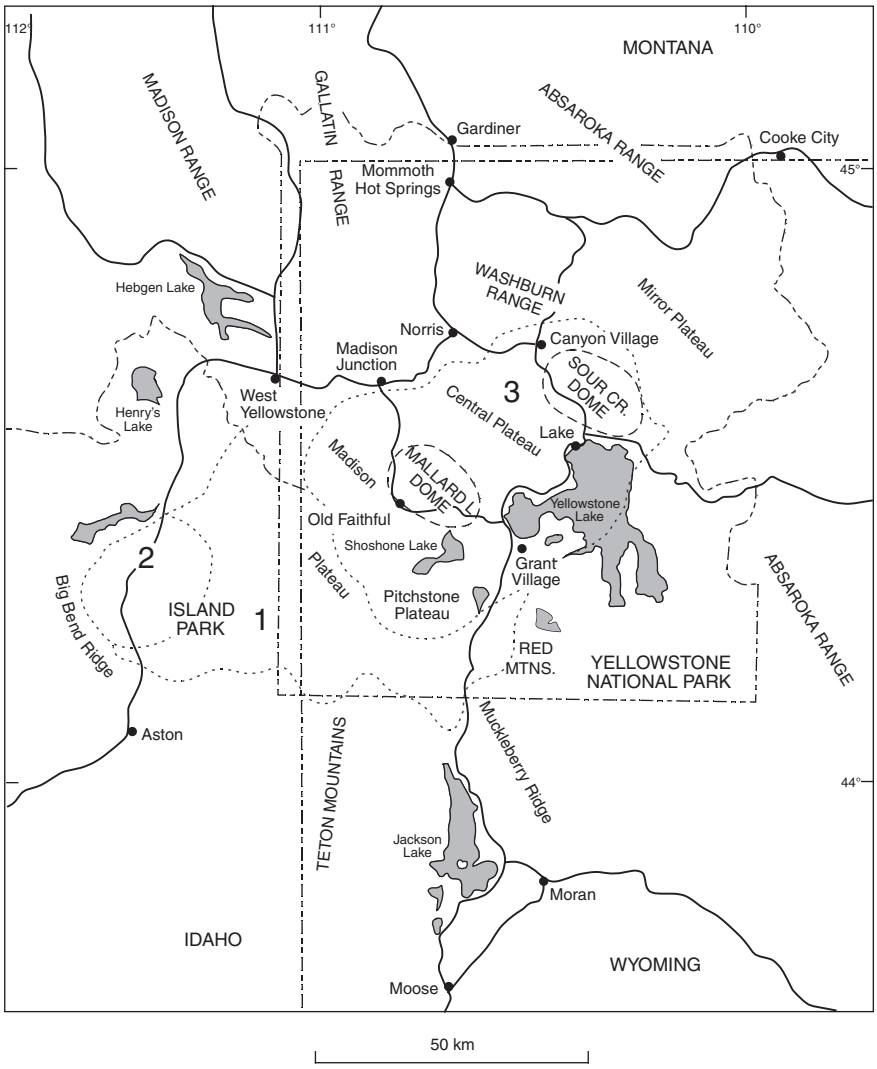


Fig. 5.54 Location and calderas of the Yellowstone National Park; 1, 2 and 3 are first, second and third cycle calderas. After Fournier et al. (1994b)

Norris Geyser Basin, Mammoth Hot Springs (both outside the caldera; see Fig. 5.54), Clearwater Springs, Sheepeater Canyon Hot Spring, Hot River. Total fluid discharges average 800 litres/second (l/s). The highest hot water and gas discharges are recorded from Mammoth Springs with more than 100 springs from which travertine terraces are deposited. The fluid flux from the Mammoth Springs system is estimated at a staggering 500–600 l/s and a gas flux of ~33 moles/s. In the Norris Geyser Basin and Clearwater Springs Na–Cl–K

hot waters discharges deposit silica sinters. In the Norris-Mammoth corridor the dominant gas is CO_2, locally with significant H_2S and N_2. The values of $^3He/^4He$ (R) ratios relative to air (R_A) of gas samples ranging from <1 to >6 (up to 8.1–8.4 R/R_A) suggest a mantle source for the CO_2. Kharaka et al. (2000) suggested that the Mammoth system may be related to a separate subjacent magmatic body in the area. Seismic tomography does reveal a body with low P-waves velocity beneath the Mammoth system, but this is interpreted differently (see below).

Stable isotopic studies suggest that some 95% of the geothermal water at Yellowstone is of meteoric origin. A parent water rich in chloride, CO_2 and H_2S has been postulated to exist at depth, continuously recharged with cold meteoric water, which is heated to temperatures of about 350°C. The diversity of the chemical character of the hot springs is due to gas–water–rock interactions, mixing, boiling and dilution processes that occur en route to the local reservoirs that feed the various surface manifestations (Xu et al. 1998). Acid-sulphate springs (e. g. Frying Pan Spring) derive their water from the subsurface boiling of chloride, near neutral pH water, with the generation of steam that condenses and H_2S oxidising to sulphate, in part by way of microbial processes. Chloride-rich springs (e. g. Porkchop Spring) discharged into the Norris Geyser Basin, have an average Cl^-/SO_4^{-2} ratio of 72.5 (Xu et al. 1998). Elsewhere there are wide variations in the Cl^-/SO_4^{-2} ratios indicating mixing of acid-sulphate and chloride waters (Fournier 1989). The S isotopic compositions for waters with low Cl^-/SO_4^{-2} ratio (<3) show $\delta^{34}S$ values of around 0‰, interpreted to represent deep sulphate in equilibrium with H_2S with a $\delta^{34}S = 0$ at 360°C. Waters with higher Cl^-/SO_4^{-2} ratios (>54) have $\delta^{34}S$ values of around 18‰, attributed to non-equilibrium oxidation of H_2S. Shallow reservoirs beneath the Lower and Upper Geyser Basins have estimated temperatures ranging from 215 to 200°C, whilst outside the caldera rim, the reservoir beneath the Norris Geyser Basin has estimated temperatures of between 325 and 200°C.

Guidry and Chafetz (2003) and Hinman and Walter (2005) studied in detail the facies and microfacies of the Yellowstone sinter deposits, respectively. These studies are very important not only because of their association with ore systems but also because they give valuable insights into similar environments in the ancient geological record and early life (Chapter 10). The siliceous springs of Yellowstone can be grouped into four main types (Guidry and Chafetz 2003) Fig. 5.55A: (1) spires and cones; (2) domal mounds; (3) terraced mounds; and (4) ponds. Spires and cones are associated with both geysers and hot springs, are high-relief features, with a wide base narrowing upwards, have a conical to cylindrical shape and do not have a spring pool. Spires and cones hav also been detected in Yellowstone Lake, where they can reach heights of 5–7 m. They are the equivalent of the smoker chimneys in oceanic environments (Chapter 7). Domal mounds are characterised by a convex surface, discharge channels and debris aprons flanking the mound. Domal mounds have terminal pools, rimmed by stromatolites forming overhanging ledges and the abandoned outflow channels are covered with silicified microbial mats. The stromatolitic

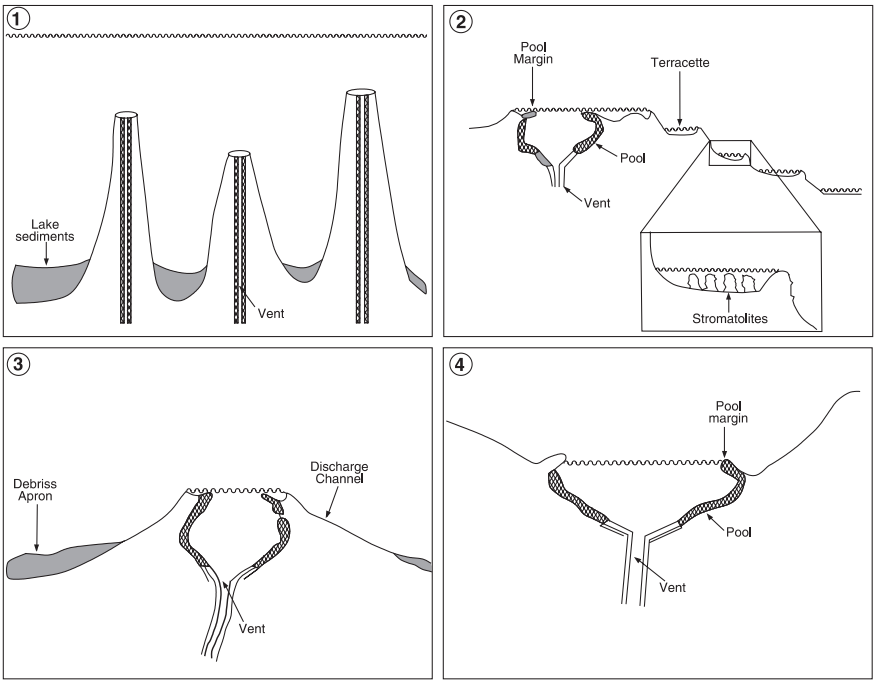


Fig. 5.55 Schematic cross-sections of four types of siliceous hot springs at Yellowstone National Park, (**1**) subaqueous siliceous spire and cones found in Yellowstone Lake; (**2**) domal mound; (**3**) terraced mound; (**4**) pond. After Guidry and Chafetz (2003) and Hinman and Walter (2005)

columns are quite small, about 3 cm in width and height, and consist of alternating black, organic-rich, material and white opal-A layers. Terraced mounds are usually made up of travertine, as described for Mammoth Springs, with each terrace having a shallow pool behind a raised rim. Siliceous terraces occur at Cistern Spring where they occupy an area of 2000 m^2. Siliceous terraces are also found at the Ohaaki pool in the Taupo Volcanic Zone (Section 5.4.2) and at El Tatio geysers in Chile. Siliceous ponds are generally geysers of hot springs that occupy a depression filled with water. These morphological types of hot springs have distinct depositional facies, also detailed by Guidry and Chafetz (2003). These facies are: vent, proximal vent, pool, pool margin, pool eddy, discharge channel or flowpath, and debris apron. The accompanying mineral species include chalcedony and opal-A with native S for vent, proximal vent and pool facies, forming mm- to μm-size aggregates and spherules. Authigenic minerals, such as opal-A, alunite, fluorite, native S, calcite and hematite characterise the pool margin facies, again forming mm- to μm-size spherules. Opal-A is typically represented in the other facies (pool eddy, discharge channel, debris apron and geyser). Commonly silicification is associated with

microbial filaments, 2–5 μm in diameter. Abiotic chalcedonic fabrics are present in high temperature hot spring vents.

XRD and petrographic analyses of sinter material from Artist Point at Yellowstone enabled Hinman and Walter (2005) to distinguish characteristic microfacies, relative to vent, splash zones, channels and pool environments of a hot spring (Fig. 5.55B). These were called mound armour, stratiform geyserite, columnar geyserite, columnar stromatolites with net fabric, columnar stromatolites with domes and spicular geyserite. Mound armour is composed of chert, characterised by 1–2 mm thick dense silica sheets, locally with ripple marks, forming near the vent. The stratiform geyserite is a well-bedded chert, with 10–50 cm-thick laminae, that may also show ripple marks. Under the microscope this geyserite is seen to consists of discontinuous sheets of quartz crystals and/or chalcedonic spherules probably precipitated from a colloidal solution. These deposits form around geysers and surging springs. The columnar geyserite microfacies is a white to grey chert, characterised by quartz crystals arranged in layered columns. These also form near vents and in splash zones (see Fig. 5.55B). Columnar stromatolite microfacies has three distinct morphologies: ridges and spines, domes and spicular. The former combines a pillared fabric with conical forms consisting of 1–10 mm wavy layers. The surface forming a series of ridges and valleys with 10–15 μm thick dendrites of opaline silica believed to be remnants of microbial filaments. Columnar stromatolites with domes consist of domical structures that are microbial mats in gently flowing sheets towards stagnant ponds. Under the microscope they consist of dense stellate dendrites. Spicular microfacies are high-relief structures (>10 cm high) that consist of botryoidal and hemispheric surfaces. A range of petrographic textures are typically present, ranging from radial or fan-shaped fabrics of alternating quartz and opal. Hinman and Walter (2005) noted that post-depositional history and diagenesis and recrystallisation, which rapidly transform silica and filling pore spaces, modify and may even destroy these microfacies, although there are cases, such as near-vent microfacies where origina textures are preserved.

Fournier et al. (1994b), who investigated the Au abundance in the opaline siliceous sinter deposits and the $^{3}He/^{4}He$ ratios of the hot spring water at Yellowstone came up with interesting results. The Au abundances in the sinters and the felsic rocks from both within and without the caldera show the same range. Both sinters and geothermal waters have relatively low Au abundances. Therefore it was considered unlikely that there was any leachable Au from the rocks through which the fluids circulated. On this basis, the authors then suggested that it is the variations in H_2S and concentration of total dissolved sulphide, resulting from diverse physico-chemical processes in different parts of the hydrothermal system that exert a control on the abundance of Au, and presumably other metallic elements. The Yellowstone hydrothermal fluids are known to convect upwards through a series of shallower and cooler reservoirs, in which gas–water–rock interactions occur in response to changing physical conditions. In some reservoirs there is decompression boiling, whereas in others

there is conductive cooling with no boiling; mixing of deep and shallow fluids also takes place. These processes lead to a general decrease of H_2S and the breakdown of dissolved Au-sulphide complexes in the reservoir waters. Consequently, different reservoirs will have waters with different H_2S and Au contents. Because the H_2S contents in hot springs as a monitor of the H_2S in the reservoir is fraught with uncertainties and changing values, due to steam loss, water–rock interaction and bacterial activity, Fournier et al. (1994b) used the $^3He/^4He$ (R) ratios, relative to the previously mentioned R_A (see also Chapter 1) as monitor of the H_2S. R values range from 2.7 to 16 times the ratio in air (R_A), reflecting a mixture of magmatic ^3He and radiogenic ^4He gained from the surrounding rocks. When boiling takes place, both He and H_2S partition into the vapour phase, with the residual liquid becoming correspondingly depleted. The residual liquid flows into shallower reservoirs, gaining ^4He from the surrounding rocks resulting in a decrease of R values. Fournier (1989) and Fournier et al. (1994b) observed that sinters deposited from waters with $R/R_A > 9$ have substantially more Au than sinters deposited from waters with R/R_A values < 9. This would indicate that subsurface processes that lead to a decrease in R/R_A values, correspond to a decrease in the H_2S fugacity and therefore less likely to carry Au in solution.

The evolution of the Yellowstone supervolcano may have occurred as shown in Fig. 5.56 and recapitulated as four end-member stages as follows (Bindeman 2006). In Stage 1, a large lower magma chamber, ponds at the base of the crust, which induces partial melting of the overlying continental crust; the newly formed magma rises to develop an upper magma chamber. Stage 2 shows that this upper chamber begins to differentiate to high-silica melts, which tend to rise resulting in surface uplift and the development of ring fractures; the viscous silica-rich magmas exsolve water and gases and explosive activity along the ring fractures occurs. In stage 3, the magmatic system evolves further with new explosive vents forming all along the ring fractures, this results in the broken ground in the middle of the evolving caldera to sink into the magma chamber, forcing more melts along the outside ring fracture; this is a catastrophic large scale eruption mostly by pyroclastic flows. In stage 4 the central part collapses to form a depression, the present-day caldera, just above the partially drained magma; the pieces of material that sunk into the magma chamber, produce new but limited eruptions, usually manifested by small rhyolitc domes (resurgent stage). This is the stage when geothermal fields become active at surface powered by large scale hydrothermal convection in the subsurface. The presence of a hot, crystallising magma chamber at depth is confirmed by tomographic imaging. Husen et al. (2004) analysed 3-D P-wave and the ratio of P- and S-wave velocities at Yellowstone, determined from local earthquakes and recorded from the seismic network in the area. The derived tomographic images show a low Vp body beneath the Yellowstone caldera at depths greater than 8 km, which the authors interpreted as an active magma chamber. In addition, a volume of anomalously low Vp and Vp/Vs ratios is also present to the northwest at a depth of < 2 km. Husen et al. (2004) interpreted this

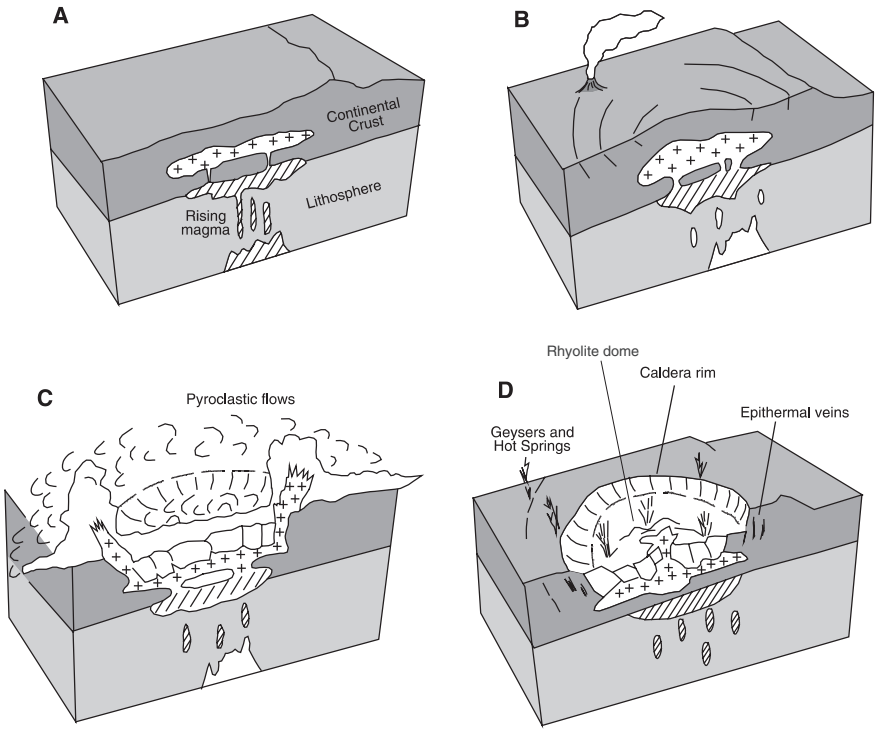


Fig. 5.56 Evolution of a caldera system of a supervolcano; (**A**) Underplating of the base of the continental crust by mantle-derived mafic melts (lower chamber) and partial meting of continental crust forms an upper magma chamber, (**B**) the upper chamber evolves and the silica-rich parts rises towards the surface, (**C**) high pressure builds up with volatile concentration and a volcanic explosive event takes place characterised by massive pyroclastic flows, along ring fractures above the upper chamber, (**D**) following the eruption of pyroclastic material, a caldera is formed, above the partially drained upper magma chamber; smaller and highly evolved batches of magma develop in collapsed blocks in the central parts of the caldera, this evolved magma erupts to form domes of rhyolitic composition; low-sulphidation epithermal veins develop in this stage in the evolution of the caldera system. After Bindeman (2006)

to represent a porous, gas-filled reservoir and suggested that the gas, probably CO_2, may have originated from the degassing of the magma chamber beneath the caldera.

5.4.5 Salton Sea

The Salton Sea geothermal field is situated near the southeastern edge of the Salton Sea, on the north slope of the Colorado River delta in southern California. It is near the axis of a major structural trench that extends

northwestward from the Gulf of California. The depression is a rift in the San Andreas fault system in a highly fractured and structurally complex region. The field is one of several within the Imperial Valley (USA) and the Mexicali Valley (Mexico), where the Cerro Prieto geothermal system is situated. In the Imperial Valley geothermal power plants produce electricity for more than 100 000 homes. Details of the Salton.

Sea system may be found in McKibben and Elders (1985) and McKibben et al. (1988). Seeps of mud, gas and dominantly polyaromatic hydrocarbons are common in the Salton Sea geothermal field, where wells drilled for geothermal power recorded temperatures of up to 350°C at depths ranging from 1500 to 2500 m (Svensen et al. 2007). The above mentioned hydrocarbons appear to originate from hydrothermal activity rather than thermal maturation of organic compounds (Svensen et al. 2007). Hydrocarbon seeps are also found in the hydrothermal fields of the Guaymas Basin in the Gulf of California, discussed in Chapter 7.

The lithologies in the Salton Sea area include an alternating sequence of fluvial and lacustrine deltaic deposits of Pliocene-Pleistocene age with a thickness of about 4500 m above the basement, as well as rhyolitic and basaltic rocks. Within the field, a number of Late Quaternary domes of rhyolitic rocks are aligned along a northeast trend for a distance of approximately 8 km, nearly perpendicular to the main structural trends. The Salton Buttes is a group of five rhyolitic domes that were extruded onto the Quaternary sediments of the Colorado River delta. Beneath the Salton Buttes is a 5 x 8 km magnetic high, interpreted to represent either a granitic pluton or a swarm of dykes (for more details see the website http://vulcan.wr.usgs.gov/Volcanoes/California/SaltonButtes/ (last accessed in April 2008). In addition, sills and dykes have been intersected in drillholes. The sedimentary rocks have been progressively metamorphosed to greenschist facies by burial and thermal metamorphism; this thermal activity is probably related to buried intrusive rocks. The chloride- and metal-rich brines, containing up to 26 wt% of dissolved solids, have temperatures of 300°C at 1000 m and 365°C at depths of 2000–3000 m. Hydrological studies have established that groundwater flow is from the southeast, and that, based on Cl/Br ratios which are three times higher than sea water, all subsurface waters in the Imperial Valley are Colorado River waters (White 1981). It has also been suggested that the Pb of the brines is possibly leached from the Colorado River sediments by interaction with the thermal brines (McKibben and Elders 1985). Geochemical and isotopic studies have indicated the presence of two distinct and stratified geothermal fluids: one is a deep hypersaline metamorphic brine and the other a low-salinity fluid of shallower origin, separated by a brine interface (McKibben et al. 1988). Textural features and distribution of Fe sulphides indicate a broad zoning as a function of temperature and depth. Thus, there are three zones of mineralisation in the Salton Sea field. The first occurs at depths of less than 760 m, where the Fe sulphides form fine-grained disseminations in an essentially unaltered host rock; the second zone, which occurs at depths of greater than 760 m, is characterised by extensive

alteration of the sediments; the third zone occurs at depths of approximately 1000 m and forms fracture and pore space fillings in sandstone and siltstone. The genetic processes that account for this mineralisation include diagenesis (temperatures of less than 250°C), metamorphism (200–300°C) and hydrothermal activity, which accounts for the fracture fillings with ore minerals such as chalcopyrite, sphalerite, pyrite, pyrrhotite and galena. The host rocks are altered and the alteration assemblages include calcite, quartz, adularia, epidote, anhydrite, chlorite and actinolite. There are two types of vein assemblages (McKibben and Elders 1985). One is sulphide–carbonate–silicate with minerals such as chalcopyrite + sphalerite + calcite + epidote ± adularia ± pyrite ± quartz ± galena. The other is hematite–silicate–sulphide–sulphate and contains principally hematite + epidote ± chalcopyrite ± pyrite ± anhydrite. A model by McKibben et al. (1988) to explain the mechanisms of brine upwelling and mineral deposition, proposed that an intrusion caused the expulsion of reduced connate fluids in an upper zone of low-salinity fluids, forming the first type of veins discussed above. With the rise of the thermal front, hypersaline brines ascend from depth to interact with moderate- to low-salinity fluids in the upper zones, forming the second type of veins. On cooling of the geothermal system, oxidised surface waters are drawn in and form the late-stage hematite veinlets. The authors further speculate that if the hypersaline brines of the Salton Sea system were to vent in a body of water, the development of a stratiform metalliferous deposit could result. In 1962, over a 3-month period, fluid discharge from boreholes at temperatures of 130–170°C precipitated several tonnes of sulphide minerals and opaline silica having a bulk composition of up to 20% Cu, 7% Ag, and 7% Fe (Weissberg et al. 1979). An estimate of the size and content of the brine reservoir by White (1981) gives the following: 5 Mt of Zn metal, 9 Mt of Pb, 120 000 t of As, 60 000 t of Cu, 20 000 t of Cd and 10 000 t of Ag, contained in a brine volume of about 11.6 km^3 to a depth of 3 km and with a mean reservoir temperature of 300°C.

5.4.6 Lake Tanganyika

Lake Tanganyika is in the western branch of the East African Rift System (Chapter 8_Fig. 10.2). In the northern part of the lake, hydrothermal activity is present both on- and off-shore. In this region, Tiercelyn et al. (1989, 1991) and Pflumio et al. (1994) studied three hydrothermal fields, Pemba, Cape Banza and Cape Kalamba, where hydrocarbons, sulphide and carbonates are being deposited. Lake Tangayika has a complex geological structure. It consists of northern and southern basins that can be further subdivided into seven sub-basins. These basin and sub-basin structures are controlled by a complex system of faults. In the northern basin high heat flow was recorded with values of up to 320 mW m^{-2}. This high heat flow is related to magmatic activity below the floor of the lake. The waters of Lake Tanganyika are stratified with the transition between oxic and anoxic layers at water depths ranging from 50 to 100 m in the

north, to 240 m in the south. About 90% of the lake's bottom waters are anoxic, and as a result the bottom sediments, which reach a thickness of up to 6 km, have high total organic carbon (TOC) content of up to 12%. In addition, the anoxic layers have significant amounts of CO_2, H_2S, CH_4 and He. The high heat flow induces maturation of the organic matter and the formation of hydrocarbons, as revealed by oil seepages at Cape Kalamba.

Hydrothermal activity at Pemba and Cape Banza is characterised by gas emanations (mainly CO_2 and CH_4) and discharge of thermal waters on land and under water. In the Pemba field there are kaolinite-rich layers and stockworks of quartz-pyrite that cut throught the basement rocks. Blocks of massive marcasite and pyrite are associated with quartz, barite and kaolinite. Hydrothermal fluids discharge through several vents, at temperatures ranging from 60 to 90°C. The vents are surrounded by mat-forming microbial communities. At Cape Banza the hydrothermal field covers an area of 300 x 40 m to a water depth of 6 m, where a littoral plateau contains several active vents, or groups of vents, each with aragonite chimneys. Fluids have temperatures between 50 and 103°C and flow rates of 1–3 l/s. The Banza chimneys are coated with filamentous algal mats; pyrite forms films and encrustations on fractures and along the channels through which the fluids circulate. On land, fossil hydrothermal activity resulted in the deposition of Fe oxides, quartz and kaolinite veins. Analyses of the hydrothermal fluids revealed that there are two end-members: a Na–HCO_3 type and a Na–Cl type. The isotopic ($\delta\ ^{18}O$, $\delta\ ^{2}H$ and $\delta\ ^{13}C$) composition of these fluids suggests that they are of magmatic origin, but have interacted with meteoric and lake waters. A model illustrating the hydrothermal system of the northern Lake Tanganyika is shown in Fig. 8.7.

5.5 Concluding Remarks

In this chapter I have described and discussed porphyry and epithermal systems including some of the more classic examples of both. Porphyry deposits constitute an economically important category of metallic mineral resources that are typically contained in large volumes of rock. Porphyry systems are formed in subduction-related settings at continental margins and in rift-related intracontinental settings. Porphyry systems commonly reported in the literature are subduction-related and they are some of the largest and well-studied mineral systems. Subduction-related porphyries are associated with volcanic edifices and can be gradational to high-sulphidation epithermal systems and hot springs at surface. Rift-related intracontinental settings, although known for some time, have only recently been the focus of publications. Porphyry systems of non-subduction settings cover a wide range and are associated with granitic rocks that are linked with mantle upwellings in regimes of lithospheric thinning. Some of these porphyries could be considered as intrusion-related systems, as they often show features that are transitional to the latter. Examples discussed

in this book are mostly from Asia. I have included the porphyry systems of the Colorado Mineral Belt, although a non-subduction setting for these may well be debated. However, the role of mantle upwelllings cannot be underemphasised, because there are clear examples from the volcanic rifted margins of eastern Greenland and the oldest porphyry systems in the East Pilbara Craton in Western Australia, for which a mantle plume involvement is well established. Where porphyry intrusions interact with carbonate sedimentary rocks, skarns are likely to develop and these are treated in Chapter 6.

In the epithermal range, I have distinguished "fossil" and present-day systems. The latter are represented in geothermal systems in continental settings (Yellowstone) to partly continental (Taupo) to emerged volcanic arcs (Kamchatka) to partly submerged volcanic arcs (Kurile and White Island), providing the full range of epithermal settings, before heading out to the deep sea, to the submarine systems, which are the subject of Chapter 7. Epithermal deposits are associated with calc-alkaline to alkaline magmatism and constitute an important source of precious metals, but are almost always confined to geologically young terranes, due to their near-surface to shallow depth positions and therefore amenable to erosion, although there are examples of preservation of clastic sediments derived from the erosion of ancient epithermal deposits. This is the interesting case for Kanowna Bell in Western Australia.

References

Ambrus J (1978) Chuquicamata deposit. In: Sutulov A (ed) Int Molybd Encycl 1778–1978, vol 1. Santiago de Chile, pp 87–93

Arculus RJ (1994) Aspects of magma genesis in arcs. Lithos 33: 189–208

Arnórsson S (2000) Exploitation of geothermal resources. In: Sigurdson H (Chief Ed) Encyclopedia of volcanoes, Academic Press, San Diego, pp. 1243–1258

Bailey DK (1987) Mantle metasomatism – perspective and prospect. Geol Soc Lond Spec Publ 30: 1–14

Baldridge WS, Keller GR, Haak V, Wendlandt E, Jiracek GR, Olsen KH (1995) The Rio Grande rift. In: Olsen KH (ed) Continental rifts: evolution, structure, tectonics, Elsevier, Amsterdam, pp 233–324

Barbarin B (1999) A review of the relationships between granitoid types, their origins and their geodynamic environments. Lithos 46: 605–626

Barley ME (1982) Porphyry-style mineralization associated with early Archean calc-alkaline igneous activity, eastern Pilbara, Western Australia. Econ Geol 77: 1230–1236

Barnes HL (1990) Hydrothermal fluids and the deposition of ore minerals, with emphasison gold, silver and copper. Course Notes, Econ Geol Res Unit, Univ Witwatersrand, Feb 1990

Barnes HL, Seward TM (1997) Geothermal systems and mercury deposits. In: Barnes HL (ed) Geochemistry of hydrothermal ore deposits, 3rd edn, John Wiley & Sons, New York, pp 699–736

Barton PB (1970) Sulfide petrology. Mineral Soc Am Sp Pap 3: 187–198

Bartos PJ (2000) The pallacos of cerro rico de potosi, bolivia, a new deposit type. Econ Geol 95: 645–654

Baumer A, Fraser RB (1975) Panguna porphyry copper deposit, Bouganville. In: Knight CL (ed) Economic geology of Australia and Papua New Guinea. 1 Metals. Australas Inst Min Metall, Parkville, Victoria, pp 855–866

Beane RE, Titley SR (1981) Porphyry copper deposits, Part II: Hydrothermal alteration and mineralization. Econ Geol 75th Ann vol: 214–268

Beckett TS, Fahey GJ, Sage PW, Wilson GM (1998) Kanowna Belle deposit. Aust Inst Min Metall Monogr 22: 179–206

Berger BR, Eimon P (1982) Comparative models of epithermal gold–silver deposits. Soc Min Eng Reprint 82–13

Berzina AP, Borisenko AS (2007) Porphyry Cu–Mo mineralization and mantle plumes, in: Abs Vol Large Igneous provinces of Asia, mantle plumes and metallogeny Inter Symp, Novosibirsk, pp 214–216

Bindeman IN (2006) The secrets of supervolcanoes. Sci Am June Iss: 27–33

Bindeman IN, Ponomareva VV, Bailey JC, Valley JW (2004) Volcanic arc of Kamchatka: a province with high-$\delta^{18}O$ magma source and large-scale $^{18}O/^{16}O$ depletion of the upper crust. Geochim Cosmochim Acta 68: 841–865

Bird DK, Schiffman P, Elders WA, Williams AE, McDowell SD (1984) Calc-silicate mineralization in active geothermal systems. Econ Geol 79: 671–695

Bissig T, Clark AH, Lee JKW, Hodgson CJ (2002) Miocene landscape evolution and geomorphological controls on epithermal processes in the El Indio-Pascua Au–Ag–Cu belt, Chile and Argentina. Econ Geol 97: 971–996

Blisniuk PM, Hacker BR, Glodny J, Ratschbacher L, Bi SW, Wu Z, McWilliams MO, Calvert A (2001) Normal faulting in central Tibet since at least 13.5 Myr ago. Nature 412: 628–632

Bogie I, Lawless J (1987) Controls on the hydrology of large volcanically hosted geothermal systems: implications for exploration for epithermal mineral deposits. Proc Pac Rim '87 Congr Australas Inst Min Metall, pp 57–60

Bonin B, Ethien R, Gerbe MC, Cottin JY, Feraud G, Gagnevin D, Giret A, Michon G, Moine B (2004) The Neogene to recent Rallier-duBaty nested ring complex, Kerguelen Archipelago (TAAF, Indian Ocean): stratigraphy revisited, implications for cauldron subsidence mechanisms. Geol Soc, Lond, Sp Publ 234: 125–149

Bonnichsen B, Christiansen RL, Morgan LA, Moye FJ, Hackett WR, Leeman WP, Honjo N, Jenks MD, Godchaux MM (1989) Excursion 4A: Silicic rocks in the Snake River Plain-Yellowstone plateau province. New Mex Bureau Mines Min Res and New Mex Inst Min Techn Memoir 47: 135–153

Borisenko AS, Sotnikov VI, Izokh AE, Polyakov GV, Obolensky AA (2006) Permo-Triassic mineralization in Asia and its relation to plume magmatism. Russian Geol Geophys 47: 166–182

Botcharnikov RE, Shmulovich KI, Tkachenko SI, Korzhinsky MA, Rybin AV (2003) Hydrogen isotope geochemistry and heat balance of a fumarolic system: Kudriavy volcanoc, Kuriles. J Volc Geoth Res 124: 45–66

Brathwaite RL, Faure K (2002) The Waihi epithermal gold–silver-base metal sulfide quartz vein system, New Zealand: temperature and salinity controls on electrun and sulfide deposition. Econ Geol 97: 269–290

Brathwaite RL, McKay DF (1989) Geology and exploration of the Martha Hill gold-silver deposit, Waihi. Australas Inst Min Metall Monogr 13: 83–88

Brathwaite RL, Pirajno F (1993) Metallogenic Map of New Zealand. Inst Geol Nucl Sci Monogr 3

Brathwaite RL, Christie AB, Skinner DNB (1989) The Hauraki goldfield: Regional setting, mineralisation and recent exploration. Australas Inst Min Metall Monogr 13: 45–56

Brathwaite RL, Torckler LK, Jones PK (2006) The Martha Hill epithermal deposit, Waihi – geology and mining history. Australas Inst Min Metall Monogr 25: 171–178

Brooks CK, Tegner C, Stein H, Thomassen B (2004) Re–Os and $^{40}Ar/^{39}Ar$ ages of porphyry molybdenum deposits in the east Greenland volcanic-rifted margin. Econ Geol 99: 1215–1222

Browne KL (1986) Gold deposition from geothermal discharges in New Zealand. Econ Geol 81: 979–983

Bryan S (2007) Silicic large igneous provinces. Episodes 30: 20–31

Buchanan LJ (1981) Precious metal deposits associated with volcanic environments in the southwest. In: Dickinson WR, Payne WD (eds) Relation of tectonics to ore deposits in the South Cordillera. Ariz Geol Soc Digest 14: 237–262

Burnham CW (1985) Energy release in subvolcanic environments: implications for breccia formation. Econ Geol 80: 1515–1522

Camprubi A, Ferrari L, Cosca MA, Caredellach E, Canals A (2003) Ages of epithermal deposits in Mexico: regional significance and links with the evolution of Tertiary volcanism. Econ Geol 98: 1029–1037

Camus F (1975) Geology of the El Teniente orebody with emphasis on wall rock alteration. Econ Geol 70: 1341–1372

Cannell J, Cooke DR, Walshe JL, Stein H (2005) Geology, mineralization and structural evolution of the El Teniente porphyry Cu–Mo deposit. Econ Geol 100: 979–1003

Carman GD (2003) Geology, mineralization and hydrothermal evolution of the Ladolam gold deposit, Lihir Island, Papua New Guinea. Soc Econ Geol Sp Publ 10: 247–284

Carroll AR, Graham SA, Hendrix MS, Ying D, Zhou D (1995) Late Paleozoic tectonic amalgamation of northwestern China: Sedimentary record of the northern Tarim, northwestern Turpan and southern Junggar basin. Geol Soc Am Bull 107: 571–594

Carten RB, White WH, Stein HJ (1993) High-grade granite-related molybdenum systems: classification and origin. Geol Ass Can Spec Pap 40: 521–554

Chen YJ, Fu SG (1992) Gold Mineralization in West Henan, China. Seismol Press, Beijing, 234 pp. (in Chinese with English abstract)

Chen H, Xu B (1997) Isotope tracing and prospecting assessment of gold-silver deposits in Zhejiang Province. Acta Geol Sinica 71: 293–304

Chen CH, Lin W, Lu HY, Lee CY, Tien JL, Lai YH (2000) Cretaceous fractionated I-type granitoids and metaluminous A-type granites in SE China: the Late Yanshanian post-orogenic magmatism. Trans Royal Soc Edinb Earth Sci 91: 195–205

Chen YJ, Li C, Zhang J, Li Z, Wang HH (2000) Sr and O isotopic characteristics of porphyries in the Qinling molybdenum deposit belt and their implication to genetic mechanism and type. Sci in China Ser D 43(Supp.): 82–94

Chen YJ, Pirajno F, Sui YH (2004) Isotope geochemistry of the Tieluping silver-lead deposit, Henan, China: A case study of orogenic silver-dominated deposits and related tectonic setting. Mineral Depos 39: 560–575

Chouinard A, William-Jones AE, Leonardson RW, Hodgson CJ, Silva P., Tellez C, Vega J, Rojas F (2005) Geology and genesis of the multistage high-sulfidation epithermal Pascau Au–Ag–Cu deposit, Chile and Argentina. Econ Geol 100:463–490

Christie AB, Brathwaite RL (eds) (2006) Geology and exploration of New Zealand mineral deposits. Australas Inst Min Metall Monogr 25

Christie AB, Brathwaite RL, Mauk JL, Simpson MP (2006) Hauraki Goldfield – regional exploration databases and prospectivity studies. Austral Inst Min Metall Monogr 25: 73–84

Christie AB, Simposn MP, Brathwaite RL, Mauk JL, Simmons SF (2007) Epithermal Au–Ag and related deposits of the Hauraki goldfield. Coromandel Volcanic Zone, New Zealand. Econ Geol 102: 785–816

Chung SL, Chua MF, Zhang YQ, Xie YG, Lo CH, Lee TY, Lan CY, Li XH, Zhang Q, Wang YZ (2005) Tibetan tectonic evolution inferred from spatial and temporal variations in post-collisional magmatism: Earth-Sci Rev 68: 173–196

Clark GH (1990) Panguna copper-gold deposit In: Hughes FE (ed) Geology of the mineral deposits of Australia and Papua New Guinea, vol 2, Australas Inst Min Metall Monogr 14, pp 1807–1816

Cole JW (1984) Taupo-Rotorua depression: an ensialic marginal basin of North Island, New Zealand. Geol Soc London Spec Publ 16:109–120

Cole JW (1986) Volcanism in the Taupo Volcanic Zone. In: Henley RW, Hedenquist JW, Roberts PJ (eds) Guide to active epithermal (geothermal) systems and precious metal deposits of New Zealand. Monogr 26. Gebruder Borntr, Berlin, pp 23–28

Cole JW (1990) Structural control and origin of volcanism in the Taupo Volcanic Zone, New Zealand. Bull Volc 52: 445–459
Cole DR, Drummond SE (1986) The effect of transport and boiling on Ag/Au ratios in hydrothermal solutions: a preliminary assessment and possible implications for the formation of epithermal precious-metal ore deposits. J Geochem Expl 25: 45–79
Cole JW Lewis KB (1981) Evolution of the Taupo-Hikurangi subduction system. Tectonophysics 72:1–21
Cooke DR, Simmons SF (2000) Characteristics and genesis of epithermal gold deposits. Rev Econ Geol 13: 21–244
Cooke DR, Hollings P, Walshe JL (eds) (2005) A special issue devoted to giant porphyry deposits. Econ Geol 100, No. 5
Crew Gold London News Release 2005, www.crewgold.com (viewed in 2007)
Crowe D, Jordan T, Baker MS, Schroeder P (2006) Mapping the distribution of alteration minerals in an active geothermal setting using satellite-based spectral reflectance: an example from the Uzon caldera, Kamchatka, Far East Russia. Geol Soc Am 2008 Ann Meet, Abs with Programs, Sess 234, p 565
Cunningham CG, Zartman RE, McKee EH, Rye RO, Naeser CW, Sanjinés O, Ericksen GE, Tavera F (1996) The age and thermal history of Cerro Rico de Potosi, Bolivia. Mineral Depos 31: 374–385
Davies RM, Ballantyne GH (1987) Geology of the Ladolam gold deposit Lihir island, Papua New Guinea. Proc Pac Rim '87 Congr. Australas Inst Min Metall, pp 943–949
DePaolo DJ (1981) Trace element and isotopic effects of combined wallrock assimilation and fractional crystallisation. Earth Planet Sci Lett 53: 189–202
De Ronde CEJ, Stoffers P, Garbe-Schönberg D, Christenson BW, Jones B, Manconi R, Browne PRL, Hissmann K, Botz R, Davy BW, Schmitt M, Battershill CN (2002) Discovery of active hydrothermal venting in Lake Taupo, New Zealand. J Volc Geoth Res 115: 257–275
Deyell CL, Leonardson R, Rye RO, Thompson JFH, Bissig T, Cooke DR (2005) Alunite in the Pascua-Lama high sulfidation deposit: constraints on alteration and ore deposition using stable isotope geochemistry. Econ Geol 100: 131–145
Dickinson WR (2006) Geotectonic evolution of the Great Basin. Geosphere 2: 353–368
Dilles JH, Camus F (eds) (2001) A special issue devoted to porphyry copper deposits of northern Chile. Econ Geol 96, No. 2
Dilles JH, Einaudi MT (1992) Wall-rock alteration and hydrothermal flow paths about the Ann-Mason porphyry copper deposit, Nevada – a 6 km vertical reconstruction: Econ Geol 87: 1963–2001
Dong G, Morrison GW (1995) Adularia in epithermal veins, Queensland: morphology, structural state and origin. Mineral Depos 30: 11–19
Dow DB (1975) Geology of Papua New Guinea. In: Knight CL (ed) Economic Geology of Australia and Papua New Guinea. 1 Metals. Australas Inst Min Metall, pp 823–835
Eastoe CJ (1978) A fluid inclusion study of the Panguna porphyry copper deposit, Bougainville, Papua New Guinea. Econ Geol 73: 721–748
Einaudi MT, Hedenquist JW, Inan E (2003) Sulfidation state of fluids in active and extinct hydrothermal systems: transition from porphyry to epithermal environments. Soc Econ Geol Sp Publ 10: 285–313
Ellis AJ (1979) Explored geothermal systems. In: Barnes H L (ed) Geochemistry of hydrothermal ore deposits. John Wiley & Sons, New York, pp 632–683
Ellis AJ, Mahon WAJ (1977) Chemistry and geothermal systems. Academic Press, New York, London
England BM, Ostwald J (1993) Framboid-derived structures in some Tasman fold belt base-metal sulphide deposits, New South Wales, Australia. Ore Geol Rev 7: 381–412
Ericksen GE, Luedke RG, Smith RL, Koeppen RP, Urquidi BF (1990) Peraluminous igneous rocks of the Bolivian tin belt. Episodes 13:3–8

Ewers RG, Keays RR (1977) Volatile and precious metal zoning in the Broadlands geothermal field, New Zealand. Econ Geol 72:1337–1354

Fan HR, Xie YH, Zheng XZ, Wang YL (2000) Ore–forming fluids in hydrothermal breccia–related gold mineralization in Qiyugou, Henan Province. Acta Petrol Sinica 16: 559–563 (in Chinese with English abstract)

Fitton JG, James D, Leeman WP (1991) Basic magmatism associated with late Cenozoic extension in the western United States: compositional variations in space and time. J Geophys Res 96: 13693–13711

Ford JH (1978) A chemical study of alteration at the Panguna porphyry copper deposit, Bougainville, Papua New Guinea. Econ Geol 73: 703–720

Fournier RO (1989) Geochemistry and dynamics of the Yellowstone National Park hydrothermal system. Ann Rev Earth Planet Sci 17: 13–51

Fournier RO, Christainsen RL, Hutchinson RA, Pierce KL (1994a) A field-trip guide to Yellowstone National Park, Wyoming, Montana and Idaho-Volcanic, hydrothermal and glacial activity in the region. U.S. Geol Surv Bull 2099

Fournier RO, Kennedy MB, Aoki M, Thompson MJ (1994b) Correlation of gold in siliceous sinters with $^{3}He/^{4}He$ in hot spring waters of Yellowstone National Park. Geochim et Cosmochim Acta 58: 5401–5419

Frutos J (1982) Andean metallogeny related to the tectonic and petrologic evolution of the Cordillera: Some remarkable points. In: Amstutz GC, El Goresy A, Frenzel G, Kluth C, Moh G, Wauschkuhn A, Zimmermann RA (eds) Ore genesis – The State of the art. Springer, Berlin, pp 493–507

Gammons CH, Barnes HL (1989) The solubility of Ag_2S in near-neutral aqueous sulfide solutions at 25–300°C. Geochim Cosmochim Acta 53: 279–290

Gao YF, Hou ZQ, Wei RH, Zhao RS (2003) Post-collisional adakitic porhyries in Tibet: geochemical and Sr–Nd–Pb isotopic constraints on partila melting of oceanic lithosphere and crust-mantle interaction. Acta Geol Sinica 77: 194–203

Gernet J (1999) A history of Chinese civilization, 2nd edn. Cambridge University Press, Cambridge

Geyti A, Schonwandt HK (1979) Bordvika a possible porphyry molybdenum occurrence within the Oslo province, Norway. Econ Geol 74: 1211–1220

Geyti A, Thomassen B (1984) Molybdenum and precious metal mineralization at Flammefjel southeast Greenland. Econ Geol 79: 1921–1929

Giggenbach WF, Shinohara H, Kusakabe M, Ohba T (2003) Formation of acid volcanic brines through interaction of magmatic gases, seawater, and rock within the White Island volcanic-hydrothermal system, New Zealand. Soc Econ Geol Sp Publ 10: 19–40

Goff F, Janik CJ (2000) Geothermal systems. In: Sigurdson H (Chief Ed) Encyclopedia of Volcanoes, Academic Press, San Diego, pp 817–834

Grieve PL, Corbett GJ, Leach TM (2006) Explorationat Ohakuri North epithermal Au–Ag prospect, Taupo Volcanic Zone. The Aus Inst Min Metall Monogr 25: 197–202

Groves DI, Goldfarb RJ, Gebre-Mariam M, Hagemann SG, Robert F (1998) Orogenic gold deposits: a proposed classification in the context of their crustal distribution and relationship to other gold deposit types. Ore Geol Rev 13: 7–27

Guidry SA, Chafetz HS (2003) Anatomy of siliceous hot springs: examples from Yellowstone National Park, Wyoming, USA. Sedim Geol 157: 71–106

Guilbert JM, Lowell JD (1974) Variations in zoning patterns in porphyry ore deposits. Can Inst Min Metall Bull 67:99–109

Gustafson LB, Titley SR (eds) (1978) Porphyry copper deposits of the southwestern Pacific islands and Australia. Econ Geol 73, No. 5

Halter WE, Pettke T, Heinrich CA (2002) The origin of Cu/Au ratios in porphyry-type ore deposits. Science 296: 1844–1846

Han CM, Xiao, WJ, Zhao, GC, Mao, JW, Yang JM, Wang ZL, Yan Z, Mao QG (2006) Geological characteristics and genesis of the Tuwu porphyry copper deposit, Hami, Xinjiang, Central Asia. Ore Geol Rev 29: 77–94

Han YG, Zhang SH, Pirajno F, Zhang YH (2007) Evolution of the Mesozoic granites in the Xiong'ershan-Waifangshan region, Henan province, China, and its tectonic implications. Acta Geol Sinica 81: 253–265

Harrison TM, Leloup PH, Ryerson FJ, Tapponnier P, Lacassin R, Chen WJ (1996) Diachronous initiation of transtension along the Ailaoshan-Red River shear zone, Yunnan and Vietnam. In: Yin A,, Harrison TM, (eds) The Tectonic Evolution of Asia. Cambridge Univ Press, Cambridge, pp 208–226

Hedenquist JW (1983) Waiotapu geothermal field excursion handout notes on epithermal environments in New Zealand. Pt 2. Individ Geotherm Fields, Int Volcanol Congr, Auckland, NZ, pp F1–F16

Hedenquist JW (1997) Epithermal gold deposits: Styles, characteristics and exploration. Key Centre Econ Geol, Univ West Aust, Short Course Notes

Hedenquist JW, Henley RW (1985) Hydrothermal eruptions in the Waiotapu geothermal system, New Zealand: origin, breccia deposits and effect on precious metal mineralization. Econ Geol 80: 1640–1666

Hedenquist JW, Lowenstern JB (1994) The role of magmas in the formation of hydrothermal ore deposits. Nature 370: 519–527

Hedenquist JW, Simmons SF, Giggenbacj WF, Eldridge SC (1993) White Island, New Zealand, volcanic-hydrothermal system represents the geochemical environment of high-sulfidation Cu and Au ore deposition. Geology 21: 731–734

Hedenquist JW, Yukihiro Matsuhisa, Izawa E, White NC, Giggenbach WF, Aohi M (1994). Geology, geochemistry and origin of high sulfidisation Cu–Au mineralization in the Nansatsu District, Japan. Econ Geol 89: 1–30

Hedenquist JW, Izawa E, Arribas A, White NC (1996) Epithermal gold deposits: styles, characteristics and exploration. Poster Soc Res Geol Sp Publ 1

Hedenquist JW, Arribas A, Reynolds TJ (1998) Evolution of an intrusion-centered hydrothermal system: Far Southeast-Lepanto porphyry and epithermal Cu–Au deposits, Philipines. Econ Geol 93: 373–404

Hedenquist JW, Arribas A, Gonzalez-Urien E (2000) Exploration for epithermal gold deposits. Soc Econ Geol Rev 13: 245–277

Henley RW, Ellis AJ (1983) Geothermal systems ancient and modern: a geochemical review. Earth Sci Rev 19: 1–50

Henley RW, Hedenquist JW, Roberts PJ (eds) (1986) Guide to active epithermal (geothermal) systems and precious metal deposits of New Zealand. Monogr 26 Gebruder Borntr, Berlin, 211 pp

Hickman AH (2004) Two contrasting granite-greenstone terranes in the Pilbara Craton, Australia: evidence for vertical and horizontal tectonic regimes prior to 2900 Ma. Precambr Res 131: 153–172

Hildreth W, Moorbath S (1988) Crustal contributions to arc magmatism in the Andes of central Chile. Contr Miner Petr 98: 455–489

Hill KC, Hegarty KA (1987) New tectonic framework for PNG and the Caroline plate: implications for cessation of spreading in back-arc basins. In: Pacific Rim Congr '87. Australas Inst Min Metall, pp 179–182

Hinman NW, Walter MR (2005) Textural preservation in siliceous hot spring deposits during early diagenesis: examples from Yellowstone National park and Nevada, U.S.A. J Sedim Res 75: 200–215

Hochstaedter AG, Kepezhinskas PK, Defant MJ, Drummond MS, Bellon H (1994) On the tectonic significance of arc volcanism in northern Kamchatka. J Geol 102: 639–654

Hockstein MP, Browne PRL (2000) Surface manifestations of geothermal systems with volcanic heat sources. In: Sigurdson H (Chief Ed) Encyclopedia of Volcanoes, Academic Press, San Diego, pp 835–855

Hollister VF (1978) Geology of the porphyry copper deposits of the western hemisphere. Am Inst Min Metall Pet Eng, 219p

Hou ZQ, Ma HW, Zaw K, Zhang YQ, Wang MJ, Wang Z, Guitang P, Renli T (2003) The Himalayan Yulong porphyry copper belt: product of large scale strike-slip faulting in eastern Tibet. Econ Geol 98: 125–146

Hou ZQ, Gao YF, Qu XM, Rui ZY, Mo X (2004a) Origin of adakitic intrusives generated during mid-Miocene east-west extension in southern Tibet. Earth Planet Sci Lett 220: 139–155

Hou ZQ, Qu XM, Wang SX, Du A, Gao YF, Huang W (2004b) Re–Os age for molybdenite from the Gangdise porphyry copper belt on Tibetan plateau: implication for geodynamic setting and duration of the Cu mineralization: Sci China Ser. D 47: 221–231

Hou ZQ, Zaw K, Pan GT, Mo XX, Xu Q, Hu YZ, Li XZ (2007a) Sanjiang Tethyan metallogenesis in S. W. China: tectonic seting, metallogenic epochs and deposit types. Ore Geol Rev 31: 48–87

Hou ZQ, Xie YL, Xu WY, Li YQ, Zaw K, Beaudoin G, Rui ZY, Wei H, Luobu C (2007b) Yulong deposit, East Tibet: a high-sulfidation Cu–Au porphyry Cu deposit in the eastern Indo-Asian collision zone. Inter Geol Rev 49: 235–248

Hou ZQ, Pan XF, Yang ZM (in press) Porphyry Cu–(-Mo–Au) deposits unrelated to oceanic slab subduction: examples from Chinese porphyry deposits in intracontinental settings. Ore Geol Rev

Hougton BF, Nairn IA (1991) Strombolian and phreatomagmatic eruptions of White Island, New Zealand: eruption and depositional mechanisms at a "wet" volcano. Bull Volc 54: 25–49

Howell FH, Molloy JS (1960) Geology of the Braden orebody, Chile, South America, Econ Geol 55: 863–905

Hu RZ, Burnard PG, Bi XW, Zhou MF, Pen JT, Su WC, Wu KX (2004) Helium and argon isotope geochemistry of alkaline intrusion-associated gold and copper deposits along the Red River-Jinshajaing fault belt, SW China. Chem Geol 203: 305–317

Huang DH, Wang Y, Nie F, Jiang X (1985) A new type of molybdenum deposit – geological characteristics and metallogenic mechanism of the Huanglongpu carbonatite vein type of molybdenum (lead) deposit, Shanxi. Acta Geol Sinica 59: 241–258 (in Chinese with English Abstract)

Huang DH, Dong QY, Gan ZX (1990) Molybdenum deposits of China. In: Edit Comm Miner Depos China, vol 1, Geol Publ House, pp 288–355

Husen S, Smith RB, Waite GP (2004) Evidence for gas and magmatic sources beneath the Yellowstone volcanic field from seismic tomographic imaging. J Volc Geother Res 131: 397–410

Huston DL, Keillor B, Standing J, Blewett R, Mernagh TP (2000) Epithermal deposits of the central Pilbara tectonic zone; description and exploration significance. AGSO Res Newslett 32: 34–39

Huston DL, Morant P, Pirajno F, Cummins B, Baker D, Mernagh TP (2007a) Palaeoarchean mineral deposits of the Pilbara Craton: genesis, tectonic environment and comparisons with younger deposits. In: Van Kranendonk MJ, Smithies RH, Bennett VC (eds), Earth's oldest rocks, Chpt 4.4, Elsevier, Amsterdam, pp. 411–450

Huston DL, Van Kranendonk MJ, Hickman AH, Pirajno F (2007b) Change from plume to convergent tectonics in the early Archaean: metallogenic implications in the Pilbara Craton, Western Australia. In: Andrew CJ et al (eds) Proceed Ninth SGA Meeting Dublin 2007, vol 1, pp 23–26

Hutchison C S (1983) Economic deposits and their tectonic setting. MacMillan, London

Isacks BL (1988) Uplift of the central Andean plateau and bending of the Bolivian orocline. J Geophys Res 93: 3211–3231

Jahn BM (2004) The Central Asian Orogenic Belt and growth of the continental crust in the Phanerozoic. Geol Soc Lond Sp Publ 226: 73–100

Jahn BM, Zhou XH, Li JL (1990) Formation and tectonic evolution of southeastern China and Taiwan: isotopic and geochemical constraints. Tectonophysics 183: 145–160

Jannas RR (1995) El Indio district, Chile. PhD thesis, unpubl, Harvard Univ
Jannas RR, Bowers TS, Petersen U, Beane RE (1999) High-sulfidation deposit types in the El Indio district, Chile. Soc Econ Geol Sp Publ 7: 219–266
John DA (2001) Miocene and Early Pliocene epithermal gold-silver deposits in the northern Great Basin, Western United States: characteristics, distribution and relationship to magmatism. Econ Geol 96: 1827–1853
Jolley DW, Bell BR (eds) (2002) The North Atlantic Igneous Province: stratigraphy, tectonic, volcanic and magmatic processes. Geol Soc London Spec Publ 197
Kay SM, Mpodozis C (2001) Central Andean ore deposits linked to evolving shallow subduction systems and thickening of the crust. GSA Today 11: 4–9
Kawakatsu H, Watada S (2007) Seismic evidence for deep-water transportation in the mantle. Science 316: 1468–1471
Kear D (ed) (1989) Mineral deposits of New Zealand. Aus Inst Min Metall Monogr 13
Kharaka YK, Sorey ML, Thorsden JJ (2000) Large-scale hydrothermal fluid discharges in the Norris-Mammoth corridor, Yellowstone National Park, USA. J Geochem Expl 69–70: 201–205
Khashgerel B-E, Rye RO, Hedenquist JW, Kavalieris I (2006) Geology and reconnaissance stable isotope study of the Oyu Tolgoi porphyry Cu–Au system, South Gobi, Mongolia. Econ Geol 101: 503–522
Kirwin DJ (1985) Tourmaline breccia pipes. Unpubl MSc thesis, James Cook Univ, Australia
Klemm LM, Pettke T, Heinrich A, Campos E (2007) Hydrothermal evolution of the El Teniente deposit, Chile: Porphyry Cu–Mo ore deposition from low-salinity magmatic fluids. Econ Geol 102: 1021–1045
Korzhinsky MA, Tkachenko SI, Shmulovich KI, Taran YA, Steinberg GS (1994) Discovery of a pure rhenium mineral at Kudriavy volcano. Nature 369: 51–52
Lang JR, Baker T, Hart CJR, Mortensen JK (2000) An exploration model for intrusion-related gold systems. SEG Newslett 40: 1–15
Lattanzi P, Okrugin VM, Corsini F, Ignatiev A, Okrugina A, Tchubarov V, Livi S (1995) Geology, mineralogy and geochemistry of base and precious metal mineralization in the Mutnovsky area, Kamchatka, Russia. SEG Newslett 20: 1–10
Laznicka P (2006) Giant metallic deposits – future resources of industrial minerals. Springer, Berlin
Lexa J, Štohl J, Konecny V (1999) The Banska Stiavnica ore district: relationship between metallogenic processes and the geological evolution of a stratovolcano. Miner Depos: 34: 639–654
Li ZX (1998) Tectonic history of the major East Asian lithospheric Blocks since the Mid-Proterozoic – A synthesis. Am Geophys Union Geodynamic Ser 27: 221–243
Li ZX, Li XH (2007) Formation of the 1300 km-wide intracontinental orogen and postorogenic magmatic province in Mesozoic South China: a flat-slab subduction model. Geology 35: 179–182
Li YQ, Rui ZY, Cheng LX (1981) Fluid inclusions and mineralization of the Yulong porphyry copper (Mo) deposit. Acta Geol Sinica 55: 18–23 (in Chinese with English abstract)
Li C, Xu B, Jiang X, Hu Y (1993) Interval order between host magmatic rock-forming ages in hydrothermal deposits of eastern China. Res Geol 43: 339–347
Li S, Deng J, Hou ZQ, Xiao R, Yuan WM, Feng XL, Zhao Z, Shen JF, Zhou S (2001) Regional fractures and denudation of gold ore deposits in Gangdise block, Tibet: evidence of Ag/Au values: Sci China Ser. D 44: 121–127
Li SG, Huang F, Li H (2002) Post–collisional lithosphere delamination of the Dabie–Sulu orogen. Chinese Sci Bull 47(3): 259–263
Li YF, Mao JW, Guo BJ, Shao YJ, Fei HC, Hu HB (2004) Re–Os dating of molybdenite from the Nannihu Mo (-W) orefield in the East Qinling and its geodynamic significance. Acta Geol Sinica 78: 463–470

Liang HY, Campbell IH, Allen C, Sun WD, Liu CQ, Yu HX, Xie YW, Zhang YQ (2006) Zircon Ce^{4+}/Ce^{3+} ratios and ages for Yulong ore-bearing pophyries in eastern Tibet. Mineral Depos 41: 152–159

Lindgren W (1933) Mineral deposits. McGraw-Hill Book Co, New York

Long KR (1995) Production and reserves of Cordilleran (Alaska to Chile) porphyry copper deposits. Arizona Geol Soc Digest 20: 35–69

Lowell JD, Guilbert JM (1970) Lateral and vertical alteration-mineralization zoning in porphyry ore deposits. Econ Geol 65: 373–408

Luo MJ, Li SM, Lu XX, Su ZB (2000) Metallogenesis and deposit series of main minerals resources of Henan Province. Geol Publish House, Beijing 452 pp (in Chinese)

Maheo G, Guillot S, Blichert-Tofa J, Rolland Y, Pecher A (2001) A slab breakoff model for the Neogene thermal evolution of southern Karakorum and south Tibet. Earth Planet Sci Lett 195: 45–58

Mao JW, Goldfarb RJ, Zhang ZW, Xu WY, Qiu YM, Deng J (2002) Gold deposits in the Xiaoqinling-Xiong'ershan region, Qinling Mountains, central China. Mineral Depos 37: 306–325

Mao JW, Xie GQ, Bierlein F, Qü WJ, Du AD, Pirajno F, Li HM, Guo BJ, Li YF, Yang ZQ (2008) Re–Os dating of Mesozoic molybdenum deposits in the East Qinling-Dabie orogenic belt: implications for the geodynamic evolution of eastern China. Geochim Cosmochim Acta 72: 4607–4626

Martin H, Smithies RH, Rapp R, Moyen J-F, Champion D (2005) An overview of adakite, tonalite-trondhjemite-granodiorite (TTG) and sanukitoid: relationships and some implications for crustal evolution. Lithos 79: 1–24

McCallum ME (1985) Experimental evidence for fluidisation processes in breccia pipe formation. Econ Geol 80: 1523–1543

McKibben MA, Elders WA (1985) Fe–Zn–Cu–Pb mineralization in the Salton Sea geothermal system, Imperial Valley, California. Econ Geol 80:39–559

McKibben MA, Andes JP, Williams AE (1988) Active ore formation at brine interface in metamorphosed deltaic lacustrine sediments: the Salton Sea geothermal system, California. Econ Geol 83: 511–523

McMillan WJ, Panteleyev A (1980) Ore deposits models. 1. Porphyry copper deposits. Geoscie Can 7: 52–63

Meng QR, Zhang GW (1999) Timing of collision of the North and South China blocks: Controversy and reconciliation. Geology 27: 123–126

Miller LD, Goldfarb RJ, Nie FJ, Hart CJR Miller ML, Yang YQ, Liu YQ (1998) North China gold – a product of multiple orogens. Soc Econ Geol Newslett 33: 1–12

Miller C, Schuster R, Klotzli U, Frank W, Purtscheller F (1999) Post-collisional potassic and ultrapotassic magmatism in SW Tibet: Geochemical and Sr–Nd–Pb–O isopotic constrains for mantle source characteristics and petrogenesis. J Petrol 40: 1399–1424

Minnitt RCA (1986) Porphyry copper-molybdenum mineralization at Haib River. South West Africa/Namibia. In: Anhaeusser CR, Maske S (eds) Mineral deposits of southern Africa II. Geol Soc S Afr, pp 1567–1585

Misra KC (2000) Understanding mineral deposits. Kluwer Academic Publishers, Dordrecht

Mortimer C, Munchmeyer C, Urqueta I (1977) Emplacement of the Exotica orebody, Chile. Trans Inst Min Metall 86: B121–B127

Moyle AJ, Doyle BJ, Hoogvliet H, Ware AR (1990) Ladolam gold deposit, Lihir island. In: Hughes FE (ed) Geology of the mineral deposits of Australia and Papua New Guinea, vol 2. Australas Inst Min Metall Monogr 14, pp 1793–1805

Müller D, Herzig PM, Scholten JC, Hunt S (2002) Ladolam gold deposit, Lihir Island, Papua New Guinea: gold mineralization hosted by alkaline rocks. Soc Econ Geol Sp Publ 9:367–382

Mungall EJ (2002) Roasting the mantle: slab melting and the genesis of major Au and Au-rich Cu deposits. Geology 30: 915–918

Myers JS, Swager CP (1997) The Yilgarn Craton. In: de Wit MJ, Ashwal LD (eds), Greenstone Belts, pp. 640–656, Clarendon Press, Oxford
Neubauer F, Lips A, Kouzmanov K, Lexa J, Ivăşcanu P (2005) Subduction, slab detachment and mineralisation: the Neogene in the Apuseni Mountains and Carpathians. Ore Geol Rev 27: 13–44
Neumann ER (1994) The Oslo Rift: *P-T* relations and lithospheric structure. Tectonophysics 240: 159–172
Neumann ER, Wilson M, Heeremans M, Spencer EA, Obst K, Timmerman MJ, Kirstein L (2004) Carboniferous-Permian rifting and magmatism in southern Scandinavia, the North Sea and northern Germany: a review. Geol Soc London, Spec Publ 223: 11–40
Nie FJ (1994) Rare element geochemistry of the molybdenum-bearing granitoids in the Jinduicheng-Huanglongpu district, Shanxi Province, northwest China. Mineral Depos 29: 488–498
Nie FJ (1997) An overview of the gold resources of China. Intern Geol Rev 39: 55–81
Nielsen RL (1976) Recent developments in the study of porphyry copper geology: a review. In: Sutherland Brown A (ed) Porphyry deposits of the Canadian Cordillera. Can Inst Min Metall Spec Vol 15: 487–500
Nomade S, Renne PR, Mo X, Zhao ZD, Zhou S (2004) Miocene volcanism in the Lhasa block, Tibet: spatial trends and geodynamic implications: Earth Planet Sci Lett 221: 227–243
Okay AI, Sengör AMC, Görür N (1994). Kinematic history of the opening of the Black Sea and its effect on the surrounding regions. Geology 22: 267–270
Orleansky VK, Yeroschchev-Shak VA, Karpov GA, Inkova TA, Zawarzin GA (1994) Bedded bacterial-algal formation (Mats) in the Kamchatka thermal fields. Int Geol Rev 36: 298–302
Ossandón GC, Fréraut RC, Gustafson LB, Lindsay DD, Zentilli M (2001) Geology of the Chuquicamata mine: a progress report. Econ Geol 96: 249–270
Pan YM, Dong P (1999) The Lower Chiangjiang (Yangzi/Yangzte River) metallogenic belt, east central China: intrusion- and wall rock-hosted Cu–Fe–Au, Mo, Zn, Pb, Ag deposits. Ore Geol Rev 15: 177–242
Panigrahi MK, Misra KC, Bream B, Naik RK (2002) Genesis of the granitoid affiliated copper-molybdenum mineralization at Malanjkhand central India: facts and problems. Proc 11th Quadren IAGOD Symp, Windhoek, Namibia (electronic file)
Panigrahi MK, Mookherjee A (1997) The Malanjkhand copper (+molybdenum) deposit, India: mineralization from a low-temperature ore-fluid of granitoid affiliation. Mineral Depos 32: 133–148
Pei R, Hong D (1995) The granites of South China and their metallogeny. Episodes 18: 77–86
Pflumio C, Boulègue J, Tiercelin JJ (1994) Hydrothermal activity in the northern Tanganyika rift, East Africa. Chemical Geology 116: 85–109
Pirajno F (1992) Hydrothermal mineral deposits – Principles and fundamental concepts for the exploration geologist. Springer, Berlin
Pirajno F (1995) Volcanic-hosted epithermal systems in northwest Turkey. S Afr J Geol 98: 13–24
Pirajno F (2000) Ore deposits and mantle plumes. Kluwer Academic Publishers, Dordrecht
Pirajno F, Bagas L (2002) Gold and silver metallogeny of the South China fold Belt: a consequence of multiple mineralizing events? Ore Geol Rev 20: 109–126
Pirajno F, Bagas L, Hickman AH, Gold Research Team (1997) Gold mineralisation of the Chencai-Suichang Uplift and tectonic evolution of Zhejiang Province, southeast China. Ore Geol Rev 12: 35–55
Pirajno F, Mao J-W, Zhang Z-C, Zhang Z-H, Chai F-M (2008) The association of anorogenic mafic-ultramafic intrusions and A-type magmatism in the Tian Shan and Altay orogens, NW China: implications for geodynamic evolution and potential for the discovery of new ore deposits. J Asian Earth Sci 32: 165–183

Plimer IR, Andrew AS, Jenkins R, Lottermoser BG (1988) The geology and geochemistry of the Lihir gold deposit, Papua New Guinea. In: Bicentennial Gold '88. Geol Soc Aust Abstr Ser 22:139–143

Rabone SDC (1975) Petrography and hydrothermal alteration of Tertiary andesite-rhyolite volcanics in the Waitekauri Valley, Ohinemuri, New Zealand. N Z J Geol Geophys 18: 239–258

Rae AJ, Cooke DR, Phillips D, Yeats C, Ryan C, Hermoso D (2003) Spatial and temporal relationships between hydrothermal alteration assemblages at the Palinpilon geothermal field, Philippines – implications for porphyry and epithermal ore deposits. Soc Econ Geol Sp Publ 10: 223–246

Ratschbacher L, Frisch W, Chen CS, Pan GT (1996) Cenozoic deformation, rotation, and stress patterns in eastern Tibet and western Sichuan, China. In: Yin, A, Harrison, TM (eds), The Tectonic Evolution of Asia. Cambridge Univ Press, Cambridge, pp 227–249

Ratschbacher L, Hacker BR, Calvert A, Webb LE, Grimmer JC, McWilliams MO, Ireland T, Dong S, Hu J (2003) Tectonics of the Qinling (Central China): tectonostratigraphy, geochronology and deformation history: Tectonophysics 366: 1–53

Ren SK, Heithersay PS (1998) The Kanowna Belle gold deposit and its implications to Acrhaean gold metallogeny of the Yilgarn Craton, Western Australia. Proceed Ninth Quadr IAGOD Symp: 303–318

Richards JP (1995) Alkalic-type epithermal gold deposits – A review. Mineralogical Association of Canada Short Course 23: 367–400

Richards JP (2003) Tectono-magmatic precursors for porphyry Cu–(Mo–Au) deposit formation. Econ Geol 98: 1515–1533

Robertson AHF, Dixon JE (1985). Introduction: aspects of the geological evolution of the Eastern Mediterranean.Geol Soc Spec Publ 17: 1–74

Rogerson R, McKee C (1990) Geology, volcanism and mineral deposits of Papua New Guinea. In: Hughes F E (ed) Geology of the mineral deposits of Australia and Papua New Guinea, vol 2 Australas Inst Min Metall Monogr 14, pp 1689–1701

Ross AA, Barley ME, Ridley JR, McNaughton NJ (2001) Two generations of gold mineralization a the Kanowna Bell gold mine, Yilgarn Craton. Extended Abs, Fourth Inter Archaean Conf, Geosci Aust, AGSO, pp 398–399

Ross AA, Barley ME, Brown SJA, McNaughton NJ, Ridley JR, Fletcher IR (2004) Young porphyries, old zircons: new constraints on the timing of deformatyion and gold mineralization in the Eastern Goldfields from SHRIMP U-Pb zircon dating at the kanowna Belle gold mine, Western Australia. Precambr Res 128: 105–142

Rui ZY, Goldfarb RJ, Qiu YM, Zhou TH, Chen RY, Pirajno F, Yun G (2002) Palaeozoic-Early Mesozoic gold deposits of the Xinjiang Autonomous Region, northwestern China. Mineral Depos 37: 393–418

Sarkar SC, Kabiraj S, Bhattacharya S, Pal AB (1996) Nature, origin and evolution of the granitoid-hosted early Proterozoic copper-molybdenum mineralization at Malanjkhand, central India. Mineral Depos 31: 419–431

Sawkins FJ (1990) Metal deposits in relation to plate tectonics, 2nd edn. Springer, Berlin

Schneider HJ, Lehmann B (1977) Contribution to a new genetical concept on the Bolivian tin province. In: Klemm D D, Schneider HJ (eds) Time and stratabound ore deposits. Springer, Berlin, pp 153–168

Schneider GIC, Seeger KG (1993) Copper. The Mineral Resources of Namibia, 1st edn. Ministry of Mines and Energy, Geol Surv Namibia, pp 2.3/14–2.3/15

Schneider HJ, Dulski P, Luck J, Moeller P, Villapando A (1978) Correlation of trace element distribution in cassiterites and geotectonic position of their deposits in Bolivia. Mineral Depos 13: 119–122

Schonwandt HK, Petersen JS (1983) Continental rifting and porphyry-molybdenum occurrences in the Oslo region, Norway. Tectonophysics 94: 609–631

Seedorff E, Einaudi MT (2004a) Henderson porphyry molybdenum system, Colorado: I. Sequence and abundance of hydrothermal mineral assemblages, flow paths of evolving fluids and evolutionary style. Econ Geol 99: 3–37
Seedorff E, Einaudi MT (2004b) Henderson porphyry molybdenum system, Colorado: II. Decoupling of introduction and deposition of metals during geochemical evolution of hydrothermal fluids. Econ Geol 99: 39–72
Seedorff E, Dilles JH, Proffett JM, Einaudi MT, Zurcher L, Stavast WJA, Johnson, DA, Barton MD (2005) Porphyry deposits: characteristics and origin of hypogene features. Econ Geol 100th Ann vol: 251–298
Sengör AMC (1992). The Palaeo-Tethyan suture: A line of demarcation between two fundamentally different architectural styles in the structure of Asia. The Island Arc 1: 78–91
Sengör AMC, Natal'in BA (1996). Paleotectonics of Asia: fragments of synthesis. In: Yin A, Harrison TM (eds), The Tectonic Evolution of Asia. Cambridge Univ Press, Cambridge, pp 486–640
Sengör AMC, Yilmaz Y (1981). Tethyan evolution of Turkey: a plate tectonic approach. Tectonophysics 75:181–241
Sengör AMC, Cin A, Bowley DB, Nie S (1993) Space-time patterns of magmatism along the Tethysides: a preliminary study. J Geol 101: 51–84
Seward TM (1979) Hydrothermal transport and deposition of gold. In Glover JE, Groves DI (eds), Gold mineralisation, Univ West Aust Extn Publ 3, pp 45–55
Seward TM, Barnes HL (1997) Metal transport by hydrothermal ore fluids. In: Barnes HL (ed) Geochemistry of hydrothermal ore deposits, 3rd edn, John Wiley & Sons, pp 435–486
Seyitoglu G, Scott BC (1992) Late Cenozoic volcanic evolution of the northeastern Aegean region. J Volcanol Geoth Res 34: 157–176
Shenberger DM, Barnes HL (1989) Solubility of gold in aqueous sulfide solutions from 150 to 350°C. Geochim Cosmochim Acta, 53:269–278
Sheppard SMF (1986) Characterization and isotopic variations in natural waters. Rev Mineral Min Soc Am 16: 165–183
Sherlock RL (2005) The relationship between the McLaughlin gold-mercury deposit and active hydrothermal systems in the Geysers-Clear Lake area, northern Coast Ranges, California. Ore Geol Rev 26: 349–382
Sherlock RL, Tosdal RM, Lehman NJ, Graney JR, Losh S., Jowett EC, Kesler SE (1995) Origin of the McLaughlin mine sheeted vein complex: metal zoning, fluid inclusion and isotopic evidence. Econ Geol 90: 2156–2181
Silberman ML, Berger BR (1985) Relationship of trace element patterns to alteration and morphology in epithermal precious-metal deposits. Rev Econ Geol 2: 203–232
Sillitoe RH (1973) The tops and bottoms of porphyry copper deposits. Econ Geol 68: 799–815
Sillitoe RH (1985) Ore-related breccias in volcanoplutonic arcs. Econ Geol 80: 1467–1514
Sillitoe RH (1986) Space-time distribution, crustal setting and Cu/Mo ratios of central Andean porphyry copper deposits: metallogenic implications. In: Friedrich GH, Genkin AD, Naldrett AJ, Ridge JD, Sillitoe RH, Vokes FM (eds) Geology and metallogeny of copper deposits. Geol Soc Appl Min Depos Spec Publ 4: 235–250
Sillitoe RH (1991). Gold metallogeny of Chile – An introduction. Econ Geol 86: 1187–1205
Sillitoe RH (1993) Gold-rich porphyry copper deposits: geological models and exploration implications. Geol Ass Canada Spec Pap 40: 465–478
Sillitoe RH (1995) Exploration of porphyry copper lithocaps. In: Mauk JL, St George JD (eds) Proc Pacrinm Congress 95, Auckland 1995, Aus Inst Min Metall Publ Ser 9/95, pp. 527–532
Sillitoe RH (1997) Characteristics and controls of the largest porphyry copper-gold and epithermal gold deposits in the circum-Pacific region. Aust J Earth Sci 44: 373–388
Sillitoe RH (2002) Some metallogenic features of gold and copper deposits related to alkaline rocks and consequences for exploration. Mineral Dep 37: 4–13

Sillitoe RH, Hedenquist JW (2003) Linkages between volcanotectonic settings, ore-fluid compositions and epithermal precious metal deposits. Soc Econ Geol Spec Publ 10: 315–343
Sillitoe RH, Halls C, Grant JN (1975) Porphyry tin deposits in Bolivia. Econ Geol 66: 215–225
Sillitoe RH, Steele GB, Thompson JFH, Lang JR (1998) Advanced argillic lithocaps in the Bolivian tin-silver belt. Mineral Depos 33: 539–546
Simmons SF, Brown KL (2006) Gold in magmatic hydrothermal solutions and the rapid formation of a giant ore deposit. Science 314: 288–291
Simmons SF, Browne PRL (2000) Hydrothermal minerals and precious metals in the Broadlands-Ohaaki geothermal system: implications for understanding low-sulfidation epithermal environments. Econ Geol 95: 971–999
Simmons SF, Graham I (eds) (2003) Volcanic, geothermal, and ore-forming fluids: rulers and witness of processes within the Earth. Soc Econ Geol Spec Publ 10
Simmons SF, White NC, John DA (2005) Geological characteristics of epithermal precious and base metal deposits. Econ Geol 100th Ann Vol: 485–522
Simmons SF, Brown KL, Browne PRL (2006) Precious metals in hydrothermal systems of the Taupo Volcanic Zone. The Aus Inst Min Metall Monogr 25: 203–210
Singer DA, Berger VI, Moring BC (2005) Porphyry copper deposits of the world: Database, map, and grade and tonnage models. USGS Open-File Rpt 2005–1060
Slagstad T (2006) Did hot, high heat-producing granites determine the location of the Oslo Rift? Tectonophysics 412: 105–119
So CS, Zhang DQ, Yun ST, Li DX (1998) Alteration-mineralization zoning and fluid inclusions of the high sulfidation epithermal Cu–Au mineralization at Zijinshan, Fujan Province, China. Econ Geol 93: 961–980
Stein HJ, Markey RJ, Morgan JW, Du AD, Sun Y (1997) Highly precise and accurate Re–Os ages for molybdenite from the East Qinling molybdenum belt, Shaanxi province, China. Econ Geol 92: 827–835
Stein HJ, Hannah JL, Zimmerman A, Markey RJ, Sarkar SC, Pal AB (2004) A 2.5 Ga porphyry Cu–Mo–Au deposit at Malanjkhand, central India: implications for late Archean continental assembly. Precambr Res 134: 189–226
Surface V, Brumbaugh RL, Smith RP (1978) Climax molybdenite deposits. In: Sutulov A (ed) International molybdenum encyclopedia, 1778–1978, Vol 1. Resources and production. Intermet, Santiago de Chile, pp 95–107
Sutherland Brown A (1976) Morphology and classification. In: Sutherland Brown A (ed) Porphyry deposits of the Canadian Cordillera. Can J Earth Sci Spec Vol 15: 44–51
Svensen H, Karlsen DA, Sturz A, Backer-Owe K, Banks DA, Planke S (2007) Processes controlling water and hydrocarbon composition in seeps from the Salton Sea geothermal system, California, USA. Geology 35: 85–88
Tan LP (1991) The Chinkuashih gold-copper deposits, Taiwan. Soc Econ Geol Newslett 7: 22–24
Tapponier P, Molnar P (1976) Slip-line field theory and large-scale continental tectonics. Nature 264: 319–324
Tapponier P, Molnar P (1979) Active faulting and Cenozoic tectonics of the Tien Shan, Mongolia and Baykal regions. J Geophys Res 84: 3425–3459
Tapponier P, Lacassin R, Leloup PH, Scharer U, Zhong DL, Wsu HW, Liu XH, Ji SC, Zhang LS, Zhong JY (1990) The Ailao Shan/Red River metamorphic belt: Tertiary left-lateral shear between Indochina and South China. Nature 343: 431–437
Taran YA, Pilipenko VP, Rzhkov Am, Vakin EA (1992) A geochemical model for fumaroles of the Mutnovsky volcano, Kamchtaka, USSR. J Volc Geoth Res 49: 269–283
Taran YA, Hedenquist JW, Korzhinsky MA, Tkachenko SI, Shmulovich KI (1995) Geochemistry of magmatic gases from Kudriavy volcano, Iturup, Kuril Islands. Geochim Cosmochim Acta 59: 1749–1761
Taran YA, Pokrovsky BG, Volynets ON (1997) Hydrogen isotopes in hornblendes and biotites from Quaternary volcanic rocks of the Kamchatka-Kurile arc. Geochem J 31: 203–221

Tegner C, Duncan RA, Benstein S, Brooks CK, Bird DK, Storey M (1998) $^{40}Ar/^{39}Ar$ geochronology of Tertiary mafic intrusions along the East Greenland rifted margin: relation to flood basalts and the Iceland hot spot track. Earth Planet Sci Lett 156: 75–88

Tiercelyn JJ, Thouin C, Kalala T, Mondeguer A (1989) Discovery of sublacustrine hydrothermal activity and associated massive sulfides and hydrocarbons in the north Tanganyika trough, East African rift. Geology 17: 1053–1056

Tiercelyn JJ, Boulègue J, Simoneit BRT (1991) Hydrocarbons, sulphides, and carbonate deposits related to sublacustrine hydrothermal seeps in the north Tanganyika trough, east African Rift. In: Parnell J, Kucha H, Landais P (eds), Bitumen and Ore Deposits, Springer-Verlag, Berlin, pp. 96–113

Tingley JV, Berger BR (1985) Lode gold deposits of Round Mountain, Nevada. Nev Bur Min Geol Bull 100

Titley SR (1993) Characteristics of porphyry copper occurrence in the American southwest. Geol Ass Canada Spec Pap 40: 433–464

Titley SR, Beane RE (1981) Porphyry copper deposits Part I. Geologic setting, petrology and tectogenesis. Econ Geol 75th Ann Vol: 214–269

Titley SR, Hicks CL (eds) (1966) Geology of the porphyry copper deposits – Southwestern North America. Univ Arizona Press

Torckler LK, McKay D, Hobbin J (2006) Geology and exploration of the Favona Au–Ag deposit, Waihi, Hauraki Goldfield. Australas Inst Min Metall Monogr 25: 179–184

Turner S, Hawkesworth G, Liu J, Roger N, Kelley S, Calstern PV (1993) Timing of Tibetan uplift constrained by analysis of volcanic rocks. Nature 364: 50–54

Turner S, Arnaud N, Liu J, Rogers N, Hawkesworth C, Harris N, Kelley S, van Calsteren P. Deng WM (1996) Post-collisional, shoshonitic volcanism on the Tibetan Plateau: Implications for convective thinning of the lithosphere and the source of ocean island basalts. J Petrol 37: 45–71

Van Kranendonk MJ (2006) Volcanic degassing, hydrothermal circulation and the flourishing of early life on Earth: A review of the evidence from c. 3490–3240 Ma rocks of the Pilbara Supergroup, Pilbara Crato, Western Australia. Earth-Sci Rev 74: 197–240

Van Kranendonk MJ, Pirajno F (2004) Geochemistry of metabsalts and hydrothermal alteration zonesassociated with c. 3.45 Ga chert and barite deposits: implications for the geological setting of the Warrawoona Group, Pilbara Craton, Australia. Geochem Expl Envir Anal 4: 253–278

Van Kranendonk MJ, Hickman AH, Smithies RH, Nelson DR (2002) Geology and tectonic evolution of the Archean North Pilbara terrain, Pilbara Craton, Western Australia. Econ Geol 97: 695–732

Van Kranendonk MJ, Collins WJ, Hickman AH, Pawley MJ (2004) Critical tests of vertical vs horizontal tectonic models for the Archaean East Pilbara Granite-Greenstone Terrane, Pilbara Craton, Western Australia. Precambr Res 131: 173–211

Van Kranendonk MJ, Hickman AH, Smithies RH, Williams IR, Bagas L, Farrell TR (2006a) Revised lithostratigraphy of Archean supracrustal and intrusive rocks in the northern Pilbara Craton, Western Australia. Geol Surv West Aust Rec 2006/15

Van Kranendonk MJ, Hickman AH, Huston DL (2006b) Geology and mineralization of the East Pilbara — a field guide. West Aust Geoll Surv Record 2006/16

Van Leeuwen TM, Hedenquist JW, James LP, Dow JAS (eds) (1994) Mineral deposits in Indonesia – Discoveries of the past 25 years. J Geochem Expl Sp Iss 50(1–3)

Villapando A (1988) The tin ore deposits of Bolivia. In: Hutchison CS (ed) Geology of tin deposits in Asia and the Pacific. UN Econ Soc Commiss for Asia and the Pacific. Springer, Berlin, pp 201–215

Wallace RS (1995) The Climax-type molybdenite deposits: What they are, where they are, and why they are. Econ Geol 90: 1359–1380

Wallace RS, McKenzie WB, Blair RG, Muncaster NK (1978) Geology of the Urad and Henderson molybdenite deposits, Clear Creek County, Colorado, with a section on a comparison of these deposits with those at Climax, Colorado. Econ Geol 73:325–367

Walters A, Phillips J, Brown R, Field M, Sparks RSJ (2006) The role of fluidisation processes in the formation of volcaniclastic kimberlite: gran size observations and experimental investigation. J Volcan Geoth Res 155: 119–137

Wang H, Chen J, Ji JF, Qu XM (1997) Geological and geochemical characteristics of the Hetai Gold deposit, South China: Gold mineralization in an auriferous shear zones. Int Geol Rev 39: 181–190

Wang H, Zhang SH, He H (2005) China and Mongolia. In: Selley RC, Robin I, Cocks M, PLmer IR (eds) Encyclopedia of Geology, Elsevier, Oxford, vol 1, pp. 345–358

Wang DH, Mao JW, Yan SH, Yang JM, Xu J, Chen YC, Xue CJ (2005a) Episodes of Cenozoic gold mineralization on the eastern margin of the Qingai-Tibet plateau: $^{40}Ar/^{39}Ar$ dating and implication for geodynamic events. Acta Geol Sinica 79: 233–253

Wang DH, Qu WJ, Li ZW, Yin HL, Chen YC (2005b) Mineralization episode of porphyry copper deposits in the Jinshajiang-Red River mineralization belt: Re–Os dating. Sci China Ser D 48: 192–198

Weissberg BG (1969) Gold–silver ore-grade precipitates from New Zealand thermal water. Econ Geol 64:95–108

Weissberg BG, Browne PRL, Seward TM (1979) Ore metals in active geothermal systems. In: Barnes HL (ed) Geochemistry of hydrothermal ore deposits. John Wiley & Sons, New York, pp 738–780

Whalen JB, Currie KL, Chappell BW (1987) A–type granites: geochemical characteristics, discrimination and petrogenesis. Contrib Miner Petrol 95:407–419

White DE (1981) Active geothermal systems and hydrothermal deposits. Econ Geol 75th Anniv Vol: 392–423

White NC, Hedenquist JW (1995) Epithermal gold deposits: styles, characteristics and exploration. SEG Newsletter 23: 1–13

White WH, Bookstrom AA, Kamilli RJ, Ganster MW, Smith RP, Ranta DA, Steininger RC (1981) Character and origin of Climax-type molybdenum deposits. Econ Geol 75th Anniv Vol, pp 270–316

White DE, Herepoulos C, Fournier RO (1991) Gold and other minor elements associated with the hot springs and geysers of Yellowstone National Park, Wyomng, supplemented with data from Steamboat Springs, Nevada. US Geol Surv Bull 2001

White NC, Leake MJ, McCaughey SN, Parris BW (1995) Epithermal gold deposits of the southwest Pacific. J Geochem Expl 54: 87–136

Williams GJ (1974) Economic Geology of New Zealand. Australas Inst Min Metall Monogr 4

Williams-Jones AE, Heinrich CA (2005) Vapor transport of metals and the formation of magmatic-hydrothermal ore deposits. Econ Geol 100th Anniv Iss: 1287–1312

Williams H, Turner S, Kelley S, Harris N (2001) Age of composition of dikes in southern Tibet: New constraints on the timing of east-west extension and its relationship to post-collisional magmatism. Geology 29: 339–342

Wilson M (1989) Igneous petrogenesis – a global tectonic approach. Unwin Hyman Inc, Winchester

Windley BF (1995) The evolving continents. 3rd edn, John Wiley & Sons, Chichester

Windley BF, Allen MB (1993) Mongolian plateau: evidence for a late Cenozoic mantle plume under central Asia. Geology 21: 295–298

Windley BF, Allen MB, Zhang C, Zhao Z, Wang C (1990) Paleozoic accretion and Cenozoic redeformation of the Chinese Tian Shan range, Central Asia. Geology 18: 128–131

Windley BF, Alexeiev D, Xiao WJ, Kröner A, Badarch G (2007) Tectonic models for accretion of the Central Asian Orogenic Belt. J Geol Soc, London, 64: 31–47

Wood SA (ed) (1989) Experimental investigations of hydrothermal processes: applications to ore deposit genesis. Proc 3rd Int Conf Min Expl Res Inst, Can, Geochim Cosmochim Acta 53(2)

Wu C, Bai G, Xu L (1993) Types and distribution of silver ore deposits in China. Mineral Depos 28: 223–239

Wu G, Yano T, Inomata M (1998) Yanshanian orogenies in south China: a relation to Neotethyan evolution. Sci Geol Sinica 7: 1–10

Xiao L, Wang CZ, Pirajno F (2007) Is the underthrust Indian lithosphere split beneath the Tibetan Plateau? Int Geol Rev 48: 90–98

Xu B (1988) Stable isotope geochemistry of gold deposits in the Shaoxing-Longquan ore forming zone, Zhejaing Province. Mineral Deposits 3: 53–61 (in Chinese with English abstract)

Xu B, Li C, Chen H (1994) Mineralization chronology and isotopic geochemistry of the Haoshi silver deposit in Zhejiang Province. Min Deposits 13: 271–281 (in Chinese with English Abstract)

Xu B, Li C, Chen H (1995) Isotope geochemistry of the Xinchang-Yongjia silver (lead-zinc) ore belt in eastern Zhejiang Province. Acta Geol Sinica 8: 69–83 (in Chinese with English Abstract)

Xu G, Niu H, Wang Y, Fu H (1994) Tectonic framework and evolution of Precambrian on the southeastern margin of the Yangtze plate. Sci Geol Sinica 3: 255–264

Xu G, Yao S, Zhang C, Wang P (1995) A case study of the Zhilingtou gold-silver deposit, Zhejiang, China. PACIFIC RIM '95, Abs Vol Australas Inst Min Metall, pp. 645–649

Xu Y, Schoonen MAA, Nordstrom DK, Cunningham KM, Ball JW (1998) Sulfur geochemistry of hydrothermal waters in Yellowstone National Park: I. The origin of thiosulfate in hot spring waters. Geochim Comsochim Acta 62: 3729–3743

Yakubchuk A (2004) Architecture and mineral deposit settings of the Altaid orogenic collage: a revised model. J Asian Earth Sci 23: 761–779

Yakubchuk A, Shatov VV, Kirwin D, Edwards A, Tomurtogoo G, Badarch G, Buryak VA (2005) Gold and base metal metallogeny of the Central Asian Orogenic Supercollage. Econ Geol 100th Anniv Vol: 1035–1068

Ye Y, Shimazaki H, Simizu M, Hu S (1998) Tectono-magmatic evolution and metallogenesis along the Northeast Jiangxi Deep Fault, China. Resour. Geol. 48: 43–50

Yigit O (2006) Gold in Turkey – a missing link in Tethyan metallogeny. Ore Geol Rev 28: 147–179

Yilmaz Y (1989). The origin of young volcanic rocks of Western Turkey. In: Sengör AMC (ed), Tectonic evolution of the Tethyan region, Kluwer Acad Publ pp. 159–189

Yilmaz Y (1990). Comparison of young volcanic associations of western and eastern Anatolia formed under a compressional regime: a review. J Volcanol Geother Res 44: 69–87

Yilmaz H, Oyman T, Arehart GB, Colakoglu AR, Billor Z (2007) Low-sulfidation type Au–Ag mineralization at Bergama, Izmir, Turkey. Ore Geol Rev 32: 81–124

Yin A (2000) Mode of Cenozoic east-west extension in Tibet suggesting a common origin of rifts in Asia during the Indo-Asian collision: J Geophys Res105: 21745–21759

Yin A, Nie SY (1996) A Phanerozoic palinspastic reconstruction of China and its neighboring regions. In: Yin A Harrison TM (eds), The Tectonic Evolution of Asia. Cambridge Univ Press, Cambridge, pp 442–485

Zhang YH (2006) Alteration types of Qiyugou breccia-type gold deposit and its dynamic process. PhD thesis, unpubl, China University of Geosciences, Beijing

Zheng M, Liu JM (1987) Physico-chemical conditions and ore-forming process of the Zhilingtou Au–Ag deposit, Zhejiang, China. Acta Geol Sinica 3: 253–266 (in Chinese with English Abstract)

Zhang ZM, Liou JG, Coleman RC (1984) An outline of the plate tectonics of China. Geol Soc Am Bull 95: 295–312

Zhang YH, Zhang SH, Han YG, Pirajno F (2005) Low-sulphidation epithermal gold-bearing Qiyugou breccia pipes, Xiong'ershan montains, China. In: Mao JW, Bierlein FP (eds) Mineral Deposit Research: meeting the global challenge vol 2, Springer, Berlin pp 1111–1113

Zhang YH, Zhang SH, Pirajno F (2007) Fluidization: an important process in the formation of the Qiyugou Au-bearing breccia pipes in central China. Acta Geol Sinica 81: 226–238

Zhou XM, Li WX (2000) Origin of Late Mesozoic igneous rocks in Southeastern China: implications for lithosphere subduction and underplating of mafic magmas. Tectonophysics 326: 269–287

Zhou TH, Goldfarb RJ, Phillips GN (2002) Tectonics and distribution of gold deposits in China – an overview. Mineral Dep 37: 249–282

Zhu YF, Zhang LF, Gu L-B, Guo X, Zhou J (2005) The zircon SHRIMP chronology and trace element geochemistry of the Carboniferous volcanic rocks in western Tianshan mountains. Chin Sci Bull 50(19): 2210–2212

Chapter 6
Skarn Systems

6.1 Introduction

Many porphyry stocks may be sited below stratovolcanoes, and the uppermost sectors of the porphyry intrusive are transitional upward to epithermal mineralisation and laterally to skarn deposits, where carbonate rocks are present (see Fig. 5.4). Skarns are rocks dominated by calc-silicate minerals formed by replacement of carbonate lithologies either during regional metamorphism or by contact metasomatic processes related to igneous intrusions. The word "skarn" was originally used by Swedish miners to indicate Fe-rich calc-silicate gangue material and the term was first published by Törnebohm (1875; cited in Meinert et al. 2005). A brief digression into the terminology and classification of skarns is useful before proceeding with the main purpose of this section, which is to review intrusion-associated skarn-type alteration-mineralisation. The terminology and classification of skarns adopted here are those of Einaudi (1982a,b) and Einaudi and Burt (1982), further refined by Meinert and co-workers in several of their works (e.g. Meinert 1989, 1992, 1993; Meinert et al. 2000, 2005 and references therein).

Einaudi (1982a) distinguished between reaction skarns and ore skarns. The former, of limited extent, are formed along shale-limestone contacts during metamorphism. The latter, as the name implies, are the skarns that contain mineralisation, and are formed as a result of infiltration of fluids derived from igneous intrusions. A classification of skarns should take into consideration both the rock type and the mineralogical association of the replaced lithology. The terms endo- and exoskarns refer to the skarnification of igneous or aluminous rocks and carbonate rocks respectively. Exoskarns were subdivided by Einaudi (1982a) in terms of their calc-silicate mineral assemblages into calcic skarns and magnesian skarns. Calcic skarns, which are formed by replacement of limestones, contain minerals such as garnets (andradite-grossularite series), clinopyroxenes (diopside-hedenbergite series), wollastonite, scapolite, epidote and magnetite. Magnesian skarns result from the replacement of dolomitic rocks and are typified by minerals such as diopside, forsterite, serpentine, magnetite, talc in silica-poor environments; and talc, tremolite-actinolite in environments richer in silica. Silica-pyrite skarn is a third type which relates to a stage of alteration-mineralisation associated with some porphyry deposits.

F. Pirajno, *Hydrothermal Processes and Mineral Systems*,

© Springer Science+Business Media B.V. 2009

Skarnoid is a term used in connection with garnet-rich rocks whose origin is uncertain, or following Meinert et al. (2005) formed by metamorphism of impure lithologies. From the mineral system point of view skarns are classified in terms of their metal association, and the following classes may be considered: Fe skarns, Au skarns, W skarns, Cu skarns, Zn-Pb skarns, Mo skarns and Sn skarns. The main characteristics of these skarns are given in Table 6.1, and for more details the reader is referred to the works of Einaudi and coworkers cited above as well as Kwak (1987), the Special Issue of Economic Geology (Einaudi and Burt 1982) and Meinert et al. (2005).

Skarns occur in most tectonic settings where there is magmatism and development of carbonate lithologies (Figs. 5.4 and 6.1) (Einaudi et al. 1981; Meinert et al. 2005). Meinert et al. (2005) considered four main tectonic scenarios: (1) oceanic steep subduction; (2) transitional low-angle subduction; (3) continental

Table 6.1 Chief characteristics of skarn deposits. (A) Non-porphyry-related skarns; (B) porphyry-related skarns (after Einaudi et al. 1981; Einaudi and Burt 1982)

A	Fe	W	Sn-W	Mo
Size (Mt) (million tonnes)	5–200	0.1–2	0.1–3	<0.1–?
Grade	40% Fe	0.5% W	0.1–0.7% Sn	±0.1% Mo
Associated metals	Cu, Co, Au	W, Mo, Cu, Zn, Bi	Sn, F, W, Cu, Zn	Cu, U, W, Bi
Igneous rocks	Gabbro, syenite, diorite	Quartz-diorite, quartz-monzonite	Granite	Granite, quartz-monzonite
Ore minerals	Magnetite, chalcopyrite, cobaltite, pyrrhotite	Scheelite, molybdenite, chalcopyrite, sphalerite, magnetite, pyrite, bismuth	Cassiterite, scheelite, sphalerite, pyrrhotite, magnetite, pyrite,	arsenopyrite
Molybdenite, pyrrhotite,	chalcopyrite, pyrite, bismuthinite, magnetite, bornite, arsenopyrite, sphalerite			
Early minerals	Ferrosalite, grandite, epidote, magnetite	Ferrosalite, hedenbergite, grandite, idocrase, wollastonite	Idocrase, spessartine, andradite, datolite	Garnet, pyroxene, wollastonite, idocrase, olivine
Late minerals	Amphibole, chlorite, ilvaite	Spessartine, almandine, grandite, biotite, hornblende, plagioclase	Amphibole, mica, chlorite, tourmaline, fluorite	Amphibole, epidote, actinolite, chlorite

Table 6.1 (continued)

B	Cu	Zn-Pb
Size (Mt)	1–400	0.2–3
Grade	1–2% Cu	9% Zn; 6% Pb; ±15 g/tAg
Associated metals	Mo, Zn, W, Ag	Ag, Cu, W
Igneous rocks	Granodiorite, quart-monzonite stock, dykes and breccia pipes	Granite, diorite, syenite, stocks and dykes
Ore minerals	Chalcopyrite, pyrite, hematite, magnetite, pyrrhotite, molybdnite, tennantite	Sphalerite, galena, pyrhotite, pyrite, magnetite, chalcopyrite, arsenopyrite
Early minerals	Andradite, diopside, wollastonite	Mn-hedenbergite, andradite, spessartine, rhodonite
Late minerals	Actinolite, chlorite, montmorillonite	Mn-actinlite, ilvaite, chlorite, rhodocrosite

subduction; and (4) continental rifting. Oceanic steep subduction environments tend to produce Fe, Cu and Au skarns associated with diorite and granodiorite plutons; transitional low-angle subduction may be the setting for Mo, W-Mo skarns associated with monzonite and granitic plutons; continental subduction is the tectonic setting for the vast majority of skarns, including Zn-Pb, Cu, Au, W, Mo, generally associated with granodiorite and granite plutons. Finally, continental rifting, associated with mantle plumes or upwelling asthenosphere, results in the emplacement of granitic plutons and Sn-W skarns. Table 6.1 provides the chief elements of porphyry-related and non-porphyry related skarns. Depth of emplacement is also important. W skarns appear to be related to batholiths emplaced at depths of between 5 and 15 km. Intermediate to shallow-depth magmas (1–6 km) give rise to porphyry stocks with less extensive contact aureoles, and the associated skarns are sulphide-rich with Cu, Cu-Fe, Pb-Zn, and minor Mo, Au and Ag. Tungsten and Mo would become dominant in I-type magmas, which have interacted with continental crust rocks. Crustal-derived magmas emplaced in rifting environments may produce skarns of the Sn-W class with a host of other elements such as Be, B, F, Bi, Cu, Zn, Sn and U (Kwak 1987).

The depths of skarn formation is important in terms of size, geometry and alteration (Meinert et al. 2005). Deep skarns tend to be smaller and with a vertical geometry by comparirosn with shallow skarns. At depths of >12 km the ambient temperature of rocks is around 400°C, thereby reducing the reactivity of the host rocks.

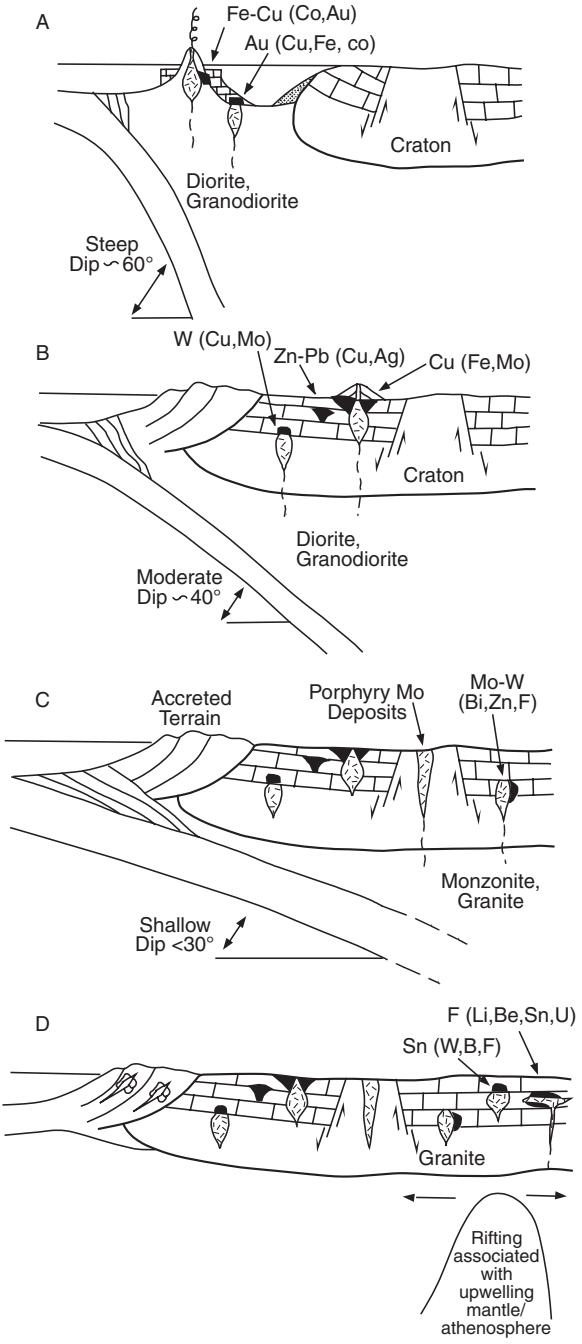


Fig. 6.1 Tectonic settings of skarn systems and environments of carbonate deposition; (**A**) oceanic island arc and associated carbonate deposits; steep (**B**) and shallow (**C**) subduction beneath a continental margin, carbonate deposits are present on the craton's margins; (**D**) Continental rift setting and granite intrusions associated with the impigment of a mantle plume. Modified after Meinert (1992) and Meinert et al. (2005)

Skarn mineralogy can be complex, and as cautioned by Meinert et al. (2005) sometimes improperly labelled due to lack of identification of end members mineral phases. Quartz and calcite are essentially ubiquitous, whereas others such as serpentine, phlogopite and talc are restricted to magnesian skarns. The main skarn minerals are given in Table 6.2.

Table 6.2 Some common skarn minerals. After Meinert et al. (2005)

Mineral phase	End Members	General formula	Abbreviation
Garnet	Grossularite	$Ca_3Al_2Si_3O_{12}$	Gr
	Andradite	$Ca_3Fe_2\ Al_2Si_3O_{12}$	Ad
	Spessartine	$Mn_3Al_2Si_3O_{12}$	Sp
	Almandine	$Fe_3Al_2Si_3O_{12}$	Al
	Pyrope	$Mg_3Al_2Si_3O_{12}$	Py
Pyroxene	Diopside	$CaMgSi_2O_6$	Di
	Hedenbergite	$CaFeSi_2O_6$	Hd
	Johannsenite	$CaMnSi_2O_6$	Jo
	Fassaite	$Ca(Mg, Fe, Al)(Si,Al)_2O_6$	Fas
Olivine	Forsterite	Mg_2SiO_4	Fo
	Fayalite	Fe_2SiO_4	Fa
	Tephroite	Mn_2SiO_4	Tp
	Monticellite	Ca_2SiO_4	Mc
Pyroxenoid	Ferrosilite	$FeSiO_3$	Fs
	Rhodonite	$MnSiO_3$	Rd
	Wollastonite	$CaSiO_3$	Wo
Amphibole	Tremolite	$Ca_2Mg_5Si_8O_{22}(OH)_2$	Tr
	Ferroactinolite	$Ca_2Fe_5Si_8O_{22}(OH)_2$	Ft
	Hornblende	$Ca_2Mg_4Al_2Si_7O_{22}(OH)_2$	Hb
	Pargasite	$NaCa_2Mg_4Al_3Si_6O_{22}(OH)_2$	Pg
	Ferrohastingsite	$NaCa_2Fe_4Al_3Si_6O_{22}(OH)_2$	Fh
	Cummingtonite	$Mg_5Fe_2Si_8O_{22}(OH)_2$	Cm
	Dannemorite	$Mn_2Fe_5Si_8O_{22}(OH)_2$	Dm
	Grunerite	$Fe_7Si_8O_{22}(OH)_2$	Gru
Epidote	Piemontite	$Ca_2MnAl_2Si_3O_{12}(OH)$	Pm
	Allanite	$(Ca,REE)_2FeAl_2Si_3O_{12}(OH)$	All
	Epidote	$Ca_2FeAl_2Si_3O_{12}(OH)$	Ep
	Pistacite	$Ca_2Fe_3Si_3O_{12}(OH)$	Ps
	Clinozoisite	$Ca_2Al_3Si_3O_{12}(OH)$	Cz
Plagioclase	Anorthite	$CaAl_2Si_2O_8$	An
Scapolite	Meionite	$Ca_4Al_6Si_6O_{24}(CO_3, OH, ClSO_4)$	Me
Other	Vesuvianite	$Ca_{10}(Mg, Fe, Mn)_2Al_4Si_9O_{34}(OH, Cl, F)_4$	Vs
	Prehnite	$Ca_2Al_2Si_3O_{10}(OH)_2$	Pr
	Axinite	$(Ca, Mn, Fe)_3Al_2BO_3Si_4O_{12}(OH)$	Ax

The alteration-mineralisation of carbonate rocks in the environment of porphyry systems constitutes a class of skarns characterised by being both economically important and the largest base metal sulphide skarn deposits. Porphyry-related skarns, whose features generally correspond to Cu and Zn-Pb skarns (see Table 6.1), have been studied in detail by Einaudi (1982a,b), and the results of his work, which focussed mainly on the North American deposits, are summarised in this section. The nature of the ore-bearing skarns in the porphyry environment depends largely on the carbonate content of the replaced units, their permeability and structural features. Carbonate rocks are decomposed according to the reaction:

$$CaCO_3 + 2H^+ = Ca^{2+} + CO_2 + H_2O.$$

The alteration-mineralisation styles also depend on the hydrothermal and metasomatic processes involved. These are responsible for the formation of the various types of skarns that Einaudi (1982a,b) called: hornfels skarnoid, calcic skarns, magnesian skarns and silica-pyrite skarns. Hornfels skarnoids originate by decarbonation and dehydration of the carbonate units without addition of components. They include wollastonite-rich lithologies developed from silica-rich limestones, and diopside hornfels developed from calcarous siltstones; calc-silicate hornfels containing quartz, tremolite-actinolite, epidote, plagioclase and diopside is commonly formed in calcareous shales. Calcic skarns are the dominant type in the porphyry systems of North America. They contain epidote, garnet ± clinopyroxene and wollastonite ± garnet ± idocrase ± clinopyroxene forming a zoned pattern from the causative intrusion outward, in the order given above. These anhydrous mineral assemblages are, at later stages and with decreasing temperatures, replaced by hydrous silicates, sulphides, oxides and carbonate minerals. The mineralisation in this system consists of sulphide and oxide disseminations, veins and massive replacement of the carbonate rocks at the skarn front. It shows a distinct zoning pattern consisting of pyrite ± chalcopyrite nearest the contact with the intrusive and associated with garnet-rich skarns, to pyrite + chalcopyrite ± magnetite associated with garnet-pyroxene skarn, to bornite + chalcopyrite ± magnetite (garnet-wollastonite skarn), to sphalerite + chalcopyrite ± magnetite ± pyrite (marble zone). This zoning is interpreted by Einaudi to be due to decreasing Fe outward from the pluton. Skarn zonation reflects fluid flow and it occurs at scales from micrometres to kilometres (Meinert et al. 2005). Commonly the contact between zonations can be sharp. In general skarns have zonations from endoskarns in the causative pluton, to proximal garnet and distal pyroxene, which also indicate the overall oxidation state of the skarn system (Fig. 6.2; Meinert et al. 2005). Magnesian skarns are usually derived from dolomitic rocks and characterised by the common presence of magnetite, while other typical minerals may include serpentine, forsterite and talc. These skarns are rich in magnetite but have relatively low sulphide contents. Silica-pyrite, mentioned

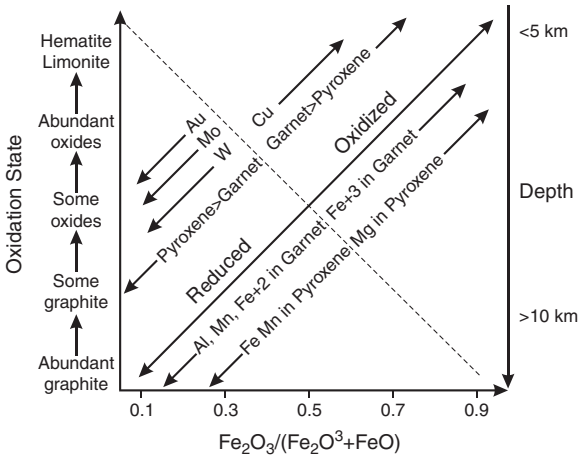


Fig. 6.2 Oxidation states of skarn systems in relation to host rock characteristics; the oxidation state of the causative plutons is given by the ratio $Fe_2O_3/(Fe_2O_3 + FeO)$; other monitors of oxidation stae are presence or absence of oxide minerals such as magnetite, hematite and ilmenite as well as the Fe content of rock-forming minerals such as pyroxene, amphibole and biotite; the oxidation state of the host rocks can be gauged by the abundance of carbon as indicated by graphite, hydrorcarbons, sulphides (pyrrhotite, pyrite) and the above mentioned oxides. Modified after Newberry (1991) and Meinert et al. (2005)

previously, is "*a common alteration feature associated with sulphide deposition in carbonate rocks of some porphyry copper districts*" (Einaudi 1982b, p. 192). Silica-pyrite forms during phases of advanced hydrogen ion metasomatism of the pluton, such as phyllic and argillic alteration stages. Silica-pyrite skarns are characterised by pyrite, quartz, various forms of silica (in some areas opal and cristobalite, in others chalcedony and jasper), clay minerals (montmorillonite, nontronite), chlorite and talc.

Skarn genesis involves a series of processes related to, and correlated with, the late magmatic and hydrothermal phases of a pluton intruding sedimentary rocks. The emplacement and cooling of the plutonic mass is accompanied by contact metamorphism and metasomatism in the wall rocks. Thus, the formation of skarns involves stages of prograde isochemical metamorphism and metasomatism. Towards the final phases of cooling a retrograde stage occurs, during which the early skarn assemblages are destroyed and replaced by hydrous minerals. Effectively, these stages of skarn formation correspond with the early potassic and later hydrolitic alteration in the porphyry stock or pluton. Skarns develop in temperatures ranging from between 700 and 200°C and at pressures of between 0.3 and 3 kbar. The metasomatic fluids have salinities that range from 10 to about 45 wt% NaCl equivalent. The hydrothermal solutions originated from the magma in the early stages with an increasingly meteoric component during the retrograde stages, as also observed for, and compatible with, the porphyry mineralising solutions. In summary, the formation of skarns can be

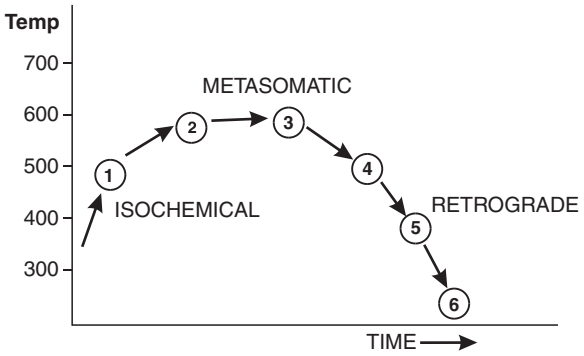


Fig. 6.3 Stages of skarn development as a function of time and temperature; 1 calcite, diopside; 2 calcite, diopside, wollastonite, vesuvianite (idocrase), grossular; 3 andradite, diopside-hedenbergite, eidote, powellite; 4 quartz, chalcopyrite, scheelite; 5 amphibole, calcite, epidote, quartz; 6 zeolites. See text for more details. After Brown et al. (1985)

related to three main stages (Fig. 6.3): (1) isochemical prograde thermal metamorphism; (2) metasomatism; and (3) retrograde hydrothermal alteration.

The diagram of Fig. 6.3 refers to a study of W (scheelite) skarns at Pine Creek in California by Brown et al. (1985). At this locality the carbonate protolith contained calcite, dolomite, quartz, K-feldspar and organic material. This protolith underwent progressive devolatilisation, which produced the mineral assemblage of calcite + diopside + K-feldspar + sphene + graphite (isochemical stage). Following the cooling of a quartz-monzonite pluton, H_2O-rich fluids were expelled and moved up along the structural break provided by the contact of the carbonate rocks with the pluton. These fluids reacted with the carbonates to release Ca and CO_2, some of which diffused back towards the pluton, forming an endoskarn. Infiltration of the metasomatising fluids into the carbonates formed Fe-poor silicates and Fe-rich garnet and pyroxene (metsaomatic stage). A light green outer skarn zone was formed containing calcite + diopside + wollastonite + idocrase + garnet + fluorite. The scheelite-bearing skarn contains garnet + pyroxene + epidote. Amphibole minerals, epidote, quartz and zeolites characterise the retrograde stage.

Metamorphic and metasomatic reactions of skarns involve the systems CaO-MgO-SiO_2-H_2O and CaO-Al_2O_3-Si_2O-CO_2-H_2O (Einaudi et al. 1981). Some typical reactions are:

$$\text{tremolite} + 3\,\text{calcite} + 2\,\text{quartz} = 5\,\text{diopside} + CO_2 + H_2O;$$

$$9\,\text{hedenbergite} + 2O_2 = 3\,\text{andradite} + 9\,\text{quartz} + \text{magnetite};$$

$$3\,\text{hedenbergite} + S_2 = \text{andradite} + 3\,\text{quartz} + FeS_2;$$

$$\text{andradite} + 3\,CO_2 + 2S_2 = 2FeS_2 + 3\,\text{quartz} + 3\,\text{calcite} + 3/2O_2;$$

$$2\,\text{andradite} + 4S_2 = 6\,\text{wollastonite} + 4_2 + 3O_2.$$

Garnets and pyroxenes are important components of skarns. Their internal zoning and various generations are a function of the changing physico-chemical

conditions of the fluids. For this reason microprobe analyses of garnets and pyroxenes are important in establishing the nature and type of skarns. Ternary plots of the compositional distribution of garnets and pyroxenes (spessartine-grandite-andradite and johannsenite-diopside-hedenbergite respectively) can be used to characterise the class of skarns. Porphyry-related Cu skarns are characterised by the presence of andradite and diopside, whereas the grossularite-hedenbergite association is more typical of W-bearing skarns (Einaudi and Burt 1982). Smirnov (1976) explained the mechanism of skarn genesis by the infiltration-diffusion model, and refined by Einaudi et al. (1981) under the name of bimetasomatic diffusion. The latter authors also mentioned other processes for the developemnt of skarns. Einaudi and Burt (1982), for example, considered infiltration to be the main mechanism of skarn genesis. All, however, refer to large-scale transfer or exchange of components during high temperature regimes. The diffusion-infiltration theory holds that skarns result from a system with imbalanced chemistry, developed in hot aqueous solutions that impregnate both the intrusive igneous rocks and the carbonate lithologies on either side of the contact (Newberry 1991). This leads to the formation of endo- and exoskarns, mentioned previously. Elements are dissolved from both sides and the solution tends to homogenise by diffusion from areas of high concentration to areas of low concentration. Exchange reactions take place along these diffusion fronts between the solutions and the enclosing lithologies. Due to the different mobilities of the elements concerned, their concentrations in the solution would fall toward the diffusion front at different rates, giving rise to well-developed zoning and distinct mineral paragenesis. Smirnov (1976) considered four groups of compounds and elements in order of decreasing mobility. They are: (1) H_2O and CO_2; (2) S, Cl, K, Na; (3) O, Si, Ca, Mg, Fe; (4) P, W, Al. Furthermore, three temperature stages are distinguished (Smirnov 1976, p. 183): (1) a high temperature stage with pyroxene + garnet and pyroxene + epidote; (2) an intermediate temperature stage with two substages, one characterised by epidote + actinolite, and the other with epidote + chlorite; (3) a low temperature stage is subdivided into six substages with prehnite, pumpellyite, calcite + albite, calcite + quartz + sericite + chlorite, calcite + quartz + sericite + dolomite, and zeolite. These stages roughly correspond to those shown in Fig. 6.3.

A sequence of events of skarn genesis in a porphyry-related system is given below and depicted in Fig. 6.4. Firstly, the intrusion of a pluton results in contact metamorphism of the carbonate wall rocks. This stage involves decarbonation and dehydration reactions to form diopside and wollastonite skarns. The timing of this stage would correspond with the crystallisation of the pluton's margins following the intrusion of the melt phase into the sedimentary lithologies. The temperature range is from 900 to 500°C. Fluids, which are released from the partially solidified intrusion, infiltrate into and along fractures of pluton and country rocks. This is the stage of potassic alteration and disseminated chalcopyrite mineralisation in the plutonic rocks. This stage corresponds to the movement of the fluids outward into the structural breaks of

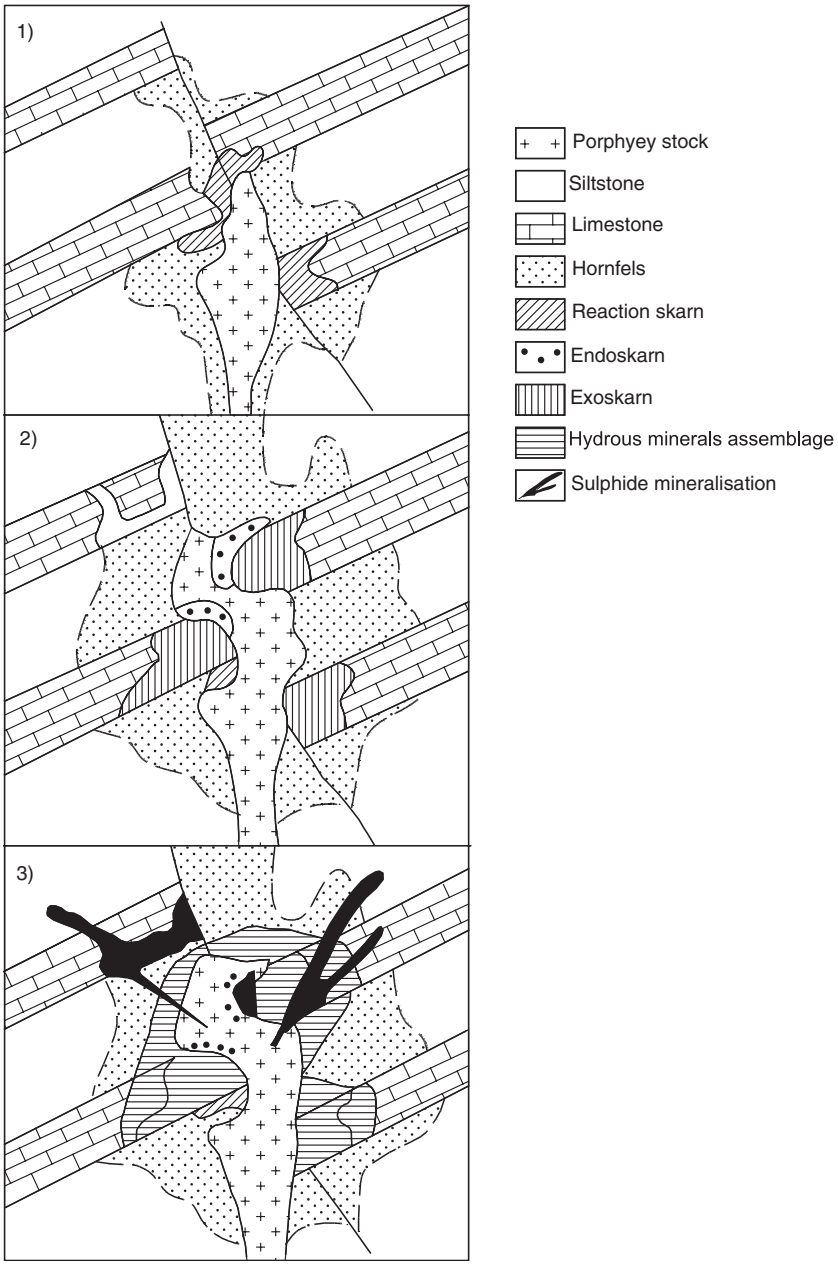


Fig. 6.4 Stages of skarn formation; (1) isochemical stage with hornfels developing in non-carbonate units and the commencement of reaction skarns in carbonate rocks; (2) this is the metasomatic stage with extensive development of exo- and endoskarns; (3) retrograde stage tends to destroy the earlier skarns and is dominated by hydrous minerals and sulphides. Modified after Einaudi et al. (1981)

the country rocks (fractures, contacts, permeable horizons) to form early skarn facies consisting of andradite, magnetite and sulphides. The temperature range is from approximately 600–400°C.

The next phase is one of ore deposition in the ongoing skarn development: andradite is replaced by magnetite, quartz, pyrite and calcite; while diopside skarn is replaced by actinolite, calcite and quartz with some chalcopyrite. This corresponds to the waning stages of potassic alteration and the beginning of the quartz-sericite-pyrite alteration in the pluton with concomitant Cu ± Mo mineralisation. The range of temperatures is from 500 to 300°C. The final stage (retrograde alteration) involves the destruction of the skarn assemblages and is characterised by the deposition of clay minerals (kaolinite, montmorillonite, nontronite), chlorite, calcite, quartz, hematite, pyrite or locally silica-pyrite. Mineralisation largely consists of pyrite, sphalerite, galena and tennantite. These sulphides tend to form veins. This stage of skarn destruction or retrograde alteration coincides with late phases of quartz-sericite-pyrite and argillic alteration of the porphyry intrusion and is therefore dominated by the incursion of meteoric waters in the system. Ore deposition in the sequence above is, in broad terms, classified by Einaudi (1982a) on a morphological and textural basis into two styles, namely: disseminated mineralisation and lode mineralisation. The former coincides with the early phases of skarn genesis (potassic event in the porphyry stock), and the latter more or less with sericitic, silicification and argillic alteration of the porphyry pluton. These two styles may occur in the same deposit. Lateral and vertical zoning of both disseminated and lode mineralisation styles may be present and is related to the distance from the porphyry pluton (Figs. 6.4 and 6.5). The nature of the zoning also depends on the nature of the replaced lithologies (e.g. limestone, calcareous siltstone). In the disseminated mineralisation styles, a zone of bornite + chalcopyrite + magnetite closest to the intrusion is followed by an intermediate zone of pyrite + chalcopyrite, a peripheral pyrite ± chalcopyrite ± tennantite ± sphalerite ± galena, hematite and/or magnetite. A distal zone occurs within the carbonate rocks and contains pyrite + chalcopyrite + magnetite ± sphalerite ± tennatite ± pyrrhotite. In the lode style of mineralisation the following zonation from the intrusive contact outward may be present: a zone of pyrite + digenite + enargite ± Sn-Bi-W minerals; an intermediate zone of pyrite + bornite + chalcopyrite + tennantite ± sphalerite; a peripheral zone of pyrite + chalcopyrite + tennantite + sphalerite + galena ± hematite; a distal zone within the carbonate rocks of pyrite + bornite + chalcopyrite + tennantite + sphalerite + galena ± magnetite or hematite. The alteration and mineralisation of carbonate rocks in the porphyry environments displays very complex features reflecting the variability of both the geological materials and the physico-chemical properties of the hydrothermal solutions. The above review is clearly generalised and focuses on the common features of porphyry-related skarn deposits. The reader should be aware that individual deposits will display many variations from the common theme. A special issue of Economic Geology (Meinert et al. 2000) is devoted to skarn deposits.

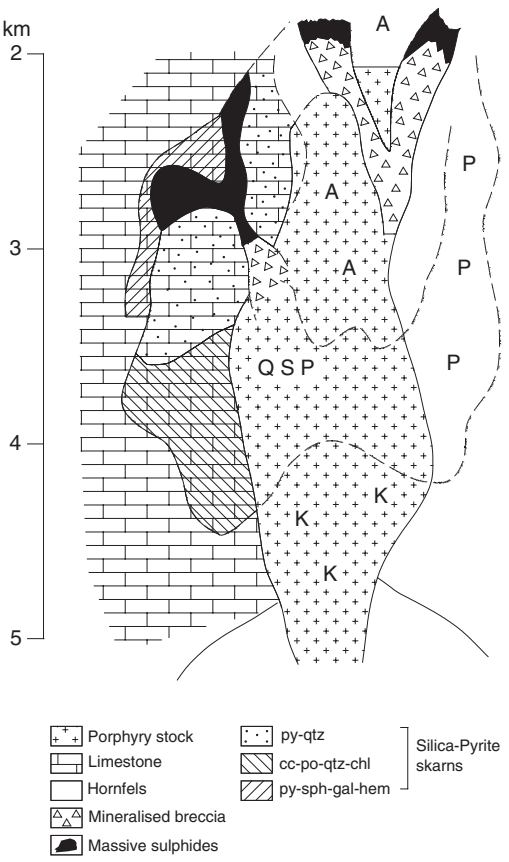


Fig. 6.5 Idealised zoning patterns of alteration-mineralisation in a porphyry-related skarn system; py-qtz pyrite and quartz, cc-po-qtz-chl chalcocite-pyrrhotite-quartz-chlorite, py-sph-gal-hem pyrite-sphalerite-galena-hematite; alteration: A argillic, QSP phyllic (quartz-sericite-pyrite), P propylitic, K potassic. Modified after Einaudi (1982b)

Skarn ore systems can also be distinguished on the basis of their metal endowment. In the following sections Cu, Sn-W, W, Au, Zn and Mo skarns are discussed largerly based on the works of Einaudi (1982a,b), Meinert (1992), Meinert et al. (2005) and others as cited in the text. In addition, I also briefly discuss some key examples for Cu, Sn-W and Au skarn deposits. Some examples of what skarn rocks look like in the field are shown in Fig. 6.6.

6.2 Copper Skarns

Copper skarns are the world's most abundant type (Meinert 1992), with 573 listed by Meinert et al. (2005). Most Cu skarns are associated with I-type, magnetite-series plutons emplaced in shallow environments and that have cogenetic stockworks and widespread and intense hydrothermal alteration (Meinert et al. 2005). The largest Cu skarns are almost invariably part of



Fig. 6.6 Field photographs of some typical skarns; (**a**) wrigglite and (**b**) wollastonite-garnet skarn from Poshi in the eastern Tian Shan orogenic belt (Xinjiang Province, NW China), the Permian Poshi mafic-ultramafic intrusion was emplaced in Proterozoic carbonate rocks producing these unmineralised skarns; (**c**) and (**d**) Navachab Au skarns, (**c**) shows a skarn vein with sulphides cutting across dolomitised marble, (**d**) is the same type of vein intersected in drill core, this section assayed 200 g/t Au

mineralised porphyry Cu systems, which exhibit K-feldspar and sericitic alteration that temporally correlate with prograde and retrograde skarn alteration (Meinert et al. 2005). These skarns are dominated by andradite garnet, diopside, vesuvianite, wollastonite, actinolite and epidote. Hematite and magnetite may be present and locally may form massive lodes. Copper skarns are zoned with massive garnetite nearest the causative pluton, followed by increasing amounts of clinopyroxene and vesuvianite and/or wollastonite in the vicinity of the marble contact. Pyrite, chalcopyrite and bornite are the most abundant sulphides, and increase away from the pluton (Meinert 1992). Einaudi (1982a,b) reviewed in detail the Cu skarns systems.

Examples of porphyry-related Cu skarns can be found in the west of the USA. The majority of these Cu skarns are located in Arizona, the most important region for porphyry Cu deposits, but important deposits also occur in Nevada (Yerington) and in Utah (Bingham, one of the largest known Cu skarns). The Cu skarns of the western USA are associated with Cenozoic calc-alkaline magmatic arcs related to complex subduction processes along the west coast of the USA (Cordilleran belt). The strong pulse of magmatism and related porphyry systems in this region during the Neogene coincides with an increase

in spreading rates along the East Pacific Rise, and changes in the angle of dip of the Benioff zone (Sawkins 1990). The Cu skarns of the western USA are associated with highly fractured subvolcanic granodiorite to quartz-monzonite porphyry displaying varying degrees of potassic and sericitic alteration. The intrusive stocks were emplaced at depths of between 5 and 1 km. Cu-skarns are of the calcic type and mineralisation consists of sulphide (2–15%) and Fe oxide (ca. 10%) disseminations, veins, and massive replacement of marble rocks at the skarn front. Ore reserves range from less than 1 to ~400 Mt at grades of approximately 1% Cu with Au, Ag, Mo, Pb and Zn being recovered locally as by-products.

6.2.1 Bingham

Bingham in the state of Utah is the largest known Cu-skarn deposit, and one of the largest porphyry Cu deposits in the world, with 2.6 Bt grading 0.67% Cu and a skarn resource of 90 Mt grading 0.8% Cu (Laznicka 2006). The discussion that follows is based on Lanier et al. (1978), Atkinson and Einaudi (1978) and Reid (1978). In the Bingham mine area a Mid-Neogene composite stock, intruded along a northeast-trending fault direction, consists of early monzonite, followed by quartz-monzonite and late quartz-latite porphyry. This composite stock was intruded into a sequence of sedimentary rocks of Upper Carboniferous age, consisting of older units of feldspathic orthoquartzite and calcareous quartzite (Butterfield Peaks Formation) and younger units of limestone, calcareous sandstone and quartzite (Bingham Mine Formation). An early stage of Mg-Si metasomatism formed diopside in quarztite and in silty limestone beds, and wollastonite in cherty limestone, up to 1500 m and 600 m from the stock respectively. A trace amount of sulphides accompanied this early metasomatic event, which was synchronous with the emplacement of the quartz-monzonite porphyry. Actinolite-biotite alteration of diopside along sulphide-bearing fractures in quartzite and garnet alteration of wollastonite-bearing marble, constitute the main-stage mineralising event, which was synchronous with the potassic alteration of the intrusive stock. The mineralised skarns vary in thickness from 15 to 60 m. The main-stage skarn consists of brown andradite, diopside, magnetite and chalcopyrite superimposed on the early-stage wollastonite up to 450 m from the porphyry intrusion. The main-stage of ore deposition culminated with the alteration of andradite to various mixtures of calcite, quartz, hematite, magnetite, siderite and sulphides. In the wollastonite zone, yellow-green garnet is accompanied by chalcopyrite and bornite with minor sphalerite and galena. Pyrite to chalcopyrite ratios, decrease from the outer margin of the andradite-diopside zone towards the intrusive contact. A late-stage alteration phase produced pyrite, chlorite, montmorillonite, sericite, talc and opal.

6.2.2 *Yerington*

The Yerington district, western Nevada, is located within a belt of Jurassic intrusive rocks comprising a northern granodiorite batholith and a southern quartz-monzonite batholith. These are separated by Triassic-Jurassic volcanic and volcaniclastic-sedimentary rocks forming an east-west-trending zone about 8 km long and 3 km wide (Einaudi 1982a). The district is an area of major porphyry Cu systems with possible total resources in excess of 1.16 Bt of Cu ore, including the Yerington, Ann Mason, Bear-Lagomarsino and MacArthur porphyry Cu deposits. Mason Valley is one of several Cu-skarn deposits in the district. The Mason Valley Cu-skarn deposit occurs within a thick sequence of volcano-sedimentary rocks of Triassic age. The lower half of the sequence is composed of metamorphosed andesite and rhyolite lavas, breccias and sediments, whereas the upper portion consists largely of massive limestone, thin-bedded black calcareous shale and siliceous volcaniclastic rocks. The limestone beds are the host of numerous small Cu skarns located on the outer margins of a hornfels-skarnoid aureole. The Jurassic Yerington batholith rocks include granodiorite intruded by quartz-monzonite and younger quartz-monzonite porphyry dykes. The youngest rocks in the area are Neogene rhyolite-dacite volcanics. The carbonate rocks are not in direct contact with the porphyry plutons but are located some 3–4 km from the outermost edge of the porphyry Cu mineralisation. The large mass of granodiorite effectively shielded the carbonate rocks from direct contact with the porphyry Cu plutons. This spatial separation resulted in a mild retrograde alteration-mineralisation event, rendering it difficult to correlate alteration-mineralisation events between the intrusive and the sedimentary rocks. Two episodes of metasomatic and hydrothermal activity have been recognised (Einaudi 1982a). An early episode produced garnet-pyroxene hornfels near the batholith contact and recrystallisation to hornblende hornfels facies further out. Garnets of the hornfels rocks belong to the grossularite-andradite series, whereas the pyroxenes belong to the diopside-hedenbergite series. The second episode involved the brecciation of the early hornfels and the development of chalcopyrite-pyrite-bearing skarns. Formed in limestone, the skarn extends along a contact zone with tuffaceous rocks for about 600 m, with an average width of 65 m. The skarn consists of a footwall zone and a hangingwall zone , the former being made up largely of garnet and containing pyrite and chalcopyrite (1–5% by volume), the latter consisting of garnet and pyroxene and approximately 20% pyrite and chalcopyrite. The hangingwall skarn is late relative to the footwall skarn and is developed along the outer edge of the footwall zone. The zoning in the hangingwall skarn outward from a centre-line towards the dolomitic marble is: garnet + pyroxene, pyroxene and tremolite + talc at the contact with the dolomitised marble. This zonal pattern reveals that the direction of the metasomatising fluids was southward away from the batholith contact and along the faulted and

brecciated limestone-tuff contact. In the later stages the fluids infiltrated along bedding planes in marble rocks, forming the hangingwall skarns.

6.3 Sn-W and W Skarns

Meinert et al. (2005) separated W skarns from Sn skarns. Tin-W and W skarn deposits have been reviewed by Kwak (1987) and Newberry (1998). Tungsten skarns are generally found in plutons of calc-alkaline composition and Meinert et al. (2005) listed 203 deposits of this type. The causative plutons for W skarns are characterised by high temperature metamorphic aureoles and pegmatites. The main Sn minerals are cassiterite and stannites, and the main W minerals are wolframite and scheelite, with the latter being more common in the late paragenetic stages. There are two varieties of scheelite: Mo-rich (powellite) and Mo-poor. Powellite is found in reduced skarn environments, whereas Mo-poor scheelite in oxidised ones (Fig. 5.23). Reduced W-skarns are dominated by hedenbergite-grandite, spessartine and almandine garnets. Sulphide minerals include pyrrhotite, molybdenite, chalcopyrite, sphalerite and arsenopyrite. Retrograde skarn minerals are epidote, biotite and hornblende. Oxidised W skarn have andradite more abundant than pyroxene, usually diopsidic (Meinert et al. 2005). Tin skarns are almost entirely confined to high-silica granites and are commonly associated with greisen type alteration and high F activity (see Chapters 2 and 4), which seems to be absent from other types of skarns (Meinert et al. 2005). It is important to note that Sn skarns tend to be related to granitic plutons formed by partial melting of continental crust in rift settings. Tin skarns commonly have a F-B-Be-Li-W-Mo elemental association. Tin skarns are zoned from calcic to magnesian, oxide-rich to sulphide-rich and from greisen to skarn proper and Kwak (1987) reported that the richer skarns are usually distal. Ore fluids characteristics as recorded by studies of inclusion fluids in cassiterite have a wide range form about 200 up to 500°C (Solomon and Groves 1994 and references therein). Aqueous ore fluids generally contain CO_2, CH_4, NaCl, KCl, FeCl, $MgCl_2$ and $CaCl_2$. There is usually a decrease of salinity with time and this may be due to the input of meteoric waters during the late stages of the ore forming process. The $\delta^{34}S$ values of sulphides in these skarns vary from near 0‰ close to the causative pluton to + 10‰ in the sedimentary rocks away from the granite (Solomon and Groves 1994).

Important W skarn deposits of Mid- to Late Cretaceous age (~92 Ma), located in Canada (North West Territories, Yukon), are the MacWilliam Pass (MacTung) deposit containing about 32 Mt of ore at 0.74% W, and the Canadian Tungsten (CanTung) deposit with approximately 116000 t of W metal. CanTung is one of the largest producers of scheelite in the world. Both deposits are hosted in carbonate units of the Lower Palaeozoic within the thermal aureole of quartz-monzonite stocks. Details of these Canadian deposits

can be found in Einaudi et al. (1981), Dick and Hogson (1982), and Mathieson and Clark (1984).

In eastern Australia Sn, W and Sn-W deposits occur in several provinces in the Tasman Fold Belt System (Solomon and Groves 1994). In this section, I discuss skarn deposits from Tasmania, namely the Sn-W Moina deposit, and the W skarn of King Island, which represent good examples for these types of skarns. These descriptions are based on the works of Kwak and Askins (1981) (Moina deposit), Kwak and Tan (1981) (King Island). For more details the reader is referred to the above, the Special Issue of Economic Geology devoted to the geology and mineral deposits of Tasmania (Solomon et al. 1981), Kwak (1987) and Solomon and Groves (1994).

6.3.1 Moina Sn-W Deposit

The Moina skarn deposit contained 25–30 Mt of ore at an average grade of 0.15% Sn, and is located near the margin of the Dolcoath granite in north Tasmania. The area is underlain by Ordovician sedimentary rocks capped by Neogene basalts. The Ordovician sediments comprise the Moina sandstone (altered to quarztite) conformably overlain by the Gordon limestone (altered to marble). The Dolcoath granite, of Devonian age, is not in contact with either the limestone or the skarn, but is separated by about 200 m of Moina sandstone. Kwak and Askins (1981) interpret the mineralising fluids to have been channelled along fracture zones through the Moina sandstone, damming up at and near the contact with the overlying limestones to form the skarn deposits. The east-west-trending fractures along the Bismuth Creek fault, filled with Sn-W-bearing quartz veins, probably provided the plumbing system for the access of the fluids. The skarn unit extends for more than 1 km and is up to 100 m thick. It is divided into a lower granular skarn unit and an overlying wrigglite skarn unit (see Fig. 6.6). Wrigglite is a dark, fine-grained rock with an irregular laminar pattern of alternating light and dark laminae up to 0.5 mm wide, which are closely related and parallel to fractures (original definition in Kwak and Askins 1981). The granular skarn is further divided into a pyroxene-rich type, a garnet-rich type and a wollastonite-rich type. All three are enriched in F, Sn, Fe, W and Cl. The primary mineralogy of the wrigglite skarn is magnetite in the dark laminae and vesuvianite and fluorite in the light laminae. The skarn unit as a whole carries up to 25% F, 0.6% Sn, 0.5% W, 0.2% Be, 27.5 Zn and 4.5 g/t Au. Primary skarn may be altered to form amphibole or sulphide-rich zones in which Sn values are low. Replacement of wrigglite skarn by base metal sulphides, Fe sulphides and hematite is generally close to the Bismuth Creek fault. It is interesting to note that Kwak and Askins (1981) reported Sn to be contained as a solid solution in garnet as well as very fine cassiterite. The genetic model for the Moina deposit is described here. The intrusion of the Dolcoath granite produced a dense hornfels unit and metamorphosed the sandstone and

limestone to quartzite and marble respectively. At the same time metasomatism produced the granular calc-silicate skarn. Aqueous fluids evolved from the crystallising pluton and were trapped below a solid carapace and the dense hornfels rocks. Rupturing of the carapace by fluid overpressure led to a pressure drop and boiling (fluid inclusion evidence suggests a temperature range from 300 to 500°C) produced an acidic and volatile-rich (HF, HCl, H_2S) vapour phase and saline phase. The vapour phase greisenised the granite and the hornfels, while the fluids were channelled along faults and fractures, eventually replacing the marble rocks to form skarns higher up in the sequence. The laminations of the wrigglite skarn remain complex and at least five models in numerous papers have been proposed in an attempt to explain this phenomenon (Kwak and Askins 1981). One of these models interprets the rhythmic nature of the wrigglite laminae as possibly due to a mechanism similar to that which produces Liesagang banding. The mechanism of Liesagang banding, though still poorly understood, probably involves diffusion of ions from supersaturated colloidal (?) solutions.

6.3.2 King Island Scheelite Deposit

The King Island mine is located in the southeastern part of the island (off the northwestern tip of Tasmania). Three orebodies originally contained about 14 Mt of ore grading 0.64% W (Kwak and Tan, 1981). The local geology consists of a sandstone-siltstone unit overlain by dolomitic siltstone and shale of the Grassy Group of Neoproterozoic to Lower Cambrian age. This in turn is overlain by a Mid(?) Cambrian volcanic sequence comprising lavas and pyroclastics, which was intruded by two granitic stocks: the Grassy granodiorite and the Bold Head adamellite (Lower Carboniferous-Devonian). In the vicinity of these intrusions the Grassy Group sediments, which are metamorphosed and metasomatised, are locally known as the Mine Series. This succession is, from the bottom upwards: lower biotite-hornfels, lower metavolcanics, finely banded hornfels and marble, C-lens skarn unit (separated into an upper and lower unit by barren marble), pyroxene-garnet ± biotite hornfels, upper biotite hornfels and upper metavolcanics. The Mine Series at the Dolphin orebody, on the northern margin of the Grassy granodiorite, strikes approximately parallel to the contact and dips from 30 to 60° towards the pluton. The W ore mineral is a Mo-bearing scheelite (powellite), which occurs as inclusions in, and interstitially to, andradite garnet. Most of the scheelite mineralisation occurs in the C-lens skarn, although some is found in the marble in the interbedded footwall rocks. The mineralogy of the primary skarn is garnet + pyroxene + scheelite, on which is superimposed a secondary assemblage of ferrohastingsite + epidote + calcite + quartz + Fe sulphides + scheelite + molybdenite. Thus two generations of scheelite are recognised: one (Mo-rich) formed by high

temperature solutions (500°C near the pluton's contact to 300°C at approximately 500 m away); the other formed as a result of the dissolution of the Mo-rich scheelite and subsequent re-distribution as Mo-poor scheelite and molybdenite. This latter constitutes most of the King Island ore.

6.4 Proterozoic W Skarns in the Gascoyne Complex, Western Australia

Most of the skarn deposits discussed above are of Phanerozoic age, but W skarns of Palaeoproterozoic age are present in the Gascoyne Complex in Western Australia. The Gascoyne Complex is part of the Capricorn Orogen, a major Palaeoproterozoic orogenic belt that separates the Archaean Pilbara and Yilgarn Cratons in Western Australia (Cawood and Tyler 2004).

The Gascoyne Complex consists of granitic rocks and low- to high-grade metamorphic rocks, extending for approximately 400 km to the northwest from the Yilgarn Craton (Fig. 6.7; Sheppard et al. 2004; 2005). The Complex is separated from the Yilgarn Craton by the Errabiddy Shear Zone (Fig. 6.7). The southern part of the Gascoyne Complex has recently been remapped, and the ages of the major magmatic and orogenic events have been constrained by SHRIMP U–Pb zircon dating (Sheppard et al. 2004, 2005). The complex contains three main lithological subdivisions, namely: (1) granitic gneisses; (2) metasedimentary rocks (Morrissey Metamorphic Suite); and (3) large plutons of tonalite through to syenogranite (including the Minnie Creek Batholith).

The southern Gascoyne Complex consists of the Glenburgh Terrane and the Camel Hills Metamorphics. The Glenburgh Terrane comprises ca. 2.54 Ga granodiorite, tonalite and monzogranite tectonically interleaved with 2.0–1.97 Ga foliated and gneissic granites of the Dalgaringa Supersuite and Palaeoproterozoic metasedimentary rocks of the Moogie Metamorphics. These latest Archaean and Palaeoproterozoic rocks are exotic to both the Yilgarn Craton to the south and the Pilbara Craton to the north. The Camel Hills Metamorphics outcrop only within the Errabiddy Shear Zone, to the south of the Glenburgh Terrane. This shear zone also contains components of the Yilgarn Craton. Protoliths to the Camel Hills Metamorphics are pelitic, psammitic and calc-silicate rocks, which were deposited between ca. 2.02 and ca. 1.96 Ga, possibly in a fold-and-thrust belt out to the northwest or west of the Yilgarn Craton.The Glenburgh Terrane, Camel Hills Metamorphics, and the northwestern margin of the Yilgarn Craton were deformed and metamorphosed at medium- to high grade during the 2.0–1.96 Ga Glenburgh Orogeny (Occhipinti et al. 2004). These three tectonic units were intruded by granite plutons (Bertibubba Supersuite; Sheppard et al. 2004) at 1.96–1.95 Ga, which mark the collision and suturing of the Glenburgh Terrane and Yilgarn Craton.

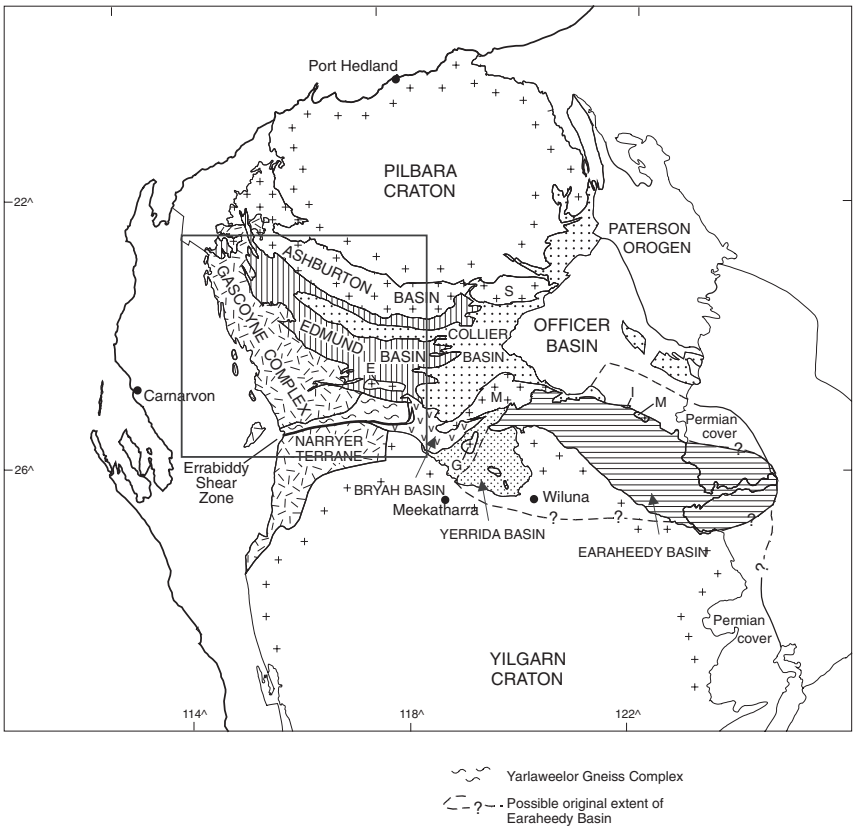


Fig. 6.7 Simplified geology of the tectonic units of the Palaeoproterzoic Capricorn Orogen in Western Australia; the Gascoyne Complex (within *square*) is at the nortwestern margin of the Yilgarn Craton (Sheppard et al. 2004, 2005). After Pirajno (2004)

During the Capricorn Orogeny at 1.83–1.78 Ga the Gascoyne Complex was extensively intruded by granitoid plutons (Cawood and Tyler 2004). At the same time, part of the northern edge of the Yilgarn Craton was deformed and metamorphosed at high-grade, and intruded by granite and pegmatite to form the Yarlarweelor Gneiss Complex. Granitic rocks have ages ranging from 2005 to 1970 Ma and are grouped under the name of Dalgaringa Supersuite (Sheppard et al. 2004). The Dalgaringa Supersuite extends for at least 100 km in an east-northeast direction, records two episodes of granitic magmatism and consists of 2005–1985 Ma gneissic diorite and monzogranite and 1975 Ma tonalite and granodiorite plutons. The Dalgaringa granites, on the basis of geochemical and isotopic data (granitic rocks of the Supersuite have SiO_2 contents from 47 to 76 wt% and ε_{Nd} values ranging from –3.4 to –6.0), have been interpreted as being part of an Andean-type batholith that was emplaced along a continental margin, before its collision with the northwestern part of

the Yilgarn Craton (Sheppard et al. 2004). Sheppard et al. (2005) identified an additional orogenic event, Mangaroon Orogeny that largely affected the northern part of the Gascoyne Complex between 1680 and 1620 Ma, during which granodiorite and biotite-muscovite monzogranite plutons were emplaced.

The W skarns of the Gascoyne Complex are discussed in some detail by Davies (1998) and reviewed by Pirajno (2004). Scheelite-bearing skarns are present in the northwestern Gascoyne Complex, are associated with highly differentiated and weakly peraluminous granitic rocks (Davies 1998). These skarn deposits (Kilba Well, described here, and Mount Alexander) are developed in calcite-tremolite-chlorite marble rocks at the contact with monzogranite and granodiorite intrusions (Fig. 6.8). The skarns, associated with greisen and sericitic alteration of the intrusives, show well-developed mineralogical zoning (prograde and retrograde stages). Scheelite is associated with fluorite, vesuvianite and epidote. The age of the Gascoyne skarns is not known with certainty, but given their spatial association with the Mangaroon granitic rocks, it is possible that their age is around 1680–1620 Ma.

The Kilba Well prospect (Fig. 6.8) is characterised by metasedimentary rocks that wrap around a central monzogranite stock. The metasedimentary rocks are mica schist, quartzite, marble, psammitic schist, amphibolite and muscovite

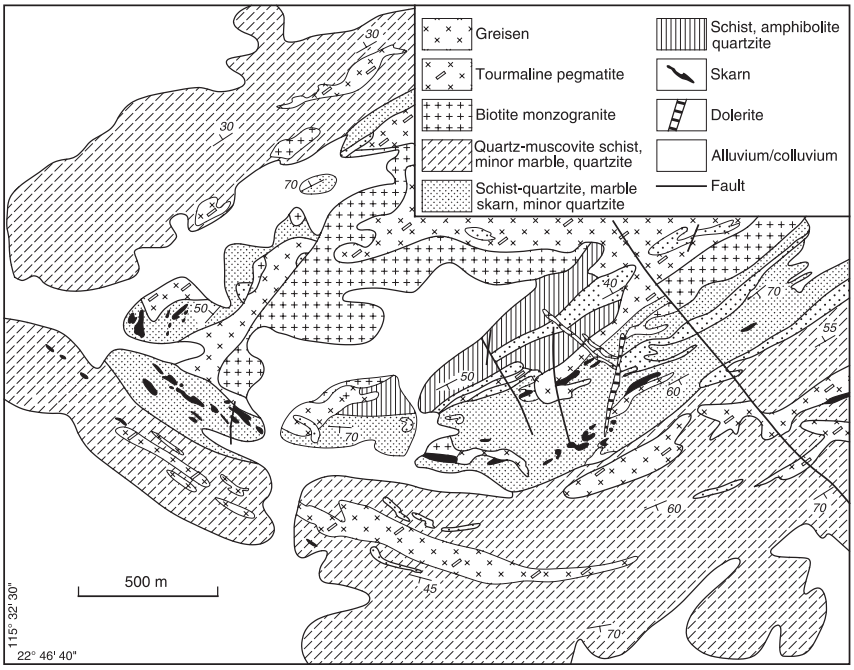


Fig. 6.8 Simplfied geology of the area around the Kilba Well skarns, Gascoyne Complex. After Davies (1998)

schist. These rocks are intruded by tourmaline-bearing pegmatites, which are probably related to the porphyritic monzogranite stock. The core of this monzogranite stock is equigranular, but its outer parts contain large (up to 2 cm) microcline phenocrysts. The marginal zones of the monzogranite stock exhibit sericitic and greisen alteration, consisting of coarse muscovite, quartz, tourmaline and clinozoisite. Quartz-tourmaline veins are present within the altered margins of the stock and, in addition to quartz and tourmaline, also contain chlorite, sericite, calcite, pyrrhotite, chalcopyrite and cassiterite. The contact metamorphic assemblages in the surrounding metasedimentary rocks constitute the Kilba Well skarns. These skarns form discontinuous bodies that surround the monzogranite stock, and are characterised by complex prograde and retrograde zones (Davies 1998) that extends from the host marble rocks to the intrusive (Fig. 6.9). The mineralogical zonation of the Kilby Well skarns are given in Table 6.3 and briefly described below.

At Kilba Well, the wollastonite zone is the outermost zone and is in contact with unaltered marble (Fig. 6.9). It consists of well-developed fibrous to columnar wollastonite aggregates with lesser garnet, pyroxene, calcite and vesuvianite. Garnet and vesuvianite occur as coarse porphyroblasts. The metamorphic tremolite, phlogopite and chlorite minerals of the marble were destroyed and their contained Mg released to form vesuvianite. The transition zone is a thin and discontinuous intermediate layer, separating the wollastonite zone from the garnet-vesuvianite zone (Fig. 6.9). This transition zone is marked by the loss of wollastonite and the increasing abundance of garnet and pyroxene. Scheelite is present in the matrix and as inclusions in the vesuvianite. The garnet-vesuvianite zone (Fig. 6.9) is characterised by garnets up to several cm across and growth-banded vesuvianite. The garnets contain inclusions of wollastonite, pseudomorphed by calcite-epidote-clinozoisite. Epidote, calcite and microcline fill interstices between the coarse garnet and the vesuvianite. Minor scheelite is

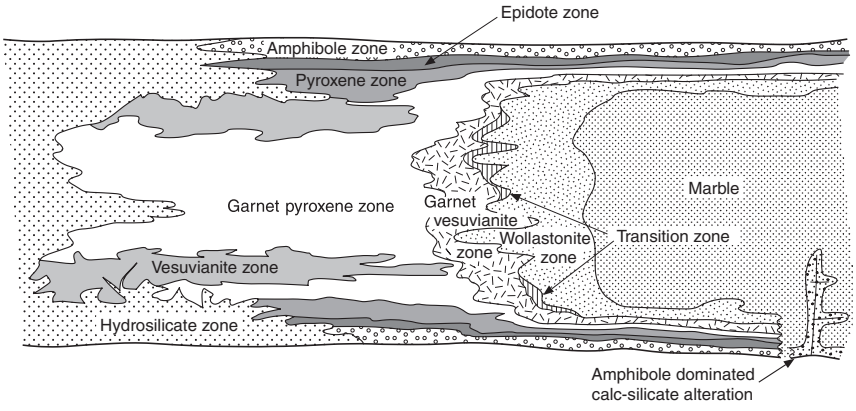


Fig. 6.9 Schematic geometry and distribution of skarn mineral zones at the Kilba Well (Gascoyne Complex). After Davies (1998)

Table 6.3 Mineral assemblages of the Kilba Well skarn in Western Australia (after Davies 1998)

Zone	Dominant assemblage	Intermediate assemblage	Minor assemblage
Prograde zone			
Wollastonite	Wollastonite	Garnet-clinopyroxene-vesuvianite	Calcite
Transition	Garnet-clinopyroxene	Vesuvianite-calcite-clinopyroxenite	Quartz-scheelite-sphalerite-pyrrhotite
Garnet-vesuvianite	Garnet or vesuvianite	Microcline-clinozoisite-quartz	Actinolite-scheelite
Garnet-pyroxene	Garnet	Clinopyroxene-vesuvianite-epidote-clinozoisite-quartz-feldspar	Actinolite-scheelite
Pyroxene	Clinopyroxene	Clinozoisite-epidote-albite-quartz-garnet	Sphalerite-muscovite-actinolite-pyrrhotite-pyrite-scheelite
Retrograde zone			
Amphibole	Actinolite	Quartz-calcite-epidote-clinozoisite-titanite	Phlogopite-apatite-alanite-clinopyroxene
Vesuvianite	Vesuvianite	Clinozoisite-calcite-feldspar	Quartz-scheelite-fluorite-apatite-actinolite

present in this zone and is associated with vesuvianite, calcite and feldspar. Garnet compositions in this zone are grossular-rich, whereas the pyroxene are diopside rich, with hedenbergite contents of 21–28 mole %. The garnet-pyroxene zone (Fig. 6.9) is present as remnants left from retrograde overprinting, although reconstructions based on drill core data suggest that this zone was far more extensive. These remnants show coarse poikiloblastic garnet and fine- to medium-grained clinopyroxene, together with minor amounts of calcite, quartz, feldspar, epidote, actinolite, fluorite and rare scheelite. Here too garnet is grossular-rich, whereas pyroxene has hedenbergite contents from 31 to 48 mole %. The pyroxene zone is best developed along the footwall and hangingwall margins (Fig. 6.9) and is characterised by an increase in pyroxene and epidote group minerals. The assemblages of this zone occur as a fine-grained granoblastic intergrowths of pyroxene with epidote, clinozoisite and minor vesuvianite, calcite, quartz, albite, scheelite and pyrrhotite. Pyroxene is diopside rich with hedenbergite contents from 22 to 42 mole %. The epidote zone has a typically green to cream colouration and is also fine-grained and granoblastic, and is best developed parallel to the pyroxene zone at the footwall and hangwall of the skarn system. The zone is banded and is defined by a granoblastic intergrowth of epidote and clinozoisite with variable proportions of quartz, calcite, clinopyroxene, albite and titanite. Zones of retrograde hydrous alteration, can be separated into an amphibolite, vesuvianite and hydrosilicate zones. The amphibolite zone borders the epidote zone and is only about 5 cm wide. It consists of actinolite laths, accompanied by calcite, phlogopite, clinozoisite, epidote, albite, quartz, titanite, pyrrhotite and chalcopyrite. The vesuvianite zone is defined, as the name

implies, by abundant coarse and poikiloblastic vesuvianite with quartz, minor calcite, epidote, clinozoisite, actinolite, albite, fluorite, microcline and apatite. Scheelite is present as inclusions in the vesuvianite or as single grains and is locally associated with fluorite. Hydrosilicate assemblages replace the prograde assemblages and are identified by the presence of hydrous mineral phases, mostly amphibole and phlogopite with varying proportions of quartz, calcite, epidote, vesuvianite, fluorite, scheelite, albite, allanite, titanite, pyrrhotite, chalcopyrite and sphalerite. Scheelite is intergrown with sericitised albite or forms selvages to veins.

The Kilba Well scheelite mineralisation is preferentially sited in the retrograde zones of skarns that are typically Fe-poor. Scheelite solubility in the ore fluids is controlled by their composition and especially Ca concentrations. Hydration of Ca-rich assemblages increases the activity of the Ca^{2+} ions in theore fluids, thereby enhancing the possibility of scheelite and fluorite precipitation.

6.5 Gold Skarns

Although Au skarns have been mined since the late 1800s, there was little published about them until recently and they were not included in the major world review of skarn deposits by Einaudi et al. (1981). In the past 20 years there have been numerous gold skarn discoveries (e.g. Red Dome, Queensland, and Navachab, Namibia), but the fact that this gold mineralisation was a type of skarn was not at first realised. In gold skarns the highest gold grades range from 5 to 15 g/t, and they are mined solely for their precious metal content, and lack economic concentrations of base metals. Other gold skarns are more oxidized, have lower gold grades (1–5 g/t Au), and contain subeconomic amounts of other metals such as Cu, Pb, and Zn. Several other skarn types, particularly Cu skarns, contain enough gold (0.01->1 g/t Au) for it to be a by-product. Most high grade gold skarns are associated with reduced (ilmenite-bearing, $Fe^{+3}/Fe^{+2} < 0.75$) diorite-granodiorite plutons and dyke or sill complexes. Such skarns are dominated by iron-rich pyroxene (typically >Hd50); proximal zones can contain abundant intermediate grandite garnet. Other common minerals include K-feldspar, scapolite, idocrase, apatite, and high-chlorine aluminous amphibole. Distal and early zones contain biotite + K-feldspar hornfels that can extend for hundreds of metres beyond massive skarn. Arsenopyrite and pyrrhotite can be dominant sulphide minerals. Most gold is present as electrum and is strongly associated with various bismuth and telluride minerals including native bismuth, hedleyite, wittichenite, and maldonite (e.g. Navachab, Namibia).

Gold skarns are generally those that contain Au as the only or main economically viable product. Meinert (2000) listed 60 world wide, ranging in age from Archaean to Mesozoic, later updating the list to 93, of which 33 are in

Canada and 26 in China (Meinert et al. 2005). A key alteration mineral assemblage common of most Au skarns is biotite±K-feldspar, resulting in rocks with hornfelsic textures (Meinert 2000). This author distinguished four main magmatic-hydrothermal associations: reduced, oxidised, magnesian Au skarns and those that are found in regionally metamorphosed terranes. These are briefly introduced here together with some key examples.

In the reduced systems, Meinert (2000) included as representative of this category the Au skarns of the Hedley District in British Columbia (Canada), the Fortitude deposit (Battle Mountain district) in Nevada, Crown Jewel in Washington and the Au skarns of the Elkhorn district in Montana (all in the USA), the skarns of the Rio Narcea district (Spain) and Junction Reef (Australia). In general Au skarns of reduced systems, although only producing Au, typically have a distinct metal association of Au-Bi-Te-As ± Co linked to the activities of reduced, ilmenite-bearing diorite-granodiorite plutons, dyke or sill complexes (Meinert et al. 2005). Reduced Au skarns are dominated by Fe-rich pyroxene, grandite garnet, K-feldspar, scapolite, vesuvinaite, apatite and amphibole. An important aspect of Au skarns is that they appear to be associated with clastic and carbonaceous protoliths and that Au is intimately associated with Bi-bearing mineral phases.

Oxidised Au skarn systems are characterised by high garnet/pyroxene ratios, low sulphide content and an association with retrograde alteration with abundant adularia and quartz as the main minerals (Meinert et al. 2005). Some of these skarns can be transitional to epithermal systems (see Chapter 5). Meinert (2000) considered the Big Gossan Cu-Au skarn in the Ertsberg district of Papua New Guinea as a representative of this category, together with the Red Dome deposit in Queensland (Australia) McCoy (Nevada) and Nambijia (Ecuador).

Magnesian Au skarns are associated with dolomitic rocks and have a diagnostic mineral assemblage dominated by forsterite, spinel and serpentine (Meinert et al. 2005). Magnetite is an important spinel phase and for this reason these skarns are usually exploited as Fe ore. The Cable mine in Montana is an example of Au magnesian skarn.

Metamorphic terranes in orogenic belts may host skarns that are associated with both plutonic rocks and high-T and high-P metamorphism, which include greenstone-hosted orogenic lode Au deposits with typical skarn type assemblage and apparent lack of associated intrusions (Mueller and Groves 1991). These greenstone-hosted lode Au deposits are present in the Yilgarn Craton and their skarn type alteration assemblages include high and low temperature (Mueller and Groves 1991). The former (350–700°C) is characterised by assemblages such as microcline + quartz + muscovite + andalusite, garnet + pyroxene + biotite and amphibole + biotite + calcite. The latter (350–200°C) may contain biotite + ankerite + albite and sericite + ankerite + albite. Sulphide minerals are stibnite, pyrrhotite and arsenopyrite-loellingite for the high temperature assemblages and pyrrhotite-arsenopyrite for the low temperature ones. Pyrite is uniquitous. The high temperature Au skarns formed at depths of 13–15 km and 3–5 kbar of pressure, wheareas the low temperature systems

formed at depths of 3–7 km and pressures of 1–2 kbar (Mueller and Groves 1991). There are several other skarn systems of this type in the Slave and Superior Provinces of Canada and the Dharwar Craton of India. In Namibia, the Navachab Au deposit, which was included in this category (Nörtemann et al. 2001), constitutes a good example of a Au-Bi-W skarn system in a region characterised by other similar but more distal skarn systems. Navachab and surrounding deposits provide a good example of a multiple skarn type hydrothermal mineral system and are discussed in more detail next.

6.5.1 Navachab, Namibia

The Navachab Au deposit and surrounding region is located in the southern Central Zone of the Damara Orogen, Namibia, which is part of a network of orogenic belts of Panafrican age (570–460 Ma) (inset of Fig. 6.10; Gray et al. 2006). The Damara Orogen developed from a triple junction rift system that is thought to have formed as a result of the impingement of a mantle plume beginning at about 800 Ma (Pirajno 2000 and references therein). Two of the Damara rift arms (northern and southern) evolved through a full Wilson cycle, while the third arm is the intracontinental branch, divided into a Northern Platform, Northern Zone, Central Zone, Southern Zone and a Southern Marginal Zone (see Miller 1983 for a comprehensive account of the geology of the Damara Orogen). The northeast-trending intracontinental branch (Damara belt) evolved to form a narrow oceanic arm (Matcheless ophiolite belt; see Chapter 7), and was subsequently involved in the collision between the Congo and Kalahari cratons forming the orogenic belt at around 570–550 Ma (Johnson et al. 2006). The Damara Orogen extends northeastward to become the Katanga Sequence of the Lufillian Orogen in Zambia-Angola-Congo (see also Figs. 8.12 and 8.14). The northeast-trending Damara Orogen originated as a series of rift structures, formed during the breakup of the Rodinia supercontinent that had amalgamated at about 1.0 Ga. This rifting was accompanied by ~750 Ma bimodal volcanism and accumulation of siliciclastic rocks that constitute the basal units (Nosib Group) of the Damara sequence.

Gold ± Cu ± Bi ± W skarn mineralisation is present in marble rocks of the Okawayo and Karibib Formations, near the towns of Karibib and Usakos. In this region there are a number of skarn style mineral occurrences (Onguati, Brown Mountain, Western Workings, Habis, Otjimboyo) in addition to the Navachab operating mine (Fig. 6.10). Mineralisation in the region is found in major northeast-trending anticlinoria within marble units at different stratigarphic levels. The regional stratigraphy includes pelitic schist, marble, calc-silicates and amphibolites, locally with well-preserved pillow structures. These rocks have undergone regional amphibolite facies metamorphism.

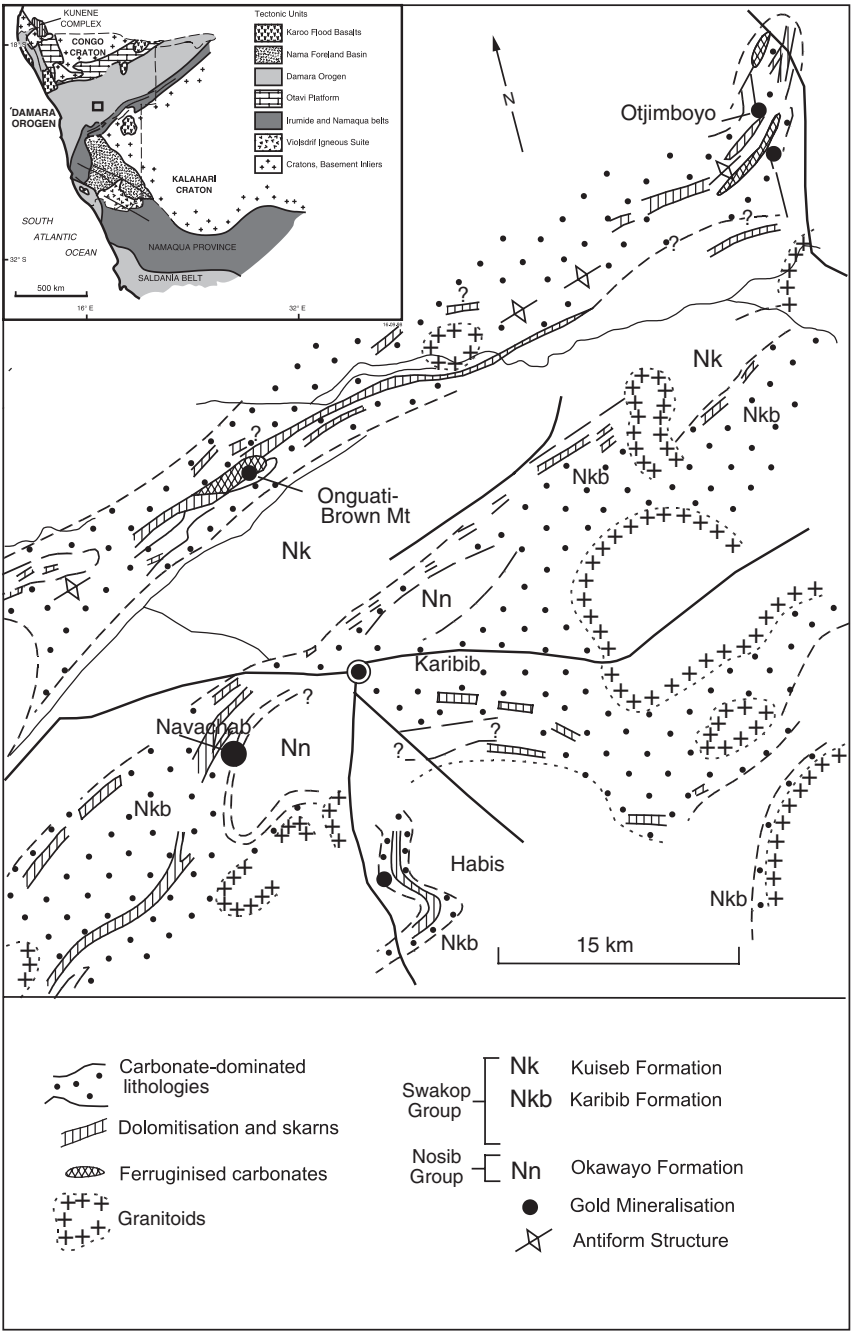


Fig. 6.10 (continued)

The Navachab mine came into production in 1989 with a resource of 11 Mt at 2.6 g/t Au, with an annual production of about 2.4 t of Au. Publications on Navachab include Pirajno et al. (1991), Meinert (1998), Nörtemann et al. (2001), Jacob et al. (2001) and Kisters (2005). The Navachab ore styles include massive skarns and structurally-controlled quartz veins, developed on the southern limb of the Karibib dome, which has a core of gneissic rocks, unconformably overlain by 1500 m of basal rift-related volcano-sedimentary succession of the Etusis Formation (Damara Sequence; Miller 1983). The Etusis Formation is successively overlain by the Chuos Formation (of international fame because of its glaciogenic diamictites that provide clues for the snowball Earth hypothesis; Hoffman et al. 1998) and the Spes Bona Formation, which forms the footwall succession of the Navachab deposit. The Spes Bona Formation consists of biotite schist, calc-silicates, metapsammite and marbles. The mineralisation is mainly hosted by the Okawayo Formation, a 100–200 m thick marble succession that consists of two units. A basal unit (called MC and the main host of the mineralisation) is 35 m thick and contains garnet-diopside-biotite calc-silicates, interlayered with marble rocks and overlain by 70–80 m of calcareous and dolomitic marbles. The Okawayo Formation is overlain by the Oberwasser (amphibolites and calc-silicates) and Karibib (marbles and calc-silicates) formations. In addition, numerous pegmatites and aplites intruded these metasedimentary rocks. Two main styles of mineralisation are present: quartz-sulphide lodes, or MC type, and shallow-dipping quartz veins that cut the host rocks (Kisters 2005). The MC type consists of bedding-parallel sulphide pods and lenses hosted by the calc-silicates and marbles of the MC unit. The sulphide-quartz lenses are cm to m thick, are also referred to as massive skarn, and are associated with calc-silicate alteration. The second type is represented by sheeted auriferous quartz veins, which extend laterally for 300–400 m and down-dip for 200–300 m. The quartz veins contain sulphides (pyrrhotite, chalcopyrite, and pyrite mainly) and exhibit thin haloes of skarn type alteration characterised by clinopyroxene, garnet, tremolite and biotite (see Figs. 6.6 and 6.11). Gold occurs as a native element and is associated with maldonite (Au_2Bi) and native Bi. The skarn is well zoned and reflects the composition of the Okawayo Formation carbonate protolith, ranging from massive skarn alteration to unaltered marble. Massive skarn consists of clinopyroxene (hedenbergite and diopside) and garnet with an almandine-rich core and spessartite- and andradite-rich rims. The mineralisation is associated with retrograde alteration, dominated by amphibole. Two paragenetic sequences for the massive skarns were determined by Nörtemann et al. (2001), who recognised an older assemblage with pyrrhotite-chalcopyrite-arsenopyrite-sphalerite

Fig. 6.10 (continued) Schematic geology of the area around Karibib (Damara Orogen, Namibia) and distribution of Au skarn systems. Inset shows simplified geology of southwestern Africa with Namibia outlined; square indicates approximate position of Karibib area. After Pirajno et al. (1991)

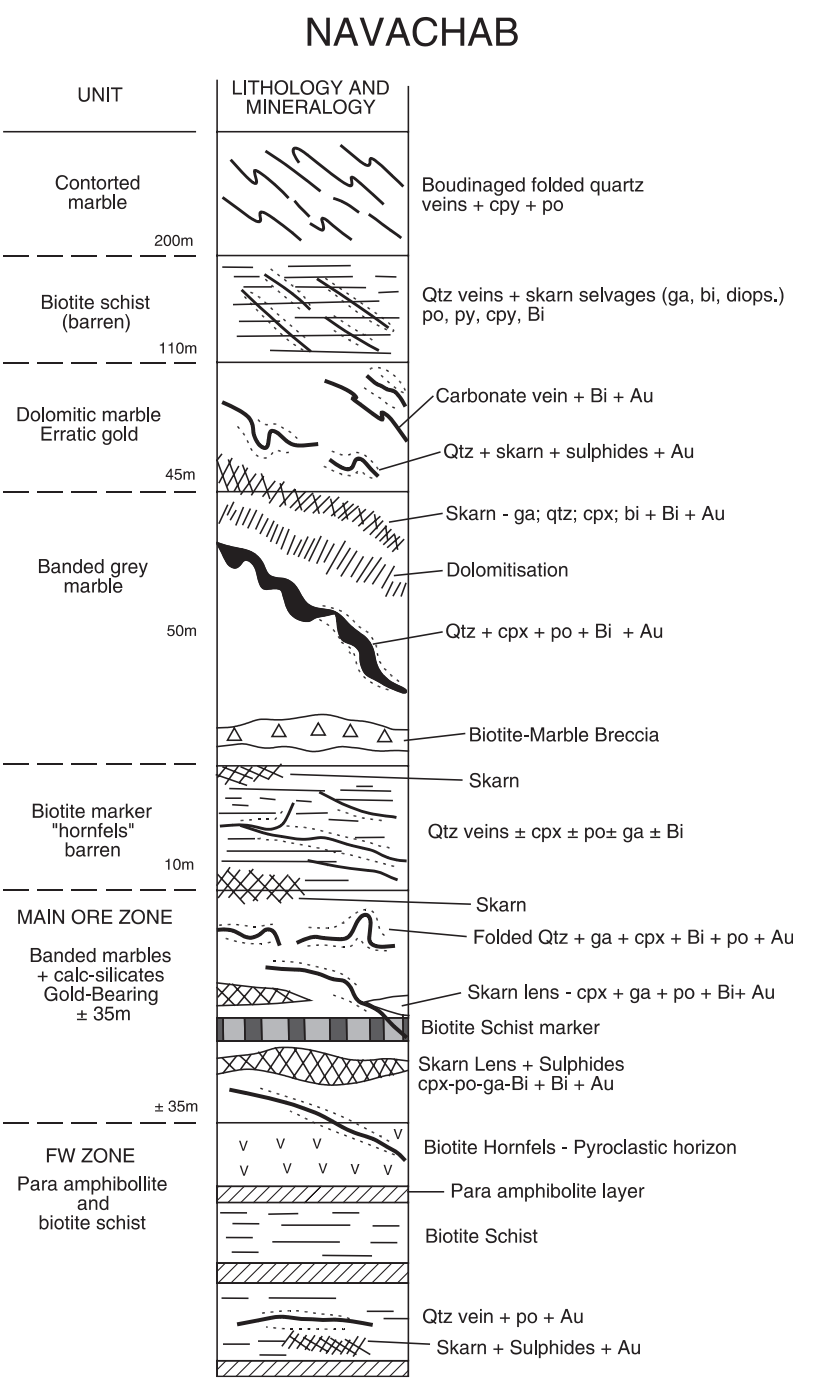


Fig. 6.11 Stratigraphic column for the Navachab area, with position of the various skarn veins (Pirajno and Jacob, unpublished data)

(± molybdenite-scheelite-uraninite) and a younger one with native Bi and Au, pyrite, bismuthinite (± pyrrhotite and chalcopyrite). The older paragenesis forms massive ores in fractures and veins emplaced during a brittle and late deformation stage. Textural and crystal features of chalcopyrite and pyrrhotite of this stage suggest temperatures of about 500°C. The younger paragenesis is a clinopyroxene skarn and it constitutes most of the economic mineralisation, which again is sited in fractures and veins. A key features of this stage is the alteration of pyrrhotite to pyrite and of bismuth to bismuthinite. Vein ore mineralogy is characterised by quartz, calcite, K-feldspar and sulphides, but is volumetrically minor although with erratic high Au values. The composition of the garnets (almandine-spessartine-andradite) suggestive of reducing conditions, while the pyrrhotite-chalocpyrite-maldonite-gold association, and lack of Te- and Sb-bearing mineral species is indicative of high temperature as well as reducing conditions. The ore and associated alteration minerals were formed at pressures of 2.5–3 kbars and temperatures of 600–570°C, corresponding to the temperature and pressure of the regional metamorphism in the area. Sulphur isotopic data shown $\delta^{34}S_{CDT}$ values of +2 to +3‰ in the main skarn, whereas the vein ore shows a wider range from +3 to +14‰. The Navachab Au skarns have features that suggest a relationship with felsic-intermediate (leucogranite and diorite) intrusions, but the deposit is sited in a high-grade metamorphic environment. SHRIMP U-Pb age data by Jacob et al. (2001) indicate two age clusters around 550 and 500 Ma, with the former possibly representing the age of the intrusions and the latter of prograde regional metamorphism. The mineralisation could be related to either (Jacob et al. 2001).

Taken in the regional context, the Navachab skarns together with other marble-hosted mineral occurrences, such as Western Workings, Onguati, Brown Mountain, Habis and Otjmboyo, represent a large mineral system (Fig. 6.12). At Onguati, Brown Mountain and Western Workings vein type Cu-Au, Cu-W-Bi mineralisation is hosted in marbles at a higher stratigraphic level than Navachab and within the Karibib Formation, which lies above the Okawayo Formation. These veins are up to 2 m thick and extend for up to 200 m along strike. Gold is associated with pyrrhotite, chalcopyrite, pyrite and arsenopyrite. The Au values are generally low (0.6–6 g/t), although in places reach very high grades (80 g/t). Gold correlates with anomalous Cu, As, Bi and W.

Pirajno et al. (1991) proposed multistage processes of ore formation occurred during regional metamorphism and the emplacmenet of felsic-intermediate pluton(s). In a first stage, deformation and prograde metamorphism resulted in dehydration reactions and the production of metamorphic hydrothermal fluids, which may have leached Mg from amphibolites (mafic volcanics) that are present in the sequence and perhaps some of the ore metals. In a second stage, intrusion of post-tectonic felsic-intermediate magmas occurred and provided the themal energy to drive large scale hydrothermal cells, which produced the observed skarn systems in the region.

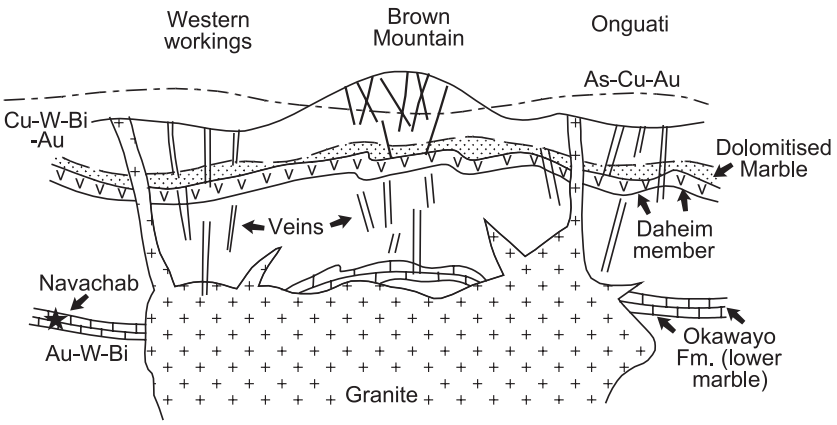


Fig. 6.12 Schematic model of spatial relationships of the skarn systems in the Karibib region with granitic intrusions. After Pirajno et al. (1991)

6.5.2 Gold Skarns in China

In China gold skarns contain a total resource of approximately 1,000 tonnes of gold, accounting for 20% of China's gold reserves. Chen et al. (2007) identified and listed 70 Au skarns or Au-bearing skarns including Cu, Fe and Pb-Zn deposits. One of these ranks as super-large (>100 t Au), nineteen are large (20–100 t Au) and twenty-four are medium-sized (5–20 t Au). The distribution of Chinese Au skarns is shown in Fig. 6.13, and the following is summarised from Chen et al. (2007). The skarn Au systems in China are located in collisional orogenic belts, intracontinental fault-controlled magmatic belts and reactivated cratonic margins. These skarns are contained in various lithotectonic units within ten metallogenic provinces (Fig. 6.13), namely: (1) Qiangtang Block (Tibet-Sanjiang region); (2) southern margin of the Yangtze Craton (northern Ailaoshan-Dayaoshan region); (3) Huanan Orogen (South China Fold Belt); (4) The eastern part of the Yangtze Craton; (5) Central China (Qinling) Orogen; (6) Tan-Lu fault zone; (7) Taihang fault zone; (8) Yan Shan; (9) Hingan Orogen (northeastern China); and (10) Tian Shan-Altay orogenic belts (northwestern China). The largest and economically most important skarn deposits are in the Yangzte Craton, Huanan Orogen and Central China Orogen.

Collisional orogenic belts in China all contain skarn gold deposits (Fig. 6.13). The Tibet-Sanjiang orogenic belt hosts the Yulong porphyry Cu-(Mo-Au) deposits and a group of porphyry-skarn Cu-Au systems. Although regarded as a porphyry Cu belt (see Section 5.2.2.4), the Tibet-Sangjiang region may also be considered as an important skarn Au belt. The Central China (Qinling) Orogen, contains the Baxi, Deerni, Saishitang, Yemaquan, Kendekeke and Yinjiagou deposits; the Tian Shan-Altay orogenic belts in northwest China contain four

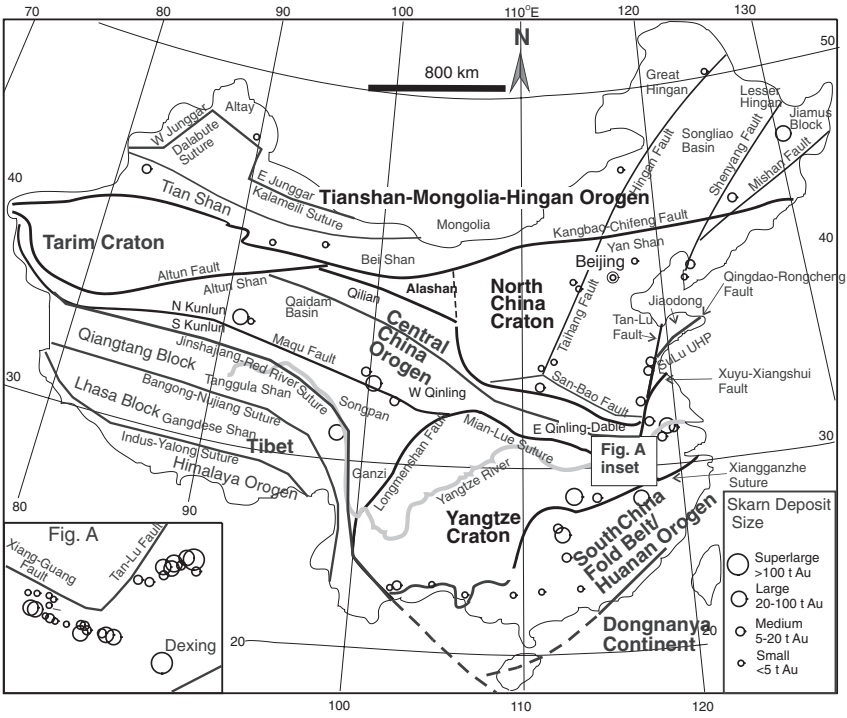


Fig. 6.13 Simplified map of mainland China showing tectonic provinces and distribution of Au skarn systems and deposit size (see inset at *right*); (**A**) shows the distribution of Au-dominated skarns in the Yangzte River Valley, described in Section 6.9. After Chen et al. (2007)

skarn Au deposits; the Hingan orogenic belt hosts the Chaobuleng, Laozhashan, Sankuanggou and Lanjia deposits. The Huanan Orogen contains the important Dabaoshan and Kanjiawan deposits, the collisional zone between the Qiangtang-Indochina block and the Yangtze Craton (Fig. 6.13) includes the Jinping and Qinjia deposits.

Igneous activity in intracontinental fault-controlled magmatic belts and reactivated cratonic margins is contemporaneous with that in the collisional orogens. Some additional explanation is needed for skarn Au deposits along the Tan-Lu and Taihang fault-controlled magmatic belts, since these are discordant to the dominant orogenic trends. During the Triassic-Early Jurassic north-south collision took place between the North China and Yangzte Cratons, and these two major fault zones were accommodated by strike-slip motion and east-west extension (possibly as pull-apart). In addition, during the decompression-extension stage that affected East China in the Mesozoic, these fault zones again acted as extensional structures. The Taihang and Tan-Lu fault zones (Xu and Zhu 1994) are examples of intracontinental fault-controlled magmatic belts in the North China Craton. These fault zones trend north-northeast or northeast and

are nearly perpendicular to collisional orogenic belts, such as the Qinling-Dabie and the Mongolia-Hingan Orogens (Fig. 6.13). As mentioned above, following the Mesozoic collision between the Yangtze and the North China Cratons, these fault zones accommodated intracontinental extension and emplacement of large volumes of intermediate and felsic magmas that are associated with skarn-type metallic deposits, including Au-bearing skarns. The Lanjia, Laozuoshan, Qianchang, Yinan deposits, and the Xi'nancha porphyry-skarn Au-copper deposit (38 t Au, 0.18 Mt Cu) are present along the Tan-Lu fault magmatic belt and its northern extension, the Shenyang fault (Fig. 6.13). Along the Taihang fault-controlled magmatic belt, skarn Au deposits include the Fenghuangzui, Sijiawan, Diaoquan, and Tainashui deposits, and along its northern extension (the Hingan fault) are the Chaobuleng and Sankuanggou skarn Au and the Duobaoshan porphyry Cu-Au (73 t Au) deposits.

During Phanerozoic collisions, ancient cratonic margin sequences were affected by magmatism that produced skarn Au deposits. For instance, the southern margin of the Yangtze Craton, was involved in collisions along the Jinshajiang-Red River fault in the Late Triassic (see also Section 5.2.2.4), and hosts the Jinping, Jixinnao, Qinjia, Liuhe, Dulong and Kafang skarn Au deposits. Similarly, the eastern margin of the Yangtze Craton (the Lower Yangtze River region), one of the most important skarn Au belt in China, with more than 30 deposits (Fig. 6.13), was intensely reactivated in the Mesozoic.

Along the southern margin of the North China Craton, skarn Au deposits are hosted in the Mesoproterozoic-Neoproterozoic carbonate-clastic lithofacies developed in a marginal basin, but were formed during the Mesozoic Yanshanian tectono-thermal event (see below). In the Yan Shan region, on the northern margin of the North China Craton (Fig. 6.13), are the Huatong and Shouwangfen deposits hosted in the Proterozoic or Palaeozoic evaporite-carbonate-clastic lithofacies. As indicated previously, all of the above cratonic margins underwent reactivation during Late Palaeozoic, Mesozoic and Cenozoic collisional and extensional tectonics. Indeed, some workers regard these marginal tracts as orogenic belts in their own right. For example, the Huaxiong block, enclosed by the San-Bao Fault and the Luanchuan Fault (Fig. 6.13), is regarded as part of the Qinling Orogen. Likewise, the Yan Shan region (Fig. 6.13), the type locality of the Yanshanian event, is now interpreted in terms of the deformation that resulted from the collision of the Siberia and North China Plates during the Mesozoic closure of the Mongol-Okhotsk Ocean (Davis et al. 1996).

6.6 Zinc Skarns

Most Zn skarns occur in continental settings associated with either subduction or rifting. They are mined for ores of Zn, Pb, and Ag although Zn is usually dominant. They are also high grade (10–20% Zn + Pb, 30–300 g/t Ag). Related igneous rocks span a wide range of compositions from diorite through

high-silica granite. They also span diverse geological environments from deep-seated batholiths to shallow dyke-sill complexes to volcanic extrusions. The common thread linking most Zn skarn ores is their occurrence distal to associated igneous rocks. A review of Zn skarn deposits can be found in Einaudi et al. (1981). Most Zn skarn districts grade outward from skarn-rich mineralisation to skarn-poor ores, veins, and massive sulphide bodies that may contain few if any skarn minerals. Incompletely explored districts may only have some of these zones exposed. Besides their Zn-Pb-Ag metal content, Zn skarns can be distinguished from other skarn types by their distinctive Mn- and Fe-rich mineralogy, by their occurrence along structural and lithologic contacts, and by the absence of significant metamorphic aureoles centered on the skarn. Almost all skarn minerals in these deposits can be enriched in manganese including garnet, pyroxene, olivine, ilvaite, pyroxenoid, amphibole, chlorite, and serpentine. A typical zonation sequence from proximal to distal is: altered/endoskarned pluton, garnet, pyroxene, pyroxenoid, and sulphide/oxide replacement bodies (occasionally referred to as mantos and chimneys based upon geometry). The occurrence of Zn skarns in distal portions of major magmatic-hydrothermal systems may make even small deposits potentially useful as exploration guides in poorly exposed districts. Thus, reports of Mn-rich mineral occurrences may provide clues to districts that have not yet received significant exploration activity.

6.7 Molybdenum Skarns

The majority of Mo skarns are associated with leucocratic granites and range from high grade, relatively small deposits to low grade, bulk tonnage deposits (Meinert et al. 2005). Numerous small occurrences are also found in Precambrian stable cratons, where they occur in pegmatite, aplite, and other leucocratic rocks. Molybdenum skarns have metal associations including W, Cu, Zn, Pb, Bi, Sn, and U, with Mo-W-Cu being the most common. Hedenbergitic pyroxene is the a common calc-silicate mineral reported from several Mo skarns with lesser grandite garnet, wollastonite, amphibole, and fluorite. This skarn mineralogy indicates a reducing environment with high F activity. Einaudi et al. (1981) described the main features of Mo skarns, using examples from Australia, the USA and Morocco, as follows. The causative intrusive rocks are generally granite, granite porphyry and quartz-monzonite. Common prograde mineral assemblages include: garnet-pyroxene-wollastonite, garnet-hedenbergitic pyroxene-vesuvianite-wollastonite, pyroxene-andradite garnet. Retrograde minerals are mainly epidote, actinolite, serpentine, muscovite, chlorite, fluorite and tremolite. The chief ore minerals, apart from molybdenite, are powellite, pyrrhotite, arsenopyrite, chalcopyrite, pyrite, sphalerite, magnetite and in some cases pitchblende. Amongst the largest Mo skarns mentioned by Einaudi et al. (1981) include Yangchiaachangtze in China (7 Mt with 0.5% MoS_2), Mount Tennyson

(New South Wales, Australia; about 7 Mt with 0.2% MoS_2) and Little Boulder Creek (Colorado, USA, labelled as very large and with 0.15% MoS_2).

6.8 Iron Skarns

The largest skarn deposits are the Fe skarns (Meinert et al. 2000). Iron skarns are mined for their magnetite content and although minor amounts of Cu, Co, Ni, and Au may be present, Fe is typically the only commodity recovered. Many deposits are very large (>500 million tons, >300 million tons contained Fe) and consist dominantly of magnetite with only minor silicate gangue. Some deposits contain significant amounts of Cu and are transitional to more typical Cu skarns. Meinert et al. (2000) distinguished calcic and magnesian Fe skarns.

Calcic Fe skarns tend to occur in oceanic island arcs and are associated with Fe-rich plutons intruded into limestone and volcanic wall rocks. Russian researchers, cited by Einaudi et al. (1981) distinguished magnetite calc-skarn, scapolite-albite-magnetite and Fe-Co skarn deposits. These skarns are found in island arc terranes such as those of the Urals, the Philippines, Japan, Cuba and northern Cordillera. The intrusive are generally dioritic, but also include gabbro and syenite. In some deposits, the amount of endoskarn may exceed exoskarn. The prograde skarn mineralogy consists dominantly of ferrosalite, salite, magnetite, grandite garnet, epidote and actinolite; all being iron-rich. The retrograde assemblage is dominated by amphibole, chlorite and ilvaite. Magnetite is the chief ore mineral and may be accompanied by varying quantities of chalcopyrite, cobaltite and pyrrhotite. Alteration of igneous rocks is common with widespread albite, orthoclase, and scapolite veins and replacements. In contrast, magnesian Fe skarns are associated with diverse plutons (granodiorite mostly) forming small stocks, dykes, breccia pipes and sills, in a variety of tectonic settings; the unifying feature is that they all form in dolomitic wall rocks. Calcic skarns magnetite deposits mentioned by Einaudi et al. (1981) include the Empire mine in Vancouver Island (Canada) and Larap in the Philippines.

Magnesian skarns are dominated by magnetite ores and tend to form in silicic monzogranite and granodiorite stocks and dykes of Cordilleran style orogenic belts (Einaudi et al. 1981). These skarns are especially common in dolomitic rocks. In magnesian skarns, the main skarn minerals, such as forsterite, diopside, periclase, talc, and serpentine, do not contain much iron; thus, the available iron in solution tends to form magnetite rather than andradite or hedenbergite. A typical magnesian skarn association is spinel-pyroxene-forsterite±calcite, with distinct zoning from the granite towards the marble front. Hydrothermal fluids of magnesian skarns can precipitate mineral phases containing both Sn and B (Einaudi et al. 1981). Borates are present in the innermost prograde magnetite-phlogopite zones, in which Sn occurs in magnetite or

borate minerals. However, the Sn content decreases with time as the fluid becomes more Fe-rich. In the final stage of acidic activity, Sn is released from the borates to precipitate cassiterite, as in the following reaction (Einaudi et al. 1981):

$$\underset{\text{Sn-bearing ludwigite}}{(Fe^{2+}, Mg)_2(Fe^{3+}, Sn^{4+})BO_5} + HF \rightarrow \underset{\text{fluoborite}}{Mg_3(BO_3)(F, OH)_3} + Fe_3O_4 + SnO_2$$

Stratiform magnetite orebodies of magnesian skarns can reach large sizes up to hundreds of m in thickness and several km in strike lengths (Einaudi et al. 1981). These large stratiform magnetite ores are found in Russia (Teya deposit with 144 Mt and 33% Fe, and the Sheregosh with 234 Mt and 35% Fe).

6.9 Iron, Au, Cu-Mo Skarns in the Yangzte (Chiangjiang) River Valley, China

In the middle-lower Yangtze (Chiangjiang) River valley, East China, there are numerous stratabound pyrite- and magnetite-rich and polymetallic skarns constituting a metallogenic belt that also includes porphyry and Kiruna-style magnetite deposits. The Yangzte River Valley metallogenic belt was described in detail by Pan and Dong (1999) and Mao et al. (2006). The polymetallic skarn deposits can be considered as Fe-dominated, Au-dominated and Cu-Mo skarns (Fig. 6.14). The Yangzte River valley metallogenic belt is situated on the northern margin of the Yangtze Craton (Figs. 6.13 and 6.14), where Palaeozoic lithostratigraphic successions overlie a metamorphic basement and comprise Cambrian and Ordovician siltstone, shale and dolomitic limestone, in turn overlain by clastic and dolomite rocks of Sinian and Silurian ages. During the Late Silurian and Devonian, uplift occurred with deposition of terrestrial thick successions including sandstone, conglomerate, coal and hematite-rich clastic rocks. The Carboniferous and Permian are characterised by a succession of littoral to shallow marine carbonate, with various intercalations of shales and clastic rocks (Mao et al. 2006). During the Lower-Mid Triassic, shallow marine to littoral carbonate beds and minor evaporites were again deposited, which culminated with terrestrial sandstone and coal seams. During the Triassic collision between the North China and the Yangzte cratons occurred, with the formation of a foreland basin. A series of fault-bound basins were then formed in the Jurassic-Cretaceous heralding a regime of extensional tectonics throughout the Lower-Mid Yangtze River valley, with lake- and swamp-facies sandstone, siltstone and shales, followed by volcanic and volcaniclastic rocks. This volcanism produced andesite, rhyolite, shoshonite and alkali basalt (Mao et al. 2006). In the upper Cretaceous and Neogene red bed clastic rocks with volcanic and evaporitic intercalations complete the local extension-dominated geological history. As is the case for the Au skarns, the Yangzte River Valley

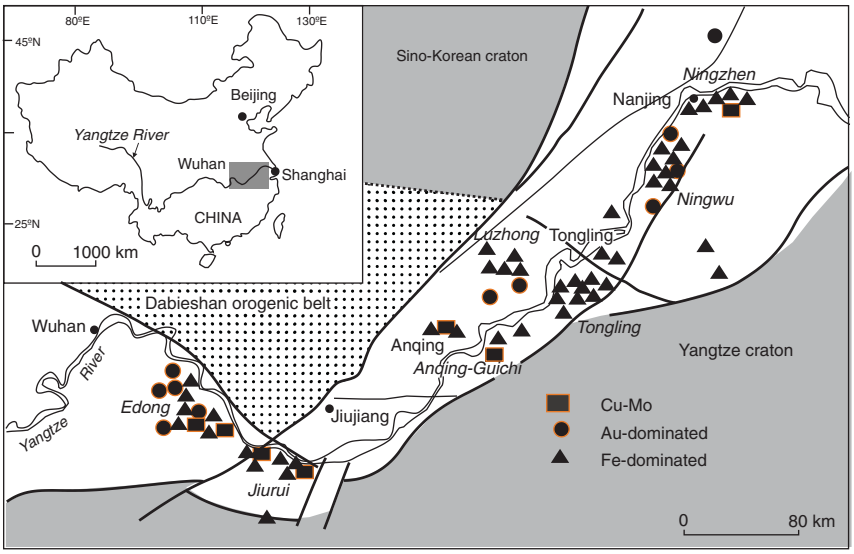


Fig. 6.14 Schematic representation of the Yangzte River Valley metallogenic belt at the boundary between the Yantze Craton and the Sino-Korean Craton of which the North China Craton is part (see also Fig. 6.13), and distribution of polymetallic skarn ore systems. After Pan and Dong (1999)

skarns are also related to phases of Yanshanian magmatism, dominated by I-type high K-calc-alkaline granitic rocks (gabbro, diorite, granodiorite), Na-rich calc-alkaline dioritic intrusions and A-type granites (Mao et al. 2006 and references therein). This magmatism in the region mainly developed in two stages, at 160–135 Ma with I-type intrusions and a later phase at about 120 Ma dominantly with A-type granitoids (Mao et al. 2006). These intrusions were emplaced during stages of extension and lithospheric delamination with upwellings of asthenospheric material, which resulted in the emplacement first of the I-type and later A-type granitoids. These intruded into above-mentioned thick carbonate sucessions of various ages, resulting in the widespread formation of skarn systems. Pan and Dong (1999) noted an apparent increase in alkalinity eastward, because large calc-alkaline granitic intrusions (Edong, Jiurui, Anqing-Guichi and Tongling) give way to sub-alkaline to alkaline volcanic and sub-volcanic complexes (Luzhong, Ningwu, Ningzhen) (Fig. 6.14), probably reflecting different levels of exposure.

The skarn systems of the Yangzte River Valley exhibit a range of ore styles, from disseminated to stratabound massive sulphides and magnetite. The Longgiao Fe deposit is a stratabound and stratiform magnetite skarn with a resource of approximately 100 Mt, grading 44% Fe (mine staff pers. comm. 2007). The ore zone extends for 2200 m, is associated with a 131 Ma syenitic intrusion and consists of pyroxene-magnetite ± epidote ± calcite skarns and magnetite bands

replacing a calcic sandstone (personal observations 2007). The Jiurui district (Fig. 6.14) contains thirteen Cu-Mo and Au skarn deposits all associated with stocks and dykes of granodiorite porphyry, diorite, quartz-porphyry and monzogranite. The diorite and granodiorite porphyry have K-Ar ages of 135–205 Ma (early Yanshanian), whereas the quartz porphyries are younger with ages ranging from 120 to 98 Ma (Pan and Dong 1999). The ore systems in the Juirui district include porphyry, stratabound ores and skarns. The latter are developed at the contact between the intrusions and Carbonifeorus-Triassic carbonate successions. The skarn ores contain chalcopyrite, pyrite, marcasites, bornite, magnetite, molybdenite, chalcocite, native Au, galena and sphalerite. The skarn rocks exhibit a well-developed zonation from endoskarn in the causative intrusion to exoskarns with andradite garnet, diopside, actinolite-tremolite, wollastonite, calcite, epidote, talc and serpentine and silicified marble outward from the intrusion. In the Anqing-Guichi Cu-Fe-Au-Mo district (Fig. 6.14) are small stocks of diorite, granodiorite anad alkali-rich granite with K-Ar ages ranging from 118 to 138 Ma (Pan and Dong 1999). Here the main deposits are stratabound massive sulphides hosted in Carboniferous carbonate rocks. The Tongling Cu-Au district contains 45 deposits.One of these is the interesting ore system at Dongguashan, where skarn-hosted magnetite and sulphides (pyrite + chalcopyrite + pyrrhotite) almost entirely surround and cap a dioritic cupola. These skarns formed in Carboniferous and Devonian dolomites and limestones, which along the Carboniferous-Devonian boundary developed retrograde wriggly-type skarns (Mao JW pers. comm. 2007).

The Ningwu Fe ore district occurs along northeast and northeast-trending volcano-sedimentary basin structures. Volcanic and sub-volcanic rocks are present and consist of alkaline basalt, andesite, trachytes, dacite and phonolite, gabbro-diorite, gabbro, diorite, monzonite all with well developed porphyritic textures and with K-Ar ages ranging from 137 to 90 Ma (Pan and Dong 1999). Iron ores are sited in the middle to upper parts of sub-volcanic gabbro-diorite intrusions and the skarn ores consist of massive, banded and brecciated to disseminated magnetite, siderite, hematite, pholgopite, actinolite, apatite, albite, chlorite, quartz and carbonate. Other Fe ores (magnetite-hematite) are located in fractures and faults in the aureoles of the intrusions. Hydrothermal alteration is extensive and mainly represented by scapolite and albite. Alteration zoning is characterised by albite-pyroxene-sericite-pyrite-titanite in the lower parts of the subvolcanic intrusion to a middle zone of diopside-garnet-apatite-scapolite-magnetite to an upper zone of argillic and propylitic alteration. The Fe skarns are lenticular and located at the contact between the sub-vocanic intrusions and Triassic calcareous shale and gypsum-bearing carbonates.

Pan and Dong (1999) compiled an extensive dataset of stable isotope analyses (S, O, C). Sulphur isotopic compositions show $\delta^{34}S$ values of –0.9–8.7‰ in sulphides from the Yanshanian intrusive rocks and from –1.0 to 8‰ in sulphides from the skarn ores, indistinguishable from the host intrusions and indicating a dominantly magmatic sulphur in the orebodies. The $\delta^{34}S$ values

of pyrite from individual deposits show systematic variations from proximal (2.3–4.1‰) to distal (9.9‰) skarns and up to 16‰ in the stratabound massive sulphide ores. Strongly negative $\delta^{34}S$ values (–35 to –15‰) are recorded from the Mesozoic sedimentary rocks.

6.10 The Geodynamic Setting of Skarn (and Porphyry) Metallogenesis in China

Mesozoic-Cenozoic intraplate tectonism and magmatism affected much of the eastern margin of mainland Asia, extending from Far East Russia, through the Baikal and Mongolia regions, to north-eastern and eastern China. These phenomena are broadly linked with a complex series of events, involving subduction, collision, post-collision collapse and rifting. The Mesozoic (and Cenozoic) extensional tectonics of mainland China and the rest of eastern Asia are the surface expressions of shallow mantle dynamics in the region. These may relate to asthenospheric upwellings linked to lithospheric delamination in response to rifting following collision between Siberia and Mongolia-North China (Jurassic-Cretaceous) and subduction systems in the western Pacific (Cenozoic) (Barry and Kent 1998). In eastern China this is the extensive and dominantly Cretaceous Yanshanian tectono-thermal event that affected a large region extending for about 1000 km inland from the coastal areas. This event produced vast amounts of granitic intrusions that invaded Palaeozoic shallow-water dolomitic and limestone strata and resulting in widespread porphyry (see Chapter 5), Au and Fe skarn systems. I return to this topic in Chapter 9 when discussing orogenic Au lodes in eastern China.

Chen et al. (2007) proposed that the space-time relationships of the skarn Au systems in China are more consistent with the geodynamics of post-orogenic extensional collapse that commonly follows collision tectonics.

In northwestern China, the Paleoasian Ocean closed at the end of the Early Carboniferous (>322.8 Ma), and was followed by collision between the Siberian (or Angara Craton) and Tarim-North China Plates. According to Jahn et al. (2000) and Zhang et al. (2003), peraluminous granites are intruded by K-rich granites, with ages clustering between 300 and 260 Ma, followed by A-type granites of ~260 Ma. These K-rich granitoids and shoshonitic volcanic rocks were probably developed in a regime of decompression and increasing geothermal gradient; with the A-type granites probably marking the end of collision, because they are overlain by Late Permian basalts and coal-bearing strata (Zhang et al. 2003). Hence, the magmatism and associated skarn Au deposits in northwestern China most probably formed in a regime of decompression and increasing geothermal gradient, during the transition from collisional shortening to extension.

In the western portion of the Central China Orogen (Kunlun-West Qinling orogenic belts), skarn deposits are hosted in Triassic strata deposited in a

foreland basin, on south side of the north-dipping Maqu-Mian-Lue Fault (Fig. 6.13) interpreted as the suture derived from an oceanic closure. This setting rules out the possibility of relating skarnst and associated intrusions to north-directed oceanic subduction.

Age data for the Yulong porphyry system (Chapter 5) show that granitic magmatism and metallogenesis postdated the onset of the collision between the Lhasa and Qiangtang-Indochina blocks. Here too magmatism is K-rich and includes rocks of shoshonitic affinity (Rui et al. 1984). The dextral strike-slip Jinshajiang-Red River fault-systems (Yin and Nie 1996; Harrison et al. 1996) may have facilitated the emplacement of these shoshonitic intrusions. The India-Eurasia collision began between 66 and 50 Ma (Yin and Nie 1996). Immediately south of the Indus-Yalong suture (Himalaya Orogen), there are peraluminous leucogranites and coeval Sn deposits, yielding isotopic ages ranging from 22 to 8 Ma, peaking at 15.5 Ma (Yang and Jin 2001), whereas porphyries and associated Cu-Au deposits of the Gangdise metallogenic belt (Section 5.2.2.4) are present north of the suture (Lhasa Block in Fig. 6.13) and yield isotope ages ranging ca. 17–15 Ma (Rui et al. 2003).

As the southeastern portion of Eurasia continent, East China was affected by the Eurasia-Pacific interaction. This has led many geologists (Quan et al. 1992; Zhao et al. 1999) to consider that East China is part of the Circum-Pacific metallogenic belt, and consequently the Mesozoic magmatism and metallogenesis of the East China region may be associated with the northwestward subduction of the Pacific plate beneath the Eurasia plate. However, this relationship is not consistent with: (1) large-scale metallogenesis and granitic magmatism in East China, which occurred during the Yanshanian and peaked around 130 Ma, contrasting in time with the Cenozoic metallogenesis that took place in Korea, Japan, Taiwan and other islands in western Pacific Ocean; (2) important metallogenic provinces, such as the Yan Shan, Lower Yangtze River region, southern China, East Qinling (Mo, Au, Ag; see Section 5.2.2.3) and Jiaodong (Au) (Chen et al. 2004), all trend perpendicular, and not parallel to the Mesozoic and present-day trenches (Sengör and Natal'in 1996).

All of these features confirm that the Yanshanian granitic magmatism and related metallogenesis in East China probably occurred in a geodynamic regime of post-orogenic extension. The continental collisions in East China began in Permo-Triassic times along the Solonker suture, followed by Triassic continental collisions to the south, and the Early Jurassic Dongnanya-Eurasia collision. During this sequence of collisional events, the whole of East China was subjected to strong compression, which resulted in the development of peraluminous granites. In the subsequent period from 180 Ma to 98 Ma, no significant collisions occurred and the geodynamic conditions involved a change to an extensional regime. Fluid generation and hydrothermal metallogeny, including skarn-type mineralisation, occurred between 180 and 98 Ma, and peaked around 120–130 Ma.

A model that could explain the post-orogenic extensional metallogenesis of the Mesozoic skarn systems in China is lithospheric delamination and

asthenospheric upwelling, as already mentioned in Sections 5.2.2.3 and 5.2.2.4 (see also Chapter 3). The thermo-tectonic evolution of the lithospheric mantle beneath eastern China between the Ordovician and present day is envisaged to have resulted from lithospheric extension, delamination and asthenospheric upwelling, with the possibility of deep mantle plumes being ruled out, given the nature of the volcanism (diffuse and alkaline) in the region. The onset of this lithospheric extension can be linked to the Triassic collision between the North China block (part of the Sino-Korean Craton) and the Yangzte Block, along the Qinling orogenic belt (Xu, 2001) and the collision of the North China block in the Jurassic-Cretaceous with the Siberian Craton (Wang et al. 2006). Lithospheric thermal weakening and erosion proceed as a result of conductive heating by the upwelling asthenosphere. Importantly, this asthenospheric upwelling was most likely affected by the existing lithospheric and lower crustal heterogeneities, with the result that the flow of hot mantle was preferentially channelled along major discontinuities and lithospheric breaks, such as the Tan-Lu fault and tectonic boundaries (Fig. 6.15). The tectonic boundary between the North China and the Yangzte Cratons is an important crustal break, which is where an abundance of skarn systems, as well as other deposit types, are found, thus explaining the observation made by Chen and co-workers of the perpendicularity of Mesozoic-Cenozoic magmatic products and ore systems in relation to the subducting plates of the Pacific Ocean beneath the east Asian margins. Figure 6.15 shows assumed paths of asthenospheric melts channelled along crustal breaks.

The 210–90 Ma Yanshanian tectono-thermal event is part of and a manifestation of the above-mentioned intraplate geodynamic evolution and is characterised by a range of intrusives from gabbro to granitic rocks, including A-type alkaline rocks and Basin-and-Range style rifting with volcano-sedimentary basins (Shanxi Rift System). Volcanic rocks are bimodal in composition but dominated by alkali basalt. Intrusive activity particularly affected regions along major zones of weakness, such as the boundaries between the North and South China Cratons and the North China and Siberian Cratons, and the above-metnioned crustal-scale north-northeast-trending Tan Lu Fault (Fig. 6.15).

Wang et al. (2006) linked the nature of Mesozoic magmatism in northeastern China (Great Xing'an range) with a geodynamic scenario spanning the Jurassic-Cretaceous. They recorded an age progression from 160 to 140 Ma, 130–120, ~100 to ~80 Ma, from the northeast China interior towards Japan and attribute it to retreat and delamination of the subducting slab, with upwelling of asthenospheric mantle under each window created by each slab retreat. It may be that metallogenesis, both for porphyry and skarn systems, was related to this regime of delamination tectonics and mantle upwelling and extension, during which magmatism and large scale flow of hydrothermal fluids occurred. The geodynamics of mantle upwelling and lithospheric extension created a favourable environment for the development of granitic magmas and the generation of hydrothermal fluids.

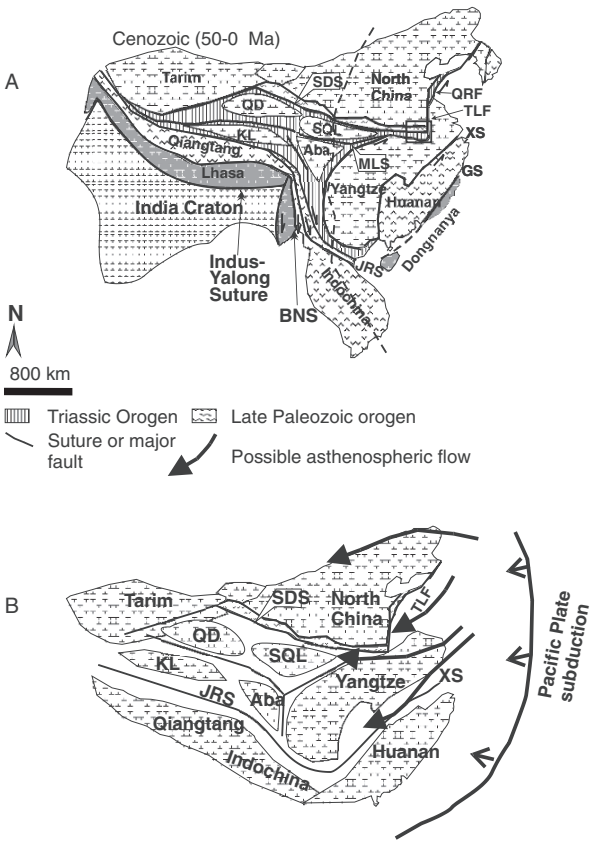


Fig. 6.15 (**A**) cartoon schematically depicting the major tectonic units of mainland China; after Chen et al. (2007); (**B**) shows exaggerated breaks between the various tectonic units and the flow paths that asthenospheric melts may have followed, westward and northeastward along the structural breaks provided by the boundaries between the tectonic units. BNS Bangong-Nujiang suture, GS Gunanhai suture, JRS Jinshanjiang-Red River fault, KL Kunlun terrane, MLS Mian-Lue suture, QD Qiadam Block, SDS Shang-Dan suture, SQL, Southern Qinling terrane, TLF Tan-Lu fault, XS Xiangganzhe suture

6.11 Concluding Remarks

Skarn systems form in any rock type so long as these are affected by thermal metamorphism associated with igneous intrusions or high temperature regional metanorphism, although economic skarns are usually formed in carbonate rocks. The development of skarns involves extensive metasomatic processes that results in complex calc-silicate mineralogical assemblages, exhibiting distinct zoning, from endoskarns (within the margins of the intrusion), progressively to proximal and distal, generally reflecting variations due to decreasing temperature away from the intrusive contacts. Retrograde alteration commonly overprints the primary zoning and is related to the influx of meteoric fluids. As discussed in this chapter, skarns can be distinguished on the basis of their dominant metals (Fe, Au, Cu, Zn, W, Mo and Sn). The Chinese skarns present an interesting case of polymetallic and complex ore systems that exhibit a variety of styles including disseminated, breccias and stratabound massive magnetite and sulphides. These are intimately associated with granitic plutons

in which endoskarns are developed that commonly seem to merge with porphyry style mineralisation so that, in places it is difficult to decide whether the mineral system is a porphyry or an endoskarn. To add to these uncertainties are the stratabound massive magnetite lenses, which in some cases bear resemblance to Kiruna-style mineralisation. The mineral systems of the Qinling Orogen and the Yangzte River Valley present cases in which the distinction between porphyry, endoskarn, intrusion-related and even IOCG mineral system types is somewhat blurred. In all cases, however, these mineral systems are linked to mantle upwellings and associated development of granitic magmatism. These are related to a complex interaction of delamination and subduction tectonics linked to subduction of the Pacific plate beneath the east Asian continental margin. The Chinese skarn systems highlight the variability of tectonic settings in which skarns may be developed.

References

Atkinson WW, Einaudi MT (1978) Skarn formation and mineralization in the contact aureole at Carr Fork, Bingham, Utah. Econ Geol 3:1326–1365

Barry TL, Kent RW (1998) Cenozoic magmatism in Mongolia and the origin of central and east Asian basalts. Am Geophys Union, Geodyn Ser 27:347–364

Brown PE, Bowman JR, Kelly WC (1985) Petrologic and stable isotope constraints on the source and evolution of skarn-froming fluids at Pine Creek, California. Econ Geol 80:72–95

Cawood PA, Tyler IM (2004) Assembling and reactivating the Proterozoic Capricron Orogen: lithotectonic elements, orogenies and significance. Precambr Res 128:201–218

Chen YJ, Pirajno F, Sui YH (2004) Isotope geochemistry of the Tieluping silver-lead deposit, Henan, China: A case study of orogenic silver-dominated deposits and related tectonic setting. Mineral Depos 39:560–575

Chen YJ, Chen HY, Zaw K, Pirajno F, Zhang ZJ (2007) Geodynamic settings and tectonic model of skarn gold deposits in China: an overview. Ore Geol Rev 31:139–169

Davies BM (1998) Proterozoic zoned tungsten-bearing skarns and associated intrusives of the northwest Gascoyne Complex, Western Australia. Geol Sur West Aus Rpt 53

Davis GA, Qian XL, Zheng YD, Tong HM, Wang C, Gehrels GE, Shafiquallah M, Fryxell J (1996) Mesozoic deformation and plutonism in the Yunmeng Shan: a metamorphic core complex north of Beijing, China. In: Yin A, Harrison TM (eds) The tectonic evolution of Asia. Cambridge University Press, Cambridge, pp 253–280

Dick LA, Hogson CJ (1982) The MacTung W-Cu (Zn) contact metasomatic and related deposits of the Northeastern Cordillera. Econ Geol 77:845–867

Einaudi MT (1982a) Description of skarns associated with porphyry copper plutons. In: Titley SR (ed) Advances in geology of the porphyry copper deposits, southwestern North America. University of Arizona Press, Tucson, pp 139–184

Einaudi MT (1982b) General features and origin of skarns associated with porphyry copper plutons. In Titley SR (ed) Advances in geology of the porphyry copper deposits, southwestern North America. University of Arizona Press, Tucson, pp 185–209

Einaudi MT, Burt DM (eds) (1982) A special issue devoted to skarn deposits – Introduction, terminology, classification and composition of skarn deposits. Econ Geol 77:4

Einaudi MT, Meinert LD, Newberry RJ (1981) Skarn deposits. Econ Geol 75th Anniv Vol, pp 317–391

Gray DR, Foster DA, Goscombe B, Passchier CW, Trouw RAJ (2006) $^{40}Ar/^{39}Ar$ thermochronology of the Pan-African Damara Orogen, Namibia, with implications for tectonothermal and geodynamic evolution. Precambr Res 150:49–72

Harrison TM, Leloup PH, Ryerson FJ, Tapponnier P, Lacassin R, Chen WJ (1996) Diachronous initiation of transtension along the Ailaoshan-Red River shear zone, Yunnan and Vietnam. In: Yin A, Harrison TM (eds) The Tectonic Evolution of Asia. Cambridge University Press, Cambridge, pp 208–226

Hoffman PF, Kaufman AJ, Halverson GP, Schrag DP (1998) A Neoproterozoic snowball earth. Science 281:342–1346

Jacob RE, Moore JM, Armstrong RA (2001) Zircon and titanite age determinations from igneous rocks in the Karibib district, Namibia: implications for Navachab vein-style gold mineralization. Communs Geol Surv Namibia 12:157–166

Jahn B, Wu F, Chen B (2000) Massive granitoid generation in Central Asia: Nd isotope evidence and implication for continental growth in the Phanerozoic. Episodes 23:82–92

Johnson SD, Poujol M, Kisters AFM (2006) Constraining the timing and migration of collisional tectonics in the Damara Belt, Namibia: U-Pb zircon ages for the syntectonic Salem-type Stinkbank granite. S Afr J Geol 109:611–624

Kisters AFM (2005) Controls of gold-quartz vein formation during regional folding in amphibolite-facies, marble dominated metasediments of the Navachab gold mine in the Pan-African Damara belt, Namibia. S Afr J Geol 108:365–380

Kwak TAP (1987) W-Sn skarn deposits and related metamorphic skarns and granitoids. Developments in economic geology 24. Elsevier, Amsterdam, 415p

Kwak TAP, Askins PW (1981) Geology and genesis of the F-Sn-W (Be-Zn) skarn (wrigglite) at Moina, Tasmania. Econ Geol 76:439–467

Kwak TAP, Tan TH (1981) The geochemistry of zoning in skarn minerals at the King Island (Dolphin) mine. Econ Geol 76:468–497

Lanier G, John EC, Swanson AJ, Reid A, Bard CE, Caddey SW, Wilson JC, (1978) General geology of the Bingham mine, Bingham Canyon, Utah. Econ Geol 73:1228–1241

Laznicka P (2006) Giant metallic deposits – future resources of industrial minerals. Springer, New York

Mao JW, Wang YT, Lehmann B, Yu JJ, Du A, Mei YX, Li YF, Zang WS, Stein HJ (2006) Molybdenite Re-Os and albite 40Ar/39Ar dating of Cu-Au-Mo and magnetite porphyry systems in the Yangzte River avlley and metallogenic implications. Ore Geol Rev 29:307–324

Mathieson GA, Clark AH (1984) The CanTung E Zone scheelite skarn orebody, Tungsten, Northwest Territories. A revised genetic model. Econ Geol 79:883–901

Meinert LD (1989) Gold skarn deposits – geology and exploration criteria. Econ Geol Monogr 6:537–552

Meinert LD (1992) Skarns and skarn deposits. Geoscie Can 19:145–162

Meinert LD (1993) Igneous petrogenesis and skarn deposits. Geol Ass Can Spec Pap 40:569–583

Meinert LD (1998) A review of skarns that contan gold. Miner Assoc Can Short Cour 26:359–414

Meinert LD (2000) Gold skarns related to epizonal plutons. Rev Econ Geol v 13:347–375

Meinert LD, Lentz DR, Newberry RJ (eds) (2000) A special issue devoted to skarn deposits. Econ Geol 95:6

Meinert LD, Dipple GM, Nicolescu S (2005) World skarn deposits. Econ Geol 100th Ann Vol: 299–336

Miller McGR (1983) (ed) Evolution of the Damara orogen of South West Africa/Namibia. Geol Soc S Afr Spec Publ 11

Mueller AG, Groves DI (1991) The classification of Westen Australian greenstone-hosted gold deposits, according to wallrock alteration assemblages. Ore Geol Rev 6:291–331

Newberry RJ (1991) Scheelite-bearing skarns in the Sierra Nevada region, California. Contrasts in zoning and mineral compositions and tests of the infiltration metasomatism theory. In Barto-Kyriakidis (ed) Skarns – their genesis and metallogeny, Theophrastus Publ, Athens pp 343–384
Newberry RJ (1998) W- and Sn-skarn deposits: a 1998 status report. Miner Ass Can Short Course Ser 26:289–335
Nörtemann MFJ, Mücke A, Weber K, Meinert LD (2001) Mineralogy of the Navachab skarn deposit, Namibia: an unusual Au-bearing skarn in high-grade metamorphic rocks. Communs Geol Surv Namibia 12:149–156
Occhipinti SA, Sheppard S, Pascschier C, tyler IM, Nelson DR (2004) Palaeoproterozoic crsutal accretion and collision in the southern Capricorn orogen: the Glenburgh Orogeny. Precambr Res 128:237–256
Pan Y, Dong P (1999) The lower Chanjiang (Yangzi/Yangzte River) metallogenic belt, East China: intrusion- and wall rock-hosted Cu-Fe-Au, Mo, Zn, Pb and Ag deposits. Ore Geol Rev 15:177–242
Pirajno F (2000) Ore deposits and mantle plumes. Kluwer Academic Publishers, Dordrecht
Pirajno F (2004) Metallogeny in the Capricorn Orogen, Western Australia, the result of multiple ore-forming processes. Precambr Res 128:411–440
Pirajno F, Jacob RE, Petzel VFW (1991) Distal skarn-type gold mineralization in the central zone of the Damara Orogen, Namibia. Proc Brazil Gold'91, Ladeira EA (ed), pp 95–100
Quan H, Han QY, Ai YF, Lin YC, Wei JY (1992) The Features and prospects of metallogenesis of polymetals, Gold and Silver in Yan-Liao Area of China. Geol Publ House, Beijing, 134p (in Chinese)
Reid JE (1978) Skarn alteration of the commercial limestone, Carr Fork area, Bingham, Utah. Econ Geol 73:1315–1325
Rui ZY, Huang CK, Qi GM, Xu J, Zhang HT (1984) Porphyry Copper (Molybdenum) Deposits of China. Geol Publ House, Beijing, 350p (in Chinese with English abstract)
Rui ZY, Hou ZQ, Qu XM, Zhang LS, Wang LS, Liu YL (2003). Metallogenic epoch of Gangdise porphyry copper belt and uplift of Qinghai-Tibet Plateau. Mineral Depo 22:217–225 (in Chinese with English abstract)
Sawkins FJ (1990) Metal deposits in relation to plate tectonics, 2nd edn. Springer, Berlin
Sengör AMC, Natal'in BA (1996). Paleotectonics of Asia: fragments of synthesis. In: Yin A, Harrison TM (eds) The tectonic evolution of Asia. Cambridge University Press, Cambridge, pp 486–640
Sheppard S, Occhipinti SA, Tyler IM (2004) A 2005-1970 Ma Andean-type batholith in the southern Gascoyne Complex, Western Australia. Precambr Res 128:257–278
Sheppard S, Occhipinti SA, Nelson DR (2005) Intracontinental reworking in the Capricorn Orogen, Western Australia: the 1680-1620 Ma Mangaroon Orogeny. Aust J Earth Sci 52:443–460
Smirnov VI (1976) Geology of mineral deposits. MIR, Moscow
Solomon M, Walshe JL, Eastoe CJ (eds) (1981) An issue on the geology and mineral deposits of Tasmania. Econ Geol 76:2
Solomon M, Groves DI (1994) The geology and origin of Australia's mineral deposits. Clarendon Press, Oxford
Törnebohm AE (1875) Geognostic beskrifning ofver Persbergets Grufvefält. Sverige Geol Undersökning, Norstedt and Sons, Stockholm
Wang F, Zhou XH, Zhang LC, Ying JF, Zhang YT, Wu FY, Zhu RX (2006) Late Mesozoic volcanism in the Great Xing'an Range (NE China): timing and implications for the dynamic setting of NE Asia. Earth Planet Sci Lett 251:179–198
Xu J, Zhu G (1994) Tectonic models of the Tan-lu fault zone, eastern China. Int Geol Rev 36:771–784
Xu YG (2001) Thermo-tectonic destruction of the Archaean lithospheric keel beneath the Sino-Korean Craton in China: evidence, timing and mechanism. Phys Chem of the Earth 26:747–757

Yang XS, Jin ZM (2001) Studies on Rb-Sr and Sm-Nd isotope of Yadong leucogranite in Tibet: constraint on its age and source material. Geol Rev 47:300–307 (in Chinese with English abstract)

Yin A, Nie SY (1996) A Phanerozoic paliinspastic reconstruction of China and its neighboring regions. In: Yin A, Harrison TM (eds) The tectonic evolution of Asia. Cambridge University Press, Cambridge, pp 442–485

Zhang ZJ, Chen YJ, Chen HY, Bao JX, Liu YL (2003) The petrochemical characteristics of the Hercynian granitoids in Tianshan and its geodynamic implications. J Mineral Petro l23:15–24 (in Chinese with English abstract)

Zhao YM, Zhang YN, Bi CS (1999) Geology of gold-bearing skarn deposits in the middle and lower Yangtze River Valley and adjacent regions. Ore Geol Rev 14:227–249

Chapter 7
Submarine Hydrothermal Mineral Systems

7.1 Introduction

Present-day, active submarine hydrothermal effluents, at spreading centres (mid-ocean ridges) and in oceanic volcanic arcs and back-arcs, are of considerable interest because they provide a window into ore systems of the ancient geological record that are interpreted to have originated from submarine fluids venting. A wide range of volcanogenic, volcanic-associated or volcanic-hosted massive sulphide deposits, commonly known as VMS or VHMS, as for example the giant ore deposits of the Iberian belt, Cyprus, the Japanese Kuroko deposits and the Archaean Canadian Noranda- or Abitibi-type deposits and similar style ore systems in the very ancient ($\sim$3.25 Ga) geological record of the Pilbara Craton in Western Australia, are all explained by models of submarine venting at spreading centres, arc or back-arc rift settings.

Since the 1960s, exploration and research activity on the mid-ocean ridges in the Pacific and Atlantic oceans has led to the discovery of numerous hot spring systems, many of which produced, and still do, ore grade mineralisation. The first discovery and retrieval of hydrothermal material from a seamount located off the axis of the East Pacific Rise (EPR) was reported in 1966. In 1972 the first submarine hydrothermal field was discovered in the mid-Atlantic ridge by the NOAA Trans-Atlantic Geotraverse project (TAG), while the first direct observation of active hydrothermal vents and the discovery of new biological communities and ecosystems, associated with the deep-sea hot spring environment were made in 1977 by the crews of the ALVIN submersible. Mounds of massive sulphide deposits were observed and sampled by an international team of geoscientists using the submersible CYANA at the East Pacific Rise (EPR) near 21°N latitude. As a result of these and subsequent exciting discoveries made during many dives in the following years and continuing today, our knowledge of seafloor spreading, magmatic, hydrothermal and biological processes and ore genesis has increased considerably. Thus, in the last 25 years a great deal of research on seafloor hydrothermal systems has been carried out and published in single papers, collection of papers and books. Here I cite landmark papers by Bonatti (1975, 1978), Rona (1986, 1988, 2003), Rona et al. (1983). The collection of papers by Humphris et al. (1995a) and Parson et al.

F. Pirajno, *Hydrothermal Processes and Mineral Systems*,

© Springer Science+Business Media B.V. 2009

(1995) cover most aspects of seafloor hydrothermal activity. An excellent review encompassing submarine magmatism and seafloor volcanic activity, hydrothermal systems and aspects of microbial life and microfauna was presented by Kelley et al. (2002), to whom I refer on several occasions in this chapter and in Chapter 10. A more recent overview is provided by Hannington et al. (2005). Published volumes, detailing 40 years of research and discovery in the subject of marine geology, arising from ocean drilling programs are available from http://www-odp.tamu.edu/publications and http://www.deepseadrilling.org (accessed April 2008).

An understanding of the nature, composition and structure of the oceanic lithosphere has been largely obtained from a variety of geophysical techniques (see overview by Pratson and Haxby 1997). Satellite radar imaging measures variations in the elevation of the water at the surface of oceans, reflecting minute differences in the Earth's gravity, which cause the sea surface to have sea-surface height variations by up to 200 m. Beautiful global maps of the oceans showing, relative to scale, the detailed topography of the ocean floors, are produced by means of these measurements from orbiting satellites. Profiles of the seafloor and the construction of bathymetric charts are obtained by the use of single and multibeam echo sounding. The side-scan sonar imaging system, in conjunction with the multibeam echo sounding, provided images of the ocean floor and its main structural features. Cross-sections of the oceanic layers are obtained from refraction and reflection seismic surveys. Small variations in the shape of the ocean surfaces in relation to the geoid (surface of equal gravity) are determined by the topography of the floor, as the force of gravity gives the geoid undulations, which correspond to topographic highs and lows of the ocean floor. This radar survey filters out the effects of the motions of the sea, caused by currents, wave actions, barometric pressure etc. Light scattering measurements have been succesfully employed for the detection of hydrothermal plumes in the Kermaded volcanic arc. Suggested literature for the reader who is interested in marine geology and details of the seafloor and the evolution of ocean basins includes Kennett (1982) and Seibold and Berger (1982).

The use of both manned and unmanned submersible crafts has furnished geoscientists with direct observations of the seafloor and its geological phenomena, particularly the discharge of hot springs in the axial regions of mid-ocean ridges. Deep sea drilling has also contributed much to a growing database, where probing hundreds of metres into the seafloor has provided geological records that could be compared with that of on-land oceanic sequences. However, the most complete lithological and stratigraphic successions are still obtained from oceanic sequences tectonically emplaced on-land that is ophiolite complexes. Accordingly, for a more complete understanding of igneous and metamorphic processes and the products of hydrothermal activity in oceanic environments, in this chapter I include a discussion on ophiolitic rocks.

In this chapter I focus on two aspects of submarine hydrothermal systems. In the first a review present-day active systems is presented, in the second ore systems in the geological record that were derived from the same processes are

described. Thus, following a brief review of the main physiographic features of the ocean floor and the nature and structure of the oceanic lithosphere, I examine the hydrothermal processes that take place as a result of sea water interaction with magmatic systems in large sectors of the oceanic crust in the oceanic regions and the mineral deposits that result from this activity in the present-day seafloor. Excluded from this section are the hydrogenous seafloor deposits of Mn-rich nodules, which are believed to form by direct precipitation of metals from sea water, although the metal components are possibly derived from the hot springs that issue at mid-ocean ridges, and are subsequently dispersed in sea water. The reader is reminded that there are transitions from incipient rifts, which may initially form a narrow sea way, as exemplified by the Red Sea, where present-day hydrothermal discharge occurs at several sites resulting in syngenetic metalliferous sediments, discussed in Chapter 8, to mid-ocean ridge seafloor systems. The presence of oceanic crust in these early stages of opening of a rift is confined to narrow strips, or it has not yet made its appearance on the seafloor. I take up this topic later (Section 7.3) when discussing the development and closure of an ocean basin. A possible example, in the geological recors, of an intermediate stage of rifting with development of seafloor spreading is provided by the Matchless Amphibolite Belt in the Damara Orogen (Namibia) to be described in Section 7.6.3. Modern volcanic-associated massive sulphide deposits (VMS) form in back arc basins of two types, intraoceanic, such as the Lau back-arc basin and the Eastern Manus basin, and intracontinental, such as the Okinawa Trough. I then describe VMS from the geological record. The equivalents in the ancient geological record are the Pb-rich Kuroko systems, typically found in Japan, and the Zn–Cu-rich Archaean Abitibi or Noranda-type. There is a tendency for the VMS to exhibit a time bias with the Abitibi or Noranda time being more common in the Archaean-Palaeoproterozoic and the Kuroko type, being more common in the Phanerozoic (see Chapter 3).

7.2 Physiography of the Ocean Floor

A typical profile of the ocean floor, for example across the Atlantic ocean, clearly shows at least three principal elements in the morphology of this oceanic area, namely: continental margins, comprising a continental shelf, slope and rise; the abyssal plains; and the mid-ocean ridge (MOR). The continental margins of the Atlantic Ocean are called Atlantic-type, or aseismic or passive margins, developed initially from the rifting of a continental mass. The Red Sea represents the early stages in the making of an ocean, in which the sea has invaded the opening created by the rifting of a continent. A profile across the Pacific Ocean shows a rather different picture in which some new physiographic elements can be seen. The Pacific margins, which are of the active type and very much seismic, indicate on-going subduction-related tectonic and magmatic activity, which is topographically expressed by deep submarine trenches and

festoons of volcanic islands. The collision of oceanic and continental plates in the Pacific gives rise to Chilean-type margins, whereas collision of two oceanic plates gives rise to the Mariana- or Kermadec-type margins. Other important physiographic features to be found in all oceans are transform faults, fracture zones and seamounts. Together with the mid-ocean ridges, they constitute very important areas for hydrothermal systems and ore-making processes, owing to their permeability which allows the ingress of large amounts of sea water, and for associated magmatic activity that provides the heat source for the convective circulation of sea water. In addition to the above features, the ocean basins also contain oceanic plateaux, representing vast submarine fields of mafic and to a lesser extent silicic lavas, derived from the impingment of mantle plumes. Oceanic plateaux constitute Large Igneous Provinces (LIP) and are the oceanic equivalent of continental flood basalts (CFB). Examples of oceanic plateaux are Ontong Java-Manihiki-Hikurangi plateau system in the Pacific Ocean (Taylor 2006) and the Kerguelen plateau in the Indian Ocean (Wallace et al. 2002), which cover large areas of the ocean floor ($>2 \times 10^6$ km^2). Some of these oceanic plateaux constitute allochthonous terranes after they have accreted or obducted onto a continental margin. Examples are provided by Late Cretaceous Caribbean-Colombian igneous province along the coastal zone of Ecuador (Mamberti et al. 2003) and the Narracoota Formation, a fragment of an ancient ($\sim$2.0 Ga) plateau accreted onto the northwest margin of the Archaean Yilgarn Craton in Western Australia (Pirajno 2004).

7.2.1 Mid-Ocean Ridges

The most conspicuous topographic features of the ocean basins are the mid-ocean ridges, commonly referred to as MOR, (the word ridge, however, does not do justice to what is effectively the longest mountain range on planet Earth). MOR extend through all the oceans for a total length of approximately 75 000 km (Fig. 7.1) at an average depth of 2500 m below sea level, with widths of up to 1000 km and heights above the surrounding seafloor ranging from approximately 1000–3000 m. MOR usually occur in the middle part of an ocean basin (hence the adjective mid), except in the Pacific Ocean where they are for the most part confined to the northeast and eastern parts of the ocean basin. Only in one place does the mid-ocean ridge have a terrestrial expression, and that is Iceland, which straddles, and is part of, the mid-Atlantic ridge system. MOR are characterised by a highly rugged topography and are formed by a ridge crest and ridge flanks, which extend more or less symmetrically for hundreds of kilometres, on either side of the crest. Within the ridge crest a central rift valley, 1–2 km deep and up to 30–35 km wide, may occur. These median rift valleys are characterised by a series of inward-facing escarpments up to a few hundreds of metres high. The deepest part of a rift valley forms the inner floor, which is a flattish area where accumulation of lava flows takes

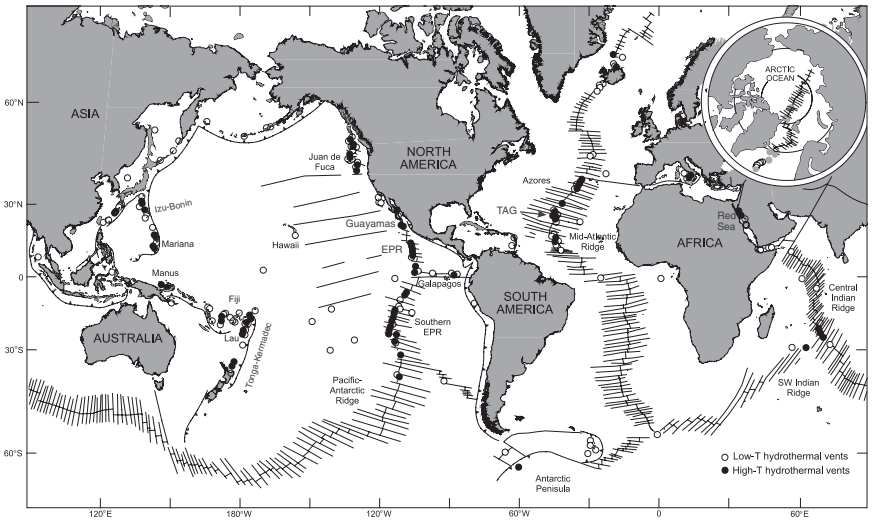


Fig. 7.1 Distribution of known submarine low and high-temperature hydrothermal systems, associated Fe-Mn, metalliferous sediments and polymetallic sulphide deposits. After Hannington et al. (2005)

place. However, the development of the rift valleys is a function of the rate of spreading. The mid-ocean ridge in the Atlantic has an average spreading rate of 1–2 cm yr^{-1} (slow-spreading centre) and the resulting median rift valleys are well developed and deep. By contrast, in the Pacific ocean where spreading rates are of the order of 5–8 cm yr^{-1} (e.g., East Pacific Rise fast-spreading centre), the resulting ridge profiles are smoother and much less rugged, and the median rift valley may be absent altogether (Fig. 7.2). Intermediate spreading centres have lower rates of magma supply and eruptions, deeper axial valleys than fast-spreading centres, as exemplified by the Juan de Fuca and Gorda ridges and the Galapagos Rift system. The MOR are seismically and volcanically active, particularly in the axial regions, which spreads apart as new crust is created by injections of magma. Most of the sub-seafloor hydrothermal discharges occur in the axial regions.

At mid-ocean spreading centres, new lithosphere is formed that consists of mafic material welled up from partially molten asthenosphere, and which forms magma chambers just below the spreading centre. This part of the lithosphere, or oceanic crust, consists of an uppermost layer of basaltic pillow lavas and associated pelagic sediments, underlain and intruded by sheeted dyke systems, passing downward into gabbroic, peridotitic, dunitic and harzburgitic rocks. Once the oceanic crust moves away from the ridge it is either consumed in a subduction zone, or it may be accreted to a continental margin. Accreted oceanic crust is known as ophiolite. This is a term of Greek derivation, meaning snake-rock because of the predominantly green colouration of ophiolitic rocks.

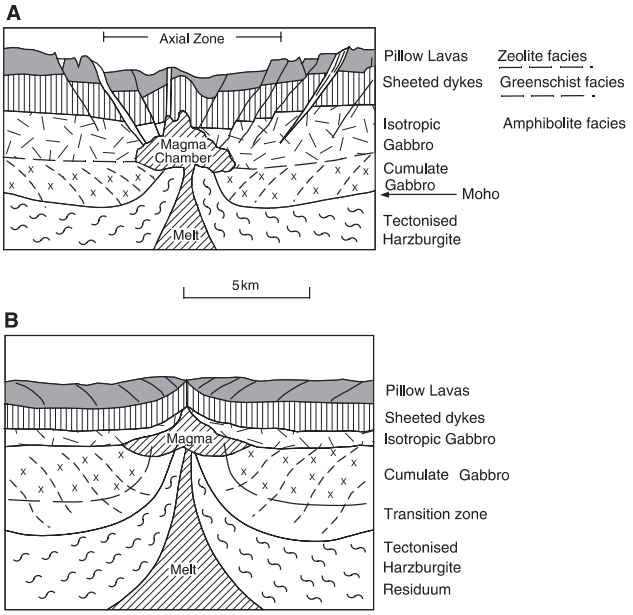


Fig. 7.2 Idealised cross-sections of (**A**) slow-spreading North Atlantic-type mid-ocean ridge and (**B**) a fast-spreading East Pacific type mid-ocean ridge (After Burke et al. 1981)

Serpentinite is the Latin-derived equivalent, but it does not necessarily imply ophiolite. Spreading centres also form in back arc or marginal basins in supra-subduction settings (a modern-day example is the Sea of Japan). Although geochemical discrimination has been attempted to differentiate between mid-ocean and back-arc spreading centres, the distinction in ancient systems is by no means clear. Typical cross-sections depicting oceanic crust are shown in Fig.7.3, bearing in mind that the overall structural configuration of a mid-ocean ridge system depends on the rates of spreading.

7.2.2 Transform Faults and Fracture Zones

The ocean floor is cut by numerous fracture zones which can be seen on modern oceanic maps as parallel lines that usually transect the mid-ocean ridges at right angles, thereby indicating the direction of seafloor spreading (see Fig. 7.1). The ridge axes are offset by transform faults, along which the lithospheric plates slide past each other. Transform faults terminate at the end of each offset spreading ridge, and beyond these points the fault becomes a fracture, as no slip movement occurs since the fracture is, by this stage, entirely situated in one plate. The transform faults therefore also mark plate boundaries, which together with their fracture zone extensions, form small circles centred on the

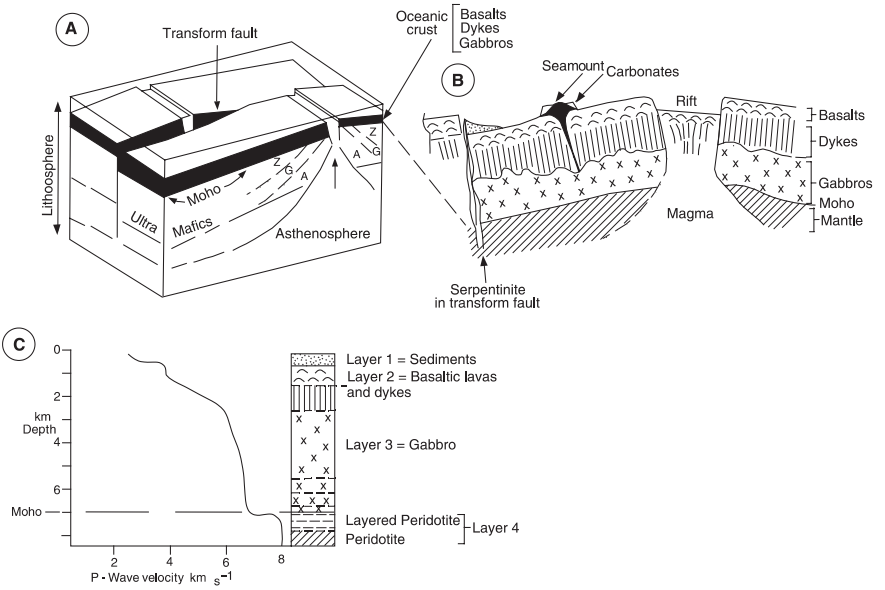


Fig. 7.3 Idealised cross-sections of oceanic lithosphere. (**A**) Block-diagram showing spreading centre and transform fault; A, G and Z indicate amphibolite, greenschist and zeolite facies respectively, with isograds shown by the dashed lines. (**B**) Detail of spreading ridge, section of oceanic crust with seamount and transform fault. A and B are after Burke et al. (1981). (**C**) Idealised stratigraphic column of oceanic lithosphere with corresponding velocity of P-waves. See text for details

rotation pole of the lithospheric plates. Fracture zones can extend from several hundreds of kilometres up to a few thousand, and can be up to 100 km wide. They also have an irregular topography characterised by escarpments and troughs. "Leaky" transform faults are those along which generation of new crust takes place by virtue of the fact that they are oblique to the direction of spreading. In this case as the plates slide past each other the transform fault has to open in order to accomodate the new geometry, thus allowing melts to rise into the opening. Transform faults can continue into continents, such as is the case for the transform boundary between the Pacific and the North American plate. Here along the Gulf of California, this transform boundary becomes the Salton trough, and further to the north the much publicised San Andreas fault. The Salton trough is the site of intense on-land hydrothermal activity, and submarine hydrothermal activity has been discovered at a number of sites in the Gulf of California (Guaymas basin, discussed in Section 7.5.2.4). Fracture zones can also continue into continental areas, where they may become the site of intracontinental alkaline volcanism, as is observed in southwestern Africa (Angola, Namibia, South Africa), where numerous alkaline complexes, carbonatites and kimberlites tend to occur along the on-land continuation of fracture zones in the South Atlantic (Marsh 1973).

7.2.3 Seamounts and Volcanic Chains

Seamounts and volcanic chains are an important part of the ocean floor physiography. Oceanic volcanic islands and seamounts are intraplate volcanic structures that occur isolated, clustered in groups, or form linear chains. All of these volcanic structures are younger than the oceanic crust on which they are built, and many of the submarine portions of these islands constitute broad volcanic constructs on the seafloor (Fig. 7.3B). Their composition ranges, in general, from tholeiitic basalt to alkalic basalt. The origin and nature of seamounts are not entirely understood, one of the questions being, for example, whether they are the product of eruptions from fractionating magma chambers that are decoupled from the main chamber beneath the axis, or whether they are connected with it. In the latter case, the magma feeding the seamount is drawn from the more fractionated sides of the axis chamber, from which more primitive melts are derived. This issue is not entirely academic because seamounts are clearly important for the formation of hydrothermal deposits, as is detailed below.

Some of the oceanic-volcanic islands are large and composite volcanic structures which, as with Hawaii, may rise to nearly 10 000 m from the seafloor, forming large shield volcanoes. Another example of an active shield volcano is Reunion Island in the Indian Ocean, approximately 240 km wide at its base and rising about 7500 m from the floor of the ocean. A special case is the previously mentioned Iceland, because it straddles a spreading centre, but evidence suggests that it originated from a mantle plume (Wolfe et al. 1997), although the hot spot path related to the Icelandic plume does not appear to form a volcanic chain with an age progression, as for the Hawaii-Emperor chain. Indeed, linear chains of seamounts and volcanic islands constitute one of the most spectacular features of the Pacific Ocean. They are represented by the Hawaiian islands-Emperor seamounts chain (with Hawaii at the younger, active southeast end), the Tuamoto-Line islands group (with Pitcairn at the younger southeast end), the Cook-Austral-Marshall chain with the active Macdonald seamount at the southeast end. In the Indian Ocean the Ninety East Ridge trends northward from the mid oceanic ridge towards India; the Mascarene Plateau estends northeast to Reunion and Mauritius at the active, younger end. A sharp bend of the Hawaii-Emperor chain is at Yuryaku island, dated at 43.4 Ma. This bend is considered to represent the time at which the Pacific plate abruptly changed direction. Similar sharp bends also characterise the Tuamoto-Line islands chain and the Cook-Austral-Marshall chain. Recently, Montelli et al. (2006), using seismic tomography, have shown that the Hawaian hot spot is due to a single conduit deep mantle plume. The age progression of the dog-legged Pacific volcanic island chains not only provides evidence for the northwesterly motion of the Pacific plate but, more importantly shows that active volcanism appears to be anchored at more or less fixed points, or hot spots, the latter being a loose term that essentially refers to the concept of a stationary heat source in the

mantle and the high heat flow that is related to magma advection (Schubert et al. 2001). For this reason, hot spots constitute one of the main tenets of the mantle plume theory, as formulated by Wilson (1963) and later by Morgan (1971). However, age progressions for oceanic islands and seamounts are not always clear cut. McNutt et al. (1997), for example, found that the Cook-Austral-Mcdonald chain consists of three distinct volcanic chains, spanning a 34 Ma range of ages. These authors proposed that diffuse mantle upwelling in the region extended over a large region, and that pre-existing lithospheric fractures controlled the eruption of basalts.

Off-axis volcanoes are fed by magma chambers at the edge of the subaxial melt zones, or that have been decoupled from it by seafloor spreading. From their submarine beginnings, off-axis volcanoes become seamounts that ride on the moving lithospheric plate until they may emerge as islands. Seamounts are submarine volcanoes, commonly characterised by flat tops owing to wave erosion of the volcano summit during and after emergence above sea-level. Eventually, these islands sink below sea-level, as the emerged part is eroded and the plate that carries them gradually subsides, as it moves further away from the spreading centre. Many atolls are coral reefs that top and surround submerged seamounts. In this context, it is appropriate to bear in mind that it was Charles Darwin (Darwin 1860), who first suggested an explanation for the formation of atolls, as coral reefs fringing subsiding volcanoes. Flat-top seamounts were called guyots by H. H. Hess (Hess 1946), who during World War II took echo-sounding of parts of the Pacific. Seamounts that are carried on the "conveyor belt" of the seafloor, may reach plate margins where they are partly subducted or accreted to the accretionary prism. This is the case for the Japan trench, where the Kashima and Erimo seamounts are in the process of being subducted (e.g., Kobayashi et al. 1998). In the Pacific, Indian and Atlantic Oceans clusters of seamounts and volcanic islands form aseismic ridges and rises. In the Atlantic Ocean, aseismic ridges and rises connect the Mid Atlantic ridge to the continental margins of Africa, the Americas and northwest Europe. Notable amongst them are the Rio Grande Rise and Walvis Ridge in the South Atlantic, which connect the Mid Atlantic ridge with the coast of South America and southwestern Africa respectively. Wessel (1997) estimated that in the Pacific Ocean alone there are more than 50 000 seamounts.

7.3 Birth, Life and Death of An Ocean Basin

I have mentioned that mid-ocean ridges are constructive margins, where new oceanic crust is more or less continuously created by the upwelling of magma in the axial rift valleys. As the size of the Earth has remained practically constant for most of its geological history, the creation of new crust at the spreading centres must be counterbalanced by the destruction of an equal amount of crustal material. This takes place in zones of subduction (Chapter 3), along which oceanic crust with its sedimentary cover plunges into the mantle. There is

evidence from seismic tomography that subduction slabs can "cascade" through the mantle to reach the core-mantle boundary, causing thermal instabilities that result in the rise of mantle plumes (see Pirajno 2007a and references therein, for an overview). The impingment of these deep mantle plumes onto the subcontinental lithospheres is thought to be the cause of rifting, which begins the life cycle of an ocean basin (Morgan 1983, Pirajno 2000).

The present-day oceanic crust is characteristically young, in fact no older than the Jurassic (about 150–160 Ma), as for example in the north–northwest of the Pacific ocean and along the eastern seaboard of North America. It has been noted that the depth of an ocean basin increases with distance from the ridge axis and with the age of the lithosphere. More specifically, the average depth away from the ridge may be expressed as a linear relationship, which varies with the square root of the age of the oceanic crust. From this figure the approximate age of the oceanic crust can be determined if the depth, corrected for sediment cover, is known. However, the age-depth relationship is not applicable beyond an age excceding 100 Ma, because on reaching thermal equilibrium the curve tends to reach a constant value. Further limitation is that the fast-spreading ridges are deeper than slow-spreading ridges. From this it is clear that the oceanic crust of a fast-spreading ridge will have a greater volume than that created by a slow-spreading ridge; also, during episodes of fast spreading, the sea level has to rise because of the bulging lithosphere (Kennett 1982). There are several lines of evidence to indicate that throughout the history of our planet oceans have formed and disappeared in a series of geotectonic cycles. Figure 7.4 illustrates the evolution of an ocean basin, which begins with the inception of rifting in a continental mass, from its embryonic stage, through to its young, mature and terminal stages, and finally to the relicts of former oceanic crust, as shown by ophiolitic rocks characteristically marking suture zones.

The East African rift valleys are zones of crustal extension and uplift heralding a rupture of the crust and perhaps its eventual spreading. The next stage is characterised by young, narrow sea arms bound by subparallel coast lines. The Red Sea and the Gulf of Aden are modern-day examples of this stage of ocean development or embryonic ocean basins. The widening of the rift between the Arabian peninsula and Africa probably began some 20 Ma ago and is continuing today. The reconstruction of the fit between the two shore lines is remarkable, except for the Afar Triangle which is overlapped by the southwest corner of Arabia. During these initial stages shallow, and locally ephemeral, marine basins form, and if the climatic conditions are right, evaporation of these lake-size seas will result in the deposition of great quantities of evaporites. This is indeed the case for the Red Sea, where evaporites up to 4 km thick are present along the flanks of the rift. As discussed in Chapter 8, the presence of evaporites may play a very important role in the genesis of some sedimentary-hosted sulphide orebodies. From this young Red Sea stage follows a mature stage, in which an ocean basin develops with an active mid-ocean ridge. This is the stage of the Atlantic Ocean today. Most geoscientists agree that in all probability the

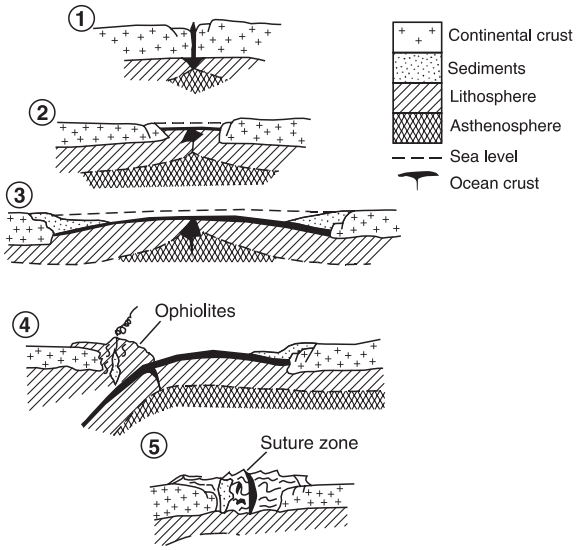


Fig. 7.4 The birth, life and death of an ocean basin. (1) A rift is formed in continental crust, and is characterised by graben structures and bimodal continental magmatism; present-day examples are the rift valleys of the East African rift system; (2) Splitting of the continental crust forms an elongate sea basin, evaporites and terrigenous sediments accumulate; a present-day example of this stage is the Red Sea; (3) Sea-floor spreading continues and an oceanic basin is formed, sedimentation takes place at the passive continental margins; this is the stage of the Atlantic Ocean; (4) The ocean basin begins to close, a subduction zone is developed and a magmatic arc forms on the overriding continental margin, oceanic crust material is intruded into wedges of trench sediments (accretionary subduction complex) forming belts of melange and ophiolites; some parts of the Pacific Ocean could be represented by this stage (e.g., Andean margin); the two continental margins continue to move towards each other, resulting in a collision orogen, a situation that could be compared to the movement of India towards Eurasia during closure of the Tethys Ocean; (5) Collision takes place and the opposing continental masses are "sutured", with only fragments of oceanic material being squeezed along the line of collision (suture zone); the ocean basin is now completely closed. Re-opening can occur and the cycle is repeated. After Pirajno (1992)

Atlantic Ocean did not exist 150 Ma ago and that it was the rifting and fragmentation of the Pangea supercontinent which began in the Mesozoic that eventually led to the opening and development of the ocean as we see it today. Prior to this, another ocean existed namely, the Iapetus Ocean, the opening and closing of which led to the formation of the Caledonides, Hercynides and the Appalachian orogens (Rogers and Santosh 2004). The Atlantic has passive, aseismic margins in which sedimentary rocks, including reef carbonates, turibidites and evaporites, predominate. Voluminous mafic extrusive and intrusive complexes may also occur along some passive margins, as is the case for East Greenland, mentioned in Chapter 5. These complexes exhibit prominent seismic seaward-dipping reflectors, or seaward-dipping layers

(Menzies et al. 2002). The seaward-dipping reflectors are present in the upper crust, at the flanks of and parallel to the continental slope. Typically, they are underlain by high-velocity crustal bodies (7.2–7.5 km s^{-1}), like those observed beneath the oceanic plateaux (Pirajno 2000).

A more mature or even declining stage is characterised by fast-spreading ridges, subduction zones and magmatic arcs. The Pacific Ocean is clearly representative of this stage of ocean development. Closure of the ocean basin is the final or terminal stage, during which shrinking, uplift and collision with the rising of young mountain ranges, take place. The Mediterranean Sea, Black Sea and Caspian Sea, together with the Alpine-Caucasus-Elburs mountain ranges, may be representative of this stage today. These seas are possibly the remnants of the great east-west-trending Tethys ocean that separated the Laurasian continents in the north from the Gondwana continent in the south (Rogers and Santosh 2004). The movement of these two large landmasses towards each other led to the gradual disappearance of Tethys during a number of complex geotectonic events and resulting in the amalgamation of accretionary orogens, whose boundaries are marked by suture zones. Finally, as collision continues, all bodies of water disappear, mountain ranges rise and develop further, so that all that remains of the former ocean are the so-called suture zones, in which slivers of oceanic crust (ophiolites) are preserved. The Indus suture in the Himalayas, separating the Indian plate from Eurasia, and the Solonker suture separating the Central Asian Orogenic Belt from the North China Craton (see Chapter 5) are examples of this stage.

7.4 Oceanic Lithosphere and Ophiolites

I have mentioned that knowledge of the structure and nature of the oceanic lithosphere is derived from geophysical, deep-sea drilling, direct observations by submersible crafts, and the study of ophiolitic rocks in collisional orogens. The integration of the data thus obtained has enabled the construction of models of oceanic lithosphere such as those shown in Figs. 7.2 and 7.3).

Oceanic lithosphere constitutes about 0.1% of the Earth's mass and has thicknesses ranging from 0 to 10 km. Much of the oceanic crust is formed at the mid-ocean ridges, a system of fractures that encircles the Earth, and through which new crust is continuously added at the rate of about 17 to 20 km^3 yr^{-1}. Present-day oceanic crust formed during the last 200 Ma or so, whilst oceanic crust older than 200 Ma is only preserved in tectonically-emplaced zones of tectonised remnants of mafic and ultramafic rocks (ophiolite belts). The oceanic crust is made up of three layers: layer 1 consists of pillow lavas, covered away from the ridge by a veneer of deep sea sediments; layer 2 comprises pillow lavas and a sheeted dyke complex, which represents the conduits for magmas to rise and erupt onto the ocean floor; layer 3 consists of gabbro, within which is lodged the magma chamber below the ridge axis, and a zone of ultramafic cumulates (olivine and pyroxene). The Layer 3 cumulate rests on upper mantle

peridotite. Here the Moho shows up as a seismological and a petrological boundary. The petrological Moho is at the base of the cumulate layer. The depth of the seismological Moho is imaged, by multichannel seismic techniques, at between about 1.5–2 and 6 km. The Moho beneath the ridge axis has widths of 2–8 km. The results of seismic reflection and tomographic imaging suggest that the Moho in the mid-ocean ridge regions marks the boundaries of relatively small magma chambers, at relatively shallow depths. These magma chambers differ in size and structure, according to whether they are associated with a slow or fast spreading ridge. Models of magma chambers in spreading ridges suggest that they have an outer zone, with small amounts of partial melt, and an inner zone of crystal mush that behaves as a viscous fluid (Sinton and Detrick 1992). With reference to Fig. 7.3, the upper portion of the oceanic lithosphere, the oceanic crust proper, is formed by basaltic and gabbroic rocks which are the products of consolidation of upwelling mantle partial melts. The rest of the lithosphere, beneath this zone of mafic rocks is essentially the refractory residue of these partial melts that have been injected into the already consolidated crust and erupted at the surface. Below the refractory layer, that is the lower lithosphere boundary, is the pristine upper mantle material, or asthenosphere, which extends down to about 300 km, and in which temperatures approach the melting point and lateral flow can occur on account of its plastic behaviour. Owing to its rheological properties the asthenosphere is identified with a low velocity zone, or attenuation of P- and S-seismic waves.

It is beyond the scope of this book to detail the igneous processes and various petrogenetic models that describe the nature and compositions of the rocks that compose the oceanic lithosphere. For this the reader is referred to Burke et al. (1981), Wilson (1989), the collection of specialised papers edited by Beccaluva (1989) and Cannat et al. (2006). Details of the geology, petrology and tectonism of ophiolitic rocks can be found in Coleman (1977), Dilek and Robinson (2003) and Dilek and Newcomb (2003). An atlas showing the distribution of ophiolites in the world was published by the Geological Society of America (1979).

For the present purpose it will suffice to say that generation of magma at mid-ocean ridges takes place by adiabatic decompression of the asthenospheric mantle, which rises below the ridge and partially melts to produce magmas of basaltic composition (Fig. 7.5). Studies of experimentally determined stability fields of minerals from mantle peridotite indicate that melting occurs at depths ranging from 90 to <10 km, beneath the seafloor (Kelley et al. 2002 and references therein). Furthermore, melts that form beneath mid-ocean ridges during adiabatic upwelling, rise through conduits and melt channels, recognisable by dunitic veins. These melt channels coalesce and eventually pond to form crustal magma chambers from 4 to 1 km beneath the ridge axis. There is evidence that zoned magma chambers may be present just below the ridge axis. According to Burke et al. (1981), olivine cumulates are deposited near the magma supply axis, which grade into clinopyroxene-rich cumulates and into clinopyroxene-plagioclase cumulates towards the edges of the chamber. The size, shape and depth of the submarine magma chambers, as shown in Figs. 7.2

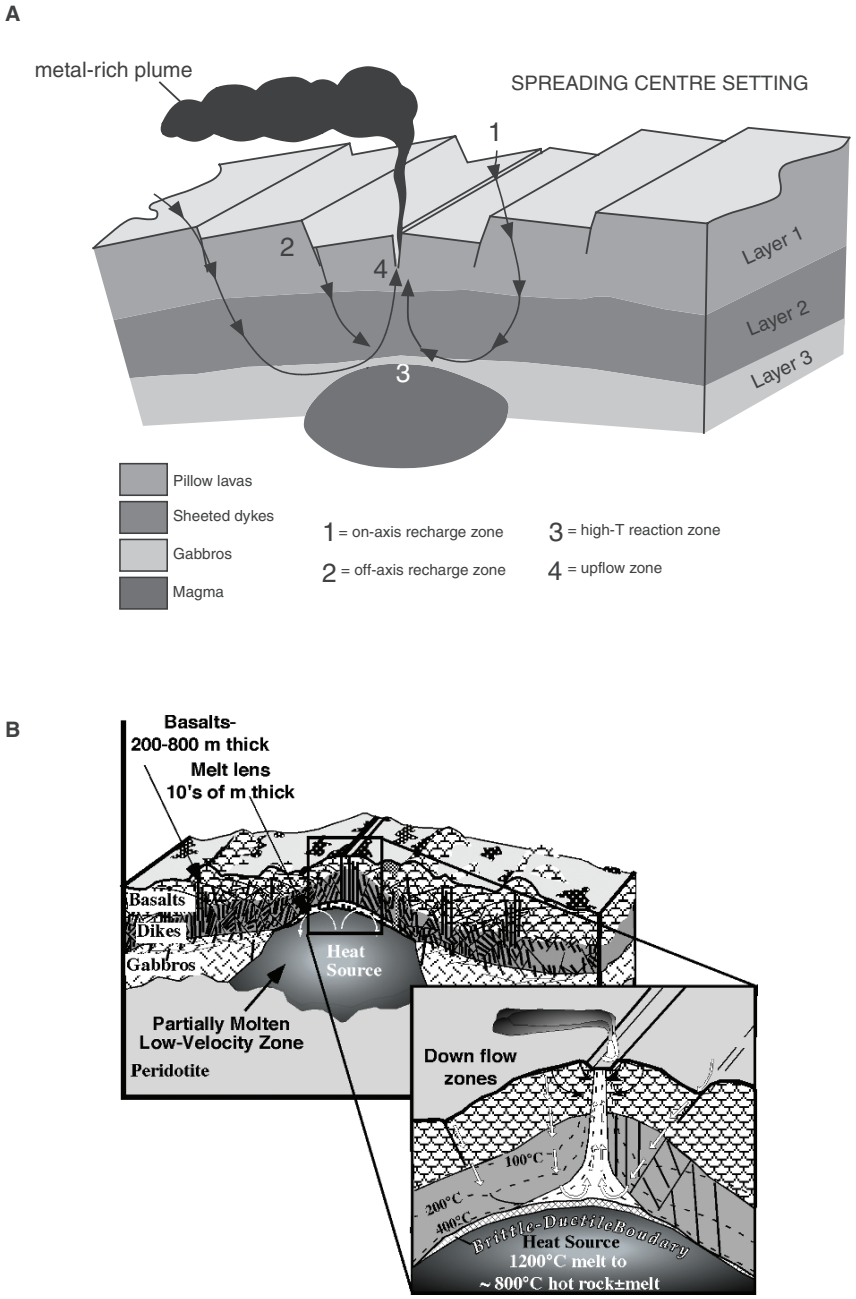


Fig. 7.5 (continued)

and 7.5, probably differ in slow- and fast-spreading ridges. These magma chambers more or less episodically inject melts along ridge-parallel fissures or conduits, which consolidates to form dykes and feed the eruption of lavas on the ocean floor. The mid-ocean ridges are in fact, the site of almost continuous volcanic and earthquake activity, with the latter allowing seismic monitoring. Underwater hydrophones record from tens to hundreds of small tremors a day, effectively recording the breaking through of discrete dykes and the arrival of new magma. Dyke propagation at mid-ocean ridges has been documented by the migration of earthquakes, using submarine hydrophone arrays. In the Juan de Fuca Ridge, these data have indicated dyke propagation of up to 60 km along a ridge in two days (Dziak et al. 1995).

In contrast, the volcanism of off-axis submarine volcanoes (sea mounts or guyots, referred to above) is short-lived, substantiating the idea that the feeding magma chambers are decoupled from the asthenospheric mantle and as such may evolve independently. The cooling and crystallisation of the chamber melt produces gabbroic rocks at the top and along the sides, with layered gabbros at the bottom. These in turn pass below the Moho into depleted harzburgite and lherzolite (upper mantle peridotite), which has led to the subdivision of the oceanic lithosphere into the four layers (Figs. 7.3 and 7.5) described below. Layer 1 is the veneer of unconsolidated oceanic sediments, including clays, siliceous and calcareous oozes. This layer is on the average about 0.5 km thick, but is absent at the ridge crest, with the possible exception of local basins. The oceanic sediments of layer 1 thicken away from the ridge areas towards the continental margins. The thickness of the oceanic sediments can reach 5 km beneath parts of the continental rise bordering the Atlantic Ocean (Bott 1982). Layer 2, comprising the basaltic lavas and dykes, is further subdivided into layer 2A (basaltic pillow lavas and sheet lava flows) and 2B (dykes). Layer 2 is between 1 and 2.5 km thick and characterised by P wave velocities of between 3.4 and 6.2 km s-1[1] (Bott 1982). The composition of the basaltic lavas, usually labelled MORB (mid-ocean ridge basalts), is variable and depends on a number of factors, such as (Wilson 1989): composition of the source mantle; degree of partial melting (about 20% partial melting is required to produce primitive compositions), depth of melting, magma segregation; and fractional crystallisation. Layer 3, which is the main oceanic layer, is between 3 and 7 km thick

Fig. 7.5 (continued) (**A**) Schematic representation of hydrothermal circulation at a spreading centre and relationships between upper mantle and oceanic crust beneath a mid-ocean ridge crest, (**A**) the magma chamber is located at depths ranging from 1 to 4 km below the seafloor, feeds the eruption of lavas through a system of sheeted dykes, (**B**) steep thermal gradients (see also Figs. 7.8 and 7.10) due to the intrusion of mafic magma with temperatures of about 1200°C into cool, water-saturated and porous oceanic crust, power the hydrothermal system at the spreading centre, resulting in the circulation and venting of acidic and metal-rich fluids to the seafloor; sulphides and sulphates precipitate following mixing with cold and oxygenated water (from Kelley et al. 2002; figure reproduced unchanged by permission of the authors)

and characterised by P wave velocities of between 6.4 and 7.7 km s^{-1} (Bott 1982). It may also be subdivided into layers 3A (isotropic gabbro) and 3B (layered gabbros), which are probably partially metamorphosed to amphibolite and greenschist facies. The Moho occurs at an average depth of 7 km, and is marked by a steep P wave velocity jump at the base of layer 3, from the values above to about 8.15 km s^{-1} (Bott 1982). Layer 4 is constituted by an upper section of layered peridotite passing downward into unlayered peridotite, dunite and harburgite.

Geophysical data suggest that partial melting beneath mid-ocean ridges probably begins at depths of 150–300 km (Gu et al. 2005). These depths are too deep for dry melting of peridotite and therefore small amounts of CO_2 and/or H_2O are needed in order to begin partial melting. Dasgupta and Hirschmann (2006), on the basis of experimental studies, suggested that melting beneath mid-ocean ridges may occur at depths of ~330 km, in which carbonatite liquids are produced. The carbonate melt moves through the mantle from depths of about 300 km, promoting dissolution of the olivines, deformation, grain coarsening and lattice preferred orientations. The carbonatite melts will be enriched in highly incompatible elements, while the residual peridotite is correspondingly depleted. The authors contended that these depletions affect a large mass of the mantle and that the carbonatite melts extracted at ~300 km will provide large amounts of C, He, Ar and incompatible elements to mid-ocean ridges. Dasgupta and Hirschmann (2006) calculated that for a source containing 120–1200 ppm CO_2, fluxes of CO_2 from 0.12 to 3.40×10^{15} g/yr can occur at mid-ocean ridges.

7.4.1 Ophiolites

The preservation of oceanic crust in the geological record is generally poor, because as pointed out in the previous discussion on the life cycle of an ocean basin, this crust tends to be destroyed in subduction zones. However, tectonic slices and fragments may survive during collision events by the process of obduction, and along the sutures that mark the line of collision between two lithospheric plates with intervening oceanic crust. These sequences of oceanic crust rocks on land are the ophiolites. But what precisely is an ophiolite, and how is it defined? In 1972, participants of the Penrose Conference agreed to define an ophiolite as follows (Penrose Conference Participants 1972): *Ophiolite refers to a distinctive assemblage of mafic to ultramafic rocks. It should not be used as a rock name or as a lithologic unit in mapping. In a completely developed ophiolite the rock types occur in the following sequence, starting from the bottom and working upward:*

- *Ultramafic complex, consisting of variable proportions of harzburgite, lherzolite and dunite, usually with a metamorphic tectonic fabric (more or less serpentinised).*

- *Gabbroic complex, ordinarily with cumulus textures commonly containing cumulus peridotites and pyroxenites and usually less deformed than the ultramafic complex.*
- *Mafic sheeted dyke complex.*
- *Mafic volcanic complex, commonly pillowed.*

Associated rock types include (1) an overlying sedimentary section typically including ribbon cherts, thin shale interbeds, and minor limestones; (2) podiform bodies of chromite generally associated with dunite; (3) sodic felsic intrusive (plagiogranite) and extrusive rocks. Faulted contacts between mappable units are common. An ophiolite may be incomplete, dismembered, or metamorphosed, in which case it should be called a partial dismembered, or metamorphosed ophiolite. Although ophiolite generally is interpreted to be oceanic crust and upper mantle the use of the term should be independent of its supposed origin. Indeed more recently, the concept of ophiolite has changed to include subduction slab material, so that the term of supra-subduction zone (SSZ) has become acceptable (Robinson and Zhou 2008), mainly because many ophiolites have the geochemical signature of subduction environments, to distinguish it from MORB ophiolites (Pearce 2003). Furthermore, several MORB ophiolites seem to represent allochthonous fragments of oceanic crust from marginal or back-arc basins (Pearce 2003). Thus, the general consensus is that ophiolites are derived from spreading processes in suprasubduction zones, perhaps in response to slab rollback (Robinson and Zhou 2008). In this context, an ophiolite can be defined as a fragment of oceanic lithosphere that has been uplifted and tectonically emplaced in an accretionary wedge or a continental margin (Robinson and Zhou 2008).

Dilek (2003) classified ophiolites into seven types. (1) Ligurian type, in the western Alps and northern Apennines, characterised by serpentinised peridotite, associated with small volumes of gabbros and pillow lavas, no sheeted dykes are present; the Ligurian ophiolites may have formed during early stages of opening of an ocean basin following rifting (Red Sea style). (2) Mediterrenean type ophiolites, found in Greece, Albania, Cyprus through to Turkey and Tibet; dominantly consist of harzburgite-lherzolite, residual to MORB melt extraction; podiform chromite deposits occur in these ophiolites. (3) Sierran type ophiolites occur along the Pacific Rim (Japan, Philippines), Cuba and the western Sierra Nevada in the USA; these contain volcanic, plutonic, hypabyssal and sheeted dyke complexes; the volcanic rocks include basalt, dacite and rhyolite; Sierran ophiolites were accreted by oblique convergence and strike-slip tectonic processes. (4) Chilean type ophiolites, represented by the well-known Rocas Verdes (green rocks; Tarney et al. 1976) in southernmost South America; these rocks are essentially MORB type and were formed in a back-arc basin within a magmatic arc and are relatively autochthonous; they consist of basaltic pillow lavas, sheeted dyke complexes and gabbro; peridotite is not exposed; Chilean type ophiolites may also be represented in parts of the Central Asian Orogenic Belt. (5) Macquarie type ophiolites, uniquely represented in the

Macquarie Island (Australia) in the Southern Ocean, where 12–9.5 Ma oceanic crust is exposed along an east–west ridge segment at the Australian-Pacific plate boundary; this ridge segment was uplifted during transpression and oblique convergence; the Macquarie ophiolite from top to bottom consists of basaltic lavas and volcaniclastics, sheeted dyke complex, microgabbro, coarse-grained massive and layered gabbro, associated with lenses of troctolite, wehrlite, dunite, peridotite and harburgite; geochemically the Macquarie rocks have MORB compositions. (6) Caribbean type ophiolite, representing fragments of an oceanic plateau accreted onto the Colombian continental margin; these rocks include pillow and massive lavas, massive and layered gabbro, dunite with bands of lherzolite, websterite and gabbronorite; sheeted dykes are not present; Kerr et al. (1998) and Kerr and Tarney (2005) published excellent papers on structure, composition and geodynamic evolution of the Caribbean-Colombian ophiolitic oceanic plateau. (7) Franciscan type ophiolites are found in accretionary complexes of active margins and are intimately associated with tectonic mélanges and high-presure rocks of subduction systems; Franciscan ophiolites consist of fragments of peridotite, gabbro and basaltic rocks, representing fragments of mid-ocean ridge; the igneous rocks are associated with pelagic chert and limestone; Franciscan rocks are best represented in the Franciscan Complex in California (USA), in Japan, in the Koyak Mountains of Kamchatka and the Palaeozoic subduction-accretion complexes in New Zealand and eastern Australia. A well-documented example of ophiolites is provided by the Papuan Ultramafic Belt (Davies and Jaques 1984). The Palaeozoic Central Asian Orogenic Belt (CAOB, referred to in Chapter 5) is a collage of terranes stitched or sutured by ophiolitic rocks, representing remnants of oceanic lithosphere that separated island arcs and microcontinents (Şengör and Natal'in 2004).

An interesting case of ophiolitic rocks was reported in Long et al. (2008). These authors worked on mafic rocks that are part of a volcanic-rifted margin succession of the Palaeo-Tethys Ocean, on the western margin of the Yangzte Craton. This succession was formed by the opening of the Jinshanjinang Palaeo-Tethyan oceanic arm, caused by the impingement of the Permian Emeishan mantle plume. The subsequent closure of the Jinshanjinang ocean occurred during westward subduction that tectonically sliced the volcanic rifted margin, resulting in the emplacement of these rocks as an ophiolite sequence (Long et al. 2008). The interesting point here is that this ophiolite-like succession represents a remnant of a mantle plume-related volcanic rifted margin, similar to that of the East Greenland margin, where porphyry systems are present (see Chapter 5). This leads to the conclusion that "there are ophiolites and ophiolites", to paraphrase the famous statement by Herbert Harold Read (1889–1970) that *there are granites and granites* (see Young 2003).

Until quite recently ophiolites were thought to be absent from rocks older than Phanerozoic, with the suggestion that plate tectonics was not operative for most of the Precambrian (e.g., Hamilton, 2003). However, ophiolitic rocks of Archaean age have recently been studied and reported from the North China Craton (Kusky et al. 2004), while Furnes et al. (2007) reported the occurrence of

sheeted dykes, pillow lavas and mafic intrusions from the ~3.8 Ga Isua supracrustal belt in Greenland. Furnes et al. (2007), on the basis of the presence of the sheeted dyke, geochemical discrimination plots (e.g., Ti, Zr, V and Y immobile elements), and oxygen isotopic data from pillow lavas and dykes ($\delta^{18}O$ = 9.9–5.7‰ SMOW), which record hydrothermal ocean-floor metamorphism, interpreted these rocks as an ophiolitic association and suggested that they formed by seafloor spreading.

7.5 Submarine Hydrothermal Systems: Spreading Centres, Island Arcs and Seamounts

Hydrothermal activity in seafloor environments around mid-ocean ridges and island arcs is very common. Hannington et al. (2005) stated that *more than 80% of the world's active volcanoes occur in the oceans and the vast majority of surficial hydrothermal activity is concentrated along the 55 000 km of mid-ocean ridges and 22 000 km of island arcs* (Fig. 7.1). In common with other hydrothermal systems, a seafloor hydrothermal system consists of a heat source (the underlying magma chamber), a recharge area, circulation cell and seafloor discharge. as hot springs through vents and fractures (Fig. 7.5). Circulation and heating of sea water takes place at depths of 2–8 km within the oceanic crust. The heated sea water-derived fluids can undergo boiling and phase separation, with development of a brine layer deep in the oceanic crust. Fluid downward penetration occurs through a network of small fractures, called a cracking front (Kelley et al. 2002). The hydrothermal fluids undergo changes in temperature, composition and volatile concentration through a series of reactions with the wall rocks, extracting metals such as Cu, Zn, Pb, Fe, at temperatures ranging from 350 to 550°C and causing alteration. Sodium, Mg and Ca are added to the rocks being altered forming greenschist facies mineral assemblages (e.g., chlorite, amphibole and albite). A combination of hydrothermal and biogenic activity on the seafloor produces sulphide and oxide mineralisation. The metalliferous fluids are highly reduced with pH of 2–6 and travel through a fracture system to discharge on the seafloor as hot springs (black and white smokers) at temperatures of 350–400°C. The discovery of seafloor hydrothermal vents, since the detection of deep sea geochemical anomalies about 40 years ago, has led to a flourishing of exciting and very fruitful research, the understanding of seafloor mineral deposition with direct application to on-land ore deposits, the existence of previously unknown ecosystems that thrive on anoxia and sulphur, the assesment of future and very valuable mineral resources, provided insights as to the possible origin of life on Earth, not to mention the advances in the technology of submersible crafts, underwater video-cameras, and so on. There are many reviews of seafloor hydrothermal systems and history of research, here I cite Rona et al. (1983), Rona (1984), the special issue of Economic Geology (Rona and Scott 1993) and the collection of papers edited by Parson et al. (1995), Herzig and Hannington (1995) and Hannington et al. (2005).

Hannington et al. (2005) provided a listing of 110 submarine hydrothermal vent sites, discovered between 1965 and 2005 (see Fig. 7.1). A good web site (and various links) to seafloor hydrothermal activity can be found at: http://www.agu.org/revgeophys/humphr01/humphr01.html (last accessed April 2008).

Hydrothermal activity and related mineralisation on the seafloor comprise a wide range, from smoker sulphide chimneys at mid-ocean ridges, through Red Sea brine pools, polymetallic shallow marine hotsprings near arc volcanoes (e.g., Conical seamount near Lihir island, mentioned in Chapter 5, Palinuro seamount in the Tyrrhenian Sea), gold-rich polymetallic sulphides in back-arc settings (e.g., Lau, Manus basins, Okinawa trough), submarine acid-sulphate epithermal types, to gold-barite deposits and sulphide-rich muds. The wide range of seafloor ore deposits can be classified into three main geoenvironments (Herzig and Hannington 1995): (1) mid-ocean ridge spreading centres; (2) intraoceanic back-arc type (e.g., Lau basin); and (3) intracontinental back-arc type (e.g., Okinawa Trough). To this one may add, seamounts and submerged volcanic centres of island arc systems. The heated sea water, having become an ore fluid, is discharged as a submarine spring on reaching the seafloor. When considering the extent of mid-ocean ridges around the globe, one realises that we are, most likely, in the presence of the most powerful and extensive mineralising systems on the planet. Unfortunately, its magnitude is not reflected in the geological record for the reason already stated: namely, poor preservation potential due to collision tectonics. Figure 7.1 illustrates the worldwide distribution of known sites of hydrothermal discharge along the mid-ocean spreading centres. In the latter it is clear, as pointed out by Rona (1984), that the distribution of discharge sites is based on current knowledge, and many more could be expected to be added as submarine exploration continues. The hydrothermal mineral deposits that are formed on the seafloor include vein stockworks and disseminated sulphides and sulphates, metalliferous encrustations and accumulation of metalliferous sediments in topographic depressions. The ore metals include mainly Fe, Cu, Zn, Pb, Mn, Au, Ag and Ba. Importantly, evolving magmatic fluids transfer CO_2, H_2O, CO and the reduced species of H_2S, H_2 and CH_4 to the oceanic crust. It is also important to bear in mind that multiple stages of magma degassing and mineral-fluid reactions result in heterogeneous isotopic compositions and for this reason, isotopic data need to be carefully evaluated in the light of actual observations. Kelley et al. (2002) suggested two possible pathways for these fluids:

1) $CO_2 + (H_2O + CO + S) \rightarrow CO_2 + CH_4 + H_2O + C \rightarrow CH_4 + H_2O + C$
2) $CO_2 + (H_2O + CO + S) \rightarrow H_2O \pm CO_2(\text{vapour}) \rightarrow H_2O \pm \text{brine} \rightarrow \text{brine}$

The circulation of ore fluids within the oceanic mass above the hydrothermal vents may also assume great importance in terms of ore genesis processes, which largely involve fallout of particles from the water column. In the geological record, massive sulphide deposits are commonly associated with lateral sedimentary rocks that contain Fe and Mn oxides, sulphides, silica, barite and

carbonates, which may represent lithified metalliferous sediments. This unusual type of hydrothermal system is called a plume which, due to bottom currents, is normally displaced relative to the underlying source. These plumes are diluted hydrothermal fluids that rise above the vents and can be detected by their anomalous temperature with respect to the ambient sea-water. Sonar scanning indicates that the plumes can be sensed up to about 80 m above the emitting vent, while their lateral displacement is detected up to 50 m away. Actively accumulating metalliferous sediments are found for several kilometres around the SuSu Knolls hydrothermal field, in the eastern Manus back-arc basin of Papua New Guinea (Hrischeva et al. 2007). The sedimentary fallout from the SuSu hydrothermal plume contains Mn oxides, barite and Cu–Fe sulphides (Hrischeva et al. 2007). As previously mentioned, I return to discuss metalliferous sediments in more detail in Chapter 8.

Far more extensive hydrothermal plumes, called megaplumes, give a thermal discharge of 10^{16}–10^{17} J, rising for more than 800 m above the seafloor and extending for 20 km along the ridge axis (Baker 1998). Megaplumes seem to be associated with major "dyking eruptive events" (Kelley et al. 2002). One of these vents was recorded at the Gorda Ridge, where a large temperature anomaly was detected for 15 km along the ridge axis and 8 km across the axis (Baker 1998). The Gorda Ridge megaplume event also generated high concentrations of CH_4, which was probably the result of hyperthermophile organisms, called methanogens, utilising CO_2 released from degassing magma to produce CH_4. Sulphide particles from the plumes of black smokers may settle around the venting area to form an "apron" of sulphide material. Stokes' law governs the settling velocity of particles in a fluid medium. This velocity is proportional to the density difference between the fluid and the particles, to the radius of the particles, gravity, and inversely proportional to the viscosity of the fluid. In general it can be shown that, for a plume height of about 50 m, sulphide particles will settle within radii ranging from 50 to 250 m of the plume (Cathles 1983). Usually substantial sulphide accumulations can only form in quiet conditions, such as those attained in a depression not influenced by bottom currents. On a global scale, the currents' induced lateral shift of the plumes are indicated by the asymmetric distribution, in relation to the ridge axis, of the metalliferous sediments (Fe and Mn oxides) on the seafloor. Also, the displaced distribution of the ^3He isotope in sea water is thought to reflect emission from hydrothermal vents on the ridge axis (Edmond and Von Damm 1983).

In the geological record seafloor mineralisation includes a mixed bag of deposit styles, such as the huge Iberian Pyrite Belt, which with a total size of about 1765 Mt, is the largest accumulation of seafloor massive sulphides on our planet; the Noranda and Bathurst camps in Canada, the Irish carbonate-hosted deposits, the Japanese Kuroko deposits, the Tasmanian massive sulphides of the Mt. Read volcanic belt and of course, the massive sulphides of the Troodos Complex in Cyprus.

Seafloor hydrothermal ore-forming processes can be summarized as follows (Rona 1984):

- Penetration of cold, dense sea water into oceanic crustal layers 2 and 3
- Heating of sea water, reaction with mafic rocks, metamorphism from zeolite to greenschist facies, with increasing T and P
- Solutions carry Mg^+ and OH^-; reactions producing H^+
- High T (200–400°C), leaching and mass transfer of Li, K, Rb, Ca, Ba, transition metals (Cu, Pb, Zn, Mn) and Si, all from oceanic crust; fluids are acidic and reducing; transfer of Mg, SO_4, Na, Cl from sea water → fluids → oceanic crust rocks
- Transport of metals and sulphur in solution as chloride complexes; S derives from reduction of SO_4, Na, Cl, from sea water
- Addition of volatile phases from the mantle: He, F, Hg, S, B, H_2, CH_4
- Ascent of metal-enriched primary hydrothermal fluids, through decreasing T and P; mixing with low T (2°C) alkaline, oxidising sea water; critical point for a 350°C fluid is at P of 1500 bars (separation of liquid-vapour phases)

Mineral phases are precipitated at the rock-water interface and within the fracture/feeder system in layer 2 and 3. The precipitation mechanisms are:

- Mixing of primary fluids with sea water → deposition of particulate, disseminated, stockworks, massive Fe, Cu, Zn sulphides under reducing conditions; and Fe-rich silicates, oxides, hydroxides, Mn-rich oxyhydroxides, sulphates (e.g., barite) and carbonates under oxidising conditions
- Decrease in T and P of fluids, during ascent and loss of heat to wallrocks; possible boiling in a two-phase system
- Precipitation of amorphous Fe sulphides, with high colloidal adsorption capacity in the overlying water column; subsequent scavenging of Fe, Mn and other metals in sea water; flocculation follows and metalliferous sediments are deposited on the seafloor at some distance (km- 10 s of km) from the vents.

High-temperature (> 300°C) venting results in the construction of chimneys (black smokers), made up mainly of Cu sulphides and sulphates. Individual chimneys coalesce to form large mounds. Low-temperature (< 200°C) fluids precipitate (white smokers) Zn sulphides, together with Fe sulphides around tubes of animals (tubeworms *Vestimentifera*). Vent biomass communities have been found in the fossil record from a number of volcanogenic massive sulphide deposits (Little 2002). Circulation of fluids in the fracture/feeder systems precipitates sulphide veins and produces intense alteration of the wallrocks. This activity eventually declines, usually due to the filling of fractures and pore spaces. The hydrothermal edifice thus constructed will consist of (inner to outer): Cu sulphides, Zn and Fe sulphides, colloform sulphides, sulphates (barite, anhydrite, commonly associated with Au). Movements due to seafloor spreading will fracture the hydrothermal construct and a new cycle of hydrothermal venting begins; this can go on for several hundred or thousands of years resulting in the formation of a large massive sulphide orebody. Figure 7.6 illustrates the main features and components of submarine hydrothermal vent systems.

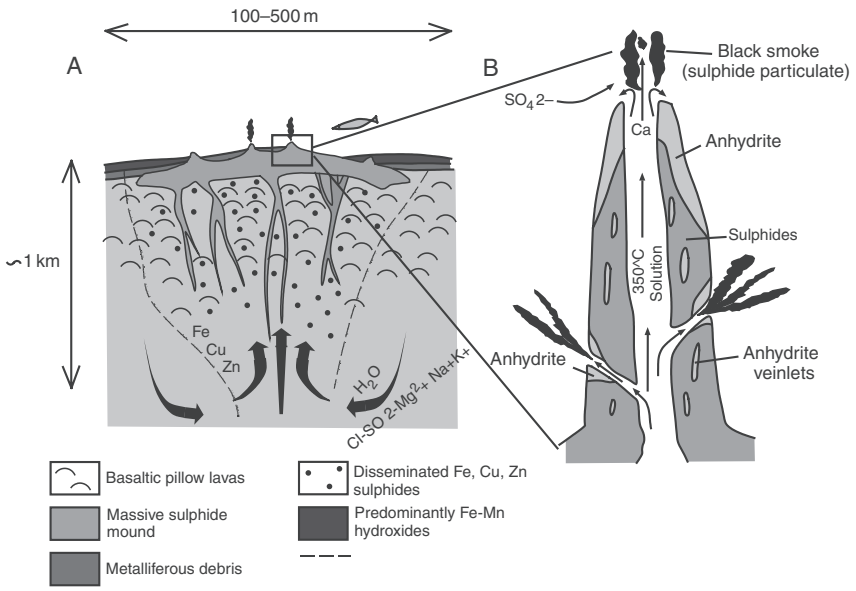


Fig. 7.6 (**A**) Schematic representations of (**A**) sulphide mound and (**B**) cross-section of a black smoker; anhydrite precipitates first, forming a leading edge, followed and replaced by hotter fluids from which sulphides are precipitated. After Edmond and Von Damm (1983)

In the sections ahead, I describe the geometry of hydrothermal circulation in the above-mentioned environments, as deduced from studies of modern systems. In particular, I examine hydrothermal systems at mid-ocean ridges, at spreading ridges close to land masses, in volcanic islands and in submarine volcanic constructs such as those that are responsible for the VMS ore systems in the geological record.

7.5.1 Hydrothermal Processes, Nature of Submarine Hydrothermal Fluids and Anatomy of a Seafloor Sulphide Deposit

The oxygenated and alkaline sea water, with a pH of about 8, becomes a reduced (pH 4–6), Cl-rich brine capable of leaching and transporting significant quantities of metals. The high temperature solutions (200–400°C) leach out of the mafic rocks, elements such as Li, K, Rb, Ca, Ba, the transition metals (Cu, Fe, Mn, Zn), and Si. Keays (1987) suggested that at least part of the ore-forming metals, in particular precious metals may be leached out from the magmatic sulphides disseminated in the mafic and ultramafic rocks of layers 3 and 4. Addition of volatile phases (He, F, Hg, S, B, H and CH_4) to the hydrothermal fluids may. They may originate either from the degassing of the underlying

magma chambers, or indirectly as by-products of the hydrothermal alteration of the mafic rocks (Rona 1984). Transport of metals and S in the solutions is probably by chloride complexes in the higher temperature fluids and by thio-sulphide complexes in the lower temperature range, with the S largely being derived from reduction of SO_4 from sea water. Huston and Large (1989) who studied the chemistry and behaviour of Au in the volcanogenic massive sulphide deposits from Tasmania and elsewhere, showed that Au is transported as $Au(HS)^-_2$, while metals such as Ag, Pb and Zn are transported as chloro-complexes during the early stages of fluid evolution (200–250°C). Whereas the chemical modelling of Huston and Large (1989) is specifically directed at Kuroko-type deposits, its general principles may well be applicable also to mid-ocean-ridge hydrothermal systems. The metals precipitate as a result of oxidation by mixing with sea water, and reduced S activity. As the fluids reach higher salinity and temperatures of 300°C or more, chloride complexing takes over and Au is transported as $AuCl_2^-$, as are Cu and other metals. Precipitation occurs as a result of pH increase and decrease in both temperature and f_{O2} (reducing conditions). For this reason, Au is commonly associated with pyrite-chalcopyrite stringers and massive lenses, which replace the earlier sulphides at the base of volcanogenic sulphide deposits. The upper parts of the sulphide deposits, on the other hand, are dominated by lower temperature Zn–Pb–Ag-rich sulphide assemblages, and, in the event that Au is present, then it would have been transported by sulphide complexing. The two associations, Cu–Au and Zn–Pb–Ag–Au are usually mutually exclusive.

The chemistry of hydrothermal fluids, venting at four sites in the East Pacific Rise (EPR; Section 7.5.2.1) at 21°N, was assessed by Von Damm et al. (1985). Manganese, Fe, Co, Cu, Zn, Ag, Cd, Hg, Pb, and As are all to a greater or lesser degree enriched in the EPR hydrothermal solutions. Lithium is found to be enriched in all four vent areas, whereas Na is enriched at one locality and depleted in the other three. The Na depletion is considered by the authors as due to the formation of albite from anorthite at depth in the system, so that by the time the fluids reach the seafloor they are depleted in this element. By contrast, the conversion of albite to chlorite higher in the system is possibly the reason for the Na enrichment in one of the vents. Experimental evidence indicates that Na is leached from the rocks and taken into solution at water/rock ratios greater than 10, to be taken up by the wallrocks at ratios less than 10. Chlorine, like Na, is both enriched and depleted in the solutions; although the behaviour of Cl is not entirely clear, it is possible that a sink for this element is provided by its substitution for hydroxyl groups (OH). Also, about 10% loss of water by hydration could account for both the Na and Cl depletion in the solutions. Potassium and Rb values, while found to be somewhat variable, are generally higher than sea water. The generally low concentrations of these elements may be a function either of original composition of the mafic rocks or of the uptake of these metals to form mineral phases, or both. Calcium is enriched in the solutions by variable amounts, in some cases Ca showing only a small increase. Low Ca concentrations are attributed to precipitation of

Ca-silicates at depth, such as epidote. As previously indicated, Ca is released into the solution during H^+ metasomatism and albitisation of the anorthite molecule, or during the conversion of epidote to chlorite. Von Damm et al. (1985) pointed out that the Ca cycle is a complex one with *numerous source and sink reactions available*. Magnesium is depleted in all vent fluids, which is in agreement with an assumed end-member solution value of zero. Magnesium and sulphate show a negative correlation with temperature, and extrapolation to the zero values of Mg and SO_4 intersects the temperature axis at 350°C, which is considered to be an end-member solution (Von Damm et al. 1983). Barium is enriched in all solutions examined, but the concentration of this element may be underestimated due to the precipitation of barite in the chimneys. Silica is enriched in the solutions and its presence is largely controlled by the solubility of quartz in the system, which is dependent on temperature and pressure. The Si content of the solutions in the EPR shows a regular decrease from north to south in the four vents examined by the authors, which is thus interpreted as indicating an increase in the depth of the hydrothermal circulation. Using the measured Si content, temperature of the EPR vents, solubility curves of quartz as a function of temperature and pressure, and by removing the pressure of the water column (2500 m = 250 bar), Von Damm and co-authors were able to estimate the pressure and depth at which the fluids are in equilibrium with quartz. They found pressures of between 300 and 600 bar, corresponding to depths of 0.5–3.5 km below the seafloor. Total S occurs as the two species of SO_4 and H_2S. The latter is present in all the vent solutions examined, while, as stated previously, sulphate has zero concentration in the end-member solution. The behaviour of S in the hydrothermal solutions is both complex and critical. The S cycle is determined by the presence of two sources and two sinks (Von Damm et al. 1985). The source of S resides in both sea water and the mafic rocks, whereas sinks are provided by the deposition of sulphates (barite, anhydrite) and its precipitation as sulphides. The S that is contained in the fluids discharged at the seafloor is derived from both sea water sulphate and mafic rocks. Sulphur-isotope systematics are also difficult to interpret because sea water sulphates contains +20‰ $\delta^{34}S$, and basaltic S has ~0‰ $\delta^{34}S$. During reduction of sulphate to sulphide the first sulphide formed will have near 0‰ values of $\delta^{34}S$, so that if the sulphate is partially reduced the resulting $\delta^{34}S$ will have a range from 0 to +20‰. In general, S isotope measurements indicate a range of values for $\delta^{34}S$ of between + 1.7 and + 5.8‰ in sulphide samples and of between + 0.5 and + 4.6‰ in the H_2S of the hydrothermal fluids of the EPR (see Fig. 1.7), with some of the S contributed by sea water and some by the mafic rocks of the oceanic crust. Reduced S is clearly important for the transport of metals, as discussed in Chapter 1. At any rate, S is used up in the precipitation of sulphides and sulphates, which contribute to the build up of mounds and chimneys.

Quite apart from circulating sea water, fluids emanated from the magma chambers beneath the spreading centres need also to be taken into

consideration. Yang and Scott (1996) showed evidence of the presence of magmatic fluids in the lavas of the eastern Manus back-arc basin, offshore Papua New Guinea, where seafloor hydrothermal systems are actively forming, at about 1700 m of water depth, polymetallic sulphide deposits (PACMANUS vent field; Binns and Scott 1993). Melt inclusions from the lavas that host the sulphide mineralisation, contain silicate glass, minerals and gas bubbles, with CO_2 being the main volatile phase, which by analogy with subaerial volcanic system is likely to have derived from early magma degassing (Yang and Scott 1996). In addition, the bubbles also contained amorphous precipitates that have Cu, Zn, Ni, Fe, Na, S and Cl, probably as sulphides and chlorides. Yang and Scott (1996) pointed out that the discovery of this metal-rich volatile phase is suggestive of metal transport by high-temperature magmatic fluids, as commonly observed for subaerial volcanoes. The metal- and CO_2-rich melt inclusions trapped in the phenocrysts provide direct evidence of these high-temperature magmatic fluids that separated from the magma through degassing. The authors also noted that compared with the dilute fluids that vent on the seafloor of the East Pacific Rise at 21° N, the magmatic volatile phases of the PACMANUS system have a much higher concentration of metals. Therefore, it is likely that these magmatic fluids are major contributors of metals, such as Cu and Zn. Of the volatile phases (CO_2, H_2S, H_2, CH_4), CO_2 is perhaps the most abundant dissolved gas in submarine hydrothermal effluents. Intense CH_4 degassing has been recorded along the Mid-Atlantic ridge at sites where serpentinised peridotite is present. Development of CH_4, C_2H_6 and H_2 fluids result from serpentinisition reactions, as discussed in Section 7.5.2.3.1. A number of sites have been reported where CO_2 occurs in the liquid state in submarine hydrothermal systems. One of these sites, called Champagne, is located in the Mariana island arc at about 1600 m of water depth, near the summit of a small volcano, named Eifuku (Lupton et al. 2006). Another site is in the Okinawa Trough, where vents emitting liquid CO_2 droplets were found at a number of hydrothermal sites on top of the Yonagumi Knoll IV (Konno et al. 2006). Beaudoin et al. (2007) examined the ore metals budget of melt inclusions in seafloor settings (back arc, mid-ocean ridge and seamounts) and found that ore elements, such as Pb and Cu, may also have been contributed from subduction slabs.

The internal geometry and the deep-structure of a seafloor hydrothermal sulphide deposit, based on the work of Herzig and Hannington (1995) is shown in Fig. 7.7. Zierenberg et al. (1998) also provided insights into the internal structure of a seafloor sulphide deposits in the Juan de Fuca Ridge and this is presented in Section 7.5.2.2. Humphris et al. (1995b) examined core samples from a series of holes drilled into the TAG hydrothermal field (see Section 7.5.2.3) at a water depth of 3650 m, where high-temperature episodic venting in the past 20 000 years has built a mound about 200 m in diameter. On the surface of the mound mineralogical zoning reflects different types of venting, with chalcopyrite-anhydrite chimneys produced by >300°C Cu-rich fluids and sphalerite-dominated material formed through

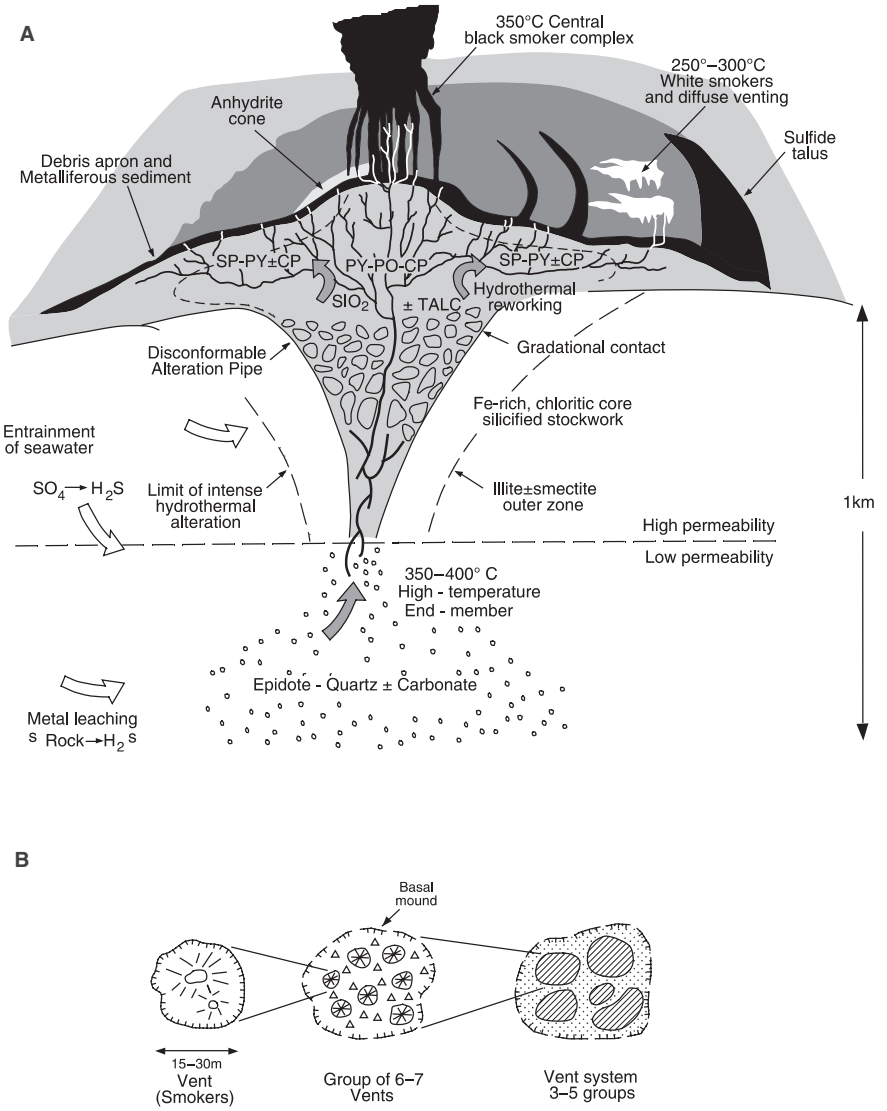


Fig. 7.7 (**A**) Components of a seafloor hydrothermal system; see text for details, after Herzig and Hannington (1995) and (**B**) clusters of smokers and mounds, after Pirajno (1992)

the action of white smokers venting Zn-rich fluids at temperatures of 260–300°C. Seventeen holes drilled at five locations of this TAG active mound enabled the detailed reconstruction of the hydrothermal system to depths of 125 m. The internal structure of the mound consists of four zones or lenses, from top to bottom: (1) clast-supported massive pyrite breccia in

the upper 10–20 m; (2) a discontinuous anhydrite-rich zone, consisting of at least two breccia types, a matrix-supported pyrite-anhydrite breccia to about 30 m below-seafloor (b.s.f.) and a pyrite-silica-anhydrite breccia to about 45 m b.s.f. to the base of zone 2; (3) the third zone is represented by intensely silicified and brecciated wallrocks in the upper part of upflow zone, below the hydrothermal mound. Below about 100 m b.s.f. the wallrock breccia grades into the hydrothermally altered (chlorite mainly) and weakly mineralised basalt (Zone 4).

The seafloor hydrothermal system illustrated in Fig. 7.7 consists of a basal mound, topped by a central black smoker complex, lateral white smokers with diffuse venting and talus material forming an apron of metalliferous sediments (Herzig and Hannington 1995). The mound is underlain by a subseafloor funnel-shaped zone of vein stockworks and disseminated sulphides, within and surrounded by an alteration pipe characterised by Mg-rich chlorite. The mineralogy of these seafloor sulphide deposits consists of assemblages related to a range of temperatures from about 400–300°C to less than 150°C. Black smokers are the highest temperature channelways formed by sulphides, such as isocubanite-chalcopyrite, pyrrhotite, pyrite and bornite. Lower temperature precipitates characterise the outer parts of the chimneys, which consists of sphalerite, marcasite, pyrite, amorphous silica and barite. At sediment-covered mid-ocean ridges, such as the Guaymas (Section 7.5.2.4), the sulphide assemblages reflect the interaction of the hydrothermal fluids with turbiditic and hemipelagic sediments, resulting in the precipitation of complex sulphide assemblages, including galena (Pb probably leached from the sediments), arsenopyrite, tetrahedrite, loellignite, boulangerite, stannite, jordanite, native bismuth, together with barite and amorphous silica (Herzig and Hannington 1995). Back-arc spreading centres, such as the intraoceanic Lau back-arc in the southwest Pacific or the intracontinental Okinawa Trough (Figs. 7.1 and 7.17), sulphide assemblages include pyrite-marcasite, chalcopyrite-isocubanite, sphalerite-wurtzite, galena, tennantite, tetrahedrite, Pb–As sulphosalts, barite, amorphous silica and native sulphur (Herzig and Hannington 1995). In some systems, cinnabar, stibnite and realgar and orpiment may also be present.

The ascent of the metal-rich fluids along channelways occurs through decreasing temperature and pressure gradients. Separation of liquid and vapour phases (critical point) for a 350°C solution is at a pressure of about 1500 bar. However, boiling does not occur at depths below sea level of more than 2000–1500 m, or >200–150 bar pressure (1 bar = a water column 10 m high). Boiling could nevertheless take place at shallower depths where the adiabatic curve for the ascending fluids intersects the liquid–vapour curve for sea water (Bonatti 1983). Mixing of these primary solutions with sea water (which is alkaline, oxidising, and at temperatures of approximately 2°C) causes the rapid precipitation of disseminated stockworks and massive sulphides along the route of the fluids, and at the seafloor, under

predominantly reducing conditions. Under more oxidising conditions various Fe-rich silicates, Fe and Mn oxides and hydroxides, sulphates and carbonates are precipitated above the sulphide zones and further away from the vents. The injection of hydrothermal plumes into the water column will result in the precipitation of amorphous ferric oxide particulate matter with high colloidal adsorption capacity. It is therefore possible that this will cause the scavenging of Fe and Mn as well as other metals from the sea water. Flocculation would thus follow, causing metalliferous sediments to be deposited distally from the discharge sites. As previously mentioned, the discharge of the primary solutions on the seafloor occurs through vents or chimneys or smokers. As previously mentioned, there are two types: black and white. In black smokers the fluids, which emerge at temperatures of $\geq$350°C, are characterised by black clouds of sulphide material (see above)-which precipitates immediately as the hot fluid comes into contact with the cold sea water (about 2°C). Primary fluids, discharging through white smoker chimneys at temperatures of between 100 and 350°C, precipitate white clouds of dominantly barite and silica with minor pyrite. The chimneys can grow by several centimetres per day and the fluid velocity is from tens of cm s^{-1} in white smokers to 2–3 m s^{-1} in black smokers. The activity of an individual smoker is usually short, as the feeding channels become sealed by the deposition of minerals, until a new channel opens up and a new smoker chimney is formed. Models of sulphide deposits (mound) formed by a vent system which, as previously stated can be formed by several chimneys are schematically illustrated in Figs. 7.6 and 7.7.

The mineral deposits formed by the venting of hydrothermal fluids at spreading centres can occur either as mounds or as pool-like stratified accumulations (Fig. 7.8). The shape of the deposits is essentially related to the dynamics of the discharging fluids (Rona 1988). Hydrothermal solutions that are less dense than sea water tend to rise as buoyant plumes up to 300 m above the vents, and their equilibrium level is primarily related to the flux of the vent. This is the case for both the Pacific and Atlantic discharge sites, where the salinities of the solutions are usually close to that of sea water. Salinities of the fluids discharging in the EPR range from 2 to 4.9 wt.% NaCl equivalent, about 4 wt.% in the Guaymas basin, and in the Juan de Fuca ridge vents they reach salinities of approximately 7 wt.%. In the brine pools of the Red Sea the discharging fluids are extremely saline (range is from 4 to 32 wt% NaCl equivalent) and therefore much denser than sea water. The discharging solutions tend to accumulate in submarine depressions and are density-stratified (see Fig. 8.2). It must be reiterated that the range of salinities varies in space and time, with higher salinities (and temperatures) usually being found deeper in the crust and in the early stages of the developing ore fluids; a general decrease both in the salinity and temperature of the fluids also occur with time. However, certain factors may serve to alter this simple evolutionary trend, for example, the presence of evaporites in the path of the moving fluids (Rona 1988).

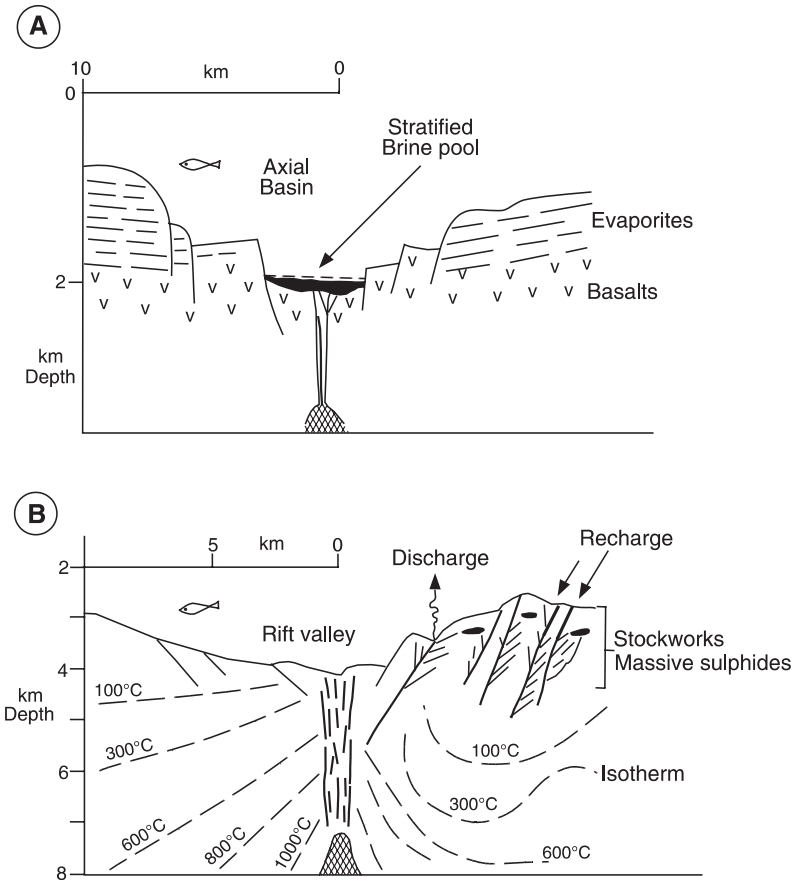


Fig. 7.8 Slow-spreading centres. (**A**) Early stage of opening; narrow sea arm bounded by continental crust (e.g., Red Sea); a basin is formed in the axial zone in which hydrothermal fluids are discharged and form a stratified deposit, characterised by a lower zone of metalliferous muds and sulphides and an upper zone of oxides, hydroxides, silicates and sulphates. (**B**) Advanced stage of opening; crestal area of a mid-ocean ridge transected by transform faults (e.g., TAG area, see also Fig. 7.12); hydrothermal discharge is along faults in the walls of the rift, forming encrustations of Fe-Mn oxides and sulphide stockworks. The matrix of talus material along the fault scarps may become impregnated with sulphides. Note bending of isotherms due to cooling effect of convecting sea water (After Rona 1984)

7.5.2 Hydrothermal Systems at Spreading Centres

Oceanic crust rocks are well endowed with both magmatic segregations and hydrothermal mineral deposits. The former comprise podiform chromite deposits, disseminations of magmatic Ni±Cu sulphides and PGE, Fe–Ti oxides and Au, associated with tectonised peridotites, as found in the

dunite–gabbro–plagiogranite intrusions in the Urals platinum belt, the Alpine-peridotite-chromite deposits of the Moa district in Cuba and the chromitites in the ophiolites of the North China Craton. Relevant references for the interested reader can be found in Sawkins (1990), Li et al. (2002) and Naldrett (2004). The hydrothermal mineral systems of the oceanic crust, discussed here, are confined to the upper layers (generally layers 1 and 2, and less commonly layer 3) (Figs. 7.3 and 7.5).

Hydrothermal systems that originate at spreading centres, whether in marginal basins, in mid-ocean ridges, or in narrow oceanic arms, have been recognised in the geological record of the emerged lands. It is appropriate to point out here that for several reasons the recognition in the geological record of subseafloor hydrothermal systems is by no means simple. This is because oceanic crust tends to be destroyed at convergent plate boundaries, so that only tectonic slices and fragments may survive embedded in a melange of highly tectonised lithologies, as discussed in the preceding sections. In some cases, during obduction tectonic process, whole sections of oceanic crust may be preserved, thereby increasing the possibility of having well-preserved fossil hydrothermal systems, and hence ore deposits. The overall preservation of ancient oceanic crust, or ophiolites, is further constrained by the depth of erosion and therefore the age of the terrane in which it occurs.

Penetration of sea water through oceanic crust results in convective systems which have been modelled to take place as flow in discrete cracks, or as flow in porous media. As mentioned above, the discharge of the return flow takes place at localised vents, or clusters of vents (Figs. 7.5 and 7.7), and is episodic in character with a very short life span (usually only a few years). Sleep (1983) estimated that the total mass of water which escapes through a venting system during its average life of 10 years is in the region of some 3×10^{10} kg , or a cube of water with sides of 300 m. Hannington et al. (2005) reported that on the basis of geophysical measurements, about 3 to 6×10^{13} kg/year of sea water circulates through the spreading centres of the world; whereas estimates based on geochemical mass balances can be as high as 1.5×10^{15} kg/year. Hannington et al. (2005) also noted that, taking into account both low- and high-temperature fluids, the combined fluid flux is probably $>10^{14}$ kg/year, implying that the entire mass of the world's oceans, 1.37×10^{21} kg, passes through the axial zones of the spreading centres every 5–10 Myrs. The estimated convective heat loss at ridge axes is about 1.8×10^{12} W, with less than 10% being discharged at high temperature vents (black smokers), which discharge at a rate of 1–2 kg/sec (Hannington et al. 2005 and references therein). Thus, it is estimated that 10% of 1.8×10^{12} W, would be equivalent to between 50 000 and 100 000 black smokers, or one per 1 km of ridge. However, Hannington et al. (2005) pointed out that a more realistic estimate would be one large vent field, with up to 100 individual black smokers and a heat output of 200–500 W, would occur every 50–100 km. Evidence indicates that sea water circulates and interacts with oceanic rocks to depths of between 5 and 10 km, with overall high water/rock ratios and temperatures probably in excess of 500°C. In a porous medium the

flow of the fluid must be dispersive and slow, so that a parcel of fluid moving laterally or vertically should mix with fluid still retained in the pore spaces. Sleep (1983) pointed out that there is little evidence of this mixing and therefore fluid flow is more likely to occur through cracks and fractures. Nevertheless, in the case of oceanic crust overlain by land-derived sediments, porosity assumes great importance, as discussed later. The simplified geometry and components of a hydrothermal system on the seafloor is shown in Fig. 7.7. The discharge is through vents which are presumed to feed on fracture zones, while recharge occurs along fault scarps near the axial zone (Fig. 7.5).

A model of a sub-seafloor geothermal system proposed by Bischoff and Rosenbauer (1989), invokes *layered double-diffusive convection*, in which a lower brine layer transfers heat and dissolved constituents to an upper sea-water-dominated convective cell (Fig. 7.9). The idea of double-diffusive

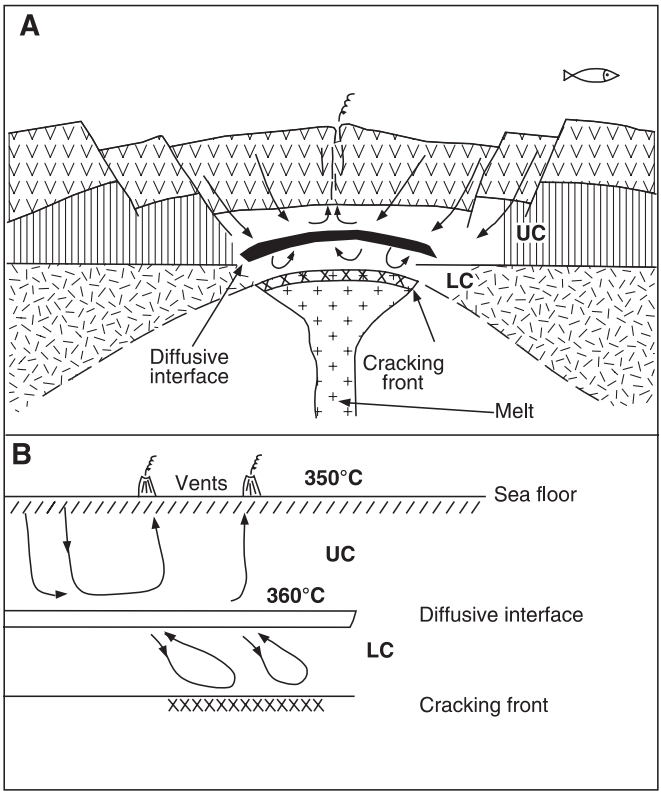


Fig. 7.9 Model of sub-seafloor hydrothermal systems; (**A**) Cross-section of oceanic crust (basaltic lavas, sheeted dykes and mafic rocks) and associated circulation of sea water; LC and UC lower brine and upper cell, respectively; (**B**) Double-diffusive convection model, lower cell (LC) transfer heat and solutes to the upper cell (UC), which discharges on the seafloor. After Bischoff and Rosenbauer (1989)

convection is, at least in theory, well constrained and it has been used to explain certain features of magma differentiation (e.g., Huppert and Sparks 1984, Irvine et al. 1983). The geometry of the sub-seafloor coupled two-layer system as envisaged by Bischoff and Rosenbauer (1989) consists of *nested convection cells* in which the lower cell is formed by a continuously recycled brine located just above a cracking front. This lower brine cell draws heat and dissolved components by circulating through the plutonic rocks, and it transfers heat and part of the solutes to the upper sea-water convective cell across a diffusive interface (Fig. 7.9). When the upper cell reaches the temperature of 360°C, it rises to debouch through vents at the seafloor. The process is used by these authors to explain the salinity variations of the vent fluids. Lower salinity vent fluids are believed to be related to the boiling of the lower brines which results in the dilution of the upper fluids through the transfer of solute-poor vapours into them. Thus, low-salinity vents would coincide with the down-flow regions of the brine cell, while high-salinity vents would correspond with zones of brine upwelling.

There are five main geological environments where mid-ocean ridge-related hydrothermal systems occur: (1) in the axial zones (rift valley) of a spreading ridge; (2) at off-axis seamounts; (3) on the ridge flanks where there may be a thin sedimentary cover; (4) spreading centres close to land, and (5) away from spreading centres where there may be a substantial thickness of deep-sea sedimentary material. Fe- and Mn-rich clays are typical of the latter situation, and these clays may also contain trace amounts of other metals such as Ni, Cu and Co. The origin of the metalliferous clays is not clear, but it is thought that they may be related to distal deposition of particulate matter issued from the seafloor hot springs at mid-ocean ridges and/or localised hydrothermal activity. Metalliferous sediments are treated in Chapter 8.

The nature of the mineralising systems that are formed in the environments of oceanic crust and the size of their mineral deposits is related to the stage of opening of an oceanic basin and the rate of seafloor spreading. Rona (1988) pointed out that sulphide deposits at slow-spreading centres tend to be larger than those at fast-spreading centres, because of the longer residence time of a parcel of oceanic crust within the region of high heat flow. Thus, one can consider slow, intermediate and fast spreading ridges within the framework of early and advanced stages of opening of ocean basins. In each of these situations local conditions must also be considered, such as depth to magma chamber, thermal gradient, permeability, the geometry of the convective system and timing of geological events. Geophysical evidence suggests that magma chambers at slow-spreading ridges (< 2 cm y^{-1}, e.g., Atlantic) are at depths ranging from 3 to 10 km, while at intermediate to fast-spreading ridges (>2 cm y^{-1}, e.g., Pacific) the magma chambers appear to be much closer to the seafloor, at depths of betwen 1 and 3 km.

Slow spreading and early stages of opening are illustrated in Fig. 7.8. This is characterised by a narrow sea bounded by rifted continental margins. The Red Sea is an embryonic ocean in its early stages of opening, locally floored by

basaltic rocks along narrow sectors corresponding to its axial regions from which slow spreading is currently active. The shoulders of the Red Sea rift consist of continental sedimentary rocks including thick evaporite beds. In this setting, hydrothermal fluids have high salinities due to the presence of the evaporites. Iron–Cu–Pb–Zn sulphides precipitate under reducing conditions in restricted basins forming pool-like stratified sulphide deposits. Polymetallic sulphates, silicates, oxides, hydroxides and carbonates precipitate at the interface between the hypersaline solutions and the overlying normal sea water. A more comprehensive description of the Red Sea mineralised pools is given in Chapter 8. Figure 7.8B illustrates a cross-section at a slow-spreading mid-ocean ridge, such as the Trans-Atlantic Geotraverse field (TAG) in the Atlantic Ocean. Hydrothermal circulations is within linear sections of the axial rift are cross-cut by transform faults. Discharges, which occur along fractures and faults in the walls of the rift valley, also impregnate talus material forming a breccia with a mineralised matrix. Recharge is higher up on the shoulders of the central rift valley as shown in Fig. 7.8A, B. A dispersion halo of Mn, Fe, Cu and Zn can extend up to 4 km from the active vents (Rona 1984). In 2005 a newly discovered active hydrothermal field along the Mid-Atlantic Ridge system, is Turtle Pits at about 2990 m of water depth, where fluids emanates with the highest temperature (407°C) so far recorded in submarine vents (Pašava et al. 2007). Turtle Pits, discovered by using plume surveys and unmanned submersibles from the Woods Hole Oceanographic Institution, consists of black smoker chimneys and mounds of sulphide talus material, containing pyrrhotite-chalcopyrite-isocubanite assemblages with anomalous contents of Rh, Pd and Pt (Pašava et al. 2007). Other vent fields in the Mid-Atlantic Ridge are Lucky Strike, Menez Gwen and Rainbow (Douville et al. 2002).

The East Pacific Rise (EPR) is the type example of a fast spreading ridge, illustrated in Fig. 7.10. Here, there are numerous hydrothermal fields in which discharge of fluids takes place along linear zones (faults), and at point sources, located within an inner zone of active extension in a terrain characterised by horst-graben structures. Hydrothermal vents (smokers) may form bands

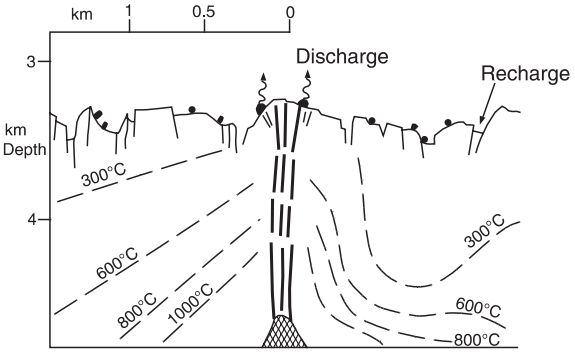


Fig. 7.10 Intermediate to fast spreading ridge and advanced stage of opening (e.g., East Pacific Rise). Sulphide deposits (clusters of smokers and mounds) are shown by the black dots; bending of isotherms as in Fig. 7.8; after Rona (1984)

20–500 m wide and up to 6 km long. The vents rise up to 10 m on a base with a diameter of 15–30 m, and may be arranged in groups of six or seven. These, in turn, may form a vent system containing three to five groups, as schematically illustrated in Fig. 7.7B. Massive sulphide and stockwork deposits are formed containing mainly Fe–Cu–Zn–Ba–Ag. Seismic and tomographic imaging of parts of the EPR, between the Clipperton and Siqueiros transforms enabled Toomey et al. (2007) to study the relationship between mantle upwelling and ridge crest processes. Toomey et al. (2007) found that mantle upwelling and asthenospheric flow is not always centered beneath the spreading axis. This asymmetric delivery of mantle melts results in segmentation of the ridge axis and more importantly in differences in the intensity of volcanic eruptions and hydrothermal activity. Thus, where magma plumbing is located beneath the centre of the ridge axis, volcanic activity and hydrothermal venting are frequent and vigorous, spawning thriving biological systems. By contrast, where melt delivery is off-axis, the melt is forced to migrate laterally to feed the ridge crest and this results in less frequent volcanic seafloor eruptions and less vigorous hydrothermal venting and biological activity. Furthermore, the authors contended that this magma plumbing model predicts that magma entering an axis-centered site is less differentiated than its off-centre equivalent, which is more differentiated and enriched in volatiles. Axis-centered melt will also have higher temperature and for this reason feed high-temperature vents, whereas off-axis melt delivery will be more amenable to differentiation, will be cooler with more common lower temperature venting. Toomey et al. (2007) concluded that the "skew" of magma delivery to the ridge crest influences segmentation and variations in hydrothermal venting.

Fast spreading and early stages of opening is a setting characterised by a narrow oceanic arm bound by continental areas and the active spreading centres are segmented by numerous en echelon transform faults. An example of this setting is the Gulf of California (Guaymas basin, to be discussed below). Abundant terrigenous and/or biogenic sediments are deposited in these basins, resulting in the rapid burying of the mineralised zones. Heat sources are thought to be cooling dykes and sills emplaced into the wet sedimentary pile. The mineralisation consists of metallic oxides, silicates, sulphides and sulphates which accumulate along fault scarps and on the seafloor. Massive and disseminated sulphide bodies occur within the sedimentary column.

In the pages that follow, I describe the hydrothermal fields from four spreading ridges: the fast-spreading East Pacific Rise, intermediate-spreading Juan de Fuca, slow-spreading TAG and the Guaymas system in the Gulf of California.

7.5.2.1 The East Pacific Rise; a Fast-Spreading Ridge

The EPR is an active, fast-spreading (approximately 10–16 cm y^{-1}) mid-ocean ridge which separates the Pacific, Nazca and Cocos lithospheric plates,

extending from the Gulf of California to the Pacific-Antarctic Ridge (Fig. 7.1). The EPR is characterised by high eruption rates, which result in a nearly continuous disruption of vent systems and associated mineralisation, contributing to the generally small volumes of sulphide deposits that form at fast-spreading ridges. About half of the known black smokers occur along the 7000 km of the East Pacific Rise (EPR). At the EPR, the subaxial magma chambers are comparatively shallow, 1.4–1.6 km below the seafloor.The areas studied in some detail are located between 11 and 13° N latitude and between 17 and 21° N latitude. The seminal works of Francheteau et al. (1979), Hekinian et al. (1980, 1983), Haymon and Kastner (1981), Hekinian and Fouquet (1985), Fouquet et al. (1988) and Graham et al. (1988), form the basis of the present discussion on the EPR at 13° N.

Near 13° N, a large number of hydrothermal deposits are present over an area approximately 20 km long and 150 m wide, and along a section of the axial zone of the mid-ocean ridge, together with a substantial mineral deposit located on a nearby seamount. The EPR at 13° N is characterised by an axial graben, 600–200 m wide and about 20 to 50 m deep, and bounded by normal faults. The average water depth at the graben floor is 2630 m. About 6 km east of the axis are two volcanic edifices (seamounts) which rise 350 (southeast seamount) and 250 (northeast seamount) m above the seafloor. Basaltic rocks in the axial zone consist of three main morphological types, namely: (1) elongated collapsed lava lakes, located in the centre of the graben; (2) lobate lava flows, occurring on the sides of the lava lakes; and (3) pillow lavas which occur in the graben, along fault scarps and at the top of the ridge. In general, the on-axis basaltic rocks have more primitive compositions (low Ti, high Mg and Ca) than those on the seamounts (enriched in Ti and K, and poorer in Mg).

The on-axis deposits form chimneys, up to 25 m high, arranged in clusters about 50 m in diameter. They are made up largely of Fe, Cu and Zn sulphides. The active and non-active chimneys have an early coating of anhydrite and Fe sulphides which is thought to act as an insulant, thus enabling the precipitation of higher temperature sulphides in the centre of the chimney. The succession of mineral phases observed towards the centre of a chimney is marcasite, Zn-sulphide, pyrite $\pm$ chalcopyrite $\pm$ pyrrhotite. The off-axis deposit is located on the southeastern seamount and is about 800 $\times$ 200 m. If a depth of 1 m is assumed and an average specific gravity of 3 g/cm^3, this deposit would contain approximately 0.5 Mt of ore. The hydrothermal material of this deposit has been categorised into four groups: (1) Fe-rich massive sulphides, consisting of pyrrhotite, colloform and layered pyrite, Zn and Cu sulphides, opal and barite; (2) Fe–Cu massive sulphides; (3) silica-rich sulphides, consisting of dark grey material containing sulphides in various stages of replacement and dissolution by silica-rich fluids (the main sulphide phases are chalcoyrite, digenite, bornite and idaite); (4) Fe-hydroxides, which are the major constituents of this seamount deposit, cover the massive sulphides and form interstitial material in the pillow lavas. Hekinian and Fouquet (1985) suggested that the off-axis seamount

mineralisation is formed by a more extended and lower temperature hydrothermal event than the on-axis deposits. Also, the discharge of hydrothermal fluids on seamounts may form lenses of sulphides which accumulate on top of one another to form more extensive deposits. The Fe-hydroxides appear to have formed as alteration products of the sulphide minerals. The alteration of chalcopyrite to goethite is prominent and is associated with chalcocite as an intermediate product. Cobalt-bearing phases are locally present as inclusions in pyrite and chalcopyrite.The general succession in these massive sulphide deposits (on- and off-axis) is colloform pyrite, pyrite ± pyrrhotite ± Zn-sulphide, chalcopyrite, marcasite, opal. This paragenesis indicates that there may have been three stages of deposition: massive sulphide stage, silica-rich stage and weathering of sulphides. The evolution of the sulphide constructs formed on both on- and off-axis is illustrated in Fig. 7.11.

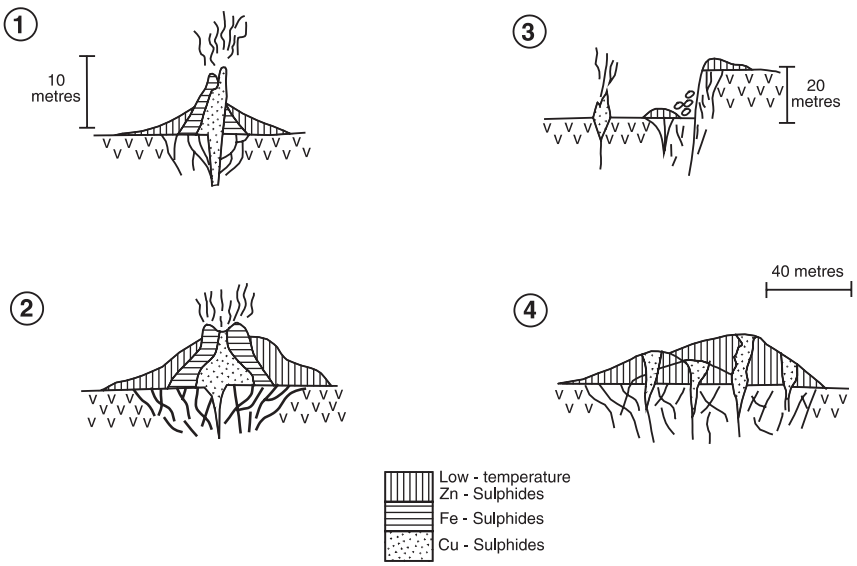


Fig. 7.11 Evolution of seafloor hydrothermal vents and chimneys; (1) Low-temperature phases of Fe and Zn sulphides are deposited on the seafloor, these may inlcude at first, pyrite, marcasite, colloform pyrite, silica, followed by Zn-sulphide and more pyrite. Mineral constructs begin to form (chimneys, or smokers if they are actively venting). A subsequent pulse of deposition results in the precipitation of Fe and Cu sulphides at higher temperatures. (2) At this stage hydrothermal venting begins to decline, but localised discharge, at lower temperature, results in the further building up of the chimney with Fe-rich phases. (3) Fracturing and collapse of the mineral construct may follow, while emission from a new vent begins nearby. (4) Illustration of the type of massive sulphide mound that may form in an off-axis situation; the mound is made up of a series of lens-shaped bodies formed by low-temperature Zn–Fe phases and high-temperature Cu-rich phases and underlying stockwork (for details on the makeup of an individual chimney see Fig. 7.6). After Hekinian and Fouquet (1985)

A number of submersible-based investigations (ALVIN and CYAMEX) led to the discovery of a large hydrothermal field near 21° N latitude. The hydrothermal field in this part of the EPR is formed by a zone, 1.5 km wide, fractured and faulted horst-graben terrain. The field consists of both active and inactive vents and associated sulphide mounds and chimney constructs. The sulphide mounds include accumulated sulphide debris that overlie the basaltic lavas, extend over areas of 15 × 30 m and are up to 2 m high. The mounds are cross-cut by networks of tubular structures, 0.5–3 cm in diameter, which are interpreted as fossilised worm tubes and mineralised channels. These tubular structures have alternating lamellae of pyrite, hydrous amorphous silica, hydrous Fe oxide, sphalerite, gel-like wurtzite and small lenticles of clay material. On top of the basal mound are the smokers. Black smokers emit, at several cm s^{-1}, dark clouds of precipitates consisting of pyrrhotite, pyrite and sphalerite suspended in hot water at a temperature of about 350°C. The black smokers consist of an exterior zone made up of anhydrite, gypsum, sphalerite, pyrite, pyrrhotite, wurtzite and covellite; and an interior zone made up of chalcopyrite, cubanite and bornite (see also Fig. 7.11). White smokers are cooler (<300°C), have slower flow rates, emit amorphous silica, barite and pyrite, and are built of the material mentioned above plus sphalerite, wurtzite, marcasite and sulphur. The white smokers are also characterised by the presence of a biomass containing numerous organisms including clams, mussels and vestimentiferan tube worms that survive on chemosynthetic products derived from H_2S, NH_4^+ and Fe_2^+, which are used as a source of energy by chemosynthetic micro-organisms (Grassle 1983). Non-active chimneys have an interior zone made up of sphalerite, sulphur, pyrite, chalcopyrite, wurtzite, marcasite, galena, bornite, cubanite and chalcocite. The exterior zone consists of amorphous silica, barite, goethite, natrojarosite and corundum. Fallout from the smokers and their fragmentation result in sulphide and sulphate sediments which accumulate to form part of the basal mounds. Bulk analyses of sulphide material give the following range of metal values: 0.20–1.5% Cu, 0.05–50% Zn, 83–480 ppm Ag, up to 640 ppm Pb, 700 ppm Cd and 500 ppm Co. High levels of Au (up to 9600 ppm) and Pt (up to 1.17%) have been detected by electron microprobe analyses of wurtzite gel material, pyrite, marcasite and chalcopyrite.

In 1991 a volcanic eruption was observed between 9° 45' N and 9° 52' N, reported by Haymon et al. (1993). This eruption was followed by a re-distribution of, and a change in the temperature and chemistry of the hydrothermal discharges, associated with the new submarine lava flows. The lavas buried the existing biological communities, but were soon followed by extensive growth of new bacterial mats. These changes were ascribed to a large flux of phase separation and vapour-rich fluids. Within a year, the vent system evolved to more focused and newly developed black smokers, with fluid temperatures decreasing from an initial 403 to 332°C, but with a chlorinity increase from 35 to 250 mmoles/kg, at the same time bacterial mats became reduced, while abundant megafauna consisiting of tube worms up to 30 cm long had appeared (Von Damm et al. 1992, 1995 and http://www.agu.org/revgeophys/humphr01/humphr01.html

(last accessed in April 2008). The 1991 eruption and subsequent changes in the nature of the discharge vents illustrate the rapidity with which a hydrothermal system can develop and evolve, as a result of a volcanic event.

7.5.2.2 Juan de Fuca: an Intermediate Spreading Ridge

The Juan de Fuca ridge in the northeast Pacific Ocean has a spreading rate of approxcimately 5–6 cm y^{-1}. Most studies have focused on three segments of the ridge: Endeavour, Axial Seamount and Cleft. One of the most active hydrothermal fields is the Endeavour segment, where 100–150 black smokers are distributed in six vent fields, along 15 km of the spreading ridge (Hannington et al. 2005). At one locality, submersible studies have revealed an active vent field, 350 m long and 180 m wide, including more than 15 individual vents, up to 30 m in diameter and >20 m in height, which occur together with a number of inactive structures (Delaney et al. 1992). In these fields there are multiflanged sulphide mounds, characterised by vigorous black smoker venting, with fluids reaching temperatures of >400°C. One of these structures is called "Godzilla" that rose 45 m above the seafloor and comprising at least 15 tiers of flanges, giving it the appearance of a tree. Godzilla collapsed in 1996 (Kelley et al. 2002). Low-temperature vents emit nutrient-rich hydrothermal fluids that support a rich and varied ecosystem.

Axial Seamount is a volcano, located in the central parts of the Ridge, which has both low- and high-temperature vents within the caldera, as well as fracture-controlled high-temperature vents along the margins of the caldera. The ASHES (Axial Seamount Hydrothermal Emission Study) field, with several active white and black vent chimneys of 4–5 m height, is located near the base of the southwestern part of the caldera wall. Gravity surveys, carried out from the Alvin submersible, detected a higher porosity in the upper parts of the volcanic edifice, related to lava tubes, lava drains and fractures (Gilbert et al. 2007). These high-porosity zones contribute to the upflow of hydrothermal fluids and are effectively large hydrothermal reservoirs. In 1986–1987 hydrothermal plumes, >20 km in diameter, were discovered in the water column above the north end of the Cleft segment (Baker et al. 1987). These "megaplumes" are the result of voluminous fluid discharges, resulting in a hydrothermal plume that can be detected for several tens of metres above the source which, as mentioned previously, can rain sulphide particles onto the seafloor forming aprons of detritus downcurrent from the vents. A breached caldera, about 7 km ×3 km, characterises the Axial Seamount. In the flat floor of the caldera a number of small depressions, 15–25 m wide and up to 30 m deep, extend for about 300 m along a north–south fissure. Along this fissure hydrothermal vents discharge fluids at temperatures of approximately 29–35°C, although extrapolation to the end-member primary fluid gives a value of 532°C. A few chimney structures are present in the vicinity of this north–south fissure. Sulphides, amorphous silica and barite are the main constituents of the hydrothermal deposit. Sulphide phases are sphalerite, marcasite, pyrite, wurtzite and traces of galena and tetrahedrite.

As for the EPR, hydrothermal activity at the Juan de Fuca Ridge is also subject to frequent changes, with some vents becoming clogged, new ones developing and fluids changing their chemistry. Butterfield et al. (1990) investigated a vent field in the southwest corner of Axial Seamount, where four large sulphide mounds, called Inferno, Hell, Hillock and Mushroom, vent fluids at temperatures ranging from 328 to 136°C. Other vent structures emit fluids of up to 299°C, precipitating pure anhydrite. Butterfield et al. (1990) measured high concentrations of CO_2 and He, probably derived from magmatic degassing, presence of H_2S, chloride, bromide, sulphate, silica, B, Li, Na, K. Mg, Ca, Sr, Zn , Fe, Mn and Cu.

On the northern Juan de Fuca spreading centre is Middle Valley along the northern extension of the Endeavour segment, where the Bent Hill massive sulphide deposit is located. The deposit was investigated by Zierenberg et al. (1998) through boreholes drilled during Legs 139 and 169 of the Ocean Drilling Program (ODP). These workers were able to reconstruct the geometry of the deposit through to its feeder zone and an extract of the results of their work is presented here. The spreading centre of Middle Valley is covered by turbiditic sediments sourced from the nearby continent, so that this section of oceanic crust is interlayered with these sediments, forming a basalt-sill-sediment complex somewhat similar to that of the Guaymas Basin (Section 7.5.2.4). The Bent Hill sulphide deposit is a 35-m-high mound with oxidised sulphide material at the top and surrounded by turbidite sediments. Most of the sulphide mound was deposited above the seafloor, with pyrrhotite being the main sulphide, followed by lesser amounts of isocubanite, sphalerite and wurtzite. Much of this deposit was later recrystallised to a pyrite-magnetite assemblage with the sulphides showing evidence of dissolution and replacement. The massive sulphide mound has a minimum thickness of 100 m, a subhorizontal base and steep flanks, with the basal zone interpreted to represent a time-marker of the onset of hydrothermal venting. The massive sulphide mounds, probably contains approximately 9 Mt of ore material. To the south of Bent Hill is a smaller sulphide mound, called ODP in which a single vent was discharging fluids at about 264°C. Since the Bent Hill sulphide mound lacks sedimentary intercalations, the deposit must have been formed during an intense and uninterrupted pulse of hydrothermal activity. This contrasts with the ODP mound in which three stacked sulphide lenses, each underlain by sediment-hosted feeder zones, testifying to intermittent venting. The feeder zone underlying the Bent Hill deposit was intersected by a drillhole, which showed that this zone can be subdivided into three units. An upper, 45 m-thick of subvertical veins, from >8 cm to >1 mm wide, containing chalcopyrite-isocubanite and pyrrhotite, hosted by turbidite rocks altered to chlorite, quartz, rutile and titanite. The next interval, from 145 to 200 m b.s.f. is less intensely veined, locally with bedding-parallel disseminated sulphides and vertical veins branching into subhorizontal sulphide impregnation in the more permeable horizons. The deepest unit, between 200 and 210 m b.s.f. was called deep copper zone (DCZ) and it consists of 50 vol% of sulphides, mainly chalcopyrite and lesser pyrrhotite, with grades

of up to 16% Cu. The feeder zone as a whole has a N–S trend, probably representing a structural control of the hydrothermal fluid flow. Interestingly, a similar high grade Cu zone was intersected in below the ODP mounds, in the same stratigraphic position, which Zierenberg and co-authors suggested that it may be a potential target for similar style deposits in the geological record on land. Two drillholes sunk on the flanks of the Bent Hill mound encountered a silicified mudstone horizon, approximately at the same depth as the DCZ. This suggests that when the veins were sealed, fluids were forced to move laterally into the more permeable horizons, where silica was precipitated. Television cameras lowered with the drillholes showed vigorous fluid venting and the intensity of the fluid flow out of the 25 cm-diameter borehole was such that it expelled coarse drill cuttings and fragments of massive sulphides, indicating that the borehole penetrated a zone of high pressure. Below the feeder zones, boreholes encountered interlayered basaltic sills and turbidite and finally a layer of pillow basalts, which is probably the top of the oceanic crust basement. Geophysical data indicates that the Bent Hill deposit formed near the transition from oceanic crust to turbidite sediment covered crust and that only after 350 m of sediments had accumulated, hydrothermal fluids began to precipitate sulphides. The sediment cover acted as a thermal and hydrological seal, forcing overpressured fluids to debouch to the seafloor.

7.5.2.3 The Trans-Atlantic Geotraverse (TAG) Hydrothermal Field at a Slow-Spreading Ridge

This is one of the largest active hydrothermal fields on the mid-ocean ridge of the Atlantic Ocean, located between the Atlantis (in the north) and the Kane (in the south) fracture zones (Figs. 7.1 and 7.12). The field, which has been the focus of several studies since its discovery in 1972 (Rona 1980, Thompson et al. 1985, 1988), covers an area of approximately 100 km^2 mostly along the eastern wall of the rift valley between two short transform faults. This wall rises for about 2000 m above the rift valley floor, and it forms a series of steps due to normal block faulting. These faults are probably the channelways for hydrothermal fluids, and it is theorised that the geometry of the block-faulted terrain is such that sea water is forced to percolate downward in the valleys and upward along the walls and rises, where an exceptional number of faults and fractures are present subparallel to the rift valley floor. The TAG field comprises an area of low-temperature discharges along the higher slopes of the eastern wall and a high-temperature discharge zone lower down, where the east wall and the rift valley floor, closer to the axis of the mid-ocean ridge. South of the TAG field a high temperature hydrothermal field, called the Snakepit, was discovered in 1985 (Thompson et al. 1988).

The low-temperature zone of TAG consists of massive stratiform deposits of Mn- and Fe-oxides and Fe silicates (nontronite), from about 1 m to 15–20 m across. The high-temperature field consists of a black-smoker system approximately at a depth of 3600 m, and is located on oceanic crust estimated to be

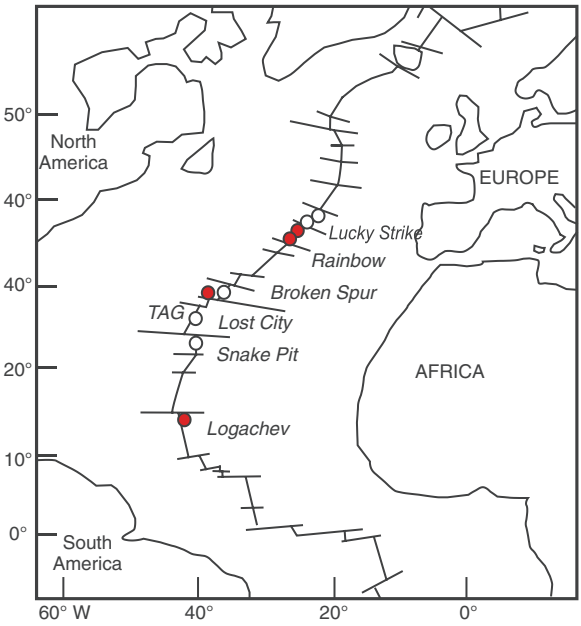


Fig. 7.12 The Mid-Atlantic Ridge; hosts numerous hydrothermal fields, such as those of TAG (Trans-Atlantic GeoTraverse), Logatchev, Rainbow and Saldahna. Red dots indicate hydrothermal fields underlain by peridotite and gabbros, the other fields are hosted on spreading ridge basaltic rocks. After an image on the web site of the University of Washington (http://www.oceanexplorer.noaa.gov/explorations/05lostcity/background/overview/overview.html last accessed in April 2008)

0.1 Ma old. The smokers are on a large outer mound 580 m wide, on which is a smaller inner mound about 250 m wide. The entire structure is approximately 80 m high. The outer mound is formed by basaltic talus and blocks of massive sulphides covered in carbonate ooze material. The inner mound has steep walls about 30 m high and composed of weathered massive sulphide debris. On the mound are inactive and active chimneys, as well as various organisms (crabs, gastropods, eels and worm tubes); chimney structures are up to 10 m high and are located on a construct about 30–40 m in diameter. Discharge of black clouds takes place from fissures at the base of the chimney structures, and the researchers reported that the whole system appears enveloped in a dense cloud of smoke (Thompson et al. 1988). One of the active chimneys of this central structure is composed of an exterior zone of pyrite ± marcasite; and chalcopyrite + anhydrite ± pyrite ± marcasite in the interior. Other chimneys emit white smoke and are composed of mixtures of sphalerite and anhydrite on the outside, and sphalerite ± chalcopyrite ± pyrite ± anhydrite on the inside. The inner parts of these chimneys are characterised by a network of discharge channels lined with chalcopyrite, pyrite and sphalerite. Other mineral phases of the high-temperature TAG hydrothermal system include Fe oxides, orange to red in colour, and they are similar to those found in the low-temperature field. Anhydrite and aragonite are the main sulphate and carbonate phases respectively. The TAG inner mound is estimated to contain some 5 Mt of ore material (Thompson et al. 1988). Humphris et al. (1995b) estimated that the TAG field contains about 2.7 Mt of massive sulphides above the seafloor and about 1.2 Mt below it, with bulk Cu metal content of 30 000 to 60 000 tonnes.

The Snakepit field is located at approximately 23° N latitude and lies in the axial zone of the rift valley, on a ridge made up of pillow basalts. The field itself is characterised by ridges, 20–30 m high and about 100 m long, parallel to the volcanic ridge. They are composed of sulphide talus and chimney material and the areas between the ridges are covered by metalliferous sediments, mainly pyrrhotite, chalcopyrite, marcasite and pyrite. Active black and white smokers are present on these ridges with solution temperatures measured at 350–335°C and 226°C, respectively. The chimneys are made up of an outer portion of fibrous pyrite ± marcasite, and inner pyrrhotite ± chalcopyrite ± pyrite, or outer pyrite + anhydrite, and inner sphalerite + pyrite ± marcasite. The talus material consists of inner pyrite + marcasite and outer native S + jarosite + Fe oxides.

The TAG hydrothermal fields differ from those of fast-spreading ridges because they last longer as a result of the penetration and contact of sea water with hot rocks to great depths. Hannington et al. (2005) called attention to the fact that some parts of the Mid-Atlantic ridge system, such as the Reykjanes Ridge, near Icaland, characterised by abundant magmatic activity, there are no major hydrothermal fields. This is likely due to shallow water depths and the lack of large faults (Hannington et al. 2005).

7.5.2.3.1 Off-Axis Hydrothermal Fields: Lost City

In December 2001, a team of scientists on the research vessels Atlantis and using the submersible craft Alvin, discovered the Lost City hydrothermal field. Other fields on the TAG ridge include Logatchev and Broken Spur (Fig. 7.12). Lost City is an extensive hydrothermal structure situated between Broken Spur and Snake Pit in TAG (Figs. 7.1 and 7.12), discovered and described by Kelley et al. (2001) and summarised here (see also the relevant web site http://www.oceanexplorer.noaa.gov/explorations/05lostcity/background/overview/overview.html last accessed in April 2008). The Lost City low-temperature hydrothermal field is one of the many that are known to occur at mid-ocean ridge-transform faults (Fig. 7.12), where vertical relief can be of few kilometres, resulting in the exposure of the deeper section of oceanic crust to sea water.

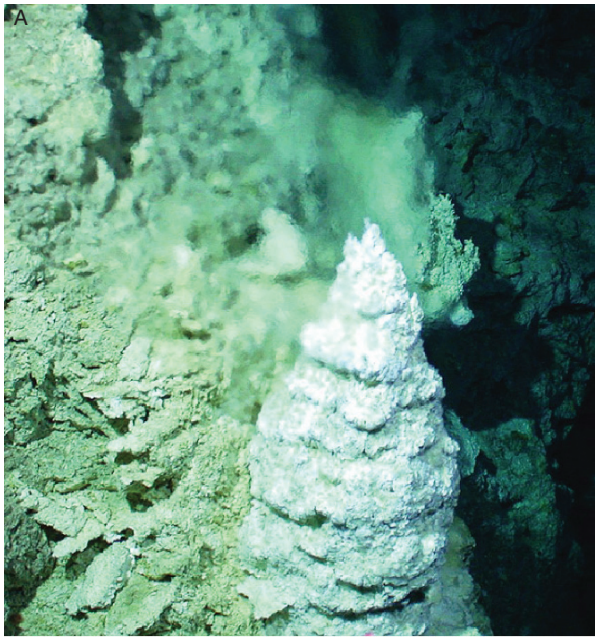
Lost City is a low-temperature vent system, built on 1.5 Ma oceanic crust, and characterised by numerous active venting structures forming pinnacles and flanges composed of carbonate and Mg hydroxide minerals. One of these active vents reaches a height of 60 m. The hydrothermal field is located at the intersection of the Mid-Atlantic Ridge with a transform fault, in the dome-shaped Atlantis Massif. The Massif is about 15 km across with a steep southern escarpment reaching 3800 m of relief and with metamorphosed peridotite and gabbro at the top of the dome. The top of the southern steep escarpment is marked by an unconformity with carbonate-cemented breccias and bedded carbonates, overlain by nearly consolidated pelagic ooze and blocks of mafic and ultramafic rocks. Kelley and co-authors suggested that the unconformity

may have been above sea level, before subsiding to its present depth of 700 m. On the southern wall of the Massif is the Lost City hydrothermal field, lying on a terrace at water depths of 700–800 m, along a south-trending spur, and overlying mafic and ultramafic rocks that are also exposed along the cliffs below the edge of the scarp. These rocks consist of serpentinised and deformed peridotite and gabbro. The Lost City field extends for at least 400 m across the terrace and has about 30 active and inactive structures, some of which form massive pinnacles or chimneys made up of calcite, aragonite and brucite (Fig. 7.13); in one case aragonite and brucite flange vent fluids at 40°C, with the carbonate growing horizontally from the chimney walls (Fig. 7.14).

Analyses of samples collected from several chimneys and flanges showed that these structures are composed of mixtures of calcite, aragonite and brucite ($Mg(OH)_2$). The pH of the fluids at 25°C is between 8 and 10, and the temperature of the vent fluids is between 40 and 75°C. These high pH and Ca-rich fluids are typically derived from serpentinised ultramafic rocks, which on mixing with sea water precipitate the above mentioned carbonates. The Lost City hydrothermal field is the result of the interaction of ultramafic rocks with sea water during serpentinisation processes (see Chapter 2). Methane and H_2S anomalies are commonly detected in the water columns above uplifted serpentinite massifs, because during serpentinisation reduced gas species, such as H_2, CH_4 and H_2S are also produced, providing the necessary energy source for microbial life (Fig. 7.14). The diffuse venting at Lost City supports dense microbial communities, characterised by white to grey filamentous strands several cm long, or forming biofilms on the surface of the carbonate deposits. The abundance of microbial life associated with hydrothermal venting caused by serpetinisation processes, raises the question as to whether submarine ultramafic lithologies of Hadean Earth (4.5–3.8 Ga) could have been a site or one of the sites in which the first living cells were formed (see Chapter 12).

The uplift of serpentinite massifs is linked to the change in the density of the rocks, from about 3.3 g/cm^3 in ultramafic rocks to about 2.7 g/cm^3 in serpentinites. This density change results in expansion and uplift of the rocks affected, which also creates extensive fracturing that allows sea water to further penetrate into the rocks below, producing more reactions with the infiltrated ultramafic rocks. These serpentinite massifs are commonly intruded by gabbro plutons, resulting in an increase in temperatures, which enhances hydrothermal circulation. Furthermore, the ultramafic environment causes enrichment of the venting fluids in Ni, Co and platinum group elements (PGE) (Pašava et al. 2007).

Serpentinisation processes could produce the heat that drives the Lost City hydrothermal system, because the alteration reactions associated with serpentinisation are exothermic, as they consume water and produce heat during the alteration of olivine to serpentine and magnetite. It is calculated that serpentinisation can consume about 300 litres of water per 1 m^3 of rock, releasing about 660×10^6 joules of heat, which can raise the temperature of the rocks by about 260°C (www.oceanexplorer.noaa.gov/accessed in April 2008). The discovery of Lost City suggests that in addition to magmatic heat, large scale



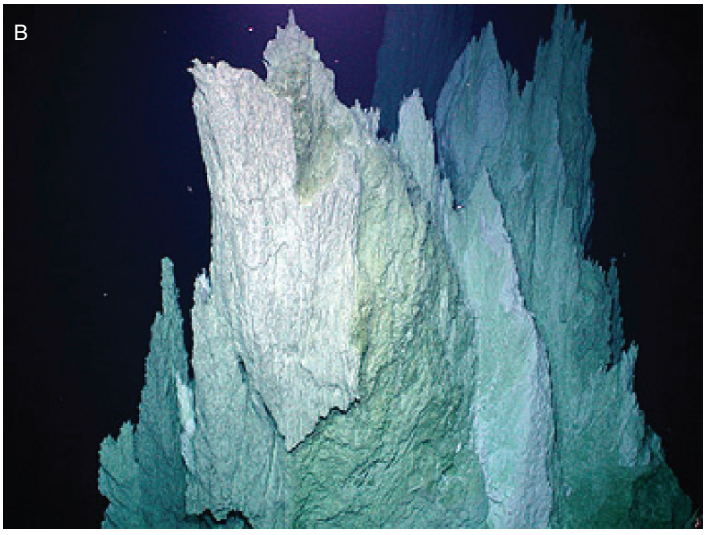


Fig. 7.13 (**A**) The beehive chimney emanating particulate-free fluids with pH of ~10 at 90°C; (**B**) Typical morphpology of Lost City active chimneys, made up of carbonates. Images courtesy of Lost City 2003, University of Washington, (http://www.oceanexplorer.noaa.gov/explorations/05lostcity/background/overview/overview.html last accessed in April 2008)

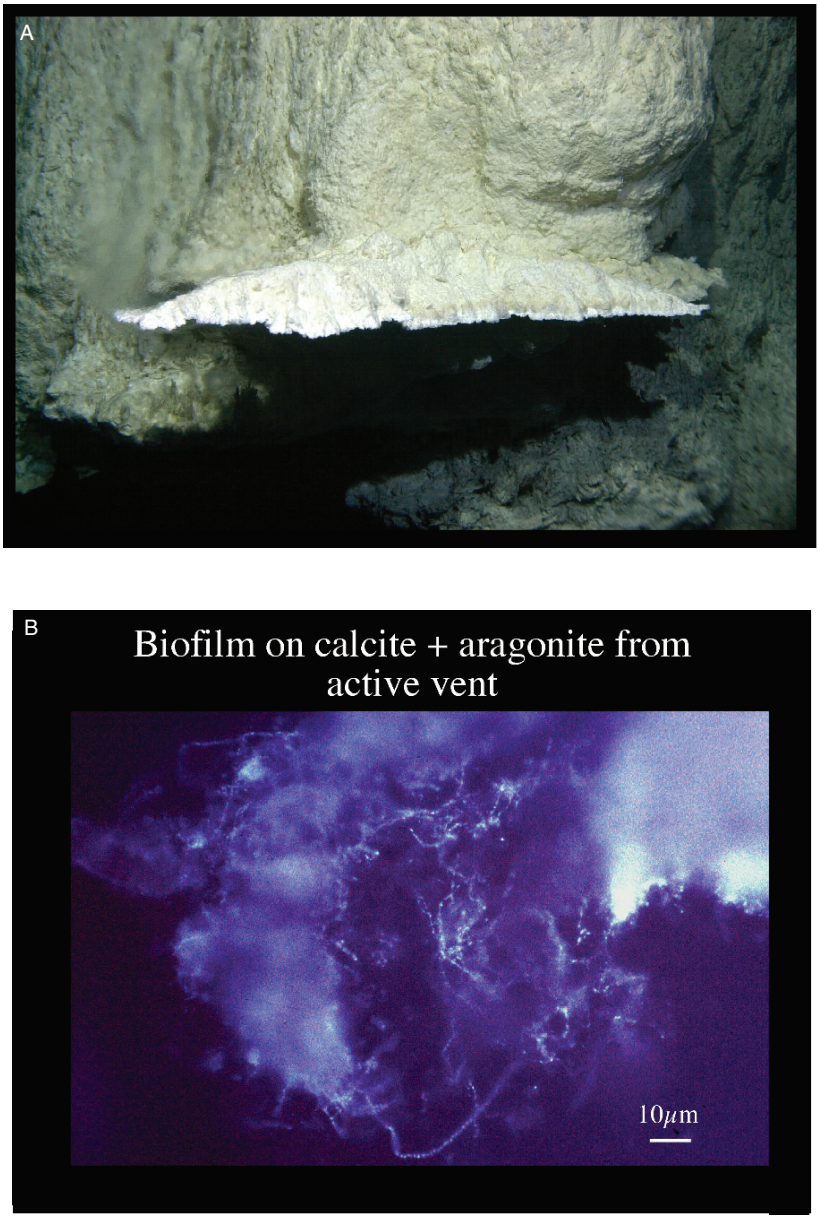


Fig. 7.14 (**A**) Horizontal ledges of aragonite and brucite formed from 40°C fluids that can be seen venting on left side of the photographs; (**B**) Photomicrograph of filamentous microbial communities from the aragonite-brucite flange shown in A; individual dots are single cells about 1 micron across. Both images downloaded from the web site cited in the text; images courtesy of University of Washington

serpentinisation processes can be an important heat engine to power hydrothermal systems. However more recently, McCaig et al. (2007) proposed a new model to explain the low temperature ultramafic-hosted Lost City hydrothermal field. These authors used Sr, O isotope systematics and REE geochemistry to show that black smoker fluids discharging at a TAG-type ocean ridge can be channelled along a low-angle detachment fault. Variable $\delta^{18}O$ values and very high $^{87}Sr/^{86}Sr$ ratios, considered together with depleted REE and negative Eu anomalies are indicative of evolved hydrothermal fluids and not just heated sea water. McCaig et al. (2007) explained these isotopic and REE characteristics by changing hydrothermal fluid systems in relation to the evolution of the detachment fault. Thus, with advancing spreading, the deep seated gabbro intrusions of the oceanic crust move away from the ridge axis, but continue driving hydrothermal circulation below and along the detachment fault causing intense talc-tremolite alteration in serpentinised peridotite. The fluids circulate through the ultramafic footwall to discharge along the boundaries of the mid-ocean rift valley ridge axis to form Rainbow-type vents (Douville et al. 2002). Several kilometres away from the ridge axis, low-temperature fluid circulation in serpentinite rocks forms Lost City-type venting. McCaig et al. (2007) suggested that the gabbro intrusions into the footwall of the detachment fault drive hydrothermal cells and the enhanced permeability provided by the fault zone focuses hydrothermal reactions, intense metasomatism and fluid discharge.

7.5.2.4 The Guaymas Basin, Gulf of California, a Modern Example of Besshi-Type Ore Systems

Besshi-type is a comprehensive name given to a class of hydrotherml mineral deposits characterised by massive sulphide lenses, generally Cu–Zn-rich, formed within terrigenous sedimentary sequences associated with intercalated sills and flows of basaltic rocks of oceanic affinity, and which provide the heat source responsible for the hydrothermal activity (Fox 1984). These geological conditions represent a setting in which the spreading centre is situated within a narrow oceanic arm between emerged lands nearby, from where abundant clastic sediments are shed off and tend to "swamp" the ridge basaltic rocks. Modern-day examples of this particular situation are strung out along the eastern side of the Pacific Ocean and along the western margin of the North American continent and include the Middle Valley, Escanaba Trough and the Guaymas Basin in the Gulf of California, all three sites reviewed by Goodfellow and Zierenberg (1999). The Grimsey hydrothermal field north of Iceland, which consists of sediment-hosted anhydrite and talc mounds associated with sulphide-absent vents, may also be considered in the same catgory (Kuhn et al. 2003). The essential prerequistes of these sediment-hosted seafloor ore systems, is that they form in active spreading centres, which are covered by hemipelagic and turibiditic sediments derived from a nearby continental landmass. As pointed out by Goodfellow and Zierenberg (1999), the sedimentary cover must play an important role in the evolution of the hydrothermal system.

The sediments have an insulating effect, resulting in a more focused discharge, as well as flow of fluids along the more permeable and receptive horizons, resulting in sulphide replacement bodies. The sediments will also react with the fluids and ultimately influence their composition. The heat source is provided by mafic sills emplaced in the sedimentary pile. A model showing the main features of an ore system in a sediment-covered speading centre is shown in Fig. 7.15. In this model there are six main elements (Goodfellow and Zierenberg (1999): (1) a sulphide vent complex or stockwork zone cutting through the sediments, with local sulphide impregnation of altered sediments; (2) a sulphide replacement zone at the base of; (3) a massive sulphide lens; (4) a zone-refined vent complex, characterised by replacement of a pre-existing massive sulphide

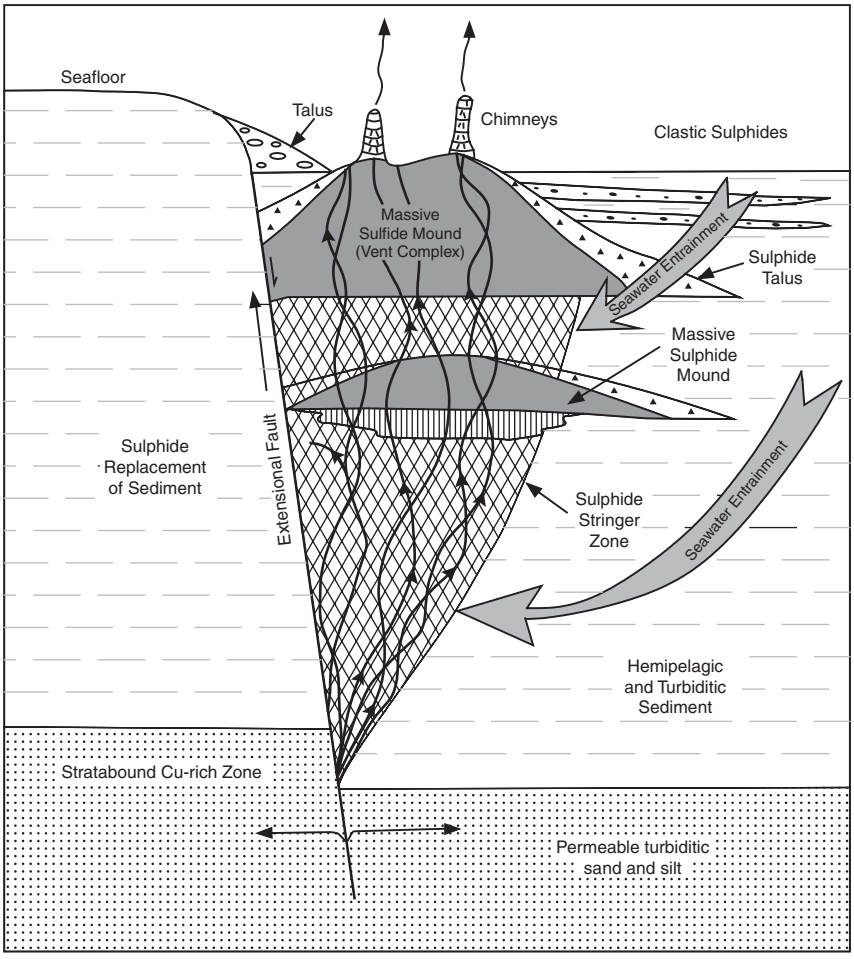


Fig. 7.15 Model of ore system in sediment-covered spreading centre (details in text). After Goodfellow and Zierenberg (1999)

replacement body; (5) sulphide talus shed off the active mounds and interbedded with incoming sediments; (6) sulphide and sulphate chimneys.

Fossil equivalents of ore systems in sediment-covered spreading centres are the above mentioned Besshi district on Shikoku Island in Japan (Slack 1993), the Windy Craggy deposit in British Columbia (Peter and Scott 1999) and the massive sulphide deposits of the Matchless Amphibolite Belt in Namibia (described in Section 7.6.3). In the North China Craton, Li et al. (2004) recognised and reported a sediment-hosted black smoker and sulphide mound complex at Wutai, in a 2.5 Ga ophiolite complex of the Central Orogenic Belt. The origin of the 1.9 Ga Outukumpu Cu–Co–Zn–Ni–Ag–Au sulphide deposits (Finland), has been re-assessed by Peltonen et al (2007) and considered to be a re-worked turbidite-hosted ore system, tectonically emplaced onto the margin of the Karelian Craton.

In the Gulf of California spreading ridges, transform faults and pull-apart basins are buried in mud and silt (Figs. 7.15 and 7.16). One of these basins is the Guaymas Basin first studied by means of sonar scans and submersible craft by Lonsdale et al. (1980), Lonsdale and Becker (1985) and Peter and Scott (1988). The Guaymas Basin extends on land into the Salton Sea through, itself a major site of geothermal activity (Chapter 5). The morphology of the Basin is that of a flat seafloor, covered by sediments and bounded by uplifted blocks also covered by sediments (Fig. 7.16). The sediments in the Guaymas Basin consist of turbidites, pelagic and hemipelagic muds, with the unaltered turbidites being composed of quartz, feldspar, minor chlorite, muscovite and clay (Goodfellow and Zierenberg 1999). These sediments are intruded by mafic sills (basaltic magma), which are emplaced in the sedimentary pile and flow laterally due to loss of buoyancy because of the low-density of the water saturated sediments (Goodfellow and Zierenberg 1999). The entire package is a sill-sediment complex. Along a section extending over more than 120 km, well over 100 hydrothermal sites were detected by side-scan sonar, with sulphide mounds from 5 to 25 m high and up to 25 m across (Peter and Scott 1991). Side-scan sonar surveys of the Guaymas basin, showed the presence of two active spreading segments, Northern Trough and Southern Trough, in which sediments up to 500 m thick have accumulated. These sedimentary accumulations are rich in planktonic carbon, which is "cracked" to form hydrocarbons by the heat of the hydrothermal activity (Edmond and Von Damm 1983), comparable to the formation of hydrocarbons in the Salton Sea (Chapter 5). In the Northern Trough a deposit containing mainly talc and pyrrhotite was discovered (Sea Cliff hydrothermal deposit), whereas more than 120 discharge sites are located in the Southern Trough, a 30-km-long axial rift valley, characterised by fault scarps. One deposit sampled by dredge was found to contain sulphates (anhydrite and barite), talc, calcite, pyrrhotite, sphalerite, chalcopyrite and galena, all "soaked in hydrothermal petroleum condensates" (Lonsdale and Becker 1985). The muddy accumulations of the Guaymas basin are in fact rich in planktonic carbon, and this is cracked by the heat of the hydrothermal fluids to form hydrocarbons. The surveying carried out by Lonsdale's team has indicated that

the shallowest intrusions of magma are buried in up to 400 m of sediment. From mineralogic and isotope systematics Lonsdale and coworkers deduced the presence of three distinct and superimposed hydrothermal systems. One is characterised by expulsion of pore water following the intrusion of a shallow mafic sill. The discharge is at low temperature (about 100°C). The other is a deep-seated hydrothermal circulation that cools a magma chamber. This fluid discharges at high temperature through fractures in overlying sills. A third type is due to convection of water within the sediments above a cooling sill, which provides the necessary thermal energy. The high temperature discharges are possibly driven by a magma chamber about 1 km wide and between 3 and 4 km long. Intrusion of mafic sills into highly porous marine sediments results in decrease of porosity above and below the sill, which drives water away from it. Soon after the intrusion, the temperature at the sill-sediment contact may rise to a maximum 400°C, and the pore water in that region can reach boiling point. The amount of pore water expelled following the intrusion of the sill may be quite considerable: for example an area of 2 km^2 intruded by sills could expell

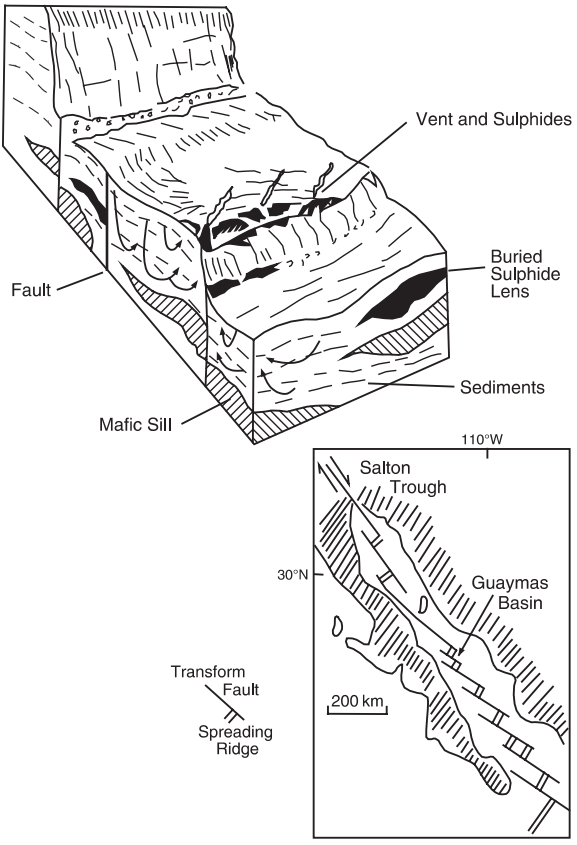


Fig. 7.16 Hydrothermal system (fluid flow indicated by arrows), and mineral deposits in the Guaymas basin, as envisaged by Lonsdale et al. (1980). The inset shows the Gulf of California and location of the Guaymas basin (after Lonsdale et al. 1980)

some 40×10^6 m^3 of pore water. This heated water would then be set into convective motion facilitated by the high permeability of the sediments above the zone of porosity reduction. The hydrothermal fluids can then be channelled along faults and discharge as hot springs at the sediment-water interface.

The surveying carried out by Lonsdale and Becker (1985) indicated that the shallowest intrusions of magma occur below a cover of sedimentary material about 400 m thick. The sites of hydrothermal discharge in the Southern Trough form clusters, with several clusters forming a hydrothermal field. At each site hydrothermal constructs include chimneys, mounds and spires, locally clogged up by tube worms. Some chimneys are composed of a mixture of anhydrite and pyrrhotite. Condensed hydrocarbons are associated with spires of barite in anhydrite-sulphide mounds. Others have their orifices sealed by horizontal precipitates of anhydrite, barite, calcite and sulphides. These horizontal caps force the fluids to discharge downward, precipitating more anhydrite. During their underwater observations, the researchers occasionally punctured the floor covered by hydrothermal material, resulting in hot hydrothermal fluid being emitted at temperatures of about 300°C. The chimneys grow to a height of up to 5 m, on mounds that are between 5 and 25 m high, until they become unstable and collapse. This, in turn, causes the broken vent to re-open and to start discharging again; a new chimney is once more formed which grows until it collapses. The end result is that the seafloor is strewn with talus of hydrothermal material which contributes to the building of a mound. Other types of constructs are columns 10–50 m wide and 25 m high, with smaller vents at their summit. The whole hydrothermal field is therefore made up of clusters of active and inactive mounds, embedded in sheets of cemented talus material. The sulphide mineralogy of the Guaymas deposits consists of pyrrhotite, marcasite, pyrite, sphalerite, wurtzite, isocubanite and chalcopyrite. Anhydrite, barite, calcite, silica, stevensite (a Mg-smectite), Fe oxides and clays constitute other important mineral phases of these deposits (Peter and Scott 1988). The mineral distribution differs between mounds and chimneys and between active and inactive chimneys. Marcasite occurs only in mounds, while chalcopyrite and wurtzite are found in the spires; amorphous silica and barite are more abundant in the mounds than in the spires. Anhydrite is usually absent in inactive constructs because this mineral, which is precipitated in sea water at temperatures greater than 140°C, becomes unstable at lower temperatures. Sulphur isotopic values for the sulphate minerals range from + 20.7 to + 26.4 $\delta 34S‰$, interpreted as having derived from the reduction of sea water sulphate in the vent fluid (Peter and Scott 1988). The presence of calcite in the system is interpreted as due to CO_2 degassing from the vent fluids.

A model for the formation of the Guaymas hot spring constructs, as worked out by Peter and Scott (1988), is summarised here. Venting of fluids on the seafloor begins with the precipitation of stevensite, anhydrite and pyrrhotite around the margins of the vents. This forms an impermeable crust,

which subsequently fractures and allows the fluids to form spire structures. The mineral constructs continue to grow upwards and outwards at the seafloor-sea water interface, which results in less mixing of sea water with the hot fluids, thus allowing the precipitation of the sulphides. As venting continues, the walls of the constructs become thicker and the fractures tend to be sealed by mineral deposition, so that the fluids become hotter and more sulphides precipitate and replace earlier mineral phases. When the central orifice of a chimney is sealed, the fluids escape laterally forming spires. Amorphous silica is precipitated as the system cools. Clusters of tube worms and other organisms play a role in the mineral deposition by insulating the vent fluid from the cold ambient sea water, promoting deposition of sulphides, as indicated by sulphide-replaced tube worms. The mounds are thought to be constructed in a manner analogous to chimneys but with the addition of detritus derived from the collapse of the spires and chimneys.

7.5.3 Subduction-Related Submarine Hydrothermal Systems (Island Arcs, Intraoceanic and Intracontinental Back-Arc Basins)

Hydrothermal activity both on-shore and on the seafloor around submerged volcanic structures of island arcs, intraoceanic and intracontinental back-arc basins, is the expression of volcanogenic submarine hydrothermal systems. Present-day manifestations of this type of activity, are recorded in the Hellenic Volcanic Arc (e.g., islands of Santorini and Milos in the Aegean Sea), in the Kermadec, Kurile and Izu-Bonin submarine arc volcanoes in the western Pacific (Fig. 7.17) and in the back-arc or marginal basins of the Okinawa Trough, Manus Basin, Woodlark Basin, Mariana Basin, Lau Basin and North Fiji Basin. Tables 7.1 and 7.2 lists volcanic arcs and active vent sites, discovered between 1984 and 2002 in island arcs and related trenches.

There is a total of nearly 22 000 km of combined intraoceanic and island arcs, of which about 20 000 km (93%) are in the Pacific Ocean, with a total of 696 volcanoes, of which 209 are submarine (De Ronde et al. 2003a, b). In the geological record some of these hydrothermal systems are probably represented by the volcanic-hosted massive sulphide deposits (VMS) (Kuroko- and Noranda-style ore deposits, to be described in Section 7.7, which are known to form within submarine calderas in rifted back-arc settings. As is the case for epithermal subaerial deposits, these mineral deposits appear to form during the late stages of caldera development, through the activity of hot springs and fumaroles taking place along the flanks of rhyolitic domes and/or the depressions of the seafloor. Stable isotope systematics generally confirm that the VMS ore fluids have a major component of sea water, and the interaction of pore sea water with hot volcanic and

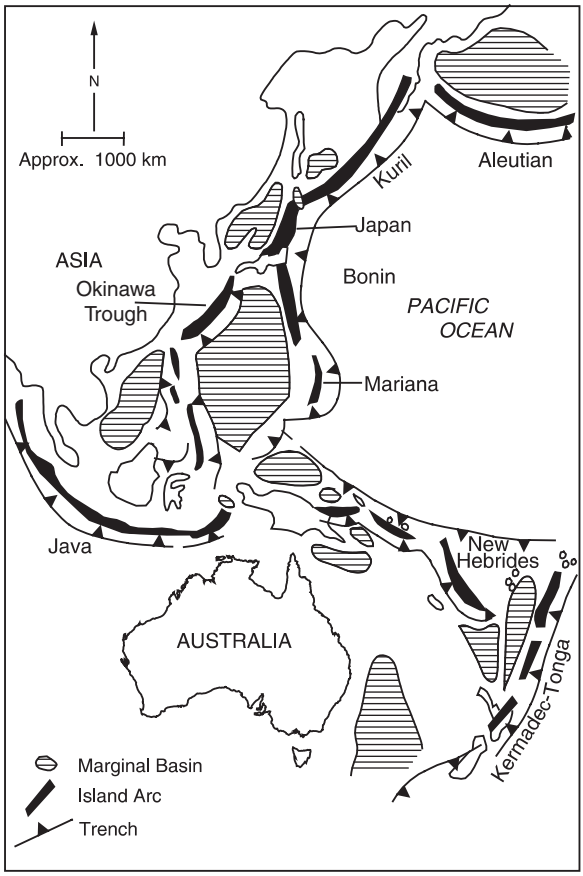


Fig. 7.17 Island arcs, marginal basins and trench systems of the western Pacific Ocean. After Pirajno (1992)

subvolcanic rocks generates hydrothermal convection systems. VMS hydrothermal activity is thought to be characterised by short (a few thousands of years) and vigorous pulses. Present-day submarine hydrothermal systems provide invaluable insights into our understanding of ancient ore systems, and for this reason I describe below the hydrothermal venting in the southern Kermadec volcanic arc, which has been the subject of research for the past ten years.

The Pacific Ocean is well-endowed with archipelagos that form volcanic arcs, which generally girdle the margins of continents and have a basement of continental crust (Figs. 7.1 and 7.17). Intraoceanic arcs, on the other hand, have a basement of oceanic crust and a cumulative length of about 7000 km and (Hannington et al. 2005). de Ronde et al. (2003a) further distinguished transitional island arcs, which are developed along the margins of island chains with a basement of young continental crust. These authors cited the

Table 7.1 List of volcanic arcs that are partly subaerial and partly submarine. After de Ronde et al. (2003a)

Name	Type	Length (km)	Number of volcanoes	Volcano frequency	Evidence for hydrothermal venting
Aeolian	Island arc	180	13	14	Yes
Lesser Antilles	Island arc	730	26	28	Yes
West Aleutian	Island arc	2200	46	48[6]	Yes
Kuriles	Island arc	1120	48	23	?
Izu-Bonin	Intra-oceanic	1200	45	27	Yes
Mariana	Intra-oceanic	1400	50	28	Yes
Luzon	Island arc	1200	55	22	Yes
Bicol	Island arc	1650	38	43	Yes
Sangihe	Island arc	580	31	19	Yes
Halmahera	Island arc	320	17	19	?
Sumatra	Island arc	1620	33	49	?
Sunda	Island arc	2200	71	31	?
Banda	Island arc	580	9	64	?
Bismark	Island arc	930	30	31	?
Solomonis	Island arc	1080	16	68	Yes
TLTF[1]	Island arc	270	10	27	Yes
New Hebrides	Intra-oceanic	1250	47	27	Yes
Tonga	Intra-oceanic	1310	56	23	Yes
Kermadec	Intra-oceanic	1220	38	32	Yes
Puysegur	Island arc	130	5	26	No
S. Sandwich	Intra-oceanic	520	12	43	?
Total		21 690	696	31	

Sunda arc as an example. Volcanic arcs represent the convergence of two plate boundaries and are the surface manifestation of magmatism related to the subduction of an oceanic plate. The Izu-Bonin arc is 1300 km long and contains 45 major stratovolcanoes, of which 26 are submarine. The Tonga-Kermadec intraoceanic arc system is 1700 km long, with at least 90 volcanoes, of which more than 70 are submarine (de Ronde et al. 2003a). The Tabar-Lihir-Tanga-Feni island arc is part of the New Ireland arc system, and in addition to several large porphyry systems, is expecially renowned for the giant Ladolam porphyry-epithermal system on Lihir island discussed in Chapter 5. In all cases, igneous rock types are of the calc-alkaline series, ranging from basalt, andesite, to dacite and rhyolite. Subduction-related magmas can be distinguished from mid-ocean ridge magmas (MORB) for their higher volatile concentrations (H_2O and CO_2, as would be expected because of the flux of sediments and biological matter in the subducting slab), higher Fe_2O_3/FeO and large ion lithophile elements (LILE; Ca, Rb, K, Ba, Sr and Pb), relative to light REE and to the high field strength elements (HFSE; Hf, Nb, Ta, Ti, Zr).

Table 7.2 List of active arc-related submarine vent sites. After de Ronde et al. (2003a)

Arc[1]	Volcano (lat/long)	Location to venting[2] (m)	Depth	Evidence for venting
Aeolian	Panarea	38°41′N/15°08′E	150	1-m high Fe oxide-rich chimneys on submerged slopes of volcano
Lesser Antilles	Kick 'em Jenny	12°17′N/62°25′W	180	Commonly volcanically active; gas discharge and discoloration of seawater
West Aleutian	Piip	55°22′N/167°16′E	390	Echo soundings show large gas-rich (CH_4, H_2) plume over summit
Izu-Bonin	Myojin Knoll	32°06′N/139°51′E	1240	High-temperature (up to 278°C) vents; huge Sunrise massive sulphide deposit
	Myojinsho	31°53′N/139°59′E	330	Volcanically active in historical time; discoloured seawater above summit
	Suiyo	28°34′N/149°39′E	1370	High-temperature (up to 317°C) vents; sulphide chimneys >1 m high
	Mokuyo	28°19′N/140°34′E	1210	Diffuse, low-temperature (max 40°C) venting; calm colony; high $^3He/^4He$
	Doyo	27°41′N/140°49′E	540	Diffuse venting observed
	Kaikata	26°43′N/141°04′E	920	Diffuse venting observed; crabs/mussels/native sulphur/sulphides around vents
Mariana	Esmeralda Bank	14°58′N/145°15′E	110	Plumes with elevated C_4, Fe, and Mn anomalies; 80°C pore fluids
	Kasuga 2	21°35′N/143°37′E	400	Diffuse venting (max 39°C); CO_2 and SO_2 rich
	Kasuga 3	21°23′N/143°36′E	1140	Diffuse venting (max 9.3°C); numerous hydrothermal deposits around vents
	Forecast	13°24′N/143°55′E	1470	White smoker chimneys (max 202°C); chimneys ~1 m high
Sangihe	Banua Wuhu	03°09′N/125°26′E	50	Weak particulate plume
Solomons	Grover	10°28′S/164°15′E	600	Venting observed by cameras; CH_4, Mn, and temperature anomalies
	Kavachi	08°59′S/157°58′E	<250	Weak evidence for elevated ^3He, Fe, and Mn in volcanic plumes
TLTF[1]	Edison	03°18′S/152°35′E	1450	Elevated CH_4 anomalies; observation of diffuse venting with clam beds
New Hebrides	Oscostar	20°59′S/170°17′E	100	Elevated CH_4 in plume above caldera floor
	Cioan (Epi)	16°41′S/168°24′E	300	Discoloration of water above summit; elevated CH_4 anomaly at caldera floor
	Kuwae	16°49′S/168°30′E	270	Anomalous CH_4 in plume above caldera floor

Table 7.2 (continued)

Arc[1]	Volcano (lat/long)	Location to venting[2] (m)	Depth	Evidence for venting
	Starfish	12°12′S/167°35′E	450	Weak local plume; anomalous temperatures
	Stanton	10°52′S/166°42′E	800	Observed shimmering water, vent biota; CH_4 and Mn anomalies in plumes
Tonga	Monowai	25°53′S/177°11′W	120	Observation of diffuse venting; temperature and/or light-scattering anomalies
Kermadec	Vulkanolog	30°41′S/178°27′W	130	Temperature and light-scattering anomalies; bubble plumes over summit
	Brothers	34°51′S/179°03′E	1650	Two distinct sites (other 1,150 m atop cone); chemically heterogeneous
	Healy	35°00′S/179°00′E	1600	Distinct ^{3}H, Fe, Mn plume anomalies; high temperature
	Rumble II West	35°21′S/178°32′E	1450	^{3}He plume; weak Fe, Mn anomalies; gas rich, probably diffuse venting
	Rumble III	35°52′S/178°26′E	250	Gas-rich venting; moderate H_2S concentrations; high Fe/Mn values
	Rumble V	36°08′S/178°11′E	440	Extremely gas-rich venting; abundant H_2S; low Fe/Mn values for plumes
	Tangaroa	36°19′S/178°02′E	890	Moderately gas-rich venting (CO_2); no H_2S; high Fe concentrations
	Clark	36°28′S/177°52′E	880	^{3}He anomaly; no light scattering; moderately gas-rich (CO_2) venting

7.5.3.1 Kermadec-Tonga Intraoceanic Arc System

The Kermadec-Tonga intraoceanic arc system extends for about 2500 km and is the magmatic expression of the subduction of the Pacific plate under the Australian plate, flanked on the western side by the Havre Trough and Lau Basin, where rifting of arc crust occurs (back-arcs), changing to continental crust rifting in the Taupo Volcanic Zone (Figs. 7.17 and 7.18; see also Fig. 5.52). The arc is estimated to contain at least 94 volcanoes, mostly submarine (de Ronde et al. 2003a, b). The southern sectors of the Kermadec-Tonga arc have been extensively studied by de Ronde and co-workers who reported the results of their research in a number of excellent papers. In this section, de Ronde (2006) and de Ronde et al. (2001, 2003a, b, 2005), constitute the basis of the present discussion. The southern sector extends for about 1200 km from the North Island of New Zealand (Fig. 7.18) with irregularly distributed volcanoes, such as Brothers, Healy, Rumble West, Rumble III and V, Tangaroa and Clark, all with active hydrothermal systems and with basalt, andesite, locally with rhyolite and dacite as rock types. Their summit depths range from 220 m (Rumble III) to 1350 m (Brothers Volcano). Systematic mapping and surveying was carried out by the New Zealand American Plume Mapping Expedition (NZAPLUME) in 1999, during which hydrothermal plumes were detected by means of light-scattering profiles by deep-tow surveys and water samples collected for He isotope analyses. Hydrothermal plumes are a mixture of suspended particulate material and dissolved chemical species generally derived from hydrothermal emissions. The analysis of He isotopes enables confirmation of the hydrothermal origin of a plume, with elevated He signals indicating plumes that contain both gas and suspended particulates, which SEM analyses show to contain Fe, S, pyrite and anhydrite. Light-scattering anomalies were detected up to 5 km from their sources with corresponding maxima of δ^3He ($\delta^3He = 100[(R/R_A)–1]$, where $R = {}^3He/{}^4He$ and $R_A = ({}^3He/{}^4He)_{air}$ (see also Chapter 1). However, predominance of gas emissions (e.g., CO_2-rich plumes) may result in high δ^3He, but poor light-scattering anomalies, as exemplified by Clark volcano, which shows a prominent ^3He anomaly but lacks a particle plume and therefore a light-scattering anomaly. Seven of the 13 volcanoes surveyed by the NZAPLUME teams in the southern Kermadec arc showed active hydrothermal veinting. de Ronde et al. (2001) estimated that at least 35 of the 60 submarine volcanoes of the Kermadec-Tonga intraoceanic arc should be hydrothermally active, thus injecting large amounts of hydrothermal fluids into the ocean and precipitating sulphides and sulphate minerals. Massive sulphides were recovered from the calderas of Brothers and Rumble II West volcanoes. Brothers has a 2 km diameter caldera floor at a water depth of 1850 m, surrounded by walls 35–450 m high; the Rumble II West 3–3.5 km diameter caldera lies at a water depth of 1450 m with 50–250 m high walls. Rock types from Brother are predominantly dacitic in composition, whereas Rumble II West is predominantly basaltic, with minor dacite and andesite. Both active and inactive black smokers and diffuse venting were found on the nortwestern

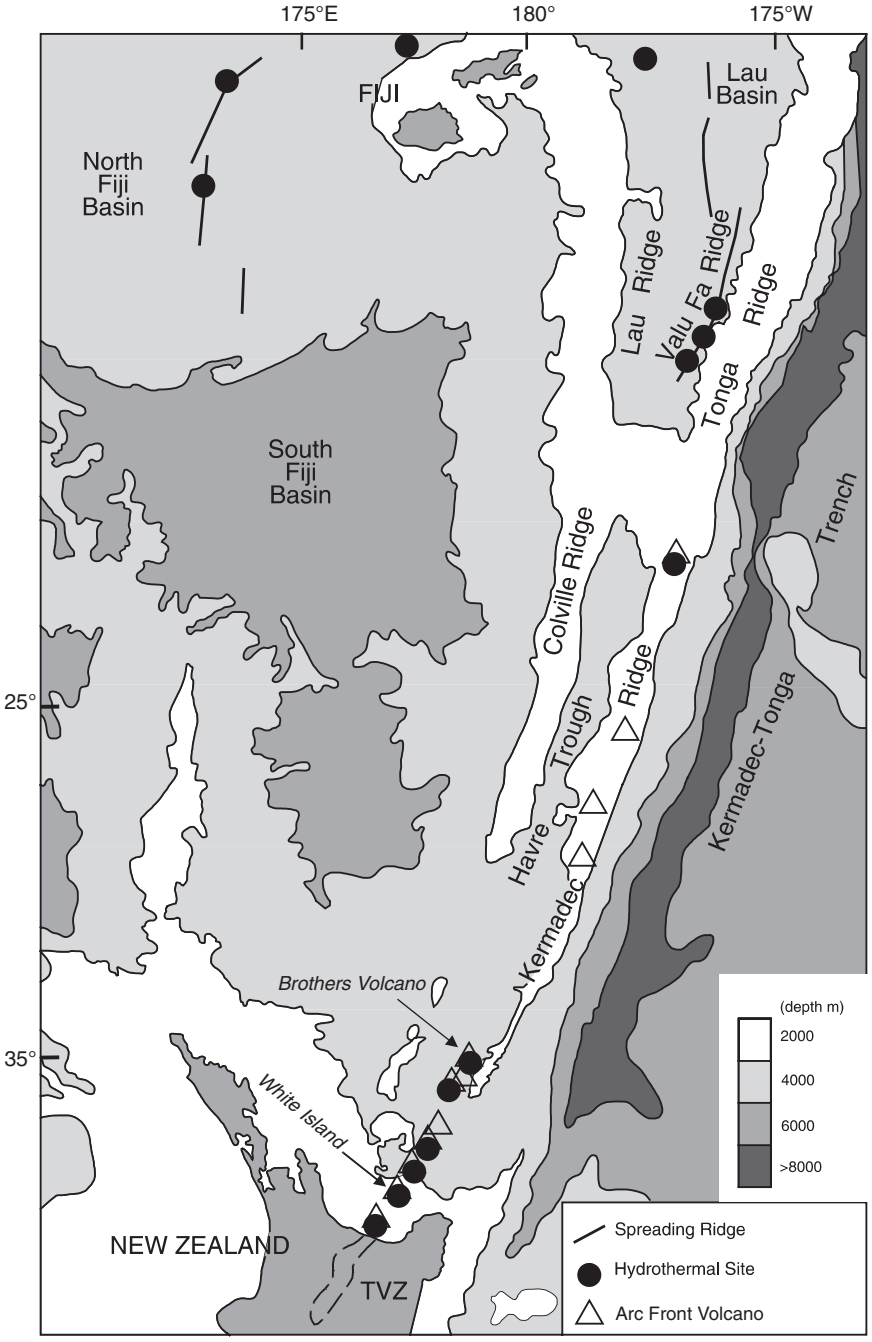


Fig. 7.18 The Kermadec-Tonga arc system, Havre trough and Lau basin-ridge system; TVZ Taupo Volcanic Zone. After de Ronde et al. (2005); see also Fig. 7.17

wall of the Brothers caldera. Hydrothermal plumes were detected during NZAPLUME surveys in 1999, 2002 and 2004 and these plumes were found to rise 750 m through the water column. The results of these surveys suggested to de Ronde et al. (2005) that Brothers volcano hosts vigorous and extensive submarine hydrothermal systems (Fig. 7.19). Hydrothermally altered rocks, stockworks, massive sulphides and pieces of smokers were recovered from the Brothers caldera. Sulphide mineralisation, associated with chimneys and spires is present at 1650 m of water depth, on a ledge and extends for about 600 m and is up to 50 m wide and is surrounded by sulphide debris and subcropping sulphides. This mineralisation and associated venting are structurally controlled by caldera ring faults. The vents are also associated with filamentous bacteria and some macrofauna, including barnacles and crabs. Hand specimens of recovered samples from Brothers, contain massive sulphides and barite. Sulphides are chalcopyrite and sphalerite, commonly intergrown with barite. Other sulphide phases include pyrite, marcasite, galena and covellite. The mineralised samples have been divided into six types (de Ronde et al. 2005): (1) pyritic stockworks; (2) massive pyrite breccia; (3) pyrite-anhydrite breccia; (4) massive pyrite; (5) Fe oxide-silica crusts; and (6) massive sphalerite-rich chimney (Fig. 7.20). A paragenetic sequence for the massive sulphides is as follows (de Ronde et al. 2003b): an early, lower-temperature barite + marcasite $\rightarrow$ sphalerite $\pm$ gold, a late, higher temperature chalcopyrite + pyrite $\pm$ galena $\pm$ gold and a later marcasites $\pm$ pyrite $\rightarrow$ covellite + Fe oxides + atacamite. Electron microprobe analyses showed that Au is primarily associated with galena. The relative abundance of barite suggests that initially the hydrothermal vents were white smokers with temperatures of $<300^{\circ}C$. Deposition of barite was then followed by marcasite and sphalerite, which acted as a seal, allowing the ingress of hotter fluids that precipitated chalcopyrite. Microthermometric studies from chalcopyrite-pyrite samples indicate average homogenisation temperatures of 254–256°C for Brothers and 237°C for Rumble II West, with salinities in the order of about 3.2–3.5 wt% NaCl equivalent. Fluid inclusion volatiles include 99% H_2O, with lesser CO_2, N_2 and CH_4. Sulphur isotopic compositions of sulphides fall into two groups: (1) $\delta^{34}S$ of between –0.2 and 2.1‰ from the sphalerite-rich chimney and from –0.5 to 3‰ from chimney sulphides from the northwest caldera and from Rumble II West; and (2) $\delta^{34}S$ from –4.7 to 0.3‰ from breccias and stockworks from Brothers caldera (northwest rim) and from other sites of the volcano. Native S $\delta^{34}S$ range from –3.9 to – 4.8‰. $\delta^{34}S$ values for sulphate range from 20 to 23.8‰. Hydrothermal alteration consists of both replaced original volcanic rocks and precipitates and even sublimates, such as native S. the most common alteration minerals are illite, illite-smectite, chlorite, saponite, epidote, corensite, celadonite, kaolinite, opal-A, zeolites, stilbite, leucoxene, hematite and goethite. Opal-A, smectite, quartz and zeolites occur as veins and in vugs. Sulphates include anhydrite, barite, natroalunite and jarosite.

The occurrence of sulphides, such as chalcocite, bornite, chalcopyrite, pyrite and enargite veins, associated with advanced argillic assemblages, such as

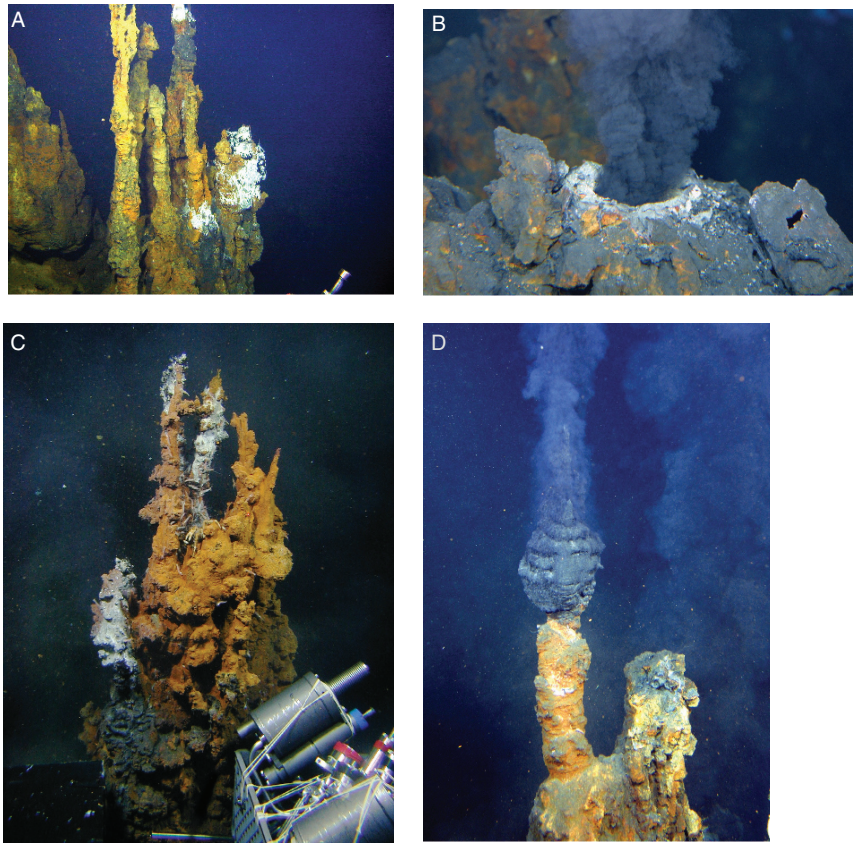


Fig. 7.19 Black smokers from the northwest caldera vent field of Brothers Volcano of the Kermadec volcanic arc (see Fig. 7.18; see de Ronde et al. 2005); (**A**) example of a group of spires from an extinct vent field that have reached heights of 4–5 m above the seafloor. (**B**) hydrothermal vent emitting fluids at a temperature of 274° that have mixed with ambient sea water, forming the black smoke that is commonly detected in surveys to locate vent fields; minerals around the margin of the vent are dominated by pyrite and sphalerite, with a thin zone of chalcopyrite nearest the vent orifice. (**C**) Close-up of an inactive chimney; this is the top of a chimney complex that stands ~4 m above the seafloor; here colonies of shrimp and scale worms congregate around vents that are emitting diffuse (low temperature) hydrothermal fluids. The exterior of the chimney is covered by Fe oxides and silica-rich precipitates. (**D**) Active venting chimney, at a depth of ~1650 m, the top part of the chimney shows a"beehive"-type structure with 302°C fluids being emitted producing the typical black smoke associated with these high-temperature vents. The vent in the photograph sits on top of a larger ~5 m tall chimney. Photographs taken on May 1st 2005 by the DSV Pisces V; photographs and captions courtesy of Cornel de Ronde (GNS Science and NOAA/PMEL, Lower Hutt, New Zealand)

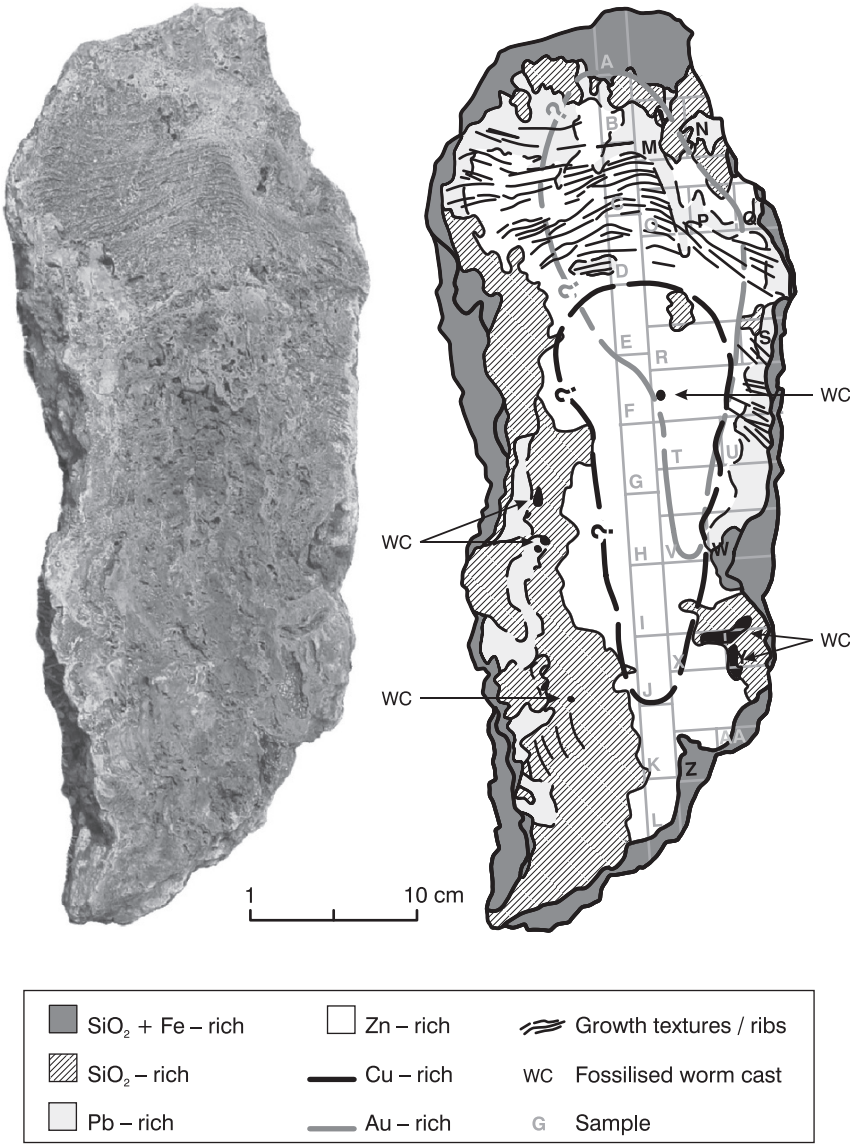


Fig. 7.20 Sphalerite-rich chimney (sample DR04004JV_NZAPII) recovered from the northwest rim of Brothers caldera; the chimney, about 60 cm long and 20 cm in diameter, is zoned with a core of sphalerite + pyrite±chalcopyrite and an outer zone of silica + barite + pyrite + marcasite containing fossil worm tubes; a galena-rich zone is at the top of the chimney. From de Ronde (2006); reproduced with permission of the author

natroalunite, native S suggest high-sulphidation. The presence of abundant native S can be explained by reactions of oxidation or hydrolysis, such as (de Ronde et al. 2005 and references therein):

$$2H_2S + SO_2 \rightarrow 2H_2O + 3S^0$$

or

$$3SO_2 + 2H_2O \rightarrow 2H_2SO_4 + S^0$$

Submarine sulphur deposits are not uncommon and have also been recorded in the Mariana arc.

The evolution of the Brothers submarine hydrothermal systems, discussed by de Ronde et al. (2005), is reported here. Alteration, sulphide, sulphate, oxide and oxyhydroxide minerals at Brothers are indicative of temperatures of the hydrothermal fluids from near-ambient seawater to 300°C. The alteration mineral phases were formed by varying degrees of interaction between seawater and magmatic fluids and changing oxidation-reduction conditions, as well as temperature. These parameter apparently changed in both time and space. Temperature is a key parameter, because as the system heats up as a result of the magmatic pulse, incursion of seawater through thermally induced cracks in the rock considerably decreases the temperature, till the next input of magmatic-hydrothermal fluids, with fluid-rock interactions changing accordingly. High-temperature conditions in the Cu–Fe–S system favour the precipitation of chalcopyrite, bornite and enargite. Decreasing temperature are indicated by mineral assemblages such as zeolites + opal-A + smectite and celadonite + pyrite + hematite + goethite. The Brothers hydrothermal system is driven by the underlying magma chamber with initially dominant high-temperature magmatic-hydrothermal fluids, which move up along the caldera ring fractures along a zone cracking that, the authors suggested, migh extend all the way to the crystallising magma. A dacite intrusion formed a cone within the Brothers caldera on the southern wall, associated with high temperature vent fluids. Cyclic volcanism rejuvenates the seawater-dominated hydrothermal system. Age dating by de Ronde and co-workers suggested that the Brothers hydrothermal system has been active for at least 1200 years.

7.5.3.2 Hydrothermal Fields in the Izu-Bonin Arc

Izu-Bonin is an intraoceanic volcanic arc marks the bouyndary between the Pacific and Philippines plates and extends north–south for about 1200 km from the Izu peninsula of Japan to the island of Iwo-Jima (Fig. 7.1). The Izu-Bonin arc has three main geotectonic units, from east to west: a volcanic front defined by the Shichito-Iwojima Ridge, a back-arc rift and the Nishi-Shichito Ridge. A series of northeast-trending seamount chains, roughly perpendicular to the

trend of the volcanic arc, are present on its west side. On the Shichito-Iwojima Ridge are the Myojin Knoll and Suiyo volcanoes, where massive sulphide deposits are being actively formed (Glasby et al. 2000; de Ronde et al. 2003a, b and references therein). To the west in a back-arc rift zone is the Bayonnaise knoll caldera, with its hydrothermal field being considered a modern analogue of Kuroko-type mineral system (Iizasa et al. 2004). All these hydrothermal mineral systems have been considered as modern analogues of Kuroko-type sulphide deposits, discussed in Section 7.7.1.

Myojin Knoll is a rhyolitic volcano with a base of 22 × 18.5 km, rising 950 m above the seafloor and has a ~5-km diameter caldera with its floor at a water depth of 1400 m and a central cone. The steep walls of this caldera rise 520 and 900 m above the floor, exposing rhyolite lavas, breccias and pumice deposits. Anomalous concentrations of CH_4 and Mn in the water column, about 300 m above the caldera provided the first clues of a hydrothermal system associated with the volcano. This was followed by 23 manned submersible investigations, reported by Iizasa et al. (1999). The hydrothermal field of Myojin Knoll produced the Sunrise massive sulphide deposit measuring 400 m in diameter and 30 m in thickness, extending upslope from the caldera floor and estimated to contain about 9 Mt of ore. The deposit consists of numerous overlapping and coalescing sulphide mounds with chimneys up to 30 m tall. More than 100 chimneys were observed with about 70% being inactive. Active chimneys emit black fluids at maximum temperatures of 278°C and are associated with macrofauna consisting of mussels, crabs, barnacles, sea anemomes and gastropods. Ore minerals are pyrite, sphalerite, chalcopyrite, galena, marcasite, orpiment, covellite, realgar and fahlore. Sulphates include barite and anhydrite. Other minerals are cerussite, jordanite, pyrargyte, in addition to native S and native As (Iizasa et al. 1999). The sulphide chimneys are up to 30 high and have a chalcopyrite conduit with sphalerite interiors and siliceous rinds. The Myojin Knoll chimneys are rich in Au (up to 49 ppm), Ag (up to 3400 ppm) and Cu (up to 20%). Fluid inclusions in barite and pyrite show that these minerals were formed at temperatures of 290 to 180°C from fluids with salinities of between 3.5 and 2.9 wt% NaCl equivalent (Iizasa et al. 1999). Sulphur isotopic values of chalcopyrite show a narrow range from +5.5 to +5.0‰. Iizasa et al. (1999) interpreted the $\delta^{34}S$ values as being derived from the hot volcanic rocks that host the hydrothermal system. Barite, on the other hand, showed $\delta^{34}S$ values of +21.0‰, suggesting that the S in the barite was sourced from seawater.

The Suyo flat-topped volcano was first formed as a dacite-rhyolite volcanic cone, which collapsed to form a horseshoe-shaped caldera. A dacite cone was later built on the collapsed northern caldera wall and then a new crater was formed by subsequent eruptions. On the flanks of this youngest crater, at water depths of 1320–1370 m hydrothermal vents are present consisting of numerous small chimneys (~1 m high). These chimneys contain sphalerite, galena, pyrite, barite, anhydrite and here too the ore is Au-rich (up to 75 ppm) and Cu-rich (up to 10%). Silver averages about 176 ppm.

The Bayonnaise knoll caldera is host to a large hydrothermal field, discovered in 2003 and called Hakurei, where polymetallic sulphide deposits are being formed that have the characteristics of Kuroko-type ores. This relatively new discovery was also reported by Iizasa et al. (2004) and is summarised here. The Bayonnaise volcano is the Quaternary back-arc rift zoone, west of the Izu-Bonin volcanic front, at the northeastern end of the northeast-trending Neogene Enpo seamount chain. The caldera has an elliptical shape and its rim is 3×2.5 km wide, with a floor that is 840–920 m deep. The caldera walls consist of dacite lavas and pyroclastics, whereas the floor contains sandy-clay sediments and pumice material. The main Hakurei hydrothermal field is 700×500 m at water depths of 820 and 680 m on the southeastern margin of the caldera floor and wall. On the southwest side, this field contains a sulphide mound 200 m long and 10 m high, topped with both active and inactive sulphide chimneys. The minerals that make up the chimneys include mainly sphalerite (associated with barite), pyrite, galena, tennantite, covellite, marcasite, jordanite and amorphous silica. Tabular barite crystals, from 5 to 2 mm long, are present in the chimneys' conduits and are thought to be the result of interaction of the hot fluids with cold seawater. Thermometric measurements from both in primary and pseudosecondary liquid-rich with small gas bubbles fluid inclusions in sphalerite crystals, showed temperatures ranging from 255 to 210°C and salinities from 4.2 to 3.2 wt% NaCl equivalent. The homogenisation temperatures and salinities of the Hakurei deposit are similar to those of the Sunrise deposit, discussed above. Chemical analyses of chimney materials and massive sulphideshow that these are enriched in Zn (average 37%), have moderate Pb contents (average 3.1%), Cu averages about 1%, Au averages 6 ppm and Ag 692 ppm. Barium can reach values of up to 23.7%, averaging 5.6%. Other metals that are present are As (34–5020 ppm) and Hg 1.6–57.2 ppm). These metal abundances are somewhat different from the sulphide deposits of mid-ocean ridges, most notably with Cu being depleted in the hydrothermal systems of the Izu-Bonin arc compared to mid-ocean ridge sulphides.

7.5.3.3 Lau Basin

Fouquet et al. (1991a, b, 1993) discovered a number of active hydrothermal fields in a spreading centre of the back-arc Lau basin, in the southwest Pacific (Figs. 7.17 and 7.18). The following is condensed from Fouquet and co-authors. The Lau basin, situated west of the Kermadec-Tonga subduction zone, is being formed by behind-arc spreading between the Lau ridge in the west and the Tonga ridge in the east. The roughly triangular shape of the basin, 600 km side to the north and 200 km side to the south, suggests that basin opening propagates southward. The basin began opening between 3 and 5 Ma ago and the spreading centre is composed tholeiitic basalts with a typically MORB signature. Along the Valu Fa active spreading centre, southwest of the island of Tonga, there are at least three active hydrothermal fields, Hine Hina, White

Chruch and Vai Lili, characterised by low- to high-temperature discharges of hydrothermal fluids depositing Fe–Mn oxides encrustations, sulphates (white smokers) and sulphides (black smokers). One of the most active and extensive of these discharge areas is the Vai Lili hydrothermal field, which was traced for approximately 400 m along strike and is 100 m wide. Rock types in the field include basalt, basaltic andesite, andesite and dacite. Hydrothermal discharges occur at temperatures ranging from 400 to 320°C in black smokers, whilst white smokers discharge occurs at temperatures of 320 to 250°C. The solutions are extremely acid with measured pH values as low as 2. The low pH is explained as due to precipitation of Cu–Fe sulphides, which has the effect of lowering both pH and H_2S contents of the fluids, according to the reaction:

$$Me^{2+} + H_2S \rightarrow MeS + 2H^+$$

Active smokers can be up to 17 m high and are surrounded by taluses of sulphide material. A sulphide mound about 200 m long and 50 m wide occupies the space between the white and black smokers. In some localities the sulphides are overlain or surrounded by Fe–Mn oxides crusts formed by extensive diffuse discharge. Hydrothermal plumes from the Vai Lili field rise up to 200 m above the seafloor. Compared with MOR-type hydrothermal discharges the Vai Lili fluids contain unusual concentrations of B, Ba, Zn, Pb, As, Au and Cd. Fouquet and co-workers were able to sample a cross-section through a massive sulphide deposit. From top to bottom this deposit consists of: (1) Ba–Cu black smoker chimneys, in which barite takes the place of anhydrite in the outer parts of the chimney, whereas in the inner parts is chalcopyrite; other minerals include bornite and covellite, derived from the oxidation of chalcopyrite, sphalerite, tennantite, galena, gold, opal; (2) Ba–Zn chimneys containing barite, sphalerite, galena, tennantite and native Au; (3) massive Cu-rich sulphides, with chalcopyrite as the dominant sulphide, pyrite, tennantite and lesser sphalerite; (4) stockworks in altered andesitic rocks with veinlets of chalcopyrite, silica, barite and sphalerite.

The high Au concentrations (locally Au is visible in the sulphide chimneys) of the poymetallic deposits of the Vaulu Fa Ridge hydrothermal fields may be the result of the dynamic nature of the hydrothermal fluids, characterised by repeated venting through the sulphide deposits, in other words some form of zone refining (Herzig et al. 1993). Gold tends to occur in the low-temperature sphalerite-barite assemblages and is more commonly associated with platy barite. Herzig et al. (1993) determined that the deposition of Au occurs during the initial stages of fluid mixing with seawater and that it was precipitated from sulphur complexes $[Au(HS)^-_2]$.

The three hydrothermal fields of Hine Hina, Vai Lili and White Church show changing styles of hydrothermal discharge and morphology from south to north. These variations can be related to the position of the individual filed within the Valu Fa Ridge and its progressive northward opening. The southernmost field is Hine Hina (south of and ~22°30' S), where volcanic activity is

characterised by autobrecciated volcanic rocks and volcaniclastics underlain by lava. The hydrothermal system here consists of two sections: a lower one controlled by faults within the underlaying lavas and an upper section within the overlying brecciated material with diffuse venting, due to lack of focusing structures. The fluids from the diffuse venting mix with seawater, resulting in low-temperature discharges with precipitation of Fe–Mn oxides, which form crusts and/or cement the surrounding sediments. These Fe–Mn oxides eventually seal the system, preventing further mixing of the fluids with seawater, leading to circulation of higher temperature fluids that flow below the Fe–Mn hard crust, precipitating Cu–Fe sulphides and forming massive subhorizontal ore. The above described Vai Lili field, at about 22°15' S, exhibits a more evolved hydrothermal system than that at Hine Hina to the south. The Vai Lili field also contains volcaniclastic sediments and is characterised both by diffuse and focused venting, with the former typically associated with Fe–Mn oxides. Focused discharge along faults produces sulphide stockworks, sulphides within the volcaniclastics and also forms smokers and massive sulphides mounds. The White Church hydrothermal field is in the northern portion of the Valu Fa Ridge (between ~22° S and 21° 45" S), is controlled by a fault and does not exhibit widespread Fe–Mn oxides deposits. Barium-Zn chimneys and massive sulphides, probably underlain by stockworks along the fault conduit, characterise this field.

Thus, all three fields exhibit sulphide deposits within altered dacitic, andesitic, basaltic andesite volcanic rocks and associated volcaniclastics. An idealised reconstruction of the southern Lau Basin hydrothermal system, consist of an underlying magma chamber at 3 km, from which magmatic-hydrothermal fluids originate and are channelled along dyking zones, mixing with deep circulating seawater along the dykes; supercritical phase separation follows to produce high salinity brines. A reaction zone is present about 1 km below the seafloor, situated at the boundary between the dyke complex and the andesitic lava flows; faults and fractures in these lavas provide the channelways for the fluids to flow upward and Cu–Fe sulphide stockworks form along the main conduits. These have the effect of lowering both pH and H_2S (see reaction above) and massive Cu–Fe sulphides are deposited through focused discharge at the base of a Ba–Zn mound. Laterally from the massive sulphides are impregnation of volcaniclastic sediments and autobrecciated lavas by sulphides, while diffuse discharges through this material forms crusts of Fe–Mn oxides.

Fouquet and co-authors noted a positive correlation between silica and Pb, Zn and Ba and a negative correlation between silica and Cu. They suggested that leaching of more differentiated and silica rich rocks may provide metals, such as Pb and Zn. The authors further considered that the setting of the Lau basin is intermediate between oceanic and continental back-arc environments. This and the nature of the mineralisation suggest that the massive sulphide deposits of the southern Lau Basin hydrothermal fields may have some similarities with, or are transitional to Kuroko-type massive sulphide deposits, which

are also enriched in Ba, Zn, Cu and Pb, as well as Au and are associated with calc-alkaline volcanic rocks (andesite and dacite) in back-arc settings. The nature and type of massive sulphide deposit appears to be controlled by the composition of the basement rocks, which in turn are related to the maturity of the back-arc system, so that in nascent or immature back-arcs the hydrothermal system is related to partial melting of continental crust with the production of felsic magmas associated with mid-ocean ridge basalts and suites of calc-alkaline volcanics (bimodal magmatism). Therefore, the Ba–Zn–Pb–Au metals associations reflect their source rock compositions. By contrast, in more mature back-arc basins, basaltic oceanic crust will produce sulphide deposits that are similar to those of mid-ocean ridges.

7.5.3.4 Seafloor Mineralisation Associated with Seamounts

Hydrothermal discharges on seamounts have been recorded and investigated at a number of sites at mid-ocean ridges, in the above discussed 21°N EPR (Alt et al. 1987) the Juan de Fuca ridge (Canadian American Seamount Expedition 1985), in the Hawaiian chain (Malahoff et al. 1982) and in the Tyrrhenian Sea (Minniti and Bonavia 1984). Two seamounts (Larson's Seamounts), located about 20 and 30 km west of the EPR at 21°N, have hydrothermal deposits within caldera-like structures (Alt et al. 1987). Larson's Seamounts, including the Red Volcano and the Green Volcano, are about 700 m high and of tholeiitic composition. Both are characterised by the presence of semicircular calderas approximately 2 km in diameter, within which are a number of small cones, or nested small craters. Alt et al. (1987) identified four types of hydrothermal material: massive sulphides, material containing opal-barite-atacamite, Fe and Mn oxides and clay minerals. In Green Volcano sulphide chimneys and mound deposits, Fe–Mn sediments and crusts, together with massive deposits of opal-barite occur in the crater inside the caldera and on the caldera rim. In Red Volcano Fe–Mn red-orange muds and crusts, nontronite and talc occur within the caldera. The sulphide material includes spherulitic marcasite and pyrite, chalcopyrite, covellite and Zn sulphide. Illite, opal, chalcedony and barite are also present in the chimney material. Sulphides are locally replaced by Fe oxyhydroxides which, together with jarosite, natrojarosite, and opal intergrown with barite and atacamite, occurin fractures, pores and cover surfaces. The association opal-barite-atacamite may be due to oxidation of primary Cu sulphides. Fe and Mn oxides and silicates include goethite, amorphous Fe oxyhydroxide, birnessite, todokorite, nontronite and Fe-rich talc. The latter forms spherules and sheafs in veinlets and fractures. Most of the non-sulphide materials are the result of either oxidation of sulphides or low-temperature (170–30°C) hydrothermal precipitates. Alt et al. (1987) concluded that the hydrothermal deposits of Green and Red Volcanoes were formed between 140 000 and 70 000 years ago and are related to the volcanic activity of the seamounts.

The Loihi Seamount, located at the southernmost end of the Hawaiian hot spot track, is an active submarine volcano (Malahoff et al. 1982). The volcanic

edifice, similar to the subaerial Hawaiian volcanoes, is characterised by an elongated caldera, within which are two craters and two associated rifts. Hydrothermal deposits in the Loihi volcano consist of yellow–brown goethite-Fe-montmorillonite-nontronite, occurring as precipitates on talus material. They are thought to represent the alteration products of high-temperature sulphide assemblages which may occur at depth.

In the Tyrrhenian Sea, Minniti and Bonavia (1984) reported the presence of hydrothermal mineralisation associated with the Palinuro seamount, a submarine volcanic edifice to the north of the Aeolian island arc. The nature of the volcanic products of this seamount (within plate basaltic rocks of alkaline to tholeiitic affinity) suggests a marginal basin setting. Sampling of the crater of the Palinuro seamount revealed massive sulphide mineralisation consisting of tennantite-tetrahedrite, luzonite and lesser amounts of pyrite, barite, native Ag, bismuthinite and stibnite. The authors argued that this unusual mineral assemblage is reminiscent of that which characterises the high level portions of porphyry systems.

7.5.3.5 Chimneys and Mounds in the Geological Record

The descriptions of seafloor hydrothermal constructs have logically resulted in an attempt to recognise similar structures in ancient hydrothermal mineral deposits which are thought to have formed in the same way. Fragments of black smoker chimneys have been recognised by Oudin and Constantinou (1984) in the brecciated ore of the Troodos massive sulphide deposits in Cyprus. Fossil chimneys and mounds have also been recognised in the 360-Ma-old sulphide and barite sedimentary-exhalative deposits in Ireland, namely, at the Tynagh Pb–Zn deposit (Banks 1985), and at one of the Silvermines orebodies (Boyce et al. 1983). In the latter, a fossil hydrothermal mound has been recognised in an open-pit barite deposit. However, the Silvermines fossilised hydrothermal constructs show marked differences from those typical of a mid-ocean-ridge setting, being smaller, composed almost entirely of pyrite, with minor sphalerite and barite, and having a distinct S-isotopic signature. The differences noted by the authors are ascribed to the diverse tectonic settings and hence the environment of the hydrothermal discharge. The Irish deposits are thought to have formed by hydrothermal discharge in a structural depression or brine pool, at temperatures of approximately 150°C. Sulphur isotope determinations ($\delta^{34}S$ of between –8 and –42‰) of fossil tubes suggest the involvement of micro-organisms that have reduced sea-water sulphate. Pyritic fossil worm tubes have been reported from the Bayda sulphide orebody of the Samail ophiolite (described below) in northern Oman (Haymon et al. 1984). These fossil worms are characterised by moulds and casts preserved in massive sphalerite and pyrite with some quartz. The tube-like fossils are 1–5 mm in diameter, are randomly oriented and have concentric mineral layering from pyrite, on the exterior, to quartz (or void), to pyrite, sphalerite and quartz. The authors compared these fossilised tubes with the worm-tube structures of the EPR. In

the Matakaoa Volcanics, North Island (New Zealand), an allochthonous block of oceanic crust of Neogene age contains small pods of Au-bearing barite and sulphide mineralisation. The study of this mineralisation revealed structures reminiscent of seafloor chimneys (Pirajno 1980).

7.6 Oceanic Crust-Related (Ophiolite) Hydrothermal Mineral Systems in the Geological Record

In this section I describe examples of hydrothermal mineral deposits, the genesis of which is generally recognised to have been in an oceanic crust environment, at or near a spreading centre. As described in Section 7.4, oceanic crust sequences that are tectonically transported, obducted onto continental crust, or marking the closure of an oceanic basin between two plates, are generally known as ophiolites. There are about 200 known ophiolite sequences, of which at least 25 have significant massive sulphide deposits. A review of ophiolite-hosted sulphide deposits can be found in Galley and Koski (1999), who also provide a list of 73 known ophiolite-hosted deposits world-wide. In this section, I describe the deposits of the Samail ophiolites in Oman, the Cyprus Cu deposits, which have been used as one of the type examples for a category of deposits also known as volcanogenic massive sulphides, and the Besshi-type Cu–Zn–Ag deposits of the Matchless Amphibolite Belt of the Damara orogen in Namibia. However, I consider these massive sulphide deposits as distinct from the VMS or Kuroko types, which are associated with submarine caldera complexes in back-arc rifting environments or in oceanic plateaux that have formed through mantle plume processes, as exemplified in the VMS of the Pilbara Craton in Western Australia.

7.6.1 Massive Sulphide Deposits of the Samail Ophiolite, Oman

Since 1975 a multidisciplinary research and exploration programme has been conducted by various British, French and American universities and institutions, in the Oman mountains in the Arabian peninsula. This work, which was primarily directed at evaluating the mineral resources of the region, also provided invaluable information on the geology, geochemistry, tectonism and ore genesis in ophiolitic rocks. Further, the data gained from this multidisciplinary study permitted an in-depth comparison between the Oman ophiolite mineral systems and those that are generated in modern spreading centres. There are several publications dealing with aspects of the geology, geochemistry and mineralisation of the Samail ophiolite; those that provided the basis for the following discussion are Fleet and Robertson (1980), Smewing et al. (1984), Coleman (1984), Ixer et al. (1984), Alabaster and Pearce (1985) and Nehlig and Juteau (1988). A special issue of Tectonophysics (Boudier and Nicolas 1988) is devoted to the ophiolites of Oman.

The Samail ophiolite is situated in northern Oman, on the east–southeastern side of the Arabian peninsula, extending for about 500 km. It forms a well-defined belt which is part of a great ophiolite system that extends from the Mediterranean Sea across Turkey and the Middle East, and marks the boundary, or the suture zone, along which the Tethys Ocean closed towards the end of the Cretaceous period. The igneous stratigraphy of the Samail rocks fits the definition of ophiolites as given by the Penrose Conference participants in 1972, and is essentially made up of a plutonic sequence and a sheeted intrusive complex, followed upward by a sequence of lavas and metalliferous sediments. Alabaster and Pearce (1985) explained the magmatic history of the region in terms of distinct volcanic units and associated high-level intrusives. The Geotimes Unit, consisting of basaltic pillow lavas up to 1.5 km thick, forms the volcanic basement upon which later units accumulated. Geochemical and petrological data suggest that the Geotimes Unit is part of a fractionation trend from cumulate gabbro, through isotropic gabbro, tonalite and trondhjemite of the Main Plutonic Sequence. It is argued that the Geotimes Unit may have formed the crust of a marginal basin rather than an open ocean. The Lasail Unit overlies the Geotimes Unit and consists of mafic to felsic lavas up to 750 m thick. This Unit is cut by andesitic cone sheets which appear to centre over a major intrusion, the Late Intrusive Complex, forming a closed system with a gabbro-diorite-trondhjemite fractionation sequence. The Alley Unit consists of basaltic pillow lavas and minor rhyolitic rocks, related to high-level gabbroic plutons. The last igneous event produced the Clinopyroxene-phyric Unit, made up of basaltic lavas fed by mafic and ultramafic intrusions. The work of Alabaster and Pearce (1985) revealed a coherent picture of ocean floor hydrothermal and ore genesis processes in the Lasail area. In the Lasail area hydrothermal metamorphism produced mineral assemblages characteristic of greenschist facies, chlorite and albite, interpreted as being the result of a multipass fluid flow beneath a sedimentary cover. The Geotimes Unit displays an alteration assemblage of brown smectite + chlorite + albite + calcite + quartz + Fe hydroxides ± actinolite ± epidote ± sphene ± prenhite ± stilbite. Albitisation of the feldspars is typical in the Unit; chlorite is particularly abundant, whereas prehnite and epidote are usually found only in vesicles and veinlets. Traces of jasper and sulphides are locally present and a zone of stockwork veining may represent the feeder to the Lasail massive sulphide deposit. The Lasail basalts have an alteration assemblage of epidote + chlorite + albite + prehnite + quartz + calcite ± actinolite ± sphene ± pyrite ± laumontite ± Fe hydroxides. Chlorite and epidote usually replace the olivines, whereas albite ± prehnite ± epidote replace the plagioclases. The Lasail Unit is interpreted to represent off-axis volcanic seamounts developed on oceanic crust. The alteration assemblage that characterises the basaltic rocks of the Alley Unit includes stilbite + celadonite + albite + chlorite + smectite + calcite ± mesolite ± quartz ± Fe hydroxides. Albite replaces plagioclase and is in turn replaced by the zeolite minerals. The clinopyroxene-phyric Unit has an alteration assemblage of chlorite + epidote + albite + smectite ± prehnite ± calcite ± sphene ± Fe hydroxides.

The predominance of albite and chlorite is indicative of widespread greenschist facies, which in present-day oceanic crust is restricted to hydrothermal discharge zones. Analyses of chlorites and zeolites show a uniform composition for these minerals and this too contrasts with oceanic greenschist rocks in which the chlorites, for example, show strong variations in Mg/Fe ratios. Alabaster and Pearce (1985) advocated a *sealed, multipass hydrothermal system*, due to repeated fluid circulation through the crust. The greenschist facies assemblages are thought to represent prograde metamorphism, while the assemblages containing zeolites and clay minerals possibly represent retrograde reactions due to the cooling phases of the hydrothermal system. The seal of the convective circulation could have been provided by the sedimentary cover of radiolarian mudstones, pelagic sediments and volcanoclastics.

More than 150 massive sulphide prospects have been identified in the Samail ophiolite (Galley and Koski 1999). There are also numerous Fe–Mn-rich sediments which occur as lenses intercalated in the lavas of the Geotimes Unit. These metalliferous sediments are red–brown in colour, composed mainly of radiolarians, and contain quartz, hematite, goethite, Mn oxihydroxides, carbonates (calcite, dolomite, ankerite), epidote, pumpellyite, apatite and natroalunite (Karpoff et al. 1988). Two end members are considered by Karpoff et al. (1988), Fe–Mn types and Si–Ca types, the former having a greater recognisable hydrothermal component than the latter, which contains more biogenic materials. Economically more important are the massive sulphide deposits, such as those of the Lasail area, where three main deposits have been identified: Lasail, Aarja and Bayda, described by Ixer et al. (1984). All three are pyrite-rich, but contain enough chalcopyrite and sphalerite to attain the necessary ore grades for Cu. The larger Lasail deposit has about 8 Mt of ore, Aarja approximately 3 Mt, and Bayda 0.75 Mt; all with an average Cu grade of approximately 2% (Ixer et al. 1984). At Aarjia the sulphide-quartz-chlorite stockwork zone was traced to a depth of 3000 m and is up to 500 m wide (Galley and Koski 1999). The Lasail massive sulphide deposit is approximately 50 m thick and extends to a depth of at least 200 m. The mineralisation consists of a massive sulphide saucer-shaped lens underlain by a stockwork of quartz-pyrite-chlorite in the Geotimes footwall lavas. The massive sulphide lens consists mainly of pyrite with intercalations of chalcopyrite, magnetite-hematite $\pm$ chalcopyrite bands. Minor quantities of sphalerite, marcasite, bornite and traces of cubanite, pyrrhotite, mackinawite and carrollite are also present. The gangue mineralogy includes quartz, calcite, chlorite, epidote and gypsum. The massive sulphide lens is overlain by gossan material containing Fe oxides and hydroxides, jarosite, kaolinite, malachite, azurite and native Cu. Geological evidence suggests that rocks of the Lasail Unit may represent off-axis volcanic seamounts (Alabaster and Pearce 1985), and the mineralogical and geochemical character of the Lasail mineralisation points to certain differences with typical on-axis mineralisation. Ixer et al. (1984) suggested that some of these differences are the higher pyrite content, the overall Zn and Cu depletion, and the higher Co content of pyrites of the Lasail mineralised material compared to the on-axis

mineralisation. Pyrites of mineralised material associated with seamounts may contain up to 17% Co (Hekinian et al. 1983), whereas pyrites from the EPR and the Juan de Fuca ridge have Co contents of less than 40 ppm (Ixer et al. 1984).

7.6.2 The Cu Deposits of Cyprus Island

Copper (cuprum) may have derived its name from the island of Cyprus, or vice versa. What is certain, however, is that Cu has been mined on Cyprus since ancient times (~5000 years BP). The Cyprus Cu deposits, from which also Zn and precious metals are locally recovered, having undergone only minor metamorphism and deformation are ideally suited for study. For this reason they have been used as a type example of ophiolite-related massive sulphide deposits. The geology, geochemistry and tectonic evolution of the Cu deposits of Cyprus are described in the works of Govett and Pantanzis (1971), Robertson (1975), Constantinou and Govett (1972), Constantinou (1980) and Adamides (1984). The main geological feature, and the host of the Cu deposits, is the Troodos Igneous Complex, one of the best exposed and documented ophiolite complexes of the world (Fig. 7.21). It represents the exposed portion of a much larger igneous complex that probably extends beneath most of the island. Although unanimously recognised as an ophiolite, the precise origin of the Troodos Complex remains a matter of controversy. It may be part of oceanic crust thrust up to its present position from a mid-ocean-ridge in the Tethys Ocean, or it may be an off-axis part of the Tethyan oceanic crust, or it may be part of a back-arc marginal basin. The Complex is divided into: (1) The Troodos Plutonic Complex; (2) Sheeted Intrusive Complex; and (3) Troodos Pillow Lavas. The Plutonic Complex is composed of ultramafic rocks, including harzburgite and

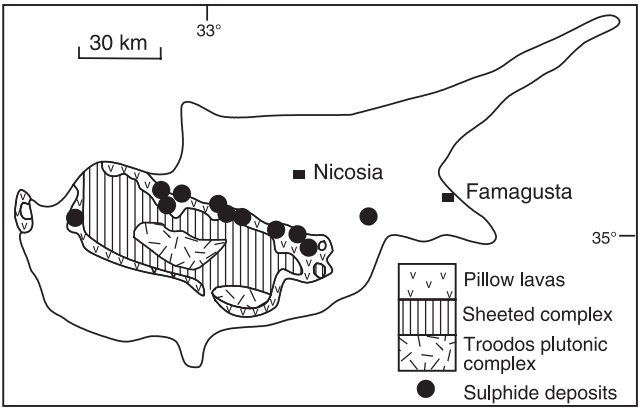


Fig. 7.21 Simplified geology of the Troodos Igneous Complex, Cyprus, and distribution of the main massive sulphide deposits. After Searle (1972)

dunite, interpreted as depleted mantle material, and a gabbroic suite, including peridotite and pyroxenite, intepreted as components of the magma chambers that fed the overlying basalts. The gabbroic rocks and part of the overlying Sheeted Intrusive Complex are correlated with layer 3 of the typical oceanic lithosphere sequence. The upper part of the Sheeted Complex, which consists almost entirely of dolerite dykes, and the overlying pillow lavas of tholeiitic basaltic composition, are correlated with layer 2 of oceanic crust. The Troodos Complex is overlain by marls and limestones which are correlated with layer 1 of a typical oceanic crust.

7.6.2.1 The Sulphide Orebodies

The sulphide mineralisation is restricted to the Troodos Pillow Lavas, which consist of three units: Upper and Lower pillow lavas and the Basal group. This mineralisation occurs as massive sulphides and stockworks forming clusters of three or more bodies in five major mining districts. More than 90 orebodies are known, their size varying from about 50 000 tonnes to 20 Mt and Cu grades ranging from 0.3 to 4.5%. Reconstruction of the orebodies shows that they are saucer-shaped, and most of them characterised by a distinct vertical zoning comprising, in downward succession, an ochre horizon, a zone of massive ore (Zone A), a pyrite-silica zone (Zone B) and a stockwork zone (Zone C; Fig. 7.22). Zone A massive ore is the most economic and comprises two structural types: conglomeratic ore and hard-compact ore. The former is made up of spheroidal, or pillow-shaped, blocks of sulphide material in a gritty matrix of sulphide grains. The size of the blocks tends to increase downward with a concomitant decrease in the matrix material. The increase in the matrix material affects tonnage calculations on account of its lower specific gravity. Hard-compact ore underlies the conglomeratic ore and comprises large blocks of sulphides separated by fractures, several centimetres wide, along which there is a soft and friable pyrite. The dominant ore mineral is pyrite, of which three paragenetic types are recognised. Pyrite I, which is euhedral to subhedral; pyrite II is anhedral and overgrows pyrite I; and pyrite III forming colloform bands mainly in the conglomeratic ore. Chalcopyrite and minor sphalerite are more abundant in the conglomeratic ore, and are rare in the compact ore where they occur as inclusions along the pyrite growth zones. The pyrite-silica zone (Zone B) is characteristically very hard and, in addition to pyrite, has small and variable amounts of chalcopyrite and sphalerite. The silica component is represented by quartz, chalcedony and red jasper. The stockwork zone (Zone C) extends to depths greater than 700 m. It contains small amounts of chalcopyrite and sphalerite, mostly confined to pyrite veins. Pyrite, on the other hand, occurs as veins and veinlets and is disseminated throughout the lavas, which are intensely silicified. The stockworks pass downward into hydrothermally altered and mineralised lavas in which the pillow structures are still recognisable. The hydrothermal mineral assemblage is quartz-chlorite-epidote-illite-kaolinite. Laumontite, celadonite and mordenite are common in both Lower and Upper

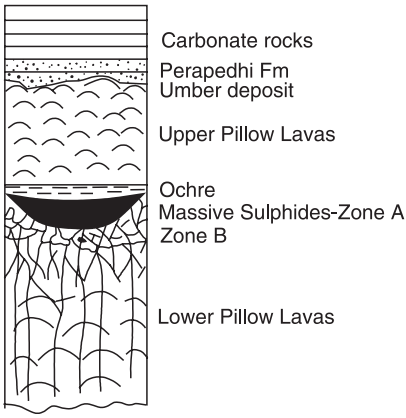


Fig. 7.22 Schematic section through a typical Cyprus-type sulphide deposit, and relationships with overlying rocks. After Hadjistavrinou and Constantinou (1982)

pillow lavas. Deeper down, chlorite, albite, epidote, calcite and pyrite become the dominant alteration minerals. Ochre material, conformably overlies the ore (Fig. 7.22) and is a Mn-poor, Fe-rich, bedded deposit with varying proportions of chert, tuffaceous material and limestone. Ochre contains bands or fragments of sulphides and is enriched in Cu and Zn, with low Ni/Co ratios (<1). It should not be confused with umber, which is a fossiliferous, siliceous fine-grained Mn–Fe-rich sediment, with high Ni/Co ratios (>1). Umber lies unconformably above the sequence of pillow lavas, away from or around the massive sulphide orebodies and at the base of the overlying sedimentary sequence. Umbers post-date the formation of the sulphides and are concentrated in off-axis half-graben structures and are locally enriched in Au (Prichard and Maliotis 1998).

Hydrothermal alteration and the nature of the mineralisation are consistent with seafloor hot spring activity in which pyrite is the dominant primary mineral with lesser quantities of chalcopyrite and sphalerite. As mentioned above for the Samail deposits this may be indicative of an off-axis origin. After formation of the sulphide mineralisation, oxidation of pyrite at the sea water-mineralisation interface produced H_2SO_4, causing acid leaching of pyrite I. This leaching process resulted in the vertical zonation of the ore, from an upper zone of complete leaching, through a zone of partial leaching (conglomeratic ore), to a lower zone where leaching was minimal (compact ore). Some of the products of leaching were lost to sea water, while some were precipitated as secondary sulphides in a zone of secondary enrichment within the conglomeratic ore. The degree to which secondary enrichment progressed was largely dependent on the precipitation and removal rates of the Fe hydroxides because, as layers of the Fe hydroxides accumulated on top of the sulphides, these were protected from further oxidation. The Fe hydroxides are now preserved as layers of ochre material. Continuing volcanic activity deposited fresh basalts over the sulphide mineralisation, and when volcanism ceased oceanic weathering resulted in the formation of umbers, and thereafter a normal marine sedimentary sequence began to accumulate.

7.6.3 The Besshi-Type Cu Deposits of the Matchless Amphibolite Belt, Namibia

The Matchless Amphibolite Belt (MAB) occurs in the Southern Zone of the intracontinental branch of the Damara orogen, Namibia (see also Chapter 6). The MAB is clearly visible in satellite imagery as a dark northeast-trending line, extending for about 350 km from the southwest in the Namib desert to the northeast in the highlands around the capital city of Windhoek.

Rocks of the MAB are lithostratigrahically included in the Matchless Member of the Kuiseb Formation (Khomas Subgroup, Damara Sequence; see also Chapter 6) and comprise amphibolite, metagabbro, minor talc schist, quartz-sericite schist and chlorite schist, intercalated within quartz-biotite schist, garnet, staurolite and kyanite schist. The metasedimentary rocks are indicative of terrigenous-dominated sedimentation in a deep and narrow trough (Khomas Trough), which may have been underlain by oceanic crust. The mafic rocks of the MAB form discontinuous lenses within these metasediments (Fig. 7.23), aggregating a total exposed width of approximately 3 km.

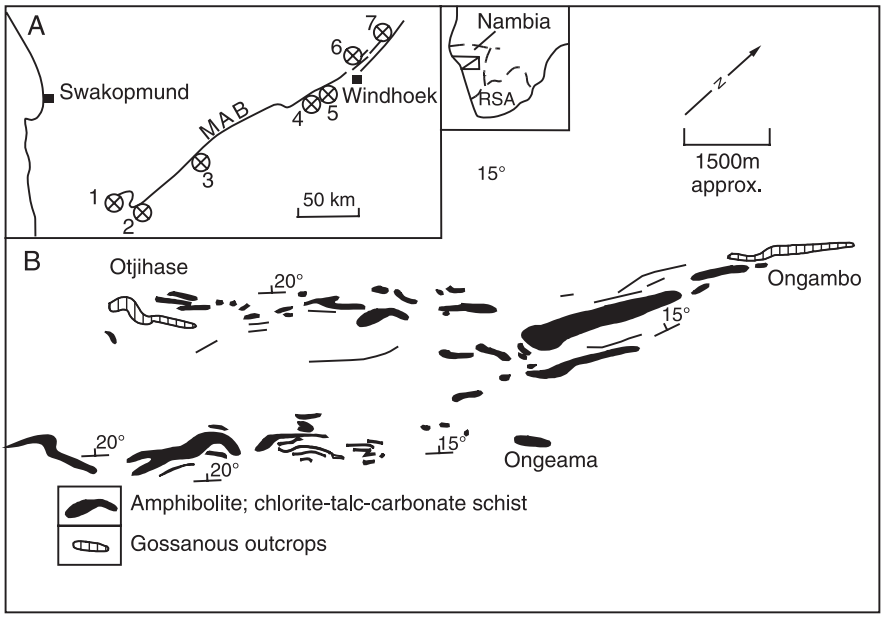


Fig. 7.23 (**A**) Schematic representation of the Matchless Amphibolite Belt (MAB) in the intracontinental branch of the Damara Orogen, Namibia, and location of associated massive sulphide deposits, 1 Hope; 2 Gorob; 3 Niedersachsen; 4 Matchless; 5 Kupferberg; 6 Otjihase; 7 Ongeama and Ongambo. After Breitkopf and Maiden (1988). (**B**) Distribution of the Matchless amphibolite and allied lithologies around the Otjihase, Ongeama and Ongambo sulphide deposits near Windhoek

Attention focused on the MAB because the interpretation of the nature of its lithologies may help in elucidating the tectonic setting of the Belt and hence the geodynamic evolution of the Damara orogen as a whole. Three tectonic settings have been considered: intracontinental, oceanic and one of small and restricted ocean basins where spreading was active (Red Sea style?). The amphibolites have been interpreted as metalavas of tholeiitic composition with petrological and geochemical affinities to mid-ocean ridge basalts (MORB). However, there is evidence for a syn-sedimentary submarine extrusive origin for the amphibolites, such as interfingering with the metasediments and their common association with magnetite quartzite, whose precursor lithology was probably a chemical sediment formed near hydrothermal discharge vents. Also, the position of the MAB, high in the Kuiseb stratigraphy, together with the lack of evidence of a tectonic melange and recognisable sheeted dykes, do not suggest that the MAB is a typical ophiolite. Breitkopf and Maiden (1988) and Klemd et al. (1989) interpreted the tectonic setting of the MAB on the basis of the trace element geochemical signature of the mafic rocks and the character of the associated sulphide mineralisation. These authors consider that along the length of the MAB, and the Khomas trough, there may be at least two main tectonic subsettings. One is in the western sector of the Belt, where the Gorob and Hope Cu deposits are located (Fig. 7.23), in which the mafic rocks show degrees of fractionation compatible with within-plate basalts. This is shown by their Ti, Ti/Cr and FeO/MgO ratios, which are higher, and Ni/Ti ratios, which are lower, than the mafic rocks of the other subsetting in the central and eastern sectors. In the eastern sector MAB rocks have compositions consistent with mid-ocean-ridge tholeiitic basalts. The Matchless, Otjihase and Ongambo Cu deposits occur in this eastern sector (Fig. 7.23). Thus, the scenario envisaged is one of extensional tectonics, characterised by continental rifting with thinning and stretching of the crust, which resulted in the development of a series of small, elongated basins or troughs. In the western sectors, the basins were formed above the thinned and stretched continental crust in which mafic magmas ascended and fractionated within this crust. In the central sectors there was possibly less continental crust, as suggested by the systematic variations in Ti, Ni, Cr, Fe and Mg indicated above. According to this model, a basin in the eastern sector of the Khomas trough was probably floored by oceanic crust, and mafic magmas were being injected into wet and unconsolidated terrigenous sediments. The western basin could have been formed by strike-slip movements which resulted in a pull-apart basin (Breitkopf and Maiden 1988). Breitkopf and Maiden (1988) also contended that the size of the associated massive sulphide deposits appears to correlate with the stage of opening of these basins. The larger deposits (Matchless, Otjihase) are located in the eastern basin floored by oceanic crust, and the smaller (Gorob, Hope) in areas underlain by continental crust. The Otjihase and Gorob ore systems are discussed next.

7.6.3.1 Mineralisation

A number of massive sulphide deposits containing Cu–Zn–Ag–Au, occur along the MAB (Fig. 7.23). These include Gorob, Hope, Luigi and Vendome in the southwestern part of the Belt, Niedersachsen in the central part and Matchless, Kupfeberg, Otjihase, Ongeama and Ongambo in the northeast, near Windhoek. The MAB mineralisation was reported by Killick (1983, 2000), Adamson and Teichmann (1986), Klemd et al. (1987, 1989). Moroni (1990) studied the Ongeama and Ongombo deposits. A comprehensive review of the MAB mineral deposits can be found in Schneider and Seeger (1992). In this section I describe the Otjihase and Gorob deposits.

Dynamothermal metamorphism obliterated the original structures and bedding of the sedimentary layers. Intense compression of the MAB and Kuiseb Formation rocks resulted in isoclinal to recumbent folding and the development of a dominant penetrative S_2 foliation which dips to the northwest. The shape and present attitude of the massive sulphide bodies, which are cigar-shaped and have steep northerly plunges reflect the deformation history of the area. Mineral lineations are present which parallel the ore shoots and as such provide a useful guide for the intepretation of geophysical surveys and for establishing of drill targets (Fig. 7.24).

7.6.3.1.1 Otjihase

The Otjihase deposit is located 20 km northeast of Windhoek, capital city of Namibia. At the end of 1991 ore reserves were approximately 10 Mt at 2.6% Cu, 0.3–0.6% Zn, 9–10 ppm Ag and 0.35–0.5 ppm Au, with pyrite concentrates containing 50% S (Killick 2000). The mineralisation is hosted in quartz-biotite schists of the Kuiseb Formation, but in the vicinity of the orebodies the host rocks also include garnetiferous quartz-biotite schist and chlorite schist, talc-carbonate schist and actinolite schist. The rocks strike northeast, dipping northwest at about 15°. The deposit is dividedinto different fault-bounded blocks, by north- and northeast-trending faults. The orebody is closely associated with a magnetite-quartzite unit of the Matchless Member, which here consist of layers and lenses of amphibolite and talc-chlorite schist, within garnet-biotite-quartz schist and biotite-chlorite schist of the Kuiseb Formation. Surface expressions

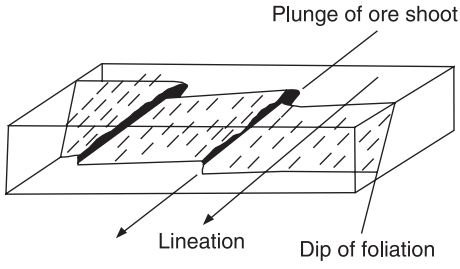


Fig. 7.24 Block diagram showing location of ore shoots in drag-fold closures and plunge of lineations (details in text). After Pirajno (1992)

of the mineralisation are characterised by four distinctive gossanous magnetite quartzite outcrops which can be traced for a distance of at least 1.5 km (Fig. 7.23). These outcrops are up to 12 m thick and have a downdip extent of about 4 km. The gossan material is red-brown in colour and consists of leached limonite, goethite and siliceous material in which Cu values are only about 0.1%. Oxidation of the sulphide zones extends down to a depth of about 50 m in places, where there is an abrupt change to sulphides without a zone of secondary enrichment. The mineralisation is situated some 300–200 m structurally and possibly also stratigraphically, above the MAB rocks (Fig. 7.23). The main orebody (northern oreshoot) is narrow, elongate and lenticular. As already mentioned, an important feature both of the Otjihase deposit (and of Gorob, described below) is that the plunge of the long axis of the ore shoots is defined by a prominent D_2 mineral lineation, which parallels the direction of minor fold axes seen on the surface in the footwall magnetite quartzite. The northeastern limit of the orebody is sharp and represents a possible fold closure, while on the southwestern side the ore zone interfingers with schists and the cutoff is determined by assay values. The hangingwall contact is usually transitional, whereas the footwall contact is sharp. Therefore a footwall contour map provides a useful picture of the mineralisation and also aids in stope planning. The orebody averages 2.5 m in width, but may locally thicken to 7 m. A representative cross-section of an ore lens of the Otjihase deposit is shown in Fig. 7.25. Goldberg (1976) divided the ores into massive, disseminated and stringer. The massive ore is composed of more than 80% sulphides and 20% magnetite quartzite gangue. Sulphides are fine- to coarse-grained and form massive bands composed of pyrite + chalcopyrite or alternating bands of pyrite and chalcopyrite. Disseminated ore contains up to 50% sulphides in a gangue of sericitised chlorite-biotite schist and magnetite quarztite. Stringer sulphides form narrow veins of either pyrite or chalcopyrite. The mineralisation consists of pyrite and chalcopyrite mainly, with varying minor quantities of sphalerite, galena, pyrrhotite and electrum. Silver and Au are also associated with the chalcopyrite. The sulphides form disseminations in magnetite quartzite and quartz + biotite + chlorite + garnet + feldspar schist and as massive bodies in association with the above lithologies. Metamorphism and deformation have substantially modified the orebodies with noticeable boudinaging of the magnetite quartzite, flowage of the more ductile schists, and doubling-up of layers which have resulted in local thickening of the orebodies. Annealing of the sulphide grains has resulted in the development of coarse-grained sulphide aggregates and mosaics. Because of deformation it is difficult to recognise pristine vertical and lateral zonations within the ore lenses. Looking at the representative cross-section of Fig. 7.25A and the semi-quantitative geochemical profiles along the mineralisation (Fig. 7.25B), two interpretations may be advanced, depending on whether the mineralisation was formed as a convex lens, or mound, or as a sulphide pool. In the first case, (as suggested by the mine geologists; A.Thomson pers. comm. 1989), the entry point of the hydrothermal fluids was at the site of the magnetite quartzite, which would then represent the

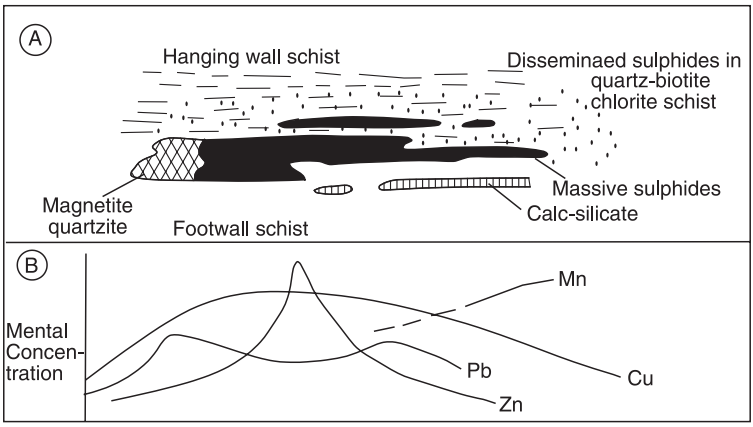


Fig. 7.25 Schematic cross-section of (**A**) Otjihase-type orebody and (**B**) semi-quantitative lateral distribution of selected elements (see text for details). After Pirajno (1992)

waning stage of the sulphide deposition, with the sulphide lenses occurring laterally to the magnetite-quartzite. In this case, the present footwall would also be the stratigraphic footwall. The other possibility is that the original mineralisation was formed in a structural depression as in a brine pool. The magnetite quartzite would still represent waning hydrothermal activity, but would have formed in the oxygenated environment above the sulphide pool. In this case the magnetite quartzite would represent the stratigraphic top with the whole ore lens, as seen now, lying on its side, with the stratigraphic footwall on the right-hand side of Fig. 7.25A.

Hydrothermal alteration is not readily apparent, either mineralogically or geochemically, because of metamorphism and deformation. However, in their study of the Matchless ore lenses, Klemd et al. (1989) proposed that the chlorite-quartz-ankerite schist, with intercalated bands of magnetite quartzite and lenticles of sulphides at the immediate structural hangingwall of the orebody, may represent an original footwall feeder zone, and therefore the sequence would be overturned. In their model, the magnetite quartzite is interpreted as the metamorphosed equivalent of a ferruginous cherts deposit around the exhalative vents on the seafloor. By contrast, the pyrite-quartz-muscovite (or sericite) rocks, which occur in the structural footwall, are interpreted as exhalites forming as a result of waning hydrothermal activity, and they appear to decrease in number away from the mineralisation, that is upward in the stratigraphic hangingwall. Geochemically, the assumed footwall feeder zone rocks show depletions in Na, Ca and Sr, and enrichment in Rb, Ba, Fe and S as well as Cu, Zn and Pb. The local exploration geologists (T.Smalley and D.Corbett pers. comm. 1990), however, do not support the model proposed by Klemd et al. (1989), but instead regard the magnetite quartzite bands as the top of the mineralised system, in which case the sequence would be the right way up (Smalley 1990).

7.6.3.1.2 Gorob

The Gorob prospect is located at the southwestern end of the MAB (Figs. 7.23 and 7.26), where a number of similar deposits (the above-mentioned Luigi, Vendome and Hope), occur around a major synform which closes to the west

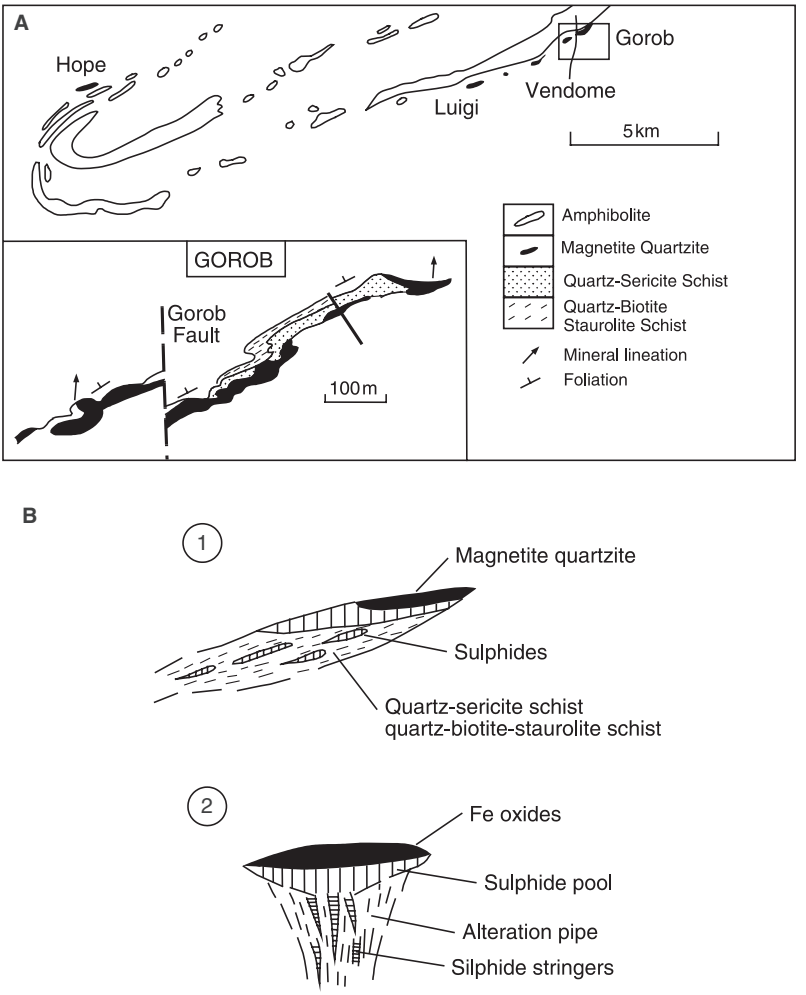


Fig. 7.26 (**A**) Schematic illustration of distribution of Matchless Amphibolite Belt outcrops at the southwestern end of the belt in the Namib desert; inset shows details of the Gorob prospect. After Killick (1983). (**B**) Reconstruction of an idealised mineralised lens at Gorob; (1) Observed field relationships of a deformed mineralised lens showing the succession of magnetite quartzite, sulphide mineralisation (gossan) and a zone of quartz-sericite schist and quartz-biotite-staurolite schist enclosing sulphide lenses and stringers; (2) Reconstructed mineralised lens, based on the interpretation that the quartz-sericite and quartz-biotite-staurolite schists represent the metamorphic equivalent of a siliceous and potassic alteration envelope containing sulphide stringers (possible feeder channels to the mineralised lens). After Pirajno (1992)

near the Hope deposit (Fig. 7.26A). The Gorob deposit is separated by approximately 200 m of quartz-biotite schist from the base of the MAB rocks in the north. The ore lens is hosted by a unit of quartz-sericite schist up to 12 m thick, underlain by massive magnetite quartzite from 0 to 8 m thick. The hangingwall of quartz-sericite schist contains disseminations and veins of sulphides, with a thickness of up to 200m above an amphibolite lens. Grades, as determined by exploration drilling, vary from 4.4 to 1.7% Cu over thicknesses of about a metre or slightly more. Ore reserves were estimated at ~3.3 Mt, with an average grade of 1.93% Cu. The surface expression of the deposit is a gossanous outcrop of magnetite quartzite and quartz-sericite schist, stained by secondary Cu minerals such as malachite and chrisocolla. The gossanous outcrops dip approximately 45° to the northwest. Drilling revealed that the ore shoots are contained in drag-fold closures that parallel a prominent D2 mineral lineation which indicates the plunge of the shoots at 45° towards 356° (Fig. 7.24). Below the level of oxidation, pyrite is the dominant sulphide followed by chalcopyrite, pyrrhotite, sphalerite, galena and rare molybdenite (Killick 1983). Killick (1983) also reported a metal zoning from a Cu-rich hangingwall to a Zn-rich footwall, as well as a sharp footwall contact and a gradational hangingwall contact as observed at Otjihase. This would indicate that the younging direction is towards the south and that in the Gorob area the succession is probably overturned. A reconstruction of an idealised mineralised lens at Gorob is shown in Fig. 7.26B.

7.6.3.2 Comparison with Besshi-Type Deposits and Ore Genesis

The affinity of the MAB massive sulphide deposits with Besshi-type deposits (Fox 1984) is generally accepted (Breitkopf and Maiden 1988; Klemd et al. 1989). These deposits are formed when a ridge axis is proximal to a source of terrigenous sediments, so that the axial region is rapidly covered in silty material, as exemplified by the Gulf of California and the Guaymas basin described in Section 7.5.2.4 (see also Section 7.7.1.1). The ascending magmas are intruded into the sedimentary material as sills (see Fig. 7.16), with the hydrothermal convection cells developing above the intruded sill, which acts as a heat source. These features distinguish Besshi-type deposits from the massive sulphides of the Cyprus-type (Section 7.6.2). Besshi-type ores are usually tabular in shape, or cigar-shaped where deformed. The metal association is typically Cu–Zn–Ag–Co, and Sn, Mo and W may be enhanced, possibly due to the nature of the sedimentary host rocks. Carbonate material of exhalative origin is usually present, and, as in the Matchless Belt, oxide–silicate Fe formation (metamorphosed to magnetite quartzite) may also occur. Three S isotope analyses of sulphide samples (pyrite and chalcopyrite) from the Otjihase deposit (see below) returned $\delta^{34}S$ values ranging from + 7.8 to + 9.4‰ (Pirajno et al. 1992), which compare well with the S isotopic composition of a sulphide deposit in a "sedimented ridge crest" in the Northern Juan de Fuca ridge (Franklin et al. 1990). Here these authors reported $\delta^{34}S$ values ranging from + 6 to + 15‰, which are

interpreted to be the result of interaction of hydrothermal fluids with sediments in the sub-seafloor environment (Franklin et al. 1990).

The Besshi deposits occupy a tectonic setting, which is transitional between rift-related sedimentary exhalative, the Red Sea rift setting (Chapter 8) and the Cyprus-type volcanic-hosted massive sulphide deposits. In the classification adopted by Rona (1988) for present-day oceanic crust-related mineralisation, the sediment-hosted deposits of the Salton Sea area, Guyamas basin in the Gulf of California, Bauer Deep on the east flank of the EPR and others cited by Rona (1988), (Table 1, p. 440–442) could all be the modern equivalent of the Besshi-type deposits of the geological record. Fox (1984) listed a number of Besshi-type deposits, ranging in age from the Lower Proterozoic to the Upper Paleozoic. They include the type area in Japan, known as Sambagawa belt (Upper Palaeozoic) with more than 100 deposits, of which the Besshi mine is the largest containing 33 Mt at 2.6% Cu, 20 ppm Ag and 0.05% Co; the deposits of the lower Proterozoic Outukumpu region in Finland (Peltonen et al. 2007), with the Kerretti mine (31 Mt at 3.5% Cu, 0.5% Zn, 0.12% Co, 10 ppm Ag and 1 ppm Au) and the Vuonos mine (6.6 Mt at 2.1% Cu, 1.2% Zn, 0.11% Co, 38 ppm Ag), and others in Canada, USA and Norway (Fox 1984). The world's largest Besshi-type deposit is Windy Craggy (British Columbia), containing approximately 300 Mt of ore, grading 1.38% Cu (Peter and Scott 1999).

As mentioned previously, sea water-dominated hydrothermal convection cells develop in the semi-consolidated sediment pile above mafic intrusions, discharging as submarine hot springs at the seafloor. Feruginous cherts are characteristically developed and generally cap the sulphide mineralisation. Carbonate lenses or layers in the silty sediments are formed perhaps from the dissolution of organic material by the convecting fluids. Ferruginous cherts are the precursor rocks of magnetite quartzite and the carbonates are possibly the precursor rocksof the calc-silicate lenses (hornblende-garnet) commonly seen intercalated with the Kuiseb schist. The quartz-sericite schists associated with the MAB deposits are possibly the metamorphosed equivalent of clay-rich altered sediments.

7.7 Volcanic-Associated Massive Sulphide Ore Systems (VMS)

Hydrothermal polymetallic mineral systems associated with submarine calderas are generally known as volcanogenic or volcanic-associated massive sulphide deposits (VMS), or volcanic-hosted massive sulphides (VHMS). In the same category are also generally included mineral systems at mid-ocean ridge spreading centres. Volcanogenic massive sulphide deposits have been classified in terms of their metal content (Franklin et al. 1981), geological environment (Sangster and Scott 1976), composition of host rocks and tectonic setting (Sawkins 1990), whereas Barrie and Hannington (1999) drawing on a database of 878 deposits (excluding China and former ex-Soviet bloc countries)

used a five fold classification based on host rock compositions. Franklin et al. (2005) considered VMS in terms of five lithostratigraphic types: (1) bimodal-mafic; (2) mafic; (3) pelitic-mafic; (4) bimodal felsic; (5) siliciclastic felsic. These authors defined volcanogenic massive sulphide deposits as *strata-bound accumulation of sulphide minerals that precipitated at or near the seafloor in spatial, temporal and genetic association with contemporaneous volcanism* (Franklin et al. 2005, p. 524).

In my opinion, Sawkins (1990) perhaps enabled a clearer subdivision, which to a large degree encompasses the criteria used in other classification schemes. Thus, in adopting the plate tectonic approach of Sawkins, one can distinguish three main types of volcanogenic massive sulphide deposits: (1) Kuroko-type, which form in subduction-related back-arc settings; (2) Cyprus-type, formed at mid-ocean ridges, or suprasubduction spreading centres, discussed in Section 7.6.2; and (3) Besshi-type, which also form at spreading centres, but is sediment-hosted because of the proximity of these centres to landmasses. As mentioned earlier, I prefer to separate polymetallic massive sulphide ore system that form at spreading centres from those that are associated with volcanic edifices, such as calderas, not only because of the diverse tectonic environment, but also because of host rock compositions, as already pointed out in the preceding sections in relation to modern analogues. In this section, therefore, I confine my discussion to the Kuroko-type (Kuroko literally means "black ore" in Japanese) polymetallic massive sulphide deposits, but I will also interchangeably use the acronym VMS for all these polymetallic hydrothermal ore systems that are associated with submarine dominantly silicic volcanism in rift-related settings, whether these were formed behind a volcanic arc (back-arc) or in settings that may be associated with oceanic plateaux formed by mantle plume activity, as for example the VMS deposits in the Archaean Pilbara Craton of Western Australia (see Section 7.7.4). Furthermore, cases are made for VMS forming in marine continental margin rift basins, where volcanism is alkaline to subalkaline in composition and may have been a product of upwelling asthenosphere related to rifting rather than in a subduction-related magmatism (Barrett and MacLean 1999). Many VMS can be considered as the submarine equivalent of subaerial low-sulphidation epithermal systems (Sillitoe and Hedenquist 2003). Both VMS and subaerial low-sulphidation epithermal systems are associated with rhyolitic or rhyodacitic domes, usually in caldera volcanoes in rift-related settings. Transitional VSM-epithermal systems may also exist in situations where a caldera system is submerged in shallow water. Sillitoe and Hedenquist (2003) mentioned that the Esky Creek VMS in British Columbia has features, including high Au and Ag grades, as well as high contents of As, Sb and Hg, as being transitional to a subaerial low-sulphidation system. Also quoted by Sillitoe and Hedenquist (2003) is the Conical Seamount, 20 km south of the giant Ladolam low-sulphidation epithermal deposit, discussed in Chapter 5. At the Conical Seamount Au-rich veins of black amorphous silica with disseminated polymetallic sulphides and an earlier pyrite stockwork system are located at about 1050 m of water depth (Petersen et al. 2002). The sulphides comprise

sphalerite, galena, pyrite, marcasite and chalcopyrite, accompanied by varying amounts of Cu–Pb–As–Sb sulphosalts. Gold occurs as discrete grains of electrum and native Au, with whole-rock values of up to 230 ppm and associated with high concentrations of As, Cd, Hg, Sb and Tl. The mineralised veins overprint the stockwork system and are flanked by alteration comprising illite, chlorite, smectite, amorphous silica and K-feldspar, whereas the overprinted pyrite stockwork is associated with platy alunite, kaolinite and other clay minerals. Petersen et al. (2002) put forward the idea that the mineralisation of Conical Seamount has mineralogical, chemical and textural features that are typical of subaerial epithermal systems and that both the giant Ladolam epithermal deposit and Conical Seamount are part of the same magmatic-hydrothermal system.

Another example of a hybrid or transitional VMS is provided by the low-sulphidation epithermal systems of the emerging volcanic complex of Milos Island in the Pliocene Aegean volcanic back-arc. The Aegean back-arc is located 150–250 km north of the Ellenic trench, is built on continental crust and comprises seven andesitic and dacitic volcanic centres (Naden et al. 2005). Epithermal mineralisation is hosted by rhyolitic pyroclastic with extensive silica, sericite and adularia alteration associated with crustiform and banded quartz or chalcedony + adularia + barite veins. An active geothermal system on Milos is located about 1–2 km below sea level with reservoir temperatures of 350–250°C, venting fluids that are enriched in Fe, Mn, Si and Ba and locally depositing pyrite, marcasite, barite, gypsum and calcite. Naden et al. (2005), on the basis of stable isotope systematics (δD and $\delta^{18}O$), determined that the Milos active geothermal system is sourced by meteoric, seawater and magmatic fluids. The Milos geothermal fluids are discharged in an emergent environment and where these fluids boil they form quartz veins with typical epithermal textures (see Chapter 2 for details of vein styles and textures), associated with adularia alteration, sericitic and distal propylitic alteration. The authors argued that Milos is a good example of a hybrid or transitional epithermal-VMS system.

VMS that occur in the Archaean greenstone belts, such as those in Canada (Noranda-type in the Abitibi belt) and in Western Australia (Mons Cupri and the Panorama district in the Pilbara Craton (Section 7.7.6), and Scuddles-Golden Grove in the Yilgarn Craton), have been considered as ancient analogues of Kuroko-type systems. Hutchinson (1980), however, considered them a separate class of deposits, which he called "primitive type". The distinction between the Phanerozoic Kuroko deposits and the VMS deposits of Precambrian age is essentially one of metal contents, with Pb appearing to be a dominant metal in the former, whereas it is scarcer in the latter, which in turn appears to be related to the immaturity (Zn–Pb–Cu–Ba–Au–Ag systems) or maturity (Zn–Cu–Au–Ag systems) in the geodynamic evolution of the rift regime. Thus, the metal association of the Phanerozoic volcanogenic massive sulphide deposits is Zn–Pb–Cu–Ba–Au–Ag, whereas the Precambrian deposits are dominated by Zn–Cu–Au–Ag. In addition, Gifkins et al. (2005) pointed out that the Australian Palaeozoic VMS and the Japanese Kuroko deposits are

characterised by footwall alteration typically more sericitic and quartz rich, whereas the Archaean Canadian, Noranda-type VMS, are characterised by dominant chlorite in the footwall alteration pipes. These differences are ascribed to the thinner crust and larger high-level felsic plutons in the Archaean, compared to Phanerozoic conditions, which have less extensive and lower temperature alteration pipes (Gifkins et al. 2005). The time distribution of VMS deposits is shown in Fig. 3.8. Groves et al. (2005) showed that major peaks of VMS deposits, in terms of ore production, are at ~2.7 Ga, ~1.9 Ga and between ~0.6–0.25 and ~0–0.03, with an apparent gap between 1.7 Ga and 0.6 Ga, which they attributed to loss due to erosion.

Both Kuroko and Noranda-type VMS were comprehensively reviewed by Large (1992a). This review, in which styles, genetic models and factors that influence metal associations and ratios, apply to Australian deposits, but its concepts can be extended to other VMS deposits.

7.7.1 Kuroko-Type Mineral Systems

The Kuroko polymetallic massive sulphide deposits form at the discharge site of submarine hydrothermal systems associated with silicic caldera structures. A monograph issue of the Society of Economic Geologists is devoted to the geology of Kuroko deposits (Ohmoto and Skinner 1983), whereas an overview of Kuroko systems is provided by Ohmoto (1996). Some Kuroko systems may be considered the submarine equivalent of the subaerial epithermal systems, as mentioned in the preceding section. Fluid inclusion data indicate that Kuroko ores form at temperatures ranging from 100 to approximately 330°C (Pisutha-Arnond and Ohmoto 1983) and according to Ohmoto and Takahashi (1983) Kuroko mineralisation requires relatively deep marine conditions (>1000 m), because in shallower environments boiling solutions would result in the dispersion of the mineralisation with the subsequent development of veins and/or disseminated sulphides. Examples of present-day hydrothermal systems that can be considered as modern analogues of Kuroko-type deposits have been described in Section 7.5.3. The Kuroko deposits, such as those of the well-known HoKuroko district in Japan are related to bimodal volcanic sequences generally consisting of tholeiitic basalts at the base followed upwards by dacite, rhyodacite, rhyolite and related pyroclastic rocks. This bimodal sequence is usually superimposed on calc-alkaline volcanic piles typical of magmatic arcs formed above subduction zones. Sillitoe (1982) proposed inter-arc and back-arc extensional settings for most Kuroko-type deposits, characterised by rifting and dominant bimodal volcanism. Rifting of an island arc could, according to Sillitoe (1982), occur as a result of oblique subduction, and it is also possible that this rifting may evolve into a marginal basin. An intracontinental extensional environment is also considered by Sillitoe (1982) for rhyolite-hosted massive sulphide deposits that are generally associated with bimodal sequences,

such as those of Bathurst, New Brunswick in Canada, Captains Flat and Woodlawn in Australia, and the Iberian Pyrite Belt (Section 7.7.5).

The association of massive sulphide ore deposits with caldera structures and resurgent rhyolite domes has been noted by several authors. The most important role of caldera formation is thought to be the creation of depressions, which become the loci for discharging hydrothermal fluids. In addition, faulting associated with caldera formation is largely responsible for providing channelways for the circulating fluids. In most cases the mechanism of caldera formation is preceded by voluminous eruptions of pyroclastic material, resulting in the rapid emptying of the magma chamber and subsequent collapse of the volcanic structure. Kuroko-type deposits usually occur in clusters, each of which is associated with a caldera structure. They also tend to occur along particular stratigraphic intervals within a volcanic sequence, such as the final stages of major pulses of volcanic activity.

Modern examples suggest that Kuroko systems form through discharge of hydrothermal fluids, which take place on caldera floors and walls and along the flanks of rhyolitic domes (Eldridge et al. 1983). It must be pointed out, at this juncture, that the density and pressure of the hydrothermal fluids in relation to the density and hydrostatic pressure of the sea water at the point of discharge, are important factors in determining the style and morphology of the orebodies. We may consider three cases. In the first, the hydrothermal fluid density and pressure are greater than the surrounding medium, the ore solutions are injected into the sea water and the resulting mineralisation is dispersed over a fairly wide area, forming layered horizons. In the case of Kuroko mineralisation, the orebodies would then be largely composed of sulphates with minor sulphides. In the second case, the density and pressure of the ore solutions are at near equilibrium with the surrounding medium, resulting in the formation of well-zoned, stratabound black and yellow ores under relatively stable conditions. In the third case, the ore fluids have density and pressure less than the surrounding sea water; thus veins and stringer deposits form instead of massive sulphide and sulphate bodies. In models of Kuroko ore genesis, leaching of metals from the wall rocks is generally implied; however, some studies indicate that the metals are, at least in part, derived from high level magma chambers underlying and feeding the volcanic system (Urabe et al. 1983). Stable isotope systematics confirm that Kuroko ore fluids have a major component of sea water, but mixing with magmatic waters is nevertheless not entirely excluded. Sulphur isotope compositions of Kuroko systems are generally in the positive range of $\delta^{34}S$ values. Ohmoto (1996) examined in some detail the systematics of sulphur isotopes in Kuroko deposits and these, with reference to Fig. 7.27, are described here. The $\delta^{34}S$ values for pyrite and pyrrhotite are close to 0‰, with these values, however, increasing to about 5‰ by interaction with biogenic pyrites in the wallrocks. Interestingly, this change in $\delta^{34}S$ values is accompanied by a change in pyrite morphology from fine-grained framboidal of biogenic pyrite to coarse-grained euhedral pyrite in the hydrothermal pyrite. Changes in pyrite morphology and internal fabrics, which can be readily assessed in a preliminary

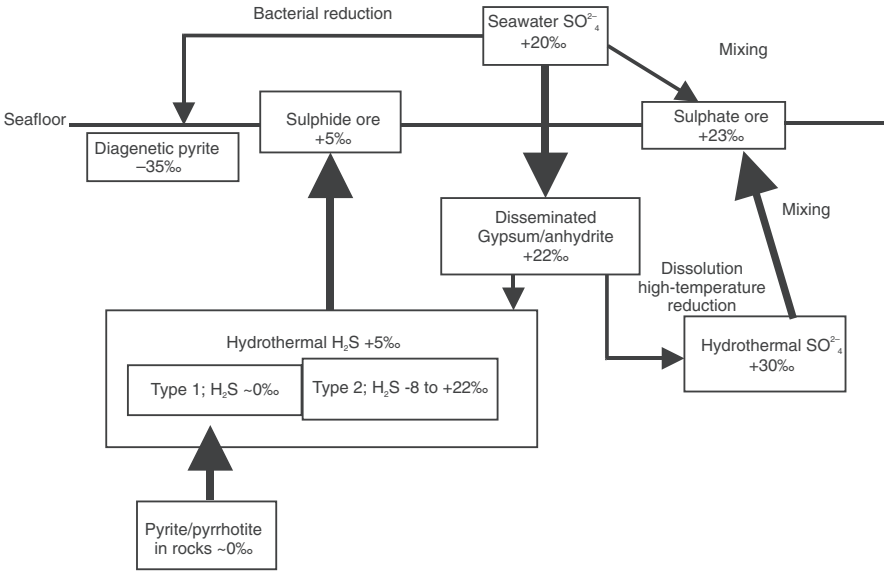


Fig. 7.27 A "flow chart" of interactive $\delta^{34}S$ systematics in a Kuroko ore system. After Ohmoto (1996)

fashion under a polarising microscope and by SEM analysis, seem to monitor changes in fluid compositions and regime in hydrothermal systems. A case of pyrite morphology and internal fabric changes are taken up again in Chapter 9. Ohmoto (1996) suggested that hydrothermal H_2S in Kuroko systems, with $\delta^{34}S$ of 5±3‰, is a mixture of H_2S derived from the leaching of sulphides in the wallrocks (0 to +5‰) and H_2S derived by non-bacterial reduction of seawater (+20 to 22‰). The seawater SO_4^{2-} would have been fixed in the footwall rocks as anhydrite and/or gypsum, through a reaction of the type:

$$Ca^{2+} + SO_4^{2-} \Leftrightarrow CaSO_4$$

during downward percolation of seawater at temperatures of about 150°C; dissolution of the sulphates occurs at higher temperatures and are eventually reduced to H_2S. Sulphate reduction also occurs by Fe^{2+}-bearing minerals at temperatures above 200°C. The $\delta^{34}S$ values of the second type of H_2S ranging from –8 to +22‰, can be explained considering the pathways above described and shown in Fig. 7.27. Ohmoto concluded that the range of S isotopic values is largely dependant on the degree of sulphate reduction during the generation of the second H_2S type, referred to above, the mixing ratios of the two types and importantly the $\delta^{34}S$ value of seawater, which varied between +10 and +30‰ during Phanerozoic and Phanerozoic, but was only about 2‰ in the Archaean (Ohmoto et al. 1993).

Modelling of Kuroko hydrothermal systems was carried out by Pisutha-Arnond and Ohmoto (1983) and Cathles (1983). Here I report in Cathles' modelling, shown in Fig. 7.28. In this exercise Cathles used a series of calculations, together with geological, geochemical and isotopic data to constrain the convective cooling of a small intrusive body, the related flow of fluids around it and the changes in the chemical and isotopic nature of both fluids and rocks. The author begins by considering the relationship between the size of the igneous intrusion and the total mass of hydrothermal fluid that can be convected by its thermal energy. A simple formula is used to express this relationship:

$$Mw = Mi\ Ci/Cw\ \ln T_0/T$$

where Mw represents the mass of hydrothermal fluid circulated, Mi the mass of the intrusion, Ci its heat capacity (cal/g/°C), Cw the heat capacity of water, T_0 is the initial difference in temperature between the igneous body and the surrounding environment, and T the temperature difference after cooling to a certain level (i.e. 300°C). If a pluton at a temperature of 700°C is intruded at a depth of 4 km, where the ambient temperature is 100°C and cooled to 300°C, the mass of fluid circulated is 22% of the pluton's mass. If the intrusion is at 1300°C, a mass of hydrothermal solution hotter than 300°C would be about 36% of the pluton's mass. Using the above formula, Cathles' calculations indicate that an intrusion of between 1.5×10^{11} to about 10^{13} tonnes is necessary to account for the metal resources estimated at 4.7 Mt and 4.5 Mt of combined Cu + Pb + Zn metals for the Noranda (Canada) and Kuroko (Japan) districts respectively.

Also interesting is that the amount of silica deposited at the surface can be used to estimate the size of the intrusion and the amount of fluid involved. Using an example from the Noranda area, where a silicified basalt containing approximately 20% silica is present, and taking into account the solubility of silica in a 300°C fluid and the volume of the area affected by the silicification, Cathles estimates that some 2.3×10^{15} kg of hydrothermal fluid at above 300°C would have been required to produce this silicification. This in turn requires an igneous mass of about 10^{13} at 700°C. Comparatively small magma chambers (approximately 2 km wide by 3 km high) are considered in modelling their cooling history by convective circulation of fluids. This modelling indicates firstly that fluids at 600°C should be vented after 5000 years after the intrusive event, and since observation of black and white smokers at mid-ocean ridges indicates venting temperatures of about 350°C, it is concluded that a very hot rock (>350°C) is probably quite impermeable. Permeability is therefore a key factor in that it allows penetration of water and cooling of the igneous body. Convective cooling of a magma chamber 1 km wide by 3.25 km high by inflow of fluids is shown in Fig. 7.28. The flow lines in this figure represent the idealised geometry of the hydrothermal circulation system. This modelling (Cathles 1983) shows that initially fluids move up the temperature gradient, and then

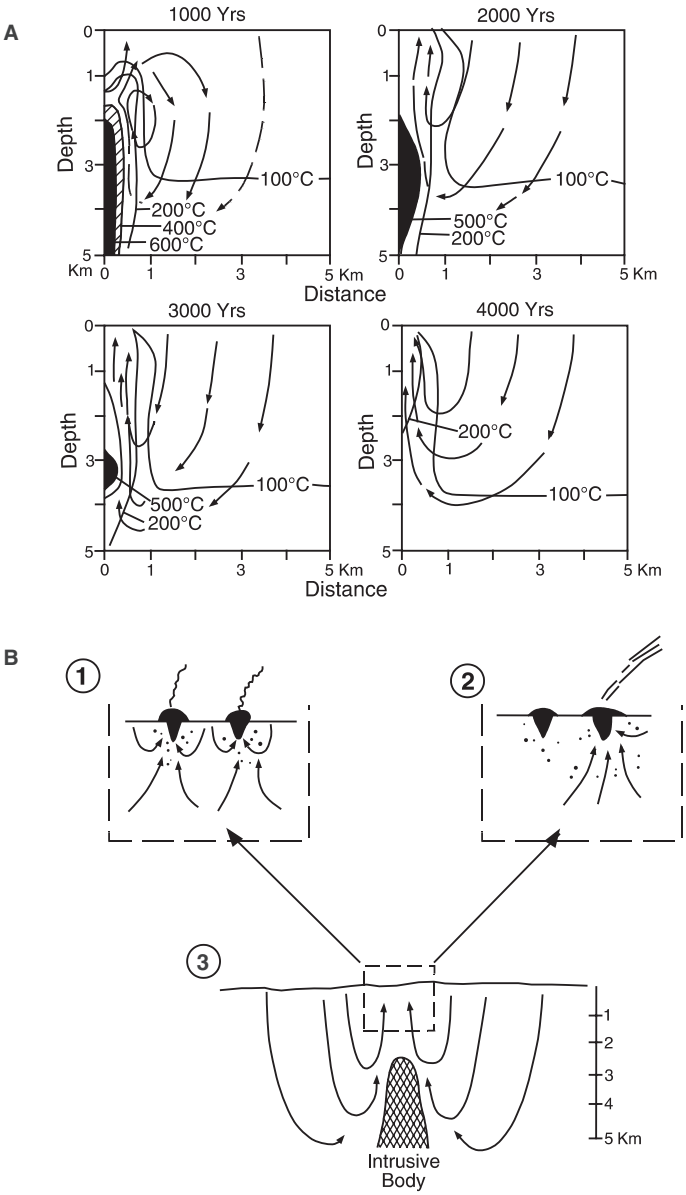


Fig. 7.28 (**A**) Computer model of convective cooling of a magma chamber; permeability is set at 5 millidarcy; arrows indicate fluid flow, after Cathles (1983) and see text for details. (**B**) Evolutionary stages of hydrothermal fluid circulation; stage 1 low-temperature white smokers, with silica, sulphate and disseminated sulphides deposition; stage 2 relates to high-temperature black smokers with precipitation of massive and disseminated (*dots*) sulphide. One vent (*on the left*) is sealed by the precipitated mineral phases; 3 represents the overall view, with the dashed box showing the position of 1 and 2 in the system (after Cathles, 1983)

back down as they move into the thermal anomaly generated by the pluton. The model also shows that the fluids only gain access to the intrusive mass after it has cooled to approximately 350°C in about 5000 years. During this cooling it is estimated that over 8000 tonnes of solution at a temperature of about 300°C are circulated. Considering the 40 km long Hokoruka basin in Japan, Cathles estimated that the total mass of water vented would have been of the order of 3.3×10^{10} tonnes at a temperature greater than 300°C. The speed with which this water circulates through the entire system is probably around 2000 years (intake and discharge). Finally, two main stages of fluid circulation and ore deposition are considered (Fig. 7.28B). Fluids penetrate to a depth of about 5 km and form two convective cells, one nearer the surface and the other deeper down. During the first stage, lower and shallower circulating fluids discharge at the rock-water interface to precipitate sulphates. In stage two, more reduced and higher temperature conditions prevail. The previous vent may have been sealed by mineral precipitation and the fluids vent at a new locale, where they deposit massive sulphides.

Hydrothermal alteration processes of a Kuroko system, and indeed for all submarine hydrothermal systems, are linked to the dynamics of heated seawater-rock interactions. The system is open to seawater flowing in and out, that is seawater is continuously supplied in low-temperature regions and removed from high-temperature regions. Seawater-rock interactions are rock-dominated for a single parcel of water moving through the rocks ($\sim$10–100 years), but tends to become water-dominated for the duration of the hydrothermal activity ($\geq$10 000 years). Reactions that take place during these interactions include hydration, dehydration, cation exchange, redox reactions, precipitation and dissolution, all of which are part of the hydrothermal alteration processes discussed in Chapter 2. A special issue of Economic Geology is devoted to hydrothermal alteration associated with VMS deposits (Gemmell and Herrmann 2001). Here, I draw attention to some specific reactions that are especially important in terms of the isotopic and chemical compositions of the fluids during different stages of alteration-mineralisation processes, as envisaged by Ohmoto (1996).

In a first stage and prior to the initiation of hydrothermal activity, rocks react with pore seawater at low temperatures resulting in dehydration of volcanic glass forming zeolites and smectite. Cation exchange between pore fluids and smectite clays, result in the addition of seawater Mg to the volcanic rocks, while the Ca released during these reactions will form sulphates (gypsum or anhydrite), or calcite. The rocks of the seafloor become gradually heated following the intrusion of magma enhancing the progress of first stage reactions to form zeolites, but also inducing the breakdown of organic matter to produce CO_2, as in the reaction:

$$CH_2O(s) \rightarrow CO_2 + CH_4$$

which in turn may induce the formation of calcite:

$$Ca^{2+} + H_2O + CO_2 \rightarrow CaCO_3 + 2H^+$$

The breadown of organic matter will increase the CO_2 content of the fluid causing more reactions converting zeolites, such as clinoptilolite and mordenite to analcime, adularia, quartz and calcite:

$$KNaAl_2Si_{10}O_{24}\,8H_2O(\text{clinoptilolite}) + Ca^{2+} + CO_2 \rightarrow NaAlSi_2O_6H_2O$$
$$(\text{analcime}) + KAlSi_3O_8(\text{adularia}) + 5SiO_2 + CaCO_3 + 2H^+ + 6H_2O$$

A third stage, called montmorillonite stage by Ohmoto (1996), results from increasing temperatures to about 200°C, resulting in the conversion of zeolites and smectites to Mg–Ca smectite and quartz. Plagioclase is also affected and converted to Ca montmorillonite:

$$\text{plagioclase} + H^+ \rightarrow \text{Ca montmorillonite} + SiO_2 + Na^+$$

A stage of mixed-layer clay follows at temperatures above 250°C, with montmorillonite and plagioclase further becoming unstable and replaced by mixed layer montmorillonite-illite clays and sericite:

$$9\text{Na-montmorillonite} + 7K^+ \rightarrow 7\ \text{sericite} + 12SiO_2 + 4H^+ + 3Na^+$$

and:

$$3NaAlSi_3O_8 + K^+ + 2H^+ \rightarrow KAl_3Si_3O_{10}(OH)_2(\text{sericite}) + 6SiO_2 + 3Na^+$$

The above reactions continue as temperatures increase to about 300°C, resulting in the formation of abundant sericite and the Mg–Ca smectite is converted to Mg-rich chlorite. All these reactions lead to an increase in the K and Mg contenst of the rocks (sericite-chlorite zone) and a corresponding depletion in Na and Ca.

7.7.1.1 Ore Genesis Models and Processes

Figure 7.29 show two ore genesis models as envisaged by Sato (1974) and Ohmoto and Rye (1974). In the first (Fig. 7.29A, B) the massive sulphide ores lie on top of rhyolitic domes, in the second model (Fig. 7.29C), the massive sulphides were accumulated in depressions and more specifically on the floor of submarine calderas. The recent discoveries of seafloor mineral systems in submerged calderas, described in Section 7.5.3, indicate that the Ohmoto and Rye's model is more accurate. As is the case for subaerial epithermal systems, the Kuroko-type deposits also form during the late stages of caldera development, through the activity of submarine hot springs taking place along caldera walls or ring fractures and in depressions in the caldera floor, as elaborated below.

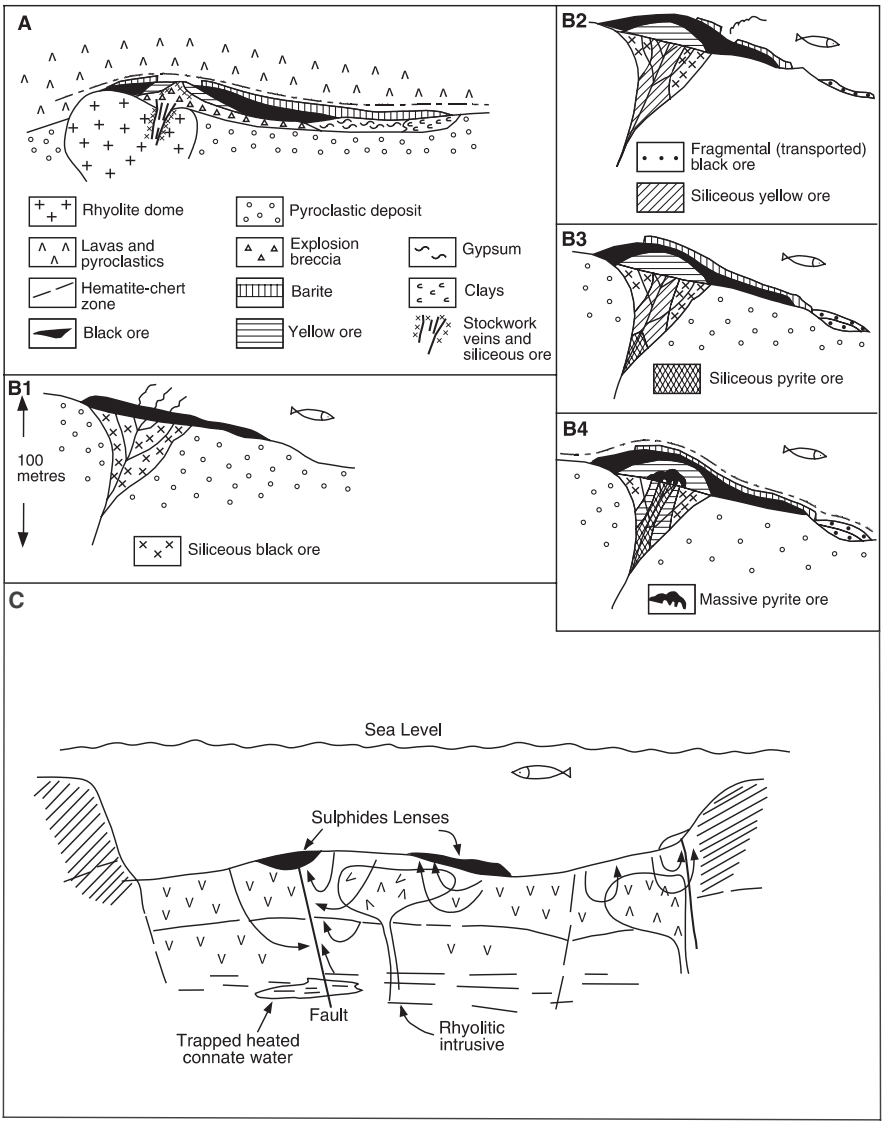


Fig. 7.29 Evolutionary stages of a Kuroko system; (**A**) according to Sato (1974); (**B**) cartoons, 1–4 after Eldridge et al. (1983); (**C**) shows the formation of a Kuroko system in a submarine caldera, after Ohmoto and Rye (1974)

There is general agreement that all VMS districts are related to episodes of extension tectonics, graben subsidence and bimodal volcanism with development of submarine calderas. Stix et al. (2003) discussed the link between caldera-forming processes and the origin of VMS deposits. These authors correctly argued that calderas, submarine and subaerial, are one of the most

important ore-forming environments, where subsurface magma chambers provide the thermal energy to drive hydrothermal circulation and are the host for a wide range of ore systems including epithermal, porphyry, polymetallic veins and the subject of this section, VMS deposits. Stix et al. (2003) further argued that the caldera-forming processes are key factors for the genesis of all these deposits. In the case of VMS, hot fluids are generally focused along the caldera's inner ring faults, while cold seawater recharge occurs along the outer faults. In all cases, seawater interacts with the degassing magma to produce a hydrothermal system. Subsidence and asymmetric caldera collapse are important factors, because these tend to expose the underlying magmatic-hydrothermal system. Subsidence may result in a horst-graben structure along which fluids are channelled and will affect the kind of VMS deposit that is generated, depending on water depths and different amounts of boiling fluids. In two end-member cases, at deeper levels (100–1000s of metres), fluids will either not boil or undergo little boiling resulting in Cu–Zn enriched VMS deposits. On the other hand, at shallower levels greater boiling of fluids will result in Au and Hg enrichment. Renewed magmatism causes resurgence, a common feature of most caldera volcanoes, with localised uplift in the affected part of the caldera. This resurgence may cause further inflow of seawater and the generation of a VMS deposit in the central part of the caldera. Stix and co-authors' model is shown in Fig. 7.30. An excellent example of studies of the evolution of submarine calderas was presented by Mueller et al. (2008), with one of these examples illustrated in Fig. 7.31.

Figure 7.32 shows a genetic model as proposed and discussed in detail by Franklin et al. (2005), which is discussed here. The main features of this model are the magmatic heat and source at depths of 1–3 km; this magma would also contribute to the metal budget of the VMS. Above and around the magma chamber is a high-temperature reaction zone, in which some metals are leached from the surrounding volcanic and sedimentary rocks by interaction with heated seawater. An impermeable barrier or cap rock could be present, which may insulate the hydrothermal system. The hydrothermal fluids are focused along synvolcanic faults and fractures and discharge on the seafloor. Below the zone of discharge, the footwall rocks become extensively altered by reaction of mixed seawater and magmatic fluids. These alteration zones are discussed in some detail in Chapter 2, but I point out here the chemical gains and losses that affect the system. In the reaction zones, elements such as Cu, Zn, Fe, K, Ba are leached out of the wallrocks by up to 90%. Calcium and silica are generally added, as shown by epidote, carbonate and quartz as alteration minerals. Gains in silica and carbonate occur near the palaeoseafloor and at the top of the reaction zone. The channelways through which the fluids flow form the alteration pipe and a zone of stockwork sulphide mineralisation, leading upward and the surface to fluid venting and the deposition of massive sulphide lenses at or near the seafloor. At the seafloor, as for mid-ocean ridge systems, the development of the sulphide body proceeds by a combination of continuing chimney growth and collapse, cementation and replacement of the chimney debris, until

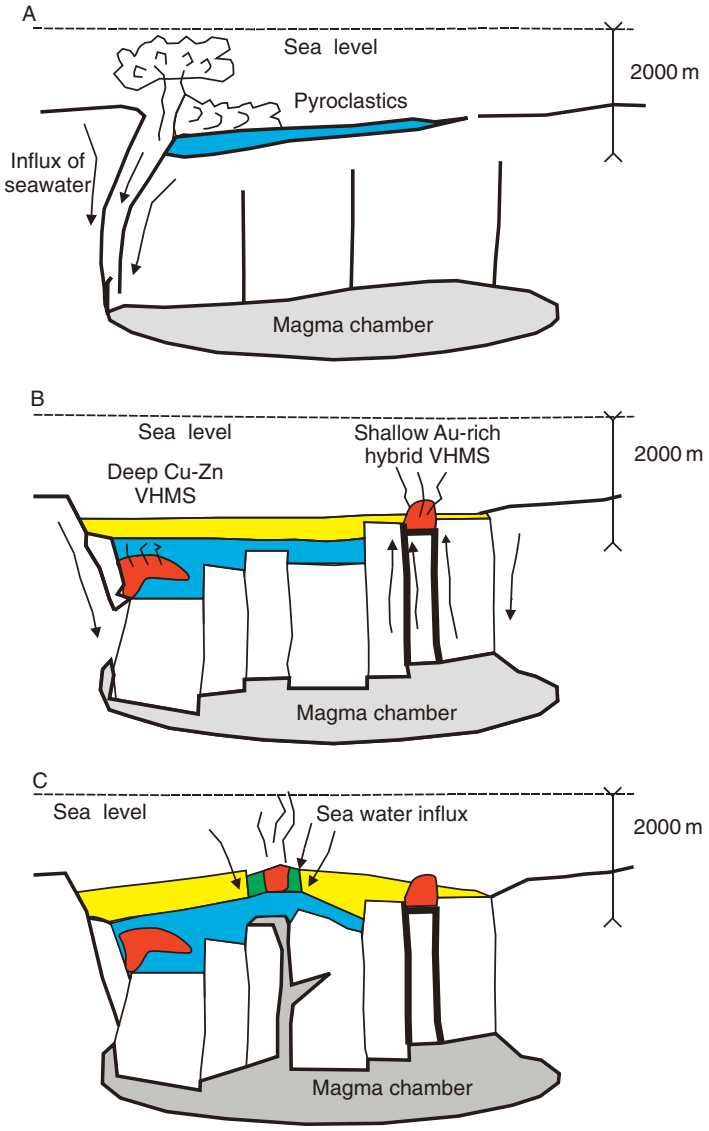


Fig. 7.30 Conceptual model of caldera evolution and formation of two types of VMS deposits; deep water Zn-rich and shallow water transitional to low-sulphidation epithermal (after Stix et al. 2003)

the system effectively clogs and shuts down. Chimneys grow by inflation through internal additions, with the growth process being disturbed by microseismic events, fracturing and thermal rejuvenation. Within each mound, created by a series of chimneys, progressive heating leads to outward displacement of the lower-temperature sulphides (pyrite-sphalerite), by the

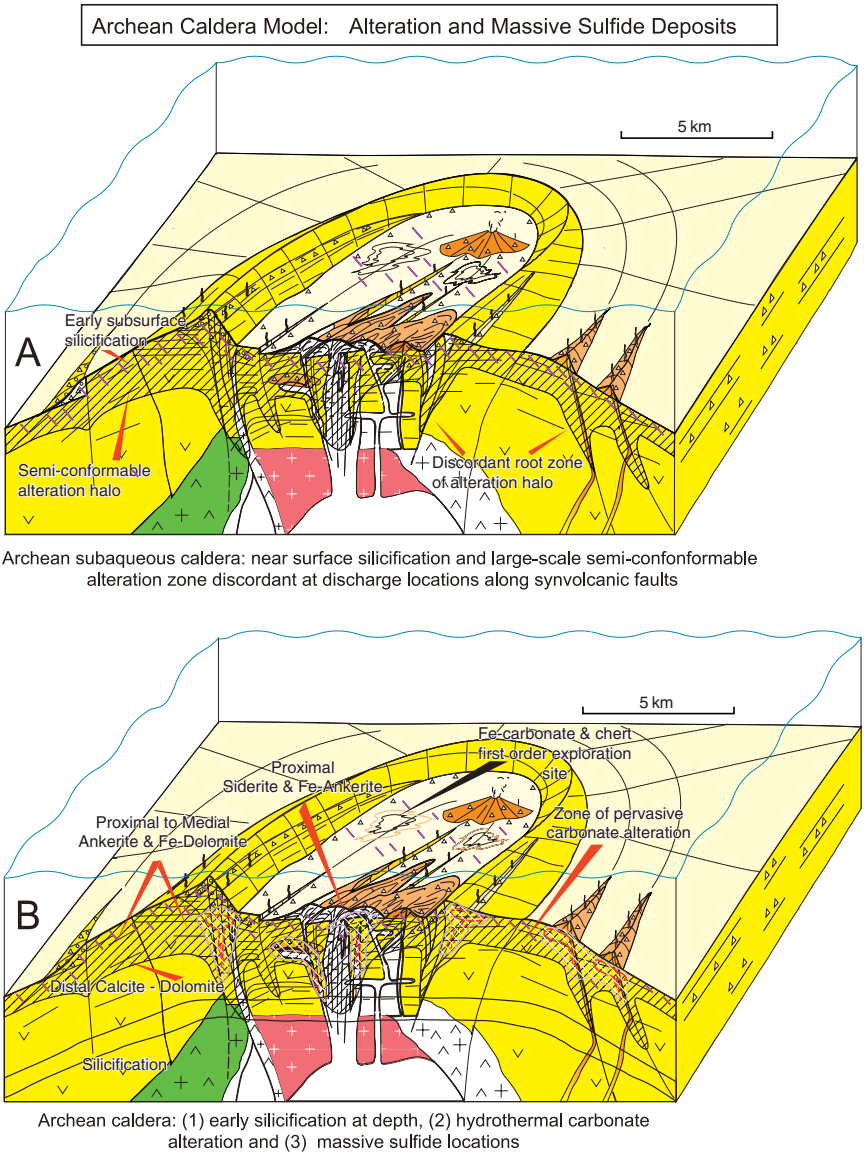


Fig. 7.31 Hydrothermal carbonate alteration model of a submarine caldera is primarily based on the Hunter Mine caldera with attributes of the Normetal and Sturgeon Lake calderas. (**A**) General alteration patterns with an early phase of near surface silicification and an extensive semi-conformable alteration zone which discordant at discharge zones. (**B**) Carbonate alteration pairings indicate lateral change across strike of the caldera from focused to more distal reaches. Silicification at depth is shown in this diagram but is contemporaneous with the near-surface silicification shown in A. Note the importance of the subenvironments and the polymetallic deposits in the volcaniclastic deposits, wherein the largest VMS deposits are favoured at the caldera wall. Reproduced unchanged from Mueller et al. (2008), figure and caption courtesy of the authors

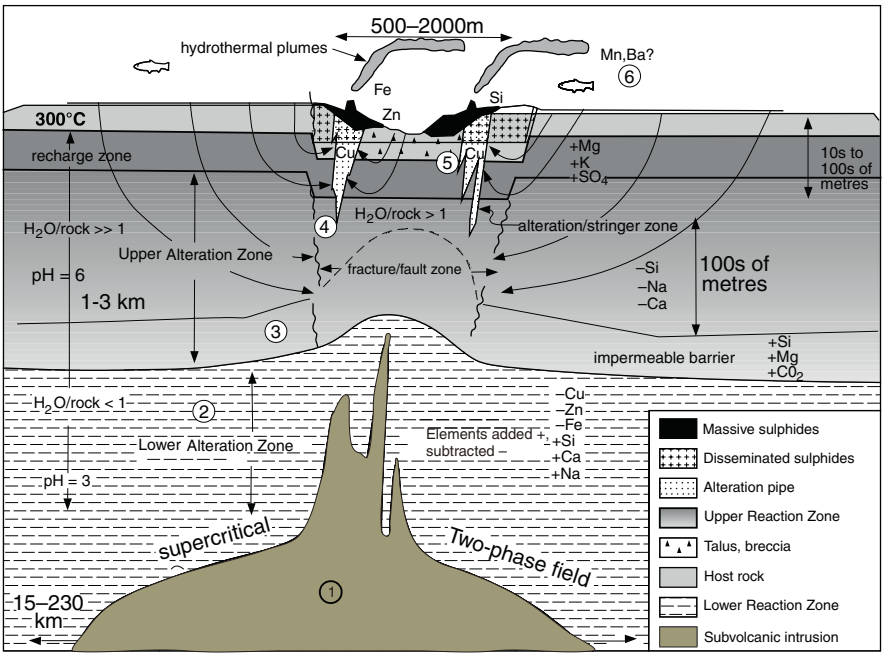


Fig. 7.32 Genetic model for the formation of VMS deposits; (1) heat source; (2) high-temperature reaction zone; (3) synvolcanic faults; (4) footwall zone; (5) alteration pipes, stockworks and massive sulphides; (6) distal mineralisation, as a fallout from hydrothermal plumes. After Franklin et al. (2005)

higher-temperature Cu sulphides, resulting in a kind of zone refining, resulting in a metal zonation with the central parts of the sulphide mounds being Cu-rich, with Zn on the outside. This zone refining process reflects a change with time in the composition and temperature of the fluids and perhaps a change in the source. In addition, Franklin and co-authors pointed out that large sulphide bodies may draw in more heated seawater resulting in the destabilisation of the sulphide species and their large scale recrystallisation, which will overprint the primary assemblages. Sulphide bodies also form below the seafloor (sub-seaflor sulphide deposits). The mechanism responsible for the formation of sub-seafloor massive sulphides is infiltration of hydrothermal fluids and precipitation of sulphides in pore spaces and fractures of permeable lithofacies, resulting in cementation by sulphides. This cementation, in turn, will result in the building up of fluid pressure, hydraulic fracturing and further precitation of sulphides in jigsaw fractures. Sub-seafloor VMS, including the Besshi-type described in Section 7.6.3, form in volcaniclastic and/or terrigenous sedimentary rocks, such as sandstone, wacke and mudstones. Thick, pumice-rich pyroclastic successions are especially favourable, due to their greater permeability and seawater-saturated pore space. The magmatic-hydrothermal fluids are channelled along

synvolcanic faults, flowing laterally along these permeable lithofacies, where they mix with cooler pore and/or percolating seawater, causing the precipitation of sulphides in stratabound or sheet-like lenses, surrounded by hydrothermally altered wallrocks, with quartz, smectite, carbonate and barite. Carbonate rocks, if present, will act as chemical traps that preferentially concentrate metals by processes of open space filling, neutralisation, replacement and dissolution or combinations thereof. Impermeable cap rocks, such as fine-grained argillites, chert, felsic domes, may also force the flow of fluids laterally into permeable lithofacies.

Another mechanism for the generation of VMS is by precipitation of sulphides from a brine pool (see Fig. 7.29C), similar to those that occur in the Red Sea, discussed in Chapter 8. As shown in Fig. 7.29C, brine pools can form on the floor of submarine calderas, and are characterised by stratabound sulphides, general absence of debris breccias, and a distinct vertical zonation from Cu-rich base to Zn-rich top, reflecting a combination of relative solubility of chalcopyrite and sphalerite during cooling and bacteria induced S saturation.

The fallout on the seafloor from hydrothermal plumes emitted by the smokers will carry particulate material in suspension and form both proximal and distal deposits (exhalites; generally Ba and Mn enriched). Exhalites can extend for tens of km from the plume source and their presence could be a powerful vector to locate new massive sulphide mineralisation. Franklin and co-workers noted that extensive, low-temperature and diffuse submarine discharges, can be synchronous or post-date the deposition of massive sulphides and their products may surround the deposits for 100s of metres and more importantly, provide vital nutrients and energy for microbial life. VMS-associated Fe-rich cherts in the geological record probably represent nucleation of silica and Fe oxides associated with microbial mats. Similarly, barite may be precipitated by these exhlative processes on the seafloor and rise as large caps for hundreds of metres over the vent sites, and/or be dispersed by fallout in distal deposits in sedimentary layers.

Figure 7.32, shows two sources of metals and suphur, the magma chamber and the high-temperature deep reaction zone in the footwall rocks, where metals are derived by interaction of seawater-modified fluids with the wallrocks. In the high-temperature reaction zone, metal solubility is largely pH dependant. As the temperature increases the pH decreases resulting in greater solubility of metals. Experimental runs with evolved seawater and basalt indicate that at temperatures of 385–375°C and pressures of 500–300 bars, the metal content of the fluids and reactions that produce assemblages, such as epidote-albite-quartz-actinolite match those in basalt-hosted seafloor deposits. By contrast, reactions in felsic and/or sedimentary rocks produce fluids with lower temperatures of around 300–250°C, also attaining low pH values and solubility of metals, except that these are Zn–Pb-rich and Cu-poor, by comparison with basalt-dominated successions, because Zn and Pb are soluble at lower temperatures compared with Cu. This may be one of the reasons for the presence of Zn–Pb-rich sulphide deposits in siliciclastic and felsic-dominated environments,

as opposed to Cu-rich deposits in mafic rocks dominated environments. This in turn may provide an explanation for the tendency of the Archaean, Noranda-type VMS to be Cu-rich, compared to the Miocene Kuroko-type VHSM deposits. The former are basalt-dominated in a tectonic setting influenced by mafic oceanic plateaux formed by mantle plume activity, versus the felsic and sediment-dominated arc-related settings for the more recent Kuroko VMS.

Metals and S are also provided during magma degassing, as in subaerial systems and the composition of the gases will reflect the composition of the magmas in question. These can be determined from high-salinity fluid inclusions and stable and radiogenic isotope systematics. Metal-rich melt inclusions in footwall rocks are also indicative of magmatic metalliferous fluid phases, as well as Au–Bi–Te–Cu–Co-rich VMS deposits associated with advanced argillic alteration zones, by comparison with low-sulphidation epithermal Au–Cu systems. Variations in the S isotopic compositions for VMS through time are shown in Fig. 7.33 (Huston 1999). These indicate that Precambrian sulphides are closer to magmatic values (closer to 0‰) than Phanerozoic sulphides, which tend to parallel sulphate and seawater values. Sulphur isotopic compositions of Phanerozoic VMS sulphides average about 17.5‰, whereas values of sulphates

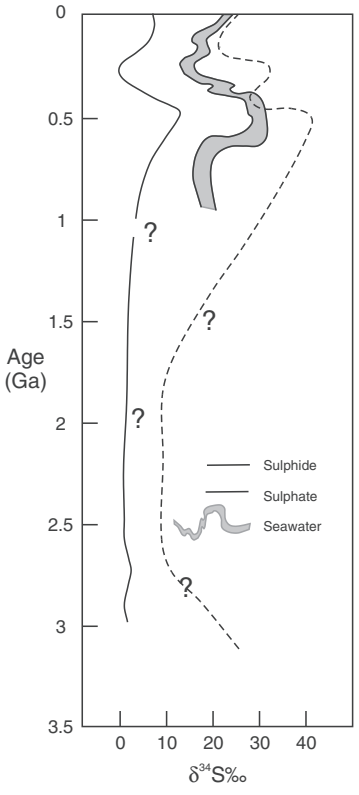


Fig. 7.33 Trends of suphur isotopic compositions through time; question marks indicate uncertainties, due to poor records. After Huston (1999)

(barite and gypsum, up to 40‰) are closer to contemporaneous seawater (Fig. 7.33). The heavy S isotopic composition of the Phanerozoic sulphates can be attributed to a dominant biogenic reduction of seawater sulphate.

The tectonic controls of VMS range from collisional environments (subduction related volcanic arcs) to rifting (back-arc). Rifting occurs as a result of slab rollback, due to steep subduction of cold and old oceanic slabs, which tend to create back-arc basins. Mantle plumes may also induce rifting under the subduting plate or the overriding plate. In these cases, rifting leads to subsidence and thinning of the crust and the rise of asthenopheric mantle onto the base of the continental or oceanic crust, with underplating and partial melting of crustal materials to produce hot felsic melts that are erupted together with mafic melts produced by adiabatic decompression of the upwelling asthenosphere, resulting in the bimodal magmatism that accompanies rifting.

Ore genesis models of individual VMS fields are also discussed in the appropriate sections below.

7.7.2 The Kuroko Deposits of Japan

The Kuroko deposits of Japan have been well studied and documented by several workers, because of their young age (16–11 Ma) and lack of significant deformation and metamorphism. For details the reader is referred to the classic publications of Tatsumi (1970), Sato (1974), Lambert and Sato (1974), Ishihara (1974) and Ohmoto and Skinner (1983).

The Japanese Kuroko deposits are hosted by the Green Tuff belt and the type area is in the Hokuroko district. In this district about 100 or more orebodies aggregate 140 Mt, with an average grade of 3% Zn, 1.5% Cu and 1% Pb (Laznicka, 2006). An important element of the district is the Hokuroko Basin, containing a volcanic succession, 3–6 km thick and of bimodal composition (tholeiites and rhyolites mainly) and is part of the Green Tuff belt. The Green Tuff belt extends across te western part of Honshu, parts of Hokkaido and Kyushu islands of Japan, and is the result of tectonic and igneous activity that formed the Japan Sea and the Japanese island arc during the period from about 65 Ma ago to the present (Ohmoto 1983). The onset of the back-arc extension in Japan is postulated to be related to the steepening of a northwesterly dipping subduction zone beneath the Japanese island arc 65 Ma ago (Outer Honshu province). Subduction of oceanic crust below the Outer Honshu province resulted in calc-alkaline magmatic activity in the inner zone of the province. Continued magmatic activity, uplift and back-arc spreading in the Yamato basin between 25 and 5 Ma ago was accompanied by bimodal volcanism, subsidence and caldera formation in the inner Honshu and Yamato provinces (Ohmoto 1983). Kuroko-type deposits were formed during this period within the deep marine basins that resulted from rapid subsidence. The deposits were localised by calderas within these basins.

Numerous massive sulphide and barite deposits of Miocene age occur in the Hokkaido and Honshu islands of Japan. The Okuroku district (Honshu) is particulary well endowed with Kuroko deposits. The Miocene geology of the district was described in detail by Ishikawa et al. (2004, in Japanese) and is condensed here, as reported in English by Morozumi et al. (2006). The Miocene of the Hokuroko district is divided into four formations: Menaichizawa, Ohkuzu, Ohtaki and Tobe. The Menaichizawa Formation overlies a pre-Neogene basement and consists of andesitic welded tuff and lapilli with fossil flora in the lower part and by fossiliferous sandstone. Stratigraphic and fossil data indicate a transition from inland fluvio-lacustrine environment to marine conditions. The Ohkuzu Formation is entirely submarine and contains bimodal volcanic rocks intercalated with mudstones and is host to major Kuroko systems, which are associated with the late felsic phases of this volcanism, dated at 14 Ma. Felsic volcanism is dominantly dacitic in composition, but rhyolite domes overlie the dacitic lavas. The Ohtaki Formation also contains rocks that are of bimodal composition, but are dominantly dacitic pyroclastics intercalated with mudstone and only minor dacite lavas. The Onnawaga Stage of the Ohtaki Formation indicates a shallowing of the seafloor, based on the presence of pisolites and mudballs. The Tobe Formation mainly comprises dacitic tuff. Granitic rocks with ages ranging from 10 to 6 Ma intrude the succession. The Ohkuzu and Ohtaki Formations are interepreted to represent an extensional tectonic setting with widening of an oceanic basin and submarine bimodal volcanism, characterised by deep-sourced basalts and dacites, erupted from shallow magma chambers lodged in continental crust. As mentioned above, the main period of Kuroko development was during deposition of the Ohkuzu Formation, with lesser hydrothermal activity during deposition of the next two formations (Ohtaki and Tobe). However, Morozumi et al. (2006) studying the distribution of vein systems in the district, generated during the Nishikurosawa (Ohkuzu) and Funakawa Stages (Ohtaki), noted that the granitic rocks and associated vein systems were fractured and are linked with large scale explosive dacitic volcanism, after the main Kuroko period. The authors suggested that a change in tectonic regime from extension and weakly compressive regime to a full extensional regime during which there was intensive submarine volcanism. The Kuroko mineralisation would have been enhanced or favoured during the mildly compressive regime, because this would have increased the residence time of the magmas in the crust allowing further differentiation and the evolution of hydrothermal fluids.

As mentioned above, Kuroko means black ore in Japanese and generally consists of sphalerite, galena, pyrite, chalcopyrite and barite stratiform ore zones (Sato 1974). Other Japanese terms are herein explained (Sato 1974): Keiko refers to siliceous ore consisting of pyrite, chalcopyrite and quartz stockworks; Sekkoko is an assemblage of gypsum, anhydrite with varying amounts of chalcopyrite, pyrite, sphalerite, galena, quartz, clay minerals, forming stratabound zones above or laterally to keiko ores; Ryukako is pyrite ore with lesser chalcopyrite and forming veins and/or disseminations; Oko ore is stratiform

pyrite, chalcopyrite with lesser sphalerite and barite; Tetsusekiei beds refer to ferruginous chert (cryptocrystalline quartz with hematite. Barite ore commonly occurs as well defined beds, locally with minor amounts of calcite, dolomite and/or siderite.

As an example of Japanese Kuroko mineralisation I describe some of the key geological features of the Shakanai deposit, located about 4 km from the town of Ohdate, Akita Prefecture. Detailed information on this deposit can be found in Ohtagaki et al. (1974). The Shakanai mine area comprises a cluster of 11 orebodies, defined from 763 surface drillholes. Total reserves were approximately 30 Mt, grading 2.5% Cu, 4.2% Zn, 1.3% Pb, 75 g/t Ag and 0.7 g/t Au. In the mine area, the 500 m thick Shakanai Formation consists of mudstone, brecciated rhyolite and pyroclastics in its lower part (first 250 m), and brecciated rhyolite and dacite with associated pyroclastics in its upper part. The orebodies are situated within the upper part of the Formation at the contact with the overlying Sainokami Formation which includes mudstone, pyroclastics and minor rhyolites. Intrusive rocks include chloritised dolerite sills and dykes which cross-cut both formations. Several rhyolite or dacite bodies of uncertain age are present, of which two phases are altered and mineralised, while a third and later dacitic body is unaltered. The mineralisation at Shakanai is well zoned with black ore at the top, followed downward by yellow ore, siliceous ore and gypsum ore at the bottom. The No. 1 orebody consists of a number of unit bodies of black ore interbedded with mudstone and pumiceous tuff. The massive black ore is composed of fine-grained sphalerite, galena and barite with minor quantities of chalcopyrite, pyrite, bornite, germanite, argentite and tetrahedrite-tennantite. Native Au is associated with galena. This ore grades into brecciated ore composed of round black ore fragments, less than 1 m in diameter, in a matrix of clay. The No. 2 orebody is composed of gypsum in footwall tuffs surrounded by sericitic alteration. Gypsum ore consists of alabaster, anhydrite, satinspar and clay, with grades of approximately 30% $CaSO_4$. The No. 4 orebody, which is the largest of the cluster, is composed of three main zones of yellow ore with minor amounts of marginal black ore forming small pods in clay-altered tuffs. The upper portions of the yellow ore consist of graded aggregates of chalcopyrite, pyrite, sphalerite and quartz. The remaining lower portions of this ore zone consist of pyrite breccias with stockworks of chalcopyrite and pyrite. The No. 11 orebody is formed by three stacked ore lenses hosted in tuffs. The lower zone contains black ore and gypsum, the middle zone Cu-rich black ore, and the upper zone is formed by mixed yellow and black ore. Hydrothermal alteration surrounding the ore zones is characterised by Mg-chlorite, sericite and montmorillonite. Al-chlorite occurs in the footwall gypsum zones. The footwall volcanic rocks show varying degrees of diagenetic alteration represented by minerals of the zeolite group, such as mordenite and heulandite. Alteration zoning is used as a guide by the local geologists to locate new orebodies.

Ohmoto (1996) reviewed the nature and composition of the ore-forming fluids of the Japanese Kuroko systems. Primary fluid inclusions have salinities

ranging from ~8 to ~2 wt% NaCl equivalent that are close to that of normal seawater as are the δD and $\delta^{18}O$ values, which range from –20 to + 20‰ and –8 to + 4‰, respectively. Ohmoto (1996) also observed a change of the $\delta^{18}O$ values with time and temperature. These increased from –8‰ at ~100°C in the first mineralising stages to about + 2‰ at ~350°C during the middle stage, to values of –10‰ in the final stages. This temporal variation has been interpreted as due to mixing of three types of water: (1) meteoric, with $\delta^{18}O$ of <0‰; (2) seawater with $\delta^{18}O$ of ~0‰; and (3) magmatic water with $\delta^{18}O$ of + 8‰. Ohmoto pointed out that given the submarine setting of the Kuroko ores, it is unlikely that meteoric water would have been involved in the ore-making process. However, contribution of meteoric water was recognised in pseudosecondary inclusions, suggesting that the deposits were uplifted to subaerial conditions, after their formation.

7.7.2.1 Ore Genesis

A model of ore genesis for the Japanese Kuroko systems is detailed in Ohmoto (1996). Black ore minerals (sphalerite, galena, tetrahedrite, barite, pyrite) were formed in the early stages of hydrothermal activity at temperatures ranging from ~300 to ~200°C, with most of the Cu minerals (yellow ore), such as chalcopyrite and bornite, formed as replacement of the black ore minerals, during a stage of maximum temperatures from about 380 to 280°C (Fig. 7.34). Minor amounts of black ore minerals can form again during the wanng stages at temperatures from ~300 to 150°C. Replacement of the black ore minerals by chalcopyrite is indicated by the small inclusions of chalcopyrite

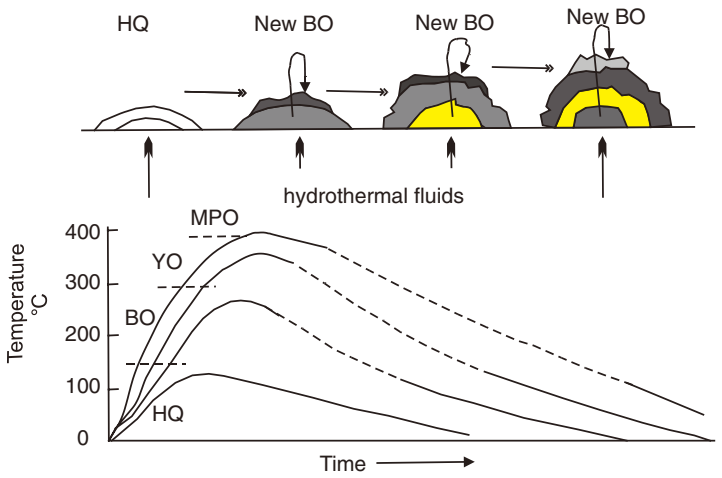


Fig. 7.34 Model showing the evolution of a Kuroko massive sulphide (**A**) and thermal history of the hydtrothermal fluids (**B**). HQ hematite-quartz, BO black ore. YO yellow ore, MPO massive pyrite ore. After Ohmoto (1996)

along fractures and in patches of Fe-rich sphalerite (called chalcopyrite disease). The first stage is the deposition of black ore, which results from the rapid mixing of cold seawater with the hot hydrothermal fluids. This forms mixtures of anhydrite-barite-sphalerite-galena-pyrite-tetrahedrite. The second stage is replacement of the black ore minerals by hotter fluids that deposit yellow ore (chalcopyrite mainly). During this stage, the dissolved black ore minerals are partially re-deposited where fluids mix with cold seawater on the outer parts of the sulphide body. The next stage involves the dissolution of chalcopyrite, which is replaced by newly formed pyrite. These processes result in the continuous addition of elements, such as Ca, Ba, Zn, Pb and Fe to the exterior of the sulphide body, whereas Cu and Fe are added to the interior (Fig. 7.34). An interesting and novel idea by Ohmoto (1996) is that the chert layers (silica-hematite-barite) that commonly overlie the sulphide ores also formed by mixing of the hydrothermal fluids with seawater, but within the unconsolidated sediments and not on the seafloor. In other words, Ohmoto suggested that the cherts originated during diagenetic processes involving precipitation of silica from the fluids.

7.7.3 Noranda or Abitibi-Type Type Massive Sulphide Deposits

The Noranda-type (or Abitibi-type) VMS deposits are generally hosted in sequences ranging from tholeiites at the base to andesite-dacite-rhyolite at the top and are characterised by deep, semi-conformable alteration zones in the footwall, cut by discordant stockworks and alteration pipes beneath the massive sulphide deposits. Volcanic rocks include lavas and associated pyroclastic rocks (fragmentals) generally associated with immature volcanoclastics. Many deposits of this type occur in Archaean greenstone belts and in the Palaeoproterozoic. Good examples are Noranda, Matagami, Snow Lake, Sturgeon Lake, Kidd Creek and Flin Flon in Canada (Franklin et al. 1981), and the Panorama district (see Section 7.7.6) and Golden Grove in Western Australia (Sharpe and Gemmell 2001, Ashley et al. 1988). Less commonly this type of Kuroko-style mineralisation is also found in Phanerozoic island arc terranes such as the deposits in the Canadian Palaeozoic terranes of Newfoundland and the Bathurst mining fields of New Brunswick (Lentz 2006). As mentioned previously, the main difference with the Phanerozoic Japanese-style Kurokos is the metal association which, for Noranda-type, is essentially Cu–Zn-rich with higher Ag/Au ratios. Another important difference between the Noranda-type and the younger Japanese Kuroko deposits is that the former contain a much smaller proportion of felsic volcanics. In the Abitibi greenstone belt of Canada, for example, felsic rocks constitute less than 4% of the entire volcanic pile. These differing proportions of mafic and felsic rocks may account for the metal associations and the observed increase in Pb content of the volcanogenic deposits with decreasing age. The Canadian Noranda-type VMS are hosted by felsic and mafic volcanics and typically occur close to small, locally steep-sided,

felsic domes composed of rhyolitic and fragmental rocks and quartz-feldspar porphyries in submarine caldera settings. The domes are usually underlain by rhyolitic dykes, and subvolcanic intrusions of tonalitic and trondhjemitic compositions may be present in the footwall stratigraphy, as for example, at Noranda, Sturgeon Lake, Matagami, Flin Flon and Bathurst. The presence of pillow lavas, graded bedding, great lateral extent of the lava flows, and paucity of pyroclastic material are all indicative of submarine conditions. The general lack, or scarcity, of oxide facies rocks such as sulphates (barite and gypsum) or banded iron formation rocks may be indicative of an oxygen-deficient environment. The deposits display a close association with coarse felsic pyroclastic rocks. The orebodies are nearly circular or lensoid in shape and contain greater than 50% by volume of sulphides. The size of Noranda-type VMS deposits in terms of tonnage and grades, although variable, is much greater than the younger Kuroko orebodies. The Gossan Hill and Scuddles VHSM deposits at Golden Grove in Western Australia, for example, contained reserves of 21 Mt tonnes grading 1.2% Cu, 8.2% Zn, 0.6% Pb, 1 g/t Au and 67 g/t Ag (Ashley et al. 1988, Barley 1992). These massive sulphide deposits are underlain by footwall breccia zones or pipes shaped as an inverted cone, with sulphides occurring as disseminations and veinlets (stringer ore). The footwall pipes, interpreted as the feeder channels for the mineralising fluids, are fairly well defined and vertically extensive. In the Vauze deposit (Noranda; Spence 1975), for example, the alteration pipe extends over 1000 m below the massive sulphide lens. Many pipes appear to be structurally controlled by faults and/or fractures. Alteration patterns are largely confined to the footwall pipes, unlike the younger Japanese Kurokos, and are characterised by chlorite, sericite, silica and carbonate assemblages. The Millenbach pipe, Noranda, exemplifies a typical alteration sequence, with its chlorite-rich core which is surrounded by a halo of sericite and an outermost silicified zone. The chloritic alteration of the pipes is therefore the most prominent feature of the Precambrian volcanogenic deposit. Thus, chloritic alteration and Mg-metasomatism are the main features of these deposits, and in extreme cases this may lead to cordierite or anthophyllite rocks, locally known as "dalmatianite" because of their spotted appearance. Important chemical changes in the alteration pipes are enrichments in Fe and Mg and depletions in Ca, Na, Si and K.

7.7.3.1 The Noranda Deposits of the Abitibi Belt, Canada

The Abitibi Archaean greenstone belt, taken together with the adjacent Wava greenstone belt in the Canadian shield is the largest in the world and, like other granite-greenstone terranes, hosts a variety of ore systems including orogenic Au lodes, Ni sulphides associated with komatiites, porphyry Mo deposits and the VMS discussed here. In the Abitibi belt, some 3000 occurrences and 265 past and present mines, record the second largest Au endownment, after the Witwatersrand fields in South Africa (Laznicka, 2006). A comprehensive collection of papers detailing the evolution of the Abitibi greenstone belt can be found in

Mueller et al. (2002). The Abitibi-Wawa greenstone belt was accreted with volcanic arcs forming a cratonic nucleus between 2.9 and 2.65 Ga. Wyman et al. (2002) interpreted the lithotectonic association as a series of intraoceanic arcs, consisting of: 2.75–2.7 Ga arc tholeiites and calc-alkaline rocks; a 2.71 Ga, depleted tholeiite-boninite suite; plume-related oceanic plateaux (2.73–2.705 Ga tholeiites and komatiites); adakites or high Mg andesites (slab melting in arc settings); and syn-late tectonic batholitic tonalite-trondjemite-granodiorite (TTG) intrusions, reflecting melting of subducted oceanic crust or plateau material. Shoshonites are also present and are interpreted as late-tectonic, second-stage melting of refractory sub-arc mantle, fertilised by late fluids developed during arc uplift and extensional collapse. A different interpretation was proposed by Ayer et al. (2002) who, using U-Pb geochronological data and focussing on the southern Abitibi greenstone belt, instead of a collage of terranes, favoured an autochthonous lithotectonic assemblage, which comprises nine supracrustal assemblages. These assemblages would effectively represent a nearly continuous volcanism, ranging in composition from mantle plume-related komatiitic and tholeiitic basalts to calc-alkaline mafic to felsic subduction-related volcanic rocks. Ayer et al. (2002) advocated a large scale and long-lived interaction between mantle plume magmatism and subduction zone related volcanic arcs, accompanied by extensive mixing of different magmas. In the Abitibi belt, komatiite lavas stratigraphically interlayered with Mg- and Fe-rich tholeiitic basalts are attributed to mantle plume activity. The tholeiitic basalts of this association have a geochemical signature that is similar to that of Phanerozoic plateau basalts (e.g., flat REE patterns). The boninite-depleted tholeiite association is interlayered with the basalt-komatiite association. This interfingering relationship has been interpreted as evidence of contemporaneous mantle plume and volcanic arc magmatism. The adakitic-high Mg andesite-basalt association is temporally and spatially linked with the calc-alkaline island arc volcanic rocks and appears to be related to intra-arc extension and rifting. It is interesting to note that the Noranda-type VMS deposits are numerous within this setting. Wyman et al. (2002) found that the Abitibi-Wawa volcanic arc and oceanic plateau lithologies, when plotted on Nb/U vs. La/Sm_{PM} diagrams, form a line that passes through the average Archaean continental crust. These researchers reiterated that this, in conjuction with other trace element systematics and field observations, support a model of tectonically imbricated intraoceanic volcanic arcs and oceanic plateaux formed during a "hybrid" tectonic process that involves both subduction systems and mantle plumes.

The Abitibi greenstone belt is approximately 750 km long and between 150 and 100 km wide and contains 11 major mafic-to-felsic volcanic piles or complexes, within which are the important Zn–Cu dominated VMS deposits of the Noranda, Timmins and Matagami Lake mining camps. In the Noranda area, the Blake River Group, consisting of felsic lavas and pyroclastics, hosts the Horne, Vauze, Millenbach, Norbec, Amulet, Lake Dufalt and Waite deposits. The ore deposits occur within a steeply dipping series of folded and faulted

rhyolitic rocks, and the mineralisation is associated with sequences of rhyolite lavas, breccias, tuffs and quartz-porphyry intrusions. A network of dykes of dioritic composition, intrude the sequence and locally completely surround the mineralised zones. Five zones of rhyolitic rocks mark successive periods of volcanic activity. The ore deposits and underlying chloritic pipes occur near the top of the rhyolitic formations and are associated with domes and explosive breccias. There is evidence of fragmentation of the sulphides prior to their being covered by later lavas.

The Vauze deposit (Spence 1975; Spence and de Rosen-Spence 1975) is associated with a rhyolite breccia located on the flank of a domal structure. In this deposit two types of ore are recognised: (1) massive stratiform lens on the flank of the dome, known as the B1 Zone; and (2) a steeply plunging pipe with disseminations and stringers of sulphides (B2 Zone), accompanied by chloritic and sericitic alteration. The massive sulphide lens (B1 zone) has a length of approximately 140 m, with an average thickness of about 2 m thinning out towards the edges where it merges with mineralised chert. The lens overlies a rhyolite breccia and is overlain in turn by an andesite flow. In this massive sulphide lens three main subzones of sulphide mineralisation are distinguished. The first is a massive sulphide subzone consisting of pyrrhotite, chalcopyrite, pyrite and sphalerite. It is crudely banded and thickest towards a postulated discharge vent area where it consists almost exclusively of chalcopyrite. Gangue material is composed of chlorite, quartz and carbonates. This massive ore grades into a breccia of sulphide clasts mixed with rhyolite fragments, which forms the second subzone of mineralisation. The third subzone stratigraphically overlies both the massive and brecciated subzones and consists of sulphide-bearing cherty tuff. It thickens away from the vent and is overlain by andesite. Within the chert layer pyrite, sphalerite and minor chalcopyrite occur as discontinuous layers. The B2 ore zone consists of two pipe-like shoots of sulphide mineralisation which occur in a more or less circular zone of strongly chloritised and sericitised rock. The mineralisation, which is concentrated mainly in these two shoots, consists of disseminations and stringers of mainly pyrite and chalcopyrite, with minor sphalerite, bornite, pyrrhotite, magnetite, Ag and Au. Pyrite and chalcopyrite are associated with the more pervasive chloritic alteration towards the centre of the pipe.

The Horne Cu–Au–Zn deposit, with a total production of 60 Mt grading 2.2% Cu and 5.3 g/t Au, is characterised by at least 30 individual massive sulphide orebodies of cylindrical, podiform to tabular shapes, associated with stringer sulphides zones (chalcopyrite-pyrite-pyrrhotite-quartz) forming subvertical structures. The ores are hosted in rhyolitic breccias and tuff that are pervasively altered to quartz-sericite and sericite-chlorite (Maclean and Hoy 1991).

Kidd Creek in Ontario, with production and resources totalling 156 Mt, grading 6.5% Zn, 2.35% Cu, 0.23% Pb, 89 g/t Ag, 0.1% Sn, is probably the largest of the Noranda-type VMS (Laznicka, 2006). The orebody is 700 m long, up to 150 m wide, extending for at least 3000 m downdip, lies in a graben

structure withn the Kidd-Munro volcanic series (Laznicka 2006). This volcanic series comprises tholeiitic basalts, komatiites and rhyolites. The rhyolitic rocks are massive to flow-banded lavas and pyroclastics, associated with epiclastic units that consist of polymictic conglomerate. The rhyolitic rocks are altered with silica, sericite, chlorite and carbonate and surround the stringer zone pipe below the massive sulphides. The massive sulphides have a Cu-rich lower part and a Zn-rich upper part. The Flin Flon Zn–Cu–Au–Ag ore field in Manitoba is actively being explored with new ores being found under the inhabited centre, contains the Flin Flon deposit with a total past production of 64 Mt, grading 4.4% Zn, 2.2% Cu, 2.6 g/t Au (Laznicka 2006).

Important points to consider in formulating a genetic model for the Canadian deposits are the stratiform and stratabound nature of the massive sulphide; their stratigraphic position at a time break within the depositional sequence; association of the ore with fragmental rhyolitic rocks and a dome-like structure; and the lateral and vertical zoning. In summary, the following sequence of events is envisaged. The ore-bearing hydrothermal solutions moved up along and through channelways of fractured rock, forming what now appears as a breccia pipe and causing alteration mainly in the form of Mg metasomatism, subsequently depositing sulphides as disseminations and veinlets. The emergence of the mineralising fluids from a vent on the flank of the rhyolitic dome resulted in the precipitation of sulphide layers as lenses along the steep sides of the dome. Slumping of the sulphide material along these steep sides resulted in the formation of the breccia ore zones. With time, this hydrothermal activity waned with the concomitant impoverishment in their metal content, causing the deposition of siliceous layers (chert) covering the sulphide mineralisation. Renewed volcanism resulted in the outpouring of pillowed lava flows which covered the massive sulphide deposit.

7.7.4 The VMS Deposits of Tasmania, Australia

The Cambrian Mount Read Volcanics in western Tasmania (Australia) host a number of complex and fascinating Kuroko-style VMS and hybrid VMS-high sulphidation epithermal systems, including Mount Lyell, Hercules, Rosebery, Que River and Hellyer, described in Large (1992a), Solomon and Groves (1994), Large et al. (2001) and Gifkins et al. (2005). The following discussion is derived from these sources.

The ~502 Ma Mount Read Volcanics form a narrow belt, east of the Proterozoic Tyennan Block in western Tasmania (Fig. 7.35), comprise the following lithostratigraphic units: Tyndall Group, Western volcano-sedimentary sequences, Central Volcanic Complex, Eastern sequence and the basal units of Sticht Range Beds. The Mount Read Volcanics are a succession of submarine basaltic to rhyolitic rocks, intrusions and variable amounts of intercalated sedimentary rocks, interpreted to be the result of post-collisional volcanism, following arc-continent collision. Solomon and Groves (1994) considered the ore

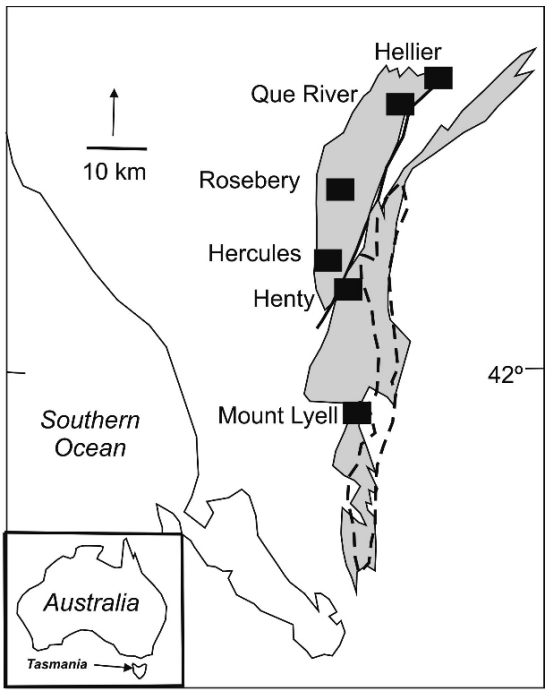


Fig. 7.35 Extent of Mount Read Volcanics and distribution of main VMS deposits; dashed line represents the inferred outline of subsurface synvolcanic granitic intrusions. After Large et al. (2001)

deposits of the Mount Read Volcanics within the following lithostratigraphy: a Northern Central Complex, hosting the Rosebery ore system, the Que-Hellyer Volcanics with Hellyer-Que River deposits, and the Southern Central Volcanic Complex with the Mount Lyell ore system. These lithostratigraphic units are separated by major faults. The dominant volcanic facies consists of dacites and rhyolites lavas, domes, associated pyroclastic rocks, syn-volcanic sills and sedimentary rocks, which comprise black pyritic mudstone, mudstone and sandstone. Granitic sills are present at depth on the eastern margin of the Mount Read Volcanics belt (Fig. 7.35) and a genetic relationship has been proposed by Large and co-workers between these intrusions the Mount Read Volcanics and related ore systems. The Mount Read Volcanics were subjected to diagenetic processes, extensive hydrothermal alteration, at least two deformation events, regional greenschist facies metamorphism and were intruded by Cambrian and Devonian granites.

Solomon and Groves (1994) discussed a possible analogy of the Mount Read Volcanics with the modern-day back-arc basin Okinawa Trough, west of the Ryuku subduction zone and trench (see Fig. 7.17), where sites of hydrothermal activity have been discovered (see also Section 7.53). One of these is the Jade field, located in a submarine caldera, and containing massive sulphides mounds (pyrite-sphalerite-galena-chalcopyrite) underlain by stockwork veins, reported by Halbach et al. (1989), who considered the Jade hydrothermal field a modern analogue of Kuroko-type VMS.

The ore systems of the Mount Read Volcanics exhibit a range of styles from lenses, sheet-like polymetallic massive Zn-rich (Rosebery and Hellyer), to massive and disseminated pyritic Cu–Au ores, to disseminated stratabound in the Mount Lyell district. Large et al. (2001) suggested that the ore systems of the Mount Read Volcanics represent a spectrum from classic VMS to replacement, intrusion-related Cu–Au ores that may by trasitional to high-sulphidation epithermal systems, to shallow water Au-rich stratabound replacement ores that resemble low-sulphidation epithermal systems. The Que River polymetallic massive sulphide ores consist of five steeply dipping lenses, Hellyer is a polymetallic mound-shaped orebody and Rosebery is the largest ore system in the belt consisting of sheet-like ore lenses extending for 1.5 km along strike. The Hercules polymetallic ore field comprises numerous, deformed ore lenses, about 100 m long; the Mount Lyell field contains 21 orebodies and has the oldest mine in Tasmania, which started operations as a Au mine in 1893. The Mount Lyell field produced a total of 113 Mt of ore. The ore systems of the Mount Read province are described in detail in the special issue of Economic Geology, edited by Large (1992b) , whereas a selection of deposits are described in Solomon et al. (2004) and Gifkins et al (2005). For this section I have chosen to briefly describe Hellyer, Rosebery and Western Tharsis.

The Hellyer polymetallic deposit (Figs. 7.35 and 7.36) is the northernmost in the Mount Read belt, with a pre-mining resource of 16.2 Mt, grading 13.9% Zn, 7.1% Pb, 0.4% Cu, 2.5 g/t Au and 168 g/t Ag. The orebody is a north-trending lens of massive sulphides, about 800 m long and 200 m wide and an average thickness of 45 m and is hosted by volcaniclastic rocks. The footwall rocks comprise andesitic and basaltic lavas and sills, whereas the hangingwall units consist of basalt and mudstone. The mineralisation is hosted by intermediate to mafic calc-alkaline Que-Hellyer Volcanics of the Mount Charter Group, equivalent of the Western volcano-sedimentary sequence. The massive sulphide ore consists of pyrite-sphalerite-galena-arsenopyrite-chalcopyrite assemblage, overlain by a cap of quartz + pyrite and flanked by lenses of barite. Below the massive sulphide lens is a carrot-shaped footwall alteration pipe that extends to a depth of about 500 m. The alteration pipe is composed of a central silica-rich zone with quartz-sericite-pyrite in which all primary texterus are destroyed, enveloped by successive zones of chlorite-sericite and sericite-quartz and carbonate. The hangingwall alteration forms an upward flaring zoned system above the massive sulphides, with a central pervasive fuchsite zone, flanked by chlorite–carbonate, followed by albite-quartz and sericite. The S isotopic composition of sulphides and barite is highly variable, with $\delta^{34}S$ values ranging from 5.7 to 27.4‰ in pyrite and sphalerite, 3.8 to 8.9‰ in chalcopyrite. Delta^{34}S values of between 42.9 and 44.7‰ were recorded from the barite cap (Solomon and Groves 1994). This range of values has been interpreted as due to complex rock-fluid interactions, oxidation of reduced S and reduction of seawater sulphate.

The Rosebery polymetallic massive sulphide deposit in the Central Volcanic Complex has a resource of 32 Mt, grading 14.7% Zn, 4.5% Pb, 0.6% Cu, 146 g/t

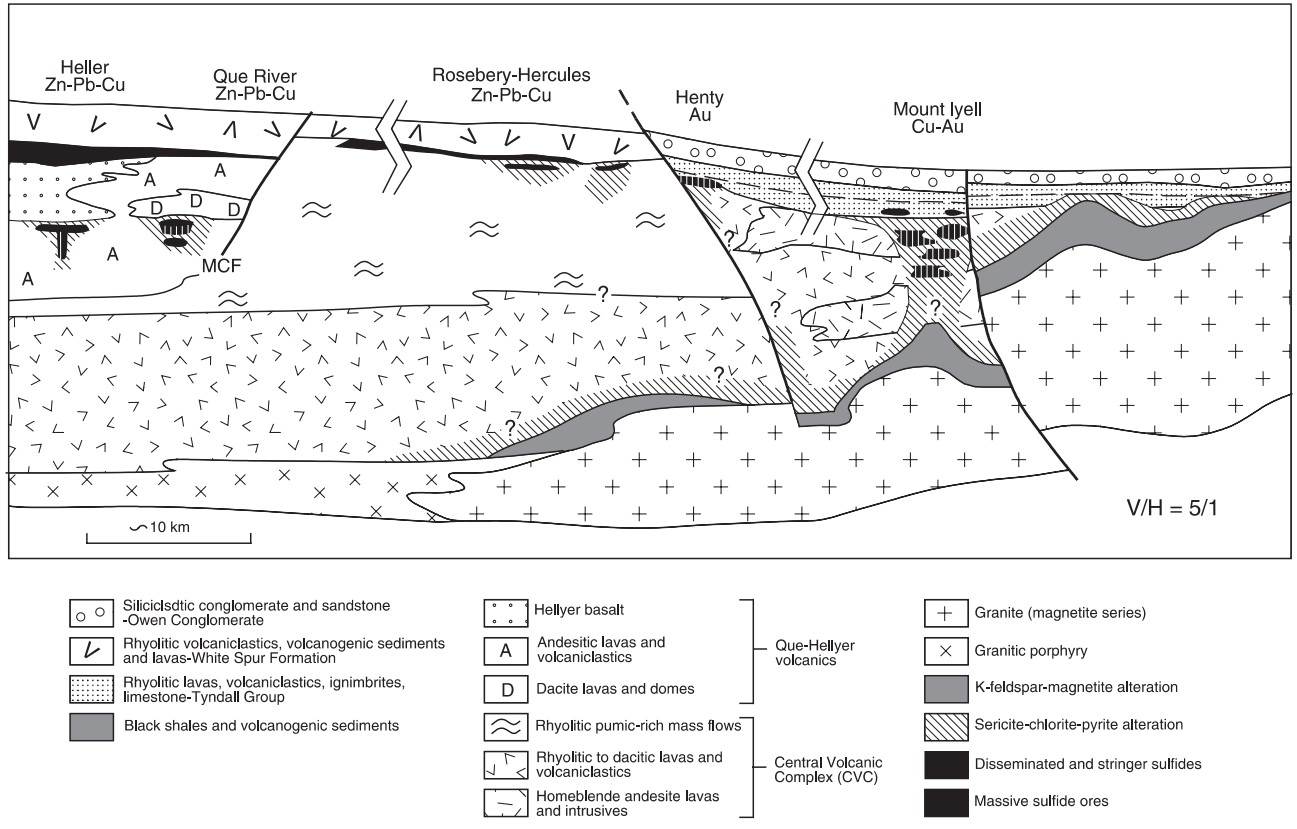


Fig. 7.36 Long-section across the Mount Read Volcanics, showing interpreted distribution and styles of VMS deposits. After Large et al. (2001)

Ag and 2.6 g/t Au. This ore system comprises at least 16 sheet-like ore lenses, varying in size from 0. 5 to 5 Mt. The Rosebery (Figs. 7.35 and 7.36) ore lenses are composed of massive and banded assemblages of sphalerite, galena, pyrite, chalcopyrite and barite, associated with subparallel barite lenses, all enclosed in stratabound alteration zones. Minor amounts of tetrahedrite, arsenopyrite, pyrrhotite, hematite and magnetite are also present. Some lenses are dominated by pyrite, sphalerite, galena, chalcopyrite and arsenopyrite. Massive sulphide lenses display distinct zoning with Cu-rich ore (chalcopyrite-pyrite) at the base and Pb-Zn-rich ore (pyrite-sphalerite-galena) at the top and may be well banded, with the banding being subparallel to bedding of the host rocks. The ore lenses were complexly deformed during the Devonian and exhibit mesoscale folds. The footwall rocks comprise a rhyolitic-dacitic succession, which is interpreted to have resulted from voluminous submarine caldera eruptions. The ore lenses are hosted in a sequence of pumiceous siltstone, sandstone, crystal-rich volcaniclastic and pumice breccias and carbonaceous shales (referred to as black slate; Solomon et al. 2004). These rocks are overlain by black mudstone, representing a hiatus in volcanism. The hangingwall rocks comprise rhyodacitic volcaniclastic units, interbedded with mudstone. As mentioned above, the Rosebery sulphides are enclosed in stratabound alteration zones, which consist of a broad outer sericite zone, followed inward by quartz-sericite, chlorite and Mn-carbonate. The Mn-carbonate alteration overlies the ore lenses and can be up to 10 m thick, but can extend laterally well beyond the ores. These carbonates include rhodocrosite ($MnCO_3$), manganosiderite [$Mn,Fe(CO_3)$] and kutnahorite [$CaMn(CO_3)$]. The strike extent of the black slate rocks is about the same as that of the ore lenses, a feature that led Solomon et al. (2004) to suggest that these slates may have been deposited in a basin structure.

The Western Tharsis deposit (Figs. 7.35 and 7.36) is in the Mount Lyell mining camp and consist of subvertical stratabound pyrite-chalcopyrite with resources of 12.4 Mt, grading 1.3% Cu and 0.3 g/t Au, but as yet not mined. The Mount Lyell camp ores occur west of the Great Lyell Fault, at various stratigraphic levels of the Central Volcanic Complex. The Western Tharsis ore lens is about 150 m thick and is one of several of the Mount Lyell ore system shown in Fig. 7.37. The ore systems consist of disseminated pyrite-chalcopyrite in a gangue of quartz-sericite-chlorite, locally associated with magnetite. The footwall rocks comprise several hundred metres of rhyolitic volcaniclastics and interbedded volcanogenic clastic sedimentary rocks, andesitic volcaniclastics, lavas and sills. The hangingwall consists of 300–200 m thick succession of felsic and intermediate volcaniclastic rocks. The Western Tharsis ore is enclosed within a 500–400 m wide zone of quartz-sericite-pyrite schist adjacent to the Great Lyell Fault, grading outward to sericite-chlorite (Fig. 7.37). In the upper parts of the mineralised system is a 150 m wide zone of intense, proximal quartz-pyrophyllite-pyrite and quartz-topaz alteration, associated with bornite-chalcopyrite. This is also enclosed by an alteration halo of quartz-sericite-pyrite, followed outward by a weak chlorite-sericite-carbonate alteration.

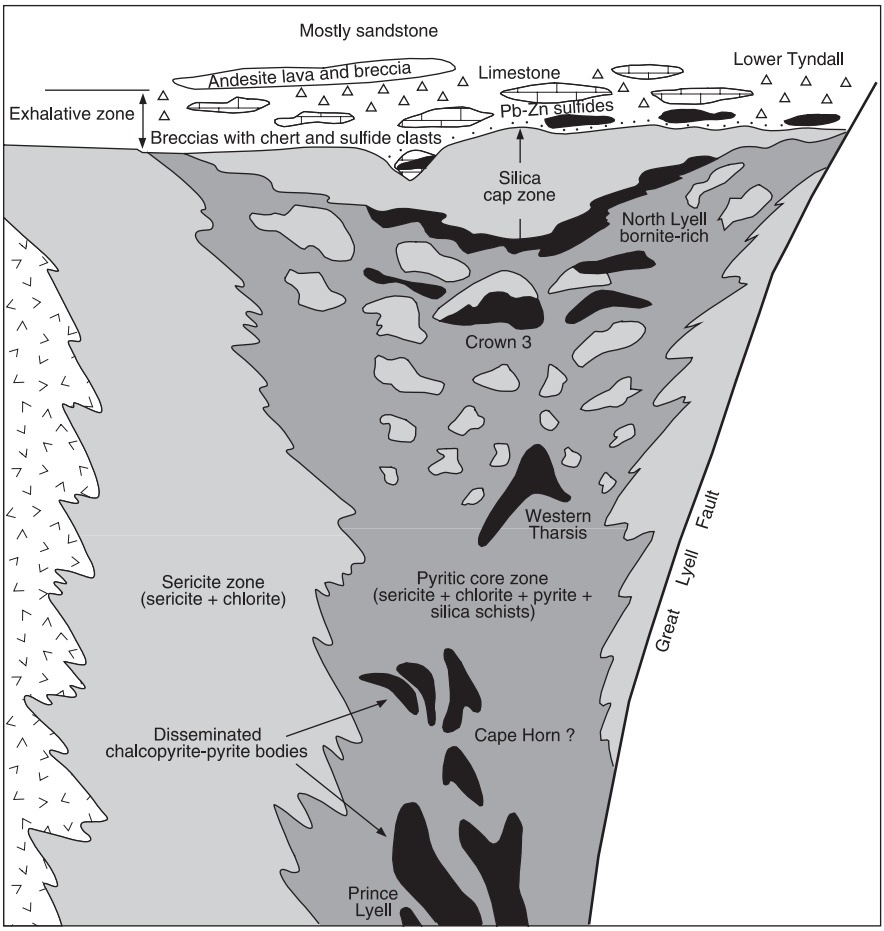


Fig. 7.37 Schematic cross-section model of the Mount Lyell VMS system. After Corbett (2001) and Gifkins et al. (2005)

7.7.4.1 Ore Genesis and Mineralisation Styles

The mineral systems, briefly described above, provide three examples of VMS of diverse style and origin. Large (1992a), while acknowledging a complete spectrum of shapes and forms exhibited by Australian VMS, considered three main groups: (1) lensoid deposits, exemplified by Rosebery; (2) mound deposits, and (3) pipe and stringer deposits, both these styles exemplified by the Hellyer system.

The Hellyer massive sulphide deposit was probably formed as a classic Kuroko-type mound in a seafloor depression, and exhibits a zone refining type of metal zonation from Cu to Pb–Zn to Ba. Alternatively, it could have formed in a brine pool, above a feeder pipe. The polymetallic sheet-like

Rosebery massive sulphide deposit, was initially interpreted as synvolcanic-exhalative, but again the size and stratiform nature suggested to some researchers (e.g., Solomon and Groves, 1994) that it also formed in a brine pool, from high-salinity fluids and as such was similar to a sedimentary exhalative ore system (SEDEX; Chapter 8). However, Large and co-workers, pointing out the lack of alteration pipes and stringer zones and the presence of disseminated sulphides parallel to the ore lenses, suggested that this ore system formed by lateral flow of hydrothermal fluids, on or just below the seafloor, with pervasive replacement of permeable pyroclastic rocks. The Western Tharsis, on the other hand, is different from the other two. This ore system is associated with mineral assemblages that are typical of advanced argillic alteration, consistent with acidic fluids of magmatic origin, similar to those of high-sulphidation epithermal systems. Because of this, the Western Tharsis is considered as a hybrid VMS, transitional to epithermal (see Fig. 7.30). Large (1992a) considered two alternative metal sources for the Tasmanian VMS deposits: leaching of metals from footwall rocks by heated seawater convecting above a sub-volcanic magma chamber, or direct input of both metals and fluids from the magma chamber. Many workers, cited by Large (1992a), support the seawater convection and leaching model, nevertheless significant inputs due to release of metal-rich volatiles from magmas is also likely to have been an important factor in the genesis of the Tasmanian VMS. The nature, style and isotopic composition of the ore system, and by analogy with modern-day submarine caldera hydrothermal fields, indicate that in the final analysis the ore fluids are a mixture of heated seawater and magmatic fluids, the proportions of which depend on the levels of hydrothermal activity. As concluded by Large (1992a), seawater may dominate in the upper levels of the volcanic pile, where the more soluble metals, such as Zn, Pb, Ba, As, Sb, Hg, may be leached out and are part of the ore fluids. In the lower sectors, fluids will have a greater magmatic component and enriched with the less soluble metals, such as Cu, Bi, Sn, Mo and Te. Gold, could be linked to both systems, namely convecting seawater, at lower temperature and transported as sulphide complex [$Au(HS)_2^-$], or in higher temperature magmatic fluids as a chloride complex ($AuCl_2^-$).

7.7.5 The Iberian Pyrite Belt Massive Sulphide Deposits

The Iberian Pyrite Belt (IPB) is one of the largest metallogenic provinces in the world forming an east-west-trending belt about 250 km long with a maximum width of 60 km, extending from southwestern Spain to southern Portugal (Fig. 7.38) and containing in excess of 1600 Mt of polymetallic massive sulphides and about 250 Mt of stockwork ores (Tornos, 2006). This astounding sulphide endownment is concentrated in 90 known orebodies, of which 20% have been mined and 10–15% are estimated to have been lost to erosion (Carvalho et al. 1999). Some of the more important ore fields include Lousal, Neves-Corvo, Cerro Colorado, La Zarza and the world-famous Rio Tinto ore

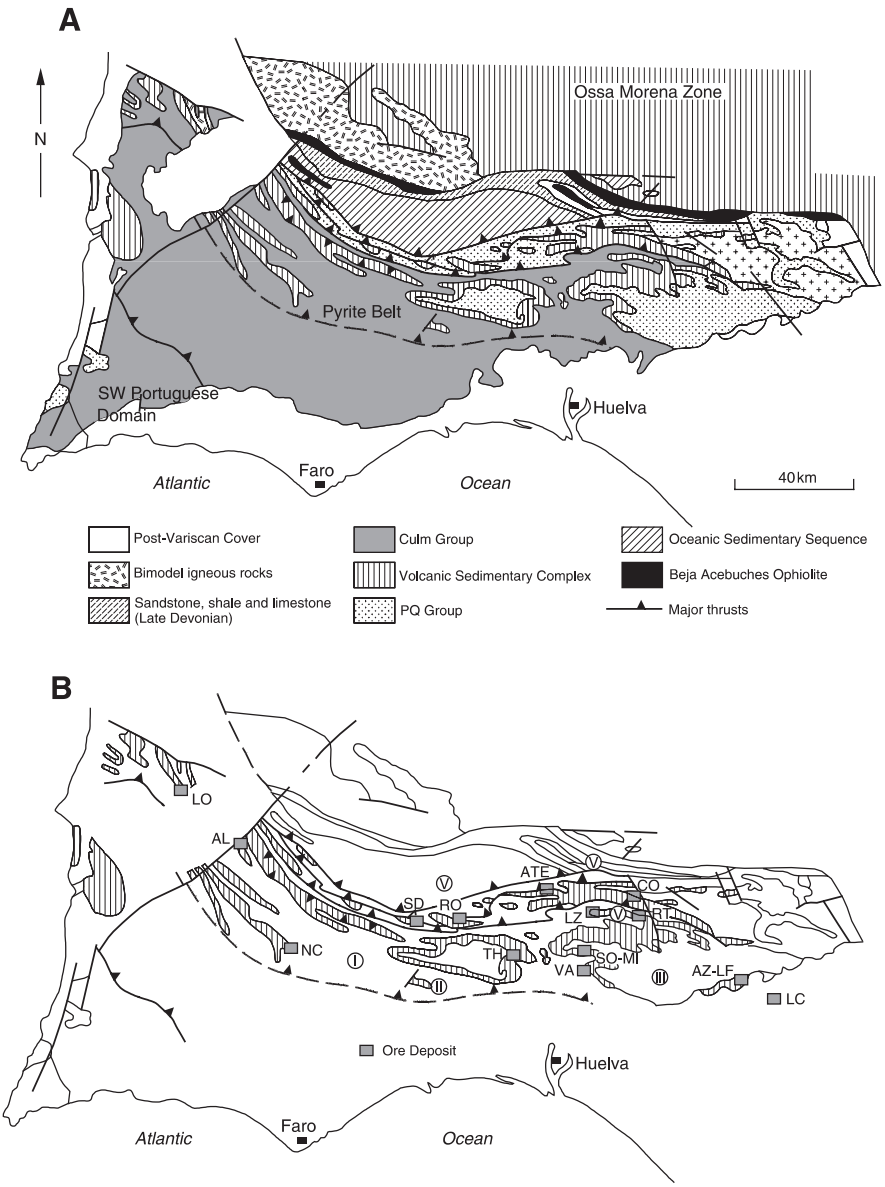


Fig. 7.38 (**A**) Simplified geology of the Iberian Pyrite Belt (IPB) and (**B**) distribution of selected massive sulphide deposits; metallogenic domains shown in B are I Western; II Puebla de Guzman; III Sotiel-Aznalcóllar; IV Rio Tinto; V Paymogo; VI Northern. Both A and B are after Tornos (2006)

field (Fig. 7.38). However, despite the large size of the IPB deposits, most massive sulphides are dominated by pyrite. The IPB has been, and still is the subject of numerous research studies and is considered as a distinct type of VMS. For the present purpose I make use of two outstanding papers, Carvalho et al. (1999) and Tornos (2006), who provided comprehensive reviews of the IPB and many key references of previous works.

The IPB is part of the great Variscan-Hercynian fold belt that forms a broad arc from the Moldavian and Saxo-Thuringian zones in central-western Europe, to the Central Armorican Zone through to the South Portuguese Zone, where the IPB is located. The South Portuguese Zone is separated to the north from the Ossa Morena Zone by a belt of ophiolitic rocks (Beja Acebuches Ophiolite) (Fig. 7.38). The general lithostratigraphy of the IPB, as presented by Carvalho et al. (1999), consists of autochthnous units of Upper Devonian-Lower Carboniferous age and allochthnous units of Lower Carboniferous age, separated by a major thrust. from base to top, the autochthonous units are represented by the Phyllite-Quartzite Group (PQ, more thn a 200 m thick), a Volcanic Siliceous Complex (VS, from 100 to 1000 m thick) and a Flysch Group (>3000 m thick). Black shales, exhalites, massive sulphides and stockworks occur at the top of the Volcanic Siliceous Complex, which largely contains felsic, mafic and sedimentary rocks. The felsic rocks are dominantly pyroclastics with some rhyolite and dacite lavas and domes. The allochthonous units are represented by a succession of black and grey shales, purple shales, siliceous tuffs, pyretic shales and greywackes. Tornos (2006), on the other hand, provided a somewhat simpler lithostratigraphy (used here), in which the PQ Group (Fammenian age) contains about 2000 m of mudstones and sandstones, and discontinuous layers of limestone, debris flows and delta deposits at the contact with the overlying Volcanic Sedimentary Complex (VS; Upper Fammenian-Early-Late Visean) consisting of up to 1300 m of mudstones, dacite, rhyolite, basalt, volcaniclastics and near the top levels of purple shales, jasper rocks and Mn deposits. The felsic volcanics form dome complexes and the basaltic rocks form sills or small stocks; locally subaqueous pillow lava flows are present in the Rio Tinto area. The mafic rocks have an alkaline tholeiitic composition. Overlying the VS are about 3000 m of turbidites of the Culm Group of Middle-Upper Pennsylvanian. Plutonic rocks are uncommon, only found north of the IPB, and consist of diorite, tonalite, gabbro and granite and may be synvolcanic, although this relationship has not been confidently ascertained. One of these plutons was dated by the U-Pb method, yielding an age of ~354 Ma. One of the puzzling features of the IPB is the absence of dykes, significant hydrothermal alteration and stockworks in the PQ Group, below the VS units. Tornos (2006) pointed out that, unlike other VMS provinces that formed in oceanic or continental back-arcs, the tectonic setting of the IPB is that of an intracontinental pull-apart basin, characterised by crustal thinning and underplating of mafic intrusion, which induced widespread melting and ascent of felsic magmas into the upper crust.

Most of the IPB massive sulphides are underlain by stockworks, surrounded by hydrothermal alteration. Tornos (2006) pointed out that previously it was

believed that shale-hosted sulphides did not have an underlying stockwork zone and as such these sulphide bodies were interpreted as distal facies. This view is now revised, because structural work has shown that shale-hosted sulphides not underlain by stockworks are structurally unrooted and bound by a fault. The stockworks are not pipe- or funnel-shaped, but have an irregular to stratabound morphology. The stockworks have an ore mineralogy that differs from the pyrite-dominated overlying massive sulphides. The ore minerals in the stockwork system comprise arsenopyrite, cobaltite, bismuthinite, Bi-tellurides and Bi–Cu–Pb sulphosalts. The ore systems of the IPB can be grouped into shale-related massive sulphides, felsic volcaniclastic-hosted massive sulphides and massive sulphides hosted by both shale and volcanic rocks (Rio Tinto district).

The shale-related sulphide bodies, as the name imply are associated with shale units that overlie the PQ Group and can either occur as a thick package, or may simply form a thin envelope around the ores. Six of the supergiant deposits belong to this group, characterised by large tonnages but dominated by pyrite and therefore have low base metal grades, except for Neves Corvo, briefly described below. The shale-related massive sulphides are underlain by zones of irregular stockworks that have been locally traced to a depth of 200 m, cross-cutting shale of the VS complex and the underlying sandstone and shale of the PQ Group. The massive sulphides generally consist of fine-grained pyrite, hosting sulphide-rich and shale-bearing breccias. The sulphides are overlain by unaltered pyrite-rich dark shale beds and a layer of grey chert. In the footwall there are carbonates, which consist of siderite-cemented sulphides breccias, or these may form zones of pervasive carbonate alteration. There is no significant hangingwall hydrothermal alteration in these shale-hosted ore systems. In most of these deposits, sedimentary structures are common and appear to be related to slumping or debris flow processes in a tectonically unstable environment. The felsic volcaniclastic-hosted massive sulphides are dominant in the Paymogo nd the Western metallogenic domains (Fig. 7.38). The host rocks generally consist of fragmental volcanic rocks, intruded by rhyolite domes with marginal hyaloclastites and the ore deposits lie within an east-west-trending tectonised zone about 18 km long. Although there is a general lack of footwall stockworks, at one mine the footwall rocks exhibit asymmetric zones of pervasive hydrothermal alteration, which from core to edge comprise quartz, chlorite, sericite-chlorite and sericite-quartz. Some of the large pyrite orebodies can contain high base metal and Au grades. The giant La Zarza deposit is located at the margins of a dacite dome and associated hyaloclastites and sills of the same composition, characterised by an extensive stockworks. Massive sulphides of the volcaniclastic ore system form tectonically stacked lenses of high aspect ratios, in which the ores can be several hundred metre long, but only 1–10 m thick. Extensive deformation hampers efforts to unravel the original geometries of the ore systems. For example, stockworks and footwall alteration pipes, although locally well developed, in most instances these are difficult to see. In other cases, a tectonic

or primary origin of the sulphides bands is hard to interpret either way. Contacts with host rocks are always discordant and replacive and the massive sulphides have interstitial silicates and remnants or fragments of chloritised host rocks. Sulphates are present as barite or gypsum ores, usually above the sulphide lenses; Fe oxides (mostly magnetite) can be locally abundant, but their relationship to the sulphide ores is uncertain. The third ore system is that of the Rio Tinto-type massive sulphides hosted both by shale and volcanic rocks. The massive sulphides form a series of dismembered lenses, which could have been part of a single, large, sheet covering an area of about 4 km^2 and a total tonnage estimated at 500 Mt. There are two types of Rio Tinto massive sulphides. In one, as at Filón Sur, San Dionisio, Planes and San Antonio, massive sulphides are interbedded with shales and are underlain by hydrothermally altered rocks. The sulphides consist of massive pyrite with primary sedimentary banding and lenses of sedimentary breccias. Also present are mm-size sphalerite veins with colloform textures, cross-cutting the massive sulphides. A 0.5–1 m thick white chert, green and purple shales occur in the hangingwall. The second type, exemplified by deposits in the north of the Rio Tinto district, consists of tabular bodies if massive and semi-massive sulphide hosted by dacites, surrounded by pervasive sericitic alteration, stockwork veins and disseminated sulphides. The massive and semi-massive sulphides are composed of coarse-grained pyrite and chalcopyrite, intergrown with varying amounts of quartz, sericite and chlorite and with fragments of host rocks. Two stages of mineralisation have been recognised: (1) an early stage with quartz-sericite-chlorite veining and sulphides filling open spaces; and (2) replacement of the altered rocks by sulphides, ending up in the massive and semi-massive sulphide lenses.

7.7.5.1 Neves Corvo and Rio Tinto Ore Fields

The Neves Corvo ore field is in southern Portugal, discovered in 1977 by drilling through 300 m of cover into a Bouguer gravity anomaly and is characterised by large amounts of cassiterite, with 4.3 Mt grading 2.5% Sn (Laznicka 2006). The ore field comprises a cluster of five massive sulphide lenses hosted by black shale rocks with a total tonnage of 219 Mt, averaging 1.9% Cu and 0.13% Sn. The massive sulphides are mostly pyrite (called pyritite by Laznicka 2006), but with a resource of Cu ore and lesser quantities of Pb and Zn ores. These ores are zoned with Cu in the basal portions, followed upward by Pb and Zn. Apart from the dominant pyrite, base metal sulphides are galena, sphalerite, chalcopyrite, with lesser amounts of tetrahedrite, bornite. Cassiterite and stannite are the Sn ore minerals. Gangue and alteration minerals include quartz, chlorite, sericite, dolomite, siderite and barite. The footwall rocks are hydrothermally altered with quartz, chlorite and sericite and the associated stockworks contain veins and disseminations of chalcopyrite, locally with cassiterite and sphalerite. In the hangingwall are bands of pyrite, chalcopyrite, sphalerite and cassiterite

alternating with the black shales. This banding is interpreted as due to tectonic interleaving.

The Rio Tinto ore field is in southwest Spain (Fig. 7.38), and as mentioned above, has the largest metal endownment in the IPB, covering an area of at least 8 km^2 and with 513 Mt of ore material, averaging 1.36% Cu. One of the largest the San Dionisio orebody, which is a folded massive pyritite mass, with minor chalcopyrite, sphalerite and galena. The footwall stockworks have stringers and disseminations of pyrite and chalcopyrite with quartz, and sericite hydrothermal alteration minerals, enveloped by a zone of chloritic alteration.

7.7.5.2 Ore Genesis and the IPB Hydrothermal System

Tornos (2006) listed the main features that set the IPB ore systems apart from other VMS. They are: (1) a pull-apart basin tectonic setting; (2) thick siliciclastic succession below the VS; (3) small thickness of the VS Complex (0–1300 m); (4) abundance of shale in the VS rocks; (5) clustering of large deposits and high proportion of supergiant deposits; (6) characteristic geochemical and isotopic compositions, as discussed below.

Sedimentary structures in footwall and hangingwall rocks, presence of carbonaceous shales, high aspect ratios of the ore lenses, lack of vent constructs above the sulphides and lack of alteration in the hangingwall rocks, are indicative of sulphide deposition in a brine pool, in a model that is comparable to that of a Red Sea type SEDEX ore system (Solomon et al. 2004; Tornos, 2006). The Atlantis II Deep (described in Chapter 8) has metal contents comparable to those of the IPB deposits, but is formed on a spreading ridge and lacks felsic volcanic rocks. Therefore, although both ore systems are exhalative in nature, the comparison is more one of geometry rather than genetic. For the IPB, it is thought that the sulphides were precipitated on the seafloor when S saturation was reached and that reduce sulphides were formed by sulphate-reducing bacteria communities that would thrive at the temperature range of the shale-hosted massive sulphides (120–70°C). In addition, the fine-grained nature of the sulphides is interpreted as having originally been gel-like, with precipitation caused by supersaturation induced by biogenic H_2S. Continuous supply of sulphate-rich seawater is needed to feed the system and Tornos (2006) suggested that there must have been active circulation of seawater in the more oxygenated upper parts of the basin. The fact that the lowermost parts of the massive suphides show evidence of epigenesis is taken to indicate that this mineralisation was formed by a combination of pore-filling and replacement of the footwall rocks. The felsic volcanic-hosted massive sulphides show no evidence of having been exhaled on the seafloor. Here there is lack of sedimentary structures, presence of alteration surrounding the orebodies and of replacive fronts are suggestive of stratabound replacement of favourable host lithologies. The favourable lithologies include the hyaloclastite marhins of felsic domes and the porous and chemically reactive volcaniclastic rocks. A suggested ore-forming

mechanism is by mixing of hot deep fluids with cool seawater-derived fluids confined to stratabound aquifers.

The IPB fluids, as characterised by fluid inclusion studies, were CO_2-poor and saline brines (up to 24 wt% NaCl equivalent; see Table 7.3), which are similar to those of the Tasmanian deposits (e.g., Hellyer), but significantly higher that the Japanese Kuroko systems (8–2 wt% NaCl equivalent). The stable isotopic compositions, in terms of δD and $\delta^{18}O$ values (see Table 7.3), are inconclusive in that these values are compatible with a variety of fluid reservoirs, including magmatic, metamorphic, connate and mixtures thereof with seawater. Tornos (2006) emphasised that the only by comparing $\delta^{18}O$ analyses of quartz with independent geothermometres can provide some realistic estimates of $\delta^{18}O$ values. The $\delta^{18}O$ data, salinities and temperature estimates for the IPB systems are given in Table 7.3. The S isotopic compositions, from a large number of analyses, show a wide range of $\delta^{34}S$ values from –34 to 21‰, contrasting with that of other VMS in the geological record. The $\delta^{34}S$ data indicate derivation of the S from a variety of sources, such as the host volcanic rocks, leaching of basement rocks and thermochemical sulphate reduction or a combination of the above.

The IPB hydrothermal system is unlike that of other VMS and Tornos' preferred model is that of forced convection in a basin, with the heat engine being provided by deep plutonic intrusions, for example Sn-rich granites could be present at depth as the roots of the VS Complex rocks. However, a direct role of magmatic fluids is unlikely because of the absence of high temperature alteration assemblages, such as feldspar-chlorite-magnetite-apatite, potassic and/or sodic alteration and heavy $\delta^{18}O$ values. The IPB orebodies were subjected to extensive deformation during the Variscan orogenesis (Late Palaeozoic). Thrust-and-fold tectonics resulted in the displacement or decoupling of the massive sulphides from the stockwork feeder zones, tectonic stacking and dismembering of the ore lenses with some metal enrichment along deformation bands. Syntectonic pyrite-rich vein systems, unrelated to the IPB hydrothermal systems were also formed during the Variscan event and. The tectonic metal enrichment produced Cu, Zn, Pb, Au and Ag mineralisation in faults that cut the orebodies, would explain the high base metal content in the more deformed orebodies. In conclusion the IBP originated in a pull-apart basin of a transpressive orogen and within a thin volcanic succession. Tornos and Heinrich (2007) reviewed the essential elements for the genesis of IPB ores as follows (see also section 7.7.5.3): (1) suitable source provided by a thick package of sedimentary rocks with disseminated sulphides; (2) high geothermal gradient provided by underlying igneous intrusions; (3) efficient chemical trap by the addition of biogenically-derived H_2S near the sediment-water interface. A model of ore genesis, as envisaged by Tornos (2006) is shown in Fig. 7.39.

Finally, a comparison of selected features between IPB, Japanese Kurokos and Tasmanian deposit is provided in Table 7.4.

Table 7.3 Compilation of fluid inclusion and oxygen-deuterium isotope data of the Iberian Pyrite Belt; after Tornos (2006 and references cited therein); values in parentheses are averages; **stw** is stockwork and **to** is tin ore

Locality	Homogenization temperatures (°C)	Salinity wt.% NaCl eq.	Interpretation	Isotopic temperatures	O–H isotopes	Interpretation
Aznalcóllar	139–345	0.4–12.4	Modified seawater. Low salinities due to input of meteoric water or condensation of gas Local boiling.			
Las Cruces	109–287 (155)	0.8–9.8 (5)	Modified seawater with late mixing of meteoric fluids		$\delta^{18}O_{fl} = -2.5\%$ to 0.8%	Modified seawater
Rio Tinto	130–230 140–260 (160)	2–10 3–6.5 (5.3)	Boiling deep fluids Modified seawater + magmatic fluid.	stw: 210–230	$\delta^{18}O_{fl} = 5.5$–7.7%[3] $\delta^{18}O_{fl} = 0$–1.3%[4] $\delta D_{fl} = -5\%$ to -8%[4]	[3] Modified seawater + magmatic fluid [4]Seawater
Valverde	139–387	1.9–12.4	Boiling deep fluids			with minor deep fluids
San Miguel	160–240 (188)	5.2–9.7 (6.9)	Modified seawater + magmatic fluid		$\delta^{18}O_{fl} = -2.3\%$ to 7.2% $\delta D_{fl} = -12\%$ to -10%	Modified seawater + magnetic fluid
Aquas	168–261 (201)	4.0–6.9 (5)	Modified seawater		$\delta^{18}O_{fl} = -3.0\%$ to 3.8%[1]	[1] Modified seawater
Teñidas Este	82–240	5–24	Modified seawater + magmatic fluid		$\delta^{18}O_{fl} = -2.7\%$ to 9.6%[2] $\delta D_{fl} = -45\%$ to 36%[2]	[2] Modified seawater + magnetic fluid
San Telmo	200–285 (243)	6.7–9.2 (7.5)	Modified seawater + magmatic fluid		$\delta^{18}O_{fl} = 3.9\%$ to 5.6% $\delta D_{fl} = -10.2$	Modified seawater + magnetic fluid

Table 7.3 (continued)

Locality	Homogenization temperatures (°C)	Salinity wt.% NaCl eq.	Interpretation	Isotopic temperatures	O–H isotopes	Interpretation
Salgadinho Neves Corvo	222–235	2.6–5.7	Seawater + magmatic fluid	to: 112–196 to: 167–188 stw: 259–402	$\delta^{18}O_{fl}$ = –3.1% to 10.2% (1)	Modified seawater + magmatic fluid
Aljustrel	270–305	2.6–6.7	Slightly modified seawater	ms: 170–245 stw: 160–175	$\delta^{18}O_{fl}$ = 0.0% to 6.1% (2) δD_{fl} = 0 to 15% (2)	(2) Mixing of seawater with minor amounts of deep fluids
Lagoa Salgada	159–348	3.2–7.4				

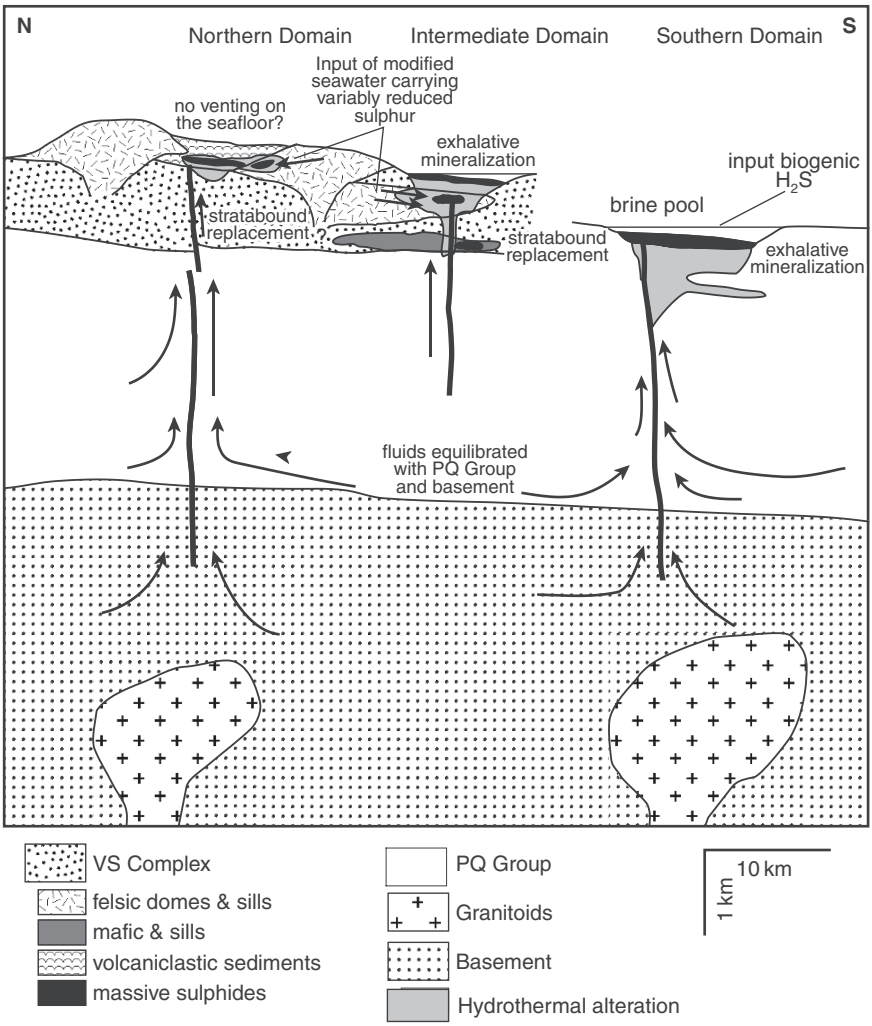


Fig. 7.39 Conceptual model for three types of Iberian Pyrite Belt ore systems, as proposed by Tornos (2006). In this model the basement rocks (PQ Group) were the source of fluids and metals; widespread convective hydrothermal circulation occurred, together with compaction and dewatering of the siliclastic sedimentary pile and the synchronous emplacement of igneous intrusions, which provided the heat engine; style and nature of the IPB orebodies was dicated by local palaeogeographic features. The ores formed in two main hydrothermal regimes: (1) exhalative ores deposited in brine pools (intermediate and southern domains) and (2) as replacement below the seafloor (northern domain)

Table 7.4 Comparison of selected features between IBP, and VMS in Tasmania and Japan. After Solomon et al. (2004)

Features	Iberian Pyrite Belt	Tasmania (Hellyer)	Japanese Kurokos
Ore type	Low Zn and Pb contents; Cu enrichment near base; footwall stockworks, sericite and chlorite alteration in footwall rocks	Barite-sulphide ores; Zn-Pb ores; Cu enriched in core of massive sulphides, pyrite at base; footwall alteration with siliceous core, chlorite-sericite	Barite present, but less than Tasmanian deposits; oko (yellow ore)
Textures	Common framboids, banding	Framboids, veinlets and banding	Framboids; veinlets and banding locally present
Chimneys	Not present	Not present	Yes
Massive sulphides ore minerals	Pyrite»sphalerite> galena>chalcopyrite> arsenopyrite±pyrrhotite	Pyrite>sphalerite> galena> Arsenopyrite> chalcopyrite	Kuroko:Barite> sphalerite> Galena>pyrite> Chalcopyrite; Oko: chalcopyrite-pyrite
Bacteria present	Suggested by isotopic fractionation	Suggested by isotopic fractionation	No evidence
Fluid inclusion salinity	Up to 14 wt% NaCl equivalent	Up to 15 wt% NaCl equivalent	~5.5 wt% NaCl equivalent

7.7.5.3 The Abra Polymetallic Deposit in Western Australia: a Possible Proterezoic IPB Analogue?

Abra is a blind, stratabound sedimentary rock-hosted Fe–Pb–Cu–Ba ± Ag ± Au ± W deposit, discovered in 1981, located within the easterly trending Jillawarra rift sub-basin of the Mesoproterozoic Edmund Basin, situated between the Pilbara Craton in the north and the Yilgarn Craton in the south (Western Australia). The Edmund Basin is part of the Capricorn Orogen and contains the Edmund Group, which consists mainly of siltstone, dololutite, stromatolitic dolomite and sandstone, grouped into ten formations which can be subdivided into four unconformity-bounded sequences. The Discovery Chert Formation in the Edmund Group, is an important stratigraphic marker consisting predominantly of silicified carbonaceous siltstone. Detrital zircons from the Edmund Group have ages greater than 1.46 Ga; (Martin and Thorne, 2004). A number of fault-bounded sub-basins developed subparallel to and controlled by the regional structural grain. One of these is the Jillawarra sub-basin referred to above, within which is the polymetallic Abra deposit. Initial rifting occurred in the central part of the Edmund Basin (Collins and McDonald l994, Vogt 1995) and along the northern margin of the Gascoyne Complex. Igneous activity in the Jillawarra sub-basin includes high-K rhyolite,

with a possible U-Pb age of 1.64 Ga. Elsewhere in the Edmund Basin dykes and sills of alkaline affinity are present (Gifford Creek Complex; Pearson et al. 1996).

The Abra deposits, as yet unmined and at the time of writing still in an exploration stage, is estimated to contain approximately 50 Mt of ore, grading 5.5% Pb equivalent and 10 Mt at 0.8% Cu equivalent, beneath a 200–500 m cover of lower Edmund Group rocks (Jillawara Sub-basin; Martin and Thorne 2004). Recent drilling results confirm the giant status of this deposit, with some intersections yielding 58 m at 9.7% Pb and 4.5 g/t Ag; 12.8 m at 9.5% Pb, 15.5 g/t Ag and 2.8% Zn; 56 m at 3.4% Pb, 15 g/t Ag and 0.3 g/t Au (Media release to the Australian Stock Exchange, January 2008). The Abra mineralisation was described by Vogt and Stumpfl (1987), Boddington (1990), Collins and McDonald (1994) and Vogt (1995). More recently, the Abra mineralisation was investigated as part of an MSc project by Austen (2007). This polymetallic deposit is hosted in dolomitic siltstone and shale of the Gap Well Formation and is characterised by a funnel-shaped brecciated (feeder) zone, possibly a breccia pipe, overlain by stratabound mineralisation (Pirajno, unpublished data). The stratabound mineralisation includes an earlier Red zone, cut by a later Black zone that may be part of the breccia feeder pipe. The Red zone is characterised by jaspilite, hematite, galena, abundant barite and siderite. The Black zone consists of hematite, magnetite, carbonate, barite, scheelite and Pb, Zn and minor Cu sulphides. The ore minerals are galena, sphalerite, with minor tetrahedrite, chalcopyrite and scheelite. The feeder zone or breccia pipe merges with Black Zone and is estimated to contain about 150 Mt of base metals, including 0.13 g/t Au. This zone consists of a stockwork of carbonate-quartz veins, with abundant fluidised and/or jigsaw textures and that cut through an alteration envelope of chlorite and siderite in siltstone units of the Gap Well Formation, which is enriched in silica and Fe, and depleted in Al, Ca and Rb in relation to unaltered rocks. Boddington (1990) noted that the upper part of the stringer zone contains higher Ba–Ag–Pb than the lower parts, which is enriched in Cu–Au. The Abra mineral system is multiphase, in that it is characterised by several overprinting phases of hydrothermal activity, from several stages of brecciation and fluidisation, barite and sulphide veining to barren low-temperature chalcedonic (epithermal style) veining (Pirajno, unpublished data). Hydrothermal alteration consists of pervasive to non-pervasive silicification, and chloritisation. Locally albitic alteration (Na metasomatism) is present and is associated with sulphides. Isotopic (O, D and Sr) and fluid inclusion studies by Austen (2007) suggest that the metals may have been derived from the sedimentary rocks and that the ore fluids had temperatures ranging from 162 to 250°C, with salinities ranging from 5.8 to about 20 wt% NaCl.

Vogt and Stumpfl (1987) and Collins and McDonald (1994) linked the genesis of the Abra deposit to ca 1.64 Ga rift-related tectonics and felsic magmatism. Vogt and Stumpfl (1987) also suggested that the source of the Pb and Ba may have been the associated arkosic sediments. The association of the

deposit with felsic magmatism in a rift setting, together with Fe-rich and chlorite alteration of the host sedimentary rocks, raises the possibility that the Abra deposit may be a variant of the IBP deposits, which typically are associated with thick siliciclastic successions in a rift setting and exhibit widespread chloritic alteration. Recent work on IBP systems by Tornos and Heinrich (2007) using thermodynamic modelling, support the idea of a genetic relationship between the sulphide mineralisation and siliciclastic sedimentary successions as a metal source. Tornos and Heinrich (2007) also envisaged that the heat energy my be provided by an underlying igneous source and a mechanism of sulphide precipitation by mixing of S-deficient metalliferus brines with biogenic H_2S-rich fluids at or near the seafloor. These authors suggested that single-pass dewatering and diagenetic maturation and compaction of siliciclastic sequences can release enough fluids and metals to generate large orebodies.

Tornos and Heinrich (2007), quoting Saez et al. (1996), pointed out that the IPB (and Abra) mineral systems also share features that are common to SEDEX systems, rather than volcanogenic. However, the IPB deposits have an undeniable link with coeval felsic magmatism and this militates in favour of a volcanogenic association. The case is less clear for Abra, although there appears to be a link with felsic volcanism, represented by the Tangadee Rhyolite, that outcrops in the vicinity of the deposit. The Tangadee Rhyolite and the Abra mineralisation are, at the time of writing, being studied by geoscientists of the Geological Survey of Western Australia. For this deposit, the jury is still out.

7.7.6 The Oldest VMS: Pilbara Craton, Western Australia

The Pilbara Craton, spanning a geological history of more than 800 million years from about 3.65 to 2.83 Ga, contains the oldest known hydrothermal mineral systems. The Craton is made up of two main tectonic units: the North Pilbara, represented by Palaeoarchaean granite-greenstone rocks and the overlying Neoarchaean Mount Bruce Supergroup deposited in the Hamersley Basin, the repository of the vast Fe ore province to be discussed in Chapter 8. The geology and distribution of mineral deposits of the North Pilbara terrain are shown in Figs. 7.40 and 5.47).

In Chapter 5, I discussed the oldest epithermal systems and mentioned the VMS of the Warrawoona Group of the East Pilbara Terrane, in this section I continue with a more detailed look at the VMS in the Panorama District in the Archaean North Pilbara Terrain. In the North Pilbara terrain there are several deposits that bear the hallmark of VMS systems, such as Whim Creek, Mons Cupri and Salt Creek in the West Pilbara Terrane and hosted by the ~3.0 Ga Whim Creek greenstone belt, the Big Stubby, Lennon's Find, the Panorama Zn–Cu–Pb deposits, all hosted by the 3.53–3.42 Ga Warrawoona Group of the East Pilbara Terrane (Fig. 7.40). Relevant literature for the Pilbara geology and VMS deposits include Solomon and Groves (1994), Vearncombe et al. (1995, 1998), Vearncombe (1999), Vearncombe and Kerrich (1999), Rasmussen

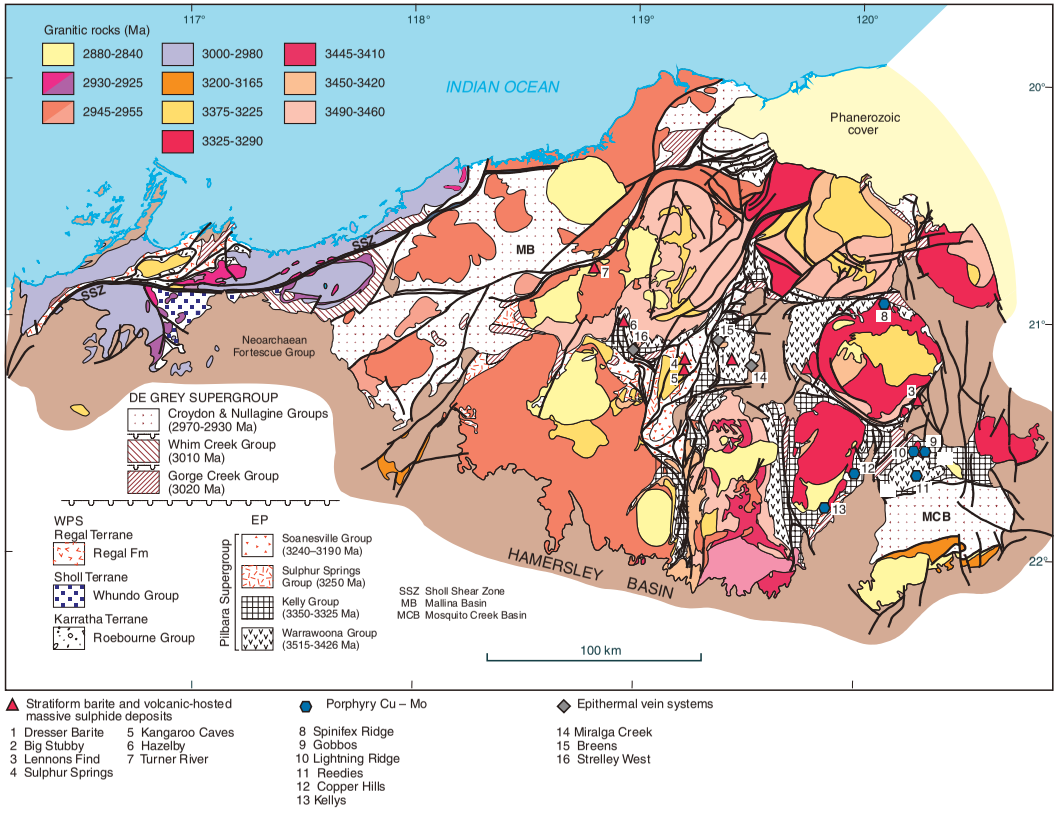


Fig. 7.40 Simplified geological map of the north Pilbara Craton and distribution of porphyry, epithermal and VMS deposits, formed before 3.2 Ga; MB Mallina Basin, MCB Mosquito Creek Basin, SSZ Shoal Shear Zone. After Huston et al. (2007)

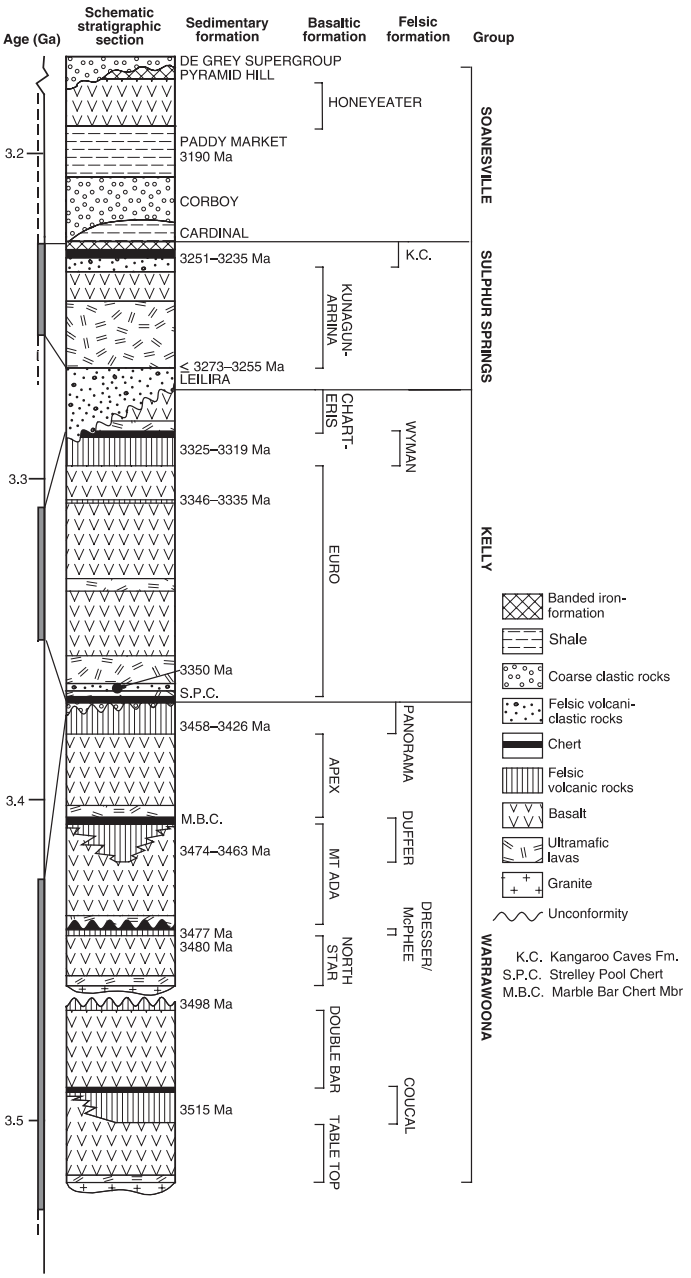


Fig. 7.41 Lithostratigraphic column of the Pilbara Supergroup in the East Pilbara Terrane and position of VMS deposits. After Van Kranendonk et al. (2006a)

(2000), Huston et al. (2001, 2007), Huston (2006), Van Kranendonk et al. (2006a, b). For a comprehensive account of the geology and tectonic evolution of the North Pilbara terrain, the interested reader is referred to the special issue of Economic Geology edited by Huston et al. (2002). These works constitute the database of the discussion that follows, in which I focus on the Panorama district VMS mineral systems.

The East Pilbara Terrane, briefly described in Chapter 5, is the ancient cratonic nucleous of the Pilbara Craton, which is the host not only of the oldest mineral systems, but also contains evidence of the oldest life on Earth (Van Kranendonk et al. 2002). The Warrawoona Group and Sulphur Springs Group of the East Pilbara Terrane, contain the oldest epithermal and VMS ore systems. The 3.53–3.42 Ga Warrawoona Group is made up of a bimodal succession of mafic (Table Top, Double Bar, North Star, Mount Ada and Apex formations) and felsic (Dressser, Coucal, McPhee, Duffer and Panorama formations) volcanic rocks. The 3.27–3.23 Ga Sulphur Springs Group, overlies the Euro Basalt and is a succession of dominantly volcanic rocks and is divided into four formations (Lelira, Kunagunarrina, Kangaroo Caves and Budjan Creek). A lithostratigraphic column of the East Pilbara Terrane is shown in Fig. 7.41. The world's oldest base metal accumulations are hosted by the 3.47–3.46 Ga Duffer Formation, with the Big Stubby and Lennon's Find deposits; the 3.49 Ga Dresser Formation hosts massive barite lenses and the Sulphur Springs Group hosts the Panorama Zn–Cu–Pb deposits (Huston et al. 2007). The northern Pilbara's VMS deposits (and porphyry and epithermal systems) are important, not only because they are the oldest in the world, but also because these hydrothermal systems were formed during intraplate tectono-magmatic processes related to mantle plumes and are not related to subduction zone magmatism as is the case for most, but by no means all, post-Archaean porphyry and epithermal systems, as discussed in Chapter 5.

7.7.6.1 Big Stubby and Lennons Find

The Big Stubby VMS Zn–Pb–Ag–Ba deposit is small with only 100 000–200 000 tonnes of ore grading 13.8% Zn, 4.5% Pb, 350 g/t Ag and 20% Ba. The deposit consists of six stacked lenses of massive sulphides and jaspilite associated with tuff-breccia and rhyolite domes. The ore mineralogy is simple and consists of sphalerite, pyrite, galena, minor chalcopyrite. Gangue and alteration minerals include tourmaline, barite, quartz, sericite, chlorite and calcite. Fluid inclusion studies gave homogenisation temperatures of 290–230°C (Huston et al. 2007).

The Lennon's Find is probably the oldest known VMS in the world (~3470 Ma) comprises five mineralised zones over a strike length of about 5 km and is poorly documented. The Duffer Formation in the area is characterised by a basal quartzo-feldspathic schist, overlain by clastic metasedimentary rocks, in turn overlain by quartz-muscovite schist. One of the mineralised zones has a small resource of about 1.2 Mt, grading 0.43% Cu, 7.76% Zn, 1.94% Pb and 100 g/t Ag. The five mineralised zones are found in two horizons.

In the upper part of the Duffer Formation, which consist of quartz-muscovite schist, probably a metamorphosed and/or hydrothermally altered felsic volcanic rock and a lower horizon of metamorphosed clastic sedimentary rocks. The Hammerhead mineralised zone is better documented, consisting of thin lenses of semi-massive to massive sulphides. The Hammerhead ore minerals comprise sphalerite, chalcopyrite and galena mainly, associated with barite and pyrite. Massive banded ore contains 25–80% sulphides in a gangue of quartz, barite, chlorite, carbonate, tourmaline, muscovite and biotite. This massive sulphide ore overlies thinly banded and disseminated sulphide ore with mainly pyrite. This zone of thinly banded ore has been interpreted as a stringer or feeder zone. Alteration facies in the Lennon's Find area are represented by pyrite and quartz-sericite. Massive barite is present at the contact between the Duffer Formation and the Apex Basalt (Fig. 7.41).

7.7.6.2 The VMS of the Panorama District, Sulphur Springs Group

The Sulphur Springs Group hosts a number of VMS deposits in the Panorama district, of which Sulphur Springs and Kangaroo Caves are economically more important (Figs. 7.40 and 7.42; Huston et al. 2007). The Sulphur Springs Group is described in detail by Van Kranendonk et al. (2006a) (Fig. 7.41; see also Chapter 10 and Figs. 10.12, 10.13 and 10.14). In the Panorama district the Sulphur Springs Group reaches a thickness of about 3000 m and consists of three volcano-sedimentary successions, flanking the Strelley Monzogranite on its eastern side (Fig. 7.42). The rocks of the Sulphur Springs Formation are tilted to between 30 and 80°, thereby providing a cross-sectional view (Vearncombe et al. 1995). The lowermost succession (Leilira Formation) consists of turbidites and chert beds, locally intruded by rhyolitic rocks. The Kunagunarrina Formation comprises mafic and komatiitic volcanic rocks, associated with thin volcaniclastic horizons and chert. The uppermost Kangaroo Caves Formation is represented by basalt, andesite, dacite and rhyolite volcanic rocks, epiclastic and banded iron formation units. At the top of this formation is a marker chert unit, up to 100 m thick, with abundant kerogen chert veining (Huston et al. 2007). The Strelley Monzogranite is coeval with the volcanics of the Kangaroo Caves Formation and its intrusion resulted in the inflating of the Sulphur Springs Group successions (Van Kranendonk et al. 2006a). The Strelley Monzogranite is composed of three phases: porphyritic biotite-hornblende monzogranite, a leucocratic quartz-plagioclase granodiorite and a leuco-monzogranite and is considered to have been the heat engine that powered the hydrothermal system responsible for the VMS deposits of the Panorama district.

The VMS mineralisation in the district (Sulphur Springs and Kangaroo Caves) is associated with laterally extensive zones of hydrothermal alteration and comprises stratabound Cu–Zn massive sulphide lenses with barite, developed above stringer zones with veins of pyrite, chalcopyrite, minor sphalerite and carbonate. The Sulphur Springs prospect has resources of 10 Mt, grading 1.4% Cu, 3.5% Zn, whereas the Kangaroo Caves prospect has 1.7 Mt grading

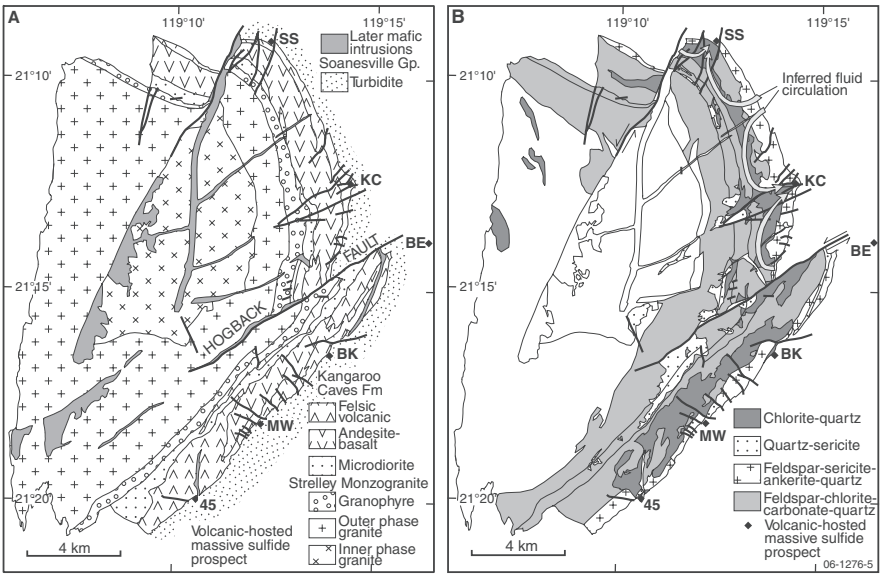


Fig. 7.42 Simplified geology of the Panorama district and distribution of VMS deposits (**A**) and alteration facies (**B**). After Brauhart et al. (1998) and Huston et al. (2007)

0.6% Cu, 9.8% Zn, 0.6% Pb, 18 g/t Ag and 0.1 g/t Au (Huston et al. 2007). The massive sulphides exhibit an upward zonation from Cu to Zn–Pb, compatible with other VMS systems and contain an ore assemblage of pyrite, sphalerite, chalcopyrite, galena, tennantite, arsenopyrite, barite and pyrrhotite (Vearncombe et al. 1995). Chalcopyrite is more common in the stringer zones, whereas barite, sphalerite and galena are more abundant in the sulphide lenses.Vearncombe et al. (1995) examined in some detail the textural features of the mineralisation. These authors noted spherulitic, dendritic or arborescent and colloform sulphide textures, including banded and stromatolite-like features. Barite commonly occurs as tabular blades and rosettes. These textures have been interpreted as having formed from progressive growth in small conduits and are suggestive of black smokers' textural characters and growth. The spherical textures are similar to the amorphous silica spherules which coat filamentous bacteria. Indeed, Rasmussen (2000) discovered pyritic filaments, located in the siliceous cores and bands of the colloform textures. The filaments are up to 300 μm long and 2–0.5 μm thick, are quite abundant have straight, curved and sinuous shapes and occur parallel to the banding or oriented perpendicular to it. Rasmussen (2000) inferred a biogenic origin for these filaments and suggested the possibility of micro-organisms growing in the pore spaces and microfractures of rocks at shallow depth with the hydrothermal fluids delivering the necessary nutrients, including metals that are essential for the growth of microbial life.

Hydrothermal alteration has regional extent was described in detail by Brauhart et al. (1998) and is schematically shown in Fig. 7.42. Feldspar-destructive sericite-quartz and chloritic alteration occurs 2–1.5 km below the sulphide lenses. There are four main regional alteration assemblages: (1) feldspar-chlorite-carbonate-quartz; (2) feldspar-sericite-quartz-ankerite in the Strelley Monzogranite only; (3) feldspar-destructive sericite-quartz; and (4) chlorite-quartz. In the hanging wall, the alteration transgresses into the overlying Soanesville Group and comprises an inner zone of silica-sericite-chlorite-pyrite and an outer carbonate and silica-carbonate zones.

Huston et al. (2001) suggested that the metals fo the Panorama VMS were leached from the base of the volcanic succession. Furthermore, they pointed out that unlike the younger Neoarchaean Noranda-type deposits, the common presence of barite in the Panorama VMS is indicative of sulphate in the ancient seawater. Thus, these Palaeoarchaean VMS are more similar to the Japanese Kuroko, except that the S isotopic composition of the Panorama VMS is different having a narrow range of $\delta^{34}S$ (~4 to –3‰), unlike the Phanerozoic which have a wider range (+20 to –5‰). The $\Delta^{34}S_{\text{sulphate-sulphide}}$ values are also lower in the Palaeoarchaean (5–10 ‰) than those in the Neoarchaean and the Phanerozoic (–20 to +27‰). Sulphur isotopic compositions reported for the Kangaroo Caves deposit (Huston et al. 2001) gave $\delta^{34}S$ values for pyrite ranging from –1.0 to +0.7‰ and for barite from +4.9 to +5.6‰. On the basis of these S isotopic data and the Fe_2O_3/FeO, Huston and co-workers suggested that seawater sulphate reduction took place. The Panorama rocks are enriched in Fe_2O_3 (hematite present), relative to FeO at the base of the volcanic succession, becoming more FeO rich towards the upper levels (chlorite-quartz zone and pyrite). Thus, base of the volcanic succession is a zone of high Fe_2O_3/FeO, low S, but high whole-rock $\delta^{34}S$ values (+3.7 to 10.0‰), but outside this zone whole-rock $\delta^{34}S$ values, range from –1.8 to 0.6‰. With these data in hand, Huston and co-workers reasoned that Fe was oxidised and S depleted at the base of the volcanic pile and that the presence of hematite and increase in Fe_2O_3/FeO suggested that sulphate reduction occurred by oxidation of FeO, according to the following reaction:

$$HSO_4^- + 8FeO_{\text{rock}} + H^+ = H_2S + 4Fe_2O_3$$

Thus, sulphate (as barite) would have been a significant component of the Palaeoarchaean seawater, at least in the upper levels of a layered ocean, in contrast to the lack of barite in the Neoarchaean and Palaeoproterozoic VMS, which is indicative of an anoxic ocean. Palaeoarchaean barite is characterised by negative mass-independent ^{33}S fractionation, implying photochemical dissociation of SO_2 in the atmosphere (see Farquhar et al. 2000 for details of mass-independent isotopic signatures in the Precambrian). The Panorama S isotopic data are also consistent with the derivation of the S from magmas and/or leaching from the volcanic rocks, again unlike the Phanerozoic VMS for which S is largely derived from reduction of seawater sulphate.

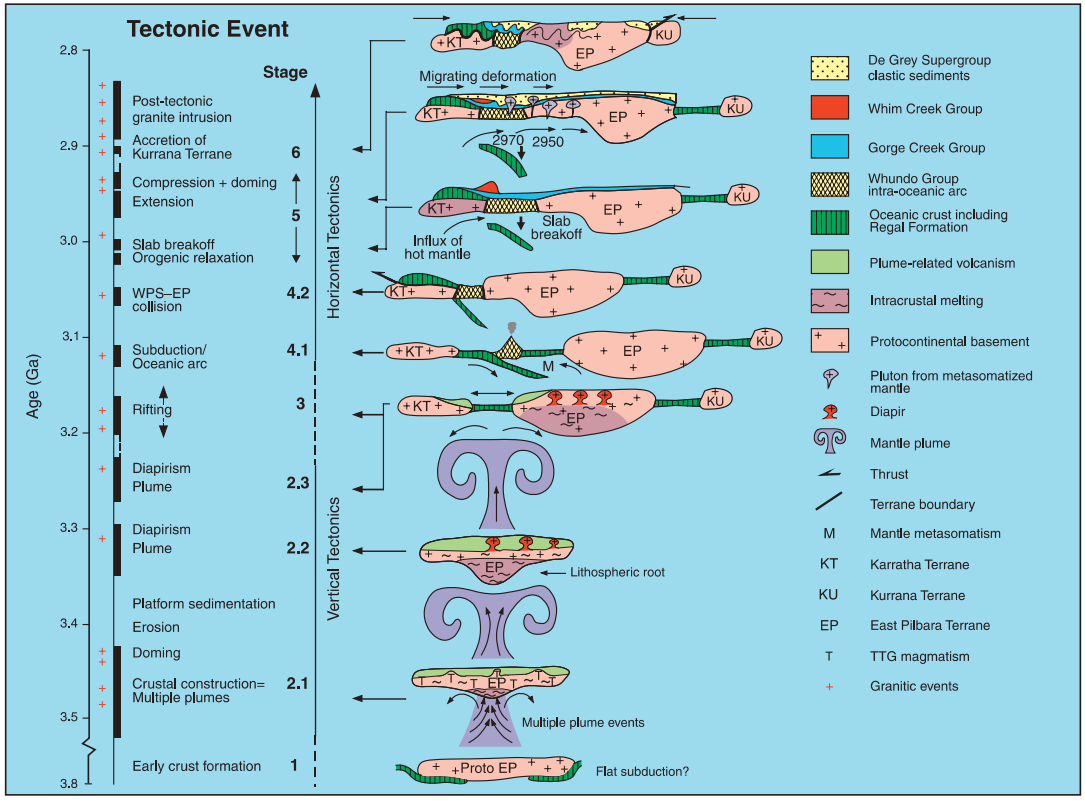


Fig. 7.43 Model illustrating the geodynamic evolution and tectonic events of the northern Pilbara Craton, between 3.8 G and 2.8 Ga; note changes with time from mantle plume-related vertical tectonics to subduction-style horizontal tectonics. After Van Kranendonk et al. (2006a, b)

Finally, the restriction of banded and granular iron formations in the period from 2.5 to 1.8 Ga is roughly coincident with the period of VMS with no barite, this because iron formations and sulphate-free seawater require anoxic conditions, whereas lack of iron formations and presence of seawater sulphates indicate oxic conditions (Huston et al. 2001).

7.7.6.3 Tectonic Setting

In Chapter 5 I mentioned the role of intraplate magmatism and mantle plume events for rift-related porphyry systems and the northern Pilbara Craton. The geodynamic evolution and crustal growth of the East Pilbara Terrane is linked with mantle plume that impinged on subcontinental lithospheric mantle, producing a series of oceanic plateaux (Fig. 7.43; Smithies et al. 2005, Van Kranendonk et al. 2002, 2006a, b, Pirajno 2007a, b). By analogy with modern oceanic plateaux (e.g., Kerguelen; Taylor 2006), which can reach depths of 1330–500 m below sea level with local emergent caldera-style volcanism, the formation of ore systems in this environment would include VMS in shallow water submarine calderas.

7.8 Concluding Remarks

In this chapter I described submarine hydrothermal mineral systems, which form at spreading centres in classic oceanic crust, as exemplified by the Cyprus massive sulphide deposits and those that are associated with submarine calderas in volcanic arcs and others that formed in very ancient greenstone terranes, many of which are interpreted as mantle plume-related oceanic plateaux, similar to the more recent ones (Cretaceous) in the Pacific and Indian oceans (e.g., Kerguelen, Ontong Java-Hikurangi). These massive sulphide deposits are variably called in the literature as VHMS, VMS, Kurokos, Noranda-type. As explained at the beginning of Section 7.7, I prefer to distinguish those that form at spreading centres from those that occur in volcanic arcs and oceanic plateaux. The setting is different, as are the host rocks and the nature of the sulphide systems. Massive sulphides from mid-ocean ridge spreading centres, following closure of the oceanic basin, are tectonically emplaced on land through accretion and collision processes. These are the ophiolitic sequences, generally marking the closure of oceanic arms and forming suture zones between accreted plates. In some instances, spreading centres are in proximity of land masses, as is the case for the Guaymas Basin in the Gulf of California, where the products of spreading are covered with sediments eroded off the nearby lands. The Gulf of California and its on-land continuation of the Salton Sea, presents us with very complex and varied hydrothermal systems, from oceanic to a land rift setting. Ancient analogues of these settings are the so-called Besshi type sulphide deposits, of which the type area is the Besshi district

in Japan. In this chapter I described the massive sulphide deposits of the Matchless Amphibolite Belt (MAB) in Namibia, as perhaps one of the best examples of ancient Besshi type systems. These general comparisons between modern and ancient hydrothermal systems are very useful, not only for the understanding of ore genesis processes, but also because clearer insights can and do provide useful vectors for the discovery of new ore deposits.

The last few decades have seen flourishing and ground-breaking research on the seafloors of our oceans. This research, involving earth and life sciences has led to the astounding discovery of previously unsuspected ecosystems, both macrofauna and microbial, that thrive in anoxic and hot environments. Interwoven with these discoveries is also the link between the origin of the sulphides and microbial communities, with cases where it is the microbial communities that induce S reduction and precipitation of sulphides. Furthermore and of wide interest to all scientists, is the almost inescapable conclusion that seafloor hydrothermal venting systems may have provided the cradle for the origin of early life. Back to our submarine mineral systems: the seafloor discoveries both at spreading centres and in volcanic arcs, such as Izu-Bonin, Kuril, Tonga-Kermadec, have given us powerful insights for the understanding of ancient VMS, as analogues of present-day systems. And viceversa, ancient VMS give insights for those parts of submarine vents that are below the seafloor. This is all exciting and far-reaching research work, both on land and in the deep sea.

The Kuroko polymetallic ore systems, as described from the Miocene rocks of the Hokuroku district in Japan, are formed in submarine silicic calderas, generally in back-arc settings, and are the archetype of VMS. The heat source for these systems comes from the magma chambers that underlie these volcanoes, resulting in convection cells of magmatic-hydrothermal fluids that rise and mix with seawater. The hydrothermal circulation thus generated is very dynamic, resulting in several phases of mineral precipitation. The fluids leach metals from the crustal rocks through which they flow, along fissures and faults. The fluids carry the metals to the seafloor where, as these interact with cold seawater, precipitate polymetallic sulphides contaning varying amounts of metals, such as Cu, Pb, Zn, Au, Ag, Ba, As, Sb, Cd, and even Hg and native S. VMS that form in shallow submarine calderas are transitional to epithermal systems. Modern examples are provided in the Aegean and Tyrrhenian seas, whereas ancient analogues can be found in some of the VMS in Tasmania.

The Iberian Pyrite Belt (IPB) is a type of VMS, characterised by abundant pyrite, barite and lesser Cu, Pb and Zn sulphides, which recent research suggests formed in a pull-apart basin tectonic setting, associated with thick siliciclastic sequences and only minor felsic magmatism. The IPB is one of the largest massive sulphides repositories in the world and there are, so far, no clear analogues in present-day settings or in the ancient record, although I suggested that Abra (Fe–Ba–Pb–Cu–Ag–Au) deposit in Western Australia might represent an IPB style mineral system. Research on Abra is on its infancy, but regional features and alteration-mineralisation characteristics suggest a similar tectonic environment and mineral system. The origin of the IPB is still

uncertain, but forced convection in a basin, with the heat engine being provided by deep plutonic intrusions and a hydrothermal stratabound replacement model seems to provide a reasonable explanation.

Finally, the oldest (~3.4 Ga) VMS in the North Pilbara terrain are small, but important for at least for two reasons. One is that they provide evidence of VMS formed in oceanic plateau settings, and second the abundance of barite in these Palaeoarchaean systems is evidence of seawater sulphates and oxygenated upper levels of oceanic waters, which as pointed out in a number of publications by Huston and co-workers, contrast with the general lack of barite in Noranda-type and Palaeoproterozoic VMS systems. Interesting the observation made by Huston et al. (2001) that Superior type iron formations are largely restricted to the Palaeoproterozoic, in concert with VMS with no barite, for both of which an anoxic ocean is required. Presence of seawater sulphates, hence oxic conditions, is not conducive to the formation of iron formations. I return to this topic in more detail in the next chapter.

References

Adamides NG (1984) Cyprus volcanogenic sulfide depositsin relation to their environment of formation. Unpubl PhD thesis, University of Leicester

Adamson RG, Teichmann RFH (1986) The Matchless cupreous pyrite deposit, South West Africa/Namibia. In: Anhaeusser CR, Maske S (eds) Mineral deposits of Southern Africa, vol 2. Geol Soc S Afr, pp 1755–1760

Alabaster T, Pearce JA (1985) The interrelationship between magmatic and ore-forming hydrothermal processes in the Oman ophiolite. Econ Geol 80: 1–16

Alt JC, Lonsdale P, Haymon R, Muehlenbachs K (1987) Hydrothermal sulfide and oxide deposits on seamounts near 21°N, East Pacific Rise. Geol Soc Am Bull 98: 157–168

Ashley PM, Dudley RJ, Lesh RH, Marr JM, Ryall AW (1988) The Scuddles Cu-Zn prospect, an Archean volcanogenic massive sulfide deposit, Golden Grove district, Western Australia. Econ Geol 83: 918–951

Austen S (2007) Isotopic and thermal constraints on the origin and formation of the Abra polymetallic deposit, Jillawara Sub-basin, Western Australia. Unpub MSc thesis, School Ocean Sci, Univ Southampton

Ayer J, Amelin Y, Corfu F, Kamo S, Ketchum J, Kwok K, Trowell N (2002) Evolution of the southern Abitibi greenstone belt based on U-Pb geochronology, autochthonous volcanic construction followed by plutonism, regional deformation and sedimentation. Precambr Res 115: 63–96

Baker ET, Massoth GJ, Feely RA (1987) Cataclysmic venting on the Juan de Fuca Ridge. Nature 329: 149–151

Baker ET (1998) Patterns of event and chronic hydrothermal venting following a magmatic intrusion: new perspectives from the 1996 Gorda Ridge eruption. Deep Sea Res II 45: 2599–2618

Banks DA (1985) A fossil hydrothermal worm assemblage from the Tynagh lead-zinc deposits in Ireland. Nature 313:128–131

Barley ME (1992) A review of Archean volcanic-hosted massive sulfide and sulfate mineralization in Western Australia. Econ Geol 87: 855–872

Barrett TJ, MacLean WH (1999) Volcanic sequences, lithogeochemistry, and hydrothermal alteration in some bimodal volcanic-associated massive sulfide systems. Rev Econ Geol 8: 101–131

Barrie CT, Hannington MD (eds) (1999) Volcanic-associated massive sulphide deposits: processes and examples in modern and ancient settings. Rev Econ Geol 8

Beaudoin Y, Scott SD, Gorton MP, Zajacz Z, Halter W (2007) Pb and other ore metals in modern seafloor tectonic environments: evidence from melt inclusions. Marine Geol doi: 10.1016/j.margeol.2007.04.004

Beccaluva L (ed) (1989) Ophiolites and lithosphere of marginal seas. Chem Geol 77

Binns RA, Scott SD (1993) Actively forming polymetallic sulfide deposits associated with felsic volcanic rocks in the Eastern Manus back-arc basin, Papua New Guinea. Econ Geol 88: 2226–2236

Bischoff JL, Rosenbauer RJ (1989) Salinity variations in submarine hydrothermal systems by layered double-diffusive convection J Geol 97: 613–623

Boddington TDM (1990) Abra lead–silver–copper–gold deposit. In: Hughes, FE (ed), Mineral deposits of Australia and Papua New Guinea. Aus Inst Min Metal, Monograph 14: 659–664

Bonatti E (1975) Metallogenesis at oceanic spreading centres. Earth Planet Sci Lett 3: 401–431

Bonatti E (1978) The origin of metal deposits in the oceanic lithosphere. Sci Am 238: 54–61

Bonatti E (1983) Hydrothermal metal deposits from the ocean rifts: a classification. In: Rona PA, Bostrom K, Laubier L, Smith KL (eds) Hydrothermal processes at seafloor spreading centers. Plenum, New York, pp 491–502

Bott MHP (1982) The interior of the Earth: its structure, constitution and evolution. Arnold, London

Boudier F, Nicolas A (eds) (1988) The ophiolites of Oman. Tectonophysics Spec Issue 151

Boyce AJ, Coleman ML, Russell MJ (1983) Formation of fossil hydrothermal chimneys and mounds from Silvermines, Ireland. Nature 306: 545–550

Brauhart CW, Groves DI, Morant P (1998) Regional alteration systems associated with volcanogenic massive sulfide mineralization at Panorama, Pilbara, Western Australia. Econ Geol 93: 292–302

Breitkopf JH, Maiden KJ (1988) Tectonic setting of the Matchless Belt pyritic copper deposits, Namibia. Econ Geol 83: 710–723

Burke KC, Kidd WSF, Turcotte L, Dewey JF, Mouginis-Mark PJ, Parmentier, EM, Šengör AMC, Tapponier PE (1981) Tectonics of basaltic volcanism. In: Basaltic volcanisn on the terrestrial planets. Lunar Planet Inst (ed), Houston. Pergamon, New York, pp 803–898

Butterfield DA, Massoth GJ, McDuff RE, Lupton JE, Lilley M (1990) Geochemistry of hydrothermal fluids from Axial Seamount hydrothermal emission study vent field, Juan de Fuca Ridge: subseafloor boiling and subsequent fluid-rock interaction. J Geophys Res 95: 12895–12921

Canadian American Seamount Expedition (1985) Hydrothermal vents on an axis seamount of the Juan de Fuca ridge. Nature 313: 212–214

Cannat M, Sautre D, Ruellan E, Okino K, Escartin J, Combier V, Baala M (2006) Modes of seafloor generation at a melt-poor ultraslow-spreading ridge. Geology, 34: 605–608

Carvalho D, Barriga FJAS, Munhá J (1999) Bimodal siliciclastic systems – the case of the Iberian Pyrite Belt. Rev Econ Geol 8: 375–408

Cathles LM (1983) An analysis of the hydrothermal system responsible for massive sulfide deposition in the HoKuroko basin of Japan. Econ Geol Monogr 5: 439–487

Coleman RG (1977) Ophiolites. Springer-Verlag, New York

Coleman RG (1984) Ophiolites and the tectonic evolution of the Arabian peninsula. Geol Soc Special Publ 13: 359–366

Collins PLF, McDonald IR (1994) A Proterozoic sediment-hosted polymetallic epithermal deposit at Abra in the Jillawarra sub-basin of the central Bangemall Basin, Western Australia. Geol Soc Aus Abs 37: 68–69

Constantinou G (1980) Metallogenesis associated with the Troodos ophiolite. In: Panayioutou A (ed) Ophiolites. Int Symp Cyprus 1979, Proc Cyprus Minist Agric Nat Resourc, pp 663–674

Constantinou G, Govett GJS (1972) Genesis of sulphide deposits, ochre and umber of Cyprus. Trans Inst Min Metall 81: B34–B36
Corbett KD (2001) New mapping and interpretation of the Mount Lyell mining district, Tasmania: A large hybrid Cu–Au system with an exhalative Pb–Zn top. Econ Geol 96: 1089–1122
Darwin C (1860) The origin of the species – by means of natural selection. 2nd edn, John Murray, London
Dasgupta R, Hirschmann MM (2006) Melting in the Earth's deep upper mantle caused by carbon dioxide. Nature 440: 659–662
Davies HL, Jaques AL (1984) Emplacement of ophiolite in Papua New Guinea. Geol Soc Spec Publ 13: 341–349
de Ronde CEJ (2006) Mineralisation associated with submarine volcanoes of the southern Kermadec arc, New Zealand. Aus Inst Min Metall Monogr 25: 333–338
de Ronde CEJ, Baker ET, Massoth GJ, Lupton JE, Wright IC, Feely RA, Greene RR (2001) Intraoceanic subduction-related hydrothermal venting, Kermadec volcanic arc, New Zealand. Earth Planet Sci Lett 193: 359–369
de Ronde CEJ, Massoth GJ, Baker ET, Lupton JE (2003a) Submarine hydrothermal venting related to volcanic arcs. Soc Econ Geol Spec Publ 10: 91–110
de Ronde CEJ, Faure K, Bray CJ, Chappell DA, Wright IC (2003b) Hydrothermal fluids associated with seafloor mineralization at two southern Kermadec arc volcanoes, offshore New Zealand. Miner Depos 38: 217–233
de Ronde CEJ, Hannington MD, Stoffers P, Wright IC, Ditchburn RG, Beyes Ag, Baker ET, Massoth GJ, Lupton GJ, Walker SL, Greene RR, Soong CWR, Ishibashi J, Lebon GT, Bray CJ, Resing JA (2005) Evolution of a submarine magmatic-hydrothermal system: Brothers Volcano, southern Kermadec arc, New Zealand. Econ Geol 100: 1097–1133
Delaney JR, Robigou V, McDuff RE, Tivey MK (1992) Geology of a vigorous hydrothermal system on the Endeavour Segment, Juan de Fuca Ridge. J Geophys Res 97: 19663–19682
Dilek Y (2003) Ophiolite concept and its evolution. Geol Soc Am Spec Pap 373: 1–16
Dilek Y, Robinson PT (eds) 2003, Ophiolites in Earth history. Geol Soc, Lond, Spec Publ 218
Dilek Y, Newcombe S (eds) (2003) Ophiolite concept and the evolution of geological thought. Geol Soc Am Spec Pap 373
Douville E, Charlou JL, Oelkers EH, Bienvenu P, Jove Colon CF, Donval JP, Fouquet Y, Prieur D, Appriou P (2002) The Rainbow vent fluids (36 14' N, MAR): the influence of ultramafic rocks and phase separation on trace metal content in Mid-Atlantic Ridge hydrothermal fluids. Chem Geol 184: 37–48
Dziak RP, Fox CG, Schreiner AE (1995) The June–July 1993 seismo-acoustic event at Co-Axial segment, Juan de Fuca Ridge: evidence for a lateral dike injection. Geophys Res Lett 22: 135–138
Edmond JM, Von Damm K (1983) Hot springs on the ocean floor. Sci Am 248: 70–85
Eldridge CS, Barton PB, Ohmoto H (1983) Mineral textures and their bearing on formation of the kuroko orebodies. Econ Geol Monogr 5: 241–281
Farquhar J, Bao HM, Thiemens M (2000) Atmospheric influence of Earth's earliest sulphur cycle. Science 289: 756–758
Fleet AJ, Robertson AHF (1980) Ocean-ridge metalliferous and pelagic sediments of the Semail Nappe, Oman. J Geol Soc London 137: 403–422
Fouquet Y, Auclair G, Cambon P, Etoubleau J (1988) Geological setting and mineralogical and geochemical investigations on sulfide deposits near 13°N on the East Pacific Rise Marine. Geology 84: 145–178
Fouquet Y, von Stackelberg V, Charlou JL, Donval JP, Erzinger J, Foucher JP, Herzig P, Mühe R, Sokai S, Wiedicke M, Whitechurch H (1991a) Hydrothermal activity and metallogenesis in the Lau back-arc basin. Nature 349: 778–781
Fouquet Y, von Stackelberg U, Charlou JL, Donval JP, Foucher JP, Erzinger J, Herzig P, Mühe R, Wiedicke M, Soakai S, Whitechurch H (1991b) Hydrothermal activity in the Lau back-arc basin: sulfides and water chemistry. Geology 19:303–306

Fouquet Y, von Stackelberg U, Charlou JL, Erzinger J, Herzig PM, Mühe R, Wiedicke M (1993) Metallogenesis in back-arc environments: the Lau Basin example. Econ Geol 88: 2154–2181

Fox JS (1984) Besshi-type volcanogenic sulphide deposits – a review. Can Inst Min Metall Bull 77: 57–68

Francheteau J, Needham HD, Choukroune P, Juteau T, Seguret M, Ballard RD, Fox PJ, Normark W, Carranza A, Cordoba D, Guerrero J, Rangin C, Bougault H, Cambon P, Hekinian R (1979) Massive deep-sea sulphide ore deposits discovered on the East Pacific Rise. Nature (London) 277: 523–528

Franklin JM, Sangster DM, Lydon JW (1981) Volcanic-associated massive sulfide deposits. Econ Geol 75th Anniv Vol: 485–627

Franklin JM, Goodfellow WD, Lydon JW, Jonasson IR, Davis EE (1990) Middle valley; a major center of hydrothermal activity in a sedimented ridge crest, Northern Juan de Fuca Ridge. Abstracts with Programs. Geol Soc Am Annu Meet, Dallas, p A9

Franklin JM, Gibson HL, Jonasson, IR, Galley AG (2005) Volcanogenic massive sulfide deposits. Econ Geol 100th Ann Vol: 523–560

Furnes H, de Witt M, Staudigel H, Rosing M, Muehlenbachs K (2007) A vestige of Earth's oldest ophiolite. Science 315: 1704–1707

Galley AG, Koski RA (1999) Setting and characteristics of ophiolite-hosted volcanogenic massive sulfide deposits. Rev Econ Geol 8: 221–246

Gemmell JB, Herrmann W (eds) (2001) A special issue devoted to alteration associated with volcanic-hosted massive sulphide deposits, and its exploration significance. Econ Geol 96, No 5

Geological Society of America (1979) International Atlas of Ophiolites. Geol Soc Am Map and Chart Ser MC-33

Gifkins C, Herrmann W, Large R (2005) Altered volcanic rocks – A guide to description and interpretation. Centre Ore Dep Res, Univ Tas

Gilbert LA, McDuff RE, Johnson HP (2007) Porosity of the upper edifice of Axial Seamount. Geology 35: 49–52

Glasby GP, Iizasa K, Yuasa M, Usui A (2000) Submarine hydrothermal mineralization of the Izu-Bonin arc, south of Japan: an overview. Marine Geores Geotech 18: 141–176

Goldberg I (1976) A preliminary account of the Otjihase copper deposit, South West Africa. Econ Geol 71: 384–390

Goodfellow WD, Zierenberg RA (1999) Genesis of massive sulfide deposits at sediment-covered spreading centers. Rev Econ Geol 8: 297–324

Govett GJS, Pantanzis TM (1971) Distribution of Cu, Zn, Ni and Co in the Troodos pillow lava series, Cyprus. Trans Inst Min Metall 80: B1327–B1346

Graham UM, Bluth GJ, Ohmoto H (1988) Sulfide-sulfate chimneys on the East Pacific Rise, 11 and 13°N latitudes. Part I: mineralogy and paragenesis. Can Mineral 26: 487–504

Grassle JF (1983) Introduction to the geology of hydrothermal vents. In: Rona PA, Bostrom K, Laubier L, Smith KL (eds) Hydrothermal processes at seafloor spreading centers. Plenum, New York, pp 665–676

Groves DI, Vielreicher RM, Goldfarb RJ, Condie KC (2005) Controls on the heterogeneous distribution of mineral deposits through time. Geol Soc Lond Spec Publ 248: 71–101

Gu Y-J, Lerner-Lam AL, Dziewonski AM, Ekstrom G (2005) Deep structure and seismic anisotropy beneath the East Pacific Rise. Earth Planet Sci Lett 232: 259–272

Hadjistavrinou Y, Constantinou G (1982) Cyprus. In: Dunning, FW, Mykura W, Slater D (eds) Mineral deposits of Europe, Vol 2. Inst Min Metall, London, pp 255–277

Halbach P, Nakamura K, Washner M, Lange J, Sakai H, Kaselitz L, Hansen RD, Yamano M, Post J, Prause B, Seifert R, Michaelis W, Teichmann F, Kinoshita M, Märten A, Ishibashi J, Czerwinski S, Blum N (1989) Probable modern analogue of Kuroko-type massive sulphide deposits in the Okinawa Trough back-arc basin. Nature 338: 496–499

Hamilton WB (2003) An alternative Earth. GSA Today 13: 4–12

Hannington MD, de Ronde CEJ, Petersen S (2005) Seafloor tectonics and submarine hydrothermal systems. Econ Geol 100th Ann vol: 111–141

Haymon RM, Kastner M (1981) Hot spring deposit on the East Pacific Rise at 21°N: preliminary description of mineralogy and genesis. Earth Planet Sci Lett 53:363–381

Haymon RM, Koski RA, Sinclair C (1984) Fossils of hydrothermal vent worms from Cretaceous sulfide ores of the Samail Ophiolite, Oman. Science 223:1407–1409

Haymon RM, Fornari DJ, Von Damm KL, Lilley MD, Perfit MR, Edmond JM,. Shanks WC, Lutz RA, Grebmeier JM, Carbotte S (1993) Volcanic eruption of the mid-ocean ridge along the East Pacific Rise crest at 9° 45' 52" N: Direct submersible observations of seafloor phenomena associated with an eruption event in April 1991. Earth Planet Sci Lett 119: 85–101

Hekinian R, Fevrier M, Bischoff JL, Picot P, Shanks WC (1980) Sulfide deposits from the East Pacific Rise near 21°N. Science 207:1433–1444

Hekinian R, Fevrier M, Avedik F, Cambon P, Charlou JL, Needham HD, Raillard J, Boulegue J, Merlivat L, Moinet A, Manganini S, Lange J (1983) East Pacific Rise near 13°N: geology of the hydrothermal fields. Science 219:1321–1324

Hekinian R, Fouquet Y (1985) Volcanism and metallogenesis of axial and off-axial structures on the East Pacific Rise near 13°N. Econ Geol 80: 221–249

Herzig PM, Hannington MD, Fouquet Y, Von Stackelberg U, Petersen S (1993) Gold-rich polymetallic sulfides from the Lau back arc and implications for the geochemistry of gold in sea-floor hydrothermal systems of the Southwest Pacific. Econ Geol 88: 2182–2209

Herzig PM, Hannington MD (1995) Polymetallic massive sulphides at the modern seafloor: A review. Ore Geol Rev 10: 95–115

Hess HH (1946) Drowned ancient islands of the Pacific Basin. Am J Sci 244: 722–791

Hrischeva E, Scott SD, Weston R (2007) Metalliferous sediments associated with presently forming volcanogenic massive sulfides: the SuSu Knoll hydrothermal field, eastern Manus Basin, Papua New Guinea. Econ Geol 102: 55–73

Humphris SE, Zierenberg RA, Mullineaux LS, Thomson RE (eds) (1995a) Seafloor hydrothermal systems – Physical, chemical, biological and geological interactions. Am Geophys Union, Monogr 91

Humphris SE and 24 others (1995b) The internal structure of an active seafloor massive sulphide deposit. Nature 377: 713–716

Huppert HE, Sparks RSJ (1984) Double-diffusive convection due to crystallization in magmas. Annu Rev Earth Planet Sci 12:11–37

Huston DL (1999) Stable isotopes and their significance for understanding the genesis of volcanic-hosted massive sulfide deposits: a review. Rev Econ Geol 8: 157–179

Huston DL (2006) Mineralization and regional alteration at the Mons Cupri stratiform Cu-Zn-Pb deposit, Pilbara Craton, Western Australia. Mineral Depos 41: 17–32

Huston DL, Large RR (1989) A chemical model for the concentration of gold in volcanogenic massive sulphide deposits. Ore Geol Rev 4: 171–200

Huston DL, Brauhart CW, Drieberg SL, Davidson GJ, Groves DI (2001) Metal leaching and inorganic sulfate reduction in volcanic-hosted massive sulfide mineral systems: Evidence from the paleo-Archean Panorama district, Western Australia. Geology 29: 687–690

Huston DL, Hickman AH, Collins PLF (eds) (2002) A special issue devoted to the Early to Middle Archean mineral deposits of the North Pilbara terrain, Western Australia. Econ Geol 97, No 4

Huston DL, Morant P, Pirajno F, Cummins B, Baker D, Mernagh TP (2007) Palaeoarchean mineral deposits of the Pilbara Craton: genesis, tectonic environment and comparisons with younger deposits. In: Van Kranendonk MJ, Smithies RH, Bennett VC (eds), Earth's oldest rocks, Chpt 4.4, Elsevier, Amsterdam, pp 411–450

Hutchinson RW (1980) Massive base metal deposits as guides to tectonic evolution. In: Strangeway D W (ed) The continental crust and its mineral deposits. Geol Ass Can Spec Pap 20: 659–684

Iizasa K, Fiske RS, Ishizuka O, Yuasa M, Hashimoto J, Ishibashi J, Naka J, Horii Y, Fujiwara Y, Imal A, Koyama S (1999) A Kuroko-type polymetallic sulfide deposit in a submarine silicic caldera. Science 283: 975–977

Iizasa K, Sasaki M, Matsumoto K, Shiokawa S, Tanahashi M and on-board scientists (2004) A first extensive hydrothermal field associated with Kuroko-type deposits in a silicic submarine caldera in a nascent rift zone, Izu-Ogasawara (Bonin) arc, Japan. Oceans 2004 MTS/EEE Conference: Techno-Ocean '04, Bridges across the oceans: Kobe, Japan, Marine Techn Soc pp 991–996

Irvine TN, Keith DW, Todd SG (1983) The J-M platinum-palladium reef of the Stillwater Complex, Montana: II Origin by double-diffusive convection magma mixing and implications for the Bushveld Complex. Econ Geol 78: 1287–1348

Ishihara S (ed) (1974) Geology of kuroko deposits. Min Geol Spec Issue 6

Ishikawa Y, Mikami S, Hashimoto K (2004) Volcanic rock facies and volcano stratigraphy of the lower to middle Miocene in the Hokuroko District. Rpt on Region Surv, Ministry Econ Trade Ind Japan (in Japanese)

Ixer RA, Alabaster T, Pearce JA (1984) Ore petrography and geochemistry of massive sulphide deposits within the Semail ophiolite, Oman. Trans Inst Min Metall 93: B114–B124

Karpoff AM, Walter AV, Pflumio C (1988) Metalliferous sediments within lava sequences of the Sumail ophiolite (Oman): mineralogical and geochemical characterization, origin and evolution. Tectonophysics 151: 223–246

Keays RR (1987) Principles of mobilization(dissolution) of metals in mafic and ultramafic rocks. The role of immiscible magmatic sulphides in the generation of hydrothermal gold and volcanogenic massive sulphide deposits. Ore Geol Rev 2: 47–63

Kelley DS, Karson JA, Blackman DK, Fruh-Green G, Butterfield DA, Lilley MD, Olson EJ, Schrenk MO, Roe KK, Lebon GT, Rivizzigno P & the AT3-60 Shipboard Party (2001) An off-axis hydrothermal vent field near the Mid-Atlantic Ridge at 30° N. Nature 412: 145–149

Kelley DS, Baross JA, Delaney JR (2002) Volcanoes, fluids and life at Mid-ocean ridge spreading centers. Ann Rev Earth Planet Sci 30: 385–491

Kennett J (1982) Marine Geology. Prentice-Hall, Englewood Cliffs

Kerr AC, Tarney J (2005) Tectonic evolution of the Caribbean and northwestern South America: the case for accretion of two Late Cretaceous oceanic plateaus. Geology 33: 329–332

Kerr AC, Tarney J, Nivia A, Marriner GF, Saunders AD (1998) The internal structure of oceanic plateaus: inferences from obducted Cretaceous terranes in western Colombia and the Caribbean. Tectonophysics 292: 173–188

Killick AM (1983) Sulphide mineralization at Gorob and its genetic relationship to the Matchless Member, Damara Sequence, SWA/Namibia. Geol Soc S Afr Spec Publ 11: 381–384

Killick AM (2000) The Matchless Belt and associated sulphide mineral deposits, Damara Orogen, Namibia. Commun Geol Surv Namibia 12: 73–80

Klemd R, Maiden K J, Okrusch M (1987) The Matchless copper deposit, South West Africa/Namibia: A deformed and metamorphosed massive sulfide deposit. Econ Geol 82: 587–599

Klemd R, Maiden KJ, Okrusch M, Richter P (1989) Geochemistry of the Matchless metamorphosed massive sulfide deposit, South West Africa/Namibia: wall-rock alteration during submarine ore-forming processes. Econ Geol 84: 603–617

Kobayashi K, Nakanishi M, Tamaki K, Ogawa Y (1998) Outer slope failure associated with the western Kuril and Japan trenches. Geophys J Inter 134: 356–372

Konno U, Tsunogai U, Nakagawa F, Nakaseama M, Ishibashi J-I, Nunoura T, Nakamura K-I (2006) Liquid CO_2 venting on the seafloor: Yonaguni KKnoll IV hydrothermal system, Okinawa Trough. Geophys Red Lett 33: L16607, doi:10.1029/2006GL026115

Kuhn T, Herzig PM, Hannington MD, Garbe-Schönberg D, Stoffers P (2003) Origin of fluids and anhydrite precipitation in the sediment-hosted Grimsey hydrothermal field north of Iceland. Chem Geol 202: 5–21

Kusky TM, Li JH, Glass A, Huang XN (2004) Origin and emplcament of Archaean ophiolites of the central orogenic belt, North China Craton. In Kusky TM (ed) Precambrian ophiolites and related rocks, Elsevier, Dev Precambr Geol 13: 223–274

Lambert IB, Sato T (1974) The kuroko and associated deposits of Japan: a review of their features and metallogenesis. Econ Geol 69: 1215–1236

Large RR (1992a) Australian volcanic-hosted massive sulfide deposits: features, styles and genetic models. Econ Geol 87: 471–510

Large RR (ed) (1992b) A special issue devoted to Australian volcanic-hosted sulfide (VMS) deposits and their volcanic environment. Econ Geol 87, No 3

Large RR, McPhie J, Gemmell JB, Herrmann W, Davidson GJ (2001) The spectrum of ore deposit types, volcanic environments, alteration halos, and related exploration vectors in submarine volcanic successions: some examples from Australia. Econ Geol 96: 913–938

Laznicka P (2006) Giant metallic deposits – future sources of industrial metals. Springer

Lentz DR (ed) (2006) Volcanic-hosted massive sulfide deposits and their geological settings in the Bathurst Mining Camp, New Brunswick. Expl Min Geol 15, Nos 3–4

Li JG, Kusky TM, Huang XN (2002) Archean podiform chromitites and mantle tectonites in ophiolitic melange, North China Craton: a record of early oceanic mantle processes. GSA Today July Iss: 4–11

Li JG, Kusky TM, Niu XL, Jun F, Polat A (2004) Neoarchean massive sulfide of Wutai mountain, North China: a black smoker chimney and mound complex within 2.50 Ga-old oceanic crust. In Kusky TM (ed) Precambrian ophiolites and related rocks, Elsevier, Dev Precambr Geol 13, pp 339–362

Little CTS (2002) The fossil record of hydrothermal vent communities. Cahiers Biol Marine 43: 313–316

Long X, Qi H, Pirajno F, Ni PZ, Du JX, Wei OR (2008) Possible correlation between a mantle plume and the evolution of the Paleo-Tethys ocean: evidence from a volcanic rifted margin in the Xiaru-Tuoding area, Yunnan, SW China. Lithos 100: 112–126

Lonsdale P, Becker K (1985) Hydrothermal plumes, hot springs, and conductive heat flow in the Southern Trough of Guaymas Basin. Earth Planet Sci Lett 73: 211–225

Lonsdale P, Bischoff JL, Burns VM, Kastner M, Sweeney RE (1980) A high-temperature hydrothermal deposit on the seabed at a gulf of California spreading center. Earth Planet Sci Lett 49: 8–20

Lupton JE and 15 others (2006) Submarine venting of liquid carbon dioxide on a Mariana Arc volcano. Geochem Geophys Geosyst G^3 7(6): Q08007, doi:10.1029/2005GC001152

Maclean WH, Hoy LD (1991) Geochemistry of hydrothermally altered rocks at the Horne Mine, Noranda, Quebec. Econ Geol 86: 506–528

Malahoff A, McMurtry GM, Wiltshire JC, Yeh HW (1982) Geology and chemistry of hydrothermal deposits from active submarine volcano Loihi, Hawaii. Nature 298: 234–239

Mamberti M, Lapierre H, Bosch D, Jaillard E, Ethien R, Hernandez J, Polve M (2003) Accreted fragments of the late Cretaceous Caribbean-Colombian plateau in Ecuador. Lithos 66: 173–199

Marsh JS (1973) Relationships between transform directions and alkaline igneous rock lineaments in Africa and South America. Earth Planet Sci Lett 18: 317–323

Martin D McB, Thorne AM (2004) Tectonic setting and basin evolution of the Bangemall Supergroup in the northwestern Capricorn Orogen. Precambr Res 128: 385–409

McCaig AM, Cliff RA, Escartin J, Fallick AE, MacLeod CJ (2007) Oceanic detachment faults focus very large volume of black smoker fluids. Geology 35: 935–938

McNutt MK, Caress DW, Reynolds J, Jordhal KA Duncan RA (1997) Failure of plume theory to explain midplate volcanism in the southern Austral islands. Nature 389: 479–482

Menzies MA, Klemperer SL, Ebinger CJ, Baker J (2002) Characteristics of volcanic rifted margins. Geol Soc Am Spec Pap 362: 1–14
Minniti M, Bonavia FF (1984) Copper-ore grade hydrothermal mineralization discovered in a seamount in the Tyrrhenian sea (Mediterrenean): is the mineralization related to porphyry-coppers or to base metal lodes? Marine Geol 59: 271–282
Montelli R, Nolet G, Dahlen FA, Masters (2006) A catalogue of deep mantle plumes: New results from finite-frequency tomography. Geochem Geophys Geosyst 7: 10 November 2006
Morgan WJ (1971) Convection plumes in the lower mantle. Nature 230: 42–43
Morgan WJ (1983) Hotspot tracks and the early rifting of the Atlantic. Tectonophysics 94:123–139
Moroni M (1990) The geology, petrology and geochemistry of the mineralization and hydrothermal alteration at Ongeama, Ongombo and the Matchless West Extension, Namibia. Unpubl MSc thesis, Rhodes University, Grahamstown, South Africa
Morozumi H, Ishikawa N, Ishikawa Y (2006) Relationship between Kuroko mineralization and paleostress inferred from vein deposits and Tertiary granitic rocks in and around the Hokuroko district, northeast Japan. Econ Geol 101: 1345–1357
Mueller WU, Marquis R, Thurston P (eds) (2002) Evolution of the Archean Abitibi greenstone belt abd adjacent terranes: New insights from geochronology, geochemistry, structure and facies analysis. Precambr Res Spec Iss 115, Nos 1–4
Mueller WU, Stix J, White JDL, Corcoran PL, Lafrance B, Daigneault R (2008) Characterization of Archean subaqueous calderas in Canada: physical volcanology, carbonate-rich hydrothermal alteration and a new exploration model. In: Gottsmann J, Martí J (eds), Caldera volcanoes: analysis, modeling and response. Developments in Volcanology 10, Chapter 5 Elsevier, pp 183–232
Naden J, Kilias SP, Fiona Darbyshire DP (2005) Active geothermal systems with entrained seawater as modern analogues for transitional volcanic-hosted massive sulfide and continental magmato-hydrothermal mineralization: the example of Milos Island, Greece. Geology 33: 541–544
Naldrett AJ (2004) Magmatic sulfide deposits – Geology, geochemistry and exploration. Springer, Berlin
Nehlig P, Juteau T (1988) Deep crustal seawater penetration and circulation at ocean ridges: evidence from the Oman ophiolite. Mar Geol 84: 209–228
Ohmoto H (1983) Geological, paleontological and tectonic studies, Pt 1. Geologic history of the Green Tuff Region. Econ Geol Monogr 5: 9–23
Ohmoto H (1996) Formation of volcanogenic massive sulfide deposits: the Kuroko perspective. Ore Geol Rev 10: 135–177
Ohmoto H, Rye RO (1974) Hydrogen and oxygen isotope compositions of fluid inclusions in the Kuroko deposits, Japan. Econ Geol 69: 947–953
Ohmoto S, Skinner B J (eds) (1983) The kuroko and related volcanogenic massive sulfide deposits. Econ Geol Monogr 5
Ohmoto H, Takahashi T (1983) Geological, paleontological and tectonic studies, Pt 3. Submarine calderas and kuroko genesis. Econ Geol Monogr 5: 39–54
Ohmoto H, Kakegawa T, Lowe DR (1993) 3.4 billion year-old biogenic pyrites from Barberton, South Africa: sulphur isotope evidence. Science 262: 555–557
Ohtagaki, T, Tsukada, Y, Hirayama, H, Fujioka, H, Miyoshi, T (1974) Geology of the Shakanai mine, Akita Prefecture. Min Geol Spec Iss 6:131–140
Oudin E, Constantinou G (1984) Black smoker chimney fragments in Cyprus sulphide deposits. Nature 308: 349–352
Parson LM, Walker CL, Dixon DR (eds) (1995) Hydrothermal vents and processes. Geol Soc Lond Spec Publ 87
Pašava J, Vymazalová A, Petersen S (2007) PGE fractionation in seafloor hydrothermal systems: examples from mafic- and ultramafic-hosted hydrothermal fields at the slow-speading Mid-Atlantic Ridge. Mineral Depos 42: 423–431

Pearce JA (2003) Supra-subduction zone ophiolites: The search for modern analogues. Geol Soc Am Spec Pap 373: 269–293
Pearson JM, Taylor WR, Barley ME (1996) Geology of the alkaline Gifford Creek Complex, Western Australia. Aus J Earth Sci 43: 299–309
Peltonen P, Kontinen A, Hhma Hm Kuronen U (2007) New mineral deposit model for the Cu–Co–Zn–Ni–Ag–Au sulphide deposits in Outukumpu, Finland. SGA News 21: 1–9
Penrose Conference Participants (1972) Penrose Field Conference Ophiolites. Geotimes 17: 24–25
Peter JM, Scott SD (1988) Mineralogy, composition, and fluid-inclusion microthermometry of seafloor hydrothermal deposits in the southern trough of Guaymas Basin, Gulf of California. Can Mineral 26: 567–587
Peter JM, Scott SD (1991) Hydrothermal mineralization in the Guaymas Basin, Gulf of California. Am Ass Pet Geol 47: 721–741
Peter JM, Scott SD (1999) Windy Craggy, northeastern British Columbia: the world's largest Besshi-type deposit. Rev Econ Geol 8: 261–295
Petersen S, Herzig PM, Hannington MD, Jonasson IR, Arribas A (2002) Submarine gold mineralzation near Lihir Island, New Ireland fore-arc, Papua New Guinea. Econ Geol 97: 1795–1813
Pirajno F (1992) Hydrothermal mineral deposits – Principles and fundamental concepts for the exploration geologist. Springer, Berlin
Pirajno F (1980) Sub-seafloor mineralisation in rocks of the Matakaoa Volcanics around Lottin Point, East Cape, New Zealand. NZ J Geol Geophys 23: 313–334
Pirajno F (2000) Ore deposits and mantle plumes. Kluwer Academic Publishers, Dordrecht
Pirajno F (2004) Oceanic plateau accretion onto the northwestern margin of the Yilgarn Craton, Western Australia: implications for a mantle plume event at ca. 2.0 Ga. J Geodyn 37: 205–231
Pirajno F (2007a) Mantle plumes, associated intraplate tectono-magmatic processes and ore systems. Episodes 30: 6–19
Pirajno F (2007b) Ancient to modern Earth: the role of mantle plumes in the making of continental crust. In: Van Kranendonk MJ, Smithies RH, Bennett VC (eds), Earth's oldest rocks, Chpt 4.4, Elsevier, Amsterdam, pp 1037–1064
Pirajno F, Kinnaird JA, Fallick AE, Boyce AJ, Petzel VWF (1992) A preliminary regional sulphur isotope study of selected samples from mineralised deposits of the Damara Orogen, Namibia. Communs Geol Surv Namibia 8(1992/93): 81–97
Pisutha-Arnond V, Ohmoto H (1983) Thermal history, and chemical and isotopic compositions of the ore forming fluids responsible for the Kuroko massive sulfide deposits in the Hokoruku district of Japan. Econ Geol Monogr 5:523–558
Pratson LF, Haxby WF (1997) Panoramas of the seafloor. Sci Am 276: 67–71
Prichard HM, Maliotis G (1998) Gold mineralisation associated with low-temperature, off-axis, fluid activity in the Troodos ophiolite, Cyprus. J Geol Soc, Lond 155: 223–231
Rasmussen B (2000) Filamentous microfossils in a 3,235-million-year-old volcanogenic masive sulphide deposit. Nature 405: 676–679
Robertson AHF (1975) Cyprus umbers: basalt-sediment relationships in a Mesozoic ocean ridge. J Geol Soc London 131: 511–531
Robinson PT, Zhou MF (2008) The origin and tectonic setting of ophiolites in China. J Asian Earth Sci 32: 301–307
Rogers JWJ, Santosh M (2004) Continents and supercontinents. Oxford Univ Press, Oxford
Rona PA (1980) TAG hydrothermal field: Mid-Atlantic Ridge crest at latitude 26°N. J Geol Soc London 137:385–402
Rona PA (1984) Hydrothermal mineralization at seafloor spreading centers. Earth Sci Rev 20: 1–104
Rona PA (1986) Mineral deposits from seafloor hot springs. Sci Am 254:66–75
Rona PA (1988) Hydrothermal mineralization at oceanic ridges. Can Mineral 26:431–465

Rona PA (2003) Resources of the seafloor. Science 299: 673–674
Rona PA, Scott SD (eds) (1993) A special issue on seafloor hydrothermal mineralization: new persectives. Econ Geol 88, No. 8
Rona PA, Bostrom K, Laubier L, Smith KL (eds) (1983) Hydrothermal processes at seafloor spreading centers. Plenum, New ork, 796 pp
Saez R, Almodavar GR, Pascual E (1996) Geological constraints on massive sulphide genesis in the Iberian Pyrite Belt. Ore Geol Rev 11: 429–451
Sangster DF, Scott SD (1976) Precambrian stratabound massive sulphide ores of North America. In: Wolf KH (ed) Handbook of strata-bound and stratiform ore deposits, vol 6. Elsevier, Amsterdam, pp 129–222
Sato T (1974) Distribution and geological setting of the kuroko deposits. Soc Min Geol Jpn Spec Issue 6:1–10
Sawkins FJ (1990) Metal deposits in relation to plate tectonics. 2nd edn, Springer, Berlin
Schneider GIS, Seeger KG (1992) Copper. In: The Mineral Resources of Namibia, 1st edn, Ministry of Mines and Energy, Geol Surv Handb
Schubert G, Turcotte DL, Olson P (2001) Mantle convection in the Earth and Planets. Cambridge Univ Press, Cambridge
Searle P L (1972) Mode of occurrence of the cupriferous pyrite deposits of Cyprus. Trans Inst Min Metall 81:B189–B197
Seibold E, Berger WH (1982) The seafloor. An introduction to marine geology. Springer, Berlin
Šengör AMC, Natal'in BA (2004) Phanerozoic analogues of Archaean oceanic basement fragments: Altaid ophiolites and ophirags. In Kusky TM (ed) Precambrian ophiolites and related rocks, Elsevier, Dev Precambr Geol 13: 675–726
Sharpe R, Gemmell JB (2001) Alteration characteristics of the Archean Golden Grove Formation at the Gossan Hill deposit, Western Australia: Induration as a focusing mechanism for mineralizing hydrothermal fluids. Econ Geol 96: 1239–1262
Sillitoe RH (1982) Extensional habits of rhyolite-hosted massive sulfide deposits. Geology 10:403–407
Sillitoe RH, Hedenquist JW (2003) Linkages between volcanotectonic settings, ore-fluid compositions and epithermal precious metal deposits. Soc Econ Geol Spec Publ 10: 315–343
Sinton JM, Detrick RS (1992) Mid-ocean ridge magma chambers. J Geophys Res 97: 197–216
Slack JF (1993) Descriptive and grade-tonnage models for Besshi-type massive sulphide deposits. Geol Ass Can Spec Pap 40: 343–371
Sleep NH (1983) Hydrothermal convection at ridge axes. In: Rona PA, Bostrom K, Laubier L, Smith KL (eds) Hydrothermal processes at seafloor spreading centers. Plenum, New York, pp 71–82
Smalley TJ (1990) The Matchless West Extension cupreous pyrite deposit, Namibia; a field-based study. In: Abstr Geocongress '90 Cape Town. Geol Soc S Afr, pp 514–517
Smewing JD, Christensen NI, Bartholomew ID, Browning P (1984) The stucture of the oceanic upper mantle and lower crust as deduced from a northern section of the Oman ophiolite. Geol Soc Spec Publ 13:41–54
Smithies RH, Van Kranendonk MJ, Champion DC (2005) It started with a plume – early Archaean basaltic proto-continental crust. Earth Planet Sci Lett 238: 284–297
Solomon M, Groves DI (1994) The geology and origin of Australia's mineral deposits. Clarendon Press, Oxford Sci Publ
Solomon M, Tornos F, Large RR. Badham JNP, Both RA, Zaw K (2004) Zn–Pb–Cu volcanic hosted massive sulphide deposits: criteria for distinguishing brine pool-type from black smoker-type sulphide deposition. Ore Geol Rev 25: 259–283
Spence CD (1975) Volcanogenic features of the Vauze sulfide deposit, Noranda, Quebec. Econ Geol 70:102–114

Spence CD, De Rosen-Spence AF (1975) The place of sulfide mineralization in the volcanic sequence at Noranda, Quebec. Econ Geol 70: 90–101
Stix J, Kennedy B, Hannington M, Gibson H, Fiske R, Mueller W, Franklin J (2003) Caldera-forming processes and the origin of submarine volcanogenic massive sulfide deposits. Geology 31: 375–378
Tarney J, Dalziel IWD, de Wit MJ (1976) Marginal basins 'Rocas Verdes' complex from S Chile: a model for Archaean greenstone belt formation. In: Windley BF (ed) The Early History of the Earth, Wiley-Interscience, London, pp 131–146
Tatsumi T (ed) (1970) Volcanism and ore genesis. Univ Press, Tokyo, Japan
Taylor B (2006) The single largest oceanic plateau: Ontong-Java-Manihiki-Hikurangi. Earth Planet Sci Lett 241: 372–380
Thompson G, Mottl MJ, Rona PA (1985) Morphology, mineralogy and chemistry of hydrothermal deposits from the TAG area, 26°N Mid-Atlantic Ridge. Chem Geol 49:243–257
Thompson G, Humphris SE, Schroeder B, Sulanowska M, Rona PA (1988) Active vents and massive sulfides at 26°N (TAG) and 23°N (Snakepit) on the Mid-Atlantic-Ridge. Can Mineral 26: 697–711
Toomey DR, Jouselin D, Dunn RA, Wilcock WSD, Detrick RS (2007) Skew of mantle upwelling beneath the East Pacific Rise governs segmentation. Nature 446: 409–414
Tornos F (2006) Environment of formation and styles of volcanogenic massive sulfides: the Iberian Pyrite Belt. Ore Geol Rev 28: 259–307
Tornos F, Heinrich CA (2007) Shale basins, sulphur-deficient ore brines and the formation of exhalative base metal deposits. Chem Geol doi:10.1016/j.chemgeo.2007.10.011
Urabe T, Scott SD, Hattori K (1983) A comparison of foot-wall rock alteration and geothermal systems beneath some Japanese and Canadian volcanogenic massive sulfide deposits. Econ Geol Monogr 5: 345–364
Van Kranendonk MJ, Hickman AH, Smithies RH, Nelson DR, Pike G (2002) Geology and tectonic evolution of the Archean North Pilbara terrain, Pilbara Craton, Western Australia. Econ Geol 97: 695–733
Van Kranendonk MJ, Hickman AH, Smithies RH, Williams IR, Bagas L, Farrell TR (2006a) Revised lithostratigraphy of Archean supracrustal and intrusive rocks in the northern Pilbara Craton, Western Australia. West Aust Geol Surv Record 2006/15
Van Kranendonk MJ, Hickman AH, Huston DL (2006b) Geology and mineralization of the East Pilbara — a field guide. West Aust Geol Surv Record 2006/16
Vearncombe S (1999) VMS potential determined via subvolcanic intrusions in Precambrian rocks: key geochemical signatures. Aust Inst Geoscie Bull 30: 97–103
Vearncombe S, Barley ME, Groves DI, McNaughton NJ, Mikucki EJ, Vearncombe JR (1995) 3.26 Ga black smoker-type mineralisation in the Strelley Belt, Pilbara Craton, Western Australia. J Geol Soc London 152: 587–590
Vearncombe S, Kerrich R (1999), Geochemistry and geodynamic setting of volcanic and plutonic rocks associated with Early Archaean volcanogenic massive sulphide mineralization, Pilbara Craton. Precambr Res 98: 243–270
Vearncombe S, Veancombe JR, Barley ME (1998) Fault and stratigraphic controls on volcanogenic massive sulphide deposits in the Strelley Belt, Pilbara Craton, Western Australia. Precambr Res 88: 67–82
Vogt JH (1995) Geology of the Jillawarra area, Bangemall Basin, Western Australia. Geol Surv West Aus, Rpt 40
Vogt JH, Stumpfl EF (1987) Abra: A stratabound Pb–Cu–Ba mineralization in the Bangemall basin, Western Australia. Econ. Geol 82: 805–825
Von Damm KL, Edmond JM, Grant B, Measures CI (1985) Chemistry of submarine hydrothermal solutions at 21°N, East Pacific Rise. Geochim Cosmochim Acta 49: 2197–2220
Von Damm KL, Grant B, Edmond JM (1983) Preliminary report on the chemistry of hydrothermal solutions at 21 North, East Pacific Rise. In: Rona PA, Bostrom K, Laubier

L, Smith KL (eds) Hydrothermal processes at seafloor spreading centers. Plenum, New York, pp 369–390
Von Damm KL, Colodner DC,. Edmonds HN (1992) Hydrothermal fluid chemistry at 9–10°N EPR '92: big changes and still changing. EOS, Trans Am Geophys Un 73: 524
Von Damm KL, Oosting SE, Kozlowski R, Buttermore LG, Colodner DC, Edmonds HN, Edmond JM, Grebmeler JM (1995) Evolution of East Pacific Rise hydrothermal vent fluids following a volcanic eruption. Nature 375: 47–50
Wallace PJ, Frey FA, Weis D, Coffin MF (2002) Origin and evolution of the Kerguelen Plateau, Broken Ridge and Kerguelen archipelago. J Pet 43: 1105–1108
Wessel P (1997) Sizes and ages of seamounts using remote sensing: implications for intraplate volcanism. Science 277: 802–805
Wilson JT (1963) A possible origin for the Hawaiian islands. Can J Phys 41: 863–870
Wilson M (1989) Igneous Petrogenesis. Unwin Hyman, London
Wolfe CJ, Bjarnason IG, VanDecar J, Solomon SC (1997) The anatomy of a mantle plume: seismic structure of the Iceland hospot. Nature 385: 245–247
Wyman DA, Kerrich R, Polat A (2002) Assembly of Archean cratonic mantle lithosphere and crust: plume-arc interaction in the Abitibi-Wawa subduction-accretion complex. Precambr Res 115: 37–62
Yang K, Scott SD (1996) Possible contribution of a metal-rich magmatic fluid to a seafloor hydrothermal system. Nature 383: 420–423
Young DA (2003) Mind over magma: The story of igneous petrology. Princeton Univ Press, Princeton
Zierenberg RA and 27 others (1998) The deep structure of a seafloor hydrothermal deposit. Nature 392: 485–488

Chapter 8
Metalliferous Sediments and Sedimentary Rock-Hosted Stratiform and/or Stratabound Hydrothermal Mineral Systems

8.1 Introduction

In this chapter I discuss and describe a range of hydrothermal mineral systems that are generated at passive margins, in basin structures of intracontinental or back-arc rifts, with or without obvious connection to igneous activity, seafloor metalliferous sediments and iron and manganese oxide accumulations. Passive margins and rift-related ore deposits include those known as Mississipi Valley-type (MVT), sedimentary exhalative polymetallic massive sulphides (SEDEX) and the Cu-rich stratabound and stratiform disseminated sulphides, all of which can be broadly grouped under the wider family of sedimentary-hydrothermal ore systems. The origin of sedimentary-hydrothermal ore systems involves a variety of processes including diagenesis, flow of brines across basins and venting of hydrothermal fluids on the floor of the sea or lakes. A schematic setting of MVT and SEDEX deposits is shown in Fig. 8.1. Several SEDEX massive sulphide deposits form on sea or lake floors by the discharge of fluids that vent through structurally controlled conduits. They are generally associated with dominantly anoxic conditions and are commomly hosted by carbonaceous shales. MVT deposits form in the shallower environments of carbonate platforms, which capture the flow of mineralising fluids. Whether or not SEDEX and MVT mineralisation form two ends of a continuum is a question that remains unanswered. In contrast to the SEDEX and MVT deposits, the Cu-rich stratabound and stratiform disseminated sulphides (Cu-Ag, Cu-Co), such as those of the Zambian and Kalahari copperbelts in southern Africa, the Kupferschiefer deposits in central Europe and Udokan in Siberia, are associated with thick oxidised siliciclastic successions (red beds, defined in Section 8.6), evaporites and shallow-marine or lagoonal environments. Many of these ore deposits are also hosted in reduced carbonaceous horizons, which are deposited during phases of minimum tectonic activity. The metalliferous brines are of diagenetic or connate basinal origin. They flow through porous continental sediments, leaching metals from rock-forming minerals (e.g. feldspar) and/or diagenetic Fe oxides and precipitating sulphides at redox interfaces, or reduced horizons, forming disseminations rather than massive concentrations.

F. Pirajno, *Hydrothermal Processes and Mineral Systems*,

© Springer Science+Business Media B.V. 2009

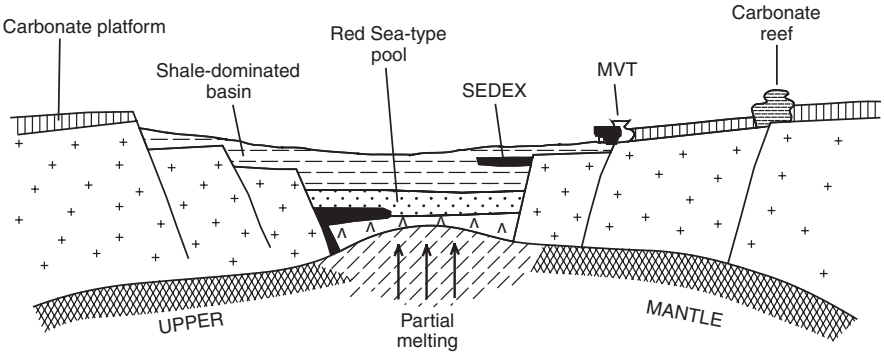


Fig. 8.1 Conceptual model linking SEDEX and MVT ore deposits in the same rift basin as suggested by Goodfellow et al. (1993). In this model these ore deposits are formed by mixing of basinal fluids with anoxic waters; discharge of Red Sea-type metalliferous brines occur in the axial rift on oceanic crust rocks (see also Fig. 8.8)

For more information on sedimentary-hosted, rift-related, metal deposits the reader is referred to Pirajno (1992), Goodfellow et al. (1993), Parr and Plimer (1993), Leach and Sangster (1993), Deb and Goodfellow (2004), Hitzman et al. (2005), Large et al. (2005), Leach et al. (2005) and Huston et al. (2006). An exhaustive treatise (10 volumes!) on stratabound and stratiform ore deposits was edited by Wolf (1981). A schematic model of SEDEX ore-forming system is shown in Fig. 8.2. A spatial, and possibly genetic, association with basinal evaporite successions is advocated by Warren (2000) for several sedimentary-hosted ore deposits including the Kupferschiefer, the Red Sea oxide-sulphide pools and some of the MVT deposits (e.g. Cadjebut in Western Australia).

Goodfellow et al. (1993) listed the following modern analogues of SEDEX environments: the great tectonic lakes, such as the East African lakes and Lake Baikal; the Red Sea metalliferous brine pools, such as Atlantis II (described in Section 8.5.1); the Salton Sea trough, in which a large hydrothermal system is active within a fluvio-lacustrine sedimentary succession, about 10 km thick (discussed in Chapter 7). Leach et al. (2005) mentioned the *historical controversy* of classification and terminology for sedimentary rock-hosted Pb-Zn deposits and used the following broad classification:

1. Mississipi Valley Type (MVT)
2. sedimentary exhalative (SEDEX)
3. sandstone lead
4. sandstone-hosted deposits

While agreeing with the difficulties of resolving the historical controversy and being fully aware that far from doing justice to what is an enormous variety of and complex mineral systems, I add to the list the stratabound and stratiform

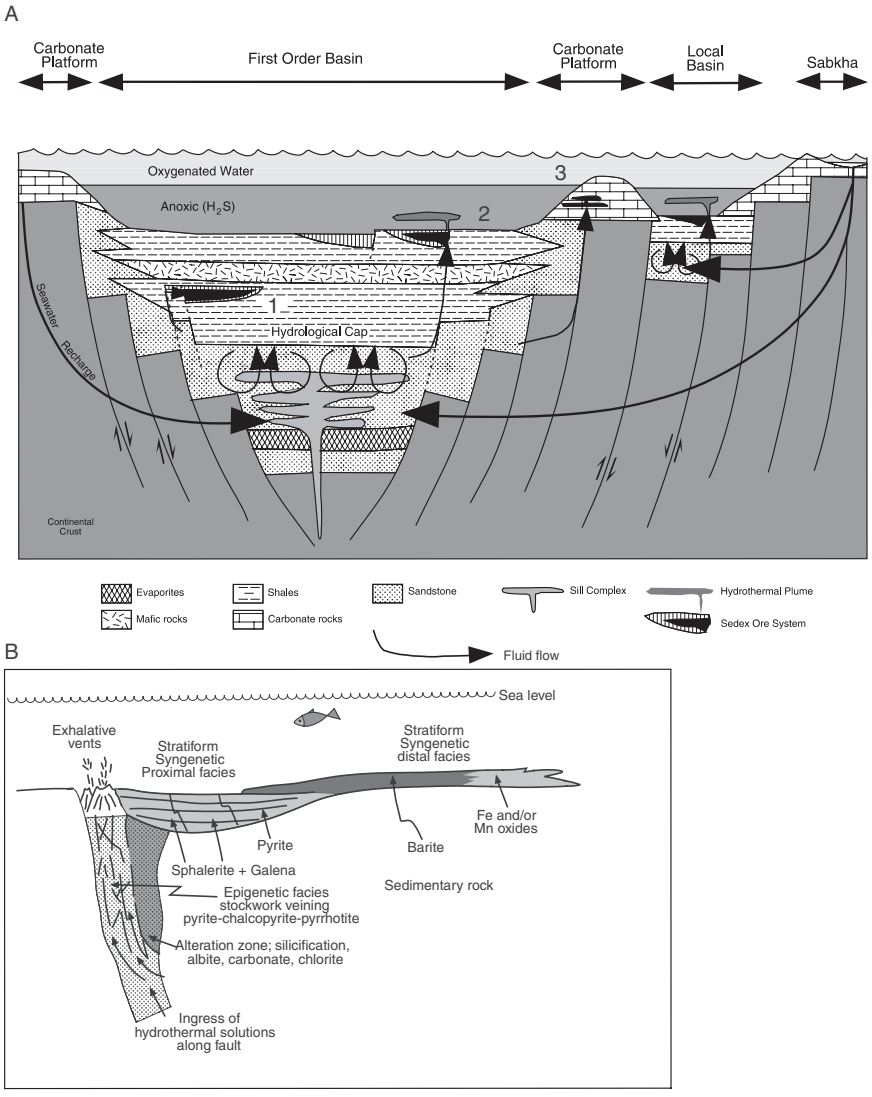


Fig. 8.2 (**A**) Generalised architecture of sedimentary basin in which SEDEX ore systems form, as replacement bodies in shale sequences (1), or in Red Sea-type brine pools (2), or in a carbonate platform (3); the latter may provide a link with Mississippi Valley-type ore systems; after Goodfellow and Lydon (2007); (**B**) Idealised model of exhalative system, as for example No. 2 in (**A**), showing the epigenetic facies and associated alteration along the conduit (feeder pipe), and the syngenetic proximal bedded facies and a distal sedimentary facies. The proximal bedded facies may be vertically zoned (sphalerite-galena at bottom to pyrite at *top*); the distal sedimentary facies is laterally zoned, from barite to Fe and Mn oxides away from the vent. Based on Large (1981) and Goodfellow et al. (1993), see also Lydon (2004)

Cu systems (Copperbelt style), iron formations and seafloor metalliferous sediments and in keeping with the title of this chapter, I use the following breakdown:

- Mineral systems associated with the East African Rift System; as a modern day example
- Red Sea brine pools, also a modern day example
- Stratiform and stratabound Cu (Kupferschiefer and Copperbelt styles)
- Sedimentary exhalative (SEDEX) systems
- Stratabound carbonate-hosted, or Mississippi Valley Type (MVT)
- Iron and manganese oxides
- Recent metalliferous sediments on seafloors

The best known and well-studied SEDEX systems are those in Australia (Broken Hill, McArthur River-Mt Isa), South Africa (Gamsberg-Aggeneys) and Sullivan in Canada. Stratabound and stratiform disseminated sulphides in sedimentary rocks of rift basins, include those of the Copperbelt in southern-central Africa and the Kupferschiefer of central Europe. The Mississippi Valley Type (MVT) ore systems, with many variants, also form in basin settings and are described in this chapter. The Red Sea brine and sulphide accumulations are forming today at an incipient spreading centre, and these are transitional to the submarine hydrothermal systems discussed in Chapter 7. SEDEX, Copperbelt-Kupferschiefer style deposits and Red Sea brines may be considered as part of a time-space continuum of hydrothermal systems, depending on the stage of development of the rift setting considered (e.g. incipient to advanced, see below).

A breakdown of sedimentary rock-hosted ore deposits in relation to evolutionary stages of rifting is presented in Table 8.1.

I begin this chapter by examining metallogeny in two modern settings, which may be considered as analogues of ancient sedimentary-hosted sulphide deposits: the lakes of East African Rift System and the Red Sea brine pools, where ore deposits are actively forming. In the great lakes of the East African rift valleys, mineral deposits are forming as a result of subaerial hot springs, exhalations at the water-sediment interface and within the thick sedimentary

Table 8.1 Evolutionary stages of rifting and associated stratiform and/or stratabound sedimentary rock-hosted mineral systems (after Sawkins 1990)

Incipient stage of rifting	Hydrothermal discharges in rift lakes (e.g. East African Rift System; transitional to or similar to SEDEX)
Intermediate stage or Failed rifts	Stratabound sediment-hosted disseminated sulphides (e.g. Copperbelt-type; Cu-Co, Cu-Ag); spatial (and genetic?) association with evaporite successions;
	SEDEX (sediment-hosted exhalative massive sulphides, Cu-Pb-Zn-Ag-Ba)
Advanced stage and rifted passive margins	Red Sea type polymetallic brine pools; Mississippi Valley Type

pile. In the Red Sea, a major submerged rift zone, in parts of which oceanic crust is being generated, brine pools and accumulations of massive sulphides are forming by discharge of highly saline brines. These brines derive much of their solutes from evaporite deposits that develop during the earliest phases of rifting, of which a present-day analogue can be found in the Afar region, discussed in Section 8.4.2. Sedimentary-hydrothermal ore deposits, SEDEX, Cu-rich stratabound sulphides and MVT are discussed next. In the last two sections of this chapter, I conclude with the giant Superior type iron and manganese formations, of great economic importance for their vast resources of iron, much in demand by the ascending giant Asian economies and the possible link that these impressive geological entities have with mantle plumes and the deposition of recent metalliferous sediments on oceanic seafloors. Leach et al. (2005) and Hitzman et al. (2005) reviewed from a global perspective the sedimentary rock-hosted ore systems, and listed 248 and 129 deposits, respectively.

8.2 Basin Formation and Volcano-Sedimentary Successions in Continental Rifts

The evolution of continental rifts, from incipient graben structures to proto-oceanic and oceanic sea-floor spreading, is accompanied by the development of sedimentary basins. Rift-related sedimentary basins are host to a variety of hydrothermal mineral systems including vein-type, stratabound and/or stratiform disseminated and massive sulphide deposits. Comprehensive studies of continental rifting and basin geology can be found in the books by Allen and Allen (1990, 2005), Busby and Ingersoll (1995), Olsen (1995), Leeder (1999) and Einsele (2000). A good collection of papers can be found in Beaumont and Tankard (1987). The geodynamics of rifts and associated basins is treated in Chapter 3, here I briefly introduce a classification of tectonic basins that can be useful in order to gain a better understanding of the environments of deposition of sedimentary-hydrothermal ore systems. A classification of rift basins is shown in Table 8.2. Continental rift basins may form as a result of mantle plume impingement onto the base of the lithosphere. The surface expression of mantle plumes is typically manifested by doming of the crust, reflected as topographic swells of 1000–2000 km in diameter and 2000–4000 m elevations (a.s.l.), and intraplate volcanism (Ernst and Buchan 2003). Uplift is followed by subsidence due to loss of buoyancy of the plume head, or removal of magma from the top of the plume, thermal decay, or a combination of all three (Condie 2001). Subsidence and crustal sagging cause the formation of sedimentary basins, characterized by the deposition of extensive aprons of siliciclastics, carbonates and evaporites, commonly overlain by continental flood basalts and/or transected by related dyke swarms. An example is provided by the Centralian Superbasin in Australia (Walter et al. 1995), where crustal sagging

Table 8.2 Basin classification; modified after Busby and Ingersoll (1995 and references therein)

	Rift type	Process	Modern example/ ancient example
Divergent Settings	Terrestrial Rift Valleys:	Rifts within continental crust, commonly associated with bimodal volcanism.	Rio Grande rift, New Mexico/ Keeweenanwan rift
	Proto-Oceanic Rift Troughs (see also Table 8.2):	Incipient oceanic basins floored by new oceanic crust and flanked by young rifted continental margins.	Red Sea/East Greenland
Intraplate Settings			
	Continental rises and Terraces; passive margins	Mature rifted continental margins in intraplate settings at continental-oceanic interfaces	East coast of USA/ Canadian Cordillera
	Intracratonic rift basins (see also Tables 8.1 and 8.3)	Broad cratonic basins floored by fossil rifts in axial zones.	Chad basin/ Witwatersrand (South Africa)
	Continental Platforms	Stable cratons covered with thin and laterally extensive sedimentary strata.	Barenst Sea/Mid-Palaeozoic North America mid-continent
Convergent Settings			
	Forearc Basins	Basins within arc-trench gaps.	Sumatra/Cretaceous Great Valley (California)
	Intra-Arc Basins	Basins along arc platform, which includes superposed and overlapping volcanoes.	Lake Nicaragua/ Sierra Nevada (California)
	Back-arc Basins	Oceanic basins behind intraoceanic magmatic arcs (including interarc basins between active and remnant arcs), and continental basins behind continental-margin magmatic arcs without foreland foldthrust belts.	Sea of Japan/ McArthur River-Mt Isa (Australia)
	Retroarc Foreland Basins	Foreland basins on continental sides of continental-margin arc-trench systems (formed by subduction-generated compression and/or collision).	Andean foothills/ Western Sn belts (SE Aasia)

Table 8.2 (continued)

	Rift type	Process	Modern example/ ancient example
Divergent Settings	Peripheral Foreland Basins	Foreland basins above rifted continental margins that have been pulled into subduction zones during crustal collisions (primary type of collision-related forelands).	Persian Gulf/Molasse basin in Switzerland
	Piggyback Basins	Basins formed and carried atop moving thrust sheets.	Peshawar Basin (Pakistan)/ Appennines (Italy)
	Foreland Intermontane Basins (Broken Forelands)	Basins formed among basement-cored uplifts in foreland settings.	Sierra Pampeanas (Argentina)/ Laramide Basin (USA)
Transform Settings (and transcurrent-fault-related basins)			
	Transtensional Basins	Basins formed by extension along strike-slip fault systems.	Salton Sea (California)/ Carboniferous Magdalen Basin (Canada)
	Transpressional Basins	Basins formed by compression along strike-fault systems.	Santa Barbara Basin (California)/ Miocene Ridge Basin (California)
Hybrid Settings			
	Aulacogens (see also Table 8.2)	Former failed rifts at high angles to continental margins, which have been reactivated during convergent tectonics, so that they are at high angles to orogenic belts.	Benue Trough (West Africa)/ Athapuscow (Canada)
	Intracontinental rift systems (see also Table 8.2)	Rifts formed during extensional; tectonics related to asthenospheric upwelling.and lithosphere thinning	Baikal rift/Rhine graben
	Successor Basins	Basins formed in intermontane settings following cessation of local orogenic or taphrogenic activity.	Southern Bains-and-Range (Arizona)/ Sustut Basin (British Columbia, Canada)

began as a result of a mantle plume activity at about 826 Ma (Zhao et al. 1994), with the deposition of thick successions of marine and fluvial sands. The evolution of this large depositional system continued through to the latest Proterozoic, culminating with the eruption of continental flood basalts from a second plume event at about 510 Ma (Kalkarindji LIP; Glass and Phillips 2006). Thus, uplifts related to mantle plumes also record pulses of sedimentary successions that are controlled by eustatic sea level fluctuations, due to an interplay of increased oceanic plateau formation (sea level rise) and supercontinent aggregation (sea level fall) (White and Lovell 1997). An overview of continental rift basins related to mantle plume activity is given in Table 8.3.

As noted above, rifting processes commonly result in the formation of basin structures within which thick successions of sediments and volcanic materials accumulate. The volcano-sedimentary successions of rift-related basins can be extremely important from the economic point of view, because they may host large ore deposits. As mentioned above, examples include the world-class Mt Isa and Broken Hill sedimentary-exhalative (SEDEX) massive sulphides in Australia; Gamsberg-Broken Hill in South Africa; Sullivan in Canada; stratabound, disseminated or massive sulphides of the Rammelsberg and Kupferschiefer type of deposits in central Europe; Udokan in Siberia; Dongchuan in China; the giant Cu-Co mineral systems of the Central African copperbelt. A point of note is that many of these ancient rift basins, hosting large sedimentary ore deposits, may have been lacustrine, a facet that is seldom mentioned in the literarure. The major Fe resources of banded iron-formations (BIF) are hosted in passive margin-related basinal volcano-sedimentary successions (e.g. Hamersley in Western Australia, Transvaal in South Africa). I examine some of these deposits in Section 8.9. Although a discussion of basin stratigraphy and associated facies models is beyond the scope of this book, it is opportune to briefly review the basic concepts of depositional styles and principal facies of basins. Details of the geology and stratigraphy of sedimentary basins are

Table 8.3 Rift basins formed as a result of lithosphere thinning and mantle plume activity; after Pirajno (2000)

Rift basin type	Ancient example	Modern example
Graben structures, rift valleys and rift zones, aulacogens, associated with bimodal volcanism	Keeweenawan (USA; Canada); Athupuscow (Canada)	Lake Baikal; Rhine Valley graben; Afar (this Chapter)
Proto-oceanic rift; incipient oceanic basin, floored by oceanic crust, flanked by rifted continental margins	Matchless Belt, Namibia (Chapter 7)	Red Sea (this Chapter); Gulf of California (Chapter 7)
Rifted continental margins; continental rises and terraces	East Greenland (Chapter 5)	East coast of USA
Intracratonic basins; basins in the interior of cratons	Ventersdorp; Soutpansberg basins (South Africa)	Chad Basin (North Africa)

available in Allen and Allen (1990), Busby and Ingersoll (1995) and Leeder (1999). The shape or geometry of an incipient basin structure, and its subsequent evolution, determines the type and facies of sedimentary and volcanic infill. This in turn is linked to eustatic sea-level changes to which facies-dependant stratigraphic units are related. The following is summarised from Allen and Allen (1990; pp. 189–259), who subdivided continental depositional systems into: fluvial, aeolian, lacustrine, coastal-near shore and continental shelf. In terms of depositional settings, there are two types of continental basins: those with a "through drainage" (perennial rivers and lakes), and those with an "internal drainage" (ephemeral rivers, lakes, sabkhas and desert environments).

Fluvial systems and related alluvial deposits are sensitive to climate and tectonism and hence topography. River channels are subject to rapid changes in response to base level changes. Alluvial fans, meandering and braided stream channels are common terms used in sedimentology. Aeolian systems include sandy and stony desert environments and dried river courses. Sandy deserts are characteristic of continental interiors (e.g. Sahara, Gobi and central Australian deserts). Aeolian deposits typically contain thick cross-bedded sandstone successions, and may be intercalated with continental evaporite and playa lake deposits.

Lacustrine systems are highly variable and sensitive to both climate and tectonism, with their associated deposits being clastic and/or chemical-biochemical. Ephemeral lakes of internal drainage basins are dominated by chemical (including hot spring precipitates), biochemical and evaporitic sediments (e.g. alkaline carbonate and evaporites of some of the lakes in the East African Rift System and Afar region), whereas through-flowing lakes of continental rift systems (e.g. Lake Baikal) are characterised by terrigenous clastic sediments. Three main depositional settings for lacustrine deposits can be distinguished: open freshwater lake, perennial saline lake and ephemeral salt lake (see Fig. 7.13 in Allen and Allen 1990). Sediments of hydrologically closed lakes (e.g. Lake Chad in Africa; Lake Carnegie in Westerrn Australia) include central and marginal facies. The central facies typically contains saline precipitates from lake brines (e.g. trona), organic-rich sediments (e.g. remains of algae) and carbonate-rich laminites. The marginal facies, reflecting periodic lake level fluctuations, includes stromatolitic carbonates, laminated marls with dessication cracks and gypsiferous sediments. In contrast, hydrologically open lake basins have offshore and nearshore facies. Offshore facies include laminites of clastic, carbonate and organic layers, fluvial thinly bedded silts and muds. Nearshore facies contain wave-rippled sandstones, cross-bedded sandstone (beach deposits) and stromatolitic bioherms. Lacustrine rift basins, generally characterised by half-graben morphologies, commonly have stratigraphy comprising three stages: early fluvial, middle lacustrine and late fluvial (Lambiase 1990). An overview of the tectono-stratigraphic architecture of lacustrine rift basins can be found in Scholz et al. (1998), who considered low- (e.g. East African lakes) and high-latitude (e.g. Lake Baikal) systems, both with early and late rift sedimentation phases.

Coastal and nearshore systems are very complex because they are influenced by the vagaries of fluvial input, base level and climatic changes as well as basin dynamics. Broadly, these systems can be classified into: siliciclastic- and carbonate-evaporite-dominated shorelines, or deltaic and non-deltaic systems. These relate to a topographically high sourceland and to a low or distant sourceland. Carbonate and evaporite systems are characteristic of arid shorelines and typically have stromatolitic carbonates (common in Precambrian and Palaeozoic times) in the tidal and lagoon zone, algal mats in the intertidal zone and evaporites in the supratidal zone. The intertidal and supratidal zones constitute the sabkha environment, which can be important for ore deposition. Similarly, continental shelf environments have siliciclastic- and carbonate-dominated systems, which are also very complex and dependant on sea-level fluctuations. The hydraulic regimes of these facies can be related to three end-members: storm-dominated, wave-dominated and tide-dominated.

8.3 Fluid Dynamics in Sedimentary Basins

In this section, I discuss the dynamics of large-scale fluid systems in sedimentary basins that are responsible for a wide range of sedimentary rock-hosted strata-bound and stratiform ore sytems. These include the Mississippi Valley Type (MVT) Pb, Zn and barite, the Kupferschiefer Cu deposits of central Europe and the sandstone-hosted roll-front and unconformity type U deposits (Chapter 13). Ore-making fluids in sedimentary basins that form the above ore systems are essentially part of, and derived from, large-scale groundwater and pore fluids in sediments. Excluded from the above are some SEDEX ore systems in rift basins, where exhalation of brines discharge on the seafloor forming deposits, such as those of the Red Sea and the Irish-style carbonate-hosted mineral systems, although transitional situations may exist.

During the evolution of a sedimentary basin, expulsion of fluids takes place as a result of burial, compaction and diagenesis. The origin of fluids, their physical and chemical properties and flow patterns in sedimentary basins were examined and discussed by Hanor (1979), later followed by Garven and Raffensperger (1997). Key aspects of the processes that generate hydrothermal fluids and their flow in sedimentary basins are taken from these two publications. Water in sedimentary basins is trapped in the pores of sediments during their accumulation in a sedimentary cycle, is produced during diagenetic reactions and introduced from outside the basin (e.g. rainfall). Diagenetic changes may be an important component of hydrothermal fluids, and in this connection it must be recalled that the boundary between diagenesis and metamorphism is by no means well defined. For practical purposes, diagenesis is essentially a sedimentary process which takes place under physico-chemical conditions not too dissimilar from those found at, or near, the surface, whereas metamorphism involves higher temperatures and pressure. Dehydration reactions during high

temperature metamorphism also produce water, but this is not considered here, as this process is discussed in Chapter 9

Diagenesis involves dehydration of clay minerals, organic matter and gypsum. In clay minerals, such as montmorillonite, the interlayered water is removed during dehydration and conversion of montmorillonite to illite. This is an important process because K is necessary for this conversion and the source of this element is provided by detrital feldspar and mica, whose diagenetic destruction also provides elements, such as Ba and Pb that are contained in the lattice of these detrital minerals. Sources of metals in basin may include the organic fraction of the sediments and/or the silicate minerals and carbonates. Doe and Delevaux (1972) showed from the isotopic composition of Pb in galena ores from Missouri, that the Pb is derived from the feldspar component of the La Motte sandstone through which the basin fluids circulated.

Hanor (1979) suggested that dehydration of clays occurs during two temperature phases: 90°C and 120°C. Diagenesis is linked to burial and porosity reduction, which results in the expulsion of water in the first instance. Thus, large volumes of water are released during compaction due to burial and diagenesis. An average shale will yield about 3.5×10^3 l/m^3 of solid deposited, whereas an average sandstone will yield 0.7×10^3 l/m^3 of solid deposited. Calculations of the volume of water that can be contained in a rock mass subject to burial was estimated by Fyfe et al. (1978), who considered a prism of sediments 5 km thick and one km on a side (5 km^3) with an initial water content of 50%. In this example there would be some 2.5 km^3 of salty water available. These authors also considered that if an element has 1 ppm solubility, then there could be $2.5 \times 10^{15}\,g \times 10^{-6} = 2.5 \times 10^9$, or 2500 tonnes, of that element in solution. During compaction dehydration adds water to the system at depths of 2–3 km, where montmorillonite is converted to illlite.

Physical parameters of fluids in sedimentary basins are temperature, pressure, density and viscosity. Temperature-depth relationships are defined by geothermal gradients, which in turn are related to heat flow and thermal conductivity of the sediments, according to:

$$Q = K(dT/dz)$$

where Q is the heat flow, dT/dz is the geothermal gradient (T temperature; z depth), K is thermal conductivity. Geothermal gradients increase with depth from <50°C at 1 km to >100°C below 4 km. Fluid pressure or formation pressure is defined as the pressure exerted by a subsurface fluid against the mineral grains. This pressure in sediments is controlled by mechanical compression, temperature increase, dewatering processes and osmotic diffusion. Density and viscosity are controlled by temperature and salinity. Increases in salinity and pressure will increase density, but temperature increase will have the opposite effect on density, so that this parameter will flatten with depth. Chemical properties of fluids are salinity, dissolved species, acidity and

oxidation states. Total dissolved solids or salinity increase with depth, but where evaporites are present salinity of waters can reach high values, typically up to or exceeding 400‰ (sea water value is 35‰). Generally, subsurface saline waters in sandstone and carbonates are enriched in Ca, Sr, Ba, F and depleted in Na, K, Mg and sulphate, compared to modern sea water and relative to chloride content. Known pH values of saline waters in sedimentary basins range from 5 to 9, as measured in wells or in laboratory experiments, but these have not been corrected for depth and temperature, which tend to decrease the pH.

The composition of basinal waters is characteristic of a given sedimentary basin. Salinity increases with depth in basins, and this is explained by a mechanism of membrane filtration, a process whereby argillaceous sediments allow the passage of neutral molecules (H_2O and H_2S), while preventing the migration of anions and cations, resulting in their downward concentration. Thus, deeper waters become saltier and enriched in cations and anions. Elements that are usually enriched in formation waters are Pb, Zn, Ba, F, Sr and S. The latter is probably derived from bacterial reduction of dissolved sulphates to sulphide during diagenesis. Sulphate is predominant in most formation waters, whereas H_2S is more common in oil field gases. In the Cheleken (Caspian Sea) and central Mississippi regions, where there is no evidence of igneous activity, brines have a high metal content. Metal-rich brines are commonly derived from dissolution of evaporites, either at depth or from hypersaline waters in surface evaporative environments. Sulphur-rich saline brines can also develop by metamorphism of evaporite sequences, discharge at surface as hot springs and deposit stratiform tourmalinites (Schmidt-Mumm et al. 1987). Metal-rich waters in the Salton Sea, the Red Sea and central Mississippi are in part derived through interaction with evaporites. In the Cheleken region, three types of formation waters were recognised (Hanor 1979). The deepest are Na-Cl-HCO_3 waters, with temperatures above 105°C, and salinities of 35–40 g/l TDS (total dissolved solids). These waters precipitated calcite and barite in well pipes. The second type are NaCl waters with high Pb and Zn concentrations, considerably more saline (150–290 g/l TDS) and with temperatures of approximately 80°C. The third and shallowest waters are contained in red beds are Na-Cl-Ca brines with salinities of about 250 g/l TDS and abundant H_2S. Hanor (1979) reported that these high- H_2S and high metal brines were mixed in a surface tank and precipitated a 2.5 mm crust of sphalerite, galena and pyrite within a 3-months period! In the central Mississippi region, oil field Na-Ca-Cl waters with 160–340 g/l TDS and temperatures of 100–140°C hosted in carbonate rocks at depths of 2700–4400 m, contain up to 370 mg/l Zn and 92 mg/l Pb. These waters precipitated barite and galena at the well-head. Organic matter can also be an important source of metals, mainly because organic complexes can be very efficient in transporting metals.

Hot brines tend to flow from regions of high fluid pressure, generally in the central and deepest parts of a basin, laterally through permeable beds,

towards regions of lower pressure, along basin margins or along faults. Faulting may enhance the release of fluids, providing major conduits for the flow and discharge of fluids from depth. Other factors that cause groundwater flow are gravitational gradients due to topographic relief and fluid buoyancy associated with temperature and salinity (Garven and Raffensperger 1997). Tectonic compression and seismic pumping also result in major flow of basin fluids. Garven and Raffensperger (1997) stressed that the dominant mechanism for the transport of chemical mass in sedimentary basins is groundwater flow and that fundamental to the understanding of sedimentary rock-hosted mineral systems is knowledge of the hydrodynamics and geochemistry of fluid flow and transport in porous and fractured lithologies. The hydrologic, thermal and tectonic regimes that cause fluid flow in a sedimentary basin are shown in Fig. 8.3. At least seven principal factors must be considered that cause large-scale fluid flow: (1) gravity due to changes in elevation; (2) fluid overpressures due to diagenetic reactions; (3) compaction associated with burial and subsidence, which causes sediment loading; (4) tectonic compression and thrusting; (5) crustal extension and normal faulting; (6) buoyancy due to thermal and salinity gradients; and (7) erosional unloading due to stress relaxation. Topographic relief is one of the dominant causes of groundwater flow in sedimentary basins (Fig. 8.3A), with maximum rates of approximately 1–10 m/year developed in deep aquifers, but much smaller rates in aquitards. The flow patterns are largely controlled by basin geometry, topography and permeability. Temperature and salinity can produce density gradients that drive convection cells with flow rates of about 0.1 m/year (Fig. 8.3B). Abnormal pressure gradients occur following compaction, diagenesis and tectonic dilation, whereas tectonic compression and thrusting results in large-scale overpressurring in fold-and-thrust belts at basin margins (Fig. 8.3C). In this regime, flow rates are estimated in the range of metres/year. Overpressures can also occur following rapid sedimentation, subsidence and compaction (Fig. 8.3D). High pressures are also produced by dehydration reactions, pressure solution and hydrocarbon generation. Seismic pumping in rift faults results in rapid fluid flow with high flow rates of >10 m/year. Sibson et al. (1975) invoked seismic pumping as a mechanism, which allows large quantities of fluids can move along a fault plane during earthquakes to form hydrothermal mineral deposits. (Fig. 8.3E). Finally, groundwaters in a basin can be compartmentalised due to dykes and/or faults that separate compartments with different permeabilties, with groundwaters forming separate convection cells in each compartment (Fig. 8.3F). All of the processes described above develop and evolve during the evolutionary history of the basin through geological time. For example, fluid migration may commence with sediment compaction in the early stages. Uplift may follow resulting in topographically gravity-driven fluid flow and/or seismic pumping along fault zones. Gravity-driven fluid migration in fold-and-thrust belts moves fluids from the zones of tectonic compression across the basin to undeformed areas at the basin margins, as is the case for Mississippi Valley-type (MVT) ore systems (Section 8.8).

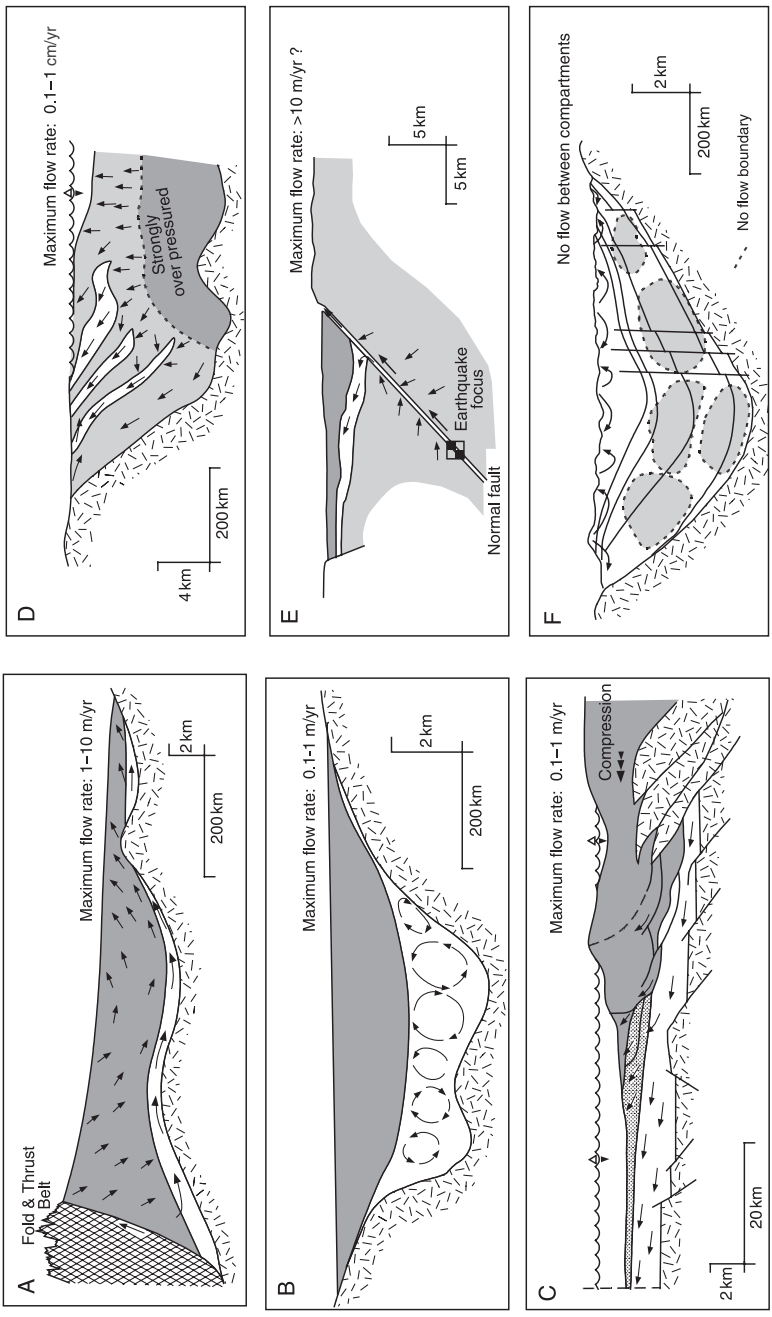


Fig. 8.3 Large-scale groundwater flow in sedimentary basins and associated hydrologic regimes and tectonic settings; (**A**) gravity-driven flow in uplifted foreland; (**B**) thermally-driven convective flow in intracratonic sag/rift basin; (**C**) groundwater flow related to tectonic compression in a fold-and-thrust belt; (**D**) overpressure-driven flow in a rapidly subsidising basin at a continental margin; (**E**) flow due to seismic pumping in fault zone; (**F**) compartmentalised basin with flow confined to individual compartments. After Garven and Raffensperger (1997)

8.4 The East African Rift System

The East African Rift System (EARS) is approximately 3000 km long, from the Afar region in Ethiopia to Lake Tanganyika and reaching as far as the Zambezi River and Okavango Delta in southern Africa (Fig. 8.4). To the north, the rift system continues beyond the Afar region into the Gulf of Aden, the Red Sea, the Sinai peninsula to the Dead Sea in Palestine, effectively adding another 2000 km to its overall extent. The rifts of East Africa are entirely continental, where blocks of continental crust are displaced and downfaulted to form depressions. In the Gulf of Aden the continental crust ruptured about 10 Ma ago, forming oceanic crust. The Red Sea, on the other hand, is in a transitional phase, because most of its floor still consists of stretched continental crust, with axial elongate zones where oceanic crust is forming. The meeting point is a triple junction, between the Red Sea, the Gulf of Aden and the Afar region, also known as Afar Triangle. Several lines of evidence suggest that a mantle plume underlies the Afar Triangle. I return to this point below. There are many articles and reviews on the African rifts in general, the EARS and sectors thereof in particular, that cover aspects of tectonism, volcanism and sedimentation in the associated basins. The following references provide useful information: McConnell (1972), Rosendahl (1987), Frostick et al. (1986), Lambiase (1989, 1990), Kampunzu and Lubala (1991), Braile et al. (1995), Schlüter (1997), Ebinger et al. (2000) and Rogers (2006).

The EARS consists of a series of graben and half-graben structures, characterised by strong uplift, normal faulting, alkaline volcanism, geothermal activity and the development of lakes and basins with thick accumulations of clastic, chemical and evaporitic sediments. Some of the EARS lacustrine rift basins are very large; Lake Tanganyika is 1470 m deep and more than 600 km long, and Lake Malawi is 700 m deep and 560 km long. The age of these African lakes is estimated at between 9 and 12 Ma. Many of the lakes (e.g. Kivu, Magadi, Bogoria, Baringo) in the EARS are characterised by high heat flow and hot springs, which discharge saline and metalliferous fluids. In several places, the pattern of the rift system tends to follow pre-existing Precambrian structural discontinuities. This is best illustrated where the rift system splits around the Tanzanian craton into two branches: western and eastern (Fig. 8.4). In the western branch, the Albert, Edward and Tanganyika rifts follow the trend of Archaean and Proterozoic orogenic belts; in the eastern branch, the Ethiopian, Lake Turkana and Gregory rifts connect with the Lake Malawi rift, following the meridional trends of the Mozambique mobile belt; the Luangwa rift valley in Zambia follows the trend of the Kibaran orogen, continuing across the Lufillian arc towards the Okavango rift system in Botswana (Fig. 8.5). Volcanism in the EARS is temporally and compositionally varied, and irregularly distributed. In the northern sectors of the EARS, from the Afar to the Ruwenzori mountains in Kenya, the rifts are characterised by Cenozoic to Recent volcanism. In the southern sectors

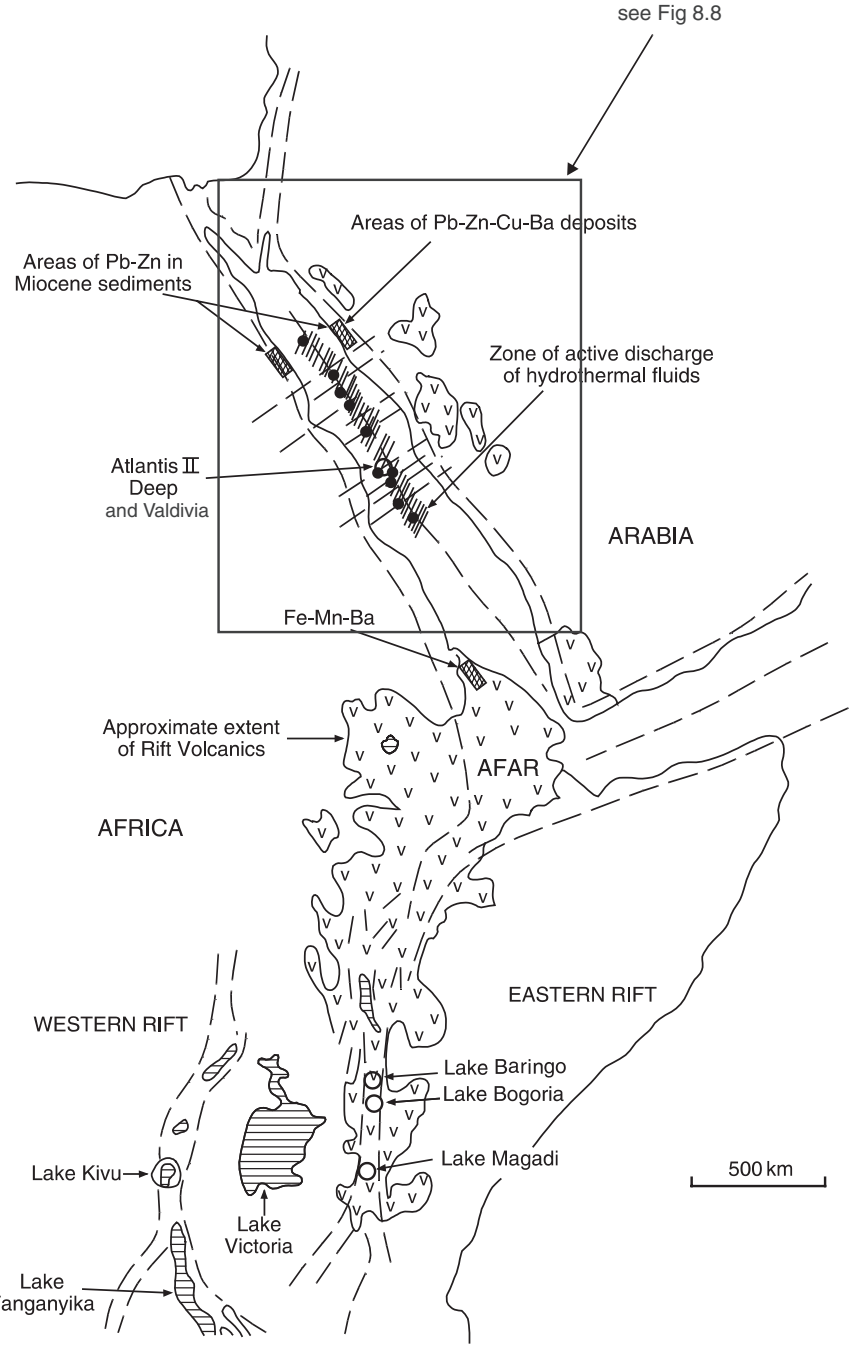


Fig. 8.4 Part of the East African Rift System, showing the Red Sea brine pools, on-land metalliferous deposits and the lakes in the eastern and western branches, where present-day hydrothermal discharges occur. After Pirajno (1992), see also Fig. 8.6

volcanism is limited or altogether absent. The Afar region and the Ethiopian and east African plateaux have the most voluminous volcanism in the form of continental flood basalts and central volcanic complexes. In these areas, the volcanic products can be classified into two associations: alkali basalt and nephelinite. The former includes alkali-olivine basalt, basanite, hawaiite, mugearite, trachyte and rhyolite, whereas the latter includes nepheline-trachyte, phonolite, carbonatite and kimberlite. It appears that in the Ethiopian and eastern rift sectors, volcanism began at about 45 Ma and preceded rifting (Ebinger et al. 2000).

The Afar region is a depression at the triple junction defined by the Red Sea, The Gulf of Aden and the Ethiopian part of the EARS. Barberi et al. (1975) and Barberi and Varet (1978) described aspects of the geology, volcanology and tectonics of the Afar. The Afar Triangle is dominated by predominantly fissure-type mafic volcanism, explosion craters, volcaniclastic deposits, hot springs and playa lakes containing thick evaporite deposits. The apex of the Afar Triangle joins the Ethiopian rift valley, which in turn connects with the Kenyan sector of the EARS. The Afar Triangle is decribed in more detail in Section 8.4.2.

One of the active volcanoes of the Ethiopian rift is Tullu Moje, for which two distinct magma series are recognised. One magma series is K_2O-rich with olivine-bearing basalt, hawaiite and trachyte. The other is K_2O-poor and includes comendite and rhyolite. The Kenyan rift province (eastern branch, comprising the Turkana and Gregory rifts) is characterised by Na-rich rocks, where volcanism started 30 Ma ago and continues to-day. Magmatism in this province shows pronounced time-space variations. In the northern sector nephelinite and carbonatite were emplaced between 24 and 10 Ma, preceded by voluminous eruptions of alkali basalt. This volcanism changed to less alkaline compositions with the development of bimodal products, namely basalt-trachyte volcanoes. During the Pliocene-Pleistocene, on the eastern flank of the rift, volcanism consisted of chains of monogenetic alkali basalt cones, shield-type volcanoes and large central volcanoes, such as Kilimanjaro (the highest peak in Africa at 5894 m above sea level) and Mt Kenya. In the southern sectors of the rift, nephelinite-carbonatite complexes are also present. Further south in Tanzania, is the most famous carbonatite in the world, namely the Oldonyo Lengai volcano, which erupted natrocarbonatite lavas, for the first time providing direct evidence of the existence of a carbonatite melt (Wooley 2001 and references therein).

The Afar region, the Ethiopian and East African plateaux is the general area, where a mantle plume is impinging beneath the continental lithosphere. This is the conclusion reached by Ebinger and Sleep (1998), who on the basis of gravity data and geochemistry of the volcanic products, numerically modelled the dynamics of the Afar-East African mantle plume. An interesting concept proposed by Ebinger and Sleep (1998) is that the effects of the Afar-east African plume might extend along the EARS, to the south, offshore to the Comoros islands, and to the west along the Darfur swell and the Cameroon Line

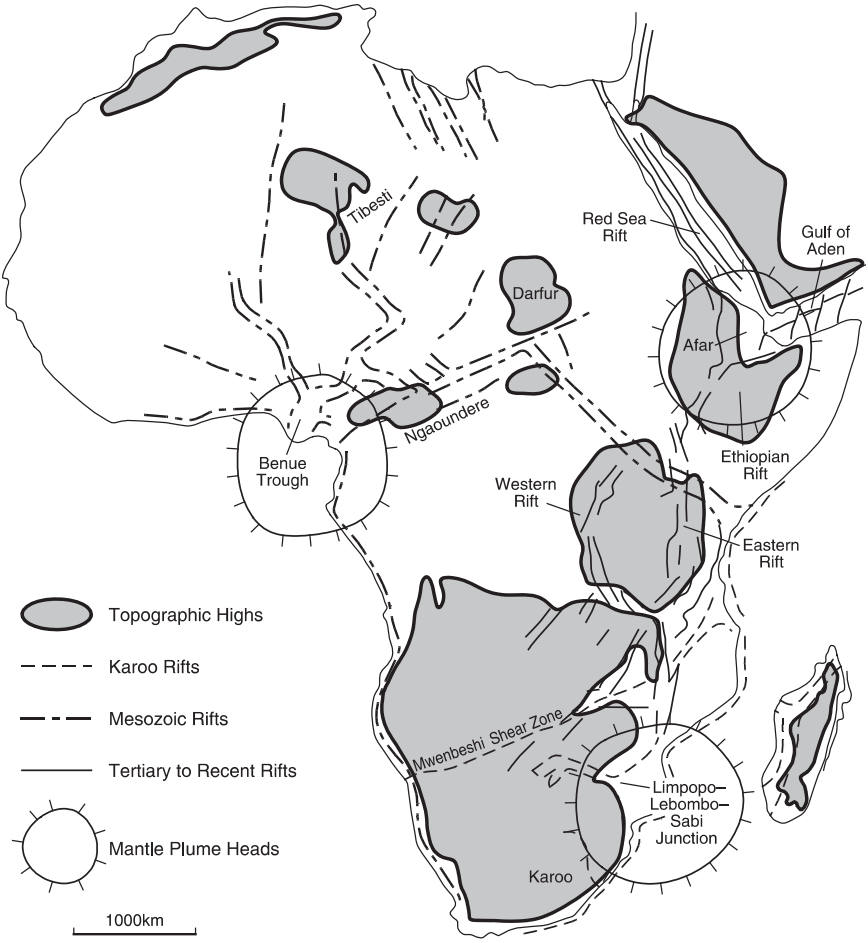


Fig. 8.5 The major Phanerozoic rift systems of Africa: Karoo rifting, associated with the opening of the South Atlantic; Mesozoic rifting in subSaharan and Saharan Africa; Neogen to Recent rifting of the East African Rift System (EARS). Note the spatial association of the rifts with continental scale topographic highs and assumed relationship with mantle plumes. After Pirajno (2000)

(Fig. 8.5). In their model, the authors suggested that the plume head flattens beneath the lithosphere, and flows laterally in zones where the lithosphere is thinner. In this way the behaviour of the plume, in terms of melting, is controlled by pre-existing variations in the thickness of the lithosphere, such as those of the west African Mesozoic rift zones (Fig. 8.5) and along the passive margins of Africa and Arabia. Ebinger and Sleep (1998) proposed that the single large plume model explains the timing of uplift and magmatism in eastern Africa. Rogers et al. (2000), on the basis of Sr, Nd, and Pb isotope systematics

and geochemical data, suggested that the EARS is underlain by two mantle plumes, one beneath the Kenya rift and the other beneath the Ethiopian rift and Afar region.

Many of the lakes of the East African Rift System (Fig. 8.4) are associated with high heat flow, thermal springs and sublacustrine hydrothermal discharges, containing dissolved organic compounds and metal complexes. Colonies of stromatolites, cyanophytes and bacteria are commonly associated with the thermal springs of the EARS, forming flat or fibrous mats (Schlüter 1997). Hydrothermal carbonate chimneys, up to several tens of metres high are present in some of the lacustrine environments. Terraces of travertine material are found between thermal springs and lakes in fluvial environments (Schlüter (1997). The hydrothermal environment of the East African lakes represents a possible present-day analogue for some of the stratiform/stratabound oxide and sulphide deposits in the geological record (Tiercelin et al. 1993 and Section 8.4.1). Studies of the East African lakes include those of Eugster (1986), Renaut et al. (1986, 2002), Tiercelin et al. (1991) and Pflumio et al. (1994). Robbins (1983) reviewed present-day hydrothermal systems in rift lakes. Schlüter (1997) reviewed hot springs, fumaroles and the East African lakes. Discharge of hot, saline and metalliferous solutions occurs in Lake Kivu, Lake Bogoria and Lake Magadi (Fig. 8.4), with temperatures ranging from 34°C to near boiling point at 97°C. Most of these thermal springs have alkaline chemistry, with pH varying from 7.8 to 9.9, and some are the source of trona deposits (Schlüter 1997). Degens and Kulbicki (1973) estimated that approximately 60 000 t of Cu, 270 000 t of Pb and 60 000 t of Zn have accumulated in Lake Kivu in about 5000 years.

Lake Magadi is an ephemeral alkaline lake, where hydrous Na silicates, such as trona and magadiite, are precipitated (Eugster 1986). The mineral magadiite ($NaSi_7O_{13}(OH)_3 \cdot 3H_2O$) is of special interest because it forms layers which grade along strike into bedded cherts. The mechanism of replacement of the magadiite by microcrystalline silica is, in the view of Eugster (1986), related to dehydration and groundwater leaching of Na. Hot springs in Lake Magadi have temperatures of about 86°C, and are enriched in Na, HCO_3^-, Cl, K, SO_4, F, SiO_2, P and B. Total dissolved solids (TDS) range form 10 000 to 35 000 ppm. Hot springs discharge into lagoons forming brine pools and precipitating silica gels. The brine pools also contain varicoloured bacteria and cyanobacteria, which give rise to black organic muds (Baker 1986). The environment of Lake Magadi has been compared to some evaporitic sequences in the ancient geological record, such as the HYC shale of the McArthur River ore systems in Australia (Eugster 1986; discussed in Section 8.7.1).

Renaut et al. (1986) investigated mineralisation in the sediments of Lake Bogoria, a saline and alkaline lake in a deep half-graben of the Kenyan rift. Lake Bogoria is fed by surface waters and approximately 200 hot springs, which are located along its shores and the floor of the lake. The lake's waters of the lake contain Si, F, Na, HCO_3 and Cl. There are two types of hot springs: low and high temperature. The former (34–48°C) have solute concentrations of about 1.0 g/l. High-temperature springs (64–98°C) have solute concentrations

ranging from 4 to 15 g/l. The origin of the hot springs is due to lake water that percolates downward through fissures and is heated by hot volcanic gases (mainly CO_2). Spring deposits consist of mounds and crusts of travertine (essentially aragonite and low-Mg calcite), which is deposited by removal of CO_2 from oversaturated solutions. This travertine is locally covered by 4 000 year old stromatolites and algae. Also present in the hot springs are white gelatinous suspensions of colloidal silica, which result in the deposition of opaline silica crusts. Other precipitates include magadiite and fluorite. Rocks around the springs are hydrothermally altered (pyrolusite, opaline silica, quartz, smectite, illite, zeolite). Iron oxide deposits are forming at water depths of less than 250 m in Lake Malawi (Müller and Förstner, 1973). These deposits consist of limonite, nontronite, vivianite (a Fe-phosphate) and opaline silica that precipitate from the discharge of hot solutions at the oxic-anoxic boundary zone. The occurrence of recent iron-formations in a rift-related lake is interesting because it may point the way to a closer understanding of Proterozoic banded iron-formation, to be discussed in Section 8.9.

Renaut et al. (2002) also studied sublacustrine sinter diatomaceous deposits along the shorelines of the Ol Kokwe volcanic island in Lake Baringo, just north of Lake Bogoria. Present day hot springs (Soro springs) on the eastern margin of the Ol Kokwe volcanic island, discharge Na-HCO_3-Cl waters with salinities of about 3 g/l^{-1} in TDS and a pH of 8.7, originating from a deep reservoir of lake water and groundwater with an estimated temperature of 180°C. The Ol Kokwe is a multivent volcano that comprises basalt, mugearite and trachyte lavas and scorias, erupted about 175 000 years ago. The Soro hot springs have a temperature range from 81 to 96°C and are locally associated with fumaroles and mud pots, with extensive hydrothermal alteration, mostly clay minerals, gypsum and native sulphur. Renaut et al. (2002) observed that this thermal activity is subject to rapid changes with time. Sublacustrine sinters were formed by thermal springs discharging on the floor of the lake and are of three types, all with well-preserved diatoms: (1) massive and structureless; (2) pore-lining silica, and (3) laminated crusts. Morphologically these form small mounds or chimneys with precipitates around the vents, both on the floor and in the surrounding sediments. Silica-rich fluids rise from depth and cool conductively until they become supersaturated when in contact with the cooler dilute lake waters. The actual state of the silica precipitates is not clear, but it is thought that it may very soft and possibly gelatinous. Filamentous cyanobacteria and microbial mats, together with other micro-organisms constitute most of the organic matter associated with the silica sinters. The origin of the thin silica laminations is ascribed by the authors to alternating gelatinous and structureless silica precipitated from the thermal waters and the colonization of the siliceous substrate by microbial mats. Renaut et al. (2002) pointed out some important differences that exist between subaerially and subaqueoulsy precipitated sinters. The former commonly have microbial crusts and have low preservation potential in the geological record. These authors observed the almost complete distruction of these crust in the time span of only two years.

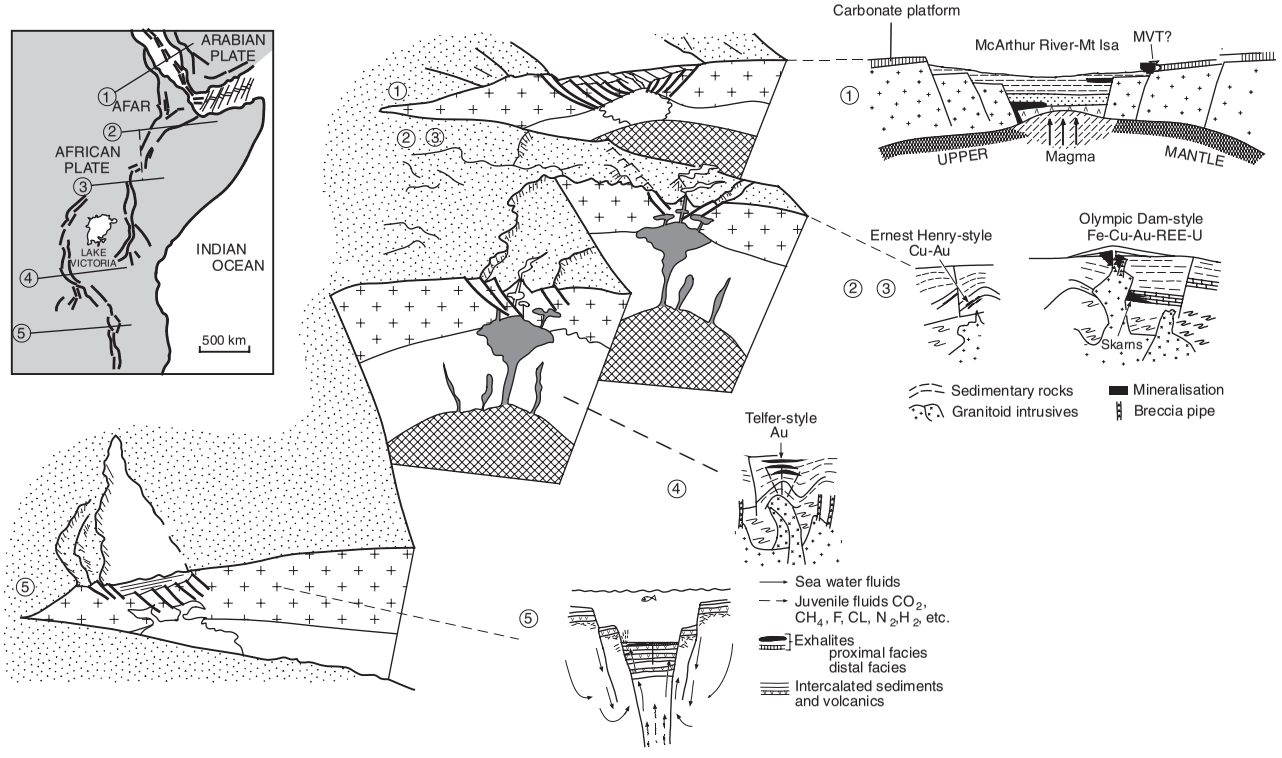


Fig. 8.6 Schematic illustration of the East African Rift System and hypothetical ore systems that may be associated with it. (1) the advanced Red Sea rift, where oceanic crust is being emplaced and where pools of brines and sulphides are actively forming; (2) and (3) represent a continental rift with anorogenic alkaline magmas at depth, from which magmatic and hydrothermal deposits of the Fe oxide-Cu-Au style may be forming (names of deposits in the figure refer to well-known Australian examples). (4) represents a rift system with a deep lake in which sediments and volcanic materials accumulate together with subaqueous exhalites. (5) also a rift-lake system, where sediments are organic-rich and where subaqueous hydrothermal venting occurs. After Pirajno (2007a)

The sublacustrine sinters, on the other hand, have high preservation potential, with the silica undergoing diagenesis to quartz and chalcedony. Important too is the fact that these deposits in the geological record could resemble silcretes. Pirajno and Grey (2002) investigated cherts in the Palaeoproterozoic Yerrida Basin (Western Australia) and using REE geochemistry and detailed petrography, were able to recognise an origin by thermal springs in a lacustrine rift environment.

Taken in terms of a "big picture", the EARS and the northward extension represented by the Red Sea (Section 8.5) may represent the ideal environment possessing all the necessary ingredients for a wide range of magmatic-hydrothermal and hydrothermal ore systems. Current and hypothetical ore systems that may be associated with the EARS and the Red Sea are shown in Fig. 8.6. It is important to consider the large-scale regional context in the understanding of mineral systems because this provides insights into the geodynamic environment of ore formation and, importantly, facilitates exploration targeting.

8.4.1 Lake Tanganyika

Lake Tanganyika is in the western branch of the EARS (Fig. 8.4). In the northern part of the lake, hydrothermal activity occurs both on and off-shore. In this region, Tiercelin et al. (1991, 1993) and Pflumio et al. (1994) studied three hydrothermal fields, Pemba, Cape Banza and Cape Kalamba, where hydrocarbons, sulphide and carbonates are being deposited.

Lake Tanganyika has a complex geological structure. It consists of northern and southern basins that can be further subdivided into seven sub-basins. These basin and sub-basin structures are controlled by a complex system of faults. In the northern basin high heat flow was recorded with values of up to 320 mW m^{-2}. This high heat flow is related to magmatic activity below the floor of the lake. The waters of Lake Tanganyika are stratified with the transition between oxic and anoxic layers at water depths ranging from 50 to 100 m in the north, to 240 m in the south. About 90% of the bottom waters are anoxic, and as a result the bottom sediments, which reach a thickness of up to 6 km, have high total organic carbon (TOC) content of up to 12%. In addition, the anoxic layers have significant amounts of CO_2, H_2S, CH_4 and He. The high heat flow induces maturation of the organic matter and the formation of hydrocarbons, as revealed by oil seepages at Cape Kalamba.

Hydrothermal activity at Pemba and Cape Banza is characterised by gas emanations (mainly CO_2 and CH_4) and discharge of thermal waters on land and under water. At Pemba, an underwater hydrothermal field extends for 180 m and is 80 m wide to a depth of 45–50 m. In the Pemba field there are kaolinite-rich layers and stockworks of quartz-pyrite that cut through the basement rocks. Blocks of massive marcasite and pyrite are associated with quartz, barite and kaolinite. Hydrothermal fluids discharge through several vents, at

temperatures ranging from 60 to 90°C. The vents are surrounded by mat-forming microbial communities. At Cape Banza, the hydrothermal field, with more than 70 active vents, covers an area of 300 × 40 m to a water depth of 6 m, where a littoral plateau contains several active vents, or groups of vents, each with aragonite chimneys. The vents consist of chimneys of various sizes, mostly made up of aragonite, emitting fluids with temperatures between 50 and 103°C and flow rates of 1–3 litres per second. The Banza chimneys are coated with

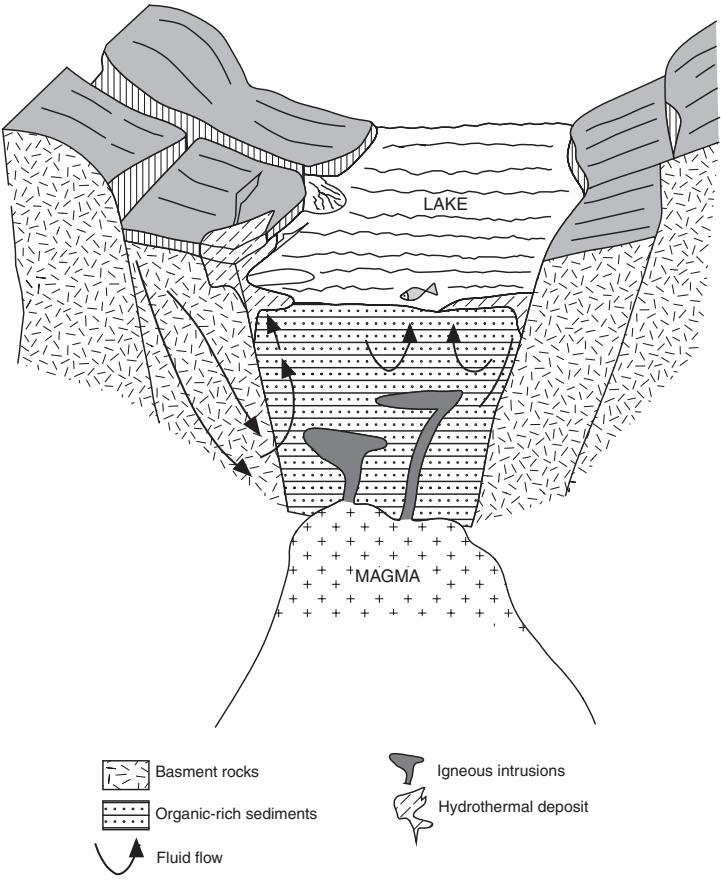


Fig. 8.7 Model of hydrothermal circulation in the northern part of Lake Tanganyika; the thick sediment pile is rich in organic material and largely anoxic, high heat flow within this pile of sediments is probably related to igneous intrusions, or a subjacent magma chamber. The high heat flow results in maturation of organic matter and production of hydrocarbons; hot fluids circulate through the sediments and along the walls of the rift and discharge at the surface as hot springs depositing sulphides, Fe oxides, clays and barite. Sulphide deposition is likely to occur also within the sedimentary pile, owing to their rich organic content. The model is based on Tiercelin et al. (1989)

filamentous algal mats; pyrite forms films and encrustations on fractures and along the channels through which the fluids circulate. On land, fossil hydrothermal activity resulted in the deposition of Fe oxides, quartz and kaolinite veins. Analyses of the hydrothermal fluids revealed that there are two end-members: a Na-HCO_3 type (Pemba site) and a Na-Cl type (Cape Banza site). The isotopic ($\delta\ ^{18}O$, $\delta\ ^{2}H$ and $\delta\ ^{13}C$) composition of these fluids suggests that they are of magmatic origin, but have interacted with meteoric and lake waters. A model illustrating the hydrothermal system of the northern Lake Tanganyika is shown in Fig. 8.7.

8.4.2 The Afar Triangle

The best modern example of a triple junction is the Afar Triangle in the horn of Africa (Figs. 8.4 and 8.5) ((Beyene and Abdelsalam 2005; Yirgu et al. 2006). The Afar is a depression at the rift-rift-rift triple junction defined by the Red Sea, the Gulf of Aden and the Main Ethiopian Rift, which is part of the EARS (McConnell 1972; Mohr 1978; Wolfenden et al. 2004). The Afar Triangle is the triple junction that marks the transition between the continental and oceanic rifts (Red Sea and the Gulf of Aden) of the EARS (Fig. 8.4). The Afar has a very special place in the evolutionary history of humans, because the geological and fossil records show that the speciation of hominids, which culminated with the advent of *Homo Sapiens,* was after all the result of the tectonic and environmental forcing at about 3.0–2.0 Ma that affected the Afar region and the branch of the main Ethiopian rift (Kimbel 1995; Redfield et al. 2003). The Afar is the birth place of humans (see also Reed 1997). The Afar depression is part of a large dome feature, about 1000 km across, that was uplifted as a result of the impingement of the Afar mantle plume, associated with the eruption of up to 2 km thick succession of flood basalts (Sengör 2001). This uplift, which elevated the Ethiopian plateau to about 2.5 km a.s.l., eventually led to the collapse of the region that now forms the Afar depression at about 24 Ma, with the Danakil block separating from the Nubian plate at about 20 Ma (Beyene and Abdelsalam 2005). The Afar depression and its continuation to the southwest into the Main Ethiopian Rift, split the original dome structure (Ethiopian plateau) into the present-day northwestern and southwestern plateaux. The Afar depression itself is defined by the Western Escarpment of the Ethiopian Plataeu and Main Border Fault at the western margin of the Somali Plateau (Keranen and Klemperer 2007). The Main Ethiopian Rift itself is a complex active system, which developed as a result of rift propagation controlled by lithospheric structures and in a second stage by magmatic processes, or magma-assisted rifting (Keranen and Klemperer 2007).

The Afar region has experienced almost continuous volcanic activity at least since 30 Ma and is characterised by tholeiitic volcanism, dyking, hot springs and playa lakes with thick evaporite deposits (Barberi and Varet 1978). Barberi and

Varet (1978) recognised three stages of magmatic activity in the Afar region. The first was a continental rift stage in the lake region of the Ethiopian rift, where basaltic lavas issued from fissure systems; felsic volcanic centres were restricted to the intersection of the main rift trend with transverse lines of weakness. The magmas of this first stage were alkaline and light REE enriched. The second stage occurred in southern Afar and at the northern termination of the Ethiopian rift, and was characterised by volcanic activity along narrow grabens. Fissure basaltic activity (flood basalts) dominated with central volcanoes becoming less common, and the magmas being moderately enriched in light REE. The third stage was the development of a proto-oceanic spreading structure in northern and central Afar. This was characterised by a narrow rift valley with fissure-fed tholeiitic volcanism, with a REE pattern of chondritic affiliation. The oceanic rift in the Gulf of Aden, where oceanic crust continues to form today, is the final stage. Dyking appears to be an important factor in the rifting process, as deduced from satellite data and three-dimensional deformation studies (Wright et al. 2006). These studies suggested that magmas under the active Gabho and Dabbahu volcanoes flowed horizontally for about 60 km, at depths of 2–9 km, resulting in faulting and displacing adjacent plates by 2–4 m in opposite directions, in less than a week (Wright et al. 2006). The Afar region is dominated by fissure-type mafic volcanism, explosion craters, volcaniclastic deposits, numerous hot springs, salt and playa lakes with thick sequences of evaporites. In the norhern Afar, hydrothermal activity is related to active volcanism and is manifested by fumaroles and hot springs that discharge along faults. Several of the salt lakes are fed by hot springs, such as the 100-m-deep Lake Giulietti, where springs along its shores have temperatures of about 40–50°C. These warm and saline waters probably derive their salinity from interaction with evaporite deposits in the region (Marinelli 1971). In this same region there are belts of fossil coral reefs and other marine deposits, indicating several stages of marine transgressions. Here, Fe-Mn-Ba deposits of hydrothermal origin are present and were formed during the last 200 000 years (Bonatti et al. 1972). The Fe-Mn-Ba deposits consist of massive Mn-oxide-rich beds aggregating about 2 m in thickness. Ore minerals include pyrolusite, manganite, rhodocrosite, strontiobarite, barite and celestite. Bonatti et al. (1972) proposed that the deposit was formed by submarine discharge of Fe-, Mn-, Ba- and Si-rich fluids.

8.5 Red Sea Brine Pools

The Red Sea is a proto-oceanic basin, is part of the African-Arabian rift system, which includes the East African Rift System (EARS), and extends for about 2000 km along a north-northwest direction, forming a relatively narrow depression between the Arabian and African plates (Figs. 8.4 and 8.5). To the north, the Red Sea splits into two smaller rifts, Gulfs of Akaba and Suez, whereas to

the south it connects with the Gulf of Aden, through the shallow Bab el Mandeb Strait. The Red Sea rift is bordered by uplifted margins, up to 2000 m high, of the Precambrian terranes on the Egyptian side and the Arabian peninsula. The rift began its development during the Oligocene (32–28 Ma), by continental thinning above a mantle plume beneath the Afar depression. Active seafloor spreading occurs in the Gulf of Aden. Rifting was followed by magmatism and seafloor spreading, which led to the formation of oceanic crust in a number of places. During the Miocene, high evaporation rates resulted in the development of evaporite deposits, which are thought to have contributed to the formation of the brines in the Red Sea depressions. Details on the geological and tectonic evolution of the Red Sea rift system can be found in Bonatti (1985), Bayer et al. (1989), Bohannon (1989) and Ghebread (1998). As mentioned above, the Red Sea is an example of advanced stages of continental rifting, and is an ocean basin in its early stage of development (see Fig. 8.1).

Volcanism associated with the Red Sea rift is alkaline, peralkaline and tholeiitic. Alkaline and peralkaline volcanism occurred mainly during the early phases of doming, uplift and rifting. Tholeiitic volcanism forms a Trap series, which extends over an area of some 700 000 km^2 and reaches a thickness of 3 km. The distribution of the volcanic rocks is somewhat asymmetric with respect to the rift axis, being concentrated in the Afar region and on the Arabian side. This asymmetry is explained by a shallower asthenosphere beneath the Arabian plate (Bayer et al. 1989). The flank areas on either side of the rift are covered by continental clastic sediments, evaporites and interbedded marine sediments of Miocene age. Based on sea-floor morphology and the nature of its crust, the Red Sea is subdivided into northern, transitional, multi-deep and rift-valley regions (Fig. 8.4). Oceanic crust is present in the rift valley region, the rest being underlain by transitional and thinned continental crust (Bonatti 1985). This, combined with the history of sedimentation and volcanism, confirms propagation of the Red Sea rift in a northerly direction.

The Red Sea brine pools, such as Atlantis II Deep, were first reported in 1948 and subsequently studied in detail by Bischoff (1969), Degens and Ross (1976), Shanks and Bischoff (1980), Pottorf and Barnes (1983), Zierenberg and Shanks (1983), Anschutz and Blanc (1995, 1996) and Pierret et al. (2001). Gurvich (2006) gave a detailed review of the geology, geochemistry and mineralogy of the Red Sea metalliferous sediments and brines. These works, in addition to specific citations, provided the information reported in this section. There are more than 20 Red Sea deeps, but not all contain brines and metallifeorus sediments. The distribution of the more important deeps is shown in Figs. 8.4 and 8.8, with some of the best studied being: Atlantis II, Suakin, Port-Soudan, Chain, Valdivia, Tethys and Nereus (Pierret et al. 2001). Base metal deposits are present on shore and are probably situated along the on-land continuation of transform faults. Several of the active geothermal brine pools are located at the intersection of transform faults with the axial zone of the rift, as shown in Fig. 8.8. The brines exhibit considerable variations in their chemistry, temperature, and the mineralogy of the metalliferous sediments. These brines have

different salinity and compositions from normal Red Sea water, with Mg^{2+} and SO_4^{2-}, being strongly depleted, but typically the brines tend to have high concentrations of dissolved Fe, Mn, Zn, Cu, Pb, Co, Ba, Li and Si. Selected details of Red Sea metalliferous sediments and brines are given in Tables 8.4 and 8.5. The metalliferous sediments of the pools (or deeps) have highly variable compositions and complex mineral associations. Some of the more common minerals include Fe oxides and oxyhydroxides (goethite, hematite, magnetite, lepidocrocite, maghemite), Fe and Mn carbonates (e.g. siderite, rhgodocrosite), Mn-oxyhydroxides (e.g. todokorite), sulphates (barite, gypsum, anhydrite) and abundant sulphide species (pyrite, greigite, sphalerite, chalcopyrite). Massive sulphides are present in the Kebrit Deep and consist of pyrite, marcasite, sphalerite and galena (Botz et al. 2007). It is useful to bear in mind the complexity and variability of the Red Sea metalliferous sediments, when evaluating a province of sedimentary-hosted (e.g. SEDEX type) mineral systems. The message to explorationists is that in spite of this complexity, the various, seemingly unrelated mineral occurrences/deposits, may in fact all belong to the same setting and system.

Pierret et al. (2001), on the basis of geochemical and isotopic data, suggested that the formation of the brines is probably the result of two main processes: (1) alteration of oceanic crust by sea water; and (2) chemical dissolution of the thick Miocene evaporites by circulating sea water. Interaction of sea water with hot oceanic crust results in hydrothermal fluids with high concentrations of Li, K, Rb, Ba, Si, Ca, Sr, Mn, Fe, Zn and Cu, but with SO_4 and Mg concentrations that decrease almost to zero. Above 150°C, anhydrite precipitation removes most of the SO_4 from sea water, whereas the removal of Mg from sea water produces smectite clays and chlorite at higher temperatures. Details of sea water-oceanic crust interaction and resulting fluids and hydrothermal minerals are given in Chapter 7. The interaction with evaporitic minerals such as gypsum, halite, anhydrite and magnesite, well explains the high salinities and enrichements of the brines in Ca, Na, Cl, Mg and SO_4 relative to se water. Pierret et al. (2001) used Zn/Cl and Fe/Mn ratios to differentiate between the oceanic and the evaporitic hydrothermal systems. High temperature hydrothermal circulation through basaltic rocks results in high Zn concentrations and hence high Zn/Cl ratios. By contrast, evaporite leaching has larger concentrations of Cl, resulting in lower Zn/Cl ratios. Similarly high Fe/Mn ratios reflect high temperature interaction with oceanic crust. Zinc/Cl ratios for Atlantis II Deep average 7.59, whereas those for the Suakin and Valdivia deeps are 0.93 and 1.15 respectively. The presence of SO_4 in the brines is derived from a combination of evaporite dissolution and oxidation of organic matter. Oxidation of organic matter occurs in the presence of sulphate-reducing bacteria, in which the sulphate ions replace oxygen as electron acceptor, according to a reaction of the type:

$$2CH_2O + SO_4^{2-} \Leftrightarrow HCO_3^- + H_2S$$

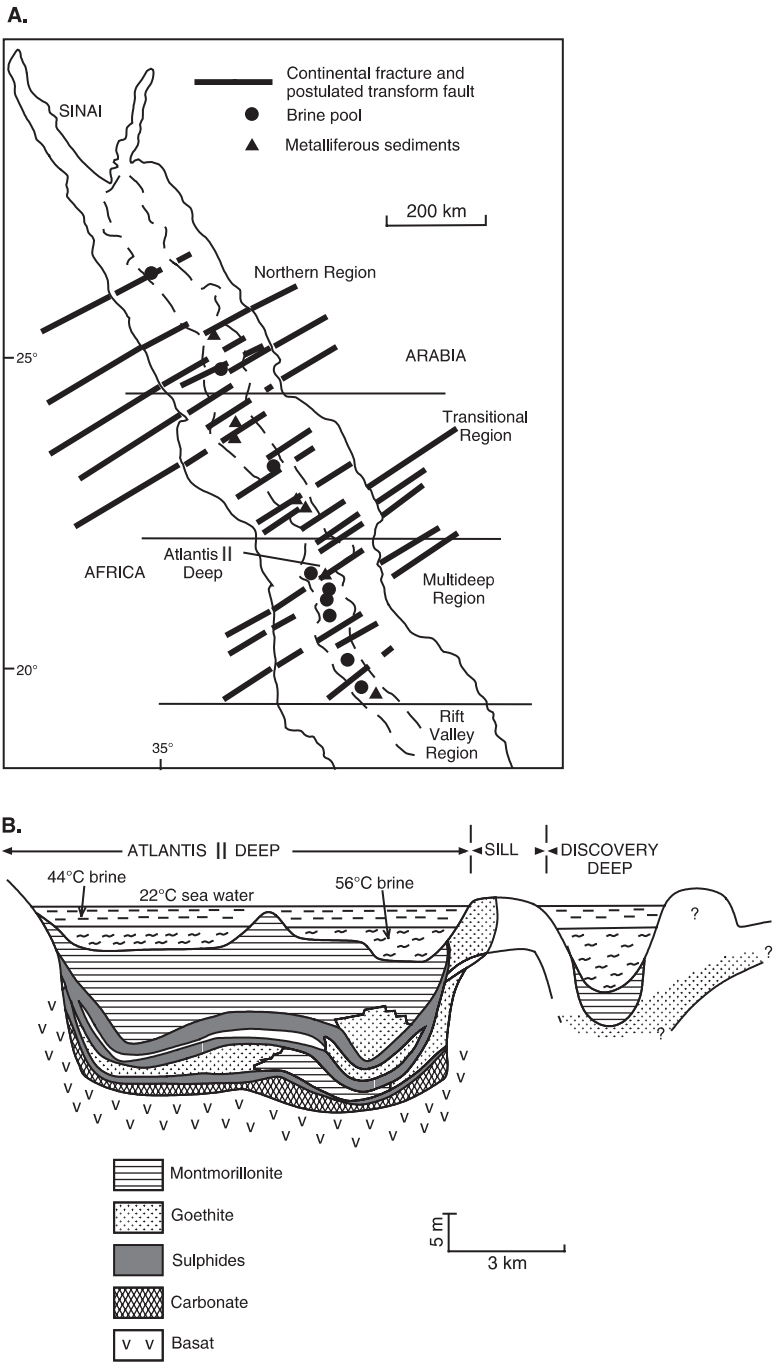


Fig. 8.8 (continued)

Table 8.4 Depth, thickness and temperatures of brines and average metal contents of selected Red Sea metalliferous sediments. After Gurvich (2006 and references therein)

Name of Deep	Maximum depth (m)	Maximum brine thickness (m)	Fe wt%	Mn wt%	Zn wt%	Cu wt%	Approx. maximum recorded temperature (°C)
Suakin SW	2850	74	6.4	1.4	0.067	0.0078	23–24
Suakin NE	2830	54	9.7	1.92	0.14	0.011	24.6
Port Soudan	2800	286	5.9	0.40	0.055	0.0086	36–36.2
Erba	2395	19	14.5	0.64	0.078	0.033	28
Shagara	2496	8	7.4	3.1	0.053	0.009	??
Albatross	2133	72	19.6	0.35	0.054	0.019	24.4
Chain A	2072	83					52–53
Chain B	2130	140					45–46.7
Discovery	2237	179	23.7	2.11	1.34	0.33	44.7–51
Wando W	2013	28	14.5	1.7	0.17	0.03	24
Valdivia	1673	123	4.5	0.3	0.024	0.0076	30
Atlantis II	2170						
AM		29–31	33.6	0.70	2.3	0.488	41–56
SU2			26.3	0.88	5.07	0.84	
CO			34.3	4.67	0.475	0.205	
SU1			33.1	1.77	3.49	1.09	
DOP			22.7	0.14	0.92	0.37	
Lower brine layer		122					56–67
Atlantis	1960	No brines	31	0.4	0.09	0.015	
Kebrit	1573	84	No analytical data, but massive sulphides are present				23
Hadarba	2200	No brines	6.3	1.3	0.057	0.012	
Tethys NE	1800	No brines	28.3	10.6	0.37	0.082	
Nereus E	2458	39	7.6	1.7	0.066	0.019	30
Vema	1611	No brines	10.5	0.29	0.025	0.0025	
Gypsum	1196	No brines	39	0.36	0.16	0.089	
Red Sea background sediments			3.5	0.41	0.032	0.0071	

This is the dominant mechanism for the production of H_2S in anoxic basins, as further discussed in Chapter 10. Organic-rich sediments are common in the Red Sea brine pools, as is the case for the Shaban and Kebrit deeps, in the

Fig. 8.8 (continued) (**A**) Distribution of brine pools and metalliferous sediments in the northern and central Red Sea region; note that the brine pools tend to be situated along the intersection of the axial rift with continental fractures and their continuation as transform faults (after Bignell 1975; Sawkins 1990; Bonatti 1985). (**B**) Schematic cross-section of Atlantis II Deep (after Bischoff 1969; Sawkins, 1990)

Table 8.5 Average composition of Red Sea brines, after Pierret et al. (2001)

	Suakin	Port Soudan	Atlantis II	Chain	Valdivia	Nereus
pH	7.85	6.43	5.21	6.48	6.21	7.43
Na mol/l	2.48	3.79	4.88	4.81	4.13	3.74
Cl mol/l	2.76	4.04	5.37	5.17	4.59	4.35
K mmol/l	38	49	69.9	66.8	52	80.2
Ca mmol/l	56.1	33.52	146.3	143.3	25	237.7
Rb μmol/l	8.2	6.7	25.3	25.1	3.1	31.1
Mg mmol/l	72.2	64.6	32.8	36.8	95.3	80.4
SO_4 mmol/l	33.3	44	6.7	8.5	72	7
Fe mmol/l	0.007	0.107	1.4	0.02	0.13	0.06
Mn mmol/l	0.48	0.12	1.52	0.71	0.06	0.94
Li μmol/l	45.7	106	563.4	429	98.1	168.7
Ba μmol/l	1.1	1.6	15.3	5.3	0.5	4.5
Cu μmol/l	0.5	4.1	3.8	6.9	Below det.	12
Zn μmol/l	2.6	4.7	41.6	9.9	Below det.	18.4

northern Red Sea, where hydrocarbons impregnate massive sulphides, which occur together with kerogen and other organic compounds (Botz et al. 2007).

8.5.1 The Atlantis II Deep

The Atlantis II Deep is the best studied of the brine pools, and so far is the only one with economic potential. Details of the Atlantis II Deep can be found in Gurvich (2006 and references therein). The Atlantis II Deep, as defined by the 2000 m isobath, is 14 km long and about 5 km wide and contains approximately 5 km^3 of density-stratified brines, which are actively accumulating through the discharge of hydrothermal solutions. The Deep is subdivided into a number of basins separated by sills, namely north and south basins, separated by the northern sill, west and east basins, separated by a central sill and a southwest basin. The Atlantis II brines are stratified with an upper and a lower layer and variable thicknesses of metalliferous muds. The lower brine is about 150 m thick, has high salinity and a temperature of 60°C; the upper brine is 50 m thick and has lower salinity and a temperature of 50°C. The lower brine is in contact with the metalliferous sediments, which in turn rest on basaltic rocks. The temperatures of the hydrothermal fluids that enter the Deep are variably estimated to range from approximately 210°C to as high as ~450°C. The brines have high concentrations of Fe, Mn, Zn, Cu, Pb, Co, Ba, Li and Si, with the lower layer being considerably richer than the upper layer.

The resources of the Atlantis pool are estimated to be about 91 Mt (dry salt-free basis), containing 2.06% Zn, 0.46% Cu, 41 ppm Ag and 0.512 ppm Au (Laznicka 2006). A generalised cross-section of the Atlantis II Deep is shown in Fig. 8.8. Syngenetic mineralisation forms the main part of the Atlantis II Deep with its bedded, laminated varicoloured metalliferous muds, which are

approximately 20–25 m thick. Epigenetic mineralisation is present in the southwestern part of the Deep, where it forms fissures filled with anhydrite, talc, smectite, pyrite, sphalerite and chalcopyrite. Pottorf and Barnes (1983) divided the metalliferous sediments into lithostratigraphic facies, as described here.

A basal detrital facies of unstratified and unconsolidated carbonate-rich sediment, approximately 2 m thick: the carbonate-rich material of this facies consists of coarse, crystalline, buff-coloured rhodocrosite, manganosiderite, siderite with quartz, feldspar and halite. A bedded sulphide facies, mostly composed of black homogeneous material, includes mainly sphalerite, lesser chalcopyrite galena and pyrite and locally barite and anhydrite. There are three sulphide layers (Fig. 8.8): a lower layer about 10 cm thick, a middle layer (about 50 cm thick) and an upper layer (about 2 m thick). Between the sulphide layers are oxide or goethite facies, which can reach a thickness of 4 m. The main mineral components of this facies are poorly crystalline goethite and amorphous limonite. Lepidocrocite and hematite are commonly mixed with goethite; black crystalline magnetite is locally present. White massive beds of anhydrite, up to 20 cm thick, are present both within the Fe-montmorillonite and the sulphide facies. Fifteen to 50 cm-thick beds of manganite are present locally in the goethite facies, and are in places associated with todokorite. In an earlier and detailed work, Bäcker and Richter (1973) subdivided the Atlantis II layers into five lithostratigraphic zones, from oldest to youngest (see also Table 8.4): (1) detrital oxide-pyrite zone (DOP); (2) lower sulphide zone (SU1); (3) central oxide zone (CO); (4) upper sulphidic zone (SU2); and (5) amorphous siliceous zone (AM). These authors recognised additional lithostratigraphic zones in the southwest basin, as follows: sulphidic-oxide-anhydrite zone (SOAN), overlain by an oxide-anhydrite zone (OAN) and a sulphidic-amorphous-siliceous zone (SAM). The abundance of sulphides in the sulphidic zones differs in each of the basins; for example pyrite is the main sulphide in the SU1 of the western, eastern and northern basins, with chalcopyrite and sphalerite being less abundant. In the southern basin sphalerite is the most abundant sulphide with chalcopyrite occurring in small amounts. In addition, other mineral phases that may accompany the sulphides include Fe-Si gel manganosiderite minerals, hematite, anhydrite, authigenic silicates, barite and lesser atacamite.

The S isotopic composition of sulphides in the SU1 ranges from $\delta^{34}S$ 0.75–7.93‰. The SU2 zone contains abundant sphalerite with lesser pyrite as well as X-ray amorphous sulphide minerals and Fe-Mn carbonates, anhydrite, gypsum and barite. In the southern basins there are more complex assemblages, comprising X-ray amorphous sulphides, sphalerite, pyrrhotite, pyrite, chalcopyrite and Cu-sulphosalts. Also present are anhydrite and gypsum. In the SU2 zone the values of $\delta^{34}S$ average +7‰. The oxide zones typically contain Fe oxyhydroxide, Mn-oxyhydroxide, manganite, todorokite and X-ray amorphous Mn-hydroxides. In addition, detrital biogenic material may be locally abundant. The amorphous silicate zone (AM), which overlies the SU2 zone, mainly consists of amorphous Fe-hydroxides and silica and the $\delta^{34}S$ values of sulphide sulphur in the AM zone range from 3.4 to 9.8‰. The precipitation of

Fe and Mn oxyhydroxides in the upper layers of the brines requires oxidation of Fe^{2+} to Fe^{3+} and of Mn^{2+} to Mn^{4+}. The redox potential is higher for Mn^{2+} to Mn^{4+} than for the oxidation of Fe^{2+} to Fe^{3+}, for this reason Mn^{4+} oxyhydroxide minerals tend to accumulate in more oxygenated areas above the brine pool or in more elevated areas on the periphery of the Deep. The effects of Mn^{4+} in the brine system are interesting. Manganese oxides and hydroxides scavenge trace elements from sea water, which are then co-precipitated with the Mn oxyhydroxides and/or sorbed by them. Subsequent dissolution of the Mn oxyhydroxides releases these trace elements in the upper brine layer. It appears that Fe^{3+} hydroxide minerals have the same effect. The formation of Si-Fe gels seems to be widespread, resulting in their great abundance not only in the Atlantis II pool, but also in other pools of the Red Sea. These Si-Fe phases not only contains Fe^{3+}, but also Fe^{2+} ions, which enter by a process of sorption and/or scavenging of Fe^{2+} by particles of Fe^{3+}-oxyhydroxides and silica. These processes result in the crystallisation of mineral phases such as, celadonite and mixed layer nontronite-celadonite. A scheme of the processes, according to Butuzova (1998, cited in Gurvich 2006), that precipitate the various mineral species in the Atlantis II Deep is shown in Fig. 8.9)

The configuration of the hydrothermal system of the Deep is depicted in Fig. 8.10. Isotope systematics suggest that the hydrothermal fluids originate as palaeo-sea water, which percolates through the evaporite deposits on the shoulders and floor of the rift basin. Leaching of the evaporite minerals (anhydrite and halite) results in high salinity of the fluids. The palaeowater is heated by the high local heat flow, and by virtue of its Cl content acquires potential for metal complexing. As this water comes into contact with the recent basalts in

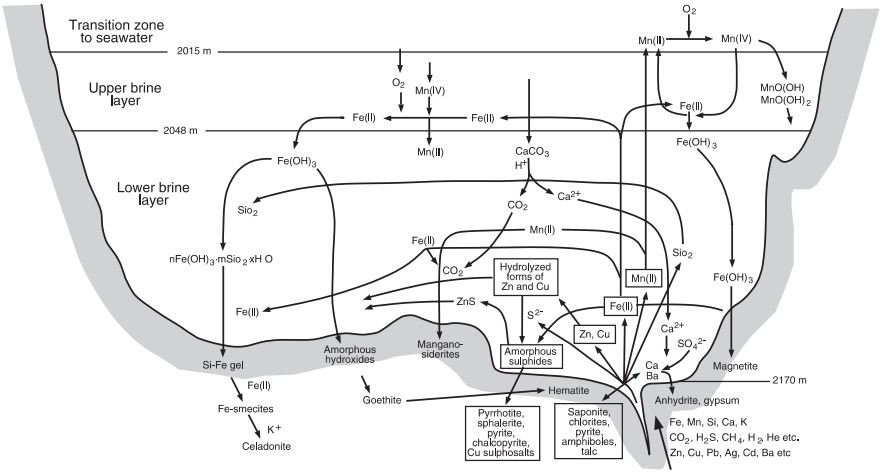


Fig. 8.9 Mineral-forming processes and pathways in the Atlantis II Deep; see details in text. After Gurvich (2006; based on Butuzova 1998)

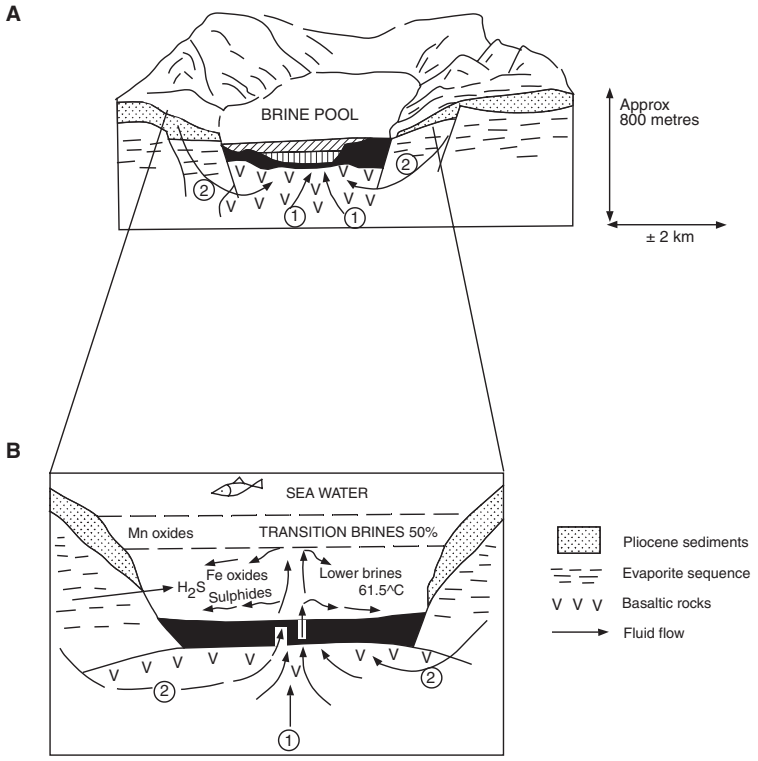


Fig. 8.10 Schematic illustration showing: (**A**) main topographic features of an Atlantis II type brine pool area of the Red Sea and (**B**) detailed cross-section of brine pool, its density, stratification and fluid flow. Numbers (1) and (2) explained in text. After Pottorf and Barnes (1983)

the axis of the rift zone, it is heated to a temperature of about 250°C and it leaches metals from the basaltic layer. The hydrothermal fluid is convected upwards, where at least two fluids can be identified in this part of the circulation system. Fluid (1) is shallow and relatively oxidised, and with a temperature of less than 250°C and high salinity. The deeper circulating fluid (2), is more reduced, maintaining a temperature of about 330°C, which is also of high salinity (Pottorf and Barnes 1983). Subsequent to passing through the basaltic layer, both these fluids discharge in the Deep and mixing occurs. No hydrothermal vents, such as those of the mid-ocean ridges, appear to be present, perhaps because vent construction is prevented by the presence of the soft muddy sediments trapped in the pool. The mixed hydrothermal fluids then discharge on to the seafloor where they precipitate metal sulphides, sulphates and silicates. The modified and cooler fluid continues to rise to the density boundary with the upper brine, where it precipitates Fe and Mn oxides.

In contrast to the brine pools, the hydrothermal fluids in the southwestern areas, where epigenetic mineralisation is formed, have salinities near that of sea water. The ore fluids in this case are not ponded in depressions, but the resulting mineralisation occurs as veins and chimney constructs and not as stratiform accumulations. This epigenetic mineralisation is dominated by sulphides, owing to the higher temperatures of the discharging fluids. The epigenetic deposits are considered to be the proximal facies, while the stratiform syngenetic mineralisation is the distal to the mineralising system.

8.5.2 Mechanisms for the Formation of the Red Sea Metalliferous Sediments

The Red Sea deeps are filled with brines that differ considerably in their composition, temperature and salinity as well as their sizes. The chemical and mineral composition of the metalliferous sediments depends on a number of factors (Gurvich 2006), including: temperature and degree of precipitation; intensity of hydrothermal effluence; presence or absence of brines in the deep; origin of the brines (direct hydrothermal circulation or fluids percolating through evaporites); distance from the emitting vent; position of the vents (in the deep or along its walls); overflow of brines to a lower level. As mentioned above, several lines of evidence indicate that the source of the salts in the brines is the evaporite deposits of the Red Sea rift system. Gurvich (2006) pointed out that there are three possible ways for the evaporite salts to enter the deeps. One is by exposure of the salt-bearing strata along the walls of the deep; the second is by percolation of sea water through the salt-bearing strata and the third by direct circulation of ascending hydrothermal fluids through these strata. In the first case, the brines would form without hydrothermal activity, whereas in the second and third cases the brines would form only during periods of hydrothermal activity in the deep. The hydrothermal fluids that are emitted from hot springs on the seafloor come into contact with bottom brines and precipitate metalliferous sediments containing sulphates, sulphides and oxides. These mineral species are zonally distributed around the emitting vents. Iron, Cu and Zn sulphides precipitate from high temperature vents, with Fe oxides, Fe oxyhydroxides, clay minerals (nontronite) and Mn-oxyhydroxides progressively away from the vents. Gurvich (2006) suggested that there are at least four groups of metalliferous sediments. In the first, metallifeorus sediments form directly from the emission of hydrothermal fluids on the seafloor with temperatures of about or greater than 300°C and without important changes in their composition taking place. There are two end-member cases. One is when the discharge of these high temperature fluids occurs in a deep already filled with stratified brines and this stratification is broken or disturbed by the entering fluids. The second is when highly saline fluids enter a deep with no brines and the discharging fluids form the brine layer. The second group of

metalliferous sediments form when the hydrothermal fluids that enter the deep have been subjected to compositional changes in relation to the primary fluids. These fluids are depleted in metals, such as Fe, Cu, Zn, presumably because of sulphide precipitation en route to the seafloor. The vents temperatures are low, from 30 to $<300^{\circ}$C and the metalliferous sediments around the vents are mainly Fe-oxyhydroxides and Fe silicate mineral species. Sulphides may be present but are in small amounts. However, in reducing environments bacterial sulphate reduction may produce abundant sulphides. Metalliferous sediments of the third group also form from hydrothermal fluids that have undergone compositional changes because of precipitation of sulphides in the sub-seafloor. The discharging residual fluids are depleted in Fe, Cu, Zn and the vents are of low temperature and sediments preferentially accumulate Mn-oxyhydroxides. However, in deeps filled with thick layers of brines, redox conditions may not be favourable for the precipitation of Mn oxyhydroxides and near the vents and some distance from them, Fe oxyhydroxides may precipitate instead and sulphides form from bacterial sulphate reduction. The Mn minerals will settle on the seafloor at or near the boundary between brines and sea water. The fourth group of metalliferous sediments form at or near the seafloor by migration of heavy and metal-rich brines. This migration occurs when the brines flow down slope into a deep with no hydrothermal vents or by overflow of brines to a deep at a lower level.

As mentioned above, these various groups are complex and there are several variants that may affect the overall picture. Gurvich (2006) listed sixteen variants from the four groups discussed.

8.6 Stratiform and Stratabound Sedimentary Rock-Hosted Disseminated Cu Sulphides Ore systems

Stratiform and stratabound Cu-Ag and Cu-Co ore deposits account for a substantial proportion of the world's production of copper and cobalt, in addition to significant amounts of silver, lead and zinc. Classic examples are the Permian Kupferschiefer (Germany and Poland), the Palaeoproterozoic Udokan deposit (Siberia), the Neoproterozoic central African Copperbelt (Zambia, Democratic Republic of Congo) and the Kalahari Copperbelt (Namibia and Botswana). Stratabound Cu-Ag and Cu-Co deposits are hosted in marine or continental (red beds) sandstone, shale and siltstone rocks; environmental associations with evaporites, basalts, conglomerates and breccias are common. Continental red beds are defined as first-cycle immature sediments, generally sourced from a crystalline basement and which contain abundant labile minerals (Metcalfe et al. 1994). Red beds are deposited in rift basins from fluvial, lacustrine and aeolian sediments, in arid to semi-arid oxidising environments and for this reason red beds are commonly associated with evaporites. Red beds are important for the genesis of stratiform and stratabound ore systems for two main reasons,

namely: they have high porosity and permeability thereby providing ideal conduits for the flow of groundwaters; and they act as a source of metals that are either bound in components minerals or are held in solution in formation waters (Metcalfe et al. 1994).

Red beds containing Fe oxyhydroxides and disseminated specularite are the main source of metals, whereas S is probably derived from multiple sources including evaporites, seawater or H_2S-bearing petroleum or gas plays. Metals are transported in oxidised, generally low-temperature (100–125°C), chloride-rich basinal saline fluids and precipitated at redox boundaries, as sulphides along faults or in permeable sedimentary beds or along palaeotopographic highs. Stratiform and stratabound sedimentary rock-hosted ore systems typically consist of disseminated and/or veinlet sulphides in siliciclastic, shale or carbonate rocks. The source of the fluids remains contentious, but could be diagenetic from arkosic sandstones or mafic volcanic rocks in the succession. Metals are sorbed to Fe oxyhydroxide and clay minerals of the source rocks (red beds) and are subsequently leached during diagenesis and interaction with basin fluids. Thus, an important aspect of these ore systems is that the basins in which they occur must contain red bed sequences (Hitzman et al. 2005). Furthermore, as pointed out by Hitzman and co-workers, many of the red beds in these rift basins are also spatially associated with bimodal volcanic rocks, which may also provide a ready source of Cu and other metals. In the Kupferschiefer and possibly in the central African Copperbelt, marine evaporites are (or were) present in the stratigraphy, usually below the red bed sequences. Anhydrite cements and nodules are also present in sandstone beds and were formed by diagenetic-related sulphate-rich brines flow, possibly from overlying evaporite units. Hitzman et al. (2005) reiterated that reduction was the principal cause of sulphide precipitation, with the reductant units being organic matter, hydrocarbons and/or pre-existing sulphides (diagenetic pyrite in shales?), and microbial algal mats in carbonate rocks. Furthermore, these authors envisaged a three-end member basin redox architecture (Fig. 8.11). The first is a basin containing oxidised red bed sediments, constituting the metal source, interbedded with evaporitic sediments, organic-rich shales and microbial lacustrine sediments. In this basin, the evaporites comprise either gypsum and anhydrite, or Na-Ca sulphates. In the second end-member basin architecture, the thick oxidised red bed succession is interbedded with microbial lacustrine sediments, which is the main source of reductants; in this case evaporites and carbonates overlie the red bed succession, providing a source of S, from the contained sulphates and high salinity brines from the halite. These brines would cause leaching of metals from the red bed and perhaps lenses of mafic volcanics that may be present in the succession. This second basin architecture would apply to the Kupferschiefer, in which the Zechstein evaporites overlie the red beds. The third redox basin architecture, the red bed sediments overlie both evaporites and organic-rich source rocks for petroleum that provide the reductants. In summary, the key features in all cases are: (1) oxidised rocks (red beds) that contain Fe oxyhydroxides capable of binding metals (metal source);

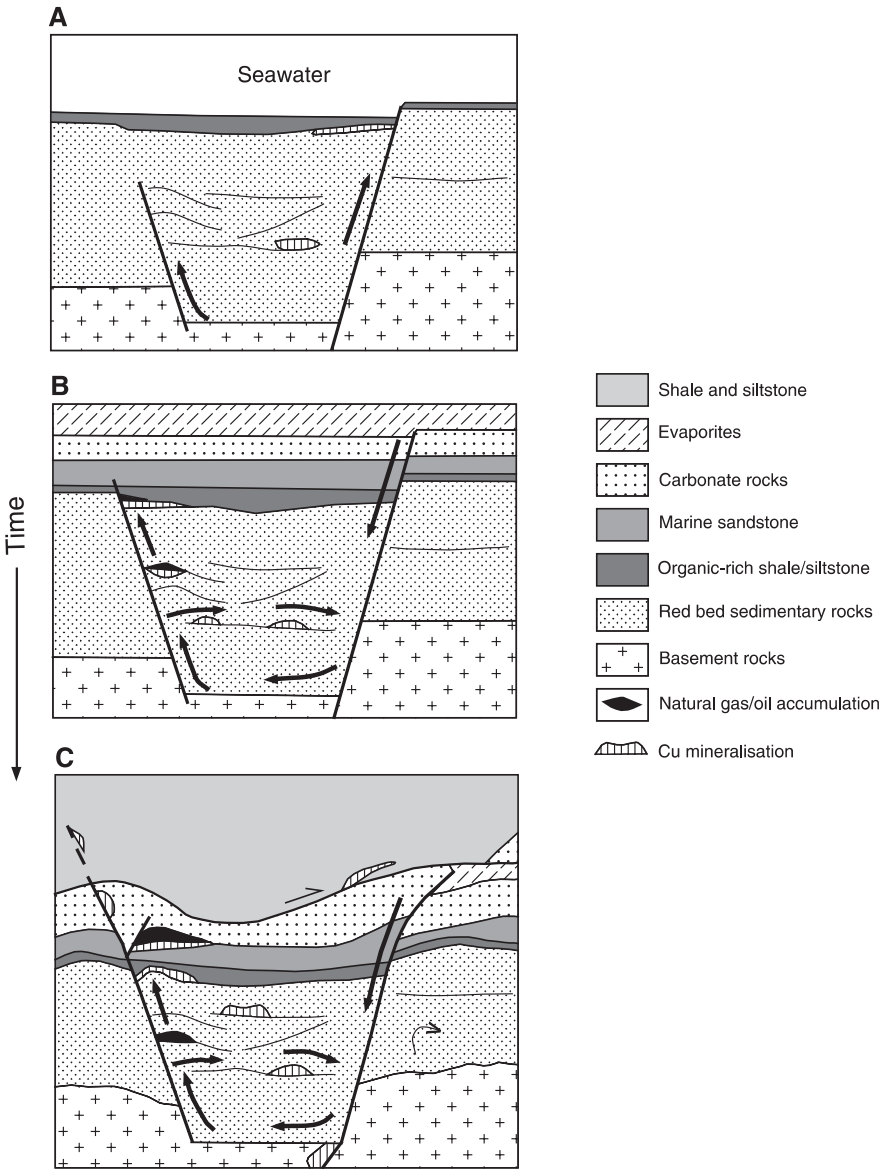


Fig. 8.11 Three-stage model of basin evolution and development of stratiform Cu ore systems; (**A**) in the first stage the basin is filled with red bed sediments overlain by organic-rich shales; compaction leads to fluid movements and production of low-temperature saline brines, which locally form disseminated Cu zones; (**B**) in the next stage, marine sandstone, carbonate rocks and evaporites are deposited in the basin overlying the red bed succession, evaporite dissolution produces saline brines, which percolate down into the red beds, leaching metals and forming late-diagenetic Cu sulphide deposits, mostly along the base of transgressive structures; (**C**) in this stage the basin is subjected to deformation and local inversion, with the evaporites largely

(2) evaporites to provide a source of salts and sulphates for the brines; (3) reductant materials, such as organic-rich sediments, microbial carbonates and hydrocarbons.

One the main features of stratabound Cu deposits is their metal zoning, which in most cases appears to be related to palaeogeographic and palaeoenvironmental controls. This zoning was realised since the early field-based detailed studies of the Zambian Copperbelt (Garlick 1961), where from palaeoshore outward, sulphides in the ore shales exhibit the following zonation: chalcocite → bornite → chalcopyrite → galena-sphalerite → pyrite. The general pattern of metal zoning, both vertically and horizontally, is Cu-Pb-Zn-Fe. Garlick (1961) advocated a syngenetic origin for the Copperbelt ores and related this zoning to cycles of transgression and regression of the shore line. These stratabound and stratiform ore systems, as the terms imply, are characterised by lateral continuity, only locally cross-cutting beds. The principal ore minerals are chalcocite, chalcopyrite, pyrite and bornite, for which textural evidence shows that these sulphides were deposited after the deposition of the host rocks. The mineral zonation, referred to above, is indicative of oxidising fluids that are progressively reduced. Hitzman et al. (2005) distinguished two types of disseminated sulphides of stratabound-stratiform ore systems. The Kupferscheifer type hosted by reduced dark shales and carbonate rocks above oxidised red bed sequences. These sedimentary rocks were deposited in shallow marine or lacustrine environments. The second type is "red bed", typically hosted by sandstone or arkosic units within red bed sequences.

Apart from the Central African and Kalahari Copperbelt, discussed in this section, stratabound and stratiform disseminated sulphides ore systems include other world-class deposits, such as White Pine in the Mid-Continent rift system (Michigan; USA), Dongchuan in Yunnan Province (China), the deposits of the vast Kupferschiefer in Europe and Udokan (Kodoro-Udokan basin in Siberia, Russia). Other basins that host these ore systems are in Kazakhastan, Afghanistan, Mongolia (see comprehensive listing provided by Hitzman et al. (2005).

In the White Pine area the mineralisation is within the Parting Shale Member of the Nonesuch Shale Formation, which overlies the basaltic lavas and minor rhyolites of the 5000 m-thick Portage Lake Formation. The Nonesuch Shale Formation is 180 m thick and consists of interbedded shale and siltstone. The main ore minerals are native copper, chalcocite, pyrite, bornite, chalcopyrite

Fig. 8.11 (continued) disappearing as a result of tectonism, brines continue to form, flowing downward along faults, fluid temperature and salinity are higher the in the previous stages and hence more fertile, stratiform Cu deposits form where fluids react with hydrocarbon sites of accumulation and fluids react with carbonaceous (reductant) lithologies. After Hitzman et al. (2005)

and native silver. There appears to be an association with the carbonaceous sedimentary rocks. A broad lateral and vertical zonation is characterised by a lower native copper zone, followed upwards by a chalcocite-native copper zone, then a chalcocite zone overlain by an extensive pyrite-dominated area (Brown 1971). Although the mineralisation is stratabound, on a regional scale the zoning patterns are transgressive to bedding. The cupriferous zones reach a maximum thickness at the intersection of the White Pine fault with a sandstone palaeohigh. Copper grades decrease away from the fault suggesting that it acted as a channel for the hydrothermal fluids. Brown (1971) suggested that the origin of the Keweenawan native copper deposits is related to chloride-rich brines (basinal and/or magmatic?). These brines leached the metals from the basement and the mafic rocks, which have an average of about 120 ppm Cu. The metals were then deposited in the porous lava flow tops and in the reducing environment of the overlying sedimentary rocks.

Dongchuan, the third largest Cu mining area in China, is hosted by the Palaeoproterozoic Luoxue Formation (Kunyang Group) and consists of stratabound disseminations of chalcocite-chalcopyrite in algal dolomites. During deformation events the Dongchuan Cu sulphide disseminations were locally redistributed to form hydrothermal vein systems (Ran 1989; Qiu et al. 2002).

The Kupferschiefer Cu deposits of central Europe have been exploited since ancient times, extending for 1500 km from southwest England through central Germany to Poland and covering an area of about 600 000 km^2 (Laznicka 2006). The Kupferschiefer is one of the largest accumulations of Cu world-wide and is located at the boundary between the Lower Permian and the Zechstein (Upper Permian), covering about 800 000 km^2, in the Rotliengendes-Zeichstein basin. Important Kupferschiefer deposits include Mansfeld-Sangerhausen and Marsberg in Germany, Lubin-Sieroszowice in Poland. Interesting to note that Au, Pt and Pd anomalous contents have been reported from the Mansfeld-Sangerhausen and the Lubin-Sieroszowice mining districts (Borg et al. 2005 and references therein). Oil and gas accumulations are also present in the basin. The Rotliengendes-Zeichstein basin contains two main successions of the same names. The Rotliengendes is essentially continental with a lower succession of clastic rocks and bimodal volcanic rocks deposited at about 300–290 Ma. The upper Rotliengendes succession consists of fluvial conglomerates, aeolian sandstone, sabkha sandstone, siltstone and claystone. The Rotliengendes was followed by the Zechstein transgression during 258–250 Ma, with sequences of shale-carbonate-evaporites. The Cu mineralisation is typically zoned from Fe^{3+} (hematite) to Cu (chalcocite → bornite → chalcopyrite → galena-sphalerite → pyrite). Although not always associated with mineralisation, the hematite alteration, known as Rote Fäule, can be an important vector to new deposits.

The ~1.9 Ga Udokan stratabound Cu deposit is located in the Olyokma Terrain of the Aldan Shield (Siberia) and is characterised by Cu-Fe sulphide disseminations in sandstone (Udokan Group) and siltstone (Alexandrov and Naminga groups) units (Larin and Mikhailov 1997). The deposit contains three mineralised zones: a lower zone is 250 m thick and consists of sandstone lenses

with weak Cu sulphide disseminations; a middle, main ore zone has thicknesses varying from 20 to about 330 m, and abundant sulphides hosted by quartz-rich sandstone units; and an upper zone about 100 m thick that is only weakly mineralised. The principal sulphide species at Udokan are: chalcocite, bornite, chalcopyrite and pyrite. Lesser quantities of native silver, and native bismuth, molybdenite, sphalerite, galena, arsenopyrite, tennantite and valeriite are also present. Hydrothermal epigenetic Cu deposits are associated with the sedimentary-hydrothermal ores and appear to be related to stages of metamorphism and intrusion of mafic dykes (Larin and Mikhailov 1997).

8.6.1 The Central African Copperbelt

The central African Copperbelt is one of the great metallogenic provinces of the world, where giant stratiform and stratabound Cu-Co-Ag deposits are hosted by a predominatly clastic sedimentary succession of the Lower Roan Group (Katanga Supergroup). In addition, the Copperbelt contains numerous vein type hydrothermal systems (Cu, U, Au, Pb, Zn) and skarns. In the northwestern part of the central African Copperbelt is the Shaba belt in the Katanga region of the Democratic Republic of Congo. This belt is about 250 km long, 70 km wide and contains more than 230 occurrences and deposits, including the Kolwezi and Kambowe ore districts, with resources of 125 Mt Cu and 10 Mt Co (Laznicka 2006; Bartholomé 1973). Little information is available from the Shaba belt deposits. Overviews of the central African Copperbelt metallogeny can be found in Unrug (1988) and more recently Hitzman et al. (2005) and Selley et al. (2005). The geology and exploration of the Copperbelt were described in detail by Mendelsohn (1961) and Fleischer et al. (1976) For this section I use the works of Selley et al. (2005) and Hitzman et al. (2005).

The central African Copperbelt extends, as a broad arc, from northern Zambia, the Katanga region of the Democratic Republic of Congo to northeastern Angola (Fig. 8.12) and is part of the Lufillian fold belt. The Lufillian fold belt is one of the Pan-African orogens, separated from the Zambezi fold belt to the south by the southwest-trending transcontinental Mwembeshi Shear Zone that reaches to the Damara belt near the Atlantic coast (Fig. 8.12). The Lufillian sedimentary successions belong to the Katanga Supergroup, deposited in an intracontinental rift basin, between 879 and 735 Ma (age of mafic lavas and intrusives), with mineralisation ages ranging from about 500–670 Ma, but largely constrained between 580 and 560 Ma, which is more or less coeval with the Lufillian deformation, metamorphism and synorogenic granitic intrusions. The Katanga Supergroup, resting on a Palaeoproterozoic basement, from 1 to 3 km thick (but could have been up to 7 km prior to erosion), is divided into Lower Roan, Upper Roan, Mwashia and Lower Kundelungu Groups (Fig. 8.13). The Lufillian belt is divided, from north to south, as follows

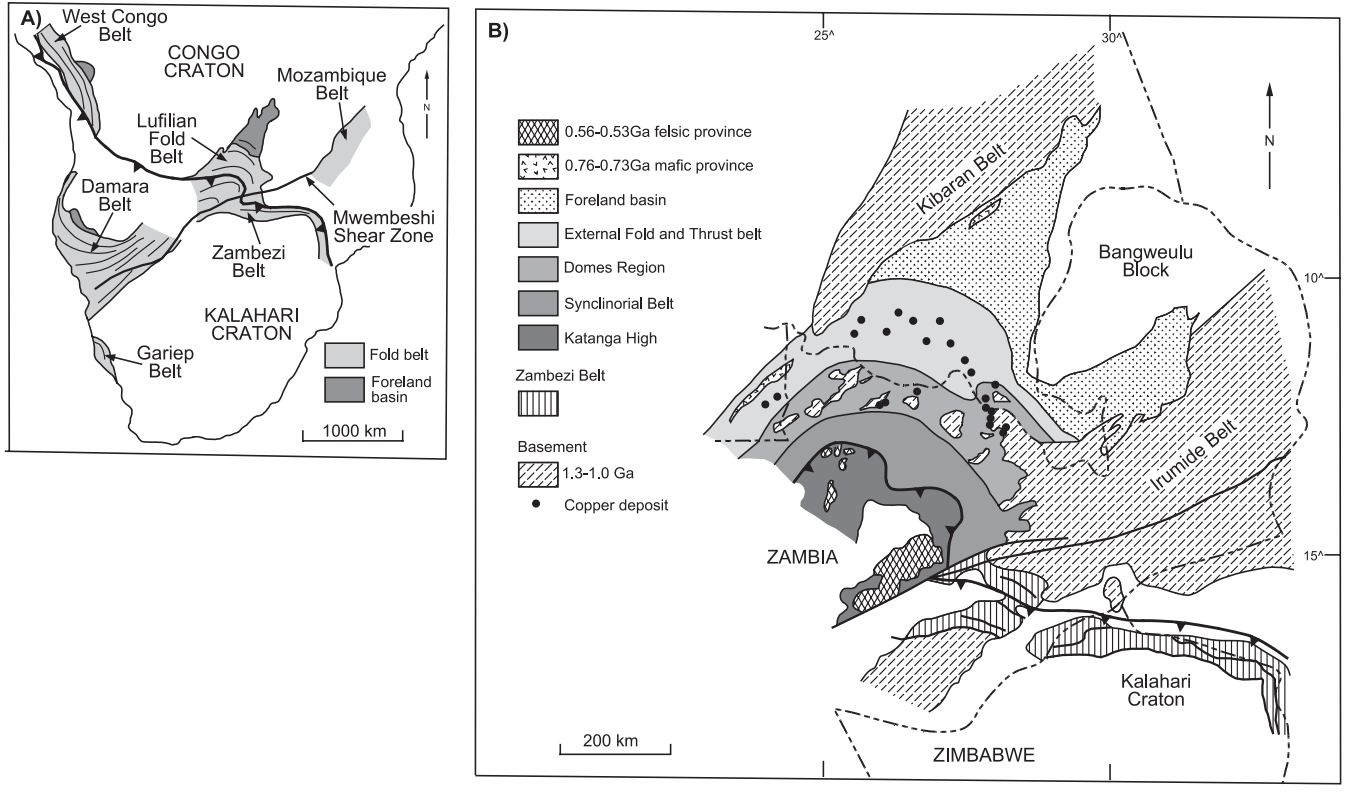


Fig. 8.12 Schematic tectonic map of central Africa (Zambia, Zimbabwe and the Congo), showing the main tectonic elements of the Lufillian fold belt and distribution of stratiform Cu deposits; inset shows the position of the Lufillian belt in relation to the Kalahari and Congo Cratons and its possible continuation to the Damara Orogen (see also Fig. 8.14). After Selley et al. (2005)

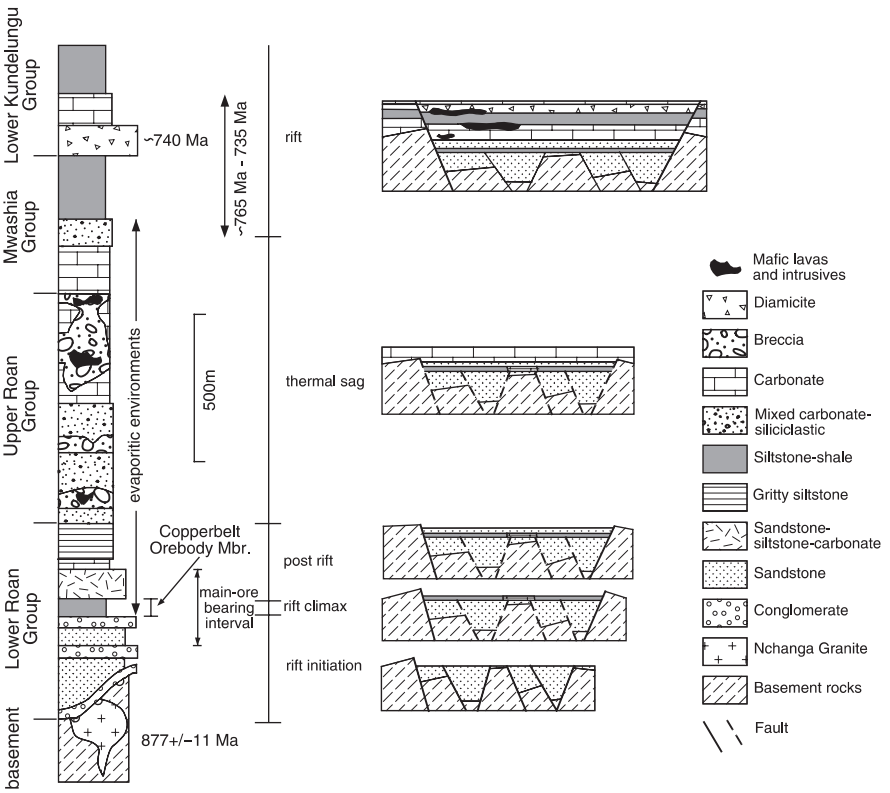


Fig. 8.13 Stratigraphy and basin evolution of the Katanga Supergroup in the Zambian Copperbelt; see text for explanation. After Selley et al. (2005)

(Fig. 8.12): (1) External fold-and-thrust belt; (2) a Domes region; (3) a synclinorial belt; and (4) the Katanga High. These tectonic units, originally established by Porada (1979), were folded and overthrust to the north and northeast. Thrusting involved mainly Katangan rocks, but in places basement slices were incorporated into the thrust packages. The Katanga High is part of an overriding plate, separated by a major thrust from the poorly known Synclinorial Belt, but probably representing thrust sheets of Upper Katangan Supergroup units. The Domes region consists of basement-cored recumbent folds and nappes that underwent upper greenschist to amphibolite facies metamorphism. The Synclinorial and External belts may represent changes in basin environments, from a marginal marine platform-lagoonal setting to deeper water basin sequence. The entire structural architecture of the Lufillian belt, taken together with the foreland basin to the northeast, containing rocks of the Kundelungu Group (Fig. 8.12), has been interpreted as a failed arm of a rift structure, or aulacogen, suggesting that it may have

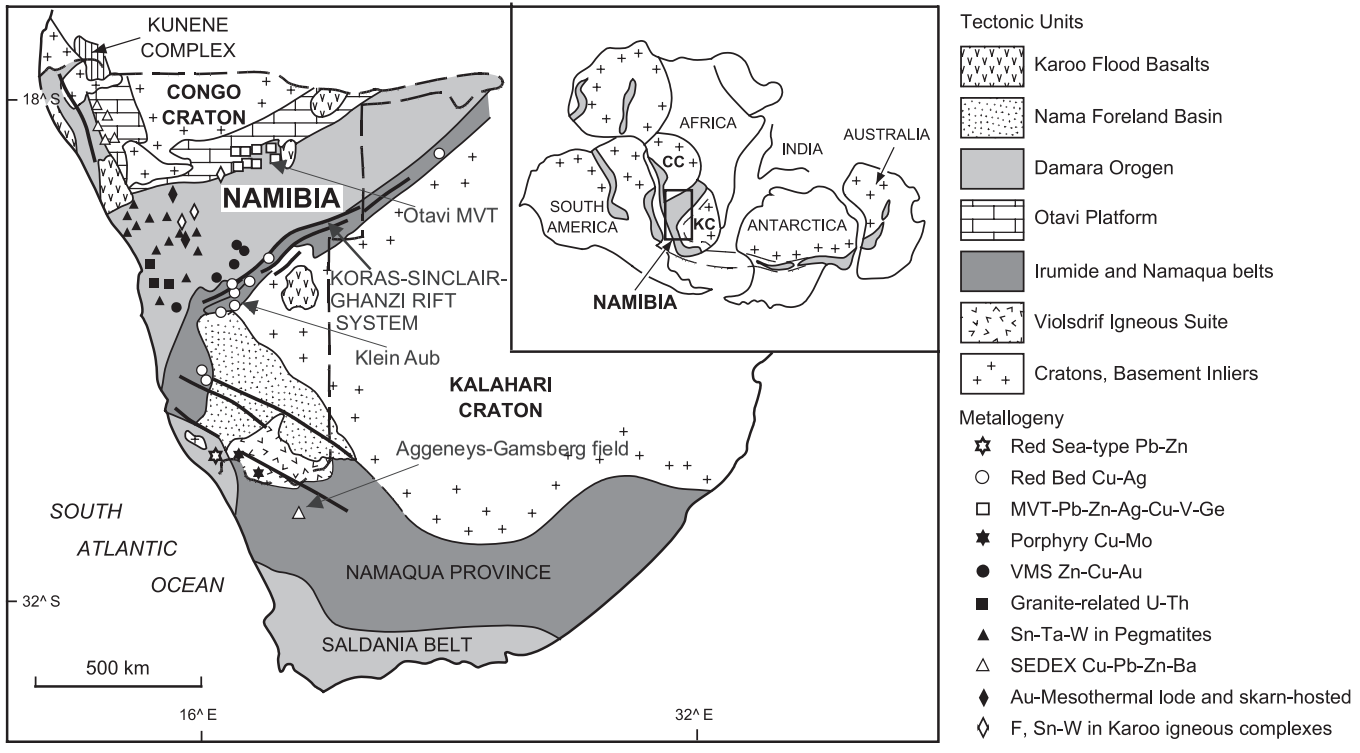


Fig. 8.14 Simplified geology of southwestern Africa, showing the distribution of selected mineral deposits in Namibian part of the Damara Orogen and associated mineral systems, including the large Otavi MVT field (Tsumeb), the adjacent Irumide Orogen, which contains stratabound base metal sulphide deposits and the Namaqua belt, which hosts the world-class Aggeneys-Gamsberg ore field; inset shows the position of these orogens in a Gondwana reconstruction

originated from a triple junction rift system (Unrug 1988; Porada 1989). Selley et al. (2005) have suggested a rift system that evolved through time, from a rift inititiation with a series of sub-basins, to post-rifting sags, to renewed rifting in Kundelungu times, as shown in Fig. 8.13. The final rifting stage was accompanied by the intrusion of 765–735 Ma gabbroic rocks and associated mafic extrusives.

Basin evolution is of primary importance for ore genesis (see Section 8.3). The Lower Roan Group contains from base to top the Mindola Clastic Formation and the Kitwe Formation. The former comprises conglomerates and subarkosic sandstone deposited in fluvial, alluvial fans and aeolian environments with strong lateral and vertical facies variations. The base of the Kitwe Formation (Copperbelt Orebody Member) is the principal host of the Cu-Co mineralisation and comprises laminated dolomitic siltstone, carbonaceous shale, sandstone and microbial dolomite. Presence of local dessicatiuon cracks and anhydrite nodules suggest subaerial exposure and evaporitic conditions. The Copperbelt Orebody Member is overlain by conglomerate, subarkosic sandstone, argillaceous sandstone, dolomitic siltstone and dolomite of marine-evaporitic facies. The Upper Roan Group is dominated by dolomite beds and consists of upward-fining cycles of sandstone, siltstone, dolomite, microbial dolomite and anhydrite beds. The Upper Roan locally hosts Cu-Co mineralisation, but of little commercial value. The carbonate dominated succession is of platform environment with thicknesses varying form 30 to 800 m. These thickness variations are associated with extensive unsorted breccia units that probably formed along evaporite horizons and may contain very large fragments (up to thousands of metres long) which, in the Congolese side, host Cu-Co orebodies. The Mwashia Group is shale-dominated, but in the Congo the Group contains breccias, dolomite and volcanic rocks. The Grand Conglomerat marks the contact between the Mwashia Group and the overlying Lower Kundelungu Group. The Grand Conglomerat is a unit of debris flows and diamictites that is correlated with the Chuos Formation (see Section 8.8.5) of the Damara sequence in Namibia and other Sturtian diamictites deposited at about 740 Ma. The Petit Conglomerat, also of possible tectonic origin, separated the Lower Kundelungu from the Upper Kundelungu, which largely consists of mudstone, siltstone and sandstone. The Kundelungu rocks occupy the northeast-trending aulacogen-like trough, referred to above.

The Zambian Copperbelt mineralisation includes disseminations, prefolding and post-folding veins and supergene styles. The primary ore minerals are chalcocite, bornite, chalcopyrite, pyrite and carrollite ($CuCo_2S_4$). Post-folding veins also contain uraninite, pitchblende, brannerite and molybdenite, which can be locally economic. The primary ore minerals are commonly replaced by supergene oxide ore minerals, mostly Cu sulphates, carbonates, cuprite and native Cu. The characteristic sulphide zoning, mentioned above, extends both vertically and horizontally up to several km. The ore paragenesis reflects this zoning with the oldest mineral (chalcocite) being also proximal and the most distal (pyrite) being the latest phase. Ore sulphides generally replace authigenic

cementing material, such as anhydrite, dolomite, quartz and feldspar, thereby indicating a late to post-diagenetic timing.

Alteration assemblages are recorded in the mineralised zones and are mainly represented by alkali metasomatism (potassic mainly with K-feldspar, sodic with albite and scapolite), tourmaline, and Ca-Mg alteration with sericite, carbonate, anhydrite and rutile (Hitzman et al. 2005). Potassic metasomatism is manifested by K-feldspar, phologopite, muscovite, sericite and is especially focused in argillaceous horizons of the Lower Roan Group. Locally K-feldspar is associated with tourmaline and in argillite-hosted deposits together with phlogopite occurs intergrown with chalcopyrite. K-feldspar tends to replace detrital plagioclase and textural evidence shows several phases of K-feldspar growths from early diagenetic to post-deformation veins. Potassic alteration tends to be pervasive and not related to fractures. K-feldspar is one of the major gangue minerals in the Copperbelt ores. Sericite alteration is very common in arenite-hosted deposits and less common in argillite-hosted deposits (see below). Sericite replaces detrital minerals and the K-feldspars and pervasively replaces the matrix of clastic rocks. Sodic metasomatism is manifested by albite replacing K-feldspar and sericite, is locally associated with scapolite and is especially evident in arenite-hosted deposits. Sodic alteration (albite and scapolite) becomes dominant in the Upper Roan Group and appears to stratigraphically coincide with former evaporite and breccia strata. In contrast to potassic alteration, albitisation is commonly most intense in fracture zones, breccias and around veins. Like for K-feldspar, albite is also a common gangue mineral, although not strictly coupled with sulphide minerals. Textural relationships indicate that albitisation overprints the potassic alteration and the sulphide mineralisation but, on the basis of geochronological data, appears to be associated with U and Mo ore veins and quartz-dolomite-Cu ores dated at 510 Ma. Given the wide extent of the alkali metasomatism (up to 2 km above the Upper and Lower Roan Groups), this type of alteration is a poor indicator for new mineral deposits (Hitzman et al. 2005). Magnesiun metasomatism (Ca-Mg alteration) is characterised by the presence of phlogopite, anhydrite, calcite and dolomite, with phlogopite being widespread and pervasive especially in argillaceous rocks. Anhydrite, dolomite and calcite tend to occur as nodules, coarse-grained recrystallised zones and as veins and are most abundant in theUpper Roan Group rocks, although anhydrite and carbonate veins are found at all stratigraphic levels.

Selley et al. (2005) conducted studies of isotopic systems applied to the Zambian Copperbelt, pointing out their extreme complexity. A general trend was observed of $\delta^{13}C$ and $\delta^{18}O$ values (–5 to –10‰ and + 19–26‰ , respectively) typical of unaltered marine carbonates, to isotopically light values (–5 to –26‰ and –5 to –23‰, respectively) in samples near or within the mineralisation. The carbonates of the Copperbelt Orebody Member have a broad range of $\delta^{13}C$ and $\delta^{18}O$ values (–26 to + 3‰ and 7–23‰, respectively), whereas the ore zones have depleted isotopic values ($\delta^{13}C < -14$‰; $\delta^{18}O < 13$‰). Sulphur isotopic values also have broad ranges with $\delta^{34}S$ of sulphides ranging from –18.4 to + 23‰.

The $\delta^{34}S$ of sulphates have a restricted range (from 14 to 19‰). These S isotopic are indicative of evaporitic sources for the basinal fluids.

In the sections that follow, I focus on the Zambian Copperbelt. The stratiform Cu deposits of the Zambian Copperbelt have resources of about 88 Mt of contained copper grading 2.68% Cu (Selley et al. 2005). As mentioned previously, the stratiform Cu orebodies are hosted in the sedimentary rocks of the Lower Roan Group, Katanga Supergroup, unconformably overlying Archaean granitic and gneissic basement rocks. The principal host rocks are euxinic argillaceous rocks, arkose and quartzite. The unconformity is extremely irregular with hills and ridges of basement, and is marked by a basal conglomerate. There are two groups of deposits: arenite-hosted and argillite-hosted.

8.6.1.1 Arenite-Hosted Deposits

The main arenite-hosted Cu-Co deposits are Bwana Mkubwa, Mokambo, Lubembe, Chibuluma South and Chibuluma, with total copper resources exceeding 100 Mt. The Lower Roan, from the base upwards, comprises: an extensively deformed basal conglomerate, up to 5 m thick, flanking basement hills and gullies; aeolian feldspathic quartzite, 0–13 m thick, unconformably overlain by 3–15 m of arkosic sediments; the Ore Formation, up to 23 m thick, consisting of arkose overlain by feldspathic arenites; and the Hanging Wall Formation, consisting of arkose with interbedded argillite. The sequence is metamorphosed to greenschist facies but the rocks retain their sedimentary structures. The ore minerals are chalcopyrite, bornite, chalcocite, carollite and pyrite and follow the stratification of the host arenites. Vertical and lateral mineral zonations are present. From top to bottom the ore zone shows pyrite in albitic arenite to chalcopyrite-sericite arenite to Co-rich "sulphidite" (a term used to indicate beds exceptionally rich in sulphides). Laterally, from margin to centre, bornite and chalcopyrite occur in cross-bedded arkose, followed by chalcopyrite, carollite and pyrite in sericitic arkose and then pyritic feldspathic arenite.

The Mufulira mine opened in 1933, with initial reserves in the order of 280 Mt at 3.5% Cu; current resources are 315 Mt, grading 2.83% Cu. The orebodies occur in three repeated sequences of the Lower Roan, which from the base upwards comprises: Foot Wall Formation, up to 150 m thick, consisting of a poorly developed boulder conglomerate, overlain by feldspathic sandstone or greywacke, and characterised by a carbonate or anhydrite cement; the Ore Formation, 30–80 m thick, which is a sequence of three transgressive cycles of arenite-argillite-greywacke-dolomite-mottled sandstone, with the ore-bearing arenites containing fairly abundant anhydrite and dolomite; Hanging Wall Formation, 60–80 m thick, which is a sequence of anhydrite-rich argillaceous quartzite and dolomite. The mineralisation occurs in 21 distinct horizons, and ore minerals include chalcopyrite, bornite, pyrite, chalcocite and carollite. A mineral zonation is present: stratigraphically, from bottom upwards, chalcocite → bornite → chalcopyrite → pyrite;

and laterally, from low-grade pyrite-rich zones over basement highs, to chalcopyrite in the greywacke, to high-grade chalcocite zones. The arrangement of metal and sulphide zones appears to be related to the palaeogeographic configuration as deduced from basement highs and the nature or facies of the host lithologies. In general, this zoning is from the oxygenated palaeoshore towards deeper anoxic parts of the depositional basin. Models explaining the origin of this zonation are discussed below.

8.6.1.2 Argillite-Hosted Deposits

Argillite-hosted deposits are confined to the souhtwest flank of the Kafue anticline. The Luanshya and the Rokana deposits are hosted mainly by shales. The mixed arenite-argillite Nchanga-Chingola on the south flank of the Chambishi-Nkama basin, has resources of 711 Mt Cu, grading 2.5% and 47 Mt Co, grading 0.38% (Selley et al. 2005). The Luanshya basin consists of an outlier of Katanga Supergroup sediments folded into a synclinorium surrounded by basement rocks. The Lower Roan Foot Wall Formation consists of argillaceous feldspathic arenites, conglomerate, sandstone, arkose and argillite. The Ore Shale unit is also part of the Lower Roan Group, and contains nearly all the Cu mineralisation in the Luanshya basin. The Ore Shale unit has a thickness ranging from 15 to 55 m. The Hanging Wall Formation consists of arkose and dark grey argillite. The orebodies comprise two Cu zones separated by a barren pyritic layer. Locally the mineralisation penetrates basement rocks, where the Ore Shale horizon rests directly on the underlying basement. Ore minerals are disseminated and include chalcocite, bornite, chalcopyrite and pyrite. Covellite, digenite, carollite and pyrrhotite occur as accessory ore minerals. The gangue mineralogy, i.e. the components of the Ore Shale, are biotite, quartz, microcline and dolomite with minor quantities of calcite, chlorite, anhydrite, sericite, scapolite, tremolite and oligoclase.

8.6.2 Stratabound Cu-Ag Deposits of the Irumide Belt in Southern Africa

In southern Africa Proterozoic tectonic provinces, or mobile belts, are situated between the Kalahari Craton in the south and the Congo Craton in the north (Fig. 8.14). The ages of the Proterozoic mobile belts in Africa cluster around 1.9 Ga (Eburnian-Ubendian), 1.05–0.95 Ga (Kibaran/Irumide) and 0.6 Ga (Pan-African). The period from 1.4 to 0.95 Ga is one of great importance in southern Africa, during which the Kibaran and Irumide fold belts were formed and overprinted older mobile belts. The Kibaran fold belt in the northwest of the orogenic system (Fig. 8.14), has a complex metallogeny that is remarkably different from the Irumide fold belt to the southwest. The Kibaran metallogeny

is dominated by Sn-bearing granitoids, pegmatites, Au-rich quartz veins and mafic-ultramafic intrusions with Ni-Cu-Co, PGE and Fe-Ti mineralisation (Pohl 2006).

The term Irumide was first applied to a belt of folded rocks in Zambia and this is correlated with folded sequences of the Kibaran-Irumide tectonothermal event of 1050–950 Ma (De Waele et al. 2006). The northeast-trending Irumide orogenic belt, or Koras-Sinclair-Ghanzi belt, can be traced for more than 2000 km in southern-central Africa, from south-central Namibia, on the northwestern margin of the Kalahari Craton, to the northeast across northern Botswana and northern Zimbabwe (Fig. 8.14). The Botswana portion of the Irumide belt is covered by much younger rocks and its geology therefore remains speculative. The Irumide belt is best exposed, relatively undeformed and little metamorphosed in south-central Namibia, along the northwestern margin of the Kalahari craton. The belt becomes buried beneath more recent strata or is overprinted by the later Damara tectonism, but re-appears in a succession of rocks between the Zambian and Zimbabwe cratons (Fig. 8.14). The Irumides are characterised by an extensive rift system (Koras-Sinclair-Ghanzi rifts; Borg and Maiden 1986; 1987), which developed around the margins of the Kalahari craton. The rift basins of the Irumide belt were formed during phase of crustal extension, and graben formation, accompanied by a high heat flow regime that caused partial melting of the lower crust. Thus, felsic melts were produced, resulting in high-level intrusions and subaerial felsic volcanism. The graben faults penetrated deep into the crust and also controlled the advection of melts towards the surface. Erosion of the uplifted blocks supplied coarse clastic sediments, which accumulated into narrow troughs. The final stage was one of thermal subsidence, producing sag structures in which low-energy sediments were deposited in shallow waters. During the Neoproterozoic, rifting shifted to the north, perhaps in response to movement of the African plate over a mantle plume, to form the Damara rift system (Pirajno 2000). In southwestern Africa, the Irumide belt is a complex zone containing igneous and metamorphic basement rocks, granitic intrusions, clastic sequences (conglomerate, sandstone, shale, carbonate rocks) and bimodal volcanic rocks (rhyolitic-basaltic) emplaced in a series of rift basins (Thomas et al. 1994). These thick (>10000 m) volcano-sedimentary successions were deposited in northwest- (Sinclair) and northeast-trending (Rehoboth) basins; the former containing dominantly volcanic rocks with subordinate amounts of sediments, whereas in the latter sediment volumes predominate over volcanic materials. The ~1200–1000 Ma Sinclair Group includes felsic volcanic rocks (rhyolitic lavas, quartz-porphyry and ignimbrite), mafic lavas, quartzite, tuffs and clastic rocks (Nuckopf and Grauwater Formations). These are intruded by granitoid rocks (~1200 Ma Gamsberg granite suite), and separated by an unconformity from the overlying Doornpoort and Klein Aub Formations, which contain mainly sedimentary units (shale, limestone, arenite, coglomerate) and some mafic and felsic volcanic rocks at the base (Borg 1988; Borg and Maiden 1987). The Sinclair Group contains stratabound Cu-Ag red-bed hosted

deposits, such as Klein Aub and Witvlei and their correlative Ghanzi and Lake N'Gami in Botswana (Kalahari Copperbelt; Borg and Maiden 1987).

The volcano-sedimentary succession of the Klein Aub basin is approximately 11 km thick, comprising three main units: (1) felsic extrusives with intercalated coarse clastic sediments; (2) mafic extrusive and red beds; and (3) shallow marine deposits. The first unit comprises rhyolitic porphyry and pyroclastics, the nature of which suggests a caldera-type volcanism. The felsic volcanics (Nuckopf Formation) are associated with lenses of continental coarse sediment (Grauwater Formation). The second unit nconformably overlies the first and comprises basic volcanic rocks and a thick sequence of coarse continental red beds (Doornpoort Formation). A change to marine conditions is indicated by rocks of the third unit, which include pyritic sandstone, shale and stromatolitic carbonate rocks (Klein Aub Formation); these rocks have been subjected to lower greenschist facies metamorphism and deformation, during the collisional phases of the Damara orogen to the north. The succession was folded and a well-developed slatey cleavage dips at 70° to the north-northwest. Mineralisation in the Klein Aub basin occurs as native Cu in the brecciated flow top of the basaltic lavas of the Doornpoort Formation and in shear zones in hydrothermally altered lavas, and as stratabound disseminated Cu-Ag in pyritic sediments of the Klein Aub Formation.

The geodynamic evolution of the Klein Aub basin, as worked out by Borg (1988), is of general interest because it offers insights in terms of rift tectonic evolution and related mineral systems. Three phases have been recognised. In the first phase, crustal extension and thinning were accompanied by a high heat flow regime which caused partial melting of the lower crust. Felsic magmas were produced, resulting in high-level intrusions and extrusion of acid volcanics. This is a stage of block faulting and formation of grabens. During the second phase, the graben faults penetrated deep below the crust into the mantle, causing the upwelling and extrusion of basaltic lavas. Erosion of the uplifted faulted blocks supplied coarse clastic sediments which accumulated into narrow depressions. The third phase is characterised by thermal subsidence and a marine transgression. In other basins, lakes were formed during this subsidence. Low-energy sediments were deposited in these shallow waters in which bacterial activity resulted in the formation of pyritic shales and sandstones.

8.6.2.1 The Klein Aub Cu-Ag Deposit

The Klein Aub deposit is located approximately 180 km south of Windhoek. In 1986 production was 19 000 tonnes per month with an average head grade of 2% Cu and 40 g/t Ag, yielding 375 tonnes of Cu and 600 kg of Ag. The mine is now closed but undergoing renewed exploration. The Klein Aub deposit contained 7.5 Mt at 2% Cu and 50 ppm Ag, of which 5.5 Mt were mined from 1966 to 1987 (Schneider and Seeger 1992). The Witvlei Cu deposits have resources of 2.98 Mt at 2.1% Cu and Witvlei Pos 9.5 Mt at 1.5% Cu

(http://www.mme.gov.na/gsn/basemetal.htm accessed in October 2007). Details of the geology of the Klein Aub deposit can be found in Ruxton (1986). The Klein Aub Formation, which is host to the Cu-Ag deposits, comprises a sequence about 3700 m thick, containing, from the base upward, conglomerate, red-brown quartzite, conglomerate with interbedded quartzite, shale, calcareous shale with lenses of limestone and fine-grained purplish quartzite. The Formation is separated by an unconformity from the underlying lithologies of the Doornpoort Formation. The Cu-bearing basaltic lavas of the Doornpoort Formation have been dated at approximately 1.1 Ga. The basement is block-faulted and in the vicinity of Klein Aub it forms a palaeotopographic high, which supplied sediments into the fault-bounded Klein Aub basin. The stratigraphic column in the mine area is shown in Fig. 8.15. The stratabound mineralisation occurs in a number of stacked bands (Fig. 8.15) in fine-grained, locally calcareous, laminated siltstone and argillites. Cross-bedded sandstone-siltstone units normally occur beneath the mineralised bands. A reverse oblique fault, with strike- and dip-slip components, truncates the mineralised bands downdip to the south. The fault is almost bedding-parallel and dips southwards slightly more steeply than the mineralised bands. Borg and Maiden (1987) recognised two types of mineralisation: one, which constitutes 60–70% of the ore, occurs along cleavage planes or bedding-plane fractures, the other occurs in a finely disseminated form in the host units. Locally, mineralised veins cut across bedding planes at steep angles. Although the fault zone itself is not mineralised, it is noted that the tenors of the mineralised bands tend to decrease away from the fault. The main ore mineral is chalcocite; subordinate amounts of hematite, pyrite, chalcopyrite, bornite, digenite, covellite and rare native Cu are also present. Sulphur isotopic values, reported by Ruxton (1986), range from –20 to –40‰ $\delta^{34}S$. Ruxton (1986) suggested this wide range of values can be explained by bacterial fractionation in an open system from an initial value of $\delta^{34}S$ of 0‰. Lead isotopic studies, also by Ruxton (1986), resulted in an isochron age of about 500 Ma, which is attributed to the late stages of deformation of the adjacent Damara Orogen (see Chapter 4).

Both syngenetic and epigenetic models have been proposed to explain the origin of the Klein Aub mineralisation. The former envisages the transport of Cu into the basin with synsedimentary precipitation caused by reducing conditions. The stratabound and finely disseminated nature of some of the mineralisation is cited as evidence in favour of the synsedimentary origin. Tregoning (1987) proposed a synsedimentary origin with later remobilisation during deformation and metamorphism, which would account for the discordant mineralisation. However, these models fail to account for the decreasing tenors away from the fault. Borg and Maiden (1987), on the other hand, favour a multistage ore genesis involving leaching of Cu and other metals from the underlying basaltic lavas, which are locally mineralised with native Cu in the amygdales of the flow tops. These authors postulated four main stages. In the first there was extrusion of the basaltic lavas and sedimentation of red beds

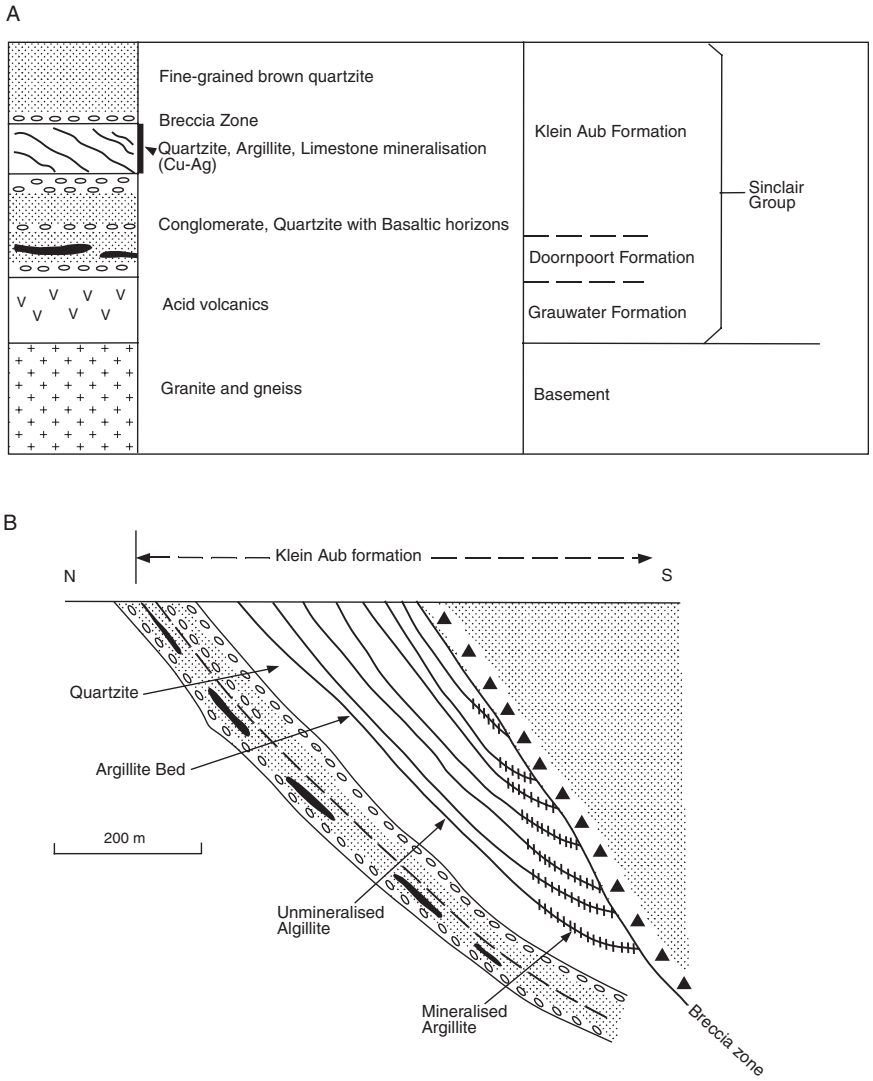


Fig. 8.15 Simplified stratigraphy of the Klein Aub area (**B**) schematic cross-section of the Klein Aub Formation showing relationship of mineralised argillite beds against the Breccia Zone, possibly a strike-slip fault. After Pirajno (1992)

in an environment of basement uplift and block faulting. In the second stage a marine transgression took place, with the change from oxidising continental conditions to a reducing shallow marine environment. At this stage organic S would have formed diagenetic pyrite, and some synsedimentary Cu sulphides may also have formed. The third stage, which involved compaction and basin dewatering, resulted in the upward movement of fluids, which leached metals from basement rocks (as suggested by Pb isotopic studies and also enriched in Cu

and other metals, such as Au), red beds and basaltic rocks. The fluids would have precipitated Cu on contact with the S-bearing sediments. The final stage would have involved devolatilisation reactions during deformation and metamorphism, with the production of hot fluids. These fluids could have leached more Cu from the basaltic lavas, precipitating Cu in the pyritic beds. The hydrothermal alteration of the basalts is used as evidence that hydrothermal solutions interacted with them. The strike-slip fault provided the main channelway for the movement of the Cu-bearing fluids.

8.6.3 Genetic Models

Stratiform and stratabound ore systems are related to the flow of fluids in sedimentary basins. The hydrodynamics of continental basins are related to topography, fluid density and rate of compaction of the sedimentary package (Person and Garven 1994). A collection of papers that deals with the origin of fluids and their migration in sedimentary basins can be found in Parnell (1994). From numerical modelling, Person and Garven (1994) proposed that two flow systems can develop in the life of a sedimentary basin. The first is during the early phases of rifting, when fluid flow is driven by gravity gradients, caused by uplift of the crystalline basement, and by compaction of the sediments. Groundwater flow is along coarse-grained alluvial fan and sand flat deposits. These fluids have the capacity of leaching metals from the silicate minerals of clastic sediments (e.g. Pb from feldspars) and/or disseminated Fe oxyhydroxides. The second flow system develops during the post-rift subsidence stages in shallow marine conditions, when erosion has reduced the hinterland relief. In this case, fluid flow is likely to be driven by density (salinity) variations (Person and Garven 1994). Dissolution of evaporites and high rates of evaporation of marine and continental waters have the effect of increasing the salinity of the basinal fluids, which then acquire enhanced capacity of transporting metals, mainly as chloride complexes (Hanor 1994). In addition to leaching of metals from clastic sediments, diagenesis plays an important role in providing both fluids and solutes. In this respect, it may be opportune to bear in mind that Fe oxides and oxyhydroxides as disseminations and cement material can form as a result of circulation of Fe-rich fluids.

The mineral zonation worked out from the detailed study of the Copperbelt mines (Garlick 1961; Fleischer et al. 1976) was explained as a zonation from shore to sea, with copper sulphides precipitating near the shore (chalcocite-bornite-chalcopyrite) to Fe (pyrite) in the deeper and anoxic waters. Later these metalliferous deposits would be capped by evaporites upon desiccation of the basin. This model has two major drawbacks: (1) the most soluble metals occur in the most basinward position, and the resultant metal zonation requires that transgression should have occurred, whereas in fact the enclosing lithofacies

reflect regressive sedimentation; and (2) the metal bearing strata extend into the overlying evaporites and into the oxidised layers below.

The sabkha model of Renfro (1974), was proposed to explain the genesis and the sulphide zonation of the central African Copperbelt deposits. This model takes cognisance of the common presence of evaporites and fossil algal mats in the sedimentary successions that host the mineralisation. A sabkha is a coastal evaporite flat bordering a body of water on one side and a desert on the other. It differs from a normal evaporite pan in that the depositional environment is subaerial whereas that of an evaporite pan is subaqueous. An incipient sabkha forms when sediment supply and subsidence reach a steady state, causing an evaporite suite (aragonite-gypsum-halite) to rest on desert continental sediments. In a coastal sabkha, groundwater evaporation causes solutes to be deposited at the sabkha surface. This results in a subsurface hydraulic gradient, which induces marine water of high pH and low Eh to flow inland towards the sabkha, while meteoric underground water of low pH and high Eh flows seaward. The sequences develop from regression-transgression to regression and the creation of a mature sabkha accompanied by precipitation of sulphides, with a zonation dictated by the affinity of the metals with sulphur. The mechanism involved is explained as follows. The body of water adjacent to tha sabkha is prolific with blue-green algae. These tend to form algal mats which, upon decay, generate much H_2S, CO_2, CH_4. The landward flowing marine waters are therefore enriched in these constituents, whereas the terrestrial meteoric waters carry traces of Cu, Ag, Zn, Pb and Fe. On transgression, the algal facies will onlap the oxygenated desert sediments, and at the same time the advancing marine water forces the meteoric waters back towards the land. During regression, the algal mat is over-ridden by the evaporites while the trailing edge is buried by desert sediments. On evaporation above the mixing zone, the metal-bearing groundwaters combine with sulphur sourced from the decay of algal mats to precipitate sulphides, whereas Mg from sea water causes dolomitisation of carbonate rocks. Reactions that produce sulphides from bacterial reduction of evaporitic sulphates are:

$$CaSO_4 + CH_4 \rightarrow CaCO_3 + H_2S + H_2O$$
$$MeCl_2 + H_2S \rightarrow MeS + 2HCl$$

The sabkha model, however, was considered "*a seductively simple vision*" by Eugster (1986), who attempted to link the relationship of sedimentary-hosted ore deposits with shales and evaporites. This author envisaged that NaCl-rich brines, derived from evaporites, and acidity resulting from oxidation of pyrite in organic-rich shales, are necessary to produce solutions that are capable to leach metals from rock-forming silicates and oxides.

Speczik (1995) reviewed the Kupferschiefer, and considered that ascent of metalliferous brines along the flanks of basement highs and their overturning beneath the Zechstein evaporite cap (Jowett's model, see below) formed the

stratabound mineralisation. A model of convective circulation of diagenetic metalliferous brines in sedimentary basin, such as the Kupferschiefer, was proposed by Jowett (1986). In this model, convecting diagenetic brines move downward into the deepest parts of the basin and upward along the flanks of basement highs, and metal deposition takes place below an impermeable cap, where the brines turn over for the return flow into the basin. Metal deposition occurred below the evaporitic sediments of the Zechstein, which is where the brines turn over for the return flow into the basin.

As already stated, there is good evidence of a spatial relationship between types of sediment-hosted mineralisation from deeper and hotter towards cooler and higher regions of a sedimentary basin or, in other words, from shale-hosted to carbonate-hosted deposits. The spatial arrangements and mineralisation styles provide a possible link between the diagenetic and the exhalative theories. Heating of the basinal fluids by a source of thermal energy (mantle?, magmatic?) creates hydrothermal convection in the deep portions of the basin, upward movement and channelling of the fluid along graben faults or other fractures to eventually exhale at, or below the water-sediment interface, where they would precipitate sulphides. A hypothetical sediment-hosted exhalative sulphide deposit and its progressive zonation away from the point of exhalation as well as its epigenetic and syngenetic facies, could form in this way.

The abundant and varied mineralisation types of the Pan-African Lufillian orogen of Zambia, D. R. Congo and Angola was explained by Unrug (1988) in a model of hydrothermal fluid circulation that combines Jowett's (1986) diagenetic brines with deep-seated fluids. Unrug's model, although disputed by Sweeney and Binda (1989) and Garlick (1989), elegantly puts the controversial Copperbelt and adjacent areas into a unified framework of rift tectonics, associated basin evolution and hydrothermal fluid development. This model is described here. The stratiform Cu-Co Copperbelt mineralisation occurs near the base of a thick stratigraphic succession of the Katangan Supergroup. Also present in the succession are other types of mineral systems, including vein and skarn deposits, containing a host of metals such as U, Au, Ag, Pb, Zn, etc. The stratiform mineralisation was emplaced before folding and metamorphism, and it is recognised that Cu and Co were probably brought into the basin at a late stage of diagenesis. The temperature of the hydrothermal fluids is estimated to have been between 200 and 250°C higher than the 100–150°C of the brines responsible for the Mississippi Valley-type deposits. Basinal brines were developed in the deepest parts of the basin, and formed convective cells driven by a high heat flow associated with the rifting event that created the basin. These brines probably originated by compaction and dewatering of the thick pelitic sequence of the Lower Kundelungu. The thermal gradient forced circulation of the fluids in the aquifers of the Roan Group sediments on the shoulders of the rifted basement blocks. The fluids in turn interacted with the lithologies containing the primary diagenetic sulphides (pyrite mainly) to give rise to the stratiform mineralisation. The fluids in the Lower Roan group were confined by the impermeable overlying units of the Grand Conglomerat, and flowed

updip along the basement highs, where they may have overturned (see Jowett 1986) to flow back into the deeper parts of the basin to complete the convection cell. At a later stage, metamorphism, compression and deformation of the sedimentary sequences produced renewed hydrothermal activity in the form of metamorphism-generated and -driven fluids. These could have formed the vein-type mineralisation also present in the region. Rift-related alkaline magmatism may have been responsible for the skarn mineralisation.

8.7 SEDEX Ore Systems

Sediment-hosted exhalative, stratiform, massive sulphide deposits, commonly referred to as SEDEX, are a major source of base metals. A selection of these ore deposits are listed in Table 8.6. The age range of SEDEX deposits is from 150 Ma to about 1800 Ma, but the largest and richest are those of Proterozoic age (see Fig. 3.8). SEDEX ore deposits are formed by fluids rich in metals, particularly Cu, Pb, Zn, Ag and Ba that ascend along graben-bounding faults to exhale at higher levels. The composition of the fluids depends on the nature of the basin lithologies (e.g. volcanic-dominated, sedimentary-dominated, presence of evaporites in the succession). The mineralisation that results from these exhalations is typically zoned outward from the point of discharge, and has vent and feeder pipe facies, a syngenetic proximal bedded facies and a distal sedimentary facies, as illustrated in Fig. 8.2. The bedded facies consists of sulphides, of which pyrite and pyrrhotite may be major components. The main Zn and Pb ore minerals are sphalerite and galena with lesser chalcopyrite. Chert, quartz, barite, fluoroapatite and various carbonates are common gangue minerals. Much of the chert is hydrothermally derived, as Jiang et al. (1994) have demonstrated in a study of the Sullivan deposit, based on silicon isotopes. This study showed that silica precipitated during hydrothermal processes has negative $\delta^{30}Si$ (–0.6 to about –3‰). Carbonates commonly include calcite, siderite, ankerite, dolomite and Ba-carbonates (Goodfellow et al. 1993). Distal facies hydrothermal sediments include barite, Fe-Mn oxides, and hematite-chert iron-formation. In many deposits massive barite reaches tonnage and grade of economic significance, as for example at Gamsberg in South Africa (McClung et al. 2007) and Meggen (Germany), where barite represents a resource of 10 Mt with a grade of 95% (Large and Walcher 1999). Feeder pipes are commonly characterised by silicification and veining.

Alteration haloes in SEDEX systems can be extensive. Leach et al. (2005) described Fe-Mn alteration, silicate, trace element and isotopic haloes. Iron-Mn alteration is usually well developed in carbonate-siltstone hosts rocks and can extend along the stratigraphy for tens of km, with Fe and Mn contents decreasing away from the ore zones. The alteration phases are Mn siderite, Mn ankerite and ferroan dolomite. At the Century deposit (Large et al. 2005), there is extensive Mn ankerite alteration along and laterally from the Termite fault zone. This Mn ankerite alteration envelops lenses of Mn siderite alteration and

Table 8.6 Age, tonnage and metal grades of selected SEDEX ore deposits

Deposit (country)	Age (~Ma)	Million tonnes(total resource)	Cu%	Zn%	Pb%	Ag ppm	Reference
HYC (Australia)	1640	227		9.2	4.1	41	Williams (1998a)
Century (Australia)	~1570	105		12	1.8	46	Huston et al. (2006)
Lady Loretta (Australia)	~1650	13.6		17	5.9	97	Huston et al. 2006)
Mount Isa (Australia)	1652	~150		7	6	150	Huston et al. (2006)
Hilton-George Fisher (Australia)	1652	228		10.8	5.5	97	Huston et al. (2006)
Cannington (Australia)	~1676	43.8		4.4	11.65	538	Walters et al. (2002)
Broken Hill (Australia)	~1690	280	0.14	8.5	10	148	Huston et al. (2006))
Rosh Pinah (Namibia)	1100	?	0.1	7	2		Goodfellow et al. (1993)
Gamsberg-Aggeneys district (South Africa)	~1650	439	0.21	3.6	1.43	21	McClung et al. (2007)
Red Dog (Alaska)	350	140		16.6	4.6	70	Edgerton (1997); Kelley and Jennings (2004)
Meggen (Europe)	370	50	0.2	8	1	14	Large & Walcher. (1999)
Rammeslberg (Europe)	370	28	1–2	17–21	7–12	80–120	Large & Walcher. (1999)
Sullivan (Canada)	1430	162		5.86	6.08	67	Goodfellow and Lydon (2007)

the laminated sulphides of the ore zone. Silicate alteration haloes are present in some siliciclastic-hosted SEDEX. Silicified wall rocks occur in the Rammelsberg and Century deposits. At Sullivan (see also below) a pipe zone, below the deposit, contains tourmaline flanked by chlorite-pyrrhotite alteration, whereas the hangingwall is characterised by a zone of chlorite-albite-pyrite, in turn enveloped by pervasive muscovite alteration. One of the most conspicuous

trace element haloes is that of Tl, which in the Australian deposits has values ranging from 100 to 1000 ppm in the ore zones, steadily decreasing laterally to values of less than 1 ppm at distances of 1–20 km along the ore horizon. Other trace element that exhibit dispersion haloes from the ore zones are As, Ba, Bi, Ge, Hg, Ni, P and Sb. Isotopic haloes mentioned by Leach et al. (2005), include variations in C, O and Sr isotopes. The HYC and Sullivan deposits exhibit ^{18}O-enriched ($\delta^{18}O$ values from 23 to 26‰) and ^{13}C depleted ($\delta^{13}C$ –2 to –3.5‰) signatures, compared to similar sedimentary rocks of the region. Strontium isotope compositions of barite and carbonates have strong radiogenic values (up to 0.718) compared to sea water values (0.708), as exemplified by $^{87}Sr/^{86}Sr$ ratios of bedded barite from the Aggeneys-Gamsberg SEDEX systems in South Africa (McClung et al. 2007). Ore textures are important in attempting to establish syngenesis versus epigenesis in SEDEX ore systems. Although SEDEX deposits exhibit substantial variations in ore textures, typical ore textures are bedding-parallel layers or laminations, alternating with the host sediments. Also present are breccias, veins, sulphide disseminations and nodular textures. Textural features of SEDEX have been variably interpreted as due to synsedimentary or replacement processes (Leach et al. 2005). Some of the evidence for synsedimentary processes includes: interlayering of sulphide bands with the host sediments (Fig. 8.16); presence of subrounded sulphide clasts in graded sediments and interpreted as due to reworking of pre-existing sulphide layers. Replacement processes are indicated by sulphide replacement of carbonate or barite layers and nodules; sulphide replacing barite crystals and glass shards. Leach and co-workers pointed out that all these textures can be explained by sub-seafloor replacement below a zone of exhalative activity (see Fig. 8.2). Mineral zonations in SEDEX are linked to the exhalative system (see Fig. 8.2), with the reduced phases along and near the discharge zone and the more oxidised phases towards and within the distal ore facies. This zoning is reflected by trends of increasing Fe/Zn, Fe/Pb, Zn/Pb ratios and decreasing Zn/Ba, Zn/Mn ratios and ore grades, from the discharge zone towards the periphery of the system (Lydon 2004). Large et al. (2005) reported zonation of ore minerals in the Mount Isa district from pyrrhotite → galena → sphalerite → pyrite, from the boundary of silica-dolomite alteration outward. Vertical metal zonation is manifested by a general upward decrease of Zn/Pb ratios and increasing Zn/Fe ratios.

The sedimentary successions of SEDEX hosting basins are in general similar and characterised by basal clastic-dominated or clastic-volcanic-dominated sequences, overlain by argillaceous rocks, carbonates and/or evaporites. The SEDEX systems tend to be sited in the upper parts of the successions, in reduced sedimentary units, such as shale, siltstone, mudstone or within intercalated carbonate rocks. SEDEX fluids have a wide range of temperature and salinities. Maximum homogenisation temperatures of approximately 400°C have been reported from fluid inclusions, but more commonly temperatures ranging from 70 to about 180°C have been recorded from a number of deposits. Similarly, maximum salinities of >45% NaCl equivalent are unusual, with most ranging

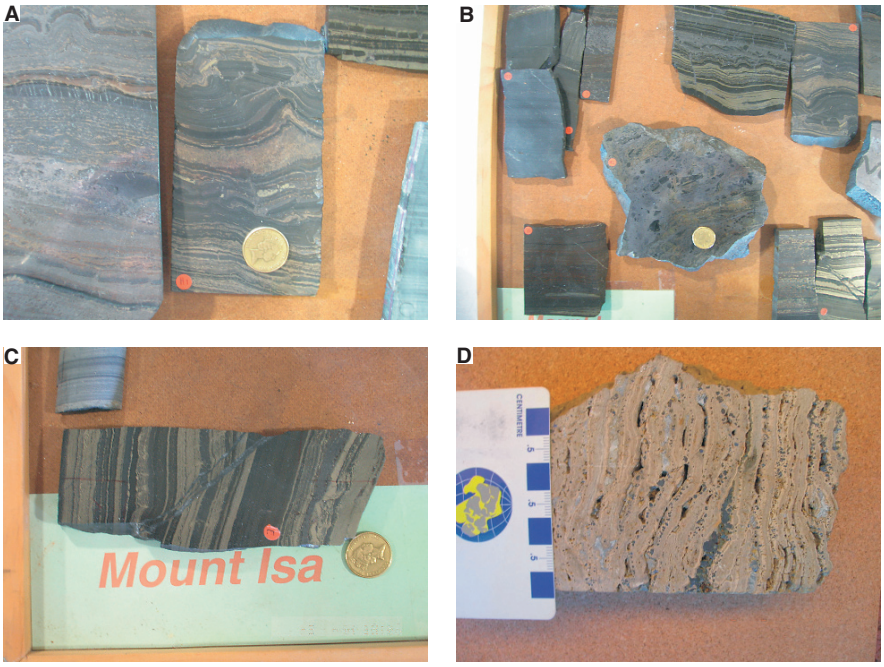


Fig. 8.16 Photographs of hand specimens from Mount Isa finely laminated ores (**A**, **B** and **C**), courtesy of Centre for Ore Deposit Research (CODES), University of Tasmania; (**D**) hand specimen of sphalerite from the Cadjebut MVT deposit, Western Australia

from about 10 to 23 wt% NaCl. At the Red Dog deposit, primary fluid inclusions in sphalerite recorded homogenisation temperatures of 100–200°C and salinities of 14–19% NaCl (Leach et al. 2004). The thermal energy that powers the ore fluids may be the result of high geothermal gradients (e.g. mantle heat in crust attenuated environments), circulation of brines to great depths, or magmatic activity at depth. The latter is probably the cases for those SEDEX systems that are temporally and spatially associated with intrusive and volcanic rocks. Sources of ore fluids are mostly basinal metalliferous brines, with the high salinities attributed to dissolution of salts from evaporite beds, although Leach et al. (2005) pointed out that many SEDEX deposits are hosted in sedimentary basins with no evaporites. In this case, these workers suggested a mechanism of gravitational settling of brines in the lower parts of the basin stratigraphy. In other cases, models of basin-hugging brines have been proposed, in which brines infiltrate sediments underlying a brine pool. The metal contents of SEDEX ore fluids is linked to S species in solution, such as H_2S for reduced, acidic with comparatively high temperature fluids (200–300°C) and SO_4 for oxidised, neutral to alkaline, lower temperature fluids (100–200°C). Sulphur isotope systematics ($\delta^{34}S$ in SEDEX range generally from –7 to +27‰) indicate that the source of S was

likely marine sulphate, followed by bacterial reduction and/or thermochemical reduction of the sulphate (see Chapter 10).

The tectonic settings of SEDEX systems are of three types (Leach et al. 2005): (1) intracontinental rift systems developed as back-arc extension; (2) continental rifts floored by oceanic crust (Red Sea type; Fig. 8.1 and Section 8.5); and (3) rifted passive continental margins. Although cases have been made for intracontinental rift basins similar to those of the EARS (Section 8.4), and therefore with lacustrine sedimentary facies, isotopic signatures of microbial carbonates suggest precipitation of carbonate sediments from sea water. If this is correct, these intracontinental basins may have been embayments connected with the open ocean, although I would not exclude EARS type lakes and/or basins in Afar-type regions, where abundant evaporites occur (Section 8.4).

Sawkins (1989) suggested that the formation of the giant base metal exhalative sedimentary rock-hosted massive sulphide deposits, such as Broken Hill, McArthur, Mt Isa (Australia), Aggeneys-Gamsberg (South Africa) and Sullivan (Canada) are related to anorogenic felsic magmatism, and that these deposits are formed during advanced phases of rifting. Plimer (1986) cited different types of ensialic rifting (failed to successful), mantle degassing, and associated magmatism to explain the development of complex exhalites at Broken Hill and Mt Isa in Australia. Plimer (1986) argued that the Mt Isa orebodies were formed in an aulacogen-type rift setting, where hypersaline brines formed hydrothermal systems that were focused and exhaled into depressions in the deep grabens, with no magmatic component. Periodic expulsion of the heated brines would have taken place in accordance with Sawkins' views. The brines would have moved along major fractures and faults at high pressure. In contrast, the Broken Hill scenario has an association with bimodal (mafic-felsic) magmatism related to deeper and more successful rifting in a thinner continental crust. Plimer's model assumes mantle fluids enriched in CO_2, F, B, H_2, P, Mn, Fe, Pb, Zn, REE to have risen along the graben faults and to have locally mixed with sea water (Section 8.7.1.2). Submarine exhalations deposited sulphides and other exhalites containing Si, Zn, Mn, Fe and B-rich minerals on the floor of the rift valleys. Both the regional and local zonations of the Broken Hill setting are interpreted in terms of distance, upward and laterally, from the conduit through which the hydrothermal fluids rose. A similar zonation at the regional scale is observed in Namaqualand (South Africa), for the Aggeneys-Gamsberg deposits.

As mentioned above, SEDEX world-wide were mainly formed in the Palaeo-Mesoproterozoic, between 1.6 and 1.0 Ga, with another group (e.g. Red Dog, Howard Pass) having developed in the lower-middle Palaeozoic (Table 8.6). Groves et al. (2005) discussed the temporal patterns of SEDEX systems and drew attention to the fact that the giant Ausralian SEDEX deposits formed during the final assembly of Australia at ~1750–1700 Ma, which was part of a supercontinent assembly that involved the collision and amalgamation of Laurentia, Baltica and Siberia. This would have provided the setting for the development of rift basins and high heat flow in the crust, due to emplacement of high heat producing granites, which Groves et al. (2005) suggested may have

been implicated in providing the necessary thermal energy for the circulation of basinal brines. Collision events along the margins of the protoAustralian continent would also have resulted in far-field extensional tectonism that formed rift basins, as also suggested by Betts et al. (2003). The topic of the temporal distribution of ore systems is discussed more fully in Chapter 3.

In the next sections, I discuss what I consider as some of the best studied and described SEDEX systems, namely those in Australia and in South Africa.

8.7.1 SEDEX Systems in Australia

Precambrian (Archaean and Proterozoic) Australia is represented by terranes and tectonic units west of the Phanerozoic "Tasmanides" (Direen and Crawford 2003). The Archaean to Palaeo-Mesoproterozoic cratonic framework of Australia consists of the West Australian Craton (WAC), North Australian Craton (NAC), and South Australian Craton (SAC) (Fig. 8.17). The geodynamic evolution of Proterozoic Australia has been discussed in some detail by Myers et al. (1996), Betts et al. (2002), Giles et al. (2004), and Betts and Giles (2006). Solomon et al. (2000) provided a detailed and comprehensive review of the Proterozoic in Australia and associated mineral deposits. Wyborn et al. (1994) and Jaques et al. (2002) reviewed the Australian Proterozoic mineral systems. A special issue of Economic Geology is devoted to Australian Zn-Pb-Ag deposits (Southgate et al. 2006a). The following summary of the geodynamic history of Proterozoic Austrtalia is taken from Pirajno and Bagas (in press, and references therein).

The geodynamic history of the NAC, WAC and SAC began with the collision of the NAC and WAC, between ~1830 and ~1760 Ma during the Capricorn-Yapungku-Stafford-Early Strangways orogenies, along the Capricorn-Rudall-Arunta orogenic belts. Between ~1760 and ~1620 Ma, much of the tectonic activity was related to the collision of the Gawler Craton, coming in from Antarctica, with the NAC (Kimban-Late Strangway orogenies). This also produced the inversion of the Leichhardt Superbasin in the Mount Isa Inlier and renewed magmatism in the Arunta Orogen at about ~1640 Ma. Şener et al. (2005), using new geochronological data, suggested that the amalgamation of the NAC, SAC and WAC was completed by ~1750–1720 Ma. The next stages saw the development of the McArthur River-Mount Isa, Broken Hill, Georgetown rift systems, accompanied by large-scale bimodal magmatism (e.g. Gawler Range Volcanics and Hiltaba Event in SAC; Giles 1988). These rift systems are considered as being intracratonic back-arc extensional structures, which were formed as a result of regional and far-field tectonic stresses (Betts et al. 2002) (Fig. 8.18).

These rift basins developed mainly in the NAC between ~1800 and 1660 Ma (Betts et al. 2003; Foster and Austin 2007), in which the SEDEX Pb-Zn-Ag deposits were formed. The McArthur River-Mount Isa Inlier intracontinental

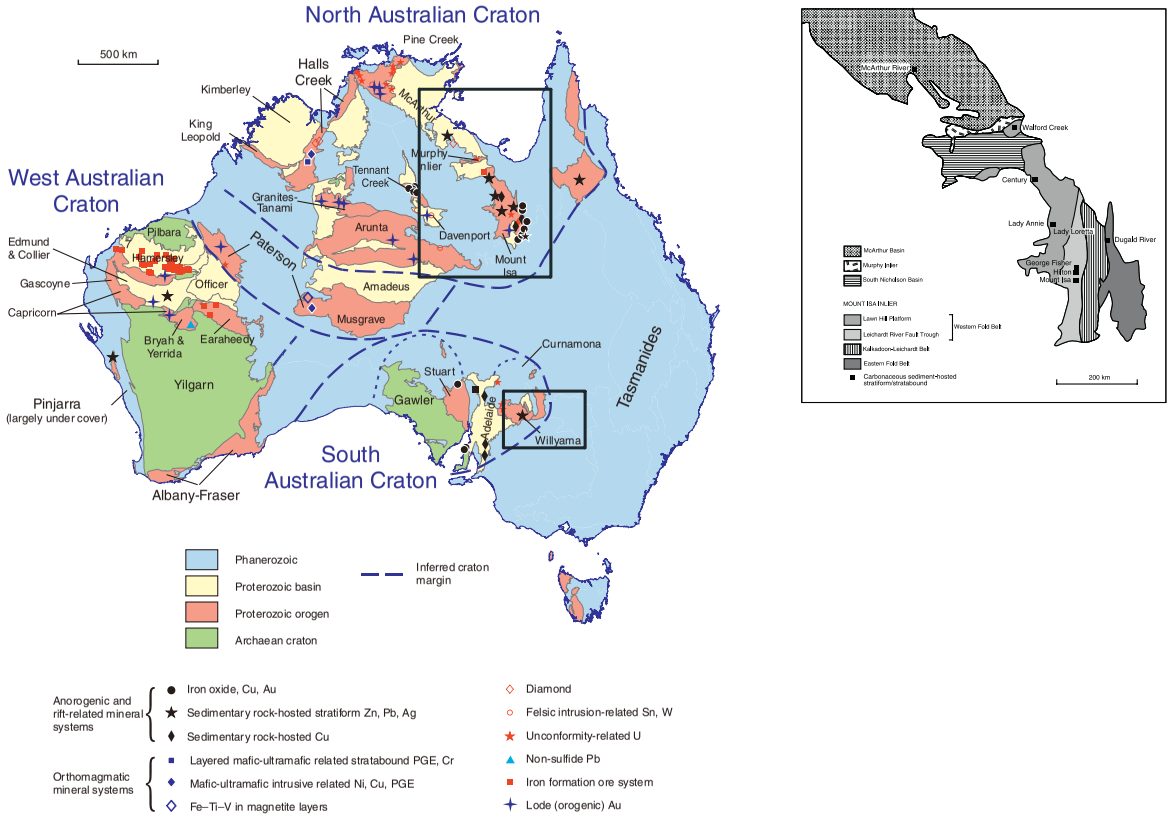


Fig. 8.17 Australia's Phanerozoic, Proterozoic and Archaean terranes and distribution of selected mineral systems of Proterozoic age (based on and modified from Jaques et al. 2002). After Pirajno and Bagas (2008). McArthur-Mount Isa and Willyama rift basins shown in the squares; map at left shows the simplified geology of the McArthur-Mount Isa rift system and distribution of Mount Isa type (MIT) ore deposits, after Williams (1998a,b)

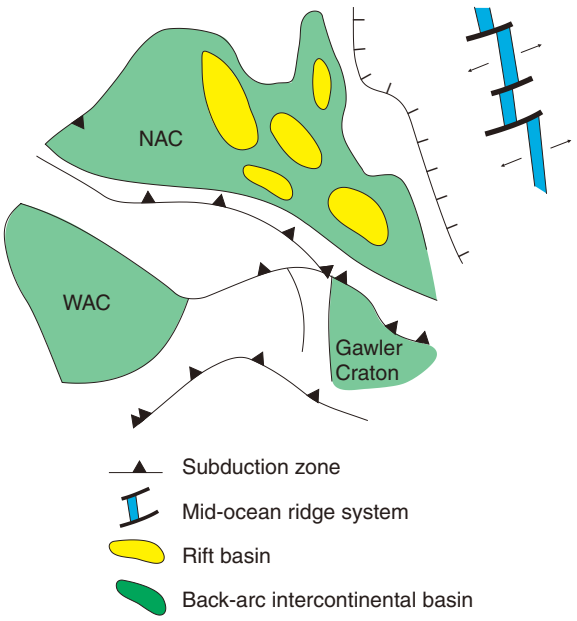


Fig. 8.18 Schematic and not-to-scale sketch showing the development of intracontinental basins in the North Australian Craton in a back-arc tectonic setting (Pirajno and Bagas 2008; based on Betts et al. 2002; Betts and Giles, 2006)

rift basin system of the NAC extends for more than 1200 km along a north-northwest trend, containing up to 15 km of sedimentary successions. The main tectonic elements of the rift basin system, from north to south are (see inset in Fig. 8.17): McArthur Basin, Murphy Inlier, South Nicholson Basin, the Mount Isa Inlier, comprising the Western Fold Belt (Lawn Hill Platform and Leichardt River Fault Trough), Kalkadoon-Leichardt Belt and the Eastern Fold Belt. These continental rift-related basins are characterised by thick clastic sedimentary sequences and bimodal (felsic-mafic) magmatism with widespread alkali metasomatism. Crustal thinning, extension and bimodal magmatism suggest some form of mantle upwelling, perhaps due to a mantle plume or to convective removal of continental lithosphere (crustal delamination; Gibson et al. 2004). In the SAC, the Olary-Willyama Block (Fig. 8.17) contains sedimentary and bimodal volcanic rocks in the ~1690–1590 Ma Willyama Supergoup, which hosts the stratiform Broken Hill massive sulphide deposits (Gibson et al. 2004). Huston et al. (2006) subdivided Australian SEDEX in two main types: Mount Isa type (MIT) and Broken Hill type (BHT).

8.7.1.1 MIT Ore Systems

The McArthur River-Mount Isa basins system cover an area of about 200 000 km^2 and includes some of the largest massive sulphide deposits in the world, namely: Mount Isa, McArthur River HYC (Here is Your Chance),

Hilton-George Fisher, Lady Loretta, and Dugald River. Together they make up the largest Zn-Pb metallogenic province in the world. Similar to these, but of different age is the ~1595 Ma Century deposit. Prior to mining, Mount Isa contained about 150 Mt @ 7% Zn, 6% Pb and 150 g/t Ag; HYC contained 237 Mt @ 9.2% Zn, 4.1% Pb, and 41 g/t Ag; Century contained 118 Mt @ 10.2% Zn, 1.5% Pb and 36 g/t Ag (Betts et al. 2003; see also Painter et al. 1999; Williams 1998a,b; Southgate 2000; Betts and Goleby 2006). Important features of these giant ore systems, as listed by Large et al. (2005), include: (1) ores located at or near basin-scale synsedimentary faults, along which fluids were channelled; (2) deposits hosted in organic-rich black shale and siltstone; (3) bedding-parallel synsedimentary sulphides; (4) stacked ore lenses separated by Fe-Mn carbonate-bearing rocks; (5) metal zonations, vertical with upward-decreasing Zn/Pb ratios, and lateral with increasing Zn/Pb ratios away from feeder structures; (6) stratabound Fe-Mn alteration haloes; and (7) lack of footwall stringer zones or vent systems. A conceptual genetic model for the McArthur River and Mount Isa ore systems is shown in Fig. 8.19.

Detailed descriptions of the MIT ore systems and North Australian tectonostratigraphy are provided by Large et al. (2005), Southgate et al. (2006b) and Huston et al. (2006). The following discussion is derived from these sources, in places combined with overviews from Pirajno (1992). The Mount Isa basin has three superbasins, bounded by unconformities, from bottom to top: ~1800–1745 Ma Leichhardt, ~1745–1690 Ma Calvert and ~1670–1575 Ma Isa. Siliciclastics bimodal volcanics and felsic magmatism dominate the two lower superbasins, whereas the Isa superbasin contains shallow-water carbonate rocks, deeper water shale and siltstone and, importantly for ore genesis, organic matter-rich shales. The stratigraphy of the three superbasin and the position of the SEDEX systems is shown in Fig. 8.20 and the general basin

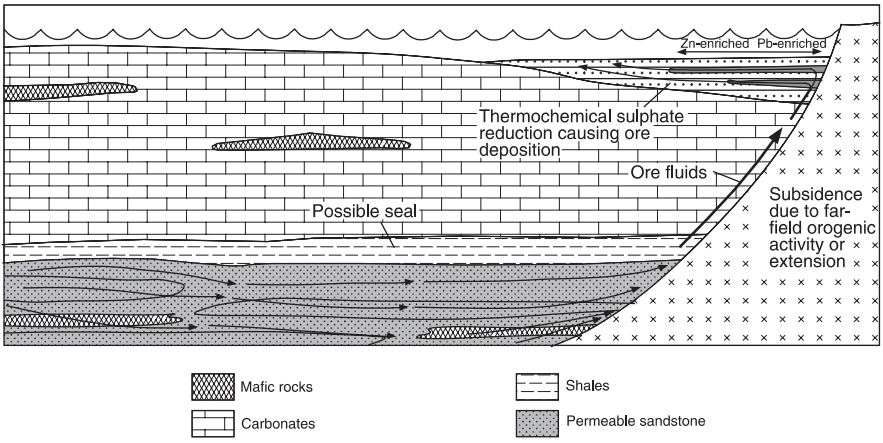


Fig. 8.19 Main components of a Mount Isa type (MIT) ore system; shaded area at base represents a zoneof metal leaching and K-feldspar-hematite alteration. After Huston (2006)

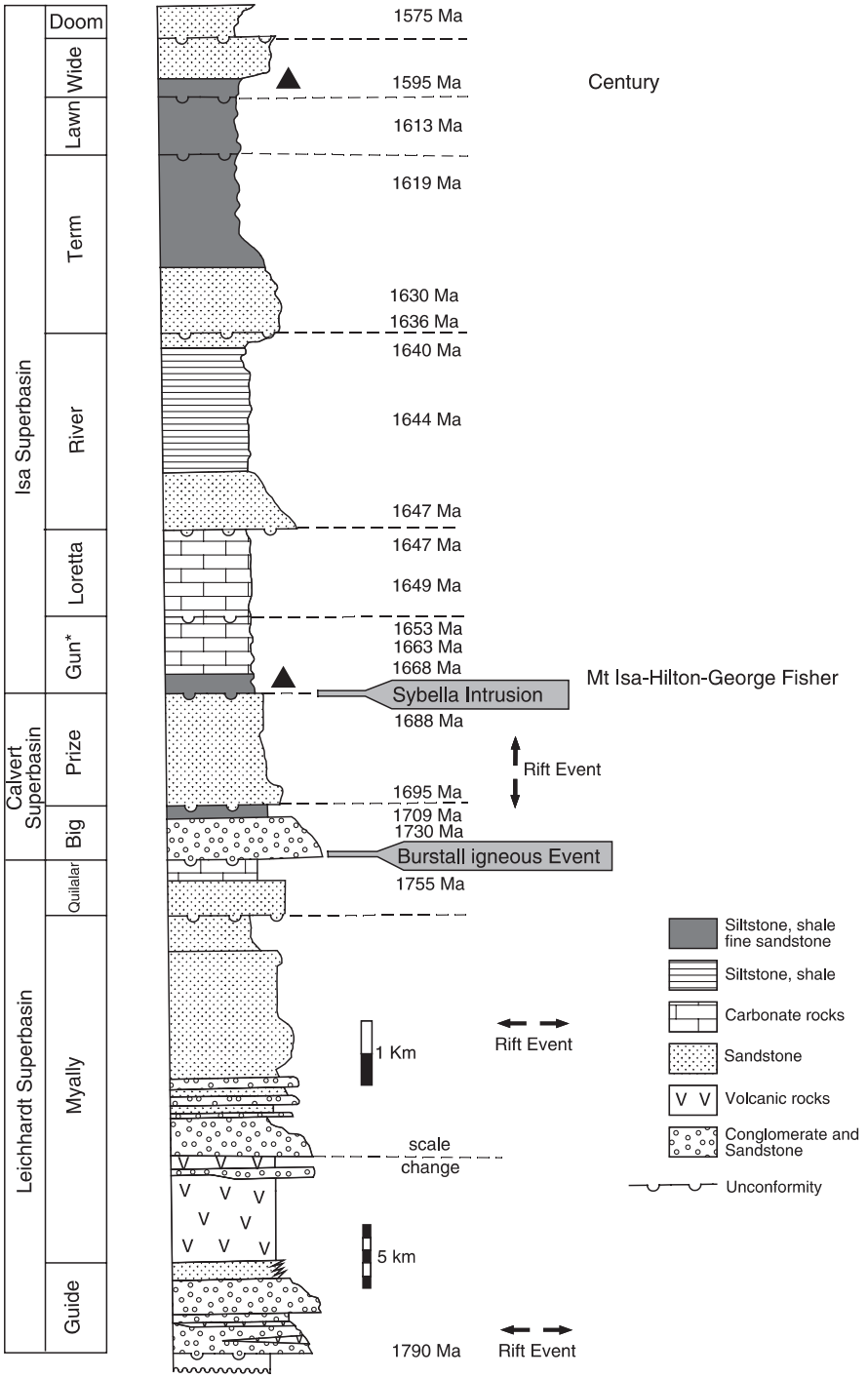


Fig. 8.20 (continued)

architecture is shown in Fig. 8.21. The MIT deposits formed in sub-basins developed by pull-apart structures along major strike-slip faults. These intracratonic basins may have developed as a result of far-field tectonism along the southern margin of the NAC, or as a result of back-arc extension (Fig. 8.18). Because the MIT are not spatially associated with igneous rocks, present in the lower two superbasins, the MIT ore systems are thought not to be related to hydrothermal fluids driven by magmatism. This is confirmed by fluid inclusion studies showing low temperatures (70–240°C) of the ore fluids. Basinal fluids interact with sedimentary mineral grains during burial and generate fertile basin brines. Flow of these basin brines can result in alteration of the more susceptible rocks, such as mafic igneous rocks. Potassium metasomatism has been recorded in dolerites and mafic volcanics in the vicinity of the HYC deposit and in the Mount Isa Western Succession, with two distinct mineral assemblages. One consists of K-feldspar, quartz, sericite, hematite, dolomite, barite and anatase, characterised by high Fe_2O_3/FeO ratios; the other assemblage consists of chlorite, K-feldspar and quartz, but with lower Fe_2O_3/FeO ratios. It appears that this type of alteration is regionally extensive, indicative of regional fluid flow largely controlled by fault zones. Hydrological modelling for MIT systems suggests fluid flow along permeable sedimentary packages along faults, such as the Termite Range Fault (Fig. 8.21B). Most researchers agree that deep penetrating faults in these basins promote fluid flow, perhaps driven by burial or magmatic heat. Alternatively, flow of basin brines may have been related to overpressuring and triggered by extension tectonics. The nature of the MIT fluids is still not entirely resolved. Fluid inclusion studies of the regional alteration zones show homogenisation temperatures ranging from 100 to 240°C and salinities of up to 20 wt% NaCl equivalent. As mentioned above, the MIT fluids are thought to be amagmatic basinal brines, with the source of the S and Cl being evaporitic units in the succession. Furthermore, it has been shown that altered volcanic rocks (Fig. 8.20) are significantly depleted in Pb and Zn, suggesting strong leaching and providing a metal source. Most evidence for the origin of the MIT ore systems supports a model of brines migration upward along faults and laterally through permeable, semiconsolidtaed sediments. This evidence includes the fine layering of the ores (Fig. 8.16). However, in the case of the Century deposit, although stratiform the finely laminated ores cross-cut the stratigraphy and geochronology work indicates that the ores postdate the age of the rocks by ~30 million years (Huston et al. 2006), suggesting that the mineralisation is post-sedimentary and epigenetic. Metal transport in MIT deposits occurs in saline conditions, with the H_2S source coming from

Fig. 8.20 (continued) Stratigraphic column for the Western succession of Mount Isa rift system, subdivided into three main sequences: Leichardt, Calvert and Isa Superbasins; and position (*black triangles*) of Mount Isa, Hilton, George Fisher and Century deposits. After Polito et al. (2006)

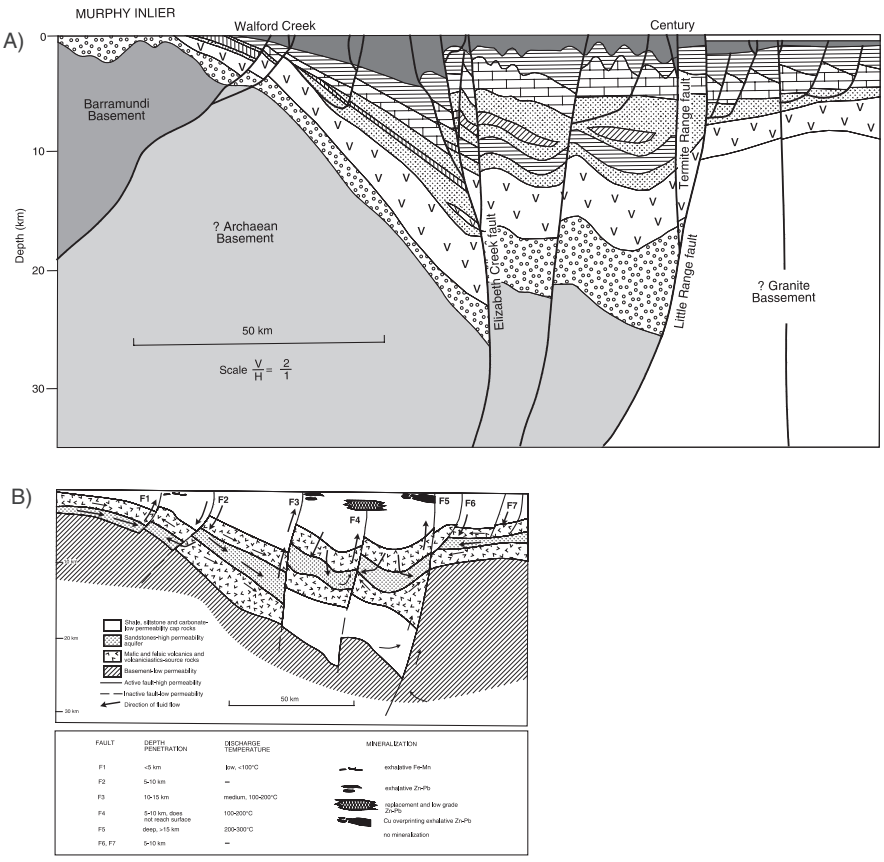


Fig. 8.21 Geological cross-section (**A**) between Murphy Inlier and Termite Range Fault, where the Century deposit is located, illustrating the architecture of the Mount Isa basin, see Fig. 8.20 for explanation of symbols; after Southgate et al. (2006b); (**B**) Main elements of Mount Isa style basin architecture, fluid flow and associated mineral systems, based on numerical modelling carried out by Zhang et al. (2006)

diagenetic pyrite, or by bacterial and/or thermal reduction of sulphates. Zones of fluid discharge, or outflow zones, must have been extensive judging by the widespread alteration haloes characterised by laterally anomalous Zn, Pb, Cu, Ag, Tl, Hg and Mn, up to 15–20 km from the ore zones.

8.7.1.1.1 McArthur River HYC

The McArthur River HYC (Here's Your Chance) deposit lies on the eastern margin of the north-trending Batten Trough, whereas Mt Isa and the close-by Hilton deposit are located further to the south in a northeast-trending trough (Fig. 8.17). The sedimentary succession within the Batten trough is essentially

unmetamorphosed, whereas those to the south around Mt Isa have undergone several periods of deformation and are variably metamorphosed. The HYC deposit was discovered in 1955 by a field assistant and exploration drilling carried out in 1959, when a mineralised zone approximately 1.65 km long, 1 km wide and 50 m thick was delineated. Development of this major deposit was initially hampered by metallurgical problems due to the very fine-grained nature of the ore. HYC has a mining resource of 125 Mt, grading 13% Zn, 6% Pb and 60 g/t Ag (Large et al. 2005; see also Table 8.6). The HYC deposit is located close to the Emu Fault and comprises at least eight stacked ore lenses hosted by a succession of dolomitic and siltstone rocks of the HYC Pyritic Shale Member, within which tuff bands were dated by U-Pb at 1640 Ma. The stratigraphic succession in the vicinity of the mineralisation represents a major transgression from subaerial red dolomitic siltstone of the Tooganinie Formation through intertidal and shallow marine carbonates of the Emmerugga and Teena Formations, to deeper water sediments of the Barney Creek Formation. Subsequent regression is represented by shallow-water and intertidal carbonates of the Barney Creek Formation and the overlying Reward Formation. The major orebody at McArthur River is the HYC orebody, which occurs in the HYC Pyritic Shale Member of the Barney Creek Formation. This unit was laid down in a sea-floor depression (Bulburra depression), whose development was controlled by syn-depositional movements along the Western and Emu faults. Other host rocks of the orebodies are dolomites of the Emmerugga and Cooley Formations, thought to represent either an algal reef complex or a near-shore carbonate bank. The HYC ore lenses vary in thickness from 3 to 12 m and consist of thin laminae of fine-grained pyrite, sphalerite and galena interbedded with shale and tuffaceous shale (Fig. 8.16). These beds show features of penecontemporaneous deformation, such as slumping.

The main sulphides of HYC ores are pyrite, sphalerite and galena, with lesser quantities of chalcopyrite, tetrahedrite, arsenopyrite, marcasite, chalcocite and covellite. As mentioned above, the main features of the HYC ores are the sulphide laminations and their bedding-parallel nature. Large et al. (2005) described four main mm-scale laminae types: (1) organic-rich mud layers; (2) quartz-illite-carbonate layers; (3) Zn-Pb sulphide-rich layers; and (4) laminae that are a mixture of the first three types. Sulphides are very fine-grained (1–10 μm) and intergrown with the laminae. Previous studies revealed distinct pyrite morphologies which, in conjunction with S-isotope systematics, were used to explain the genesis of the sulphide mineralisation. Pyrite occurs in three main forms: (1) euhedral to rounded crystals, between 2 and 5 μm in size, which were deposited first and occur as fine dissemination or laminae; (2) spherical pyrite in the size range of 5–20 μm; (3) framboidal shapes. The interpretation of pyrite morphologies and S-isotope systematics is not simple; it has been suggested that the pyrite was formed in two stages: (1) by a hot, metal-rich, but S-poor, brine, which dissolved early diagenetic pyrite; and (2) redeposition of pyrite on the earlier grains by the new S-enriched solution. Large et al. (2005 and references therein) reported two stages of pyrite (py1

and py2) and two stages of sphalerite (sph1 and sph 2), in the paragenetic order of py1 → sph1 → py2 → sph2. Latest studies show that sph1 and sph2 are texturally and isotopically distinct and that sph1 predates py2 and is syngenetic, whereas sph2 postdates py2 and is of diagnetic origin (Ireland et al. 2004; cited in Large et al. 2005).

The base metal sulphides are zonally distributed, showing decreasing Cu/Pb + Zn ratios from the Emu Fault towards the HYC orebody. This zoning, therefore, suggests that the mineralising fluids were possibly introduced along the Emu Fault and spread out away from it. Delta^{34}S values for sphalerite and galena increase westward from the Emu Fault, a feature which has been interpreted as due to cooling of the ore solutions away from the conduit represented by the Fault. The conformable nature of the ore, and its early diagenetic structures suggest a syngenetic origin for the HYC orebody. Williams (1978a,b) proposed an epigenetic model involving metal- and sulphate-rich solutions emanating from fault zones and reacting with the dolomitic rocks. In any case it is generally agreed that both the conformable and discordant deposits were formed from the same mineralising fluids, which flowed from the Emu Fault. The HYC pyritic siltstone laterally grades into nodular carbonate laminae, consisting of dolomite aggregates of 1–4 mm across that displace the siltstone and sph1 and are in turn displaced by sph2 grains and overprinted by py2. These textural features indicate that the nodular carbonate was formed sometime between the syngenetic and diagenetic stages.

Sulphur isotope systematics report a wide range of δ^{34}S values (13 to +45‰; Fig. 8.22; Large et al. 2005; Ireland et al. 2004). The δ^{34}S values are related to paragenetic stages, with the earliest sulphides (py1) having the lowest average δ^{34}S (–01‰), but with a wide range of values from –13 to +30‰, followed by the next stage of sulphide paragenesis (sph1) with a mean of 3.8‰ δ^{34}S and a much narrower range (–5 to +15‰). The next paragenetic stage is that of the diagenetic nodular sphalerite (sph2) with a mean of 9.8‰ and a range from +3 to + 19‰. The latest sulphide in the paragenesis is py2 with a mean δ^{34}S of +13.1‰ and the widest range (–5 to +45‰). These trend are interpreted as follows (Large et al. 2005; Ireland et al. 2004): py1 formed by bacterial reduction of sea water sulphate in an anoxic water column, sph1 was also produced by biogenic sulphate reduction in a transient pool of warm brines; the isotopically heavy S of sph2 formed in a closed system within muds underlying the brine pool and py2 from the remaining heavy S in the pore fluids of the sediments. Biogenetic processes are supported by the presence of microfossils (mostly cyanobacteria) in lenses of black chert that occur in the MIT ores (Logan et al. 2001). The metallifeorus brines, reacted with the organic rich muds, producing sulphides, according to the reactions (Logan et al. 2001):

$$2CH_2O + SO_4^{2-} \rightarrow 2HCO_3^- + H_2S$$

$$H_2S + M^{2+} \rightarrow MeS + 2H^+$$

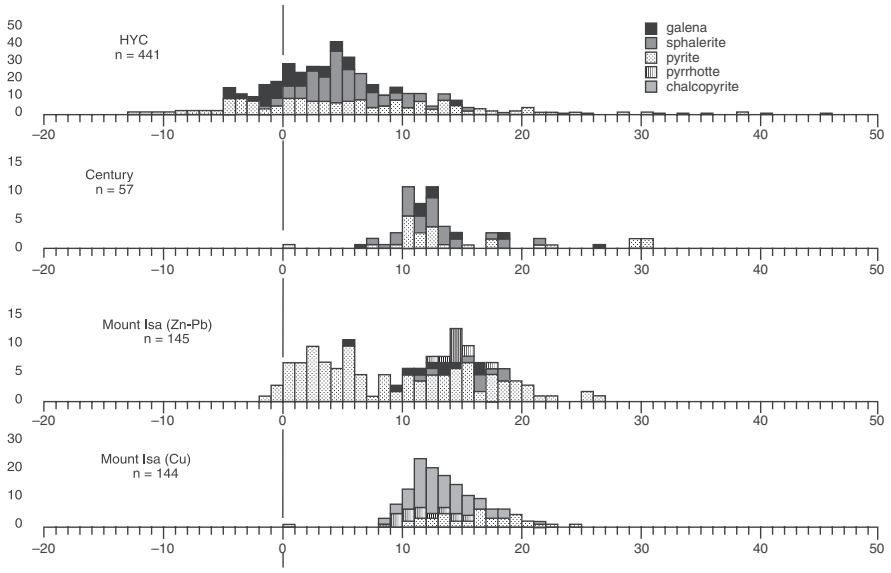


Fig. 8.22 Histograms of $\delta^{34}S$ values for sulphides from McArthur HYC, Century and Mount Isa Zn-Pb and Cu Zn-Pb-Ag ores. After Large et al. (2005 and references cited therein)

where MeS is metal sulphide.

Temperature estimates of the ore fluids are generally below 200°C, ranging from 100 to 270°C, although higher temperatures (250–400°C) have been recorded, but in the opinion of Large and co-workers these do not reflect the temperature at the site of the ore formation.

The genesis of HYC ores revolves around two models: syndiagenetic replacement and synsedimentary exhalative (Large et al. 2005). In the first model, the mineralisation would have formed within organic-rich sediments 10–20 m below the seafloor, with hot (250–400°C) metalliferous brines migrating along the more permeable sediments. In this model, biogenic pyrite was formed by diagenetic growth in the muds, followed by precipitation of Zn and Pb sulphides from metal complexes in hydrothermal fluids reacting with organic-rich compounds and sulphates. This model is not considered viable by Large and co-workers for the following reasons: the presence of laminated sulphide clasts in sedimentary breccias, close relationship of the ore lenses with the sedimentary breccias and, importantly, concentration of the Zn and Pb sulphides in the fine-grained shales and siltstone and not in the more permeable coarse-grained lithologies. In the synsedimentary exhalative model (Large et al. 1998; Ireland et al. 2004), pulses of metalliferous fluids entered the brine pool as bottom-hugging currents, with sulphides being precipitated both within and above the uppermost layer of muds on the seafloor. Stratiform py1 precipitated first due to bacterial sulphate reduction. Each pulse of fluid mixed with the existing brine

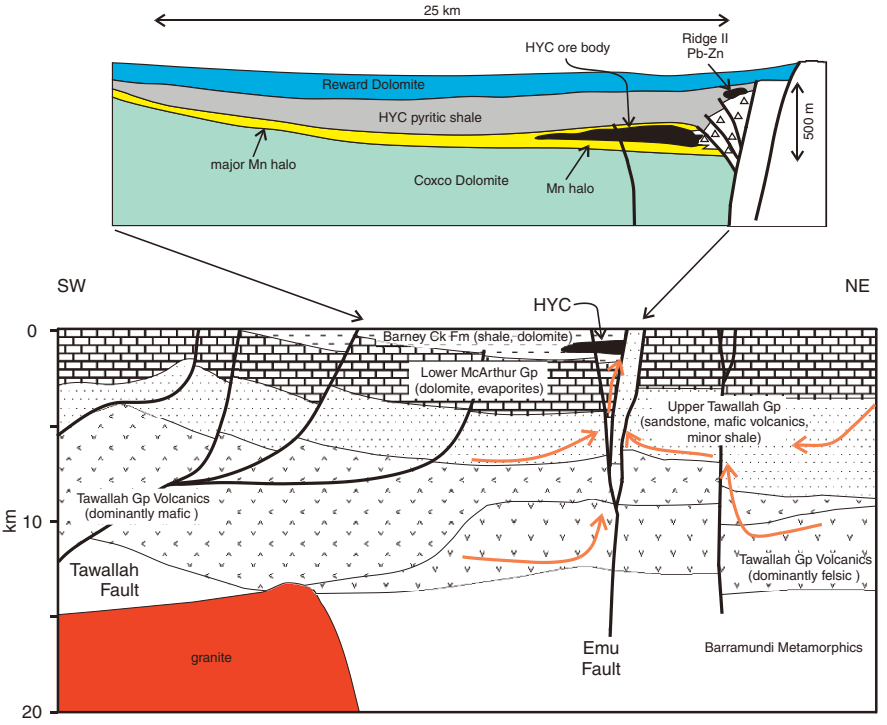


Fig. 8.23 Conceptual model schematically illustrating the genesis of the HYC ore system in the McArthur River-Mount Isa rift system; saline fluids may have derived from evaporite beds, mixing with magmatic fluids from subjacent granite plutons. From Pirajno and Bagas (in press), based on Large et al. (1998) and Large et al. (2005)

along the brine-anoxic transition zone, causing the precipitation of Zn and Pb sulphides and forming aggregates that subsequently collected on the basin floor by gravitational collapse, forming the well-known laminations. Sph2 and py2 followed with the replacement of carbonate nodules and by biogenic reduction in sulphide muds, respectively. The fine intercalated laminae of siltstone and sulphides are the result of repeated and interspersed pulses of metalliferous brines and turbidite sedimentation. A genetic model of the HYC ore system is shown in Fig. 8.23.

8.7.1.1.2 Mount Isa and Hilton-George Fisher

The Mt Isa and Hilton-George Fisher Pb-Zn-Ag deposits in the Mount Isa district, immediately east of the Mount Isa fault, are hosted by the upper part of the Urquhart Shale Formation, which is thought to be a correlative of the HYC shale at McArthur River. These three deposits have a combined pre-mining resource of >370 Mt, grading 10% Zn, 5.6% Pb, 120 g/t Ag (Large et al. 2005).

The Urquhart Shale Formation, occurs in the lower part of the Mt Isa Superbasin, and includes well-bedded carbonaceous, dolomitic, quartzo-feldspathic siltstone, dolomite and tuffite. At Mt Isa there are at least 30 stratiform ore horizons, each of which may be up to 35 m thick. The mineralisation extends for some 1600 m along the strike, discontinuously across a stratigraphic width of approximately 1200 m and downdip for about 650 m. There are 10 ore lenses at Hilton and 11 at George Fisher over 250 and 350 m of stratigraphic thickeness (Large et al. 2005). A schematic cross-section of the Mt Isa mineralisation is illustrated in Fig. 8.24. The major ore minerals, occurring as distinct concordant bands, are galena, sphalerite, freibergite, pyrite and pyrrhotite, with minor amounts of chalcopyrite, marcasite, arsenopyrite and tetrahedrite. Locally pyrite abundances of up to 50% have been recorded (Painter et al. 1999). Gangue minerals are Fe-dolomite, quartz, albite, microcline, chlorite, sericite and phlogopite. Folding has deformed the orebodies, and the re-mobilisation of sulphides during deformation events has resulted in enrichment of the mineralisation in fold hinges. Immediately adjacent to the Pb-Zn-Ag orebodies are large, non-stratiform Cu orebodies, which are confined to a silica-dolomite facies of the Urquhart Shale. The silica-dolomite consists of crystalline dolomite, re-crystallised shale and brecciated siliceous shale. The silica-dolomite orebody extends for about 2600 m and is 530 m wide at its thickest point near the greenstone basement contact. The Cu ore, which occurs as disseminations and vein fillings within the silica-dolomite rocks, includes pyrite, pyrrhotite and chalcopyrite, with minor amounts of arsenopyrite, marcasite, galena, sphalerite and a number of Co-As species. The major gangue minerals are siderite and quartz, with minor and localised talc, chlorite and K-feldspar. Chalcopyrite forms veins and irregular aggregates, usually associated with coarse-grained pyrite. Locally, bands of fine-grained chalcopyrite are associated with fine-grained framboidal pyrite. Mount Isa has high grade Cu lenses that are closer to the Paroo fault and separate from the Zn-Pn orebodies (Fig. 8.24). Copper mineralisation decreases dramatically in the Hilton deposit and attains background values only at George Fisher. Thus, there is a distinctive metal zonation from Mount Isa to Hilton to George Fisher, with marked decreases in Cu and Pb/Zn ratios. A sulphide zonation within individual lenses is present away from the silica-dolomite zone, characterised by pyrrhotite, galean, sphalerite, pyrite (Large et al. 2005).

The S isotopic composition of galena and sphalerite shows a range of $\delta^{34}S$ from 10 to 20‰, whereas the pyrite has ranges from –2 to + 28‰ (Fig. 8.22), suggesting differences in S source, but ultimately compatible with a marine sulphate source (Large et al. 2005; Painter et al. 1999). Delta^{34}S values for the Cu ores have a somewhat more restricted range, from 8 to 23‰ (Fig. 8.22). Based on the S isotopic data, Painter et al. (1999) suggested that the ores were formed at temperatures ranging from 240 to 120°C.

Large et al. (2005) discussed three genetic models for the Mount Isa-Hilton-George Fisher ore system. One model suggests a syngenetic-syndiagenetic replacement below the seafloor, with the Zn-Pb-Ag ores being analogous to

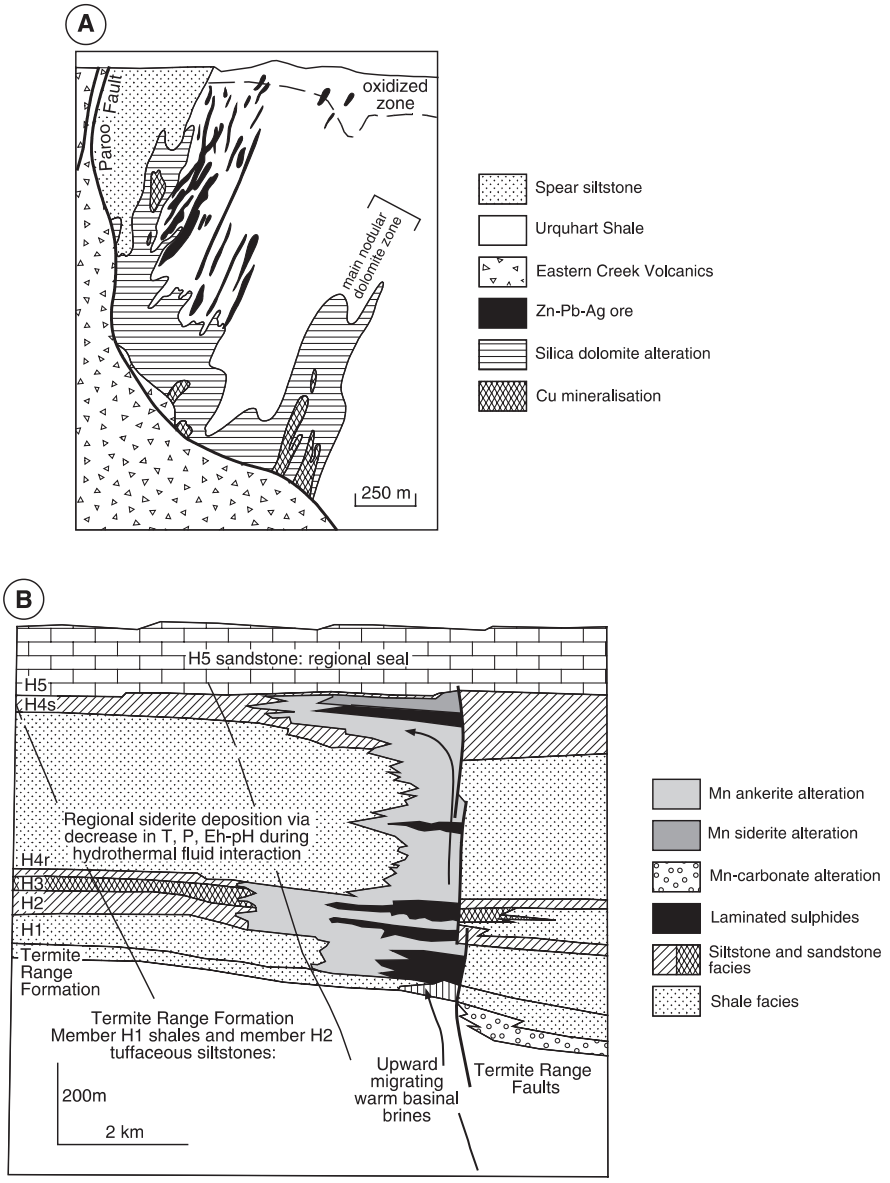


Fig. 8.24 (**A**) Simplified cross-section for Mount Isa showing stratiform Zn-Pb-Ag ore lenses, Cu orebodies and zones of silica-dolomite alteration; (**B**) model for the Century deposit, the H5 sandstone formed a barrier for the upflowing ore fluids, which moved along the Termite Range Fault zone, the ore was formed in the H4s shales, by reactions between the organic-rich shales, sulphates and metal chlorides. After Large et al. (2005)

those of HYC, whereas the Cu ores were formed by syntectonic replacement during the Isan orogeny. The second model mentioned by Large et al. (2005) suggests that both the Cu and Zn-Pb-Ag mineralisation were formed during the Isan orogenic event by syntectonic replacement. However, this model is not favoured because the age of tuff rocks in the host sequence is the same as that of the ores, indicating synchroneity of ore and sedimentation. The third model suggests that the mineralisation was formed during sedimentation and diagenesis below the seafloor, with a synsedimentary fault providing the conduit for the hydrothermal fluids. These fluids discharged on the seafloor and caused replacement below the seafloor. The silica dolomite and the Cu ores would have formed at a later time, closer to the feeder fault and by more evolved and hotter fluids that could transport Cu.

A variant of these interpretations for the genesis of the Mt Isa orebodies is that the Cu orebodies were formed syngenetically at the same time as the stratiform Pb-Zn-Ag ores, and that the silica-dolomite facies of the Urquhart Shale formed in a near-shore algal reef environment, which was sheared and recrystallised during later deformation. As for the McArthur River HYC deposit, the mineralisation may have formed by ascending mineralising solutions along channelways, probably a fault zone, which were active during deposition of the sediments. The Cu mineralisation could have been precipitated nearest the source of the fluids, with Pb, Zn and Ag further away from it, as illustrated in Fig. 8.2. An alternative hypothesis, proposed by Swager (1985), considers a hydrothermal-epigenetic origin for the Cu mineralisation in the silica-dolomite, temporally separated from the stratiform Pb-Zn-Ag mineralisation. According to Swager (1985), the silica-dolomite was formed during hydrothermal replacement processes coeval with a D_3 deformation event. On the basis of microstructural evidence, Swager (1985) recognised three stages of alteration-mineralisation: (1) silicification and dolomite re-crystallisation; (2) dolomitisation; and (3) chalcopyrite + pyrite + quartz + chlorite deposition. In conclusion, it is possible that the Mt Isa mineralisation resulted from two temporally distinct events. One, the stratiform Pb-Zn-Ag mineralisation, could have been formed during rifting by the movement of hydrothermal fluids activated by the high heat flow in the rift environment. The other, Cu and silica-dolomite, would be the result of a much later hydrothermal event connected with deformation and metamorphism. Thus, as pointed out by Large et al. (2005), the consensus seems to lie with the first model of synsedimentary Zn-Pb-Ag ores, later overprinted by syntectonic Cu mineralisation.

8.7.1.1.3 Century

The Pb-Zn-Ag Century deposit (Table 8.6), hosted by the Lawn Hill Formation in the Western Fold Belt of the Mt Isa Inlier (Fig. 8.17), is located close to the Termite Range Fault, probably the major conduit of ore fluids, on the west side of a 20-km diameter circular structure. This circular structure is recognised as a meteorite impact structure (Shoemaker and Shoemaker 1996); however, the age

of the impact structure is not known and any possible relationship to the Century deposit has not been considered. The host rocks are flat-lying to gently dipping siliceous black shales and siltstones, containing a 300 m-thick mineralised sequence, called H4. The Century deposit is spatially associated with a cluster of quartz-siderite-galena-sphalerite lodes, which formed late in the metallogenic history of the district (Broadbent et al. 2002). Importantly, a stratabound, siderite-Fe dolomite-ankerite-illite alteration is centered on Century and overlaps the surrounding vein systems, suggesting a genetic link (Broadbent et al. 2002). The Century ore lenses are bedding-parallel laminae of sphalerite and galena, with pyrite forming a halo around these ore lenses. A schematic cross-section and a model for the Century ore system is shown in Fig. 8.24.

Broadbent et al. (1998, 2002) studied this deposit and considered it as a new end-member of the hydrothermal sedimentary ore deposit family. The Century stratiform mineralisation is Zn-rich and consists of two major zones or blocks that are separated by a fault. The mineralisation transgresses the stratigraphy, in that the higher grade zones are associated with thicker black shale host rocks, indicating a replacement origin. The deposit is spatially associated with regional-scale lode mineralisation, mainly veins and breccias within fault zones. The main ore mineral is sphalerite, of which two varieties are present: one porous and associated with abundant pyrobitumen, the other is non-porous and with a low pyrobitumen content. The intergrowth of the sphalerite with hydrocarbons, suggests that thermochemical sulphate reduction (reaction of deeper sulphate and metal-bearing fluids with liquid and gaseous hydrocarbons), took place. The proposed reactions are:

$$CH_4 + SO_4^{2-} \rightarrow H_2S + HCO_{3-} + OH^-$$
$$HCO_{3-} + Me^{2+} \rightarrow MeCO_3 + H^+; \text{and}$$
$$H_2S + Me^{2+} \rightarrow MeS + 2H^+$$

where Me is a metal, such as Pb, Zn, Cu (see also Section 8.7.1.1.1).

An interesting ore genesis model, proposed by Broadbent et al. (1998), envisages that sulphate-bearing hydrothermal solutions originated from the deeper parts of the basin and were channeled along faults (Termite Range Fault system). The movement of fluids is related to phases of basin inversion and regional deformation. The hot fluids reacted with organic-rich shales, producing gas and liquid hydrocarbons. This led to the thermochemical reactions, which resulted in the precipitation of sulphides, as shown above. Suphur isotope systematics revealed progressively higher $\delta^{34}S$ values, from 5–10‰ to 20–25‰, reflecting a closed-system hydrothermal reservoir with enrichment in heavy sulphur over the life of the mineralisation event. The sulphate-bearing fluids may have derived from evaporite rocks in the deeper parts of the basin. Broadbent et al. (1998) suggested that the Century mineralisation may represent a link with MVT deposits.

8.7.1.2 BHT Ore Systems

The stratiform Broken Hill ore deposit (Broken Hill Lode) is located in the Willyama Inlier (Willyama Supergroup) of the Curnamona Province (Fig. 8.17), represents the largest accumulation of Zn, Pb and Ag in the world and is the type model for BHT systems. In the Mount Isa district, the Cannington deposit is also a BHT system (Table 8.6; see Walters et al. 2002 for a detailed description). The Willyama Supergroup, from base to top, consists of the Thackaringa, Broken Hill, Sundown and Paragon Groups. These rocks are granulite-amphibolite facies quartzofeldspathic gneisses, calc-silicates, quartzite and magnetite quartzite. Although still disputed, the protoliths of these high-grade metaomorphic rocks were probably bimodal volcanic and intrusive rocks and granitoids (Parr and Plimer 1993). The Willyama Inlier contains several ore deposits including stratiform, stratabound, vein and stockworks, and pegmatites (Solomon et al. 2000). Broken Hill and Pinnacles are representative of the stratiform deposits, which typically contain Pb and Zn sulphides in assemblages that consist of garnetite or quartz-gahnite ($ZnAl_2O_4$), garnet-quartz, iron formations and quartz-fluorite. Stratabound systems are characterised by sulphides hosted by bodies of quartz and amphibolite, quartz-feldspar-biotite gneiss and tourmalinite. Tourmalinite is thought to be of exhalative or diagenetic origin. The vein systems are polymetallic, dominantly with Ag-Pb, or Cu-siderite-quartz.

Webster (2006) produced an excellent and detailed book devoted to the Broken Hill deposit. Solomon et al. (2000) and Huston et al. (2006) described the key features of the BHT ores and the following is largely taken from these authors. The Broken Hill ore system, although subjected to intense folding and metamorphism, is considered pre-tectonic in origin and to have formed at or just below the seafloor. The principal features of the Broken Hill Lode and other BHT ore systems are: (1) metal associations that include As, Sb, Cu, as, Bi and Au; (2) presence of exhalites; (3) Fe-Mn-Ca-F-Si skarn type assemblages; (4) stacked ore lenses with low aspect ratios; (5) lack of, or minor, pyrite; and (6) large-scale alteration haloes. The alteration haloes are characterised by high K/Na ratios and Fe-Mn garnets in the host metasedimentary rocks. Some of the ore horizons have rocks of unusual composition with minerals, such as blue quartz, the above-mentioned gahnite, ferroan calcian spessartine, plumbian orthoclase, tourmaline and zincian ilmenite. These rocks are interpreted as being the metamorphosed product of hydrothermal precipitates (Parr and Plimer 1993; see also Chapter 2 for details of metamorphic precursors of metamorphosed hydrothermal alteration systems). The Broken Hill deposit is associated with metamorphic rocks of the Broken Hill Group (Willyama Supergroup), a 7–9 km thick succession of pelites, psammites, quartzofeldspathic rocks, mafic rocks and chemical sediments, interpreted to have been deposited in an epicontinental basin or intracontinental rift (Parr and Plimer 1993; Page et al. 2005). The deposit consists of a series of lenses or lodes hosted by the 1685 Ma Hores Gneiss, which comprises a

succession 60–400 thick of quartz-feldspar-biotite-garnet gneiss (Potosi Gneiss), pelitic and psammitic metasedimentary rocks, quartz-gahnite and calc-silicate. The Hores Gneiss is overlain by pelite and banded iron-formation and underlain by metapelite, banded iron-formation, metapsammite, amphibolite, feldspathic gneiss and granite gneiss. The granite gneiss and the Potosi Gneiss have been interpreted as having originated from igneous protoliths.

The Broken Hill mineralisation extends for 7 km and contains six ore lenses (A, B, C and 1, 2, 3 lodes), which are either dominated by galena (e.g. No. 2 and 3 lodes) or by sphalerite (e.g. A, B, C and No. 1 lode). Apart from galena and sphalerite, other ore minerals include chalcopyrite, pyrrhotite, loellingite, arsenopyrite and gahnite. Rhodonite, fluorite, quartz, garnet, calcite, micas and amphiboles are the more common gangue minerals. Mining grades range from 2.5 to 15% Pb, 5 to 20% Zn and 20 to 300 g/t Ag (Solomon et al. 2000). The garnet-rich rocks are a typical feature of Broken Hill and have been extensively researched (e.g. Spry and Wonder 1989; Plimer 2006; Spry et al. 2007). Spry and co-workers identified three types of garnet-rich rocks: quartz-garnetite, garnetite and garnet-rich alteration envelopes, with the first being the most common and containing between 10 and 80% garnet accompanied by varying amounts of quartz, biotite, apatite, gahnite, sphalerite, pyrhhotite, feldspars, hedenbergite and wollastonite. Quartz-garnetite is typically laminated and spatially associated with the orebodies and may extend for hundreds of metres. Spry et al. (2007) used rare earth element (REE) geochemistry to gain an insight into the origin of the garnet-rich rocks. Chondrite-normalised REE patterns of the garnetite rocks show high lightREE/heavyREE ratios, whereas the garnets show low lightREE/heavyREE ratios, generally flat heavy REE and low ΣREE contents ($<$100 ppm). The authors interpreted the whole rock and garnet REE signatures as due to the heavy REE being incorporated in the garnet and the light REE in the intergranular material. Spry et al. (2007) concluded that the REE signatures reflect variable inputs of detrital and hydrothermal sediments in the protolith and that the REE patterns of garnet reflect metamorphosed sediments formed by submarine hydrothermal processes. The laminated garnetites probably represent hydothermal precipitates at or just below the seafloor, whereas the garnetite envelopes surrounding the orebodies and the quartz veins were formed by metasomatic processes, during post-peak metamorphism (Spry et al. 2007).

The BHT deposits were probably formed in an ensialic rift setting and are typically characterised by thick siliciclastic successions, associated with felsic volcanic rocks, tholeiitic sills and granites. The presence of these igneous rocks is considered important for the genesis of the BHT deposits, as the heat source may have been linked to this magmatism. Indeed, the Broken Hill ore is hosted by metasedimentary rocks that are part of the 1686 Ma Hores Gneiss, considered to be of volcanic origin. In addition, 1682 Ma felsic sills metamorphosed to gneiss (Rasp Ridge Gneiss) were emplaced at about the same time as the ores. Tholeiitic amphibolite and mafic granulites below the ores have ages of

1690–1670 Ma. The above-mentioned Cannington BHT deposit is also spatially associated with mafic igneous rocks (metabasalt, amphibolite) and minor felsic volcaniclastics, within a predominantly metasedimetary succession. This bimodal magmatism may have been instrumental in providing the heat source for the hydrothermal circulation. The large-scale alteration haloes mentioned above are found in both the Broken Hill and Cannington deposits and are characterised by stratiform albite-rich zones occurring 500–2000 m below the ore zones. Furthermore, an extensive proximal garnet-quartzite alteration zone envelops most of the ore lenses and is characterised by Na, Ca, Sr and Mg depletion and K, Rb, Mn, Pb and S enrichment (Plimer 1979). At Cannington, on the other hand, biotite-sillimanite schist and psammite with almandine garnet is also interpreted as a proximal alteration zone, characterised by losses in Na, K, and Rb and gains in Ca, P, Mn, Fe, Pb and Zn (Huston et al. 2006 and references therein). A schematic view of a BHT ore system is shown in Fig. 8.25.

Sulphur isotopic values ($\delta^{34}S$) of the BHT ores range from 0 to 4‰, whereas Pb isotopic compositions fall on a primitive growth curve. Both the S and Pb isotope systematics suggest mantle or magmatic input for the ore fluids. The BHT stacked ore lenses are indicative of a prolonged, but episodic vent hydrothermal activity, which discharged fluids in brine pools and/or the sub-seafloor (Fig. 8.26). This model suggests that the BHT ore systems may represent an ancient Red Sea brine pool, such as Atlantis II, discussed in Section 8.5.1. The exhalites, which are commonly associated with BHT systems consist of quartz-gahnite rock, banded iron formation and tourmalinites, which are a distal facies of Fe, Mn and B-rich metalliferous sediments.

For the BHT systems Plimer (1986) proposed that these deposits are related to rift structures with bimodal volcanism, and that mantle-generated fluids are enriched in CO_2, F, Mn, P, Fe, Pb, Zn, Ag, Cu. The Broken Hill mineralisation is spatially associated with several other hydrothermal deposits, such as strata-bound Cu-Au, W, epigenetic Pb-Ag, Cu-Ag, Cu-Ni-Fe and PGE, pegmatitic Sn-Ta, U, Nb, Be and Sn deposits. By contrast, the Mt Isa Pb-Zn ore deposits appear to have a spatial and genetic association with Mississippi Valley-type (carbonate rock-hosted; see Fig. 8.2) Pb-Zn mineralisation. Plimer (1986) and Parr and Plimer (1993) proposed that the Broken Hill and Mt Isa ore deposits are related to hydrothermal systems in rift basins, and were developed during phases of maximum tectonic activity and highest geothermal gradients. The fluids had a high metal-carrying capacity, leached metals from the enclosing lithologies and exhaled in an oxygen-deficient ambient. Plimer's model suggests that the Mt Isa mineralisation was formed in a failed rift (aulacogen) setting, in which hypersaline brines flowed along major faults to exhale into depressions or deep graben structures, with no magmatic component. For Broken Hill, on the other hand, the mineralisation formed in more advanced rift settings and its association with bimodal magmatism indicates involvement of high-temperature magmatic fluids. In the model proposed by Plimer (1986), shown in Fig. 8.27, stacked and polymetallic massive sulphide lenses form within the

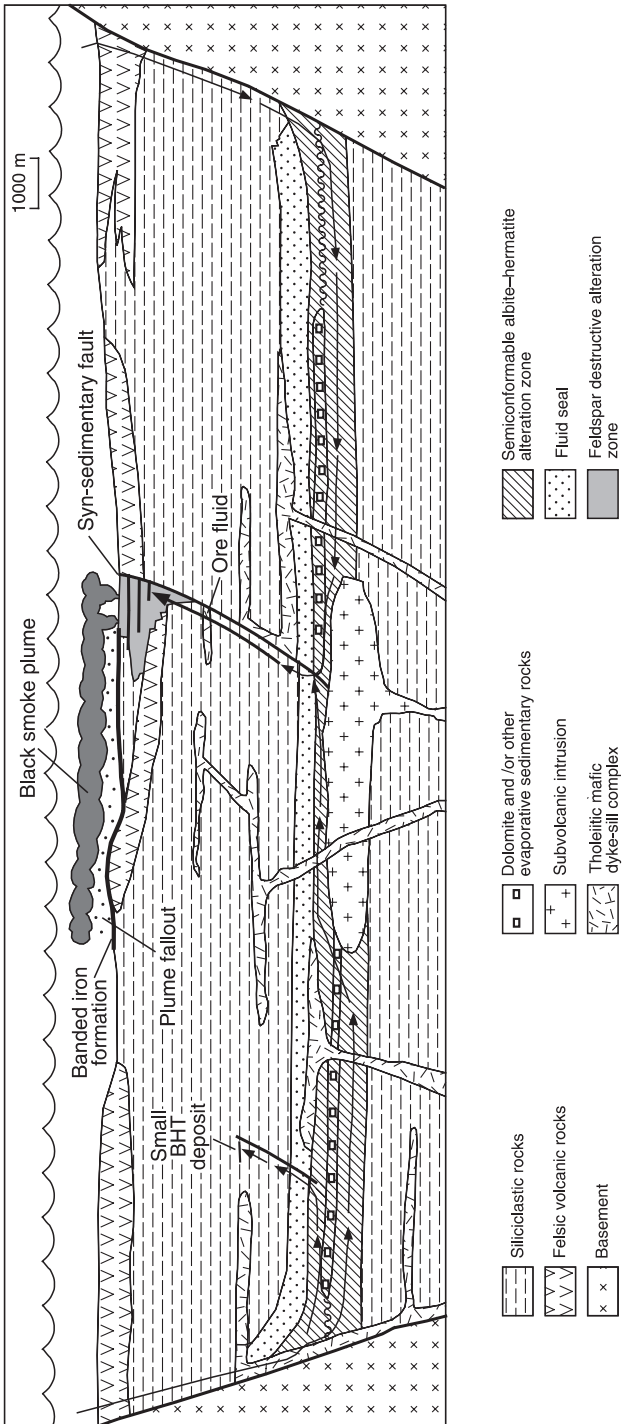


Fig. 8.25 Main components and basin architecture of BHT ore systems; hydrothermal fluids develop in an ensialic rift basin, powered by igneous intrusions and precipitating sulphides at the seafloor, below it and along the conduit; see also Figs 8.26 and 8.27. After Huston (2006)

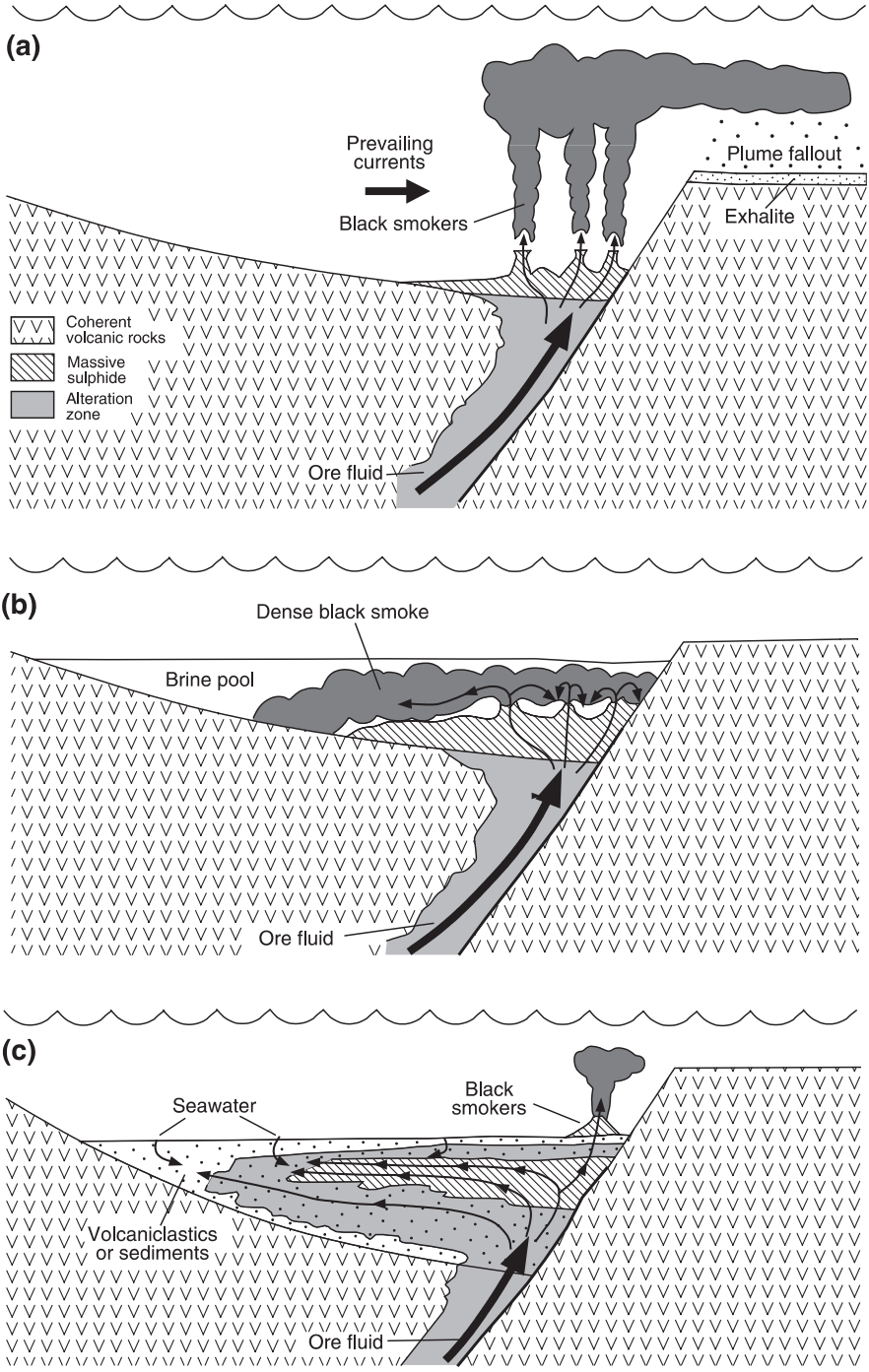


Fig. 8.26 (continued)

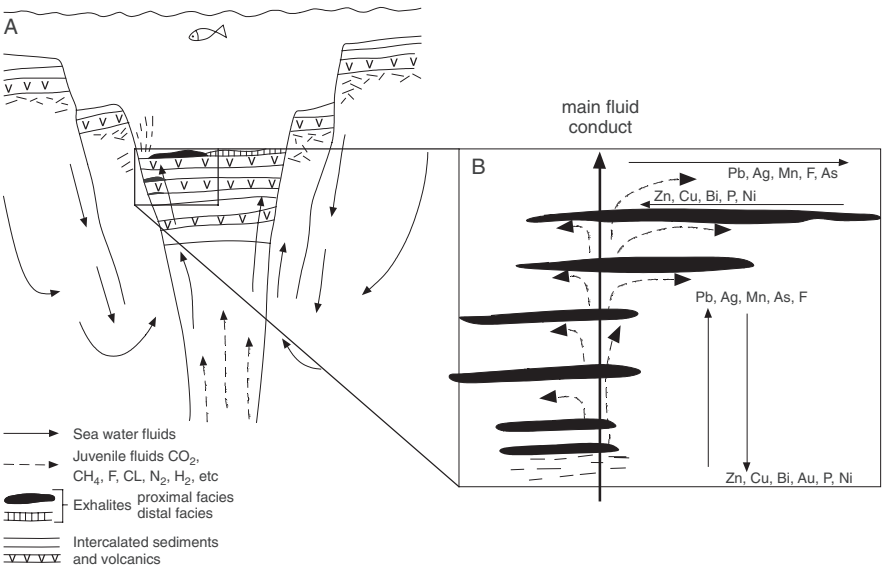


Fig. 8.27 (**A**) Hydrothermal circulation in a deep rift structure, in which magmatic and/or mantle fluids rise along faults and mix with sea or lake waters, to exhale in subaqueous environments forming sulphide and oxide deposits; (**B**) horizontal and vertical zonation from a conduit(s) result in a series of stacked sulphide-oxide lenses. This is the model proposed by Plimer (1986) to explain the Broken Hill type ore systems

sedimentary package, as a result of progressively cooling flow of hydrothermal fluids and mantle volatiles, along a major conduit, provided by a rift fault zone. The heat energy for the fluids was provided by granitic intrusions (Parr and Plimer 1993).

8.7.1.3 Overview of Main Characteristics of MIT and BHT Ore Systems and Comparison with Similar Systems in Other Parts of the World

Huston et al. (2006) reviewed the main characteristics of the MIT and BHT systems of Australia, shown in Table 8.7; Red Sea type rifts for BHT and extensional basins with thick sedimentary successions for the MIT systems. In the former fluids are probably driven by magmatic heat and mixing with evaporites finally forming brine pools, similar to those of the Red Sea (Section 8.5). The formation and evolution of basinal brines is related to compaction and

Fig. 8.26 (continued) Ore fluids depositional mechanism of a BHT system; (**a**) black smoker discharge and plume; (**b**) brine pool and bottom-hugging hydrothermal fluids; (**c**) precipitation of sulphides below the seafloor. After Huston (2006)

Table 8.7 Main characteristics of Zn-Pb-Ag MIT and BHT ore systems; modified after Huston et al. (2006)

Main features	MIT	BHT
Tectonic setting	Extensional sedimentary basins	Ensialic rift basins
Extent/size	10s of km horizontally	Up to 20 km strike length and 2–3 km vertically
Lithologies	Dominantly carbonates in upper ore-hosting stratigraphy, siliciclastic and volcanic rocks in lower parts of the stratigraphy	Siliciclastic successions with felsic volcanic rocks, mafic intrusions; high Fe^{3+}
Heat source	High geothermal gradient and crusta high heat production?	Heat flow probably associated with mafic intrusions
Plumbing system	Basin dewatering linked to far-field tectonism	Rift shoulders?
Structural controls	Basin-bounding faults	Synsedimentary faults
Aquifers/aquicludes	"Dirty" sandstone at base of stratigraphy/important for focusing fluids	Not important/possibly important
Regional-scale alteration	K-feldspar-hematite in rocks at the base of stratigraphy	Albitites below ore lenses
Ore fluids	Oxidised, H_2S-poor, T = 100–240°C; salinity 15–25 wt% NaCl eq	Reduced, H_2S-rich, T = 200–300°C; salinity 3–25 wt% NaCl eq
Water and chloride sources	Basinal brines, evaporites	Sea water, basinal brines, evaporites
Sulphur/metals	Basinal brines, evaporites/leaching of volcanic and feldspathic units at base of succession	Sea water and leaching of volcanic and sedimentary rocks
Depositional mechanisms	Thermochemical sulphate reduction	Mixing of fluids with sea water
Site of deposition	Below seafloor in reactive sediments	Sub-seafloor replacement and/or brine pools

diagenesis of suitable lithologies ("dirty" sandstone). These fluids move along aquifers and are constrained or focussed by aquitards. Temperatures and salinities reflect the origin of the fluids and the nature of the heat source, with higher temperatures and salinities for BHT compared to MIT systems.

In North America Meso- to Neoproterozoic rift systems contain several stratabound and stratiform base metal deposits. One of these is the Belt-Purcell rift-basin on the western margin of the North American craton, which hosts the world-class Sullivan Pb-Zn SEDEX deposit in British Columbia, and the Coeur d'Alene epigenetic Ag-rich veins in Idaho (USA). The Sullivan ore deposit was described Turner and Leitch (1992), Jiang et al. (1994, 1998), Beaudoin (1997) and more recently by Lydon (2007). The Sullivan deposit is hosted by clastic sedimentary rocks of the Aldridge Formation that were intruded, while still unconsolidated, by gabbro sills and dykes (Moyie sills). At Sullivan, the sulphide mineralisation consists of lenses of massive (dominantly

pyrrhotite-galena-sphalerite) and bedded (dominantly sphalerite-galena) sulphides. The sulphide ore is underlain by a vent complex made up of tourmalinite, breccias (with clasts up to 50 m across) and clastic sedimentary rocks. Tourmalinites are both discordant and concordant; stratiform tourmalinite is associated with manganiferous garnet. A network of sulphides, quartz and siderite veins cut through the vent complex. The tourmalinite zone is cut by extensive chlorite-pyrrhotite and chlorite-albite-pyrite alteration, which extends into the overlying strata (Turner and Leitch, 1992). The stratiform tourmalinites are thought to have formed from Fe-Mn-B-rich fluids discharging in a brine pool, at the same time as clastic and sulphide sedimentation (Jiang et al. 1994). The Sullivan mineralisation, tourmalinite pipe and alteration zones are the result of a complex interplay of hydrothermal fluids, some of which were syn-sedimentary, others were derived from the nearly coeval gabbroic intrusions. Post- mineralisation fluids produced the hangingwall alteration during greenschist facies regional metamorphism (Jiang et al. 1998). The ~1890–1850 Ma Bergslagen Province in Sweden contains polymetallic massive sulphides deposits that are considered to be BHT. These include the Garpenger Cu-Pb-Zn, Zinkgruvan Zn-Pb-Ag, Falun Cu-Pb-Zn-Au and others that have been mined since the Middle Ages (Parr and Plimer 1993).

SEDEX ore systems are present in the Yenisei Ridge Province and the Patom Highlands, on the western and southeastern margins of the Siberian Craton, respectively. The Yenisei Ridge Province includes clastic-carbonate-black shale successions, possibly originated at a passive margin. Within these rocks is the Angara Pb-Zn metallogenic belt, containing the ~870 Ma Gorevskoe Pb-Zn-Ag deposit, Russia's second largest Pb-Zn resource (Yakubchuk et al. 2005). The Gorevskoe ores consist of thick, sulphide-quartz-siderite-ankerite veins hosted in quartz-sericite, dolomite and quartzite. The orebodies extend for 1800 m along strike and 100 m wide zones. This deposit was classified as a BHT metamorphosed deposit (Yakubchuk et al. 2005; Smirnov 1977). The 1050 Ma Kholodninskoe deposit located in the Patom Highlands on the southeastern margin of the Siberian Craton, was also classified as a BHT system (Smirnov 1977; Yakubchuk et al. 2005). The Kholodninskoe deposit has resources of 334 Mt and economic concentrations of Pb, Zn, Cu, Ag, Cd, Se, Te and In. The mineralisation extends of 7–9 km along strike and has thicknesses of 8–65 m and is hosted by garnet-quartz-muscovite, quartz-biotite-muscovite schist, marbles, quartz-graphite-mica schist and quartzites, which have been interpreted as representing a passive margin succession (Yakubchuk et al. 2005).

A more recent analogue of MIT deposits could be the 320 Ma Red Dog district in the western Brooks Range in Alaska (see the special issue of Economic Geology edited by Kelley and Jennings 2004). In South Africa, good analogues of BHT systems are the deposits of the Aggenays district (Aggenays and Broken Hill) in the Namaqua Province, discussed next.

8.7.2 SEDEX Systems in Southern Africa

The Namaqua Province in South Africa, forms the northwestern and western portion of the Namaqua-Natal Belt, which developed along the southern flank of the Kaapvaal craton between 2.0 and 1.1Ga and connects with the Irumide Orogens (Sinclair-Rehoboth in Namibia, and Ghanzi-Chobe in Botswana; Section 8.6.1) to the west of the Zimbabwe-Limpopo-Kaapvaal cratonic block (Fig. 8.14). Cornell et al. (2006) recognised five domains in the Namaqua sector: Richterveld, Bushmanland, Kakamas, Areachap and Kaaien. The geodynamic evolution of these subprovinces and terranes, and of the Namaqua-Natal Belt as a whole, remains conjectural and controversial, in view of the polyphase deformation, high grade metamorphic imprints and extensive cover. In general, models proposed for the geotectonic evolution of the Namaqua Province involve intracratonic ensialic multi-stage processes (Kröner 1978; Botha and Grobler 1979), intracontinental rifting and subduction (van Ziji 1981), and accretionary models (Joubert 1986b). Studies of the Namaqua Province and various geological syntheses have been published by Stowe et al. (1984), Joubert (1986a,b) Hartnady et al. (1985) and more recently Eglington (2006) and Cornell et al. (2006). The Richtersveld and Bushmanland subprovinces appear to have had different evolution histories, and they also appear to have developed separately over relatively short time spans (Hartnady et al. 1985). Isotopic and structural data allow the recognition of two major crust-forming events: The Eburnian event (2.0–1.7 Ga), recognised in the Richtersveld subprovince (possibly an island arc), and the later Namaqua orogeny at about ~1.2–1.0 Ga, which has been considered as a time-equivalent of the Grenville province in North America (Clifford et al. 1981). Eglington (2006) identified juvenile mafic-intermediate igneous activity at ~1.2–1.3 Ga, and two periods of granitic intrusions at ~1.15 and ~1.03–1.08 Ga. The Bushmanland province or the Namaqua belt consists of multiply deformed and medium- to high-grade metamorphosed volcano-sedimentary rocks (Namaqua Metamorphic Complex; see Moore 1989 for a comprehensive account).

The metallogeny related to the Eburnian and Irumide orogenic cycles includes the formation of deposits of Cu, Cu-Ag, Pb-Zn-Ag, Sn-W, U-Th-REE, and Cr in a variety of tectonic settings ranging from rift-related, to collisional, to those of ophiolite obduction, as for example in the Natal subprovinces (Matthews 1976). There are at least five distinct mineral districts in the Namaqua belt: the O'Kiep Cu district (Gibson and Kisters 1996), U-Th-REE pegmatites (Boelema and Hira 1998), the BHT Aggeneys-Gamsberg Pb-Zn deposits, a Cu-Zn Besshi-type district (Geringer et al. 1987) and the Haib porphyry Cu (described in Chapter 5). In this section, I focus on the Aggeneys ore field and Gamsberg. These ore systems are polymetallic sulphide deposits, which occur within the supercrustal Bushmanland Group of the Bushmanland subprovince (Fig. 8.14). The base-metal sulphides are associated with banded-iron formations, classified by Ryan et al. (1986) as stratabound sedimentary

exhalative deposits. Rozendaal (1980) compared the Aggeneys-Gamsberg deposits with the sulphidic sediments presently forming in the Red Sea, implying an inter-continental rift environment. Indeed, sedimentary facies analyses of the Bushmanland paragneisses (Moore 1980, 1989) defined a large elongate E-W trending rift basin that includes the Aggeneys-Gamsberg area.

8.7.2.1 The Aggeneys Ore Field and Gamsberg

Four major Pb-Zn-Cu-Ag-Ba deposits, Broken Hill, Black Mountain (Swartberg), Big Syncline, constituting the Aggeneys ore field, and Gamsberg are located in the Bushmanland subprovince of the Namaqua Metamorphic Complex (NMC) (Fig. 8.14). The Gamsberg deposit was studied by Rozendaal (1986) and Stalder and Rozendaal (2004, 2005). Details of the Aggeneys orebodies can be found in Ryan et al. (1986), McGregor (1986) and Smith (1986). In the area of the mineralisation, rocks of the Bushmanland Group are exposed in a series of inselbergs, where the Gams Formation, which hosts the massive sulphides and barite, is best exposed at Gamsberg (Table 8.8. The Bushmanland Group is intruded by the pink-coloured leucocratic Hoogoor Gneiss and the 1.2 Ga syn-post-tectonic Little Namaqualand Suite (McClung et al. 2007).

The basal Hoogoor Gneiss, informally known as Pink Gneiss, has an unknown precursor, although recent work appears to indicate that it may have had a felsic volcanic parentage, and may perhaps have had extensive ignimbrite sheets as precursor rocks. On this basis, and together with other evidence, such as the bimodal composition of the gneissic rocks, the Bushmanland sequence is interpreted as a volcano-sedimentary sequence that was part of an evolving rifting system (Moore 1989; Willner et al. 1990). The rocks that underlie the Gams Formation, Namies Schist and the Pella Quartzite, were interpreted as argillaceous and arenaceous sediments respectively (Rozendaal 1986). However, based on geochemical evidence, Willner et al. (1990)

Table 8.8 Lithostratigraphy of the Gams Formation (Bushmanland Group) in the Gamsberg area. After Rozendaal (1986) and Stalder and Rozendaal (2004, 2005)

Unit	Rock types	Subunit
C	Garnet-pyroxenoid rhythmite, pyroxenoid-amphibole-garnet-clinopyroxene rock, quartz-garnet-apmphibole-magnetite rock, magnetite-hematite quartzite, barite	C2 garnet-pyroxenoid-quartz
		C1 Fe-Mn silicates and silicate-carbonate rocks
B	Quartz-sericite-sillimanite schist, quartz-grunerite-garnet rock; main horizon of massive sulphides	B2 calc-silicate-hosted sulphides
		Apatite Marker; apatite nodules
		B1 graphitic metapelite-hosted sulphides
A	Quartz-garnet-feldspar-clinopyroxen rock, carbonate-quartz-garnet-clinopyroxene marble, garnet-pyroxene-amphibole rock	A3 quartz-garnet rocks
		A2 impure marbles
		A1 Fe-Mn silicates

interpreted the sillimanite and corundum-bearing rocks of the Namies Schist as having originated from the metamorphism of Al-rich clays and hydroxides associated with exhalative products enriched in B, F and P. The precursor rocks are therefore interpreted as belonging to high-Al hydrothermal alteration systems which preceded the metalliferous event that gave rise to the SEDEX deposits of Aggeneys and Gamsberg. Above the Gams Formation are amphibolites and metapelitic and metapsammitic schist, interpreted as a unit of arenaceous sediments and basaltic lavas. Because of the isolated nature of the inselbergs, it is not possible to prove the correlation between the sequence at Gamsberg with that in the Aggeneys area. Such a correlation, however, is inferred, because of the massive sulphide deposits which are almost certainly genetically related, as indicated by the regional metal zonation. The Gams Formation comprises fine-grained pelitic and calcareous metasediments, characterised by a prominent banding and high concentrations of Fe and Mn. At Gamsberg the Formation is divided into the A, B and C members (Table 8.8), which probably represent various facies of a precursor banded iron-formation lithology. Thus, the A member may represent silicate and carbonate facies, the B member the sulphide facies and the C member a mixed silicate, oxide and carbonate facies. Barite occurs in the C member above the sulphide horizon (Fig. 8.28). A discussion on the precursor lithologies of the metamorphosed rocks at Gamsberg and Aggeneys is given in Chapter 2. The bedded barite deposits of the Aggeneys-Gamsberg ore field have recently been the subject of studies by Stalder and Rozendaal (2005) and McClung et al. (2007). At Gamsberg, the bedded barite occurs in association with hematite-quartz and manganiferous iron formations. Stalder and Rozendaal (2005), on the basis of petrographic and geochemical data, suggested that the barite layers were precipitated from hydrothermal fluids during a transition from anoxic to oxidised conditions, immediately after the deposition of the sulphides. Furthermore, the authors suggested that the widespread presence of barite and Ba-rich rocks in the region indicate that the fluids were relatively hot (200–250°C), acidic and reduced, in order to transport base metal chloride complexes and that the change from sulphide deposition to Fe-Mn-Ba-Ca-Si-rich exhalites must have been the result of lowering temperatures and oxidising conditions. McClung et al. (2007) observed that the Aggeneys-Gamsberg barites have low concentrations of SrO (~0.5%) and radiogenic $^{87}Sr/^{86}Sr$ ratios (~0.7164), accompanied by elevated $\delta^{34}S$ (~34 to ~20‰) and $\delta^{18}O$ (4.6–14.5‰) values, with these compositions being higher in the Gamsberg deposit compared to Big Syncline and Black Mountain. McClung and co-authors proposed that these values reflect lower temperatures for the Gamsberg barites, which were deposited in a distal restricted basin setting in relation to the sulphides. At Aggeneys the ores occur as stratabound lenses of massive to disseminated sulphides containing galena, sphalerite, chalcopyrite, pyrite and pyrrhotite.

The Gamsberg deposit consists of stratiform ores, up to 50 m thick, of massive to disseminate sulphides, comprising sphalerite, pyrite, galena, and pyrrhotite; chalcopyrite is minor and occurs as inclusions in sphalerite. Silver

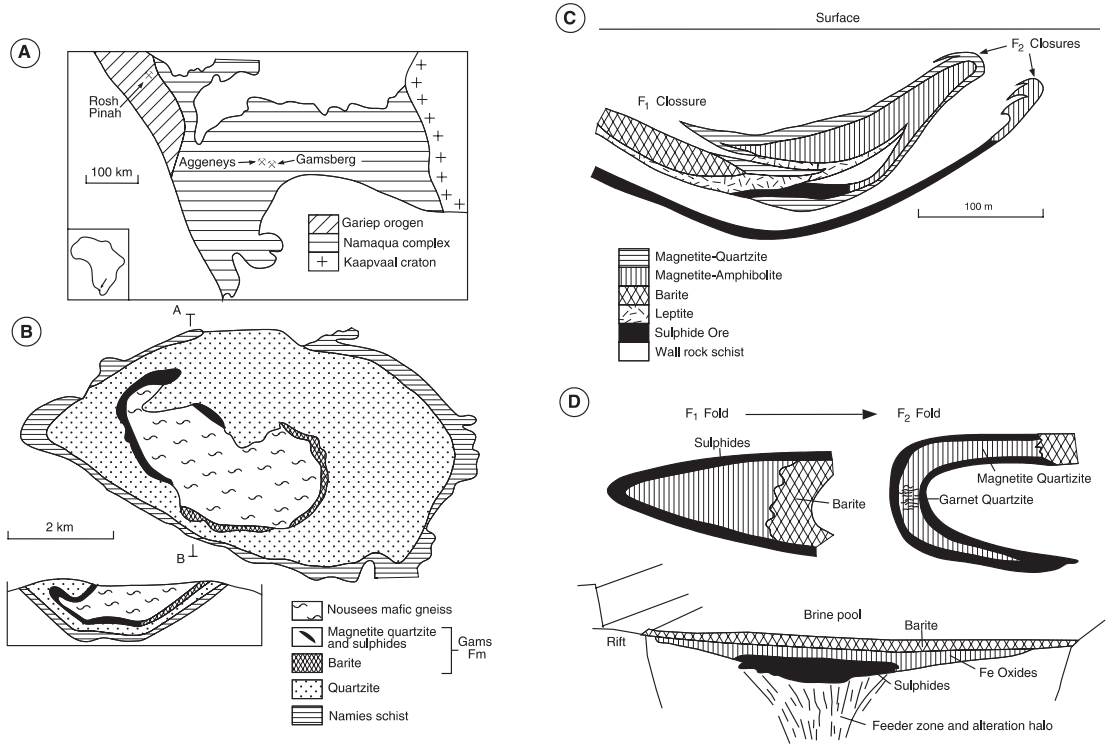


Fig. 8.28 (**A**) Location of the Aggeneys-Gamsberg deposits in the Namaqua Metamorphic Complex. To the northwest is the Rosh Pinah deposit in the Pan African Gariep Orogen, a continuation of the southern coastal arm of the Damara Orogen (Namibia); this deposit is hosted by carbonate rocks and is thought to have formed in a rift environment similar to present day Red Sea brine pools (see also Fig. 8.10); (**B**) Simplified geological map of the Gamsberg inselberg and section across the sulphide mineralisation (after Rozendaal (1986); (**C**) Schematic cross-section of the Black Mountain orebodies (Aggeneys); (**D**) A possible reconstruction of the Aggeneys mineralisation prior to F1 and F2 folding; (**C**) and (**D**) are after Ryan et al. (1986)

occurs as a substitution element in galena, with grades being much higher in the Aggeneys field (~80–50 g/t) than at Gamsberg (5 g/t). Stalder and Rozendaal (2004) reported the presence of a discrete band of apatite nodules within the massive sulphides in the Gamsberg deposit, at the transition from siliciclastic-hosted pyrite-sphalerite-graphite mineralisation to calc-silicate-hosted pyrrhotite-sphalerite mineralisation. This transition records a change from anoxic to less anoxic conditions. Apatite is also found in the oxide-facies iron-manganese formations and Stalder and Rozendaal (2004) suggested, on the basis of REE patterns, a common hydrothermal origin for both types of apatite.

Each of the base metal deposits is preserved in a synclinal fold structure (Fig. 8.28). At Broken Hill, two orebodies merge together and are interpreted as being the two limbs of a single isoclinally folded unit, but the different Pb/Zn ratios in the upper and lower orebody indicate that this may not be the case. A greater concentration of Cu in the upper orebody suggests that the sequence is inverted. A possible reconstruction of the Aggeneys mineralisation prior to deformation is illustrated in Fig. 8.28D. In all four deposits the main sulphide minerals are chalcopyrite, sphalerite, galena, pyrite and pyrrhotite; other minerals present are marcasite, hematite, magnetite, ilmenite, graphite, barite and various silicates. There is a zonation from the Cu-rich Zn-poor Black Mountain

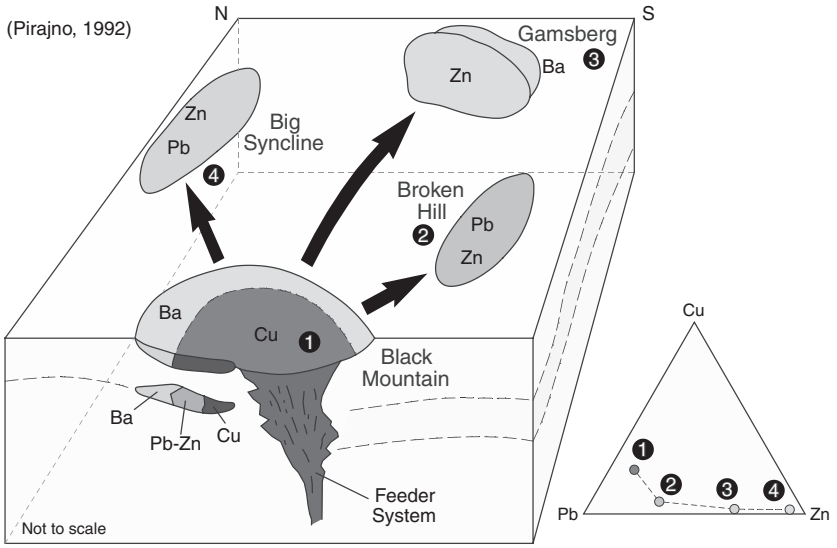


Fig. 8.29 Schematic representation of the genesis and metal zoning of the Aggeneys-Gamsberg SEDEX ore field. The garnet-quartzite beneath Black Mountain is interpreted as an alteration zone around a channelway through which mineralising fluids ascended and discharged in a structural depression. Dispersion of fluids, shown by the arrows, resulted in sulphide and oxide accumulation in other structural depressions at increasing distances (Broken Hill, Big Syncline and Gamsberg) from the vent area (Black Mountain); (**B**) Ternary plot showing relative proportions of metal contents for the Aggeneys-Gamsberg deposits (numbers correspond to those in A. After Pirajno (1992)

deposit in the west, to the Zn-rich, Pb-poor Gamsberg deposit in the east, as illustrated in Fig. 8.29. This zonation is interpreted by Rozendaal (1986) as being related to the distance from the source of the mineralising fluids. The nature of the ore ranges from undeformed, well-banded sulphides, to fine-grained sulphide breccias, to coarse-grained re-crystallised sulphides. Gossans occur above all four deposits in the Aggeneys-Gamsberg area. They vary from an orange-brown jasperoidal material with well-developed boxworks to black magnetite rubble with no sign of mineralisation. At Gamsberg the gossan contains up to 7.7% Pb and only 0.3% Zn, demonstrating the greater mobility of Zn in the oxidised environment.

8.7.2.1.1 Ore genesis

The stratiform and banded nature of the orebodies, and the intimate association with the Fe-Mn formations, suggest that the mineralisation is of syngenetic origin. The Aggeneys-Gamsberg deposits are considered to be associated with an intracontinental rift environment. The ores formed when hydrothermal fluids rich in Fe, Cu, Pb and Zn are introduced into an anoxic submarine environment. The hydrothermal fluids are envisaged as either metal-rich brines developed from formation waters, or modified highly saline sea water. Barite was deposited during and after a change to oxic conditions, by sub-seafloor replacement and/or as exhalites on the seafloor. The heat source to drive the hydrothermal system was probably related to the presence of rift-related magmas. The main channelways along which the hydrothermal fluids gained access to the region were probably synsedimentary regional faults. A possible channelway is believed to have passed near Black Mountain, because of the regional zonation referred to above, and the presence of a cross-cutting Cu-rich garnet-quartzite zone beneath the Black Mountain orebody. This zone has been interpreted as a hydrothermal alteration surrounding a feeder vent (Fig. 8.28). The scenario envisaged is that fluids were introduced along this channelway and then dispersed across the seafloor away from the Black Mountain vent. The sulphides precipitated in local depressions on the seafloor, perhaps in the manner illustrated in Fig. 8.29. The Cu/Pb/Zn ratios reflect the distance of each depression from the vent area, thus explaining the lack of recognisable feeder channels, stockworks or alteration zones (Fig. 8.29). For the Gamsberg deposit, Stalder and Rozendaal (2004) constructed a genetic model taking into consideration the presence of the apatite nodule band in the mineralisation. These authors envisaged a four-step scenario, as follows (refer also to Table 8.7): (1) the B1 subunit was deposited in a shallow anoxic third-order basin, with pulses of hydrothermal fluids resulting in the formation of low-grade disseminated sulphide mineralisation; (2) with the infilling of this third-order basin, conditions became more oxidising, while the influx of hot Pb-Zn-P-rich brines continued and diagenetic growth of apatite nodules took place at the sediment-sea water interface; (3) this is the stage of peak sulphide deposition within the B2 subunit, at the same time the metalliferous and phosphatic

brines upwelled onto the shelf shoulder of the basin, resulting in the precipitation of Fe-P formations, together with Mn; (4) sulphide deposition is terminated, due to lower temperatures in the fluid system, but with Fe and Mn still being transported and precipitating as silicate- or carbonate-facies sediments.

8.8 Stratabound Carbonate Rock-Hosted Ore Systems

Stratabound carbonate rock-hosted Pb-Zn ± Cu deposits constitute a major source of Pb and Zn in North America and Europe, where this type of deposit is represented in the MacKenzie district in Canada, the Appalachian, Tri-State, southeast and southcentral Missouri (Viburnum Trend) and the upper Mississippi Valley districts in the USA, in the Alpine, Silesian, central Irish Plain and South Pennine districts of Europe. Other important deposits also occur in southern Africa, North Africa, Russia and Australia. The deposits of the Mississippi Valley have often been considered as classic examples of stratabound carbonate rock-hosted base metal sulphide deposits, and for this reason are commonly referred to as Mississippi Valley-type, or MVT (henceforth referred to as either carbonate rock-hosted or MVT). While these deposits have a wide temporal geological distribution, they are most common in the Devonian to Permian, but also occur in the carbonate sequences of Palaeoproterozoic age, such as those of the Transvaal and Griqualand basins (Transvaal Supergroup) in South Africa (e.g. Pering, Bushy Park, Zeerust district; Wheatley et al. 1986; Kesler et al. 2007). Important Pb-Zn deposits of Neoproterozoic age are the Kabwe deposit in the Lufillian belt in Zambia (Kamona et al. 1999) and the world-famous Tsumeb and adjacent deposits in the Otavi Mountain Land in Namibia, to be discussed below in some detail. Two special publications of the Society of Economic Geologists devoted to carbonate-hosted Pb-Zn deposits have been published (Brown 1967; Sangster 1996). The contents of the papers in Brown (1967), largely based on field observations and optical microscopy work carried out more than 40 years ago, still make very interesting reading. A comprehensive review, tables and maps of world-wide distribution of MVT ore systems can be found in Leach et al. (2005).

Sangster (1983) classified carbonate rock-hosted deposits on the basis of metal ratios (Zn/Zn + Pb) and distinguished Pb-rich cratonal, Zn-Pb basinal and Zn-rich platformal deposits. Sawkins (1990) subdivided carbonate rock-hosted base metal deposits into three main groups: (1) Mississippi Valley-type; (2) Alpine type; and (3) Irish type. These deposits do not appear to have any connection with magmatic activity, nor do they have a clear connection with rifting events. Nevertheless, Sawkins (1990) noted that carbonate rock-hosted base metal deposits generally occur in shelf-facies sedimentary sequences along rifted passive margins or within intracratonic basins. An example of this relationship is provided by the presence of carbonate rock-hosted Pb-Zn deposits along the coasts of the Red Sea (see Fig. 8.1). For this reason it is also

considered possible that gradations may exist from a Red Sea-type ore system to MVT deposits on passive continental margins (Fig. 8.2). Leach and Sangster (1993) considered the main characteristics of MVT as being epigenetic, not associated with igneous activity, stratabound, locally possibly stratiform and occurring in platform carbonate sequences, formed by low temperature (75–200°C, but more commonly in the range of 90 to150°C) and salinity (10–30 wt% NaCl equivalent) basinal brines, which may have an input from evaporite dissolution (Leach et al. 2005). MVT deposits are generally small (<15 Mt) and tend to occur in clusters, forming districts that may cover hundreds of km^2, but not necessarily all at the same stratigraphic horizon. Typically, MVT ore styles are disseminated to massive sulphides and occur as replacement of carbonate rocks, as open-space fillings, as veins associated with varying degrees of hydrothermal alteration, mainly represented by dolomitisation. Hydrothermal dolomite and/or calcite replacing the host carbonate rocks and forming distinct alteration haloes are common features of MVT systems. Silicification is recognised in some deposits. Ore assemblages are generally simple and consist of galena, sphalerite, pyrite, marcasite and chalcopyrite, whereas gangue minerals are dolomite, calcite, fluorite, barite and quartz. However, more complex mineral assemblages are recorded from the Viburnum Trend in which a variety of Cu, Co, Ni, Ag and Sb sulphides and sulphosalts are present and metals, such as Cd, Ge, Ga and In, are recovered in some deposits (Leach et al. 2005). Sulphides can be coarse-, fine-grained and commonly exhibit stratiform features (Fig. 8.16D). MVT mineralisation is commonly spatially associated with basement highs, with the ore being located within carbonate reef complexes and structures, situated below an unconformity. There is always evidence that dissolution of the host carbonate rocks has taken place, as manifested by the presence of breccias and solution collapse structures. In other instances the ore fluids acted on karst structures in post-tectonic regimes (Sangster 1983).

Sangster (1983) maintained that the differences in the various carbonate rock-hosted deposits outweigh the similarities, making the attainment of a unifying genetic scheme very difficult. However, it must be pointed out that MVT deposits are probably part of the larger family of sediment-hosted base metal sulphide deposits, including the "Red Bed" disseminated Cu sulphide mineralisation, SEDEX systems and perhaps the sandstone-Pb deposits (Björlykke and Sangster 1981). Leach et al. (2005) viewed these conflicting ideas in terms of "*splitters*" and "*lumpers*", with the former focusing on differences and the latter considering the diversity of the various classes of ore systems as the norm. I prefer the latter, because within any type of ore deposit there are always differences due to unique local and regional geological features.

A possible connection between the major Pb-Zn districts and areas containing petroleum and natural gas has been suggested (Sverjensky 1986; Oliver 1986; Eisenlhor et al. 1994). In the USA, areas of MVT Pb-Zn mineralisation occur along basin margins and there is almost complete lack of overlap with the

petroliferous areas. This type of spatial arrangement may reflect differential movement of fluids in the sedimentary basins, with base metal-bearing brines moving over longer distances than the more viscous oils which require trapping in suitable structures. Mississippi oil-field brines contain appreciable amounts of Pb, Zn, Cu, Ag, Au, Co and Ni (Saunders and Swann 1990), whereas Sverjensky (1986) showed that fluids with a composition similar to Mississippi oil-field brines could become an ore solution during migration towards the basin margins. Sulphur and Pb isotope systematics and fluid inclusion studies of galenas from the Viburnum Trend corroborate Sverjensky's idea that MVT ore-forming brines originated from sedimentary basins and that they have similar composition to oil-field brines (Crocetti and Holland 1989). On the basis of Br^-, Cl^-, K^+ and Na^+ values of fluid inclusions in cubic and octahedral galenas, respectively, Crocetti and Holland (1989) also showed that the composition of oil-field brines was probably of marine-evaporite origin. The association with hydrocarbons is also recorded in Palaeoproterozoic MVT occurrences, such as those of the Earaheedy Basin in Western Australia (Pirajno 2004).

Sulphur isotopic composition of MVT sulphides show large variations (–25 to + 25 $\delta^{34}S‰$), consistent with equally variable sources, including evaporites, connate seawater and organic material. Leach et al. (2005) suggested that these variations, particularly the negative values, can be explained by bacterial sulphate reduction (BSR) although, these authors pointed out, some of the reduced sulphur can also be derived from thermochemical sulphate reduction (TSR) of organic matter (see Chapter 10 for details of TSR and BSR processes). Metal sources for MVT are likely to be the same as those of other ore systems that are formed by the flow of basinal brines, such as the stratabound Cu-Ag systems discussed above, in which labile Fe (e.g. hematite) in sandstone rocks enables the metalliferous brines to extract metals from the surronding lithologies.

Bradley and Leach (2003) eminently examined and discussed the tectonic settings of carbonate rock-hosted ore systems. As mentioned above, stratabound carbonate rock-hosted ore systems are typically located in platform carbonate successions. These successions generally form in foreland regions associated with compression tectonics in arc-passive margin collision settings, Andean-type and inversion-type orogens (Bradley and Leach 2003), but there are examples of MVT deposits that were developed in extensional settings, such as those of the Lennard Shelf in Western Australia (Section 8.8.6). In arc-passive margins of collisional orogens that develop at low latitudes, carbonate platforms are constructed and become buried by upward-shallowing siliciclastics, which derive from thrusting and orogenic uplift due to collision processes. Post-orogenic collapse and erosion unloading result in further uplift with topographic relief that helps in driving fluids towards the foreland (Bradley and Leach 2003). Andean-type orogens, which develop in continental margins above subduction zones, result in crustal thickening, formation of thrust belts and foreland basins in the back-arc region, where MVT are generated. Thus, the formation of MVT systems relates to the migration of basinal fluids towards foreland basins, where

there is a build up of carbonate sequences. The flow of fluids is aided by orogenic compression and uplift, which drive the fluids towards to the margins of the foreland basin, where they interact with the carbonate rocks to form MVT (Fig. 8.30). It is important to point out that supergene enrichment of MVT ore deposits results in a variety of Zn and Pb oxides, silicates and carbonates, such as willemite, smithsonite, hydrozincite and cerussite which may, in suitable conditions, become economically viable ores in their own right. These are generally referred to as nonsulphide ore systems and are described in Chapter 9.

Before providing descriptions of selected examples of MVT from the Viburnum Trend, Alpine, Irish Midlands, the Otavi Mountain Land in Namibia and

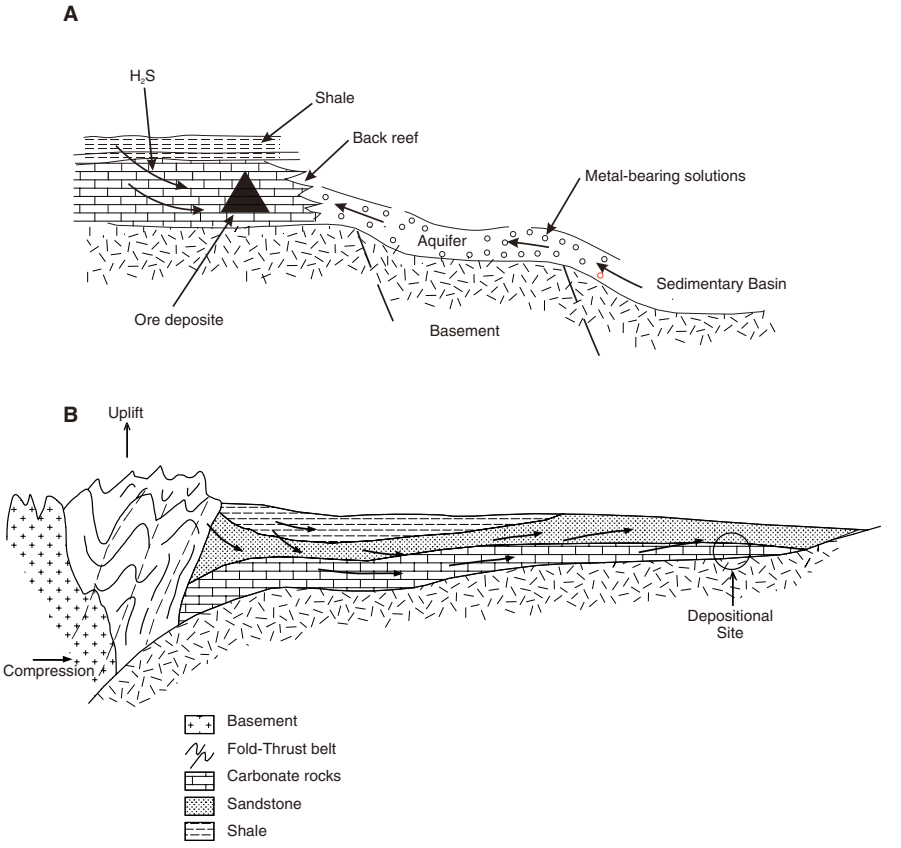


Fig. 8.30 (**A**) Model to explain the origin of stratabound carbonate rock-hosted ore systems; basinal fluids migrate from the sedimentary basin towards a carbonate reef, where they encounter a reducing environment due to the presence of H_2S in organic matter, and sulphides are precipitated in solution cavities, or along faults and other reef structures. Based on Sverjensky (1986); (**B**) Uplift and Appalachian and Ouachita mountains, during the Permian, resulted in gravity-driven groundwater flow along regional aquifers, across the Midcontinent; after Garven and Raffensperger (1997)

the Lennard Shelf in Australia, I think it opportune to make a brief mention of sandstone-hosted Pb-Zn deposits. Sandstone-hosted Pb-Zn deposits have been considered as another variant of MVT systems; classic examples are present in the 425 Ma Caledonides of Scandinavia (see Grip 1966; Rickard et al. 1979; Björlykke and Sangster 1981; Björlykke and Thorpe 1982). These Scandinivian deposits are contained within coastal-marine sandstones, deposited unconformably on a Precambrian basement. Another example is the world-class Jinding sandstone-hosted Zn-Pb deposit of Neogene age in Yunnan Province, on the western margin of the Yangtze platform, China (Kyle and Li 2002). This deposit has a resource of 16 Mt, grading 7% Pb + Zn (Kyle and Li 2002).

8.8.1 Mississippi Valley-Type Deposits of the Viburnum Trend (USA)

As its name implies, the classic area for this mineralisation is the drainage basin of Mississippi River in the central USA, where MVT deposits cluster to the west of the Appalachian Mountains mainly in Missouri, Arkansas, Kentucky and Tennessee (Fig. 8.31). Similar deposits occur in the Appalachian district where the MVT deposits are folded and at Pine Point in western Canada. The Viburnum Trend, also known as New Lead Belt, ore deposits contained the largest reserves of Pb and Zn in the USA, with approximately 450 Mt at 7% combined Pb + Zn. Significant amounts of Au, Ag and Cd are also present. Mining of Pb (Old Lead Belt district) began in 1868, but there are reports of mining which date from the 18th century. An issue of Economic Geology (Vineyard 1977) was devoted to the Viburnum Trend. Age dating shows that the mineralisation of the Viburnum Trend formed in the Late Carboniferous, between 330 and 300 Ma (Leach et al. 2001), a time interval that marks a major period of compressional tectonics associated with the amalgamation of the Pangea Supercontinent. In southeastern USA, the Ouachita collisional orogen records such events and this orogeny was probably responsible for enhancing the migration of fluids in the region (Robb 2005).

The Viburnum Trend, southeast Missouri, is approximately 65 km long and lies near the southern edge of the central stable region of the North American craton. The dominant structural feature in the region is the Ozark Dome, composed of rhyolitic and granitic rocks of Precambrian age (~1.4 Ga). The Ozark Dome (Fig. 8.31) constitutes an area of uplift that probably formed an island complex in the Cambrian seas. The stratigraphy in the region consists of six formations which are, in ascending order: Lamotte Sandstone, Bonneterre Formation, Davis Formation, Derby-Doerun Dolomite, Potosi Dolomite and Eminence Dolomite. Late Cambrian sedimentation started with the deposition of the Lamotte Sandstone on a shallow stable platform formed by a Precambrian basement. In the Viburnum Trend area these sediments have a shallow westward dip. The Lamotte Sandstone is a clean orthoquartzite, fine-grained

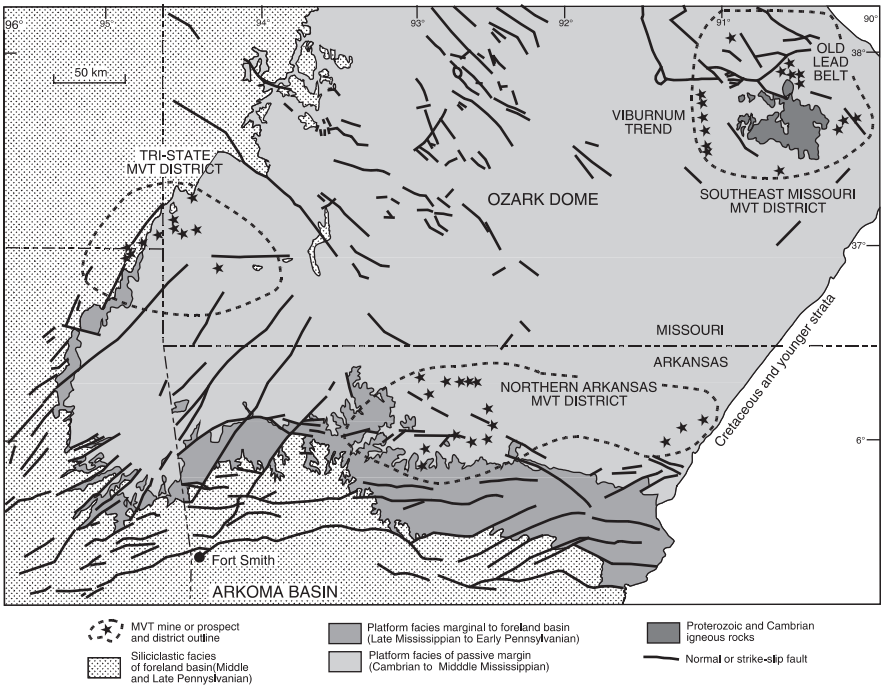


Fig. 8.31 Simplified map of the Ozark Dome and surrounding Mississippi Valley-type ore districts. After Bradley and Leach (2003)

and cross-bedded, porous and therefore permeable, with a maximum thickness of approximately 125 m. Shelf sedimentation continued with the conformably overlying Bonneterre Formation, about 90 m thick, which is the carbonate platform unit hosting the mineralisation. The impermeable Davis Shale Formation, which is 50 m thick, unconformably overlies the Bonneterre Formation and consists of alternating shales, carbonates, siltstones and some sandstones. Thin, irregularly bedded (Derby-Doerun Dolomite) and massive bedded dolomitic rocks (Potosi and Eminence Dolomites) follow upward in the sequence. The ore-bearing Bonneterre Formation has been compared to the present-day carbonate platform in the Bahamas. The Formation is divided into four facies: (1) offshore or basin facies; (2) reef facies; (3) back-reef facies; and (4) shelf facies. The offshore facies is composed of micrite and shales of a low-energy environment; the reef facies is composed of stromatolite and algal material. Erosion surfaces, surge channels and inter-reef areas, filled with clastic carbonate and reef debris, are present. Oolitic material occurs in the front and back parts of the reef. The back-reef facies is made up of light-coloured (white rock) coarse and crystalline dolomite and burrowed lime mudstones and stromatolites. The environment of deposition is probably represented by tidal flats. The reefs formed a palaeoshore line along the Viburnum Trend and coalesced to form a linear barrier reef.

8.8.1.1 Mineralisation

The feature common to all deposits in the Viburnum Trend is that they occur in the dolostone of the Bonneterre Formation, although the mineralisation is not confined to a specific horizon within the Formation, but is generally controlled by the palaeotopography of the Precambrian basement. Minor occurrences are hosted in the Lamotte Sandstone. The main deposits of the Trend are Viburnum Nos. 27, 28, 29, Magmont, Buick, Brushy, Fletcher and Ozark. The orebodies are aligned along a north-south trend (Fig. 8.31) more or less parallel to the above-mentioned palaeoshore line. The Viburnum 27 deposit (Grundmann 1977) occurs adjacent to three basement highs which probably formed islands during the Cambrian. The mine had reserves of approximately 20–23 Mt tonnes grading over 4% Pb, with minor quantities of Zn and Cu. The Bonneterre Formation dolostone is recrystallised and locally silicified in the mine area and most of the ore is associated with algal reefs, and more specifically with surge channels and troughs filled with clastic material. The contact between the reef and the channels (which vary from 1 to 10 m width) is characterised by numerous fractures which provided the pathway for the ore solutions. The ore minerals are galena, sphalerite and chalcopyrite, with a ratio of approximately 10:1:0.6, and lesser amounts of pyrite and marcasite. Gangue minerals are calcite and dolomite. The mineralisation occurs as disseminations and open-space fracture fillings. In the Ozark deposit (Mouat and Clendenin 1977) the mineralisation appears to be structurally and stratigraphically controlled. The ore is divided into four types: (1) bedded and disseminated; (2) breccia ore; (3) marginal break; and (4) fracture stockwork. The bedded and disseminated type, which is the most important, is localised along permeable horizons such as burrowed mudstone, along bedding planes, or lithological contacts. Breccia bodies are due to solution collapse and extend across the depositional strike of the sediments. Marginal breaks exist on both sides of collapse breccias, forming zones up to 50 m wide. Both solution and tensional structures are used as sites of deposition by the mineralising solutions. Fracture stockwork is commonly found below the collapse breccia, and the mineralisation occurs as veinlets and fracture fillings that cross-cut the strata. Dominant ore minerals are galena and sphalerite with a ratio of 6:1. Chalcopyrite is a minor constituent. In addition to Pb and Zn, other metals recovered from the concentrates are Ag, Cu and Cd.

8.8.2 Alpine-Type Deposits

Carbonate-hosted Pb-Zn-Ba-F deposits are present in the eastern Alps, in a metallogenic district shared by Austria, Italy and Slovenia. This district extends for approximately 450 km in an east-west direction and 250 km in a north-south direction. Four deposits, Bleiberg-Kreuth, Mezica, Raibl and Salafossa, account for most of the Pb and Zn production in the region. These deposits

occur within carbonate sequences in the Ladinian stage of the Mid-Triassic (Brigo and Omenetto 1985) and are spatially associated with the so-called Peri-Adriatic Line, a tectonic lineament active since the Palaeozoic. It appears that the main difference between the classic MVT deposits and the Alpine type is the timing of sulphide deposition relative to the host rocks. The Alpine deposits are characterised by two main mineralisation styles: stratiform and discordant. The carbonate host rocks consist mainly of shallow-water calcarenite and oolitic limestones, with stromatolites, intraformational breccias and karst structures. Tuffaceous rocks occur in the footwall sequence of most orebodies and are considered important in terms of source of metals. The Salafossa and Raibl deposits are found in a reef platform environment, whereas the Bleiberg and Mezica deposits are in a back-reef lagoonal setting. At least five styles of mineralisation are found: (1) stratiform (syngenetic?) ores; (2) stratabound vein and fissure fillings; (3) fault-related epigenetic ores; (4) ores in breccia networks; (5) orebodies in karst structures. The ore minerals are represented by galena, sphalerite, wurtzite, pyrite and marcasite. Wulfenite and descloizite are present at the Mezica deposit. Gangue minerals include calcite, dolomite, barite, fluorite and quartz. Fluorite has been mined at a number of localities in the Italian sector. In many instances ore and gangue minerals show typical sedimentary depositional structures, including rhythmic layering, graded bedding and load casts. Mining at the Raibl Pb-Zn deposit began in the 14th century, the mine closed in 1991. It is located within the Dolomia Metallifera and is characterised by filling of fissure and karst cavities which are spatially related to fault systems of Triassic age (Dondi and Puggioli 1992; Brigo and Omenetto 1985). The Raibl mineralisation is therefore epigenetic and consists of colloform sphalerite, galena, pyrite, marcasite and barite. The sphalerite contains significant amounts of Ge and Tl, whereas the galena is enriched in As, Sb and Tl, but is Ag-free. The Salafossa orebody is essentially a breccia pipe and is spatially associated with a fault in the Mid-Triassic Serla Dolomite.

In the same region, base metal sulphides, barite and fluorite mineralisation occur within a belt of Lower Carboniferous, stratabound and carbonate-hosted, pervasively silicified lithological units (Brigo et al. 2001). This belt extends for about 150 km, and is developed above a palaeokarstic unconformity on the epicontinental carbonate rocks. This unusual mineralisation is characterised by dominant tetrahedrite, with varying amounts of chalcopyrite, sphalerite, galena, pyrite, cinnabar, skutterudite, bournonite, jamesonite, enargite and arsenopyrite, in addition to barite, fluorite and detrital bitumen. The silica is represented by microcrystalline quartz and coarser quartz in vugs and fractures. Notably, chalcedonic and opaline silica are absent. Brigo et al. (2001) considered this stratabound siliceous crust type of mineralisation as a variant of MVT systems. The authors proposed that the silica was derived from clay-rich basin sediments during diagenetic changes of the clay to illite, with the silica being transported by a convective hydrological system activated as a result of transtensional tectonics.

8.8.3 Irish Midlands Deposits

At least three major metal deposits, Zn-Pb at Navan, Pb-Zn-Ag-Ba at Silvermines, and Pb-Zn-Cu-Ag at Tynagh , as well as a number of smaller deposits and occurrences (Keel, Ballinalack, Abbeytown and Moate) are present in Lower Carboniferous carbonate rocks of shelf facies situated between the Caledonides and Hercynian belt in Ireland (Boyce et al. 1983; Hitzman and Beaty 1996). Overviews of the Irish Midlands ore field can be found in Hitzman and Beaty (1996) and Wilkinson (2003). The Irish deposits have been compared to the Australian McArthur River and Canadian Sullivan Pb-Zn deposits and are considered to be the result of submarine exhalations of hydrothermal fluids in fault-controlled basins (Boyce et al. 1983, 2003; Fig. 8.2). This view is substantiated by the discovery of pyritic tubes resembling those of hydrothermal chimneys through which fluids are discharged (Larter et al. 1981). All of the major Pb-Zn orebodies occur north of the Hercynian front, where deformation was minimal, and most of the structures associated with the mineralisation are related to the Caledonian event which took place following the collision of the North American and European plates. The Caledonian suture zone remained active well into the Lower Carboniferous, and probably controlled basin development. Most deposits are situated along east-northeast and northeast-trending faults, and all appear to be associated with pre-Carboniferous basement inliers. The stratigraphic succession indicates that a Devonian red-bed sequence was deposited in a deep basin in southern Ireland. This sequence gradually thinned northwards and during the Lower Carboniferous was transgressed by marine sandstones, overlain by interbedded limestone and calcareous shale, containing algal mats and occasional gypsum pseudomorphs. This lower succession is overlain by a widespread green mudstone marker horizon, bedded shelf limestone, in turn overlain by carbonate reef bank limestone consisting of mounds and sheet-like bodies of pale- to dark-grey porous bioclastic material. There are no known post-Devonian plutonic rocks, although Lower Carboniferous volcanic centres are present.

The most common ore minerals are sphalerite and galena, accompanied by lesser amounts of tennantite, chalcopyrite and sulphosalts; barite is present in all deposits (Hitzman and Beaty 1996). The host carbonate rocks are pervasively altered to black dolomite that forms a halo around the massive sulphides. Fluid inclusion studies show that the ore fluids had temperatures ranging from 240 and 150°C, with salinities of between 10 and 23 wt% NaCl equivalent (Hitzman and Beaty 1996). Other characteristics of the Irish deposits include (Leach et al. 2005 and references therein): sulphides derived from bacterial sulphur reduction, with ore deposition resulting from the mixing of reduced fluids with metal-bearing fluids; ore zones controlled by steeply dipping normal faults; the main source of metals are basement rocks and sediments derived from them. Deposition of the ores was at or near the seafloor.

8.8.3.1 Navan

The Navan Zn-Pb deposit is located one km west of the town of Navan and 50 km northwest of Dublin and is the world's largest carbonate rock-hosted Pb-Zn deposit (Leach et al. 2005 and references therein). The mineralisation was discovered in 1969 during a follow-up on a geochemical anomaly, subsequently a drilling programme was carried out over I.P. anomalies and one of the holes intersected about 35 m of mineralised material. Approximately 70 Mt of ore were delineated grading 10.9% Zn and 2.6% Pb. There is abundant literature on the deposit; here I cite and draw from Anderson et al. (1998), Peace and Wallace (2000) and Wilkinson (2003).

The orebody occurs in bioclastic and oolitic dolomitised limestones, a shallow-water sequence called Pale Beds of Lower Carboniferous age (Courceyan; 363 Ma), unconformably overlain by deeper-water dark limestone and red beds of the Nava Group. The mineralisation is located at the intersection of a reverse northeast-trending fault and a normal east-west-trending fault. This latter fault cuts the orebody and is cut by the unconformity. The ores are complex stratabound tabular lenses, commonly truncated by erosional structures and overlain by the Conglomerate Group ore within a debris flow unit (Boulder Conglomerate), containing mineralised clasts. The orebody consists of massive sulphides and sulphide layers intercalated with layers of barren limestone. The ores, which are generally fine-grained, show bedding parallel laminations, but disseminated and fracture filling ores also present.

The main ore minerals are sphalerite and galena with minor pyrite and marcasite. Barite is also present. The sulphides were deposited in open spaces and exhibit a range of textures, from dendritic-skeletal, stalactitic, to rhythmically banded, geopetal and bladed. Sulphur isotope determinations of sulphides show three clusters of $\delta^{34}S$ values: –23 to –5‰, 0 to +15‰ and –23 to –15‰. Barite has a range of $\delta^{34}S$ values from 17.7 to 35.0‰,with an average of 21‰,which is considered to represent Lower Carbonifereous seawater sulphate. These S isotopic compositions are interpreted as the result of bacterial reduction of Carboniferous seawater sulphate (negative values) and transport of sulphides in hydrothermal fluids (positive values).

8.8.3.2 Tynagh and Silvermines

Tynagh was discovered in 1961 as a result of soil geochemistry and E.M. surveys. Subsequently, drilling outlined a primary orebody, containing approximately 8.5 Mt of 3% Pb, 3.2% Zn, 0.3% Cu and 34 g/t Ag, and a secondary orebody of 3.8 Mt grading 9% Pb, 7.4% Zn, 0.6% Cu and 110 g/t Ag (Pirajno 1992). The deposit is now worked out. The primary mineralisation is carbonate reef-bank limestone that thins laterally into a banded hematite-chert unit, and overlain by argillaceous pyritic limestone. The mineralisation consisted of three orebodies, namely: (1) residual cavity fills of Neogene age; (2) massive steeply dipping orebody close to the Tynagh Fault; (3) a bedded

orebody. The ore minerals are sphalerite, argentiferous galena, chalcopyrite, tennantite, pyrite, marcasite and barite. Secondary minerals include cerussite, smithsonite, malachite, azurite, native Cu and Ag. Ore textures vary from fine bedding-parallel laminations to disseminations and fracture filling.

The Silvermines deposits are located south of the town of Nenagh. The district has a history of mining dating to the 17th century. In the 1960s geochemical and I.P surveys followed by drilling located a number of orebodies. The "upper G and B" orebodies combined contained approximately 13 Mt grading 8.3% Zn, 2.4% Pb and 28 g/t Ag. The B orebody grades laterally into the Ballynoe barite deposit, where the fossil pyrite chimneys were discovered. The "lower G" orebody contained approximately 2 Mt at 4.5% Pb, 3.4% Zn and 39 g/t Ag. The ore mineralogy consists of sphalerite, galena, pyrite, marcasite and barite. The upper G and B orebodies consist of stratiform fine–grained massive sulphides with laminated and colloform textures. The lower G orebody consists of massive, coarse-grained sulphides with brecciated and open-space filling textures. The footwall limestone is dolomitised and brecciated, whereas the overlying bank carbonates contain disseminated mineralisation.

Boyce et al. (2003) discovered in the Ballynoe barite deposit, pyritised worm tubes hosted by massive hematite, associated with hematitic filamentous structures, interpreted as fossil bacteria. The worm tubes are very similar to those found in modern submarine volcanogenic sulphide deposits (see Chapter 7) and therefore interpreted as being part of a fossil hydrothermal vent field. Sulphur isotopic values of pyrite from the worm tubes are $\delta^{34}S$ –23.2 and –18.4‰, which fall within the range of bacteriogenic S in stratiform deposits. The filamentous structures are hosted in jasper-rich barite ore that overlies the fossil vent field. The filamentous structures consist of tubular aggregates of sub-micron scale hematite, morphologically similar to an Fe oxidising bacterium, *Gallionella feruginea*.

8.8.4 Models of Ore Genesis for MVT Ore Systems

There are a number of conceptual models that attempt to explain the origin of stratabound carbonate rock-hosted base metal deposits. As mentioned earlier, the timing of introduction of ore fluids in relation to the deposition of the host carbonates is one of the key issues, at least in the case of the Alpine deposits where, locally, ore textures suggest a syngenetic origin. Nevertheless, most models envisage an epigenetic origin for the mineralisation. One model looks at the formation of brines during compaction, dewatering and diagenesis of sediments in an evolving sedimentary basin. The brines include formation or connate waters, which would migrate from the centre towards basin margins in response to hydraulic gradients. This model is schematically illustrated in Fig. 8.30. Migration of fluids occurs along great distances by mechanisms of tectonic expulsion, following continental collision, resulting in the focusing of

the fluids along thrust faults. Another model, which may be more applicable to the Irish deposits, envisages that hydrothermal fluids would move along faults and are discharged on the seafloor where they precipitate sulphides, sulphates and oxides (see, for example, Fig. 8.2). The origin of the fluids in this case is more problematical, and a geothermal gradient, perhaps enhanced by a magmatic heat source, must be assumed. In the European deposits, peculiar submicroscopic spherical structures called "peloids" are associated with the mineralisation. In fact, peloids are predominantly composed of Zn-rich carbonate, siderite, silica, pyrite, sphalerite and galena. Detailed studies by Kucha et al. (1990) indicate that these peloids are formed through bacterial activity, and the authors suggested that the same bacteria may be responsible for converting sulphates into native sulphur. The discovery of worm tubes and filamentous fossil bacteria in the Irish deposits confirms the role of bacteriogenic activity. An exhalative hydrothermal system formed by large scale (tens of km) convection cells was proposed by Russell (1978) for the sediment-hosted mineralisation in Ireland. This model proposes a system of "*downward excavating hydrothermal cells*" in an evolving sedimentary basin. The cells shift deeper towards higher temperatures, becoming larger with time and the progressive evolution of the basin, which allows fractures to move downward as the rock packages become more brittle. In this model there are at least three major pulses, or stages of hydrothermal activity during which different metal abundances result, thus explaining the observed mineral paragenesis of early Fe-Mn-Zn-Pb to mid Zn-Pb-Fe-Mn to late Zn-Pb-Cu-Fe-Mn dominated mineral assemblages.

In all cases, however, it is clear that the carbonate host rocks play a dual role in that they constitute both physical and chemical traps. Features such as basin morphology, palaeotopographic highs, erosional surfaces and palaeoaquifers are of particular significance for the origin of these deposits. In the case of MVT and Alpine types especially, basement highs play an important role in localising the mineralisation. Thus, the main controlling parameters must include (1) carbonate lithologies, which provide suitable sites of ore deposition, and (2) palaeogeographic features, such as basement highs and unconformities. An important prerequisite for the formation of hydrothermal ore systems is the permeability of the host rocks, which must allow the passage of the ore fluids. Dissolution, brecciation (karsting, see below) and dolomitisation of the host carbonates are therefore important in this respect. Dolomitisation and silicification are characteristic features of MVT deposits. The term "dolomite" refers to the mineral species with the general formula $CaMg(CO_3)_2$, and a rock with greater than 50% dolomite is referred to as "dolostone". Dolostones are the favoured host rocks for the stratabound carbonate rock-hosted base metal deposits. Evaporite basins, if present, may be important sources of both Mg and S. Evaporation of sea water causes precipitation of gypsum ($CaSO_4\,2H_2O$), resulting in the removal of Ca, and thereby increasing the Mg^{2+}/Ca^{2+} ratio and migration of Mg, which may induce dolomitisation. Hydrothermal dolomite, or late dolomite cement (LDC), however, is also thought to form from the

migration and effervesence of CO_2-rich basinal fluids interacting with carbonate rocks (Leach et al. 1991). These authors studied fluid inclusions in LDC materials from the Ozark region (Mississippi Valley), where LDC is associated with sulphides in fractures and solution collapse structures. Apart from dolomitisation, other alteration features associated with MVT Pb-Zn deposits are silicification and potassic alteration. The latter was suggested by Hearn et al. (1987) on the basis of fluid inclusion studies of overgrowths on detrital K-feldspars and quartz grains in unmineralised rocks. Fluid inclusion studies of sphalerite and calcite in MVT deposits indicate that the fluids have temperatures in the order of 50–200°C, more commonly from 95 to 120°C. The fluids are Na-Ca-Cl sulphur-deficient brines, with salinities of approximately 20–30 wt% NaCl equivalent. Fluid inclusion studies of Irish-type deposits, however, indicate higher temperatures (approximately 260–150°C). Pb isotope studies of Viburnum Trend deposits show an anomalous radiogenic character of Pb, and it is postulated that the metal was derived from the Lamotte Sandstone, with lesser amounts having been leached from the Precambrian basement rocks and perhaps the offshore facies of the Bonneterre Formation (Doe and Delevaux 1972). At Pine Point in western Canada, isotope studies suggest a sea-water origin for the S. The similarity in the isotopic composition of S of the sulphides with that of anhydrite from the Devonian evaporites in the Elk Point Basin has led to the conclusion that sulphates in the evaporite sequence are reduced to H_2S or S by anaerobic bacteria, and that this S combines with the metals to precipitate the sulphide mineralisation (Sverjensky 1986). Chloride complexing and pH values less than neutral were probably important for the transport of Pb and Zn. Organic ligands have also been considered, as their presence has been ascertained in the brines of oil fields. Metals, possibly contained as adsorbed ions on clay minerals, or even organic matter, could have been released during burial diagenesis and introduced into highly saline pore fluids that are low in S. The low S content is possibly the result of fixing by Fe to form pyrite or marcasite during diagenesis. Movement of the metal-bearing brines occurs along permeable horizons, such as a sandstone unit, and up-dip towards the edges of the basin and the topographic highs, against which carbonate reefs are formed. In this environment there may be an influx of H_2S derived either from organic material in the carbonates or from overlying shales. The H_2S fluids mix with the metalliferous brines to precipitate sulphides in suitable traps within the carbonate lithologies.

8.8.4.1 Karsting

This is an important process of ground preparation for the localisation of most carbonate-hosted mineral deposits. Karsting provides excellent conduits and receptacles for the introduction and movement of hydrothermal fluids, and the precipitation of ore materials. The process of karsting is due to the dissolution and transport of Ca carbonate by meteoric waters in terranes predominantly underlain by carbonate rocks. The term karst is derived from the Carso region

in the Istria peninsula, a border area between Italy and Slovenia, where the phenomenon is especially well developed. Ca carbonate, which is normally insoluble in pure water, becomes soluble in meteoric water enriched in CO_2, according to:

$$CaCO_3 + H_2O + CO_2 \rightarrow Ca^{2+} + 2HCO_3^-$$

This reaction is responsible for the formation of caves, subterranean chambers and channels, created by the action of the CO_2-enriched meteoric waters along joints and fractures, which become progressively enlarged through the dissolution of the carbonate by the descending waters. In this way, a water solution is formed which contains the ions Ca^+ and HCO_3^-. On release of CO_2 (i.e. by evaporation), the above reaction is reversed and $CaCO_3$ precipitated to form the spectacular stalactites (conical constructs hanging from the roof of a cave) and stalagmites (constructs rising from the floor), cascades and myriads of other forms. The deposits thus formed are known as speleothems (Esteban and Klappa 1983). In the Istria region entire drainage systems have gone underground, as, for example, in the Timavo and Postumia districts. In general, karsting phenomena operate in the vadose zone, but, in the specific case of carbonate rock-hosted base metal deposits, dissolution of the carbonate lithologies may also have been achieved by the action of hot waters in the vadose zone, perhaps with a contribution of basinal waters. It has been proposed that the term "hydrothermal karsting" be adopted to explain and describe the brecciation and open-space filling of carbonate rocks by ore-related brines (Ohle 1985). The idea is that ground preparation of the host carbonate rocks is the result not only of karsting but also of chemical brecciation and dissolution, or hydrothermal karsting.

8.8.5 The Pb-Zn-Cu-Ag-V Deposits of the Otavi Mountain Land, Namibia

In this section I discuss the geology and mineralisation of the Otavi Mountain Land, and describe three of the most important representative deposits: Tsumeb, Kombat and Berg Aukas. The carbonate rock-hosted mineral deposits of the Otavi Mountain Land present an interesting case of multistage processes of ore genesis. As explained later, the nature and character of these deposits suggest they are the result of a number of mineralising episodes. At least three episodes are recognised (Pirajno and Joubert 1993). The first involved low-temperature and high-salinity Cu-poor basinal fluids, which formed MVT deposits. The second episode appears to have involved Cu-rich fluids with higher temperatures and salinities. The third, and last, episode is related to recent weathering processes which resulted, locally, in the re-distribution of the ores formed during the first two episodes and the inception of nonsulphide ores.

The Otavi mineralisation was described in some detail by Innes and Chaplin (1986), Lombaard et al. (1986), Misiewicz (1988) and Frimmel et al. (1996). In the discussion that follows I draw heavily from the above authors and from Pirajno (1992), Pirajno and Joubert (1993) and Chetty and Frimmel (2000).

The Otavi Mountain Land, covering approximately 10 000 km^2, is a mineral province located at the eastern end of the Northern Carbonate Platform of the Damara Orogen in northern Namibia (see also Chapter 6). In the Otavi Mountain Land there are over 600 deposits and occurrences of Cu-Pb-Zn-Ag sulphide mineralisation and V-rich nonsulphide mineralisation (Boni et al. 2007 and Chapter 9). The largest and/or more important deposits in the area are Tsumeb, Kombat, Khusib Springs, Berg Aukas and Abenab, none of which is at the time of writing, operating. The distribution of the hydrothermal mineral deposits and occurrences in the Otavi Mountain Land is shown in Fig. 8.32. Tsumeb was the largest deposit and world-renowned for the variety and beauty of its minerals. The formation of these carbonate rock-hosted deposits was largely controlled by karst structures, faults and shear zones as well as joints and fractures. Karst topography developed at two levels in the stratigraphy of the Mountain Land with both levels being marked by a disconformity. Rocks of the Otavi Group were deposited in a carbonate shelf environment. Overlying the Nosib Group, they also, in places, lie directly on pre-Damara basement rocks (Grootfontein Complex), and are overlain by the Mulden Group, a molasse-type sedimentary sequence. The Nosib Group was deposited in rift basins, which were subsequently overlain by the platform carbonates of the Otavi Group. The Otavi Group is divided into the Abenab and Tsumeb Subgroups, separated by a disconformity. The Abenab subgroup includes the Berg Aukas, Gauss and Auros Formations. The Berg Aukas Formation represents a transition facies from the coarse-grained clastic sediments of the Nosib Group to the predominantly carbonate depositional environment of the Otavi Group. Main rock types include light grey to dark grey laminated dolomites with occasional stromatolitic horizons and interbedded arkose, greywacke and shale. The Gauss Formation is characterised by a thick succession of massive fine-grained dolomite, with oolitic cherts towards the top. The Auros Formation includes dark grey to black, thinly bedded limestone and olive-green shale, overlain by grey to white massive dolomite with distinctive marker horizons of stromatolites. The stromatolitic reefs are thought to have developed adjacent to cratonic areas prior to a period of crustal disturbance and erosion. The rocks of the Tsumeb Subgroup are, from bottom to top, informally labelled T1–T8, and subdivided into the Chuos, Maieberg, Elandshoek and Huttensberg Formations. The Chuos Formation (T1; see also Chapter 6 and Section 8.6.1) consists predominantly of diamictites with lenses of dolomite and schist. Sorting of clasts is very poor and an individual clast may reach a diameter of 1 m. The clast population includes dolomite, limestone, quartzite, basement granite and gneiss. The Chuos Formation has been described as a tillite, a fluvioglacial deposit, debris or mass-flow deposit. The Maieberg Formation consists of a thick carbonate sequence containing the T2 and T3 zones. T2 includes

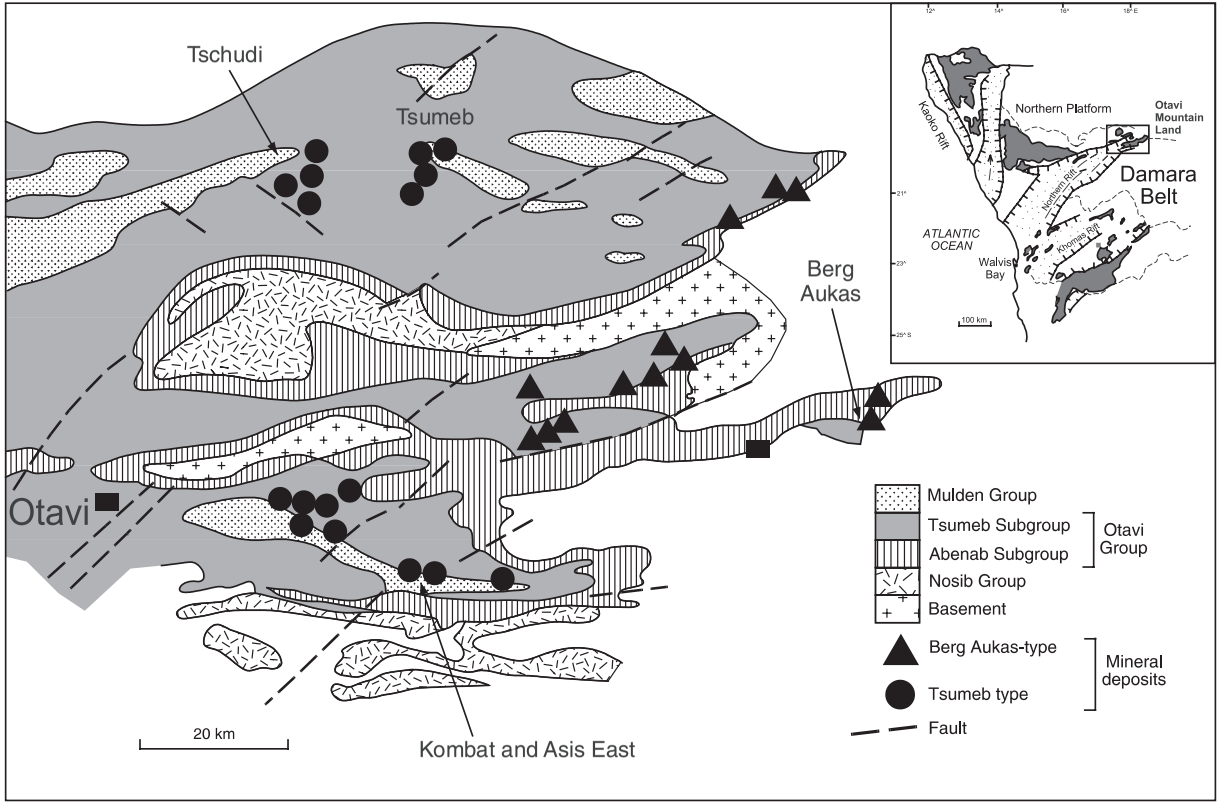


Fig. 8.32 Simplified geology of the Otavi Mountain Land and distribution of main base metal mineral deposits; after Pirajno (1992), inset shows the rifts of the Damara Orogen (after Miller 1983), basement blocks (dark shaded) and the position of the Otavi Mountain Land

laminated limestone and marl with abundant breccias and limestone conglomerates. The T3 zone consists of finely laminated grey dolomites. The Elandshoek Formation includes the T4 and T5 zones. T4 consists of massive light grey dolomite with oolitic and stromatolitic beds towards the top. It includes a stratabound zone of brecciation typified by a network of silica veinlets, subrounded blocks of dolomite within a matrix of silica and sparry calcite, This breccia zone is regionally extensive and is considered as a palaeoaquifer. Along the northern flank of the Otavi Syncline the T4 dolomites are intensely jointed and replaced by jasperoidal material. Zone T5 consists of light grey, thinly bedded dolomite with occasional oolitic lenses. The Huttenberg Formation includes zones T6, T7 and T8. Zone T6 is a light grey bedded dolomite with chert lenses and oolitic beds towards the top. Three stromatolitic horizons are well developed and used by local geologists as marker horizons. In the Tsumeb area the T6 zone also contains a 10 m-thick zone of alteration and brecciation, and it too is interpreted as a palaeoaquifer (Lombaard et al. 1986). Zones T7 and T8 consist of sedimentary sequences of lagoonal facies, including algal beds, oolitic, pisolitic and fetid carbonates. At Tsumeb a prominent marker horizon, known as the Augen Marker, comprises calcite nodules have been interpreted as pseudomorphs after anhydrite (Lombaard et al. 1986). In the Tsumeb Syncline there is evidence for a palaeokarst surface, which was probably formed during the hiatus before sedimentation of the Mulden Group commenced (Misiewicz 1988). In fact, the origin of the Tsumeb pipe is attributed to a chimney-like structure formed by dissolution of carbonate during this karsting event. The solution collapse of the Tsumeb pipe is thought to have occurred in the phreatic zone at the intersection of the karst structure with an aquifer (North Break Zone). Karst structures are also well developed at the top of the Abenab Subgroup, but their nature and timing are less well constrained. The mineralised Abenab breccia pipe is situated on the Abenab fault, which is a bedding-plane thrust along the contact between massive dolomite and laminated limestone.

In the Otavi Mountain Land there are two broad types of mineralisation: (1) Tsumeb-type and (2) Berg-Aukas type. The former (Tsumeb and Kombat deposits) is characterised by complex ores containing Cu, Pb, Zn, Ag, As, Ge, Cd and Ga. The ore minerals are generally disseminated in a variety of loci including pipes, solution breccias, shear zones, dilation fractures and breccias derived from hydraulic fracturing. The ores, which are not stratabound, are generally confined to the upper part of the Tsumeb Subgroup and have a close spatial relationship with the disconformity that separates the Tsumeb Subgroup from the Mulden Group. The most significant deposits are located close to northeast-trending fractures and faults regarded as re-activated basement structures. The Berg Aukas type is characterised by ores containing Pb, Zn and V, and is very similar to the Pb-rich members of the MVT deposits. They have little or no Cu, and although the sulphides are enriched in Ag, Ge, Ga and Cd, the abundance of these trace elements is typically much less than the sulphides of Tsumeb-type mineralisation. These deposits are generally confined to the

Abenab Subgroup and the lower part of the Tsumeb Subgroup. Also, they have a close spatial relationship with the basal unconformity between the Abenab Subgroup and the Nosib Group, or basement rocks. The two principal deposits, Berg Aukas and Abenab, while occurring at different stratigraphic levels, lie at approximately equal distances above the unconformity. However, a number of Berg Aukas-type deposits occur above the Abenab-Tsumeb Subgroups disconformity and contain minor Cu. The mineralisation occurs in breccia bodies and may be stratabound or discordant. Hydrothermal alteration around the sulphide bodies consists of dolomitisation, calcitisation, carbonate recrystallisation and silicification. Chetty and Frimmel (2000) recognised various phases of dolomitic alteration overprinting the host Dolomite I. Dolomite II is a coarse recrystallised dolomite containing hydrocarbons and sulphides; Dolomite III is the next generation and is represented by sparry dolomite. At Kombat, Calcite I consists of light pink veins associated with Fe-Mn minerals, whereas Calcite II is represented by a pervasive calcitisation of dolomite with sulphides (chalcopyrite, pyrite, bornite) and as dark-colured siliceous calcitic material forming the matrix of dolomite breccia hosting galena, chalcopyrite and bornite (Chetty and Frimmel 2000). At Berg Aukas, on the other hand, alteration of the host dolomite (Dolomite I) consists of a complex series of dolomites with different textures, namely: very coarse crystalline Dolomite II, granoblastic Dolomite II with sphalerite and galena, white sparry Dolomite IV also with sulphides and sparry Dolomite V as karst infill (Chetty and Frimmel 2000).

8.8.5.1 Tsumeb

The Tsumeb polymetallic Pb-Cu-Zn-Ag ore system consists of a pipe-like structure, situated on the northern side of a doubly-plunging synform within dolomitic rocks of the upper Tsumeb Subgroup. Details of the Tsumeb deposit can be found in Lombaard et al. (1986) and Hughes (1987). A cross-section of the Tsumeb orebody is shown in Fig. 8.33E. The Tsumeb mine closed in 1998 and recorded production was about 30 Mt, grading 10% Pb, 4.3% Cu, 3.5% Zn and 95 g/t Ag (Maiden and Hughes 2000). The age of the deposit is approximately 580–550 Ma (Lombaard et al. 1986). The Tsumeb pipe penetrates zones T8 to at least T5, and is defined by the distribution of mineralisation, dolomite breccia, feldspathic sandstone (formerly known as pseudo-aplite), alteration and arcuate fracturing. The feldspathic sandstone, found throughout the known vertical extent of the pipe (1716 m), is correlated with the Tschudi Formation that disconformably overlies the Otavi Group. The plunge of the pipe is approximately perpendicular to bedding in the lower levels and subparallel to bedding in the upper levels, and was controlled by the reaction of competent dolomites and incompetent limestones to folding. Thus, bedding slip was more pronounced in limestone lithologies of the upper levels, with the result that the pipe structure was dragged along the slips. For this reason the plan shape of the pipe is elliptical in undeformed areas and lensoid were bedding slip is prevalent. Two main types of solution-collapse breccia occur in the pipe.

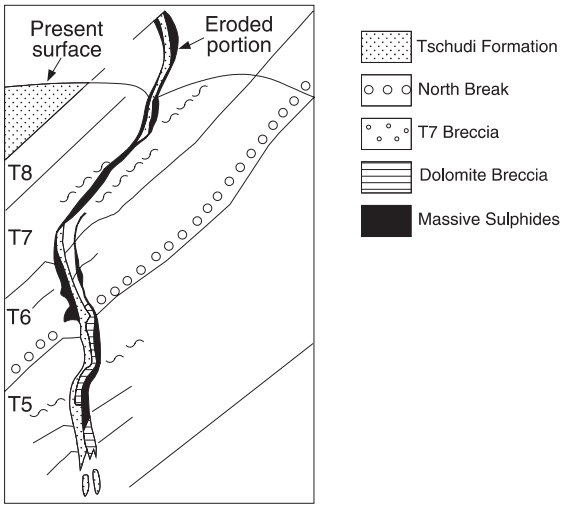


Fig. 8.33 Cross-section (not to scale) of the Tsumeb pipe; known to extend to a depth of more than 1700 m, after Lombaard et al. (1986); circulating meteoric water occurred above the North Break Zone aquifer, this resulted in a solution cavity which was infilled with dolomite fragments, mainly from the T7 zone and a collapse dolomite breccia. Sandy material from the overlying Tschudi Formation infilled the karst cavity above the North Break; this was followed by inflow of hydrothermal fluids along the North Break and deposition of Cu-Pb-Zn sulphides in the pipe and also further to the west (Tschudi)

One is attributed to solution by circulating meteoric water in folded, cleaved and fractured dolomite above and below a prominent zone of brecciation, the North Break Zone, interpreted as a palaeoaquifer, possibly a former evaporite unit (Chetty and Frimmel 2000). This channel eventually breached the basin floor in which deposition of Tschudi sediments was taking place, thus allowing the influx of unconsolidated arenaceous material to form the feldspathic sandstone. The second type of breccia resulted from subsequent solution activity associated with ascending hydrothermal fluids along fracture cleavages. The hydrothermal event induced arcuate collapse fractures in the breccia and adjoining bedded dolomite as well as alteration of the rocks. Hydrothermal alteration consists of calcitisation, which within the pipe extends upwards to about 570 m below the present surface, reaching a maximum intensity at approximately 1120 m depth. Below this level, silicification becomes the predominant alteration type. Regional deformation was active during the evolution of the pipe structure and the mineralising event was more or less synchronous with waning tectonic activity.

The main ore minerals are galena, tennantite, sphalerite, chalcocite, bornite, pyrite and enargite. Erratically distributed and lesser quantities of sulphides and sulphosalts of Ge, Ga, V, Sn, and W are also present. Massive ore is concentrated at the periphery of the deposit, or as manto-like bodies in bedded dolomite. Disseminated and stringer ores occur in the deeper part of the pipe. The manto sulphide bodies, which were of high grade, may have formed by remobilisation of sulphides into tensional fractures during folding. Massive

sulphides in the pipe display minor folding and textures indicative of deformation and partial annealing. Secondary, oxidised ores were of economic importance to a depth of approximately 300 m, and again from 750 to 1160 m, in the zone of intersection between the North Break Zone palaeoaquifer and the pipe. At surface, the North Break is visible as a solution-collapse zone with a vanadiferous calcrete infill. The North Break is associated with Cu, Pb and V mineralisation, and characterised by silicification, calcitisation, ferrusiginisation and Mn oxides alteration. The supergene ore minerals include native Cu, native Ag, cuprite, azurite, malachite, cerussite, smithsonite, anglesite, duftite, chrysocolla and dioptase. More than 200 mineral species have been recorded, of which at least 30 are unique to this deposit. The feldspathic sandstone infill is also mineralised and locally calcitised. The orebody is vertically and laterally zoned with respect to metal abundance and ore mineralogy.

8.8.5.2 Kombat

In the Otavi Valley, south of Tsumeb, are numerous carbonate rock-hosted mineral deposits including Baltika, Central, Auros, Kupferberg, Gross Otavi, Kombat and Guchab (Fig. 8.32). All lie along the northern limb of the Otavi Valley Syncline. The Kombat deposit included at least five orebodies, namely: Asis East, Kombat East, Kombat Central, Kombat West and Asis West. A detailed account of the Kombat mineralisation can be found in Innes and Chaplin (1986). The Kombat ores developed in the T7 and T8 zones at and along the contact with shales and phyllites of the Mulden Group. As is the case for Tsumeb, feldspathic sandstone material from the Tschudi Formation is found associated with the mineralisation. The contact between the phyllites and dolomites dips 40–80° to the south, and the main ore-localising features are monoclinal flexures, locally known as "roll structures", which are characterised by fissures in the footwall dolomite. The fissures strike northeast and contain lenses and stringers of the feldspathic sandstone that was locally deposited along the phyllite-dolomite contact. A schematic cross-section of a Kombat ore zone and a three-dimensional view of a roll structure and associated mineralisation are illustrated in Fig. 8.34. The origin of these roll structures is not clear, but mine geologists attributed them to flexuring, parasitic folding or to thrust tectonics. Significantly, the area is cut by numerous northeast-trending faults, which parallel a major northeasterly fracture, possibly related to an original rift shoulder. Mineralisation occurs as fracture fillings and as replacements in the dolomite and feldspathic sandstones. The mineralisation consists of sulphide bodies and overlying Fe-Mn bodies. Primary sulphides include bornite, chalcopyrite, galena, tennantite and sphalerite. In the Asis West orebody, supergene sulphides include chalcocite, cuprite, malachite, cersussite and mottramite. The sulphide orebodies are characterised by a fairly well-defined zonation; they are enriched in Cu in the centre and become Pb-, Zn- and pyrite-rich towards the periphery. Thus, a zonation of ore minerals, from the core towards the periphery, consists of bornite, chalcopyrite, galena, sphalerite and

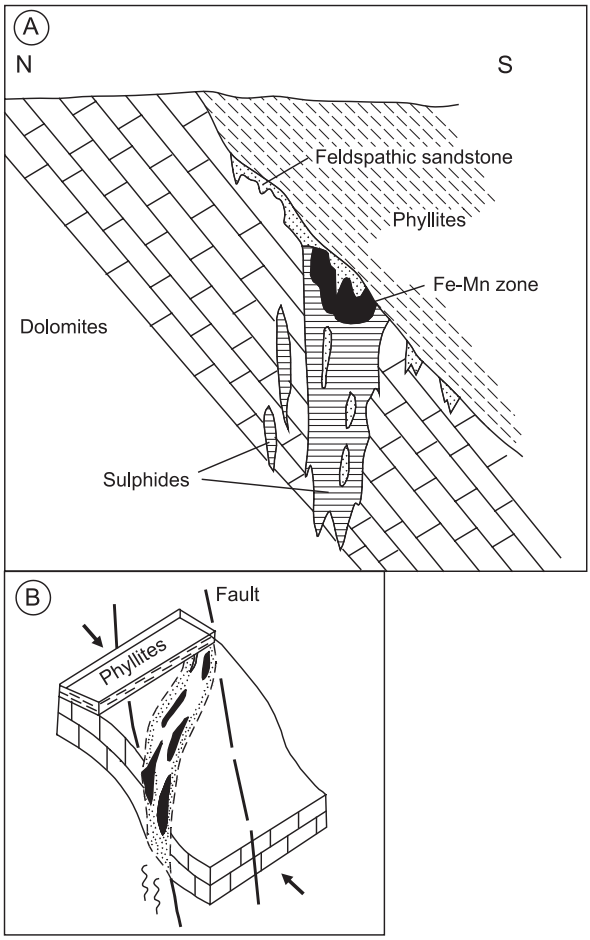


Fig. 8.34 Idealised cross-section of a Kombat orebody, showing stratigraphic relationships and position of Fe-Mn and sulphide zones; drawing not to scale. (**B**) Block diagram illustrates "roll structure" and associated mineralisation; the structure is bound by later northeast-trending faults. Structural evidence indicates that the Fe-Mn deposition was probably taking place at the same time as early Mulden Group sedimentation, whereas sulphide deposition was in progress during the development of the roll structure which enhanced the movement of the hydrothermal fluids. After Pirajno (1992)

pyrite. Ag is associated with Cu and grades at approximately 10 g/t for every 1% Cu. During mining, the ore was defined by a 1% Cu, or 3% Pb, cutoff. The average grade of ore mined in a rich zone at Asis West was 4.5% Cu, 2.3% Pb, and 42 g/t Ag.

The Fe-Mn bodies are generally separated from the sulphide ore by magnetite and hematite. The Fe-Mn ores have sharp boundaries and display pretectonic layering. They comprise oxide, silicate and carbonate facies as well as metasomatic borate and arsenate assemblages. The mineralogy of the Fe-Mn bodies is complex and some 48 Fe-Mn minerals have been identified. Some of the minerals present in the layered Fe-Mn ores include hausmannite, jacobsite, hematite, magnetite, barite, calcite, tephroite (Mn_2SiO_4), alleghanyite [$Mn_5(SiO_4)_2(OH)_2$], pyrochroite [$Mn(OH)_2$], mangonosite (MnO), galaxite ($MnAl_2O_4$), glaucochroite ($CaMnSiO_4$), spessartine, andradite and vesuvianite. The Kombat orebodies are associated with hydrothermal alteration forming

haloes up to 50 m away from the mineralisation. Alteration consists of calcitisation and re-crystallisation of the dolomite lithology, with coarsening of the carbonate grains and local replacement by Mn oxides. Calcitisation is generally fracture-controlled and is an important exploration guide. Fluid inclusion studies indicate a temperature of 300°C for early sphalerite and a range of 280–200°C for the main period of Cu mineralisation. On the basis of $\delta^{34}S$ values of about –0.8‰ and the presence of elements such as B, Li and Be, Innes and Chaplin (1986) proposed a magmatic affinity for the Kombat mineralisation.

8.8.5.3 Berg Aukas

The Berg Aukas Zn-Pb-V deposit, located approximately 20 km east-northeast of the town of Grootfontein (Fig. 8.32), is important because it contains large resources of V (Boni et al. 2007). The deposit, with an estimated resource of 3.4 Mt at 15% Zn and 4% Pb, is hosted by the Light Grey Dolostone of the Gauss Formation of the Abenab Subgroup (Cairncross 1997). Mineralisation was deposited as open-space filling created by karsting, and consists of massive sulphides, including mainly sphalerite and galena. Other sulphides are pyrite, tennantite, enargite, chalcopyrite and renierite. Circulating meteoric waters during subsequent karst activity resulted in extensive oxidation and deposition of secondary, supergene minerals which include willemite, smithsonite, cerussite and descloizite [$PbZn(VO)_4OH$]. The deposit consists of three distinct orebodies, namely: a stratabound Northern Ore Horizon, a discordant Central Orebody and a stratabound Hanging Wall Ore Horizon (Misiewicz 1988). The Northern Ore Horizon comprises three stratabound massive sulphide lenses (sphalerite and galena), of which the top portion is oxidised to willemite, cerussite and smithsonite. The ore is capped by dolomite breccia enriched in descloizite, and the ore lenses are characterised by sharp contacts with the host dolomite. Cavities of varying dimensions may occur within or adjacent to the ore, but are more common towards the hanging wall. Caliche sand and mud enriched in descloizite and ore material fill these cavities. The Central Orebody is a breccia pipe-like mineralised zone. The ore was extensively oxidised and enriched in vanadiferous muds and breccia, consisting of blocks of barren dolomite and partially oxidised sulphides mixed with vanadiferous caliche. The Hanging Wall Orebody is characterised by north-south-trending lenses of steeply dipping ore-filled fractures hosted in dolomitic rocks above the Northern Ore Horizon. Sphalerite is the dominant ore mineral and varies from a Fe-rich, fine-grained variety to an Fe-poor, honey-coloured, coarse-grained variety. Cadmium and Ge are present as traces in the sphalerite. Galena, which is more sporadically developed compared to sphalerite, also occurs in two forms, of which one is coarse-grained, while the other variety occurs intergrown with sphalerite. Ore textures indicate that the sulphide mineralisation is syn- to late-tectonic. Fluid inclusion studies (Misiewicz 1988) indicate homogenisation temperatures ranging from 205 to 97°C in sphalerite. Results of freezing experiments

suggest brine compositions containing NaCl, MgCl, $CaCl_2$ and H_2O with a salinity of approximately 23 wt% NaCl equivalent.

8.8.5.4 Ore Genesis

A genetic model for the ore deposits of the Otavi Mountain Land must explain: (1) the origin of the metals; (2) the nature and origin of the mineralising fluids; and (3) substantial differences between the Berg Aukas type and Tsumeb type. The main differences needing explanation are: (a) the timing of the mineralisation as indicated by the stratigraphic levels (i.e. Berg Aukas-type below the Abenab disconformity and the Tsumeb type above it; (b) different ore mineral assemblages and metal associations; (c) high temperature range and low salinities for the Tsumeb type, and low temperature range and high salinities for the Berg Aukas type; (d) the Fe-Mn bodies associated with the Kombat deposits; and (e) distinct Pb-isotope signatures (Allsopp et al. 1981). The Otavi deposits have been considered by local geologists to have Mississippi Valley-type affinity. Black shales, arkose and evaporites are probable source rocks for MVT deposits, but it has been proposed that most rocks represent potential sources of metals, providing a large enough volume is taken into consideration. Since the genetic model for MVT deposits favoured by most workers involves basin dewatering, the eugeosynclinal sediments of the Swakop Group would seem a likely source, with the underlying Nosib Group, which contains evaporites, as an additional source. A large layered mafic intrusion east of Berg Aukas (Grootfontein Igneous Complex, an alkaline mafic intrusion) could also be considered as a source of metals, in particular Cu and V. A basin-dewatering model involves, compaction, diagenesis and movement of fluids from the graben troughs along rift margins and towards basement highs, into karst cavities formed in carbonate rocks (see Fig. 8.30). This model seems to adequately explain most features of the Berg Aukas deposit and may be extended to include all of the Berg Aukas-type occurrences in the Otavi Mountain Land. However, the model fails to explain some important features of the Tsumeb-type mineral deposits, such as their Cu content, the presence of layered Fe-Mn bodies at Kombat and their isotopic and fluid inclusion characteristics (Pirajno and Joubert 1993). Lead isotope systematics for the Tsumeb and Berg Aukas types (Allsopp et al. 1981; Welke et al. 1983) suggest that the linear Pb-isotopic trends, represent mixing of two or more components with distinct Pb-isotopic signatures. The difference between the trends for the Tsumeb and Berg Aukas type may therefore be ascribed to the movement of the hydrothermal fluids through different lithologies. Welke et al. (1983) interpreted the observed trends in terms of a mixing model involving a common lower end member, but distinct upper end members for the two deposit types. Tsumeb and Kombat have higher Cu contents compared to Berg Aukas, implying another mineralising fluid that may have delivered Cu from a different source for the Tsumeb-type deposits. Fluid inclusion data from Tsumeb ores indicate temperatures of approximately 370–405°C and salinities of 2–8 wt% NaCl equivalent. By contrast, at Berg

Aukas, fluid inclusions have homogenisation temperatures that range from 97 to 255°C, and salinities of about 23 wt% NaCl (Misiewicz 1988; Chetty and Frimmel 2000). The temperature and salinity values for the Tsumeb type are incompatible with a basin dewatering model, and contrast with the lower temperature and higher salinities of the fluids responsible for the Berg Aukas mineralisation, which are closer to fluids derived from the compaction and diagenesis of sediments in a basin. Also, and importantly, the Berg Aukas-type deposits tend to occur beneath the Abenab Subgroup-Tsumeb Subgroup unconformity, whereas the Tsumeb-type deposits all lie above this unconformity. These results, integrated with inclusion fluids analytical data, led Chetty and Frimmel (2000) to suggest that the Berg Aukas-type system is derived from basinal brines similar to MVT, whereas the higher temperature fluids of Tsumeb-type systems are likely to have been derived or interacted with evaporite units. In view of these important differences, it is concluded that the two deposit types were formed during two distinct mineralising events, both in time and space. It can be postulated that the first event to take place was responsible for the Berg Aukas type, and involved fluids derived from basin dewatering. The ore fluids were of relatively low temperature, which is close to the range of MVT deposits. Movement of these fluids was probably along aquifers provided by clastic sedimentary horizons, breccias and contact zones. The fluids became enriched in Pb and Zn en route towards structural highs, where sulphide deposition took place in karst structures in carbonate rocks of the Abenab Subgroup. The second event took place at a later stage, and it involved Cu-rich, higher temperature and lower salinity fluids. The origin of these fluids is not known, but if one considers timing constraints, they would be compatible with an origin due to devolatilisation reactions during prograde metamorphism. The timing of the second mineralising event is constrained by isotopic dating of Pb from the Tsumeb and Kombat ores, which gives ages ranging from 580 to 550 Ma, whilst on the basis of the stratigraphic level the Tsumeb types must have formed after the Berg Aukas types. The second mineralising event is therefore postulated to be synchronous with the peak of metamorphism in the Damara orogen. Metamorphic mineral assemblages in the northern part of the Northern Zone include chlorite + muscovite + quartz, whereas in the central and southern parts of the Northern Zone these assemblages include biotite. Thus, the "biotite-in" isograd is just south of the Otavi Mountain Land. This isograd represents the boundary of lower greenschist facies metamorphism, between 300 and 400°C. Prograde metamorphism of pelitic and silicate rocks involves dehydration reactions, and abundant fluids are believed to be produced in the range of low- to medium-grade metamorphism at temperatures of approximately 350–650°C. Large-scale hydrothermal convection cells are activated during regional metamorphism, a topic to be treated in some detail in Chapter 9. Convection of metamorphic fluids can provide viable means for the leaching and transport of metals from large volumes of rocks. Chetty and Frimmel (2000) suggested that fluid flow may have been driven by thermal gradients associated with crustal thinning at around 750 Ma, which formed the

rift basins (see inset of Fig. 8.32). High-temperature metamorphic fluids would have moved along regional structures, such as graben faults, lineaments and shear zones. In some localities, focused fluid flow was discharged at the surface, or in structural traps, resulting in exhalative activity and the deposition of massive sulphides and the Fe-Mn bodies of Kombat. Innes and Chaplin

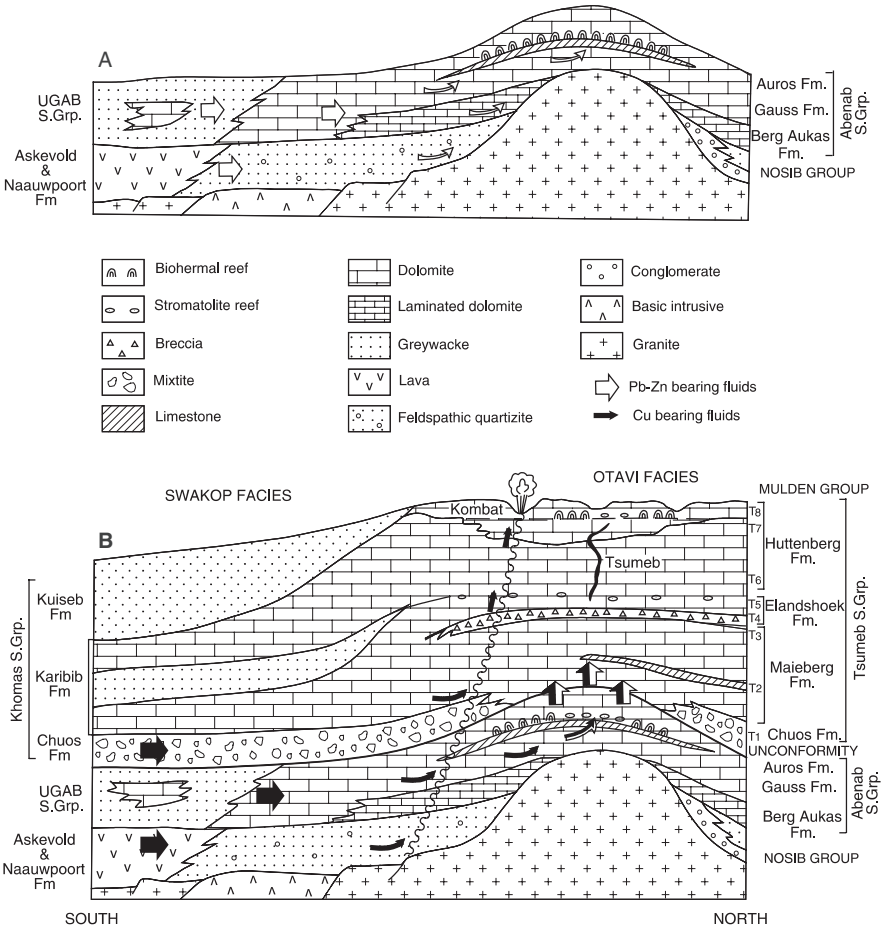


Fig. 8.35 Model of ore genesis for the Tsumeb-type and Berg Aukas-type ore systems of the Otavi Mountain Land (after Pirajno and Joubert 1993). The model shows, idealised and not-to-scale, west-facing cross-sections of the Mountain Land and the northern margin of the Northern Rift (refer to inset of Fig. 8.32), in which there is a change from (Otavi carbonate platform facies) to turbiditic conditions (Swakop facies). (**A**) The first episode which gave rise to the Pb-Zn-rich, Cu-poor Berg Aukas-type mineralisation; white arrows indicate flow of low-temperature and predominantly Pb-Zn-bearing basinal fluids. (**B**) The second episode resulted in the emplacement of the Cu-rich Tsumeb-type mineralisation; black arrows indicate flow of Cu–bearing fluids. Note the different hydrothermal character of Kombat (exhalative) and Tsumeb (pipe infill); this is confirmed by Pb isotope systematics. Local re-working of mineralisation formed during the first event is indicated by black + white arrows

(1986) gave convincing evidence for the exhalative origin of these Fe-Mn bodies, their argument being based on the presence of layering in the bodies, presence of barite and the close similarity in the trace element content with the seafloor bedded Mn oxides. During the second mineralising event in the Otavi Mountain Land, the high-temperature fluids in places may have leached, or remobilised, metals from Berg Aukas-type deposits, resulting in the formation of Cu-bearing Berg Aukas-type mineralisation in areas situated above the Tsumeb-Abenab unconformity. This model of two-stage ore genesis is illustrated in Fig. 8.35. The origin of the V mineralisation is probably not a result of hydrothermal activity, but rather of more recent (Neogene) supergene processes (Boni et al. 2007). The element V is carried in solution in the oxidised weathering environment, and deposited when the solutions encounter a reducing environment, such as a sulphide body. Thus, the concentration of V mineralisation constitutes the third mineralising episode of the Otavi Mountain Land.

8.8.6 MVT Deposits of the Lennard Shelf, Western Australia

The Lennard Shelf is on the northeastern margin of the Phanerozoic northwest-trending, rift-related, intracratonic Fitzroy Trough, a graben that is part of the Canning Basin, located between the Pilbara Craton and the North Australian Craton (Figs. 8.17 and 8.36; Kennard et al. 1994). An extensive Middle to Late Devonian carbonate reef complex fringes the Palaeozoic and Precambrian basement and a major period of extension during the Ordovician and Devonian resulted in the10 km-thick sedimentary succession that accumulated in the Canning Basin. The basin extends offshore and developed as a long-lived depositional system with a complex structural evolution history spanning 500 Myrs from the Ordovician. This protracted history resulted in the complex segmentation and faulting of the basin (Kennard et al. 1994). The Devonian reef complexes of the Lennard Shelf extend for about 350 km and are about 50 km wide and have been extensively studied by Playford (1980, 1984, 2002), and Playford and Cockbain (1992). The reef complexes were constructed as shallow reefs and fringing reefal limestone platforms and containing three basic facies: the platform, marginal-slope and basin facies. The Devonian reef complex consists of two depositional sequences: the Pillara and Nullara Sequences. The Pillara Sequence developed on Ordovician and Precambrian basement and is characterised by stromatoporoid, coral, and microbial reefs; the Nullara Sequence was developed on Precambrian basement and on the carbonates of the previous cycle and is characterised by microbial advancing reefal platforms. The total thickness of the Devonian succession is estimated to have reached up to 2000 m (Playford 1980).

The Lennard Shelf MVT deposits are spatially related to regional faults and temporally associated with a period of extensional tectonics at the end of reef development (Fig. 8.36). The Lennard Shelf contains a number of prospects and

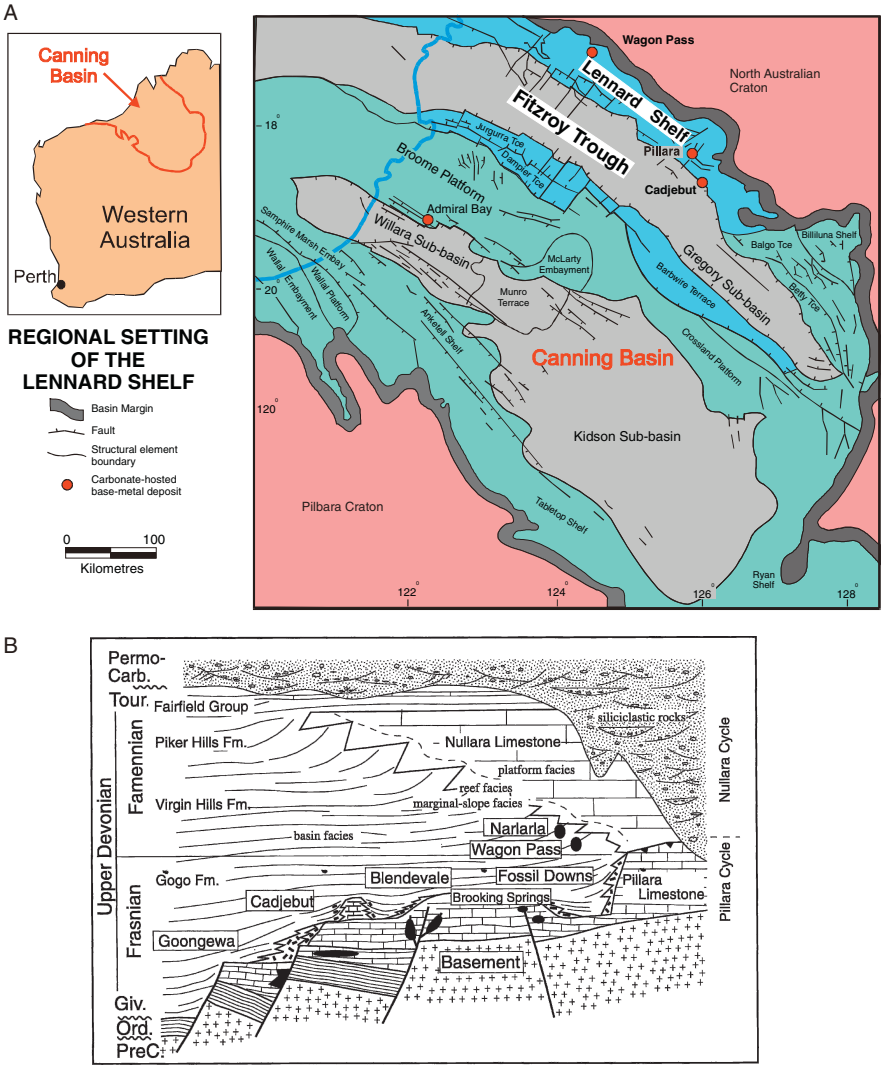


Fig. 8.36 (**A**) Canning Basin in Western Australia and position of the Lennard Shelf; (**B**) architecture of the Devonian reef complexes of the Lennard Shelf and distribution of MVT deposits (after Playford 1980)

at least six deposits, Pillara, Cadjebut, Goonjewa, Fossil Downs, Wagon Pass, and Narlarla, with individual resources ranging from 0.5 to 20 Mt, grading approximately 12% Zn + Pb and displaying a variety of mineralisation styles, hosted in dolomite and limestone of platform and marginal-slope facies. The ore minerals comprise galena and sphalerite, with lesser amounts of chalcopyrite, bornite, digenite and covellite in some deposits. Key publications on the Lennard Shelf MVT deposits include Tompkins et al. (1994a,b), Vearncombe

et al. (1996), Dörling et al. (1996, 1998), Solomon et al. (2000) and Wallace et al. (2002).

The ~325 Ma Cadjebut deposit is characterised by stratabound, almost flat-lying lenses up to 8 m thick, exhibiting rhythmically banded ore (Fig. 8.16) surrounded by a marcasite halo. The rhythmically banded ore is considered to be replacement of a primary sedimentary fabric, probably evaporitic. At least three pulses of mineralisation and several dolomitisation events have been recognised for this deposit, suggesting multiple episodes of fluid expulsion (Tompkins et al. 1994a). There are three main stages of diagenetic dolomitisation (Dolomite I, II and III) and evaporites are associated with the early stages of mineralisation, represented by fine sphalerite and marcasite. Later stages are associated with calcite replacement of the host evaporite, which retains the shapes of the original minerals (gypsum and anhydrite). The sulphides of this stage include sphalerite, galena and marcasite, contained in late clear calcite that replaces earlier cloudy calcite. Fluid inclusions in sphalerite show significant amounts of hydrocarbons (Wallace et al. 2002) and have homogenisation temperatures ranging from 200° to 70°C and salinities ranging from 7 to 25 wt% NaCl equivalent. Delta^{34}S values from sulphides of several deposits have a very wide range from –26 to + 52‰ (Solomon et al. 2000). This wide range of δ^{34}S is mostly from pyrite, whereas the range for sphalerite and galena is about 10–28‰. Barite, on the other hand, has δ^{34}S values ranging from about 33 to 50‰. Lead-isotope systematics show that all deposits have strongly radiogenic signatures, with those of Cadjebut being least radiogenic and with an overall systematic decrease of the radiogenic signature in a northwest direction along the Lennard Shelf, from Cadjebut to Wagon Pass (Dörling et al. 1996). The origin of the MVT deposits in the Lennard Shelf is linked with tectonic uplift and faulting, perhaps related to the Alice Springs Orogeny of central Australia, initiating fluid flow from the deeper parts of adjacent sub-basins, along faults and permeable lithologies. Solomon et al. (2000) also suggested that the thermal energy driving the fluids may have been derived from high heat-producing granites in the basement.

Lenticular stromatolite-barite-sulphide mounds, hundreds of metres long and tens of metres thick, are also present at several localities in the reef complexes and were studied and reported by Playford and Wallace (2001). These authors interpreted these mounds as sedimentary exhalative deposits. The mounds consist of stromatolitic limestone buildups, intergrown with barite with cross-cutting veins of marcasite and pyrite. Playford and Wallace (2001) suggested that these exhalative barite-sulphide deposits were formed by the expulsion of fluids during compaction of basinal shales. The fluids migrated along permeable beds and faults, discharging on the seafloor as fluid seepages. The fluids provided nutrients and the ideal environment for chemosynthetic bacteria, whose mediation resulted in the growth of stromatolites and the deposition of barite and sulphides. The cool-fluid seepages contrast with the hotter fluids responsible for the MVT deposits of the Lennard Shelf, which were formed

later than these exhalative mounds, perhaps, driven by the tectono-thermal Alice Springs Orogeny.

8.8.7 MVT Deposits in the North Sea?

The Mesozoic-Cenozoic North Sea rift system is a good example of links between rifting, sedimentation, hydrocarbon accumulation, and the formation of sulphide deposits (Whiteman et al. 1975; Baines et al. 1991). The North Sea rift system extends for more than 1200 km, forming a network of troughs, platforms and triple junctions in the northwestern European plate, between southeast England and the Voring Basin off the coast of Norway. The origin of the North Sea rift system has been ascribed to mantle plume-lithosphere interaction initiated in the Late Carboniferous-Early Permian (Pirajno 2000 and references therein).

Marine sediments, evaporites and volcanic rocks that accumulated in the North Sea troughs are up to 10 km thick and form uncomformity-bound successions, within which are the North Sea oil fields. Baines et al. (1991) reported the presence of Pb-Zn-Fe sulphides in the hydrocarbon reservoirs in the Mid-Mesozoic Witch Ground graben located off the northeast coast of Scotland. The hydrocarbon reservoirs are hosted in sandstone and mudstone units of Upper Jurassic age. Organic-rich mudstones show considerable enrichment in metallic elements (e.g. Mo, Ni, U, V, Co, Cu, Zn). Sulphide mineralisation is present in reservoir sandstones that have been subjected to burial diagenesis. Multiple generations of sulphide species are present and include sphalerite, galena and pyrite, associated with barite. The sulphides are closely associated with early authigenic minerals precipitated before migration of oil into the reservoirs took place. This mineralisation is structurally controlled in that it is located within fracture systems associated with fault blocks along the margins of the graben. Fluid inclusions studies suggest temperatures of formation between 70 and 120°C and salinities ranging from 7 to 25 wt% NaCl equivalent.

Baines et al. (1991) compared these North Sea sulphide occurrences to Mississippi Valley Type (MVT) deposits, for which an association with hydrocarbon-rich brines is well-established. However, the North Sea occurrences appear to be closely related to burial diagenetic processes, whereas for an MVT deposit to form, migration and entrapment of brines in suitable host lithologies (usually carbonates) is necessary. A link between MVT deposits, Carlin-type gold deposits, and oil reservoirs is possible (Hulen and Collister 1999).

8.9 Iron Formations and Manganese Deposits

Iron formations are chemical-sedimentary units containing about 30% Fe and about 50% silica (Trendall 2002; Trendall and Blockley 2004). Iron formations, consisting of Fe oxides (hematite and/or magnetite) alternating with chert and

silica bands, white or red in colour, are called banded iron formation popularly known as BIF (Fig. 8.37). These alternations have been interpreted as being the result of varve-like seasonal variations (Trendall and Blockley 1970), whereas the differences in Fe contents may have been caused by variations in the Fe input from hydrothermal sources (Morris 1993). Clastic iron formations, thought to result from the re-working of BIF in shallow waters, are known as granular iron formation (GIF; Fig. 8.37). World production of iron ore obtained from Fe formations is in excess of 31 000 Mt (Clout and Simonson 2005). In the Precambrian there are two main types of iron formations: (1) Algoma-type associated with volcanic sequences in greenstone belts; and (2) Superior-type associated with sedimentary sequences in continental shelves of passive tectonic margins. The smaller Algoma-type BIF tend to predominate in the Archaean and the transition from Algoma-type to the larger Superior-type may reflect growth of continental crust and the appearance of continental margins and stable shelves, which offer more uniform depositional environments (Clout and Simonson 2005).

Best known iron formations, both geological and for their economic value are those of the Transvaal Supergroup (Kaapvaal Craton, South Africa), the Hamersley Group (Pilbara Craton, Western Australia), Minas Gerais (Quadrilatero Ferrifero Brazil), Krivoy Rog basin (Ukraine), the BIF of the

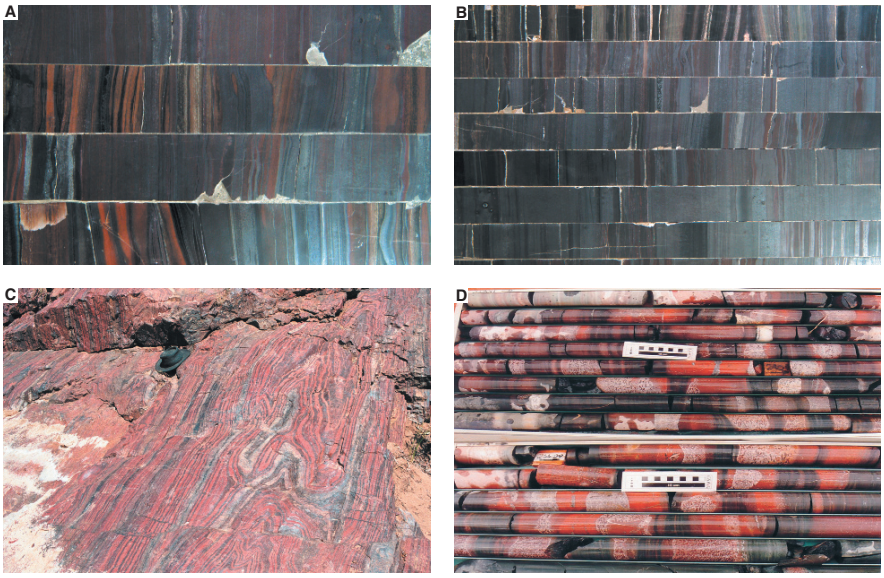


Fig. 8.37 (**A**) and (**B**) banded iron formation from the Hamersley Basin; (**C**) jaspilitic iron formation from the Cleaverville Formation of the Gorge Creek group, Coppin Gap locality, photo courtesy of Arthur Hickman (Geological Survey of Western Australia); (**D**) granular iron formation from the Earaheedy Basin, jasperoidal iron formation (*red bands*), intercalated with peloidal beds (*light colour*) and Fe-rich shales (*dark bands*)

Liaoning province (northeastern China) and the classic Gunflint, Biwabik and Sokoman iron formations of the Lake Superior region in North America. The Hamersley and Transvaal iron formations combined represent the largest accumulation of iron in the world. Literature on iron formations is very abundant commencing with the early works of Van Hise and Leith (1911) and James (1954). The following few pages hardly do any justice to one of the most intriguing geological problems, clearly linked to oxygen levels in the atmosphere, photosynthesis and the evolution of life. In this section I will not describe individual deposits, nor will I embark on stratigraphic details, but will confine this discussion to an overview on the nature and origin of Precambrian iron formations, based on the more recent publications on this vast subject. For details of typical stratigraphic columns of iron formation successions, the reader is referred to the detailed sequence stratigraphic analysis of the Brockman Supersequence (Hamersley Group) of Krapež et al. (2003). Relevant to this section are the book edited by Trendall and Morris (1983), the comprehensive papers by Kimberley (1989a,b), Morris (1985, 1993), Beukes and Klein (1990), Webb et al. (2003) and Pickard (2003). An exhaustive listing of iron formations can be found in Kimberley (1989b). Recent reviews are provided by Trendall (2002), Trendall and Blockley (2004) and Clout and Simonson (2005). All of these have been perused for this section.

Superior-type iron formations are most abundant in the Late Archaean-Early Proterozoic, although iron formations are also known from the Early Archaean and the Phanerozoic. The temporal distribution of BIF and GIF shows that they span the age range from 3.8 Ga to 1.8 Ga, with a peak of extensive development between 2.5 and 2.4 Ga (Fig. 8.38). The 2.5–2.4 Ga temporal peak seems more or less to coincide with the so-called 2.45–2.2 Ga Great Oxidation Event (GOE; Holland 2002), during which there was a rapid rise in the level of oxygen in the atmosphere. This topic is examined more fully in Chapter 10.

The Proterozoic iron formations are commonly associated with giant manganese deposits, such as those of the 2.2 Ga Kalahari Mn field in South Africa (the largest in the world with about 8 Bt of ore; see below) and Minas Gerais in Brazil. This close spatial relationship is related to the chemical affinity of Fe and Mn and therefore the same solutions that are enriched in Fe are also enriched in Mn (Frakes and Bolton 1984; Schissel and Aro 1992; Roy 1992; Cornell and Schütte 1995). Manganese is more soluble than Fe and its deposition is distal, both vertically and horizontally, with respect to Fe and the source hydrothermal vents.

James (1954) recognised four main facies of iron formations: (1) oxide (magnetite and hematite); (2) silicate (greenalite, minnesotaite, stilpnomelane); (3) carbonate (siderite and ankerite); and (4) sulphide (pyrite, pyrrhotite). Trendall and Blockley (2004) considered iron formations as "*very clean*" rocks in terms of composition. Apart from Fe oxides and Fe carbonates (ankerite, siderite), other mineral phases that can be present in minor or locally significant amounts are stilpnomelane, chlorite, greenalite, minnesotaite,

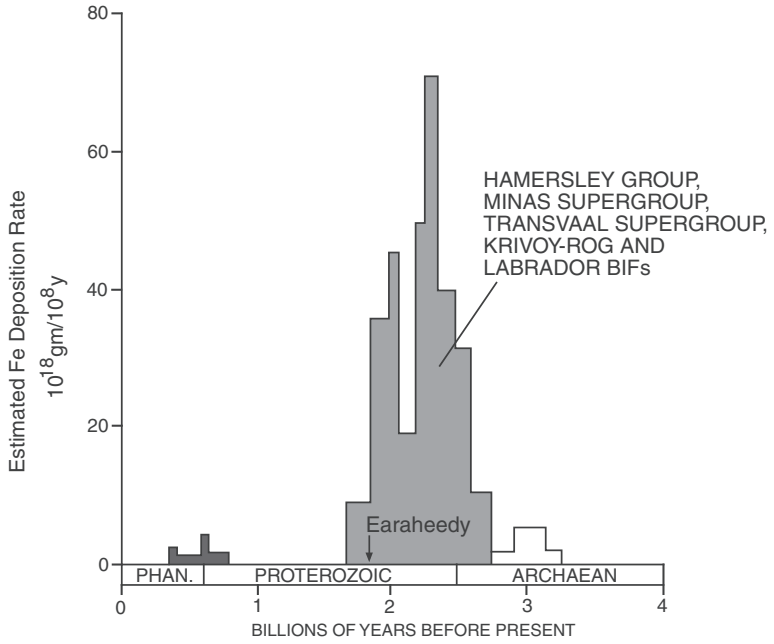


Fig. 8.38 Histogram of age distribution of iron formation in relation to deposition rate. After Isley (1995)

riebeckite, pyrite and pyrrhotite. Metamorphism of iron formation may produce mineral phases such as cummingtonite, grunerite, clino- and orthopyroxene, fayalite and almandine. Both BIF and GIF exhibit Fe-rich and Fe-poor cyclic and alternating laminae and/or beds, which as the name indicates are referred to as bands that typically can be resolved into macrobands (metre scale), mesobands (centimetre scale) and microbands (millimetre scale) (Trendall and Blockley 1970). An example is shown in Fig. 8.39. The striking feature of these bands is that they can be correlated for distances of more than 100 km in the Hamersley Basin (Trendall and Blockley 1970), although these correlations have been disputed by Lascelles (2007). The microbands have been interpreted as varves linked to climatic changes due to orbital-forcing (Clout and Simonson 2005 and references therein). Clout and Simonson (2005) pointed out the difficulties in interpreting the environmental significance of iron formations, which provide a wide range of possibilities, from open marine settings, on shelf and slope areas, below wave base, and shallow high-energy platforms in the case of GIF.

The origin of the iron and manganese formations requires that large amounts of these metals be brought into solution as reduced species (Fe^{2+} and Mn^{2+}), which are then oxidised (Fe^{3+} and Mn^{3+}, Mn^{4+}) and precipitated as Fe and Mn oxides and carbonates. Three issues are contentious for the

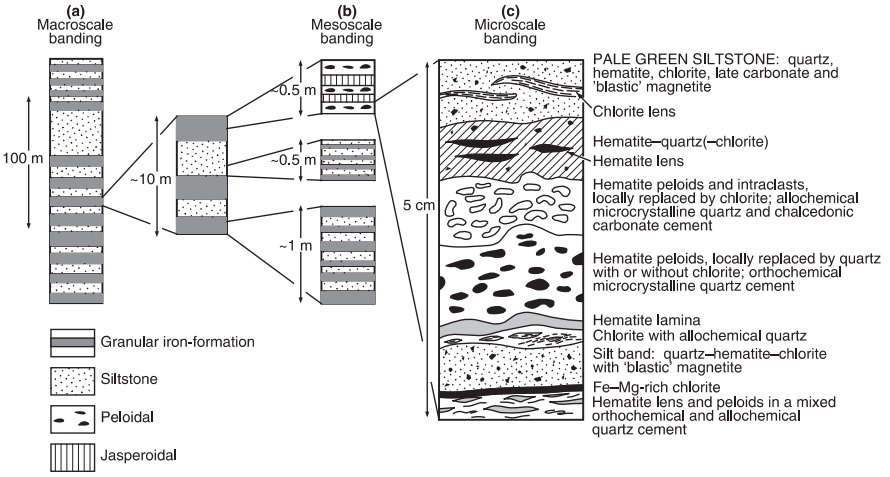


Fig. 8.39 Macroscale, mesoscale and microscale banding in the granular iron formation (GIF) of the Earaheedy Basin (Pirajno et al. submitted)

genesis of these formations: the source of the metals, the amount of oxygen in the atmosphere that is necessary to induce oxidation of the Fe and Mn and the vast areal extent and extreme regularity of the banding of the iron formations, especially the Superior-type. For the source of the metals, two possibilities are considered: one is that the Fe is derived from the weathering of iron-rich lithologies (e.g. continental flood basalts); the second is that the Fe (and Mn) is introduced by subaqueous hydrothermal discharges, in lakes or in ocean basins, or in Red Sea-type narrow rifts. Common to both theories is the necessity of a density-stratified system, in which upwelling currents bring the reduced iron from anoxic deeper waters into the oxygenated environment of near-surface waters, such as a continental shelf, where the Fe^{2+} is oxidised and precipitated as oxides or carbonates. The general consensus is that the Fe was introduced in the ocean from hydrothermal vents, followed by deposition of iron formations on continental shelf and upper slope environments in a stratified (anoxic-oxic) water column. A model of iron formation deposition is shown in Fig. 8.40. The enormous extent of Superior-type BIF is more difficult to explain. Lascelles (2007) suggested that the wide extent of BIF can be explained by a combination of turbidity and density currents, originating from seafloor hydrothermal vents.

The relationship to life of iron formations may be considered in terms of the precipitation mechanism of an original hydrous silica-iron gel (Trendall and Blockley 2004). These authors considered the oxidation of dissolved Fe^{2+} must have involved one or more of the following mechanisms: photosynthesising microbes, direct microbial oxidation and oxidation by solar ultraviolet (UV) radiation. A number of biological processes mediated by bacteria can account

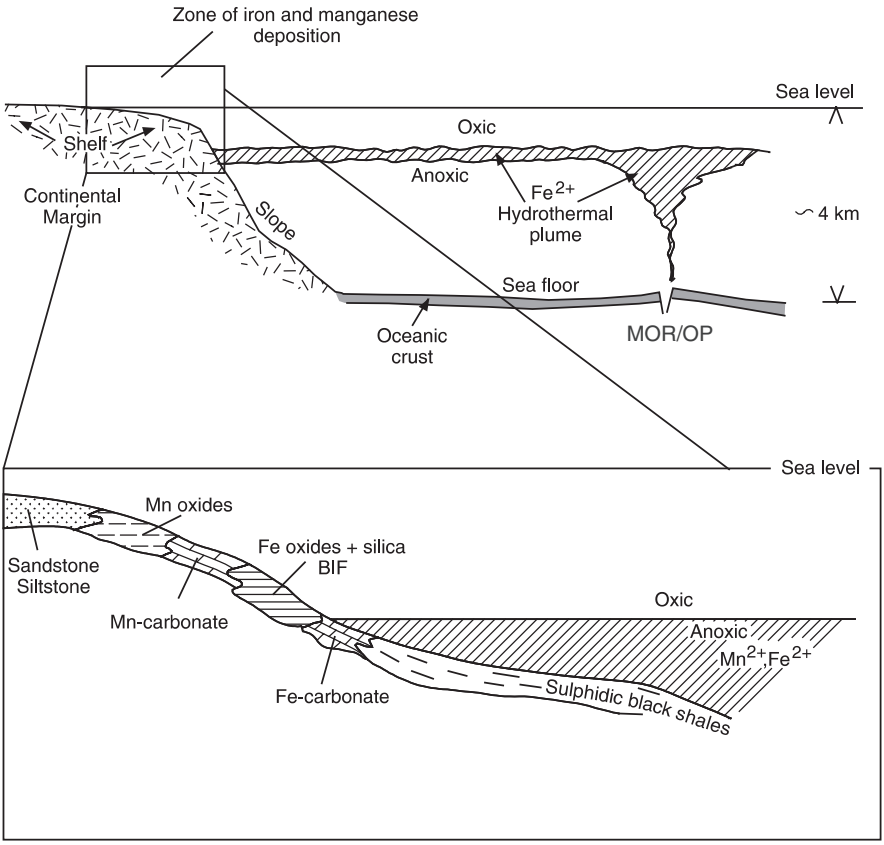


Fig. 8.40 Schematic illustrations showing models for the deposition of iron-formation. A hydrothermal plume rises, from a mid-ocean ridge (MOR) effluent or mantle plume-related oceanic plateau (OP) associated with a mantle plume, to a level of neutral buoyancy, in which Fe^{2+} is transported in solution until it reaches an oxygenated level on the continental shelf, where it is deposited as Fe^{3+} at depths of less than 1 km; the origin of the fine and regular mesoscale (cm-scale) banding of Fe oxides and silica, typical of BIF, remains unknown, but must reflect differences in the supply of Fe at the discharge vent; other metals in the hydrothermal plume include Mn, Cu, Pb, Zn; of these Mn is precipitated as oxide and carbonate facies at shallower levels in response to higher Eh values in near-surface conditions, by contrast Cu, Pb, Zn precipitate in deeper water under conditions of lower pH and Eh in black shale facies (*enlarged box*). After Isley, (1995) and Schissel and Aro, (1992)

for the oxidation of Fe^{2+} and the formation of BIF (Konhauser et al. 2002). One of the possible reactions may involve chemolithoautotrophic species (e.g. *Gallionella ferruginea*, mentioned above for the Irish Midlands MVT) with a reaction of the type (Holm 1989):

$$6Fe^{2+} + 0.5O_2 + CO_2 + 16H_2O \rightarrow CH_2O + 6Fe(OH)_3 + 12H^+$$

or by purple and green bacteria by anoxygenic photosynthesis with a reaction of the type (Konhauser et al. 2002 and references therein):

$$4Fe^{2+} + 7H_2O + CO_2 \rightarrow CH_2O + 4FeOOH + 8H^+$$

An unusual, but interesting model, is the "snowball Earth" proposed by Hoffman et al. (1998), who suggested that a build-up of Fe^{2+} in the oceans occurred during glacial periods in the late Proterozoic, when the oceans were sealed by ice. Oxidation and deposition of the iron would have occurred during the interglacial periods. Hoffman et al. (1998) used the diamictites of the Ghaub Formation, at the base of the Otavi carbonate platform in Namibia, for which they measured a change in $\delta^{13}C$ from positive (+10) to negative (−6) values at the base of the pre-glacial sequence.

The issue of when in geological time, the atmosphere became oxygen-rich is still being debated. One theory, advocated by Cloud (1973, 1976), is that the Archaean atmosphere was O_2-poor (about 1% of present level) and that the O_2 produced by an increasing abundance of photosynthetic micro-organisms could have been lethal for their survival, so that the excess O_2 had to be eliminated. This would have been achieved by oxisidising Fe^{2+} to Fe^{+3}, or in other words Fe (and Mn) was the oxygen acceptor and sink. After a time, oxygenation prevailed, leading to a gradual build-up of O_2 in the atmosphere to present-day levels. In this way, according to Cloud's model, the deposition of iron formations reached a peak at about 2000 Ma. Indeed, after this time, the geological record shows an abundance of red beds instead of iron formations, supporting the model. Additional support comes from the presence of detrital uraninite and pyrite grains in the Archaean clastic rocks of the Witwatersrand in South Africa. Unconformity-associated uranium mineralisation in the Proterozoic appears to be linked to this post-2000 Ma atmospheric oxygenation, which allowed the dissolution and transport of U as hexavalent uranyl complexes (Robertson et al. 1978; Marmont 1987). Critics of the Cloud's model pointed out that the presence of oxides, sulphates, such as barite, in some Archaean terranes, does not corroborate the view of an early reducing atmosphere. For example, significant barite mineralisation is present in the Archaean Pilbara Craton (Western Australia; Vearncombe and Kerrich 1999), and Fe oxides in the Barberton greenstone belt (South Africa; de Ronde et al. 1994). Although the issue of a reducing versus oxidising early atmosphere is not resolved, it could also be that in the Archaean, the atmosphere had not reached a uniform composition and that O_2-rich-"pockets" existed. In any case, it seems clear that the ocean became more oxic in the Neoproterozoic, thereby restricting the mobility of Fe^{2+}.

Barley et al. (1997) proposed to link flood basalt volcanism, with large input of Fe^{2+} into the ocean and the origin of the banded iron formations of the Hamersley Group in Western Australia. Isley (1995) and Isley and Abbott (1999) also suggested a link between plume-related igneous activity and the deposition of iron formations during the Archaean and Proterozoic. They used

the geochronological record of plume activity between 3.8 and 1.6 Ga, as monitored by the presence in the geological record of komatiites, flood basalt sequences, mafic dyke swarms and mafic-ultramafic layered intrusions. These rocks are an abundant and ready source of Fe through high-temperature hydrothermal effluents on the seafloor, related to volcanic activity, and through erosion. In both cases Fe goes into solution as Fe^{2+} in bodies of water (oceans or lakes) and precipitation takes place when Fe^{2+} is oxidised to Fe^{3+}. Isley and Abbott (1999) used time-series analysis to examine the possible temporal correlation between mantle plume events and the deposition of iron formations. They constructed a time-series by using the minimum and maximum ages of an event, with half the difference between the minimum and maximum ages being one standard error about the mean (Isley and Abbott 1999, p. 15466). A time-series was constructed for each data set on komatiites, flood basalts, dykes and layered intrusions. They found a remarkable correlation between the peaks of the iron formation time series and those from other data sets. Iron formations and plume events had similar patterns of occurrence, but are separated by a lag of about 1–3 Ma. They also found that certain maxima in the distribution of the proxies of plume activity (i.e. komatiite, flood basalts, dykes and layered intrusions) are present at 2.75–2.7 Ga, 2.5–2.4 Ga, 2.25–2.2 Ga and 2.0–1.86 Ga, coincident with times of major iron formation accumulations. As pointed out by Clout and Simonson (2005), the mantle plume hypothesis is consistent with the necessary vigorous output of Fe from oceanic hydrothermal systems and the widespread occurrence of Superior-type iron formations in the Neoarchaean-Palaeoproterozoic, owing to enhanced plume activity during these stages of Earth's geological history (see also Pirajno 2007b). Glikson (2006), on the other hand, noted a temporal and spatial association between ejecta units of asteroid/comet impacts and BIF. This author correlated the 2629 ± 5 Ma and 2481 ± 4 impact spherule units and tsunami-type deposits overlain by the BIF of the Marra Mamba Iron Formation and intercalated with Dales Gorge Iron Member, respectively, in the Hamersley Basin (Western Australia) and possible equivalents of the Kuruman Formation in the Transvaal (South Africa). According to Glikson (2006), the link between asteroid/cometary impacts and iron formations may be related to the denudation of uplifted mafic rocks and subsequent enrichment of soluble Fe in oxygen-poor atmosphere and hydrosphere and hydrothermal activity triggered by the impacts.

8.9.1 Iron Formation Ore Systems and Genetic Models

Clout and Simonson (2005) subdivided BIF- and GIF-hosted iron ore systems as follows: (1) primary iron formation (30–45 wt% Fe); (2) supergene-enriched iron ores with martite-goethite and hydrous Fe oxides (56–63 wt% Fe); and (3) high-grade hematite ores (60–68 wt% Fe) of supergene or modified hypogene origin. The high-grade hematite ores are further subdivided into hematite,

itabarite and microplaty hematite replacement ore. Itabarite is a metamorphosed, deformed BIF ore that was formed by supergene leaching of gangue minerals and residual accumulation of Fe oxides. The microplaty hematite typically consists of hematite plates, from 10 to 200 μm, which result from replacement of chert, Fe silicate and carbonate minerals. In addition to iron, there is evidence that, where deformed and metamorphosed, the Superior-type iron formations can also host hydrothermal Au and PGE mineralisation, as in the Itabira district of Brazil (Olivo et al. 1995). Here, Au and Pd mineralisation is hosted by quartz-hematite veins and altered rocks, which contain tourmaline, talc and phlogopite, developed within the iron formation (itabarite).

Martite-goethite ores are generally characterised by a predominance of goethite over martite and the preservation of the primary banding. In these ores the original BIF is replaced by goethite-martite and the magnetite by martite. In the ~2.60 Ga Marra Mamba Iron Formation in the Hamersley Group, martite replaces magnetite microbands, which remain preserved. Goethite occurs as a hard brown mineral or as powdery yellow ochreous goethite. Hematite and itabarite ores are formed from leaching of chert and carbonate bands, with hematite being left as an enriched residue. More recent weathering of martite-goethite ores results in the formation of a "hardcap", which may extend down to 60 m below the surface and consist of porous vitreous goethite and minor collofrom quartz (Clout and Simonson 2005). In the West Angelas deposit, also in the Marra Mamba Iron Formation, the hardcap is underlain by martite-goethite ore with >50 wt% hematite, which grades downward into friable martite-goethite ore with less than 50%wt hematite and then into friable ochreous goethite-martite ore with less than 30 wt% hematite (Clout and Simonson 2005). The high-grade hematite ores (>60 wt% Fe) contain residual martite-hematite and microplaty hematite and have less than 15 wt% goethite. A prominent example is the giant Sishen hematite deposit in the Transvaal Basin, with resources of 1690 Mt, at 64.8% Fe and grading downward into unmineralised BIF. The high-grade Sishen ores are locally slumped in karst structures of the underlying Campbellrand Dolomite, and are overlain by conglomerate ore, derived from re-worked iron ore. The Sishen hematite ore was formed by supergene enrichment during pre-Neogene times and is associated with lateritic profiles and aluminous shales. The Sishen ores are described by Beukes et al. (2002), who recognised three main ore types: hard microcrystalline, massive and laminated martite ore, both formed by supergene enrichment of BIF below a major unconformity and the above-mentioned detrital conglomeratic ore, derived from the erosion of the underlying laminated martite ore.

High-grade hematite ores make up the huge deposits of the Quadrilatero Ferrifero (Carajás District, Brazil), with resources of about 17500 Mt, grading 64% Fe. These iron ores were mostly formed by residual concentrations from supergene leaching of itabarite (metamorphosed BIF). Rosière et al. (2002) and Rosière and Rios (2004), both cited in Clout and Simonson (2005), carried out fluid inclusion studies integrated with detailed petrographic and textural data

from one of the Quadrilatero Ferrifero deposits (Conceiçao). These authors were able to establish three generations of hematite and specularite in response to deformation events. The first, Hematite I, consists of martite and hematite crystals, formed from the oxidation of magnetite at low temperature and low salinity fluids derived from surface water, during the final phases of the 2.1–2.0 Ga Transamazonian orogeny. Hematite II marks a second episode of Fe mineralisation relating to recrystallisation during regional metamorphism, resulting in a granoblastic fabric. The Hematite II stage is characterised by two-phase fluid inclusions with temperature of homogenisation (Th) ranging from 115 to 145°C and salinities of 4–10 wt% NaCl equivalent. Hematite III is tabular and formed at temperatures ranging from 120 to 140°C, during the 0.8–0.6 Ga Brasiliano Orogeny. A last stage represented by platy specular hematite has two- and three-phase fluid inclusions with Th from 140 to 205°C. Both Hematite III and the microplaty hematite are associated with high salinity fluids (>20 wt% NaCl equivalent).

Microplaty hematite ores, as the name implies, are essentially characterised by abundant hematite microplates, with or without martite. An example is the Mount Tom Price deposit in the Pilbara Craton, with resources of 900 Mt, grading 63.9% Fe. This deposit is situated in a synclinorium on the northern limb of a regional syncline, in an area of thrusts and faults paralleling the fold axes. The Mount Tom Price Fe mineralisation is hosted by the Dales Gorge Member of the Brockman Iron Formation and the Colonial Chert Member. The Tom Price microplaty hematite ranges from hard and massive to friable and powdery, to a leached blue dust ore. Dolerite dykes cut across the mineralisation and are characterised by chlorite-hematite-talc alteration. Hydrothermal alteration zoning was established in one part of the deposit (Thorne et al. 2004). This zoning consists of a proximal zone of martite-microplaty hematite-apatite, which is the main ore, grading into a zone of hematite-ankerite-magnetite, to a distal zone of magnetite-siderite-Fe silicate. Pseudoseconadry and secondary fluid inclusions from hematite-ankerite veins of the distal zone show high salinity H_2O-$CaCl_2$ of about 24 wt% $CaCl_2$ equivalent and Th of 253°C in pseudosecondary and 117°C, in secondary fluid inclusions.

Superior-type iron formations constitute the major iron resource of the world. The commercial exploitation of the iron formations is based on their subsequent enrichment to grades of up to 68% Fe, as martite-goethite and hematite ores (Clout and Simonson 2005). How this enrichment occurred is controversial, with theories invoking supergene enrichment (e.g. Morris 1985, 1993, 1998), hydrothermal processes (e.g. Barley et al. 1999), or flow of hot basinal fluids (e.g. Powell et al. 1999). Thus, there are three principal genetic models that attempt to account for the iron ores; they are: syngenetic-diagenetic, hypogene hydrothermal alteration and replacement linked either to magmatism or basinal brines and supergene. The supergene model suggests that the hematite and magnetite of the original iron formation are enriched by supergene processes to an assemblage of hematite and goethite and this is subsequently further modified by burial metamorphism to hematite-rich ores

(Morris 1993, 1998). The hydrothermal model of Barley and co-workers is essentially based on fluid inclusion and petrographic studies of the Hamersley iron ores (Barley et al. 1999; Ridley, 1999). In this model, interaction of high temperature fluids (hotter than 150°C, and possibly above 250°C) with the original BIF units, resulted in an assemblage of magnetite-hematite-siderite. Increasing oxidation at high temperature converted magnetite to martite (hematite) and microplaty hematite, and removed silica. The synorogenic hydrothermal model of Powell et al. (1999) proposes the expulsion of cool meteoric and hot basinal fluids migrating from an uplifted fold-and-thrust belt to a foreland. The model is similar to that envisaged for MVT ore systems, as shown in Fig. 8.30B. Powell et al. (1999; see also Martin et al. 1998), on the basis of oxygen isotope systematics, fluid inclusions and textural data, suggested that regional flow of high-temperature oxidising meteoric fluids occurred during orogenic activity at about 2.4–2.2 Ga (Ophthalmia Orogeny). These fluids were expelled from a fold-and-thrust belt, along low-angle faults, towards the northern, less deformed margin of the host Hamersley Basin.

The hypogene-hydrothermal model of Thorne et al. (2004) involves four stages. The first stage is related to ascending basinal brines at temperatures of 150–250°C, changing the primary BIF to an assemblage of magnetite-siderite-Fe silicate and desilication of the chert bands. Ferric oxyhydroxides can react with Fe^{2+}-rich fluids to form magnetite, according to the reaction:

$$2Fe(OH)_3 + Fe^{2+} \rightarrow Fe_3O_4 + 2H_2O + 2H^+$$

The second stage is also by hypogene basinal brines, but at higher temperatures (200–300°C) and producing hematite-siderite-magnetite alteration and microplaty hematite. The third stage is of lower temperature (about 120°C) basinal fluids, forming martite-microplaty hematite-apatite assemblages. The last stage is the supergene enrichement by descending meteoric waters during the Neogene with temperatures of less than 100°C and resulting in massive martite-microplaty hematite-goethite alteration. This model is shown in Fig. 8.41.

Krapež et al. (2003) came up with a novel and interesting model. These authors examined in great detail the sedimentology and the mineralogy of BIF successions of the 2.5–2.45 Ga Brockman Iron Formation of the Hamersley Group. The Group comprises the 2.63–2.59 Ga Marra Mamba Iron Formation at the base, followed upward by the Wittenoom Dolomite (carbonates and mudrocks), Mount Sylvia Formation (mudrocks and chert), Brockman Iron Formation, topped by the Woongarra Volcanics. Krapež et al. (2003) suggested that the precursor sediments were hydrothermal muds composed of Fe smectite, Fe oxyhydroxides and Fe carbonates, deposited on the flanks of submarine volcanoes and re-sedimented by density and turbidity currents. The fine-grained hematite is compared with the Fe oxide accumulations in the brine pools of the Red Sea (Section 8.5). These Fe oxides are the products of diagenesis of primary Fe oxyhydroxides discharged from hydrothermal vents and

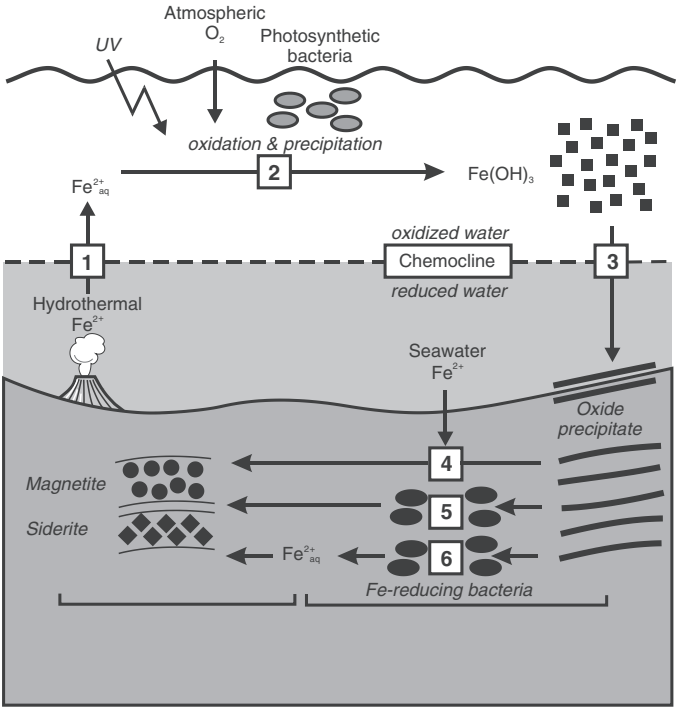


Fig. 8.41 Hypogene-supergene model for the formation of iron ores, applicable to the deposits of Tom Price (Pilbara Craton, Western Australia). The four stages shown in this figure are described in text. After Thorne et al. (2004)

deposited on the flanks of submarine volcanoes. Similarly, magnetite is considered to be a replacement of hematite and siderite. The chert matrix of BIF is also considered of diagenetic origin. Lascelles (2007) is the main proponent of the syngenetic-diagenetic model, which is probably a variant of the model proposed by Krapež et al. (2003). As mentioned previously, Lascelles advocated the action of turbidity and density currents, originating from submarine hydrothermal vents. Slumping of the hydrothermal mounds and gravity sliding, aided by seismic events, would have resulted in the formation of turbidity currents and the deposition of GIF as proximal fans, but more importantly the suspension of colloidal Fe-rich particles in density currents. These eventually deposited fine-grained BIF over large areas of the ocean, alternating with intervals of quiet pelagic sedimentation and silicification, forming interbedded shale bands. The dissociation of Al-poor hydrous Fe silicates, during diagenetic processes, results in the formation of Fe oxides, colloidal silica and bands of chert.

More recently, the use of Fe isotope systematics has been gaining momentum for the study of the origin of BIF and the possible role of bacteria. Iron participates in both biotic and abiotic redox processes and the isotopic

compositions using stable Fe isotopes is expressed as $^{56}Fe/^{54}Fe$ ratios, relative to average igneous rocks in the usual permil (‰) notation (Hoefs 2004; Johnson et al. 2007), so that:

$$\delta^{56}Fe = (^{56}Fe/^{54}Fe\ \text{sample}/^{56}Fe/^{54}Fe\ \text{igneousrocks} - 1)10^3$$

Whereas the isotopic fractionation between two composnents A and B is given by:

$$\Delta^{56}Fe_{A-B} = \delta^{56}Fe_A - \delta^{56}Fe_B \sim 103 \ln \alpha_{A-B}$$

Johnson et al. (2007) stated that the overall fractionation of ferric oxide/hydroxide-Fe^{2+}aq is similar regardless of the pathways involved, such as biotic and abiotic oxidation or even UV photo-oxidation. Based on the Fe isotope systematics, Johnson et al. (2007) suggested that at least six pathways, shown in Fig. 8.42, for the oxidation of Fe^{2+} and the formation of BIF can be considered. The first is the discharge of Fe^{2+} afrom hydrothermal vents at mid-ocean ridges and/or submarine volcanoes related to mantle plume events. The Fe^{2+} ascent across the chemocline (boundary between anoxic and oxidised water) results in pathway 2 with the formation of ferric oxides and hydroxides, such as $Fe(OH)_3$, by a combination of UV radiation (minimal) and photosynthetic bacteria (predominant). The ferric oxides and hydroxides have positive $\delta^{56}Fe$ values. Raining of the ferric oxide and hydroxides back across the chemocline to the ocean floor (pathway 3) is where BIF accumulates with conversion to magnetite, with near 0 to positive $\delta^{56}Fe$ values, by reaction with sea water (pathway 4), or by bacterial reduction (pathway 5). Pathway 6 refers to further bacterial reduction of excess Fe^{2+} (called dissimilatory iron reduction or DIR; Johnson et al. 2007).

A number of researchers (e.g. Francois 1986) suggested that the oxidation of Fe^{2+} to Fe^{3+} and $Fe(OH)^+$ in the Archaean and Palaeoproterozoic was due to the high levels of UV radiation. However, Konhauser et al. (2007), conducted experimental and thermodynamic modelling, simulating the chemistry of the Precambrian seawater mixing with Fe^{2+}-rich hydrothermal fluids, with and without UV radiation. These authors found that the amount of photochemical oxidation was in fact negligible, but when Fe^{2+} interacted with Fe-oxidising photosynthetic bacteria ferric hydroxides rapidly precipitated. Konhauser et al. (2007) concluded that the Fe oxides of BIF form by direct and/or indirect biologically mediated oxidation. Moreover, other experimental data of Konhauser et al. (2005) suggest that the biologically precipitated Fe^{3+}, can be recycled back into the water column and subsequently reduced with magnetite formation, by microbial reduction back to Fe^{2+}, so that a cyclic pathway from oxidation to reduction and back to oxidation could have occurred, providing a possible explanation for the large areal extent of BIF. Other models of BIF deposition (Kappler et al. 2005; Konhauser et al. 2002) propose a mechanism

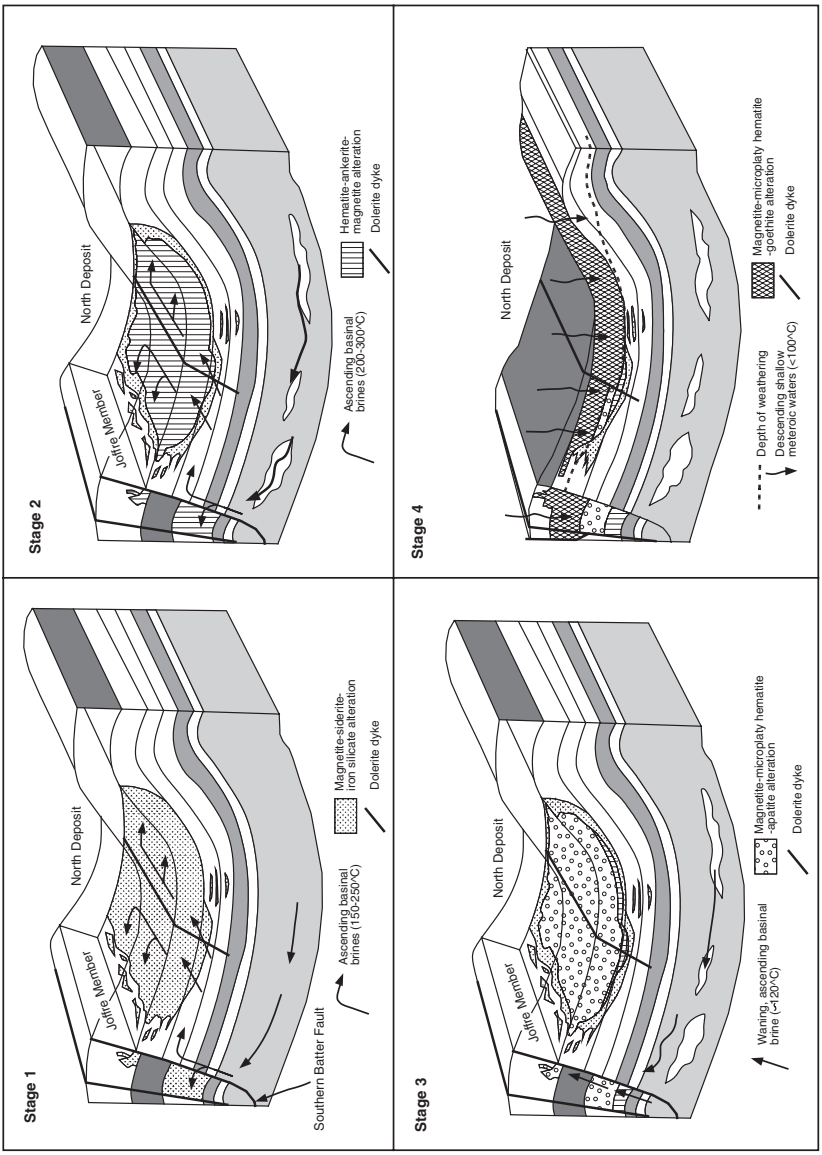


Fig. 8.42 Iron pathways (1 to 6) in BIF genesis; details in text. After Johnson et al. (2007)

for the oxidation of hydrothermal Fe(II) to Fe(III) by anoxygenic photosynthetic bacteria. A possible bacteria-mediated reaction is:

$$4Fe_2 + CO_2 + 11H_2O + \text{light energy} \rightarrow CH_2O + 4Fe(OH)_3 8H^+$$

8.9.2 *Granular Iron Formation of the Palaeoproteroroic Earaheedy Basin, Western Australia*

Clout and Simonson (2005) listed three textural components in granular iron formations (GIF): a framework of clasts, a fine-grained interstitial material or matrix and cementing authigenic minerals. Framework clasts comprise a mixture of ooids, granules and peloids of Fe oxides, Fe silicates, Fe carbonates and chert. These clasts are round to angular or elliptical and are usually concentrically laminated, locally exhibiting septarian cracks, due to post-depositional shrinkage. GIF locally display cross-stratification and beds of stromatolites. The Fe-rich bands of GIF usually consist of close-packed ooliths, about 1 mm across, but locally can reach a 3–5 cm across (Pirajno et al. submitted). Mixtures of BIF and GIF are more common than GIF alone, however an exception to this are the iron formation beds of the Palaeoproterozoic Earaheedy Basin, which consist entirely of GIF. Granular iron formation formed in shallow marine continental shelf to coastal conditions. Ferruginous peloids accreted in wave- and current-agitated iron-rich waters (Beukes and Klein 1992), and were deposited after some reworking by mechanical processes, with variable terrigenous contamination.

The Earaheedy Basin (Pirajno et al. 2004), lies at the easternmost end of the Capricorn Orogen (Cawood and Tyler 2004) (Fig. 8.43; see also Fig. 6.7). Basement to the exposed Earaheedy Basin is the Archaean Yilgarn Craton and to the west the Yerrida Basin. The Basin's regional structure is an asymmetric east-plunging syncline, with a vertical to locally overturned northern limb, due to compressive movements from the northeast, which created a zone of intense deformation, named the Stanley Fold Belt, along the exposed northern margin of the Earaheedy Basin. The Basin contains the Earaheedy Group, a 5-km-thick succession of shallow marine clastic and chemical sedimentary rocks that is divided into two subgroups, indicative of a shallow marine to coastal environment, which deepened to the north to northeast. The older Tooloo Subgroup comprises the Yelma Formation (base) and the Frere Formation, containing the GIF, with the Fe-rich shales of the Windidda Member (top). The overlying Miningarra Subgroup consists of the Chiall Formation (base), Wongawol Formation, Kulele Limestone, and Mulgarra Sandstone (top). The age of the Earaheedy Group is poorly constrained, but is younger than the underlying 1.84 Ga Mooloogool Group of the Yerrida Basin and older than 1.65 Ga, the age of the deformation of the Stanley Fold Belt (Pirajno et al. submitted).

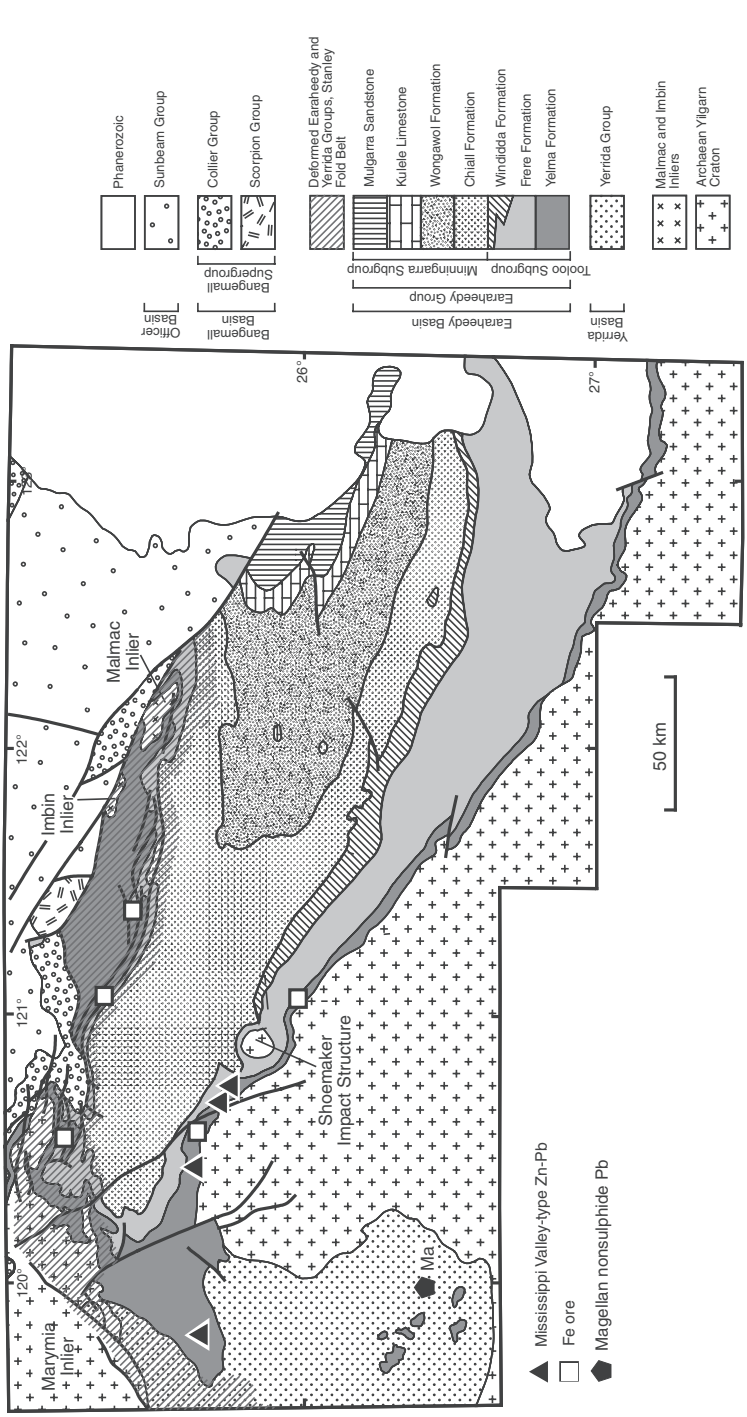


Fig. 8.43 Earaheedy Basin simplified geology and extent of the Frere granular iron formation and distribution of sedimentary ore systems. After Pirajno (2004)

The Frere Formation records the onset of major Fe oxide precipitation within the Earaheedy Basin and consists of up to four major granular iron formation intervals, separated by at least three major shale and siltstone bands, and minor carbonate. The Frere granular iron formation is an important iron resource, similar to the Superior iron formations and is one of few of this type recorded outside of North America (Trendall 2002). Walter et al. (1976) and Tobin (1990) described and compared microfossils within the Frere granular iron formation with those in the Gunflint Formation in the Superior Province (Awramik and Barghoorn, 1977). The Gunflint Iron Formation contains microfossils (Gunflint-type microbial communities) that are similar to those found in the Frere Formation (Walter et al. 1976; Tobin 1990). Gunflint-type microbiota are considered to be characteristic of marine subtidal environments. These microfossils consists of contorted and/or randomly oriented filaments and include Gunflintia *minuta*, Animikiea *septata*, Eoastrion *simplex*, Eoastrion *bifurcatum*, Huraniospora *psilate*, Kakabekia *umbellata* and Archaeorestis *schreiberensis* (Walter et al. 1976; Tobin 1990).

The Frere Formation is exposed both along the southern and northern margins of the Earaheedy Basin and is folded into a broad east-trending, south-verging asymmetric synclinal structure, with a steep to overturned northern limb. On the southern margin the Frere Formation is unmetamorphosed, undeformed or only mildly deformed, forming layers that are shallow-dipping to the north. The total thickness of the formation is estimated at about 600 m.

GIF horizons in the Frere Formation consist of jasperoidal granular iron-oxide beds, typically 0.5–20 cm in thickness, interbedded with chloritic shale and/or siltstone. Individual GIF beds consist of chert, iron oxides (hematite and/or magnetite) and jasper peloids, in a cement of microcrsytalline quartz, chalcedonic quartz (allochemical) or jasperoidal (orthochemical) cement. Hematite is replaced by microplaty hematite and/or magnetite in GIF beds deformed in the Stanley Fold Belt. In fractures and zones of deformation the iron formation beds are pervasively silicified, with the peloids and the interbedded iron-chlorite-rich shale replaced by stilpnomelane. Maghemite and martite replace the hematite and magnetite in zones of supergene alteration. Typically, the granular iron beds alternate with shale and siltstone beds, at scales ranging from hundreds of metres through metres to millimetres, similar to the macrobands and mesobands of the banded iron formation (Fig. 8. 39; Trendall 2002). Shale and siltstone units are parallel-laminated, and contain quartz, iron-rich chlorite and disseminated euhedral magnetite. The granular iron-shale/siltstone couplets of the Frere Formation are indicative of cyclic changes in primary sediment composition that probably relate to sea level changes and supply of iron and silica. Cross-bedding is locally visible in granular iron formation beds, and in general sedimentary structures indicate traction-current deposition.

The boundary between the Tooloo and Miningarra subgroups (base of Chiall Formation) reflects a change in depositional setting from a chemical, clastic-starved regime to one of abundant clastic supply. The granular iron

beds, shale, and siltstone all have different iron and silica content both within and between units. This points to a complex, varying interrelationship between clastic influx, dissolved silica and dissolved iron. The supply of dissolved silica appears to have been variable at all scales, and can be interpreted as a result of fluctuating concentrations. The supply of Fe is also interpreted as the result of fluctuating concentrations but with a high proportion of Fe remaining in suspension throughout deposition of the Frere Formation. The shale interbedded with GIF and in major shale horizons may indicate periods where the rates of silica and iron precipitation were low. GIF beds provide a reasonable indicator of depositional setting, because in order to have large scale deposition of clastic iron oxides, a shallow-water environment, probably a continental shelf (passive margin) would have been required (e.g. Trendall 2002). Thus, the lithofacies of the Earaheedy Group suggest that it was part of a trailing passive margin, characterised by low-magnitude marine transgressions and regressions in response to fluctuating sea-level changes, due to a combination of sediment supply, subsidence and eustasy (Erikson et al. 2001). The grain size (dominantly medium-fine sand to silt) indicates dominantly quiet, low-energy conditions, although this could be because coarser material was simply not available due to a low-gradient, weathered, basin hinterland. Sea-level fluctuations are envisaged to be both eustatic and tectonic, with short-term eustatic changes in a greenhouse climate producing metre-scale cyclicity in carbonates and from tens of metres to metre scale cyclicity in the iron formation (iron formation-siltstone bands), and longer term tectonism responsible for increases in sand deposition by either hinterland uplift or basin subsidence. North to northeastward deepening is consistent with the distribution of facies within the basin architecture.

The Earaheedy Basin has a special importance in the tectonostratigraphic record of Palaeoproterozoic terranes because of the presence in the basin stratigraphy of the GIF units of the Frere Formation. The presence of the Frere Formation GIF could be related to a period of mantle plume(s) breakout, which resulted in global magmatism at ca. 1.8 Ga, supercontinent breakup, trailing margins and deposition of iron-formations (cf. Barley et al. 2005). In addition, oxygenic photosynthesis associated with the GIF may have contributed to the rise of oxygen levels in the Earth's atmosphere. Granular iron-formation formed in shallow marine continental shelf to coastal conditions. Beukes and Klein (1992) and Isley (1995) considered that granular iron formation formed as the shallow water, higher energy equivalent of deeper water banded iron formations. However, it should be noted that the model for the origin of the iron formations proposed by Beukes and Klein (1992) and Isley (1995) accounts for the large volumes of iron, but it does not explain the association of iron and silica in grains of possible biogenic origin. Some of the grains classified as peloids, may have been originally oncolites (Brown et al. 1995). If this is correct, then it is possible that biogenic activity may have played a major role in the development of the Earaheedy granular iron formation, through a mechanism of bacterial Fe oxidation (Brown et al. 1995). The

northwards-deepening, passive-margin model for Earaheedy Basin of Pirajno et al. (2004) is consistent with these models.

8.9.3 Manganese Oxide Ores

Proterozoic iron formations are commonly associated with giant manganese deposits, such as those of the 2.2 Ga Kalahari field in South Africa and Minas Gerais in Brazil. Economic Geology published a special issue on Mn deposits (Frakes and Bolton 1992). The close Fe-Mn spatial relationship is related to the chemical affinity of these two elements and therefore the same solutions that are enriched in Fe are also enriched in Mn (Schissel and Aro 1992; Cornell and Schütte 1995). The origin of both the iron and manganese formations requires that large amounts of these metals be brought into solution as reduced species (Mn^{2+}), which are then oxidised (Mn^{3+}, Mn^{4+}) and precipitated as Fe and Mn oxides and carbonates. Iron and Mn are geochemically similar and in many instances they are precipitated together, but separation can and does occur during precipitation from hydrothermal solutions, depending on Eh-pH environmental conditions. Almost complete separation of these two elements is known from the Fe and Mn formation of the Transvaal Basin in South Africa (e.g. Klein and Beukes 1992). Force and Cannon (1988) suggested that at low Eh, iron solubility is low, due to the uptake of iron by sulphur ligands, precipitating sulphides. On the other hand and under the same conditions, Mn solubility is high, because there is no comparable Mn sulphide (alabandite, MnS, is uncommon in sedimentary rocks; Force and Maynard 1991). In oxic environments, Fe and Mn also tend to precipitate separately, again in response to Eh and pH conditions, with Fe oxides predominantly precipitating in deeper water (continental slope, at lower Eh for a given pH) and Mn oxides in shallower waters (on the shelf, at higher Eh for a given pH) (Schissel and Aro 1992). The association of glauconite-bearing sandstone and Fe-Mn oxides has been investigated by Ostwald and Bolton (1992). Glauconite, is a micaceous mineral with the general formula $(K,Na,Ca)_{1.2–2.0}(Fe^{+3},Al,Fe^{+2},Mg)_4$ $[Si_7AlO_{20})$ $(OH)_4.n(H_2O)$. It is generally deposited in shallow marine continental shelves (water depths of 50–500 m), and has a spatial association with Fe and Mn formations. Ostwald and Bolton (1992) found that there is a genetic relationship between them. Glauconite tends to form in deeper offshore water, whereas Mn oxide precipitation occurs along palaeoshore lines. In addition, glauconite enhances the Mn content of the water because it removes Fe from the system. In other words, glauconite fixes Fe in the clastic sediments, rather similar to pyrite fixing Fe in black shales. In this way, waters moving along the shelf are enriched in Mn, which is then precipitated as oxide (Mn^{2+}). Anoxic conditions prevail basinward from the iron-formation, iron-manganese oxides and glauconite zones, resulting in deposition of black shales.

8.9.3.1 Kalahari Manganese Field

The 2.2 Ga Kalahari manganese field is the largest Mn resource in the world with about 8 Bt at grades of between 28 and 48% Mn (Tsikos et al. 2003) and is entirely covered by the Cenozoic Kalahari Group, except for one isolated outcrop, the Voelwater jasper at Black Rock (Fig. 8.44). The succession in the Kalahari field is part of the Transvaal Supergroup (equivalent of the Hamersley Group of Western Australia), comprising three laminated Mn oxides units intercalated with BIF. The Hotazel Formation hosts the Mn ore and lies at the top of the Griqualand West Sequence, a shelf succession formed by the 2.6 Ga Campbell Dolomite, BIF and the Ongeluk basaltic lavas. The Hotazel

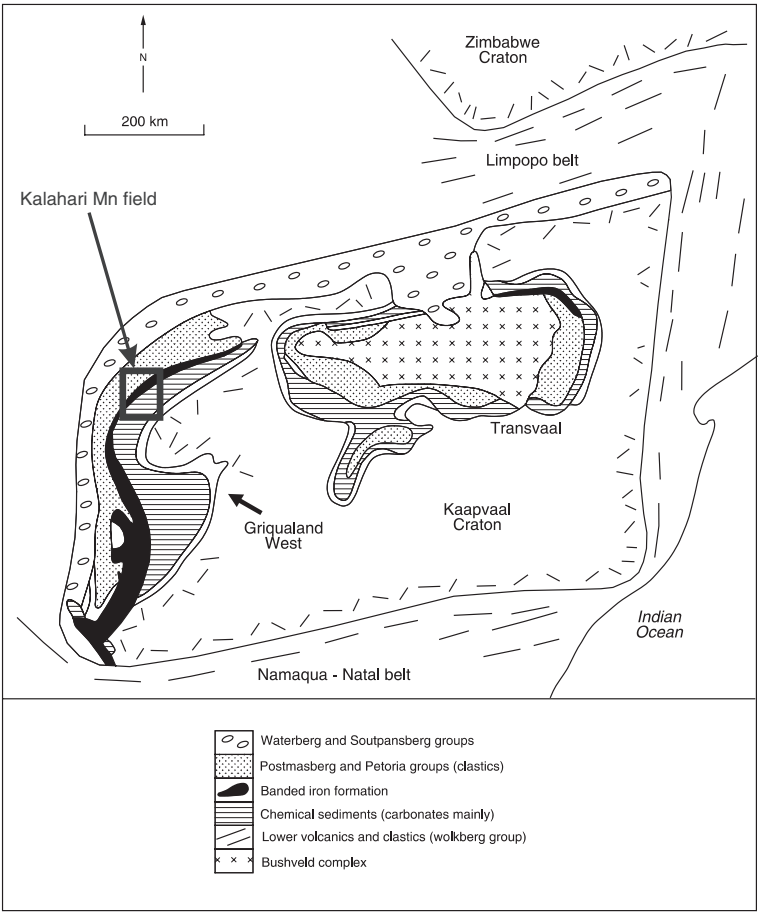


Fig. 8.44 Sketch map and simplified geology of the Kaapvaal Craton (South Africa) and position of the Kalahari Mn field. After Pirajno (1992)

Formation, estimated to be about 140 m thick, overlies the Ongeluk lavas and consists of three cycles of iron formation and associated Mn layers. A basal jaspilite is followed upward by BIF (cycle 1), a Mn-rich iron formation, a Lower Mn orebody and Mn-rich iron formation (cycle 2), BIF with intercalated middle and upper Mn orebodies (cycle 3). The cycle 3 units are unconformably overlain by limestone and sands of the Kalahari Group. The Mn ore is laterally very extensive, finely laminated and composed mainly of black braunite (locally oolitic), hausmannite and jacobsite. There are three main deposits: Wessels, Hotazel and Mamatwan. At Wessels all three Mn-bearing layers are present; at Hotazel the middle layer is discontinuous, whereas it is absent altogether at Mamatwan. The ore is finely laminated and composed of dull black semi- to non-crystalline braunite. Two types of braunite occur: braunite I ($3Mn_2O_3.MnSiO_3$) and braunite II [$(7Mn.Fe)_2O_3{\cdot}CaSiO_3$]. Other ore minerals include hausmanite (Mn_3O_4) and jacobsite ($MnO{\cdot}Fe_2O_3$). The ore, in places, has small spherical accretions, interpreted as ooliths, which may be dolomitic in compositions but are replaced by Mn. Within the Mn orebodies, occasional thin (<1 cm) hematite layers are present and one of these is continuous for several kilometres and is used as a marker horizon. Grades are very variable, from less than 7% up to 65–68% Mn. Best grades are in the basal parts of the lower and upper orebodies, although secondary enrichment occurs close to faults. Primary braunite I changes to braunite II as a fault is approached, and hausmanite is best developed next to the fault. These mineralogical changes are accompanied by concomitant changes in grade, which in places may increase by as much as 7%, to higher than 50% Mn, over a distance of a few metres. This fault-controlled epigenetic upgrading of the orebodies is particularly important at the structurally more complex Wessels mine, where up to three periods of faulting are present. There appears to be no correlation, however, between grade and any particular set of faults. Supergene enrichment resulted in the development of secondary Mn minerals such as cryptomelane [$(K{\cdot}H_2O)_2Mn_5O_{10}$] and todokorite [$(Mn,Ca,Mg)Mn_3O7{\cdot}H_2O$]. Two bostonite dykes occur at Wessels, and one at Hotazel, but the only observed effect on the orebodies is the development of a narrow aureole of jacobsite around one of the dykes at Wessels. Locally, there are zones of skarn-like assemblages, which are attributed to burial metamorphism, and are characterised by sugilite (an attractive purple-coloured mineral, $(K,Na)(H_2O,Na)_2(Fe^{3+},Na,Ti,Fe^{2+})_2$ $(Li,Al,Fe^{3+})_3(Si_{12}O_{30})$, andradite, wollastonite, pectolite, vesuvianite and quartz.

The genesis of the Mn ore is thought to be the result of sedimentation of oolitic carbonate in a matrix of gelatinous Mn and Fe hydroxides and carbonates, and locally, hydrous silicates of Mg and Fe. The limits of the known Mn field presumably represent a part of the Griqualand West basin, in which conditions were conducive to the precipitation of Mn rather than Fe. Precisely what these conditions were and what caused them is not understood. During diagenesis, crystallisation of the manganiferous gel formed braunite I, rhodocrosite, jacobsite and pyrolusite. At a later stage, perhaps during burial metamorphism, minerals like braunite II, hausmannite and those of the skarn

assemblages were formed. Nevertheless, in order to form the economic Mn orebodies, it is believed that some form of enrichment (hypogene or supergene?) must have taken place. If a manganiferous gel did exist, then it is implied that a colloidal solution must have been active. The source of so much Mn is also problematic. It has been suggested that the source of both the Mn and Fe of the Voelwater Formation may, in some way, be connected with the underlying Ongeluk andesitic lavas, perhaps through hydrothermal venting. Beukes et al. (1982) drew attention to the association of the Mn deposits with jaspers and pillow lavas. They also pointed to the presence of hematite in hyaloclastites as being indicative of hydrothermally-derived ferrous Fe, which was then rapidly oxidised and precipitated in proximity of the volcanic source. Divalent Mn ions, on the other hand, take much longer to oxidise than ferrous Fe, and are therefore deposited distally from the volcanic source.

The origin of the Kalahari manganese field and the association of Fe and Mn are still debated. Tsikos and Moore (1998), have divided the ore genesis models into: (1) epigenetic replacement; (2) volcanic-exhalative (e.g. ocean ridge submarine volcanism; and (3) chemical sedimentary (related to sea level fluctuations). Although the intimate spatial association with the Ongeluk pillow lavas invites a genetic link with volcanism, Tsikos et al. (2003) suggested that low temperature fluids were channelled along the unconformity that separates the Hotazel Formation from the overlying Olifantshoek Supergroup, perhaps associated with fault-controlled leaching and enrichment to high-grade Mn ores.

8.10 Metalliferous Sediments on Seafloors

Metalliferous sediments cover vast areas of the seafloor of the Earth's oceans. These metalliferous sediments are the product of hydrothermal plumes emitted from submarine vents and largely consist of ferromanganese oxide crusts, distal mixed clays and nodular deposits.

Literature on ferromanganese crusts and enriched pelagic clays on ocean floors, other than normal oceanic sediments, includes a United Nations report (United Nations Ocean Economics 1979), Burns and Burns (1979), Toth (1980) and Roy (1992). An exhaustive review on the metallifeorus sediments in the oceans can be found in Gurvich (2006). In the Pacific Ocean metalliferouos sediment crusts cover areas, north and south of the equator, roughly from 10° S to 40° S and from 5° N to 40° N where, according to Gurvich (2006), the thickness of the sediments, mixed with abyssal red clays and other sediments, may reach up to 30 m. An important features is that the distribution and thickness are more or less symmetrically disposed around the mid-ocean ridges. Ferromanganese crusts also cover flanks of oceanic islands, seamounts and oceanic ridges, originating from submarine vents hydrothermal precipitates. Laznicka (2006) reported a resource of crusts on the Horizon Guyot as 75.5 Mt

containing 18 Mt of Mn, 0.58 Mt Co, 0.34 Mt Ni and 46 t of Pt. The age of the metalliferous sediments ranges from about 150 Ma to present day, and as is the case for oceanic crust, this age increases away from the spreading centres. As mentioned above, the metalliferous sediments accumulate as a result of the spreading of hydrothermal plumes that arise from active submarine vents. The hydrothermal fluids at the point of emission have lower density than the cold sea water, due to their high temperature, and therefore these fluid become buoyant and mix with the sea water. A buoyant plume can attain heights of between 150 and 400 m above the emitting vents and the higher the temperature of the fluids at vent, the higher the plume will rise (Lupton 1995). The hydrothermal plume carries particulate matter in suspension that is directly derived from black and white smokers. The rising hydrothermal plume will eventually reach a level of neutral buoyancy and start to spread laterally. This is called by Gurvich (2006) a nonbuoyant plume. A nonbuoyant plume spreads laterally away from above the vents field carried by the prevailing direction of the marine current and can enrich the pelagic clays for distances of up to 600 km from a mid-ocean ridge (Laznicka 2006). It is calculated that more than 90% of the particulate material in a hydrothermal plume can be transported for more than 2 km from the vent field (Dymond and Roth 1988). The hydrothermal plume will disperse its particulate matter over large distances, till it is assimilated in the ocean water and its source no longer recognised (Gurvich 2006).

Of future economic significance are the ferromanganese nodules, largely composed of zoned segregations of Mn oxyhydroxides (e.g. todorokite, birnessite) and Fe hydroxides, round to elliptical in shape and ranging in size from a few mm up to tens of cm across or more, but most are only a few cm in across. Literature on ferromanganese nodules includes Roy (1992), Hein et al. (1997), Glasby (1976, 2000), Mukhopadhyay et al. (2002) and Graham and Wright (2007). The largest areas of ferromanganese nodules are in the Pacific Ocean, where tonnage estimations of recoverable nodules vary considerably. Laznicka (2006) quoted an estimate of Russian authors (Bezrukov et al. 1970), based on 36.13×10^6 km^2 of the Pacific Ocean abyssal floor, of 3.4 trillion tonnes of nodules, containing resources of 71 Bt Mn, 2.3 Bt Ni, 1.0 Bt Co and 1.9 Bt Cu. Another estimate (Dean 1983, also cited in Laznicka 2006) based on an area of 2.5 km^2 of Pacific Ocean floor, is of 20 Bt of nodules, grading 28.8% Mn, 1.2% Ni, 0.99% Cu, 0.23% Cu. 0.13% Zn and 0.048% Mo. Modern ferromanganese nodules rest on pelagic siliceous and carbonate oozes, red clays and hemipelagic sediments (Roy 1992).

There are two types of ferromanganese nodules: hydrogenous and diagenetic. Hydrogenous nodules are mostly composed of todorokite, buserite ($Na_4Mn_{14}O_{27}{\cdot}21H_2O$), vernadite ($\delta$-$MnO_2$) and Fe hydroxides (goethite and lepidocrocite) and form by precipitation of metals from the ocean water onto nucleii of rock fragments or shells, with slow growth rates. Todorokite has a special tunnel structure that allows the admission of Ni^{2+}, Cu^{+2} and Co^{+2} ions (Roy 1992). Diagenetic nodules have irregular shapes, botryoidal surfaces and consist of buserite and berthierine [(Fe, Fe, AlMg)(SiAl)O(OH)] and form in

seafloor sediments from seawater pore fluids (Roy 1992; Graham and Wright 2007). The growth of both types of these nodules is aided by Mn oxidising bacteria. Nodules commonly have a smooth top and more ragged bottom parts, which also differ in chemical composition reflecting different sources of metal supply. The parts of the nodules that are buried in the marine sediments, tend to receive Mn and other metals from the pore waters (diagenetic), whereas the parts from above the ocean interface receive Mn and metals from the ocean (hydrogenous). However, movements of the nodules by bottom currents can switch the supply from diagenetic to hydrogenous and those nodules that are round with concentric growth textures were probably continuously moved (Roy 1992).

Graham and Wright (2007) studied the extensive ferromanganese nodule fields of the Campbell Plateau in the southwest Pacific, within the New Zealand Exclusive Economic Zone. The Campbell Plateau, south and southeast of New Zealand, rises about 3000 m above the seafloor (4500–5500 water depth) and the nodule field is distributed along the flanks of the Plateau. The seafloor in this area is covered with a mix of biogenic calcareous ooze, fine gravel lags and ferromanganese nodules. The ferromanganese nodule field substrate forms an undulating abyssal belt 300–150 km wide, with densities of nodule abundances ranging from >75% to 25% . Variations in the extent of the field and nodule densities are related to bottom currents and seafloor topography. Graham and Wright (2007) described the nodules of the northeast Campbell field as being both hydrogenous and diagenetic, with the largest nodule examined about 20 cm in diameter and 15 Myr old. The nodules exhibit a range of internal textures, from cuspate to columnar to globular with abundant pore spaces filled with microfossils and detrital minerals, such as quartz, feldspar, pyroxene, apatite. The Ni + Cu values range from 0.06 to 1.3% Ni and Co from 0.003 to 0.46%. The growth rate of these nodules, determined using the $^{10}Be/^{9}Be$ system, is 5.5 mm/Ma. The REE pattern typically show positive Ce anomalies, a feature that is characteristic of nodules world-wide. Internal geochemical variations, from core to rim, show increasing Mn/Fe ratios and Ni + Cu and decreasing silica and Co. Graham and Wright (2007) estimated the economic potential of the 5000 km^2 northeastern Campbell field, considering a mean nodule diameter of 3 cm, mean weight of 300 g and a mean seafloor density of 50%, in the region of 2 Bt of nodules with a resource of 5 Mt of Ni, 2 Mt of Cu and 3 Mt of Co.

8.11 Concluding Remarks

Following an overview of sedimentary basin geology, I have discussed at some length the East African Rift System (EARS). This rift system, including its more advanced stage represented by the Red Sea where oceanic crust is developing and pools of brines and sulphides are actively forming, is in my opinion, the prime example of an "ore-making environment" encompassing a wide range of

ore systems, from the brine pools in a protooceanic rift (the Red Sea), to hot spring deposits and subaqueous exhalites in lakes. The range of possibilties, although purely hypothetical, is shown in Fig. 8.6. However, the message here is that it is important that each single ore deposit in the geological record be assessed and considered within a broader tectonic context. The EARS extends for more than 5000 km, from the Red Sea to the Zambezi valley, exhibiting a great variety of geological environments, from oceanic crust, to evaporite plains, alkaline volcanoes, carbonatites, central volcanoes, rift lakes with subaqueous hot springs teaming with microbial life. This inevitably leads to compare the EARS with ancient rift systems, which are commonly poorly exposed or partly eroded and hosting a variety of ore systems including stratiform-stratabound Copperbelt style, SEDEX and even some MVT deposits. The analogy could help in the understanding of these ancient rift systems. Stratiform and stratabound Cu deposits and SEDEX deposits contain large resources of base metals. These ore systems are the object of continuing studies aimed at understanding their genesis. Genetic models, range from syndiagenetic replacement to epigenetic or combinations of the two. The bottom line here is that the origin of individual deposits needs to be assessed first, followed by regional overviews with the aim of placing a given deposit or ore systems within this regional context, as discussed above using the example of the EARS. Mississippi Valley type (MVT) ore systems are equally variable in terms of their style and origin. In some examples the link with SEDEX may be valid; in others this link is not obvious. Also, MVT are clearly amagmatic and perhaps could have been discussed in Chapter 9. However, I thought that given the nature of these ore systems and their possible link with SEDEX, not to mention the evidence in some instances of seafloor venting, it is more appropriate to have MVT included in this Chapter. These uncertainties bring home the fact that ore systems are complex and often not amenable to simple pigeonholing.

The Proterozoic Fe and Mn formations constitute a remarkable and vast resource of these metals. Today, the Fe resources from banded iron formations are in very high demand by the emerging Asian economies, at the same time providing unparalled economic prosperity for all countries that are involved in its production. Finally, considering the ferromanganese nodules in the abyssal plains of the oceans, there is little doubt that these constitute a further and an immense resource for the future.

References

Allen PA, Allen JR (1990) Basin analysis – principles and applications. Blackwell Scientific Publ, Oxford

Allen PA, Allen JR (2005) Basin analysis: principles and applications, 2nd edn. Blackwell Scientific Publ, Oxford

Allsopp HL, Welke HJ, Hughes MJ (1981) Shortening the odds in exploration. Nucl Act 24:8–12

Anderson IK, Ashton JH, Boyce AJ, Fallick AE, Russell MJ (1998) Ore depositional processes in the Navan Zn-Pb deposit, Ireland. Econ Geol 93:535–564
Anschutz P, Blanc G (1995) Chemical mass balances in metalliferous deposits from the Atlantis II Deep, Red Sea. Geochim Cosmochim Acta 59:4205–4218
Anschutz P, Blanc G (1996) Heat and salt fluxes in the Atlantis II Deep (Red Sea). Earth Planet Sci Lett 142:147–159
Awramik SM, Barghoorn ES (1977) The Gunflint microbiota. Precambr Res 5:121–142
Baines SJ, Burley SD, Pize AP (1991) Sulphide mineralisation and hydrocarbon migration in North Sea oilfields. In: Pagel M, Leroy JC (eds) Source, transport and deposition of metals, Balkema, Rotterdam, 507–510
Bäcker H, Richter H (1973) Die rezente hydrothermal sedimentäre Lagerstätte Atlantis-II Tief im Roten Meer. Geologische Rundschau 62:697–741
Baker BH (1986) Tectonics and volcanism of the southern Kenya rift valley and its influence on rift sedimenation. Geol Soc London, Sp Publ 25:45–58
Barberi F, Varet J (1978) The Afar rift junction. In: Neumann R, Ramberg IB (eds) Petrology and geochemistry of continental rifts, Reidel, Dordrecht, pp55–69
Barberi F, Ferrara R, Santacroce R, Varet J (1975) Structural evolution of the Afar triple junction. In: Pilger A, Rosler A (eds) Afar depression of Ethiopia, Scheweizerbart, pp 38–54
Barley ME, Pickard AL, Sylvester PJ (1997) Emplacement of a large igneous province as a possible cause of banded iron formation 2.45 billion years ago. Nature 385:55–58
Barley ME, Pickard AL, Hagemann SG, Folkert SI (1999) Hydrothermal origin for the 2 billion year old Mount Tom Price giant ore deposit, Hamersley Province, Western Australia. Mineral Depos 34:784–789
Barley ME, Bekker A, Krapež B (2005) Late Archean to Early Paleoproterozoic global tectonics, environmental change and the rise of atmospheric oxygen. Earth Planet Sci Lett 238:156–171
Bartholomé P (ed) (1973) Gisement stratiformes et provinces cupriferes. Geol Soc Belg, Liège
Bayer HJ, El-Isa Z, Hotzl H, Mechie J, Prodehil C, Saffarini G (1989) Large tectonic and lithospheric structures of the Red Sea region. J Afr Earth Sci 8:565–587
Beaudoin G (1997) Proterozoic Pb isotope evolution in the Belt-Purcell Basin: constraints from syngenetic and epigenetic sulfide deposits. Econ Geol 92:343–350
Beaumont C, Tankard AJ (eds) (1987) Sedimentary basins and basin-forming mechanisms. Can Soc Petrol Geol Monogr 12
Betts PG, Giles D (2006) The 1800-1100 Ma tectonic evolution of Australia. Precambr Res 144:92–125
Betts PG, Goleby BR (eds) (2006) Mt Isa tectonics. Aust J Earth Sci Thematic Issue 53(1)
Betts PG, Giles D, Lister GS, Frick RL (2002) Evolution of the Australian lithosphere. Aust J Earth Sci 49:661–695
Betts PG, Giles D, Lister GS (2003) Tectonic environment of shale-hosted massive sulphide Pb-Zn-Ag deposits of Proterozoic northeastern Australia. Econ Geo 98:557–576
Beukes NJ, Klein C (1990) Geochemistry and sedimentology of a facies transition – from microbanded to granular iron-formation – in the early Proterozoic Transvaal Supergroup, South Africa. Precambr Res 47:99–139
Beukes NJ, Kleyenstuber A, Nel C (1982) Volcanogenic-sedimentary cycles in the Kalahari Manganese Field. Abstr Sedimentology 82. Geol Soc S Afr 93–97
Beukes NJ, Klein C (1992) Models for iron-formation deposition, in The Proterozoic biosphere: a multidisciplinary study. In: Schopf W, Klein C (eds) Cambridge University Press, pp 147–151
Beukes NJ, Gutzmer J, Mukhopadhyay J (2002) The geology and genesis of high-grade hematite iron ore deposits. Austr Inst Min Metall Publ Ser 7/2002:23–29
Beyene A, Abdelsalam MG (2005) The tectonics of the Afar depression: a review and synthesis. J Afr Earth Sci 41:41–59

Bezrukov PL, Petelin VP, Skorjakova NS (1970) Mineral'ney resursy okeana. Tikhii Okean 2, Nauka, Moscow
Bignell RD (1975) Timing, distribution and origin of submarine mineralisation in the Red Sea. Trans Inst Min Metall B84: B1–B6
Bischoff JL (1969) Red Sea geothermal brine deposits: their mineralogy, chemistry and genesis. In Degens ET, Ross DA (eds) Hot brines and recent heavy metal deposits in the Red Sea, Springer, Berlin, pp 368–401
Björlykke A, Sangster DF (1981) An overview of sandstone lead deposits and their relation to red-bed copper and carbonate-hosted lead-zinc deposits. Econ Geol 75th Anniv Vol: 179–213
Björlykke A, Thorpe RI (1982) The source of lead in the Osen sandstone lead deposit on the Baltic Shield. Econ Geol 77:430–440
Boelema R, Hira H (1998) Pegmatite deposits. In: Wilson MGC, Anhaeusser CR (eds) The mineral resources of South Africa, 6th edn, Handbk 16, Council Geosci, pp 509–521
Bohannon RG (1989) Style of extensional tectonism during rifting, Red Sea and Gulf of Aden. J Afr Earth Sci 8:589–602
Bonatti E (1985) Punctiform initiation of seaflor spreading in the Red Sea during transition froma continental to an oceanic rift. Nature 316:33–37
Bonatti E, Fisher DE, Joensuu O, Rydell HS, Beyth M (1972) Iron-manganese-barium deposit from the northern Afar rift (Ethiopia). Econ Geol 67:717–730
Boni M, Terracciano R, Evans NJ, Laukamp C, Schneider J, Bechstädt T (2007) Genesis of vanadium ores in the Otavi Mountain Land, Namibia. Econ Geol 102:441–469
Borg G (1988) The Koras-Sinclair-Ghanzi rift in southern Africa. Volcanism, sedimentation, age relationships and geophysical signature of a late middle Proterozoic riuft system. Precambr Res 38:75–90
Borg G, Maiden KJ (1986) A preliminary appraisal of the tectonic and sedimentological environment of the Sinclair Sequence in the Klein Aub area, SWA/Namibia. Commun Geol Surv of SWA/Namibia 2:65–73
Borg G, Maiden KJ (1987) Alteration of late Middle Proterozoic volcanics and its relation to stratabound copper-silver-gold mineralisation along the margin of the Kalahari Craton in SWA/ Namibia and Botswana. Geol Soc Spec Publ 33:347–354
Borg G, Frotzscher M, Ehling B (2005) Metal content and spatial distribution of Au and PGE in the Kupferschiefer of the Mansfeld/Sangerrhausen mining district, Germany. In: Mao JW, Bierlein FP (eds) Mineral deposit research: meeting the global challenge, vol 2. Springer, Berlin, pp 885–888
Botha BJV, Grobler NJ (1979) The geotectonic evolution of the middle to late Precambrian Namaqua Mobile Belt in eastern Namaqualand, South Africa. Precambr Res 10:33–41
Botz R, Schmidt M, Wehner H, Hufnagel H, Stoffers P (2007) Organic-rich sediments in brine-filled Shaban and Kebrit deeps, northern Red Sea. Chem Geol, doi: 10.1016/j.chemgeo.2007.07.004
Boyce AJ, Anderton R, Russell MJ (1983) Rapid subsidence and early Carboniferous base-metal mineralization in Ireland. Trans Inst Min Metall 92: B55–B66
Boyce AJ, Little CTS, Russell MJ (2003) A new fossil vent biota in the Ballynoe barite deposit, Silvermines, Ireland: evidence for intracratonic sea-floor hydrothermal activity about 352 Ma. Econ Geol 98:649–656
Bradley DC, Leach DL (2003) Tectonic controls of Mississippi Valley-type lead-zinc mineralization in orogenic forelands. Mineral Depos 38:652–667
Braile LW, Keller GR, Wendlandt RF, Khan MA (1995) The East African rift system. In: Olsen KH (ed) Continental rifts: evolution, structure, tectonics, Elsevier, Amsterdam, pp 213–232
Brigo L, Omenetto P (1985) Lithogeochemical observations on some ore-bearing Triassic sequences of the Italian southern Alps. Monograph series on mineral deposits, vol 25. Bornträeger, Berlin, pp 95–194
Brigo L, Camana, G, Rodeghiero F, Potenza R (2001) Carbonate-hosted siliceous crust type mineralization of Carnic Alps (Italy-Austria). Ore Geol Rev 17:199–214

Broadbent GC, Myers RE, Wright JV (1998) Geology and origin of the shale hosted Zn-Pb-Ag mineralization at the Century deposit, northwest Queensland, Australia. Econ Geol 93:1264–1294

Broadbent GC, Andrews SJ, Kelso IJ (2002) A decade of new ideas: geology and exploration history of the Century Zn-Pb-Ag deposity, northwestern Queensland, Australia. Soc Econ Geol Sp Publ 9:119–140

Brown JS (ed) (1967) Genesis of stratiform lead-zinc-barite-fluorite deposits (Mississippi Valley type deposits). Soc Econ Geol Monogr 3

Brown AC (1971) Zoning in the White Pine copper deposit, Michigan. Econ Geol 66:543–573

Brown DA, Gross GA, Sawicki JA (1995) A review of the microbial geochemistry of banded iron-formations. Canad Mineral 33:1321–1333

Burns RG, Burns VM (1979) Manganese oxides. In: Burns RG (ed) Marine Minerals. Mineral Soc Am Strat Course Notes 6, pp 1–46

Busby CJ, Ingersoll RV (1995) Tectonics of sedimentary basins. In: Busby CJ, Ingersoll RV (eds) Tectonics of sedimentary basins, Blackwell Science, Oxford, pp 1–51

Butuzova GYu (1998) Hydrothermal-sedimentary ore forming processes in the Red Sea rift zone. GEOS, Moscow

Cairncross B (1997) The Otavi Mountain Land Cu-Pb-Zn-V deposits. Mineral Rec 28:109–137

Cawood PA, Tyler IM (2004) Assembling and reactivating the Proterozoic Capricorn Orogen: lithotectonic elements, orogenies and significance. Precambr Res 128:201–218

Chetty D, Frimmel HE (2000) The role of evaporites in the genesis of base metal sulphide mineralisation in the Northern Platform of the Pan-African Damara Belt, Nambia: geochemical and fluid inclusion evidence from carbonate wall rock alteration. Mineral Depos 35:364–376

Clifford TN, Stumpfl EF, Burger AJ, McCarthy TS, Rex DC (1981) Mineral-chemical and isotopic studies of Namaqualand granulites, South Africa: a Grenville analogue. Contrib Mineral Petrol 77:225–250

Cloud P (1973) Paleoecological significance of the banded iron formation. Econ Geol 68:1135–1143

Cloud P (1976) Major features of crustal evolution. Trans Geol Soc S Afr LXXIX: 1–33

Clout JMF, Simonson BM (2005) Preacambrian iron formations and iron formation-hosted iron ore deposits. Econ Geol 100th Anniv Vol: 643–649

Condie KC (2001) Mantle plumes and their record in Earth history. University Press, Cambridge

Cornell DH, Schütte SS (1995) A volcanic-exhalative origin for the world's largest (Kalahari) manganese field. Mineral Depos 30:146–151

Cornell DH, Thomas RJ, Moen HFG, Reid DL, Moore JM, Gibson RL (2006) The Namaqua-Natal province. In: Johnson MR, Anhaeusser CR, Thomas RJ (eds) The geology of South Africa, Geol Soc S Afr and Council Geoscie, Pretoria, pp 325–379

Crocetti CA, Holland HD (1989) Sulphur-lead isotope systematics and the composition of fluid inclusions in galena from the ViburnumTrend, Missouri. Econ Geol 84:2196–2216

De Waele B, Liégeois JP, Nemchin A, Tembo F (2006) Isotopic and geochemical evidence of Proterozoic episodic crustal reworking within the Irumide belt of south-central Africa, the southern metacratonic boubdary of an Archaean Bangweulu Craton. Precambr Res 148:225–256

Dean WE (1983) Geochemistry of deep-sea manganese nodules-organic involvement. In:Shanks WC (ed) Cameron volume unconventional mineral deposits, AIME, New York, pp 123–132

Deb M, Goodfellow WD (eds) (2004) Sediment hosted lead-zinc sulphide deposits: attributes and models of some major deposits in India, Australia and Canada. Narosa Publ House, New Delhi

Degens ET, Kulbicki G (1973) Hydrothermal origin of metals in some East African rift lakes. Mineral Depos 8:388–404

Degens ET, Ross DA (1976) Strata-bound metalliferous deposits found in or near active rifts. In: Wolf KH (ed) Handbook of strata-bound and stratiform ore deposits, vol 9. Elsevier, Amsterdam, pp 165–202

de Ronde CEJ, de Wit MJ, Spooner ETC (1994) Early Archaean (>3.2 Ga) Fe-oxide-rich, hydrothermal discharge vents in the Barberton greenstone belt, South Africa. Geol Soc Am Bull 106:86–104

Direen NG, Crawford AJ (2003) The Tasman Line: where it is, what it is, and is it Australia's Rodinian breakup boundary? Aust J Earth Sci 50:491–502

Doe RB, Delevaux MA (1972) Source of lead in southeast Missouri galena ores. Econ Geol 67:405–425

Dondi M, Puggioli G. (1992). La mine de Raibl, Cave del Predil (UD) – 2° partie. Rivista Mineral Ital 3:153–166

Dörling SL, Dentith MC, Groves DI, Vearncombe JR (1996) Mississippi Valley-type deposits of the southeast Lennard Shelf: an example of the interplay of extensional deformation, sedimentation and mineralization. Soc Econ Geol Sp Publ 4:96–111

Dörling SL, Groves DI, Muhling P (1998) Lennard Shelf Mississippi Valley-type (MVT) deposits, Western Australia. AGSO J Geol & Geophys 17:115–120

Dymond J, Roth S (1988) Plume dispersed hydrothermal particles: A time-series record of settling flux from the Endeavour Ridge, using moored sensors. Gechim Comsochim ACta 52:2525–2536

Ebinger CJ, Sleep NH (1998) Cenozoic magmatism throughout east Africa resulting from the impact of a single plume. Nature 395:788–791

Ebinger CJ, Yemane T, Harding DJ, Tesfaye S, Kelley S, Rex DC (2000) Rift deflection, migration and propagation: Linkage of the Ethiopian and eastern rifts, Africa. Geol Soc Am Bull 112:163–176

Edgerton D (1997) Reconstruction of the Red Dog Zn-Pb-Ba orebody, Alaska: implications for the vent environment during the mineralizing event. Can J Earth Sci 34:1581–1602

Eglington BM (2006) Evolution of the Namaqua-Natal Belt, southern Africa – A geochronological and isotope geochemical review: J Afr Earth Sci 46:93–111

Einsele G (2000) Sedimentary basins – evolution, facies and sediment budget. Springer, Berlin

Eisenlhor BN, Tompkins LA, Cathles LM, Barley ME, Groves DI (1994) Mississippi Valley-type deposits: Products of brine expulsion by eustatically induced hydrocarbon generation? An example from northwestern Australia. Geology 22:315–318

Erikson PG, Martins-Neto MA, Nelson DR, Aspoler LB, Chiarenzelli JR, Catuneau O, Sarkar S, Altermann W, Rautenbach CJW (2001) An introduction to Precambrian basins: their characteristics and genesis. Sedimen Geol 141–142:1–35

Ernst RE, Buchan K (2003) Recognising mantle plumes in the geological record. Ann Rev Earth Planet 31:469–523

Esteban M, Klappa CF (1983) Subaerial exposure. Mem Am Assoc Petroleum Geol 33:1–54

Eugster HP (1986) Lake Magadi Kenya: a model for rift valley hydrochemistry and sedimentation? Geol Soc, Lond, Spec Publ 25: 177–190

Eugster HP (1986) Lake Magadi Kenya: a model for rift valley hydrochemistry and sedimentation? Geol Soc Sp Publ 25:177–190

Fleischer VD, Garlick WS, Haldane R (1976) Geology of the Zambian Copper Belt. In: Wolf KH (ed) Handbook of stratabound and stratiform ore deposits, vol 6. Elsevier, Amsterdam, pp 223–352

Force ER, Cannon WF (1988) Depositional model for shallow-marine manganese deposits around black shale basins. Econ Geol 83:93–117

Force ER, Maynard JB (1991) Manganese: Syngenetic deposits on the margins of anoxic basins. Rev Econ Geol 9:147–157

Foster DRW, Austin JR (2007) The 1800 to 1610 Ma stratigraphic and magmatic history of the Eastern Succession, Mount Isa Inlier, and correlations with adjacent Palaeoproterozoic terranes. Precamb Res doi: 10.1016/j.precamres.2007.08.010

Francois LM (1986) Extensive deposition of banded iron formations was possible without photosynthesis. Nature 320:352–354
Frakes L, Bolton B (1984) Origin of manganese giants: sea level changes and anoxic-oxic history. Geology 12:83–86
Frimmel HE, Deane JG, Chadwick PJ (1996) Pan-African tectonism and the genesis of base metal sulfide deposits in the northern foreland of the Damara orogen, Namibia. Soc Econ Geol Sp Publ 4:204–217
Frakes L, Bolton B (eds) (1992) A special issue devoted to advances in Manganese metallogenesis. Econ Geol 87(5)
Frostick LE, Renaut RW Reid I, Tiercelin JJ (eds) (1986) Sedimentation in the African rifts. Geol Soc, London, Sp Publ 25
Fyfe WS, Price NJ, Thompson AB (1978) Fluids in the Earth's crust. Elsevier, Amsterdam
Garlick WS (1961) The syngenetic theory. In: Mendelsohn F (ed) The geology of the Northern Rhodesian Copperbelt, Macdonald, London, pp 146–165
Garlick WS (1989) Mineralization controls and source of metals in the Lufillian Fold Belt, Shaba (Zaire), Zambia and Angola. Econ Geol 84:966–968
Garven G, Raffensperger JP (1997) Hydrogeology and geochemistry of ore genesis in sedimentary basins. In: Barnes HL (ed) Geochemistry of ore deposits, 3rd edn. John Wiley & Sons, New York, pp 125–189
Geringer GJ, Pretorius JJ, Cilliers FH (1987) Strata-bound copper-iron sulphide mineralization in a Proterozoic front arc setting at Boksputs, Borthwest Cape, South Africa – a possible Besshi-type deposit. Mineral Depos 22:81–89
Ghebread W (1998) Tectonics of the Red Sea region. Earth-Sci Rev 45:1–44
Gibson RL, Kisters AFM (eds) (1996) Special issue on the geology of the Okiep copper district. S Afr J Geol 99(2)
Gibson GM, Peljo M, Chamberlain T (2004) Evidence and timing of crustal extension versus shortening in the early tectonothermal evolution of a Proterozoic continental rift sequence at Broken Hill, Australia. Tectonics 23:TC5012, doi: 10.1029/2003TC001552
Giles CW (1988) Petrogenesis of the Proterozoic Gawler Range Volcanics, South Australia. Precambr Res 40/41:407–427
Giles D, Betts PG, Lister GS (2004) 1.8-1.5 Ga links between the North and South Australian Cratons and the early-Middle Proterozoic configuration of Australia. Tectonophysics 380:27–41
Glasby GP (1976) Manganese nodules in the South Pacific: a review. New Zeal J Geol & Geophys 19:707–736
Glasby GP (2000) Manganese: predominant role of nodules and crusts. In: Schulz HD, Zabel M (eds) Marine geochemistry, Springer, New York, pp 771–790
Glass LM, Phillips D (2006) The Kalkarindji continental flood basalt province in Australia with possible links to faunal extinctions. Geology 34:461–464
Glikson A (2006) Asteroid impact ejecta units overlain by iron-rich sediments in 3.5-3.2 Ga terrains, Pilbara and Kaapvaal cratons: accidental or cause-effect relationships? Earth Planet Sci Lett 246:149–160
Goodfellow WD, Lydon JW, Turner RJW (1993) Geology and genesis of stratiform sediment-hosted (SEDEX) zinc-lead-silver sulphide deposits. Geol Ass Canada Sp Pap 40:201–252
Goodfellow WD, Lydon JW (2007) Sedimentary exhalative (SEDEX) deposits. Geol Ass Canada Sp Publ 5:163–183
Graham IJ, Wright IC (2007) The Campbell ferromanganese nodule field in the southern part of New Zealand's exclusive economic zone. Aust Inst Min Metall Monogr 25:339–347
Grip E (1966) On the genesis of the lead ores of the eastern border of the Caledonides in Scandinavia. Soc Econ Geol Monogr 3:208–226

Groves DI, Vielreicher RM, Goldfarb RJ, Condie KC (2005) Controls on the heterogeneous distribution of mineral deposits through time. Geol Soc Lond Sp Publ 248:71–101
Grundmann WH (1977) Geology of the Viburnum No. 27 mine, Viburnum Trend, southeast Missouri. Econ Geol 72:349–364
Gurvich EG (2006) Metalliferous sediments of the world ocean. Springer, Berlin
Hanor JS (1979) The sedimentary genesis of hydrothermal fluids. In: Barnes HL (ed) Geochemistry of hydrothermal ore deposits, 2nd edn. John Wiley & Sons, New York, pp 137–172
Hanor JS (1994) Origin of saline fluids in sedimentary basins. Geol Soc, Lond, Sp Publ 78:151–174
Hartnady CJH, Joubert P, Stowe CW (1985). Proterozoic crustal evolution in southwestern Africa. Episodes 8:236–244
Hearn PP, Sutter JF, Belkin HE (1987) Evidence for Late-Palaeozoic brine migration in Cambrian carbonate rocks of the central and southern Apalachians: Implications for Mississippi Valley-type sulfide mineralization. Geochim Cosmochim Acta 51:1323–1334
Hein JR, Koscjinsky A, Halbach P, Manheim FT, Bau M, Kamg JK, Lubick N (1997) Iron and manganese oxide mineralization in the Pacific. Geol Soc London Sp Publ 119:23–138
Hitzman MW, Beaty DW (1996) The Irish Zn-Pb-(Ba) orefield. Soc Econ Geol Sp Publ 4:112–143
Hitzman MW, Kirkham R, Broughton D, Thorson J, Selley D (2005) The sediment-hosted stratiform copper ore system. Econ Geol 100th Ann Iss: 609–642
Hoefs J (2004) Stable isotope geochemistry. 5th edn. Springer, Berlin
Hoffman PF, Kaufman AJ, Halverson GP, Schrag DP (1998) A Neoproterozoic snowball Earth. Science 281:1342–1346
Holland HD (2002) Volcanic gases, black smokers and the Great Oxidation Event. Geochim Cosmochim Acta 66:3811–3826
Holm NG (1989) The $^{13}C/^{12}C$ ratios of siderite and organic matter of a modern metalliferous sediment and their implications for banded iron formations. Chem Geol 77:41–45
Hughes MJ (1987) The Tsumeb ore body, Namibia, and related dolostone-hosted base metal deposits of Central Africa. Univ Witwatersrand, Johannesburg, unpubl PhD thesis
Hulen JB, Collister JW (1999) The oil-bearing Carlin-type gold deposits of Yankee Basin, Alligator Ridge district, Nevada. Econ Geol 94:1029–1050
Huston DL, Stevens B, Southgate PN, Muhling P, Wyborn L (2006) Australian Zn-Pb-Ag ore-forming systems: a review and analysis. Econ Geol 101:1117–1157
Innes J, Chaplin RC (1986) Ore bodies of the Kombat Mine, South West Africa/Namibia. In: Anhaeusser CR, Maske S (eds) Mineral deposits of southern Africa, vol 2. Geol Soc S Afr, pp 1789–1805
Ireland T, Large RR, McGoldrich P, Blake M (2004) Spatial distribution patterns of sulphur isotopes, nodular carbonate and ore textures in the McArthur River (HYC) Zn-Pb-Ag deposit, Northern Territory, Australia. Econ Geol 99:1687–1710
Isley AE (1995) Hydrothermal plumes and the delivery of iron to banded iron formation. J Geol 103:169–185
Isley AE, Abbott DH (1999) Plume-related mafic volcanism and the deposition of banded iron formation. J Geophys Res 104:15461–15477
James HL (1954) Sedimentary facies of iron formation. Econ Geol 49:235–293
Jaques AL, Jaireth S, Walshe JL (2002) Mineral systems of Australia: an overview of resources, settings and processes. Aus J Earth Sci 49:623–660
Jiang SY, Palmer MR, Ding TP, Wan DF (1994) Silicon isotope geochemistry of the Sullivan Pb-Zn deposit, Canada: a preliminary study. Econ Geol 89:1623–1629
Jiang SY, Palmer MR, Slack JF, Shaw DR (1998) Paragenesis and chemistry of multistage tourmaline formation in the Sullivan Pb-Zn-Ag deposit, British Columbia. Econ Geol 93:47–67
Johnson CM, Beard BL, Klein C, Beukes NJ, Riden EE (2007) Iron isotopes constrain biologic and abiologic processes in banded iron formation genesis. Geochim Cosmochim Acta 10.1016/j.gca.2007.10.013

Joubert P (1986a) The namaqualand metamorphic complex. In: Hunter DR (ed) Precambrian of the southern hemisphere developments in precambrian geology 2, Elsevier, Amsterdam; pp 671–705
Joubert P (1986b) The namaqualand metamorphic complex. A summary. In: Anhaeusser CR, Maske S (eds) Mineral deposits of southern Africa II. Geol Soc S Afr, pp 1395–1420
Jowett EC (1986) Genesis of Kupferschiefer Cu-Ag deposits by convective flow of Rotliegende brines during Triassic rifting. Econ Geol 81:1823–1837
Kamona AF, Lévêque J, Fridrich G, Haack U (1999) Lead isotopes of the carbonate-hosted Kabwe, Tsumebr, and Kipushi Pb-Zn-Cu sulphide deposits in relation to Pan African orogenesis in the Damaran-Lufillian fold belt of central Africa. Mineral Depos 34:273–283
Kampunzu AB, Lubala RT (eds) (1991) Magmatism in extensional structural settings – the Phanerozoic African plate. Springer-Verlag, Berlin
Kappler A, Pasquero C, Konhauser KO, Newman DK (2005) Deposition of banded iron formations by anoxygenic phototrophic Fe(II)-oxidizing bacteria. Geology 33:865–868
Kelley KD, Jennings S (2004) Special issue devoted to barite and Zn-Pb-Ag deposits in the Red Dog district, Brooks Range, Alaska. Econ Geol 99:1267–1280
Kennard JM, Jackson MJ, Romine KK, Shaw RD, Southgate PN (1994) Depositional sequences and associated petroleum systems of the Canning Basin, WA. In: Purcell PG, Purcell RR (eds) The sedimentary basins of Western Australia, Proceed Petr Expl Soc Aus, Symp, pp 657–676
Keranen K, Klemperer, SL (2007) Discontinuous and diachronous evolution of the Main Ethiopian Rift: implications for development of continental rifts. Earth Planet Sci Lett doi: 10.1016/j.epsl.2007.09.038
Kesler SE, Reich M, Jean M (2007) Geochemistry of fluid inclusion brined from Earth's oldest Mississippi Valley-type (MVT) deposits, Transvaal Supergroup, South Africa. Chem Geol 237:274–288
Kimbel WH (1995) Hominid speciation and Pliocene climate change. In: Vrba ES, Denton GH, Partridge DC, Burckel LH (eds) Palaeoclimate and evolution with emphasis on human origins. Yale University Press, New Haven, pp 425–437
Kimberley MM (1989a) Nomenclature for iron formations. Ore Geol Rev 5:1–12
Kimberley MM (1989b) Exhalative origins of iron formations. Ore Geol Rev 5:13–145
Klein C, Beukes NJ (1992) Proterozoic iron-formations. In: Condie KC (ed) Proterozoic crustal evolution, Elsevier, Amsterdam, pp 383–418
Konhauser KO, Hamade T, Raiswell R, Ferris FG, Southam G, Canfield DE (2002) Could bacteria have formed the Precambrian banded iron formations? Geology 30:1079–1082
Konhauser KO, Newman DK, Kappler A (2005) The potential significance of microbial Fe(III) reduction during deposition of Precambrian banded iron formation. Geobiol 3:167–177
Konhauser KO, Amskold L, Lalonde SV, POsth NR, Kappler A, Anbar A (2007) Decoupling photochemical Fe(II) oxidation from shallow-water BIF deposition. Earth Planet Sci Lett 258:87–100
Krapež B, Barley ME, Pickard AL (2003) Hydrothermal and resedimented origins of the precursor sediments to banded iron formation: sedimentological evidence from Early Palaeoproterozoic Brockman Supersequence of Western Australia. Sedimentology 50:979–1011
Kröner A (1978) The Namaqua Mobile Belt within the framework of Precambrian Crustal evolution in Southern Africa. Geol Soc S Afr Specl Publ. 4:181–188
Kucha H, Van der Biest J, Viaene NA (1990) Peloids in strata-bound Zn-Pb deposits and their genetic importance. Mineral Depos 25:132–139
Kyle JR, Li N (2002) Jinding: A giant Tertiary sandstone-hosted Zn-Pb deposit, Yunnan, China. SEG Newslett 50:1–16
Lambiase JJ (1989) The framework of African rifting during the Phanerozoic. J Afr Earth Sci 8:183–190

Lambiase JJ (1990) A model for tectonic control of lacustrine stratigraphic sequences in continental rift basins. Am Ass Pet Geols Mem 50:265–276
Large DE (1981) Sediment-hosted submarine exhalative lead-zinc deposits-A review of their geological characteristics and genesis. In: Wolf KH (ed) Handbook of stratabound and stratiform ore deposits, vol 9. Elsevier, Amsterdam, pp 469–507
Large D, Walcher E (1999) The Rammelsberg massive sulphide Cu-Zn-Pb-Ba deposit, Germany: an example of sediment-hosted massive sulphide mineralization. Mineral Depos 34:522–538
Large RR, Bull SW, Cooke DR, McGoldrick PJ (1998) A genetic model for the HYC deposit, Australia, based on regional sedimentology, geochemistry, and sulfide-sediment relationship. Econ Geol 93:1345–1569
Large RR, Bull S, McGoldrick PJ, Waters S, Derrick GM, Carr GR (2005) Stratiform and stratabound Zn-Pb-Ag deposits in Proterozoic sedimentary basins, northern Australia. Econ Geol 100th Anniv Vol: 931–963
Larin AM, Mikhailov DA (1997) Olyokma Terrain. In: Rundqvist DV, Gillen C (eds) Precambrian ore deposits of the East European and Siberian cratons, Devel Econ Geol, Elsevier, pp 211–225
Larter RCL, Boyce AJ, Russell MJ (1981) Hydrothermal pyrite chimneys from the Ballynoe baryte deposit, Silvermines, County Tipperary, Ireland. Mineral Depos 16:309–318
Lascelles DF (2007). Black smokers and density currents: a uniformitarian model for the genesis of banded iron-formations. Ore Geol Rev 32:381–411
Laznicka P (2006) Giant metallic deposits – Future sources of industrial metals. Springer, Berlin
Leach DL, Plumlee GS, Hofstra AH, Landis GP, Rowan EL, Viets JG (1991) Origin of late dolomite cement by CO_2-saturated deep basin brines: evidence from the Ozark region, central United States. Geology 19:348–351
Leach DL, Sangster DF (1993) Mississippi valley-type lead-zinc deposits. Geol Ass Can Sp Pap 40:289–314
Leach DL, Bradley DC, Lewchuk M, Symons DTA, Brannon J de Marsily G (2001) Mississippi Valley-type lead-zinc deposits through geological time: inplications from recent age-dating research. Mineral Depos 36:711–740
Leach DL, Marsh E, Emsbo P, Rombach C, Kelley KD, Reynolds J, Anthony M (2004) Nature of hydrothermal fluids at the shale-hosted Red Dog Zn-Pb-Ag deposits, Brooks Range, Alaska. Econ Geol 99:1449–1480
Leach DL, Sangster DF, Kelley KD, Large RR, Garven G, Allen CR, Gutzmer J, Walters S (2005) Sediment-hosted lead-zinc deposits: A global perspective. Econ Geol 100th Ann Iss: 561–607
Leeder M (1999) Sedimentology and sedimentary basins – from turbulence to tectonics. Blackwell Science, Oxford
Logan GA, Hinman MC, Walter MR, Summons RE (2001) Biogeochemistry of the 1640 Ma McArthur River (HYC) lead-zinc ore and host sediments, Northern Territory, Australia. Geochim Cosmochim Acta 65:2317–2336
Lombaard AF, Gunzel A, Innes J, Kruger TL (1986) The Tsumeb lead-copper-zinc-silver deposit, South West Africa/Namibia. In: Anhaeusser CR, Maske S (eds) Mineral deposits of southern Africa, vol 2. Geol Soc S Afr, pp 1761–1787
Lupton JE (1995) Hydrothermal plumes: near and far field. Am Geophys Union Monogr 91:317–346
Lydon JW (2004) Genetic models for Sullivan and other SEDEX deposits. In: Deb M, Goodfellow WD (eds) Sediment hosted lead-zinc sulphide deposits: attributes and models of some major deposits in India, Australia and Canada. Narosa Publ House, New Delhi, pp 149–190
Lydon JW (2007) Geology and metallogeny of the Belt-Purcell Basin. Geol Ass Canada Sp Publ 5:581–607

Maiden K, Hughes M (2000) Mount Isa and Tsumeb: a comparative metallogenic study. Commun Geol Surv Namibia 12:167–177
Marinelli G (1971) La province géothermique de la dépression Danakil. Annales Mines 12:123–133
Marmont S (1987) Ore deposit models #13. Unconformity-type uranium deposits. Geosci Can 14:219–229
Martin DMcB, Li ZX, Nemchin AA, Powell CMcA (1998) A pre-2.2 Ga age for giant hematite ores of the Hamersley Province, Australia. Econ Geol 93:1084–1090
Matthews PE (1976) Possible Precambrian obduction and plate tectonics in South Eastern Africa. Nature 240:37–39
McClung CR, Gutzmer J, Beukes NJ, Mezger K, Strauss H, Gertloff E (2007) Geochemistry of bedded barite of the Mesoproterozoic Aggeneys-Gamsberg Broken hill-type district, South Africa. Mineral Depos 42:537–549
McConnell RB (1972) Geological development of the rift system of Eastern Africa. Geol Soc Am Bull 83:2549–2572
McGregor GJ (1986) Geology of the Black Mountain ore body- Aggeneys. In: Abstr Geocongress '86 Johannesburg. Geol Soc S Afr, pp 1025–1028
Mendelsohn F (ed) (1961) The geology of the Northern Rhodesian Copperbelt. MacDonald, London
Metcalfe R, Rochelle CA, Savage D, Higgo JW (1994) Fluid-rock interactions during continental red bed diagenesis: implications for theoretical models of mineralisation in sedimentary basins. Geol Soc Lond Sp Publ 78:301–324
Miller RMcG (1983) The Pan-African damara orogen of South-West Africa/Namibia. Geol Soc S Afr Sp Publ 11:431–515
Misiewicz JE (1988) The geology and metallogeny of the Otavi Mountain Land, Damara Orogen, SWA/Namibia, with particular reference to the Berg Aukas Zn-Pb-V deposit – A model of ore genesis. MSc Thesis, Rhodes University, Grahamstown
Mohr P (1978) Afar. Ann Rev Earth Planet Sci 6:145–172
Moore JM (1980) A study of certain paragneiss associations and their metallogenic characteristics in Namaqualand and Bushmanland. Ann Rep Precambr Res Unit, Univ Cape Town 17:65–73
Moore JM (1989) A comparative study of metamorphosed supracrustal rocks from the Western Namaqualand Metamorphic Complex. Precambr Res Unit, Dept Geol, Univ Cape Town, Bull 37
Morris RC (1985) Genesis of iron ore in banded iron-formation by supergene and supergene-metamorphic process – a conceptual model. In: Wolf KH (ed) Handbook stratabound and stratiform ore deposits 13**,** Elsevier, pp 73–235
Morris RC (1993) Genetic modelling for banded iron-formation of the Hamersley Group, Pilbara Craton, Western Australia. Precambr Res 60:243–286
Morris RC (1998) BIF-hosted iron ore deposits – Hamersley style. AGSO J Aust Geol & Geophys 17:207–211
Mouat MM, Clendenin CW (1977) Geology of the Ozark Lead Company mine, Viburnum Trend, Southeast Missouri. Econ Geol 72:398—407
Mukhopadhyay R, Iyer SD, Ghosh AK (2002) The Indian Ocean nodule field: petrotectonic evolution and ferromanganese deposits. Earth-Sci Rev 60:67–130
Müller G, Förstner U (1973) Recent iron formation in Lake Malawi, Africa. Mineral Depos 8:278–290
Myers JS, Shaw RD, Tyler IM (1996) Tectonic evolution of Proterozoic Australia. Tectonics 15-6:1431–1446
Ohle EL (1985) Breccias in Mississippi Vally-type deposits. Econ Geol 80:1736–1752
Oliver J (1986) Fluids expelled tectonically from orogenic belts: their role in hydrocarbon migration and other geological phenomena. Geology 14:99–102

Olivo GR, Gauthier M, Bardoux M, De Sa EL, Fonseca JTF, Carbonari Santana F (1995) Palladium-bearing gold deposit hosted by Proterozoic Lake Superior-type iron-formation at the Cauê iron mine, Itabira district, southern San Francisco Craton, Brazil: geologic and structural controls. Econ Geol 90:118–134

Olsen KH (ed) (1995) Continental rifts: evolution, structure, tectonics. Devlpmt Geotect, Elsevier, Amsterdam

Ostwald J, Bolton BR (1992) Glauconite formation as a factor in sedimentary manganese deposit genesis. Econ Geol 87:1336–1344

Page RW, Stevens BPJ, Gibson GM (2005) Geochronology of the sequence hosting the Broken Hill Pb-Zn-Ag orebody. Econ Geol 100:633–661

Painter MGM, Golding SXD, Hannan KW, Neudert MK (1999) Sedimentologic, petrographic, and sulfur isotope constraints on fine-grained pyrite formation at Mount Isa mine and environs, northwest Queensland, Australia. Econ Geol 94:883–912

Parnell J (ed) (1994) Geofluids: origin, migration and evolution of fluids in sedimentary basins. Geol Soc Lond Sp Publ 78

Parr JM, Plimer IR (1993) Models for Broken Hill-type lead-zinc-silver deposits. Geol Ass Can Sp Pap 40:253–288

Peace WM, Wallace MW (2000) Timing of mineralization at the Navan Zn-Pb deposit: A post-Arundian age for Irish mineralization. Geology 28:711–714

Person M, Garven G (1994) A sensitivity study of the driving forces on fluid flow during continental-rift basin evolution. Geol Soc Am Bull 106:461–475

Pflumio C, Boulègue J, Tiercelin JJ (1994) Hydrothermal activity in the northern Tanganyika rift, East Africa. Chem Geol 116:85–109

Pickard AL (2003) SHRIMP U-Pb zircon ages for the Palaeoproterozoic Kuruman iron formation, Northern Cape Province, South Africa: evidence for simultaneous BIF deposition on Kaapvaal and Pilbara Cratons. Precambr Res 125:275–315

Pierret MC, Clauer N, Bosch D, Blanc G, France-Lanord C (2001) Chemical and isotopic ($^{87}Sr/^{86}Sr$, $\delta^{18}O$, δD) constraints to the formation of Red Sea brines. Geochim Cosmochim Acta 65:1259–1275

Pirajno F (1992) Hydrothermal ore deposits – Principles and fundamental concepts for the exploration geologist. Springer-Verlag, Berlin

Pirajno F (2000) Ore deposits and mantle plumes. Kluwer Academic Publ., Dordrecht

Pirajno F (2004) Metallogeny in the Capricorn Orogen, Western Australia, the result of multiple ore-forming processes. Precambr Res 128:411–439

Pirajno F (2007a) Mantle plumes, associated intraplate tectono-magmatic processes and ore systems. Episodes 30:6–19

Pirajno F (2007b) Ancient to modern Earth: the role of mantle plumes in the making of continental crust. In: Van Kranendonk MJ, Smithies RH, Bennett VC (eds) Earth's oldest rocks, Dev Precambr Geol 15, Elsevier, Amsterdam, pp 1037–1064

Pirajno F, Joubert BD (1993) An overview of carbonate-hosted mineral deposits in the Otavi Mountain Land, Namibia: implications for ore genesis. J Afr Earth Sci 16:265–272

Pirajno F, Bagas L (2008) A review of Australia's Proterozoic mineral systems and genetic models. Precambr Res, doi:10.1016/j.precamres.2007.05.008

Pirajno F, Grey K (2002) Chert in the palaeoproterozoic bartle member, killara formation, Yerrida Basin, Western Australia: a rift-related playa lake and thermal spring environment? Precambr Res 113:169–192

Pirajno F, Jones JA, Hocking RM, Halilovic J (2004) Geology and tectonic evolution of Palaeoproterozoic basins of the eastern Capricorn Orogen, Western Australia. Precambr Res 128:315–342

Pirajno F, Hocking RM, Reddy S, Jones AJ (submitted) The geology and mineral systems of the Earaheedy Basin, Western Australia. Geol Surv West Aust Rpt and Earth Sci Rev

Playford PE (1980) Devonian "Great Barrier reef" of Canning Basin, Western Australia. Am Ass Petr Geol Bull 64:814–840
Playford PE (1984) Platform margin and margina-slope relationships in Devonian Reef complexes of the Canning Basin. Geolo Soc Aus-Petr Expl Soc Aus Symp, Proceed, pp 191–214
Playford PE, Cockbain AE (1992) Devonian reef complexes of the Canning Basin, Western Australia. Petr Expl Ass Aus and Am Ass Petr Geol Field Trip Guidebk 1
Playford PE (2002) Palaeokarst, pseudokarst, and sequence stratigraphy in Devonian reef complexes of the Canning Basin, Western Australia. In: Keep M, Moss J (eds) The sedimentary basins of Western Australia 3, Proceed Petrol Expl Soc Aust Symp, Perth, Western Australia, pp 763–793
Playford PE, Wallace M (2001) Exhalative mineralization in Devonian reef complexes of the Canning Basin, Western Australia. Econ Geol 96:1595–1610
Plimer IR (1979) Sulphide rock zonation and hydrothermal alteration at Broken Hill, Australia. Inst Min Metall Trans 88: B161–B176
Plimer IR (1986) Sediment-hosted exhalative Pb-Zn deposits; products of contrasting ensialic rifting. Trans Geol Soc S Afr 89:57–73
Plimer IR (2006) Manganoan garnet rocks associated with the Broken Hill Pb-Zn-Ag orebody, Australia. Mineral Petrol 88:443–478
Pohl W (2006) Metallogeny of the northeastern Kibaran belt, Central Africa. Geol J 22:103–119
Polito PA, Kyser TK, Southgate PN, Jackson MJ (2006) Sandstone diagenesis in the Mount Isa basin: an isotopic and fluid inclusion perspective in relationship to district-wide Zn, Pb and Cu mineralization. Econ Geol 101:1159–1188
Porada H (1979) The Damara-Ribeira orogen of the Pan-African Brasiliano cycle in Namibia (Southwest Africa) and Brazil as interpreted in terms of continental collision. Tectonophysics 57:237–265
Porada H (1989) Pan-African rifting and orogenesis in southern to equatorial Africa and eastern Brazil. PrecambrRes 44:103–136
Pottorf RJ, Barnes HL (1983) Mineralogy, geochemistry and ore genesis of hydrothermal sediments from the Atlantis II Deep, Red Sea. Econ Geol Monogr 5:198–223
Powell McA, Oliver NHS, Li ZX, Martin D McB, Ronaszeki J (1999) Synorogenic hydrothermal origin for giant Hamersley iron oxide ore bodies. Geology 27:175–178
Qiu HN, Zhu BQ, Sun DZ (2002) Age significance interpreted from $^{40}Ar/^{39}Ar$ dating of quartz samples from the Dongchuan copper deposits, Yunnan, SW China, by crushing and heating. Geochem J 36:475–491
Ran CY (1989) Dongchuan-type stratabound copper deposits, China: a genetic model. Geol Ass Can Sp Pap 36:667–678
Redfield TF, Wheeler WH, Often M (2003) A kinematic model for the development of the Afar Depression and its palaeogeographic implications. Earth Planet Sci Lett 216:383–398
Reed KE (1997) Early hominid evolution and ecological change through the African Plio-Pleistocene period. J Human Evol 32:289–322
Renaut RW, Tiercelin JJ, Owen RB (1986) Mineral precipitation and diagenesis in the sediments of Lake Bogoria basin, Kenya rift valley. Geol Soc London, Sp Publ 25:159–176
Renaut RW, Jones B, Tiercelin JJ, Tarits C (2002) Sublacustrine precipitation of hydrothermal silica in rift lakes: evidence from Lake Baringo, central Kenya Rift Valley. Sed Geol 148:235–257
Renfro AR (1974) Genesis of evaporite-associated stratiform metalliferous deposits – a sabkha prccess. Econ Geol 15:362–366
Rickard DT, Wilden MY, Marinder NE, Donnelly TH (1979) Studies on the genesis of the Laisvall sandstone lead-zinc deposit, Sweden. Econ Geol 74:1255–1285
Ridley M (1999) Evidence for the hydrothermal origin of iron ore, Southern Ridge, Mt Tom Price, Western Australia. Univ West Australia, BSc Hon thesis (unpublished)

Robb L (2005) Introduction to ore-forming processes. Blackwell Publ, Oxford
Robbins IE (1983) Accumulation of fossil fuels and metallic minerals in active and ancient rift lakes. Tectonophysics 94:633–658
Robertson DS, Tisley JE, Hogg GM (1978) The time-bound character of uranium deposits. Econ Geol 73:1409–1419
Rogers NW (2006) Basaltic magmatism and the geodynamics of the East African Rift System. Geol Soc London, Sp Publ 259:77–93
Rogers NW, Macdonald R, Fitton JG, George R, Smith M, Barreiro B (2000) Two mantle plumes beneath the East African rift system: Sr, Nd and Pb isotope evidence from Kenya rift basalts. Earth Planet Sci Lett 176:387–400
Rosendahl BR (1987) Architecture of continental rifts with special reference to East Africa. Ann Rev Earth Planet Sci 15:445–503
Rosière CA, Rios FJ (2004) The origin of hematite in high-grade iron ores based on infrared microscopy and fluid inclusion studies: the example of the Conceição mine, Quadrilatero Ferrifero, Brazil. Econ Geol 99:611–624
Rosière CA, Siemes H, Rios FJ, Quade H (2002) Deformation-controlled high-grade iron ores. Ext Abs Quadriennal IAGOD Symp and Geocongress 11th, Windhoek, Geol Surv Namibia, CD-ROM
Roy S (1992) Environments and processes of manganese deposition. Econ Geol 87:1218–1236
Rozendaal A (1980) The Gamsberg zinc deposit, South Africa: a banded stratiform base-metal sulphide deposit. Proc Fifth IAGOD Symp, pp 619–633
Rozendaal A (1986) The Gamsberg zinc deposit, Namaqualand district. In: Anhaeusser CR, Maske S (eds) Mineral Deposits of southern Africa, vol 2. Geol Soc S Afr, pp 1477–1488
Russell MJ (1978) Downward-excavating hydrothermal cells and Irish-type ore deposits: importance of an underlying thick Caledonian prism. Trans Inst Min Metall B87:B168–B171
Ruxton P (1986) Sedimentology, isotopic signature and ore genesis of the Klein Aub Copper Mine, South West Africa/Namibia. In: Anhaeusser CR, Maske S (eds) Mineral deposits of southern Africa, vol 2. Geol Soc S Afr, pp 1725–1738
Ryan PJ, Lawrence DL, Lipson, RD, Moore JM, Paterson A, Stedman DP, Van Zyl D (1986) The Aggeneys base metal sulphide deposits, Namaqualand District. In: Anhaeusser CR, Maske S (eds) Mineral deposits of Southern Africa, vols I and II. Geol Soc S Afr, pp 1447–1474
Sangster DF (1983) Mississippi Valley-type deposits: a geological melange. In: Kisvarsanyi G, Grant SK, Pratt WP, Koenig JW (eds) International conference on Mississippi Valley-type lead-zinc deposits. Proc Vol Univ Missouri, Rolla, pp 7–19
Sangster DF (ed) (1996) Carbonate-hosted lead-zinc deposits. Soc Econ Geol Sp Publ 4
Saunders JA, Swann CT (1990) Trace-metal content of Mississippi oil field brines. J Geochem Explor 37:171–183
Sawkins FJ (1989) Anorogenic felsic magmatism, rift sedimentation and giant Proterozoic Pb-Zn deposits. Geology 17:657–660
Sawkins FJ (1990) Metal deposits in relation to plate tectonics. 2nd ed. Springer-Verlag, Berlin
Schissel D, Aro P (1992) The major early Proterozoic sedimentary iron and manganese deposits and their tectonic setting. Econ Geol 87:1367–1374
Schmidt-Mumm A, Behr HJ, Horn EE (1987) Fluid systems in metaplaya sequences in the Damara Orogen (Namibia): evidence for sulphur-rich brines – general evolution and first results. Chem Geol 61:135–145
Schlüter T (1997) Geology of East Africa. Gebrüder Borntraeger, Berlin
Scholz CA, Moore TC, Hutchinson DR, Golmshtok AJa, Klitgord KD, Kuotchkin AG (1998) Comparative stratigraphy of low-latitude versus high latitude lacustrine rift basins: seismic data examples from the East African and Baikal rifts. Palaeogeog, Palaeoclim, Palaeoec 140:401–420

Schneider GIC, Seeger KG (1992) Copper. In: The Mineral Resources of Namibia, 1st edn. Geol Surv Namibia, pp 2.3–4.3
Selley D, Broughton D, Scott R, Hitzman M, Bull S, Large RR, McGoldrick P, Croaker M, Pollingotn N, Barba F (2005) A new look at the geology of the Zambian Copperbelt. Econ Geol 100th Ann Iss: 965–1000
Şener AK, Young C, Groves DI, Krapež B, Fletcher IR (2005) Major orogenic gold episode associated with Cordilleran-style tectonics related to the assembly of Palaeoproterozoic Australia. Geology 33(3):225–228
Sengör AMC (2001) Elevation as an indicator of mantle plume activity. Geol Soc Am Sp Pap 352:183–225
Shanks WC, Bischoff JL (1980) Geochemistry, sulfur isotope composition and accumulation rates of Red Sea geothermal deposits. Econ Geol 75:445–459
Shoemaker EM, Shoemaker CS (1996) The Proterozoic impact record of Australia. AGSO J Geol & Geophys 16:379–398
Sibson RH, Moore JMcM, Rankin AH (1975) Seismic pumping- a hydrothermal fluid transport mechanism. J Geol Soc London 131:653–659
Smirnov VI (ed) (1977) Ore deposits of the USSR. Pitman Publ, London
Smith P (1986) The geology of the Broken Hill Pb-Ag-Zn-Cu deposit. In: Abstr Geocongress '86 Johannesburg, Geol Soc S Afr, pp 881–884
Solomon M, Groves DI, Jaques AL (2000) The geology and origin of Australia's mineral deposits. Centre for Ore Deposits Research, Univ West Australia and Univ Tasmania Centre Global Metall, Publ 32
Southgate PN (ed) (2000) Carpentaria-Mt Isa zinc belt: basement framework, chronostratigraphy and geodynamic evolution of Proterozoic successions. Aus J Earth Sci Thematic Issue 47
Southgate PN, Kyser TK, Large RR (eds) (2006a) A special issue devoted to Australian Zn-Pb-Ag deposits: A basin systems and fluid-flow analysis. Econ Geol 101(6)
Southgate PN, Kyser TK, Scott DL, Large RR, Golding SD, Polito PA (2006b) A basin system and fluid-flow analysis of the Zn-Pb-Ag Mount Isa-type deposits of northern Australia: identifying metal sources, basinal brine reservoirs, times of fluid expulsion, and organic matter reactions. Econ Geol 101:1103–1116
Speczik S (1995) The Kupferschiefer mineralisation of Central Europe: new aspects and major areas of future research. Ore Geol Rev 9:411–426
Spry PG, Wonder JD (1989) Manganese-rich garnet rocks associated with the Broken Hill lead-zinc-silver deposit, New South Wales, Australia. Canad Mineral 27:275–292
Spry PG, Heimnann A, Messerley JD, Houk RS (2007) Discrimination of metamorphic and metasomatic processes at the Broken Hill Pb-Zn-Ag deposit, Australia: Rare earth element signatures of garnet-rich rocks. Econ Geol 102:471–494
Stalder M, Rozendaal A (2004) Apatite nodules as an indicator of depositional environment and ore genesis for the Mesoproterozoic Broken Hill type Gamsberg Zn-Pb deposit, Namaqua Province, South Africa. Mineral Depos 39:189–203
Stalder M, Rozendaal A (2005) Distribution and geochemical characteristics of barite and barium-rich rocks associated with the Broken Hill-type Gamsberg Zn-Pb deposit, Namaqua Province, South Africa. Sth Afr J Geol 108:35–50
Stowe CW, Hartnady CJH, Joubert P (1984) Proterozoic tectonic provinces of Southern Africa. Precambr Res 25:229–231
Sverjensky DA (1986) Genesis of mississipi valley-type lead-zinc deposits. Ann Rev Earth Planet Sci 14:177–199
Swager CP (1985) Syndeformational carbonate-replacement model for the copper mineralization at Mount Isa, northwest Queensland: a microstructural study. Econ Geol 80: 107–125
Sweeney MA, Binda PL (1989) Mineralization controls and source of metals in the Lufillian Fold Belt, Shaba (Zaire), Zambia and Angola – A discussion. Econ Geol 84:963–964

Thomas RJ, Agenbacht ALD, Cornell DH, Moore JM (1994) The Kibaran of southern Africa: tectonic evolution and metallogeny. Ore Geol Rev 9:131–160
Thorne WS, Hagemann SG, Barley ME (2004) Petrographic and geochemical evidence for the hydrothermal evolution of the North deposit, Mt Tom Price, Western Australia. Mineral Depos 39:766–783
Tiercelin JJ, Thouin C, Kalala T, Mondeguer A (1989) Discovery of sublacustrine hydrothermal activity and associated massive sulfides and hydrocarbons in the north Tanganyika trough, East African rift. Geology 17:1053–1056
Tiercelin JJ, Boulègue J, Simoneit BRT (1991) Hydrocarbons, sulphides, and carbonate deposits related to sublacustrine hydrothermal seeps in the north Tanganyika trough, east African Rift. In: Parnell J, Kucha H, Landais P (eds) Bitumen and ore deposits, Springer-Verlag, Berlin, pp 96–113
Tiercelin JJ, Pflumio C, Cartec M, Boulègue J, gente P, Rolet J, Coussement C, Stetter KO, Huber R, Buku S, Mifundu W (1993) Hydrothermal vents in Lake Tanganyika, East Africa Rift System. Geology 21:499–502
Tobin KJ (1990) The paleoecology and significance of the Gunflint-type microbial assemblages from the Frere Formation (Early Proterozoic), Nabberu Basin, Western Australia. Precambr Res 47:71–81
Tompkins LA, Pedone VA, Roche MT, Groves DI (1994a) The Cadjebut deposit as an example of Mississippi Valley-type mineralization on the Lennard Shelf, Western Australia – single episode or multiple events? Econ Geol 89:450–466
Tompkins LA, Rayner MJ, Groves DI, Roche MT (1994b) Evaporites: in situ sulphur source for rhythmically banded ore in the Cadjebut Mississippi Valley-type Zn-Pb deposit, Western Australia. Econ Geol 89:467–492
Toth JR (1980) Deposition of submarine crusts rich in manganese and iron. Geol Soc Am Bull 91:44–54
Tregoning TD (1987) The tectono-metallogenesis during the Irumide and Pan African events in South West Africa/Namibia. MSc Thesis, Rhodes University, Grahamstown
Trendall AF (2002) The significance of iron-formation in the Precambrian stratigraphic record. Spec Publ Int Ass Sediment 33:33–66
Trendall AF, Blockley JG (1970) The iron formation of the Precambrian Hamersley Group, Wetsern Australia. Geol Surv West Aust Bull 119
Trendall AF, Blockley JG (2004) Precambrian iron formation. In: Erikson PG, Altermann W, Nelson DR, Muller WU, Catuneau O (eds) The precambrian earth: tempos and events, Elsevier, Amsterdam, pp 403–421
Trendall AF, Morris RC (eds) (1983) Iron-formation: facts and problems. Elsevier, Amsterdam
Tsikos H, Moore JM (1998) The Kalahari manganese field: an enigmatic association of iron and manganese. S Afr J Geol 101:287–290
Tsikos H, Beukes NJ, Moore JM, Harris C (2003) Deposition, diagenesis and secondary enrichment of metals in the Paleoproterozoic Hotazel Iron Formation, Kalahari Manganese Field, South Africa. Econ Geol 98:1449–1462
Turner RJW, Leitch CHB (1992) Relationship of albitic and chloritic alteration to gabbro dykes and sills at the Sullivan deposit and nearby area, southeastern British Columbia. Geol Surv Canada Current Res Paper 92–1E 95–105
United Nations Ocean Economics (1979) Manganese nodules: dimensions and perspectives. Springer, Berlin
Unrug R (1988) Mineralization controls and source of metals in the Lufillian Fold Belt, Shaba (Zaire), Zambia and Angola. Econ Geol 83:1247–1258
Van Hise CR, Leith CK (1911) The geology of the Lake Superior region. US Geol Surv Monogr 52
Van Ziji CZ (1981) Structural and metamorphic evolution in the transitional zone between craton and mobile belt. Precambr Res Unit Univ Cape Town Bull 31

Vearncombe JR, Chisnall AW, Dentith MC, Dörling SL, Rayner MJ, Holyland PW (1996) Structural controls on Mississippi Valley-type mineralization, the southeast Lennard Shelf, Western Australia. Soc Econ Geol Sp Publ 4:74–93
Vearncombe S, Kerrich R (1999) Geochemistry and geodynamic setting of volcanic and plutonic rocks associated with Early Archaean volcanogenic massive sulphide mineralization, Pilbara Craton. Precambr Res 98:243–270
Vineyard JD (ed) (1977) An issue devoted to the Viburnum Trend, Southeast Missouri. Econ Geol 77(3)
Wallace MW, Moxham H, Johns B, Marshallsea S (2002) Hydrocarbons and Mississippi Valley-type sulfides in the Devonian reef complexes of the Eastern Lennard Shelf, Canning Basin, Western Australia. In: Keep M, Moss SJ (eds) The sedimentary basins of Western Australia 3, Proceed Petrol Expl Soc Aust Symp, Perth, Western Australia, pp 795–815
Walter MR, Goode ADT, Hall JA (1976) Microfossils from the newly discovered Precambrian stromatolitic iron formation in Western Australia. Nature 261:221–223
Walter MR, Veevers JJ, Calver CR, Grey K (1995) Neoproterozoic stratigraphy of the Centralian Superbasin, Australia. Precambr Res 73:173–195
Walters S, Skrzeczynski B, Whiting T, Bunting F, Arnold G (2002) Discovery and geology of the Cannington Ag-Pb-Zn deposit, Mount Isa Eastern Succession, Australia: development and application of an exploration model for Broken Hill-type deposits. Soc Econ Geol Sp Publ 9:95–118
Warren JK (2000) Evaporites, brines and base metals: low-temperature ore emplacement controlled by evaporite diagenesis. Aus J Earth Sci 47:179–208
Webb AD, Dockens GR, Oliver NHS (2003) From banded iron-formation to iron ore: geochemical and mineralogical constraints from across the Hamersley Province, Western Australia. Chem Geol 197:215–251
Webster AE (2006) The geology of the Broken Hill lead-zinc-silver deposit, New South Wales, Australia. CODES Monogr 1, University of Tasmania, Burnie
Welke HJ, Allsopp HL, Hughes M J (1983) Lead isotopic studies relating to the genesis of the base metal deposits in the Owambo basin, Namibia. Geol Soc S Afr Spec Publ 11:321
Wheatley CJV, Whitfield GG, Kenny KJ, Birch A (1986) The Pering carbonate-hosted zinc-lead deposit, Griqualand West. In: Anhaeusser CR, Maske S (eds) Mineral deposits of southern Africa, Geol Soc S Afr, pp 867–874
White N, Lovell B (1997) Measuring the pulse of a plume with the sedimentary record. Nature 387:888–891
Whiteman AJ, Naylor D, Pegrum R, Rees G (1975) North Sea troughs and plate tectonics. Tectonophysics 26:39–54
Wilkinson JJ (2003) On diagenesis, dolomitisation and mineralisation in the Irish Zn-Pb orefield. Mineral Depos 38:968–983
Williams N (1978a) Studies of the base metal sulfide deposits at McArthur River, Northern Territory, Australia: I. The Cooley and Ridge deposits. Econ Geol 73:1005–1035
Williams N (1978b) Studies of the base metal sulfide deposits at McArthur River, Northern Territory, Australia: II. The sulfide-S and organic-C relationships of the concoradnt deposits and their significance. Econ Geol 73:1036–1056
Williams PJ (1998a) An introduction to the metallogeny of the McArthur River-Mount Isa-Cloncurry minerals province. Econ Geol 93:1120–1131
Williams PJ (1998b) (ed) A special issue on the McArthur River-Mount Isa-Cloncurry minerals province. Econ Geol 93(8)
Willner A, Schreyer W, Moore JM (1990) Peraluminous metamorphic rocks from the Namaqualand Metamorphic Complex (South Africa): Geochemical evidence for an exhalation-related sedimentary origin in a Mid-Proterozoic rift system. Chem Geol 81:221–240
Wolf KH (ed) (1981) Handbook of stratabound and stratiform ore deposits: Elsevier, Amsterdam

Wolfenden E, Ebinger C, Yrgu G, Deino A, Ayalew D (2004) Evolution of the northern Main Ethiopian rift: birth of a triple junction. Earth Planet Sci Lett 224:213–228
Wooley AR (2001) Alkaline rocks and carbonatites of the world. Part 3. Africa. Geol Soc Publ House, London
Wright TJ, Ebinger C, Biggs J, Ayele A, Yirgu G, Keir D, Stork A (2006) Magma-mantained rift segmentation at continental rupture in the 2005 Afar dyking episodes. Nature 442:291–294
Wyborn LAI, Heinrich CA, Jaques AL (1994) Australian Proterozoic mineral systems: essential ingredients and mappable criteria. Australas. Inst Min Metall Publ Ser 5/94:109–115
Yakubchuk AS, Shatov VV, Kirwin D, Edwards A, Tomurtogoo O, Badarch, G, Buryak VA (2005) Gold and base metal metallogeny of the Central Asian Orogenic Collage. Econ Geol 100th Ann Iss: 1035–1068
Yirgu G, Ebinger CJ, Maguire PKH (eds) (2006) The Afar volcanic province within the East African Rift System. Geol Soc Lond Sp Publ 259
Zhang Y, Sorjonen-Ward P, Ord A, Southgate PN (2006) Fluid flow during deformation associated with structural closure of the Isa Superbasin at 1575 Ma in central and northern Lawn Hill Platform, Northern Australia. Econ Geol 101:1293–1312
Zhao JX, McCulloch MT, Korsch RJ (1994) Characterisation of a plume-related ~800 Ma magmatic event and its implications for basin formation in central-southern Australia. Earth Planet Sci Lett 121:349-367
Zierenberg RA, Shanks WC (1983) Mineralogy and geochemistry of epigenetic features in metallifeorus sediments, Atlantis-II Deep, Red Sea. Econ Geol 78:57–73

Chapter 9
Orogenic, Amagmatic and Hydrothermal Mineral Systems of Uncertain Origin

9.1 Introduction

In the preceding chapters I have discussed, what I would consider main-stream hydrothermal systems responsible for a wide range of ore deposits. In this section, I discuss a range of hydrothermal mineral systems, for which a link with magmas or magmatic activity is either missing or uncertain, hence the title of this chapter. In this category fall the economically very important orogenic Au lodes, ranging in age from Neogene to Palaeoarchaean and providing large gold outputs, not only in countries normally well-endowed with mineral resources, such as Canada, South Africa, Australia, Russia, but also to countries less fortunate in this respect, as for example New Zealand and Uzbekistan. Orogenic hydrothermal systems form in all stages of convergent, collisional to post-collision tectonics (Fig. 9.1). These are hydrothermal systems related to devolatisation reactions during prograde regional metamorphism, with some fluid derived from mantle sources and/or magmas (some mixing with meteoric waters can occur). Ore deposition is almost invariably post-peak metamorphism, spanning the ductile, brittle-ductile to brittle regimes. In some cases there is no obvious temporal and/or spatial relationship with igneous intrusions, in other cases this relationship with granitic intrusives is inferred but by no means established. Yet in other instances the distinction between orogenic lode systems and intrusion-related veins is even less clear. In this chapter, I have chosen to include the Carlin-style ore systems, which although exceptionally well described in the literature, continue to defy the geological community as to how they formed. As pointed out by Goldfarb et al. (2001), a genetic distinction between orogenic lodes, some Carlin-like and intrusion-related Au ore systems remains problematic, although a link with magmatism is perhaps more acceptable for Carlin-style ores than for orogenic lodes.

In addition to orogenic Au lodes and Carlin-type ores, I think that it is important and opportune to describe, albeit briefly, amagmatic hydrothermal systems, such as those associated with black shales and those that derive from intense oxidation of sulphides (nonsulphide ore systems). Unconformity-related U deposits fall in the amagmatic group, but they are discussed in Chapter 13, devoted to hydrothermal uranium ore systems. Other amagmatic

F. Pirajno, *Hydrothermal Processes and Mineral Systems*,

© Springer Science+Business Media B.V. 2009

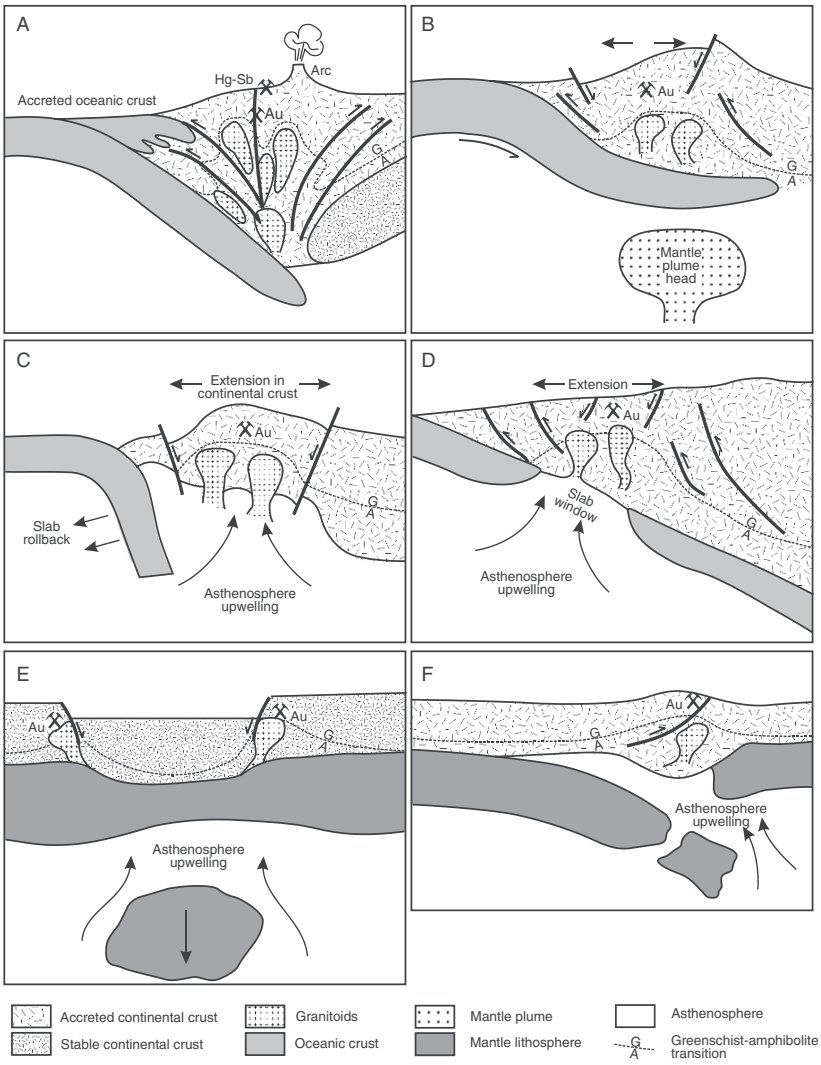


Fig. 9.1 Scenarios of tectonic settings and mantle thermal anomalism that may be responsible for the generation of orogenic lode systems; after Goldfarb et al. (2001 and references therein). (**A**) plate subduction, crustal thickening, formation of magmatic arc; increased geotherms drive circulation of fluids that form orogenic lodes over a wide range of crustal depths with epizonal Hg-Sb near the surface (see also Fig. 9.2); (**B**) mantle plume impacting a subduction systems, as envisaged for some Neoarchaean lode systems in the Yilgarn Craton (Australia) and Superior Province (Canada) (see Barley et al. 1998); (**C**) subduction rollback, oceanic ridge subduction and slab window (**D**), both allowing asthenospheric upwelling, crustal melting, granite emplacement and spatially associated orogenic lodes; scenarios of lithospheric delamination and resulting astehnospheric upwellings (**E**) subcontinental lithospheric delamination and asthenospheric upwelling, extension and lode systems spatially associated with granitic intrusions; (**F**) delamination of mantle lithosphere, crustal melting, emplacement of A-type granitoids and generation of lode systems

ore systems may be less economically important at this point in time, but in the future could become important sources of metals and energy are the hydrothermal systems related to high heat producing granites (HHP) that result from radioactive decay of U, Th and K.

9.2 Orogenic and Metamorphism-Related Lode Systems

Orogenic lodes are exclusively found in metamorphic terranes, whose principal characteristic is their strong structural control and whose genesis is attributed to the action of deep-circulating crustal fluids. Many of the orogenic deposits, especially those of Archaean age, have a spatial relationship to igneous rocks, while for others there is no clear connection with igneous activity. However, even in the former case the precise role of the igneous activity in the genesis of the mineralisation remains uncertain. Orogenic Au ore systems constitute a "coherent group of deposits" consistently found in collisional orogens (Groves et al. 1998, 2000, 2003; Goldfarb et al. 2001, 2005), with the mineralisation hosted in a variety of lithologies metamorphosed to lower-upper greenschist facies, and less commonly to lower amphibolite facies. The deposits are found within high strain zones in brittle (lower greenschist facies), brittle-ductile structures (mid-upper greenschist facies) to ductile (amphibolite facies). In the literature they have also been called metamorphogenic or metamorphic vein deposits (e.g. Groves et al. 1989). Nesbitt (1988) and Nesbitt and Muehlenbachs (1989) referred to these deposits, in which Au is the chief economic metal, as "mesothermal lode gold". However, recent research showed that the label of mesothermal is not appropriate, because the temperatures in which orogenic lodes form spans the range from hypothermal to epithermal (Groves et al. 1998). Nesbitt (1988) proposed that lode deposits in the continental crust form a continuum of at least three principal end members, namely: volcanic-hosted epithermal, sediment-hosted (Carlin-type) epithermal and mesothermal deposits. According to Nesbitt (1988), these reflect increasing depth and temperature of dominantly meteoric fluid circulation, and decreasing water/rock ratios, from shallow (2–3 km) for epithermal deposits, to deep (15–20 km) for mesothermal deposits. Using isotope systematics (particularly variations in δD) Nesbitt and Muehlenbachs (1989) recognised a major role for meteoric fluids in the Canadian Cordillera mesothermal deposits rather than metamorphic, although they also postulated that metamorphic fluids may participate in the overall mineralising event by mixing with the meteoric waters. A similar idea was proposed by Craw and Koons (1989) and Craw et al. (1987a, b) for the vein mineralisation in the Southern Alps of New Zealand and Chen et al. (2004) for orogenic lodes in the Qinling Orogen in China. However, as is pointed out below, the role of meteoric fluids, particularly in mesozonal to hypozonal systems is debated.

Within the category of orogenic Au lodes are included the mineralised quartz vein systems in Archaean granite-greenstone terranes, well exemplified in the Yilgarn Craton of Western Australia, the Abitibi Belt in the Superior Province

of Canada, the Murchison and Barberton greenstone belts in the Kaapvaal Craton of South Africa. Phanerozoic turbidite-hosted lode Au deposits are found in the Canadian Cordillera, Nova Scotia and Alaska in North America, in Victoria in Australia, and the Otago-Marlborough districts in New Zealand. Orogenic Au-Ag and Ag lodes of Mesozoic age are present in the Qinling and in the Archaean rocks of the Shandong districts of China. The weight of the evidence from field and laboratory data indicates that metamorphic devolitilisation reactions were responsible for a substantial component of the mineralising fluids. In fact, the best field evidence of fluid generation and flow during regional prograde metamorphism is the common presence of quartz and carbonate veining in the rocks of the metamorphic terranes hosting the orogenic ore systems. In the Southern Alps of New Zealand it has been shown that metamorphic quartz veinlets carry Au (Craw et al. 1987; Craw and Koons 1988). Deep-circulating meteoric waters played an important role, particularly in Phanerozoic orogenic belts, such as the New Zealand Southern Alps and the Canadian Cordillera. The case for hydrothermal fluids of magmatic origin is less compelling, although, at least on a local scale, this is not ruled out. Orogenic lodes are hosted in variably metamorphosed rocks with dominant alteration minerals represented by carbonate-sulphide $\pm$ sericite $\pm$ chlorite. Elements usually found in orogenic lode deposits are Au, Ag, As, Sb, Hg, W, Mo, Te and B, in various combinations, such as Au-Ag, Au-Te, Sb-W, Au-W, Au-Sb-W, or Hg-Sb. The nature of the fluids, as deduced from fluid inclusion studies, is characterised by low salinities (up to 12 wt% NaCl equivalent), high H_2O and CO_2 content (> 4 mol%), with lesser amounts of CH_4 and N_2 and near-neutral pH. Gold transport is by sulphur complexes and depositional conditions are characterised by temperature and pressure ranges of approximately 250 and 350°C at pressures of between 1 and 3 kbar, but can reach up to 650°C and 4–5 kbar for some deposits and as low as 150°C and 0.5 kbar for some near surface lodes (Groves et al. 2000). The styles of mineralisation of lode systems reflect the rheological regime (ductile, brittle-ductile and brittle) and variations in pressure and temperature conditions, under which they form (Goldfarb et al. 2005), within the crustal continuum model of Groves (1993) (Fig. 9.2). Under hypozonal ductile conditions (high temperature and pressure) mineralisation is dominated by bedding- or foliation-parallel deformed veins and replacement textures. Typically in the ductile regime, quartz grains are extensively recrystallised. Brittle-ductile conditions (mesozonal) span the greatest range of temperatures and pressures (Fig. 9.2C), mostly characterised by concordant or discordant laminated crack-seal quartz-carbonate veins and sigmoidal vein arrays. Crack-seal textures are typical of hydraulic fracturing, a topic further examined in Section 9.2.3. The brittle epizonal regime is conducive to vein stockworks, breccia veins and saddle reefs, such as those of world-famous Victorian goldfields in eastern Australia (e.g. Phillips and Hughes 1998). In the brittle-epizonal regime, vein styles exhibit open-space fillings (comb, cockade, crustform and colloform textures), which are also typical of volcanic-related epithermal systems. Individual veins or groups of veins can extend

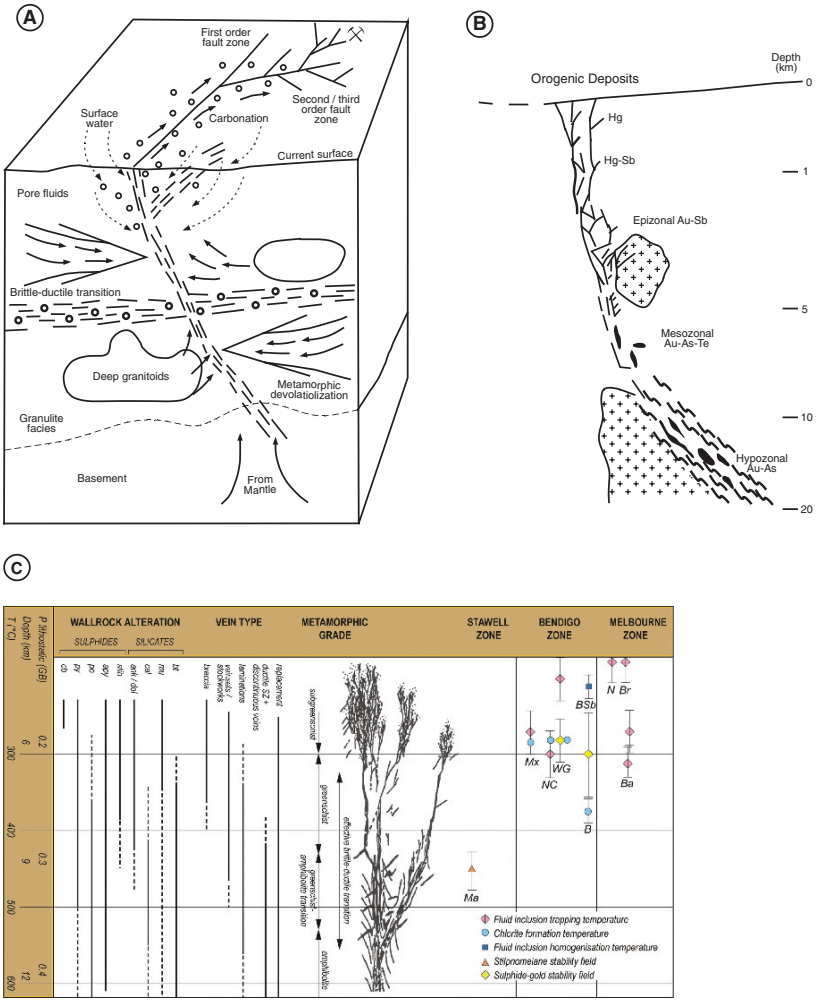


Fig. 9.2 (**A**) Fluid sources for the formation of lode Au deposits in metamorphic terranes, these sources include meteoric, metamorphic, magmatic, and mantle reservoirs. Stable isotope data (see Fig. 9.3) seem to rule out significant inputs of meteoric waters, whereas other geochemical data are not consistent with fluid components being derived from the mantle (after Goldfarb et al. 2005, Appendix Figures), however, there are cases where, on the basis of $^{3}He/^{4}He$ systematics mantle fluids are considered permissive (Mao et al. 2007); (**B**) the crustal-continuum model, based on Colvine (1989), Groves (1993), Groves et al. (1998); (**C**) another view of the crustal-continuum model, as applied to the lode systems of Victoria (Australia), also showing patterns of wall rock alteration, vein type, metamorphic grade and the position of individual gold fields, B Central Deborah-Bendigo, Ba Ballieston; Br Brunswick, BSb antimony mineralisation in the Bendigo zone, Ma Magdala-Stawell, Mx Maxwell-Inglewood, N Nagambie, Nc New Cambrian-Tamaguilla, Wg Wattle Gully-Castlemain. This diagram is reproduced by courtesy of Peter O'Shea, Minerals Geosciences, Victoria, based on Vanderberg et al. (2000)

along strile for hundreds of metres or even kilometres, with widths ranging from less than a metre to tens of metres to combined widths of up to a kilometre. Depths range from a few hundred metres up to 3 km, although theoretically a crustal scale lode system could be developed over a depth range of 10–15 km (Colvine 1989; Groves 1993; Goldfarb et al. 2005). The types of ore assemblages are also dependent on depths of formation, temperature and pressure, as well as the nature of the wall rocks (Fig. 9.2C). Arsenopyrite and pyrite are common sulphides, with the former being dominat in lode systems hosted in metasedimentary rocks and the latter in igneous rocks. At high temperatures ($> 400^{\circ}C$) and lower crustal levels, loellingite and pyrrhotite may become the dominant sulphide species, whereas in the epizonal range stibnite becomes the common sulphide. Stibnite may be accompanied by various amounts of cinnabar, tellurides and bismuthinides. Less commonly, scheelite and Pb-Zn and Cu sulphides may be present. Gangue minerals are the same as those of the associated alteration haloes and include quartz, albite, muscovite, sericite, fuchsite, chlorite, tourmaline, biotite and carbonates.

Hydrothermal alteration generally includes carbonitisation, silicification, sulphidisation and varying degrees of alkali metasomatism. Alteration haloes around a vein have widths of few centimetres up to several kilometres. A common feature to almost all orogenic Au lodes is the presence of widespread the carbonate alteration zones (Groves et al. 2000; see also Dubé and Gosselin 2007). The carbonate minerals include ankerite, ferroan dolomite, siderite and calcite, whereas the mineral phases that characterise alkali metasomatism of the Au lodes are albite, fuchsite, biotite and K-feldspar. Sulphidation is widespread in banded iron-formation and Fe-rich mafic rocks (Groves et al. 1984). Sulphidation reactions involving Fe-rich host rocks are (Phillips and Groves 1984):

$$\underset{\text{Chlorite}}{Fe_6Si_4O_{10}(OH)_8} + 12H_2S + 3O_2 \rightarrow \underset{\text{pyrite}}{6FeS_2} + 4SiO_2 + 16H_2O$$

$$\underset{\text{Chlorite}}{Fe_6Si_4O_{10}(OH)_8} + 12HS^- + 3O_2 \rightarrow \underset{\text{pyrite}}{6FeS_2} + 4SiO_2 + 4H_2O + 12(OH)^-$$

Quartz is the dominant mineral in the veins, accompanied by varying amounts of chlorite, carbonate minerals and sulphides (< 3–5%). Fluid interactions with Fe-rich mafic rocks results in alteration assemblages that are dominated by carbonate minerals, suggesting extensive addition of CO_2 and to a lesser extent H_2S (Phillips 1986). Wall-rock alteration of the Golden Mile Dolerite in the Kalgoorlie goldfield in Western Australia is characterised by the following reactions (Phillips 1986):

$$\underset{\text{Actinolite}}{6Ca_2Fe_5Si_8O_{22}(OH)_2} + 12CO_2 + 14H_2O \rightarrow \underset{\text{chlorite}}{5Fe_6Si_4O_{10}(OH)_8} + \underset{\text{calcite}}{12CaCO_3} + \underset{\text{quartz}}{28SiO_2}$$

$$\underset{\text{Chlorite}}{Fe_6Si_4O_{10}(OH)_8} + 6CO_2 \rightarrow \underset{\text{siderite}}{6Fe(CO_3)_2} + \underset{\text{quartz}}{4SiO_2} + 4H_2O$$

$$\underset{\text{Siderite}}{FeCO_3} + 2H_2S + 1/2O_2 \rightarrow \underset{\text{pyrite}}{FeS_2} + CO_2 + 2H_2O$$

$$\underset{\text{Magnetite}}{Fe_3O_4} + 3CO_2 \rightarrow 3\underset{\text{siderite}}{FeCO_3} + 1/2O_2$$

Goldfarb et al. (2005) pointed out that because fluids that form orogenic lodes are generally in equilibrium with the surrounding rocks, being developed under ambient metamorphic temperature and pressure conditions, the alteration haloes are not as conspicuous or evident as they are in other hydrothermal systems. The exception to this general situation is where the fluids interact with a chemically reactive rock, such as granites or iron formations. Importantly in all cases, the alteration minerals overprint the metamorphic minerals. Of the carbonate minerals, ankerite and ferroan dolomite, accompanied by pyrite and Au, are the dominant phases in rocks with $Fe/(Fe+Mg) \geq 0.5$; for lower values of this ratio the available Fe is incorporated in magnesite or siderite. Apparently this is important because where magnesite-siderite are present there is not enough Fe to form pyrite and consequently little or no disseminated Au can be precipitated due to desulphidation reactions (Goldfarb et al. 2005). Carbonate minerals in proximal alteration zone commonly occur as porphyroblasts. In greenschist facies sedimentary and mafic rocks (mesozonal, brittle-ductile domains) proximal alteration assemblages consist of ankerite and/or ferroan dolomite, quartz, chlorite, muscovite, pyrite, arsenopyrite and albite. Alteration in rocks of mid-greenschist facies is shown by strong bleaching due to sericitisation and/or clay weathering of feldspars and chlorite. Intermediate zones of alteration can extend for up to 100 m from the orebody dominantly have albite and chlorite, whereas distal zones exhibit chlorite, calcite, quartz and epidote.

The ore-hosting structures are subsidiary shear zones or normal to reverse faults, which are always related to a major regional-scale structure such as a transcurrent fault or a crustal lineament or a thrust. Nesbitt and Muehlenbachs (1989), for example, drew attention to the close spatial association of mesothermal lode Hg, Sb and Au deposits of the Canadian Cordillera with right-lateral strike-slip fault systems. As is the case with most of these deposits, the mineralisation is not exactly on the fault structure but occurs on secondary or subsidiary faults or shear zones, although in some areas of the Cordillera Hg deposits do occur within the main strike-slip fault zone. This clearly suggests that both the main fault and its subsidiary structures have acted as conduits for the mineralising fluids. The fluids are channelled into these structures during the late stages of deformation and metamorphism of a compressive tectonic cycle, in which temperature and pressure conditions, at or below the amphibolite facies transition, favoured the development of brittle to brittle-ductile structures (Groves et al. 1989).

Stable isotope systematics of orogenic lode deposits are also reviewed in Goldfarb et al. (2005). The $\delta^{18}O$ and δD values of orogenic lodes have been

variously interpreted and their significance debated. The role of meteoric waters is controversial as is that of deeply-sourced fluids. Ore fluid $\delta^{18}O$ values of between 6 and 11‰ seem to characterise Archaean lodes, whereas values of 7–13‰ are more commonly found in Phanerozoic deposits. Most δD values range from –80 and –20‰. A plot of $\delta^{18}O$ and δD values for some lode systems is shown in Fig. 9.3. Sulphur isotopic values vary widely (–20 to +25 $\delta^{34}S$‰) between different lode systems and the source of the S remains equivocal at best. In Archaean and Proterozoic lodes, $\delta^{34}S$ values range from 0 to 10‰. A similar problem of wide variations is encountered with carbon isotopes from ore-related carbonate minerals. Values of $\delta^{13}C$ have been recorded from near 0 to –32‰. Mantle signatures have been recorded from stable isotope systematics. This is discussed in Section 9.3.5.

As mentioned above fluid inclusion studies all seem to show that orogenic fluids are aqueous and carbonic and of low salinity. Other nonaqueous volatiles include CH_4, N_2 and H_2S. Salinities range from 3 to 12 wt% NaCl equivalent. It is of interest to note that fluid inclusions with lessser amounts of CO_2 gas appear to be more common in Phanerozoic systems, which form at lower temperatures (250–350°C) than those of Archaean age (325–400°C), which are also more gas rich (Goldfarb et al. 2005). This difference could be related to the metamorphic grades and erosion levels. Gold in lode deposits is transported as bisulphide

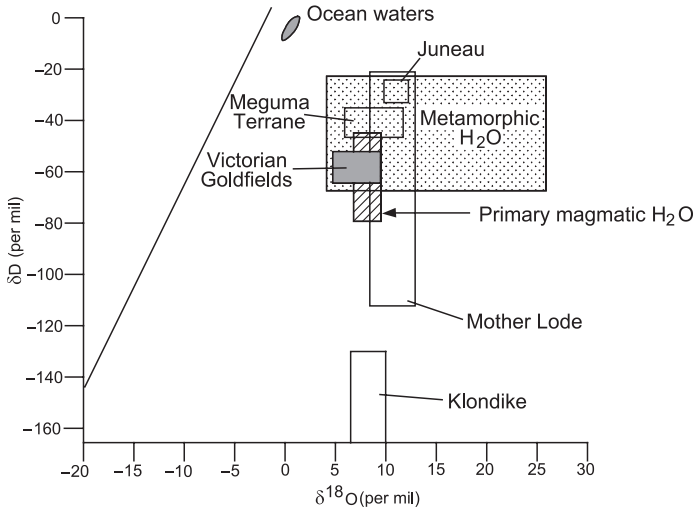


Fig. 9.3 Oxygen-hydrogen isotope diagram of ore-forming fluids for some Phanerozoic lode gold deposits, such as the Victorian goldfields (Australia), Juneau (Alaska), Meguma (Nova Scotia, Canada), the Mother Lode (USA), after Goldfarb et al. (2005, Appendix Figures). Isotopically heavy fluids contrast with those characteristic of meteoric water. The D-depleted values for the Klondike and, to a lesser extent, some of the Mother Lode deposits, reflect measurements of bulk fluid inclusion waters that contain fluids from abundant secondary inclusions unrelated to the ore-forming process

complex in near-neutral pH and slightly reduced fluids. The dominant Au species is $AuHS^0$ in hydrothermal fluid at less than 300°C (see Chapter 1). In Fe-rich rocks (mafic igneous, banded iron-formations), sulphidation of the wall rocks causes the destabilisation of the bisulphide complex, resulting in precipitation of Au.

In any case, the general association of the Au with sulphides, the Fe-rich nature of the host rocks and the lack of mobility of Fe are taken as evidence that Au deposition was related to sulphidisation of wall rocks. In fact, many Au deposits are believed to have formed as a result of sulphidisation of wall rock, and the contemporaneous deposition of Fe-sulphides and Au in those channelways which intersect Fe-rich lithologies within greenschist facies domains. Groves and Phillips (1987) suggested that stratabound, or locally stratiform, ores may also form as a result of replacement and sulphidisation adjacent to fractures in oxide facies BIF units (Fig. 9.4). Interaction of Fe-rich host rocks and S-bearing fluids would result in the formation of pyrite and the breakdown of sulphide complexes to precipitate Au. One of the possible reactions is (Phillips and Groves 1984):

$$FeO + HAu(HS)_2 + 1/4O_2 \rightarrow FeS_2 + 3/2H_2O + Au$$

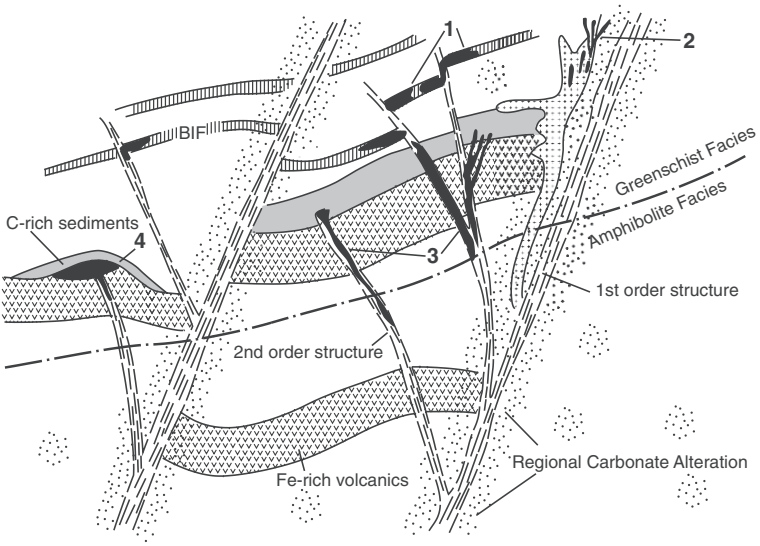


Fig. 9.4 Schematic representation of the metamorphic-replacement model of Groves and Phillips (1987). H_2O-CO_2 fluids gain access through first- and second-order structures, causing extensive carbonitisation (*dot pattern*) and the formation of orogenic lodes above the greenschist-amphibolite facies transition. (1) Replacement BIF-hosted Au-sulphide deposit; (2) stockworks; (3) vein lodes; (4) Au-Te lodes. Drawing not to scale

Orogenic processes which favour large-scale generation and transport of hydrothermal fluids are subduction systems and collision orogens. Fluids are generated during convergent processes, which result in compression, deformation and prograde metamorphism of sedimentary wedges and subducted oceanic crust. Conceptual models of fluid generation and migration in these tectonic environments have been investigated, among others, by Oliver (1986), Duane and de Witt (1988), Langseth and Moore (1990a, b) and Torgersen (1990). In a subduction system, such as that depicted in Fig. 9.5, the accretionary prims are subject to intense deformation. The prism comprises thick sedimentary packages, including turbidite-facies sequences, which by virtue of their depositional environment are sea-water-saturated.

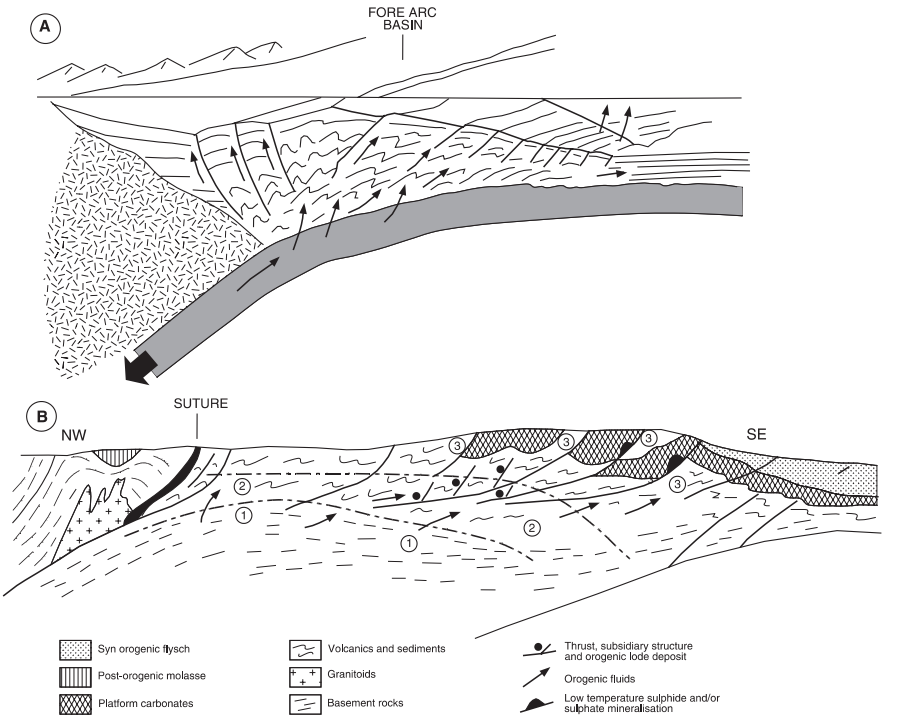


Fig. 9.5 (**A**) Subduction system and accretionary prism. Arrows indicate paths of fluid movement; dewatering of sediments predominates in the upper sectors and oceanward, while devolitisation reactions dominate at depth. Fluids are also derived from dehydration of oceanic crust; drawing is not to scale (after Langseth and Moore 1990a, b). (**B**) Schematic representation of the eastern Alps orogen, which is the result of the collision between two continental plates: Noric and Austroalpine; metamorphic zones in the collision zone are indicated by the *dash-dot lines*. (1) amphibolite facies domain; (2) greenschist facies domain; (3) zone of mixing between metamorphic and meteoric fluids. Orogenic lode deposits are formed along subsidiary shear zones branching off the main thrust faults, after Frimmel (1990)

Subduction processes result in deformation, increasing temperature and pressure and the expulsion of sea water incorporated in the sediments as well as the water released from the dewatering of clays. Tectonic compaction of the accretionary prism commences near the oceanward portion, where the fluids derived from the dewatering of the sediments, move along permeable beds and are expelled along thrusts and faults. Towards the trench, at the rear of the prism, fluids are generated at deeper levels by dehydration reactions. These fluids move along thrust faults and along the interface between the prism sediments and oceanic crust (basalt-sediment interface). Release of fluids also occurs in the underlying oceanic crust material and these may mix with those generated within the accretionary prism. Kerrich and Wyman (1990) in reviewing the geodynamic setting of orogenic lode mineralisation noted that, at least for Phanerozoic times, there is a distinct spatial association between lode deposits and regional structures in allochthonous terranes which have accreted onto continental margins or island arcs. The common features (nature of fluids, structure, metal association) between Phanerozoic and Archaean lode deposits confirms a common and coherent mechanism of ore deposition. Kerrich and Wyman (1990) developed a "transpressive accretion hypothesis", whereby the lode mineralisation is the result of subduction-related crustal underplating and prograde metamorphism in subduction complexes. These orogenic fluids form through processes of tectonic burial, compression and prograde dehydration reactions in the collision zone. As collision proceeds the fluids, according to the model, are effectively "squeezed out" and expelled towards the foreland. The paths followed by the orogenic hydrothermal fluids are mainly along decollement zones and thrust faults. Frimmel (1990) proposed that some fluids produced in the collision zone may facilitate thrusting and during their propagation or expulsion towards the fold belt (foreland), the orogenic fluids may remobilise metals from existing syngenetic deposits (Fig. 9.1B). If the foreland contains platform sequences, such as evaporites and/or carbonate shelf sediments, these fluids would mix with percolating meteoric waters, become oxidised and result in the precipitation of epigenetic sulphide and sulphate (e.g. barite) deposits in veins or pre-existing cavities.

9.2.1 Metamorphism and Fluid Generation; Metamorphogenic Hydrothermal Systems

There is ample evidence that fluids exist in deep levels of the crust. The presence of veins in metamorphic rocks is direct proof of fluid flow along fractures and tectonite fabrics. Helium isotope systematics ($^3He/^4He$) have been used to investigate fluxes of amagmatic mantle fluids in the ductile lower crust in the northern Basin-and-Range province of the western USA (Kennedy et al. 2007). This study clearly demonstrated that mantle volatiles (H_2O and CO_2) play an

important role in fault-controlled fluid penetration in the crust, even in region where there is no recorded magmatism (Kennedy et al. 2007). Superdeep continental drilling programmes in Russia and Germany have confirmed the presence of crustal fluids at depths of 9–12 km, particularly along shear and fault zones (Kremenetsky and Ovchinnikov 1986; Möller et al. 1997; Emmermann and Lauterjung 1997). Free fluids detected during the German superdrilling programme included, in addition to formation H_2O, highly saline fluids and gases such as CH_4, He and Rn. Analysis of the saline fluids yielded 7160 mg/l Na, 15 700 mg/l Ca, 44 100 mg/l Cl, and lesser quantities of Sr, Br, SO_4 (Emmermann and Lauterjung 1997). The temperature at the bottom of the hole (9100 m) was 265°C and with a surprisingly high value of heat flow of 85 mW/m^2 (Emmermann and Lauterjung 1997).

Phillips et al. (1994) examined the role of metamorphic fluids in the formation of hydrothermal ore deposits. These authors pointed out that the loss of volatiles during metamorphism is related to the metamorphic mineral assemblages, which lose volatiles as the metamorphic grade increases. The generation of fluids during metamorphism is important for metallogenesis, because they dissolve metals from large volumes of rocks and flow through networks of microcracks and fractures, constituting giant hydrothermal systems. Metamorphic fluids acquire the capacity of leaching, transporting and depositing metals in structurally and/or lithologically controlled locales. The generation of metamorphic fluids is related to dehydration and decarbonation reactions, which allow fluid flow, generally in the direction of increasing temperature (Ferry 1994; Oliver et al. 1998). The dominant species of volatiles that are present in metamorphic environments are H_2O, CO_2, CO, H_2, Cl, F, S, CH_4, NH_3, inert gases and hydrocarbons. Details on the origin, nature and flow of fluids in the crust can be found in Fyfe et al. (1978); other important works on the topic include those of Etheridge et al. (1983), Kerrich (1986), Fyfe (1987, 1997), Ferry (1994), Oliver et al. (1998), the collection of papers edited by McCaffrey et al. (1999) and Jamtveit and Yardley (1997). A collection of papers on the dynamics of metamorphism and metamorphic reactions is edited by Treloar and O'Brien (1998).

Sedimentary sequences contain large quantities of aqueous fluids, mainly within pores spaces and fractures. These sedimentary brines are driven out during compaction (burial), and by means of gravity and tectonic compression. The flow of these brines in basin structures, prior to the onset of regional prograde metamorphism, may result in the development of low-temperature sulphide and oxide mineralisation in structural and lithogical traps (e.g. MVT deposits). However, much of the released fluids originate from increasing temperature and pressure, which drive dehydration reactions. In this way, bound water and other volatiles are released from the lattice of rock-forming minerals, mainly clays, micas and carbonates. Fyfe et al. (1978) calculated that an average aluminous pelite can lose 2.7 wt% of H_2O during the transition from the biotite isograd to the K-feldspar isograd. This would correspond to a lake 300 m deep above a column of pelitic rocks 5 km thick. Fyfe et al. (1978) also

calculated fluid release curves for pelitic sediments and mafic rocks. These fluid release curves, at geothermal gradients ranging from 20 to 100° C, shown in Fig. 9.6, indicate that the quantity of fluids released is a function of metamorphic grade and geothermal gradient. The release of fluids from the mineral lattices is a continuous process, which eventually leads to partial melting (Fig. 9.6). Materials and minerals that are largerly responsible for the

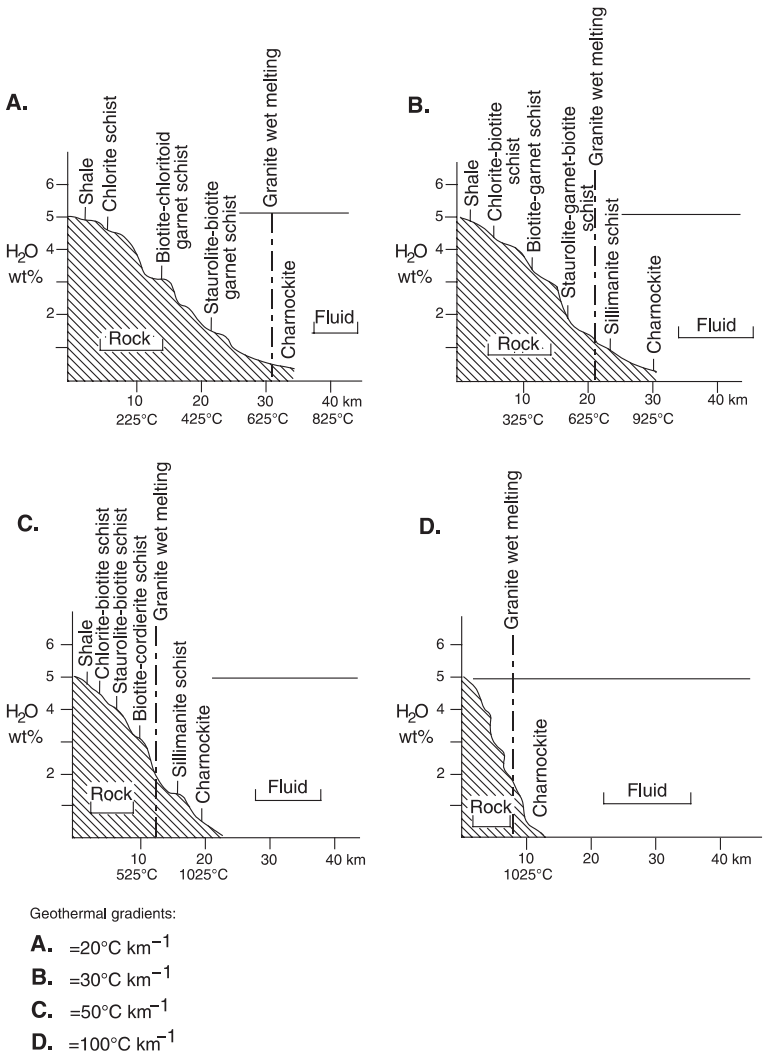


Fig. 9.6 Fluid release curves (**A–D**) for pelitic sediments at four geothermal gradients as shown (see text for details). After Fyfe et al. (1978)

generation of fluids and some of the more common dehydration reactions that occur during metamorphis are considered below.

Etheridge et al. (1983) envisaged convective circulation above a large heat source, such as a mantle diapir. In their model, shown in Fig. 9.7, zones of hydrothermal circulation exist above a region of crustal melting induced by the mantle heat source. A lower zone, corresponding to amphibolite facies conditions, contains less active circulation than an overlying zone of more active circulation and corresponding to greenschist facies conditions. The boundary between the two zones is the metamorphic facies boundary as well as the

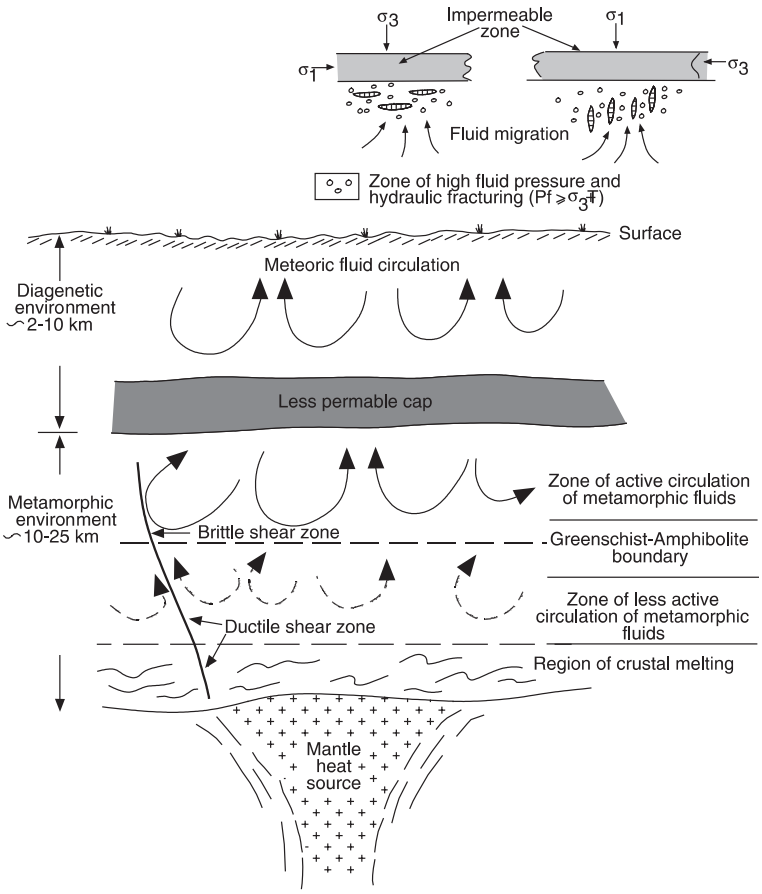


Fig. 9.7 Model of metamorphic fluid generation above a mantle heat source (after Etheridge et al. 1983). Inset above shows a model of fluid movement below an impermeable layer in the crust (after Cox et al. 1986); fluid pressure in the rocks below the barrier builds up to equal the lithostatic pressure (see also Sibson and Scott 1998). Hydraulic fracturing will occur when the fluid pressure (P_f) exceeds or equals the tensile strength of the rocks (T) and the least principal stress (σ_3), as shown in the figure

boundary between ductile and brittle crustal environments. These zones of metamorphic fluid circulation are confined by a less permeable cap, above which is the diagenetic environment, where meteoric water circulation dominates with pore fluids being liberated by burial and compaction. The less permeable cap is a seal that results from the precipitation of mineral phases at the interface between the two hydrothermal systems, cool-meteoric above and hot-metamorphic below. The cap can be breached by overpressuring of metamorphic fluids. Also, the fluids can be channelled through ductile, brittle-ductile to brittle shear zones, where hydrothermal vein deposits would form. Etheridge et al.'s (1983) model is not too different from that proposed by Fyfe and Kerrich (1985) to explain the Au mineralisation of Archaean granite-greenstone terranes. Fyfe and Kerrich's model envisaged extensive dewatering of metabasaltic and metasedimentary rocks during prograde metamorphism, which would be triggered by granitic intrusions.

The implications of these models for metallogeny are important, and discussed below. Underplating of the base of the crust by mantle melts causes a large thermal anomaly. These mantle melts assimilate metal-rich components from crustal materials, including greenstone rocks, and induce metamorphic degassing of CO_2, H_2O and S from the crust. Ore elements can be transported upward by complexes of these volatile components. Fyfe (1987) estimated that if greenschist rocks with an initial water content of 4 wt%, are heated to amphibolite facies with a water content of about 1 wt%, and if the total volume of the affected zone is 1000 km^3, the water released from this heating event would be around 100 km^3. The fluids would be of low salinity and dominated by H_2O and CO_2, as suggested by numerous fluid inclusion studies of mesothermal Au deposits.

Oliver et al. (1998) examined the role of metamorphism and crustal fluid flow in the genesis of Australian vein or shear zone-hosted metamorphogenic ore deposits. According to these authors hydrothermal systems develop, in which regional-scale fluid flows are thermally and dilatancy driven. Thermally driven fluid flow is caused by metamorphic dehydration reactions, with associated metal dissolution. The flow of these fluids is "up-temperature", that is from regions of lower temperature towards zones of higher temperature probably related to late-tectonic magmas. From this zone of higher temperatures, the flow of fluids is "down-temperature". Here, fluids are also dilatancy-driven and are channelled along major structures, where metals are deposited to form vein- and shear zone-hosted metamorphogenic metalliferous deposits. Most probably, some contribution to these fluids comes from the late-tectonic magmas. Mixing with meteoric waters can occur in the upper levels in the structures along which the fluids are focused. The down-temperature channelised fluid flow, suggested by Oliver et al. (1998) is considered to be the main process of metamorphogenic ore-forming systems, which results in the genesis of vein- and shear zone-hosted mineralisation. The main mechanisms that account for the dissolution, transport and precipitation of metals in these structures are: decreasing temperature and pressure gradients; change in the chemistry of the

fluids and their mixing. Down-temperature fluid flow results in changes from prograde to retrograde metamorphism. Prograde greenschist to amphibolite facies metamorphism would induce metal dissolution, while during retrograde phases of metamorphism metals are precipitated. Temperature and pressure, during peak metamorphism range from 350 to 650°C and 3–5 kbar.

Circulating metamorphic fluids are preferentially channelled through pathways determined by breccia, cataclastic or mylonitic zones associated with major faults or structural breaks. The influence of rock type may also be important, either in terms of primary porosity, or because of secondary porosity enhancement due to metamorphic or other processes. Major structural features such as faults, shear zones and thrusts are perhaps the most important channelways, at least in terms of ore deposition, for the movement and focusing of hydrothermal fluids (Fig. 9.4). Large-scale fluid movement is thought to be associated with steep shear zones, because fluids are focused in a highly permeable and restricted zone (Etheridge et al. 1983). Movement of hydrothermal fluids also occurs along detachment zones that separate tectonic plates in metamorphic core complexes, as for example in the western USA (Coney 1980; Reynolds and Lister 1987). These detachment zones are low-angle normal faults along which there is strong brecciation and mylonitisation. Hydrothermal alteration and the presence of mineralisation in the tectonic plates testify to the movement of fluids. The upper plate is characterised by potassic (K-feldspar) and hematitic alteration, whereas the lower plate has propylitic-type alteration and is composed mainly of the minerals epidote and chlorite. Reynolds and Lister (1987) proposed that two regimes of fluid flow are present in core complexes. One, in the upper plate, is associated with meteoric and connate waters; the other, related to the shear zone, migrates from deep-seated regions. The latter fluids could derive from either an igneous or a metamorphic source (Kerrich 1986), or even possibly from a mantle source, if one assumes that the detachment zone extends into the mantle above a section of thinned crust, as suggested by Wernicke (1981).

The role of collision tectonics and thrust faulting in the generation and movement of fluids is widely recognised. Hubbert and Rubey (1961) were perhaps the first to realise the importance of high fluid pressures for the translation of large overthrust masses. A detailed analysis of these effects was described by Fyfe and Kerrich (1985). In major thrusts, such as those described for the Himalayas, with long distances (hundreds of km) and thick plates (15–30 km) involved, thermal equilibrium is not attained during the time of thrusting. Where one continental block 30 km thick has been thrust upon another, the overthrust continental block is initially hotter than the underthrust block, but with time, equilibrium temperature is determined according to erosion rates and melting at the base. During thrusting, pore water is expelled and prograde metamorphism occurs over the entire thickness of the underplate. On average it is estimated that about 4% H_2O may be lost from the underplate, and these fluids either penetrate the overthrust plate, or flow along it during thrusting. Penetration of fluids in the overplate is generally by hydraulic fracturing

mechanisms, resulting in swarms of veins and shear zones. The once near-surface rocks will be relatively more oxidised, so that the fluids will tend to oxidise the overplate and, consequently will not precipitate silica but rather dissolve it. Massive veining occurs, with the possible formation of Au deposits. In time, smaller regions of the inverted gradient become exposed (due to erosion effects), so that even mineralisation processes will eventually progress. Near the thrust surface the most dramatic prograde and retrograde changes occur, including partial melting. The model for the generation of crustal fluids outlined above was utilised by Le Fort et al. (1987) to explain the origin of Himalayan leucogranites. They associate thrusting on the continental scale, with the inception of inverted metamorphism and the liberation of large quantities of fluids, followed by anatectic melting of crustal material, with the production of geochemically specialised leucogranites. Thrusting, as described above, results in the superpositioning of hot, deep continental crust, over little metamorphosed lithologies. Heating then proceeds from top to bottom, inducing inverted metamorphic grades. Also, during the metamorphism of the lower and colder formations, metamorphic reactions release a large amount of fluids, particularly H_2O and CO_2. The fluids move along and above the thrust inducing melting close to minimum melt compositions. Another interesting case of metamorphic fluid movement associated with faulting and uplifting has recently been proposed in a number of papers by Craw and co-workers (Craw et al. 1987a, b; Craw and Koons 1989). These authors postulated infiltration of hot metamorphic fluids to shallow levels of the crust by rapid uplift on the east side of the Alpine transcurrent fault, in the South Island of New Zealand. The H_2O-CO_2-rich metamorphic fluids eventually mix with meteoric waters to precipitate silica and gold (this is discussed further below). The main feature of this model is that a metamorphic-meteoric hydrothermal system can be activated as a result of high heat flow due to rapid uplift which brought hot rocks to shallow levels.

9.2.1.1 Dehydration Reactions

Metamorphic dehydration (devolatilisation) reactions provide abundant fluids that result in advective mass transport during regional prograde metamorphism. The fluid budget is commonly greater than that expected from dehydration or compaction dewatering. The apparent discrepancy is probably related to permeability enhancement such as porosity networks, dilatancy and hydraulic fracturing (Rumble 1994). Time-integrated fluxes of pervasive fluid flow of up to 10^6 cm^3 water/cm^3 rock in shear zones have been calculated by Ferry (1994). Fluid flow in metamorphic rocks occurs through networks of microfractures and along mineral grain boundaries. It is important to remember that the volume of reaction products is smaller than that of the mineral reactants, in some case reaching a difference of about 33%, so that devolatilisation reactions tend to produce a continuous network of fluid flow (Ferry 1994). Fluid release curves for initially dry mafic rocks suggest first a hydration process, followed by

dehydration, which increase and become steeper with increasing geothermal gradients, as is also observed for pelitic rocks (Fig. 9.6). Near-surface hydration of mafic rocks result from equilibration with the hydrosphere and hydrate minerals are zeolites, carbonates, chlorite and clays. With increasing temperature, progressive dehydration takes places, with the following typical reactions (Fyfe et al. 1978):

$$\text{Analcite} + SiO_2 \rightarrow \text{albite} + H_2O$$
$$\text{Laumontite} \rightarrow \text{wairakite} + 2H_2O$$
$$2\text{Wairakite} \rightarrow \text{prehnite} + \text{kaolinite} + 3SiO_2$$

and if CO_2 is present:

$$\text{Laumontite} + CO_2 \rightarrow \text{calcite} + \text{kaolinite} + 2SiO_2 + 2H_2O$$

Greenschist facies mineral assemblages such as quartz + chlorite + albite + epidote + calcite ± actinolite develop by alteration of Fe-Mg minerals and plagioclase. Muscovite and biotite may be formed if more potassic rocks are present (e.g. andesite, dacite). Fluids that evolve from mafic rocks are generally H_2O-rich, with only limited development of CO_2, due to the good stability of carbonate phases in the temperature-pressure range of mafic rock dehydration. The breakdown of carbonate minerals during metamorphism results in the release of CO_2 and H_2O. The amount of H_2O that is released from the devolatisation of carbonates is largely dependant on the presence of impurities, such as clays. Fyfe et al. (1978) emphasized that the presence of impurities in carbonate rocks have an important effect in metamorphic reactions, because they can occur at lower temperatures than those required by reactions such as:

$$\text{Calcite} + SiO_2 \rightarrow \text{diopside} + CO_2$$

The above reaction takes place at temperatures greater than 600°C. Dehydration of dolomitic rocks by reaction with quartz take place at much lower temperatures, and produce clinopyroxene or tremolite, with release of CO_2, as shown below:

$$\text{Dolomite} + 2SiO_2 \rightarrow \text{diopside} + 2CO_2$$
$$5\text{Dolomite} + 8SiO_2 + H_2O \rightarrow \text{tremolite} + 3\text{calcite} + 7CO_2$$

Inverse reaction can occur if CO_2 is flushed through metamorphosed impure calcitic marbles, such as calc-silicates, to produce dolomite and quartz. The presence of impurities in carbonate rocks (clays, micas) is clearly important because they provide the H_2O necessary for decarbonation reactions to occur. Fyfe et al. (1978) considered three main categories of carbonate sediments from which CO_2 can be released: (1) dolomitic marble with quartz, which will release

a CO_2-rich fluid at high metamorphic grades; (2) carbonate rocks with clays and/or micas will release H_2O-rich fluids; and (3) pelitic sediments with carbonate interbeds will tend to release H_2O-rich and CO_2-poor fluids.

9.2.1.2 Mobilisation and Transport of Metals

Metalllic elements are mobilised, transported and precipitated as sulphides or oxides whenever a pile of rocks is subjected to heating, either because of regional prograde metamorphism or by igneous intrusions. The precise mechanisms of mobilisation and transport are poorly known. In general, the composition and nature of rock successions determines the type of volatiles released and metal complexing agents (Phillips et al. 1994). Thus, mafic rocks produce metamorphic low-salinity fluids containing H_2O, H_2S and CO_2, and for this reason they promote Au-S complexing and the formation of gold-only lode deposits. Highly saline fluids, on the other hand, can result from dehydration of evaporite sequences, which can produce fluids containing Na and Cl and promote base metal-Cl complexes. High chlorinity fluids have the capacity of transporting several metals, including gold and generate polymetallic ore deposits. The nature of the fluids also influences the type and style of hydrothermal alteration of wallrocks. Details on the control of metal solubilities in hydrothermal fluids can be found in Crerar et al. (1985).

On the basis of microstructural evidence, Etheridge et al. (1983) envisaged mass transport of elements through a metamorphic fluid phase that results in up to 50% volume loss from mica-rich domains in cleaved rocks, whereas quartz-rich domains tend to remain unaffected. These domains undergo substantial loss of Si and Na, with concomitant gains in Ti, Al, K, Y and Zr. This in situ Si depletion allows transport of this element in fluid phases and its subsequent precipitation within relatively short distances, which accounts for the presence of quartz veins in greenschist facies metamorphic rocks. Mobilisation of metals, such as Ba, Pb, Bi, Ag, Cu, Zn, is particularly efficient from pelitic rocks during regional metamorphism as large amounts of H_2O and CO_2 are liberated at the same time. Estimated yields per km^3 of aluminous pelitic rocks during prograde metamorphism, calculated by Haack et al. (1984), are in the order of 280 000 t of Ba, 16 000 t of Pb and 83 000 t of Cu.

Gold is carried in solution mainly as AuHS(aq) at low pH and as $AuHS^-$ at near-neutral pH and at temperatures below 400°C. In the temperature range of 400–300°C these complexes are destabilised and Au is precipitated. At higher temperatures, Au tends to be transported as a chloride complex ($AuCl_2^-$) Loucks and Mavrogenes (1999) on the basis of experiments on chloride brines saturated with Au, magnetite, Fe sulphides, K-feldspar and muscovite at 550–725°C and 100–400 megapascals, demonstrated that the solubility of Au as sulphide species is much higher than expected. Metamorphic fluids undergo strong decompression from lithostatic to hydrostatic regime, during their passage through the ductile-brittle transition at about 425–375°C. This is probably the reason why some 90% of the Au mined from orogenic systems is

in greenschist facies metamorphic terranes and in the brittle-ductile transition regime (Kerrich 1999). The tendency of Au to be preferentially transported as a sulphide complex also explain the near-absence of base metals (Cu, Pb, Zn) in the same mineral systems, because these metals form complexes with Cl rather than S.

9.2.2 Fluid Paths: Shear Zones, Faults and Thrust Faults

The deformation systems with which orogenic ore systems are spatially associated include faults, fractures, bedding-controlled slip and dilation zones, brittle and brittle-ductile shear zones. The latter are especially important because they are the most common ore-hosting structures. It is therefore appropriate to consider briefly the geometry of shear zones and the formation of veins and related mineralisation. Details on the topic can be found in Ramsay (1980), Hodgson (1989) and Passchier and Trouw (1996), whose work provided most of the information provided here. Tectonic deformation processes cause strain in rock bodies. For the effects of deformation on the microscale and resulting microstructures the reader is referred to Vernon (2004). Passchier and Trouw (1996) defined a shear zone as "deformation in high strain zones usually contains a rotation component, reflecting lateral displacement of wall rock segments with respect to each other". Strain or the change in the shape of a body as a result of applied stress, can be described in terms of three orthogonal axes: (1) principal maximum stress (σ_1); (2) intermediate stress (σ_2); and (3) minimum stress (σ_3) (see Figs. 9.7 and 9.8). The change in the shape (deformation) of a body can occur by compression, for which $\sigma_1 > \sigma_2 = \sigma_3$ (pure shear), or by torsion or rotation, in which $\sigma_1 > \sigma_2 > \sigma_3$ (simple shear), a combination of the two, or by extension ($\sigma_3 > \sigma_1 = \sigma_2$). Failure by fracturing takes place at low mean stress and high strain rate. Fractures are developed parallel to the maximum principal stress σ_1. As stress increases and strain rate decreases tensile fracturing gives way to shear fracturing and eventually to ductile flow. The presence of pore fluids in rocks undergoing deformation is very important because it counteracts the effects of the confining pressure and it also influences and promotes mineral reactions, which in turn affect the mechanical properties of the rocks. Ramsay (1980) classified shear zones into three types: brittle, brittle-ductile and ductile. Recognition of these three types is based on the type of markers' displacement across the shear zone. Thus, brittle shears are characterised by the abrupt offset of markers. In brittle-ductile shear zones external markers show both continuous and discontinuous offsets along discrete slip surfaces, whereas rocks in ductile shears are mylonitic and external markers show continuous offsetting. The character of shear zones reflects the temperature, pressure and fluid regime of the environment and the rheological properties of the rocks affected. In terms of geometrical features Hodgson (1989) distinguished internal features and external forms of shear

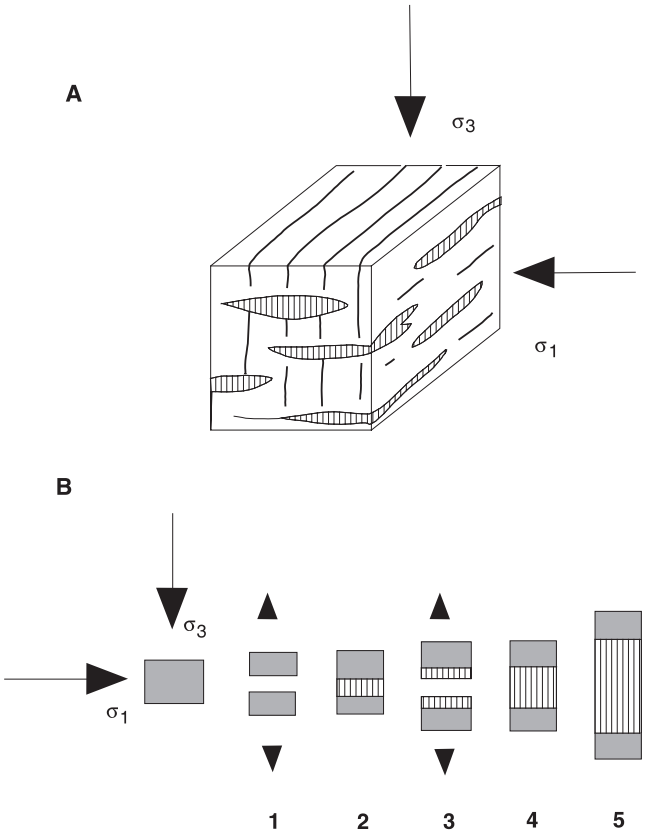


Fig. 9.8 Metamorphic vein system resulting from fluids that flow from cleavage zones perpendicular to σ_1, to tensile fractures perpendicular to σ_3, into which solutes are precipitated to form veins (**A**); these veins grow by a process of crack-seal (**B**), as explained in text. (**A**) is after Etheridge et al. (1984), (**B**) is after Cox et al. (1986)

zones. The former include microscopic to mesoscopic fabrics which can be recognised at the thin-section to hand-specimen scale. Cataclasites or rocks with cataclastic textures are characterised by non-foliated fragments produced by fracturing in the brittle regime. They form breccias, microbreccias and gouges, which through pseudotachylites (microbreccias cemented by frictionally produced melt; see Vernon 2004 for details on pseudotachylites), pass into mylonite, formed in the brittle-ductile to ductile regime. Quartz-rich rocks are most sensitive to strain. In quartz, low angle sub-grain boundaries develop and are shown by bands of undulose extinction. Soft minerals in the rock tend to recrystallise into matrix material, hence the proportion of soft minerals in the rock before shearing will influence the proportion of matrix that will eventually develop into a mylonite. The development of mylonitic rocks follows a trend from protomylonite, through mylonite to ultramylonite, as indicated by the

progressive increase of granulated and shaered matrix material (grain-size reduction). The nature of the lithology being sheared has a marked effect on the development of mylonitic fabrics. Thus, lithologies with a high proportion of "hard" minerals (e.g. feldspar, garnet, amphibole or pyroxene) tend to have limited bulk ductility with the deformation being to a large extent controled by the hard minerals. On the other hand, lithologies with a high proportion of "soft" minerals (e.g. quartz and mica) tend to deform in a plastic manner. The external form of shear zones and shear zone systems are characterised by anastomosing patterns visible on hand specimen to map scale. The anastomosing geometry shows many fractures whose inclination towards the trend of the shear zone enables one to distinguish the following types: low-angle and high-angle Riedel shears (R), pressure or P shears, C- and S-type shear bands. Shear zone systems often form intersecting sets or networks of planar deformed zones which wrap around areas of low deformation. Sets of subparallel shears in a system, which have an opposite sense of movement and are developed in the same stress regime, are called a conjugate system.

The principles of fluid flow in fractured and porous rocks have been investigated in detail by Cox et al. (2001) and Sibson (2001). These authors emphasised that fluid pathways between ore metal sources and depositional site are governed by fluid pressure, buoyancy and permeability. The driving force of fluid flow is related to pressure gradients and buoyancy, which can be thermally controlled or chemically induced (Cox et al. 2001). Pressure-driven flow can be related to topography, deformation or draining of reservoirs. Topographic relief is one of the important factors because it establishes pressure gradients from topographically high towards lower topography areas. Equally important can be regional deformation, which induces pore pressure changes, resulting in vertical and lateral hydraulic gradients at all crustal depths (Cox et al. 2001). Sibson (2001) highlighted the importance for mineralisation of the pressure exerted by fluids in pores and fracture spaces. Hydrostatic pressure is where pore and fracture space is saturated with aqueous fluids that are connected with the water table. Where this connection is missing such as in rock compartments sealed by impermeable horizons, then fluids are overpressured to suprahydrostatic values. These seals break during faulting and fracturing, allowing the overpressured fluid to escape with the rapid pressure drop causing mineral precipitation. Fluid overpressure also arises as a result of compressional deformation, as in accretionary wedges; by igneous intrusions into fluid saturated crust and in zones linked to mantle degassing (Sibson 2001; see also Fig. 9.7). Near-lithostatic to lithostatic fluid pressures characterise regions of prograde metamorphism at depth, overlain by a brittle carapace, providing a transitional regime to hydrostatic pressures above it (Sibson and Scott 1998).

The movement of fluids in a rock mass is attained and enhanced by permeability. Permeability is dependent on, and due to rock type, fractures, foliation, shear zones and faults. Any steeply inclined plane (e.g. foliation) will constitute a pathway for the migration of fluids, and of particular importance therefore are the pipe-like structures formed at the intersection of two planes.

Deformation-induced permeability, such as fractures formed during seismic events and aseismic faults and folds. Mineral precipitation is linked to seismic slips and mechanisms of suction-pump and fault-valve action, due to rapid slip transfer across dilational jogs and subsequent drop in fluid pressure at these sites, which trigger precipitation of mineral phases during postseismic periods (Sibson 2001). Networks of faults, fractures and shear zone are the principal channelways for the movement of fluids in the crust and the site of ore deposition. Mineralisation can be restricted to jogs and bends in shear zones or faults, or fold structures (saddle reefs) (Cox et al. 2001). Sibson (2001) and Sibson et al. (1975) proposed seismic pumping as a mechanism whereby large quantities of fluids can move along a fault plane during earthquakes to form hydrothermal mineral deposits. Their model assumes that just before seismic failure along a strike-slip fault a regime of dilation surrounds the area of the focus. This would be due to increasing shear stress by the opening of vertical fractures normal to the least principal stress (σ_3), which in the case of strike-slip faults is horizontal. Sibson et al. (1975) argued that the development of these fractures allows the fluid pressure to decrease in the region of dilatancy, resulting in fluid movement along these fractures. Fluid pressure then rises again, accompanied by a decrease in the frictional resistance, so that seismic failure takes place with partial stress relief. The result is the expulsion of the fluids upward in the direction of the pressure relief. This flow of fluids takes place along the fault and nearby fractures, and mineral deposition occurs above the dilation zone. To support their model, Sibson et al. (1975) drew attention to the common observation of hot springs along active faults. They cited the example of an earthquake in Japan, which resulted from movements along a buried wrench fault about 10 km long. The earthquake was accompanied at the surface by the expulsion for 1 year of some 10^{10} l of warm brine containing Na, Cl and Ca, and saturated with CO_2. The authors further proposed that if the fault intersects a suitable source region, then metals could be leached out by the moving fluids, transported by seismic pumping and deposited above the dilatant zone.

9.2.3 Veins in Metamorphic Rocks

Veins in metamorphic rocks are evidence of fluid flow in fracture systems (Ferry 1994). Veins range in size from a few millimeters to several metres thick and are the consequence of the flow of fluids, which carry solutes that subsequently precipitate in the conduits through which flow occurs. Focussing of fluids along faults and shear zones may enhance the dissolution and mobilisation of material. The precipitation of solutes takes place in chemically or mechanically developed sites, such as fractures or penetrative fabrics, whose orientation is related to the dominant stress field in the rock body. Dewatering due to prograde metamorphism and igneous intrusions are important sources of fluids and dissolved silica, leading to the formation of quartz veins in metamorphosed rocks. Bons (2001) examined the effects of fluid flow in

fractures and suggested that batches of fluids move very fast by a process of hydrofracturing. This fast ascent enables hot fluids with dissolved silica and metals to precipitate upon arrest of the moving hydrofracture – fluid system, resulting in a mineralised quartz vein. Bons (2001) calculated that a single large vein can experience a very large number of fluid ascent in mobile hydrofractures, with repeated opening and closing of the fractures, thus explaining the deformation of the quartz grains and wall rock alteration commonly associated with veins. The veins are preferentially oriented perpendicular to least compressive stress (σ_3). Jébrak (1997) reviewed the nature of the brecciation that characterise vein systems in response to propogation processes, based on the morphology of the fragments and particle size distribution. This author recognised the following: tectonic comminution, hydraulic fluid-assisted brecciation, wear abrasion, volume reduction, impact, collapse and corrosive wear.

High fluid pressure causes hydraulic fracturing, which can be expressed by:

$$P > \sigma_3 + T$$

In the equation above, a fracture is formed when the fluid pressure exceeds the minimum principal stress σ_3 and the tensile strength of the rocks T. If σ_3 is vertical, then a system of horizontal fractures, parallel to σ_1, develops, whereas if σ_3 is horizontal, as in most extensional situations, inclined or vertical fractures would form (Fig. 9.8).

Metamorphic veins can be classified into two main types: replacement and hydrothermal filling. The first is generated by diffusion processes with precipitation of solutes into small dilatancy sites (Fyfe et al. 1978). The second type is important for the origin of mineralised vein systems and is formed by the flow of hydrothermal solutions along larger scale fractures, faults or shear zones.

Vein growth in the metamorphic environment takes place either by a mechanism of crack-seal and fibre growth or by simple growth (Cox et al. 1986, 2001). In the process of crack- seal and fibre growth, fluids migrate from cleavage zones perpendicular to σ_1 into tensile fractures perpendicular to σ_3. The process of crack-seal and fibre growth is shown in Fig. 9.8. Mineral phases are precipitated on the walls of the fracture, which is then sealed (steps 1 and 2 in Fig. 9.8); in a subsequent phase of fracturing, the growth of the same or new mineral phases along the older minerals takeplace (steps 3 and 4 in Fig. 9.8). The process can be repeated several times (step 5 in Fig. 9.8), resulting in multiphase vein fillings characterised by fibrous textures. Mesothermal veins, which are characterised by sheeted vein systems, showing ribbon or laminated structures are an example of this process. Veins that are formed by a process of simple growth are the result of continuous fracture opening, accompanied by concomitant and continuous deposition of solutes, due to constant high fluid pressure. Typically, the resulting textures are banded, crustified or comb-like. This type of open-space filling is more common in epithermal veins systems. A discussion on types of quartz morphology in mineralised vein systems is presented in Chapter 2.

9.2.4 Oxygen and Hydrogen Isotope Systematics

The isotopic compositions of metamorphic waters are obtained from the isotopic values of whole rocks, mineral phases and fluid inclusions contained in quartz vein material in metamorphic rocks. The field of metamorphic waters is shown in Fig. 9.3, where it can be seen that these waters are $\delta^{18}O$-enriched and δD-depleted with respect to SMOW and the meteoric water line. The calculated field for metamorphic waters is δD 0 to –70 and $\delta^{18}O$ of +3 to +20‰ (Sheppard 1986). In general metasediments have δD from –40 to –100‰, $\delta^{18}O$ of between +8 and +26, and $\delta^{18}O$ of +3 to +14‰. The range of these values in metamorphic rocks is probably related to the precursor rocks. Kerrich (1986) reported on the isotope systematics of a number of mineral provinces in North and South America. The results of these studies, which focused on hydrogen and oxygen isotopes, indicate that for many of the mineralised localities, metamorphic or mixed metamorphic and meteoric fluids were responsible for the deposition and concentration of metals. One of the cases discussed in detail by Kerrich (1986), refers to the Grenville Front mylonitic zones, which separate the Grenville high-grade gneisses from the low-grade sediments of the Southern Province. Two mylonitic zones, MZI and MZII, associated with the Grenville Front were investigated. MZI shows retrograde metamorphic reactions and has $\delta^{18}O$ values of +7‰ for the associated fluids, with isotopic temperatures estimated at 420–490°C, which are in good agreement with the results of garnet-amphibole thermometry (540°C). MZII shows prograde metamorphic reactions and the $\delta^{18}O$ of quartz ranges from +9.6 to +11.8‰, with isotopic temperatures of 580–640°C, also in good agreement with garnet-biotite thermometry, and which gave a deformation temperature of around 600°C. Quartz-hematite veins, emplaced in fractures overprinting the deformation fabrics of MZI, have $\delta^{18}O$ (quartz) of –0.8 to –1.3‰. This quartz crystallised at temperatures of 200–350°C with fluids depleted in $\delta^{18}O$ (–8 to –14‰). In Kerrich's view the MZI and MZII were formed at high temperatures in the presence of metamorphic fluids (positive $\delta^{18}O$ values). The high grade rocks (gneisses) were tectonically placed into contact with low-grade rocks (metasediments) which had been subjected to brittle fracturing and had interacted with continental meteoric waters (negative $\delta^{18}O$ values). Sporadic $\delta^{18}O$ - depleted mineral phases may be indicative of incursions of meteoric waters into the upper plate (Kerrich 1986).

9.3 Orogenic Lodes

Goldfarb et al. (2001) and Groves et al. (2005) have shown that the temporal distribution of orogenic lodes is characterised by peaks at 2.7–2.5 Ga, 21.–2.0 Ga, 1.8 Ga, 0.8 Ga and 0.7–0.6 Ga and that orogenic lodes of all ages record high fluxes of deeply-sourced fluids during accretionary and subduction processes at convergent margins. The works of these authors have been perused

for this section. The oldest recognised orogenic lodes are those of the 3.57–3.08 Ga Barberton greenstone belt in the eastern part of the Kaapvaal Craton in South Africa, where significant Au lodes, related to accretionary tectonics, formed at 3126–3084 Ma. The Fairview, New Consort, Bonanza, Agnes, Golden Quarry and Sheba Au deposits are representative of orogenic lode systems in the Barbeton belt. Similarly, in the Murchison greenstone belt, about 50 km north of Barberton, a number of orogenic Sb-Au lodes, are hosted in a sequence of talc-carbonate, chlorite schist, banded iron formations, fuchsitic and siliceous carbonate rocks along the east-northeast-trending Antimony Line. Here the largest Sb-Au deposit is Alpha-Gravelotte, where stibnite is associated with varying amounts of scheelite and gold. More orogenic lodes are present in the Pietersburg greenstone belt, west of Barberton. A review of these South African deposits can be found in Ward and Wilson (1998). The Late Archaean was especially prolific in the generation of orogenic mineral systems. World-class deposits are present in the 3.0–2.6 Ga Yilgarn Craton (see below), the 3.1–2.6 Ga Superior Province in central Canada, where the giant Hemlo Au-Mo deposit is located (Corfu and Muir 1989; Pan and Fleet 1995). Other Au deposits in the Province include the Timmins-Hollinger-McIntyre goldfield, Kirkland Lake, Val d'Or, Balmerton and Red Lake districts (Dubè and Gosselin 2007 and references therein). Other orogenic systems in Canada occur in the 2.7–2.6 Ga greenstone belts of the Slave Province. Elsewhere in the world, Archaean greenstone belts well-endowed with orogenic Au mineralisation are found in the Quadrilatero Ferrifero in Brazil, in the Kwekwe and Kadoma districts in the Zimbabwe Craton, in the Dharwar Craton in India, in the Aldan-Stanovik and Anabar shields in Siberia.

The Palaeoproterozoic (2.5–1.6 Ga), punctuated by global orogenies at 1.9–1.8 Ga, saw the formation of the world-class Ashanti goldfields in the 2.2–2.0 Ga West African Craton, the 2.2–1.9 Ga Rio Itapicuru greenstone belts in Brazil, accompanied by Witwatersrand-style palaeoplacer deposits in Serra de Jacobina. In Australia, Palaeoproterozoic orogenic Au systems are present in the Arunta Orogen and the Pine Creek Inlier. In the Arunta Orogen, orogenic lode-Au deposits are concentrated around the Granites and Tanami Au province in the Northern Territory and include the world-class Callie deposit, which has a resource of 188 t Au (Huston et al. 2006). Gold deposits in the Granites–Tanami Orogen are hosted by a variety of rock types, including carbonaceous siltstone, iron formation, basalt, dolerite, and turbiditic sedimentary rocks. Most deposits are associated with relatively late oblique strike and reverse faults, and many are localized where the late faults intersect anticlines. These structures provided the environment that allowed pressure fluctuations and the focussing of ore into chemically reactive rocks, producing large, high-grade deposits such as Callie (Huston et al. 2006). Most of the gold in the Granites–Tanami Orogen is hosted by carbonaceous siltstone and iron formation in the Dead Bullock Formation, which are extensively hydrothermally altered. At Callie, carbonaceous siltstone is decarbonized and bleached in ore zones, which appears to have accompanied gold deposition. Decarbonization

leads to reduction of the ore fluid and the production of CO_2(g) and H_2(g) (Huston et al. 2006). Several orogenic Au deposits are located around the Cullen Batholith in the Pine Creek Inlier. The Pine Creek goldfield is about 1 km wide and 6 km long and includes 15 mines (Ahmad et al. 1999). The Pine Creek Shear Zone is a complex zone of faults that extend SE through the Cullen Batholith in the vicinity of the Yimuyn Manjerr gold mine, and lies in the Noonamah-Katherine Lineament Zone. Many of the deposits are Au-bearing quartz veins forming saddle reefs, concordant and discordant veins, and stockworks along axial planes of anticlines.

Important Au mineral systems in the Meso- and Neoproterozoic (1.6–0.6 Ga) include those that formed in the deformed terranes of the Baikal fold belt, with the giant Sukhoi Log Au deposit as the best representative (see below). Goldfarb et al. (2001) included in this period the world-class 650 Ma Telfer Au deposit in the Paterson Orogen, situated between the North and West Autsralian Cratons, where extensive deformation and thrusting occurred. Genetic models emphasize the importance of structural controls on mineralization that is hosted by a series of vertically stacked, stratabound quartz-carbonate-sulphide reefs, and centred on the anticlinal hinge zone of the Telfer Dome. Other styles of mineralization include stockworks, pods, and vein systems in faults. The reefs are typically linked by stockworks of quartz-sulphide veins and sheeted vein sets. However, the genesis of the Telfer Au-Cu deposit has also been explained by a syngenetic exhalative model, based on the observations that the mineralization is stratabound in the Malu Formation of the Lamil Group and pyrite is usually laminated (Pirajno and Bagas, in press and references therein). The sulphide minerals are mainly pyrite and chalcopyrite, and form either aggregates or disseminations in carbonate and argillic veins in the quartz reefs. Gold is found in pyrite as small inclusions and in fractures, and is generally associated with small amounts of chalcopyrite and trace amounts of pyrrhotite (Dimo 1990). Wallrock silica-dolomite (-sericite-tourmaline-rutile-xenotime-monazite) alteration is restricted to narrow zones at the reef margins, which contain disseminations of fine-grained gold with disseminated euhedral to subhedral pyrite, and minor chalcopyrite and galena. The quartz veins are up to 0.2 m thick and contain up to 10 g/t Au; the laminated veins are up to 0.3 m thick with grades up to 160 g/t Au. High-grade mineralization is due to supergene enrichment that extends to 300 m below the surface (Dimo 1990). Fluid inclusion studies show that the ore fluids were rich in H_2O-CO_2-CH_4-NaCl, and reached temperatures between 225° and 450°C (Dimo 1990; Goellnicht et al. 1991; Rowins et al. 1997). Goellnicht et al. (1991) suggested that the mineralizing fluid was a mixture of fluids derived from magma and host or basin rocks, and mineralization is related to a distal Au-halo of a giant porphyry Cu-Au system. Goldfarb et al. (2001) suggested that the Sabie-Pilgrim's Rest Au deposits in South Africa bear some similarities with Telfer. Sabie-Pilgrim's Rest in this book is considered as an intrusion-related system (due to the emplacement of the Bushveld Igneous Complex) and is discussed in Chapter 4.

The Palaeozoic (570–250 Ma) abounds with orogenic Au-forming events, mostly due to subduction zones encircling the Gondwana and Laurasia continents, separated by the Palaeotethys Ocean. In this environment, the orogenic lodes of the Lachlan fold belt in eastern Australia and the Westland goldfields and Reefton district of the South Island in New Zealand, were formed along the Gondwana active margin. Subduction of the Palaeotethys Ocean beneath the Kazakhstan and Siberian sides of Laurasia, produced the orogenic lodes of the Tian Shan, Kazakhstan, Altaids, Mongol-Zaibaikal belt (Zorin et al. 2001) (Fig. 9.9). The Tian Shan orogenic belt in central Asia extends for 3500 km, from northwestern China westward to Tajikistan, Kyrgyzstan and Uzbekistan, where the giant Muruntau Au deposit is located (see below). The

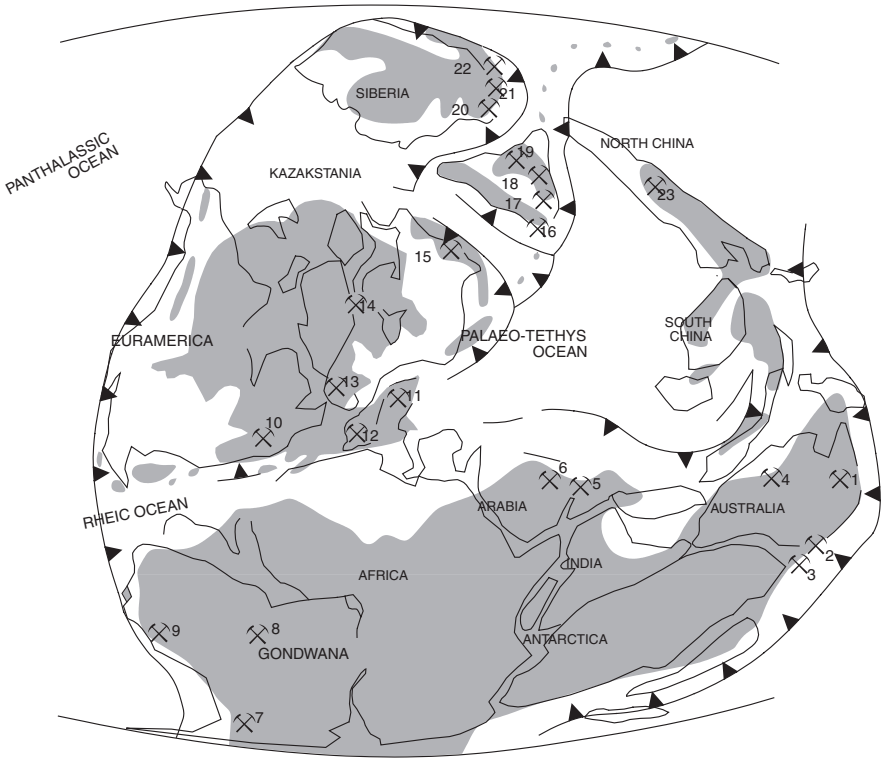


Fig. 9.9 Mid-Palaeozoic supercontinents reconstruction (after Scotese 1997) and distribution of major orogenic Au provinces on continental margins of Gondwana, Euramerica, Kazakstania, Siberia and North China; (1) Thomson fold belt; (2) Lachlan fold belt; (3) South Island, New Zealand; (4) Telfer; (5) Arabian-Nubian shield; (6) Hoggar; (7) Sierra Pampeana; (8) Brasilia fold belt; (9) Eastern Cordillera; (10) Southern Appalachian; (11) Bohemian Massif; (12) Iberian Massif; (13) Meguma; (14) Caledonides; (15) Ural mountains; (16) Western Tian Shan; (17) Eastern Tian Shan; (18) Altaids; (19) Kazakhstan; (20) Sayan; (21) Mongol-Zaibakal belt; (22) Baikal; (23) Northern China Craton. After Goldfarb et al. (2001)

belt of orogenic lodes of the eastern Tian Shan in Xinjiang Autonomous Region (China) continues eastward along the northern margin of the North China Craton (Fig. 9.9).

A comprehensive review of the Tian Shan Au deposits can be found in Rui et al. (2002), from whom I have drawn the following regarding the orogenic lodes of the Chinese Tian Shan. In the Chinese Tian Shan, the Wangfeng deposit and adjacent smaller prospects are restricted to the NW-striking Bingdaban or Shenglidaban mylonitized shear zone, which separates Proterozoic to Ordovician, and perhaps Silurian, orthogneiss, schist and marble from mainly Early Carboniferous granitoids, within the northern part of the Yili block (central Tian Shan). The Wangfeng deposit consists of two distinct and parallel, 1300-m-long orebodies that are about 10 m apart, characterised by silicified, ductile shear zones, with 1–2% pyrite and pyrrhotite in the gold-bearing veinlets. The Dashankou deposit, south of the Wangfeng deposit consists of large quartz veins, smaller stockwork systems, and gold-enriched altered rock along a major east- to southeast-trending brittle-ductile shear zone, exposed over a length of almost 2 km and a width of 300 m in the mine area. The auriferous quartz contains minor pyrite, with common sericite and ankerite in ore-hosting, altered Late Silurian to Early Devonian metamorphosed clastic rocks. The Sawayaerdun gold deposit, along the China-Kyrgyzstan border, is the largest recognized orogenic gold deposit in Xinjiang, with a geologically inferred resource of at least 300 t of Au. This deposit within the eastern Kokshaal area of the southern Tian Shan province is hosted by Late Silurian slates and carbonaceous phyllites. The middle Paleozoic rocks are part of a complex sequence of allochthonous slices, with thrusting having occurred during Variscan collisions (Rui et al. 2002). Gold mineralization at Sawayaerdun is localized over a 70-km-long by 50- to 600-m-wide zone between two regional faults, perhaps representing sutures between accreted oceanic terranes. Quartz, sericite, siderite, calcite, and chlorite are commonly associated with the gold. Pyrite, pyrrhotite, and arsenopyrite are the main ore-associated sulphides, with less common stibnite, chalcopyrite, galena, sphalerite, and marcasite. Except for a few small mafic dikes, no igneous rocks have been recognized in this gold-rich zone. Fluid inclusions homogenize at two modes of 155–220°C and 260–290°C, and contain abundant CO_2 and significant CH_4 and N_2. Fluid inclusion waters from ore-related gangue at the Sawayaerdun deposit have δD values of –59 to –84‰, and $\delta^{34}S$ data for sulphide minerals range between about –3 and + 1‰. Many of these features, including a probable Permo-Triassic age of formation, suggest that the deposit is similar to the giant Muruntau deposit located farther to the west in the southern Tian Shan, described in Section 9.3.3.

The Mesozoic heralded the great subduction systems of the Pacific Ocean. Whereas the South American Andean margin is effectively free of orogenic Au lodes, by contrast the Pacific margin along western North America (from California to Alaska) and eastern Asia (Far East Russia to eastern China) is remarkably well endowed by numerous orogenic lode systems. Along the western North American margin are the Cordilleran orogens characterised by

the accretion of allochthonous terranes with the eastern cratonic margins of the continent. These events led to the development of the well known Au districts, including Klondike, the Juneau gold belt (Goldfarb et al. 1988; Light et al. 1990) and the famous Mother Lode. In Russia, are the numerous orogenic lodes and associated placer deposits of the Transbaikalia Au belt, with the Allakh-Yun and Mongol-Okhotsk fold belts, bordering the eastern margin of the Siberian platform (Zorin et al. 2001; Spiridonov et al. 2006). The Mongol-Okhotsk fold belt was formed during the collision between the North China Craton and the Siberian Craton. This collision formed the orogenic lodes of northeast China (Wulashan district) and the districts east of Lake Baikal (Mogocha, Selemdzha, Niman, Kerbi). The eastern and northeastern Asian orogenic lodes extend from Far East Russia through to eastern China, in the Jiadong peninsula. In Far East Russia, lode deposits form the 1000 km long Yana-Kolyma metallogenic belt, also associated with numerous placer deposits. Comprehensive listings and databases providing details of the orogenic deposits and associated placers in northeast Asia can be found in USGS open file reports (Nokleberg et al. 2003, 2006).

In eastern China Cretaceous orogenic lodes are present in the Qinling-Dabie orogenic belt on the southern margin of the North China Craton, in the Jiaodong peninsula, (both described in Section 9.3.6) and along the 5000-km-long Tan Lu fault zone, which formed during the oblique collision between the Izangi and Eurasian plates in the northwest Pacific basin. It is interesting to note that although these Chinese orogenic lodes are located within terranes of various ages in the Qinling-Dabie orogen accreted onto the southern margin of the North China Craton and within Jurassic granitic plutons in the Jiaodong peninsula, the age of the lodes is 130–120 Ma (Early Cretaceous). These ages correspond to the great Yanshanian tectono-thermal event and associated large scale hydrothermal activity (see also discussion on Chinese skarn systems in Chapter 6), which is also coeval with the circum-Pacific subduction tectonism and with mantle plume (superplume) events (e.g. Kerguelen and Ontong-Java-Hikurangi oceanic plateaux; Pirajno 2000). This large scale Au (and Ag) forming event in eastern China and along the northern margin of the North China Craton are all of the same age, as are several porphyry and skarn systems in the same areas. The "orogenic" label for the Chinese lodes may have to be revised, because evidence shows that the Yanshanian event is related to mantle dynamics. Griffin et al. (1998) showed that during the Jurassic-Cretaceous, some 80–140 km of Archaean lithosphere was removed from beneath the North China Craton, followed by asthenopsheric upwelling and magmatic underplating. This lithospheric erosion may have been linked to delamination processes, due either to the Qinling-Dabie orogeny or to the circum-Pacific tectonism, or both may have been responsible for the large scale Yanshanian magmatism and high crustal temperatures that may have been responsible for the circulation of hydrothermal fluids. I return to this argument in Section 9.3.5.

9.3.1 Yilgarn Craton, Western Australia

The Yilgarn Craton in Western Australia, together with the Superior province in Canada, is one of the most intensively mineralised areas of continental crust. The Yilgarn Craton contains world-class Ni, Zn-Cu and orogenic Au lodes, on which much has been published over the last 30 years. Here I cite the following papers, which I consider relevant for this particular section: Phillips and Groves (1984), Phillips (1986), Solomon and Groves (1994), Groves et al. (1995), Phillips et al. (1996), Groves et al. (2000) and Cassidy et al. (2005). The latest (at the time of writing) collection of papers dealing with the geology and mineral systems of the Craton can be found in the Proceedings of the Kalgoorlie '07 Conference (Geoscience Australia 2007). The simplified geology and distribution of Au lode deposits in the Yilgarn Craton is shown in Fig. 9.10.

It is now recognised that the Yilgarn Craton is a collage of autochthonous and alllochthonous crustal fragments, ranging in age from 3.4 to 3.8 Ga to about 2.6 Ga, with a complex history of accretion events (Cassidy et al. 2005; Wyche 2007). Voluminous granite intrusions occurred between 2.76 and 2.62 Ga, associated with orogenic events that resulted in the final assembly of the terranes that form the present day configuration of the Craton (Cassidy et al. 2005; Champion and Cassidy 2007). The granitic magmatism constitutes a larger proportion of Yilgarn rocks, accounting for more than 70% of the Craton. Champion and Cassidy (2007) provide an up to date listing of the various granite groups. High-Ca granodiorite, granite and trondhjemite dominate and are distributed both within and externally to greenstone belts; low-Ca granodiorite and granite, mostly external to greenstone belts; high HFSE granite and granodiorite, mostly internal to greenstone belts; mafic granitoids (diorite, granodiorite, granite, tonalite, trondhjemite) and finally volumetrically minor syenitic rocks. The mafic granitoids and syenitic rocks have a spatial association with the Au lodes. An overview of the tectonic assembly of the Yilgarn Craton, taken from Cassidy et al. (2005) and Wyche (2007), follows (Fig. 9.10). The Yilgarn is subdivided into fault-bounded terranes and domains, which from west to east include: Narryer and South West Terranes, Youanmi terrane, containing the Cue, Murchison and Southern Cross Domains, the north-northeast-trending Eastern Goldfields Superterrane (EGST) containing three fault-bounded tectonostratigraphic terranes: Kurnalpi, Kalgoorlie Terrane, each with a number of domains, and the Burtville Terrane. The 3.0–2.9 Ga Cue Domain represents a rifted crustal block and is an exotic terrane, containing the 2.81 Ga Windimurra mafic-ultramafic layered intrusion associated with felsic volcanic rocks, suggesting that the Domain originated in a rift environment. The Kalgoorlie Terrane (Eastern Goldfields Terrane) is interpreted to represent either an exotic block or a crustal fragment rifted off the Youanmi Terrane that forms the central portion of the Craton (Fig. 9.10) and is dominated by 2.76–2.73 Ga felsic volcanism and high-Al TTG (tonalite-trondhjemite-granite) granitic rocks. At about 2.75 Ga, convergent tectonics

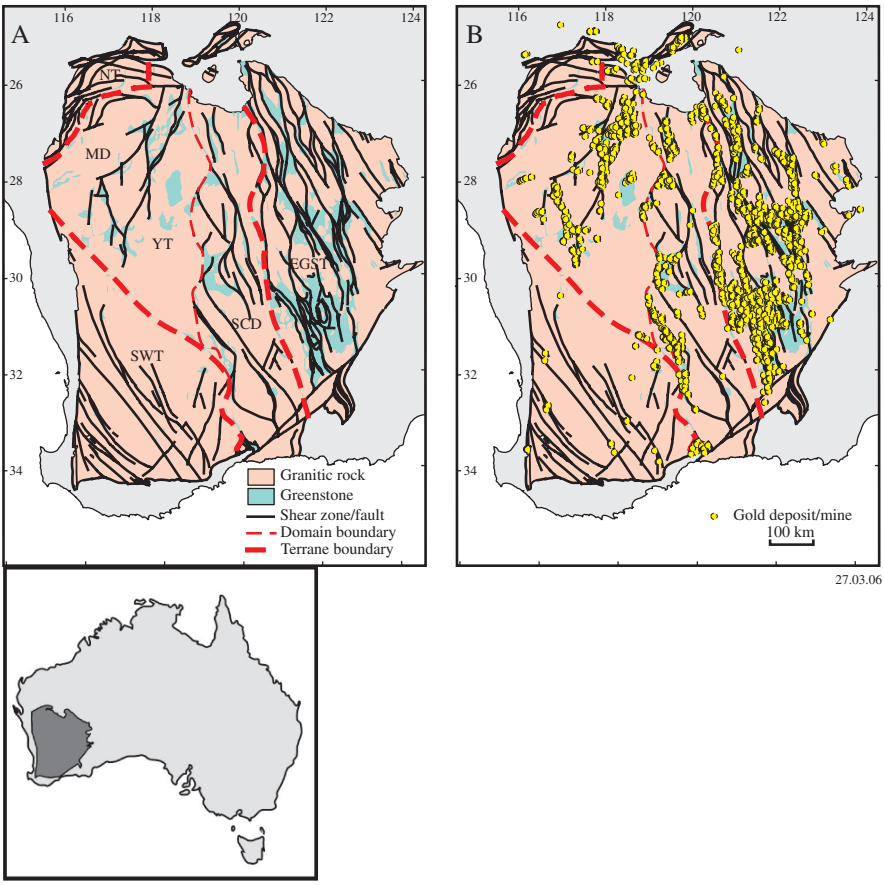


Fig. 9.10 (**A**) Simplified geological map of the Yilgarn Craton and terrane boundaries; (**B**) distribution of principal Au deposits discovered since 1986. YT Younami Terrane, MD Murchison Domain, SWT Southwest Terrane, NT Narryer Terrane, SCD Southern Cross Terrane, ESGT Eastern Goldfields Superterrane Based on Wyche (2007) and Geological Survey of Western Australia database

resulted in the allochthonous 3.8–3.3 Ga Narryer Terrane (Narryer Gneiss Complex) being emplaced over the Youanmi Terrane. The Kalgoorlie Terrane contains the youngest (2.71–2.66 Ga) greenstone belts, formed as a result of submarine eruptions of mafic-ultramafic volcanic rocks (basalt, high Mg-basalt and komatiite), related to mantle plume events (Barley et al. 1998). This was followed by arc-related felsic volcanism. The Kurnalpi Terrane is made up of crustal fragments comprising 2.72–2.70 Ga calc-alkaline volcanic rocks of intermediate composition, overlain by mafic-ultramafic rocks. Also part of this Terrane a series of rifted arc successions and 2.69 Ga bimodal volcanic rocks on the western margin of the Terrane. The ages of the rifted arc sequences progressively change from ~2.72 to ~2.68 Ga in a westward direction, which led

Cassidy et al. (2005) to suggest eastward subduction beneath the margin of an older continental fragment. In the eastern Yilgarn between 2.68 and 2.69 Ga abundant high Al and TTG granites and high Mg monzodiorite and granodiorite (sanukitoid-type) plutons were emplaced. At 2.65 Ga sanukitoids and transitional TTG and low-Ca granitic and syenitic rocks were emplaced in the Kalgoorlie Terrane. These intrusions post-dated the greenstone rocks, but were contemporaneous with deposition of submarine felsic volcanic and sedimentary rocks in back-arc basins in the Kalgoorlie Terrane. The low-Ca intrusions have been interpreted as representing a change in the thermal regime, reflecting extensional tectonics and perhaps lithospheric delamination, associated with melting of older crust. This appears to be a common theme even in younger terranes, as described in Section 9.3.5.

9.3.1.1 The Lode Au Deposits of the Yilgarn Craton

There are more than 2000 lode deposits in the Yilgarn Craton, most found in the Kalgoorlie, Kurnalpi and the Younami Terrane (Fig. 9.10). The source of the Au is likely to be the abundant mafic-ultramafic greenstone sequences in these terranes, whereas the abundance of Au lodes may be linked to accretionary fluid events and lithospheric scale plumbing systems provided by terrane boundaries. Review papers on several of the Yilgarn goldfields can be found in the monographs of the Australasian Institute of Mining and Metallurgy (Hughes 1990; Berkman and Mackenzie 1998). The Kalgoorlie goldfield (Golden Mile and Mount Charlotte) contains a giant lode system and is the largest producer (production + reserves totalling about 2380 t of gold; Laznicka 2006). Several papers have been published on the Kalgoorlie goldfield, beginning with the classic publications by Woodall (1965) and Travis et al. (1971), followed by Phillips (1986), Boulter et al. (1987) and Clout et al. (1990), Gauthier et al. (2004, 2007) to mention a few. The goldfield was discovered in 1893 by Patrick Hannan, Thomas Flanagan and Dan Shea, leading to the exploitation of numerous individual veins and culminating in the currently operating Superpit, the largest opencast mining operation in Australia. The Golden Mile and Mount Charlotte lode systems extend for about 10 km along strike and are up to 2 km wide. The Golden Mile orebody is affectionately called and quite appropriately the "richest mile on Earth". The main host is the 2675±2 Ma Golden Mile Dolerite, a sill-like layered mafic intrusion about 20 km long and up to 700 m thick, which is metamorphosed to greenschist facies and hydrothermally altered (see below). The Golden Mile Dolerite was intruded along the contact between the Paringa Basalt and sedimentary rocks of the Black Flag Group. The Paringa Basalt is a 40–750 m thick sequence of high Mg basalts at the base to high Fe tholeiites towards the top. Synvolcanic basaltic and andesitic dykes are associated with the Paringa volcanism (Gauthier et al. 2007).

The Golden Mile shear zone is characterised by numerous north-northwest striking lodes, dipping to the southwest (Fig. 9.11). The strike lengths of the

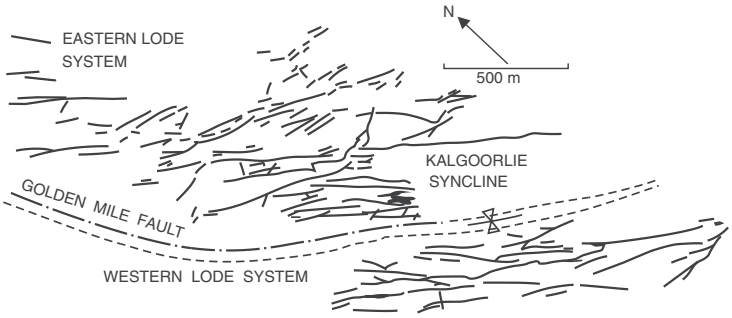


Fig. 9.11 The lode systems of the Golden Mile. After Boulter et al. (1987)

lodes range from 30 m to 1.8 km, up to 10 m wide and extending vertically to at least 1.1 km (Clout et al. 1990). Lode styles are variable and comprise mylonitic rocks, phyllonite, and ductile brecciated material. The Au is contained in pyrite, which occurs as disseminations, veinlets to massive sulphide lenses. Some Au and Ag are contained in telluride minerals. At the northern end of the superpit is the Mount Charlotte orebody, which consist of a low-grade stockwork systems hosted in a granophyre phase of the Golden Mile Dolerite. The Mount Charlotte stockworks consist of quartz veins surrounded by ankerite, sericite and pyrite alteration haloes (Laznicka 2006). The bulk of the Golden Mile system is the Fimiston-style mineralisation (Fimiston lodes), showing high level veins and breccias, subdivided into four stages (Gauthier et al. 2007): (1) carbonate-magnetite ± chlorite, hematite breccias and veins with cockade and crustiform textures; (2) pyrite-tourmaline-magnetite-chlorite-carbonate disseminations and replacement veins hosting Au and tellurides; (3) quartz-carbonate veinlets and quartz replacements, with open space filling textures, also hosting Au and tellurides; and (4) carbonate-quartz veins (2–20 cm thick), usually barren, or with selvages of sericite-carbonate carrying Au and tellurides.

Interaction of the hydrothermal fluids with the Golden Mile Dolerite resulted in a series of reactions, in part controlled by the mineralogical changes of the original igneous layering. Some of these reactions are discussed in Chapter 2. Phillips (1986) recognised three distinct alteration zones within the Golden Mile Dolerite, which overprint the metamorphic assemblages of the sill. Alteration assemblages reflect not only different degrees of alteration intensity, but also the Fe/Mg ratios of the host rocks, and the CO_2/H_2O ratios of the hydrothermal fluids. Throughout the Golden Mile, the outermost wall-rock alteration halo is the chlorite zone which, in the area studied by Phillips (1986), is estimated to be at least 1 km wide and 3 km long. This zone is characterised by the assemblage chlorite + calcite ± ankerite ± albite ± paragonite ± quartz ± magnetite ± siderite ± pyrite. This is followed by the carbonate zone, forming 100-m thick areas around the Eastern and Western Lode Systems, along strike lengths of up to 2 km. This zone, which parallels the stratigraphy and is

influenced by the main ductile shear zones, is characterised by the assemblage ankerite ± quartz ± muscovite ± albite ± siderite ± pyrite. Within the carbonate alteration and controlled by ductile shear zones, are 1–5 m thick zones of pyritic alteration, which contain the Au lodes. These are characterised by the assemblage pyrite ± quartz ± ankerite ± albite ± muscovite ± siderite ± dolomite ± tourmaline. Other sulphide minerals are chalcopyrite, arsenopyrite and minor pyrrhotite. Studies of geochemical changes in the host rocks during the chlorite, carbonate and pyritic alteration indicate that CO_2, S, K, Rb, Si, B, Ba, W and Au were added, while there was a moderate loss of H_2O and Li. The geochemical nature of the alteration zones indicates that only one hydrothermal fluid was involved, whose introduction into the shear zone system post-dated the peak of regional metamorphism. It is concluded that the alteration – mineralisation event was probably part of a single and progressive episode, which began with pyrite + Au, during a deformation stage of a transitional ductile regime, leading to a brittle regime, and the deposition of late veins containing telluride + Au. The giant size of the deposit is attributed to the large volume of hydrothermal fluids, the exceptional permeability of the host lithologies due to intense development of shear zones, and their Fe-rich character.

9.3.1.2 Ore Genesis

In the Yilgarn Craton, lode Au deposits form a broadly synchronous (2635–2680 Ma) group, over a range of epithermal to mesothermal styles, metamorphic environments from greenschist to granulite facies, and hosting lithologies (Groves 1993; Groves et al. 1995, 2000). The mineralising fluids are typically deeply sourced, of low-salinity, containing H_2O, CO_2 and CH_4, with temperatures ranging widely from 180°C to more than 700°C, and pressures of 1–5 kb (Groves et al. 1995). Mixing with cooler meteoric waters is suggested in some cases, especially for those deposits that are hosted in brittle structures and low-grade metamorphic rocks. The timing of the Archaean Au mineralisation is syn- to post-peak metamorphism. Data integrated from regional, structural, mineralogical, isotopic, fluid inclusion, geochemical, alteration and tectonic setting studies have led to the crustal continuum model advocated by Groves (1993) and shown in Fig. 9.2.

A direct genetic link, if any, between granitoid intrusions and the Archaean Au mineralisation remains elusive. The spatial and temporal relationship of the lode mineralisation to granitic rocks in Western Australia was investigated by Witt (1991), who noted the association of the lode mineralisation with K-metasomatism (muscovite, biotite, K-feldspar) in the thermal aureoles of late syntectonic granitoids emplaced in the final stages of the tectonic history of greenstone belts. This work led to the "synmetamorphic lateral fluid flow" genetic model of lode Au mineralisation in the Kalgoorlie and Norseman terranes in Western Australia (Witt and Davy 1997; Witt et al. 1997). In this model, large-scale fluid flow systems are envisaged in two main stages. In the

early stage, pervasive deeply-sourced fluid flow is channeled along shear zones; in a later stage, tectonic uplift and granitic intrusions promote lateral flow of fluids first towards areas of high heat flow and then along structural paths of decreasing temperature (Witt et al. 1997). On the other hand, Smithies and Champion (1999) noted that crustal-scale hydrothermal activity appears to be associated with volumetrically minor felsic alkaline plutons, which were intruded along major crustal structures at 2650–2630 Ma, during peak metamorphism. Smithies and Champion (1999) suggested that this crustal-scale hydrothermal activity resulted from metamorphic dehydration of the crust, associated with an input of volatiles from the mantle. Qiu and Groves (1999) proposed that unstable thickened crust, due to a continental collision event in the southwest Yilgarn Craton, was followed by lithospheric delamination and extensional collapse, which resulted in a major tectonomagmatic event between 2640 and 2630 Ma. This was a craton-scale thermal anomaly that would have been responsible for much of a giant hydrothermal system, resulting in the widespread Au mineralisation of the Yilgarn Craton. This collision event in the southwest Yilgarn Craton produced suites of granitic rocks, ranging from A-to I- and S-type, which are interpreted by Qiu and Groves (1999) as representing massive melting of the lower crust. These authors suggested that asthenospheric mantle upwelling due to lithospheric delamination occurred towards the end of the collision event. This mantle activity, according to these authors, could have been related to processes of crustal delamination, similar to those described below for the Au lodes in China.

However, the ultimate origin of the Archaean fluids remains contentious. Two end-member theories may be considered. One is that the large volumes of fluids were generated during the tectonic assembly of a cratonic province, of which the present-day Yilgarn is but a remnant. This is the view suggested by Myers (1995) and supported by Qiu and Groves (1999), who postulated that the Yilgarn craton was formed through the collision and amalgamation of accreted island-arc terranes. After the assembly of these terranes, the fluids passed through dextral transcurrent fault zones, which mark terrane boundaries. The other theory, perhaps implied in the crustal-continuum model is that fluids may be linked to interaction of mantle plumes with the lithosphere (Barley et al. 1998). Interaction of a mantle plume with an island arc has been suggested for the Archaean Au mineralisation of the Abitibi greenstone belt in Canada (Wyman et al. 1999).

9.3.2 Hemlo Au-Mo Deposit, Abitibi-Wawa Greenstone Belt, Superior Province, Canada

The Hemlo Au-Mo-Ba deposit, discovered in 1982, is located near the northern shore of Lake Superior (Ontario) in the Abitibi-Wawa greenstone belt. The Abitibi-Wawa greenstone belt in the Superior Province of the Canadian shield

is the largest in the world and was accreted with volcanic arcs forming a cratonic nucleus between 2.9 and 2.65 Ga. Details on geology and evolution of the Superior Province and Abitibi-Wawa greenstone belt can be found in a special issue of Precambrian Research edited by Mueller et al. (2002) and Percival (2007). The Abitibi-Wawa greenstone belt is subdivided into a Northern Volcanic Zone and a Southern Volcanic Zone, with the former consisting of autochthonous arc sequences and the latter of allochthonous mafic-ultramafic lithotectonic assemblages (Wyman et al. 1999). Wyman et al. (2002) interpreted the lithotectonic associations of the greenstone belt as a collage of intraoceanic arcs, consisting of: 2.75–2.7 Ga arc tholeiites and calc-alkaline rocks; a 2.71 Ga, depleted tholeiite-boninite suite; mantle plume-related oceanic plateaux (2.73–2.705 Ga tholeiites and komatiites); adakites (high Mg andesites); and syn-late tectonic batholitic TTG intrusions, both reflecting melting of subducted oceanic crust slab or plateau material. Shoshonites are also present and are interpreted as late-tectonic, second-stage melting of refractory sub-arc mantle, fertilised by late fluids developed during arc uplift and extensional collapse. A different interpretation was favoured by Ayer et al. (2002), using U-Pb geochronological data and focussing on the southern Abitibi greenstone belt. Instead of a collage of terranes, these authors favoured an autochthonous assemblage, which comprises nine supracrustal assemblages, effectively representing nearly continuous volcanism ranging in composition from mantle plume-related komatiitic and tholeiitic basalts to calc-alkaline mafic to felsic subduction-related volcanic rocks. Ayer et al. (2002) advocated a large scale and long-lived interaction between mantle plume magmatism and subduction zone related volcanic arcs, accompanied by extensive mixing of different magmas.

The Abitibi-Wawa belt has the world's second largest Au endownment after the Witwatersrand in South Africa (Laznicka 2006). The greenstone belt contains world-class and world-renowned metallogenic districts, such as Timmins-Porcupine, Holinger-McIntyre, Kirkland Lake, Val d'Or and the giant Au-Mo-Ba Hemlo deposit, discussed in this section.

The Hemlo Au camp is located in the 2.69 Ga Hemlo-Heron greenstone belt (Wawa terrane), a sequence of east-west-trending volcano-sedimentary units enclosed by granitic rocks (Fig. 9.12). Metamorphism ranges from greenschist facies in the eastern part of the belt, near Heron Bay, to amphibolite facies in the Hemlo area, where metamorphic assemblages consist of biotite + garnet + quartz + plagioclase ± muscovite ± kyanite ± sillimanite ± staurolite ± cordierite. However, this grade of metamorphism was possibly followed by hydrothermal minerals of lower grades, in association with the development of low-temperature ore minerals such as cinnabar, realgar and orpiment. The Hemlo Au-Mo deposit does not conform to the more common Archaean lode type, but is an unusual type of mineralisation, spanning the range from mesothermal to epithermal (350–175°C; based on the thermal stability of some of its ore minerals), paucity of quartz veins and lack of carbonate alteration. Details of the geology, geochemistry and mineralisation of the Hemlo

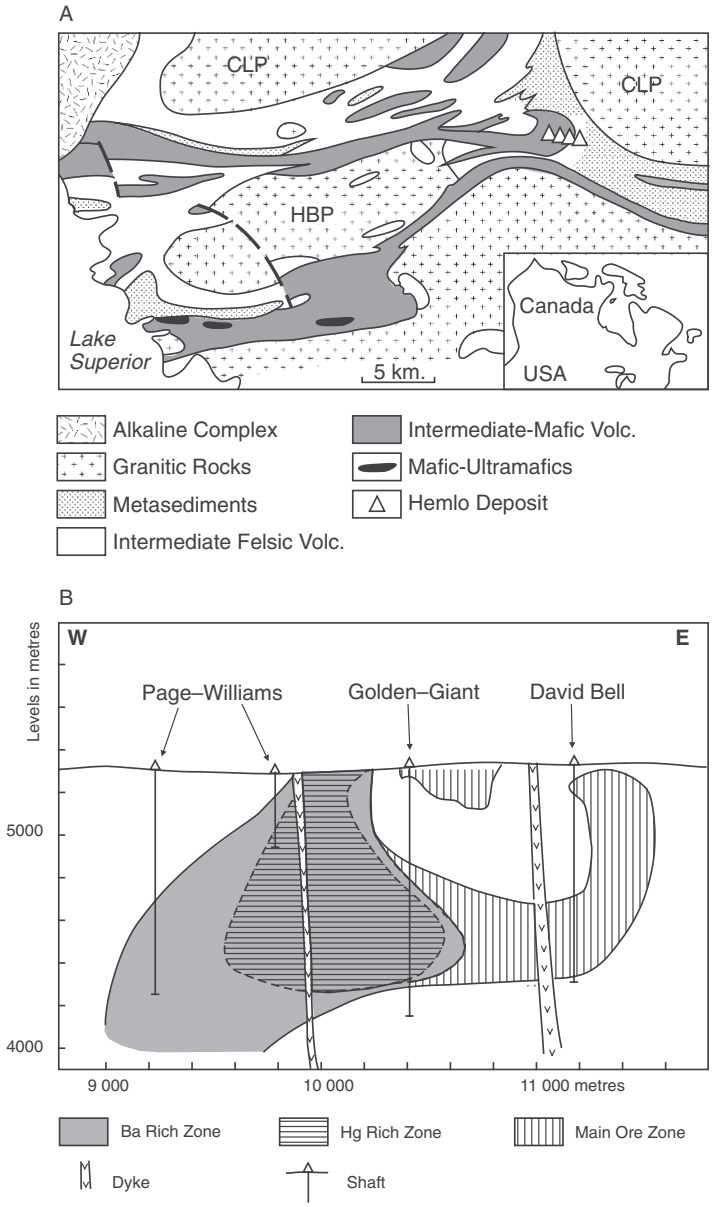


Fig. 9.12 (**A**) Simplified geological map of part of the Hemlo-Heron greenstone belt, showing location of the Hemlo Au-Mo deposits. GLP Gowan Lake Pluton; HBP Heron Bay pluton; CLP Cedar Lake pluton (After Corfu and Muir 1989); (**B**) Schematic longitudinal section showing outline of the Hemlo main ore zone and distribution of Ba- and Hg-rich areas (After Harris 1989)

deposit can be found in Harris (1989), Muir et al. (1988), Corfu and Muir (1989) and Pan and Fleet (1995). These works constitute the basis of this short review.

The Hemlo deposit contains several ore zones, with the main ore zone estimated to contain 80 Mt grading approximately 8 g/t Au. In one of the orebodies (Golden Giant) the MoS_2 content reaches an average of 0.16%. In addition to Au and Mo the ore zone contains Sb, As, Hg, Tl, V and Ba. The deposit extends for approximately 3 km along the strike, with thicknesses of 3–45 m and a vertical extent of 1.5 km, situated within the ductile Hemlo Shear Zone in tightly folded metavolcanic rocks (Fig. 9.12). Three mine properties are developed, which from east to west are: David Bell, Golden Giant and Page Williams (Fig. 9.12). The dominant type of mineralisation consists of a laminated quartzo-feldspathic rock, characterised by the presence of laminae of a green vanadian muscovite, 5–10 wt% pyrite and up to 0.5% MoS_2 with grades of approximately 12 g/t Au. On the Golden Giant property from hangingwall to footwall the ore zone consists of (Laznicka 2006 and references therein): (1) banded quartz, biotite schist and granofels with garnet and staurolite porphyroblasts and bands of chloritic alteration; (2) quartz-muscovite schist (possibly a metarhyolite) with Ba-rich microcline porphyroblasts; (3) phyllonite with disseminated molybdenite, granofels with Ba-microcline, quartz, muscovite and roscoelite, locally brecciated with the fragments cemented by barite and sulphides; in this zone are also quartz pods with stibnite or cinnabar; (4) chert with moybdenite, pyrite and bands of barite, disseminated pyrite with Au, native Au and aurostibnite; and (5) schist with feldspar porphyroblasts and porphyry sills. The host rocks at the David Bell property and in the upper levels are biotite schist and a quartz-feldspar porphyry, at depth these pass into muscovite-rich rocks and feldspathic rocks.

The mineralisation forms irregularly shaped tabular to lensoid orebodies, characterised by the presence of abundant pyrite (average 8 wt%), native Au accompanied by lesser amounts of aurostibite, molybdenite, sphalerite, arsenopyrite, stibnite, tetrahedrite, tennantite, realgar, cinnabar, V-Sb-W-bearing rutile, and a host of other ore minerals some of which have been recognised as new species, such as hemloite $[(Ti,V,Fe,Al)_{12}(As,Sb)_2(O,OH)_{24}]$ (Harris 1989). Native Au occurs as disseminated grains at grain boundaries of silicate minerals and only rarely as inclusions in sulphides. Microprobe analyses show that it is Hg-rich (up to 27 wt%). Characteristically, sphalerite and tetrahedrite-tennantite also contain Hg in amounts of up to 29.5 and 18 wt%, respectively. Common gangue minerals include quartz, muscovite, phlogopite, barian feldspar (microcline with up to 17 wt% Ba) and barite. Tourmaline (dravite variety) is present as an accessory gangue mineral and is essentially confined to the footwall rocks and in the areas of quartz veining.

The deposit is crudely zoned with a central As- and Hg-rich portion, within which are also deformed quartz veins and pods. These are enriched in realgar, stibnite, cinnabar and Tl-bearing minerals. Barite occurs as massive zones (up to 70 wt%) extending from the central zone to the peripheral regions of the deposit, which are depleted in As and Hg minerals. Hydrothermal alteration

is characterised by three main types: (1) potassic; (2) quartz-muscovite; and (3) calc-silicate alteration. Potassic alteration is dominated by K-feldspar, of which four generations have been recognised, from early metamorphic to late vein filling. The K-feldspar is the above-mentioned Ba-rich microcline and the following reaction for the development of microclone was proposed by Walford et al. (1986):

$$\text{Biotite} + \text{oligoclase} + \text{quartz} + K^+ + S^{2-} \rightarrow \text{microcline} + \text{albite} + \text{quartz} + \text{phlogopite} + \text{pyrite}$$

Muscovite alteration is characterised by two varieties, a V-rich and a Cr-rich muscovite, with the former being spatially associated with the Au mineralisation. Calc-silicate rocks form lenses and thin layers, replacement aggregates and veins. Early and higher temperature calc-silicate lenses and layers have mineral assemblages of garnet, diopside, hornblende, plagioclase, biotite, scapolite, anhydrite, barite, quartz and calcite. Late and lower temperature calc-silicate replacement aggregates and veins contain prehnite, epidote, actonoite, chlorite, pumpellyite, vesuvianite, garnet, diopside, tourmaline, allanite, quartz, albite, microcline, calcite and pyrite. Unusual at Hemlo is the relative deficiency of carbonate alteration compared to other Archaean Au deposits in the Abitibi-Wawa belt (Dubé and Gosselin 2007). The Au-Mo mineralisation appears to be related to the potassic alteration of the host rocks as well as to areas of most intense deformation. There is also a close relationship between V and Au, while the precise relationship between Au and Mo is not clear, except that the presence of molybdenite is also indicative of the presence of Au. It appears that the early potassic alteration was associated with the influx of Au into the system, while later, the formation of quartz (+microcline +albite) veins was associated with an influx of Mo. Sulphur isotopic compositions show a wide range of $\delta^{34}S$ values from –17.5 to +12.6‰ whereas barite $\delta^{34}S$ values range from +1.8 to +12‰. The $\Delta\delta^{34}S$ (fractionation between barite and pyrite) has a mean value of +12.70‰, corresponding to a mean exchange temperature of 504°C, consistent with metamorphic temperature of ~550°C at pressures of 3–4 kbar, based on mineral equilibria of coexisting hornblende-plagioclase and scapolite-plagioclase pairs.

9.3.2.1 Ore Genesis

Because of its unusual features, the origin of the Hemlo deposit has been vigorously debated. Genetic models include syngenetic processes, hot spring model, structural model, metamorphic replacement, porphyry and multistage late replacement. A syn-volcanic origin was postulated first. The stratiform nature of portions of the ore zone was used to suggest that the mineralisation was formed syngenetically and was only later deformed during orogenic events. The presence of muscovite and Al-rich minerals (e.g. kyanite) was interpreted to

reflect argillic-type hydrothermal alteration. It was also suggested that the mineralising event may have been related to rifting, with circulation of hydrothermal solutions along growth faults and precipitation of Au-bearing material. The Au-As-Sb-Hg-Tl element association was also called upon to postulate a syngenetic origin for the mineralisation by comparing it with the sinters of the Taupo Volcanic Zone in New Zealand (Goldie 1985). Although by no means resolved, the evidence from petrographic studies suggests that the hydrothermal alteration-mineralisation is epigenetic, structurally controlled, and is probably related to stages of dextral shearing and to calc-silicate and K metasomatism. On the basis of U-Pb dating, it is estimated that the hydrothermal activity was episodic and may have occurred over a period of some 40–50 Ma (Corfu and Muir 1989). The multistage model is advocated by Pan and Fleet (1995), who envisaged that the Au mineralisation occurred during the late calc-silicate alteration event, at temperatures ranging from 200 to 400°C and 1–2 kbar of pressure, with high salinity fluids (indicated by limited fluid inclusion data). Good evidence for this hypothesis is provided by the association of native Au with low-temperature calc-silicate minerals. The temperature of the early calc-silicate and potassic alteration events (~500°C) would have been too high for the precipitation of Au, but quite suitable for the deposition of moybdenite. The Hemlo Shear Zone was active for a long time and fluids were focussed along the conduit during metamorphism, magmatic activity and periods of dylatancy. The first event is linked to the early high-temperature calc-silicate alteration, closely followed by more extensive anhydrous potassic (microcline) and hydrous (muscovite) lower temperature (400–500°C) alteration events, associated with Ba, V, Cr and pyrite mineralisation. Pan and Fleet (1995) suggested that the Au mineralisation event took place about 40 Ma later and at higher crustal levels from fluids that could have had a magmatic source, as indicated by the Mo-Au association and by protracted felsic magmatism in the region. Gold precipitation was aided by reactions of the ore fluid with pyrite. Thus, as in other orogenic-associated ore systems (e.g. Sukhoi Log discussed below), the Hemlo deposit is the result of multistage events.

9.3.3 Muruntau, Uzbekistan

The giant Muruntau Au deposit in Uzbekistan was discovered in 1957 during an exploration program aimed at finding uranium. The deposit has huge reserves, probably in excess of 5100 t of Au metal (Morelli et al. 2007). Muruntau is located within the Tian Shan orogen, in which a metallogenic province, comprising not only orogenic Au, but also porphyry and epithermal systems, extends for about 2000 km in a broad arc from Uzbekistan, Kazakhstan, Kyrgizstan to Xinjiang Province in northwest China (Fig. 9.13; Yakubchuk et al. 2005). In the Muruntau area major shear zones and nappe structures developed as a result of continent-continent collision between the Karakum

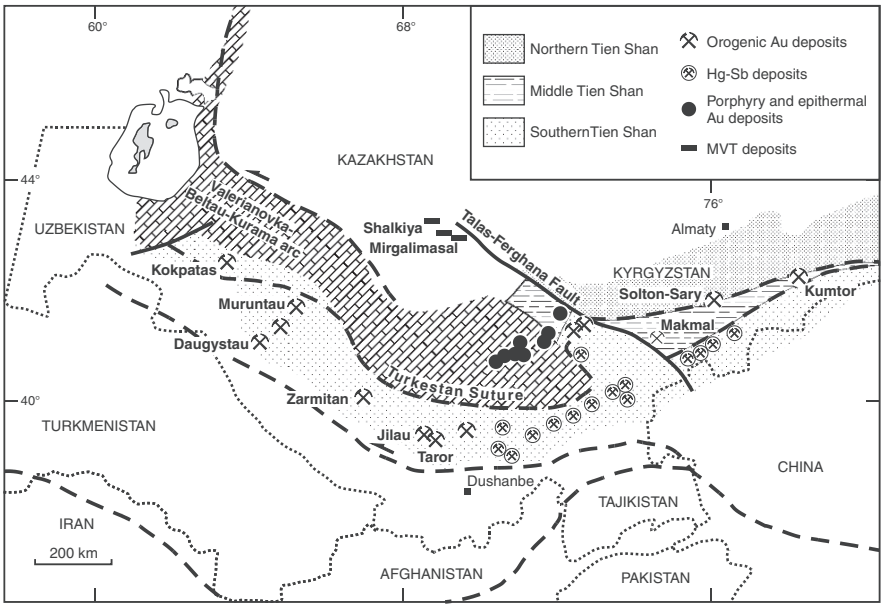


Fig. 9.13 The Tian Shan orogenic belt and distribution of mineral systems orogenic lodes, porphyry and epithermal deposits. After Yakubchuk et al. (2005)

plate and the North Tian Shan orogen. This collision event was accompanied by calc-alkaline volcanis of the Valerianovsky volcanic belt (Drew et al. 1996). Carbonate and turbiditic sequences were deposited on passive margins in Mid-Late Carbonifeous and Carbonifeours-Permian granitic intrusions were emplaced into the nappe structures and shear zones.

The mineralisation is hosted by metamorphosed Cambrian-Ordovician shales and carbonaceous siltstone with a close spatial relationship to 285–280 Ma granite, quartz diorite, syenite and lamprophyre dykes (Drew et al. 1996; Yakubchuk et al. 2005). In fact, the deposit is within the thermal aureole of a leucocratic granite pluton, which lies about 4000 m beneath the deposit, although the precise relationship of this granite with the mineralisation is not clear. However, hydrothermal activity occurred together with the the intrusive activity and was confined in ductile shear zones (Drew et al. 1996). A Sm-Nd isochron age of 279±18 Ma was obtained from scheelite (Kempe et al. 2001), whereas $^{40}Ar/^{39}Ar$ of sericite in vein selvages gave ages of 245 and 220 Ma (Wilde et al. 2001). Re-Os dating of arsenopyrite yielded model ages of 287.5 Ma and 290.3 Ma, assumed to relate to the main stage of the mineralisation (Morelli et al. 2007). The spread of ages, from as young as 245 Ma to ~280 Ma, suggests a series of ore-forming events. Furthermore, the dated arsenopyrite has unradiogenic initial Os and elevated $^{3}He/^{4}He$ ratios of 0.23–0.33 R_A.

The Muruntau deposit is associated with two major faults (North-East and South faults) and is hosted by the Muruntau-Daugyztau brittle-ductile shear zone, in which are northwest-trending areas of intense hydrothermal alteration, including zones of pervasive silicification (Fig. 9.14; Drew et al. 1996). The Muruntau mineralisation consists of Au-bearing quartz veins of two styles: (1) flat to shallow dipping, deformed and boudinaged veins with low-grade Au; and (2) steeply dipping stockwork veins with high-grade Au. The latter vein systems crosscuts and displaces the flat vein system (Kempe et al. 2001). The

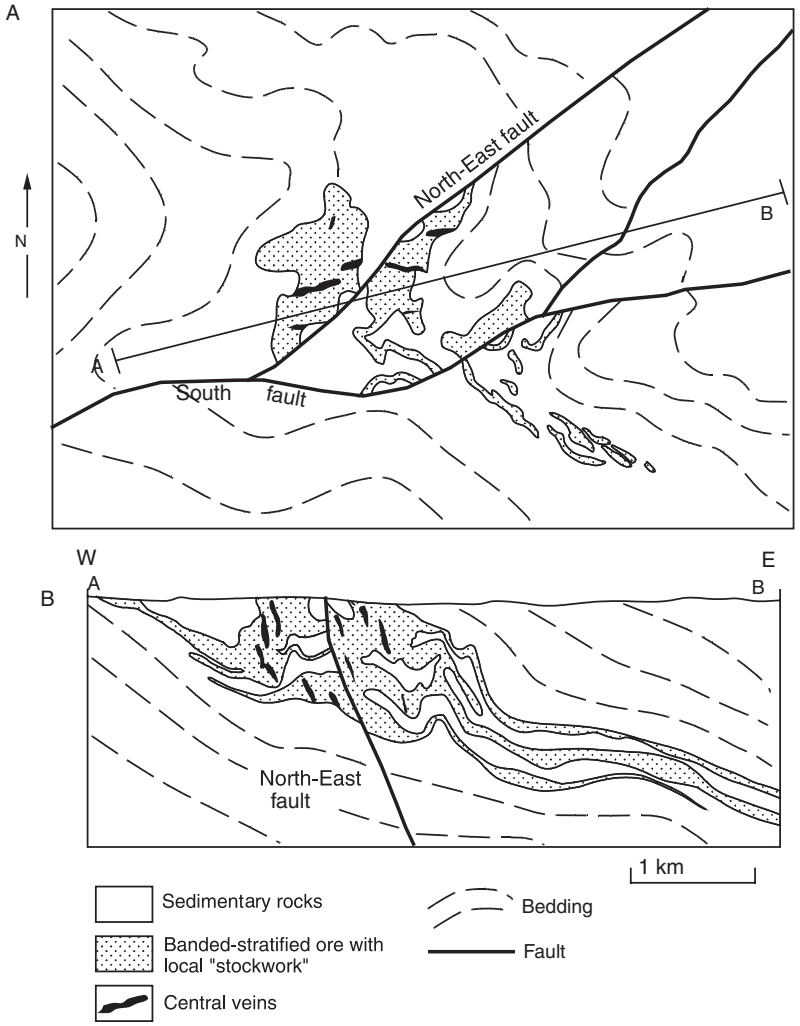


Fig. 9.14 Simplified geology of the Muruntau mine area (**A**) and east-west cross section (**B**). After Drew et al. (1996)

low-grade flat veins contain grey quartz, pyrite, pyrrhotite, K-feldspar, chlorite, apatite, scheelite and calcite. The high-grade stockworks contain white quartz, sericite, pyrite, molybdnite, scheelite and carbonates (Kempe et al. 2001). As observed with all orogenic lode systems, calcite forms in the latest stages of hydrothermal activity. The ore minerals include mainly native Au, pyrite and arsenopyrite, with minor quantities of scheelite, bismuthinite, pyrrhotite, marcasite, chalcopyrite, molybdenite, galena, sphalerite, tetradymite, Au and Bi tellurides, selenides, wolframite and native bismuth. Gangue minerals are quartz, K-feldspar, biotite, tourmaline, actinolite, hornblende, muscovite, Fe-carbonate and apatite. Although variable for each vein, three stages of hydrothermal alteration can be distinguished, from earliest to latest, as follows: (1) sodic alteration with albite, quartz, biotite, K-feldspar, chlorite and carbonates; (2) sericitic alteration with muscovite, Mg chlorite, quartz, phlogopite, K feldspar and carbonates; (3) potassic alteration with quartz, K-feldspar, muscovite, carbonate and sulphides. Spotted schist related to thermal metamorphism is overprinted by the shear zone-controlled quartz veins and veinlets mineralisation with quartz-albite-biotite-chlorite-oligoclase. The pre-hydrothermal alteration spotted schist, appear to be confined within the Muruntua area and change with depth from greenschist facies to amphibolite and garnet-bearing calc-silicate rocks. Alteration minerals are characterised by high Mg contents, which enable to distinguish them from mineral phases related to regional metamorphism (Drew et al. 1996). The element association of the ore is Au-Ag-W-As-Bi-Sb. Preliminary studies of fluid inclusions from the early stage veins (Berger et al. 1994) showed that ore fluids are aqueous and carbonic, with minor amounts of N and CH_4 and homogenisation temperatures ranging from 350 to 400°C. $\delta^{18}O$ values range from +15‰ in the early stage veins, to +7.8‰ in the stockwork veins and assuming a temperature of 400°C for all veins, the $\delta^{18}O_{fluid}$ would range from +4 to +9‰ (Berger et al. 1994). Sulphur isotopic values from pyrite and aresonpyrite from stockwork veins range from +2.8 to +5.5‰ (Berger et al. 1994).

The origin of the Muruntau ore system remains unresolved. However, the studies of Re-Os and He systematics by Morelli et al. (2007) suggest a mantle source for the ore fluids. Although acknowledging the uncertainties, Morelli et al. (2007) integrating the timing of the granitic magmatism, which overlaps that of the mineralisation, and the spatial association with lamprophyre dykes, with the results of the juvenile Os abundances and He isotopic compositions, suggested that the Muruntau ore system has a component of mantle derived fluids and metals. Whereas these results are in disagreement with previous findings invoking a crustal source for the fluids (Wilde et al. 2001), the mantle contribution, as revealed by He isotope systematics, is compatible with results from other provinces of orogenic Au, such as the Jiaodong province in China, discussed below.

9.3.4 Sukhoi Log Au-PGE Deposit of the Lena Goldfield, Russia; Multi-Stage Origin with a Late Metamorphic Overprint

The Lena Goldfield, on the eastern margin of the Siberian Craton, is a major mining district where alluvial gold has been exploited for some 150 years. This alluvial gold is sourced from metamorphosed sedimentary rock-hosted Au deposits that include the world-class Sukhoi Log Au-PGE and smaller similar deposits, all of which are located in a deformed passive margin succession. The Siberian Craton (also known as Angara Craton; Şengör and Natal'in 1996) is a major Precambrian continental nucleus comprising the Archaean Anabar and Aldan shields and covered by Proterozoic platform sedimentary rocks. The Siberian Craton, is surrounded by Atlantic-type margins and large rift systems (e.g. Permo-Triassic Khatanga trough), which were reactivated time and again by collision and extension tectonics, resulting in the orogenic belts that surround the Craton, including the Neoproterozoic Yenisei Ridge Orogen on the western margin and the Patom Highlands, north of Lake Baikal, on the southeastern margin (Fig. 9.15). For overviews and details of the geology, mineralisation and geodynamic evolution of this, comparatively poorly known (at least in Western literature) but extremely interesting part of Siberia, the reader is referred to Şengör and Natal'in (1996) and Rundquist and Gillen (1997). World class orogenic Au and placer deposits, as well as base metal ore systems, abound in both the Yenisei Ridge and Patom Highlands orogens (see Yakubchuk et al. 2005 for reviews). The Lena goldfield, of which the giant Sukhoi Log deposit is part, occurs in the Patom Highlands orogen, a deformed passive margin sequence bound by ophiolites, thrust northward onto the Siberian Craton and intruded by granites of Mid-Palaeozoic age. The ore-hosting rocks consist of a 15–20-km thick clastic-carbonate succession, metamorphosed to greenschist and amphibolite facies (Yakubchuk et al. 2005). The orogenic Au deposits, including Sukhoi Log, occur in a series of east-west subparallel belts within the Boidabo Synclinorium characterised by a complex geometry, which may have been a major factor in the channelling of mineralising fluids. The overall structure, shown in Fig. 9.15B, is dominated by core complexes north of the Boidabo Synclinorium and a divergent structure with northward-dipping thrusts that run opposite to the regional thrust movement. Rocks in the central parts of the synclinorium are metamorphosed to greenschist facies, whereas rocks in the peripheral parts are metamorphosed to amphibolite facies, associated with granite-gneiss domes (Distler et al. 2004) These thrust faults and associated folds constituted, according to Yakubchuk and co-authors, an ideal trap for hydrothermal fluids generated during metamorphism and granite magmatism. The Konstantinovsky Granite is a small pluton, about 6 km south of Sukhoi Log, is dated at 290±20 Ma. Other intrusions in the region are granite plutons with ages of 350–330±10 Ma, 313±59 Ma lamprophyre dykes, cut by 290±20 Ma granite porphyry dykes (Wood and Popov 2006).

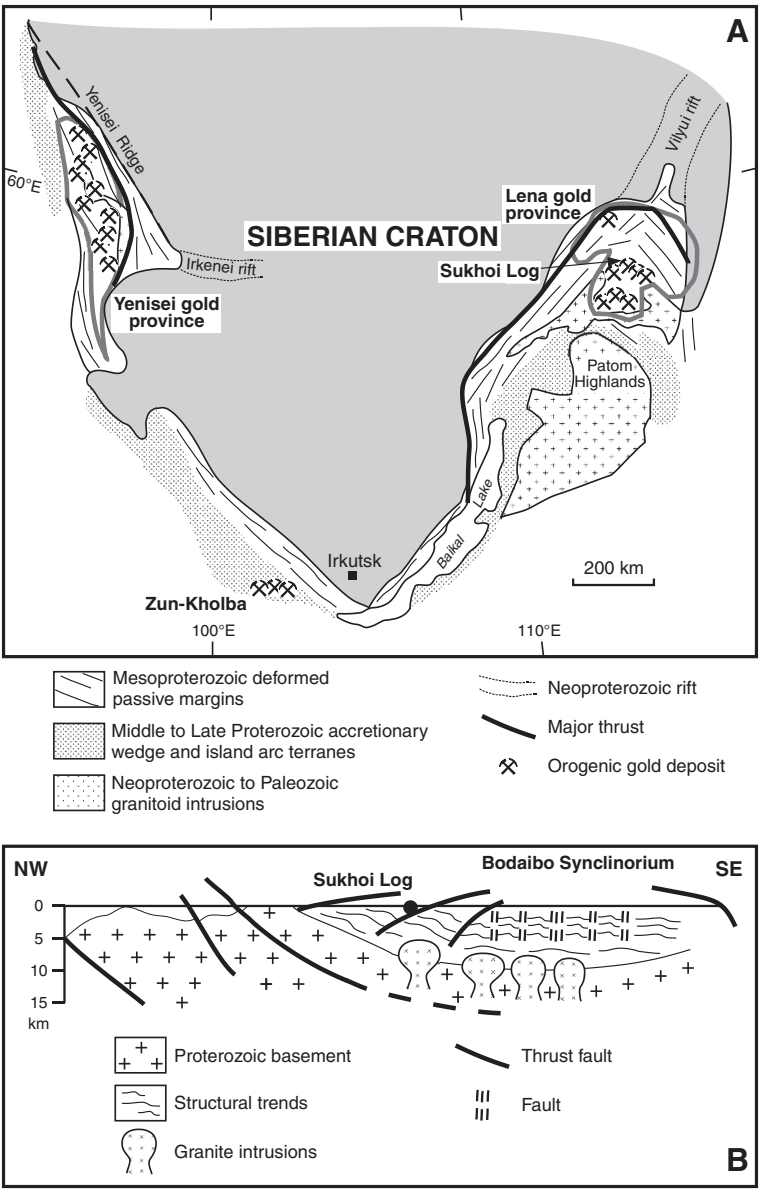


Fig. 9.15 (**A**) Part of the Siberian (or Angara) Craton with marginal orogenic belts and distribution of orogenic Au deposits; (**B**) cross-section through the central part of the Lena goldfield, showing core complex, the Bodaibo synclinorium and position of Sukhoi Log. After Yakubchuk et al. (2005)

The Lena goldfield has been known since the 1840s when alluvial gold was discovered in river valleys near the Sukhoi Log deposit. The Sukhoi Log Au-PGE deposit has no surface expression, was discovered in the 1960s, lies 850 km northeast of the town of Irkutsk and is reported to contain a resource of about 1500 tonnes of Au (Wood and Popov 2006). A detailed account of the Sukhoi Log deposit, including interesting historical notes can be found in Wood and Popov (2006) and Distler et al. (2004), whose works I have perused for this section. Wood and Popov (2006) proudly stated that the discovery of Sukhoi Log was made by geologists who used new conceptual models, state-of-the art geochemical methods and diamond drilling. Rb-Sr dating method on quartz yielded an age of 320±16 Ma for the Sukhoi Log mineralisation (Distler et al. 2004).

The Au orebody, 40–60 m below the surface, hosted in black shales of the Khomolko Formation (Patom Group), is an elongate lens, dipping north at 15–30°, with a thickness of 15–140 m and extending downdip for about 400 m, based on a cutoff grade of 1 ppm Au. The ore zone is within the core of an overturned anticlinal fold. Following this folding, the sequence was intruded by the Konstantinovsky Granite. The ore is characterised by disseminated pyrite, thin bedding-parallel quartz-sulphide veinlets and quartz veins hosted in black shale and siltstone. Pyrite occurs as disseminations, veinlets, porphyroblasts and as nodular clusters. Other ore minerals, constituting less than 2% of the total sulphides, include pyrrhotite, chalcopyrite, sphalerite, galena, gesdorffite, millerite, pentlandite, rutile, magnetite and traces of arsenopyrite, argentite, cubanite, scheelite, molybdenite and acanthite. There are several generation of pyrite, as detailed below. Gold is present in pyrite and quartz-pyrite-carbonate veins. There are at least two generations of Au: drop-shaped particles in pyrite with a 900–920 fineness and a later less pure Au (840–880 fineness) occurring as coarser grains in veins and veinlets. The drop-shaped purer Au is thought to be of syngenetic origin and encapsulated by metamorphogenic pyrite. PGE mineralisation is peripheral to the Au orebody and consists of native Pt, Pt-Cu-Fe alloys, sperrylite and cooperite. Also present are native Fe, Cr, Cu, Ni, Sn, W, Ti and Te and assorted alloys of these metals. Distler et al. (2004) recognised six morphological types of Au mineralisation: (1) interlayers and lenticles of diagenetic pyrite; (2) stratified zones of ovoid pyrite; (3) fine-grained pyrite and pyrrhotite along cleavage planes; (4) coarse euhedral pyrite; (5) granoblastic pyrite aggregates; (6) quartz-sulphide stockworks. The ore-hosting black shales of the Khomolko Formation have high S and organic C contents (up to 20% and 2.7%, respectively) and have a metamorphic assemblage of quartz, sericite and carbonate with minor quantities of rutile, tourmaline, zircon, monazite and albite. The ore-forming process was accompanied by multistage hydrothermal alteration, characterised by ankerite and porphyroblasts of Mg-siderite, associated with the quartz-sulphide veinlets and quartz veins. Other alteration minerals comprise monazite and magnetite, with lesser scheelite, wolframite, baddeleyite and xenotime. The zone of hydrothermal alteration also tends to contain most of the PGE

mineralisation, with Pt concentrations reaching 3–5 ppm and as mentioned above the PGE ores lie outside of the zone with highest Au concentrations.

Stable isotopic (C, O and S) composition of the ores and host rocks were determined and reported by Distler et al. (2004). The $\delta^{34}S$ values of pyrite range from 3.5 to 15.3‰; pyrite from the quartz-sulphide veinlets has $\delta^{34}S$ from 8.0 to 11.1‰ (average 9‰); the sedimentary pyrite has values of 3.5‰ and the pyrite from quartz veins $\delta^{34}S$ values of 15‰. The $\delta^{13}C$ values of the Fe-Mg carbonates range from –0.12 to –6.17‰ and the $\delta^{18}O$ has ranges of 24–30‰; the $\delta^{13}C$ values of the organic carbon in the host rocks range from –6.7 to –42‰. The $\delta^{18}O$ values of the quartz, from the quartz-sulphide veinlets has a narrower range from 8.8 to 13.5‰. Five types of primary and pseudosecondary fluid inclusions were recognized in quartz and carbonates from the veinlets and veins (Distler et al. 2004). Type 1 fluid inclusions contain dense CH_4-CO_2-rich fluids; type 2 are vapour-rich also with N_2-CH_4-CO_2 gas mixture; type 3 are two phase vapour-rich aqueous inclusions; type 4 also vapour-rich are filled with N; type 5 are two-phase dilute aqueous. Homogenisation temperatures range from 130 to 385°C and salinities of between 3.7 and 8.6 wt% NaCl equivalent in quartz and 185–340°C with salinities of 5.0–6.7 wt% NaCl in the carbonate minerals.

An interesting and detailed study of auriferous pyrite from the Sukhoi Log deposit conducted by Large et al. (2007) has unravelled a complex series of events that eventually led to the formation of a metamorphism-related Au mineral system. The results of this work demonstrate the complexity of ore making processes and that although what is observed today is the last episode, careful and detailed work can reconstruct the series of events that led to the last episode. Large et al. (2007) identified six generations of pyrite (Py1 to Py6) each with different features and trace element endowment as outlined below. Py1 is very fine-grained, forms nodular assemblages or is concentrated in bedding-parallel layers in black shales. Py1 comprise three types, micron-size crystals, framboidal aggregates and pyrite with a "sooty appearance". These are interpreted to be syn-sedimentary and diagenetic, similar to the framboidal pyrite commonly found in black shales. LA-ICPM spot analyses of Py1 show that this pyrite is enriched in elements, such as Mo, Sb, Te, Pb, Ag, Ni, Co, Se, Zn, Ba, Mn, U and V. Gold contents range from 0.44 to 12 ppm with an average of 3.32 ppm; As values range from 180 to 14 000 ppm with an average of 1900 ppm. This Au correlates well with Cu and Te, but less so with As. The authors noted that these elements are those that are typically enriched in euxinic sediments (organic-rich shales). Py2 forms euhedral pyrite crystals, ranging from 30 to 300 μm across, that overgrow and surround or replace Py1. Py2 may be early diagenetic and may have formed from the recrystallisation of Py1. In contrast to Py1, Py2 is depleted in metallic elements such as Au, Ag, Cu, Pb, Te, Zn and Sb. Gold contents range from 0.02 to 13 ppm with an average of 1.02 ppm; As remains enriched in Py2, varying from 2 to 18 550 ppm with a mean of 4260 ppm. Py3 is confined to sandy units intercalated with the black shales, has a porous texture forming aggregates with irregular outlines and no obvious

fabric. Py3 is coarser grained, reaching up to 5 mm across, and contains inclusions of country rocks, gold and sulphides (pyrrhotite, chalcopyrite and sphalerite). Etching with HNO_3 (nitric acid) revealed that Py3 has a well defined internal fabric and that this stage of pyrite formation was by replacement of the sedimentary materials. Py3 has gold inclusions, but LA-ICPM analyses show that Py3 is itself depleted in Au, which has a range of 0.05–2.2 ppm and a mean of 0.16 ppm. A second but minor population (20%) of higher Au shows values ranging from 4 to 82 ppm with a mean of 30 ppm. Arsenic values range form 7 to 31 000 with a mean of 2900 As. Other elements, Bi, Se, Mo, Sb, Ba, Pb, Co etc., are depleted compared to Py1. Py4 is hosted in the shale beds and has higher contents of Au, As, Sb compared to Py3. Gold contents range from 0.02 to 1.3 ppm with a mean of 0.25 ppm; As varies from 400 to 5560 ppm and a mean of 2270 ppm. Py4 has high values of Ti (up to 15 000 ppm) probably because of its abundant inclusions. Py4 is characterised by isolated large euhedral crystals, with pressure shadows and exhibits strong internal fabric and microinclusions when acid etched. As for Py3 the internal fabric of Py4 shows that it must have replaced the host sedimentary rock. Py4 is interpreted to have formed late in the deformation history of the host rocks. Py5 and Py6 are post-peak metamorphism, they are clear and featureless and replace or cut Py3 and Py4 and are the most depleted in trace elements, although As, Ni and Se remain enriched. Gold contents of Py5 range from 0.01 to 0.2 pm with a mean of 0.07 ppm. Finally, Py6 is the last generation of this sulphide and is post-metamorphism and hydrothermal. Thus, the late generations of pyrite, Py4, 5 and 6 become progressively depleted in trace elements, including Au. The release of lattice-bound Au and other metallic elements from the early pyrite generations (Py1 and Py2) resulted in their concentration as inclusions (free gold and sulphides) in structural sites. Gold, As, Pb, Cu, Sb, Mo, Bi, Te, Ag are all enriched during the early stages of sedimentation and diagenesis only to be released during stages of metamorphism. The ore fluids are then channelled into the hinge of a tight anticlinal fold, where they now form the ore zones.

9.3.4.1 Ore Genesis

The original composition of the host rocks may have been important for the genesis of the Sukhoi Log mineralisation (Yakubchuk et al. 2005 and references therein). These rocks are carbonaceous and fine-grained and were deposited in small anoxic basins and a first stage of sulphide mineralisation may have been related to exhalative synsedimentary processes. The exhalative fluids may have introduced Au, S, Fe and As. Background Au values are estimated to be in the range of 3–8 ppb and the content of organic carbon from 1 to 5%. Yakubchuk et al. (2005) supported the idea that the Sukhoi Log mineral system was the result of multistage processes, beginning with syngenetic sulphide deposition, followed by remobilisation of the syngenetic sulphides and their recrystallisation during metamorphism. This resulted in pyritic lenses having Au concentrations

of as much as 350 ppm. This view follows on that of Buryak (1982), who proposed that the Au was remobilised and concentrated in anticlinal traps during regional metamorphism. Nevertheless, as Yakubchuk and co-workers pointed out, the role of the Konstantinovskiy granite intrusion remains unresolved and the respective roles of metamorphic and magmatic processes still unknown. Distler et al. (2004) integrating ore compositions, element associations, fluid inclusions and stable isotopic and pointing out to a number of key features of the Sukhoi Log mineralisation proposed an infiltration metasomatism genetic model, as follows. The mineralisation, controlled by a high strain zone along the axis of an anticline, exhibits an early mineral assemblage preserved along the flanks and a late assemblage in the central and most altered parts of the orebody. There are two distinct element associations that do not occur together: (1) Fe-Ni-Co-Cr-Ti-Pt-Pd and (2) Sn-W-REE-Zr. The first is typical of mafic-ultramafic rocks and the second is more typically associated with granitic magmas, furthermore the central parts of the orebody are rich in Au, whereas the outer parts are enriched in PGE. The mineralisation is the result of complex interactions of deeply sourced hydrothermal CO_2 and N_2-rich fluids that interacted with organic matter in the black shales. As indicated above, the element associations suggest two fluid and metal sources; mafic-ultramafic and granitic. Thus, the main events can be described as follows. A Neoproterozoic rift system developed on the margin of the Siberian Craton, in which organic rich sediments accumulated in an anoxic basin. Regional metamorphism followed linked to deformation and thrusting of the sedimentary sequence onto the Craton's margins at about 516 Ma. During the Mid-Palaeozoic granite plutons were intruded into the deformed sequence (palingenetic granites of Distler et al. 2004). Fluids associated with this granitic magmatism as well as mantle fluids may have been implicated and interacted with mafic-ultramafic rocks, scavenging PGE and other elements typically associated with these rocks. Wood and Popov (2006) added to this scenario, suggesting that seafloor Au-PGE exhalative mineralisation was formed first and later redistributed during deformation and metamorphism.

Large et al. (2007), on the basis of the above-outlined paragenetic study of pyrites, proposed a three-stage scenario for the origin of the Sukhoi Log mineralisation. In the first stage, sedimentation of organic-rich shales and exhalation of reduced basinal H_2S-rich and Au-As-bearing fluids along east–west rift faults occurred, producing syngenetic py1 and py2. In a second stage, late diagenesis, folding and deposition of carbonates followed, while basinal fluids carrying Au-As-Te-Pb flowed laterally through the organic-rich shales, near the feeder faults and below an impermeable cap provided by the carbonate rocks. This stage deposited bedding-parallel py3. Deformation and metamorphism followed during a final but multiphase stage, with tight folding and thrusting. Metamorphic fluids were produced, which dissolved the early pyrites and re-distributed lattice-bound Au, resulting in overprinting of py1, py2, py3 and py4. The released Au formed inclusions of free Au, Au tellurides and dissolved Ag-Bi-Te in the latest pyrite generations.

9.3.5 Orogenic Au Lodes of the South Island, New Zealand

Orogenic (mesothermal) Au lodes in the South Island of New Zealand occur in Palaeozoic metasedimentary rocks such as the Reefton district, west of the Alpine Fault (Christie and Brathwaite 2003; Christie et al. 2006) and in Mesozoic metasedimentary rocks, east of the Alpine Fault (Fig. 9.16). These include the deposits of the Reefton district, hosted in turbidite rocks (Greenland Group) of Ordovician age that are part of the Western Belt (Buller Terrane), an accretionary complex intruded by Carbonifeours and Cretaceous granites (see Brathwaite and Pirajno 1993 for an overview). The Reefton district from 1870 to 1951 had a total production of nearly 66 000 kg of Au (Christie et al. 2006). Scheelite, Au and stibnite mineralisation occurs in quartz vein lodes in the Mesozoic metamorphosed turbidite sequences of Otago, the Southern Alps and the Marlborough district (Fig. 9.16). These sequences are part of the Torlesse and Caples terranes, which form a complex belt of schist (Otago Schist) displaced by the Alpine Fault. Williams (1974) provided details of individual lodes and lode fields. Reviews and works on individual lodes of the Southern Alps and Otago Schist that are useful in the context of this section, can be found in Paterson (1986), Craw et al. (1987a, b), Brathwaite and Pirajno (1993), De Ronde et al. (2000), Craw and Campbell (2004) and Mitchell et al. (2006) and the collection of papers in Christie and Brathwaite (2006). Although the production from these lodes was historically relatively small, approximately 10 000 kg of Au and 3000 tonnes of scheelite (Paterson 1986), larger quantities of Au were, and are currently being won from Tertiary and Quaternary placer deposits derived from the erosion of uplifted segments of mineralised schists. The placers of Otago and Westland, which are mainly fluvial, fluvio-glacial and beach deposits, have past production + reserves of approximately 1478 tonnes of Au (Laznicka 2006). Between 1988 and 2004 the Westand placers produced a total of 21 130 kg of Au (Cotton and Rose 2006). The South Island placers have had a long history of continuous reworking of auriferous conglomerate. In this context it is worth mentioning the concept proposed by Henley and Adams (1979), who suggested that giant placers are formed in response to tectonic uplifts of Au-bearing source terranes and consequent reworking of alluvial accumulations. The Otago, Westland in New Zealand, the Lena goldfield, the Yukon and California placers also fall into this category, and it is possible that the much larger and richer Witwatersrand palaeoplacers, in South Africa, may have originated in the same fashion.

9.3.5.1 Reefton Goldfield

The Reefton goldfield comprises the largest group of mesothermal lode deposit west of the Alpine Fault in the South Island (Fig. 9.16). For this section I have drawn from the works of Brathwaite and Pirajno (1993), Christie and Brathwaite (2001) and Christie et al. (2006). North of Reefton, other lodes hosted in Palaeozoic metasedimentary rocks are the Lyell and Golden Blocks fields, Mount Greenland to the south and Preservation Inlet in Fiordland.

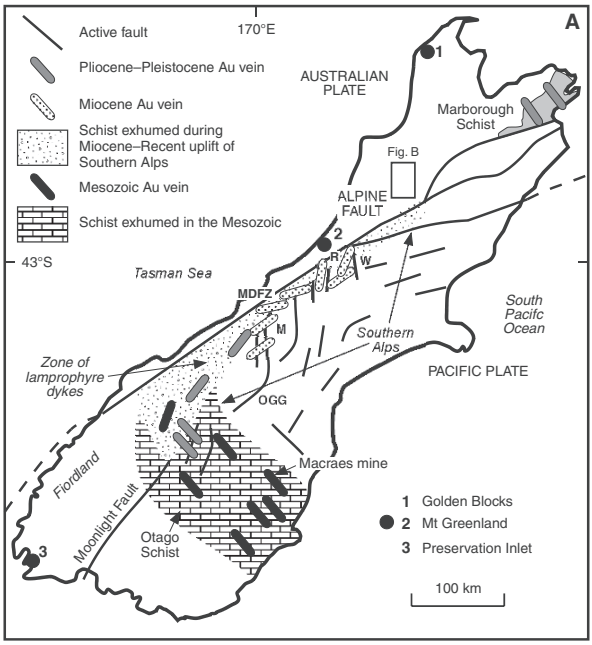


Fig. 9.16 (**A**) The South Island (New Zealand) with locations and simplified orientation of mesothermal lode systems, after Craw et al. (2002); (**B**) Reefton gold field and distribution of orogenic lode deposits, after Christie and Brathwaite (2003)

The Au lodes of the Reefton district are hosted in turbidite facies rocks of the Cambrian-Ordovician Greenland Group, a monotonous succession of alternating sandstone and shale, tightly folded and metamorphosed to greenschist facies. The Greenland Group was intruded by plutons of the Karamea Batholith, producing narrow thermal aureoles. The Karamea Batholith is composed of Devonian granitic rocks of the Karamea Suite and various plutons of Cretaceous age. Locally roof pendants of Greenland Group rocks are present in the batholith and one of these contains a lode deposit (Alexander; Fig. 9.16B). The rocks of the Greenland Group are folded into a series of upright to west-verging tight folds, with overturned and faulted limbs. The line of lodes follows shear zones developed along the overturned limbs of these folds. The Au-bearing quartz lodes are within a north-trending 34-km-long corridor and include deposits, such as Ajax, Globe-Progress, Big River and Blackstone (Fig. 9.16B). The Au lodes, range in width from 0.6 to 3.2 m, have strike lengths of 100–1000 m, down-plunge extents of up to 1200 m and consist of a series of quartz shoots, within north to north-northeast trending shear zones. The veins are characterised by ribbon banded and crack seal textures. Gold occurs as free grains or associated with arsenopyrite and pyrite. In some cases, zones of disseminated Au are hosted in clay-rich fault breccias, containing fragments of quartz veins and wall rocks. Other ore minerals include stibnite (locally making up 10–30% of the vein material), chalcopyrite, sphalerite, galena and various sulphosalts. Gangue minerals are carbonates, sericite and chlorite. Hydrothermal alteration is generally marked by intense bleaching of the wall rocks, with development of carbonate porphyroblasts and increasing amounts of disseminated pyrite and arsenopyrite and of thin carbonate, quartz and sulphide veinlets. Hydrothermal mineral phases include muscovite, sericite, dolomite-ankerite, siderite, quartz, chlorite and the above-mentioned sulphides. There is a general lack of vertical zonation. The Reefton lodes have been compared with those of the Victoria goldfields in Australia and Nova Scotia in Canada, where similar hydrothermal alteration, vein structure and texture and mineralisation styles have been noted (Christie et al. 2006 and references therein).

The origin of the Reefton lodes was attributed by Brathwaite and Pirajno (1993) to stages of folding and faulting associated with regional greenschist facies metamorphism. Another view is that this mineralisation may be related to the Cretaceous granitic magmatism of the Karamea Batholith or post-Jurassic mafic dykes (Leach et al. 1997).

9.3.5.2 Gold-Scheelite Lodes in the Otago Schist

The Otago Schist consists of metagreywacke, metapelite, with minor intercalations of mafic metavolcanic and pyroclastics rocks and cherts. The metamorphic grade increases from prehnite-pumpellyite facies to greenschist facies (chlorite and biotite zones), to narrow bands of amphibolite facies metamorphism (garnet and garnet-oligoclase zones) along the Alpine Fault. It

is worthy of mention that this region also provided the ground for classic studies of regional prograde metamorphism (Turner 1935; Hutton and Turner 1936). The Au-W-Sb mineralisation occurs in quartz vein lodes which tend to form major systems, or lode fields. In Otago these appear to be concentrated in a central area within textural zones III and IV of greenschist facies rocks which have been exposed by uplift. In this area are the well-known Glenorchy and the Macraes Flat lode fields, described by Lee et al. (1989), Begbie and Sibson (2006), De Ronde et al. (2000) and Mitchell et al. (2006). The lodes are emplaced within crush or shear zones, which can be up to 350 m wide and 10 km long, and are characterised by quartz veins, predominantly set in the hinge zone of recumbent folds (Paterson 1986). Individual lodes generally cut the deformation fabrics at a high angle, although at Macreas the lodes are subparallel to the main fabric of the host lithologies. The thickness of the veins ranges from a few centimetres to approximately 6 m, but more commonly around 1–2 m. Veins are irregular and discontinuous, and arranged in zones of up to a few 100 m in strike length.

The Glenorchy lode field consists of an extensive quartz vein system and arrays of hydrothermal fractures covering an area of about 1500 km^2 (Begbie and Sibson 2006). The Glenorchy vein system contains about 60 quartz-scheelite-Au quartz veins, from which approximately 2200 tonnes of 70% WO_3 concentrates have been produced (Begbie and Sibson 2006). The mineralisation is mainly scheelite, contained in laminated and massive quartz with minor pyrite, arsenopyrite, sphalerite, rare Au, calcite, kaolinite, sphene and clinozoisite. The Otago Schist in this area consists of metavolcanic rocks, Fe-Mn-bearing chert and sulphide-rich metapelitic schist. Fluid inclusion studies by Paterson (1986) indicate that the fluids contained about 4 mol% CO_2 with salinites of approximately 6–7 wt% NaCl equivalent. Trapping temperatures are estimated to have been at least 290°C. Hydrothermal alteration of wall rocks at Glenorchy consists of a change in colouration of the schist from grey to greenish and black, and there is a decrease, or loss, of some of the metamorphic minerals such as actinolite and epidote, whereas calcite, pyrite, arsenopyrite and kaolinite are added. Figure 9.17 illustrates these mineralogical and geochemical variations, associated with the ingress of the hydrothermal fluids in the shear zone at Glenorchy.

The Round Hill Au-W deposit is part of the Macraes Flat field, hosted in the northwest-trending Hyde-Macraes Shear Zone, a low-angle duplex thrust system (Lee et al. 1989; De Ronde et al. 2000). This deposit is characterised by Au-scheelite-arsenopyrite-pyrite within shear zone-hosted quartz veins. The Macraes deposit has estimated resources of 87 Mt of ore gradding 1.4 g/t Au (Mitchell et al. 2006). Mitchell et al. (2006) described four mineralisation styles: (1) hydrothermal replacement of the host schist rocks by sulphides and microcrystalline quartz; (2) black sheared schist, represented by microshears with fine graphite and sulphide; (3) shear-parallel veins of massive quartz, with some internal laminations and breccia; (4) stockworks, in which individual veinlets range in thickness from 1 to 30 cm and are strongly laminated. The Round Hill

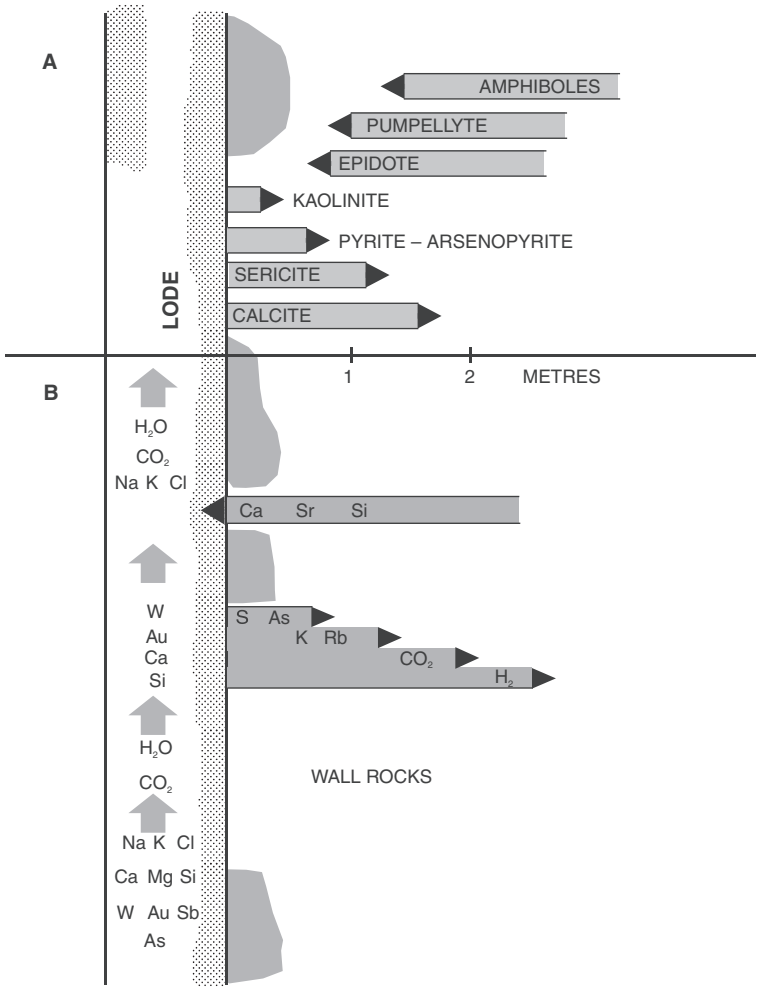


Fig. 9.17 Glenorchy hydrothermal alteration and elemental exchange system (**A**) Distribution of alteration minerals from the margins of a lode vein to wall rocks; (**B**) exchange of elements between the fluid conduit (lode vein) and wall rocks. After Paterson (1986)

orebody is characterised by nearly flat veins, cut by later hanging wall shear veins. The mineralisation is hosted by a carbonaceous intrashear metapelite unit, about 100 m wide (De Ronde et al. 2000). Fluid inclusion studies on quartz show that dominant volatiles are H_2O (99 mol %) and CO_2 (0.14–0.76 mol %). Two main types of fluid inclusions were recognised (De Ronde et al. 2000): type 1 are primary two-phase aqueous with negative crystal inclusions; type 2 are secondary and also two-phase. Microthermometric measurements gave homogenisation temperatures in the flat veins from 110 to 188°C, whereas the stockwork veins gave values ranging from 125 to 179°C; corresponding salinities are

from 0.2 to 3.7 and 0.2 to 3.1 wt% NaCl equivalent, respectively. A pressure correction to the hongenisation temperatures raises the overall value to 300°C. The $\delta^{18}O$ values in quartz are consistent and have a narrow range from 15.6 to 16.7‰; calculated values for the hydrothermal fluids, based on an average $\delta^{18}O$ of 16.1‰ at 300°C gives a $\delta^{18}O_{H2O}$ value of 9.2‰.The $\delta^{18}O$ values of scheelite range from 4.1 to 5.2‰ (average 4.8‰), whereas those of calcite have a wider range from 14.3 to 20.8‰. Application of the $\Delta_{calcite\text{-}H2O}$ fractionation curve at 300°C, gave $\delta^{18}O_{H2O}$ for calcite values of between 8.7 and 10.2‰. The δD_{H2O} values for fluid inclusions in stockwork veins average –75‰, whereas for the flat veins the average is –58‰. Thus, on the basis of fluid inclusions and stable isotope systematics, De Ronde et al. (2000) argued for a large component of meteoric fluids for the stockwork veins mixing with fluids having a substantial magmatic component.

The Endeavour Inlet Sb-Au deposit in the Marlbourough district consists of a series of irregular quartz veins, arranged en echelon within a 300 m wide northeast-trending shear zone. The thickness of individual veins range from 0.2 to 1.9 m, with strike lengths of up to 65 m. The main feature of this deposit is that it is vertically zoned with an upper stibnite-rich zone grading down, approximately 200 m below, into an arsenopyrite-pyrite-marcasite-Au zone (Pirajno 1979). The stibnite zone is considered to have formed late in the paragenetic sequence at shallower depths and lower temperatures than the Au-bearing assemblages (Brathwaite and Pirajno 1993).

In the Mount Cook region, thin quartz-calcite veinlets in the schist contain traces of scheelite, sulphides and native Au. These occurrences have been studied by Craw and Koons (1988, 1989) and Johnstone et al. (1990) and reviewed in Craw (2006). The mineralised localities are distributed close to the Alpine Fault and within amphibolite and greenschist facies domains. The Southern Alps veins are less than 1 m thick and 10 m long and may contain visible Au associated with calcite, pyrrhotite, scheelite and biotite. Locally these veins are post-dated by sets of veins with adularia, quartz and bladed calcite, indicative of boiling fluids. Johnstone et al. (1990) noted that older Au-bearing veins are confined to areas of greenschist facies, while younger veins containing base metals, mainly Cu, occur closer to the Fault and are restricted to amphibolite facies rocks. Gold, arsenopyrite and scheelite occur in quartz-calcite ± epidote ± actinolite veinlets which are from 1 to 10 cm thick and contain Au where they cut graphitic horizons. Craw et al. (1987b) recognised at least three types of veinlets. One contains rhombohedral calcite and prismatic quartz crystals with minor chlorite. The second type, with Au and sulphides, consists of massive quartz-calcite veinlets in which the grain size of the mineral components is much smaller than in the first type. The wall rocks show some degree of hydrothermal alteration with arsenopyrite, biotite and chlorite. The third type of veins consists of open-space filling with quartz, platy calcite and adularia, and is associated with the second type. Fluid inclusions studies indicate that these three types represent precipitation products from fluids of different character. Type 1 veins were probably formed from H_2O-CO_2 fluids at 270°C and

2–3 km of depth; type 2 veins were formed from fluids with temperatures in excess of 320°C, which may have mixed with cooler and less saline fluids, whereas type 3 veins were formed from low salinity fluids which boiled at about 240°C.

9.3.5.3 Ore Genesis

The Southern Alps represent an active compressional orogen, characterised by rapid uplift, which brings hot rocks closer to the surface. The abundant rainfall on the western side of the mountain range, provides a plentiful source of meteoric water, (Craw and Koons 1989; Craw 2006). The high geothermal gradients close to the surface heat the meteoric water resulting in large scale hydrothermal circulation, producing lode systems at depth and hot springs at surface. The heated meteoric waters then mix with deeply-sourced fluids that are generated by dehydration reactions arising from prograde metamorphism, which in turn will have mobilised metals, such as Au, As, W, from the rocks through which they circulate. The uplift of the Southern Alps was initiated in the Miocene and moved northward through the Pliocene and continues today. Lamprophyre dykes were intruded in the Miocene and were accompanied by more fluids and hydrothermal alteration (mostly ankeritic carbonate), suggesting perhaps a localised link with mantle fluids. Magnetotelluric soundings along a 150-km-long transect across the central part of the Southern Alps, revealed the presence of a deep crustal conductor (Wannamaker et al. 2002). This conductor has been interpreted to represent the presence of interconnected crustal fluids. The geometry of the crustal conductor based on an electrical resistivity profile nicely portrays what is likely to be a pattern of upwelling fluids towards the Alpine Fault, the Main Divide and other faults to the east, associated with fault-fracture meshes formed by the upwelling fluids in the brittle environment (Wannamaker et al. 2002).

On the basis of geological, fluid inclusion data and stable isotope systematics, Craw and coworkers proposed an interesting model (Fig. 9.18) to explain the Alpine Schist occurrences (see Craw and Koons 1989 and Craw et al. 2002 for details). In their model, these authors take cognizance of the tectonic environment, in which the Southern Alps represent a major zone of collision between the Pacific and the Indo-Australian plates. As mentioned previously, this resulted in considerable uplift, and the presence of a thermal anomaly, manifested by the numerous hot springs which issue along and close to the Alpine Fault. The authors point out that during uplift, temperatures as high as 300°C can occur at depths of less than 5 km. This constitutes a very powerful heat engine, for which no igneous activity is needed. This system is capable of activating hydrothermal convection for a longer time than shallow igneous intrusions, which tend to decay much more rapidly as heat sources. Another key facet of the model is that uplift occurs at a rate greater than that at which rocks cool by conduction. In this way a complex hydrothermal convective system develops at depths ranging from 1 to 6 km. In this system, rising and

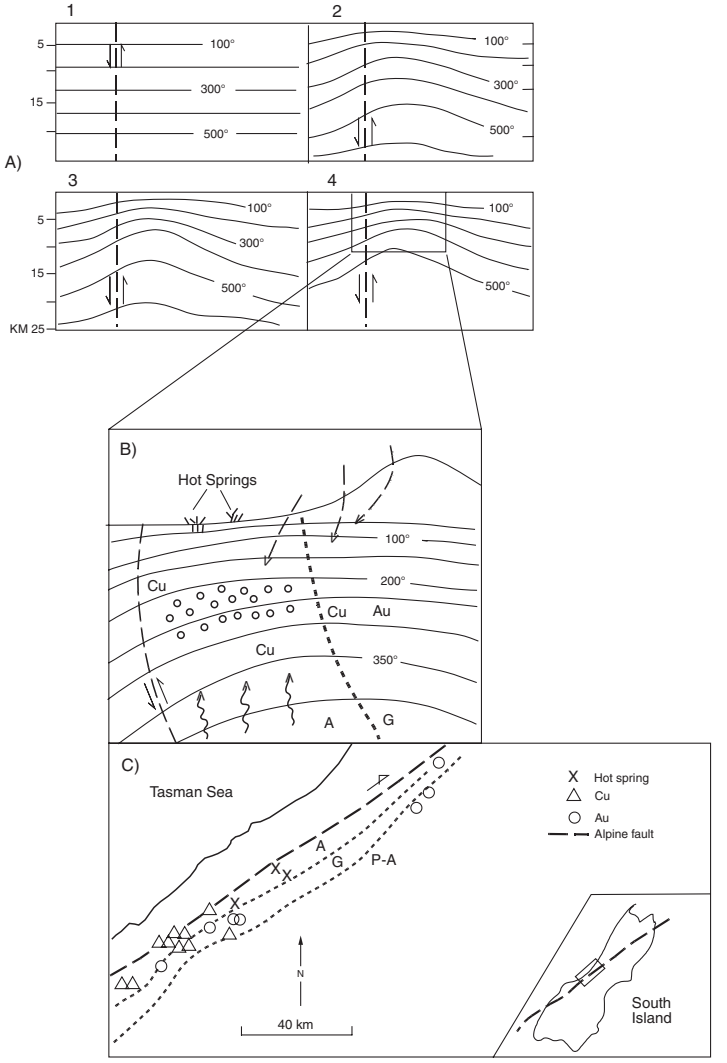


Fig. 9.18 (**A**) Modelled thermal profiles at t = 0 Ma 1, t = 2 Ma 2, t = 3 Ma 3 and t = 4 Ma 4 After 4 Ma the 300 and 400°C isotherms are raised to within 5–10 km of the surface on the upthrown block (*right hand side* of the fault, shown by *dashed lines*). Isothermal intervals are 100°C. (**B**) Portion of thermal profiles (*outlined* in (**A**)) showing movement of metamorphic fluids (*wavy arrows*, H_2O-CO_2) and meteoric fluids (*dashed arrows*). Boiling zone illustrated by *bubbles*; *dotted line* represents the boundary between amphibolite facies A and greenschist facies G domains. Au and sulphides are preferentially precipitated within the greenschist facies domain, while Cu sulphides are deposited closer to the fault within amphibolite facies rocks. Cu sulphide assemblages of amphibolite facies include chalcopyrite + pyrrhotite, and chalcopyrite + pyrite as late veins; in the greenschist facies domain ore assemblages are mainly chalcopyrite + pyrite, bornite + hematite and Au + pyrrhotite or pyrite. (**C**) Schematic map showing location of veinlet occurrences and hot springs. A Amphibolite facies; G greenschist facies; P-A pumpellyite-actinolite facies. (**A**) and (**B**) and (**C**) are after Craw and Koons (1988, 1989)

hot metamorphic fluids leach out Au and base metals (e.g. Cu), boil and mix in the upper levels with descending cool meteoric fluids. This hydrothermal activity results in the formation of various generations of veins and veinlets as discussed above. Type 1 veinlets would be the product of CO_2-rich metamorphic fluids. Type 2 veinlets result from mixing of these fluids with cooler metoric waters, whereas those of type 3 result from possible boiling, as indicated by the presence of platy calcite and adularia. The earlier generations of quartz-calcite veinlets contain Au and scheelite, are probably the result of hot and reduced fluids of metamorphic origin, and are restricted to domains of greenschist facies. Greenschist facies rocks, in the opinion of the authors, are particularly ideal as a source of fluids because of their chlorite content, which would provide abundant H_2O on devolatilisation. The hydrothermal fluid thus formed is capable of leaching Au, As and W from the surrounding lithologies, some of which might include bands of fertile metavolcanics and manganiferous cherts. A later generation of veinlets, emplaced at shallower levels and closer to the Fault, contain mainly Cu sulphides, and result from cooler and more oxidised fluids (Fig. 9.18B). The implications of the model of Craw and coworkers are important because they highlight the role of uplifted segments of crust at collision plate boundaries, past and present, in the localisation of orogenic ore systems and their derived placers. In these regions thermal anomalies are associated with the rise of isotherms (hot lower crust) due to rapid uplift, which in the Southern Alps is estimated at between 8 and 10 mm yr^{-1}. In the light of fluid inclusion and stable isotope data, it is reasonable to assume that at least two sources of fluids are involved. One source is in that sector of the crust where sedimentary packages are being deformed and metamorphosed to release H_2O-CO_2-rich fluids. Waters of meteoric origin constitute the other source; they are able to penetrate deep into the crust due to the inherent intense deformation associated with the collisional boundaries. Therefore, young mountain ranges, formed at collision boundaries, are prime targets for both mesothermal lodes and placer deposits but, as briefly discussed below, not in all cases.

Craw et al. (2002) made an interesting comparison between the hydrothermal activity of the Southern Alps and that of the western Himalaya, both young collisional mountain belts. Whereas the Southern Alps hydrothermal system is Au- As- and W-rich, the hydrothermal activity in the western Himalaya did not produce Au mineralisation. In the western Himalaya, the discharge of several hot springs testify to hydrothermal circulation, but with no traces of metallic mineralisation and quartz veins have negligible alteration haloes and no sulphides. This lack of orogenic lodes in the western Himalaya is, according to Craw et al. (2002) due to CO_2-rich metamorphic fluids derived from dehydration of amphibolite-granulite facies rocks. These CO_2-rich fluids cannot dissolve Au and other metals, while contemporaneous meteoric waters are too hot, have low reduced sulphur content, which also restrict the solubility of metals.

9.3.6 *Precious Metal Lode Deposits in the North China Craton and Qinling Orogen*

The North China Craton contains a large number of precious metal deposits, clustered in nine metallogenic provinces, all located along or close to major structural breaks or sutures (see review by Yang et al. 2003). Two of the major Au provinces in the North China Craton are the Qinling (Xiaoqinling) orogenic belt in Henan Province and the Jiadong peninsula (Fig. 9.19), estimated to contain about 12% and 25% of the total Au resources of China, respectively (Zhou et al. 2002; Chen et al. 2005). Both contain lode systems of approximately the same age (Cretaceous) associated with theYanshanian tectono-thermal event. In the Qinling belt precious metal lodes are hosted by the Taihua Supergroup and the Xiong'er Group, whereas the lodes in the Jiaodong province are for the most part hosted in Cretaceous granitic plutons. Although, the precious metal lodes of these two provinces are clearly linked to the Yanshanian magmatism, they present two different aspects of ore genesis, as detailed in the sections that follow. The precious metal lode systems of the North China Craton have often been considered to belong to

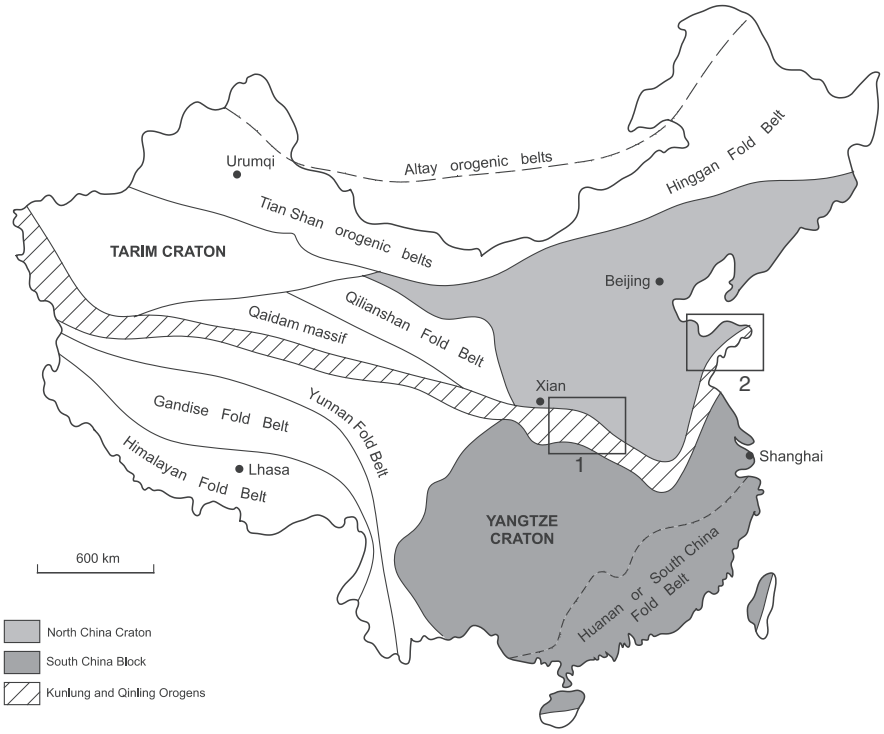


Fig. 9.19 Simplified tectonic map of China and position of the two Au provinces discussed in this chapter, (1) Qinling; (2) Jiaodong. After Chen et al. (2004)

the orogenic class, as defined in Groves et al. (1998) and Goldfarb et al. (2001). However, there are considerable differences between the lode systems of central and eastern China and the orogenic class, which as detailed in Sections 9.2 and 9.3, is associated with regional scale deformation and metamorphism. Goldfarb et al. (2007; see also Nie et al. 2004) recognised the unusual patterns of the Chinese lode systems, pointing out that these deposits are hosted in faults and shear zones within Archaean basement rocks and Mesozoic granitoids and that the ages of lode deposits cluster between 130 and 120 Ma. Importantly, there is no evidence of regional compressional tectonics and regional metamorphism that can be associated with the Cretaceous tectono-thermal events in central and eastern China (unpublished field observations, 2004–2008). The only evidence of Cretaceous deformation is recorded in brittle and brittle-ductile shear zones, faults and strong multi-stage, locally basement-cored, uplifts. In addition, rift basin-and-range style structures associated with basaltic volcanism were also formed during these Cretaceous events. Thus, hydrothermal fluid flow and the development of Au lode systems were linked with a series of magmatic and structural events during uplift, exhumation and collapse. These events have been attributed to upwelling asthenospheric mantle during delamination processes, resulting from changes in subduction direction of the Izanagi (Pacific) plate beneath east Asia, perhaps in conjunction or aided by the impingement of the Cretaceous superplume that formed the Ontong-Java oceanic plateau in the Pacific Ocean (Goldfarb et al. 2007). Based on geochemical and stable isotope studies, it appears that the origin of the mineralising fluids is essentially magmatic, although there are many cases in which the mineralisation was formed through processes of hydrothermal activity related to the influx of meteoric waters and their mixing with high-temperature fluids of magmatic origin. The ore-forming processes are always accompanied by alteration of the host rocks, including alkali metasomatism, silica and phyllosilicate alteration. Furthermore, fluorite is a very common mineral phase in most of these lode mineral systems, and also forming numerous occurrences and economic deposits as A-type alkali granite-hosted veins (unpublished field observations, 2004–2008). This suggests a link between the precious metal lodes with A-type magmatism. In other cases it can be argued that magmas may have locally interacted with volatile-rich sedimentary rocks, producing volatile-charged hydrothermal fluids that formed numerous breccia pipes in the Qinling region (see Chapter 5) and carbonate strata that formed skarn systems in the Yangzte River Valley (Chapter 6). Weakly negative $\delta^{34}S$ values commonly recorded in sulphides from lodes, breccia pipes and porphyry systems, could be derived from a memory of a sedimentary source (Chen et al. 2004).

Below I discuss the geological, isotope systematics and fluid inclusions data from key deposits, leading to models of ore genesis. These accounts are largely based on the works of Chen et al. (2004, 2005, 2006, 2008) and Mao et al. (2002a, b; 2007).

9.3.6.1 Precious Metal Lodes in the Qinling Orogen

The Qinling Orogen (also called Qinling-Dabie) is introduced in Chapter 5 (Section 5.2.2.3). A variety of hydrothermal ore deposits including, precious metal vein lodes, porphyry Mo, breccia pipes containing Au and Mo, and base metal skarns are present in the Qinling orogenic belt. Geochronological data, structural and geological constraints show that all these deposits, although hosted in rocks of Archaean to Palaeo-Mesoproterozoic age, are Mesozoic in age and their genesis is related to collisional and extensional tectonics during the Yanshanian 208–290 Ma tectono-thermal event.

Chen et al. (2004, 2006, 2008) studied two lode deposits in the eastern Qinling orogen: the Ag-dominated Tieluping and the Au-dominated Shanggong (Fig. 9.20). The Tieluping Ag-Pb ± Au deposit has reserves of 1217 t Ag grading 293 g/t, and 186 772 t Pb at an average grade of 3.1% Pb. Gold grade is uneconomic (<1 g/t), although this metal is recovered as a by-product. The Shanggong Au deposit has a resource of about 30 t of Au metal with ore grades averaging 6.9 g/t Au. These two deposits, together with other lode systems and the Yinjiagou gold skarn belt in the Xiong'er Terrane, the Jinduicheng porphyry Mo and the Qiyugou Au-Mo breccia pipes are all controlled by northeast-trending structures (Fig. 9.20).

The regional setting is dominated by the Xiong'er Terrane (Fig. 9.20), which is a northeast-trending, roughly wedge-shaped area, containing two main lithostratigraphic units: the Neoarchaean-Palaeoproterozoic Taihua Supergroup and the overlying Palaeoproterozoic Xiong'er Group. The Terrane is intruded by a suite of granitoids of Jurassic-Cretaceous age (described in Chapter 5). To the south and in contact with the Machaoying Fault are the sedimentary successions of the Guandakou and Luanchuan Groups. Subsidiary fault-splays of the Maochaoying fault are common in the Xiong'er Terrane, which served as major conduits for both granitic intrusions and hydrothermal fluids. The east-west-trending Machaoying fault (Fig. 9.20), with a strike length of over 200 km and inferred depth of 34–38 km, has been interpreted as the trace of a major north-dipping thrust, formed during the continental collision that in the Triassic sutured the North China and the Yangzte Cratons, resulting in the Qinling-Dabie orogenic belt. The Taihua Supergroup is a high-grade metamorphic sequence of amphibolite to granulite facies rocks (2.55∼2.3 Ga Beizi Group Dangzehe greenstone belts) and a passive margin succession of graphite schist, marble and iron-formation rocks (2.3∼2.2 Ga Shuidigou Group). The Xiong'er Group, is up to 7600 m thick (Zhao et al. 2002), and is a well-preserved unmetamorphosed and only slightly deformed predominantly bimodal volcanic sequence with well-constrained ages of 1826 ± 32 Ma to 1840 ± 14 Ma (Peng et al. 2005) that unconformably overlies the metamorphic basement (TaihuaSupergroup) and is overlain by Mesoproterozoic carbonate rocks. The origin of the Xiong'er volcanic rocks is controversial. Kusky and Li (2003), suggested that the Xiong'er volcanic rocks are a bimodal succession formed in a NE- trending rift system related to the opening of the Qinling ocean.

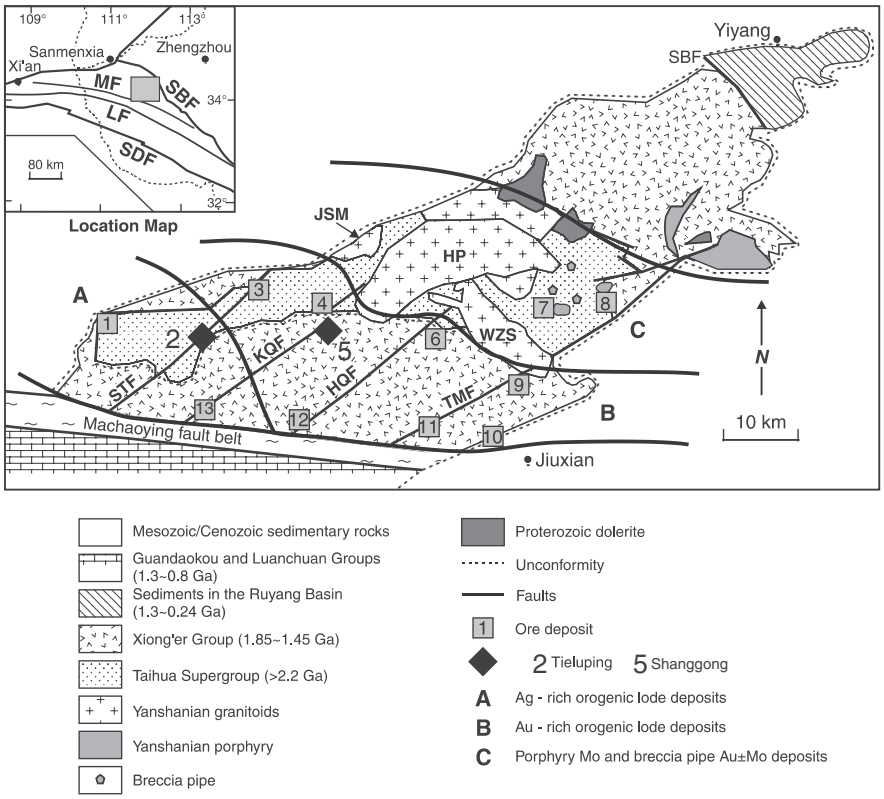


Fig. 9.20 Simplified geological map of the Xiong'er Terrane in the East Qinling and location and geological setting of the Tieluping and Shanggong deposits. Other hydrothermal ore deposits: (1) Haopinggou (Ag-Pb); (2) Tieluping Ag-Pb; (3) Xiaochigou (Au); (4) Hugou Au; (5) Shanggong Au; (6) Qinggangping (Au); (7) Leimengou (Mo-Au); (8) Qiyugou (Au-Mo); (9) Yaogou (Au); (10) Qianhe Au; (11) Tantou (Au); (12) Hongzhuang (Au); (13) Kangshan (Au-Ag-Pb); **A**, **B**, and **C** metallogenic districts, Ag-rich, Au-rich and Mo-rich, respectively; JSM Jinshanmiao granite; HP Haoping granite; WZS Wuzhangshan granite. Faults: STF Sanmen-Tieluping; KQF Kangshan-Qiliping; HQF Hongzhuang-Qinggangping; TMF Tao-chun-Mayuan. Location inset: LF Luanchuan fault; MF Machaoying fault; SBF San-Bao-fault; SDF Shang-Danfault. After Chen et al. (2004, 2005)

Peng et al. (2005, 2008), on the other hand, showed that the Xiong'er volcanic rocks and dyke swarms are part of a 1.78 Ga large igneous province emplaced in a north-south-trending rift system developed across the North China Craton (see Fig. 4.50). The Guandaokou and Luanchuan Groups, south of the Machaoying fault (Fig. 9.20) contain carbonaceous carbonate rocks, quartz sandstones, shales and cherts (CSC sequence). The CSC rocks were largely sourced from the Taihua Supergroup and the Xiong'er Group and deposited in a forearc basin between 1.3 and 0.8 Ga. The CSC sequence appears to be associated with the breakup of the Rodinia supercontinent (Zhang et al. 2000).

The lithostratigraphic units discussed above were intruded by Jurassic to Cretaceous (~160 Ma to ~110 Ma) granitoids, including the 200 km^2 Haoping batholith, the Huashan Complex and a number of mineralized porphyry intrusions, diatremes and the Qiyugou Au-bearing breccia pipes (described in Chapter 5).

9.3.6.1.1 Tieluping Ag-Pb

The Tieluping Ag-Pb ± Au deposit is controlled by the NE-trending sinistral Tieluping fault (Fig. 9.20) and hosted byplagioclase-amphibole gneisses, amphibolites and biotite-plagioclase gneisses of the Taihua Supergroup. The ore bodies are associated with a group of subsidiary, parallel fractures on the west side of the Tieluping fault that dips 50–80° west-northwest.

The two largest orebodies are 730 m long and 390 m deep, with average thickness of 4.6 m and an average grade of 347 g/t Ag; and 780 m long and 310 m deep, with average thickness of 4.7 m and an average grade of 303 g/t Ag. Although vertical zonation in alteration assemblages is not observed, lateral zoning is pronounced (Fig. 9.21). This zoning is gradational

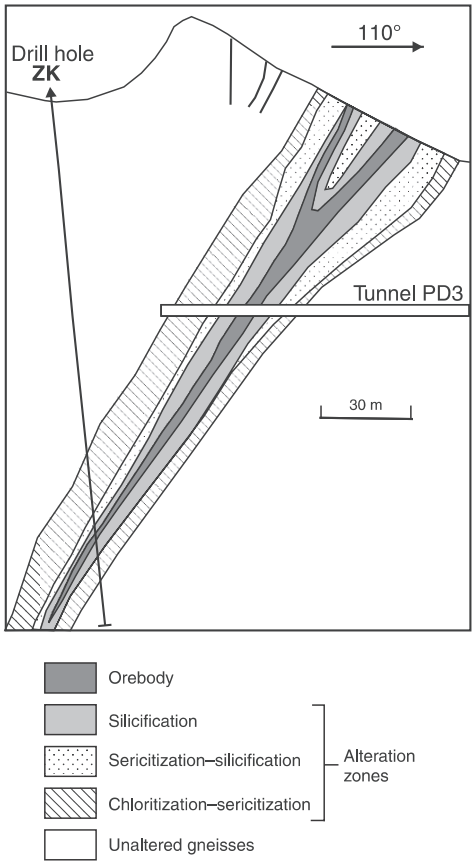


Fig. 9.21 Cross-section through the Tieluping orebody and wall-rock alteration zones. After Chen et al. (2004)

and is characterized by silicification proximal to the ore, through a zone of sericite-quartz grading into a distal chlorite-sericite zone. Orebodies are usually within multistage silicified zones that only locally form coarse-grained quartz veins. These veins commonly have cataclastic, banded, stockworks, or massive structures. Ore textures are highly variable. For example, brecciated quartz grains are replaced by galena and chalcopyrite; tetrahedrite is replaced and armoured by digenite; early formed pyrite and galena are usually brecciated, and replaced by galena or tetrahedrite; locally, embayed sphalerite and chalcopyrite are replaced by galena.

Three paragenetic stages, from early (E), middle (M) to late (L), are recognized on the basis of crosscutting relationships. They are: (1) E-stage fault-controlled pyrite-quartz veins, locally containing some galena, and pyrite-sericite-quartz assemblage in the wall rocks; (2) M-stage, with the assemblage quartz + sericite + galena + chalcopyrite + sphalerite + tetrahedrite + pyrite, is present in veinlets that cut the E stage assemblages; (3) L-stage veinlets of calcite ± quartz ± sericite ± chlorite ± digenite ± galena ± pyrite, with comb textures, crosscuts the E-and M-stage minerals and wall rocks. These paragenetic stages are in broad agreement with the results of fluid inclusion studies, in which homogenization temperatures (uncorrected for pressure) fall into three groups: ~370°C (E stage), ~250–165°C (M stage) and ~135–203°C (L stage). Microscope and electron microprobe studies indicate that Ag is present as native metal and within tetrahedrite, freibergite, polybasite, and galena. These minerals mostly formed during the M-stage. The E-stage massive galena and L-stage disseminated galena do not contain significant silver.

The results of C, S and Pb isotope systematics of ores and minerals from Tieluping enabled important constrains for understanding the genesis of this lode system. Depleted $\delta^{13}C$ values of CO_2 gas and carbonate minerals in hydrothermal ore deposits generally suggest a deep-seated juvenile source for the carbon (Faure 1986), however fluids from the Tieluping deposit have much higher $\delta^{13}C_{CO2}$ values, which decrease with time, indicating a significant difference in fluid nature and source. In the E-stage, $\delta^{13}C_{CO2}$ values range from 0.3 to 4.0‰, and averages 2.0‰, higher than those of organic matter (average –27‰), CO_2 in fresh water (–9 to –20‰), igneous rocks (–3 to –30‰), continental crust (–7‰), and mantle (–5 ~ –7‰) (Faure 1986; Hoefs 2004). This indicates that, whereas at Tieluping the CO_2 in the E-stage fluids could not be sourced from one or a mixture of the above-mentioned materials, they could be dominantly sourced from marine carbonates by metamorphic devolatilisation processes. $\delta^{13}C_{CO2}$ values of L-stage fluid range from –0.3 to –2.0‰ (average –1.3‰), lower than that of E-stage. Therefore, L-stage $\delta^{13}C$ values imply an atmospheric CO_2 component, which may have entered the crust with meteoric water and probably mixed with hydrothermal fluids of the Tieluping ore-fluid system. This may have led to the $\delta^{13}C$ values to decrease from E-stage to L-stage. One $\delta^{13}C_{CO2}$ value for the M-stage sample, overprinted by L-stage, is 0.1‰, which is between those of E-and L-stages. This suggests the M-stage fluid is a mix of meteoric and metamorphic fluids, or marks the transition from the

E-stage metamorphic fluid to the L-stage meteoric fluid. Chen et al. (2004) concluded that the carbon isotope compositions suggest that the E-stage fluid originated from metamorphic devolatilisation of marine carbonates, the L-stage fluid mainly from meteoric water containing atmospheric CO_2, and the M-stage fluid, although based only on one value, would suggest a mix of metamorphic and meteoric fluids or the transition from early metamorphic to late meteoric fluids.

The $\delta^{34}S$ ratios of galena separates and ores range from –8.8 to –0.6‰ and average –4.3‰. As no sulphate minerals have been observed in the Tieluping deposit, a reduced system can be inferred for the deposition of sulphides. The histogram of the $\delta^{34}S$ values for Tieluping, the Xiong'er Group and the granitic rocks of the Huashan Complex, shown in Fig. 9.22, indicates that the sulphur in the ore-forming fluid could not have been sourced from the Huashan Complex. The data also preclude a mantle source, because such a source would have $\delta^{34}S$ between 0 and 2‰ (Hoefs 2004).

Lead isotope analyses of the ores from the Tieluping deposit show that the ores have higher ratios of $^{207}Pb/^{204}Pb$, $^{206}Pb/^{204}Pb$ and $^{208}Pb/^{204}Pb$ than the Huashan granite, Xiong'er Group and Taihua Supergroup. The Taihua Supergroup, the Xiong'er Group and the Huashan Complex, as well as the lower crust and mantle beneath the Xiong'er Terrane have previously been considered as the sources of ore-forming fluids and metals. However, the lower crust and mantle should possess even lower contents of U, Th and lower lead isotope ratios than the upper crust (Taylor and McLennan 1985, 1995). Chen et al. (2004) ruled out the possibility of the lower crust and/or mantle as a source of the ore lead, pointing out that together with the evidence of carbon and sulphur isotopic systems, the radiogenic lead characteristic of the Tieluping deposit may have been derived from the northward underthrusting of the CSC sequence.

9.3.6.1.2 Shanggong

The Shanggong Au deposit, discovered in 1982, and hosted in volcanic rocks of the ~1.8 Ga Xiong'er Group, has a resource of about 30 t of Au metal with ore grades averaging 6.9 g/t Au. Since its discovery, more than 10 large (>20 t) and medium (10–20 t) Au deposits and one large Ag deposit (>1000 t Ag) have been found in the region (Fig. 9.20).

The Shanggong deposit, contains 30 orebodies within a horsetail-like dilational jog (Fig. 9.23), all located in high strain zones and distributed in a northeast-trending array, about 2200 m long and 600 m wide (Fig. 9.23). The ore zones have irregular and gradational borders, depending on cut-off grades, but are commonly more or less lenticular or tabular, both in plan and section views. Orebodies are usually within silicified zones that contain thin (mostly > 1 mm) quartz veins. These veins have brecciated, mylonitic and banded structures and form stockworks, disseminated veinlets and locally massive veins. The Shanggong orebodies are laterally zoned, from the centre outward: a Au-bearing sulphide-quartz-ankerite-sericite zone (usually 1–3 m wide; >3 g/t Au); a

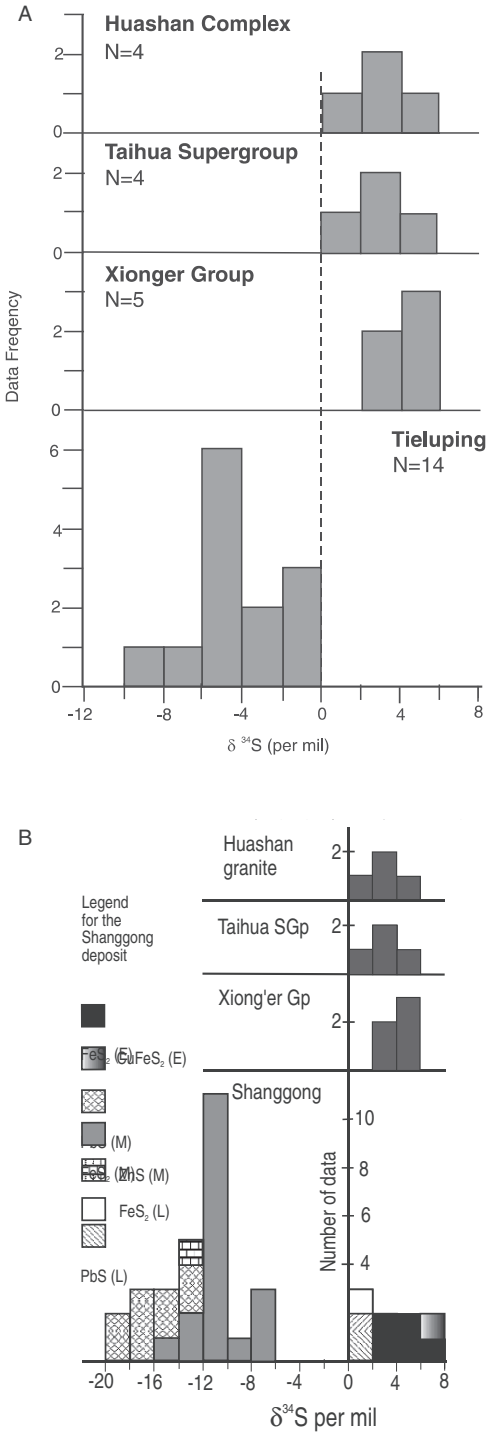


Fig. 9.22 $\delta^{34}S$ histogram for (**A**) Tieluping Ag deposit and associated rocks; (**B**) Shanggong Au deposit and associated lithologies, the Taihua Supergroup, Xiong'er Group and Huashan Complex have similar $\delta^{34}S$ values; the $\delta^{34}S$ values of E-and L-stages sulphides of the ores are similar to those of the wall rocks, the Xiong'er Group, whereas M-stage sulphides have negative $\delta^{34}S$ values suggesting a source characteristic of biogenic sulphur. Inset show position of area studied in the Qinling Orogen. After Chen et al. (2004, 2008)

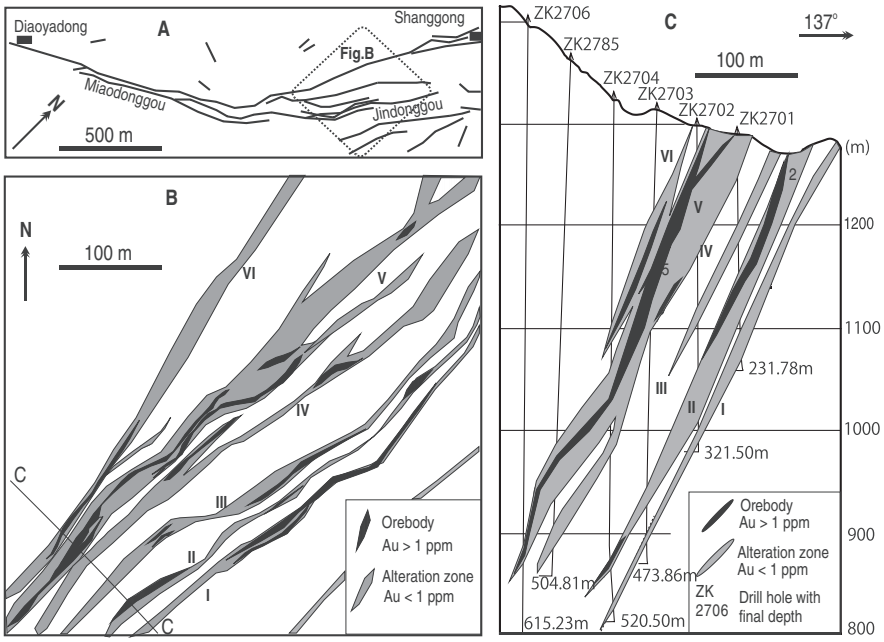


Fig. 9.23 Structurally-controlled Au orebodies and associated alteration zones; (**A**) The Shanggong Au deposit is located in a horsetail-like dilational jog of the Kangshan-Qiliping faul system. (**B**) At the 1111 m level, the dilational fracture splays control the alteration and ore occurrence. (**C**) A profile along No. 27 *exploration line*, showing the vertical geometry of the orebodies and surrounding altered wall rocks. Roman numerals in (**B**) and (**C**) indicate the six main ore-hosting tectonite zones. After Chen et al. (2008)

1 to 20-m wide, pervasively altered, pyrite-carbonate-sericite-chlorite-epidote zone (0.5–3 g/t Au), grading outward to; a 50 m-wide of weakly altered pyrite-carbonate-sericite-chlorite-epidote zone (<1 g/t Au); and finally unaltered country rock of the Xiong'er Group (averaging 0.7 ppb Au). No vertical zoning is observed. Gangue minerals comprise quartz, ankerite and sericite, chlorite, epidote and fluorite, with lesser calcite, kaolinite, smectite, albite, apatite and tourmaline. Major ore minerals are pyrite and galena. Other ore minerals include magnetite, hematite, chalcopyrite, sphalerite, wolframite, scheelite, chalcocite, tetrahedrite, argentite, bornite, pyrrhotite, molybdenite, native Au, electrum, calaverite, hessite, petzite, altaite, melonite and siderite. In addition, limonite, jarosite, cerusite, anglesite, covellite, malachite, azurite and hydrocerussite are present in the weathering zone.

As is the case for the Tieluping lode deposit, field data, petrographic observations and textural relationships, show that the mineralization and alteration can be divided into: an early (E), middle (M) and late (L) stages. The E-stage is further subdivided into an older substage characterized by sericite, albite, quartz, ankerite, chlorite, epidote, pyrite and minor tourmaline, which form infills or replaces fine-grained (<2 mm) minerals, and a younger substage, of

coarse-grained, milky quartz veins that contain ankerite, coarse-grained cubic pyrite, and locally, fluorite, scheelite, wolframite and molybdenite. The alteration assemblages and veins of E-stage are locally mylonitized with development of corona-like textures. The M-stage is characterized by stockworks of pyrite, galena, sphalerite, chalcopyrite, tetrahedrite and minor tellurides and native elements (Au, Ag, Cu and Te). M-stage gangue minerals include quartz, chlorite, sericite, epidote and ankerite, which also filled the brecciated E-stage coarse-grained milky quartz veins. The M-stage minerals are fine-grained, including fine-grained pentagonal dodecahedron pyrite and quartz and do not show any deformation. The L-stage is dominated by quartz-carbonate veinlets (1–30 mm), locally associated with chlorite, sericite and fluorite. These L-stage veinlets penetrate fracture zones in the country rocks, and quartz crystals typically grew from both walls towards the center, which is filled with calcite crystals. It is pertinent to note that E-stage anhedral quartz with undulose extinction, was replaced by L-stage euhedral unstrained quartz.

Stable isotope systematics and the geochemistry of ore fluids from the Shanggong Au deposits have been reported by Chen et al. (2006, 2008). $\delta^{13}C$ values for ankerite range from –2.2 to 1.5‰, (average –0.8‰), whereas $\delta^{13}C_{CO2}$ values for inclusion fluids released from M-stage quartz, range from –1.2 to 0.5‰ (average –0.2‰). The range of the high $\delta^{13}C$ values of the Shanggong ankerite are interpreted to reflect decarbonation of the marine carbonates of the underthrust Guandaokou and Luanchuan Groups (CSC sequence referred to above). Qi et al. (2005) reported $\delta^{13}C_{Carbonate}$ values for these rocks, which range from –2.8 to 0.8‰ (average –0.9‰). According to calculations of fractionation factors for dolomite-CO_2 and calcite-CO_2 the $\delta^{13}C_{CO2}$ values of metamorphic fluids equilibrated with the CSC sequence at 400°C, would be in the range of –1 to 2.7‰, similar to the measured $\delta^{13}C$ of ankerite in the Shanggong ore system.

The E-stage sulphides have positive $\delta^{34}S$ values (average 4.3‰), which are similar to the rocks of the Xiong'er Group (average 4.1‰) (Fig. 9.22). Therefore, it is likely that the Xiong'er Group contributed much of the sulphur to the E-stage sulphides during fluid-rock interaction. This interpretation is also consistent with the observations that the E-stage sulphides are disseminated in the altered andesites and in lenticular quartz-veins. The $\delta^{34}S$ values of M-stage pyrite, galena and sphalerite range from –19.2 to –6.3‰ and are quite different from the $\delta^{34}S$ values of both the E- and L-stage sulphides (Fig. 9.22). This $\delta^{34}S$ variation shows that the S-isotope fractionations, among coexisting pyrite, galena and sphalerite, were not equilibrated, possibly due to rapid precipitation of the M-stage minerals. The M-stage mineral assemblage, which also contains native metallic elements, indicates that the M-stage sulphides were formed in a reducing environment, relative to the E- and L-stage fluids. In the Xiong'er terrane, only the CSC sequence contains organic material, which can be considered as a possible source of the biogenic sulphur of the Shanggong hydrothermal system. The average $\delta^{34}S$ value of sulphides of the L-stage is 1.1‰, suggests that this sulphur may have been sourced either from igneous rocks or from the immediate host rocks by meteoric water circulation.

Chen et al. (2006) found that the $\delta^{18}O$ values of ore fluids, extracted from fluid inclusions, systematically increase from unaltered volcanic rocks (6.7–8.0‰), through altered volcanic rocks (8.5–8.9‰) to ores (12.7‰). These values show that ^{18}O was added to the wall rocks during fluid-rock interaction. Calculated $^{18}O_W$ values for E-stage fluids average 8.1‰, which is in the range of metamorphic water. δD values for inclusion fluids of E-stage mineral separates range from –66 to –88‰, which plot in the magmatic box and below the metamorphic water box. Chen et al. (2006) concluded that the E-stage fluids show characteristics of magmatic and/or metamorphic fluids. Calculated values of $\delta^{18}O_w$ of L-stage fluids range from –2.4 to –1.1‰. These low values show that the L-stage fluids had a large meteoric water component. In addition, the δD_{H2O} value of the L-stage fluid, extracted from fluid inclusions in fluorite, is –56‰, which together with the $\delta^{18}O_w$ value, would plot towards the meteoric water line. $\delta^{18}O_W$ values for M-stage fluids range from 1.9 to 4.5‰, are intermediate between those for E-stage (8.1‰) and L-stage (–2.4 ∼ –1.1‰). These trends may be interpreted to indicate a mixing of deep-sourced metamorphic fluids with meteoric water.

9.3.6.1.3 Chen's CMF Model of Ore Genesis for Precious Metal Lode Systems in the Qinling Orogen

Chen and co-workers proposed a holistic model that links metallogenesis, fluid generation and fluid flow (CMF) to collisional and extensional tectonics (Chen 1998; Chen et al. 2004; 2005). Pirajno and Chen (2005) refined the CMF model, as explained below. Age constraints suggest that the origin of the Tieluping Ag-Pb and Shanggong Au deposits is related to thermal relaxation and extension, following the collision between the North China and Yangtze Cratons, which formed the Qinling Orogen, now marking the tectonic boundary between the Cratons (Fig. 9.19). The Orogen is the result of a complex geodynamic history, including divergence and convergence of continental blocks, spanning a period from the Late Neoproterozoic to the Cretaceous (Xue et al. 1996; Yan et al. 2004) The latest events in the geodynamic evolution of this Orogen can be divided in three main stages (Ratschbacher et al. 2003): (1) an early compressive stage, during the Triassic to middle Jurassic; (2) a transitional stage from compression to extension in the late Jurassic to early Cretaceous; and (3) a late extensional stage in the Cretaceous. Studies of metamorphic *PTt*-path and magmatic evolution of the Qinling-Dabie Orogen suggest that the most extensive granitic magmatism, generation of hydrothermal fluids and metallogenesis took place during Late Jurassic-Early Cretaceous time in response to lithospheric extension. The onset of this lithospheric extension can be linked to the Triassic collision between the North China Craton and the Yangzte Craton, along the Qinling orogenic belt (Xu 2001), and the collision of the North China Craton with the Siberian Craton in the Jurassic-Cretaceous (Wang et al. 2006).

The timing of the orogenic lodes metallogenesis in the Qinling orogen during the geodynamic processes from collisional compression to extension in the Mesozoic, is in agreement with the following key aspects: (1) decrease in

regional pressure and temperature from early to late ore-forming stages, probably related to uplift and mountain-building; (2) precious metals-hosting structures changed from reverse faults in the Triassic to tensional in the Jurassic-Cretaceous; (3) ore fabrics changed from E-stage compressive shearing to L-stage open space filling textures, quartz changed from E-stage anhedral and stressed crystals to L-stage unstressed euhedral crystals; (4) ore-forming fluids changed from magmatic and/or metamorphic to meteoric water dominant; and (5) the composition of Mesozoic granitoids in the Xiong'er Terrane changed from peraluminous to K-rich and K-feldspar porphyritic calc-alkaline series. Chen and co-workers, on the basis of isotope systematics, proposed that carbonate-bearing sedimentary rocks containing biogenic matter could have been a likely source of fluids, even though the ore-bodies are hosted in volcanic rocks of the Xiong'er Group or the Taihua Supergroup. The H-O and C isotope data suggest that the ore fluids of these deposits were derived from devolatilization of a source with high $\delta^{18}O$ and $\delta^{13}C$. The major inflow of fluids, especially E-stage, was probably derived from the metamorphic devolatilization of the carbonate-rich rocks of the CSC succession.

The CMF model applied to the above-described Tieluping and Shanggong lode systems envisages that during the early compression stage (Fig. 9.24B), the CSC sequence (Guandaokou and Luanchuan Groups) was thrust northwards beneath the Xiong'er Terrane (Fig. 9.24C). Devolatilisation of C-rich rocks in the crustal slab provided both S and Cl-complexing agents, resulting in the transport and deposition of Au, Ag and some base metals in lode deposits. The temperature and pressure of the thrust slab increased with depth, resulting in metamorphism and partial melting of subducted materials (G1 syncollisional peraluminous granites; Fig. 9.24C1). Water, other volatiles (e.g. CO_2), silica and organic matter were mobilized during devolatilization processes forming metamorphic fluids, moved upward together with some ore-forming elements (e.g. Te). These fluids also mobilized and extracted ore elements (e.g. Au) from the wallrocks (e.g. the Xiong'er Group) during their upward movement. When the fluids reached favorable sites, e.g. lithological discontinuities, dilatant fault-jogs and the ductile-to-brittle transitions, the ore-forming components were precipitated. This is the E-stage in the mineralization paragenesis of the Tieluping and Shanggong deposits. During the transition stage, *P-T* conditions (from P_{max} to T_{max}, i.e., decompression–rising geotherms, possibly due to upwelling asthenospheric mantle) (Fig. 9.24B) resulted in decompression melting in the deep levels, providing energy, fluids for metallogenesis and melts (G2 metaluminous granites; Fig. 9.24C2). Structures would dilate due to regional (terrane- or orogen-scale) decompression and uplift, providing good conduits for fluid circulation. These upward-flowing, deeply-sourced, fluids would mix with the downward-flowing, shallow-sourced, fluids in fractures and other favorable loci (Fig. 9.24C2). Upon mixing, the upward-flowing, deep-sourced fluids and the downward-flowing shallow-sourced fluids change their physico-chemical character, resulting in the most intensive mineralization that is characteristic of the M-stage. During the late extensional stage

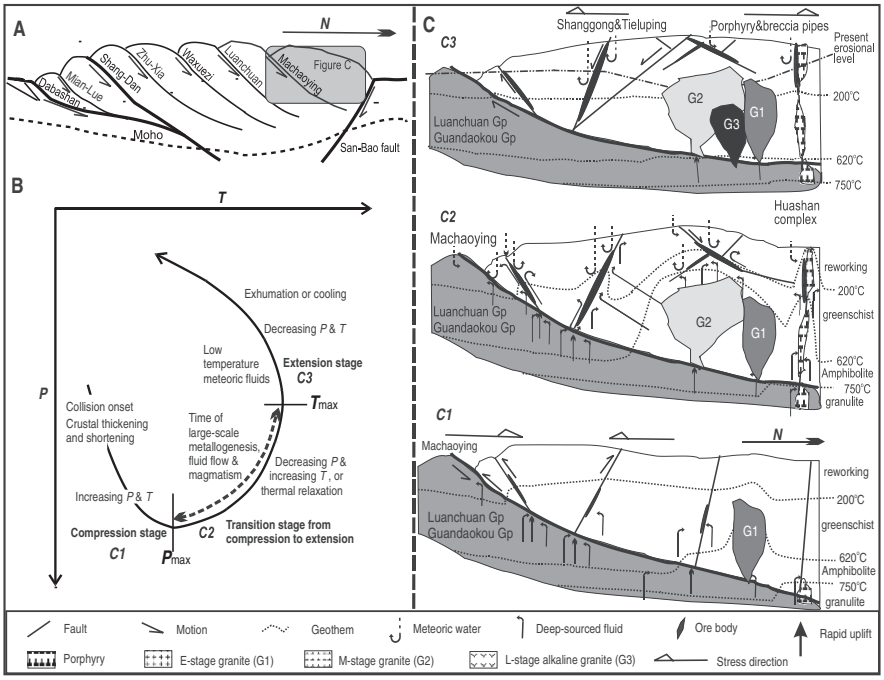


Fig. 9.24 CMF model of ore genesis in the Qinling Orogen; (**A**) Simplified tectonic structure of the Qinling Orogen; (**B**) Typical *PTt* path of a collisional orogen, such as the Qinling, showing that a collision process includes three progressive geodynamic regimes (compression, transition to extension, extension), which are responsible for fluid generation, large scale fluid flow, metallogenesis and magmatism. (**C**) Schematic diagram illustrating the regional tectono-thermal, fluid flow and ore-forming processes, the position of the Tieluping-Shanggong hydrothermal Au-Ag belt and its spatial and temporal relationships with A-subduction, ore-hosting structures, various generations of granitoids (G1, G2, G3; see text for details), the porphyry and Qiyugou Au-bearing breccia pipes. C1, C2 and C3, correspond to compression (crustal thickening, shortening), transition (uplift and beginning of extension) and final extensional stages as shown in (**B**), respectively. See detailed discussion in text; see also Fig. 3.4. After Chen et al. (2004, 2005, 2006)

and thermal relaxation (after T_{max}; Fig. 9.24B), heat energy and the mobilized ore components became less and the deep-sourced fluids became negligible, with only the shallow-sourced fluid-systems acting weakly and restrictedly (Fig. 9.24C3). Therefore, this latest stage is characterized by low-temperature and shallow-sourced fluids and contributed little to Au mineralization. This is the L-stage recognised in both deposits. This late extensional stage is also characterized by A-type alkaline granitoids typically associated with the final stages of extension in rift settings (G3 granites; Fig. 9.24C3).

9.3.6.2 Lode Au in the Jiadong Peninsula: Possible Mantle Contribution

The Jiaodong province is the largest Au producer with a resource of more than 1000 t (Mao et al. 2007). There are seven major orogenic lodes in the province

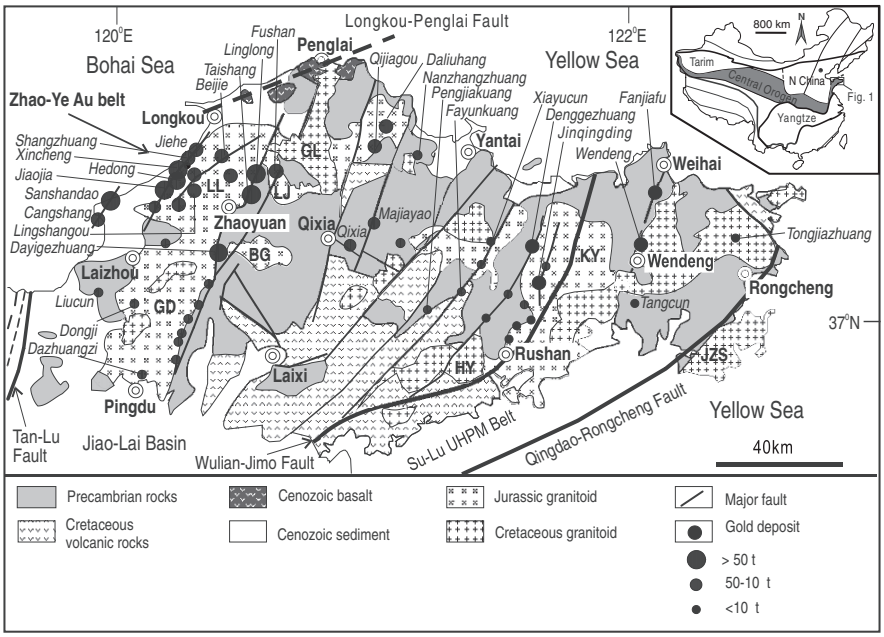


Fig. 9.25 Geology and distribution of gold deposits in the Jiaodong province; abbreviations for granitoid intrusions: BG, Biguo; GD, Guojiadian; GL, Guojialing; HY, Haiyang; KY, Kunyushan; LJ, Luanjiahe; LL, Linglong. After Chen et al. (2005)

(Sanshandao, Jiaojia, Xinncheng, Linglong, Fushan, Taishang, Daingezhuang) and about 300 smaller deposits and occurrences (Fig. 9.25). Zhou et al. (2002) recognised two main styles of lode Au in Jiaodong, namely: (1) large quartz veins hosted in granites and (2) disseminated veinlets in fractures and shear zones at the contact between granites and Archaean greenstone rocks. The former are best represented in the Linglong gold fields and the latter in the Jiaojia-Xincheng field. Mao et al. (2007) added a third style: breccia ores hosted in detachment fractures and northeast-trending faults on the margins of the Cretaceous Jiaolai Basin. These authors carried out a comprehensive study of ten deposits in the Jiaodong province using stable isotope systematics, as discussed hereinafter.

The Jiaodong peninsula is located along the southeastern margin of the North China craton and at the western margin of the Pacific Plate (Fig. 9.19). It is bounded to the west by the north-northeast-trending Tan-Lu fault zone that extends for thousands of kilometres from the Yangtze River north to Far East Russia. The Jiaodong peninsula is divided into two-Jurassic tectonic units: the Jiaobei Terrane in the north and Sulu Terrane in the south. These terranes are separated by the Wulian-Yantai suture. The Sulu Terrane is at the eastern end of the Qinling – Dabie – Sulu diamond- and coesite-bearing ultra-high pressure metamorphic belt. The Jiaobei Terrane consists of the Jiaobei uplift in

the north and the Jiaolai basin in the south. Three pulses of magmatic activity in the Mesozoic resulted in the intrusion of the Linglong, Luanjiahe and Kunyushan granites, Guojialing granodiorite, and a series of dolerite, lamprophyre and felsic dykes. The Linglong biotite granite, Guojialing granodiorite, Luanjiahe biotite granite, and Kunyushan biotite granite were intruded into the Archaean rocks. The Linglong, Luanjiahe and Kunyushan biotite granites are metaluminous-peraluminous, and are mainly composed of plagioclase, K-feldspar, quartz and biotite, with accessory garnet and muscovite. Dykes are present in the Jiaodong area, especially in the Linglong gold field, and include several types (lamprophyre, dolerite, diorite, granite, granite porphyry and pegmatite). The dykes were emplaced in several stages, which preceded and postdated the gold mineralisation event. Dyke emplacement shows a temporal trend from early lamprophyre to later intermediate-felsic dykes. Zircon SHRIMP U-Pb and ^{40}Ar-^{39}Ar dating of these dykes, revealed ages ranging from 120 Ma for granite porphyry dykes in the Oujiakuang gold deposit to 103–123 Ma for lamprophyre and mafic dykes, which are spatially associated with mineralized veins. Based on textural and cross-cutting relationships, Mao et al. (2007) recognized two main mineral stages: (1) quartz-pyrite or quartz sulphides, and (2) carbonate veins. The carbonate veins include calcite, quartz-calcite, ankerite, and a few siderite veins, which commonly contain disseminated macrocrystalline pyrite, but without gold. The carbonate veins crosscut the orebodies, granite, granodiorite, and some of the lamprophyre and mafic-intermediate dykes. Therefore, as observed for the Qinling lode systems, the carbonate veins represent the latest stage of hydrothermal activity in the metallogenic event of the Jiadong province.

Mao and co-workers also carried out stable isotopic studies on several of the Jiaodong Au deposits, integrated with data from published works. $\delta^{34}S$ of all three types of deposits show values increasing from the quartz vein ores (6.8–9.3‰, averaging 8.3‰) to altered fracture ores (8.5–12.5‰ averaging 10.9‰) and breccia ores (9.9–12.7‰, averaging 11.0‰). The $\delta^{34}S$ values of pyrite in the Jiaodong greenstone rocks range from 7.2‰ to 9.8‰, whereas the average $\delta^{34}S$ values of pyrite in the Linglong biotite granite is 7.3‰, for the Luanjiahe biotite granite 8.9‰, for the Guojialing granodiorite 6.7%, and for the mafic-intermediate dykes 6.9‰.

The $\delta^{18}O_{SMOW}$ and δD values of sericite from the three types of ore are quite similar, i.e. 10.5‰ and –55‰ on average for altered fracture-type ore, 9.3‰ and –61‰ for quartz vein-type ore, and 8.8‰ and –83‰ for breccia-type ore. Both $\delta^{18}O_{SMOW}$ and δD values decrease from altered fracture, quartz vein to breccia-type ores. The $\delta^{18}O_{SMOW}$ values of K-feldspar in the three type of ores also indicate the same character, i.e. from 10.1‰, 8.8‰ to 6.8‰, but the δD values do not show much difference. The $\delta^{18}O_{SMOW}$ and δD values of K-feldspar from the granodiorite and biotite granite are 9.7‰ and –80.2‰, and 10.1‰ and –84.8‰, respectively (Fig. 9.26). Carbon isotopic compositions for the late-stage carbonates from the Linglong deposit yielded $\delta^{13}C_{PDB}$ values of –3.4‰ to –6.4‰ (average –5.4‰). The values of $\delta^{13}C_{PDB}$ and $\delta^{18}O_{SMOW}$ of dolomite from the

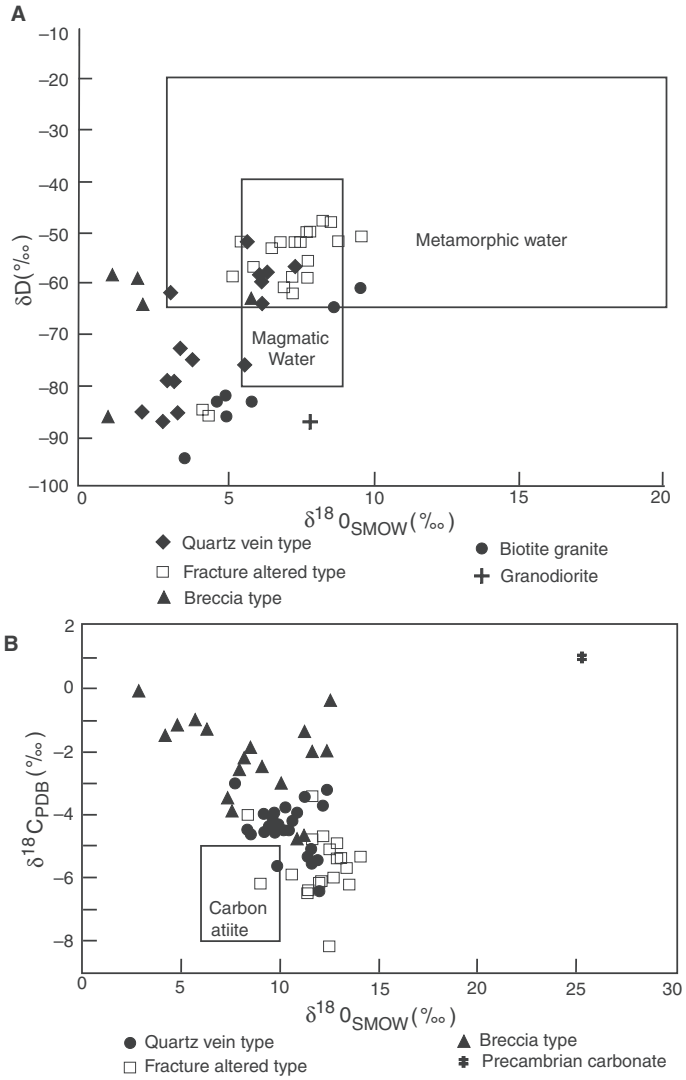


Fig. 9.26 Isotopes Diagrams of (**A**) δD‰ vs $\delta^{18}O_{WATER}$‰ for the three types of ores and Jurassic biotite granite and Cretaceous granodiorite; (**B**) $\delta^{18}O_{SMOW}$‰ vs $\delta^{13}C_{PDB}$‰ for the late-stage carbonate veins without gold systems. After Mao et al. (2007)

Jiaojia deposit are –5.3‰ and + 14.1‰, respectively and from calcite grains from the Dazhuangzi deposit –0.4‰ to –2.0‰ (average –1.5‰).

Several studies of fluid inclusions have been carried out on the gold deposits of the Jiaodong district. Fan et al. (2003) reported three types of fluid inclusions for the Sanshandao deposit: CO_2-H_2O, CO_2-H_2O-CH_4 and aqueous. The first type (CO_2-H_2O) is associated with the early metallogenic stage, the second

(CO_2-H_2O-CH_4) with the main metallogenic stage, and the last with the quartz-calcite or calcite veins of the post-metallogenic stage. Yang (1998) suggested that the dominant components of fluid inclusions in the Jiaodong district are CO_2 and H_2O, and the content of H_2O is normally higher than that of CO_2. Because the fluid inclusions are rich in CO_2, Sun and Shi (1995) referred to these as C-H-O fluids, similar to mantle-derived fluid with H, alkali components, CO_2, N, and S-rich (HACONS) as suggested by Menzies and Hawkesworth (1987). Homogenization temperatures range from 180 to 350°C: 280–350°C for the K-feldspar alteration, 240–275°C for pyrite-sericite-quartz alteration and quartz vein ore, and 180–250°C for quartz-carbonate and calcite veins. The salinities of the ore fluids are in the range of 7–17 wt% NaCl equivalent (Fan et al. 2003). The salinities of fluid inclusions containing daughter minerals can be up to 30–46 wt% NaCl equivalent (Yang 1998), which is different from the shear zone-type gold deposit with lower salinities in the range of 5–7 wt% NaCl equivalent, as documented for example by Groves et al. (1998) and Goldfarb et al. (1998). The δD values of inclusion fluids range from –57‰ to –85‰ for quartz vein ores, –48‰ to –87‰ for altered fracture ores, and –58‰ to –86‰ for breccia ores, with corresponding $\delta^{18}O_{water}$ values of 2.1‰–7.4‰, 2.8‰–9.7‰, and 1.0‰–5.9‰, respectively. These hydrogen and oxygen isotopic data are consistent with those of magmatic water, as suggested by Sheppard (1986). The fluids of the quartz-veins and altered fracture types ores may represent magmatic water mixed with some meteoric water. The fluids of the breccia-type ores is mixed with greater quantities of meteoric water, suggesting that this mineralisation developed in a relatively open system.

The $\delta^{18}O_{SMOW}$ and $\delta^{13}C_{PDB}$ values average 10.4‰ and –4.4‰ for quartz vein ores; 12.0‰ and –5.5‰ for altered fracture ores; 8.5‰, and –2.2‰ for breccia ores. These $\delta^{18}O_{SMOW}$ and $\delta^{13}C_{PDB}$ values of carbonates in quartz vein-type are close to those of the fracture-type, whereas the values of carbonate in breccia ores are of lower in $\delta^{18}O$ but higher in δ^{13}. These data are close to that of mantle-sourced carbonatite and almost overlap with those of calcites from the Cretaceous lamprophyre and mafic dykes. The character of carbon isotope compositions of the Au ores in the Jiaodong suggest that these ores formed by mixing of magmatic or mantle fluids with CO_2-bearing meteoric fluids.

Zhou et al. (2002) reported the Sr-Nd isotopic compositions of the Xincheng, Linglong, and Mouping gold deposits in the Jiaodong peninsula. The $^{87}Sr/^{86}Sr_i$ values of pyrite-sericite-quartz altered rock in the Xincheng deposit range from 0.71074 to 0.71189, and from 0.71019 to 0.71089 for the pyrites in the Linglong deposit. These values are similar to those of the Linglong granite (0.710498–0.712286), the Guojialing granodiorite (0.709361–0.711419), and lamprophyre dykes, gabbro, and porphyritic diorite (0.708926–0.710698). The ϵ_{Nd} values of gold ores range from –15.5 to –20.6, from –19.7 to –20.1 for the granite country rocks, and –12.5 to –16.9 for the lamprophyre dykes. The Sr and Sm-Nd isotopic systems suggest multiple sources for the ore metals, and that mantle-derived fluids experienced strong interaction with the country

rocks, leading to variable additions of crustal materials into the metallogenic system.

Helium isotopes provide an efficient way to trace mantle-derived fluids. Zhang et al. (2002) carried out a preliminarily study of the noble gas isotopes of the Denggezhuang, Jiaojia, Pengjiakuang, and Fayunkuang gold deposits. Their results show that the $^3He/^4He$ ratios of inclusion fluids in pyrite are 0.40–2.36 Ra. More specifically, the $^3He/^4He$ ratios of Denggezhuang (quartz vein-type) and Jiaojia (fracture-type) are 1.64–2.36 Ra, but 0.43–0.79 Ra for the breccia type in the Pengjiakuang-Fayunkuang deposits. These He isotope systematics suggest that mantle-derived fluids were involved in the metallogenic process.

The above mentioned fluid inclusion studies show that the gold deposits in the Jiaodong district are commonly rich in CO_2. The source of CO_2 in orogenic Au deposits is still a matter of debate and with inconclusive results. As mentioned previously, orogenic Au deposits have been documented to be associated with metamorphic fluids, magmatic fluids, meteoric water, or mantle degassing. The metallogenic system of the Jiaodong gold district is enriched in CO_2, suggesting that the Au mineralisation may be related to mantle fluids. This is supported by the presence of CO_2 gas pools in the Shengli oilfield adjacent to the Jiaodong area (Zheng et al. 2001; He et al. 2001), which are part of the several thousand-kilometre-long He and CO_2 gas pool belt dated to be Cretaceous to Tertiary, distributed along the Tanlu Fault zone (Mao et al. 2002c). Helium and C isotope systematics have shown that $R/Ra = 3.1–4.9$ and $\delta^{13}C_{PDB} = -3.8‰$ to $-9.9‰$ for the He and CO_2 gas pools, indicating that these result from vigorous mantle degassing. He et al. (2001) further suggested that the fluids enriched in Au and CO_2 in the Shengli oil field formed during processes of mantle metasomatism and ascended into the crust by magma advection and degassing, and then mixed with crustal fluids, subsequently involved in mineralisation events.

9.3.6.2.1 Geodynamic Setting and Ore Genesis

There are four principal views on the geodynamic setting of the Jiaodong lode Au mineralisation: (1) Sun et al. (2000) suggested that the Jiaodong Au district developed in a back-arc extensional area, during subduction of the Palaeo-Pacific plate (Kula or Izanagi) under the Eurasian plate; (2) Chen et al. (2005) proposed that gold mineralisation occurred during periods of transition from compression to extension during the collision of the Yangtze and North China Cratons; (3) Zhai et al. (2004) argued that the gold mineralisation occurred during a period of geodynamic changes between 120 and 130 Ma in eastern China; (4) Mao et al. (2002a, c; 2006) suggested that large-scale Mesozoic mineralisation in the North China craton and adjacent areas occurred during three main periods: 200–160 Ma, ~140 Ma, and ~130–110 Ma, which correspond to geodynamic settings of post-collisional extension in the North China and South China cratons and east–west lithospheric extension

caused by subduction of the Palaeo-Pacific plate. Regardless of the differences, all agree that the large-scale mineralisation in the Jiaodong region is linked to extension and/or lithosphere thinning.

Studies on Palaeozoic kimberlite intrusion in eastern China inferred that the lithospheric root was at least 180 km-thick in eastern China in the Palaeozoic, in accordance with the stability field of diamond-bearing peridotite. Studies on mantle xenoliths in Cenozoic alkaline basalts show that the lithosphere of eastern China, thinned by about 100 km from the Palaeozoic to the Cenozoic (Xu 2001; O'Reilly et al. 2001). Niu et al. (2004) and Hu et al. (2006) argued that the North China craton was affected by the impingement of a mantle plume in the Mesozoic, and that the core of the plume was located in the Bohai Sea, while mantle plume branches were active in the Jiaodong and Luxi areas (western Shandong province). The alkali ring complexes in the Luxi area, and a SHRIMP zircon U-Pb age of 177 Ma recorded for the granodiorite in the alkaline complexes (Hu et al. 2005), suggest that mantle plume activity and/or lithospheric thinning began in the Mid-Jurassic. Volcanic eruptions migrated from the circum-Bohai basins to the Luxi uplift, with ages ranging from 136–135 Ma to 124–115 Ma for the volcanic rocks in the Luxi area (Mao et al. 2007 and references therein). Several carbonatite dykes in Badou and Xueye, Luxi area, have K-Ar ages of ~123 Ma, have also been recorded and are coeval with those of lamprophyre dykes, felsic dykes, and Guojialing-type granodiorite. Therefore the period from 135 to 115 Ma is important and appears to mark a series of intracontinental thermal events, which are temporally associated with the Au mineralisation in the Jiaodong province.

Volcanism in the Cenozoic Bohai basin, gravity and magnetic anomalies, seismic profiling and hydrothermal activity, all reflect a shallow Moho depth (Xiao et al. 2004). In addition, the Bohai basin shows early Tertiary radiating and annular fault systems, from the center of the Bozhong depression (Mao et al. 2007). These features are suggestive of mantle upwelling, lithospheric thinning and crustal extension. A synoptic geodynamic model, as proposed ny Mao et al. (2007) is shown in Fig. 9.27. At ~120 Ma, lithospheric delamination and thinning, abundant lamprophyre dykes, emplaced along a group of paralleling north-northeast-trending faults, imply that the mantle magmas and fluids continuously advected into the crust (Fig. 9.27). Most of gold deposits in both Jiaodong and Eastern Qinling, and skarn-magnetite system along the Middle-Lower Yangtze belt, discussed in Chapter 6, occurred in this period. The carbon, oxygen, hydrogen, and sulphur isotopes systematics of the three types of gold ores in the Jiaodong area, show that they were formed from water-rock interaction and mixing of fluids derived from the same reservoir. The metallogenic conditions of quartz vein-type and fracture altered-type ores are basically similar, with the only difference being the different locales in the fault system (Fig. 9.27). As for the breccia-hosted gold deposits in the detachment zone at the north margin of the Jiaolai basin, fluid mixing and water-rock interaction led to more crustal fluids with greater input of carbon and sulphur

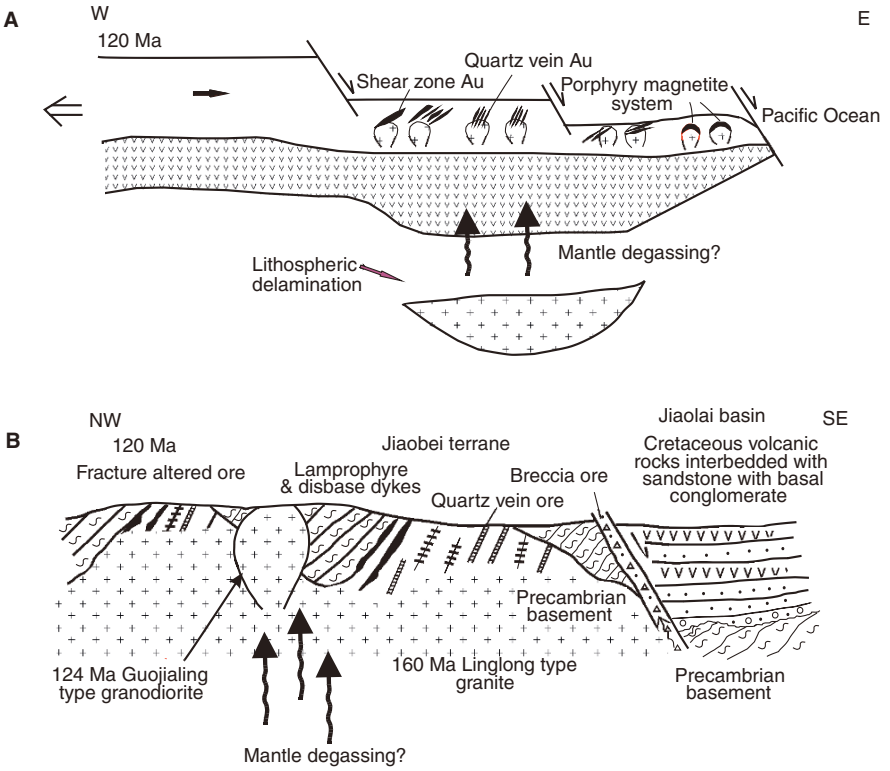


Fig. 9.27 Geodynamic model of ore formation, as proposed by Mao et al. (2007); (**A**) lithospheric thinning event during the Cretaceous caused by delamination with possibly mantle degassing, and was accompanied by intrusions and volcanic eruptions, related skarns and lode style Au mineralisation (~120 Ma); (**B**) Quartz vein, fracture altered and breccia type orogenic Au deposits in the Jiaodong area formed at ~120 Ma, their ore-forming materials probably derived from mantle fluids, which ascended together with lamprophyre and dolerite dykes, and interacted with crustal fluids and host rocks. After Mao et al. (2007)

from the crust in the ore fluids. The data show high ^{34}S values, and hydrogen and oxygen isotopic shift towards meteoric water, and the fluid mixing nature of magmatic or mantle fluids with CO_2-bearing meteoric fluids, possibly derived from the leaching of Precambrian carbonates.

9.3.7 Orogenic Lodes and Lamprophyres

From the preceding sections it is clear that there is a widespread space-time association between orogenic Au deposits and lamprophyres. Rock (1987) gave a comprehensive review of the nature and origin of lamprophyric rocks. Lamprophyres represent a diverse clan of ultramafic to mafic, porphyritic, volatile-rich, alkaline igneous rocks, subdivided by Rock (1987) into five groups: calc-alkaline,

alkaline, ultramafic, lamproites and kimberlites. Rock and Groves (1988) and Rock et al. (1989) provided data to show that the lamprophyres contain from one to three orders of magnitude more Au than other common igneous rocks. Mean values for lamprophyres range from 1.6 to 99 ppb with a global average of 43 ppb. These high values are unlikely to represent secondary Au for a number of reasons including the fact that many samples analysed were petrographically fresh and that high Au also occurs in those lamprophyres which are nowhere associated with Au. Rock et al. (1989) gave at least four explanations for the high Au contents in lamprophyres: (1) lamprophyric melts are highly enriched in H_2O, CO_2, F, K, Ba, Rb and minerals, such as biotite, chlorite and carbonates that are also present in the alteration haloes of Au deposits; (2) lamprophyres are enriched in S, an element needed to complex Au; (3) lamprophyres occur in metasomatised mantle material at depths in excess of 150 km under volatile-rich conditions, which are ideal for concentrating Au; (4) the metasomatised mantle is thought to be formed by fluids rising from core-mantle areas, these fluids would produce an Au-enriched metasomatised mantle, from which lamprophyric melts are generated. However, although all lamprophyres groups are enriched in Au, the orogenic Au-lamprophyre association seems to be restricted to calc-alkaline lamprophyres, which are spatially and perhaps genetically, associated with post-orogenic granitic intrusions.

The Au-calc-alkaline lamprophyres model "suggests that lamprophyres are part of large scale crust-mantle events in which they may contribute at least some Au, S and CO_2 to complex, crustal, metamorphic-hydrothermal systems" (Rock et al. 1989, p. 620). In the model, lamprophyre melts, produced by partial melting of a Au-enriched metasomatised mantle, underplate the crust. From this, two end members are considered. In the first, the ascending lamprophyres interact with the crust to produce granitoid-porphyry magmas, in which case Au mineralisation could form according to the magmatic model. Because lamprophyres are both very hot and enriched in volatiles, they have an enhanced capacity to melt crustal material, although it must be borne in mind that lamprophyres are not the parental melts to all granitoids, but only to the volumetrically smaller felsic stocks and dykes with which the mineralisation is associated. In the second case, the intrusion of lamprophyres would promote devolitilisation reactions and set up hydrothermal circulation in the crust, with Au being leached from the lamprophyric rocks, as well as the surrounding country rocks. Lamprophyre-derived fluids could mix with metamorphism-generated fluids. In this case the metamorphic-replacement model is satisfied. The authors also draw attention to the narrow temporal span of Au deposition, in which it appears that the auriferous fluids only enter the structural conduits during specific times which, as they speculate, could coincide with the emplacement of the lamprophyric magmas. Clearly, all intermediate stages would exist between these two end members, implying that both the magmatic and metamorphic-replacement models are partly correct. Wyman and Kerrich (1989) disputed the genetic relationship of lamprophyres with Au. They suggested that the anomalous Au present in these rocks is the result of secondary overprinting, and that a lack of correlation between Au and LREE in lamprohyres precludes

mantle metasomatism as a main process for generating Au-rich melts. Wyman and Kerrich (1989) contended that the association between lamprohyric rocks and Au is the result of a common geotectonic setting, but otherwise represent distinct processes, with the Au-bearing hydrothermal systems being largely confined to continental crust regions.

9.4 Carlin-Type Gold Deposits

Since its discovery in 1962 the Carlin deposit, of Neogene age, in Nevada (western USA) has lent its name to a type of fine-grained disseminated Au-Ag (other associated elements are As, Sb, Tl, Hg, W, Te) hydrothermal replacement mineralisation, hosted by carbonate rocks. The Carlin-type (also known as sediment-hosted disseminated gold) deposits in the western USA contain resources that are in excess of 3300 t of gold (Laznicka 2006). The discovery of similar deposits in the region and elsewhere, made it clear that Carlin is most probably an end-member of a group of deposits that displays considerable variations in their geological, mineralogical and geochemical features. Carlin-type deposits are present in Italy (Lattanzi 1999) and in China, in the western Qinling orogen and in southern and southwestern China (Mao et al. 2002b; Peters et al. 2002). Tooker (1985) edited an authoritative collection of works on Carlin-type deposits. Economic Geology published a special issue on Carlin deposits in northern Nevada (Hofstra et al. 2003). Good reviews are by Arehart (1996) and Hofstra and Cline (2000) and more recently Cline et al. (2005).

Hofstra and Cline (2000) defined Carlin-type Au deposits as "epigenetic, disseminated auriferous pyrite (marcasite or arsenopyrite) deposits characterised by carbonate dissolution, argillic alteration, sulfidation, and silicification of typically calcareous sedimentary rocks". Bagby and Berger (1985) defined two subsets: (1) jasperoidal and (2) Carlin sensu stricto. There is a complete gradation between the two, and both have a strong correlation of Au with Hg, As, Tl and Sb. The jasperoidal subset includes deposits hosted in jasperoid, quartz veins and silicified wall rocks. The term jasperoid refers to an epigenetic body that consists of fine-grained ferruginous chert, which has replaced a pre-existing rock. Most jasperoid bodies are structurally controlled or located at contacts between carbonate rocks and shale. The Carlin subset is characterised by evenly disseminated Au and Ag in rocks that are not obviously silicified. The ore zones are tabular or pod-like and extend several tens of metres from the controlling structures. The association of gold with organic carbon, and locally with hydrocarbons, is typical of most Carlin-type deposits. This organic carbon consists of veinlets, seams and particles of amorphous carbon. The precise relationship between gold and carbon is unknown, although the reducing power of the carbon may have been the catalyst for the precipitation of the gold. Organic carbon was probably introduced with the main-stage hydrothermal fluids, but in terms of ore genesis the role of the carbonate rocks is of greater importance. The removal of calcite and its replacement by silica-rich

gold-bearing ore fluids was a key factor in the formation of the orebodies. Thus, the main stage of hydrothermal activity consisted of decalcification, argillisation, silicification and pyritisation. In the Alligator Ridge district (Nevada) Carlin-type ores are associated with liquid hydrocarbons, where it is found as fluid inclusions in calcite and realgar and in vugs (Hulen and Collister 1999). Homogenisation temperatures of the oil-bearing inclusions are lower than 150°C. Hulen and Collister (1999) suggested that the Alligator Ridge (Yankee Basin) fossil hydrothermal system is similar to active, but Au-poor, geothermal system that are associated with oil reservoirs. Hulen and Collister's work has important implications because it may provide a link between Carlin-type gold deposits with Mississipi Valley Type (MVT) base metal deposits, which are also known to be associated with rift-basin settings containing oil reservoirs (Chapter 8).

Carlin-type deposits in the USA are located in the Basin and Range province, situated between the Colorado plateau in the east and the Sierra Nevada in the west. The Basin and Range province was formed by extensional tectonics, associated with mantle plume activity (see Chapter 5). Evidence of Late Cenozoic extension is provided by the presence of bimodal (basalt-rhyolite) volcanism and the development of normal faults. Precious metal mineralisation appears to be related to hydrothermal processes associated with this tectonothermal event. Carlin-type Au-Ag deposits are of Eocene age, shallow-seated, and spatially related to normal faults, which are generally occupied by pre-ore dykes (Radtke et al. 1980). Important structural controls are intersections between high-angle normal faults and minor fractures with brecciated, permeable, thin-bedded carbonate units. The orebodies are tabular, stratiform and irregularly shaped masses, passing upward into zones of argillic alteration (acid leaching) and supergene oxidation. The geometry of the mineralised zones is a function of the permeability and the nature of the bedding of the host lithologies, but in all cases it is assumed that the mineralised zones have structurally controlled feeders. Hydrothermal alteration is prominent in these deposits, the main types being argillic alteration near the surface, silicification and dolomitisation. Silicification is particularly well developed along fault zones in the vicinity of the mineralisation. Tonnages and grades of these deposits are highly variable, ranging from less than 1 Mt up to 160 Mt, with Au tenors from a fraction of g/t up to 10 g/t (Bagby and Berger 1985). Fluid inclusion studies indicate that the temperature and pressure during ore deposition are in the epithermal range, from surface hot spring conditions (100°C) to about 225°C and 30 bar. At Carlin, temperatures and salinities of the fluids were approximately 175–200°C and from 3 to 15 wt% NaCl equivalent (Radtke et al. 1980).

9.4.1 Carlin Deposits of Nevada, Western USA

Hofstra and Cline (2000) and Cline et al. (2005) reviewed the Carlin-type deposits in Nevada, where they are aligned along four trends: Getchell, Battle

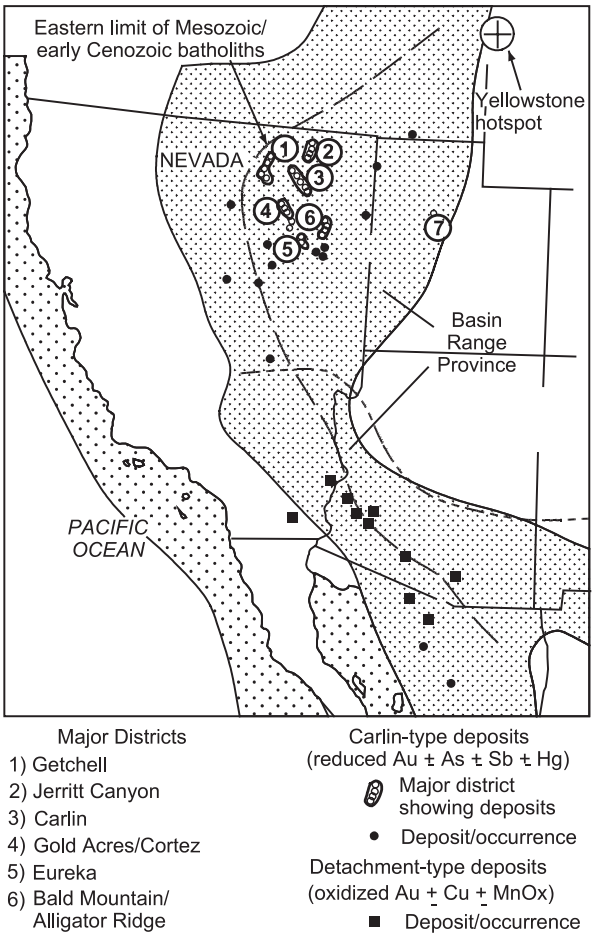


Fig. 9.28 Schematic map showing extent of the Basin-and-Range province in the western USA and Mexico; and location of major districts containing Carlin-type deposits in Nevada; note position of the Yellowstone hotspot (after Ilchik and Barton 1997)

Mt-Eureka, Jerritt Canyon and Carlin (Fig. 9.28). The work of Cline et al. (2005) is summarised in this section, followed by a short review of the classic Carlin deposit in the following section.

Individual orebodies have a variety of shapes (tabular, stratabound, carrot-like, T-shape and irregular), all resulting from zones of porosity and permeability that allowed replacement of favourable lithologies by hydrothermal fluids. Most deposits have strike lengths of up to 3 km, with depth extensions of up to 1 km or more, although the ores are stacked and do not form vertically continuous zones. An idealised cross-section of a Carlin-type deposits is shown in Fig. 9.29. Cline and co-workers pointed out that although igneous rocks are present in the area, mostly Jurassic to Neogene dykes and sills, there is no evidence of a genetic link with the mineralisation, as shown by the lack of hydrothermal alteration zoning in relation to the intrusions. Ore stage minerals

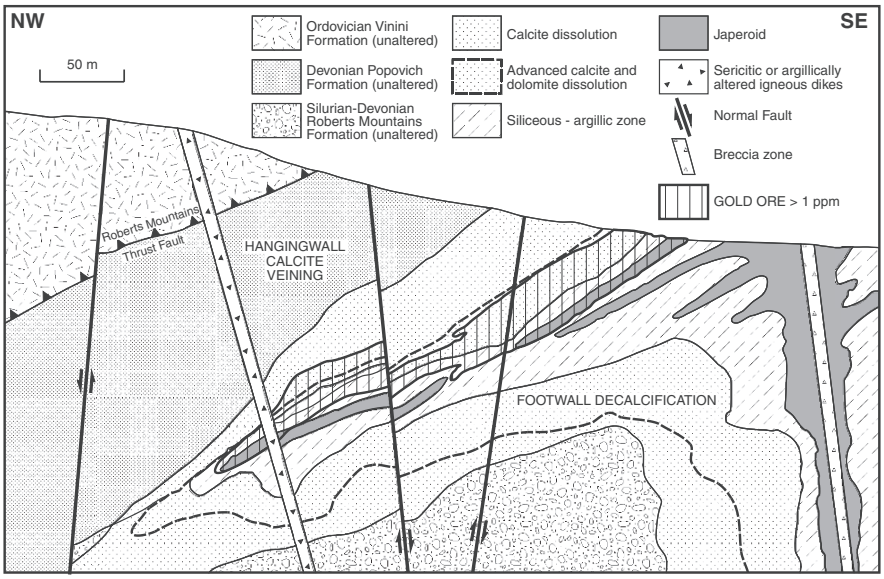


Fig. 9.29 Idealised cross section through a Carlin-type ore zone, illustrating spatial relationship between ore and alteration assemblages. After Figure A5 of Cline et al. (2005)

comprise Au- and As-bearing pyrite, marcasite, quartz, kaolinite, dickite and illite; late ore-stage minerals include calcite, pyrite, marcasite, quartz, orpiment, realgar and stibnite. Other and minor minerals are cinnabar, sphalerite and tellurides. Barite can be abundant as both a late- or post-ore stage mineral. The host carbonate rocks are dissolved and replaced by quartz and jasperoid. Where intense, carbonate dissolution may result in collapse breccias, which in turn increase permeability promoting fluid-rock interaction and the formation of high grade mineralisation. Outward from fluid conduits, mineral zoning is from dolomite to calcite, whereas calcite, siderite, ankerite, dolomite, reflecting the original composition of the wall rocks, are formed by release of CO_2 from the dissolution of carbonates. Argillic alteration results from the activity of acidic fluids and reaction with alumino-silicate minerals to form kaolinite, dickite and illite. Kaolinite and dickite are proximal to the fluid conduits, grading outward to muscovite-illite, or smectite and further out to K-feldspar. Cline et al. (2005) reported that dating of these clay minerals gave ages that are older and seemingly unrelated to Au, further adding to the debate surrounding Carlin-type deposits. Silicification is typically represented by jasperoid and to a lesser extent quartz veins. Jasperoidal textures have been interpreted to indicate temperature and depth of formation. Thus, reticulate and xenomorphic textures due to replacement are suggestive of higher temperatures ($>180^{\circ}C$) and greater depths, whereas jigsaw and chalcedonic textures with opaline silica suggest lower temperatures and shallower depths. Gold in Carlin-type deposits is typically of submicron size in pyrite and marcasite, hence the popular label of

invisible gold, although visible Au has been reported in places. Ore-stage arsenian pyrite can carry as much as 9000 ppm Au, 15 wt% As and variable amounts of Sb, Hg, Tl, Te and Cu. Carbonaceous rocks deposited in anoxic basins are very common and, as mentioned above, organic carbon and hydrocarbons are associated with the mineralisation. This carbon occurs as intergranular films and particles in pores, fractures, in quartz and calcite veins. In the Carlin trend C-rich rocks show evidence of petroleum generation, whereas in other localities, organic carbon has overmatured and converted to graphite. The organic matter may also have provided a source of H_2S by thermochemical sulphate reduction.

Thermometric measurements from main ore-stage minerals show temperatures ranging from 180 to 240°C and salinities of 2 to 3 wt% NaCl equivalent. Aqueous fluids contain CO_2, CH_4 and H_2S, with CO_2 in the fluids exerting an important control on their pH, which decreased as these fluids moved upward and cooled, causing more carbonate dissolution and engendering the formation of alteration minerals, such as kaolinite, illite and dickite. The Carlin ores do not show evidence of boiling, which together with fluid inclusion data, suggest a range of depths of ore formation somewhere between 2 and 8 km. However, apatite fission-track studies indicate that the upper parts of the deposits may have formed at depths from 300 m to about 3 km.

9.4.2 The Carlin Deposit

The Carlin deposit is situated in northern Eureka County, Tuscarora Mountains, Nevada. A brief history of the discovery of the deposit, its mining, leaching and milling operations is given by Jackson (1983). The deposit contained approximately 10 Mt grading about 10 g/t Au. The geological characteristics of the deposit have been published by Adkins and Rota (1984) and Bagby and Berger (1985), who provided the basis for the present discussion. The Carlin orebodies consist of tabular and irregularly shaped zones in the upper portions of the autochthonous Roberts Mountains Formation of Silurian age. This Formation strikes northeast and dips beneath the Roberts Mountains Thrust which is the oldest and most prominent structure in the area. Numerous high-angle faults of various ages disrupt this thrust fault. All these structures are considered to predate the mineralising event, the high-angle normal faults clearly served as channels for the hydrothermal fluids, resulting in the shattering and brecciation of the upper portions of the Roberts Mountains Formation, which was also chemically favourable and suitably positioned for ore deposition. The upper portions of the Roberts Mountains Formation are composed of two main facies of carbonate rocks. One consists of laminated, argillaceous to arenaceous dolomite with a high content of organic carbon (up to 0.8 wt%); the other is characterised by thin-bedded arenaceous rock with a low content of organic carbon (0.2–0.4 wt%). The rocks of the first type appear to have higher permeability, making them thus more suitable both for the dissolution of carbonate

and for the introduction of the hydrothermal fluids. Igneous rocks in the Carlin pit occur as fault-filling dykes of dacitic or quartz-latitic composition. In the district, however, numerous dykes and two granodioritic to dioritic stocks of Late Jurassic and Early Cretaceous age are present. The mine dykes are altered and locally mineralised.

The mineralisation occurs in several stratigraphic zones defining a northeast trend of about 2.8 km and forming three recognisable mine units: the Main Ore Zone, the East Ore Zone and the West Ore Zone. Since the ore is difficult, if not impossible, to distinguish from waste, ore control is totally dependent on assay values. The unoxidised ore is classified into five types: normal, siliceous, pyritic, carbonaceous and arsenical. Normal ore accounts for nearly 60% of the total unoxidised ore, in which some 25–50% of the original calcite was removed by the hydrothermal fluids, while small amounts of pyrite, fine quartz, Au, Hg, Tl, Sb and As were introduced. Small amounts of Au are associated with organic carbon. Siliceous ore, which accounts for approximately 5% of the primary mineralisation, contains large amounts of introduced silica and grades from normal type to jasperoidal type. Most of the Au occurs on the surfaces of fine-grained pyrite, while small amounts of very fine Au are dispersed in the hydrothermal quartz grains. Stibnite, realgar and pyrite are the sulphide minerals present in this ore type. Pyritic ore (5–10% of the primary ore) is characterised by the high pyrite content (up to 10% by volume). Pyrite occurs as euhedral to subhedral grains forming disseminations or small veinlets. Locally pyrite forms clusters of framboidal-like structures associated with organic material and quartz. Some of this framboidal pyrite is coated by Au. Small quantities of other sulphides include realgar, stibnite, sphalerite, galena, molybdenite and chalcopyrite. Hydrocarbons are also present as dissemination in the rock matrix. Carbonaceous ore, which makes up approximately 15–20% of the unoxidised ore, contains between 1 and 5 wt% organic carbon, is dark grey to black in colour and has small veinlets of hydrocarbons and other organic material. In addition to pyrite the carbonaceous ore also contains realgar, orpiment, stibnite, cinnabar, sphalerite, galena and a mineral called carlinite (Tl_2S). Au occurs both with the carbonaceous material and as coatings on pyrite grains. Arsenical ore constitutes 5–10% of the primary ore and contains high concentrations of As (0.5–10 wt%), mainly as realgar and orpiment.

Gold is associated with the carbonaceous material, as coatings on the surface of pyrite grains and as inclusions in realgar. The arsenical ore also contains unusually high concentrations of Hg, Sb and Tl, together with a wide variety of sulphides and sulphosalts. Organic carbon compounds that occur in the unoxidised Au-bearing carbonate rocks at Carlin, and in fact in many of the other disseminated sediment-hosted precious metal deposits in Nevada, consist of veinlets, seams and particles of amorphous carbon, hydrocarbons and a substance resembling humic acid. The precise nature of the Au-C association is not clear. The organic material was probably introduced with the main-stage hydrothermal solutions. In terms of ore genesis, it appears that the role of the carbonate rocks is of far greater importance due to the replacement of calcite

grains by silica containing pyrite and micron-sized Au grains. The removal of the calcite therefore created the necessary permeability for the silica-rich ore fluids. The main hypogene hydrothermal alteration at Carlin, as distinguished from the supergene alteration, is characterised by decalcification, argillisation, silicification and pyritisation, which correspond to stages of hydrothermal activity. These stages include an early hydrothermal stage, a main and late hydrothermal stage, an acid-leaching stage and, finally, a stage of supergene oxidation. Decalcification represents the earliest stage of alteration in which carbonate minerals were selectively removed and re-distributed. The initial penetration of the fractured rocks was probably made by low temperature fluids which dissolved the calcite, resulting in the increase of permeability previously mentioned. Argillisation accompanied the pre-Au decalcification stage, resulting in the formation of clay minerals. Silicification was a bulk replacement process at Carlin and is closely related to the introduction and concentration of the Au mineralisation. Pyritisation is common to most deposits of this type. Pyrite-rich rocks are locally auriferous and the pyrite grains contain Au in cavities and fractures. There are two stages of pyrite formation, the second generation of pyrite being associated with the Au mineralisation. Post-Au mineralisation hydrothermal activity is the acid-leaching stage, which resulted in the prominent alteration of the upper portions of the ore zones. This stage is characterised by the effects of the oxidation of H_2S exsolved during boiling of the fluids towards the end of the main-stage mineralising event. During this phase most of the remaining calcite together with large amounts of dolomite, were removed from the host lithologies (upper portion of the Roberts Mountains Formation and lower parts of the Popovich Formation). Organic carbon compounds and pyrite were oxidised and removed, and kaolinite and anhydrite developed.

Following the cessation of hydrothermal activity, rocks and ores underwent supergene alteration brought about by cool meteoric waters. Supergene alteration is deepest along faults and lithological/formation contacts. The oxidised ore contains varying amounts of quartz, clay (illite, kaolinite and montmorillonite) and dolomite. Small particles of Au are scattered through the rock and locked in fine-grained quartz, with lesser amounts associated with the secondary Fe oxides and clays.

9.4.3 Genetic Models

The genesis of Carlin-type ore deposits has been controversial for many years and the most recent reviews on the topic can be found in Hofstra and Cline (2000) and Cline et al. (2005). Genetic models that have been proposed for the origin of Carlin-type deposits include magmatic and non-magmatic models.

Cline et al. (2005) listed three possible models: meteoric water model, epizonal intrusion model and deeply sourced ore-fluid model. Ilchik and Barton (1997) proposed that meteoric fluids were heated by high thermal gradients

during crustal extension and the Au was scavenged by interaction of the fluids with the sedimentary rocks at depth. The meteoric water model, whilst consistent with isotopic and geochemical data, does not account for the presence of magmatic and/or metamorphic fluids identified by isotopic data in some deposits, not to mention the temporal relationship with extensive magmatism. The epizonal intrusion model puts forward that Carlin deposits may be the sedimentary-hosted equivalent of volcanic epithermal systems or even the distal expression of porphyry systems. In one epizonal magmatic model, the mineralisation is the result of distal deposition from magmatic hydrothermal fluids that originate in porphyry stocks (Sillitoe and Bonham 1990). Berger and Bagby (1991) considered that the Carlin deposits were formed as a result of granodioritic or alkaline intrusions, which produced stockworks and skarn deposits just above their roof zones. Deeply circulating meteoric waters mixed with the magmatic-hydrothermal solutions, to rise along faults and to form jaspers first. At a later stage replacement ore zones affected the finely laminated sedimentary rocks, whose carbonate and organic-rich composition was particularly favourable for the precipitation of gold and associated sulphides. The magmatic models are supported by the element association of Carlin-type deposits. Isotopic data from some deposits together with the large scale of the hydrothermal activity and the role of crustal-scale structures support the role of metamorphic and/or magmatic fluids generated at depth and channelled along crustal faults to shallower levels in the crust. Asthenospheric mantle and magmatic heat may have provided the necessary thermal energy to drive hydrothermal circulation.

Isotopic age determinations of igneous rocks and hydrothermal minerals, constrain the age of the Carlin deposits at between 32 and 42 Ma, coinciding with the magmatic events in the Great Basin (Hofstra and Cline 2000). Oppliger et al. (1997) linked the Carlin-type deposits with the Yellowstone hotspot. They argued that the impingement of the Yellowstone mantle plume beneath north-central Nevada in the Eocene, resulted in metasomatism, thermal weakening of the lithosphere and magmatism. This, in turn, caused metamorphic devolitilasation of the lower crust and widespread hydrothermal convective circulation in the upper crust. They also argued, that the source of gold and associated elements, may have been the core-mantle boundary, where the plume originated. However, Cline et al. (2005) attributed the magmatism in the Great Basin region to flat subduction of the Farallon and Kula plates beneath North America between the Late Cretaceous and Mid-Eocene, with a slab window forming under the Nevada area. High K calc-alkaline magmatism within the northern Great Basin area of Nevada initiated at ~42 Ma, culminating in Oligocene-Miocene volcanic activity in central Nevada. The southward younging of this calc-alkaline magmatic activity may have been the result of the progressive removal of the northern margin of the Farallon plate from the base of the overriding North American lithosphere, resulting in asthenosphere upwelling, magmatism and increased heat flow. The intrusion of mafic magmas into the lower crust caused partial melting of crustal material and prograde

metamorphism with generation of metamorphic and magmatic fluids, which carry the signature of mantle components.

Thus, in both cases (mantle plume or asthenospheric upwelling) magmatic and/or metamorphic fluids may have been the primary cause for the transport of metals, but progressively these fluids mixed to varying degrees with meteoric waters, during the main ore-stages. Stable isotope systematics for the Carlin ore materials, support a meteoric source for the hydrothermal fluids, which contained sedimentary sulphur and carbon. The δD values of fluid inclusions are strongly negative (–139 to –160‰), suggesting that major amounts of meteoric water were present during the alteration processes. However, high δD_{H2O} values from fluid inclusions, coupled with the presence of mantle He determined from the Getchell deposit, indicate a deep seated source for the fluids. The $\delta^{34}S$ values of different sulphides average +11‰, which is close to the average of $\delta^{34}S$ of +13‰ for the diagenetic pyrite in the Roberts Mountains Formation rocks. This would indicate that the S in the Carlin deposit was probably derived by dissolution of the diagenetic sulphides in the Formation. The $\delta^{13}C$ values of hydrothermal calcite also indicate that the carbon in the ore fluids was derived from the host rocks. Hofstra et al. (1991), using geochemical, fluid inclusion and stable-isotope data from jasperoidal, barite and calcite and chemical-reaction-path modeling, determined that mixing of two fluids and sulphidisation were responsible for the Au mineralisation of the Carlin-type deposits in the Jerritt Canyon district in Nevada. These authors propose that one fluid was evolved meteoric water, enriched in CO_2 and H_2S, characterised by δD of ~ –111‰, $\delta^{18}O$ of ~5‰ and with a temperature of 225°C, and a salinity of 6 wt% NaCl equivalent. The other fluid was dilute unexchanged meteoric water characterised by δD of ~ –118‰, $\delta^{18}O$ of ~ –16‰ and with temperatures of less than 200°C. Hofstra et al. (1991) proposed that the Au was transported as a sulphide complex, which broke down by reacting with the Fe content of the wall rocks, precipitating Au according to the reaction:

$$Au(HS)_2^{-1} + FeO + H^+ \rightarrow FeS_2 + Au + H_2O + 0.5H_2$$

where FeO is the reactive Fe contained in the wall rocks. It is interesting to note that sulphidisation of Fe-rich lithologies as a Au precipitating mechanism is also advocated to explain some of the Au mineralisation in Archaean lode deposits.

Finally, Emsbo et al. (2003, 2006) drew attention to a "protracted interplay" that involved periodic activation of basement faults and a succession of superimposed hydrothermal events in the Great Basin, from SEDEX to porphyry to epithermal and hot spring deposits, all of which would have contributed to the large Au endowment of the Carlin province in Nevada. Remobilisation of Au would have occurred especially from Palaeozoic syngenetic Au deposits (SEDEX), by interaction with meteoric fluids, powered by heat sources linked to Mesozoic magmatism. The interaction of these heated meteoric waters with the Au-rich pre-existing deposits would have generated H_2S, which suppressed the solubility of base metals, but enhancing the uptake of Au, As and other trace

elements in the ascending hydrothermal fluids and their migration into reactive Fe-rich rocks, resulting in the formation of the epigenetic Carli-type deposits (Emsbo et al. 2003).

9.5 Metalliferous Black Shales

Black shales are sediments rich in organic carbon that accumulate under anoxic conditions. It must be emphasised that these anoxic conditions are created through oxygen consumption of decaying organic matter, so anoxia is not necessarily a deep-water condition, as is commonly perceived, except for density-stratified silled basins, such as the Black Sea (Wignall 1994).

Black shales are economically very important, not only because they are the source of hydrocarbons, but also because they are commonly enriched in several trace metals (Zn, Cu, Pb, Mo, Ag, Au, V, Ni, PGE, Mn, U and REE). Black shales also host a range of exhalative type mineral systems, as for example black shale-hosted Cu and Cu-Pb-Zn deposits, such as those of the Copperbelt and the Kupferschiefer, in which the ores are hosted in reduced black mudstone, dolomite or sandstone, typically associated with red bed successions in rift basins. These ore systems are discussed in Chapter 8. Here I discuss metalliferous or polymetallic black shales, of which those of southern China constitute a good example, where metal concentrations attain grades amenable to exploitation. There is abundant literature on metalliferous black shales, which are defined as "a black shale that is enriched in any given metal by a factor of two (except for Be, Co, Mo and U, for which 1X is sufficient) relative to the U. S. Geological Survey Standard SDO-1" (Huyck 1990; Schultz 1991; Pašava, 1993, 1996). Coveney and Glascock (1989), Coveney et al. (1992, 1994), Hulbert et al. (1992), Gauthier et al. (1994), Murowchick et al. (1994), Urban et al. (1995) and Lott et al. (1999) have studied various aspects of Phanerozoic black shale-hosted ore deposits from southern China, Pennsylvania (USA), Yukon and Quebec region (Canada), and Germany. Black shale-hosted ores are also known from older rocks, such as the Palaeoproterozoic Willyama Supergroup in South Australia (Bierlein 1995). Pašava (1993) listed the depositional environments of metalliferous black shales to include: intracontinental rift-related sedimentary basins, without igneous rocks (e.g. southern China, Selwyn basin in the Yukon, Canada) and intracontinental rift basins associated with mafic volcanism. Metamorphosed black shales in the Fennoscandian shield are rich in graphite and sulphides and are spatially associated with massive sulphide deposits such as the Cu-Co-Zn Outukumpu and the Zn-Cu-Pb Vihanti in Finland (Arkimaa et al. 1999; Loukola-Ruskeeniemi 1999). A special issue of Mineralium Deposita is devoted to metalliferous black shales (Mineralium Deposita 1991).

The reason for the metal enrichment of black shales is not entirely clear. An interesting possibility, advanced by Coffin and Eldholm (1993, 1994), is that the deposition of black shales may be correlated with mantle plumes and associated emplacement of large igneous provinces (oceanic plateau and continental flood

basalt eruptions). The implication arises that black shales may owe their anomalous metal content to these vast volcanic eruptions. The indirect relationship between mantle plumes and the deposition of black shales is illustrated in Fig. 9.30. The

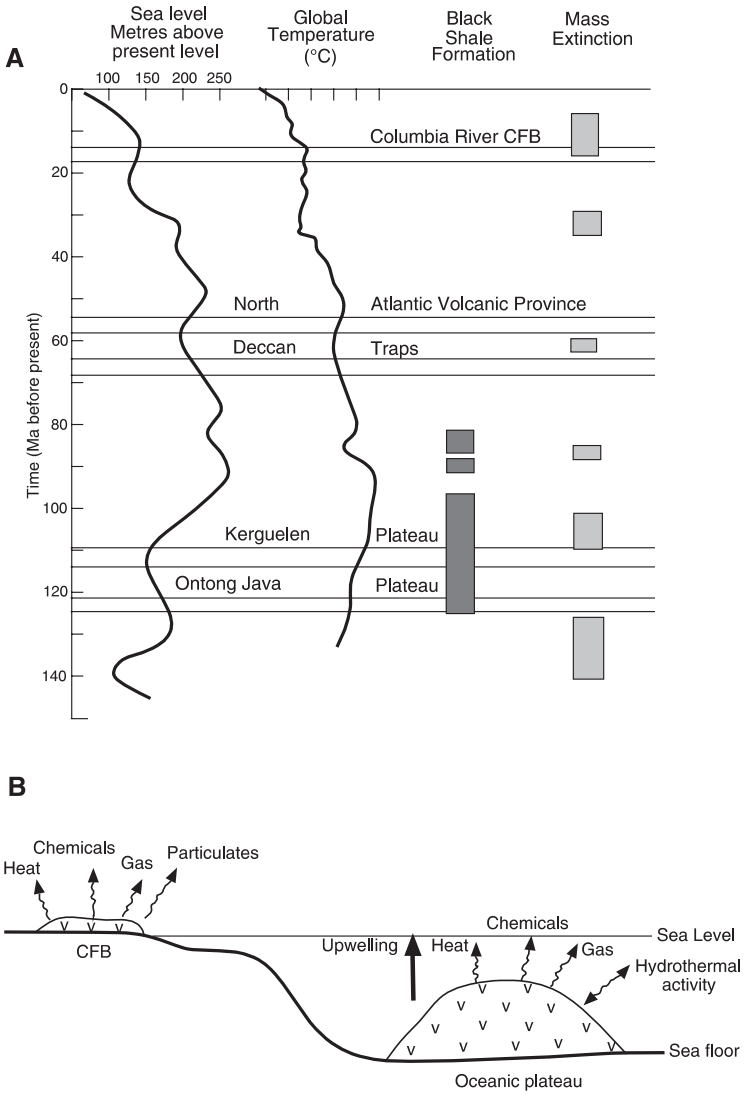


Fig. 9.30 Environmental effects due to mantle plume-related large scale eruptions that form large igneous provinces (LIPs): (**A**) correlation of sea level fluctuations, global temperatures, mass extinctions and deposition of black shales; release of CO_2 during volcanic activity promotes greenhouse warming, which enhances biomass production, and in turn, formation of organic-rich sediments (black shale); mass extinctions also appear to correlate well with the emplacement of LIP (**B**) Environmental parameters associated with the emplacement of LIP. After Coffin and Eldholm (1993, 1994)

essential element of this relationship is the reduction of the O_2 content in bottom waters. There are at least two possible reasons for this. One is the release of CO_2 in the atmosphere, caused by the eruptions of continental flood basalts, which induces global warming and reduces the amount of O_2 in bottom waters. This, in turn, contributes to anoxic conditions and the deposition of black shales. The near-contemporaneous emplacement of the Ontong Java Plateau and the deposition of black shales lend support to the idea (Coffin and Eldhom 1994). The second reason may be that oceanic plateau volcanism causes global anoxia due to increased hydrothermal venting on the seafloor, which results in a reduction of the O_2 content of bottom waters (Sinton and Duncan 1997). At present, geoscientists, mainly focusing on the polymetallic blacks shales of southern China, consider two main models: submarine hydrothermal discharge (exhalative type) and synsedimentary deposition in euxinic basin (seawater precipitation). The two models have been the topic of interesting debates (Coveney 2003; Lehmann et al. 2003). The metalliferous black shales of southern China are described below, for which in addition to the above-mentioned models, I raise the possibility of an origin associated with meteorite impact.

9.5.1 Mo-Ni-V-PGE-Au in Black Shales, Southern China: Seafloor Venting, Seawater Precipitation, or Impact-Related?

The lower Cambrian black shales in the Yangzte Platform (southern China) are enriched in Mo, Ni, PGE, Au, Ag, Zn, V and As and were first reported by Fan et al. (1973). Continental rifting on the southern and northern margins of the Yangzte Craton, controlled the platform Neoproterozoic to Cambrian carbonate-dominated depositional systems of the Craton (Wang et al. 2005). Oceanward, the platform developed a series of deep basins, which were filled with organic-rich sediments. These constitute the vast black shale province that borders the northern and southern margins of the Yangzte Craton, covering about 10^6 km^2 (Emsbo et al. 2005). The metalliferous shales horizon, which includes phosphorite and stone coal, extends along a belt 1600 km long, from Yunan Province in the south-southwest to Zhejiang Province in the east-northeast (Fig. 9.31). The metalliferous shales form a unit that is from 1 to 30 cm thick, and is underlain by 3–15 cm-thick phosphorite beds and Neoproterozoic dolomite rocks. The shale sequence is part of the Niutitang Formation (Mao et al. 2002d). The Niutitang Formation is underlain by the Neoproterozoic carbonate succession of the Dengying Formation, which in turn is underlain by a succession of black shale, locally hosting V-Ag mineralisation, chert and dolomite rocks of the Doushantau Formation. The latter rests on the 590–575 Ma tillites of the Nantuo Formation, correlated with the global Marinoan glaciation (Mao et al. 2002d and references therein). The entire

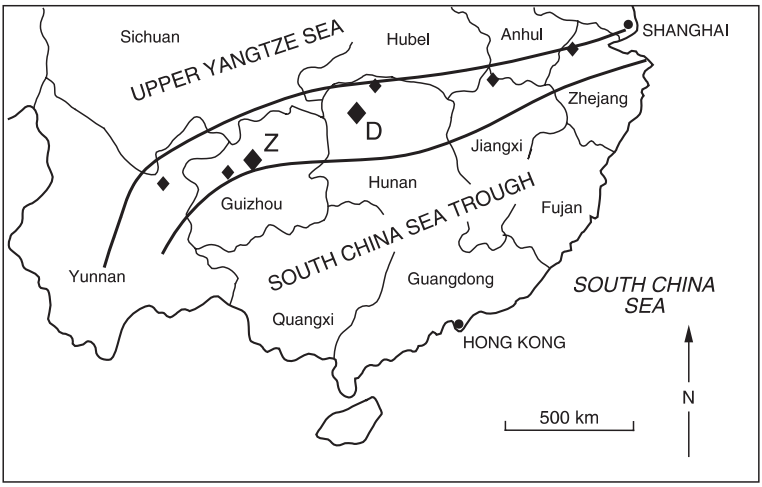


Fig. 9.31 Distribution of major black-shale hosted Ni-Mo-Au-PGE deposits in south China; the larger symbols marked Z and D, indicate deposits near Zunyi and Dayong, respectively. After Coveney et al. (1992, 1994)

sedimentary package was deposited in a sedimentary shelf environment, built on Precambrian basement of the Yangzte Craton. Rocks of the Niutitang Formation, described in Mao et al. (2002d), from older to younger, consists of:

- 0–0.3 m discontinuous lenses of Fe-Mn palaeoweathering crust, resting on undulating palaeosurface of the Duoshatau Formation;
- 0.5 m U-rich phosphorite;
- 0.5–2.5 m organic C-rich shale with lenses of phosphorite, containing collophane with 200–300 ppm U and locally economic concentrations of Mo, Ni, V, Y and light REE;
- 5 cm to 2 m Ni-Mo-PGE-Au ore unit, continuous for several kilometres, locally with flat-pebble conglomerate, colloidal Ni-Mo sulphides with nodular textures;
- Mo-V-Ni-bearing stone coal layer, consisting of organic C-rich hydromica claystone-shale with up to 35% C_{org}, 0.3% Mo, 0.2% Ni and 0.9% V;
- 100 m carbonaceous hydromica claystone-shale. The ore nodules, mentioned above, are 1–3 mm long and consist of microcrystalline Fe, Mo and Ni sulphides, a colloidal Mo-S-C phase, mixed with organic debris, quartz, carbonate, clay minerals and apatite.

The colloidal material has a composition that can be approximated by the formula (Mo, Fe, Ni) $(S, As)_2C_2$ (jordisite), a mineral phase with a layered structure that pseudomorphoses fossil bacteria and is thought to have replaced sedimentary organic material (Kao et al. 2001).

This metalliferous shale horizon probably represents a change, along a transitional shelf zone, from platform sedimentation in the northwest to a

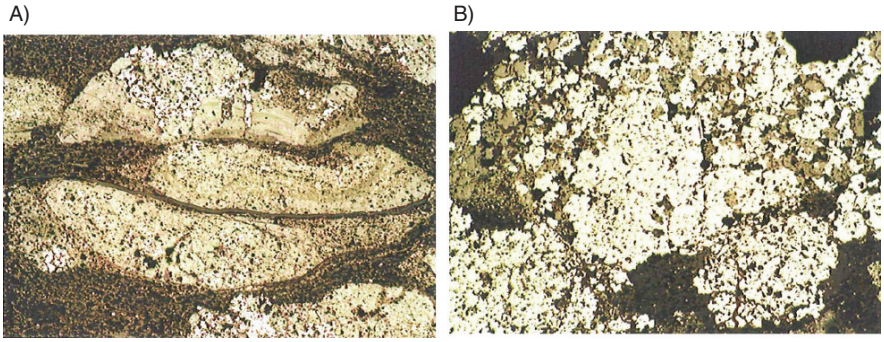


Fig. 9.32 Photomicrographs of Ni-Mo ore in black shales from Huangjiawan; (**A**) Ni-Mo-ch sulphide nodules and pyrite in carbon-rich shale and clastic debris; (**B**) recrystallised pyrite and Ni-bearing pyrite in colloidal Ni-Mo-S nodules. Base of photomicrographs is 1mm photomicrographs courtesy of Prof Mao Jingwen, Institute of Mineral Resources, Chinese Academy of Geological Sciences. See also Mao et al. (2002d)

deeper foreland setting in the southeast (Murowchick et al. 1994). These metalliferous shale beds are stratigraphically correlated with apropelic alginate or combustible shale with organic C in excess of 30%, barite and phosphorate deposits and V- and U-rich shales (Lehmann et al. 2007; Coveney et al. 1994). The sulphidic rocks are characterised by unusual textures, including polymictic mm-size pebbles, sulphide clasts or nodules in a siliceous-carbonaceous matrix and microlaminated sulphidic sediments (Lehmann et al. 2007). The sulphide nodules consist of micron-size globular aggregates (Fig. 9.32). The sulphur isotopic composition of the nodular sulphides has a wide range of $\delta^{34}S$ values, from +30 to –30‰ (Lehmann et al. 2007). The concentrations of selected elements (Ni, Cu, Zn, Mo, Ba) of black shales and associated ores are shown in Table 9.1.

At Zunyi (Guizhou Province; Fig. 9.31), the ores average 4% Mo and contain up to 7% Ni, 2% Zn, 2% As, 2% V, 1.4 ppm PGE + Au and 50 ppm Ag (Coveney et al. 1992, 1994). In the Hubei Province, black shales are enriched in Ag and V and are associated with intraclastic phosphorite, illitic shale and dolostone, at the same stratigraphic horizon as the Zunyi shales. Vanadium is contained in the illite, whereas Ag is present as sulphide, selenide and native metal (Fan et al. 1992). The ores consist of sulphides and phosphates that form laminae and nodules up to 10 mm across. The principal sulphides are pyrite, vaesite (NiS_2), gersdorffite (NiAsS) and jordisite, associated with fluorapatite, dolomite, calcite, fluorite and sulphates (barite and gypsum) (Murowchick et al. 1994; Coveney et al. 1994). The Ni-Mo-(PGE-Au) ores of the Huangjaiwan mine (Guizhou province) are characterised by a complex assemblage of sulphides and sulpharsenides, together with gersdorffite, millerite, polydymite, pyrite, sphalerite, chalcopyrite, galean and calusthalite (Belkin and Luo 2007). The paragenetically late assemblages gersdorffite- millerite-ploydymite

Table 9.1 Concentration (ppm) of selected elements in black shale (a) and sulphidic material (b) from the Niutitang Formation, Zunyi, Guizhou Province. After Jiang et al. (2006)

(a)

Element	1	2	3	4	3	4	5	6	Mean value
V	538	1629	8232	3168	8603	11 339	15 652	16 515	8209.5
Cr	218	1234	397	1591	5157	5686	2455	3153	2486.4
Co	0.21	1.8	0.26	0.83	3.53	4.03	5.96	4.89	2.689
Ni	26.1	186	42.6	124	254	308	399	337	209.6
Cu	140	524	731	379	434	1392	312	187	512.4
Zn	114	259	443	357	774	1490	3189	2318	1118
Mo	41.9	70.2	53.9	74.4	80.5	132	315	261	128.6
Ba	5231	13 686	11 384	4804	5276	5919	7163	6497	7495
Pb	23.3	32.2	21.3	27.5	30.4	36.1	44.3	51.8	33.36
U	41.2	31.6	80.9	57.1	81	71.5	66.7	80.9	63.86

(b)

Element	1	2	2	3	4	5	6	7	Mean value
V	52.8	14.9	358	149	25.4	10.4	152	102	108.06
Cr	22.9	6.73	39.7	17.6	13.1	6.5	23.2	16.8	18.32
Co	9.62	0.45	42.6	3.52	8.49	0.57	41.8	3.66	13.84
Ni	9237	615	7381	595	8789	751	9792	688	4731
Cu	814	68.7	248	24	429	74.9	451	40.4	268.7
Zn	1284	204	390	39.7	1739	194	374	39.7	533.05
Mo	2027	552	26 973	1407	1203	490	19 677	10 107	7804.5
Ba	27	66.6	40.3	128	40	25	8.64	119	56.82
Pb	61.4	5.75	137	8.05	55.7	9.79	86.8	6.46	46.37
U	57.2	16.6	90.6	5.72	61.9	34.2	123	6.8	49.5

and millerite-gersdorffite indicate temperatures of 200–300°C, which Belkin and Luo (2007) interpreted as having precipitated from hydrothermal fluids.

Re-Os isotope systematics indicate ages for the sulphide material ranging from 541±16 Ma (Mao et al. 2002d), whereas Pb-Pb isochrons yielded ages of 531±24 and 521±54 Ma (Jiang et al. 2006). Fluid inclusion studies (Lott et al. 1999) of quartz and fluorite in black shale ores in Guizhou and Hunan provinces, indicate that the minimum temperature of deposition was between 65 and 187°C. Lott et al's study also revealed that there are negative correlations between homogenisation temperature and salinity upward in the stratigraphy, suggesting boiling of fluids. This led the authors to argue for a sedimentary exhalative origin for the Chinese black shale ores. The presence of quartz veining and stockworks in the underlying dolomite units was cited in support of the model.

9.5.1.1 Genesis of Metalliferous Black Shales in China

Mao et al. (2002d) and Lehmann et al. (2007) suggested a model involving precipitation from seawater enriched in metals. According to these authors, localised euxinic basins developed in the Yangzte carbonate platform, had

stagnant water that was episodically replenished by upwelling oxidised sea water. The upwelling oxidised sea water deposited phosphorites along the raised edges of these basins, where oxidised conditions prevailed, while synsedimentary polymetallic sulphides were deposited at the bottom of the euxinic basins. Lehmann et al. (2007) used the Mo isotopic composition of sulphides from the Huangjiawan mine to monitor the isotopic signature of seawater at the time these sulphides were precipitated. The $\delta^{98/95}Mo_{MOMO}$ values (relative to modern ocean water, MOMO = mean ocean molybdenum) have a narrow range, averaging –1.24‰, quite different from that of modern oxic oceans (about –3.0 to –2.5‰). This average value of the $\delta^{98/95}Mo_{MOMO}$ in the Early Cambrian sulphides is indicative that the ocean Mo sinks were predominantly anoxic. The model calls for a seawater column similar to that of present-day Black Sea, where metal-rich sediments are in contact with a metal-depleted water column (see Einsele 2000 for an overview of the geology of the Black Sea). Bacterial sulphate reduction produces H_2S, which in the specific case of the Chinese black shales, resulted in the sulphidation of a MoO_4^{2-} ligand (Mao et al. 2002d).

The role of organic matter, principally cyanobacterial and algal mats, was emphasised by Murowchick et al. (1994). Bacterial decomposition of the organic debris may have caused deposition of metal sulphide and phosphorite beds, through replacement processes. The metals would have been introduced by hydrothermal fluids discharging into the basin either through vents or by diffuse seepage (Murowchick et al. 1994). Coveney (2003), citing Lott et al. (1999), pointed out the presence of quartz stockworks and fluid inclusions with homogenisation temperatures of up to 290°C, below the ore beds at Daping (Hunan), to suggest a hydrothermal origin for the mineralisation. Jiang et al. (2006) used REE geochemistry and the positive Eu anomaly in the sulphide ores, to infer a submarine hydrothermal origin. Their genetic model proposes venting of Ni-Mo-PGE-bearing hydrothermal fluids in a euxinic basin filled with organic-rich sediments. In this setting a hydrothermal plume rises above the vent, precipitating and adding the metals to the organic-rich muds. Polymetallic sulphides could have formed by the action of anaerobic bacteria by sulphate reduction producing H_2S that interacted with the metallic elements in the organic-rich muds.

Fan (1983), on the basis of high Ir values, first suggested the possibility of an extraterrestrial source for the southern China metaliferous black shales. This however, was rejected by Coveney et al. (1992) who found that Ir concentrations only averaged 1.7 ppb. Nevertheless, the extraordinary extent, nature and textures of the metalliferous horizon of the black shales and their equally unusual metal endownment are suggestive of extraordinary circumstances. There are no known meteorite impact that match the ~530 Ma age of the South China metalliferus black shales. The closest, but substantially older the Acraman meteorite impact in South Australia has a poorly constrained age of ~580 Ma (Grey et al. 2003; Williams and Wallace 2003). The Acraman bolide diameter is estimated to have been approximately 5 km with a collapse crater 85–90 km across, and the known

ejecta spread over a radius of greater than 560 km (Williams and Wallace 2003). The estimated impact energy was greater than 106 megatons, which exceeds the threshold for global catastrophe. The Acraman impact event occurred just prior to the evolution of animals, which preceded the Cambrian biotic explosion (Grey et al. 2003).

Examples of meteorite impact ejecta are well documented from Early Precambrian impact ejecta units. These have been carefully investigated and there is good evidence that they formed during large scale tsunami events linked to meteorite impact into the ocean (Simonson et al. 1998; Simonson 2003; Glikson 2004, 2005). Effects of mega-impacts span the range of proximal and distal features. Most proximal effects are commonly eliminated by erosion, burial and/or tectonism. However, distal effects may include widespread distribution of olistostromes, diamictites, turbiditic and tsunami deposits, and stratigraphic horizons containing microtektites and microkrystites. Spherule-rich layers have been found in the late Archaean and Palaeoproterozoic successions of the Hamersley (Western Australia) and Griqualand West (South Africa) basins (Simonson 2003). The 3.26 Ga spherule units at the base of the Fig Tree Group (Kaapvaal craton, South Africa) and the Gorge Creek Group (Pilbara craton, Western Australia) consist of vapour-condensate spherules, called microkrystites. Microkrystites are millimeter-size spherules that predominantly consist of K-feldpspar. In the Barberton greenstone belt (South Africa) spherules-rich layers, with individual spherules up to 3 mm in diameter, have Cr isotopic signatures consistent with a chondritic source and are enriched in Ir (up to >1500 pbb) (Reimold et al. 2000). In the ejecta units of the Pilbara region, in addition to vapour-condensate spherules, rip-up clasts and fragmented textures are present and they strongly resemble tsunami deposits. These ejecta units have high abundances of siderophile elements (Ni, Co and PGE), as well as V and Cr in some cases (Glikson 2005). In the light of the above, it is conceivable that the Chinese metalliferous black shales may represent the distal effects of a mega-impact(s) that occurred in the ocean and for which there is no geological record. It is also possible that the original ejecta layer could have been overprinted during subsequent tectonic and hydrothermal processes.

9.6 Nonsulphide Mineral Systems

Nonsulphide mineral systems include a range of mineralisation types that are related to supergene processes and weathering. These would also include lateritic bauxites, Fe, Ni and Au deposits, most of which are confined within a world-wide broad equatorial belt of lateritic weathering that roughly corresponds to areas of humid tropical climate. A comprehensive review of these deposits is by Freyssinet et al. (2005). In this section, however, I confine the discussion to those deposits, more strictly defined as nonsulphide ore systems, which derive from the oxidation of sulphides by supergene processes or may be of hypogene origin. A special issue

of Economic Geology is devoted to Zn nonsulphide deposits (Sangster 2003), in which classification and genetic models are given in Hitzman et al. (2003). More recently, a number of Zn-Pb nonsulphide ore systems are described in a special issue of Ore Geology Review (Gilg et al. 2008).

The supergene environment is largely controlled by the mineralogy and fabric of the primary rock type, by climate, topography, access to water and oxygen and biological activity. During weathering Fe sulphides produce significant amounts of acid causing leaching of metals (Pb, Zn, Cu) in the near surface environment. This results in a Fe-oxide rich (mostly goethite) outcrop, popularly known as gossan, typically with boxwork textures. Gossan are commonly associated with quartz, due to the release of silica during the oxidation process. For the sake of completion, it may be useful to mention that not all Fe oxides + quartz outcrops are gossans. Thus, there are false gossans, in which Fe oxides are transported along linear structures (e.g. shear zones) to form elongate outcrops; barren gossans resulting from the weathering of pyrite bodies and transported gossans, in which parts of a true gossan may have moved down a topographic slope. Trace element geochemical analyses can help in distinguishing true gossans from other types of gossan-like outcrops.

During weathering processes, Eh-pH conditions control the position and distribution of the resulting Fe oxides in what is referred to as the redox front. The oxidation of pyrite produces strong acid solutions that further promote weathering, acid attack and solubility of cations. Common weathering reactions involving pyrite are:

$$\underset{\text{pyrite}}{4FeS_2} + 10H_2O + 15O_2 \rightarrow \underset{\text{goethite}}{4FeOOH} + 8SO_4^{2-} + 16H^+$$

$$\underset{\text{pyrite}}{4FeS_2} + 8H_2O + 15O_2 \rightarrow \underset{\text{hematite}}{2Fe_2O_3} + 8SO_4^{2-} + 16H^+$$

The supergene alteration of a mineral deposit depends on the nature of the primary ore assemblage and therefore on susceptibility of being more or less weathered. Therefore deposits can be resistant to weathering, as for example the Fe oxides of banded iron formations; or susceptible to weathering, as is the case for disseminated sulphides, or highly susceptible to weathering, such as massive sulphides and/or carbonate minerals. Oxidised ore deposits typically are associated with sub-horizontal and sub-vertical zones of trace element anomalism in the weathering profile, with elemental distribution controlled by climate and topography (Granier et al. 1989; see also Butt and Zeegers 1992).

9.6.1 Classification and Genetic Models

Hitzman et al. (2003), considered nonsulphide Zn deposits for their classification, but I suggest that this is equally valid for a general case of nonsulphide deposits.

These authors divided this family of ore systems into two types: supergerne and hypogene. The supergene type is perhaps the most common and is further subdivided into: direct replacement, wallrock replacement and residual karst-fill. Supergene nonsulphide deposits can include more than one of these subtypes and are located in areas that have been subjected to extensive Neogene-Quaternary weathering. The hypogene types are dominantly silicates and oxides, occurring as pipes and veins (structurally controlled) or as stratiform lenses. Table 9.2 lists some of the more common mineral species found in nonsulphide ores. Key factors in the development of nonsulphide ore systems are the presence of a pre-existing sulphide body, strong oxidation enhanced by tectonic uplift, permeable wall rocks and efficient focussing of fluids. The role of thermophilic bacteria can be very important, particularly in highly oxidising, sulphate rich environments at temperatures ranging from 30 to 50°C (Hitzman et al. 2003).

A model for the formation of supergene nonsulphide ores and the sequence of mineralogical changes are shown in Fig. 9.33. The following is taken from the work of Hitzman et al. (2003). Direct replacement deposits are gossans (Fig. 9.33). Sphalerite is replaced by smithsonite and hemimorphite, whereas galena and chalcopyrite are replaced by carbonates, oxides and chalcocite. Mississippi Valley type ores oxidise to form simple assemblages containing smithsonite, hemimorphite and hydrozincite. Complete leaching can result in the formation of vuggy jasperoidal gossans consisting of Fe oxides, cerussite, plumbojarosite, hemimorphite and various Cu carbonates. Complete removal of Zn in areas of deep weathering results in residual Pb deposits hosted in a clay-rich gangue, as is the case for the Magellan deposit, described in the next section. Wallrock replacement deposits (Fig. 9.32) derive from the weathering of a sulphide body or a direct replacement body, in which the flow of acidic ground water moves the solutions into the carbonate wallrocks to precipitate metal carbonates. The development of a replacement deposit is favoured by the descent of the phreatic zone or tectonic uplift. Hitzman and co-authors

Table 9.2 Pb and Zn carbonate and silicate minerals commonly found in replacement nonsulphide mineral systems. From http://webmineral.com/data/ and http://www.mindat.org/index.php (both accessed in April 2008)

Mineral name	Empirical formula
Cerussite	$Pb(CO_3)$
Coronodite	$MnPbMn_6O_{14}$
Descloizite	$PbZn(VO_4)(OH)$
Franklinite	$Zn_{0.6}Mn^{2+}{}_{0.3}Fe^{2+}{}_{0.1}Fe^{3+}{}_{1.5}Mn^{3+}{}_{0.5}O_4$
Hydrozincite	$Zn_5(CO_3)_2(OH)_6$
Hemimorphite	$Zn_4Si_2O_7(OH)_2 \cdot (H_2O)$
Sauconite	$Na_{0.3}Zn_3Si_3AlO_{10}(OH)_2 \cdot 4(H_2O)$
Smithsonite	$Zn(CO_3)$
Willemite	$Zn_2(SiO_4)$
Zincite	(Zn, Mn)O

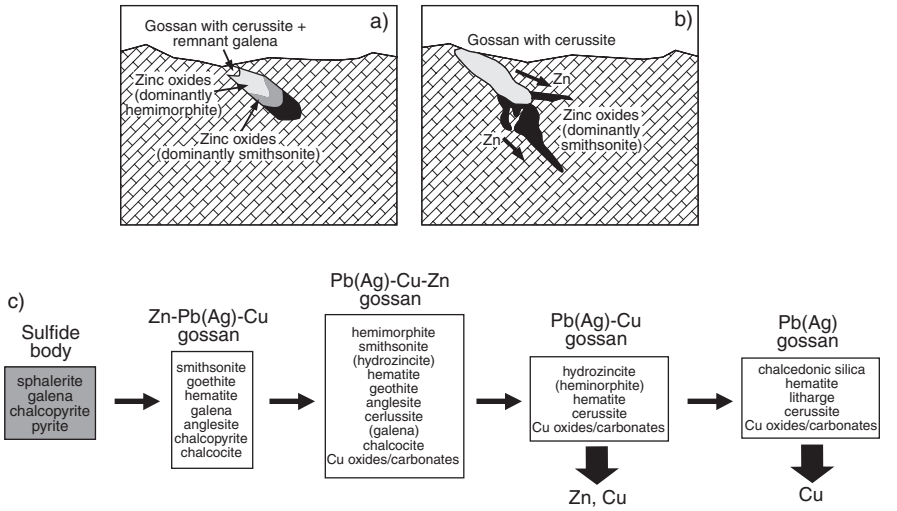


Fig. 9.33 Formation of nonsulphide ore system, after Hitzman et al. (2003); (**a**) direct replacementt; (**b**) wallrock replacement; (**c**) mineralogical changes of sulphide ore during supergene processes

pointed out that due to different metal solubilities and multicycling oxidation and leaching, Zn, Cu, Ag Fe and Pb are separated during processes of dissolution, transport and precipitation, with Zn moving farther away down the ground water gradient due to this element's greater mobility. Secondary leaching of pre-existing nonsulphide bodies involves a series of progressive mineralogical and colour changes. For example, leaching of a massive white-brown smithsonite body, produces a porous red brown Fe smithsonite-hemimorphite-hematite-goethite assemblage. Continuing leaching will produce a pale brown to red brown hemimorphite-sauconite-hematite-goethite-chalcedonic quartz, which may end up to a barren goethite-chalcedonic quartz-calcite body. During this process, Zn can migrate down ground water flow gradient to form a new secondary body containing smithsonite, minerecordite and Mn-siderite. Manto type deposits fall in the category of replacement deposits and many of these are formed in MVT and porphyry systems. An example of wallrock replacement nonsulphide deposit is Skorpion, described below.

Hypogene nonsulphide systems are not directly derived from associated sulphide bodies, or in some case they are co-precipitated, as suggested by intergrowth textures (Hitzman et al. 2003). They occur as structurally controlled veins and pipe-like bodies The main oxide minerals in these deposits include willemite, zincite, smithsonite, hemimorphite, hydrozincite, sauconite, desclozite and cerussite. Structurally controlled nonsulphide deposits are not especially common and Hitzman et al. (2003) list amongst them the Kabwe

Zn-Pb-V deposit in Zambia and Berg Aukas, described in Chapter 8. Stratiform nonsulphide deposits are mainly known from the USA (e.g. Franklin) and contain franklinite and willemite. Willemite is found in several carbonate rock-hosted Pb-Zn deposits and is commonly associated with high Zn grades. Brugger et al. (2003) modelled the formation of willemite under hydrothermal conditions and showed that, under alkaline and oxidising conditions and in the presence of sulphur and quartz in fluids, precipitation of willemite will occur rather than sphalerite. Furthermore and using the Beltana nonsulphide Zn-Pb deposit (South Australia) as an example, Brugger and co-workers were able to show that willemite can form at temperatures above 120°C as a result of fluid mixing and interaction with wallrocks. Thus, it appears that oxidised and alkaline fluids and with low activity of sulphur can precipitate willemite. Hitzman et al. (2003) noted that hypogene nonsulphide deposits, exhibit a continuum from willemite (sphalerite, galena) to sphalerite (willemite).

9.6.2 Magellan Pb Deposit, Western Australia

The stratabound Magellan nonsulphide Pb deposit is hosted in an outlier of the Earaheedy Group in the southeast of the Yerrida Basin (see Chapter 8 and Fig. 8.43) and located about 30 km northwest of the town of Wiluna in Western Australia. Its discovery was announced by Renison Goldfields Consolidated in 1993, with resources estimated at approximately 220 Mt at 2.2% lead. A feasibility study of the Magellan prospects was completed in 2001, with latest reserves (January 2007) from three operating pits (Magellan, Cano and Pinzon) totalling approximately 10 Mt, grading 6.8%, using a 3.2% Pb cut-off (http://www.ivernia.com/magellan/index.html accessed in April 2008). The deposit is currently in production and is the world's largest "pure" lead mine (Ivernia 2006). A carbonate Pb-Pb model age of 1.65 Ga was reported in Le Blanc Smith et al. (1995).

The mineralisation is hosted in variably silicified and weathered clay-quartz breccia, stromatolitic dolomite (Sweetwaters Well Member), siltstone and sandstone rocks of the Yelma Formation close to the disconformity with the underlying 2.2 Ga Windplain Group (Yerrida Basin) (Fig. 9.34; Pirajno et al. 2004). The host succession comprises, from top to bottom: a lateritic unit overlying a complex zone of silicified quartz-clay breccia, in turn overlying a progressively less weathered saprolitic clay breccia and siltstone. The footwall consists of unweathered black shales of the Maraloou Formation (Windplain Group). In this area, basement rocks, represented by Archaean granite-greenstones of the Yilgarn Craton, are unconformably overlain by sedimentary rocks of the Windplain Group, comprising a basal mature sandstone and stromatolitic carbonate, dolomite, siltsone and shale. Disconformably overlying these beds are stromatolitic dolomite, quartz-wacke, sandstone, siltstone and minor conglomerate of the Yelma Formation, the basal unit of the Earaheedy Group, forming in the Magellan area a series of outliers (Fig. 9.34). The outlier of the Yelma Formation that hosts Magellan forms a gentle syncline with a

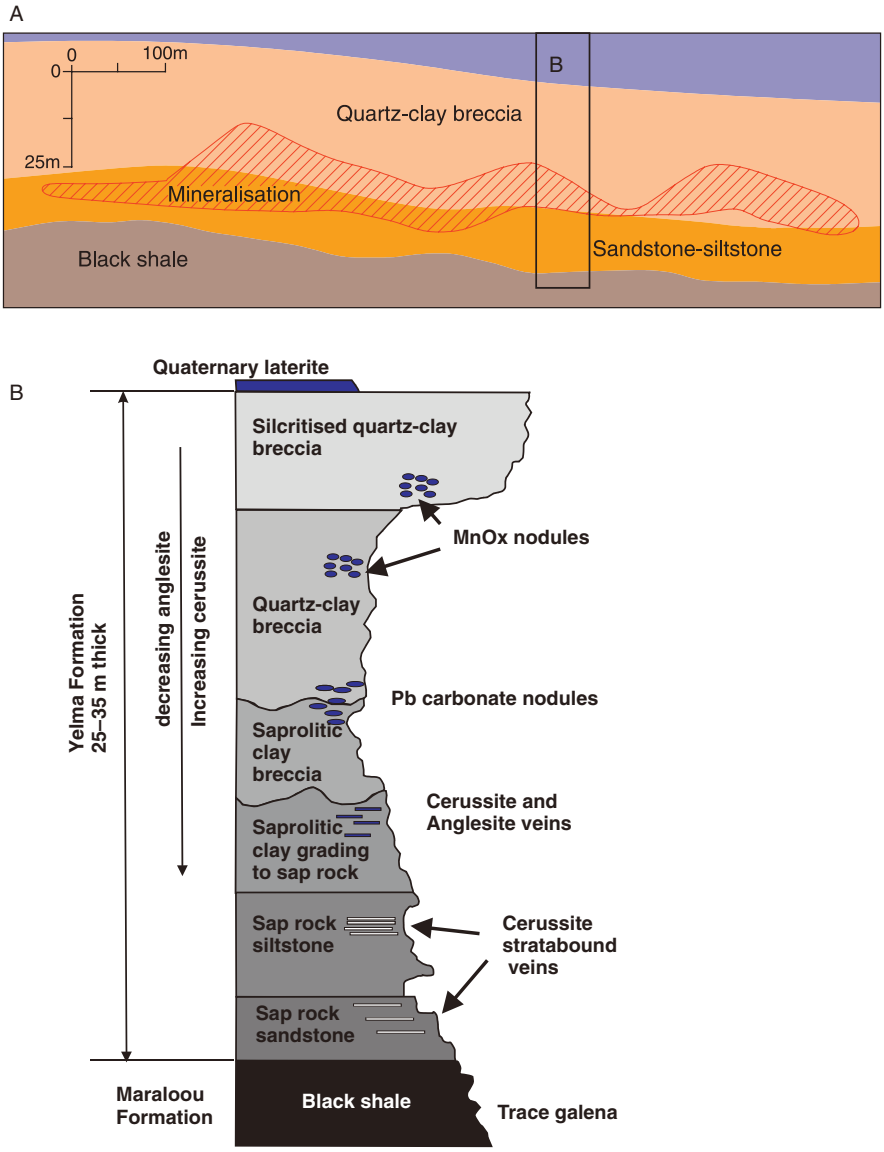


Fig. 9.34 (**A**) Cross section of the Magellan orebody, looking north, based on McQuitty and Pascoe (1998) and http://www.ivernia.com/; (**B**) Mine stratigraphy, details in text (after R. Burlow of Magellan Metals Pty Ltd, unpublished)

northwest-trending axis. In this part of the Yerrida Basin, north-northwest faults and east-west-trending fractures and mafic dykes are also present.

Magellan is an unusual mineral deposit, first described by McQuitty and Pascoe (1998), and containing cerrusite ($PbCO_3$), anglesite ($PbSO_4$), plattnerite

(PbO_2), coronadite ($PbMn_8O_{16}$), plumbogummite [$PbAl_3(PO_4)_2$] and pyromorphite [$(PbCl)Pb_4(PO_4)_3$] as ore minerals. The lead minerals are paragenetically late and form replacement mineral of the matrix of the host rocks. An idealised section of the mine stratigraphy is shown in Fig. 9.34B. The ore section is from 25 to 35 m thick and consists of the above-mentioned quartz-clay breccia, which contains clasts of silicified stromatolitic carbonate, chert, siltstone, in a clay matrix and locally cemented by crustiform and/or colloform banded quartz. Breccia clasts are from 10 mm to about 10 cm across. Neogene weathering resulted in intense silicification of the upper part of the quartz-clay breccia, forming a layer of silcrete. The quartz-clay breccia becomes progressively more clay rich downward (saprolitic) and through a highly irregular contact passes into a saprock, derived from the intense weathering of sandstone and siltstone units. The disconformity contact with the underlying black shales of the Maraloou Formation (Yerrida Group) is sharp and little affected by weathering or alteration.

Trace element analyses of ore materials indicate anomalous abundances of barium (1000–1828 ppm), manganese (1900–3672 ppm), and copper (257–400 ppm). No sulphides or other metals are present. The ore zone is a subhorizontal sheet with a high aspect ratio (Fig. 9.34), exhibiting weak vertical zoning with an anglesite zone in the upper part progressively replaced by cerussite at the lower levels. Zinc grades are very low, with a Zn/Zn + Pb ratio of about 1:1000 and with Zn contents strongly depleted (about 13 ppm) in the upper parts of the ore sheet, tending to increase downward towards the base of the oxidation to about 310 ppm (McQuitty and Pascoe 1998). Homogenisation temperatures of primary fluid inclusions in mineralised quartz range from 180 to 220°C, with salinities of 9–15 wt% NaCl equivalent (McQuitty and Pascoe 1998). The host quartz-clay breccia unit is interpreted to have originated by solution collapse of an original carbonate-hosted Pb-Zn sulphide deposit. The lack of sulphides and the unique presence of oxide minerals would suggest that the deposit might be somehow related to palaeo-weathering processes, under physico-chemical conditions, which were conducive to the oxidation and subsequence mobilisation of Pb, which could have been sourced from the breakdown of K-feldspar during weathering and then mobilised as a soluble complex in groundwater. Alternatively and more likely and as explained below (Pirajno, work in progress), the mineralisation is the residue from pre-existing MVT mineralization hosted in the Sweetwaters Member of the Yelma Formation. The Pb carbonate probably resulted from the intense and deep weathering of the precursor Pb-Zn MVT deposit, in which the sulphides were completely weathered out with removal of the more mobile elements such as Fe and Zn. The Pb was re-precipitated first as a sulphate (anglesite) and oxide (plattnerite) with reactions, such as:

$$PbS + 4H_2O \rightarrow \underset{\text{anglesite}}{PbSO_4} + 8H^+$$

$$PbS + 4H_2O \rightarrow \underset{\text{plattnerite}}{PbO_4} + H_2S + 6H^+$$

This was followed, through a combination of degassing of CO_2, derived from the dissolution of the carbonate sulphide host, and progressive weathering, leading to the formation of cerussite with a reaction of the type:

$$PbSO_4 + H_2O + CO_2 \rightarrow PbCO_3 + H_2SO_4$$

Prevailing acidic conditions continuously and progressively altered the clastic beds, stratigraphically below the dissolved carbonate rocks, to clay (kaolinite mostly). Reactions of the type shown above and the associated chemical processes have been modelled by Reichert and Borg (2008) for nonsulphide Zn-Pb ore systems. These authors envisaged two stages, which may be at least in part, applicable to Magellan. In stage 1, oxidation processes take place, possibly enhanced by bacterial activity, during which sulphides are oxidised forming sulphates and hydrous ferric oxides. This promotes a highly acidic environment, in spite of the neutralisation tendency of carbonates. The ferric oxides adsorb metals (Pb^{2+}, Ca^{2+}, Zn^{2+} and Mg^{2+}), but Pb is removed from the fluids due to the formation of anglesite (see reaction above). The important phase of this model is the neutralisation of the H_2SO_4 by carbonates, resulting in the liberation of large quantities of CO_2. Stage 2 is the post-oxidation phase, resulting in a drastic change of the entire geochemical system. The neutralisation of the acidic fluids results in an increase of the solubility of sulphates, promoting the dissolution of anglesite, which is now replaced by cerussite (see reaction above). At Magellan, however, H_2O and atmospheric CO_2, may have played an important role during progressive weathering, typically resulting in the formation of saprolite and saprock. The reader interested in weathering profiles and associated terminology is encouraged to consult Taylor and Eggleton (2001).

This model is supported by the fact that there are several MVT occurrences, east and north of the Magellan deposit, all hosted in the stromatolitic dolomite of the Sweetwater Well Member (Pirajno 2004). Another possible interpretation is that the Magellan deposit may represent the relic of a palaeo-redox front, comparable to a roll-front type uranium deposit. This interpretation is based on the nature of the quartz-clay breccia, which contains pebbles and boulders of metamorphic quartz, suggesting that it could have been a debris unit derived from greenstone rocks, and the clays in the host succession, which are indicative of a weathered palaeoregolith profile. Whereas nonsulphide Zn ore systems are well known (Hitzman et al. 2003), with most characterised by various combination of Cu, Zn, and Pb oxides and/or carbonates, Magellan remains the only one of its kind, as far as I am aware. Only one other deposit has been reported to contain cerussite ore hosted in sandstone, the Rio Pischinappiu occurrence in Italy (Fadda et al. 1998). However, the setting of this occurrence is different from that of Magellan, being hosted by volcaniclastic rocks related to a felsic volcanic complex, which is part of a calc-alkaline Oligocene-Miocene volcanic arc (Fadda et al. 1998). Furthermore, the Magellan Pb ore was formed through

dissolution of precursor sulphides, above the current ore zone, with increasing acidic conditions that resulted in the deposition of Pb sulphate first, followed by and through a progressively downward moving weathering front, the deposition of Pb carbonate (cerussite).

9.6.3 Skorpion, Namibia

The nonsulphide Skorpion Zn deposit in Nambia, is located in the Neoproterozoic Gariep fold belt of the southern branch of the Damara orogen and has a resource of 24.6 Mt grading 10.6% Zn (Borg et al. 2003). Details of the Panafrican Gariep belt and the Damara Orogen can be found in Frimmel and Frank (1998) and Miller (1983), respectively (see also Chapter 6). The following account is taken from the comprehensive work of Borg et al. (2003). The setting of the Skorpion deposit is a rift basin containing clastic sedimentary and bimodal volcanic rocks, for which an age of 751.9±5.5 Ma was determined by SHRIMP zircon dating. This volcano-sedimentary sequence was affected by Panafrican tectonic and metamorphic events at 550–545 Ma, with metamorphism reaching upper greenschist to lower amphibolite facies, accompanied by intense deformation with folding, thrusting and faulting. In the region, the development of the Gariep fold belt began with rifting that led to the opening of the Adamastor Ocean, which separated the Rio de la Plata Craton (on the present-day South American side) from the Congo Craton. Closure of the Adamastor Ocean and subduction of oceanic rocks occurred at 575 Ma, followed by the collision event at 550–545 Ma that produced strong deformation and metamorphism.

In the Skorpion area there are four major lithological units. At the base is a mafic metavolcanic unit with minor siliciclastic and carbonate intercalations, hosting disseminated and stringer sulphides and magnetite. This is followed by a barren massive dark grey marble unit, a siliciclastic unit with minor metarhyolitic volcaniclastic rocks hosting Fe hydroxides pseudomorphs after sulphides and the nonsulphide minerals. At the top is a felsic metavolcanic unit with disseminated and stringer sulphides and secondary sulphides. The lowermost sulphide mineralisation occurs as disseminations and stringers of pyrrhotite and semimassive layers of magnetite. The siliciclastic unit hosting the nonsulphide ore consist of metaarkose, quartzite and metavolcaniclastic rocks, characterised by encrustations of Fe and Mn hydroxides, interpreted as remnants of former sulphides. Sulphides occur in the uppermost felsic metavolcanic unit and consist of stringer and semimassive pyrite-sphalerite, minor galena and chalcopyrite. These sulphides also bear the imprint of oxidation and leaching.

The nonsulphide orebody is irregularly shaped and is transgressive to the layers. The main ore mineral is sauconite (Table 9.2), occurring as coatings of in intergranular spaces and voids that formed from the breakdown of detrital feldspar. The second most common nonsulphide mineral is hemimorphite, occurring as replacement and impregnation of lapilli-bearing siliciclastic

rocks. Also present is smithsonite, which together with hemimorphite is found as euhedral crystals in open spaces and fractures. All nonsulphide minerals are post-metamorphism as they do not show any deformation fabric. There are also nonsulphide Cu and Mn minerals, such as malachite, chrysocolla, atacamite, psilomelane and hydroheterolite ($Zn_2Mn_4O_8{\cdot}H_2O$). The Skorpion orebody is characterised by three styles of mineralisation: high-grade fracture fill, massive colloform and low-grade disseminations. High-grade fracture fill ores consist of silicified breccia cemented by the mineral tarbuttite [$Zn_2(PO_4)(OH)$] and scholzite ($CaZn_2(PO_4)_2{\cdot}2H_2O$), which also occur as veins and in open spaces. The massive colloform ores consist of hydrozincite and smithsonite, associated with an amorphous Mn-Zn-Ba oxide. The low-grade ores contain disseminated sauconite, which replaces feldspar and mica in the host quartzite rocks. A paragenetic sequence indicates an earlier hypogene assemblage of pyrite, sphalerite, chalcopyrite, titanomagnetite and minor galena. The oxidation and dissolution of these sulphide minerals led to at least two distinct paragenetic associations. An earlier association has secondary sulphides such as galena, chalcocite, covellite, greenockite (CdS) and brunckite (ZnS) and barite, but volumetrically more important in this paragenetic group are the nonsulphide minerals, sauconite, hemimorphite and smithsonite. The second paragenetic association manly consists of hydrozincite and hemimorphite.

As mentioned above, the Skorpion nonsulphide ores are massive, undeformed and characterised by low temperature euhedral to subhedral crystals, precipitated by meteoric fluids in pore spaces, fractures and as veins and breccia cements. Open spaces and breccias were formed as a result of sulphuric acid derived from the oxidation of sulphides and the subsequent selective dissolution of primary minerals in the host rocks. Alteration associated with the precipitation of the nonsulphide minerals is mainly silicification due to the breakdown of the feldspars.

9.7 Amagmatic Hydrothermal Systems Related to High Heat Producing Granites

> So for all you green punters, remember: wind is good when it blows, sun is hot when it shines, but hot rocks are hot all the time(M. Nahan, The West Australian, October 20th, 2007).

Highly incompatible and heat producing elements, U, Th and K are concentrated in the continental crust, with estimates varying considerably between different authors. The energy produced by the decay of these radioactive elements accounts for a large fraction of the heat flow at the surface of continents. Surface heat flow is expressed by:

$$Q = K(\delta T/\delta z)$$

where K is the thermal conductivity of the rocks, T is the temperature and $(\delta T/\delta z)$ the vertical thermal gradient (Morgan 2000). Taylor and McLennan

(1985) estimated that the upper continental crust contains 2.8 ppm U, 10.7 ppm Th and 2.80% K. Assuming a thickness of 30 km for the upper crust, the heat flow at Earth's surface is 60 mW/m^{-2} (W is watt), without taking mantle heat into account. The total heat flow from the Earth is estimated at 31±1 TW (TW = terawatt = 10^{12} watt; Hofmeister and Criss 2005). The decay energy of radioactive elements is an effective source of heat and on a geological time scale radiogenic heat comes from the decay of four isotopes, with half lives of about 10^9 years. These isotopes are ^{238}U, ^{235}U, ^{232}Th and ^{40}K. Potassium, a powerful heat producing element, contained mainly in K-feldspars and leucite, has three isotopes, ^{39}K (93.25%), ^{40}K (0.012%) and ^{41}K (6.7%). Of these only ^{40}K is radioactive, emitting β or γ radiations and it is calculated that ordinary K will release 0.27 cal/g yr^{-1}. The energy release of ^{232}Th is 0.20 cal/g yr^{-1} and of ordinary U 0.73 cal/g yr^{-1} (Heier 1978). Crustal heat production constants are presented in Table 9.3 and the mean heat flow in selected Archaean and Proterozoic provinces in Table 9.4.

Granites, especially post-orogenic and anorogenic A-type granites, and felsic alkaline volcanic rocks contain appreciable amounts of U, Th and K and therefore can generate significant heat over geological time. This has led to the term of High Heat Production (HHP) granites. A typical HHP granite containing 20 ppm U, 50 ppm Th and about 4% K would generate about 10 mW/m^3 and this multiplied many times to take into account the usual large size of a granite body, amounts to a substantial heat production over geological time (Tyler 2006). This has important implications, because HHP rocks can provide the necessary thermal energy to power hydrothermal circulation in the crust. Indeed, it can be safely assumed that the emplacement of HHP granites will result in two hydrothermal systems (McLaren et al. 1999): (1) one due to the advective heat caused by the intrusion; and (2) radiogenic decay of heat producing elements contained in the granite. The former will cause a large thermal anomaly around the intrusion, causing thermal metamorphism and heating of meteoric and/or connate fluids up to several kilometres from the intrusion. However, hydrothermal fluids may circulate long after the granitic intrusion has cooled and crystallised and this is due to high concentrations of U, Th and K, producing enough heat by radiogenic decay to enable continuing hydrothermal circulation over a period of time. In Australian Proterozoic terranes several hydrothermal deposits formed 20–40 million years after the granite intrusions, as noted for the Burnside Granite in the Pine Creek Inlier

Table 9.3 Heat production constants of natural isotopes; after Jaupart and Mareschal (2003)

Isotope	Natural abundance (%)	Half life (year)	Heat production per unit mass of isotope (W kg^{-1})
^{238}U	99.27	4.46×10^9	9.17×10^{-5}
^{235}U	0.72	7.04×10^8	5.75×10^{-4}
^{232}Th	100	1.40×10^{10}	2.56×10^{-5}
^{40}K	0.0117	1.26×10^9	2.97×10^{-5}

Table 9.4 Mean heat flow (Q) in selected provinces, after Jaupart and Mareschal (2003)

Province	Mean heat flow Q (mW m^{-2} ± one standard error)
Arhaean	
Dharwar, India	36 ± 2.1
Wiwatersrand, South Africa	51 ± 0.7
Western Australian shield	49 ± 2.1
Superior, Canada	42 ± 1.0
Proterozoic	
Central shield, Australia	78 ± 2.2
Baltic shield	31 ± 1.2
North China block	50 ± 1.1
Yangzte block, China	53 ± 0.8
Tarim block, China	44 ± 2.1
Grenville, North America	41 ± 2.0

(northern Australia) around which numerous Au deposits are distributed in a halo of about 5 km from the granite margins (McLaren et al. 1999). Numerical modelling shows that the thermal perturbation caused by radiogenic heat can extend up to 10 km from the granite margins (McLaren et al. 1999, 2003). As mentioned above, the implications of this concept is that many hydrothermal deposits that are spatially associated with HHP granites may owe their genesis or at least their late paragenetic assemblages to radiogenic heat emanated from them. Although the convective hydrothermal system generated by radiogenic heat is likely to be less vigorous than that associated with cooling magmas, it would nevertheless provide low temperature convection of considerable magnitude and for long periods of time.

There are many areas in the world that have HHP rocks and potentially amagmatic hydrothermal systems, for example the anorogenic alkaline province of Nigeria (Kinnaird and Bowden 1987), the Massif Central and Bohemian Massif in western Europe, the granites of the Bushveld Igneous Complex in South Africa, the granites of the Arabian shield (see Chapter 4), the Proterozoic granites of Australia (Wyborn et al. 1992) and those of southwest England and Cornwall, to name a few. For this section I have chosen southwest England-Cornwall and south-central Australia to discuss the post-magmatic hydrothermal fluids generated as a result of radiogenic heat.

9.7.1 Southwest England and Cornwall High Heat Producing Granites and Associated Hydrothermal Systems

An overview of the geology of southwest England and Cornwall is given in Chapter 4 and the simplified distribution of HHP granites shown in Fig. 4.13. A series of papers specifically dealing with HHP in the region include Fehn

(1985), Rankin and Alderton (1985) Stone and Exley (1985) and Shepherd et al. (1985), all contained in a special issue on high heat producing granites (The Institution of Mining and Metallurgy 1985).

Southwest England and Cornwall are well known for their 300–260 Ma granitic intrusions and associated ore systems. There are six main outcropping granitic intrusions, from Dartmoor in the east to Lands End in the west-southwest (Fig. 4.13). These granitic bodies are thought to coalesce at depth into a much larger granitic body, the Cornubian batholith. Granite types include coarse-grained megacrystic biotite granite, fine-grained biotite granite, tourmaline-bearing microgranite, megacrystic Li-mica leucogranite and fluorite-bearing granite. As outlined in Chapter 4, Sn-W and U deposits are spatially associated with these granitic bodies, as well as large kaolinite deposits, which may have had a hydrothermal component. The high temperature Sn and W ore systems are undoubtedly related to magmatic fluids and the cooling stages of the granites. However, dating of U-bearing veins indicates ages ranging from 280 to 75 Ma, suggesting that hydrothermal convection continued to operate well after the magmatic stage, and it is possible that the large kaolinite deposits developed during low-temperature amagmatic processes (Fehn 1985; Stone and Exley 1985). Present-day thermal groundwaters, with a temperature of 52°C, in the Carnmenellis Granite are indicative of this ongoing hydrothermal circulation. Fehn's (1985) numerical modelling showed that, under present day conditions, hydrothermal convection with temperatures of around 50°C is operative and in agreement with the present day thermal groundwaters of the Carnmenellis Granite.

Stone and Exley (1985) compiled a generalised paragenetic sequence of ore minerals, reproduced here as Table 9.5, which shows four mineralisation stages from early high temperature greisen to progressively younger hypothermal, mesothermal and epithermal.

Thermometric measurements give the temperatures of the mesothermal and epithermal stages at 350–150°C and <150°C, respectively, with dominant U, Pb, Ni, Bi, Co, Ag and Cu, As, Fe and Sb ore minerals. The mesothermal zone is surrounded by the epithermal zone. Age dating revealed at least four main mineralisation pulses at 290–270 Ma (magmatic main mineralisation stage), 225–215 Ma, 170–160 Ma and 75 Ma (Stone and Exley 1985). During each of these mineralisation pulses, some of the earlier minerals were dissolved and redistributed, resulting in chronologically and spatially complex sequences and multistage ore systems. Most of the exposed granites of southwest England and Cornwall exhibit degrees of kaolinisation, with the main pits extracting china-clay distributed around Dartmoor, Bodmin Moor and St Austell (Fig. 4.13). The kaolinisation process involved replacement of plagioclase and K-feldspar progressively by sericite, montmorillonite, illite and finally kaolinite. Kaolinite bodies occur as pipes and troughs, extending to depths of up to 400 m (Stone and Exley 1985). The kaolinisation is controlled by the circulation of hot acidic fluids in fractures, joints and faults, with zones of extreme kaolinisation associated with closely spaced fractures and joints. Stable isotope systematics

Table 9.5 Paragenetic sequence of vein mineralisation associated with HHP granites in southwest England; after Stone and Exley (1985)

Paragenetic Stages	GREISEN VEINS	HYPOTHERMAL				MESOTHERMAL		EPITHERMAL	
		1	2	3	4	5a	5b	6	7
T_h°C of fluid inclusions		500–250				350–150		150>	
Salinity of fluids Equiv. Wt% NaCl		40–8				10–0.1		-25	
Gangue Minerals		Quartz Feldspar Muscovite Tourmaline Chlorite Fluorite Haematite Chalcedony Barytes, Dolomite, Calcite							
Ore Minerals		Arsenopyrite Wolframite Cassiterite Molybdenite Specularite Scheelite Stannite Chalcopyrite Pyrite Sphalerite				Pitchblende Niccolite Smaltite Cobaltite Bismuthinite Argentite Galena		Tetrahedrite Bournonite Siderite Haematite Marcasite Jamesonite Sibnite	
Economically important elements		As W Sn Cu				U Ni Co Bi Zn Ag Pb		Fe Sb	
Typical form of emplacement	Sheeted veins, Stockworks, Fault-related fractures	Main Lodes, Caunter Lodes Fault-related veins, breccias, Stockworks and Carbonas				Lodes, Caunter Lodes, Faults Cross-Courses		Mainly Cross-Courses and Faults	
Wall-rock alteration		Greisenization Tourmalinization Silicification Feldsdpathization Chloritization Haematization							

provided strong evidence for the involvement of meteoric water during the kaolinisation process. The $\delta^{18}O$ values of kaolinite range from +17.9 to 20.48‰ and of δD from –60 to –66‰ (Stone and Exley 1985 and references therein), well within the range of meteoric fluids (see Fig. 1.12). These values suggest that kaolinisation is largely related to weathering, however evidence of hydrothermal kaolinite is provided by the presence of saline solutions, up to 25 wt% NaCl equivalent in fluid inclusions (Table 9.5). Stone and Exley (1985)

concluded that the obvious source of heat to generate the low-temperature and latest stages of mineralisation in the region is likely to be radiogenic due to the high abundances of heat producing elements in the Cornubian granites. For example the mean contents of U in granitic rocks range from about 3–5 ppm (Levinson 1974), whereas in the Cornubian granites U abundances range from 11 to 15 ppm, with local high values of up to 66 ppm (Simpson et al. 1979). Potassium and Th concentrations average 4.32% and 19 ppm, respectively. A geothermal gradient of 40°C km^{-1} and a heat flow of 120 mW m^{-1}, was determined for the Cornubian granites (Tammenagi and Wheildon 1977; and compare this value with those of Table 9.4). Whilst recognising that the main and initial pulses of mineralisation are related to the 290–270 Ma magmatic-hydrothermal fluids, followed by the influx of and mixing with meteoric waters (?225–215 Ma), the recurrence of mineral systems at 170–160 and 75 Ma must implicate thermal energy unrelated to magmatic activity, leaving the only alternative to radiogenic heat.

9.7.2 Central Australian Heat Flow Province

Anomalous high heat flow is recorded central Australia, where average surface heat flow is in the order of ~80 mWm^{-2} (McLaren et al. 2003). The source of this anomalous heat flow, which has been termed the Central Australian Heat Flow Province (McLaren et al. 2003), is related to high K, Th and U contents of high heat producing (HHP) Proterozoic granites. One of the outcomes of this anomalous high heat flow is the presence of amagmatic hydrothermal systems and associated surface manifestations, such as hot springs in the Curnamona Province. Brugger et al. (2005) reported and assessed the significance of the Paralana hot springs in the Northern Flinders Ranges of South Australia, a region characterised by numerous occurrences of hydrothermal mineral systems, with a wide range of ages from Palaeozoic to Neogene and including Fe oxides-U-Mo siliceous sinters, epithermal Cu-Au-Bi-V-As-U and U in sands of Neogene age, located 15 km east of the Paralana springs. In addition, the region is also the focus of current exploration for the production of geothermal energy.

In the Northern Flinders Ranges of South Australia is the Mt Painter Domain (Mt Painter and Mt Babbage Inliers), which consists of Mesoproterozoic granites and gneisses overlain by the sedimentary rocks of the Adelaide Geosyncline. Basement and the cover rocks were affected by The Cambro-Ordovician Delamerian Orogeny. The inliers of the Mt Painter Domain are charaterised by HHP granites and also characteristic is a halo of high-grade metamorphism that overprints low-grade metamorphism of the Delamerian Orogeny. Sandiford et al. (1998) attributed this unusual high-grade metamorphism, which is spatially associated with the Mt Painter Inlier, to the high concentration of HHP elements. Two important features in the region are the Lake Frome embayment, on the southern margin of the Great Artesian Basin (Habermehl 1980; visit http://www.nrw.qld.gov.au/water/gab/ (last accessed in

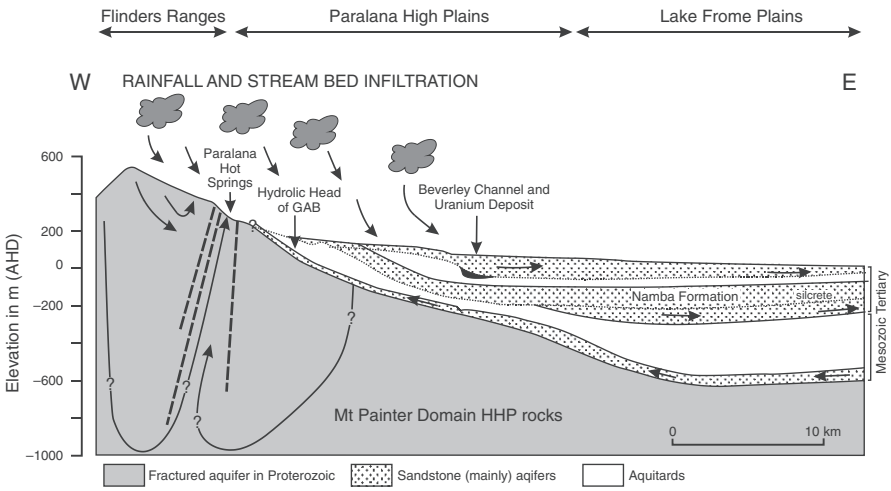


Fig. 9.35 Schematic cross-section of the Mt Painter Domain and its groundwater circulation system and Paralana hot springs. After Brugger et al. (2005)

May 2008) for information on the GAB) and the Paralana fault system. The Lake Frome embayment created during recent tectonic uplift contains Neogene marine, fluviatile and lacustrine sediments and is one of the main discharge areas of the Great Artesian Basin, through a continental sandstone aquifer (Fig. 9. 35). The long-lived northeast-trending Paralana fault system, separates the Adelaide Geosyncline from the Proterozoic Curnamona Province (see Chapter 4), with numerous splays branching off the main fault zone. The Paralana hot springs are located on this fault system, in a dilational structure associated with a deflection in one of the splays, the Lady Buxton Fault. The Paralana fault and Mt Painter Domain are within the South Australian heat flow anomaly, identified and reported by Neumann et al. (2000), where the highest surface heat flow is recorded at 126×10^{-3} W m^{-2}. The heat production of the Mt Painter Domain was estimated at 9.9×10^{-3} W m^{-3}, which is four times the heat production of average granites (Sandiford et al. 1998).

The Mt Painter Domain is host to a number of epithermal mineral systems, of which two types are recognised. One system is represented by deposits along the Paralana fault system, consisting of jasperoidal rocks, laminated and brecciated quartz veins, chalcedonic quartz and high concentrations of Au, As, Cu, Se, Te, U, Bi and V. The other epithermal system consists of quartz-hematite veins and sinter material, containing fluorite, barite, bladed calcite (indicative of boiling fluids) and late stage quartz veins with laumontite crystals. The hematite material has high concentrations of monazite and torbernite [$Cu(UO_2)_2P_2O_8.12H_2O$], whereas minor Au and roescolite have been detected in drill core. This epithermal system is associated with the U-REE-Cu-Mo-Nb Radium Ridge hematite breccia of the Mt Painter deposits (Drexel and Major 1990). The origin of these mineralised breccias was interpreted as having

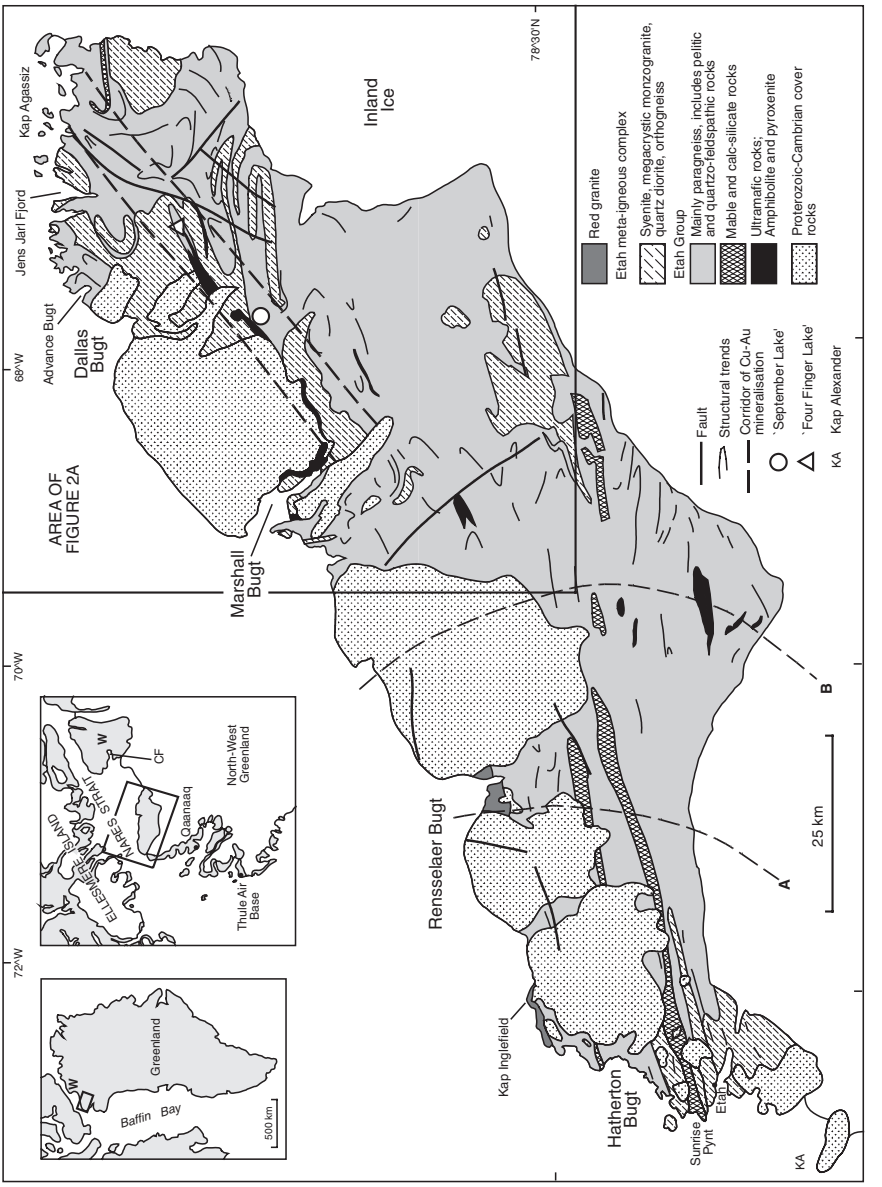
resulted from high pressure fluids related to hot spring activity. The Paralana hot springs have temperatures of 56–62°C, a pH of 6.4 and high contents of He and Rn. Field evidence shows that the Paralana fault system is a long-lived fluid conduit, along which high and low temperature fluids have been channelled with deposition of opaline silica, chalcedonic quartz and gypsum. Geothermometric calculations indicate that water-rock interaction may have reached temperatures of 95±5°C, using chalcedony, illite, K-feldspar and muscovite as minerals that have equilibrated with the hydrothermal water. Local groundwater carry high U concentrations, in which this metal is probably transported as a uranyl carbonate complex [$UO_2(CO_3)_2^{2-}$] and Brugger et al. (2005) suggested that this U may derive from the U-rich granitic rocks and may be the source of the Beverley U mineralisation in Neogene sands of Lake Frome.

Figure 9.35 depicts a model of groundwater and hydrothermal circulation in the Lake Frome embayment and along the Paralana fault system, where radiogenic heat powers the fluids that discharge as hot springs and likely produced the above mentioned epithermal style mineralisation.

9.8 An Unusual Amagmatic Mineral System in Inglefield Land, NW Greenland

Inglefield Land in North-West Greenland is an ice-free 7000 km^2 region underlain by the high-grade, polydeformed Palaeoproterozoic rocks of the Inglefield mobile belt, which extends into Ellesmere Island, Arctic Canada (Fig. 9.35). The belt consists of quartzo-feldspathic gneisses, meta-igneous and supracrustal rocks, unconformably overlain by an umetamorphosed cover containing the successions of two sedimentary basins: the sedimentary–igneous rocks of the Mesoproterozoic Thule Basin and the Lower Palaeozoic sedimentary rocks of the Franklinian Basin (Dawes et al. 2000). The Inglefield mobile belt is interpreted as the remnant of a Paaleoproterozoic juvenile arc, which collided with Archaean crustal blocks at about 1.92 Ga (Nutman et al. 2008). Aspects of the geology, geophysics, geochemistry and mineralisation of the Inglefield mobile belt are described in Dawes (1997, 1999), Henriksen et al. (2000), Dawes et al. (2000), Thomassen and Appel (1997), Nutman et al. (2008). Thomassen et al. (2000a, b) reported on the economic geology, including details of soil and rock geochemistry. Details of the unusual mineral Cu-Au system described in this section can be found in Pirajno et al. (2003) from whose work the following account is extracted.

Various expeditions by the Geological Survey of Denmark and Greenland work led to the discovery of a number of interesting Au occurrences in the northeastern part of the Inglefield mobile belt, with several rock samples assaying up to 12.5 ppm Au. In many of these occurrences Au is typically associated with Cu, with the mineralised localities being distributed along a 70 × 4 km northeast-striking corridor, which coincides with a conspicuous aeromagnetic lineament, interpreted as a deep-seated crustal structure (Figs. 9.36 and 9.37).


Kap Agassiz
Jens Jarl Fjord
Advance Bugt
Dallas Bugt
Inland Ice
78°30'N
68°W
70°W
72°W
AREA OF FIGURE 2A
Marshall Bugt
Rensselaer Bugt
Kap Inglefield
Hatherton Bugt
Sunrise Fynt
KA
Red granite
Etah meta-igneous complex
Syenite, megacrystic monzogranite, quartz diorite, orthogneiss
Etah Group
Mainly paragneiss; includes pelitic and quartzo-feldspathic rocks
Mable and calc-silicate rocks
Ultramafic rocks; Amphibolite and pyroxenite
Proterozoic-Cambrian cover rocks
Fault
Structural trends
Corridor of Cu-Au mineralisation
'September Lake'
'Four Finger Lake'
Kap Alexander
A
B
25 km
Greenland
Baffin Bay
500 km
ELLESMERE ISLAND
NARES STRAIT
CF
Qaanaaq
North-West Greenland
Thule Air Base

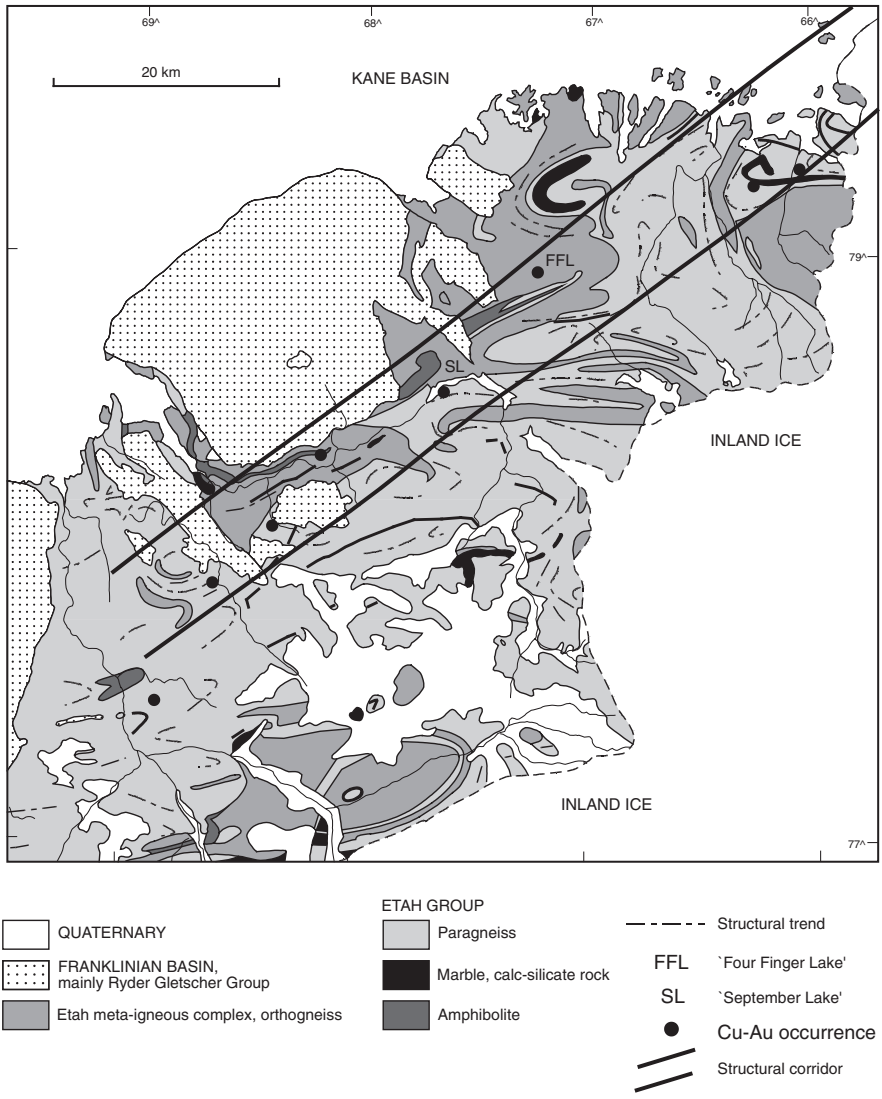


Fig. 9.37 (**A**) Simplified geological map of northeastern Inglefield Land, showing structural corridor and distribution of the main Cu-Au occurrences, after Thomassen et al. (2000a, b)

Fig. 9.36 (continued) Simplified geological map of Inglefield Land showing the Inglefield corridor (*straight dashed lines*), and localities discussed in text. *Dashed lines* labelled A and B indicate eastern limit of Mesoproterozoic basaltic sills and Thule Supergroup feather-edge limit, respectively. KA Kap Alexander, that is positioned on Fig. 9.37, W on the inset map marks Cass Fjord and Washington Land. Modified from Dawes et al. (2000)

The copper-gold mineralisation in this corridor is mainly hosted by paragneiss and is associated with sulphides and graphite.

The oldest rocks in Inglefield Land belong to the Etah Group consisting of supracrustal units containing a variety of quartzo-feldspathic and pelitic gneisses, dominated by garnet-sillimanite paragneiss, as well as marble and calc-silicate rocks, amphibolite, metapyroxenite, and intermediate to mafic orthogneiss. In several places metapelitic and quartzo-feldspathic rocks underwent in situ partial melting, producing granitic leucosomes (segregations of quartz + feldspar), veins, bands, pods and lenses of aluminous garnetiferous leucogranite, that are now exposed over areas ranging in size from a few centimetres to kilometres across. This anatectic granite, locally coalesces into larger bodies that become intrusive and discordant to the gneissic foliation. The Etah Group is intruded by the Etah meta-igneous complex, a polyphase igneous suite that mainly includes orthogneisses of dioritic, quartz-dioritic, tonalitic and gabbroic composition, late-tectonic pink granite or quartz-syenite, megacrystic monzogranite and pegmatitic granite. Post-tectonic reddish granite and quartz-syenite dykes cut all rocks. The Etah Group was deposited between 2.0 and 1.95 Ga, with the main episode of the Etah meta-igneous complex being intruded between 1.95 and 1.91 Ga. Rocks of the Etah Group exhibit intense deformation and high-grade metamorphism, in the upper amphibolite-granulite facies domain. Retrograde metamorphism is locally present, but is generally non-pervasive and more focused, and as such is confined to shear zones and faults. Retrograde metamorphism is probably associated with the influx of a fluid phase, which is discussed more fully below. Two distinct regional structural patterns characterise the Inglefield mobile belt: a dominant linear east–west trend in a southern and southwestern zone, whereas complex fold patterns characterise a central and northeastern zone.

9.8.1 Mineralisation in Northeastern Inglefield Land

The Cu-Au mineralisation is hosted by graphite-bearing garnetiferous paragneiss. Bands of sulphide ± graphite-bearing paragneiss informally referred to as "rust zones", are intercalated with a succession of garnet-sillimanite quartzo-feldspathic and pelitic paragneisses and calc-silicate rocks (Fig. 9.37). As the name implies, the rust zones typically exhibit a brown to reddish colour. These rust zones are commonly parallel to or slightly discordant with the paragneiss main foliation, suggesting a close genetic relationship. The rust zones have strike lengths from a few metres to more than 5 km, and widths from a few centimetres to 200 m. They are commonly flanked by altered wallrocks, which show bleaching due to weathering. This alteration is characterised by a bright red to red-brown coloured coarse biotite, anhedral quartz and chlorite, which replace the host mineral assemblage (plagioclase-quartz-sillimanite-garnet). Biotite and quartz are also present within the rust zones. Two localities where

paragneiss-hosted copper-gold mineralisation is well-represented are September Lake and Four Finger Lake (Fig. 9.37).

In the September Lake area a number of major rust zones, up to 200 m wide, strike eastnortheast to northeast (Fig. 9.37). In one locality the host paragneiss is associated with lenses of pyroxenite, containing disseminated and semi-massive sulphides (pyrrhotite and lesser chalcopyrite). The September Lake rust zones exhibit a mylonitic texture associated with dominant red-brown biotite. In places the rust zones show metre-sized mounds of massive pyrrhotite + graphite covered by black, white and yellow oxidation products revealed by XRD analyses to be rozenite ($FeSO_4.4H_2O$), jarosite ($KFe_3(SO_4)_2(OH)_6$), cacoxenite ($Fe_9(PO_4)_4(OH)_{15}.8H_2O$ and jahnsite ($CaFe(Fe,Mg)_2Al_2(PO_4)_2\ (OH)_2.8H_2O$.

The most conspicuous rust zones occur south of Four Finger Lake (Fig. 9.36) hosted within a 1 km-wide band of eastnortheast-striking paragneiss containing lenses of amphibolite and intruded by syenite dykes. These rust zones are all conformable with the paragneiss foliation. The sulphides include pyrrhotite, pyrite, cubanite and minor yellow-brown chalcopyrite. The yellow-brown colour of the chalcopyrite is attributed to the presence of Se. The rocks of the rust zones exhibit mylonitic to cataclastic textures, with non-pervasive, fracture-controlled potassic alteration (red biotite, sericite and minor chlorite). The sulphides in the rust zones are mainly pyrrhotite, pyrite and chalcopyrite, all spatially associated with graphite. Graphite contents range from less than 0.5–5 vol%. A common association is pyrrhotite-chalcopyrite-graphite. Other, but minor, sulphide species include sphalerite, galena, pentlandite, arsenopyrite, cubanite and marcasite. Locally native Cu is present. In some cases the sulphides are distributed along microfractures, or form networks around silicate grains. Textural relationships suggest that graphite post-dates the sulphides. Sulphides are in places associated with Fe-Ti oxides and/or magnetite. The sulphides form disseminations up to 30% vol% but in places they are massive pods or lenses up to 20–30 m, and about 0.1–0.5 m wide. The sulphides are strongly oxidised, and products include Fe oxyhydroxides, sulphates and locally native sulphur. As mentioned above, whole-rock XRD analyses revealed the presence of hydrous Fe sulphate, hydrous Fe phosphate and jarosite.

A rust zone is typically made up of a polygonal mosaic of quartz-plagioclase (oligoclase-andesine)-red-brown biotite, with intergranular graphite flakes and pyrrhotite. The biotite is commonly located along microfractures and is associated with strained and fractured quartz. In other examples, the coarse red-brown biotite is associated with poikilitic-like large K-feldspar and/or quartz crystals (enclosing quartz and biotite). Plagioclase, where still recognisable, is fractured and altered to a fine aggregate of sericite crystals. Other, but less common alteration minerals are chlorite and epidote. Monazite and apatite are locally present. Many rust zones in the localities described above, exhibit mylonitic or cataclastic textures.

Whole rock assays of samples from the rust zones show values of up to 0.4% Cu and 8.6 ppm Au. Samples that contain elevated abundances of Cu and Au

also have anomalous Zn, Mo, Ni, Co, Ba, La, Th, but the highest Cu values do not necessarily correspond with the highest Au values. However elevated Au always has corresponding elevated Cu. Statistical analyses indicate that correlations above 0.45 exist between Ag, As, Se, Pt, S, Y, U and Th. No statistical correlation is present between Cu and Au.

The crystallinity or structural order of graphite is a function of temperature, with high degrees of ordering reflecting high metamorphic grade. The use of graphite geothermometry was tested by Luque et al. (1993), who established by means of X-ray diffraction a relationship between the structural ordering of graphite (d-spacing and c dimension) and temperature. X-ray powder diffractometry and using the calibrations of Luque et al. (1993) the estimated graphite c dimensions for the Inglefield Land graphite indicate temperatures of formation of between 650 and 700°C, which are within the range of upper amphibolite facies metamorphism. Luque et al. (1993) pointed out that graphitisation is also related to shear stress and frictional heat and that the highest graphite crystallinities are observed in areas of higher shear stresses. Sulphur isotope analyses of pyrrhotite give $\delta\ ^{34}S$ values ranging from – 6.2 to + 9.3‰, with two values close to 0 (0.1 and 0.2‰). The relatively narrow range of the $\delta\ ^{34}S$ values would suggest no bacterial sulphate reduction. This range of $\delta\ ^{34}S$ values of the Inglefield Land pyrrhotites is similar to that recorded for sulphides of the Macraes Au deposit (Section 9.3.5.2 and Craw et al. 1995). The limited or absence of S isotope fractionation and given the age of the host rocks (~1.9 Ga) indicates a reducing or oxygen-deficient and a high-temperature environment, as well as a single source for the sulphur (Craw et al. 1995).

9.8.2 Origin of the Rust Zones and Ore Genesis: A New Mineralisation Style?

The main features of the rust zones can be summarized as follows:

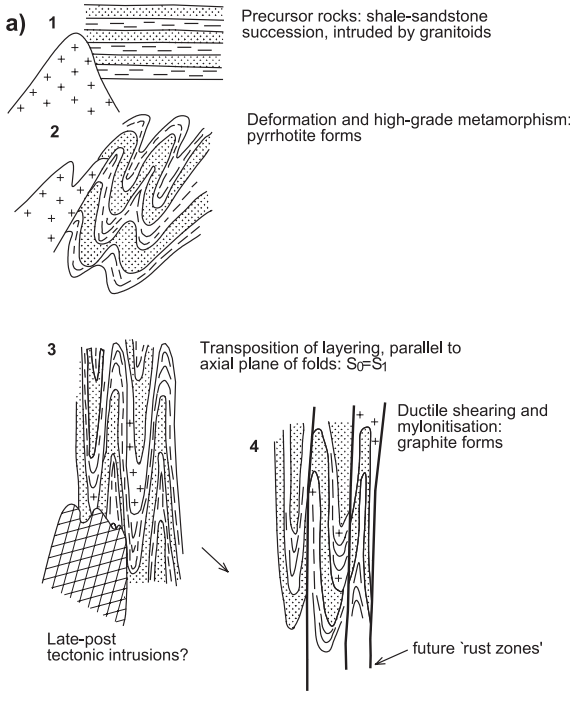
- The rust zones form well-defined bands predominantly parallel to the regional foliation of the paragneiss
- Presence within the rust zones of mylonitic and/or cataclastic textures
- Copper-gold association in rust zones is essentially confined within a NE-trending corridor
- Silicification, and hydrolitic (chlorite and biotite) alteration assemblages overprint of the rust zones and wallrocks and this alteration is retrograde with respect to the regional granulite facies metamorphism
- Narrow range of $\delta\ ^{34}S$ values
- Pyrrhotite-graphite association

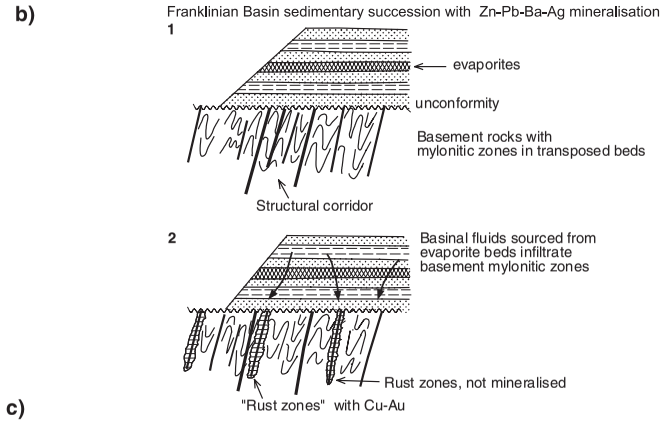
The association of graphite with Au mineralisation in metamorphic rocks is fairly well documented. Dissanayake and Rupasinghe (1992) reported on the gold-graphite association in granulite rocks in Sri Lanka, where numerous gold

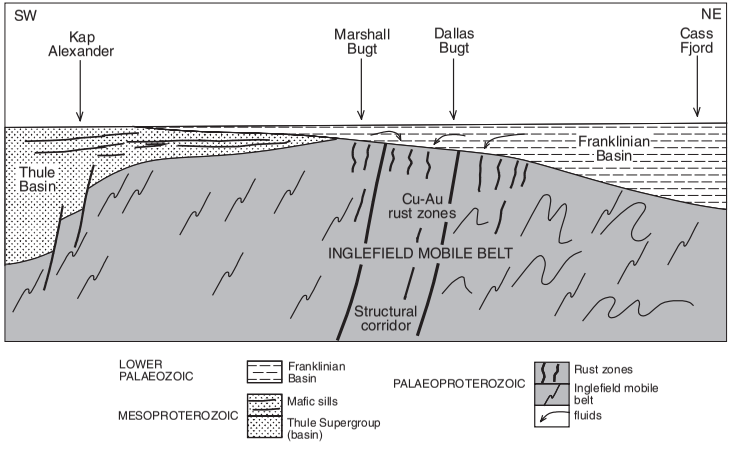
occurrences are present in narrow bands containing graphite, sulphides and sulphates. Interestingly, the Sri Lankan graphites are also enriched in Ba, Mn, Mo, Ni and Cu. Dissanayake and Rupasinghe (1992) suggested that these gold-graphite deposits may be related to mantle-derived CO_2 fluids that moved along major deep-seated fractures during metamorphism and deformation events. An association of graphite + pyrrhotite in quartzo-feldspathic gneiss of granulite facies metamorphism, that appears to be similar to the Inglefield mobile belt occurrences is reported from New Jersey (USA) by Volkert et al. (2000). These authors, taking into account the negative $\delta\ ^{13}C$ values (–6‰) of the graphite and the comparatively narrow range of $\delta\ ^{34}S$ values (0 to +9‰), attributed the origin of the graphite to high-grade metamorphism of organic matter in the sedimentary precursor, possibly algal mats. The previously mentioned mineralisation in the Macraes Au-W deposits is hosted by graphitic schist (biotite-grade metamorphic zone, Otago Schist) within a low-angle thrust system. Craw et al. (1995) attributed the origin of this graphite to metamorphism of carbonaceous material in pelitic rocks and suggest a link between the graphite and the Au mineralisation. Graphite forms at high temperatures (>500°C) and is probably also related to shear stresses. Graphite tends to buffer the fO_2 to low values and is stable with magnetite and Fe-Mg silicates in reduced fluids (Spear 1993). Gold can be precipitated, owing to decreasing values of fO_2 in carbon-rich ore fluids, in which the graphite acts as a reductant of Au complexes, such as $AuCl_4$ (Dissanayake and Rupasinghe 1992). The origin of graphite in high-grade quartzo-feldspathic gneisses is controversial (biogenic versus abiogenic C), with the source of the C being attributed either to metamorphic devolatilisation reactions from organic materials (biogenic C; e.g. Volkert et al. 2000), or mantle degassing (abiogenic C; Dissanayake and Rupasinghe 1992). In conditions of high T and high P, and of low-oxygen, the CO_2 is converted to graphite. One possible reaction that could account for the origin of graphite is:

$$CO_2 + CH_4^- \rightarrow 2C + H_2O$$

In the Inglefield Land rust zones, there is evidence that graphite cross-cuts pyrrhotite and is therefore of later generation. On the basis of the points outlined above Pirajno et al. (2003) proposed a model, in which mylonitised or sheared paragneiss rocks provided the channelways for the infiltration of hydrothermal fluids. The model is shown in Fig. 9.38 and discussed below. The precursor rocks of the quartzo-feldspathic and pelitic gneisses were probably alternating sandstone and organic-rich (carbonaceous) argillaceous sediments (shale). Upon high-grade metamorphism and under dominant reducing conditions, these rocks converted to paragneiss, with the original diagenetic sulphides changing to pyrrhotite. Deformation events caused transposition of the precursor sandstone-carbonaceous shale beds parallel to the axial plane of folds. With ongoing deformation, shear or mylonitic zones formed along the transposed layers, especially or exclusively along the less competent carbonaceous shale beds. Thus, a first-step in the origin of rust zones may be linked to a


a)
1
Precursor rocks: shale-sandstone succession, intruded by granitoids
2
Deformation and high-grade metamorphism: pyrrhotite forms
3
Transposition of layering, parallel to axial plane of folds: S_0=S_1
4
Ductile shearing and mylonitisation: graphite forms
Late-post tectonic intrusions?
future `rust zones'


b)
Franklinian Basin sedimentary succession with Zn-Pb-Ba-Ag mineralisation
1
evaporites
unconformity
Basement rocks with mylonitic zones in transposed beds
Structural corridor
2
Basinal fluids sourced from evaporite beds infiltrate basement mylonitic zones
Rust zones, not mineralised
"Rust zones" with Cu-Au


c)
SW
NE
Kap Alexander
Marshall Bugt
Dallas Bugt
Cass Fjord
Franklinian Basin
Thule Basin
Cu-Au rust zones
INGLEFIELD MOBILE BELT
Structural corridor
LOWER PALAEOZOIC
Franklinian Basin
Mafic sills
MESOPROTEROZOIC
Thule Supergroup (basin)
PALAEOPROTEROZOIC
Rust zones
Inglefield mobile belt
fluids

precursor lithology such as black shales, which originally contained organic matter and diagenetic sulphides. Ductile shearing during transposition of carbonaceous matter-rich layering converted organic matter to graphite. Therefore the rust zones are interpreted as replacement sulphide-graphite deposits. This replacement is generally pervasive, so that the structure and textures of the mylonite or shear zone are almost completely obliterated. However, the association with a possible regional crustal structure, and cataclastic/mylonitic textures of the rust zones and the retrograde metamorphism or hydrothermal alteration of the wallrocks, suggest that the introduction of fluids into these structures occurred after the formation of graphite-pyrrhotite replacement zones. These zones of ductile shearing and mylonitisation represent the future rust zones, which acted as channelways for infiltration of cooler fluids at later stages. Fluid flow in the crystalline basement that constitutes the Inglefield mobile belt had to be structurally-controlled, because porosity in high-grade metamorphic rocks is very low, effectively restricting fluid flow to intergranular porosity (Cox et al. 2001). Whatever the origin of the fluids, their infiltration caused stages of retrograde potassic (biotite), chloritic alteration and silicification, engendering remobilisation of sulphides, and introducing elements such as Cu, Au, Pb, Mo, etc. depending on the nature of the lithologies with which the fluids interacted. With regard to the infiltrating fluids, Pirajno et al. (2003) advanced two possibilities: (1) metamorphic and/or igneous-related fluids and (2) deep-penetrating surface waters and/or external brines. Metamorphic fluids derive from dehydration reactions during prograde metamorphism, producing both H_2O and CO_2 (if carbonate rocks are present). Details on the circulation of metamorphic fluid systems and their role in metallogenesis are discussed in Section 9.2.1. Oliver et al. (1998), pointed out that during prograde metamorphism metals, such as Cu and Au, are dissolved, whereas their precipitation

Fig. 9.38 (continued) Model to explain origin of the rust zones and the Cu-Au mineralisation. (**a**) Precursor rocks are a succession of sandstone, carbonaceous shale and possibly marl (1); these are intruded by granitoids and subjected to polyphase deformation and metamorphism up to granulite facies; pyrrhotite is formed from early diagenetic sulphides, (2) resulting in transposition of layering parallel to the axial plane of folds, late-post tectonic granitoids may have intruded at this stage (3), with ongoing deformation ductile shearing and mylonitisation occurs along limbs of the less competent lithologies, such as carbonaceous shale; graphite forms from carbonaceous shale (4). (**b**) Franklinian sediments are deposited in a basin that unconformably overlies rocks of the Inglefield mobile belt (1); during compaction of the sediments, evaporite-sourced fluids flow downward to the hot basement and infiltrate the mylonitised zones, resulting in remobilisation of sulphides; precipitation of the ore elements preferentially occurred in the rust zones within a structural corridor (2). (**c**) Schematic cross-section across the Inglefield mobile belt, showing assumed original extent of the overlying Thule and Franklinian Basins. In the west the sedimentary succession of the Thule Basin was intruded by mafic sills, which may have acted as impermeable barriers to descending basinal fluids. Most rust zones occur east of the Thule Basin onlap to the Inglefield mobile belt basement, and beneath the Palaeozoic sedimentary succession of the Franklinian Basin. After Pirajno et al. (2003)

occurs during stages of retrograde metamorphism. The narrow range of S isotopes values could point to fluids originating from an igneous source. The only igneous source in the region that could have introduced fluids into the rust zones are the late-tectonic megacrystic monzogranite intrusions. However, no alteration patterns were noted that could be associated with the granitoid rocks. Moreover, the Cu-Au mineralisation in the rust zones is effectively confined within the structural corridor shown in Fig. 9.37 and is not spatially associated with the granitoids that crop out outside of the corridor. Yardley et al. (2000) stressed that retrograde alteration of high-grade metamorphic basement rocks is related to infiltration of fluids along fractures and shear zones and that this retrogression is associated with the hydration of high-temperature anhydrous mineral phases. In discussing possible sources of the fluids, Yardley et al. (2000) suggested that there are settings in which this retrograde alteration could be caused by basinal brines that infiltrate the basement from above, and concluded that fractures in brittle, dry crust would "pull water down" from overlying sedimentary basins.

In western and southwestern Inglefield Land the shield rocks are unconformably overlain by Mesoproterozoic deposits of the Thule Basin (Thule Supergroup; Dawes 1997) disconformably overlain by Cambrian rocks of the Franklinian Basin. In Inglefield Land the Thule Supergroup represents a marginal wedge succession, 0–300 m thick, composed of siliciclastic rocks with prominent and regionally persistent basaltic sills up to 70 m thick (Fig. 9.38). The Cambrian section, cut by the present erosion surface, represents only the lowermost strata of the shelf succession of the Franklinian Basin that, to the north in Washington Land and in the west in Canada, is up to 3 km thick comprising dolomites and limestones with important intervals of evaporite, shale and siliciclastics (Henriksen et al. 2000). Farther north, the trough deposits of the Franklinian Basin have a total thickness of at least 8 km. Units in the shelf succession can be traced over long distances, for example the Ordovician evaporite formations can be traced through Canada and Greenland for over 1000 km. Based on regional geology it is assumed that Cambrian, Ordovician and Silurian shelf rocks once covered Inglefield Land. The Franklinian Basin succession would have provided an ideal source of brines as well as complexing ligands, such as Cl^-, which transported metals and infiltrated into the crystalline basement. The idea of external basinal brines causing hydrothermal alteration (and therefore retrogression) and mineralisation has been examined and modelled, in connection with Fe oxide-Cu-Au hydrothermal systems, by Barton and Johnson (2000), who proposed that evaporite-derived brines can cause deep-seated alkali metasomatism, with no magmatic water being necessary. Pirajno et al. (2003) envisaged that external brines derived from the Franklinian succession, infiltrated the basement into the structural channels provided by the shear/mylonitic zones, created during advanced transposition of sandstone-shale layers. At the regional scale, this infiltration was facilitated by the northeast-trending corridor, postulated to be a regional crustal structure spatially associated with the Cu-Au occurrences in the rust zones and a regional break outlined by total magnetic intensity imaging . The lack of apparent isotopic age

resetting younger than the disturbances at 1.8 and 1.75 Ga mentioned earlier can be explained by assuming that since fluid flow is focussed into discrete structures, the isotopic systems of the surrounding rocks are not affected.

The Franklinian succession in Washington Land hosts fault-controlled MVT mineralisation at two stratigraphic levels: Pb-Zn-Ba mineralisation in the Upper Cambrian Cass Fjord Formation and Pb-Zn-Ag mineralisation in the Lower Ordovician Cape Clay Formation (Jensen and Schønwandt 1998; Dawes et al. 2000). The youngest strata preserved in Inglefield Land are stratigraphically below these levels containing enrichments in the same elements, in addition to Au. A key factor for the understanding of the Inglefield Land rust zones is the nature and origin of the fluids that caused the mineralisation. The proposed model, Palaeozoic brines acting on Proterozoic structures, although isotopically and geochemically poorly constrained, is viable on the basis of the available evidence. The closest analogue to the Inglefield Land rust zones is the graphite + pyrrhotite mineralisation in quartzo-feldspathic rocks of New Jersey (Volkert et al. 2000). The Inglefield Land rust zone may well represent an amagmatic new mineralisation style.

9.9 Concluding Remarks

In this chapter I have dealt at some length with orogenic lode systems that formed in two different geodynamic settings. One is that of accretionary tectonics and subduction-related collision zones, whereas the other is an intracontinental setting, associated with collision events, but followed by extensional tectonics, asthenospheric upwelling, granitic magmatism and metamorphic devolatilisation. The orogenic and metamorphism-related lode systems, although a "coherent group of deposits" as correctly labelled by Groves and co-workers, still present unsolved issues, particularly with regards to the involvement of magmatism in providing a source of fluids and metals. I have used examples from the Yilgarn Craton, Muruntau, Sukhoi Log, lode deposits in New Zealand and in China, all of which have clear similarities in the style of mineralisation. One of the common features, not often considered, is the association of orogenic lodes with calc-alkaline (shoshonitic) lamprophyric magmatism. This possibility was first advanced by Rock and Groves (1988), who argued that this spatial and temporal association may be linked with the mantle or perhaps a mantle plume (e.g. Barley et al. 1998). Rock and Groves (1988) pointed out that lamprophyres are Au-rich and that Au-bearing lodes in metamorphic terranes occur along major structural discontinuites as calc-alkaline lamprophyres. In addition, both lamprophyres and Au lodes exhibit carbonate alteration again implying some commonality. The spatial-temporal and carbonate alteration association is well exhibited in the central part of the South Island (New Zealand), a feature pointed out by Craw et al. (2002). Craw et al. (2002) used the example of the New Zealand Southern Alps to emphasize that orogenic lodes formed in subduction settings exhibit different mineralisation

styles according to the level of exposure, following on the crustal continuum model of Groves (1993), from shallow (epizonal) to intermediate (mesozonal), to deep (hypozonal). Although convergent tectonics seems to be the common factor to all orogenic lode systems, there are examples in China, where post-orogenic extensional regimes and magmatism are implicated in the development of vein systems that share the characteristics and styles of those formed in subduction and accretionary settings. Recent studies used He isotope systematics to support the idea of mantle sources for intraplate lode deposits (e.g. Mao et al. 2007).

The Carlin-type ore systems remain a puzzle, with ideas on their origin ranging from distal epithermal to a variant of intrusion-related to a complex sequence of magmatic and mineralising events related to the impingement of a mantle plume. Similar types or style deposits occur in China, where post-orogenic magmatism associated with astehnospheric upwelling is invoked to explain a wide range of ore systems from porphyry to orogenic to Carlin-type.

Metalliferous black shales in China present a most unusual style of mineralisation also found in Canada. Black shales are enriched in several trace metals and are commonly associated with SEDEX ore systems. However, the black shales in south China have high grades of metals such as Ni, Mo, PGE, coupled with unusual textures. There are two main schools of thought to explain their genesis; one suggests direct precipitation from sea water, the other calling on hydrothermal vents on the seafloor. A third, perhaps less likely but still worthy of further investigations, suggests that the globular textures in these black shales represent distal effects of a giant meteorite impact.

Nonsulphide ore systems are becoming increasingly popular in the literature, due to a growing economic interest. Some of these ore systems are formed through weathering and oxidation of pre-existing sulphide bodies, in other words they are "giant" gossans; others are considered as originating from hypogene hydrothermal processes. The Magellan nonsulphide Pb in Western Australia is a world-class deposit and perhaps unusual in the nonsulphide family, because it was formed by acidic dissolution of an MVT sulphide protore that lay above the nonsulphide ore zone. The ore was formed by a combination of CO_2-rich fluids, derived from the acidic dissolution of carbonate beds, and downward moving weathering front, resulting in intense clay-alteration and deposition of Pb sulphate and carbonate.

There is good evidence that high heat production (HHP) from rocks containing high concentrations of radioactive elements (U, Th, K) provide the thermal energy for low temperature hydrothermal systems. Of considerable interest is also the likelihood that the late low temperature complex paragenetic sequences that characterise mineral systems associated with HHP rocks are related to radiogenic heat production. In addition, HHP rocks are acquiring more and more importance as a potential source of geothermal energy.

Finally, the Inglefield Land "rust zones" also a very unusual mineralisation style, whose origin is by no means clear. A model suggested in Pirajno et al. (2003) proposed that basin brines descended into the underlying metamorphic

basement, infiltrating mylonitic structures in which sulphides precipitated within a structural corridor.

References

Adkins AR, Rota JC (1984) General geology of the Carlin gold mine. In: Johnson JL (ed) Exploration for ore deposits of the North American Cordillera. Field Trip Guide Book, Ass Expl Geochem Reg Symp, Reno, Nevada, pp 17–23

Ahmad M, Wygralak AS, Ferenczi PA (1999) Gold deposits of the Northern Territory. Northern Territory Geol Surv Rpt 11

Arehart GB (1996) Characteristics and origin of sediment-hosted disseminated gold deposits: a review. Ore Geol Rev 11:383–403

Arkimaa H, Hyvönen E, Lerssi J, Loukola-Ruskeeniemi K, Vanne J (1999) Compilation of maps of black shales in Finland: applications for exploration and environmental studies. Geol Surv Finland, Current Res 1997–1998, Sp Pap 27:111–114

Ayer J, Amelin Y, Corfu F, Kamo S, Ketchum J, Kwok K, Trowell N (2002) Evolution of the southern Abitibi greenstone belt, based on U-Pb geochronology: autochthonous volcanic contsurction followed by plutonism, regional defomrtaion and sedimentation. Precambr Res 115: 63–95

Bagby WC, Berger BR (1985) Geologic characteristics of sediment-hosted, disseminated precious-metal deposits in the western United States. Rev Econ Geol 2:169–202

Barley ME, Krapež B, Groves DI, Kerrich R (1998) The Late Archaen bonanza: metallogenic and environmental consequences of the interaction between mantle plumes, lithospheric tectonics abd global ciclicity. Ore Geol Rev 91:65–90

Barton MD, Johnson DA (2000) Alternative brine sources for Fe-oxide-(Cu-Au) systems: implications for hydrothermal alteration and metals. In: Porter TM (ed) Hydrothermal iron oxide copper-gold & related deposits: a global perspective. Aust Min Found, Adelaide, pp 43–60

Begbie MJ, Sibson RH (2006) Structural controls on the development of fault-hosted scheelite-gold mineralisation in Glenorchy, northwest Otago. Australs Inst Min Metall Monogr 25:291–298

Belkin HE, Luo K (2007) Late-stage sulfides and sulfarsenides in Lower Cambrian black shale (stone coal) from the Huangjiawan mine, Guizhou Province, People's Republic of China. Mineral Petrol doi:10.1007/s00710-007-0201-9

Berger BB, Drew LJ, Goldfarb RJ, Snee LW (1994) An epoch of gold riches: the late Paleozoic in Uzbekistan, Central Asia. SEG Newslett 16:1–11

Berger BR, Bagby WC (1991) The geology and origin of Carlin-type gold deposits. In: Foster RP (ed) Gold metallogeny and exploration, Blackie, pp 210–248

Berkman DA, Mackenzie DH (eds) (1998) Geology of Australian and Papua New Guinean mineral deposits. Australas Inst Min Metall Monograph 22, Carlton, Victoria

Bierlein FP (1995) Metalliferous anoxic sediments in the Willyama Supergroup, South Australia. In: Pašava J, Kříbek B, Žak K (eds) Mineral deposits: from their origin to their environmental impacts, Balkema, Rotterdam, pp 931–934

Bons PD (2001) The formation of large quartz veins by rapid ascent of fluid in mobile hydrofractures. Tectonophysics 336:1–17

Borg G, Kärner K, Buxton M, Armstrong R, van der Merwe SW (2003) Geology of the Skorpion supergene zinc deposit, southern Namibia. Econ Geol 98:749–771

Boulter CA, Fotios MG, Phillips GN (1987) The Golden Mile, Kalgoorlie: a giant gold deposit localized in ductile shear zones by structurally induced infiltration of an auriferous metamorphic fluid. Econ Geol 82:1661–1678

Brathwaite RL, Pirajno F (1993) Metallogenic map of New Zealand. Inst Geol & Nuclear Sci Ltd, Monogr 3, Lower Hutt, New Zealand
Brugger J, McPhail DC, Wallace M, Waters J (2003) Formation of willemite in hydrothermal environments. Econ Geol 98:819–835
Brugger J, Long N, McPhail DC, Plimer I (2005) An active amagmatic hydrothermal system: the Paralana hot springs, Northern Flinders Ranges, South Australia. Chem Geol 222:35–64
Buryak VA (1982) Metamorphism and ore formation. Moscow, Nedra (in Russian)
Butt CRM, Zeegers H (eds) (1992) Regolith exploration and geochemistry in tropical and subtropical terrains. Handbook Expl Geochem, Elsevier, Amsterdam
Cassidy KF, Champion DC, Huston DL (2005) Crustal evolution constraints on the metallogeny of the Yilgarn Craton. In: Mao J-W, Bierlain F (eds) Mineral deposits research: meeting the global challenge 2:901–904, Proceedings SGA 2005 Beijing
Champion DC, Cassidy KF (2007) An overview of the Yilgarn Craton and its crustal evolution. Proceed Kalgoorlie '07, Geosci Aust Rec 2007/14:8–13
Chen YJ (1998) Fluidization model for continental collision in special reference to study ore-forming fluid of gold deposits in the eastern Qinling mountains, China. Progress Nat Sci 8: 385–393
Chen YJ, Pirajno F, Sui YH (2004) Isotope geochemistry of the Tieluping silver-lead deposit, henan, China: a case study of orogenic silver-dominated deposits and related tectonic setting. Mineral Depos 39:560–575
Chen YJ, Pirajno F, Qi JP (2005) Origin of gold metallogeny and sources of ore-forming fluids, Jiaodong Province, Eastern China. Int Geol Rev 47:530–549
Chen YJ, Pirajno F, Qi JP, Li J, Wang HH (2006) Ore geology, fluid geochemistry and genesis of the Shanggong gold deposit, eastern Qinling Orogen, China. Res Geol 56:99–116
Chen YJ, Pirajno F, Qi JP (2008) The Shanggong gold deposit, Eastern Qinling Orogen, China: isotope geochemistry and implications for ore genesis. Asian J Earth Sci doi:10. 1016/jseas.2007.12.002
Christie AB, Brathwaite RL (2003) Hydrothermal alteration in metasedimentary rock-hosted orogenic gold deposits, Reefton goldfield, South Island, New Zealand. Mineral Depos 38:87–107
Christie AB, Brathwaite RL (eds) (2006) Geology and exploration of New Zealand mineral deposits. Australas Inst Min Metal Monogr 25, Carlton, Vic, Aust
Christie AB, Cox SC, Rattenbury MS, Brathwaite RL, Whetter N (2006) Orogenic (mesothermal) gold deposits of the Reefton goldfield, West Coast – A review of exploration and geology. Australas Inst Min Metall Mongraph 25:255–262
Cline JS, Hofstra AH, Muntean JL, Tosdal RM, Hickey KA (2005) Carlin-type gold deposits in Nevada: critical geologic charateristics and viable models. Econ Geol 100th Ann Iss: 451–484
Clout JMF, Cleghorn JH, Eaton PC (1990) Geology of the Kalgoorlie gold field. Australas Inst Min Metall Monogr 14:411–432
Coffin MF, Eldholm O (1993) Large igneous provinces. Sci Am 269:26–33
Coffin MF, Eldhom O (1994) Large igneous provinces: crustal structure, dimensions and external consequences. Am Geophys Un, RevGeophys 32:1–36
Colvine AC (1989) An empirical model for the formation of Archean gold deposits – products of final cratoniastion of the Superior Province, Canada. Econ Geol Monogr 6:37–53
Coney PJ (1980) Cordilleran metamorphic core complexes: an overview. Mem Geol Soc Am 153:7–31
Corfu F, Muir TL (1989) The Hemlo-Heron Bay greenstone belt and Hemlo Au-Mo deposit, Superior Provice, Ontario, Canada 2. Timing of metamorphism, alteration and Au mineralization from titanite, rutile and monazite U = Pb geochronology. Chem Geol (isot geosci) 79:201–223

Cotton RJ, Rose RV (2006) Alluvial gold mining on the West Coast, South Island, 1988–2004. Australas Inst Min Metall Monogr 25:269–274
Coveney RM (2003) Re-Os dating of polymetallic Ni-Mo-PGE-Au mineralization in Lower Cambrianbalck shales of South China and its geological siginificance – A discussion. Econ Geol 98:661–665
Coveney RM, Glascock, MD (1989) A review of the origins of metal-rich Pennsylvanian black shales, central U.S.A., with an inferred role for basinal brines. Applied Geochem 4:347–367
Coveney RM, Murowchick JB, Grauch RI, Chen NS, Glascock M D (1992) Field relations, origins, and resource implications for platiniferous molybdenum-nickel ores in black shales of south China. Expl Min Geol 1:21–28
Coveney RM, Grauch RI, Murowchick JB (1994) Metals, phosphate and stone coal in the Proterozoic and Cambrian of China: the geologic setting of precious metal-bearing Ni-Mo ore beds. SEG Newsletter 18:1–11
Cox SF, Etheridge MA, Wall VJ (1986) The role of fluids in syntectonic mass transport, and the localisation of metamorphic vein-type ore deposits. Ore Geol Rev 2:65–86
Cox SF, Knackstedt MA, Braun J (2001) Principles of structural control on permeability and fluid flow in hydrothermal system. SEG Rev Econ Geol 14:1–24
Craw D (2006) Gold-bearing veins in the Southern Alps. Australas Inst Min Metall Monogr 25:285–288
Craw D, Johnstone RD, Rattenbury MS (1987a) Gold mineralisation in a high uplift rate mountain belt, Southern Alps, New Zealand. Proc Pac Rim '87 Congr. Australas Inst Min Metall, Parkville, Victoria, pp 95–98
Craw D, Rattenbury MS, Johnstone RD (1987b) Structural geology and vein mineralisation in the Callery River headwaters, Southern Alps, New Zealand. N Z J Geol Geophys 30:273–286
Craw D, Koons PO (1988) Tectonically induced gold mineralisation adjacent to major fault zones. In: Bicentennial Gold '88. Geol Soc Aust Abst Ser 22:338–343
Craw D, Koons PO (1989) Tectonically induced hydrothermal activity and gold mineralisation adjacent to major fault zones. Econ Geol Monogr 6:471–478
Craw D, Hal, AJ, Fallick AE, Boyce AJ (1995) Sulphur isotopes in a metamorphogenic gold deposit, Macraes mine, Otago Schist, New Zealand. NZ J Geol Geophys 38:131–136
Craw D, Koons PO, Horton T, Chamberlain CP (2002) Tectonically driven fluid flow and gold mineralisation in active collisional orogenic belts: comparison between New Zealand and western Himalaya. Tectonophysics 348:135–153
Craw D, Campbell JR (2004) Tectonic and structural setting for active mesothermal gold vein systems, Southrn Alps, New Zealand. J Struct Geol 26:995–1005
Crerar DA, Wood S, Brantley S, Bocarsly A (1985) Chemical controls on solubility of ore forming minerals in hydrothermal solutions. Can Mineral 23:333–351
Dawes PR (1997) The Proterozoic Thule Supergroup, Greenland and Canada: history, lithostratigraphy and development. Geol Greenland Surv Bulletin 474
Dawes PR (1999) A review of geoscientific exploration and geology in the Kane Basin region of Greenland, central Nares Strait. Danmarks og Grønlands Geologiske Undersøgelse Rapport 1999/32
Dawes PR, Frisch T, Garde AA, Iannelli TR, Ineson JR, Pirajno F, Sønderholm M, Stemmerik L, Stouge S, Thomassen B, van Gool JAM (2000) Kane Basin 1999: mapping, stratigraphic studies and economic assessment of Precambrian and Lower Palaeozoic provinces in north-west Greenland. Geol Greenland Surv Bull 186:11–28
De Ronde CEJ, Faure K, Braw CJ, Whitford DJ (2000) Round Hill shear zone-hosted gold deposit, Macreas Falt, Otago, New Zealand: evidence of a magmatic ore fluid. Econ Geol 95:1025–1048
Dimo G (1990) Telfer gold deposits. In: Hughes FE (ed) Geology of the mineral deposits of Australia and Papua New Guinea. Australas Inst Min Metall Monog 14:643–651

Dissanayake CB, Rupasinghe MS (1992) Gold-graphite association in granulite terrains – implications for ore genesis. Cheml Geol 97:265–272
Distler VV, Yudovskaya MA, Mitrofanov GL, Prokof'ev VY, Lishnevskiy EN (2004) Geology, composition and genesis of the Sukhoi Log noble metals deposit, Russia. Ore Geol Rev 24:7–44
Drew LJ, Berger BR, Kurbanov NK (1996) Geology and structural evolution of the Muruntau gold deposit, Kyzulkum desert, Uzbekistan. Ore Geol Rev 11:175–196
Drexel JF, Major RB (1990) Mount Painter uranium-rare earth deposits. Aust Inst Min Metall Monogr 14:993–998
Duane MJ, de Witt MJ (1988) Pb-Zn ore deposits of the northern Caledonides: Products of continental-scale fluid mixing and tectonic expulsion during continental collision. Geology 16:999–1002
Dubé B, Gosselin P (2007) Greenstone-hosted quartz-carbonate vein deposits. Geol Ass Can Sp Publ 5:49–73
Einsele G (2000) Sedimentary basins – evolution, facies and sediment budget. Springer, Berlin
Emmermann R, Lauterjung J (1997) The German continental deep drilling program KTB: overview and major results. J Geophys Res 102:18179–18201
Emsbo P, Hofstra AH, Lauha EA, Griffin GL, Utchinson RW (2003) Origin of high-grade gold ore, source of ore fluid components and genesis of the Meikle and Neighboring Carlin-type deposits, Northern Nevada Trend, Nevada. Econ Geol 98:1069–1105
Emsbo P, Hofstra AH, Johnson CA, Koenig A, Grauch R, Zhang XC, Hu RZ, Su WC, Pi DH (2005) Lower Cambrian metallogenesis of south China: interplay between diverse basinal hydrothermal fluids and marine chemistry. In: Mao JW, Bierlein FP (eds) Mineral deposit research: meeting the global challenge, Beijing, Springer, pp 115–118
Emsbo P, Groves DI, Hofstra AH, Bierlein FP (2006) The giant Carlin gold province: a protracted interplay of orogenic, basinal and hydrothermal processes above a lithospheric boundary. Mineral Depos 41:517–525
Etheridge MA, Wall J, Vernon RH (1983) The role of the fluid phase during regional metamorphism and deformation. J Metam Geol 1:205–226
Fadda S, Fiori M, Pretti S (1998) The sandstone-hosted Pb occurrence of Rio Pischinappiu (Sardinia, Italy): a Pb-carbonate end-member. Ore Geol Rev 12:355–377
Fan D (1983) Polyelemets in the Lower Cambrian black shale series in southern China. In: Augustithis SS (ed) The significance of trace elements in solving petrogenetic problems & controversies, Theophrastus Publ SA, Athens, pp 447–474
Fan D, Ye J, Lui TB (1992) Black shale series-hosted silver-vanadium deposits of the upper Sinian Doushantuo Formation, western Hubei province, China. Expl Min Geol 1:29–38
Fan HR, Zhai MG, Xie YH, Yang JH (2003) Ore-forming fluids associated with granite-hosted gold mineralisation at the Sanshandao deposit, Jiaodong gold province, China. Mineral Depos 38:739–750
Fan TL, Yang HC, Wang FL, Chen NC (1973) Petrologic and geochemical characteristics of a nickel-molybdenum-multi-element-bearing lower Cambrian black shale from a certain district in south China. Geochimica 9:143–164 (in Chinese)
Faure G (1986) Principles of isotope geology, 2nd edn. John Wiley & Sons, New York
Fehn U (1985) Post-magmatic convection related to high heat production in granites of southwest England: a theoretical study. Proceed Conf, Austell, Cornwall Sp Iss:99–112
Ferry JM (1994) A historical review of metamorphic fluid flow. J Geophys Res 99:15487–15498
Freyssinet Ph, Butt CRM, Morris RC, Piantone P (2005) Ore-forming processes related to lateritic weathering. Econ Geol 100th Ann Iss:681–722
Frimmel HE (1990) Ore mineralization in platform sediments: passive or active continental margin features? Abstr Geocongress '90 Cape Town, Geol Soc S Afr, pp 165–168
Frimmel HE, Frank W (1998) Neoproterozoic tecton-thermal evolution of the Gariep belt and its basement, Namibia and South Africa. Precambr Res 90:1–28

Fyfe WS (1987) Tectonics, fluids and ore deposits: mobilisation and remobilisation. Ore Geol Rev 2:21–36
Fyfe WS (1997) Deep fluids and volatile recycling: crust to mantle. Tectonophysics 275:243–251
Fyfe WS, Price NJ, Thompson AB (1978) Fluids in the Earth's crust. Elsevier, Amsterdam
Fyfe WS, Kerrich R (1985) Fluids and thrusting. Chem Geol 49:353–362
Gauthier M, Chratrand F, Trotter J (1994) Metallogenic epochs and metallogenic provinces of the Estrie-Beauce region, Southern Quebec Appalachians. Econ Geol 89:1322–1360
Gauthier L, Hagemann SG, Robert F, Pickens G (2004) New constraints on the architecture and timing of the Giant Golden Mile gold deposit, Kalgoorlie, Western Australia. In: Muhling J, Goldfarb RJ, Vielreicher N, Bierlein F, Stumpfl E, Groves DI, Kenworthy S, Knox-Robinson CM (eds) SEG 2004: Predictive mineral discovery under cover. Extended abstracts, Univ West Australia Publ 33:353–356
Gauthier L, Hagemann S, Robert F (2007) The geological setting of the Golden Mile gold deposit, Kalgoorlie, WA. Proceed Kalgoorlie '07, Geosci Aust Rec 2007/14:181–185
Geoscience Australia (2007) Proceedings of Geoconfrences (WA) Inc, Kalgoorlie '07 Conference. Geosci Aus Record 2007/14
Gilg HA, Boni M, Cook NJ (eds) (2008) A special issue devoted to nonsulfide Zn-Pb deposits. Ore Geol Rev 33
Glikson AY (2004) Early Precambrian asteroid impact-triggered tsunami: excavated seabed, debris flows, exotic boulders and turbulence features associated with 3.47–2.47 Ga-old asteroid impact fallout units, Pilbara Craton, Western Australia. Astrobiology 4:19–50
Glikson AY (2005) Geochemical signatures of Archean to Early Proterozoic maria-scale oceanic impacts. Geology 33:125–128
Goellnicht NM, Groves DI, McNaughton NJ (1991) Late Proterozoic fractionated granitoids of the mineralized Telfer area, Paterson Province, Western Australia. Precambr Res 51:375–391
Goldfarb RJ, Leach DL, Pickthorn WJ, Paterson CJ (1988) Origin of lode gold deposits of the Juneau gold belt, southeastern Alaska. Geology 16:440–443
Goldfarb RJ, Phillips GN, Nokleberg WJ (1998) Tectonic setting of synorogenic gold deposits of the Pacific Rim: Ore Geol Rev 13:185–218
Goldfarb RJ, Groves DI, Gardoll S (2001) Orogenic gold and geologic time: a global synthesis. Ore Geol Rev 18:1–75
Goldfarb RJ, Baker T, Dubé B, Groves DI, Hart CJR, Gosselin P (2005) Distribution, character, and genesis of gold deposits in metamorphic terranes. Econ Geol 100th Ann Iss:407–450
Goldfarb RJ, Hart C, Davis G, Groves DI (2007) East Asian gold: deciphering the anomaly of Phanerozoic gold in Precambrian Cratons. Econ Geol 102:341–345
Goldie R (1985) The sinters of the Ohaki and Champagne pools, New Zealand: possible modern analogues of the Hemlo gold deposits, Northern Ontario. Geosci Can 12:60–64
Granier C, Hartley J, Michaud JC, Troly G (1989) Contribution of three-dimensional geochemical exploration to the discovery of extension of the Thalanga polymetallic deposit under Tertiay cover rocks (Queensland, Australia). J Geochem Expl 32:467–475
Grey K, Walter MR, Calver CR (2003) Neoproterozoic diversification: snowball Earth or aftermath of the Acraman impact? Geology 31:459–462
Griffin WL, Zhang AD, O'Reilly SY, Ryan G (1998) Phanerozoic evolution of the lithosphere beneath the Sino-Korean Craton. In: Flower M, Chng SL, Lo CH, Lee TY (eds) Mantle dynamics and plate interactions in East Asia, Am Geophys Union Geodyn Ser 27:107–126
Groves DI (1993) The crustal continuum model for late-Archean lode gold deposits of the Yilgarn block, Western Australia. Mineral Depos 28:366–374
Groves DI, Phillips GN, Ho SE, Henderson CA, Clark ME, Woad GM (1984) Controls on distribution of Archaean hydrothermal gold deposits in Western Australia. In: Foster RP (ed) Gold '82: The geology, geochemistry and genesis of gold deposits, Proceed Symp Gold '82, Zimbabwe, AA Balkema, Rotterdam, pp 689–711

Groves DI, Phillips GN (1987) The genesis and tectonic control on Archean gold deposits- A metamorphic replacement model. Ore Geol Rev 2:287–322
Groves DI, Barley ME, Ho S (1989) Nature, genesis and tectonic setting of mesothermal gold mineralization in the Yilgarn Block, Western Australia. Econ Geol Monogr 6:71–85
Groves DI, Ridley JR, Bloem EMJ, Gebre-Mariam M, Hageman SG, Hronsky JMA, Knight JT, McNaughton NJ, Ojala J, Vielreicher RM, McCuaig TC, Holyland PW (1995) Lode-gold deposits of the Yilgarn block: products of late Archaean crustal scale overpressured hydrothermal systems. Geol Soc, London, Sp Publ 95:155–172
Groves DI, Goldfarb RJ, Gebre-Mariam M, Hagemann SG, Robert F (1998) Orogenic gold deposits: a proposed classification in the context of their crustal distribution and relationship to other gold deposit types: Ore Geol Rev 13:7–27
Groves DI, Goldfarb RJ, Knox-Robinson CM, Ojala J, Gardoll S, Yun GY, Holyland P (2000). Late-kinematic timing of orogenic gold deposits and significance for computer-based exploration techniques with emphasis on the Yilgarn Block, Western Australia. Ore Geol Rev 17:1–38
Groves DI, Goldfarb RJ, Robert F, Hart CJR (2003) Gold deposits in metamorphic belts: overview of current understanding, outstanding problems, future research, and exploration significance. Econ Geol 98:1–29
Groves DI, Vielreicher RM, Goldfarb RJ, Condie KC (2005) Controls on the heterogeneous distribution of mineral deposits through time. Geol Soc Lond Sp Publ 248:71–101
Haack U, Heinrichs H, Bones N, Schneider A (1984) Loss of metals from pelites during regional metamorphism. Contrib Mineral Petrol 85:116–132
Habermehl MA (1980) The great artesian basin. BMR J Aust Geol Geophys 5:9–38
Harris DC (1989) The mineralogy and geochemistry of the Hemlo gold deposit, Ontario. Geol Surv Can Rep 38
He Y, Mao JW, Wang RT, Zhang ZJ (2001) Carbon dioxide rich and gold bearing fluids degassed from mantle derived magma-reality and possibility. Earth Sci Frontiers (China Univ Geosciences) 8:265–270 (in Chinese with English abstract)
Heier KS (1978) Potassium. In: Wedepohl KH, Correns CW, Shaw DM, Turekian KK, Zemann J (eds) Handbook of geochemistry, vol II/2, Springer-Verlag, pp 19-B-1/19-B-2
Henley RW, Adams J (1979) On the evolution of giant gold placers. Trans Inst Min Metall 88:B41–B50
Henriksen N, Higgins AK, Kalsbeek F, Pulvertaft TCR (2000) Greenland from Archaean to Quaternary: descriptive text to the Geological map of Greenland 1: 2 500 000. Geol Greenland Surv Bull 185
Hitzman MW, Reynolds NA, Sangster DF, Allen CR, Carman CE (2003) Classification, genesis and exploration guides for nonsulfide zinc deposits. Econ Geol 98:685–714
Hodgson CJ (1989) The structure of shear-related, vein-type gold deposits: a review. Ore Geol Rev 4:231–273
Hoefs J (2004) Stable isotope geochemistry, 5th edn. Springer-Verlag, Berlin
Hofmeister AM, Criss RE (2005) Earth's heat flux revised and linked to chemistry. Tectonophysics 395:159–177
Hofstra AH, Leventhal JS, Northrop HR, Landis GP, Rye RO, Birak DJ, Dahl AR (1991) Genesis of sediment-hosted disseminated gold deposits by fluid mixing and sulfidization: chemical-reaction-path modelling of ore-depositional processes documented in Jerritt Canyon district, Nevada. Geology 19:36–40
Hofstra AH, Cline JS (2000) Characteristics and models for Carlin-type gold deposits: Rev Econ Geol 13:163–221
Hofstra AH, John DA, Theodore TG (eds) (2003) A special issue devoted to gold deposits in Northern Nevada: Part 2. Carlin-type deposits. Econ Geol 98(6)
Hu HB, Mao JW, Liu DY, Niu SY, Wang YB, Li YF, Shi RR (2005) SHRIMP zircon U-Pb dating of the Tongshi magmatic complex in western Shandong and its implication. Acta Geol Sinica 79:401–406

Hu HB, Mao JW, Niu SY, Li YF, Li MW (2006) Geology and geochemistry of telluride- Au deposits in the Pingyi area, western Shandong, China. Miner Petr 87:209–240
Hubbert MK, Rubey WW (1961) Role of fluid pressure in mechanics of overthrust faulting. Bull Geol Soc Am 70:1581–1594
Hughes FE (ed) (1990) Geology of the mineral deposits of Australia and Papua New Guinea. Australas Inst Min Metal lMonogr 14, Parkville, Victoria
Hulbert LJ, Carne RC, Gregoire DC, Paktune D (1992) Sedimentary nickel, zinc, and platinum-group-element mineralization in Devonian black shales at the Nick property, Yukon, Canada: a new deposit type. Expl Min Geol 1:39–62
Hulen JB, Collister JW (1999) The oil-bearing Carlin-type gold deposits of Yankee Basin, Alligator Ridge district, Nevada. Econ Geol 94:1029–1050
Huston DL, Vandenberg LC, Wygralak A, Mernagh T, Bagas L, Crispe A, Lambeck L, Cross A, Fraser G, Williams N, Worden K, Meixner T, Goleby B, Jones L, Lyons P, Maidment D (2006) Lode gold mineralization in the Tanami region, northern Australia. Mineral Depos 42:175–204
Hutton CO, Turner FJ (1936) Metamorphic rocks in northwest Otago. Trans R Soc NZ 65:405–406
Huyck HLO (1990) Proposed definition of "black shale" and "metalliferous black shale" for IGCP # 254. Eighth IAGOD Symp, Geol Surv Can:A183–184
Ilchik RP, Barton MD (1997) An amagmatic origin of Carlin-type gold deposits: Econ Geol 92:269–288
Ivernia (2006) Magellan Metals Pty ltd Annual Rpt (unpublished)
Jackson D (1983) Carlin gold: a Newmont money generator keeps on renewing itself after sparking the rebirth of gold mining in Nevada. Eng Min J 184:38–43
Jamtveit B, Yardley BWD (eds) (1997) Fluid flow and transport in rocks. Chapman & Hall, London
Jaupart C, Mareschal JC (2003) Constraints on crustal heat production from heat flow data. Treatise in geochemistry, vol 3, Elsevier, Amsterdam, pp 66–84
Jébrak M (1997) Hydrothermal breccias in vein-type ore deposits: a review of mechanism, morphology and size distribution. Ore Geol Rev 12:111–134
Jensen SM, Schønwandt HK (1998) A new carbonate-hosted Zn-Pb-Ag occurrence in Washington Land, western North Greenland. Danmarks og Grønlands Geologiske Undersøgelse Rapport 1998/3
Jiang SY, Chen YQ, Ling HF, Yang JH, Feng HZ, Ni P (2006) Trace- and rare-earth element geochemistry and Pb-Pb dating of black shales and intercalated Ni-Mo-PGE-Au sulfide ores in lower Cambrian strata, Yangzte Platform, South China. Mineral Depos 41:453–467
Johnstone RD, Craw D, Rattenbury MS (1990) Southern Alps Cu-Au hydrothermal system, Westland, New Zealand. Mineral Depos 25:118–125
Kao LS, Peacor DR, Coveney RM, Zhao G, Dungey KE, Curtis MD, Penner-Hahn JE (2001) A C/moS, mixed-layer phase (MoSC) occurring in metalliferous black shales from southern China, and new data on jordisite. Am Mineral 86:852–861
Kempe U, Belyatsky BV, Krymsky RS, Kremenetsky AA, Ivanov PA (2001) Sm-Nd and Sr isotope systematics of scheelite from the giant Au)-W) deposit Muruntau (Uzbekistan): implications for the age and sources of Au mineralization. Mineral Depos 36:379–392
Kennedy BM, Matthjs C, van Soest C (2007) Flow of mantle fluids through the ductile lower crust: helium isotope trends. Science 318:1433–1436
Kerrich R (1986) Fluid transport in lineaments. Phil TransRoy Soc, Lond, Ser A 317:219–251
Kerrich R (1999) Nature's gold factory. Nature 284:2101–2102
Kerrich R, Wyman D (1990) Geodynamic setting of mesothermal gold deposits: an association with accretionary tectonic regimes. Geology 18:882–885
Kinnaird JA, Bowden P (1987) African anorogenic alkaline magmatism and mineralization – a discussion with reference to the Niger-Nigerian province. Geol J 22:97–340

Kremenetsky AA, Ovchinnikov LN (1986) The Precambrian continental crust: its structure, composition and evolution as revealed by deep drilling in the USSR. Precambr Res 33:11–43
Kusky TM, Li JH (2003) Paleoproterozoic tectonic evolution of the North China Craton. J Asian Earth Sci 22:383–397
Langseth MG, Moore CJ (1990a) Introduction to special section on the role of fluids in sediment accretion, deformation, diagenesis and metamorphism in subduction zones. J Geophys Res 95:8737–8741
Langseth MG, Moore CJ (1990b) Fluids in accretionary prisms. EOS Am Geophys Un 71:245–247
Large R, Maslennikov V, Robert F, Danyushevsky L, Chang ZS (2007) Multi-stage sedimentary and metamorphic origin of pyrite and gold in the giant Sukhoi Log deposit, Lena gold province, Russia. Econ Geol 102:1233–1267
Lattanzi P (1999) Epithermal precious metal deposits of Italy: an overview. Mineral Depos 34:630–638
Laznicka P (2006) Giant metallic deposits – future sources of industrial metals. Springer, Berlin
Leach T, Corbett GJ, Magner P, McKenzie M (1997) A geological model for gold mineralisation at Reefton, New Zealand. Proceed 1997 New Zealand Minerals and Mining conference, Ministry Commerce, pp 159–165
Le Blanc Smith G, Pirajno F, Nelson D, Grey K (1995) Base metal deposits in the early Proterozoic Glengarry terrane, Western Australia. Geol Surv West Aust Ann Rev 1993–94:59–62
Le Fort P, Cuney M, Deniel C, France-Lanord C, Sheppard SMF, Upreti BN, Vidal P (1987) Crustal generation of the Himalayan leucogranites. Tectonophysics 134:39–57
Lee MC, Batt WD, Robinson PC (1989) The Round-Hill gold-scheelite deposit, Macraes Flat, Otago, New Zealand. Australas Inst Min Metall Monogr 13:173–180
Lehmann B, Mao JW, Li SG, Zhang GD, Zeng MG (2003) Re-Os dating of polymetallic Ni-Mo-PGE-Au mineralization in Lower Cambrian black shales of South China and its geological significance – A reply. Econ Geol 98:661–665
Lehmann B, Nägler TF, Holland HD, Wille M, Mao JW, Pan JY, Ma DS, Dulski P (2007) Highly metalliferous carbonaceous shale and Early Cambrian. Geology 35:403–406
Levinson AA (1974) Introduction to exploration geochemistry. Applied Publ, Calgary, Can, 614 pp
Light TD, Brew DA, Ashley RP (1990) The Alaska-Juneau Treadwell lode gold systems, southeastern Alaska. US Geol Surv Bull 1857:D27–D36
Lott DA, Coveney RM, Murowchick JB, Grauch RI (1999) Sedimentray exhalative nickel-molybdenum ores in south China. Econ Geol 94:1051–1066
Loucks RR, Mavrogenes JA (1999) Gold solubility in supercritical hydrothermal brines measured in synthetic fluid inclusions. Nature 284:2159–2163
Loukola-Ruskeeniemi K (1999) Origin of black shales and the serpentinite-associated Cu-Zn-Co ores at Outokumpu, Finland. Econ Geol 94:1007–1028
Luque FJ, Barrenechea JF, Rodas M (1993) Graphite geothermometry in low and high temperature regimes: two case studies. Geol Mag 130:501–511
Mao JW, Goldfarb RJ, Zhang ZW, Xu WY, Qiu YM, Deng J (2002a) Au deposits in the Xiaoqinling-Xiong'ershan region, Qinling Mountains, central China. Mineral Depos 37:306–325
Mao JW, Qiu YM, Goldfarb RJ, Zhang ZC, Garwin S, Ren FS (2002b) Geology, distribution and classification of gold deposits in the western Qinling Belt, central China. Mineral Depos 37:352–377
Mao JW, Zhang ZH, Wang YT, Jia YF, Rober, K (2002c) Nitrogen isotope and content record of Mesozoic orogenic gold deposits surrounding the North China craton. Sci China (Series D) 46:231–2457

Mao JW, Lehmann B, Du AD, Zhang GD, Ma DS, Wang YT, Zeng MG, Kerrich R. (2002d). Re-Os dating of polymetallic Ni-Mo-PGE-Au mineralization in Lower Cambrian black shales of South China and its geologic significance. Econ Geol 97:1051–1061

Mao JW, Wang YT, Lehmann B, Yu JJ, Du AD, Mei YX, Li YF, Zang WS, Stein HJ, Zhou TF (2006) Molybdenite Re-Os and albite $^{40}Ar/^{39}Ar$ dating of Cu-Au-Mo and magnetite porphyry systems in the Yangtze River valley and metallogenic implications. Ore Geol Rev 29:307–324

Mao JW, Wang YT, Li HM, Pirajno F, Zhang HQ, Wang RT (2007) The relationship of mantle-derived fluid to gold metallogenesis in the Jiadong peninsula: evidence from D-O-C-S isotope systematics. Ore Geol Rev. doi:10.1016/j.oregeorev.2007.01.003

McCaffrey K, Lonergan L, Wilkinson J (eds) (1999) Fractures, fluid flow and mineralization. Geol Soc Lond, Sp Publ 155

McLaren S, Nemann N, Sandiford M, Wyborn L (1999) Post-intrusion heating associated with high-heat-producing Proterozoic granites – implications for mineralisation? AGSO Res Newslett 30:23–26

McLaren S, Sandiford M, Hand M, Neumann N, Wyborn L, Bastrakova I (2003) The hot southern continent: heat flow and heat production in Australian Proterozoic terranes. Geol Soc Aus Spec Publ 22 and Geol Soc Am Spec Pap 372:157–167

McQuitty BM, Pascoe DJ (1998) Magellan lead deposit. Australas Inst Min Metall Monogr 22:293–296

Menzies MA, Hawkesworth CJ (1987) Mantle Metasomatism. Academic Press, London

Miller McGR (ed) (1983) Evolution of the Damara orogen of South West Africa/Namibia. Geol Soc S Afr Spec Publ 11

Mineralium Deposita (1991) Black shales. Mineral Depos 26(2)

Mitchell M, Maw L, Angus PV, Craw D (2006) The Macraes gold deposit, East Otago. Australas Ins Min Metall Monogr 25:313–318

Möller P, Weise SM, Althaus E, Bach W, Behr HJ, Borchradt R, Bräuer K, Drescher J, Erzinger J, Faber E, Hansen BT, Horn EE, Huenges E, Kämpf H, Kessels W, Kirsten T, Landwehr D, Lodemann M, Machon L, Pekdeger A, Pileow HU, Reutel C, Simon K, Walther J, Weinlich FH, Zimmer M (1997) Paleofluids and recent fluids in the upper continental crust: results from the German continetal deep drilling program (KTB). J Geophys Res 102:18233–18254

Morelli R, Creaser RA, Seltmann R, Stuart FM, Selby D, Graupner T (2007) Age and source constraints for the giant Muruntau gold deposit, Uzbekistan, from coupled Re-Os-He istopes in arsenopyrite. Geology 35:795–798

Morgan P (2000) Heat flow. In: Veevers JJ (ed) Billion-year history of Australia and neighbours in Gondwanaland, GEMOC Press, Sydney, pp 82–90

Mueller WU, Marquis R, Thurston P (eds) (2002) Evolution of the Archean Abitibi greenstone belt and adjacent terranes: new insights from geochronology, geochemistry, structure and facies analysis. Precambr Res 115

Muir TL, Elliott CG, Corfu F (1988) The tectono-stratigraphic setting of the Hemlo Au-Mo deposit, Ontario, Canada. In: Bicentennial Gold '88. Geol Soc Aust Abstr Series 23:95–97

Murowchick JB, Coveney RM, Grauch RI, Eldridge CS, Shelton KL (1994) Cyclic variations of sulphur isotopes in Cambrian stratabounds Ni-Mo-(PGE-Au) ores of southern China. Geochim Cosmoch Acta 58:1813–1823

Myers JS (1995) The generation and assembly of an Archaean supercontinent: evidence from the Yilgarn craton, Western Australia. Geol Soc Lond Sp Publ 95:143–154

Nesbitt BE (1988) Gold deposit continuum: a genetic model for lode Au mineralization in the continental crust. Geology16:1044–1048

Nesbitt BE, Muehlenbachs K (1989) Evidence for ore formation from evolved meteoric water. Econ Geol Monogr 6:553–563

Neumann N, Sandiford M, Foden J (2000) Regional geochemistry and continental heat flow: implications for the origin of the South Australian heat flow anomaly. Earth Planet Sci Lett 183:107–120

Nie FJ, Jiang SH, Liu Y (2004) Intrusion-related gold deposits of North China craton, People's Republic of China. Res Geol 54:299–324

Niu SY, Hu HB, Mao JW, Sun AQ, Xu CS, Hou QL (2004) Structure in western Shandong and its genetic mechanism. Geol China 31:34–39 (in Chinese with English abstract)

Nokleberg WJ, Bounaeva TV, Miller RJ, SEminskiy ZV, Diggles MF (eds) (2003) Significant metalliferous and selected non-metalliferous lode deposits and selected placer districts for northeast Asia. USGS Open File Rpt 03–220

Nokleberg WJ, Miller RJ, Diggles MF (eds) (2006) Geographic Information System (GIS), spatial data compilation of geodynamic, tectonic, metallogenic, mineral deposits and geophysical maps and associated descriptive data for northeast Asia. USGS Open File Rpt 2006–1150

Nutman AP, Dawes PR, Kalsbeeek F, Hamilton MA (2008) Palaeoproterozoic and Archaean gneiss complexes in northern Greenland: palaeoproterozoic terrane assembly in the High Arctic. Precambr Res 161:419–451

Oliver J (1986) Fluids expelled tectonically from orogenic belts: their role in hydrocarbon migration and other geological phenomena. Geology 14:99–102

Oliver NHS, Rubenach MJ, Valenta RK (1998) Precambrian metamorphism, fluid flow and metallogeny of Australia. AGSO J Geol & Geophys 17:31–53

Oppliger GL, Murphy JB, Brimhall GH (1997) Is the ancestral Yellowstone hotspot responsible for the Tertiary "Carlin" mineralisation in the Great Basin of Nevada? Geology 25:627–630

O'Reilly SY, Griffin WL, Poudjom-Djomani YH, Morgan P (2001) Are lithospheres forever? Tracking changes in subcontinental lithopsheric mantle through time. GSA Today 11:4–10

Pan Y, Fleet ME (1995) The late Archean Hemlo gold deposit, Ontario, Canada: a review and synthesis. Ore Geol Rev 9:455–488

Pašava J (1993) Anoxic sediments – an important environment for PGE; an overview. Ore Geol Rev 8:425–445

Pašava J (ed) (1996) A group of papers devoted to the metallogeny of black shales. Econ Geol 91(1)

Passchier CW, Trouw RAJ (1996) Micro-tectonics. Springer, Berlin

Paterson CJ (1986) Controls on gold and tungsten mineralisation in metamorphic-hydrothermal systems, Otago, New Zealand. Geol Ass Can Sp Pap 32:25–39

Peng P, Zai MG, Zhang HF, Guo JH (2005) Geochronological constraints on the Paleoproterozoic evolution of the North China Craton: SHRIMP zircon ages of different types of mafic dikes. Int Geol Rev 47:492–508

Peng P, Zhai, MG, Ernst RE, Guo JG, Liu F, Hu B (2008) A 1.78 Ga large igneous province in the North China Craton: the Xiong'er Volcanic Province and the North China Dyke Swarm. Lithos 101:260–280

Percival JA (2007) Geology and metallogeny of the Superior Province, Canada. Geol Ass Can Sp Publ 5:903–928

Peters SG, Huang JZ, Li ZP, Jing CG (2002) Introduction to and classification of sedimentary rock-hosted Au Deposits in P.R. China. USGS Open File Rpt 02-131

Phillips GN (1986) Geology and alteration of the Golden Mile, Kalgoorlie. Econ Geol 81:779–808

Phillips GN, Groves DI (1984) Fluid access and fluid-wallrock interaction in the genesis of the Arcahean gold-quartz vein deposit at Hunt Mine, Kambalda, Western Australia. In: Foster RP (ed), Gold '82, The geology, geochemistry and genesis of gold deposits, Balkema, Rotterdam, pp 389–416

Phillips GN, Williams PJ, De Jong G (1994) The nature of metamorphic fluids and significance for metal exploration. Geol Soc, Lond Sp Publ 78:55–68

Phillips GN, Groves DI, Kerrich R (1996) Factors in the formation of the giant Kalgoorlie gold deposit. Ore Geol Rev 10:295–317
Phillips GN, Hughes MJ (1998) Victorian gold province. The Australas Inst Min Metall Monogr 22:495–506
Pirajno F (1979) Geology, geochemistry and mineralisation of the Endeavour Inlet antimony-gold prospect, Marlborough Sounds, New Zealand. NZ J Geol Geophys 22:227–237
Pirajno F (2000) Ore deposits and mantle plumes. Kluwer Academic Publishers, Dordrecht
Pirajno F (2004) Oceanic plateau accretion onto the northwestern margin of the Yilgarn Craton, Western Australia: implications for a mantle plume event at ca. 2.0 Ga. J Geodyn 37:205–231
Pirajno F, Thomassen B, Dawes PR (2003) Copper-gold occurrences in the Palaeproteroic Inglefield mobile belt, northwest Greenland: a new mineralisation style? Ore Geol Rev 22:225–249
Pirajno F, Jones JA, Hocking RM, Halilovic J (2004) Geology and tectonic evolution of Palaeoproterozoic basins of the eastern Capricorn Orogen, Western Australia. Precambr Res 128:315–342
Pirajno F, Chen YJ (2005) Hydrothermal ore systems associated with the extensional collapse of collision orogens. In: Mao J-W, Bierlain F (eds) Mineral deposits research: meeting the global challenge 2:1045–1048. Proceedings SGA 2005 Beijing
Qi JP, Zhang J, Tang GJ (2005) Carbon and oxygen isotope composition of the Meso-Neoproterozoic strata south of the Xiong'er Terrane: evidences of the CMF model. Acta Petrol Sinica 21:1365–1372 (In Chinese with English abstract)
Qiu YM, Groves DI (1999) Late Archean collision and delamination in the southern Yilgarn Craton: the driving force for Archean orogenic lode gold mineralization. Econ Geol 94:115–122
Radtke AS, Rye RO, Dickson FW (1980) Geology and stable isotope studies of the Carlin gold deposit, Nevada. Econ Geol 75:641–672
Ramsay JG (1980) Shear zone geometry: a review. J Struct Geol 2:83–100
Rankin AH, Alderton DHM (1985) Fluids in granites from southwest England. Proceed Conf, Austell, Cornwall Sp Iss:287–300
Ratschbacher L, Hacker BR, Calvert A, Webb LE, Grimmer JC, McWilliams MO, Ireland T, Dong S, Hu J (2003) Tectonics of the Qinling (Central China): tectonostratigraphy, geochronology and deformation history. Tectonophysics 366:1–53
Reichert J, Borg G (2008) Numerical simulation and a geochemical model of supergene carbonate-hosted non-sulphide zinc deposits. Ore Geol Rev 33:134–151
Reimold WU, Koeberl C, Johnson S, McDonlad I (2000) Early Achean spherule beds in te Barberton Mountain Land, South Africa: impact or terrestrial origin? In: Gilmour I, Koeberl C (ed) Impacts and the early earth. Springer, Berlin, pp 117–180
Reynolds SJ, Lister GS (1987) Structural aspects of fluid-rock interactions in detachment zones. Geology 15:362–366
Rock NMS (1987) The nature and origin of lamprophyres: an overview. Geol Soc London Spec Publ 30:191–226
Rock NMS, Groves DI (1988) Can lamprophyres resolve the genetic controversy over mesothermal gold deposits? Geology 16:538–541
Rock NMS, Groves DI, Perring CS, Golding SD (1989) Gold, lamprophyres, and porphyries: what does their association mean? Econ Geol Monogr 6:609–625
Rowins SM, Groves DI, McNaughton NJ, Palmer MR, Eldridge CS (1997) A reinterpretation of the role of granitoids in the genesis of Neoproterozoic gold mineralization in the Telfer Dome, Western Australia. Econ Geol 92:133–160
Rui ZY, Goldfarb RJ, Qiu YM, Zhou, TH, Chen RY, Pirajno F, YUn G (2002) Paleozoic-eraly Mesozoic gold deposits of the Xinjiang Autonomous region, northwestern China. Mineral Depos 37:393–418

Rumble D (1994) Water circulation in metamorphism. J Geophys Res 99:15499–15502
Rundquist DV, Gillen C (eds) (1997) Precambrian ore deposits of the East European and Siberian Cratons. Devopmt Econ Geol, Elsevier, Amsterdam
Sandiford M, Hand M., McLaren S (1998) High geothermal gradient metamorphism during thermal subsidence. Earth Planet Sci Lett 163:149–165
Sangster DF (ed) (2003) A special issue devoted to nonsulfide zinc deposits: a new look. Econ Geol 98(4)
Schultz RB (1991) Metalliferous black shales: accumulation of carbon and metals in cratonic basins. Rev Econ Geol 5:171–176
Scotese CR (1997) Paleogeographic Atlas. PALEOMAP Project, Arlington, Texas
Şengör AMC, Natal'in BA (1996) Paleotectonics of Asia: fragments of a synthesis. In: Yin A, Harrsion M (eds) The tectonic evolution of Asia, Cambridge Univ Press, Cambridge, pp 486–640
Shepherd TJ, Miller MF, Scrivener RC, Darbyshire DPF (1985) Hydrothermal fluid evolution inrelation to mineralization in southwest England with special reference to the Dartmoor-Bodmin area. Proceed Conf, Austell, Cornwall Sp Iss:345–364
Sheppard SMF (1986) Characterization and isotopic variations in natural waters. Rev Mineral, Min Soc Am 16:165–183
Sibson RH (2001) Seismogenic framework for hydrothermal transport and ore deposition. SEG Rev Econ Geol 14:25–50
Sibson RH, Moore JM, Rankin AH (1975) Seismic pumping: a hydrothermal fluid transport mechanism. J Geol Soc, Lond, 131:653–659
Sibson RH, Scott J (1998) Stress/fault controls on the containment and release of overpressured fluids: examples from gold-quartz vein systemsin Juneau, Alaska; Victoria, Australia and Otago, New Zeland. Ore Geol Rev 13:293–306
Sillitoe RH, Bonham HF (1990) Sediment-hosted gold deposits: distal products of magmatic-hydrothermal systems. Geology 18:157–161
Simonson BM (2003) Petrographic criteria for recognising certain types of impact spherules in well-preserved Precambrian successions. Astrobiology 3:49–65
Simonson BM, Davies D, Wallace M, Reevs S, Hassler SW (1998) Iridium anomaly but no shocked quartz from late Archean microkrystite layer: oceanic impact ejecta? Geology 26:195–198
Simpson PR, Brown GC, Plant J, Ostle D (1979) Uranium mineralization and granite magmatsim in the British Isles. Phil Trans Roy Soc, London, A291:385–412
Sinton CW, Duncan RA (1997) Potential links between ocean plateau anoxia at the Cenomanian-Turonian boundary. Econ Geol 92:836–842
Smithies RH, Champion D (1999) Late Archaean felsic alkaline igneous rocks in the Eastern Goldfields, Yilgarn Craton, Western Australia: a result of lower crustal delamination? J Geol Soc London 156:561–576
Solomon M, Groves DI (1994) The geology and origin of Australia's mineral deposits. Oxford Science Publ, Clarendon Press, Oxford
Spear FS (1993) Metamorphic phase equilibrium and pressure-temperature-time paths. Mineral Soc Am Monogr, Washington
Spiridonov AM, Zorna LD, Kitaev NA (2006) Gold-bearing ore-magmatic systems of Transbaikalia. Novosibirsk Acad Publ House "Geo" (in Russian)
Stone M, Exley CS (1985) High heat production granites of southwest England and their associated mineralization: a review. Proceed Conf, Austell, Cornwall Sp Iss:571–593
Sun FY, Shi ZL (1995) On the mantle-derived C-H-O fluid system and its significance to some geologic processes within continental plate. Earth Sci Frontiers (China Univ Geosciences) 2:167–174 (in Chinese with English Abstract)
Sun JG, Hu SX, Ling HF (2000) Study on the geochemistry and subduction-crust mantle interaction of the high potassium dyke rocks in gold deposits concentration zone of east Shandong, China. Acta Petr Sinica 16:401–412 (in Chinese with English abstract)

Tammenagi HY, Wheildon J (1977) Further data on the SW England heat flow anomaly. Geophys J Roy Astron Soc 49:531–539
Taylor G, Eggleton RA (2001) Regolith geology and geomorphology. Wiley & Sons Ltd, Chichester
Taylor SR, McLennan SM (1985) The continental crust: its composition and evolution. Blackwell Scientific, Boston, Mass
Taylor SR, McLennan SM (1995) The geochemical evolution of the continental crust. Rev Geophys 33:241–265
The Institution of Mining and Metallurgy (1985) High heat production (HHP) granites, hydrothermal circulation and ore genesis. Proceed Conf, St Austell, Cornwall, Inst Min Metal, September 22–25, 593 pp
Thomassen B, Appel PW (1997) Ground check of airborne anomalies and regional rust zones in Inglefield Land, North-West Greenland. Danmarks og Grønlands Geologiske Undersøgelse Rapport 1997/141
Thomassen B, Dawes PR, Iannelli TR, Pirajno F (2000a) Gold indications in northern Inglefield Land, North-West Greenland: a preliminary report from project Kane Basin 1999. Danmarks og Grønlands Geologiske Undersøgelse Rapport 2000/9
Thomassen B, Pirajno F, Iannelli TR, Dawes PR, Jensen SM (2000b) Economic geology investigations in Inglefield Land, North-West Greenland: part of the project Kane Basin 1999. Danmarks og Grønlands Geologiske Undersøgelse Rapport 2000/100
Tooker EW (1985) Geologic characteristics of sediment- and volcanic-hosted disseminated gold deposits – search for an occureence model. USGS Bull 1646
Torgersen T (1990) Crustal scale fluid transport – magnitude and mechanisms. EOS Am Geophys Un 71:11–13
Travis GA, Woodall R, Bartram GD (1971) The geology of the Kalgoorlie goldfield. Geol Soc Aust Spec Pub l3:175–190
Treloar PJ, O'Brien J (eds) (1998) What drives metamorphism and metamorphic reactions? Geol Soc, Lond, Sp Publ 138
Turner FJ (1935) Metamorphism of the Te Anau Series in the region northwest of Lake Wakatipu. Trans R Soc NZ 65:329–349
Tyler J (2006) Hot-rock energy steaming up. The Aust Geol Newslett 140:22–25
Urban H, Stribrny B, Zereini F, Ye Y (1995) Geochemistry and metallogenesis of Lower Carboniferous black shale-hosted ore deposits, NE Rhenish Massif, FR Germany. Ore Geol Rev 9:427–443
Vanderberg AHM, Willman CE, Maher S, Simons BA, Cayley RA, Taylor DH, Morand VJ, Moore DH, Radojkovic A (2000) The Tasman fold belt system in Victoria. Geol Surv Vic Sp Publ
Vernon RH (2004) A practical guide to rock microstructure. Cambridge Univ Press, Cambridge
Volkert RA, Johnson CA, Tamashausky AV (2000) Mesoproterozoic graphite deposits, New Jersey Highlands: geologic and stable isotopic evidence for possible algal origins. Can J Earth Sci 37:1665–1675
Walford P, Stephens J, Skrecky G, Barnett R (1986) The geology of the "A" zone, Page-Williams mine, Hemlo, Ontario, Canada. In: Macdonald AJ (ed) Proceed Gold '86, Toronto, pp 362–378
Wang H, Zhang SH, He GQ (2005) China and Mongolia. In: Selley RC, Robin L, Cocks M, PLimer IR (eds) Encyclopedia of geology, vol 1. Elsevier, Oxford, pp 345–358
Wang F, Zhou XH, Zhang LC, Ying JF, Zhang YT, Wu FY, Zhu RX (2006) Late Mesozoic volcanism in the Great Xing'an Range (NE China): timing and implications for the dynamic setting of NE Asia. Earth Planet Sci Lett 251:179–198
Wannamaker PE, Jiracek GR, Stodt JA, Caldwell TG, Gonzalez VM, McKnight JD, Porter AD (2002) Fluid generation and pathways beneath an active compressional orogen, the New Zealand Southern Alps, inferred from magnetotelluric data. J Geophys Res 107. doi 10.1029/2001JB000186

Ward JHW, Wilson MGC (1998) Gold outside the Witeatersrand Basin. In: Wilson MGC, Anhaeusser CR (eds) The mineral resources of South Africa, 6th edn, Council for Geoscience, Handbk 16, pp 350–386
Wernicke B (1981) Low-angle normal faults in the Basin and Range Province: nappe tectonics in an extending orogen. Nature (London) 291:645–647
Wignall PB (1994) Black shales. Clerendon Press, Oxford
Wilde AR, Layer P, Mernagh T, Foster J (2001) The giant Muruntau gold deposit: geologic, geochronologic, and fluid inclusion constraints on ore genesis. Econ Geol, Bull Soc Econ Geol 96:633–644
Williams GE, Wallace MW (2003) The Acraman asteroid impact, South Australia: magnitude and implications for the late Vendian environment. J Geol Soc 160:545–554
Williams GJ (1974) Economic geology of New Zealand. Australas Inst Min Metall Monogr 4, Parkville, Vic, Aust
Witt WK (1991) Regional metamorphic controls on alteration associated with gold mineralization in the Eastern Goldfields province, Western Australia: implications for the timing and origin of Archean lode-gold deposits. Geology 19:982–985
Witt WK, Davy R (1997) Geology and geochemistry of Archaean granites in the Kalgoorlie region of the Eastern Goldfields, Western Australia: a syn-collisional tectonic setting? Precambr Res 83:133–183
Witt WK, Knight JT, Mikucki EJ (1997) A synmetamorphic lateral fluid flow model for gold mineralization in the Archean southern Kalgoorlie and Norseman terranes, Western Australia. Econ Geol 92:407–437
Wood BL, Popov NP (2006) The giant Sukhoi Log gold deposit, Siberia. Russ Geol Geophys 47:315–341
Woodall R (1965) Structure of the Kalgoorlie goldfield. In: Modigan RT (ed) 8th Common Min Metall Cong Aust & NZ, vol 1. Australas Inst Min Metall, Parkville, Victoria, pp 71–79
Wyborn LA, Wyborn D, Warren RG, Drummond BJ (1992) Proterozoic granite types in Australia: implications for lower crust composition, structure and evolution. Trans Roy Soc Edinburgh: Earth Sci 83:201–209
Wyche S (2007) Towards a unified stratigraphy for Yilgarn greenstones. Proceed Kalgoorlie'07 Conference, Geosci Aust Rec 2007/14:18–22
Wyman D, Kerrich R (1989) Archean shoshonitic lamprophyres associated with Superior Province gold deposits: distribution, tectonic setting, noble metal abundances and significance for gold mineralization. Econ Geol Monogr 6:661–667
Wyman DA, Kerrich R, Groves DI (1999) Lode gold deposits and Archean mantle plume-island arc interaction, Abititbi subprovince, Canada J Geol 107:715–725
Wyman DA, Kerrich R, Polat A (2002) Assembly of Archean cratonic mantle lithosphere and crust: plume-arc interaction in the Abitibi-Wawa subduction-accretion complex. Precambr Res 115:37–62
Xiao L, Wang FZ, Wang H, Pirajno F (2004) Mantle plume tectonics constraints on the formation of Songliao and Bohaiwan basins. Earth Sci J China Univ Geosci 29:283–292
Xu YG (2001) Thermo-tectonic destruction of the Archaean lithospheric keel beneath the Sino-Korean Craton in China: evidence, timing and mechanism. Phys Chem Earth 26:747–757
Xue F, Kroner A, Reischmann T, Lerch F (1996) Palaeozoic pre- and post-collision calc-alkaline magmatism in the Qinling orogenic belt, central China, as documented by zirocn ages on granitoid rocks. J Geol Soc London 153:409–417
Yakubchuk AS, Shatov VV, Kirwin D, Edwards A, Tomurtogoo O, Badarch G, Buryak VA (2005) Gold and base metal mteallogeny of the Central Asian Orogenic Supercollage. Econ Geol 100th Ann Iss: 1035–1068
Yan QR, Hanson AD, Wang ZQ, Druschke PA, Yan Z, Wang T, Liu DY, Song B, Jian P, Zhou H, Jiang CF (2004) Neoproterozoic subduction and rifting on the northern margin

of the Yangtze platem China: implications for Rodinia reconstruction. Int Geol Rev 46:817–932
Yang MZ (1998) Geochemistry of wall alteration zone of gold deposits: from Jiaodong gold deposits. Beijing Geol Publ House, pp 1–20 (in Chinese with English Abstract)
Yang JH, Wu FY, Wilde SA (2003) A review of the geodynamic setting of large scale Late Mesozoic gold mineralization in the North China Craton: an association with lithospheric thinning. Ore Geol Rev 23:125–152
Yardley B, Gleeson S, Bruce S, Banks D (2000) Origin of retrograde fluids in metamorphic rocks. J Geochem Expl 69/70:281–285
Zhai MG, Fan HR, Yang JH, Miao LC (2004) Large scale cluster of gold deposits in East Shandong: anorogenic metallogenesis. Earth Sci Front (China Univ Geosciences, Beijing), 11:85–98 (in Chinese with English abstract)
Zhang LC, Shen YC, Li HM, Zeng QD, Li GM, Liu TB (2002) Helium and argon isotopic compositions of fluid inclusions and tracing to the source of ore-forming fluids for Jiaodong gold deposits. Acta Petr Sinica 18:559–565 (in Chinese with English abstract)
Zhang SH, Li ZX, Wu HC, Wang HZ (2000) New paleomagnetic results from the Neoproterozoic successions in southern North China Block and paleogeographic implications. Sci China, Ser D 43 (suppl):233–244
Zhao TP, Zhou MF, Zhai M, Xia B (2002) Paleoproterozoic rift-related volcanism of the Xiong'er Group, North China Craton: implications for the breakup of Columbia. Inter Geol Rev 44:336–351
Zheng L, Wang S, Liao YS, Feng ZJ (2001) CO_2 gas pools in Jiyang sag, China. Applied Geochem 16:1033–1039
Zhou T, Goldfarb RJ, Phillips GN (2002) Tectonics and distribution of gold deposits in China – An overview. Mineral Depos 37:249–282
Zorin YuA, Zorina LD, Spiridonov AM, Rutshtein IG (2001) Geodynamic settings of gold deposits in the Transbaikal region (eastern Siberia, Russia). Ore Geol Rev 17:215–232

Chapter 10
Hydrothermal Systems and the Biosphere

10.1 Introduction

In this chapter I present an overview of the links between life and hydrothermal systems, a topic that is experiencing a revolutionary rise in popularity and importance, involving and uniting, perhaps for the first time in the history of science, scientists from a wide range of disciplines, from Astronomy to Geology and the new exciting field of Astrobiology. For the first time in the last twenty years or so, we are reconsidering life, not just on Earth and the Solar System, but also beyond. It is, in my opinion, a revolution comparable to the great voyages of discovery and of scientific observations of the Europeans between the 14th to the 19th centuries, which culminated with Charles Darwin and his revolutionary book "The Origin of the Species" (Darwin 1859). For this reason, and before embarking on treating the main topic of this chapter, I think it opportune to discuss, however briefly, the emergence and physical limits of life.

To write about the emergence or origin(s) of life is fraught with a great deal of difficulty, to put it mildly. Nevertheless, to make a short trip into the topic is exciting and stimulating. We have a greater understanding on the physical limits of life, at least on Earth, than we had only two decades ago. Recent advances in biological research has established that present day bacteria, and presumably ancient bacteria too, can withstand extreme ambient conditions, including temperatures in excess of 100°C, such as exist around hot springs and high temperature submarine hydrothermal discharges (black smokers). Bacteria are also found in drillholes sunk to several km below the surface, under pressures greatly in excess of 1 atm, and in lakes beneath the Antarctic ice (see Chapters 1 and 12). Most importantly, the most ancient of extant bacteria are heat-loving, or thermophiles. In other words there are indications that Earth's most primitive life, not only survived the many changes that affected our planet, but also thrives in the same extreme conditions that must have been present in the ancient Earth. The deep sea hydrothermal vents are therefore prime candidates for having been the cradle of life.

I begin this Chapter by briefly examining the emergence of life on Earth, the hypotheses that attempt to shed some light on the origin of life, and the first signs of life in the fossil record of the oldest rocks of our planet. In a second part

F. Pirajno, *Hydrothermal Processes and Mineral Systems*,

© Springer Science+Business Media B.V. 2009

of this chapter, I examine the relationships between life and present-day and ancient hydrothermal systems. The evidence is overwhelming that heat-loving extremophile bacteria abundantly inhabit the deep sea hydrothermal vents and clear isotopic signatures and even fossilised forms are found in ancient hydrothermal systems.

10.2 The Emergence of Life on Earth

> *The notion of a Creator is non-scientific principally because there is no type of evidence that cannot be explained as the work of a Creator. Falsification of the creation hypothesis, or creationism, is impossible, therefore the whole idea lies beyond the purview of science. However, it is certainly possible to test, at least in principle, hypotheses that life originated as a result of some particular natural event. It is a perfectly legitimate scientific occupation to seek to identify processes and conditions for the origin of life through natural causes* (Dobzhansky et al. 1977, p. 149).

To this day, fundamental questions on the definition and origin of life on Earth are a grey area between science and philosophy, and in reality no one knows how life first formed. It is generally assumed that the first single-cell organisms developed through a series of chemical steps that eventually led to C-rich molecules assembling to form amino acids, which then linked to form proteins, the building blocks of life, as we know it. Numerous attempts have been made to give a scientific definition of life and speculate on its origins. Books, special issues of journals and papers on this prodigious and vast subject and one of fundamental importance in human societies, abound (Oparin 1961; Dobzhansky et al. 1977; Folsome 1979; Bengtson 1994; Cronin 1998; Davies 1998; Lahav 1999; Smil 2002; Lurquin 2003; Knoll 2003; Ward and Brownlee 2004; Bada 2004).

Simply put, life can be defined as "*an open, coherent, spacetime structure maintained far from thermodynamic equilibrium by a flow of energy through it – a carbon-based system operating in a water-based medium, with higher forms metabolising oxygen*" (astrophysicist Eric Chaisson, cited in Lurquin, 2003, p. 7). Davies (2007) wrote that a definition of life must include the ability to metabolise (draw nutrients from the environment, convert these nutrients into energy and excrete waste products) and the ability to reproduce. Another, apparently simpler but perhaps hiding a more complex definition was decided by a NASA panel in 1994 in which life was defined as "*a chemical system capable of Darwinian evolution*" (Benner et al. 2004).

On Earth, the unit of life is the cell. Cells extract energy and manufacture their constituents from the surrounding ambient; unicellular life is most abundant and includes bacteria and some marine algae, which can grow to several metres; multicellular life is more complex and includes jellyfish and *Homo sapiens*. Extraction of energy and manufacture of constituents is called metabolism, which relies on a precise code of instructions in order to function. These instructions are stored in genes that are made of DNA (see below).

Cells regulate their metabolic functions to fit the environment and reproduce themselves; in other words they multiply. Most importantly, mutating genes allow cells to adapt to an ever changing environment. The fundamental requirements for life, as we know it, are liquid water and organic polymers (Bada 2004). Polymers are substances of high molecular mass, made by combining small molecular units called monomers. A typical polymer molecule may contain a chain of monomers several thousand units long; some polymers are derived from a single monomer unit repeated several times; others may contain different kinds of monomer units (olygomers). Natural polymers are essential to all forms of life.

In thermodynamic terms, life is constantly in disequilibrium with its surroundings, whereas equilibrium means death. In fact, thermodynamic disequilibrium is considered as a basic requirement for life, and this link between hydrothermal activity and life is perhaps best exemplified by black smokers. in deep sea environments at spreading centres (Chapter 7), where hydrothermal fluid flow and associated fluxes of nutrients and energy are capable of supporting diverse microbial communities, as well as macrofaunas (e.g. Benner et al. 2004). Kelley et al. (2002, p. 409) stated that "*Of all the impressive natural phenomena that researchers have witnessed on the seafloor, the massive effusions of biogenic particles emitted from fissures, cracks and pits, following an eruptive event must be one of the most remarkable and important of the past decade*".

Subaerial hot springs, such as those of the Yellowstone National Park (Chapter 5), also support dense colonies of microbes. Evidence of microbial life is also found in deep aquifers and from deep boreholes (Pedersen 1993).

Details on the topic of the role of the biosphere in the genesis of hydrothermal ore deposits can be found in Bock and Goode (1996), Glikson and Mastalerz (2000), Wilcock et al. (2004). Table 10.1 presents a glossary of terms that are used by bioscientists and that are now commonly encountered in the geological literature.

Table 10.1 Glossary of selected terms commonly used in relation to micro-organisms and microbial life. After McCollom and Shock (1997)

Metabolism	Chemical reactions by which cells process matter and energy from the environment
Methanogen	Cells that through metabolism can generate methane (CH_4)
Autotroph	A cell that can synthesise cellular material from CO_2
Heterotroph	Bacteria that require organic carbon for metabolism
Chemotroph	Microorganisms that can use chemical energy for metabolism
Phototroph	Microorganisms that use light energy for metabolic processes
Lithotroph	Microorganism that use non organic compounds, such as H_2S and Fe^{2+}, as the electron donor for its metabolism
Organotroph	Microorganism that use organic compounds forthe electron donor for its metabolism
Chemosynthesis	Cellular material synthesised by using chemical energy from CO_2
Thermophile	Organisms that are able to live at temperatures above 50°C
Hyperthermophiles	Organisms that are able to live at temperatures above 80°C

As stated above, the definition and origins of life are very much a grey area between science and philosophy, and here I believe it appropriate to exercise freedom of expression and dwell on a science-based philosophical topic. I suggest that there may be no clear boundary between living and non-living matter and that perhaps gradations exist between the two. Perhaps in a most extreme and atheistic view, living beings are nothing more than one form of a wide variety of products that originate from the dynamic interaction of atmosphere-hydrosphere-crust over geological time. As such, living matter is just another product of planetary evolution, where C and liquid water may be present. Once established, life may take active part in the interactive phenomenology of a planet's engine and shape its evolutionary patterns in a continuosly changing environment. A good example is viruses, which appear to be the connecting link (van Loon 2005). Viruses can occur in a frozen crsytalline state and may contain DNA or RNA (see below), but never both and are incapable of reproduction except as parasites in a living host.

The basic molecules of life are proteins and nucleic acid. They have complex structures and large molecular weights. Nucleic acid, which is present in all living cells and is a blueprint carrying all necessary information that will shape the organism to which it belongs and is called either DNA, or deoxyribose nucleic acid, and RNA, or ribose nuclei acid. DNA is made of nucleotides (complex organic molecules) and proteins. Proteins are made of aminoacids and are formed following instructions encoded in DNA. Shapiro (2007) stated that this brings to mind the old riddle of which came first: the chicken or the egg? One solution may be provided by RNA which, if involved in the origin of life, must have appeared before DNA. Since aminoacids and nucleic acids are present in all living beings, these must have had a common genesis.

In the so-called RNA world, five steps can be considered that led to DNA (Horgan 1991). In the first step, RNA forms from organic compounds, as the RNA molecules evolve they learn to make copies of themselves (step 2); the RNA molecules synthesise proteins (step 3), which then help the RNA to make double strand versions that evolve to DNA (step 4). DNA takes over, using RNA to make proteins, copies of itself and transfer its genetic information to RNA.

But, all of the above begs the question: how did the first RNA form? Like for DNA, RNA building blocks are nucleotides, each being made of C, N, P and O atoms, linked in a three-dimensional pattern. How did this linkage come about? There are thousands of possible combinations, and is only one the right link for life? Shapiro (2007) listed five essential requirements for the origin of life: (1) a boundary to separate life from non-life; (2) energy source to drive the organisation process; (3) a coupling mechanism to link the release of energy to the system that produces and sustains life; (4) a chemical system that allows adaptation and evolution; (5) this system must be able to reproduce and evolve. Shapiro (2007) suggested a "small molecule" approach for the origin of life, in which the demands of the above-listed five requirements must be met. These requirements, Shapiro contended, are readily available in nature and no

elaborate steps would be needed to form the first replicating molecule. He concluded his article by quoting biologist Stuart Kauffman that "*... life is vastly more probable than we have supposed. Not only we are at home in the universe, but we are far more likely to share it with as yet unknown companions*".

The Tree of Life, a model of life's evolution and the phylogenetic grouping of all known living organisms, is based on DNA and molecular sequence comparison of genes that code for ribosomal RNA (Fig. 10.1). The Tree of Life, first proposed by Woese et al. (1990), groups all living organisms in three branches, Archaea, Bacteria and Eukarya (or Eucarya), all sharing a common, but unknown ancestor. The fundamental facets of life's origins are that it almost certainly arose quite early in the Earth's geological history, likely before 3.8 Ga,

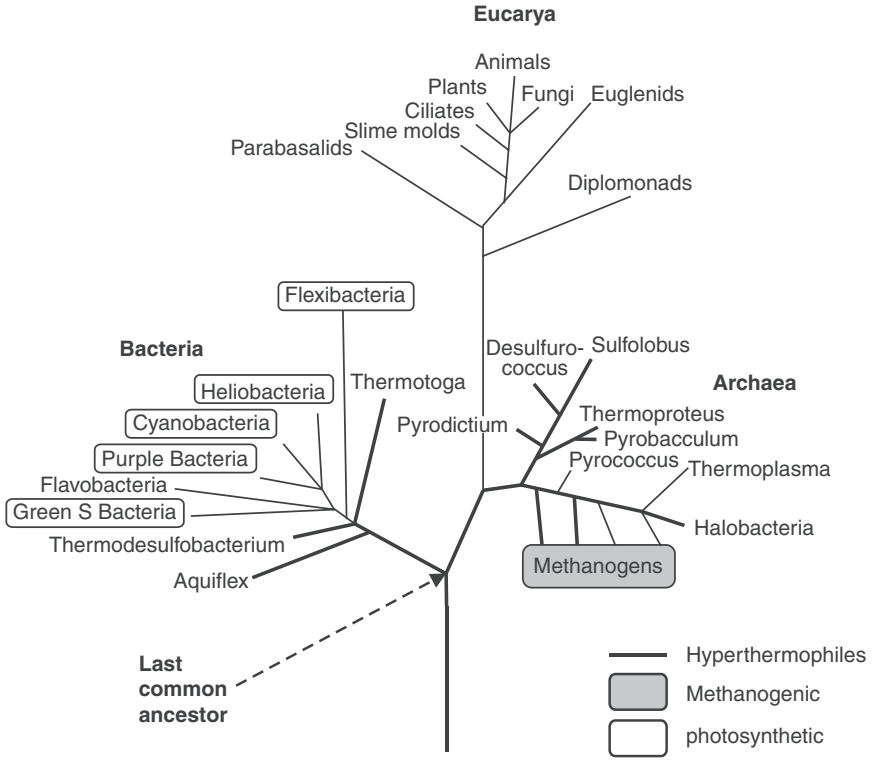


Fig. 10.1 The universal philogenetic tree (Tree of Life) is based on 16S rRNA sequence comparisons, showing the genealogical relationship of all living organisms (Stetter 2002). It shows an arboreal figure, divided into three branches: Archaea, Bacteria and Eukaria. Although the details are being argued by biologists, all agree on its general outlines. Note that the length of each branch indicates the degree of difference between gene sequences. Also indicated are photosynthetic bacteria and methanogens, whereas the heavy lines indicate hyperthermophiles, which occupy the lower sections of the three branches, suggesting that life began with chemolithotroph hyperthemophiles. This figures is after Knoll (2003, p. 25; see also Skinner and Jahren 2003)

Table 10.2 Gases emitted during early volcanic outgassing of the primitive Earth. After Folsome (1979)

Major gases	Minor gases	Trace gases
Hydrogen (H_2)	Carbon dioxide (CO_2)	Methane CH_4)
Water vapour (H_2O)	Sulphur (S_2)	Sulphur dioxide (SO_2)
Nitrogen (N_2)		
Carbon monoxide (CO)		
Hydrogen sulphide (H_2S)		

through chemical reactions that produced organic molecules and other building blocks of life in the presence of stable surface water (Davis and McKay 1996).

On early Earth, the primeval atmosphere consisted mostly of CH_4, NH_3, H_2O and volcanic outgassing was intensive (Table 10.2).

Apart from the brief overview given below, it is beyond the scope of this book to elaborate fully on the origin of life, suffice to say that theories that attempt to explain the origin of life on Earth are based on four models (Orgel 1998): (1) organic molecules were transported by cometary and/or asteroidal impacts (panspermia hypothesis); (2) synthesis of prebiotic molecules in a reducing atmosphere; (3) prebiotic organic molecules formed on metal sulphides bubbles in deep sea hydrothermal vents; (4) clay minerals may have been the catalysts for prebiotic synthesis (Ferris 2005). The reader should be aware that the different lengths of the sections below do not imply a favoured view on my part.

10.2.1 Panspermia

The idea that the origin of life might be connected with interplanetary transport of micro-organisms within the Solar System and perhaps from beyond is a theoretical proposition that is being seriously considered (Wickramasinghe 2006). The original suggestion was made by Lord Kelvin in 1865 and further taken up by Arrhenius (1903). The panspermia hypothesis postulates that organic molecules, or even micro-organisms, may disperse in space by radiation pressure or via asteroid impacts from one planet to another or even from one solar system to another (Horneck et al. 2002). Indeed, the Murchison meteorite, for example, is known to have several classes of complex organic compounds (Cronin 1998). In one view, panspermia may have been brought about during the early accretion stages of Earth. The gravitational collapse of dust particles under temperatures in excess of 1000 °K was followed by the late addition of volatile and organic compounds presumably from early cometary contributions. Horneck et al. (2002 and references therein) list a number of recent discoveries that enhance the possibility that panspermia may be a valid concept. Amongst others, they cite the detection of organic molecules in the above-mentioned Murchison meteorite; the ability of bacteria to survive the shock

of impacts; the high ultraviolet radiation resistance of micro-organisms at the low temperatures of deep space; the survival of bacteria enclosed in amber or salt, over millions of years. A collection of papers that deal with various aspects of the role that comets may have played in the origin of life was published by Thomas et al. (2006). Interstellar ice consists of water, methanol, hydrocarbons, carbon monoxide and dioxide and silicate granules, but under the onslaught of ultraviolet radiation the chemical bonds of the frozen compounds are broken. Nevertheless, it is possible that some of these organic compounds could have provided life's precursor molecules, through conversion of interstellar hydrocarbons to complex alcohol, ethers, and quinones (Bernstein et al. 1999). The latter is especially significant because it is present in living systems today and is essential for converting light into chemical energy as in photosynthesis (Bernstein et al. 1999).

However, interesting and intriguing as it may be, the panspermia hypothesis (also mentioned in Chapter 1) encounters some problems. The oldest traces of terrestrial life, still hotly debated, are found in 3.85 Ga rocks, therefore if organic molecules or proteins were transported by comets or meteorites this must have occurred during the 4.2–3.8 Ga Late Heavy Bombardment (LHB), of which the maria basin on the Moon are representative. How organic molecules or proteins could have survived prolonged cosmic radiations presents a problem. In addition, the essential ingredients of life, DNA and RNA have not been found in meteorites and the steps required to make these self-replicating nucleic acids from simple organic molecules is unknown. Also, amino acids found in carbonaceous chondrites are of a type unknown in terrestrial materials. Another problem is that terrestrial amino acids, with some minor exceptions, possess only left-handed symmetry, whereas extraterrestrial materials possess equal amounts of left-handed and right-handed symmetry molecules. Therefore, if large-scale cometary contributions of amino acid with right-hand symmetry had been common, these molecules should have been preserved or metabolised by terrestrial micro-organisms. This is not the case. Organic compounds are continuously synthesised during terrestrial hot spring hydrothermal processes, such as seafloor systems (see Chapter 7). Volatile fractions of volcanic emissions, such as those of Kilauea, consist predominantly of H_2O (30%), H_2 (0.35%), CO_2 (40%), CO (1.2%), SO_2 (28%), S_2 (0.04%), HCl (0.034%), contrast sharply in terms of their proportions from the volatile fractions of some comets (H – (56%), O– (31%), C – (10%), N – (2.7%) and S – (0.3%) (A. Y. Glikson, written comm., 2004). It is more likely that extraterrestrial compounds would have been destroyed on entry as a result of meteoritic disentegrations.

An interesting variant of the panspermia model is the hypothesis that some of the influenza outbreaks may be caused by viruses from space that coincide with the 11-year cycles of sunspot activity (Belisheva 2005). Microbial growth in humans could be affected by extraterrestrial agents, such as solar wind and cosmic rays. Belisheva (2005) suggested that growth of pathogenic microbial organisms with solar wind and cosmic rays could indicate the possibility of bacteria coming from space.

10.2.2 Synthesis of Prebiotic Molecules, Organic Soups and Warm Little Ponds?

But how did then the critical organic molecules form? Laboratory experiments are consistent with the syntheis of organic molecules in the early terrestrial environments. Starting conditions are assumed to have been a reducing atmosphere enriched in CH_4, NH_3, H_2, H_2S and H_2O, in which the essential building blocks of life, the amino acids, would have been synthesised by lightning. This hypothesis stemmed from the brilliant and famous experiments performed in the early 1950s at the laboratory for Planetary studies, Cornell University, by Stanley Miller and Harold Urey (Miller 1953; Miller and Urey 1959). Briefly, these experiments consisted of sparking electrical discharges, to simulate lightning, in a glass flask containing a mixture of CH_4, NH_3, H_2S and H_2O, assumed to be components of the early atmosphere. After continuous sparking for several days at a high voltage (30 000–60 000 volts), the interior of the glass flask was coated with a variety of organic molecules, including amino acids. Sagan (1981) reported that Harold Urey was asked what he thought could be achieved by such an experiment. He replied: *Beilstein*, referring to the 28 volume German compendium listing all organic molecules known to chemists at the time. Effectively the Miller-Urey experiments shifted the debate on the origins of life from the speculative and philosophical realm to experimental science.

Since the first Miller-Urey experiments, other workers have performed similar experiments with varying input of gases and types of energy such as shock waves, beta and gamma rays. Other experiments involved heating the gas mixtures to high temperatures (up to 900°C) in the presence of metallic catalysts to simulate interactions of a primitive atmosphere with lava flows. Taken together, the results of all these experiments produced a great variety of organic compounds, in addition to amino acids. The principal products obtained from these experiments include hydrogen cyanide (HCN), formaldehyde (HCOH), and formic acid (HCO_2H) as intermediate products, and dicyanamide ($HN(CN)_2$), glycoaldehyde ($HOCH_2CHO$), acetic acid (CH_3CO_2H), several hundred amino acids, fatty acids, hydrocarbons and a host of other small organic compounds as end products (Folsome 1979). Importantly, if these synthetised organic materials did form in the primeval atmosphere, some would have remained in the atmosphere, others would have gone into solution in water pools or lakes, fatty acids and hydrocarbons would have floated as a scum on water, but all would have been subject to intense solar ultraviolet radiation and other energy sources, so that if on the one hand the synthesis continued, their degradation would also have occurred, so that there was a continuous cycling of components from gases to organic compounds and back:

$$H_2 + CO + CO_2 + N_2 + H_2 + CH_4 + H_2S \leftrightarrow \text{organic compounds}$$

It can be concluded that it is likely that biological organic materials were synthetised from mixtures of gases in the primeval atmosphere. If this is the

case, life would have arisen from abiotically produced organic materials (Kral et al. 1998). Therefore, it is also likely that the first living organisms would have been autotrophs using chemical energy. This energy could have been provided by H_2, a gas commonly associated with hydrothermal fluids and volcanic emissions. Indeed, a H_2-rich early Earth atmosphere is considered likely, taking into account a balance between H_2 escape and volcanic outgassing (see Table 10.2; Tian et al. 2005).

This may have favoured the production of prebiotic organic compounds more efficiently than cometary delivery or synthesis in hydrothermal systems, according to Tian et al. (2005), who suggested that the "*organic soup in the oceans and ponds on early Earth*" were favourable sites for the origin of life. Hydrogen-consuming reactions by methanogenic bacteria, with reduction of CO_2 to produce CH_4, with the reaction (Kral et al. 1998; Chapelle et al. 2002):

$$CO_2 + 4H_2 \rightarrow CH_4 + 2H_2O$$

This reaction would have been a sink of geologically produced H_2 by methanogens and a source of CH_4 as a by-product. This chemosynthesis could have been the basis for the inception of H_2-based microbial ecosystems on Earth and perhaps Mars and Europa (Kral et al. 1998; Chapelle et al. 2002).

However, the brilliant simplicity of the Miller-Urey experiments, which led to a general acceptance of the "primordial soup" hypothesis, was more recently queried on the basis of given assumptions that may not have been correct. Cairns-Smith et al. (1992) doubted the presence of a strongly reducing atmosphere in the early Earth, which would have been essential for the Miller-Urey model to function. While the question of the composition of the early Earth atmosphere is by no means resolved, Cairns-Smith et al. (1992) considered more likely that there was an atmosphere more like that of Mars or Venus with CO_2, H_2O and N_2, rather than CH_4 and NH_3 as the main constituents.

10.2.3 Sulphide Bubbles in Seafloor Hydrothermal Vents

As mentioned previously, the physical limits of life are quite extraordinary. Bacteria can survive, indeed thrive, in extreme environmental conditions, such as several km beneath the surface under pressures in excess of 1 kbar, in hot springs at temperatures well above 100°C (hyperthermophiles) and in frozen lakes beneath the Antarctic ice sheet, as in Lake Vostok (see Chapter 1). The discovery of hydrothermal vents on the seafloor in the 1970s that support thriving living communities, such as tube worms, clams, and bacteria whose energy source is not light but sulphur compounds emitted from the vents, has opened a new chapter in the quest on the origins of life. The vent hypothesis captured the imagination of a German lawyer with a PhD degree in organic chemistry, Günter Wächtershäuser, who proposed

that pyrite (FeS_2) would provide a positively charged surface that would attract organic compounds (reported in Horgan 1991). Furthermore, the formation of pyrite from Fe and S, yields energy that would promote reactions between organic compounds.

Cairns-Smith et al. (1992), Russell et al. (1988; 1994) and Russell and Hall (1997), taking the cue from the synthesis of organic compounds in high-temperature submarine hydrothermal vents, proposed that life emerged in submarine hot springs in a Fe-rich ocean in Hadean Earth (4.4–3.85 Ga). The following is summarised from the work of these authors.

Just as hydrothermal fluids are very effective in concentrating metallic elements to form orebodies, so these fluids could glean organic molecules originally provided by cometary impacts and the constant rain of interplanetary debris during the early meteoritic bombardment. It has been suggested that these organic molecules in hydrothermal fluids could have reacted to produce further organic molecules and finally a protocell of sorts. For example, Russell and co-workers envisaged that Fe monosulphide bubbles formed at an alkaline submarine hot spring at about 4.2 Ga, were responsible for the creation of the first organic protocells. The premise put forward by these researchers is that continuing attempts to attain geochemical equilibrium by the hydrothermal fluids with the Hadean ocean were effectively impeded by the precipitation of Fe monosulphide membranes and that the Hadean atmosphere was not reduced and that there was no organic soup. In addition, given that living cells contain abundant water, then life must have originated in water, which in the early Earth would have been the Hadean ocean. Russell and co-workers suggested that the Hadean water, together with CO and CO_2 most probably was derived in part from asteroid contributions and in part by volcanic degassing. The presence of CO and CO_2 would have induced a greenhouse effect, similar to present-day Venus, and high ocean temperatures (85–110°C). The Hadean ocean water was continuously recycled in part by acid rain and in part by acidic submarine hot springs (>400°C) as well as by numerous hot ($\leq$ 200°C) alkaline seepages on the ocean floor. The model, shown in Fig. 10.2, suggests that these low-temperature alkaline and reduced springs, in which Fe in solution precipitated as Fe monosulphide by mixing with HS^- in the hydrothermal fluids on the ocean floor. Laboratory experiments were conducted in which a solution of ferrous chloride was introduced into a vessel containing sodium sulphide so that:

$$FeCl_2 + Na_2S \rightarrow FeS + 2NaCl$$

resulting in the formation of monosulphide bubbles. The researchers reasoned that the sodium sulphide solution represented the Hadean ocean and the ferrous chloride the hydrothermal solution. They suggested that the Ni-rich Fe monosulphides formed bubbles with membranes (Fig. 10.2) that acted as an interface between the hydrothermal solutions and the ocean water. These Fe monosulphide bubbles were therefore a catalytic boundary encouraging the synthesis of

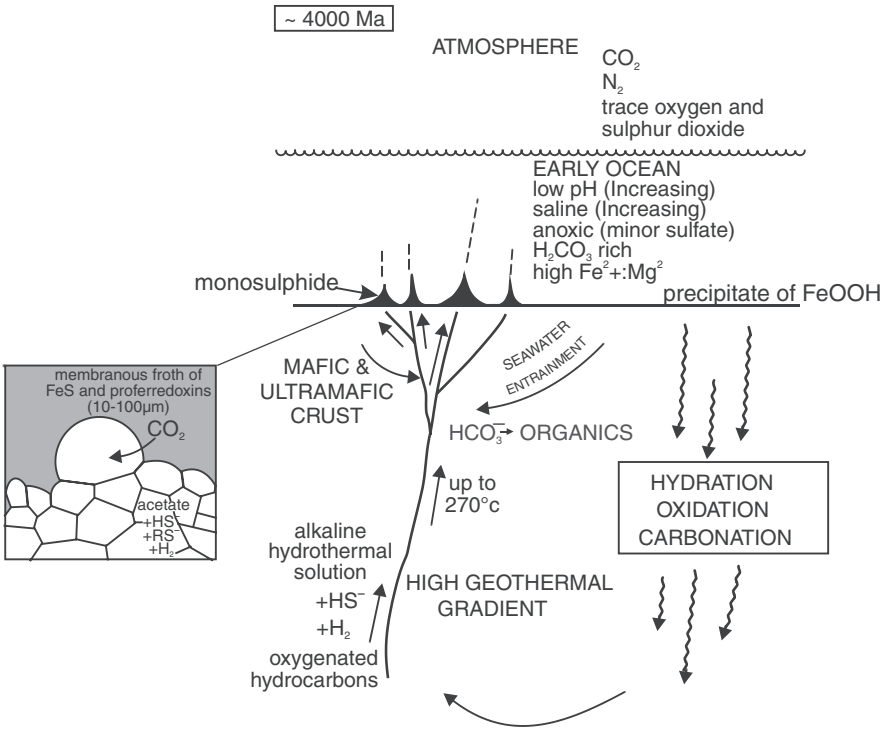


Fig. 10.2 Simplified sketch depiciting a model of alkaline submarine hot spring in the Hadean ocean (> 4.0 Ga). The hydrothermal fluids are rendered alkaline by interaction with mafic-ultramafic rocks; discharge on the ocean floor formed chimney spires similar to those of modern submarine hot springs (see Chapter 7). On the leading edge the chimneys precipitate monosulphide (FeS) bubbles or a froth-like assemblage, whose membrane exchanged with ambient seawater. This figure combines figures 1 and 5 from Russell and Hall (1997) and Cairns-Smith et al. (1992), respectively

organic molecules, with the hydrothermal solutions providing the necessary organic ingredients, such as C, N, P, NH_3, HS^-, H_2. Condensation of organic molecules to organic sulphides was facilitated by protons (H^+) or protonmotive force, which is the universal energy mechanism of life. This is exemplified by ferrous iron oxidising bacteria such as *Thiobacillus ferrooxidans*, which uses natural protonmotive force to form adenosine triphosphate (ATP), according to Russell and Hall (1997):

$$2Fe^{2+} + {}^1/_2\,O_2 + 2H^+ \rightarrow 2Fe^{3+} + H_2O$$

Finally, in these "*chemical gardens*", as put it by Cairns-Smith et al. (1992), the role of the monosulphide membrane was taken over by the synthesised organic sulphides.

10.2.4 Models Based on Minerals Other than Sulphides

Hazen (2001) described five possible situations in which organic molecules could form and assemble on crystal faces. Crystals could act as: (1) containers; (2) templates; (3) catalysts; (4) scaffolds; and (5) reactants. In the case of container minerals, submicroscopic pits are present for example in the weathered surfaces of the mineral feldspar, and these act as tiny chambers that could harbour organic materials. Template minerals, such as calcite, tend to attract left- and right-handed amino acids to specific crystal faces. It is well known that amino acids come in mirror image forms; left-handed, or simply L, and right-handed, or D. It is an enduring mystery that living organisms have nearly 100% L amino acids. Hazen ran experiments with calcite crystals because of their mirror-image faces and found that L faces of calcite crystals tend to "select" L amino acids and vice versa. The mystery remains, but it is possible that pure chance allowed a successful organic molecule to develop on crystal faces that selectively attracted L amino acids. Magnetite is capable of catalysing some biochemical reactions, as for example nitrogen and hydrogen into ammonia, an essential compound of living cells.

10.2.4.1 Clay Minerals

Clay minerals, such as zeolites and montmorillonite, are of considerable interest to origin of life discussions because they are capable of interacting with organic molecules (Cairns-Smith et al. 1992). This interaction consists of adsorbtion of biochemicals from dilute aqueous solutions. Montmorillonite clays exert a control on polymerisation of amino acids. Zeolites are known to be almost ubiquitous in moderate temperature hydrothermal systems and have good adsorptive and catalytic properties. Cairns-Smith et al. (1992) also list phosphates as possible catalysts for the synthesis of prebiotic molecules.

Ferris (2005) discussed the role of montmorillonite in catalysing reactions of organic compounds and the assembly of nucleotides that result in the formation of RNA polymers. The main points of his paper follow. The stochiometric formula of montmorillonite is $Al_4Si_8O_{20}(OH)_4$, but this allows the substitution of Al^{3+} by ions such as Mg^{2+}, Fe^{2+} and Fe^{3+} in octahedral layers and Al^{3+} for Si^{+4} in tetrahedral layers. These substitutions result in a negative charge, which tends to be neutralised by the substitution of cations. The crystalline geometry of montomorillonite is like a deck of cards consisting of platelets that stack on top of each other when dry. When H_2O is added, the ions in the interlayer become hydrated and this results in the expansion of the distance between the platelets. In a similar fashion, adsorbtion of organic compounds takes place in these interlayers as the clay mineral expands. This tendency of clays to adsorb organic molecules contributes to their propensity to catalyse organic reactions that, in Ferris' view, are critical to life's origins. Some of these are redox reactions, mentioned in Chapter 1, which involve the donation and acceptance

of electrons, in this case from the clay interlayers. Ferris (2005) cited the example of the redox reaction of the organic compound diaminomaleonitrile (DAMN), which oxidises to diminosuccinonitrile (DISN) and binds to the Fe^{3+} of montomorillonite. Apparently, this redox reaction is typical of metabolic processes in many cells. In addition, clays have the capacity to accelerate organic reactions through the action of metal ion complexes.

In his quest to understand the origin of life, Ferris (2005) makes the important premise that DNA is necessary to make proteins, but on the other hand proteins are needed in order to make DNA. So, which came first? Once again a chicken and egg conundrum. This led to the concept of RNA first, because RNA has the ability to play the role of both DNA and protein as well to store genetic information. RNA consists of a sugar molecule, a phosphate group, and other organic compounds (bases that are called A, C, G and U). These bind together to form a phosphate-sugar-base unit called nucleotide (a ribose molecule linked to other carbon and phosphate based compounds, also known as RNA monomer). Nucleotides, in turn, link to each other forming a kind of RNA chain, which can carry information. However, there are problems with the RNA hypothesis for the orgin of life in that no mechanism has been found for the prebiotic synthesis of RNA. This is where montmorillonite could fill the gap as a potential prebiotic catalyst.

Experiments showed that RNA monomers (one unit of an RNA polymer) can bind to clays. These montmorillonite-catalysed reactions yielded RNA olygomers of up to 10 mers (small molecules that are chemically bonded to monomers or polymers). However, the RNA that functioned as an early life holder of genetic information needs to be olygomers with more than 40 mers in order to function as catalysts. These experiments opened the way for a better understanding of the role of lifeless minerals and metal ion catalysis in the formation of complex organic structures that enventually may have led to the first living cell.

Experiments by Hanczyc et al. (2003) can be seen as a combined clay model with alkaline submarine discharges on a 4.3 Ga ocean floor (Russell 2003). These experiments require initial alkaline conditions where clays can catalyse and nucleate lipid vesicle growth. Russell (2003) suggested that alkaline (pH $\sim$10) hydrothermal fluids that flow through precipitated clays, Fe-Ni sulphides and hydroxides, such as brucite [$Mg(OH)_2$], to discharge into an acidic ocean, favour phosphate chemistry, acid-base catalysis and provide a sink for protons, essential to a "*protonmotive force that is required for all cells*" (Russell 2003).

10.2.5 The First Signs of Life on Earth and the Great Oxidation Event

The identification of microbial life in the geological record, especially that of Precambrian, is a difficult task and its results are usually open to debate. There

are several papers that deal with aspects for (Hofmann et al. 1999; Westall, 2001, 2005; Van Kranendonk et al. 2003; Furnes et al. 2004, 2007; Allwood et al. 2006; Van Kranendonk 2007) and against (Brasier et al. 2002, 2004, 2005; Garcia-Ruiz et al. 2003) early life in Archaean greenstone rocks, providing much food for thought and interesting debates (see also Whitehouse and Fedo, 2007, who discuss evidence for early life from Greenland). Only with the Cambrian Explosion, at about 540 million years ago, did the first skeletal organisms appear, examples of which are beautifully preserved in the world-famous Burgess Shale of British Columbia (see Conway Morris 1992). Therefore, over more than 3.5 billion years of geological history, living organisms had no hard or skeletal parts that could be preserved as fossils.

The fossil record before 540 Ma is entirely represented by silicified forms or casts that only locally preserve a biogeochemical signature (see Knoll 2003), although some ancient microbial commuities precipitated minerals and left diagnostic shapes in carbonate rocks called stromatolites (Kalkowsky 1908).

Bona fide morphological evidence of ancient life forms falls into four categories, according to Westall (2005): (1) small (+10 μm long) and larger (up to 100 μm long) filaments; (2) curved rod structures, 2 to ~4 μm long and 1 μm wide; (3) spheroidal structures from about 0.4 to 1.3 μm in diameter; and (4) straight rods about 1 μm in length. Stromatolite morphology, although not exclusively accepted (e.g. Grotzinger and Rothman 1996), can also be used as an indicator of biogenicity in well preserved ancient rocks (e.g. Altermann 2007; Van Kranendonk 2007). Stromatolites span the entire geological record and today they can be seen in the quiet, warm and brine-rich waters of Shark Bay in Western Australia, ironically not too far from the Pilbara region (visit http://pilbara.mq.edu.au/wiki/Images, last accessed in February 2008, for a full range of images of Strelley Pool Chert and Shark Bay stromatolites).

In any case, biomineral signatures and stromatolite-like structures need to be considered, not in isolation, but in the geological context (e.g. Van Kranendonk 2006). For example, as well illustrated in Westall (2005), the laterally extensive laminated domed structures found in the greenstone belts of the Pilbara Craton (see Fig. 10.3) and in the Barberton greenstone belt (Kaapvaal Craton, South Africa), interpreted as being the silicified remnants of microbial mats replaced by silica, are almost identical to those of modern day algal structures in sea lagoons (Fig. 10.3) and in hot springs (e.g. Walter 1972).

Another potential indicator of biogenicity is isotopic signals, although these are controversial and subject to post-depositional processes that may alter the original isotopic compositions. Carbon isotopic values, ranging from –14 to –42‰ are commonly attributed to biological activity, but again these isotopic fractionations can also be produced abiotically by the Fischer-Tropf synthesis (see Brasier et al. 2002). The Fischer-Tropf synthesis is a series of abiotic reactions that can be described by the following equation:

$$2nH_2 + nCO = n(-CH_2^-) + nH_2O$$



Fig. 10.3 Stromatolites from the Warrawoona Group, Pilbara Craton; (**A**) wrinkly laminated mat of oldest stromatolites in the world, dated at ca. 3.49 Ga (Pb-Pb on syn-genetic galena in barite), from the Dresser Formation (penknife is 15 cm long) (**B**) the "egg-carton" stromatolites of the Strelley Pool Chert. (**C**) Palaeoproteozoic stromatolites in the Yelma Formation (Earaheedy Basin, see Chapter 8); (**D**) present-day stromatolites, Shark Bay Western Australia. (**A**) and (**B**) courtesy of Martin J Van Kranendonk

and is a way of producing hydrocarbons from the combustion of coal (see Potter and Konnerup-Maiden 2003 and references therein). Similar problems are encountered with sulphur isotopic compositions (see references in Westall 2005).

Earth's earliest life was probably established soon after the cessation of the heavy asteroid bombardment at about 3.8 Ga. Before that time, only hyperthermophiles could have existed in hot hydrothermal vents and may have survived the heavy meteoritic bombardment.

The earliest evidence of putative life comes from the 3.8 Ga Isua greenstone belt in southwest Greenland, where carbonates and graphite globules with an organic $\delta^{13}C$ signature ($\sim$19‰) occur in water-lain sediments (Nisbet and Sleep 2001). The biological origin of the Isua carbonates and graphite remains, however, heavily disputed, although banded iron formations that are present in the Isua belt could be considered as a valid biomarker (see Schopf 2004 and Whitehouse and Fedo 2007 for reviews).

The region of the world where the oldest fossils, in the form of stromatolites (Walter et al. 1980; Hofmann et al. 1999; Allwood et al. 2006; Van Kranendonk 2006, 2007), putative microfossils (Awramik 1983; Schopf 1993; Ueno et al.

2001), and chemical signatures (Shen et al. 2001; Ueno et al. 2004, 2006; Marshall et al. 2007; Philippot et al. 2007) can be found is the ~3.5–3.35 Ga rocks of the Warrawoona and Kelly Groups in the Pilbara Craton, Western Australia (see Van Kranendonk 2007 for a review).

The history of the Pilbara's oldest traces of life are not without controversy, however, because the Pilbara's stromatolite forms have been considered by some scientist to represent deposition of abiotic chemical sediments (Buick et al. 1981; Brasier et al. 2004; Lindsay et al. 2005), and others have questioned the evidence for the biogenicity of proposed microfossils (Brasier et al. 2002; Garcia-Ruiz et al. 2003). Nevertheless, the overwhelming evidence is that stromatolites, when viewed in detail, in combination with a thorough knowledge of geological setting, and a host of other tests, remain our best and most conspicuous fossils and as such do provide a record of evidence of early life (Van Kranendonk 2007).

This issue is well argued and presented by Allwood et al. (2006), who studied several kilometres of stromatolitic outcrops of the ~ 3.4 Ga Strelley Pool Chert, at the base of the Kelly Group (Van Kranendonk et al. 2002) (see Figs. 5.47 and 7.41 and discussions of the Warrawoona Group in Chapters 5 and 7). Although, the authors acknowledged that the biogenicity of the Pilbara stromatolites is not proven, there is compelling field evidence that stromatolites in the Strelley Pool Chert do represent ancient microbial mats. Coniform, and weakly branching stromatolites (Fig. 10.3) were first described by Lowe (1980), based on their morphology, a claim re-iterated by Hofmann et al. (1999). However, Lowe (1994) and Lindsay et al. (2005) considered that the stromatolite forms were the results of abiotic chemical processes, precipitated from hydrothermal fluids. Subsequent rare earth elements geochemistry and detailed morphological studies showed that an origin of stromatolites as quiet water hydrothermal precipitates could not be sustained (Van Kranendonk et al. 2003).

The palaeoenvironment of the Strelly Pool Chert was a peritidal carbonate platform, a depositional setting that is common in several recognised stromatolites of later ages. The detailed stratigraphy of the area consists of four members (Van Kranendonk 2006, 2007; Allwood et al. 2006): a basal M1 member represented by a thin discontinuous jasperoidal and cherty boulder conglomerate; member 2 (M2) is a 10–20 m thick layer of stromatolitic carbponate/chert; member 3 (M3) is a bedded black chert; and member 4 (M4) is a fining upward volcaniclastic unit. The palaeoenvironmental settings of these units range from a rocky coastal setting (M1), to a southward deepening peritidal carbonate platform due to transgression (M2), to clastic sedimentation, volcanism and hydrothermal activity in a southward-deepening basin (M3-M4).

Allwood et al. (2006) identified six stromatolite types in M2, consisting of pseudocolumnar structures associated with rhythmic chert/carbonate laminae. M3 contains a seventh stromatolite type consisting of laminated ironstone in chert (Van Kranendonk 2007). M2 exhibits evaporite crystal casts and

intraclast conglomerates, features of intertidal to supratidal carbonate facies. M2 also has facies associations of four stromatolite types, namely: "*egg-carton laminites*", "*large complex cones*" in the central and southern areas, and "*large cuspate swales*", and "*small crested conical laminites*" in the north. Van Kranendonk et al. (2003) and Van Kranendonk (2007) presented evidence for stromatolite deposition under high-energy conditions including the presence of granular sediments in the laminites, indicating a microbial mat that trapped the sediment grains, as is observed in modern stromatolites. These authors concluded, in support of Hofmann et al. (1999) that morphological features were sufficient proof of biogenicity.

Allwood et al. (2006) argued that the stromatolite facies associations are inconsistent with either mechanical or chemical deposition; for example, they show that "*large complex cones*" are not isopachous (points of equal thickeness) and therefore cannot be chemically precipitated, and also that the nearly vertical conical pseudocolumns of other forms require vertical growth, a feature not known in abiogenic models. The other stromatolite facies have attributes that confirm their true origin, such that Allwood et al. (2006) concluded by saying that an abiogenic model for the Strelley Pool Chert stromatolites is an "*extraordinary claim*" that requires "*extraordinary proof*". I have visited the Strelley Pool locality on a number of occasions, during field trips organised by the Geological Survey of Western Australia, led by Martin Van Kranendonk, and I entirely agree with the above conclusion.

10.2.5.1 The Great Oxidation Event (GOE)

The initiation of an oxygenated atmosphere-ocean system was probably the most significant event that transformed and created new biotic niches, culminating with the advent of metazoa. Some of the interesting works that furnish insights on the evolutionary trends of the atmosphere are those of Canfield (2005) and Canfield et al. (2000).

Ohmoto (2004) classified models for the evolution of atmospheric oxygen into two groups: (1) the Cloud-Walker-Holland-Kasting (CWHK) model and (2) the Dimroth-Ohmoto (DO) model. The CWHK model is based on the concept that life originated in a reducing atmosphere and that, as discussed below, the Great Oxidation Event (GOE) occurred at around 2.3 Ga, triggering the emergence of eukarya (Holland 2002), although it is now known that eukaryotes originated much earlier (Brocks et al. 1999). The model further implies that the oceans, except for a shallow photic zone, were mostly anoxic till about 600 Ma. The geological evidence for a reduced environment throughout most of the Archaean is provided by (Ohmoto 2004): (1) presence of detrital pyrite, uraninite and siderite in continental sediments; (2) behaviour of Fe in subaerial (e.g. paleosols, red beds) and marine (e.g. iron formations) environments; (3) the geochemical cycle of sulphur (Fig. 10.4); (4) the geochemical cycle of C ($\delta^{13}C$).

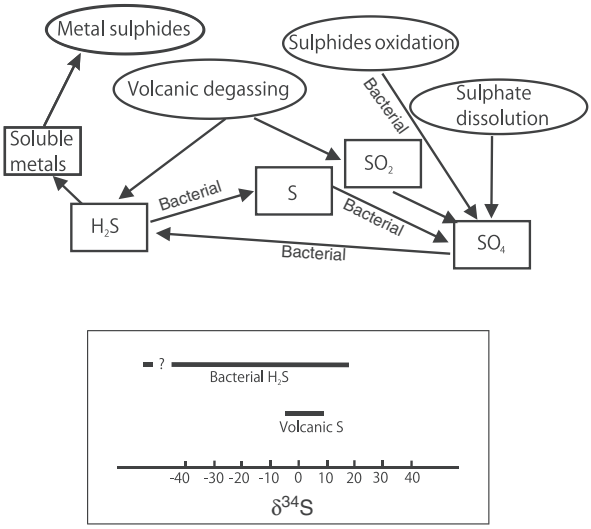


Fig. 10.4 Simplified sulphur cycle for mineral systems. Modified from C. Mills' web site http://technology.infomine.com/enviromine/ard/Microorganisms/roleof.htm#Role%20of%20Bacteria (last accessed in May 2008). Inset box shows the range of volcanic and bacterial $\delta^{34}S$ values (‰); see also Fig. 1.14. For details of the terrestrial sulphur cycle see Brimblecombe (2003)

In stark contrast to the generally accepted model above, the DO model postulates that the emergence of oxygenic photosynthetic micro-organism (cyanobacteria) occurred after the formation of oceans and continents at about 4 Ga, triggering a rise of atmospheric oxygen to about 50% of PAL, thereafter rising gradually to present atmospheric level (PAL; present atmospheric level of oxygen is 0.21×10^6 ppm). Support for an early (at least partly) oxidizing environment has been confirmed by recent studies of S isotopes (Anbar et al. 2007; Kaufman et al. 2008). Photosynthesis is the mechanism by which organisms capture sunlight's energy to perform metabolic reactions, as in the well known equation:

$$6CO_2 + 6H_2O(+\text{light energy}) \rightarrow C_6H_{12}O_6 + 6O_2$$

This metabolic reaction is the product of billions of years of microbial respiration and the ultimate source of the oxygen we breathe today. It was this vast production of photosynthetic oxygen that induced new adaptations and the evolutionary changes in Earth's living systems.

In the DO model, the oceans would have been oxygenated since about 4.0 Ga, except for enclosed local basins, which were anoxic (e.g. today's Black Sea). Ohmoto (2004) reviewed the interaction of life with atmospheric and oceanic chemistry in the Archaean, stressing that all of the atmospheric O_2 was produced through biological activity and photosynthesis, at the same time

influencing the amount of atmospheric CO_2 and CH_4. In closed bodies of sea water, the deceased biomass decomposes by reaction with O_2 and sinks, causing a stratified water body that is an oxygenated upper layer and an anoxic bottom layer. The sulphur chemistry is linked to sulphate-reducing bacteria (SRB) and the atmospheric O_2 level. Under an anoxic atmosphere, the SO_4^{-2} content of sea water was much lower than the present value (corresponding to ~900 ppm S). In the Archaean oceans the SO_4^{-2} was generated by photochemical reactions of volcanic gases (Farquhar and Wing 2003). At temperature below 250°C, aqueous solutions cannot contain large amounts of Fe^{2+} and H_2S, because Fe_2S will precipitate. In the DO model, the Fe^{2+} and H_2S contents of ocean waters remained low since about 4.0 Ga except in anoxic basins, in which abundant Fe^{2+} was supplied through hydrothermal vents and large amounts of H_2S produced by SRB processes.

The CWHK model is discussed in Holland (2002) and Barley et al. (2005). There is good evidence that between 2.3 and 2.1 Ga the oxidation state of the atmosphere changed dramatically. The presence of biomarkers in the 2.7–2.8 Ga geological record that are characteristic of cyanobacteria (Brocks et al. 1999), suggests that the 2.3–2.1 Ga change in the oxidation of the atmosphere may have taken place for reasons, other than photosynthesis. This is supported by non-mass dependant fractionation (NMDF) $\Delta^{33}S$ values of sulphides and sulphates that range from –2.5 to +8.1‰, whereas the $\Delta^{33}S$ in post 2.3 Ga sulphides and sulphates are <0.4‰. The >0.4‰ $\Delta^{33}S$ values are indicative of an anoxic atmosphere, contrasting with those of sulphides and sulphates in rocks younger than 2.3 Ga, which suggest quantities of oxygen in the atmosphere greater than 10^{-5} PAL.

The oxidation state of the atmosphere is linked to H_2, CO_2, CO, SO_2 and H_2S volcanic degassing. These volatiles are removed from the atmosphere-ocean system by deposition of organic matter and carbonate (CO and CO_2) and sulphides and sulphates (H_2S and SO_2), whereas H_2 is removed by reduction reactions and by loss from the atmosphere to space. The H_2 loss to space becomes significant only when the required amount of H_2 to convert CO_2 and CO to organic matter and all of the SO_2 and H_2S to sulphide (pyrite) is exceeded. The amount of H_2 needed to convert volcanic CO_2 and CO to organic carbon is estimated at about 20% and this value is considered to have been more or less constant throughout geological time. Consequently, the quantity of H_2 needed to remove volcanic sulphur gases is determined by the available H_2 required to form pyrite. If the amount of available H_2, is less than that required to produce sulphides, then some of the available sulphur will be used to form sulphates, such as gypsum and anhydrite. If, however, the amount of H_2 is greater than that needed to form pyrite, then the excess H_2 escapes to space (Holland 2002). Other sources of reduced elements to the atmosphere-ocean system include Fe^{2+}, emitted from black smokers and, according to Holland (2002), also from serpentinisation processes. The important point here is that before oxidation of the atmosphere-ocean system, Fe^{2+} was removed through the precipitation of FeS_2, $FeCO_3$ and Fe oxides and hydroxides, with the last

two represented by the giant Proterozoic Fe formations (see Fig. 3.8). Oxidation of Fe^{2+} to produce magnetite is:

$$3Fe^{2+} = 4H_2O \rightarrow Fe_3O_4 = 6H^+ + H_2$$

The above reaction shows that precipitation of magnetite in either Fe formation or during serpentinisation generates H_2 and H^+, with the latter being used up by reactions with Mg silicates, or it escapes to space. The $\delta^{13}C$ values of carbonates associated with Fe formations and marine carbonate sedimentary rocks show a remarkable world-wide positive excursion between 2.2 and 2.05 Ga (Karhu and Holland 1996). At the peak of the excursion, $\delta^{13}C$ values in carbonate rocks was about + 12‰, whereas carbon in organic matter was about –24‰, allowing an estimate that at least 50% of the carbon in the exogenic cycle was removed as organic carbon (see Melezhik et al. 2005, 2007). The large positive $\delta^{13}C$ excursion is therefore considered the result of high rates of organic carbon deposition, which in turn generated excess O_2 production. At the same time the large amount of carbon burial would have also enhanced the amount of PO_4^{-3}, because phosphate is released during weathering which is proportional to the rate of CO_2 addition to the atmosphere and oxidation of pyrite to form H_2SO_4. These processes would have made more available PO_4^{-3} for photosynthesis. Holland (2002) pointed out that there was an increase in phosphatic Fe formations and phosphates at the beginning of the GOE.

Barley et al. (2005) suggested that the GOE occurred between 2.47 and 2.4 Ga, coinciding with the assembly of a supercontinent and following a time of widespread mantle plume events at 2.72–2.65 Ga (plume breakout). Oxygen sinks, largely provided by reduced volcanic volatiles and Fe formations, were especially powerful during this plume breakout thereby favouring anerobic production of CH_4 and increasing levels of atmospheric CO_2 and CH_4. Furthermore, the increased hydrothermal emission of Fe^{2+} and deposition of Fe formations would have limited the abundance of PO_4^{-3} and inhibited photosynthesis with continuing low levels of atmospheric O_2 ($<10^{-5}$ PAL). The large flux of reduced volcanic gases, hydrothermal activity and oxidation of Fe to form the extensive Fe formations must have had a substantial effect in filling the available oxygen sinks. The filling or exhaustion of these oxygen sinks together with loss of H_2 to space led to the irreversible oxidation of the atmosphere. The decreased global emission rates of volcanic gases and the exhaustion of the oxygen sinks also greatly contributed to photosynthetic oxygen production, finally leading to the rise of atmospheric oxygen to $>10^{-5}$ PAL.

More recently, Kaufman et al. (2007), using high resolution $\delta^{34}S$ and $\Delta^{33}S$ data from the 2.5 Ga Mount McRae Shale in the Hamersley Basin in the Pilbara Craton, found positive correlation between $\delta^{34}S$ and $\Delta^{33}S$ in the lower parts of the Mount McRae Shale, whereas in the upper parts positive $\Delta^{33}S$ values are coupled with negative $\delta^{34}S$ values. The negative $\delta^{34}S$ suggest microbial sulphate reduction, coupled with increasing sulphate production, whereas the positive

$\Delta^{33}S$ values would reflect reduced sulphur. To account for these two contrasting isotopic signatures, Kaufman et al. (2007) proposed that the sulphate formed through oxidation processes (positive $\delta^{34}S$ and $\Delta^{33}S$) and was re-reduced by microbial activity, which resulted in the negative $\delta^{34}S$ whilst retaining the positive $\Delta^{33}S$. This implies a stratified water column with oxygenated top layers and anoxic bottom layers. The authors also compared the sulphur isotopic composition between the Mount McRae Shale and the equivalent units of the Gamohan and Kuruman Formations in South Africa. The two areas show remarkable similarities in their sulphur isotopic signatures, supporting the idea of atmospheric and oceanic homogeneity. The conclusion of this important work is that oxygenation of the surface ocean preceded the rise of atmospheric oxygen by more than 50 million years.

10.2.6 Is Life Being Created Today?

Is life still being created on Earth? This is the acute question posed by van Loon (2005). The answer hinges on whether the environmental conditions that created life in the first place still exist somewhere on Earth. As van Loon (2005) stated, as far as he (and I) are aware, the question has rarely, if ever, been addressed by the scientific community, except for Fridriksson (1975), who in his book on the Surtsey volcanic island, which began as a submarine eruption in November 1963 off the south coast of Iceland, invited the question: was life produced? If one accepts that life did not originate in a subaerial environment and that the original habitat was associated with hot hydrothermal effluents on the seafloor, then it is, at least theoretically, possible that microbial life is still being created today. Van Loon (2005) cited the example of the discovery of a primitive micro-organism, *Nanoarchaean equitans*, in a submarine hot vent recently reported by Huber et al. (2002) and described as "*weird*". Perhaps the genesis of life may be more common than hitherto accepted, and the synthesis of organic molecules may even be a frequent process in submarine hot springs. Protocells containing hydrothermally derived organic compounds could form in large quantities around submarine vents. In these hydrothermal systems it is not unlikely that the synthetised organic molecules can form polymers.

From another angle, the question on whether life is still being created today may be rephrased: are there different forms of life among us? In an article published in Scientific American, Paul Davies, cosmologist and astrobiologist and authors of several books, explored the possibility that perhaps life may have arisen on our planet more than once and that there may be alternative life forms that are radically different from all other living organisms (Davies 2007). If these alternative life forms are still present would they not have been already discovered? According to Davies (2007) the answer is emphatically no, as the majority of organisms are microbes and it would be quite impossible to tell by

simply looking through a microscope. The genetic sequence of an organism needs to be determined and its position on the tree of life established. All known organisms are descended from a common ancestor(s), share a similar biochemistry and use an almost identical genetic code and, as Davies (2007) pointed out, that the procedures used by microbiologists to analyse new organisms are deliberately customised to detect life as we know it. Thus, if an alien form of life exists, could it be in an isolated niche that could not be used by known life? Life, as we know it, needs liquid water, but would it be possible that ecosystems isolated from the biosphere exist and use some other substance instead of water? (See also discussion in Chapter 12).

Other liquids may be used as the solvent for biochemical reactions. Liquid methane and ethane have been detected on Titan and this possibility is addressed in Chapter 12. Another possibility is that instead of the normal vital elements (C, H, O, N and P), different element(s) may substitute for one of these. Arsenic is a possible candidate, as it may substitute for phosphorus. Phosphorus would not have been especially abundant in the early history of the Earth and As could have take the role of the element P for some organisms and provide a distinctive advantage in ancient Earth. Another possibility examined by Davies (2007) is that his "*shadow life*" might share the same biochemistry with known life, but employ different set of aminoacids, the building blocks of DNA. Although these views are clearly speculative, some life scientists are seriously considering the possibility. For more information on this topic, the interested reader is referred to Davies and Linewaever (2005) and Cleland and Copley (2005).

10.3 Hydrothermal Systems and the Biosphere; the Role of Bacteria in Ore Genesis

Life on Earth is largely based on C, H and O (about 80% of dry weight in a bacterial cell), with other constituents being N and P (Knoll and Grotzinger 2006). Other elements that are required for life include Fe, Mo, Mg and Mn. Of these, Fe is the main element in haemoglobin and Mg is important for chlorophyll. Ultimately, pre-biotic compounds and life require metallic elements for several of their biochemical reactions. In the preceding chapters, reference to microbial or biological activity associated with ore systems has been made several times. In this section, I explore in more detail the relationship between certain types of mineral systems and biological, mainly bacterial, activity. A collection of works on the evolutionary trends of the atmosphere, hydrosphere and biosphere and their relationship to ore systems was edited by Kesler and Ohmoto (2006).

Bacteria are single cell micro-organisms, some species of which can survive at very high temperatures ($>100^{\circ}C$) and at temperatures below the freezing point. As shown in the Tree of Life (Fig. 10.1), there are two categories of bacteria: prokaryotes and archaea. Although there are thousands of species of bacteria,

most have one of three basic morphologies: (1) rod-like (bacilli); (2) spheroidal (cocci); (3) helical or spiral. An important phylum of bacteria is cyanobacteria, which obtain their energy requirements through photosynthesis (see reaction in Section 10.2.5.1). Microbially mediated processes can be fingerprinted by the stable isotopic record (Lyons et al. 2003).

Microbes have the ability to bind metals as part of their metabolism and therefore the solution and precipitation of metallic elements may be controlled by bacterial mediation through processes of oxidation and reduction. The source of H_2S in many hydrothermal systems is from the reduction of dissolved sulphate, derived from seawater or evaporite brines or dissolution of sulphates (anhydrite, gypsum). The topic of sulphate reduction was treated by Machel et al. (1995) and is summarised here.

Sulphate reduction (see also Section 10.3.1.1) can occur in two different and mutually exclusive processes: bacterial sulphate reduction (BSR) and thermochemical sulphate reduction (TSR). Both these processes are very important because the H_2S produced reacts with metal-bearing fluids to precipitate sulphides. Other common reaction products include calcite, dolomite, native sulphur and oxidised hydrocarbons. A common reaction is:

$$2CH_2O + SO_4^{2-} \rightarrow 2HCO_3^{-} + H_2S$$

Criteria that may enable to distinguish BSR from TSR include textural features and sulphur isotopic compositions. In the first, pyrite framboids (equidimensional, raspberry-shaped spheroids found in many and diverse environments, both modern and in the ancient geological record; Rickard 1970) are commonly a texture resulting from BSR, whereas for TSR pyrite tends to be euhedral or a replacement of other minerals. Finely disseminated stratabound pyrite associated with kerogen is likely to have formed by BSR processes. The best indicator for biogenic sulphides is the sulphur isotopic composition of minerals. The fractionation of sulphur isotopes during dissimilatory sulfate reduction produces sulphides that are depleted in ^{34}S. Thus, strong negative fractionations, ranging from –15 to –65‰ characterise BSR, whereas for TSR negative fractionations are smaller and temperature dependant with –20‰ at 100°C, –15‰ at 150°C and 10‰ at 200°C and decreasing further with increasing temperature. Sulphate-reducing anaerobic bacteria include *Desulphibrio* and *Desulphotomaculum*. A web site that describes the role of micro-organisms in the sulphur cycle is http://technology.infomine.com/enviromine/ard/Microorganisms/roleof.htm#Role%20of%20Bacteria (last accessed in February 2008). Trudinger (1971) provided details of BSR as follows. Sulphates are activated by reaction with an energy-transferring compound called adenosine triphosphate (ATP), producing a compound called adenylylsulphate, which contains a phosphorous-oxysulphur bond. The reaction is:

$$\text{Sulphate} + \text{ATP} \rightarrow \text{APS} + \text{pyrophosphate}$$

The APS is then reduced to sulphite and adenosine monophosphate, and subsequently the sulphite is reduced to sulphide, according to:

$$SO_3^{2-} + 6e + 8H^+ \rightarrow H_2S + 3H_2O$$

Thermophilic chemolithoautotrophic micro-organisms in modern deep-sea hydrothermal-vent ecosystems are sulphur- and sulphate-reducing micro-organisms. A thermophilic chemolithotrophic sulphate-reducing bacterium from a deep-sea hydrothermal vent is *Thermodesulfatator indicus*.

Southam and Saunders (2005) reviewed the role and effects of bacteria on the geochemistry of dissolved metals and minerals. The following is taken from their paper. Bacteria are prokaryotic micro-organisms that are found in the surface and subsurface and are subdivided into aerobic and anaerobic, according to their oxygen tolerance, with the latter being the only extant bacteria before the onset of photosynthesis. Autotrophic or chemolithotrophic bacteria (Table 10.1) need elements such as Fe, Mn and S for their metabolism. Sulphur-oxidising anaerobic bacteria can synthetise carbohydrates at deep seafloor hydrothermal vents in anoxic conditions. Bacteria that oxidise Fe and Mn results in the precipitation of Fe- and Mn oxyhydroxides, together with precipitation of other elements, such as As, Co, Cu, Ni, Ba, V, U and REE in the near surface and in ferromanganese nodules (Chapter 8). The mechanisms that lead to precipitation of these metals involve the stripping of electrons from the carbon of organic matter and their transfer to Mn^{4+} and Fe^{3+} and their reduction to Mn^{2+} and Fe^{2+}, which then go into solution. The dissolution of Mn, Fe and bicarbonate by reducing bacteria can result in the precipitation of magnetite, siderite and rhodocrosite. Similarly, metals such as U are precipitated from U^{+6} to U^{+4} as UO_2(s). Sulphate reducing bacteria release H_2S and bicarbonate as metabolic products;

$$2CH_2O + SO_4^{2-} \rightarrow H_2S + 2HCO_3^-$$

Methane production is linked to anaerobic bacterial processes, which brings inorganic carbon into the organic carbon cycle:

$$2CO_2 + 6H_2 \rightarrow CH_2O + CH_4 + 3H_2O$$

This methane, in turn, can become a source of organic carbon to heterotrophic bacteria. A zonation of decreasing redox potential, from aerobic to Mn- and Fe- reduction, to sulphate reduction is thought to characterised aquifers with increasing depth. Two important processes are metal sorption and mineral nucleation onto bacterial cell envelopes. The first is related to competition

between hydrogen ions, alkaline earth ions and metals to occupy anionic sites on bacterial surfaces. Mineral nucleation on bacteria occurs through metal adsorption on the bacterial surface. Bacterial metabolism, therefore, can release metals from rocks and minerals and as a result play an important role in ore genesis, especially in low-temperature systems. This is particularly evident in sedimentary Fe formations, sedimentary U and native sulphur deposits. Bacteria such as *Acidithiobacillus thiooxidans* and *A. ferrooxidans* are commonly found in acid mine drainages and under acidic conditions these bacteria can cause strong oxidation, as exemplified by the blankets of supergene Cu oxides of porphyry Cu deposits. The bacteria effectively and selectively colonise sulphides that are oxidised as a source of energy, with estimates that a few kilograms of thiobacilli can leach up to 0.87 tonnes of Cu per year. Also important is the rate of erosion in these deposits, which exposes the primary sulphides to the oxidising bacteria near surface. There is evidence that chemical weathering of silicate minerals can be caused by bacterial activity, resulting in the dissolution of quartz and feldspars, further enhanced by organic acids produced from the decay of bacteria. It is well known that hydrous ferric oxides and Mn oxyhydroxides, also products of chemical weathering aided by bacteria, have the great capacity of adsorbing metals. Many Fe and Mn oxyhydroxides that look like gossans turn out to be false gossan precisely because of this process. On the other hand, continental sandstone known as red beds (Chapter 8) constitute a good source of metals for the same reason.

The precipitation of secondary minerals via bacterial mediation can be divided into two categories: intracellular and extracellular (Skinner and Jahren 2003). Intracellular is bacteria-controlled produces nanometre-scale precipitates that are unlikely to play an important role in metal deposition. Extracellular precipitation is directly induced by bacteria, is accelerated by H_2S and, as the name implies, is not limited by the space inside the cell, but can and does expand and plays a siginifcant role in the genesis of some ore systems. Sulphate-reducing bacteria are thought to play a major role in the genesis of many sedimentary ore deposits, commonly characterised by typical textures, such as peloidal, oolitic and framboidal, although these can also be produced by inorganic reactions. Southam and Saunders (2005) pointed out that although it may not always be possible to be able to distinguish between biotic and abiotic textures, light sulphur isotopic compositions are associated with sulphate-reducing bacteria. Gong et al. (2008) documented pyrite framboids from Middle Permian glaciomarine greywacke in the Sydney Basin (Australia) and interpreted them as the pyritised remains of microbial colonies. These microbial colonies had a symbiotic relationship with burrowing organisms called *Zoophycos*.

Good examples of mineral systems associated with bacterial activity are provided by banded iron formations, placer Au deposits, SEDEX systems, Irish-type deposits and volcanogenic massive suphides (VMS). Photosynthetic reactions (see above) have been suggested as having provided the major source of oxygen for the deposition of banded Fe formations in the

Archaean and Proterozoic. The oxidation of ferrous Fe to ferric Fe and reaction with water would produce Fe hydroxide on bacterial surfaces, according to:

$$Fe^{2+} + {}^{1}/_{4}\,O_2 + H^+ \rightarrow Fe^{3+} + {}^{1}/_{2}H_2O \text{ and}$$

$$Fe^{3+} + 3H_2O \rightarrow Fe(OH)_3$$

In the Precambrian oceans, bacteria and adsorbed metal ions to Fe hydroxides would have produced metal-rich sediments and some authors suggested that banded iron formation could have been precipitated by Fe-oxidising bacteria together with trace metals, such as Mn, Co, Zn, V and Mo. The characteristic laminae of BIF would relate to seasonal effects of bacterial growth. Placer native gold consists of octahedral crystals, nuggets and aggregates commonly coated with secondary gold. The origin of nuggets is considered to be of supergene origin and resulting from the precipitation of the element Au and/or accretion of smaller nuggets onto one another. This traditional view, however, has been challenged by Hough et al. (2007) who, on the basis of detailed investigations, suggested that the polycrystalline Au of nuggets is of hypogene origin and exposed to the surface as a result of prolonged erosion. Nevertheless, according to Southam and Saunders (2005) there is the possibility that under surface conditions, bacterial oxidation of sulphides can produce thiosulphate, which is a powerful complexing agent that would promote transport and precipitation of Au as octahedral crystals. Biological processes may also be implicated in the formation of colloidal Au from the near-surface dissolution of Au-bearing minerals.

Bacterial activity may have played an important role in the genesis of MVT deposits. This is suggested by the common observation of organic matter being associated with the ores. Some genetic models for MVT deposits suggest that H_2S formed by bacterial sulphate reduction was transported to the site of ore deposition where it precipitated sulphides by reaction with metal-bearing fluids. Light $\delta^{34}S$ compositions in the sulphide ores of the Irish-type deposits are consistent with bacterial sea water sulphate reduction. Sulphate reducing and Fe-oxidising bacteria have been found in modern VMS systems. A model of ore genesis for the McArthur River HYC SEDEX deposit in Australia (Chapter 8) suggests bacterial oxidation of organic matter with sulphate to produce sulphides (Logan et al. 2001). This is supported by the presence of abundant microfossils in lenses of black chert within the orebodies. The ore genesis model proposed by Logan et al. (2001) involves redox reactions between organic matters and brine sulphate, resulting in the production of H_2S and subsequent reaction with metal-bearing fluids to precipitate sulphides. One of the products of sulphate oxidation is bicarbonate, which precipitated to form the nodular carbonate that characterises lateral facies of the HYC siltstone.

10.3.1 High-Temperature Ecosystems Associated with Mineralisation

The discovery of hydrothermal vent communities on the Atlantic and East Pacific mid-ocean ridges (Chapter 7), has contributed enormously to our view of life and the energy sources that allow life to thrive in conditions other than oxygen-rich environments. Submarine environments that support a great diversity of microbial and macrofaunal life are black and white smokers, microbial mats, seafloor sediments, the surfaces of rocks and animals. Microbes are present in hydrothermal plumes emanating from the smokers and in channels of diffuse hydrothermal circulation and in the sub-seafloor. Kelley et al. (2002) described in detail the life systems at mid-ocean ridges, whereas the fossil record in submarine hydrothermal systems is discussed in Little (2002). Holm (1992) edited a collection of papers on the topic of submarine hydrothermal systems and life. Subaerial hot springs also support abundant microbial life, as can be seen by visiting some of the well known and easily accessible localities, such as the Taupo Volcanic Zone in New Zealand or the Yellowstone National Park in the western USA. For more information on life systems associated with submarine hot springs the interested reader is referred to Van Dover (2000) and Gargaud et al. (2005). A special issue of the Canadian Journal of Earth Sciences deals with bacterial communities of subaerial hot springs (Renaut and Jones 2003). The volume of the Cyba Foundation Symposium 202 provides a very interesting collection of work on hydrothermal systems and related ecosystems (Bock and Goode 1996).

10.3.1.1 On the Ocean Floor and Sub-Seafloor

Stoffers et al. (2006) studied submarine volcanoes of the Tonga arc (SW Pacific) and reported on the occurrence of submarine hydrothermal vents and extensive biological communities from the shallow submarine Volcano 19 and Volcano 1. Volcano 19, is a caldera complex with dimensions of 14×12 km, within which is a 3.5×2.5 km western caldera and central cone complex that rises to a minimum water depth of 385 m. Volcano 19 has two hydrothermal fields, one near the summit between 385 and 540 m depths and the other at a depth of 970 m. The upper part of the central cone is covered with bright orange to brown Fe oxyhydroxides, underlain by green clays. These Fe oxyhydroxides originate from venting of fluids at temperatures of about 70°C. High temperature (245–265°C) vents occur along a ridge and form clusters of up to 10 m-high chimneys composed of barite and anhydrite, locally associated with chalcopyrite, sphalerite and wurtzite. Chimneys in the deeper hydrothermal field are also composed of barite and anhydrite, associated with pyrite, marcasite and sphalerite and coarse chalcopyrite, Although crabs, worms and shrimps and sea stars are present in these hydrothermal fields, they are less abundant than the macrofauna of mid-ocean ridges. At the base of the caldera edifice, at depths

of 985–850 m, diffuse venting of warm fluids (~30°C) is associated with mats of Fe-oxide-stained filamentous bacteria, associated with large clusters of 1–2 m high Fe oxyhydroxides and silica chimneys, forming a distinct field of about 200 × 300 m in extent. Volcano 1 has a basal diameter of 28 km and rises from a depth of 1800 m to only 65 m below sea level. Volcano 1 is characterised by a caldera, scoria cones and small explosion craters, around which there is widespread hydrothermal venting. Ash beds around the explosion vents are cemented by native sulphur and although no chimneys were seen in this area, vigorous gas discharges occur through holes and fissures in the sulphur-encrusted material. This field is covered by mussels of the *Bathymodiulus* genus and around the chain of craters, the seafloor is almost entirely covered by white fields of filamentous bacteria.

Kelley et al. (2002) emphasised the scientific impact of the discovery in the last few decades of the *massive effusion of biogenic particles* and of the *diverse populations of single-celled, heat-loving organisms that thrive in the absence of sun light and oxygen*.

For this section, I have condensed the following from the above authors. Massive effusions of microbial material is are associated with seafloor eruptions and degassing, resulting in large plumes that can disperse for kilometres away from the eruption sites. Importantly, there is good evidence that the energy requirements of these microbial communities is derived from volatiles emitted during the eruptions and from high-temperature hydrothermal fluids, thereby confirming that submarine volcanoes support life in the absence of sunlight and oxygen. First evidence of bacterial activity came in the late 1980s from dives in the Juan de Fuca Ridge and the MacDonald seamount, followed by more discoveries in the East Pacific Rise. At the MacDonald seamount, Huber et al. (1990) reported that immediately following an eruption event, a surface slick of hyperthermophile bacteria was detected up to 1 km from the vent, with a bacterial cell count of $>10^9$/litre of sea water. Similarly, eruptions at the 9°N East Pacific Rise are associated with widespread effusion of microbial particles that are entrained in the vented hydrothermal fluids. The microbial, dominantly white, particle-laden hydrothermal effusion was dubbed "*snowstorm*", reaching 50 m above the seafloor. Furthermore, mats of filamentous bacteria from 1 to 10 m thick accumulated on lava flows and in fractures. At the Co-axial Segment (Juan de Fuca Ridge), following an eruption, extensive venting (with temperatures ranging from 50 to 36°C) occurred for some 4 km along a fissure. Although no hyperthermophiles were isolated from collected samples, yellow-orange bacterial mats, up to 10 cm thick and composed of Fe oxidising bacteria, were observed coating fresh lava flows (Holden et al. 1998). At the same time and about 20 km to the south of the eruption site, a *blizzard-like storm of flocculated mat fragments* dominated the water column for hundreds of metres on both sides of the axial valley. Dyke intrusions (dyking events of Kelley and co-workers), are equally prolific in providing energy and nutrients for micro-organisms. Dyking events episodically perturb (or even

destroy) and enrich the thermophilic zones and plumes. Days and weeks after a dyking event, C and energy from magmatic volatiles and hydrothermal fluids mix with oxygen, sulphate and nitrates from the sea water, resulting in the establishment of the massive white floc material composed of mesophilic S, Fe and CH_4 micro-organism oxidisers. Within a year, macrofaunal communities, represented by tubeworms, crabs, clams, etc., thrive by exploiting the chemical energy and nutrients provided by the microbial communities. Both micro- and macrofaunas tend to die or become dormant, following the cessation of seafloor hydrothermal activity.

The environments of seafloor hydrothermal venting that harbour life include sulphide mounds, chimneys, the sub-seafloor and hydrothermal plumes. In these environments, physico-chemical conditions span a range of extreme regimes in temperature, Eh, pH and metal concentrations which, it is widely recognised, limit the environmental requirements within which life can exist (Fig. 10.5). In all cases, micro-organisms and macrofaunas, life at seafloor hydrothermal vents exploits energy and C sources derived from hydrothermal processes and inhabit both the anaerobic and aerobic environments with temperatures that range from 2°C to greater than 110°C. Microbes utilise C and energy from minerals and volatiles, such as CO_2, H_2S, CH_4 and H_2 (Fig. 10.5). Microbial communities use a range of electron acceptors and donors (e.g. Fe^{3+} and Fe^{2+} are a donor and acceptor, respectively), whereas the macrofaunas feed on the microbes or live in symbiotic association with sulphur and CH_4 oxidising bacteria, while at the same time developing mechanisms to balance or avoid the toxicity of high metal concentrations. Tables 10.3 and 10.4 provide details of biological chemical species and microbial processes associated with seafloor hydrothermal vents. From Table 10.3 it can be seen that in addition to carbon there are other chemical species that are essential to some micro-organisms and these include N, P, Fe, Mn, Mo, W, Ni and Zn. High

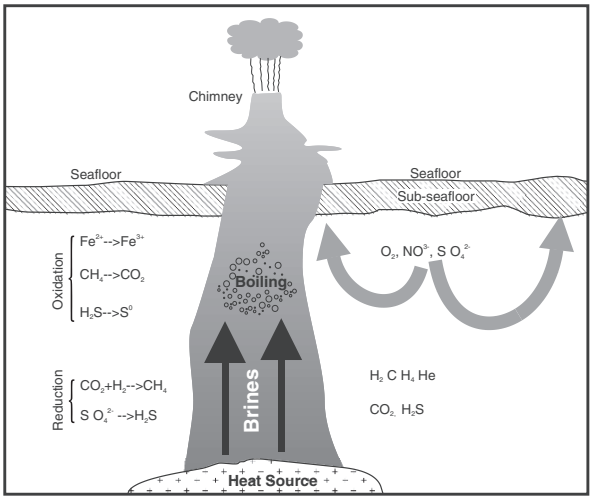


Fig. 10.5 Chemical and volatile components, redox reactions during mixing with seawater and by microbial mediation in submarine hydrothermal systems (compare with Fig. 2.16). Modified after Kelley et al. (2002)

Table 10.3 Sources of biological chemical species and their significance. After Kelley et al. (2002)

Chemical species	Sources in vents	Biological significance
CO_2	Magma degassing, water/rock reactions	Carbon source for chemoautotrophs and methanogens
CH_4	Magma degassing, reduction of CO_2, methanogenesis	Aerobic and anaerobic microbial oxidation
H_2	Magma degassing, water/rock reactions, microbial fermentation	Methanogenesis, aerobic and anaerobic oxidation by bacteria
H_2S	Water/rock reactions, chemical reduction to anhydrate, microbial reduction of SO_4^{2-}	Primary energy source for aerobic chemoautotrophs including symbionts; oxidized sulphur species reduced by high diversity of micro-organisms
NH_3 or NH_4^+	Organic-N in buried sediments, possibly N_2-fixation by micro-organisms and/or chemical reduction of N_2	A source of nitrogen for subsurface micro-organisms; oxidation to NO_3 or NO_2 by nitrifying bacteria
PO_4^{2-}	Water/rock reactions (P_2O_5 in basalts), seawater PO_4^{2-}	All organisms require P for nucleic acids, energy reactions and fatty acids; animals and aerobic microbes use seawater-PO_4^{2-} and/or detrital organic PO_4^{2-} compounds
Fe	Water/rock reactions, major component of sulphides as pyrite	Energy source for Fe(II) oxidizing bacteria Fe(III) as electron acceptor for some groups of vent microbes. Trace element required by all organisms
Mn	Water/rock reactions	Energy source for Mn(III) oxidizing bacteria. Trace element required by all organisms
Si	Water/rock reactions, seawater entrainment, major component of outer layers of sulphide deposits	Some evidence for microbially mediated Si precipitation in sulphides
Zn	Water/rock reactions, major component of sulphides as pyrite	Trace element required for key enzymes including alkaline phosphatise and RNA
Cu	Water/rock reactions, major component of sulphides, such as chalcopyrite	Trace element required for enzymes including oxidative enzymes involved in electron transfer; toxic in μ mol concentrations
Co	Water/rock reactions	Trace element required by all organisms
Cd	Water/rock reactions	Toxic to all organisms in nmol levels
Pb	Water/rock reactions	Toxic to all organisms in nmol levels
Mo	Water/rock reactions	Trace element required for specific enzymes
W	Water/rock reactions	Trace element required for specific enzymes by hyperthermophilic archaea
Ni	Water/rock reactions	Important component in coenzymes of methanogens and enzymes of hyperthermophilic archaea

Table 10.4 Metabolic processes of microbes in submarine hot spring environments. After Kelley et al. (2002)

Conditions	Electron donor	Electron acceptor	Carbon source	Metabolic process	Habitat	Groups of micro-organism
Aerobic	HS^-, S^o, $S_2O_3^{2-}$ $S_4O_6^{2-}$	O_2, possibly NO_3^-	CO_2	Sulphur oxidation	Diffuse-flow vent fluids, sulphides,e basalts, microbial mats, smoker plume fluid, symbionts of tube-worms, clams and mussels, gut flora of heterotrophic macrofauna	Mesophilic bacteria, proteobacteria in microbial mats at vents presumed to be S-oxidizers
	H_2	O_2, possible NO_3^-	CO_2	Hydrogen oxidation	Diffuse-flow vent fluids, smoker plumes	Mesophilic bacteria
	Fe^{2+}, Mn^{2+}	O_2	CO_2	Metal oxidation	Diffuse-flow vent fluids, sulphides and some basalts, microbial mats, surface of tubes and shells of some animals	Mesophilic bacteria
	CH_4 and other C_1 compounds	O_2	CH_4, CH_3OH, CO, CO_2	Methanotrophy	Diffuse-flow vent fluids, sulphides, surface of tubes and shells of some animals, smoker plume fluid,	Mesophilic proteobacteria
	NH_4, NO^{2-}	O_2	CO_2	Nitrification	Diffuse-flow vent fluids	Mesophilic bacteria
	Organic compounds	O_2, NO_2^-	Organic compounds	Heterotrophy	Ubiquitous at vents	Many different genera of mesophilic and thermophilic bacteria
Anaerobic	H_2	S^o, SO_4^{2-}, $S_2O_3^{2-}$	CO_2	Sulphur and sulphate reduction	Diffuse-flow vent fluids, sulphides, microbial mats, sediments	Mesophilic and thermophilic bacteria and hyperthermophilic archaea
	H_2	CO_2	CO_2	Methanogenesis	Ubiquitous in anaerobic biotopes	Mesophilic, thermophilic, and hyperthermophilic archaea

Table 10.4 (continued)

Conditions	Electron donor	Electron acceptor	Carbon source	Metabolic process	Habitat	Groups of micro-organism
	H_2	NO_3^-	CO_2	Hydrogen oxidation	Diffuse-flow fluids	Identified from molecular analyses of vent samples
	Organic acids	Fe^{3-} (iron oxyhydroxides)	Organic acids	Iron reducers	Crustal fluids from new eruptions, subsurface fluids, and sediments	Mesophilic bacteria and hyperthermophilic archaea
	CH_4	SO_4^{2-}?	CH_4?	Anaerobic methane oxidation	In methane hydrate sediments and from enrichment culture with high-temperature hydrothermal fluids	Methanosarcina spp., oxidizes CH_4 anaerobically
	Organic compounds	S^o, SO_4^{2-}	Organic compounds	Sulphur and sulphate reduction	Hyperthermophilic archaea isolated from diffuse-flow vent fluids, sulphides and guts of sulphide-dwelling animals	Mesophilic and thermophilic bacteria and hyperthermophilic archaea

microbial concentrations can be enriched in metallic elements, such as As, Au, Ag, Th and Sb.

The chemical energy of the submarine hydrothermal vents effectively substitutes for light energy, whereas volcanic gases (Fig. 10.4) provide the necessary energy and nutrients below the seafloor. Aerobic micro-organisms derive energy from the oxidisation of reduced sulphur compounds and CH_4, H_2, NH_4^+, or other organic compounds and use O_2 and NO_3^- as the electron acceptor. Oxidation of sulphur compounds is a very important process in symbiotic associations and is represented by:

$$S^{2-}(HS^-, H_2S, S) + CO_2 + O_2 + H_2O \rightarrow SO_4^{2-} + CH_2O$$

Other reactions involving methane, hydrogen and ammonia oxidisers, which coat surfaces of animals and rocks and are present in hydrothermal plumes, are:

$$CH_4 + O_2 \rightarrow CH_2O + H_2O$$

$$4H_2 + O_2 + CO_2 \rightarrow CH_2O + 3H_2O$$

$$NH_3 + O_2 + CO_2 \rightarrow CH_2O + HNO_3$$

There are many other and diverse groups of aerobic heterotrophic micro-organisms that utilise a variety of organic compounds. A common feature of these oxidising microbes is that they require the presence of organic compounds.

Anaerobic micro-organisms include both bacteria and archaea, some of which are happy to grow and function at temperatures above 100°C. There are three significant anaerobic microbial groups: sulphate reducers, methanogens and fermenters. The first is of great significance for ore systems, as highlighted in several instances in this book. Sulphate reduction, already mentioned in the preceding pages, takes places by two processes, one involving energy from chemical reactions obtained from inorganic compounds and CO_2 as the only carbon source (chemolithotrophy) and the other by heterotrophy, involving existing organic compounds. Key SO_4^{2-} reduction reactions are:

$$\text{chemolithotrophic} : CO_2 + SO_4^{2-} + 6H_2 \rightarrow CH_2O + S^{2-} + 5H_2O$$

and

$$\text{heterotrophic} : CH3COOH(\text{acetate}) + SO_4^{2-} \rightarrow 2CO_2 + S^{2-} + 2H_2O$$

Methanogens (see also Section 10.4) are Archaea and typically reduce CO_2 to CH_4:

$$2CO_2 + 6H_2 \rightarrow CH_2O + CH_4 + 3H_2O$$

Many methanogens are hyperthermophiles capable of living at temperatures in excess of 80°C and are exceptionally fast-growing, with some species doubling their numbers in less than 30 min. Anaerobic heterotrophic Archaea

constitute another group, characterised by having nutrient requirements that include amino acids and sulphur, with the source of organic materials being provided by dead animals and other microbes. Anaerobic Archaea are indicators of hot sub-seafloor ecosystems, because they have minimum growth temperatures in excess of 50°C.

Kelley and co-workers cited evidence (e.g. McCollom and Seewald 2001) that amino acids, petroleum hydrocarbons and organic acids, can be synthetised from volcanic gases and metal catalysts using heat as energy source. Experimental simulations of submarine hydrothermal vent conditions have shown that abiotic synthesis of organic compounds can be realised and, significantly, that the presence of a sub-seafloor biosphere is consistent with field observations, showing that the seafloor hydrothermal vents are in fact open systems, with continuous input of seawater and the effluence of hydrothermal fluids that flow through oceanic crust rocks, Kelley et al. (2002) rightly stated that these seafloor systems are chemical reactors and, I would add, factories not only of ores but also of microbial communities. In terms of subsurface hydrothermal circulation, the authors also pointed out that this is more effective as a diffuse flow on the flanks of ridges and not with the more visually stimulating outflow associated with the vent systems.

It has been pointed out above the extraordinary diversity of the micro-organisms that live in submarine hydrothermal ecosystems. Although beyond the scope of this book, I will briefly mention some of the more important groups of bacteria, again referring the reader to the detailed work of Kelley et al. (2002 and references cited therein). Micro-organisms that live symbiotically with macrofaunal animals (e.g. tube worms) also constitute a significant fraction of microbes in diffuse flow and in microbial mats and include *Thiobacillus*, *Thiomicrospira* and *Ferrobacillus*. Micro-organisms that are present in low-temperature vent fluids can survive in environments with high salt concentrations (up to 25%), are called halotolerant and include *Halomonas* and *Marinomonas*. Amongst the hyperthermophiles are *Thermococcus*, *Hyperthermus* and *Staphylothermus* requiring growth temperatures of less than 105°C; the methanogen *Methanopyrus* growing at 100°C and *Pyrolobus fumarii* at 113°C. The majority of hyperthermophiles are anaerobic using S° as an electron acceptor, as well as SO_4^{2-} and $S_2O_3^{2-}$, with notable species including *Pyrodictium occultum* and *Thermoproteus tenax*. The order of Thermococcales includes microbes that can be used as tracers of seafloor and sub-seafloor ecosystems, as exemplified by *Thermococcus* and *Pyrococcus*. Within the sulphide constructs are sulphur-dependent heterotroph and metahongens and hyperthermophiles have been isolated from the digestive system of worms, such as *Alvinella* and *Paralvinella*.

10.3.1.2 On land

As mentioned previously, subaerial hot springs also team with microbial life and consequently have biomineralisation processes. The intrinsic ability of

microbes to bind and precipitate metals, under a wide range of environmental conditions, discussed for submarine systems is equally valid for subaerial hot springs. Present-day subaerial hot springs are also ideal sites for studying the effects of microbial activity, and they provide invaluable insights for ancient analogues, as described in Section 10.5. Here, I review some examples of ecosystems that are commonly found in subaerial hot springs. Apart from Renaut and Jones (2003), other publications of interest are Cady and Farmer (1996), Konhauser et al. (2003), Jones et al. (2001, 2004).

Opaline silica and carbonate form extensive deposits around hot springs and geysers and in near-neutral and alkaline waters thick sinter deposits have abundant and well-preserved silicified microbes. Iron precipitates are generally less common. By contrast, carbonate and Fe precipitates generally lack preserved microbes. It follows that the mechanism of silicification is important for the preservation of cell structures. Konhauser et al. (2003) recognised three important factors that lead to the preservation of microbes during silicification processes: (1) rapid silicification helps to keep intact cell morphologies, prevents heterotrophic micro-organisms from degrading other cells and does not allow time for cells to degrade after death; (2) microbial species with thick cell sheets are more resistant to degradation and as such become more prone to silicification; (3) retarded cell degradation seems to be linked to the ability of metal ions, especially Fe, to bind on bacterial cell surfaces, and this again promotes silicification. Silica sinters can form both biogenically and abiogenically with resulting deposits being architecturally complex and exhibiting several vertical and lateral lithofacies and biofacies variations such as, geyserite, oncoids and coccoid microbial mats, spicules, columnar and tabular or stratiform stromatolites (Konhauser et al. 2003). Yee et al. (2003) carried out experimental runs of silica precipitation at neutral pH, using cyanobacteria, concluding that in hydrothermal waters silica precipitation is abiogenic and cyanobacteria have negligeable effect on silica nucleation. However, this find is not consistent with the ubiquitous presence of microbial activity associated with hot spring silica precipitates. Geyserite has a typically laminated structure and may be covered by biofilms as observed in the Yellowstone and Taupo geothermal areas. Biogenic sinters form by silica growing around the microbes and in the more distal parts from the discharge area complex biogenic fabrics form, with some microbial species responding to the rapid silica encrustations by moving ahead of the rate of silica deposition. In the Yellowstone geothermal area sinter laminae are tens of micrometre thick and are attributed to nocturnal growths of *Chlorofexus* and during the day by rapid growths of *Synechococcus* (Walter et al. 1972).

Siliceous sinters and silicified microbes have been well studied in the geothermal areas of the Taupo Volcanic Zone, one of the world's best studied geothermal areas (Chapter 5). Here I use the works of Jones et al. (2004, 2001) and Campbell et al. (2001) for the following. The Iodine Pool in the Waimangu geothermal area, hot spring waters have temperatures ranging from 69 to 100°C, a pH of 8.3 to 9.0 and about 450 ppm SiO_2. Jones and co-workers

carried out experiments with glass slides placed in the Pool for 90 h. On retrieval, the glass slides were covered with thin layers of opaline silica, opal-A spherules, pseudofilaments, unsilicified, partly silicified and silicified microbes. The unsilicified microbes, which are found on top of the opal-A precipitates and of silicified filaments, consist of at least five types of filamentous structures (called CM-A to CM-E), ranging in size from 4–8 to > 500 μm in length and 300 nm to 350–500 μm in diameter. Silicified microbes form complex colonies associated with opal-A spherules, which encase or are built around microbes, or form multiple layers encrusting filamentous bacteria. An important conclusion of Jones et al. (2004) is that the silicification of microbes in modern hot springs, although useful for providing an analogue of ancient systems, cannot provide a precise identification of microbes. The authors found that the silicification process tends to destroy key taxonomic features. The Champagne Pool hot spring (Waiaotapu geothermal area, Taupo Volcanic Zone) has neutral-chloride anaerobic waters with a temperature of 75°C (Jones et al. 2001). Sinter deposits surrounds the Pool and a shallow subaqueous shelf is composed of an orange sinter material, which together with an orange siliceous floc suspended in the spring water, is rich in sulphides and metals, such as As, Sb, Tl, Hg, Au and Ag (see Table 1.6 and Chapter 5). The orange sinterous material of the subaqueous shelf also exhibits domal and semispheroidal structures, up to 10 cm high that are considered to be stromatolite forms. Jones et al. (2001) determined that opaline silica and amorphous sulphides precipitate on filamentous microbes and biofilms. The subaqueous orange sinter is composed of loose soft sediments and detritus covered by the orange siliceous precipitate. The orange colouration is thought to be due to As sulphides. Microbes in the stromatolitic sinter consist of filamentous shapes up to 8.25 μm long and with diameters of 170–1250 nm; bacilliform microbes, up to 2.5 μm long and 0.85 μm in diameter; rods, 4 μm long, 600–650 nm long and with a curious spherical body at one end, about 2 μm in diameter; 1 μm long coccoids; biofilms and 12 μm long diatoms. The orange sinter and suspended flocs contain intertwined sulphur-oxidising thermophilic anaerobic filamentous microbes, encrusted and/or replaced by metal-rich silica. The orange sinter microbes were tentatively identified on the basis of their morphology as *Chloroflexus, Thermothrix thioparus, Thermus aquaticus, Thermoproteus* and *Pyrobaculum*. The presence of Au in the neutral-chloride of Champagne Pool is attributed to processes that include boiling, cooling of the fluids near the surface, mixing with steam-heated waters and adsorption of Au onto As sulphides. Gold in the epithermal environments is transported as sulphide complexes, which would require the presence of H_2S gas in the fluids. Loss of H_2S occurs with boiling and pressure reduction, which break the ligand and precipitate Au (and Ag) on a favourable substrate (see also Chapter 5). CO_2 may also participate in destabilising the H_2S ligands, causing the co-precipitation of colloidal As and Sb sulphides, which in turn may scavenge Au, and silica. The metal-rich orange sinters of Champagne Pool were mediated by microbial activity, with the microbes providing the templates upon which silica and metals precipitated (Jones et al. 2001).

Campbell et al. (2001) investigated in detail the mineralogy and sedimentary facies of the Umukuri sinter deposits (also in the Taupo Volcanic Zone). X-ray diffraction analyses show that silica phases in this sinter are dominantly opal-CT (or α-cristobalite), opal-C (tridymite) and microcrystalline quartz. Campbell et al. (2001) recognised nine microfacies, representing primary depositional textures, although the authors caution that in ancient sinters later overprints and diagenesis will obscure the original textures of a sinter deposit. These microfacies are: (1) fine porous palisade, vertical pillar-like structures encrusted with spherules; (2) thinly laminated, continuous undulose layers and parallel laminae about 1 mm thick; (3) wavy laminated, alternating laminae of vitreous and porous silica, with open spaces and linking to from micro-stromatolite structures; (4) curved laminae with lenticular voids, consisting of smooth silica layers, 03 to 3 mm thick; (5) fine-grained spheroidal to irregularly shaped golden-brown clots of silica with filamentous microfossils; (6) plant-rich, containg silicified plant material; (7) peloidal, consisting of layers, up to 15 cm thick, of closely packed elliptical grains, associated with silica spheroids, similar structures (chert ooids) were reported from the Devonian sinter in the Drummond basin, described below; (8) pisoidal, 1–20 mm diameter, angular to subrounded grains containing nuclei of opaline silica fragments and organic detritus; (9) sinter breccia, mostly transported sinter fragments, cemented by later silicification. The microfacies are intercalated both laterally and vertically and are all to a greater or lesser degree modified by diagenesis, with the fabric of the silica matrix ranging from least modified, in which microbial filaments can still be recognised, to a partly modified dense vitreous fabric, to a late stage with extensive modification that results in crystalline quartz that obliterates the primary textures. It is critical to be aware of these changes when attempting to recognise microbial traces in ancient sinters, as repeated solution-precipitation, replacement and re-crystallisation are likely to occur.

Cady and Farmer (1996) aware of the problem in recognising microbial communities in ancient hot spring precipitates, studied siliceous sinter of the Yellowstone National Park to understand the relationship between microorganism and sinter morphologies and recogmised that both abiotic and biotic processes contribute to the morphology of sinter deposits. They distinguished high temperature, near-vent environments, moderately high temperature pools and channels, mid-temperature pools and channels and low temperature terraces (see Fig. 5.55). Gesyerite, typically with laminated fabrics, forms in high temperature, near vent environments with a lower temperature limit of 73°C and thought to form abiogenically, although Cady and Farmer found that micro-organisms contribute by providing a substrate for the precipitation of opaline silica. In addition, spicular geyserites examined with the scanning electron microscope revelead micron-thick biofilms and submicron-size filament in the surface of the spicular geyserites. In moderately high temperature (~60–73°C) pools and channels, thin yellow to orange mats formed by the cyanobacterium *Synechoccus* and the filamentous photosynthetic bacterium *Chloroflexus* cover the surfaces of ponds and outflow channels. Coniform

stromatolites represented by *Phormidium* and thick gelatinous, green to orange mats dominated by filamentous cyanobacterium *Phormidium* are observed in mid-temperature (~35–59°C) pools and channels. Brown-green mats of *Calothrix*, forming vertical palisades, cover low temperature terraces (<35°C). The *Calothrix* palisades, in turn, are covered by filamentous and coccoid microorganisms, diatoms and protozoans. These sinters deposits thermophiles are preserved through processes of replacement, encrustation and permineralisation, with the latter being somewhat similar to silicification of wood in which the vascular tissue of the plant provides a template for the deposition of silica, perhaps through a reaction of the type (my suggested reaction):

$$H_2SiO_3 \rightarrow SiO_2 + H_2O$$

Douglas (2005) reported the association between microbial life and minerals. She investigated the relationship between bacteria and sulphur minerals in evaporite deposits, the geomicrobiology of minerals in non-photosynthetic cave environments, microbial involvement in the formation of dolomite in hypersaline lagoons and silicified microbial mats.

Konhauser and Ferris (1996) examined microbial mats of hot springs in Iceland using electron microscopy (TEM) and energy-dispersive X-ray spectroscopy (EDS) and found that bacterial surfaces bind significant amounts of Fe and silica. Complete encrustations of bacterial cells by spheroids composed of amorphous Ferric hydroxides and acicular goethite were detected by EDS. The authors suggested that precipitation of Fe can occur as an amorphous ferric hydroxides on bacterial nucleation sites and/or through Fe oxidising bacteria, which oxidise Fe as an energy source. Konhauser and Ferris (1996) contended that the precipitation of Fe and silica on these Icelandic extant microbial mats may represent a biomineralisation process that could explain the origin of the Precambrian banded iron formations, following the model originally advocated by Cloud (1973) and discussed in Chapter 8.

Senko et al. (2004) studied the precipitation of barite through biological oxidation of sulphides in the Zodletone spring in the Anadarko Basin in Oklahoma (USA), from which abundant Ba and sulphides are carried in spring waters. Here, sulphide-rich spring water flows downstream where anaerobic, anoxygenic and phototrophic bacteria oxidise the sulphide to sulphate, producing barite sinters or travertines, crusts and accumulations on microbial mats.

10.3.2 Microbes Inside Rocks and in the Deep Subsurface

Walker et al. (2005) documented endolithic (inside rocks) communities of microbes from the Yellowstone geothermal area. Photosynthetic, endolithic microbial communities live in the pore spaces of rocks in chalcedonic sinters of the Norris Geyser Basin in the Yellowstone National Park. Here, fractured

rocks show 1–15 mm-thick green bands, 2–10 mm beneath the surface, caused by photosynthetic pigments of red algae. The pore waters from the chalcedonic sinter material have been found to contain high concentrations of sulphuric acid, silica and metals (e.g. up to 983 ppm Mn, 551 ppm Cu and 1038 ppm As). These rocks contain from 10 to 32 wt% of pore waters, whose evaporation results in silica precipitation and continuous encrustation of microbes. Using DNA-sequence and SEM imaging methods Walker et al. (2005) were able to isolate and identify a variety of acid-tolerant genera of photosynthetic bacteria, including filamentous and spherical forms that resemble the microbial mats of *Cyanidium caldarium*, typically of hot springs in Hokkaido, Japan. Mycobacterium was also identified as one of the dominant species in the Norris Geyser sinters which, the authors pointed out, is one of the pathogens responsible for tubercolosis in humans. Importantly, the mineralisation of endolithic microbial communities of geothermal environments may provide identifiable biomarkers that can be used in the recognition of similar structures in the geological record, as shown by the 2.0 Ga Gunflint microbiota, for which an environment similar to that of the Yellowstone geothermal area was proposed (Walter 1972). In deep aquifers, chemolithotrophic micro-organisms metabolise H_2 and CO_2 and can be primary producers of organic carbon and CH_4 (Kotelnikova 2002).

There is now evidence that microbial ecosystems live in the deep subsurface, mostly in the spaces between mineral grains of igneous and sedimentary rocks, as well as deep ground water (Gold 1992, Fredrickson and Onstott 1996). These are autotrophic microbes that derive nutrients and energy from the inorganic elements of rocks or organic material trapped at the time of deposition and, in turn, these autotrophic micro-organisms provide nutrients to other microbes. Stevens and McKinley (1995) discovered flourishing lithoautotrophic microbial ecosystems at depths of 1.5 km in basaltic rocks of the Columbia River plateau in western USA. They are archaea autotrophs that manufacture organic material using H_2 and CO_2 in the rock and producing CH_4. These microbial communities were dubbed SLiME for "*subsurface lithoautotrophic microbial ecosystem*". Pedersen (1993) reviewed the microbiology of the deep subterranean environments and parts of this work are summarised here. In Sweden, a borehole was drilled to a depth of 6779 m and thermophilic bacteria, possibly identified as *Termoanaerobium*, were isolated from depths of 3900–4000 m. Still in Sweden, construction of tunnels for disposal of nuclear waste in crystalline bedrock at two sites, the Stripa Fe mine and at Äspö, revealed the presence of anaerobic and methanogenic bacteria. Microbial life was also detected in the Atlantic coastal plains of South Carolina (USA), where fluvial, deltaic and marine sediments were deposited in the Late Cretaceous. Samples of ground water and sedimentary rocks were found to contain high counts of bacteria. In addition, algae, fungi and protozoa were also observed. In the Dreifontein Au mine in the Witwatersrand (South Africa), samples were collected from depths of 3200 m at ambient rock temperatures of 50–60°C (DeStefano et al. 2000). These samples showed bacterial life and biofilms, as well as rod-shaped possible fossils about 2 μm in size with high concentrations of Au and U.

Bacterial communities cannot possibly withstand the high temperatures and pressures of the deep crust, following burial and magmatic intrusions. However, tectonic uplift brings rocks closer to the surface, and infiltration by ground waters will lead to renewed colonisation by microbial communities in a continuing cycle.

Cockell et al. (2006) studied endolithic microbial communities associated with the ~23 Ma Haughton meteorite impact structure in Canada. The Haughton crater is about 23–24 km in diameter and was formed in sedimentary rocks of Ordovician-Silurian age overlying Precambrian gneisses. Cockell et al. (2006) divided the microbial colonisation of impact-shocked rocks into two categories: (1) phototrophic micro-organisms that live near the surface within a few mm inside the shocked rocks, and (2) non-phototrophic communities that live deeper inside the shocked rocks, well away from the photosynthetic zone, but still limited by the depth of water penetration. The former are represented by cyanobacteria and the latter are heterotrophic and chemolithotrophic micro-organisms. The authors were able to isolate 27 bacteria including genera, such as *Planococcus*, *Bacillus*, *Caulobacter*, *Arthobacter* and *Stenotrophonomas*, which closely resembles bacteria that are found in soils, polar and marine environments. Cockell and co-workers suggested that these micro-organisms may have been transported below the surface and into impact-induced fractures by meltwater, but more importantly, they also suggested that the endolithic environment of impact-shocked rocks may have provided an ideal refugium from UV radiations, and as such would have been a favourable habitat for the early primitive micro-organisms.

10.3.3 Role of Bacteria in the Weathering Profile

In the supergene environment Au is readily mobilised as a chloride or thiosulphate complexes (Mann 1984), under acidic and oxic conditions or mildly acidic to alkaline reducing conditions, respectively. Lengke and Southam (2006, 2007 and references therein) have shown that bacteria have the ability to precipitate colloidal Au and influence the change from colloidal to crystalline octahedral Au. Some of the key aspects of these workers' experiments and results, based on bacterial cultures isolated from the Driefontein Au mine in the Witwatersrand Basin (South Africa) are briefly described here.

Thiosulphate is an effective complexing agent for Au in near-surface and surface conditions. The thiosulphate is generally produced through the formation of sulphoxyanions by oxidation of sulphides and the reaction of Au-bearing thiosulphate complexes with sulphur-reducing bacteria (BSR) may be responsible for the precipitation of Au in the weathering profile. Lengke and Southam produced micrometre-scale Au particles by interaction of Au-thiosulphate with the bacterial constituents of the experimental growth media. The biogenic colloidal Au produced was observed both within the cells and at

the cell surface of the species *Desulphovibrio*, a characteristic BSR. The authors suggested that the Au-thiosulphate complex may have entered the bacterial cells through the pores of the cell envelope or actively transferred by the bacteria. Destabilisation of the Au-thiosulphate complex occurs and Au is released:

$$Au(S_2O_3)_2^{3-} \rightarrow Au^+ + 2SO2/3^-$$

Gold is subsequently precipitated (reduced), by reaction with an organic electron donor. Furthermore, octahedral Au can form from the thiosulphate, in the presence of and if catalysed by bacteria. Octahedral Au is a common in palaeoplacer deposits, such as the Mother Lode in California, in the Witwatersrand deposits and in the weathering profiles in Western Australia.

10.4 Gas Hydrates, Mud Volcanoes, Seafloor Seeps, Methanogens and Chemosynthetic Communities

In this section I present an overview on the so-called cold seeps, mud volcanoes and associated mineral constructs and ecosystems. Cold seeps are emissions of H_2S, NH_3, CO_2, CH_4 and hydrocarbons on the ocean floor, resulting in a variety of features, including mud volcanoes, hard ground, carbonate crusts, chimneys, veins, stromatolitic mats and pyritic carbonate nodules. Chemoautotrophic organisms, methanogenic bacteria, massive barite deposits and carbonate (calcite, dolomite, aragonite) crusts are found around seafloor vents that emit gas hydrates. Gas hydrates are ice-like crystalline compounds in which methane (Fig. 10.6A), other hydrocarbon gases are contained in rigid cages of water molecules that are found in low-temperature permafrost regions and in the deep oceans within the gas hydrate stability zone (Fig. 10.6B and C) (Milkov et al. 2003; Zhang and Lanoil 2004a; Osegovic et al. 2006). Methane is by far the most common gas (up to 99%) in natural gas hydrates (Max et al. 2006). The source of CH_4 in gas hydrates is from bacterial activity and/or thermal maturation of organic matter. In marine settings, methane hydrates are stable at a range of temperatures between 0°C and 15°C, water depths greater than 500 m and depths below the seafloor of up to 300 m. Gas hydrates are also known as "flammable ice" because potentially these compounds may provide an alternative and very abundant source of energy for the future and a previously unsuspected component of the global carbon cycle (Suess et al. 1999). Details on this subject can be found in several papers and books. Here I cite those that I believe appropriate in the topic of this book, such as the collection of papers edited by Henriet and Mienert (1998), Max et al. (2006) and the special issue of Chemical Geology (Zhang and Lanoil 2004a). Gas hydrates are commonly associated with deep-water mud volcanoes, defined by Milkov (2000) as a seafloor edifice from which mud, water, brine, gas and oil are erupted. Milkov (2000) emphasised not to confuse mud volcanoes with shale/mud diapirs, pointing out that whereas all mud volcanoes are associated with

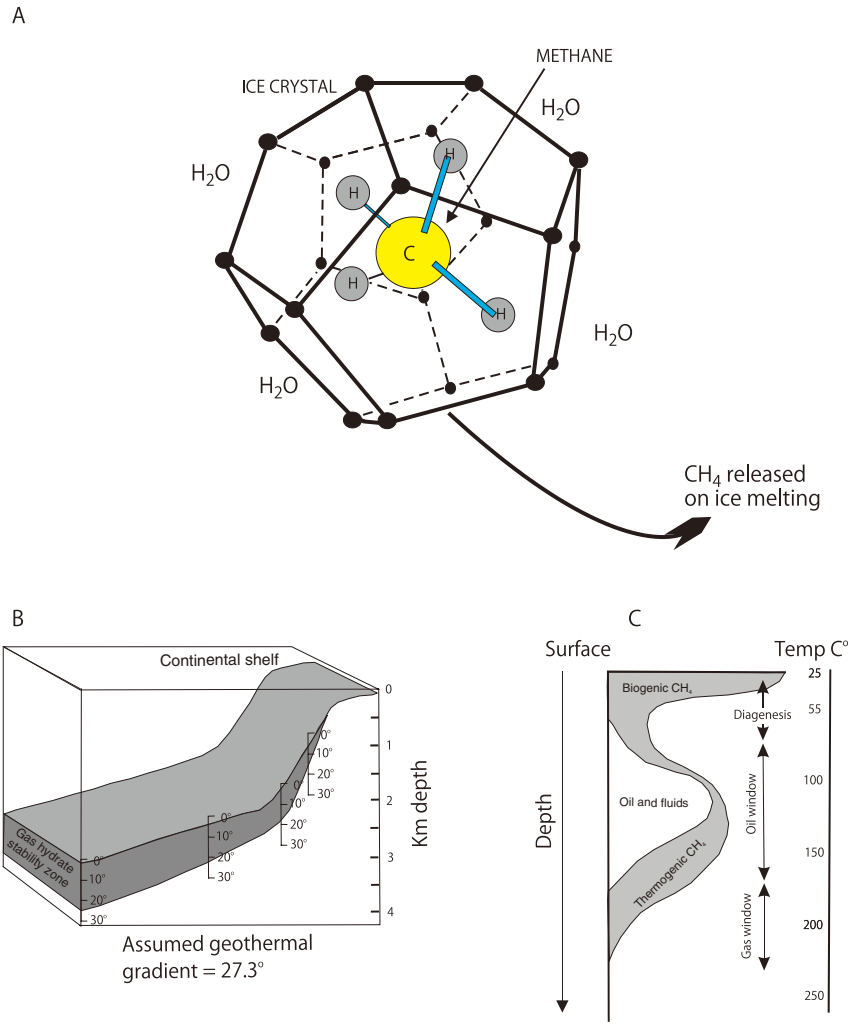


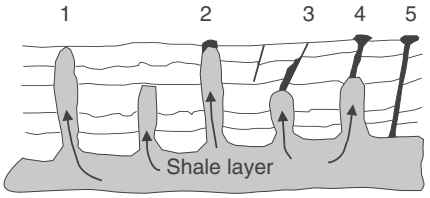
Fig. 10.6 (**A**) Gas hydrate cage; CH_4 and other gases released on ice crystal melting (after Suess et al. 1999); (**B**) gas hydrate stability zone, lowering of sea level will alter the hydrate stability zone resulting in ice cage melting and release of CH_4 into the atmosphere; (**C**) gas, oil and biogenic CH_4 as a function of temperature and pressure (**B** and **C** after Max et al. 2006)

diapirs, the opposite is not true. According to Dimitrov (2002) there are more than 900 subaerial and 800 offshore mud volcanoes; the subaerial mud volcanoes are subdivided into three classes: Lokbatan, Chikishlyar and Schugin. The Lobkatan class is characterised by explosive activity and ignition of the emitted gases; the Chikishlyar class is characterised by weak but persistent activity, emitting mostly mud and water; the Schugin class is a transitional type with intermittent eruptive periods and weak activity. Dimitrov (2002) does not

classify submarine mud volcanoes, which are gas hydrates emitters and characterised by carbonate build-ups, bacterial mats and chemosynthetic ecosystems. Subaerial mud volcanoes are common along the coast of the Caspian Sea (Baku region, Azerbajan), in Sicily, southern and northern Italy, Albania and in Romania. The subaerial mud volcanoes can reach heights of 300–400 m and in some cases more than 500 m, with craters of 500 m diameter and bases of 3–4 km across (Dimitrov 2002).

Milkov's model of mud volcanoes and cold seeps is shown in Fig. 10.7; the world-wide distribution of cold seeps and associated mud volcanoes is shown in Fig. 10.8. Milkov et al. (2003) estimated that between 2100 and 3600 Gt of methane are contained within marine gas hydrates. In the Gulf of Mexico there are numerous gas hydrate and hydrocarbon sites, where anaerobic microbial activity provides H_2S, deposit authigenic carbonates, sulphides and native sulphur (Sassen et al. 2004). The geological record of gas hydrates is not particularly bountiful, but this is probably due to a lack of recognition rather than actual dearth of fossiliferous bodies representing the activity of gas hydrates and associated methanogens. A short review of ancient gas hydrates and mud volcanoes is provided in Section 10.4.2.

The formation of gas hydrates is associated with accretionary sedimentary prisms at convergent margins, where there is active folding and strong compression. These processes cause compaction of the sediments, intense early diagenesis and dehydration (Boetius and Suess 2004). Warm hydrocarbon fluids are produced from the fermentation of micro-organisms and thermal maturation of organic matter, resulting in the expulsion of these fluids from the sedimentary accretionary prism. Fluid expulsion of the hydrocarbons, CH_4 and other gases is through seafloor vents, which support and fuel a variety of ecosystems, resulting in the deposition of authigenic carbonates, barite deposits, sulphides and sub-seafloor gas hydrates. The deposition of carbonates reperesents a good sink for carbon gases, however sea level fluctuations can release large amounts of CH_4 into the atmosphere, where it converts to CO_2, another greenhouse gas. Greinert et al. (2002) reported the presence of massive barite and



1 Diapir without mud volcano

2 Mud volcano on top of seafloor-piercing diapir

3 Seafloor seep

4 Fluidised sediments, fluids and gases rise along fault to form mud volcanoes

Fig. 10.7 Model for the origin of diapirs, mud volcanoes and seafloor gas hydrate seeps. After Milkov (2000)

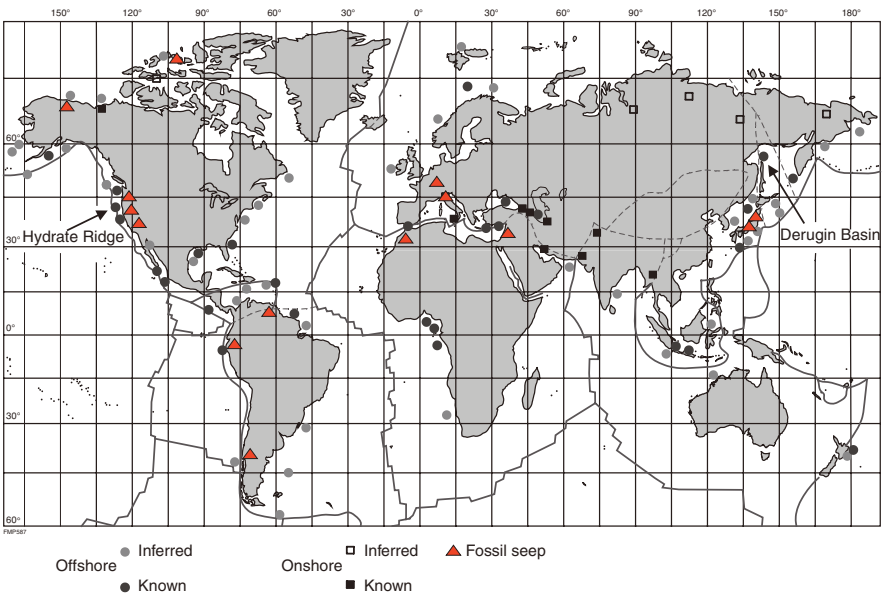


Fig. 10.8 World distribution of cold seeps and gas hydrate deposits. After Milkov (2000) and Zhang and Lanoil (2004b)

authigenic carbonate at 1500 m water depth in the Derugin Basin, Sea of Okhosk, associated with a large cold seep with chemoautotrophic clams (*Calyptogena*) and CH_4 emissions (Fig. 10.8). A schematic model of seafloor gas hydrate venting system is shown in Fig. 10.9.

Melting of the hydrate layer liberates not only CH_4, but also H_2S and NH_3, which then provide abundant nutrients to chemosynthetic communities and colonies of clams and tube worms. Subsequent oxidation of CH_4 produces carbonate chimneys and mounds, such as those found at Hydrate Ridge, off the Oregon coast, (Juan de Fuca plate, North America; see Fig. 10.8) where these features were first observed by Erwin Suess in 1984 (Suess et al. 1985). Hydrate Ridge is discussed in the next section, as an example of venting of hydrates and the chemosynthetic organisms that metabolise CH_4. Max et al. (2006) considered gas hydrates as a mineral resource, comparing it to some stratabound metalliferous deposits. They classified hydrate deposits into two main classes: concentrated and dispersed, with the former corresponding to high grade deposits and the second to low grade deposits.

10.4.1 Hydrate Ridge

Hydrate Ridge, along the Cascadia subduction zone, about 100 km off the coast of Oregon, is an accretionary ridge, about 25 km long and 15 km wide, with

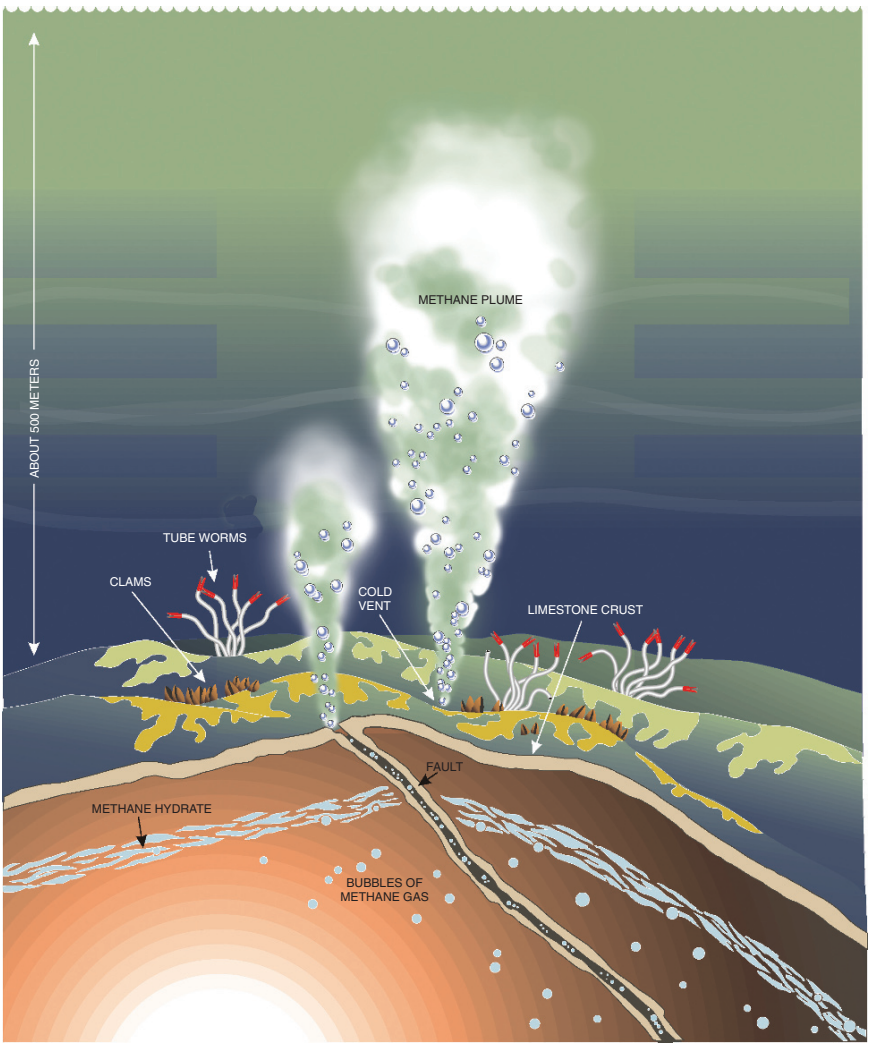


Fig. 10.9 Seafloor vent system expelling CH_4 and other gases and supporting microbial chemosynthetic communities; heat melts the hydrate layer releasing CH_4 from the sub-seafloor hydrate layer is oxidised by bacteria and form carbonate crusts; some of the CH_4 rises as plumes in the ocean and escapes into the atmosphere. Modified after Suess et al. (1999)

seafloor gas vents associated with authigenic carbonates and chemosynthetic communities. Hydrate Ridge was studied during a number of expeditions, using submersibles and reported by Suess et al. (1985, 1999), Milkov et al. (2003) and Boetius and Suess (2004). These works have been perused for this section.

Hydrate Ridge sub-seafloor gas hydrates are mapped by seismic reflection methods, with the gas hydrates becoming visible 20–100 m above a strong bottom simulating reflectors (BSR), forming layers to about 150 m below the

seafloor and reaching concentrations of about 20–30% of the pore volume. In 100 $km^2$of the surveyed area a reservoir is estimated to contain 6.4 billion m^3 of gas hydrate. Sediments in Hydrate Ridge comprise hemipelagic clays and silty clays intercalated with silty and volcanic ash units of turbidite facies. These sediments have mm- to cm-scale Fe sulphide nodules. Lenses of gas hydrate occur within these sediments and are several metres thick, with horizontal or vertical orientations. The Hydrate Ridge area is characterised by a northern and southern summits, typically with rough topography and an undulating morphology of mounds and depressions with patchworks of thick and dense white or orange microbial mats, which also cover the hydrate mounds and are associated with clam and benthic communities that include giant sulphide-oxidising bacteria (*Beggiatoa*). The clam fields contain *Calyptogena*, which has in its gills sulphide-oxidisers. Other macrofaunas are represented by mussels and tubeworms. Gas samples collected from a bacterial mat on the southern summit contain 97% CH_4, <3% sulphides and minor amounts of hydrocarbons. The CH_4 with a strong biogenic signature of –65‰ $\delta^{13}C$ is transported from depth in fluids and as free gas bubbles through channels. Carbonate deposits form according to the reaction:

$$CH_4 + SO_4^{2-} + Ca^{2+} \rightarrow CaCO_3 + H_2S + H_2O$$

have $\delta^{13}C$ compositions ranging from –38 to –65‰ and consist of aragonite and Mg-calcite, forming large chemoherms with chimney structures up to 40 m high. There are four settings of chemosynthetic benthic communities: (1) areas of gas expulsion; (2) areas of microbial mats; (3) macrofauna fields; and (4) background sediments containing chemosynthetic sulphide-oxidising clam *Acharax* to depths of 5–30 cm below the seafloor. The sulphide fluxes are related to the supply of CH_4 and seawater sulphate and the production of sulphides supports *Beggiatoa*, *Calyptogena* and *Acharax* benthic communities.

Larrasoaña et al. (2007) reported on the presence of authigenic greigite and monoclinic pyrrhotite from Hydrate Ridge and attributed their formation to anaerobic oxidation of methane (OAM) in the gas hydrate zone, below the seafloor. Samples examined by these authors also contain framboidal and euhedral pyrite. Larrasoaña et al. (2007) suggested the following sequence of events to account for the precipitation of sulphides. Metabolic activity drives progressive degradation of buried organic matter, involving consumption of oxygen, under oxic conditions, and of Mn and Fe oxides, under suboxic conditions. Sulphate-reducing microbes first release suphides in the form of pyrite. When all the sulphate is exhausted, at depths below the sulphate zone, CO_2 reduction results in the formation of CH_4. When CH_4 reaches saturation, gas hydrate will form, but some CH4 will also migrate upward into the sulphate zone, where it is aneorobically oxidised, a processs that is mediated by consortia of sulphate-reducing bacteria and results in the precipitation of Fe sulphides, such as pyrrhotite and greigite.

10.4.2 Mud Volcanoes and Gas Hydrate Constructs in the Geological Record

Campbell (2006) listed known fossil hydrocarbon vents and seeps (Fig. 10.8) and hydrothermal vent sites associated with microbial communities, ranging in age from Pleistocene to Early Archaean. She makes the distinction between seeps and vents, with the former being of slow emission rate and the latter characterised by vigorous and fast emissions with the development of chimneys and mud volcanoes. Examples of low-temperature hydrate discharges and related lithological products in the geological record are herein discussed.

The identification of biotic, lithological and tectonic setting (continental margins, accretionary prisms) associations in ancient hydrate seeps is very important for their correct recognition. Late Jurassic to Cretaceous fossil seeps are characterised by macrofaunas that largely includes vestimentiferan, tube worms and bivalves. Extinct fauna comprise brachiopods, bivalves and worm tubes and vestimentiferan resembling those of modern day vent and seep sites. Microbial stromatolitic fabrics are common in both present and fossil seeps, generally forming laminated crusts and peloidal beds. Depleted $\delta^{13}C$ values (see above) retain a record of microbial CH_4 mediation. Indeed, this is the most common tool used to trace the source of C of carbonate rocks formed through microbial activity at seep sites. Methane formed by thermal maturation will have $\delta^{13}C$ values ranging from –30 to –50‰, whereas biogenic CH_4 formed by microbial degradation of organic matter will have $\delta^{13}C$ values of between –20 and –25‰ (Campbell et al. 2002). Authigenic carbonate and barite deposits, formed by microbial processes, are good markers for hydrate seeps, providing they are stratigraphically isolated and/or associated with diapiric structures, mud rocks, serpentinite. Features related to fluid flow include pipe and chimney structures, tubular concretions and breccias. Campbell (2002) reported palaeogeographic locales that typically have numerous fossil hydrate seeps. These include the Jurasssic-Cretaceous and Palaeocene seeps of California, Cretaceous seeps in Japan and those of Miocene age in Italy. Below I discuss fossil seeps of Cretaceous age in Morocco.

Barbieri et al. (2004) described a limestone unit of Silurian age from the Middle Atlas, Morocco, which they interpreted as having formed by fluid seepage and associated microbial chemosynthetic activity. The limestone unit, named El Borj, contains both fossil stromatolites and brachiopods communities, is 15 m thick, extends for a few tens of metres and is embedded within shale rocks. The stratigraphy of the El Borj limestone body consist of three units, A, B and C, which from base to top comprises: a basal unit (A) of interbedded limestone and marls with micritic and ferruginous limestone beds that at the microscopic show features related to etxsnive microbial activity; unit A is gradational to the overlying unit B, which consists of poorly defined layers with brachiopods fauna, intercalated with thin layers of hematitic micrite; the overlying unit C is characterised by stromatolitic laminae and

oncolite structures (concentric growths up to 30 cm across). Barbieri et al. (2004) also distinguished, within the above stratigraphic framework, a hematite facies (unit A), brachiopod facies (unit B) and a stromatolite facies (unit C). The hematite facies, as the name implies, consist of reddish and ferruginous mudstone and mudstone recrystallised into microsparite, which preserves concentrations of fecal pellets. The hematite patches consist of globular aggregates that are interpreted to be of microbial origin, initially concentrated in microfractures, from which they spread into the micritic rock. Also present in the hematite facies are ferruginous crusts and rims, merging into oucrop-scale crenulated structures. Features called alveoli, consist of hematite and aragonite crystals forming stellate clusters. Quartz and framboidal pyrite are also present in the hematite facies. The structures of the hematite facies have been interpreted as being related to biological activity and mediation by Fe bacteria. The authors compared the alveoli mentioned above to *Beggiatoa* mats, composed of filamentous cyanobacteria, typical of oxygen-depleted environments. The brachiopod facies consists of concentrations of fossil shells, within a fine calcitic matrix and filled with spar, drusy calcite and associated with filamentous fabrics of probable microbial origin. The dense packing of the brachiopod shells suggests that they accumulated in situ and represent a community that formed around the original seepage. The stromatolite facies also consists of brachiopods concentrations, in this part of the stratigraphy associated with laminar and oncoids structures. Barbieri et al. (2004) concluded that the El Borj limestone body exhibits abundant evidence of microbial textures and macrofaunas that can be compared to those of modern gas hydrate seeps. Compelling evidence for microbial processes include: presence of pyrite framboids in the hematite facies, ferruginous crusts and rims, also in the hematite facies, filamentous fabrics and biofilms.

Beauchamp et al. (1989) described cold-seep fossil communities from the Lower Cretaceous of the Canadian Arctic in the Ellef Ringnes Island and Prince Patrick Island. Here are circular mound-like carbonate units within siltstone and shale rocks. The mounds have diameters of up to 60 m and rise from 1 to 8 m above ground level. Fossils communities consist of bivalves, worm tubes, ammonites, gastropods, foraminifera and fish teeth. The carbonate rocks of these ancient seep sites comprises three authigenic carbonate phases: a brecciated dark micrite with organic matter, pyrite framboids and fecal pellets ranging in length from 0.02 to 1 mm; yellow calcite associated with abundant pyrite, commonly coating the worm tubes; and botryodal calcite alternating with layers of yellow calcite. $\delta^{13}C$ values of micrite, calcite and yellow calcite range from –35 to –50‰, carbonate of worm tubes have a range of $\delta^{13}C$ values from –24 to –44‰. The carbon isotopic data conforms to those of CH_4-derived carbonate rocks, in which the CH_4 forms by oxidation of bacterially mediated processes. Beauchamp et al. (1989) suggested that the fossil seep communities of the Canadian Arctic formed during seepages of CH_4 along faults. The CH_4 was then oxidised by bacteria, producing $\delta^{13}C$-depleted CO_2 that became incorporated in organic-rich mud. The carbonate crusts, built on

pockmark-like depressions on the seafloor created by gas overpressure, became populated by the macrofauna communities. The authors argued that the presence of pyrite is indicative of intermittent H_2S emissions. The ultimate source of the CH_4 and H_2S remains uncertain and these could be derived either from a deep thermogenic or a shallow biogenic source, with the $\delta^{13}C$ data being somewhat inconclusive in this respect, because $\delta^{13}C$ values for these two source overlap (–35 to –50‰ and –35 to –60‰, respectively).

10.5 Hydrothermal Ecosystems in the Geological Record

These are several examples of hydrothermal systems in the geological record, in which bacterial activity may have been implicated in ore genesis processes. In the sections that follow, I discuss examples from the Plio-Pleistocene, Cretaceous, Palaeozoic and Archaean. Ore deposits from two of these, the Plio-Pleistocene Rio Tinto Basin (Iberian Pyrite Belt) and the epithermal systems of the Archaean Pilbara Craton, are described in Chapters 7 and 5, respectively.

10.5.1 The Rio Tinto Basin, Spain

Fernández-Remolar et al. (2005) compared the Plio-Pleistocene Fe oxides and sulphate deposits of the Rio Tinto Basin in southwestern Spain with the Meridiani Planum rocks on Mars (see Chapter 12 for details of Meridiani Planum). In this section, I present a synopsis of Fernández-Remolar et al's work as an example of an ecosystem related to the oxidation of the massive pyrite bodies of the Rio Tinto ore field in the Iberian Pyrite Belt. The Rio Tinto drainage system consists of a series of "iron terraces", ranging in age from Upper Neogene ($\sim$2.1 Ma; older terrace) to Pleistocene (60–30 ka; intermediate age terrace) to Holocene ($<$10 ka; lower terrace) and comprising laminated facies, various cemented breccias, plant-rich sandstone, cross-bedded and rippled sandstone, white, yellow and orange precipitates, iron crusts with laminated structure and black laminates with botryoidal textures. The Rio Tinto waters (Rio Tinto is Spanish for red river) have an acid-sulphate chemistry, with pH values ranging from 0.9 to 3, high Fe^{3+}, Al^{3+}, Mg^{2+} Ca^{2+} and Na^{+} Ba^{2+} concentrations, reflecting interaction of groundwaters with a sulphide substrate and the activity of chemolithotrophic micro-organisms, according to the reaction;

$$FeS_{2(s)} + 15/4O_{2(aq)} + 7/2H_2O_{(l)} \rightarrow Fe(OH)_{3(s)} + 2H_2SO_{4(aq)}$$

In the headwaters of the drainage system the pH is between 0 and 2, with the following hydrolysis reaction:

$$Fe^{3+} + 3H_2O \leftrightarrow Fe(OH)_3 + 3H^+$$

The precipitation of sulphates and Fe hydroxides is largely controlled by pH and by seasonal conditions. Evaporative water loss during the dry and hot season, precipitation of sulphates occurs, for example:

$$8Fe^{3+} + SO_4{}^{-2} + 14H_2O \leftrightarrow Fe_8O_8(OH)_6(SO_4) + 22H^+$$

But, during the wet season, higher pH and lower sulphate concentrations engendered the precipitation of ferric hydroxides:

$$Fe^{3+} + 2H_2O \rightarrow FeOOH + 3H^+$$

The Rio Tinto waters support photosynthetic eukaryotes and chemolithotrophic bacteria and various species of heterotrophs. Red and green algae and diatoms are present as diverse assemblages. The chemolithotrophs are dominated by Fe and S oxidising bacteria, such as *Leptospirillum ferroxidan* and *Acidithiobacillus ferrooxidans*. Filamentous fungi are represented by several genera and laminated domal structures along the river strongly resemble stromatolites. Fe sulphates are seen to encrust plant remains, whereas filamentous fungi, bacteria, algae and domal "blisters", due to emission of biogenic gas, are preserved on the surface of the Upper Neogene terrace, providing clear biosignatures in the sediments. Precipitating minerals, especially Fe hydroxides, tend to preserve biological forms as casts and moulds, down to the cellular details (Fig. 10.10). Efflorescent sulphate precipitates identified by Fernández-Remolar and co-workers, using XRD and Mössbauer spectra, include minerals of the copiapite group [$(AR_4\ (SO_4)_6(OH)_2 \cdot 20\ H_2O$], where R = Fe^{3+} and A = Mg^{2+}, $Al_{2/3}{}^{3+}$ and $Fe_{2/3}{}^{3+}$, gypsum, epsomite, natrojarosite [$NaFe_3(OH_6)(SO_4)_2$] and alunogen [$Al_2(SO_4)_3 \cdot 17H_2O$]. The evolutionary sequence from the headwaters through to the lower terraces is shown in Fig. 10.11. Biosignatures are clearly shown by textural features in which single cells, multicellular tissues and filamentous bacteria are replaced by Fe oxyhydroxides (goethite), but preserved in fine detail. Diagenetic conversion of goethite to hematite can locally destroy the signal, but microbial casts and moulds can still be preserved and recognised. At the macroscopic scale, plant matter, mostly leaves, also exhibits clear imprints. As mentioned above, Fernández-Remolar et al. (2005) drew a comparison with the Meridiani Planum depositional system noting that the suite of minerals identified in the Rio Tinto drainage is remarkably similar to that of Meridiani Planum and that this is suggestive of similar conditions. Therefore if micro-organisms thrive in the Rio Tinto valley, then it is reasonable to assume that similar micro-organism may have existed in Meridiani Planum (Chapter 12).

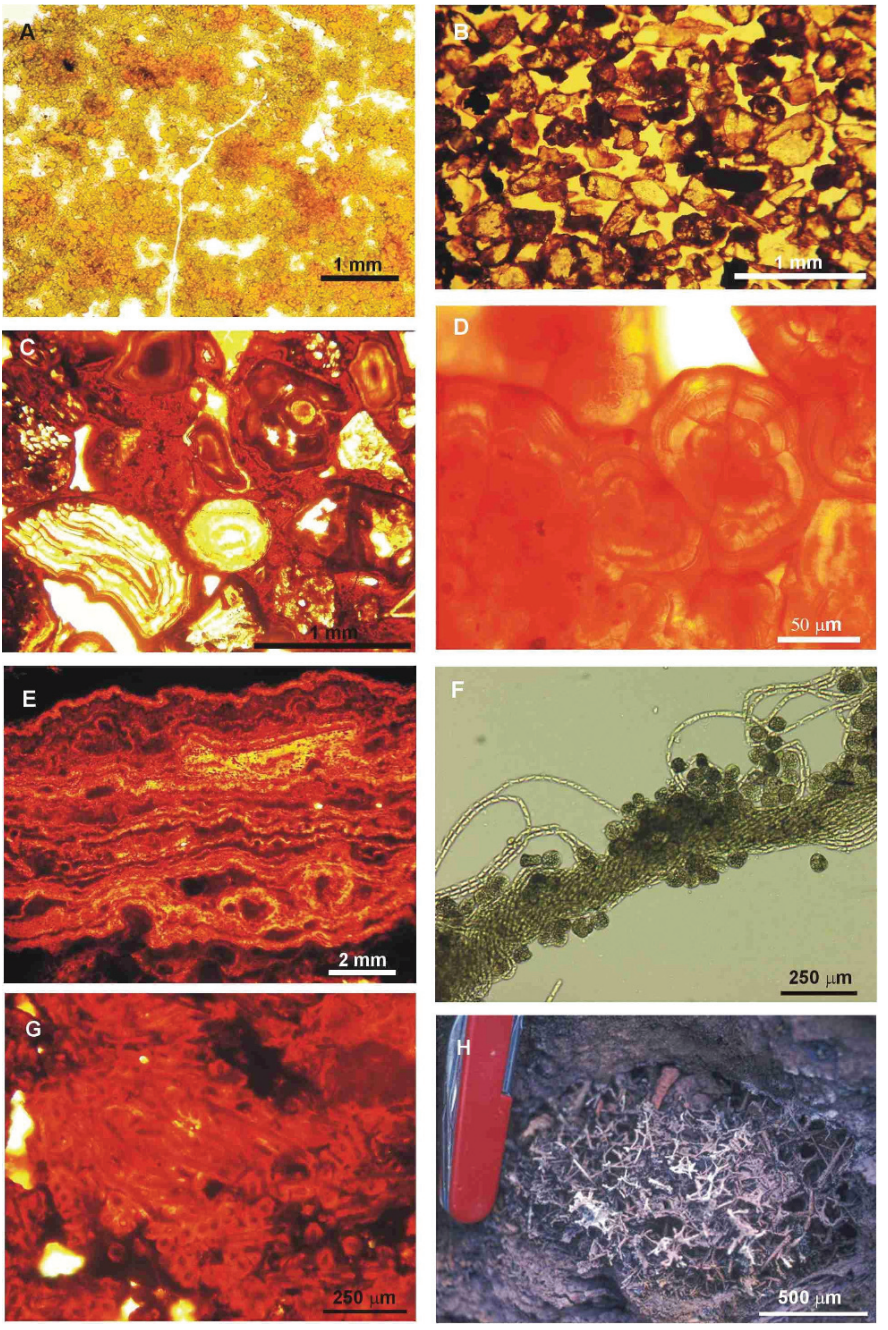


Fig. 10.10 (continued)

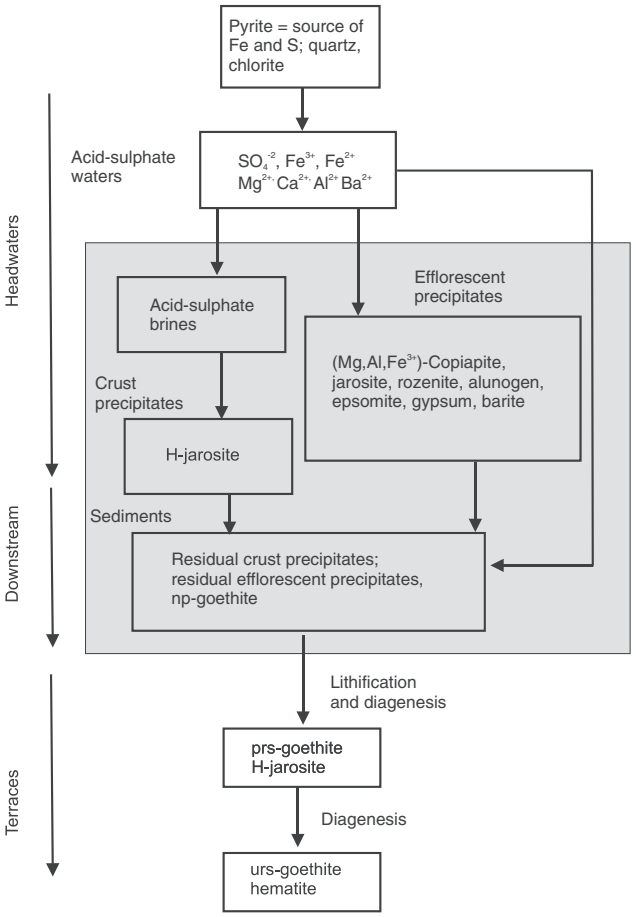


Fig. 10.11 Evolutionary sequence of minerals that form from sulphides and acid-sulphate sources in the Rio Tinto; mineral species determined by XRD and Mössbauer spectra, np nanophase, prs partially relaxed sextet, urs unrelaxed sextet are spectra terms (Fernández-Remolar et al. 2005)

Fig. 10.10 (continued) (**A**) jarosite in modern deposits along the headwaters of Rio Tinto; (**B**) sandstone cemented by Fe oxyhydroxides; (**C**) bioclasts cemented by goethite; (**D**) goethite textures; (**E**) laminated ironstone facies in the older terrace; (**F**) living algal filaments associated with isolated cells sampled at the Rio Tinto headwaters; (**G**) filamentous microfossils preserved in goethite; (**H**) macroscopic fossil of fungal network in a sediment cavity, previously occupied by a tree branch. This figure is reproduced by permission of the authors (Fernández-Remolar et al. 2005)

10.5.2 Cretaceous Polymetallic Ore Deposit in Georgia

Little et al. (2007) described the occurrence of hydrothermal vent fauna from a submarine Cretaceous polymetallic ore deposit. The Madneuli polymetallic deposit, estimated to contain more than 70 Mt of ore, is located in the Bolnisi district in the Republic of Georgia. Madneuli is a volcanogenic massive sulphide (VMS) system, hosted in andesitic and rhyodacitic rocks that belong to a volcanic arc in the Transcaucasus-eastern Pontides, extending from northeastern Turkey through southern Georgia, Armenia and Azerbaijan. The deposit consists of stockworks and stratiform orebodies. The latter exhibit zonation patterns that from the base upward are: pyrite-chalcopyrite-quartz with minor sphalerite, galena and epidote, anhydrite and fluorite; barite-sphalerite-pyrite-galena with minor chalcopyrite and marcasite; Au-bearing quartz-barite-calcite-pyrite. Fluid inclusion studies show two ranges of homogenisation temperatures, 370–260°C and 270–180°C, but fluids trapped in the barite associated with the tube fossils show temperatures of less than 60°C. A block of quartz-barite ore, examined by Little et al. (2007) contains tubular fossils that are about 35 and 96 mm long and 11–13 mm in diameter and consist of quartz with euhedral pyrite and framboids, overprinted by barite and galena. These tubular structures were identified as fossils rather than fluid conduits on the basis of the regular, cylindrical shapes. The authors tentatively identified these fossils as vestimentiferan, which may represent the closest analogue of similar structures at modern vent sites, such as tubes called *Riftia* and *Alvinella* and also similar to other fossils from another VMS deposit in Russia, where tubular shapes were identified as *Yamankasia rifeia*. The Madneuli vent community was probably formed at depths of <1 km, as the associated volcanics show a shallow to subaerial depositional environment. The authors pointed out that the Madneuli vent fauna is the first ancient example from a volcanic arc, as most other fossil sites are from back-arc settings. The volcanic arc, where Madneuli is located, had a complex configuration similar to that of present-day western Pacific, with subduction zones, island arcs, microcontinental blocks and marginal basins.

10.5.3 Mid-Palaeozoic Hot Spring Deposits and Associated Ecosystems, Queensland, Australia

Devonian to Carboniferous sinter deposits have been described from the Drummond Basin, Queensland, where they developed in association with continental felsic volcanism (White et al. 1989) and in northeast Scotland (Trewin 1996). The Early Devonian Rhynie cherts in Scotland exhibit well-preserved fossilplants, fungi, algae and cyanobacteria, all well documented by Trewin (1996). The sinter deposits of the Drummond basin are associated with a widespread area of hydrothermal alteration of the footwall rocks, and contain zones of low-grade Au mineralisation that have textures indicative of epithermal

conditions. Walter et al. (1996, 1998) carried out detailed investigations of these sinter deposits and the following is extracted from these works.

The Drummond Basin is a back-arc basin of Late Devonian to Early Carboniferous age in northeastern Queensland, within the Tasman Orogenic Belt and divided by the north-south trending basement Anakie Inlier. Between 305 and 290 Ma, the basin was affected by extensive subaerial volcanism with the eruption of rhyolites and ignimbrites, forming the Bulgonunna Volcanic Group. Deep erosion has exposed underlying high level plutons, comprising high K granites and monzogranites. A number of epithermal Au systems and siliceous sinter deposits occur in the eastern part of the Drummond Basin along a north-south trend and extending for approximately 10 km. Walter and co-authors focused their studies on two sinter localities: Verbena and Conway. The Conway hydrothermal system occupies a 4–5 km wide subcircular area, in which are rhyolitic and andesitic lavas and volcaniclastic rocks of the Bimurra Volcanics at the base of the Drummond Basin succession. The Conway system is characterised by zones of extensive hydraulic fracturing, breccias, silicic, propylitic and argillic-phyllic alteration associated with quartz veins. Thin sinters, less than 1 m thick, are interbedded with volcaniclastic rocks and diamictites (possible lahars) and extend along strike for no more than 100 m. The quartz veins have colloform and comb textures, and chalcedonic quartz. Argillic-phyllic alteration consists of sericite, mixed layer illite-smectite; carbonate-epidote-quartz-chlorite assemblages define zones of propylitic alteration. Pyrophyllite, K-felspar, kaolinite, alunite and jarosite, calcite and zeolite are other alteration phases present in the Conway system. Gold and Ag mineralisation is hosted by the quartz veins and zones of intense silica alteration.

The sinters of the Verbena hydrothermal system are hosted in tuffaceous sandstone, tuff and ignimbrite. A flow-banded rhyolite plug is present some 2 km to the southeast. Quartz veins, stockworks, hydrothermal breccias and sinters occur along a zone 1.5 km long and 400–600 m wide. The sinters consist of microcrystalline quartz, quartz tabular crystals up to 0.2 mm long, fibrous and spherulitic quartz (length-fast chalcedony).

Thirteen sinter microfacies were recognised at the Conway and Verbena localities. These include: massive white to grey chert with sub-horizontal laminae; brecciated with angular clasts; finely laminated chert forming spicular and botryodal structures, similar to those forming around modern spring and geyser vents; ooids about 1 mm and pisoids 1–3 cm in diameter; thin flat bedded chert similar to high-temperature Yellowstone National Park geyserites; finely laminated chert with tubular and laminar fenestrae and elongate filamentous features (streamers) parallel to the laminae, interpreted as flow-oriented micro-organisms, the laminar fenestrae are abundant and may represent cyanobacteria similar to those of modern springs; various types of thinly bedded cherts associated with microstructures that are interpreted as representing fossil micro-organisms, including *Calothrix*, conical features built by the cyanobacterium *Phormidium*, in addition to a number of fossil plant stems.

The Conway and Verbena systems are fossil hot spring sinters showing many features that can be compared to those of the Yellowstone National Park except, as Walter and co-authors pointed out, for the veins and hydrothermal breccias which may represent unexposed levels in the Yellowstone analogy. Furthemore, the authors were able to relate the various microfacies to proximal and distal settings from the hot spring orifice to vent margins, to channels and outflow ponds to distal terraces and ponds (see Fig. 5.55). For example, columnar and spicular features represent splash zones of geysers and hot springs, whereas sinters with wavy laminae would represent high temperature ($>70^{\circ}C$) pool floors and thinly bedded and conical laminated cherts represent distal facies filamentous bacteria and stromatolites.

10.5.4 Palaeo- to Mesoarchaean Ecosystems Associated with Hydrothermal Activity in the East Pilbara Terrane

The 3.53–3.165 Ga Pilbara Supergroup in the East Pilbara Terrane of the Pilbara Craton hosts several epithermal and VMS mineral systems from 3.49 to 3.24 Ga, described in Chapters 5 and 7, respectively (see Huston et al. 2007). In these hydrothermal environments, the presence of filamentous micro-organisms and fossil stromatolites, for which there is convincing evidence of biogenicity, have been extensively documented in numerous papers. For this section, I briefly describe the intimate association of hydrothermal fluids with microbial life.

10.5.4.1 The 3.24 Ga Sulphur Springs Deposits

Rasmussen (2000) reported that probable bacterial features occur in the Sulphur Springs VMS deposit, in very low metamorphic grade and low strain rocks of the 3.24 Ga Sulphur Springs Group (see Figs. 7.41 and 7.42). The massive sulphide deposit contains textures similar to those of modern black smokers and filamentous microfossils interpreted to have been thermophilic chemotropic prokaryotes. The Sulphur Springs hydrothermal fluid circulation developed in response to intrusion of the contemporaneous, subvolcanic Strelley Granite laccolith, emplaced just 1.5 km beneath the paleosurface towards the end of volcanism (Fig. 10.12). Hydrothermal circulation resulted in extensive alteration of the footwall rocks and precipitation of volcanogenic massive sulphide deposits, beneath a 1–30 m thick unit of silicified epiclastic and siliciclastic sedimentary rocks at the top of the group that acted as an impermeable cap to fluid circulation.

Using optical microscopy and SEM, this author was able to identify in core samples, from depths of 300 to 500 m below the present day surface, and therefore with no evidence of weathering or contamination. The filaments are contained in the colloform structures that are associated with replacive pyrite, sphalerite, chalcopyrite, tennantite, arsenopyrite, galena, chlorite, carbonate and chert. The colloform structures are composed of inclusion-rich

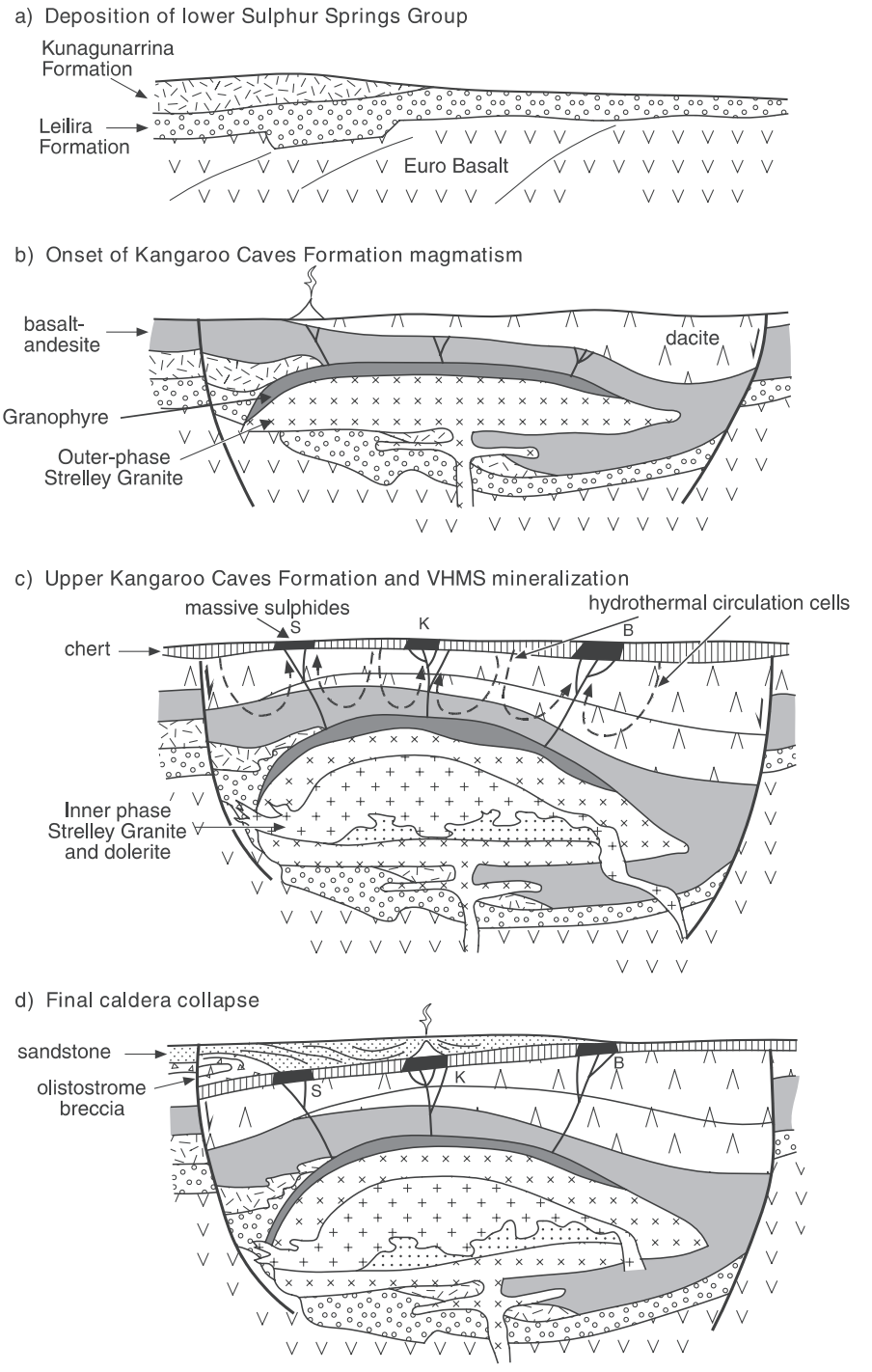


Fig 10.12 (continued)

pyrite, enclosed by paragenetically late chert material. The pyrite is mostly recrystallised by later hydrothermal fluids and partly replaced by later sulphides. The colloform banding is typically defined by inclusions following the replacement of the original inclusion-rich chert, quartz crystals and carbonate by pyrite. Where these original minerals are preserved, fine banding consists of laminae defined by dark and light zones and trails of pyrite crystals. The filaments are straight or sinuous and occur in the early chert and quartz and absent from later silica phases and have uniform thickness, up to 300 μm long and 0.5–2 μm in diameter. Their biogenic origin is based on morphology, uniform lengths and intertwined habit, all features that are comparable with younger fossil microbes and quite different from abiogenic filamentous microstructures. Also important is Rasmussen's observation that changes in the preferred orientation of the filaments is similar to those of modern hot spring microbial mats, suggesting a biotic response to fluctuating environmental conditions. Rasmussen (2000) further suggested that the Sulphur Springs micro-organisms probably lived in pores and crevices of the rocks, through which hydrothermal fluids circulated and provided the necessary nutrients and metals. The filaments were nucleation sites for early silica, later replaced by lower temperature fluids from which sulphides were precipitated. The filaments replaced by paragenetically early silica within a VMS style deposit indicates that the Sulphur Springs biota were thermophiles ($<100^{\circ}C$) in a typically hydrothermal ecosystem, in which sulphur was likely the main energy provider.

Duck et al. (2007) studied in detail carbonaceous material obtained from drill core samples of the hanging wall rocks of the Sulphur Springs VMS deposit. In their study these authors used conventional transmitted and reflected light petrography, carbon isotopic analyses, transmission electron microscopy (TEM), organic reflectance (%Ro) and total organic content (TOC) measurements. Duck et al. (2007) recognised and isolated black organic matter and well preserved filamentous, tubular and spherical structures that closely resemble modern-day microbial forms. Samples examined included highly opaque black organic-rich sulphidic material with dominant,

Fig. 10.12 (continued) Schematic evolution of the Sulphur Springs Group and Strelley Granite: (**a**) unconformable deposition of the lower part of the Sulphur Springs Group on the Euro Basalt; (**b**) intrusion of the outer phase of the Strelley Granite and deposition of intermediate to felsic volcanic rocks in the lower part of the Kangaroo Caves Formation, during the onset of block faulting; (**c**) intrusion of the inner phase of the Strelley Granite during continued block faulting and felsic volcanism. Extensive hydrothermal circulation is instigated during the late stage of magmatism, resulting in precipitation of massive sulphides with contained microfossils beneath an impermeable marker chert unit of silicified epiclastic sediments; (**d**) asymmetrical (north-side-down) late stage caldera collapse results in deposition of an olistostrome breccia at Sulphur Springs (**S**) and coarse sandstone turbidites that onlap the marker chert between Sulphur Springs and a late volcanic dome at Kangaroo Caves (**K; B** = Breakers prospect). After Van Kranendonk et al. (2001), Van Kranendonk and Pirajno (2004) and Van Kranendonk (2006)

in places framboidal, pyrite. TEM images show closely packed bundles of filaments and tubular structures up to 100 μ long and ranging from 1 to 5 μm in width, with the individual tubes about 0.3 μm in diameter. Spherical forms, vary in size from 100 to <50 nm, are of pure carbon composition, are hollow and consist of clusters and aggregates attached to a substrate of amorphous organic material. Duck et al. (2007) found that the thermally more mature organic material (Ro values > 2.0), no longer exhibit microbial-like forms or structures. They showed that the reflectivity of organic matter is affected by separate episodes of hydrothermal heat with the lowest Ro representing the latest event. The highest Ro value is 2.95%, which is equivalent to a temperature of 250°C, whereas low thermal maturity of microbial material has Ro values of 0.2–0.3%, representing temperatures of 90–100°C, which the authors interpreted as the last temperature regime of a hydrothermal cycle, before the resumption of sedimentation. The range of Ro values of the Sulphur Springs organic material is indicative that the rocks were subjected to intense hydrothermal metamorphism (described in Chapter 7). The C isotopic compositions show a restricted range of $\delta^{13}C$ values from –26.8 to 34.0‰ and these values are consistent with biological isotopic fractionations. Furthermore down-hole profiling shows a trend to heavier values with depth, with two of the heaviest values of –26.8 and 26.9‰ occurring above the contact with the underlying footwall dacitic rocks (Kangaroo Caves Formation), attributed to thermal effects that result in enrichment of ^{13}C with high temperatures. Duck et al. (2007) compared the microbial forms of the Sulphur Springs VMS to those found at the Mid-Atlantic Ridge, where tubular hyperthermophilic microbes, *Pyrodictium abyssi* are present (Rieger et al. 1995). Finally, the authors also reflected on the resemblance of the larger hollow spherical structures with similar structures in carbonaceous chondrites (Garvie and Buseck 2004) and pointed out that meteorite impact signatures have been documented in the sedimentary rocks of the Sulphur Springs Group (Glikson and Vickers 2006) some of these spherical bodies may have been carried into the microbial depositional environment; an intriguing possibility.

10.5.4.2 Dresser Formation: A Shallow Water Hydrothermal Ecosystem

This example of a shallow water ecosystem associated with hydrothermal circulation is described in Van Kranendonk and Pirajno (2004) and Van Kranendonk (2006). The following is an abridgment from these papers. The Dresser Formation is between 6 and 30 m thick and consists of layered grey, white, and black chert, bedding-parallel horizons of coarsely bladed barite, jaspilitic chert, clastic sedimentary rocks and minor carbonate rocks, with layers of fine wrinkly laminates that have been interpreted as stromatolites (Walter et al. 1980; Van Kranendonk 2006, 2007). Stromatolites have a variety of forms including wrinkled mats, broad, low-amplitude domes, steep-sided domes with wrinkly lamination, and conical forms (Fig. 10.3). Some of the stromatolites lie on silicified calcareous sandstone with ripple marks, indicative

of shallow water conditions. The presence of oncolitic structures and desiccation cracks also support a shallow-water, carbonate environment of deposition for at least part of the formation (Lambert et al. 1978; Shen et al. 2001). Previously, this evidence was used to suggest a restricted shallow-marine carbonate environment of deposition, based on analogy with Shark Bay, Western Australia, where living stromatolites thrive in the absence of predators caused by the high salinity (Groves et al. 1981).

Recent studies, however, have shown that there is a significant hydrothermal component to deposition of the Dresser Formation (Nijman et al. 1998; Van Kranendonk 2000, 2006; Van Kranendonk and Pirajno 2004; Ueno et al. 2004). Field observations show that the sedimentary rocks of the Dresser Formation are fed by a large (up to 2 km deep), and voluminous swarm of hydrothermal feeder veins that are composed of black to grey silica, barite, and pyrite, the same principal components that form most of the bedded material (Van Kranendonk 2000, 2006). These veins, although previously thought to postdate the bedded cherts during periods of doming (Buick and Dunlop 1990), are demonstrably contemporaneous with sediment accumulation and stromatolite growth (Nijman et al. 1998; Van Kranendonk 2006). The black silica-barite veins represent a massive feeder swarm that resulted from multiple pulses of hydrothermal fluids in an epithermal, high-sulphidation environment (Van Kranendonk and Pirajno 2004). Hydrothermal circulation accompanied normal faulting and basin development within a footwall of pillow basalts. Footwall basalts were affected by extensive hydrothermal alteration including zones of propylitic, phyllic, and advanced argillic alteration that, together with the local development of hydrothermal kaolinite, indicates alteration in a steam-heated acid-sulphate volcanic caldera type geothermal system (Van Kranendonk and Pirajno 2004). Thus the chert-barite succession of the Dresser Formation has all the features of brine pool-type (low-temperature, white-smoker (sulphate)) sulphide deposition.

Stromatolites in the Dresser Formation occur in two main settings. Lower in the formation, wrinkly laminates and broad domes are associated with massive barite and layered grey and white cherts, and are locally developed immediately upon large fallen panels of chert and barite (Fig. 10.13) and at vents of hydrothermal barite veins that indicate growth directly in a hydrothermal environment. Higher up in the formation, wrinkly stromatolite mats and conical forms occur immediately on rippled carbonate sandstones. Primary carbonates are Fe-rich dolomite or ankerite with REE data indicative of precipitation from a seawater source (Van Kranendonk et al. 2003) that may have been as warm as 30–50 $^{\circ}$C (Ohmoto et al. 2004). Putative spheroidal microfossils have been described from bedded cherts in the Dresser Formation (Dunlop et al. 1978). Putative filamentous microfossils have also been described from the black silica hydrothermal veins immediately beneath the bedded rocks (Ueno et al. 2001, 2004, 2006), from which carbon isotopic signatures suggest methanogenesis.

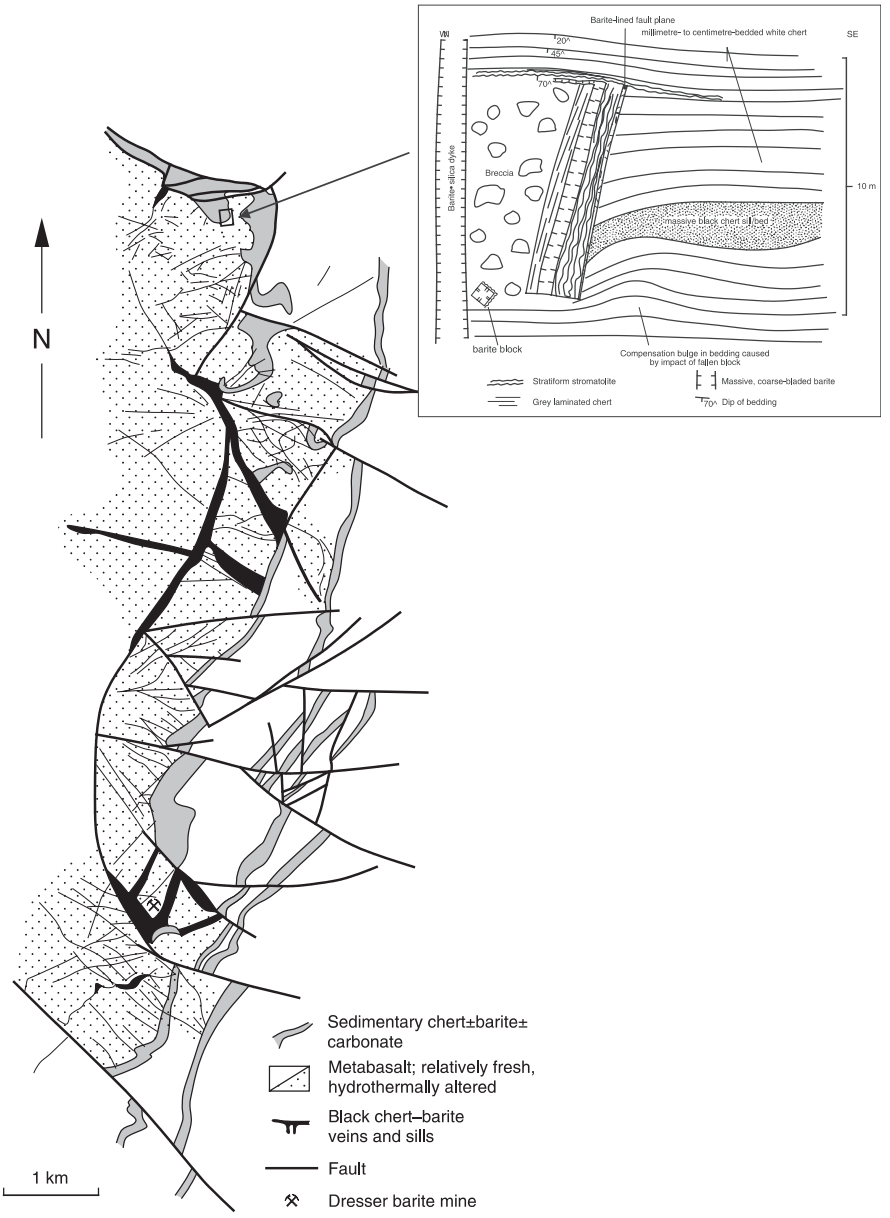


Fig. 10.13 Simplified geological map of part of the Dresser Formation, showing the relation between bedded chert-barite, swarms of hydrothermal silica-barite feeder veins, and hydrothermal alteration of footwall pillow basalts; inset is a sketch map of area outlined in the square, showing details of the Dresser Formation barite veining and stromatolites. After Van Kranendonk and Pirajno (2004) and Van Kranendonk (2006)

Van Kranendonk (2006) detailed a model for the evolution of the Dresser Formation hydrothermal processes. Van Kranendonk's model, shown in Fig. 10.14, suggests that felsic magmas would contribute either or both H_2S and SO_2 to the hydrothermal fluids. Hydrothermal circulation was highly dynamic and subject to changes in pressure linked with rates of normal faulting and sealing due to silicification of cap rocks. Data from fluid inclusions indicate that the magmatic component introduced H_2S into the system together with varying amounts of liquid CO_2, H_2O and traces of CH_4. At the same time, the large volumes of barite are indicative of SO_2, during low-pressure venting in shallow water conditions. The volume of dissolved SO_2 in felsic magmas in shallow crustal settings can reach concentrations of up to 28 vol%, together with significant amounts of H_2S. These high volumes of volatiles would have resulted in volcanic eruptions and the release of SO_2 into the atmosphere, where photolytic dissociation to HSO_3, SO_4 and S^0, would readily account for the non-mass dependant ^{33}S fractionation, resulting in the $\Delta^{33}S$ anomalies, recorded in the barites and cherts of the Dresser Formation (see Farquhar et al. 2001). The eruption cloud also explains the concentration of sulphates in a restricted basin at North Pole although, as pointed out by Van Kranendonk (2006), much sulphate was also produced by acid-sulphate alteration. Sulphide laminations alternate with barite and the complexity of feeder veins, suggest a highly complex and dynamic hydrothermal system, perhaps related to several hydrothermal cells with variable chemistries and fluid components and continuous recycling of meteoric and sea waters. The magmatic fluids leached Ba, Fe and Si from the footwall rocks by acid-sulphate alteration processes. The leached Fe combined with H_2S to produce laminated pyrite, typically with $\delta^{34}S$ values of around –0.9‰. The H_2SO_4 formed by the interaction of H_2S with heated sea water, resulted in intense and pervasive phyllic alteration, with the process also resulting in the release of SO_4^{2-} ions and leaching of Ba^{2+} from the feldspars in the footwall basalts to form hydrothermal barite at shallow levels.

Suphur isotope systematics ($\delta^{34}S$ values of $+3.7$‰) show that the North Pole barite is not related to biogenic processes. However, the presence of minute pyrite grains within growth zones of barite crystals have been shown to derived from microbial processing of elemental sulfur (Philippot et al. 2007).

In the final analysis, the Dresser Formation hydrothermal system was characterised by intermittent reducing and oxidising conditions, reflecting changing magmatic volatile discharges and near-surface recharge (H_2S forming sulphides and SO_2 resulting in process leading to barite precipitation). The wrinkly stratiform stromatolites of the Dresser Formation were probably anaerobic chemoautotrophs that developed near seafloor hydrothermal vents, whereas the conical forms and pseudocolumnar stromatolites in the Strelley Pool Chert (see Fig. 10.3) were deposited in a shallow marine carbonate platform, possibly under sunlight and a CO_2-rich atmosphere conditions, which would have been conducive to photolysis.

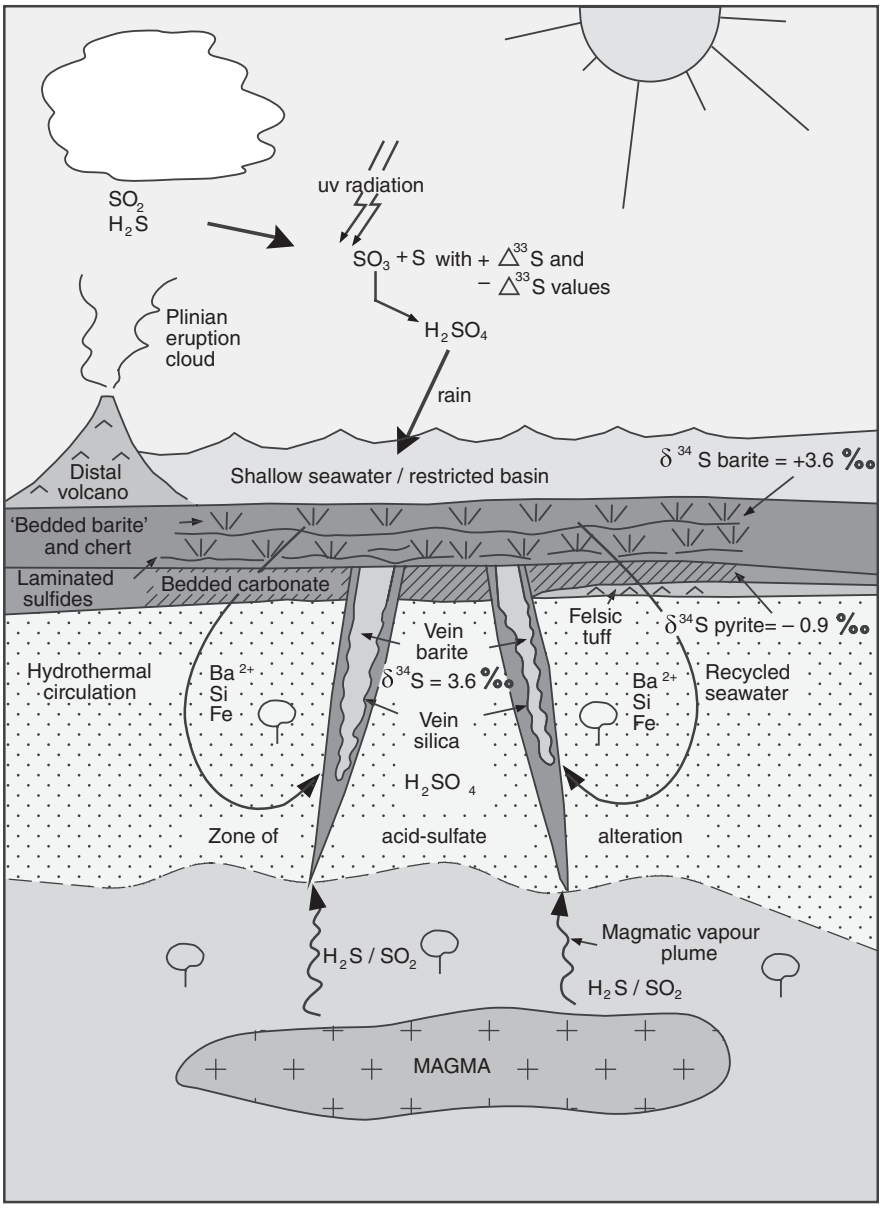


Fig. 10.14 Model for the evolution of the 3.49 Ga Dresser Formation hydrothermal and ecological systems, according to Van Kranendonk (2006). See text for details. Figure reproduced by permission of the author

10.6 Concluding Remarks

In this chapter, I have presented a panoramic of ecosystems that are associated with hydrothermal systems and also participate in the making of ore minerals. In so doing, I thought to delve first into the emergence of life on Earth and review the main theories on the origin of life. This was in order to provide the background on the role of bacteria in ore genesis. It is also intriguing to realise that primitive life forms — bacteria and archaea — did not undergo great evolutionary changes, nor were they subjected to mass extinctions, through nearly four billion years of Earth history. Mass extinctions seem to be confined to eukaryotes and the risk of extinction is greater with more complex organisms (Ward and Brownlee 2004). The Great Oxidation Event was the most significant event in the history of life on Earth, again due to bacterial metabolic activity, in which the use of sunlight, H_2O and CO_2 pumped large volumes of oxygen into the atmosphere, effectively leading to greater biotic diversity, as well as crises. Thus, microbial life has given us the oxygen we breathe, the opportunity to evolve and many of the ores we exploit.

In Hadean and Archaean times submarine volcanism was very common and deep-sea ridges and oceanic plateaux would have been much more extensive that today's or in later geological times. This, volcanically active, submarine environment must have been energy rich, with widespread hydrothermal activity with abundant emissions of elements and volatiles from the mantle. The chemistry of the ocean would have been quite different than it is now and it is likely that the ocean was largely reducing and at higher temperatures. The brief overviews on microbial life in the hot springs of the ocean floor and of on-land geothermal areas give invaluable insights on many fronts, including ore genesis. Gas hydrates at cold seeps constitute a major energy resource as well as potential climate greenhouse gas, as CH_4 converts to CO_2 in the atmosphere. Sea level fluctuations can bring gas hydrates out of their stability zone, pumping greenhouse gases into the atmosphere. The role of gas hydrate destabilisation on climate changes is poorly known, but may have been, and may still be, of paramount importance in the global climate cycles. The spatial association of salt domes, oil traps, hydrate seeps, sulphur-oxidising and sulphate-reducing chemosynthetic microbial communities, related precipitation of carbonates and sulphides, explain the common link between hydrocarbons and sulphides in Mississippi Valley type (MVT) deposits (Chapter 9). Finally, many dedicated bio- and geoscientists are steadily making progress in the study and recognition of fossil microbes in the geological record. Nowhere this is more evident than the vibrant and stimulating studies conducted and still in progress in the Pilbara Craton in Western Australia and the Barberton greenstone belt in South Africa, where the oldest life forms are there for all to see.

References

Altermann W (2007) The early Earth's record of enigmatic cyanobacteria and supposed extremophilic bacteria at 3.8 to 2.5 Ga. In: Seckbach J (ed) Algae and cyanobacteria in extreme environments. Cellular Origin, Life in Extreme Habitats and Astrobiology (COLE) vol 11. Springer Verlag, Berlin, pp 759–778

Allwood AC, Walter MR, Kamber BS, Marshall CP, Burch IW (2006) Stromatolite reef from Early Archaean era of Australia. Nature 441:714–718

Anbar AD, Duan Y, Lyons TW, Arnold GL, Kendall B, Creaser RA, Kaufman AJ, Gordon GW, Scott C, Garvin J, Buick R (2007) A whiff of oxygen before the Great Oxidation Event? Science 317:1903–1906

Arrhenius S (1903) Die Verbreitung des Lebens im Weltenraum. Die Umschau 7:481

Awramik SM, Schopf JW, Walter MR, (1983) Filamentous fossil bacteria from the Archean of Western Australia. Precambr Res 20:357–374

Bada JL (2004) How life began on Earth: a status report. Earth Planet Sci Lett 226:1–15

Barley ME, Bekker A, Krapež B (2005) Late Archean to Early Proterozoic global tectonics, environmental changes and the rise of atmospheric oxygen. Earth Planet Sci Lett 238:156–171

Barbieri R, Ori GG, Cavalazzi B (2004) A Silurian cold-seep ecosystem from the Middle Atlas, Morocco. Palaios 19:527–542

Beauchamp BK, HR, Harrison JC, Nassichuk WW, Eliuk LS (1989) Cretaceous cold-seep communities and methane-derived carbonates in the Canadian Arctic. Science 244:53–56

Belisheva N (2005) Extraterrestrial agents dependence of terrestrial microbial survival. Geol Soc Am Ann Meeting, SLC 2005, Abstracts with Programs:206

Bengtson S (ed) (1994) Early life on Earth. Proceed Nobel Symposium 84, Coumbia University Press, New York

Benner SA, Ricardo A, Carrigan MA (2004) Is there a common chemical model for life in the Universe? Curr Opin Chem Biol 8:672–689

Bernstein MP, Sandford SA, Allamandola LJ (1999) UV irradiation of polycyclic aromatic hydrocarbons in ices: production of alcohols, quinones and ethers. Science 283:1135–1138

Bock GR, Goode JA (eds) (1996) Evolution of hydrothermal ecosystems on Earth (and Mars?). Ciba Found Symp 202, John Wiley & Sons, Chichester

Boetius A, Suess E (2004) Hydrate Ridge: a natural laboratory for the study of microbial life fueled by methane from near-surface gas hydrates. Chem Geol 205:291–310

Brasier MD, Green OR, Jephcoat AP, Kleppe AK, Van Kranendonk MJ, Lindsay JF, Steele A, Grassinau N (2002) Questioning the evidence for Earth's oldest fossils. Nature 416:76–81

Brasier MD, Green O, Lindsay J, Steele A (2004) Earth's oldest (~3.5 Ga) fossils and the 'Early Eden hypothesis': questioning the evidence. Orig Life Evol Biosph 34:257–269

Brasier M, Green O, Lindsay J, McLoughlin N, Steele A, Stoakes C (2005) Critical testing of Earth's oldest putative fossil assemblage from the ~3.5 Ga Apex chert, Chinaman Creek, Western Australia. Precambr Res 140:55–102

Brimblecombe P (2003) The global sulphur cycle. Treatise Geochem vol 8. Elsevier, Amsterdam, pp 645–682

Brocks JJ, Logan GA, Buick R, Summons RE (1999) Archean molecular fossils and the early rise of eukaryotes. Science 285:1033–1036

Buick R, Dunlop JSR, Groves DI (1981) Stromatolite recognition in ancient rocks: An appraisal of irregularly laminated structures in an early Archaean chert-barite unit from North Pole, Western Australia. Alcheringa 5:161–181

Buick R, Dunlop JSR (1990) Evaporitic sediments of early Archaean age from the Warrawoona Group, North Pole, Western Australia. Sedimentology 37:247–277

Cady SI, Farmer JD (1996) Fossilization processes in siliceous thermal springs: trends in preservation along geothermal gradients. In: Evolution of hydrothermal ecosystems on Earth (and Mars?), Ciba Found Symp 202, John Wiley & Sons, pp 150–169

Cairns-Smith AG, Hall AJ, Russell MJ (1992) Mineral theories of the origin of life and an iron sulfide example. Orig Life Evol Biosph 22:161–180
Campbell KA (2006) Hydrocarbon seep and hydrothermal vent paleoenvironments and paleontology: Past developments and future research directions. Palaeogeogr, Palaeoclim, Palaeoecol 232:362–407
Campbell KA, Farmer JD, Des Marais D (2002) Ancient hydrocarbon seeps from the Mesozoic convergent margin of California: carbonate geochemistry, fluids and palaeoenvironments. Geofluids 2: 63–94
Campbell KA, Sannazzaro K, Rodgers KA, Herdianita NR, Browne PRL (2001) Sedimentary facies and mineralogy of the Late Pleistocene Umukuri silica sinter, Taupo Volcanic Zone, New Zealand. J Sedim Res 71:7 28–747
Canfield DE (2005) The early history of atmospheric oxygen: Homage to Robert M. Garrels. Ann Rev Earth Planet Sci 33:1–36
Canfield DE, Habicht KS, Thamdrup BO (2000) The Archean sulfur cycle and the early history of atmospheric oxygen. Science 288:658–661
Chapelle FH, O'Neill K, Brdaley PM, Methé BA, Clufo SA, Knobel LL, Lovley DR (2002) A hydrogen-based subsurface microbial community dominated by methanogens. Nature 415:312–318
Cleland CE, Copley SD (2005) The possibility of alternative microbial life on Earth. Astrobiology 4:165–173
Cloud P (1973) Paleoecological significance of the banded iron formation. Econ Geol 68:1135–1143
Cockell CS, Fike DA, Osinski GR, Lee P (2006) Geomicrobiology of impact-altered rocks. In: Cockell CS, Koeberl C, Gilmour I (eds) Biological processes associated with impact events, Springer, Berlin, pp 21–40
Conway Morris S (1992) Burgess Shale-type faunas in the context of the "Cambrian explosion": A review. J Geol Soc London 149:631–636
Cronin JR (1998) Clues from the origin of the solar system. In: Cronin JR (ed) The molecular origins of life: assembling pieces of the puzzle, Cambridge University Press, New York, pp 119–146
Darwin C (1859) On the origin of the species by means of natural selection, or the preservation of favoured races in the struggle for life. John Murray, London
Davies P (1998) The fifth miracle: the search for the origin of life. Simon & Schuster, New York
Davies P (2007) Are aliens among us? Sci Am 297:36–43
Davies P, Lineweaver CH (2005) Finding a second sample of life on Earth. Astrobiology 5:154–163
Davis WL, McKay CP (1996) Origins of life: A comparison of theories and applications to Mars. Origins Life Evol Biosph 26:61–73
DeStefano AL, Ford JC, Winsor SK, Allen CC, Miller J, McNamara KM, Gibson EK (2000) Microbial life in the terrestrial deep subsurface: deep, hot and radioactive. Lunar Planet Sci XXXI:1702.pdf
Dimitrov LI (2002) Mud volcanoes – the most important pathway for degassing deeply buried sediments. Earth-Science Rev 59:49–76
Dobzhansky T, Ayala FJ, Stebbins GL, Valentine JW (1977) Evolution. WH Freeman and Company, San Francisco, 572p
Douglas S (2005) Mineralogical footprints of microbial life. Am J Sci 305:503–525
Duck LJ, Glikson M, Golding SD, Webb RE (2007) Microbial remains and other carbonaceous forms fromte3.24 Ga Sulphur Springs black smoker deposit, Western Australia. Precambr Res 154:205–220
Dunlop JSR, Muir MD, Milne A, Groves DI (1978) A new microfossil assemblage from the Archaean of Western Australia. Nature 274:676–678
Farquhar J, Savarino J, Airieau S, Thiemens M (2001) Observations of wavelength-sensitive mass-independent sulphur isotope effects during SO_2 photolysis: implications for the early atmosphere. J Geophys Res 106:32829–32839

Farquhar J, Wing BA (2003) Multiple sulphur isotopes and the evolution of the atmosphere. Earth Planet Sci Lett 213:1–13
Fernández-Remolar DC, Morris RV, Gruener JE, Amils R, Knoll AH (2005) The Rio Tinto Basin, Spain: Mineralogy, sedimentary geobiology, and implications fro interpretation of outcrop rocks at Meridiani Planum, Mars. Earth Planet Sci Lett 240:149–167
Ferris JP (2005) Mineral catalysis and abiotic synthesis: montmorillonite-catalyzed formation of RNA. Elements 1:145–149
Folsome CE (1979) The origin of life. WH Freeman and Company, San Francisco, 168p
Fredrickson IK, Onstott TC (1996) Microbes deep inside the Earth. Sci Am 275:42–47
Fridriksson S (1975) Surtsey – evolution of life on a volcanic island. Halsted Press, John Wiley & Sons, New York
Furnes H, Banejee NR, Muehlenbachs K, Staudigel H, de Wit M (2004) Early life recorded in Archean pillow lavas. Science 304:578–581
Furnes H, Banejee NR, Staudigel H, Muehlenbachs K, McLoughlin N, de Wit M, Van Kranendonk MJ (2007) Comparing petrographic signatures of bioalteration in recent to Mesoarchean pillow lavas: tracing subsurface life in oceanic igneous rocks. Precambr Res 158:156–176
Garcia-Ruiz JM, Hyde ST, Carnerup AM, Christy AG, Van Kranendonk M.J, Welham NJ (2003) Self-assembled silica-carbonate structures and detection of ancient microfossils. Science 302:1194–1197
Gargaud M, Barbier B, Martin H, Reisse J (eds) (2005) Lectures in Astrobiology, vol I. Springer, Berlin
Garvie LAJ, Buseck PR (2004) Nanosized carbon-rich grains in carbonaceous chondrite meteorites. Earth Planet Sci Lett 224:431–439
Glikson AY, Vickers J (2006) The 3.26-3.24 Ga Barberton asteroid impact cluster: tests of magmatic and tectonic consequences, Pilbara Craton, Western Australia. Earth Planet Sci Lett 241:11–20
Glikson M, Mastalerz M (eds) (2000) Organic matter and mineralisation: thermal alteration, hydrocarbon generation and role in metallogenesis. Kluwer Academic Publ, Dordrecht
Gold T (1992) The deep, hot biosphere. Proceed Nat Acad Sci 89:6045–6049
Gong YM, Shi GR, Weldon E, Du YS, Xu R (2008) Pyrite framboids interpreted as microbial colonies within the Permian *Zoophycos* spreiten from southeastern Australia. Geol Mag 145:95–103
Greinert J, Bollwerk SM, Derkachev A, Bohrmann G, Suess E (2002) Massive barite deposits and carbonate mineralization in the Derugin Basin, Sea of Okhotsk: precipitation processes at cold deep sites. Earth Planet Sci Lett 203:165–180
Grotzinger JP, Rothman DH (1996) An abiotic model for stromatolite morphogenesis. Nature 383:423–425
Groves DI, Dunlop JSR, Buick R, (1981) An early habitat of life. Sci Am 245:64–73
Hanczyc MM, Fujikawa SM, Szostak JW (2003) Experimental models of primitive cellular compartments: encapsulation, growth and division. Science 302:618–622
Hazen RM (2001) Life's rocky start. Sci Am 284:62–71
Henriet JP, Mienert J (eds) (1998) Gas hydrates – relevance to world margin stability and climatic change. Geol Soc Sp Publ 137
Hoffman HJ, Grey K, Hickman AH, Thorpe R (1999) Origin of 3.45 Ga coniform stromatolites in Warrawoona Group, Western Australia. Geol Soc Am Bull 111: 1256–1262
Holden JF, Summit M, Baross JA (1998) Thermophilic and hyperthermophilic microorganisms in 3–30°C fluids following a deep-sea volcanic eruption. FEMS Microbiol Ecol 425:533–41
Holland HD (2002) Volcanic gases, black smokers and the Great Oxidation Event. Geochim Cosmochim Acta 66:3811–3826
Holland HD (2003) The geologic history of seawater. Treatise on Geochemistry 6, Elsevier, Amsterdam, pp 583–625

Holm NG (ed) (1992) Marine hydrothermal systems and the origin of life. Kluwer Academic Publ, Dordrecht
Horgan J (1991) In the beginning. Sci Am 264:100–109
Horneck G, Mileikowsky C, Melosh HJ, Wilson, JW, Cucinotta, FA, Gladman B (2002) Viable transfer of microorganisms in the Solar System and beyond. In: Horneck G, Baunstark-Khan C (eds) Astrobiology – the quest for the conditions of life. Springer, Berlin, pp 57–76
Hough RM, Butt CRM, Reddy SM, Verrall M (2007) Gold nuggets: supergene or hypogene? Aust J Earth Sci 54:959–964
Huber R, Stoffers P, Cheminee JL, Richnow HH, Stetter KO (1990) Hyperthermophilic archaebacteria within the crater and open sea plume of erupting MacDonald Seamount. Nature 345:179–182
Huber H, Hohn MJ, Rachel R, Fuchs T, Wimmer VC, Stetter KO (2002) A new phylum of Archaea represented by a nanosized hyperthermophilic symbiont. Nature 417:63–67
Huston DL, Morant P, Pirajno F, Cummins B, Baker D, Mernagh TP (2007) Palaeoarchean mineral deposits of the Pilbara Craton: genesis, tectonic environment and comparisons with younger deposits. In: Van Kranendonk MJ, Smithies RH, Bennett VC (eds) Earth's oldest rocks, Developm Precambr Geol, Elsevier, Amsterdam, pp 411–450
Jones B, Renaut RW, Rosen MR (2001) Biogenecity of gold- and silver-bearing siliceous sinters forming in hot (75°C) anaerobic spring-waters of Champagne Pool, Waiotapu, New Zealand. J Geol Soc Lond 158:895–911
Jones B, Konhauser KO, Renaut RW, Wheeler RS (2004) Microbial silicificcation in Iodine Pool, Waimangu geothermal area, North Island, New Zealand: implications for recognition and identification of ancient silicified microbes. J Geol Soc Lond 161:983–993
Kalkowsky E (1908) Oolith und stromatolith im norddeutschen Buntsandstein. Zeitschrift der Deutschen Gesellschaft für Geowissenschaften Band 60:68–125
Karhu JA, Holland HD (1996) Carbon isotopes and the rise of atmospheric oxygen. Geology 24:867–870
Kaufman AJ, Johnston DT, Farquhar J, Masterton AL, Lyons TW, Bates S, Anbar AD, Arnold GL, Garvin J, Buick R (2007) Late Archean biospheric oxygenation and atmospheric evolution. Science 317:1900–1903
Kaufman AJ, Johnston DT, Farquhar J, Masterson AL, Lyons TW, Bates S, Anbar AD, Arnold GL, Garvin J, Buick (2008) Late Archean biospheric oxygenation and atmospheric evolution. Science 317:1900–1903
Kelley DS, Baross JA, Delaney JR (2002) Volcanoes, fluids and life at Mid-ocean ridge spreading centers. Ann Rev Earth Planet Sci 30:385–491
Kesler SE, Ohmoto H (eds) (2006) Evolution of early Earth's atmosphere, hydrosphere and biosphere – constraints from ore deposits. Geol Soc Am Mem 198
Knoll AH (2003) Life on a young planet. Princeton University Press, Princeton NJ
Knoll AH, Grotzinger J (2006) Water on Mars and the prospect of Martian life. Elements 2:169–173
Konhauser KO, Ferris FG (1996) Diversity of iron and silica precipitation by microbial mats in hydrothermal waters, Iceland: Implications for Precambrian iron formations. Geology 24:323–326
Konhauser KO, Jones B, Reysenbach AL, Renaut RW (2003) Hot spring sinters: keys to understanding Earth's earliest life forms. Can J Earth Sci 40:1713–1724
Kotelnikova S (2002) Microbial production and oxidation of methane in deep subsurface. Earth-Sci Rev 58:367–395
Kral TA, Brink KM, Miller Sl, McKay CP (1998) Hydrogen consumption by methanogens on the early Earth. Origins of Life Evol Biosph 28:311–319
Lahav N (1999) Biogenesis: theories of life's origin. Oxford University Press, New York

Lambert I, Donnelly T, Dunlop J, Groves DI (1978) Stable isotope compositions of early Archaean sulphate deposits of probable evaporitic and volcanogenic origins. Nature 276: 808–811

Larrasoaña JC, Roberts Ap, Musgrave RJ, Gràcia E, Piñero E, Vega M, Martinez-Ruiz F (2007) Diagenetic formation of greigite and pyrrhotite in gas hydrate sedimentary systems. Earth Planet Sci Lett, doi: 10.1016/j.epsl.2007.06.032

Lengke MF, Southam G (2006) Bioaccumulation of gold by sulfate-reducing bacteria cultured in the presence of gold(I)-thiosulfate complex. Geochim Cosmochim Acta 70:3646–3661

Lengke MF, Southam G (2007) The deposition of elemental gold from gold(I)-thiosulfate complexes mediated by sulphate-reducing bacterial conditions. Econ Geol 102:109–126

Lindsay JF, Brasier MD, McLoughlin N, Green OR, Fogel M, Steele A, Mertzman SA (2005) The problem of deep carbon – an Archaean paradox. Precambr Res 143:1–22

Little CTS (2002) The fossil record of hydrothermal vent communities. Cahiers Biol Marine 43:313–316

Little CTS, Magalashvili AG, Banks DA (2007) Neotethyan Late Creatceous volcanic arc hydrothermal vent fauna. Geology 35:835–838

Logan GA, Hinman MC, Walter MR, Summons RE (2001) Biogeochemistry of the 1640 Ma McArthur River (HYC) lead-zinc ore and host sediments, Northern Territory, Australia. Geochim Comsochim Acta 65:2317–2336

Lowe DR (1980) Stromatolites 3,400 Myr old from the Archaean of Western Australia. Nature 284:441–443

Lowe DR (1994) Abiological origin of described stromatolites older than 3.2 Ga. Geology 22:387–390

Lurquin PF (2003) The origin of life and the universe. Columbia University Press, New York

Lyons TW, Zhang CL, Romanek CS (eds) (2003) Isotopic records of microbially mediated processes. Chem Geol 195(1–4)

Machel HG, Krouse HR, Sassen R (1995) Products and distinguishing criteria of bacterila and thermochemical sulphate reduction. Applied Geochem 10:373–389

Mann AW (1984) Mobility of gold and silver in lateritic weathering profiles: some observations from Western Australia. Econ Geol 79:38–50

Marshall CP, Love GD, Snape CE, Hill AC, Allwood AC, Walter MR, Van Kranendonk MJ, Bowden SA, Sylva SP, Summons RE (2007) Characterization of kerogen in Archaean cherts, Pilbara Craton, Western Asutralia. Precambr Res 155:1–23

Max MD, Johnson AH, Dillon WP (2006) Economic geology of natural gas hydrate. Springer, Berlin

McCollom TM, Shock EL (1997) Geochemical constraints on chemolithoautotrophic metabolism by microorganisms in seafloor hydrothermal systems. Geochim Cosmochim Acta 61:4375–4391

McCollom TM, Seewald JS (2001) A reassessment of the potential for reduction of dissolved CO2 to hydrocarbons during serpentinization of olivine. Geochim Cosmochim Acta 21:3769–3778

Melezhik VA, Fallick AE, Hanski EJ, Kump LR, Lepland A, Prave AR, Strauss H (2005) Emergence of the aerobic biosphere during the Archean-Proterozoic transition: challenges of future research. GSA Today 15:4–11

Melezhik VA, Huhma H, Condon DJ, Fallick AE, Whitehouse MJ (2007) Temporal constraints on the Paleoproterozoic Lomagundi-Jatuli carbon isotopic event. Geology 35:655–658

Milkov AV (2000) Worldwide distribution of submarine mud volcanoes and associated gas hydrates. Marine Geol 167:29–42

Milkov AV, Claypool GE, Lee YJ, Dickens GR, Xu W, Borowski WS, ODP Leg Scientific Party (2003) In situ methane concentrations at Hydrate Ridge offshore Oregon: new

constraints on the global gas hydrate inventory from an active margin. Geology 31:833–836
Miller SL (1953) A production of amino acids under possible primitive Earth conditions. Science 117:528–529
Miller SL, Urey HC (1959) Organic compound synthesis on the primitive Earth. Science 130:245–251
Nijman W, De Bruin K, Valkering M (1998) Growth fault control of early Archaean cherts, barite mounds, and chert-barite veins, North Pole Dome, Eastern Pilbara, Western Australia. Precambr Res 88:25–52
Nisbet EG, Sleep NH (2001) The habitat and nature of early life. Nature 409:1083–1091
Ohmoto H (2004) The Archaean atmosphere, hydrosphere and biosphere. In: Eriksson PG, Altermann W, Nelson DR, Mueller WU, Catuneanu O (eds) The Precambrian Earth: tempos and events, Dev Precambr Geol, Elsevier, Amsterdam, pp 361–388
Ohmoto H, Watanabe Y, Kumazawa K (2004) Evidence from massive siderite beds for a CO_2-rich atmosphere before ~1.8 billion years ago. Nature 429:395–399
Oparin AI (1961) Life, its nature, origin and development. Oliver Boyd, Edinburgh
Orgel LE (1998) The origin of life – a review of facts and speculations. Trends Biochem Sci 23:491–495
Osegovic JP, Tatro SR, Holman SA (2006) Physical chemical characteristics of natural gas hydrate. In: Max MD, Johnson AH, Dillon WP (eds) Economic geology of natural gas hydrate, Springer, Berlin, pp 45–104
Pedersen K (1993) The deep subterranean biosphere. Earth-Science Rev 34:243–260
Philippot P, Van Zuilen M, Lepot K, Thomazo C, Farquhar J, Van Kranendonk M (2007) Early Archean microorganisms preferred elemental sulphur, not sulphate. Science 317:1534–1537
Pirajno F, Van Kranendonk MJ (2005) Review of hydrothermal processes and systems on Earth and implications for martian analogues. Aust J Earth Sci 52:329–352
Potter J, Konnerup-Maiden (2003) A review of the occurrence and origin of abiogenic hydrocarbons in igneous rocks. Geol Soc London Sp Publ 214:151–173
Rasmussen B (2000) Filamentous microfossils in a 3,235-million-year-old volcanogenic massive sulphide deposit. Nature 405:676–679
Renaut RW, Jones B (eds) (2003) Sedimentology of hot spring systems. Can J Earth Sci 40, No 11
Rickard DT (1970) The origin of framboids. Lithos 3:269–293
Rieger G, Rachel R, Hertmann R, Stetter KO (1995) Ultrastrcture of the hyperthermophilic Archeon *Pyrodictium abyssi*. J Struct Biol 115:78–87
Russell MJ (2003) The importance of being alkaline. Science 302:580–581
Russell MJ, Hall AJ, Cairns-Smith AG, Braterman PS (1988) Submarinehot springs and the origin of life. Nature 336:117
Russell MJ, Daniel RM, Hall AJ, Sherringham J (1994) A hydrothermally precipitated catalytic iron sulphide membrane as a first step toward life. J Molec Evol 39:231–243
Russell MJ, Hall AJ (1997) The emergence of life from iron monosulphide bubbles at a submarine hydrothermal redox and pH front. J Geol Soc Lond 154:377–402
Sagan C (1981) Cosmos. Macdonald Futura Publ, London
Sassen R, Roberts HH, Carney R, Milkov AV, DeFreitas DA, Lanoil B, Zhang CL (2004) Free hydrocarbon gas, gas hydrates, and authigenic minerals in chemosynthetic communities of the northern Gulf of Mexico continental slope: relation to microbial processes. Chem Geol 205:915–217
Schopf JW (1993) Microfossils of the Early Archaean Apex Chert: new evidence of the antiquity of life. Science 260:640–646
Schopf JW (2004) Earth's earliest biosphere: status of the hunt. In: Eriksson PG, Altermann W, Nelson DR, Mueller WU, Catuneanu O (eds) The Precambrian Earth: tempos and events, Dev Precambr Geol, Elsevier, Amsterdam, pp 516–538

Senko JM, Campbell BS, Henriksen JR, Elshahed MS, Dewers TA, Krumholz LR (2004) Barite deposition resulting from phototrophic sulfide-oxidizing bacterial activity. Geochim Cosmochim Acta 68:773–780

Shapiro R (2007) A simpler origin for life. Sci Am 296:24–31

Shen Y, Buick R, Canfield DE (2001) Isotopic evidence for microbial sulphate reduction in the early Archaean era. Nature 410:77–81

Skinner HCW, Jahren AH (2003) Biomineralization. Treatise Geochem, vol 8, Elsevier, pp 117–184

Smil V (2002) The Earth's biosphere: evolution, dynamics, and change. MIT Press, Cambridge, Mass

Southam G, Saunders JA (2005) The geomicrobiology of ore deposits. Econ Geol 100:1067–1084

Stetter KO (2002) Hyperthermophilic microorganisms. In: Horneck G, Baunstark-Khan C (eds) Astrobiology – the quest for the conditions of life. Springer, Berlin, pp 168–184

Stevens TO, McKinley JP (1995) Lithoautotrophic microbial ecosysystems in deep basaltic aquifers. Science 270:450–454

Stoffers P, Worthington TJ, Schwarz-Schampera U, Hannington,MD, Massoth GJ, Hekinian R, Schimdt M, Lundtsen LJ, Evans LJ, Vaiomo'unga R, Kerby T (2006) Submarine volcanoes and high-temperature hydrothermal venting on the Tonga arc, southwest Pacific. Geology 34:453–456

Suess E, Carson B, Ritger S, Moore JC, Jones M, Kulm LD, Cochrane G (1985) Biological communities at vent sites along subduction zones off Oregon. Bull Biol Soc Wash, Washington DC, 6:475–484

Suess E, Bohrmann G, Greinert J, Lausch E (1999) Flammable ice. Sci Am 281:52–59

Thomas PJ, Hicks RD, Chyba CF, McKay CP (eds) (2006) Comets and the origin of life. Springer, Berlin

Tian F, Toon OB, Pavlov AA, De Sterck H (2005) A hydrogen-rich early Earth atmosphere. Science 308:1014–1017

Trewin NH (1996) The Rhynie cherts: an early Devonian ecosystem preserved by hydrothermal activity. In: Bock GR, Goode JA (eds) Evolution of hydrothermal ecosystems on Earth (and Mars?). Ciba Found Symp 202, John Wiley & Sons, Chichester, pp 131–145

Trudinger PA (1971) Microbes, metals, and minerals. Minerals Sci Engng 3:13–25

Ueno Y, Maruyama S, Isozaki Y, Yurimoto H (2001) Early Archaean (ca. 3.5 Ga) microfossils and ^{13}C depleted carbonaceaous matter in the North Pole area, Western Australia: Field occurrence and geochemistry. In: Nakashima S, Maruyama S, Brack A, Windley BF (eds) Geochemistry and the origin of Life. Universal Acad Press, Tokyo, Japan, pp 203–236

Ueno Y, Yoshioka H, Maruyama S, Isozaki Y (2004) Carbon isotopes and petrography in ~3.5 Ga hydrothermal silica dykes in the North Pole area, Western Australia. Geochim Cosmochim Acta 68:573–589

Ueno Y, Yamada K, Yoshida N, Maruyama S, Isozaki Y (2006) Evidence from fluid inclusions for microbial methanogenesis in the early Archaean era. Nature 440:516–519

Van Dover CI (2000) The ecology of deep sea hydrothermal vents. Princeton University Press, New Jersey

Van Kranendonk MJ (2000) Geology of the North Shaw 1:100 000 sheet. Geol Surv West Aust, 1:100 000 Geol Ser Explan Notes

Van Kranendonk MJ (2006) Volcanic degassing, hydrothermal circulation and the flourishing of early life on Earth: A review of the evidence from c. 3490–3240 Ma rocks of the Pilbara Supergroup, Pilbara Crato, Western Australia. Earth-Sci Rev 74:197–240

Van Kranendonk MJ (2007) A review of the evidence for putative Paleoarchean life in the Pilbara Craton, Western Australia. In: Van Kranendonk MJ, Smithies RU, Bennett VC (eds) Earth's oldest rocks, Develop Precambr Geol 15, Elsevier, Amsterdam, pp 855–878

Van Kranendonk MJ, Hickman AH, Williams IR, Nijman W (2001) Archaean geology of the East Pilbara Granite-Greenstone Terrane, Western Australia; A Field Guide. Geol Surv West Aust, Record 2001/9

Van Kranendonk MJ, Hickman AH, Smithies RH, Nelson DR, Pike G (2002) Geology and tectonic evolution of the Archaean North Pilbara terrain, Pilbara Craton, Western Australia. Econ Geol 97:695–732

Van Kranendonk MJ, Webb GE, Kamber BS (2003) Geological and trace element evidence for a marine sedimentary environment of deposition and biogenicity of 3.45 Ga stromatolitic carbonates in the Pilbara Craton, and support for a reducing Archean ocean. Geobiology 1:91–108

Van Kranendonk MJ, Pirajno F (2004) Geochemistry of metabasalts and hydrothermal alteration zones associated with c. 3.45 chert and barite deposits: implications for the geological setting of the Warrawoona Group, Pilbara Craton, Australia. Geochem Expl, Environ, Analys 4:253–278

van Loon AJ (2005) The needless search for extraterrestrial fossils on Earth. Earth-Sci Rev 68:335–346

Walker JJ, Spear JR, Pace NR (2005) Geobiology of a microbial endolithic community in the Yellowstone geothermal environment. Nature 434:1011–1014

Walter MR (1972) A hot spring analog for the deposiional environment of Precambrian iron formations of the Lake Superior region. Econ Geol 67:965–980

Walter MR, Bauld J, Brock TD (1972) Siliceous algal and bacterial stromatolites in hot spring and geyser effluents of Yellowstone National Park. Science 178:402–405

Walter MR, Buick R, Dunlop JSR (1980) Stromatolites, 3,400-3,500 Myr old from the North Pole area, Western Australia. Nature 284:443–445

Walter MR, DesMarais D, Farmer JD, Hinman NW (1996) Lithofacies and biofacies of Mid-Paleozoic thermal spring deposits in the Drummond Basin, Queensland, Australia. Palaios 11:497–518

Walter MR, Mcloughlin S, Drinnan AN, Farmer JD (1998) Palaeontology of Devonian thermal spring deposits, Drummond Basin, Australia. Alcheringa 22:285–314

Ward PD, Brownlee D (2004) Rare Earth – why complex life is uncommon in the Universe. Copernicus Books, Springer Science, New York

Westall F (2005) The geological context for the origin of life and the mineral signatures of fossil life. In: Gargaud M, Barbier B, Martin H, Reisse J (eds) Lectures in Astrobiology, vol I. Springer, Berlin, pp 195–226

Westall F, de Witt MJ, Dann J, van der Gaast S, de Ronde CEJ, Gernecke D (2001) Early Archean fossil bacteria and biofilms in hydrothermally-influenced sediments from the Barberton greenstone belt, South Africa. Precambr Res 106:93–116

White NC, Wood DG, Lee MC (1989) Epithermal sinters of Paleozoic age in north Queensland, Australia. Geology 17:718–722

Whitehouse MJ, Fedo CM (2007) Searching for Earth's earliest life in southern west Greenalnd – history, current status, and future prospects. In: Van Kranendonk MJ, Smithies RH, Bennett VC (eds) Earth's oldest rocks. Developm Precambr Geol 15. Elsevier, Amsterdam, pp 841–853

Wilcock WSD, Delong EF, Kelley DS, Baross JA, Cary SC (eds) (2004) The subseafloor biosphere at mid-ocean ridges. American Geophysical Union 144, 408p

Woese CR, Kandler O, Wheelis ML (1990) Towards a natural system of organisms. Porposal for the domains Archaea, Bacteria and Eucarya. Proceed Nat Acad Sci, USA 87:4576–4579

Wickramasinghe C (2006) Astrobiology, comets and the origin of life. World Scientific Publishing, Singapore

Yee N, Phoenix V R, Konhausser KO, Benning LG, Ferris FG (2003) The effect of cyanbacteria on silica precipitation at neutral pH: implications for bacterial silicification in geothermal springs. Chem Geol 199:83–90

Zhang CL, Lanoil B (eds) (2004a) Geomicrobiology andbiogeochemistry of gas hydrates and cold seeps. Sp Iss Chem Geol 205
Zhang CL, Lanoil B (2004b) Editorial on Geomicrobiology andbiogeochemistry of gas hydrates and cold seeps. Sp Iss Chem Geol 205:187–194

Chapter 11
Hydrothermal Processes Associated with Meteorite Impacts

11.1 Introduction

The study of asteroid impacts has gained considerable momentum in the last 30 years or so, following the pioneering works of Eugene (Gene) Shoemaker (1928–1997) who, with his wife Carolyn and Edward Chao, discovered shock features diagnostic of very high pressures that can only be attained by hypervelocity impacts. They were instrumental in the recognition by the geological community of asteroidal impacts as a major planetary process. Other pioneers included Robert Dietz (1914–1995) and Richard Grieve, who realised the impact origin of Sudbury, Bevan French, Michael Dence and Dieter Stoffer.

Our planet was subjected to a great meteorite flux between 4.3 and 3.8 Ga during the late heavy bombardment (LHB), when Earth was impacted by no less than 20 000 meteorites larger than 1 km in diameter, 100 meteorites with diameters in excess than 10 km and several planetesimals 20–40 km across (Glikson 1998). Today, geomicrobiology, astrobiology and the study of impact structures have enormously enriched and contributed to our knowledge of the Earth and planets, resulting in teams of scientists from several disciplines working together with geologists. Papers and books that treat the topic of asteroid impacts abound. The reader interested in looking beyond these pages, should consult Melosh (1989), French (1998), Grady et al. (1998), Dressler and Sharpton (1999), Gilmour and Koeberl (2000), Buffetaut and Koeberl (2002) and Koeberl and Henkel (2005). The study of asteroidal impacts has revolutionised our view of planet Earth and the role of impacts as a major factor in the early evolution of Earth and other planets in the solar system and the biological effects on our planet, dramatically exemplified by the Cretaceous/Tertiary (K/T) mass extinction.

Hypervelocity impacts cause melting of the target rocks and form a crater resulting in the conversion of kinetic to thermal energy, which in turn causes thermal perturbations and heat release particularly in the central structural uplifts, which bring near the surface deeper and hotter crust. These thermal effects result in a spectrum of phenomena from partial melting to high-temperature metamorphism and hydrothermal fluid flow. In general, the transformation of kinetic energy into heat will take place mainly at sub-crater levels, where

F. Pirajno, *Hydrothermal Processes and Mineral Systems*,

© Springer Science+Business Media B.V. 2009

hydrothermal circulation would be focussed, although impact-related hydrothermal circulation can extend well below the crater floor to depths of several kilometres (Komor et al. 1988). It is also likely that impact-related hydrothermal fluids can vent at the surface as hot springs and geysers, forming silica-rich deposits (Newsom 1980). The effects of hydrothermal fluid flow would be presumably greatly enhanced if the impact occurs in ocean, where seawater would rush into the heated and fragmented target rocks, as probably was the case for Chicxulub (Goto et al. 2004). The flow of hydrothermal fluids leaves its mark on the rocks through which they pass in the form of new mineral assemblages, with processes that involve cation and H^+ metasomatism and resulting in hydrothermal alteration (see Chapter 2).

In this chapter I discuss hydrothermal and metasomatic processes that have taken place in impact structures, subsequent to the collapse of the transient cavity and the cooling of the melt sheet and melt rocks. Most of what follows is drawn from Pirajno et al. (2003), Pirajno (2005) and Pirajno and Van Kranendonk (2005), particularly for the Australian examples (Section 11.4). The flow of hot aqueous solutions commonly results in the formation of mineral deposits. Therefore, knowledge of post-impact hydrothermal activity is important because it may have resulted in economic mineral deposits. The world-class and widely known Sudbury mineral deposits (Ni, Cu, PGE, Pb, Zn, Au) are perhaps the best and most celebrated expression of mineralisation directly related to a meteorite impact. Several lines of evidence suggest that the giant gold deposits of the Witwatersrand in South Africa may have had an indirect relationship to the large Vredefort impact structure. Both these cases are examined briefly in the sections that follow. Hydrothermal circulation systems associated with impact events have been reported from the Ries (Germany), Puchezh-Katunki (Russia), Jämtland and Lockne (Sweden), Roter Kamm (Namibia), Manson (USA), the above-mentioned Vredefort, Kärdla (Estonia), Sudbury and Haughton (Canada) structures (Newsom et al. 1986; Koeberl et al. 1989; Naumov 1993; Sturkel et al. 1998; Ames et al. 1998; McCarville and Crossey 1996; Grieve and Thierriault 2000; Osinski et al. 2001; Molnár et al. 2001; Puura et al. 2000 2002). Recently, aspects of hydrothermal alteration in the Chicxulub impact structure have been published in Meteoritic and Space Science (Ames et al. 2004; Lüders and Rickers 2004; Zürcher and Kring 2004; Goto et al. 2004).

11.2 Asteroid and Cometary Impacts and Hydrothermal Circulation

Allen et al. (1982) studied hydrothermally altered melt rocks and breccias from twelve impact structures, including Ries, Manicouagan and Sudbury, and suggested possible analogues at Martian impact sites. These authors recorded dominant assemblages consisting of clay minerals, chlorite, mixed layer illite-chlorite,

silica, K-feldspar and zeolites, which they estimate to have formed at low pressures and at temperatures between 100 and 300°C. Commonly, impact-related hydrothermal systems result in the remobilization and deposition of sulphides in breccias or fracture zones. Naumov (2002) provided a detailed account of impact-related hydrothermal processes in three major impact structures: Kara, Popigai and Puchezh-Katunki, briefly introduced below, together with other examples.

In the Ries impact structure, hydrothermal alteration minerals include illite, montmorillonite, analcite, calcite, siderite, K-feldspar, quartz, barite and chlorite (Newsom et al. 1986). The Puchezh-Katunki 80-km diameter impact crater (Russia) is characterised by widespread hydrothermal alteration, mainly concentrated within the central uplift, which is composed of brecciated Archaean basement rocks. At this impact site, Naumov (1993) recognized the following hydrothermal assemblages: (1) chlorite + albite + epidote + calcite, associated with andradite garnet, epidote and prehnite in fractures; (2) prehnite + calcite + pyrite, absence of Ca-Fe silicates; (3) zeolites + apophyllite + calcite + anhydrite + pyrite in vugs and fractures. Masaitis and Naumov (1993) modelled the hydrothermal convection for the Puchezh-Katunki structure and suggested that the fluids originated by infiltration of water from a crater lake towards a lens of hot impact breccia and basement rocks. These fluids would have reached the surface along the uplifted margins. Masaitis and Naumov (1993) proposed three stages of hydrothermal activity: (1) an initial stage, with temperatures in the region of 400–500°C, decreasing downward and outward from the impact site; (2) a main stage, with maximum temperatures of 200–300°C, and fluids circulating at depths of 2.5–4 km; and (3) a final stage, in which circulation is restricted to the uppermost parts of the basement rocks, with temperatures of 150–100°C.

Alkali metasomatism at deep levels is followed by a lower temperature hydrothermal regime, which partially obliterates the alkali-rich rocks, but is best manifested at higher levels, possibly because of downward flow of meteoric water-dominated hydrothermal circulation. A view of this lower temperature regime at higher levels is provided by the central uplift of the Woodleigh structure, where the dominant alteration minerals are phyllosilicates with carbonate overprints. Impact-induced alkali metasomatism and the presence of syenite-like rocks in impact structures may be more common than realised (see Section 11.4.1). Puura et al. (2000, 2002) studied impact-induced K metasomatism in sub-crater basement granitoids for the Kärdla Crater in Estonia. These authors found strong chemical and mineralogical alteration of the sub-crater lithologies. Chemical alteration includes K enrichment and Na and Ca depletion, whereas the mineralogical alteration results in changes in the structural state of the feldspars (related to K enrichment, Na and Ca removal) and decomposition of hornblende to Fe-rich chlorite and quartz. Puura et al. (2000) concluded that these changes took place as a result of post-impact alteration processes, but that the source of K is unknown. However, the authors also pointed out that geochemical studies of impactites indicate selective

mobility of alkalis with loss of K and Na in strongly shocked rocks from large craters. The K and Na lost from shocked rocks could be mobilized, during phases of post-impact hydrothermal action, resulting in the enrichment of the surrounding and/or deeper lithologies. Three possibilities are considered for the selective mobility of alkalis (Puura et al. 2000): (1) impact-induced high temperature hydrothermal system; (2) ultrahigh-temperature and pressure mobilization of fluids; and (3) action of low-temperature post-impact hydrothermal system.

11.2.1 A Working Model

A working model of a hydrothermal system that may develop within, and as a result of meteorite impacts on land is shown in Fig. 11.1. This model schematically shows two stages of the hydrothermal processes, which clearly represent end members of a continuum. In stage 1, hydrothermal fluids are primarily derived from heat supplied by the melt sheet and melt injected into the surrounding target rocks. This is a magmatic-hydrothermal stage during which alkali metasomatism is dominant. This is the stage of highest temperature (probably 500–600°C) in which mineral reactions result in the formation of K-feldspar and/or albite (potassic and sodic metasomatism), resulting in the modification of protoliths to a rock of syenitic affinity. In addition to the alkali metasomatism previously mentioned for the Kärdla structure, impact-related Ca-Na-K metasomatism has also been well-documented at Chicxulub by Zürcher and Kring (2004). These authors reported the occurrence of the same alteration phases as those found in Shoemaker and Yarrabubba (Section 11.4), namely albite, K-feldspar, titanite, diopside-hedenbergite, amphibole, biotite and epidote.

This type of alteration affects the shattered target rocks well below the melt sheet and are best manifested at the lower levels of an impact structure. Progressive cooling of the melt sheet, decaying of the high-temperature magmatic fluid system and inflow of meteoric waters, lead to stage 2. In this lower temperature regime (<500°C), the flow of hydrothermal fluids is dominantly fracture-controlled. Much of the thermal energy for this stage could be provided by the hot rocks of the central uplift. The uplifted central peak is therefore especially affected, as is shown in the Woodleigh structure (Section 11.4.3). Quite possibly, hot springs discharge at surface, within remnants of the crater, and along its walls, with their pathways bearing the signs of the passage of hot solutions, resulting in hydrothermal mineral assemblages that form alteration types like those found in volcanic epithermal systems. These include phyllic, propylitic, argillic, silicification and carbonatisation types including mineral phases such as sericite, chlorite, epidote, calcite, hematite, iron carbonates, and quartz. These alteration types overprint the earlier assemblages of the alkali metasomatic stage. Boiling of fluids in the hot spring system, forms veins of

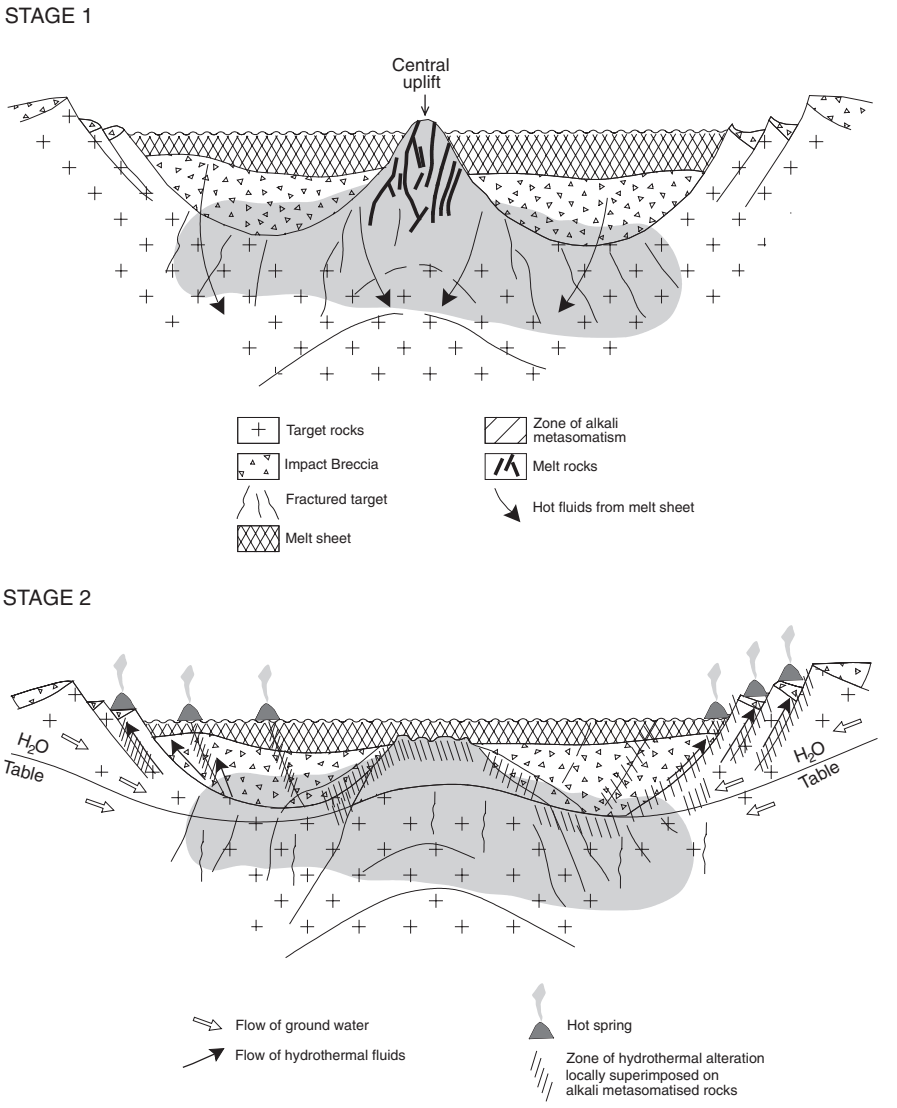


Fig. 11.1 Model of hydrothermal fluid circulation in impact structure; details in text. After Pirajno (2005)

bladed calcite within zones dominated by silicified rocks. This may have been the case at Yarrabubba (Section 11.4.2). Phase separation is potentially a very important mechanism for the precipitation of metal sulphides and gold. The presence of hot springs also constitutes an ideal environment for microbial life, and this too may lead to metal precipitation by biologically mediated processes (Chapter 10).

The activity of a hydrothermal system in impact structures is effectively no different from those formed in magmatic settings, except perhaps in terms of duration. The largest impacts (e.g. Vredefort, Sudbury, Chixulub) would have had hydrothermal systems operating for long periods of time (hundreds of thousands of years; Rowe et al. 2004), whereas hydrothermal activity in smaller impacts is likely to be short-lived. It is estimated that melt pools can provide the heat source necessary to drive hydrothermal circulation systems for some 100 000 years (Kring 1995; McCarville and Crossey 1996). The depth extent of hydrothermal flow is also related to the size of the impact structure. Depths of 2–4.5 km have been recognised by Naumov (1993), whereas a depth of 5 km has been estimated for the 80-km diameter Puchezh-Kantunki impact crater (Pevzner et al. 1992; Zürcher and Kring 2004). In this light, it is also possible that for the larger impacts (megaimpacts; e.g. Vredefort, Sudbury) the thermal effects could spatially extend well beyond the crater's limits, with impact-induced fluids circulating in prexisting fractures and faults in country rocks and around the crater for several kilometres.

11.3 Mineral Deposits and Impact Structures

The inception of impact-induced hydrothermal activity may have important consequences in terms of ore formation or modification of existing mineralisation. There is already a substantial body of evidence to suggest that economically important mineral deposits owe their existence, directly or indirectly, to impact events. A review of economic mineral deposits associated with impact structures can be found in Reimold et al. (2005), who also provided a list of all impact structures that are associated with mineral systems and hydrocarbons. A key paper detailing the economic potential of impact structures is that of Grieve and Masaitis (1994), who classified impact-associated ore deposits, as follows.

Progenetic mineral deposits are those that existed before the impacting event, but subsequently modified during and after the impact. Examples are: (1) the Fe and U ores at the Ternovka structure (age ~375 Ma, 15-18 km diameter) in the Ukraine; (2) U ore at the Carswell structure (age ~115 Ma, 39-km diameter) in Canada; (3) Au and U associated with the Vredefort multi-ringed structure (Section 11.3.3). In Australia, a possible example of redistribution of ore minerals as a result of impact-related hydrothermal fluids is provided by MVT type sulphide deposits around the Shoemaker structure (Pirajno et al. 2003).

S*yngenetic* deposits are those that are formed as a direct consequence of the impact, either during or soon afterwards. They include magmatic type Cu-Ni-PGE and diamonds. The best known example is above-mentioned Sudbury Igneous Complex with its world-class Ni-Cu sulphide deposits (Naldrett 2002). The high pressure of shock metamorphism (greater than 30 GPa) can produce diamonds from pre-existing carbon in the target rocks, such as graphite and coal. Impact diamonds are known from a number of localities. These

include the Kara (68 Ma and a 65 km-diameter) and Popigai (~35.7 Ma and a 100 km-diameter) structures, in Russia; the Ries crater in southern Germany. The Popigai impact-formed diamonds are polycrystalline, not of industrial quality, but they are harder than mantle-derived diamonds (Koeberl et al. 1997). The Ries crater is 24 km in diameter and was formed 15 Ma ago; here the occurrence of diamond and lonsdaleite (a polymorph of diamond) and silicon carbide was reported by Hough et al. (1995). A speculative corollary is that, since most mantle-derived diamonds are known to be approximately 3.3 Ga old (e.g. Phillips et al. 1989), could it be that they may be associated with Eoarchaean mega-impacts?

Epigenetic deposits form as a result of hydrothermal circulation within and around the structure, caused by cooling of impact melt sheets or by related magmatic activity. Examples of hydrothermal ores are numerous. They include Pb, Zn, Ag, Ba at Siljian in Sweden (Johansson 1984), Serpent Mound, USA, and Cu, Zn, Pb, Au at Vermilion in the Sudbury structure. Always in the Sudbury structure, a number of Zn-Cu-Pb massive sulphides deposits can be ascribed to post-impact hydrothermal activity (see Naldrett 2002 and references therein; Golightly 1984). Hildebrand and Pilkington (2002) on the basis of seismic and aeromagnetic data suggested that the floor of the Chicxulub crater may contain exhalative sulphide deposits and calculated a possible metalliferous concentration of 50 Mt. It is interesting to note that Zürcher and Kring (2004) likened the Chicxulub hydrothermal system to that which is characteristic of Fe oxide-Cu-Au-REE deposits, such as Olympic Dam in South Australia.

Included in epigenetic deposits are hydrocarbon occurrences related to the formation of impact basins with restricted sedimentation. This is because impact events induce considerable fracturing, thus enhancing the permeability of the target rocks, this may result in the formation of oil and gas traps. The Ames buried structure (~450 Ma, 14-km diameter in Oklahoma, USA) contains important reserves of hydrocarbons (Carpenter and Carlson 1992; Donofrio 1998). The 25 km-diameter Steen River impact structure in Canada has an estimated 3 billion barrels of oil along the rims of the structure (Grieve 2003). Chicxulub offshore has reserves of 30 billion barrels. In Queensland, Australia, the 55 km-diameter Tookoonooka structure also contains hydrocarbons (Gorter 1998). Impact structures associated with productive oil fields are found in the Cretaceous Avak (Alaska) and the late Cambrian Newporte structures (Kirschner et al. 1992; Forsman et al. 1996).

In the sections that follow, I describe examples of epigenetic and progenetic deposits, in which the hydrothermal activity is linked with impact events.

11.3.1 The Sudbury Hydrothermal System

Sudbury (Ontario, Canada) is an 1850 Ma deformed impact structure whose original diameter was about 140 km (Melosh 1989; other estimates consider diameters of 200–250 km, Dressler and Sharpton 1999). Sudbury or more accurately the Sudbury Igneous Complex is probably best known for its mineral

wealth, which includes world-class Ni-Cu ores as well as a number of Zn-Cu-Pb massive sulphides deposits (see Naldrett 2002 and references therein; Golightly 1984).

Ames et al. (1998) recognised regional-scale semi-conformable hydrothermal alteration in the Sudbury structure, more specifically in the Onaping Formation, which represents crater-fill rocks (Fig. 11.2). This alteration is pervasive and consists of silicification, albitisation, chloritisation, calcitisation and complex phases of feldspathisation (microcline, hyalophane and celsian). The authors linked this alteration to a basin-wide hydrothermal circulation, which resulted in the formation of the above-mentioned Zn-Cu-Pb massive sulphide deposits (Fig. 11.2). On the basis of geochronological data Ames et al. (1998) argued that this extensive alteration lasted from tens to hundreds of thousand years and is related to conductive heat loss of the Sudbury Igneous Complex. The authors concluded that this comparatively short-lived impact-induced hydrothermal system resulted in the alteration zones and mineralisation similar to the VMS of volcanic terranes.

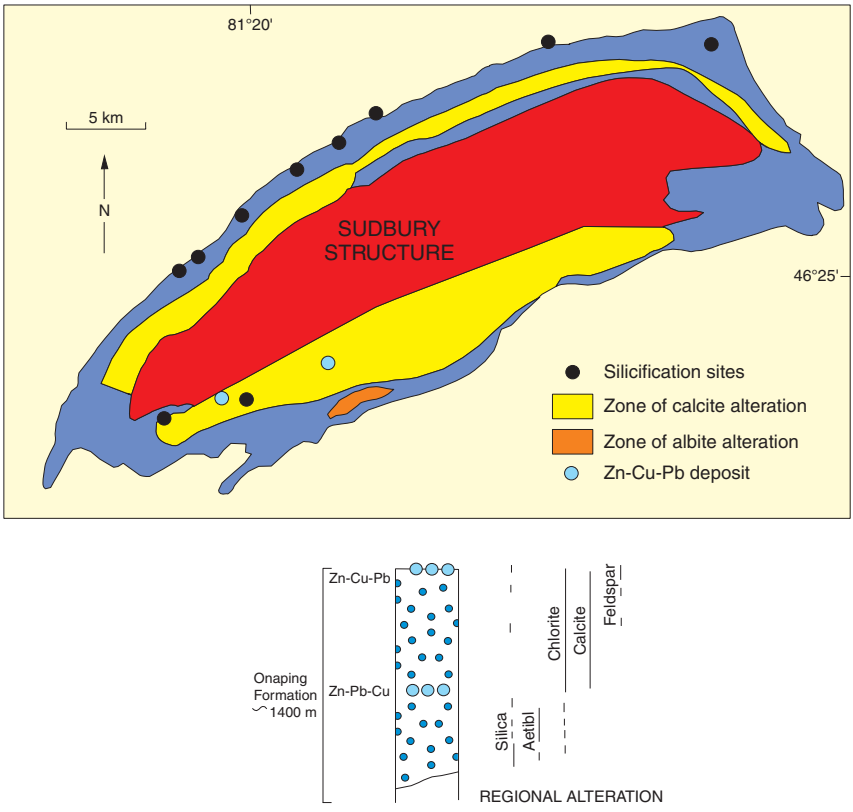


Fig. 11.2 Outline of the Sudbury impact structure showing distribution of mineral deposits and alteration zones. After Molnár et al. (2001)

Molnár et al. (2001), based on a systematic fluid inclusion study of samples along the contacts of the Sudbury Igneous Complex with the North Range footwall rocks, recognised that post-impact hydrothermal processes were responsible for vein type Cu-Ni-PGE mineralisation. These authors established at least three stages of hydrothermal activity. Early stage high temperature (> 400°C) fluids, resulted in hydrothermal assemblages of epidote-quartz-actinolite-chlorite, which form vein selvages, where Cu, Ni and PGE occur as veins and disseminations. A second stage of hydrothermal activity is characterised by carbonic-aqueous fluids (at least two coexisting fluids; 20–26 wt% and 6–12 wt% NaCl equivalent), which caused the formation of carbonate-epidote-actinolite-chlorite veins, overprinting the earlier assemblage. These fluids also precipitated Cu, Ni, Bi sulphides and native silver. Fluid inclusions indicate that these fluids boiled at about 300–350°C, during uplift from 6 to 3–4 km. A final stage of hydrothermal activity was dominated by aqueous solutions (20–40 wt% salinity) and with temperatures of between 150 and 250°C. These late fluids were channelled along fractures more or less parallel to the Sudbury Igneous Complex and footwall contacts. They formed late veinlets containing chalcopyrite-epidote-quartz-chlorite. However, Molnár et al. (2001) related this late stage hydrothermal activity to a tectonothermal event linked to the emplacement of dykes at 1.24 Ga.

11.3.2 The Lockne Impact Structure

This ~455 Ma structure in central Sweden was formed in a marine environment, with seawater depths of about 200 m, with the final crater being at a depth of 500 m (Sturkel et al. 1998). The 13.5-km diameter Lockne structure provides an excellent example of an impact structure in which hydrothermal processes took place in a marine setting and with seawater as the source of the fluids.

Sturkel et al. (1998) conducted a comprehensive study of fluid inclusions and stable isotopes from drill core samples. The Lockne impact breccia and the fractured basement contain cavities filled with hydrothermal minerals that include calcite, quartz, chalcopyrite, pyrite, galena and zeolites, as well as solid bitumen. At least three phases of fluid activity are recognised in fluid inclusion trapped in quartz crystals (phase 1), calcite and sulphides (phase 2) and late calcite (phase 3). Gaseous inclusions in quartz consist of CH_4 and other hydrocarbons, whereas aqueous inclusions in sulphides and calcite contain $CaCl_2$-NaCl-H_2O, with salinities ranging from 28.8 to 20.5 wt % NaCl equivalent. Temperatures of liquid–vapour homogenistation range from 77 to 218°C, with most values between 100 and 180°C. Fluid inclusion studies of samples collected from outcrops also showed the presence of $CaCl_2$-NaCl-H_2O-rich solutions, which homogenise between 136 and 169°C. The presence of CH_4 in the fluid inclusions is interpreted by the authors as the result of organic-rich clay in the Cambrian shales of the target which were thermally altered and decomposed by impact-heated basement rocks to form hydrocarbons and CH_4-rih

fluids. Sulphides have $\delta^{34}S$ values ranging from +1 to +5.5%. The authors suggested that the S was largely derived from the fractured mafic volcanic basement. $\delta^{13}C$ determinations for the hydrothermal calcite yielded values of –2 to 14‰, suggestive of a mixed marine and organic source. Sturkel et al. (1998) concluded that the impact-induced hydrothermal convection system of the Lockne structure was short lived and low-temperature, but nevertheless capable of generating sulphides and hydrocarbons.

Uranium-Th-rich bitumen nodules are present in the matrix of finely crushed granitic rocks of the Lockne structure (Lindgren et al. 2007). The U-Th-rich bitumen nodules would form from coatings of hydrocarbons around radioactive minerals. The radiation from the minerals breaks the C-H bonds of the hydrocarbons, releasing H and C, resulting, down the line, in complex organic polymers (Lindgren et al. 2007). The nodules are from 50 to 400 μm across and are rimmed by calcite. The U-Th phase occurs as small inclusions in the bitumen, other minerals are thorite, coffinite, uraninite and monazite. Lindgren et al. (2007) interpreted this unusual occurrence as due to a post-impact hydrothermal system that allows circulation of fluids in the fractured and brecciated target rocks, where organic molecules are polymerised by interaction with pre-existing U-Th radioactive minerals.

11.3.3 The Vredefort Meteorite Impact and the Case for Witwatersrand Gold

The greatest concentration of Au in the world is in the Witwatersand Basin (Witwatersrand Supergroup), South Africa (Fig. 11.3), where in the order of 50 000 tonnes of Au have been mined between 1886 and 2004, or about 40% of all the gold mined in recorded history (Frimmel et al. 2005). Overviews of the geology of the Witwatersrand are provided by Frimmel et al. (2005) and Law and Phillips (2005). The Witwatersrand Supergroup is subdivided into the West Rand (older) and Central Rand (younger) Groups, overlying the Dominion Group and all lying on a basement of Archaean granite-greenstone rocks (Kaapvaal Craton). The Witwatersrand rocks are predominantly clastic sediments, which include the ore-bearing fluvial conglomerates. The maximum ages of the West Rand and Central Rand Groups, provided by detrital zircons are 2914±8 Ma and 2902±13 Ma, respectively. Xenotime dating yielded a minimum age of 2780±3 Ma for the Central Rand Group. The exceptional Au endownment of the Witwatersrand goldfields has fascinated geologists for well over a century. Ideas on the origin of the "Wits gold" range the full span from placer (alluvial, lacustrine delta and even marine), to placer subsequently modified through hydrothermal circulation (modified placer model) to purely hydrothermal and other genetic models. Enter the catastrophic event of a meteorite impact to add to the complicated and fascinating geological history of this part of the world, where the largest layered intrusion with the largest Cr and Pt deposits in the world and the basin with

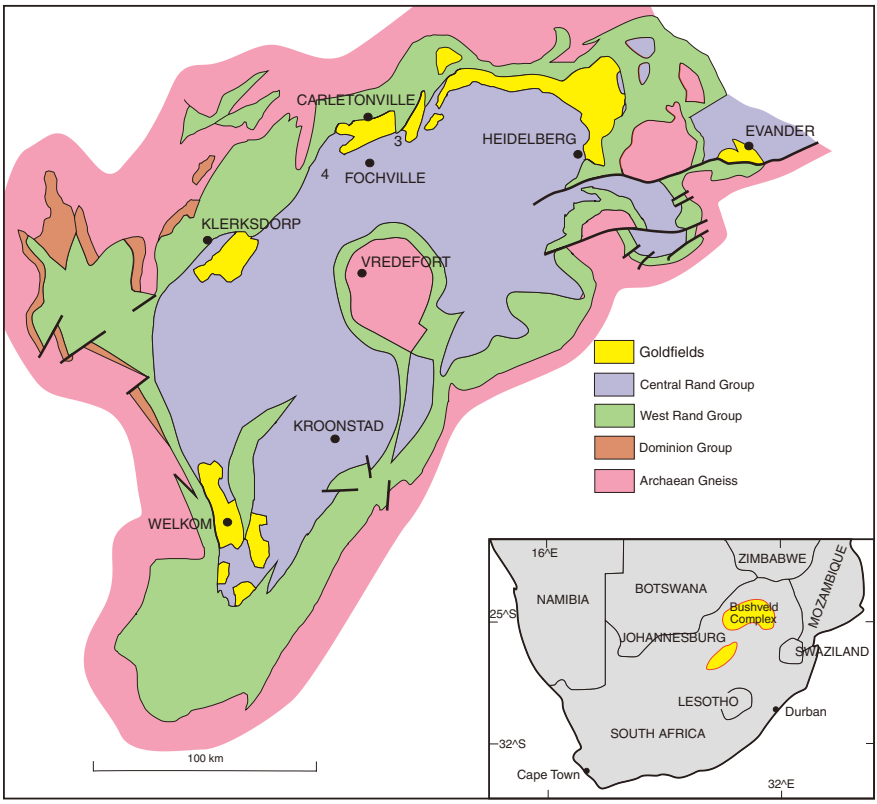


Fig. 11.3 Simplified map of the gold fields of the Witwatersrand Basin (South Africa) and position of the Vredefort Dome. After Reimold et al. (1999)

largest Au accumulation in the world occur in the same region: the Kaapvaal Craton.

The Witwatersrand goldfield is generally considered a palaeoplacer deposit, based on evidence provided by the presence of detrital uraninite and pyrite (buckshot pyrite), studies of detrital zircons showing that detrital gold and pyrite have pre-sedimentation ages and the fact that most gold is associated with fluvial conglomerates. However, Au is also found redistributed in micro-fractures and associated with hydrothermal minerals and this has been taken to signify that the original placers were subsequently modified by hydrothermal activity (modified palaeoplacer model). Frimmel and co-workers suggested that the uniqueness of the Witwatersrand goldfields is linked to strong reworking of sediments, shed from rapidly exhumed greenstone belts containing orogenic and perhaps also porphyry-epithermal systems (as suggested by the presence of blue opalescent quartz in the conglomerates), and by braided rivers and streams in a region that must have been devoid of vegetation and with intense chemical weathering under an acidic and anoxic Archaean atmosphere. The palaeoplacer

model was challenged by Neil Phillips in a series of papers published from 1987 onward (e. g. Phillips 1987, 1988), presenting arguments for a role of metamorphic fluids in the genesis of the Au mienralisation. Law and Phillips (2005) reiterated the viability of the hydrothermal model pointing out that regional metamorphism with peak temperatures of 300–400°C, generated mineral assemblages including pyrophyllite, chloritoid, chlorite, muscovite and pyrite and that this metamorphism extended for up to 300 km around the basin margins. Furthermore, the extent of this regional metamorphism coincides with the distribution of the Au mineralisation. Hydrothermal CO_2-H_2S aqueous fluids carrying Au would have been introduced along thrust faults and controlled by bedding-parallel fracture networks and unconformity surfaces. Critical to the hydrothermal replacement model is the timing of the metamorphism and associated hydrothermal alteration. Law and Phillips (2005) considered the thermal effects of the 2.05 Ga Bushveld Igneous Complex and of the 2.02 Ga Vredefort Dome, as possible candidates for Au remobilisation in the Witwatersrand Basin. In addition, due consideration should also be given to the heat generated by the 2.7 Ga Ventersdorp igneous province (Ventersdorp Supergroup; an 8 km thick succession of dominantly sub-aerially erupted tholeiitic basalts, komatiites, andesites and pyroclastics; see Pirajno (2000) and references cited therein).

The ~2020 Ma Vredefort Dome in South Africa is an 80 km-wide central uplift of a large impact structure with a possible original diameter of 300 km. Remarkably, and perhaps not coincidentally, the Vredefort structure is at the centre of the Witwatersrand Basin (Figs. 11.3 and 11.4). Reimold (1995), Reimold and Gibson (1999), Gibson amd Reimold (2001) have described the impact origin of the Vredefort structure, which is one of the largest and the

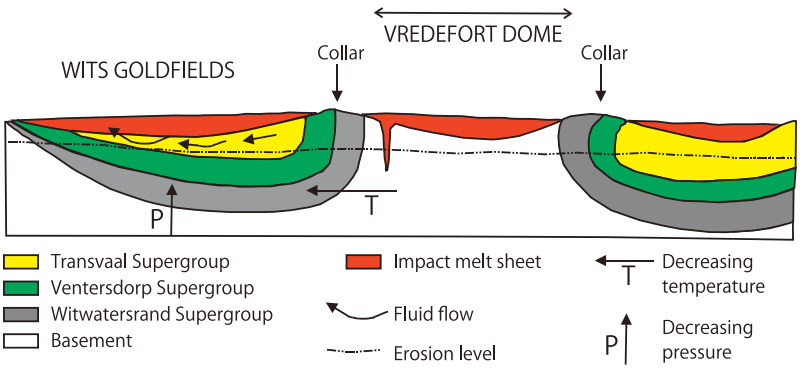


Fig. 11.4 Idealised cross-section of the Witwatersrand Basin and Vredefort Dome, with hydrothermal fluid flow generated by the impact event. Heat from the overlying melt sheet and the hot central uplift (Vredefort Dome) powered the circulation of hydrothermal fluids. The highest shock pressures and temperatures were in the central uplift, decreasing away from it, as shown by the arrows. After Reimold et al. (2005). See also Fig. 11.1

oldest known terrestrial impact structure. An excellent and well-illustrated book on the Vredefort structure was published by Reimold and Gibson (2005). The core of the Dome consists of pre 3.1 Ga granitic and gneissic rocks, supracrustals and mafic rocks. These are further subdivided into an inner zone of leucogneisses (Inlandsee Leucogranofels) and an outer zone of granitic rocks. The central uplift of the Dome represents rocks of the upper and mid crust. The core is surrounded by collars of rocks of the Transvaal, Ventersdorp and Witwatersrand Supergroups, These volcano-sedimentary successions are nearly vertical or overturned, and form a regional rim synclinorium around the Dome. In the core of the synclinorium is the mafic-ultramafic Losberg Complex, whereas alkali and basic igneous complexes are present near and along the contact between the Ventersdorp and Transvaal Supergroups. Rocks around the Vredefort Dome are metamorphosed to lower greenschist facies (about 350°C and 2–3 kbar). The metamorphic grade increases towards the dome, so that the corresponding greenschist, amphibolite and granulite facies are concentrically arranged around it.

The greenschist facies zone, in the outer collar pelites of the Transvaal Supergroup, is characterised by chloritoid, biotite, chlorite and muscovite. The amphibolite facies zone lies between the rocks of the upturned collar and the core of the Dome. The collar rocks include pelite, quartzite, and banded iron-formations of the Witwatersrand Supergroup, and basaltic lavas of the Dominion Group and the Ventersdorp Supergroup. Amphibolite facies minerals are: biotite, muscovite, chlorite, cordierite, andalusite, garnet and staurolite, all of which form various assemblages, depending on the composition of the precursor material. In the core, which is made up of Archaean rocks, mafic xenoliths contain an upper amphibolite facies assemblage, consisting of hornblende + biotite + plagioclase + quartz. The granulite facies zone is between the Outer Granite Gneiss and the Inlandsee Leucogranofels. This zone is poorly defined, due to the intense structural disruption caused by the impact event. Nevertheless, Gibson and Stevens (1998) recognised within pelitic stromatic migmatites, coarse-grained garnet, cordierite and orthopyroxene. In mafic rocks, the assemblage that characterises the granulite facies is represented by clinopyroxene + hornblende + plagioclase + magnetite ± orthopyroxene. Although, the high-grade metamorphic assemblages detailed above were affected by a post-impact retrograde event, Gibson and Stevens (1998) were able to filter out retrograde assemblages, and recognised peak metamorphic reactions, which define an anticlockwise P-T path for the amphibolite facies, with peak temperatures of around 570–600°C at pressures of 4–4.5 kbar. The anticlockwise P-T path for granulite facies rocks is estimated to have reached peak temperatures in excess of 900°C, marking the transition from spinel + quartz to garnet + sillimanite, at pressures of 4–5 kbar. Textural evidence suggests that metamorphic peak conditions occurred prior to the impact event, although current geochronological data are unable to distinguish between the two events (U-Pb zircon age of 2017±5 Ma in granulite facies rocks, and 2023±4 Ma for the impact event). Nevertheless, estimates of

pre- and post-impact geothermal gradients indicate that these had elevated values. The pre-impact prograde metamorphism of the Vredefort Dome could be related to the emplacement of the Bushveld Igneous Complex at about 2.05–2.06 Ga, which predated the impact by approximately 30 Ma.

Thus, the Witwatersrand was subjected to at least two important metamorphic-hydrothermal events. One is pre-impact, as discussed above and documented by Phillips and co-workers, the other is post-impact with metamorphic grades decreasing away from the Vredefort Dome. Grieve and Masaitis (1994) suggested that the Witwatersrand Au-U ores, which are distributed in a semicircular fashion around the Vredefort structure, owe their preservation and present-day exposure, to the downdropped annular ring away from the central uplifted core. Reimold et al. (1999) carried out petrographic and geochemical studies of the pseudotachylite breccias in the fault zones of the Witwatersrand Basin, where they are associated with gold and uranium mineralisation. These pseudotachylite breccias are related to the Vredefort impact event and were found to have acted as major channels for hydrothermal fluids that resulted in the remobilisation of Au, U and base metals along the fault zones. Along these lines, Hayward et al. (2003) suggested that the Vredefort impact had a direct influence on the distribution of the Witwatersrand gold mineralisation. These authors contended that Vredefort-related post-impact metamorphism, driven by the heat energy of the melt sheet and the uplift of deep crustal rocks, caused the hydrothermal remobilisation of the gold, at least on a small scale, along late brittle fractures in sulphides, quartz and zircons, whereas the Au is associated with prograde chlorite.

In conclusion, the Witwatersrand Au mineral system is of the progenetic type in the classification of Grieve and Masaitis (1994) and its preservation was largely due to the Vredefort impact. Whereas a post-impact hydrothermal overprint of the Witwatersrand rocks is yet to be proven, there are indications of hydrothermal activity at about 2.0 Ga (e. g. Gibson and Reimold 1999). At least two thermal events are recognised in the Vredefort Dome. The first is linked with the Bushveld magmatism at around 2.06 Ga, causing greenschist facies metamorphism. The second, centered on the Dome and was caused by the uplift of hot rocks, due to the impact's shock wave. This thermal event may have attained temperatures ranging from 1400 to 1000°C in the Dome and of 300–500°C in the Witwatersrand rocks (Reimold et al. 2005). Hydrothermal circulation associated with this event extended to the areas of Au mineralisation on the northwestern margin of the Basin. There is evidence that some ore textures in the Witwatersrand Au were formed during post-impact times, such as widespread brittle deformation, pseudotachylite breccias and Au remobilisation (Reimold et al. 2005 and references cited therein). It is envisaged that the high temperatures in the central uplift and the region of the surrounding collar, powered hydrothermal circulation that extended throughout the Witwatersrand Supergroup, resulting in the redistribution of Au (Fig. 11.4).

11.4 Australian Examples of Impact-Related Hydrothermal Activity

In the following I describe three Australian impact structures, which exhibit evidence of post-impact hydrothermal fluid flow, namely the Shoemaker structure (Pirajno 2002; Pirajno et al. 2003), the recently discovered Woodleigh (Mory et al. 2000, 2001) and Yarrabubba structures (Macdonald et al. 2003) (Fig. 11.5). Petrographic observations of altered impactites from Shoemaker, Woodleigh and Yarrabubba allow some insights into complex but widespread hydrothermal and metasomatic processes that are associated with meteorite impacts on land. The present day outcrops of these three structures represent levels of exposure ranging from deep (Yarrabubba, Shoemaker) to nearer the surface (Woodleigh). Woodleigh is a buried structure but, as suggested from the interpretation of geophysical data (Iasky et al. 2001), its level could be higher than the other two. Assuming that this is correct then a generalised sequence of time-space alteration events can be reconstructed. At the deepest level (Yarrabubba and Shoemaker), complete replacement of a granitic protolith takes place by processes of alkali metasomatism, similar to magmatic-hydrothermal

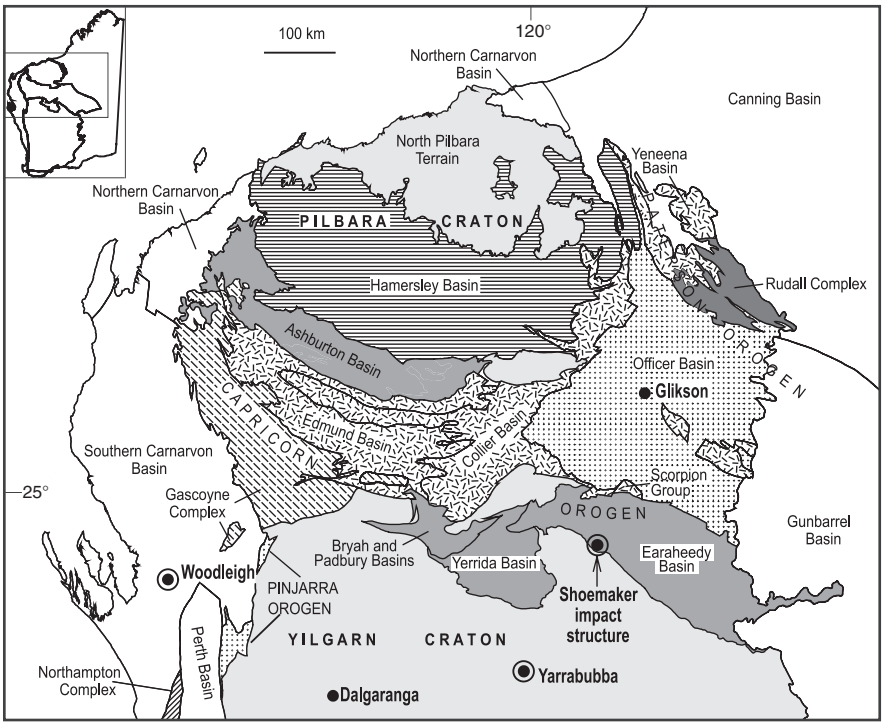


Fig. 11.5 Location of three major impact structures in Western Australia: Shoemaker, Yarrabubba and Woodleigh

systems associated with anorogenic granite systems (Chapter 4), resulting in rocks of syenitic appearance. Alkali metasomatism at deep levels is followed by a lower temperature hydrothermal regime, which partially obliterates the alkali rocks, but is best manifested at higher levels, probably because of downward flow of the hydrothermal circulation. A view of this lower temperature regime at higher levels is provided by the central uplift of the Woodleigh structure, where the dominant alteration minerals are phyllosilicates with carbonate overprints.

11.4.1 Shoemaker Impact Structure

The Shoemaker impact structure, with a diameter of about 30 km, is located on the southern edge of the Palaeoproterozoic Earaheedy Basin, which overlies the northern margin of the Archaean Yilgarn Craton (Fig. 11.5; see also Fig. 8.43). Details of the geology and geochemistry of the Shoemaker structure are provided in Pirajno (2002) and Pirajno et al. (2003). The structure is topographically well-defined by two concentric rings of low hills that interrupt the continuity of the west-northwest-trending Frere Range. The target rocks consist of strata that are shallowly dipping to the northeast (about 10–15°), including essentially undeformed and unmetamorphosed sedimentary rocks of the Earaheedy Group, overlying Archaean granite-greenstone basement of the Yilgarn Craton. Basement granitic rocks are only exposed within the eastern part of the central structure, on the inside of the inner ring of the Shoemaker impact structure. These granitic rocks are grouped under the name of Teague Granite. The central and the western parts of the inner structure are entirely covered by Quaternary lake sediments and sand dunes (Fig. 11.6). However, aeromagnetic data indicate that granitic rocks (possibly monzogranite) and greenstone rocks are present beneath these surficial deposits, representing the northern continuation of the Yilgarn Craton beneath the sedimentary cover of the Earaheedy Basin (Chapter 8). The presence of diagnostic impact indicators, suggest that granitic and greenstone rocks form an impact-induced central structural uplift and possibly the basement core of the original crater. This central uplift has a diameter of about 12 km. The eastern side of the structural uplift is characterized by high total magnetic intensity (TMI), hydrothermal alteration and the only exposures of the granitic rocks (Teague Granite). The TMI pattern suggests not only that the upper parts of the original impact structure were eroded away, but also that the entire structure is probably tilted towards the east.

The age of the Shoemaker impact is not resolved, because of thermal and tectonic resetting of the isotopic systems of the target rocks at 1670–1620 Ma (reactivation of the Capricorn Orogen; Tyler 2005), 1076 Ma (age of a large igneous province in the region; Wingate et al. 2004) and ~550 Ma (age of the 560 Ma Petermann Orogeny; Scrimgeour et al. 1999). The magmatic age of the Teague Granite is Archaean (2648 ± 8 Ma; Nelson 1999), which is within the range of other granitic rocks in the Yilgarn Craton (Smithies and Champion

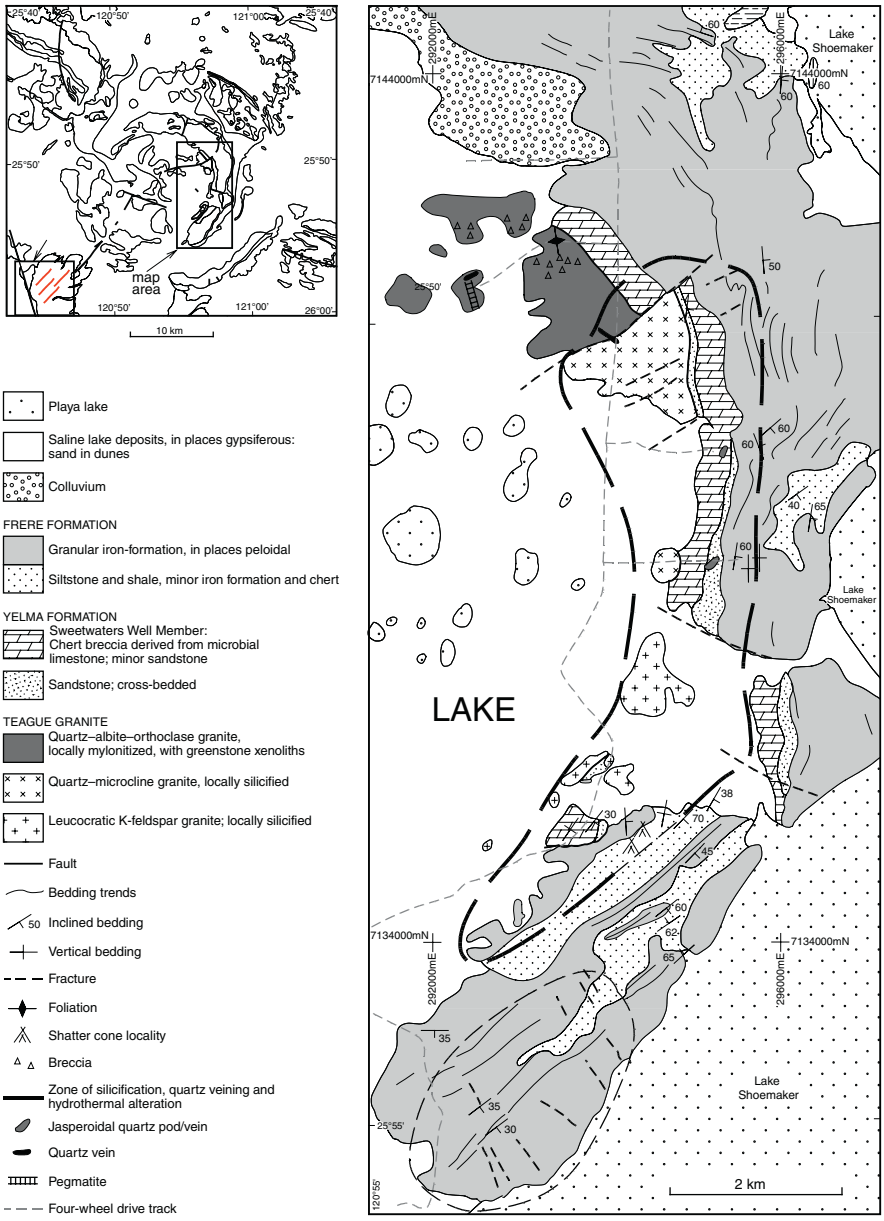


Fig. 11.6 Simplified geological map of the eastern inner ring of the Shoemaker structure, showing the extent of hydrothermal alteration, silica pods and shatter cone localities. Inset shows full extent of the impact structure; the smaller square in the bottom left corner of the inset shows northeast trending quartz veins, which were formed as a result of impact-related hydrothermal activity. After Pirajno (2002)

1999). Bunting et al. (1980) obtained two whole-rock Rb-Sr isochron ages of 1630 and 1260 Ma from samples Teague Granite. Pirajno et al. (2003) reported K-Ar and $^{39}Ar/^{40}Ar$ determinations on K-feldspar and illite-smectite separates also from the Teague Granite. The $^{39}Ar/^{40}Ar$ system yielded unreliable results, only providing broad constraints as to a maximum age (<1300 Ma). The K-Ar system gave two ages: 694±25 Ma and 568±20 Ma for K-feldspar and illite-smectite separates, respectively. It was concluded that the 568±20 Ma K-Ar age determined on illite could represent either resetting due to the Petermann Orogeny, or the formation of illite as a result of post-impact hydrothermal activity.

11.4.1.1 Hydrothermal Alteration

In the Shoemaker impact structure the effects of impact energy-induced hydrothermal circulation within the impact aureole are evident in the Teague Granite and in the sedimentary rocks of the Yelma and Frere formations (Earaheedy Group) exposed in the eastern inner ring. The extent of the hydrothermal alteration in the eastern rim of the structure is shown in Fig. 11.6. Outcrops of Teague Granite in the east and southeast are fractured, hydrothermally altered and partially to pervasively silicified. The rocks of the Teague Granite were studied as part of a regional investigation of felsic alkaline rocks of the Yilgarn Craton by Johnson (1991), who concluded that the granitic rocks that outcrop in the Shoemaker structure were modified by alkali metasomatism resulting in a granitoid of syenitic composition. Johnson's conclusion was confirmed in subsequent studies (Pirajno and Glikson 1998; Pirajno 2002; Pirajno et al. 2003), in which the Teague Granite was subdivided into three units: syenite, quartz syenite and leucocratic alkali feldspar granite.

The syenite is medium-grained and pink to brick-red in colour, and it contains up to 55% orthoclase phenocrysts and up to 15% zoned alkali pyroxene (sodic hedenbergite or aegirine-augite), with albite (~25%) as small grains forming a groundmass. Accessories include green fibrous amphibole, zircon and andradite garnet. The quartz-syenite is also medium-grained, pink to brick-red in colour, fractured and characterized by a distinct polygonal and granoblastic texture, and is transitional to the syenite. This rock is dominated by euhedral to subhedral albite and quartz, roughly in equal proportions, overprinted by perthitic microcline crystals. Accessory minerals include alkali pyroxene (aegirine-augite or sodic hedenbergite), actinolite-tremolite, zircon and titanite. The leucocratic alkali feldspar granite is coarse- to medium-grained, locally brecciated, and consists an assemblage quartz + K-feldspar (microcline) ± albite ± biotite ± sericite. Where it is least altered, it contains about 30% by volume quartz, 40% albite and 30% K-feldspar. Generally, this granitic rock has a cataclastic to mylonitic fabric and/or brecciated texture. Unlike the syenitic rocks, the overall texture of the leucocratic granite is distinctly cataclastic. This cataclastic deformation suggests that this type of Teague Granite is a remnant of an original Archaean, which underwent deformation during the impact event.

The leucocratic alkali feldspar granite is probably the result of stages of silicification of the Teague Granite. This silicification was in places pervasive, whereby the granitic rock is almost entirely replaced by quartz (silica flooding). In places, fibrous amphibole (actinolite-tremolite) infills microfractures in the rock and in a network of cracks in andradite garnet crystals that are locally present in the Teague Granite. Andradite garnets have also been found in hydrothermally altered rocks in the Manson impact structure for which a reaction of the type given below is postulated (McCarville and Crossey 1996):

$$3Ca_2{}^{+} + 2Fe_3{}^{+} + 3H_4SiO_4 + O_2 \rightarrow \underset{\text{andradite}}{Ca_3Fe_2Si3O_{12}} + 12H^{+}$$

Greenstone enclaves in the Teague Granite are cut by quartz-albite veinlets, associated with selvages of diopside. All these features are evidence that hydrothermal minerals were precipitated during phases of post-impact hydrothermal activity. Some of the mineral phases associated with this hydrothermal activity are illustrated in Fig. 11.7.

A tentative paragenetic sequence based on textural relationships and assuming that the mineral assemblages observed, replaced those of an original granite (monzogranite?) is shown in Fig. 11.8. The three columns in Fig. 11.8 indicate mineral assemblages that are present in the Teague Granite and in greenstone xenoliths within it. It is not known whether or not these represent different protolith compositions. It can be concluded, however, that the protolith(s) was completely modified by an early Na-K-Ca metasomatic processes, followed by hydrous alteration with deposition of silica and phyllosilicate phases.

The petrography and overall chemistry of the Teague Granite shows that it is of syenitic affinity and alkaline composition, with the mineral assemblages and textural relationships suggesting that it is derived from alkali metasomatism of a precursor granitoid (Johnson 1991; Pirajno 2002). The syenitic rocks of the Teague Granite are strongly enriched in Na_2O, K_2O, Rb, Sr, Y, Zr, Nb, Ba, and REE compared to high-Ca granite and alkaline rocks of the Yilgarn Craton. The REE patterns of the Teague Granite are similar to the average alkaline rocks of the Yilgarn Craton (Witt and Davy 1997). However, the syenite is enriched in REE by almost one order of magnitude compared to the average Yilgarn alkaline rock, whereas the leucocratic alkali granite shows REE depletion. The quartz syenite is close to the average Yilgarn syenite (Witt and\ Davy 1997). The strong REE enrichment of the Teague Granite syenite, compared to average Yilgarn Craton high-Ca granite, confirms that the precursor granitoid was modified by alkali alteration.

Pervasive silicification affected rocks of the Yelma Formation (Sweetwaters Well Member), whereas the granular iron formation rocks of the Frere Formation exhibit cross-cutting quartz veining and are partially silicified. In the same area, pods of chert and jasperoidal quartz are present along the eastern margin of the central uplift (Fig. 11.6). The chert material consists mainly of brecciated microcrystalline quartz cemented by chalcedonic quartz. Open spaces are filled

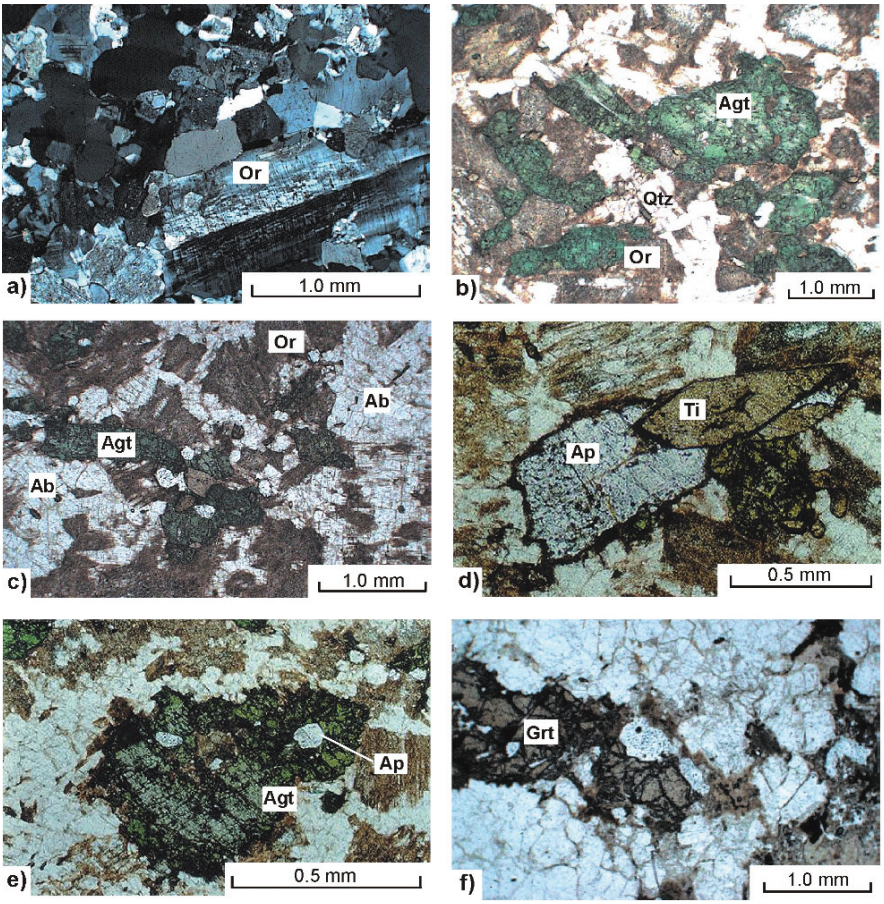


Fig. 11.7 Photomicrographs showing mineralogical assemblages of the Teague Granite (syenite): (**a**) orthoclase (Or) phenocryst in a matrix of quartz-albite; (**b**) orthoclase (Or), aegirine-augite (Agt) and quartz (Qtz); (**c**) orthoclase (Or), aegirine-augite (Agt) and albite (Ab) assemblage; (**d**) apatite (Ap) and titanite (Ti) crsytals; (**e**) aegirine-augite crystal (Agt) with apatite (Ap) inclusion; (**f**) garnet (Grt) crystal associated with a quartz-albite assemblage. b, c, d, e and f in plane polarized light, a with crossed polars. After Pirajno (2002)

with euhedral quartz crystals. These chert pods are interpreted to have formed by precipitation from hydrothermal fluids that circulated along faults and fractures in the eastern sector of Shoemaker impact structure.

To the southwest of Shoemaker impact structure, a number of northeast-trending milky white quartz veins are associated with and parallel to northeast and north-northeast-trending fractures in hornblende quartz-monzonite granite (see inset of Fig. 11.6). The attitude of the veins and associated fractures suggests a pattern that converges towards the centre of Shoemaker impact structure. The quartz veins post-date the hornblende quartz-monzonite that

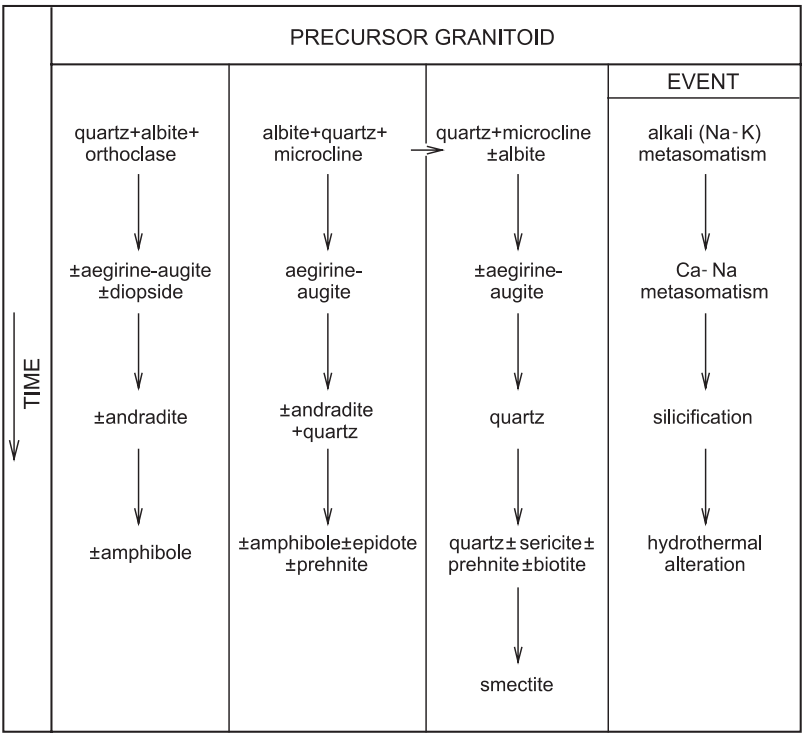


Fig. 11.8 Mineral assemblages and tentative paragenetic sequence of the Teague Granite. After Pirajno (2002)

was emplaced at 2664 ± 4 Ma (Nelson 1999) and again are evidence of unusual hydrothermal activity in the area. Other Archaean granitic rocks in the region do not display the same intensity and regular pattern of quartz veins and fractures. It is therefore concluded that the northeast-trending fractures are impact-related and that their local infilling with quartz may have resulted from impact-induced circulation of hydrothermal fluids.

It is likely that the meteorite impact that created the Shoemaker impact structure formed a melt sheet which, together with impact-released heat in the central uplift, gave rise to a hydrothermal convection system, within and around the central uplift zone. The melt sheet would have acted as a magma-like heat source within the crater structure and would have formed several hot springs in the crater and surrounding areas. Fluid channels and degassing pipes have been reported from the Ries impact crater in Germany (Newsom et al. 1986). Hydrothermal pods are present in the annular structures associated with the Haughton impact structure in Canada that has been interpreted as hydrothermal pipe structures (Osinski et al. 2001). Similarly, the pods of quartz-jasperoidal material that are present along structural breaks in the eastern rim of the Shoemaker impact structure may the eroded remnants of fluid channels that fed thermal springs.

11.4.2 Yarrabubba Impact Structure

The Yarrabubba impact structure, a recent discovery (Macdonald et al. 2003), is situated about 100 km southeast of Meekatharra in Western Australia in Archaean granite-greenstone rocks of the Yilgarn Craton (Fig. 11.5). The structure is highly eroded and no readily visible topographic or geological expression can be discerned, except for an elliptical zone (15 km long axis) of low magnetic signature roughly centred around the Barlangi Granophyre and shocked granitic rocks (Yarrabubba Granite). Within this magnetic low and surrounding the main outcrop of the Barlangi Granophyre (discussed below), is a circular high-frequency magnetic anomaly, about 2 km in diameter. An east-west-trending linear magnetic anomaly, interpreted as a mafic dyke, traverses the zone of low magnetic signature and is assumed to be of post-impact age (Fig. 11.9).

Macdonald et al. (2003) reported on the age constraints of the Yarrabubba structure, largely based on field, and limited and inconclusive U-Pb SHRIMP dating of xenocrystic zircons from the Barlangi Granophyre. These zircons yielded ages of around 2715 Ma. Dating carried out by the Geological Survey of Western Australia (DR Nelson, unpublished data) revealed two populations of xenocrystic zircons in the Barlangi Granophyre, which yielded ages of 2689±7 and 2647±11 Ma). *In situ* ultra-violet laser Ar-Ar dating was reported in Pirajno (2005) for one pseudotachylite sample that had been altered to sericite. A weighted mean of the 7 youngest ages yielded an Ar-Ar age of 1134 ± 26 Ma (95% confidence). However, the Ar-Ar pseudotachylite age may possibly reflect a younger resetting or partial resetting age, as a result of the alteration of the original pseudotachylite material to sericite, or a later thermal event. Macdonald et al. (2003) concluded that a Proterozoic age for Yarrabubba is indeed likely and this is supported by the observation that the central region of the structure is cut by the above-mentioned east-trending dyke, assumed to be of Proterozoic age, as are most east-trending dykes in the Yilgarn Craton.

The rock type that enabled the recognition of the Yarrabubba structure is the Barlangi Granophyre (Fig. 11.10). This is a pink-brown coloured rock containing xenocrysts and lithic fragments of granite. In thin section the Barlangi granophyre exhibits typical K-Na-feldspar-quartz granophyric intergrowths, as well as silica spherules and nucleation textures indicative of rapid quenching. Macdonald et al. (2003) interpreted the Barlangi Granophyre as an impact melt injected along a fault or fracture. As mentioned previously, large impact structures generate impact melts, which generally collect within the crater and/or form sill-like and dyke-like igneous bodies that penetrate into the basement below the crater floor (French 1998). The REE and normalised trace element abundance patterns of the Barlangi Granophyre and the Yarrabubba Granite are almost identical and this confirms that the granophyre was formed by melting of granitic target rocks. The Barlangi Granophyre is surrounded by shocked granitic rocks (Yarrabubba Granite) displaying classic shatter cones and pseudotachylite veins. Petrographic

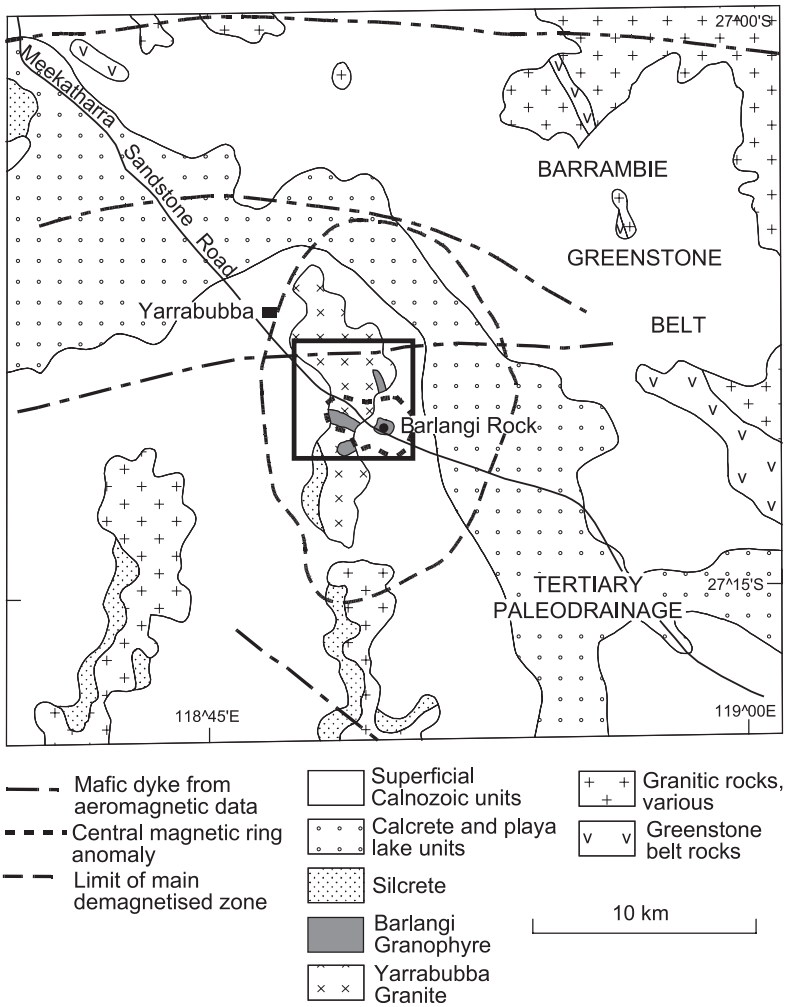


Fig. 11.9 Simplified geology of the Yarrabubba region, square indicates area of Figure 11.10. After Pirajno (2005)

work on the Yarrabubba Granite revealed common quartz grains with multiple sets of planar deformation lamellae or features (PDFs). Pseudotachylites form injection veins, locally showing flow-banded micro- to cryptocrystalline quartz and sericite aggregates with plastically deformed shapes (lithic fragments).

11.4.2.1 Hydrothermal Alteration

Petrographic work revealed evidence of post-impact hydrothermal fluid flow in both the Yarrabubba Granite and the Barlangi Granophyre. The most

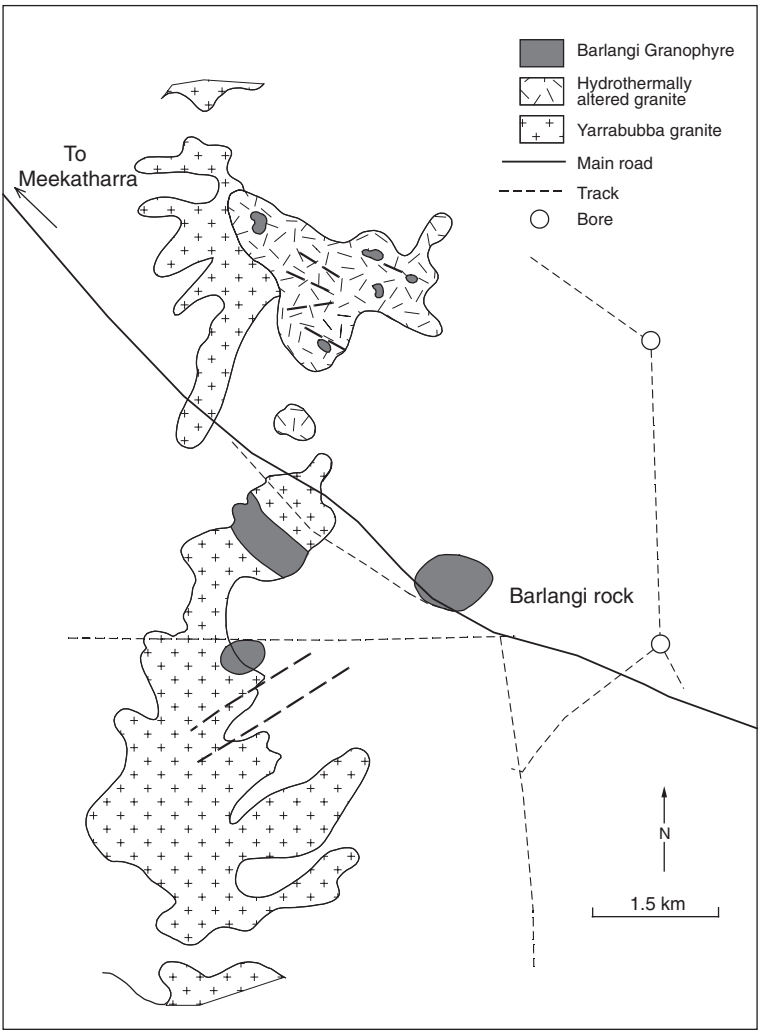


Fig. 11.10 Simplified geological map of Barlangi area. After Pirajno (2005)

conspicuous features of this hydrothermal circulation can be seen in the Yarrabubba Granite and include veins of bladed calcite (Fig. 11.11a) similar to those found in volcanic epithermal systems. Bladed calcite, commonly replaced by quartz, is indicative of boiling of CO_2-bearing fluids (Chapter 5). Reddish-brown alkali feldspar granite of the Yarrabubba Granite consists of a granoblastic aggregate of K-feldspar and quartz (Fig. 11.11b, c, d). In places, the Yarrabubba Granite appears modified by coarsening and absence of FeMg silicates and exhibits cross-cutting veins of K-feldspar. This rock is interpreted as representing the complete replacement of a granitic protolith, similar to that

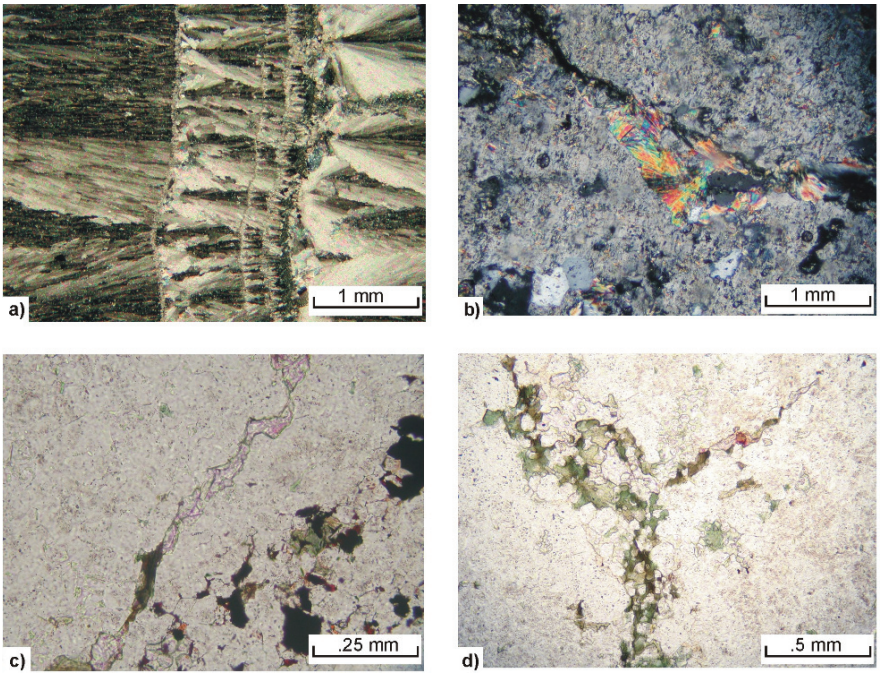


Fig. 11.11 Photomicrographs showing (**a**) aggregates of bladed calcite crystals (*crossed polars*; (b), (c) and (d) syenitic like Yarrabubba Granite composed of a granoblastic aggregate of K-feldspar and quartz is cut by a vein of prehnite and lesser chlorite (**b**), a vein containing green biotite and fluorite (**c**) and veins of chlorite (**d**); b at crossed polars, c and d in plane polarised light

observed in the syenitic rocks of the Teague Granite in the Shoemaker structure. Fluorite + biotite and chlorite + prehnite occur as veinlets (Fig. 11.11b, c, d) cutting through the granoblastic aggregate of K-feldspar and quartz of the Yarrabubba Granite. Macdonald et al. (2003) recognized that the presence of K-feldspar (microcline) and albite together with muscovite is indicative of strong K metasomatism. These authors also suggested that the central demagnetized zone may be the effect of this metasomatism, which resulted in the destruction of Fe-bearing mineral phases. As also observed for the Shoemaker structure, these assemblages suggest that an early alkali metasomatism was followed by hydrous fluids that infiltrated fractures in the metasomatically altered target rocks. Pervasive sericitic alteration and green mica overprint the granophyric textures in the Barlangi Granophyre

11.4.3 Woodleigh Impact Structure

Woodleigh is a buried, multi-ring impact structure, approximately 160 km south-southeast of Carnarvon, east of Shark Bay (Fig. 11.5; Mory et al. 2000,

2001). The structure was first identified as a possible impact crater in late 1997, during a geological review of the Gascoyne Platform, from the coincidence of shallow granitic rocks in a drillhole over the centre of a circular gravity anomaly (Fig. 11.12). The hole was later deepened to verify the impact interpretation. The new Woodleigh 1 core shows extremely well preserved shock metamorphic features in granitic rocks, including veins of pseudotachylite, breccia, and planar deformation features, thereby providing indisputable evidence of an impact origin. Subsequently, a second drillhole (Woodleigh 2A) was sunk 13 km to the west to sample the crater-infill section (Fig. 11.13). Woodleigh 2A intersected a substantial thickness of paraconglomerate, overlain by lacustrine strata of the Woodleigh Formation. The paraconglomerate contains lithic fragments of shocked granitic rocks and sandstone, and is interpreted as the re-working of shocked material that filled the impact crater. The Woodleigh Formation probably represents a later crater-lake fill. The structure is most clearly shown on the first vertical derivative of the Bouguer gravity as a series of annular ridges and troughs (Fig. 11.12). The central gravity high, about 25 km in diameter, is interpreted as the central uplift of the impact. The adjacent gravity "trough" probably corresponds to a ring syncline filled with strata

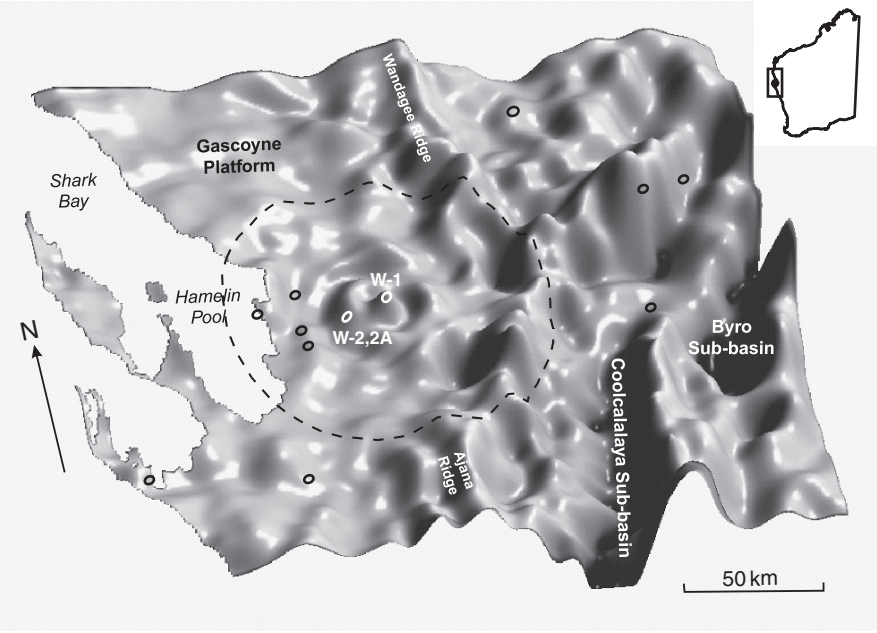


Fig. 11.12 Woodleigh impact structure: isometric view of first vertical derivative of the Bouguer gravity (after Mory et al. 2001); small circles indicate position of drillholes and the dashed line shows the inferred extent of the structure

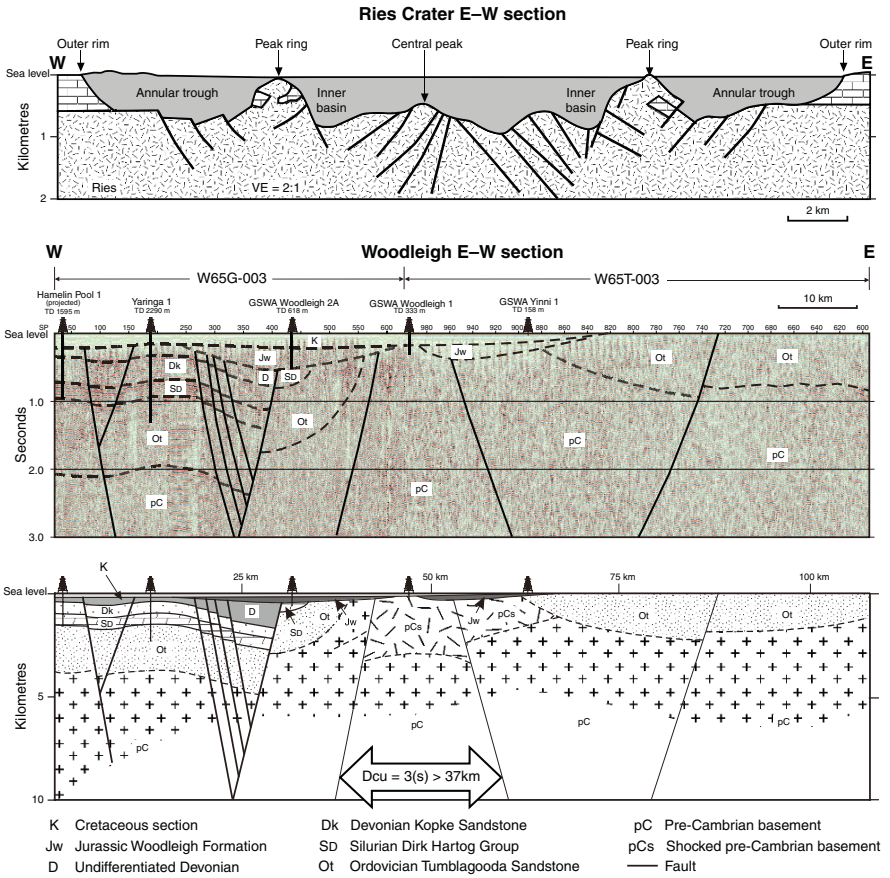


Fig. 11.13 Woodleigh impact structure: seismic reflection east-west cross section and geological interpretation, compared with a section of the Ries impact structure in Germany. After Glikson et al. (2005 and references cited therein)

similar to those in Woodleigh 2A. The diameter of the Woodleigh structure remains controversial. Estimates range from a maximum of 120 km (Mory et al. 2000; Glikson et al. 2005) to 60–70 km (Reimold et al. 2003).

Gravity and seismic data indicate that the structure is asymmetric with basement east of the central peak being about 2 km shallower than to the west. The asymmetry is interpreted as due to tilting during Early Cretaceous. Initial studies constrain the age of the Woodleigh impact to between Early Permian and Early Jurassic (290–200 Ma). K–Ar isotope dating of clay minerals within shocked granitic rocks from Woodleigh 1, and from transported shocked material in Woodleigh 2A have yielded ages clustering around 359 Ma (Uysal et al. 2001, 2002), near the Devonian-Carboniferous boundary.

11.4.3.1 Hydrothermal Alteration

The extensively fractured and brecciated granitic rocks cored in Woodleigh 1 show clear evidence of post-impact hydrothermal alteration and sulphide mineralisation. This is shown by the presence of mineral phases, such as albite, quartz, muscovite, illite, chlorite, calcite, which overprint the primary and/or impact-modified mineralogy and infill microfractures (Fig. 11.14a, b). Uysal et al. (2001) reported on the occurrence of illitic clays and their textural relationships, which indicate that these clays represent phases precipitated from hydrothermal fluids and are not pre-existing clay minerals. Furthermore, the presence of abundant fluid inclusions (liquid and liquid + gas) within impact-related microstructures (Fig. 11.14c) is evidence that substantial volumes of fluids circulated through the impact-modified target rocks. Sulphides that have been recognised by reflected light optical microscopy include pyrite, marcasite and chalcopyrite. Typically, these sulphides fill microfractures in the silicate matrix and in pre-existing ore minerals, such as ilmenite. Examples are shown in Fig. 11.14d, e.

Hydrothermal alteration is especially common in rocks that are extensively fractured and/or have pseudotachylite veinlets. Textural relationships gleaned from petrographic work suggest a possible alteration paragenesis, as follows: quartz + albite → muscovite or sericite ± epidote → silica flooding− → calcite.

The pervasive shock-thermal alteration has produced distinctly re-constituted leucocratic medium-grained granitic rocks with rust-coloured patches (Fig 11.14f). Magmatic biotite, where present, exhibits kink bands, edge resorption, and concordant to transgressive pseudotachylite veins; locally PDFs are also present. Fresh and undeformed biotite may be the product of post-impact potassic alteration. Some of the pseudotachylite veinlets show devitrification features characterised by nucleation of quartz and alkali feldspar (usually microcline) with a spherulitic appearance and/or granophyric texture. Isolated corundum crystals locally replace feldspar, suggesting re-concentration of alumina as a refractory element. Accessory phases in the shocked granitic include zircon, monazite and apatite, whereas post-impact hydrothermal alteration effects include calcite veinlets, pyrite growth in pseudotachylite veins and microfractures, epidote, and fine sericite aggregates replacing shocked feldspar grains.

Both in Woodleigh 1 and 2A altered zones in shocked quartz and feldspars take on a reddish-brown colour due to oxidation of iron and the presence of numerous fluid inclusions. Woodleigh 1 shows features of melt devitrification, which involves nucleation of quartz and alkali feldspar (generally microcline) and results in a spherulitic and/or a granophyric texture. The spherulitic texture is more common and generally consists of blebs, or roundish bodies of quartz and feldspar.

Major and trace element analyses of core samples from Woodleigh 1 were reported by Mory et al. (2001). These were used to show if changes can be detected in the chemistry of the target rocks (central uplift granite). The data were normalised against average granite, in absence of comparable granites in

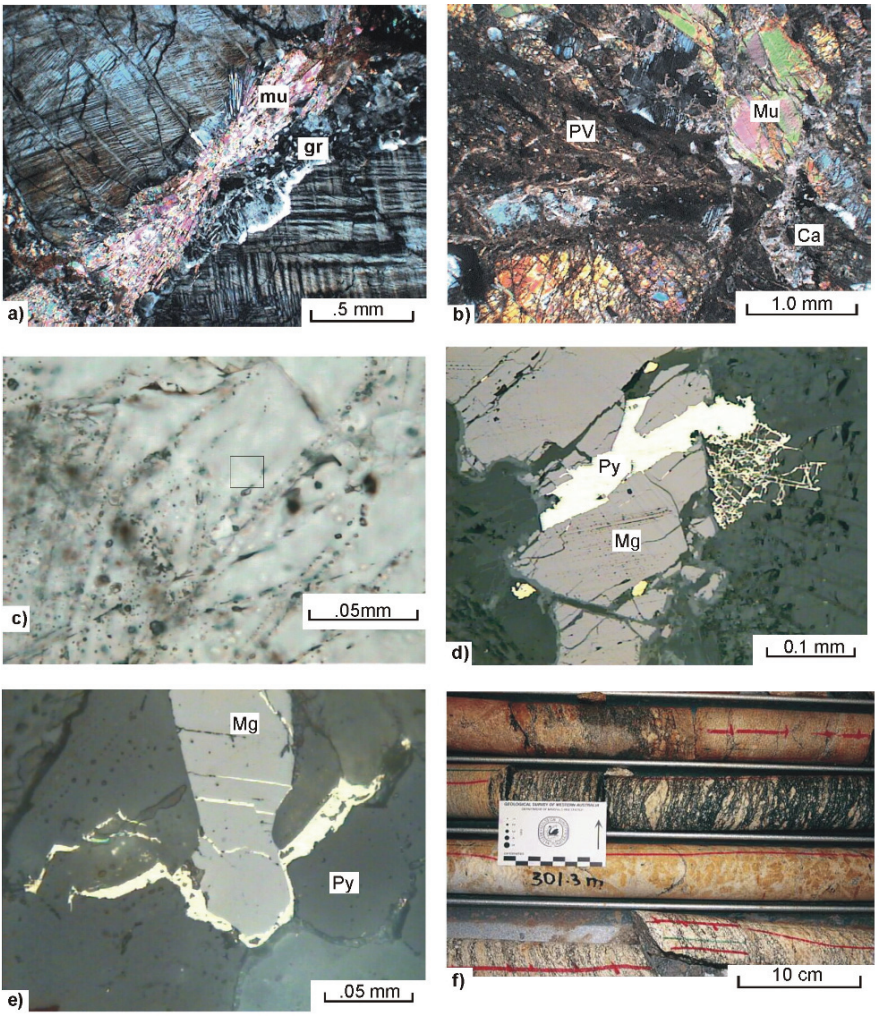


Fig. 11.14 (**a**) photomicrographs taken with crossed polars, showing sheaves of muscovite (mu) overprinting granophyric material (gr) at the boundary between quartz (with PDFs) and microcline; (**b**) photomicrographs taken with crossed polars, pseudotachylite veinlet (PV) displaced by a late microfracture and overprinted by calcite (Ca), there are also large muscovite (Mu) crystals in the brecciated groundmass material; (**c**) photomicrographs taken with crossed polars, showing PDfs in quartz decorated with fluid inclusions, boxed area shows a two-phase inclusion; (**d**) reflected light photomicrograph showing magnetite (Mg), cut by pyrite (Py), associated with fine pyrite filling a network of microfractures and chalcopyrite blebs (at margins of the magnetite); (**e**) reflected light photomicrograph showing magnetite (Mg) and pyrite filling small fractures in silicate minerals and the magnetite; (**f**) core (about 301 m) of shocked granitoid rock with yellow-brown (*rusty*) patches and brecciated biotite-gneissic granite

the region. Results indicate that while the lithophile and chalcophile trace metals (Pb, Sn, W, Mo, Bi, Ag, Sb, Zn, Cu, Au) vary by factors in the range of 0.1–10 times relative to average granite. Siderophile trace metals, however, are strongly enriched (V, 6–20 times; Cr, up to 30 times; Co, 10–50 times; Ni, up to 120 times). Major elements show moderate to strong K_2O enrichment, associated with depletions in SiO_2, Na_2O, TiO_2, MgO and P_2O_5 (Mory et al. 2001).

11.5 Concluding Remarks

The possibility of hydrothermal ore deposits, directly or indirectly related to impacts is a good catalyst to encourage geoscientists to investigate impact-induced hydrothermal systems. An asteroid or a comet, say 10–15 km in diameter, travelling at a rate of 10–12 km/sec, crushing into the Earth's crust would produce an explosion equivalent to 10 000 times a simultaneous blast produced by the entire world's nuclear arsenal (Ward and Brownlee 2004). An enormous volume of rock is melted instantly constituting a large magma lake or chamber, followed in the next instant by an elastic rebound that would bring hot rocks from several km of crustal depth to the surface. In this scenario, it is difficult not to imagine large scale hydrothermal activity operating for thousands of years in the aftermathg of such an impact.

The heat engine is provided by either the melt sheet of large impact structures and/or the hot sections of the central uplift. This is probably followed by the influx of meteoric fluids into the highly fractured rocks, which also make available an ideal reservoir for hydrocarbons. The role of the Vredefort large impact structure in the development of the Witwatersrand Au mineralisation remains uncertain, mainly because of the difficulty in separating the metamorphic-hydrothermal signatures of two or even three thermal events that affected the region at around 2.05–2.02 Ga.

Up till now, impact-related hydrothermal activity has been studied in comparatively large impact structures, all of which have a central uplift. More recently, however, Glikson et al. (2008) have shown that a low-temperature hydrothermal system can be activated in simple (no central uplift) small-diameter ($\sim$260 m) impact structures. Impact structures will continue to surprise the geoscientific community.

References

Allen CC, Gooding JL, Keil K (1982) Hydrothermally altered impact melt rock and breccia: contributions to the soil of Mars. J Geophys Res 87: 10083–10101.

Ames DE, Watkinson DH, Parrish RR (1998) Dating of a regional hydrothermal system induced by the 1850 Ma Sudbury impact event. Geology 26: 447–450

Ames DE, Kjarsgaard IM, Pope KO, Dressler B, Pilkington M (2004) Secondary alteration of the impactite and mineralization in the basal Tertiary sequence, Yaxcopoil-1, Chicxulub impact crater, Mexico. Meteor Planet Sci 39: 1145–1167

Buffetaut E, Koeberl C (eds) (2002) Geological and biological effects of impact events. Springer, Berlin
Bunting JA, De Laeter JR, Libby WG (1980) Evidence for the age and cryptoexplosive origin of the Teague Ring structure. Geol Surv West Aust Ann Rep 1980: 125–129
Carpenter BN, Carlson R (1992) The Ames impact carter: Oklahoma Geol Surv 52: 208–223
Donofrio RR (1998) North American impact structures hold giant field potential Oil and Gas J, May 11, pp 69–83
Dressler BO, Sharpton VL (eds) (1999) Large meteorite impacts and planetary evolution II. Geo Soc Am Sp Pap 339
Forsman NF, Gerlach TR, Anderson NL (1996) Impact origin of the Newporte structure, Williston Basin, North Dakota. Am Ass Petrol Geol Bull 80: 721–730
French BM (1998) Traces of catastrophe – a handbook of shock-metamorphic effects in terrestrial meteorite impact structures. Lunar Planet Ins Contr 954, Lunar and Planetary Institute, Houston, Texas
Frimmel HE, Groves DI, Kirk J, Ruiz J, Chesley J, Minter WEL (2005) The formation and preservation of the Witwatersrand goldfields, the world's largest gold province. Econ Geol 100th Ann Vol: 769–797
Gibson RL, Stevens G (1998) Regional metamorphisn due to anorogenic cratonic magmatism. Geol Soc Lond, Spec Publ 138: 121–135
Gibson RL, Reimold WU (1999) Significance of the Vredefort Dome for metamorphic-mineralization studies in the Witwatersrand Basin. Miner Petr 66: 25–53
Gibson RL, Reimold WU (2001).The Vredefort impact structure, South Africa – The scientific evidence and a two-day excursion guide. Council Geosci S Afr Memoir 92
Gilmour I, Koeberl C (2000) Impacts and the early Earth. Springer, Berlin
Glikson A (1998) Eugene Shoemaker and the impact paradigm in Earth and planetary science. Celes Mechan Dynam Astron 69: 1–7
Glikson A, Mory AJ, Iasky RP, Pirajno F, Golding SD, Uysal LT (2005) Woodleigh, Southern Carnavon Basin, Western Australia: history of discovery, Late Devonian age, and geophysical and morphometric evidence for a 120 km-diameterimpact structure. Aust J Earth Sci 52: 545–553
Glikson A, Hickman A, Vickers J (2008) Hickman Crater, Ophthlamia Range, Western Australia: Evidence supporting a meteorite impact origin. Aust J Earth Sci 55: 1107–1117
Golightly JP (1984) The Sudbury Igneous Complex as an impact melt: evolution and ore genesis. Ontario Geol Surv Sp Vol 5: 105–118
Gorter JD (1998) The petroleum potential of Australian Phanerozoic impact structures. APPEA J 38: 159–187
Goto K, Tada R, Bralower TJ, Hasegawa T, Matsui T (2004) Evidence for ocean water invasion into the Chixculub crater at the Cretaceous/Tertiary boundary. Meteor Planet Sci 39: 1233–1247
Grady MM, Hutchinson R, McCall GJH, Rothery DA (eds) (1998) Meteorites: flux with time and impact effects. Geol Soc Lond Spec Publ 140
Grieve RAF (2003) Extraterrestrial triggers for resource deposits. Ext Abs Appl Earth Sci 112(2): B145–B147
Grieve RAF, Masaitis VL (1994) The economic potential of terrestrial impact craters. Int Geol Rev 36: 105–151
Grieve RAF, Thierriault A (2000) Vredefort, Sudbury and Chixculub: three of a kind? Ann Rev Earth Planet Sci 28: 305–338
Hayward CL, Reimold WU, Robb LJ, Gibson RL (2003) The Witwatersrand gold deposit, South Africa: an impact-modified metamorphosed placer. In: McDonald I, Annels AE, Bevins RE, Boyce AJ, Brabham PJ, Butler IB, Herrington RJ, Polya DA (eds), World Class Mineral Deposits, Extended Abstracts, The Geological Society's 2003 Fermor Flagship Meeting, B147–B148
Hildebrand AR, Pilkington M (2002) Crater floor exhalative (Crafex) sulphide deposits at the Chicxulub crater, Yucatan, Mexico. Lunar Planet Sci XXXIII, p 2031

Hough RM, Gilmour I, Pillinger CT, Arden JW, Glikes KWR., Yuan J, Milledge HJ (1995) Diamond and silicon carbide of impact melt rock from the Ries crater. Nature 378: 41–44
Iasky R, Mory AJ, Blundell K (2001) The geophysical interpretation of the Woodleigh impact structure, southern Carnavon Basin, Western Australia. Geol Surv West Aust Report 79
Johansson Å (1984) Geochemical studies on the Boda Pb-Zn deposit in the Siljan astrobleme, central Sweden. Geologiska Föreningens I Stockholm Förhandlingar 106: 15–25
Johnson GI (1991) The petrology, geochemistry and geochronology of the felsic alkaline suite of the eastern Yilgarn block, Western Australia: PhD thesis (unpublished), University of Adelaide, Adelaide, p 192
Kirschner CE, Grantz A, Mullen MW (1992) Impact origin of the Avak structure, Arctic Alaska and genesis of the Barrow Gas Fields. Am Ass Petrol Geol Bull 76: 651–679
Koeberl C, Fredrikson K, Götzinger M, Reimold WU (1989) Anomalous quartz from the Roter Kamm impact crater, Namibia: evidence for post impact hydrothermal activity? Geoch Cosmoch Acta 53: 2113–2118
Koeberl C, Masaitis VL, Shafranovsky GI, Gilmour I, Langenhorst F, Schrauder M (1997) Diamonds from the Popigai impact structure, Russia. Geology, 25: 967–970
Koeberl C, Henkel H (eds) (2005) Impact tectonics. Springer, Berlin
Komor SC, Valley JW, Brown PE (1988) Fluid-inclusion evidence for impact heating at the Siljan Ring, Sweden. Geology 16: 711–715
Kring DA (1995) The dimension of the Chicxulub impact crater and impact melt sheet. J Geophys Res 100: 16979–16989
Law JDM, Phillips GN (2005) Hydrothermal replacement model for Witwatersrand gold. Econ Geol 100th Ann Vol: 799–811
Lindgren P, Parnell J, Norman C, Mark DF, Baron M, Ormo J, Sturkel E, Conliffe J, Fraser W (2007) Fromation of uranium-thorium-rich bitumen nodules in the Lockne impact structure, Swede: A mechanism for carbon concentration at impact sites. Meteor Planet Sci 42:1961–1969
Lüders V, Rickers K (2004) Fluid inclusion evidence for impact-related hydrothermal fluid and hydrocarbon migration in Cretaceous sediments of the ICDP-Chicxulub drill core Yax-1. Meteor Planet Sci 39: 1187–1198
Macdonald FA, Bunting JA, Cina SE (2003) Yarrabubba – a large, deeply eroded impact structure in the Yilgarn Craton, Western Australia. Earth Planet Sci Lett, 213: 235–247
Masaitis VL, Naumov MV (1993) Puchezh-Katunki impact crater: preliminary model of hydrothermal circulation system. Meteor 7: 390–391
McCarville P, Crossey LJ (1996) Post-impact hydrothermal alteration of the Manson impact structure. Geol Soc Am Sp Pap 302: 347–379
Melosh HJ (1989) Impact cratering – A geologic process. Oxford Univ Press, New York, Clarenodn Press, Oxford
Molnár F, Watkinson DH, Jones PC (2001) Multiple hydrothermal processes in footwall units of the North Range, Sudbury Igneous Complex, Canada, and implications for the genesis of vein-type Cu-Ni-PGE deposits. Econ Geol 96: 1645–1670
Mory AJ, Iasky RP, Glikson AY, Pirajno F (2000) Woodleigh, Carnarvon Basin, Western Australia: a new 120 km-diameter impact structure. Earth Planet Sci Lett 177: 119–128
Mory AJ, Pirajno F, Glikson AY, Coker J (2001) GSWA Woodleigh 1, 2, and 2A well completion report: Woodleigh impact structure, Southern Carnarvon Basin, West Aust Geol Surv West Aust Record 2001/6
Naldrett AJ (2002) From impact to riches: evolution of geological understanding as seen at Sudbury, Canada. GSA Today 13: 4–10
Naumov MV (1993) Zonation of hydrothermal alteration in the central uplift of the Puchezh-Katunki astrobleme. Meteoritics 28: 408–409
Naumov MV (2002) Impact-generated hydrothermal systems: data from Popigai, Kara and Puchezh-Katunki impact structures. In: Plado J, Pesonen LJ (eds), Impacts in precambrian shields, impact studies series, Springer-Verlag, Berlin, pp 117–171

Nelson DR (1999) Compilation of geochronology data (2000). Geol Surv West Aust Record 1999/2
Newsom HE (1980) Hydrothermal alteration of impact melt sheets with implications for Mars. Icarus 44: 207–219
Newsom HE, Graup G, Sewards T, Keil K (1986) Fluidization and hydrothermal alteration of the suevite deposit at the Ries Crater, West Germany, and implications for Mars. J Geophys Res 91: E239–E251
Osinski GR, Spray JG, Lee P (2001) Impact-induced hydrothermal activity within the Haughton impact structure, arctic Canada: generation of a transient, warm, wet oasis. Meteor Planet Sci 36: 731–745
Pevzner LA, Kirjakov AF, Vorontsov AK, Masaitis VL, Mashchak MS, Ivanov BA (1992) Vorotilovskaya drillhole; first deep drilling in the central uplift of large terrestrial impact crater. 23rd Lunar Planet Sci Conf, Houston, Abs Vol, pp 1063–1064
Phillips D, Onstott TC, Harris JW (1989) 40Ar/39Ar laser-probe dating of diamond inclusions from the Premier kimberlite. Nature 340: 460–462
Phillips GN (1987) Metamorphism of the Witwatersrand gold fields: conditions during peak metamorphism. J Metamorph Geol 5:307–322
Phillips GN (1988) Widespread fluid infiltration during metamorphism of the Witwatersrand gold fields: generation of chloritoid and pyrophyllite. J Metamorph Geol 6:311–332
Pirajno F (2000) Ore deposits and mantle plumes. Kluwer Academic Publ, Dordrecht
Pirajno F (2002) Geology of the Shoemaker impact structure, Western Australia. Geol Surv West Aust Rep 82
Pirajno F (2005) Hydrothermal processes associated with meteorite impact structures: evidence from three Australian examples and implications for economic resources. Aust J Earth Sci 52: 587–620
Pirajno F, Glikson AY (1998) Shoemaker Impact Structure, Western Australia. Celest Mechanics Dyn Astron 69: 25–30
Pirajno F, Hawke P, Glikson AY, Haines P, Uysal T (2003) Shoemaker impact structure, Western Australia. Aust J Earth Sci 50: 775–796
Pirajno F, Van Kranendonk MJ (2005) Review of hydrothermal processes and systems on Earth and implications for Martian analogues. Aust J Earth Sci 52: 329–352
Puura V, Kärki A, Kirs J, Kirsimäe K, Kleesment A, Konsa M, Niin M, Plado J, Suuroja K, Suuroja S (2000) Impact-induced replacement of plagioclase by K-feldspar in granitoids and amphibolites at the Kärdla Crater, Estonia. In Gilmour I, Koerberl C (eds) Impacts and the early Earth, Springer-Verlag, Berlin pp 417–445
Puura V, Koeberl C, Kärki A, Juvonen R, Konsa Plado JM, Suuroja K, Kirs J, Huber H (2002) Geochemistry of K-enriched impactites, based on drillings into the Kärdla Crater, Estonia. Geol Soc Am Abs with Programs, Denver, Oct. 2002, p 341
Reimold WU (1995) Impact cratering – A review, with special reference to the economic importance of impact structures and the southern African impact crater record. Earth, Moon Planets 70: 21–45
Reimold WU, Gibson RL (1999) Geology and evolution of the Vredefort impact structure, South Africa. J Afr Earth Sci 23: 125–162
Reimold WU, Gibson RL (2005) Meteorite impact! The danger from space and South Africa's mega-impact – The Vredefort structure. Chris van Rensburg Publ Pty Ltd, Johannesburg
Reimold WU, Köeberl C, Fletcher P, Killick AM, Wilson JD (1999) Pseudotachylite breccias from fault zones in the Witwatersrand Basin, South Africa: evidence of autometasomatism and post-brecciation alteration processes. Mineral Petr 66: 25–53
Reimold WU, Koeberl C, Hough R, Mcdonald I, Bevan A, Amare K, French BM (2003) Woodleigh impact structure: shock petrography and geochemical studies: Meteor Planet Sci 7: 1109–1130
Reimold WU, Koeberl C, Gibson RL, Dressler BO (2005) Economic mineral deposits in impact structures: a review. In: Koeberl C, Henkel H (eds), Impact tectonics. Springer, Berlin, pp 479–552

Rowe AJ, Wilkinson JJ, Coles BJ, Morgan JV (2004) Chicxulub: testing for post-impact hydrothermal input into the Tertiary Ocean. Meteor Planet Sci 39: 1223–1231

Scrimgeour IR, Close DF, Edgoose CJ (1999) Petermann Ranges SG52-7 Explanatory Notes. Northern Territory Geol Surv Dept Mines and Energy

Smithies RH, Champion DC (1999) Late Archean felsic alkaline igneous rocks in the Eastern Goldfields, Yilgarn Craton, Western Australia: a result of lower crustal delamination? J Geol Soc Lond 156: 561–579

Sturkel FF, Broman C, Forsberg P, Torsander P (1998) Impact-related hydrothermal activity in the Lockne impact structure, Jämtland, Sweden. Eur J Mineral 10: 589–609

Tyler IM (2005) Australia: Proterozoic. In Encyclopedia of Geology RC Selley, LRM Cocks, IR Plimer (eds) , vol. 1. Elsevier, Oxford, pp 208–221

Uysal IT, Golding S, Glikson AY, Mory M, Glikson M (2001) K-Ar evidence from illitic clays of a Late Devonian age for the 120 km diameter Woodleigh impact structure, southern Carnavon Basin, Western Australia. Earth Planet Sci Lett 192: 281–289

Uysal IT, Golding S, Glikson AY, Mory M, Glikson M, Iasky RP, Pirajno F (2002) Reply to "Comment on: K-Ar evidence from illitic clays of a Late Devonian age for the 120 km diameter Woodleigh impact structure, southern Carnavon Basin, Western Australia. Earth Planet Sci Lett 201: 253–260

Ward PD, Brownlee D (2004) Rare Earth – why complex life is uncommon in the Universe. Copernicus Books, Springer Science, New York

Wingate MTD, Pirajno F, Morris PA (2004) Warakurna large igneouys province: a new Mesoproterozoic large igneous province in west-central Australia. Geology 32: 105–108

Witt WK, Davy R (1997) Geology and geochemistry of Archaean granites in the Kalgoorlie region of the Eastern Goldfields, Western Australia: a syn-collisional tectonic setting? Precambr Res 83: 133–183

Zürcher L, Kring DA (2004) Hydrothermal alteration in the core of the Yaxcopoil-1 borehole, Chicxulub impact structure, Mexico. Meteor Planet Sci 39: 1199–1222

Chapter 12
Hydrothermal Processes and Systems on Other Planets and Satellites: Clues for the Search of Extraterrestrial Life

12.1 Introduction

In this chapter, I discuss hydrothermal processes that almost certainly operate, or have operated, on other planets and satellites in our Solar System, including Mars, where liquid water is, or was, present (Baker 2001). In addition, the possible nature of hydrothermal systems on satellite bodies of Jupiter (Europa and Ganymede) and Saturn (Enceladus and Titan), are also briefly considered. Studies that focus on analogue processes and the potential for hydrothermal systems on other planetary bodies in the Solar System are important because these will play a crucial role not only on future exploration missions to Mars and the search for extraterrestrial life, but will also provide new insights and new dimensions on regions of hydrothermal activity on Earth (Walter and Des Marais 1993). For this reason terrestrial analogues are discussed where considered appropriate.

Given the above, I also embark on a speculative note of where to search for life, as we know it, in other planetary bodies. This, by default, necessitates a definition of life and some idea of how life might have originated, a topic that is addressed in Chapter 10. Furthermore, life links with hydrothermal systems are well established both on modern Earth in its geological record, therefore the search for extraterrestrial primitive life can be paired to searching for hydrothermal systems.

12.2 Extraterrestrial Water

Water ice is abundant in the Solar System, with most of the icy planetesimals forming between Jupiter and Saturn (Zolensky 2005). It is thought that condensation of water ice could only have occurred from about 5 astronomical units (1 AU = distance between Earth and Sun), which is inside from Jupiter's orbit (Zolensky 2005). Earth is situated in a favourable life (as we know it)-supporting zone in the Solar System. This is the Habitable Zone, a region where the distance from the Sun is such that the temperature in the planetary surface

F. Pirajno, *Hydrothermal Processes and Mineral Systems*,

© Springer Science+Business Media B.V. 2009

allows a water ocean to neither freeze nor boil (Ward and Brownlee 2004). The Habitable Zone can shift as the Sun (or a central star of any planetary system) evolves with time.

Spectroscopic observations confirm that water ice is one of the dominant components of the satellites of Jupiter, Saturn, Uranus and Pluto. Europa is almost entirely covered by water ice, which would be the equivalent of a crust and for this reason many planetologists speculate that it may overlie salty liquid water, the equivalent of a terrestrial asthenosphere or partially melted mantle. Europa's icy crust is revealed in the spectacular images provided by the Galileo mission. I return to discuss Europa in Section 12.5.1. Similarly, Some of Saturn's moons also contain some water ice. In addition to water ice, methane (CH_4) and ammonia (NH_3) have been detected, together with several other constituents (Table 12.1).

Asteroids are small bodies from as little 50 m to 1000 km in diameter, orbiting inward from Neptune, although the majority form a belt between Mars and Jupiter. About 80 000 have been identified. Asteroids are divided into classes according to a concentric pattern, named E, M, S, C, D, and P, with increasing distance from the Sun. The asteroids that are closest to the Sun (E, M, S, C) are bone dry, whereas those that are volatile rich and may have water ice are those that are farthest (P and D). Some asteroids may have contained water ice initially, but this was later driven off (Zolensky 2005). Closer to home, there is now no doubt that Mars had surface water, and may still preserve frozen water in the subsurface, as discussed in the next section. Perhaps, Mars was near the outer edge of the Habitable Zone, early in its history.

Table 12.1 List of ices that have been detected or suspected to be present on satellites of the outer planets. After Geissler (2000)

Compound	Formula	Freezing point in degrees Kelvin
Water	H_2O	273.2
Hydrogen peroxide	H_2O_2	272.7
Sulphur dioxide	SO_2	200.5
Ammonia	NH_3	195.5
Carbon dioxide	CO_2	194.7
Hydrogen sulphide	H_2S	190.3
Formaldehyde	H_2CO	181.2
Methanol	CH_3OH	175.4
Methane	CH_4	90.7
Ozone	O_3	80.7
Carbon monoxide	CO_2	68.1
Nitrogen	N_2	63.3
Oxygen	O_2	54.8

12.3 Mars

Mars, named after the god of war (Mars) of ancient Latin tribes in central Italy, is a terrestrial-type planet, fourth from the Sun, with a diameter of 6371 km, about half that of the Earth, a mean density of 3.94 g/cm^3, an axis inclined at 25° to the ecliptic and a 24.5 h day (called sol). For this reason Mars has seasons similar to the Earth's, but with a thin (P = 6 mbar), CO_2-rich atmosphere. An overview of the geology of Mars is used to develop ideas as to what type of hydrothermal systems may have been or may be present there and where to search for signs of extinct and possibly extant life, most notably around the volcanoes of the Tharsis Rise, including caldera floors, channels, valley networks and in rift systems. The interaction of ascending magmas with the cryosphere (ice-rich layer and permafrost) is proposed as a mechanism to explain some of the surface features of Mars (Head and Wilson 2002). As on Earth, potential hydrothermal systems on Mars must be primarily linked to magmatic systems and the interaction of melts with ice and water near and around volcanoes and dyke swarms. On Earth, the African plate can be considered as the closest analogue to a "one plate" planet like Mars, because Africa has been stationary for at least 65 Ma (Burke 1996), so that crustal uplifts, rifts and intraplate volcanism have not been recycled by convergent margin tectonics. The East African Rift System could be an analogue for the great rift system of Valles Marineris on Mars. Apart from volcanoes, Valles Marineris could represent a likely setting for hydrothermal processes, similar perhaps to those that characterise lakes and geothermal springs in the East African Rift System (Chapter 8). The discovery of crystalline hematite and sulphate deposits on Mars points to chemical precipitation analogous to that of banded iron-formation and/or hot spring sinter-like deposits, as explained in Section 12.3.4.1.

The first surface feature of Mars, Sirtis Major, was identified by the Dutch astronomer Christiaan Huygens in 1659; about seven years later the ice caps were identified by the Italian astronomer Giovanni Cassini. In 1877 another Italian astronomer, Giovanni Schiaparelli, saw straight linear features, which he thought might be artificial channels, or canali, translated as canals in English. Soon after Schiaparelli's putative discovery, the American astronomer Asaph Hall discovered the two tiny Martian satellites, Deimos, about 10 × 12 × 16 km, and Phobos, about 20 × 23 × 28 km. These two tiny moons are pockmarked with numerous impact craters. Meanwhile, Schiaparelli's interpretation of Martian canals was enthusiastically taken up by the American astronomer Percival Lowell, in 1894, who opened an observatory at Flagstaff in Arizona and in studying the Martian surface became convinced that the canals were made by a civilised society for irrigation purposes. It was not until the first images of Mars were acquired by the flybys of Mariner 4 in 1965, soon followed by further Mariner missions 6, 7, and 9 in the period 1969, 1971 and 1972, and then the Viking missions (1 and 2) in 1976, that the surface features of Mars were shown with amazing clarity and revealing a planet

with a desert landscape, hardly different from some desert areas of our planet, spectacular volcanic edifices, rift valleys and dry valleys networks. Some of the modern literature on the surface features and geology of Mars relevant for the purpose of this book can be found in, Carr et al. (1993), Carr (1981, 1990, 1996a, b; 1999), McSween (2003), Walter et al. (2005), Bibring (2005). More recently, a systematic analysis of the surface of Mars, encompassing the information that has accumulated in the last decade as a result of the various Mars spacecrafts, is presented in Carr (2006). A book edited by Chapman (2007) provides a wide range of articles on the geology of Mars and terrestrial analogues.

Mars is currently geologically mostly inactive, although the presence of volcanoes, sedimentary successions and rifts indicates that it was geologically active in the relatively recent past. The current inactivity is due to its smaller size that caused Mars to cool down more rapidly than Earth, so that its mantle may no longer be convecting (Harder and Christensen 1996; Schubert et al. 2000). On the basis of its impact cratering size-frequency record, an approximate geological time scale for Mars recognises three eons, namely: Noachian (named after Noachis Terra, 4.6 – ~3.6 to 3.5 Ga; correlating with our Hadean), Hesperian (named after Hesperia Planum, 3.6–2.9 Ga, corresponding with the early Archaean) and Amazonian (named after Amazonis Planitia, 2.9 Ga-present). No doubt this time scale will be refined and further subdivided as more data are aquired by space missions. An early geological map of Mars was published by Pollack (1975) and shown in Fig. 12.1, where most geological features are shown, but with no age subdivisions. Valles Marineris and the Tharsis bulge and its volcanoes prominently displayed, as is the hemispheric dycothomy, discussed below. A fairly detailed geological map by Yenne (1990) shows the time divisions of Noachian, Hesperian and Amazonian and landform based lithostratigraphic subdivisions, namely plains materials, constructional volcanic materials, channel and canyon materials and rough terrain materials. As well, in this map are shown dyke swarms radiating from Tharsis Montes and Alba Patera. Another compilation, presented by Nimmo and Tanaks (Fig. 12.2), showed nine geological units, which from younger to older, include Amazonian layered deposits, Early Amazonian Vastitas Borealis, Lower Amazonian-Lower Hesperian volcanic materials, Hesperian materials, Lower Noachian-Early Hesperian knobby materials, Lower Noachian-Early Hesperian materials, Noachian-Early Hesperian materials, Noachian materials, early Noachian materials. The Noachian period is characterised by the formation of the northern lowlands and impact basins, including Hellas and Argyre (Figs. 12.1 and 12.2). Also attributable to the Noachian is the early Tharsis tectono-thermal activity. The presence of valley networks (see below) suggests that this early time was wet and warmer than present-day Mars; and it is also reasonable to assume that hydrothermal systems may have been active at this time. In the Hesperian period, significant volcanism occurred in the Tharsis, Syrian and Elysium regions, the great Valles Marineris rift system, filled with sedimentary layers, and major outflow channels were formed. Other volcanic

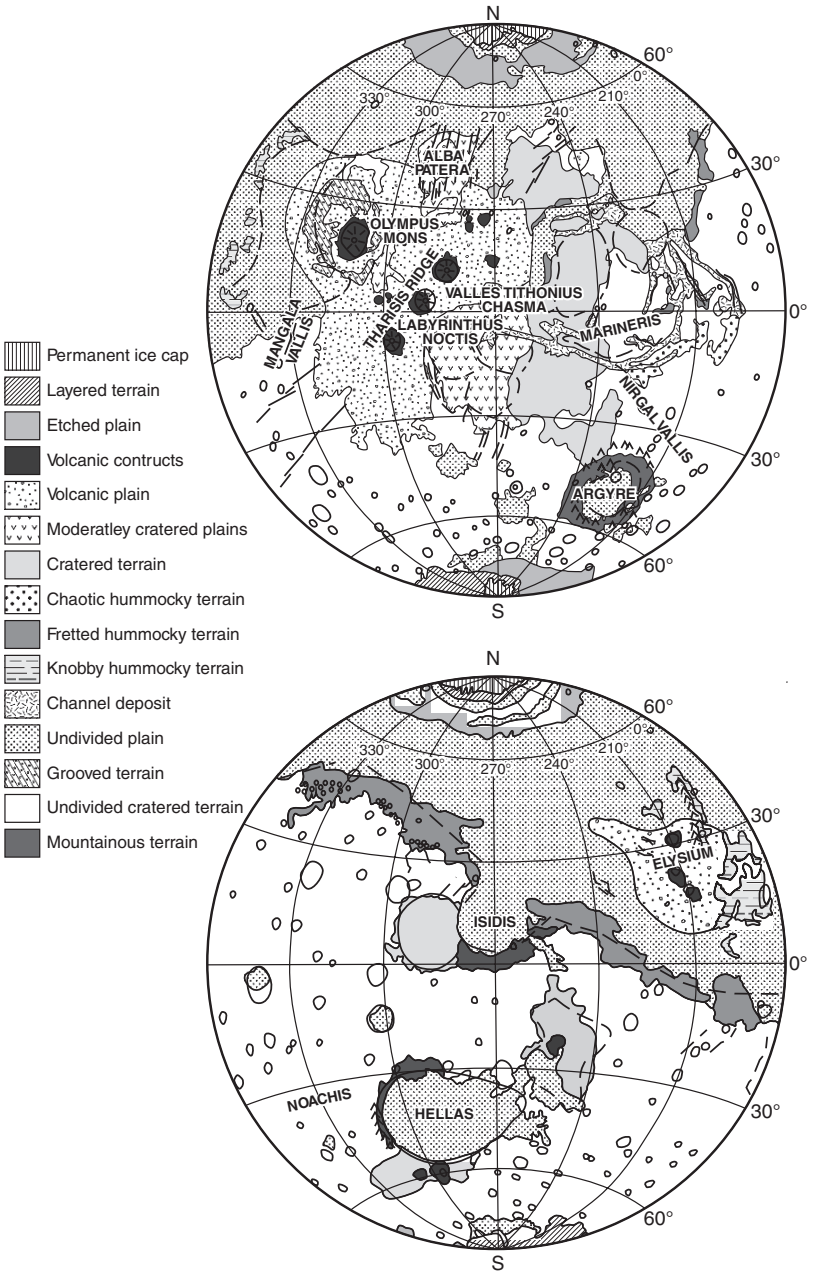


Fig. 12.1 An early geological map published by Pollack (1975)

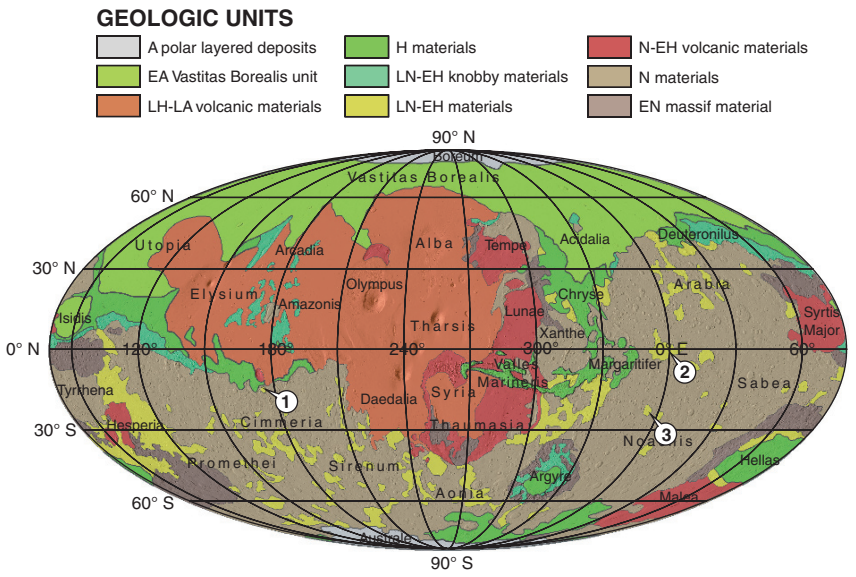
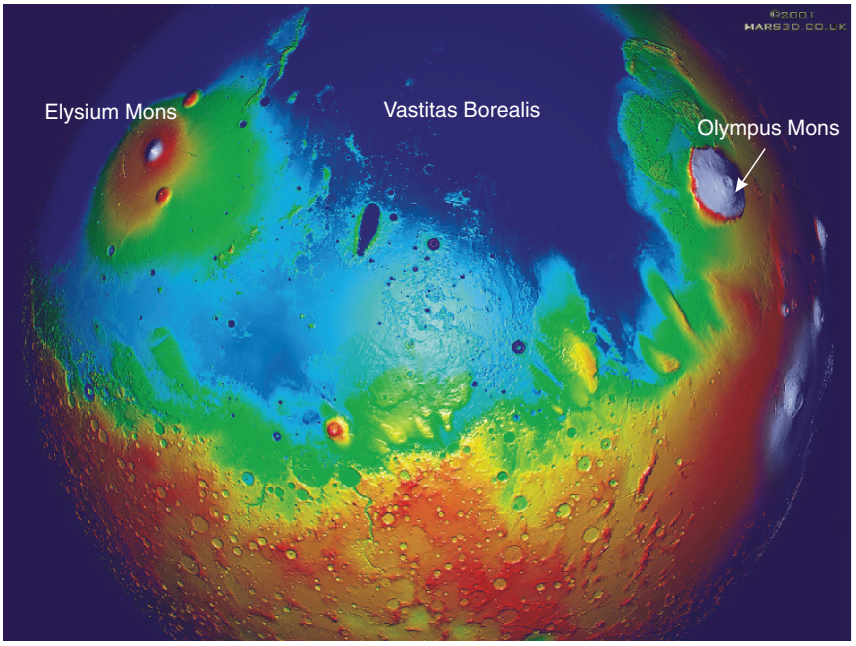


Fig. 12.2 A more recent geological compilation by Nimmo and Tanaka (2005); showing position of some of the features discussed in this chapter, 1 Gusev crater; 2 Meridiani Planum; 3 Holden crater

centres of this period are characterised by a morphology of low-lying edifices, suggestive of magma-water and/or ice interaction (see section 12.3.4) and explosive eruptions, from which ejecta material was widely dispersed around the volcanic centres (Head and Wilson 2002). At least three major trends characterise the Hesperian period (Head and Wilson 2002): (1) change from regional to local volcanism and associated decrease in magmatism; (2) this was accompanied by a decrease in heat flux with corresponding increase in cryosphere thickness; and (3) large scale water movement with formation of outflow channels, breaching of the cryosphere and transfer of water from the subsurface to the surface. During the Amazonian both tectonism and volcanism decreased in Tharsis and Elysium and there was a change of style of volcanic eruptions from explosive to effusive, perhaps reflecting the depletion in the supply of groundwater. The cryosphere reached its maximum thickeness in the Amazonian. The Amazonian is also characterised by late phases of channel formation, lobate debris-flow deposits in Elysium and Utopia regions, aeolian activity and formation of polar deposits, as seen today. Also in the Amazonian, magma-water interactions become less frequent, due to less groundwater and magmatic flux, but where this occurred with penetration of igneous system of the cryopshere, release of sediment-charged groundwater resulted in lahar-type deposits (Head and Wilson 2002).

The surface of Mars shows a distinct hemispheric dichotomy (Figs. 12.2 and 12.3), represented by: (1) ancient heavily cratered highlands covering most



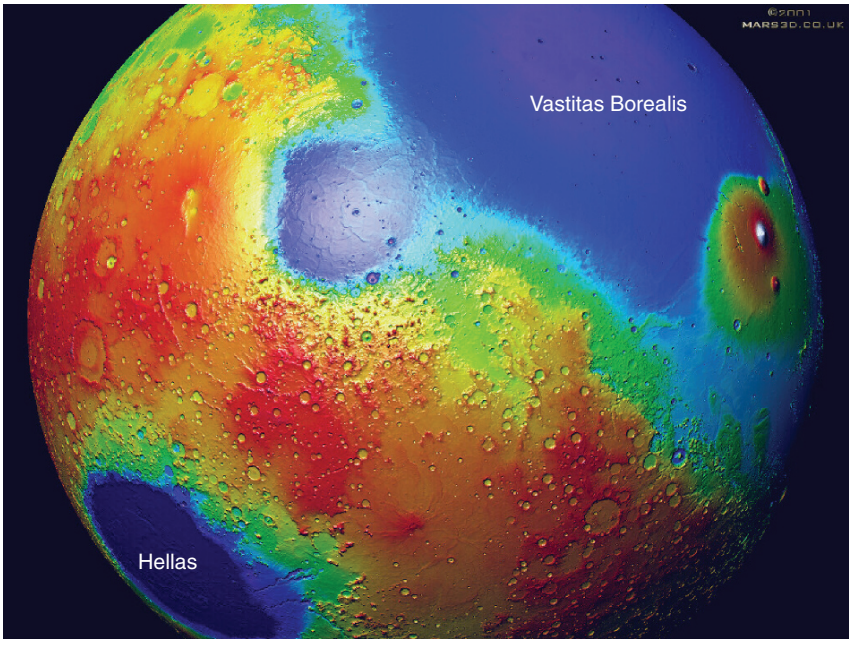


Fig. 12.3 (continued)

of the southern hemisphere and parts of the northern hemisphere that rise between 1 and 4 km above; (2) lowland plains in the northern hemisphere, referred to as Vastitas Borealis (Latin for vast northern plains), which occupy about one third of the planet's surface. The reasons for this dichotomy are not known, but some suggest that the northern plains may have been covered by a shallow ocean (Head et al. 1999; Clifford and Parker 2001). The flatness and smoothness of the northern lowlands, ringed by surface features for thousands of kilometres, as revealed by high-resolution altimetric data from Mars Global Surveyor and Mars Orbiter Laser Altimeter (MOLA), can be interpreted as shorelines and could have enclosed a large body of standing water or ocean, and this would have played and important role in the climatic history of the planet (Head et al. 1999). Although the shorelines hypothesis has been disputed, on the basis of long-wavelength trends of the topographic profiles, Perron et al. (2007, and references therein) reinforced the ocean hypothesis by proposing that the long wavelength topography can be interpreted as due to deformation caused by true polar wander, or in other words a change of the orientation of the planet with respect to the pole of rotation. Outflow channels appear to empty into the lowlands. However, the young appearance of these lowlands is deceptive because quasi-circular depressions first spotted by MOLA (Frey 2006), turn out to be subsurface large-diameter impact basins. Watters et al. (2006) analysed data from the Mars Advanced Radar for Subsurface and Ionospheric Sounding (MARSIS) and produced "radargrams" that show parabolic features of possible impact basins with diameters between ~200 and ~310 km. These buried basins have no surface expression in the lowlands.

In the cratered southern hemisphere are two very large circular basins, Argyre and Hellas, both of impact origin and in some way similar to the mare basins of the Moon. The Hellas basin (Hellas Planitia) with a diameter of about 2300 km, a relief of about 9 km is the largest known impact structure in the Solar System. To the west is the 1500-km diameter Argyre basin (Argyre Planitia).

Baker (2006a) advocated that plate tectonics occurred early in the geological history (Early Noachian) of Mars. Baker (2006a) proposed that in the early stages of planet formation a steam atmosphere rich in CO_2 and H_2O would have been generated above a magma ocean, which then formed a crust. With progressive cooling there was condensation of the steam atmosphere forming a water ocean. Baker reasoned that the juxtaposition of a water ocean on hot

Fig. 12.3 (continued) The crustal dichotomy of Mars is dramatically shown in the topography images obtained from MOLA (Mars Orbiter Laser Altimeter on the Mars Global Surveyor); elevations shown by colours, from lowest as deep blue (eg Vastitas Borealis), to grey-white being the highest (eg Olympus Mons). Image credit MOLA science team (http://ltpwww.gsfc.nasa.gov/tharsis/mola.html last opened in 2007), but no longer available, see web site http://ssed.gsfc.nasa.gov/tharsis/mola.html (last opened in April 2008)

crust would have been ideal for subduction, thereby initiating plate tectonic processes. This early phase of plate tectonics occurred during a phase of heavy meteorite bombardment and was associated with a strong core dynamo, as indicated by the remanent magnetism observed today in the southern highlands. More importantly, the subduction of slabs conveyed H_2O, CO_2 and sulphates down to the core mantle boundary layer. The impingement of these subducted materials would have promoted the growth of a solid core. With progressive cooling and core solidification the dynamo effects were terminated. Some time after termination of the core dynamo, plate tectonic processes also came to an end, perhaps about 4 Ga ago, when Mars become a one-plate planet with stagnant lid convection and mantle plume activity. Anguita et al. (2006) carried out a detailed structural analysis of the Thaumasia region (Fig. 12.2) focusing on previously studied north-trending compressional and extensional structures such as grabens, strike-slip faults, normal faults, folds and thrusts (Plescia and Saunders 1982), and compared them to those of the Iberian chain in central Spain and the Cantabrian alpine belt of northern Spain. Anguita et al. (2006) suggested that these tectonic structures are the result of an Earth-style orogenic belt, named the Thaumasia-Aonia Orogen. This orogenic chain extends for at least 5000 km, is 2000 km wide and, based on crater counts, was formed between 4 and 3 Ga (Noachian-Hesperian), prior to the inception of the Tharsis bulge. The authors concluded that the Thaumasia block has some similarities with the southeastern sector of the Eurasia plate, with zones of compression along the margins and strike-slip and extensional structures in the interior.

Finally, for a brief mention of the Martian regolith. This consists of high-albedo fine-grained dust and low-albedo (dark) sand dunes and drifts, indurated soils and rock fragments (Wyatt and McSween 2006). The northern lowlands have Hesperian to Amazonian materials that make up the Vastitas Borealis Formation, mostly re-worked sediments and residues derived from the sublimation of frozen water (Wyatt and McSween 2006 and references cited therein). Metre-thick ice-rich sediments form a more or less continuous mantle towards the polar regions (Mustard et al. 2001).

12.3.1 Volcanism, Rifting and Mantle Plumes

Important geological and morphological features of Mars include rises and volcanoes associated with narrow graben and fracture systems, channels and valley networks, and impact craters. A dominant feature of Mars is Tharsis Rise, an elevated domal feature about 4000 km wide, which comprises 25% of the planet's surface and rises to about 10 km above the mean surface in the central part (Figs. 12.1 and 12.2). The Tharsis Rise is coincident with a large gravity anomaly and constitutes a large igneous province of some 6.5×10^6 km^2 (Head and Coffin 1997). On Earth, igneous provinces of large extent and emplaced in the interior of tectonic plates, that is not related to convergent

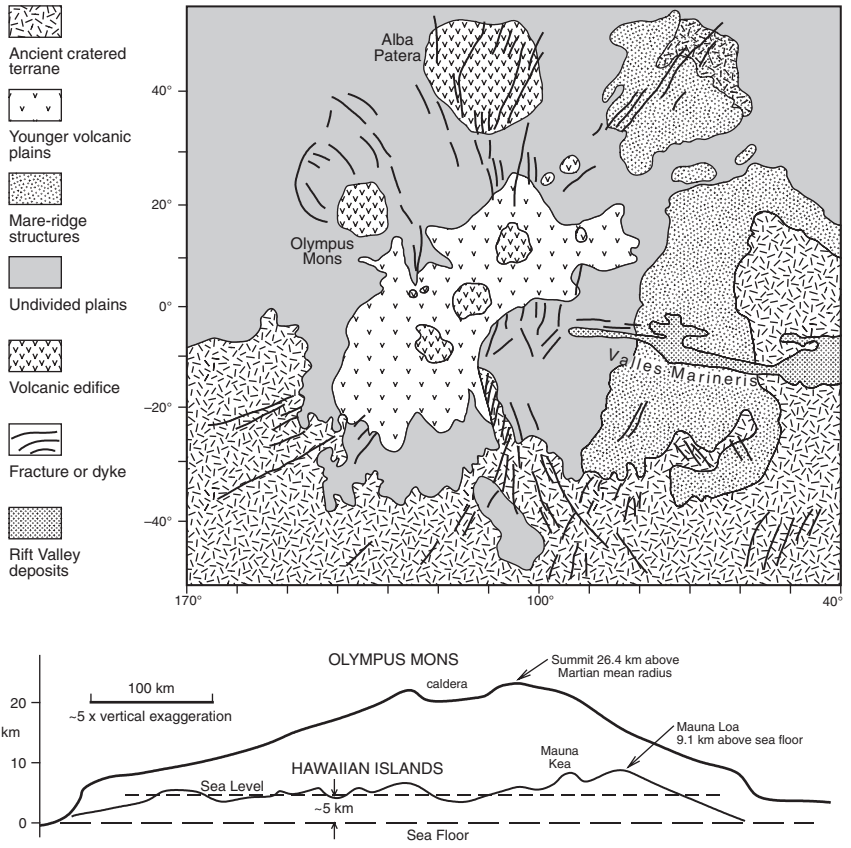


Fig. 12.4 Simplified geological map of the Tharsis province (after Head and Solomon 1981); below the geological map are the profiles, at the same scale, of Olympus Mons and the Hawaiian volcanic system (after Carr 1990)

margins, are called LIPs for large igneous provinces (see Chapter 3). On its northwest flank are Tharsis Montes, formed by three large shield volcanoes: Ascraeus Mons, Pavonis Mons and Arsia Mons, which are aligned along a northeast-trending line (Figs. 12.4 and 12.5). The Tharsis volcanoes are associated with giant radiating dyke swarms. To the northwest of Tharsis is Olympus Mons, the largest known volcano in the Solar System. Olympus Mons is a shield volcano, 24 km high and 550 km in diameter, surrounded by an escarpment 6 km high. By comparison, the largest volcano on Earth is Mauna Loa, which rises about 10 km above the ocean floor and is 120 km at its base (Fig. 12.4). Both Olympus Mons and Mauna Loa have summit calderas. Another major dome feature on Mars is Elysium Planitia, 1700 by 2400 km, and comprising three volcanoes: Hecates Tholus, Elysium Mons and Albor Tholus. North of the Tharsis region lies Alba Patera, a volcano about 7 km high

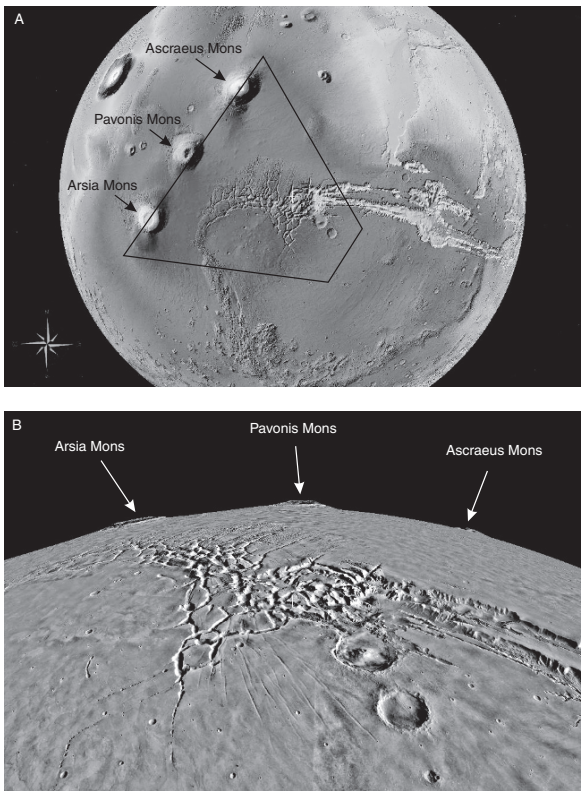


Fig. 12.5 (**A**) MOLA image of Mars centered at about S Lat 9.40475621 E Long 910.53755816, western end of Valles Marineris exhibits a frayed or multifractured pattern, possibly due to repeated and progressive catastrophic sappings; (**B**) inclined perspective of area shown by polygon in (**A**); height exaggeration is 5X. Images obtained from NASA World Wind. The Mars Global Surveyor spacecraft was launched by NASA in November 1996, MOLA-2 or Mars Orbiter Laser Altimeter, has a laser altimeter with a range precision of 37 cm and a vertical accuracy of about 1 m. The original MOLA instrument was described by Zuber et al. (1992), other relevant papers from the MOLA team include Carr and Garvin (2001) and Zuber (2001)

and with a base diameter is 1500 km (Fig. 12.4). It is estimated that the Tharsis rise volcanism on Mars covered a period from about 1.0 to 0.1 Ga, a time span which is much longer that equivalent terrestrial LIPs (1–2 Ma). It is estimated that the volume of Martian flood volcanism is in the region of 26×10^6 km^3, corresponding to a mean thickeness of 200 m if averaged over the entire surface of the planet (Greeley 1987). There is general consensus that the Tharsis Rise, together with its principal features that include the large shield volcanoes (Olympus Mons, Alba Patera, Tharsis Montes) and the great rift system of Valles Marineris (see below) is the surface expression of a deep mantle plume (Mège and Masson 1996). This mantle superplume could have been induced by a large asteroid impact (Reese et al. 2002), or the initiation of the Tharsis superplume could have been initiated by focused subduction, according to Baker (2006a). This author suggested that some form of subduction was taking place early in the evolution of the planet, with cool plate slabs sinking to the core mantle boundary. Partial melting of the volatile-rich material would have initiated the rise of the Tharsis superplume. Flood volcanism may be an important component of the Martian surface, as it is estimated that at least

82% of the planet's surface is covered by volcanic plains and plateaux (McEwen 1999; Keszthelyi and McEwen 2007). Some of the flood lavas appear fresh and with only few impact craters and for this reason considered to be less than 10 Ma. This may be the case for an extensive region, about the size of Canada, in the Cerberus and Amazonis plains, where a radar-rough area is interpreted to represent flood lava flows (Keszthelyi et al. 2000).

Williams and Greeley (1994) examined the hypothesis that large asteroid impacts can cause enough antipodal disruption to cause mantle upwelling and volcanism. These reseachers observed that the Hellas impact basin which lies at 40° S 292° W was its antipodal 40° N 112° W site that corresponds to the large volcanic construct of Alba Patera (Figs. 12.1, 12.2 and 12.3). They suggested that this volcanism could be the result of focussing of seismic energy caused by the large impact that formed the Hellas basin. Similarly, the Isidis and Argyre basins (Figs. 12.1, 12.2 and 12.3), have corresponding antipodes characterised by Hesperian volcanic features and fractured units. Similar observations were made for the moon in respect of the Mare Imbrium basin with antipodal disrupted formations, possibly produced by impact-induced seismic activity. The Mare Imbrium impact would have caused a 600 km deep excavation cavity and would have produced strong ground movement at the antipodes. Mathematical modelling further indicates that these seismic effects can be much stronger in a planet with a molten interior than in a completely solid planet (Schultz and Gault 1975; Hughes et al. 1977; Williams and Greeley 1994). On the other hand, Reese et al. (2002, 2004), suggested that a mantle plume generated from the core-mantle boundary and participating in mantle convection would be unlikely in a small planet like Mars. According to Reese and co-workers large quantities of melt generated by an asteroid impact would have obliterated the initial impact crater. A mathematical model was advanced to show that localised mantle upwelling results in decompression melt volumes on the order of those observed for Tharsis. These same concepts have been applied to planet Earth, with several studies using computational simulations exploring the cause-and-effect connection that could account for close temporal relationship of some large igneous provinces with asteroid impact events (Abbott and Isley 2002; Ingle and Coffin 2004; Elkins-Tanton and Hager 2005). The evidence in all cases is not well constrained. Nevertheless, there are a number of intriguing features that provide much food for thought on this topic, here I will only mention the antipodal effects of asteroid impacts studied by Boslough et al. (1996) and Hagstrum (2005), because these may furnish more insights on planetary analogues, such as the above mentioned Martian and Lunar cases. Seismological simulations of the distribution of impact energy indicate that the locus of maximum energy lies along the antipodal axis and that the most intense focusing is actually within the asthenosphere at the antipode (Boslough et al. 1996). Boslough et al. (1996) made the point that the convergence of surface and body waves at the antipode of earthquakes is a well-known phenomenon that has been and is being used by seismologists in order to obtain information on the Earth's interior. The focussing of seismic energy along a planetary axis

does provide a mechanism to produce a thermal anomaly in the antipodal asthenophere that could trigger large scale volcanism. Hagstrum (2005) reviewed the distribution of 45 terrestrial hot spots and found that 49% of these have antipodal pairs and that all have one oceanic hotspot that are opposite to a continental one. Hagstrum (2005) suggested that an oceanic hot spot can be formed by asteroid impact into the ocean and that a second antipodal hot spot may result from focused seismic energy in the lithosphere and asthenosphere, resulting in a continental large igneous province.

The Valles Marineris rift system extends for some 4500 km, is in places 600 km wide and as much as 10 km deep (Fig. 12.5) (Carr 1999). The rift system consists of numerous canyons that from the Syria Planum merge into a series of outflow channels and chaotic terrains. High-resolution images from the Mars Orbital Camera revealed that the walls of Valles Marineris consist of layered successions, about 8 km thick, including basaltic flood lavas (McEwen 1999). These layered successions are contained within trough structures and one of these is a marginal depression, just south of the trough called Melas Chasma, where there are well-exposed sedimentary layers, forming depositional sequences bounded by unconformities quite similar to terrestrial deposits (Dromart et al. 2007). Whereas earlier I suggested that the Tharsis Rise and Valles Marineris could be comparable to the African Plate and the East African Rift System, Komatsu et al. (2004a, b) compared the Tharsis Rise to the Mongolia-southern Siberia plateau and the Valles Marineris to the Baikal rift system. These authors suggested that tectonic and magmatic processes in these two areas on Mars and Earth are comparable, especially in terms of dynamic uplift, drainage systems, rifting, sub-ice volcanism and associated cataclysmic floods. The Mongolian plateau has an average elevation of 2000 m and is characterized by a basin-and-range topography, presence of major domes with altitudes in excess of 3000 m, anomalous low seismic velocities, high heat flow and is dissected by rifts of Cenozoic age that define a triple junction (Windley and Allen 1993). The Mongolian plateau and the Baikal rift zone are also the focus of intraplate alkaline basaltic volcanism. All these features (uplift and doming, high heat flow, rifts, alkaline volcanism) are indicative of lithospheric thinning and extension above a hot asthenospheric mantle and are consistent with the plateau representing the initial stages of mantle plume-lithosphere interaction (Windley and Allen 1993; Zorin et al. 2003). In the Baikal rift region, Cenozoic-Quaternary basaltic volcanism is typically governed by ice-magma interactions (sub-ice volcanoes called "tuyas", dominated by hyaloclastite accumulations and layered deposits related to flooding; Komatsu et al. 2004b). Similarly in the Valles Marineris on Mars, interior layered deposits (ILD; Komatsu et al. 2004b) are interpreted as volcanic sheet flows and distal volcanic turbidites. In addition, other volcanic landforms such as dykes, vents and volcanic necks are recognised. Komatsu et al. (2004b) suggested that the ILD in Valles Marineris are related to sub-ice volcanic processes similar to those observed in the Baikal rift zone. Komatsu et al. (2004a, b) also hinted at the possibility of hydrothermal systems related to

sub-ice volcanic processes. Other examples of terrestrial sub-ice volcanoes that can have Martian analogues, can be found in southern Siberia (Tuva volcanic province) and Iceland, where they form tuyas and hyaloclastite ridges, due to eruptions that melt ice and generate large outburst mudflows (Chapman 2002a; Komatsu et al. 2006). These tuyas are geomorphic features, sometimes referred to as table mountains, because they are characterised by a flat-topped mesa. Volcanic tuyas are formed in four stages (Chapman 2002a): (1) eruption of pillow lavas beneath the ice; (2) overlain by a hyalotuff cone; (3) slope failure by gravitational collapse forming on the flanks of the tuff cone a; (4) hyaloclastite delta; (5) subaerial lava may cap the tuff cone giving the final shape the tuya. Ridges of hyaloclastite material, which can be capped by lavas, are similar to tuyas, except that they have a linear form. Rocks of these tuyas consist of sublalkaline basalt, hawaiite and basanite. A comprehensive review of the Tuva volcanism is provided by Sugorakova et al. (2003). Chapman (2002a) noted that features similar to terrestrial sub-ice volcanoes could exist on Mars. Landforms that resemble tuyas can be seen in Acidalia Planitia, in Utopia Planitia, both in the northern plains (Vastitas Borealis) and possible hyaloclastite ridges on the northwest flank of Elysium Mons volcano (Figs. 12.1. and 12.2). Chapman (2002b) suggested that lacustrine and other layered sediments on Mars may represent tephra deposits formed during volcano-ice interactions.

To the south of the Valles Marineris rift valley is another volcanic plateau region, the Thausamia plateau, which has a close temporal association of volcanism, rift systems, networks of erosional valleys and impact craters (Dohm and Tanaka 1999). Uplift of the Thaumasia plateau is believed to be related to deep intrusions. It is of interest to note that the erosional valleys have been interpreted to be the result of hydrothermal activity due to magmatic intrusions into groundwater systems (Farmer 1996; Gulick 1998).

As mentioned above, most planetary scientists favour the idea that Tharsis is a large hotspot, and as such the surface expression of a mantle plume on a stationary one-plate lithosphere. This contrasts with terrestrial hotspots, which move away from the source plume due to lateral movement of the tectonic plates, as exemplified by the Hawaiian chain. On the basis of gravity data and distribution of volcanic features on Mars, which are largely restricted to the Tharsis region, Harder and Christensen (1996) suggested a one-plume model of mantle convection, forming a single and large upwelling beneath Tharsis. Other authors (e.g. Schubert et al. 1990) invoked cylindrical plumes as the probable form of mantle upwelling, which are counteracted by planar downwellings. Mège and Masson (1996) discussed details of a plume model for the Tharsis region. Models of Martian mantle convection and the rise of plumes and their role in establishing surface topography and volcanic flux can be found in Schubert et al. (2001). One of the major features of the Tharsis Rise is the presence of radial graben and fracture systems, which extend for as much as 3000–4000 km (Wilson and Head 2002). These graben and fractures radiate southwest, south and southeast from Arsia Mons and Syria Planum (Figs. 12.4 and 12.5). Wilson and Head (2002), on the basis of numerical

modelling and geological relationships obtained from MOLA, suggested that these radial graben and fractures represent a giant dyke swarms analogous to the Mackenzie dyke swarm in Canada (Ernst and Baragar 1992; Ernst et al. 2001). These processes of dyke intrusions and interaction with the cryosphere (subsurface frozen ground, estimated to range from ~2 to ~13 km thick; Clifford and Parker 2001), could also result in the inception of giant hydrothermal circulation cells (Wilson and Head 2002).

An extensive area of narrow ridges is present northeast of the Huygens crater and was interpreted by Head et al. (2006) as representing a major dyke swarm. On the basis of relationships with other features, such as valley networks and impact craters, this dyke swarm is thought to have been emplaced near the Noachian-Hesperian boundary (~3.6 Ga) and may have been linked to extensive surface volcanism that, as speculated by Head et al. (2006), would have placed large amounts of volatiles into the Martian atmosphere producing sufficient warming that in turn would have resulted in pluvial or surface sublimation to cause extensive melting and/or runoff conditions.

12.3.2 The Findings by the Spirit and Opportunity Rovers

The sensational findings of NASA's rovers Spirit and Opportunity, have been reported and documented in detail by the mission's planetary scientists (e.g. Bell et al. 2004; Christensen et al. 2004a, b; Gellert et al. 2004; Morris et al. 2004; Herkenhoff et al. 2004a, b; Rieder et al. 2004; Squyres et al. 2004a, b; Klingelhöfer et al. 2004; McSween et al. 2004). The rovers, equipped with a Microscopy Imager, Alpha Particle X-ray spectrometer, Mössbauer and Miniature Thermal Emission (Mini-TES) spectrometers, provided information on the textures, partial chemical analyses of rocks and soils, Mössbauer and Mini-TES spectra at Gusev crater and Meridiani Planum (Fig. 12.2). A panoramic camera (Pancam) furnished details of the landscape. Table 12.2 lists acronyms and explanations used by the imaging teams.

12.3.2.1 Spirit Rover at Gusev Crater

The Microscopy Imager detected volcanic textures, alteration rinds and veins of possible secondary mineralisation as well as weathering textures due to impacts, wind and perhaps water. The Alpha Particle X-ray spectra are consistent with rocks of basaltic composition and revealed high abundances of bromine. The elevated Br abundances have been interpreted as alteration due to water (Gellert et al. 2004). Olivine, pyroxene and ferric-bearing phases were detected in Mössbauer spectra, whereas the Mini-TES was able to provide some details of the mineralogical composition of the rocks (Ca-rich pyroxene, pigeonite, forsterite, sodic to intermediate plagioclase; Christensen et al. 2004a). The Gusev basaltic rocks are geochemically primitive (Mg-rich and K-poor),

Table 12.2 List of selected acronyms commonly used by the NASA and European Space Agency (ESA) imaging teams (in part from McSween 2006)

Acronym	Significance	Explanation
MOLA	Mars Orbiter Laser Altimeter	Measures topography using laser reflections
MOC	Mars Orbiting Camera	High resolution digital imaging
Mini TES	Miniature Thermal Emission Spectrometer	Spectrometer device to identify minerals using lattice vibrational motions
TES	Thermal Emission Spectrometer	Measures infrared spectra
Mössbauer	Mössbauer spectrometer	Spectrometer that identifies Fe-bearing minerals by measuring nuclear oscillations
Pancam	Panoramic camera	Colour imaging device
THEMIS	Thermal Emission Imaging System	Imaging system to record heat emitted from the surface
OMEGA	Observatoire pour la Mineralogie, l'Eau, les Glaces et l'Activité	Visible and near infrared (IR) reflectance spectrometer for the identification of minerals by using absorptions due to electronic transitions and molecular vibrations
APXS	Alpha particle X-ray Spectrometer	Measures bulk rock chemistry using interactions of alpha particles with the target
GRS	Gamma ray spectrometer	Measures abundance of H and other elements by their interactions with neutrons
VNIR	Visible Near Infrared spectra	
MGS	Mars Global Surveyor	
MO	Mars Odyssey	
MEX	Mars Express	
MAWD	Mars Atmospheric Water Detector	
MRO	Mars Reconnaissance Orbiter	
MARSIS	Mars Advanced Radar for Subsurface and Ionospheric Sounding	Multifrequency synthetic aperture orbital sounding radar, can "see" the subsurface through "radargrams"
HiRISE	High resolution Imaging Science Experiment	

indicating that they were produced by a high degree of partial melting and therefore they may be comparable to terrestrial komatiites or picrites. Chemical analyses of lavas in the Gusev crater by the Alpha Particle X-ray spectrometer indicated compositions that are consistent with picritic basalt, and containing olivine, pyroxene, plagioclase and FeTi oxides.

Mössbauer spectra measurements by Spirit rover indicate that rocks and soils in the Gusev crater contain olivine, pyroxene, magnetite and hematite. The rocks are olivine-rich basalts, as revealed by the Mini-TES spectra, with a mineralogy, calculated from soils, averaging 20% Ca-rich pyroxene, 25% pigeonite, 40% plagioclase and 15% olivine. These basaltic rocks have coatings or rinds of Fe oxides, suggesting surface alteration or weathering.

12.3.2.2 Opportunity Rover

Opportunity travelled several hundreds metres across Meridiani Planum (so named because this site is at the intersection of the equator with the prime meridian; Squyres et al. 2004a), from the landing site at Eagle crater (20 m diameter), eastward to Endurance crater (156 m diameter). The Pancam showed flat-lying sedimentary rocks, finely laminated (mm scale) and cross-stratified. Hematite spherules (called blueberries by the mission scientists; Fig. 12.6A), typically 4–6 mm in diameter, are embedded in the rocks and are interpreted as concretions (Fig. 12.6B), formed by aqueous fluids (Squyres et al. 2004a). Vugs are also present in some units and consist of tabular prismatic shapes that cut across the laminations to form openings of about 1 cm long and 1–2 mm wide. Vugs' shapes are consistent with a sulphate precursor mineral, gypsum or kieserite, which must have been dissolved by fluids, leaving behind voids.

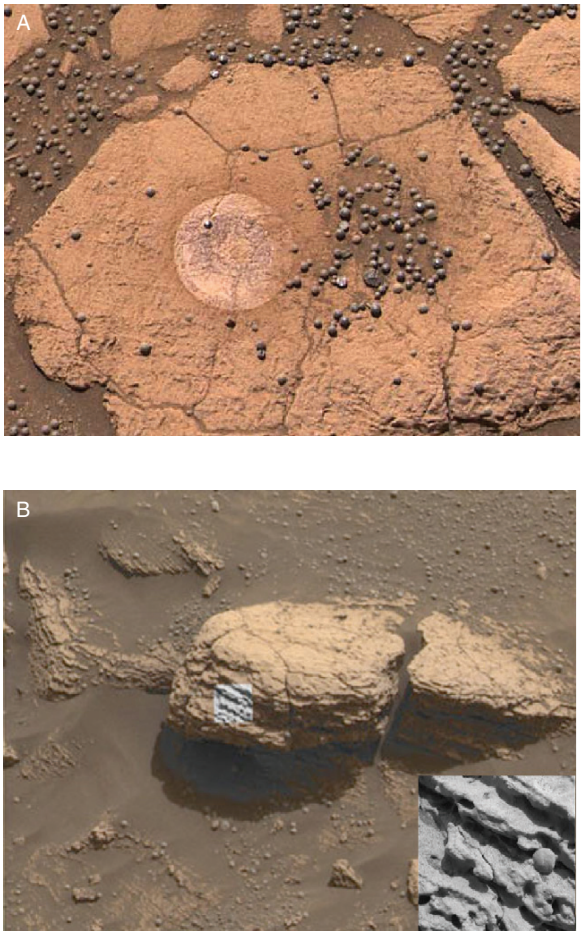


Fig. 12.6 Hematite spherules, called "blue berries", are found strewn across large areas of Mars. They are also found embedded as concretions in the rocks. The spherules in (**A**) have a diameter of about 4 mm; (**B**) sherules embedded in rock, here a 3 cm inset shows the details of an embedded spherule. Credit: Mars Exploration Rover Mission, NASA/JPL, both pictures obtained from the website http://antwrp.gsfc.nasa.gov/aopd/ap040210.html (last opened in 2007, but no longer available). For an exhaustive atlas of Pancam pictures visit http://pancam.astro.cornell.edu/pancam_instrument/true_color2.html (last opened in April 2008)

Hematite spherules are also found as surficial lags in the soils of the landing site, and were probably derived from the erosion of spherule-bearing rocks (Squyres et al. 2004b; Christensen et al. 2004b). These Martian spherules have been compared to concretions in terrestrial sandstone, as explained in Section 12.3.4.1. A very important finding is that the rocks at Meridiani Planum are also enriched in jarosite and other sulphates as detailed below (Squyres et al. 2004a). In addition to hematite and sulphates, Mini-TES spectra also revealed the presence of feldspar, olivine, and pyroxene. A final analysis of the Meridiani Planum sedimentary rocks showed that they consist of 50 wt% fine-grained siliciclastics, derived from the weathering of basalt, about 20–40 wt% Mg and Ca sulphates and jarosite and about 10 wt% hematite concretions (Squyres et al. 2004a). Examination of the soils at the landing site revealed that these are dominated by fine-grained basaltic sands and that hematite in the soils is concentrated as spherules, referred to above, and fragments thereof. Outcrops in the Eagle crater have embedded spherules, showing a uniform spatial distribution. These rocks have high abundances of SO_3, up to 25 wt%, and this is probably present as sulphates, as detected by the Mössbauer spectra. The spherules, having more than 80% hematite by mass, have a different composition than the rocks in which they occur. These spherules have been interpreted as having formed by precipitation from aqueous fluids, within the rock after it was formed. The sedimentary rocks exhibit laminations and cross-stratification, which are interpreted as a combination of aeolian and aqueous processes.

Near the rim of Eagle Crater a 40 cm high rock, named Bounce Rock by the team investigators, whose composition as revealed by Mössbauer spectra is distinct from the rocks of the crater. Bounce Rock consists clinopyroxene (55%), orthopyroxene (5%), plagioclase (20%), olivine (5%) and 10% oxides. The chemical and mineralogical composition of Bounce Rock is essentially similar to a shergottite, a meteorite found on Earth but that originated from Mars (see Section 12.3.4). Therefore, the distinct characteristics of Bounce Rock together with its isolated position, indicate that it may be one of the ballistic ejecta from a nearby impact crater. Colour Pancam multispectral observations in the visible and near-infrared, in the Eagle crater, are consistent with ferric and ferrous Fe oxides, which possibly include mixtures of hematite, jarosite and goethite. Spectra of dark spherules also exhibit ferric Fe signatures. Mini-TES spectra of outcrops indicate 20–40 wt% of Ca and Mg sulphates. As mentioned above, the element Br is present in substantial concentrations, which in outcrop rocks range from 30 to 440 ppm. The hematite spherules are strewn across the Opportunity landing area and are found inside the Eagle crater and the surrounding plains. These spherules are considered the primary carriers of the grey hematite detected from orbit by the Mars Globa Surveyor and reported by Christensen et al. (2001). Photographs of Martian spherules are shown in Fig. 12.6. Mini-TES observations of rocks and soils at Meridiani Planum have also shown that other mineral phases, such as quartz, chert and carbonate are not present at abundances greater than 5%.

Mission investigators have proposed that the materials of Meridiani Planum are a mixture of chemical and siliciclastic sediments derived from basaltic rocks and that have undergone complex diagenetic processes, under environmental conditions characterised by episodic flooding, followed by evaporation and desiccation. The hematite concretions formed in this environment through precipitation from groundwater. Following this activity of aqueous deposition and diagenetic processes, a thin layer of basaltic sand was deposited on the sulphate-rich sedimentary material. This evolutionary sequence clearly points to a stage in the geological history of Mars when liquid water was an active player on its surface. But exactly when, was liquid water running on the Martian surface? The OMEGA mission, discussed in the Section that follows, may have provided an answer.

12.3.3 The Findings of the OMEGA Mission and Their Implications

Mineralogical mapping of Mars was conducted by OMEGA (Table 12.2), an instrument on board the Mars Express of the European Space Agency (ESA). The OMEGA instrument covered more than 75% of the surface of Mars at a resolution of 0.3–4.8 km per pixel, using visible-near-infrared hyperspectral reflectance imagery. The results, integrated with the data provided by Mars Global Surveyor (MGS) and THEMIS (Thermal Emission Imaging System), reported by Poulet et al. (2005), Langevin et al. (2005), Gendrin et al. (2005), Bibring et al. (2005, 2006) and Wyatt and McSween (2006), are outlined here.

The OMEGA team identified mafic and ultramafic minerals including high-Ca and low-Ca pyroxene, and olivine, suggesting basalt and andesitic basalt rock types. Olivine-rich surfaces were found in crater floors and rims around Syrtis Major and in craters with diameters $<$20 km an their lobate ejecta in the Vastitas Borealis region (Figs. 12.1, 12.2 and 12.3). Sulphate minerals, probably gypsum and possibly also bassanite ($2CaSO_4 \cdot H_2O$), were detected in the north polar regions, correlating with dark longitudinal dune fields of Olympia Planitia. Absorption bands corresponding to other sulphates, kieserite and epsomite ($MgSO_4 \cdot 7H_2O$), in addition to gypsum, were also found in the light-toned layered deposits of Valles Marineris, Margaritifer Terra and Terra Meridiani. In a locality, known as Candor Chasma, in Valles Marineris, kieserite was observed on a 4 km high hill of layered deposits, whereas at another site, Juventae Chasma, gypsum and kieserite occur in horizontal layers, hundreds of metres thick. The OMEGA investigators have pointed out that the sulphates detected by instruments are unlikely to represent simple surface or soil coatings, but are rather a bulk component of the deposits. By analogy with terrestrial environments, the Martian sulphate deposits could have originated by evaporation of water in playa-type lakes (see Section 12.6.2.1), or lagunas connected to sea (sabkhas; see Chapter 8). Furthermore, because of the dominant basaltic component for the Martian rocks, sulphate minerals are likely to be richer in

Fe and Mg relative to Earth sulphates. Sulphates, however, can also be produced by magmatic-sourced S-rich hydrothermal fluids, as explained in Chapter 5 and Section 12.3.4. In addition, the widespread presence of sulphates suggests an acidic environment, which is not conducive to the formation of carbonates that, in fact, have not been identified on Mars. The lack of carbonate deposits on Mars is attributed to the displacement of CO_2 in waters rich in sulphuric acid, but as pointed out by Catling (2007), the temporal evolution of the CO_2 in the planet's atmosphere remains elusive, although the discovery of phyllosilicates in the ancient terrains of the planet may provide an answer, as dicussed below.

The OMEGA Mars Express mission also identified water-bearing phyllosilicates in layered deposits in Valles Marineris, Aram Chaos, Terra Meridiani and areas near the north polar cap, although the presence of phyllosilicates had been previously reported through in situ analyses by the Viking landers. Mineral identification by the OMEGA instrument is in a spectral domain of the solar reflected light with wave lengths of 0.3–3.0 μm, in which minerals exhibit well-defined absorption bands, followed by standard procedures aimed at isolating absorption features relating to water and OH vibrations (for details of remote sensing systems and their use for acquiring information about planets, the interested reader is referred to Rees 2001 and Short 2006). The identified phyllosilicates include the Fe-rich smectite, nontronite, Fe-Mg chlorite, chamosite and Al-rich smectite, montmorillonite. The phyllosilicates were detected in two types of terrains: low albedo (percentage of incoming radiation reflected from a surface) dark deposits and eroded outcrops. The former are mainly found in Arabia Terra, northern Syrtis Major and Terra Meridiani, where absorption features are compatible with the presence of Fe-Mg smectites. Eroded outcrops, first seen in Syrtis Major, and later in Nili Fossae, Mawrth Vallis, around Terra Meridiani and northern Hellas, are characterised by Fe-rich clays. Iron-rich smectite clays, such as nontronites are typically found in hydrothermally altered mafic rocks, and are common on Mars. An interesting case is that of Nili Fossae, a region that experienced strong erosion, as indicated by terrains with chaotic texture, isolated mesas and eroded craters. In this region, areas with olivine were detected not only by OMEGA, but also by TES and THEMIS (Christensen et al. 2006). The areas of high olivine abundance are spatially distinct from those that have high abundances of hydrated mineral phases. Close examination reveals that olivine-rich outcrops actually lie above clay-rich areas, suggesting either that the olivine-rich rocks were deposited on top of the clays, or in other words an earlier water-altered crust, or that olivine-bearing rocks were altered to clays and later exposed by erosion. A large accumulation of phyllosilicates was found in the Mawrth Vallis region in light-toned outcrops in the flanks of the Vallis and on a plateau, but not in the valley itself. These features led the OMEGA team to conclude that these Martian clays were formed as a result of water-based alteration processes. The clays predate the volcanism of Syrtis Major and the Noachian-Early Hesperian cratering; they are not a

surface coating but are a major constituents of the rocks and layered sediments. The formation of clays is generally controlled by rock composition, to some extent by climatic conditions and long-term availability of water. Therefore, the presence of these clays on Mars is indicative that conditions must have been very different from those observed in present day Mars. In Noachian times, Mars must have had an active and sustained hydrological system in order to alter the mafic igneous rocks to clays. Furthermore, the Martian climate must have been considerably warmer or alternatively the fluids that produced the clays must have been hot. Surface formation of clay minerals would have to involve a long permanence of surface and alkaline water. But, clay minerals can also be formed in the subsurface by hydrothermal activity, by one of two processes; (1) impact cratering delivering groundwater to the surface and producing clay alteration; (2) volcanic hydrothermal fluids.

It was emphasised by the OMEGA team that phyllosilicate deposits are distinct from sulphate deposits and that sulphate formation involves acidic water and does not require the long-term residence of water. This is a very important facet, as eloquently discussed by Newsom (2005) on his commentary of the first paper of the OMEGA team (Poulet et al. 2005). Although acid-sulphate conditions on Mars, as detected by the Spirit and Oportunity rovers must have been prevalent for a good part of Mars' geological history, the presence of phyllosilicates in the ancient cratered highlands of Mars is indicative of the fact that Earth-like conditions existed before ~3.7–3.5 Ga. At later stages, however, the Martian surface became more acidic, impeding the formation of phyllosilicates (and of carbonates), leading instead to the deposits of hematite and sulphates, as documented by the Mars rovers. Chevrier et al. (2007) worked on the thermodynamic equilibria of smectites in order to gain some insights as to the geochemical and environmental conditions on the surface of Mars during the Noachian, based on the fact that smectites and phyllosilicates in general, apart from hydrothermal processes are also produced through weathering processes, as a result of the interaction between atmosphere, hydrosphere and lithosphere. Consequently, where hydrothermal processes are not involved, the widespread presence of phyllosilicates is indicative of ion leaching from the primary silicates by liquid water on the surface of Mars. Phyllosilicates, as well as sulphates and carbonates, then precipitate from the leaching fluids. Critically, the precipitation of these secondary minerals is dependent on composition, temperature and pH of the leaching fluids. Chevrier and co-workers' calculations showed that Fe^{3+} phyllosilicates precipitated under weakly acidic to alkaline conditions and that the precipitation of these clay minerals occurred under very low partial pressure of CO_2 and in equilibrium with the atmosphere. This, in turn, would suggest that the absence of carbonates on Mars, is the result of low levels of CO_2 in the atmosphere and therefore greenhouse gases (e.g. CH_4, SO_2), other than CO_2, may have played a role in sustaining the warmer and wet climate in Noachian times (Chevrier et al. 2007). Catling (2007) in his "*News and Views*" commentary of Chevrier et al's paper, argued that the lack of CO_2 could be attributed to early atmospheric loss

(by hydrodynamic escape or planetary wind). The principal issue of Chevrier et al's paper is that the neutral to alkaline conditions necessary to form the phyllosilicates do not require the presence of H_2SO_4 to explain the absence of carbonates on Mars. Instead and as, explained above, the formation of sulphates is associated with more acidic conditions, which developed later in the geological history of the planet. OMEGA did not detect any carbonate minerals, although these should have been present if Mars had a CO_2-rich atmosphere early in its history. Explanations for the absence of carbonates according to Bibring et al. (2006), include: (1) liquid water did not remain on the surface for enough long time to enable the CO_2 from the atmosphere to precipitate carbonates; (2) clay minerals were formed by impact or subsurface hydrothermal processes that did not involve surface liquid water, so that most of the primordial CO_2 remained in the atmosphere; (3) carbonates were precipitated but were subsequently removed by acid weathering; and (4) Mars never did have a CO_2-rich atmosphere. The jury on this issue is still out.

The analysis of OMEGA's data led to further insights on the geological history of Mars. Bibring et al. (2006) proposed that Mars underwent three evolutionary stages, as shown in Fig. 12.7: (1) an early stage, during the Noachian, of non-acid aqueous alteration, traced by phyllosilicate minerals; (2) a stage dominated by acidic alteration in the Hesperian, probably caused by S outgassed by volcanic eruptions, traced by sulphate deposits; and (3) atmospheric aqueous-free alteration, traced by Fe oxides, characterised by lack of hydration, which markedly contrasts with the first two stages, which required abundant liquid water. These stages have been named by Bibring et al. (2006), phyllosian, theiikian and siderikian, respectively (Fig. 12.7). The first stage (phyllosian) has implications for the possibility of extinct life, because it would have offered through the presence of clay minerals the right conditions for the biochemical development of micro-organisms (see relevant discussion in Chapter 10). The second and third stages, however, locally may have been contemporaneous or the siderikian stage may have immediately followed the theiikian (Bibring et al. 2007).

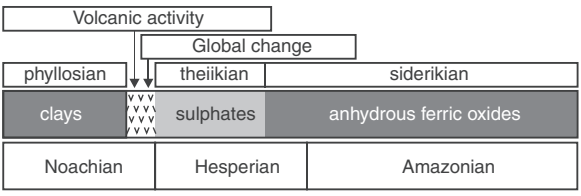


Fig. 12.7 Sketch illustrating the timing of the principal alteration minerals, phyllosilicates, sulphates and Fe oxides, on Mars. Adapted from Bibring et al. (2006)

12.3.4 Water and Potential Hydrothermal Systems on Mars

Evidence of past and/or recent water on Mars is now beyond dispute, as shown in part by geomorphological features such as outflow channels, valley networks



Fig. 12.8 Examples of liquid water flows on Mars; (**A**) valley network and drainage system at mouth of Ares Vallis, teardrop-shaped island in the centre is about 50 km long (Carr 1996)

(Fig. 12.8), giant polygonal patterned terrains and alluvial fans (Carr 1996a, b; Jaumann et al. 2002; Baker 2006b). There is evidence that in the geological past Mars must have had surface temperatures above the freezing point of water, to allow liquid precipitation and runoff. Evidence from the OMEGA findings, shows that surface water was probably quite abundant during the Noachian (4.55–3.7 Ga). This was followed by arid conditions in the Hesperian period (~3.7 to ~3.0 Ga), which allowed the deposition of sulphate-rich and hematite-rich layered sediments at Meridiani Planum. Other important features are recent gullies, glaciers and the polar ice caps, which are believed to be composed of both water and CO_2 ices. The polar regions are also characterised by layered terrains consisting of alternating bands of bright and dark material, probably sedimentary strata formed during cyclical climatic changes (Carr 1999). The recent gullies are associated with debris-flow fan deposits. Glaciated landforms include polygonally patterned ground, frost mounds, debris flows, all consistent with ice-related processes (Baker 2006b). In addition, there may have been at various stages in the planet's history, lakes as documented with compelling evidence by Cabrol and Grin (2002). A special issue of the journal Elements is devoted to water on Mars (McSween 2006).

The polar caps of Mars have been known since the earliest telescope observations, and they are assumed to be composed of H_2O and CO_2 ice. The volume of H_2O estimated in the seasonal caps is about $3 \times 10^{-2}\,km^3$ (Christensen 2006). The size of the polar ice caps of Mars varies seasonally, that is they retreat to a perennial size during the summer seasons (northern and southern). Well-layered sedimentary deposits extend for up to 600 km outward from the polar caps and the layers are defined by dust that is included in the ice (Christensen 2006). The presence of subsurface ice is deduced from the mapping of high hydrogen abundances in the uppermost metres and extending from both poles to about 50° of latitude. In addition, ice-rich materials in mid-latitudes is substantiated by the presence of lobate, grooved and ridge textures that are interpreted from the flow of ice-rich soils and other glacial landforms (Clifford et al. 2000). Ice-rich material is also seen flowing from mesas in the northern

hemisphere, a process that is detected as being currently active (Christensen 2006). Evidence of H_2O on Mars is also provided by Martian meteorites (Leshin and Vicenzi 2006). Martian meteorites, called SNC for shergottite-nakhlite-chassignite, of which the most famous is undoubtedly ALH84001 (discussed further in Section 12.6.2.3), are essentially igneous rocks. The SNC have ages ranging from about 4.5 Ga (ALH84001) to 175–575 Ma for the shergottites. The Martian origin of these meteorites is primarily based on the presence of N_2, Ar and Xe gases trapped in impact-produced glasses, whose isotopic compositions match those of the present-day Martian atmosphere (Leshin and Vicenzi 2006). The nakhlites exhibit the best mineralogical evidence of aqueous alteration, such as presence of iddingsite, a hydrous phase that results from the hydrous breakdown of olivine, and gypsum and halite salts within veinlets that cut the olivine crystals. Hydrogen, O and C isotope systematics provide further evidence of aqueous alteration of Martian meteorites. For example, deuterium (D) enriched water of hydrous minerals (δD values of + 2000 ‰), ^{13}C-enriched CO_2 (δ^{13}C values of + 42 ‰) and δ^{18}O values of 20–30 ‰ (Leshin and Vicenzi 2006).

A recent paper published in Nature by Andrews-Hanna et al. (2007) and commented on by Baker (2007) in the same issue, presents a hypothesis, based on numerical modelling, that early in its history Mars did not have large standing bodies of water, but rather had a globally connected groundwater system, which was probably continuously supplied from the subsurface. This groundwater system was linked to the development of the Tharsis Rise magmatism, responsible for injecting large quantities of H_2O and CO_2 into the Martian atmosphere. The numerical modelling of Andrews-Hanna et al. (2007) focused on the fact that terrestrial non-marine evaporites are deposited in enclosed basins (lakes), following evaporation of the meteoric water and concentration of solutes leached from the surrounding rocks. The Meridiani Planum evaporitic deposits are not situated in an enclosed basin in which bodies of water could have evaporated, but on a tilted plain. Therefore, the Meridiani Planum evaporitic deposits must have formed in a different way. In their modelling the authors considered three scenarios, regarding the Meridiani Planum 7 m thick evaporitic layers of the Burns Formation: (1) they were formed before the Tharsis event; (2) they were formed after the Tharsis event; and (3) they were formed within a steady rate of Tharsis construction over a period of 500 Myrs. In the pre- and post-Tharsis simulation models the water table intersects the surface in most of the northern lowlands, the larger impact basins and Meridiani Planum, where the evaporitic deposits would be formed. In the third scenario, there is a lag between the construction of Tharsis and the migration of the brittle-plastic transition level which, due to loss of porosity and permeability, regulates the groundwater depth. With the uplift of the Tharsis construct, the brittle-plastic transition level migrates downward, resulting in the lowering of the water table in the Tharsis region. This, Andrews-Hanna and co-authors reasoned, must have produced upwelling of groundwater from the subsurface, resulting from the lithostatic pressure of the Tharsis growth.

Groundwater moved through the aquifers to discharge at various sites, such as the Meridiani Planum.

Several of the Martian valley networks exhibit a morphology that is consistent with slow drainage of groundwater and erosion, or in other words sapping processes. These sapping structures probably formed by catastrophic discharges, either seasonal or accidental (Cabrol and Grin 2002; Baker 2006b). These episodic releases of groundwater were common in the geological history of the planet. Each episode was probably short lived, as shown by streamlined islands and striated floors and the resulting flows were likely like giant mudflows. It has been calculated that flow velocities ranged from 4.7 to 27 ms^{-1} (Cabrol and Grin 2002 and references therein). In some cases, valleys have channels comparable to active river channels on Earth (Irwin et al. 2005) and erosion of craters and impact basins by surface run off have called for Earth like precipitations (Cradock and Howard 2002; Baker 2006b). Martian light coloured gullies have been imaged on impact crater walls and have been interpreted as due to present-day flow of liquid water or water-laden debris, with the water coming from groundwater, melting ground ice or snow (Malin et al. 2006). Squyres et al. (2004b), in reviewing the geological record of Meridiani Planum, suggested that the sedimentary rocks have a complex diagenetic history and were formed through episodic inundation of surface water, followed by evaporation and desiccation. Jarosite, identified by Mössbauer spectra, is a H_2O-bearing Fe sulphate, and therefore not only good evidence of water on Mars, but also of aqueous acid sulphate activity under oxidising conditions (Klingelhöfer et al. 2004). These workers calculated an average of 2 wt% H_2O in the jarosite-bearing outcrops of Meridiani Planum. On Earth, jarosite forms in high sulphidation epithermal systems, discussed in Chapter 5.

Burr et al. (2002), examining the data obtained from MOC and MOLA, proposed that the erosional streamlined geomorphic features along the southeast margins of Elysium Mons (Athabasca Valley, Cerberus Fossae) were formed by floodwaters. These floodwater-carved channels are geologically young with possible ages, calculated from crater counts, ranging from 10 to 140 Ma. The origin of the water is not clear, but it considered possible that it may have derived from deep frozen aquifers, melted and mobilised as a result of tectonism and/or magmatic heat. Wyatt and McSween (2006) reviewed the evidence from the identification of surface compositions and mineral phases by TES and VNIR. These authors considered high-albedo and low-albedo surfaces, with the former being consistent with oxidised fine-grained materials probably composed of Fe oxides and perhaps hydroxyl-bearing phases. Low-albedo surfaces are attributed to presence of Fe^{2+} in pyroxene and hematite. High-albedo surface compositions measured by TES, which is sensitive to the chemistry and structure of rock-forming minerals, showed spectral absorptions that are consistent with zeolite and Mg-carbonate, probably magnesite. Wyatt and McSween (2006) pointed out that zeolites are commonly produced on Earth in the cold and dry environment of Antarctica, whereas Mg-carbonates are found as aqueous precipitates in a variety of terrestrial environments.

Low-albedo surface compositions measured by TES showed two spectral end members, called ST1 and ST2 (surface type 1 and 2). ST1 is similar to terrestrial continental flood basalts and consists of plagioclase, high Ca-pyroxene and olivine, whereas ST2 with plagioclase, abundant volcanic glass but less high-Ca pyroxene is similar to andesites and/or altered basalts (Bandfield et al. 2000). The above TES lithological identifications are important because andesites and altered basalts imply some interaction with H_2O. ST1 basalt and ST2 altered basalt seem to dominate in equatorial and mid-latitude, and high-latitude northern lowlands and southern highlands, respectively. Wyatt et al. (2004) interpreted this distribution to ice-rich mantle deposits and suggested a topographic and latitude influence on the surface alteration of the planet. Again due to the cold and dry environment, permafrost and ground ice, there is some analogy with the Dry Valleys of Antarctica.

The sedimentary rocks in Meridiani Planum, as revealed by the rover Opportunity, consists of 30–50% siliciclastic minerals, 20–30% Mg and Ca hydrous sulphates, 15–25% various silica-bearing minerals, 10% jarosite and 6% hematite (Chavdarian and Sumner 2006 and references cited therein). These sedimentary rocks exhibit structures including cross-stratifications that typically form by Aeolian processes, and concretions that are interpreted as evaporite pseudomorphs formed as a result of aqueous alteration. These structures are indicative of a dune field or playa environment (Squyres et al. 2004a, b). Chavdarian and Sumner (2006) examined polygonal cracks and fins in the gypsum-rich dunes of the White Sands National Monument in the USA and suggested that these may be an analogue of similar structures in the sulphate-rich sedimentary rocks imaged by Opportunity on Meridiani Planum. The White Sands sulphate dunes were formed in an evaporitic and aeolian environment similar to that interpreted for the Meridiani Planum rocks. The formation of polygonal cracks is generally ascribed to evaporation and shrinkage of sand. The processes that lead to the formation of fins are less clear, but Chavdarian and Sumner (2006) proposed that water from frost first percolates into the sand and shrinkage cracks. The water in the cracks evaporates and cementing material is precipitated in the crack. When the dune surface is eroded it leaves behind the cemented crack whose strength is increased by adhesion of wind-borne particles. The final result is the protruding of fin-shaped structures. The implications for similar structures in Meridiani Planum (McLennan et al. 2005) is that they are formed by similar processes that involve interaction with liquid water.

All these features on Mars indicate that it must have had abundant liquid water and perhaps a warmer climate. However, and as previously mentioned, many of these drainage systems seem to have formed by spring sapping and not surface run off (Carr 1981), which would perhaps preclude atmospheric precipitations (Farmer 1996), although this has been recently disputed (Segura et al. 2002). Some of the largest channels have a morphology that is suggestive of catastrophic release of water, probably from underground reservoirs (Hartmann 1979). Hynek and Phillips (2001), examining MOLA data,

concluded that the morphology in the southern highlands could only have been derived from "*precipitation-fed runoff*". A mechanism invoking bursts of water released from hydrothermal circulation of groundwater could result from the high heat flow associated with plume magmatism (Baker et al. 1991). As on Earth, internal heat energy (radioactivity and residual) advected by upwelling magmas must have had an important role in the inception of hydrothermal convection. Possible mechanisms of fluid circulation patterns resulting from the interaction of rising magmas with the cryosphere are schematically illustrated in Fig. 12.9. With this figure Pirajno and van Kranendonk (2005) proposed a model to explain the widespread deposition of sulphates on Mars as hydrothermal precipitates, generated through the interaction of magmatic H_2S in hydrothermal solutions, with water in the cryosphere. This fluid circulation would produce sulphate-rich hydrothermal solutions. The general view is that Martian water is now present as ground ice and permafrost (cryosphere), because liquid water would be unstable on the Martian surface (Carr 1996a, b), although it is possible that in the past it may have existed on the surface and as mentioned previously, may even have formed oceans (Fig. 12.3; Baker et al. 1991; Baker 2006b).

Farmer (1996) provided an assessment of possible hydrothermal systems on Mars, referring to geomorphic features obtained from orbital images during the Viking missions in the 1970s. Farmer's assessment is still valid and recently confirmed during the latest missions. Potential hydrothermal systems on Mars could form in and around volcanoes (as on Earth), caldera floors, fractures, and rift valleys. A good candidate for hydrothermal activity is the Tharsis region, described above and shown in Fig. 12.4, where hydrothermal convective cells would have been active around and within the volcanic edifices, along the major fracture and dyke systems, and in the Valles Marineris rift system. Emplacement of the giant dyke swarms on Tharsis must have produced a large thermal

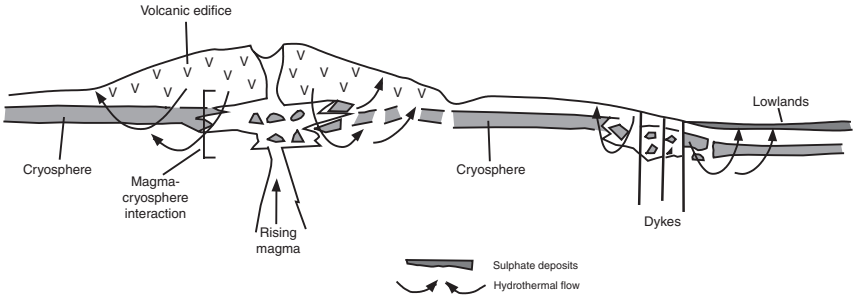


Fig. 12.9 Schematic model illustrating patterns of hydrothermal circulation in the subsurface of Mars; sulphate deposits could form in lowlands due to reaction of volcanic H_2S with water derived from the melting of the cryosphere to produce sulphate-rich hydrothermal solutions, which then discharge at the surface forming sinter-like deposits. After Pirajno and Van Kranendonk (2005)

anomaly that caused extensive hydrothermal circulation, which could have resulted in surface discharges of hot springs and surface deposits of chemical sediments. This thermal anomaly would have heated the groundwater systems beneath the cryosphere, resulting in its fracturing and catastrophic release of the groundwater, forming outflow channels (Wilson and Head 2002). More recently, Okubo and McEwen (2007) using images returned from the High resolution Imaging Science Experiment (HiRISE) reported the presence of fracture sets, from hundreds of metres to kilometres long, surrounded by light-coloured haloes in western Chandor Chasma region, one of the Valles Marineris canyons (Figs. 12.2 and 12.5). These fractures are interpreted as joints because of the lack of displacement of the darker surrounding materials through which they cut and their slightly smooth and positive relief. The light-coloured haloes are probably bleached material interpreted to be the result of chemical precipitation of minerals from circulating fluids. In other words, as on Earth, the haloes of bleached material are the product of hydrothermal alteration due to the joints acting as conduits for circulating fluids and their interaction within the fracture with the wallrocks. Okubo and McEwen (2007) suggested that this kind of geochemical bleaching or alteration implies large-scale subsurface migration of fluids. These authors also noted that not all joints have haloes of bleached material, indicating a difference in the age of the joints. The non-haloed joints probably formed when fluids were no longer circulating in the subsurface.

Release of hydrothermal fluids may also be associated with the formation of lakes, following impact cratering and the breaching of the cryosphere and local groundwater, as postulated by Newsom et al. (1996), who suggested that heat sources in craters of more than 50-km diameter can drive hydrothermal convection for thousands of years. Cabrol and Grin (2002) suggested that fault systems in volcanic regions may generate outflow channels from the emergence of groundwater along the Memmonia fault in the Tharsis volcanic region. This outflow rushed for several hundred kilometres to debouch into Amazonis Planitia to the west of Olympus Mons, destroying on the way some craters and forming lakes in others.

12.3.4.1 Hematite and Sulphate Deposits; Magma-Ice Interactions

The discovery, by thermal infrared mapping, of widespread crystalline hematite deposits, extending for an area of 500 × 250 km in Sinus Meridiani and Valles Marineris, as well as other localities, is of enormous interest because they are of possible hydrothermal origin (Christensen et al. 2000, 2001). The OMEGA spectrometer revealed spectral features that are common to a variety of ferric oxides and oxyhydroxides (hematite, goethite, lepidocrocite, ferrihydrite) and ferric sulphates, such as jarosite. The Valles Marineris hematite is associated with interior layered deposits (ILD), and therefore associated with sedimentary units. Iron is soluble in water as Fe^{2+} and precipitates as ferrihydrate, $Fe(OH)_3$, in alkaline and oxidising conditions, then dehydrates to goethite (FeOOH) and finally to hematite (Fe_2O_3) (Catling 2004). Christensen et al. (2000) suggested

that the Mars hematite was chemically precipitated from standing oxygenated water in a manner perhaps similar to terrestrial banded iron-formations. If this is correct, the implications could be far reaching because there is evidence that in terrestrial iron-formation, Fe oxides precipitation is bacterially mediated (Huston and Logan 2004; Inskeep et al. 2004; and Chapter 8). Chan et al. (2004) on the other hand, proposed a mechanism for the origin of the Martian hematite spherules similar to that which formed the hematite concretions in the very permeable Jurassic Navajo Sandstone, in which disseminated Fe oxides are brought into solutions by reducing fluids resulting in a bleaching of the sandstone. When the Fe-rich fluids mix with oxidising meteoric water, hematite precipitates typically as round concretions, but also in other forms, such as pipes and sheets. These authors go on to say that presence of bacteria can increase the rate of Fe precipitation. More recently, Bowen et al. (2008) examined spheroidal hematite concretions in subsurface sediments of Lake Brown, one of Western Australia's acid saline lakes and drew anologies with the Martian "blue berries". At Lake Brown, in addition to hematite spherules, the intergranular material of the lake's sediments also include gypsum, halite and jarosite. The hematite concretions at Lake Brown are from 2 mm to 4 cm in diameter and have a radiocarbon age of about 2913 years before present (BP). Detailed studies by these authors, revealed that the hematite concretions were formed during several stages over the last ~3000 years. Bowen and co-authors also pointed out that in modern terrestrial settings where these concretions are present, microbial activity is likely to have been involved in their formation. In most cases, the presence of liquid water is essential for the formation of these extensive hematite deposits, whereas the possibility of these spherules being melt droplets from meteorite impacts or volcanic lapilli is ruled out, on the basis of thermal infrared spectral characteristics (Bowen et al. 2008).

Bibring et al. (2007) examined the OMEGA spectral signatures for oxides and sulphates and suggested that, at least locally, these may have formed contemporaneously. These authors found that ferric oxides and sulphates occur in close spatial association in Valles Marineris and Margaritifer Terra, and suggested that ferric oxides may have formed by near-surface fluid circulation at the same time as the sulphates or sightly later by diagenetic alteration. The overall acidic environment is confirmed for the precipitaton of both oxides and sulphates, as also occurs on Earth during acid-sulphate hydrothermal alteration processes. Bibring et al. (2007) also proposed an alternative hypothesis of oxides forming by diagenetic processes from the circulation of Fe-rich fluids. The lag deposits of hematite spherules are likely the result of wind erosion that removed the softer sulphates.

Sulphates were also detected by the Mars Express of the European Space Agency using the Visible and Infrared Mineralogical Mapping Spectrometer (Kerr 2004). One of the sulphate minerals detected is kieserite ($MgSO_4 \cdot H_2O$) in lowlands. Kerr (2004) suggested that these sulphates might be the outcome of volcanic degassing of sulphuric acid mixing with water. Pirajno and Van Kranendonk (2005) suggested two alternative explanations, based on the

possibility that interaction of magmatic S_2, SO_2 and H_2S with the cryosphere results in hydrothermal circulation, transport of H_2S in much the same way as in terrestrial high sulphidation epithermal systems (discussed in Chapter 5), reaction with water, and deposition of transported S as sulphates (Fairén et al. 2004). In the first alternative, deposition of sulphates, which is predominant in lowlands, could occur as in terrestrial saline lake evaporitic sediments, commonly characterised by evaporite salts-clastic couplets produced by ephemeral storm runoffs (Leeder 1999). The interior layered deposits (ILD) in Valles Marineris described by Komatsu et al. (2004b), which the authors ascribe to effects of sub-ice volcanism, could be explained as large hydrothermal-evaporite deposits. The second alternative suggests that the Martian sulphates could represent chemical hydrothermal precipitates, formed through the same oxidative process of volcanic H_2S on Earth, its reaction with water to produce sulphate-rich hydrothermal solutions, which then discharge at the surface as thermal springs, forming sinter-like deposits.

Head and Wilson (2002) examined in some detail the interaction of magmas with the cryosphere and an underlying megaregolith, which may contain groundwater and/or ice. Magma and water-ice interactions result from the rising of plutons, sills and dykes in the subsurface. These intrusions into the regolith and the cryosphere will cause ice melting and circulation of hot fluids with ensuing hydrothermal activity. Head and Wilson (2002) drew attention to the emplacement of dykes, because they can be emplaced laterally for thousands of kilometres, interacting all the way with aquifers, groundwater and the cryosphere, setting up hydrothermal convection cells and locally forming outflow channels and lahars. In some cases, the authors contended, melted ice can be incorporated into the magma, resulting in explosive hydromagmatic eruptions. The low-relief volcanic structure Tyrrhena Patera was possibly generated by hydromagmatic eruptions, with water flow rates calculated at 10^5–10^6 m^3 s^{-1} and water volumes of $\sim 7.5 \times 10^{16}$ kg (Head and Wilson 2002 and references therein). The emplacement of plutons, cause a more localised but nevertheless potent hydrothermal field, distributed above and around the magma body, much as it happens on Earth (see Chapters 4 and 5). Head and Wilson (2002) reported calculations for a 10 km-wide magma body emplaced at a depth of 10 km, will result in a thermal pulse capable of melting ice within an area of 25 km in diameter above the intrusion. In addition, the interaction of these plutons with water will almost certainly also modify the composition of the pluton and its differentiation during cooling. These workers suggested that for the major volcanic centres, such as Tharsis and Elysium (Figs. 12.1 and 12.2), the depths of the associated plutons may be between 9 and 13 km below the summits, which means that the thermal effects would have to cause extensive disruption of the cryosphere and ice melting, possibly leading to extensive hydrothermal circulation within the volcanic edifice itself and locally causing mass movements (land slides) as observed for the western flanks of Arsia Mons (Head and Wilson 2002). Sills and lava flows can also be efficient in melting near-surface ice and release groundwater; in the case of sill intrusions, heat is

generally lost upward from the top, rather than downward. A sill intruding the megaregolith and emplaced at the base of the cryosphere could produce about 10^4 km^3 of meltwater, induce uplift, fracturing, collapse of the roof materials and outflow channels. It is possible that hot fluids under pressure vent as steam in the collapse zone and the head of the outflow channels.

The combination or association of sulphate and hematite and other Br, S and Cl-rich minerals discovered on Mars is not a common feature on Earth, except in alteration zones within and around fumaroles in volcanic craters, where S-rich volcanic gases that condense or dissolve in groundwaters form acid fluids that cause extensive leaching of the surrounding rocks, resulting in argillic alteration and deposition of minerals such as hematite, various forms of silica, gypsum, alunite and jarosite (see Chapter 2). Furthermore, hot springs discharge these volcanic hydrothermal reservoirs and transport extremely acidic (pH $>$ 1) sulphate-chloride brines. An example is provided by the Capahue Volcano in Argentina, which Varekamp (2004) suggested as a possible analogue of the Opportunity landing site. The Capahue Volcano has a crater with an acid lake and hot springs, with pH ranging from 1.7 to 2.4, as measured in 1999 and 2003. The hot springs discharge into the Upper Rio Agrio, which in turn discharges into a glacial lake (Lake Caviahue). The chemistry of the hot springs tends to change with each new eruption as fresh magma invades the hydrothermal reservoir. When visited in 2004, the rocks in the headwaters of the Upper Rio Agrio were coated with bright red hematite. The main hot springs had a pH of 1.3 and a temperature of about 80°C, but a few tens of metre downstream the temperature decreased to about 40°C with a pH of 1.45. Prior to the last eruption the spring waters were saturated with silica, anhydrite, hematite, alunite and jarosite and Cu-bearing minerals, suggesting the activity of a subvolcanic high-S epithermal system. Varekamp (2004) noted that these mineral associations are similar to those found at the Opportunity Rover landing site. He further pointed out that the Copahue hot spring fluids contain 50–70% magmatic water that are subsequently quenched by melt waters from the summit glacier of the volcano and that a similar scenario could exist on Mars, where volcanic fluids would be quenched by the Martian cryosphere, then forming small streams from which the above mineral phase precipitate. Apart from the small streams, Lake Caviahue, with a surface area of 10 km^2 could also provide an analogue for more extensive areas of volcanic-related sulphate and hematite mineralisation on Mars.

Dohm et al. (2008) suggested that the Tharsis-Elysium region, including the Valles Marineris rift system has been, and may still be, geologically active in the past 10–100 Ma. Dohm et al. (2008) proposed that the Solfatara Crater in Italy may be a possible terrestrial analogue for this region. The Solfatara Crater is part of a 12 km wide Phlegrean Field nested caldera system, where active fumarolic discharges are linked to a vapour-dominated hydrothermal systems of mixed meteoric-magmatic origin and emitting fluids rich in H_2S, CO_2, HCl, CH_4 and depositing native sulphur, gypsum, barite, alunite and pyrite (Valentino et al. 1999).

12.3.5 Impact Craters

Several Martian impact structures exhibit distinctive patterns of lobate ejecta blankets termed by Carr (1981) "*splosh craters*" (Fig. 12.10). The lobate margins probably formed as a result of fluidisation due to impact kinetic energy (fluidised ejecta due to mixing with groundwater or water-ice) and a depositional regime characterised by debris flow rather than ballistic, as is normally the case (Carr 1981). Interestingly, small craters (few km) do not have lobate ejecta, suggesting a certain depth of groundwater that can only be breached by larger impacts. Assuming that water is the cause of the fluidisation, then it is possible that subsequent hydrothermal circulation might be activated from the thermal effects inherent to the conversion of kinetic energy to thermal energy (cf. Kring 2000) or by the heat source that can be provided by impact melt bodies. Farmer (1996) and Newsom et al. (2001) included meteorite impacts and as one of the major heat sources for Martian hydrothermal systems, something that is sometimes overlooked for ancient Earth systems and further elaborated in Chapter 11. Crater lakes may form as a result of water derived from deep aquifers that were penetrated by the impact, with freezing being retarded due to impact-related heat (Rathburn and Squyres 2002). Long-lived lakes on Martian impact craters have been predicted by Rathburn and Squyres (2002) using a numerical model developed to simulate multiphase groundwater flow and heat transport to temperatures of 1200°C in a 180-km diameter complex crater. These researchers reported that in their modelling small diameter (e.g. 7 km or less) craters do not sustain enough flow of liquid water to create a long-lived lake system. The formation of a lake in an impact crater has important implications for sedimentary processes, hydrothermal convection, hot springs and hyperthermophilic chemolithoautotrophic life forms.

I return to discuss the potential link between impact-induced hydrothermal systems and life in Section 12.5.2.

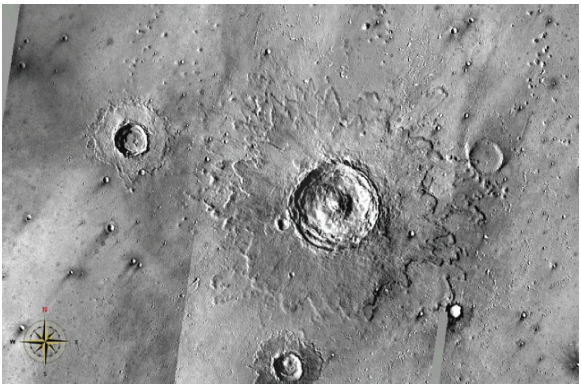


Fig. 12.10 "Splosh" craters on Mars; the larger crater in this image is about 30 km in diameter and is centred at lat N26.392° Long W38.675°; altitude 1710.63 km; the distinctive lobate ejecta patterns testify to debris being saturated with liquid water that flowed mud-style outward from the impact site (Carr 1999)

12.4 Europa, Ganymede, Enceladus and Titan

Europa and Ganymede together with Io are the three inner so-called Galilean satellites (because they were discovered by Galileo Galilei in 1610) that orbit Jupiter. The Galilean satellites are geologically active, as spectacularly shown by the Voyager images of erupting volcanoes on Io, with no impact craters on its surface and therefore the most geologically active planetary body in the Solar System (Johnson 1999). Enceladus is one of the smaller Saturn's 35 moons. Europa, Ganymede and Enceladus share features that make them very interesting in terms of possible hydrothermal systems and exobiological potential. All three satellites are internally well differentiated and layered, with a Fe core, a silicate shell overlain by a liquid ocean and an icy crust.

The heat sources that power volcanism on Io and cryovolcanism on other satellites are (see Johnson 1999 for an overview): (1) heat released by colliding planetesimals (accretionary heat); (2) radioactive decay of short-lived radionuclides, such as ^{26}Al, and long-lived isotopes, such as those of U, Th and K; and (3) tidal energy. The latter is of special interest in the context of this section, because it is probably the main heat source responsible for the observed geological, volcanic and hydrothermal features of the Europa, Ganymede and Enceladus, as well as volcanism on Io. Tidal energy is the result of gravitational interaction or friction between bodies that orbit close to one another. This interaction produces distortion, essentially because gravitational attraction is stronger on one side than the other (Johnson 1999); when the gravitational field changes, the body will distort in response, producing heat in its interior. Johnson (1999) gave a practical example by comparing planetary tidal heating with the continuous squeeze and release of a rubber ball. Because Io is very close to Jupiter its tides are very large during its 42.5 hour day. The thermal energy released on Io has been calculated at a global average greater than 2.5 watts/m^2. By comparison, Earth has a global heat flow of 0.06 watts/m^2, with the geothermal field of Wairakei in New Zealand, having an average heat flow of 1.7 watts/m^2 (Johnson 1999). The continuing and widespread volcanic activity on Io makes this satellite a poor candidate for hydrothermal activity, since no water or water-ice can possibly exist.

NASA's Galileo spacecraft, after a 6 year journey from Earth, reached the Jovian system in 1995. The Galileo mission very successfully imaged the Jovian satellites and in addition to images previously acquired by the Voyager missions (Voyager 1 and 2 1979) the spacecraft returned a wealth of remote sensing data acquired from solid state imaging (SIS), near-infrared mapping spectrometry (NIMS), photopolarimeter-radiometer (PPR) and ultraviolet spectrometer (UVS), in addition magnetic and gravity data were also obtained. NASA's Voyager spacecraft flew past Enceladus in 1980 and returned the first images of the satellite. Between December 2004 and December 2005, the Cassini-Huygens mission to Saturn and Titan began its examination of the major icy satellites of Saturn (Porco et al. 2006). For more information about the

Cassini-Huygens mission, a cooperative project of NASA, the European Space Agency and the Italian Space Agency, the interested reader can visit the mission web site at http://saturn.jpl.nasa.gov and the imaging team homepage at http://ciclops.org (both last accessed in April 2008). The Cassini spacecraft was equipped with the Huygens probe, which in December 2004 carried out a 20 day trip to Titan (see Sotin et al. 2005 and Tobie et al. 2006 for more information on the Huygens probing of Titan). Amongst other achievements the Cassini-Huygens mission resulted in the discovery of 13 more satellites orbiting Saturn, bringing the total to 35.

12.4.1 Europa

Europa, the smallest of the Galilean group is a Jovian satellite about 3130 km in diameter, has a smooth surface criss-crossed by lines and bands, peculiar cracks, curved black lines and scalloped ridges (Fig. 12.11), with only three large impact craters, suggesting that its surface is continuously renewed by some form of dynamic geological activity, probably dominated by outpourings of flood "volcanism" of liquid water. Europa's surface has a mean age ranging from 30 to 70 Ma, based on cratering rates (Zahnle et al. 2003). The linear markings, thousand of kilometres long and called by the Latin term *lineae* are thought to be ridges and/or fractures. Some form unusual structures called "*triple bands*", in which the darker parts are probably areas of non-ice. Images from the Galileo spacecraft showed features that are very similar to the ice floes

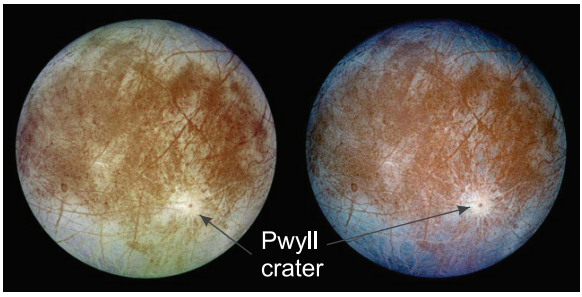


Fig. 12.11 Two images of Europa taken by the Galileo spacecraft in November 1996 from about 41 000 km; on the left is an image in natural colour, on the right is a false-colour composite, which combine violet, green and infrared to enhance colour differences. The regions coloured blue represent the water ice crust, whereas the brown coloured regions represent predominantly rocky material. Where asteroids have impacted the rocky crust, this was breached and the underlying water ice ejected. This is shown by the 50 km in diameter impact structure on the bottom right, named Pwyll (Celtic god of the underworld). The long, dark lines are fractures and rifts. See also Fig. 12.12. Courtesy of Calvin Hamilton (http://www.solarviews.com/eng/europa.htm#calvin last opened in April 2008) and NASA/JPL public domain

that cover the arctic regions on Earth. The high reflective surface of the satellite, together with data from interferometer spectrometers which show strong absorption bands of infrared light with wavelengths of 1.4 and 1.8 μm, are indicative of water ice. The presence of water on Europa makes this satellite one of the prime candidates for harbouring extraterrestrial life. Papers that describe the known geology of Europa include Greeley (1999), Pappalardo et al. (1999), Greenberg et al. (2002), Greeley et al. (2004) and Lowell and DuBose (2005) from whom the overview that follows is taken.

First images of Europa were those obtained from the flybys of Pioner 10 and 11 spacecrafts in 1973 and 1974. These were followed by the Voyager 1 and 2 flybys in 1979 during which about 70 images were obtained that enabled the identification of the Europa's main surface features. In 1995 the Galileo mission returned high resolution images (6–13 m pixels for most of the satellite surface) from 18 flybys. The imaging, gravity and magnetic data allowed a first look into the composition of Europa, based on its gravity, mass and density, suggesting that it has a layered structure with a small metallic core, surrounded by a rocky layer, covered by a mantle of liquid water, and an icy crust. The thickness of the icy crust is possibly around 15–20 km, but other calculations suggest that it could be as thin as 2 km (Nimmo 2004).

Greeley et al. (2004, p. 330) stated that "*the surface of an object is a window to its interior*". This is certainly the case for Europa and indeed the other two satellites considered in this book. The surface of Europa is characterised by bright plains and mottled terrains and areas that display considerable tectonic disruption. Two categories of terrain stand out: tectonic crustal cracking and chaotic. All these regions are criss-crossed by bands, ridges and linear markings (Fig. 12.12). Multispectral mapping by the Galileo spacecraft showed infrared bright and dark or mottled regions. The bright regions consist of multiple sets of ridges and grooves pockmarked by pits and depressions. The dark or mottled regions are a patchwork of dark zones that grade into the bright areas. One of these areas is the Conamara Chaos (Fig. 12.13) where, as the name implies, chaotically disposed, rotated and tilted blocks resemble a breccia or more appropriately a jumbled arrangement of ice blocks, with intervening non-ice material, punctured here and there by impact structures. These impact structures are interpreted to have formed by large blocks of ice thrown out by the large Pwyll impact, some 1000 km to the south, and clearly visible because of its bright ejecta (Fig. 12.11). A possible explanation for the Conamara Chaos is initial upwarping resulting from buoyant, low-density diapirs of "magma" that rise from convective upwelling towards the surface. This upwelling would form a series of surface parallel ridges that progressively extend, allowing more upwelling. The extended ridges then collapse to form the chaotic terrain. This mechanism would also be responsible for surface eruptions of liquid water (magma), producing what has been called cryovolcanism, that is the eruption of liquid water and other volatiles, with or without entrained solids that become frozen because of normal temperature of the planetary icy surface (Geissler 2000). Dome features near Conamara Chaos suggest that these may represent

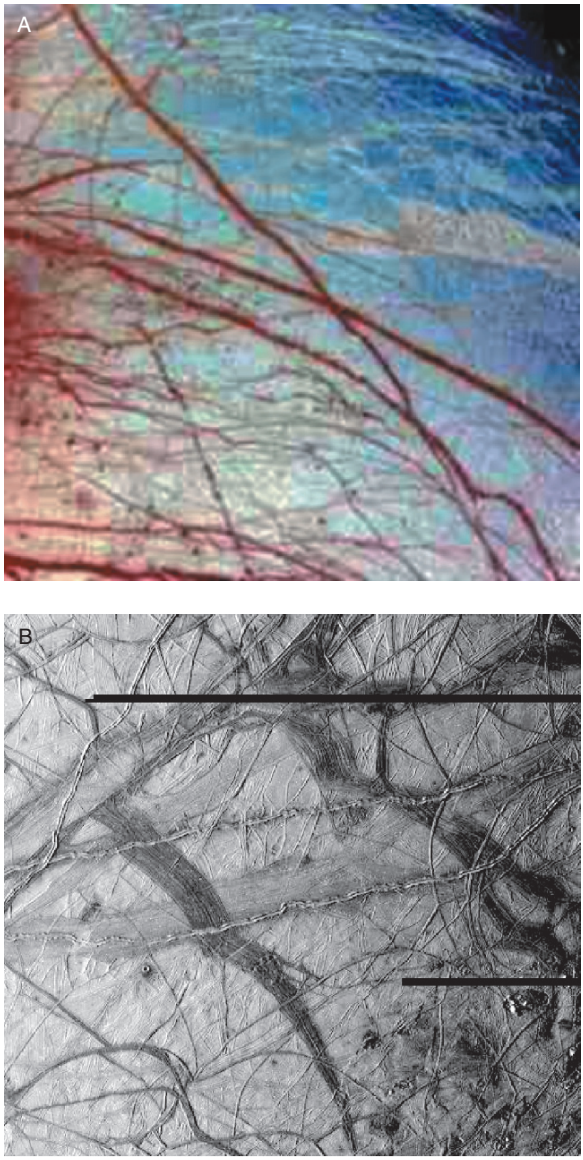


Fig. 12.12 (**A**) is a composite false colour image at wavelengths of 989, 757 and 559 nm, of the Minos Linea region, taken by the Galileo spacecraft in 1996, the area shown in this image is 1260 km across. The triple bands, linae (lines in Latin) and mottled terrain appear in brown and reddish colours, which indicate rocky material mixed with ice. The icy areas are shown in bluish colours (after Greeley 1999). (**B**) In this image, which covers an area of 238 km across, dark bands, sinuous and curved lines, ridges and fractures can be seen. The complete absence of impact craters, apart from a few very small ones, indicate a geologically young terrain. Courtesy of Calvin Hamilton (http://www.solarviews.com/eng/europa.htm#calvin (last opened in April 2008) and NASA/JPL public domain

volcanic structures resulting from the surface venting of diapiric intrusions. Flow like features have also been imaged, up to 20 km long that cut through the ridges, but these flows do not appear to be connected to source vents. Another, and still enigmatic feature, is a dark, smooth "puddle" that overprints ridges and grooves. This "puddle" has been interpreted to have formed as a result of melting of ice from a subjacent hot spot (Greeley 1999). Another area of doming

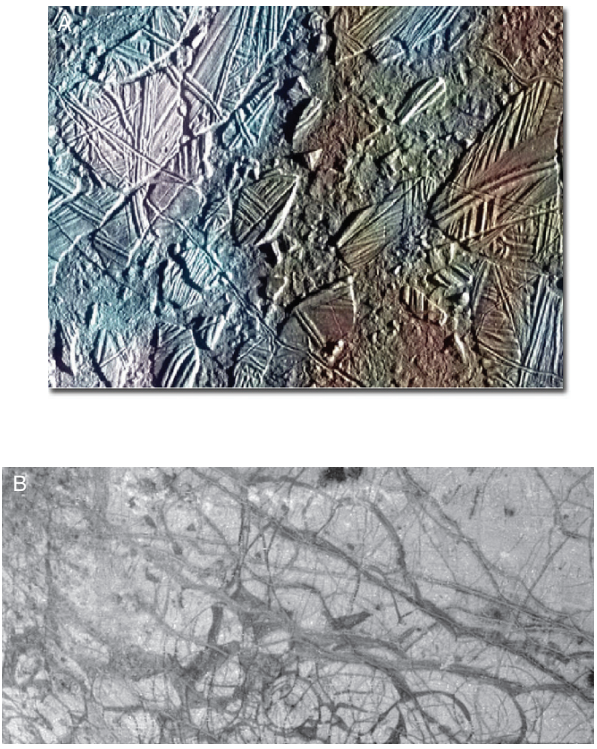


Fig. 12.13 Image of (**A**) Conamara Chaos, a region of disrupted ice crust, broken plates and ice slabs in the Conamara region, not too dissimilar from the ice floes of our polar regions; note criss-crossing ridges and double ridges, this image covers an area about 70 km across; (**B**) image taken by the Galileo spacecraft in June 1997 exhibits curved, wedge-shaped and dark linear bands, which have broken the icy crust into plates and fragments up to 30 km across; the dark areas bounding the plates are possibly fractures along which gases and rocky materials have been erupted; note that some plates appear to have been rotated; the area shown is in the equatorial region of Europa and is 989 × 510 km, taken from a distance of 156 000 km. NASA/JPL public domain

and cryovolcanism is a nearly circular, slightly elongate, feature named Thera Macula (Mével and Mercier 2007). This structure measures 140 × 80 km and is located in the southern hemisphere and studies of the Galileo's images have led Mével and Mercier (2007) to propose an interesting cryomagmatic and diapiric mechanism for the formation of Thera Macula that resembles that of terrestrial upwelling mantle material resulting in doming, rifting, and subsequent collapse of the rift with formation of tilted blocks, followed by eruption of lavas. Thera Macula consists of a smooth bright area and a chaotic dark area, with the latter apparently flowing out of the structure through its southern rim. In the southern chaotic and dark area, blocks of various sizes are elevated and tilted above the dark matrix. Mével and Mercier (2007) explain the features of Thera Macula as due to doming or uplift resulting from the rise of "warm" material

from the underlying liquid ocean and its impingement on to the brittle icy crust. This doming produces tensile stresses forming fractures that define tilted blocks, forming a chaotic terrain bound on one side by a major median fracture. Gravity collapse of the tilted blocks occurred allowing the eruption of liquid material (cryovolcanism), which flowed southward. The final collapse of the structures may have been enhanced by the emptying of the cryomagmatic reservoir.

A major problem with cryovolcanism is that the hexagonal structure of ice makes it less dense than liquid water. This makes it difficult for liquid water to rise through an icy crust. This density problem can be overcome if gases are present, perhaps in the form of clathrates, ice cagelike structures that trap gases (Geissler 2000; see also Chapter 10). In this case, the trapped volatiles would drive explosive volcanism similar to terrestrial pyroclastic eruptions (Geissler 2000). As for Earth, the necessary conditions for cryovolcanism to occur are the generation of liquids in the interior and their migration to the surface. As mentioned previously, the necessary energy sources to produce internal liquids (or magmas) in the satellites of the outer planets are gravitational, radiogenic and tidal (frictional heating due to gravitational interaction with other satellites, which cause an increase in orbital eccentricity).

The bands and stripes of Europa's surface are probably of extensional origin, locally with a strike-slip component, with a morphological symmetry that resembles the seafloor spreading ridges and valley of Earth (Nimmo 2004). There are several types and complex patterns of linear features on Europa. They include straight ridges, scalloped ridges, multiple ridges and grooves cross-cutting one another and bright and dark bands of ridges (triple bands). These triple bands could have formed by a graben-style rift mechanism, in which the sunken parts were flooded by a slush composed of ice mixed with non-ice material. Another and perhaps more likely mechanism could be a form of cryovolcanism. In this model, explosive venting of geysers emitting CO_2 and other volatiles erupt through the icy crust along a linear fracture, resulting in a continuous line of geysers (Greeley 1999). In these geyser-like jets the non-ice component would form deposits around the fracture that progressively thin out away from the fissure. With depletion of the volatiles, cleaner ice oozes out to form a central ridge system (Greeley 1999). The global lineaments patterns of Europa are dominated by double ridges, which are thought to derive by diurnal tides (Greenberg et al. 2002). In this scheme, diurnal tides open the cracks and water flows in to the surface where in the vacuum boils and freezes. With the closure of the crack, a slurry of ice, slush and water is squeezed upward and erupts to the surface, spilling over on both sides of the crack.

12.4.1.1 Hydrothermal Systems and Life

The liquid mantle of Europa and its frozen surface is about 100 km thick and, as mentioned above, is considered to result from the heat generated by tidal forces (Lowell and DuBose 2005). The total volume of water is estimated at 3×10^9 km^3, which is twice that of Earth. Tidal heat is transferred from the

rocky core to the liquid water layer above it through hydrothermal discharges. Terrestrial seafloor-like hydrothermal systems (see Chapter 4) are thought to be present and to discharge plumes enriched in H_2S, H_2, and CH_4, which may vent to the surface as geyser-like jets, to eventually freeze and add to the icy crust (McCollom and Shock 1997). A conceptual model of this system is shown in Fig. 12.14. Lowell and DuBose (2005) estimated that Europa's hydrothermal system may have temperatures of 100°C, with a global hydrothermal heat flux of about 5×10^{12} Watts (Earth's is about 10^{13} Watts), a total hydrothermal mass flux of about 10^7 kg s^{-1} (Earth's is about 2.5×10^8 kg s^{-1}), and a number of high temperature hydrothermal systems from about 5000 to 250 000 (Earth has from about 300 to 3000 on mid-ocean ridges).

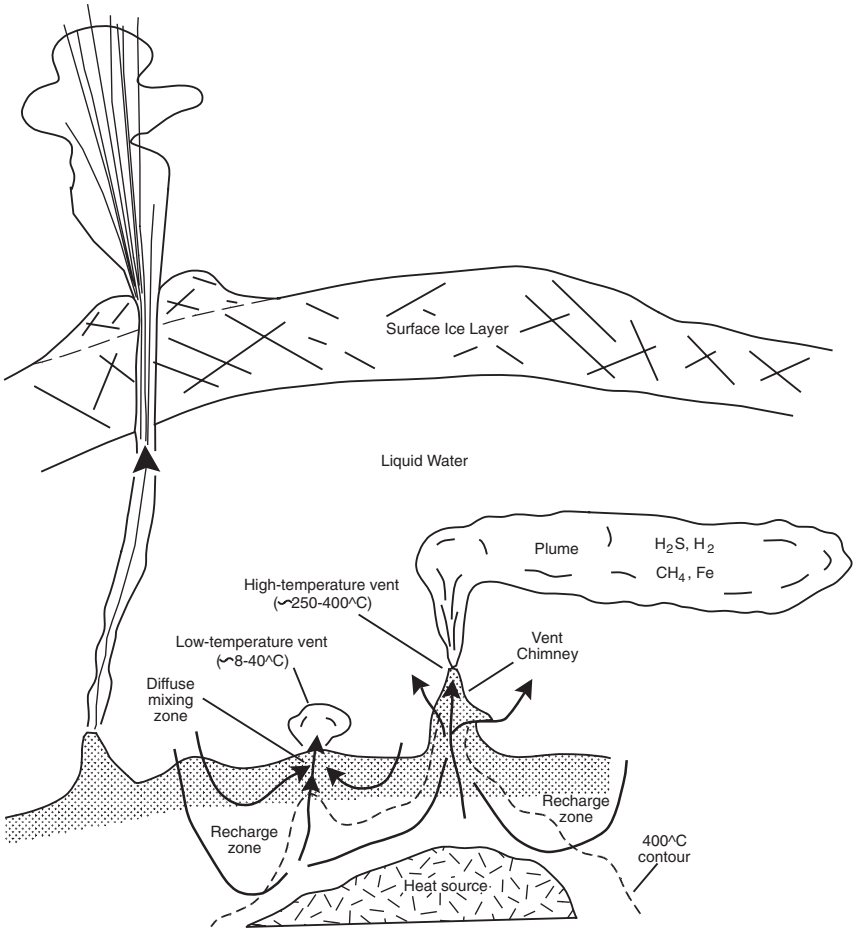


Fig. 12.14 Model of hydrothermal system on Europa or Enceladus. Details in text. After McCollom and Shock (1997) and McCollom (1999)

As mentioned above, the paucity of impact craters is indicative of a geologically active and young surface. The resurfacing processes are explained as due to the interaction of a liquid water ocean (a magma equivalent) with the surface. The few craters that are present on Europa have allowed an estimate of the thickness of the icy crust to be in the order of a few km, although this is likely to vary. The underlying liquid water ocean may have hydrothermal vents, by analogy with those that exist on the seafloor of our oceans. If this is correct, then it was thought that ecosystems may be present that derive metabolic energy from chemolithotrophic reactions, again by analogy with hyperthermophiles at the high-temperature black smoker chimneys on Earth (Chapter 5). A possible habitable setting on Europa was modelled by Greenberg et al. (2002), who envisaged that cracks would penetrate to the liquid water ocean and that they would open and close during diurnal tides, and as mentioned above, with crushed ice and slush being forced to the surface. This daily tidal flow would transport heat and organic compounds between the ocean and the surface. At the surface radiation effects (solar ultraviolet radiaton) can produce oxidants, as spectrally detected in the form of CO_2, H_2O and H_2SO_4, as well as perhaps molecular O_2. Cometary impacts can deliver further organic materials to the surface. Chemical and thermodynamic disequilibria at various levels in the crack would provide a setting conducive to life. While, no organism could survive a surface temperature of about 170°C and the constant bombardment of energetic charged particles from the Jovian magnetosphere, organisms could nevertheless survive deeper down in the crack. Greenberg et al. (2002) suggested that different ecosystems could exist at different levels of the crack, as shown in their model reproduced in Fig. 12.15.

12.4.2 Ganymede

Ganymede with its 5276-km diameter is the Solar System's largest satellite, in fact larger than the planet Mercury. The surface of this satellite is characterised by dark and bright grooved terrains, with the latter being ice-rich. Its mean density, gravity and magnetic data from the Galileo mission suggest that Ganymede is a well differentiated body that consists of a Fe core, and a rocky silicate mantle overlain by an ice-liquid water shell approximately 800 km thick. Ganymede has an internally generated magnetic field and the magnetic data further imply that an ocean of liquid water of several tens of kilometres might be present at a depth of 170 km (Pappalardo et al. 2004). Ganymede's magnetic field is probably derived from a dynamo action within the liquid part of its Fe core. The surface features and geology of Ganymede have been reviewed by Pappalardo (1999) and Pappalardo et al. (2004) and summarised below.

The geological units recognisable on Ganymede's surface are dark and bright terrains. The dark terrain is pockmarked with impact craters, suggesting that this is an old surface, and is traversed by bright 5 to10 km-wide depressions

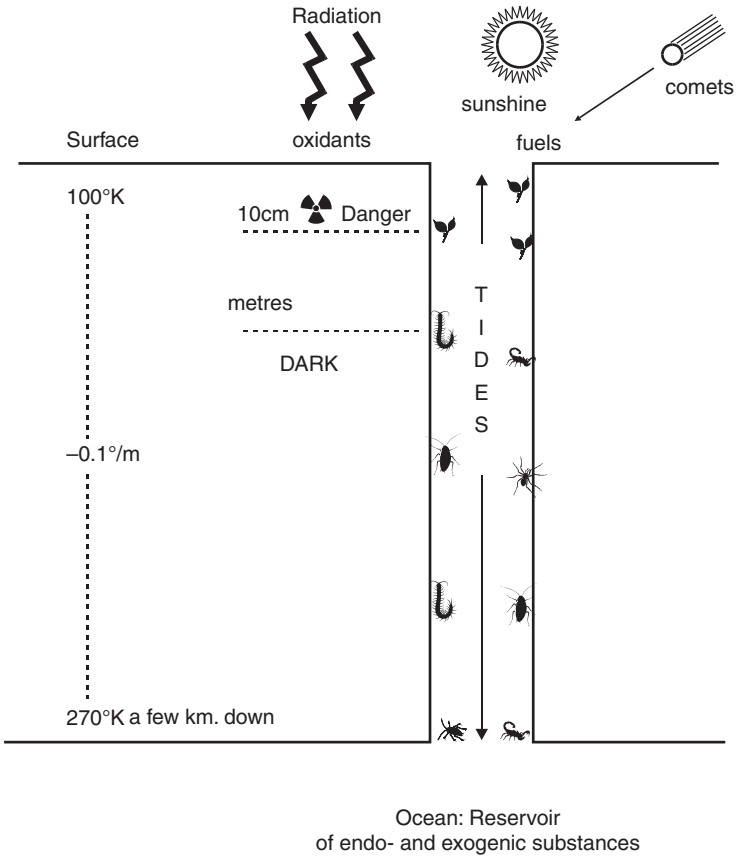


Fig. 12.15 Possible habitable setting on Europa, as envisaged by Greenberg et al. (2002). The habitable zone is provided by a fracture or crack in the icy surface that reaches the layer of "warm" liquid water ocean, where the liquid state is maintained by heat created by tidal energy dissipation. Photosynthetic organism might survive by exploiting a zone just below the surface radiation, while other organisms that do not require O_2, could survive further down and use the energy provided by the chemical disequilibrium and the diurnal flow of water along the conduit. When the crack closes and freezes, the organism would die unless, as so typical of life, they developed hibernating strategies

or furrows, which appear to trace the outline of concentric structures (Fig. 12.16). The craters have variable sizes, with dark or bright floors; the latter perhaps bringing up icy material. In detail, images of the dark terrain reveal complex checkerboard patches of darker and bright to less dark material. This checkerboard pattern appears to be a thin layer of silicate-rich lag overlying ice, with the darkest material occupying topographic lows. It is possible that the dark terrain might contain clays and organic materials which, Pappalardo and co-workers suggest, may indicate the composition of the impactors from which the satellite accreted. Images show that the dark

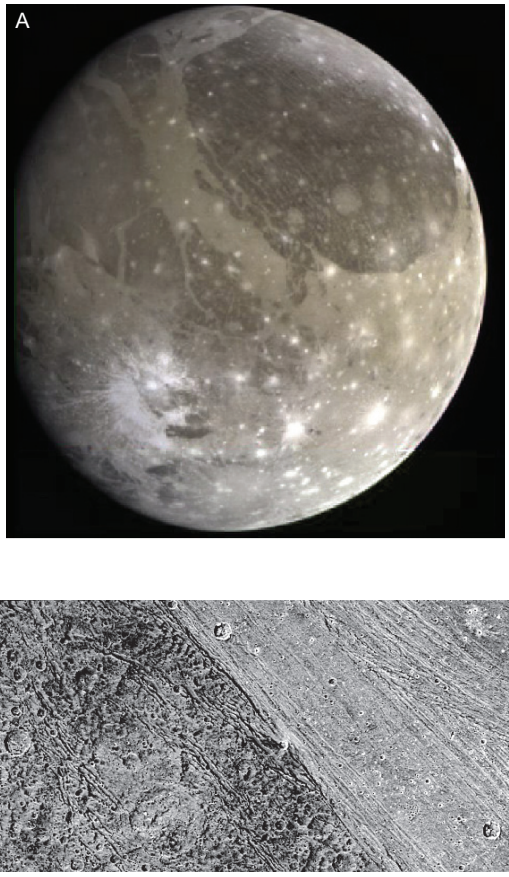


Fig. 12.16 (**A**) True colour image of Ganymede acquired by the Galileo spacecraft. NASA/JPL image. Impact craters show as white spots because of ejecta ice. The circular dark terrain is called Galileo Regio at right is surrounded by swaths of bright grooved terrain. (**B**) This image taken from 11 800 km with a resolution of 121 m per pixel, shows the boundary between two very distinct terrains on Ganymede to the left is an older, dark terrain with numerous craters; to the right is a younger, bright terrain characterised by subparallel ridges and grooves. Images taken on May 20th, 2000. NASA/JPL public domain

terrain has undergone some form of tectonic activity. The furrows that cut the dark terrain form sub-concentric systems, which could be the remnants of large impacts early in the satellite's history. These early impacts would have broken through a thin brittle silicate-rich crust into a warmer icy layer, creating a crater, exposing a slush of icy material and forming layers of ejecta. A central uplift is formed as a result of elastic rebound and slushy subsurface ice flows toward it, resulting in a series of concentric faults or rings that develop in the brittle crust. Tectonism was probably the main cause of Ganymede's curved and disrupted grooved terrains, which cut and straddle the dark regions. The possible presence of icy volcanism on Ganymede has been hypothesised (Schenk et al. 2001) but, as cautioned by Pappalardo et al. (2004) there is no structure that could be unequivocally interpreted as due to volcanism.

The bright terrain is less cratered than the dark terrains, and therefore must be geologically younger. The swaths of bright grooved terrain (or sulci, singular sulcus, from the Latin word for groove or furrow) can be up to 100 km wide

and, as mentioned above, form intricate patterns. One of these is Uruk Sulcus, which is 2500 km long and 300 km wide and consisting of horst-graben style normal faulting. This type of terrain is characterised by subparallel ridges and troughs that can be continuous for hundreds of kilometres. The regions of bright grooved terrains have impact crater densities 2–10 times less than in the dark terrains. Studies of the bright grooved terrains have helped in constraining models of Ganymede's surface geology as well as its interior structure. Importantly for genetic models, is the fact that the bright grooved terrains display a continuum of structures from a single trough to ridge-trough set to extremely complex grooved terrains. The bright areas are interpreted as graben structures that are infilled with liquid water and icy slush that froze to the surface's ambient temperature. A three-step rift model was proposed to explain the grooved terrain: (1) formation of a fault-bounded graben in the dark terrain; (2) eruption of water and icy slush floods the floor of the graben; (3) narrow sub-parallel structures are formed due to continuing extension. The observations from the Galileo mission allowed the refinement of this rift model to a four-step evolution of the grooved terrain, in the following sequence: (1) normal faults develop in the dark terrain and are subsequently reactivated (dark terrain tectonism); (2) extensional tectonism and disruption of the existing fault zones; (3) continuing faulting is accompanied by icy volcanism, which smooths the graben's floors and produces bright surfaces; (4) more bright terrain swaths are formed and cross-cut one another, resulting in the observed complex polygonal patterns. High resolution images (86, 74–47 m pixels) show examples of impact craters that have been extensionally strained during the formation of the grooved terrain. Also in these cases all stages of strain deformation can be observed.

As mentioned above the presence of icy volcanism on Ganymede is uncertain. However, scalloped depressions (called paterae, Latin for saucer) have been identified that could be interpreted as caldera structures (Schenk et al. 2001). A number of these paterae are seen in an area named Sippar Sulcus, where a prominent patera exhibits a flow-like lobate structure that is consistent with the flow of lava-like icy material (Schenk et al. 2001).

Impact structures on Ganymede display a great variety of morphologies. They include bright ray, dark ray, craters with dark floors and bright ejecta, craters with central pits and domes, multi-ring structures characterised by subconcentric furrows and low-relief ancient structures, called palimpsests. Palimpsests can be up to 100 km in diameter and were formed during the resurfacing of the bright grooved terrains and have a basin-like morphology.

Water ice is the major constituent of Ganymede's surface. Evidence of water ice on Ganymede is provided by infrared reflectance spectra (as it did for Europa and Enceladus). Pappalardo and co-workers suggested that this water ice is the result of thermal processing of water and water-bearing materials from which the satellite was originally formed. The spectral signatures of this water ice indicate variations in particle size and degree of crystallinity. Non-ice components are also abundant and largely constitute the dark regions, but

remain unidentified. Other compounds, as revealed by NIMS infrared spectra, include SO_2, CH and possibly HCN. Interestingly, the NIMS data are consistent with the spectra of organic residues produced in laboratory experiments by the discharge of energy into mixtures of C-, H-, N- and O-bearing molecules. Furthermore, on Ganymede the presence of these organic molecules could be the result of cometary impacts, because interstellar ice grains show very similar absorption spectra that are interpreted as due to CO_2, CN and CH, perhaps synthetised by ultraviolet irradiation of C-bearing ices (Pappalardo et al. 2004).

The well differentiated and layered structure of Ganymede is in stark contrast to its neighbour Callisto with its lack of magnetic field, poorly differentiated structure and an ice-rich outer layer densely packed with impact structures (Pappalardo 1999). The difference between the two satellites may be the greater size of Ganymede, which allows for more impact generated kinetic energy as well as more radiogenic heat. However, these two elements alone cannot explain the extreme differences of Ganymede and Callisto. More likely is the explanation offered by tidal heating. Together with Io and Europa, Ganymede is forced into an eccentric, rather than circular, orbit. This eccentrity induces tidal heating and is more pronounced for Io, the most volcanically active body in our Solar System.

In view of the above features, what are the possibilities for the presence of hydrothermal activity on Ganymede? Although to date, no evidence of live geyser like eruptions as observed for Enceladus has been detected, there are a number of scenarios in which hydrothermal systems may be operating or have operated in the past on Ganymede. Firstly, a liquid ocean like that of Europa, could support similar "seafloor" style hydrothermal venting. Secondly, the rift structures of the bright grooved terrain, with its sub-parallel faults could provide channelways for rising warmer liquid water from the internal liquid ocean (see Fig. 12.14). If flooding of water ice lavas did occur in the grooved terrain, then it would be possible that hot spring type systems could have been associated with this volcanic activity.

12.4.3 Enceladus

Enceladus, one of the smaller Saturnian moons (499 km across), was discovered by William Herschel in 1789. An overview of the geology of Enceladus is provided by Kargel and Pozio (1996) and is discussed here. Enceladus is largely composed of ice, water ice and silicate rock and it has a surface that is characterised by numerous impact craters and smooth plains with sinuous fracture zones (Fig. 12.17). The smooth plains indicate active resurfacing and young volcano-tectonic activity. The fracture zones in the smooth plains, named "*tiger stripes*" by the Cassini imaging team, may be associated with liquid water welling up from the interior and spilling over the surface to solidify as ice. The ice pours out of the tiger stripes and it forms new fresh crystalline ice,

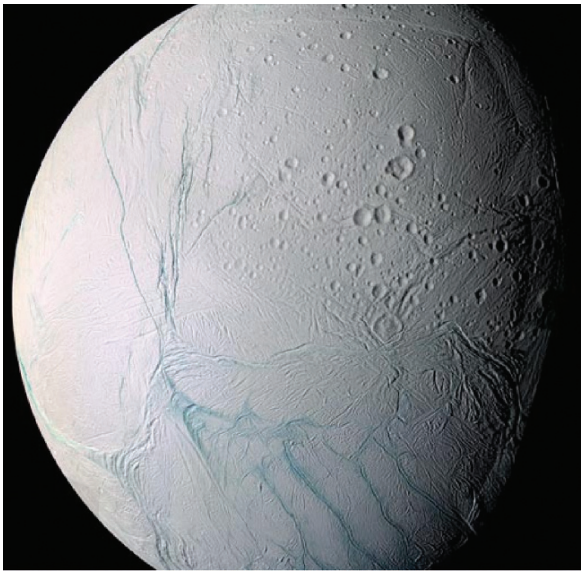


Fig. 12.17 Enceladus shown by a Voyager 2 image mosaic (NASA/JPL's image No 1234421mainPIA06254-516). The satellites is one of the most reflective bodies in the Solar System. The youthful and geologically complex terrains are shown on side, where the surface is scarred by linear rifts and ridges, contrasting with the other side which is older and dominated by impact craters. NASA/JPL public domain

converting to amorphous ice with age, a process that is thought to take some tens of years, thereby suggesting that the tiger stripes are very young features (the interest reader should visit www.nasa.gov/home/hqnews/2005/aug/HQ_05237_Cassini_Tiger_Stripes.html last accessed in April 2008).

Figure 12.18 shows some of the more exciting features of Enceladus, such as fractures zones and impact craters that have been modified by the satellite's tectonic activity. This tiny satellite has a geological history of cryovolcanism, extensional and compressional tectonics and intensive impact cratering. The cratered surface is bordered by sinuous ridge and rift belts (called sulci and fossae, respectively). These, according to the interpretation of Kargel and Pozio (1996) and by analogy with similar features on Earth, are probably indicative of major lateral lithospheric motions. The recent images returned by NASA's Cassini spacecraft have revealed in stunning details a complex system of fractures, ridges and a resurfaced terrain. Image analysis confirm that the surface is composed of pure water ice.

Latest images from the Cassini spacecraft show what must be geyser-like jets emanating from the south pole of Enceladus (Fig. 12.19). A preliminary analysis by the Cassini imaging team, suggested that these geysers erupt from magma-like chambers of liquid water below the icy surface of the satellite. The latest images show an individual plume as tall as the satellite's diameter.

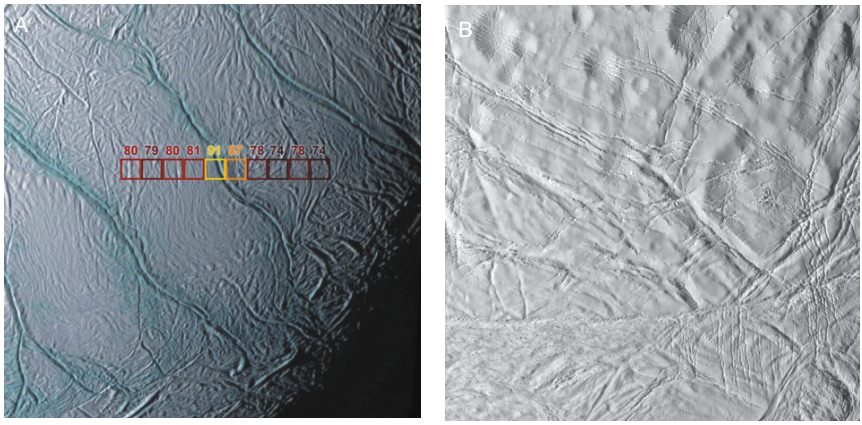


Fig. 12.18 (**A**) This Cassini's image of "*warm fractures*" shows what is possibly the warmest place in the southern polar region of Enceladus. The region covered by this image is about 125 km across and was taken from a distance of 21 000 km. An infrared spectrometer instrument measured the infrared radiation of the surface between wavelengths of 9 and 16.5 μm within each of the squares shown in the bar scale, in which each square is 6 km across, and the number above a square indicates the temperature in Kelvin. The warmest temperatures measured are 91 and 89 K (about –183°C). This indicates that a small area near the sinuous rift has a much higher temperature than the surrounding terrain. The Cassini imaging team suggested that these "warm" temperatures are due to internal heat leaking out of the sinuous rift. These sinuous rifts and ridges have been named "tiger stripes" by the imaging team. Image courtesy of NASA/JPL/GSFC/Space Science Institute. Cassini's images are available at http://www.nasa.gov/cassini or http://saturn.jpl.nasa.gov or http://ciclops.org (all last opened in April 2008); (**B**) This high resolution image (67 m per pixel) of Enceladus taken in visible light at a distance of about 11 500 km. "Softened" impact craters cut by fractures are shown in this image, fractured plains and wrinkled terrain, clearly demonstrating considerable past geological activity that has resulted in the "softening" of impact craters. Image courtesy of NASA/JPL/Space Science Institute. Cassini's images are available at http://www.nasa.gov/cassini or http://saturn.jpl.nasa.gov or http://ciclops.org (all last opened in April 2008)

As for Europa, the hydrothermal system is probably generated by tidal heat of a rocky core, which then produces a pocket or chamber of pressurised liquid water, which vents to the surface as water vapour and ice. More specifically, Hurford et al. (2007) proposed that the tiger stripes open and close in response to varations in tidal stresses and at the same time the shear stress generates heat. During each orbit the tiger stripe rifts are in tension for half the time, opening the rift and allowing eruptions to occur. In the same issue of Nature, Nimmo et al. (2007) proposed that heating is caused by tidally-driven strike-slip movements along the tiger stripes and that this heating results in the production of vapour that escapes as plumes from the fractures that are opened and re-opened by these tidal stresses. Furthemore, these authors calculated, on the basis of tidal displacements, that the ice shell of Enceladus is about 5 km thick and is decoupled from a silicate interior by a subsurface liquid layer or ocean. A model proposed for Enceladus by the Cassini imaging team is shown in Fig. 12.20.

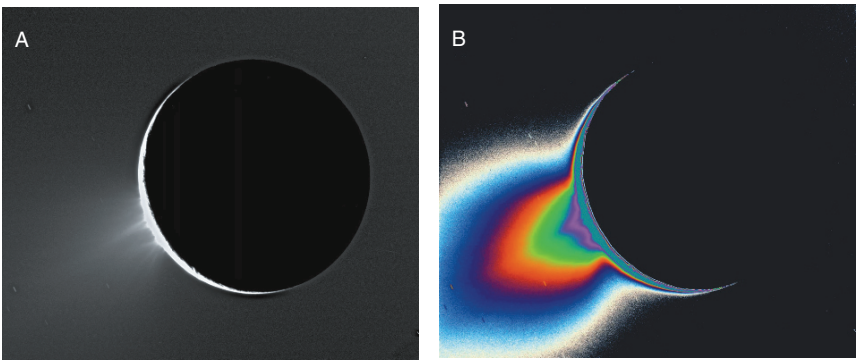


Fig. 12.19 The Cassini imaging team appropriately labelled these images "*the fountains of Enceladus*", which emanate from the south polar region of Enceladus (**A**). It is not clear whether these fountain-like sprays are of water vapour escaping from "warm" ice, or whether they originate from depth where higher temperatures allow water to become liquid, which then escapes under pressure in geyser-like fashion. The image in (**B**) is colour coded to show the weakening of the jets with height. The Cassini imaging team satisfactorily showed that the images of Enceladus fountains were not a camera artefact, by taking images of other moons, such as Tethys and Mimas, with similar lighting, viewing geometries and camera parameters. Image courtesy of NASA/JPL/Space Science Institute. Cassini's images are available at http://www.nasa.gov/cassini or http://saturn.jpl.nasa.gov or http://ciclops.org (all last opened in April 2008)

12.4.4 Titan

Titan was discovered by Christian Huygens in 1655, but only named some 200 years later by Sir John Hesrchel. The first images were obtained by Voyager 1 in 1980. This Saturnian satellite has a diameter of 5150 km, bigger than the planet Mercury and second largest satellite, after Jupiter's Ganymede, in the Solar System. The bulk density of Titan indicates that it is composed of 0.5–0.7 by mass silicate with the rest being water-ice (Tobie et al. 2006). Recent work on the Cassini's data seems to confirm that Titan might have a water ocean beneath its icy crust. This is the conclusion reached by Lorenz et al. (2008), who observed differences in the rotational and orbital periods of this satellite, which would be consistent with a crust decoupled from the core by an internal water ocean. Titan is the only satellite with a very dense atmosphere (about 10 times than Earth's) that mostly consists of molecular N_2, probably sourced from NH_3, followed by CH_4 and other hydrocarbons, such as acetylene (C_2H_2), propane (C_3H_8) and ethane (C_2H_8), as well as hydrogen cyanide (HCN) and molecular H_2. These hydrocarbons and other organic molecules in Titan's atmosphere are thought to form by the breakup of N_2 and CH_4 molecules due to the bombardment of photons from ultraviolet rays (photolysis) and high-energy electrons ejected from Saturn's magnetosphere (Owen 1982, 1999). As aptly put by Owen (1982), Titan offers an immense natural laboratory, in which these organic compounds may well provide clues as to the prebiotic origin of molecules that eventually gave origin to life.

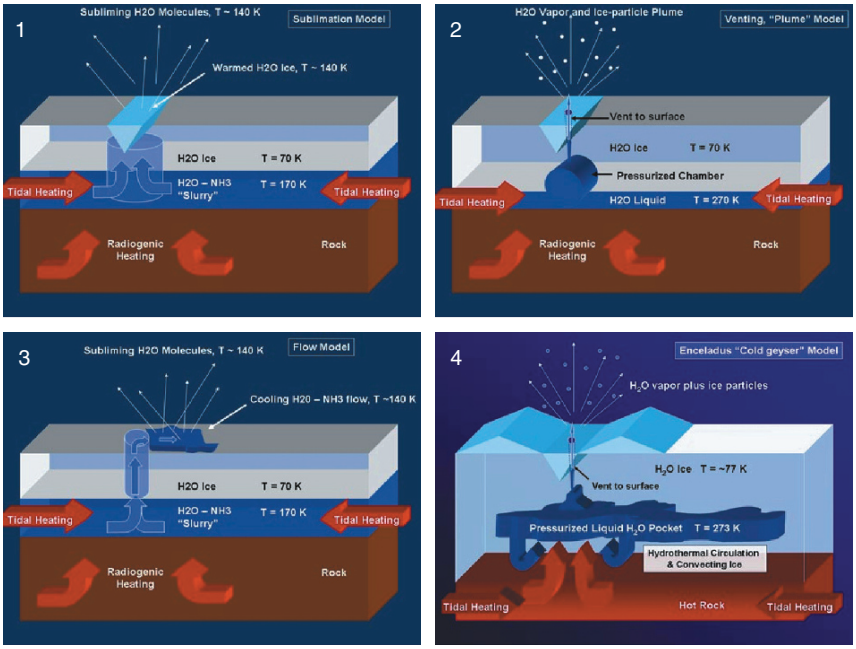


Fig. 12.20 Models of mechanisms to explain the "*fountains of Enceladus*", which could represent a form of hydrothermal system, as suggested by the Cassini imaging team (see also Porco et al. 2006). These models (sublimation, plume venting, flow-sublimation, cold geyser) are based on the assumption that reservoirs of warm (above 273 K or 0°C) pressurised liquid water are present at depth, which vent to the surface as fountains of water vapour and ice particles. The water is warmed through a combination of tidal and radiogenic heating. In the sublimation model of Panel 1, a slurry of H_2O and NH_3 is propelled towards the surface, resulting in the sublimation (change from solid to gas without passing through the liquid phase) of surface ice. In Panel 2, a model of venting of H_2O ice is envisaged involving plumes from a pressurised chamber. In Panel 3 the flow-sublimation model suggests flow of a H_2O-NH_3 slurry and its subsequent sublimation. Finally, the cold geyser model shown in Panel 4, depicts the underground reservoir of a pressurised liquid water at a temperature above 0°C, which erupts to the surface in geyser-like style with jets of icy material. Interestingly, the fountains of Enceladus are spatially associated with fractures in the southern polar region (tiger stripes discussed in text). Image courtesy of NASA/JPL/Space Science Institute. Cassini's images are available at http://www.nasa.gov/cassini or http://saturn.jpl.nasa.gov or http://ciclops.org (all last opened in April 2008)

The Cassini Titan Radar Mapper (Elachi et al. 2005) on board NASA's Cassini-Huygens mission spacecraft imaged small swaths of Titan's surface at a resolution of about 0.5 km/pixel. Images of Titan are frequently being posted on the web site http://saturn.jpl.nasa.gov/home/index.cfm (last accessed in April 2008). The Cassini data, so far, has only revealed three impact craters, the largest about 60 km in diameter and with a bright surrounding blanket of ejecta, which has an asymmetric appearance, suggesting some form of wind erosion. The lack of numerous craters is a clear indication that Titan's surface is

relatively young, a characteristic feature of a dynamic planet with ongoing geological activity.

One of the four modes operated by the Titan Radar is synthetic aperture radar (SAR) imaging, which provided amazing details of the satellite's surface along a 4000 km-long swath. Among the features identified by SAR is a 180 km-diameter circular structure, which could be a volcano construct. At the centre of the structure is a depression, about 20 km wide, which resembles a crater, with sinuous channels and ridges radiating from it. Other saturnian satellites show heavily cratered terrains typically with 200–400 craters per 10^6 km^2 that are larger than 20 km in diameter, Elachi et al. (2005) calculated that the Titan swath scanned by the radar should have 100–200 craters. No recent impact craters were found by Elachi and co-workers, who concluded that the resurfacing rate must have been higher than the impact rate.

Sotin et al. (2005), using near-infrared images obtained during a flyby in October 2004, reported identifying a 30-km diameter circular structure or dome. The instruments used was the Visual and Infrared Mapping Spectrometer (VIMS), which observes in the 0.35–5.2 μm wavelengths, particularly suitable to reduce the scattering noise of the satellite's dense atmosphere. The radar-bright circular or dome-like feature and has a central dark pixel surrounded by curved lineaments, was interpreted as a caldera-like volcanic edifice. Other linear features are east-west trending and have been interpreted as representing zone of extension similar to Ganymede's grooved terrains. Sotin and co-workers suggested that these lineaments may be related to upwelling of "*hot ice*" which also contains hydrocarbons that vaporise immediately into the atmosphere. As for other satellites, tidal heating is a source of energy that could drive cryovolcanism on Titan. The 30 km-diameter radar-bright circular feature is interpreted as a cryovolcano in an area of tectonic extension.

Tobie et al. (2006) modelled the interior of Titan using laboratory experiments and assuming, as noted above, a silicate core surrounded by shells of $H_2O + NH_3$. These researchers predicted three major episodes of CH_4 outgassing, in response to a sequence of silicate core formation, onset of convection in this core, cooling and crystallisation of the outer layers. Methane was probably accumulated in Titan's core at the end of the accretion process; alternatively it is argued that this CH_4 could have formed by conversion of CO_2 through serpentinisation of the silicate core, as in terrestrial hydrothermal systems (see Chapters 2 and 7). Titan's CH_4 would combine with the overlying water to form methane clathrate hydrates. The accumulation of the methane clathrate near the surface results in an increase of the surface ocean temperature. In the second episode the silicate core is sufficiently hot to initiate convection, CH_4 now accumulates at the base of the outer layer and it ascends along fractures. In the third episode, hot plumes, induced by tidal energy, penetrate through the clathrate layer producing the thermal destabilisation of the clathrate to form liquid CH_4 chambers, which then erupt to the surface to form the observed cryovolcanic constructs. The erupted liquid CH_4 would be the equivalent of terrestrial flood lavas. Titan is thought to have a methanological cycle akin to

Earth's hydrological cycle (Atreya et al. 2006). As hinted above, the source of CH_4 is probably deep in the interior and Atreya and co-authors suggested that serpentinisation could have been a viable process in Titan's interior during accretion and asteroidal bombardment.

Evidence of liquid CH_4 or C_2H_6 (ethane) on the surface of Titan is provided by fluvial-like channels, dramatically revealed in the July 2006 Cassini's radar images of the Xanadu region (Fig. 12.21). Mission scientists speculated that liquid CH_4 and C_2H_6 might form lakes near the polar regions of Titan. The radar images cover a swath, about 4500 km long and 490 km wide, to show a dark terrain, with river networks that flow into possible lakes. The dark to black radar response, indicating that no radar signal is reflected back and this implies that extremely smooth surfaces, which have been interpreted by the mission scientists as lakes' surfaces. These CH_4 rivers may be the equivalent of lava flows or they may originate from springs that feed the lakes; visit this web site for more information, http://www.jpl.nasa.gov/news/news.cfm?release=2006-093 (last accessed in April 2008). The abundant CH_4 on Titan's atmosphere would be stable as a liquid, unlike H_2O which cannot exist as a liquid on Titan. The existence of methane lakes on Titan was finally confirmed by detailed studies of the radar-dark patches by Stofan et al. (2007). These authors reported that in the northern hemisphere of the satellite there are a number of such lakes in various states from partly dry to liquid-filled. The origin of the lakes would be either by methane precipitation and/or by river influx, or the depressions are filled from underground reservoirs of a liquid methane



Fig. 12.21 Cassini's radar image of Xanadu (Titan); note well formed river channels, probably of liquid methane. Image from NASA/JPL News Release July 20th, 2006. NASA Ames Research Center scientists suggested that liquid methane drizzles from clouds of liquid methane-nitrogen on the surface of Titan; this constant drizzles makes the ground on Titan saturated with liquid methane; the surface temperature is estimated to be around −149°C. The fluvial features shown in this image may be the result of this uninterrupted methane rain. NASA/JPL public domain and news release No. 06_57AR (July 27th 2006)

table. The underground reservoirs would deliver methane to the surface through cryovolcanism or when the surface is impacted by meteorites. Indeed, it is also considered possible that Titan's atmosphere is replenished in methane by cryovolcanism. This is suggested by the fact that methane has a short lifetime of a few tens of million years on the geological scale, because it is rapidly dissociated by sunlight (Sotin 2007). In any case, the presence of these lakes further suggests, as pointed out by Sotin (2007), that methane on Titan plays a similar role to that of water on Earth, in other words CH_4 participates in a condensable-liquid cycle in the atmosphere and the surface.

The combined radar and infrared data provide a powerful high resolution system to unravel the mysteries of this satellite. During a flyby on the 25th of October 2006, a tall mountain range was revealed, covered with several layers of organic materials (NASA mission news on http://www.nasa.gov/mission_pages/cassini/media/cassini-20061212.html, last accessed in April 2008). The mountain range is about 150 km long and 30 km wide and almost 1.5 km high. In addition, a fan-shaped feature appears to be a lava flow associated with a circular structure that has been tentatively interpreted as a volcanic edifice.

12.5 Where to in the Search for Extraterrestrial Life?

The search for life in other planetary bodies of our Solar System and indeed in the Milky Way galaxy is today actively being pursued. This, seemingly purposeless, but ambitious challenge strikes at the very heart of the fundamental question: are we alone in the universe? Given the accidental and random character of life's evolutionary processes, it is very unlikely, if not impossible, that anything like humans could possibly have emerged or are emerging on other planetary bodies. In our search we are clearly biased towards life forms that are carbon-based, a fact that is encouraged by the common occurrence of organic molecules in comets and asteroids. But, if production of organic molecules is common in asteroids and comets, then it is reasonable to assume that these exist on planets that are in any case formed by accretion of planetesimals, asteroids and comets. The crucial point is to find a site or sites where these organic molecules might have formed from clay minerals or perhaps from monosulphide bubbles vented through hydrothermal discharges (see discussion in Chapter 10), then followed the required chemical reactions to increasing degrees of complexity till they evolved into organic complexes capable of reproduction.

The next step in the search for extraterrestrial life involves a two-pronged strategy. In one, we search for traces of organic compounds either directly or indirectly through lithologies that required liquid water and biological mediation (eg sulphates, Fe oxides) for their formation. In the other, we search for technologically advanced life forms. The Search for Extraterrestrial Intelligence (SETI, see below) began in the USA in the 1950s, is an effort in trying to detect the existence of a techonologically advanced community in some distant planet

of our galaxy. This search is based on the detection of signals and patterns in the electromagnetic spectrum that might suggest trasmissions that could be characterised as intelligent. One of the SETI programs include SERENDIP (Search for Extraterrestrial Radio Emissions from Nearby Developed Intelligent Populations) launched at the University of California, Berkeley. SERENDIP instruments are installed at the Arecibo observatory in Chile, the Parkes Radio Telescope in Australia and the Very Long Baseline Interferometry (VLB) telescope in Medicina, Italy. An informative website for the interested reader is http://www.seti.org/ (last accessed in May 2008). In section 12.6.2, I examine the first alternative, which barring surprises, has a good chance of being successful in the foreseeable future. However, it is worthy of note that it may also be pertinent to ponder on whether or not some life forms actually need water, or in other words is the old dictum, where there is water there is life, valid in all instances?

12.5.1 Where There is Water There is Life?

Liquid water on Earth co-exists with gases, such as CO_2, N_2, H_2S, NH_3 and can accumulate CO_3^{2-}, HCO_3^-, HS^-, NH_4^+ Fe^{2+} and other ions in solution and it can have dissolved organic molecules (Knoll and Grotzinger 2006). Water, therefore, is the medium in which organic compounds interact and organisms live. However, Knoll and Grotzinger (2006) pointed out that water may not be unique in this respect. Ball (2005), reporting on the outcomes of a meeting held in 2005 in Varenna, Italy, quoted one of the biochemist delegates, Steven Benner, as maintaining that "*water is terrible solvent for life*" and therefore is water really essential for life to form and exist? A most intriguing question is that there may be some kind of biochemistry that uses a different solvent system (see also Chapter 10). A general agreement amongst the biochemists at the meeting was that life on Earth adapted to water and not the other way around! Benner et al. (2004) suggested that liquid ammonia (NH_3) could be an alternative to water. Ammonia is liquid at temperatures ranging from –78 to –33°C at the pressure of 1 atmosphere, can dissolve organic compounds and is able to form hydrogen bonds. The liquid range of NH_3 is even greater at higher pressures, for example at 60 atm NH_3 is liquid between –77 and + 97.8°C (Benner et al. 2004). Liquid NH_3 is common on Jupiter and perhaps beneath the surface of Titan. Also on Titan, as mentioned above, rivers of liquid methane or other hydrocarbons may be present. Another compound, formamide, which forms by reaction of hydrogen cyanide (HCN) with water, is polar like water and is liquid over a wide range of temperatures and pressures and might be present on Mars. Liquid N, or even supercritical liquid H on planets such as Saturn, Uranus and Neptune could be permissible. Ball (2005) pointed out that while NASA's quest remains focussed on looking for liquid water, the mission called Terrestrial Planet Finder (TPF), will employ space-based telescopes to

detect and analyse reflected light from extra-solar system planetary bodies, and this mission could perhaps explore the possibility of life forms that do not require water.

Another aspect to note is: water is the aqueous solution containing ions, organic molecules and organisms, but the actual content of water in a solution is of great importance for cellular physiological processes. The equation (Knoll and Grotzinger 2006; Grant 2004).

$$a_W = n_1/(n_1 + n_2)$$

where n_1 represents moles of water, n_2 moles of solute and $a_W$is water activity. Most living organisms cannot survive at a_W below 0.9, some bacteria survive at a_W ranging from 07.5 to 0.85 and some fungi at a_W as low as 0.61 (Grant 2004). Knoll and Grotzinger (2006) stressed that if a_W is too low, such as in brines, water although present may not harbour life.

12.5.2 The Search for Extraterrestrial Life

Carl Sagan in one of his many popular books "Cosmos" (Sagan 1981, p. 298) wrote:

> But is anyone out there to talk to? With a third or half a trillion stars in our Milky Way Galaxy alone, could ours be the only one accompanied by an inhabited planet? ... Perhaps when we look up at the sky at night, near one of those faint pinpoints of light is a world on which someone quite different from us is the glancing idly at a star we call the Sun and entertaining, for just a moment, an outrageous speculation. It is very hard to be sure. There may be severe impediments to the evolution of a technical civilization. Planets may be rarer than we think. Perhaps the origin of life is not so easy as our laboratory experiments suggest. Perhaps the evolution of advanced life forms is improbable. Or it may be that complex life forms evolve readily, but intelligence and technical societies require an unlikely set of coincidences – just as the evolution of the human species depended on the demise of the dinosaurs or the ice-age recession of the forests in whose trees our ancestors screeched and dimly wondered.

In the same chapter, Sagan (1981) continued by attempting to estimate the number N of technologically advanced civilisations, defined as those capable of radio astronomy, in the Milky Way Galaxy. For this Sagan (1981) utilised the famous Drake equation (developed by Frank Drake in 1961, during the first SETI meeting):

$$N = N * f_p\ n_e\ f_l\ f_i\ f_c\ f_L$$

Where N is the number of stars in the Milky Way Galaxy, with an estimate being around 4×10^{11} or 400 billion (Sagan 1981; but other estimates suggest 100 billion), f_p fraction of stars that have planetary systems, n_e the number of planets that are suitable for life, f_l fraction of suitable planets on which life

exists, f_i fraction of inhabited planets on which an intelligent life has evolved, f_c fraction of inhabited planets where intelligent life has developed a communicative technical civililisation, f_L the fraction of the planet's life during which the communicative technical civilisation survives. Sagan (1981) then estimated that the fraction of stars with a planetary system at about 1/3 of the 4×10^{11} stars of the Milky Way Galaxy, therefore $N{*}f_p$ would be roughly 1.3×10^{11}. If each planetary system were to contain, say 10 planets, the total number of "worlds" in the Milky Way alone would be around 1 trillion. In our Solar System, apart from Earth, life could have developed on Mars, and some of the outer planets satellites, like those discussed in this chapter (Europa, Ganymede and Enceladus). Assuming that life did originate in these planetary bodies and assuming the uniqueness of life's tenacity to survive and evolve, the value of n_e could be at least 2, in which case the number of planets that are suitable for life in the Galaxy would be $N{*}f_p\, n_e \sim 3 \times 10^{11}$. If it is assumed that f_l is $\sim$1/3, then the total number of planets where life originated at least once is $N{*}f_p\, n_e\, f_l \sim 1 \times 10^{11}$ (a hundred billion inhabited planets!). In his philosophical pursuit Sagan (1981) recognised that to assign numbers to the next fractions, f_i and f_c, is extremely difficult. Nevertheless, if a number is to be assigned he chose that only about 1% of the planets on which life originated actually produced a technological civilisation ($f_i \times f_c = 1/100$). This would be bring the total for $N{*}f_p\, n_e\, f_l\, f_i\, f_c$ to about 1×10^9, a billion planets on which a technical civilisation arose at least once. But, as pointed out by Sagan (1981), this does not mean that these civilisations exist as I am writing this book. This is where f_L comes in, the most difficult if not intractable fraction. Consider the Earth as an example; the lifetime of the Sun and the Earth is about 10 billion years, but so far we have been communicating with radio waves for about 100 years, if we survive self-destruction, then our communicative technical civilisation could last 10 000 years. If, self-destruction is assumed the final $N{*}f_p\, n_e\, f_l\, f_i\, f_c\, f_L$ could range from 1 to 10. If, however, the alternative is considered in which technological civilisations do not self-destruct, then $f_L \sim 1/100$ and N becomes about 10^7, the number of extant civilisations in our Galaxy alone. I make a more conservative estimate as follows: $N{*} = 100$ billion; $f_p = 50\%$; $n_e = 1$; $f_l = 50\%$; $f_i = 10\%$; $f_c = 10\%$; $f_L = 10\,000$ years, then $N = 250$: in our galaxy alone!

The estimates arising from Drake's equation are disputed by Taylor (1999) who believed that technological civilisations may be unique or exceedingly rare in the Universe. Although this view might bring to mind the case of the worm inside an apple: the worm believes it is the only being in the only apple that exists in the Universe. Furthermore, due consideration must be given to the previously mentioned, Habitable Zone in a given planetary system, as well as in the Milky Way Galaxy. The galactic Habitable Zone (GHB), proposed by Gonzales et al. (2001), defines the most hospitable places for life in the Milky Way. The boundaries of the GHZ are constrained by the availability of the right elements that can be assembled to form Earth-like planets. In addition, the size of the planet is important for it to retain an atmosphere and sustain geological processes related to mantle dynamics. This GHB is what astronomers refer to as

the "metal" rich zone. Since the big bang initially produced H and He and only after billions of years this initial mix changed into a mix in which the ratio of metallic atoms to the number of H atoms was increased. In this way the GHB has to exclude innermost regions (too hot) and inner regions of the Milky Way, where too much metallicity is detrimental (larger planets, stronger gravity). By the same token, the outer regions of the Milky Way will be metal poor and therefore unsuitable. The GHZ is a broad belt with diffuse boundaries, roughly in the middle of the Milky Way. Within the GHZ are planetary systems, which like for the Solar System, would have a Habitable Zone. In the Solar System, the habitable zone is probably somewhere between the orbit of Venus and just short of, or slightly beyond, the orbit of Mars.

The topic of the search for life in the Solar System and the Universe is a burgeoning field and textbooks have already been published (Westall 1999; Davies 1999; Schulze-Makuch et al. 2002; Clancy et al. 2005; Seckbach et al. 2005; Brack 2005). The biological potential of planetary bodies requires surface or subsurface liquid water and C-based organic molecules. The distinctive properties of H_2O are fundamental for the survival of known biological molecules. As already discussed in Chapter 1, a water molecule has a tetrahedral geometry, with an oxygen atom at the centre linked to two hydrogen atoms on one side of the tetrahedron, and two unshared electron pairs on the other side. This results in the water molecule having a slight negative polarity around the oxygen atom and a slight positive polarity around the hydrogen atoms. It is this polarity that allows H_2O to readily interact with other polar molecules including salts, sugars, various proteins and DNA. Water can dissolve polar molecules, termed hydrophilic (water loving), but does not interact with nonpolar molecules (eg fats, oil), termed hydrophobic (water fearing). DNA molecules contain both hydrophilic and hydrophobic arranged with the former on the surface, where they can interact with H_2O and the hydrophobic groups in the interior, where they are shielded from H_2O. In living organisms the space not occupied by the biological molecules is filled with H_2O (human cells are mostly H_2O).

The possible presence of liquid water, cryovolcanism and hot spots on Europa can provide environments that could sustain primitive life forms. There is no direct evidence of organic compounds on Europa but, and according to the Panspermia hypothesis discussed in Chapter 10, these could have been delivered to the satellite by cometary impacts. In any case, and as pointed out by Greeley (1999) all three basic conditions for the establishment of life are present on Europa (and Enceladus, Ganymede and Titan): heat, liquid water and organic compounds.

12.5.2.1 Diversity of Environmental Conditions

On Earth, micro-organisms that can survive maximum temperatures of $>110^{\circ}C$, such as the deep-sea microbe *Pyrolobus fumarii*, are known as hyperthermophiles. At higher temperatures organic molecular systems become

thermally unstable. Hyperthermophiles include bacteria that are able to grow at temperatures of between 80 and 110°C and some are not even able to survive below 80°C. Hyperthermophilic bacteria have been recognised in deep sea hydrothermal vents and also from continental solfatara fields and geothermal power plants (Stetter et al. 1990). However, a "hot" origin of life (hyperthermophiles) is probably not possible because RNA breaks down at high temperatures and therefore it is more likely that life first appeared in a less extreme environment (Brack 2005). As mentioned in Chapter 10, micro-organisms are also known to survive extremes of cold, with a lower limit for bacterial growth reported as low as –12°C (Brack 2005 and references therein). Apart from temperature extremes, pressure is another physical parameter in which many micro-organisms seem to be able to comfortably withstand. Pressures greater than 1000 bars occur in the deep ocean, where micro-organisms thrive in and around hot hydrothermal discharges. Similarly, micro-organisms have been found in subterranean environments, oil fields and deep marine sediments down to depths of 750 m below the seafloor (Brack 2005). Methane, a green house gas and a minor constituent of our atmosphere, is commonly found in the subsurface, where it is generated by microbial processes. It is estimated that subsurface microbes are present to depths of more than 3 km (Kotelnikova 2002). This subterranean microbial life does not depend on the sun's energy (photosynthesis) for energy and respiration. Instead these anaerobic autotrophic micro-organisms (methanogens; sulphate-reducing and Fe-reducing bacteria) produce CH_4 from the respiration of H_2 and CO_2 gases that are ultimately derived from mantle magmas. The presence and distribution of biogenic CH_4 is of considerable economic importance as a source of energy. Biogenic CH_4 has been detected in a wide variety of environments: marine and lake sediments, marine subsurface (down to 7 km of depth), in carbonate rocks (to depths of 6 km), in Permian sandstone associated with oil fields at a depth of 2 km, as well as onshore gas seeps (Kotelnikova 2002). The biogenicity of this CH_4 is determined through geochemical and carbon isotope systematic studies. Methane of biogenic origin generally has $\delta^{13}C$ values ranging from –60 to –90‰ compared to PDB standard (the $\delta^{13}C$ is defined by $R_{sample} - R_{PDB} \times 1000$, where $R = {}^{13}C/{}^{12}C$ and PDB is the Pee Dee belemnite standard = 0.0112372). Although, the isotopic composition of the biogenic CH_4 is ultimately dependant on the nature of the source of CO_2, which can be derived from a variety of rocks and minerals, and therefore the isotopic signature needs to be evaluated with caution. Biogenic production of CH_4 is accomplished by *Archaea* methanogens, such as *Methanobacterium thermoautotrophicum*, isolated from a hydrothermal vent in the Yellowstone National Park (USA) and *Methanothermus fervidus*, isolated from deep hydrothermal vents in Iceland (Kotelnikova 2002).

Some halophiles (salt loving) micro-organisms thrive in salt-rich environments, where salt concentrations can reach as high as 20% NaCl, such as those found in salt lakes. Best examples of this type of environment can be found in Western Australia, where ephemeral salt lakes provide a haven for halophiles (Benison et al. 2005). Halite and gypsum are common precipitates in these lakes,

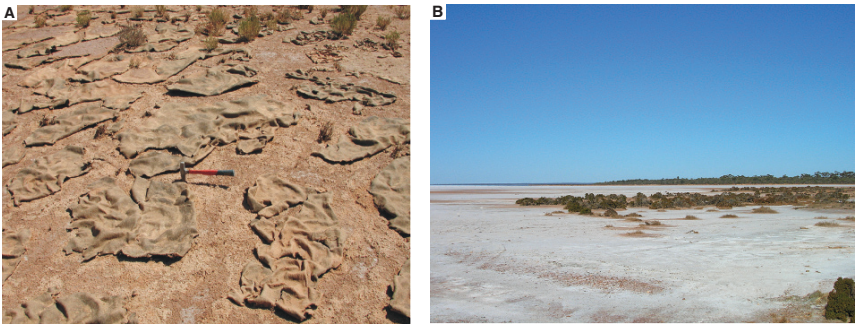


Fig. 12.22 (**A**) Remnants of microbial mat, dessicated by the sun, on the northern shore of the saline Lake Carnegie, Western Australia; (**B**) Lake Goongarrie, a saline lake about 100 km north of the mining town Kalgoorlie in Western Australia. Playa lakes on Mars could harbour primitive life

where the presence of microbial life is revelead by filamentous and algal mat structures (Fig. 12.22A), as well as production of gases such as H_2S. Terrestrial life is generally adapted to environments with neutral pH, but again there are micro-organisms that are able to adapt under extreme pH conditions, from very acidic (pH = 0) to very alkaline (pH = 12.5), although these micro-organisms manage to keep the intracellular fluids to at near neutral pH. Extreme acidophiles are found amongst the hyperthermophiles and include genera such as *Sulfolobus*, *Metallosphera*, *Acidiunus* and *Sesulfurolobus* (Stetter et al. 1990). A listing of common hyperthermophile micro-organisms can be found in Stetter (1996).

12.5.2.2 Biosignatures

The search for extraterrestrial life will have to rely on remote sensing methodologies for the next few years till such time when samples can be obtained from the Martian surface. What can be detected to tells us that there may be life, as we know it, beyond Earth? Schulze-Makuch et al. (2002) listed the following bio- and geosignatures: (1) atmospheric gases, such as O_2 and CH_4, which may the products of biogenic processes; (2) rock types that are known on Earth to be associated with biogenic mediation, such as iron-formations and stromatolites; (3) presence of biogenic substances, like chlorophyll, that are not formed by inorganic processes. Other features listed by these authors, but much less likely at least in the foreseeable future are: geometric regularities or aggregates, such as insect colonies or cities and regular radiowave emissions.

The Earth's atmosphere is best example of a biosignature. We know that our atmosphere is the result of the photosynthesis process. The high amount of O_2, with the presence of CH_4, NH_3, various sulphur gases and organic compounds are the result of life processes. Signature of chemotrophic life, chemosynthesis, is reflected in large expanses of rock types such as iron-formation and carbonates generated as a chemical end-product of microbial activity. Biochemical

products such as stromatolite colonies and coral reefs are detectable from space. Chlorophyll is easily detectable by spectra in the visible range. More difficult is the remote sensing detection of fossil remnants or isotopic fractionations caused by biological processes (Schulze-Makuch et al. 2002). But, as the reader would certainly realise, life could exist in a form that is not familiar or known to us in which case the bio- and geosignatures that are familiar in our understanding of life, may not be present. Therefore other features must be taken into account. Schulze-Makuch et al. (2002) list the following: (1) maintenance of disequilibrium with the environment, energy gradients for sustaining low-entropy states; (2) chemical complexities which require to transform and store energy and that require a fluid medium where molecular mobility can be maintained; (3) storage and transmission of information, which would require polymeric chemistry. Thus, energy flow, fluid medium or media and polymeric chemistry, together with the presence of an atmosphere, are the essential ingredients for the existence of some form of extraterrestrial life. Remote detection of these life indicators would include molecular absorption spectra, surface reflectance spectra, radar measurements, detection of alteration minerals, imaging spectroscopy, polarimetry, infrared radiation, radiometry, infrared to visible spectra imaging, and microwave radiometry to detect geothermal heat flow. Chemical complexity of polymeric molecules is C-based and organic C molecules are known to be widely present throughout the observable universe. Although we assume that any form of life has to be C-based but, as pointed out by Sagan (1994), other polymer forming elements are possible, as for example Si-based polymers under high pressure and high to low temperatures. Polymeric compounds can be detected by absorption spectra.

In our Solar System, Mars, Europa, Ganymede, Enceladus and also Titan are all good candidates for the possible existence of some form of microbial life, fossil or extant. As discussed in the preceding sections of this chapter, the reasons for their suitability to harbour or to have harboured life are the past or current presence of liquid water and sources of thermal energy that drive or may have driven hydrothermal circulation, as well as mineral species, such as hematite, whose formation may have been mediated by bacterial organisms. On Earth, both submarine and subaerial hydrothermal systems support prolific biological communities and it is assumed that if these systems are or were present on Mars, Europa, Ganymede and Enceladus, the same conditions may have existed to create and support life.

With the above in mind, McCollom (1999) examined the potential for the possible development of biological communities on Europa by assuming that chemolithoautotrophic ecosystems, which derive energy from chemical reactions, exploit chemical disequilibria to gain metabolic energy. This author suggested that methanogenesis, conversion of CO_2 to CH_4, is this possible source of energy, according to the reaction:

$$CO_{2aq} + 4H_{2aq} = CH_{4aq} + 2H_2O$$

This reaction is used by autotrophic methanogens on Earth, which utilise CO_2 to synthesise organic compounds. These are chemolithoautotrophs (see Table 10.1, in Chapter 10, for nomenclature). Methanogenesis is a powerful source of chemical energy in terrestrial hydrothermal vents and one for which oxygen is not required. Methanogens in submarine hydrothermal vents are thermophiles capable of growth at temperatures from 50 to $>100^{\circ}C$, in contrast to aerobic chemolithoautotrophs that can only survive at temperatures of 40–50°C or less. McCollom (1999) proposed a similar mechanism for hypothetical hydrothermal sites on Europa, a conceptual model of which is shown in Fig. 12.14. In this model heated water from the European liquid ocean layer reacts with the surrounding rocks and the modified solutions discharge through vents on the seafloor, where the hydrothermal solutions mix with the liquid ocean, creating a potential habitat for chemolithoautotrophic organisms that derive their energy from the redox disequilibria (McCollom 1999).

Westall (1999) set out criteria for the search of extraterrestrial life based on the identification of fossil bacteria. She reviewed the ways in which fossil bacteria are preserved and examined the problem of misidentification of non-microbial structures. Size, shape, cellular outer wall features, organisation and distribution being important aspects to consider. Bacteria range in size from 0.5 to 100 μm or more, with shapes varying from spherical, rod-like, filamentous to spiral. Filamentous and rod-shaped bacteria may exhibit branching. Most important is the fact that bacteria tend to form colonies consisting of coexisting species or consortia that are attached to a substrate, creating a slime layer or biofilm, which is what commonly remains in the fossil record after the colony dies out. The preservation of bacteria is by a process known as permineralisation and by mineral replacement. Permineralisation acts on the dead micro-organisms and involves a process whereby silica in solution nucleates on active organic templates, such as CO, or PO_3, forming a mineral matrix. Permineralisation is especially efficient after degradation has occurred, because this releases more active groups (Westall 1999). Permineralisation was common in the Precambrian, as observed in the Duck Creek Dolomite in Western Australia in which the permineralised micro-organisms changed to kerogen after diagenesis (Knoll et al. 1988). Other classic examples of Precambrian permineralised and mineralised bacteria are the Gunflint Formation in the Lake Superior region (Ontario, Canada) and the Frere Formation of the 1.8 Ga Earaheedy Basin in Western Australia (Chapter 8).

By contrast, in the Phanerozoic permineralisation in marine sediments is not common, largely because the silica is utilised by organisms with a siliceous test, such as diatoms. Permineralisation may lead to mineral replacement, in which the entire organic structure of the bacterium is replaced by silica or carbonate minerals, phosphates, Fe sulphides, Fe or Mn oxides. Westall (1999) pointed out that permineralisation and mineral replacement are two end-stages of a continuum. It must be borne in mind that permineralisation and mineral replacement are not to be confused with biomineralisation, which is a metabolic process that micro-organisms use, resulting in the precipitation of a mineral or minerals.

There remains the problem of misidentification of non-biological structures that may exhibit bacterial shapes, called bacteriomorphs. Biogenicity has to be demonstrated. This includes establishing size, shape, cellular complexity, organisation, colony, and cell wall texture. Spherical structure can be easily confused with bacteria. Abiogenic macromolecule vesicles, such as lipids and proteins can produce sphere of bacterial size surrounded by a membrane. Furthermore these abiogenic spherules can also become mineralised and preserved like fossils. Amorphous minerals and gas bubbles can also form spheres and even appear to divide due to spherical growth around seed nuclei, so that the spheres interfere with one another forming aggregates. Abiogenic spherules can be distinguished by their generally larger size. Westall (1999) cited the example from volcanic lake sediments containing rod-shaped phosphatised bacteria as well as abiogenic spherules, probably gas bubbles, exhibiting a wide size range. Rod-shaped bacteria (bacilli) or filamentous bacteria are less of a problem because abiogenic organic structures have a greater tendency to be round. Interestingly, mineralised bacteria can become enclosed in crystals, such as aragonite and calcite. The biogenicity of bacterial forms can be tested by using carbon isotopic fractionation. Evidence of life in Precambrian sedimentary rocks, apart from the recognition of micro-organisms, can be deduced from the enrichment of reduced carbon in $\delta^{13}C$. The isotopic compositions of reduced carbon in Precambrian sedimentary rocks indicate a wide range of $\delta^{13}C$ values from –15 to –40‰ relative to PDB (see Chapter 1), and therefore there is a strong enrichment in $\delta^{12}C$, suggesting photosynthetic reactions (Faure 1986). However, some enrichment in $\delta^{13}C$ does appear with metamorphism and this is possibly due to formation of CH_4.

12.5.2.3 Potential Sites on Mars

Liquid water cannot exist on present-day Mars and it is highly unlikely that micro-organisms could survive on the surface. The study of geological processes on Mars that may have possible analogues on Earth ideally would restrict the choice of potential sites that could have been conducive to the formation of organic molecules and eventually life. "Terrestrial Analogs to Mars" was a study commissioned and formalised by the US National Science Foundation (Farr 2004 and references therein). A special issue of Planetary and Space Science is devoted to Mars and Earth analogues (Marinangeli et al. 2004).

Of the similar geological processes that can be considered to exist between Mars and Earth, the first that come to mind and perhaps the easiest to recognise are volcanoes (Fig. 12.4). Other obvious geomorphological and geological features include landforms that are created by sedimentary processes, by aeolian action, such as desert sands, or by liquid water, such as river valley networks and drainage systems and sedimentary layers in lacustrine deposits (delta deposits, alluvial fans; Malin et al. 2003). Examples of desert sites, where geological and geomorphological processes are reasonably well-known on our planet, can be found on all continents, (e.g. central Australian deserts, the

Sahara, Namib and Kalahari in Africa, the Gobi desert in south-central Asia). One of the features of many deserts are playa lakes, which can serve as excellent analogues to Martian areas that have been proposed as having contained palaeolakes and evaporite deposits (Farr 2004), discussed in more detail below. Ice fields, faults and fractures, rift systems and meteorite impact structures are other sites of considerable interest to planetologists. Ice sheets, glaciers, volcanoes and hot springs are well known and within easy reach in Iceland and Alaska, and Martian analogues could include the polar regions as well as several areas in the northern hemisphere, where permafrost, periglacial and glacial processes can be seen (Farr 2004). Knowledge of volcanic processes, including associated hydrothermal systems, from Iceland, Alaska and particularly the previously mentioned East African Rift System, with its arrays of volcanic constructs, lakes, evaporite deposits, playas, hot springs, all teeming with primitive life forms. Martian rift zones, such as the giant Valles Marineris and its many branches provide good sites for investigation. Over 200 impact craters are now known on Earth, and more are being discovered as geophysical techniques improve that allow us to see beneath surficial covers (e.g. Woodleigh impact structure in Western Australia; Chapter 11). Again, Australia provides easily accessible sites for comparative studies (Glikson and Haines 2005). Hydrothermal systems are known in terrestrial impact structures (Pirajno 2005) as mentioned in Section 12.3.4 and discussed below.

It is not known if life on Mars arose and if so whether it existed continuously or it was time and again terminated during catastrophic events only to reappear again. The meteorite found in Allan Hills in Antarctica in 1984 and called ALH 1984 #001, shortened to ALH84001, sparked a flood of papers and debates. ALH84001 is an orthopyroxenite and one of the NSC meteorites, so-called after Shergottites, Nakhlites and Chassigny, a group of Martian meteorites, which have a volcanic or plutonic origin, young crystallisation ages (1.3 Ga to about 180 Ma) and with a unique oxygen isotopic signature and FeO/MnO ratios, indicating that they are not from the Earth or the moon. This is further confirmed by the isotopic character of N_2 and noble gases, which are identical to those of the Martian atmosphere as analysed by the Viking landers. For a comprehensive overview on the classification of meteorites the interest reader should consult Krot et al. (2003).

The ALH84001 orthopyroxenite with an age of about 4.5 Ga is probably a fragment of Mars' ancient crust (Krot et al. 2003). McKay et al. (1996) found orange coloured carbonate globules in ALH84001, for which an age of 3.9 Ga was determined (Borg et al. 1999). It was suggested that these globules resemble terrestrial carbonate spherules where bacteria are common. The ALH84001 carbonate globules also contain magnetite crystals that are very similar to those found in bacterial cells and have rod-like shapes closely resembling terrestrial bacteria, as revealed by the electron microscope (Fig. 12.23). This finding was disputed by Kirkland et al. (1999) others on the basis that mineral surfaces in many terrestrial rocks are decorated with spherical, rod-shaped, and ovoid shaped objects of 25–300 nm (nanometers) size and that these bacteria-shaped

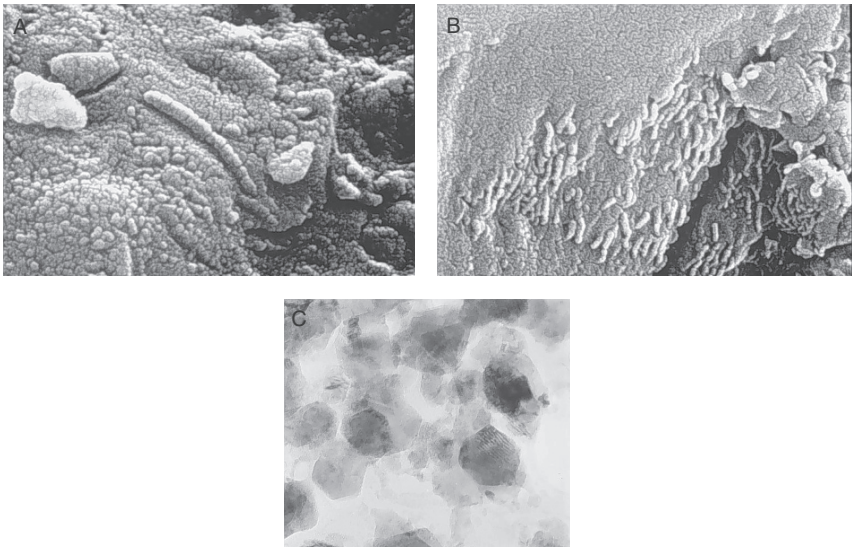


Fig. 12.23 (**A**) and (**B**) Scanning electron microscope photomicrographs of putative bacterial fossils on ALH84001; (**C**) transmitted electron microscope photomicrograph of aggregate of magnetite crystals (a single crystal is about 40 nanometre across), extracted from carbonate globules in ALH84001. Field of view of A and B is about 800 nanometres. After Thomas-Kerpta et al. (2000), McKay et al. (1996), Bradley et al. (1996)

objects can be inorganic mineral structures. Nevertheless, McKay et al.'s (1996) claim led to dozens of papers being presented at the 29th Lunar and Planetary Science conference in 1998, and hot debates for and against the biogenicity of ALH84001 bacteria-like shapes, as outlined below.

ALH84001 contains at least two types of organic carbon. One is terrestrial contamination, and is associated with the carbonate globules. The second is associated with the pyroxene minerals in the meteorite, and includes polycyclic aromatic hydrocarbons (PAH) and high-mass polymerized organic molecules (kerogen). This organic material has a carbon isotope composition that is not consistent with terrestrial contamination, and is inferred to be Martian. However, it is similar to organic material in carbonaceous meteorites, and therefore it represents meteorite material that fell onto Mars, not Martian life (Becker et al. 1999). But, on the other hand, the carbonate globules in ALH84001, may still provide evidence of possible ancient Martian life, because they could have precipitated from pore water fed from a saline lake (McSween and Harvey 1998). Some deposits from saline lakes show sequences of minerals like those in the globules, and most other data on the globules are consistent with this evaporitic origin. Bacteria and other microbes are abundant in evaporite lakes on Earth, but are not necessary for precipitation of the carbonate minerals. Thus, this model does not necessarily support the hypotheses of McKay et al. (1996), although it does suggest that evaporite lakes on Mars might be

good targets for spacecraft exploration in the search for Martian life. The carbonates globules in ALH84001 differ from known terrestrial evaporite deposits in several respects: some of these carbonates are rich in Fe and they have layers rich in magnetite. Magnetite grains are abundant in the carbonate globules, and McKay et al. (1996) suggested that the grains were formed by bacteria on Mars. However, shapes of some ALH84001 magnetite is not known from terrestrial bacteria. Magnetite crystals in terrestrial bacteria are all "single magnetic domain" sized-lengths and widths so the grains spontaneously become strongly magnetic. Bradley et al. (1996) disputed the biogenic origin of the ALH84001 magnetite crystals, largely because they thought that the temperature of magnetite formation is too high for any form of life. But the counter-argument has it that these grains are ideal for bacteria that need to sense magnetic fields around them (Thomas-Keprta et al. 1998). More recent further work on the sub-micron hexa-octahedral magnetite crystals within the carbonate globules of ALH84001 suggested an origin by magnetotactic bacteria (Fig. 12.23; Thomas-Keprta et al. 2000, 2004).

On Mars, potential sites where primitive life could have formed include areas where active or fossil hydrothermal systems may be present in rift systems, such as Valles Marineris, or where springs discharge, or along the flanks of volcanic edifices, or in palaeolake systems. Bacterial communities exist on Earth within the pore spaces of rocks near and well below the surface. The endolithic habitat is protected from solar radiation and is common in terrestrial extreme climates, especially hot and cold deserts (Walker et al. 2005). Pedersen (1993) provided a detailed review of the deep subterranean biosphere. This author listed lithofacies environments and depths where bacterial communities were found, including ashfall tuff (400 m), crystalline granitic basement rocks (129–1240 m), dolomitic limestone (1264–1752 m), oil-bearing sedimentary rocks (29–1690 m). The possibility of endolithic or subterranean micro-organism communities on Mars cannot be excluded.

The combination of past widespread volcanic activity and liquid water is the correct recipe that inevitably results in large scale hydrothermal circulation, which may have operated in the Martian subsurface at some stage during the geological history of the planet. Sulphate minerals and Fe oxides can be precipitated from hydrothermal fluids and mediated by metabolic processes of micro-organisms. Various lines of evidence indicate that Mars was warmer and wetter and with a CO_2-rich atmosphere in the early stages of its geological history and perhaps even in recent times (Kargel 2004; Tokano 2004). The loss of its atmosphere led to the freezing of its water and although the there is clear evidence of water activity on the planet's surface, this may have been somewhat episodic and catastrophic, perhaps as a result of asteroid impacts and/or rising magma heating the subsurface ice. It is therefore possible that life arose in the early environment of Mars, which was similar to that of early Earth or, given the ample demonstrations of life's tenacity to survive in extreme conditions, the possibility exists, as mentioned above, that organisms might be present in the subsurface layer.

Chemosynthesis may be the form of energy source utilised by putative Martian micro-organisms and hydrothermal systems provide the only plausible environment where a source of chemical energy is abundant and readily available. Geochemical and numerical models developed by Varnes et al. (2003) explore the consequences of mixing Martian hydrothermal fluids with groundwaters. In the absence of O_2 in the Martian environment, important sources of metabolic energy for chemosynthetic microbes are methanogenesis (see reaction above) and sulphate reduction:

$$SO_4^{2-} + 2H^+ + 4H_2 \rightarrow H_2S + 4H_2O$$

The results of this modelling suggest that while chemical energy is plentiful for microbial metabolism, the potential biomass that can be created in Martian hydrothermal systems, largely associated with the predominantly basaltic crust, is substantially lower compared with that of the Earth. Varnes et al. (2003) suggested that the best targets would be provided by extinct hydrothermal systems hosted in ultramafic rocks. This is because the large concentrations of H_2 needed to drive the above reactions, can be produced by serpentinisation of Fe-Mg silicate phases, such as:

$$3Mg^{2+} + 2SiO_{2(aq)} + 5H_2O \rightarrow Mg_3Si_2O_5(OH)_4$$

Given the abundance of Fe oxides found on Mars (Section 12.3.2.2), electron donors (Fe^{2+}) and acceptors (Fe^{3+}) can also provide metabolic energy, albeit in lesser amounts. The necessary energy for the reduction of H_2O to H_2, which in turn can support production of biomass, as in the oxidation reaction of fayalite to hematite (Jakosky and Shock 1998):

$$Fe_2SiO_4 + H_2O \rightarrow Fe_2O_3 + SiO_2 + H_2$$

or, the reaction of magnetite to hematite

$$2Fe_3O_4 + H_2O \rightarrow 3Fe_2O_3 + H_2$$

As mentioned in Section 12.3.5, large asteroid impact craters may induce hydrothermal activity and hence provide potential sites for extinct or extant life. Apart from the evidence of lake sediments in Martian impact craters, hydrothermal processes could have occurred soon after impacts. Impact-induced hydrothermal circulation, whose surface discharges, by analogy with Earth's impact craters, will produce siliceous and/or calcareous deposits, such as sinters and travertines, respectively. Newsom et al. (2001) suggested that these have the best chance of preserving microbial biosignatures. An assessment of impact craters as possible repositories of hydrothermal systems and primitive life needs to take into account, the magnitude and duration of the heat source, and the size

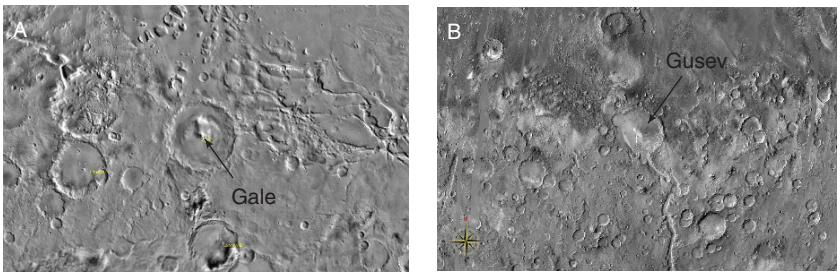


Fig. 12.24 (**A**) View of Gale Crater, 120-km diameter; Lat 5.5° S Long 1310.99° E; altitude 693.9 km;). Note drainage system in the vicinity to the east of the crater; (**B**) Gusev crater, 150-km diameter; –110.798° S Lat 172.696° W Long; altitude 976 km, both thought to have sediments related to playa-type lakes; from NASA World Wind

and exposure time of the crater's lake sediments. The primary heat sources of large impact structures, both on Mars and on Earth, are the melt bodies created by the kinetic energy of the impact and the heat from the central uplift. Newsom et al. (2001) estimated that large craters, such as Gale and Gusev (Fig. 12.24), may have had as much as 20 000 km^3 of impact melt, corresponding to a melt layer 900 m thick, from which the total heat available would be in the order of 2×10^{22} to 2×10^{23} Joules. The duration of hydrothermal activity in an impact structure depends on the size and cooling rate of the causative melt sheet, which in turn is also dependant on the amount of down-flowing groundwater, the ensuing convective fluid system and the permeability of the rocks through which the fluid circulate and deposit minerals that may be causing sealing. Sealing is an important aspect of hydrothermal systems and may result in boiling, due to build-up of hot fluids pressure below the seal, and/or horizontal flow. Horizontal flow may cause the discharge of the fluids well away from the impact crater. Newsom et al. (2001) reported that the duration of hydrothermal systems in impact structures can be up to 10^5 years for 100-km diameter craters and 10^6 years for 180 km craters. The rocks with which hydrothermal fluids interact are subjected to the effects of alteration which in terrestrial cases, range from high temperature alkali metasomatism to the development of low temperature hydrothermal minerals (Pirajno 2005). Mineral phases that typically form include various clays (smectite, kaolinite), quartz, K-feldspar, chlorite, epidote, carbonates and zeolites. In the case of Mars where basaltic rocks appear to predominate alteration minerals could include celadonite, and Fe-saponite as shown by the 2-km diameter Lonar Crater in India that formed in basaltic rocks of the 65 ma Deccan Traps (Newsom et al. 2001). Focusing of hydrothermal fluids can occur at the boundary between the walls and the floor of the crater, where emerging groundwater may create a fluvial system as seen for the Aram Chaos structure shown in Fig. 12.25A. Aram Chaos, a 250-km diameter round depression that was probably originated by a meteorite impact, is linked with the Ares Valley by a deep channel that flows into the depression and form a delta structure (Fig. 12.25). Cabrol and Grin (2002) suggested that

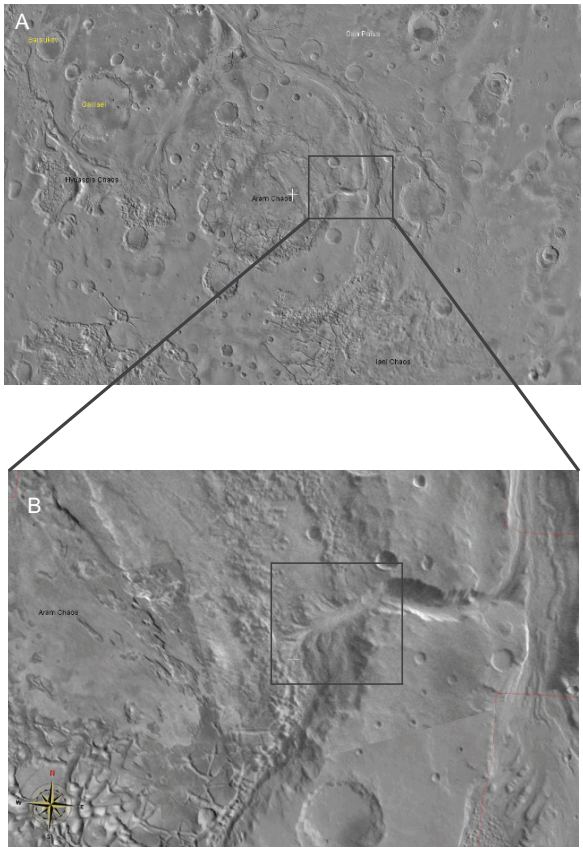


Fig. 12.25 Aram Chaos structure, 250 km in diameter, (lat 2.709 N long 20.349 W; altitude 9710.59 km), is a partially eroded impact crater with distinct dendritic channel networks due to the sapping of ground water (**A**); this area could be the site of hydrothermal discharges; (**B**) shows in some detail the deltaic structure (about 40 km across), formed as a result of the breaching of the eastern rim by Ares Vallis outflow channel. After Cabrol and Grin (2002); image obtained from NASA World Wind

this deltaic structure has the characteristics of a sub-lacustrine delta with a platform, a prodelta slope, tributary channels and deposits of finely laminated sediments. The Aram Chaos delta is about 40 km long and 25 km wide (Fig. 12.25B). Importantly, the Aram Chaos is one of the areas where hematite was discovered (Christensen et al. 2000, 2001).

Newsom et al. (2001) argued that some large impact craters on Mars that may contain hydrothermal silica deposits should be targeted for the search of extraterrestrial life. These authors suggested that the most important parameters to consider are: large diameter craters, identification of hydrothermal deposits, presence of outflow channels, presence of lacustrine deposits. Examples of craters that conform to these requirements are the Holden-Eberswalde and Gusev craters. The Holden crater, imaged in amazing details (Fig. 12.26A), is 154 km in diameter and contains site of water-flow deposits, consisting of layered sediments, channels and alluvial fans, suggesting a long history of water-induced deposition (Christensen et al. 2006). The Holden Crater is breached by the Uzboi Vallis large fluvial system (Fig. 12.26B), which flowed into the crater, depositing sediments. Just north of Holden is the 65-km diameter

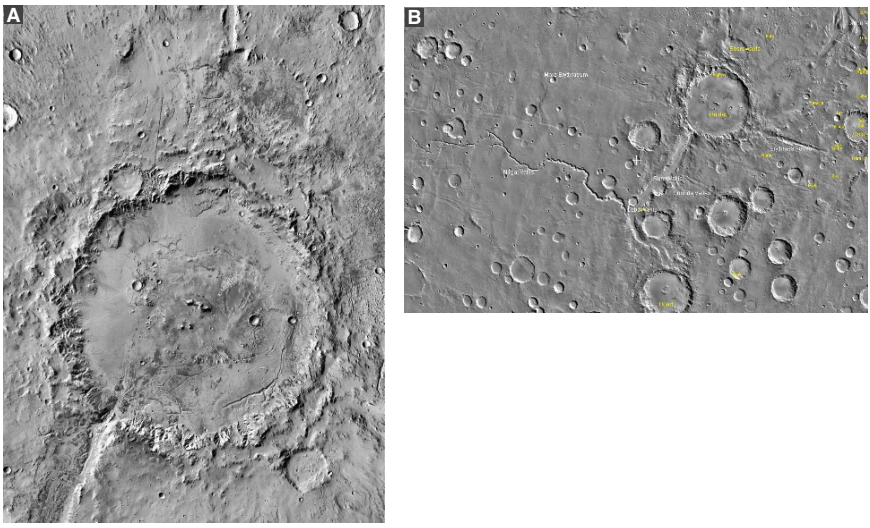


Fig. 12.26 (**A**) Infrared image of Holden Crater, 154 km in diameter, (lat 25.5 S long 326.0E); image size is 214 × 291.4 km; resolution is 100 m. Image from NASA/JPL/ASU (Christensen et al. 2006); (**B**) shows an image of the Nirgel Vallis, a long meandering fluvial channel, that joins the Uzboi Vallis and the Uzboi-Holden crater systems

Eberswalde crater, in which the remnants of a river delta can be seen (Christensen et al. 2006). The delta has layered sediments and meandering channels, similar to when a terrestrial river empties into a standing body of water.

The 150-km diameter Gusev crater (Section 12.3.2.1) and the 900-km long Ma'adim Vallis, together form a hydrogeological system, studied in detail by Grin and Cabrol (1997) and Cabrol et al. (1996) (Fig. 12.24), using terrestrial analogues, such as those provided by sub-glacial Antarctic lakes and deltas. These authors suggested that Gusev crater hosted a series of lakes and playas. Bathymetric modelling by Grin and Cabrol (1997) indicates that the sedimentary material deposited in the crater's floor is in the order of 500 m with a volume of water of about 11 300 km^3 and that the Gusev palaeolake history developed in two episodes. In the first, the crater floor was filled by groundwater from drainage that resulted from the impact, generating an intracrater lake. In a second stage, water from Ma'adim Vallis breached the southern rampart of the crater and flowed into the earlier lake, forming a sublacustrine delta deposit. Playas were formed at the end of the life of lake Gusev, with the waning of flow from Ma'adim Vallis and the aquifer drainage. The Gusev palaeolake system is considered by Grin and Cabrol (1997) to have been a sub-ice lake similar to Lake Vostok in Antarctica (see Chapter 1). Cabrol and Grin (2002) identified 180 palaeolakes in Martian impact craters using Viking data and classified them in three categories: open lakes, closed lakes and lake chain systems. The open lakes have inflow and outflow channels, closed lakes do not have outlets, lake chain system refer to a series of impact

crater palaeolakes that are connected to one another through channels. The distribution of Martian palaeolakes covers a wide range of latitudes and is more related to the cratered terrains rather than simply geographic and climatic parameters as is the case for Earth. These lakes could have harboured forms of primitive life.

The discovery of sulphate minerals by Opportunity Rover lends further support for the possibility of life on Mars in palaeolakes. Aubrey et al. (2006) found evidence that organic molecules can be deposited with evaporite minerals in playa lakes. These authors examined sulphate minerals (gypsum, anhydrite and jarosite) from evaporite deposits from the ~4 Ma Anza-Borrego desert, the ~40 Ma Panache Valley, both in California, and the ~23 Ma Haughton impact crater in Canada. The sulphate minerals revealed significant amounts of total organic carbon and nitrogen (TOC and TON) and detected organic compounds including amino acids, adenine, methylamine and ethylamine. Aubrey et al. (2006) concluded that amino acids provide an excellent biosignature and should be searched for on Martian sulphate deposits for possible traces of life. Aubrey et al's (2006) results complement those of Benison (2006), who found similar sedimentary structures, such as ripple marks, cross-bedding and mud cracks, in saline palaeolake deposits of Permian age (Nippewalla Group, Kansas, USA), and modern saline lakes of Western Australia (Fig. 12.22B) and those exposed in the Burns Cliff within the Endurance impact crater, Meridiani Planum, on Mars. The Western Australian lakes are typically shallow, mostly ephemeral, acidic (pH 1.5–4.0) and precipitate, in addition to hematite, abundant sulphate minerals, generally halite, gypsum, but also jarosite and alunite. In addition, features such as filamentous structures, subaerial and subaqueous mat structures (Fig. 12.22A), H_2S emanations, are clear indications of microbial life (Benison et al. 2005). Both the Meridiani Planum outcrops and the Nippewalla Formation have hematite and sulphate minerals (e.g. jarosite, gypsum, anhydrite). In addition, hematite concretions, coatings and cement found in both the Nippewalla Group and in the Burns Cliff strata, are probably formed by diagenetic growth from Fe-rich fluids (Benison 2006). The Western Australian saline lakes and the palaeolake deposits now preserved in the Nippewalla Group, could represent analogues of Martian strata in Meridiani Planum and in the palaeolakes of impact craters. The presence of sulphate minerals on the Martian surface provide some evidence that saline lakes similar to those in Australia could have existed.

Russell et al. (1999) suggested that terrestrial lacustrine evaporitic sedimentary successions may provide suitable analogues for some of the Martian putative palaeolakes. These authors examined the microbial mounds of Salda Gölü (lake) in southwestern Turkey, an alkaline magnesian lake that covers an area underlain by partially serpentinised ultramafic rocks, mostly harzburgite and dunite. In this lake hydromagnesite stromatolites, probably associated with warm seepages, are present around the lake and the submerged parts of the microbial mounds are covered by centimetre-thick biofilm of green cyanobacteria filaments

(Russell et al. 1999). Hydromagnesite forms from the release of Mg from lizardite serpentine reacting with H_2O and CO_2, according to:

$$5Mg_3Si_2O_5(OH)_4 + H_2O + 6CO_2 \rightarrow 3Mg^{++} + 2SiO_2 + 6HCO_3^-$$

and precipitation of hydromagnesite follows according to:

$$5Mg^{++} + 4HCO_3^- + 6OH^- \rightarrow Mg_5(CO_3)_4(OH)_2^4H_2O$$
(hydromagnesite)

Sampling of waters entering the lake indicate that they are Mg-rich and with a pH of 11.8–10. The precipitation of the hydromagnesite of Salda Gölü is mediated by photosynthetic bacteria and driven by evaporation.

Russell et al. (1999) suggested that the White Rock structure on Mars (Fig. 12.27) could represent stromatolitic mounds broadly similar to the hydromagnesite stromatolites of Salda Gölü. White Rock is a mound-like structure that covers about 200 km^2 and is located on the floor at the western margin of a 100-km diameter crater, that lies about 400 km from the southern rim of the large Schiaparelli crater (350 km in diameter). The White Rock has been interpreted as an erosional remnant of an evaporite deposit approximately 700 m thick and compared with sulphate deposits of terrestrial playa lakes and its yarding topography has been interpreted as the result of wind erosion.

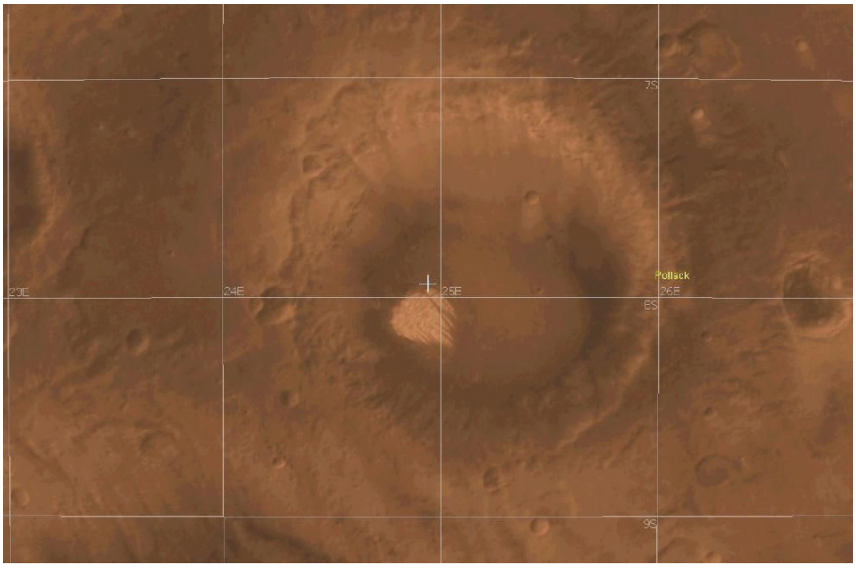


Fig. 12.27 The White Rock mound inside a 100-km diameter crater in Sabaea Terra;. note the stripe texture of the mound-like deposit possibly sculpted by wind; image from NASA World Wind

Absorption bands obtained from Mariner 6/7 infrared spectra indicate that the White Rock could be hydrous magnesium carbonates, not unlike hydromagnesite. On Mars, this hydrous carbonate could have precipitated by evaporation from Mg bicarbonate leached from olivine and pyroxene rocks, on the assumption that surface water was present on early Mars and that atmospheric CO_2 was more abundant than it is today. CO_2-bearing ground waters could have reacted with the Fe-Mg silicates and dissolved large quantities of Mg as carbonate or as bicarbonate. Russell et al. (1999) proposed that the investigation of Mg carbonate outcrops on Mars, such as those of White Rock, is warranted for these would have provided the right nutrients for the growth of photosynthetic microbes.

On the other hand, Shock (1997) maintained that life can exist in the subsurface environment of Mars without exhibiting a surface expression. The abundant evidence of surface and subsurface water activity on Mars and the presence of volcanoes, inevitably lead to the conclusion that some form of hydrothermal systems must have been operating on the planet. Subsurface hydrothermal circulation is likely to have occurred, thereby forming a chemical system that is in thermodynamic disequilibrium. Reactions that attempt to reach an equilibrium state take place in this hydrothermal regime. This is witnessed on Earth, where geochemical and biological processes take advantage of this disequilibrium to gain energy, either as heterotrophs (gain energy involving organic compounds created by other organisms) or as autotroph (generate their own energy). On early Earth and possibly Mars, hyperthermophilic chemolithoautotrophs took energy for their metabolic functions by taking H_2 from the hydrothermal fluids and reduce CO_2 to form CH_4 and H_2O, in the well established methaonogenic reaction:

$$CO_2 + 4H_2 \rightarrow CH_4 + 2H_2O$$

Discharge of groundwater in the proximity of volcanic constructs and of subsurface hydrothermal fluids as hot springs on Mars may have produced siliceous sinter deposits like those that characterise terrestrial hot springs (e.g. Yellowstone in the USA, Taupo in New Zealand and Iceland; see Chapter 5). Amorphous opaline silica is typically a product of hot springs on Earth, accompanied by a host of other hydrothermal minerals such as sulphides, carbonate, clays, zeolites (Chapters 2 and 5). Silica commonly is deposited from near-neutral to alkaline thermal springs that also support a wide range of biological communities as shown by extensive microbial mats by filamentous cyanobacteria. These siliceous deposits preserve micro-organisms, such as bacteria, cyanobacteria and algae, remarkably well. The search for fossil life on Mars could be directed to areas of volcanism associated with groundwater discharges and attempt to detect chemical precipitates such as clays, Fe oxides, silica, carbonate. As mentioned previously many of the Martian valleys and fluvial networks formed by headwater sapping on volcanic regions may have preserved evidence of life.

Fernández-Remolar et al. (2005) suggested that the Rio Tinto river system in southwestern Spain with its sulphate- and biologically-rich environment may provide a possible analogue of Meridiani Planum. I find that the analogy suggested by Fernández-Remolar et al. (2005) is interesting in the context of possible microbial life on Mars. Their paper is summarised in Chapter 10 (see also Figs. 10.10 and 10.11). Finally, Crumpler et al. (2007) in their assessment of terrestrial volcanic features that may have analogues on Mars, drew attention to hot spring deposits associated with volcanism in the Rio Grande rift (New Mexico, USA). These deposits typically form mound structures topped by small craters, thus mimicking the characteristics of small volcanic vents. On Mars, the authors showed, numerous pitted mounds can be seen within the Isidis Basin and in other areas as isolated cratered mounds. If these mound features on Mars are in fact hot spring deposits, they will add to the list of possible sites for microbial life.

12.6 Concluding Remarks

Spacecraft missions to Mars, Jupiter and Saturn and their satellites have shown that a number of planetary bodies are geologically active (Io, Europa, Ganymede, Enceladus) or have been in the recent past (Mars). The interior heat energy of the outer planets' satellites is largely derived from tidal frictional heating, resulting from gravitational interactions between the satellites and the mother planet. The case for Mars is, like for the Earth, different in that the heat energy is partly residual (accretion and impact heat), partly radiogenic. In all cases, however, the silicate interior of these planetary bodies provides the heat energy that drives hydrothermal systems, which are probably not much different from those that occur on Earth. If these hydrothermal systems are similar to those found on Earth, the possibility exists that primitive forms of life could have formed and that either extinct or extant life may be present. Hot springs on Earth, whether subaerial or submarine, host truly astonishing and thriving ecosystems, with bacterial forms that are able to live in a temperature range from near 0 to $>100^{\circ}$C (hyperthermophilic).

Mars, although a one-plate planet, was geologically active and the evidence gained from the latest space missions indicate that the planet had abundant liquid water and that three distinct geological periods (Noachian, Hesperian and Amazonian) were characterised by non-acid aqueous alteration during the earliest stages (Noachian) with the formation of hydrous phyllosilicates. This was followed by large scale volcanic activity (e.g. Tharsis Rise), which led to the deposition of sulphates and finally a time of oxidation, with the precipitation of Fe oxides, mostly corresponding to the latest geological period, the Amazonian. These exciting developments in our knowledge of the "red planet" also opened a window into our understanding of terrestrial geodynamics. Hydrothermal systems were or are almost certainly present on Mars and, by analogy with

Earth systems, a variety of settings are conducive to have had circulation of hydrothermal solutions. Apart from magmatic activity and associated S degassing (Fig. 12.9), other settings include impact craters, with heat energy provided by melt sheets, the giant Valles Marineris rift system, which I am keen to compare with the East African Rift System, or as suggested by others, with rifts and sub-ice volcanism that characterises regions of Mongolia. The possibilities are many and all open to exciting research, by remote sensing, robotic devices, or indeed directly by humans in the not too distant future.

More spectacular findings continue to come in from other space missions, like the Galileo to the Jovian satellites (Europa, Ganymede, Io) and Cassini-Huygens to Saturn, Enceladus and Titan. It turns out that Europa and Ganymede have a layered structure with an iron core, surrounded by a rocky silicate mantle, a shell of ice-liquid water and an icy crust. The surface of these satellites reveals intense and on-going geological activity, characterised by long linear rift zones, ice floes type structures, perhaps volcanic edifices. The ice-liquid water beneath the crust can be considered as the equivalent of the Earth's low-velocity zone or asthenospheric mantle. This ice-liquid water erupts to the surface giving rise to icy volcanism. Space mission scientists have proposed models that could predict the existence of hydrothermal effluents similar to those on terrestrial seafloor (Fig. 12.14) and of possible primordial ecosystems that could thrive in them, as is the case for Earth. The case for Enceladus is particularly interesting. Infrared data indicate the presence of "warm" fractures (Fig. 12.18), and dramatic images of geyser-like jets (the fountains of Enceladus) emanating from the south polar region. These are jets of water, maintained in the liquid state by tidal heat. The Cassini team came up with four possible scenarios, shown in Fig. 12.20, that could explain the origin of the jets. On-going excitement keeps coming in. Rivers of liquid methane have been shown by the Cassini Titan Radar Mapper. The images could well be those of a terrestrial drainage system.

The search for life is a compelling and irresistible quest as we cannot help but wonder whether we are alone in the Universe. The models mentioned above, although viable, are speculative and up until now no evidence of life, as we know it, has been detected. With the data so far gained, Mars provides the best chance. Running water, volcanism, rift valleys, phyllosilicates, sulphates and Fe oxides, all give us tantalizing hints. The discovery of bacilli-like forms on ALH84001 in 1996 caused a remarkable output of studies and publications and whether or not they are real fossil bacteria, these studies resulted in renewed interest in the search for extraterrestrial life.

In closing this chapter, as a field geologist I can confidently state that theories and speculations borne out of remotely sensed data will be substantially modified, if not altogether thrown out, by ground truth evidence. Future manned explorations of Mars will undoubtedly produce more surprises that surely will fuel more and new exciting research for future generation of planetary scientists.

References

Abbott DH, Isley E (2002) Extraterrestrial influences on mantle plume activity. Earth Planet Sci Lett 205: 53–62

Andrews-Hanna JC, Phillips RJ, Zuber MT (2007) Meridiani Planum and the global hydrology of Mars. Nature 446: 163–166

Anguita F, Fernandez C, Cordero G, Carrasquilla S, Anguita J, Nunez A, Rodriguez S, Garcia J (2006) Evidences for a Noachian-Hesperian orogeny in Mars. Icarus 185: 331–357

Atreya SK, Adams EY, Niemann HB, Demick-Montelara JE, Owen TC, Fulchignoni M, Ferri F, Wilson EH (2006) Titan's methane cycle. Planet Space Sci 54: 1177–1187

Aubrey A, Cleaves HJ, Chalmers JH, Mathies RA, Grunthaner FJ, Ehrefreunbd P, Bada JL (2006) Sulphate minerals and organic compounds on Mars. Geology 34(5): 357–360

Baker VR (2001) Water and the Martian landscape. Nature 412: 228–236

Baker VR (2006a) Water and the evolutionary geological history of Mars. Boll Soc Geol It 125: 357–369

Baker VR (2006b) Geomophological evidence for water on Mars. Elements 2: 139–143

Baker VR (2007) Water cycling on Mars. Nature 446: 150–151

Baker VR, Strom RG, Gulick VC, Kargel JS, Komatsu G, Kale VS (1991) Ancient oceans, ice sheets and the hydrological cycle on Mars. Nature 352: 589–594

Ball P (2005) Seeking the solution. Nature 436: 1084–1085

Bandfield JL, Hamilton VE, Christiensen PR (2000) A global view of Martian surface compositions from MGS-TES. Science 287: 1626–1630

Becker L, Popp B, Rust T, Bada JL (1999) The origin of organic matter in the Martian meteorite ALH84001. Earth Planet Sci Lett 167: 71–79

Bell JF and 39 others (2004) Pancam multispectral imaging results from the Opportunity rover at Meridiani Planum. Science 306: 1703–1709

Benison KC (2006) A Martian analog in Kansas: comparing Martina strat with Permian acid saline lake deposits. Geology 34(5): 385–388

Benison KC, Mormile MR, Oboh-Ikuenobe FE, Bowen F, Hong B-Y, Jagniecki EA, Story SL (2005). Modern microbial life in saline lakes and pans in Australia: a field perspective. Geol Soc Am Ann Meeting, SLC 2005, Abstracts with Programs: 124

Benner SA, Ricardo A, Carrigan MA (2004) Is there a common chemical model for life in the Universe? Curr Opin Chem Biol 8: 672–689

Bibring JP (2005) Comparative planetology, Mars and exobiology. In: Gargaud M, Barbier B, Martin H, Reisse J (eds) Lectures in astrobiology, vol I. Springer, Berlin, pp 352–383

Bibring JP, Langevin Y, Gendrin A, Gondet B, Poulet F, Berthé M, Soufflot A, Arvidson R, Mangold N, Mustard J, Drossart P and the OMEGA Team (2005) Mars surface diversity as revealed by the OMEGA/Mars express observations. Science 307: 1576–1581

Bibring JP, Langevin Y, Mustard, JF, Poulet F, Arvidosn R, Gendrin A, Gondet B, Mangold N, Pinet P, Forget F & the OMEGA team (2006) Global mineralogical and aqueous Mars history derived from OMEGA/Mars Express data. Science 312: 400–404

Bibring JP, and 11 others (2007) Coupled ferric oxides and sulfates on the Martian surface. Science 317: 1206–1210

Borg LE, Connelly JN, Nyquist LE, Shih CY, Wiseman H, Reese Y (1999) The age of the carbonate in Martian meteorite ALH84001. Science 286: 90–94

Boslough MB, Chael EP, Trucano TG, Crawford DA, Campbell DI (1996) Axial focusing of impact energy in the Earth's interior: a possible link to flood basalts and hotspots. Geol Soc Am Spec Pap 307: 541–50

Bowen BB, Benison KC, Oboh-Ikuenobe FE, Story S, Mormile MR (2008) Active hematite concretion formation in modern acid saline lake sediments, Lake Brown, Western Australia. Earth Planet Sci Lett doi:10.1016/j.epsl.2007.12.023

Brack A (2005) From the origin of life on Earth to life in the Universe. In: Gargaud M, Barbier B, Martin H, Reisse J (eds) Lectures in astrobiology, vol I. Springer, Berlin, pp 3–23
Bradley JP, Harvey RP, McSween HY (1996) Magnetite whiskers and platelets in the ALH84001 Martian meteorite: evidence of vapour phase growth. Geochim Cosmochim Acta 60: 5149–5155
Burke K (1996) The African plate. S Afr J Geol 99: 341–409
Burr DM, Grier JA, McEwen AS, Keszthelyi L (2002) Repeated aqueous flooding from the Cerberus Fossae: evidence for very recently extant, deep groundwater on Mars. Icarus 159: 53–73
Cabrol NA, Grin EA, Dawidowicz G (1996) Ma'adim Vallis revisited through new tpographic data: evidence for an ancient intravalley lake. Icarus 123: 269–283
Cabrol NA, Grin EA (2002) Overview on the formation of paleolakes and ponds on Mars. Glob Planet Change 35: 199–219
Carr, MH (1981) The surface of Mars. Yale University Press, New Haven and London
Carr, M H (1990) Mars. In: Beatty JK, Chaikin A (eds) The New Solar System, Cambridge Univ Press, Sky Publishing Corp, Cambridge, pp 53–76
Carr MH (1996a) Water on early Mars. In: Bock GR, Goode JA (eds), Evolution of hydrothermal systems on Earth (and Mars), Ciba Foundation Symposium 202, John Wiley & Sons, Chichester, pp 249–264
Carr MH (1996b) Water on Mars. Oxford University Press, Oxford
Carr MH (1999) Mars. In: Beatty JK, Petersen CC, Chaikin A (eds) The New Solar System, Cambridge Univ Press, Sky Publishing Corp, pp. 141–156
Carr MH (2006) The surface of Mars. Cambridge Univ Press, Cambridge
Carr MH, Garvin JB (2001) Mars exploration, Nature 412: 250–253
Carr MH, Kuzmin RO, Masson P (1993) Geology of Mars. Episodes 16: 307–315
Catling DC (2004) On Earth as it is on Mars? Nature 429: 707–708
Catling DC (2007) Ancient fingerprints in the clay. Nature 448: 31–32
Chan MA, Beitler B, Parry WT, Ormö J, Komatsu G (2004) A possible terrestrial analogue for haematite concretions on Mars. Nature 429: 731–734
Chapman MG (2002a) Sub-ice volcanoes and ancient ocean/lakes: a Martian challenge. Glob Planet Change 35: 185–198
Chapman MG (2002b) Layered, massive and thin sediments on Mars: possible Late Noachian to late Amazonian tephra? Geol Soc Lond. Spec Publ 202: 273–293
Chapman MG (ed) (2007) The geology of Mars – evidence from Earth-based analogs. Cambridge University Press, Cambridge
Chavdarian GV, Sumner DY (2006) Cracks and fins in sulphate sand: evidence for recent mineral-atmospheric water cycling in Meridiani Planum outcrops? Geology 34: 229–232
Chevrier V, Poulet F, Bibring JP (2007) Early geochemical environment of Mars as determined from thermodynamics of phyllosilicates. Nature 448: 60–63
Christensen PR (2006) Water at the poles and in permafrost regions of Mars. Elements 2: 151–155
Christensen PR, Bandfield JL, Clark Edgett KS, Hamilton VE, Hoefen T, Kieffer HH, Kuzmin RO, Lane MD, Malin MC, Morris RV, Pearl JC, Pearson R, Roush TL, Ruff SW, Smith MD (2000) Detection of crystalline hematite mineralization on Mars by the Thermal Emission Spectrometer: evidence for near-surface water. J Geophys Res 105: 9623–9643
Christensen PR, Morris R, Lane MD, Bandfield JL, Malin MC (2001) Global mapping of Martian hematite mineral deposits: remnants of water-driven processes on early Mars. J Geophys Res 106: 23873–23885
Christensen PR and 26 others (2004a) Initial results from the Mini-TES experiment in Gusev crater from the spirit rover. Science 305: 837–842
Christensen PR and 26 others (2004b) Mineralogy at Meridiani Planum from the Mini-TES experiment on the Opportunity rover. Science 306: 1733–1739

Christensen PR, Gorelick NS, Mehall GL, Murray KC (2006) THEMIS public data release. Planetary Data System Node, Ariz State University, http://themis.data.asu.edu
Clancy P, Brack A, Horneck G (2005) Looking for life, searching the Solar System. Cambridge University Press, Cambridge
Clifford SM, Parker TJ (2001) The evolution of the Martina hydrosphere: implications for the fate of a primordial ocean and the current state of the northern plains. Icarus 154: 40–79.
Clifford SM and 52 others (2000) The state and future of Mars polar science and exploration. Icarus 144: 210–242
Cradock RA, Howard AD (2002) The case for rainfall on a warm, wet early Mars. J. Geophys Res 107(E11): 5111, doi:10.1029/2001JE001505
Crumpler LS, Aubele JC, Zimbelman JR (2007) Volcanic features of New Mexico analogous to volcanic features on Mars. In: Chapman M (ed) The geology of Mars – evidence from Earth-based analogs, Cambridge University Press, Cambridge, pp 95–125
Davies P (1999) The fifth miracle: the search for the origin of life. Simon Schuster, New York
Dohm JM, Tanaka KL (1999) Geology of the Thaumasia region, Mars: plateau development, valley origins, and magmatic evolution. Planet Space Sci 47: 411–431
Dohm JM and 21 others (2008) Recent geological and hydrological activity on Mars: the Tharsis/Elysium corridor. Planet Space Sci, doi:10.1016/j.pss.2008.01.001
Dromart G, Quantin C, Broucke O (2007) Stratigraphic architectures spotted in southern Melas Chasma, Valles Marineris, Mars. Geology 35: 363–366
Elachi C and 34 others (2005) Cassini radar views the surface of Titan. Science 308: 970–974
Elkins-Tanton L, Hager BH (2005) Giant meteoroid impacts can cause volcanism. Earth Planet Sci Lett 239: 219–32
Ernst RE, Baragar WRA (1992) Evidence from magnetic fabric for the flow pattern of magma in the MacKenzie giant radiating dyke swarm. Nature 356: 511–513
Ernst RE, Grosfils E, Mège D (2001) Giant dyke swarms: Earth, Venus and Mars. Ann Rev Earth Planet Sci 29: 489–534
Fairén AG, Fernández-Remolar D, Dohn JM, Baker VR, Amils R (2004) Inhibition of carbonate synthesis in acidic oceans on early Mars. Nature 431: 423–426
Farmer JD (1996) Hydrothermal systems on Mars: an assessment of present evidence. Evolution of hydrothermal ecosystems on Earth (and Mars?) In: Bock, GR, Goode, JA eds., Evolution of hydrothermal systems on Earth (and Mars). Ciba Foundation Symposium 202, John Wiley & Sons, Chichester, pp 273–299
Farr TG (2004) Terrestrial analogs to Mars: the NRC community decadal report. Planet Space Sci 52: 3–10
Faure G (1986) Principles of isotope geology, 2nd edn. John Wiley & Sons, New York
Fernández-Remolar DC, Morris RV, Gruener JE, Amils R, Knoll AH (2005) The Rio Tinto basin, Spain: mineralogy, sedimentary geobiology, and implications for interpretation of outcrop rocks at Meridiani Planum, Mars. Earth Planet Sci Lett 240: 149–167
Frey HV (2006) Impact constraints on the age and origin of the lowlands of Mars. Geophys Res Lett 33: L08S02, doi:1029/2005/GL024484
Geissler P (2000) Cryovolcanism in the outer Solar System. In: Sigurdsson H (ed) Encyclopedia of Volcanoes. Academic Press, San Diego, pp 785–802
Gellert R and 14 others (2004) Chemistry of rocks and soils in Gusev crater from the Alpha particle X-ray spectrometer. Science 305: 829–832
Gendrin A, Mangold N, Bibring JP, Langevin Y, Gondet B, Poulet F, Bonello G, Quantin C, Mustard J, Arvdison J, LeMoulélic S (2005) Sulfates in Martian layered terrains: the OMEGA/Mars Express view. Science 307: 1587–1591
Glikson AY, Haines PW (eds) (2005) Shoemaker memorial issue on the Australian impact record: 1997–2005 update. Aust J. Earth Sci 52(4/5)
Gonzales G, Brownlee D, Ward PD (2001) The Galactic Habitable Zone: Galactic chemical evolution. Icarus 152: 185–200

Grant WD (2004) Life at low water activity. Phil Trans Roy Soc B359: 1249–1267
Greeley R (1987) Release of juvenile water on Mars: estimated amount and timing associated with volcanism. Science 236: 1653–1654
Greeley R (1999) Europa. In: Beatty JK, Chaikin A (eds) The New Solar System. Cambridge University Press, Sky Publishing Corp, Cambridge, pp 253–262
Greeley R, Chyba CF, Head JM, McCord TB, McKinnon WB, Pappalardo RT, Figueredo PH (2004) Geology of Europa. In: Bagenal F, Dowling TE, McKinnon WB (eds) Jupiter – the planet, satellites and magnetosphere. Cambridge: Cambridge University Press, pp 329–362
Greenberg R, Randall Tufts B, Geissler P, Hoppa GV (2002) Europa's crust and ocean: how tides create a potentially habitable physical setting. In: Horneck G, Baumstark-Khan C (eds) Astrobiology – the quest for the conditions of life, Springer, Berlin, pp 111–124
Grin EA, Cabrol NA (1997) Limnological analysis of Gusev crater paleolake, Mars.Icarus 130: 461–474
Gulick VC (1998) Magmatic intrusions and a hydrothermal origin for fluvial valleys on Mars. J Geophys Res 103: 19365–19387
Hagstrum JT (2005) Antipodal hot spots and bipolar catastrophes: were oceanic karge-body impacts the cause? Earth Planet Sci Lett 236: 13–27
Harder H, Christensen UR (1996) A one plume model of Martian mantle convection. Nature 380: 507–509
Hartmann W (1979) The watery past of Mars. New Sci, 82: 1083–1085
Head JW, Solomon SC (1981) Tectonic evolution of the terrestrial planets. Science 213: 62–76
Head JW, Coffin MF (1997) Large igneous provinces: a planetary perspective. Am Geophys Union Monograph 100: 411–438
Head JW, Hiesinger H, Ivanov MA, Kreslavsky MA, Pratt S, Thomsom BJ (1999) Possible ancient oceans on Mars: evidence from Mars Orbiter Laser Altimeter data. Science, 286: 2134–2137
Head JW, Wilson L (2002) Mars: a review and synthesis of general environments and geological settings of magma-H_2O interactions. Geol Soc Lond Spec Publ 202: 27–57
Head JW, Wilson, L, Dickson J, Neukum G (2006) The Huygens-Hellas giant dike system on Mars: implications for Late Noachian-Early Hesperian volcanic resurfacing and climatic evolution. Geology 34: 285–288
Hedenquist JW, Thompson JFH, Goldfarb RJ, Richards JP (eds) (2005) Economic Geology 100th Anniversary Volume
Herkenhoff KE and 22 others (2004a) Textures of the soils and rocks at Gusev Crater from Spirit's microscopic imager. Science 305: 824–827
Herkenhoff KE and 32 others (2004b) Evidence from Opportunity's microscopic Imager for water on Meridiani Planum. Science 306: 1727–1729
Hughes HG, App FN, McGetchin TR (1977) Global seismic effects of basin forming impacts. Phys Earth Planet Int 15: 251–263
Hurford TA, Helfenstein P, Hoppa GV, Greenberg R, Bills BG (2007) Eruptions arising from tidally controlled periodic openings of rifts on Enceladus. Nature 447: 292–294
Huston DL, Logan GA (2004) Barite, BIFs and bugs: evidence for the evolution of the Earth's early hydrosphere. Earth Planet Sci Lett 220: 41–55
Hynek BM, Phillips RJ (2001) Evidence for extensive denudation of the Martian highlands. Geology 29: 407–410
Ingle S, Coffin MF (2004) Impact origin for the greater Ontong Java Plataeu? Earth Planet Sci Lett 218: 123–34
Inskeep WP, Macur RE, Harrison G, Bostick B, Fendorf S (2004) Biomineralization of As(V)-hydrous ferric oxyhydroxide in microbial mats of an acid-sulphate-chloride geothermal spring, Yellowstone National Park. Geoch Cosmochim Acta 68: 3141–3155
Irwin RP, Craddock RA, Howard AD (2005) Interior channels in Martian valley networks: discharge and runoff production. Geology 33: 489–492

Jakosky BM, Shock EL (1998) The biological potential of Mars, the early Earth and Europa. J Geophys Res 103: 19359–19364
Jaumann R, Hauer E, Lanz J, Hoffmann H, Neukum G (2002) Geomorphological record of water-related erosion on Mars. In: Horneck G, Baunstark-Khan C (eds), Astrobiology. Springer, Berlin, pp. 89–109
Johnson TV (1999) Io. In: Beatty JK, Chaikin A (eds) The New Solar System. Cambridge University Press, Sky Publishing Corp, Cambridge, pp 241–252
Kargel JS (2004) Mars – A warmer, wetter planet. Springer, Berlin, 605p
Kargel JS, Pozio S (1996) The volcanic and tectonic history of Enceladus. Icarus 119: 385–404
Kerr RA (2004) Rainbow of Martian minerals paints picture of degradation. Science 305: 770–771
Keszthelyi L, McEwen A (2007) Comparison of flood lavas on Earth and Mars. In: Chapman M (ed) The geology of Mars – evidence from Earth-based analogs, Cambridge University Press, Cambridge, pp 126–150
Keszthelyi L, McEwen AS, Thordarson TH (2000) Terrestrial analogs and thermal models for Martian flood lavas. J Geophys Res 105: 15027–15050
Kirkland BL, Lynch FL, Rahnis MA, Folk RL, Molineux IJ, McLean RJC (1999) Alternative origins for nannobacteria-like objects in calcite. Geology 27: 347–350
Klingelhöfer G and 18 others (2004) Jarosite and hematite at Meridiani Planum from Opportunity's Mössbauer spectrometer. Science 306: 1740–1745
Knoll AH, Grotzinger J (2006) Water on Mars and the prospect of Martian life. Elements 2: 169–173
Knoll AH, Strother PK, Rossi S (1988) Distribution and diagenesis of microfossils from the Lower Proterozoic Duck Creek Dolomite, Western Australia. Precambr Res 38: 257–279
Komatsu G, Dohn JM, Hare TM (2004a) Hydrogeologic processes of large-scale tectonomagmatic complexes in Mongolia-southern Siberia and on Mars. Geology 32: 325–328
Komatsu G, Ori GG, Ciarcelluti P, Litasov YD (2004b) Interior layered deposits of Valles Marineris, Mars: analogous sub-ice volcanism related to the Baikal rifting, southern Siberia. Planet Space Sci 52: 167–187
Komatsu G, Ori GG, Arzhannitkov SG, Arzhannitkova AV (2006) The Azas plateau in southern Siberia: a proposed terrestrial analogue site for ice-magma-flood processes. Lunar Planet Sci XXXVII: 1065.pdf
Kotelnikova S (2002) Microbial production and oxidation of methane in the deep subsurface. Earth Sci Rev 58: 367–395
Kring DA (2000) Impact events and their effect on the origin, evolution and distribution of life. GSA Today 10: 1–7
Krot AN, Keil K, Goodrich CA, Scott ERD, Weisberg MK (2003) Classification of meteorites. In; Davis AM (ed) Treatise on Geochemistry, Elsevier, Oxford, pp 83–128
Langevin Y, Poulet F, Bibring JP, Gondet B (2005) Sulfates in the north polar regions of Mars detected by OMEAG/Mars Express. Science 307: 1584–1586
Leeder MR (1999) Sedimentology and sedimentary basins. Blackwell Science, Oxford
Leshin LA, Vicenzi E (2006) Aqueous processes recorded by Martian meteorites: analyzing Martian water on Earth. Elements 2: 157–162
Lorenz RD, Stiles BW, Kirk RL, Allison MD, Persi del Marmo P, Iess L, Lunine JI, Ostro SJ, Hensley S (2008) Titan's rotation reveals an internal ocean and changing zonal winds. Science 319: 1649–1651
Lowell RP, DuBose M (2005) Hydrothermal systems on Europa. Geophys Res Lett 32: L05202, doi:10.1029/2005GL022375
Malin MC, Edgett KS, Posiolova (2003) Evidence for persistent flow and aqueous sedimentation on early Mars. Science 302: 1931–1934
Malin MC, Edgett KS, Posiolova LV, McColley SM, Noe Dobrea EZ (2006) Present-day impact cratering rate and contemporaneous gully activity on Mars. Science 314: 1573–1577

Marinangeli L, Flamini E, Espinasse S (eds) (2004) Exploring Mars surface and its Earth analogues. Planet Space Sci 52(1/3)
McCollom TM (1999) Methanogenesis as apotential source of chemical energy for primary biomass production by authotrophic organisms in hydrothermal systems on Europa. J. Geophys Res 104: 30729–30742
McCollom TM, Shock EL (1997) Geochemical constraints on chemolithoautotrophic metabolism by micro-organisms in seafloor hydrothermal systems. Geochimica et Cosmochimica Acta 61: 4375–4391
McEwen AS (1999) Flood lavas on Mars. The Geological Society of America, 1999 Annual Meeting, Abstracts with Programs, A-131
McKay DS, Gibson EK, Thomas-Keprta KL, Vali H, Romanek CS, Clemett SJ, Chillier XDF, Maechling CR, Zare RN (1996) Search for past life on Mars: possible biogenic activity in martian meteorite ALH84001. Science 273: 924–930
McLennan SM and 31 others (2005) Provenance and diagenesis of the evaporite-bearing Burns Formation, Meridiani Planum, Mars. Earth Planet Sci Lett 240: 95–121
McSween HY (2003) Mars. In: Davis AM (ed) Treatise on Geochemistry, Elsevier, Oxford, pp 601–621
McSween HY (ed) (2006) Water on Mars. Elements 2(3): 135–137
McSween HY and 34 others (2004) Basaltic rocks analysed by the Spirit Rover in Gusev Crater. Science 305: 842–845
McSween HY, Harvey RP (1998) An evaporation model for formation of carbonates in the ALH84001 martian meteorite. Intl Geol Rev 40: 774–783
Mège D, Masson P (1996) A plume tectonics model for the Tharsis province, Mars. Planet Space Sci 44: 1499–1546
Mével L, Mercier E (2007) Large-scale doming on Europa: A model of formation of *Thera Macula*. Planet Space Sci, doi:10.106/j.pss.2006.12.001
Morris R and 16 others (2004) Mineralogy at Gusev crater from the Mössbauer spectrometer on the Spirit rover. Science 305: 833–836
Mustard JF, Cooper CD, Rifkin MK (2001) Evidence for recent climate change on Mars from the identification of youthful near-surface ground ice. Nature 412: 411–413
Newsom EH (2005) Clays in the history of Mars. Nature 438: 570–571
Newsom EH, Britelle GE, Hibbits CA, Crossey LJ, Kudo AM (1996) Impact cratering and the formation of crater lakes on Mars. J Geophys Res 101: 14951–14955
Newsom EH, Hagerty JJ, Thorsos IE (2001) Location and sampling of aqueous and hydrothermal deposits in Martian impact craters. Astrobiology 1(1): 71–88
Nimmo F (2004) Dynamics of rifting and modes of extension on icy satellites. J Geophys Res 109: E01003, doi:10.1029/2003JE002168
Nimmo F, Spencer JR, Pappalardo RT, Mullen ME (2007) Shear heating as the origin of the plumes and heat flux on Enceladus. Nature 447: 289–291
Nimmo F, Tanaka K (2005) Early crustal evolution of Mars. Ann Rev Earth Planet Sci 33: 133–161
Okubo CH, McEwen AS (2007) Fracture-controlled paleo-fluid flow in Candor Chasma, Mars. Science 315: 983–985
Owen T (1982) Titan. In: The Planets, Sci Am, WH Freeman and Co, New York, pp 84–93
Owen T (1999) Titan. In: In: Beatty JK, Chaikin A (eds) The New Solar System. Cambridge University Press, Sky Publishing Corp, Cambridge, pp 276–284
Pappalardo RT (1999) Ganymede and Callisto. In: Beatty JK, Chaikin A (eds) The New Solar System. Cambridge Univ Press, Sky Publishing Corp, Cambridge, pp 263–276
Pappalardo RT and 31 others (1999) Does Europa have a subsurface ocean? Evaluation of the geological evidence. J Geophys Res 104: 24015–24055
Pappalardo RT, Collins GC, Head JW, Helfenstein P, McCord TB, Moore JM, Prockter LM, Schenk PM, Spencer JR (2004) Geology of Ganymede. In: Bagenal F, Dowling TE,

McKinnon WB (eds) Jupiter – the planet, satellites and magnetosphere. Cambridge University Press, Cambridge, pp 363–396
Pedersen K (1993) The deep subterranean biosphere. Earth Sci Rev 34: 243–260
Perron TJ, Mitrovica JX, Manga M, Matsuyam I, Richards (2007) Evidence for an ancient martian ocean in the topography of deformed shorelines. Nature 447: 840–843
Pirajno F (2004) Hotspots and mantle plumes: global intraplate tectonics, magmatism and ore deposits. Mineral Petrol 82: 183–216
Pirajno F (2005) Hydrothermal processes associated with meteorite impact structures: the evidence from three Australian examples and implications for economic resources. Aust J Earth Sci 52: 587–605
Pirajno F, Van Kranendonk MJ (2005) Review of hydrothermal processes on Earth and implications for Martian analogues. Aust J Earth Sci 32: 329–351
Plescia JB, Saunders RS (1982) Tectonic history of the Tharsis region, Mars. J. Geophys Res 87: 9775–9791
Pollack JB (1975) Mars. Sci Am 233: 106–117
Porco CC and 24 others (2006) Cassini observes the active south pole of Enceladus. Science 311: 1393–1425
Poulet F, Bibring JP, Mustard JF, Gnedrin A, Mangold N, Langevin Y, Arvidson RE, Gondet B, Gomez C & the Omega Team (2005) Phyllosilcates on Mars and implications for early martian clmate. Nature 438: 623–627
Rathburn JA, Squyres SW (2002) Hydrothermal systems associated with Martian impact craters. Icarus 157: 362–372
Rees WG (2001) Physical principles of remote sensing. Cambridge University Press
Reese CC, Solomotov VS, Baumgardner JR (2002) Survival of impact-induced thermal anomalies in the Martian mantle. J Geophys Res 107, E10, 5082, doi:10.1029/2000JE001474
Reese CC, Solomatov VS, Baumgardner JR, Stegman DR, Vezolainen AV (2004). Magmatic evolution of impact induced Martian mantle plumes and the origin of Tharsis. J Geophys Res 109: E08009
Rieder R and 14 others (2004) Chemistry of rocks and soils at Meridiani Planum from Alpha particle X-ray spectrometer. Science 306: 1746–1749
Russell MJ, Ingham JK, Zedef V, Maktav, Sunar F, Hall AJ, Fallick AE (1999) Search for signs of life on Mars: expectations from hydromagnesite microbialites, Salda Lake, Turkey. J. Geol Soc Lond 156: 869–888
Sagan C (1981) Cosmos. Macdonald Futura Publ, London
Sagan C (1994) Pale blue dot. Random House, New York
Schenk PM, McKinnon WB, Gwynn D, Moore JM (2001) Flooding of Ganymede's bright terrains by low-viscosity water-ice lavas. Nature 410: 57–60
Schubert G, Bercovici D, Glatzmaier GA (1990) Mantle dynamics in Mars and Venus: influence of an immobile lithosphere on three-dimensional mantle convection. J Geophys Res 95: 14105–14130
Schubert G, Russell CT, Moore WB (2000) Timing of the Martian dynamo. Nature 408: 666–667
Schubert G, Turcotte DL, Olson P (2001) Mantle convection in the Earth and planets. Cambridge University Pres, Cambridge
Schultz PH, Gault DE (1975) Seismic effects from major basin formations on the Moon and Mercury. The Moon 12: 159–177
Schulze-Makuch D, Irwin LN, Guan H (2002) Search parameters for the remote detection of extraterrestrial life. Planet Space Sci 50: 675–683
Seckbach J, Chela-Flores J, Owen T, Raulin T (2005) Life in the Universe – from the Miller experiment to the search for life on other worlds. Kluwer Academic Publ, Dordrecht
Segura TL, Toon OB, Colaprete A, Zahnl EK (2002) Environmental effects of large impacts on Mars. Science 298: 1977–1980
Shock EL (1997) High-tempertaure life without photosyntheis as a model for Mars. J. Geophys Res 102: 23687–23694

Short NM (2006) Remote Sensing Tutorial; http://rst.gsfc.nasa.gov/
Squyres SW and 48 others (2004a) The Opportunity rover's Athena science investigation at Meridiani Planum, Mars. Science 306: 1698–1703
Squyres SW and 18 others (2004b) In situ evidence for an ancient aqueous environment at Meridiani Planum. Science 306: 1709–1714
Solomon SC and 16 others (2005) New perspective on ancient Mars. Science 307: 1214–1220
Sotin C and 25 others (2005) Release of volatiles from a possible cryovolcano from near-infrared imaging of Titan. Nature 435: 786–789
Sotin C (2007) Titan's lost seas found. Nature 445: 29–30
Stetter KO (1996) Hyperthermophiles in the history of life. In: Bock GR, Goode JA (eds), Evolution of hydrothermal systems on Earth (and Mars). Ciba Foundation Symposium 202, John Wiley & Sons, Chichester, pp 1–10
Stetter KO, Fiala G, Huber G, Huber R, Segerer A (1990) Hyperthermophilic micro-organisms. FEMS Microbiol Rev 78: 117–124
Stofan ER and 37 others (2007) The lakes of Titan. Nature 445: 61–64
Sugorakova AM, Yarmolyuk VV, Lebedev VI (2003) The Cenozoic volcanism of Tuva. Tuvinian Inst Expl Natural Res SB RAS (in Russian)
Taylor SR (1999) Destiny or chance: our Solar System and its place in the Cosmos. Cambridge University Press, Cambridge
Thomas-Keprta KL, Bazylinski DA, Golden DC, Wentworth SJ, Gibson EK, McKay DS (1998) Magnetite from ALH84001 carbonate globules: Evidence of biogenic signatures? (abstract). Lunar Planet. Sci. XXIX, Abstract #1494
Thomas-Keprta KL, Bazylinski DA, Kirschvink JL, Clemett SJ, McKay DS, Wentworth SJ, Vali, H, Gibson EK, Romanek CS (2000) Elongated primastic magnetite crystals in ALH84001 carbonate globules: potential Martian magnetofossils. Geochim Cosmoch Acta 64: 4049–4081
Thomas-Keprta KL, Clemett SJ, Schwartz C, McIntosh JR, Bazylinski DA, Kirschvink J, McKay DS, Vali H, Romanek CS (2004) Truncated hexa-octahedral magnetite crystals in Martian meteorite ALH84001: evidence of biogenic activity on early Mars. Geophys Res Abs 6: 05283
Tobie G, Lunine JJ, Sotin C (2006) Episodic outgassing as the origin of atmospheric methane on Titan. Nature 440: 61–64
Tokano T (2004) Water on Mars and life. Springer, Berlin 248p
Valentino GM, Cortecci G, Franco E, Stanzione D (1999) Chemical and isotopic compositions of minerals and waters from Campi Flegrei volcanic system, Naples, Italy. J Volc Geoth Res 91: 329–344
Varekamp JC (2004) Copahue Volcano: a modern terrestrial analog of the Opportunity landing site? Am Geophys Union EOS 85(41): 401 and 407
Varnes ES, Jakosky BM, McCollom TM (2003) Biological potential of Martian hydrothermal systems. Astrobiology 3(2): 407–414
Walker JJ, Spear JR, Pace NR (2005) Geobiology of a microbial endolithic community in the Yellowstone geothermal environment. Nature 434: 1011–1014
Walter MR, Brown AJ, Chamberlain SA (2005) Geology of Mars. Encyclopedia of Geology, Elsevier, Amsterdam
Walter MR, Des Marais DJ (1993) Preservation of biological information in thermal spring deposits: developing a strategy for the search for fossil life on Mars. Icarus 101: 129–143
Watters TR, Leuschen CJ, Plaut JJ, Picardi G, Safaeinli A, Clifford, SM, Farrell WM, Ivannov AB, Phillips RJ, Stofan ER and the MARSIS science team (2006) Evidence of buried basins in the northern lowlands of Mars from the MARSIS radar sounder. Lunar Planet Sci Abs XXXVII: 1693.pdf
Ward PD, Brownlee D (2004) Rare Earth – why complex life is uncommon in the Universe. Copernicus Books, Springer Science, New York

Westall F (1999) The nature of fossil bacteria: a guide to the search for extraterrestrial life. J. Geophys Res 104: 16437–16451
Williams DA, Greeley R (1994) Assessment of antipodal-impact terrains on Mars. Icarus 110: 196–202
Wilson L, Head JW (2002) Tharsis-radial graben systems as the surface manifestation of plume-related dike intrusion complexes: models and implications. J Geophys Res 107, 10.1029/200IJE001593
Windley BF, Allen MB (1993) Mongolian plateau: evidence for a late Cenozoic mantle plume under central Asia. Geology 21: 295–298
Wyatt MB, McSween HY, Tanaka KL, Head JW (2004) Global geologic context for rock types and surface alteration on Mars. Geology 32: 645–648
Wyatt MB, McSween HY (2006) The orbital search for altered materials on Mars. Elements 2: 145–150
Yenne B (1990) The atlas of the Solar System. Bison Books, Hong Kong
Zahnle K, Schenk PM, Levison HF, Dones L (2003) Cratering rates in the outer Solar System. Icarus 163: 263–289
Zolensky ME (2005) Extraterrestrial water. Elements 1(1): 39–43
Zorin YuA, Turtanov EK, Mordvinova VV, Kozhevnikov M, Yanovskaya TB, Teusso A (2003) The Baikal rift zone: the effect of mantle plumes on older structure. Tectonophysics 371: 153–173
Zuber MT (2001) The crust and mantle of Mars. Nature 412: 220–227
Zuber MT, Smith DE, Phillips RJ, Solomon SC, Banerdt WB, Neumann GA, Aharonson O (1992) Shape of the northern hemisphere of Mars from the Mars Orbiter Laser Altimeter (MOLA). Geophys Res Lett 25: 4393–4396

Chapter 13
Uranium Hydrothermal Mineral Systems

13.1 Introduction

A chapter specifically dealing with uranium hydrothermal mineral systems is appropriate, not only because of its inherent scientific value, but also because of the evolving economic, social and political paradigms at the start of the 21st century. Uranium, not withstanding its belligerent and senseless use (why thousands of nuclear warheads are made and stored is quite beyond comprehension), has awesome energy potential that can be relatively easily harnessed. The uranium story, as is the case for some other human enterprises, is largely one that is linked to emotional and often irrational issues as well as political plays. For this reason, studies of uranium deposits dramatically declined in the second half of the 20th century, and it is only very recently owing to the above mentioned shifting paradigms, research on and exploration of uranium mineral systems is experiencing an exciting and strong revival. The importance of uranium as a source of clean energy is gathering fast momentum, particularly in the face of climate change. Newton et al. (2006) provided an excellent and acute update on nuclear power. Following an initial upsurge in the 1950s which was largely focussed on military ventures, the last 60 years or so have witnessed cycles of U mining and production that are best expressed by the rise and falls of the prices for the commodity, from US$40 per pound (1 pound = 453.592 grams) in 1979, to about US$7 per pound in the 1980s, to $10.90/lb in 2003 to US$52/lb at the time of writing this chapter. Newton et al. (2006) reported that as of April 2006, a total of 441 nuclear reactors were operating in 30 countries, supplying 16% of the world's electricity, with another 27 under construction in 13 countries, and another 60 planned over the next 15 years. France leads the charge by having some 78% of its electricity generated by nuclear power. Australia and Canada are the largest uranium producers with 23 and 28%, respectively. Amazingly, Australia has no operating nuclear power plants, although at the time of writing this situation is under review. World production in 2005 was 108.5 Mlb (49 215 tonnes), estimated to increase dramatically over the next few years. The most comprehensive and detailed information on uranium mineral deposits can be found in Dahlkamp (1993). A special issue of Economic Geology was devoted to uranium geology (Nash 1978).

F. Pirajno, *Hydrothermal Processes and Mineral Systems*,

© Springer Science+Business Media B.V. 2009

In this chapter, I present an overview of the geochemistry of U, the decay schemes of the important radioactive isotopes (^{235}U, ^{238}U and ^{232}Th) and discuss some of the more common and economically important U hydrothermal systems, namely: unconformity-related, roll front, vein type U deposits and alaskite-hosted. The latter cannot be strictly considered hydrothermal, however these pegmatitic-style systems are formed during the very late stages of the magmatic fractionation of igneous bodies in the sub-solidus regime, at the boundary with a magmatic-hydrothermal stage.

13.2 Uranium Geochemistry and Decay Schemes

Some of the constraints on the physico-chemical conditions of U transport and deposition are related to the geochemical cycle and behaviour of the lithophile element U. There are many works that deal with this topic, but for a short and comprehensive review the reader is referred to Nash et al. (1981). By and large, the chemical behaviour of U can be explained in terms of its two most common ions, the reduced form U^{6+} and the oxidised form U^{4+}. All U ions tend to combine with oxygen even in the reduced form (e.g. uraninite UO_{-2}), and this tendency allows the U ions to form soluble complexes with anions such as CO_3^{2-}, $PO_4^{2-}SO_4^{4-}$ and AsO_4^{3-}. Therefore redox conditions are important in determining the environment of solution and precipitation of U-bearing minerals. In passing from its hexavalent state to the tetravalent state, oxidising to reducing conditions, and in the presence of metal ions, such as Na^{+}, K +, Ca^{2+}, Cu^{2+}, the solubility of the uranyl complexes decreases and very complex U salts are precipitated (Nash et al. 1981).

Uranium is a lithophile and oxyphile element whose ionic radii and charge makes it something of a "misfit" element during the genesis of mineral deposits (Morton 1979), as shown in Table 13.1

Table 13.1 Coordination number and ionic radius of selected elements. After Morton (1979)

Species	Coordination	Ionic radius (Å)
U^{4+}	8	1.08
U^{6+}	6	0.81
Th^{6+}	8	1.12
Th^{4+}	6	1.08
Ca^{2+}	6	1.08
Y^{3+}	6	0.98
Zr^{4+}	8	0.92
Zr^{4+}	6	0.80
Ta^{5+}	8	0.77
Nb^{5+}	6	0.77
W^{4+}	6	0.73
Mo^{4+}	6	0.73
Ti^{4+}	6	0.69

Thus, there is a common diadochy between U^{4+} and Th^{4+} (e.g. uraninite-thorianite-uranothorite). A substitution of U^{4+} for Ca^{2+} and Ti^{4+} is clearly possible, but is limited due to the charge discrepancy on the one hand and size differences on the other (e.g. apatite, sphene, fluorite, brannerite, davidite). The rest of the elements in the list of Table 13.1 will exhibit only very limited substitution for U^{6+} or U^{4+} due to their differences in ionic size and to the resultant structural defects they induce in the lattice. U^{3+}, U^{4+}, U^{5+} and U^{6+} exist in nature. The quadrivalent (reduced form) and hexavalent (oxidised form) states are of geological importance. The reduced form U^{4+} is represented in the mineral uraninite, pitchblende and coffinite. The uranyl U^{6+} has a large variety of minerals, however a general formula can be:

$$(Me^{+})_2\ (\text{divalent metal})\ (U^{6+}O_2)^{2+}\ (R^{5+}O_4)_2{}^{3-} \pm nH_2O \quad \text{or}$$

$$(Me^{2+})\ (\text{monovalent metal})\ (U^{6+}O_2)^{2+}\ (R^{5+}O_4)_2{}^{3-} \pm nH_2O$$

Where Me can be K, Na, Ca, Mg, Cu and R is V, As, P; for example if Me = K and R = V, the mineral carnotite is formed. Thus, U is the classic incompatible element, strongly lithophile and for this reason U does not tend to form its own minerals, but substitutes for other elements in other minerals, such as apatite, titanite and zircon. Uranium will also enter in Th-bearing minerals, such as thorite and monazite, or it may enter REE minerals, for example xenotime. Niobates and tantalates may contain U and one of the niobates, pyrochlore, with the general formula $(Na,Ca)_2Nb_2O_6(OH,F)$, if containing more than 15% U is called betafite. Pyrochlore is found in carbonatites, alkaline systems and pegmatites. Due to its incompatible character U is commonly found along grain boundaries, small cracks and microfractures of minerals (labile U). This is an important aspect of U mineral systems, because this is a common form of occurrence, usually in the U^{6+} form and as films and coatings of oxide minerals. A list of the more common U-bearing minerals is given in Table 13.2. A far more exhaustive list can be found in Dahlkamp (1993).

In a H_2O-bearing granitic melt, residual liquids may contain U in the U^{6+} form and these will develop hydrothermal fluids, from which vein deposits can form within the granite and the surrounding country rocks. There are at least two types of vein deposits: simple and complex. The simple type contains uraninite + pyrite or marcasites ± quartz ± hematite ± carbonate ± minor base metal sulphides. The complex type is essentially the same as the simple type, but with more base metal sulphides and Co-Ni arsenides. In all cases hematite is abundant and can be used as a prospecting tool. The relationship with hematite is not clear, but it is possible that oxidation of Fe causes the reduction of U from its +6 to +4 state, facilitating its precipitation, according to:

$$3H_2O + Fe^{2+} + (U^{6+}O_2)^{2+} \rightarrow Fe_2O_3 + 6H^{+} + U^{4+}O_2\ (\text{uraninite})$$

Uranium is soluble over a wide range of pH and Eh conditions due to the formation of stable complexes of UO_2^{2+} ions with the most abundant anions in water, such as carbonate, sulphates, chlorides. In particular it forms tri- and bi-carbonate complexes which are very stable and soluble, thereby giving rise to kilometre-wide dispersion aureoles around the mineralisation. Equilibrium Eh-Ph diagrams are shown in Fig. 13.1.

13.2.1 Organic Geochemistry of Uranium

The affinity of U for organic materials has been known for a long time. Uraniferous coals and lignites have been mined in the USA and Canada. One of the important groups of organic materials that captures and precipitate U compounds, are humic acids and humates, derived form the breakdown of plant

Table 13.2 Some common U-bearing mineral species

Category	Minerals	Chemical composition
Oxides	Uraninite	UO_2
	Thorianite	ThO_2
	Gummite	Hydrated uranyl oxides
	Pitchblende	Botryodal/cryptocrystalline form of uraninite
	Fourmarierite	$PbO.4UO_3.5H_2O$
Carbonates	Schroeckingerite	$NaCA_3(UO_2)(CO_3)_3(SO_4F.10H_2)O$
Sulphates	Zippeite	$ZUO_3.SO_3.5H_2O$
Phosphates and Arsenates	Monazite	$(Ce,La,Th)(PO_4)$
	Autunite	$Ca(UO_2)_2(PO_4)_2{\cdot}10\text{-}12H_2O$
	Meta-autunite	$Ca(UO_2)_2(PO_4)_2{\cdot}8H_2O$
	Torbernite	$Cu(UO_2)_2(PO_4)_2{\cdot}10H_2O$
	Metatorbernite	$Cu(UO_2)_2(PO_4)_2{\cdot}8H_2O$
	Uranothallite	$Cu(UO_2)_2(CO_3)_2{\cdot}11H_2O$
	Salecite	$Mg(UO_2)_2(PO_4)_28\text{-}10H_2O$
	Zeunerite	$Cu(OU_2)_2(AsO_4)_2{\cdot}10\text{-}16H_2O$
	Metazeunerite	$Cu(UO_2)_2(AsO_4)_2{\cdot}8H_2O$
	Phosphuranylite	$Ca(UO_2)_4(PO_4)(OH)_4{\cdot}7H_2O$
Vanadates	Carnotite	$K_2(UO_2)_2(VO_4)_2{\cdot}1\text{-}3H_2O$
	Tyuyamunite	$Ca(UO_2)_2(VO_4)_2{\cdot}5\text{-}8H_2O$
Silicates	Coffinite	$U(SiO_4)_{1-x}(OH)_{4x}$
	Uranophane	$Ca(UO_2)_2Si_2O_7{\cdot}6H_2O$
	Beta-uranophane	$Ca(UO_2)_2(SiO_3)_2(OH)_2{\cdot}5H_2O$
	Sklodowskite	$Mg(UO_2)_2(SiO_3)_2(OH)_2{\cdot}6H_2O$
	Kasolite	$Pb(UO_2)(SiO_3)(OH)_2$
Multiple oxides	Betafite	$(U,Ca)(Nb,Ta,Ti)_3O_9{\cdot}H_2O$
	Pyrochlore-microlite	$NaCaNb_2O_6F\text{-}(Na,Ca)_2Ta_2O_6(O,OH,F)$
	Brannerite	$(U,Ca,Fe,Th,Y)_3Ti_5O_{16}$
	Davidite	$(Fe,Ce,La,Y,U,Ca,Zr,Th.)(Ti,Fe,V,Cr)_3(O,OH)$

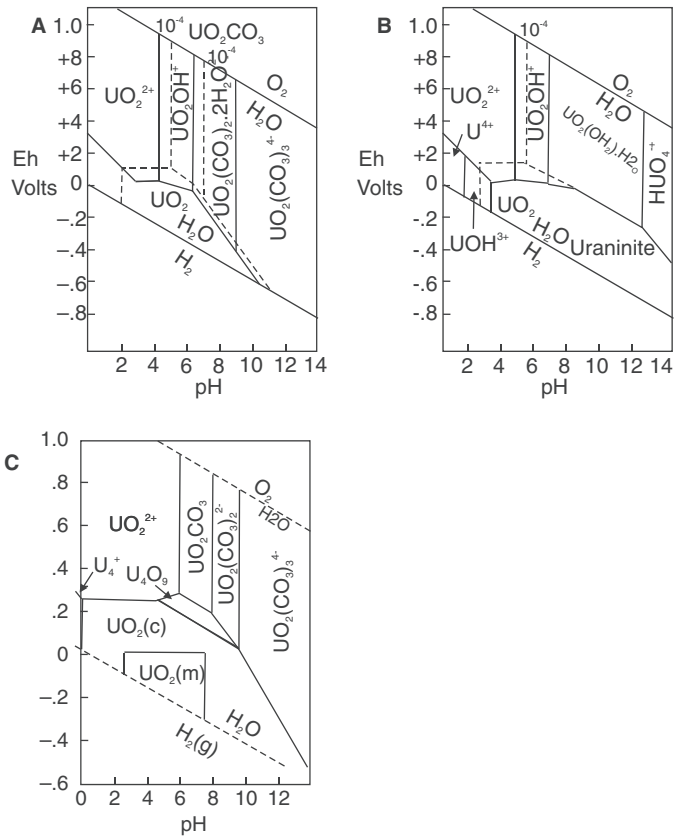


Fig. 13.1 Eh-pH diagrams of (**A**) U-O_2-H_2O-CO_2 system at 25°C and 1 atm pressure; alkaline conditions favour the uranyl tri-carbonate complex ($UO_2(CO_3)_3^{4-}$), which is 10 times more soluble than uranyl ions, the uranyl complex (UO_2^{2+}) is stable under oxidising ande acid conditions; (**B**) U-O_2-H_2O systems at 25°C and 1 atm pressure, uraninite is stable in reducing and neutral to alkaline conditions; (**C**) U-O_2-CO_2-H_2O system at 25°C for $P_{CO2} = 10^{-2}$ atm; stability fields for amoprohus UO_2(am) and ideal uraninite UO_2(c). A and B after Hosteler and Garrels (1962), C after Langmuir (1978)

material (peat and coals). Humic acids and humates have multiple roles, such as adsorption, as reactants and reductants. Reduction results in the precipitation of uraninite and this in organic materials is probably mediated by bacterial colonies, which reduce sulphates to H_2S and causing precipitation of uraninite, according to:

$$UO_2F^+ + HS^- \rightarrow UO_2 + HF + S$$

Plant decay products and bacterial activity play a major role in the generation of sedimentary U deposits. The presence of "thucolite" (a mixture of

carbonaceous matter, hydrocarbons, U and Th minerals, first described by Ellsworth 1928) in the Witwatersrand conglomerates suggests that organic matter and bacteria were present in the Neoarchaean and may have cause the initial precipitation of U compounds. However, high-rank coals and petroleum have little affinity for U. In black shales the organic material is vitrain and bituminous coal, derived from algae and plant debris in post-Ordovician shales.

13.2.2 Decay Schemes

It is perhaps appropriate in this section to briefly look into some fundamental concepts before proceeding further, for those who, like me, may be a bit "rusty" on the subject. The reader who may wish to know more on the fundamentals of nuclear science and the structure of the atom can consult the authoritative books of Shultis and Faw (2002) and Faure (1986).

The atomic number Z indicates the number of protons in the nucleus of the atom, it is also the nuclear charge number (number of positive charges). The range of Z is from 0 to >100. The number of neutrons in the nucleus is the neutron number N, with a range of 0 (H) to 149 (^{244}Am). Thus, the total number of nucleons is Z + N = A, which is the mass number and the difference N-Z is the isotopic number. The familiar notation $_8{}^{16}$O means that the nuclide of an atom of oxygen has 8 protons and 8 electrons in the neutral state and a total of 16 nucleons (8 neutrons + 8 protons). It follows that isotopes are elements which have the same proton number Z, but different neutron numbers and hence different atomic mass, which is what is utilised in isotope geology. All elements of Z > 83 (^{83}Bi) are *radioactive* in that they decay towards stable daughter nuclide by emitting alpha and/or beta particles or by electron capture. There are three main forms of radiations: alpha (α), beta (β) and gamma (γ). The α particle is $_2{}^4$He, it has an energy of approximately 4 MeV (1 million electron Volt or eV, which is the kinetic energy gained by an electron accelerated through the potential difference of 1 Volt) and it has a short range in air (2–4 cm) and only about 50 μm in solids. The β particle is equivalent to an electron therefore its mass is very low and its penetration in solids is generally less than 2 cm. The range of energies of a β particle is from about 0.10 to >3 MeV. The γ ray is an electromagnetic wave phenomenon that originates in the nucleus, following α and/or β emissions and its charge and mass are zero. The γ ray is highly energetic and therefore highly penetrative, from 2 to 4 cm in lead and 10–50 cm in soil. An α particle ($_2{}^4$He; two protons and two neutrons) is ejected from the nucleus during the α-decay and after the event the daughter nucleus will have two fewer protons than the parent:

$$_{92}{}^{238}\mathrm{U} \rightarrow {}_{90}{}^{234\mathrm{Th}} + \alpha$$

The beta (β) decay, on the other hand is the emission of a negative electron from an unstable parent nucleus. This results in the charge of the nucleus to

Table 13.3 Decay series of U and Th; a year, d day, m minute, s second, ms millisecond, μs microsecond. After Plant et al. (1999) and Kaye and Laby (1986)

^{235}U decay series			^{238}U decay series			^{232}Th decay series		
Isotope	Half-life	Principal decay mode	Isotope	Half-life	Principal decay mode	Isotope	Half-life	Principal decay mode
^{235}U	7.0×10^8 a	alpha	^{238}U	4.5×10^9a	alpha	^{232}Th	1.4×10^{10} a	alpha
^{231}Th	26 h	beta	^{234}Th	24 d	beta	^{228}Ra	5.8 a	beta
^{231}Pa	3.3×10^4 a	alpha	^{234}Pa	6.8 h	beta	^{228}Ac	6.1 h	beta
^{227}Ac	22 a	beta	^{234}U	2.4×10^5 a	alpha	^{228}Th	1.9 a	alpha
^{227}Th	19 x	alpha	^{230}Th	7.3×10^3 a	alpha	^{224}Ra	3.7 d	alpha
^{223}Ra	11.4 d	alpha	^{226}Ra	1.6×10^3 a	alpha	^{220}Rn	56 s	alpha
^{219}Rn	4.0 s	alpha	^{222}Rn	3.8 d	alpha	^{216}Po	0.15 s	alpha
^{215}Po	1.8 ms	Alpha	^{218}Po	3.1 m	alpha	^{212}Pb	11 h	beta
^{211}Pb	36.1 m	Beta	^{214}Pb	27 m	beta	^{212}Bi	61 m	beta
^{211}Bi	2.2 m	Alpha	^{214}Bi	20 m	beta	^{212}Po	0.30 μs	alpha
^{207}Tl	4.8 m	Beta	^{214}Po	160 μs	alpha	^{208}Pb	Stable	–
^{207}Pb	Stable	–	^{210}Pb	22 a	beta			
			^{210}Bi	5.0 d	beta			
			^{210}Po	138 d	alpha			
			^{206}Pb	Stable	–			

increase by one unit, therefore the atomic number increase by one because there is now one more proton, but there is no significant change in mass, so that:

$$_{82}{}^{214}\mathrm{Pb} \rightarrow {}_{83}{}^{214}\mathrm{Bi} + \beta$$

Important in geochronology is the decay of $_{19}{}^{40}\mathrm{K}$ to $^{40}\mathrm{Ca}$ by β emission and to $^{40}\mathrm{Ar}$ by electron capture and γ emission. The decay schemes for the naturally occurring isotopes $_{92}{}^{238}\mathrm{U}$, $_{92}{}^{235}\mathrm{U}$ and $_{90}{}^{232}\mathrm{Th}$ are given in Table 13.3. These isotopes decay to final daughter nuclides as follows:

$$^{238}\mathrm{U} \rightarrow {}^{206}\mathrm{Pb}\ (t_{1/2} = 4.51 \times 10^9\ \mathrm{yr})$$

$$^{235}\mathrm{U} \rightarrow {}^{207}\mathrm{Pb}\ (t_{1/2} = 7.04 \times 10^8\ \mathrm{yr})$$

$$^{234}\mathrm{U} \rightarrow {}^{238}\mathrm{U} + \alpha, \beta\ (t_{1/2} = 2.48 \times 10^5\ \mathrm{yr})$$

It is clear, from a comparison of the half lives ($t_{1/2}$ see below), that the ratio $^{238}\mathrm{U}/^{235}\mathrm{U}$ must have changed considerably during the history of the Earth; 4.5 billion years ago the ratio would have been 3.45, whereas today it is almost always 137.5 ± 0.5.

13.2.2.1 Half Life

The decay of any nucleus can be described by the exponential law. Starting with N_0 radioactive atoms at time $t = 0$, at any subsequent time there will be (see also Chapter 1):

$$N = N_0{}^{-\lambda t}$$

Where λ is the decay constant, or the probability of decay per nucleus per unit time, which is related to the half life t½:

$$t\tfrac{1}{2} = \ln 2/\lambda = 0.693/\lambda$$

13.3 Uranium Hydrothermal Mineral Systems

The abundances of radioactive elements in the Earth are shown in Table 13.4.

The data on the average concentrations of uranium and thorium in terrestrial rocks are worthy of brief consideration and some immediate implications are:

(i) Anatexis (partial melting) probably fractionates both U and Th into the melt.
(ii) Igneous differentiation processes are effective means of concentrating U selectively into the late-stage residua.

(iii) The reaction between sea water (or meteoric water) and basalts is one process for the mobilization of uranium.
(iv) Uranium has an affinity for organic materials.
(v) Prograde regional metamorphism might be an effective means for the natural mobilization and concentration of U in the crust. Repeated metamorphism may thus have depleted older crustal segments.

Uranium, REE and Nb minerals are normally enriched in alkaline igneous rocks and carbonatites, which commonly occur as intracontinental ring complexes, such as those of the Damara province in Namibia (Chapter 4) and the Jos Plateau in Nigeria (Kinnaird and Bowden 1987). Anorogenic magmatism (A-type granitic rocks, anorogenic, anhydrous and generally alkaline) is typically associated with post-orogenic and/or intracontinental rift settings. Anorogenic magmatism is especially common in the Mesoproterozoic and is linked to the emplacement of high-heat producing granites (HHP), which may host world-class U and REE ore systems including Fe oxides-gold-copper deposits (IOCG) such as Olympic Dam in South Australia (Chapter 8). In addition, the emplacement of HHP results in the inception of large scale hydrothermal

Table 13.4 Distribution of radioactive elements (ppm) in the Earth and their heat production. After Plant et al. (1999 and references cited therein)

	K	U	Th	Th/U	K/U	Total heat production	
						($W\ kg^{-1}$)	($W\ m^{-3}$)
CI carbonaceous chondritis	545	0.0074	0.029	3.92	73 649	1.54×10^{-12}	4.00×10^{-9}
Primitive mantle	250	0.021	0.085	4.05	11 905	4.37×10^{-12}	1.14×10^{-8}
Bulk silicate earth	240	0.023	0.0795	3.46	10 435	4.42×10^{-12}	1.15×10^{-8}
Continental crust							
Upper	27 500	2.5	10.5	4.20	11 000	5.30×10^{-10}	1.38×10^{-6}
Middle (Archaean)	17 500	2.2	8.4	3.82	7 954	$4.44 \times 10^{1-10}$	1.15×10^{-6}
Lower (Archaean)	8333	0.05	0.42	8.40	166 660	1.67×10^{-11}	4.33×10^{-8}
Lower and Middle (post Archaean)	20 000	1.25	6	4.80	16 000	2.86×10^{-10}	7.43×10^{-7}
Average (1)	17 500	1.3	5.7	4.38	13 461	2.82×10^{-10}	7.34×10^{-7}
Average (2)	12 500	1.25	4.8	3.84	10 000	2.53×10^{-10}	6.58×10^{-7}
Oceanic crust							
Normal Mid-ocean ridge basalt	600	0.047	0.12	2.55	12 766	7.88×10^{-12}	2.05×10^{-8}
Ocean island basalt	12 000	1.02	4	3.92	11 765	2.09×10^{-10}	5.43×10^{-7}

convection long after magmatic cooling with the development of polymetallic hydrothermal systems and hot springs, as discussed in Chapter 9. Apart from Dahlkamp (1993), recent papers documenting U deposits can be found in Mao and Bierlein (2005) and Cuney et al. (2007). The world-wide distribution of uranium mineral systems, following Dahlkamp's classification (see below), is shown in Fig. 13.2

A general and simplified classification of U mineral systems can be as follows: in granitic rocks, metamorphic rocks, hydrothermal veins, at unconformities, in conglomerates (Witwatersrand type), in sandstone, in phosphorites, black shales, coal etc. Dahlkamp (1993) in his book divided U deposits into 16 types and several sub-types. The 16 types are: (1) unconformity contact, (2) subconformity, (3) vein, (4) sandstone, (5) collapse breccia pipe, (6) surficial, (7) quartz-pebble conglomerate (Witwatersrand type), (8) breccia complex, (9) intrusive (alaskite, porphyry, carbonatite, peralkaline syenite, pegmatite), (10) phosphorite, (11) volcanic, (12) metasomatite, (13) synmetamorphic, (14) lignite, (15) black shale and (16) strata-controlled.

The Organisation for Economic Co-operation and Development (OECD), Nuclear Energy Agency (2004) classified uranium mineral systems in order of economic importance, as follows: (1) Unconformity-related; (2) sandstone-hosted; (3) hematite breccia complex (Olympic Dam style or IOCG, see Chapter 4); (4) Witwatersrand type (quartz pebble conglomerate); (5) hydrothermal veins; (6) intrusive deposits; (7) volcanic and caldera-related; (8) metasomatite deposits; (9) surficial; (10) collapse breccia; (11) phosphorites; (12) other types and rocks with elevated U content. Details from the OECD classification are given below:

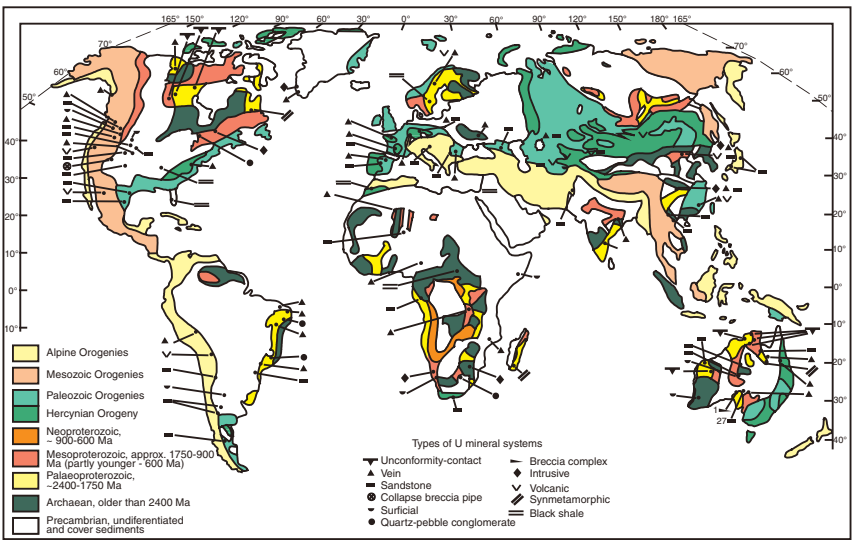


Fig. 13.2 World distribution of U mineral systems. Modified from Dahlkamp (1993)

- Unconformity-related U systems, as the name implies, occur at, above and below an unconformity that separates a basement from an overlying sedimentary succession. Two sub-types are recognised: (1) unconformity contact including fracture-controlled within metasediments below the unconformity and clay-bound deposits, which occur directly above the unconformity and are associated with clay alteration, an example is Rabbit Lake in Canada; (2) sub-conformity-post-metamorphic deposits are stratabound in metasediments below the unconformity, this style is polymetallic and of high grade; an example is Cigar Lake in Canada.
- Sandstone U deposits are hosted in medium-coarse sandstones deposited in continental fluvial or marginal marine environments. There are four subtypes: roll front, tabular, basal channel deposits and tectonic/lithologic. Roll front typically have mineralised zones that are convex down the hydrological gradient, with diffuse boundaries on the convex side with the reduced sandstone and sharp with the oxidised sandstone on the concave side. The mineralisation is parallel to the strike and perpendicular to the direction of groundwater flow. Examples can be found at Crow Butte in the USA and at Bukinay, Sugraly in Uzbekistan. Tabular deposits form irregularly shaped masses in reduced sediments, where U occurs as impregnations and the mineralised zones are oriented parallel to the depositional trend. Examples can be found in Australia (Westmoreland) and in the Colorado Plateau. Basal channel U deposits occur in palaeodrainge systems consisting of several hundred metres wide channels filled with alluvial-fluvial sediments. The mineralisation occurs as elongate lenses or ribbon-like shapes. Examples can be found at Beverley in Australia and in the Vitim district in Russia. Tectonic/lithologic U deposits are in sandstone and related to a permeable zone, where U is precipitated in open spaces. An example is Mikouloungou in Gabon.
- Hematite breccia complex, best exemplified by the Olympic Dam IOCG system, described in Chapter 4.
- Quartz-pebble conglomerate U deposits are typically represented by the Witwatersrand Au-U ore systems, briefly described in Chapter 11. The main features are the presence of detrital uraninite grains in quartz pebble conglomerates of fluvial and lacustrine braided river systems. Apart from the Witwatersand in South Africa, another example is Elliot Lake in Canada.
- Vein deposits consist of fracture-controlled carbonate or quartz veins containing pitchblende. The vein deposits of the Massif Central in France are a good example (see Chapter 4).
- Intrusive deposits are associated with a variety of highly differentiated and/or alkaline granitic rocks (leucogranites, peralkaline syenite, carbonatite, pegmatites). Examples are the Rössing deposit, described in this chapter, Palabora in South Africa (Chapter 4), Ilimaussaq in Greenland. Pegmatite-hosted and carbonatite-hosted U occurrences are present in the Gascoyne Complex in Western Australia (Pirajno et al. 2008).

- Volcanic and caldera-related U deposits are within mafic to felsic volcanic complexes and associated clastic sediments. The mineralisation is controlled by structures at several stratigraphic levels and may extend into the fractured basement rocks. Uranium minerals are accompanied by sulphides and fluorite. Examples include the Strelsovsk caldera in Russia, Nopal in Mexico and Michelin in Canada.
- Metasomatite deposits are confined to Precambrian shields hosted by granites, migmatites, gneisses and ferruginous quartzite, metasomatically altered to albitites and alkali amphiboles. The mineralisation consists of uraninite and brannerite and examples include the Valhalla deposit in Australia and several deposits in Ukraine.
- Surficial deposits are near surface concentrations in sediments and soils of Neogene to Recent age. The calcrete-hosted deposits belong to this type, of which Yeelirrie In Western Australia and Lange Heinrich in Namibia are good examples. Surficial U deposits also occur in valley-fill sediments and Neogene drainage channels and in playa lake sediments, such as in Lake Maitland in Australia.
- Collapse breccia pipe deposits occur in vertical pipes filled with down-dropped clasts and uraninite is found in the breccia matrix and in ring fracture zones around the pipe. Examples are in Arizona (USA)
- Phosphorite deposits consist of continental shelf marine deposits of phosphorite containing stratiform disseminated U and fine-grained apatite. Uranium can be recovered as a by-product. These deposits constitute large resources of U. Examples are at Gantour, Morocco and Uncle Sam (USA).
- Other deposits include metamorphic, limestone and uranium coals and various rock types that have elevated U and may become economic in the future. These include rare metal pegmatites, such as Greenbushes in Western Australia, HHP granites (Chapter 9) and uraniferous black shales, such as the Lower Cambrian Zunyi Formation in southern China (also in Chapter 9).

Plant et al. (1999) distinguished two main associations of U ore systems: (1) plutonic and volcanic associations; (2) sedimentary. A more detailed classification from these authors is shown in Table 13.5.

13.3.1 Plutonic Associations

These U ore systems are associated with a variety of evolved intrusive rocks in which differentiation leads to unusual U concentrations. Commonly these intrusions also develop hydrothermal systems from which various types of vein deposits are formed. Anorogenic alkaline complexes including peralkaline syenitic rocks, carbonatites, alaskite and pegmatites are probably related to mantle plume magmatism in rift settings and provide numerous examples of U ore systems. Examples of U mineral systems of the plutonic associations include the above-mentioned Ilimaussaq syenite complex in Greenland with U concentrations of U that can reach 300 ppm and the Palabora carbonatite

Table 13.5 Classification of U ore systems. Modified after Plant et al. (1999)

1. Plutonic associations
Magmatic ore systems in alkaline complexes
Magmatic-hydrothermal vein deposits
2. Anorogenic granitic and felsic volcanic magmatism
Breccia complex deposits (Fe oxides-copper-gold or IOCG systems)
Deposits associated with high-level felsic volcanism
3. Formed from metamorphic fluids derived from igneous and/or sedimentary rocks previously enriched in U
Synmetamorphic
Vein deposits in metamorphic rocks
4. Late-post-orogenic continental sedimentary basins
Quartz-pebble conglomerate deposits
Unconformity-related
Sandstone-hosted
Vein deposits in sedimentary rocks
Collapse breccia
Lignite deposits
5. Surficial deposits formed during surface weathering
6. Marine deposits
Phosphorite
Black shales

complex in South Africa which averages 40 ppm U and is described in Chapter 4. Herein I describe the alaskite-hosted Rössing U deposit and those of Limousin region in France.

13.3.1.1 Rössing U Deposit, Namibia

The Rössing U deposit in the Damara orogenic belt in Namibia had total resources of 138 kt of U with grades ranging from 280 to 360 ppm U (Laznicka 2006), with a current production of 4 000 t/yr of uranium oxide, but scheduled to increase to 4 500 t/yr uranium oxide, extending the life-of-mine by five years to 2021 (*Mining Weekly*, March 10th 2008). Uranium deposits similar to Rössing are present at other localities in the region (Goanikontes, Ida Dome and Valencia). Publications on the Rössing U mineralisation include Jacob et al. (1986), Berning (1986) and more recently Kinnaird and Nex (2007). The following synopsis is obtained from these works.

The Rössing U deposit is characteristically hosted in late-post-orogenic highly fractionated leucogranites, also known as alaskites, a type of unzoned pegmatite that were probably formed, at least initially, by partial melting of U-rich igneous, metamorphic and sedimentary protoliths. These alaskites are in the Neoproterozoic intracontinental Damara belt of the Damara Orogen. The

belt trends northeast, is about 400 km wide and, on the basis of structural, tectonic and metamorphic patterns, is subdivided into a Northern Platform, Northern Zone, Central Zone, Southern Zone and a Southern Marginal Zone (Chapter 4). The stratigraphy of the Damara sequence is fairly well-established and can be considered in terms of a basal, dominantly classic succession (the Nosib Group) overlain in the Northern Platform by the carbonate-dominated Otavi Group (host of the MVT deposits discussed in Chapter 8), and in the other Zones by the Swakop Group. For details of the stratigraphy the reader is referred to Miller (1983). The Nosib Group lies unconformably on a gneissic basement, the Ababis Complex, which occurs as cores to domal structures. The Abbabis Complex has a range of ages, with a strong Pan-African overprint at ~560 Ma. The basal Nosib Group consist of quartzite, arkosic rocks and conglomerates of the Etusis Formation, overlain by the Khan Formation consisting of pelitic rocks and carbonates, in turn overlain by the Rössing Formation, a succession of marbles, cherts, conglomerates, quartzite and cordierite gneiss. The age of the Nosib rocks is constrained between ~752 and ~710 Ma. Damaran granitic and volcanic rocks were emplaced during three major episodes. The first relates to the early rifting phase at about 950 Ma and is characterised by the emplacement of felsic volcanic rocks and volumetrically minor alkaline rocks. The second episode took place between 650 and 540 Ma and is characterised by the intrusion of calc-alkaline granitic rocks of I-type affinity. The third episode of igneous activity is post-tectonic and occurred between 540 and 450 Ma and is related to closure of the rifts and continental collision, resulting in a range of S-type granitic rocks, including the U-rich Rössing alaskites sheets and two-mica granites (Miller 1983; Kinnaird and Nex 2007). The alaskites have ages ranging from ~542 to ~505 Ma, are located on the margins of basement domes and are hosted in rocks at the Nosib-Swakop Groups boundary. Six types of alaskites have been recognized, ranging in composition from tonalite to alkali feldspar granite and referred to by Kinnaird and Nex (2007) as sheeted leucogranites. The six types of sheeted leucogranites, as identified in the Goanikontes area are: (A) pale pink, irregular, folded, fine-medium-grained; (B) white, fine-pegmatitic, folded and boudinaged, contains garnet, biotite and tourmaline; (C) pale, pink-cream, medium-pegmatitic, clear quartz and two feldspars; (D) white, irregular, anastomosing, medium-coarse-grained, granular texture and with smoky quartz; (E) pink, variable colour and grain size, locally boudinaged; and (F) red, tabular, coarse-pegmatitic with mily quartz. Of these, type D has the highest U and Th concentrations, averaging 204 and 97.6 ppm, respectively. Textures are variable, ranging from granophyric, aplitic to coarse-grained granitic to pegmatitic. Not all alaskites are U-bearing, with only those that post-date the latest deformation event (D_3) being mineralized. The leucogranite sheets occur as irregular, cross-cutting, anastomosing dykes and/or concordant bodies (Fig. 13.3) and can reach more than 90 m in thickness. In one area an alaskite plug is 500 m long and 200 m across and containing mostly betafite as ore mineral. The leucogranites consist mainly of quartz and K-feldspar with less than 5% mafic minerals. Albite and

oligoclase may be also be present. The main ore minerals are uraninite, thorite and betafite. Secondary U minerals include uranophane, thorogummite, gummite, coffinite, autunite, monazite, torbenite, rössingite, uranothallite, carnotite and some niobates. These secondary minerals occur in the leucogranites and in cracks and fractures of the surrounding rocks and in quartz and carbonate veins. Uraninite occurs as intragranular and intergranular grains, up to 0.01 mm, in quartz and feldspar. High U concentrations are associated with smoky quartz, a feature usually attributed to radiation damage, but interestingly detailed studies have shown that the smoky quartz has a better defined structure than clear quartz (Kinnaird and Nex 2007). Fluid inclusion studies show that there is a correlation between the abundance of inclusions and U concentrations. Most inclusions are secondary and are of two types: carbonic and aqueous. Carbonic inclusions contain liquid and vapour CO_2. Aqueous inclusions have homogenisation peaks between 170 and 220°C; salinities range from 5 to 18 wt% NaCl equivalent. A few inclusions have halite as daughter crystal, which dissolves between 200 and 450°C, equivalent to a range of salinities between 30 and 48 wt%, NaCl equivalent (Kinnaird and Nex 2007).

The origin of the mineralisation is related to partial melting of Nosib Group and/or U-enriched basement rocks, resulting in A-type granitic melts. Kinnaird and Nex (2007) cited previous work suggesting that the leucogranite sheets were

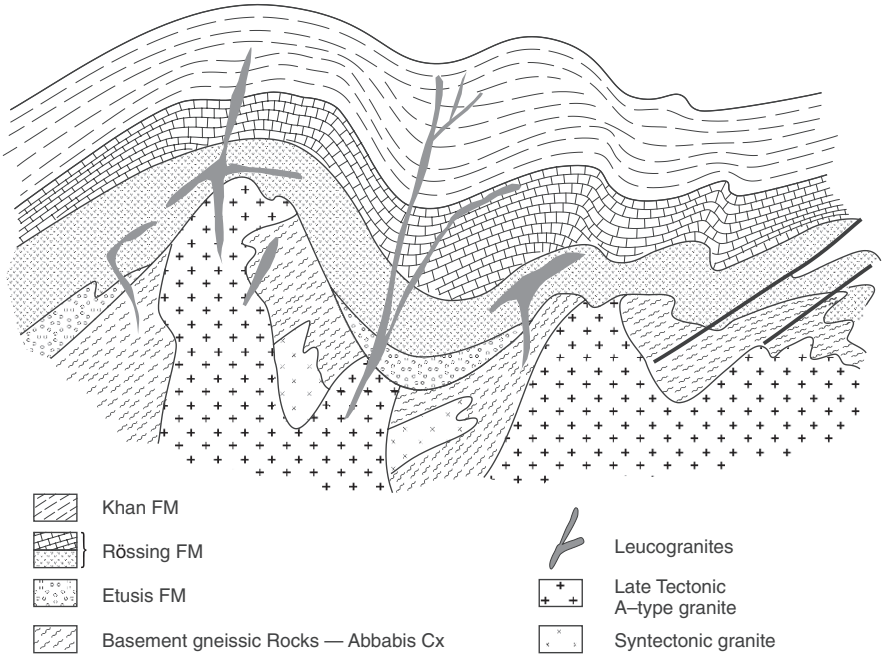


Fig. 13.3 Conceptual model of leucogranite (alaskite) emplacement and associated U mineralisation

derived from partial melting of high heat producing syn-tectonic granites (HHP), which may have localized heat generation. Post-tectonic events (post-orogenic collapse?) created dilation zones allowing the access of the magmas in areas of minimum stress. Kinnaird and Nex (2007) also pointed out that there is evidence of sub-solidus hydrothermal overprints at Rössing, suggesting fluid flow and re-distribution of U both within the leucogranites and the country rocks. However, there is also evidence of limited fluid-host rock interaction and that the U-rich type D leucogranites at Goanikontes are primarily magmatic. Another important aspect is that the alaskite magmas become U-rich where they cross-cut the metasedimentary rocks of the Khan and Rössing Formations. Furthermore, de-carbonation of marble rocks released CO_2, which was transferred to vapour phase of the magma resulting in its boiling. The role of hydrothermal fluids for the primary U mineralisation remains uncertain, except for the secondary U minerals for which there is evidence of fluid circulation.

13.3.1.2 Limousin, Massif Central, France

The U deposits of the Limousin region of the Massif Central in France are similar to those of Rössing (Dahlkamp 1993; Plant et al. 1999), briefly introduced in Chapter 4. The Limousin deposits have reserves estimated at 34 000 tonnes with ore grades ranging from 0.1 to 0.5% U and are hosted in highly evolved leucogranitic rocks of Hercynian age, which also contain anomalous abundances of Th, Be, F, Sn and W. These granites commonly have aureoles of Sn-W vein systems. The granitic intrusions are called episyenites (a term used by uranium geologists referring to U-bearing altered syenitic rocks), where mineralisation is hosted in pipes and lenses, with vertical extents from 30 to 200 m and diameters of up to 10 m. Locally uraniferous veins intersect pipes, in which case the ore grade increases substantially to up to 10% U_3O_8. The ore minerals of the uraniferous veins are pitchblende and coffinite mainly, with variable amounts of Cu, Pb, Zn sulphides, fluorite and barite. Pitchblende, pyrite, coffinite and fluorite als occur in fractures. Autunite and torbenite are secondary U minerals in the oxidation zone. The veins, localised along major fractures, are cm to about 5 m thick, are discontinuous with pinch-and-swell structures, and may also form stockworks or breccias. The host leucogranites are hydrothermally altered with greisen (quartz-muscovite), albite, chloritic and argillic alteration. Hydrothermal alteration extends for less than 0.5 m from the vein margins into the wall rocks. There are two stages of hydrothermal alteration: an early stage of muscovite, chlorite and pyrite, followed by hematite, montmorillonite, adularia and microcrystalline silica in the wallrocks around the fractures. The alteration assemblage that accompanies coffinite consists of hematite, montmorillonite, adularia and quartz. Resources of individual veins, as reported by Dahlkamp (1993), range from less than 10 Mt to hundreds Mt U_3O_8 with grades ranging from 0.15 to 40% U_3O_8.

The uraniferous magmas were possibly formed by anhydrous melting of lower crust and/or upper mantle under conditions of high F and CO_2 pressure,

during or after extensional collapse of the Variscan orogen. Fluid inclusion studies showed the presence of CO_2-rich fluids and temperatures of about 350°C, for the first stage of alteration associated with pitchblende mineralisation and lower temperatures (120°C maximum) and aqueous fluids for the second stage of alteration associated with coffinite mineralization (Turpin et al. 1990). Anatectic melting of U-rich sedimentary rocks gave rise to granitic melts, which during crystal fractionation enriched the magmas in U and was further enriched through hydrothermal processes with fluids precipitating ore minerals in regional fracture systems.

13.3.2 Unconformity-Related U Deposits

Unconformity-related U deposits constitute a major source of U. Most of these deposits occur in the 1650–1350 Ma Proterozoic terranes of the province of Saskatchewan in Canada and the Northern Territory in Australia. Works that describe this class of U mineralisation include the collection of papers edited by Evans (1986), reviews by Marmont (1987) and Jefferson et al. (2007). The latter authors prefer to refer to these mineral systems as unconformity-associated. Apart from their age, one of the chief characteristics of unconformity-related U deposits, as the name implies, is that they tend to occur close to a major unconformity. The mineralisation therefore is located both above and below a palaeosurface, separating predominantly metasedimentary sequences of Proterozoic age, deposited on metamorphic basement. The basement rocks are typically palaeoweathered, forming a clay-altered, hematite-rich palaeoregolith grading, through chlorite-altered rocks, into fresh basement. In Canada, the unconformity at the top of the sequence is characterised by a 220 m thick paleoregolith, which consists of chloritic material, illite, kaolinite and hematite. This regolith is interpreted to be either a palaeosol or a palaeolateritic horizon. Basement rocks also include U-rich granites and pegmatites, generated by anatexis of metasedimentary rocks. Evidence indicates that the unconformity acts as a redox front between oxidising (above) and reducing (below) domains. Another important feature is that the mineralisation is spatially associated with fractures, reverse and normal faults. Jefferson et al. (2007) distinguished two types of unconformity-related ore systems: monometallic consisting of pods, veins and breccias in fault zones, generally in basement rocks and polymetallic consisting of sub-horizontal lenses, at the unconformity, and replacing sandstone and basement rocks and containing, in addition to U, Ni, Co, As, traces of Au, PGE, Cu, REE and Fe. Figure 13.4 illustrates an idealised cross-section of unconformity-related U mineral systems.

13.3.2.1 Canadian Deposits

In Canada, the unconformity-related U deposits of the Athabasca Basin, such as Cigar Lake and McArthur River, are the world's largest (Jefferson et al. 2007).

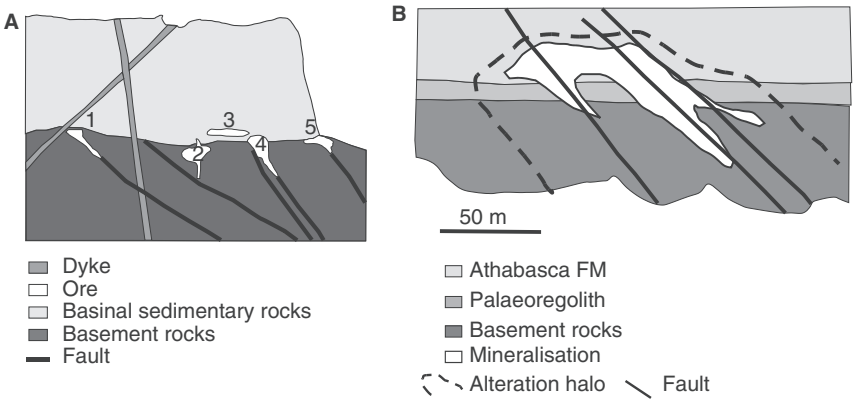


Fig. 13.4 (**A**) Idealised cross-section of Athabasca-type and range of unconformity-related U ore systems; (1) polymetallic (U, Ni, Co, As, PGE, Au) ore, (2) U in palaeokarst marble (not discussed in text), (3) U oxides in sandatone above unconformity, (4) combination of 1 and 3, (5) polymetallic (U, Ni, Co, As, PGE, Au) ore; After Laznicka (2006). (**B**) Cross-section of idealised unconformity-related U deposit, based on Canadian examples; After Hoeve and Sibbald (1978)

Similar basins in Canada, but with lesser U mineralisation, include the Thelon and Martin Basins. Basins structures located on the western Churchill Province, are considered as "*lakes of gravel and sand*". Other important Canadian deposits are Key Lake (Dahlkamp 1978), Rabbit Lake (Hoeve and Sibbald 1978) and McClean (Wallis et al. 1986). The following summary is take from Jefferson et al. (2007 and references therein). The Athabasca Basin contain the Athabasca Group, which consists of at least six sedimentary Formations, grouped into four depositional sequences separated by unconformities, totalling some 3.5 km in thickness and resting on a basement of Archaean and Palaeoproterozoic gneisses with late intrusions dated at ~1750 Ma. The sedimentary rocks are dominated by fluvial, conglomeratic sandstones and red beds. The clastic rocks that overlie the palaeoweathered basement gneisses and host part of the polymetallic mineralisation are red beds that have been subjected to complex and multiphase diagenetic and hydrothermal alteration processes. Basin-wide alteration includes pre-ore diagenetic alteration and alteration haloes specifically associated with the U deposits. The diagenetic alteration, called the Q1 event, consist of quartz overgrowths around hematite coating clastic quartz grains. The Q1 event was followed by a complex diagenetic sequence that includes kaolinite, chlorite, montmorillonite and low-Fe-Mg-illite. With progressive diagenesis this assemblage was overprinted by a mixture of dickite and minor amounts of chlorite and illite. Illite crystallinity indicates burial temperatures of around 200°C. Regional illite is an important diagenetic-alteration phase, probably derived from detrital K-feldspar and mica; locally this illite is associated with zones containing chlorite and blue-green dravite. The illite is

expressed in spectral gamma-ray surveys as a K anomaly. Geochronological constraints, based on fluoroapatite ages, indicate ages of 1640–1620 Ma for the regional hydrothermal event in the Athabasca Basin, whereas hydrothermal ore-related events show ages of 1600–1500 Ma and 1460–1350 Ma, overprinted by a series of U mineralisation events at 1176, 900 and 300 Ma. A similar punctuated history of U mineralisation events is also found in the Australian deposits.

In Canadian deposits exhibit two main ore styles. One is fracture-controlled and breccia-hosted and the other is clay-bounded massive ore. Fracture controlled ore is characterised by steeply to moderately dipping brittle shears, fractures and breccia zones that can extend for hundreds of metres into the basement. Fracture-controlled and breccia-hosted ore consist of disseminated and massive uraninite-pitchblende, with grades of up to 2% U. Lenses and pods of ore can be up to100 m in vertical extent, 90 m in length and 50 m in width. Clay-bounded ore is along the unconformity and forms elongate pods or linear ore zones with a high grade core (>1–15% U_3O_8), enveloped by lower grades haloes. In places, ore zones of disseminated pitchblende extend into the overlying sedimentary rocks along breccias and fracture zones, thought to have formed by remobilisation processes. These ore zones are uneconomic but are good indicators of ore grades at depth.

The ore minerals of polymetallic deposits are disseminated uraninite and pitchblende, accompanied by other ore minerals such as pyrite, arsenopyrite, chalcopyrite, galena, molybdenite, rammelsbergite, gersfordite and millerite. Au and PGE may occur as tellurides. Secondary minerals may also be present and include coffinite, uranophane, torbenite and autunite. Hydrothermal alteration is prominent and forms haloes of up to a few hundred metres around the orebodies. Alteration consists of chloritisation, argillisation, dolomitisation and silicification. Usually chlorite is the most abundant alteration mineral, but sericite, tourmaline, apatite and hematite are also part of the alteration assemblage. There are also phosphate minerals, such as xenotime, apatite and C-Sr-REE-Al phosphate minerals, involving multistage events of precipitation, dissolution and re-precipitation. These phosphate minerals, referred to as AP, are present in minor amounts in the Athabasca Basin, but they provide some constraints on diagenetic and hydrothermal processes. Some of these AP minerals have been referred to as "crandallite group" and identified as florencite, intergrown with illite, dickite, anatase and hematite (Mwenifumbo and Bernius 2007). As mentioned above, stages of quartz dissolution and cementation were important and responsible for volume reduction and subsequent collapse of the sedimentary strata. Jefferson et al. (2007) described two main forms of alteration in the Canadian deposits: egress and ingress types. Egress alteration haloes form in both basement and overlying sandstone rocks and comprise illite, Q1 and Q2 silica and a later illite-kaolinite-chlorite-dravite assemblage. This later assemblage can form a bell-shaped halo of up to 400 m at the base of the Athabasca Group rocks, tapering upwards and downwards into the basement. In the ingress style, oxidising U-rich fluids move downwards along faults and fractures into the basement, where they are reduced to precipitate uraninite.

Cathelineau et al. (2007) reported on the compositions of fluid inclusions from the McArthur River field in Saskatchewan and Alligator Rivers in Australia (see below), using a Raman microprobe and Laser Induced Breakdown Spectroscopy (LIBS). These authors found that in the McArthur River field there are two types of brines in the Athabasca sandstones and the underlying basement. One type is represented by ~190°C brine containing ~25 wt% NaCl, up to 14 wt% $CaCl_2$ and 1 wt% $MgCl_2$; the other is a cooler (~140°C) brine consisting of up to 20 wt% $CaCl_2$, 11 wt% $MgCl_2$ and 5–8 wt% NaCl. The hotter NaCl-rich brines were the earliest regional basinal fluids, which were still active during and after U deposition. A cooler NaCl-rich brine percolated into the basement from the upper levels of the sedimentary pile and exchanged with Ca to form the $CaCl_2$-rich brines. This brine was injected into faults and fractures and was associated with silica cementation events, of which Cathelineau et al. (2007) recognised at least four (Qz1 to Qz4). The mixing of Ca and Na brines occurred in breccia zones during periods of high fluid influx and may have been instrumental not only in the various stages of quartz deposition, but also in the formation of the U mineralisation.

13.3.2.2 Australian Deposits

In northern Australia there are three uranium districts: Alligator Rivers uranium field, the Westmoreland district and Mount Isa. In the Mount Isa district the Valhalla U deposit is hosted in rocks of the Eastern Creek Volcanics. In the Alligator Rivers and Westmoreland districts there are five major U deposits: Naberlek, Jabiluka, Ranger, Westemoreland and Koongarra. The U minealisation is located in structural traps at or close to the unconformity between the Mesoproteozoic Cahill and Kombolgie Formations and basement metasedimentary and amphibolite rocks. The metamorphic grade of these rocks ranges from amphibolite to granulite facies. The Cahill Formation is approximately 3000 m thick and is divided into two members: a lower member comprising Mg-rich marble, graphitic schist and gneisses and an upper member comprising quartz-biotite schist and gneiss. The Kombolgie Formation is the equivalent of the Athabasca Group rocks in Canada. Details of the geology, mineralisation and alteration at Koongarra, Ranger, Jabiluka and Nabarlek can be found in Wilde and Wall (1987), Wilde et al. (1989) and Nutt (1989).

At Nabarlek, where the mineralisation is hosted by amphibolite and pelitic schist, hydrothermal alteration is very extensive, up to 1 km from the main mineralised conduit, and consists of concentric haloes (Wilde and Wall 1987). The outer halo, which is clearly fracture-controlled, is defined by silicified and hornblende-deficient lithologies. In the amphibolite and schist rocks, hornblende is replaced by chlorite and sericite, biotite by chlorite and rutile and plagioclase by sericite. Other alteration minerals are quartz, dolomite and prehnite. The inner zones are characterised by removal of quartz, presence of pervasive hematite, clay-sized chlorite and sericite. Detailed studies of alteration mineralogy at Jabiluka by Nutt (1989) revealed that sericitic alteration

preceded chloritisation, and that there are several types and generations of chlorite. The presence of this mineral is indicative of intense Mg metasomatism which is associated with the U mineralisation. The reason for this association is not clear but it is possible that chlorite may have lowered the pH of the solutions destabilising U carbonate or phosphorous U complexes causing precipitation of reduced U minerals. Mg metasomatism and the release of H^+ ions are therefore invoked as the main agents for causing chloritisation and a concomitant depletion in silica. Dolomite is thought to have provided much of the Mg needed to form the chlorite. The reaction, as proposed by Nutt (1989) is:

$$\text{quartz} + \text{muscovite} + \text{K-feldspar} + Mg^{2+} + H_2O \rightarrow \text{Mg-chlorite} + K^+ + H_4SiO_4 + H^+$$

The world class Jabiluka U deposit is located in the Alligator Rivers uranium field in the Nimbuwah Domain. There are two mineralised areas, Jabiluka I and Jabiluka II, with the latter being the largest with a resource of 31 Mt @ 0.53% U_3O_8 and 4.6 Mt @ 3.07 g/t Au (Polito et al. 2005). The ores are hosted by shallow-to-steeply dipping graphitic units of chlorite-biotite-muscovite schist in the Neoarchaean Nanambu Complex. The host rocks are unconformably overlain by shallowly dipping, coarse-grained sandstone of the Kombolgie Formation. Uranium ore is located in semi-brittle shears and breccia that is subparallel to the units in the Nanambu Complex and developed at the hinge zones of fault-related folds (Polito et al. 2005). Uraninite veins are intimately associated with chlorite, sericite, hematite, quartz, and illite veins, which extend in to the basal 2 m of the Kombolgie Formation (Gustafson and Curtis 1983). Post-diagenetic alteration has also taken place above the unconformity, suggesting that there were periods of remobilization and that the initial mineralisation was early in the history of the Kombolgie Formation. Electron microprobe and X-ray diffraction analysis of syn-ore illite and chlorite indicate a mineralisation temperature of 200°C and fluid inclusion studies suggest that the mineralising brines were saline (Polito et al. 2005). Isotopic (U-Pb and $^{207}Pb/^{206}Pb$) studies show that uraninite first precipitated at ~1680 Ma, which is coincident with the $^{40}Ar/^{39}Ar$ ages of 1683 ± 11 Ma age of brine migration out from the Kombolgie Formation (Polito et al. 2005).

At the Ranger deposit, a Paleoproterozoic sequence of volcanic and metasedimentary rocks unconformably overlie Neoarchaean granitic gneiss of the Nanambu Complex. The Paleoproterozoic rocks are folded, faulted and sheared, and crosscut by east-trending ~1870–1860 Ma granite dykes and pegmatite veins, and gently dipping N-NE trending mafic dykes of the ~1690 Ma Oenpelli Dolerite (Hein 2002). Regional metamorphism is greenschist facies and contact metamorphism is hornblende-hornfels facies. The rocks were deformed before or at the time of deposition of the Kombolgie Formation (Hein 2002). The initial deposition of the U is dated at ca. 1740 Ma (Maas 1989).

Several small U(-Au) deposits are located in the Paleoproterozoic Murphy Inlier bordering the southern McArthur Basin. The inlier comprises a greenschist facies sequence of wacke, siltstone, and shale that is intruded by

1840–1820 Ma granite and unconformably overlain by ~1773 Ma felsic volcanics (Ahmad et al. 1999). These rocks are unconformably overlain by conglomerate and sandstone included in the McArthur Basin. The mineral deposits are located in the basal sandstone and conglomerate in the McArthur Basin and consist of pitchblende-uraninite and minor brannerite with traces of galena, pyrite, marcasite, chalcopyrite, bornite and gold. The U mineralisation followed a regional sericite-illite-chlorite-haematite alteration. The mineralisation was leached either from the basal units of the McArthur Basin, presumably by the action of oxidized solutions and deposited in reducing environments, or from the basement.

The ~800 Ma Kintyre U deposit is in the Paleoproterozoic Rudall Complex in Western Australia. Jackson and Andrew (1990) described the deposit as an unconformity-related, vein-type deposit, and compared it to the East Alligator Rivers uranium deposits of the Northern Territory. The mineralization at Kintyre is hosted by chlorite (-carbonate)-quartz schist and chert in the hinge zone of an east-northeasterly plunging F_2 antiform, close to the unconformably overlying Neoproterozoic Coolbro Sandstone of the Throssell Range Group in the Yeneena Basin. At Kintyre pitchblende veins contain chlorite, dolomite, ankerite, and calcite, with accessory bismuthinite, chalcopyrite, bornite, and galena, and locally significant gold and platinum group elements (Pirajno and Bagas 2008).

Cathelineau et al. (2007) identified three types of brines from fluid inclusions in quartz from Jabiluka and Nabarlek: (1) a Ca-rich brine with 14–23 wt% $CaCl_2$ and 1–8 wt% NaCl; (2) a Na-rich brine with 10–19 wt% NaCl, 4–11 wt% $CaCl_2$ and 0–6 wt% $MgCl_2$; and (3) a fluid containing 3–13 wt% NaCl, 1–13 wt% $CaCl_2$ and 0–0.6 wt% $MgCl_2$. As is the case for the Canadian deposits, mixing of brines may have been implicated in the genesis of the U ores.

13.3.2.3 Genetic Models

Genetic models which attempt to explain the origin of unconformity-related U ore systems regard the role of U-enriched lithologies (protore), such as the Archaean basement, to be an important factor in processes of ore genesis. Two basic models are considered. In one, the source of the mineralising fluids is thought to be metamorphic or magmatic or a combination of both, while in the other, the fluids are believed to be of diagenetic or meteoric derivation.

The available data suggest that the diagenetic-hydrothermal hypothesis is perhaps more likely. However, it must be remembered that the mineralisation event, or events, appear to extend over a large time span, during which tectonism metamorphism and magmatism took place. In the Alligator Rivers deposits, for example, U-Pb isotopic dating indicates mineralisation ages ranging from 1737 ± 20 Ma to 1437 ± 40 Ma, metamorphism and magmatism have been dated from approximately 1900 to 1690 Ma, whereas the Kombolgie Formation has a Rb-Sr date of 1648 ± 29 Ma (Nutt 1989). Another important factor to bear in mind is that oxygen would have been required to move U in solution,

and once in solution a reducing environment is needed to precipitate U. This redox front was probably present in the vicinity of the unconformity (e.g. graphitic schist). For these reasons a multistage genetic model is perhaps more feasible. Stages of ore genesis can be summarised as follows. Mobilisation and pre-concentration of uraninite occurred during deformation and metamorphism of the basement lithologies as mesothermal vein-type deposits in Archaean-Palaeproterozoic basement rocks. Uplift and erosion followed with formation of a regolith, weathering and leaching with re-concentration of U in structural traps within the regolith. Sedimentation above the unconformity (Athabasca and Kombolgie sequences) took place and was accompanied by generation of oxygenated diagenetic brines, which remobilised U and associated metals, carried them along structural zones and re-distributed the mineralisation at a redox front, represented by the unconformity. Fluid mixing occurred near the unconformity, especially where cut by faults, depositing reduced U. Continuing uplift, erosion and dyke intrusions induce several cycles of re-distribution of U along structural traps above and below the unconformity. A model of unconformity-type U mineral systems is shown in Fig. 13.4.

13.3.3 Sandstone-Hosted/Roll Front U Deposits

Sandstone-hosted Permian to Cretaceous-Tertiary U deposits are comparatively common. They are found in sedimentary basins in Wyoming and in Colorado (USA), in the Karoo Basin in South Africa and in Europe. Roll front U deposits are also present in South Australia in the Frome Embayment field (Elmer et al. 2007). Dahlkamp (1993) subdivided these U mineral systems into three sub-types: tabular/peneconcordant, roll front or roll-type and tectonic-lithologic. In this section, I focus on the roll-type and tabular/peneconcordant sub-type. A review of genetic concepts of sandstone-hosted and roll front U systems is provided by Adams (1991).

Roll front U deposits are elongate in plan view and exhibit a characteristic crescent-shaped cross-section normal to their length (Fig. 13.5). The ore zones occur along curvilinear or irregular interfaces between tongues of altered sedimentary rocks and unaltered and reduced organic-rich sedimentary rocks. The altered rocks behind the roll front are commonly red, brown or yellow in colour due to the presence of hematite or goethite, forming liesagang-style rings. In other instances the rocks behind the roll front are bleached white. The concave side of the roll is usually sharp and define the limits of the richest ore, whereas the convex side has diffuse boundaries that fade into the unaltered rocks. Four variants of roll front deposits have been recognised (Morton 1979): (1) Wyoming type, in which the reductants and U complexes are within the host rocks and consist of plant debris, biogenic H_2S, pre-existing pyrite, marcasites, chalcopyrite; (2) Coast Plain type, in which the mineralisation is hosted in marine and coastal bar sediments and the ore is generated by the incursion of H_2S into U^{6+}-bearing aquifers; (3) Entrada-type, found in the Entrada

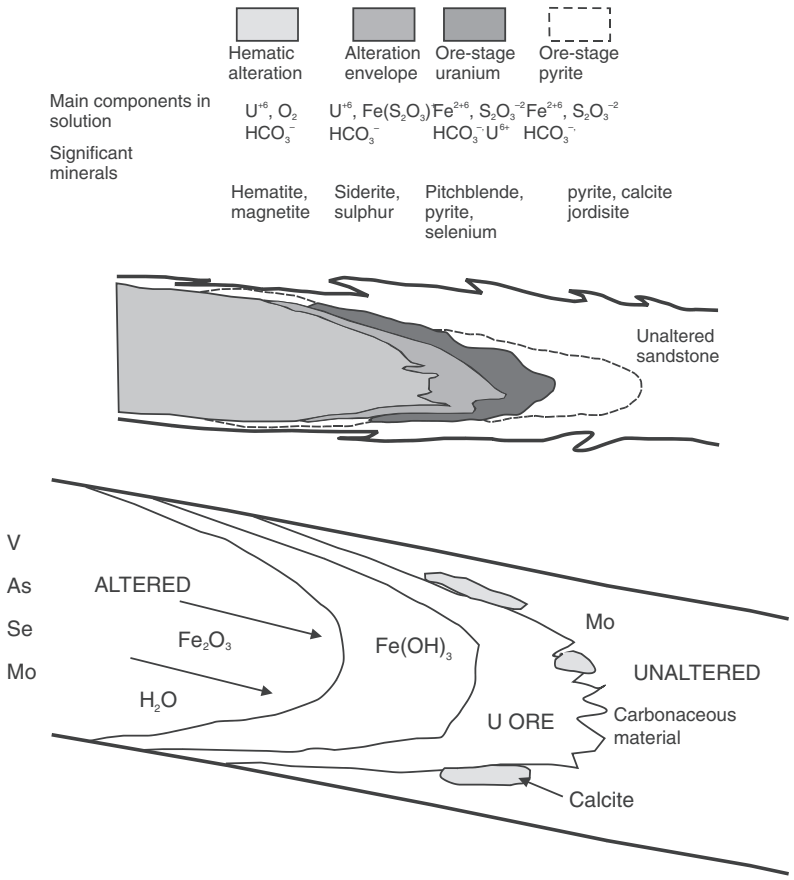


Fig. 13.5 (**A**) Geometry of roll front U mineral system with alteration zones and metal components (after Dahlkamp 1993); (**B**) schematic distribution of ore elements in a roll front U system

Sandstone in the Colorado Plateau, are V-rich and the reductants were introduced into the uraniferous aquifer, causing reduction of U^{6+}; (4) Colorado Plateau marginal rolls, developed on the margins of larger tabular orebodies; host rocks are fluvial, channel-margin, organic debris-rich fine-grained sandstones.

The tabular/peneconcordant U deposits are lenticular and quasi-concordant with host strata. Classic localities in the USA for these deposits are the Uravan Belt in Utah and Colorado, the Lisbon Valley district in Utah and the Grants district in New Mexico. They tend to form linear belts several tens of kilometres long and several kilometres wide. They are elongate in plane view and tend to conform to the trend of the host palaeochannels. The U mineralisation is in grey to black carbonaceous lithologies. As for the roll front type, two principal

genetic types are recognised for the tabular/peneconcordant deposits. One in which deposits are formed from *in situ* reductants and complexing agents, such as plant debris, bacterial communities producing H_2S, humate solutions and Fe oxyhydroxides. In the other, deposits are generated by introduced reductants, such as H_2S, hydrocarbons and Fe^{2+}. An example of peneconcordant U mineral systems, other than those in the USA, occurs in the Roman Volcanic Province (Italy; Avanzinelli et al. 2007), where alkaline volcanic rocks have U-bearing layers (Locardi 1973). The mineralisation is hosted in pyroclastic and epiclastic rocks that are extensively clay-altered and impregnated with sulphides. Uranium tenors range from 100s to 1000s ppm, and the mineralised peneconcordant layers are laterally quite extensive. According to Locardi (1973), the mineralisation was formed by groundwaters that leached U from the pyroclastic and epiclastic rocks, which then became reduced by volcanic H_2S and precipitated U minerals. The host rocks are bleached and altered to opaline silica and clay.

The following criteria are required for the generation of tabular/peneconcordant U deposits: (1) a source of U^{6+}; (2) groundwaters with Eh-pH that allows the transportation of species, such as UO_2^{2+}, $UO_2(OH)_3^-$, $U(OH)^{3+}$, UO_2OH^+, $UO_2(HPO_4)_2^{2-}$, $UO_2(CO_3)_2^{2-}$, $UO_2F_3^-$, $UO_2F_2^+$, UO_2SO_4 etc.; (3) a permeable aquifer or a fluvial or limnic system; (4) reactive minerals or compounds that might capture U, such as zeolites, humic acids or humates of low rank ($<100^\circ C$), clays, chlorites; (5) a mechanism that allows the reduction of U^{6+} to U^{4+} in the solutions, for instance H_2S from sulphides or organic degradation, Fe^{2+} released from the breakdown of sulphides, bacterially generated CH_4 or H_2.

Genetic models applicable to USA deposits suggest that the source of U was provided by volcaniclastic rocks, from which U was dissolved and transported as a bi-carbonate complex and precipitated as oxide in a reducing environment. This could also have been the case for the occurrences in the Roman Volcanic Province, whereas in South Australia the primary source of U was likely the HHP granites in the region (Elmer et al. 2007). In all cases, at redox fronts the oxidised U encounters a reducing agent and is precipitated as uraninite.

13.3.4 Time-Bound Character of U Mineral Systems

The time-bound character of some uranium mineralisation is a striking feature (Fig. 13.6, see also Fig. 3.8). This was recognised and discussed by Toens and Andrews-Speed (1984), Marmont (1987) and reviewed by Dahlkamp (1993) and Groves et al. (2005). In contrast to the earlier U mineralisation of the Witwatersrand and Elliot Lake basins, in which the uranium was mechanically transported as detrital uraninite grains thanks to an oxygen-poor atmosphere, the Proterozoic U mineralisation developed in response to atmospheric oxygenation. If one considers only hydrothermal U concentrations in the Earth's crust, then the physico-chemical conditions for the dissolution, transport in solution and deposition of U must have been particularly favourable at least

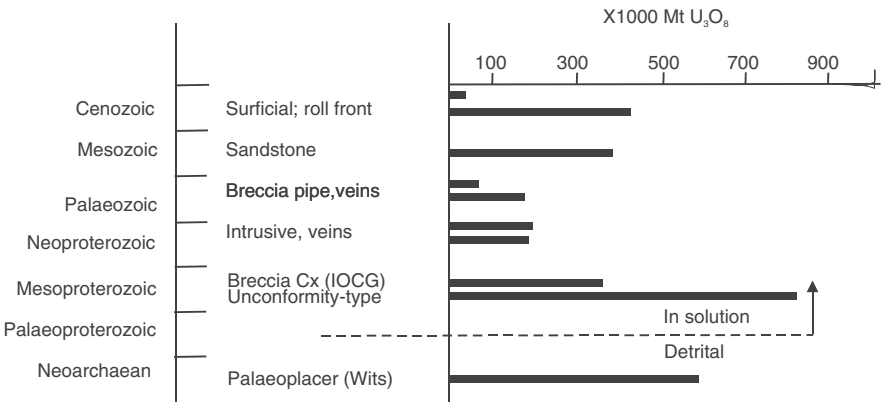


Fig. 13.6 Time-distribution of principal U mineral systems. This diagram is semi-quantitative and only designed to portray the time-bound character of uranium, the bars represent past production and total uranium resources as shown in Dahlkamp (1993)

twice in the geological history of our planet. The first time between ~1.64 and 1.35 Ga, when the majority of unconformity-related U and Olympic Dam style deposits were formed, and the second time between the Permian-Cretaceous and Cenozoic (Neogene to Recent) when sandstone-hosted (or roll front) and phosphorite U mineralisation were developed. It is estimated that unconformity-related deposits have about 30% of the global U resources (Ruzicka 1996) and the associated Proterozoic sedimentary cycles were established by ~2.0 Ga following supercontinent assembly, lower mantle plume activity and increasing continental freeboard all contributing to the accumulation of extensive siliciclastic sediments in fluvial and lacustrine environments (Kerrich et al. 2005). Mesozoic and Cenozoic roll front U deposits also account for about 30% of the global U resources and these were formed as a result of development of extensive upland forest cover and intracratonic basins with both oxidised and reduced fluvial and lacustrine sedimentary accumulations, followed by tectonic uplifts, which allowed rainfall and strong hydraulic gradients (Nash et al. 1981).

13.4 Concluding Remarks

This book concludes with a brief panoramic on uranium mineral systems to encourage research and allow more geoscientific knowledge in a subject that has been neglected in the recent past, largely for misguided political reasons. There is now a world-wide upsurge in uranium exploration, even in countries where uranium mining is, for the moment, not allowed. Rising petrol prices, apparently unstoppable, concern on greenhouse gases emissions, make nuclear power generation an attractive proposition and, as mentioned in the Introduction, there are countries such as France that make extensive use of nuclear power to

generate electricity, which is then purchased by neighbours where nuclear power is not allowed.

There are several types of U mineral systems, but only a few are at present economically viable. These include quartz conglomerate-hosted, unconformity-type, alaskite-hosted and sandstone-hosted, although others may well become viable in the future as demands increase.

Mesoproteozoic unconformity-associated U deposits of the Athabasca Basin in Canada and those of northern Australia such as the Ranger, Jabiluka, Nabarlek in the Pine Creek geosyncline, contain most of the U resources in the world. An oxidising atmosphere allowed the dissolution of U and its transport as hexavalent uranyl complexes, from either the underlying basement rocks, or the basins' sequences. The U was deposited and re-distributed during several cycles by circulating hydrothermal fluids of meteoric-connate origin, with precipitation occurring near and below an unconformity where these oxygenated fluids encountered a reducing environment such as carbonaceous material. A common feature of alaskite and unconformity-related U systems is the fact that basement rocks are commonly enriched in U and that this enrichment is due to high-grade metamorphism and partial melting of fertile sedimentary and granitic rocks, due to the strongly lithophile behaviour of the U element.

References

Adams SS (1991) Evolution of genetic concepts for principal types of sandstone uranium deposits in the United States. Econ Geol Monogr 8: 225–248

Ahmad M, Wygralak AS, Ferenczi PA (1999) Gold deposits of the Northern Territory. Northern Territory Geol Surv Report 11

Avanzinelli R, Elliott T, Tommasini S, Conticelli S (2007) Contsraints on the genesis of potassium-rich Italian volcanic rocks from U/Th disequilibrium. J Petr, doi:10.1093/petrology/egm076

Berning J (1986) The Rössing uranium deposit, South West Africa/Namibia. In: Anheusser CR, Maske S (eds) Mineral deposits of Southern Africa, vol II, Geol Soc S Afr, pp 1819–1832

Cathelineau M, Cuney M, Boiron MC, Derome D, Fabre C, Richard A, Banks DA (2007) Fluid mixing and uranium deposition in unconformity type deposits (Saskatchewan, Canada, Northern Territory, Australia). In: Andrews et al. (eds) Digging deeper., Proceed Ninth Biennial SGA Meet, Dublin 2007, vol 2, pp 1137–1140

Cuney M, McCready A, Annesley I (eds) (2007) Uranium deposits. In: Andrews et al. (eds) Digging deeper., Proceed Ninth Biennial SGA Meet, Dublin 2007, vol 2, pp 1105–1212

Dahlkamp FJ (1978) Geologic appraisal of the Key Lake U-Ni deposits, Northern Saskatchewan. Econ Geol 73: 1430–1449

Dahlkamp FJ (1993) Uranium ore deposits. Springer-Verlag, Berlin

Ellsworth HV (1928) I. Thucolite, a remarkable primary carbon mineral from the vicinity of Parry Sound, Ontario. II. Cytolite intergrowth associated with the Parry Sound thucolite. Am Miner 13: 419–441

Elmer FL, Cleverley JS, Potma W (2007) Reactive transport modelling of roll front (sandstone) uranium deposits. In: Andrews et al. (eds) Digging deeper., Proceed Ninth Biennial SGA Meet, Dublin 2007, vol 2, pp 1157–1160

Evans EL (ed) (1986) Uranium deposits of Canada. Can Inst Min Metall Spec Vol 33

Faure G (1986) Principles of isotope geology, 2nd edn. John Wiley & Sons, New York
Groves DI, Vielreicher RM, Goldfarb RJ, Condie KC (2005) Controls on the heterogenous distribution of mineral deposits through time. Geol Soc Lond Sp Publ 248: 71–101
Gustafson LB, Curtis LW (1983) Post Kombolgie metasomatism at Jabiluka, Northern Territory, Australia, and its significance in the formation of high-grade uranium mineralisation in lower Proterozoic rocks. Econ. Geol. 78: 26–56
Hein KAA (2002) Geology of the Ranger Uranium Mine, Northern Territory, Australia: structural constraints on the timing of uranium emplacement. Ore Geol Rev 20: 83–108
Hoeve J, Sibbald TI (1978) On the genesis of Rabbit Lake and other unconformity-type uranium deposit in Northern Saskatchewan, Canada Econ Geol 73: 1450–1473
Hosteler PB, Garrels RM (1962) Transportation and precipitation of uranium and vanadium at low temperatures, with special reference to sandstone-type uranium deposits. Econ Geol 57: 139–167
Jackson DG, Andrew RL (1990) Kintyre uranium deposit. In: Hughes, FE (Ed.), Geology of the mineral deposits of Australia and Papua New Guinea. Aust Inst Min Metall Monogr 14: 653–658
Jacob RE, Corner B, Brynard HJ (1986) The regional geological and structural setting of the uraniferous granitic provinces of southern Africa. In: Anheusser CR, Maske S (eds) Mineral deposits of Southern Africa, vol II, Geol Soc S Afr, pp 1807–1818
Jefferson CW, Thomas DJ, Gandhi SS, Ramaekers P, Delaney G, Brisbin D, Cutts C, Quirt D, Portella P, Olson RA (2007) Unconformity-associated uraniumdeposits of the Athabasca Basin, Saskatchewan and Alberta. Geol Ass Can Sp Publ 5: 273–305
Kaye GWC, Laby TH (1986) Tables of physical and chemical constants and some mathematical functions, 15th edn, Longmam Group, London, Bath Press, Avon
Kerrich R, Goldfarb RJ, Richards J (2005) Metallogenic provinces in an evolving geodynamic framework. Econ Geol 100th Ann Iss: 1097–1136
Kinnaird JA, Bowden P (1987) African anorogenic alkaline magmatism and mineralization – a discussion with reference to the Niger-Nigerian province. Geol J 22: 97–340
Kinnaird JA, Nex PAM (2007) A review of geological controls on uranium mineralisation in sheeted leucogranites within the Damara Orogen, Namibia. Trans Inst Min Metall, Appl Earth Sci B, 116: 68–85
Langmuir D (1978) Uranium solution-mineral equilibria at low temperature with application to sedimentary ore deposits. Mineral Ass Can 3: 17–55
Laznicka P (2006) Giant metallic deposits – future resources of industrial metals. Springer, Berlin
Locardi E (1973) Mineralizzazioni ad uranio in vulcanite quaternarie del Lazio. Bull Soc Geol It 92: 541–566
Maas R (1989) Nd-Sr isotope constraints on the age of unconformity-type uranium deposits in the Alligators Rivers uranium field, Northern Territory, Australia. Econ Geol 84: 64–90
Mao JW, Bierlein FP (eds) (2005) Mineral deposits research: meeting the global challenge, Proceed Eigth Bien SGA eeting, Beijing, vol 1
Marmont S (1987) Unconformity-type uranium deposits, Ore deposit models #13. Geosci Can 14: 219–229
Miller McGR (1983) (ed) Evolution of the Damara orogen of South West Africa/Namibia. Geol Soc S Afr Spec Publ 11
Morton RD (1979) Uranium geology – An introductory short course for industry. Course Notes, Rhodes University, Grahamstown, South Africa
Mwenifumbo CJ, Bernius G (2007) A th rich crandallite group mineral: a source of thorium enrichment in the Athabasca Group, Saskatchewan. Geol Ass Can Sp Publ 4 and Saskat Geol Soc Sp Publ 18: 521–532
Nash JT (ed) (1978) Special issue on uranium geology in resource evaluation and exploration. Econ Geol 73(8)
Nash JT, Granger HC, Adams SS (1981) Geology and concepts of genesis of important types of uranium deposits. Econ Geol 75th Anniv Vol, pp 63–116

Newton FT, Collings SP, Little BC (2006) Nuclear power update. SEG Newslett 67: 1–15
Nutt CJ (1989) Chloritization and associated alteration at the Jabiluka unconformity-type uranium deposit, Northern Territory, Australia. Can Mineral 27: 41–58
Organisation for Economic Development (OECD), Nuclear Energy Agency and International Atomic Energy (2004). Uranium 2003: Resources, production and demand, Nuclear Energy Agency, Organisation for Economic Development, 288pp
Pirajno F, Sheppard S, Groenewald PB, Johnson SP (2008) Mineral systems in the Gascoyne Complex, Western Australia. Geol Surv West Aust Record 2008/2: 4–7
Pirajno F, Bagas L (2008) A review of Australia's Proterozoic mineral systems and genetic models. Precambr Res, doi:10.1016/j.precamres.2007.05.008
Plant JA, Simpson PR, Smith B, Windley BF (1999) Uranium ore deposits products of the radioactive Earth. Rev Mineral 38: 255–319
Polito PA, Kyse, TK, Thomas D, Marlatt J, Drever G (2005) Re-evaluation of the petrogenesis of the Proterozoic Jabiluka unconformity-related uranium deposit, Northern Territory, Australia. Mineral Depos 40: 257–288
Ruzicka V (1996) Unconformity-associated uranium. Geol Surv Can, Geology of Canada 8: 197–210
Shultis JK, Faw RE (2002) Fundamentals of nuclear science and engineering. CRC Press, Taylor and Francis, Boca Raton, London
Toens PD, Andrews-Speed CP (1984) The time-bound character of uranium mineralising processes with special reference to the Proterozoic of Gondwana. Precambr Res 25: 13–36
Turpin L, Leroy JL, Sheppard SMF (1990) Isotopic systematic (O, H, C, Sr, Nd) of superimposed barrenand U-bearing hydrothermal system in a Hercynian granite, Massif Central, France. Chem Geol 88: 85–98
Wallis RH, Saracoglu N, Brummer JJ, Golightly JP (1986). The geology of the McClean uranium deposits, northern Saskatchewan In: Evans EL (ed) Uranium deposits of Canada. Can Inst Min Metall Spec Vol 33: 193–217
Wilde AR, Wall VJ (1987) Geology of the Nabarlek uranium deposit, Northern Territory, Australia. Econ Geol 82: 1152–1168
Wilde AR, Bloom MS, Wall VJ (1989) Transport and deposition of gold, uranium and platinum-group elements in unconformity-related uranium deposits. Econ Geol Monogr 6: 637–660

Index

Note: Page numbers in *italics* refer to citation in figures and/or tables

A

A-type granite, magmatism, xxviii, 107, 166, 168, 175, 177, 190, 192, 198, 206–211, 275, 280–281, 290, 304, 305–307, 315, 318, 335, 381, 390, 400, 467, 571, 573, *885*, 945, 991, *1227*
Abitibi, xxix, 77, 188, *191*, 260, 581, 583, 664, 683–685, 887, 920–921, 924
Abra deposit, xxix, *276*, 703–705, 714
Afar Triangle, 750–751
Aggeneys, 810–814
Alaska, xxiii, 171, 260, 262, *263*, 358, *782*, 808, 888, *892*, 913, 1103, 1191
Alba Patera, 1134, *1135*, 1140, 1142
Alkali metasomatism, 89, 91, 95, *96*, 104–107, 218, 220, 224, 241, 286, 296, 303, 304, 305, 307, 360, 362, 389, 771, 788, 890, 945, 1006, 1099, *1101*, 1112, 1121, 1195
Alligator River U field, 1232
  Jabiluka and Nabarlek, 1233–1234
Anatolia (Turkey), 456, *457*, 458, *462*
Anorogenic, xxiv, xxvii, 132, 157, *167*, 187–188, 190, *191*, 194–196, 199, 205, 220, 228, 236, 258, 262290, *308*, *310–311*, 315, 328, 401, 467, *747*, 785, *787*, 991–992, 1112, 1221
  Alkaline intrusions, 157, 168
  Ring complexes, 73, 106–109, 206, 280, *282*, *284*, 285–289, *290*, 296, 303, 306, 340, 398,
Antarctica, 14, 197, 786, *912*, 1155–1156, 1191, 1197
Arsia Mons, 1140, 1141, 1144, 1160
Ascraeus Mons, 1140, 1141
Asgat-Ozernoe, 278–280
Asteroid(s), 3, 6, 8, 850, 1030, 1034, 1039, 1097, 1098, 1132, 1141–1143, *1164*, 1180–1181, 1193–1194
Atlantis II Deep, *see* Red Sea
Australia, 10, 14, 77, 141, 184, 196, 260, 269, 289, 309, 311, *320*, 460, *782*, 786, 806, 885, *912*, 1198
  Queensland, 269, 1077
  Northern Territory, 136
  South Australia, 135, 155, 190, 198, 312, 995, 1221, 1235
  Tasmania, 687
  Western Australia, *80*, 110, *123*, 133, 137, 154, 181, 187, 197, 262, 275, 297, 302, 419, 486, 492, *554*, 581, 664, 703, 705, 734–735, *784*, 890, 985, 1041, 1065, *1187*, 1198, 1234

B

Bacteria, *see* Microbes
Baikal, 573, 728, *733*, 911, *912*
  Rift system, 1143, 179, 182, 409
  Lake, 14, 181, 497, 500, *734*, 735, 914, 929, *930*,
Banded iron formation (BIF), xxviii-xxix, 9, 51, 76, 141, 169, 179, 192, 195, 198, 323, 684, 709, 713, 730, 734, 746, 781, *787*, 802–803, 809, 811, 843–845, *846*, 847, 849–850, 860, 890–891, 893, 910, 946, 982, 1039, 1049, 1062, 1159, 1187
  Genetic models, 850
  Superior type and Gunflint, 859
Basins, *see* Sedimentary basins
Basin-and-Range province, 181–182, 186–189, 303, 309, 467, 481–482, 484, 575, 895, 945, 1143

Basin-and-Range province (*cont.*)
See also Great Basin
Bayan Obo, xxiv, 187, 303, 306, 311, 328–335, *330*, *333–334*, 340
Berg Aukas, 828–829, *830*, 831–832, 836–839, *839*, 985
See also Breccia pipe
Besshi ore system, 179, 627, 649, 655, 661–663, 676, 714, 809
Bingham, 85, 547–548
Biosignatures, 1187–1194
Biosphere, xxvii, 8, 198, 1027, 1044, 1046–1050
Boiling fluids, 22–23, 36, 40, 41, 48–51, *75*, *79*, 97, 113, *121*, 122–124, 225, 248, 308, 356, 361, 370, 376, 405, *406*, 416, 423, 426, *430*, 433, 434–435, *436*, 438–439, 445–447, 455–456, 480, 486, 494–496, 499, 503–504, 506–509, 512, 552, 599, 602, 608, 613, 630, 665, 673, *700*, 745, 940, *942*, 969, 971, 979, 996, *1053*, 1060, 1100, 1120, 1195
Second (retrograde) boiling, 82, 88, 214, 241, 376, 403, 407,
Brandberg (West; alkaline complex), 136, 250–258, *252*, *253*, *257*, 286, *287*, *290*, 292
Breccia pipe, 82, 114, 116, 124, 132, 178, 206, *215*, 216, 226, 244, 260–261, 269, *360*, 374–375, 377, *400*, 403–405, *406*, 407–414, 418, 431, 443, 477, *537*, 569, 704, *747*, 822, 831, 946, 948, 1222, 1224, *1238,*
Berg Aukas, 836, *839*
Tsumeb pipe, 832, *833*, *839*
Broadlands, *33*, 47, 500–503
Bougainville, 368–369
Broken Hill (Australia), 801–806
Bushveld Igneous Complex, 132, 135, 165–166, 192, 196, 220, 230–238, 262, 273, 275, 298, *299*, 322, 324, *1107*, 1108, 1110

C

Caldera (volcanic, structure), 13, 31, 107, 152, 210, 252, 292–294, 300, 304, *311*, 314, 379, 398, 425, *430*, 447, 448, *449*, 472, 482, *485*, 487, 490, 497, *513*, 619, 632, *635*, 641–643, 647, 662, 665–666, 671–673, *674, 675*, 677, 679, 684, 688, 693, 775, 1051, *1081*, 1083, *1140*, 1157, 1161, 1173, 1179, 1222, 1224
Axial Seamount caldera, 619
Brothers caldera, 637, 639, *641*
Luise Caldera, 446
Uzon Caldera, 499
Valles Caldera, 392, *393*
Waihi Caldera, 448
Yellowstone Caldera, 507–509, 512
Cannakale Volcanic Field, 456, *457*
Candelaria, 336–339
Capricorn Orogen, *see* Orogen
Carbon isotopes, 63–64, 134, 892, 960, 1071, 1186, 1192
Carbonate-hosted ore systems, *see* MVT
Carbonatite, 106–110, 148, *191*, 272, 281, *282*, 285–286, 288, *290*, 292, 296–297, 300, *301*, 303, 309, 335, 587, 596, 743, 867, 962, 1215, 1221–1224
Mountain Pass carbonatite, 303
Palabora (Lolekop) carbonatite, 326, 1224
Carlin (ore deposits; Carlin-style), xxiii, 153, 169, 216, 261, 355, 400, 482, 843, 885, 965–968, 1008
Carlin deposit, 969
Genetic models, 971
Central Asian Orogenic Belt (CAOB), 173, 258, 381, *382*, 387, 427, 592, 597, 598
Century deposit, 799–800
Cerro Rico deposit, 378
Champagne Pool, 31, *32*, 33, *34*, 503, 606, 1060
Chimney (sulphide, vents, smokers), *603*, *617*, *625–628*, *640–641*, 648
Chuquicamata porphyry system, *371*, 372–373
Classification of ore deposits, xxiii, xxv
Climax porphyry system, 392, *393*, 395–396
Cloncurry (IOCG district), 190, 306, *311*, 319, 325
Coastal Volcanic Belt, *466*, 468, 472
Complex ions, xxvii, 44– 47, 50, 178, 434–438
See also Ligands
Continental flood basalts, 183, 188, 192, 195, 285, 281, *310*, 332, 334, 425, 584, 731, 734, 974, 976, 1156
Deccan, 286
Etendeka (Paraná), 290, 314
Ethiopian, 743
Siberian Traps, 310

Copperbelt
Central African, 764, 766, *767*,
Kalahari, 764
Zambian, 764, 770
Coromandel Volcanic Zone, *123*, 448, *449*, *451,*
Cornwall, 238–242, 992
Cyprus Island, 652
Sulphide ores, 653–654

D
Damaraland, 289–292
Decay series of U and Th, *1219*
Delamination (lithospheric, tectonics), 184–186, 571, 573, 574, 575, *886*, 917, 920, 945, 962, *963*
Deuterium, 52–57, *55*, *257*, 325, *441*, 445–446, *470*, *892*, 909, 958, *959*
Dogancilar, *see* Kirazli
Dongchuan, 765
Dresser Formation, 1082, *1084*, *1086*

E
Earaheedy Basin, *276*, *787,* 817, *844*, *846*, *847*, 857, *858*, 860, 985, *1039*, 1112, 1189
East African Rift System, xxix, 14, 38, 179, 182, 187, 281, 282, 288, *320*, 494, 515, *554,* 590, 730, 741–748, *747*, 751, 1133, 1143, 1191, 1202
East Greenland, 417–419
East Pacific Rise, 548, 581, 604, 606, 614, *614*, 615–619, 620. 1052
Ecosystems, xxix-xxx, 31, 38, 581, 599, 714, 1033, 1045, 1047, 1050, 1058, 1063, 1067, 1077, 1079, 1082, *1086*, 1170, 1188
El Indio-Pascua belt, 475–480, *476*, *478*
Epithermal systems, 120–122, 422–426
Active epithermal systems, 493
Alkalic type, 431
Caldera setting, *491*, *495*, *513*,
Classification and models, *428, 432,*
Fossil epithermal system, 426
High sulphidation, 430
Hot spring type *see* Hot spring
Low sulphidation, 429, 484
Etendeka, *291*
See also Continental flood basalts
Erongo (volcanic complex), 286, *287*, *290*, 292–296
Evaporite(s), 10, 11, *12*, 12, 62, 132, 136, 184, 219, 309, 319, 494, 567, 590, 609, 614, 727, *730*, 731, 735, 736, 738, 750, 752, 753, 758, 760, 762, 764, 778, 806, *807*, 816, 817, 826–827, 833, 842, 867, 895, 903, *1004*, 1006, 1040, 1046, 1062, 1154, 1156, 1160, 1191, 1192, 1198
In ore genesis, 837–838
In SEDEX ore systems, 781, 783–785, *796*
Zeichstein evaporate, 779
Extraterrestrial life, 1181–1187

F
Fenite, 89, 106–111, *327*
See also Alkali metasomatism
Fluid inclusions, 38–42, *40*, 244, 266–267, 318, *325*, 335, 370, 389, 403, 445, *700*
Fugacity (oxygen), 26, 28, 29, 213, 228, 414, 427, *437*
Fumaroles, 31, 36–38, 50, 84, 94, 387, 423, *425*, 439, *447*, 490, 495, 496, 499, 500, 504, 507, 632, 745, 751, 1161

G
Gamsberg, *810*, *812–813*
See also Aggeneys
Gangdise porphyry belt, *410*, 412–413
Gascoyne Complex, 110, *123*, 133, 275, *276*, 553, *554*, 555, 703, 1223
Gas Hydrates, xxx, 1065, 1067, 1069
Hydrate Ridge, 1068
Gawler Craton, 198, *311*, 312, *313*, 315, 319, 321, 786, *788*
Geothermal system, *see* Epithermal
Geysers-Clear Lake, 505–507
Granular iron formation (GIF), 198, 713, 844, *847*, 857, 859, 860, *1113*, 1115
Great Basin, 181, 187, 189, 424, 481–484, *485*, 972
See also Basin-and-Range
Great Oxidation Event (GOE), 1041–1044
Greisen, 101, 206, *217*, 218–230, *222*, *223*, *226*, 248
Endogreisen, 231
Exogreisen, 236, 246
Groundwater, *4*, 6, 15–17, 120, 319, 356, 407, 422, 439, 455, 472, 496, 503, 514, 736, 739, 745, 778, *818*, 987, 993, 997, 1073, 1136, 1144, 1149, 1154–1155, 1158, 1160–1162, 1194, 1200, 1223, 1237
Guaymas Basin, 179, 609, 627, *630*

Gulf of California, 615, 616, 620, 627–629, *630*, 661
Gusev crater, 1136, 1145, 1195

H
Haib porphyry system, *357*, 421–422
Hauraki, 448–453
Hemlo deposit, 920
High Heat Production Granites, 990
  Central Australian Heat province, 995
  Heat production constants, 991
Helium isotopes, 57–61, 413, 511–512, 895, 961
Hitalba Suite, 315–316
Hot spring, xxvii, 9, 16, 19, 22, 30–33, 38, 42, 55, 94, *121*, 142, 287, 297, 303, 411, 423, *425*, *430*, 431, 439, 442, 446, 447, 489, 494, 499, 501, 581, 599, 613, 631, 730, 735, 738, 907, 941, *942*, 973, 1027, 1031, 1038, 1045, 1050, 1058–1063, 1077, 1100, 1191, 1222
  in East African rifts, 745–748, *749*, 750
  Hot spring-type epithermal system, *432*, 433
  on Mars, 1133, 1158, 1161, 1200
  Paralana hot springs, 995, *996*
  Red Sea, 760, 867
  Seafloor/submarine hot springs, 654, 662, 671, 1034
  Yellowstone National Park hot springs, *508*, 509–511
    see also Yellowstone National Park
  See also epithermal
Huangshan Complex, *471*
Hydrogen, 1, 17–18, 23, 25, 51–54, 111, *1030*, 1033, 1036, 1048, *1055*, 1057, 1153, 1182, 1185
  Ion metasomatism, 91–92, 127, 218, 541
Hydrolysis, 1, 17–18, 51, 91, 111, 128, 642, 1073
Hydrosphere, xxvii, xxix, 2–3, 5–7, 9, 13, 198, 850, 902, 1028, 1046, 1151
Hydrothermal (system, definition), 74, 80–86
  Breccia, 122–124, *236*,
  Breccia pipe, 269–272
  Hydrothermal systems and life, 1168
  on Mars, 1152, *1157*
  on Titan, *1178*
  Sudbury, 1103
  Terminology, *98–99*
  Uranium, 1220, *1222, 1230, 1238 (time distribution)*
  Vein, 76–79
Hydrothermal Alteration, 90–91, 94–94, *93*
  Alteration pipe, 142, 608, 665, 673, *676*, 683, 684, 689, 693, 696
  Alteration in Kuroko systems, 125
  Argillic, 51, *83*, *96*, 103–104, 115, *118*, 120, *215*, 224, *363*, *364*, 384, 399, 416, 445, 455, 459, 541, *546*, 911, 966, 968, 1078, 1161, 1228
  Carbonate, 136–137
  Greisen alteration *see* Greisen
  Hematitic, *123*, 135, 316, 900, 1071
  Hydrogen metasomatism, 91
  Hydrolitic, 91, *357*, 541, 1002
  in impact structures, 1114–1117, 1119, 1124
  Phyllic (sericitic, QSP), 83, 95, *96*, *99*, 101–103, *112*, 114, 116, 147, 240, 246, 272, *360*, 370, 389, 402, 420, 459, *546*, 1078,
  in porphyry systems, 111
  Potassic, *83*, *96*, 97–101, 105–106, *112*, 115, *118*, 308, 336, *361*, *364*, 370, 375, 384, 403, 420, 455, 548, 699, 771, 924, 1001, 1124
  Serpentinisation, 133, 624, 1043, 1179, 1194
  Terminology, *98–99*
  Skarn type *see* Skarn
  Talc-carbonate, xxvii, 133, 910
  Tourmalinisation, *123*, *217*, 132, 241, 295

I
Iberian Pyrite Belt, 197, 693–697
  Neves Corvo, 697
  Rio Tinto, 697
  Model, *702*
Impact structures (meteorites)
  Lockne, 1105
  on Mars 1162, *1195*, *1196*, *1197*
  Shoemaker, 1112
  Sudbury, 1003
  Vredefort, 1106
  Woodleigh, 1121
  Yarrabubba, 1119
Inglefield Land (Greenland), 997
  Rust zones and ore genesis, 1002
Iron formations, *see* Banded and granular
  Genetic models, 850–857

Iron oxide copper gold (IOCG), 166, *167*, 168, 190, 192, 198, 206, 306–311, *313*, *320*, 328, 336, 1221, *1225, 1238*
Districts, *310*
Island arcs, 14, *30*, 117, *168*, 171, 173, *209*, 306, 358, 632, *633–636*, 368–369, 390, 465, *538*, 599, 606, 632, 683, 1077
Izu-Bonin arc, 642
List of volcanic arcs, *634*

J
Jinduicheng porphyry deposit, *357*, 402–403
Juan de Fuca, 585, 595, 606, 619–620, 647, 661, 1068

K
Kaapvaal Craton, 192, 196, 809, 844, *862*, 888, 910, 981, 1038, 1106, 1107
Kalguta, 258–259
Kalahari Manganese field, 845, 862–864
Kamchatka peninsula, 497–499
Kanowna Bell, 492–493
Kemptville, 248–249
Kermadec-Tonga, 637, *638*
Kidston, 269–272
Kilba Well prospect, 555
Mineral assemblages, *557*
Kimberlite, 288–289
King Island, 552–553
Kirazli, 459–461
Klein Aub, 775–778
Kombat (Otavi Mountain Land), 834–836
Kruidfontein, 287, *299*, 300–303
Kupferschiefer, 190, 727, 730, 736, 761–765, 779, 974
Kuril, *498*
See also Kamchatka peninsula
Kuroko ore systems, 125–126, 197, 665, *667*, *672*, *682*
Kuroko deposits in Japan, 679

L
Ladolam, 442–445
Lamproite, 288–289
Lau Basin, 169, 632, 637, 644
Lead isotopes, 63, 837, 842, 950
Leimengou, *400*
Lena goldfield (Sukhoi Log), 929
Lennard Shelf, 817, 819, 840, *841*, 842
Life on Earth, 1037–1041
Ligands, 44–47, 434–438
Lihir island, *443*
See also Ladolam
Limousin (Massif Central), 1228
Lockne, *see* Impact structures
Lode Au (orogenic/mesothermal), *42*, 262, 493, 559, 888, *889*, 910, 917, 919, 961
Alteration, *939*
Golden Mile, 917, *918*
in Jiadong peninsula, 956
Orogenic lodes, 909
in New Zealand, 935
Lost City, 623–624, *625–626*
Lufillian arc/orogen, 197, *310*, 560, 741, 766, 780, 815

M
Macraes Flat (Round Hill), 938
Magellan deposit, 985–989
See also Nonsulphide
Malanjkhand porphyry, 420–421
Manganese oxide ore, 861–864
See also Iron formation
Mantle plume, *180*, 187, *191*, 282, 290, *320*, 713, 1139
Martha Hill, 453–456
Matchless Amphibolite Belt, 655–656
Gorob, 660
Otjihase mineralisation, 657–659
McArthur River (and HYC), 792–796
Metalliferous sediments, 864–866
Black shales, 974
Metamorphism
of altered rocks, 137–142
hydrothermal, 74, 124, 130, 650, 1082
metamorphic minerals, *139–140*
metamorphic fluid generation, 895–901
ocean floor, 127, 599
Metasomatism
Potassic, 88, *100*, 106, 331
Sodic, 104, 305, 1100
Metasomatic reactions in skarns, 542
See also Hydrothermal alteration
Microbes (microbial life/bacteria), 32, 33, 745, 825, 847, 1025, *1029*, 1033, 1047, 1051–1058, 1060, 1062, 1070, 1186, 1192, 1194, 1200, 1217, 1237
Bacteria in ore genesis, 1046
Glossary of terms, 1027
Metabolic processes, *1055–1056*
Microbial mats, 503, 618, *1187*
Oxidising, 38, 61–62, 1048, 1062

Microbes (microbial life/bacteria) (*cont.*)
Photosynthetic, 38, 849, *854*, 1063
Reducing, 38, 61–62, *667*, 753–754, 794, 980
in the weathering profile, 1064
Mid ocean ridge, 178, *209*, 583, 584–586, *586*, *587*, 589, 592, 596, 599, 613, 616, 662, *788*, *848*, 864, 1051, 1169
See also Spreading centre
Mineral deposit
definitions, xxi, xxii
See also Ore deposit
Missouri, 15, 44, 306, *311*, 737, 815, 819
Moina, 551
Mount Bischoff, 244–248
Mount Isa, *311*, 319, *782*, *784*, 786, *787*, 788, *789,* 791, *792*, *795*, 796–799, 801, 1232
Mount Lyell, 687, *688*, 691, *692*
Mount Read Volcanics, 687–688, *690*
Mud volcanoes, 1071–1073
Muruntau deposit, 927
MVT (Mississippi Valley type), 170, 171, *730*, *769*, 819–820
Alpine type, 821
Irish type, 823
Otavi field (Mountain Land), *769*, 828–832
Viburnum Trend, 819

N
NASA acronyms, *1146*
Navachab, *547*, 560–564
Neodymium (Samarium), 259, 307, 328, 412–413, 960
New Zealand, *32*, 36, 38, *43*, *123*, 134, 423, 426, 448, 500, *640*, 866, 935, 1200
Noble gas isotope systematics, *see* Helium isotopes
Nonsulphide ore systems, xxx, 818, 828, 981, 983–985, 989, 1008
Genetic models, 982
Noranda, 683, 684–687
North China Craton, 329, *330*, 331–332, *334*, 381, 399, 566–567, *571*, 913, 944, 957, 961, *992*

O
Oceanic crust, 126–131, 590
Ocean floor, 583, 586, 588, 592, 864, 1034, 1065
Olympic Dam, *311*, 312–319
Olympus Mons, 1135, 1137, *1140*, 1158
Ophiolite, 592, 596–599
Samail ophiolite, 649
Ore system, *98*, *167*, 192, *216*, 218, 285, *308*, 362, 403, *425*, 627, 662, 688, *729*, 736, 781, *789*, *796*, 808, 825, 887, 981, 1221, *1225*, *1230*
Orogen, orogenesis, 175, *176*, 554
Capricorn orogen, 275, *276*, *554*, 703
Central China Orogen, 573
Collisional, *170*, 174, 175
Damara orogen, 137, 184, 250, 257, 272, 560, *562*, 655, *767*, *769*, 775, *812*, 829, 838
Irumide, 197, *769*, 773–775, 809
Oslo graben, *see* Rifting
Otavi, *see* MVT
Ozernoe, *see* Askat-Ozernoe
Oxygen isotopes, 52–57, *55*, 151–153, *257*, 266, 318, 325, 328, 338, *386*, 402, *441*, 445–446, *470*, *700*, 771, *892*, 909, 928, 958, *959*
Oyu Tolgoi, 381, 383–387

P
Palabora, 283, *287*, *299*, 307, 326–328
Panasqueira, 242–244
Panguna, 368–370
Panorama district, 664, 709, *710*
Panspermia, 1030–1031
Passive margin, 178, 192
Pavonis Mons, 1140, *1141*
Permeability, 15, *16*, 75
Pilanesberg, *287*, 298, *299*
Pilbara, 10, 196–197, 486, 664, 705, *706*
Pilgrim's Rest, *see* Sabie-Pilgrim's Rest
Pipe, *see* Breccia pipe
Porphyry system
Alkaline porphyry, *417*
Classification, *358*
Distribution, *359*, *368*
Lowell-Guilbert model, *361*
Cu-Au, 368–370
Cu-Mo, 370, 420, 421
Mo, 117–119, 371, 396
Sn-Ag, 376
System, 111, 356
Alteration, *112–113*

Q
Qinling orogen, 399, 408, 565, 567, 573, 944, 946, *951*, 954, *956*, 965

R
Rapakivi granite, 191, 210
Red Beds, 191, 761, 762, *763*, 775, 824, 849, 1041, 1049, 1230
Red River fault, 413
Red Sea, 179, 187, 283, 583, 590, *591*, 614, 698, 728, 730, 736, 741, 750–752, 806, *812*
  Atlantis II Deep, 752, 756–760, *758*
  Metalliferous sediments, 134, *755*, 760
Redox, 24–26, *27*, 198, 205, *216*, 435, 758, *1053*, 1214
Reefton goldfield, 935
Remote sensing, 153–156
Rift, rifting
  Baikal rift system *see* Baikal
  Continental, *12*, 179, *180*, 181–184
  African rifts, *744*
  Evolutionary stages, *730*
  on Mars, 1139
  Oslo graben (rift), 396, *397*, 398
  Passive and active, 182
  Rio Grande rift, *393*
  Volcanic rifted margins, 390, 517
Ring complexes, *see* Anorogenic
Rodinia, 195–197
Roll-front (uranium), 17, 736, 988, 1223, 1235
Rooiberg, 236–238
Rosebery, 142, 687
Rössing (Namibia), 1225
Roxby Downs Granite, 316

S
Sabie-Pilgrim's Rest, 273–275
Salton Sea, 513–515
Samail, *see* Ophiolite
San Juan volcanic field, 152, 392, *393*
Scheelite Dome, 262–268
Seafloor hydrothermal system, 601, 603, *607*, 610, *612*, *628*, 647, *667*, 976, 1033, 1051, *1067*
Seamount, *587*, 588, 599, 616, 647–648
  Axial Seamount, 619
  Conical, Seamount, 61, 443, 600, 663
  Emperor Seamount, 588
  MacDonald Seamount, 588, 1052
Seawater, 9, *11*, 12–13, *447*, *628*, *667*, 670, *701*, *854*, 976
SEDEX (sedimentary exhalative), 165, 190, 196, 727
  Deposits, *782*
  Mount Isa type (MIT) and Broken Hill type (BHT), 806–808
  Ore systems, 781
  South African, 809
Sedimentary basin, *729*, 736, *740*
  Classification, *732–733*
  Evolution, *763*
  Rift basins, *734*
Shanggong Au lodes, 950
Siberian Craton, *930*
Skarns, 119–120, 216, 265–266
  Alteration, 540–546
  Characteristics, *536–537*
  Common minerals, *539*
  Gold skarns, 558–561
  Iron skarns, 569
  Molybdenum skarns, 568
  Sn-W skarns, 550
  Tectonic settings, *538*
  Zinc skarns, 567
  Yangzte River Valley skarns, 570–573
Skorpion deposit, 989
  See also Nonsulphide
Smokers, *see* Chimneys
Solar system, 3, 7, 1025, 1030, 1097, 1131, 1138, 1163, 1170, 1174, 1181, 1184, 1185, 1188
South China Fold Belt, 463, *464*, *466*, 473
Spinifex Ridge, 419–420
Spreading centre (ridge), *128*, 178, 599, 610, 615, 619, 621
Strelley Pool Chert, 490
Sudbury, 1098, 1102–1103, *1104*
  See also Hydrothermal
Sulphide chimney, *see* Chimney
Sulphur isotopes, 61–62, 266, 338, *385*, *470*, 605, *666*, 678, *795*, 797, 928, 950, *951*, *1053*
Sulphur Springs deposits, 1079
Supercontinent, *191*, 192–199, *912*
Sukhoi Log, *see* Lena Goldfield

T
Tanganyika (Lake), 515–516, 741, 748–750, *749*
Taupo
  Lake, 30
  volcanic zone, *14*, 32, 500–504
Tennant Creek, 321
Terrestrial planets, 3, 7, 192, 1182

Tharsis Montes (province), 1133, 1134, 1139, 1140, 1144, 1154, 1157
Tibet, 409, *410*, *411*
Tieluping deposit, 948
Tombstone-Tungsten Belt, 268–269
Trans-Atlantic Geotraverses (TAG), 614, 621–622
Transform fault, 586–587
Travertine, 36, 510
Tree of Life, *1029*
Tsumeb, *769*, 832–834
  See also Breccia pipe
Tubeworms (*vestimentifera*), 602, 618, 1052, 1070, 1071, 1077
Turkey, *see* Anatolia
Tuwu porphyry deposit, 387–390

U
Unidirectional solidification textures (UST), *217*
Urad-Henderson porphyry system, 392, *393*, 394–395

V
Valles Marineris, 1133, *1136*, 1141, 1143, 1149, 1157, 1191
Veining
  Quartz veins, *78–79*,
  Veins in metamorphic rocks, 907
Vergenoeg, 322–325
VMS (volcanogenic/volcanic-hosted/volcanic associated massive sulphides), 76, *99*, 124, 145, 153, 169, 188, 197, *276*, 381, 581, 583, 603, 632, 649, 662–665, 670, 672, 673, *676*, *675*, *676*, 677–679, 683, *703*, 711, 1049, 1077, 1079–1082, 1104
  Iberian type *see* Iberian Pyrite Belt
  Kuroko type *see* Kuroko
  Noranda (Abitibi) type, 683–686
  Oldest VMS, 705–711, *710*
  Tasmanian VMS, 687–693, *690*,
Vostok
  Lake, 14–15, 1033, 1197

W
Wairakei, 35, 424, 442, 501, 502, 1163
Water
  circulation, *4*,
  connate, 19, 53, 56, 74, 218, 440, 507, 699, 727, 817, 825, 900, 991, 1239
  extraterrestrial, 1131, 1165, 1182,
  juvenile, 2, 19–20, 54–56, 64, 74
  meteoric, 3, *4*, 13, 16, 19, 36, 53–56, 60, 74, 82, 111, 120, 206, 224, 241, *257*, 318, *364*, 376, 403, 422, 442, 495, 509, *833*, 836, 887, *942*, 971, 994, 1099, 1159
  metamorphic, 19–20, *55*, 56–57, 64, 74, 134, *170*, 218, 309, 469, *470*, 507, 514, 699, 839, 887, 896, *898*, 899, 900–903, 909, *942*, 943, 949–950, 953–955, 961, 972–973, 1108, *1225*,
White Island, 504–505
Witwatersrand, xxvi, xxx, 76, 171, 181, 190, 197–198, 684, 849, 910, 921, 935, 1063, 1065, 1098, 1106–1110, *1108*, 1218, 1222–1223, 1237

Y
Yangzte Craton, 400, 464, 475, 565, 566, 570, 575, 598, 946, 954, 976, 977
Yangzte River Valley, *see* Skarn
Yellowstone National Park, 507–517
Yerington, 549
Yilgarn Craton, 110, 133, 260, 275, 297, 419, 486, 492, 533, *554*, 555, 559, 584, 664, 703, 857, *886*, 910, 915, 985, 1112, 1115, 1118
  Lode Au in the Yilgarn Craton, 917, 919
Yukon, 262, *263*
Yulong ore belt, 414–416, 574
Yustid rift, 277

Z
Zaaiplaats, 231
Zambian Copperbelt, *see* Copperbelt
Zhilingtou, 468–473
Zijinshan, 472